ISBN: 978-3-95450-227-1 ISSN: 2673-5490 doi:10.18429/JACoW-IPAC2022-MOPLXGD1

THE SuperKEKB HAS BROKEN THE WORLD RECORD OF THE LUMINOSITY

Y. Funakoshi*, T. Abe, K. Akai, Y. Arimoto, K. Egawa, S. Enomoto, H. Fukuma, K. Furukawa, N. Iida, H. Ikeda, T. Ishibashi, S. Iwabuchi, H. Kaji, T. Kamitani, T. Kawamoto, M. Kikuchi, T. Kobayashi, K. Kodama, H. Koiso, M. Masuzawa, K. Matsuoka, T. Mimashi, G. Mitsuka, F. Miyahara, T. Miyajima, T. Mori, A. Morita, S. Nakamura, T. Nakamura, K. Nakanishi, H. Nakayama, A. Natochii, M. Nishiwaki, S. Ogasawara, K. Ohmi, Y. Ohnishi, N. Ohuchi, K. Oide, T. Okada, T. Oki, M. A. Rehman, Y. Seimiya, K. Shibata, Y. Suetsugu, H. Sugimoto, H. Sugimura, M. Tawada, S. Terui, M. Tobiyama, R. Ueki, X. Wang, K. Watanabe, R. Yang, K. Yoshihara, S. Yoshimoto, T. Yoshimoto, D. Zhou, X. Zhou, and Z. Zong,
KEK, 1-1 Oho, Tsukuba, Ibaraki 305-0801, Japan

Abstract

The SuperKEKB broke the world record of the luminosity in June 2020 in the Phase 3 operation. The luminosity has been increasing since then and the present highest luminosity is $4.65 \times 10^{34}\mathrm{cm}^{-2}\mathrm{s}^{-1}$ with β_y^* of 1 mm. The increase of the luminosity was brought with an application of crab waist, by increasing beam currents and by other improvements in the specific luminosity. In this paper, we describe what we have achieved and what we are struggling with. Finally, we mention a future plan briefly.

INTRODUCTION

The purpose of SuperKEKB is to search for a new physics beyond the standard model of the particle physics in the B meson regime. SuperKEKB consists of the injector Linac, a damping ring for the positron beam, two main rings; *i.e.* the low energy ring (LER) for positrons and the high energy ring (HER) for electrons and the physics detector named Belle II. The beam energies of LER and HER are 4 GeV and 7 GeV, respectively. The design beam currents of LER and HER are 3.6 A and 2.6 A, respectively. The design luminosity is $8 \times 10^{35}\mathrm{cm}^{-2}\mathrm{s}^{-1}$. More detailed parameters of SuperKEKB is described elsewhere [1]. The Phase 3 beam operation started in March 2019 and has continued until now. An initial report on the Phase 3 operation is shown elsewhere [2]. In this report, we summarize the progress of SuperKEKB after IPAC2020.

OPERATION HISTORY

The history of machine operation in Phase 3 is shown in Figure 1. In the figure shown are the history of the HER beam current, the LER beam current, the peak luminosity and the total integrated luminosity (delivered and recorded values) from the top to the bottom, respectively. Both in the beam currents and the luminosity, there has been a great progress since IPAC2020 held in May 2020. Table 1 shows a comparison of machine parameters in 4 cases. In comparison between the parameters at present (June 8th 2022) with those on May 1st 2020, the peak luminosity has increased about

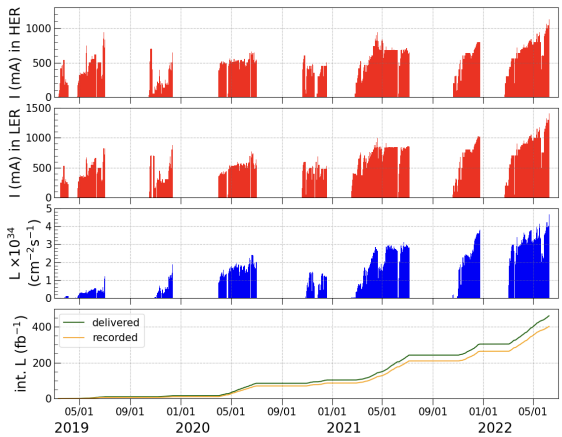

Figure 1: Operation history in Phase 3.

by a factor 3. This increase of the luminosity has been mainly brought by the increase in the beam currents and the improvement in the specific luminosity. In both cases β_y^* is the same value, 1 mm. With the similar bunch currents, the vertical beam-beam parameters have been improved. This indicates that the specific luminosity has been improved. In comparison between the parameters at present with those achieved by KEKB, the peak luminosity at present is more than twice higher than the achieved value at KEKB. But if we compare the present beam performance with the design values of SuperKEKB, we are still at an early stage of the project.

A comparison of the peak luminosity of various colliders as the function of the CMS (center-of-mass system) energy is shown in Figure 2. On June 17th 2009, KEKB set an luminosity record of $2.11 \times 10^{34}\mathrm{cm}^{-2}\mathrm{s}^{-1}$. This record was bettered by LHC in May 2018. On June 15th 2020, the luminosity of SuperKEKB broke the world records which had been set by LHC. The highest luminosity accomplished by SuperKEKB on June 8th 2022 is $4.65 \times 10^{34}\mathrm{cm}^{-2}\mathrm{s}^{-1}$.

* yoshihiro.funakoshi@kek.jp

ISBN: 978-3-95450-227-1 ISSN: 2673-5490 doi:10.18429/JACoW-IPAC2022-MOPLXGD2

PROGRESS TOWARDS DEMONSTRATION OF A PLASMA-BASED FEL

E. Chiadroni*
Dept. of Basic and Applied Sciences for Engineering - Sapienza, University of Rome
and INFN-LNF, Italy

Abstract

Plasma-based technology promises a revolution in the field of particle accelerators by pushing beams to gigaelectronvolt energies within centimeter distances. Several experiments are ongoing world-wide towards demonstration of a plasma based FEL enabling the realization of ultra-compact facilities for user applications like Free-Electron Lasers (FEL). The progress towards a plasma based FEL user facility is here reported, with particular focus on the recent results about the first experimental evidences of FEL lasing by both a particle beam-driven plasma accelerator at the SPARC_LAB test facility and a laser-driven plasma accelerator at SIOM. The status in the International scenario and prospects toward a plasma-based FEL are discussed.

MOTIVATION

Plasma-based accelerators, both laser and beam driven, have already demonstrated the ability to accelerate multi-GeV electrons in cm-scale plasma structures [1–4]. The current goal of the worldwide plasma, laser and photo-injector communities is to demonstrate the stable and repeatable acceleration of high brightness beams to drive a plasma-based user facility.

Owing to ultra-high accelerating gradients, combined with injection into micrometer-scale accelerating wakefield structure, plasma-based accelerators hold great potential to drive novel, smaller footprint light sources. Several advances, in particular focused on the optimization of the energy spread, have been done toward high quality plasma-accelerated beams paving the way to new generation of compact Free-Electron Lasers (FELs) based facilities. Two promising results on this topic are shown in Figs. 1 and 2, highlighting experiments performed at FLASHForward (DESY) [5] and at SPARC_LAB (LNF) [6].

Figure 1 demonstrates the preservation of the energy spread and the high efficiency acceleration, exploiting a strong beam loading when accelerating bunches with peculiar charge density profiles [7]; while Fig. 2 shows the reduction of the energy spread based on the assisted-beam loading technique: during the acceleration, the witness longitudinal phase space (LPS) is rotated and energy spread reduced by 40% with respect to the initial value. The energy chirp imprinted on the witness is thus used to both improve its beam loading and compensate the slope of the plasma wakefield, so that it can be considered an assisted beam-loading energy spread compensation [8].

To drive a plasma-based FEL facility the quality of the accelerated beam must not be degraded in the plasma, since

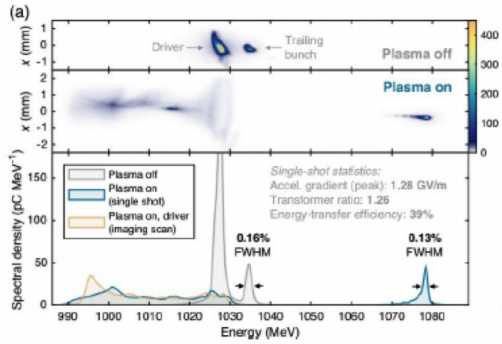

Figure 1: Preservation of the energy spread and the high efficiency acceleration based on strong beam loading induced by peculiar charge density profiles [7].

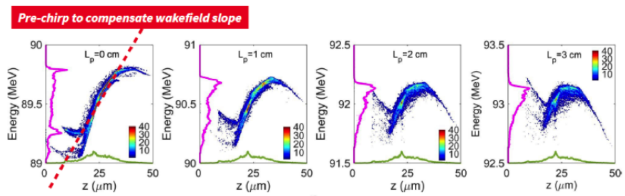

Figure 2: Witness beam longitudinal phase space: minimization of energy spread based on assisted beam loading technique [8].

the requirements on the 6D phase space to operate a FEL must be guaranteed. In particular, the following conditions on transverse normalized emittance, peak current and energy spread must be satisfied:

$$\varepsilon_n \ll \text{mm mrad}, \text{I} \approx \text{kA}, \frac{\Delta\gamma}{\gamma} \ll 1\%.$$

Indeed many of these properties are described by the 1D model of the FEL interaction and are related to the so-called Pierce parameter

$$\rho = \frac{1}{2\gamma}\left[\frac{I}{I_A}\left(\frac{\lambda_u K[JJ]}{\sqrt{8}\pi\sigma_x}\right)^2\right]^{1/3}, \quad (1)$$

which determines the 1D gain length, $L_g = \frac{\lambda_u}{4\sqrt{3}\pi\rho}$, giving an estimation of the saturation power, $P_{sat} = P_{in}e^{z/L_g}$; γ is the Lorentz factor of the beam, I the peak current, $I_A = 17$ kA the Alfven λ_u the undulator period, K defines the maximum angle of the emitted radiation with respect to the axis, $[JJ]$ is the Bessel factor, defined as the difference between the J_0 and J_1 Bessel functions of an argument ξ that depends on K, and σ_x the rms beam transverse size.

In addition for driving plasma-based FEL, the long term and the shot-to-shot stability and reproducibility are issues to overcome and finally the high repetition rate would be

* enrica.chiadroni@uniroma1.it

ISBN: 978-3-95450-227-1 ISSN: 2673-5490 doi:10.18429/JACoW-IPAC2022-MOPLXGD3

THE ACCELERATOR AND BEAM PHYSICS OF THE MUON g-2 EXPERIMENT AT FERMILAB

D. A. Tarazona*, Cornell University, Ithaca, NY, USA

Abstract

The physics case of the Muon g-2 Experiment at Fermilab is outstanding and has recently attracted significant attention from its first official results. Although its measurements involve high energy physics methods, such as counting positron production rates with the use of calorimeters and beam diagnostics with tracking detectors, this experiment is strongly bound to accelerator and beam physics. This paper reviews the principles of the experiment and the details necessary to provide a solid ground for the beam-dynamics uncertainties and the corrections of the systematic effects influencing the output of the experiment: a single numerical value, which may unveil new physics.

INTRODUCTION

The Fermi National Accelerator Laboratory (Fermilab) Muon g-2 Experiment (E989) recently yielded its first measurement of the positive muon magnetic anomaly, $a_\mu \equiv (g_\mu - 2)/2$, with an experimental relative uncertainty of 0.46 parts per million (ppm) [1]. This result from the "Run-1" dataset, combined with the previous result from Brookhaven National Laboratory (BNL) [2], differs from the current Standard Model (SM) prediction [3] by 4.2 standard deviations. The error budget of the g-2 experiment (0.14 ppm to strongly establish evidence for new physics) requires the production of a highly polarized muon beam with momentum 3.094 GeV/c and sufficient intensity to collect more than twenty times the number of recorded high-energy positrons from the previous experiment at BNL [4].

In addition, the storage ring is designed to allow for precise measurements and maintain a uniform evolution of the two main frequencies from which a_μ is extracted, i.e., $a_\mu \propto \omega_a/\tilde{\omega}'_p(T_r)$. The frequency $\tilde{\omega}'_p(T_r)/2\pi \approx 61.7$ MHz is the proton Larmor frequency measured in a spherical water sample at a temperature $T_r = 34.7\,^\circ$C, weighted by the muon distribution [5]. Such frequency, directly proportional to the magnetic field experienced by the stored muons, regulates the magnitude of the anomalous precession frequency, $\omega_a/2\pi \approx 0.23$ MHz, which, under design conditions, corresponds to the spin-precession frequency relative to the cyclotron frequency in the laboratory frame [6].

In the following sections, an overview of the accelerator complex at Fermilab, the Muon Campus, for the production and delivery to the storage ring of the muon beam; a description of the main components of the storage ring directly related to the goals of the muon g-2 experiment from the beam dynamics front; and the beam-dynamics systematic corrections in the experimental measurement are presented.

* dtarazona@cornell.edu

MUON CAMPUS

The Muon Campus at Fermilab, depicted in Fig. 1, is a series of approximately 1 km-long beamlines between a "pion production" target and the entrance of the Muon g-2 Storage Ring that was designed to meet the statistical goal and deliver $(0.5\text{–}1.0)\times10^5$ highly polarized muons per 10^{12} protons that arrive at the pion production target [4]. Batches of four/eight

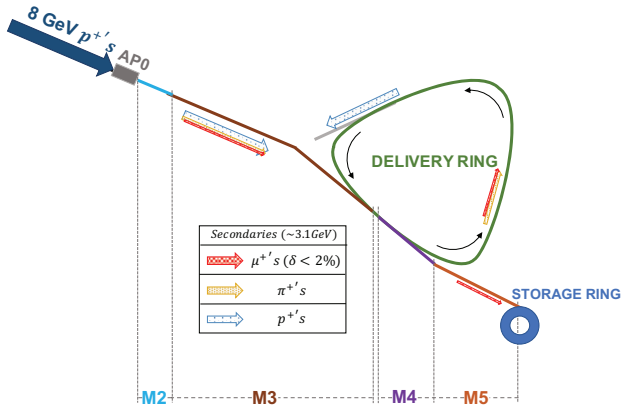

Figure 1: A schematic layout of the Muon Campus [7]. Secondary particles (mostly pions, muons, and protons) downstream of the target station at AP0 are canalized through the M2/M3 lines and injected into the Delivery Ring (DR), where protons are discarded and most of the remaining pions decay after four turns. A beam of mostly muons is extracted to the M4/M5 lines and ultimately delivered to the Muon g-2 Storage Ring.

8.9 GeV/c proton bunches are directed to an Inconel-600 pion production target—an alloy of iron, chromium, and nickel—located at Fermilab's AP0 target hall from which positive secondary particles emerge. A magnetic quadrupole triplet focuses the proton pulses upstream of the production target to a transverse size of about 150 µm to minimize beam loss. Mostly pions with momentum acceptance of ±2 % around 3.094 GeV/c are collected and transported along FODO channels, bending magnets, and quadrupole arrangements for dispersion suppression, with an overall transverse acceptance of 40π mm.mrad, supported by the beamline apertures of the Muon Campus.

Most of the muon beam emerges via the $\pi^+ \rightarrow \mu^+\nu_\mu$ weak-decay channel. As the emitted muons are completely polarized in the pion rest frame and the Muon Campus beamlines impose a stringent momentum acceptance, only highly polarized muons are transported to the storage ring.

ISBN: 978-3-95450-227-1 ISSN: 2673-5490 doi:10.18429/JACoW-IPAC2022-MOIYGD1

PROGRESS IN DEVELOPING AN ACCELERATOR ON A CHIP*

R. J. England†, SLAC National Accelerator Laboratory, Menlo Park, CA USA
P. Hommelhoff, Friedrich Alexander University, Erlangen, Germany
R. L. Byer, Stanford University, Stanford, CA USA

Abstract

Acceleration of particles in photonic nanostructures fabricated using semiconductor manufacturing techniques and driven by ultrafast solid state lasers is a new and promising approach to developing future generations of compact particle accelerators. Substantial progress has been made in this area in recent years, fueled by a growing international collaboration of universities, national laboratories, and companies. Performance of these micro-accelerator devices is ultimately limited by laser-induced material breakdown limits, which can be substantially higher for optically driven dielectrics than for radio-frequency metallic cavities traditionally used in modern particle accelerators, allowing for 1 to 2 order of magnitude increase in achievable accelerating fields. The lasers required for this approach are commercially available with moderate (micro-Joule class) pulse energies and repetition rates in the MHz regime. We summarize progress to date and outline potential near-term applications and offshoot technologies.

INTRODUCTION

Constraints on the size and cost of accelerators have inspired a variety of advanced acceleration concepts for making smaller and more affordable particle accelerators. The use of lasers as an acceleration mechanism is particularly attractive due to the intense electric fields they can generate combined with the fact that the solid state laser market has been driven by extensive industrial and university use toward higher power and lower cost over the last 20 years. Dielectrics and semiconductor materials have optical damage limits corresponding to acceleration fields in the 1 to 10 GV/m range, which is orders of magnitude larger than in conventional accelerators. Such materials are also amenable to rapid and inexpensive CMOS and MEMS fabrication methods developed by the integrated circuit industry. These technological developments over the last two decades, combined with new concepts for efficient field confinement using optical waveguides and photonic crystals, have inspired an international community of university, government laboratory, and industrial researchers to develop on-chip integrated particle accelerators driven by micro-Joule to milliJoule class infrared lasers, which we refer to as *dielectric laser accelerators* (DLA).

As an advanced accelerator concept, the DLA approach offers some unique advantages. The acceleration mechanism is inherently linear and occurs in a vacuum region in a static structure. In addition to the stability benefits this affords, the acceleration effect is inherently dependent on the phase of the laser field, which makes it possible to dynamically fine-tune accelerator performance by manipulation of the incident laser phase profile. Gradients on the GV/m scale have already been demonstrated with energy gains exceeding 0.3 MeV for a few-fC beam, and wall plug efficiencies comparable or superior to conventional approaches appear feasible. The primary supporting technologies (solid state lasers and nanofabrication) are mature and already at or near the capabilities required to develop an integrated on-chip accelerator based on this approach. Development of near-term applications in medicine, science, and industry could utilize the unique capabilities of these sources while providing platforms for further technological development.

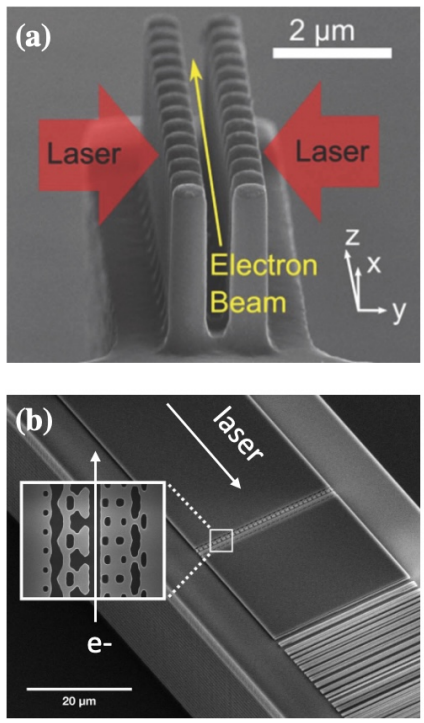

Figure 1: Recently demonstrated DLA structures based on (a) the dual-pillar design [1] and (b) an optical waveguide-coupled approach utilizing computer-aided *inverse design* to produce highly optimized structures [2].

STATE OF THE ART IN ON-CHIP PARTICLE ACCELERATORS

The field of particle acceleration using laser-driven dielectric structures has undergone significant experimental progress within the last decade. In 2013, the first demonstra-

* Work supported by the Gordon and Betty Moore Foundation
† england@slac.stanford.edu

ISBN: 978-3-95450-227-1 ISSN: 2673-5490 doi:10.18429/JACoW-IPAC2022-MOOYGD2

THE AWAKE EXPERIMENT IN 2021: PERFORMANCE AND PRELIMINARY RESULTS ON ELECTRON-SEEDING OF SELF-MODULATION

E. Gschwendtner†, L. Verra, G. Zevi Della Porta, CERN, Geneva, Switzerland
P. Muggli, Max-Planck Institute for Physics Munich, Munich, Germany
for the AWAKE Collaboration

Abstract

The future programme of the Advanced Wakefield (AWAKE) experiment at CERN relies on the seeded self-modulation of an entire proton bunch, resulting in phase-reproducible micro-bunches. This important milestone was achieved during the 2021 proton run by injecting a short electron bunch ahead of the proton bunch, demonstrating for the first time the electron-seeding of proton bunch self-modulation [1]. This paper describes the programme, performance and preliminary results of the AWAKE experiment in the 2021 proton run and introduces the programme of the 2022 proton run.

INTRODUCTION

AWAKE is an accelerator R&D experiment to demonstrate plasma wakefield acceleration of electrons in wakefields driven by a proton bunch and, in the future, take advantage of the large energy store in the proton bunch to reach very high energy gain in a single plasma for first particle physics applications using plasma wakefield acceleration. During its first run period (2016 – 2018) AWAKE observed the strong modulation of high-energy proton bunches in plasma, which demonstrated for the first time that strong wakefields are generated by proton beams [2-4]. In addition, the acceleration of externally injected electrons to multi-GeV energy levels in the proton driven plasma wakefields [5] was demonstrated.

The goal of the AWAKE Run 2 programme [6, 7] which started in 2021, is to produce high-charge bunches of electrons accelerated to high energies (~10 GeV) while maintaining beam quality as well as to demonstrate the scalability of this process.

In order to accelerate with low energy spread, an accelerated bunch charge of at least 100 pC and an emittance control at the 10 mm-mrad level, the scheme of AWAKE Run 2 includes two plasma sources, i.e. a self-modulator and an accelerator, and a new electron beam system. In the first plasma source the proton beam self-modulation (SM) is seeded by an electron bunch [6] and modulates along the entire bunch. The self-modulation process must reach saturation before electrons are injected for acceleration in the second plasma source.

The roadmap for AWAKE Run 2 is well-defined and is subdivided in four phases spanning over several years [7].

The programme of the first phase, Run 2a (2021-2022), focusses on the demonstration of the self-modulation of the entire proton bunch reproducibly seeded by an electron bunch.

† edda.gschwendtner@cern.ch

Seeded Self-Modulation

The self-modulation instability (SMI) is a self-consistent process, where the wakefields driven in plasma by a long, narrow, relativistic, charged particle bunch act back on the bunch itself, modulating its transverse distribution along the bunch. The modulated distribution drives enhanced wakefields, initiating a feed-back loop that converts the bunch into a train of micro-bunches. Hence, the timing of the micro-bunch train along the bunch is tied to that of the transverse wakefields: the micro-bunches develop in their focusing phase. When a long ($\sigma_t \sim 240$ ps) proton bunch enters a pre-ionized plasma with a much shorter plasma wavelength, it undergoes the self-modulation instability. SMI develops from the noise [8] or from the imperfections [4] in the proton bunch charge distribution. Thus, it is neither reproducible in amplitude nor in timing from event to event [4]. However, when a seed wakefield is applied, SM grows from the initial modulation of the radius along the bunch caused by the seed wakefields: the timing and initial amplitude of SM is then defined by the seed wakefields.

During AWAKE Run 1, seeding was obtained by placing the ionizing laser pulse (that generates the plasma) within the proton bunch. The fast onset of the beam-plasma interaction was therefore driving the seed wakefields. This method has the advantage of the inherent alignment between the proton bunch and the plasma, avoiding the hosing instability, but it has the disadvantage of leaving the front of the bunch unmodulated, because it travels as if in vacuum. Since the final stage of the AWAKE experiment (Run 2c and Run 2d) is composed by two plasmas (the first one being the modulator, the second the accelerator [7]), the unmodulated front of the bunch may self-modulate in the second (preformed) plasma and disrupt the structure of the self-modulated back of the bunch. Therefore, the entire proton bunch must be self-modulated with reproducible timing and amplitude, when entering the accelerator section. This can be obtained only if the seed wakefields act on the entire proton bunch.

In AWAKE Run 2, the SM process is achieved by seeding SM with an electron bunch preceding the proton bunch.

Experimental Layout

The experimental layout is shown in Fig. 1. For the experiments during 2021/22 the same infrastructure as that of AWAKE Run 1 can be used. In addition, the 18 MeV electron beam coming from the existing electron injector of Run 1 can be used for seeding. The experiment uses a 400 GeV/c proton bunch from the CERN SPS, with a rms bunch length of ~240 ps, to drive wakefields in a 10 m-long rubidium plasma section with a plasma electron

ISBN: 978-3-95450-227-1 ISSN: 2673-5490 doi:10.18429/JACoW-IPAC2022-MOIYSP2

TOUSCHEK AND INTRABEAM SCATTERING IN ULTRALOW EMITTANCE STORAGE RINGS

R. Bartolini, DESY, Hamburg, Germany

Abstract

In next-generation synchrotron radiation sources targeting extremely low emittance around the so-called diffraction limit, the Touschek and intrabeam scattering (IBS) effects are important factors determining the performance of the facility. As the emittance decreases, the bunch volume decreases and the Touschek beam lifetime also decreases. However, this downward trend in beam lifetime is expected to turn to increase in the emittance region below a certain threshold. Since this threshold is determined by the emittance at equilibrium including the IBS effect, a self-consistent treatment is necessary for a correct and unified understanding of the beam characteristics. In currently operating facilities, such as MAX-IV, or in next-generation light sources under construction or in the planning stages, it is expected that such effects may be observed depending on the operating conditions. This talk will be reviewing Touschek and IBS Effects in terms of how these effects limit the ring performance.

INTRODUCTION

In the last 10 years the synchrotron light sources community has taken a decisive step towards the construction or the upgrade of facilities operating quasi-diffraction limited storage rings. Design emittance in the order of 100 pm are common to many lattice designs, exploiting the concept of multi-bend achromats (MBA) or variations thereof. The optimisation of such ring design is notoriously difficult in terms of single particle dynamics to guarantee basic operational parameters such as injection efficiency and beam lifetime. At the same time operation at high current poses further challenges in the control of collective effects and IBS. Two basic limitations in the performance of such rings, namely the Touschek lifetime and the emittance growth due to IBS, stem from the same basic physics mechanism, i.e. electron-electron scattering within the electrons in a bunch.

TOUSCHEK AND IBS THEORY

Electron-electron scattering occurring between electrons performing betatron oscillations within a bunch can transfer significant momentum from the transverse to the longitudinal plane. The analysis of the scattering in the CM of the two electrons show that the conservation of momentum allows event where the whole transverse momentum px is scattered in the longitudinal plane. When transferred back to the LAB frame the longitudinal component acquires a multiplicative factor γ, given by the relativistic factor of the electron bunch. This can be a significant portion of the total energy E_0 of the beam. If the acquired longitudinal momentum is outside the momentum aperture ε_{MA} of the lattice, the particles are lost. This is the Touschek scattering. If the momentum acquire is within ε_{MA}, the particles survive the scattering event but the sudden exchange in momentum creates an excitation effect on the dynamics which is the core reason for the IBS effect. In short

$p_x\gamma > \varepsilon_{MA}$ Touschek scattering
$p_x\gamma < \varepsilon_{MA}$ Intrabeam scattering

Touschek Scattering

The analysis of Touschek scattering aims at providing expression for the rate of particle loss and the Touschek lifetime of the beam. Starting from the electron-electron differential scattering cross section, we compute the total cross section for the events that produce a longitudinal momentum outside of the momentum aperture. Since the total cross section refers to a fixed momentum incident flux on a single target, the calculation for a real beam requires its computation over the phase space distribution of the electrons to yield the rate of particle loss. A common expression for the Touschek lifetime is given by the celebrated Bruck formula [1] cast in the form

$$\frac{1}{\tau} = \frac{N r_0^2 c}{8\pi\sigma_x\sigma_y\sigma_s}\frac{1}{\gamma^2\delta_{MA}^3}D(\xi) \qquad (1)$$

where N is the number of electrons per bunch, $\sigma_{x,y,s}$ the rms dimension of the bunch, δ_{MA} the momentum aperture, and

$$\xi = \left(\frac{\delta_{MA}}{\gamma\sigma_{p_x}}\right)^2$$

where $D(\xi)$ is the function

$$D(\xi) = \sqrt{\xi}\left[-\frac{3}{2}e^{-\xi} + \frac{\xi}{2}\int_{\xi}^{\infty}\frac{\ln u \times e^u}{u}du + \frac{1}{2}(3\xi - \xi\ln\xi + 2)\int_{x}^{\infty}\frac{e^{-u}}{u}du\right]$$

Equation (1) provides the dependence of the Touschek lifetime over the electron beam parameters and the main machine parameters. It is proportional to the current stored in the bunch via N, to the bunch volume $V = \sigma_x\sigma_y\sigma_s$, to the momentum aperture δ_{MA} appearing also in the argument of D, and on the rms of the transverse momentum σ_{px}. This last term can be expressed in terms of the emittance and the optics functions, e.g. neglecting dispersion it is simply $\sigma_{px} = \sqrt{(\varepsilon_x/\beta_x)}$ whereby $\xi = \delta_{MA}^2\beta_x/\gamma^2\varepsilon_x$. It is interesting to observe that the function $D(\xi)$ reported in Figure 1, has a relatively flat behaviour for values of x that are typical of third generation light sources, while it shows a sharp decrease

ISBN: 978-3-95450-227-1 ISSN: 2673-5490 doi:10.18429/JACoW-IPAC2022-MOOYSP1

IMPACT OF LONGITUDINAL GRADIENT DIPOLES ON STORAGE RING PERFORMANCE*

F. Zimmermann†, Y. Papaphilippou, A. Poyet, CERN, Meyrin, Switzerland

Abstract

Innovative new magnets with longitudinally varying dipole field are being produced for installation in a few modern light-source storage rings. We investigate some of the associated beam-dynamics issues, in particular the photon spectrum and quantum fluctuation associated with such magnets, and we study whether the resulting equilibrium emittance may deviate from the value expected in the long-magnet limit.

INTRODUCTION

Dipole magnets with longitudinally varying bending field are proposed to minimise the emittance, or cost, of linear collider damping rings [1] and storage-ring light sources [2–6]. A "trapezium" magnet was designed that could provide a factor ~7 emittance reduction for the CLIC Damping Rings [7, 8]. A similar magnet is being considered for reducing the horizontal emittance of the ELETTRA 2.0 light source by almost a factor of two [9].

The approach of tailoring the dipole field with longitudinal position is based on the standard expression for the horizontal equilibrium emittance (assuming separate function magnets and no linear coupling)

$$\varepsilon_x = C_q \gamma^2 I_5 / I_2 \ , \tag{1}$$

with $C_q = (55/(32\sqrt{3})\hbar c/(m_e c^2)$ (m_e electron mass, c speed of light, $\hbar$ the reduced Planck constant), the radiation integrals [10] $I_2 = \int 1/\rho(s)^2 ds$ and $I_5 = \int \mathcal{H}_x(s)/\rho(s)^3 \ ds$, where the integrals are evaluated around the storage ring, $\rho(s)$ designates the local bending radius, and $H_x(s) = \beta_x D_x'^2 + 2\alpha_x D_x D_x' + \gamma_x D_x^2$ the value at location s of the "curly-H" function defined by Sands [11]. The integral I_2 is related to the energy loss per turn, and the integral I_5 describes the quantum excitation. The dipole field is varied longitudinally to minimise the ratio I_5/I_2 and, hence, the emittance.

Specifically, when choosing the same cell length and betatron phase advances as in a conventional lattice and assuming a practical maximum field, the variational bend "TME" lattice was shown to reduce the storage ring emittance by a factor of 2–3, without a significant change in the dynamic aperture [1]. Reference [1] also pointed out that, alternatively, one could use variational bends to obtain the same emittance as with constant bends, while reducing the number of cells by 25% to 30%, which might lead to a larger dynamic aperture, a larger momentum compaction, and shorter circumference, as was achieved for the CLIC Damping Rings [8].

CLASSICAL QUANTUM EXCITATION

The radiation integral I_5 in Eq. (1) stems from the classical quantum excitation due to photon emission in a constant magnetic field [11]

$$\Delta\varepsilon_x = \int \dot{N}_{\rm ph} \left\langle u^2 \right\rangle \mathcal{H}_x \ ds \ . \tag{2}$$

The "long-magnet" photon spectrum for a single electron passing through a magnet with constant field B_0 and length $2L$ is given by

$$\frac{dN_{\rm ph}}{d\nu} = \frac{4 r_e e}{9\hbar} \frac{B_0 2L}{\nu} S\left(\frac{\nu}{\nu_c}\right) \ , \tag{3}$$

with

$$S\left(\frac{\nu}{\nu_c}\right) = \frac{9\sqrt{3}}{8\pi} \frac{\nu}{\nu_c} \int_{\nu/\nu_c}^{\infty} K_{5/3}(x') dx' \ , \tag{4}$$

$\nu_c = (3/2) c\gamma^3 B_0 e/p$, and r_e the classical electron radius.

The mean-square photon energy is $\left\langle u^2 \right\rangle = (11/27)\epsilon_{\rm cr}^2$ with critical photon energy $\epsilon_{\rm cr} = (3/2)\hbar c\gamma^3/\rho$, and $\dot{N}_{\rm ph} = (15\sqrt{3}/8) P_\gamma/\epsilon_{\rm cr}$, with $P_\gamma = cC_\gamma/(2\pi)E^4/\rho^2$, E the beam energy, $C_\gamma = (4\pi/3) r_e/(m_e c^2)^3$ and $1/\rho = B_0 e/p$. Note that $S(u)$ is normalized such that $\int_0^\infty S(u) du = 1$ and $\int_0^\infty (1/u) S(u) du = 45/(8\sqrt{3})$.

LONGITUDINAL GRADIENT DIPOLES

For a magnet with varying dipole field $B_y(s)$, from Eq. (3) the magnetic field variation can be taken into account as

$$\frac{d^2 N_{\rm ph}}{d\nu \ ds}(s) = \frac{4 r_e e}{9\hbar} \frac{B_y(s)}{\nu} S\left(\frac{\nu}{\nu_c(s)}\right) \ , \tag{5}$$

where now $\nu_c(s) = (3/2) c\gamma^3 B_y(s) \ e/p$. Integrating over the magnet length $2L$ we obtain the classical photon spectrum for this dipole

$$\frac{dN_{\rm ph}}{d\nu} = \int_{-L}^{L} \frac{d^2 N_{\rm ph}}{d\nu \ ds}(s) ds \ . \tag{6}$$

However, there may be a limitation to this approach. For a dipole magnet with non-constant field, we can define an effective "local" magnet length as

$$l_{\rm eff}(s) \approx B_y(s) / \left| dB_y(s')/ds' \right|_{s'=s} \ , \tag{7}$$

while the emission "source length" of synchrotron radiation is of order $l_{\rm source} \sim \pm\rho/\gamma$, where $\rho(s) = p/(eB_y)$. In the

* Work partially supported by the European Union's Horizon 2020 Research and Innovation programme under Grant Agreement No. 101004730 (iFAST).
† frank.zimmermann@cern.ch

ISBN: 978-3-95450-227-1 ISSN: 2673-5490 doi:10.18429/JACoW-IPAC2022-MOOYSP2

MEASUREMENTS OF COLLECTIVE EFFECTS RELATED TO BEAM COUPLING IMPEDANCE AT SIRIUS

F. H. de Sá*, M. B. Alves, L. Liu, Brazilian Synchrotron Light Laboratory, Campinas, Brazil

Abstract

SIRIUS is the new storage-ring-based 4th generation synchrotron light source built and operated by the Brazilian Synchrotron Light Laboratory (LNLS) at the Brazilian Center for Research in Energy and Materials (CNPEM). In ultralow emittance storage rings such as SIRIUS, the small radius of the vacuum chamber gives rise to strong beam coupling impedances which significantly alter the beam dynamics. In this work, we present the single-bunch measurements made so far to characterize such effects and compare the results with those simulated using the impedance budget built during the storage ring design.

INTRODUCTION

SIRIUS is the new Brazilian synchrotron light source based on a 3 GeV electron storage ring, comprising a 20-cell 5BA magnetic lattice with 250 pm rad emittance. It is one of the three 4th generation storage-ring-based light sources in operation worldwide. Information regarding the commissioning results and current operation status can be found in references [1, 2].

The standard storage ring vacuum chamber is cylindrical with 12 mm of inner radius and made of copper. Almost all chambers are coated with non-evaporable getter (NEG) [3, 4] with a thickness of 1.0 µm, including all five 6 mm-gap aluminum chambers for the commissioning undulators [5]. Such small chambers give rise to strong beam coupling impedances not only due to the finite conductivity of the materials, but also because of inner transitions and cross section changes originated by special devices. For this reason, the design of every device of the storage ring was optimized not only based on its vaccum performance but also on the additional impedance it creates [6–11].

Details about the impedance budget can be found in references [12, 13]. The resistive wall and longitudinal coherent synchrotron radiation impedances and wakes were evaluated using semi-analytical approaches [14, 15] and refer to the system response to a point-like charge, which may turn time-domain simulations challenging due to the longitudinal grid discretization. For this reason all these wakes were convoluted with a 40 µm Gaussian distribution to remove high frequency components. On the other hand, the geometric wakes were computed using numerical solvers of Maxwell equations [16–19] and thus refer to the system response to a Gaussian bunch. Since in this work we will deal with single-bunch effects, all simulations were performed with a wake-length of 0.4 m and a source bunch with length of 0.5 mm. They were used as it is in time-domain simulations and their impedances were calculated up to 150 GHz for frequency domain simulations. The impedance budget used here reflects the current status of the machine, including models for all in-vacuum components, except one: the temporary Petra 7-Cell cavity that is currently being used. Instead, the broadband contribution of the still not installed superconducting cavities is included.

It is important to note that all comparisons of the results predicted by the impedance budget with measurements presented in this work were performed using the impedances and wakes calculated directly from 2D and 3D models of the vacuum chamber components, without any kind of fitting of effective models such as resonators, resistive and inductive impedances or scaling of the budget to fit the data. The main idea is not only to characterize the storage ring and create a model to describe its dynamics, but also to evaluate the methodology applied along the last few years to compose the impedance budget and to have an indication of how predictive this kind of approach could be for future machines and also for the next components to be installed in the storage ring.

LONGITUDINAL DYNAMICS

We performed bunch length measurements with a recently installed Hamamatsu C5680 dual-axis streak camera in two occasions. The first data set (Data Set 1) was acquired with a single-bunch in the machine using the streak camera in single scan mode in its highest resolution configuration. The bunch charge was varied by inducing partial current losses with our horizontal pinger and the bunch distribution was retrieved as function of the current. The second data set (Data Set 2) was acquired with a different setup: two bunches were injected, one in bucket 1 with high initial charge (2.3 mA) and other in bucket 431 with very low current (20 µA). Since the fast scan frequency of our camera is 1/4 of the RF frequency, it is possible to see every other bucket simultaneously with alternating vertical positions on the camera. With this setup we can not only measure the longitudinal distribution of the high charge bunch, but also its synchronous phase variation with current, since the low charge bunch serves as a time reference. This idea was already discussed in the literature [20] and it is known for compensating jitter between the RF system and the synchroscan unit of the camera, so that the average position of both bunches provide the synchronous phase shift information of the high charge one. The disadvantage of this setup is that the resolution for bunch length is compromised because we need to operate the camera with a different scale to see both bunches.

In both scenarios the measurements were performed with an integration time of 100 ms to improve resolution. Even though this long exposure time does increase the measured

* fernando.sa@lnls.br

ISBN: 978-3-95450-227-1 ISSN: 2673-5490 doi:10.18429/JACoW-IPAC2022-MOPOST001

PERFORMANCE OF AUTOMATED SYNCHROTRON LATTICE OPTIMISATION USING GENETIC ALGORITHM*

X. Zhang†, S. L. Sheehy[1], The University of Melbourne, Melbourne, Australia
[1]also at Australian Nuclear Science and Technology Organisation (ANSTO), Sydney, Australia

Abstract

Rapid advances in superconducting magnets and related accelerator technology opens many unexplored possibilities for future synchrotron designs. We present an efficient method to probe the feasible parameter space of synchrotron lattice configurations. Using this method, we can converge on a suite of optimal solutions with multiple optimisation objectives. It is a general method that can be adapted to other lattice design problems with different constraints or optimisation objectives. In this method, we tackle the lattice design problem using a multi-objective genetic algorithm. The problem is encoded by representing the components of each lattice as columns of a matrix. This new method is an improvement over the neural network based approach in terms of computational resources. We evaluate the performance and limitations of this new method with benchmark results.

INTRODUCTION

The high level goal of this work is to assess whether the 'art' of lattice design can be economically achieved by a computer without assuming existing standard lattice configurations known to accelerator physicists. This paper is a continuation of the effort to develop an automated lattice optimisation algorithm. In the previous implementation of this algorithm [1], a neural network based approach was used to generate new lattice structures. There were two main problems with the neural network based approach. Firstly, new lattices were generated piece-wise based on a feedback loop controlled by tracking the motion of a test particle. This required each successful neural network to have *a priori* encoded values to produce the exact feedback values in order to create a desirable lattice. This is possible in principle, however this system is an overly complicated mapping between the optimisation quantities and the actual machine lattice structure. Secondly, the neural networks are very sensitive to small perturbations of the node values and resulted in drastically different lattice structures. Therefore it becomes computationally expensive to optimise the neural network values for target lattice structures with a large number of elements. The work for this paper tackles both of these problems by introducing a different method for generating lattices. In addition, the newest version of the genetic algorithm was implemented to improve the performance when optimising higher dimensional objectives.

* Work supported by Australian Government Research Training Program
† xuanhaoz@student.unimelb.edu.au

LATTICE MATRIX ENCODING

One major challenge with applying any kind of optimisation algorithm is how to represent the problem and parse it to the algorithm, this is referred to as the encoding of the problem. A matrix encoding method was used in this work, such that any lattice structure with n elements and at most p attributes per element can be represented by a $p \times n$ matrix. For example, a simple FODO cell with separate function dipole magnets is represented by an 8×4 matrix as shown in Fig. 1. Each column explicitly represents a different element of the lattice including empty drift spaces (E). The rows encapsulate all the attributes needed to describe every element in the lattice, where *k0* and *k1* are the dipole and quadrupole coefficients as used by MADX [2].

Element	QF	E	B	E	QD	E	B	E
k0	0	0	1.07	0	0	0	1.07	0
k1	0.23	0	0	0	-0.23	0	0	0
Length	0.3	0.43	0.87	0.43	0.3	0.43	0.87	0.43

Figure 1: Example matrix encoding of a FODO cell with separate function dipoles.

It should be noted that this matrix encoding can include any number of attributes by adding more rows, such as higher order coefficient terms of non-linear magnets. Also, it does not matter to the optimisation algorithm where the actual starting point of the lattice is defined. This property is particularly useful when optimising for a periodic structure such as a ring.

As part of the optimisation algorithm, the aim is to probe as much of the available parameter space as possible. In other words: to explore lattice configurations that we might not think would be stable based on our experience. This calls for a method to randomly sample from the entire parameter space that is bounded by a few basic design requirements such as the total bending angle or betatron tune. Note that there is no constraint on the number of magnetic elements or the total length of arc. Using the matrix encoding method, it is possible to initialise a collection of random lattice structures by building the lattices one element at a time. This means, starting each lattice matrix from a randomly chosen element (drift, dipole, quadrupole, or combined function dipole) and randomly choosing the attribute values necessary for that element. This process is repeated by adding new columns to the lattice matrices until the total bending angle of the lattice exceeds the requirement.

ISBN: 978-3-95450-227-1 ISSN: 2673-5490 doi:10.18429/JACoW-IPAC2022-MOPOST003

BBQ AND DOUGHNUT BEAMS: A TASTY RECIPE FOR MEASURING AMPLITUDE DEPENDENCE OF THE CLOSEST TUNE APPROACH

E. H. Maclean F. S. Carlier, T. H. B Persson, R. Tomás, CERN, Geneva, Switzerland

Abstract

Beam-based observations and theoretical studies have demonstrated the existence of a significant amplitude dependence of the closest tune approach (ADECTA) in the LHC. This effect has the potential to generate significant distortion of the tune footprint and thus is of interest in regard to Landau damping. Conventionally ADECTA has been studied through saturation of tune separation with action during amplitude-detuning type measurements. In this paper, an alternative measurement technique is proposed and results of initial tests with beam are presented. The novel technique attempts to measure ADECTA by performing a classical closest approach tune scan, using proton beams in the LHC, which have been kicked and allowed to decohere, effectively giving a large action doughnut beam. It is shown that the tune and closest approach of the doughnut beams can be measured using the existing LHC Base-Band tune (BBQ) measurement system, and an amplitude dependence can be observed.

AMPLITUDE DEPENDENT CLOSEST TUNE APPROACH

Linear coupling creates a closest tune approach (ΔQ_{min}) of the fractional tunes ($Q_{x,y}$), equal to the linear coupling coefficient ($|C^-|$) [1]. During amplitude detuning measurements of the LHC at injection in 2012, a highly non-linear change of $Q_{x,y}$ with action ($J_{x,y}$) was seen for kicks detuning towards $Q_x - Q_y = 0$, with similar effects observed in best-knowledge LHC models [2]. The nonlinearity of detuning was sensitive to initial working point and not explained by expected dodecapole or higher-order errors [2]. By observing the change of tune-split with action ($\frac{\partial|Q_x-Q_y|}{\partial 2J}$) as opposed to detuning with action ($\frac{\partial Q_{x,y}}{\partial 2J}$) this unexpected pattern of detuning was identified with a saturation of the fractional tune-split as a function of kick amplitude. An example of saturation of tune-split versus J_y is shown in Fig. 1. The observed saturation however, occurred for ΔQ far in excess of the measured $|C^-|$. It was therefore proposed that the measurements could be interpreted as an amplitude dependence of the closest tune approach [2]. That is: $\Delta Q_{min} \neq |C^-|$ but instead is a function of the linear coupling and actions $\Delta Q_{min}(J_x, J_y)$.

Simulation studies subsequently identified the main source of amplitude dependent closest tune approach (ADECTA) as the combination of linear coupling with strongly powered Landau octupoles '*MO*' (used for damping of instabilities) [3]. A theory for the mechanism was proposed via the interaction of linear coupling with the h_{1111} Hamiltonian coefficient generated by normal octupoles [4]. h_{1111} (related to cross-term detuning, $\partial Q_{x,y}/\partial J_{y,x}$) can be easily compensated in the LHC by powering the focusing ('*MOF*') and defocusing ('*MOD*') MO with opposite polarity. Predictions that compensating h_{1111} would suppress ADECTA were validated by beam-based measurements [5, 6].

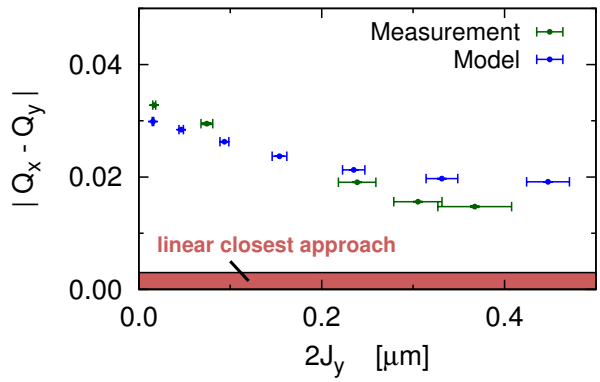

Figure 1: Beam-based observation of amplitude dependent closest tune approach [2].

Simulation also showed ADECTA was generated by the combination of normal- (b_4) and skew-octupole (a_4) sources (a_4 alone did not generate ADECTA) [7]. ADECTA from $a_4 + b_4$ sources was demonstrated with beam in the LHC [8]. This is of interest to LHC and HL-LHC at top-energy, where large a_4 errors are generated in the low-β^* insertions. Such ADECTA can distort the Q-footprint, which may be detrimental to Landau damping [9]. Figure 2 (bottom) shows the footprint-distortion expected in the LHC ($\beta^* = 0.25$ m) if a_4 errors are uncompensated, at typical MO powering. Distortion is large compared to that from typical $|C^-| \approx 0.001$ (Fig. 2, top). Measurement would thus be of interest at top-energy. The conventional technique (saturation of $Q_{x,y}$-separation with $J_{x,y}$) is impractical however, given the need to dump and re-inject/ramp (taking several hours) after every kick, while methods using AC-dipole kicks do not generate ADECTA [6]. Given the reliance on octupolar detuning to drive $Q_{x,y}$ towards the coupling resonance, the conventional technique is also highly limited in terms of the multipole and J_x, J_y parameter space which can be explored. As such, alternative methods of measurement are of interest.

BBQ WITH DOUGHNUT BEAMS

LHC proton beams suffer minimal radiation damping, especially at injection. Consequently when a single-kick is applied to a bunch, constituent particles remain at the kick

ISBN: 978-3-95450-227-1 ISSN: 2673-5490 doi:10.18429/JACoW-IPAC2022-MOPOST004

BEAM-BASED MEASUREMENT OF SKEW-SEXTUPOLE ERRORS IN THE CERN PROTON SYNCHROTRON

S.J. Horney[1,2], A. Huschauer[1], E.H. Maclean[1]
[1]CERN, Geneva, Switzerland, [2]University of Bristol, UK

Abstract

During Proton Synchrotron (PS) commissioning in 2021, beam losses were observed when approaching the $3Q_y$ resonance if the Beam Gas Ionization (BGI) profile monitor was enabled. This indicated the presence of a strong skew-sextupole source in this instrument. Beam-based measurements of the skew-sextupole component in the BGI were performed, to benchmark the BGI magnetic model and provide quantitative checks of sextupole corrections determined empirically to minimize the beam-losses. In this contribution, results of the successfully performed measurements are presented, including tune feed-down, chromatic coupling and resonance driving terms (RDT).

SKEW-SEXTUPOLE IN THE PS BGI

Since 2021 a Beam Gas Ionization monitor is installed in the CERN PS to provide non-destructive emittance measurement [1, 2]. In the BGI, interaction between protons and residual gas generates charged ions. An external electric field accelerates the ionization electrons to a detector system, while a 0.2 T magnetic field (parallel to the electric field) confines the electrons along the plane of interest. A triple-dipole design is employed, where a central dipole provides the instrumental field, and dipoles either side compensate the orbit distortion. Fields inside the BGI are shielded from stray fields of the PS Main Unit magnets (MU) by shielding plates on either side. A schematic of the BGI instrument is shown in Fig. 1.

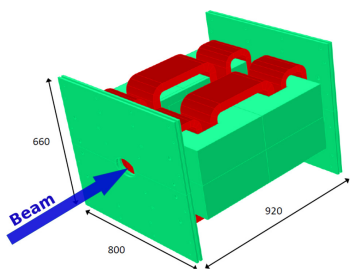

Figure 1: Schematic of the PS BGI and shielding plates [3].

During 2021 PS commissioning tune-scans were performed across the $3Q_y$ resonance. With the BGI magnet disabled minimal beam-losses were observed, but with the BGI enabled it was observed that $\approx 50\,\%$ of the beam was lost upon crossing the $3Q_y$ resonance [4].

Observation of losses at the $3Q_y$ upon enabling the BGI indicated the presence of a significant skew-sextupole (a_3) source generated by the BGI instrument [4]. Studies of the magnetic model [3, 5] indicated that an a_3 can be generated by the interplay of the BGI magnet with the shielding plates, but was highly dependent on the aperture design. A series of beam-based measurements were then performed in the PS at injection (magnetic rigidity $B\rho = 9.3$ [Tm]) to attempt to measure the skew-sextupole generated by the BGI in order to compare to the magnetic model prediction. Studies of chromatic-coupling, tune feed-down and the $3Q_y$ RDT were performed. Results of the beam-based studies are presented in this paper.

CHROMATIC-COUPLING MEASUREMENT

Chromatic coupling is the momentum dependence of linear coupling, generated by skew-sextupoles in regions of non-zero horizontal dispersion. It is characterized [6] via the change with $\delta p/p$ of the f_{1001} RDT (driving the $Q_x - Q_y$ linear coupling resonance), where the closest tune approach ($|C^-|$) is related to the RDT as

$$|C^-| \approx 4|Q_{x,frac} - Q_{y,frac}||f_{1001}| \quad (1)$$

and $Qx, y, frac$ are the fractional tunes. The BGI model predicts an integrated skew-sextupole ($n = 3$) field at the reference radius ($R_{ref} = 20$ mm)

$$A_n L = \int \mathrm{d}s \frac{R_{ref}^{n-1}}{(n-1)!} \frac{\partial^{n-1} B_x}{\partial x^{n-1}} = -5.5 \times 10^{-4}\ [\mathrm{Tm}] \quad (2)$$

By contrast magnetic measurement of the skew-sextupole field of a PS MU at injection powering (404 A) gives $A_3 L = 1.2 \times 10^{-6}$ [Tm] at the same R_{ref} (2 orders of magnitude smaller) [7]. As such the BGI when powered should represent the dominant source of chromatic coupling.

The PS is not equipped with dedicated kicker magnets for optics studies. Beams can be excited however using the transverse damper (ADT) to drive forced oscillations at a frequency (Q_{AC}) close to the natural tunes (Q_{nat}). This is known as ADT-AC-dipole type excitation, and coupling measurement can be performed as for a conventional AC-dipole [8, 9]. An example of turn-by-turn (TbT) BPM data during an ADT-AC-dipole kick is shown in Fig. 2.

To provide an initial qualitative check of the PS skew-sextupole model chromatic coupling was measured using the PS ADT. Figure 3 shows the real and imaginary parts of f_{1001} linear coupling RDT (expressed in C^- units) measured on-momentum, and then upon application of $\Delta p/p = 0.001$ offset. With the BGI unpowered the coupling measurement is unchanged by the momentum trim. With the BGI enabled however, a clear shift in the linear coupling is observed. This confirms the expectation from magnetic models that the BGI skew-sextupole should represent the dominant skew-sextupole source in the PS ring.

ISBN: 978-3-95450-227-1 ISSN: 2673-5490 doi:10.18429/JACoW-IPAC2022-MOPOST005

THE HL-LHC PROJECT GETS READY FOR ITS DEPLOYMENT

O. Brüning, B. Di Girolamo, P. Fessia, C. Gaignant, H. Garcia Gavela, E. Maclean, M. Modena, T. Otto, L. Tavian, G. Vandoni, M. Zerlauth, CERN, Geneva, Switzerland

Abstract

Following the successful completion of the second long shutdown (LS2), the Large Hadron Collider (LHC) is preparing for its final operational run before the majority of the High Luminosity Upgrade (HL-LHC) will be installed during the third Long Shutdown starting in 2026. The HL-LHC upgrade will enable a further tenfold increase in integrated luminosity delivered to the ATLAS and CMS experiments, starting by an upgrade of the machine protection, collimation and shielding systems in LS2, and followed by the deployment of novel key technologies, including Nb3Sn based insertion region magnets, cold powering by MgB2 superconducting links and integration of Nb crab-cavities to compensate the effects of a larger crossing angle. After a period of intensive R&D and prototyping, the project is now entering the phase of industrialization and series production for all main components. In this contribution, we provide an overview of the project status and plans for deployment and performance ramp-up. Progress on the validation of key technologies, status of prototypes and series production as well as the final integration studies for the HL equipment are summarized. These are accompanied by the imminent completion of major civil engineering work and the start of infrastructure installations. Initial operational experience will be gained at the Inner Triplet (IT) String, presently in assembly at CERN's Superconducting Magnet Test Facility, which will enable a fully integrated test of the main magnets, powering, and protection systems in the actual HL-LHC insertion configuration.

INTRODUCTION

The second run of CERN's LHC was successfully completed in 2018, producing 160 fb^{-1} of integrated luminosity over the 4 year long run, with 70 fb^{-1} attained in 2018. During the following Long Shutdown 2 (LS2), primarily devoted to the LHC Injector Upgrade (LIU) [1], the first deliverables of the HL-LHC upgrade project were installed in the LHC, including passive absorbers, secondary low impedance collimators and crystal collimators. These have been fully commissioned for the third operational run of the LHC, planned to last until the end of 2025 at a beam energy of 6.8 TeV, to potentially cumulate an additional 210 fb^{-1} and thus bringing the total integrated luminosity in the LHC well above the initial design value of 300 fb^{-1}. The third long-shutdown, starting in 2026 and lasting for three years will be devoted to the installation of the HL-LHC upgrade, before exploitation will start in 2029 (see Figure 1).

Today, the project is in the transition from prototyping to series production for all key technologies (see Figure 2), nearing completion of the important civil engineering work on the surface as well as underground and gearing up for a full-scale test of a complete insertion magnet string at CERN's Superconducting Magnet Test Facility SM18.

KEY TECHNOLOGIES

Large aperture Nb_3Sn focusing quadrupole magnets will be installed around the high luminosity experiments ATLAS and CMS, representing one of the cornerstones of the HL-LHC upgrade. They will provide the larger aperture as well as higher integrated field required to reach the nominal β^* of 15 cm at the collision points. The inner triplet magnets are designed and constructed in collaboration with the HL-LHC Accelerator Upgrade Project (AUP) in the USA [2]. The Q1 and Q3 magnets (MQXFA) will be provided as in-kind contribution from AUP, while the longer version for Q2 (MQXFB) will be produced at CERN.

At AUP, coil production is progressing at BNL and FNAL, with 70% of the coils and 40% of the magnets completed [3]. An endurance test on magnet MQXFA05 has been recently completed in vertical position to gather more information on the long-term behaviour of Nb_3Sn magnets. The test involved five thermal cycles and a total of 50 high current quenches, eight during training and 42 being provoked at nominal current via the quench heaters. At the end of this campaign, the magnet reached the required nominal performance without quenching, both at 1.9 K and at 4.5 K, confirming the large temperature margin already observed during the first powering [4]. At FNAL, the construction of the first cryostated horizontal cold mass is ongoing, integrating the first two series magnets that were successfully tested in the BNL vertical setup by fall 2020.

The CERN-AUP joint short model program has been successful, with 5 assemblies out of 6 reaching operation at 7.5 TeV, and record peak fields above 13 T in two models [5]. The short model program allowed to verify the dependence of performance on preload, make endurance tests, and validate the assembly of the stainless steel shell around the magnet. CERN has produced two full scale prototypes MQXFBP1 and MQXFBP2, both of which have shown performance limitations to 6.5 TeV and 6.8 TeV respectively. MQXFBP1 has been disassembled, and MQXFBP2 will be used as a prototype cold mass and possibly installed in the IT string. MQXFBP2 went through a thermal cycle and a total of 50 quenches, without showing signs of degradation. Investigations on the possible causes of the performance limitations are ongoing. Tomographies and metallographic inspection revealed filament breakage in a localized region of the cross-section [6]. The next prototype MQXFBP3 has been assembled with a revised strategy for the shell welding, minimizing the mechanical coupling to the magnet. The following magnet MQXFB02 has been assembled with a revised procedure minimizing the peak load during bladdering. Both magnets will be tested in 2022. Magnet MQXFB03 will make use of coils manufactured with improvements in procedures and handling; it will be tested in 2023.

ISBN: 978-3-95450-227-1 ISSN: 2673-5490 doi:10.18429/JACoW-IPAC2022-MOPOST006

BEAM COMMISSIONING AND OPTIMISATION IN THE CERN PROTON SYNCHROTRON AFTER THE UPGRADE OF THE LHC INJECTORS

A. Huschauer*, M. Coly, D. Cotte, H. Damerau, M. Delrieux, Y. Dutheil, S. Easton, J.-C. Dumont, M.A. Fraser, O. Hans, G. Imesch, S. Joly, A. Lasheen, C. Lombard, R. Maillet, B. Mikulec, J.-M. Nonglaton, S. Sainz Perez, B. Salvant, R. Suykerbuyk, F. Tecker, R. Valera Teruel
CERN, Geneva, Switzerland

Abstract

The CERN LHC injector chain underwent a major upgrade during the Long Shutdown 2 (LS2) in the framework of the LHC Injectors Upgrade (LIU) project. After 2 years of installation work, the Proton Synchrotron (PS) was restarted in 2021 with the goal to achieve pre-LS2 beam quality by the end of 2021. This contribution details the main beam commissioning milestones, difficulties encountered and lessons learned. The status of the fixed-target and LHC beams will be given and improvements in terms of performance, controls and tools will be described.

LS2 UPGRADES IN THE PS

In the PS, the main LIU activities [1] were related to the upgrade of the injection energy to 2 GeV kinetic energy to mitigate space charge issues and to improvements of the radio-frequency (RF) systems by reducing their impedance or implementing additional feedback systems (see also [2]). New beam instrumentation devices, such as new wire scanners, beam gas ionisation (BGI) monitors and beam loss monitors (BLMs) were installed to improve the diagnostic capabilities. Furthermore, important consolidation activities were performed during LS2, such as the renovation of 43 out of the 100 combined function main magnet units (MUs).

PS BEAM COMMISSIONING

Following a shutdown period of two years and three months, beam was again injected into the PS on the evening of 3 March 2021. Despite the many modifications during LS2, it took less than half a day to accelerate the beam to the maximum flat top momentum of 26 GeV/c and to extract it towards the external dump. During the following five days, commissioning progress was even faster than anticipated and low-intensity variants of the main beam types were quickly set up.

This initial quick progress was slowed down by a breakdown of the newly installed injection septum, requiring a stop of beam operations for eight days to repair the device and re-establish operational vacuum conditions. This inadvertent stop was also used to perform a first iteration of beam-based alignment of the combined function MUs, which was required due to the extensive consolidation campaign of the magnets during LS2. Following a second iteration, a total of eight MUs were aligned to improve the orbit, reducing the root mean square orbit excursions from 3.3 to 1.6 mm in the horizontal and from 1.9 to 0.9 mm in the vertical plane.

After this first phase of commissioning low-intensity beams, PS operations entered into the intensity ramp-up phase. During this period various issues were encountered, the majority of them related to unexpected beam loss at various locations along the accelerator.

Beam Loss Around Straight Section 88

The versatility of the PS is closely related to a multitude of RF cavities used for acceleration and longitudinal gymnastics such as bunch splittings or bunch rotations [3]. During the beam commissioning, one of the cavities used for bunch rotation, an 80 MHz system installed in straight section 88, could not be reliably used due to a high pressure level. In addition, increased beam losses were measured on the BLMs especially around this region, but also elsewhere in the accelerator delaying the intensity ramp-up.

Introducing a local vertical orbit bump at this specific cavity could reduce but not completely remove the losses. Therefore, an aperture restriction at the cavity was expected to be the source of both the beam loss and the increased pressure. A small misalignment of the cavity was subsequently corrected, but did not improve the issues described before. Furthermore, a radiation hot spot of 42 mSv/h at contact on top of the vacuum chamber just downstream of the RF cavity was observed. All these observations led to the suspicion of an obstacle inside the vacuum chamber and hence the decision was taken to break the vacuum and perform an endoscopy. Indeed, a sponge-like object was located just upstream of the RF cavity. This piece obstructed the lower half of the vacuum chamber and was a leftover from the MU consolidation program, where it was used to protect the vacuum chambers while they were stored in the workshop. In hindsight, all the observations were well explained by the presence of this object. The object actually acted as a scatterer and the interaction of the beam with it caused the increased vacuum pressure in the cavity as well as the increased beam losses. The radiation hot-spot, however, was generated by the local bump that was introduced to pass the object. Removal of the object allowed the beam commissioning activities to be pursued.

Electron Cloud Effects and Scrubbing

The first observation of electron cloud (EC) effects in the PS dates back to the early 2000s, during the commissioning of LHC-type beams in the PS. At that time the beam quality

* alexander.huschauer@cern.ch

ISBN: 978-3-95450-227-1 ISSN: 2673-5490 doi:10.18429/JACoW-IPAC2022-MOPOST007

SUMMARY OF THE FIRST FULLY OPERATIONAL RUN OF LINAC4 AT CERN

P. K. Skowroński, G. Bellodi, B. Bielawski, R. Borner, G.P. Di Giovanni, E. Gousiou, J.-B. Lallement, A. Lombardi, B. Mikulec, J. Parra-Lopez, F. Roncarolo, R. Scrivens, J.-L. Sanchez Alvarez, L. Timeo, R. Wegner, CERN, 1211 Geneva 23, Switzerland

Abstract

In December 2020 the newly commissioned LINAC4 started delivering beam for the CERN proton accelerator chain, replacing the old LINAC2. LINAC4 is a 352 MHz normal conducting linac, providing a beam of negative hydrogen ions at 160 MeV that are converted into protons at injection into the PS Booster (PSB) synchrotron. In this paper we report on the achieved beam performance, availability, reproducibility and other operational aspects of LINAC4 during its first fully operational year. We also present the machine developments performed and the plans for future improvements.

INTRODUCTION

In LINAC4 negative hydrogen ions (H^-) are accelerated to a kinetic energy of 160 MeV [1]. It is a normal conducting linear accelerator operating at a frequency of 352 MHz. It consists of the following building blocks: caesiated RF source, Low Energy Beam Transport (LEBT), RFQ, Medium Energy Beam Transport (MEBT) including a chopper and 3 bunching cavities, 3 Drift Tube Linac (DTL) accelerating structures, 7 Cell-Coupled Drift Tube Linac (CCDTL) structures and 12 PI Mode Structures (PIMS). The 170 meter transfer line to the PSB is equipped with an additional PIMS cavity known as the debuncher located 42 m from the last accelerating cavity. It operates at zero crossing phase and is used to regulate the beam energy spread.

The project started in 2008 [2]. The commissioning took place from 2013 to 2016 and it was interleaved with installation phases [2–5]. Reliability runs took place in 2017 and 2018. These revealed several issues that would otherwise impossible to discover during commissioning [6, 7]. In December 2020 the beam was injected for the first time into the PSB using a charge exchange technique [8].

The source produces 800 μs long pulses at 35 mA intensity every 1.2 s, resulting in a beam of 28 mA at 3 MeV out of the RFQ (transmission 80-82%). So far, the source was exchanged once per year with one of its 2 identical spares. At every exchange the resulting beam is somewhat different and the LEBT settings need to be slightly re-optimized. The beam chopper defines the accelerated beam pulse length (maximally 600 μs) and, therefore, the total intensity injected into the PSB, which is different for each user. For the operational cycles it ranges from $5 \cdot 10^{10}$ protons per pulse (LHC pilot beam) up to $4 \cdot 10^{13}$ (ISOLDE beam), and it could be increased to a maximum of $6.8 \cdot 10^{13}$. The first 200 μs, called the pulse head, are removed by the chopper because in this part the intensity is not constant, due to the time required for space charge compensation and to ramp-up the intensity of the source. The beam is injected into the 4 superposed PSB rings over a maximum of 150 turns per ring. The chopper removes the bunches falling on the edges of the PSB longitudinal acceptance, which would therefore be lost during the energy ramp, as well as the ones produced while the PSB injection switches from one ring to another.

TRANSFER LINE COMMISSIONING

The commissioning of the transfer line took place during the CERN Long Shutdown 2 (LS2) in 2019-2020. In the first stage, in 2019, when the PSB was still undergoing renovation, the beam was operated up to a dedicated measurement line (the LBE line) located approximately 40 meters upstream from the PSB injection.

For the first time the beam setup was performed as for operational machines with the help of newly developed tools and procedures that were implemented aiming at thorough and time efficient machine commissioning. This included automatised cavity phasing, trajectory steering, optics control using high level parameters, and software applications for the beam measurements of: trajectory response matrix, transverse and longitudinal profiles (showing comparisons to reference curves), emittance and Twiss parameters. As the result of this exercise, the time required for the machine restart after a shutdown has now been determined to be 5 days for the linac and 3 days for the transfer line.

The beam setup went smoothly. Discrepancies in the vertical plane between the optics measurements and the model expectations were found to be due to an error in modelling of the edge focusing of the dipole magnets. They were removed by implementing the correct magnet gap height in the model. With recomputed optics the mismatch factor (Eq. (7.98) in Ref. [9]) was reduced to 0.08, see Fig. 1. The normalised emittance with a beam current of 25 mA was measured to be below 0.3 $\pi \cdot \mu$m in both transverse planes. The design value is 0.4 $\pi \cdot \mu$m for a 40 mA beam current.

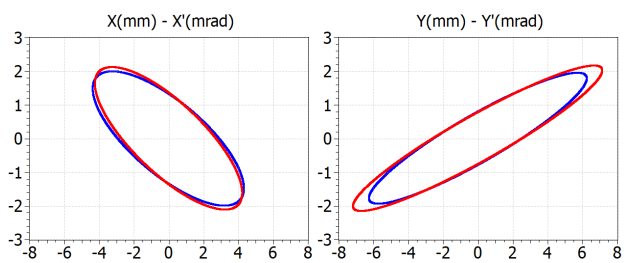

Figure 1: Comparison of the design (blue) and measured (red) phase space ellipses in LBE.

ISBN: 978-3-95450-227-1 ISSN: 2673-5490 doi:10.18429/JACoW-IPAC2022-MOPOST008

SIMULATIONS OF PROTONS TO EXTRACTION AT $G\gamma = 7.5$ IN THE AGS BOOSTER

Kiel Hock, Haixin Huang, François Méot
Brookhaven National Laboratory, Upton, NY 11973

Abstract

To prepare for polarized helion collisions at the Electron Ion Collider (EIC), polarization transmission at the injectors for the Hadron Storage Ring must be studied and optimized. To this effect, an AC dipole has been installed in the AGS Booster to maximize polarization transmission of helions through several intrinsic resonances. This installation also allows polarized protons to be extracted at higher energy without polarization loss. By increasing the proton extraction energy from $G\gamma = 4.5$ to $G\gamma = 7.5$, protons will cross the $G\gamma = 0 + \nu_y$ and $G\gamma = 12 - \nu_y$ depolarizing vertical intrinsic resonances, the $G\gamma = 5$, 6, and 7 imperfection resonances in addition to the $G\gamma = 3$, 4 that are crossed in the present configuration, and be injected into the AGS at a higher rigidity. By simulation, it is determined that there is sufficient strength of the AC dipole to full spin-flip through each of the intrinsic resonances, and there is sufficient corrector current to preserve polarization through the three additional imperfection resonances. The higher injection rigidity facilitates the horizontal and vertical tunes being placed inside the AGS spin-tune gap at injection due to a substantial improvement on the AGS admittance at injection.

INTRODUCTION

The two types of resonances encountered by polarized beams in the injectors are imperfection resonances, which occur when

$$G\gamma = M \tag{1}$$

where M is an integer, G is the anomolous magnetic moment, and γ is the Lorentz factor, and intrinsic resonances, which occur when

$$G\gamma = mP \pm \nu_y \tag{2}$$

where m is an integer, P is the superperiodicity ($P = 6$ for the Booster, $P = 12$ for AGS), and ν_y is the vertical betatron tune. Imperfection resonances are the result of non-zero closed orbits that are primarily caused by misaligned quadrupoles. Intrinsic resonances occur when the spin precession is in phase with the particles betatron motion.

To preserve polarization in the AGS, there are two partial snakes whose settings allow for imperfection resonances to be avoided by prohibiting $\nu_s = M$, where ν_s is the spin tune. The betatron tunes can be placed near the integer ($\nu_y > 8.9$) to mostly avoid intrinsic resonances by prohibiting $\nu_s = \nu_y$ for vertical, which is referred to as being inside the spin-tune gap [1]. Due to the geometrical location of the two snakes, the stable spin direction in the AGS is nearest vertical every $G\gamma = 3n + 1.5$, where n is an integer. The cold snake in particular has strong optical distortions which decrease exponentially with energy [2]. These optical distortion adversely affect the admittance and how the tunes can be configured [3]. In efforts to further improve the polarization transmission of protons in the injectors, protons can be injected into the AGS at higher rigidity which can hypothetically allow for stronger snakes and allow both the horizontal and vertical betatron tunes to be set inside the spin-tune gap.

Protons are presently injected into the Booster at $G\gamma = 2.19$ and extracted into the AGS at $G\gamma = 4.5$. At injection both betatron tunes are kept above the half-integer ($\nu_y, \nu_x > 4.5$) and quickly moved near 4.9 to minimize effects from the space charge [4]. In this configuration, the $G\gamma = 0 + \nu_y$ resonance is avoided by keeping $\nu_y = 4.8$. In order to match the stable spin direction from the Booster to AGS, protons can be extracted at $G\gamma = 7.5$. This higher extraction energy will cause protons to cross the $G\gamma = 3$ through 7 imperfection resonances and the $G\gamma = 0 + \nu_y$ and $G\gamma = 12 - \nu_y$ intrinsic resonances. Simulations of intrinsic resonance crossing, imperfection resonance crossing, and AGS admittance at injection are performed using Zgoubi [5].

INTRINSIC RESONANCE CROSSING

An AC dipole has been installed in the Booster to overcome vertical intrinsic resonances that polarized beams will encounter as they are accelerated [6, 7]. It is able to induce a full spin-flip of all particles in the bunch by driving high amplitude vertical coherent oscillations, causing all particles of the bunch to sample the strong horizontal fields in the quadrupoles. The amplitude of these oscillations follows [8]

$$Y_{coh} = \frac{B_m l}{4\pi B\rho \delta_m}\beta_y \tag{3}$$

where $B_m l$ is the AC dipole strength, $B\rho$ is the rigidity, $\delta_m = \nu_m - \nu_y - n$ is the separation between the AC dipole tune (ν_m) and the vertical betatron tune, and β_y is the vertical beta function. The AC dipole tune is

$$\nu_m = f_m / f_{rev} \tag{4}$$

with f_m being the AC dipole oscillation frequency and f_{rev} is the revolution frequency. The AC dipole system is designed with a maximum $B_m l = 25$ Gm and an oscillation frequency of $f_m = 250$ kHz.

For protons crossing the $G\gamma = 0 + \nu_y$ resonance, the configuration is $\nu_y = 4.8088$ and $\nu_m = 0.1812$ which requires $B_m l = 12.3$ Gm at $\delta_m = 0.01$ to full spin-flip (as shown in Table 1). Protons crossing the $G\gamma = 12 - \nu_y$ resonance will require $\nu_y = 4.8161$ with $\nu_m = 0.1739$. In order to have a full spin-flip, the AC dipole strength $B_m l = 28.0$ Gm at

ISBN: 978-3-95450-227-1 ISSN: 2673-5490 doi:10.18429/JACoW-IPAC2022-MOPOST009

EIC CRAB CAVITY MULTIPOLE ANALYSIS AND THEIR EFFECTS ON DYNAMIC APERTURE*

Q. Wu†, Y. Luo, B. Xiao, Brookhaven National Laboratory, Upton, NY, USA
S. U. De Silva, Old Dominion University, Norfolk, VA, USA
Z. Li, SLAC, Menlo Park, CA, USA

Abstract

Crab cavity is essential for retrieving the loss in luminosity due to the large crossing angle in the two colliding beam lines of the Electron Ion Collider (EIC). Due to the asymmetric design of the proton beam crab cavity, the fundamental mode consists of contributions from higher order multipoles. These multipole modes may change during fabrication and installation of the cavities, and therefore affect the local dynamic aperture. Thresholds for each order of the multipoles are applied to ensure dynamic aperture requirements at these crab cavities. In this paper, we analysed the strength of the multipoles due to fabrication and installation accuracies and set limitations to each procedure to maintain the dynamic aperture requirement.

INTRODUCTION

The concept of using an RF deflector to compensate for the geometrical loss in the colliding beams due to fast sep-aration from the designed crossing angle has been intro-duced by Robert Palmer in 1988 [1]. As concept only relates to colliders that pursue high luminosity, these RF deflectors are not developed as popular as other RF resonators in traditional accelerators. Figure 1 shows the various crab cavities that have been built and operated in the past [2-5].

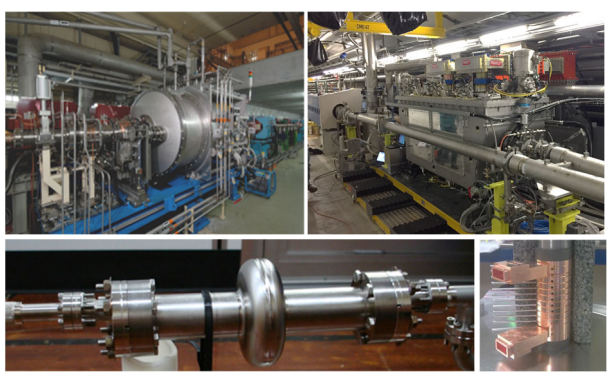

Figure 1: Difference crab cavities fabricated and operated. Top left: Squashed crab cavity at 509 MHz operated in the HER ring @ KEK. Top right: Double Quarter Wave crab cavity at 400 MHz operated in the SPS ring @ CERN. Bottom left: Single-cell prototype of the 3.9 GHz 9-cell crab cavity for ILC. Bottom right: 12-cell copper travelling-wave structure for crabbing in CLIC.

The future Electron Ion Collider [6] has a design goal of reaching a luminosity of 10^{34} cm^{-2} sec^{-1}. The EIC interaction region has a crossing angle of 25 mrad, Fig. 2 which is more than 40 times larger than the LHC. With such a large crossing angle, the EIC benefits from the LHC experience as well as encounters many challenges while demonstrating the crabbing scheme. The crab cavity of the EIC will have a full SRF system with 197 MHz and 394 MHz resonators combined. To reach the peak luminosity, both frequencies must be considered for beam-cavity interaction studies. This paper will focus on the main crab cavity of 197 MHz for hadron storage ring, as shown in Fig. 3. The 394 MHz crab cavity requires future work.

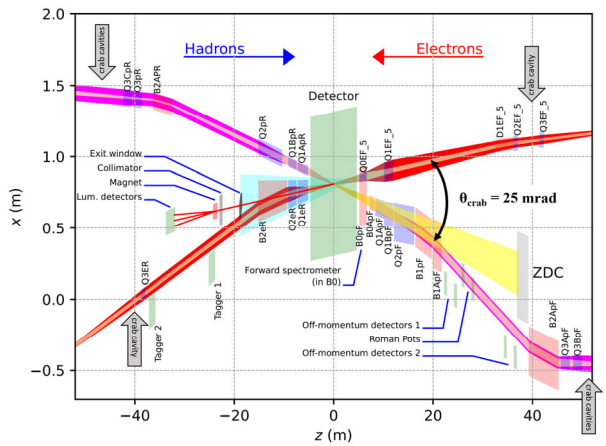

Figure 2: EIC interaction region layout with 25 mrad full crossing angle.

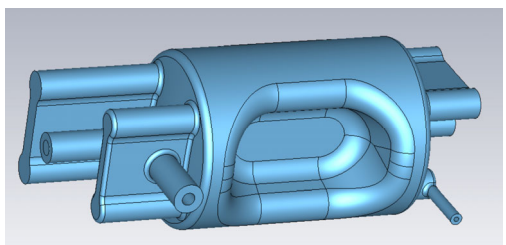

Figure 3: 197 MHz crab cavity model with horizontal coupling for EIC.

CRAB CAVITY MULTIPOLES

The transverse crabbing effect in the RF structure can be decomposed into a series of EM fields that imitate the magnets in the machine, with the time-dependent dipole mode (crabbing mode) dominating. The coefficient of each mode can be evaluated through the Lorentz force of the transverse EM field or analysing the longitudinal electric field using the Panofsky-Wenzel Theorem [7].

* Work supported by Brookhaven Science Associates, LLC under Contract No. DE-SC0012704 with the U.S. Department of Energy.
† qiowu@bnl.gov

ISBN: 978-3-95450-227-1 ISSN: 2673-5490 doi:10.18429/JACoW-IPAC2022-MOPOST010

DEUTERON BEAM POWER RAMP-UP AT SPIRAL2

A.K. Orduz*, M. Di Giacomo, R. Ferdinand, J-M. Lagniel, G. Normand
Grand Accélérateur National d'Ions Lourds (GANIL), Caen, France
D. Uriot, IRFU, CEA, Université Paris-Saclay, F-91191 Gif-sur-Yvette, France

Abstract

The SPIRAL2 linac commissioning started on 8 July 2019 after obtaining the authorisation to operate by the French Safety Authority. The tuning of the two Low Energy Beam Transport (LEBT), Radio Frequency Quadrupole (RFQ), Medium Energy Beam Transport (MEBT), Superconducting (SC) linac and High Energy Beam Transport (HEBT) was done with H^+, $^4He^{2+}$ and D^+ beams during three periods of six months each in 2019, 2020 and 2021. The results obtained in 2021 with a D^+ beam are presented. The strategy for the tuning of the MEBT, including three rebunchers, is described. The comparison between the beam parameter measurements and reference simulations are also presented. The main results of the power ramp-up to 10 kW in the linac with a 5 mA D^+ beam are next reported. Finally, the extrapolation from the nominal power (200 kW) to the obtained results is analysed.

INTRODUCTION

SPIRAL2 is the major recent upgrade made of the GANIL facility [1]. The linear accelerator is composed of two LEBT lines, one for heavy ions ($A/Q < 3$) and one for H^+/D^+, followed by a third one that collects the beam from the first two and matches it to the RFQ [2]. The MEBT to match the beam to the SC linac, is also designed to host a dipole to insert a heavier ion beam coming from a second injector (NEWGAIN project) [3] and includes a bunch selection system [4] allowing to inject from 1/100 to 1/1000 bunch in the linac for the Time of Flight (ToF) experiments in Neutron For Science (NFS) room.

The SC linac is composed of a low β section ($\beta = 0.07$) with 12 single-cavity cryomodules [5], and a high β section ($\beta = 0.12$) with 7 two-cavity cryomodules [6]. Finally, three HEBT lines deliver the beam to the linac Beam Dump (SAFARI) [7], NFS and S3 (Super Separator Spectrometer) experimental rooms as shown in Figure 1.

The different ions can be accelerated up to 14.5 MeV/A, 20 MeV/A and 33 MeV/A with a maximum beam power of 45 kW, 200 kW and 165 kW for mass to charge ratios (A/Q) 3, 2 and 1 respectively.

The ECR sources, LEBT lines and the RFQ were commissioned before getting the authorisation to operate the SC linac in July 2019 [2]. During the second semesters of 2019, 2020 and 2021, the MEBT, SC linac and HEBT lines were commissioned, the first NFS experiments were also done [1, 8].

The main 2020 objective was to perform a power ramp-up for a nominal current H^+ beam (5 mA) to validate the whole accelerator before taking the risk of activating it with the deuterons. This target has been achieved on November 18, 2020, with a beam power of ~ 16 kW (4 mA, 12.6 % duty factor) [9]. Two measurements were very useful to control the beam loss variations during the power ramp-up: the pressure variations mainly along the low β section, and the count rate in the BLMs along the high β section and in the HEBT area.

The last part of the linac commissioning started in July 2021 with the tuning of the LEBT, MEBT, linac and HEBT lines for a $^4He^{2+}$ beam. The same tuning was then validated with a D^+ beam. The tuning was then optimised with the D^+ beam and the power was increased to 10 kW. One of the objectives for the commissioning team at this step was to increase the beam power in order to validate the tuning and detect problems (e.g. related to diagnostics or cavities).

The next section of this paper presents the strategy carried out to achieve this goal. The results obtained during the different optimization steps and their analysis are next also presented.

STRATEGY

The commissioning of SPIRAL2 in 2021 took place between July and December and was divided into four stages. In the first stage , the tuning of the LEBT, RFQ, MEBT, and linac with a $^4He^{2+}$ beam were carried out. The second stage consisted to drive the D^+ beam to SAFARI without optimising the linac tuning. Afterwards, the objective was to reduce the beam losses optimising the beam transport in the MEBT and SC linac before starting the power ramp-up to 10 kW with a 5 mA D^+ beam.

MEBT Tuning

The tuning of the MEBT, including the three rebunchers and the Single Bunch Selector (SBS), was carried out with a 1.2 mA $^4He^{2+}$ beam. The transverse rms emittance measured in the MEBT was 0.2 π.mm.mrad. Two methods called "simplified" and "zero-crossing" were used for the rebuncher tunings. The simplified method uses phase measurements on the pick up at the end of the MEBT, first with the three rebunchers off and detuned. Then, the first rebuncher is turned on at its theoretical voltage value and a phase scan is performed. The cavity phase and amplitude are found comparing the phase measurements and computations done tracking a reference particle in the rebuncher field map. The process is replicated for the next two rebunchers. The issue with this method comes from phase measurement shifts induced by a strong debunching due to the long distance between the RFQ output and the pick-up, as well as between the first and second rebunchers and the pick-up.

* angie.orduz@ganil.fr

ISBN: 978-3-95450-227-1 ISSN: 2673-5490 doi:10.18429/JACoW-IPAC2022-MOPOST011

CEA CONTRIBUTION TO THE PIP-II LINEAR ACCELERATOR

N. Bazin†, S. Arsenyev, J. Belorgey, S. Berry, Q. Bertrand, P. Bredy, E. Cenni, C. Cloue, R. Cubizolles, J. Drant, H. Jenhani, S. Ladegaillerie, A. Le Baut, A. Moreau, O. Piquet, A. Raut, P. Sahuquet, C. Simon and O. Napoly*, Université Paris-Saclay, CEA, Département des Accélérateurs, de la Cryogénie et du Magnétisme, Gif-sur-Yvette, France

Abstract

The Proton Improvement Plan II (PIP-II) that will be installed at Fermilab is the first U.S. accelerator project that will have significant contributions from international partners. CEA joined the international collaboration in 2018, and will deliver 10 low-beta cryomodules as In-Kind Contribution to the PIP-II project, with cavities supplied by LASA-INFN and power couplers and tuning systems supplied by Fermilab. This paper presents the CEA scope of work that includes the design, manufacturing, assembly and tests of the cryomodules and the upgrade of the existing infrastructures to the PIP-II requirements.

INTRODUCTION

The PIP-II project is an upgrade of the accelerator complex of Fermilab to enable the world's most intense neutrino beam for the Long Baseline Neutrino Facility (LBNF) and the Deep-Underground Neutrino Experiment (DUNE) located in South Dakota, 1200 km from the neutrino production in Illinois.

PIP-II will deliver 1.2 MW of proton beam power from the injector, upgradeable to multi-MW capability. The central element of PIP-II is an 800 MeV linear accelerator, which comprises a room temperature front end followed by a superconducting section. The superconducting section consists of five different types of cavities and cryomodules, including Half Wave Resonators (HWR), Single Spoke and elliptical resonators operating at state-of-the-art parameters [1].

PIP-II is the first U.S. accelerator project that will be constructed with significant contributions from international partners, including India, Italy, France, United Kingdom and Poland [2].

OVERVIEW OF THE CEA CONTRIBUTION TO THE PIP-II PROJECT

CEA is designing, building, testing, installing and commissioning superconducting linear accelerators (or part of them) for others labs since 20 years. It includes the development of a wide range of cryomodules with different frequencies, different types of cavities (low beta ones – half-wave and quarter-wave resonators – and high beta ones – elliptical cavities), different types of supports and insertion modes of the cold mass: 352 MHz cryomodule for SOLEIL, 88 MHz QWR cryomodules for Spiral2, 1.3 GHz cryomodules for XFEL, 175 MHz HWR cryomodules for IFMIF/EVEDA, IFMIF-DONES and SARAF, 704 MHz cryomodules for ESS [3, 4].

Thanks to this expertise, CEA joined the PIP-II collaboration in 2018. The involvement of CEA in the PIP-II Linac construction was formally approved by the French Ministry of Research in July 2020 with the definition of the scope of work and the budget envelope.

CEA contribution focuses on the 650 MHz superconducting accelerating section, with the design, fabrication, assembly and test of 1 pre-production and 9 production low-beta 650 MHz cryomodules (called “LB650” hereafter) according to the PIP-II project specified requirements. This includes:

- The design of the LB650 cryomodule.
- The procurement of most of the components of the cryostat (i.e. the cryomodule without the cavities, the tuning systems, the power couplers and some standard components provided by the PIP-II collaboration).
- The assembly and cold RF tests of the 10 LB650 cryomodules.
- The design of the transport frame for the LB650 cryomodules, fabrication of 2 units and road test of the pre-production cryomodule.
- The preparation for shipment before the transfer title from CEA to the U.S Department of Energy and the overseas transportation from France to the USA.

DESIGN OF THE LB650 CRYOMODULE

The LB650 cryomodule houses four 5-cell β=0.61 cavities (developed by Fermilab, INFN, and VECC for the pre-production cryomodule and series cryomodules [5]). The frequency tuning systems and the power couplers for the low beta and high beta cavities are identical. They are under the responsibility of Fermilab, with CEA contribution on the design studies of the power couplers. Each cavity is connected to the a supporting system that stays at room temperature , the strongback, using two support posts made of low thermal conductivity material to limit the thermal load between the room temperature strongback and the helium temperature devices. The posts have two thermal intercepts, one connected to the thermal shield (cooled around 40 K) and the 5 K line where liquid helium flows inside.

The LB650 cryomodule is similar to the HB650 cryomodule that is being developed by Fermilab [6]. In order to benefit from the HB650 cryomodule to the LB650 one, CEA is part of the integrated design team with Fermilab,

* Now at Fermilab, Batavia IL 60510, USA
† nicolas.bazin@cea.fr

ISBN: 978-3-95450-227-1 ISSN: 2673-5490 doi:10.18429/JACoW-IPAC2022-MOPOST012

HIGH CURRENT HEAVY ION BEAM INVESTIGATIONS AT GSI-UNILAC

H. Vormann[1], W. Barth[1, 2, 3], M. Miski-Oglu[1, 2], U. Scheeler[1], M. Vossberg[1], S. Yaramyshev[1],
Presenting Contributor M. Vossberg,
[1]GSI Helmholtzzentrum fuer Schwerionenforschung GmbH, Darmstadt, Germany
[2]HIM Helmholtz Institute Mainz, Mainz, Germany
[3]JGU Johannes-Gutenberg-University Mainz, Mainz, Germany

Abstract

The GSI Universal Linear Accelerator UNILAC and the synchrotron SIS18 will serve as injector for the upcoming FAIR-facility. The UNILAC-High Current Injector will be improved and modernized until FAIR is commissioned and the Alvarez post stripper accelerator is replaced.

The reference heavy ion f[l]or future FAIR-operation is uranium, with highest intensity requirements. To re-establish uranium beam operation and to improve high current beam operation, different subjects have been explored in dedicated machine investigation campaigns. After a beam line modification in 2017 the RFQ-performance had deteriorated significantly; new rods have been installed and the RF-working point has been redefined. Also the Superlens-performance had become unsatisfactory; improved with a modified RF-coupler. With a pulsed hydrogen gas stripper target the uranium beam stripping efficiency could be increased by 65%. Various work has already been carried out to establish this stripper device in routine operation. With medium heavy ion beams a very high beam brilliance at the end of transfer line to SIS18 was achieved.

Results of the measurement campaigns and the UNILAC upgrade activities will be presented.

INTRODUCTION

Before the year 2021, high current uranium beam machine experiments were conducted in October 2015 and July 2016 for the last time, only at the GSI-High Current Injector (HSI) and the gas stripper section. At this time only three of the five Alvarez DTL post stripper tanks were available, due to work on the post stripper RF-amplifier systems of the UNILAC (Fig.1). The achievable high current beam brilliance at injection into the heavy ion synchrotron SIS18 was estimated only by using front-to-end high-current measurements with a proton beam performed in 2014 [1-14].

During the long shutdown in the whole year 2017 there was no beam operation at all. After this shutdown, the beam times 2018 and 2019 had to be re-organised, as the HSI-RFQ performance had decreased strongly and required a time-consuming repair. In 2020 uranium beam operation was skipped due to the Corona crisis (Fig. 2).

The measurement campaigns in 2021 and 2022 have been conducted with high intensity heavy ion beams (uranium, bismuth, tantalum, xenon) and with medium and light ion beams (Argon, p+), to fully characterize the high intensity beam properties of the UNILAC.

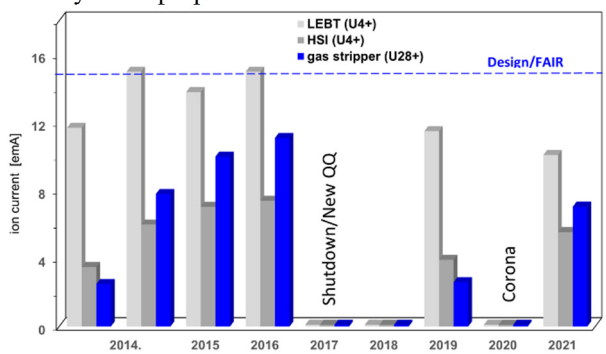

Figure 2: Uranium beam intensity at the UNILAC HSI [4].

HSI RFQ OPTIMISATION

The RF performance of the HSI-RFQ had decreased strongly after a beam line modification during the shutdown 2017, when the RFQ had been kept under atmosphere conditions for almost one year. During the re-commissioning campaign in 2018 only 70% of the nominal RF-voltage could be reached. Apparently the copper surface conditions were significantly degraded, due to many years of operation and additional humidity influence. Therefore new electrodes (rods) have been produced and installed (2018-2019). After successful recommissioning with light ions and also with U^{5+}, the working point of the HSI-RFQ has been re-defined: With a medium heavy ion beam (Ar^{2+} and Ar^{1+}), applying different RF-voltages for acceleration, the transmission through the HSI has been scanned in a wide range from voltages far below the working point to

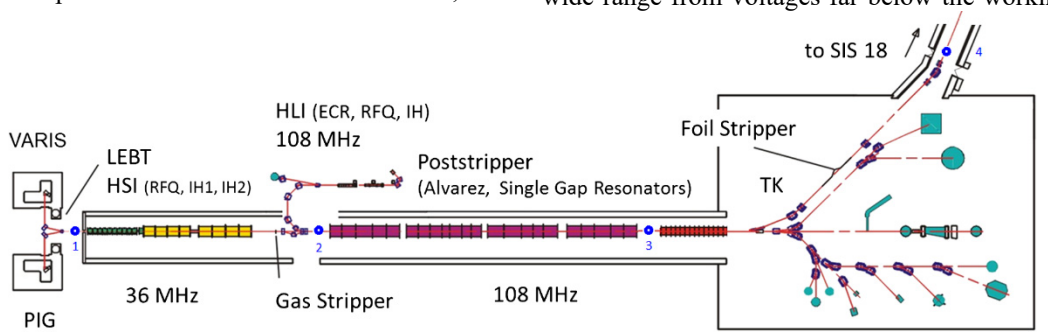

Figure 1: Overview of the GSI Universal Linear Accelerator UNILAC [4].

ISBN: 978-3-95450-227-1 ISSN: 2673-5490 doi:10.18429/JACoW-IPAC2022-MOPOST014

THE 325 MHz FAIR pLinac LADDER RFQ - FINAL ASSEMBLY FOR COMMISSIONING

M. Schuett*[1,2], U. Ratzinger[1], C. Kleffner[2], K. Knie[2]
[1] Institute for Applied Physics, Goethe University, Frankfurt, Germany
[2] GSI Gesellschafft für Schwerionenforschung, Darmstadt, Germany

Abstract

Based on the positive results of the unmodulated 325 MHz Ladder-RFQ prototype from 2013 to 2016, we developed and designed a modulated 3.4 m Ladder-RFQ. The Ladder-RFQ features a very constant voltage along the axis as well as low dipole modes. The unmodulated prototype accepted 3 times the operating power of which is needed in operation corresponding to a Kilpatrick factor of 3.1 with a pulse length of 200 µs. The 325 MHz RFQ is designed to accelerate protons from 95 keV to 3.0 MeV according to the design parameters of the proton linac within the FAIR project. This particular high frequency for a 4-ROD-RFQ creates difficulties, which triggered the development of a Ladder-RFQ with its high symmetry. The results of the unmodulated prototype have shown, that the Ladder-RFQ is very well suited for that frequency. For the applied cooling concept, the Ladder-RFQ can be driven up to a duty factor of 10%. Manufacturing has been completed in September 2018. The final flatness & frequency tuning as well as the final assembly have been completed. We present the final RF measurements and assembly steps getting the Ladder-RFQ ready for shipment and high power RF test prior to assembly.

INTRODUCTION

The idea of the Ladder type RFQ firstly came up in the late 1980s [1, 2] and was realized successfully for the CERN Linac3 operating at 101 MHz [3] and for the CERN antiproton decelerator ASACUSA at 202 MHz [4].

Due to its high symmetry, this Ladder-RFQ features a very constant voltage along the axis well-suited for high frequency operation and duty factors up to 10%. A modified short (0.7 m) and non-mudulated Ladder-RFQ prototype was high power tested at the GSI test stand [5]. It accepted three times the RF power level needed in operation [6, 7]. That level corresponds to a Kilpatrick factor of 3.1 with a pulse length of 200 µs.

According to the design parameters of the proton linac within the FAIR project, the 325 MHz RFQ [6] (see Fig. 1) is designed to accelerate protons from 95 keV to 3.0 MeV [8, 9]. This particular high frequency creates difficulties for a 4-ROD type RFQ. Yet the results of the unmodulated prototype have shown, that the Ladder-RFQ is a suitable candidate for that frequency, which triggered the development of a classical Ladder-RFQ with its higher symmetry. The basic design and tendering of the RFQ have been successfully completed in 2016 [6]. Manufacturing and copper-plating of the tank have been succeeded in September 2018. The final machining step for both flatness and frequency tuning has been finished in April 2019. Afterwars, the final assembly including vacuum components, frequency plungers, motor-driven plungers, RF coupler and cooling has been completed (see Figs. 2 and 3).

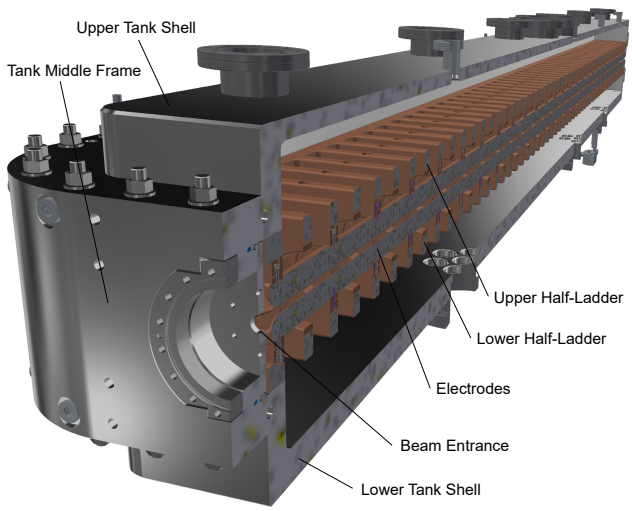

Figure 1: Cut view of the Ladder RFQ showing the individual components.

DESIGN AND MANUFACTURING

The mechanical design consists of an inner copper ladder structure mounted into an outer stainless steel tank. The tank is divided into three parts - the lower and upper shells and a middle frame (see Fig. 1). The lower shell of the tank carries and fixes the position of the inner resonating ladder structure. Due to manufacturing reasons, the ladder structure is divided into two lower and two upper half-ladder elements, which are precisely aligned via guide pins. The half-ladders themselves are machined from solid copper blocks. Between the half-ladder elements, the electrodes are precisely fixed via carrier-rings [10] (see Fig. 4). Those carrier-rings furthermore guarantee a seamless RF connection between the electrodes and the ladder structure.

The RF features are mainly determined by the resonating structure, while the dimensions of the tank have no significant influence on the frequency. Based on the successful high power tests of the unmodulated prototype, we decided to develop a new beam dynamics for a vane-vane voltage of 88 kV. For details of the final beam dynamics and error studies, see [11, 12]. The basic physical and mechanical

* schuett@iap.uni-frankfurt.de / m.schuett@gsi.de

ISBN: 978-3-95450-227-1 ISSN: 2673-5490 doi:10.18429/JACoW-IPAC2022-MOPOST015

BEAM DYNAMICS SIMULATIONS FOR THE SUPERCONDUCTING HELIAC CW LINAC AT GSI*

M. Schwarz†[1], K. Aulenbacher[2,3,4], W. Barth[2,3,4], M. Basten[2,4], C. Burandt[2,4], T. Conrad[1], F. Dziuba[2,3,4], V. Gettmann[2,4], M. Heilmann[4], T. Kürzeder[2,4], S. Lauber[2,3,4], J. List[2,3,4], M. Miski-Oglu[2,4], H. Podlech[1,5], A. Rubin[4], S. Yaramyshev[2,4]
[1]IAP, Goethe University, Frankfurt, Germany, [2]HIM, Helmholtz Institute Mainz, Germany
[3]Johannes Gutenberg University, Mainz, Germany, [4]GSI Helmholtzzentrum, Darmstadt, Germany
[5]Helmholtz Research Academy Hesse for FAIR (HFHF), Frankfurt, Germany

Abstract

The superconducting (SC) continuous wave (CW) heavy ion linac HELIAC (HElmholtz LInear ACcelerator) is a common project of GSI and HIM under key support of IAP Frankfurt. It is intended for future experiments with heavy ions near the Coulomb barrier within super-heavy element (SHE) research and aims at developing a linac with multiple CH cavities as key components downstream the High Charge State Injector (HLI) at GSI. The design is challenging due to the requirement of intense beams in CW mode up to a mass-to-charge ratio of 6, while covering a broad output energy range from 3.5 to 7.3 MeV/u with minimum energy spread. In 2017 the first superconducting cavity of the linac has been successfully commissioned and extensively tested with beam at GSI. In the light of experience gained in this research so far, the beam dynamics layout for the entire linac has been updated and optimized in the meantime. This contribution will provide a brief overview of the recent progress on the project, as well as a potential modification to the linac layout.

BEAM DYNAMICS CONCEPT

A preliminary beam dynamics design - based on the EQUUS (Equidistant Multigap Structure) concept - has been published in 2009 [1]. Meanwhile many experiences have been gained at GSI/HIM [2–7] and IAP [8–16] in design, fabrication and operation of superconducting CH (Crossbar *H*-mode) cavities (Fig. 1) and the associated components. In this context, a revision of the beam dynamics concept was strongly recommended and has been published in 2020 [17]. The EQUUS beam dynamics concept differs from the widely used constant phase approach in a way that the gap center distances in a cavity are equidistant. As the velocity of a bunch increases inside a cavity, EQUUS leads to a varying synchronous phase of the bunch for each gap.

RECENT PROGRESS

In the current advanced demonstration stage, an extended beam test with a first fully equipped series cryomodule is planned to take place shortly at GSI. In recent years, the corresponding infrastructure at GSI has been built and expanded. Among other things, this includes a radiation-shielding area with a connection to the existing 4 K helium liquefier. In addition, the commissioning of an ISO-class 4 clean room at the Helmholtz Institute Mainz (HIM) providing the high-purity environment required for the adequate assembly of superconducting RF structures took place.

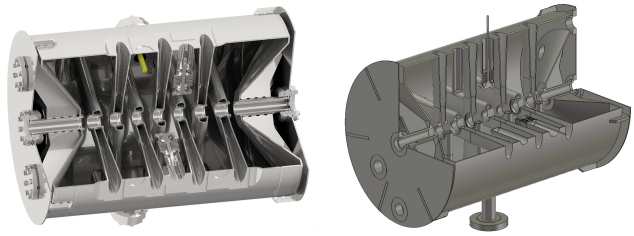

Figure 1: Two of the twelve CH cavity models used to obtain realistic assumptions of gap and drift lengths, as well as gap voltage distributions. Autodesk Inventor rendering of CH1 *(left)* and CST model of CH4 *(right)* [12].

Furthermore, activities on the normal-conducting HLI-injector are underway: This includes R&D for the existing and for a new HLI-RFQ [18] as well as the started tendering for two IH structures for acceleration from 300 keV/u to 1.4 MeV/u by means of an APF beam dynamics concept [19]. Finally, there are considerations regarding an upgrade of the ECR ion source from 14 GHz to 18 GHz to fulfill demands for higher charge states.

Table 1: Basic HELIAC Design Parameters [1]

Parameter	Value
W_{in}	1.4 MeV/u
W_{out}	3.5–7.3 MeV/u
ΔW_{out}	±3 keV/u
I	≤ 1 mA
A/z	≤ 6

The main requirements and boundary conditions for the linac design are summarized in Table 1. With a relatively low beam current, CW-operation and limited longitudinal space, this linac is predestined to be operated in the superconducting mode. Further thoughts on the choice of technology with regard to superconducting or room-temperature operation can be found in [20].

* Work supported by the German Federal Ministry of Education and Research (BMBF, contract no. 05P21RFRB2)
† schwarz@iap.uni-frankfurt.de

ISBN: 978-3-95450-227-1 ISSN: 2673-5490 doi:10.18429/JACoW-IPAC2022-MOPOST016

PROTON LINAC DESIGN FOR THE HIGH BRILLIANCE NEUTRON SOURCE HBS

M. Schwarz[1*], J. Baggemann[2], T. Brückel[2], Q. Ding[2], M. Droba[1], T. Gutberlet[2], K. Kümpel[1], S. Lamprecht[1], J. Li[2], Z. Ma[2], E. Mauerhofer[2], O. Meusel[1], N. Petry[1], H. Podlech[1,4], U. Rücker[2], A. Schwab[2], P. Zakalek[2], C. Zhang[3]
[1]Institute for Applied Physics (IAP), Goethe University Frankfurt, Frankfurt, Germany
[2]JCNS, Forschungszentrum Jülich GmbH, Jülich, Germany
[3]GSI Helmholtzzentrum für Schwerionenforschung GmbH, Darmstadt, Germany
[4]also at Helmholtz Research Academy Hesse for FAIR (HFHF), Frankfurt, Germany

Abstract

Due to the decommissioning of several reactors, only about half of the neutrons will be available for research in Europe in the next decade despite the commissioning of the ESS. High-Current Accelerator-driven Neutron Sources (HiCANS) could fill this gap. The High Brilliance Neutron Source (HBS) currently under development at Forschungszentrum Jülich is scalable in terms of beam energy and power due to its modular design. The driver linac will accelerate a 100 mA proton beam to 70 MeV. The linac is operated with a beam duty cycle of up to 13.6 % (15.3 % RF duty cycle) and can simultaneously deliver three pulse lengths (208 µs, 833 µs and 2 ms) for three neutron target stations. In order to minimize the development effort and the technological risk, state-of-the-art technology of the MYRRHA injector is used. The HBS linac consists of a front end (ECR source, LEBT, 2.5 MeV double RFQ) and a CH-DTL section with 44 room temperature CH-cavities. All RF structures are operated at 176.1 MHz and are designed for high duty cycle. Solid-state amplifiers up to 500 kW are used as RF drivers. Due to the beam current and the high average beam power of up to 952 kW, particular attention is paid to beam dynamics. In order to minimize beam losses, a quasi-periodic lattice with constant negative phase is used. This paper describes the conceptual design and the challenges of a modern high-power and high-current proton accelerator with high reliability and availability.

DESIGN PHILOSOPHY

The High Brilliance Neutron Source HBS [1,2] belongs to the HiCANS class. Their beam energy is significantly lower than the one of spallation neutron sources and therefore opens up other research areas. The beam is sent simultaneously to three different targets by means of a multiplexer in the High Energy Beam Transfer (HEBT) [3]. Each individual beam behind the multiplexer must have a specific time structure in order to use the optimum resolution of the different instruments behind a specific target. The beam macro pulse lengths result from the experimental requirements and are envisaged at 208 µs (96 Hz), 833 µs (24 Hz) and 2 ms (48 Hz), see Fig. 1, resulting in a total average beam power of up to 952 kW (13.6 % beam duty factor).

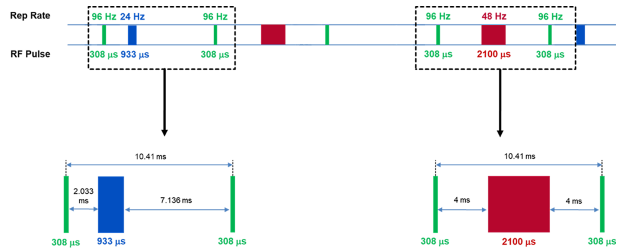

Figure 1: Possible HBS proton pulse structure as generated by the chopper.

Because of the filling time of the cavities the RF duty factor is about 15.3 %. Table 1 summarizes the top-level requirements of the HBS linac.

One of the most important issues of high-power hadron linacs is the choice of technology with respect to superconducting or room-temperature operation. In general, the higher the duty factor and the lower the beam current, the smaller the transition energy between room temperature and superconducting cavities [4]. Because of the high beam current for HBS the required RF power is dominated by the beam power even for room temperature cavities. Because of the much simpler technology avoiding a cryogenic plant, the development of cryomodules and suitable power couplers a room temperature solution has been chosen for HBS.

Table 1: HBS Top-Level Requirements

Parameter	Specifications
Particle type	Protons
Peak beam current	100 mA
Final energy	70 MeV
Duty cycle (beam/RF)	13.6/15.3 %
Beam pulse length	208/833/2000 µs
Repetition rate	96/24/48 Hz
Peak beam power	7 MW
Average beam power	952 kW

The realization of high-power proton accelerators is usually associated with a large R&D effort with corresponding resources regarding man power, prototyping and testing infrastructure. In the case of HBS, this development effort should be minimized by using already developed technology.

* schwarz@iap.uni-frankfurt.de

ISBN: 978-3-95450-227-1 ISSN: 2673-5490 doi:10.18429/JACoW-IPAC2022-MOPOST017

DESIGN AND BEAM DYNAMICS STUDY OF DISK-LOADED STRUCTURE FOR MUON LINAC

K. Sumi*, T. Iijima, K. Inami, Y. Sue, M. Yotsuzuka,
Nagoya University, Nagoya, Aichi, Japan
H. Ego, M. Otani, N. Saito, T. Mibe, M. Yoshida,
High Energy Accelerator Research Organization (KEK), Tsukuba, Ibaraki, Japan
Y. Kondo, K. Moriya, Japan Atomic Energy Agency (JAEA), Tokai, Naka, Ibaraki, Japan
Y. Takeuchi, Kyushu University, Fukuoka, Japan
Y. Nakazawa, Ibaraki University, Mito, Ibaraki, Japan
H. Yasuda, University of Tokyo, Tokyo, Japan

Abstract

The disk-loaded structures (DLS) in the muon LINAC are under development for the J-PARC muon g−2/EDM experiment. Four DLSs with an accelerating gradient of 20 MV/m take charge of muon acceleration from 40 MeV to 212 MeV, which corresponds to 70% to 94% of the speed of light. The quasi-constant gradient type TM01-2π/3 mode DLSs with gradually varying disk spacing was designed and it was confirmed that the cumulative phase slip due to the mismatch between muon and phase velocity can be suppressed to less than 2 degrees at the frequency of 2592 MHz. In addition, the optimum synchronous phase and the lattice were investigated to satisfy the requirements of the total emittance less than 1.5π mm mrad and the momentum spread less than 0.1% in RMS.

INTRODUCTION

The world experimental average value of the muon anomalous magnetic moment, g−2, deviates from the standard model prediction by 4.2 times the standard deviation [1]. This discrepancy may be a sign of new physics beyond the standard model. The muon electric dipole moment, EDM, which is unobserved, could also be enhanced if new physics exists.

The experiment in J-PARC plans to validate the discrepancy of muon g−2 and to search muon EDM with novel techniques: low emittance muon beam, compact storage magnet, no electrostatic focusing, and three-dimensional spiral injection [2]. The low emittance muon beam is generated by thermalized muonium ionization followed by their acceleration by the muon LINAC. The requirements for beam quality are low transverse normalized emittance of approximately 1.5π mm mrad and momentum of 300 MeV/c with a small spread of less than 0.1% in root-mean-square (RMS).

The muon linac consists of four kinds of structures: radio frequency quadrupole (RFQ), inter-digital H-mode drift-tube linac (IH-DTL), disk and washer coupled cavity linacs (DAW-CCL), and disk-loaded traveling wave structures (DLS), matching the varying muon velocity for the short-time — sufficiently shorter than the muon lifetime of 2.2 µs — acceleration to suppress decay loss. The DLS section consists of four DLSs approximately 2 m in length and takes charge of acceleration from 40 MeV to 212 MeV in kinetic energy, corresponding velocity range of 70-94% of the speed of light. The transport line includes two quadrupole magnets between each DLS. The requirement for the DLS is a high accelerating gradient of 20 MV/m.

STRUCTURE DESIGN

Since DLS is an accelerating structure that has been in use for relativistic electron acceleration and has proven to have a sufficiently high gradient, we apply it for high-velocity muon acceleration. The essential feature of DLS for muon acceleration, different from DLS for electron acceleration, is that disk spacing (cell length) varies proportionally to muon velocity [3]. Since assuming a constant gradient is convenient for the velocity calculation of muon through the DLS section, a quasi-constant gradient type with linear tapering iris apertures is adopted.

Table 1: Parameters of the First Cell in the DLS Section of Two Different Frequencies

Parameters	**L-band** [5]	**S-band**
Structure type	disk-loaded traveling wave quasi-constant gradient type	
Resonant mode	TM01-2π/3	
Frequency [MHz]	1296	2592
Muon velocity ($\beta = v/c$)	0.695	
Cell length (D) [mm]	53.698	26.885
Iris aperture ($2a$) [mm]	43.370	25.875
Cylinder diameter ($2b$) [mm]	181.147	92.070
Disk thickness [mm]	5.000	
Quality factor (Q)	17116	11289
Shunt impedance (Z) [MOhm/m]	29.15	31.16
Group velocity (v_g/c) [%]	1.22	1.52
Field attenuation factor (α) [/m]	0.0648	0.163
Cell accelerating gradient (E_{acc}) [MV/m/MW$^{1/2}$]	1.94	3.13

* ksumi@hepl.phys.nagoya-u.ac.jp

ISBN: 978-3-95450-227-1 ISSN: 2673-5490 doi:10.18429/JACoW-IPAC2022-MOPOST020

IN-KIND CONTRIBUTIONS: THE PIP-II PROJECT AT FERMILAB

L. Lari†, Fermilab, Batavia, IL, USA
L. Merminga, A. Rowe, Fermilab, Batavia, IL, USA

Abstract

The Proton Improvement Plan II (PIP-II) Project is the first U.S. accelerator project with significant contributions from International Partners. A project management framework was created to fully integrate and make consistent across all partners the design, development, and delivery of In-Kind Contributions (IKC) to PIP-II. This framework consists of planning documentation, procedures, and communication and assessment processes to control schedule, risk, quality, and technical integration over the lifetime of the project. The purpose of this paper is to present the PIP-II IKC model put in place to properly integrate the IKC deliverables into the PIP-II Linac and share experience and lessons learned from its early implementation.

INTRODUCTION

The PIP-II Project [1,2] is an essential upgrade of the Fermilab accelerator complex. An all-new, leading-edge superconducting linear accelerator located in new buildings, combined with a comprehensive overhaul of the laboratory's existing circular accelerators, will deliver multimegawatt proton beam power and, in turn, enable the world's most intense beam of neutrinos for the international Long Baseline Neutrino Facility (LBNF) and Deep Underground Neutrino Experiment (DUNE) [3]. The PIP-II Project is also designed with scalability in mind to enable future upgrades with a broad spectrum of scientific opportunities.

A unique aspect of the PIP-II Project is that it is the first U.S. Department of Energy (DOE) funded particle accelerator to be built with significant international participation. Figure 1 shows a schematic overview of the PIP-II Linac IKC from partner countries indicated by flag. PIP-II will be the highest-energy and highest-power continuous-wave (CW) proton Linac ever built, capable of delivering both pulsed and continuous particle beams.

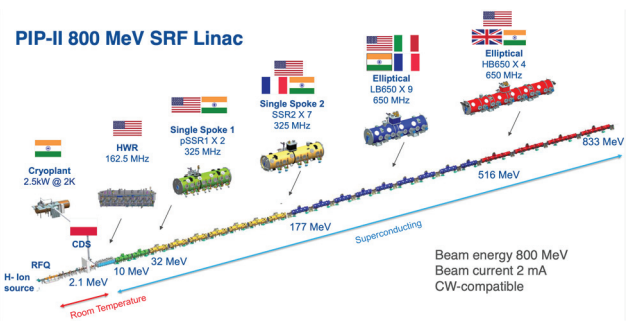

Figure 1: Overview of the significant IKC for PIP-II. Flags highlight which country plans to contribute to PIP-II Project. The flags are in the areas of the specific contribution.

† llari@fnal.gov

With major IKC from institutions in India [1], Italy [1,4], UK [1], France [1,5] and Poland [1], the project's international partners bring wide-ranging expertise and know-how in core particle accelerator technologies along with an established track-records in big-physics initiatives.

PIP-II IKC MODEL

The PIP-II Project was baselined in December 2020 and in April 2022 received the approval from DOE to start construction. The DOE portion of the PIP-II Project cost is approximately one billion dollars (i.e., $978M). The IKC cost is estimated to be approximately one third of the DOE approved project cost. The PIP-II Project is planned to be completed at the end of 2028. This date represents the early completion target date.

The IKC size and the international nature of the PIP-II Project required the development of a special planning framework to properly integrate the Partner deliverables into the PIP-II Project scope and schedule. Figure 2 shows a schematic of the IKC life cycle implemented in the PIP-II Project.

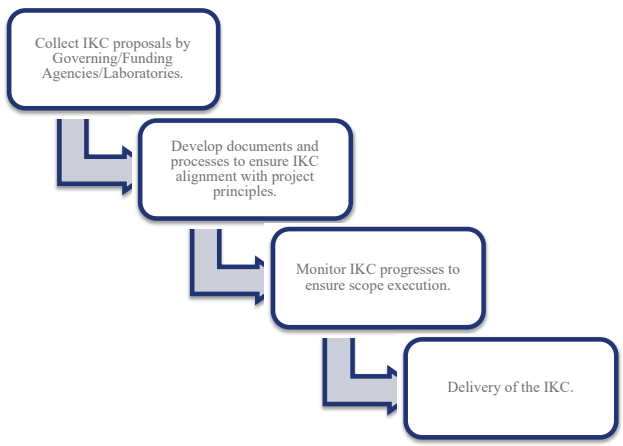

Figure 2: PIP-II Life cycle of IKC.

- Collect IKC proposals by Governing/Funding Agencies/Laboratories is the initial phase for starting the evaluation of any possible IKC to the PIP-II Project. If IKC are selected on the basis on expertise/know-how in a specific technical field, Agency-Level Agreements or other legally binding agreements are typically established between DOE and the Partner funding agency. These legally binding documents outline the high-level management structure for activities to be undertaken under the agreement and/or its subsidiary agreements. At this stage, it is imperative to clearly define the IKC high-level deliverables.

ISBN: 978-3-95450-227-1 ISSN: 2673-5490 doi:10.18429/JACoW-IPAC2022-MOPOST021

REACCELERATOR UPGRADE, COMMISSIONING AND FIRST EXPERIMENTS AT THE NATIONAL SUPERCONDUCTING CYCLOTRON LABORATORY (NSCL) / FACILITY FOR RARE ISOTOPE BEAMS (FRIB)*

A.C.C. Villari†, B. Arend, G. Bollen, D.B. Crisp, K.D. Davidson, K. Fukushima, A.I. Henriques, K. Holland, S-H. Kim, A. Lapierre, T. Maruta, D.G. Morris, D.J. Morrissey, S. Nash, P.N. Ostroumov, A.S. Plastun, J. Priller, B.M. Sherrill, M. Steiner, R. Walker, T. Zhang, Q. Zhao
Facility for Rare Isotope Beams, Michigan State University, East Lansing, MI, U.S.A.

Abstract

The reaccelerator ReA is a state-of-the-art super-conducting linac for reaccelerating rare isotope beams produced via inflight fragmentation or fission and subsequent beam stopping. ReA was subject of an upgrade that increased its final beam energy from 3 MeV/u to 6 MeV/u for ions with charge over mass equal to 1/4. The upgrade included a new room-temperature rebuncher after the first section of acceleration, a new beta = 0.085 QWR cryomodule and two new beamlines in a new experimental vault. During commissioning, beams were accelerated with near 100 percent transport efficiency through the linac and delivered through beam transport lines. Measured beam characteristics match those calculated. Following commissioning, stable and long living rare isotope beams from a Batch Mode Ion Source (BMIS) were accelerated and delivered to experiments. This contribution will briefly describe the upgrade, and results from beam commissioning and beam delivery for experiments.

INTRODUCTION

The reaccelerator (ReA) at NSCL/FRIB [1] is a worldwide unique facility accelerating rare isotope beams, which are initially produced by projectile fragmentation or fusion-fission and stopped in gas cells. ReA has been operated since 2015 accelerating rare or stable isotope beams from 0.3 MeV/u to 3 MeV/u for the mass to charge ratio (Q/A) of 4 and 6 MeV/u for Q/A of 2.

Low-energy beams from the beam stopping facilities are mass separated and injected into a beam-cooler-buncher (BCB). The BCB is a radio-frequency quadrupolar trap with axial and radial confinement of ions in a buffer gas, designed to improve the optical properties by cooling and to convert the incoming continuous beam into bunches for efficient injection and capture in the Electron Beam Ion Trap (EBIT) [2]. In the EBIT, the beam is charge breed for achieving charge states compatible with the needs for acceleration and beam purity. After the EBIT, the beam is mass selected in the achromatic Q/A separator and injected at the energy of 12 keV/u in a multi-harmonic buncher, where it is buched to the operation frequency of the Radio Frequency Quadrupole (RFQ) at 80.5 MHz [3]. Following the RFQ, the beam is injected into the first superconducting quarter wave resonator (QWR) with beta = 0.041 acting as a rebuncher. Two superconducting solenoids (SS) with a maximum field of 9 T are installed in this cryomodule. Following the rebuncher, a first accelerating cryomodule has six QWRs with beta = 0.041 and three SS. The third and last cryomodule of ReA3 has eight QWRs with beta = 0.085 and three SS. Following the accelerator, the beam is energy analyzed and sent to an experimental area with three beam lines, one dedicated to the spectrometer SECAR for astrophysics studies, and two others general purpose without permanent experimental setups.

For providing broader opportunities for nuclear physics experiments with higher beam energies, an upgrade of ReA was started in May 2019 with the goal to double the final beam energy and add new experimental stations with equipment adapted to the new scientific areas. The upgrade, which was completed in April 2021, included a new room-temperature rebuncher at 161 MHz after the first section of the accelerator, a new FRIB-style cryomodule [4] with beta = 0.085 quarter wave resonators and two beamlines in a new experimental vault adapted to higher energies.

Simultaneously, a Batch-mode-ion source (BMIS) was completed. BMIS is based on the ISOLDE/VADIS target/ion source [5]. Its purpose is to provide beams of stable of long-lived rare isotope beam for reacceleration during the time NSCL's coupled cyclotron facility was shut down in the transition phase of FRIB project completion and start of operation.

In this contribution we'll briefly present the new rebuncher as well as the new cryomodule and beam lines, the beam optics calculations and commissioning results. Finally, we'll provide information regarding beams used for experiments after the commissioning of the upgrade.

THE REA6 PROJECT

The low energy and reaccelerator areas as well as the new upgrade of the reaccelerator (called ReA6) is shown in Fig. 1. Labels 1, 2, 3 and 4 indicate the location of the batch mode ion source, the new room-temperature rebuncher, the new cryomodule and the new experimental area. The new cryomodule for ReA6 is identical to the ones

* Work supported by the NSF under grant PHY15-65546 and DOE-SC under award number DE-SC0000661
† villari@frib.msu.edu

ISBN: 978-3-95450-227-1 ISSN: 2673-5490 doi:10.18429/JACoW-IPAC2022-MOPOST022

UPGRADE OF THE RADIO FREQUENCY QUADRUPOLE OF THE REACCELERATOR AT NSCL / FRIB*

A. S. Plastun, S. Nash, J. Brandon, A. Henriques, S.-H. Kim, D. Morris,
P. N. Ostroumov, A. C. C. Villari, Q. Zhao, S. Zhao, D. Crisp, D. Sanderson
Facility for Rare Isotope Beams, Michigan State University, East Lansing, MI 48824, USA

Abstract

The ReA-RFQ is a four-rod radio frequency quadrupole (RFQ) structure of the MSU rare isotope Reaccelerator.

Since the commissioning in 2010 the original ReA RFQ experienced some operational problems. The design voltage was never reached, and continuous wave (CW) operation was never achieved due to cooling issues. In 2016, a new design including trapezoidal modulation was proposed, which permitted achieving increased reliability, and would allow reaching the original required specifications. The new rods were built, installed and commissioned in 2019. Since then, the RFQ has been working successfully, and recently it was opened for inspection and verification of its internal status. No damage and discoloration were observed.

This paper describes the RFQ rebuild process, involving specific RF protections and other technical aspects related to the assembly of the structure.

INTRODUCTION

The MSU reaccelerator started user operation as ReA3 in 2015 [1]. The facility is being continuously upgraded to enhance its scientific capabilities and reliability. Recent upgrades include: (a) replacement of the ReA3 RFQ electrodes to improve their cooling and provide high capture of pre-bunched 16.1 MHz beams with $A/Q = 5$ [2], as well as CW operation, (b) installation of a room-temperature rebuncher cavity and another superconducting RF (SRF) cryomodules after the ReA3 linac, (c) installation of the new high-current electron-beam ion source (EBIS) for stable and rare-isotope beams, (d) installation of the new RF controllers.

Although the nominal range of mass-to-charge ratios is from 2 to 4, the operation with ions of $A/Q = 5$ is considered to best match the EBIT performance [3]. The original ReA3 RFQ was commissioned in 2010 and has been in service until April 2019. Several issues related to the RF contacts between various parts of the structure became apparent upon commissioning. After the modification of the tuning plates, their RF contacts, and the electrodes' water line clamps, we had to limit the average power to 40 kW. This could provide the CW operation only with beams of $A/Q = 2$. Higher voltages, required for the beams with A/Q above 4, were possible at reduced duty factors. Thanks to the natural pulsed operation of the EBIT, this was not a problem for the facility, except for the inability to accelerate beams of $A/Q = 5$ due to the sparking issues. Despite the multiple upgrades and improvements, the operational reliability of the RFQ was gradually reducing.

The CW operation of the reaccelerator facility is essential for its future multi-user upgrade, when pulsed rare-isotope and stable beams will be simultaneously accelerated in the linac and delivered to different users in an alternate manner [4,5]. Until recently, the RFQ has been the only part limiting the CW performance of the facility.

UPGRADE STRATEGY

In 2016, the original vendor of the ReA3 RFQ proposed a new design of the electrodes' stems. The proposal included the modification of cooling channels, tuning plates, and the angle brackets connecting the tuning plates to the vertical stems of the four-rod RF structure.

The FRIB/NCSL scientists also proposed to re-designed the quadrupole electrodes in order to reduce the inter-electrode voltage. First, this allowed for the reduction of the RF power consumption. Second, the peak surface electric fields also decreased. To recover some energy gain after the voltage got reduced, a trapezoidal modulation of the electrodes was employed [6]. Table 1 summarizes the main design parameters that have been changed. Some design considerations are presented in [2].

Table 1: Modifications of the RFQ (for $A/Q = 5$ beam)

Parameter	**Original RFQ** [7]	**New RFQ**
Output energy	600 keV/u	538 keV/u
Voltage	86.5 kV	70.0 kV
Average radius R_0	7.3 mm	6.56 mm
RF power	120 kW	80 kW
Peak surface field	1.6 Kp	1.4 Kp
Synch. phase	−20°	−60° to −20°
Modulation	1.15 – 2.6	1.13 – 2.5
Transmission of:		
80.5-MHz beam	82%	89%
16.1-MHz beam	N/A	78%

SIMULATIONS

Analysis of the Four-rod RF Structure

The design upgrade started from analysis of the original four-rod ReA3 RFQ to find reasons for sparking. It required an accurate simulation of the electric field distribution on the surfaces of the electrodes. Rather than simulating the whole four-rod RF structure, we created an electrostatic model of

* WORK SUPPORTED BY THE NATIONAL SCIENCE FOUNDATION UNDER GRANT PHY15-65546

ISBN: 978-3-95450-227-1 ISSN: 2673-5490 doi:10.18429/JACoW-IPAC2022-MOPOST024

A LOCAL MODIFICATION OF HL-LHC OPTICS FOR IMPROVED PERFORMANCE OF THE ALICE FIXED-TARGET LAYOUT*

M. Patecki†, D. Kikoła, Warsaw University of Technology, Faculty of Physics, Warsaw, Poland
A. Fomin, P. Hermes, D. Mirarchi, S. Redaelli, CERN, Geneva, Switzerland

Abstract

The Large Hadron Collider (LHC) at the European Organization for Nuclear Research (CERN) is the world's largest and most powerful particle accelerator colliding beams of protons and lead ions at energies up to 7 TeV and 2.76 TeV, respectively. ALICE is one of the detector experiments optimised for heavy-ion collisions. A fixed-target experiment in ALICE is considered to collide a portion of the beam halo, split using a bent crystal, with an internal target placed a few meters upstream of the detector. Fixed-target collisions offer many physics opportunities related to hadronic matter and the quark-gluon plasma to extend the research potential of the CERN accelerator complex. Production of physics events depends on the particle flux on target. The machine layout for the fixed-target experiment is being developed to provide a flux of particles on a target high enough to exploit the full capabilities of the ALICE detector acquisition system. In this paper, we discuss a method of increasing the system's performance by applying a local modification of optics to set the crystal at the optimal betatron phase.

INTRODUCTION

Advancements in the knowledge of fundamental constituents of matter and their interactions are usually driven by the development of experimental techniques and facilities, with a significant role of particle accelerators. The Large Hadron Collider (LHC) [1] at the European Organization for Nuclear Research (CERN) is the world's largest and most powerful particle accelerator colliding opposite beams of protons (p) and lead ions (Pb), allowing for unprecedentedly high centre-of-mass energies of up to 14 TeV and 5.5 TeV, respectively. The ALICE fixed-target (ALICE-FT) programme [2] is proposed to extend the research potential of the LHC and the ALICE experiment [3]. The concept is based on steering onto a solid internal target a fraction of the proton beam halo split by means of a bent crystal, similar to crystals being developed for beam collimation at the LHC [4–6]. Splitting the beam is performed by exploiting the channelling process occurring inside a bent crystal, resulting in a trajectory deflection equivalent to the geometric bending angle of a crystal body [7]. Such a setup, installed in the proximity of the ALICE detector, would provide the most energetic proton beam ever in the fixed-target mode with centre-of-mass energy per nucleon-nucleon ($\sqrt{s_{NN}}$) of 115 GeV. By using high-density targets, a high luminosity, in the order of an inverse femtobarn, can be achieved, allowing for an intensive study of rare processes, quark and gluon distributions at high momentum fraction (x), sea quark and heavy-quark content in the nucleon and nucleus and the quark-gluon plasma, including the QCD phase transition. Most of these phenomena are not accessible otherwise. Details on the physics potential of the ALICE-FT programme are summarised in the AFTER@LHC study group [2, 8].

The problem that we address is to design the machine layout that provides a number of protons on a target high enough to exploit the full capabilities of the ALICE detector acquisition system without affecting the LHC availability for regular beam-beam collisions. Our proposal of the ALICE-FT layout [9] follows general guidelines on technical feasibility and impact on the LHC accelerator of potential fixed-target experiments provided by the LHC Fixed Target Working Group of the CERN Physics Beyond Colliders forum [10, 11]. We also profit from the preliminary designs reported in [12, 13] and from the design study of an analogous fixed target experiment at the LHC proposed to measure electric and magnetic dipole moments of short-lived baryons[14]. In this paper, we give an update on the ALICE-FT machine layout. We report on a local optics modification in the insertion hosting the ALICE experiment (IR2) that provides an increased flux of particles on a target by setting the crystal at the optimal betatron phase. This method is independent of the crystal location, allowing for a crystal installation in a place with good space availability.

MACHINE CONFIGURATION

A potential installation of the ALICE-FT setup will coincide with a major LHC upgrade in terms of instantaneous luminosity, commonly referred to as the High-Luminosity LHC (HL-LHC) [15], taking place in the Long Shutdown 3 (2025-2027), to make it ready for Run4 starting in 2027. Some of the expected beam parameters, having a direct impact on the ALICE-FT experiment performance, are given in Table 1. Among beam parameters being a subject of the upgrade, we highlight the total beam current increase nearly by a factor of two, up to about 1.1 A, leading to more than 0.7 GJ of total beam energy stored in the machine. A highly efficient collimation system is therefore present in the LHC [16] to protect its elements, especially superconducting, from impacts of particles from the beam. The collimation system is organised in a precise multi-stage hierarchy (see Table 2) over two dedicated insertions (IRs): IR3 for momentum cleaning and IR7 for betatron cleaning. Each collimation insertion features a three-stage cleaning based on primary collimators (TCP), secondary collimators (TCSG)

* This project has received funding from the European Union's Horizon 2020 research and innovation programme, acronym: FixedTargetLand, grant agreement: 101003442.
† marcin.patecki@pw.edu.pl

ISBN: 978-3-95450-227-1 ISSN: 2673-5490 doi:10.18429/JACoW-IPAC2022-MOPOST025

INFLUENCES OF THE TRANSVERSE MOTIONS OF THE PARTICLES TO THE RECOMBINATION RATE OF A CO-PROPAGATING ELECTRON-ION SYSTEM*

G. Wang†, V. N. Litvinenko[1], D. Kayran, I. Pinayev, P. Thieberger,
Collider-Accelerator Department, Brookhaven National Laboratory, Upton, NY USA
[1]also at Department of Physics and Astronomy, Stony Brook University, Stony Brook, NY USA

Abstract

For a system with the ion beam co-propagating with the electron beam, such as a traditional electron cooler or a Coherent electron Cooler (CeC), the recombination rate is an important observable for matching the energy of the electrons with the ions [1, 2]. In this work, we have developed the analytical expressions to investigate how the recombination rate depends on the energy difference of the two beams, with the influences from the transverse motions of the particles being considered. The analytical results are then applied to analyse the measured recombination data collected during the CeC experiment in RHIC run 21 and RHIC run 22.

INTRODUCTION

The CeC experiment at RHIC targets on cooling of Au^{+79} ions with electrons at the energy of $\gamma = 28.5$ [3]. One of the major challenges in the experiment is to ensure that the electron beam has the same energy as that of the ion beam. A common technique employed for the energy matching is by measuring the recombination rate. Since the recombination rate is maximized when the velocities of the two beams coincide, the optimal energy of the electrons can be identified by scanning the energy of the electrons while monitoring the recombination rate. How fast the recombination rate drops with the energy deviation from the optimal energy depends on the 3D velocity spreads of the electrons and the ions. During RHIC run 21, it was found in the CeC experiment that the measured recombination rate drops much slower than what one would expect solely from the measured energy spread of the electrons and the ions. One of the major candidates responsible for the discrepancy is the transverse motion of the particles which had been neglected from the analytical estimates.

In this work, we derived analytical formula to calculate the recombination rate with transverse motion of the particles taken into account. The analytical results are then used to fit the data collected during the CeC experiment in run 21 and run 22.

DERIVATION OF RECOMBINATION RATE

The general form of the recombination rate is given by the following integral over the velocity distribution of the electrons and the ions [2].

$$\alpha_r = \frac{\int_{-\infty}^{\infty} d^3v_i d^3v_e f_e(v_e) f_I(v_i) |\vec{v}_e - \vec{v}_i| \sigma(|\vec{v}_e - \vec{v}_i|)}{\int_{-\infty}^{\infty} d^3v_i d^3v_e f_e(v_e) f_I(v_i)}, \quad (1)$$

where $\sigma(|\vec{v}_e - \vec{v}_i|)$ is the recombination cross section which depends on the relative velocity of an ion with respect to an electron, and $f_e(v_e)$ and $f_I(v_i)$ are the velocity distributions of the electrons and the ions.

Gaussian Transverse Velocity Distribution

We assume that the velocity distribution of electrons is

$$f_e(v_e) = \frac{1}{2\pi\beta_{e,\perp}^2} \exp\left(-\frac{v_{e,x}^2 + v_{e,y}^2}{2\beta_{e,\perp}^2}\right) f_{e,z}(v_{e,z}) \quad (2)$$

and that of ions is

$$f_I(v_i) = \frac{1}{2\pi\beta_{i,\perp}^2} \exp\left(-\frac{v_{i,x}^2 + v_{i,y}^2}{2\beta_{i,\perp}^2}\right) f_{i,z}(v_{i,z}), \quad (3)$$

with $\beta_{e,\perp}$ and $\beta_{i,\perp}$ being the transverse velocity spread of the electrons and the ions. Inserting Eq. (2) and Eq. (3) into Eq. (1) yields

$$\alpha_r = \frac{\int_{-\infty}^{\infty} d^3v v\sigma(v) e^{-m_e\left(v_x^2+v_y^2\right)/2kT_{ei}} \int_{-\infty}^{\infty} f_{e,z}(v_z + v_{i,z}) f_{i,z}(v_{i,z}) dv_{i,z}}{(2\pi kT_{ei}/m_e) \int_{-\infty}^{\infty} f_{e,z}(v_z + v_{i,z}) f_{i,z}(v_{i,z}) dv_z dv_{i,z}} \quad (4)$$

where we defined the effective temperature parameter

$$T_{ei} = \frac{m_e}{2k}\left(\beta_{e,x}^2 + \beta_{e,y}^2 + \beta_{i,x}^2 + \beta_{i,y}^2\right). \quad (5)$$

Longitudinally Cold Electrons and Ions

Typically, the longitudinal velocity spread in the beam frame is much smaller than the transverse velocity spread and hence we can take the delta function for the longitudinal velocity distribution, i.e. $f_{e,z}(v_{e,z}) = \delta(v_{e,z} - v_{z0})$ and $f_{i,z}(v_{i,z}) = \delta(v_{i,z})$. In this case, Eq. (4) becomes

$$\alpha_r = \frac{1}{2\pi kT_{ei}/m_e} \int_{-\infty}^{\infty} d^3v v\sigma(v) e^{-m_e\left(v_x^2+v_y^2\right)/2kT_{ei}} \delta(v_z - v_{z0}). \quad (6)$$

The recombination cross section for an electron moving with velocity $\vec{v}$ with respect to the ion is [2]

$$\sigma(v) = A\frac{2h\nu_0}{m_e v^2}\left[\ln\left(\sqrt{\frac{2h\nu_0}{m_e v^2}}\right) + \gamma_1 + \gamma_2\left(\frac{m_e v^2}{2h\nu_0}\right)^{1/3}\right], \quad (7)$$

where $A = 2.11\times10^{-22} cm^2$, $h\nu_0 = Z^2 \times 13.6eV$, Z is the

* Work supported by Brookhaven Science Associates, LLC under Contract No. DE-SC0012704 with the U.S. Department of Energy.
† gawang@bnl.gov

ISBN: 978-3-95450-227-1 ISSN: 2673-5490 doi:10.18429/JACoW-IPAC2022-MOPOST026

INFLUENCES OF THE ENERGY JITTER TO THE PERFORMANCE OF THE COHERENT ELECTRON COOLING*

G. Wang†, V. N. Litvinenko[1], J. Ma,
Collider-Accelerator Department, Brookhaven National Laboratory, Upton, NY USA
[1]also at Department of Physics and Astronomy, Stony Brook University, Stony Brook, NY USA

Abstract

The bandwidth of a coherent electron cooling (CeC) system is typically two to three orders of magnitude higher than the traditional RF based stochastic cooling system, which make it possible to cool the ion bunches with high energy and high intensity. However, for such broad bandwidth, jitters in the energy of the cooling electron bunches present a serious challenge to the performance of the cooling system. In this work, we present simulation studies about the influences of the energy jitter to a CeC system with parameters relevant to the on-going CeC experiment at RHIC.

INTRODUCTION

As one of the candidates for cooling high energy proton beam with high intensity in a collider, the principle of CeC has not been demonstrated experimentally. To test its feasibility, the CeC experiment at RHIC has been developed with the goal of cooling of Au^{+79} ions with electrons at the energy of $\gamma = 28.5$ [1]. During the CeC experiment in RHIC run 21, it had been measured that the RMS pulse-to-pule jitter in the energy of the electron bunches was in the level of 0.1%, which was significantly larger than the slice energy spread of the electron bunch, i.e. 0.02% (RMS). It was suspected that such an energy jitter was responsible for the absence of the expected cooling from the CeC.

In this work, we investigate how the CeC rate is affected by the level of energy jitter in the electrons' energy through numerical simulations. Firstly, we validate the simulation code by benchmarking it with the analytical results for an infinitely long electron bunch. Then we simulated the evolution of the ion bunch profile in the presence of the CeC with realistic electron bunch for various level of energy jitter in the electron bunches.

REDUCTION OF LOCAL COOLING RATE DUE TO ENERGY JITTER

During the cooling process of the PCA based CeC, each ion creates an electron density perturbation in the modulator, which is then amplified in the PCA and generates an electric field in the kicker section to cool the ion. Figure 1 (red triangles) shows the cooling electric field in the kicker section as predicted by 3D simulation for the CeC experiment at RHIC. The arrival time of the ion with respect to the cooling field depends on the energy of the electrons and the ions. In the presence of an energy jitter in the electron bunches, the arrival time of the ions with respect to the cooling field that they generate varies from turn to turn, which leads to a reduction of the cooling rate.

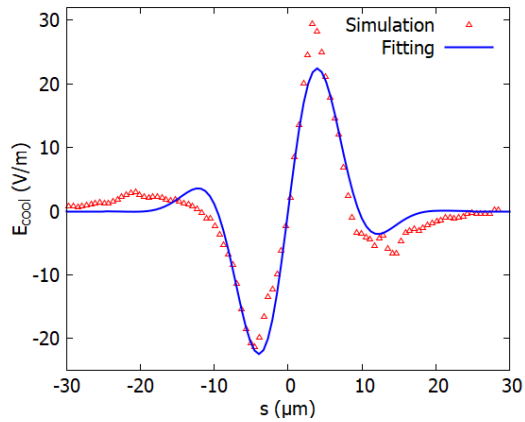

Figure 1: Cooling field initiated by an ion in the electrons of the CeC experiment at RHIC. The red triangles are data from the 3D simulations with code SPACE and the blue solid curve is the fitting from Eq. (1).

To simplify the analytical derivation and long-term cooling simulation, we fit the cooling field with the following expression (see the blue curve in Fig. 1) [2]:

$$E_{fit}(z) = E_A \exp\left(-\frac{z^2}{2\sigma_c^2}\right)\sin(k_0 z), \quad (1)$$

with $\sigma_c = 6.475\mu m$, $E_A = 28.1V/m$ and $k_0 = 3.28\times10^5 m^{-1}$. We assume that the energy jitter of the electron bunches has Gaussian distribution, i.e.

$$f(\delta_e) = \frac{1}{\sqrt{2\pi}\delta_{jit}}\exp\left(-\frac{\delta_e^2}{2\delta_{jit}^2}\right), \quad (2)$$

where $f(\delta_e)$ is the probability function to find the electron bunch has energy of $E_0 + \delta_e E_0$, E_0 is the designed energy of the electrons, and δ_{jit} is the R.M.S. spread of the energy jitter. In the presence of the energy jitter of the electron bunches, the effective energy kick received by an ion for cooling should be averaged over the distribution function of the energy jitter, i.e.

$$\langle\delta\gamma\rangle = Zel_k\int_{-\infty}^{\infty} f(\delta_e)E_{fit}(\Delta z)d\delta_e, \quad (3)$$

where $\Delta z = R_{56}(\delta_e - \delta_h)$ is the longitudinal location of the ion with respect to the cooling electric field, l_k is the length of the kicker section, R_{56} is the longitudinal dispersion from the modulator to the kicker and δ_h is the relative

* Work supported by Brookhaven Science Associates, LLC under Contract No. DE-SC0012704 with the U.S. Department of Energy.
† gawang@bnl.gov

ISBN: 978-3-95450-227-1 ISSN: 2673-5490 doi:10.18429/JACoW-IPAC2022-MOPOST027

THE ZGOUBIDOO PYTHON FRAMEWORK FOR RAY-TRACING SIMULATIONS WITH ZGOUBI: APPLICATIONS TO FIXED-FIELD ACCELERATORS

M. Vanwelde *, C. Hernalsteens[1], R. Tesse, E. Gnacadja, E. Ramoisiaux, N. Pauly,
Université libre de Bruxelles, Brussels, Belgium
[1]also at CERN, Geneva, Switzerland

Abstract

The study of beam dynamics in accelerators featuring main magnets with complex geometries such as Fixed Field Accelerators (FFAs) requires simulation codes allowing step-by-step particle tracking in complex magnetic fields, such as the Zgoubi ray-tracing code. To facilitate the use of Zgoubi and to allow readily processing the resulting tracking data, we developed a modern Python 3 interface, Zgoubidoo, using Zgoubi in the backend. In this work, the key features of Zgoubidoo are illustrated by detailing the main steps to obtain a non-scaling FFA accelerator from a scaling design. The results obtained are in excellent agreement with prior results, including the tune computation and orbit shifts. These results are enhanced by Zgoubidoo beam dynamics analysis and visualization tools, including the placement of lattice elements in a global coordinate system and the computation of linear step-by-step optics. The validation of Zgoubidoo on conventional scaling and non-scaling FFA designs paves the way for future uses in innovative FFA design studies.

INTRODUCTION

The magnetic field of FFAs is constant in time, which allows rapidly accelerating different kinds of beams, in particular high-intensity beams (high repetition rate), in a wide energy range (variable energy beam). Their magnetic structure also enables strong focusing, either focusing using alternating fields or focusing using spiral magnet edges. These key points allow FFAs to be accelerators of choice for some applications: FFAs have already been considered for neutron spallation, muon accelerators, and medical applications [1–5]. There are two main variants of FFAs: scaling FFAs and non-scaling FFAs. Scaling FFAs, which were the first to be studied, allow having constant tunes with energy by imposing a strong condition on the magnetic field, while non-scaling FFAs relax this condition to have easier to build magnets and to reduce the orbit shift at the expense of a non-zero tune variation. The complex geometry and magnetic fields and the absence of a true reference trajectory due to its energy dependence make simulation codes featuring step-by-step tracking the tools of choice. The Zgoubi ray-tracing code [6–8] allows tracking particles in any magnetic and electric field, particularly in highly non-linear magnetic fields, which is the case for FFAs. In addition, Zgoubi realistically models the magnet fringe fields and allows the user to implement complex and arbitrary misalignment of the magnetic elements, and shape of the magnet edges. It can be used for the optics study, helpful for the accelerator design, but also for the final study of the lattice, using measured field maps with realistic fringe fields and possible magnetic imperfections. Because of these advantages, Zgoubi has been extensively used to study FFA lattices [5, 9]. To facilitate the use of Zgoubi and allow data analyzes and simplified visualizations, we developed a modern Python 3 interface using Zgoubi in the backend: Zgoubidoo [10]. This library provides a fully featured and easy-to-use interface to Zgoubi. It can be used both to generate Zgoubi input files and run the simulations in parallel, as well as to perform more advanced tracking results analyzes, including linear and non-linear beam dynamics studies. Additionally, Zgoubidoo also has modules ensuring the correct placement of the lattice elements in space and the plotting of the beamline and tracking results, including particle trajectories in the global reference frame. Zgoubidoo thus has all the necessary tools to study all kinds of accelerators, especially FFAs. This work illustrates the main features of Zgoubidoo on well-known scaling and non-scaling FFA designs [11, 12]. First, the main steps to model and simulate a scaling lattice with a large field index [11] are presented. Then, the magnet simplification steps allowing to transform this scaling design into a non-scaling one following the steps presented in Ref. [12] are detailed. The complete analysis of conventional FFA lattices with Zgoubidoo, from the closed orbit search to the linear tune computation, validates its different modules and paves the way for further studies of FFA designs.

MODEL DEFINITION OF THE SCALING LATTICE

The first lattice studied with Zgoubidoo is scaling and consists of 12 identical triplet cells, with radial focusing (sector-alternating field) and a nominal energy of 250 MeV. The working point of this lattice is chosen in the second stability region of Hill's equations, with a phase advance per cell larger than 180°, which implies choosing a large field index. It allows reducing the orbit shift while remaining a scaling lattice and therefore having energy-independent tunes [11]. Zgoubidoo allows studying this lattice: closed orbit search, particle tracking, linear and non-linear beam dynamics, and parametric study to set the working point. Zgoubidoo's class structure makes it straightforward to create the lattice with a few efficient commands: it is possible to build a Zgoubi input file with realistic default values for the

* marion.vanwelde@ulb.be

ISBN: 978-3-95450-227-1 ISSN: 2673-5490 doi:10.18429/JACoW-IPAC2022-MOPOST028

TUNE CONTROL IN FIXED FIELD ACCELERATORS

A. F. Steinberg*[1,2], R. B. Appleby[1], University of Manchester, Manchester, UK
S. L. Sheehy[3], University of Melbourne, Melbourne, Australia
[1]also at Cockcroft Institute, Warrington, UK
[2]also at University of Melbourne, Melbourne, Australia
[3]also at Australian Nuclear Science and Technology Organisation (ANSTO), Australia

Abstract

Fixed Field Alternating Gradient Accelerators have been proposed for a wide range of challenges, including rapid acceleration in a muon collider, and large energy acceptance beam transport for medical applications. A disadvantage of these proposals is the highly nonlinear field profile required to keep the tune energy-independent, known as the scaling condition. It has been shown computationally that approximately constant tunes can be achieved with the addition of nonlinear fields which do not follow this scaling law. However the impacts of these nonlinearities are not well understood. We present a new framework for adding nonlinearities to Fixed Field Accelerators, seeking a constant normalised focusing strength over the full energy range, and verify the results by simulation using Zgoubi. As a model use case, we investigate the degree of tune compensation that can be achieved in a Fixed Field Accelerator for ion cancer therapy.

INTRODUCTION

In synchrotrons, the tune working point is dominated by linear quadrupole focusing, and is kept approximately independent of energy by ramping the fields of all magnets up during acceleration. The tune shift can be taken to be small, in part because the energy deviation δ is small. In many cases, corrections can be performed by the placement of low-field sextupole or octupole magnets around the lattice [1], giving overall tune shifts that are small enough for machine operation. However, this is not feasible in Fixed Field Accelerators (FFAs) [2, 3], where momentum acceptance can be as much as ± 50 %, and small corrections to chromaticity are insufficient. In addition, the orbit excursions in FFAs are generally large, and the closed orbit can vary significantly between the lowest and highest energy: this can complicate attempts at tune compensation, as the field gradient varies with amplitude when nonlinearities are included.

Multiple methods have been proposed to control the tune in FFAs. The most widely known approach is for the field to follow a 'scaling law' [3], a highly nonlinear profile which was first proposed before the formulation of linear beam dynamics. Although this will produce a lattice where the tune is not a function of rigidity, a downside is that all closed orbits must be scale enlargements of one other. Also, to ensure strong focusing, either the magnets must have a large spiral angle (as in spiral-sector cyclotrons [4]), or the lattice must include reverse-bending defocusing magnets. Although these challenges make scaling FFAs unfavourable when compared with synchrotrons or cyclotrons, there are other Fixed Field Accelerator designs available.

One attempt to control the tune in an FFA without strictly adhering to the scaling law was used for PAMELA [5], which began with a scaling lattice, but truncated the multipole field expansion to decapole order and used rectangular rather than sector magnets. However, the design is still similar to a scaling FFA, with the same issues as previously discussed. Another method, which fixes tunes by modifying orbit shapes directly [6], works well for constant-field isochronous cyclotrons but imposes restrictions (such as no orbit crossing) that make synchrotron-like lattices difficult.

An alternative option is to begin with a simple linear lattice with rigidity-dependent tunes, and to add nonlinearities to combat this. Previous studies [7, 8] have achieved moderate success by performing numerical optimisations to flatten the tune, at the expense of a reduction in dynamic aperture and high error sensitivity. Results from this purely numerical approach are difficult to interpret, with no clear link between the tunes and field strengths. Instead of optimising the tunes themselves, we propose a lattice where the focusing strength is approximately constant for every energy, for each magnet individually: this is determined by the local magnetic field gradient along the closed orbit trajectories. An ion therapy accelerator is used to demonstrate this method, using the PyZgoubi wrapper for the tracking code Zgoubi [9, 10]. The resulting lattice has dynamics that are almost energy-independent, with tunes that are robust against magnet errors.

TUNES IN LINEAR FFAS

Where there is no overall bending – either from dipole fields, or from a rotation of the reference axis – all closed orbit trajectories go directly through the magnet centres, with the same path length. For a synchrotron, increasing the magnetic fields keeps the normalised gradient constant: this in turn leads to constant tune and dynamics. However, this is not the case when fields are fixed, as higher rigidity (P/q) beams feel a weaker focusing force: this was observed in the linear FFAs EMMA and CBETA [11, 12]. In the straightforward case of a FODO cell with drift length l_d, quadrupole length l_q, normalised quadrupole strengths $k_\pm = \pm\frac{g}{(P/q)}$ for gradients $\pm g$, and negligible fringe fields, we find from the the overall linear transfer matrix that

* adam.steinberg@manchester.ac.uk

ISBN: 978-3-95450-227-1 ISSN: 2673-5490 doi:10.18429/JACoW-IPAC2022-MOPOST029

FAST CYCLING FFA PERMANENT MAGNET SYNCHROTRON*

D. Trbojevic†, S. Brooks, J.S, Berg, M. Blaskiewicz, BNL, Upton, NY, USA

Abstract

We present a novel concept of the Fixed-Field-Alternating (FFA) small racetrack proton accelerator 10x6 size, with kinetic energy range between 30-250 MeV made of permanent magnets. The horizontal and vertical tunes are fixed within the energy range, as the magnets The combined function magnets have additional sextupole and octupole multipoles the chromatic corrections, providing very fast cycling with a frequency of 1.3 KHz. The injector is 30 MeV commercially available cyclotron with RF frequency of 65 MHz. The permanent magnet synchrotron RF frequency is 390 MHz and acceleration uses the phase jump scheme.

INTRODUCTION

This is a proposal based on the existing patent on permanent magnet Fixed Field Alternating Gradient accelerator [1]. This is a Non-Scaling Fixed Field Alternating (FFA) gradient accelerator with fixed vertical and horizontal tunes with an estimated RF power of 400 kW.

The proposal follows the successful commissioning of the Cornell Brookhaven Electron Test Accelerator (CBETA) [2-7]. The electrons were transported though the single beam line from the superconducting accelerator starting with energy of 36 MeV and finishing with 150 MeV, passing 4 times through the linac in acceleration mode and 4 times in decelerating mode making full energy recovery.

This is a proposal of an extraordinary synchrotron as acceleration time does not depend on limited speed of magnet response. The acceleration cycle is imitated only by the RF. In the present design the accelerator cycle frequency is 1.3 kHz. This represents at the same time a proof of principle for the future proton drivers – an essential element in a chain of synchrotrons in any collider. The proposal uses permanent combined function magnets lay out in a racetrack and occupying a very small area of 10 x 6 m. The proton beam is accelerated in a kinetic energy range between 10 MeV and 250 MeV with three Pill Box cavities with synchronous voltage of 25 kV. The total number of turns is ~3600.

The synchrotron permanent magnets are significantly smaller than warm iron synchrotron magnets. This specific energy range is very important for the proton cancer therapy and recent FLASH cancer radiation therapy [8]. The FLASH therapy occurs when the large radiation dose is delivered in controlled way during a very short time ~100 ms.

* This manuscript has been authored by employees of Brookhaven Science Associates, LLC under Contract No. DE-SC0012704 with the U.S. Department of Energy.
†dejan@bnl.gov

The other possible applications are the fast-cycling synchrotrons for protons, muons, or other hadron drivers like the Proton Driven Fusion systems and colliders.

APPLICATION FOR 'FLASH' THERAPY

The 'FLASH' cancer therapy is a relatively new possibility in treating the cancer tumours if the radiation is required. Multiple biological studies and even few patients' treatments around the world in recent years confirmed significant improvements in the cancer treatment results by delivering the radiation dose *in much shorter time intervals* — fractions of a second as opposed to minutes — and in far fewer fractions or even a single fraction and therefore at dose rates that are thousands of times higher [9]. All cancer particle radiation facilities in the world are presently not capable of delivering the radiation dose within 100 ms as it is very difficult to get such a fast response from the magnets in such a short time. The cyclotron-based proton therapy facilities have an additional problem with necessary energy degraders as the proton energy from the cyclotrons is fixed ~230 MeV. The degraders significantly reduce the intensity of the beam and enhance the beam size-emittance. The fast-cycling FFA synchrotron, made of permanent magnets, can extract very fast the required proton energies for the patient's treatment and can transport all energies without changing the magnetic field. In addition, the delivery system-gantry is made as well of permanent magnets and can accurately transport protons of all energy range between 70-250 MeV to the patients.

FFA FAST CYCLING SYNCHROTRON

The proton therapy accelerator from 10 MeV to 250 MeV is designed using the racetrack lattice made of Non-Scaling Fixed Field Alternating Gradient (FFA) arcs and two parallel straight sections. The layout of the accelerator is shown in Fig. 1.

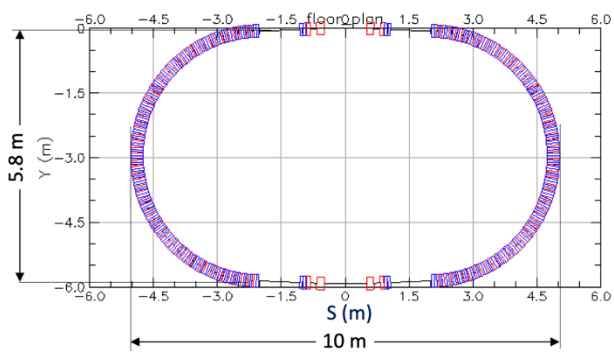

Figure 1: Layout of the Fast-Cycling FFA synchrotron.

The injector for this accelerator could be one of the 10-30 MeV cyclotrons available on the market (CYCLONE 10/2) [10]. The racetrack accelerator magnets in the arcs

ISBN: 978-3-95450-227-1 ISSN: 2673-5490 doi:10.18429/JACoW-IPAC2022-MOPOST030

PROTON IRRADIATION SITE FOR Si-DETECTORS AT THE BONN ISOCHRONOUS CYCLOTRON

D. Sauerland,*R. Beck, P.D. Eversheim, Helmholtz-Institut f.Strahlen- u. Kernphysik, Bonn,Germany
J. Dingfelder, P. Wolf, Silizium Labor Bonn, Physikalisches Institut, Bonn, Germany

Abstract

The Bonn Isochronous Cyclotron provides proton, deuteron, alpha particle and other light ion beams with a charge-to-mass ratio Q/A of $\geq 1/2$ and kinetic energies ranging from 7 to 14 MeV per nucleon[1]. At a novel irradiation site, a 14 MeV proton beam with a diameter of a few mm is utilized to homogeneously irradiate silicon detectors, so-called devices under test (DUTs), to perform radiation hardness studies. Homogeneous irradiation is achieved by moving the DUT through the beam in a row-wise scan pattern with constant velocity and a row separation smaller than the beam diameter. During the irradiation procedure, the beam parameters are continuously measured non-destructively using a calibrated, secondary electron emission-based beam monitor, installed at the exit window of the beamline. The diagnostics and the irradiation procedure ensure a homogeneous irradiation with a proton fluence error of smaller than 2 %. In this work, an overview of the accelerator facility is given and the irradiation site with its beam diagnostics is presented in detail.

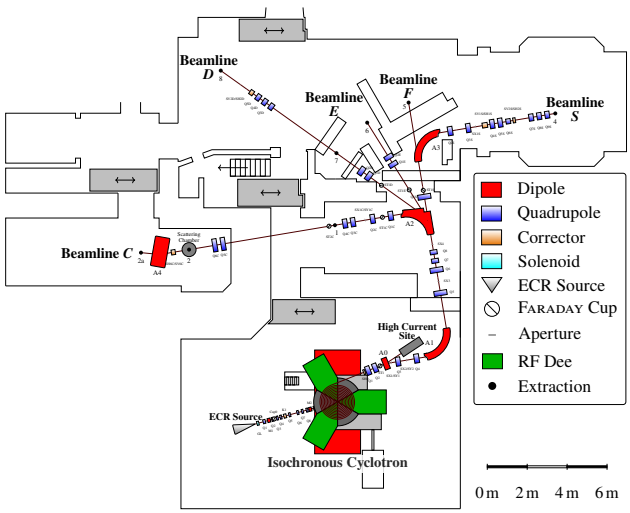

Figure 1: Overview of the accelerator facility.

BONN ISOCHRONOUS CYCLOTRON

The accelerator facility of the Bonn Isochronous cyclotron is shown in Fig. 1. Here, light ions, like protons, deuterons or alpha particles with a kinetic energy of 7 to 14 MeV/A, are provided to five experimental sites. The ions are generated by two external electron cyclotron resonance (ECR) sources.

* sauerland@hiskp.uni-bonn.de

[1] Operating at the third cyclotron harmonic ($h = 3$). For the acceleration of heavier ions up to $^{16}O^{6+}$, see Fig. 2.

Table 1: Parameters of the Bonn Isochronous Cyclotron

available ions	p, d, α, …, $^{16}O^{6+}$
energy ($h = 3$, $Q/A \geq \frac{1}{2}$)	7 to 14 MeV/A
beam current (ext.)	$\lesssim 1\,\mu A$
injection / extraction radius	38 mm / 910 mm
number of revolutions	approx. 120
hill sectors	3 × 40°, 0° spiral angle
hill / valley field strength	1.9 / 0.7 T (max.)
flutter factor	0.62
dees	3 × 40°, 40 kV (max.)
cyclotron harmonic h	3, 9
RF frequency ν_{RF}	20.1 to 28.5 MHz
hor. / vert. emittance	16 / 22 mm mrad
relative energy spread	4×10^{-3}

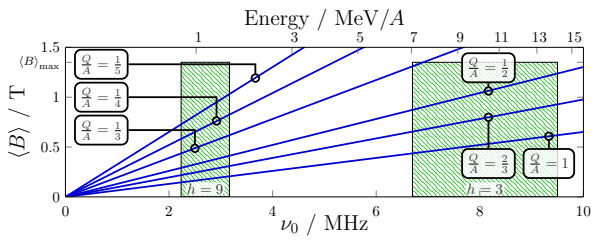

Figure 2: Parameter space of possible cyclotron operation (green) with average magnetic flux density $\langle B \rangle$ and ν_0.

A two-stage 5 GHz source is located beside, whereas a single-stage, polarized 2.5 GHz source is situated underneath the cyclotron. The generated 2 to 8 keV beam is guided below and is injected vertically into the cyclotron's magnetic center using an electrostatic hyperboloid inflector.

The Bonn Isochronous Cyclotron [1] is an isochronous AVF cyclotron with a 120°-symmetric magnetic field configuration in the azimuthal plane. Its magnet yoke therefore is separated into three hill-and-valley sectors with 0° spiral angle. In the valleys, three broadband dees are located, providing an acceleration voltage of up to 40 kV. The main parameters of the cyclotron are shown in Table 1. Due to its symmetry, the cyclotron normally operates at the third cyclotron harmonic $h = 3$, where the RF frequency ν_{RF} equals three times the ions' cyclotron frequency ν_0, but also an operation at $h = 9$ is possible. The RF frequency range and the maximum average magnetic flux density $\langle B \rangle_{max}$ of approx. 1.4 T define the cyclotron's mass-to-charge acceptance, as shown in Fig. 2. After approx. 120 revolutions, the beam is extracted to a field-compensated channel in a single-turn extraction, using an electrostatic septum. The

ISBN: 978-3-95450-227-1 ISSN: 2673-5490 doi:10.18429/JACoW-IPAC2022-MOPOST032

A NEW APPROACH TO CYCLOTRON DESIGN

O. Karamyshev†, JINR, Dubna, Russia

Abstract

Cyclotrons are the oldest type of circular accelerators, with many applications, design of the majority of cyclotrons nowadays follow has become a standard for most of developers, and there is a clear trend for switching towards superconducting magnets to increase the magnet field level and decrease the size and weight. A new approach, described in this paper allowed the author to design a line-up of cyclotrons from 15 to 230 MeV as compact and power efficient as superconducting cyclotrons, but using resistive copper coil.

INTRODUCTION

Every day more and more cyclotrons for medical and industrial applications are being produced. Especially in the energy range between 10-70 MeV proton (mostly) beams for medical isotopes production such as PET, SPECT isotopes. Also recently discovered FLASH [1] proton therapy created a demand for 230 MeV proton accelerator which can produce beams with higher current then existing accelerators. Cyclotrons seems to be a good choice for such task. The modern trend in cyclotrons is to apply superconducting coils to increase magnetic field strength of the cyclotron in order to make the accelerator more compact, and thus reduce the overall cost of the cyclotron complex.

Why is it important to make cyclotron compact:

- Compact mean less materials (steel and copper) used for production
- Compact means that the bunker is smaller, and for medical equipment it is very important, as usually space around medical facilities is restricted.

How can we make cyclotron more compact?

- Higher magnetic field makes poles smaller
- Higher frequency of RF system
- Smaller coil

Increase of magnetic field leads to problems with flutter, it becomes more difficult to manage shimming of the magnet, and injection and extraction becomes way more challenging. That is why author has decided to follow other 2 options to make cyclotrons more compact and cheaper.

If we look at frequency allocation chart [2] we will find out that the highest frequency in medical cyclotrons is 106.8 MHz, used by IBA C235 [3] is also the end of the lane dedicated for FM Radio, but between 108 and 136 MHz there are frequencies dedicated for aeronautical navigation, therefore it is not suitable for cyclotron. Author believes that the optimal frequency is 145 MHz, which is dedicated for amateur use. If we use 145 MHz as harmonic 6 the central field would be 1.55 Tesla.

Harmonic 6 means that about 30 degrees of azimuthal width is required for each cavity. But what if we don't use all 6 cavities, but instead have 3 sectors of 90 degrees and 3 valleys of 30 degrees for RF system. In this case more steel means less amper-turns in coil needed, meaning smaller coil. As the result we get a much more compact cyclotron. The 15 MeV cyclotron (see Fig. 1, Table 1) in more details presented in [4]. For the 230 MeV [5] cyclotron 3 sectors is not a suitable option due to resonances induced by 3rd harmonic of magnetic field. Instead, 4 sectors were used and same 6th harmonic 4x145 MHz RF cavities were used operating in push-pull mode. The goal is to create maximal level of unification between all cyclotrons in the line-up between 15 MeV and 230 MeV covering all the range, used in medical applications.

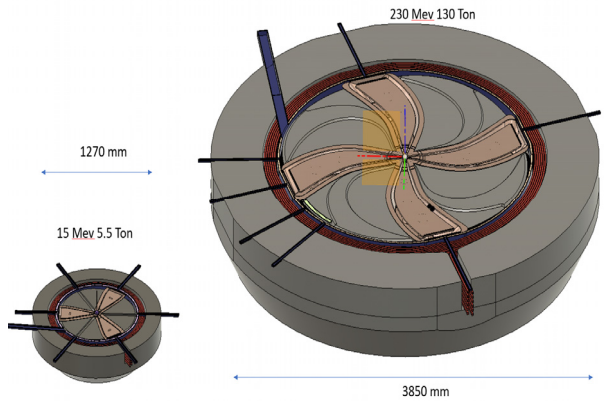

Figure 1: Overview of 15 MeV and 230 MeV cyclotrons.

Table 1: Parameters of 15 MeV Cyclotron

Parameter	
Magnet type	Compact, copper coils
Number of sectors	3
Ion source	Internal/External
Final energy MeV	15
Final radius, mm	360
Mean magn. field, T	1.55
Dimensions (height×diameter), mm	750 × 1290
Weight, kg	5500
Hill/Valley field, T	2.1/0.3
Hill/Valley gap,mm	25/210
A*Turn number	27 000
Magnet power consumption, kW	25
RF freq., MHz	145
Harmonic number	6
Voltage, kV	30-50
Turn number	120
RF power, kW	8
Beam intensity, μA	Up to 1000
Extraction type	Stripping foil

† olegka@jinr.ru

ISBN: 978-3-95450-227-1 ISSN: 2673-5490 doi:10.18429/JACoW-IPAC2022-MOPOST033

BETATRON TUNE CHARACTERIZATION OF THE RUTGERS 12-INCH CYCLOTRON FOR DIFFERENT MAGNETIC POLES CONFIGURATIONS

Cédric Hernalsteens, CERN, 1211 Geneva 23, Switzerland
Michelle Miller, Brown University, Providence, Rhode Island, USA
Timothy S. Ponter, Ion Beam Applications, Louvain-la-neuve, Belgium
Brian Beaudoin, Timothy W. Koeth, University of Maryland, College Park, Maryland, USA
Kiersten Ruisard, Oak Ridge National Laboratory, Oak Ridge, TN, USA
Robin Tesse, ULB, Bruxelles, Belgium

Abstract

The Rutgers cyclotron is a small 12-Inch, 1.2 MeV proton cyclotron. Sets of magnet pole-tips were designed to demonstrate different cyclotron focusing options: weak focusing, radial sector focusing and spiral sector focusing. The purpose of this paper is to experimentally characterize the transverse dynamics provided by different types of focusing. Magnetic field measurements provide insight into the as-built properties of these magnetic poles configurations. First we discuss the axial betatron tune measurements as a function of the beam energy towards outer radii, which agree well with the values expected from measured magnetic data. Turn-by-turn betatron envelope oscillation measurements are also reported and compared with the tune measurements. Excellent agreement is once again found.

THE RUTGERS 12-INCH CYCLOTRON

The Rutgers cyclotron is a 12-Inch, 1.2 MeV proton cyclotron built out of passion and intended for instructional use. It saw first beam in 1999 [1] and since has been the host of multiple students projects, contributing to the improvement of the machine and its subsystems. In particular, different sets of magnet pole-tips have been designed and built. These different magnetic configuration illustrate the main aspects of the cyclotron focusing theory: weak focusing, radial sectors (Thomas focusing) and spiral sectors (Kerst and Laslett focusing effects) [2–4]. The transverse betatron motion of the beam accelerated with the weak focusing pole configuration has been observed in the past [5] using the main diagnosis tool available at the cyclotron: a phosphor coated screen mounted on a radial probe instrument observed with a DSLR camera.

We make two independent tune calculations based on two sets of measured data: a mapping of the magnetic field in the mid-plane of the magnet and transverse betatron centroid and envelope oscillations data extracted from beam images.

To carry out the measurements discussed below, we used a modified source chimney featuring an aperture offset along the vertical axis in order to provide a beam with an initial axial offset to drive large axial oscillations. The design of the source, a cold cathode Penning Ion Gauge (PIC) source, is reported in Ref. [6]. Additionally, the aperture is circular with a 0.8 mm radius, and it can sustain a current of 5 mA. A picture of the modified aperture source is shown in Fig. 1 (left). The off-centered aperture is clearly identified.

Magnetic Field Focusing

The cyclotron magnet features flat poles with a maximum B-field of about 1 T. The magnetic field can be shaped using pole-tips that are fixed on the flat poles. Magnetic maps have been measured using a home-made magnetic measurement table and stepper motors electronics with a digital Gaussmeter. The magnetic centers of the sector focusing pole-tips are identified using a field harmonic analysis on a set of circles with different radii; indeed the non-structure harmonics are minimal at the magnetic center.

The so-called weak-focusing poles have azimuthal symmetry (see Fig. 1 (right)). The axial magnetic field decreases with the radius, the gradient of which provides axial focusing. The radial focusing comes from the usual dipole

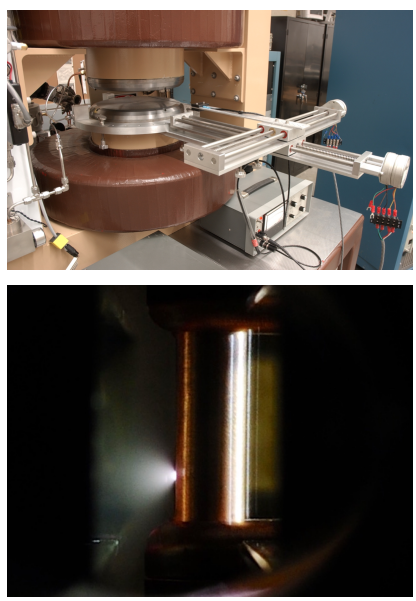

Figure 1: (top) Weak focusing pole-tips on magnet, with magnetic measurement stage. (bottom) Glow of the plasma out of the source chimney aperture. The symmetry plane of the cyclotron lies in the axial center of the chimney. The offset of the aperture with respect to that plane is directly visible.

ISBN: 978-3-95450-227-1 ISSN: 2673-5490 doi:10.18429/JACoW-IPAC2022-MOPOST035

OPERATIONAL EXPERIENCE AND PERFORMANCE OF THE REX/HIE-ISOLDE LINAC

J.A Rodriguez†, N. Bidault, E. Fadakis, P. Fernier, M. Lozano Benito, S. Mataguez, E. Piselli, E. Siesling, CERN, Geneva, Switzerland

Abstract

Located at CERN, ISOLDE is one of the world's leading research facilities in the field of nuclear science. Radioactive Ion Beams (RIBs) are produced when 1.4 GeV protons transferred from the Proton Synchrotron Booster (PSB) to the facility impinge on one of the two available targets. The RIB of interest is extracted, mass-separated and transported to one of the experimental stations, either directly, or after being accelerated in the REX/HIE-ISOLDE post-accelerator. In addition to a Penning trap (REXTRAP) to accumulate and transversely cool the beam and a charge breeder (REXEBIS) to boost the charge state of the ions, the post-accelerator includes a linac with both room temperature (REX linac) and superconducting (HIE-ISOLDE linac) sections followed by three HEBT lines to deliver the beam to the different experimental stations. The latest upgrades of the facility as well as a comprehensive list of the RIBs delivered to the users of the facility and the operational experience gained during the last physics campaigns will be presented in this contribution.

THE REX/HIE-ISOLDE LINAC

The REX linac consists of seven room temperature accelerating structures (Fig. 1). A four-rod RFQ followed by a buncher, an IH structure, three spiral resonators and a second IH structure accelerate the beam from an injection energy of 5 keV/u to 2.8 MeV/u [1]. REX is a 101.28 MHz pulsed machine with a maximum repetition rate of 50 Hz and 2 ms RF pulse length. However, it is generally operated at lower duty cycles (typically 1.0-1.6 ms pulses at 2-25 Hz depending on the optimum breeding time of the particular RIB). It is capable of accelerating beams with mass to charge ratios (A/q) between 2.5 and 4.5.

The HIE-ISOLDE linac [2] is the superconducting extension of the REX room temperature linac. It consists of four cryomodules and the corresponding inter-tank sectors. Each cryomodule is equipped with a superconducting solenoid and five superconducting Quarter Wave Resonators (QWR) made of a copper substrate coated with niobium. The geometrical beta of the QWRs is 0.103 and the maximum gradient is 6 MV/m with a nominal quality factor higher than $5 \cdot 10^8$. The final energy of the beam (Fig. 2) depends on its A/q since each QWR can be phased independently (e.g. 9.2 MeV/u for A/q = 4.5 if all QWRs could be operated at 6 MV/m).

Three HEBT lines are used to deliver the beam to different experimental stations: the Miniball spectrometer, the ISOLDE Solenoid Spectrometer (ISS) and the Scattering Chamber (SEC). The latter is occasionally replaced by different travelling experimental stations increasing the flexibility of the facility.

The diagnostic boxes (DB), distributed along the linac and HEBT lines, are equipped with Faraday cups, scanning slits, collimators, silicon detectors, beam attenuators and carbon stripping foils (50 and 75 ug/cm^2).

Electrostatic quadrupoles (before the RFQ), superconducting solenoids (inside the cryomodules) and magnetic quadrupoles (in the rest of the linac and HEBT lines) are used for transverse focusing. Two 45 deg. dipoles in each of the HEBT lines can be used as spectrometers to measure

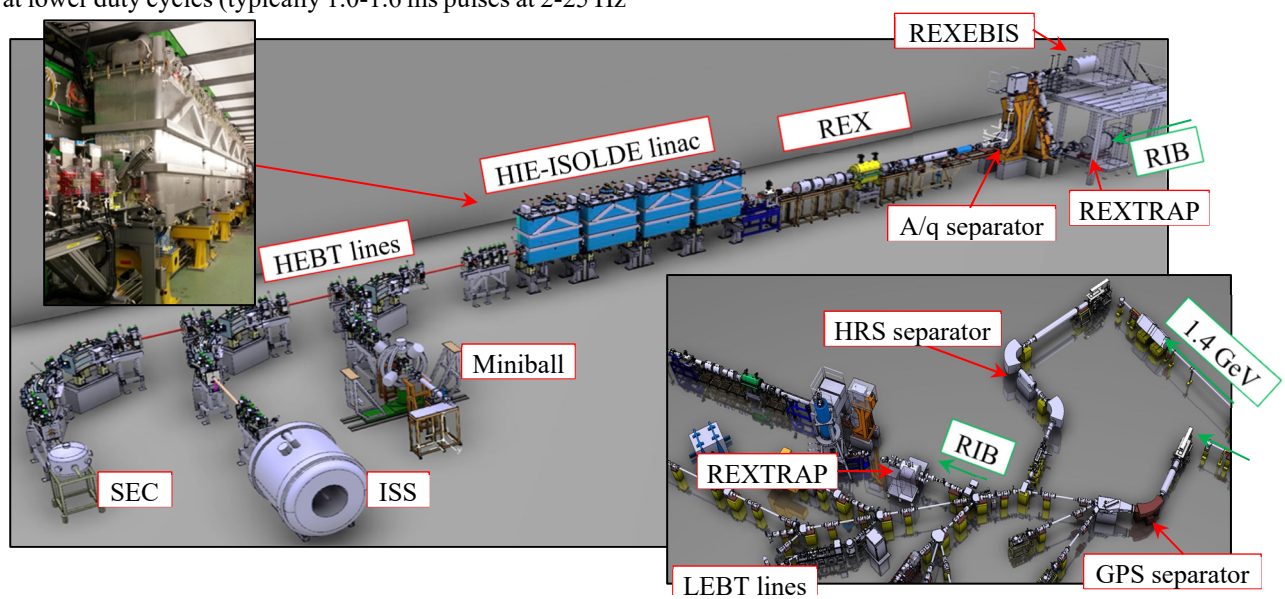

Figure 1: Layout of the ISOLDE separators and LEBT lines (bottom right) and the REX/HIE-ISOLDE post-accelerator.

† alberto.rodriguez@cern.ch

ISBN: 978-3-95450-227-1 ISSN: 2673-5490 doi:10.18429/JACoW-IPAC2022-MOPOST036

TRANSVERSE EMITTANCE MEASUREMENTS OF THE BEAMS PRODUCED BY THE ISOLDE TARGET ION SOURCES

N. Bidault*, CERN, CH-1211 Geneva, Switzerland

Abstract

The Isotope mass Separator On-Line DEvice (ISOLDE) is a Radioactive Ion Beam (RIB) facility based at CERN where rare isotopes are produced from 1.4 GeV-proton collisions with a target. The different types of targets and ion sources, operating conditions and ionization schemes used during the physics campaign results in extracted beams with various emittances. Characterizing the beam emittance allows deducing the transport efficiency to low-energy experimental stations (up to 60 keV) and the mass resolving power of the separators.

We report on emittance measurements for different beams of stable elements extracted from surface and plasma ion sources. The dependence of the emittance on the different conditions of operation of the ion sources is investigated and the results are compared to previous measurements.

INTRODUCTION

Motivation

Radionuclei are produced, ioniozed and accelerated in two separate frontends at ISOLDE before transport towards either the High-Resolution Separator (HRS) or the General Purpose Separator (GPS) [1]. The mass-resolving power of the separators is to first order, inversely proportional to the horizontal emittance of the beam. The characterization of the transverse beam properties is essential to determine the quality of beam transport to the low energy experimental stations, including the efficiency of trapping devices. The objective is to maximize the beam's brightness, which is proportional to the intensity and is inversely proportional to horizontal and vertical emittances.

Recent changes in the extraction electrodes and focusing elements of the frontends, coupled with the growing use of different types of target ion sources, motivated a review of the transverse properties of the beams produced at ISOLDE.

Definitions

We define the assumptions and sometimes necessary conventions used for describing the transverse properties of an ion beam.

The transverse projections are shown in the trace space $(u, u' = \frac{du}{dz})$ - non-normalized by the beam energy - with $u = x, y$ respectively for the horizontal and vertical plane. Using the Courant-Snyder invariant, the contours (u, u') of ion beams propagating through a focusing lattice describe ellipses [2]. The lengths of the beam ellipses' semi-axes are hereafter derived using the root-mean-square (1-rms) norm. When assuming a bi-Gaussian density distribution, a beam ellipse of size 1-rms encloses 39% of the particles. The value of the emittance $\varepsilon_{x,y}$ is calculated as the product of the semi-axes of the beam ellipses, and displayed in units of π.mm.mrad.

The effect of space charge on the particle motion is neglected after investigating the perveance of the beams used. The generalized perveance parameter K appearing in the Courant-Snyder equation is:

$$K = \frac{q \cdot I}{2\pi\epsilon_0 m(\gamma\beta c)^3} \quad (1)$$

The relativistic term $(\gamma\beta c)$ is evaluated for beam energies between 30 to 60 keV/u and a mass 200 amu. With peak current values I limited to 1 μA during the measurements and considering singly-charged ions, the generalized perveance remains below 10^{-9}.

EXPERIMENTAL SETUP

A schematic of the frontends installed at ISOLDE is shown in Fig. 1, it displays the target ion source vessel, the extraction electrodes, and the first electrostatic elements used to steer and focus the beam post-acceleration.

Target Ions Sources

The transverse properties of extracted beams were measured for three types of ion sources differentiated by the scheme of ionization and selection: surface ionizing, plasma ionizing and Laser Ion Source and Trap (LIST). The first type of ion source listed is efficient for alkalis, rare earth elements and molecules with low ionization potentials. The second type of ion source listed involves the creation of a plasma in a chamber between the line and extraction electrode. The region is subject to a magnetic field and an anode voltage to ionize a mixture of noble gases and generate secondary electrons adding the scheme of electron impact ionization at energies of a few hundred eV. Finally, the LIST-type of targets is a recent upgrade of the Resonance Ionization Laser Ion Source (RILIS), with the addition of an RFQ serving as an ion guide and repellers to suppress isobaric contaminants stemming from surface ionization. After extraction from the ion source, the beam is centred and sent parallel to the first quadrupole triplet via a pair of electrostatic steerers. A selective overview of the ISOLDE literature on ion sources can be found in [3] [4].

Quadrupole Scan Method

The principle behind the quadrupole scan method is to measure multiple transverse profiles for different known transformations of the beam ellipse and apply a fitting to deduce the emittance and Twiss parameters. The first

* niels.killian.noal.bidault@cern.ch

ISBN: 978-3-95450-227-1 ISSN: 2673-5490 doi:10.18429/JACoW-IPAC2022-MOPOST037

CHARACTERISATION OF BUNCH-BY-BUNCH TUNE SHIFT EFFECTS IN THE CERN SPS

I. Mases Solé*, H. Bartosik, V. Kain, K. Paraschou, M. Schenk, C. Zannini,
CERN, Geneva, Switzerland.

Abstract

After the implementation of major upgrades as part of the LHC Injector Upgrade Project (LIU), the Super Proton Synchrotron (SPS) delivers high intensity bunch trains with 25 ns bunch spacing to the Large Hadron Collider (LHC) at CERN. These beams are exposed to several collective effects in the SPS, such as beam coupling impedance, space charge and electron cloud, leading to relatively large bunch-by-bunch coherent and incoherent tune shifts. Tune correction to the nominal values at injection is crucial to ensure beam stability and good beam transmission. During the beam commissioning of the SPS, measurements of the bunch-by-bunch coherent tune shifts have been conducted under different beam conditions, together with appropriate corrections of the average tunes at each injection. In this paper, we describe the methodology that has been developed to acquire bunch-by-bunch position data and to perform online computations of the coherent tune spectra of each bunch using refined Fourier transform analysis. The experimental data are compared to multiparticle tracking simulations using the SPS impedance model, in view of developing an accurate model for tune correction in the SPS.

INTRODUCTION

In preparation of the high luminosity upgrade of the LHC (HL-LHC), the LHC injectors including the SPS have been upgraded in the framework of the LIU project [1] to enable the production of high intensity and high brightness beams. Due to the high intensity of the bunches, there is a strong bunch-by-bunch coherent and incoherent tune shift in the SPS caused by the impedance. Furthermore, at injection energy the proton beam is sensitive to instabilities induced by the resistive wall impedance. Thus it is necessary to measure the horizontal and vertical bunch-by-bunch tunes and correct the average coherent tunes such that they are close to the central tunes programmed for the bunch-by-bunch transverse damper in order to stabilize the beam. The nominal values of the horizontal and vertical tunes (in the SPS Q20 optics [2]) are $Q_x = 20.13$ and $Q_y = 20.18$.

The bunch-by-bunch transverse tune shift depends strongly on the beam configuration. The most important parameters are the intensity per bunch, and the total intensity of the beam through the number of bunches and the number of batches (i.e. bunch trains from the injector), as illustrated schematically in Fig. 1. In particular, the broadband impedance sources in the SPS (mostly kicker magnets) result in a relatively large tune shift already for single bunches in the machine [3], denoted in the graph as ΔQ_{SB}.

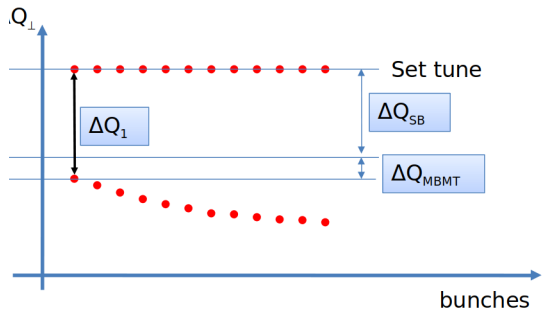

Figure 1: Schematic view of transverse tune shift along the bunch train (explanation in the text).

Due to the resistive wall impedance and other narrow-band impedances in the machine, the wakefield builds up along the train, resulting in a growing tune shift for the trailing bunches. Moreover, if the wakefield does not fully decay within one turn of the machine, an additional tune shift from these long range wakefields is experienced even by the first bunch of the train denoted as ΔQ_{MBMT} in Fig. 1.

The aim of the bunch-by-bunch tunes study is to be able to predict the transverse tune shifts as a function of the beam characteristics. For this purpose, tune shift measurements and adjustments have been carried out in the SPS at different intensities. The methodology followed to carry out the measurements is detailed in the following sections. In addition to the measurements, impedance induced tune shifts as function of intensity have been determined with PyHEADTAIL [4] simulations using the SPS impedance model. Finally, the tune shifts from measurements and simulations are compared at different intensity values.

TUNE SHIFT MEASUREMENTS

The beam position is recorded for several turns after injection into the SPS using the LHC prototype Beam Position Monitors (BPMs) installed in the SPS, as those are the only ones capable of acquiring bunch-by-bunch data. Residual injection oscillations are generally not providing enough signal to noise ratio in the recorded turn-by-turn position data. For this reason, a controlled excitation is applied with a kicker magnet at injection so that the beam oscillations are enhanced. A beam in standard configuration (four trains of 72 bunches each) was used in the measurements. The trains are injected consecutively and, at injection of each train, a kick to all bunches in the beam is applied in order to induce transverse oscillations. This allows measuring the bunch-by-bunch tunes of every train circulating in the machine through a refined Fourier analysis, as described later

* ingrid.mases.sole@cern.ch

ISBN: 978-3-95450-227-1 ISSN: 2673-5490 doi:10.18429/JACoW-IPAC2022-MOPOST038

EXCITATION OF THE $\sigma_{l\_l} = 90°$ RESONANCE BY THE CAVITY RF ACCELERATING FIELDS

J-M. Lagniel†, GANIL, Caen, France

Abstract

In rf linacs the longitudinal focalization is done by sinusoidal forces and at high accelerating fields the zero-current longitudinal phase advance per longitudinal focusing period σ_{0l_l} can be high. The nonlinear components of the sinusoidal rf field (sextupolar, octupolar and higher order components) can then excite parametric resonances, including the 4th-order resonance ($\sigma_{l\_l} = 90°$) when σ_{0l_l} is higher than 90°, inducing strong longitudinal emittance growths and acceptance reductions. As pointed out in previous papers, the longitudinal beam dynamics is therefore complex, even when the space-charge forces are ignored. The parametric resonance excitation by the rf field is analyzed before discussing the additional effect of the space-charge forces, in particular to explain why the zero-current longitudinal phase advance per transverse focusing period σ_{0l_t} is not a relevant parameter. Examples are given in the SPIRAL2 linac case.

PARAMETRIC RESONANCES, BASIC DEFINITIONS

As done in [1, 2], the choice done here is to study the parametric resonances in the longitudinal plane independently of the study of the radial-longitudinal coupling resonances in order to avoid unnecessary complications and confusions. As usual (e.g. [3] chapter X, section IV), the resonance zoology is defined considering the linear equation of motion of individual particles perturbed by linear (n = 1) or nonlinear (n > 1) periodic perturbing forces

$$\frac{d^2\delta\varphi}{dz^2} + \sigma_l{}^2\,\delta\varphi + a_{n,k}\,\frac{[\delta\varphi_0 \sin(\sigma_l z)]^n}{[\delta\varphi_0 \cos(\sigma_l z)]^n}\cos(k\sigma_p z) = 0 \qquad (1)$$

with σ_l the phase advance per unit of length of the unperturbed particle motion, σ_p and k the phase advance per unit of length and the harmonic number of the perturbing force respectively. Considering that a resonance condition is fulfilled when a component (n, k) of the perturbing force has a "frequency" equal to the unperturbed particle oscillation "frequency" σ_l [3], a resonance occurs when

$$(i+1)\,\sigma_l = k\,\sigma_p$$

with i even integer from 0 to n for n even and i odd integer from 1 to n for n odd.

Using $\sigma_{l\_l} = \sigma_l\,L_l$ the longitudinal phase advance per period of the longitudinal focusing system (gaps or cavities), $\sigma_{l\_p} = \sigma_l\,L_p$ the longitudinal phase advance per period of the perturbation and $\sigma_p = 2\pi/L_p$ with L_p the period of the perturbation, the resonance condition is

$$\sigma_{l\_p} = (L_p/L_l)\,\sigma_{l\_l} = \frac{2\pi k}{i+1} \qquad (2)$$

$(i+1)$ is the order of the resonance and k is the harmonic of the perturbation.

For example, particles with $\sigma_{l\_l} = 90°$ can be excited by the $a_{n=3,k=1}$ component of the perturbing force when $L_p = L_l$ (fourth order resonance), or can be excited by the $a_{n=1,k=1}$, $a_{n=3,k=1}$ and $a_{n=3,k=2}$ components of the perturbing force when $L_p = 2L_l$ (half integer and fourth order resonances).

EXITATION BY THE CAVITY RF FIELD

Following [1, 2], the non-linear components of the rf accelerating field must be considered as main perturbing forces in the parametric resonance studies. This can be understood starting from the equation of motion of the phase oscillations around the synchronous particle obtained in smooth approximation ([3], chapter XVI section II-D).

$$\frac{d^2\delta\varphi}{dz^2} + K_{dp}\,\frac{d\delta\varphi}{dz} + \left[\frac{2\pi q\,E_0\,\mathrm{T}_{\beta_s}}{m_0c^2\lambda\,\beta_s^3\gamma_s^3}\right][\cos(\Phi_s+\delta\varphi) - \cos\Phi_s] = 0 \qquad (3)$$

The effect of the damping term K_{dp} which has a great importance on the longitudinal dynamics at high acceleration rates [1, 2] is not discussed here to focus the analysis on the rf field nonlinear focusing force which can be expressed by its Taylor series

$$\begin{aligned}[\cos(\Phi_s+\delta\varphi) - \cos\Phi_s] = \\ -[\sin\Phi_s]\,\delta\varphi \quad &\text{"quadrupole" (linear focusing)} \\ -[\cos\Phi_s/2!]\,\delta\varphi^2 \quad &\text{"sextupole"} \\ -[\sin\Phi_s/3!]\,\delta\varphi^3 \quad &\text{"octupole"} \\ +[\cos\Phi_s/4!]\,\delta\varphi^4 \quad &\text{"decapole" + ...}\end{aligned} \qquad (4)$$

Equation (3) is obtained using the smooth approximation, then averaging the effect of the rf field over the longitudinal period L_l. The effect of the gap or cavity periodicity must be analyzed including the harmonics of the rf field $E_z(z) = E_0 + \sum E_k\,cos(k\,2\pi z/L_l)$ in the longitudinal focusing force of Eq. (3), then to each term of the Taylor series of Eq. (4). The longitudinal focusing of the rf field can then be seen as a nonlinear focusing Eq. (4) and with $k = 0$ in Eq. (1), plus $\delta\varphi^n\,cos(k\,2\pi z/L_l)$ perturbing

† lagniel@ganil.fr

ISBN: 978-3-95450-227-1 ISSN: 2673-5490 doi:10.18429/JACoW-IPAC2022-MOPOST039

ALGORITHM TO MITIGATE HYSTERESIS IN MAGNETS WITH UNIPOLAR POWER SUPPLIES*

J. Nasser†, R. Baartman, O. Kester, S. Kiy, T. Planche, S. D. Rädel, O. Shelbaya,
TRIUMF, V6T 2A3 Vancouver, Canada

Abstract

The effects of hysteresis on the fields produced by magnetic lenses are not accounted for in TRIUMF's models of the accelerators. Under certain conditions, such as quadrupoles with unipolar power supplies operating at low currents, these effects have introduced significant field errors with consequences upon transverse tunes. To combat these uncertainties and make the fields more reproducible and stable, a technique new to TRIUMF has been implemented. This technique ramps the current cyclically about the desired setpoint to reach a reproducible field that is independent of its history. Results of magnetic measurements at TRIUMF using this technique are presented, as well as the expected improvements to the accuracy of the beam optics model, particularly for unipolar quadrupoles.

INTRODUCTION

The beam optics models for quadrupoles in TRIUMF's ISAC (Isotope Separator and Accelerator) facility were calibrated using the initial magnetization curves of the magnets during machine commissioning, circa 2000. However, many of the quadrupoles have been installed with unipolar power supplies due to cost considerations and cannot be degaussed during beam delivery. Without degaussing, the fields of a quadrupole are constrained to be within the hysteresis loop bounded by the lower and upper branches shown in Fig. 1. The lower and upper branches are defined as the curves followed by either increasing from 0 to 60 Amps or decreasing from 60 to 0 Amps respectively.

There is a significant offset from the calibrated B-I relationship and the measured quadrupole fields due to hysteresis, as shown in Fig. 1. We can call this offset the *systematic error*, which will be calculated as the error between the calibration curve and the centre of the hysteresis loop in Fig. 1.

Furthermore, all points within the bounded area are possible depending on the magnet's history and the rate at which the power supply is ramped, both of which are not accounted for during machine tuning. Therefore, this error will be referred to as the *random error* and will be calculated as half the width of the hysteresis loop.

In this proceeding we will discuss a ramping technique that can mitigate these errors, and present the expected improvements to the beam optics models at TRIUMF.

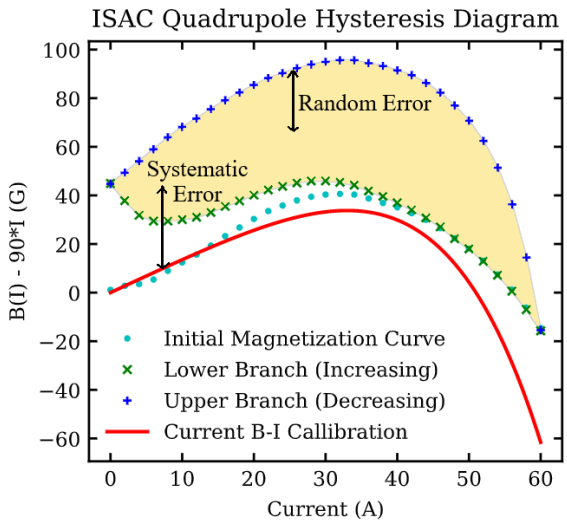

Figure 1: Diagram showing the hysteresis curve of a magnetic quadrupole with the systematic and random errors labeled. Y-axis is the tip-field with the linear portion subtracted.

RAMPING TECHNIQUE

The ramping technique originally described by Decker [1] involves cycling the current about the desired setpoint. TRIUMF's adaptation of this technique is programmed within a python package called Accpy [2] and called with a subroutine developed for this work, dubbed fancy_set. By using this technique, the field of the magnet is brought near the centre of the hysteresis curve regardless of the initial state. fancy_set also allows user control of the ramp rate, the number of periods, and the amplitudes of the cycles.

Figure 2 shows an example of the fancy_set ramping technique applied for a desired current setting of 30 A, starting from the lower branch of the hysteresis curve. As shown in Fig. 2 Top, the ramp rate is held constant throughout the process, and this constant can be maximized for each magnet to optimize the runtime and reproducibility of the technique. The field during this ramp is shown in Fig. 2 Bottom as the green dashed line which starts on the bottom branch and spirals toward the centre.

For each magnet, fancy_set is applied for various current settings within the range of the power supply to construct a full model of the middle branch. This is shown in Fig. 3 for a 52 mm diameter aperture, 325 mm effective length quadrupole in use at TRIUMF. The reproducibility of the technique is shown as error bars at each point, which is obtained by applying it for various initial condi-

* Funded under a contribution agreement with NRC (National Research Council Canada).
† j2nasser@uwaterloo.ca

ISBN: 978-3-95450-227-1 ISSN: 2673-5490 doi:10.18429/JACoW-IPAC2022-MOPOST040

ON A FRAMEWORK TO ANALYZE SINGLE-PARTICLE NON-LINEAR BEAM DYNAMICS: NORMAL FORM ON A CRITICAL POINT*

M. Titze†, Helmholtz-Zentrum Berlin, Germany

Abstract

Normal form analysis around a stable fixed point is a well-established tool in accelerator physics and has proven to be invaluable for an understanding of non-linear beam dynamics.

In this work we present progress in developing a modular Python framework to analyze some of the non-linear aspects of a storage ring, by directly operating with the given Hamiltonians.

Hereby we have implemented Birkhoff's normal form and Magnus expansion. This leads to a flexible framework to perform calculations to high order and, moreover, to relax the constraint of stability to also include certain unstable fixed points in the analysis.

INTRODUCTION

During the course of last year, two promising candidates for a successor of the third-generation light source BESSY2 have been singled out by the HZB machine development group [1, 2].

To study and answer questions concerning their dynamic aperture, Touschek-lifetime, IBS[1], error-response, chromaticity, momentum compaction factors and a possible future TRIB[2]-like operation mode, it soon became clear that there is a need for a deeper understanding of the non-linear aspects of these candidates.

Programs typically used for such tasks at HZB are OPA [4], Elegant [5, 6] and MAD-X/PTC [7, 8].

While these codes have the advantage of being developed over a relatively long period of time, and therefore can be considered as fairly robust, they also share some disadvantages concerning their flexibility and I/O formats. Often there is demand to access their internal objects from a modern, more interactive environment, which is usually not possible or only with great effort. These difficulties are well known in the community, and spurred the development of various projects as a result [9–11].

Here we have chosen a modular strategy in form of Python packages, each dedicated to specific tasks. Hence, the project takes full advantage of the Python syntax, while working along the custom user scripts (and the large pool of Python community scripts). Consequently, there is natural access to all its internal objects, leading to vast flexibility.

Work on the project commenced in October 2021 with the main focus on Hamilton mechanics. In this regard there are currently three packages under active development and maintenance [12–14].

CONCEPTS

Magnus Expansion

Consider the one-turn map $\mathcal{M}$ of a beam line consisting of n elements, each of which can be written in terms of an s-indepdendent Hamiltonian $\mathcal{H}_k$ and having length L_k[3]:

$$\mathcal{M} = \exp(-L_n : \mathcal{H}_n :) \cdots \exp(-L_1 : \mathcal{H}_1 :). \tag{1}$$

It is well known that already for two of these elements, the combination $\#(A, B) =: C$ with $\exp(C) = \exp(A)\exp(B)$ rapidly becomes complicated due to the amount of nested commutators involved.

However, for a qualitative analysis, already the lowest order[4] terms in Eq. (1) can be worthwhile to study and investigate, as shown in e.g. [15]. Moreover, it is possible to perform normal form analysis on such an effective Hamiltonian. For these reasons we have turned our attention to the Magnus expansion, which includes the Hamiltonian $\#_{k=1}^{n} : \mathcal{H}_k :$ as a special case, if considering hard-edge elements.[5]

More recently it has been outlined in [18, 19] that the Magnus expansion can formally be computed in terms of binary rooted trees. Specifically, if $X = \exp(: \Omega(s) :)$ is a solution to the equation $\dot{X} = : \mathcal{H} : X$, $X(0) = 1$,[6] with s-dependent Hamiltonian $\mathcal{H}$, then [19, 20]

$$\Omega(s) = \sum_{m=0}^{\infty} \sum_{\tau \in \mathcal{T}_m} \alpha(\tau) \int_0^s \mathcal{H}_\tau(s_1) ds_1, \tag{2}$$

$$\mathcal{H}_\tau(s) = \left\{ \int_0^s \mathcal{H}_{\tau_1}(s_2) ds_2, \mathcal{H}_{\tau_2}(s) \right\}, \tag{3}$$

$\tau = (\tau_1, \tau_2)$ denotes a binary tree with leaves τ_1 and τ_2 and

$$\mathcal{T}_m := \{(\tau_1, \tau_2); \tau_1 \in \mathcal{T}_{k_1} \wedge \tau_2 \in \mathcal{T}_{k_2} : k_1 + k_2 = m - 1\} \tag{4}$$

denotes a set of trees, called *forest*, containing trees τ involving exactly m nested commutators of $\mathcal{H}$ with $\tau \in \mathcal{T}_0 \Leftrightarrow \mathcal{H}_\tau \equiv \mathcal{H}$. The coefficients $\alpha(\tau)$ are given by

$$\alpha(\tau) = \frac{B_w}{w!} \prod_{k=0}^{w} \alpha(\tau_w), \tag{5}$$

* Work supported by German Bundesministerium für Bildung und Forschung, Land Berlin, and grants of Helmholtz Association.
† malte.titze@helmholtz-berlin.de

[1] Intra-beam scattering.

[2] Transverse Resonance Island Bucket, see e.g. Ref. [3].

[3] Without loss of generality we consider the independent variable s to agree with the position variable along the ring; s-dependent Hamiltonians can be modeled in a similar fashion by a suitable phase space extension.

[4] 'Order' is to be understood here as the number of involved operators within a nested commutator expression.

[5] Note that $\#(A, \#(B, C)) = \#(\#(A, B), C)$, so dropping the brackets in the #-expression makes sense.

[6] Including the minus sign inside $\mathcal{H}$ for brevity here.

ISBN: 978-3-95450-227-1 ISSN: 2673-5490 doi:10.18429/JACoW-IPAC2022-MOPOST041

DYNAMIC APERTURE STUDIES FOR THE TRANSFER LINE FROM FLUTE TO cSTART

J. Schäfer *, B. Haerer, A. Papash, R. Ruprecht, M. Schuh,
A.-S. Müller, Karlsruher Institute of Technology, 76131 Karlsruhe, Germany

Abstract

The compact STorage ring for Accelerator Research and Technology cSTART project will deliver a new KIT accelerator test facility for the application of novel acceleration techniques and diagnostics. The goal is to demonstrate storing an electron beam of a Laser Plasma Accelerator (LPA) in a compact circular accelerator for the first time. Before installing an LPA, the Far-Infrared Linac and Test Experiment (FLUTE) will serve as a full energy injector for the compact storage ring, providing stable bunches with a length down to a few femtoseconds. The transport of the bunches from FLUTE to the cSTART storage ring requires a transfer line which includes horizontal, vertical and coupled deflections which leads to coupling of the dynamics in the two transverse planes. In order to realize ultra-short bunch lengths at the end of the transport line, it relies on special optics which invokes high and negative dispersion. This contribution presents dynamic aperture studies based on six-dimensional tracking through the lattice of the transfer line.

INTRODUCTION

Making future accelerators more compact and energy efficient is a global goal of general interest. A key technology for achieving this goal are Laser Plasma Accelerators (LPA) [1]. These new accelerator structures promise to be much smaller and come with new characteristic beam properties. Especially the typical short bunch lengths makes them interesting for applications like the generation of coherent synchrotron radiation (CSR). The compact STorage ring for Accelerator Research and Technology cSTART [2] project at KIT will provide the first storage ring for LPA-like bunches. It serves as a test bench for manifold R&D topics e.g. the non-equilibrium evolution of an ultra-short bunch length or the development of dedicated diagnostic devices. The linac-based test experiment, the Far-Infrared Linac and Test Experiment (FLUTE) can produce electron bunches with a wide parameter range, especially the expected bunch length of down to 3 fs allows to mimik an LPA accelerator. This makes FLUTE the first full-energy injector for this project [3]. For injecting the bunches into the storage ring a complex 3D transfer line (TL) is required. As a solution to this problem, a systematic study was proposed on the lattice design with suitable optics to support the injection of ultra-short bunches into the storage ring [4]. A sketch of the geometrical arrangement with best result for the transfer line is shown in Fig. 1. This contribution briefly summarizes the beam dynamics in the transfer line and furthermore presents the dynamic aperture (DA) studies.

* jens.schaefer2@kit.edu

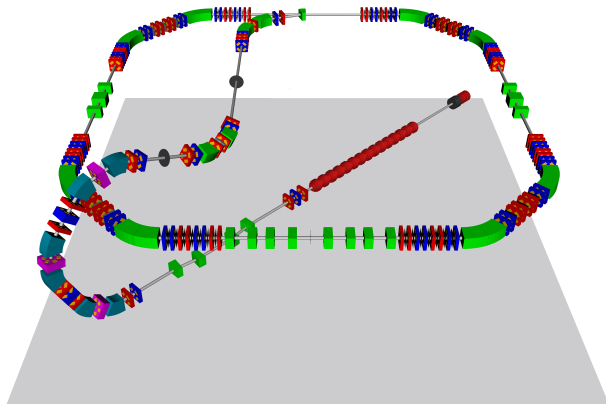

Figure 1: In grey, the footprint of the experimental hall, with FLUTE orientated diagonally, starting in the top right corner on the ground floor. The TL guides the bunches from the end of FLUTE to the injection point of the storage ring, which is horizontally aligned above FLUTE in the first floor. Dipoles are shown in green (h)/turquoise (v), quadrupoles in red (h)/blue (v), combined-function magnets in pink. The FLUTE RF components are also shown in red, the solenoid in grey. Two grey discs in the TL represent rotations of the Frenet-Serret coordinate system.

OPTICS IN THE TRANSFER LINE

FLUTE can create electron bunches with a wide range of parameters. For the design of the TL and the DA studies only one specific parameter set is picked out and referred to as the FLUTE example bunch. The example bunch parameters lead to peak performance in the longitudinal bunch compression with a final RMS bunch length of 3 fs by passing the FLUTE bunch compressor. Table 1 summarizes the beam parameters after the linac to include the optics of the FLUTE bunch compressor into the optics calculations for the TL.

Table 1: Beam Properties of FLUTE Example Bunch

Parameter	value
E	42 MeV
δE	0.25 %
q	1 pC
$\epsilon_{x,y}$ (norm)	193 nm rad
σ_t	173 fs
$\sigma_{x,y}$	1.4 mm

ISBN: 978-3-95450-227-1 ISSN: 2673-5490 doi:10.18429/JACoW-IPAC2022-MOPOST042

USING DYNAMIC INDICATORS FOR PROBING SINGLE-PARTICLE STABILITY IN CIRCULAR ACCELERATORS*

C.E. Montanari[1], A. Bazzani, G. Turchetti, Bologna University, Bologna, Italy
M. Giovannozzi, CERN Beams Department, Geneva, Switzerland
[1]also at CERN Beams Department, Geneva, Switzerland

Abstract

Computing the long-term behaviour of single-particle motion is a numerically expensive process, as it requires a large number of initial conditions to be tracked for a large number of turns to probe their stability. A possibility to reduce the computational resources required is to provide indicators that can efficiently detect the chaotic character of the orbits, which is considered a precursor of unbounded motion. These indicators could allow skilful selection of sets of initial conditions that are then considered for long-term tracking. The chaotic nature of each orbit can be assessed by using fast-converging dynamic indicators, such as the Fast Lyapunov Indicator (FLI), the Reversibility Error Method (REM), and the Smallest and Global Alignment Index (SALI and GALI). These indicators are widely used in the field of celestial mechanics, but not so widespread in accelerator physics. We have studied their efficiency by applying them both to a modulated Hénon map, as a toy model, and to realistic lattices of the High-Luminosity LHC. In this paper, we discuss the results of detailed numerical studies, focusing on their performance in detecting chaotic motions.

INTRODUCTION

The chaotic character of the orbits of a Hamiltonian system, such as the $4d$ modulated Hénon map [1], which describes the transverse motion in a circular accelerator [2] or a realistic accelerator lattice such as that of the HL–LHC [3], can be analysed by means of dynamic indicators. These are quantities that probe the linear response to an initial small random displacement or to random displacements along the orbit. Dynamic indicators have been one of the main tools for studying the chaotic character and long-term stability in many specific problems in celestial mechanics [4–6].

As direct tracking of realistic accelerator lattices on timescales of physical interest, i.e. 10^8 turns, is not an option for several initial conditions, there is a strong interest in tools that can probe the long-term behaviour of initial conditions at lower numbers of turns. Well-established dynamic indicators, like the Fast Lyapunov Indicator (FLI) [6], have been applied to accelerator physics, together with indicators based on harmonic analysis [7]. Recently, studies based on the Reversibility Error Method (REM) [5] have also been performed [8]. However, modern dynamic indicators such as the Smallest and Global Alignment Index (SALI and GALI) [9] have not yet been extensively considered in accelerator studies. Moreover, a general overview of different dynamic indicators in accelerator models is not available. The study presented here is a first step in assessing the performance of these indicators for accelerator-related studies.

OVERVIEW OF DYNAMIC INDICATORS

Lyapunov-based Dynamic Indicators

Given a non-autonomous Hamiltonian map $M(\mathbf{x}, n)$ in $\mathbb{R}^{2d}$, $DM(\mathbf{x}, n)$ denotes the symplectic Jacobian matrix $(DM)_{ij} = \partial M_i / \partial x_j$ at the point $\mathbf{x}$, then the orbit of the map $\mathbf{x}_n$ and the recurrence for the tangent map L_n are given by

$$\begin{aligned} \mathbf{x}_n &= M(\mathbf{x}_{n-1}, n-1) & \mathbf{x}_0 &= \mathbf{x} \\ \mathrm{L}_n(\mathbf{x}) &= DM(\mathbf{x}_{n-1}, n-1)\,\mathrm{L}_{n-1}(\mathbf{x}) & \mathrm{L}_0 &= \mathrm{I}\,. \end{aligned} \tag{1}$$

Note that in the autonomous case $\mathrm{L}_n(\mathbf{x}) = DM^{\circ n}(\mathbf{x})$. For any initial condition $\mathbf{x}$ we consider a small stochastic deviation $\epsilon\xi$, where ξ is a random vector with zero mean and unit covariance matrix. Letting $\mathbf{y}_n = M(\mathbf{y}_{n-1}, n-1)$ be the orbit with initial condition $\mathbf{y}_0 = \mathbf{x} + \epsilon\xi$, the linear response vector $\Xi_n(\mathbf{x})$ is defined by

$$\Xi_n(\mathbf{x}) = \lim_{\epsilon\to 0} \frac{\mathbf{y}_n - \mathbf{x}_n}{\epsilon} = DM(\mathbf{x}_{n-1}, n-1)\,\Xi_{n-1}\,. \tag{2}$$

The FLI after n iterations is defined as $\mathrm{FLI}_n(\mathbf{x}) = \log \|\mathrm{L}_n(\mathbf{x})\xi\| / n$, and can be easily implemented with the 'shadow particle' method [10], i.e. estimating $\|\mathrm{L}_n(\mathbf{x})\xi\|$ by explicitly taking a companion particle with initial condition $\mathbf{y}_0$ and computing the displacement after n turns, while performing norm renormalizations every m turns.

As FLI can be affected by the choice of ξ [11], a novel method consists in evaluating the eigenvalues and invariants of $\mathrm{L}_n\mathrm{L}_n^T$ given by

$$\mathrm{L}_n(\mathbf{x})\mathrm{L}_n^T(\mathbf{x}) = \left\langle \Xi_n(\mathbf{x})\Xi_n^T(\mathbf{x}) \right\rangle \quad \text{with} \quad \left\langle \xi\, \xi^T \right\rangle = \mathrm{I}\,. \tag{3}$$

This provides interesting results [12] as it is equivalent to considering all possible directions of the initial displacement vector. However, for complex maps, such as the Poincaré map of a realistic lattice, an analytical expression of the tangent map is not available, and the use of this method requires further considerations. A possible alternative is provided by the Orthogonal Fast Lyapunov Indicator (OFLI) [13], which consists in computing different FLI values along an orthonormal base of displacements. We refer to OFLI MAX as the maximum value obtained along the tracking and to OFLI MEAN as the mean of the computed values.

* Research supported by the HL–LHC project

ISBN: 978-3-95450-227-1 ISSN: 2673-5490 doi:10.18429/JACoW-IPAC2022-MOPOST043

TESTING THE GLOBAL DIFFUSIVE BEHAVIOUR OF BEAM-HALO DYNAMICS AT THE CERN LHC USING COLLIMATOR SCANS*

C.E. Montanari[1], A. Bazzani, Bologna University, Bologna, Italy
M. Giovannozzi, A. Gorzawski[2], S. Redaelli, CERN Beams Department, Geneva, Switzerland
[1]also at CERN Beams Department, Geneva, Switzerland
[2] now at ESS, Lund, Sweden

Abstract

In superconducting circular particle accelerators, controlling beam losses is of paramount importance for ensuring optimal machine performance and an efficient operation. To achieve the required level of understanding of the mechanisms underlying beam losses, models based on global diffusion processes have recently been studied and proposed to investigate the beam-halo dynamics. In these models, the building block of the analytical form of the diffusion coefficient is the stability-time estimate of the Nekhoroshev theorem. In this paper, the developed models are applied to data acquired during collimation scans at the CERN LHC. In these measurements, the collimators are moved in steps and the tail population is reconstructed from the observed losses. This allows an estimate of the diffusion coefficient. The results of the analyses performed are presented and discussed in detail.

INTRODUCTION

In high-energy colliders or storage rings bound to use superconducting magnets, the beam dynamics is extremely complex and intrinsically nonlinear, due to the unavoidable magnetic field errors. This might generate beam losses or emittance growth that affect the accelerator performance, either because of a reduction of the luminosity or due to a reduction of the operational efficiency. A link between dynamic aperture (DA), i.e. the extent of the phase-space region in which bounded motion occurs, and beam lifetime has been established [1] and successfully used to measure DA [2]. However, this approach does not give any hint on the evolution of the beam distribution, which provides means to predict the beam losses and lifetime, and, more importantly, also the evolution of the beam emittance. This is crucial to assess the presence of emittance growth phenomena, which play a role in determining the actual performance of the collider or storage ring.

In this respect, the development of a framework based on diffusive models of the non-linear beam dynamics is particularly useful. The approach followed is to construct a Fokker-Planck (FP) equation that gives access to the evolution of the beam distribution over time scales compatible with those of physical interest (direct tracking of 10^8 turns for several initial conditions for a complex lattice like the LHC one is still not an option nowadays). The development of diffusive models of the transverse beam dynamics is not new for accelerator physics (see, e.g. [3–10] and references therein). However, recently a new framework has been developed [11–13], in which the functional form of the diffusion coefficient is derived from the optimal estimate of the perturbation series provided by the Nekhoroshev theorem [14–16]. The FP equation describes the time evolution of the beam distribution ρ according to

$$\frac{\partial \rho(I,t)}{\partial t} = \frac{1}{2}\frac{\partial}{\partial I} D(I) \frac{\partial}{\partial I} \rho(I,t) \qquad D(I) \propto \exp\left[-2\left(I_*/I\right)^{\frac{1}{2\kappa}}\right], \tag{1}$$

where $D(I)$ is the diffusion coefficient as a function of the action variable I. Equation (1) is suitable for studying the evolution of beam distributions in the presence of collimators with jaws that provide absorbing boundary conditions necessary to solve the FP equation. Note that the so-called collimator scans, i.e. the controlled movement of the jaws of the LHC collimators, can be used to study beam-halo dynamics and, in particular, to reconstruct the diffusion coefficient behaviour as a function of transverse amplitude [5, 9, 17, 18]. The collimator scan method is widely used in LHC operation and is based on small jaw displacements at different amplitudes I, combined with measurement of beam losses. Displacements can be inward or outward, causing different characteristic profiles of beam losses.

The special functional form of the diffusion coefficient is related to the functional form provided by the estimate of the optimal perturbation series, according to the Nekhoroshev theorem [15, 16]. The parameters κ, I_* have a physical meaning that stems from the Nekhoroshev theorem: the exponent κ is related to the analytic structure of the perturbative series and to the dimensionality of the system [12]; I_* is related to the asymptotic character of the perturbative series.

PROBING $D(I)$ FROM LOSS DATA

A recent work [13], considered a measurement protocol for probing a Nekhoroshev-like diffusive behaviour of the beam halo. It is based on alternating inward and outward jaw movements during collimator scan measurements. The idea behind the proposed protocol is that the observed current loss signal $J(t)$ can be divided into two separate processes with different timescales: (1) a global process $J_{\mathrm{eq}}(t)$ generated by exponentially slow erosion of the beam core and (2) a recovery current $J_{\mathrm{R}}(t)$ generated by changes in jaw position that occur on time scales shorter than (1). The latter causes the system to relax into a new semi-stationary equilibrium.

* Research supported by the HL–LHC project

ISBN: 978-3-95450-227-1 ISSN: 2673-5490 doi:10.18429/JACoW-IPAC2022-MOPOST045

A NOVEL TOOL FOR BEAM DYNAMICS STUDIES WITH HOLLOW ELECTRON LENSES*

P. D. Hermes†, R. Bruce, R. De Maria, M. Giovannozzi, G. Iadarola, D. Mirarchi, S. Redaelli
European Organization for Nuclear Research (CERN), Geneva, Switzerland

Abstract

Hollow Electron Lenses (HELs) are crucial components of the CERN LHC High Luminosity Upgrade (HL-LHC), serving the purpose of actively controlling the population of the transverse beam halo to reduce particle losses on the collimation system. Symplectic particle tracking simulations are required to optimize the efficiency and study potentially undesired beam dynamics effects with the HELs. With the relevant time scales in the collider in the order of several minutes, tracking simulations require considerable computing resources. A new tracking tool, Xsuite, developed at CERN since 2021, offers the possibility of performing such tracking simulations using graphics processing units (GPUs), with promising perspectives for the simulation of hadron beam dynamics with HELs. In this contribution, we present the implementation of HEL physics effects in the new tracking framework. We compare the performance with previous tools and show simulation results obtained using known and newly established simulation setups.

INTRODUCTION

The CERN Large Hadron Collider (LHC) is designed to store and collide hadron beams of unprecedented intensities and particle energies up to 7 TeV [1]. The High-Luminosity LHC (HL-LHC) [2] upgrade, foreseen for installation after the LHC Run 3 (2022-25), aims to increase the collider's luminosity by reducing the value of β^* at the ATLAS and CMS insertions and an increase in beam brightness and intensity, thanks to the LHC Injectors Upgrade project [3], up to a total stored beam energy of 684 MJ per circulating beam. Such intense beams have a large damage potential in the event of uncontrolled beam losses. A high-performance multistage collimation system is installed in the LHC [4–6] and is being upgraded for the HL-LHC [7], in order to keep the collider protected against beam losses.

Measurements in the LHC [8,9] have shown that the transverse beam halo at amplitudes greater than 3 σ can constitute up to 5% of the total beam intensity. Estimated by simple scaling to the intensity of the desired proton beam, the energy in the beam halo of HL-LHC could reach the order of 34 MJ. Different failure scenarios could cause orbit offsets of up to 2 σ within a few turns [10], which could induce very high beam losses. Hollow electron lenses (HELs) have been integrated in the HL-LHC baseline to mitigate this risk by active depletion of the beam halo [10–12]. A HEL generates a hollow cylindrical shaped electron beam (e-beam) and steers it through a solenoid in the centre of which they move coaxially and oppositely directed to the proton beam. Perfectly symmetric hollow electron beams would leave particles at amplitudes smaller than the inner radius of the e-beam unaffected, while particles in the beam halo would be subject to a transverse kick from the electromagnetic field created by the e-beam. Exploiting this behavior allows to drive halo particles towards larger amplitudes in a controlled way, such that they are intercepted and disposed of by the collimators, whereby the population of the halo is reduced.

Operational scenarios for HEL are studied using symplectic tracking simulations, computing particle trajectories over a large number of turns (up to several millions) [13]. Of particular interest is the classification of turn-by-turn pulsing schemes in which the HEL is switched on and off according to a pre-defined time pattern. Examples of figures of merit to be studied in such simulations are the depletion efficiency, quantifying the percentage of the beam halo that is removed, and the emittance growth, a detrimental effect caused by the residual kick acting on the core of the main proton beam.

SixTrack [14–16], a single-particle symplectic tracking tool, provides the functionality of simulating HEL kicks [17], allowing the user to select different profiles $\rho(r)$ of the e-beam, and to simulate turn-by-turn pulsing of the HEL [18]. Simulation results obtained using this framework were presented in [13]. Since 2021, a new symplectic tracking framework, Xsuite [19], a collection of Python packages that can be run on CPUs and GPUs, is being developed. Simulations over a large number of turns in machines like the LHC can be carried out at significantly shorter simulation times when using GPU platforms. The Xtrack (XT) tracking package in Xsuite contains the symplectic tracking maps used in the simulation process.

This contribution describes the implementation of HEL physics in the Xtrack framework and the benchmark against SixTrack. Besides comparing the amplitude-dependent kick in the HEL, we verify the equivalence of both codes focusing on the two physical figures of merit: halo depletion efficiency and beam-core emittance growth.

HEL KICK

From Biot-Savart's law, one can derive the transverse kick θ that a hadron receives from the interaction with the oppositely directed HEL electron beam [20] as follows:

$$\theta(r) = \frac{1}{2\pi\epsilon_0 c^2} \frac{LI(1+\beta_e\beta_p)}{(B\rho)_p \beta_e \beta_p} \frac{1}{r} f(r)\,, \qquad (1)$$

where L is the active length of the HEL, β_e and β_p are the relativistic factor of the electrons and protons, respectively, $(B\rho)_p$ is the magnetic rigidity of the proton beam

* Research supported by the HL–LHC project
† pascal.hermes@cern.ch

ISBN: 978-3-95450-227-1 ISSN: 2673-5490 doi:10.18429/JACoW-IPAC2022-MOPOST046

ENFORCING THE CONVERGENCE OF LONGITUDINAL BUNCH DENSITY CALCULATION IN THE PRESENCE OF A HARMONIC CAVITY THROUGH ANDERSON ACCELERATION METHOD

I. C. Almeida*, A. P. B. Lima, M. H. Wallner
Brazilian Center for Research in Energy and Materials, Campinas, Brazil

Abstract

Sirius is a 4th generation synchrotron light source at the Brazilian Center for Research in Energy and Materials in Campinas, Brazil. A passive superconducting third harmonic cavity is planned to be installed in the storage ring in order to lengthen the bunches and increase beam lifetime by reducing Touschek scattering while keeping its high brightness. This paper presents the results obtained in applying Anderson acceleration method to enforce the convergence of the self-consistent algorithm used for calculation of the equilibrium longitudinal bunch density in the presence of a harmonic cavity.

INTRODUCTION

New generation synchrotron light sources require low-emittance storage rings in order to increase radiation brightness, which reduces beam lifetime due to Touschek scattering. A common approach to increase beam lifetime without affecting the brightness is to include a higher harmonic cavity in the system in order to lengthen the bunches and reduce the longitudinal bunch density [1]. For Sirius, which has a natural emittance of 0.250 nm–rad and a fundamental RF frequency of 500 MHz, a 1.5 GHz passive superconducting third harmonic cavity is planned to be installed and a beam lifetime increase around 4.5 times the current value is expected.

Since it is known that the maximum lifetime increase is obtained with bunch overstretching , *i.e.*, with a harmonic voltage higher than the one calculated for flat potential [2], a voltage sweep was carried on to find the maximum beam lifetime working point using the self-consistent approach described in [3, 4]. It was observed that above a threshold voltage value the algorithm could not converge and the longitudinal bunch density started to bounce between different fixed states. In this paper, Anderson acceleration method is adopted to enforce the convergence of the self-consistent equilibrium bunch density calculation based on the approach presented in [5].

ANDERSON ACCELERATION

In a passive harmonic cavity the voltage is due only to beam loading, which means that amplitude and phase cannot be controlled independently [3]. Hence, for a given harmonic voltage amplitude, the self-consistent bunch density calculation should converge to an equilibrium state and provide the corresponding cavity detune. However, as will be later shown, above a threshold voltage amplitude, the algorithm does not converge and an equilibrium bunch density cannot be obtained. To overcome this issue, the bunch densities from previous iterations started being used through Anderson acceleration method.

For each iteration k, the electron bunch density of a storage ring is given by:

$$\rho_k(\tau) = Ae^{-\frac{\Phi_k(\tau)}{\alpha^2\sigma_e^2}}, \tag{1}$$

where A is a normalization constant, α is the momentum compaction factor, σ_e is the energy spread, τ is the time deviation with respect to the synchronous particle and $\Phi(\tau)$ is the voltage dependent potential function.

Since the voltage of a harmonic cavity depends on the bunch density, a fixed point problem is established and the following map can be defined:

$$g_k = g(\rho_k) = Ae^{-\frac{\Phi(\tau,\rho_k)}{\alpha^2\sigma_e^2}}. \tag{2}$$

The new bunch density can be calculated as a linear combination of the maps of previous iterations. Anderson acceleration method solves a constrained linear least-squares problem to find the coefficients of the linear combination [5]:

$$f_k = g_k - \rho_k,$$
$$(\alpha_0^k, \alpha_1^k, ..., \alpha_{m_k}^k) = \text{argmin}\left|\sum_{j=0}^{m_k}\alpha_j^k f_{k-m_k+j}\right|^2, \tag{3}$$
$$\sum_{j=0}^{m_k}\alpha_j^k = 1.$$

Therefore,

$$\rho_{k+1} = \sum_{j=0}^{m_k}\alpha_j^k g_{k-m_k+j} \quad \text{for} \quad k \geq 0, \tag{4}$$

where $m_k = \min(k, m)$ with $m \geq 1$ being the number of previous iterations desired to be taken into account in the the current step. For $k = 0$, an initial condition must be given and the constraint relation provides $\alpha_0^0 = 1$.

An extra degree of flexibility can be added by introducing the relaxation parameter $\beta_k \leq 1$:

$$\rho_{k+1} = \beta_k\sum_{j=0}^{m_k}\alpha_j^k g_{k-m_k+j} + (1-\beta_k)\sum_{j=0}^{m_k}\alpha_j^k\rho_{k-m_k+j}. \tag{5}$$

* iago.almeida@cnpem.br

ISBN: 978-3-95450-227-1 ISSN: 2673-5490 doi:10.18429/JACoW-IPAC2022-MOPOST047

DETERMINATION OF THE PHASE-SPACE STABILITY BORDER WITH MACHINE LEARNING TECHNIQUES

F.F. Van der Veken*, R. Akbari, M.P. Bogaert, E. Fol, M. Giovannozzi, A.L. Lowyck, C.E. Montanari, W. Van Goethem, CERN, Meyrin, Switzerland

Abstract

The dynamic aperture (DA) of a hadron accelerator is represented by the volume in phase space that exhibits bounded motion, where we disregard any disconnected parts that could be due to stable islands. To estimate DA in numerical simulations, it is customary to sample a set of initial conditions using a polar grid in the transverse planes, featuring a limited number of angles and using evenly distributed radial amplitudes. This method becomes very CPU intensive when detailed scans in 4D, and even more in higher dimensions, are used to compute the dynamic aperture. In this paper, a new method is presented, in which the border of the phase-space stable region is identified using a machine learning (ML) model. This allows one to optimise the computational time by taking the complex geometry of the phase space into account, using adaptive sampling to increase the density of initial conditions along the border of stability.

INTRODUCTION

When studying the non-linear beam dynamics in a circular hadron ring in numerical simulations, one of the key concepts is that of dynamic aperture (DA). It represents the smallest, simply-connected volume in the $2n$-dimensional phase space that is stable (where n is the number of degrees of freedom), i.e. that exhibits bounded motion over a given time interval [1, 2]. More precisely, it is defined as the radius of the $2n$-sphere with the same volume V_{2n} as the bounded region:

$$\mathrm{DA} = \sqrt[2n]{\frac{\Gamma\left(n+1\right) V_{2n}}{\pi^n}}\,. \tag{1}$$

The DA is a useful quantity, not only in accelerator design, but also because it can be linked to measurable quantities such as the time evolution of the beam intensity [3, 4] or luminosity [5, 6] of a storage ring or collider.

In practice, computational limitations make us consider the DA in two dimensions only, instead of six (the dimension of the phase space of a particle beam). The transverse momenta and longitudinal position coordinates are typically set to zero, while the longitudinal momentum coordinate is typically set at a non-zero value that is deemed representative for the longitudinal beam distribution under consideration.

An important aspect in the definition of DA, is that it excludes disconnected stable islands from the calculation of the volume. To consider this in simulations, traditionally the DA is calculated by sampling initial conditions in a polar grid, over a certain number of angles [2]. The stability border is given, for each angle θ_i, by the largest connected stable amplitude r_i. After integrating r_i over angles, the DA is approximated by [2]:

$$\mathrm{DA} \approx \sqrt{\frac{2}{\pi}\Delta\theta \sum_i^{N_\theta} c_i\, r_i^2} \qquad \Delta\theta = \frac{1}{N_\theta+1}\frac{\pi}{2}\,, \tag{2}$$

where c_i are the constants of the chosen open integration method and N_θ the number of angles. This calculation has an error that scales with $\sim \Delta r \Delta\theta$, hence ideally one would like to keep $\Delta r \sim \Delta\theta$ to minimise the error associated to the DA estimate [2].

It is also clear that the overall strategy to compute the DA of a given accelerator lattice would gain in efficiency if the initial conditions could be chosen to probe with high density the region of the stability border, only. In this paper, we explore an alternative to the polar sampling, where an initial set of particles is sampled uniformly and machine learning (ML) is applied to recognise the stability border at a given number of turns. In a second step, we resample a larger set of particles focused around the border region.

MACHINE LEARNING

To find the stability border at a given number of turns N, we divide the particles into those that survived at least N turns, meaning their motion remains bounded for at least this time, and those that did not, and then train an ML model as a classifier. While in theory it would be feasible to divide the particles in multiple groups for different number of survived turns, it would not be an optimal division to train the ML algorithm on.

We opted to use a support-vector machine (SVM) model [7, 8], which is a supervised learning algorithm that is one of the most robust prediction methods available. Because of its (by default) binary classification, it is well-suited for our particular data structure if split as described in the previous paragraph. Though SVM is by default a linear classifier, it can be used to classify data that are separated by a non-linear boundary by using a kernel transformation: in our case, a radial basis function is most suited due to the radial nature of the data. It is an exponential kernel that maps two vectors $\mathbf{v}$ and $\mathbf{w}$ as a function of the hyperparameter γ:

$$K(\mathbf{v},\mathbf{w}) = \mathrm{e}^{-\gamma\,\|\mathbf{v}-\mathbf{w}\|}\,, \tag{3}$$

where $\|\cdot\|$ stands for the vector norm. In ML training, the different hyperparameters have to be tuned to get optimal results. Like in classical statistics, a model that is not adequately tuned can lead to under- or over-fitting the data. In our case, there are two hyperparameters to tune: the above-mentioned γ that represents the convolution of the curve

* frederik.van.der.veken@cern.ch

ISBN: 978-3-95450-227-1 ISSN: 2673-5490 doi:10.18429/JACoW-IPAC2022-MOPOST048

EFFICIENT REPRESENTATION OF REALISTIC 3D STATIC MAGNETIC FIELDS FOR SYMPLECTIC TRACKING AND FIRST APPLICATIONS FOR FREQUENCY ANALYSIS AND DYNAMIC APERTURE STUDIES IN ELENA

Lajos Bojtár, CERN, Geneva, Switzerland

Abstract

The algorithm called SIMPA has a new and unique approach to long-term 4D tracking of charged particles in arbitrary static electromagnetic fields. Field values given on the boundary of the region of interest are reproduced by an arrangement of hypothetical magnetic or electric point sources surrounding the boundary surface. The vector and scalar potentials are obtained by summing the contributions of each source. The second step of the method improves the evaluation speed of the potentials and their derivatives by orders of magnitude. This comprises covering the region of interest by overlapping spheres, then calculating the spherical harmonic expansion of the potentials on each sphere. During tracking, field values are evaluated by calculating the solid harmonics and their derivatives inside a sphere containing the particle. Frequency analysis and dynamic aperture studies in ELENA is presented. The effect of the end fields and the perturbation introduced by the magnetic system of the electron cooler on dynamic aperture is shown. The dynamic aperture calculated is the direct consequence of the geometry of the magnetic elements, no multipole errors have been added to the model.

INTRODUCTION

In recent papers [1, 2] we described a new algorithm allowing long-term symplectic integration of charged particle trajectories in arbitrary static magnetic and electric fields. The approach to particle tracking we described naturally includes the end fields for all kinds of elements with the same treatment.

THE TRACKING ALGORITHM

A Short Summary

We recommend reading the previous papers [1,2] to understand the algorithm in detail, as only a summary is provided here.

Symplectic integrators keep the conserved quantities bounded, but cannot cure the errors coming from the representation of the fields. These are two separate sources of errors. It is crucial to have a physically valid representation of the fields, otherwise there is a spurious energy drift during the tracking. The potentials are expressed analytically in terms of their sources. These sources are placed outside of the volume of interest, at some distance from the boundary, and their strength is set such that they reproduce the magnetic or electric field at the boundary by solving a system of linear equations. After the potentials are reproduced at the boundary by the sources, they can be evaluated analytically anywhere inside the volume. However, this method is too slow to be practical.

Several orders of magnitude improvement can be achieved by using a local description of the potentials. Spherical harmonics scaled appropriately are called solid harmonics. Regular solid harmonics are the canonical representation for harmonic functions inside a sphere. A key characteristic of the algorithm is the description of vector and scalar potentials by solid harmonics inside a set of overlapping spheres covering the volume of interest.

The potentials satisfy exactly the Laplace equation inside the spheres. The discontinuity between the spheres decrease exponentially with the degree of solid harmonics expansion and can be easily kept close to machine precision. The representation of the potentials in terms of solid harmonics is optimal in terms of memory and allows fast evaluation.

The name of our software is SIMPA [3], an abreviation of Symplectic Integration through MonoPole Arrangements. The workflow starts with modeling individual magnets with CAD software or measurement data, then the strengths of the point sources are calculated for each type of magnet. The next step is to assemble these sources according to the lattice of the machine. Finally, the solid harmonics coefficients of each sphere covering the volume of interest are calculated, providing a field map for the fast evaluation.

The boundary of the volume of interest is described by a Standard Tessellation Language (STL) file in SIMPA. The next step is to fill it with overlapping spheres, such that the entire beam region is covered without gaps. The spheres should be small enough to not overlap with the sources.

It is practical to place the center of the spheres onto a regular lattice. The coordinates of the sphere centers on an infinite HCP lattice can be obtained by three simple expressions. We keep only those spheres from the infinite lattice which are necessary to cover the beam region. Figure 1 shows the ELENA beam region and the centers of the covering spheres. The radius of the spheres was 1 cm in this study and about 76000 of them were needed to cover the aperture.

Preparing the Field Maps

As a first step, the field of each type of magnet in ELENA has to be expressed as a collection of point sources. This provides continuous and analytic potential everywhere in the beam region. To do so, the magnetic field values have been obtained from the CAD software OPERA for each magnet at specific points on a surface surrounding the beam region. This surface is close to the poles of the magnet. The point sources are placed outside of the surface at 2.5 cm distance. Then a system of linear equation is solved to find

ISBN: 978-3-95450-227-1 ISSN: 2673-5490 doi:10.18429/JACoW-IPAC2022-MOPOST049

ELECTRON CLOUD BUILD-UP FOR THE ARC SEXTUPOLE SECTIONS OF THE FCC-ee

J. E. Rocha-Muñoz*, G. H. I. Maury-Cuna, Universidad de Guanajuato, León, México
K. B. Cantun-Ávila, Universidad Autónoma de Yucatán, Mérida, México
F. Zimmermann, CERN, Geneva, Switzerland

Abstract

In particle accelerators that operate with positrons, an electron cloud may occur due to several mechanism. This work reports preliminary studies on electron cloud build-up for the arc sextupole sections of the positron ring of the FCCe+e- using the code PyECLOUD. We compute the electron cloud evolution while varying strategic parameters and consider three simulation scenarios. We report the values of the central density just before the bunch passage, which is related to the single-bunch instability threshold and the electron density threshold for the three scenarios. In addition, we compare the simulated electron distribution across the central circular cross-section for a chamber with and without winglets.

INTRODUCTION

The electron-cloud (EC) effect is a phenomenon that occurs in high-energy particle accelerators that operate with positrons (or positively charged beams). It consists of the accumulation of electrons inside the machine vacuum chamber produced by a secondary emission process, where seed electrons come from the residual gas ionization or a photoemission process due to the beam-induced synchrotron radiation. Commonly electrons generated by this last mechanism constitute the main source of primary electrons in high-energy accelerators, such as the Future Circular electron-positron Collider (FCC-ee).

In the positron ring of the FCC-ee, it is expected that the electric field of the beam would accelerate these electrons to energies of up to several hundred eV [1]. Once the beam passes, these electrons will collide with the chamber walls and, depending on their speed, position, direction, and the beam pipe surface conditions, can generate new electrons. This process is repeated with each new bunch passage, and, due to the multipactor effect induced by the beam, an avalanche growth of the number of electrons may arise generating an electron cloud [2]. The EC density in the chamber can reach high levels and drive instabilities in the beam, such as the single-bunch head-tail instability [3].

The EC density is a critical aspect in order to avoid this instability. It depends on parameters such as the bunch spacing, the geometry of the vacuum chamber, photoelectron generation rate (n_γ), and the secondary emission yield (SEY) [4]. In this work, we present an analysis of the dependence of the electron density for three different scenarios to determine which presents the broadest range of variation of the aforementioned parameters below the instability threshold.

ELECTRON DENSITY THRESHOLD AND SIMULATION SCENARIOS

Scenarios

The FCC-ee is a proposed first stage post-LHC particle accelerator with energy significantly above that of previous circular colliders [5]. It is still in the design stage, and its operating parameters are constantly updated. We consider three scenarios for the EC build-up simulations of the main arc sextupole sections. The first one considers the design parameters extracted from the 2019 conceptual design report (CDR) to be used as a reference [6] (named *Scenario A*). In November 2021, a careful review of the parameters presented in the CDR resulted in an update, starting with a smaller circumference and only eight arc sections [7], these updated parameters make up our *Scenario B*; however, this set cause coherent beam instability issued, including high impedances [8], consequently in March 2022 an alternative set of parameters with slight changes was presented, which we named *Scenario C*.

Electron Density Threshold

The electron cloud acts as a short range wake field with frequency [9]:

$$\omega_e = \sqrt{\frac{2\lambda_p r_e c^2}{\sigma_y(\sigma_x + \sigma_y)}} \tag{1}$$

where $\lambda_p = \frac{N}{4\sigma_z}$ is the line charge density, N the bunch population and σ_z bunch length, r_e is the classical electron radius and $\sigma_{x,y}$ are the transverse beam dimensions.

The threshold density for the single-bunch head-tail instability is given by:

$$\rho_{th} = \frac{2\gamma Q_s}{\sqrt{3} Q r_e \beta_y C} \tag{2}$$

where Q_s is the synchrotron tune, C the machine circumference, γ the Lorentz factor and $Q = min\left(7, \frac{\omega_e \sigma_z}{c}\right)$.

The electron density threshold and the values used to compute them using Eqs. (1) and (2) are listed in Table 1 for each scenario.

The smallest threshold is found with the data extracted from the CDR with a value of $2.99 \times 10^{10}\ e^-/m^3$, while the threshold for scenarios B and C is essentially the same, with a value of $4.75 \times 10^{10}\ e^-/m^3$.

* je.rochamunoz@ugto.mx

ISBN: 978-3-95450-227-1 ISSN: 2673-5490 doi:10.18429/JACoW-IPAC2022-MOPOST050

THIRD-ORDER RESONANCE COMPENSATION AT THE FNAL RECYCLER RING

C. E. Gonzalez-Ortiz*, P. N. Ostroumov[1], Michigan State University, East Lansing, USA
R. Ainsworth, Fermilab, Batavia, USA
[1]also at FRIB, East Lansing, USA

Abstract

The Recycler Ring (RR) at the Fermilab Accelerator Complex performs slip-stacking on 8 GeV protons, doubling the beam intensity delivered to the Main Injector (MI). At MI, the beam is accelerated to 120 GeV and delivered to the high energy neutrino experiments. Femilab's Proton Improvement Plan II (PIP-II) will require the Recycler to store 50% more beam. Simulations have shown that the space charge tune shift at this new intensity will lead to the excitation of multiple resonance lines. Specifically, this study looks at normal sextupole lines $3Q_x = 76$ and $Q_x + 2Q_y = 74$, plus skew sextupole lines $3Q_y = 73$ and $2Q_x + Q_y = 75$. Dedicated normal and skew sextupoles have been installed in order to compensate for these resonance lines. By measuring and calculating the Resonance Driving Terms (RDT), this study shows how each of the resonance lines can be compensated independently. Furthermore, this study shows and discusses initial investigations into compensating multiple lines simultaneously.

INTRODUCTION

The Fermilab accelerator complex under the current Proton Improvement Plan II (PIP-II) aims to reliably deliver a 1.2 MW proton beam to the DUNE (Deep Underground Neutrino Experiment) experiment. The addition of an 800-MeV superconducting linear accelerator along with improvements to the existing Main Injector (MI) and Recycler Ring (RR) will allow this facility to achieve such a goal [1].

The Recycler Ring at the Fermi National Accelerator Laboratory (Fermilab or FNAL) receives twelve batches of proton beam from the Booster. Once in the Recycler, a slip-stacking procedure is performed in order to double the bunch intensity and, consequently, beam is sent to the Main Injector. In the MI, beam is accelerated to 120 GeV and sent to either NuMI (Neutrinos at the Main Injector) or other experiments via Switchyard. The RR also sends beam to the muon campus after rebunching the proton buckets from 53 MHz to 2.5 MHz [2].

In order to achieve the PIP-II beam power objective, the Recycler will be required to store and accumulate 50% more beam than current operations. Simulations have shown that space charge tune shifts at such intensities will lead to the crossing of multiple betatron resonances, and consequently, this will lead to beam loss. Of particular interest are third order resonance lines which significantly reduce the dynamic aperture of the Recycler Ring [1].

* gonza839@msu.edu

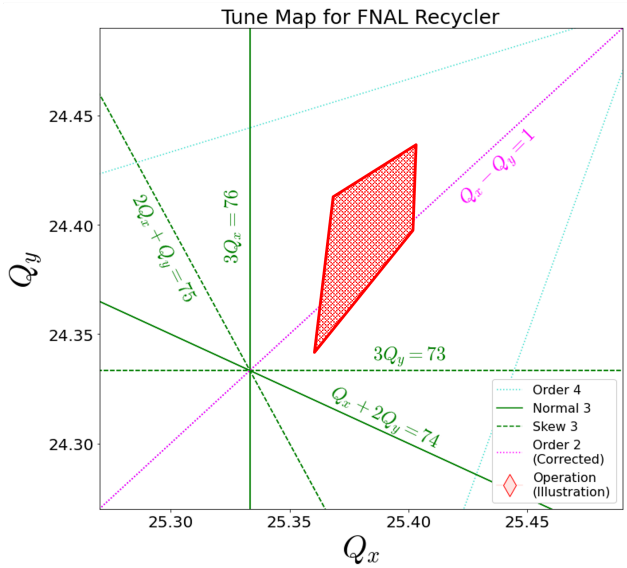

Figure 1: Tune map illustration of relevant resonance lines in present RR operation.

Figure 1 shows the tune map for the present RR operation, including an approximate tune footprint (filled diamond shape) for an approximate intensity of 5×10^{10} particles per bunch (ppb). As intensity is increased in the Recycler, the tune footprint area will increase to the point of intersecting the third order resonance lines. Resonance lines driven by normal sextupole components include $3Q_x = 76$ and $Q_x + 2Q_y = 74$. Skew sextupole lines include $3Q_y = 73$ and $2Q_x + Q_y = 75$. It is also worth pointing out that the coupling line $Q_x - Q_y = 1$ is already being corrected for with dedicated skew quadrupoles. The present work will describe how by measuring and controlling the resonance driving terms in the Recycler, we can use dedicated normal and skew sextupoles to compensate third order resonances.

RESONANCE COMPENSATION

Resonance Driving Terms

The Courant-Snyder variables $(\hat{x},\hat{p}_x,\hat{y},\hat{p}_y)$ or normalized phase space coordinates can be written to first order as:

$$\hat{u} = \sqrt{2J_u}\cos\left(\phi_u + \phi_{u_0}\right); \quad (1)$$

$$\hat{p}_u = -\sqrt{2J_u}\sin\left(\phi_u + \phi_{u_0}\right), \quad (2)$$

where u can stand either for the x or y coordinate, J_u and ϕ_u correspond to the action-angle variables and ϕ_{u_0} corresponds to the initial phase. It is worth pointing out that J_u is

ISBN: 978-3-95450-227-1 ISSN: 2673-5490 doi:10.18429/JACoW-IPAC2022-MOPOST051

STUDY OF TRANSVERSE RESONANCE ISLAND BUCKETS AT CESR*

S. T. Wang†, V. Khachatryan, CLASSE, Cornell University, Ithaca, NY, USA

Abstract

A 6-GeV lattice with the horizontal tune near a 3rd-order resonance line at $3\nu_x$=2 is designed for studying the transverse resonance island buckets (TRIBs) at the Cornell Electron Storage Ring (CESR). The distribution of 76 sextupoles powered individually is optimized to maximize the dynamic aperture and achieve the desired amplitude-dependent tune shift α_{xx} and the resonant driving term h_{30000}, which are necessary conditions to form stable island buckets. The particle tracking simulations are developed to check and confirm the formation of TRIBs at different tunes with clearing kicks in this TRIBs lattice. Finally, the lattice is loaded in CESR and the TRIBs are successfully observed when the horizontal fractional tune is adjusted to 0.665, close to the 3rd-order resonance line. Bunch-by-bunch feedback is also explored to clear the particles in the main bucket and the island buckets, respectively.

INTRODUCTION

Nonlinear resonances are critical topics in the beam dynamics of accelerator physics, which have been studied theoretically and experimentally for many years [1]. Normally a storage ring operates at tunes far away from resonant lines to avoid the negative impact such as instability, poor lifetime, and increased emittance. However, by taking advantage of the resonance nature, one application of the ring operating at the 3rd-order resonance line is to extract particles in multi-turns at CESRN-PS and ELSA [2]. Recently, MLS and BESSY-II have demonstrated the stable two-orbit operation by utilizing the transverse resonance island buckets (TRIBs) [3, 4]. The second orbit for the beam in the island decreased the x-ray pulse frequency by 3 or 4 times which expands the possibilities for timing experiments [5].

TRIBs form in the vicinity of a resonance line, which can be achieved by adjusting the horizontal tune along with the familes of sextupoles (harmonic and normal) to tune the amplitude-dependent tune shift (ADTS) to stabilize the beam [3]. This approach is effective but empirical tuning of the sextupoles may be required. With this method, TRIBs have been successfully observed at MLS, BESSY-II, and MAX-IV [6]. To understand how TRIBs can form at CESR, a relatively high-energy (6-GeV) storage ring, we choose a different approach by designing a lattice with the horizontal tune near the 3rd integer line and a new sextupole distribution, at which TRIBs could form easily by adjusting the horizontal tune only.

In this paper, we discuss the criteria of optimizing the sextupoles for the TRIBs. A particle tracking simulation is developed to demonstrate the formation of TRIBs at different tunes. The lattice is then loaded into CESR and the TRIBs are successfully observed while adjusting horizontal tune to 0.665. Clearing kicks using feedback kicker is explored to clear the particles in the core or island buckets.

LATTICE DESIGN

Cornell Electron Storage Ring (CESR) is a 6-GeV accelerator located on the Cornell University campus. Since 2008, CESR serves as a dedicated light source for x-ray users, namely Cornell High Energy Synchrotron Source (CHESS). In 2018, one sextant of the ring was upgraded with double bend acromat to reduce the emittance and accommodate more compact undulators [7]. The main accelerator parameters are listed in Table 1. CESR magnets including 113 quadrupoles, 12 dipole quadrupoles, and 76 sextupoles are all individually powered, which provides great flexibilty for lattice design and complex nonlinear dynamics studies. Details of CESR lattice are described in Ref [7].

As shown in Table 1, the nominal horizontal fractional tune (Q_x) during CHESS operation is 0.556, far from the 3rd-order line $3\nu_x$=2 (0.667). It is very unlikely that TRIBs would appear by only adjusting the tune near 0.667. Thus, we first optimize quadrupoles to create a linear lattice with the design tunes at (16.643, 12.579) closer to the 3rd-order line while preserving most optics parameters as the normal lattice. Then 76 sextupoles are optimized to meet the conditions of forming TRIBs as well as maxmizing the dynamic aperture (DA).

The formula of the stable fixed points (SFP) have been derived in Reference [1] as shown in Eq. (1),

$$J_{SFP}^{1/2} = \frac{3G_{3,0,l}}{4\alpha_{xx}}\left(1 \pm \sqrt{1 - \frac{16\alpha_{xx}\delta}{9G_{3,0,l}^2}}\right), \qquad (1)$$

where J_{SFP} is the particle's action at the SFP, $G_{3,0,l}$ is the resonance strength at the 3rd-order resonance $3\nu_x$=l, α_{xx} is the detune coefficient of ADTS, and δ=$Q_x - \frac{l}{3}$. As Eq. (1) implys, the formation of TRIBs depends on three variables

Table 1: CESR Parameters

Beam Energy (GeV)	E_0	6.0
Circumference (m)	L	768.438
Transverse Damping time (ms)	$\tau_{x,y}$	12.0, 14.6
Longitudinal Damping time (ms)	τ_z	8.2
Synchrotron tune	Q_s	0.027
Horizontal tune	Q_x	16.556
Vertical Tune	Q_y	12.636
Horizontal Emittance (nm·rad)	ϵ_x	~ 28
Energy spread	σ_p	8.2×10^{-4}

* Work supported by NSF PHYS-1757811 and DMR-1829070.
† sw565@cornell.edu

ISBN: 978-3-95450-227-1 ISSN: 2673-5490 doi:10.18429/JACoW-IPAC2022-MOPOST053

TRANSVERSE RESONANCE ISLANDS BUCKETS AT SPEAR3*

Jaehyun Kim†, J. Safranek, K. Tian
SLAC National Accelerator Laboratory, CA, USA

Abstract

We have explored a possible operation mode for timing experiments at SPEAR3 by populating a single bunch into the transverse resonance islands buckets (TRIBs), driven either by the multi-bunch feedback kicker over multiple turns or by one of the injection kickers within a single turn. In this paper, we present both experimental observations and numerical simulations for TRIBs studies at SPEAR3.

INTRODUCTION

Beam resonance in a storage ring is generally considered as a limiting factor for the beam performance. Therefore, operational betatron tunes are chosen to avoid harmful resonance lines such as those of integer tunes and half-integer tunes. When a potential-well is formed around a certain resonance, a bunch can be trapped inside the potential-well. This transverse resonance islands buckets (TRIBs) can be exploited to provide a bunch which has a different repetition rate and a spatial separation from the bunch circulating the ring on the nominal orbit. The TRIBs can be useful for some timing experiments in the beam line.

TRIBs have been studied and demonstrated at BESSY II [1] and MAX-IV [2]. Both studies focused on the 3rd order horizontal resonance by moving the horizontal tune, ν_x, close to 0.3333 (or 0.6666) and driving the beam to the TRIBs with the bunch-by-bunch (BxB) feedback kicker. Since the kick amplitude generated by the BxB kicker is small, a bunch will be diffused to the 3 islands evenly.

In this paper, we present experimental and numerical studies on TRIBs at SPEAR3. It was found that the beam can be driven to the TRIBs by using either the BxB feedback kicker or one of the injection kickers, K1. In either approach, instead of being populated to three islands, the beam was completely driven to one of the resonant islands.

SPEAR3 TRIBS MODE

SPEAR3 is a 3 GeV storage ring based on the double bend achromat (DBA) lattice with a circumference of 234.144 m. The 6-nm latice is an operational mode under development. Though it is not ready for user operations, the 6-nm lattice provides adequate lifetime and injection efficiency for accelerator physics experiments. In addition, the designed ν_x is 15.32, convenient for the TRIBs studies. As a result, the 6-nm lattice was chosen for this work. The nominal chromaticity of the 6-nm lattice is +2 for both the horizontal and the vertical planes. During our TRIBs study, the horizontal chromaticity was reduced to 0 using a chromaticity response matrix to avoid tune shifts caused by momentum deviation when driving the beam horizontally. We were able to drive the TRIBs mode either with the BxB feedback kicker or the injection kicker, K1, however, with the BxB feedback kicker, ν_x was increased to 0.3297 from the design value of 0.32 due to the relatively weak strength of the kicker [3].

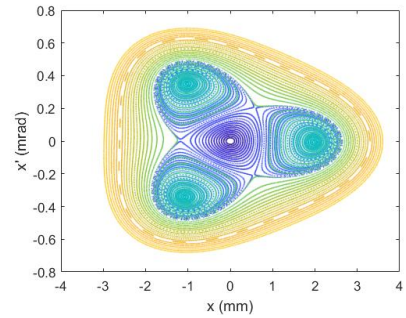

Figure 1: Contours on the x-x' phase space at s = 0 position.

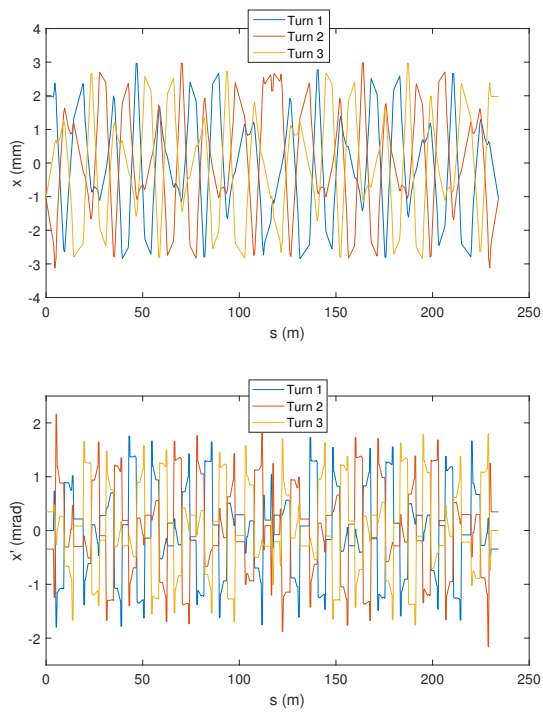

Figure 2: Closed orbit of SPEAR3 TRIBs optics.

Using ELEGANT [4], single particles with varied initial offsets were tracked in a lattice obtained from optics fitting with LOCO [5]. The distribution of resonance islands is visualized in Fig. 1 as three potential wells around ν_x = 0.3333. Once the electron beam is trapped in one of these islands, the new orbit (x, x'), passing through the centers of the 3 islands as shown in Fig. 2, is closed every 3 turns. The

* Work supported by U.S. Department of Energy under Contract No. DEAC02-76SF00515
† jaehyun@slac.stanford.edu

ISBN: 978-3-95450-227-1 ISSN: 2673-5490 doi:10.18429/JACoW-IPAC2022-MOPOST054

A HYBRID MULTI-BEND ACHROMAT LATTICE DESIGN FOR SSRL-X*

J. Kim†, X. Huang, K. Tian, M. Song, J. Safranek, P. Raimondi
SLAC National Accelerator Laboratory, CA, USA

Abstract

We present a lattice design for SSRL-X which is a green-field low-emittance storage ring proposal. The lattice is based on the hybrid multi-bend achromat and has natural emittance of 63 pm with 24-cells and 570 m circumference under 3.5 GeV energy. Insertion of damping wigglers on dedicated straight sections futher reduces natural emittance to 34 pm, which yields 18 pm under the full-coupling condition. Performance of the lattice and preliminary optimization study is given.

INTRODUCTION

We are exploring options to provide more bright and reliable synchrotron light source which can serve Stanford Synchrotron Radiation Lightsource (SSRL) for next decades. It includes upgrade of existing SPEAR3 storage ring into a multi-bend achromat lattice, a ring fits the 2.2-km PEP tunnel and a 570-m green-field storage ring.

SSRL-X is a green-field low-emittance storage ring proposal with 3.5 GeV energy and 63 pm natural emittance. Design of the storage ring is based on the hybrid multi-bend achromat which is widely adopted for 4th generation storage rings. Emittance of the storage ring is further reduced to 32 pm with additional damping from damping wigglers. The ring can achieve minimum emittance with the full-coupling condition which divides emittance as much as $\varepsilon_x \frac{J_x}{J_x+1}$ on both transverse planes. The value is 18 pm and it is close to diffraction-limit of 10-KeV photon beam, 10 pm.

In this paper, we present characteristics and matching constraints of SSRL-X, and show nonlinear performance. Preliminary optimization based on 2D scanning is given. Performance limit due to intrabeam scattering (IBS) is also investigated.

SSRL-X OPTICS

Twiss-functions of one standard cell and SSRL-X ring are shown in Fig. 1. It is a hybrid multi-bend achromat which has strong FODO region at the middle and two large dispersion bumps where chromatic sextupole magnets are located. Phase advances between adjacent dispersion bumps are satisfying $\psi_x = 3\pi$ and $\psi_y = 3\pi$ for local cancellation of resonance driving terms caused by chromatic sextupole magnets. Bending magnet region near the dispersion bumps consists of longitudinal gradient bending magnets to suppress emittance increase in the large dispersion region. A quadrupole is added inside the outer longitudinal gradient bending magnet region to match horizontal and vertical beta-functions to $L/2$ where L is length of straight section.

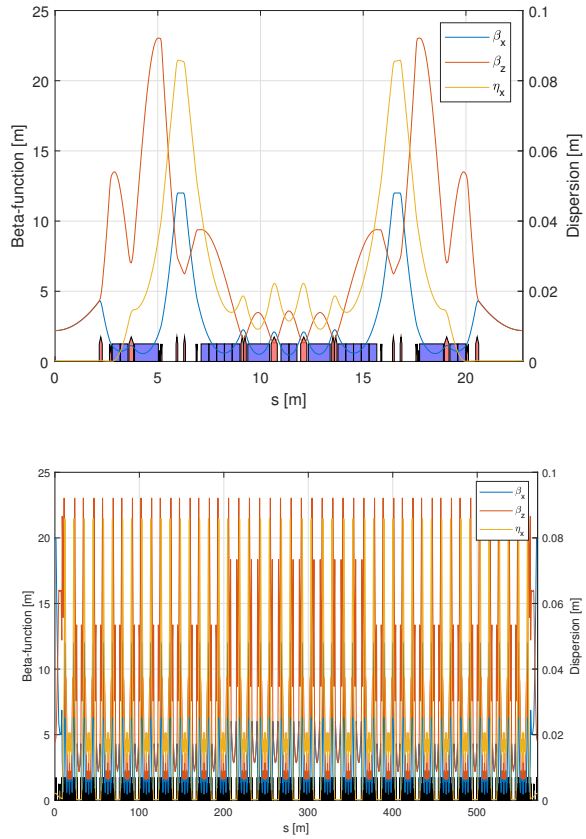

Figure 1: Twiss functions of a unit cell (upper plot) and a ring (lower plot).

A ring consists of 17 standard cells, 5 long-straight cells, and 1 injection cell (Fig. 1 lower plot). Long-straight cells and an injection cell are modifications of the standard cell. Long-straight sections are dedicated for damping wigglers. Additional damping from wigglers reduces the natural emittance from 63 pm to 34 pm. The injection cell provides large horizontal beta-function region which makes off-axis injection feasible. Although these cells have different lengths compared to the standard cell, 24-cell periodicity is preserved in terms of phase advance. They have same phase advance with the standard cell and satisfy $\psi_x = 3\pi$ and $\psi_y = 3\pi$ between the adjacent dispersion bumps. The ring also has one octupole family and one decapole family in each cell to effectively cancel detuning coefficients. Lattice parameters are listed in Table 1.

* Work supported by U.S. Department of Energy under Contract No. DEAC02-76SF00515
† jaehyun@slac.stanford.edu

ISBN: 978-3-95450-227-1 ISSN: 2673-5490 doi:10.18429/JACoW-IPAC2022-MOPOST055

THE EIC RAPID CYCLING SYNCHROTRON DYNAMIC APERTURE OPTIMIZATION

H. Lovelace III*, C. Montag, V. Ranjbar, Brookhaven National Laboratory, Upton, NY, USA
F. Lin, Oak Ridge National Laboratory, Oak Ridge, TN, USA

Abstract

With the design of the Electron-Ion Collider (EIC) [1], a new Rapid Cycling Synchrotron (RCS) is designed to accelerate the electron bunches from 400 MeV up to 18 GeV. An optimized dynamic aperture with preservation of polarization through the energy ramp was found. The codes DEPOL [2], MADX [3], and BMAD [4] are used in modeling the dynamics and spin preservation. The results will be discussed in this paper.

INTRODUCTION

The EIC will be built at BNL by modifying the Relativistic Heavy Ion Collider (RHIC) [5] existing straight sections. The a new hadron storage ring (HSR) will be built from the arcs of the existing RHIC. The HSR will store polarized protons with energies up 275 GeV and heavy ions up to a beam rigidity of 917 Tm. A new electron storage ring (ESR) [6] has been designed to store electron beams of energies ranging from 5 GeV to 18 GeV. An electron linear accelerator pre-injector will inject a 400 MeV electron beam into the RCS. The RCS, with a circumference ratio to the ESR of approximately 316/315, will accelerate the electron beam to a maximum energy of 18 GeV and will transfer electron bunches to the ESR. Both the RCS and ESR will join the HSR within the existing RHIC tunnel. A schematic of the EIC is seen in Fig. 1.

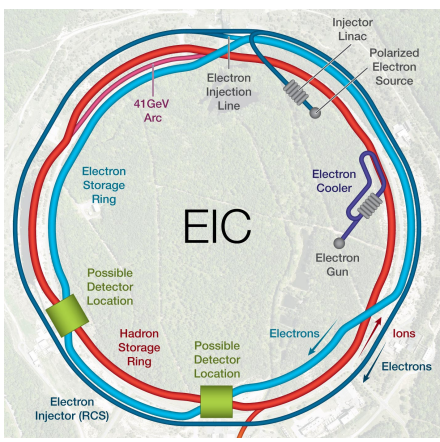

Figure 1: Overhead schematic of EIC electron accelerator.

MAGNETIC LATTICE

The magnetic lattice of the RCS has three distinct sections due to the need for high periodicity [7]. The arcs of the RCS contains four interleaved sextupole families, labeled *sxfa, sxda, sxfb,* and *sxdb*, to correct the chromaticity of a $\pi/2$ phase advance, $\phi_{x,y}$ FODO cell. The RCS has two unique straight section designs. In the 6 o'clock and 8 o'clock regions of the lattice, the dipoles are arranged such that the beam line bypasses the detectors with the lattice centerline 5 m away from the centerline of the tunnel. In both straight section configurations, the magnetic lattice is symmetric about the midpoint. In the 10 o'clock straight section, ten 591 MHz cavities are located split with five cavities on one side of the midpoint and five cavities on the other side of the midpoint. In the experimental bypass straight sections the number of sextupole families is eleven while in the other straights the number of families is four. Figure 2 shows the arrangement of the sextupoles in each of the three lattice sections. Each of the lattice quadrupoles have a effective length of 0.6 m and the sextupole effective length is 0.5 m.

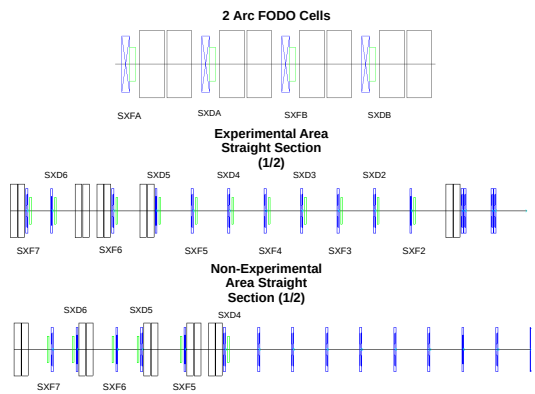

Figure 2: Lattice layout of the arc cells, spin transparent experimental bypasses, and the utility straight sections. Dipoles (black), quadrupoles (blue), and sextupoles (green) are shown. Each straight section is symmetric about the midpoint of the lattice.

OPTICS

The optical design of the RCS was based upon the need to minimized the intrinsic and imperfection depolarization resonances through the energy ramp and to provide at least a 5σ beam envelope that fits within the 32.9 mm diameter beam pipe. Thus, with a 40 mm-mrad injection rms emittance, the $\beta_{max(x,y)}$ is 120 m. The dispersion, η_x, at the center of the non-experimental straight sections was constrained to be zero. Figure 3 shows the β functions, η, and 5σ beam envelopes of the RCS. The fractional tunes, $\nu_{x,y}$, were selected to be far from the half integer and third integer

* hlovelace@bnl.gov

ISBN: 978-3-95450-227-1 ISSN: 2673-5490 doi:10.18429/JACoW-IPAC2022-MOPOST056

INTERPLAY BETWEEN SPACE CHARGE AND INTRA-BEAM SCATTERING FOR THE CERN ION INJECTORS

M. Zampetakis*[1], F. Antoniou, F. Asvesta, H. Bartosik, Y. Papaphilippou,
CERN, Geneva, Switzerland
[1]also at Department of Physics, University of Crete, Heraklion, Greece

Abstract

The CERN ion injectors, SPS and LEIR, operate in a strong space charge and intra-beam scattering regime, which can lead to degradation of their beam performance. To optimize machine performance requires thus to study the interplay of these two effects in combined space charge and intrabeam scattering tracking simulations. In this respect, the kinetic theory approach of intra-beam scattering has been implemented in pyORBIT and benchmarked against analytical models. First results of combined space charge and intra-beam scattering simulations for SPS and LEIR are presented in this contribution. The simulation results are compared with observations from beam measurements.

INTRODUCTION

In the CERN ion injectors, such as the Low Energy Ion Ring (LEIR) and Super Proton Synchrotron (SPS), lattice imperfections can excite resonances and eventualy limit the machine performance. In addition, in this regime of low kinetic energies, incoherent effects like Intra-Beam Scattering (IBS) and Space Charge (SC) can be strong enough to further degrade the quality and the lifetime of the beam.

Each of these effects has been intensively studied in several regimes and accelerators. In particular, IBS plays an important role in ion and proton storage rings where the beam is stored for many hours [1–3]. Moreover, SC has been studied in many low-energy machines where the induced SC tune spread may result in particle losses and emittance increase in the vicinity of resonances [4–13].

The interplay between IBS and SC can further enhance particle diffusion in phase space, as was shown for the Compact LInear Collider Damping Rings (CLIC DRs) using a simplified IBS kick [14]. However, similar studies for the ion injectors that operate below transition are not trivial. In this regime, IBS can lead to emittance exchange which could not be simulated with the already implemented simplified kick in Ref. [14]. Therefore, a more general IBS kick was implemented based on the Kinetic Theory and Nagaitsev's formalism [15–17].

In this contribution, the general IBS kick based on the Kinetic Theory is benchmarked against analytical predictions and used for studying the interplay between SC and IBS in the CERN ion injectors LEIR and SPS. First comparisons between beam measurements and simulation results are also discussed.

COMBINED SIMULATIONS FOR SPS

The SPS is the last accelerator of the LHC ion injector chain and the second largest machine in CERN's accelerator complex, with a circumference of 7 km. Even though the SPS is a high-energy machine, in the case of heavy ions SC induces a considerable tune shift of $\Delta Q_{x,y} = (-0.2, -0.29)$ for the case of Pb ions at injection energy, making the beam susceptible to resonances.

In operational conditions, an emittance exchange between horizontal and vertical planes, followed by a large emittance blow up in both planes was observed along the acceleration cycle, as shown in Fig. 1 (lines with point markers). A simulation campaign performed in 2016 could not explain the observed behavior neither from standalone SC or IBS simulations, nor from the sum of them [18].

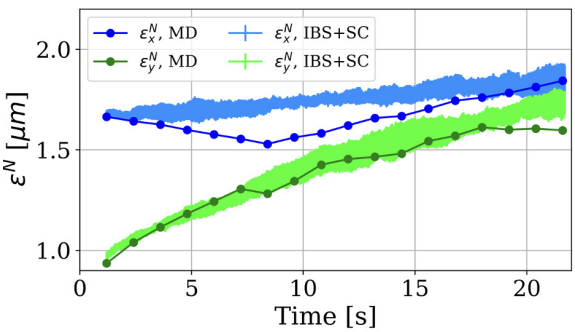

Figure 1: Evolution of the horizontal (blue) and vertical (green) emittance as observed in operation (dotted lines) and from combined SC and IBS simulations (solid line with errorbars) in PyORBIT (averaged over 3 different runs). The error bars correspond to the one standard deviation.

To this end, a simulation campaign was initiated to investigate the impact of the interplay of SC and IBS. The simulations were performed using the pyORBIT tracking code [19] with the "frozen" potential SC kick acting on the particles. The kicks are computed analytically using the Bassetti-Erskine formula [20], taking into account the local longitudinal density and the transverse beam sizes of a chosen distribution. In this case, the SC potential is re-evaluated every 1000 turns, based on the evolution of the tracked particles. A quadrupolar error is included in the ideal lattice, inducing a 5-10% beta-beating, similar to what is observed in the real machine in operational conditions.

The IBS effect was included in the simulation model based on the Kinetic Theory and is applied with a similar form to

* michail.zampetakis@cern.ch

ISBN: 978-3-95450-227-1 ISSN: 2673-5490 doi:10.18429/JACoW-IPAC2022-MOPOST057

CHARACTERIZATION OF THE VERTICAL BEAM TAILS IN THE CERN PS BOOSTER

T. Prebibaj*[1], F. Antoniou, F. Asvesta, H. Bartosik,
C. Bracco, G. P. Di Giovanni, E. Renner[2],
CERN, Geneva, Switzerland
[1]also at Goethe University, Frankfurt, Germany, [2]also at TU Wien, Vienna, Austria

Abstract

The CERN Proton Synchrotron Booster (PSB) went through major upgrades in the framework of the LHC Injectors Upgrade Project (LIU) aiming to double the brightness of the LHC beams. Operation restarted in early 2021, demonstrating the expected performance improvement. The high-brightness beams, nevertheless, appear to have overpopulated tails in the vertical beam profiles, both at injection and at extraction energies. In an attempt to understand the origin and evolution of the observed tails, systematic profile measurements were performed for different machine and beam configurations using Wire Scanners (WS). The results are presented in this report and compared to simulations. The effect of the Coulomb scattering of the wire to the beam distribution is also addressed.

INTRODUCTION

Following the implementation of the LHC Injectors Upgrade (LIU) project [1], the Proton Synchrotron Booster (PSB) delivered beams that were well within the project's requirements. The optimization of the resonance compensation schemes and tune evolution along with the beta-beating compensation contributed to an increased beam brightness [2, 3], going beyond the initial predictions.

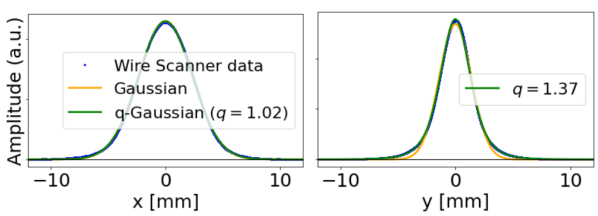

Figure 1: Ring 3 horizontal (left) and vertical (right) beam profiles of an LHC25-type beam close to extraction (t = 770 ms) in blue, Gaussian and q-Gaussian fits in orange and green respectively.

Measurements of the transverse beam profiles using Wire Scanners (WS) [4], revealed that the high-brightness beams have tails that differ from the ones of a normal distribution. These tails appear to be mostly in the vertical plane. Figure 1 shows an example of the transverse profiles close to extraction of the PSB Ring 3 for a bunch population of $N_b \approx 270 \cdot 10^{10}$ protons. The tails in the vertical plane are overpopulated. In order to investigate the possible sources of beam tail enhancement and to eventually improve the quality of the delivered beams, a measurement campaign was initiated. Beam profiles were acquired for different beam intensities, working points and energies during the acceleration cycle. This report summarizes the main results of these measurements focusing on the PSB ring 3. The measurements in the other PSB rings are similar.

FITTING NON-GAUSSIAN PROFILES

To characterize bunch profiles that follow a non-Gaussian shape, the q-Gaussian function [5] was used. The q-Gaussian is a generalized Gaussian function that incorporates a parameter q to model the weight of the distribution's tails. For $q = 1$, the q-Gaussian distribution coincides with a Gaussian distribution, for $1 < q < 3$ the distribution's tails are overpopulated, while if $q < 1$ the tails are underpopulated. The q-Gaussian function has been used in the past to model non-Gaussian beam profiles in the LHC [6]. The q-factor will be used throughout this report as an observable for the beam tail population.

BEAM TAILS AT INJECTION

Non-Gaussian beam tails are observed already at injection energies of the PSB. A typical vertical beam profile close to injection, for a low bunch population of $N_b \approx 10 \cdot 10^{10}$ protons, is shown in Fig. 2. The working point of this measurement is set to $(Q_x, Q_y) = (4.17, 4.23)$, which is a resonance free region. The beam tails are overpopulated ($q = 1.5$) but the tail population is not symmetric with respect to the beam core. At low beam energies, heavier tails are observed on one side of the profile compared to the other. This effect has been seen in previous studies [7], which suggest that the main contributor for this is the measuring instrument itself. In this study, an attempt to quantify and remove the undesired effects that the WS causes to the beam profile is made.

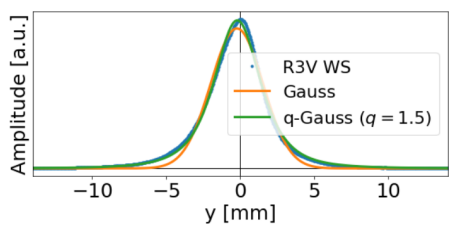

Figure 2: Ring 3 vertical beam profile of an LHC25-type beam close to injection (t = 290 ms) in blue, Gaussian and q-Gaussian fits in orange and green respectively.

* tirsi.prebibaj@cern.ch

ISBN: 978-3-95450-227-1 ISSN: 2673-5490 doi:10.18429/JACoW-IPAC2022-MOPOST058

STUDIES ON THE VERTICAL HALF-INTEGER RESONANCE IN THE CERN PS BOOSTER

T. Prebibaj*[1], F. Antoniou, F. Asvesta, H. Bartosik
CERN, Geneva, Switzerland
G. Franchetti[1]
GSI Helmholtzzentrum für Schwerionenforschung, Darmstadt, Germany
[1]also at Goethe University, Frankfurt, Germany

Abstract

Following the upgrades of the LHC Injectors Upgrade Project (LIU), the Proton Synchrotron Booster (PSB) at CERN successfully delivers beams with double brightness. An important contributing factor for this was the dynamic correction of the beta-beating induced by the injection chicane which allowed stable operation closer to the half-integer resonance. Ideally, injection above the half-integer resonance could further improve the beam brightness. In this context, a series of studies were initiated in order to characterize the effects of space charge when crossing the half-integer resonance. In this contribution, the first results of these investigations are reported.

INTRODUCTION

The brightness of the PSB beams is limited by space charge effects at injection [1]. In the framework of the LHC Injectors Upgrade (LIU) project [2], the PSB injection energy was increased from 50 MeV to 160 MeV, which allowed doubling the beam intensity while having similar space charge detuning and transverse emittances.

Stable beam operation with higher working points, that are closer to the vertical half-integer resonance $2Q_y = 9$, further mitigated the space charge effects at injection and contributed to an increased beam brightness [3]. On the same principles, injection above the half-integer resonance could result to an even higher brightness. However, the extraction working point of the PSB is set at $(Q_x, Q_y) = (4.17, 4.23)$ and thus the half-integer resonance needs to be crossed during the acceleration cycle. This can result in particle losses and/or emittance growth.

The effects of the half-integer resonance crossing on the beam will depend on the resonance strength, the crossing speed and the space charge detuning. At the end of 2021, systematic studies were initiated in the PSB to understand the beam behaviour under these conditions.

The PSB is an excellent machine for performing these studies. The multi-turn H^- injection scheme [4] allows producing a large variety of transverse emittances and beam intensities, which enables the control of the space charge tune footprint. In addition, the recently implemented tune control system [5] allows machine operation in a wide range of working points below and above the half-integer resonance and also the dynamic change of tunes along the acceleration cycle. Finally, the identification and compensation of resonances up to fourth order has been extensively studied in the PSB [6]. As a result, the half-integer resonance not only can be compensated to a good extent, but can also be excited in a controlled manner by deliberately degrading the compensation scheme.

This contribution focuses on the characterization of the half-integer resonance for different excitation amplitudes.

HALF-INTEGER RESONANCE CORRECTION AND EXCITATION

The PSB is equipped with a set of multipole corrector magnets that are used for the compensation of the naturally excited resonances. The half-integer resonance $2Q_y = 9$ is compensated by two families of normal quadrupole correctors, illustrated in Fig. 1. The first family consists of quadrupoles in the fourth and in the twelfth section of the machine (QNO412) and the second family of quadrupoles in the eighth and sixteenth section (QNO816). The driving term generated by QNO412 is orthogonal with respect to the driving term of QNO816. The optimal strength of the quadrupoles that cancels the driving term of the naturally excited half-integer resonance is determined experimentally [7]. The quadrupole families are configured such that they do not change the tune.

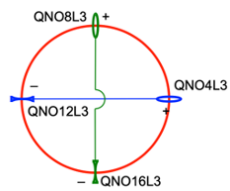

Figure 1: The two orthogonal families of quadrupole correctors and their corresponding polarities.

By slightly varying the strength of the QNO412 and QNO816, with respect to their compensating value, the half-integer resonance is excited. Since the orientation of the two families is orthogonal, the half-integer resonance can be excited with any phase and amplitude, within the limits of the quadrupole currents.

The excited resonance is characterized by its stopband width. Inside the stopband the particle motion is unstable and losses occur. Outside but near the stopband, the motion is stable but the growth in amplitude of the betatron oscillations (β-beating) can drive particles to large amplitudes

* tirsi.prebibaj@cern.ch

ISBN: 978-3-95450-227-1 ISSN: 2673-5490 doi:10.18429/JACoW-IPAC2022-MOPOPT002

IMPROVEMENTS ON SIRIUS BEAM STABILITY

S.R. Marques†, M.B. Alves, F.C. Arroyo, G.O. Brunheira, M.P. Calcanha, H.F. Canova, A.C.T. Cardoso, R.B. Cardoso, F.H de Sá, R.J. Leão, L.R. Leão, B.E. Limeira, L. Lin, P.H.S. Martins, S.S. Moreira, R.T. Neuenschwander, R.O. Neto, A.G.C. Pereira, M.G. Siqueira, D.O. Tavares, LNLS, Campinas, Brazil

Abstract

Sirius is a Synchrotron Light Source based on a 3 GeV electron storage ring with 518 meters circumference and 250 pm.rad emittance. The facility is built and operated by the Brazilian Synchrotron Light Laboratory (LNLS), located in the CNPEM campus, in Campinas. A beam stability task force was recently created to identify and mitigate the orbit disturbances at various time scales. This work presents studies regarding ground motion (land subsidence caused by groundwater extraction), improvements in the temperature control of the storage ring (SR) tunnel air conditioning (AC) system, vibration measurements in accelerator components and the efforts concerning the reduction of the power supplies' ripple. The fast orbit feedback implementation and other future perspectives will also be discussed.

INTRODUCTION

Since late 2020 the SR has operated for beamline commissioning and more recently for external users. The routine operation has started with 40 mA and 30 hours lifetime. Currently, 100 mA is provided with 16 hours lifetime, with two injections per day.

Beamlines are observing slow photon beam movements with periods of hours and others from 60 Hz mains frequency present in both planes of the beam orbit spectrum.

Future matters of concern are the horizontal orbit perturbation in the SR due to booster ramping at 2 Hz and its harmonics and the fast orbit transients caused by injection pulsed magnets. Both need to be addressed, as top-up operation is planned to start soon.

KNOWN INSTABILITIES

We separated the phenomena into 3 categories: short, medium, and long-term disturbances. Long-term ones show time scales greater than many minutes or hours, like temperature variations, and must be attenuated as much as possible, as they usually affect the readings of sensors used in feedback systems. Mid-term disturbances comprise the low-frequency phenomena up to the upper limit of the fast orbit feedback system (FOFB) system actuation range. Short-term instabilities are those on the scale of milliseconds or less. Most of the ground settlement has already occurred allowing two important girder alignment campaigns in 2021 and 2022 for SR and booster, respectively [1–4].

Long-term Disturbances

Sirius counts on a network of 20 hydrostatic leveling system (HLS) sensors installed on the roof of the tunnel that allowed us to detect 2-4 hours oscillations also noticed in the beamline experiments' data. The oscillation patterns were present in the SR radio frequency (RF) when the slow orbit feedback system (SOFB) is ON and in the BPMs and tunes with the SOFB OFF. The horizontal plane was more affected in the SR, while the vertical one was in the beamlines.

Slightly more intense oscillations were detected by HLS sensors on SR sector 11. Observing the surroundings of the building, a drilled water well with 180 meters in depth was found near the long beamlines, 20 meters apart from the building. Tests were performed by turning the water well pump off to check its influence on Sirius stability (Fig. 1). After turning off the source of the few-hour period oscillations, a 24-hour period disturbance is clearly seen, which indicated the existence of more sources of instability.

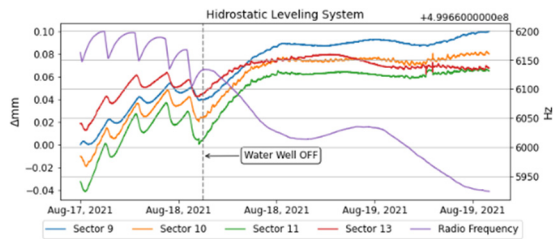

Figure1: RF readback and HLS sensors around sector 11. SOFB system ON.

A test where a second water well, with similar characteristics to the disturbing one, inside CNPEM (250 meters far from the Sirius building) was activated intermittently showed no measurable effect on the HLS sensors, orbit stability, or RF frequency. More distant wells, outside the institute should not affect the stability. Variations in the water level of the aquifer, influenced by rainfall will possibly cause much a smaller and slower effect.

As a temporary solution, a new operation mode was implemented in which the water is pumped every 10 minutes, with a constant duty cycle calculated to provide an average flow that meets the consumption demands.

Terrestrial tidal effects were expected to affect horizontal and vertical planes likewise, thus not being able to explain the large RF frequency variations when the well operated in modes other than the standard one (Fig. 2). Therefore, the possibility of some effects being related to temperature variations and possible deformations caused by thermal dilatation started being considered.

Sirius' concrete slabs have a network of temperature and strain gauge sensors installed in several layers around the building (Fig. 3, left). To check the correlation between the Sirius concrete temperature and the RF oscillation we developed a simple model of concrete ring expansion based

† Sergio.marques@cnpem.br

ISBN: 978-3-95450-227-1 ISSN: 2673-5490 doi:10.18429/JACoW-IPAC2022-MOPOPT003

STUDYING INSTABILITIES IN THE CANADIAN LIGHT SOURCE STORAGE RING USING THE TRANSVERSE FEEDBACK SYSTEM

S. Martens, D. Bertwistle, M. J. Boland*[1], Canadian Light Source, Saskatoon, Canada
[1]also at University of Saskatchewan, Dept. of Phys. and Eng. Phys., Saskatoon, Canada
P. Hartmann, DELTA, TU Dortmund University, Germany

Abstract

The transverse feedback system at the Canadian Light Source (CLS) can identify, categorize, and mitigate against periodic instabilities that arise in the storage ring beam. By quickly opening and closing the feedback loop, previously mitigated instabilities will be allowed to grow briefly before being damped by the system. The resulting growth in the beam oscillation amplitude curve can be analyzed to determine growth/damp rates and modes of the coupled bunch oscillations. Further measurements can be collected via active excitement of modes rather than passive growth. These grow/damp and excite/damp curves have been collected and analyzed for various storage ring beam properties, including beam energy, machine chromaticity, and in-vacuum insertion device gap widths.

OVERVIEW AND MOTIVATION

A third-generation synchrotron storage ring is subject to several instabilities arising from the electromagnetic interaction between the stored electron bunches and the vacuum chamber. These instabilities can grow over time and, without intervention, can increase the size of the beam, reducing the brilliance of the synchrotron radiation supplied to beamlines, or in extreme cases cause the loss of the beam entirely. The addition of multiple in-vacuum insertion devices in third generation synchrotron storage rings can further compound the effect of these instabilities. Intervention via active feedback systems can be used to mitigate against these instabilities. A transverse feedback system (TFBS) produced by the commercial supplier Dimtel Inc. was recently installed at the CLS that uses a beam position monitor (BPM) and response network to identify, categorize, and mitigate against these coupled bunch instabilities [1].

By quickly opening and closing the feedback loop, previously mitigated instabilities will be allowed to grow briefly before being damped by the system. The resulting growth in the beam oscillation envelope can be analyzed to determine growth/damp rates and modes of the coupled bunch instabilities. These results can provide better understanding of the storage ring's behavior and may influence the design of future storage rings at the CLS2 and elsewhere.

THEORY

Wake fields arise in a storage ring via interaction between the fields generated from a relativistic charge bunch and the vacuum chamber. Radiation will scatter when encountering metallic objects or changes in the boundary conditions of the ring. Scattered radiation will then interact with subsequent bunches and perturb their motion.

Wake fields give rise to coupled bunch instabilities. When M Bunches oscillate at the tune frequency of the synchrotron, they give rise to M modes via a phase difference between bunches $\delta\phi$:

$$\delta\phi = \frac{2\pi n}{M} \tag{1}$$

Where n is the mode number. The CLS storage ring operates with 285 bunches which yields 285 modes. The growth/damping rate T, of these modes over time can modelled as an exponential [2] of the form:

$$y = Ae^{\tau T} \tag{2}$$

EXPERIMENT

Grow Damp Measurements

Experiments with the transverse feedback system were conducted during development shifts throughout 2021. The storage ring was set up in its standard operating mode with top-up disabled. A chromaticity of $\xi_{x,y} = 0$ was used, and all insertion device gaps not actively being experimented with were left fully opened. The TFBS was set up in Grow/Damp mode. This operation mode disables the feedback network which allows instabilities to grow briefly before re-enabling the feedback which dampens the instability. Custom code was written to connect to existing Dimtel MATLAB code to collect and sort data from the TFBS and any Process Variables (PVs) of interest during measurements. Five grow damp measurements were taken at each step during each experiment. Measurements were performed while varying the insertion device (ID) gap width for the five in-vacuum insertion devices with adjustable gap-widths. In addition, measurements were done while varying the horizontal and vertical machine chromaticity.

Excite Damp Measurements

Results from grow damp measurements showed large growth in the highest and lowest modes, typically the product of resistive wall instabilities. As a consequence, the structure of the remaining modal growths were lost beneath the much larger amplitudes of the highest and lowest modes. To view the modal structure of the remaining modes, a series of excite damp measurements were deemed necessary. The storage ring was set up identically to the grow damp measurements performed previously. The TFBS software

* mark.boland@lightsource.ca

ISBN: 978-3-95450-227-1 ISSN: 2673-5490 doi:10.18429/JACoW-IPAC2022-MOPOPT004

DEVELOPMENT OF A NEW CLUSTERIZATION METHOD FOR THE GEM-TPC DETECTOR

M. Luoma*[1], F. García, T. Grahn[1], A. Jokinen[1], R. Turpeinen, J. Äystö[1]
Helsinki Institute Of Physics, Helsinki, Finland
S. Rinta-Antila, University of Jyvaskyla, Jyvaskyla, Finland
T. Blatz, H. Flemming, K. Götzen, C. Karagiannis, N. Kurtz, S. Löchner
C. Nociforo, C.J. Schmidt, H. Simon, B. Voss, P. Wieczorek, M. Winkler
GSI, Darmstadt, Germany
D. Chockeli, Georgian Technical University, Tbilisi, Georgia
[1]also at University of Jyvaskyla, Jyvaskyla, Finland

Abstract

The GEM-TPC detector in a twin field-cage configuration will be used as one of the Super-FRS particle identification detectors. It aims to provide the position information at up to a 1 MHz counting rate, with a position resolution less than 1 mm, and with close to 100 % tracking efficiency. In a single field-cage configuration, the GEM-TPC was tested at the FRS with a newly integrated AWAGS ASIC readout electronics, with a uranium beam at 850 MeV/u. The obtained results show that the new clusterization method developed for the analysis works on an event-by-event basis. The spatial resolution of 0.80 - 0.82 mm and cluster strip multiplicity of 14.3 - 8.6 strips were obtained for digitization with a decreased number of bits, starting from 13 bits which was the original number of bits during data taken, and then applying software conversion to 8 and 4 bits. The presented paper describe the methodology followed to reach such results in detail.

INTRODUCTION

Superconducting FRagment Separator (Super-FRS) [1] will be an extremely powerful in-flight magnetic separator for producing, separating, and delivering high-energy radioactive beams. It will be one of the main parts of the Facility for Antiproton and Ion Research (FAIR) [2] at GSI in Darmstadt, Germany.

In the future, the tracking at the Super-FRS will be done in an event-by-event basis by Time Projection Chambers (TPC) with a Gas Electron Multipliers (GEM-TPC) in a twin field-cage configuration [3] to cope with the high particle rate. The GEM-TPC in twin configuration will provide position information of traversing particles.

The twin GEM-TPC includes two single GEM-TPCs inside the same vessel, with one of them rotated 180 degrees with respect to the other in such a way that the electric fields of the field-cages are in opposite directions (see Figure 1). The GEM-TPC detector consists of a field cage and Gas Electron Multiplier (GEM) [4] stack, a pad plane, and readout electronics.

It is required at the Super-FRS that such tracking detectors have a position resolution <1 mm, dynamic range suitable for particles from protons up to uranium, and tracking efficiency >95 %.

In the present in-beam test, the GEM-TPC prototype in the single field-cage configuration [5] was tested with a newly integrated Low Noise Amplifier With Adaptive Gain Settings - (AWAGS) ASIC [6] readout electronics. One of the goals was to test a newly developed clusterization method for its data analysis, which can be integrated into the analysis framework of future experiments. The following chapters describe the experimental setup, the clusterization method, and the results of the data analysis for different digitization of the signal amplitude.

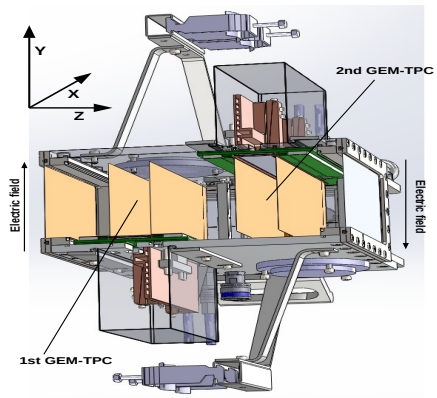

Figure 1: The layout of the GEM-TPC detector in the twin field-cage configuration.

EXPERIMENTAL

The setup of the present in-beam test included a plastic scintillator for triggering, thus setting the starting time of each event, and two conventional Time Projection Chambers (TPC) [7] used as reference trackers. The whole setup was located at the final focal plane S4 of the GSI FRagment separator (FRS) [8].

The primary beam used was ^{238}U at 850 MeV/u, with a varied intensity of 100 - 1k ions/s and with a spill length of 2 s to 8 s. The detector was filled with P10 gas (90% Ar, 10% CH4), and the electric field strength varied from 90 V/cm to 320 V/cm.

* mianmalu@jyu.fi

ISBN: 978-3-95450-227-1 ISSN: 2673-5490 doi:10.18429/JACoW-IPAC2022-MOPOPT005

BUNCH MEASUREMENTS WITH BPM AT LOW ENERGY HADRON ACCELERATORS

Dr. Ben Abdillah†, Université Paris-Saclay, CNRS/IN2P3, IJCLab, Orsay, France
S. Boussa, A. Gatera, F. Pompon, SCK CEN, Brussels Belgium

Abstract

Beam Position Monitors (BPM) are one of the key diagnostics use in LINACs, BPMs should ensure a continuous monitoring of the beam position and energy. BPMs also give an indication of the beam transverse shape. For electron LINACs, beam longitudinal length is measured with BPMs. However, in hadron LINACs, it is performed with intrusive modules (wire scanners, beam shape monitors) This document relates the measurement of beam longitudinal length with BPMs. It is divided in two parts: first, a theoretical model of the BPM operation and the formulas driving the measurement of beam longitudinal length from BPM output signals. Second, an experimental study run at MYRRHA LINAC facility and showing good agreement between estimated values of beam longitudinal length from Tracewin simulations and BPM measurements.

INTRODUCTION

It is important to know the bunch longitudinal length for beam dynamics optimization and loss reduction in linear accelerators. This is especially true for accelerators with flexible longitudinal settings like superconducting linacs having large numbers of independently powered accelerating cavities and uncorrelated amplitude and phase set points. Typically, the superconducting part of a linac has strong limitations on the use of interceptive diagnostics due to concerns regarding contamination of superconducting surfaces. This precludes the use of conventional longitudinal bunch profile diagnostics such as bunch shape monitors (BSM) [1] or similar devices. There are non-interceptive methods [2] [3] but they are either intended for electrons or not too precise particularly at low beam energies.

The main purpose of this article is to evaluate the measurement of the bunch longitudinal length with a non-interceptive method using button BPM.

BUTTON BPM MECHANICAL MODEL

Button BPM is sketched in Figure 1. It is equipped with 4 identical feedthroughs attached to electrodes. The sets (feedthrough + electrode) are identical and symmetrical regarding the centre of the BPM.

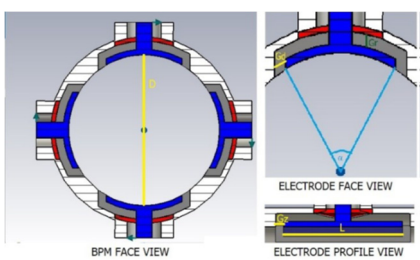

Figure 1: Layout of button BPM.

† sidi-mohammed.ben-abdillah@ijclab.in2p3.fr

Where D is the BPM diameter, L the BPM longitudinal length and α the BPM angular width.

BUTTON BPM THEORETICAL MODEL

The LINAC RF structure generate a periodical beam bunches. The beam current or bunch I_b may be represented by a Fourier series expansion in the frequency domain [4].

$$I_b(t) = \langle I_b \rangle \left(1 + 2\sum_{0}^{\infty} A_n \cos\left(2\pi n F_{acc} t + \varphi_n\right)\right) \quad (1)$$

Where $< I_b >$ is the average dc current, A_n is a bunch-shape-dependent form factor, F_{acc} is the bunching frequency, n is the harmonic number, and φ_n is the phase of the n^{th} harmonic.

The beam distribution is supposed Gaussian; the beam current is modelled as:

$$I_b(x,y,t) = \langle I_b \rangle \frac{e^{-t^2/2\sigma_t^2} e^{-x^2/2\sigma_x^2} e^{-y^2/2\sigma_y^2}}{\sqrt{2}\pi\sigma_t \sqrt{2}\pi\sigma_x \sqrt{2}\pi\sigma_y} \quad (2)$$

The beam induces a wall current I_{wall} on the on the BPM electrodes: for a line current I_b at (r,θ), the rms image current density I_w at the n^{th} harmonic frequency and azimuthal position φ on the conducting cylindrical beam tube is given by

$$I_{w,n} = \sqrt{2}\langle I_b \rangle A_n \sum_{m=-\infty}^{\infty} \frac{I_m(ngr)}{I_m(ngD/2)} \cos\left(m(\varphi - \theta)\right) \quad (3)$$

Where I_m represents the modified Bessel function of order m and $g = 2\pi F_{acc}\sqrt{(1-\beta^2)}/(\beta c)$ with c the light speed and β the relative velocity of the beam.

Figure 2 illustrates the different parameters in (3).

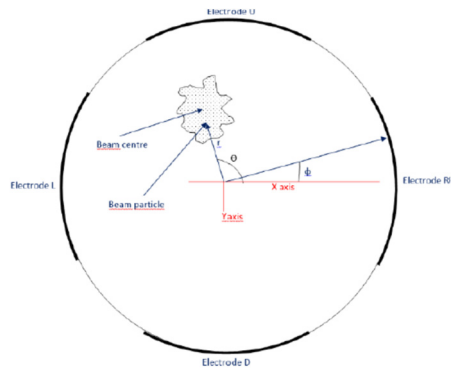

Figure 2: 2D presentation showing the parameters in (3).

ISBN: 978-3-95450-227-1 ISSN: 2673-5490 doi:10.18429/JACoW-IPAC2022-MOPOPT006

CHARACTERIZATION OF THE ELECTRON BEAM VISUALIZATION STATIONS OF THE ThomX ACCELERATOR*

Alexandre Moutardier†, Christelle Bruni, Jean-Noël Cayla, Iryna Chaikovska, Sophie Chance, Nicolas Delerue, Hayg Guler, Hugues Monard, Maher Omeich, Scott David Williams[1]
Université Paris-Saclay, CNRS/IN2P3, IJCLab, 91405, Orsay, France,
on behalf of the ThomX collaboration‡
[1]now at the University of Melbourne, Melbourne, Australia

Abstract

We present an overview of the diagnostics screens stations - named SSTs - of the ThomX compact Compton source. ThomX is a compact light source based on Compton backscattering. It features a linac and a storage ring in which the electrons have an energy of 50 MeV. Each SST is composed of three screens, a YAG:Ce screen and an Optical Transition Radiation (OTR) screen for transverse measurements and a calibration target for magnification and resolution characterisation. The optical system is based on commercial lenses that have been reverse-engineered. An Arduino is used to control both the aperture and the focus remotely, while the magnification must be modified using an external motor. We report on the overall performance of the station as measured during the first steps of beam commissioning and on the optical system remote operations.

OVERVIEW OF THE OPTICAL DIAGNOSTICS AT THOMX

The ThomX Compact Compton source is a novel accelerator which is being commissioned in Orsay [2, 3]. We report here on the optical diagnostics used in this accelerator.

The overall diagnostics layout is shown in Fig. 1. There are five screens stations. They are located near the RF Gun, at the end of the linac, in the transfer line (twice) and in the extraction line. The current operation permit from the Nuclear Safety Authority only allows commissioning of the straight part of the accelerator after the photo-cathode (upper part of the drawing), hence this paper will focus on the two first screens stations, named LI/DG/SST.01 and TL/DG/SST.01.

Each screens station is made of a vacuum vessel with a UHV-compatible actuator to move the screens in vacuum. The visualisation is made using a Basler scA640-70gm CCD camera equipped with a commercial lens. A drawing of these diagnostic stations can be seen in Fig. 2. There are three types of screen for each station: a YAG:Ce screen, an Optical Transition Radiation (OTR) screen and a calibration target. Those screens are at a 45° from both the beam trajectory and the camera axis. Each screen is separately described in the following sections.

The TL/DG/SST.01 has also a sapphire screen used to generate Cerenkov light and allow longitudinal length measurement. This feature is not yet commissioned and will not be mentioned further in this paper.

COMMERCIAL LENS REVERSE-ENGINEERING

Lens Characteristics

The lens used in both SSTs is a Tamron : 18-400mm F/3.5-6.3 Di II VC HLD. Those lens have a focal length of 18 mm to 400 mm and an apperture going from f/3.5 (f/6.3) to f/22 (f/40) at a focal length of 18 mm (400 mm).

Reverse-engineering

This kind of lens allows auto-focus and aperture control by photographer's cameras, but the ThomX cameras do not have the required outputs. To remotely control both those parameters, an Arduino Uno circuit controlled by a web interface has been developed [4].

A 3D printed structure is under test to remotely control the magnification by adding an external motor.

CALIBRATION TARGET

Before using a scintillation screen to evaluate beam size, some calibrations must be done. For that purpose, a specific calibration target, named USAF1951 calibration chart, is used (see Fig. 3). Nine identical calibrated targets allow the measurement of the magnification and resolution at each target position. Two numbers - group and element - are use to characterise each triplet of vertical and horizontal lines [5]. The width of a line - or a fifth of its length - may be computed using Eq. (1).

$$d[\text{mm}] = 2^{-1\times(1+group+(element-1)/6)} \quad (1)$$

From the size of the largest element, one may compute the pixel/millimetre ratio needed to compute the beam size - hence the magnification - while the resolution comes out from the smallest element's triplet of lines that one can discriminate. Table 1 show the resolution and magnification computed for both images of Fig. 3. The magnification computation give a 2x2 matrix used to compute, from horizontal (h) and vertical (v) pixel length on the image, the horizontal (x) and vertical (y) physical length of the beam (in mm) as show un Eq. (2).

* Work supported by the French "Agence Nationale de la Recherche" as part of the program "investing in the future" under reference ANR-10-EQPX-51 and by grants from Région Ile-de-France
† moutardier@ijclab.in2p3.fr
‡ For ThomX collaboration members, see Ref. [1]

ISBN: 978-3-95450-227-1 ISSN: 2673-5490 doi:10.18429/JACoW-IPAC2022-MOPOPT009

NEW BUNCH-BY-BUNCH FILLING PATTERN MEASURING SYSTEM AT ELSA

A. Wald*, K. Desch, D. Elsner, D. Proft, Physics Institute, University of Bonn, Germany

Abstract

The electron accelerator facility ELSA at the University of Bonn, Germany, can accelerate and store electrons with a final energy from 0.8 GeV up to 3.2 GeV. To routinely determine the filling pattern in the storage ring, a new measuring system has been developed. For hadron physics experiments the filling pattern, which is influenced by the injection from the pre-accelerating synchrotron, should be as homogeneous as possible. The new measurement system should provide a real-time measurement of the filling pattern, so that the injection can be continuously optimized. Moreover, a position measurement for each individual bunch is provided, from which the two transverse and the longitudinal tunes can be deduced. To measure the bunch-by-bunch intensity and position, the signals of the existing button-type BPMs will be digitized by fast 12-bit ADCs synchronized to the 500 MHz ELSA radio frequency. The fast pre-processing and intermediate storage of the data is realized with a 500 MHz clocked FPGA and transfers the data to a PC for further processing. First results of measurement system developed in-house will be presented.

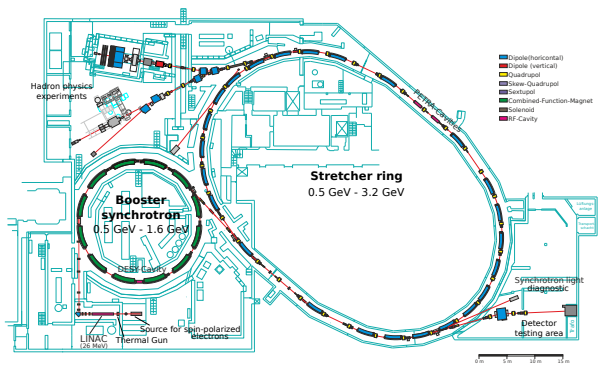

Figure 1: Overview map of ELSA.

THE ELSA ACCELERATOR

The electron accelerator ELSA (short for **El**ectronen **S**tretcher **A**nlage, *English: electron stretcher facility*, overview map is shown in Fig. 1) consists of three accelerator stages: the linear accelerator, the booster synchrotron and the stretcher ring, giving the entire facility its name. In the stretcher ring, a electron beam with a beam energy between 0.8 GeV and 3.2 GeV and a total beam current typically up to 30 mA, can be stored for minutes or up to hours and be extracted to one of the two hadron physics experiments or to the detector testing area. In the booster synchrotron and in the stretcher ring, the electrons are accelerated by 500 MHz cavities, leading to a bunched beam structure with 2 ns bunch separation.

To measure the beam position, a system of 32 Beam Position Monitors (BPM) has been installed in the beam pipe. Until now the electrodes are read out slowly, indicating that only the average position of the beam can be determined with a frequency of 1 kHz. More information can be found in [1].

MOTIVATION FOR A NEW BPM-READOUT SYSTEM

Because of the slow processing of the analog electrode signals, information about individual bunches is not available. This allows a lower sampling frequency and fewer data points are recorded.

A BPM consists of four button electrodes isolated from the beam pipe arranged around the center of it. While a ultra-relativistic bunch of electrons is passing the BPM, a charge is induced on the electrodes, whereby the corresponding voltage can be measured via a resistor. For a beam pipe with infinite conductivity, the induced signal depends on the BPM geometries, the bunch position and the beam filling pattern, i.e. the charge per bucket. This electrode signal, containing information about each individual bunch, is shown in Fig. 2. After 2 ns the signal amplitude is negligibly small, indicating no signal interference between two consecutive bunches.

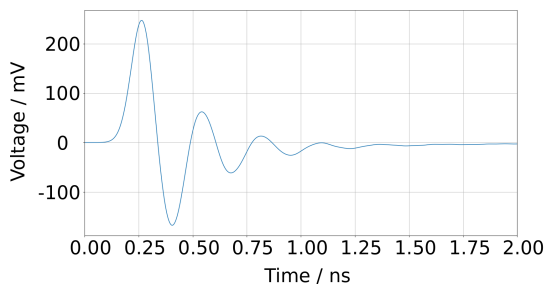

Figure 2: Example for a voltage signal induced by a bunch containing 37 pC charge and a length of 15 mm, corresponding to a beam energy of about 1.7 GeV (see [2]), on the electrode, simulated with the wakefield solver of CST-Studio [3].

In the new readout system, the information for the individual bunches is preserved by a proper pre-processing of the analog signal and the digitization. It is mandatory that the bandwidth of the used components must be large enough and the sample frequency must be sufficiently high. Due to information preservation, the position for all individual bunches, the beam filling pattern and also the tunes in the horizontal, vertical and longitudinal direction, respectively, can be deduced.

* wald@uni-bonn.de

ISBN: 978-3-95450-227-1 ISSN: 2673-5490 doi:10.18429/JACoW-IPAC2022-MOPOPT010

STATUS OF DIAMOND AND LGAD BASED BEAM-DETECTORS FOR THE mCBM AND CBM EXPERIMENTS AT GSI AND FAIR

A. Rost[1*], I. Deppner[2], J. Frühauf[3], T. Galatyuk[3,4], N. Herrmann[2], V. Kedych[4], M. Kis[3], W. Krüger[4], P.-A. Loizeau[1], J. Pietraszko[3], E. Rubio[2], M. Träger[3], F. Ulrich-Pur[3]
[1]FAIR GmbH, Darmstadt, Germany
[2]Physikalisches Institut, Universität Heidelberg, Heidelberg, Germany
[3]GSI Helmholtzzentrum für Schwerionenforschung GmbH, Darmstadt, Germany
[4]Institut für Kernphysik, TU Darmstadt, Darmstadt, Germany

Abstract

The Compressed Baryonic Matter (CBM) experiment is currently under construction at the Facility for Antiproton and Ion Research (FAIR) in Darmstadt. The aim of the experiment is the exploration of the Quantum Chromodynamics (QCD) phase diagram of matter at high net-baryon densities and for moderate temperatures.

In this contribution a beam monitoring (BMON) system will be presented which will include a high-speed time-zero (T0) detector. The detector system must meet the requirements of the CBM time-of-flight (ToF) measurement system for proton and heavy-ion beams and should also allow for beam monitoring. The detector technology is planned to be based on chemical vapor deposition (CVD) diamond basis but also new Low Gain Avalanche Detector (LGAD) developments are evaluated. In this contribution the beam detector concept will be presented and the results of first prototype tests in the mini-CBM setup will be shown.

INTRODUCTION

The future CBM Experiment [1] at the Facility for Antiproton and Ion Research (FAIR) in Darmstadt will be a fixed-target multi-purpose detector with the aim to explore the QCD phase diagram of nuclear matter at high net-baryon densities and for moderate temperatures. The detectors will detect hadrons, photons, electrons and muons in elementary and heavy-ion collisions over the entire energy range provided by the heavy-ion synchrotron SIS100, i.e. 3 - 11*A* GeV for heavy-ion and 29 GeV for proton beams. The measurements will be performed at event rates from 100 kHz up to 10 MHz using free-streaming readout electronics and fast online event reconstruction. The miniCBM (mCBM) programme at the already existing heavy-ion synchrotron SIS18 provides ideal experimental conditions in order to benchmark CBM sub-detectors at realistic beam conditions.

In this contribution the current development status of the high-speed time-zero (T0) and beam monitoring system (BMON) for the CBM experiment will be presented. This detector must meet the requirements of the time-of-flight (ToF) measurement system for beams of protons and heavy ions. The system should have a time precision of better than 50 ps (sigma) and allow stable long-term detector operation at high interaction rates of 10^7 particles/s with a detection efficiency of almost 100%. The detector technology is currently planned on chemical vapour deposition (CVD) diamond [2] basis but also new Low Gain Avalanche Detector (LGAD) [3] developments are under consideration.

* a.rost@gsi.de

THE CBM BEAM MONITORING SYSTEM

The BMON system will consist of two detector stations located in front of the CBM target chamber. The T0-station is foreseen to measure the start time of the reaction, while the halo-station will be used for beam halo monitoring. Both detectors will be mounted inside a beam-pipe using commercially available vacuum elements, as schematically shown in Fig. 1.

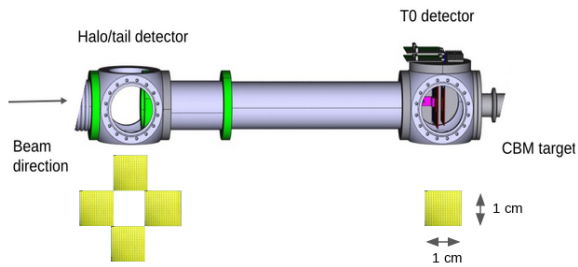

Figure 1: Schematic illustration of the CBM BMON system. Two stations of beam detectors will be used for beam halo and T0 measurement and are mounted in standard CF 100 vacuum chambers. For the T0 measurement a single sensor will be used and for the halo measurement a mosaic structure of four sensors is foreseen.

The sensor of the T0-station, currently planned on polycrystal CVD (pcCVD) diamond technology, will cover the area of $1 \times 1\,\mathrm{cm}^2$ and is equipped with a metallization arranged in 16 strips on both sides. The strip segmentation and orientation, aligned in x and y-directions, will allow to extract a position information of the beam particles.

The halo-station is foreseen to be used as an independent beam monitoring system. The halo detector will consist of a mosaic arrangement of four sensors, each metallized with four strips on both sides. The sensor arrangement is schematically shown in Fig. 1. This arrangement allows to monitor the beam position and its rate during the extraction process. This information will be used for securing sensible CBM detectors as part of a fast beam-abort-system.

ISBN: 978-3-95450-227-1 ISSN: 2673-5490 doi:10.18429/JACoW-IPAC2022-MOPOPT011

TRANSVERSE EXCITATION AND APPLICATIONS FOR BEAM CONTROL

P. J. Niedermayer*, R. Singh,
GSI Helmholtzzentrum für Schwerionenforschung, Darmstadt, Germany

Abstract

Transverse excitation of stored particle beams is required for a number of applications in accelerators. Using a time-varying, transverse electric field with a dedicated frequency spectrum, the amplitude and coherence of betatron oscillations can be increased in a controlled manner. This allows for determination of the betatron tune from turn-by-turn position measurements, control of transverse beam shapes, as well as extraction of stored beams. For studies of beam excitation, a custom signal generator is being developed. It is based on software-defined radio (SDR) which allows for configurable signal characteristics and tuneable spectra. This approach enables usage for multiple applications in beam diagnostics and control. To determine appropriate excitation spectra, studies of particle dynamics in presence of excitation are being carried out. Nonlinear fields are also incorporated to account for beam extraction conditions, which affects frequency spectra of beam motion due to detuning effects.

PARTICLE DYNAMICS SIMULATIONS WITH SIMPLIFIED MODEL

To study the effect of excitation on the dynamics of particles in a circular accelerator, a simplified model is used. In this model, the linear ion optics are described by a linear transfer map with machine tune q. Nonlinear contributions are condensed in a single virtual sextupole magnet in thin-lens approximation, which drives a 3rd order resonance hence allowing to model conditions typical for beam extraction. A dipole kicker excites the transverse betatron oscillations with a dedicated, time-dependent kick. The particle motion is studied in 2D (flat beam approximation) with zero chromaticity. By making use of normalized phase space coordinates $X = \sqrt{2J}\cos(\theta)$ and $X' = -\sqrt{2J}\sin(\theta)$ as well as normalized kick strengths, the simulation is independent of local twiss parameters.

The simulations presented in this paper use a machine tune of $q = r + d$ with small distance $d = -0.003$ to the resonance $r = 2/3$, but the results are valid for the $1/3$ resonance as well. The 3rd order resonance is driven by a sextupole with normalized strength $S = -0.45\,\mathrm{m}^{-1/2}$. The free particle dynamics of such a system is well described by the Kobayashi theory [1] with Hamiltonian:

$$H = 3\pi d\left(X^2 + X'^2\right) + \frac{S}{4}\left(3XX'^2 - X^3\right) \qquad (1)$$
$$H_{\mathrm{sep}} = (4\pi d)^3 / S^2$$

The equipotentials of H are shown in Fig. 1 (left).

* p.niedermayer@gsi.de

SINUSOIDAL EXCITATION

We consider a dipolar deflector with a time-variant, sinusoidal transverse field. A traversing particle experiences a kick $\Delta X' = K\sin(2\pi f_{\mathrm{ex}} t)$ where $K = -k_0 l\sqrt{\beta_x}$ is the normalized strength of the deflector and f_{ex} the excitation frequency. A typical use case of such a sinusoidal excitation is a beam transfer function (BTF) measurement [2] of a linear machine, where the beam response is measured as function of the excitation frequency. In the case of linear dynamics, this allows to determine the resonant tune.

Beating

If the excitation frequency f_{ex} is near but different from the betatron oscillation frequency $f_{\mathrm{q}} = qf_{\mathrm{rev}}$, a beating can be observed, leading to large transverse beam oscillations, where f_{rev} denotes the revolution frequency. In linear beam dynamics this beating motion is simply the consequence of the superposition of the two oscillating terms which are periodically in and out of phase. This leads to a period in- and decrease of the particle oscillation energy at the beating frequency $|f_{\mathrm{q}} - f_{\mathrm{ex}}|$, causing the beam to spiral in- and outwards in phase space. The particle oscillation energy is thereby quantified by the value of the Hamiltonian H.

For nonlinear dynamics and excitation in the vicinity of the driven 3rd order resonance however, detuning with action J and angle θ plays a major role [3,4]. In this case, the betatron oscillation frequency and therefore its phase advance

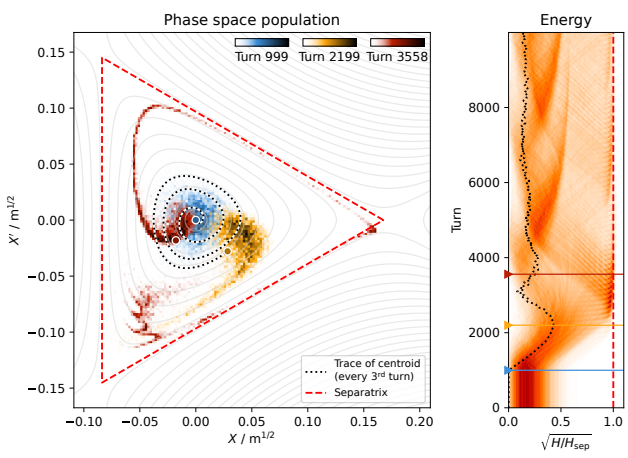

Figure 1: Particle beam dynamics during sinusoidal excitation with frequency $f_{\mathrm{ex}}/f_{\mathrm{rev}} = 0.6641$. The excitation with strength $K = 10^{-4}\,\mathrm{m}^{-1/2}$ starts in turn 1000. The color shading represents particle density; the dotted black line the centroid motion; and the red dashed line the separatrix. Left: Phase space image for three distinct turns and trace of centroid in between. Right: Energy according to Eq. (1).

ISBN: 978-3-95450-227-1 ISSN: 2673-5490 doi:10.18429/JACoW-IPAC2022-MOPOPT012

CONCEPT OF A BEAM DIAGNOSTICS SYSTEM FOR THE MULTI-TURN ERL OPERATION AT THE S-DALINAC*

M. Dutine†, M. Arnold, R. Grewe, L. Jürgensen, N. Pietralla, F. Schließmann, M. Steinhorst
Technische Universität Darmstadt, Dept. of Phys., Institute for Nuclear Physics, Darmstadt, Germany

Abstract

The S-DALINAC is a thrice-recirculating electron accelerator operating in cw-mode at a frequency of 3 GHz. It is possible to operate the accelerator as an Energy-Recovery LINAC, due to the implementation of a path-length adjustment system capable of a 360° phase shift. The multi-turn ERL operation has been demonstrated in 2021. While operating the accelerator in this mode, there are two sets of bunches, the still-to-be accelerated and the already decelerated beam. Effectively, they act as a 6 GHz beam with largely different absolute longitudinal coordinates in the same beamline. For this mode, a non-destructive, sensitive beam diagnostics system is necessary in order to measure the position of both beams simultaneously. The status of a 6 GHz resonant cavity beam position monitor (cBPM) will be given together with the results of a wire scanner measurement of the multi-turn ERL beam.

INTRODUCTION

The Superconducting Darmstadt Linear Accelerator (S-DALINAC) is a thrice-recirculating linear electron accelerator operating in cw-mode at a frequency of 2.997 GHz [1]. It has been upgraded in 2016 by the installation of a third recirculation beamline. A path-length adjustment system included in the newly built beamline allows the change of the path-length by up to 100 mm corresponding to a phase shift of 360° in beam phase [2]. It is therefore possible to operate the S-DALINAC as an Energy-Recovery-Linac (ERL) by shifting the beam phase by 180° which was first demonstrated in 2017 [3]. A floorplan of the S-DALINAC is shown in Fig. 1.

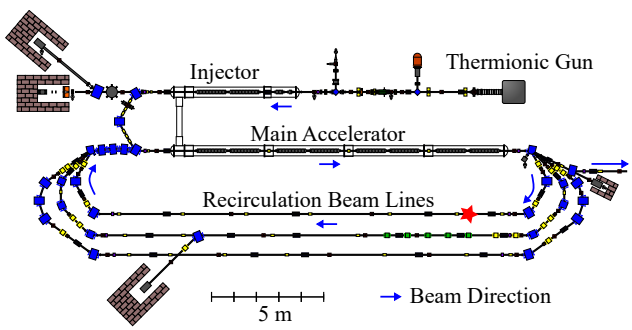

Figure 1: Floorplan of the S-DALINAC. The red star marks the position of the wire scanner and the planned cavity beam position monitor.

* Work supported by DFG (GRK 2128), BMBF (05H21RDRB1), the State of Hesse within the Research Cluster ELEMENTS (Project ID 500/10.006) and the LOEWE Research Group Nuclear Photonics.
† mdutine@ikp.tu-darmstadt.de

In 2021, the multi-turn ERL operation was demonstrated at the S-DALINAC [4,5]. During this operational mode, the beam was accelerated twice and subsequently decelerated twice again. In this mode, the once accelerated beam and the once decelerated beam share the same beamline (first recirculation) but do not necessarily have the same orbit in this beamline. Therefore, a beam position measurement capable of determining the positions of both beams simultaneously is required. In addition, a beam phase and current measurement is desired. The measurement has to be non-destructive as it would otherwise interrupt the ERL mode. A particular challenge is the operation at low beam currents of 100 nA, which corresponds to bunch charges of about 30 aC, while the beam is tuned. As conventional pick-ups are not suitable for these low bunch charges, two solutions are pursued:

1. A resonant cavity beam position monitor (cBPM) operated at 6 GHz.
2. A wire scanner measurement.

6 GHz RESONANT CAVITY BEAM POSITION MONITOR

In ERL mode, the beam has an effective bunch repetition frequency of 5.995 GHz in the first recirculation beamline. The first concept is a position measurement using a resonant cavity BPM with its TM_{110} mode at the doubled fundamental frequency of nearly 6 GHz. The TM_{110} mode is the so called dipole mode. It can be used for position measurement as the field strength depends linearly on the beam current and the transverse offset to the cavity center for small offsets. In order to distinguish between a change of the beams position and its current, a non-destructive current measurement is necessary.

Design and Construction

The required cavity radius R_{res} for a simple pillbox cavity without beampipes can be calculated to

$$R_{res}^{110} = \frac{c_0 \cdot a_{mn}}{2\pi \cdot f_{res}} \approx 30.5\,\text{mm}, \quad (1)$$

where $f_{res} = 6\,\text{GHz}$ is the resonance frequency, c_0 is the speed of light and a_{mn} is the nth zero of the Bessel function of mth order [6]. However, simulations using CST Microwave Studio [7] have been carried out in order to determine the geometrical parameters of the cBPM. The monitor has been designed with two separate cavity cells, one for the horizontal and one for the vertical position measurement. To ensure the excitation of the TM_{110} mode along the desired axis, mode separators were included. Two capacitive antennas

ISBN: 978-3-95450-227-1 ISSN: 2673-5490 doi:10.18429/JACoW-IPAC2022-MOPOPT013

COMPARATIVE STUDY OF BROADBAND ROOM TEMPERATURE THz DETECTORS FOR HIGH AND INTERMEDIATE FREQUENCY RESPONSE*

R. Yadav†,1,2, S. Preu [1], A. Penirschke [2]
[1]Terahertz Devices and Systems, TU Darmstadt, 64283 Darmstadt, Germany
[2] High Frequency Technology, Mittelhessen University of Applied Sciences, Friedberg, 61169 Friedberg,Germany

Abstract

Room temperature terahertz (THz) detectors based on Field effect transistors (FETs) and Zero-bias Schottky diodes (SD) are prominent members for the temporal-spatial characterization of pulses down to the picosecond scale generated at particle accelerators. Comparative study of in house developed THz detectors both at higher and intermediate frequency (IF) is carried out using table top THz systems and commercially available sources. In this paper, we present high frequency and intermediate frequency (IF) response of Gallium Arsenide (GaAs) FET and Zero-bias Schottky diode THz detectors. The IF results obtained are helpful for understanding and designing of optimized IF circuit with broader bandwidth.

INTRODUCTION

The generation of THz radiation in particle accelerators allows for prospective applications in the THz domain [1]. Coherently generated picosecond scale THz pulses can be used for various applications such as spectroscopy, imaging [2]. In order to explore the inter and intra molecular moments of molecules, highly sensitive, accurate, stable and fast detectors are the key elements. The Gallium Arsenide (GaAs) based high electron mobility transistors, commonly known as field effect transistors (FETs) and Zero-bias Schottky diode based THz detectors are prominent members as the heterodyne detectors [3–5]. In order to optimize the detectors, it is required to understand the active channel characteristics of FETs [6] and designing the optimal readout IF circuitry for packaging.

In this paper, the IF and THz characteristics of these in house developed THz detectors is presented. The IF characterization is done from 0 - 30 GHz and the THz characterization from 50 GHz to 1.2 THz. The technical and incremental results shown in this paper are essentials for optimizing the detectors to best of their level.

EXPERIMENTAL SETUP

The THz and IF experiments were performed in order to understand the frequency response of the detectors. The detailed experiment setup is explained below.

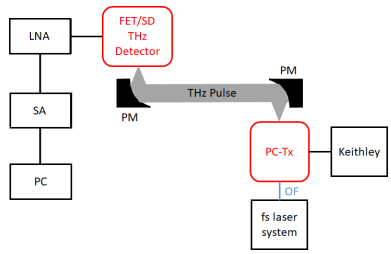

Figure 1: Experimental setup for IF frequency response measurements.

Intermediate frequency measurements

The experimental setup used for IF characterisation is shown in Fig. 1. A THz pulsed laser system from Menlo Systems GmbH was used along with in housed developed photomixer transmitter [7] as a source (PC-Tx). A keithley is used to bias the photomixer. The optical fiber (OF) was used to connect the photomixer to the laser source. Low noise amplifier (LNA) working between 50 kHz - 17 GHz was used after the detector followed by a handheld spectrum analyzer (SA) from Anritsu, as shown in Fig. 1.

High frequency measurements

The THz characterization experimental setup is shown in Fig. 2. A Continuous Wave (CW) laser system from TOPTICA Photonics AG was used. The P-I-N diode continuous wave emitter (CW-Tx) from TOPTICA Photonics AG / Fraunhofer Heinrich Hertz institute was used as a source. On the detector side, the Trans-Impedance Amplifier (TIA) followed by the lock-in is used in order to measured the detected signal.

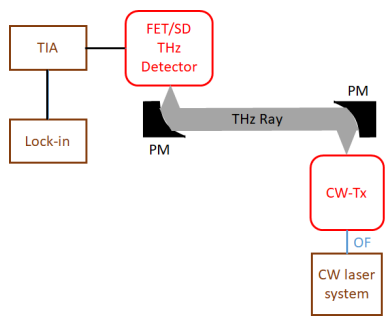

Figure 2: Experimental setup for THz frequency response measurements.

* We are grateful to the Hesse ministry of science and culture (HMWK) for funding the position of Mr. Rahul Yadav. We are thankful to ACST GmbH for providing the Schottky diode.
† yadav@imp.tu-darmstadt.de

ISBN: 978-3-95450-227-1 ISSN: 2673-5490 doi:10.18429/JACoW-IPAC2022-MOPOPT016

UPDATE OF THE BUNCH ARRIVAL TIME MONITOR AT ELBE

M. Kuntzsch†, K. Zenker, A. Maalberg, A. Schwarz, Helmholtz-Zentrum Dresden-Rossendorf HZDR, Dresden, Germany

M.K. Czwalinna, J. Kral, Deutsches Elektronen-Synchrotron DESY, Germany

Abstract

The bunch arrival time monitor (BAM) at the radiation source ELBE has been upgraded twofold. In order to achieve a higher precision a new frontend has been designed, based on a development by DESY, that uses state of the art 50 GHz electro-optical modulators (EOMs). The frontend allows for thermal control of critical components and monitoring of system parameters. The modulated EOM signals and monitoring data are distributed to a new readout electronic. The new MicroTCA-based receiver is based on a dedicated FMC card developed at DESY that is installed on an FMC25 carrier board. The arrival time is calculated on a FPGA with low latency and can be used for machine diagnostic. The code has been adapted to enable the processing of a data stream of the continuous train of electron bunches, allowing for the implementation of a cw beam based feedback in a later step.

INTRODUCTION

ELBE Accelerator

ELBE is a superconducting linear accelerator in user operation since 2002. It generates electron bunches with an energy up to 40 MeV in continuous wave mode (cw) up to a repetition rate of 26 MHz. A thermionic DC gun can inject up to 100 pC bunches, while a superconducting RF gun (SRF Gun) is used for high charge mode up to 300 pC. The main accelerator consist of two superconducting modules, housing two TESLA-type cavities each.

ELBE can drive various secondary sources, like a neutron source, a positron source, a bremsstrahlung setup, two infrared free electron lasers and a THz facility.

BAM Principle

The described bunch arrival time monitor is using an actively stabilized reference signal, provided by a laser-based synchronization system and distributed over polarization maintaining optical fibers. The laser pulse signal is fed into an electro optical modulator (EOM). The RF input of the EOM is connected to a broadband beamline pickup, which takes a probe of the electric field of the electron bunches passing by. The two signals are aligned in time such, that the most pronounced slope of the pickup signal coincide with one of the pulses in the laser pulse train. This leads to a strong intensity modulation change of a single laser pulse when the timing between laser reference signal and pickup signal is changed. By using this scheme, the arrival time information is mapped into an amplitude modulation of all laser pulses that coincide with the pickup signal in the EOM [1]. Figure 1 shows a block diagram of the BAM system.

BAM Upgrade Motivation

The old BAM setup was using custom hardware for the signal conditioning and National Instruments PXI hardware for the digital data processing [2]. This configuration allowed no fast data transfer to the digital low level radio frequency (LLRF) controller, which is needed to apply a feedback controller to stabilize the arrival time actively.

For the EuropeanXFEL a BAM frontend and readout electronics has been developed which enables arrival time measurements with high accuracy [3] and fast data transfer to connected clients. This system has been adapted for the use at ELBE. The firmware was modified to enable the processing of continuous wave data.

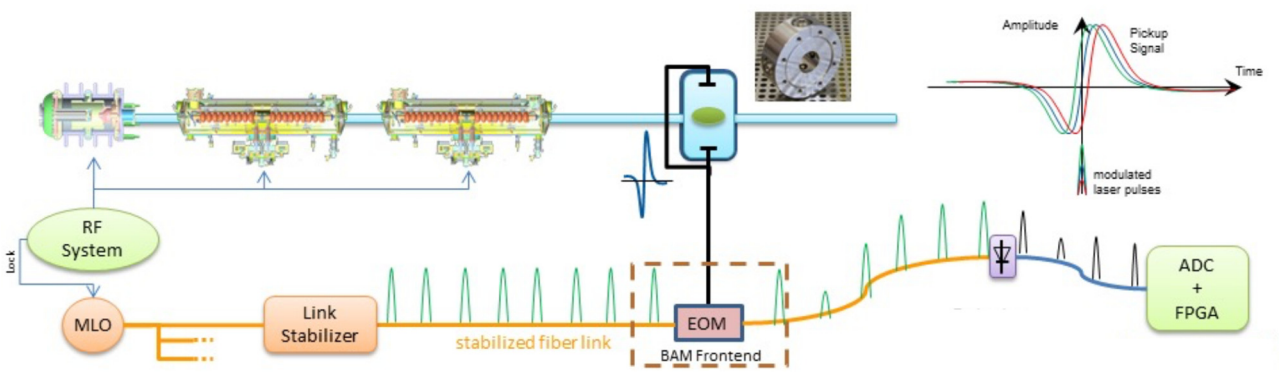

Figure 1: Bunch arrival time measurement scheme.

† m.kuntzsch@hzdr.de

ISBN: 978-3-95450-227-1 ISSN: 2673-5490 doi:10.18429/JACoW-IPAC2022-MOPOPT017

TERAHERTZ SAMPLING RATES WITH PHOTONIC TIME-STRETCH FOR ELECTRON BEAM DIAGNOSTICS

O. Manzhura[1*], M. Caselle[1†], S. Bielawski[2], S. Chilingaryan[1], S. Funkner[1], T. Dritschler[1], A. Kopmann[1], M. J. Nasse[1], G. Niehues[1], M. M. Patil[1], J. L. Steinmann[1], E. Bründermann[1], E. Roussel[2], C. Szwaj[2], A.-S. Müller[1]
[1]Karlsruhe Institute of Technology, Eggenstein-Leopoldshafen, Germany
[2]PhLAM/CERLA, Villeneuve d'Ascq cedex, France

Abstract

To understand the underlying complex beam dynamics in electron storage rings often large numbers of single-shot measurements must be acquired continuously over a long period of time with extremely high temporal resolution. Photonic time-stretch is a measurement method that is able to overcome speed limitations of conventional digitizers and enable continuous ultra-fast single-shot terahertz spectroscopy with rates of trillions of consecutive frames. In this contribution, a novel ultra-fast data sampling system based on photonic time-stretch is presented and the performance is discussed. THERESA (TeraHErtz REadout SAmpling) is a data acquisition system based on the recent ZYNQ-RFSoC family. THERESA has been developed with an analog bandwidth of up to 20 GHz and a sampling rate of up to 90 GS s^{-1}. When combined with the photonic time-stretch setup, the system will be able to sample a THz signal with an unprecedented frame rate of 8 Tf s^{-1}. Continuous acquisition for long observation times will open up new possibilities in the detection of rare events in accelerator physics.

INTRODUCTION

Many scientific applications and experiments, especially in particle accelerator physics, require the continuous observation of non-repetitive and statistically rare events occurring on very short time scales. This imposes high technological challenges on Data Acquisition (DAQ) systems such as oscilloscopes. One of them is the limited temporal resolution of commercially available Analog-to-Digital-Converters (ADCs) [1]. In 1999 a first demonstration of a concept to overcome this limitation was presented [2]. To relax the demands on the data converter performance, prior to digitization, the signal under investigation is stretched in time using chirped optical pulses and the chromatic dispersion in optical fibers. This concept, also called Photonic Time-Stretch (PTS), is already successfully employed in combination with a real-time oscilloscope at the SOLEIL (Source optimisée de lumière d'énergie intermédiaire du LURE) synchrotron facility [3].

The second limitation is the short contiguous acquisition time of commercially available oscilloscopes, which is in the range of few milliseconds. Therefore, the continuous acquisition over long observation time (up to hours), e.g. for the study of the evolution of electron bunch profiles on a turn-by-turn basis, is not possible. To overcome these limitations THERESA, a new digitizer system suitable for PTS measurements, has been developed. THERESA consists of sixteen parallel sampling channels operating in time-interleaved mode, which enables a sampling rate of over 90 GS s^{-1} [4]. In the next sections an overview of the system is given and a description of the firmware architecture and calibration strategy is discussed.

ARCHITECTURE

The digitizer architecture with the photonic time-stretch system is shown in Fig. 1. It consists of an optical time-stretching path, developed at Lille University [3], a fast photo-detector and the THERESA sampling system. THERESA contains a wideband power-divider, a sampling board and a readout card based on the recent ZYNQ-RFSoC technology.

Time-Stretch Setup

The general principle of PTS is shown in Fig. 1. A broadband, chirped carrier laser pulse is fed through an electro-optical crystal which encodes the ultra-fast signal to be sampled onto to the laser pulse. The modulated laser pulses are then stretched in time by means of a long dispersive fiber until their duration is in the order of nanoseconds. The factor S, by which the pulse is slowed down, can be calculated by

$$S = 1 + \frac{L_2}{L_1}, \tag{1}$$

where L_1 and L_2 are the lengths of the two fibers [1, 3].

Sampling Board

The stretched and modulated pulse from the PTS is split into 16 identical signals by an active power divider. Each signal is fed into the individual channels on the THERESA card. High-bandwidth Track-and-Hold Amplifiers (THA) [5] device are employed to sample the input signal at a high rate. The sampling clock of the THAs is individually delayed by picosecond programmable delay chips [6]. One key feature of the THERESA architecture is its high flexibility in the sampling operation. The system can operate either in continuous or in single-shot sampling mode. In continuous mode, the phase of the sixteen parallel sampling channels are equally distributed over the sampling interval, which can

* olena.manzhura@kit.edu
† michele.caselle@kit.edu

ISBN: 978-3-95450-227-1 ISSN: 2673-5490 doi:10.18429/JACoW-IPAC2022-MOPOPT018

ADVANCING TO A GHz TRANSITION RADIATION MONITOR FOR LONGITUDINAL CHARGE DISTRIBUTION MEASUREMENTS*

S. Klaproth†[1], A. Penirschke, Thechnische Hochschule Mittelhessen, 61169 Friedberg, Germany
R. Singh, T. Reichert, GSI Helmholtzzentrum für Schwerionenforschung, 64291 Darmstadt, Germany
H. De Gersem, Technische Universität Darmstadt, 64289 Darmstadt, Germany
[1]also at Technische Universität Darmstadt, 64289 Darmstadt, Germany

Abstract

In the past, longitudinal beam profiles have been measured with e.g., Feschenko monitors, Fast Faraday Cups (FFC) and field monitors. Feschenko monitors usually examine an average shape over several pulses and FFCs are interceptive devices by design. In this work we want to present the progress in the development of a novel GHz diffraction radiation monitor which shall be able to measure the longitudinal charge distribution of single bunches within Hadron beam LINACS non-destructively. A proof-of-concept measurement has been performed at GSI. We aim for a resolution of 50 ps to 100 ps at beam energies of $\beta = 0.05$ to 0.74. electronic field simulations were performed using CST Particle Studio® to determine an optimal RF-Window, which also suits as vacuum chamber and the beam energy and angular dependencies of the diffraction radiation for different materials were analyzed.

INTRODUCTION

The longitudinal bunch shape is of interest for conditioning and verification of the beam dynamics of LINACs. While for relativistic particles pick-ups may be used to observe the longitudinal shape, non-relativistic particles self field spreads significantly along the beam axis, so that a direct correlation of the self fields and the actual charge distribution becomes ambiguous. The very same problem is given for field monitors. They also depend highly on the transverse field component which increases with the Lorentz factor γ. The response of the field monitor becomes more flattened for slower beams cause of the stretched field distribution [1].

However, there are other ways to measure the longitudinal beam profiles of non-relativistic particles like e.g., Feschenko monitors [2], which rely on beam interactions with a wire to create secondary electrons. Unfortunately, only average measurements are possible [3]. So changes of the shape from shot-to-shot measurements might not be visible. Another option to measure longitudinal beam profiles are Fast Faraday Cups (FFC). Nevertheless, those have two major disadvantages. The first is its destructive nature towards the beam itself and the second is the field elongation for non-relativistic beams, where the self field of the beam interacts with the FFC before the beam actually hits the FFC. Meanwhile, there are designs to reduce the effect of the self field [4–6], but careful handling of secondary electrons is still necessary for a longitudinal charge profile measurement.

In the following sections we will discuss the next step on advancing to a novel longitudinal beam shape monitor based on diffraction radiation. The diffraction radiation of the beam passing an aperture from the outside of the beam pipe, it is essential that the diffraction radiation can exit the vacuum system through the vacuum chamber. Hence, selecting a well-suited material is crucial for the operation of this type of monitor. The presented effect of different materials on the diffraction radiation is examined with the particle in cell solver of the simulation software CST Particle Studio®.

THEORY

A summary of the theory of the normal incident radiation (NIR) and the angular distribution of the radiated electric field [3] is given, before discussing the results of the simulation.

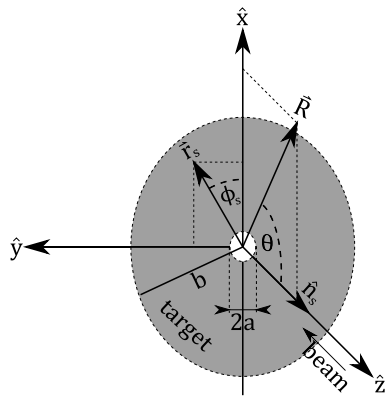

Figure 1: Coordinate system and target plane [3].

Figure 1 shows the idealized setup for the diffraction radiation simulations. The perpendicular incident bunch is passing through the aperture of radius a of the perfect electric conducting (PEC) target of radius b with velocity $\vec{v}_e = -\beta c_0 \hat{e}_z$. If the field monitor, located at $\vec{R}$, is in the x-z plane, then it should be sensitive to the emitted radiation of the field components E_x and E_z. Meaning that the relevant signal components would be $k_x \hat{e}_x + k_z \hat{e}_z$, which are generated at the surface location $\vec{r}_s$ on the target plane [3]. The angle ϕ_s describes a rotation in the target plane and θ the angle between beam axis and the position vector of the field monitor.

* This work is supported by the German Federal Ministry of Education and Research (BMBF) under contract no. 05P21RORB2. Joint Project 05P2021 - R&D Accelerator (DIAGNOSE)
† Stephan.Klaproth@iem.thm.de

ISBN: 978-3-95450-227-1 ISSN: 2673-5490 doi:10.18429/JACoW-IPAC2022-MOPOPT019

WAKEFIELD STUDIES FOR A BUNCH ARRIVAL-TIME MONITOR CONCEPT WITH ROD-SHAPED PICKUPS ON A PRINTED CIRCUIT BOARD FOR X-RAY FREE-ELECTRON LASERS*

B. E. J. Scheible[1†], A. Penirschke, Technische Hochschule Mittelhessen, Friedberg, Germany
M. K. Czwalinna, H. Schlarb, Deutsches Elektronen-Synchrotron DESY, Hamburg, Germany
W. Ackermann, H. De Gersem, Technische Universität Darmstadt, Darmstadt, Germany
[1]also at Technische Universität Darmstadt, Darmstadt, Germany

Abstract

The European XFEL (EuXFEL) and other notable X-ray Free-Electron Laser facilities rely on an all-optical synchronization system with electro-optical bunch arrival-time monitors (BAM). The current BAMs were benchmarked with a resolution of 3.5 fs for nominal 250 pC bunches at the EuXFEL, including jitter of the optical reference system. The bunch arrival-time jitter was reduced to about 5 fs with a beam-based feedback system. For future experiments at the EuXFEL the bunch charge will be decreased to a level where the existing system's accuracy will no longer be sufficient. In simulations a concept based on rod-shaped pickups mounted on a printed circuit board indicated its potential for such low charge applications. For the feasibility of the proposed design, its contribution to the total impedance is essential. In this work the design and an intermediate version are compared to state-of-the-art BAM regarding their wake potential. Furthermore, measures to mitigate wakefields are discussed.

INTRODUCTION

X-ray Free-Electron Lasers (XFELs) are 4$^{\text{th}}$ generation light sources for experiments with high temporal and spatial resolution [1]. A major challenge in utilizing the XFEL's full potential is fs-precision synchronization of subsystems in a several km-long facility [2]. The synchronization includes high-precision arrival-time measurements [3].

Sufficient precision can be achieved by an all-optical synchronization system [3, 4], which contains bunch arrival-time monitors (BAMs) with the electro-optical (eo) detection scheme described in [4]. They provide non-destructive measurements of individual bunch arrival times with high precision. The European XFEL (EuXFEL) [3] recently reported an eo-BAM resolution of 3.5 fs at nominal 250 pC [5] with cone-shaped pickups [6].

In order to reach single-digit fs measurement resolution below 20 pC, the BAMs have to be improved. A proposed design will potentially extract a voltage signal ten times higher as the current pickups [7].

Since some of the beam energy is extracted, the invasiveness due to wakefield should be evaulated. Bunch-to-bunch and short-range interaction might be problematic in the updated pickup, because of the sharp edges in the cross-section. Additionally striving for higher signal intensity will also extract more energy. Therefore, it is necessary to check the wake potential while evaluating the design options.

Wakefields

Wakefields emerge from interaction between a charged particle and its surroundings [8]. Finite conductivity and geometric changes in the beam pipe are sources of wakefields [8, 9], which affect source and trailing particles [8].

The wake function describes the response to a pulse excitation [10], which, separated by orientation, is‡

$$w_\nu\left(\vec{r}_0,\vec{r},z\right)=\frac{1}{q_0 q}\int_{-\infty}^{\infty}\vec{F}_{\mathrm{L}}\left(\vec{r}_0,s,\vec{r},z\right)\cdot\vec{e}_\nu \mathrm{d}s\,, \tag{1}$$

where ν is either $\parallel$, x or y and $\vec{e}_\nu$ the corresponding standard basis vector in $\mathbb{R}^3$. $\vec{r}_0$, q_0 and $\vec{r}$, q are transverse position and charge of source respectively test particle, z is the longitudinal distance between them, s the trajectory and $\vec{F}_{\mathrm{L}}$ the Lorentz force [8, 9]. Sometimes it is convenient to use the Fourier transform, called wake impedance Z_ν [8].

The effect on a test charge by wakefields of the entire bunch is defined as the convolution of the bunch's linear charge distribution $\lambda(z)$ and the wake function normalized to the bunch charge Q_{B} [10]. For longitudinal wakes this is

$$W_\parallel(z)=\frac{1}{Q_{\mathrm{B}}}\int_{-\infty}^{\infty}w_\parallel\left(z'-z\right)\lambda\left(z'\right)\mathrm{d}z'\,. \tag{2}$$

The total wake loss factor (WLF) [11–13], which is the energy lost by the bunch per squared charge, is‡

$$k_\sigma=\frac{\Delta E}{Q_{\mathrm{B}}^2}=-\frac{1}{Q_{\mathrm{B}}}\int_{-\infty}^{\infty}\lambda\left(z\right)W_\parallel\left(z\right)\mathrm{d}z\,. \tag{3}$$

The rms energy spread per charge [12], referred to as energy spread factor (ESF), is calculated by‡

$$ESF\left(\sigma\right)=\sqrt{\frac{1}{Q_{\mathrm{B}}}\int_{-\infty}^{\infty}\lambda\left(z\right)\left[W_\parallel\left(z\right)+k_\sigma\right]^2\mathrm{d}z}\,. \tag{4}$$

Numerical Field Calculation

In this work the wakefield solver of CST Particle Studio® (PS) was applied with integration method "Indirect Interfaces", at least 300 mm simulated wakelength and a Gaussian excitation. CST PS uses the finite integration technique

* Work supported by the German Federal Ministry of Education and Research (BMBF) under contract No. 05K19RO1.
† bernhard.scheible@iem.thm.de

‡ It is common to add a minus sign in the longitudinal wake function to associate energy loss with a positive value. The (total) WLF in Eq. (3) then also has an opposite sign, e.g. in [11,12]. Likewise the sign in Eq. (4) would switch. In this work we follow the definition used by CST® [13].

ISBN: 978-3-95450-227-1 ISSN: 2673-5490 doi:10.18429/JACoW-IPAC2022-MOPOPT020

LONGITUDINAL PHASE SPACE DIAGNOSTICS WITH CORRUGATED STRUCTURE AT THE EUROPEAN XFEL

S. Tomin*, W. Decking, N. Golubeva, A. Novokshonov, T. Wohlenberg, I. Zagorodnov
Deutsches Elektronen-Synchrotron DESY, Hamburg, Germany

Abstract

Characterization of the longitudinal phase space (LPS) of the electron beam after the FEL process is important for its study and tuning. At the European XFEL, a single plate corrugated structure was installed after the SASE2 undulator to measure the LPS of the electron beam. The beam passing near the plate's corrugations creates wakefields, which induce a correlation between time and the transverse distribution of the beam. The longitudinal phase space of the beam is then analyzed on a scintillating screen monitor placed in the dispersion section. In this paper, we present the result of commissioning the corrugated structure and the first LPS measurement.

INTRODUCTION

Longitudinal phase space (LPS) measurements after the undulator are of high interest for FEL and beam dynamics studies and facility operation. The standard way to measure LPS is to use the Transverse Deflection Structure (TDS) [1, 2]. The TDS is powered by a klystron and streaks the electron beam in the transverse plane. The streaked beam is observed on a scintillating screen monitor. The TDS-screen system will allow observation of the longitudinal phase space of the beam if the screen is located in the dispersion section and the dispersion is orthogonal to the direction of TDS deflection. However, the size and complexity of such diagnostics grows with increasing electron beam energy. Therefore, the development and installation of TDS requires a significant investment of time (years) and manpower [3], especially for the European XFEL, which operates with the beam energies up to 17.5 GeV [4].

Another way is to use a corrugated structure. A corrugated structure - a corrugated pipe of small radius or two corrugated metal plates with an adjustable gap - has been proposed in [5] to remove linear energy correlation (chirp) in a relativistic electron beam and first confirmed experimentally in [6]. When an electron beam is displaced relative to the center of the corrugated structure and passes near the corrugated wall, it experiences a time-correlated transverse kick in the direction of the wall. However, the transverse kick is not linear unlike the TDS. This makes it difficult to analyze the measurements obtained due to non-linearity of the time axis, and the time resolution is poor at the beam head. A corrugated structure is a type of wakefield structure along with, for example, dialectic structures. Nevertheless, the simplicity of passive streamers based on wakefield structure is attractive for electron beam manipulation both for FEL techniques, e.g. [7], and for diagnostic purposes [8–10].

* sergey.tomin@desy.de

LPS DIAGNOSTICS WITH CORRUGATED STRUCTURE

At the European XFEL, the development of LPS diagnostic based on a corrugated structure was started in October 2020 and commissioned in January 2022. The new device is a metal corrugated plate, consisting of 5 segments of length of 1 m each. The corrugated structure is installed after the SASE2 undulator and, together with the GAGG:Ce screen installed in the downstream arc, forms a diagnostic system for measuring the LPS of the electron beam. The strength of the transverse kick of the corrugated plate depends on the beam current distribution and the distance between the beam and the corrugated plate. Unlike the corrugated structures in PSI [10] or SLAC [11], which use movable jaws with appropriate mechanics to change the distance between the beam and the corrugated plate, we control the distance with a trajectory bump. This significantly simplifies the design of the entire system. The trajectory bump is created by 4 vertical correctors, with maximum amplitude 4 mm – distance between the plate and reference beam trajectory. A simplified layout of the diagnostic beam line is shown in Figure 1 and the corrugated structure installed in the tunnel is shown in Figure 2.

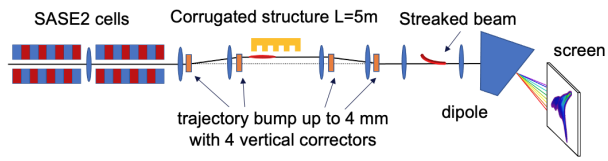

Figure 1: Simplified layout of the diagnostic beam line for LPS measurement after SASE2 undulator.

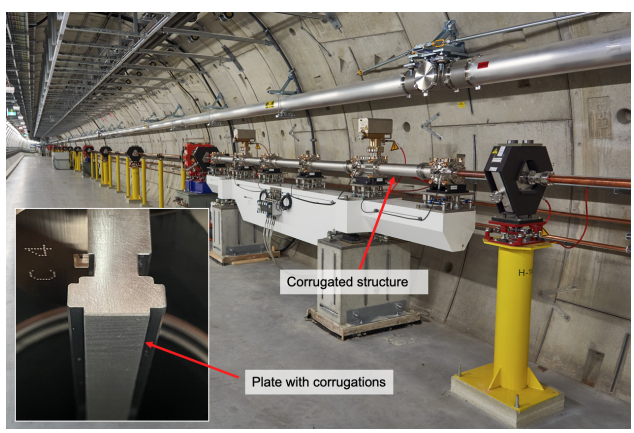

Figure 2: Installed corrugated structure in the tunnel.

ISBN: 978-3-95450-227-1 ISSN: 2673-5490 doi:10.18429/JACoW-IPAC2022-MOPOPT021

5D TOMOGRAPHY OF ELECTRON BUNCHES AT ARES

S. Jaster-Merz*[1], R. W. Assmann[2], R. Brinkmann, F. Burkart, T. Vinatier,
Deutsches Elektronen-Synchrotron DESY, Germany
[1]also at Department of Physics Universität Hamburg, Germany
[2]also at Laboratori Nazionali di Frascati, Italy

Abstract

The ARES linear accelerator at DESY aims to deliver stable and well-characterized electron bunches with durations down to the sub-fs level. Such bunches are highly sought after to study the injection into novel high-gradient accelerating structures, test diagnostics devices, or perform autonomous accelerator studies. For such applications, it is advantageous to have a complete and detailed knowledge of the beam properties. Tomographic methods have shown to be a key tool to reconstruct the phase space of beams. Based on these techniques, a novel diagnostics method is being developed to resolve the full 5-dimensional phase space (x, x', y, y', z) of bunches including their transverse and longitudinal distributions and correlations. In simulation studies, this method shows an excellent agreement between the reconstructed and the original distribution for all five planes. Here, the 5-dimensional phase space tomography method is presented using a showcase simulation study at ARES.

INTRODUCTION

Advanced accelerator research and development benefits greatly from stable and well-characterized electron bunches. Undesired correlations between the two transverse planes can arise due to unnoticed rotated beamline elements or stray fields on the photocathode and in the gun region and can lead to 2D emittance growth [1, 2]. Longitudinal-transverse correlations are introduced due to space-charge forces [3] in the low energy region, a transverse dependent energy gain which evolves into a longitudinal-transverse correlation over a drift, or coherent-synchrotron radiation in, for example, bunch compressors in the beamline which can introduce longitudinally dependent transverse offsets [4]. In simulations, the full 6-dimensional phase space is available at any location in the beamline and such effects can be monitored and minimized. However, in reality, such diagnostics of the bunch is not as straightforward and requires advanced methods. A measurement of the 6-dimensional charge density has been performed for a H^- beam in a dedicated beamline using slit masks [5]. In operating accelerators, tomographic methods are a useful tool to obtain detailed knowledge of the beam distribution [6–10]. Methods to measure multi-dimensional distributions such as the full transverse phase space [11–14] as well as the 3-dimensional charge-density distribution [15–18] exist. Here, a tomographic method to reconstruct the 5-dimensional charge-density distribution (x, x', y, y', z) of an electron bunch is introduced. It combines a quadrupole-based tomography of the 4-dimensional transverse phase space with the variable streaking direction of a PolariX X-band transverse deflecting structure (TDS) – a device developed in collaboration between CERN, DESY, and PSI [18–20]. The method allows to reconstruct correlations between the horizontal and vertical positions x,y and divergences x',y' as well as the longitudinal position z in the bunch. Such information is useful to identify undesired correlations and therefore enables the optimization and improvement of the accelerator performance and beam quality.

The method is tested on an example case based on the ARES linear accelerator at DESY. ARES [21–23] is a normal conducting S-band linear electron accelerator designed for accelerator research and development. It operates at up to 50 Hz, 155 MeV and charges from 0.05 pC to 200 pC. ARES is designed to produce and measure bunches with sub-fs durations [16, 17, 24–26]. Additionally, it focusses on the study of novel dielectric-based acceleration techniques [27–30] and electron radiotherapy, the development of diagnostics devices and methods [31–34] and the application of machine learning to accelerator operation [35, 36]. Furthermore, it serves as a general test bed for new accelerator components [37]. For the simulations, a Gaussian particle distribution with ARES-compatible beam parameters for a fully on-crest working point is chosen. To demonstrate the potential of the method, an artificial longitudinal sinusoidal oscillation of the transverse beam size and divergence in the x-plane is imprinted on the bunch. The Courant-Snyder parameters [38], the alpha $\alpha_{x,y}$ and beta $\beta_{x,y}$ functions, are kept constant. Together with the geometric emittance $\epsilon_{x,y}$ these functions describe the statistical beam parameters.

The present study aims to demonstrate the working principle of the method by utilizing the ARES beamline. Furthermore, a simulated reconstruction of a particle distribution is presented and compared to the input distribution.

WORKING PRINCIPLE

The 5-dimensional phase space (x, x', y, y', z) of electron bunches is reconstructed using a tomographic method. In general, a tomography uses low-dimensional projections of an object along different angles to reconstruct a higher-dimensional distribution. This can be applied to bunches in an accelerator. The transverse information is obtained by scanning the transverse phase advances $\mu_{x,y}$ with, e.g., quadrupoles. The longitudinal information is obtained by streaking the beam with a TDS. To also resolve the correlations between the two transverse planes, their phase advances are controlled simultaneously. Furthermore, the streaking

* sonja.jaster-merz@desy.de

ISBN: 978-3-95450-227-1 ISSN: 2673-5490 doi:10.18429/JACoW-IPAC2022-MOPOPT022

BEAM DYNAMICS OF THE TRANSPARENT INJECTION FOR THE MAX IV 1.5 GeV RING

M. Apollonio*, Å. Andersson, M. Brosi, D. K. Olsson,
P. F. Tavares, A. Vorozhstov
MAX IV Laboratory, Lund University, Lund, Sweden

Abstract

Following the successful operation of the Multipole Injection Kicker in the MAX IV 3 GeV storage ring, we plan to introduce a similar device in the MAX IV 1.5 GeV ring. In order to assess the effectiveness of such device and to define its working parameters, we performed a series of studies aimed at understanding the beam dynamics related to the injection process. In this paper we describe the optimisation of the MIK working parameters, we study the resilience to tune shifts for a chosen injection scheme and illustrate some tests conducted to evaluate the ring acceptance. We conclude with remarks about the effects of magnet errors on key performance parameters such as the injection efficiency and perturbations to the size and divergence of the stored beam and a brief discussion on future work.

INTRODUCTION

At the MAX IV complex in Lund, Sweden [1, 2], two storage rings (SR) are operated, fed by a common LINAC injector. The first ring, R1, receives a 1.5 GeV beam, while the 3 GeV ring, R3, is injected further downstream. Both SRs operate in top-up mode, albeit at different rates (half an hour for R1, 10 minutes for R3) and currents (400 mA and 300 mA respectively). To allow injection and alleviate the effects of top-up transients on the stored beam, R3 makes use of a Multipole Injection Kicker (MIK), thoroughly described in [3]. These pulsed magnets generate strong spatially dependent multipole fields, mainly acting on the off-axis injected beam, whereas the nearly zero field at the nominal orbit highly suppresses any disturbance on the circulating beam. This is highly valued by photon beamlines, especially at fourth generation SRs, where beam reduced dimensions can exacerbate the perturbations produced in the top-up phase. After the early implementations at KEK, first with a pulsed quadrupole [4] and then with a pulsed sextupole [5], whose use was initially considered at MAX IV [6] instead of a more conventional four-bump injection, studies at BESSY [7] first demonstrated a scheme based on a 8-wire iron-free concept, further developed through a collaboration with SOLEIL and installed and commissioned at MAX IV in 2018. Since then, the MIK has been working very successfully, being the first application of this technology on a fourth-generation SR.

A Multipole Injection Kicker for R1

Following the positive results with R3 MIK, MAX IV has recently considered to adopt the same technology for the low-energy ring R1, a 12-DBA lattice [1], whose main parameters are summarized in Table 1. The beam from the LINAC proceeds towards an extraction line (TR1) located below the ring main floor, hence it is deflected vertically by means of a chicane set-up, reaching a septum whose inner wall is 13.5 mm in the horizontal plane from the nominal orbit. At the septum exit we expect a horizontal separation of 17 mm between the incoming beam and the stored one. The injected beam is then strongly deflected while crossing the magnets in achromats one and two, until reaching a dipole kicker (DK) located in straight 3, 14.8 m from the centre of the injection straight, imparting a correction while also disturbing the incoming stored beam. The aperture sharing regime allows an effective stacking, however beam stability is lost at each top-up. The R1-MIK will be located 90 cm past the DK, in the same straight.

Table 1: MAXIV R1 Ring Global Parameters

E_e (GeV)	1.5
L (m) / T (μs)	96 / 320
ϵ_x (nm)	5.9
$\nu_{x,y}$	11.22 / 3.15
$\xi_{x,y}$	1.5 / 1.8
$\Delta E/E$ (%)	0.075
α_C	3.05e^{-3}

Injection Dynamics

Accelerator Toolbox (AT) [8] was used to investigate the beam dynamics of R1 when injecting with the MIK. The model for the multipole was introduced as a rescaled kick-map after a campaign of measurements by SOLEIL done to characterize the kicker for R3 [9]. A matlab [10] script utilizing AT was developed to visualize the process of injection and correction of the incoming beam, as illustrated in Fig. 1. On the top-left we see a beam of 100 electrons with a phase-space distribution taken from the LINAC parameters as it enters R1 from the outer part of the septum (cyan tracks), −17 mm from the nominal orbit. In addition to the (B_x, B_y) field map as a function of the position of the beam, the model comprises a time wave-form (bottom-left), taking into account the duration of the pulse, here set at 1.28 µs or four periods of the ring. Past the septum, electrons undergo strong deflections due to the magnets crossed at large horizontal displacements, until they reach the MIK where they receive a first kick (K1) imparting an initial correction to the injected beam. On the following turn the beam reaches the crossing point at another horizontal position

* marco.apollonio@maxiv.lu.se

ISBN: 978-3-95450-227-1 ISSN: 2673-5490 doi:10.18429/JACoW-IPAC2022-MOPOPT023

IMPROVED EMITTANCE AND BRIGHTNESS FOR THE MAX IV 3 GeV STORAGE RING

M. Apollonio*, Å. Andersson, M. Brosi, R. Lindvall, D. K. Olsson,
M. Sjöström, R. Svärd, P. F. Tavares,
MAX IV Laboratory, Lund University, Lund, Sweden

Abstract

At MAX IV Laboratory, the Swedish Synchrotron Radiation (SR) facility, the largest of two rings operates at 3 GeV with a bare lattice emittance of 330 pmrad. Upgrade plans are under consideration aiming at a gradual reduction of the emittance, in three stages: a short-term with an emittance reduction of 20% to 40%, a mid-term with an emittance reduction of more than 50% and a long-term with an emittance in the range of the diffraction limit for hard X-rays (10 keV). In this paper we focus on the short-term case, resuming previous work on a proposed lattice that can reach 270 pmrad emittance, with only minor modifications to the gradients of the magnets of the present ring, *i.e.* without any hardware changes and all within the present power supply limits. Linear lattice characterisation and calculations of key performance parameters, such as dynamic aperture and momentum aperture with errors, are described and compared to the present operating lattice. Experimental tests of injection into this lattice are also shown.

INTRODUCTION

The MAX IV complex in Lund, Sweden, comprises a LINAC used for injection and also feeding a Short Pulse Facility (SPF), and two storage rings (SR) operating at 1.5 GeV (R1) and 3 GeV (R3). Made of 20 7BA achromats with a circumference of 528 m, R3 is credited to be the first 4th generation electron SR, with a nominal bare-lattice equilibrium emittance of 330 pmrad [1]. The R3 ring provides daily synchrotron light to 10 beamlines at 300 mA, in a 10 minutes top-up mode, with a typical lifetime of 20 hours. Since its first light delivery to beamlines in 2016 [2], studies were made towards a further improvement in its performances. The time has come to consider a testable reduction in emittance and increase in brightness at the ID straights in an operating machine. This paper takes inspiration from a study dating back to 2014 [3] and, after a revision of the case, focuses on the implementation of a lattice into the present ring. For this study only the currents of quadrupoles, sextupoles and octupoles were altered, with no hardware modification. We first discuss the drive behind the linear characterization, illustrating the optimisation procedure towards a lower emittance and the differences in dynamics between the new and the baseline lattice. After that we describe how the new lattice is implemented in the real machine, and the threading technique adopted to capture the first beam. We then discuss the LOCO fits used to define the lattice in the ring, and conclude with the present status of the implementation and with a discussion of the possible further steps.

LATTICE DESIGN

The main drive in the characterization of the new lattice is the reduction of the natural emittance. Another desirable parameter to consider, not directly targeted in the optimisation, is the brightness at the ID straights. The strategy adopted was to start from the present machine and act on four quadrupole families (QF, QDE, QFE, QFM) to gradually reduce the natural emittance while preserving the non-integer parts of the tunes. The process utilized the MAX IV cluster to exploit the parallel optimisation capabilities of the tracking code elegant [4]. The obtained results, with Twiss parameters shown in Fig. 1, were surprisingly well matched to the initial studies, confirming a natural tendency of the system when optimsation is driven by only the four aforementioned quadrupole families. The code OPA [5] was utilized to tune sextupoles and octupoles in order to improve the non-linear dynamics of the lattice, such as the dynamic aperture (DA), the control of the tune shift with amplitude and with energy deviation. Table 1 summarizes the result of this process, as compared to the present lattice[1]. Magnet variations for quadrupoles, sextupoles and octupoles can be found in Table 2. Figure 2 shows a calculation of DA over 10 seeds with the tracking code elegant [4], where errors on magnet gradients and positions were introduced, and a physical aperture of 22 mm diameter was considered. The DA of the new lattice is clearly penalized in both planes. For the vertical one this is due to the 25 m beta function at both edges of the achromat, a typical feature of the new lattice, together with an important reduction of the horizontal dispersion inside the achromat

Table 1: Comparison of the R3 Parameters for the Baseline Lattice and the Low-Emittance Case

R3	baseline	low-emittance
ϵ (pm rad)	328.18	269.14
ν	(42.20, 16.28)	(44.1997, 14.2793)
ξ (natural)	(-49.98, -50.08)	(-50.72, -76.47)
α_C ($\times 10^6$)	305.97	259.69
$\tau_{x,y,E}$ (ms)	15.7, 29.0, 25.2	16.9, 29.0, 22.7
$\beta_{x,y}^{straight}$ (m)	9.0, 2.0	7.47, 1.04
brightness increase (%)	-	+22
RF_{height}(1.2 MV) (%)	5.19	5.64

* marco.apollonio@maxiv.lu.se

[1] brightness increase computed for a 4m long 1Å source

ISBN: 978-3-95450-227-1 ISSN: 2673-5490 doi:10.18429/JACoW-IPAC2022-MOPOPT024

MEASURING THE COHERENT SYNCHROTRON RADIATION FAR FIELD WITH ELECTRO-OPTICAL TECHNIQUES

C. Widmann*, M. Brosi, E. Bründermann, S. Funkner, M. J. Nasse, G. Niehues, M. D. Noll, M. M. Patil, M. Reissig, J. L. Steinmann, A.-S. Müller, Karlsruhe Institute of Technology, Karlsruhe, Germany

Abstract

For measuring the temporal profile of the coherent synchrotron radiation (CSR) a setup based on electro-optical spectral decoding (EOSD) will be installed as part of the sensor network at the KIT storage ring KARA (Karlsruhe Research Accelerator). The EOSD technique allows a single-shot, phase-sensitive determination of the complete spectrum of the CSR far-field radiation at each turn. Therefore, the dynamics of the bunch evolution, e.g. the micro-bunching, can be observed in detail. Especially, in synchronized combination with the already established near-field EOSD, this method could provide deeper insights in the interplay of bunch profile and CSR generation for each individual electron bunch.

For a successful implementation of the EOSD single-shot setup, measurements with electro-optical sampling (EOS) are performed. With EOS the THz pulse shape is scanned over several turns by shifting the delay of laser and THz pulse. In this contribution, different steps towards the installation of the EOSD far-field setup are summarized.

INTRODUCTION

The KIT storage ring KARA (Karlsruhe Research Accelerator) can be operated in a short-bunch mode, the so-called low-α_c mode, in which the bunch self-interaction with its emitted coherent synchrotron radiation (CSR) leads to microstructures in the bunch profile and the micro-bunching instability. In this low-α_c mode, the bunch length is reduced to a few picoseconds at a beam energy of ≤ 1.3 GeV and a beam current of some milliamperes. Coherent synchrotron radiation (CSR) in the THz range is emitted in intense bursts. These dynamics of the micro-bunching instability are studied continuously [1–7]. Sophisticated measurement techniques are necessary to take a snapshot of the bunch at every turn, i.e. at MHz repetition rates. Therefore, several synchronized detectors are implemented in the distributed sensor network at KARA to measure the longitudinal bunch profile, the energy spread and the temporal profile and spectrum of the THz pulses.

The longitudinal bunch profile is measured using electro-optical spectral decoding (EOSD) of the near-field of the electron bunch. With this near-field EOSD setup the evolution of the longitudinal bunch profile in low-α_c operation mode at KARA could be studied in detail [2] and a 2D image of the longitudinal phase space could be reconstructed by tomography [8].

The energy distribution is measured indirectly by measuring the horizontal bunch profile in a dispersive section of KARA [5]. The change in the energy spread can be deter-mined from the change in the horizontal bunch size.

The intensity of the emitted THz radiation is measured with fast THz detectors and KAPTURE or KAPTURE-2 as readout system [3, 4, 9]. With the EOSD far-field setup [10], the temporal resolution of the THz bunch profile measure-ment will be increased and, therefore, the THz spectrum can be determined.

For the EOSD near-field, the EOSD far-field and the horizontal bunch profile measurements different versions of KALYPSO, a fast line array detector developed at KIT, are implemented [11, 12]. KALYPSO features a frame rate of 2.7 MHz, allowing the continuous resolution of each turn in single-bunch operation.

EOSD FAR-FIELD SETUP FOR KARA

With EOSD, a method originally applied in THz spec-troscopy [13], the temporal profile of the THz pulse is en-coded on the spectrum of an ultra-short laser pulse. The laser pulse is stretched to a pulse length of a few picoseconds and is overlapped collinearly with the THz pulse inside an electro-optical (EO) crystal (see also Fig. 1). The Pockels-effect causes a change of the birefringence of the EO crystal scaling linearly with the electrical field strength of the THz pulse. This results in a change of the polarization of the laser pulse from linear to elliptical. By analyzing this polarization change, the electrical field strength of the THz pulse can be determined. The complete profile of the THz pulse can be analyzed in a single shot using an optical spectrometer. This method is applied to measure the far-field of the CSR at ac-celerators [14]. To increase the sensitivity of the system, the changes in both polarization planes - horizontal and vertical - can be analyzed using a balanced detection scheme [15].

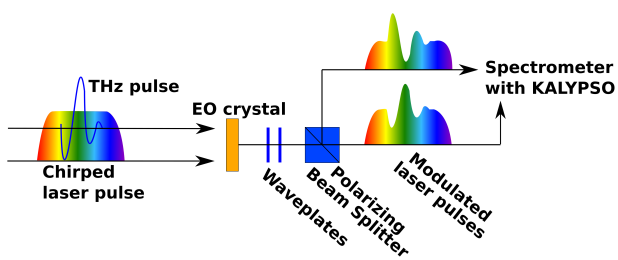

Figure 1: EOSD to measure the THz pulse shape with a chirped laser pulse: THz pulse and laser pulse are overlapped in the EO crystal. The electrical field of the THz pulse generates a modulation of the laser pulse spectrum. Both polarization directions are analyzed in a spectrometer.

* christina.widmann@kit.edu

ISBN: 978-3-95450-227-1 ISSN: 2673-5490 doi:10.18429/JACoW-IPAC2022-MOPOPT025

DEVELOPMENT OF AN ELECTRO-OPTICAL LONGITUDINAL BUNCH PROFILE MONITOR AT KARA TOWARDS A BEAM DIAGNOSTICS TOOL FOR FCC-ee

M. Reißig*, M. Brosi†, E. Bründermann, S. Funkner, B. Härer, G. Niehues, M. M. Patil, R. Ruprecht, C. Widmann, A.-S. Müller, Karlsruhe Institute of Technology, Karlsruhe, Germany

Abstract

The Karlsruhe Research Accelerator (KARA) at KIT features an electro-optical (EO) near-field diagnostics setup to conduct turn-by-turn longitudinal bunch profile measurements in the storage ring using electro-optical spectral decoding (EOSD). Within the Future Circular Collider Innovation Study (FCCIS) an EO monitor using the same technique is being conceived to measure the longitudinal profile and center-of-charge of the bunches in the future electron-positron collider FCC-ee.

This contribution provides an overview of the EO near-field diagnostics at KARA and discusses the development and its challenges towards an effective beam diagnostics concept for the FCC-ee.

INTRODUCTION

An electro-optical near-field monitor can be used as a non-destructive method to measure the longitudinal bunch profile at high resolution and high repetition rate. The Karlsruhe Research Accelerator (KARA) at KIT has been the first electron storage ring to successfully perform single-shot bunch profile measurements using electro-optical spectral decoding (EOSD) in 2013 [1]. Since then, the setup has been improved to enable observations of the longitudinal electron bunch dynamics on a turn-by-turn basis using the KIT-developed ultra-fast line camera KALYPSO (KArlsruhe Linear arraY detector for MHz rePetition-rate SpectrOscopy) [2]. With a tomographic imaging technique, it is also possible to observe the dynamics of the longitudinal Phase-Space Distribution (PSD) including formation of microstructures caused by the microbunching instability [3]. As a result, EOSD is a promising technique for new particle accelerators like the future circular collider FCC-ee. It can be used as a non-destructive beam diagnostic tool to perform longitudinal bunch profile measurements with sub-picosecond resolution and the potential to observe phase-space dynamics on a microsecond time scale. In context of the Future Circular Collider Innovation Study (FCCIS), an adaption of the KARA EO setup is under investigation to be optimized for FCC-ee beam parameters.

REQUIREMENTS FOR FCC-ee

The FCC-ee is an electron-positron collider planned as a successor to the LHC at CERN with a circumference of around 100 km that operates at 4 different energies for precision measurements of different elementary particles [4].

Table 1: Comparison of KARA in Low-Alpha Mode and Extrema of FCC-ee Parameters (Based on 2 IP layout [5])

	KARA low-alpha mode	FCC-ee extrema
Beam energy / GeV	1.3	182.5
Bunch charge / nC	2.2	38.0
Bunch length / mm	3	12.1

It starts with a centre-of-mass energy at the Z-boson pole of 45.6 GeV and increases later to the WW threshold, ZH production peak and finally the $t\bar{t}$ threshold at 182.5 GeV. In order to achieve high luminosities, the accelerator holds up to 12 000 bunches in which the number of particles is held constant with top-up injection [5]. This requires monitoring of the bunch profile and its center of charge for every bunch. EOSD has the potential to fulfill these requirements, but a detailed investigation is needed to adapt the setup at KARA to the demanding FCC-ee beam parameters.

A comparison of the most interesting parameters for EOSD measurements of KARA and FCC-ee are presented in Table 1, where the extrema out of all operation modes of FCC-ee are shown.

EO NEAR-FIELD SETUP AT KARA

The EO near-field setup at KARA is driven by a 1030 nm laser producing chirped ultra-short pulses in the range of some 10 fs. The modulation and detection of the laser pulse, which enables the measurement of the electron bunch profile, can be divided in three major steps as shown in Fig. 1.

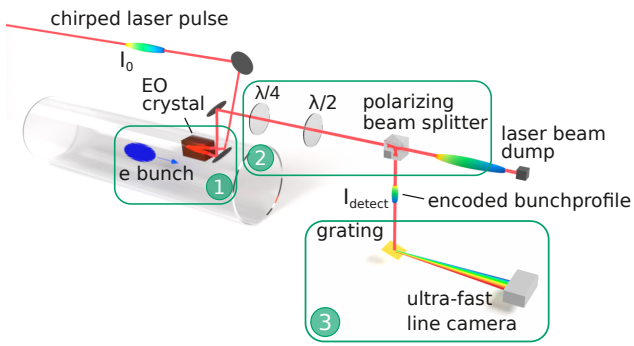

Figure 1: Scheme of the EO setup. Adapted from [3].

At first, the bunch profile is encoded in the polarization of the laser pulse. This is caused by the Pockels effect, where the birefringence of the crystal changes proportional to the

* micha.reissig@kit.edu
† Now at MAX IV Laboratory, Lund, Sweden

ISBN: 978-3-95450-227-1 ISSN: 2673-5490 doi:10.18429/JACoW-IPAC2022-MOPOPT026

BEAM DIAGNOSTICS FOR THE STORAGE RING OF THE cSTART PROJECT AT KIT

D. El Khechen*, E. Bründermann, A. Mochihashi, M.-D Noll, A. Papash, R. Ruprecht, M. Schuh, P. Schreiber, J.L. Steinmann and A.-S. Müller,
Karlsruhe Institute of Technology, Karlsruhe, Germany

Abstract

In the framework of the compact STorage ring for Accelerator Research and Technology (cSTART) project, which will be realized at Karlsruhe Institute of Technology (KIT), a Very Large Acceptance compact Storage Ring (VLA-cSR) is planned to study the injection and the storage of 50 MeV, ultra-short (sub-ps) electron bunches from a laser plasma accelerator (LPA) and the linac-based test facility FLUTE. For such a storage ring, where a single bunch with a relatively wide range of bunch charge (1 pC - 1000 pC) and energy spread (10^{-4} - 10^{-2}) will circulate at a relatively high revolution frequency (7 MHz), the choice of beam diagnostics is very delicate. In this paper, we would like to discuss several beam diagnostics options for the storage ring and to briefly report on several tests that have been or are planned to be realized in our existing facilities.

INTRODUCTION

A lot of R&D studies nowadays are being conducted on new ideas and technologies for future light sources. In this context, KIT plans to build a large acceptance storage ring to demonstrate the injection and storage of ultra-short and LPA-like electron bunches. The research and studies on this project will be exploited for the development of the infrastructure and technology for compact LPA-based future light sources.

The cSTART project (see Fig. 1) employs two different injectors, which will provide ultra-short bunches: the KIT photoinjector FLUTE [1] and an LPA injector [2]. The electron bunches will be transported from the two different electron sources to the storage ring at 3 m height via a transfer line [3]. The storage ring consists of four double-bend-achromat (DBA) arcs with 45° bending magnets [4], separated by four straight sections, amongst which two have space available for one RF station per section, one section will be dedicated for the injection and the other one for beam diagnostics. The magnetic elements in the arc are very close to each other and might be realised e.g. as solid blocks (adopting the MAX-IV magnetic design [5]), leaving nearly no space for beam diagnostics in the arcs. This along with other bunch parameters, e.g. bunch charge, bunch length, repetition rate (see Table 1), bring some challenges when choosing the type and the design of diagnostic tools in the arc, and impose high-standard requirements on dynamic ranges and electronics. In this paper, we will give an overview of the most important beam diagnostics planned for the cSTART storage ring and highlight the challenges of some existing designs. Furthermore, we will point out few experimental tests which are and will be taking place at our KIT facilities to test some of these diagnostics.

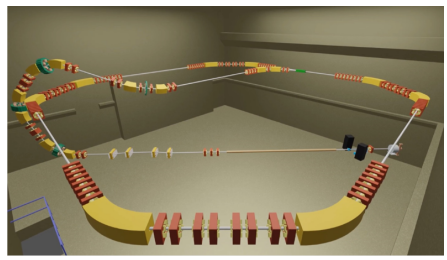

Figure 1: A 3D artistic view of the whole cSTART project: sextupoles and octupoles and the LPA injector are not included, courtesy to J. Schäfer

Table 1: Important Beam Parameters of the cSTART Storage Ring

Parameter	Value
Operation mode	single bunch
Energy	50 MeV
Revolution frequency	7 MHz
Bunch charge	1 pC to 1000 pC
Bunch length	10 fs to 1000 fs
Momentum acceptance	± 5.5%
SR losses/turn	< 1 eV
Energy spread	0.01% - 1%
Lifetime	from 100 ms to 10 s

A DESCRIPTION OF THE DIFFERENT DIAGNOSTICS TOOLS

In the very first stages of running a new machine, many unknowns will be encountered. The very important role of the beam diagnostics tools is to unmask the conditions of the machine and to help improve the operation efficiency. Within the project, we aim to perform turn-by-turn, as well as bunch-by-bunch, measurements of the beam parameters. In this section, we will discuss mainly the most important beam diagnostics tools for early stage commissioning and we will comment on the challenges of their application and design.

* dima.khechen@kit.edu

ISBN: 978-3-95450-227-1 ISSN: 2673-5490 doi:10.18429/JACoW-IPAC2022-MOPOPT027

TRANSVERSE AND LONGITUDINAL PROFILE MEASUREMENTS AT THE KARA BOOSTER SYNCHROTRON

D. El Khechen*, E. Blomley, E. Bründermann, E. Huttel, A. Mochihashi, M.-D. Noll, R. Ruprecht, M. Schuh, P. Schreiber, J.L. Steinmann, C. Widmann and A.-S. Müller,
Karlsruhe Institute of Technology, Karlsruhe, Germany

Abstract

In the booster synchrotron of the Karlsruhe Research Accelerator (KARA), the beam is injected from the microtron at 53 MeV and ramped up to 500 MeV. Though the injected beam current from the microtron to the booster seems good, the injection efficiency into the booster is currently low due to various effects. Consequently, an upgrade of the whole beam diagnostics system is taking place in the booster, in order to improve the injection efficiency through understanding the loss mechanisms and the behavior of bunches. Among these diagnostics tools are beam loss monitors, a transverse profile monitor and a longitudinal profile monitor. In this paper, we will describe the setups used for bunch profile measurements in both transverse and longitudinal planes and report on first data analysis results.

INTRODUCTION

The injection complex of KARA [1](see Fig. 1) consists of a thermal DC electron gun (CW and pulsed mode), which generates a 90 keV electron beam, a racetrack microtron, which increases the beam energy to 53 MeV, and an injection line, which transports the beam to the booster where it is injected off-axis on a multi-turn scheme. The booster then ramps up the beam energy from 53 MeV up to 500 MeV in a cycle of 1 s. The booster parameters are summarized in Table 1. Recently, an upgrade of the booster's diagnostics system took place. This includes the installation of a new beam position monitor (BPM) readout electronics based on Libera Spark [2], a Dimtel Bunch-By-Bunch feedback system [3] in both horizontal and vertical planes, four Libera beam loss scintillators [2] near the injection and extraction septa, a CCD camera for transverse profile measurements and the preparation of infrastructure and equipment for longitudinal profile measurements. Moreover, various measurements and beam diagnostics tests are planned in the booster to predict the expected behaviour of some diagnostic tools in cSTART [4], a KIT project. In the following, we will describe the experimental setups for transverse and longitudinal profile measurements and report on recent results.

TRANSVERSE PROFILE MEASUREMENTS

Two synchrotron light ports (vacuumed) exist in the booster on two bending magnets, one after the injection point and one after the extraction point. For our transverse profile measurements we used the optical window near to the injection point, on which we mounted directly a prism and a CCD camera at 90° (see Fig. 2). The CCD camera is powered with a power-over-ethernet (PoE) scheme and synchronized to the injection trigger. We used two types of filters, a neutral-density (ND) filter and a broadband filter (model: FB500-40 [5]) for the transmission of green light in the range of 480 nm to 530 nm. It is worth mentioning that these filters needed to be removed when taking data at the fixed energy of 53 MeV, as due to the lower critical frequency of the SR radiation at injection energy the intensity of the radiation in the spectral range of the camera was too low with the filters. Furthermore, to avoid saturation

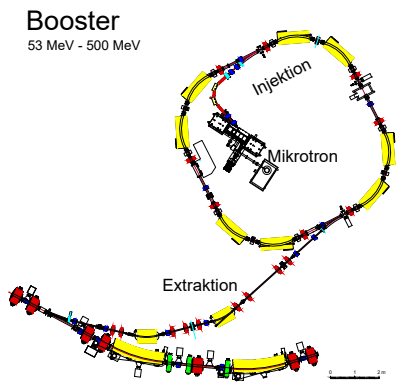

Figure 1: The schematic of the injection complex of KARA storage ring. Courtesy of U. Herberger, KIT.

Table 1: Important Parameters of the KARA Booster Synchrotron

Parameter	KARA booster
Filling pattern	CW or single bunch
Energy	53 MeV to 500 MeV
Circumference	26.4 m
Revolution frequency	11.36 MHz
RF frequency	499.74 MHz
Harmonic number	44
Beam current	5 mA

* dima.khechen@kit.edu

ISBN: 978-3-95450-227-1 ISSN: 2673-5490 doi:10.18429/JACoW-IPAC2022-MOPOPT028

BEAM DIAGNOSTICS AND INSTRUMENTATION FOR MESA*

M. Dehn†, K. Aulenbacher[1,2], J. Diefenbach, F. Fichtner, P. Heil, R. Heine,
R. Kempf, C. Lorey, C. Matejcek, JGU, Johannes Gutenberg-Universität Mainz, Germany
[1]also at HIM, Helmholtz-Institut Mainz, Germany
[2]also at GSI, Helmholtzzentrum für Schwerionenforschung, Darmstadt, Germany

Abstract

For the new Mainz Energy recovering Superconducting Accelerator (MESA) a wide range of beam currents is going to be used during machine optimization and for the physics experiments. To be able to monitor beam parameters like beam current, phases and beam positions several different kinds of beam instrumentation is foreseen. Some components have already been tested at the Mainz Microtron (MAMI) and others have been used at the MELBA test accelerator. In this paper we will present the current status of the instrumentation.

INTRODUCTION

During different phases of operation (optimization, experimental beam time, machine test and diagnostics) the beam diagnostics systems have to deliver important information about the state of the accelerator. It may be helpful to selectively record rarely occurring phenomena with high time resolution while during experimental beam times the same monitors should deliver continuous data streams for offline data analysis.

In the following section the most important requirements to operate the accelerator and to provide important data for the experiments are presented.

Beam Diagnostics

The beam position relative to the reference particle can be described by three coordinates x, y and phase ϕ along with their corresponding x', y' and energy deviation ΔE to propagate the coordinates along the different elements of a beam line. It is also important to monitor the dimensions σ_x and σ_y of the bunch in each coordinate and the density distribution σ_ϕ and energy spread σ_E.

This can be achieved by using different kinds of beam monitors. A rough overview for the placement of beam position monitors (either screens or radio frequency monitors) and phase/intensity RF monitors is illustrated with red dots in Fig. 1.

The following sections will give an overview about the instrumentation at MESA.

Screens and Wire Scanners

At MESA different kind of screens will be used. The most important ones are installed within the MESA low energy beam line (MELBA). The design of the devices as shown in

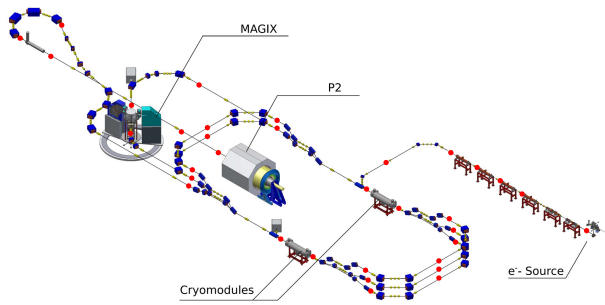

Figure 1: Placement of most important diagnostics at MESA. The red dots mark possible installation locations for diagnostic systems (screens, wire scanners, RF monitors).

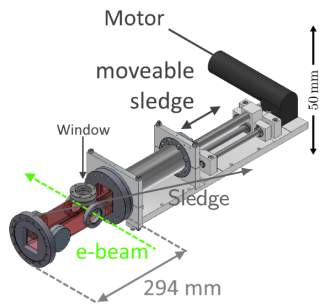

Figure 2: CAD drawing of the scanners used in MELBA to hold a view screen and wires from profile measurements.

Fig. 2 combines a view screen (luminescence or transition radiation) and wires to be able to image the beam spot and measure the dimensions with a very good resolution [1].

Radio Frequency Monitors

Bunched beams induce electromagnetic fields along the beam pipe which can be used to monitor some beam parameters. To amplify the signal output usually cavities can be used where the beam excites resonant fields at harmonic frequencies of the bunch repetition rate. To reduce the size of the installed cavities at MESA the second harmonic (i.e. 2.6 GHz) will be used.

RF cavity monitors have a limited time resolution depending on the loaded quality factor Q_L of the resonant system. Individual bunches cannot be resolved by such types of monitors, only short bunch trains with a minimum spacing of several 10 ns can be distinguished [2]. The signals also do not contain information about the distribution of the measured parameter (i.e. only horizontal position but not the horizontal beam size). It is not possible to distinguish the accelerated and the decelerated beam in CW mode.

* Work supported by PRISMA and the German federal state of Rheinland-Pfalz
† dehn@kph.uni-mainz.de

ISBN: 978-3-95450-227-1 ISSN: 2673-5490 doi:10.18429/JACoW-IPAC2022-MOPOPT029

LONGITUDINAL PHASE SPACE BENCHMARKING FOR PITZ BUNCH COMPRESSOR

A. Lueangaramwong*, N. Chaisueb, O. Lishilin, X. Li, P. Boonpornprasert, M. Krasilnikov, Z. Aboulbanine, G. Adhikari, N. Aftab, G. Georgiev, J. Good, M. Gross, C. Koschitzki, D. Melkumyan, H. Qian, G. Shu, G. Vashchenko, T. Weilbach, F. Stephan, DESY Zeuthen, Zeuthen, Germany

Abstract

The longitudinal phase space characteristics of space-charge dominated electron beams are keys to achieving bunch compression for the accelerator-based THz source at the Photo Injector Test facility at DESY in Zeuthen (PITZ). Such a THz source is proposed as a prototype for an accelerator-based THz source for pump-probe experiments at the European XFEL. A start-to-end simulation has suggested the settings of the phase of booster linear accelerator manipulating longitudinal beam characteristics to optimize the performance of the THz FEL. Although beam diagnostics after compression at PITZ are limited, the longitudinal beam characteristics as a function of the booster phase have been measured and compared with the corresponding simulations. The benchmark involves measurements of longitudinal phase space distribution for bunch charges up to 2 nC. The measurement technique assigned uses 50-μm slits to achieve higher momentum and time resolution (1.8 keV/c and 0.5 ps, respectively).

INTRODUCTION

The Photo Injector Test Facility at DESY in Zeuthen (PITZ) is established for the commissioning and testing of electron sources with various diagnostic systems from measurement of beam charge, beam momentum to transverse and longitudinal phase space characterization [1]. At PITZ, an accelerator-based THz source prototype for pump-probe experiments at the European XFEL is under development to achieve a THz Self-amplified spontaneous emission (SASE) free electron laser (FEL) [2]. A bunch compressor using a magnetic chicane has been considered as an additional part of the prototype to provide an alternative option using ~17 MeV/c electron beams with bunch charge under 2.5 nC and an average bunch current near 200 A [3, 4]. Moreover, it has been foreseen for other applications at PITZ such as seeded FEL, superradiant radiation, etc.

The chicane consists of four rectangular dipole magnets identical in strength and dimensions. In order to fit in the available space of the original PITZ beamline components, this chicane has a vertical bending plane with an angle of 19 degrees, and its estimated R_{56} is 0.215 m. Furthermore, the performance of the PITZ bunch compression affected by coherent synchrotron radiation (CSR) effects is studied via start-to-end beam dynamics simulation combining the use of programs ASTRA [5], OCELOT [6], and IMPACT-t [7].

* anusorn.lueangaramwong@desy.de

In [4], simulation results of fully-compressed electron bunch with different corresponding booster phases ϕ_2 for an initial Gaussian laser pulse with a pulse length of 8 ps in full width at half maximum (FWHM) are discussed. The booster phase becomes a beam-momentum-chirp tuning knob to optimize the performance of the SASE FEL and the other applications.

A challenge arises as the bunch compressor is installed downstream of a longitudinal bunch profile measurement station [8]. In other words, experimental results of the bunch profile after compression are not able to be measured. Thus, a measurement plan has been initiated to benchmark the simulation results. In the plan's first step, the beam momentum chirps dp/dt (with different booster phases) prior to the chicane are measured to benchmark ASTRA simulations. In the second step, a coherent transition radiation (CTR) measurement station will be installed between the chicane and LCLS-I undulator [2, 8]. The CTR measurement is expected to indicate the fully-compressed-bunch booster phases for the beam with bunch charge up to few hundred pC.

This paper discusses the first step of the measurement plan, which implies a characterization of the beam longitudinal phase space (LPS) distribution.

LONGITUDINAL PHASE SPACE MEASUREMENT

An LPS measurement setup at PITZ consists of a transverse deflecting system (TDS) and a dipole spectrometer (HEDA2), respectively (see details in [9, 10]). Note that the TDS is located between the CDS booster cavity and the chicane; see LPS measurement scheme at PITZ in Fig. 1, and longitudinal positions of the TDS, the HEDA2, and the chicane in Table 1.

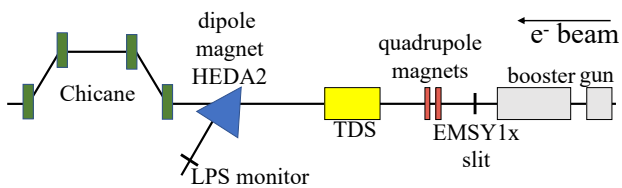

Figure 1: Longitudinal phase space measurement scheme at PITZ.

According to Table 1, the distance between the TDS and HEDA2 is approximately 7 m. Thus, it is considered that the space charge effects cause a significant change in the LPS of the beam, thereby modifying the momentum chirp. This

ISBN: 978-3-95450-227-1 ISSN: 2673-5490 doi:10.18429/JACoW-IPAC2022-MOPOPT031

RENOVATION OF THE SR BEAM PROFILE MONITORS WITH NOVEL POLYCRYSTALLINE DIAMOND MIRRORS AT THE SuperKEKB ACCELERATOR

G. Mitsuka*, T. Mitsuhashi, H. Ikeda, KEK, 1-1 Oho, Tsukuba, Ibaraki 305-0801, Japan

Abstract

Synchrotron radiation (SR) beam profile monitors are fundamental to performing the stable beam operation of SuperKEKB. To suppress thermal deformation of SR extraction mirrors, a long-standing issue in SR monitors, we developed platinum-coated diamond mirrors in 2019. The diamond mirrors were made with an optical-quality polycrystalline-diamond substrate with extremely high thermal conductivity and have a size of 20 mm (W) × 30 mm (H) × 1.2 mm (D). We found surface flatness better than $\lambda/5$ in optical testing with a laser interferometer. The diamond mirrors have been installed in HER and LER in the 2020 summer and 2021 summer, respectively. Though irradiation for a year at the beam current greater than 1050 mA, we found no significant deformation of the diamond mirrors.

INTRODUCTION

Synchrotron radiations produced from the 5 mrad bends are emitted into the 23 m away extraction mirrors in each of the straight sections of the positron Low Energy Ring (LER) and the electron High Energy Ring (HER). Table 1 summarizes the source bend parameters in SuperKEKB. SR visible lights reflected by the extraction mirrors are further relayed 30 m into the corresponding optics hut above ground. SR beam profile monitors, such as interferometers and streak cameras, are located in each optics hut. For the use of the SR visible lights, thermal deformation of the extraction mirrors has been a long-standing problem not only at the preceding KEKB collider [1] but also at many synchrotron radiation facilities. Thermal deformation of the beryllium extraction mirrors at KEKB was so significant that one needed real-time measurements and complicated compensations of the distortion to correct for the beam-current dependence of the measured beam size.

Table 1: SR Source Parameters in LER and HER at SuperKEKB

Parameters	LER	HER
Energy (GeV)	4	7
Current (A)	3.6	2.6
Bending radius (m)	177.4	580
SR power (W/mrad)	72	149

Since the beginning of SuperKEKB, we have used the single-crystalline diamond mirrors to deal with even higher SR heat loads expected due to twice the beam currents than KEKB [2]. Single-crystalline diamond has extremely high heat conductivity and a lower thermal expansion coefficient than beryllium. As presented in Ref. [2], we found the thermal deformation of the first generation diamond mirrors seemed satisfactory below 900 mA, horizontally < 1 % and vertically < 4 % compared with that at zero current. However, at the designed current 2.6 A in HER, the deformation was expected to increase up to 2.5 % and 10 % and come to require unwanted compensations as we did in KEKB. In addition to the current-dependent tilt, we found some initial deformation along the horizontal direction: a cylindrically-curved surface with the cylindrical axis in the vertical direction.

To further suppress the thermal deformation of SR extraction mirrors, we developed the second-generation diamond mirrors in 2019. Hereafter, we see the design and construction of platinum-coated polycrystalline-diamond mirrors and current-dependent deformation measurements by a Hartmann test using a square array screen.

POLYCRYSTALLINE DIAMOND MIRRORS

Single-crystalline diamond mirrors previously used in SuperKEKB in 2016-2019 showed the thermal deformation of a few percent levels at < 900 mA relative to that at zero current. Though we did not yet analyze it in detail, the initial surface flatness was roughly a level of λ. These two rather unsatisfactory performances were caused by, primarily the structure consisting of six 10 mm × 10 mm single-crystalline sections fused at each edge, and second a thinner diamond substrate of 0.5 mm [2].

On the other hand, we made a new diamond mirror (20 mm (W) × 31 mm (H)) based on a polycrystalline diamond substrate having no connected subsection. A single substrate should improve surface flatness. The polycrystalline diamond we use in SuperKEKB has thermal conductivity 1800 W/mK at 300 K which is comparable to that of a polycrystalline diamond 2000 W/mK. Also, we changed the surface coating material to platinum which had 20 % higher reflective coefficient at < 500 nm than the gold used in the previous mirrors.

MIRROR HOLDER

The mirror holder is a water-cooled split cylinder of copper. The right panel of Fig. 1 shows the mirror mounted in water-cooled copper holder. The holder grips the mirror on one edge only to minimize applying extraneous strain to the mirror surface due to the thermal deformation of the copper holder itself. The use of copper enables good heat-sinking contact with the portion of the mirror surface gripped within

* gaku.mitsuka@kek.jp

ISBN: 978-3-95450-227-1 ISSN: 2673-5490 doi:10.18429/JACoW-IPAC2022-MOPOPT032

IMPROVEMENT OF MATCHING CIRCUIT FOR J-PARC MAIN RING INJECTION KICKER MAGNET

T. Sugimoto*, K. Ishii, T. Shibata, S. Iwata, H. Matsumoto, KEK, Tsukuba, Japan

Abstract

This paper describes the improvements achieved in the impedance matching circuit for the 1.3 MW beam operation of the Japan Proton Accelerator Complex main ring injection kicker magnet. In this regard, the number of paralleled resistors was doubled, and the volume of each resistor was enlarged 2.6 times to lower the temperature of the resistors under the higher repetition rate pulse excitation. In addition, the resistor cylinders were filled with ceramic-based beads of 3 mm diameter to increase the heat conductivity. Moreover, an aluminum-made water-cooled heat sink was attached to the resistors directly, and an air-cooling fan was mounted on the side of the box containing the resistors. All resistors and their support structure in the matching circuit were replaced in May 2022. The temperature increment of resistors during continuous pulse excitation was measured using a thermography camera, and the measured value was compared with numerical calculations. Finally, the prediction results related to the beam image current obtained with the simulation model were discussed.

INTRODUCTION

J-PARC (Japan Proton Accelerator Complex) consists of three accelerators, a 400-MeV Linac, a 3-GeV Rapid Cycle Synchrotron (RCS), and a 30-GeV Main Ring (MR). The MR provides a high-intensity proton beam to the long baseline neutrino experiment (T2K) and the hadron experiments. In 2019, the beam intensity provided to the neutrino experiment was 495 kW corresponding to 2.56 $\times 10^{14}$ proton per pulse (ppp) for a repetition rate of 2.48 s [1]. However, a stable operation for high-intensity beams is required to achieve an accurate measurement of the neutrino oscillation and observe the neutrino CP violation. In particular, in the late 2020s, high intensity operation of 1.3 MW beam power will be achieved by shortening the repetition period from 2.48 sec to 1.16 sec and increasing the number of protons from 2.4 $\times 10^{14}$ to 3.34 $\times 10^{14}$ ppp [2, 3]. Including the margin, the hardware is developed to operate within a repetition period of 1 s. Proton beams extracted from the RCS were injected into the MR by four kicker magnets [4–6]. The harmonic number of the MR is nine. One RF bucket was left empty for the extraction kickers to ease the requirement of the field rise time. Four successive batches from the RCS were injected into the MR to fill 8 RF buckets spaced at 300 ns interval. Circulating bunches were deflected additionally by the residual field of the reflection pulses. It caused the coherent oscillation which induced the beam loss during the injection period. Thus, an impedance matching circuit should be implemented in the injection kicker magnet to reduce the reflection pulses. The circuit consists of a non-inductive ceramic resistor [7] and a high voltage ceramic capacitor. These elements are contained in the dedicated steel-made boxes. A maximum temperature of the resistor is recommended to operate within 150 °C to prevent degrading of the resistance. However, previous studies have suggested that the temperature of the resistor exceeded 350 °C during the continuous 1.3 MW operation [8, 9]. Therefore, a large diameter ceramic resistor should be developed to lower the temperature, and these larger ceramic resistors were installed into new boxes in May 2022. In this report, the new resistor and the matching circuit are detailed, and the temperature measurements are reported.

MATCHING CIRCUIT REPLACEMENT

Resistors

Figure 1 shows the equivalent circuit of the injection kicker magnet. The impedance matching resistor R_1 is connected to the kicker coil L_1 to reduce the reflection pulse. The resistance is 9.3 Ω, optimized by measuring the pulse shape [6]. Fifteen non-inductive ceramic resistors are connected in parallel (called "resistor-unit"). The resistors unit is contained in an individual box settled on the vacuum chamber (named the "matching box"). Resistors (R_2) and capacitors (C_2) are connected to the coil in parallel both to reduce the beam coupling impedance [4, 5] and to match the impedance for the high frequency region. The resistor electrodes were brazed at both ends of the conductive ceramics to avoid discharge [7]. The typical excitation current of the pulse is 2640 A, and the pulse width is 1.5 μsec. The pulse energy is approximately 100 J. A pulse was fed into the coil to deflect the orbit of 2 bunches to the circular orbit. The kicker magnet was excited in four times during the injection period to inject in total 8 bunches in the MR. When the circulating beam passes through the kicker aperture, an image current flows through the coil. Subsequently, the current flows in the matching circuit connected to the coil (i.e., R_1, R_2 and C_1). Therefore, the resistor R_1 is heated by both the excitation pulse current and the beam image current, while the resistor R_2 is heated only by the beam image current. The temperature rise of the resistor ΔT can be estimated as follows:

$$\Delta T = \frac{1}{N}\frac{Q_{pulse} + Q_{beam}}{hA} \quad (1)$$

$$= \frac{1}{NhA}\left(\int I^2(t)dt\frac{R}{T_{rep}} + \int E_b(t)dt\right) \quad (2)$$

where N is the number of resistors connected in parallel, Q_{pulse} is the power of the excitation pulse of the kicker magnet, Q_{beam} is the power of the beam image current, h is the

* takuya.sugimoto@j-parc.jp

ISBN: 978-3-95450-227-1 ISSN: 2673-5490 doi:10.18429/JACoW-IPAC2022-MOPOPT033

STUDY OF CHRENKOV DIFFRACTION RADIATION FOR BEAM DIAGOSTICS*

H. Hama†, K. Nanbu,
Research Center for Electron Photon Science, Tohoku University, Sendai, Japan

Abstract

Vavilov-Cherenkov diffraction radiation (ChDR) has been paid attention to non-beam-destructive diagnostics [1,2,3]. The physical understanding of ChDR is, however, not well satisfied yet because precise experimental measurement is not much easier than one expects. Although we do not deny the Cherenkov radiation and ChDR are fully explained by the classical electromagnetism, we encounter a couple of difficulties in actual applications. For instance, the theory is usually established for the far-field observation, in spite of that the radiation is often observed near-field in the realistic beam diagnostic tools employing photon measurements. In addition, the theory, as a matter of course, includes some assumptions which is sometimes not valid for the specific experiments. We have carried out test experiments for observation of coherent ChDR in a THz frequency region emitted from ultra-short electron bunches supplied by the t-ACTS accelerator at Tohoku University [4]. In this manuscript, a concept of ChDR as a probe of the beam diagnostics is discussed and some experimental results are shown.

INTRODUCTION

Diffraction radiation (DR), which is emitted from charged particles passing through in the close vicinity of a metallic or dielectric medium, is a beam diagnostic probe without beam interception [5,6]. Considering the beam is passing through the centre of a circular aperture in a screen perpendicular to the beam trajectory, radiation cones appear in both backward and forward directions with an opening angle of ~1/γ with the relativistic factor γ of charged particle. The backward DR is a reflected electromagnetic field of the beam itself, it can be teared off from the beam line by tilting the screen. The backward DR is often used as beam diagnostic tools. However, the opening angle is still very small. According to the theoretically deduced DR intensity [7], the well-known Ginzburg-Frank formula for transition radiation (TR) is attenuated in accordance with an aperture radius function K [8,9],

$$K = \exp\left(-2\xi\right) \text{ with } \xi \equiv \frac{h\omega}{\beta\gamma c}, \tag{1}$$

where ω, β and c are the angular frequency of the radiation, the relative velocity of the charged particle and the velocity of light. The aperture radius, h, is therefore an impact parameter that is a distance between the charged particle and the boundary of medium. The function $K(\xi)$ is usually called the coupling factor, and it should be noted that the Eq. (1) is valid for $\xi \gg 1$, and in case of $\xi \ll 1$, K~1.

Here we consider a cylindrical hollow dielectric for a ChDR radiator as shown in Fig. 1. Cherenkov angle, the opening angle of Cherenkov radiation (CR), is given by

$$\cos\theta_C = \frac{1}{n\beta}. \tag{2}$$

The refractive index n of dielectric medium is usually larger than 1, so that the larger opening angle can be obtained. Since the manner of the coupling factor K is essentially identical for the ChDR, the radiation intensity may depend on the azimuthal angle because the distance between the beam and the inner wall surface of dielectric dominates K, so that it would be expected an azimuthal angle dependence of ChDR contains information of the beam position inside of the aperture.

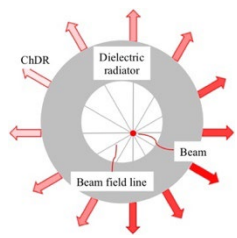

Figure 1: Cross section view of cylindrical hollow radiator and ChDR.

THEORETICAL BACKGROUND

Intensity of CR

The speed of light in the dielectric medium is varied as $c_n = c/n$ and the relative velocity of the particle becomes $\beta_n = n\beta$. Evaluating the Lienard-Wiechert potential with some math, the intensity of CR per unit frequency and per unit solid angle is written as,

$$\frac{d^2W}{d\omega d\Omega} = \frac{\mu_0}{4\pi}\frac{e^2\omega^2}{4\pi^2 c_n}\sin^2\theta\left(\frac{\sin\alpha}{\alpha}\right)^2(\Delta z)^2, \tag{3}$$

with

$$\alpha = \frac{1}{2}\left(1-\beta_n\cos\theta\right)\omega\Delta t \tag{4}$$

where μ_0, e, Δz and Δt are magnetic permeability in the vacuum, elementary charge, trajectory length of the particle in the dielectric and its duration, respectively. Eq. (3) is consistent with Tamm's formula [10]. One can find the CR intensity is roughly proportional to the square of the particle trajectory length, which is preferable for beam diagnostics because the intensity can be enhanced by using a long dielectric radiator. Although one can simply

* Work supported by JSPS KAKENHI grant number 22K12660 and 18K11915.
† hama@lns.tohoku.ac.jp

ISBN: 978-3-95450-227-1 ISSN: 2673-5490 doi:10.18429/JACoW-IPAC2022-MOPOPT034

SURROGATE-BASED BAYESIAN INFERENCE OF TRANSVERSE BEAM DISTRIBUTION FOR NON-STATIONARY ACCELERATOR SYSTEMS

H. Fujii*, N. Fukunishi, RIKEN Nishina Center, Wako, Japan
M. Yamakita, Tokyo Institute of Technology, Meguro-ku, Japan

Abstract

Constraints on the beam diagnostics available in real-time and time-varying beam source conditions make it difficult to provide users with high-quality beams for long periods without interrupting experiments. Although surrogate model-based inference is useful for inferring the unmeasurable, the system states can be incorrectly inferred due to manufacturing errors and neglected higher-order effects when creating the surrogate model. In this paper, we propose to adaptively assimilate the surrogate model for reconstructing the transverse beam distribution with uncertainty and under-specification using a sequential Monte Carlo from the measurements of quadrant beam loss monitors. The proposed method enables sample-efficient and training-free inference and control of the time-varying transverse beam distribution.

MATHEMATICAL BACKGROUND

Accelerator Systems with Unknown Drift and Parameter Uncertainties

The dynamical system of the accelerator with measurement error can be written as

$$\dot{\boldsymbol{x}} = f(\boldsymbol{x}, \boldsymbol{u}) \quad (1)$$
$$\boldsymbol{y} = h(\boldsymbol{x}, \boldsymbol{u}) + \boldsymbol{\epsilon}, \quad (2)$$

where $\boldsymbol{x} \equiv \boldsymbol{x}(t) \in \mathbb{R}^n$ is the vector of the time-varying hidden states, $\boldsymbol{u} \in \mathbb{R}^m$ is the control input state, t is the time. $\boldsymbol{y} \in \mathbb{R}^d$ is the measurement, and $\boldsymbol{\epsilon} = [\epsilon_1, ..., \epsilon_d]^T$ is the independent measurement noise.

To produce a quality beam of interest by inferring hidden states $\boldsymbol{x}$, we introduce a surrogate model as

$$\dot{\hat{\boldsymbol{x}}} = \hat{f}(\hat{\boldsymbol{x}}, \boldsymbol{u}) \quad (3)$$
$$\hat{\boldsymbol{y}} = \hat{h}(\hat{\boldsymbol{x}}, \boldsymbol{u}), \quad (4)$$

where $\hat{\boldsymbol{x}} \equiv \hat{\boldsymbol{x}}(t) \in \mathbb{R}^n$, and $\hat{\boldsymbol{y}} \in \mathbb{R}^d$ are the counterpart of the real system Eq. (1)(2) built based on the parameterized system model. One may infer the hidden state by simply minimizing the loss function

$$C(\boldsymbol{y}) = \|\boldsymbol{y} - \hat{\boldsymbol{y}}\|_2^2. \quad (5)$$

However, the accurate state $\boldsymbol{x}$ cannot be necessarily obtained due to the model uncertainties and possible multiple hidden states when the measurement is sparse. The goal of the following Approximate Bayesian Computation (ABC) framework [1] is to sequentially filter and track the time-varying hidden state estimates $\hat{\boldsymbol{x}}$ by minimizing the expectation of the cost function in Eq. (5) throughout the operation of the accelerator complex.

* hiroki.fujii@riken.jp

Markov-Chain Monte-Carlo (MCMC) for the Initial Posterior Inference

Given an observation $\boldsymbol{y}$, the initial posterior distribution of interest for a given fixed control input $\boldsymbol{u}$ can be given by

$$p(\hat{\boldsymbol{x}}|\hat{\boldsymbol{y}}) = \frac{p(\hat{\boldsymbol{y}}|\hat{\boldsymbol{x}})p(\hat{\boldsymbol{x}})}{p(\hat{\boldsymbol{y}})}, \quad (6)$$

here subscripts for denoting the time steps are omitted in this section, e.g., $\hat{\boldsymbol{x}} = \hat{\boldsymbol{x}}_{k=0}$. Since $p(\hat{\boldsymbol{x}}|\hat{\boldsymbol{y}})$ is a probability distribution, we can rewrite this equation as

$$p(\hat{\boldsymbol{y}}) = \int p(\hat{\boldsymbol{y}}|\hat{\boldsymbol{x}})p(\hat{\boldsymbol{x}})d\hat{\boldsymbol{x}}. \quad (7)$$

The probability density function $p(\hat{\boldsymbol{y}})$ given a measurement $\boldsymbol{y}$ with normally distributed sensor noise with standard deviation $\boldsymbol{\sigma}_n = \{\sigma_{n1}, ..., \sigma_{nd}\}$ is expressed as

$$p(\hat{\boldsymbol{y}}) = \prod_j^d \frac{1}{\sqrt{2\pi}\sigma_{nj}} \exp\left(-\frac{|\hat{y}_j - y_j|^2}{2\sigma_{nj}^2}\right) \quad (8)$$

and $p(\hat{\boldsymbol{y}}|\hat{\boldsymbol{x}})$ drawn by surrogate model equation Eq. (4). Then, the proposal $p(\hat{\boldsymbol{x}})$ of a general nonlinear system can be sampled using MCMC [2]. In this work, the parallel tempering MCMC (PT-MCMC) algorithm is adopted to efficiently find the optimal and promote mixing across the state spaces. Details on PT-MCMC can be found in [3].

Particle Filtering for Tracking Hidden States

The sequential importance resampling is a class of particle filter algorithm. The sequence is initialized with a set of N particles representing $p(\hat{\boldsymbol{x}})$, and assign the normalized weights $W_{k=1}^s = 1/N$, for all $s = 1, ..., N$. Then particles at a discrete time step $k-1$ are sequentially propagated for a new time step k to update prior $p(\hat{\boldsymbol{x}}_k^s|\hat{\boldsymbol{x}}_{k-1}^s, \boldsymbol{u}_{k-1})$. The weight update of s-th particle is performed based on the measurement and cosine similarity

$$p(\hat{\boldsymbol{y}}_k^s|\hat{\boldsymbol{x}}_k^s, \boldsymbol{u}_k, \boldsymbol{u}_{k-1}) \propto \mathrm{sim}_k(\Delta_k\hat{\boldsymbol{y}}^s, \Delta_k\boldsymbol{y}) \prod_j^d \exp\left(-\frac{|\hat{y}_j^s - y_j|^2}{2\sigma_{nj}^2}\right). \quad (9)$$

Here, $\mathrm{sim}_k(\Delta_k^s\hat{\boldsymbol{y}}, \Delta_k\boldsymbol{y})$ is a similarity measure between the responses of the actual system $\Delta_k\boldsymbol{y} \equiv \boldsymbol{y}_k - \boldsymbol{y}_{k-1}$ and the surrogate model $\Delta_k^s\hat{\boldsymbol{y}} \equiv \hat{\boldsymbol{y}}_k^s - \hat{\boldsymbol{y}}_{k-1}^s$ expressed by

$$\mathrm{sim}_k(\Delta_k^s\hat{\boldsymbol{y}}, \Delta_k\boldsymbol{y}) = \begin{cases} \frac{1+\tau(\Delta_k^s\hat{\boldsymbol{y}}, \Delta_k\boldsymbol{y})}{2} & (\|\Delta_k^s\hat{\boldsymbol{y}}\| > 2\sigma_n) \\ 1 & (\|\Delta_k^s\hat{\boldsymbol{y}}\| \leq 2\sigma_n) \end{cases} \quad (10)$$

ISBN: 978-3-95450-227-1 ISSN: 2673-5490 doi:10.18429/JACoW-IPAC2022-MOPOPT037

BEAM MEASUREMENT AND APPLICATION OF THE METAL VAPOR VACUUM ARC ION SOURCE AT KOMAC

S.-H. Lee, H.-S. Kim, H.-J. Kwon†
Korea Multi-purpose Accelerator Complex,
Korea Atomic Energy Research Institute, Gyeongju, Korea
Department of Accelerator and Quantum Beams in Radiation Science,
University of Science and Technology, Daejeon, Korea

Abstract

The metal ion beam facility is developed including the metal vapor vacuum arc (MEVVA) ion source at the KOMAC (Korea multi-purpose accelerator complex). The MEVVA ion source has advantage that it can be extract almost metal ion species as well as high current ion beam. After the installation, we measured beam properties such as the beam profile and peak beam current depending on the operation condition, average charge state and cathode erosion rate. In addition, as one of the application fields, we irradiate the metal beam on the air electrode of the fuel cell and measured the performance. In this paper, the beam measurement results, are summarized and solid oxide fuel cell (SOFC) performances after metal beam irradiation are described.

BACKGROUND

The MEVVA ion source generates metal plasma through vacuum arc discharge between electrode [1]. This kind of ion source does not require gaseous operation to produce metal plasma, and uses bulk metallic cathode [2]. The arc current is concentration at a tiny spot on the cathode surface, it is called a cathode spot. This micro size spot is vaporized and ionized to metal plasma [3]. It can generate almost metal io species in Periodic table [4].

In this work, the possibility is studied that the (SOFC) efficiency improvement through the beam irradiation. Nobel metal ions are difficult to extract ion beam. They are extracted and irradiated on the SOFC. Before the irradiation beam properties are measured such as stability, peak beam current and beam profile. Then the average charge state is estimated to determine the total dose. From the above experimental process, beam properties are checked, and the irradiation condition is optimized to SOFC. The electrochemical performance of irradiated SOFC is analysed and compared through current density-voltage measurement and electrochemical impedance spectrometry (EIS) analysis.

METAL ION BEAM TEST

Stability

The metal ion beam facility is developed including the MEVVA ion source at KOMAC. It consists of the MEVVA ion source, the chamber for beam irradiation, power supplies, evacuation pump, the diagnostic system and remote controller. The integrity of ion beam facility was evaluated using chromium ion species, which is one of the universal species in MEVVA ion source, in previously study [5]. The extraction voltage is stable at the 3.75 kW of arc power. Experimental conditions were 4 Hz of repetition rate, 700 μs of the pulse width and 30 kV of the extraction voltage. When the silver and copper ion beam extract, the fluctuation of extraction voltage is 30.0±2.3% and 29.9±4.7%.

Properties

Beam properties of the silver and copper ion species are measured in the same process as before study. Irradiation parameters will be determined to improve the SOFC. Fig. 1 shows the peak beam current of the silver and copper depending on the arc power and the extraction voltage. The experimental conditions were 4 Hz of repetition rate and 900 μs of pulse width. The peak beam current of both ion species is increased as the arc power and extraction voltage increase.

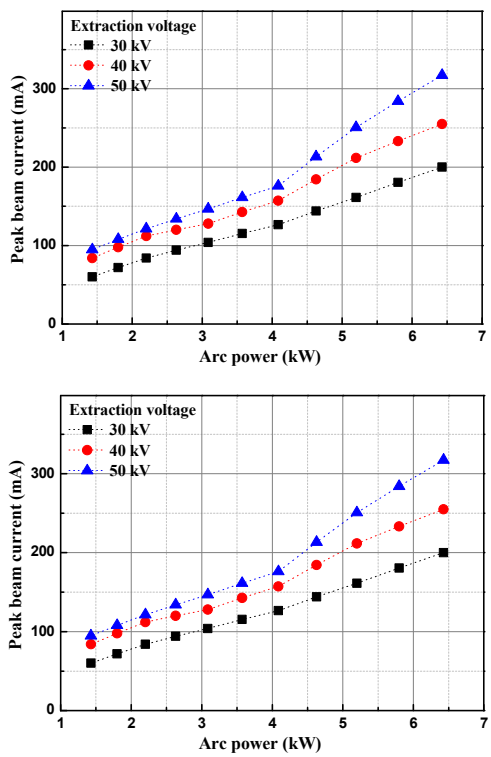

Figure 1: Peak beam current depending on the arc power and extraction voltage (a) silver (b) copper.

Figure 2 shows the beam profile and RMS radius depending on the arc power of silver and copper. The

ISBN: 978-3-95450-227-1 ISSN: 2673-5490 doi:10.18429/JACoW-IPAC2022-MOPOPT038

DEVELOPMENT OF BUTTON BPM ELECTRONICS FOR THE BUNCH BY BUNCH FEEDBACK SYSTEM OF 4GSR

S.W. Jang†, Department of Accelerator Science, Korea University, Sejong, South Korea

Abstract

With the advent of the fourth-generation storage ring, the size of the vertical emittance of the electron beam is expected to be about 100 times smaller than that of the existing generation. By advanced of synchrotron light source performance, the resolution of the beam position monitor (BPM) should also be further improved, and it can be providing a more stable and uniform beam to end station users through improved bunch by bunch (BbB) feedback system compared to a system called turn by turn or fast feed-back [1-4]. A developed BPM electronics for BbB feedback will be installed in Bessy II booster ring at HZB (Helmholtz-Zentrum Berlin) Research Institute in Germany [5]. BbB feedback BPM electronics with an improved three button BPMs will be used to measure beam position resolution and calculate an information for BbB feedback, and then it will apply to the BbB feedback system. In this proceeding, we will describe the development of button BPM electronics for BbB feedback.

INTRODUCTION

Brightness and stability are key specifications of the light source accelerator storage ring. Continuous efforts are made to achieve high current, high brightness and beam stability. The limitation of the performance of storage ring due to coupling impedance is one of issue for the next generation light source accelerator storage ring.

What made the coupled beam instability and how to treat it is a key question that accelerator researcher for light source storage ring around the world must face. Observing and measuring the bunch by bunch beam in real time helps researchers analyze the stored beam status of storage ring. As much as more precise beam bunch measurements for beam position and charge helps to quantitatively study beam impedance, coupling instability, and nonlinear dynamics, and can provide. In particular, bunch by bunch feedback is widely used as a method to solve the transverse coupled beam instability that occurs in many of light source accelerator storage ring.

With the rapid advances of DAQ devices by relate industry companies, the performance of ADC and FPGA systems has improved incredibly. High sampling rates with large memory capacities, multi-channel broadband ADC can be providing an ideal tool for obtaining raw data information of beam signal from BPMs. Bunch-by-Bunch beam position and relative charge can be obtained through the FPGA online algorithm process.

Using the high-performance uTCA board with ADC and FPGA as above, it is intended to implement the BBB feedback system by using the time domain processing (TDP) logic using raw signals without a separate FIR filter and down converting. The most important key element of this system is to obtain the same time resolution and high vertical resolution as the raw signal of the beam from BPM by interpolating the data between insufficient sampling through up-sampling technique using FPGA.

MAIN IDEA OF BBB FEEDBACK ELECTRONICS

The parameters of the BESSY II storage ring and booster ring were used to design the BbB feedback algorithm. HZB also developing their own BbB feedback system based on frequency domain processing (FDP) logic for the storage ring [1]. To compare with frequency domain processing logic, BbB electronics using time domain processing logic and also newly upgraded three beam position monitors are will be installed to booster ring. We will measure beam position resolution by using BbB electronics and three button BPM, after changing the operation mode of the booster to storage ring mode. The main parameters of BESSY II accelerator, which are used for BbB feedback signal processing logic, are summarized in Table 1.

Table 1: Main Parameters of BESSY II ofBooster Ring & Storage Ring

Parameters [unit]	Booster	Storage
Energy [GeV]	0.05 to 1.7	1.7
Circumference [m]	96	240
RF frequency [MHz]	499.622801	499.622801
Beam current [mA]	3	300
Harmonic number	160	400
T_rf [ns]	2.0015	2.0015
Sampling ratio	2048/1020	2048/1025
Sampling freq. [MHz]	1003.16421	988.270728
Sampling time [ns]	0.99684577	1.0017
Rev. frequency [MHz]	3.12264251	1.249057
T_rev [ns]	320.24159	800.603974
Integer sample turns	51	41
Samples/51 or 41 turns	16384	32768

Beam position measurement using TDP has the advantage of analyzing the beam position by using the whole information of the signal output from the beam position monitor as it is without distorting it. However, the RF frequency of a light source accelerator storage ring, such as BESSY II, usually used around 500 MHz, so the length of one bunch signal is about 2 ns. In order to measure a signal

†siwony@korea.ac.kr

ISBN: 978-3-95450-227-1 ISSN: 2673-5490 doi:10.18429/JACoW-IPAC2022-MOPOPT040

SUMMARY OF THE POST-LONG SHUTDOWN 2 LHC HARDWARE COMMISSIONING CAMPAIGN

A. Apollonio, M. Bednarek, O. Andreassen, A. Antoine, T. Argyropoulos, M. Cerqueira Bastos, B. Bordini, K. Brodzinski, A. Calia, Z. Charifoulline, G.-J. Coelingh, G. D'Angelo, D. Delikaris, R. Denz, L. Fiscarelli, V. Froidbise, M.-A. Galilée, J.-C. Garnier, R. Gorbonosov, P. Hagen, M. Hostettler, D. Jacquet, S. Le Naour, D. Mirarchi, V. Montabonnet, B. Panev, T. Persson, T. Podzorny, M. Pojer, E. Ravaioli, F. Rodriguez-Mateos, A. Siemko, M. Solfaroli, J. Spasic, A. Stanisz, J. Steckert, R. Steerenberg, S. Sudak, H. Thiesen, E. Todesco, G. Trad, J. Uythoven, S. Uznanski, A. Verweij, S. Yammine, J. Wenninger, G. Willering, V. Vizziello, D. Wollmann
CERN, Geneva, Switzerland

Abstract

In this contribution we provide a summary of the LHC hardware commissioning campaign following the second CERN Long Shutdown (LS2), initially targeting the nominal LHC energy of 7 TeV. A summary of the test procedures and tools used for testing the LHC superconducting circuits is given, together with statistics on the successful test execution. The paper then focuses on the experience and observations during the main dipole training campaign, describing the encountered problems, the related analysis and mitigation measures, ultimately leading to the decision to reduce the energy target to 6.8 TeV. The re-commissioning of two powering sectors, following the identified problems, is discussed in detail. The paper concludes with an outlook to the future hardware commissioning campaigns, discussing the lessons learnt and possible strategies moving forward.

INTRODUCTION

The LHC underwent an extensive period of maintenance in 2019-2021, the so-called Long-Shutdown 2 (LS2), in preparation for its third beam run (Run 3) in the years 2022-2025. This extensive maintenance involved many systems, related to both the accelerator and the particle detectors.

In particular, for what concerns the LHC superconducting circuits, a significant effort was devoted to the Diode Insulation and Superconducting MAgnet Consolidation (DISMAC) project [1]. Several other interventions took place, including the replacement of 19 LHC dipoles, due to known quench heater failures or high internal splice resistances [2].

Once interventions on the accelerator were finalized, a full re-commissioning of the LHC superconducting circuits for operation at the desired current levels was necessary. The initial energy target for the commissioning campaign was set to 7 TeV, which was then reduced to 6.8 TeV, as explained in detail later in the paper.

POWERING TESTS: STRATEGY

In order to fully qualify the LHC superconducting circuits for safe operation, a well defined sequence of tests needs to be performed. The tests aim at verifying the correct behaviour of the circuits, including both the warm and cold parts, from the powering scheme to the related interlock and protection systems and the ancillary systems. The LHC counts a total of 1572 superconducting circuits, including low-current circuits (60 A, 80-120 A, 600 A) and high-current circuits, i.e. Inner Triplets (ITs), Individually Powered Quadrupoles and Dipoles (IPQs and IPDs), main Dipole and main Quadrupoles (RBs and RQs), with nominal currents ranging from 4 kA to 11.6 kA.

The LHC is divided in 8 powering sectors and 28 powering sub-sectors [3], which can be independently powered and tested. Circuits within a powering sub-sector should in general not be tested in parallel, as interaction between tests may affect the efficiency of the testing process.

The following steps describe the general strategy for the commissioning of the LHC superconducting circuits:

1. Electrical Quality Assurance (ElQA): verification of the electrical integrity of the superconducting circuits before powering [4]
2. Quench Protection System (QPS) tests: verification of the correct detection and reaction to possible magnet quenches before powering
3. Powering Interlock System (PIC) tests: verification with limited or no circuit current of the correct propagation of interlock signals to all the required clients
4. Tests with increasing current levels, defined depending on the circuit type
5. Circuit powering to nominal current (including magnet training, if necessary)
6. Simultaneous powering of all circuits in a powering sub-sector, for validation of their collective behaviour in view of nominal operation
7. Tests of the connections of the PIC with the Beam Interlock System (BIS)

Tests are executed from the CERN Control Center (CCC). They are launched via the Accelerator Test Tracking framework (AccTesting) [5] and executed by the hardware commissioning sequencer.

SCHEDULE EVOLUTION

Based on the testing strategy outlined above, a baseline duration for the tests in each of the eight LHC powering

ISBN: 978-3-95450-227-1 ISSN: 2673-5490 doi:10.18429/JACoW-IPAC2022-MOPOPT041

ARTIFICIAL INTELLIGENCE-ASSISTED BEAM DISTRIBUTION IMAGING USING A SINGLE MULTIMODE FIBER AT CERN

G. Trad*, S. Burger, CERN, Geneva, Switzerland

Abstract

In the framework of developing radiation tolerant imaging detectors for transverse beam diagnostics, the use of machine learning powered imaging using optical fibers is explored for the first time at CERN. This paper presents the pioneering work of using neural networks to reconstruct the scintillating screen beam image transported from a harsh radioactive environment over a single, large-core, multimode, optical fiber. Profiting from generative modeling used in image-to-image translation, conditional adversarial networks have been trained to translate the output plane of the fiber, imaged on a CMOS camera, into the beam image imprinted on the scintillating screen. Theoretical aspects, covering the development of the dataset via geometric optics simulations, modeling the image propagation in a simplified model of an optical fiber, and its use for training the network are discussed. Finally, the experimental setups, both in the laboratory and at the CLEAR facility at CERN, used to validate the technique and evaluate its potential are highlighted.

INTRODUCTION

The Beam TV observation system (BTV) is the most widely used devices for beam image observation at CERN [1]. It is an imaging system that collects the visible light emitted by the particle beam crossing a phosphor screen, or other radiator inserted in its path, inside the vacuum chamber. The optical system relays the beam distribution image imprinted on the screen through a viewport to a detector, often a camera. In harsh radioactive environments, in-house developed cameras based on VIDICON tubes are currently in use. With the production of the tubes being discontinued worldwide, image transportation through fibers is one of the options currently being investigated as a replacement at CERN [2].

In this framework, pioneering work to reconstruct the beam's transverse distribution using a single, large-core, multimode optical fiber began in 2020. It takes advantage of advances in generative modeling using deep learning methods, such as convolutional neural networks, and attempts to apply them to beam diagnostics. In this paper the possibility of converting back the patterns at the output of the multimode fiber imaged on a camera into beam distributions is explored and the performance of such a detector in measuring beam centroid and width is assessed. Finally an outlook for the future developments will be presented.

WORKING PRINCIPLE

The proposed solution is based on an "extended" optical system that is meant to replace the rad-hard detector. The scintillating screen light is collected and its image is relayed away from the radiation area where it can be acquired using a standard CMOS camera. The system logically is split in three parts:

- a first stage refractive system, imaging the beam screen and coupling the image into an optical fiber,
- a multimode large core fiber transporting the light away from the harsh radioactive environment,
- a final single stage optical system, relaying the exit of the optical fiber onto a CMOS camera placed in a lower dose area of the accelerator.

Optical Constraints

The first stage magnification is dictated by the chosen fiber core diameter and the field of view requested to cover the dynamics of the beam. A minimum magnification of 0.05 is needed for stage 1 in order to fit a typical working area of the screen (30 mm x 30 mm) onto the entrance of the multimode fiber *FP1500ERT* [3] with a core diameter of 1500 µm (used throughout the tests). Given its Numerical Aperture (NA) of 0.5, a typical light coupling efficiency of a few percent is to be expected. Finally, a 5x amplification is needed to relay the fiber output to a typical CMOS sensor (6.6 mm x 4.1 mm). In and out optical coupling are optimized using high NA microscope objective lenses. The pair of images obtained for the beam image and fiber output will be analyzed using machine learning algorithms.

PIX2PIX CGAN MODEL

The problem under discussion could be formulated as an "Image-to-Image" translation. A classical problem that is addressed with Generative Adversarial Networks (GAN) that consist of a generator and discriminator network that improve mutually in the adversarial evolution. The state-of-the-art framework for general purpose image translation is Pix2Pix [4], a "conditional" GAN since the generator model is provided with a target image and trained to both fool the discriminator model and to minimize the loss between the generated image and the expected target image. A slightly modified version of the Pix2Pix network is used in this study:

Generator U-Net

The U-Net [5] model architecture is very similar to autoencoders, as it involves downsampling to a bottleneck and upsampling again to an output image, but links or skip-connections are made between layers of the same size in the encoder and the decoder, allowing the bottleneck to be circumvented. For our application, the input image is passed in 6 consecutive convolutional layers of size 64, 128, 128,

* georges.trad@cern.ch

ISBN: 978-3-95450-227-1 ISSN: 2673-5490 doi:10.18429/JACoW-IPAC2022-MOPOPT042

RECENT AWAKE DIAGNOSTICS DEVELOPMENT AND OPERATIONAL RESULTS

E. Senes* [1], S. Burger [1], P. N. Burrows[2], D. A. Cooke[3], T. Lefevre[1], M. Krupa[1], S. Mazzoni[1], C. Pakuza [1,2], E. Poimenidou[1,5], A. Topaloudis[1], M. Wendt[1], J. Wolfenden[4], G. Zevi Della Porta[1]
[1] CERN, Geneva, Switzerland
[2] JAI and University of Oxford, Oxford, United Kingdom
[3] University College London, London, United Kingdom
[4] University of Liverpool, Liverpool, United Kingdom
[5] Aristotle University, Thessaloniki, Greece

Abstract

The Advanced Wakefield Experiment (AWAKE) at CERN investigates the plasma-wakefield acceleration of electrons driven by a relativistic proton bunch. After successfully demonstrating the acceleration process in Run 1, the experiment has now started Run 2. AWAKE Run 2 consists of several experimental periods that aim to demonstrate the feasibility of the AWAKE concept beyond the acceleration experiment, showing its feasibility as accelerator for particle physics applications. As part of these developments, a dramatic effort in improving the AWAKE instrumentation is sustained. This contribution reports on the current developments of the instrumentation pool upgrade, including the digital camera system for transverse beam profile measurement, the beam halo measurement and the spectrometer upgrade studies. Studies on the development of high-frequency beam position monitors are also described.

INTRODUCTION

The Advanced Wakefield Experiment (AWAKE) at CERN successfully demonstrated plasma-wakefield acceleration (PWFA) of an electron bunch driven by a proton bunch [1] during AWAKE Run 1. The success of the acceleration, and the considerable experience developed [2], paved the way for the current experimental program, known as AWAKE Run 2 [3]. AWAKE Run 2 is formed of four operational periods, that plan to investigate different aspects of proton-driven PWFA between 2021 and 2028. The current period is known as Run 2a (2021-2022), investigates electron bunch seeding of plasma wakefields.

During AWAKE Run 1, an intense laser pulse was used to form the plasma by means of the relativistic ionization front and seed the proton bunch self-modulation of the cm-scale proton bunch into mm-scale micro-bunches. The anticipation of the laser pulse position in the proton bunch head, resulted in unseeded self-modulation, not reproducible event-to-event [4]. During Run 2a, the possibility to send the electron beam ahead of the proton bunch is explored. The role of the preceeding electron bunch is to seed the wakefields, allowing the self-modulation of the whole proton bunch [5]. The core experimental setup of AWAKE Run 1 is maintained for Run 2a, with the addition of a number of operational and R&D instruments.

This contribution describes a number of instrumentation projects that are currently taking place at AWAKE, for both upgrade and R&D purposes. A schematic layout of the AWAKE beamline is shown in Fig. 1. Numerous systems benefit from the upgrade of the camera system to digital cameras in terms of increase of resolution and dynamic range. This concerns the laser delivery and alignment, electron and proton transverse beam profile and halo measurement, and the spectrometer readout (items 1-6 in Fig. 1). Additionally, considerable effort has been put into the development of high frequency BPMs for the common beamline upstream of the plasma cell (items 7-8 in Fig. 1).

DIGITAL CAMERA SYSTEM

AWAKE is a demanding environment for a digital camera acquisition system, that must read out several devices with a fast repetition rate of 10 Hz and large image sensors, resulting in a large data throughput. Two independent camera acquisition systems are currently under commissioning in the experiment: one for the laser, with 8 cameras, and one for the beamline, with 18 cameras.

Each system is designed to handle up to 23 cameras. A 10 Hz physical trigger is distributed to the cameras. The large data volume is handled in two steps: all the cameras are connected via ethernet to a 24 port PoE switch; The switch forwards the data to a 64 core server for processing, via a 10 Gb fibre link roughly 2 km-long. Example features of some supported cameras are listed in Table 1.

The laser beam camera system is mainly devised to monitor the UV and IR laser beams delivery. The UV beam is observed on the electron injector virtual cathode [7], while a fraction of the IR beam is sent to the so-called "virtual beamline" (item 1 in Fig. 1). The virtual beamline relays the

Table 1: Cameras in use in the AWAKE camera system. All the cameras are manufactured by Basler AG [6].

Camera model	Format	Pixel size (μm^2)
acA1920-40gm	1920 × 1200	5.86 × 5.86
acA1600-60gm	1600 × 1200	5.3 × 5.3
acA1300-60gm	1280 × 1024	4.5 × 4.5

* eugenio.senes@cern.ch

ISBN: 978-3-95450-227-1 ISSN: 2673-5490 doi:10.18429/JACoW-IPAC2022-MOPOPT043

RECENT DEVELOPMENTS IN LONGITUDINAL PHASE SPACE TOMOGRAPHY

S. Albright*, A. Lasheen, CERN, Geneva, Switzerland
C. Grindheim, NTNU: Norwegian University of Science and Technology, Trondheim, Norway
A. Lu, KTH Royal Institute of Technology, Stockholm, Sweden

Abstract

Longitudinal phase space tomography has been a mainstay of beam diagnostics in most of the CERN synchrotrons for over two decades. For most of that time, the reconstructions have been performed using a highly optimised Fortran implementation. To facilitate increased flexibility, and leveraging the significant increase in computing power since the original development, a new version of the code has now been developed. The new version implements an object-oriented Python API, with the computationally heavy calculations in C++ for increased performance. The Python/C++ implementation is designed to be highly modular, enabling new and diverse use cases. For example, the tracking can now be performed externally and the results used for tomography, or a single set of tracked particles can be used for multiple reconstructions without needing to repeat the tracking. This paper summarises the functionality of the new implementation, and some of the applications that have been enabled as a result.

INTRODUCTION

Longitudinal phase space tomography (hereafter, tomography) is a method of reconstructing the longitudinal phase space distribution from a set of measured longitudinal profiles [1]. As the bunch undergoes synchrotron oscillations, the line density gives a one-dimenstional (1D) projection of the two-dimensional (2D) phase space distribution. Over the course of a full synchrotron period, the phase space distribution will be seen from all angles. By recording a number of beam profiles, which are projections of the distribution, it is therefore possible to perform tomographic reconstruction of the phase space distribution.

The reconstruction is an iterative process. On each iteration, the weighting of the reconstructed distribution is adjusted. First, the difference between the measured and reconstructed profiles is measured. Then, this difference is used to adjust the weighting such that it is minimised. Figure 1 shows the measured bunch profiles (left column) of a bunch undergoing synchrotron oscillations, the center column is the reconstructed profiles and the right column is the difference.

In Fig. 2 the reconstructed phase space distribution part way through the quadrupole oscillations in Fig. 1 can be seen. The measured profile is shown in black on the upper plot, the reconstructed reconstructed profile is in red, as can be seen they are in very close agreement as is the case on all measured profiles.

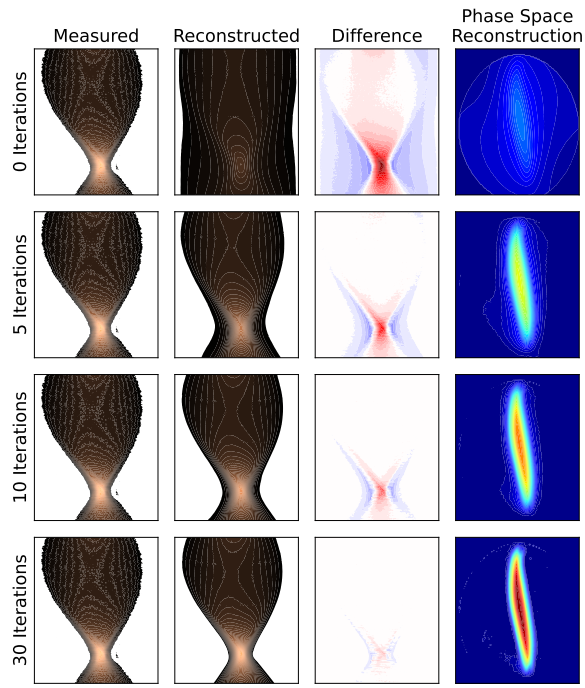

Figure 1: First Column: Waterfall plots showing measured bunch profiles during quadrupole oscillations. Second Column: Reconstructed waterfall plots produced by tomographic reconstruction. Third Column: Difference between measured and reconstructed profiles showing the error getting small as the number of iteration increases. Fourth Column: Reconstructed phase space distribution.

Tomography is a vital part of the beam diagnostics in the CERN accelerator complex. Recently, to allow further developments and new applications, a new version has been developed in mixed Python/C++. This paper outlines the changes introduced in the new version, and highlights two examples of new applications that were not previously possible. These changes have also simplified existing applications of tomography, such as RF voltage calibration [2, 3].

ALGORITHM MODIFICATIONS

Originally, the tomography software was written in Fortran95 and optimised using the High Performance Fortran (HPF) extension [4]. The software was designed for optimal speed and memory usage, which were significant considerations due to the computing power available at the

* simon.albright@cern.ch

ISBN: 978-3-95450-227-1 ISSN: 2673-5490 doi:10.18429/JACoW-IPAC2022-MOPOPT045

BEAM LOSS LOCALISATION WITH A OPTICAL BEAM LOSS MONITOR IN THE CLEAR FACILITY AT CERN

S. Benítez*[1], B. Salvachúa, M. Chen[1], E. Effinger, J. C. Esteban, W. Farabolini[2], P. Korysko[3], A. T. Lernevall. CERN, Geneva, Switzerland, also at
[1] University of Huddersfield, Huddersfield, United Kingdom
[2] CEA-Saclay, IRFU, 91191, Gif-sur-Yvette, France
[3] University of Oxford, Oxford OX1 3PU, United Kingdom

Abstract

A prototype of a Beam Loss Monitor based on the detection of Cherenkov light in optical fibres is being developed to measure beam losses in the CERN Super Proton Synchrotron. Several testing campaigns have been planned to benchmark the simulations of the system and test the electronics in the CLEAR facility at CERN. During the first campaigns, the emission of Cherenkov light inside optical fibres and the photodetector characterisation were studied. Fibre-based Beam Loss monitors continuously monitor beam losses over long distances. The localisation of the beam loss could be calculated from the timing of the signals generated by the photosensors coupled at both ends of the optical fibre. The experimental results of an optical fibre Beam Loss Monitor installed in the CLEAR facility are reported in this paper.

INTRODUCTION

An optical fibre Beam Loss Monitor (BLM) [1] is composed of a several tens of meters long quartz optical fibre equipped with a photodetector on each end. They could be installed alongside the beamline to increase the detection distance. When particles are lost, the shower of secondary particles reaching the fibre produces Cherenkov photons. Part of the emitted light is captured and transported through the fibre in both directions. The photons are collected by the photosensors at the extremities of the fibre. Hence, optical fibre BLMs are suitable and cost-effective for measuring beam losses across long distances.

A first serie of beam tests [2], were performed at the CLEAR facility with the aim to characterise the Cherenkov light produced in silica fibres. The light attenuation and the Cherenkov capture angles in optical fibres were studied in detail, as well as the saturation effect of the Silicon Photo-Multiplier (SiPM) detectors. These initial results have been used to benchmark simulation models developed for the design of an optical fibre Cherenkov monitor in the CERN accelerator complex. In this contribution, new experiments were performed to study the precision of such a monitor to localise beam losses, produced in this case intentionally. The position of the loss is calculated by measuring the arrival time of the signals measured at both ends of the fibre. Different setups were investigated varying the distance between the fibre and the beamline and also measuring with amplified and non amplified SiPMs.

* sara.benitez.berrocal@cern.ch

METHOD

In the CLEAR experimental setup, the fibre is installed parallel alongside the beamline. Because the Cherenkov photons travel in both directions inside the fibre, signals at both ends, downstream and upstream[1], can be used to calculate the loss location. However, the upstream signal gives a better longitudinal resolution than the downstream one [3]. Therefore the loss location calculation from the upstream signal is preferable.

Figure 1 illustrates the arrival times at the upstream end of two different beam losses at A and B locations.

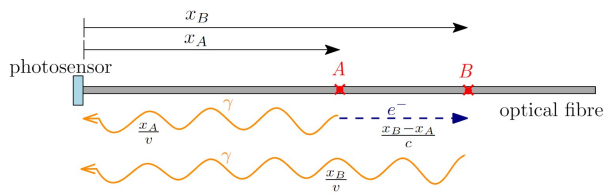

Figure 1: Arrival time between two signals at the upstream fibre end [4].

Particle A reaches the fibre at the moment $t = 0$, right before particle B. The time difference between the two particles is $(x_B - x_A)/c$. Each particle produces photons that arrive at the photosensor at $t_A = x_A/v$ and $t_B = x_B/v$ times, respectively. The photon velocity can be calculated by $v = c/n$, where $c = 0.3$ m/ns is the speed of light in a vacuum and $n = 1.46$ the average refractive index of silica in the visible spectrum. Therefore, in our system, the velocity of the photons is $v = 0.2055$ m/ns.

The arrival time difference between the two photons is given by:

$$\Delta t = t_B - t_A = \frac{x_B - x_A}{c} + \frac{x_B}{v} - \frac{x_A}{v} \quad (1)$$

From Eq. 1, the upstream arrival time difference can be expressed as:

$$\Delta t_{up} = \frac{\Delta x}{c} \cdot (1 + n) \quad (2)$$

Similarly, the expression for the downstream arrival time difference is:

[1] Downstream corresponds to the beam direction, and Upstream is the opposite direction.

ISBN: 978-3-95450-227-1 ISSN: 2673-5490 doi:10.18429/JACoW-IPAC2022-MOPOPT046

LINEARITY AND RESPONSE TIME OF THE LHC DIAMOND BEAM LOSS MONITORS IN THE CLEAR BEAM TEST FACILITY AT CERN

S. Morales*[1], B. Salvachua, E. Calvo, L. Dyks, E. Effinger, W. Farabolini, P. Korysko, A. Lernevall, C. Zamantzas, CERN, Geneva, Switzerland
C.P. Welsch[1], J. Wolfenden[1], [1]Cockcroft Institute, Warrington, Cheshire, United Kingdom

Abstract

Chemical Vapour Deposition (CVD) diamond detectors have been tested during the Run 2 operation period (2015-2018) as fast beam loss monitors for the Beam Loss Monitoring (BLM) system of the Large Hadron Collider (LHC) at CERN. However, the lack of raw data recorded during this operation period restrains our ability to perform a deep analysis of their signals. For this reason, a test campaign was carried out at the CLEAR beam test facility at CERN with the aim of studying the linearity and response time of the diamond detectors against losses from electron beams of different intensities. The signal build-up from multi-bunched electron beams was also analyzed. The conditions and procedures of the test campaign are explained, as well as the most significant results obtained.

INTRODUCTION

The LHC is the largest and most powerful particle accelerator ever built. Sitting in a tunnel located around 100 m underground and with a circumference of 27 km, it is designed to accelerate protons up to an energy of 7 TeV. The LHC beams are foreseen to contain up to 2 700 bunches with up to 1.4×10^{11} protons each during the first year of the Run 3 operation period, starting in 2022 [1].

The LHC BLM system is in charge of actively protecting the machine against energy deposition from beam losses, which could provoke a quench in the superconducting magnets, leading to an accelerator downtime in the order of weeks [2]. The LHC BLM system provides updated beam loss signals every 40 µs that may trigger a fast extraction of the beams from the main ring towards beam dumps when losses are measured above predetermined thresholds. Around 4 000 BLM detectors, most of them Ionization Chambers (ICs), are part of the system and installed downstream from the most probable loss locations [3].

Additionally, a set of CVD diamond detectors has been installed in specific LHC locations during Run 2 (2015-2018) with the aim of studying their feasibility as fast beam loss monitors. They are commonly referred to as diamond Beam Loss Monitors (dBLMs). Considering their high-radiation tolerance and their time resolution in the order of ns, they resolve bunch-by-bunch losses, being the LHC bunches typically spaced by 25 ns [4].

A signal-to-beam-loss global calibration of a set of LHC IC BLM detectors has proven to be useful to follow-up the performance of the machine, e.g. by online beam lifetime calculation [5]. However, a similar calibration of the LHC dBLMs was not able to reach the same level of accuracy, i.e. it overestimated the beam losses by a factor of approximately 4, while the calibration of the LHC IC BLMs also overestimates the beam losses, but only by a factor of 1.25 [6].

Later on, a comparison between beam losses obtained by integrating IC BLM and dBLM signals suggested a potential non-linearity of the latter with increasing beam losses. Unfortunately, the unavailability of unprocessed data prevented us from finding if this was due to the response of the detectors themselves, the presence of high levels of noise in the signals or if it was related to a possible bias induced during the pre-processing of the signals.

Taking advantage of the fact that the stand-alone electron beam facility CLEAR was operational during CERN's accelerator complex shutdown period, we had the opportunity to perform a series of beam tests with relativistic electrons. The purpose of these tests was to study the dBLM signal linearity, its response function and the signal build-up from multi-bunched beams.

The tests setup and procedures are detailed in this paper, together with the most significant observations.

DIAMOND BEAM LOSS MONITORS

The dBLM is based on a squared, 10-mm side, 0.5-mm thick CVD diamond detector. It is coated on each side with an 8-mm long and 200-nm thick squared gold electrode. The whole is protected by an RF-shielding aluminium housing and operated with a bias voltage of 500 V.

The resulting signal is connected to an AC-DC splitter that decouples the DC part from the AC part and at the same time divides the AC part into two equivalent output signals. One of them is then connected to a 40-dB amplifier, which amplifies the signal by a factor of approximately 100 and saturates at ±1 V. This allows to increase the dynamic range of the system, being sensitive to single MIP particles.

The raw signal is digitised by an ADC at a frequency of 650 MHz. It is then pre-processed by an FPGA, which sends the resulting values to be saved for offline analysis. Among the different measurement modes provided, the most useful for our studies is the so-called Integral mode, which performs a bunch-by-bunch integration of the measured beam losses approximately every second. At the same time, the signal's baseline, i.e. the amplitude of the signal in between bunches, is measured and subtracted from the integrated signal.

* sara.morales.vigo@cern.ch

ISBN: 978-3-95450-227-1 ISSN: 2673-5490 doi:10.18429/JACoW-IPAC2022-MOPOPT047

EXPERIMENTAL DEMONSTRATION OF MACHINE LEARNING APPLICATION IN LHC OPTICS COMMISSIONING

E. Fol*, R. Tomás, F. Carlier, J. Dilly, M. Hofer, J. Keintzel, M. Le Garrec, E.H. Maclean, T. Persson, F. Soubelet, A. Wegscheider, CERN, 1211 Geneva 23, Switzerland
J. Cardona, Universidad Nacional de Colombia

Abstract

Recently, we conducted successful studies on the suitability of machine learning (ML) methods for optics measurements and corrections, incorporating novel ML-based methods for local optics corrections and reconstruction of optics functions. After performing extensive verification on simulations and past measurement data, the newly developed techniques became operational in the LHC commissioning 2022. We present the experimental results obtained with the ML-based methods and discuss future improvements. Besides, we also report on improving the Beam Position Monitor (BPM) diagnostics with the help of the anomaly detection technique capable to identify malfunctioning BPMs along with their possible fault causes.

INTRODUCTION

Machine Learning (ML) techniques recently have demonstrated a great potential to improve the optics measurements and corrections in terms of measurements data quality, speed and level of automation [1, 2]. Previous works utilized simulations and historical data to verify the performance of developed ML-techniques. The successful restart of the LHC in 2022 made it possible to apply the developed methods during LHC optics commissioning, for the first time, under challenging optics settings where the beams are squeezed to β^*=30 cm [3]. In this paper we summarize the results obtained in operation and discuss future improvements. First, we present the results of turn-by-turn data cleaning, including hardware verification performed by beam instrumentation experts. Second, we compare triplet magnet errors identified by pre-trained ML estimator to local corrections found by traditional techniques. Then, we present another application of supervised learning, namely a virtual diagnostic tool to predict β-functions next to Interaction Points (IPs) and horizontal dispersion, without performing dedicated measurements. Finally, we explore future improvements of presented ML-based methods and potential new applications.

DIAGNOSTICS OF FAULTY BEAM POSITION MONITORS

Turn-by-turn data (TbT) for optics analysis is cleaned by the means of SVD-based algorithm, simple thresholds-based filtering and Isolation Forest (IF) anomaly detection [2]. During the LHC long shutdown, extensive work in collaboration with CERN's beam instrumentation experts allowed to verify the findings of cleaning methods against actual instrumentation issues. Several sets of historical measurements from the past years have been analysed, in order to identify the BPMs marked as faulty in most of the measurements and BPMs which cause unphysical outliers in the optics functions if remaining in TbT-data. In total, out of more than a thousand LHC BPMs, we identified 116 faulty BPMs which are critical for the optics measurements. Remarkably, 50 % of the BPMs reported by combined SVD and IF cleaning, revealed hardware or signal processing issues which otherwise stay hidden. In the commissioning, we applied SVD and IF cleaning with the settings refined on simulations, which demonstrated that cleaning does not affect the measurements in a negative way in terms of false positive classification as shown in Fig. 1. This is important in light of BPM upgrades performed by beam instrumentation experts to solve the identified problems, fewer faulty BPMs are expected to appear in TbT data.

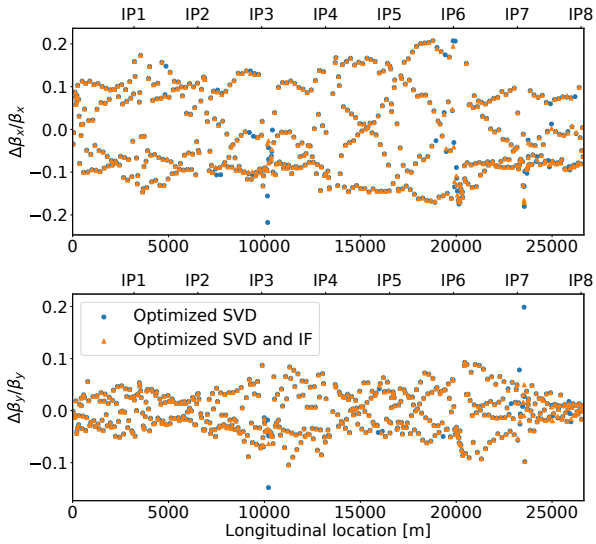

Figure 1: β-beating computed with and without IF-cleaning.

QUADRUPOLE ERRORS PREDICTION

Supervised learning based quadrupole errors prediction allows to reconstruct individual magnet gradient field errors along the whole LHC lattice, correcting the linear optics errors in both beams simultaneously [1]. However, optics corrections using quadrupoles in the arcs are possible only by trimming the circuits, i.e. several quadrupoles powered in series. Therefore, we verify the new concept first for the local corrections in the IRs, since the triplet quadrupoles, whose

* elena.fol@cern.ch

ISBN: 978-3-95450-227-1 ISSN: 2673-5490 doi:10.18429/JACoW-IPAC2022-MOPOPT048

DESIGN OF A PROTOTYPE GAS JET PROFILE MONITOR FOR INSTALLATION INTO THE LARGE HADRON COLLIDER AT CERN*

R. Veness†, M. Ady, T. Lefevre, S. Mazzoni, I. Papazoglou, M. A. Rossi, G. Schneider, O. Sedlacek[1], C. Castro Sequeiro, K.Sidorowski CERN, 1211 Geneva, Switzerland
A. Salehilashkajani[1], N. Kumar[1], O.Stringer, C. P. Welsch[1], H. D. Zhang[1], The Cockcroft Institute, Daresbury, Warrington WA4 4AD, United Kingdom
P. Forck, S. Udrea, GSI Helmholtzzentrum für Schwerionenforschung, 64291 Darmstadt, Germany
[1]also at Department of Physics, University of Liverpool, Liverpool L69 3BX, United Kingdom

Abstract

The Beam-Gas Curtain or BGC is the baseline instrument for monitoring the concentricity of the LHC proton beam with a hollow electron beam for the hollow e-lens (HEL) beam halo suppression device which is part of the High-Luminosity LHC upgrade.

The proof-of-principles experiments of this gas-jet monitor have now been developed into a prototype instrument which has been built for integration into the LHC ring and is now under phased installation for operation in the upcoming LHC run.

This paper describes the challenges overcome to produce a gas-jet fluorescence monitor for the ultra-high vacuum accelerator environment. It also presents preliminary results from the installation of the instrument at CERN.

INTRODUCTION

The High Luminosity upgrade to the Large Hadron Collider (HL-LHC) is the flagship project at CERN [1]. The higher luminosity delivered to the experiments require higher bunch intensities which in turn imply more energy and particles in the beam halo, which must be managed. One solution to this problem is to locally pass the circulating beam through a hollow electron beam which interacts electro-magnetically with the protons in the halo and diverts them into an upgraded system of classical physical collimators [2]. For such a hollow electron lens (HEL) device to operate effectively, an overlap instrument which can observe both proton beam centroid and a 2D image of the electron beam is a requirement, both for commissioning and for monitoring during operations. The intense 5 A / 10 keV hollow beam is constrained by a 2 T solenoid field created by two 4.5 K superconducting magnets with the overlap instrument in between. As such, this instrument must also operate in the intense stray fields of these magnets, making observables based on charged particles practically impossible. This has led to the development of a beam-gas curtain (BGC) concept, where a 2D supersonic gas sheet is projected across the aperture at 45 degrees to the proton beam. Interactions between both the proton and electron beams create fluorescence photons which are not influenced by the magnetic field and can be observed by an ex-vacua optical system. This creates a direct image of the two beams, similar in concept to a physical beam observation screen. Following a period of development and collaboration between the Cockcroft Institute (CI), GSI Helmholtzzentrum für Schwerionenforschung (GSI) and CERN [3], [4], a prototype designed for installation in the LHC environment, called BGCv3 has been constructed and successfully commissioned at CI [5].

COMPARISONS WITH EXPERIMENTAL DATA FOR PROTONS

The Image Intensifier is designed for single-photon detection; it comprises a photo-cathode (UV Enhanced S20) with a quantum efficiency of aprox. 8 % for the Ne-transition at 585 nm and aprox. 12 % for the N2+ transition at 391 nm and reasonable dark-count rate of 500 counts/s/cm^2 [6]. Photo-electrons are amplified by a double MCP leading to separated light spots for each photo-electron on the subsequent phosphor screen. A regular CMOS camera records the image and the centre of the spot is evaluated; the actual system is described in [7]. The Image Intensifier is an optimized version used at GSI-LINAC for regular operation [8]. The photon yield was investigated for several parameters such as gas pressure, gas species (such as N2, Ne, Ar, and Xe), beam ion, and beam energies; tests with the highest proton energy of 450 GeV were performed at CERN SPS [9]. It can be concluded that the photon yield scales basically with the energy loss in the residual according to the Bethe Equation; however, an uncertainty of at least a factor 5 remains related to systematic experimental imperfections. The signal strength at LHC top energy will be determined with the BGCv3 using a local pressure bump produced by a regulated gas inlet valve instead of the gas jet. At LHC energies, background contributions might be significantly different from lower energy investigations. The emitted synchrotron light is more intense and must be absorbed by the inner vacuum pipe [10]; methods for black coating were investigated in detail [11], and the LHC vacuum chamber was prepared accordingly. Optical interference filters with the passband centred at the florescence transitions will suppress this background in addition. Ionizing radiation from beam losses causes further background; in particular, neutrons or fast charged particles might penetrate the Image Intensifier body and cause secondary electron emission from the photo-cathode or within

* This work was supported by the HLLHC-UK project and the STFC Cockcroft core grant
† veness@cern.ch

ISBN: 978-3-95450-227-1 ISSN: 2673-5490 doi:10.18429/JACoW-IPAC2022-MOPOPT049

STUDY ON ENERGY SPECTRUM MEASUREMENT OF ELECTRON BEAM FOR PRODUCING MIR-FEL AT PBP-CMU ELECTRON LINAC LABORATORY

P. Kitisri*[1], K. Techakaew[2], S. Rimjaem†[3],
PCELL, PBP, Faculty of Science, Chiang Mai University, Chiang Mai, Thailand
[1]also at Master Program in Physics, Chiang Mai University, Chiang Mai, Thailand
[2]also at Ph.D. Program in Physics (Intl. Program), Chiang Mai University, Chiang Mai, Thailand
[3]also at ThEP Center, MHESI, Bangkok, Thailand

Abstract

At the PBP-CMU Electron Linac Laboratory (PCELL), we aim to produce a mid-infrared free-electron laser (MIR-FEL) for pump-probe experiments in the future. The electron beam is generated from a thermionic cathode radio-frequency (RF) gun with a 1.5-cell cavity before going to an alpha magnet. In this section, some part of the beam is filtered out by using energy slits. The selected part of the beam is then further accelerated by an RF linear accelerator (linac) to get higher energy. This work focuses on the measurement of energy spectrum of electron beam for producing mid-infrared free-electron laser (MIR-FEL). Since our bunch compressor (BC) for the MIR-FEL beamline is an achromat system, the longitudinal distributions of electron beam at the entrance and the exit of the BC are almost the same. Thus, we can measure the longitudinal properties of the beam before it travels to the BC. By using a dipole magnet and a Faraday cup with a slit, we can measure energy spectrum of electron beam before entering the BC. In this study, the ASTRA code is used to investigate the properties of electron beam as well as to design the measuring system. The design results including systematic error of the measuring system are presented and discussed in this contribution. The results from this work can be used as the guideline for the measuring system construction as well as the beam operation.

INTRODUCTION

At the PBP-CMU Electron Linac Laboratory (PCELL) of the Plasma and Beam Physics (PBP) Research Facility, Chiang Mai University (CMU), a mid-infrared free-electron laser (MIR-FEL) has been developed. In the accelerator system, electrons are emitted from a thermionic cathode and are accelerated by a radio-frequency (RF) gun to reach a kinetic energy of about 2-2.5 MeV. Then, the beam passes through the first magnetic bunch compressor in a form of an alpha magnet, which has energy slits for filtering electrons for desired energy and charge. After that, the beam is further accelerated by an RF linac to have the final energy of up to 25 MeV. Then, the beam enters either a dipole beam dump 1 (BD1) or magnetic bunch compressor (BC) for MIR-FEL or THz-FEL beamline. Presently, the commissioning of the electron accelerator is underway at PCELL.

To produce the MIR-FEL, electron beam parameters with proper energy, energy spread, transverse beam size and emittance are required [1, 2]. This work concentrates on the characterization of electron beam energy and energy spread. Since the BC system is an achromat system, the energy and energy spread of the beam upstream and downstream of the BC will be the same. Thus, we can obtain the beam energy and energy spread upstream the undulator entrance by measuring the beam downstream the linac exit.

This research focuses on design of the measuring system for electron beam energy, energy spread and energy spectrum downstream the linac exit. This system should be able to measure the beam with energy of 25 MeV, energy spread of 0.1%, and bunch charge of 60 pC [1, 2].

DESIGN OF MEASURING SYSTEM

To measure electron beam energy downstream the linac exit, we use the beam dump dipole 1 (BD1) and Faraday cup 1 (FC1), which is installed at the end of the straight section beamline as shown in Fig. 1. To measure energy distribution and energy spectrum of the beam with an average energy of 25 MeV and an energy spread of 0.1%, we decided to add a single slit mask in the measuring system for increasing the resolution of the measuring system. To design the slit mask, the following conditions are taken into consideration:

- The slit opening aperture must be small for measuring the beam with energy spread of 0.1%, but it should be big enough to let electrons passing through with the charge higher than the Faraday cup sensitivity.
- The slit thickness must be thick enough to block the electrons, but not too thick to avoid the electron scattering inside the aperture.
- The slit width must be large enough to block the electrons in the horizontal axis, but not larger than the vacuum chamber.

We optimized the slit opening aperture based on following equation [3]:

$$\theta\ [\mathrm{rad}] = \frac{0.2998 \int B_x(z) d_z [\mathrm{T \cdot m}]}{\beta E_{tot}\ [\mathrm{GeV}]}, \qquad (1)$$

where θ is the electron effective bending angle, E_{tot} is the total energy of electron, β is the ratio of the electron velocity

* pitchayapak_ki@cmu.ac.th
† sakhorn.rimjaem@cmu.ac.th

ISBN: 978-3-95450-227-1 ISSN: 2673-5490 doi:10.18429/JACoW-IPAC2022-MOPOPT050

SYSTEMATIC STUDY OF ELECTRON BEAM MEASURING SYSTEMS AT THE PBP-CMU ELECTRON LINAC LABORATORY

K. Techakaew*[1], S. Rimjaem†[2], PCELL, PBP, Faculty of Science,
Chiang Mai University, Chiang Mai, Thailand
[1]also at Ph. D. Program in Physics (Intl. Program), Chiang Mai University, Chiang Mai, Thailand
[2]also at ThEP Center, MHESI, Bangkok, Thailand

Abstract

The linear accelerator system at the PBP-CMU Electron Linac Laboratory (PCELL) is used to produce electron beam with suitable properties for generating coherent teragertz (THz) radiation and mid-infrared free-electron laser (MIR FEL). Optimization of machine parameters to produce short electron bunches with low energy spread and low transverse emittance was focused in this study. We conducted ASTRA simulations including three-dimentional (3D) space charge algorithm and 3D field distributions for radio-frequency (RF) electron gun and all magnets to develop measuring systems. Electron beam energy and energy spread were investigated downstream the RF gun and the RF linac using an alpha magnet and a dipole spectrometer, respectively. The transverse beam emittance was studied using the quadrupole scan technique. By filtering proper portion of electrons before entering the linac, the beam with average energy of 20 MeV and energy spread of 0.1-1% can be achieved for a bunch charge of 100 pC. The systematic error is less than 10% for measuring average energy and energy spread while it is less than 31% for measuring transverse emittance when placing the screen of at least 1.0 m behind the scanning quadrupole magnet. The results of this study were used to develop the measuring setups in our system.

INTRODUCTION

The aim of research activities PCELL is to develop an electron accelerator and experimental apparatus for producing coherent MIR and THz radiation. The MIR radiation will be generated by using the oscillator FEL technology and the THz radiation will be produced from femtosecond electron pulses via the transition radiation (TR) and the super-radiant undulator radiation techniques. The layout plan of the injector system is shown in Fig. 1. There are two sections for accelerating the electron beam. Firstly, electrons produced from the thermionic cathode are accelerated inside the RF cavities to reach the maximum energy of about 2-2.5 MeV at the gun exit. Secondary, the electrons are accelerated in the RF linac structure to reach the average energy in a range of 10 - 25 MeV depending on the linac accelerating gradient. The considered electron beam properties for generation of high quality radiation in both MIR and THz wavelengths are bunch charge, electron bunch length, energy spread, transverse emittance.

* kittipong_techakaew@hotmail.com
† sakhorn.rimjaem@cmu.ac.th

In this work, we focus on the energy and emittance measurements. The design beam diagnostic setups and measuring procedures for energy and emittance measurement in the injector system were performed based on the results from beam dynamic simulation using A Space Charge Tracking Algorithm (ASTRA) code [1] to obtain the suitable conditions with low systematic measurement error. The 3D electric and magnetic field distributions inside the RF-gun, steering magnets, the alpha magnet, quadrupole magnets, and dipole magnet were obtained from the simulations with software CST Studio Suit [2] and were imported to the ASTRA code. In the simulations, we optimized all magnetic fields to meet the appropriate electron beam properties for producing coherent THz TR at the experiment station, which are the beam average kinetic energy of 20 MeV and a electron bunch charge of about 100 pC [3]. The energy and energy spread of electron beam downstream the electron gun were measured using a low energy slit located inside the alpha magnet vacuum chamber and a current transformer (CT2). The spectrometer system consisting of a dipole magnet (DP1) and a screen station (SC6) was used to measure energy and energy spread of electron beam after the linac acceleration. The beam emittance was measured by using quadrupole scan technique [4-6] utilizing a quadrupole magnet (Q6) and a screen station downstream linac (SC4). The results from the computer simulation can be used to estimate the electron beam properties, which are expected to be produced from the accelerator system.

ENERGY AND ENERGY SPREAD MEASUREMENT

Energy Measurement after RF Gun Acceleration

Energy spectrometer in this section consists of alpha magnet and current transformer. The path length of electrons are different depending on their energy. When they travel through an alpha magnet's field. The maximum distance of the electron in horizontal direction a_{max} can be written as [7]

$$a_{max}[\mathrm{cm}] = 75.051\sqrt{\frac{\beta\gamma}{g[\mathrm{G/cm}]}}, \quad (1)$$

where g is the magnetic field gradient, $\beta = v/c$ is the relative velocity of electron, and γ is the Lorentz's factor.

In this study, we used the alpha magnet's low energy slit with known calibrated energy to select a part of electron bunch and used the current transformer CT2 to measure the

ISBN: 978-3-95450-227-1 ISSN: 2673-5490 doi:10.18429/JACoW-IPAC2022-MOPOPT051

OPTICAL FIBER BASED BEAM LOSS MONITOR FOR SPS MACHINE

T. Pulampong*, W. Phacheerak, N. Suradet, P. Sudmuang,
Synchrotron Light Research Institute, Nakhonratchasima, Thailand

Abstract

At the Siam Photon Source (SPS) beam loss monitors based on PIN diode have been used. The existing system allows beam loss detection very locally at the monitor position close to the vacuum chamber. For optical fiber, Cherenkov radiation can be detected when a lost particle travels in the fiber. Thus optical fiber based loss monitor with sufficient length can cover parts of the machine conveniently. Fast beam loss event can be detected with more accurate position. In this paper, the design and result of the optical fiber based beam loss monitor system at SPS machine are discussed. The system will be a prototype for the new 3 GeV machine SPS-II.

INTRODUCTION

Siam Photon Source (SPS) has been operating to provide photon beam for users. Beam loss is one of the undesirable events for accelerator operation. It can be irregular major losses or normal losses due to the beam lifetime. The ability to measure beam losses can provide valuable understanding of the machine condition when some components are broken, vacuum has some problems or some obstacle exists in the beam path, for example.

Previously Beam Loss Monitor (BLM) system at SPS is based on Bergoz Instrumentation PIN diodes [1]. However, it is almost impossible to cover all parts of the machine. In addition, in a tight space, the BLM cannot be fitted into the spot. To overcome these limitations, optical fiber beam loss monitor has been investigated. Optical fiber based beam loss monitor uses the generated Cherenkov radiation from a charged particle traveling in a medium with a refractive index (n) with the speed (v_p) greater than the phase velocity of light ($c_o/n < v_p < c_0$).

Optical fiber based beam loss monitor is gaining more popularity due to its flexibility and continuity for losses detection. The system allows good details of the losses event spots and it has been applied in many facilities [2] [3].

SYSTEM DESIGN

There are three main components in the system. Optical fiber plays a role of sensor. Photo Multiplier Tube (PMT) is a data collector. Finally, the collected data can be sent to an oscilloscope for processing.

Optical Fibers

Optical fiber is the main sensor in the beam loss system. To allow sufficient probability to detect beam losses event, the fiber properties has to be taken into account. Core diameter of the fiber is basically the sensor size which cover the path of the secondary particles. Thus larger core is more preferable. Numerical Aperture (NA) is the measure of the angle that light can be accepted and it depends on the refractive index of the fiber. For beam loss application large NA is better. Multimode step-index fibers providing larger NA were used. Transmission of the specific wavelength of light can be affected by water content or Hydroxyl group (OH) in the fiber. Pure Silica providing low OH is suitable for visible light produced by Cherenkov radiation. FC connector was used at both ends in order to conveniently connect the fiber to PMT via FC adapter. Thorslabs's pure silica fibers giving appropriate properties and large NA were selected. The specification for the fibers are described in Table 1. For installation, bend radius has to be carefully taken into account. For larger core diameter, the bend radius is larger at about 80 mm for FP1000ERT (48 mm for FP600ERT).

Table 1: Optical Fiber Specifications [4, 5]

Type	Core Diameter	Core / Cladding Material
FP600ERT	600 μm	Pure Silica / Hard Polymer
FP1000ERT	1000 μm	Pure Silica / Hard Polymer

PMT and Processing

To capture the light from Cherenkov radiation, the cathode spectral response for the PMT H10720-110 ranges from 230 to 700 nm as shown in Fig. 1.

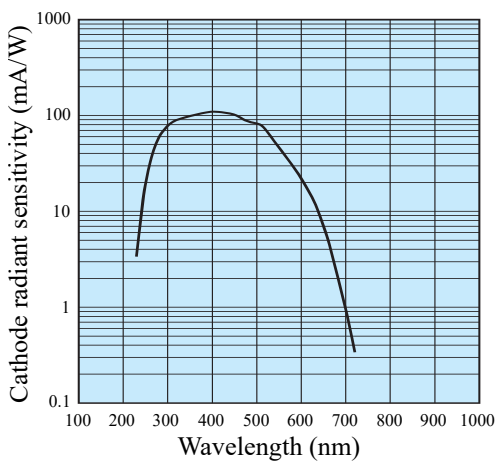

Figure 1: Cathode sensitivity for PMT [6].

* thapakron@slri.or.th

ISBN: 978-3-95450-227-1 ISSN: 2673-5490 doi:10.18429/JACoW-IPAC2022-MOPOPT052

BEAM-BASED ALIGNMENT FOR LCLS-II CuS LINAC-TO-UNDULATOR QUADRUPOLES*

Xiaobiao Huang†, Dorian Bohler
SLAC National Accelerator Laboratory, Menlo Park 94025, USA

Abstract

An advanced method for beam-based alignment that can simultaneously determine the quadrupole centers of multiple magnets has been applied to the LCLS-II CuS linac-to-undulator (LTU) section. The new method modulates the strengths of multiple quadrupoles and monitor the induced trajectory shift. Measurements are repeated with the beam trajectory through the quadrupoles steered with upstream correctors, from which the quadrupole centers can be obtained. Steering of the trajectory to minimize the induced trajectory shift is also done for finding the quadrupole centers.

INTRODUCTION

Steering the beam through the centers of quadrupole magnets in a linac or transport line has many benefits, for example, reducing spurious dispersion and reducing emittance dilution. While mechanic alignment and survey are a critical step to establish the beam path, it is usually necessary to perform beam-based alignment (BBA) measurements during the commissioning stage of a new accelerator. Beam-based measurements not only can identify potential alignment errors, but also determine the actual quadrupole centers as seen by nearby beam position monitors (BPM), which can be used as steering targets. The orbit target obtained by BBA automatically includes both the mechanic errors and the electronic errors.

The usual model dependent method initially proposed for rings [1–3] is applicable for one-pass systems as well. The method modulates the strength of a quadrupole magnet and observes the orbit shift on a BPM. Using the orbit response from a kick by the quadrupole to the BPM, the kick angle change due to the modulation can be obtained from the orbit shift, which can then be converted to beam orbit offset at the quadrupole with the known change of integrated gradient on the magnet. Mathematically, we have

$$\Delta x_b = R_{bq}\theta_q, \qquad \theta_q = \Delta K L x^{\text{off}}, \tag{1}$$

where Δx_b is the orbit shift at the BPM, θ_q is the kick angle due to modulation, R_{bq} is the orbit response from the quadrupole to the BPM, ΔK is the change of quadrupole gradient, L is the length of the magnet, and $x^{\text{off}} = x_{\text{center}} - x_{\text{beam}}$ is the horizontal distance of the quadrupole center measured from the beam trajectory. A similar formula applies to the vertical plane, but with the sign of integrated gradient reversed. The orbit response is calculated with a lattice model. Lattice errors and calibration errors of magnet strengths and BPM readings have an impact on the quadrupole center measurement.

One can steer the beam through the center of the quadrupole to minimize the orbit shift due to quadrupole gradient modulation [4]. As this can be done empirically, the quadrupole center can be determined without a lattice model. The quadrupole modulation system (QMS) method, also known as the "bow tie" method [5], is based on the same principle. It scans the orbit at the quadrupole to find the point with zero orbit shift with interpolation. The quadrupole centers found with these model independent methods are not affected by lattice errors or calibration errors.

The above methods target one quadrupole at a time. In reality, sometimes a number of quadrupoles are powered by a common power supply. In such a case, current shunting can be used to change the strength of one quadrupole. However, shunting a quadrupole is a slow and relatively complex process. A method to simultaneously determine the centers of multiple quadrupoles was recently proposed in Ref. [6]. It uses the response matrix method to correct the induced orbit shift with corrector magnets.

In this study, we applied a new method that can also perform BBA for a number of quadrupoles simultaneously. They not only address the challenge of BBA for quadrupoles on a serial power supply, but also can speed up the BBA process. The method is described in details in the next section and its application to the copper LTU section of the Linac Coherent Light Source (LCLS)-II in experiments is used as an illustration in the section following that. A method to scan the trajectory at the quadrupoles with combined knobs to minimize the induced orbit shift is also discussed.

METHOD

The model dependent method as described in Eq. (1) can be readily extended to multiple quadrupoles. Multiple BPMs are included to measure the trajectory shifts due to quadrupole modulations. In this case, the equations become

$$\Delta x_i = R_{ij}\theta_j, \qquad \theta_j = [\Delta K L]_j x_j^{\text{off}}, \tag{2}$$

where $i = 1, 2, \cdots, M$ are indices for the BPMs, $j = 1, 2, \cdots, N$ are indices of quadrupoles. If the BPMs and quadrupole are properly chosen, the kick angles by the quadrupoles for a certain modulation pattern can be obtained by inverting the response matrix $\mathbf{R}$,

$$= (\mathbf{R}^T\mathbf{R})^{-1}\mathbf{R}^T\Delta\mathbf{x}, \tag{3}$$

where ^{T} is to take transpose of a matrix. For the scheme to work, the matrix $\mathbf{R}^T\mathbf{R}$ needs to be full rank. Therefore, one

* Work supported by DOE Contract No. DE-AC02-76SF00515
† xiahuang@slac.stanford.edu

ISBN: 978-3-95450-227-1 ISSN: 2673-5490 doi:10.18429/JACoW-IPAC2022-MOPOPT053

A BEAM POSITION MONITOR FOR ELECTRON BUNCH DETECTION IN THE PRESENCE OF A MORE INTENSE PROTON BUNCH FOR THE AWAKE EXPERIMENT

C. Pakuza†, P.N. Burrows, John Adams Institute for Accelerator Science, Oxford, United Kingdom
R. Corsini, W. Farabolini, P. Korysko, M. Krupa, T. Lefevre, S. Mazzoni, E. Senes, M. Wendt, CERN, Geneva, Switzerland

Abstract

The Advanced Proton Driven Plasma Wakefield Experiment (AWAKE) at CERN uses 6 cm long proton bunches extracted from the Super Proton Synchrotron (SPS) at 400 GeV beam energy to drive high gradient plasma wakefields for the acceleration of electron bunches to 2 GeV within a 10 m length. Knowledge and control of the position of both copropagating beams is crucial for the operation of the experiment. Whilst the current electron beam position monitoring system at AWAKE can be used in the absence of the proton beam, the proton bunch signal dominates when both particle bunches are present simultaneously. A new technique based on the generation of Cherenkov diffraction radiation (ChDR) in a dielectric material placed in close proximity to the particle beam has been designed to exploit the large bunch length difference of the particle beams at AWAKE, 200 ps for protons versus a few ps for electrons, such that the electron signal dominates. Hence, this technique would allow for the position measurement of a short electron bunch in the presence of a more intense but longer proton bunch. The design considerations, numerical analysis and plans for tests at the CERN Linear Electron Accelerator for Research (CLEAR) facility are presented.

INTRODUCTION

The AWAKE experiment uses the wakefields generated by a long proton bunch with length of the order of a few hundred ps to accelerate short electron bunches [1]. The set-up is shown in Figure 1. The proton bunches arrive every 15-30 s from the SPS and their typical parameter ranges are given in Table 1. They then propagate colinearly with a 120 fs long, 780 nm central wavelength laser pulse inside a 10 m long rubidium (Rb) vapour source. The laser is used to singly ionise the Rb vapour to a plasma with the same density as the vapour. This density can be chosen in the range $1\text{-}10\times10^{14}$ cm^{-3} required for the generation of wakefields of the order of 1 GV/m [2]. To effectively drive large amplitude wakefields, the drive bunch should have transverse and longitudinal sizes of the order of the plasma wavelength which for the given plasma density range is ~1 mm. Since the proton bunch is several cm long, the generation of large amplitude wakefields relies on a process called seeded self-modulation (SSM). Here, the proton bunch is divided into a train of micro-bunches with longitudinal size less than and period equal to the plasma wavelength [3]. The relativistic ionisation front of the laser pulse seeds the self-modulation process creating a reference phase for the correct injection of electrons in order for them to be focussed and accelerated. During Run 1 (2016-2018), the self-modulation of an SPS proton bunch into a train of over 20 micro-bunches and the acceleration of electrons from 19 MeV to 2 GeV in a 10 m plasma cell was successfully demonstrated [1]. The goals for Run 2 (2021-2024) include SSM via electron bunch seeding and the addition of a density step in the vapour source for maintaining wakefield amplitudes at maximum level over longer distances [4].

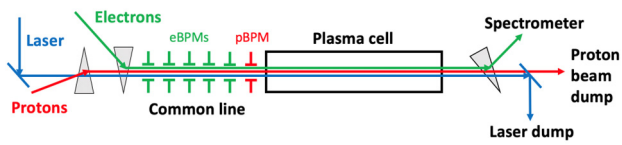

Figure 1: Schematic of the AWAKE experiment.

Amongst the diagnostics for measuring the occurrence of SSM in the proton bunch and the electron beam parameters after acceleration, the measurement of the beam position of the electron and proton bunches before the plasma cell for alignment purposes is a crucial aspect of the experiment. The beam position monitoring system for the protons is composed of 21 dual plane button-style beam position monitors (BPMs) between the extraction point from the SPS to downstream of the plasma cell [5]. For the electrons, there are 5 shorted stripline BPMs in the common beam line as shown in Figure 1. The electron BPMs operate at 404 MHz with position resolution of 10 μm in both planes [6].

Table 1: Proton and Electron Parameters at AWAKE [7]

Parameter	Protons	Electrons
Energy/GeV	400	0.01-0.02
Bunch length/ps	200-400	0.3-10
Bunch charge/nC	48	0.1-1

MOTIVATION FOR A HIGH FREQUENCY ELECTRON BEAM POSITION MONITOR

In the common beam line at AWAKE, both proton and electron bunches are present. The electron BPM system operating at 404 MHz are able to detect electrons when the protons are not present. If both beams are present, the proton signal dominates and prevents the position

† collette.pakuza@physics.ox.ac.uk

ISBN: 978-3-95450-227-1 ISSN: 2673-5490 doi:10.18429/JACoW-IPAC2022-MOPOPT054

A MODIFIED NOMARSKI INTERFEROMETER TO STUDY SUPERSONIC GAS JET DENSITY PROFILES

C. Swain*, J. Wolfenden, A. Salehilashkajani, H. D. Zhang, O. Apsimon, C. P. Welsch,
Cockcroft Institute and University of Liverpool, Warrington, Cheshire

Abstract

Gas jet-based non-invasive beam profile monitors, such as those developed for the high luminosity Large Hadron Collider (HL-LHC) upgrade, require accurate, high resolution methods to characterise the supersonic gas jet density profile. This paper proposes a modified Nomarski interferometer to non-invasively study the behaviour of these jets, with nozzle diameters of 1 mm or less in diameter. It discusses the initial design and results, alongside plans for future improvements. Developing systems such as this which can image on such a small scale allows for improved monitoring of supersonic gas jets used in several areas of accelerator science, thus allowing for improvements in the accuracy of experiments they are utilised in.

INTRODUCTION

The beam gas curtain (BGC) under development by the Cockcroft Institute, CERN, and GSI utilises a supersonic gas jet to monitor the beam with minimal invasiveness [1] [2]. The main working principles of this monitor which are being tested are ionisation and fluorescence [3]; the signal intensity produced by both of these processes are proportional to the density of the gas jet. Therefore, this a priori characterisation of the gas jet density profile is critical to the operation of a BGC and its behaviour must be studied. For this purpose, a modified Nomarski interferometer [4] has been designed to conduct non-invasive interferometric imaging. The entire optical system has been constructed on a single optical path, which connects directly to the outside of the vacuum chamber. The Nomarski style was chosen due to the single laser path, reducing the system size and chance of calibration errors. This specific design utilises a Wollaston prism to create the interferogram [5]. Following initial calibration, single shot measurements can be analysed instantly using a standard Fourier analysis methodology [6, 7]. This paper presents the design and set up of the current interferometer, alongside initial images, limitations, and planned improvements for the system.

INTERFEROMETRY THEORY

The modified Nomarski interferometer used for this design utilises a Wollaston prism, two triangular prisms made of birefringent material which create a polarising beam splitter when placed together [8]. The two sections are oriented such that the optical axes are perpendicular. A beam hitting the prism and crossing the boundary between the two halves diverges into an ordinary and extraordinary ray with orthogonal polarisations. As the two beams are from a single point source, they are coherent and therefore capable of interference. Interferometers utilise this interference to generate images (or interferograms) which show changes in phase shift that have occurred to the waves.

The phase shift of a light wave propagating through a material is caused by the change in the effective refractive index it experiences. The Lorentz-Lorentz equation states that for gases with a refractive index (η) close to 1, the number density is related via Eq. (1) [9].

$$\rho \approx (\eta - 1)\frac{2}{3}\frac{N_A}{A} \tag{1}$$

where the density is given in cm^{-3}, N_A is Avogadro's constant ($6.022 \times 10^{23}\ \mathrm{mol}^{-1}$), and A is the molar refractivity (for nitrogen, $A = 4.46\ \mathrm{cm}^3\ \mathrm{mol}^{-1}$ [10]). This equation can then be used to show how the phase shift is directly dependant on the density of the gas flow [5]:

$$\Delta\phi = l\frac{3\pi}{\lambda}\frac{A}{N_A}\rho \tag{2}$$

where λ is the laser wavelength and l is the laser path length through the gas jet, in this case taken as equal to the nozzle throat. As the density and phase shift are linked, interferograms can therefore be used to calculate the changing density profile of a gas jet.

EXPERIMENTAL SET UP

Figures 1 and 2 show the components of the interferometer system before and after the chamber. In Fig. 1, a 532 nm laser propagates through a linear polariser and beam expander before passing through the chamber. A 10x beam expander was introduced to the set up as the Gaussian profile of the laser caused changes in intensity, which created irregularities at the edges of the interferograms, affecting the accuracy of the results. In Fig. 2, after the chamber, an achromatic doublet lens with a focal length of 150 mm focused the laser onto a CMOS camera. The lens also provided a magnification factor of 2. The Wollaston prism was adjustable across a range of 180 mm to allow for fringe spacings (δ_f) to be altered, as shown in Eq. (3) [11].

$$\delta_f = \frac{\lambda b}{\epsilon a} \tag{3}$$

where λ is the wavelength of the laser, ϵ is the separation angle of the Wollaston prism, b is the distance between the prism and the imaging plane (in this case the CMOS), and a is the distance between the focusing lens and the prism. The secondary polariser was set orthogonal to the first. This meant that any light from the laser which was not refracted

* Catherine.Swain@liverpool.ac.uk

ISBN: 978-3-95450-227-1 ISSN: 2673-5490 doi:10.18429/JACoW-IPAC2022-MOPOPT055

A GAS JET BEAM PROFILE MONITOR FOR BEAM HALO MEASUREMENT

O. Stringer†, H. Zhang[1], N. Kumar[1], C. Welsch[1]
University of Liverpool, Liverpool, United Kingdom
[1]also at Cockcroft Institute, Warrington, United Kingdom

Abstract

The gas jet beam profile monitor is a non-invasive beam monitor that is currently being commissioned at Cockcroft Institute. It utilises a supersonic gas curtain which transverses the beam at an angle of 45 degrees and measures beam-induced ionisation interactions of the gas to produce a 2D transverse beam profile image. This paper builds upon previously used single-slit skimmers and improves their ability to form the gas jet into a desired distribution for imaging beam halo. A skimmer device removes off-momentum gas particles and forms the jet into a dense thin curtain, suitable for transverse imaging of the beam. The use of a novel double-slit skimmer is shown to provide a mask-like void of gas over the beam core, increasing the relative intensity of the halo interactions for measurement. Such a non-invasive monitor would be beneficial to storage rings by providing real time beam characteristic measurements without affecting the beam. More specifically, beam halo behaviour is a key characteristic associated with beam losses within storage rings.

INTRODUCTION

Beam halo is typically regarded as a region of particles outside the beam core but the distinction of the boundary between beam profile and beam halo is highly dependent on the application. Differing machines and the perspectives between instrumentation specialists and accelerator physicists give a range of definitions. A geometric perspective could be chosen, describing it as density distributions beyond n sigma or from a formation perspective, as a function of the space charge or parametric resonance [1]. In this paper, beam halo shall be defined simply by a low-density region surrounding the central beam core. Further expansion upon this definition is not required due to the proof of concept diagnostics device utilised, and a low energy, 5 keV electron beam used to demonstrate the available imaging region intended on capturing the halo.

Typical diagnostics methods for beam halo include wire scanners, scrapers and screens [1]. These are all inherently destructive in nature, especially when one regards their cumulative effects in storage rings. As such, non-invasive techniques are required for halo monitoring, such as coronagraphing synchrotron radiation with optical masks [2,3]. The Beam Gas Curtain (BGC) aims to provide an alternative method of non-invasive beam diagnostics that may be more suited to specific beam conditions.

The BGC diagnostics tool utilises a thin, supersonic gas curtain inclined at a 45-degree angle to provide ionisation and fluorescent interactions between the working gas and beam [4-6]. The setup used here was configured as an Ionisation Profile Monitor (IPM). The gas ions created can be collected upon a phosphor screen and Micro Plate Channel (MCP) above the interaction point to provide a real-time recreated 2D image of the beam at the location of interaction

The gas used is accelerated to a supersonic speed in the continuum flow regime and propagates through three

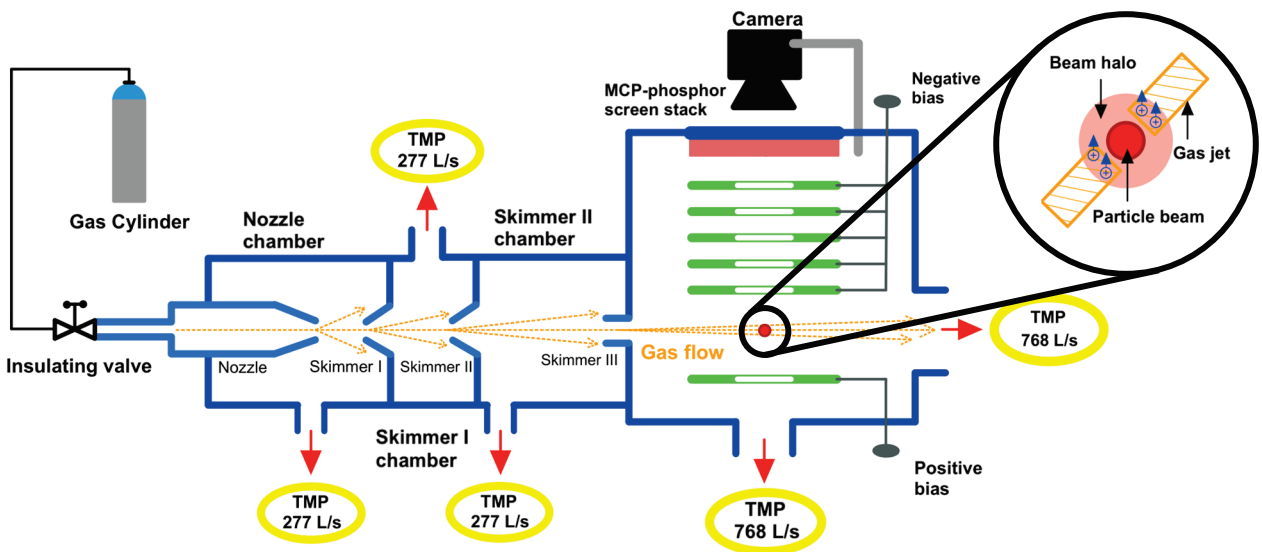

Figure 1: The layout of the Beam Gas Curtain setup configurated as an Ionization Profile Monitor for halo monitoring.

† O.Stringer@liverpool.ac.uk

ISBN: 978-3-95450-227-1 ISSN: 2673-5490 doi:10.18429/JACoW-IPAC2022-MOPOPT056

COMMISSIONING OF A GAS JET BEAM PROFILE MONITOR FOR EBTS AND LHC

H.D. Zhang*, N. Kumar, A. Salehilashkajani, O. Sedlacek, O. Stringer, C.P. Welsch,
Cockcroft Institute and University of Liverpool, WA4 4AD Warrington, United Kingdom
M. Ady, T. Lefevre, S. Mazzoni, I. Papazoglou, A. Rossi, G. Schneider, K. Sidorowski, R. Veness
CERN, 1211 Geneva, Switzerland
P. Forck, S. Udrea
GSI Helmholtzzentrum für Schwerionenforschung GmbH, 64291 Darmstadt, Germany

Abstract

A gas jet beam profile monitor was designed for measuring the electron beam at the electron beam test stand (EBTS) for the Hollow electron lens (HEL) and the proton beam in the large hadron collider (LHC). It is partially installed in the LHC during the second long shutdown. The current monitor is tailored to the accelerator environment including vacuum, geometry, and magnetic field for both the EBTS and the LHC. It features a compact design, a higher gas jet density, and a wider curtain size for a better integration time and a larger detecting range. In this contribution, the commissioning of this monitor at the Cockcroft Institute will be discussed.

INTRODUCTION

A Beam Gas Curtain (BGC) instrument is currently under development in the framework of the HL-LHC beam diagnostic upgrade. This instrument aims to develop a versatile beam profile monitor for the LHC and an overlap monitor for the Hollow Electron Lens (HEL)[1]. The HEL will be used to actively scatter the halo particles of the LHC beams by letting them interact with a hollow electron beam confined in an high magnetic field superconducting solenoid. Therefore, the homogeneity and the position of the hollow electron beam will be crucial for the successful operation of the HEL and is intended to be measured by the BGC instrument.

For the LHC and HEL, the destructive power of the beams makes all intercepting instruments fragile and thus not applicable. The widely used ionisation profile monitors (IPM)[2–4] and beam-induced fluorescence monitors (BIFs)[5, 6] based on the interaction of charged particle with the residual gas in the vacuum vessel would also be perturbed by space charge effect and the high external magnetic field. In addition, the ultrahigh vacuum environment in the LHC would also limit the sensitivity of such instruments.

To increase the signal level for IPMs and BIFs, one idea is to introduce the gas into the diagnostics chamber with needle valves[7]. More efficiently, one can use a gas jet [8–10] which is more controllable, with higher local density and easier to pump out. The latter feature will help maintain an ultrahigh vacuum environment.

Previously, an IPM based on the supersonic gas jet [11, 12], was demonstrated for detecting a two-dimensional beam profile and the vacuum feature [13] was proved. Recently, a BIF monitor based on a similar supersonic gas jet [14, 15] showed that by using a short-lived or neutral light emitters, the distortion due to the space charge effect and external magnetic field can be minimized. In both applications, the supersonic gas jet was generated by letting the working gas, usually, nitrogen or neon with a stagnation pressure of 5 bar from the gas bottle, flow through a 30 µm flat nozzle continuously into a nozzle chamber where the background pressure is maintained at $\sim 5\times10^{-3}$ mbar. Then the generated jet will be collimated through 2 conical skimmers with opening diameters of 180 µm and 400 µm and shaped into a curtain-like jet with either a pyramid or flat third skimmer which has a slit opening with a size of 0.4 mm×4 mm tilted at 45°. As shown in Fig. 1, the charged particle beam will interact with the molecules in the jet and generate secondaries such as electrons, ions and fluorescent photons which can be detected to represent the original beam profile with two-dimensional information. The gas jet density at the interaction point can reach $\sim 1\times10^{16}$ m^{-3}[16], which gives an estimation of the integration time of ~1 s for both the LHC and HEL applications. These discoveries pave the way for designing beam profile monitors for the LHC and the Electron Beam Test Stand (EBTS) for the HEL.

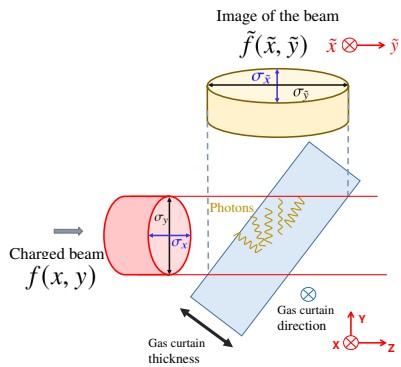

Figure 1: The principle of the gas jet curtain beam profile monitor[15].

To satisfy the LHC installation requirement, the device is redesigned to fit into the tunnel and the design principle has been discussed in [14]. Compared with the previous version [15, 17] developed in the Cockcroft Institute (CI), it features a compact overall structure with a modified geometry of the

* haozhang@liverpool.ac.uk

ISBN: 978-3-95450-227-1 ISSN: 2673-5490 doi:10.18429/JACoW-IPAC2022-MOPOPT057

UPDATES IN EFFORTS TO DATA SCIENCE ENABLED MeV ULTRA-FAST ELECTRON DIFFRACTION SYSTEM

T. B. Bolin†, S. G. Biedron[1,2], M. Martínez-Ramón, S. I. Sosa,
Department of Electrical and Computer Engineering, University of New Mexico, NM 87131, USA
M. Babzien, K. Brown, M. Fedurin, J. Li, M. Palmer,
Brookhaven National Laboratory, Upton, NY 11973, USA
D. E. Martin, M. E. Papka[3],
Argonne National Laboratory, IL 60439, USA
[1]also at Department of Mechanical Engineering, University of New Mexico, NM 87131, USA
[2]also at Element Aero, Chicago, IL 60643, USA
[3]also at Department of Computer Science, Northern Illinois University, IL 60115, USA

Abstract

A MeV ultrafast electron diffraction (MUED) instrument is a unique characterization technique to study ultrafast processes in materials by a pump-probe method. This relatively new technology can be advanced further into a turn-key instrument by using data science and artificial intelligence (AI) techniques in conjunctions with high-performance computing (HPC). This can facilitate auto-mated operation, data acquisition and real-time or near-real-time processing. AI-based system controls can pro-vide real-time feedback on the electron beam which is currently not possible due to the use of destructive diagnostics. Deep learning can be applied to the MUED diffraction patterns to recover valuable information on subtle lattice variations that can lead to a greater understanding of a wide range of material systems. A data science enabled MUED facility will also facilitate the application of this technique, expand its user base, and provide a fully automated state-of-the-art instrument. We will pro-vide updates on research and development efforts the MUED instrument in the Accelerator Test Facility of Brookhaven National Laboratory.

INTORDUCTION

MeV ultrafast electron diffraction (MUED) is a pump-probe characterization technique for studying ultrafast processes in materials. The use of relativistic beams leads to decreased space-charge effects compared to typical ultrafast electron diffraction experiments employing energies in the keV range [1, 2]. Compared to other ultrafast probes such as X-ray free electron lasers, MUED has a higher scattering cross section with material samples and allows access to higher order reflections in the diffraction patterns due to the short electron wavelengths.

However, this is a relatively new technology and several factors contribute to making it challenging to utilize, such as beam instabilities which can lower the effective spatial and temporal resolution. In the past years, machine learning (ML) approaches to materials and characterization techniques have provided anew path towards unlocking new physics by improving existing probes and increasing the user's ability to interpret data. Particularly, ML methods can be employed to control characterization probes in near-real time, acting as virtual diagnostics, or ML can be deployed to extract features and effectively denoise acquired data. In this later case, convolutional neural network architectures such as auto encoder models are an attractive and more powerful alternative to conventional denoising techniques. The autoencoder models provide a method of unsupervised learning of latent space representation of data that can help reduce the noise in the data. By supplying a paired training dataset of "noisy" and "clean" data, these ML models can denoise measurements quite effectively [3, 4]. This method relies on the existence of an ideal dataset with no noise which can be obtained by simulation or by averaging existing noisy datasets. However, in some cases these are not accessible or practical to use. Generative adversarial networks (GANs) are a more suitable option when no "clean" data are available and have been proven to perform well for blind image denoising [5]. They can be trained to estimate and generate the noise distribution, thus producing paired training datasets that can be fed to an autoencoder model. These approaches can lead to increased resolution if employed to denoise, for example, diffraction patterns. In addition, deep convolutional neural network architectures can be used for data analysis. Laanait et. al., for instance, measured diffraction patterns of different oxide perovskites using scanning transmission electron microscopy and, by applying a custom ML algorithm, were able to invert the materials structure and recover 3-dimensional atomic distortions [6]. ML has yet to be applied to the MUED technique, where it can certainly enable advances that can further our understanding of ultrafast material processes in a variety of systems.

EXPERIMENTAL

The MUED instrument is located at the Accelerator Test Facility at Brookhaven National Laboratory. A schematic representation of the experimental setup is presented in Fig.1. The details of data collection are very briefly. described here. The femtosecond electron beams are generated using a frequency-tripled Ti:Sapphire laser that illuminates a copper photocathode, generating a high brightness beam. The electrons are then accelerated and

† tbolin@unm.edu.

ISBN: 978-3-95450-227-1 ISSN: 2673-5490 doi:10.18429/JACoW-IPAC2022-MOPOPT058

MACHINE LEARNING TRAINING FOR HOM REDUCTION IN A TESLA-TYPE CRYOMODULE AT FAST*

J. Diaz Cruz[1†], A. Edelen, J.P. Sikora, B. Jacobson, SLAC, Menlo Park, CA 94720, USA
A. Lumpkin, D. Edstrom, R. Thurman-Keup, FNAL, Batavia, IL 60510, USA
[1]also at University of New Mexico, Albuquerque, NM 87131, USA

Abstract

Low emittance electron beams are of high importance at facilities like the Linac Coherent Light Source II (LCLS-II) at SLAC. Emittance dilution effects due to off-axis beam transport for a TESLA-type cryomodule (CM) have been shown at the Fermilab Accelerator Science and Technology (FAST) facility. The results showed the correlation between the electron beam-induced cavity high-order modes (HOMs) and the Beam Position Monitor (BPM) measurements downstream the CM. Mitigation of emittance dilution can be achieved by reducing the HOM signals. Here, we present a couple of Neural Networks (NN) for bunch-by-bunch mean prediction and standard deviation prediction for BPMs located downstream the CM.

INTRODUCTION

Low emittance electron beams are of high importance in accelerating structures at large facilities like the LCLS-II at SLAC. With a set of experiments performed at FAST, it was shown that off-axis beam transport may result in emittance dilution due to transverse long-range (LRW) and short-range wakefields (SRW) [1, 2]. A set of LRWs known as Higher-Order Modes (HOM) have amplitudes that are proportional to beam offset, charge and coupling impedance (R/Q). Therefore, reducing HOM signals may help to mitigate emittance dilution effects.

In order to further investigate the relation between HOMs and beam offset, a new set of experiments were performed at FAST. This time, two 4-channel HOM detectors were used to measure signals at the upstream (US) and downstream (DS) couplers of 8 superconducting RF (SRF) cavities inside a Tesla-type CM [3]. The new results showed a correlation between the electron beam-induced cavity HOM signal levels and bunch-by-bunch mean and centroid slewing at 11 BPMS located downstream of the CM [4]. In this paper, we evaluate two NN models for bunch-by-bunch mean prediction and centroid slewing prediction based on HOM signals, with the goal of using them for a controller that can drive the steering magnets to minimize beam offset and HOM signals.

* Work supported under contract DE-AC02-76SF00515 with the U.S. Department of Energy.
Work supported by Fermi Research Alliance, LLC under Contract No. DE-AC02-07CH11359 with the U.S. Department of Energy
† dejorge@slac.stanford.edu

EXPERIMENTAL SETUP AND DATA ACQUISITION

The Hardware

The Integrable Optics Test Accelerator (IOTA) at the FAST facility has a unique configuration of two TESLA-type SRF cavities after a photocatode RF gun, followed by an 8-cavity CM, similar to the LCLS-II CMs. Four meters US the CM, there is a set of horizontal and vertical correctors (H/V125) used to steer the electron beam and there are 11 BPMs DS the CM over a 80 m length.

Two 4-channel chassis were built to detect the magnitude of the HOMs at the US and DS couplers of each SRF cavity. Each channel has a 1.3 GHz notch filter to reduce the nominal resonant frequency, a bandpass filter centered at 1.75 GHz with 300 MHz bandwidth to emphasize the main TE111 HOM dipole modes, and a Schottky diode for HOM detection. More details are found in [3].

The Experiment

An electron beam of 50 bunches and 3 MHz bunch repetition rate is produced at the RF gun with an energy of <5 MeV. This bunch pattern repeats at 1 Hz and each repetition is called a "shot". After the two capture cavities (CC1 and CC2), the 25 MeV beam is transported to and through the CM with an exit energy of 100 MeV. HOM waveforms and BPM data are capture while steering the beam using the H/V125 corrector magnets, for different values of bunch charge. First, a "reference" trajectory is found manually by minimizing as many US HOM signals as possible by steering the beam. Then, we capture HOM and BPM data for this reference trajectory and for several values of bunch charge. We then repeat the previous measurements for values of the corrector currents from -1.5 A to 1.5 A in 0.5 A steps.

The Data

An US HOM waveform example for all 8 cavities is shown in Fig. 1. Although several features can be extracted from each of these waveforms (rising time, oscillation frequency, decaying time), we decided to use the peak value as a representative number. Averaging the peak value over 300 shots, the relation between V125 corrector current and HOM signal peaks average is shown in Fig. 2.

BPM average measurements over 300 shots are shown in Fig. 3. Removing the mean of each curve to center them at zero, the evolution of the relative beam centroid position can be seen in Fig. 4. A clear slew is present in the centroid position measurements, which is proportional to the V125

ISBN: 978-3-95450-227-1 ISSN: 2673-5490 doi:10.18429/JACoW-IPAC2022-MOPOPT062

FOIL FOCUSING EFFECT IN PEPPER-POT MEASUREMENTS IN INTENSE ELECTRON BEAMS*

S. Szustkowski†, M. A. Jaworski, D. C. Moir,
Los Alamos National Laboratory, Los Alamos, NM, USA

Abstract

Thin conducting foils, such as pepper-pot masks, perpendicular to an oncoming intense electron beam acts like an imperfect axisymmetric lens. The beamlets distribution from a pepper-pot mask varies based on if the mask hole radius is smaller or larger than the beams Debye length. Correcting for focusing effect is necessary for measuring transverse emittance with pepper-pot technique for intense electron beams. The Dual Axis Radiographic Hydrodynamic Test Facility (DARHT) Axis-I produces a 20 MeV, 2 kA, 80 ns FWHM electron beam for flash radiography. In this paper, we explore the effect of foil focusing due to various pepper-pot masks at DARHT Axis-I injector region from a 55 mm velvet cathode.

INTRODUCTION

Diagnostics of charged particle beams is a critical component in accelerators in understanding the underlying physics and attributes of the beam such as the emittance. One such diagnostic is pepper-pot emittance measurements, where a single shot is used to obtain data [1], whereas a solenoid scan requires several shots [2]. In the regime of intense relativistic electron beams (IREB), thin conducting foils, such as a pepper-pot mask, shorts out the transverse electric field of the beam. This causes a pinching effect to the beam due to its self-magnetic field. The transverse radial momentum receives a kick, thus the beam will have a focusing effect [3,4].

For a thermal distribution the normalized thermal beam emittance, for a given effective beam radius a, is defined as [5]

$$\epsilon_n = 2a\sqrt{\frac{k_B T\gamma}{mc^2}}, \tag{1}$$

where T is the beam transverse temperature in the laboratory frame. The beam acts like a non-neutral plasma, with density n_e, such that local charge perturbation of the beam distribution in an external focusing field will be shielded off at a distance corresponding to the Debye length λ_D. The Debye length is defined as

$$\lambda_D = \sqrt{\frac{\epsilon_0 k_B T\gamma^2}{n_e q^2}}. \tag{2}$$

When self-field effects dominate the beam, the beam radius is larger compared to the Debye length ($\lambda_D \ll a$), and the distribution is uniform. Whereas if the Debye length is larger compared to the beam radius ($\lambda_D \gg a$), the beam will be emittance dominated, exhibiting single particle behavior, and the distribution is Gaussian [6].

Using the definition of the Alfvén current limit, $I_A = 4\pi\epsilon_0 mc^3\beta\gamma/q$, and beam current, $I_B = n_e q a^2 \pi\beta c$, combining them with Eqs. (1) and (2) the Debye length can be rearranged in terms of the normalized emittance and beam current as

$$\lambda_D = \frac{\epsilon_n}{4}\sqrt{\frac{I_A}{I_B}}. \tag{3}$$

For the same initial beam attributes in varying external focusing field, the Debye length remains constant. In IREBs the Debye length is on the same order as machined holes in a pepper-pot mask. The evolution of beamlets that are produced by the mask will propagate differently based on the hole diameter.

EXPERIMENTAL ARRANGEMENT

The experiment was taken in the injection region of DARHT Axis-I, where a 55 mm velvet cathode was used. The electron beam energy during measurements was 3.25 MeV, with a current of 1.6 kA. A pepper-pot mask was placed at 41.3 cm, and 13.9 cm respectively, from an optical transition radiation (OTR) screen. The OTR screen is situated 50° to the beamline. During the run with a Debye mask it was placed 13.9 cm away from the OTR detector as illustrated in Fig. 1.

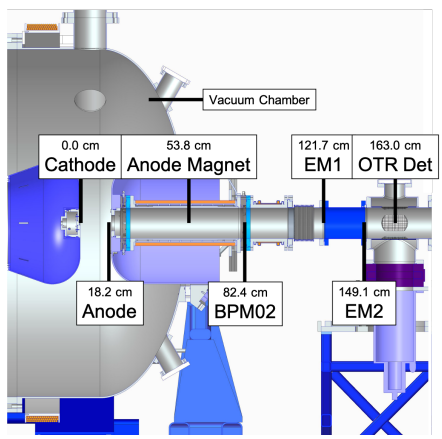

Figure 1: DARHT Axis-I injector region.

The pepper-pot mask has hole diameter of 2.0 mm with a rectangular grid spacing of 7.5 mm. The Debye mask

* Work supported by the US Department of Energy through the Los Alamos National Laboratory. Los Alamos National Laboratory is operated by Triad National Security, LLC, for the National Nuclear Security Administration of the U.S. Department of Energy (Contract No. 89233218CNA000001).
† sszustkowski@lanl.gov

ISBN: 978-3-95450-227-1 ISSN: 2673-5490 doi:10.18429/JACoW-IPAC2022-MOPOPT063

RECONSTRUCTION OF BEAM PARAMETERS FROM BETATRON RADIATION USING MAXIMUM LIKELIHOOD ESTIMATION AND MACHINE LEARNING

S. Zhang[1*], M. Yadav[1,2†], C. Hansel[3], M. H. Oruganti[1], B. Naranjo[1],
P. Manwani[1], G. Andonian[1], O. Apsimon[1,2], C. Welsch[1,2], James Rosenzweig[1]
[1]Department of Physics and Astronomy, University of California Los Angeles, CA, USA
[2]Department of Physics, University of Liverpool, Liverpool, UK
[3]Department of Physics, University of Colorado Boulder, CO, USA

Abstract

Betatron radiation that arises during plasma wakefield acceleration can be measured by a UCLA-built Compton spectrometer, which records the energy and angular position of incoming photons. Because information about the properties of the beam is encoded in the betatron radiation, measurements of the radiation can be used to reconstruct beam parameters. One method of extracting information about beam parameters from measurements of radiation is maximum likelihood estimation (MLE), a statistical technique which is used to determine unknown parameters from a distribution of observed data. In addition, machine learning methods, which are increasingly being implemented for different fields of beam diagnostics, can also be applied. We assess the ability of both MLE and other machine learning methods to accurately extract beam parameters from measurements.

INTRODUCTION

In plasma wakefield acceleration, a dense drive beam generates a linear focusing force by repelling the plasma electrons away from its path while leaving the much heavier plasma ions uniformly distributed. Subject to this focusing force in plasma frequency k_β, electrons inside the witness beam then undergo harmonic transverse betatron oscillations, giving rise to betatron radiation. Because information about the properties of the beam is encoded in betatron radiation, measurements of this radiation can be used to reconstruct beam parameters, allowing devices which record information about betatron radiation, such as the UCLA-built Compton spectrometer, to be used for beam diagnostics. A variety of beam diagnostic devices and techniques already exist, such as the beam current transformer, used to measure beam intensity and charge, and LASER-Compton scattering, used to measure beam emittance and spot size[1]. Machine learning (ML) methods are also implemented for different fields of beam [2]. For example, the application of convolutional neural networks at FAST is able to produce a prediction for various downstream beam parameters from simulated datasets[3], and ML may also have the potential to be applied to betatron radiation diagnostics. Another method of extracting information about beam parameters from measurements of radiation is maximum likelihood estimation (MLE), a statistical technique used to determine unknown parameters from a given distribution of observed data. The goal of this work is to assess the ability of both maximum likelihood estimation and machine learning as methods for accurately extracting a beam parameters from measurements of betatron radiation.

MAXIMUM LIKELIHOOD ESTIMATION

The method of maximum likelihood estimation involves some probability distribution function $f(x|\sigma)$, which specifies the probability of observing a data vector x given the parameter σ. The probability distribution function is related to a likelihood function $L(\sigma|x)$ by $L(\sigma|x) = f(x|\sigma)$, where $L(\sigma|x)$ specifies the likelihood of σ given x. Given a set of N observations of data vectors, the overall likelihood is the product of the likelihoods for each individual data vector [4], and the value of the parameter σ which is most likely to have produced the set of observed data is determined by maximizing the likelihood with respect to σ. Because working with log-likelihood, rather than raw likelihood, avoids possible problems with arithmetic underflow [5], this work performs MLE with the log-likelihood, which is given by

$$\ln L(\sigma|x_1, x_2, ..., x_N) = \sum_{n=1}^{N} \ln L(\sigma|x_n), \qquad (1)$$

where the product of likelihoods has been converted into a sum of log-likelihoods.

BEAM PARAMETER RECONSTRUCTION USING MLE

The first task tackled by this work was to correctly identify a beam's spot size from its radiation spectrum using MLE. The process described here is easily applied to other beam parameter reconstruction tasks.

First, several simulations of betatron radiation from beam particles in a plasma wakefield accelerator were run for beams of different spot sizes. The results of these simulations, plotted as 1D energy spectra, are shown in Fig. 1. This work uses a simulation in which particles are sampled from a beam and tracked through idealized fields. Betatron radiation was computed for a single particle using Lié-

* s.ziqianzhang@gmail.com
† monika.yadav@liverpool.ac.uk

ISBN: 978-3-95450-227-1 ISSN: 2673-5490 doi:10.18429/JACoW-IPAC2022-MOPOPT066

GAS SHEET DIAGNOSTICS USING PARTICLE IN CELL CODE

M. Yadav[1,2,3*], N. Cook[4], A. Diaw[4], C. Hall[4], N. Norvell [6], O. Apsimon [1,2], P. Manwani [3], J. Rosenzweig[3], C. Welsch[1,2], and G. Andonian[3,5]
[1]University of Liverpool, Liverpool, United Kingdom
[2] Cockcroft Institute, Warrington, United Kingdom
[3]University of California Los Angeles, Los Angeles, CA, USA
[4]RadiaSoft LLC, 3380 Mitchell Lane, Boulder, CO, USA
[5]Radiabeam Technologies, Santa Monica, CA, USA
[6]UC Santa Cruz, Santa Cruz, CA, USA

Abstract

As intense particle beams propagate in dense plasma or gas, ionization effects play an important role in the particle dynamics. Due to Ammosov-Delone-Krainov (ADK) ionization mechanisms, plasma electrons are generated, causing different instabilities, and difficulties, in achieving overarching physics goals of wakefield accelerators. Advanced accelerator experimental tests with high energy, high charge, and low mm-mrad emittance beams, require sophisticated beam diagnostics. Here, we will discuss ADK ionization using the fully parallel PIC code OSIRIS. Specifically, we focus on investigation of gas sheet ionization diagnostics for characterizing high intensity charged particle beams. The behavior of the ionization contains critical information on the parameters of the drive beam, which are unveiled by using sophisticated reconstruction algorithms or a spatial imaging detector. For the gas sheet, a 150 µm wide gas sheet of uniform density is generated for ionization. We study the ion profile that was generated in order to reconstruct the driver beam transverse profile. In future work, we investigate a device to detect the photons from the gas recombination that is induced in the interaction.

INTRODUCTION

Beam diagnostics play a vital role in secure and reliable operations of any particle accelerator. For high energy beams at the Facility for Advanced Accelerator Experimental Test (FACET-II)[1], non-destructive beam profile monitoring is critical. There are several methods available to measure the beam profile but, due to the high intensity beams at FACET-II (see Table 1), a sophisticated method for effectively measuring bunch parameters prior to, or at, interaction points is needed. In this paper, we examine ADK ionization using the fully parallel PIC code OSIRIS. We focus on understanding ionization of a thin gas sheet. Detection of ionization in a gas sheet interacting with the driver electron beam using sensitive monitors allows for minimally invasive measurements of the ions. Gas sheet ionization diagnostics, either by tunnel ionization or ADK ionization, are prime methods available to provide real time spot size information for intense beams at focal points where other techniques are unfeasible.

* monika.yadav@liverpool.ac.uk

INSTRUMENT OVERVIEW

The gas sheet ionization monitor is depicted in Fig. 1. The sophisticated imaging system consists of a high-pressure conical nozzle, shaping conical and rectangular skimmers, turbomolecular pumps for differential pumping, and an ion microscope (discussed in Ref. [2]). The gas jet generation and injection mechanism is relatively straightforward to implement compared to other complex injection schemes, such as optical or gas density down-ramp injections. The imaging system is based on an ion microscope subsystem, that is responsible for transporting, and imaging the ion beam that is generated at the gas sheet interaction region.

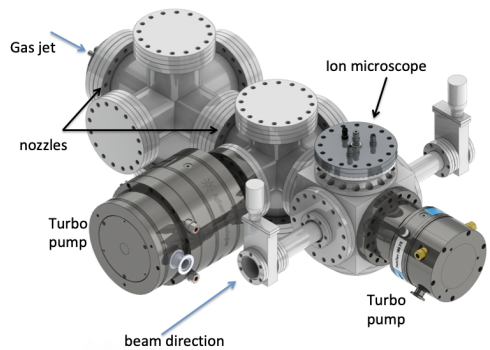

Figure 1: Gas sheet ionization monitor model. The system incorporates a series of skimmers and pumps to deliver a precision gas sheet at the interaction point.

The beam profile monitor under development is based on the experimental setup in Ref. [3]. The supersonic gas sheet, or gas curtain, enters the interaction chamber at a 45° orientation, where a beam of charged particles passes through the curtain perpendicular to its flow. The ions, and electrons, generated by the interaction between the neutral gas and the beam can then be detected using a dedicated imaging system to determine the transverse profile of the drive beam. Depending on the beam and gas sheet characteristics, transmission of ions varies from 50-100 percent for the range of interest. The primary factor in reduced transmission is the total charge of the ion beam, which increases space charge effects and drives expansion of the ion beam during transport. Simulations are used to generate training

ISBN: 978-3-95450-227-1 ISSN: 2673-5490 doi:10.18429/JACoW-IPAC2022-MOPOPT067

ELECTRON BEAM PHASE SPACE RECONSTRUCTION FROM A GAS SHEET DIAGNOSTIC

N. M. Cook*, A. Diaw, C. C. Hall, RadiaSoft LLC, Boulder, CO, USA
G. Andonian, RadiaBeam Technologies, Santa Monica, CA, USA
M. Yadav, The University of Liverpool, Liverpool, UK
N. P. Norvell, The University of California Santa Cruz, Santa Cruz, CA, USA

Abstract

Next generation particle accelerators craft increasingly high brightness beams to achieve physics goals for applications ranging from colliders to free electron lasers to studies of nonperturbative QED. Such rigorous requirements on total charge and shape introduce diagnostic challenges for effectively measuring bunch parameters prior to or at interaction points. We report on the simulation and training of a non-destructive beam diagnostic capable of characterizing high intensity charged particle beams. The diagnostic consists of a tailored neutral gas curtain, electrostatic microscope, and high sensitivity camera. An incident electron beam ionizes the gas curtain, while the electrostatic microscope transports generated ions to an imaging screen. Simulations of the ionization and transport process are performed using the Warp code. Then, a neural network is trained to provide accurate estimates of the initial electron beam parameters. We present initial results for a range of beam and gas curtain parameters and comment on extensibility to other beam intensity regimes.

INTRODUCTION

Next generation accelerator facilities necessitate novel diagnostics to characterize the transverse and longitudinal profiles for ultrashort, high brightness electron beams[1]. Typical methods employ intercepting monitors such as phosphor screens, scintillators, or wire scanners[2]. These techniques are unsuitable for facilities requiring non-intercepting diagnostics, or for which beam intensities exceed damage thresholds for the requisite monitors, as well as for novel plasma-based beam sources[3]. Noninvasive gas-based monitors have been explored as residual ionization profile monitors and induced fluorescence monitors, but are limited in their sensitivity for low charge, ultrashort bunches [4, 5]. Recent work has demonstrated the viability of an intense gas column and ion transport system to provide sufficient sensitivity and resolution to meet these demands[6].

In this paper, we describe simulation studies of a non-destructive single shot diagnostic and the development of a machine learning (ML) based reconstruction algorithm capable of characterizing beam parameters from the resulting ionization measurement. The design leverages a tailored gas curtain positioned at 45° angle with respect to the incoming beam. The incident beam ionizes the gas in the curtain, and the ion products are subsequently transported and magnified through an electrostatic microscope, consisting of a triplet of annular electrostatic plates accelerating and expanding the beam until it reaches an imaging system combining a micro-channel plate detector, phosphor screen, and camera[7]. Below we describe the simulation and analysis pathway developed to describe (1) the beam-gas interaction and ionization products, (2) the transport of the ions to an imaging system, and (3) an ML-based reconstruction algorithm for determining beam parameters based on the resulting image.

BEAM-INDUCED IONIZATION

Simulations of the beam-gas interaction were performed using the Warp particle-in-cell code[8]. Warp provides support for fully self-consistent electromagnetic propagation of intense beams in two and three-dimensional geometries, as well as support for external field maps to capture an arbitrary lens configuration. Warp also includes support for several relevant ionization models. In this paper, collisional ionization was captured using a binary-electron-dipole model with relativistic corrections[9], while tunneling ionization was captured using an ADK model implementation[10]. For extremely intense beams, tunneling ionization can become the dominant mechanism, resulting in aberrations in the ion distribution consistent with the electric field profile of the beam[11]. For most of the parametric regimes under consideration for initial tests, ADK ionization rates are insignificant and impact ionization is the principal mechanism.

TRANSPORT

Beam transport through the electrostatic lens was modeled again using the Warp code along with the ion distributions generated by the electron beam and gas sheet interaction. Electrostatic fields generated from CST Microwave Studio simulations of the ion microscope were imported into Warp alongside the initial ion profile. The beam was transported 170 mm from the beam axis and magnified ~10x through the imaging plane, where a synthetic diagnostic was applied to capture the 2D profile of the beam as it would be seen on the phosphor screen. To expedite simulations, a moving window was used, and a radial aperture condition was applied to remove electrons which would otherwise collide with the electrostatic column. Figure 1 depicts a typical beam envelope as it travels along the ion microscope.

* ncook@radiasoft.net

ISBN: 978-3-95450-227-1 ISSN: 2673-5490 doi:10.18429/JACoW-IPAC2022-MOPOPT069

A DATA-DRIVEN BEAM TRAJECTORY MONITORING AT THE EUROPEAN XFEL

A. Sulc*, R. Kammering, T. Wilksen, DESY, Hamburg, Germany

Abstract

Interpretation of data from beam position monitors is a crucial part of the reliable operation of European XFEL. The interpretation of beam positions is often handled by a physical model, which can be prone to modeling errors or can lead to the high complexity of the computational model. In this paper, we show two data-driven approaches that provide insights into the operation of the SASE beamlines at European XFEL. We handle the analysis as a data-driven problem, separate it from physical peculiarities and experiment with available data based only on our empirical evidence and the data.

INTRODUCTION

The European Free Electron Laser (EuXFEL) has been running with very high availability for several years. This high reliability put a lot of attention on the analysis of the operations on various levels. EuXFEL is a pulsed machine with a repetition rate of 10Hz and the properties of each shoot may change. Therefore, anomaly detection on linacs is still very limited. For beam trajectories, this is given by a very limited ability to explain how beam positions are affected by an ongoing anomaly since the beam trajectory changes for each injection. What makes the analysis of the beam even more challenging is that its trajectory can further vary from pulse to pulse due to various circumstances.

At the EuXFEL we are currently operating 103 beam position monitors (BPMs) at three SASE beamlines to measure the position of the beam passage through the undulator lines. All BPMs measure position and charge of up to 2700 bunches in a single bunch train. The absolute beam position is, unlike many other predictive maintenance tasks, a rather more approximate and global indicator, since the contribution of an issue on the beam position is often unknown.

The beam optics in the undulator lines is controlled by the use of a so-called FODO lattice. These alternating magnetic fields can introduce a periodic variation of the trajectory named betatron oscillation [1]. We can observe a specific periodic pattern of the electron bunches passing through the FODO lattice as shown in Fig. 1. This evidence imposes an assumption about the beam irrespective of its trajectory since the β-function of electron bunches will always follow the symmetry of the FODO lattice and should therefore preserve its period.

An ongoing problem might be indicated in various ways. For instance, if there is an anomaly on a magnet, the trajectory might be noticeably affected by an increased jitter.

One of the common approaches is modeling the beam trajectory and its comparison with a physical model [2].

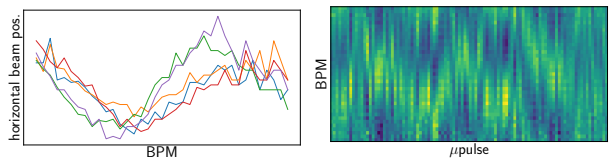

Figure 1: An example input to our methods. The left figure shows a series of the first five bunch trajectories at the SASE1 beamline after the mean of 600 bunches is subtracted. The right figure shows a series of bunches after substraction of mean. Each column is one μpulse.

A promising data-driven anomaly detection approach on synchrotons at LHC on BPM data was shown by Fol *et al.* [3, 4] to identify faulty BPMs.

We show two data-driven approaches based on our empirical evidence of the beam data at EuXFEL. The first use our assumption of the periodicity imposed by the FODO lattice and fits trajectories using a simplified assumption about the beam dynamics - mainly fitting a periodic - sine - function. The latter is a purely data-driven machine learning approach that trains to map a set of beam positions in arbitrarily long sequences to a common mode and any deviation from the mode is treated as an anomaly. This allows more flexibility in handling the input and can eventually reveal relations between bunch trains.

Our contributions can be summarized as follows: We show two data-driven approaches for the analysis of beam trajectories at the EuXFEL. The first is a method that takes into consideration a simplified empirical model of the lattice and measures the residual of this model. The second is a completely model-free approach based purely on data that models inputs from a set of multiple bunches.

In the following section, we introduce the notation and explain both proposed models. After, we show some experiments on the real data we experience at EuXFEL at SASE beamlines, and in the last section, we conclude our evaluation of the available real data.

METHOD

EuXFEL produces trains of electron bunches at a frequency up to 4.45MHz at a repetition rate of 10 Hz. These consecutive pulses vary in their individual properties and the resulting trajectory can vary from train to train. If a mean beam position is subtracted over a certain time range, we can obtain the underlying pattern formed by the magnets, as described in the introduction. Visually, it forms a characteristic periodical pattern, which can be seen after subtracting a mean trajectory which we consider as an input, see Fig. 1. Understanding these patterns provides important insights into underlying beam dynamics. The EuXFEL can

* antonin.sulc@desy.de

ISBN: 978-3-95450-227-1 ISSN: 2673-5490 doi:10.18429/JACoW-IPAC2022-MOPOTK001

THE INFLUENCE OF SOLENOID FIELD ON OFF-AXIS TRAVELLING BEAM IN AREAL ACCELERATOR

H.D. Davtyan*, A.H. Asoyan, G.A. Amatuni, M.G. Yazichyan, A.H. Grigoryan[1], Center for the Advancement of Natural Discoveries using Light Emission (CANDLE SRI), Yerevan, Armenia
[1]also at Yerevan State University, Yerevan, Armenia

Abstract

A wide range of experiments are being held at AREAL accelerator in the fields of materials science and life science by generating ultra-short 5 MeV electron beams. Beam parameter formation and stability preservation during the experiments are one of the key tasks of stable operation of the accelerator. Laser spot displacement on the photocathode could be one of the beam parameter distortion sources, which causes off-axis bunch travel also through the solenoid. The influences of laser spot horizontal displacement and the solenoid horizontal misalignment on the beam position at the experiment location are investigated separately via computer simulations. Using a laser spot mover and solenoid movers, an experiment has been carried out to compare simulation results with experiment.

INTRODUCTION

AREAL (Advanced Research Electron Accelerator Laboratory) is an RF gun-based laser-driven 20-50 MeV electron linear accelerator with low emittance (<0.3 mm-mrad) and ultrashort bunches (~500 fs) for advanced experimental studies in the area of novel accelerator concepts and coherent radiation sources, material and life science [1]. The AREAL RF gun operated in the S-band frequency (2.998 GHz), with the accelerating section 1.5 cell (total length 7.5 cm) and the maximum 110 MV/m accelerating gradient field. The RF gun, resulting to beam energies with up to 5 MeV energy. The focusing solenoid magnet is located in 0.586 m from the cathode (Fig. 1).

The off-axis beam can be the result of both laser spot displacement on photocathode and solenoid misalignment. For well aligned solenoid field the laser spot misalignment causes an off-axis traveling of electron bunches, due to initial offset and non-zero RF cavity radial field influence. The misaligned from the cathode beam is passing off-axis through the solenoid, thus causing additional distortion from magnetic fields. Besides, in the off-axis beams solenoid magnet causes the beam parameters distortion [2,3]. In the case of solenoid misalignment, only solenoid magnet causes beam parameters distortion. And therefore, the beam-based alignment of solenoid magnets is of great importance.

The integral distortions due to laser spot offset and off-axis magnetic fields were considered both by simulations and by experiments, as well. The beam centroid position and transfer rms sizes were in focus for observations. For the simulations, the ASTRA particle tracking code has been used [4].

davtyan@asls.candle.am

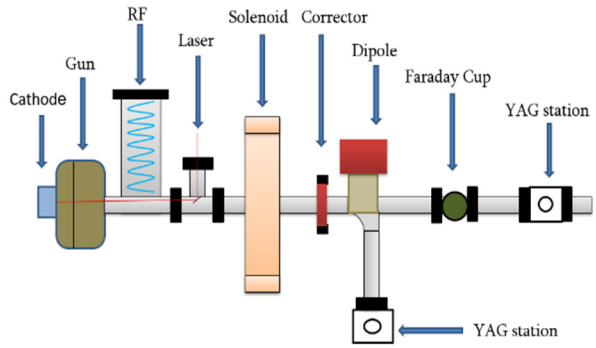

Figure 1: AREAL RF Gun layout.

THEORETICAL BASES

The transportation of electron beams in accelerator sections can be described by transfer matrices. The transfer matrices of a solenoid magnet cannot be divided into vertical and horizontal matrices, because there is a coupling between the two transverse planes in the solenoid magnet. For the hard-edge solenoid magnets, the rotational and focusing transverse matrix is well known [5]. The position of the particle with the initial coordinate of $X_0 = (x_0, x_0', y_0, y_0')$ at the exit of solenoid magnets can be found by relation

$$X_f = M_{rot} M_f X_0$$

where M_{rot} and M_f are rotational and focusing transfer matrices accordingly. The real solenoid can be presented by a series of hard-edge solenoids with various magnetic fields.

In a case of off-axis beams, the positions of particle will be

$$\check{X}_0 = X_0 + \delta X$$

where δX is deviation of the beam center from the axis. And hence δX is driving the beam center and rms sizes deviation respect to on-axis ones.

It is important to note that δX is a deviation of position and the momentum. It means that even if position deviations are zero, the slops can drive the beam position and emittance distortions.

COMPARISONS OF SIMULATION AND EXPERIMENTAL RESULTS

ASTRA Simulations

ASTRA particle tracking code based on non-adaptive Runge-Kutta integration of 4th order [4]. The

ISBN: 978-3-95450-227-1 ISSN: 2673-5490 doi:10.18429/JACoW-IPAC2022-MOPOTK002

FAST ORBIT RESPONSE MATRIX MEASUREMENT VIA SINE-WAVE EXCITATION OF CORRECTORS AT SIRIUS

M. M. S. Velloso*, F. H. de Sá, M. B. Alves
Brazilian Synchrotron Laboratory (LNLS), Campinas, Brazil

Abstract

Sirius is the new 4th generation storage ring based synchrotron light source built and operated by the Brazilian Synchrotron Light Laboratory (LNLS). In this work, we report on the implementation at Sirius of a fast method for orbit response matrix (ORM) measurement which is based on sine-wave parallel excitation of orbit corrector magnets' strength. This "AC method" has reduced the ORM measurement time from ~ 25 minutes to 2.5–3 minutes and displayed increased precision if compared to the standard serial measurement procedure. When used as input to the Linear Optics from Closed Orbits (LOCO) correction algorithm, the AC ORM yielded similar optics corrections with less aggressive quadrupoles strength changes.

INTRODUCTION

Orbit Response Matrix and Sirius' Setup

At Sirius, 160 *beam position monitors* (BPMs) read horizontal and vertical displacements of the electron beam. The BPMs data is arranged in a 320-component vector $\mathbf{u} = (x_1, x_2, \ldots, x_{160}, y_1, y_2, \ldots, y_{160})^\top$. A $\Delta\theta_j$ kick from the j-th corrector magnet (CM) causes an orbit distortion which is measured by the i-th BPM as the combination

$$\Delta u_i = \sum_{j=1}^{n} M_{ij} \Delta\theta_j. \tag{1}$$

M_{ij} are the entries of the orbit response matrix (ORM), which relates the orbit change due to CMs strength variations. At Sirius, $n = n_x + n_y = 280$ is the total number of CMs, with $n_x = 120$ and $n_y = 160$ being the number of horizontal (CHs) and vertical correctors (CVs), respectively. In matrix notation, the orbit distortion reads

$$\begin{bmatrix} \Delta\mathbf{x} \\ \Delta\mathbf{y} \end{bmatrix} = \begin{bmatrix} M_{xx} & M_{xy} \\ M_{yx} & M_{yy} \end{bmatrix} \begin{bmatrix} \Delta\theta_{\mathrm{CHs}} \\ \Delta\theta_{\mathrm{CVs}} \end{bmatrix}, \tag{2}$$

which highlights the diagonal blocks M_{xx} and M_{yy}, and off-diagonal blocks M_{xy} and M_{yx} of the ORM.

The ORM is essential to orbit correction, where we wish to minimize $\chi^2 = |\mathbf{u} - \Delta\mathbf{u}|^2 = |\mathbf{u} - M\Delta\theta|^2$, $\Delta\theta$ being the vector with entries $\Delta\theta_j$. The matrix also encodes information about the storage ring linear optics and is the input to the model-based correction algorithm LOCO [1, 2]

Fast Measurement Procedure: The "AC Method"

If we perform kicks to the beam using only one CM, say, the j-th CM, Eq. (1) reduces to $\Delta u_i = M_{ij}\Delta\theta_j$, giving $M_{ij} = \Delta u_i / \Delta\theta_j$. Therefore, by serially kicking the beam corrector by corrector and measuring the corresponding orbit distortions we can reconstruct the ORM column by column. This is the traditional procedure for measuring the ORM. At Sirius, it usually takes about 25 up to 30 minutes to be completed.

The alternative method we report here is based on the parallel, alternating excitation of the beam. This "AC method" was first implemented at the Diamond Storage Ring [3] and later at ALBA [4] and NSLS-II [5], where it proved to be a faster and reliable ORM measurement method. The general idea is to sinusoidally drive the beam by CMs at different frequencies so the harmonic signature in the BPMs readings holds information about several CMs' excitation at the same acquisition.

In the i-th BPM time series, we fit the beam motion to harmonic components at the CMs frequencies by solving the linear problem

$$\begin{bmatrix} \cos(2\pi f_1 t_1) & \sin(2\pi f_1 t_1) & \ldots \\ \cos(2\pi f_1 t_2) & \sin(2\pi f_1 t_2) & \ldots \\ \vdots & \vdots & \\ \cos(2\pi f_1 t_n) & \sin(2\pi f_1 t_n) & \ldots \end{bmatrix} \begin{bmatrix} b_{i1} \\ c_{i1} \\ \vdots \\ b_{im} \\ c_{im} \end{bmatrix} = \begin{bmatrix} u_i(t_1) \\ u_i(t_2) \\ \vdots \\ u_i(t_n) \end{bmatrix}, \tag{3}$$

where the cosines and sines columns at frequencies f_j repeat up to frequency f_m. We solve for the Fourier components $b_{i,j}$ and $c_{i,j}$ by least-squares, thus extracting the amplitudes $a_{i,j} = \sqrt{b_{i,j}^2 + c_{i,j}^2}$ and phases $\phi_{i,j} = \mathrm{atan2}(b_{i,j}, c_{i,j})$ from the beam motion imprinted by the CM oscillating at frequency f_j. The expected orbit distortions are $\Delta u_i(t_n) =$

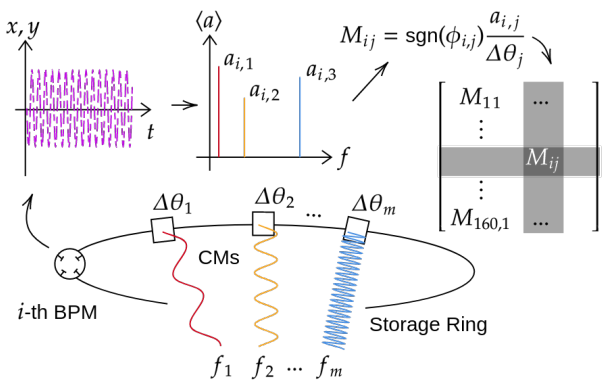

Figure 1: Parallel AC measurement of ORM: beam is excited by different CMs, each one at a different frequency. Spectral signature in beam motion reveals the amplitudes $a_{i,j}$, induced by the j-th CM to the beam as read by the i-th BPM.

* matheus.velloso@lnls.br

ISBN: 978-3-95450-227-1 ISSN: 2673-5490 doi:10.18429/JACoW-IPAC2022-MOPOTK003

ABSORBED DOSE CHARACTERISTICS FOR IRRADIATION EXPERIMENTS AT AREAL 5 MeV ELECTRON LINAC

V. Khachatryan*, Z. Amirkhanyan, H. Davtyan, B. Grigoryan, M. Ivanyan, V. Petrosyan, A. Vardanyan, A. Yeremyan, A. Grigoryan[1], CANDLE Synchrotron Research Institute, Yerevan, Armenia
[1]Also at Yerevan State University, Yerevan, Armenia

Abstract

Existing electron photogun facility at the CANDLE SRI currently can provide electron beam with the energy up to 5 MeV. The beam is being used as an irradiation source in the number of material science and life science experiments. Performed beam particle tracking simulations along with intensive application of the beam diagnostic instruments (bending magnet, YAG stations, Faraday cups) allow control of the experimental samples' irradiation parameters, particularly exposure times for given dose as well as absorbed dose spatial distribution.

Direct application of the electron beam for the irradiation experiments allows achievement of high absorbed dose. For the calculation of the irradiation parameters of the experimental sample particle transport simulation results should be combined with the beam current measurements by Faraday Cup (FC). Dose measurements and the comparison with digital simulations using various initial parameters (Transverse size, divergence and energy spread) permit to pin down their actual values.

INTRODUCTION

Numerous experiments on material science and radiation biology have been carried out at the AREAL linear accelerator aiming at investigation of the effect of the irradiation by the 5 MeV electron beam on the material or on organic sample [1]. The experimental programs scope includes though not limited to the issues a) The production of point defects (NV centres) in diamonds for hypersensitive magnetometry; b) The study of ultrafast electron beam induced non-equilibrium processes in semiconductors; c) Dose-rate effects of ultrashort pulsed electron beam irradiation on DNA damage/repair in human cancer cells [2-5]. The paper is focused on the methods of the calculation of experimental sample irradiation parameters based on beam parameters measurement and numerical simulation study of the electron beam interaction with the medium.

ELECTRON BEAM PARAMETERS AND ABSORBED DOSE

AREAL electron linac can produce clean and controllable 2-5 MeV electron beam with 30- 250 pC pulse charge and 1- 20 Hz repetition rate [6]. The main parameters of the electron beam are can be monitored and manipulated to apply precise irradiation dose for the experimental sample. AREAL uses photogun driven by 0.45 ps laser pulses thus conditioning short bunch duration taking into account that RF wavelength is 0.1 m. Main parameters of the AREAL electron beam are presented in Table 1.

Table 1: AREAL Beam Parameters

Energy	2–5 MeV
Pulse charge	30–250 pC
Pulse length	0.45 ps
Norm. emittance	≤ 0.5 mm-mrad
RMS energy spread	≤1.5 %
Pulse repetition rate	1-20 Hz
RF frequency	3 GHz

Following the recommendations of the International Commission on Radiation Units and Measurements (ICRU) one can find out absorbed dose from electrons by the formula $D = \varphi\left(S/\rho\right)_{col}$, where φ is electrons fluence (in 1/cm^2 units) and $\left(S/\rho\right)_{col}$ (in MeV cm^2/g units) is the mass collision stopping power, resulting from electron interactions with the orbital electrons in atoms [7,8]. The resulting formula for the absorbed dose rate will be:

$$\dot{D}\left[\frac{Gy}{s}\right] = \frac{Q[pC]\cdot n[Hz]}{e[C]\cdot A[\mathrm{cm}^2]} \times \left(\frac{S}{\rho}\right)_{col}\left[\frac{MeV\cdot cm^2}{g}\right] \times 10^{-3}.$$

Here $Q[pC]$ is the pulse charge in picocoulombs, $n[Hz]$ is repetition rate $e[C]$ is electron charge and $A[\mathrm{cm}^2]$ is beam spot size area at the sample surface. Since particles distributions are nearly Gaussian both in transverse vertical and horizontal directions A can be calculated as the area limited by ellipse $A = \frac{\pi}{4}XY$, where X *and* Y are beam spot sizes (FWHM) in horizontal and vertical directions.

BEAM PARAMETERS MEASUREMENTS

Advanced Research Electron Accelerator Laboratory (AREAL) based on photo cathode RF gun has been constructed at CANDLE.

The AREAL RF photogun experimental operation provides the electron bunches with up to 4.8 MeV energy and 5 nC mean current. The gun section contains the focusing solenoid, magnetic spectrometer, horizontal/vertical corrector magnet, Faraday Cups (FC) and YAG screens with cameras. The charge of individual bunches was measured using two FCs.

The beam energy and the energy spread measurements have been performed using the magnetic spectrometer

* khachatryan@asls.candle.am

ISBN: 978-3-95450-227-1 ISSN: 2673-5490 doi:10.18429/JACoW-IPAC2022-MOPOTK004

STATUS OF THE SOLEIL UPGRADE LATTICE ROBUSTNESS STUDIES

O.R. Blanco-Garcia*, D. Amorim†, M. Deniaud‡, A. Loulergue, L. S. Nadolski, R. Nagaoka
Synchrotron SOLEIL, L'Orme des Merisiers Saint-Aubin, BP 48 91192 Gif-sur-Yvette Cedex, France

Abstract

The SOLEIL synchrotron has entered its Technical Design Report (TDR) phase for the upgrade of its storage ring to a fourth generation synchrotron light source. Verification of the equipment specifications (alignment, magnets, power supplies, BPMs), and the methodology for optics corrections are critical in order to ensure the feasibility of rapid commissioning restoring full performance for daily operations. The end-to-end simulation, from beam threading in the first turns to beam storage and stacking, should be handled with a comprehensive model close to the actual commissioning procedure, taking into account all practical steps. During 2021 and 2022, the CDR lattice has undergone significant modifications in response to additional constraints. In this paper, we present an update of the robustness studies for the TDR baseline lattice.

INTRODUCTION

The SOLEIL Upgrade project aims to design and build a 2.75 GeV diffraction-limited synchrotron light source preserving the actual infrastructure, 29 beamlines (far-IR to hard X-rays) and the 500 mA uniform filling pattern. The lattice of the new storage ring presented in CDR report [1] is built over a non-standard combination of twelve 7BA cells and eight 4BA cells compliant with strong geometric constraints to produce a 80 pm rad natural emittance. The lattice can accommodate 20 straight sections (18 devoted for insertions devices) where the betatron functions at their centers are minimized to be closed to the matching value [1]. The compact injection uses a Multipole Injection Kicker (MIK) to inject the beam off-axis in the horizontal plane in a quasi-transparent way [2]. During the TDR phase significant modifications have been introduced leading to a new reference lattice [3]. The short straight sections were extended in order to allow the use of the existing in-vacuum insertion device, the tunability of the lattice has been improved, first mechanical integrations were considered, two double-waist mini-beta sections were introduced with addition of a quadrupole triplet at their centers and a magnetic chicane for one of them to host canted in-vacuum undulators. Table 1 shows the main parameters of the new TDR lattice (see [3]).

As a part of the study program for the new storage ring, the robustness studies have been refined from the work already presented in the CDR phase [4]. The present study should analyze the impact of assumed errors on the ring performance. In particular: a) ensure the possibility of on-axis (first day) and then off-axis injection (standard operation) b) guarantee the feasibility of the storage ring commissioning [orbit correction, Beam Based Alignment (BBA), correction of beta-beating, restoration of lifetime, emittance, coupling, etc.] to achieve full performance for daily operation, c) validate the selected correction schemes and corrector maximum strengths via end-to-end simulations, d) verify that the equipment tolerance specifications are consistent with commissioning and future operation, e) identify possible showstoppers and additional equipment constraints. We present in this article preliminary results on the best performance achievable under the current assumptions.

Table 1: Parameters of the SOLEIL TDR lattice

Parameter, Unity	**Value**
Lattice	TDR V0356 7BA/4BA
Energy, GeV	2.75
Circumference, m	353.92
Symmetry/Cell Number	2/96
H. Natural Emittance, pm rad	84.4
V. Emit. (30 %H. Emit), pm rad	25.3
Tunes (H/V/L)	54.2/18.3/0.00210
Energy Spread, %	0.091
Bunch Length, ps	8.5
Harmonic Number	416
Main RF Frequency, MHz	352.382
Energy Loss per turn, keV	458.5
Main RF Voltage, MV	1.8
Natural Chromaticities H/V	-118.1/-56.2
Operation Chromaticities H/V	+1.6/+1.6
Momentum Compaction Factor	1.05×10^{-4}
Damping Time H/V/L, ms	7.7/14.4/12.2
Touschek Lifetime (500 mA), h	2.5

LATTICE LAYOUT

The studied lattice is a composition of twelve 7BA, eight 4BA arc sections and two mini-beta sections with chicanes, where all dipoles and reversed bends are permanent magnets. Quadrupole magnets are either permanent or electromagnetic. The maximum current is 500 mA in a uniform filling pattern. An initial (first day) on-axis injection, with no possibility of beam accumulation, can achieve maximum 1 to 3 mA in the ring on 104 consecutive bunches. After the initial steps in the ring commissioning, the Multipole Injection Kicker (MIK) is expected to be used for off-axis as principal injection and to allow accumulation.

For this study we consider 214 girders, 180 BPMs, 180(180) dipolar horizontal(vertical) correctors, and 412(412) normal(skew) quadrupolar correctors (Fig. 1).

* oscar-roberto.blanco-garcia@synchrotron-soleil.fr
† now at CERN
‡ now at Royal Holloway, University of London

ISBN: 978-3-95450-227-1 ISSN: 2673-5490 doi:10.18429/JACoW-IPAC2022-MOPOTK006

OFF-ENERGY OPERATION FOR THE ESRF-EBS STORAGE RING

L. Hoummi*, T. Brochard, N. Carmignani, L.R. Carver, J. Chavanne, S.M. Liuzzo, T. Perron, R. Versteegen, S. White, ESRF, Grenoble, France
P. Raimondi, SLAC, Menlo Park, California, USA

Abstract

The ESRF-EBS is the first 4th generation source making use of the Hybrid Multi-Bend Achromat (HMBA) lattice cell [1], reaching an equilibrium horizontal emittance of 140 pm.rad in user mode (insertion devices (ID) gaps open). The injection in the storage ring (SR) is conducted with a short booster, operated off-energy. The RF frequency is increased compared to the nominal one to put the beam on a dispersive orbit, thus going off-axis in quadrupoles. The induced dipolar feed down effects reduce the booster horizontal emittance [2, 3].

The same strategy is extended to the ESRF-EBS SR, for an expected emittance reduction of about 20 pm rad. A first approach shifts the RF frequency by +300 Hz to operate at -1% energy offset. Optimal quadrupole and sextupole settings are defined for this off-energy operation based on simulations. The settings are then tested in the SR in terms of dynamic aperture and injection efficiency.

INTRODUCTION

The ESRF-EBS SR provides a 6 GeV electron beam of low equilibrium emittance of 140 pm.rad (insertion devices (ID) gaps open) to 44 beamlines, with canted cells and the inclusion of bending magnet (BM) sources [4] since the end of its commissioning in 2020 [5, 6]. Further reduction of its equilibrium emittance may be achieved by operating on a dispersive orbit, by going off-axis in high-gradient quadrupoles. To do so, the RF frequency is shifted by about 300 Hz, according to:

$$\delta = \frac{\Delta p}{p} = -\frac{1}{\alpha_C}\frac{\Delta f_{RF}}{f_0} \tag{1}$$

with f_0 the synchronous frequency, Δf_{RF} the frequency shift and $\alpha_C = 8.62 \times 10^{-5}$ the momentum compaction factor, under the assumption that it varies slowly with the momentum.

The emittance reduction was first tested on the ESRF-EBS storage ring, by varying its RF frequency within ±500 Hz. No correction was done on the optics. Figure 1 illustrates the variation of the horizontal emittance and the energy spread for different RF frequency shifts. A reduction of about 20 pm rad can be achieved with a RF shift of 300 Hz, which corresponds to about -1% energy deviation, and could increase the photon beam brilliance by about 5-15%.

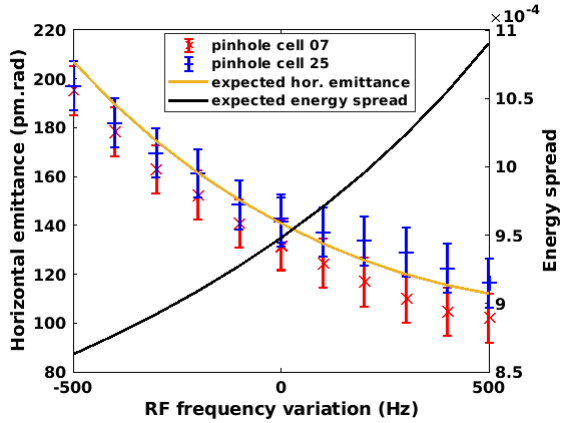

Figure 1: Expected and measured variations of the equilibrium horizontal emittance and energy spread with RF frequency shift, without optics correction.

OFF-ENERGY LATTICE OPTION FOR ESRF-EBS

The RF frequency shift introduces off-axis orbit in the quadrupoles and the sextupoles. This yields to an additional quadrupolar effect in the sextupoles,

$$k_1^{sext} = 2k_2 D_x \delta \tag{2}$$

with k_2 the sextupole strength and D_x the dispersion at the sextupole. This effect introduces beta functions and dispersion modulations that are detrimental in terms of lifetime and injection efficiency. For simplicity, the on-energy optics parameters were taken as a reference for good performances. As such, the off-energy optics were matched to the on-energy ones. Figure 2 compares the Twiss functions and dispersion of the nominal optics and its off-energy option.

The additional quadrupolar strength in the sextupoles binds the tunes and chromaticity corrections and could be compensated using the nearby quadrupoles. Nevertheless, such compensation removes two knobs from the optics matching, required to match the $-I$ transformation between sextupoles. To conserve the tunes and keep chromaticities higher than (6,6) for operation, the sextupole were included in the matching of the optics of the standard cell. The EBS injection cell [7], 2PW and SB insertions and canted cells [4] are also taken into account in the matching.

Table 1 lists the main parameters of the 6 GeV ESRF-EBS HMBA lattice and its off-energy option. The off-energy optics correction and especially the conservation of the horizontal tune decreased the overall dispersion levels and the momentum compaction factor. From (1), the RF shift corre-

* lina.hoummi@esrf.fr

ISBN: 978-3-95450-227-1 ISSN: 2673-5490 doi:10.18429/JACoW-IPAC2022-MOPOTK007

REVERSE BEND OPTION FOR A 6 GeV STORAGE RING LATTICE

L. Hoummi*, N. Carmignani, L.R. Carver, F. Cianciosi, S.M. Liuzzo, T. Perron, S. White,
ESRF, Grenoble, France

Abstract

Several high-energy synchrotron facilities adopted the Hybrid Multi-Bend Achromat scheme (HMBA) developed for the ESRF-EBS [1]. The considered lattice has been developed for a generic 6 GeV storage ring (SR) of 1100 m circumference [2]. It includes a short bending (SB) magnet at the center of the cell, and achieves a ~70 pm rad equilibrium horizontal emittance. The optics of such SR are modified introducing reverse bending magnets [3, 4] to further reduce the natural horizontal emittance to 53 pm rad. The impact of such modification on dynamic aperture and lifetime is assessed and optimized.

INTRODUCTION

The present work has been developed for a generic high-energy storage ring of 6 GeV and 1100 m circumference [2]. The lattice considered is an adaptation of the ESRF-EBS H7BA lattice [5] with 40 cells, achieving ~70 pm rad horizontal emittance. Figure 1 displays the optics of a standard cell of the presented ring.

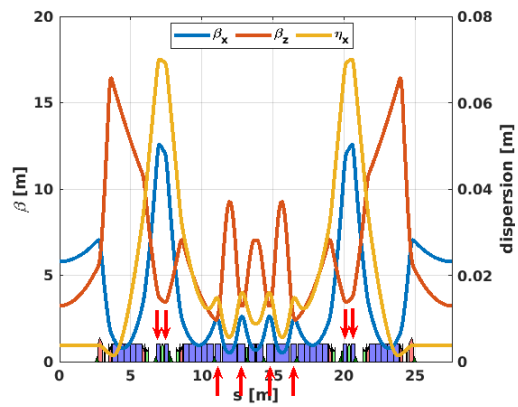

Figure 1: Location of the reverse bends (red arrows) in the lattice. All dipoles are represented in blue.

Further reduction of the horizontal emittance is achievable with a fixed lattice layout, by controlling the dispersion function at the entrance of the dipole magnets, to approach the Theoretical Minimum Emittance (TME) conditions [6]. Reverse bends (RB), which are mechanically displaced quadrupoles with regards to the machine axis, generate a negative dipolar field of resulting angle [4]:

$$\theta^{RB} = -k_1 l \Delta x \tag{1}$$

with k_1 the strength of the quadrupole, l its length and Δx the horizontal displacement. Such quadrupoles help modulate the dispersion function and derivative to approach the TME in the dipoles [3]. Previous attempts were conducted on a similar lattice [7].

ANGULAR CORRECTION

All focusing quadrupoles in the dispersive area were used as reverse bends to optimise the emittance reduction. Their location is displayed in Fig. 1. The introduction of negative angles perturbs both the geometry and the dispersion in the standard cell, reducing the total angle per cell. The correction of the total angle is pursued using two methods:

- **Transposed method** The total reverse bending angle per cell θ^{RB}_{tot} is defined as the sum of all negative bending angles, expressed per RB in Eq. 1. It is compensated by shifting the standard dipole angles to recover the geometry of the cell. The angular distribution along the cell simply becomes $\theta^{RB} = -\frac{|\theta^{RB}_{tot}|}{N_{RB}}$ for RB and $\theta_{dip} = \theta_0 + \frac{|\theta_{tot}|}{N_{dip}}$ for the standard bending magnets, where N_{RB}, N_{dip} are respectively the number of RB and dipoles in the cell, and θ_0 the bending angle of the dipoles in the nominal lattice.
- **Proportional method** The total angle is restored proportionally over the whole cell, applying the following operation on all bending magnets: $\theta_{new} = \frac{2\pi\theta_{old}}{N_{cells}*a}$, where a is the cell angle before correction, and N_{cells} the number of cells of the machine. This method conserves the perturbation of the dispersion of the reverse bends, for which we expect a stronger emittance reduction.

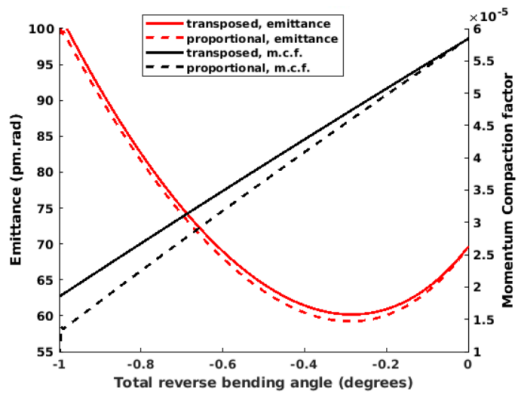

Figure 2: Evolution of the emittance and the momentum compaction factor (m.c.f.) with the total reverse bending angle, for the two methods of angle restoration.

Both methods were tested and compared in Accelerator Toolbox (A.T.) [8], for different total reverse bending angles

* lina.hoummi@esrf.fr

ISBN: 978-3-95450-227-1 ISSN: 2673-5490 doi:10.18429/JACoW-IPAC2022-MOPOTK008

OPTIONS FOR A LIGHT UPGRADE OF ESRF BOOSTER SYNCHROTRON LATTICE

T.Perron*, N. Carmignani, L.Carver, L.Hoummi, S. Liuzzo, S.White, ESRF, Grenoble, France.
P. Raimondi, SLAC, California, USA.

Abstract

The EBS 6 GeV electron storage ring recently commissioned at ESRF, in Grenoble, France, is still operated using the old injector hardware. It is now one of the limiting factor of the facility. The large horizontal emittance of the booster beam affects injection efficiency, preventing from reaching 100% transfer efficiency between the 299.8 m long booster and the storage ring. Different lattice modifications going from minor optics changes to full machine renewal are considered [1] . In this paper we will discuss different options of a "light" upgrade of the FODO lattice, keeping the RF system, vacuum chamber, power supplies, and most of the magnets. The upgrade then consists in creating a few new quadrupole families in the straight section vicinity and remove them from the main QF/QD families.

"LIGHT" UPGRADE AND IT'S LIMITATIONS

PS Limitations

The ESRF booster synchrotron is accelerating electrons from 0.2 Gev to 6 Gev following a 250 ms cycle driven by a ramped power supply (PS) feeding all magnets. This PS is based on H bridge rectifiers using IGBT's switches, and feeds three different magnet chains: Dipoles (D), Focussing Quadrupoles (QF) and Defocussing Quadrupoles (QD). The power supply, commissioned in 2015, has been tailored to the present booster layout and offers very little flexibility for improvement of output current/voltage (presently 500 A/1500 V) and number of output channels. The light version of the upgrade uses of current magnets type, with eventually minor modifications in the design of quadrupoles. It enables to keep most of present magnets, girders and vacuum chambers. New families can then be obtained either by removing some quadrupoles from the present chains, and feed them via dedicated PS, or by introducing magnets with different designs in the same chain. Expected saturation curve for current magnets is presented in Fig. 1.

Magnet Design Limitations

Additional quadrupole families can be obtained by modifying the number of turns on the coils in the magnet design. Sevral families can then be powered by a single chanel output of the ramped PS and no additional PS is requiered. Comsol [2] simulations have been performed to evaluate the impact of magnet saturation. It was coherent with the PS limitation of 500 A. These simulations were used as well to evaluate the field errors induced by a non even distribution of excitation coils. Modification of coils can only be done by removing, or adding, a full turn. Present coils have 12 turns fixing the discreet step in gradient change to 8.3% of the initial value. Removing one turn on only two over the four coils of the magnet, this step is reduced by a factor 2. The field quality is then slightly degraded because of the different current repartition in the coils. Harmonic analysis performed on a circle of 50 mm diameter, for the pole and coil geometry of Fig. 2 indeed shows the presence of a skew octupole for the geometry presented in Fig. 2. Nevertheless the relative amplitude of this component with respect to the main quadrupole gradient is of 4×10^{-4} even for the saturated case (as shown in Fig. 3). It is therefore negligible with respect to other sources of errors. For non uniform chains of magnets, saturation is a concern as well because, for this configuration, it cannot be compensate for all magnets via the power supply waveform anymore.

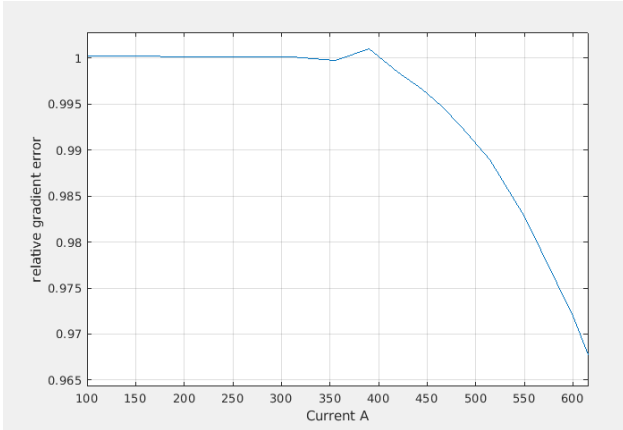

Figure 1: Simulated normalised gradient as a function of current for the present booster quadrupoles.

Extraction

Extraction hardware and layout is strongly lattice dependent. For a given lattice the ability to extract properly the beam using existing layout/hardware must be assessed and potential modifications are foreseen.

LATTICES TO BE COMPARED

Figure 4 displays how the new magnet families are labeled. The figure shows 1/6 of booster circumference. Three new lattices (PR, 3F, and 5F) with new families are compared with two lattices that do not require any hardware change: the one in operation (OP) today, and the same one with an increased horizontal tune (HT). For each lattice, analysis is done considering a 40 kHz shift on the RF frequency. Indeed EBS machine length is not in accordance with booster

ISBN: 978-3-95450-227-1 ISSN: 2673-5490 doi:10.18429/JACoW-IPAC2022-MOPOTK009

BASIC DESIGN CHOICES FOR THE BESSY III MBA LATTICE *

B. C. Kuske†, M. Abo-Bakr, P. Goslawski, Helmholtz-Zentrum Berlin, 12489 Berlin, Germany

Abstract

Lattice development for the 2.5 GeV, low emittance successor of BESSY II, are ongoing at HZB since 2 years, [1]. The choice of a multi-bend achromat lattice is indispensable due to the emittance goal of 100 pm, required to generate diffraction limited radiation up to 1 keV. Hard boundary conditions for the design are a relatively short circumference of ≈ 350 m due to the accessible construction property in vicinity to Bessy II and 16 super-periods to not step behind the number of existing experimental stations. The configuration of the two building blocks of MBA lattices - unit cell and dispersion suppression cell - has been thoroughly studied from basic principles. It was found that gradient free bending dipoles are the better choice for the BESSY III lattice, opposite to the concepts of comparable projects.

INTRODUCTION

Since the successful operation of MAX IV in Lund, Sweden [2], the innovative idea of multi-bend achromat (MBA) lattices entered basically every new low emittance storage ring design. In 2014, A. Streun, PSI, analysed the concept of reverse bends (RB) in the MBA unit cell [3]. RBs are usually realized by an off-axis placement of the focusing quadrupole. They help to detach the matching of the dispersion from that of the beta function and significantly reduce the emittance. In 2017, J. Bengtsson and A. Streun adopted the Higher-Order-Achromat approach to MBA-lattices [4, 5], where the linear lattice is constructed such, that all 1st and 2nd-order sextupole terms are completely suppressed by phase cancellation.

The BESSY III lattice design intends to integrate all three concepts from the very beginning. To this end, the basic building blocks of MBA lattices, i.e. unit cell (UC), and dispersion suppression cell (DSC) are analysed under the given constraints and with the goals of reaching 100 pm emittance, lowest chromaticity, a momentum compaction factor $\alpha > 10^{-4}$ and a short circumference. It was found, that much orientation in the vast parameter space of lattice design can be gained. By successively stepping though the different options for the design of UC and DSC a baseline version for BESSY III was developed deterministically that fulfills all demands and shows a good non-linear behavior. This approach also puts various commonplace convictions of MBA lattice design into perspective.

CHOICES FOR THE UNIT CELL

The generic, symmetric UC consists of the central dipole, two quadrupoles, QF/RB and QD, and two sextupoles, SF and SD. Drifts are initially set to 0.1 m. The three symmetry conditions $\alpha_{x,y} = \eta' = 0$, are fitted using QF, QD and the RB angle. There are several choices for the UC setup: a) include QD into the main bend (combined function cell, CF-UC) or a separate function cell (SF-UC) b) place the RB or SF at the outside, and, in case of the SF-UC, place QD or SD next to the central dipole. Table 1 lists the emittance, chromaticity and integrated sextupole strength for the six UC options.

Table 1: Features of UC Permutations

UC	Order	ε	ξ_x	ξ_y	SF [1/m²]	SD [1/m²]
CF	SF last	97	-0.7	-0.4	-1.3	1.6
CF	RB last	96	-0.8	-0.3	-2.0	2.2
SF	SF last SD central	94	-0.7	-0.3	-1.0	1.2
SF	RB last SD central	94	-0.8	-0.2	-1.7	1.7
SF	SF last QD central	96	-0.7	-0.3	-1.6	1.8
SF	RB last QD central	97	-0.8	-0.2	-3.5	-3.6

The emittance in all cases is comparable. The critical horizontal chromaticity varies only little, while the sextupole strength varies by more than a factor of 3. The reason lies in the strongly different separation of the beta functions at the location of the sextupoles, see Fig. 1. Interestingly, the length of the CF-UC is close to that of the SF-UC. The bend's gradient reduces the accessible bending field, increasing the dipole length and the stronger sextupoles need additional space. The sextupole strength of a CF-UC lies at least 30 % over the best SF-UC solution, which is chosen for the further analysis.

Effect of the Reverse Bend

The RB has been integrated into the UC from the beginning: without the additional 'knob' of the RB bending field, the UC would increase in length in order to fulfill the symmetry conditions. The deflection angle is ≈ 5 % of the main bend, but needs to be optimized. For a homogeneous dipole, the theoretical minimal emittance, TME, as well as the optimal β_0 and η_0 at the center of the dipole can be calculated [6, 7], using

$$\beta_{0,TME} = \frac{L}{\sqrt{15}}, \quad \eta_{0,TME} = \theta\frac{L}{6}, \quad \varepsilon_{0,TME} \propto \theta^3\frac{2}{3\sqrt{15}},$$

where L denotes half the dipole length and θ half the bending angle. For a main bend of $\theta = 4.5°$, 0.27 m, the TME is 130 pm and is achieved at $\beta_0 = 0.07$ m and $\eta_0 =$

* Work supported by German Bundesministerium für Bildung und Forschung, Land Berlin, and grants of Helmholtz Association
† bettina.kuske@helmholtz-berlin.de

ISBN: 978-3-95450-227-1 ISSN: 2673-5490 doi:10.18429/JACoW-IPAC2022-MOPOTK011

GENERALISATION AND LONGITUDINAL EXTENSION OF THE GENETIC LATTICE CONSTRUCTION (GLC) ALGORITHM

S. Reimann* [1,2], M. Droba[1], O. Meusel[1], H. Podlech[1,3],
[1]IAP, Frankfurt am Main, Germany
[2]GSI, Darmstadt, Germany
[3]HFHF, Helmholtz Forschungsakademie Hessen für FAIR

Abstract

The GLC algorithm allows the construction of efficient transfer lines with defined imaging properties using a minimum number of quadrupole elements. This work describes a generalisation of this algorithm to make it applicable to the use of arbitrary beam optical elements. This includes an extension to longitudinal phase space.

INTRODUCTION

The design of a matching section of a particle accelerator can be formulated as an optimisation problem that can be solved algorithmically. The goal of such an optimisation is to achieve an optimal fit of a given particle distribution to an arbitrary acceptance, with minimum energy and material requirements (i.e., with the lowest possible field strengths and the fewest possible elements). The formulation of the individual problem can be reduced to the problem of minimising a single-valued fitness function over a multidimensional cube. This requires finding a suitable, unambiguous parameterisation to encode both the transfer line geometry and the field strengths used (phenotype) by a list of numbers (genotype) [1].

PARAMETRISATION

Given a general unspecific transport line of length L, in which at least one section of length L_{opt} can be equipped with new elements. If $L = L_{\mathrm{opt}}$, then there are no constraints on the position of new elements. Furthermore, there is a set of μ freely positionable beam manipulating components $\{C_1, \cdots, C_\mu\}$. These can also be meta-elements consisting of a fixed combination of components. In addition, there are those ν components whose positions are fixed from an optimisation point of view, which means that they are located outside L_{opt}. In sum, this gives $N = \mu + \nu$ components. Each of these components $C_n \in \{C_1, \cdots, C_{\mu+\nu}\}$ has a certain number of λ_n free parameters $x_{n,1} \cdots x_{n,\lambda_n}$. These parameters can be e.g. quadrupole strengths, accelerating gap voltages, but also the lengths of the respective elements. The total number of free parameters is then

$$\eta_p = \sum_{n=1}^{N} \lambda_n \,. \tag{1}$$

A position must now be defined for each free component from $\{C_1, \cdots, C_\mu\}$. The possibility of arbitrary permutations of the components should be implicitly included. For this purpose, a relative position $s_n \in [0, 1]$ is defined for each component. The actual position l_n results then from

$$l_n = s_n \cdot \left(L_{\mathrm{opt}} - \sum_{n=1}^{\mu} L_n \right), \tag{2}$$

where L_n is the length of the component C_n. Due to free positioning, the number of free parameters increases by μ to $\eta = \eta_p + \mu$.

Every possible realisation of a transport path that satisfies the given boundary conditions can be assigned to a point in an η-dimensional subspace of $\mathbb{R}^\eta$. The parameters are normalised to the range $[-1, 1]$ with respect to the individual device limits. So this corresponds to a point

$$\boldsymbol{x} = \left(\tilde{x}_1 \ \ldots \ \tilde{x}_{\eta_p} \ \tilde{s}_1 \ \ldots \ \tilde{s}_\mu \right) \tag{3}$$

in the η hypercube. Here $\tilde{x}_n$ and $\tilde{s}_n$ are respectively the values of x_n and s_n normalised to the interval $[-1, 1]$. I want to emphasise that each design solution for such a transfer line corresponds to a point in this space. There is a distinct assignment. Each of these points can now be assigned a value of a fitness function

$$F(\boldsymbol{x}) = 1 - T(\boldsymbol{x}) + \epsilon(\boldsymbol{x}) \tag{4}$$

that describes the performance of the associated transfer line with respect to beam transmission T. Its minimum F_{min} corresponds to the largest transmission T_{max}. The term $\epsilon(\boldsymbol{x})$ represents the parameterisation of further optimisation goals, such as lowest possible field strengths or minimum component dimensions, and is defined as a sub-norm in the simplest case, e.g.

$$\epsilon(\boldsymbol{x}) = ||(\tilde{x}_1, \cdots, \tilde{x}_{\eta_p})|| = \sqrt{\tilde{x}_1^2 + \cdots + \tilde{x}_{\eta_p}^2} \,. \tag{5}$$

The minimum of the fitness function encodes the optimal design solution for any given problem.

Example: A Single Quadrupole

A drift section of length $L = 20\,\mathrm{m}$ is given at the end of which an aperture limitation is attached. This has a diameter of 4 cm horizontally and 10 cm vertically. An asymmetric, divergent particle distribution is chosen such that most of the beam is lost on the aperture limitation. For a quadrupole of length $L_q = 1\,\mathrm{m}$, the goal is to find a position $l = s \cdot (L - L_q)$ within this distance and a gradient (kL_q) at which the transmission becomes maximum (Fig. 1).

* s.reimann@gsi.de

ISBN: 978-3-95450-227-1 ISSN: 2673-5490 doi:10.18429/JACoW-IPAC2022-MOPOTK012

CONCEPT OF A POLARIZED POSITRON SOURCE FOR CEBAF

S. Habet[1,2], Y. Roblin[2], R.M. Bodenstein[2], S.A. Bogacz[2], J. Grames[2], A. Hofler[2], R. Kazimi[2], F. Lin[2], M. Poelker[2], A. Seryi[2], R. Suleiman[2], A. Sy[2], D. Turner[2], A. Ushakov[1], C.A. Valerio-Lizarraga[3], E. Voutier[1]
[1]Université Paris-Saclay, CNRS/IN2P3/IJCLab, 91405 Orsay, France
[2]Thomas Jefferson National Accelerator Facility, Newport News, VA 23606, USA
[3]Universidad Autónoma de Sinaloa, 80010 Culiacáan, México

Abstract

Polarized and unpolarized positron beams are essential for the future hadronic physics experimental program at the Thomas Jefferson National Accelerator Facility (JLab). The main challenge is to produce high duty-cycle and high intensity polarized positron beams. The JLab positron source uses the Polarized Electrons for Polarized Positrons (PEPPo) technique to create either a low intensity, high polarization positron beam (I > 100 nA, P=60%), or a high intensity unpolarized positron beam (I > 3 µA), from an intense highly polarized electron beam (I=1 mA, P=90%). The current design involves a new injector dedicated to positron production, collection, and shaping suitable for acceleration through the Continuous Electron Beam Accelerator Facility (CEBAF). The optimization of the layout and the performance of the positron source are explored in this paper.

INTRODUCTION

Positron beams can be used to probe physics phenomena. For instance, high energy beams allow to investigate the structure of nuclei while low energy beams access the distribution of electrons inside materials [1]. One interest at JLab is the study of the partonic structure of the nucleon from the scattering of highly polarized electron and positron beams. For instance, the comparison between the two beam species allows to isolate the different components of the deeply virtual Compton scattering cross section, and provides more pertinent and sensitive experimental observables [2, 3].

In this context, we may refer to the PEPPo experiment [4, 5], which demonstrated at the CEBAF injector the efficient polarization transfer from longitudinally polarized electrons to positrons [6]. Initial beam electrons generate elliptical polarized photons within a tungsten target via bremsstrahlung. These polarized photons then create in the same target positron and electron pairs. The main concern of the JLab positron project is to generate high-duty cycle longitudinally polarized positron beams from a 120 MeV/c electron beam with as high as possible an efficiency. The essential difficulty is to keep a high positron efficiency all along the collection and transport line of the positrons to the main accelerator, and to permit polarized or unpolarized dual operation with a small momentum dispersion delivered to experimental halls. The positron injector layout design, the target thickness optimization, and the positron beam optics are described in the following sections.

POSITRON INJECTOR LAYOUT

The positron injector is designed to provide an efficient number of positrons suitable for CEBAF injection. The transverse and longitudinal dynamics of the positron beam are optimized to stay within the acceptance limits. A positron collection system composed of high magnetic field lenses [7] is essential to decrease the large transverse momentum spread at the target exit. A conceptual layout of the injector is shown in Fig. 1. A moderate energy electron beam interacts within a tungsten target (T) to produce positrons that are collected with an Adiabatic Matching Device (AMD). A four quadrupoles matching section (MS) and a magnetic chicane (CP) select further the central momentum and the momentum bite of the positron population. A decelerating/accelerating section (DeAc) reduces then the momentum dispersion. Finally, a chirping cavity (ChC) correlates the momentum dispersion with the positron time-of-flight, and a second chicane (CC) compresses the positron bunch length to match with the CEBAF injection acceptance. We have determined the maximum bunch length acceptance is 4 ps, and our strategy is to further reduce this towards the nominal 12 GeV e- bunch length as possible, of 0.3 ps through compression techniques.

POSITRON TARGET OPTIMIZATION

Geant4 [8] simulations are used to optimize the positron production considering a 120 MeV/c electron beam 100% longitudinally polarized hitting a tungsten target. The analysis of simulated data follows the evolution of the positron production efficiency ϵ and of the Figure-of-Merit FoM=$\epsilon P_{e^+}^2$ as function of the target thickness. ϵ is the quantity of interest for an unpolarized positron source. The FoM further combines the average polarization to maximize the statistical precession of an experiment in the minimum amount of time. This investigation aims to optimize the target thickness for the production of unpolarized and polarized positrons. The Fig. 2 shows ϵ (left) and FoM (right) simulations for a 4 mm thick target, within a selected momentum bite $\Delta p/p$=±10% at each central momentum p_0 and within the angular acceptance $\Delta\theta_{e^+}$. The efficiency decreases when the angular aperture decreases, describing a large positron momentum spread in the transverse plane. The essential difference between unpolarized and polarized operation modes is the positron energy to be selected for optimum collection: about a sixth of the primary electron beam energy for optimized efficiency, and a half for optimized FoM. The maximum value

ISBN: 978-3-95450-227-1 ISSN: 2673-5490 doi:10.18429/JACoW-IPAC2022-MOPOTK013

MACHINE LEARNING BASED SURROGATE MODEL CONSTRUCTION FOR OPTICS MATCHING AT THE EUROPEAN XFEL

Z. H. Zhu[1,2,3*], S. Tomin[3], Y. Chen[3], W. L. Qin[3], M. Scholz[3]
[1]Shanghai Institute of Applied Physics, Chinese Academy of Sciences, Shanghai 201800, China
[2]University of Chinese Academy of Sciences, Beijing 100049, China
[3]Deutsches Elektronen-Synchrotron DESY, Notkestr. 85, 22607 Hamburg, Germany

Abstract

Beam optics matching is a daily routine in the operation of an X-ray free-electron laser facility. Usually, linear optics is employed to conduct the beam matching in the control room. However, the collective effects like space charge dominate the electron bunch in the low-energy region which decreases the accuracy of the existing tool. Therefore, we proposed a scheme to construct a surrogate model with nonlinear optics and collective effects to speed up the optics matching in the European XFEL injector section. Furthermore, this model also facilitates further research on beam dynamics for the space-charge dominated beam.

INTRODUCTION

The X-ray free-electron laser facilities around the world aim at generating high-brightness and coherent X-ray pulses [1], which facilitate the ultra-fast scientific research with atomic spatial resolution [2–4]. The European X-ray Free-Electron Laser (EuXFEL), which is in the operational stage since 2017, is designed to generate X-rays from 0.25 to 25 keV[5]. It is driven by a superconductive accelerator that is able to produce up to 27,000 electron bunches per second with maximum electron beam energy up to 17.5 GeV. As the source of electron bunches, the photoinjector section aims at generating the bunches with low emittance and matched optics with design values which is essential to the downstream beam delivery to the undulators. Therefore, it is required to measure and optimize these transverse phase space parameters by tuning the several injector settings, which is one of the routine procedures of accelerator operation.

Usually, the multi-quadrupole scan method is applied to optics measurement. These optical functions are calculated based on the beam size measurement on the intercepting screen whilst varying the upstream machine lattice. The deduction is based on the linear optics model to track the beam from the first matching quadrupole to the final reference point. However, collective effects such as space charge and wakefields are not taken into account in this approach, which might lead to inaccuracy. Moreover, the beam tracking with these collective effects would take more computational resources for one single simulation, making it not applicable to be introduced in the online optimization of beam optics matching. Therefore, the machine learning-based approach is proposed to construct the surrogate model to deal with this problem. The model involves the second-order optics and the beam collective effects, aiming to act as an alternative to the existing tool to execute the optics matching in the control room.

The machine learning technique has been applied to power many scientific domains in these two decades due to the improvements in computational resources and the theory of algorithms. As one of the classical approaches in machine learning, supervised learning builds a function that maps the input features to the output parameters using the sample set. In the accelerator community, this method has been introduced to tackle system modeling in several projects. Its most useful strength is the fast execution of high-fidelity beam simulations with sufficient accuracy. Based on it, it facilitates the fast offline beam dynamics optimization and design (i.e. dynamics aperture maximization for storage ring, the emittance, and energy spread in wakefield accelerator linacs) [6, 7], as well as providing on-the-fly prediction of the realistic machine, for instance, switching between different operation modes [8]. Hence, the machine learning-based surrogate model is introduced to assist the online optics matching at the injector section to replace the time-consuming beam tracking with collective effects, as presented in Fig. 1. The proof-of-principle experiment in the control room demonstrates the accuracy of the surrogate model and it paves the path for further exploration of machine learning applications on accelerators.

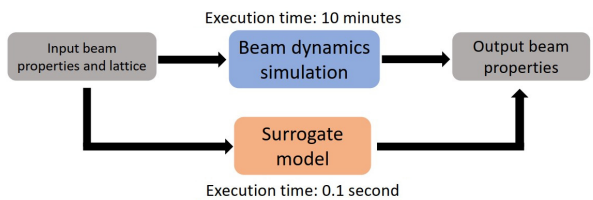

Figure 1: The built surrogate model can substitute the slow physical simulation and largely improve the evaluation efficiency, which facilitates the beam dynamics optimization both in offline design and online control.

SURROGATE MODEL CONSTRUCTION

The injector section of the EuXFEL consists of a photocathode electron gun, a booster accelerator, a third harmonic cavity, and a laser heater chicane. In the following beam diagnostic section, the transverse deflecting cavity is deployed to resolve the beam longitudinal properties. The surrogate model is constructed under a deep neural network with the

* zihan.zhu@deys.de

ISBN: 978-3-95450-227-1 ISSN: 2673-5490 doi:10.18429/JACoW-IPAC2022-MOPOTK014

OPTICS OF A RECIRCULATING BEAMLINE FOR MESA

Christian P. Stoll*, Atoosa Meseck[1]
Institut für Kernphysik der JGU Mainz, Germany
[1]also at Helmholtz Zentrum Berlin, Berlin, Germany

Abstract

The Mainz Energy-recovering Superconducting Accelerator (MESA) is an Energy Recovery Linac (ERL) facility under construction at the Johannes Gutenberg-University in Mainz. It provides the opportunity for precision physics experiments with a 1 mA c.w. electron beam in its initial phase. In this phase experiments with unpolarised, high density ($\rho \approx 10^{19}$ atoms/cm^2) gas jet targets are foreseen at the Mainz Gas Internal Target Experiment (MAGIX). To allow experiments with thin polarised gas targets with sufficiently high interaction rates in a later phase, the beam current has to be increased to up to 100 mA, which would pose significant challenges to the existing ERL machine. Thus it is proposed here to use MESA in pulsed operation with a repetition rate of several kHz to fill a storage ring, providing a quasi c.w. beam current to a thin gas target. The optics necessary for this recirculating beamline are presented here.

MESA

MESA is a small-scale, multi-turn, double-sided recirculating linac with vertical stacking of the return arcs currently being built at the Johannes Gutenberg-University Mainz. The layout of the facility can be seen in Fig. 1. The accelerator features superconducting cavities of the TESLA type [1], housed in an ELBE type cryomodule [2] and operated at 1.3 GHz. The possible modes of operation are a thrice

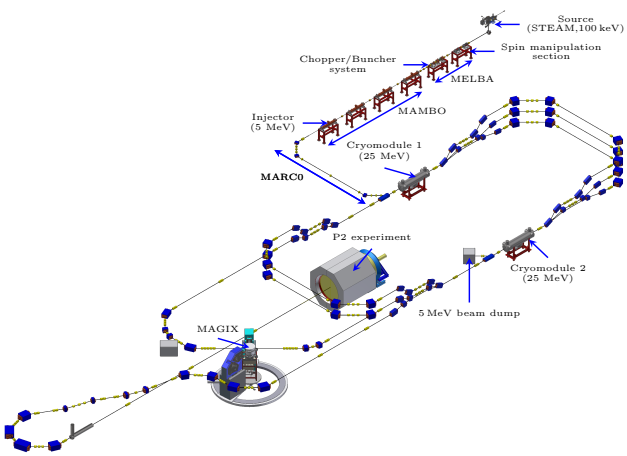

Figure 1: Rendering of the layout of the MESA facility. The injection beam line can be seen on the top right. The pseudo internal gas jet target of the MAGIX experiment is located in the fourth arc of the energy recovery mode on the bottom left.

recirculating external beam mode (EB) with 150 µA current and 155 MeV particle energy or a twice recirculating energy recovering mode (ER) with 1 mA and in a later phase 10 mA current at a beam energy of 105 MeV, where 100 MeV of beam energy can be recovered from the beam and fed back into the cavities. Further information on the facility and the planned experiments can be found in [3–5].

RING BEAMLINE

The maximum achievable beam current in ERL machines is limited for example by the Beam Breakup (BBU) instability as was investigated for MESA in [6] or the heating of the Higher Order Mode couplers. Scattering experiments in search for rare processes however would benefit from an increase in luminosity. Since the density of the minimally invasive windowless gas target for MAGIX is limited, the remaining option is to increase the beam current to further increase the luminosity. This is especially true for polarised gas targets, with target densities of the order of 1×10^{14} atoms/cm^2 [7]. One way to circumvent the BBU limit is to use MESA as an injector for a ring beamline, where high intensity bunches would recirculate in quasi c.w. operation through the experiment multiple times and be dumped afterwards. In such a configuration ERL operation of MESA would not be needed and the accelerator would be used as a pulsed injector to fill the ring. The pulsed beam will then have to be extracted and dumped at 105 MeV but with a duty cycle of the order of 0.1 %.

In the area where the beamline has to be closed in order to loop back to the MAGIX experiment a lot of the infrastructure of the P2 Experiment is housed, consisting mainly of the superconducting solenoid, the backscattering detectors, the cryogenic infrastructure for the liquid hydrogen target and the helium distribution system for the solenoid. Several options are available to install an additional beamline. The simplest of them with a small vertical offset and a closed loop above of the P2 Experiment superconducting solenoid might face complications due to space constraints. However there is an alternate option passing over and behind the P2 Experiment superconducting solenoid, since the available vertical space is close to 6 m. The ring of option 1 has a circumference of 53.87 m, which is ≈234 times the radio frequency wavelength. At a repetition rate of 6 kHz and 210 buckets filled with $Q_{\text{bunch}} = 77$ pC the average current in the ERL would be 0.1 mA, while the stored beam in the ring would provide 100 mA for the experiment. Each bunch train would be 0.153 µs long and would spend 167 µs in the ring, being stored for only 1000 turns. This is well below the estimated damping times ($\tau_i \approx 2$ s) of such a ring. Approximately 1.5 W are emitted as synchrotron radiation at 100 mA of stored beam. The first design goal of such a beamline was

* stollc@uni-mainz.de

ISBN: 978-3-95450-227-1 ISSN: 2673-5490 doi:10.18429/JACoW-IPAC2022-MOPOTK015

ENUBET'S MULTI MOMENTUM SECONDARY BEAM LINE

E. G. Parozzi*[1,2,3], G. Brunetti[3], N. Charitonidis[1], A. Longhin[4,5], M. Pari[4,5], F. Pupilli[5], F. Terranova[2,3]
[1]CERN, 1211 Geneva 23, Switzerland
[2]INFN, Sezione di Milano-Bicocca, piazza della Scienza 3, Milano, Italy
[3]Phys. Dep. Università di Milano-Bicocca, piazza della Scienza 3, Milano, Italy
[4]Phys. Dep. Università di Padova, via Marzolo 8, Padova, Italy
[5]INFN Sezione di Padova, via Marzolo 8, Padova, Italy

Abstract

In order to study the remaining open questions concerning CP violation and neutrino mass hierarchy, as well as to search for physics beyond the Standard Model, future experiments require precise measurements of the neutrino interaction cross-sections in the GeV regime. The absence of a precise knowledge of the neutrino flux (mainly due to uncertainties on the parent hadrons production cross sections) currently limits this measurement to a 5-10% uncertainty level. The ENUBET project is proposing a novel facility, capable of constraining the neutrino flux normalization through the precise monitoring of kaon decay products in an instrumented decay tunnel. The collaboration has conducted numerous studies using a beamline with a central kaon momentum of 8.5 GeV/c and a ±10% momentum spread. We present here an alternative beam-line design, broadening the range of kaons to include momenta of 4, 6, and 8.5 GeV/c, thus allowing ENUBET to explore cross sections over a much larger momentum range. Specifically, we discuss the status of this design, the optimization studies performed, the early results, and the expected performance in terms of kaon mesons and neutrino rates.

THE ENUBET PROJECT OVERVIEW

The ENUBET project [1] aims to develop an experimental facility that will provide a beam of ν_e originating essentially only from the decays of positively charged kaon mesons (K^+), more specifically from the semi-leptonic decay $K^+ \to \pi^0\, e^+\, \nu_e$ (K_{e3}), and that will be monitored by measuring the associated positrons in the decay tunnel. More recently the monitoring technique has been extended to ν_μ from $K_{\mu 3}$ and $K_{\mu 2}$. The project's physics goal is to improve the precision of the existing cross section measurements [2] by one order of magnitude. In this work, we present the design of a novel secondary beamline that will provide a secondary beam of charged kaons and therefore a narrow-band neutrino beam. The ENUBET beamline design has various stringent requirements, among them being the production and acceptance of kaons from a high intensity (O(10^{13}) protons/spill), 400 GeV/c proton beam impinging on a target. An extensive overview of the challenges that accelerator-driven neutrino beams present can be found in [3]. The momentum selection, transport, collimation, and focusing of the produced kaon beam (with an intensity $O(10^{11}$ kaons/spill) are the key parameters of the work showcased in this R&D project. The instrumentation details of the decay tunnel are not discussed in this paper but can be found in other dedicated works [4, 5].

MULTI MOMENTUM BEAMLINE

As discussed in the introduction, the "multi-momentum" line will transport secondary particles of 4, 6, and 8.5 GeV/c momenta, allowing the exploration of a larger phase-space of neutrino cross-section measurements, including the region of interest of T2K/HyperK [6, 7]. The multiple momenta will be transported through the electromagnet's field scaling in dedicated runs for each momentum bin. It must be made clear that for each momentum, the "momentum-bite" (dp/p) acceptance of the line is ±10% around the central value. Also, all other momenta between ≈1 and 8.5 GeV/c can be transported theoretically towards the decay tunnel; however the beamline parameters have been optimized further for these three momenta, and results for those momenta are presented in this paper.

Proton Extraction

To monitor the decay products of kaons on a particle by a particle basis, while maintaining a local rate at the level of ∼1 MHz/cm^2 inside the instrumented decay tunnel, ENUBET's ideal operation is based on a slow-extraction scheme. Therefore, the total intensity of the extracted proton beam should be slowly and homogenously extracted on the target over several seconds, enabling event-by-event reconstruction at the detector level. The front-end focusing using quadrupoles (as an alternative to a pulsed horn) would allow extraction of protons (and therefore the production of kaons) for up to several seconds, reducing the instantaneous rate of particles reaching the decay tunnel by almost two orders of magnitude compared to extraction in burst mode. Both static (with quadrupoles) and horn focusing options are being studied by ENUBET, and the corresponding proton extraction methods have been developed and tested at the CERN Super Proton Synchrotron - SPS [8].

Target Studies

The secondary mixed-hadron beam of ENUBET will be generated by a high-energy proton beam impinging on a solid

* E-mail: elisabetta.giulia.parozzi@cern.ch, on behalf of the ENUBET collaboration

ISBN: 978-3-95450-227-1 ISSN: 2673-5490 doi:10.18429/JACoW-IPAC2022-MOPOTK016

ARC COMPRESSOR TEST IN A SYNCHROTRON - THE ACTIS PROJECT

M. Rossetti Conti*, A. Bacci, I. Drebot, A. R. Rossi, V. Petrillo[1], M. Ruijter[2], L. Serafini,
INFN - Sezione di Milano, [20133] Milano and LASA, [20090] Segrate (MI), Italy
[1]also at Università degli Studi, [20133], Milano, Italy
[2]also at Università Sapienza, [00185], Roma, Italy
A. Curcio, Centro de Láseres Pulsados, CLPU, [37185] Villamayor, Salamanca, Spain
S. Di Mitri, Elettra - Sincrotrone Trieste S.C.p.A., [34149] Basovizza (TS), Italy
G. Kowalski, R. Panaś, A. I. Wawrzyniak, Solaris National Synchrotron Radiation Centre, Jagiellonian University, [30-392] Kraków, Poland
E. Puppin, Politecnico di Milano, [20133] Milano, Italy

Abstract

ACTIS (Arc Compressor Test In a Synchrotron) is an experiment aimed to demonstrate the reliability of arc compressors as lattices capable to increase peak current and brightness of an electron beam as it is bent at large angles. This kind of devices has been proposed at theoretical level in several works over the past decades and could be the key to achieve compact and sustainable Free Electron Lasers in the near future. The experiment has been developed since 2019 in the joint effort between INFN, Solaris National Synchrotron Radiation Center and Elettra - S.T. S.C.p.A. The experiment will take place at Solaris (Krakow). Solaris is a synchrotron whose ring is injected by a 550 MeV linac that will be used to prepare the beam with a proper chirp. ACTIS involves also the commissioning of two beam length detectors to be installed downstream of the linac and of the first ring lap. In addition, the low energy model of the machine was built to identify the optimal working point for the experiment and to foresee the longitudinal profile of the beam that will be measured. In this work we present the experiment and report first results obtained in the study phase.

INTRODUCTION

Studies on the beam dynamics of arc compressors (AC) have been performed in the last two decades mainly in the context of designs of Free Electron Lasers (FELs) based on energy-recovery linacs (ERLs) [1–4] and, more recently, on a Two-Pass Two-Way linac (TPTW) [5–8].
The lattice of these arc compressors is based on a serie of achromatic cells, typically Double Bend Achromats (DBAs) or Triple Bend Achromats (TBAs), where optical functions have to be precisely tuned. The use of arcs as compressors allows to correct chromatic aberrations, cell by cell considering Coherent Synchrotron Radiation (CSR) emission betatron kicks arising in the bending magnets [9, 10]. A review article published in 2015 [11] contains very important studies in the frame of this activity. In these studies it is shown the use of arcs to perform a longitudinal compression of the bunches (up to a compression factor of 30) in the 0.2-7 GeV energy range keeping the growth of the normalized emittance under 0.1 mm-mrad, considering bunches with total charge up to 150 pC.

A new type of arc compressor was presented in 2019 in the context of the Conceptual Design Report (CDR) of the MariX FEL [12, 13] co-funded by the INFN and University of Milan. The CDR of this innovative machine presents a bubble shaped arc compressor (BAC) used to increase the beam peak current, up to 100 multiplication factor, while the beam is u-turned and re-injected in the cryogenic booster operated in continuous wave in the way to double the energy gain from the same booster. The scheme based on the double acceleration stage in the booster plus the compression and u-turn stage in the BAC is the so called two-pass two-way (TPTW) scheme.

Up to now, the possibility of compressing bunches into magnetic arcs has been predicted only theoretically also because of costs of a dedicated machine, therefore no demonstrators were built.

ACTIS would be the first experimental proof of the proper functioning of these promising devices. In addition, the results obtained would be the cornerstone for the realization of future highly sustainable machines based on the TPTW scheme, such as BriXSinO [14–16].

THE EXPERIMENT

The ACTIS experiment can count on the support of four different institutions interested in the project:
The **INFN - Milan** that is the proposing institution and is strongly interested in the demonstration of the principle behind the TPTW scheme developed in recent years.
The **Solaris National Synchrotron Radiation Centre** that hosts the experiment, provides the machine, local expertise and experience in synchrotron radiation detection.
The **Elettra - Sincrotrone Trieste S.C.p.a.** that has great experience in arc compressor beam dynamics and synchrotron machines. It is interested in experimental demonstration of the operation of these devices as a natural continuation of theoretical studies done previously.
The **INFN - Frascati Lab.** that offer a collaboration with SPARC_LAB dedicated to the detection of THz and sub-THz coherent radiation produced in bending magnets by compressed bunches.

* marcello.rossetti@mi.infn.it

ISBN: 978-3-95450-227-1 ISSN: 2673-5490 doi:10.18429/JACoW-IPAC2022-MOPOTK017

UPDATE OF LATTICE DESIGN OF THE SPring-8-II STORAGE RING TOWARDS 50 pmrad

K. Soutome[†1], T. Hiraiwa, H. Tanaka, RIKEN SPring-8 Center, Hyogo, Japan
[1]also at JASRI, Hyogo, Japan

Abstract

The storage ring lattice of SPring-8-II has been under optimization towards a low emittance of around 50 pmrad, which was initially set at 150 pmrad [1]. The optimization concept is based on the effective use of extra-radiation damping by damping wigglers that can be installed in the four long straight sections each 30 m long in length. For this purpose, we have been re-optimizing the linear and nonlinear optics so as to reduce the radiation loss from the bending magnets. In parallel, since the emittance variation due to the gap change of the IDs can be an obstacle for conducting precise experiments, we are investigating a new passive method to suppress the emittance variation without any feedback system.

INTRODUCTION

As is the case with other facilities around the world, the upgrade plan for the SPring-8 storage ring is being studied with the goal of achieving an extremely low emittance [1] by adopting a multi-bend (MB) lattice with longitudinal field-gradient dipoles [2-4]. Recent advances in undulator technology make it possible to shorten the undulator period length and we lower the stored beam energy from 8 GeV to 6 GeV. This also contributes to lower the emittance since it is proportional to the square of the beam energy. In our previous studies [1, 5], bending magnets of separate-function type were used and the target emittance was set around 150 pmrad. However, users have asked for more emittance reduction and we decided to introduce new concepts to reach the 50 pmrad level in user operation.

Our lattice design is characterized by the following features. (i) The combined-function dipoles are used to increase the horizontal damping partition number and hence to reduce the emittance. (ii) The dipole field distribution within a unit cell is optimized to reduce the total radiation loss. This enhances the effectiveness of radiation damping. (iii) The lattice nonlinearity is well suppressed by adjusting the betatron phase between two arc sections where sextupoles are localized. (iv) Damping wigglers (DWs) are planned to be installed in some of long straight sections (LSSs) to lower the emittance further. (v) Matching conditions of optical functions at the boundary of LSS are met for on- and off-momentum electrons. This allows us to redesign the LSS lattice locally according to users' requirements. (vi) A transparent beam injection is possible without giving perturbation to the stored beam.

For the newly designed lattice, the natural emittance is 108 pmrad, and by using DWs the emittance is expected to be reduced to the level of 50 pmrad in user operation. By doing nonlinear optimization we have a large enough dynamic aperture (DA) for off-axis beam injection and momentum acceptance (MA) of about 3%. As for the beam injection, the SPring-8 has an advantage that we have an XFEL facility SACLA on the same campus and its linac has already been used as a high quality beam injector in the top-up operation of the present SPring-8 storage ring [6]. With only a few modifications, this high quality beam injection system can be used for the SPring-8-II.

LATTICE DESIGN

Emittance Reduction

In Fig.1 we show the design of a unit cell of the SPring-8-II storage ring. The cell structure is of the five-bend achromat type, and dipoles with longitudinal field-gradient are used to achieve a target emittance value [3], except for the one in the center of the cell. This central dipole is for generating hard x-rays and its field strength is fixed at 0.953 T. The field distribution of other dipole segments are optimized so that the lowest possible emittance are obtained under a given magnet arrangement. At the same time, we take care to minimize the radiation loss as much as possible, which is important for enhancing the effects of radiation damping. The dipole segment on the side near the peak of the dispersion (blue filled squares in Fig.1) is of the combined-function type by which the horizontal damping partition number is increased from 1.0 to 1.39. The maximum values of the quadrupole, sextupole and octupole fields are 55.7 T/m, 2.7e3 T/m^2 and 8.0e4 T/m^3, respectively, and these can be realized with ordinary electromagnet technologies. In Table 1 we compare machine parameters of the new storage ring with those of the present SPring-8 storage ring.

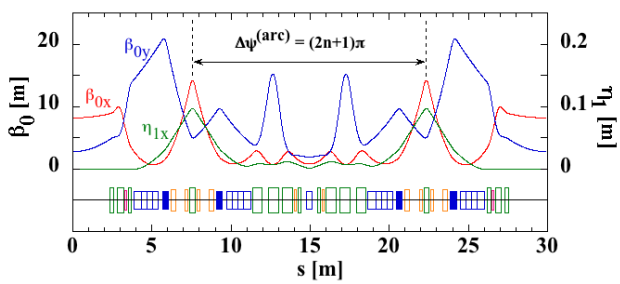

Figure 1: The optics and magnet arrangement of a unit cell. The squares shown at the bottom of the figure represent bending (blue), quadrupole (green), sextupole (orange) and octupole (red) magnets. Blue filled squares are bending magnets of the combined-function type.

† soutome@spring8.or.jp

ISBN: 978-3-95450-227-1 ISSN: 2673-5490 doi:10.18429/JACoW-IPAC2022-MOPOTK018

PARALLELIZATION OF RADIA MAGNETOSTATICS CODE*

Anushka Banerjee†, Stony Brook University, Stony Brook, NY 11794, USA
Oleg Chubar,Brookhaven National Laboratory, Upton, NY 11973, USA
Gaël Le Bec, Joel Chavanne, ESRF, 38000 Grenoble, France
Boaz Nash, Christopher Hall, Jonathan Edelen, RadiaSoft LLC, Boulder, CO 80301, USA

Abstract

Radia 3D magnetostatics code has been used for the design of insertion devices for light sources over more than two decades. The code uses the magnetization integral approach that is efficient for solving permanent magnet and hybrid magnet structures. The initial version of the Radia code was sequential, its core written in C++ and interface in the Mathematica language. This paper describes a new Python interfaced parallel version of Radia and its applications. The parallelization of the code was implemented on C++ level, where the semi-analytical calculations of interaction matrix elements and resultant magnetic fields were parallelized using the Message Passing Interface. The parallel performance results are encouraging, particularly for magnetic field calculation post relaxation where a ~600 speedup with respect to sequential execution was obtained. The new parallel Radia version facilitates designs of insertion devices and lattice magnets for novel particle accelerators.

INTRODUCTION

The Radia code has been continuously improved for nearly two decades since its inception and development in the Insertion Devices laboratory of the European Synchrotron Radiation Facility (ESRF). From establishing boundary integral method-based calculations as an alternative and better approach than the conventional finite element, for e.g., FLUX3D [1], Radia has been widely used to compute fields for undulators. Over the last few years, Radia has not only provided better time performance and precision results when compared to FEM codes [2], it provides excellent agreement between the calculated and measured field values corresponding to relatively simple structures like quadrupole and sextupole [3], or complicated structures like the iron-dominated electromagnetic structure: SOLEIL Undulator HU256 [4].

Following the concepts of object-oriented programming, the core part of Radia is written in C++ and was initially interfaced to run serially on Wolfram Mathematica and Igor Pro only. Currently, the new, open-source version of Radia is already available in Python interface [5], with ongoing developments to make it executable on web-based graphical interface like Jupyter Notebook [6]. Radia's Python interface has been used for magnetic "cross talk" computations of the recent ESRF-Extremely Brilliant Source upgrade, where a large number of sequential calculations with different input parameters were performed in parallel at the ESRF cluster. The calculated values had good agreement with the measured values (relative errors in the 10^{-4} range) [7].

METHODS USED FOR PARALLELIZATION

With an increased development in the field of light sources, the importance of magnetostatics code has increased by manifolds compared to what it was a few decades earlier. Despite Radia's stellar performance when compared to conventional FEM based code, the target computations involving 3D magnetic simulations of the insertion devices and accelerator magnets are quite complicated and CPU-intensive, with further increasing complexities. With an aim to further improve Radia's overall performance, parallelization tasks were undertaken.

MPI is a communication protocol and is used as the industry standard for the message passing model where a certain application comprises of a set of tasks which are assigned their own local memory whose location can be in the same machine or across several machines. Data exchange to conduct the operation by tasks is established by sending and receiving messages [8]. MPI provides programmers the flexibility to use it as a low-level approach with a detailed control on the flow of data, or as a high-level programming approach with parallel libraries designed to provide optimized performance without going into the depths of the MPI algorithm [9].

Solving any 3D magnetostatics problems in Radia comprises of 3 subsequent steps: calculation of elements of a large (often tens GBs memory size) matrix called Interaction Matrix and describing magnetic interaction between 'active' sub-volumes of a magnet geometry, created by segmentation (1), performing a relaxation procedure on it to determine values of the magnetization vector in all the "active" sub-volumes (2), and computing magnetic field and/or field integrals or other characteristics of magnetic fields, created by the sub-volumes with magnetization or current density (3). The two sections– the generation of the interaction matrix (1) and the calculation of magnetic field values after relaxation (3) are 'embarrassingly parallel' algorithms and hence have been parallelized using MPI at the C++ level.

Interaction matrix is a dense matrix in Radia, that may occupy a large memory, depending on geometry and its segmentation. Relaxation of this matrix may require a large number of iterations, in particular when solving complicated iron-dominated geometries [2,4]. At each of these iterations, a relatively small number of multiplications needs to be done to take into account (or update) magnetization vector in each

* Work supported by the US DOE BES SBIR grant no. DE-SC0018556.
† anushka.banerjee@stonybrook.edu

ISBN: 978-3-95450-227-1 ISSN: 2673-5490 doi:10.18429/JACoW-IPAC2022-MOPOTK022

A DESIGN STUDY OF INJECTOR SYSTEM FOR SYNCHROTRON LIGHT SOURCE

Chanmi Kim, Eun-San Kim*, Chong Shik Park†
Department of Accelerator Science, Graduate School, Korea University, Sejong, Korea

Abstract

This work presents a design study of a 200 MeV electron linear accelerator consisting of an electron gun, bunchers, and accelerator structures. We aimed to design the linac with low emittance and low energy spread. A coasting beam from a thermionic electron gun is bunched using a series of buncher cavities: sub-harmonic buncher (SHB), a pre-buncher (PB), and a Buncher. The bunched beam is then accelerated up to 200 MeV with 4 cascaded accelerating structures. The SHB was designed with one-cell standing wave structure for improving the bunching efficiency. The two types of the 500 MHz SHB were considered: elliptical and coupled-cavity linac types. We also investigated constant-gradient and constant-impedance types of 3 GHz multi-cell traveling wave resonators for following buncher cavities and accelerating structures. Depending on the type, geometries of each traveling wave structure (TWS) cavity were determined, and then the electromagnetic fields were calculated. RF powers and phases of each cavity along this linac system were optimized using beam dynamics simulation. Furthermore, the beam distributions in the transverse direction are adjusted using solenoid magnets in the low-energy section as well as quad triplets in the high-energy section.

INTRODUCTION

We designed an electron linac as an injector to the storage ring based light source. Between linac and storage ring there will be a full energy booster ring. Therefore, our linac is required to accelerate the beam energy up to 200 MeV. There are two types of electron sources used in our linac system thermionic gun and RF photoinjector gun. In the linac systems such as NSLS II [1] and swiss light source (SLS) [2], the thermionic gun is used. The RF photoinjector gun is used in Advanced Photo Source (APS) and European X-ray Free Electron linac (EXFEL), etc [3, 4]. In this paper, the electron linac using a 90 keV thermionic gun was studied. The electron gun was modeled, the elective field was calculated, and the particle tracking simulation was done using CST's particle studio [5, 6]. In order to bunch a CW beam from the thermionic gun, buncher systems are needed. The buncher system is composed of SHB, PB, and Buncher. To accelerate the beam energy, four accelerating structures were used. The geometries of these RF structures were optimized and the eletric field were computed, using the Superfish code [7]. The layout of this eletron linac can be seen in Fig.1. Beam dynamics study explores the optimized parameters in the design of beam line for high quality beam delivery. In this paper, we present Parmela code [8] simulation results and beam dynamics study in the 200 MeV linac structure.

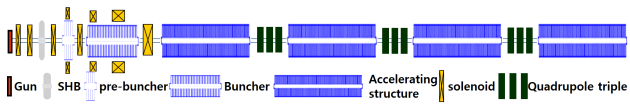

Figure 1: Electron linac layout.

DESIGN OF THE CAVITY

This injector linac has 4 types of cavities: SHB, PB, Buncher, Accelerating structures. The frequency of SHB is 500 MHz, while those of other cavities are 3 GHz. The main purpose of SHB is bunching of the continuous beam from the gun. In doing so, the standing wave structure(SWS) is chosen for SHB. Its design beta is 0.5 since the beam energy from the gun is 90 keV. Therefore, the cell length of SHB is $\beta\lambda/2 \approx 15$ cm. We considered two types of SHB shapes: Elliptical and CCL. The geometries of each type of SHB is described in Fig.2 [9]. Using the automatic design tool in Superfish, we modeled the geometries of the SHBs. These parameters are listed in Table 1. As a result of designing the cavity, the elliptical type has a larger Q value, while CCL has a larger transit time factor (TTF) and shunt impedance.

PB and Buncher are used for beam bunching and acceleration at the same time, while 4 accelerating structures are used only for beam acceleration. In these purposes, the TWS with a disc-loaded type is chosen for these cavities. In order to increase the bunching efficiency, the number of cells in PB and Buncher are 4 and 31, respectively. Also, the number of cells in 4 acceleraing structures is 94. The geometry of the TWS can be determined by cell length(d),

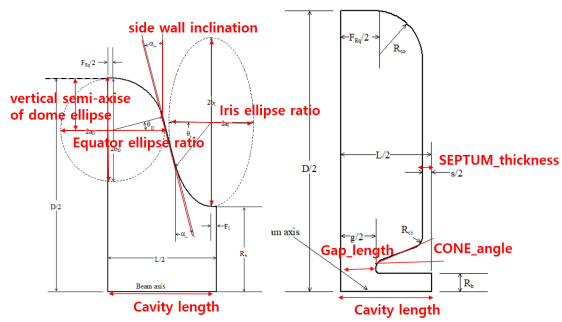

Figure 2: The sub-harmonic buncher geometry. (right: elliptical type , left: CCL type) [7].

* eskim1@korea.ac.kr
† kuphy@korea.ac.kr

ISBN: 978-3-95450-227-1 ISSN: 2673-5490 doi:10.18429/JACoW-IPAC2022-MOPOTK023

BEAM DYNAMICS STUDIES ON THE 50 MeV ELECTRON LINEAR ACCELERATOR FOR ULTRA-HIGH DOSE RATES

Yumi Lee*, Eun-San Kim,
Dept. of Accelerator Science, Korea University Sejong Campus, Sejong, Republic of Korea
Heung-Soo Lee, Hyunseok Shin, VITZRONEXTECH, Ansan-si, Gyeonggi-do, Republic of Korea

Abstract

Electron beams with ultra-high dose rates (> 40 Gy/s), which enable effective radiotherapy to act on deep-seated tumors in less than a second, can be generated by linear accelerators. To successfully achieve FLASH radiotherapy, we have performed the 50 MeV linear accelerator design studies. The designed electron accelerator consists of a thermionic electron gun, sub-harmonic buncher, buncher and 2.856 GHz traveling wave structure. In this report the design layout and particle tracking simulation results of the 50 MeV electron linac with high beam current are presented in detail.

INTRODUCTION

Electron beams with low dose rates and energy are mainly used in conventional radiotherapy. Therefore, the number of treatments received increases, and there is a limit to treatment for deep-seated tumors. In contrast to conventional radiotherapy, FLASH radiotherapy uses ultra-high dose rates and high energy of electron beams, so the number of treatments received can be reduced and even deep-seated tumors can be treated by FLASH radiotherapy. The side effects can also be reduced because damage to healthy tissues decreases. To accomplish FLASH radiotherapy, it is necessary to design a linear accelerator for the electron beams suitable for FLASH radiotherapy.

Design Goals

The dose rate and penetration depth of the electron beams are related to the beam current and energy, respectively. FLASH radiotherapy requires the electron beam current of > 15 A and beam energy of 50 MeV for ultra-high dose rates (> 40 Gy/s) and deep penetration depth [1]. The design goals of the electron linear accelerator are as follows. The electron linac must :

- be capable of accelerating the electron beams with high current (~15 A).
- be able to accelerate the electron beam energy up to ~50 MeV.
- have a high transmission rate.

DESIGN LAYOUT

The linear accelerator is made up of a 200 keV thermionic electron gun, a 476 MHz sub-harmonic buncher (SHB), a 2856 MHz buncher and a 2856 MHz acceleration structure for effective bunching and accelerating of the electron beams. Three solenoids (SOL01, SOL02, SOL03) and four coils (CO01, CO02, CO03, CO04) are used as the focusing elements of the linear accelerator. Figure 1 shows the schematic layout of electron linear accelerator.

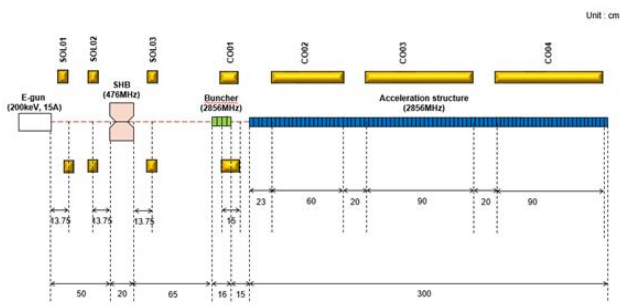

Figure 1: Schematic layout of electron linear accelerator.

MAIN COMPONENTS

The main features of the sub-harmonic buncher, buncher and acceleration structure are described in this section.

Electron Gun

The electron gun is a thermionic cathode gun, and the voltage between the cathode and the anode is 200 kV. Figure 2 shows the electrons flow in the gun with the cathode with a radius of 10 mm and the beam parameters emitted from the electron gun are listed in Table 1.

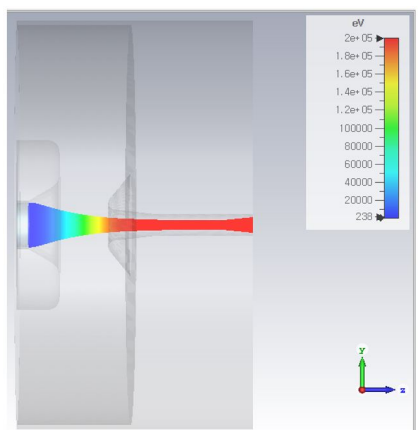

Figure 2: Electrons flow in the gun.

Sub-harmonic Buncher

A sub-harmonic buncher with a standing wave structure with a resonance frequency of 476 MHz is used to send a

* leeyumi812@gmail.com

ISBN: 978-3-95450-227-1 ISSN: 2673-5490 doi:10.18429/JACoW-IPAC2022-MOPOTK024

QUASI-FROZEN SPIN CONCEPT OF MAGNETO-OPTICAL STRUCTURE OF NICA ADAPTED TO STUDY THE ELECTRIC DIPOLE MOMENT OF THE DEUTERON AND TO SEARCH FOR THE AXION

Y. Senichev, A. Aksentyev, S. Kolokolchikov, A. Melnikov, Institute for Nuclear Research of Russian Academy of Sciences, Moscow, Russia
V. Ladygin, E. Syresin, Joint Institute for Nuclear Research, Dubna, Russia
N. Nikolaev, Landau Institute of Theoretical Physics, Chernogolovka, Russia

Abstract

The "frozen spin" method is based on the idea that at certain parameters of the ring, the particle spin rotates with the frequency of the momentum, creating conditions for the continuous growth of the electric dipole moment signal. The Nuclotron-based Ion Collider fAcility (NICA) is under construction in Joint Institute for Nuclear Research [1]. Since a straightforward implementation of the frozen spin regime at NICA is impossible, we suggest an alternative "quasi-frozen spin" concept. In this new regime, the reference particle's spin-vector precesses with a spin phase advance $\pi \cdot \gamma G/2$ per beam revolution, locally recovering the longitudinal orientation at the location of the electric-magnetic elements, Wien filters, placed in the straight sections. In the deuterons case, thanks to the small magnetic anomaly G, the spin-vector continuously oscillates relative to the direction of the momentum-vector with a small amplitude of a few degrees and the expected EDM effect is reduced only by a few percent. In this paper, we study the spin-orbital motion with the aim of using the NICA collider to measure the EDM. We also comment on the potential of NICA as an axion antenna in both the quasi-frozen spin regime and beyond.

"FROZEN SPIN" CONCEPT

The idea of searching for the electric dipole moment (EDM) of the proton and the deuteron using polarized beams in a storage ring is based on the "frozen spin" method and was originally proposed at the Brookhaven National Laboratory (BNL) [2]. The concept of the "frozen spin" (FS) lattice consists of deflectors with electric and magnetic fields incorporated in one element, in which the spin vector of the reference particle is always orientated along the momentum vector. This is clearly evident from the Thomas–Bargmann–Michel–Telegdi equation:

$$\frac{d\vec{S}}{dt} = \vec{S} \times \left(\vec{\Omega}_{mdm} + \vec{\Omega}_{edm}\right),$$
$$\vec{\Omega}_{mdm} = \frac{e}{m\gamma}\left\{(\gamma G + 1) - \left(\gamma G + \frac{\gamma}{\gamma+1}\right)\frac{\vec{\beta}\times\vec{E}}{c}\right\},$$
$$\vec{\Omega}_{edm} = \frac{e\eta}{2m}\left(\vec{\beta}\times\vec{B} + \frac{\vec{E}}{c}\right), G = \frac{g-2}{2}, \quad (1)$$

where G is the magnetic anomaly, g is the gyromagnetic ratio, Ω_{mdm} is the spin precession frequency due to the magnetic dipole moment, Ω_{edm} is the spin precession frequency due to the electrical dipole moment, and η is the dimensionless coefficient defined in (1) by the relation $d = \eta e\hbar/4mc$. The advantages of purely electrostatic machines are especially evident at the "magic" energy, when angle:

$$G - 1/\left(\gamma_{mag}^2 - 1\right) = 0, \quad (2)$$

and the spin vector initially oriented in the longitudinal direction rotates in the horizontal plane with the same frequency as the momentum Ω_p, i.e., $\Omega_{mdm} - \Omega_p = 0$.

In the case of deuterons, whose $G = -0.142$ the only possible method to EDM measurement is a hybrid storage ring with both electric and magnetic fields. This can be done by applying a radial electric field E_r to balance the contribution effected by the vertical magnetic field B_v to the frequency Ω_{mdm}^p, as shown in Eq. (1):

$$E_r = \frac{GBc\beta\gamma^2}{1-G\beta^2} \approx GB_v c\beta\gamma^2. \quad (3)$$

Thus, the only reason one might want to closely adhere to the "frozen" spin condition is to maximize the EDM signal growth.

"QUASI-FROZEN SPIN" CONCEPT

In the NICA ring, the implementation of the FS concept would require a complete upgrade of the optics. However, suppose the spin would oscillate in the horizontal plane with respect to the frozen spin direction with small amplitude of angle $(\Phi_s)^2 \ll 1$. This could be done by placing special, electric-field elements in the straight accelerator sections, which would bring the spin vector back in alignment with the momentum after it moved away from it in the magnetic arc. Then the EDM growth would decrease proportionally to the factor $J_0(\Phi_s) \approx 1 - (\Phi_s)^2/4$. Since the deuteron's magnetic anomaly $G = -0.142$ has a small value and since, in the imagined case, the spin oscillates around the momentum direction within a half value of the advanced spin phase in the magnetic arc $\Phi_s = \pi \cdot \gamma G/2 \approx 0.2$, it is obvious that the effective contribution to the expected EDM effect is reduced by only a few percent at the optimal parameters for the EDM measurement $\gamma = 1.12$.

The mental experiment described above gives the gist of the "quasi-frozen" spin (QFS) concept [3]: here the spin is not frozen with respect to the momentum vector, but continually oscillates around some average fixed direction

ISBN: 978-3-95450-227-1 ISSN: 2673-5490 doi:10.18429/JACoW-IPAC2022-MOPOTK026

4-DIMENSIONAL EMITTANCE MEASUREMENTS AND CORRECTION OF UED OPTICS UP TO SEXTUPOLE ORDER*

W. H. Li[1], M. Gordon[2], M.B. Andorf[1], A. C. Bartnik[1], C. J. R. Duncan[1], M. Kaemingk[1], S. J. Levenson[1], C. A. Pennington[1], I. V. Bazarov[1], Y.-K. Kim[2], J. M. Maxson[1]
[1]Cornell Laboratory for Accelerator-Based Sciences and Engineering, Ithaca, NY 14853, USA
[2]University of Chicago Department of Physics, Chicago, IL 60637, USA

Abstract

Ultrafast electron diffraction imposes stringent constraints on the full 6D brightness of the probe electron beam. The desired normalized emittance, often in the few-nanometer regime and below, renders the beam very sensitive to field aberrations and space charge effects. In this proceeding, we report the correction of normal quadrupole, skew quadrupole, and sextupole aberrations in the MEDUSA ultrafast electron micro-diffraction beamline and measurements of the subsequent emittance. This low emittance is enabled by alkali-antimonide photocathodes driven at the photoemission threshold. We demonstrate that the measured emittance is consistent with that of optimized simulations with these cathodes, indicating that low emittance beams from high quality photocathodes can be preserved and used in practical applications.

INTRODUCTION

Ultrafast electron diffraction(UED), ultrafast electron microscopy (UEM), and X-ray free electron lasers are some of the most important modern tools for the study of non-equilibrium processes in crystals on the picosecond scale and below [1–11]. The spatial and temporal resolution of these devices is determined by the electron beam quality.

For UED in particular, the relevant metrics, the probe beam size and divergence, can be collectively represented in the emittance. The emittance of the electron beam can be degraded in transport by non-linear fields coming from space charge and electron optics, as well as stray fields from electron optics[12]. Correcting these stray fields is common up to quadrupole fields in photoinjectors [13–15]. As beam emittance is pushed ever smaller, emittance contributions from stray fields will matter increasingly more, and unless corrected, can become the dominant contribution to the final emittance of the beam. The effects of non-linear fields are especially important for beams with larger size, as the emittance contribution grows super-linearly with the beam size.

We have implemented stray field correction of quadrupole, skew quadrupole, and sextupole moments in order to preserve the emittance in MEDUSA, a keV UED microdiffraction beamline described in [16]. A schematic of the main elements of the beamline are shown in Fig. 1.

* This work was supported by the U.S Department of Energy, grant DE-SC0020144 and U.S. National Science Foundation Grant PHY-1549132, the Center for Bright Beams.

PHASE SPACE RECONSTRUCTION

We can characterize the quality of the beam by reconstructing the beam in the 4d phase space defined by x, x', y, and y'. This reconstruction is performed by scanning the electron beam across a 10 µm aperture placed at the sample location. The x and y coordinates are determined by the beam position on the aperture. The beam is then imaged on a downstream screen. With a sufficiently large distance between the aperture and screen and a small aperture, the distribution of the beam on the screen is dominated by the momentum at the aperture, not the position. Thus, the x' and y' distribution is determined by the distribution of the beam on the final screen.

Each pixel on the final screen at a particular aperture position, therefore, corresponds to a 4d "voxel" in 4d phase space. We can build up the 4d volume voxel by voxel by scanning the beam on the aperture and measuring the intensity at each pixel, which produces a full 4d phase space. Example 2d projections of the 4d measurement in a stray field corrected beam are shown in Fig. 2.

With the phase space in hand, we can calculate the 4d sigma matrix, defined as:

$$\Sigma_{4d} = \begin{pmatrix} < x^2 > & < xx' > & < xy > & < xy' > \\ < x'x > & < x'^2 > & < x'y > & < x'y' > \\ < yx > & < yx' > & < y^2 > & < yy' > \\ < y'x > & < y'x' > & < y'y > & < y'^2 > \end{pmatrix}. \quad (1)$$

We can quantify the preservation of beam quality by calculating the normalized 4d emittance, defined as:

$$\varepsilon_{n,4d} = (\beta\gamma)^2\sqrt{\det(\Sigma_{4d})}. \quad (2)$$

To more easily compare the 4d emittance with the 2d emittance, for the rest of this paper, the square root of the 4d emittance will be reported.

QUADRUPOLE CORRECTION

One important benefit of measuring the entire 4d phase space and calculating the 4d emittance lies in the ability to measure x-y correlations. These x-y correlations can be used to reveal the presence of stray quadrupole fields along the beamline. Such stray quadrupoles commonly require corrections in photoinjectors, as the induced skew correlations can significantly degrade the 2d emittance.

Large quadrupole moments can be most easily seen in the beam size and shape. Figure 3 (a) shows the beam size as a function of solenoid current, and there is a clear asymmetry

ISBN: 978-3-95450-227-1 ISSN: 2673-5490 doi:10.18429/JACoW-IPAC2022-MOPOTK027

CHARACTERIZATION OF VARIOUS GaN SAMPLES FOR PHOTOINJECTORS

S.J. Levenson*, M.B. Andorf, I.V. Bazarov, J. Encomendero, D. Jena,
J.M. Maxson, V. V. Protasenko, and H. G. Xing, Cornell University, Ithaca, NY, USA

Abstract

Photoemission properties (quantum efficiency, spectral response, and lifetime) of various GaN based photocathodes are summarized, including p-doped samples in its hexagonal phase, cubic GaN and a more exotic 2-D hole gas sample. The 2-D hole contains no dopant impurity but achieves high conductivity via polarization fields produced at the heterojunction of GaN and AlN. For efficient electron production, cesium is used to achieve Negative Electron Affinity.

INTRODUCTION

Galium-Nitride (GaN) photocathodes have many interesting properties which make them exceptional candidates for the use of a variety of photoinjector applications. With reported quantum efficiencies exceeding 50% [1] and a high thermal conductivity, they may be suitable for high-current applications where thermal degradation of the QE can be a limiting factor. For high brightness applications, GaN has a prompt response time [2] and the Mean Transverse Energy of N-polar GaN has been reported to be 50 meV at 300 nm [3]. Ordinarily GaN is grown with a hexagonal crystal structure but can also be grown as a cubic structure from which it may be possible to produce spin-polarized electrons.

For efficient electron production, GaN must be brought to Negative Electron Affinity (NEA). Typically this is done by exposing the surface to Cs or Cs and oxygen. The activation layer forms a strong electric dipole on the GaN surface bringing the electron affinity level at the surface below the bulk conduction band minimum. Although this yields efficient electron production, it makes the photocathode very sensitive to vacuum conditions. Interestingly, N-polar GaN photocathodes have been engineered to achieve NEA in the absence of Cs [4], pointing to a potentially extremely robust photocathode. However, to date, the QE of N-polar GaN photocathodes has been limited to $\approx$ 1% for photon energies below 4.8 eV.

In this work we present measurements of the spectral response and lifetime of three novel GaN based photocathodes: (i) a sample grown in a cubic phase, (ii) a sample grown on a single-crystal Ga-polar GaN substrate resulting in a significantly lower dislocation density at the surface and (iii) a 2D Hole Gas (2DHG) which contains no doping but obtains high conductivity via polarization fields produced at a heterojunction of GaN and Aluminum Nitride [5]. All other samples are p-doped with a Mg concentration of $\approx 3 \times 10^{19}$ cm^{-3} in accordance with the results published in [1]. For comparison, a hexagonal p-GaN sample grown on a GaN template on sapphire was used. Schematics of the cathodes tested are shown in Fig. 1.

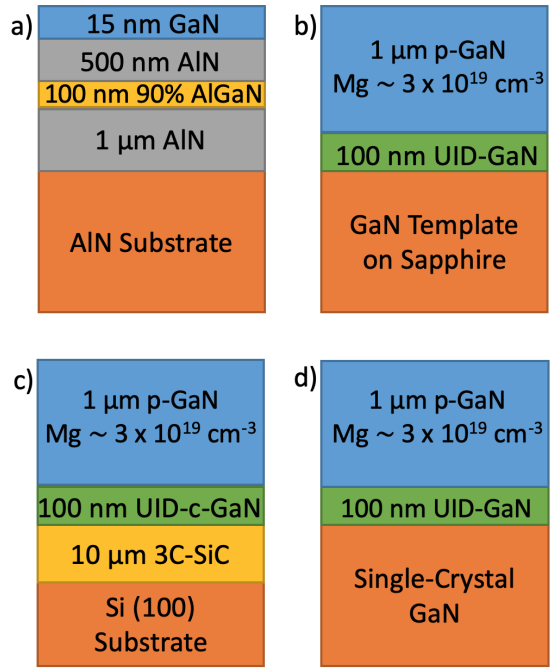

Figure 1: The four samples grown and tested in this work. *a)* The 2DHG sample, the 2DHG is found between the top GaN layer and AlN layer. *b) - d)* The hexagonal (template), cubic and single-crystal GaN samples, respectively.

Methods

The samples were grown using a Veeco Gen10 molecular beam epitaxy system equiped with standard efussion cells for elemental Gallium, Aluminum and Magnesium. Before epitaxy, the substrates were ultrasonicated in acetone, methanol and isopropanol for 10 min each, and then outgassed at 200 C for 7 hours. All the layers in each sample were grown within the step-flow growth mode and maintaining metal-rich conditions throughout the whole epitaxial process.

After growth, each of the samples were transferred into the Cornell Photoemission Laboratory main test chamber [6]. Each sample was mounted onto a sample holder compatible with the photoemission test chamber. Thermal contact was established between the samples and the holder with indium foil. During mounting and transferring of the samples between the growth and photoemission chamber, the samples were exposed to air for 5-10 minutes. The photoemission chamber has a base pressure of approximately 2×10^{-10} Torr.

* sjl354@cornell.edu

ISBN: 978-3-95450-227-1 ISSN: 2673-5490 doi:10.18429/JACoW-IPAC2022-MOPOTK028

ZERO DISPERSION OPTICS TO IMPROVE HORIZONTAL EMITTANCE MEASUREMENTS AT THE CERN PROTON SYNCHROTRON

W. Van Goethem*,[1], F. Antoniou, F. Asvesta, H. Bartosik, A. Huschauer
CERN, Geneva, Switzerland
[1]also at Goethe-University, Frankfurt, Germany

Abstract

In modern particle accelerators, the horizontal dispersion function is forced to zero at locations with instrumentation measuring the transverse beam distribution, in order to remove the dispersive contribution to the horizontal beam size. The design of the CERN Proton Synchrotron (PS) did not foresee such a zero-dispersion insertion, making it challenging to get a good precision on the beam emittance measurements. In this contribution, we present a new optics configuration, which allows to reach zero horizontal dispersion at the locations of different beam size measurement locations. This can be achieved by powering a set of trim quadrupoles, the so-called Low Energy Quadrupoles (LEQ). We investigate how the resulting optics perturbation affects beam parameters.

INTRODUCTION

The emittance is one of the most important beam parameters for accelerators. Its value must be well known along the injector chain, as a means to identify and study errors that could lead to unexpected emittance blow-ups, as it was observed at PS injection from the PSB for high-brightness beams during Run 2 [1]. The emittance ϵ can be calculated at locations where the beam size $\sigma(s)$ is measured and other parameters are known using the following equation:

$$\epsilon = \frac{\sigma^2(s) - D^2(s)\left(\frac{\Delta p}{p_0}\right)^2}{\beta(s)}\,, \tag{1}$$

with $D(s)$ the dispersion function, $\frac{\Delta p}{p}$ the relative momentum spread and β the optical beta function.

Research accelerators that are built in recent times usually contain dispersion suppressors. These are sections of the machine where the dispersion is brought to zero, removing the dispersive contribution from the expression above. The PS does not have such a section and therefore there is a non-zero horizontal dispersion along the whole ring, introducing additional errors in emittance calculations [2, 3]. In this study, the LEQs are used to induce a dispersion oscillation leading to zero dispersion at specific beam measurement locations in the PS. This dispersive oscilliation must be optimised so the other optics functions are minimally perturbed while zero dispersion is reached. The optimisation uses the single particle simulation toolkit MAD-X [4, 5] to identify the corresponding LEQ-strengths. Going from nominal optics to zero dispersion optics is initially tested using a simulation framework that allows including space charge effects in time dependent optics configurations, here implemented using PyOrbit. [6, 7]. The optics are then used in an experimental setting to see if zero dispersion is reached at the desired beam measurement location and to investigate what the effects are on the beam size and emittance while the optics are changed between the nominal and the zero-dispersion configuration.

SINGLE PARTICLE STUDY

The zero dispersion optics are abstracted into a numerical optimisation problem. The quadrupole strengths are a clear choice as optimisation variables for this study. In this manner, the change in optics can be minimised using a quadratic objective function since the induced tuneshift and beta-beating from a quadrupolar variation is directly proportional to that variation:

$$\text{minimize } \delta k_1^2 + \delta k_2^2 + \ldots + \delta k_n^2\,,$$

where δk_i are the strength variations of the individual LEQs. On top of having the quadrupole strength limits as bounds, an additional boundary condition needs to be placed on this objective function that forces the dispersion to zero at a specific location. This bound is created by superimposing the effects of each quadrupole on the dispersion at that location. This bound is of the form

$$D^* = D_0 + \Delta D_{k_1} \times \delta k_1 + \Delta D_{k_2} \times \delta k_2 + \ldots + \Delta D_{k_n} \times \delta k_n, \tag{2}$$

where D^* is the dispersion after varying the quadrupoles which will be equated to zero, D_0 is the initial dispersion and ΔD_{k_i} are the scalars proportional to the effect of a quadrupole variation of size δk_i on the dispersion. A small study was performed to prove that the dispersion beating is directly proportional to the quadrupole variation [8], validating the expression above. Thus a convex quadratic optimisation problem is formed which will force the dispersion to zero and minimally affect the other optics functions. This optimisation problem is solved using CVXOPT [9].

Initially, all 40 LEQs are used in the optimisation. However, the same result can be achieved by using less active quadrupoles. The active number of LEQs is iteratively reduced by one until the quadrupole strength limit is reached. The reduction is realised with the following reasoning: if $|\delta k_i|$ is large for a certain quadrupole, that quadrupole heavily forces the dispersion to zero. Hence, the LEQ with the lowest $|\delta k_i|$ has the least influence in this problem and can be removed from the equations.

* wietse.van.goethem@cern.ch

ISBN: 978-3-95450-227-1 ISSN: 2673-5490 doi:10.18429/JACoW-IPAC2022-MOPOTK029

IMPROVED LOW-ENERGY OPTICS CONTROL FOR TRANSVERSE EMITTANCE PRESERVATION AT THE CERN PROTON SYNCHROTRON

W. Van Goethem*,[1], F. Antoniou, F. Asvesta, H. Bartosik, A. Huschauer
CERN, Geneva, Switzerland
[1]also at Goethe-University, Frankfurt, Germany

Abstract

Preservation of the transverse emittances across the CERN accelerator chain is an important requirement for beams produced for the Large Hadron Collider (LHC). In the CERN Proton Synchrotron (PS), high brightness LHC-type beams are stored on a long flat bottom for up to 1.2 seconds. During this storage time, direct space charge effects may lead to resonance crossing and subsequent growth of the transverse emittances. Previous studies showed an important emittance increase when the PS working point is moved near integer tune values. Subsequent simulation studies confirmed that this observation is caused by an interplay of space charge effects and the optics beatings induced by the Low Energy Quadrupoles (LEQ). A new optics configuration using these quadrupoles to reduce the optics beating and the emittance growth was developed and experimentally validated. The results of simulation and experimental studies are presented in this contribution.

INTRODUCTION

The initial tune correction scheme of the PS consisted of 50 LEQs placed symmetrically around the machine, which consists of 100 combined function magnets. As a result, the beta beatings induced from quadrupoles with a 90° phase advance between them would compensate for eachother [1–3]. During the course of the PS' runtime new installations required 10 LEQs to be removed, breaking the lattice symmetry and increasing the optics beatings. Previous studies have shown that the large emittance blow-up generated at working points near integer values in the PS are caused by an interplay of the increased optics beatings due to the irregular distribution of the LEQs and space charge effects [4–7]. Beams with high tune-spread will cross the integer resonance which is the case for the high-brightness beams that are used in the LHC. These beams are therefore limited to the usable working point range [8]. In the presented study a new LEQ-configuration was explored to reduce the optics beatings and increase the flexibility of the PS in terms of working point control.

The optics beatings will be reduced by various optimisation techniques using the single particle simulation tool MAD-X [9, 10]. All promising configurations will then be tested in a simulation framework that includes space charge effects by tracking a particle bunch using PyORBIT [11] through a magnetic sequence with nodes for space-charge calculations. At the nodes, the beam distribution is calculated and dependent on the distribution, the particles receive a coulomb kick [12]. This framework is used to correctly model the direct space charge tune spread and hence investigate the effect on emittance growth. Finally, the most promising LEQ configuration is tested experimentally.

LEQ OPTIMISATION

In the current operational configuration, the LEQs are installed at the end of 40 out of 100 straight sections, just before the combined function magnet units. Of the 100 straight sections, 12 have room for a quadrupole to be installed. Additionally, many of the straight sections that are unoccupied could house two LEQs. These additional possibilities are considered in the presented calculations. The working point of all configurations are moved close to integer resonance ($Q_x = 6.1, Q_y = 6.1$) using the LEQs where the focusing and defocusing quadrupoles respectively have the same strengths. This ensures that the optics beating is large causing and increased emittance growth to be observed in the space charge simulations.

Parameterisation of the Optics Beatings

For the following optimisations, the amplitude of the beating of the three main optics functions in the PS (β_x, β_y, D_x) need to be represented by a single real value. Presuming that if a minimum of this value is found, the optics beatings for the corresponding configuration is minimised. The following representation is used here:

$$\xi = \frac{\sigma(\beta_x) + \sigma(\beta_y) + \sigma(D_x)}{3}, \quad (1)$$

Where σ is the standard variance of the optics function between brackets. Other representation were tested but this one gave better representations. Since the beatings are essentially describing large variations of the optics functions, large beatings will result in increased standard variations. The effectiveness of this representation is shown in Fig. 1 where the ideal 50-LEQ and current 40-LEQ configuration are compared.

For extra clarity, ξ is normalised to $\xi^* = \frac{\xi}{\xi_0}$ where ξ_0 is the bare machine lattice where no optics beating is present at a working point of ($Q_x = 6.21, Q_y = 6.24$).

Optimisation Algorithm

The formulation of ξ^* allows the optimisation of the LEQ positions to be solved by a numerical constrained optimisation algorithm, such as the Zeroth-Order Optimization (ZOOpt) package for Python [13]. The positions of the 40

* wietse.van.goethem@cern.ch

ISBN: 978-3-95450-227-1 ISSN: 2673-5490 doi:10.18429/JACoW-IPAC2022-MOPOTK030

BEAM OPTICS MODELLING THROUGH FRINGE FIELDS DURING INJECTION AND EXTRACTION AT THE CERN PROTON SYNCHROTRON

E. P. Johnson*, M. A. Fraser, M. G. Atanasov, Y. Dutheil, E. Oponowicz,
CERN, 1211 Geneva 23, Switzerland

Abstract

As the beam is injected and extracted from the CERN Proton Synchrotron (PS), it passes through the fringing magnetic fields of the Main bending Units (MUs). In this study, tracking simulations using field maps created from a 3D magnetic model of the MUs are compared to beam-based measurements made through the fast injection and slow extraction regions. The behaviour of the fringe field is characterised and its implementation in the MAD-X model of the machine is described.

INTRODUCTION

When protons and ion beams are injected and extracted into the PS ring, they travel through the non-linear stray fields produced by the PS MUs. In these regions, an accurate optical model is imperative to ensure high transmission and preservation of transverse emittance. Scaling of the model with energy is required, as the injection occurs at 2 GeV, and the extractions to the East Area and to the Super Proton Sychrotron (SPS) are at 24 GeV and 26 GeV, respectively. The stray field depends on the level of saturation in the MU and must be included in the model to accurately parameterise the effect on the beam over the wide range of beam energies provided by the PS. The model will be used by the Charm High-energy Ions for Micro Electronics Reliability Assurance (CHIMERA) project, which aims to deliver heavy-ion beams over a wide range of energies to study the effect of single event effects on electric, electronic, and electromechanical devices, both for research and industry users [1]. This study describes a proposed model based on particle tracking through field maps of the PS MUs.

FIELD MAPS

PS Main Units

The CERN PS is composed of 100 combined-function MU magnets that produce dipolar and quadrupolar fields simultaneously to provide strong focusing. Each magnet is divided into two half-units with quadrupole gradients of opposite polarity. Half-units are composed of five blocks, either closed (focusing) or open (defocusing); see Fig.1.

There are four types of magnets: R, S, T and U, depending on the arrangement of the half-units (FD or DF) and whether the main coil is on the inside or outside of the ring [2]. Additional coils named the Pole Face Windings (PFW) and Figure-of-eight Loop (F8L) are inserted between the yoke and the vacuum chamber to control the tune and chromaticity. Although the nominal field region of the combined function magnet extends over a large part of the magnet aperture around the circulating beam orbit, see Fig. 2, the injection and extraction trajectory of the beam travels through strong regions of fringing or stray field. This is a consequence of the PS not being built with straight sections long enough for injection or extraction, forcing the beam to travel through the stray fields of the MUs [3].

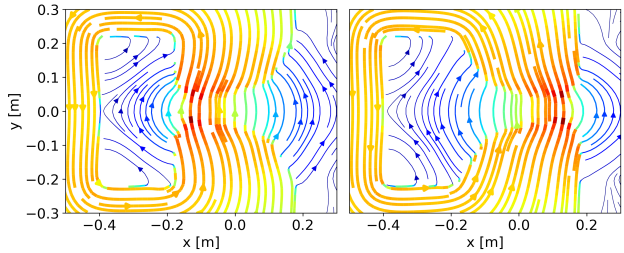

Figure 1: Vector flow of an open defocusing block (left) and a closed focusing block (right).

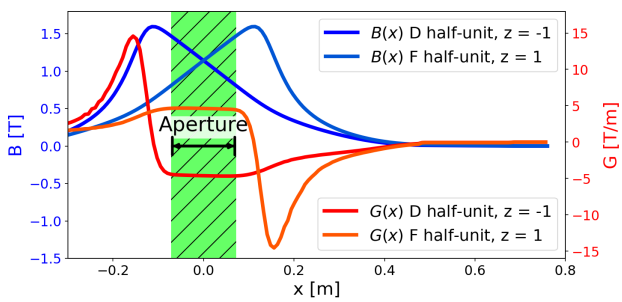

Figure 2: Dipole and gradient component of a PS U-type MU centered in the vertical plane in both half-units at 24 GeV. The green-shaded region of 14.4 cm shows where the gradient is constant to within 5% of the central and nominal gradient. A width similar to the beam pipe aperture in MU62 of 14.6 cm [4]. Outside this region, the gradient is non-linear and, at its maximum, is almost three-fold higher in amplitude.

The OPERA Model

A finite element magnetic model of the PS MU was developed using Cobham's `Opera-3D` [5,6] to generate field maps at different energies (different current in the main coils), different PFW, different F8L settings, and for all four magnet types. The model includes the main junction gap of 20 mm

* eliott.philippe.johnson@cern.ch

ISBN: 978-3-95450-227-1 ISSN: 2673-5490 doi:10.18429/JACoW-IPAC2022-MOPOTK031

10 TeV CENTER OF MASS ENERGY MUON COLLIDER

K. Skoufaris*, C. Carli, D. Schulte
European Organization for Nuclear Research (CERN), Geneva, Switzerland

Abstract

A Muon collider can provide unique opportunities in high-energy physics as an energy frontier machine. However, a number of challenges have to be addressed during the design process primarily due to the short lifetime of muons. In this work, a lattice for a 10 TeV center-of-mass energy collider is presented. Some of the more important challenges faced are: the design of an interaction region with β^* values of the order of a few millimeters and an adequate chromatic compensation without sacrificing the physical and dynamic aperture, the flexibility to control the momentum compaction factor and the radiation generated where neutrinos from muons decays reach the surface. These issues are addressed with the development of a new chromatic correction scheme, the extensive use of flexible momentum compaction factor cells and the efficient control of the optical parameters.

INTRODUCTION

Although CERN's Large Hadron Collider (LHC) [1] and its High Luminosity upgrade (HL-LHC) [2] will continue collecting experimental data until the beginning of the forties (Run 5), the new long-term strategy for the field is prepared. Thus, different new collider projects, which could be constructed after the LHC era, the IMCC [3], the FCC [4] and the CLIC [5] are performing their feasibility studies and exploring their capability to discover new physics.

The future colliders are either steered to develop precision machines (use of fundamental particles) or to reach high energy (multi-TeV) collisions to probe the energy frontier. Given that muons are fundamental particles and about 200 times heavier than electrons (less energy losses due to synchrotron radiation), the muon colliders could provide high precision physics measurements at multi-TeV collision energies. The idea of using muons is not new and it was initially discussed in [6]. The present study shows the current status of the 10 TeV collider building blocks (interaction region, chromatic correction scheme and arcs) and is based on former works [7–9].

COLLIDER RING DESIGN

An illustration of the muon accelerator complex can be seen in Fig. 1 while in Table 1 the main parameters of the collider ring are shown. Many challenges of a muon collider [10] are related to the short lifetime of the muons ($\tau_0 \approx 2.2$ s) and the radiation generated from their decay process ($\mu^+ \rightarrow \overline{\nu}_\mu + \nu_e + e^+$ and $\mu^- \rightarrow \nu_\mu + \overline{\nu}_e + e^-$). Due to this unstable nature of muons, the cooling and acceleration stages should perform fast while the collider circumference must be kept short requiring the use of high magnetic fields. The

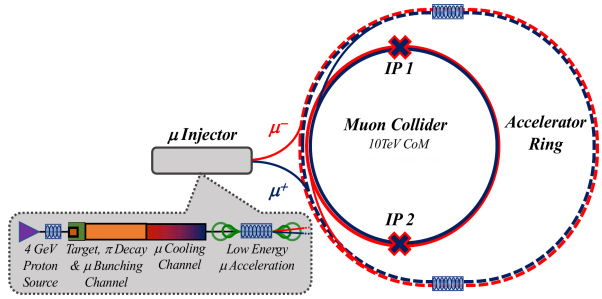

Figure 1: A conceptual scheme of the muon collider complex.

heat load and radiation driven by the muons decay can cause damage around the whole circumference of the collider. Additionally, the muons decaying around the interaction region (IR) generate an intense beam-induced background (BIB) at the detectors which is primarily formed by the secondary and tertiary interactions of the decay products. In order to mitigate the BIB (improve the accuracy of physics measurements), techniques like the addition of nozzles [11] right before and after the interaction point (IP) and special designs of the final focusing (FF) scheme are needed. Another issue from the decay of muons is the neutrino radiation. The large amount of muons used in the bunches ($N_p = 1.8 \times 10^{12}$), generates a large number of neutrinos which reach the earth surface far away from the decay within a small region. The cross section for interaction between these neutrinos and matter is such that the earth does not act as shield thus, mitigation measures are needed to keep doses below legal limits. One such measure is to avoid sections without deflection outside the IR by using combined function magnets (dipole plus a higher order multipole) for focusing and chromatic corrections and limiting straight sections to 30 cm. As a result of the extensive use of dipole fields, the collider ring has a similar shape with a racetrack where the two IRs and any insertion devices are located at the two straight sections.

In order to retain the high precision for physics discovery, the 10 TeV center of mass energy ($\sqrt{s} = 10$ TeV) muon collider ring aims to produce integrated luminosity equal to 10 ab^{-1}. In favor of the high luminosity production, only two high intensity bunches ($N_p = 1.8 \times 10^{12}$) of μ^+ and μ^- will be injected at a time and two interaction points (IPs) with very small β^* values ($\beta^*_x = \beta^*_y = 1.5$ mm) and zero crossing angle will be used. The small β^* values in combination with the large energy spread ($p_T = 0.1\%$) and the lack of a radio frequency system (RF) for longitudinal stability (due to excessive RF voltages and very high frequencies needed) requires a good control of the chromatic phenomena (linear and non-linear ones). A modest RF system without particular contsraints on the frequency is needed to compensate

* kyriacos .dot. skoufaris .at. cern .dot. ch

ISBN: 978-3-95450-227-1 ISSN: 2673-5490 doi:10.18429/JACoW-IPAC2022-MOPOTK032

AN N-BPM MOMENTUM RECONSTRUCTION FOR LINEAR TRANSVERSE COUPLING MEASUREMENTS IN LHC AND HL-LHC

A. Wegscheider and R. Tomás, CERN, Geneva, Switzerland

Abstract

The measurement and control of linear transverse coupling is important for the operation of an accelerator. The calculation of the linear transverse coupling resonance driving terms (RDTs) f_{1001} and f_{1010} relies on the complex spectrum of the turn-by-turn motion. To obtain the complex signal, a reconstruction of the particle motion is needed. For this purpose, the signal of a second BPM with a suitable phase shift is usually used. In this work, we explore the possibility of including more BPMs in the reconstruction of the transverse momentum, which could reduce the effects of statistical errors and systematic uncertainties. This, in turn, could improve the precision and accuracy of the RDTs, which could be of great benefit for locations where an exact knowledge of the transverse coupling or other RDTs is important. We present the development of a new method to reconstruct the particle's momentum that uses a statistical analysis of several nearby BPMs. The improved precision is demonstrated via simulations of LHC and HL-LHC lattices.

COUPLING FROM TURN-BY-TURN DATA

Calculating Coupling Resonance Driving Terms

The measurement and control of linear transverse coupling is important for the operation of an accelerator. In the LHC, the target is usually to completely eliminate coupling, which makes a high precision of the measurement crucial. Coupling measurements were steadily improved over the first two operational runs [1–6] and advanced coupling measurement techniques were proposed in recent years [7–9].

The coupling RDTs

$$f_{1001} = |f_{1001}|e^{iq_{1001}} \quad \text{and} \tag{1}$$
$$f_{1010} = |f_{1010}|e^{iq_{1010}} \quad , \tag{2}$$

can be calculated from the turn-by-turn spectrum [10] by

$$|f_{1001}| = \frac{1}{2}\sqrt{\left|H^+_{0,1}V^+_{1,0}\right|}\,, \tag{3}$$
$$|f_{1010}| = \frac{1}{2}\sqrt{\left|H^+_{0,-1}V^+_{-1,0}\right|} \quad , \tag{4}$$

where $H^+_{n_x,n_y}$ and $V^+_{n_x,n_y}$ are the complex horizontal and vertical spectral lines with frequencies $n_xQ_x + n_yQ_y$. Q_x and Q_y are the horizontal and vertical tunes. $H^+_{n_x,n_y}$ and $V^+_{n_x,n_y}$ are normalised by the amplitudes of the main lines with frequencies Q_x for H and Q_y for V, such that $H^+_{1,0} = V^+_{0,1} = 1$. The phase of the RDTs can be retrieved – from either the horizontal or vertical signal – by

$$\begin{aligned} q_{1001} &= -\arg(H^+_{0,1}) - \varphi^{\mathrm{m}}_{x,ab} + \frac{\pi}{2} \\ &= \arg(V^+_{1,0}) + \varphi^{\mathrm{m}}_{y,ab} - \frac{\pi}{2}\,, \end{aligned} \tag{5}$$
$$\begin{aligned} q_{1010} &= -\arg(H^+_{0,-1}) + \varphi^{\mathrm{m}}_{x,ab} + \frac{\pi}{2} \\ &= -\arg(V^+_{-1,0}) + \varphi^{\mathrm{m}}_{y,ab} + \frac{\pi}{2} \quad , \end{aligned} \tag{6}$$

where the phase advance φ_{ab} between two locations a and b is defined as $\varphi_{ab} = \varphi(s_b) - \varphi(s_a)$ and s_a denotes the longitudinal position of location a.

Unfortunately we cannot measure the particle's relative transverse momentum required to construct the complex signal. A *reconstruction* of the real spectrum using the position data at two nearby BPMs is possible, using the following equations:

$$H^+_{n_x,n_y} = \frac{1}{2}\left[(1-\tan\Delta)H^a_{n_x,n_y} - \frac{i}{\cos\Delta}H^b_{n_x,n_y}\right], \tag{7}$$
$$V^+_{n_x,n_y} = \frac{1}{2}\left[(1-\tan\Delta)V^a_{n_x,n_y} - \frac{i}{\cos\Delta}V^b_{n_x,n_y}\right], \tag{8}$$

where $H^a_{n_x,n_y}$ is the real horizontal spectral line at position s_a, analogously for the vertical signal and Δ is the deviation of the phase advance from $\pi/2$:

$$\Delta = \varphi_{ab} - \frac{\pi}{2} \quad . \tag{9}$$

Equations (7) and (8) assume that there are no additional coupling sources in between the positions a and b [11].

Phase Measurement Errors

Equations (7) and (8) are sensitive to phase measurement errors which get enhanced when the model phase advance is near a root of the cos term in the denominator. To avoid exploding errors, the conventional method is a careful selection of suitable BPM pairs.

The current implementation of the calculation of coupling in our python tool set [12, 13] features two different modes of selecting BPM pairs. The first one pairs each BPM with a second BPM j positions downstream. In the LHC arcs the phase advance between one BPM and the one 2 positions downstream is close to $\pi/2$, which is optimal for the momentum reconstruction.

The second method pairs each BPM with a second BPM downstream which has a phase advance of approximately $\pi/2$ with respect to the first one. This selective method guarantees that the pairing uses optimal phase advances. Since Eqs. (7) and (8) assume no coupling sources in between positions a and b, skipping too many BPMs increases the chances of picking up coupling errors in between, so a limit in the maximum amount of skipped BPMs has to be set.

ISBN: 978-3-95450-227-1 ISSN: 2673-5490 doi:10.18429/JACoW-IPAC2022-MOPOTK033

BEAMLINE DESIGN AND OPTIMISATION FOR HIGH INTENSITY MUON BEAMS AT PSI

Eremey Valetov*, Paul Scherrer Institut, CH-5232 Villigen PSI, Switzerland
(for the HIMB project)

Abstract

The High Intensity Muon Beams (HIMB) project at the Paul Scherrer Institute (PSI) will provide muon intensities of the order of 10^{10} muons/s for particle physics and material science experiments, two orders of magnitude higher than the state of the art, which is currently available also at PSI. In particle transport simulations for the HIMB, we use *G4beamline* with measured π^+ cross-sections and with variance reduction. We also use the codes *COSY INFINITY*, *TRANSPORT*, and *TURTLE* for some studies. We perform asynchronous Bayesian optimisation of the beamlines on a computing cluster using *G4beamline* and the optimisation package *DeepHyper*. We performed numerous studies for the design of the HIMB, and we produced various results, including the muon transmission, beam phase space, polarisation, and momentum spectrum.

INTRODUCTION

Next-generation muon experiments at the Paul Scherrer Institute (PSI), such as Mu3e phase II, require muons to be delivered at unprecedented rates. The Mu3e experiment [1] searches for indications of Beyond-Standard-Model physics by attempting to detect the neutrinoless decay of a muon into three electrons, which would be practically unobservable (at the 10^{-55} level) in the Standard Model of particle physics as a charged lepton flavour violation (cLFV) [2].

A next-generation $\mu \rightarrow e\gamma$ (MEG) experiment [3], searching for the highly suppressed cLFV decay of a muon into an electron and a photon, would also benefit from the substantially higher muon rates. Other intensity frontier particle physics experiments that would rely on an increase in the available muon rates are envisaged [3].

In addition to particle physics, novel concepts for performing characterisations of samples using the muon spin rotation method (μSR) such as pixel-based detectors or microbeams also require an increase in available muon rate [3].

With the presently available rate of $\sim 10^8$ muons/s, to achieve the sensitivity of 10^{-16}, phase II of the Mu3e experiment would have to run for more than 13 years. The High Intensity Muon Beams (HIMB) project [4] seeks to deliver muons at $\sim 10^{10}$ muons/s at a proton current of 2.4 mA, making such sensitivities feasible [3].

To provide a high-intensity muon beam at 10^{10} muons/s into the experimental areas, the HIMB project will use a new graphite target "TgH" with a slanted target design, which increases the surface muon rate; high-acceptance capture solenoids close to the target; and solenoid focusing instead of quadrupole focusing in the beamlines MUH2 and MUH3 for a higher transmission rate. A partial layout of the HIMB is shown in Fig. 1. The MUH2 beamline has only solenoid focusing, while the MUH3 beamline has solenoid focusing in the first two straight sections and conventional quadrupole focusing further downstream. The HIMB will also benefit from a newly designed layout that uses lower bending angles and large-aperture dipoles.

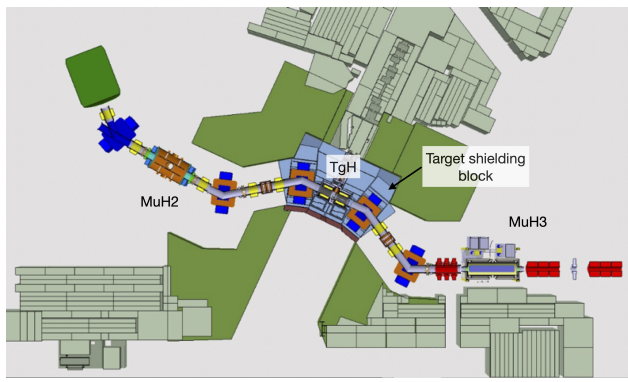

Figure 1: Layout of the HIMB target station and beamlines. The MUH3 beamline is not fully shown; it extends about 38 m from target TgH to the final focus of its branch MUH3.3 and also has a branch MUH3.2.

We performed optimisations, studies, modelling, and simulations for the target station and the muon beamlines of the HIMB project.

The scope of this paper is the author's collaborative contributions to the HIMB project. For further information about the project, please see the IMPACT conceptual design report [4]. The IMPACT project comprises the HIMB and the TATTOOS projects.

PARTICLE TRANSPORT

For simulations of particle transport and the production of surface muons at the target station, we mainly use *G4beamline* [5], based on a custom build of *Geant4* [6] with PSI's own measured π^+ cross-sections [7] and a splitting factor for π^+ production and decay for variance reduction. The measured cross-sections were found to be more precise than the default *Geant4* cross-sections, which deviated from the experimental data by a factor of up to ten (see Ref. [7]). The new target station was simulated with an equivalent of 10^{11} protons, and the produced muons were then used as the initial beam in particle transport simulations of the beamlines delivering the beam to the MUH2 and MUH3 experimental areas and the beamlines' final foci.

* eremey.valetov@psi.ch

ISBN: 978-3-95450-227-1 ISSN: 2673-5490 doi:10.18429/JACoW-IPAC2022-MOPOTK034

ENERGY RAMPING PROCESS FOR SPS-II BOOSTER*

S. Jummunt†, T. Pulampong, P. Sudmuang, P. Klysubun, S. Klinkhieo
Synchrotron Light Research Institute, Muang District, Nakhon Ratchasima, Thailand

Abstract

In order to provide synchrotron light with higher photon energy and more brilliant synchrotron light than that of the existing Siam Photon Source (SPS) machine, the possibility of constructing the new 3 GeV SPS-II has been proposed. For SPS-II, the synchrotron source with in-tunnel booster is a good candidate. The booster synchrotron has been designed in order to accelerate an electron beam of 150 MeV to 3 GeV before extracted to storage ring. For a clean injection in top-up operation, the aim in the design of the booster is to achieve the electron beam with a small emittance less than 10 nm-rad and to obtain a large dynamic aperture. The energy ramping process and related effects during the energy ramp are discussed in this paper.

INTRODUCTION

The existing machine of Siam Photon Source (SPS) in Thailand is a dedicated 1.2 GeV synchrotron radiation source. It has been in operation for synchrotron radiation users since 2003. There are several experimental techniques available for Thai and international users in many fields of scientific research and industrial development. In order to provide synchrotron light with higher photon energy and more brilliant synchrotron light than that of the existing machine, the new light source (SPS-II) is in process of the consideration of construction. The SPS-II project is located in the Eastern Economic Corridor of Innovation (EECi), in the Rayong province in Thailand.

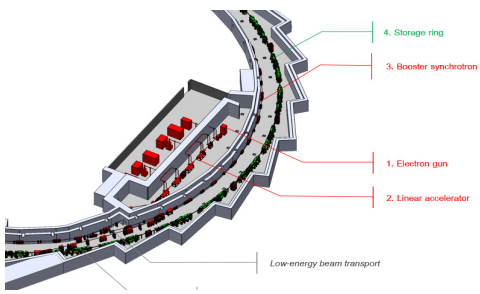

Figure 1: Layout of SPS-II source.

At present, the SPS-II source is in the process of being designed. The storage ring of SPS-II with the circumference of 327.502 m is a Double Triple Bend Achromat (DTBA) lattice, which not only obtains a beam emittance below 1 nm-rad, but also provides the sufficient spaces for the insertion devices [1]. An injector mainly consists of a 150 MeV linac as pre-injector and a 3.0 GeV booster synchrotron. The layout of SPS-II booster is shown in Fig. 1.

* Work supported by Synchrotron Light Research Institute, Thailand
† siriwan@slri.or.th

In this paper, the booster requirement, lattice consideration, the energy ramping process and related effects during the energy ramp from 150 MeV to 3 GeV are described.

BOOSTER REQUIREMENT

An RF frequency is one of the main parameters used to consider the booster circumference. The main RF frequency for SPS-II booster and storage ring was selected at a low-frequency range of 119 MHz on account of having a high RF acceptance. With the RF frequency of 119 MHz and a harmonic of 121, the total circumference is 304.829 m and the average distance between the booster and the storage ring is about 3.6 m. This distance could be suitable to mitigate the stray fields from booster magnets, and comfortable for equipment installation and transportation. To minimize stray field, our choice for the booster bending magnet is an H-type dipole. The space between STR and BS should be comfortable and enough for equipment installation and transportation.

For SPS-II storage ring, the target of beam current will be stored at 300 mA. Uniform fill with the ion-clearing gap of about 20% is a good candidate. The bucket is filled only 104 bunches (from 130 bunches) or 3.27 nC charge in each top-up cycle. With the kicker flat top width of 500 ns, the number of 52 bunches is injected bunches from linac. The required maximum bunch charge delivered to the booster from the linac should not be less than 3.3 nC for compensating the transmission efficiency of 50%. Thus, the possibility to obtain beam current provided in booster is 3.25 mA maximum. That is enough to obtain our target of 2 mA beam current for booster operation. An electron beam energy will be ramped from 150 MeV to 3 GeV with a repetition rate of 2 Hz.

LATTICE CONSIDERATION

Since the FODO lattice with combined function magnets is suitable to achieve a low-emittance beam [2], it is a good candidate for SPS-II booster synchrotron. The main advantages of combined function magnet not only can be used in limited space but also provides low-cost magnet. There are two types of combined function magnets, one is the combined dipole magnet (BD), and the other one is the combined quadrupole magnet (QF) that includes focusing quadrupole and sextupole fields. For the BD magnets, the terms of dipole field, defocusing quadrupole field, and the defocusing sextupole field are combined. The magnetic field of dipole should be about 1.0 Tesla, which can alleviate concerns of dipole magnet design. The magnetic field of about 1.0 Tesla can be achieved with the magnet length of 1.5 m and bending angle of 9 degree. The bending radius of 9.55 m can be obtained. Therefore, the 40 number of combined function dipole magnets can meet our

ISBN: 978-3-95450-227-1 ISSN: 2673-5490 doi:10.18429/JACoW-IPAC2022-MOPOTK035

BEAM-BASED DIAGNOSTICS OF ELECTRIC GUIDE FIELDS AND LATTICE PARAMETERS FOR RUN-1 OF THE MUON *g*-2 STORAGE RING AT FERMILAB

D. A. Tarazona*†, M. Berz, K. Makino, Michigan State University, East Lansing, MI, USA
J. Mott, Boston University, Boston, MA, USA[1]
V. Tishchenko, Brookhaven National Laboratory, Upton, NY, USA
J. D. Crnkovic, Fermi National Accelerator Laboratory, Batavia, IL, USA
M. J. Syphers, Northern Illinois University, DeKalb, IL, USA[1]
K. S. Khaw, Shanghai Jiao Tong University, Shanghai, China
J. Price, University of Liverpool, Liverpool, United Kingdom
[1]also at Fermi National Accelerator Laboratory, Batavia, IL, USA

Abstract

A portion of the Muon *g*-2 Storage Ring electric system, which provides vertical beam focusing, exhibited an unexpected time dependence that produced a characteristic evolution of the stored beam during Run-1 of the Muon *g*-2 Experiment at Fermilab (E989). A method to reconstruct the Run-1 electric guide fields has been developed, which is based on a numerical model of the muon storage ring and optimization algorithms supported by COSY INFINITY. This method takes beam profile measurements from the Muon *g*-2 straw tracking detectors as input, and it produces a full reconstruction of the time-dependent fields. The fields can then be used for the reproduction of detailed beam tracking simulations and the calculation of ring lattice parameters for acceptance studies and systematic error evaluations.

INTRODUCTION

During Run-1 data collection, straw tracking detector [1] measurements of the transverse muon beam revealed unexpected drifting in the beam centroid and width at early times after beam injection into the ring (i.e., $t \lesssim 200\,\mu s$). This peculiarity was observed for all Run-1 datasets: 1a, 1b, 1c, and 1d. Furthermore, coherent betatron oscillation (CBO) frequencies of the radial centroid motion were also found to evolve during the data taking period, which slowly converged to their nominal values over the course of data taking, introducing systematic effects in the Muon *g*-2 Experiment [2].

The electric guide field generated by the Electrostatic Quadrupole system (ESQ) [3] is utilized for vertical beam confinement, and under nominal conditions, the field (i.e. the optical lattice) becomes constant after stabilizing at $t \approx 30\,\mu s$ posterior to beam injection. In this normal scenario, CBO frequencies do not change while the stable lattice provides constant betatron tunes. Also, closed orbits are expected to be stable, and, consequently, the fixed points around which beam centroids oscillate should not drift over the data taking period.

* dtarazona@cornell.edu
† Currently at Cornell University.

However, one of the eight ESQ stations (see Fig. 1) exhibited an unexpected behavior during Run-1.

Figure 1: Photograph of one ESQ station. The top and bottom plates are held at positive voltages and the lateral plates are held at negative voltages for the vertical confinement of positive muons. The vertical magnetic field in the storage ring largely contributes to stable motion in the horizontal direction, in spite of the defocusing radial gradient from the ESQ inner and outer plates.

As shown in Fig. 2, the high voltage (HV) applied to a top plate and a bottom plate did not follow the nominal time evolution per storing cycle. The problem was due to corona discharges on the resistors that connected these plates to the HV source; the resistors outgassed while their temperature was increasing, which would lead to discharges at low voltages. This problem was fixed prior to Run-2.

The method described in the following section was developed to "reverse engineer" the unmeasured HV of the misbehaving ESQ plates throughout Run-1. The ESQ station that includes these plates is commonly labeled as "Q1L," which is an abbreviation that derives from its location and longitudinal dimensions within the storage ring. Based on the changing oscillation frequency of the radial centroid and vertical centroid drifts of the beam measured at the azimuthal acceptance regions of the *g*-2 straw tracking detectors, the HV of interest is reconstructed. As shown in the next section, the full ring optical functions for the Run-1 systematic-error analysis are calculated from the reconstructed HV traces and the COSY-based *g*-2 storage ring model [4].

ISBN: 978-3-95450-227-1 ISSN: 2673-5490 doi:10.18429/JACoW-IPAC2022-MOPOTK036

STUDIES OF THE VERTICAL EXCURSION FIXED FIELD ALTERNATING GRADIENT ACCELERATOR

M. Topp-Mugglestone*, S. Sheehy[1], John Adams Institute, University of Oxford, Oxford, UK
J.-B. Lagrange, S. Machida, ISIS Department, RAL, STFC, UK
[1]also at University of Melbourne, Victoria, Australia and ANSTO, Sydney, Australia

Abstract

The Vertical Excursion Fixed Field Alternating Gradient Accelerator (VFFA) concept offers a number of advantages over existing accelerator archetypes, as discussed in previous works [1, 2]. However, the VFFA has nonplanar orbits by design and unavoidable transverse coupling. Hence, current understanding of the dynamics of this machine is limited; this paper presents some in-depth study of its behaviour using a combination of analytical and numerical techniques.

INTRODUCTION

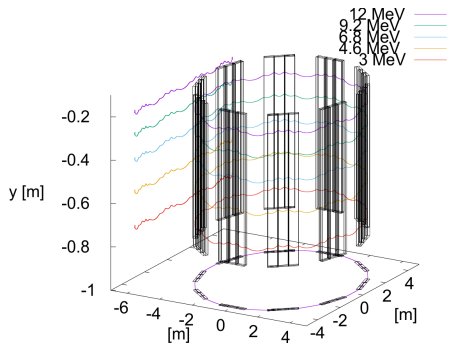

Figure 1: Closed orbits in a 10 cell VFFA FDF triplet ring at a variety of energies, showing how orbits increase in vertical height as energy increases.

In the VFFA, successive higher-energy orbits appear as vertically translated copies of lower-energy orbits (Figure 1).To ensure constant tune, magnetic fields scale as

$$\vec{B}(X,Y,Z) = \vec{B}(X,Y_0,Z)e^{m(Y-Y_0)}, \tag{1}$$

in which X, Y, and Z represent the transverse horizontal and vertical axes and the longitudinal direction respectively. m is the VFFA field index, with units m^{-1}, and defines the spatial separation of successive orbits.

Substituting this scaling criterion into Maxwell's equations, the following polynomial expansion for the magnetic fields associated with a VFFA magnet can be derived:

$$\begin{aligned} B_X &= B_0 e^{mY} \sum \frac{n+1}{m} f_{n+1} X^n \\ B_Y &= B_0 e^{mY} \sum f_n X^n \\ B_Z &= B_0 e^{mY} \sum \frac{1}{m} \frac{df_n}{dZ} X^n \end{aligned} \tag{2}$$

$$\begin{aligned} f_0 &= f(Z), f_1 = 0 \\ f_{n+2} &= -\frac{1}{(n+1)(n+2)} \left(\frac{d^2 f_n(Z)}{dZ^2} + m^2 f_n(Z) \right), \end{aligned} \tag{3}$$

in which $f(Z)$ denotes the distribution of the field along the magnet's longitudinal axis.

Several properties with notable implications for the dynamics of the VFFA can be observed from the above field expansion. Firstly, the horizontal B-field is nonzero away from the midplane, and where $f(Z)$ is increasing or decreasing (i.e. in the fringe field regions) there will exist longitudinal field components. This means, in practice, that any VFFA will have an orbit with significant vertical deviation from a horizontal plane, and that its optics are fundamentally coupled in a nontrivial manner.

An ideal model of this machine would be completely analytic, able to determine the machine's properties purely from the input parameters of the lattice. This would lead to rapid design and optimisation processes across the parameter space, and reduce the need for intensive simulations. However, the complexities discussed above render the development of an analytic model challenging, and as such we turn to numerical studies to inform the construction of an analytic approach.

There are two key elements in understanding the behaviour of any accelerator: the determination of the closed orbit; and the optics associated with the magnetic field about the closed orbit. We begin with a numerical study of the multipole fields about a pre-determined closed orbit.

NUMERICAL STUDIES

First, the closed orbit of a cell is determined using an existing tracking code such as FIXFIELD [3]. This tool is also used to compute a pair of tunes in the decoupled u and v planes of motion. The closed orbit evaluated from the tracking code then forms the basis for a technique we term harmonic analysis: at each point along the closed orbit, magnetic fields are evaluated around a circle of radius dr in a plane perpendicular to the orbit. The field at the centre of the circle (i.e. on the closed orbit) is subtracted from the fields on its circumference and divided by the radius to calculate the relative field gradient. These fields are then decomposed into horizontal and radial components, and the Fourier transform of the radial field gradient is taken. By applying an appropriate normalisation, this then allows us to obtain the multipole coefficients of a decomposition of the focussing fields about the closed orbit. The longitudinal field with respect to the closed orbit is also measured, in order to evaluate any solenoid-type effects.

* max.topp-mugglestone@physics.ox.ac.uk

ISBN: 978-3-95450-227-1 ISSN: 2673-5490 doi:10.18429/JACoW-IPAC2022-MOPOTK037

IMPACT OF INSERTION DEVICES ON DIAMOND-II LATTICE

B. Singh, H. Ghasem, J. Kallestrup, T. Olsson, R. Fielder, I. Martin
Diamond Light Source, Oxfordshire, UK

Abstract

DIAMOND-II lattice is based on the ESRF-EBS cell with the central dipole replaced by a (chromatic) mid-straight, and a -I transformer, higher order achromat and dispersion bumps are used to control the nonlinear dynamics. The majority of insertion devices currently in operation in Diamond will be either retained or upgraded as part of the Diamond-II programme, and the new mid-straights allow the total number of ID beamlines to be increased from 28 to 36. Therefore, it is important to investigate how the IDs will affect the emittance, energy spread, linear and nonlinear beam dynamics. The kickmap approach has been used to model all IDs, including the APPLE-II IDs and APPLE-II-Knot with active shim wires. In this paper, the outcome of these investigations will be presented and discussed.

INTRODUCTION

The existing Diamond storage ring contains 28 insertion devices, the majority of which will be either retained or upgraded for Diamond-II [1]. In addition, several new insertion devices are to be installed in the new mid straights, and the RF cavities in straight 17 will be removed creating space for an additional beamline. The effect that these IDs will have on beam injection and lifetime needs to be investigated and suitable solutions must be found to overcome any negative impact. Insertion devices are known to introduce linear and nonlinear perturbations in the machine optics, and significant experience with operating them has been gained from Diamond. The impact of IDs in Diamond-II can be summarised as follows:

- The IDs produce linear tune-shifts. These tune-shifts are proportional to beta functions at the ID location and its length and inversely proportional to square of energy of the ring. The higher energy of Diamond-II (3 to 3.5 GeV) helps to reduce the impact.
- The linear tune-shifts cause beta-beat and break the symmetry of ring. This may excite additional sextupolar resonances and can reduce the dynamic aperture. The beta-beat is proportional to the linear tune-shifts produced by an ID.
- IDs also introduce octupole-like nonlinear magnetic fields. These can excite 4th order resonances (4Qx, 4Qy, 2Qx±2Qy) and alter the amplitude-dependant tune-shifts, potentially driving the working point to dangerous resonances.
- Planar insertion devices produce linear and nonlinear tune-shifts only in the vertical plane whereas helical undulators can affect both planes.

IDs will change beam parameters such as energy spread, emittance, damping times and energy loss per turn. The impact on the emittance is particularly significant for high-field wigglers and IDs located in dispersive straights. Whereas wigglers in dispersion-free straights will tend to reduce the emittance, IDs in dispersive straights can cause an increase. Overall, the insertion devices in Diamond-II will reduce the emittance but increase the energy loss per turn and energy spread. Damping times are also reduced by the introduction of the IDs, which has a positive benefit both for helping to damp instabilities and to reduce the effects from intra-beam scattering.

When modelling the nonlinear effects of insertion devices, a kick-map approach has been used [2]. Kickmaps for all the Diamond-II IDs have been produced using RADIA [3], in formats for use in ELEGANT [4] and AT [5]. In all other cases, the standard linear model including radiation effects has been used.

ID COMPENSATION STRATEGY

A variety of methods exist to compensate for the effects of insertion devices. Typically, the optics perturbation is compensated by adjusting the local quadrupoles using alpha-matching with global tune correction [6] or a global optics correction using LOCO [7]. Alternatively, for more complex devices such as APPLE-II or APPLE-II KNOT insertion devices, active shim wires can be used [8, 9]. For each case, care must be taken that the combination of ID plus correction scheme does not break any of the phase advance constraints required for the -I transformation, Higher Order Achromat (HOA) and 24-fold symmetry used during optimization of the lattice optics. The choice of which correction scheme to employ depends both on the ID type and on its location.

A global tune correction has been found to be sufficient for the weak to moderate strength planar undulators such as the HPMUs or CPMUs. For high-field devices such as the super-conducting wigglers (SCW) or helical undulators such as the APPLE IDs, a local feed-forward optics correction scheme will be required. Detailed studies of the different types of ID have been conducted, the results of which are summarised in the following sections.

IDs IN MID-STRAIGHTS

The mid-straights all have moderate dispersion and so IDs located here will increase the emittance by an amount that depends on their magnetic field. The equilibrium energy spread will also be affected. Figure 1 shows how an insertion device in a mid-straight affects the main lattice parameters. In particular, the emittance grows

ISBN: 978-3-95450-227-1 ISSN: 2673-5490 doi:10.18429/JACoW-IPAC2022-MOPOTK038

BPM ANALYSIS WITH VARIATIONAL AUTOENCODERS

C. C. Hall*, J. P. Edelen, J. Einstein-Curtis, M. Kilpatrick, RadiaSoft LLC, Boulder, CO, USA

Abstract

In particles accelerators, beam position monitors (BPMs) are used extensively as a non-intercepting diagnostic. Significant information about beam dynamics can often be extracted from BPM measurements, and used to tune the accelerator. Common measurement tools such as measurements of kicked beams may become more difficult when very strong nonlinearities are present or generally when data is very noisy.

In this work we examine the use of variational autoencoders (VAEs) as a technique for extracting measurements of the beam from simulated turn-by-turn BPM data. In particular we show that VAEs may have the possibility to outperform other dimensionality reduction techniques that have historically been used to analyze such data. When the data collection period is limited, or the data is noisy, VAEs may offer significant advantages.

INTRODUCTION

The beam position monitor (BPM) is a ubiquitous diagnostic tool in particle accelerators for monitoring the transverse position of a passing charged particle beam. Source separation techniques such as independent component analysis (ICA) are commonly used [1] on data from sets of BPMs to extract measurements of an accelerator's operating point, beyond what might be available from raw BPM signals.

Autoencoder (AE) neural networks seek to create a reduced-dimensionality representation of their input by training to reproduce that input after data is compressed to a latent space at lower dimension than the input. The variational autoencoder (VAE) can be seen as an adaptation of the vanilla AE structure that instead seeks to represent a parameterization of the input data as distributions over the latent space. This representation by distribution allows for smooth interpolation over the latent space, and makes the VAE a useful tools for performing inference to make measurements of the accelerator.

In this work we demonstrate the ability of VAEs to measure tune from an analytic, continuous focusing model that is representative of the idealized transverse dynamics of a charge particle beam in an accelerator. In particular we explore the use of variational autoencoders for this task due to their ability to smoothly interpolate between latent space values. The capabilities of the VAE are compared against a vanilla autoencoder, and against a typical ICA analysis. Even when given data with a very short measurement period, or noisy measurements VAE models are shown to give good tune measurements.

* chall@radiasoft.net

METHODOLOGY

Analytic Accelerator Model

For exploration of this technique we use data generated from a simplified model of a circular (periodic) accelerator with analytic solutions [1]. Rather than composing the accelerator of discrete focusing magnets we consider a uniform focusing channel with coupled optics. This reduces the problem to that of a coupled harmonic oscillator. We consider only motion in the transverse plane so that we have coupled differential equations:

$$\begin{aligned} \frac{d^2x}{d\theta} + \nu_x x + Cy = 0 \\ \frac{d^2y}{d\theta} + \nu_y y + Cx = 0. \end{aligned} \tag{1}$$

Where C is the coupling strength and $\theta = 2\pi f t$ is the fractional revolution period. The solutions to the coupled equations of motion will then be:

$$\begin{aligned} x(\theta) &= A_x cos(\nu_+ \theta) + B_x cos(\nu_- \theta) \\ y(\theta) &= A_y cos(\nu_+ \theta) + B_y cos(\nu_- \theta), \end{aligned} \tag{2}$$

with the coupled oscillation frequency given by:

$$\nu_\pm^2 = \frac{1}{2}\left(\nu_x^2 + \nu_y^2 \pm \sqrt{\left(\nu_x^2 + \nu_y^2\right)^2 + 4C^2}\right). \tag{3}$$

The principal goal of the analysis tools developed in this paper will be to extract the correct independent frequencies from noisy, periodic measurements of x and y. These are referred to as the tunes, ν_x and ν_y in Equation 1. The amplitude coefficients may be uniquely determined from the initial x and y positions, but are not included here as we do not use them in analyzing performance of the methods presented.

To create test and training data the continuous x and y position data generated from the model is sampled as if from M BPMs placed around a ring so that BPM m will have a phase offset of $\varphi = 2\pi m/M$. Noise in the measurements at each turn N is sampled from a normal distribution $\mathcal{N}(0, \sigma_M)$. Where the variance σ_M, representing the noisiness of each BPM, has been set by sampling from a normal distribution $\mathcal{N}(0, \sigma_{noise})$. An example of data produced from the model is shown in Fig. 1.

Variational Autoencoders Model

For the VAE model, since we are analyzing time series data, we use a recurrent network architecture for the encoder and decoder. The implementation of the VAE architecture is based on [2] and uses Long Short-Term Memory (LSTM) units for both the encoder and decoder. A schematic of the VAE is shown in Fig. 2 together with the regressor for

ISBN: 978-3-95450-227-1 ISSN: 2673-5490 doi:10.18429/JACoW-IPAC2022-MOPOTK039

IRON YOKE EFFECTS IN QUADRUPOLE MAGNETS FOR HIGH RIGIDITY ISOTOPE BEAMS*

D.Greene[1†], Y. Choi[1], J. DeKamp[1], S. Manikonda[2], P. Ostroumov[1], M. Portillo[1], J. Wenstrom[1], T. Xu[1]
Facility for Rare Isotope Beams, Michigan State University, East Lansing, USA
Advanced Magnet Lab Inc., Melbourne, USA

Abstract

Iron-dominated superconducting magnets are one of the most popular and most used design choices for superconducting magnetic quadrupoles for accelerator systems. While the iron yoke and pole tips are economic and effective in shaping the field, the large amount of iron also leads to certain drawbacks, namely, unwanted harmonics from the sextupole correctors nested inside of the quadrupole. Additional problems include the nonlinear field profile present in the high-field regime engendered by the presence of steel, and the mechanical and cryogenic design challenges of the entire iron yoke being part of the cold mass. The presented work discusses these effects and challenges by comparing an iron-dominated quadrupole model to an equivalent coil-dominated quadrupole model. The comparison of their respective magnetic harmonics, integrated strength, multipole effects, and mechanical challenges demonstrates that the coil-dominated design is a more favorable choice for select accelerator systems.

INTRODUCTION

The Facility for Rare Isotope Beams (FRIB) requires the transport of secodnary rare isotope beams with high emittance and high magnetic rigidity. The magnetic rigidity of the beam can reach as high as 8 Tm. For beams that require large apertures, that is, apertures on the scale of 0.4 m, large iron yokes for the quadrupole magnets are required in order to have sufficient strength and uniformity [1]. A number of issues are introduced when using large iron yokes on this scale. These include cool down that span weeks and difficulties with alignment of the magnet due to transportation or thermal cycles. The primary issue with using iron yokes, in this application is their undesirable interaction with magnetic sextupole correctors. This effect is the main consideration of the work presented.

An iron yoke with four pole tips, for quadrupole coils, interacts with a sextupole inside of the pole tips due to the difference in their symmetry. This interaction generates a non-zero dipole component that causes a deflection of the beam that can be identified from a harmonic analysis [1]. Our group proposes replacing the iron-dominated quads of the FRIB fragment separator with coil-dominated, iron-free quads in order to minimize this effect.

* Work supported by the U.S. Department of Energy Office of Science under Cooperative Agreement DE-SC0000661, US Department of Energy Office of Science, High Energy Physics under Cooperative Agreement award number DE-SC0018362, and Michigan State University.
† greene@frib.msu.edu

QUAD STEEL AND SEXTUPOLE INTERACTION

FRIB's Ferric Superconducting Quadrupole Type-C (FSQC) is one of the primary magnet types used in the second and third stage of FRIB's fragment separator, sextupole model used can be seen in Fig. 1 [1]. For this reason, it is used to study the effect of the interaction between sextupole and the quad steel. The operating parameters of FSQC as well as the other FSQ magnets can be found in Table 1 and Table 2.

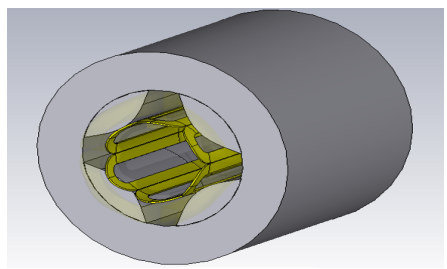

Figure 1: 3D model of FSQC's Sextupole nested inside of the quad iron yoke in CST Studio Suite®.

Table 1: Operating Parameters of FSQA, FSQB, & FSQC [1]

Type	FSQA	FSQB	FSQC
Effective Length (m)	0.723	0.400	0.790
Full Aperture (m)	0.20	0.20	0.20
Max Quad Gradient (T/m)	13.2	17	14
Max Sext. Gradient (T/m^2)	NA	9.6	6.8
Max Oct. Gradient (T/m^3)	NA	48.9	48.5

Table 2: Operating Parameters of FSQD & FSQE [1]

Type	FSQD	FSQE
Effective Length (m)	0.486	0.700
Full Aperture (m)	0.34	0.23
Max Quad Gradient (T/m)	11.9	16.6
Max Sext. Gradient (T/m^2)	NA	NA
Max Oct. Gradient (T/m^3)	NA	NA

Sextupole Field Analysis

The field of FSQC's sextupole was evaluated with CST Studio Suite® with quad coil current at zero. From the field

ISBN: 978-3-95450-227-1 ISSN: 2673-5490 doi:10.18429/JACoW-IPAC2022-MOPOTK040

PROGRESS ON THE MEASUREMENT OF BEAM SIZE USING SEXTUPOLE MAGNETS

J. A. Crittenden, H. Duan, A. Fagan, G. H. Hoffstaetter, V. Khachatryan and D. C. Sagan
CLASSE, Cornell University, Ithaca, New York

Abstract

Variations in strength of a sextupole magnet in a storage ring result in changes to the closed orbit, phase functions and tunes which depend on the position of the beam relative to the center of the sextupole and on the beam size. Such measurements have been carried out with 6 GeV positrons at the Cornell Electron Storage Ring. The initial analysis presented at IPAC21 has been extended to both transverse coordinates, introducing additional tune shifts and coupling kicks caused by skew quadrupole terms arising from the vertical position of the positron beam relative to the center of the sextupole. Variations of strength in each of the 76 sextupoles provide measurements of difference orbits, phase and coupling functions. An optimization procedure applied to these difference measurements determines the horizontal and vertical orbit kicks and the normal and skew quadrupole kicks corresponding to the the strength changes. Continuously monitored tune shifts during the sextupole strength scans provide a redundant, independent determination of the two quadrupole terms. Following the recognition that the calculated beam size is highly correlated with the calibration of the sextupole, a campaign was undertaken to obtain precise calibrations of the sextupoles and to measure their offsets relative to the reference orbit, which is defined by the quadrupole centers. We present the measured distributions of calibration correction factors and sextupole offsets together with the accuracy in their determination.

2D ANALYTIC DERIVATION FOR BEAM SIZE DETERMINATION USING SEXTUPOLE STRENGTH CHANGE

Following the line of argument of our IPAC21 paper [1] to derive the quadrupole kick $\mathrm{d}k_1 l$ and the dipole kicks $\mathrm{d}x'$ and $\mathrm{d}y'$ from a change in sextupole strength $\mathrm{d}k_2 l$ using the sextupole field components $\frac{ql}{p_0}B_\mathrm{x} = k_2 xy$ and $\frac{ql}{p_0}B_\mathrm{y} = \frac{1}{2}k_2(x^2-y^2)$, we obtain three equations with four unknowns:

$$\mathrm{d}k_1 l = \mathrm{d}k_2 l\,(X_0 + \mathrm{d}x) \tag{1}$$

$$\mathrm{d}y' = \mathrm{d}k_2 l\,(X_0 + \mathrm{d}x)\,(Y_0 + \mathrm{d}y) \tag{2}$$

$$2\,\mathrm{d}x' = \mathrm{d}k_2 l\left[\left(\frac{\mathrm{d}y'}{\mathrm{d}k_2 l}\right)^2\left(\frac{\mathrm{d}k_1 l}{\mathrm{d}k_2 l}\right)^{-2} + \sigma_\mathrm{Y}^2 - \left(\frac{\mathrm{d}k_1 l}{\mathrm{d}k_2 l}\right)^2 - \sigma_\mathrm{X}^2\right] \tag{3}$$

We note that these quantities are differences, not differentials. The equations are exact; there is no expansion.

Assuming initial $k_2 l = 0$ and including all terms:

$$\sigma_\mathrm{X}^2 - \sigma_\mathrm{Y}^2 = -2\,\frac{\mathrm{d}x'}{\mathrm{d}k_2 l} + \left(\frac{\mathrm{d}y'}{\mathrm{d}k_2 l}\right)^2\left(\frac{\mathrm{d}k_1 l}{\mathrm{d}k_2 l}\right)^{-2} - \left(\frac{\mathrm{d}k_1 l}{\mathrm{d}k_2 l}\right)^2 \tag{4}$$

Including only terms linear in $\mathrm{d}k_2 l$, we have:

$$\sigma_\mathrm{X}^2 - \sigma_\mathrm{Y}^2 = -2\,\frac{\mathrm{d}x'}{\mathrm{d}k_2 l} + Y_0^2 - X_0^2, \tag{5}$$

where X_0, Y_0 is the initial position of the beam relative to the center of the sextupole. The is the two-dimensional generalization of Eq. (5) in our IPAC21 paper.

ANALYSIS OF DIFFERENCE ORBIT AND PHASE MEASUREMENTS: EXAMPLE

Record phase and orbit measurements for eleven sextupole settings. Reference the ten sets of measurements with nonzero K_2 settings to the K_2=0 orbit and phase measurements. Fit for the linear terms in $\Delta b_1(\Delta k_2 l)$, $\Delta y'(\Delta k_2 l)$ and $\Delta x'(\Delta k_2 l)$. We obtain an estimate for the measurement uncertainties in Δb_1, $\Delta y'$ and $\Delta x'$ by setting them such that the χ^2/NDF is unity. The results are shown in Fig. 1 .

The linear term for Δb_1 gives the initial horizontal position of the beam relative to the sextupole center: $X_0 = 4.943 \pm 0.029$ mm. The linear term for Δp_y gives the initial value for the product of horizontal and vertical beam positions relative to the sextupole center: $X_0 Y_0 = 3.79 \pm 0.13$ mm^2. From this we obtain $Y_0 = 0.766 \pm 0.26$ mm. The linear term for Δp_y ($-12.45 \pm 0.28 \times 10^{-6}$ rad/m^{-2}) and Eq. (5) are used to calculate the value $\sigma_x^2 - \sigma_y^2 = 1.03 \pm 0.53$ mm^2. The vertical beam size is typically 20x smaller than the horizontal, so we can deduce with good accuracy $\sigma_x = 1.01 \pm 0.26$ mm. This result is consistent with the value expected from the optics.

FIRST-ORDER 2D ANALYSIS OF TUNE SHIFTS FROM NORMAL (b_1) AND SKEW QUAD (a_1) TERMS

Defining the normal and skew quad multipole coefficients,

$$b_1 = \frac{1}{2!}\frac{qL}{P_0}\frac{\mathrm{d}B_\mathrm{Y}}{\mathrm{dx}} = \mathrm{K}_2 L\,\mathrm{x} \tag{6}$$

$$a_1 = \frac{1}{2!}\frac{qL}{P_0}\frac{\mathrm{d}B_\mathrm{X}}{\mathrm{dx}} = \mathrm{K}_2 L\,\mathrm{y} \tag{7}$$

we have the familiar results for the tune shifts from the normal quad term:

$$\Delta\mu_x = -b_1\beta_x/2 \tag{8}$$

$$\Delta\mu_y = b_1\beta_y/2 \tag{9}$$

The tune shifts from the skew quad terms can be shown [2] to be

$$\Delta\mu_x = -a_1^2\frac{\beta_x\beta_y\sin\mu_y}{4\left(\cos\mu_x - \cos\mu_y\right)} \tag{10}$$

ISBN: 978-3-95450-227-1 ISSN: 2673-5490 doi:10.18429/JACoW-IPAC2022-MOPOTK041

MAGNETIC FIELD NOISE SEARCH USING TURN-BY-TURN DATA AT CESR*

V. A. Khachatryan†, J. J. Barley, M. H. Berry, A. T. Chapelain, D. L. Rubin, J. P. Shanks, S. T. Wang
CLASSE, Cornell University, Ithaca, New York, USA

Abstract

A method for locating for magnetic field noise has been developed using the CESR beam turn-by-turn beam position data. The technique was validated using Monte-Carlo samples and turn-by-turn real data with induced noise in one of the CESR dipole magnets. We estimate the analysis sensitivity for the noise sources slower than 4 kHz (or 100 CESR turns) with the current CESR BPM system on the level of 1 μrad or 0.2 Gs×m field integral. In this work we report the observed noise sources and the improvements achieved by applying this technique. Long-term, several hours, beam stability analysis is also performed using the same method.

INTRODUCTION

Cornell Electron Storage Ring (CESR) [1], was constructed as an electron-positron collider operating at a center-of-mass energy in the range of 3.5-8 GeV. CESR is now used as an x-ray source for a state-of-the-art x-ray facility, known as the Cornell High Energy Synchrotron Source (CHESS, or CHESS-U after the recent upgrade).

CHESS-U beams are considered fully "stable" in the vertical plane if the vertical position of the centroid at the light observation points drift less than 3 μm over all time scales, and the beam trajectory simultaneously varied by less than 1 μrad. The equivalent numbers in the horizontal direction would be 60 μm and 5 μrad. These stability requirements come from the 10% stability requirement standard used at many light sources.

Our aim is to develop methods to improve the CESR beam stability. In this paper we will discuss one of the techniques based on turn-by-turn beam data analysis, its sensitivity, and the stability improvements achieved by applying the technique.

ANALYSIS METHOD, SIMULATIONS AND VALIDATION

The positron beam stability depends on the stability of the magnetic fields and positions of the ring magnets. The beam is also sensitive to the environment where the beam components are installed.

For the beam coordinate measurements CESR Beam Position Monitors (BPM) [2] are used. Along the CESR ring there are 110 BPMs, their four-electrode design allows measurements of both the horizontal and vertical coordinates with 10 μm single-turn precision. The BPM system data acquisition (DAQ) allows accumulation of data for up to 300k turns from each BPM.

In this work the noise frequency is divided into three ranges:

- high – periodicity corresponds to several turns (tens of kHz);
- medium – from several tens of turns to thousands of turns (~ 10 kHz to a few Hz);
- low – from minutes to days.

This division important since the method being discussed can only be applied to the medium and low frequency ranges. For the medium frequency noise search the input is CESR BPM turn-by-turn data files, while for the low frequency noise, the data is averaged over 1024 turns.

The inductance of the magnets, as well as the vacuum chambers will prevent the high frequency noises from penetration into the beam pipe. Previous studies showed that frequencies above 360 Hz are suppressed significantly by the CESR aluminum vacuum chamber which cover most of the CESR ring. Noise suppression by the stainless steel vacuum chamber is not observed for the frequencies up to 720 Hz. However, only a few short (no more than 5-10 m) CESR sections are covered by stainless steel chambers. Therefore, the medium and low frequency magnetic noise searches are prioritized. For such frequency ranges, the orbit distortion due to localized kicks can be described by the following formula [3]

$$f(s) = \sum_{i=1}^{N} \theta_i \frac{\sqrt{\beta(s)\beta(s_i)}}{2sin(\pi Q)} cos(|\phi(s) - \phi(s_i)| - \pi Q), \quad (1)$$

where $f(s)$ is the closed orbit function for N kicks, i is the index of kicks, θ_i is the beam deflection angle by the i-th kick, $\beta(s)$ and $\beta(s_i)$ are the ring lattice beta functions at location s and at the kick location s_i, the CESR betatron tunes are 16.556 and 12.636 for horizontal and vertical planes respectively, $\phi(s)$ and $\phi(s_i)$ are the lattice betatron phase advances at locations s and at the location of the kicker s_i.

The analysis code is written using the ROOT package [4], and it uses Minuit-Migrad [5] minimization method to fit the data with (1) formula. The fit parameters are the kick s-coordinates and angles θ. We allow the code to increase the number of kicks as far as the fit χ^2 improvement is more than the specified threshold (default is 15). And it stops adding more kicks when the total number of the kicks reaches the maximum number (default is 8), or if there is no χ^2 improvement more than the threshold. A fit example is shown on Fig 1.

In the analysis each consecutive group of 50 turns is averaged and a fit is performed for them (50 turns is just an

* Work supported by NSF PHYS-1416318 and DMR-1829070
† vk348@cornell.edu

ISBN: 978-3-95450-227-1 ISSN: 2673-5490 doi:10.18429/JACoW-IPAC2022-MOPOTK043

WAKEFIELD EFFECTS EVALUATION ON NANOMETER SMALL BEAM AT KEK-ATF

Y. Abe*, SOKENDAI, Tsukuba, Japan
K. Kubo, T. Okugi, N. Terunuma, KEK and SOKENDAI, Tsukuba, Japan

Abstract

The KEK Accelerator Test Facility (ATF) is an R&D facility for the final focus system to develop the nanometer beam technology required for the International Linear Collider. We have confirmed 41 nm vertical beam size at the focal point of the KEK-ATF final focus test beamline, while the original designed goal is 37 nm. However, strong intensity dependence of the beam size exists due to wakefield. In order to produce the small beam stably, clear understanding of wakefield effects is necessary. In past studies, simulation results were compared with experiments and showed that the influence of some vacuum components and BPMs were significant. However, these results did not well agree quantitatively. Further investigations of the wakefield effect to the beam are being performed with more realistic simulations of the wakefield calculation including some wakefield sources, which were not considered in the past studies. This report presents the current status of the research.

INTRODUCTION

The Accelerator Test Facility (ATF) at KEK is a R&D facility for beam control and measurement techniques to develop nanometer level beam required for the International Linear Collider (ILC) [1]. The goal is to realize 37-nm vertical beam size and develop beam position control technology in the nanometer level (ATF2 project). The facility consists of an injector, a LINAC, a Damping Ring, and an extraction (EXT) and a final focus (FF) beamline (ATF2 beamline shown in Fig. 1). In 2016, it was confirmed that the beam size reached 41 nm. The beam size at ATF depends on the bunch intensity mainly due to wakefield. In November 2016, the ATF2 beamline was substantially modified to investigate the effect of wakefield. The intensity dependence was mitigated after removal of some wakefield sources and modification of some vacuum components from the FF beamline. Understanding the effects of wakefield is important for realizing stable nanometer beam [2].

The simulation results were compared with experimental results and shown that some vacuum components and BPMs had significant effect [3–5]. However, the experimental results were twice as large as the simulation results [5]. We suspect some non-negligible wakefield sources exist which had not been included in the simulations. Our past analysis considered only the major wake sources (bellows, cavity BPM and vacuum flanges). Therefore, we performed simulations reproducing more realistic beamlines to confirm more detailed effects on the beam. We considered some vacuum components located in EXT line and shielded components in FF line, and their misalignment and deformation. This paper reports updated wakefield calculations and their effects on the beams.

* abeyuki@post.kek.jp

WAKEFIELD CALCULATION

A wakefield is an excited electromagnetic field generated by a beam passing through a structure. A particle at a longitudinal position s_w with respect to the bunch center will be kicked by $\Delta p_{x,y}$, expressed as $q_1 W_{x,y}(x, y, s_w)$ where the transverse wakepotential is defined as:

$$W_{x,y}(x, y, s_w) \equiv \frac{e}{q_1} \int \{E_z(x, y, z, t) \mp cB_{y,x}(x, y, z, t)\} \mathrm{d}z \,, \tag{1}$$

where we assume an ultra-relativistic beam passing transverse position x and y, the bunch center passes $z = 0$ at time $t = 0$, q_1 is the total bunch charge, and $t = (z + s_w)/c$.

The excited wakefield is calculated by GdfidL [6] which is an electromagnetic field simulation code. Wakefield sources at ATF2 beamline is shown in Fig. 1. The 3D models were constructed to reproduce the actual geometrical shape of the wakefield souces. For example, a model of 5-mm deforming bellows with RF shield is shown in Fig. 2. We assumed that a normal distribution bunch with root mean square (RMS) length of 7.0 mm. Figure 3 shows the calculated wake potentials. The vertical axis shows the wake potential of the beam passing $y = 1$ mm offset from the geometrical center, and the horizontal axis shows the distance from the beam center s_w. Table 1 shows the peak of the wakepotential, quantity and location of wakefield sources.

We evaluated the beam size by using the position of simulated particles at virtual interaction point (IP),where the beam size is minimized at ATF2 beamline, to evaluate the effects on small beam. The position change of the particle at the IP, Δy_{IP}, is calculated approximately as Eq. 2, where i is the index for all wakefield sources, a_i is the vertical misalignment of the source, β_i the beta-function at the source, β_{IP} the beta-function at IP, and $\Delta\phi_i$ is the phase advance from the source to IP [8]:

$$\Delta y_{\mathrm{IP}} \simeq \frac{q_1}{E} W_y(x = 0, a_i, s_w) \sqrt{\beta_{\mathrm{wake}}\beta_{\mathrm{IP}}} \sin \Delta\phi_i \,. \tag{2}$$

The wakefield effect of each type of source can be expressed by $W_{\text{s-eff}}$, from the RMS of Eq. 2, considering many beamlines with different sets of random misalignments with RMS a in a unit of mm, as:

$$\begin{aligned} (\text{RMS of } \Delta y_{\mathrm{IP}}) &\approx \frac{q_1}{E}\sqrt{\beta_{\mathrm{IP}}}\, W_{\text{s-eff}} \\ W_{\text{s-eff}} &\equiv a\, W_y(0, 1) \sum_i \sqrt{\beta_i} \sin \Delta\phi_{\mathrm{i}} \end{aligned} \tag{3}$$

ISBN: 978-3-95450-227-1 ISSN: 2673-5490 doi:10.18429/JACoW-IPAC2022-MOPOTK045

GENERATION OF HIGH EMITTANCE RATIOS IN HIGH CHARGE ELECTRON BEAMS AT FACET-II*

O. Camacho†, UCLA Department of Physics and Astronomy, Los Angeles, CA, USA
A. Halavanau, R. Robles, Stanford University Department of Applied Physics
and SLAC National Accelerator Laboratory, Menlo Park, CA, USA

Abstract

Experiments foreseen at FACET-II, including dielectric plasma wakefield acceleration and linear collider tests, call for electron beams with highly asymmetric transverse emittances - so called "flat beams". A canonical recipe for the generation of such beams is injecting a magnetized beam at a waist into an appropriately tuned skewed quadrupole triplet channel. However, due to the intense non-linear space-charge forces that dominate nC bunches, this method presents difficulties in maintaining the flatness. We proceed with generalized round-to-flat-beam (RTFB) transformation, which takes into account the non-negligible divergence of the beam at the channel entrance, using a quartet of skewed quadrupoles. Our analytical results are further optimized in ELEGANT and GPT simulation programs and applied to the case of the FACET-II beamline. Non-ideal cathode spot distributions obtained from recent FACET-II experiments are used for accurate numerical modeling. Tolerances to quadrupole strengths and alignment errors are also considered, with an eye towards developing hardware specifications.

INTRODUCTION

Beam transport in PWA schemes is susceptible to transverse wakefields excited by particles far from the nominal axis. These wakefields have the potential to induce instabilities that spoil or even disintegrate the beam, and their presence therefore presents a strict limiting factor on the distances over which bunches can be immersed in intense accelerating gradients. It has been shown [1], [2] however, that such instabilities may be mitigated by employing a combination of a horizontal slab geometry in the accelerating structure and a matching transverse beam distribution. That is, an asymmetric flat beam. At a waist, $\sigma_i \sim \epsilon_i$, so that the product $\sigma_x \sigma_y \sim \epsilon_\perp$ is fixed, while the ratio $\frac{\sigma_x}{\sigma_y}$ ought to be maximized. Optimal stability requires that emittance from one transverse phase space plane be transferred into the other, thus achieving the desired asymmetry condition while respecting preservation of 4D emittance. This is achieved by exploiting conservation of canonical angular momentum $\mathbf{L_c} = \mathbf{r} \times (e\mathbf{A} + \mathbf{p})$. Imparting a beam with angular momentum, then removing, one can produce a beam which is much larger in one transverse dimension than the other, as desired. Real experimental conditions, of course, cause deviation from this ideal target. We therefore deem it worthwhile to benchmark error tolerance to ensure that the optimum found is a relatively stable one.

Modeling the FACET-II Injector

The highly nonlinear dynamics involved in modeling the emission and acceleration of a high-charge bunch necessitate a full 3-d treatment of space-charge and image-charge effects, for which the General Particle Tracer (GPT) code [3] is well suited. The bunch and low-energy beamline are therefore modeled in GPT; once the beam energy reaches 134 MeV, space-charge forces are sufficiently suppressed to permit the use of the ELEGANT [4] tracking code for further optimizations. The beam spot on the cathode is generated from experimentally measured images of the UV laser spot to be used at FACET-II to ensure fidelity between the dynamics in simulation and experiment.

In practice, the initial canonical angular momentum of the beam is supplied by immersing the cathode in an axial magnetic field $B_{z,M}$, provided by a solenoid around a 1.5 cell S-band photo-gun. Upon exiting the gun at an energy of 6 MeV, the beam is then focused by a second solenoid located in a drift space between the photo-gun exit and first travelling wave accelerating structure, the so-called L0AF, about 1.10 m from the cathode. The phase of the L0AF is optimized to simultaneously minimize the beam energy spread and normalized transverse emittance at its exit. The beam energy upon traversing this structure is brought up to 64 MeV.

Table 1: Injector Parameters

Symbol	Description	Value
$\epsilon_{\perp,0}$	Thermal emittance	3.3 mm-mrad
$B_{z,M}$	Magnetization solenoid	0.265 T
$B_{z,f}$	Focusing solenoid	0.189 T
$E_{z,g}$	Peak gun field	125 MV/m
ϕ_g	Gun launch phase	0 deg
$E_{z,L0AF}$	L0AF average accelerating gradient	20 MV/m
ϕ_{L0AF}	L0AF phase	0 deg
$E_{z,L0BF}$	L0BF average accelerating gradient	24 MV/m
ϕ_{L0BF}	L0BF phase	0 deg
E_f	Final bunch energy	134 MeV
$\epsilon_{n,\perp F}$	Final emittance	4.9 mm-mrad

The following accelerating structure (L0BF) is also phased to minimize emittance and energy spread, producing a 134 MeV beam with $\frac{\sigma_\gamma}{\bar{\gamma}} = 0.15$ % energy spread and 4.90 mm-mrad normalized emittance. This is the beam we match

* This work is supported by the U.S. Department of Energy Office of Science under Contract No. DE-AC02-76SF00515
† laotraemail14@gmail.com

ISBN: 978-3-95450-227-1 ISSN: 2673-5490 doi:10.18429/JACoW-IPAC2022-MOPOTK046

DESIGN CONCEPT FOR A SECOND INTERACTION REGION FOR THE ELECTRON-ION COLLIDER*

B.R. Gamage†, V. Burkert, A.K. Draees, R. Ent, Y. Furletova, D. Higinbotham, T. Michalski, R. Rajput-Ghoshal, D. Romanov, T. Satogata, A. Seryi, A. Sy, C. Weiss, W. Wittmer, Y. Zhang, Jefferson Lab, Newport News, VA, USA
E.-C. Aschenauer, J.S. Berg, A. Jentsch, A. Kiselev, C. Montag, R. Palmer, B. Parker, V. Ptitsyn, F. Willeke, H. Witte, Brookhaven National Lab, Upton, NY, USA
V.S. Morozov, F. Lin, Oak Ridge National Lab, Oak Ridge, TN, USA
C.E. Hyde, Old Dominion University, Norfolk, VA, USA
P. Nadel-Turonski, Stony Brook University, Stony Brook, NY, USA

Abstract

In addition to the day-one primary Interaction Region (IR), the design of the Electron Ion Collider (EIC) must support operation of a 2nd IR potentially added later [1, 2]. The 2nd IR is envisioned in an existing experimental hall at RHIC IP8, compatible with the same beam energy combinations as the 1st IR over the full center of mass energy range of ~20 GeV to ~140 GeV. The 2nd IR is designed to be complementary to the 1st IR. In particular, a secondary focus is added in the forward ion direction of the 2nd IR hadron beamline to optimize its capability in detecting particles with magnetic rigidities close to those of the ion beam. We provide the current design status of the 2nd IR in terms of parameters, magnet layout and beam dynamics.

INTRODUCTION

A preconceptual design of the second IR must satisfy the physics requirements with magnets consistent with NbTi superconducting magnet technology, and with a footprint fitting in the RHIC IP8 experimental hall along with other beam lines. Here we focus on the design of the hadron beamline since it includes a special feature of the secondary focus for detection of particles with low transverse momentum and near or above the beam magnetic rigidity. The design is constantly evolving to better accommodate the secondary focus along with the required accelerator components necessary to accommodate the detector [3]. The current layout of the EIC is shown in Fig. 1. The IRs are specified by their locations in the tunnel with the primary IR being at IP6 and second IR being at IP8. Table 1 shows a comparison of some of the critical parameters of the two IRs. Some of the key design differences of the IR8 from the IR6 are the addition of a second focus and a larger crossing angle.

Crossing Angle

One of the geometrical differences between IR8 and IR6 is that the hadron beam crosses the electron beam going from the outer to the inner wall of the tunnel [4]. The interaction point (IP) is moved radially inwards from the hall center toward the center of the ring to accommodate the RCS bypass (as shown in Fig. 1). This shortens the distance before the downstream hadron beamline reaches the inner wall of the experimental hall. A large crossing angle such as 50 mrad is undesirable mainly due to the hall geometry and the issues arising due to the crab cavities. The beta functions at the crab locations are optimized to reduce the required crabbing voltage while keeping the beam size consistent with the crab cavity aperture limit. Any increase in the crossing angle would require additional crab cavities, straining the space requirements. Extra crab cavities would also introduce more impedance and cause other dynamical issues.

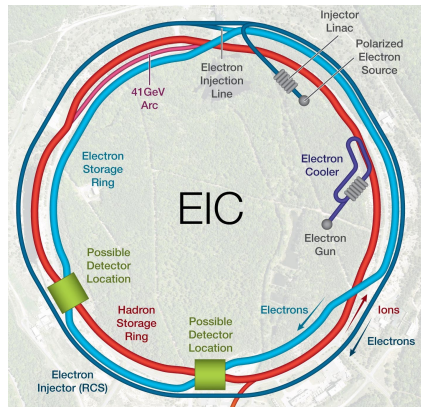

Figure 1: Layout of the EIC complex indicating the hadron storage ring (HSR), electron storage ring (ESR) and rapid cycling synchrotron (RCS). The primary IR is located at the 6 o'clock position while the second IR is located in the 8 o'clock position.

A lower crossing angle such as 25 mrad as in IR6 is more favorable from this point of view. However, the beam crossing configuration and the hall geometry prevent one from bending hadrons away from electrons as in IR6. For this reason, a larger crossing angle is needed to accommodate the hadron and electron magnets and keep the magnetic cross-talk between them at an acceptable level. This also results in placement of the zero degree calorimeter (ZDC) in IR8 on the inside of both beam lines as opposed to between

* This material is based upon work supported by Jefferson Science Associates, LLC under Contract No. DE-AC05-06OR23177, Brookhaven Science Associates, LLC under Contract No. DE-SC0012704 and UT-Battelle, LLC, under contract No. DE-AC05-00OR22725 with the U.S. Department of Energy.
† randika@jlab.org

ISBN: 978-3-95450-227-1 ISSN: 2673-5490 doi:10.18429/JACoW-IPAC2022-MOPOTK047

COOLING PERFORMANCE IN A DUAL ENERGY STORAGE RING COOLER*

B. Dhital†[1,2], Y.S. Derbenev[2], D. Douglas[2], G.A. Krafft[1,2], H. Zhang[2], F. Lin[3], V.S. Morozov[3], Y. Zhang[2]
[1]Center for Accelerator Science, Old Dominion University, Norfolk, VA 23529, USA
[2]Thomas Jefferson National Accelerator Facility, Newport News, VA 23606, USA
[3]Oak Ridge National Laboratory, Oak Ridge, TN, 37830, USA

Abstract

The longitudinal and transverse emittance growth in hadron beams due to intra-beam scattering (IBS) and other heating sources deteriorate the luminosity in a collider. Hence, a strong hadron beam cooling is required to reduce and preserve the emittance. The cooling of high energy hadron beam is challenging. We propose a dual energy storage ring-based electron cooler that uses an electron beam to extract heat away from hadron beam in the cooler ring while the electron beam is cooled by synchrotron radiation damping in the high energy damping ring. In this paper, we present a design of a dual energy storage ring-based electron cooler. Finally, the cooling performance is simulated using Jefferson Lab Simulation Package for Electron Cooling (JSPEC) for proton beams at the top energy of 275 GeV for Electron-Ion Collider.

INTRODUCTION

The method of electron cooling was first introduced by G. I. Budker in 1966 [1]. Later this method became one of the most powerful technique to shrink the size and momentum spread of the stored heavy charged particles (ions, protons, etc.) beams through their interaction with cold electron beam co-propagating at the same average velocities. After first successful demonstration of this cooling method at NAP-M ring in 1974, later this method was widely applied and developed in many heavy ion accelerators around the world [2–4].

An Electron-Ion Collider (EIC) is to be built at Brookhaven National Laboratory (BNL) [5]. In such a collider to maintain a higher luminosity during long collision runs, it is desirable to cool the hadron beams to balance the emittance growth rates due to intra-beam scattering (IBS). The proposed highest proton beam energy in EIC is 275 GeV and this requires some cooling mechanism with cooling rates which exceed the IBS growth rates. A single ring-based electron cooler for high energy beam cooling has been proposed [6], where the electron beams which continuously interact with the hadron beams to extract heat away are being cooled by synchrotron radiation damping. This single ring-based electron cooler concept make use of damping wigglers to enhance the radiation damping in a storage ring. To cool the hadron beam in the energy range 41-275 GeV, the required cooling electron beam energy is in the range 22-150 MeV. At such a low electron beam energy, the IBS effect is very strong giving very short IBS times of the order of tens of millisecond. Further, the synchrotron radiation damping effect is very weak giving long damping times of the order of seconds up to a minute. To get a balance between IBS and radiation damping, we proposed a dual energy storage ring with a high energy section to enhance the synchrotron radiation and a low energy section for the cooling [7, 8]. To enhance the damping effect, the use of wigglers in the high energy section may be another option, but it is known that for damping ring designs above around 350 MeV, it is less costly to omit wigglers and increase the energy of the high energy ring to achieve a required radiation damping rate. So, instead of using wigglers, our design uses Radio Frequency (RF) cavities to increase the energy of the high energy ring to 500 MeV which provides the enough damping to the electron beam to reach the equilibrium.

BEAM COOLING REQUIREMENT

Cooling methods enhance the beam quality and provides sharply collimated beams that is required for precise high energy physics experiments. Beam cooling aims at reducing the size and energy spread of a particle beam circulating in a storage ring and consequently enhance the luminosity. The luminosity in a collider is defined by [9]

$$L = \frac{N_1 N_2 f_0}{4\pi \sigma_x \sigma_y} \approxeq \frac{N_1 N_2 f_0}{\varepsilon \beta_y^*} \tag{1}$$

where N_1 and N_2 are particle densities, f_0 is revolution frequency, σ_x, σ_y are the horizontal and vertical beam sizes and ε is the emittance of the beam respectively. The luminosity L will be higher if ε or the corresponding beam sizes are smaller and N_1, N_2 are bigger values. Hence the goal is to 'compress' the same number of particles into a beam of smaller size and energy spread, i.e. to increase the particle density. The phase space density is a general figure of merit of a particle beam. And cooling technique greatly improves this figure of merit.

DUAL ENERGY STORAGE RING COOLER

A high current electron storage ring cooler may provide a solution to cool the hadron beams at higher energy. To cool the hadron beam at energy range of few hundred GeV,

* Work supported by U.S. DOE Contract Nos. DE-AC05-06OR23177, DE-AC02-06CH11357, DE-AC05-00OR22725, and Jefferson Lab EIC Fellowship2020.
† bdhit001@odu.edu

ISBN: 978-3-95450-227-1 ISSN: 2673-5490 doi:10.18429/JACoW-IPAC2022-MOPOTK050

LINAC OPTICS OPTIMIZATION WITH MULTI-OBJECTIVE OPTIMIZATION*

I. Neththikumara† [1], T. Satogata[1,2], S.A. Bogacz[2], R.M. Bodenstein[2], and A. Vandenhoeke[3]
[1]Old Dominion University, Norfolk, USA
[2]Jefferson Lab., Newport News, USA
[3]Artificial Intelligence Lab, Brussels, Belgium

Abstract

The beamline design of recirculating linacs requires special attention to avoid beam instabilities due to RF wakefields. A proposed high-energy, multi-pass energy recovery demonstration at CEBAF uses a low beam current. Stronger focusing at lower energies is necessary to avoid beam breakup (BBU) instabilities, even with this small beam current. The CEBAF linac optics optimization balances over-focusing at higher energies and beta excursions at lower energies. Using proper mathematical expressions, linac optics optimization can be achieved with evolutionary algorithms. Here, we present the optimization process of North Linac optics using multi-objective optimization.

INTRODUCTION

A multi-pass energy recovery (ER) experiment proposed at Jefferson Lab's CEBAF accelerator uses a high-energy electron beam. This aims to explore a new regime in ER history, an efficient energy recovery of electrons in the presence of substantial incoherent synchrotron radiation (ISR) [1].

Two superconducting linacs, connected by five vertically stacked arcs at both sides, make up the racetrack shape of CEBAF. Electron bunches accelerate on RF crest through eleven linac passes up to 12 GeV; these bunches are used and dumped at any or all of four experimental halls at intermediate energies.

Reuse of the RF energy of the accelerated beam increas the overall efficiency of the RF system. ER capability c be incorporated into CEBAF with the addition of a new pa length chicane, adding a path length of $\lambda_{rf}/2$ after the fif accelerating pass. This would shift bunches into the R minima, and would allow the transfer of their energy ba to RF during deceleration. After five decelerating pass bunches would be dumped at a low energy dump at t end of the South Linac (SL). A schematic of the propos modifications is shown in Figure 1. The additional chica and dump will not affect routine CEBAF operations.

MULTIPASS LINAC OPTICS

ERLs with racetrack topology require that both accelerating and decelerating beams share the same arcs corresponding to their energy. This requirement imposes a specific constraint in Twiss functions at the linac ends. Linac-end

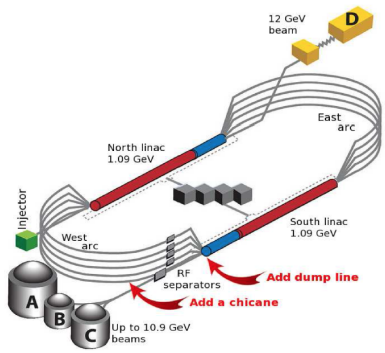

Figure 1: CEBAF accelerator, with arrows indicating new hardware installation sites.

Twiss values must be identical for both accelerating/decelerating passes that share an arc. The work presented here will focus on North Linac (NL) studies, where ten total passes (five accelerating and five decelerating) will pass through the linac. For these simulations, the accelerating beam uses the beamline elements as they are normally arranged. Decelerating bunches pass through the elements in reversed order. Graphically, the accelerating and decelerating passes are alternately connected at places of equal energy with a special matrix, M, to match with arc-end optics as illustrated in Figure 2. Here, blue arrows denote accelerating linac optics and red arrows denote decelerating linac optics. At

Figure 2: 10 pass beamline arrangement [2].

For this study, the 13-FODO-cell CEBAF NL lattice is considered. A previous, manual optimization is shown in Figure 3, for a symmetric FODO-like layout with 60° phase advance per cell.

In recirculating linacs, beam break-up (BBU) instabilities limit the threshold beam current, I_{th} [3]. For a single pill box cavity in TM_{00} mode, I_{th} is given as,

$$I_{th} = \frac{2pc}{e\omega Q\frac{R}{Q}} \frac{1}{|T_{12}|\sin\omega T_{tr}} . \quad (1)$$

Here, Q is the cavity quality factor, $\frac{p}{e}$ is beam rigidity, ω is the HOM angular frequency, and $|T_{tr}|$ is the transfer matrix

* This material is based upon work supported by the U.S. Department of Energy under contract DE-AC05-06OR23177.
† ineth001@odu.edu

ISBN: 978-3-95450-227-1 ISSN: 2673-5490 doi:10.18429/JACoW-IPAC2022-MOPOTK051

MODELING A Nb_3Sn CRYOUNIT IN GPT AT UITF*

S. Pokharel†[1], G. A. Krafft[1]
Center for Accelerator Science, Old Dominion University, Norfolk, Virginia, 23529, USA
A. S. Hofler
Thomas Jefferson National Accelerator Facility, Newport News, Virginia 23606, USA
[1]also at Thomas Jefferson National Accelerator Facility, Newport News, Virginia 23606, USA

Abstract

Nb_3Sn is a prospective material for future superconducting radio frequency (SRF) accelerator cavities. Compared to conventional niobium, the material can achieve higher quality factors, higher temperature operation, and potentially higher accelerating gradients ($E_{acc} \approx 96$ MV/m). In this work, we performed modeling of the Upgraded Injector Test Facility (UITF) at Jefferson Lab utilizing newly constructed Nb_3Sn cavities. We studied the effects of the buncher cavity and varied the gun voltage from 200 –500 keV. We have calibrated and optimized the SRF cavity gradients and phases for the Nb_3Sn five-cell cavities' energy gains with the framework of the General Particle Tracer (GPT). Our calculations show the beam goes cleanly through the unit. There is full energy gain out of the second SRF cavity but not from the first SRF cavity due to non-relativistic phase shifts.

INTRODUCTION

The desire to reduce construction and operating costs of future SRF accelerators motivates the search for higher-performing alternative materials. Nb_3Sn is a very promising alternative material for SRF accelerator cavities. Nb_3Sn possesses a high critical temperature ($T_c \approx 18.3$ K) and superheating field ($H_{sh} \approx 425$ mT) [1,2] giving it the potential for higher intrinsic quality factor (Q_0) than niobium (Nb), 4.2 K operations, and accelerating gradients of ≈ 96 MV/m. Nb_3Sn has a critical temperature about twice that of Nb, allowing it to achieve a high $Q_0 > 10^{10}$ at approximately two times higher operating temperatures than Nb. Changing the operating temperature from 2.0 K, typical for Nb, to 4.3 K for Nb_3Sn while maintaining Q_0 in the 10^{10} to 10^{11} range would reduce energy consumption and thus cryogenic operating costs by as much as an order of magnitude, and would substantially decrease infrastructure costs for the cryogenic plant. Nb_3Sn cavities have a very high quality factor even above 4 K. They can be cooled with cryocoolers for cavity cooling, which significantly cuts capital and installation costs, enabling compact and potentially even mobile applications. Many studies and tests have been done at Thomas Jefferson National Laboratory (JLab) [3–5] for Nb_3Sn and we performed the numerical simulation study of two 5-cell cavities coated with Nb_3Sn through the accelerator layout at UITF for the first time.

* Work supported by U.S. DOE, Office of Science, Office of Nuclear Physics under contract DE-AC05-06OR23177
† spokh003@odu.edu

Based on the UITF beamline layout with a new SRF booster that eliminates the need for a warm capture section, this paper describes the transport of the electron beam through the elements of a 12 m beamline which consist of the photocathode electron gun, solenoids and magnets, buncher cavity, and accelerating superconducting radio frequency (SRF) cavities. With the General Particle Tracer (GPT) [6] simulations, we will describe the designed beam size, the initial electron beam distribution, calibration, and optimization of the Nb_3Sn cryounit using different gun voltages 200 keV, 350 keV, and 500 keV. Also, we will describe the beam properties that would be expected without a capture section.

BEAMLINE SETUP AND SIMULATION DETAILS

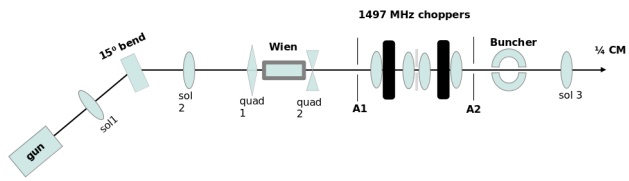

Figure 1: Cathode to the quarter cryomodule (QCM) layout of the Upgraded Injector Test Facility (UITF) at JLab.

Figure 1 is the schematic representation of the keV beamline at the Upgraded Injector Test Facility (UITF) at JLab. The beam dynamics simulation was performed by General Particle Tracer (GPT) [6]. For the simulation, we have used a straight beamline; 15° dipole, RF choppers, beam diagnostics, Wien apertures, etc. are omitted. The laser pulses are getting absorbed by the photocathode inside the electron gun cavity causing the gun to emit the electrons. The electrons are then accelerated to 200 keV initially by the electric field in the DC gun. The electron beam is transported through the solenoids, quadrupoles, and buncher cavity of 750 MHz before reaching the SRF cavities of 1497 MHz. There are two cavities inside the SRF cryomodule, both of them are 5-cell Nb_3Sn cavities separated by 792.79 mm between their centers as shown in Fig. 2. Again, we performed simulations with a different DC gun electric fields to accelerate the beam to 300 keV and 500 keV.

INITIAL DISTRIBUTION

For the particle distribution at the cathode in simulation, the beam is assumed to have a Gaussian distribution in t, x, y, p_x, and p_y following the profile of the laser. The transverse

ISBN: 978-3-95450-227-1 ISSN: 2673-5490 doi:10.18429/JACoW-IPAC2022-MOPOTK052

CEBAF INJECTOR FOR K_L BEAM CONDITIONS*

S. Pokharel†[1], G. A. Krafft[1]
Center for Accelerator Science, Old Dominion University, Norfolk, Virginia, USA
A. S. Hofler, R. Kazimi, M. Bruker, J. Grames, S. Zhang
Thomas Jefferson National Accelerator Facility, Newport News, Virginia, USA
[1]also at Thomas Jefferson National Accelerator Facility, Newport News, Virginia, USA

Abstract

The Jefferson Lab K_L experiment [1] will run at the Continuous Electron Beam Accelerator Facility with a much lower bunch repetition rate (7.80 MHz or 15.59 MHz) than nominally used (249.5 MHz or 499 MHz). While the proposed average current of 2.5 - 5.0 µA is relatively low compared to the maximum CEBAF current of approximately 180 µA, the corresponding bunch charge is atypically high for CEBAF injector operation. In this work, we investigated the evolution and transmission of low-rep-rate, high-bunch-charge (0.32 to 0.64 pC) beams through the CEBAF injector. Using the commercial software General Particle Tracer, we have simulated and analyzed the beam characteristics for both values of bunch charge. We performed these simulations with the existing injector using a 130 kV gun voltage. We have calculated and measured the transmission as a function of the photocathode laser spot size and pulse length. We report on the findings of these simulations and optimum parameters for operating the experiment.

INTRODUCTION

The K_L experiment (a new nuclear physics experiment) at Jefferson Lab in Hall D requires time-of-flight measurements which in turn requires substantially lower bunch repetition rates in Continuous Electron Beam Accelerator Facility (CEBAF) than the nominal 249.5 MHz or 499 MHz. The momenta of K_L particles will be measured using the time-of-flight between RF signal of CEBAF accelerator and start counters surrounding LH_2 target. A schematic view of beamline is presented in Fig. 1. At 12 GeV an average current of 2.5 - 5.0 µA corresponds to 30 - 60 kW of beam power, which will converted by the CPS to illuminate the Be target. Table 1 summarizes the individual bunch charges corresponding to these beam requirements for the K_L experiment.

We are developing new operating parameters of the CEBAF injector for the K_L experiment. This experiment requires relatively low rep rate but the bunch charge at the high end of what CEBAF delivers to achieve its goals. This paper describes the evolution and transmission of low-rep-rate, high-bunch-charge (0.32 to 0.64 pC) beams through the CEBAF injector. Using the computational software packages, we will describe designed beam size, the initial electron beam distribution, and analyze the beam characteristics for both values of bunch charge for 130 kV gun voltage. We characterize the transmission as a function of the photocathode laser spot size and pulse length. Finally, we describe measurement for two injector laser drive frequency modes : one with 500 MHz, and another with 250 MHz.

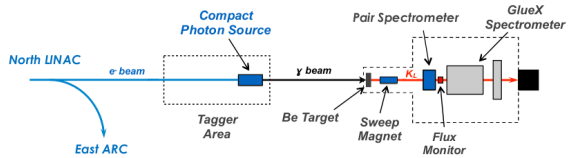

Figure 1: Schematic view of Hall D beamline on the way $e \to \gamma \to K_L$. Electrons first hit the copper radiator inside the Compact Photon Source (CPS). Then photons illuminate the Be target, and finally, neutral kaons hit the LH_2/LD_2 cryogenic target. Beam goes from left to right [1].

Table 1: CEBAF Injector bunch currents and repetition rates for K_L experiment [1].

Current (A)	Repetition Rate (MHz)	Subharmonic of 499 MHz	Bunch Charge (pC)	Equivalent 249.5 MHz current (A)
2.5	15.59	32nd	0.16	40
2.5	7.80	64th	0.32	80
5.0	15.59	32nd	0.32	80
5.0	7.80	64th	0.64	160

BEAMLINE SETUP AND SIMULATION DETAILS

Figure 2 shows the general layout of the CEBAF injector, showing the elements related to bunching, timing and focusing the beam. Our injector model for K_L beam conditions focuses on the beam line between the gun and the captured solenoid S6 (MFA0I03) upstream of the Chopper 1 RF cavity and retains the pre-upgraded injector beam line downstream from S6 (MFA0I03) onward [2]. The beam originates on a 130 keV photocathode. Then the beam transits through the elements of a 30 m beamline which consist of 1 pre-buncher cavity, 1 buncher cavity, 5-cell capture section, 1/4 cryomodule booster (2 Cornell-style 5-cell cavities), focusing solenoids, and quadrupoles. We performed the simulations using the commercial software General Particle Tracer (GPT) [3].

For the particle distribution at cathode in simulation, the beam is assumed to have a Gaussian distribution in t, x, y

* Work supported by U.S. DOE, Office of Science, Office of Nuclear Physics under contract DE-AC05-06OR23177
† spokh003@odu.edu

ISBN: 978-3-95450-227-1 ISSN: 2673-5490 doi:10.18429/JACoW-IPAC2022-MOPOTK053

RLAs WITH FFA ARCS FOR PROTONS AND ELECTRONS*

V. S. Morozov†, Oak Ridge National Lab, Oak Ridge, TN, USA
J. F. Benesch, R. M. Bodenstein, S. A. Bogacz, A. M. Coxe, K. E. Deitrick, D. R. Douglas, B. R. Gamage, G. A. Krafft, K.E. Price, Y. Roblin, A. Seryi, Jefferson Lab, Newport News, VA, USA
J. S. Berg, S. J. Brooks, F. Meot, D. Trbojevic, Brookhaven National Lab, Upton, NY, USA
G. H. Hoffstaetter, Cornell University, Ithaca, NY, USA

Abstract

Recirculating Linear Accelerators (RLAs) provide an efficient way of producing high-power, high-quality, continuous-wave hadron and lepton beams. However, their attractiveness had been limited by the cumbersomeness of multiple recirculating arcs and by the complexity of the spreader and recombiner regions. The latter problem sets one of the practical limitations on the maximum number of recirculations. We present an RLA design concept where the problem of multiple arcs is solved using the Fixed-Field Alternating gradient (FFA) design as in CBETA. The spreader/recombiner design is greatly simplified using an adiabatic matching approach. It allows for the spreader/recombiner function to be accomplished by a single beam line. The concept is applied to the designs of a high-power hadron accelerator being considered at ORNL and a CEBAF electron energy doubling project, FFA@CEBAF, being developed at Jefferson lab.

HIGH-POWER HADRON ACCELERATOR DESIGN STUDY AT ORNL

Introduction

Recent advances in the SRF technology allow for increasingly more reliable and higher power hadron linacs. Due to slow increase of the proton velocity and each RF structure being efficient only in a narrow range of velocities, hadron linear accelerators require several SRF cavity types to cover these ranges and a large number of cavities in total. There are multiple projects in all parts of the world that are already being constructed or proposed [1]. The number of different types of accelerating structures used by these projects varies from 4 to 7. Figure 1 summarizes the beam energy gain per cavity for all types of cavities against their velocity ranges for seven typical projects, namely, SNS [2], ESS [3], MYRRHA [4], Project-X [5], JAEA ADS [6], CiADS [7], and HC HP-SPL [8, 9]. Notably, all of these and other explored projects are straight linacs.

The data in Fig. 1 is described well by the exponential fit

$$\frac{\Delta E}{cav} = 0.6 \exp\left(\frac{\beta}{0.26}\right) \left[\frac{\text{MeV}}{\text{cav}}\right] \quad (1)$$

shown by the green solid line. Only SC cavity data was used in the fit, since high-power CW machines tend to have no or short warm accelerating sections after an RFQ. In anticipation of 50% or so further improvement of SRF performance in the next few years, we scale the fit line by a factor of 1.5 and adopt it for our below estimates.

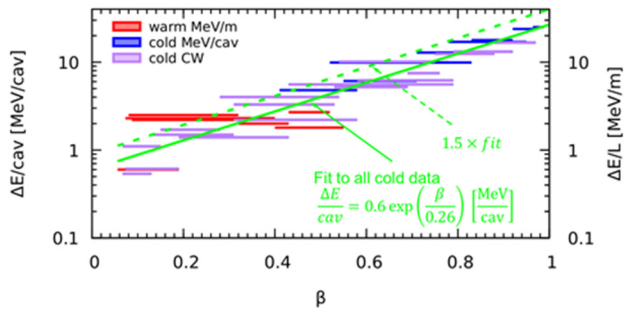

Figure 1: Summary of the energy gains per cavity versus the cavity's velocity range for the seven selected projects. The warm linac data is shown in red on the right vertical scale in terms of the energy gain per unit length.

We next conservatively assume 300 kW for the maximum power that can be coupled into a cavity for all cavity types over the entire relativistic β range. In combination with the extrapolated survey data from Fig. 1, we obtain the optimum current as a function of β

$$I(\beta) = \left[\frac{\Delta P}{cav}\right] / \left[\frac{\Delta V}{cav}\right](\beta) = 330 \exp\left(-\frac{\beta}{0.26}\right) \text{ [mA]} \quad (2)$$

shown by the green line in Fig. 2.

A point above the green line means that a cavity is running at its power limit but below its maximum voltage while a point below the green line means that a cavity is running at its maximum voltage but below the maximum power that can be made available to it. The magenta line in Fig. 2 illustrates the operation regime of a straight 1 GeV 10 MW proton linac of particular interest for the Accelerator-Driven Subcritical reactor application. Clearly, it is far from the optimum line.

Concept

The power bottleneck set by the high-β cavities in a straight linac is overcome by recirculating the beam through the lower-energy sections up to their cavity power limits. The energy boundaries shown by the red vertical lines in Fig. 2 are chosen so that each section doubles the beam momentum. This is a comfortable parameter range for an FFA arc design as shown later. Under these assumptions, the number of SRF cavities in an RLA design can be

* Authored in part by UT-Battelle, LLC, LDRD, LOIS 10908, under Contract No. DE-AC05-00OR22725, Jefferson Science Associates, LLC under Contract No. DE-AC05-06OR23177, and Brookhaven Science Associates, LLC under Contract No. DE-SC0012704 with the US Department of Energy (DOE).
† morozovvs@ornl.gov

ISBN: 978-3-95450-227-1 ISSN: 2673-5490 doi:10.18429/JACoW-IPAC2022-MOPOTK054

REVIEW OF ALIGNMENT AND STABILITY TOLERANCES FOR ADVANCED LIGHT SOURCES

A. Khan*, S. Sharma, V. Smaluk, BNL, NSLS-II, Upton, NY, 11973-5000, USA

Abstract

Alignment and mechanical-stability specifications are essential to the performance of low-emittance storage rings. Beam dynamics simulations are usually performed to establish these specifications. However, the simulation procedures and the input parameters related to magnet positions are not well established which leads to differences in the final specifications. In this paper we discuss important parameters of the mechanical/structural systems of the storage ring that impact on the alignment and stability specification. We reviewed the alignment and stability specifications used at modern light sources across the world that will help to propose an efficient model for a low-emittance upgrade of NSLS-II.

INTRODUCTION

Achieving a good level of performance in the low-emittance light sources places demanding requirements on the field quality and alignment precision of the magnets. Identifying and rectifying the major sources of machine errors is a major task during the commissioning of a new accelerator, and efforts to reduce errors and improve machine performance are frequently continued throughout the facility's lifetime. Modeling the sensitivity to various errors is also an important part of the design process, which includes studies of diagnostics to identify the sources of errors and the correction systems to compensate for them. Thus, to ensure any facility will perform as expected by reducing uncertainty, advancing design in a cost-effective way requires finding the proper alignment and stability tolerances. This is achieved by considering the work of others, and developing the suitable models for accommodating results.

There are two types of errors, static and dynamic, concerning lattice magnets. Static errors, such as misalignment and field errors, are time independent or change slowly over time. These affect dynamic aperture, dispersion, beta beating, lifetime and chromaticity. We can reduce the impact of such errors by deploying a diagnostic and corrective system. Dynamic errors, such as jitter in the power supply, floor motion, girder vibrations, and temperature variations, are ones that change with time on a scale of milliseconds to hours, as discussed in the section on noise sources. These errors affect a variety of beam properties, including orbit stability, and if we can monitor them in real time, the correction can be implemented in real time as well. Detailed beam dynamics simulations give the specification of upper limits on these errors in a machine.

It is also necessary to think through the specification of tolerances in order to avoid unnecessary costs. In this report, we discuss the alignment and stability tolerances of different light sources.

OVERVIEW OF ALIGNMENT TOLERANCES

The misalignment can be caused by the occurrence of some mounting errors and other errors in the manufacturing and assembly process of the magnets. Considering the parameters change (for convenience from the computational viewpoint) and the physical meaning of the parameter deviations, the random nature of errors is assumed [1].

There are three most important factors from beam dynamics point of view to decide the alignment tolerances for a light source: *beta beating, beam orbit and dynamic aperture*. The general steps for such simulations are as outlined in Refs. [2, 3]:

- Apply misalignment errors and beam-offset to the lattice model
- Perform trajectory correction until the beam reaches one turn
- Perform global trajectory correction until sufficient multi-turn transmission is achieved
- Perform global trajectory correction including RF cavities until closed orbit is found

Table 1 summarizes the magnet-to-magnet and girder-to-girder alignment specifications in advanced light sources around the world, including ALS-U [4], APS-U [5], Diamond-II [6], ESRF-EBS [7], NSLS-II [8], SIRIUS [9], MAX-IV[10] and SOLEIL-II [11].

Alignment specifications at APS-U are specified for two different stages: (1) the alignment requirements that have to be achieved as a zeroth-order machine alignment prior to the beam commissioning, and (2) the requirements that have to be ensured during standard machine operation [12]

The ESRF-EBS facility described that girder-to-girder tolerances are not of particular significance to the facility with loose magnet-to-magnet tolerance. From a beam dynamics perspective, as long as magnet-to-magnet tolerances (single magnet rms position errors) are met at every location in the machine, including between magnets standing on adjacent girders, the desired dynamic aperture and lifetime are achievable. It worked effectively for ESRF-EBS, well beyond expectations/simulations [13].

At SOLEIL-II, magnet tolerances are tight 30 µm and much tighter for neighboring girders (50 µm in H and 30 µm in V). The major issue is that machine lattice is so compact that considerable offset in sextupole magnets would have a significant impact on the lattice performance [14].

* akhan1@bnl.gov

ISBN: 978-3-95450-227-1 ISSN: 2673-5490 doi:10.18429/JACoW-IPAC2022-MOPOTK055

DESIGNING LINEAR LATTICES FOR ROUND BEAM IN ELECTRON STORAGE RINGS USING SLIM*

Yongjun Li†, Robert Rainer, Brookhaven National Laboratory, Upton 11973, New York, USA

Abstract

For some synchrotron light source beamline applications, a round beam is preferable to a flat one. A conventional method of obtaining round beam in an electron storage ring is to shift its tune close to a linear difference resonance. The linearly coupled beam dynamics is analyzed with perturbation theories, which have certain limitations. In this paper, we adopt the Solution by LInear Matrices (SLIM) analysis to calculate exact beam sizes to design round beam lattices. The SLIM analysis can deal with a generally linearly coupled accelerator lattice. The effects of various coupling sources on beam emittances and sizes can be studied within a self-consistent frame. Both the on- and off-resonance schemes to obtain round beams are explained with examples. Commonly used radiator devices, such as planar wigglers and undulators, can be incorporated.

INTRODUCTION

Round beam rather than a flat one is preferable for some beamline applications in the synchrotron light source community. Concurrently, an increased vertical beam size can significantly improve beam lifetime as well, particularly in extremely low emittance rings. Therefore, some future diffraction-limited light sources, such as ALS-U [1] and APS-U [2], are planning to operate with a round beam mode. Most of light source rings only have horizontal bending magnets, which leads to an intrinsically flat beam. Either dedicated devices, such as skew quadrupoles, or some imperfections in magnets, such as normal quadrupole roll errors, can couple the beam motion transversely. Conventionally, a geometric round beam in an electron machine is obtained by: (1) equally distributing the natural horizontal emittance into the horizontal and vertical planes $\epsilon_x = \epsilon_y$ through shifting the machine's tune close to a linear difference resonance $\nu_x - \nu_y = n$, with n an integer, (2) adjusting the envelop Twiss functions so that $\beta_x = \beta_y$ at the locations of radiators. Here we also assume that radiators are located at non-dispersive sections, because achromat lattices are often adopted for light source rings. The beam emittances and sizes for this on-resonance coupling case were often analyzed with perturbation theories, such as [3–5] etc. However, when the linear coupling is sufficiently strong, such perturbation analyses might not be accurate any longer and a more accurate analysis might be considered necessary.

In the presence of linear coupling, the uncoupled 2-dimensional Courant-Synder parameterization [6] can be generalized to the 4-dimensional coupled motion. Such parameterizations, proposed by Ripken and his colleagues [7,8] and further developed by Lebedev and Bogacz [9] are already available. There are also some other exact parameterizations [10–12]. These analyses only deal with linear Hamiltonian systems, the radiation damping and quantum excitation diffusion for electron beams are not considered. Therefore, the equilibrium emittance for electron storage rings has not been derived here. Instead, the following emittance re-distribution approximation [4],

$$\epsilon_x = \frac{1+2k^2}{1+4k^2}\epsilon_{x,0},\ \epsilon_y = \frac{2k^2}{1+4k^2}\epsilon_{x,0} \tag{1}$$

is often used. Here $k = \frac{|\kappa|}{\Delta\nu}$, κ is the well-known coupling coefficient given in ref. [4, 13], $\Delta\nu = \nu_x - \nu_y - p$ is the distance from the resonance, $\epsilon_{x,0}$ is the horizontal emittance for the uncoupled motion, and the natural vertical emittance $\epsilon_{y,0}$ is negligible. Eq. (1) is only valid by assuming: (1) coupling coefficient κ are sufficiently weak to be considered as perturbations, (2) the total transverse emittance remains as a constant, and (3) the coupling is caused by a single isolated resonance, (4) the vertical dispersion is negligible. Exact computations as shown later in this paper indicate that the approximation in Eq. (1) can break down when these assumptions are violated, particularly when vertical dispersion is blown up.

In this paper, to design round beam lattices for light source rings, we adopt an exact and self-consistent analysis – the Solution by LInear Matrices (SLIM) technique, developed by Chao back in the 1970–1980s [14–16]. This analysis can yield fruitful results such as the trajectory of the electron distribution center and the beam sizes and shapes in phase space. Linear coupling effects among the horizontal, vertical, and longitudinal motions are included in a straightforward manner even without introducing the auxiliary Twiss functions. Alternate, and also exact approaches, such as [17, 18] have been implemented in the code SAD [19], AT [20] and OPA [21] which could also be used for this purpose. We used AT and SLIM to compute a same coupled NSLS-II lattice and confirmed that their emittance computations are equivalent.

SLIM AND TWISS FUNCTIONS

The detailed SLIM formalism can be found in the references [14–16, 22]. It deals with the motion of a charged particle in a linear electromagnetic device by purely using their transport matrices. First, symplectic one-turn linear matrices for a storage ring are used to compute the eigenvalues and eigenvectors. The eigenvalues indicate whether the linear motion is stable or not, and provides the fractional parts of the tunes when the motion is stable. The eigenvectors evolving along the ring provide information about closed

* Work supported by US DOE Office of Science operated by BNL under Contract No. DE-SC0012704
† yli@bnl.gov

ISBN: 978-3-95450-227-1 ISSN: 2673-5490 doi:10.18429/JACoW-IPAC2022-MOPOTK056

DATA-DRIVEN CHAOS INDICATOR FOR NONLINEAR DYNAMICS AND APPLICATIONS ON STORAGE RING LATTICE DESIGN*

Yongjun Li†, Robert Rainer, Brookhaven National Laboratory, Upton, New York, USA
Jinyu Wan[1], Yi Jiao[1], Institute of High Energy Physics, Beijing, China
Allen Liu, Dept. of Ele. Comp. Engr., Purdue University, W. Lafayette, Indiana, USA
[1]also at University of Chinese Academy of Sciences, Beijing, China

Abstract

A data-driven chaos indicator concept is introduced to characterize the degree of chaos for nonlinear dynamical systems. The indicator is represented by the prediction accuracy of surrogate models established purely from data. It provides a metric for the predictability of nonlinear motions in a given system. When using the indicator to implement a tune-scan for a quadratic Hénon map, the main resonances and their asymmetric stop-band widths can be identified. When applied to particle transportation in a storage ring, as particle motion becomes more chaotic, its surrogate model prediction accuracy decreases correspondingly. Therefore, the prediction accuracy, acting as a chaos indicator, can be used directly as the objective for nonlinear beam dynamics optimization. This method provides a different perspective on nonlinear beam dynamics and an efficient method for nonlinear lattice optimization. Applications in dynamic aperture optimization are demonstrated as real world examples.

INTRODUCTION

It is well-known that the predictability of motion in a nonlinear dynamical system is closely associated with its degree of chaos. Given an initial condition, although its motion is deterministic, its long-term prediction might not be quantitatively accurate because numerical errors can be cumulative and amplified. The Lyapunov exponent [1], i.e., the exponential growth of separation of infinitesimally close trajectories, is often used as a chaos indicator to characterize the sensitivity of chaotic motion to its initial condition.

Consider a different scenario: an unknown nonlinear dynamical system is encapsulated into a blackbox and only an ensemble of trajectories (input and output data) are available. Comparing actual trajectories to interpolated trajectories is one way to gauge chaos. A typical method to interpolate from known trajectories is to build a surrogate model with machine learning techniques. A surrogate model needs to be established first, then predictions can be made by evaluating trajectories with given initial conditions. This procedure is known as "supervised learning" [2]. To validate the model, the data is often randomly split into two clusters: a large training set and a small testing set. A model is then constructed from the training set. The performance of the model, i.e., the prediction accuracy, is measured by comparing the testing data against its prediction. The performance of the model depends on the type and complexity of the model, the volume of training data, the algorithm used for training, etc. Nevertheless, the prediction accuracy depends greatly on the degree of chaos. Therefore, an intuitive method for detecting chaos directly, purely from data is possible. In other words, predictability itself can act as a chaos indicator. From our studies we observed that by using the predictability of less-complex surrogate models, and a small volume of training data, some nonlinear behaviors in a dynamical system can be well characterized.

Surrogate models have been widely used in studying nonlinear dynamical systems [3–8], including charged particle motion in modern accelerators [9–15]. These models are obtained by training on either simulated data or experimental data, which have a high computational demand or require complicated experimental processing. If models can predict the dynamical system properties accurately with reduced resource requirements, they can be used for more efficient applications, such as optimization problems. Improving the prediction accuracy is the highest priority in these applications. In contrast to these existing approaches, the main advantage of using data-driven chaos indicators is that the requirement on the absolute accuracy of surrogate models is less demanding, and therefore can be structured with less complexity and data.

DATA-DRIVEN CHAOS INDICATOR FOR HÉNON MAP

The well-studied quadratic Hénon map, as shown in Eq. (1), is used as an example to demonstrate how to construct a data-driven chaos indicator for tune-scanning. It represents a thin sextupole kick followed by a linear rotation in a 2-dimensional phase space,

$$\begin{pmatrix} x \\ p \end{pmatrix}_{n+1} = \begin{pmatrix} \cos 2\pi\nu & \sin 2\pi\nu \\ -\sin 2\pi\nu & \cos 2\pi\nu \end{pmatrix} \begin{pmatrix} x \\ p - \lambda x^2 \end{pmatrix}_n , \quad (1)$$

where, n is a non-negative integer, ν is known as the linear tune of the transformation, and the sextupole strength λ is set as one for this demonstration. We assume the map in encapsulated as a blackbox with its tune as the control knob. For a given tune, some known trajectories that start with initial conditions (x_0, p_0) (input data) within a specific area, end with (x_n, p_n) (output data) after a limited number of turns. Based on the data, we can extract some parameters to characterize its long-term stability such as, the location of resonance lines and their stop-band widths, the relative size of the stable region, etc. This is accomplished by carrying

* Work mainly supported by US DOE Office of Science operated by BNL under Contract No. DE-SC0012704
† yli@bnl.gov

ISBN: 978-3-95450-227-1 ISSN: 2673-5490 doi:10.18429/JACoW-IPAC2022-MOPOTK059

IMPLEMENTATION OF THE VICO-GREENGARD-FERRANDO POISSON SOLVER IN SYNERGIA2 *

Chong Shik Park†, Korea University, Sejong, South Korea

Abstract

Computation of space charge fields in accelerator simulations is one of the most challenging tasks. The algorithm proposed by Hockney and Eastwood is the fastest method for numerically solving Poisson equations with open boundaries and has been implemented in various accelerator simulation codes. Recently, Vico-Greengard-Ferrando proposed a new hybrid fast algorithm for computing volume potentials. The new algorithm is promising higher accuracy and faster error convergence than that of Hockney-Eastwood. This study presents the implementation of the Vico-Greengard-Ferrando solver in Synergia and shows a comparison of results with these Poisson solvers.

INTRODUCTION

Particle-in-Cell (PIC) methods are commonly used to compute space charge effects, beam-beam effects, etc. in high-intensity accelerator modeling. In PIC calculations, particles are deposited on a spatial grids and the electrostatic field on these grids is calculated by solving the Poisson equation. Finding solutions of Poisson's equations for all time steps is the most time-consuming part of full-beam dynamics simulation. Several numerical methods for solving Poisson equations in multi-particle simulations have been developed and are widely used, such as FFT-based methods [1,2], spectral finite difference methods [3], and multi-grid spectral finite difference methods [4,5].

Among them, the FFT-based Green's function method is widely used to solve the Poisson equation in the open boundary condition when the size of the beam is generally smaller than the radius of the vacuum pipe. The Green's function and charge density are computed in the doubled-domain with zero-padding [1]. In order to calculate the Green's function efficiently with high accuracy, several techniques were developed, such as the integrated Green's function [6] and the shifted Green's function [7].

Recently Vico *et al.* developed a new Green function technique for fast convolution computation [8]. This method introduces a truncated Green's function by cutting of a region beyond the domain of interest. The Fourier transform of this Green function can be solved analytically and shows higher accuracy at the cost of the additional FFT. In this study, the Vico-Greengard-Ferrando algorithm was implemented for FFT-based Green function calculation. Numerical simulations show improved accuracy with smaller grid sizes.

* Work supported by the National Research Foundation of Korea (NRF) grant funded by the Korea Government (MSIT) (No. 2020R1A2C1014675)
† kuphy@korea.ac.kr

POISSON SOLVERS

For a given charge distribution, ρ, the Poisson equation of an open boundary condition:

$$\vec{\nabla}^2\phi = -\frac{\rho}{\epsilon_0}$$

has a solution expressed with Green's function as

$$\begin{aligned}\phi(\vec{r}) &= \frac{1}{\epsilon_0}\int G(\vec{r},\vec{r}')\,\rho(\vec{r}')d^3\vec{r}' \\ &= \frac{1}{4\pi\epsilon_0}\int \frac{1}{|\vec{r}-\vec{r}'|}\rho(\vec{r}')d^3\vec{r}'\end{aligned}$$

The electric fields can be easily computed using $\vec{E} = -\vec{\nabla}\phi$. However, the Green's function above is defined in long range and has singular at $\vec{r} = \vec{r}'$. These make it difficult to calculate accurate solution of the potential in Particle-in-Cell simulations, and require fast algorithms and special and accurate quadrature techniques.

One of most popular techniques in accelerator physics codes is Hockney-Eastwood(HE) algorithm, which uses the Fast Fourier Transform(FFT) with zero-padding. In this algorithm, the charge distribution is zero-padded in the doubled domain, and then aperiodic convolution is applied using FFT as in Eq. (1).

$$\phi(\vec{r}) = \frac{1}{\epsilon_0}h_x h_y h_z \mathscr{F}^{-1}\left\{\mathscr{F}\{\hat{G}\}\mathscr{F}\{\hat{\rho}\}\right\}, \qquad (1)$$

where $\hat{G}$ is the Green's function on the extended domain, $\hat{\rho}$ is the padded charge distribution, h_x, h_y, and h_z are grid spacings on each spatial dimensions. Here, $\mathscr{F}\{\cdot\}$ represents a Fourier transformation in all spatial dimensions, whereas $\mathscr{F}^{-1}\{\cdot\}$ represents an inverse Fourier transformation in all spectral dimensions. This algorithm is scaled like $\mathcal{O}\left((2N)^d(\log(2N))^d\right)$, where N is the number of grid points in each direction before padding and d is the dimension size.

Vico *et al.* introduced a truncated spectral kernel for Green's function by replacing it as follows [8,9]:

$$G(\vec{r}) \Rightarrow G^L(\vec{r}) = G(\vec{r})\mathrm{rect}\left(\frac{r}{2L}\right),$$

where $L > \sqrt{d}$ and the indicator function, $\mathrm{rect}(x)$, is defined as

$$\mathrm{rect}(x) = \begin{cases} 1 & \text{for} \quad |x| < 1/2 \\ 0 & \text{for} \quad |x| > 1/2. \end{cases}$$

Then, the potential solution can be rewritten as

$$\phi(\vec{r}) = \frac{1}{\epsilon_0}\int G^L(\vec{r},\vec{r}')\,\rho(\vec{r}')d^3\vec{r}'.$$

ISBN: 978-3-95450-227-1 ISSN: 2673-5490 doi:10.18429/JACoW-IPAC2022-MOPOTK060

AN INDUCTION-TYPE SEPTUM MAGNET FOR THE EIC COMPLEX*

N. Tsoupas†,B. Bhandari, D. Holmes, C. Liu, I. Marneris,
C. Montag, V. Ptitsyn, V. Ranjbar, J. Tuozzolo
Brookhaven National Laboratory Upton NY, USA

Abstract

The electron Ion Collider (EIC) project has been approved by the Department of Energy to be built at the site of Brookhaven National Laboratory (BNL). Part of the EIC accelerator complex and more specifically the Rapid Cycling Synchrotron (RCS) which accelerates the electron beam up to 18 GeV and the electron Storage Ring (ESR) which stores the electron beam bunces for collisions with the hadrons, will be built inside the same tunnel of the Relativistic Heavy Ion Collider (RHIC). This technical note provides information on the electromagnetic design of the induction-type septa magnets which will be employed to extract the beam from the RCS and inject into the ESR synchrotrons.

INTRODUCTION

The EIC accelerator complex [1] will collide various ions species at energies up to 270 GeV/amu with electrons at energies 5, 10, and 18 GeV. A schematic diagram of the EIC complex is shown in Fig. 1. The ions will be injected and accelerated to the final energy in the hadron acceleration complex with the final acceleration stage, the Hadron Storage Ring (HSR) [2], and the electrons will be accelerated in the electron acceleration complex which consists of a 400 MeV LINAC, the RCS ring which will accelerate the electrons up to 18 GeV and the ESR storage ring which will store the electron bunches for collisions with the hadrons. This paper discusses the electromagnetic design of the septa magnets for the RCS extraction and the ESR injection systems. A mechanical description of an induction type of magnet is given in [3]. The electromagnetic study was performed with the AC-module of the electromagnetic code OPERA [4]. Two AC-frequencies were used, 625 Hz and 835 Hz, to excite the magnet and compare some of the results in this paper.

THE SEPTA MAGNETS

Two similar induction septa magnets will be used in the electron accelerators of the EIC; one septum magnet in the beam extraction system of the RCS and the other in the beam injection system of the ESR [5]. The septum thickness will be 3 to 4 mm to minimize the strength of the kicker magnets. A detailed description of the extraction and injection systems is given in [5]. Fig. 2 shows the location of the RCS extraction septum in reference to the hadron beam lines which are located below the RCS ring.

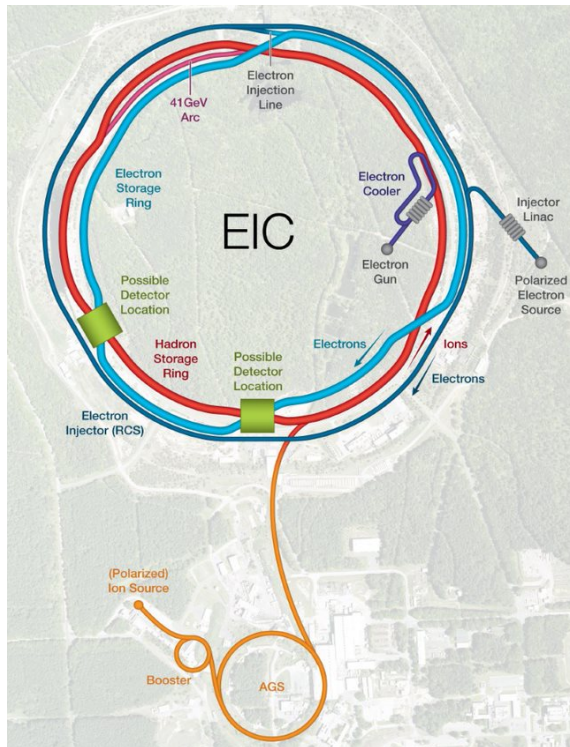

Figure 1: Schematic diagram of the EIC complex.

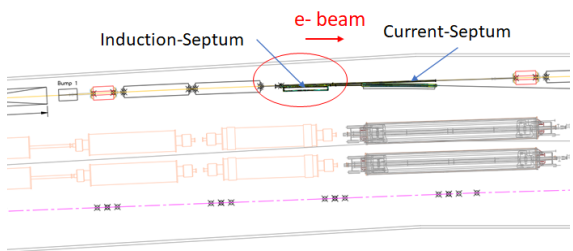

Figure 2: The location of the RCS Induction Septum.

MECHANICAL DESIGN OF THE MAGNET

Fig. 3 shows some views of the induction septum magnet. The coil of the magnet is wound around the back leg of the magnets, The magnetic iron core is made of laminations 0.35 mm thick to minimize the eddy currents. The septum plate shown in Fig. 3 is fused with the vacuum pipe of the circulating beam. The eddy currents generated in the plate and in the pipe create a uniform field in the injected beam region and also minimize the stray field in the circulating beam region.

* Work supported by Brookhaven Science Associates, LLC under Contract No. DE-SC0012704 with the US Department of Energy.
† tsoupas@bnl.gov

ISBN: 978-3-95450-227-1 ISSN: 2673-5490 doi:10.18429/JACoW-IPAC2022-MOPOTK062

NUMERICAL CALIBRATION OF THE BEAD-PULL SETUP FOR BEAM COUPLING IMPEDANCE EVALUATION

D. El Dali*, E. Metral, C. Zannini, CERN, Geneva, Switzerland
G. De Michele, S. Fanella, ADAM SA, Meyrin, Switzerland

Abstract

The bead-pull method is a commonly used electromagnetic field measurement technique exploited to tune a radiofrequency cavity to achieve design specifications. The frequency of a resonant cavity is perturbed by inserting a metallic or dielectric bead. For a given electromagnetic field, the amplitude of the perturbation depends only on the geometry of the perturbing object. Therefore, the calibration of the bead can be done in different resonant structures without loss of generality. In this paper a method to perform an accurate calibration of the bead with electromagnetic simulations is proposed. Compared to the common practice of measuring a reference cavity, the flexibility given by the simulation method to study different bead shapes and sizes could be advantageous to optimize the measurement setup. A calibrated bead-pull setup allows to quantify the electric field and, therefore, the shunt impedance of the resonant modes of the cavity. As experimental benchmark the beam coupling impedance measured with the calibrated bead-pull setup is compared with electromagnetic simulations.

INTRODUCTION

Beam coupling impedance measurements of a device are usually made by exploiting bench measurements techniques. A common and appreciated choice is to simulate the excitation due to a relativistic beam in the Device Under Test (DUT) by means of a conductive wire stretched along the axis of the structure, the so-called Wire Method (WM).

The WM is not recommended for cavity-like structures. The simple example of a pillbox with resistive walls can clarify the reason. Let us consider a cavity mode below the cut-off frequency of the attached beam pipe. In the real configuration of the structure (without wire) this mode can only get dissipated on the cavity wall. By introducing a conductive wire, the beam pipe is turned into a coaxial cable and its cut off frequency vanishes. The mode, which would be otherwise trapped in the cavity, will be able to lose power also through TEM propagation. Therefore, the quality factor measured with wire could be significantly lower than the actual quality factor of the mode (without wire) [1].

In this paper, the bead-pull method is explored as a method to measure the beam coupling impedance of structures, avoiding the issue of the conductive wire.

BEAD-PULL METHOD

Bead-Pull Radio Frequency (RF) measurement systems consist of a small dielectric or metallic bead being pulled through a cavity while electric field measurements in the cavity are taken. Bead-pull measurements involve two types of perturbations:

1. Small material perturbation, like a small dielectric bead enters a large volume of cavity.
2. Small cavity volume change, like a small metallic bead enters a large volume of cavity.

The bead-pull method is widely used in the tuning of cavities to obtain the desired accelerating field. The method is based on the classical Slater perturbation theory which states that if any resonant cavity is perturbed by a small bead, its resonant frequency shifts from the original frequency. This frequency shift is proportional to the combination of the squared amplitudes of the electrical and magnetic fields at the location of the bead [2].

This relationship is given by the equation

$$\frac{\Delta\omega}{\omega_o} = \frac{\omega_p - \omega_o}{\omega_o} = k_{SLH}\frac{|H|^2}{U} - k_{SLE}\frac{|E|^2}{U} \qquad (1)$$

where ω_p and ω_0 are the perturbed and the original resonant angular frequencies respectively, k_{SLE} and k_{SLH} are the constants determined by the shape and material of the bead, U is the energy stored in the cavity while E and H are the electric and magnetic field amplitudes at the location of the perturbation, respectively.

Therefore, if the magnetic field or k_{SLH} is zero, the electric field is directly proportional to the change in resonant frequency. Hence, if the change in resonant frequency is known, the electric field can be determined by moving the bead along a line in the cavity. For calibrated beads (knowing the bead constants) and controlled bead speed in the traversal of the structures, the bead-pull method allows a full characterization of resonances.

NUMERICAL CALIBRATION OF THE BEAD

The bead-pull technique is a perturbative method. The dimension of the perturbing object must be chosen so that the field does not vary significantly over its largest linear dimension and at the same time introduces a disturbance large enough to be distinguishable from the measurement noise. Shaped beads are used to enhance perturbation and give directional selectivity among different field components.

Since the amplitude of the perturbation depends only on the shape, material and size of the bead, a resonant cavity

* dalia.mahmoud.el.dali@cern.ch

ISBN: 978-3-95450-227-1 ISSN: 2673-5490 doi:10.18429/JACoW-IPAC2022-MOPOTK065

MINIMISING TRANSVERSE MULTIPOLES IN ACCELERATING RF CAVITIES VIA AZIMUTHALLY MODULATED DESIGNS

L. M. Wroe*, M. Dosanjh[1], S. L. Sheehy[2], John Adams Institute, University of Oxford, Oxford, UK
R. J. Apsimon[3], Cockcroft Institute, Lancaster University, Lancaster, UK
[1]also at CERN, Geneva, Switzerland, [2]also at University of Melbourne, Victoria, Australia

Abstract

In this paper, we build upon previous work of designing RF structures that support modes with tailored multipolar fields by applying the concept to negate the transverse multipoles in accelerating RF cavities caused by the incorporation of waveguide slots and tuning deformations. We outline a systematic method for designing structures that minimise these transverse multipoles and present analysis of simulations of two different minimisation designs.

INTRODUCTION

RF cavities designed to longitudinally accelerate beams of charged particles typically operate in fundamental, transverse magnetic TM_{010}-like modes [1–3]. The longitudinal monopolar term dominates in such modes but they also include transverse multipole terms as the addition of slots for power coupling [4] and components for tuning [5] break azimuthal symmetries. These transverse multipoles influence transverse beam dynamics and must not exceed the tolerances of the accelerator [6]. This can restrict the possible designs of the RF cavity, for example it may be necessary to incorporate a dual-slot coupler rather than a single-slot to negate dipolar components [7].

Previous work [8–11] has shown that azimuthally modulated RF cavities can be designed that support tailored modes with user-specified multipolar content of the form:

$$E_z(r,\theta,z) = \tilde{g}_0 J_0(kr) + \sum_{m=1}^{\infty} \tilde{g}_m J_m(kr)\cos(m\theta + \phi_m), \tag{1}$$

where the magnitude and orientation of the multipoles are denoted by $\tilde{g}_M$ and ϕ_M, J_M is the Bessel function of the first kind of order M and k is the wavenumber of the mode. Such modes are denoted as $TM_{\{M\}\eta 0}$ where $\{M\}$ denotes the set of integers for which $\tilde{g}_M \neq 0$, η denotes the radial order of the mode, and 0 denotes that the field is constant with z. The azimuthally modulated cavity cross-section, $r_0^{(\eta)}(\theta)$, that supports a desired $TM_{\{M\}\eta 0}$ mode is determined by solving:

$$0 = \tilde{g}_0 J_0(kr_0^{(\eta)}(\theta)) + \sum_{m=1}^{\infty} \tilde{g}_m J_m\left(kr_0^{(\eta)}(\theta)\right)\cos(m\theta + \phi_m). \tag{2}$$

We also note that the multipolar components in Eq. (1) can be explicitly calculated for a given electric field by undertaking a Helmholtz decomposition, as described in [6], and that a TM_{010}-like mode can be defined as a mode for which $\tilde{g}_0 \gg \tilde{g}_m$ for all m.

* laurence.wroe@physics.ox.ac.uk

In this paper, we apply this concept to minimise the magnitude of transverse multipoles in the TM_{010}-like mode of an RF cavity coupled to a power source by a slot. We present a systematic method for doing this minimisation and give an example of two different minimisation designs. We also investigate the effect of one-way tuning pins on the transverse multipoles for both designs.

PILLBOX DESIGNS

It is well-known [12] that a perfectly sealed pillbox cavity supports a non-degenerate, fundamental TM_{010} mode that can be used for the longitudinal acceleration of charged particles as its longitudinal electric field, E_z, is of the form:

$$E_z(r,\theta,z) = \tilde{g}_0 J_0(kr). \tag{3}$$

In order to exploit this mode for use in a particle accelerator, the fundamental mode must be excited by incorporating slots into the design that couple RF power into the cavity. Figure 1a shows the design of a 3 GHz RF cavity coupled to an RF input port via a single-slot design whose width has been optimised to minimise power loss in the waveguide. The single-slot breaks the azimuthal symmetry of the pillbox and Fig. 1b shows the electric field seeps into the slot. This breaking of the azimuthal symmetry of the fundamental accelerating mode means it must contain transverse multipoles and so is TM_{010}-like.

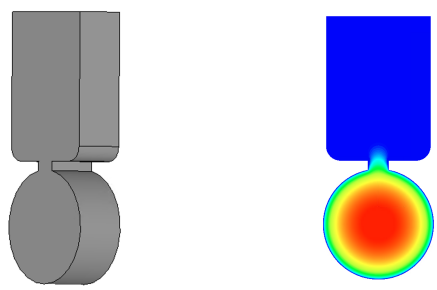

(a) Off-axis view. (b) Contour log-plot of E_z.

Figure 1: Pillbox cavity coupled to an RF input port via a single-slot that supports a 3 GHz fundamental accelerating mode.

Cavities may also require tuning post-manufacture as finite tolerances on the accuracy of machining mean the fabricated cavity may have a different resonant frequency to the ideal design. One method for tuning is to oversize the designed cavity by the upper bound of the machining tolerance, guaranteeing its resonant frequency will be lower than

ISBN: 978-3-95450-227-1 ISSN: 2673-5490 doi:10.18429/JACoW-IPAC2022-MOPOTK066

DAMPING-RING-FREE INJECTOR DESIGN FOR LINEAR COLLIDERS

T. Xu[1*], M. Kuriki[2], S. Kim[3], P. Piot[1,3], J. G. Power[3],
[1]Northern Illinois University, DeKalb, IL, USA
[2]Hiroshima University, Higashi-hiroshima, Hiroshima, Japan
[3]Argonne National Laboratory, Lemont, IL, USA

Abstract

The current designs of future electron-positron linear colliders incorporate large and complex damping rings to produce asymmetric beams for beamstrahlung mitigation at the interaction point. This paper presents the design of an damping-ring-free electron injector capable of delivering flat electron beams with phase-space partition comparable to the electron-beam parameters produced downstream of the damping ring in the proposed international linear collider (ILC) design. The performance of the proposed configuration, its sensitivity to jitter along with its impact on spin-polarization is discussed.

INTRODUCTION

A technique to mitigate beamstrahlung in linear colliders consists in using flat beams $\sigma_y \ll \sigma_x$ [1]. Flat beams are naturally produced in damping rings (DRs) which generate a beam with asymmetric transverse-emittance partition. It was first recognized in Ref. [2] that a linear transformation exploiting initial cross-plane correlation provides a path to producing flat beams ($\varepsilon_y \ll \varepsilon_x$) in a photoinjector, i.e. without the need for a DR. In Ref. [2] the achievable emittance ratio was comparable to the ones needed for ILC albeit at a much lower (0.5 nC) charge than the required 3.2 nC [3]).

This paper summarized the main results of Ref. [4] where we further expand the technique developed in [2] by combining two cross-plane phase-space manipulations: a round-to-flat beam transformer (RFBT) [2] followed by a transverse-to-longitudinal emittance exchanger (EEX) [5,6]. These phase-space manipulations were developed and experimentally demonstrated over the last two decades [7–11]. It should be noted that a similar approach employing cross-plane phase-space manipulations was proposed in a different parameter range to mitigate the micro-bunching instability in X-ray free-electron lasers (FELs) [6]. Our approach confirms that emittance partition commensurate with requirements for an LC can be attained with a simple and compact (< 50 m) beamline redistributing emittance typically produced in a conventional RF photoinjector.

START-TO-END SIMULATION

The design philosophy focuses on designing an injector capable of minimizing the beam emittance along all d.o.f's upstream of the RFBT, and then optimizing the emittance repartitioning in the RFBT and emittance-exchange process in the EEX beamlines.

* xu@niu.edu

Beam Generation

The conceptual design of the photoinjector beamline from the photocathode surface up to the entrance of the RFBT is diagrammed in Figure 1. The injector beamlines was

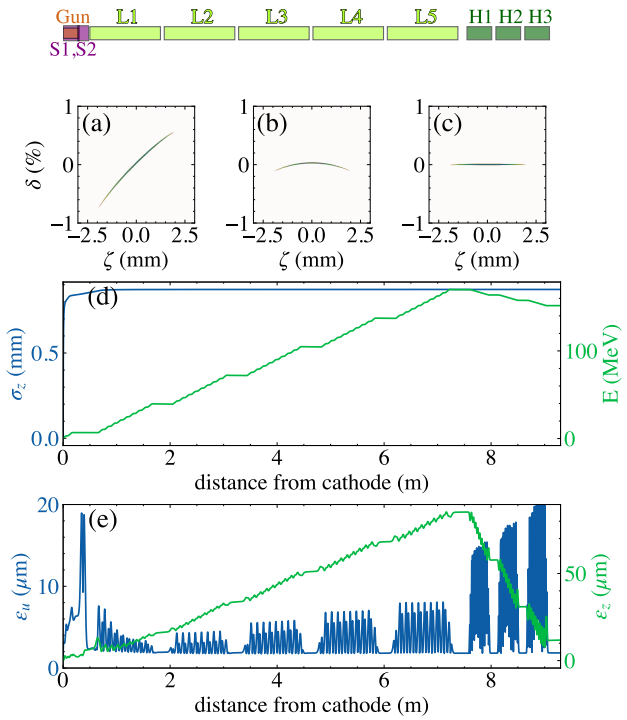

Figure 1: Photoinjector diagram (upper schematics) and snapshots of the LPS distribution at $z = 1.88$ (a), 7.48 (b), and 9.3 m (c) from the photocathode. Evolution of the beam energy and RMS bunch length (d) and corresponding 4D transverse and longitudinal emittances (e). In the upper block diagram, S1 and S2 respectively refer to the solenoidal magnetic lenses, L1-5 are the 1.3-GHz SRF cavities, and H1-3 represent the 3.9-GHz SRF cavities. In plots (a-c) and throughout this paper, $\zeta > 0$ corresponds to the head of the bunch.

modeled using the particle-in-cell beam-dynamics program IMPACT-T [12]. The electron source consists of a $1 + \frac{1}{2}$-cell RF gun operating at $f_0 = 1.3$ GHz operating with a peak field on the cathode of $E_c = 60$ MV/m. The downstream linac consists of five TESLA-type 9-cell superconducting RF (SRF) cavities operating at a peak field of $E_L = 60$ MV/m (corresponding to an accelerating gradient $G_L \simeq E_L/2 \simeq 30$ MV/m consistent with ILC demonstrated requirement of $G_L = 31.5$ MV/m [13]). The RF gun is nested in a pair of solenoidal lenses to control the beam emittance. The

ISBN: 978-3-95450-227-1 ISSN: 2673-5490 doi:10.18429/JACoW-IPAC2022-MOPOTK067

HIGH-CHARGE TRANSMISSION DIAGNOSTICS FOR BEAM-DRIVEN RF STRUCTURES

E.E. Wisniewski*[1],G. Chen, D.S. Doran, S.Kim, W. Liu,
J.G. Power, C.Whiteford, Argonne National Laboratory (ANL), Argonne, IL, USA
X.Lu, ANL, Argonne, IL USA and Northern Illinois University, Dekalb, IL, USA
D. Merenich, Northern Illinois University, Dekalb, IL, USA
F. Stulle, Bergoz Instrumentation, Saint Genis Pouilly, France
[1]also at Illinois Institute of Technology, Chicago, IL, USA

Abstract

The Argonne Wakefield Accelerator group (AWA) has been using high charge bunch-trains (>450 nC) for structure wakefield RF power generation and high power testing (100s of MW) for many years. These experiments involve fast beam-tuning for high charge transmission through small aperture wakefield structures over a large range of charge levels. The success of these experiments depends on real-time, non-destructive, fast charge measurements with devices that are robust in the high-charge and high-powered RF environment. AWA uses Bergoz Integrating Current Transformers (ICT) which are ideal for these critical charge measurements. The devices used, the method developed and their application are detailed.

INTRODUCTION

The Argonne Wakefield Accelerator (AWA) facility is dedicated to novel and advanced accelerator research, with particular attention to Structure Wakefield Accelerators (SWFA) for future colliders [1]. One of the unique challenges of the experimental program is the difficult task of tuning the beamline in order to ensure that the 65 MeV high-charge, short pulse electron bunch-trains are transmitted through SWFA devices with transmission approaching 100%. An example is wakefield generated Two-beam Acceleration (TBA) [2]. The charge is high (often hundreds of nC per pulse), and the structures have small apertures. The potential wakefield power generated per nC transmitted increases with the length of the structure. The power potential also increases as the beam aperture is made smaller for a given charge [3]. Therefore the transmission difficulty increases with the potential for power generation. To ensure the best results, it is necessary to be able to effectively monitor the charge at the input and output of the structure. In fact, it is essential to the success of these experiments. The scheme that has been developed to do this is described herein, which will be referred to as the ICT monitor scheme diagnostic.

THE EXPERIMENTAL SETUP

AWA conducts many different types of SWFA experiments, however there is one category, the high-power RF test, that will serve to illustrate the beauty and simplicity of the ICT monitor scheme diagnostic for tuning the beam for good transmission and stable high-power extraction. The goal of this type of experiment is to use the AWA drive beam to drive a Power Extraction and Transfer Structure (PETS) with a high-charge bunch train, a recent example is described in Ref. [4]. A metallic PETS which is currently in service will produce more than 400 MW RF power in each approximately 10 ns pulse at 11.7 GHz (X-band) from an 8-bunch train. Extracted power is transmitted through evacuated WR90 waveguides to the device under test (DUT), some type of Structure Wakefield Accelerator (SWFA) or related RF device. These may be metallic, dielectric, metamaterials or a hybrid such as the dielectric disk acclerator (DDA). Experiments are executed in order to study different structure design performance under high RF power and the associated high-gradients occurring within the structure, pushing them to the breakdown limits. The structures vary widely in frequency with AWA covering the range from 11.7 GHz to more than 100 GHz. Since there is an inverse relationship of structure frequency to the beam aperture, the higher frequency structure with aperture of less than 1 mm will see maximum charge transmission limited to 4 bunch trains totaling 20 nC compared to the 8 bunch, 500 nC transmitted through the 17 mm aperture of an X-band metallic structure. But monitoring and assuring good transmission is essential in all cases. The AWA drivebeam photo-injector [5]

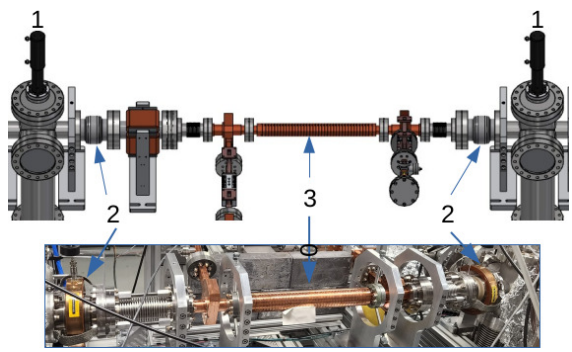

Figure 1: Experiment layout: Top: PETS vacuum installation drawing, Bottom: an installation photo illustrating the X-band PETS at AWA with some important diagnostics. Total distance from YAG to YAG is 144.5 cm. 1) YAG station 2) top: ceramic break for ICT 2) bottom: ICT as installed over ceramic break 3) PETS

is the source of high-charge bunch-trains. The photoinjector

* ewisniew@anl.gov

ISBN: 978-3-95450-227-1 ISSN: 2673-5490 doi:10.18429/JACoW-IPAC2022-MOPOMS001

PROGRESS ON DEVELOPMENT OF AXSIS: A FEMTOSECOND THz-DRIVEN MeV ACCELERATOR AND keV X-RAY SOURCE

N. H. Matlis, M. Fakhari, T. Rohwer, T. Kroh, M. Vahdani, R. Bazrafshan, D. Zhang, M. Pergament, & F. X. Kärtner[1]
Center for Free-Electron Laser Science CFEL, Deutsches Elektronen-Synchrotron DESY, Germany
[1]also at The Hamburg Centre for Ultrafast Imaging, University of Hamburg, Hamburg, Germany

Abstract

We report on the design and progress on construction of a first prototype demonstrating the concept of a THz-driven relativistic electron accelerator and an associated X-ray source. The nascent technology of THz-driven acceleration offers several key advantages over conventional accelerators, including order-of-magnitude increases in driving field, to the GV/m range; short, mm-scale wavelengths enabling ultra-high-gradient manipulations of electrons, as well as a compact foot print. Combined, these features enable electron sources with unique capabilities, including sub-10 fs bunch durations and intrinsic synchronization to laser source resulting in the capability to create electron and diffraction instruments of exceptional temporal resolution beyond the state of the art. Our machine is designed to reach 20 MeV electrons, using several-mJ pulses of THz radiation generated via nonlinear down conversion of customized lasers, and X-rays in the few keV range will be created by counter-propagating them with an "optical undulator" laser.

INTRODUCTION

The development of an electron acceleration technology driven by terahertz radiation (THz) [1,2,3,4] brings unique advantages for creation of electron and light sources with properties that are well adapted for studying material structure and dynamics on atomic scales at the limits of temporal and spatial resolution. In particular, the short wavelength of THz waves enables the possibility of sustaining electric and magnetic fields as well as field gradientsorders of magnitude higher than those in conventional accelerators yielding strong acceleration and manipulation electron beams. Over the last decade, THz-driven accelerator technology has emerged from a novelty to a fast-growing research field aimed at exploring the benefits not only for fully THz-driven accelerators and associated light sources, but also for performing high-field manipulations of electrons in conventional accelerator systems. Recent

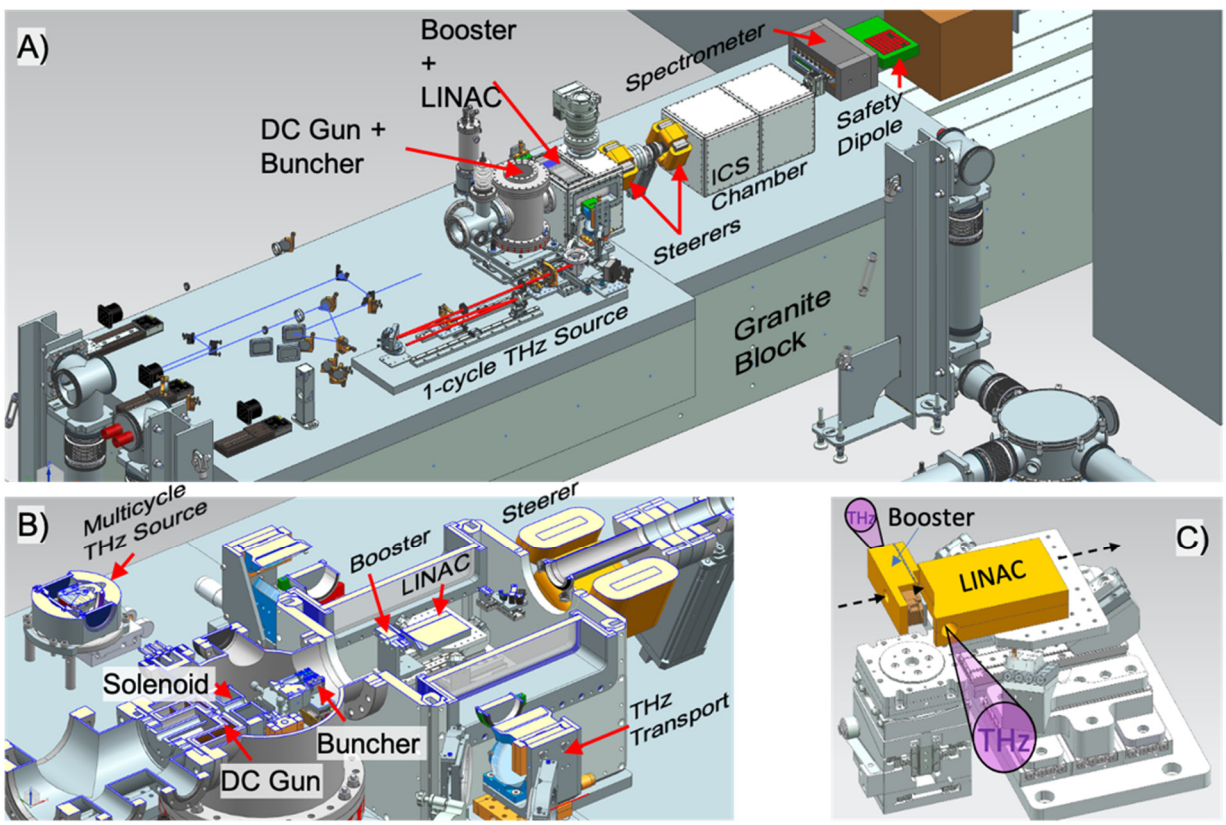

Figure 1: (A) 3D CAD Layout of the AXSIS THz-Driven X-ray Light Source Prototype. (B) Detail of the THz-Accelerator. (C) THz-driven Booster and LINAC.

ISBN: 978-3-95450-227-1 ISSN: 2673-5490 doi:10.18429/JACoW-IPAC2022-MOPOMS003

SINGLE-SIDED PUMPED COMPACT TERAHERTZ DRIVEN BOOSTER ACCELERATOR

T. Kroh[†,1], R. Bazrafshan, M. Fakhari, F. X. Kärtner[1], K. Kawase[2], N. H. Matlis, M. Pergament, T. Rohwer, M. Vahdani, D. Zhang
Center for Free-Electron Laser Science CFEL, Deutsches Elektronen-Synchrotron DESY, Germany
[1]also at The Hamburg Centre for Ultrafast Imaging, University of Hamburg, Hamburg, Germany
[2]also at Quantum Beam Science Research Directorate, National Institutes for Quantum Science and Technology, Shirakata 2 – 4, Tokai, 3191106 Ibaraki, Japan

Abstract

Here, we present on the progress of developing a multi-layered accelerator structure designed to boost the 50 keV output of a DC electron gun to energies of ~ 400 keV powered by a single high-energy terahertz ("THz") pulse. An integrated piezo-actuated mirror inside the matchbox sized structure enables fine-tuning of the electric field in the interaction region for efficient acceleration and helps reduce the complexity of the optical setup. Such a compact booster accelerator is very promising as electron source in ultrafast electron diffraction experiments and as booster stage prior to THz based LINACs.

INTRODUCTION

Scaling the RF-accelerator concept to terahertz ("THz") frequencies brings several compelling advantages, including compactness, intrinsic timing between the photoemission and driving field sources, and high field gradients associated with the short THz wavelength and high breakdown threshold [1]. Some recent demonstrations of such THz powered accelerators and beam manipulators relied on two counter-propagating single-cycle THz pulses [2-4]. However, to achieve high energy gains in the acceleration process THz pulses of high energy are needed which in turn require complex optical setups and optimization procedures [5-7]. Here, we present on the development of a multi-layered accelerator structure which only requires a single THz pulse to be powered and is designed to boost the 50 keV output of a DC electron gun to energies of up to ~ 400 keV. An integrated tunable mirror inside the matchbox sized structure interferes the front of the driving THz pulse with its rear part such that the magnetic field in the interaction region is cancelled and the electric field is optimized for efficient acceleration. This approach reduces the required number of driving THz pulses from two to one and consequently reduces the complexity of the optical setup.

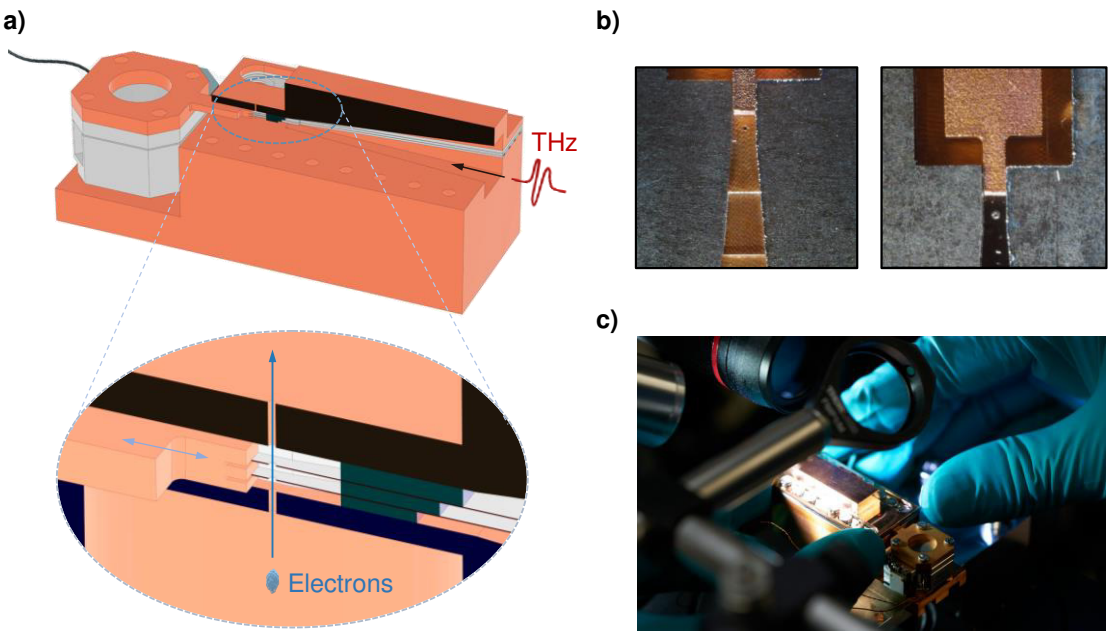

Figure 1: (a) 3D-model of the compact booster accelerator pumped transversely by a single-cycle THz pulse (red). This pumping scheme is enabled by a piezo-actuated mirror integrated into the device. (b) Top-view close-up pictures of the 1st and 2nd layer. Fused silica inserts delay the THz pulse in each consecutive layer such that efficient acceleration is achieved. (c) Assembly of the booster device under an optical microscope with an integrated alignment laser.

† tobias.kroh@desy.de

ISBN: 978-3-95450-227-1 ISSN: 2673-5490 doi:10.18429/JACoW-IPAC2022-MOPOMS004

OPTIMIZING ACTIVATION RECIPE WITH Cs, Te, O FOR GaAs-BASED PHOTOCATHODES

J. Bae*, M. Andorf, I. Bazarov, J. Maxson, Cornell University, Ithaca, USA
L. Cultrera, Brookhaven National Laboratory, Upton, USA
A. Galdi, University of Salerno, Fisciano (SA), Italy

Abstract

GaAs-based photocathodes are the most popular electron sources for producing highly spin-polarized electron beams in accelerator physics and condensed matter physics. Spin-polarized photoemission requires activation to achieve Negative Electron Affinity (NEA). Conventional NEA surfaces such as CS-O/NF_3 are extremely vacuum sensitive, and this results in rapid QE degradation. In this work, we activated GaAs with various recipes using Cs, Te, and oxygen. We demonstrate NEA activation on GaAs surfaces. Among Cs-Te activated samples, the oxidized sample showed the highest QE and longest lifetime at 780 nm.

INTRODUCTION

GaAs-based photocathodes are considered state-of-the-art for producing highly spin-polarized electron beams for accelerator and microscopy applications. Negative Electron Affinity (NEA) activated surfaces are required to extract highly spin-polarized electron beams from GaAs-based photocathodes. Activation to NEA is traditionally achieved by exposing the GaAs sample surface to cesium vapor. The deposited cesium layer forms a dipole moment that brings the vacuum level below the bulk conduction band minimum [1]. If an oxidant is included, a stronger, double-dipole layer is formed, that can further enhance the NEA [2].

NEA layers on the surface of GaAs-based photocathodes are notorious for the extreme vacuum sensitivity, and this results in rapid degradation of QE during beam operations. Conventional activation layers, such as Cs-O_2 and Cs-NF_3, are monolayers weakly bound to the GaAs surface with high chemical reactivity. Therefore, GaAs photocathodes are typically operated under extreme high vacuum (XHV) conditions and, even so, still suffer from rapid degradation [3]. Recently, activation with alternative semiconductor layers was proposed to improve the robustness [4]. It has been shown that when Te element is used for activation along with Cs vapors, the robustness of the NEA layer can be improved without negatively affecting spin polarization [5]. Variations of this approach were studied by multiple labs. Cs-K-Te activation was demonstrated to improve lifetime by more than an order of magnitude [6]. Similar to the standard activation method with Cs and oxidants, it has been shown that usage of oxygen during unconventional activation with Te or Sb can increase the QE (Quantum Efficiency) while preserving improved lifetime of GaAs photocathodes. Cs-Sb-O activation improved the photocathode lifetime at 780 nm by a factor of 7 [7, 8]. Lastly, Cs-Te-O activation at room temperature also showed an improved lifetime at 532 nm compared to the standard activation method [9]. In this work, we tested various NEA activation recipes with Cs, Te and O to understand the impact on QE and lifetime at low voltage. The activation temperature, usage of oxygen and thickness of the Te layer were varied.

EXPERIMENT

NEA Activation

Highly *p*-doped (Zn 5×10^{18} cm^{-3}) GaAs (100) wafers were cleaved in air with a diamond scribe. Prepared samples were solvent cleaned with isopropanol and rinsed in de-ionized water. Wet-etching was performed with 1% HF solvent for 30 s and samples were rinsed again with de-ionized water before loading under vacuum. The activation chamber has a base pressure of 10^{-9} Torr, and Cs and Te effusion cells are installed with shutters that control the flux on the sample. Each sample was heat cleaned at ~ 500 °C for ~ 12 hours. Five samples were grown:

1. Sample #0 was activated with the standard method using Cs and oxygen.
2. Sample #1 was activated with Cs-Te at 120 °C. 1.3 nm of Te was deposited.
3. Sample #2 was activated with Cs-Te-O at 120 °C. 1.3 nm of Te was deposited.
4. Sample #3 was activated with Cs-Te at room temperature. 1.3 nm of Te was deposited.
5. Sample #4 was activated with Cs-Te at 120 °C. 2.5 nm of Te was deposited.

Sample #1 was activated with the same recipe from our previous work [5], and Sample #2-4 are departures from this recipe. Compared to Sample #1, oxygen was additionally used for Sample # 2, the activation temperature was lowered to room temperature for Sample # 3, and twice the amount of Te was deposited for Sample #4.

In Fig. 1, we monitored the infrared QE during the activation process of Sample #1. Initially, the sample is seen to photoemit at 780 nm due to residual Cs vapors in the growth chamber. The sample is activated with only Cs until QE reaches a plateau. Then, the shutter in front of Te effusion cell is opened for deposition. QE immediately drops below a noise level. Deposited Te thickness was monitored by a quartz crystal microbalance during Cs-Te codeposition. Te

* jb2483@cornell.edu

ISBN: 978-3-95450-227-1 ISSN: 2673-5490 doi:10.18429/JACoW-IPAC2022-MOPOMS005

START-TO-END SIMULATIONS OF A THz-DRIVEN ICS SOURCE

M. Fakhari†, Y. -K. Kan, M. Vahdani, N. H. Matlis, and F. X. Kärtner[1,2]
Center for Free-Electron Laser Science, DESY, Hamburg, Germany
[1]also at Department of Physics, University of Hamburg, Hamburg, Germany
[2]also at The Hamburg Centre for Ultrafast Imaging, Hamburg, Germany

Abstract

We present start-to-end simulations for a fully THz-driven table-top X-ray source. A 1-pC electron bunch is generated via photo emission from a copper cathode embedded in a dielectric-loaded metallic cavity where the emitted electrons are accelerated up to 430 keV average kinetic energy. Instead of the conventionally used fundamental mode, a higher order mode (HOM) of the cavity (TM_{012} mode) at 300 GHz is used in order to keep the electrons phase matched with the oscillating THz field inside the gun.

The output beam of the gun is injected into a dielectric-loaded metallic waveguide operating as a linear accelerator. The phase velocity of the traveling wave inside the linac is adjusted in such a way that electrons see an accelerating field all the way along the tube resulting to an 18.5-MeV output beam which is then transported to an inverse Compton scattering (ICS) stage. The injection phase of the electrons into the linac can be tuned to introduce a negative longitudinal energy chirp to the electron bunch leading to a ballistic bunch compression after the linac. In addition to the longitudinal compression a set of permanent magnet quadrupoles (PMQ) is designed to focus the beam transversely at the ICS interaction point where the electron beam scatters off a 100-mJ, 1-µm laser beam and generates an X-ray beam with 2.6×10^7 photons per shot containing photon energies 2 keV < E_{ph} < 8 keV in a beam with 50 mrad half opening angle.

The required terahertz waves to power the gun and linac are 550-ps pulses at 300 GHz containing 5 mJ and 23 mJ energies respectively. These THz pulses can be generated using difference frequency generation (DFG) of two 1 J laser beams. Since all of the components in the proposed X-ray source are driven by the same 1-µm laser technology, it offers the unique possibility of inherent synchronization.

INTRODUCTION

Over the past decades demands for compact X-ray radiation sources have grown considerably due to their vast applications. Shrinking accelerator-based X-ray sources can be achieved either by making the accelerator and/or the undulator section compact. Operating at high frequencies, e.g. THz range, allows applying higher accelerating gradients which leads to high energy particles over a shorter distance [1, 2]. On the other hand, using optical undulators makes it possible to get X-ray radiation with relatively low energy electrons (few MeV range) due to their much shorter undulator period compared with permanent magnet undulators, of course at the expense of larger opening angles [3]. Here we introduce a THz driven Inverse Compton Scattering (ICS) source which layout is schematically illustrated in Fig. 1. Electrons are generated via photo emission from a metallic cathode embedded in a THz cavity operating at on of its higher order modes. The cavity delivers electrons with above 430 keV average kinetic energy. The electrons then traverse through a dielectric-loaded metallic waveguide, which operates as a linear accelerator (linac) and boosts the electron energy up to 18.5 MeV. A set of quadrupole magnets is used to focus the electron bunch and transport it to the ICS interaction section.

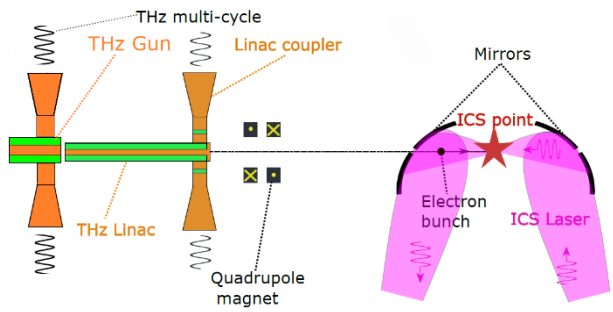

Figure 1: Schematic layout of the THz-driven compact X-ray source.

THz INJECTOR

Here, we introduce a THz gun which consists of a dielectric loaded cylindrical cavity operating at one of its higher order modes (HOM) to ensure that electrons are continuously phase matched with the oscillating electric field [4]. Figure 2 schematically illustrates the HOM gun, which consists of the main cavity and its horn coupler. The cavity itself is a cylindrical copper cavity loaded with quartz (electric permittivity of 3.85 at 300 GHz). A cross sectional view of the electric field distribution at the operating mode is also depicted in Fig. 2. The ASTRA particle tracking code [5] is used to simulate the acceleration of the 1-pC electron bunch in the gun. A 47-fs FWHM UV pulse is assumed to illuminate the cathode with a spot size of 70 µm (FWHM). Considering 5 mJ injected THz energy, the peak electric field on the axis of the gun becomes 1.4 GeV which accelerates the electrons up to 435 keV. On the other hand, the transverse field of the coupler region, focuses the beam exiting the gun to below 3 µm at a distance of 2.5 mm from the cathode. The output normalized transverse emittances are evaluated as 87 nm rad in both x and y directions, while the longitudinal emittance is 14 nm rad. The results of the ASTRA simulations are shown in Fig. 3.

† moein.fakhari@desy.de

ISBN: 978-3-95450-227-1 ISSN: 2673-5490 doi:10.18429/JACoW-IPAC2022-MOPOMS007

OPTIMIZED DIELECTRIC LOADED WAVEGUIDE TERAHERTZ LINACS

M. Vahdani[1,2], M. Fakhari[1], F. X. Kärtner[1,2,3],
[1] Center for Free-Electron Laser Science, DESY, Hamburg, Germany
[2] Department of Physics, University of Hamburg, Hamburg, Germany
[3] The Hamburg Centre for Ultrafast Imaging, Hamburg, Germany

Abstract

Dielectric loaded waveguides (DLW) powered by multi-cycle terahertz (THz) pulses have shown promising performance as a compact Linear Accelerator (LINAC) due to higher breakdown fields at THz frequencies compared to conventional RF components. By changing the dielectric dimensions one can control phase and group velocities of the THz pulse inside the DLW. Since optimum waveguide dimensions are dependent on initial electron energy, THz pulse energy, and etc., it is worthwhile to determine optimum values for different conditions in order to maximize final kinetic energy. In this work, we present a combined analytical/numerical guide to determine the optimum DLW parameters for single on-axis electron acceleration. We also introduce graphic representations to visualize optimum designs for different initial electron and THz pulse energies.

INTRODUCTION

Due to low breakdown electric fields in the RF regime, conventional Radio Frequency (RF) accelerators need to operate at limited acceleration gradient. By increasing the frequency one can take advantage of operating at higher fields [1]. Therefore, THz driven LINACs offer new capabilities when compared to RF- and optical driven accelerators. So far different techniques have been used to accelerate electrons by THz radiation [2-7]. Among these methods, cylindrical DLWs are very attractive due to easier fabrication and better field uniformity in comparison with rectangular ones [5]. Since the phase velocity of usual metallic waveguides is higher than the speed of light, a dielectric layer is added to reduce the phase velocity. Also, the group velocity is significantly lower than the phase velocity. Therefore, in this case a multi-cycle pulse is ideal to increase the interaction length between electron bunch and electromagnetic fields. In the following, we propose a method to optimize cylindrical DLW LINACs. In the simulations we assume a rectangular THz pulse powering the DLW. If this pulse is long enough and narrow band, we can neglect the dispersion effects in the waveguide but we must still take into account the envelope velocity, i.e. group velocity, of the pulse within the waveguide.

ELECTROMAGNETIC CALCULATION

We assume low bunch charge, such that beam loading and wakefields can be neglected. In this case, Maxwell's equations decouple from the equation of motion of charges. We use an analytical/numerical method to analyse the performance of a cylindrical DLW LINAC. The TM_{01} mode of a DLW is the optimum mode for acceleration with the highest longitudinal electric field on axis.

The fields of the TM_{01} mode can be written as follows [8]:

$$E_z(z,t) = \left[A_i J_0(k_{\rho i}\rho) + B_i Y_0(k_{\rho i}\rho)\right] e^{j(\omega t - k_z z)} \quad (1)$$

$$E_\rho(z,t) = -\frac{jk_z}{k_{\rho i}}\left[A_i J_1(k_{\rho i}\rho) + B_i Y_1(k_{\rho i}\rho)\right] e^{j(\omega t - k_z z)} \quad (2)$$

$$H_\phi(z,t) = -\frac{j\omega\varepsilon_{di}}{k_{\rho i}}\left[A_i J_1(k_{\rho 2}\rho) + B_i Y_1(k_{\rho i}\rho)\right] e^{j(\omega t - k_z z)} \quad (3)$$

Where i=(1,2) represents the layer number. $k_{\rho i}$ and k_z are the transverse and longitudinal components of the wave vector k. J_m and Y_m are the first and second kind of Bessel functions of order m and ε_{di} is the permittivity of the i-th layer. This formula can be used for each layer of a cylindrical concentric structure. By applying boundary conditions for continuity of the tangential fields on the interface of the layers, we are able to write the dispersion relation. By solving the dispersion relation for a given frequency, we can calculate the mode distribution and wave vector $k_z$within the DLW. Subsequently, phase velocity, group velocity, and absorption coefficient are given directly by the following equations.

$$v_{ph} = \frac{\omega}{\beta} \quad (4)$$

$$v_g = \frac{\partial\omega}{\partial\beta} \quad (5)$$

$$\beta = Re\{k_z\}, \alpha = Im\{k_z\} \quad (6)$$

Figure 1 shows phase and group velocity for a DLW loaded by a dielectric with a refractive index of 1.95 (fused silica) surrounded by a copper layer with conductivity 6e7 S/m at the frequency of 300 GHz. The DLW thickness is designed such that the phase velocity is optimized for maximum energy gain. Therefore, we need to know the field amplitude to be able to calculate the energy gain

In order to calculate the electric field on a cross section we must know the total Energy coupled to the DLW. Total power flow from a cross section is calculated by integrating the z-component of the Poynting vector over the total cross section area.

Figure 2 shows the longitudinal component of the electric field on axis of the DLW for a total input power of 1W. So far, we have calculated electromagnetic fields inside the DLW. We are now prepared to solve the equation of motion for a single on axis electron.

$$P_z = \int \frac{1}{2} E_r \times H_\varphi^* \quad (7)$$

ISBN: 978-3-95450-227-1 ISSN: 2673-5490 doi:10.18429/JACoW-IPAC2022-MOPOMS008

DIAGNOSIS OF TRANSVERSE EMITTANCE IN LASER-DRIVEN ION BEAM

T. Miyatake[1], H. Sakaki[1], I. Takemoto[1], Y. Watanabe, Kyushu University, Kasuga, Hukuoka, Japan
T. H. Dinh, S. Kojima, Ki. Kondo, Ko. Kondo, M. Kando, M. Nishikino, M. Nishiuchi, National Institutes for Quantum and Radiological Science and Technology KPSI, Kizugawa, Kyoto, Japan
[1]also at National Institutes for Quantum and Radiological Science and Technology KPSI, Kizugawa, Kyoto, Japan

Abstract

Ion beam produced in laser-driven ion acceleration by ultra-intense lasers has characteristics of high peak current and low emittance. These characteristics become an advantage to operate the request for the beam application. Therefore, we study how to control the parameters with the laser-plasma interaction.

Here, we used 2D Particle-in-Cell code to simulate the laser-driven ion acceleration and investigated the results in terms of transverse emittance, beam current, and brightness. The laser spot size and target thickness were changed in the simulation. And, these qualitative results show that interaction target thickness is a major factor in controlling beam characteristics.

INTRODUCTION

A laser-driven ion acceleration by ultra-intense lasers [1-3] is expected to be applied to various applications such as down-size of particle accelerators, hadron therapy [4], and physical property experiments including PIXE [5, 6]. In the Target Normal Sheath Acceleration (TNSA) scheme which is a well-known mechanism of laser-driven acceleration, an ultra-intense laser is focused on a solid thin foil target to accelerate electrons, and generate a charge-separating electric field gradient of ~TV/m. This field accelerates ionized hydrogen, carbon, and oxygen in a contaminant layer on the rear side of a target in ~MeV. The transverse proton emittance diagnosis is smaller than 0.004 mm-mrad (normalized RMS value) for 10 MeV protons [7], and the emittance of the laser-accelerated proton beam is much lower than that of existing RF accelerators [8, 9]. An emittance growth of the accelerated proton beam is discussed by Andreas J. Kemp *et al.*, that is caused by the filamentation of the laser-generated hot-electron jet [10].

Low emittance and high peak current, high-quality beam, become an advantage to operate the request for the beam application. Therefore, we study how to control the parameters with the laser-plasma interaction which is to clarify the correlation between laser irradiation parameters and beam characteristics of laser-accelerated ions. To understand these correlations, we can optimize the conditions for generating a high-quality beam. Generally, such as emittance and current are estimated analytically from the plasma density of an ion source and conditions of the extraction electrode [11, 12] in a typical ion source, ECR source. However, it is not easy to make an analytical model such as typical accelerator ion source for the laser-accelerated ion beams. In this paper, we systematically diagnose the correlation between laser parameters and generated beam quality.

PARTICLE-IN-CELL SIMULATION

An ideal beam is close to zero transverse emittance, but a real beam has a non-zero emittance generated while laser-plasma interaction process. We have to understand the contributing factors to control the beam quality such as emittance and beam current. Here, we focus on and evaluate two contributing factors, interaction target thickness and spot size of a laser as shown in Fig. 1.

Generating of low emittance and high peak current proton beams in TNSA scheme is simulated with a 2D Particle-in-Cell (PIC) code, EPOCH code version 4.17.10 [13], by changing a target thickness and spot size of a laser. To simplify the analysis, it is assumptive to collisionless in the simulation conditions. The diagnostic divergence angle is limited to ±50 mrad, due to the aperture of the beam transport system [9, 14]. The proton beam energy to be observed is 2 MeV with ±5 % energy dispersion. The dimensions of the simulation box are 80 μm x 80 μm and the cell size is 0.042 λ_L x 0.042 λ_L where λ_L is the laser wavelength. The laser has linearly polarized. The laser spatial distribution is assumed to be a single Gaussian distribution which is a longitudinal profile with 80 fs (FWHM). The electron density of target is set to $n_e = 40\ n_c$, where $n_c = \varepsilon_0 m_e \omega^2 / e^2$

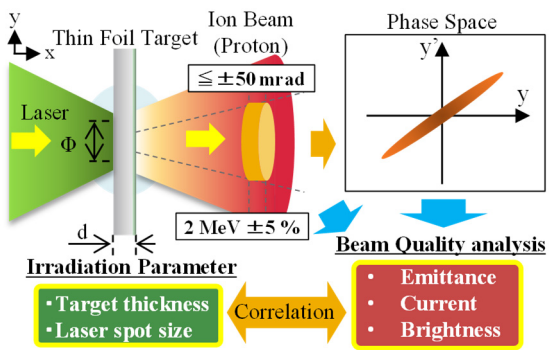

Figure 1: Overview of the calculation scheme. The phase space is created to calculate the emittance, d is the target thickness, and φ is the laser spot diameter.

ISBN: 978-3-95450-227-1 ISSN: 2673-5490 doi:10.18429/JACoW-IPAC2022-MOPOMS010

BEAM DYNAMICS AND DRIVE BEAM LOSSES WITHIN A PLANAR DIELECTRIC WAKEFIELD ACCELERATOR *

T.J. Overton† [1] , G. Xia[1], The University of Manchester, Manchester, UK
T.H. Pacey[1], Y. Saveliev[1], ASTeC/STFC, Daresbury, UK
[1] also at The Cockcroft Institute, Daresbury, UK

Abstract

Beam-driven dielectric wakefield accelerators (DWA) have the potential to provide accelerating gradients in the GV/m range. The transverse dynamics in such devices need to be understood to avoid instabilities over long transport distances and facilitate beam matching to specific applications (e.g. FELs). This presentation details simulation studies of the magnitude of beam-breakup instability (BBU) in planar dielectric lined waveguides (DLWs). These are for DWA drive beams, with high charge and momentum that can be produced at current facilities. Using a series of perpendicular DLW segments has been proposed to control instabilities over larger distances. Using self-developed software, the beam dynamics of a drive beam within a DLW are simulated and the magnitude of beam losses along a DLW of varying lengths calculated and beam quality preservation investigated. Methods to reduce transverse instabilities have been explored, and the impact of these on the length of a possible DWA acceleration stage are investigated. An acceleration stage with m-scale length, consisting of multiple alternating planar DLWs, is suggested and preservation of beam quality along this distance is shown.

INTRODUCTION

Dielectric wakefield acceleration (DWA) is a method suggested to produce high gradient acceleration of charged particles at future facilities. DWA exploits the Cherenkov radiation generated by a drive beam of charged particles inside a dielectric lined waveguide (DLW) to accelerate a trailing main (witness) bunch [1].

DWA experiments have shown that electron bunches produced by conventional accelerators can excite fields of upto 850 MV/m before strong damping is observed [2], with charge symmetry demonstrated between electron and positron drive bunches [3]. Witness electron bunches have been accelerated with gradients of 300 MV/m [4]. Shaping the drive beam longitudinally, it is possible to increase the transformer ratio (accelerating to decelerating field ratio) [5]. Whilst this comes at the expense of the maximum accelerating field obtainable it does increase the efficiency of main bunch acceleration [6].

Experimental and theoretical studies of dielectric wakefield acceleration have either focused on cylindrical DLWs [4, 7, 8], or planar structures with just a single orientation [9]. Planar structures have been suggested as potentially advantageous due to the transverse fields being approximately quadrupole-like. This allows for the use of alternating, horizontal and vertical (H+V), akin to a FODO cell, to control transverse beam size while propagating through the structure [10, 11]. In these proceedings, simulations of drive beams in planar structures are presented. Beam losses in a single planar DLW determine the total length of acceleration that can be maintained, and a H+V setup is then used to determine the extent to which beam quality can be preserved.

SIMULATION METHODOLOGY

A fully three-dimensional greens function approach has been used for these studies. Beams generated with initial parameters, or beams from other accelerator simulation tools, can be used as inputs and beam dynamics within a DLW calculated using a Boris pusher method [12]. Fields are calculated using the transverse operator method outlined in [13], which have been bench-marked against commercial codes CST and VSim. By specifically modelling DWA effects this increases efficiency compared to the commercial alternatives, allowing for computational time to be reduced by orders of magnitude. The number of modes used for each calculation is automatically chosen to ensure full convergence, and thus all higher order fields are automatically included.

SINGLE STAGE DYNAMICS

Beam and structure parameters, listed in Table 1, have been chosen to match those expected for a drive beam at a future DWA accelerator and achievable at current facilities. A beam is chosen with 2 nC charge and 1 GeV/c beam momentum to generate large longitudinal fields and facilitate ~m scale transportation. Beams with a larger charge density towards the tail are needed for a higher transformer ratio. For a maximal transformer ratio, a longer bunch with a 'double-triangular' or 'doorstop' shape would be used [14, 15]. We have chosen to simulate a highly skewed gaussian (with skewness $\alpha = -4$), so any beam losses at the tail are immediately evident.

Experimental and theoretical results have shown that transverse fields can be mitigated by using an elliptically shaped beam [9, 16]. We will compare the feasibility of a beam shaped in this way to a symmetric (circular) drive beam. Behind the drive bunches, these beam and structure parameters lead to peak accelerating fields of 78 MV/m and 62 MV/m for the circular and elliptical beams respectively.

In a realistic machine, small uncertainties in the initial beam position cannot be avoided. In Fig. 1, the charge transported in a single DLW stage is shown for the elliptical and

* Work supported by The Cockcroft Institute Core Grant and the STFC
† toby.overton@cockcroft.ac.uk

ISBN: 978-3-95450-227-1 ISSN: 2673-5490 doi:10.18429/JACoW-IPAC2022-MOPOMS012

SIMULATION STUDIES OF DRIVE-BEAM INSTABILITY IN A DIELECTRIC WAKEFIELD ACCELERATOR

W. H. Tan*, P. Piot[1], Northern Illinois University, DeKalb, IL 60115, USA
A. Myers, W. Zhang, T. Rheaume, R. Jambunathan, A. Huebl, R. Lehe, J.-L. Vay,
Lawrence Berkeley National Laboratory, Berkeley, CA 94720, USA
[1] also at Argonne National Laboratory, Lemont, IL 60439, USA

Abstract

Beam-driven collinear wakefield acceleration using structure wakefield accelerators promises a high gradient acceleration within a smaller physical footprint. Sustainable extraction of energy from the drive beam relies on precise understanding of its long term dynamics and the possible onset or mitigation of the beam instability. The advance of computational power and tools makes it possible to model the full physics of beam-driven wakefield acceleration. Here we report on the long-term beam dynamics studies of a drive beam considering the example of a dielectric waveguide using high fidelity particle-in-cell simulations performed with WarpX.

INTRODUCTION

In a beam-driven collinear wakefield accelerator (CWA), a high-charge drive beam propagates through a slow-wave medium to generate wakefields, which then accelerate a trailing witness beam. The slow wave medium can be plasma, dielectric waveguides or metallic waveguides with corrugation. In the case of using electromagnetic waveguides. Large amplitude wakefields can be generated using waveguides with a small aperture excited by a high-charge bunch. For example, the loss factor κ of a cylindrical waveguide is inversely proportional to the square of its aperture size a, $\kappa \propto a^{-2}$ [1]. In addition to using high charge, drive beams with asymmetric current profile are being considered in CWAs to enhance the transformer ratio, $\mathcal{R} \equiv |E_+/E_-|$, where E_+ is the maximum accelerating field behind the drive bunch, and E_- is the maximum decelerating field within the drive bunch. However, beam-breakup (BBU) instability caused by associated strong transverse wakefields (with transverse loss factor $\kappa_\perp \propto a^{-3}$) is one of the main challenges toward the practical realization of a CWA. Hence, efficient modeling of the beam dynamics inside a CWA is important for designing and building a practical CWA.

Advances in computer simulation software in accelerator modeling along with the availability of large computing resources are enabling first-principle electromagnetics simulations of beam dynamics in a CWA. For such simulations, particle-in-cell (PIC) simulations is a popular technique being used to model beam dynamics. In this paper, we report preliminary simulation studies of the drive-beam dynamics inside a CWA consisting of dielectric waveguides with superimposed external focusing. The model is implemented using a finite-different time-domain (FDTD) PIC algorithm in the WarpX open-source electromagnetics framework being developed for accelerator modeling [2].

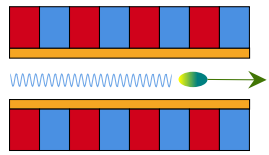

Figure 1: A dielectric wakefield accelerator consists of a dielectric waveguide embedded in a series of interleaving focusing (red) and defocusing (blue) quadrupole magnets. A drive beam (green ellipse) generates wakefields (blue sinusoidal waves) by passing through the waveguide.

DIELECTRIC-WAKEFIELD ACCELERATOR

We considered a CWA with dielectric waveguides, which we shall refer as a dielectric wakefield accelerator (DWA). This accelerator consists of a dielectric waveguide embedded in a series of interleaving focusing and defocusing (FD) quadrupole magnets for beam transport. Wakefields are generated by propagating a drive beam inside the accelerator. A schematic diagram of a DWA appears in Fig. 1. Earlier studies of a DWA were performed in Ref. [3] using a two-particle model tracking code to address the limit of accelerating gradient. In addition, simulation performed with the particle-tracking program elegant [4] indicates that a FODO lattice with a tapered quadrupole-magnet strength and asymmetric shaped drive beams with a large energy chirp can suppress the BBU instability [5]. Further investigation performed using a two-particle model provided further guidance on possible external-focusing configurations [6]. The latter paper specifically demonstrated that a drive beam with a large energy chirp and a tapered focusing-defocusing (FD) channel could suppress the BBU instability. Correspondingly, we considered a drive beam with an asymmetric current profile and a DWA with FD channels to conduct our simulation studies.

The dielectric waveguide considered throughout this paper is a multi-mode structure with fundamental-mode frequency $f \simeq 148$ GHz; see the structure parameters listed in Table 1. We considered using quadrupole without tapering focusing strength to test the limit of the drive beam stability. Table 1 shows properties of a DWA that we used in

* z1829753@students.niu.edu

ISBN: 978-3-95450-227-1 ISSN: 2673-5490 doi:10.18429/JACoW-IPAC2022-MOPOMS013

TOWARD EMITTANCE MEASUREMENTS AT 11.7 GHz SHORT-PULSE HIGH-GRADIENT RF GUN*

Sergey Kuzikov†, Chunguang Jing[1], Ernie Knight, Euclid Techlabs LLC, Bolingbrook, IL, USA
[1]also at Euclid Beamlabs LLC, Bolingbrook, IL, USA
Chen Gonxiaohui, Philippe Piot[3,4], Eric Wisniewski, ANL, Lemont, Illinois, USA
[3]also at Fermilab, Batavia, IL, USA
[4]also at Northern Illinois University, DeKalb, IL, USA
Wei Hou Tan, Northern Illinois University, DeKalb, IL, USA

Abstract

A short pulse high gradient RF gun (see Fig. 1) has been recently tested at Argonne Wakefield Accelerator (AWA) facility. The carried-out test showed that the 1,5-cell gun was able to inject 3 MeV, up to 100 pC bunches at room temperature being fed by 9 ns up to 300 MW 11.7 GHz pulses. The cathode field was as high as about 400 MV/m. So high field is aimed to mitigate repealing Coulomb forces substantially. In accordance with simulations the emittance could be as low as less than 0.2 mcm. To obtain so low emittance in the experiment, the gun is assumed to be equipped with a downstream linac to be fed from the same power extractor as the gun itself. Here we report design of the RF power distribution system splitting RF power among the gun and the linac, results of low-power tests, and emittance measurement plans for upcoming new experiment at AWA.

A CONCEPT FOR HIGH GRADIENT X-BAND GUN

High brightness beams appealing for XFELs and UEM essentially consist of a large number of electrons in a small phase space volume, i.e. a high peak current [1-2]. When such beams are generated from the cathode, there is a strong space charge force, which elongates the bunch and reduces its brightness. An optimal solution is to raise the accelerating voltage in the gun to mitigate repealing Coulomb forces. However, the maximum gradient is limited by the effects of RF breakdown.

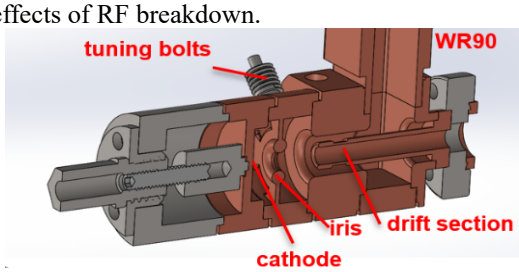

Figure 1: Engineering design of 11.7 GHz UHGPI.

We propose to utilize an ultra-high gradient and a short-pulse technology at room temperature. The probability of RF breakdown and pulse heating temperature are reduced as the RF pulse length decreases [3-4]. We present a development of an electron ultra-high gradient photoinjector (UHGPI) operating with short RF pulse (9 ns scale) that is produced by a drive beam at AWA.

The proposed 11.7 GHz gun is a 1,5 cell overcoupled resonator with the perforated iris in-between cells in order to sustain strong coupling factor [5-6]. The Q-factor is slightly below 200 to accommodate 9 ns RF pulse. The gun was fabricated two years ago. During tests the gun generated ~3 MeV electron bunches accelerated at about 400 MV/m cathode field. The gun had ~10^{-6} breakdown rate and showed a very low average dark current.

RF GUN BEAMLINE

Next experiment will include emittance measurements. For this purpose, the beamline was designed (Fig. 2). It included drive beam line with PETS connected to the gun, solenoid, and diagnostic line based on a pepper pot. In accordance with simulations the emittance could be as small as ~0.2 mm×mrad. In order to obtain so small emittance, an additional linac with ~100 MV/m gradient behind the gun will be used.

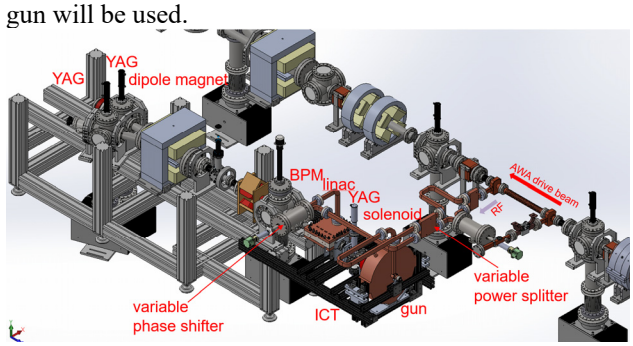

Figure 2: Beamline design for experiment #3.

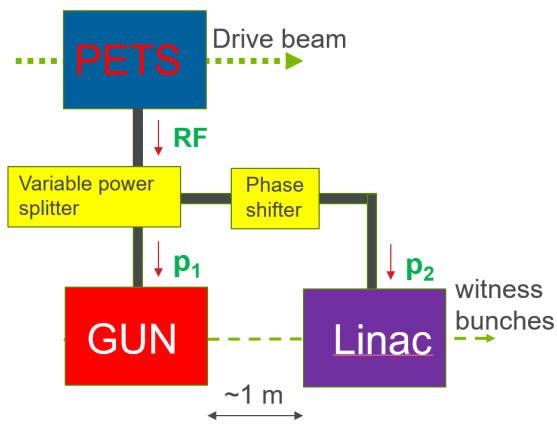

Figure 3: Scheme of gun and linac feeding.

*Work supported by DoE SBIR Phase II Grant #DE-SC0018709.
† s.kuzikov@euclidtechlabs.com

ISBN: 978-3-95450-227-1 ISSN: 2673-5490 doi:10.18429/JACoW-IPAC2022-MOPOMS014

COMMISSIONING OF A HIGH-GRADIENT X-BAND RF GUN POWERED BY SHORT RF PULSES FROM A WAKEFIELD ACCELERATOR*

W. H. Tan†, X. Lu[1], P. Piot[1], Northern Illinois University, DeKalb, IL, USA
C. Jing[1], S. Antipov, S. Kuzikov, E. Knight, Euclid Techlabs LLC, Bollingbrook, IL, USA
D. S. Doran, W. Liu, J. G. Power, C. Whiteford, E. E. Wisniewski,
G. Ha, J. Shao, Argonne National Laboratory, Lemont, IL, USA
[1] also at Argonne National Laboratory, Lemont, IL, USA

Abstract

A high-gradient X-band (11.7-GHz) photoinjector developed by Euclid Techlabs, was recently commissioned at the Argonne Wakefield Accelerator (AWA). The system comprises a 1+1/2-cell RF gun powered by short RF pulses generated as a train of high-charge bunches from the AWA accelerator passes through a slow-wave power extraction and transfer structure. The RF photoinjector was reliably operating with electric fields in excess of 300 MV/m on the photocathode surface free of breakdown and with an insignificant dark-current level. We report on the RF-gun setup, commissioning, and the associated beam generation via photoemission.

INTRODUCTION

Bright-electron sources have a wide range of applications in accelerator-based light sources and electron probes, such as free-electron lasers (FELs) and ultrafast electron diffraction. The report of Basic Energy Sciences Workshop on the Future of Electron Sources in 2016 identified *High-gradient R&D for next generation electron sources* as one of four Priority Research Directions in the future electron sources [1]. It had anticipated in 5 years the realization of a factor of two higher electric field than the well-established 100 MV/m S-band RF photoinjector thus enabling the next generation electron source with ∼ 100-pC and ∼ 30-nm emittance for the most demanding applications. A critical aspect to the generation of bright electron beams is the use of high gradient radiofrequency (RF) gun on suppressing space charge effects during the photoemission process. Accordingly, the beam peak brightness $\mathcal{B} = q/\Gamma$, where q is the bunch charge and Γ its six-dimensional phase-space volume, scales with the applied electric field E_0 on beams during emission at the emitter surface as $\mathcal{B} \propto {E_0}^{\alpha}$ where the exponent $\alpha \geq 1$ depends on the bunch's initial transverse-to-longitudinal aspect ratio [2, 3]. One path toward producing high-gradient electric fields for bright electron beam generation consists of operating a RF gun at higher frequencies. Such an approach is limited by the RF breakdowns where field-emitted electrons due to surface imperfection leads to local RF-induced heating and damage the cavity wall. The RF breakdown can be described by a phenomenological model where the breakdown rate (BDR) is described by BDR $\sim {E_0}^{30}{\tau_p}^{5}$, where E_0 is the applied electric on the surface and τ_p is the length of the RF pulse [4–6]. From the equation, it is implies that the breakdown rate of a high gradient RF gun can be reduced by shortening the RF pulse duration. Although this approach has been proposed more than a decade ago its implementation to realize short sub-100-ns RF pulse has remained elusive so far.

A high gradient X-band RF (XRF) gun was designed by Euclid Techlabs LLC and commissioned at the Argonne Wakefield Accelerator (AWA) facility [7–10]. This gun operates at 11.7 GHz driven by short RF pulses generated via the deceleration of high charge electron beams passing through a power extraction and transfer structure (PETS) available at the AWA facility. In this paper, we report the setup, commissioning of this XRF gun along with the generation of ∼ 100 pC relativistic (∼ 3 MeV) electron bunches.

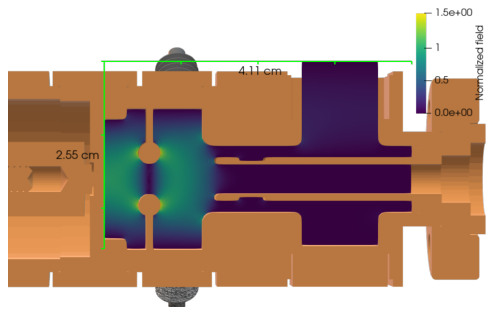

Figure 1: Cross section of the XRF gun superimposed with the applied electric field.

PHOTOINJECTOR SETUP AND DESIGN

The cut-away of the XRF gun appears in Fig. 1 with a superimposed electric-field amplitude map. The gun consists of $1 + \frac{1}{2}$-cell RF cavity oprating on the $\mathrm{TM}_{010,\pi}$ mode. The iris includes four magnetic coupling slots to increase both the RF coupling between cells and the frequency separation from the neighboring resonant $\mathrm{TM}_{010,0}$ mode. The cavity is strongly over-coupled resonator resulting in loaded Q of factor ($Q_\ell \simeq 180$), thus allowing for the rapid build-up of field inside of the cavity. The gun is made of oxygen-free copper using conventional fabrication techniques. A broadband coaxial RF-input coupler is used to ensure the field remains axi-symmetric. The X-band photoinjector beamlines is diagrammed in Fig. 2. The photoinjector consists

* This work is supported by the U.S. DOE, under award No. DE-SC0022010 to NIU, DOE SBIR grant No DE-SC0018709 at Euclid Techlabs LLC, and contract No. DE-AC02-06CH11357 with ANL.
† z1829753@students.niu.edu

ISBN: 978-3-95450-227-1 ISSN: 2673-5490 doi:10.18429/JACoW-IPAC2022-MOPOMS015

TEMPORAL AND SPATIAL CHARACTERIZATION OF ULTRAFAST TERAHERTZ NEAR-FIELDS FOR PARTICLE ACCELERATION*

A. E. Gabriel†[1], M. A. K. Othman, M. C. Hoffmann, E. A. Nanni,
SLAC National Accelerator Laboratory, Menlo Park, USA
[1]also at University of California Santa Cruz, Santa Cruz, USA

Abstract

We have measured the THz near-field in order to inform the design of improved THz-frequency accelerating structures. THz-frequency accelerating structures could provide the accelerating gradients needed for next generation particle accelerators with compact, GV/m-scale devices. One of the most promising THz generation techniques for accelerator applications is optical rectification in LiNbO3 (LN) using the tilted pulse front method. However, accelerator applications are limited by significant losses during transport of THz radiation from the generating nonlinear crystal to the acceleration structure. In addition, the spectral properties of high-field THz sources make it difficult to couple THz radiation into accelerating structures. A better understanding of the THz near-field source properties is necessary for the optimization of THz transport and coupling. We have developed a technique for detailed measurement of the THz near-fields and used it to reconstruct the full temporal 3D THz near-field close to the LN emission face. Analysis of the results from this measurement will inform designs of novel structures for use in THz particle acceleration.

MOTIVIATION

THz frequency radiation is useful for many particle acceleration and beam manipulation applications [1-4]. Optical rectification in LiNbO3 using the tilted pulse front method is routinely used to generate THz pulses with energies in the tens of micro-joules and field strengths above 1 MV/cm [5]. Despite these strong fields, current THz acceleration methods are limited by significant losses during THz transport and coupling into the accelerating structure. Using the THz near-field for particle acceleration would significantly decrease losses due to beam transport. This approach requires the design of a novel structure that would generate THz radiation and use it for acceleration immediately. Designing an accelerating structure half out of LN would allow THz to be generated by optical rectification and used for electron acceleration without the need for THz transport. This approach would remove the THz losses incurred by beam transport, and allow for a longer THz interaction length. In addition, it would allow the structure to be constructed out of dielectrics, which would facilitate the implementation of advanced machining methods, such as femtosecond laser microfabrication, that can create complex geometries. These geometries can be optimized by simulation and optimization programs to maximize accelerating gradient. Preliminary simulations of half LN half silicon accelerator structures have been carried out using an electromagnetic simulation and automatic differentiation package Ceviche [6-8]. These simulations yielded a highly optimized structure geometry that is manufacturable using available machining methods, see Fig. 1. Updated shunt impedance calculations found a shunt impedance value of 1.3×10^7 Ω/m.

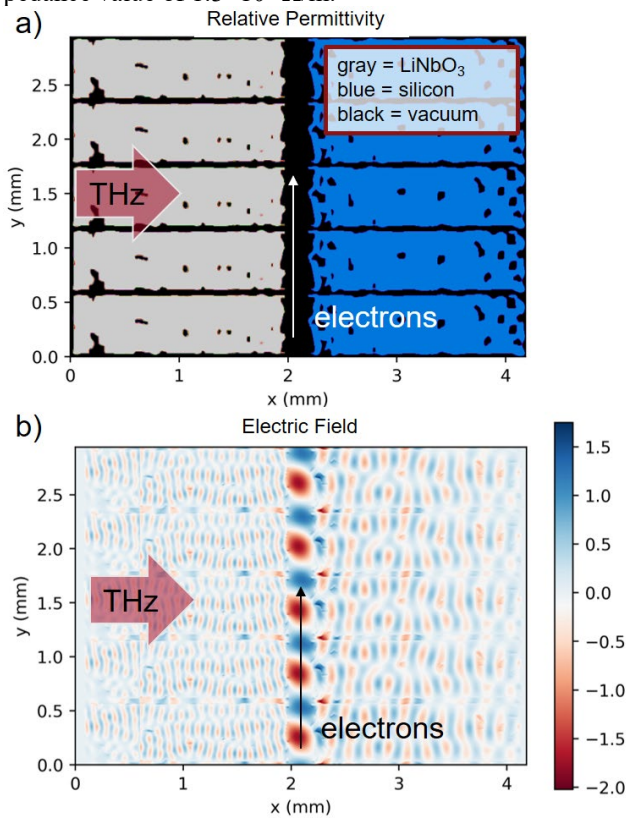

Figure 1: Final optimized geometry of a 5 period dielectric accelerator structure **(a)**. Electric fields produced by the structures in Figure 3 by a 0.5 THz continuous wave source incident from the left **(b)**. THz would be generated on the left side by optical rectification in LN. The other half of the structure would be constructed out of a material like silicon, which would act as a mirror.

A precise and robust understanding of the THz near field is needed in order to design this integrated THz generation and electron acceleration structure. We have conducted a measurement of the THz near-field from a tilted pulse front LN source in order to inform these designs, and help to develop better THz transport and coupling methods.

* Work supported by Department of Energy contract DE-AC02-76SF00515
† angabrie@slac.stanford.edu

ISBN: 978-3-95450-227-1 ISSN: 2673-5490 doi:10.18429/JACoW-IPAC2022-MOPOMS016

APPLICATION OF NANOSTRUCTURES AND METAMATERIALS IN ACCELERATOR PHYSICS*

J. Resta-López†, ICMUV – Universitat de València, Paterna, Spain
O. Apsimon, C. Bontoiu, B. Galante[1], C. P. Welsch,
Cockcroft Institute and The University of Liverpool, UK
G. Xia, Cockcroft Institute and The University of Manchester, UK
A. Bonatto, Universidade Federal de Ciências da Saúde, Porto Alegre, Brazil
[1]also at CERN, Geneva, Switzerland

Abstract

Carbon-based nanostructures and metamaterials offer extraordinary mechanical and opto-electrical properties, which make them suitable for applications in diverse fields, including, for example, bioscience, energy technology and quantum computing. In the latest years, important R&D efforts have been made to investigate the potential use of graphene and carbon-nanotube (CNT) based structures to manipulate and accelerate particle beams. In particular, the interaction of graphene and CNTs with charged particles and electromagnetic radiation might open interesting possibilities for the design of compact coherent radiation sources, and novel beam diagnostics techniques as well. This paper gives an overview of novel concepts based on nanostructures and metamaterials with potential application in the field of accelerator physics. Several examples are shown and future prospects discussed.

INTRODUCTION

Since their discovery, carbon nanotubes (CNTs) [1] and graphene [2] have found countless applications in multiple fields, e.g. electronics, photonics, bioscience, energy technology, etc. Therefore, it is worth asking about the potential of the use of graphene and carbon nanotechnology in the field of accelerator physics. Due to their special optoelectronic, thermal and mechanical properties, CNT and graphene based structures might offer novel and alternative solutions to overcome many of the present limitations of several accelerator subsystems, thus enhancing the capabilities of future accelerators. For instance, they might open new paths for manipulation and acceleration of beam particles beyond the current state-of-the-art.

In this paper we discuss potential applications of carbon based nanostructures and metamaterials in particle accelerator physics. Concretely, we give representative examples for solid-state wakefield acceleration, electron guns and beam diagnostics.

SOLID-STATE BASED ACCELERATION

In the field of accelerator physics, the channeling properties of silicon crystal have successfully been used for collimation and extraction of relativistic proton beams [3]. Solids can also provide an alternative medium for acceleration. Depending on their particular atomic configuration and electrical conduction nature, some solid-state micro- and nano-sized structures offer interesting properties to enhance electric field components or induce strong wakefields that could be useful for acceleration, as well as transverse particle guiding and radiation emission.

Semiconductor and metallic crystalline lattices have been proposed to generate a solid-state plasma medium to guide and accelerate charged particles, taking advantage of the channelling properties in crystals. High electron density in solids could be obtained from the conduction bands. Typical electron densities (n_e) in solid-state plasmas lie within the range of 10^{19} cm$^{-3} \leq n_e \leq 10^{24}$ cm^{-3} [4,5], i.e. between one and six orders of magnitude higher than the density in gaseous plasmas. Taking into account that the maximum accelerating field depends on the electron density as $E_z[\mathrm{V/m}] \approx 96\sqrt{n_e[\mathrm{cm}^{-3}]}$, solid-state based plasmas might lead to accelerating gradients 0.1 TV/m $\lesssim E_z \lesssim$ 100 TV/m.

Solid-state wakefield acceleration using crystals was proposed in the 1980s and 1990s by T. Tajima and others [4,6,7] as a technique to sustain TV/m acceleration gradients.

Wakefields in crystals can be induced by means of the excitation of high-frequency collective motion of conduction electrons through the crystalline lattice. To reach accelerating gradients on the order of ~TV/m, crystals must be excited by ultrashort X-ray laser pulses within a power range of TW– PW, which makes the practical realisation of the concept very challenging. It has only recently become a realistic possibility since the invention of the so-called single-cycled optical laser compression technique by G. Mourou et al. [8].

If natural crystals (e.g. silicon) are used for solid-state wakefield acceleration, the beam intensity acceptance is significantly limited by the angstrom-size channels. In addition, such small size channels increase the dechanneling rate and make the channels physically vulnerable to high energy interactions, thus increasing the damage probability by high power beams.

Over the past decade there have been great advances in nanofabrication techniques [9] that could offer an excellent way to overcome many of the limitations of natural crystals. Metallic nanostructures and metamaterials [10, 11] could lead to suitable ultra-dense plasma media for wakefield acceleration or charged particle beam manipulation, i.e. channelling, bending, wiggling, etc. This also includes the

* Work supported by the Generalitat Valenciana (CIDEGENT/2019/058).
† javier2.resta@uv.es

ISBN: 978-3-95450-227-1 ISSN: 2673-5490 doi:10.18429/JACoW-IPAC2022-MOPOMS017

BEAM TRANSPORT SIMULATIONS THROUGH FINAL FOCUS HIGH ENERGY TRANSPORT LINES WITH IMPLEMENTED GABOR LENSES

A. Sherjan*, K. I. Thoma [1], M. Droba, O. Meusel, S. Reimann [1],
Goethe University Frankfurt, Frankfurt a. M., Germany
[1]also at GSI, Darmstadt, Germany

Abstract

First investigations on Gabor Lens GL2000 at Goethe University have shown that it is possible to confine a 2m long stable Electron Plasma Column and to apply it as a hadron beam focusing device. With this knowledge theoretical implementations of GLs in final focus and transfer lines have started. The focusing with GLs is a weak but smooth focusing in radial direction. The GL is a suitable and inexpensive choice in addition to the existing focusing elements eg. magnetic quadrupoles. The device helps to improve beam quality and minimize losses over long distances. The investigation of relativistic hadron beams in GeV range using the example of the proposed NA61/SHINE VLE-beamline at CERN is carried out and will be presented. Thin-matrix simulations with a generated distribution as well as field map simulations with generated and realistic distributions (Geant4) at 1 - 6 GeV/c have been analysed and compared. In addition, the H4-beamline at North Area (CERN) is proposed to implement GLs for experimental tests.

VLE BEAMLINE DESIGN

Recent plans of the NA61/SHINE collaboration [1] about the conceptual design of a very low energy (VLE) beamline implemented into the H2 beamline in North Area of CERN have led to several studies to investigate possible spots for the placement of the GL and its effect on the beam properties as well as on the settings of surrounding focusing elements. The VLE beamline will guide hadrons, such as protons, pions and kaons, in a range of momenta from 1 up to 13 GeV/c from a primary target over a total distance of around 52 m to a secondary target where the NA61/SHINE experiments will take place. Along the path, the particles are first captured by an acceptance quadrupol duplet, before reaching a double bend achromat for horizontal momentum selection,

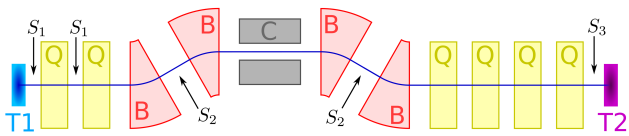

Figure 1: Conceptual design of the H2-VLE-beamline (CERN) from primary (T1) to secondary target (T2) including focusing and momentum selection devices and three possible positions for the implementation of Gabor Lenses.

followed by a final focus chain of four quadrupoles to hit the target in a matched spotsize. Due to its structure and length this beamline represents a perfect test bench to investigate the interaction of the GL as a weak radial focusing element in a HEBT line. Initial considerations included three scenarios (S1, S2, S3) in which the GL was simulated at different points on the beamline (see Fig. 1): S2 is discussed more thoroughly below, since at highly sensitive elements as an achromat the effects on the beam transport can be observed in most detail.

GABOR LENS

A Gabor lens (GL) [2] is a cylindrical device that can simply replace any drift section of a linear or circular accelerator, since it still allows plain drift when not operating (off) and radial weak focusing when fully operational (on). This is achieved by confining an electron column inside a cavity trough a superposition of electric and magnetic field along the logitudinal direction of beam propagation (see Fig. 2). For more details on GLs in general see [3]. As a result the positive space charge, which forces the beam to continously drift apart, is overcompensated by the electron density in the GL. Additionally the self electric field inside a homogenously distributed electron column is a linear radial field, so that positively charged beam particles are attracted and linearly focused towards the beam axis due to the Coulomb force.

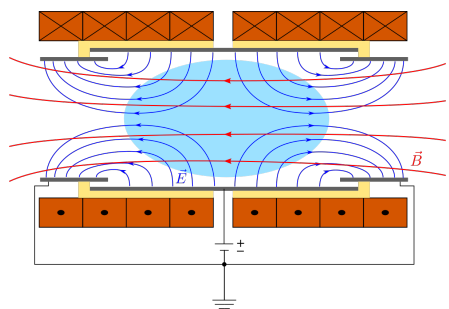

Figure 2: GL schematic setup taken from [4]: electric (blue) and magnetic field (red) confine electron cloud (light blue).

SIMULATION MODELS

Thin Lens

For the presented beam dynamics investigation the GL is a set of thin lens slices consisting of symmetrical drift-thin lens matrix-drift-combinations to approximate the focusing strength of the GL, which can be obtained geometrically:

* sherjan@iap.uni-frankfurt.de

ISBN: 978-3-95450-227-1 ISSN: 2673-5490 doi:10.18429/JACoW-IPAC2022-MOPOMS018

TUNGSTEN ELECTRON EMITTER (TE²) WITH DIRECT HEATED CATHODE BY PLASMA STREAM

K I. Thoma*[1], T. Dönges, M. Droba, O. Meusel, H. Podlech, K. Schulte-Urlichs[1]
Goethe-Universität Frankfurt am Main, Frankfurt, Germany
[1]also at GSI Helmholtzzentrum für Schwerionenforschung, Darmstadt, Germany

Abstract

At Goethe-University, a novel concept of heating metallic cathodes is currently under investigation. In the scope of the ARIES collaboration WP16, an RF-modulated electron gun was developed and manufactured for application in electron lenses for space charge compensation. The goal of this project is to increase the intensity of primary beams, especially in low energy booster synchrotrons like the SIS18 and SIS100 at GSI/FAIR or the SPS at CERN. The gun was designed to produce electron currents of 10 A at extraction voltages of 30 kV. The tungsten electron emitter (TE²) and the grid electrode were designed and manufactured to be integrated in the extractor of the original volume type ion source. Significant effort was put into a robust and flexible design with highly reliable key components. The cathode is heated by a plasma stream generated in the plasma chamber of the source. Different heating options of the cathode are currently being studied. This contribution presents the working principles of the electron gun and first measurements results of cathode heating.

INTRODUCTION

Common electron sources use oxide cathodes or photo cathodes for electron beam production [1]. Some exotic cathode materials are currently used [2]. All of these technologies are less robust against vacuum contamination, vacuum discharges (Townsend discharge) and secondary particle impact. Therefore, it was decided to use a pure tungsten cathode for the production of the intense electron beam with an emission density of J = 0.453 Acm^{-2}. The heating of the cathode is challenging, as a temperature range of 2200-2800 °C is needed for an adequate electron emission following Richardson's law. Inspired by the concept of hybrid ion sources [3], the direct heating of the cathode by the use of a plasma stream, generated by an arc discharge, was used. For the proof of concept, an existing gas discharge ion source was modified and the plasma electrode was replaced by a tungsten cathode. The flexibility of the plasma generator enables the guiding of the arc discharge to the cathode and the variation of arc power and power density distribution on the cathode. The resulting high cathode temperatures need an effective cooling of cathode and grid flange. On the other hand thermal conductivity determines the temperature distribution on the extraction surface. A careful layout of stainless steal thermal spacers led to heat balance and resulted in the desired temperature distribution. The spacers were mounted to connect the water cooled cathode flange and the tungsten cathode.

Three options to create a time structure on the extracted electron beam were discussed. The first one is a pulsed extraction voltage. This option is not favourable because of beam mismatch and the high power load. A pulsed arc discharge, leading to a pulsed heating of the cathode, is only suitable for duty cycles of a few percent with low pulse frequencies due to the thermalisation time of the cathode. Therefore, a grid modulated beam extraction is used. A high voltage modulation can be applied to synchronise the time structure of the electron beam with the ion bunch evolution during a synchrotron cycle. A careful layout protects the grid from heat load and provides a cut-off frequency of about 600 MHz. The design of the electron source presented in this paper was chosen to be the prototype of the IRME-gun [4,5]. Additionally, a research project was started for the investigation of electron emission of metal surfaces in the near of the phase transition.

DESIGN OF THE ELECTRON GUN AND TEST STAND

The design of the electron gun TE² is based on an existing volume type ion source. All parts are optimized regarding water cooling, high voltage break downs, vacuum conditions and outside isolation [6,7].

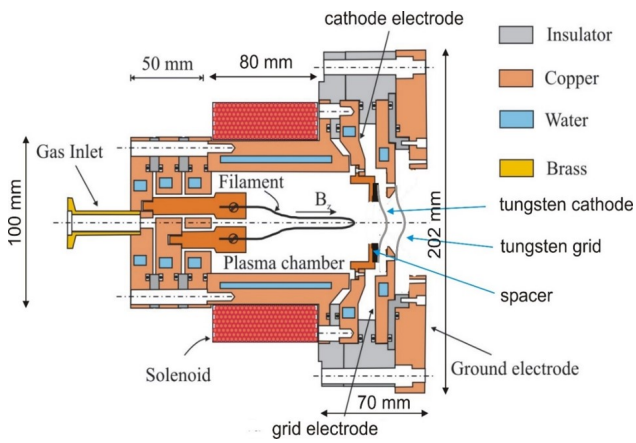

Figure 1: Cross sectional view of TE².

The ion source design was transformed into an RF modulated electron gun by replacing the plasma electrode by a copper cathode flange with tungsten cathode. The screening electrode of the former accel-decel extraction system was replaced by a grid flange with tungsten grid. The ground elec-

* thoma@iap.uni-frankfurt.de

ISBN: 978-3-95450-227-1 ISSN: 2673-5490 doi:10.18429/JACoW-IPAC2022-MOPOMS019

THE NEW SPARC_LAB RF PHOTO-INJECTOR

D. Alesini, M.P. Anania, A. Battisti, M. Bellaveglia, A. Biagioni, F. Cardelli, G. Costa, E. Chiadroni, M. Del Franco, G. Di Pirro, G. Di Raddo, L. Faillace, M. Ferrario, G. Franzini, A. Gallo, A. Giribono, A. Liedl, V. Lollo, L. Pellegrino, L. Piersanti, R. Pompili, S. Romeo, L. Sabbatini, V. Shpakov, A. Stella, C. Vaccarezza, A. Vannozzi, F. Villa
INFN-LNF, Frascati, Italy
M. Carillo, Sapienza University of Rome, Rome, Italy
A. Cianchi, M. Galletti, University of Tor Vergata, Rome, Italy

Abstract

A new RF photo-injector has been designed, realized and successfully installed at the SPARC_LAB facility (INFN-LNF, Frascati, Rome). It is based on a 1.6 cell RF gun fabricated with the new brazing-free technology, recently developed at the INFN-LNF. The electromagnetic design has been optimized to have a full compensation of the dipole and quadrupole field components introduced by the coupling hole, with an improvement of the effective pumping speed with two added pumping ports. The gun is over coupled (β=2) to reduce the filling time and to allow the operation with short RF pulses. The overall injector integrates a new solenoid with a remote control of the transverse position and a variable skew quadrupole for the compensation of residual quadrupole field components. It also allows an on axis laser injection with the last mirror in air, and the possibility of a future integration of an X/C band cavity linearizer. In the paper we report the main characteristics of the injector with particular focus on the new gun realization and final performances.

INTRODUCTION

The new injector of the SPARC_LAB Facility [1] is shown in Fig. 1. It is a complex system and has been designed to substitute the previous injector that had limitations in term of rf gun breakdown activity, solenoid alignment, laser mirror in vacuum and possibility of further improvements with the insertion of an X/C band linearizer. The injector integrates several new components, as illustrated in the next paragraph. In particular, the rf gun has been realized with the new brazing-free technology developed at INFN-LNF [2] and already adopted for the realization of new rf photo-guns [3, 4]. This technology has been demonstrated to exhibit very good performances in term of breakdown rates (BDR) and conditioning time, with a contemporary reduction of the cost and realization time. In the present paper, after a description of the overall photo-injector, we illustrate the new RF gun design, realization and performances showing preliminary measurements with beam.

NEW PHOTO-INJECTOR LAYOUT

The new injector is a complex system and integrates several different components, as given in Figs. 1 and 2 where the picture of the injector and mechanical section are reported. In particular, we have the already mentioned rf gun, the solenoid [5] with a remote control of its transverse position with a precision better than ±10 μm, the laser injection chamber that allows a laser injection with the last mirror in air, a complete diagnostic station with faraday cup, YAG screen and toroid, a skew quadrupole with variable polarity, embedded in the solenoid, for the tuning of the x-y emittances and compensation of residual asymmetries, and a corrector magnet for trajectory optimization and beam energy measurements. The injector allows also to insert, in the future, an X/C band linearizer.

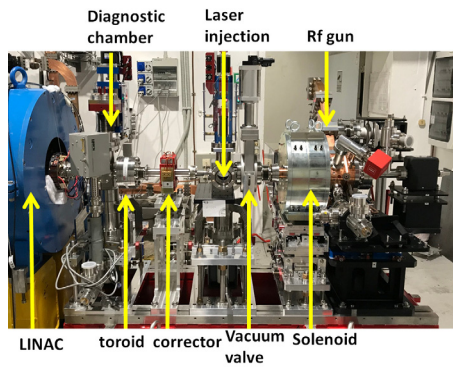

Figure 1: Picture of the new SPARC_LAB injector.

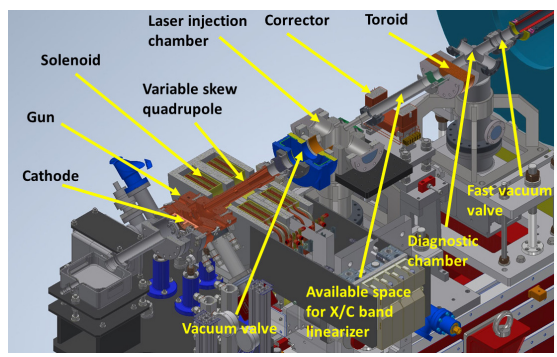

Figure 2: Mechanical section of the new photo-injector with main components.

THE NEW GUN

The gun integrates several new features both from the electromagnetic (e.m.) and the mechanical point of view. The e.m. design has been accomplished using ANSYS-HFSS [6] and the e.m. model is given in Fig. 3. It has been designed with three added holes in the coupling cell for a perfect compensation of the dipole and quadrupole e.m. field components introduced by the rf coupling hole.

The holes have been also connected to vacuum pumps allowing a strong improvement of the vacuum pressure

ISBN: 978-3-95450-227-1 ISSN: 2673-5490 doi:10.18429/JACoW-IPAC2022-MOPOMS020

DARK CURRENT STUDIES FOR A HIGH GRADIENT SW C-BAND RF GUN*

F. Cardelli†, D. Alesini, G. Di Raddo, L. Faillace, A. Giribono, A. Vannozzi
INFN - Laboratori Nazionali di Frascati, Frascati, Italy
T. G. Lucas, Paul Scherrer Institut, 5232 Villigen PSI, Switzerland

Abstract

It is now well-established that for the generation of very high brightness beams, required for fourth generation light sources, it is highly advantageous to use injectors based on Radiofrequency photo-guns with very high peak electric fields on the cathode (>120 MV/m). This very high surface electric field leads to the generation of undesirable electrons due to the field emission effect. The emitted electrons can be captured and propagate along the Linac forming a dark current beam, leading to background radiation that can damage the instrumentation and radio-activate components. Consequently, it is important that the emission of these electrons, and their subsequent transportation, is carefully evaluated. Recently, in the framework of the I-FAST project, a high gradient, standing wave, C-band (5712 MHz) RF photogun has been designed and will be realized soon. In this paper, the results of dark current studies and simulations are illustrated. The transport efficiency and the spectrum of the dark current have been evaluated by Particle-In-Cell simulations for different cathode peak field values considering also the effect of the focusing solenoid on the dark current beam.

INTRODUCTION

A few years ago, an R&D activity on C-band (5712 MHz) Radio-Frequency (RF) Gun and a full C-band Injector [1, 2] has been started at INFN-LNF. Such a system is very promising in terms of achievable beam parameters, compactness and possibility to reach very high repetition rates (up to 1kHz). Recently, this activity received new impetus with its inclusion in the european I.FAST project. I.FAST is an initiative from the European Union Horizon 2020 Research program to develop the next generation of accelerator technologies. Crucial for future light sources is the continued development of electron sources to improve beam quality, in particular higher beam brightness, while also offering more compact and cost effective solutions. As part of this project, INFN is involved in the design, realization, and low and high power RF testing of a high gradient C-band RF photo-cathode gun. It is a Standing Wave (SW) RF normal conducting Gun which aims to achieve peak cathode gradients greater than 160 MV/m (Fig. 1). The final RF test of this SW prototype will be performed at PSI. Working at very high peak fields and gradients lead to the increase of 'field emitted' electrons from the metal surfaces exposed to the field. This so called Dark Current (DC) beam can lead to transverse kicks on bunches and can damage instrumentation and produce background radiation [3]. For this reasons it has to be carefully evaluated in order to properly design radiation protection systems for instrumentation and personnel. Below the design and layout of the C-band SW Gun will briefly presented and then the preliminary dark current studies performed on this new high gradient gun are reported.

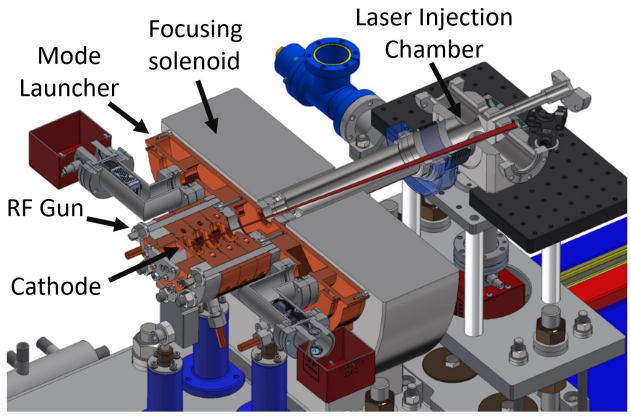

Figure 1: Section of the mechanical model of the C-band photo-injector with main components.

THE SW C-BAND GUN

To reach very high gradient fields, while keeping under control and reducing the breakdown rate (BDR), the C-band RF Gun has been designed to work with very short RF pulses (300 ns). For this purpose, the coupling coefficient β of the Gun coupling cavity has been increased and consequently also the required RF input power, taking into account the maximum sustainable reflected power. An industry-made RF isolator will be used to protect the source from the power reflected at the Gun input.

Working with such high field means that standard couplers cannot be used so a 4-port mode launcher has been integrated to lower the pulsed heating and to compensate the quadrupole field components due to the aperture in the gun cell. Design and beam dynamics simulations of this mode launcher are reported in [4,5]. In the last years many RF Gun, like the new SPARC_LAB RF Gun [6], have been fabricated with the clamping technique developed at the Frascati Laboratory of INFN demonstrating excellent performances, so the same technology has been chosen also for the realization of this gun. The clamping technology allows one to avoid

* This project has received funding from the European Union's Horizon 2020 Research and Innovation programme under GA No101004730 and INFN Commission V project TUAREG
† fabio.cardelli@lnf.infn.it

ISBN: 978-3-95450-227-1 ISSN: 2673-5490 doi:10.18429/JACoW-IPAC2022-MOPOMS021

THE NEW C BAND GUN FOR THE NEXT GENERATION RF PHOTO-INJECTORS

D. Alesini, F. Cardelli, G. Di Raddo, L. Faillace, M. Ferrario, A. Gallo, A. Giribono, A. Gizzi, S. Lauciani, A. Liedl, L. Pellegrino, L. Piersanti, C. Vaccarezza and A. Vannozzi
INFN-LNF, Frascati, Italy
M. Croia, ENEA, Casaccia, Italy
G. Castorina, AVO-ADAM, Meyrin, Switzerland
L. Ficcadenti and G. Pedrocchi, INFN Roma, Italy

Abstract

Rf photo-injectors are widely used in modern facilities, especially in FEL, as very low-emittance and high-brightness electron sources. Presently, the rf technology mostly used for guns is the S band (3 GHz) with typical cathode peak fields of 80-120 MV/m and repetition rates lower than 120 Hz. There are solid reasons to believe that the frequency step-up from S band to C band (~6 GHz) can provide a strong improvement of the beam quality due to the potential higher achievable cathode field (>160 MV/m) and higher repetition rate (that can reach the kHz level). In the contest of the European I.FAST project, a new C band gun has been designed and will be realized and tested. It is a 2.5 cell standing wave cavity with a four port mode launcher, designed to operate with short rf pulses (300 ns) and cathode peak field larger than 160 MV/m. In the paper we present the electromagnetic and thermo-mechanical design and the results of the prototyping activity with preliminary rf measurements.

INTRODUCTION

In the context of the X-band linacs of the EuPRAXIA@SPARC_LAB project [1] and XLS design study [2] the possibility to implement a full C-band injector is attractive for both the reachable beam parameters and compactness than for the possibility to operate at high repetition rate (up to 1 kHz). Since the peak field at the cathode (E_{cath}) is proportional to the achievable beam brightness [3], in the last generation of rf guns a great effort has been put to increase the field amplitude, and, at the same time, to reduce the breakdown rate probability (BDR) [4]. On the other hand, the possibility to operate such a gun at the kHz regime is very attractive for all mentioned projects. The realization and test of a C Band gun has been also funded by the EU in the framework of the I.FAST project [5] and by INFN Commission V. The gun, after its realization will be tested at PSI, Switzerland. In the present paper we illustrate the electromagnetic (e.m.) and thermo-mechanical design of the gun and the results of the prototyping activity. The gun is also attractive for its possible applications in upgrades of existing photo-injectors for FEL [6].

DESIGN CRITERIA OF THE GUN

The gun is a 2.5 cell structure and, as illustrated in [7], its design has been optimized in order to minimize the peak E field (E_{cath}), the modified Poynting vector (S_c) [8], the rf pulse length (t_p) and pulsed heating (ΔT) [9]. The gun has been designed with a coupling coefficient equal to 3 to allow operation with short rf pulses (300 ns) thus reducing the BDR, pulsed heating and the power dissipation. An elliptical profile of the iris with large aperture (diameter of 18 mm) has been also implemented to reduce the peak electric field, to increase the frequency separation with the nearest $\pi/2$-mode thus avoiding excitation of this mode with short rf pulses and to have a better pumping on the cathode cell. A four-port mode launcher [10, 11] with an on-axis coupling has been also adopted to reduce the pulsed heating on the coupler and to have a perfect compensation of the dipole and quadrupole field components. The mode launcher has been also designed to integrate two pumping ports. The e.m. design has been done with ANSYS [12] and the e.m. model is reported in Fig. 1 with the magnitude of the electric field. The final gun parameters are given in Table 1.

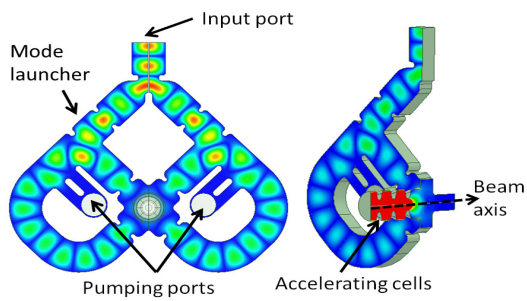

Figure 1: electromagnetic model of the gun.

Table 1: Main Parameters of the C-band Gun

Parameter	value
Resonant frequency	5.712
$E_{cath}/\sqrt{P_{diss}}$ [MV/(m·MW$^{0.5}$)]	51.4
rf input power [MW]	18
Cathode peak field [MV/m]	160
Rep. rate [Hz]	100 (400)
Quality factor	11900
Filling time [ns]	166
Coupling coefficient	3
rf pulse length [ns]	300
Mode sep. π-$\pi/2$ [MHz]	47
E_{surf}/E_{cath}	0.96
Mod. Poy. vector [W/μm^2]	2.5
Pulsed heating [°C]	16
Average diss. Power [W]	250 (1000)

ISBN: 978-3-95450-227-1 ISSN: 2673-5490 doi:10.18429/JACoW-IPAC2022-MOPOMS022

STUDIES OF A Ka-BAND HIGH POWER KLYSTRON AMPLIFIER AT INFN-LNF

M. Behtouei, B. Spataro, L. Faillace, INFN-LNF, Frascati, Italy
A. Leggieri, F. Di Paolo, F. Marrese, L. Valletti, S. Fantauzzi, Univ. di "Tor Vergata", Roma, Italy
G. Torrisi, Istituto Nazionale di Fisica Nucleare (INFN/LNS) Lab. Nazionali del Sud, Catania, Italy
M. Carillo[1], F. Bosco[1], A. Mostacci[1], L. Palumbo[1], M. Migliorati[1], INFN-Roma1, Rome, Italy
[1]also at SBAI, Sapienza University, Italy

Abstract

In the framework of the Compact Light XLS project [1], a Ka-band linearizer with electric field ranging from 100 to 150 MV/m is requested [2–4]. In order to feed this structure, a proper Ka-band high power klystron amplifier with a high efficiency is needed. This paper reports a possible solution for a klystron amplifier operating on the TM_{010} mode at 36 GHz, the third harmonic of the 12 GHz linac frequency, with an efficiency of 44% and 10.6 MW radiofrequency output power. We discuss also here the high-power DC gun with the related magnetic focusing system, the RF beam dynamics and finally the multiphysics analysis of a high-power microwave window for a Ka-band klystron providing 16MW of peak power.

INTRODUCTION

Recent developments in accelerator science require higher power at higher frequencies. At the state of the art no stand-alone power sources can respond to these requirements, with the exception of systems composed by large combination of several power sources and pulse compression devices like SLEDs and corrugated waveguide structures.

In this paper we develop the design of a Ka-band klystron amplifier with an efficiency of 44% providing 10.6 MW radiofrequency output power. The paper is organized as follows: section 1 reports the electron gun injector design and magnetostatic simulation performed with CST Particle Studio [5] , section 2 discusses the interaction structure which receives a beam current of 50 A and 480 kV with a beam radius of 1 mm confined in a drift tube of 1.2 mm radius. For the RF beam dynamics, the software KLyC [6] has been used. Much effort has been focused to obtain a sufficiently short structure suitable to accommodate a considerably narrow focusing magnet and to obtain the perveance needed for the required beam power output ensuring the maximum efficiency. In the section 3 we discusses the multiphysics analysis of a high- power microwave window for a Ka-band klystron providing 16MW of peak power.

ELECTRON GUN INJECTOR DESIGN AND MAGNETOSTATIC SIMULATION

The beam trajectory and the electric field equipotential lines are shown in Fig. (1a) and (1b). The cathode-anodes geometry was optimized to adjust the electric field equipotential lines to obtain a beam current extraction of 50A. Figs.

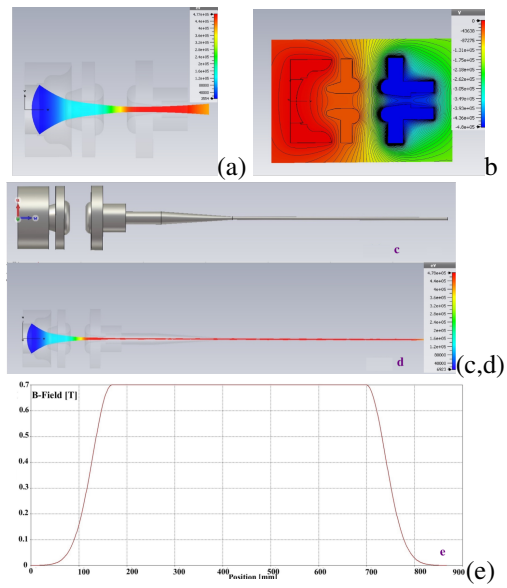

Figure 1: a) The dual anodes electron gun design from CST for a beam current of 50 A and the cathode-anode voltage of 480 kV. a) Beam trajectory b) equipotential lines c) 3D model of the gun d) beam trajectory along the propagation direction e) the axial magnetic field distribution.

(1c), (d) and (1e) show the 3D model of the gun and of the beam pipe, the beam trajectory along the propagation direction and the axial magnetic field distribution, respectively. The dual anode structure with an intermediate electrode allows us to overcome the strong space- charge force on the cathode and improve the transverse focusing [7], thus getting a low perveance. As a result, with this configuration, we are able to reduce the magnetic field value down to the normal conducting regime to confine the beam propagation in a pipe of 1.2 mm. This solution can be compared with our previous solution [8] using a magnetic focusing system working in superconducting regime. The magnetic field needed to compress the beam is reduced from 3.2 T to 0.7 T with this type of electron gun. The micro-perveance of this configuration is 0.15 $AV^{-3/2}$ which is a factor 2 less than the previous design [8]. The advantage of designing a low perveance electron gun is to get a weaker space charge, and, consequently, a stronger bunching. The maximum electric field on the focusing electrode is about 210 kV/cm almost the same of the previous configuration with standard anode.

ISBN: 978-3-95450-227-1 ISSN: 2673-5490 doi:10.18429/JACoW-IPAC2022-MOPOMS023

START-TO-END BEAM-DYNAMICS SIMULATIONS OF A COMPACT C-BAND ELECTRON BEAM SOURCE FOR HIGH SPECTRAL BRILLIANCE APPLICATIONS

L. Faillace, M. Behtouei, A. Giribono, B. Spataro, C. Vaccarezza, INFN-LNF, Frascati, Italy
L. Palumbo, F. Bosco, M. Carillo, L. Giuliano, M. Migliorati, A. Mostacci, Sapienza University of Rome Departement SBAI, Italy
J.B. Rosenzweig, O. Camacho, A. Fukasawa, N. Majernik, O. Williams, University of California, Los Angeles (UCLA) Department of Physics and Astronomy, USA
S. Tantawi, SLAC National Accelerator Laboratory, USA
R. Agustsson, D. Bruhwiler, I. Gadjev, S. Kutsaev, A. Murokh, RadiaBeam Technologies, USA

Abstract

Proposals for new linear accelerator-based facilities are flourishing world-wide with the aim of high spectral brilliance radiation sources. Most of these accelerators are based on electron beams, with a variety of applications in industry, research and medicine such as colliders, free-electron lasers, wake-field accelerators, coherent THz and inverse Compton scattering X/γ sources as well as high-resolution diagnostics tools in biomedical science. In order to obtain high-quality electron beams in a small footprint, we present the optimization design of a C-band linear accelerator machine. Driven by a novel compact C-band hybrid photoinjector, it will yield ultra-short electron bunches of few 100's pC directly from injection with ultra-low emittance, fraction of mm-mrad, and a few hundred fs length simultaneously, therefore satisfying full 6D emittance compensation. The normal-conducting linacs are based on a novel high-efficiency design with gradients up to 50 MV/m. The beam maximum energy can be easily adjusted in the mid-GeV's range. In this paper, we discuss the start-to-end beam-dynamics simulations in details.

INTRODUCTION

Electron beams with high peak currents and ultra-low normalized emittances, therefore ultra-bright, are essential for the new linear accelerator-based facilities promising numerous applications, such as electron-positron or photon-photon colliders [1,2], X-ray free-electron lasers [3,4], wakefield accelerator experimentation, coherent THz and inverse Compton scattering X-ray or γ-ray sources [5]. Other applications reside in the field of biomedical science, where low emittance photon beams are used to obtain high quality images for diagnostics due to the increased resolution and contrast they can provide [6, 7]. In order to obtain high brightness electron beams, photoinjectors [8-10], in which electron bunches are generated from the cathode metallic surface by illumination via a femtosecond-to-picosecond laser, have been the essential instrument in worldwide use for that last three decades.

RF DESIGN OF THE HYBRID PHOTOINJECTOR

The proposed *hybrid* RF photoinjector is composed of a photocathode embedded in an initial 2.5 gun cell standing-wave (SW) section connected through an input coupling cell directly to a traveling-wave (TW) section (see Fig. 1).

The are several advantages of this hybrid system compared with conventional split SW/TW injectors:

- Cancellation of RF reflections from the SW section (no circulator needed);
- Bunch lengthening effect, due to the ballistic drift, is reduced (the cell that couples the two structures replaces the long beam pipe and matching-section following the RF gun);
- The RF coupling between the SW and the TW sections optimally results in a 90 deg phase shift of the accelerating field → *strong velocity bunching* effect applied to the beam;
- Production of very short bunch lengths, over an order of magnitude smaller.

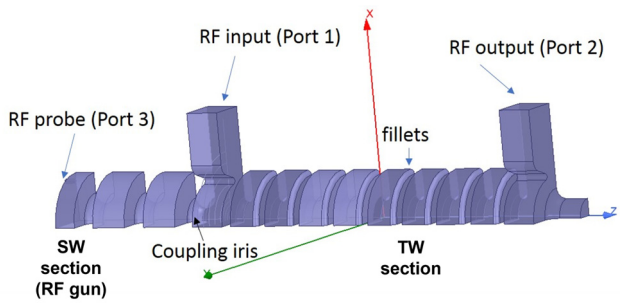

Figure 1: electromagnetic model of the gun.

The RF design was performed with the Ansys 3D code [11]. The main RF parameters are given in Table 1, and previously reported in [12-14]. The required rf input power is about 40 MW in order to obtain a peak surface electric field at the cathode equal to 120 MV/m. The ratio between the SW on-axis peak electric field and the average TW electric field is equal to $E_{z,p,SW}$ /⟨$E_{z,TW}$ ⟩ = 3.25, where

ISBN: 978-3-95450-227-1 ISSN: 2673-5490 doi:10.18429/JACoW-IPAC2022-MOPOMS025

PHOTOCATHODE PERFORMANCE CHARACTERISATION OF ULTRA-THIN MgO FILMS ON POLYCRYSTALLINE COPPER

C. Benjamin[1*], T. J. Rehaag, G. R. Bell, University of Warwick, Coventry, United Kingdom
H. M. Churn[2], L.B. Jones[2], T. C. Q. Noakes[2], ASTeC, STFC Daresbury Laboratory, United Kingdom
[1]also at ASTeC, STFC Daresbury Laboratory, United Kingdom
[2]also at Cockcroft Institute of Accelerator Science, Daresbury, United Kingdom

Abstract

The performance expected from the next generation of electron accelerators is driving research into photocathode technology as this fundamentally limits the achievable beam quality. The performance characteristics of a photocathode are most notably: normalised emittance, brightness and energy spread. Ultra–thin oxide films on metal substrates have been shown to lower the work function (WF) of the surface, enhancing commonly utilised metal photocathodes, potentially improving lifetime and performance characteristics.

We present the characterisation of two MgO/Cu photocathodes grown at Daresbury. The surface properties such as: surface roughness, elemental composition and WF, have been studied using atomic force microscopy (AFM), X-ray photoelectron spectroscopy (XPS) and ultraviolet photoelectron spectroscopy (UPS). The photoemissive properties have been characterised with quantum efficiency (QE) measurements at 266 nm. Additionally, we measure the Transverse Energy Distribution Curves (TEDC) for these photocathodes under illumination at various wavelengths using ASTeC's Transverse Energy Spread Spectrometer (TESS) and extract the Mean Transverse Energy (MTE).

INTRODUCTION

The development and improvement of the next generation electron sources require photocathodes with a high quantum efficiency (QE), low emittance, fast response times and robustness. The photoemissive properties of photocathodes are governed by its surface characteristics. The surface roughness and the work function (WF) strongly influence the quantum efficiency and intrinsic emittance. Metal photocathodes are predominantly used due to their high durability and fast response time. However, their relatively high WF leads to a low QE and the requirement for UV drive lasers [1].

The mean transverse energy (MTE) is a photoemissive property which is directly dependent on the excess energy in the photoemission process, where the excess energy is the difference between the photon energy and the WF of the sample. The MTE can be approximated using the model derived by Dowell and Schmerge [2]:

$$MTE = \frac{1}{3}(h\omega - \phi) \quad (1)$$

where $h\omega$ is the incident photon energy and ϕ is the WF of the photocathode, which was measured using ultraviolet photolectron spectroscopy (UPS) (see Table 1).

One possible method of improving the performance of photocathodes is by the use of surface preparation or treatment, lowering the surface WF and increasing the QE. Surface dielectric films on metals have been shown to produce a surface with a lower WF [3] and previous works [4, 5] on MgO thin films on Ag(100) have demonstrated this reduction in WF and the potential for QE enhancement. Therefore, MgO films have the potential to improve the QE, while simultaneously increasing the robustness of the sample due to the chemical stability of MgO forming an overlayer to protect from residual gases in the system.

EXPERIMENTAL DETAILS

Sample Preparation

Two 6 mm diameter polycrystalline copper cathodes, with a surface roughness of $R_a < 30$ nm, (labeled DaCB–7 and DaCB–14) were supplied by Surface Preparation Laboratory (SPL). Cathodes were cleaned *in situ* using cycles of Ar^+ bombardment (2 keV beam energy for 20 mins) and annealing at 500 °C, with surface contamination being assessed using X-ray photoelectron spectroscopy (XPS). Once clean, an ultra-thin MgO film layer was deposited by thermal evaporation of Mg in a Chell K-Cell Miniature Knudsen Evaporation Cell in an O_2 partial pressure of 5×10^{-7} mbar. Sample preparation, QE, XPS and ultraviolet photoelectron spectroscopy (UPS) were all conducted within the same UHV system with a base pressure of 3×10^{-9} mbar.

Surface Characterisation

XPS spectra were obtained using an non-monochromated Al K_α X-ray source (1486.7 eV) and a Thermo Alpha 110 analyser. The analyser transmission function was determined experimentally using the technique described by Ruffiuex et al. [6], and the WF of the analyser was measured using the Fermi edge of Ag. Core region spectra were acquired with a pass energy of 20 eV. Analysis was conducted using CasaXPS [7].

The surface roughness of DaCB–7 was measured using atomic force microscopy (AFM) conducted at the University of Warwick using a Bruker dimension icon AFM after all other work was completed. AFM scans over 10 μm × 10 μm and smaller were repeated over two locations on the surface. The photocathode was transported under ultra high vacuum conditions, exposed to maximum pressure of 5×10^{-10} mbar during transport. This reduced surface contamination and formation of hydroxides and carbonates.

* Christopher.Benjamin@warwick.ac.uk

ISBN: 978-3-95450-227-1 ISSN: 2673-5490 doi:10.18429/JACoW-IPAC2022-MOPOMS027

SYNTHESIS OF FIRST CAESIUM TELLURIDE PHOTOCATHODE AT ASTEC USING SEQUENTIAL AND CO-DEPOSITION METHOD.

R. Valizadeh, A.N. Hannah, STFC, WA4 4AD Warrington, UK
V.R. Dhanak, The University of Liverpool, L69 7ZF Liverpool, UK

Abstract

Caesium Telluride (Cs_2Te) photocathodes, are the electron source of choice, by many global accelerators such as European XFEL, FLASH and AWA. It offers high quantum efficiency and reasonable operational lifetime with lower vacuum requirements than multi-alkali photocathodes.

In this paper, we report on the first synthesised Cs_xTe photocathodes at ASTeC, using both sequential and co-deposition of Te and Cs on Mo substrate. Te deposition is carried out using ion beam deposition whilst the Cs is deposited using a SAES getter alkali. The ion beam deposition of Te provides a high degree of control to give a dense, smooth layer with a reproducible film thickness. The chemical state with respect to film composition of the deposited Cs_xTe is determined with in-situ XPS analyses. The films exhibit a quantum efficiency between 7.5 to 9% at 266 nm wavelength.

INTRODUCTION

The performance of a FEL is strongly related to the brightness of the electron beam generated by the photocathode. Hence, the performance of the cathode will be strongly dependent on its preparation, prior to its installation in the gun. The Linear accelerator CLARA [1], currently under development at the STFC Daresbury Laboratory will eventually drive a FEL facility in the future. At the commissioning stage, CLARA's Front End photo injector, is based on a 2.5 cell S-band photocathode RF gun, operating with a copper photocathode and driven by the third harmonic of a Ti: Sapphire laser (266 nm). It is installed in a dedicated thermally stabilized room. Light pulses with energies of up to 85 μJ are focused to a spot size of 1 mm with a timing length currently varying from 2 to 20 ps FWHM and a repetition rate of 10 Hz (eventually 400 Hz). Two class of photocathode types are envisaged to be used in CLARA mainly metallic or semiconductor.

Metallic photocathodes offer several clear advantages over semiconductor photocathodes. First, they are the most robust photocathodes against degradation caused by surface contamination and therefore do not require ultra-high vacuum conditions [1] and they can be cleaned inside the RF-gun. Second, they are robust against damage resulting from conditioning or heating. In addition, they can withstand high electric surface fields, such as those present at the cathode in RF accelerators, while other types of photocathode materials may suffer from electric breakdown. Other advantages of metallic photocathodes are their very short response time (less than picoseconds) and their very long lifetime (years or longer), which is much longer than other types of photocathodes. However, the main problem with metallic photocathodes is the rather low quantum efficiency (QE), even for UV radiation. This is due to their high reflectivity, and shallow escape depth due to electron-electron scattering. Semiconductor photocathodes have a much higher QE than metallic photocathodes, reaching values in the order of 10%. However, the lifetime is much shorter. The lifetime for semiconductor photocathodes is usually defined as the (operational) time over which the QE remains larger than 1% [2]. Another disadvantage is their high sensitivity to contamination by oxygen, CO_2 and water, which requires working in more stringent ultra-high vacuum conditions. Moreover, the response time is longer, typically in the range of tens of picoseconds. Alkali-telluride photocathodes have larger QE's and longer operational lifetimes than alkali-antimonide photocathodes. In addition, they offer the possibility of partial rejuvenation by means of heating. Among the alkali-telluride photocathodes, Cs_2Te is the most widely used one because of its relatively long potential lifetime (up to months [3]) and high QE compared to other semiconductor photocathodes [4-9]. A QE of 8 – 12% is consistently obtained at illumination with ~262 nm radiation under operational conditions (usually this means applying an RF field on the cathode while illuminating it with laser pulses, in 10^{-9} Torr vacuum conditions). Cs_2Te is less sensitive to contamination than alkali-antimonide photocathodes. In addition, it has a comparatively shorter response time (~ ps), a higher current density and a lower dark current than most other semiconductor photocathodes.

At ASTeC, the operation of CLARA has been based on metal photocathodes, however, for the future operation as a FEL injector, there is need to produce photocathodes based on Alkali-telluride. For that purpose, we have designed a new photocathode preparation facility, capable of producing a variety of photocathodes ranging from metal, metal/oxide, and caesium implanted metal to Alkali-telluride/antimonide. The versatility of the system is based on the ion beam deposition and ion beam implantation. We will report on the synthesis of Cs_xTe photocathodes, both in concurrent and sequential mode.

CATHODE PREPARATION

Molybdenum foil, 0.5 mm thick, is cut into disks and degreased in acetone, methanol and deionised water sequentially in an ultrasonic bath. The disks are dried and clamped into self-heating stubs and then introduced into a load lock, which is baked overnight, to bring the base pressure in 10^{-9} mbar. The Mo substrate is transferred on a linear sample drive, into the analysis chamber, where it is ion beam sputter cleaned to remove all oxides and carbon from the surface. Next, it is transferred to the deposition chamber and is placed onto the sample holder with the wobble stick. The

ISBN: 978-3-95450-227-1 ISSN: 2673-5490 doi:10.18429/JACoW-IPAC2022-MOPOMS028

STABILITY AND LIFETIME STUDIES OF CARBON NANOTUBES FOR ELECTRON COOLING IN ELENA

B. Galante[1, 2, 3*], G. A. Tranquille[1], C. P. Welsch[2, 3], J. Resta López[2, 3, 4]
[1]CERN SY-BI-XEI, Geneva, Switzerland
[2]The University of Liverpool, Liverpool, United Kingdom
[3]The Cockroft Institute, Sci-Tech Daresbury, Warrington, United Kingdom
[4]ICMUV-Institute of Materials Science, University of Valencia, Spain

Abstract

Electron cooling guarantees beam quality in low energy antimatter facilities. In the Extra Low ENergy Antiproton ring (ELENA), the electron cooler reduces the emittance blow-up of the antiproton beam so that a focused and bright beam can be delivered to the experiments at the unprecedentedly low energy of 100 keV. To achieve a cold beam at such low energy, the electron gun must emit a mono-energetic and relatively intense electron beam. An optimization of the electron gun involving a cold cathode is studied to investigate the feasibility of using carbon nanotubes (CNTs) as cold electron field emitters. CNTs are considered among the most promising field emitting materials. However, stability data for emission over hundreds of hours, as well as lifetime and conditioning process studies to ensure optimal performance, are still incomplete or missing. This contribution reports experiments aimed at characterizing these properties and assessing whether CNTs are suitable to be used as cold electron field emitters for many hundreds of hours.

INTRODUCTION

In ELENA the antiprotons coming from the Antiproton Decelerator (AD) with a kinetic energy of 5.3 MeV are decelerated to 100 keV [1]. Due to the deceleration process, intra-beam scattering and scattering with residual gas, the beam emittance, or transverse energy, rapidly increases leading to losses and a poor-quality beam. The electron cooling process takes place twice during the beam cycle and permits to reduce the antiproton beam emittance. During the two cooling plateaus the electron beam energy and current are E = 355 eV, I = 5 mA (first plateau), and E = 55 eV, I = 1 mA (second plateau) [2]. The thermionic gun currently used in operation limits the cooling performance due to the relatively high transverse energy of the emitted beam (> 100 meV). This is motivated by the required appliance of a high temperature enable the electron emission. The use of a cold cathode could bring several benefits regarding both the electron beam energy and the gun layout simplicity. Field emitting carbon nanotubes (CNTs) can be a promising option for fulfilling this task. CNTs are considered as the most promising field emitting materials as they can emit relatively high currents while being mechanically stable and chemically inert [3, 4]. Among all possible CNT arrangements, after several studies and tests we have chosen to focus our investigation on an honeycomb-like array, as shown in Fig. 1 [5, 6]. The CNT samples were then characterised with tests of stability, lifetime and performance during current switching in order to assess the feasibility of using such a cathode in the electron gun of ELENA's electron cooler.

EXPERIMENTS

To characterise CNT samples an apposite test bench was designed and developed, the cold cathode test bench (CCTB). The CCTB consists of a vacuum system where an experimental setup in diode configuration has been designed for each flange. The diode configuration is composed of a CNT sample, the cathode, and a Molybdenum plate, an anode. The two are 800 μm far and separated by a mica insulating spacer/mask with a center hole for allowing passage of the electron beam and delimiting the emission surface. The electrical connections are realised by means of Kapton/Copper wires and SHV feedthroughs for in-air connections. The cathode is then connected to a HV power supply and the anode to a digital multimeter for current measurements. In such a way it was possible to make DC measurements in order to test stability and lifetime of our samples [5, 6]. Furthermore, we developed a hardware current switching system for testing the current emission in pulsed mode. In ELENA, in fact, the electron beam must be turned on and off depending on the beam cycle of the antiproton beam. The current switching system was based on a Behlke push-pull [7], and the voltage on the cathode was switched between HV and ground. In this case the anode was connected to a shunt resistor and ultimately an oscilloscope was used to measure the current output as a voltage drop on the shunt resistor via the classic Ohm's law.

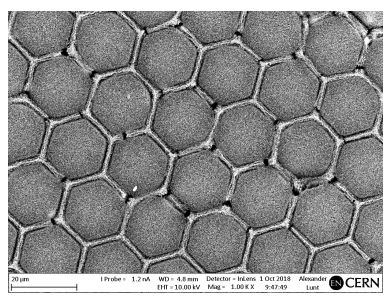

Figure 1: SEM image of a CNT honeycomb-like array.

* bruno.galante@cern.ch

ISBN: 978-3-95450-227-1 ISSN: 2673-5490 doi:10.18429/JACoW-IPAC2022-MOPOMS029

HPC MODELING OF A HIGH-GRADIENT C-BAND LINAC FOR HARD X-RAY FREE-ELECTRON LASERS*

T. B. Bolin†, S. I. Sosa, S. G. Biedron[1,2] Department of Electrical and Computing Engineering,
University of New Mexico, Albuquerque NM 87131, USA
[1]also at Department of Mechanical Engineering,
University of New Mexico, Albuquerque, NM 87131, USA
[2]also at Element Aero, Chicago, IL 60643, USA

Abstract

During the last decade, the production of soft to hard x-rays (up to 25 keV) at XFEL (x-ray free-electron laser) facilities has enabled new developments in a broad range of disciplines. However, there is great potential for new scientific discovery at even higher energies (42+ keV), such as those that can be provided by MaRIE (Matter-Radiation Interactions in Extremes) at Los Alamos National Laboratory. These instruments can require a large amount of real estate, which quickly escalates costs: The driver of the FEL is typically an electron beam linear accelerator (LINAC) and the need for higher electron beam energies capable of generating higher energy X-rays can dictate that the LINAC becomes longer. State of art accelerating technology is required to reduce the LINAC length by reducing the size of the cavities, which in turn provides for a high gradient of acceleration. Compact accelerating structures are also high-frequency (S, C, and X-bands). Here, we describe using the Argonne Leadership Computing Facility (ALCF), located at Argonne National Laboratory [1] to facilitate our investigations into design concepts for future XFEL high-gradient LINAC's in the C-band (~4-8 GHz). We investigate a Disk Loaded Wave Guide (DLWG) traveling wave (TW) structure modeled for operation at f =5.712 GHz as modelled at the ALCF using VSim software. We used an existing account under the LIGHTCONTROL project at the ALCF.

INTRODUCTION

X-ray Free Electron Lasers (XFEL) are driven by a high energy electron linear accelerator, where the need for higher energy X-rays requires higher electron beam energies. To first order, this requires longer LINACs and larger infrastructure, which quickly makes the costs prohibitive. Next generation XFELs, such as FEL projects planned at LANL [2] and UCLA [3], will take advantage of high-gradient, compact accelerating structures in the C and X-band frequency regimes, which will allow a better use of the available physical space.

The C-band frequency band ranges from 4 to 8 GHz. In this regime, cavity dimensions are on the order of a few centimeters, making them very compact as compared to cavities used in previous generation light sources. Design concepts have been discussed in [4]. It has been established that C-band design considerations must be incorporated into the actual design by using 3D EM simulations. As systems become more complex and structures require refinement, especially in a regime where particle beams must be optimized, increasing the amount of computing power needed to efficiently carry out simulations.

C-band Cavity Design

We are using VSim to investigate different geometries for accelerator applications at a C-band frequency [5]. A DLWG C-band accelerating structure is presented in Figure 1. Table 1 shows the dimensions of the array.

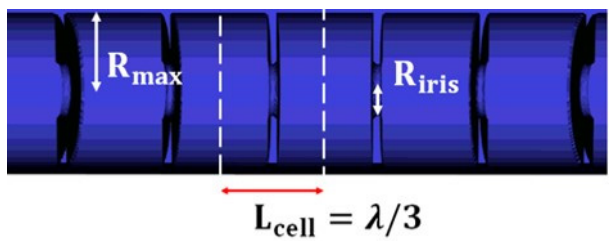

Figure 1: DLWG cavity array.

The DLWG is essentially a cylindrical waveguide structure with an added periodic array of disk loads that reduce the phase velocity of the travelling wave to match with the electron beam velocity. This structure is equivalent to a multi-cell cylindrical (pillbox) cavity. The DLWG structure has a cell length equal to $\lambda/3$ to match the phase velocity of the travelling electromagnetic wave to the velocity of relativistic electrons. This corresponds to a $2\pi/3$ phase advance between adjacent cells. The design concepts should accommodate multiple considerations including high accelerating gradient, low field breakdown rates, various fabrication techniques, choice of material, and the possibility of cryocooling [6]. Here we briefly describe the procedure to submit VSim simulations to the Argonne Leadership Computing Facility and show a simple figure as generated via the ALCF representing preliminary electromagnetic considerations of the DLWG array.

* This work was performed under Contract No. 89233218CNA000001, supported by the U.S. Department of Energy's National Nuclear Security Administration, for the management and operation of Los Alamos National Laboratory (LANL). This research also used resources of the Argonne Leadership Computing Facility, a DOE Office of Science User Facility supported under Contract DE-AC02-06CH11357.
† tbolin@unm.edu.

ISBN: 978-3-95450-227-1 ISSN: 2673-5490 doi:10.18429/JACoW-IPAC2022-MOPOMS032

COMPACT-TWO-OCTAVE-SPANNING PERPENDICULAR KICKER OF MeV ELECTRONS BASED ON A CUBIC MAGNET DIPOLE ARRAY

T. Rohwer† [1,2], P. Vagin[1], R. Bazrafshan[1,4], N.H. Matlis[1,2], F.X. Kaertner[1,2,3,4]
[1]Deutsches Elektronen Synchrotron (DESY), Hamburg, Germany
[2]also at Center for Free Electron Science (CFEL), Hamburg, Germany
[3]also at The Hamburg Center for Ultrafast Imaging
[4]also at University of Hamburg, Hamburg, Germany

Abstract

New compact particle acceleration structures, including but not limited to plasma, THz and direct laser driven accelerators, have in common that they cover a wide energy range of potential final energies and often show a large energy spread. Moreover, they may initially have a rather large emittance. To analyse the energy range of a single shot and/or to deflect the beam to safely dump the electrons away from an end-station requires an electron kicker covering a large energy range. Here, we present a magnetic dipole structure based on a 2D Halbach array. For the current experimental test accelerator in AXSIS, an electron beam in the energy range from 4 to 20 MeV is deflected by 90 degree and energetically dispersed. In direct contrast to a simple magnetic dipole, an array of cubic magnet blocks with tailored magnetization directions allows a focusing of the beam for both longitudinal and transverse directions at 90-degree bend. An genetic algorithm optimizes the magnetic field array to the predefined deflection angle and divergence. The modular array structure, in combination with the algorithm enables a simple exchange of magnets to adapt for different beam parameters.

INTRODUCTION

X-ray light sources based on large-scale linear accelerators (LINAC's), known as Free Electron Lasers have made a tremendous impact to the scientific community due to their ability to produce ultrashort (femtosecond) and ultrabright pulses that allow single shot diffractive imaging before the sample is altered.

Tremendous effort is currently put into the development of significantly more compact LINAC's by replacing the RF acceleration with plasma, THz or direct laser-driven structures. The benefits are, besides the more attractive size and costs, the potential to generate even shorter pulses in the attosecond regime. One side effect of the more compact LINAC design is that the radiation safety becomes more challenging. The electron beam and its secondary radiation is supposed to be blocked before the x-ray end station that is by design concepts only a few meters away from its generation point to maintain: a short pulse duration (lateral focussing), a good transverse focussing and to improve the overall stability. e.g., for the case of the THz powered accelerator AXSIS [1] at DESY, the entire accelerator including the experimental end-station is placed on a 10 m long granite block to circumvent any auxiliary vibrations. The area on the granite is then separated into an accelerator lab and an x-ray hutch with different radiation safety measures. Thus, the electron beam needs to be bent significantly away from the x-ray hutch by a single compact device.

Additional complexity comes from the fact that the possible beam parameters in terms of safety of these test accelerators using new acceleration techniques have to be considered to have a large energy spread and relatively large emittance as long as experimental results of these parameters are unknown.

DESIGN REQUIREMTS

The aforementioned conditions motivated us to design a bending magnet for the electron beam at 90 degrees. This way, the secondary radiation of the beam dump will stay in the accelerator lab and no direct radiation will hit the divider wall to the x-ray hutch. The challenge is that a full energy spectrum up to the maximum energy of 20 MeV has to be considered. This fixed full energy range, the compact design requirement and safety considerations all favour a permeant magnet kicker over an electromagnetic one.

A simple dipole with an exit surface of 45 degree with respect to the incident beam is a good starting point since the higher energies will propagate longer in the effective field such that all of the electrons do close to a quarter circle (90 degree) bend only limited by fringe fields, Fig. 1.

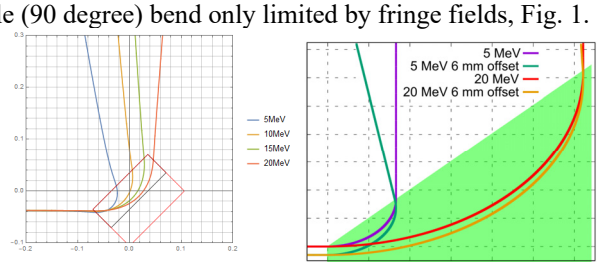

Figure 1: A dipole magnet at 45 degree with the correct field will result in about a quarter circle (90 degree) bending. However, this is very sensitive to offsets.

However, the potential divergence as well as offsets of the beam will result in different emission angles for both, within the plane of curvature and out of plane. This out-of-plane component is of particular importance since the high-energy electrons might hit the magnet and cause radiation damage, i.e., demagnetize it.

* This work has been supported by the European Research Council under the European Union's Seventh Framework Programme (FP7/2007-2013) through the Synergy Grant AXSIS (609920).
† timm.rohwer@desy.de

ISBN: 978-3-95450-227-1 ISSN: 2673-5490 doi:10.18429/JACoW-IPAC2022-MOPOMS033

EMITTANCE MEASUREMENTS OF NANOBLADE-ENHANCED HIGH FIELD CATHODE

G. E. Lawler*, N. Montanez, J. Mann, N. Majernik, J.B. Rosenzweig,
UCLA, Los Angeles, California, USA
V. Yu, RadiaBeam Technologies, Santa Monica, California, USA

Abstract

High brightness cathodes are increasingly a focus for accelerator applications ranging from free electron lasers to ultrafast electron diffraction. There is further an increasing interest in fabrication and control of cathode surface to better control the emission characteristics and improve beam brightness. One method which we can consider is based on well-known silicon nanofabrication techniques which we use to create patterned cathode surfaces. The sharp edges produced lead to field emission increases and high brightness emission. We have demonstrated that a beam can be successfully extracted with a low emittance and we have reconstructed a portion of the energy spectrum. Due to the simplicity of extended geometries in nanofabrication our beam uniquely possesses a high aspect ratio in its transverse cross section. We can begin to consider modifications for emittance exchange beamlines and having shown the patterning principle is sound we can consider additional patterns such as hollow beams. Future work will continue to characterize the produced beam and the addition of fabrication steps to remove one of the blades in the double blade geometry in order to more accurately characterize the emission.

INTRODUCTION

The National Science Foundation Center for Bright Beams is currently exploring the limits of electron beam brightness for many applications including free electron lasers, ultrafast electron diffraction, etc. One route is to increase initial brightness at the cathode through nanofabrication of cathode surfaces by reducing the emission area. We are inspired by nanotips used for electron microscopy where incident laser fields along with geometry-based field enhancement lead to electron emission via tunneling [1].

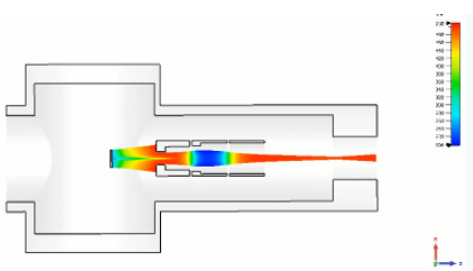

Figure 1: Cross section of vacuum chamber with electrostatic einzel lens and with example particle trajectories.

Electron rescattering processes (denoted here by the cartoon schematic in Fig. 1) after emission increase the energy of the electrons notably. Tips work well but one major drawback is the damage they sustain at higher laser intensities. The current field limits are in the 10−20 GV/m range. Instead we opt for a more robust extended geometry which is shown in the micrograph in Fig. 2. The larger surface area allows for more robustness to laser illumination and can allow us to extract higher charge which is applicable to the needs of higher current accelerators. Our recipe and further explanation for the double blade geometry are historical and further information can be found in [2, 3]. We intend to quantify the intrinsic emittance from these nanoblades in order to continue to expand the space of possible applications these cathodes.

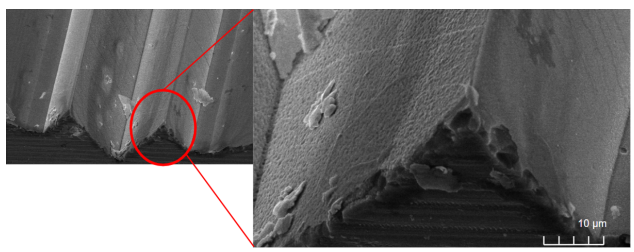

Figure 2: SEM image of nanoblades at ×5000 zoom.

EXPERIMENT

Einzel Lens

For simplification of the setup we can use a single einzel lens focusing our high aspect ratio beam on a multi-channel plate (MCP) and phosphor screen about 25 cm away from the cathode source. There does not exist a closed form solution of the focal length of a three element einzel lens but we can, for comparison, consider the limit where the lens distance is much greater than the aperture $l \gg a$ and thus can obtain a usable expression.

$$\frac{1}{f} = \frac{3\kappa^2(4-\kappa^2)}{8l(1+\kappa)} \quad \text{where} \quad \kappa = \sqrt{\frac{V_1+V_0}{V_0}} - 1 \qquad (1)$$

With regards to the experimental setup, we illuminate our cathodes with an 800 nm, 35 fs pulse of the given peak intensities and spot size. Upstream of the blade sample location we have optics to control laser fluence, polarize the beam normal to the blade surface, and focus on the sample. Downstream we have a CCD camera for initial

* gelawler@physics.ucla.edu

ISBN: 978-3-95450-227-1 ISSN: 2673-5490 doi:10.18429/JACoW-IPAC2022-MOPOMS034

MATERIAL NORMAL ENERGY DISTRIBUTION FOR FIELD EMISSION ANALYSES FROM MONOCRYSTALLINE SURFACES*

J. I. Mann†, Y. Li, J. B. Rosenzweig, UCLA, Los Angeles, CA 90024, USA
J. K. Nangoi, T. Arias, Cornell University, Ithaca, NY 14850, USA

Abstract

Electron field emission is a complicated phenomenon which is sensitive not only to the particular material under illumination but also to the specific crystalline orientation of the surface. Summarizing the ability for a crystal to emit in a particular direction would be of great use when searching for good field emitters. In this paper we propose a material normal energy distribution which describes the ability of the bound electrons to tunnel under an intense electric field. This framework breaks a computationally expensive 3-D system down to a source distribution representation applicable for more efficient 1-D models. We use the Fowler-Nordheim framework to study the yield and MTE (mean transverse energy) from sources including gold, copper, and tungsten in both monocrystalline and polycrystalline forms. We find an increase in effective work function for field emission in the (111) direction for gold and copper associated with the Bragg plane intersections of the Fermi surface.

INTRODUCTION

Electrons are commonly sourced through field emission. Nanotips, for instance, are used in a static field emission setup for electron microscopy [1]. Field emission is also the culprit of dark current [2] and may lead to breakdown [3] in RF cavities. Strong laser field emission is a growing topic of interest where a nanostructured cathode is used to enhance laser fields to field-emitting regimes [4].

Field emission is typically analyzed in 1-D using the Fowler-Nordheim (FN) framework [5] where each electron impinging on the surface has a probability of tunneling and emitting. This probability, for a transversely isotropic surface potential, is invariable on the transverse momentum and is therefore only dependent on the normal energy, summarized by the vacuum motive energy $M(x) = U(x) - E_n$ with U the vacuum potential and E_n the energy directed normal to the surface. The motive energy is integrated within the classically forbidden region to determine the tunneling probability. It is thusly important to understand the distribution of source current within the material with respect to the normal energy when finding the field emission current.

The FN model for field emission is typically considered using an isotropic free electron gas (FEG) scheme. In this case, there is a constant current density in energy space, permitting simple analytical results in the limits of low or high field strength [5]. However, we do not expect all crystalline surfaces to behave like a FEG in field emission. We thus propose a material normal energy distribution (MNED) which embodies the electron density or normal current density as a function of the energy directed towards the surface E_n.

The MNED for the FEG at zero temperature is found by integrating over slices of the Fermi sphere,

$$\frac{dj}{dT_n} = \frac{E_f - T_n}{2\pi^2} = -\frac{1}{2\pi^2}E_n \tag{1}$$

where $T_n \in [0, E_f]$ is the normal-directed kinetic energy, E_f is the Fermi energy of the material, and E_n is the normal energy relative to the Fermi level. Eqs. (1) and (2) are in Hartree atomic units (a.u.) with $\hbar = m_e = -q_e = 1$.

The MTE (mean transverse energy) as a function of the normal energy is found to be,

$$\mathrm{MTE}(T_n) = \frac{1}{2}(E_f - T_n) = -\frac{1}{2}E_n \tag{2}$$

and it is conserved in our model between bulk and vacuum due to transverse momentum conservation.

METHODS

We use density-functional theory (DFT) to determine the MNED of real materials through two approaches: slab and bulk calculations. The former is used as a direct, but coarse, calculation of the MNED so that we may verify our bulk calculation results, which attain a much higher resolution by employing some basic assumptions for an indirect approach. This verification is done only for Au (100) and (111).

We use the code JDFTx [6] for all DFT calculations. We use SG15 norm-conserving pseudopotentials [7] for all ions and the Perdew-Burke-Ernzerhof GGA exchange-correlation (XC) functional [8].

Slab System Analysis

The Au (100) and (111) slab systems consist of 15 layers where the outermost 6 layers' positions are optimized. The vacuum separation between the periodic slabs' outermost layers is 46.26 a.u. in length, about 6 lattice constants, before optimization. This slab system allows us to directly calculate the wavefunction decay rate in vacuum, κ, which may then be related to the normal energy (relative to the Fermi level) by $E_n = -\frac{1}{2}\kappa^2 + W$ for bound electronic states. To find a single value for κ for each eigenstate we average the modulus of the wavefunction in the transverse dimensions. We fit an exponential to the wavefunction starting where the potential is within 0.8 eV of vacuum level and ending before the wavefunction's magnitude falls below the noise floor.

* This research is supported by the Center for Bright Beams, U.S. National Science Foundation grant PHY-1549132.
† jomann@physics.ucla.edu

ISBN: 978-3-95450-227-1 ISSN: 2673-5490 doi:10.18429/JACoW-IPAC2022-MOPOMS036

SIMULATIONS OF LASER FIELD EMISSION FROM NANOSTRUCTURES WITH IMAGE CHARGE TRAPPING AND BAND STRUCTURE TRANSITIONS*

B. Wang†, G. E. Lawler, J. I. Mann, J. B. Rosenzweig, UCLA, Los Angeles, CA 90024, USA
S. Karkare, Arizona State University, Tempe, AZ 85287, USA
J. K. Nangoi, T. Arias, Cornell University, Ithaca, NY 14850, USA

Abstract

Laser-induced field emission from nanostructures as a means to create high brightness electron beams has been a continually growing topic of study. Experiments using nanoblade emitters have achieved peak fields upwards of 40 GV/m, begging further investigation in this extreme regime. A recent paper has provided analytical reductions of the common semi-infinite Jellium system for pulsed incident lasers. We utilize these results as well as similar previous results to further understand the physics underlying electron rescattering-type emissions. We progress in numerically evaluating the analytical solution to attempt to more efficiently generate spectra for this system. Additionally, we use the full 1-D time-dependent Schrödinger equation with a Hartree potential and a dispersion-relation transition from material to vacuum to study the same system. We determine what importance the inclusion of the material band structure may have on emissions using this computationally challenging approach.

INTRODUCTION

The bright, coherent electron beams that can be generated from nanoscale emitters have proven to be useful for such applications as electron microscopes [1], electron interferometry, nanometric imaging, synchrotrons [2], and more. A popular choice of nanostructure for electron emission, the nanotip, suffers from material breakdown when subjected to peak surface fields on the order of 10 GV/m [3, 4]. This problem of material breakdown is mitigated by the usage of a similar nanostructure, the nanoblade, which is essentially an extruded nanotip. Due to its improved thermomechanical properties, the nanoblade can survive peak surface fields over 40 GV/m and potentially even up to 80 GV/m [5, 6], allowing for higher current densities.

To investigate electron emission from nanoblades, we solve the 1-D time-dependent Schrödinger equation (TDSE), making use of recently published analytical solutions. We also perform finite difference numerical simulations investigating the effects that a collective image potential and the material's effective mass have on yields.

ANALYTICAL SOLUTION FROM REF. [7]

We use the analytical solution [7] to the TDSE,

$$i\partial_t\psi(x,t) = -\frac{1}{2}\Delta\psi(x,t) + \Theta(x)(U - Ex\cos(\omega t))\psi(x,t) \quad (1)$$

derived in Ref. [7] with the laser energy $\omega = 1.55\,\text{eV} = 0.0570$ atomic units (a.u.), total metallic potential depth $U = 10\,\text{eV} = 0.3676$ a.u., and Fermi energy $E_f = 4.5\,\text{eV} = 0.165$ a.u. to represent a gold cathode under the illumination of an 800 nm laser. In this model, the uniform cosine laser field is turned on instantaneously at $t = 0$.

The resulting yield curves exhibit the expected fourth power yield to laser intensity scaling for four-photon emission. The deviation from this power law at higher laser intensities is indicative of channel closing [8]. These features are corroborated by Fig. 4 in Ref. [9].

The difficulties that we encountered were related to computational complexity, as the required computation time increased dramatically with the temporal boundary and the electric field magnitude, which made calculations for longer periods and/or higher fields take much longer than numerical simulation. This difficulty was compounded by the fact that, in Eq. (1), there is a discontinuity caused by the instantaneous application of the cosine field at $t = 0$, which makes the results from the first few periods largely nonphysical. The termination time then needs to be somewhat large to find the asymptotic current. Reference [10] covers these findings in more detail.

ANALYTICAL SOLUTION FROM REF. [11]

A more recent paper [11] analytically solves the TDSE for periodic Gaussian pulses, so that the applied laser field is of the form,

$$F(t) = F_0 + F_1 e^{-t^2/\sigma^2}\cos(\omega t + \phi) \quad (2)$$

which resolves the discontinuity difficulty of Eq. (1). We use same parameters as before as well as static field $F_0 = 0$, carrier envelope phase (CEP) $\phi = \frac{\pi}{2}$, full-width at half-maximum (FWHM) power $\tau_p = \frac{10\pi}{\omega}$ (5 periods), and $m = 20$ cycles between pulses. Again the yield curve exhibits the expected fourth power yield to laser intensity scaling for four-photon emission, however we experience numerical issues at higher fields starting at around $F_1 = 10\,\text{V/nm}$, as can be seen in the yield curve in Fig. 1. For channel closing to be the culprit, we would expect to find a periodic drop in

* This research is supported by the Center for Bright Beams, U.S. National Science Foundation grant PHY-1549132.
† benjaminwang1@g.ucla.edu

ISBN: 978-3-95450-227-1 ISSN: 2673-5490 doi:10.18429/JACoW-IPAC2022-MOPOMS039

STUDY OF MATERIAL CHOICE IN BEAM DUMPS FOR ENERGETIC ELECTRON BEAMS

D. Zhu*, Y.-R. E. Tan, R. T. Dowd, ANSTO Australian Synchrotron, Clayton, Australia

Abstract

Lead is typically used as the initial target in a design for beam dumps for high energy electron beams (>20 MeV). Electron beams with energies above 20 MeV are usually built within concrete bunkers and therefore the design of any beam dump would just be a lead block (very cost effective) as close to the electron source as possible, after a vacuum flange of some sort. In a study of a hypothetical 100 MeV electron beam inside a concrete bunker with an extremely low dose rate constraint outside the bunker, the thickness of lead required would have been too restrictive for a compact design. In this study we investigate the potential benefits of designs that incorporate low Z materials like graphite as the primary target material in vacuum followed by progressively higher Z materials up to lead. The results show the more diffuse elastic scattering from the primary target reduces the back scattered photons and reduces the overall neutron generation. The effect was a more compact design for the beam dump to meet the same dose rate constraint.

THE AUSTRALIAN SYNCHROTRON 100 MeV LINAC

The Australian Synchrotron Light Source (ASLS) uses a full energy injector system comprising of a 100 MeV linac and 3 GeV booster synchrotron to inject beam into its 3 GeV storage ring. The linear accelerator (or linac) accelerates the electron beam to an energy of 100 MeV over about 10 metres. The linac operates in either long-pulse mode, in which up to 4 nC is generated in a bunch train of up to 150 ns with repetition rate 1 Hz, or in 1 ns short-pulse mode, in which a single bunch of up to 0.5 nC is delivered [1]. The linac is distributed inside the linac tunnel. During machine study time, the 100 MeV electron beam can be extracted for radiological study.

THE FLUKA SIMULATION CODE

In this research, the FLUKA code is used to simulate the radiological environment in the linac tunnel. FLUKA is a Monte Carlo code for calculations of particle transport and interactions with matter, covering an extended range of applications spanning from proton and electron accelerator shielding to target design, calorimetry, activation, dosimetry, detector design, accelerator driven systems, cosmic rays, neutrino physics, radiotherapy etc. [2, 3]. It has the best physics models in terms of completeness and precision, through a microscopic approach where each step has sound physics bases. FLAIR acts as an intermediate layer between the user and FLUKA. The integration of FLUKA with FLAIR provides an advanced user-friendly interface.

* dajunz@ansto.gov.au

ELECTRON BEAM INTERACTION WITH LEAD AND GRAPHITE

A geometry was created in FLUKA for the simulation of electron beam interacting with different shielding materials. The linac bunker dimensions and concrete wall thicknesses are the same as in the linac tunnel, but the target and the local shielding differs significantly. The bunker is with 100 cm thickness for the walls and 50cm thickness for the roof. The type of concrete used was Portland mixture which has a density of 2.34 g/cm^3. To change the units from 'per electron' to 'per hour' the number of electrons expected to be emitted by the electron source in one hour of constant operation is required. The number of electrons emitted by the 100MeV, 4 nC per pulse, 1 Hz repetition rate election source is 2.5×10^{10} electrons per hour. In the simulation coordinate system, X is the inboard-outboard horizontal direction, Y is the vertical direction, Z is the beam direction.

First, the penetration of electron in lead and graphite is compared. The target is a 50cm×50cm×50cm cubic block placed approximately 10 cm downstream of primary electron emitted position. The target material is lead and graphite respectively.

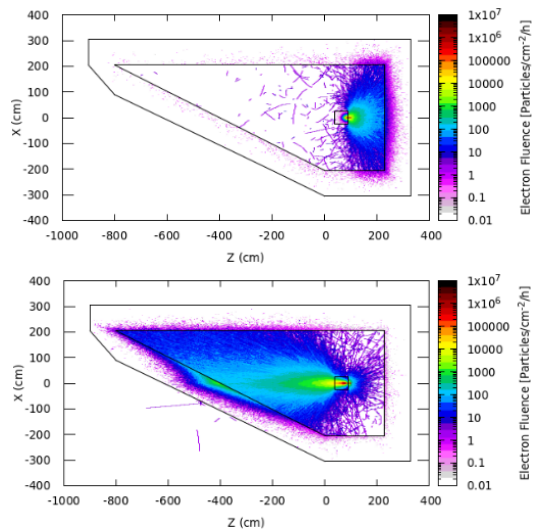

Figure 1: Electron fluence from different target, lead(top) and graphite (bottom).

Figures 1-4 provide electron fluence (track-length density), photon fluence, neutron fluence, and effective dose rate equivalent maps on horizontal cross section of the tunnel at beam height. In each figure, the top one is for lead target and bottom one is for graphite target.

From the simulation results as showing in Fig. 1, electron beam can easily penetrate through the graphite block, but the lead will stop electron after about 25 cm

ISBN: 978-3-95450-227-1 ISSN: 2673-5490 doi:10.18429/JACoW-IPAC2022-MOPOMS040

RADIATION SHIELDING DESIGN FOR THE X-BAND LABORATORY FOR RADIO-FREQUENCY TEST FACILITY –X-LAB– AT THE UNIVERSITY OF MELBOURNE

M. Volpi*[1], D. Banon-Caballero[2], M. Boronat[3], N. Catalan-Lasheras[3], R. Dowd[4], R. P. Rassool[1]
S.L. Sheehy[5,1], G. Taylor[1], S.D. Williams[1]

[1]The University of Melbourne, Melbourne, Australia
[2]IFIC, Universidad de Valencia, Valencia, Spain
[3]CERN, Geneva, Switzerland
[4]AS - ANSTO, Clayton, Victoria, Australia
[5]ANSTO, Kirrawee DC New South Wales, Australia

Abstract

Here we report radiation dose estimates calculated for the X-band Laboratory for Accelerators and Beams (X-LAB) under construction at the University of Melbourne (UoM). The lab will host a CERN X-band test stand containing two 12 GHz 6 MW klystron amplifiers. By power combination through hybrid couplers and the use of pulse compressors, up to 50 MW of peak power can be sent to any of to either of the two test slots at pulse repetition rates up to 400 Hz. The test stand is dedicated to RF conditioning and testing CLIC's high gradient accelerating structures beyond 100 MV/m. This paper also gives a brief overview of the general principles of radiation protection legislation; explains radiological quantities and units, including some basic facts about radioactivity and the biological effects of radiation; and gives an overview of the classification of radiological areas at X-LAB, radiation fields at high-energy accelerators, and the radiation monitoring system used at X-LAB. The bunker design to achieve a dose rate less than annual dose limit of 1 mSv is also shown.

INTRODUCTION

The X-LAB is being constructed in an existing radiation shielded bunker located in the basement of the School of Physics at UoM, under refurbishment after previously housing a 35 MeV electron betatron [1] until the late 1980s.

This space will become the first high-power, high-frequency accelerator laboratory in Australia. At the heart of the project is the technology transfer from the Partner Organisation CERN in the form of the multimillion dollar compact X-band accelerator radio frequency (RF) system known as XBOX3 [2, 3]. Refurbishing of the Melbourne University basement is going on, the first high power X-band pulses are planned for the end of 2022.

Conditioning of CLIC structures will take place in the X-LAB high power test stands renamed as Mel-BOX [4] (Fig. 1). Mel-BOX consists of twin low peak power, X-band (11.9942 GHz) 6 MW Toshiba E37113 klystrons and ScandiNova K1 modulators. Signals are combined in pairs allowing to sum up power of two klystrons, thus operating at 200 Hz at double power. This together with a pulse compressor on each line allows to reach the power of about 50MW for CLIC's baseline requirements [5] .

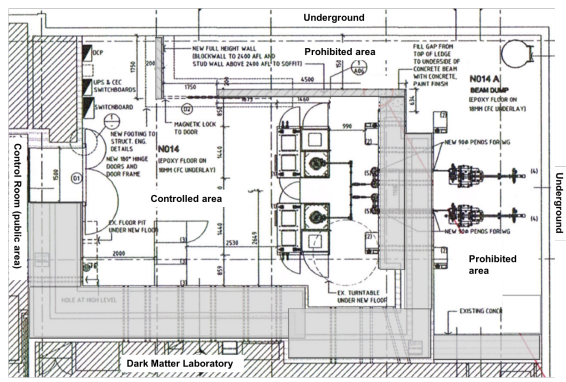

Figure 1: Layout of the new X-LAB and the configuration of the Mel-BOX test stands.

The use of high-gradient RF technology in accelerator facilities has a series of important benefits, such as compactness and cost-efficiency. However, compactness comes at the cost of having very high EM fields inside the RF cavities. High surface electric fields lead to spontaneous emission of electrons from the material surfaces, by means of quantum tunnelling of conducting layer electrons. Furthermore, this emission grows exponentially with field, becoming larger when gradients used get higher. Field emission of electrons is the origin of RF breakdown in high gradient structures' operation, but it can also cause other related problems. Field emitted electrons can be captured by the EM fields and be accelerated throughout the structures, causing the so-called dark currents [6]. If these electrons become energetic enough they can also produce ionising radiation when colliding with material walls. Dark currents can be a source of other issues, such as background noise in Beam Position Monitors (BPMs), transverse kicks of beams, and ionising radiation. To ensure adequate performance of radiation shielding in the X-LAB bunker area, the dark current of two high gradient structures has been used in this study.

* m.volpi@unimelb.edu.au

ISBN: 978-3-95450-227-1 ISSN: 2673-5490 doi:10.18429/JACoW-IPAC2022-MOPOMS041

CONCRETE SHIELDING ACTIVATION FOR PROTON THERAPY SYSTEMS USING BDSIM AND FISPACT-II

E. Ramoisiaux, C. Hernalsteens[1], R. Tesse, E. Gnacadja, N. Pauly, M. Vanwelde,
Service de Métrologie Nucléaire, Université libre de Bruxelles, Brussels, Belgium
F. Stichelbaut, Ion Beam Applications (IBA), Louvain-la-Neuve, Belgium
[1]also at CERN, Geneva, Switzerland

Abstract

Proton therapy systems are used worldwide for patient treatment and fundamental research. The generation of secondary particles when the beam interacts with the beamline elements is a well known issue. In particular, the energy degrader is the dominant source of secondary radiation. This poses new challenges for the concrete shielding of compact systems and beamline elements activation computation. We use a novel methodology to seamlessly simulate all the processes relevant to the activation evaluation. A realistic model of the system is developed using Beam Delivery Simulation (BDSIM), a Geant4-based particle tracking code that allows a single model to simulate primary and secondary particle tracking and all particle-matter interactions. The secondary particle fluxes extracted from the simulations are provided as input to FISPACT-II to compute the activation by solving the rate equations. This approach is applied to the Ion Beam Applications (IBA) Proteus®ONE (P1) system and the shielding of the proton therapy research centre of Charleroi, Belgium. Proton loss distributions are used to model the production of secondary neutrals inside the accelerator structure. Two models for the distribution of proton losses are compared for the computation of the clearance index at specific locations of the design. Results show that the variation in the accelerator loss models can be characterised as a systematic error.

INTRODUCTION

Numerous proton therapy centres have been built for patient treatment and fundamental research over the past two decades [1]. It is well known that proton therapy machines generate a large number of secondary particles, mainly neutrons, when the proton beam interacts with the beamline elements [2]. In particular, the energy degrader is the dominant source of secondary radiation. Those neutrons interact with the concrete shielding via nuclear reactions, mainly neutron capture and spallation, producing radioactive nuclides. Some are long-lived and are responsible for the long-term activation of the shielding.

When designing a new centre or preparing experimental setups, the complete modelling of proton therapy systems from the primary and secondary beam interactions to the beamline and shielding activation is a complex but necessary task. We establish a method, inspired from the Rigorous Two-Step (R2S) [3], coupling Beam Delivery SIMulation (BDSIM) [4] with the code and library database FISPACT-II [5]. BDSIM provides a full 3D model of the proton therapy system and its shielding that includes the particle-matter interactions of Geant4 and the tracking of all the particles through the beamline magnetic elements, vacuum windows and air gaps. FISPACT-II is subsequently used for the activation computation.

This methodology is thoroughly described in Ref. [6] and was applied to the shielding design of the future proton therapy centre of Charleroi, Belgium. The IBA Proteus®ONE proton therapy system that will be used in the centre was already modelled in BDSIM and validated against experimental data in Ref. [7]. The model was then used for the secondary particle generation required for shielding activation studies with FISPACT-II. The shielding activation results were fully validated against the IBA shielding design that was obtained using MCNPX [8].

During the elaboration of the BDSIM model of the future proton therapy centre of Charleroi, it was required to model in detail the proton loss pattern inside the accelerator (S2C2). Indeed, the acceleration of the primary protons is not simulated in BDSIM and therefore, the secondary neutron generation is realised by combining two different simulations. The first simulation considers the transport of the primary particles through the beamline with the secondary neutrons generated by interactions of the beam with the beamline elements. On the other hand, the second simulation simulates the propagation of lost protons inside the S2C2 structure. The S2C2 secondary neutrons generation process is presented in Fig. 1.

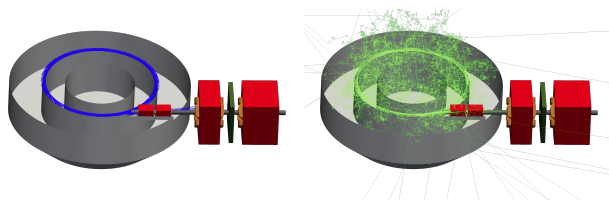

Figure 1: Illustration of the S2C2 secondary neutrons generation process in BDSIM. The protons (shown in blue) and the neutral particles, neutrons and photons (shown in green) are represented. Distribution of protons lost during the acceleration and the extraction processes serve as primary input (left). The resulting secondaries are produced by the interactions of the protons with the S2C2 structure (right).

We propose to use the BDSIM/FISPACT-II methodology to characterise the impact of two S2C2 proton loss distributions on the activation results. Figure 2 represents the BDSIM model of the vault of the proton therapy centre of Charleroi with its concrete shielding design. The concrete shielding was implemented using *Pyg4ometry*, a Python library that enables users to create GDML-based geometry rapidly [9, 10]. The S2C2 and the degrader, the two main elements of the beamline at the origin of most of the secondary particle generation, can be observed. We study the activation

ISBN: 978-3-95450-227-1 ISSN: 2673-5490 doi:10.18429/JACoW-IPAC2022-MOPOMS042

COMPARISON BETWEEN RUN 2 TID MEASUREMENTS AND FLUKA SIMULATIONS IN THE CERN LHC TUNNEL OF THE ATLAS INSERTION REGION

D. Prelipcean, G. Lerner, R. García Alía, K. Bilko, M. Sabaté Gilarte, F. Cerutti,
D. Di Francesca, D. Ricci, A. Ciccotelli, B. Humann
CERN, Geneva, Switzerland

Abstract

In this paper we present a systematic benchmark between the simulated and the measured data for the radiation monitors useful for Radiation to Electronics (R2E) studies at the Large Hadron Collider (LHC) at CERN. For this purpose, the radiation levels in the main LHC tunnel on the right side of the Interaction Point 1 (ATLAS detector) are simulated using the FLUKA Monte Carlo code and compared against Total Ionising Dose (TID) measurements performed with the Beam Loss Monitoring (BLM) system, and 180 m of Distributed Optical Fibre Radiation Sensor (DOFRS). Considering the complexity and the scale of the simulations as well as the variety of the LHC operational parameters, we find a generally good agreement between measured and simulated radiation levels, typically within a factor of 2 or better.

INTRODUCTION

The scope of this paper is to present a systematic benchmark between the simulated and the measured data for the radiation monitors useful for Radiation to Electronics (R2E) [1] studies at the Large Hadron Collider (LHC) at CERN [2]. For this purpose, the Total Ionizing Dose (TID) measurements performed with: (i) the Beam Loss Monitoring (BLM) system [3], and (ii) 180 m of Distributed Optical Fiber Sensor (OF) [4] are compared against those simulated using the FLUKA Monte Carlo code (version 4.1.1, CERN distributed) [5–7].

More specifically, the benchmark study has been performed for the Long Straight Section (LSS - up to Cell 7) and Dispersion Supressor (DS - up to Cell 11) at the high luminosity Interaction Point 1 (IP1 - ATLAS detector). Moreover, the simulation has been extended into the ARC (up to Cell 17) of IP1 to test several hypotheses. A similar approach can be used for other IPs.

RADIATION LEVELS IN LUMINOSITY-DRIVEN INTERACTION POINTS

The main source of radiation in the LHC tunnel in IP1 are inelastic proton-proton collisions in the center of the ATLAS experiment ($z = 0$ m) whose debris partially propagates in the tunnel leading to radiation showers. As anticipated, the discussion in this paper is focused on the TID, relevant for cumulated damage and lifetime degradation on machine equipment. The TID is defined as the energy deposited per unit mass by electromagnetic or hadronic showers via ionisation, and is measured by the BLM detectors and simulated with FLUKA.

Due to the origin of the showers, the BLM measurements are assumed to scale with luminosity, which is a measure of the number of inelastic collisions taking place in the IP. Still, there are several operational parameters of the LHC that can also affect the radiation levels near IP1. The ones examined in this study (but more play role, e.g. the crossing angle) are: (i) Target Collimator Long (TCL)settings: aperture size (and usage) of the collimators protecting beam elements, e.g. the cold magnets in half-cell 8 and 9, and (ii) Roman Pots (RP) [8] settings: devices used to measure the total cross section of two particle beams in a collider.

ANALYSIS STRATEGY

Experimentally, the measured data is stored continuously over the entire Run 2 period (from 2015 to 2018) of data taking. Several selection criteria are considered to identify time periods that allow for a direct comparison between measured and simulated data. The first selection criterion is for the radiation monitor data to correspond to the STABLE BEAMS beam mode, as this one corresponds to the delivery of beam to the experiments yielding collision debris. Subsequently, within this single fill, some parameters (such as the collimator settings or the roman pots usage) alternate between two predefined values (e.g., open/closed or in/out) while others are changed quasi-continuously, as the LHC performance has been improved.

The comparison of measured TID per unit integrated luminosity (fb^{-1}) for different periods of operation with the same configuration of LHC parameters exhibits a very stable profile [9]. This result allows to merge different fills corresponding to periods with identical operational conditions, yielding larger data sets (tens of fb^{-1}) per configuration. Moreover, the symmetry around IP1 allows to reduce the study to only one side of the tunnel.

The simulations employed in this study are able to (statically) replicate a given LHC configuration, meaning that quasi-continuous changes like the crossing angle anti-levelling [10] cannot be reproduced, hence the need to identify time periods with constant LHC settings as described above.

ISBN: 978-3-95450-227-1 ISSN: 2673-5490 doi:10.18429/JACoW-IPAC2022-MOPOMS043

AUTOMATED ANALYSIS OF THE PROMPT RADIATION LEVELS IN THE CERN ACCELERATOR COMPLEX

Kacper Bilko*, R. Garcia Alia, J. Potoine†
CERN, Geneva, Switzerland

Abstract

The CERN injector complex is essential in providing high-energy beams to various experiments and to the world's largest accelerator, the Large Hadron Collider (LHC). Beam losses linked to the operation of both the LHC and its injectors result in a mixed radiation field which, through both cumulative and single-event effects poses a threat to exposed electronic equipment. Therefore, detailed knowledge of the radiation distribution and evolution is necessary in order to implement adequate Radiation to Electronics (R2E) mitigation and prevention measures, resulting in an improvement in the efficiency and availability of the accelerators. In this study, we present the automated analysis scheme put in place to efficiently process and visualise the radiation data produced by various radiation monitors, distributed at the four largest CERN accelerators, namely the Proton Synchrotron Booster (PSB), Proton Synchrotron (PS), Super Proton Synchrotron (SPS), and the LHC, where proton beams are accelerated gradually from 160 MeV up to 7 TeV.

INTRODUCTION

In high energy and high intensity particle accelerators, even during nominal operation small amounts of beam are lost, leading to a mixed-field radiation, that can negatively impact the exposed electronic systems both through the stochastic Single Event Effects (SEE) and cumulative lifetime effects, such as Total Ionizing Dose (TID) and Displacement Damage (DD).

Additionally, in regions with relatively high losses, the residual radiation levels (caused by nuclear interactions induced by the prompt radiation) lead to additional Radiation Protection limitations, such as personnel access restrictions.

Therefore, a key preventive measure is the active monitoring of the prompt radiation levels in particle accelerators to i) understand the origin of beam loss mechanism, ii) forecast the future evolution, iii) detect discrepancies from the forecasted behaviour and iv) perform mitigation actions to reduce the impact, primarly on electronics. For our analysis, the four largest CERN accelerators, namely Proton Synchrotron Booster (PSB) [1], Proton Synchrotron (PS) [2], Super Proton Synchrotron (SPS) [3] and the Large Hadron Collider (LHC) [4] are considered. They are equipment with multiple radiation monitors, complimentary to each other. Primarily, the Beam Loss Monitors (BLMs) [5] provide very good time resolution (below 1 s, depending on the accelerator), whereas Distributed Optical Fibre Radiation Sensors (DOFRS) [6] allow to measure TID levels with a good spatial resolution (1 m). Finally, in selected locations, the dedicated Radiation to Electronics (R2E) monitors, RadMons [7], are deployed, to characterise the mixed field radiation not only in terms of TID, but also the fluence values relevant to radiation effects and damage.

These monitors generate relatively large amounts (over 100 GB/day) of complex and varying data, that require state-of-the-art data engineering solutions for efficient data processing and analysis. This ensures that a comprehensive insight, based on all avaliable radiation monitors, is provided instantaneously, allowing potential mitigation actions to be planned and executed effectively.

In this paper we give an overview of the radiation monitoring and the implemented automated analysis solutions that are used within the CERN's R2E project, established to reduce the impact of the radiation on the electronic systems installed in the CERN accelerators.

PROMPT RADIATION MONITORING

Beam Loss Monitors

The core of the Beam Loss Monitoring system are the Beam Loss Monitors (BLMs), ionisation chambers filled with nitrogen, that in addition to its main purpose, i.e. machine protection, can be successfully used for dosimetry. Their main advantage is a very good time resolution that, depending on the accelerator, can be as low as few μs. The system allows to measure the TID levels in terms of energy deposited in nitrogen. PSB, PS and LHC are equipped with the same generation of the ionization chambers, whereas in the SPS older detectors are used.

DOFRS

As of 2021, PSB, PS and SPS are entirely covered by the DOFRS radiation monitor, allowing to retrieve the TID (in silica) profile along the accelerator with a very good spatial resolution (as compared with point-wise measurements by BLMs), in the order of 1 m. In case of the LHC, as of 2022, there is a partial coverage of the accelerator, in the Dispersion Suppressor regions of Interaction Points 1,5 and 7. DOFRS system provides a time evolution of the levels, however, with the significantly lower time resolution as compared to the BLM. Therefore, the synergy of both monitor types is essential to build a comprehensive picture of TID levels in terms of spatial distribution (DOFRS) and their detailed time evolution (BLMs).

RadMons

In addition to BLMs and DOFRS monitors, in the CERN accelerators there are dedicated R2E detectors, RadMons,

* kacper.bilko@cern.ch
† presenter

ISBN: 978-3-95450-227-1 ISSN: 2673-5490 doi:10.18429/JACoW-IPAC2022-MOPOMS044

IMPLICATIONS AND MITIGATION OF RADIATION EFFECTS ON THE CERN SPS OPERATION DURING 2021

Y. Q. Aguiar, G. Lerner, M. Cecchetto, R. García Alía, K. Bilko, A. Zimmaro,
M. Brucoli, S. Danzeca, T. Ladzinski, A. Apollonio, J. B. Potoine
CERN, CH-1211, Geneva, Switzerland

Abstract

During the Long Shutdown 2 (LS2, 2019-2020), the CERN accelerator complex has undergone major upgrades, mainly in preparation for the High-Luminosity (HL) LHC era, the ultimate capacity for its physics production. Therefore, several novel equipment and systems were designed and deployed throughout the accelerator complex. To comply with the radiation level specifications and avoid machine downtime due to radiation effects, the electronics systems exposed to radiation need to follow Radiation Hardness Assurance (RHA) methodologies developed and validated by the Radiation to Electronics (R2E) project at CERN. However, the establishment of such procedures is not yet fully implemented in the LHC injector chain, and some R2E failures were detected in the SPS during the 2021 operation. This work is devoted to describing and analysing the R2E failures and their impact on operation, in the context of the related radiation levels and equipment sensitivity.

INTRODUCTION

Within the CERN accelerator complex, several critical systems are designed to operate under harsh environment composed of a mixed radiation field. However, besides the adoption of different radiation hardened (rad-hard) solutions for electronics, the usage of Commercial Off-the-Shelf (COTS) products is still widely exploited. This is mostly motivated by some limitations of the available rad-hard components that do not meet the specifications required for the accelerator systems, as well as by the cost of the rad-hard electronics, which can be up to a factor 100 more expensive than their COTS counterparts. Therefore, in order to prevent radiation-induced failures and their consequent impact on the accelerator availability, Radiation Hardness Assurance (RHA) methodologies are used not only to mitigate the failures during the operation lifetime, but also for the sake of prevention [1–3].

One example of a safety critical system is the Access or Personnel Protection System (PPS) which not only controls the access to the accelerator, but also interlocks its critical components in case of potential human presence underground [4]. Therefore, as will be shown in this paper, R2E failure events are capable of inducing beam dumps, negatively impacting the availability of the accelerators. In this context, this work presents the implications of the R2E failures observed during the CERN's Super Proton Synchrotron (SPS) operation in 2021 and the consequent mitigation measures taken to improve the availability of the accelerator.

SPS ACCESS SYSTEM AND R2E

The access system provides permanent protection of the personnel implementing several safety-interlock functions. It is based on a three-layer Programmable Logic Controller (PLC) architecture. The sixteen site layer controllers together with sixteen access point controllers constantly monitor some 23'000 I/O channels and make sure that whenever there is ongoing access, no beam can be present in the SPS complex. Therefore, the system has a direct impact on the operation and availability of the SPS accelerator. During the past Long Shutdown (2019 – 2020), the SPS PPS underwent a renovation campaign where the system was fully replaced [4, 5].

The PLC controllers are connected to Elements Important for Safety (EIS) such as personnel and material access devices, doors, extractor kickers, beam absorbers and etc. Given the severity of a failure occurrence and the implementation constraints, the adopted safety PLC system was designed with a Safety Integrity Level of 3. Whenever a failure is observed in the PLCs, the system goes to a fail-safe state to prevent a catastrophic event from happening as, for example, the presence of a person in the tunnel while there is beam injected in the machine. Therefore, the fail-safe state in this case is to dump the injected beam impacting on the availability of the accelerator. During the physics run in 2021, the SPS PPS has experienced an important number of failures on the input/output (I/O) cards that connect the PLC controllers to the EIS devices. Based on the failure signature, the root cause for such events was classified as radiation effects to electronics, namely, Single-Event Upsets (SEUs) in the memories. Figure 1 provides the observed number of R2E induced failures as a function of the integrated SPS injected intensity.

A total of 75 events have been recorded in the I/O cards, and, although not all of them lead to beam dumps, their occurrence can significantly increase the downtime of the machine as the modules need to be manually reset during a beam stop. Thanks to the several mitigation measures timely taken in place, the failure rate was reduced throughout the SPS operation and the annual integrated injected intensity reached $1.17 \cdot 10^{19}$ charges [6]. Table 1 provides an overview of the total number of sensitive cards in each electronics rack location in the SPS tunnel, the total number of R2E induced failures, the High-Energy Hadron equivalent (HEHeq) and thermal neutron (ThN) particle fluences measured by BatMon monitors [7, 8] and the respective R factor which is the ratio between the ThN and HEHeq particle fluences.

ISBN: 978-3-95450-227-1 ISSN: 2673-5490 doi:10.18429/JACoW-IPAC2022-MOPOMS045

VACUUM CONTROL SYSTEM UPGRADE FOR ALPI ACCELERATOR

G. Savarese, L. Antoniazzi, D. Bortolato, INFN/LNL, Legnaro (PD), Italy
A. Conte, F. Gelain, D. Marcato, C. Roncolato, INFN/LNL, Legnaro (PD), Italy

Abstract

The vacuum system of ALPI accelerator includes about 40 pumping groups based on turbomolecular pumps. The instrumentation of the accelerators complex is mainly the one installed in 90s, with consequent maintenance issues. The control and supervision systems were developed in the same period by an external company, which produced custom solutions for the HW and SW parts. Control devices are based on custom PLCs, while the supervision system is based on C and C#. The communication between the field and the supervisor is composed of multiple levels: RS-232 standard is used to transfer control parameters from the field devices up to custom multiplexers; RS-485 transmission is used from the multiplexers to two PC servers covering different sections of the installation; while Ethernet, is used to connect the servers and the operation console. Obsolescence and rigidity of the system, deficit of spare parts and impossibility of reparation or modification without external support, required a complete renovation of the vacuum system and relative controls in the next years. This paper describes the adopted strategy and the implementation status.

INTRODUCTION

The legacy ALPI-PIAVE Vacuum Control System (VCS) was developed in '90s by TELEMA company [1]. TELEMA was also in charge of maintaining and upgrading the hardware and the software. The obsolescence of the system already required the planning of an hardware replacement, which is still on-going [2]. Since at the end of 2021 TELEMA closed its business, the control system group made an immediate evaluation of the VCS software and hardware status and decided to replace as soon as possible the software [3], written in C/C#, with an EPICS [4] based control system, compatible with the existing hardware, which will be expanded to communicate with the new hardware in development.

We chose this solution for the following reasons:

- The legacy software is written in a language not used by the control system group, and it is the result of several updates not always documented or well commented. To develop an EPICS based control system from scratch will ease the software maintenance
- A working solution in a short time is required for machine protection reason and we don't have spare hardware; the control hardware should remain untouched as much as possible. EPICS IOCs creation is relatively quick, simple and adaptable to the current hardware architecture.
- The development of a new EPICS supervisor, backwards compatible, that will substitute the legacy one, was already planned.

STATE OF THE ART

Different hardware and software versions of the TELEMA Vacuum Control System (VCS) exist at the same time, but the project architecture is the same; the difference mainly impacts the controllers logic and the related graphical user interface. There are three main actors: the *controller*, the *collector* and the *supervisor*.

The *controller* represents the hardware mounted in the racks placed along the beam lines (Fig. 1). Each rack can control one or more pumping groups, and is made up of a *multiplexer* (MUX) and a custom box with microprocessor controllers called *PLC*. The MUX controls and acquires information from vacuometers and pump controllers, and forwards a subset of those data over a RS485 4-wires line. The PLC manages the valves actuation, implements the Machine Protection System (MPS) procedures, and manages high level procedures (i.e vacuum cycle). When the controller manages instruments connected to a cryostat, an additional PLC is present in the rack. This PLC is called Additional (ADD) and manages the valves, connecting the specific cryostat to the vacuum line and used for the He and N_2 inlet procedures. The vacuum line is controlled by a set of special PLCs, called Power Additional, which manage the primary pumps and the main valves connected to that line. All type of PLCs receive and send information over an RS-485 4-wires line, which is not the same of the MUXs.

Figure 1: The TELEMA rack mounted in ALPI with MUX, PLC, ADD PLC, vacuometers and pump controllers.

ISBN: 978-3-95450-227-1 ISSN: 2673-5490 doi:10.18429/JACoW-IPAC2022-MOPOMS046

RELIABILITY ANALYSIS OF THE HL-LHC ENERGY EXTRACTION SYSTEMS

M. Blaszkiewicz *, A. Apollonio, T. Cartier-Michaud,
B. Panev, M. Pojer, D. Wollmann
CERN, Geneva, Switzerland

Abstract

The energy extraction systems for the protection of the new HL-LHC superconducting magnet circuits are based on vacuum breakers. This technology allows a significant reduction of the switch opening time and increases the reliability of the overall system with reduced maintenance needs. This paper presents the results of detailed reliability studies performed for these new energy extraction systems. The study quantifies the risk of a failure preventing the proper protection of a magnet circuit and identifies the most critical components of the system. To do this, the model considers factors such as failure probabilities at the block or component level, different maintenance strategies, and repair procedures. Reliability simulations were performed using AvailSim4, a novel Monte Carlo code for availability and reliability simulations. The results are compared against the system's reliability requirements and provide insights into the most critical components.

INTRODUCTION

The Energy Extraction (EE) systems are essential elements for the protection of LHC's superconducting circuits in case of magnet quenches. Following the transition from the superconducting to the normal-conducing state, the energy stored in the magnet rapidly transforms into heat which can cause damage in a magnet, as report [1] shows. Quenches in magnets are unavoidable and, as such, are an accepted failure mode. The EE systems are responsible for extracting a maximum of the energy stored in the superconducting circuits upon receiving a signal from the Quench Detection System (QDS) [2] or the power converter [3] via the Powering Interlock Controller (PIC) [4]. The EE systems react in several milliseconds after receiving the triggering signal and redirect the circuit current into resistor banks that dissipate the remaining energy stored in the circuit.

The new EE design for HL-LHC is conceived to offer an even more resilient, reliable and maintenance-free solution that will cover the increased reliability requirements of the HL-LHC. The key design change is the circuit breaker technology: the new systems are to use vacuum interrupters instead of mechanical DC breakers. The new interrupters offer maintenance-free operation, while ensuring a better reaction time than other solutions [5, 6]. Detailed studies have been performed to validate the compliance of the new HL-LHC EE systems to the protection and reliability requirements derived in section "**RELIABILITY TARGET**".

* Research supported by the HL-LHC project

Table 1: Number of protection systems considered in this study to derive the reliability target

Magnets	Protection	Number
Inner Triplet Quadrupole	CLIQ + QH	6 × 4
2 kA orbit correctors	EE	6 × 4
600 A and 200 A high order correctors	EE	5 × 4
D1, D2	QH	2 × 4
Total		19 × 4 = 76

The EE systems for HL-LHC will exist in two versions: 2 kA and 600 A. Both are based on similar hardware.

METHODOLOGY

The reliability model of the EE system was prepared and simulated in AvailSim4 framework [7], a tool developed at CERN for availability and reliability simulations. It offers a generic Monte Carlo approach to predict system reliability and availability, while allowing for the incorporation of additional custom strategies and protection measures, specific for accelerator technologies.

The Monte Carlo approach requires performing numerous iterations, each simulating the system behavior over its expected lifetime. The occurrence of simulated events is based on failure probability distributions defined for each component based on experience, manufacturer data or the military handbook MIL-HDBK-217 [8].

The reliability model is described by a list of components, their failure dependencies and a list of failure modes with failure and repair probability distributions. Complex failure behaviors, as well as advanced repair and maintenance strategies can also be defined. High/low system loads can be simulated by means of so-called *phases*. In addition, periodic inspections and repair of *minimal replaceable units* allow to closely reproduce the adopted maintenance strategies in use for machine protection systems. More details about the methodology used with AvailSim4, a description of the tool and instructions of its usage are available in [7].

RELIABILITY TARGET

The study focused on the critical failure of a missed energy extraction upon the occurrence of a quench. Due to the high degree of redundancy implemented in the system design, this can only occur due to a combination of independent failures in different components of the system. In case of a

ISBN: 978-3-95450-227-1 ISSN: 2673-5490 doi:10.18429/JACoW-IPAC2022-MOPOMS047

CONTROL AND FUNCTIONAL SAFETY SYSTEMS DESIGN FOR REAL-TIME CONDITIONING OF RF STRUCTURES AT TEX

S. Pioli*, D. Moriggi, F. Cardelli, P. Ciuffetti, C. Di Giulio, R. Gargana, INFN-LNF, Frascati, Italy

Abstract

We report the status of the development of an High Power RF Laboratory in X-Band called TEX (TEst-stand for X-Band). TEX is part of the LATINO (Laboratory in Advanced Technologies for INnOvation) initiative that is ongoing at the Frascati National Laboratories (LNF) of the Italian Institute for Nuclear Physics (INFN) that covers many different areas focused on particle accelerator technologies. TEX is a RF test facility based on solid-state K400 modulator from ScandiNova with a 50MW class X-band (11.994 GHz) klystron tube model VKX8311A operating at 50 Hz. This RF source will operate as resource for test and research programs such as the RF breakdown on RF waveguide components as well as high power testing of accelerating structures for future high gradient linear accelerator such as EuPRAXIA and CLIC. In this context we will present the whole EPICS control system design focusing on archiving, user interfaces and custom development made as part of the functional safety to deliver real-time RF breakdown detection integrated with the timing system of the facility.

INTRODUCTION

In preparation to the activities of the EuPRAXIA@SPARC_LAB projectand the LATINO (Laboratory in Advanced Technologies for INnOvation) Initiative, a high-power test stand for X-band accelerating structures called TEX ("TEst stand for X-band") [1] is being built at LNF.

The X-band (11.994 GHz) is at present the most advanced RF technology, with demonstrated capability of providing accelerating gradients up to 100 MV/m and beyond. In this context started the implementation of a new high power X-band test stand at LNF. The area to host the new test stand within the LNF has been identified and it is presently being refurbished to provide all the required services to the facility. The concrete bunker shielding the accessible area from the radiation produced by the structures under test is also being designed and constructed.

The facility under commissioning [2] will be used for testing X-band accelerating structure prototypes (EuPRAXIA [3] and CLIC projects), RF components and sub-systems. For the rest of the time the facility will be accessible to external users, including national and international laboratories and companies.

The open-access to TEX is one of the services offered by INFN to the external community through LATINO [4], a project approved and funded by the government of "Regione Lazio" aimed at promoting and increasing the technology transfer between research centres of excellence and the surrounding economic framework.

In this document the TEX Control System will be presented with special reference to tier architecture and user tools.

CONTROL SYSTEM FRAMEWORK

The control software (CS) framework called EPICS (Experimental Physics and Industrial Control System) [5] provides an architecture for control system software to be constructed as a scalable, distributed database of control components. It is based on industry standards at all levels and includes an extensive set of tools and clients that are portable across all major architectures. TEX has selected a standardised, field-proven controls framework, EPICS, which was originally developed jointly by Argonne and Los Alamos National Laboratories, Figure 1. Complementing this selection are best practices and experience from similar facilities regarding platform standardisation, control system development and device integration and commissioning.

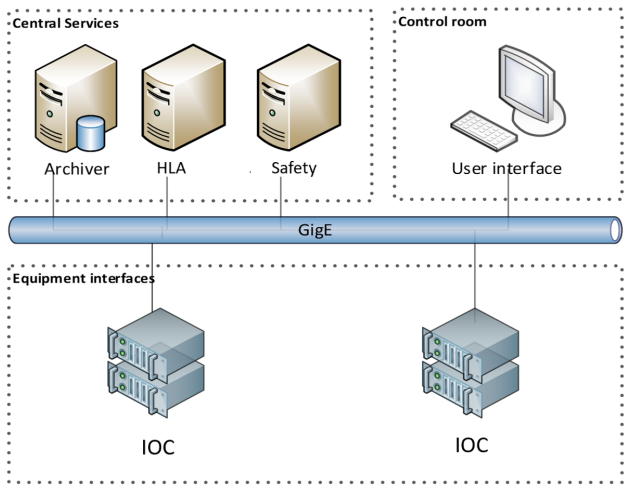

Figure 1: EPICS framework for the TEX Control System.

RESOURCE TIER

Currently we proceed in the integration of all the hardware equipment present at TEX. IOCs and support modules for any family of device have developed or acquired from repositories, as shown in Table 1.

CS hardware is composed of a standardised hardware platform, components, development tools and services. Interfaces with the equipment and parts of the facility are made through a set of analog and digital signals, real-time control loops and other communication buses.

* stefano.pioli@lnf.infn.it

ISBN: 978-3-95450-227-1 ISSN: 2673-5490 doi:10.18429/JACoW-IPAC2022-MOPOMS048

FAST TRIGGER SYSTEM FOR BEAM ABORT SYSTEM IN SuperKEKB

H. Ikeda[†,1], T. Mimashi[1], S. Nakamura[1], T. Oki[1], S. Sasaki, High Energy Accelerator Research Organization (KEK), Tsukuba, Japan
[1]also at SOKENDAI, Tsukuba, Japan

Abstract

In order to protect the hardware components of the detector and accelerator from sudden beam loss of high beam currents, the fast beam abort system is developed in the SuperKEKB. The previous abort system was not fast enough for sudden beam loss that caused QCS quench, and it gave a damage to the collimator and the Belle-II detector. A fast abort system is required to preventing such damage. The abort system consists of several sensors that generate interlock signal (the loss monitor, dose in the Bell-II detector, and the magnet failure etc.), optical cable system to transfer the interlock signal to central control room (CCR), the abort trigger signal generation system and the abort kicker. To reduce total time, we reduce transmission time from local control room to CCR by changing signal cable route. Since the interlock signal produced by magnet power supply was slow, we modified the magnet power supply. For more quick generation of abort trigger signal, we increased number of the abort gap. By these improvements, an average abort time is reduced from 31μsec to 25μsec. This improvement looks small, but it brought preventing the serious radiation damage to many hardware components. Detail of the system and result is presented in this paper.

INTRODUCTION

SuperKEK is a collider of 7GeV electrons and 4GeV positrons. KEKB was upgraded from 2011 over 5 years in order to increase the luminosity and started commissioning in 2018 after the test operation [1 - 3]. SuperKEKB is increasing the beam current and squeezing the beam size in order to obtain high luminosity. Superconducting quadrupole magnets (QCS) are installed in the interaction region (IR) in order to squeeze β*. At present, the luminosity is increased more than twice the luminosity of KEKB, by gradually reducing β, and gradually increasing the current value [4].

Accelerator and detector hardware has been upgraded and more precise handling is required for operation. In order to increase the beam current while protecting the equipment, it is necessary to strive for beam stability and abort the unstable beam as soon as possible.

ABORT SYSTEM

The beam abort kicker is composed of a tapered vertical magnet, a horizontal magnet, a Lambertson DC septum magnet, and additional pulsed quadrupole magnets for LER and a sextupole magnet for HER to increase the beam cross-section to avoid damaging the extraction window [5, 6]. It takes one revolution, i.e. 10μsec to completely extract the storage beam from the ring. The beam is distributed every 2-4 RF buckets in the ring and 200 ns is empty to cover the build-up time of the abort kicker magnet field as shown in Fig. 1. We call 200ns no beam period in the beam train “Abort Gap”.

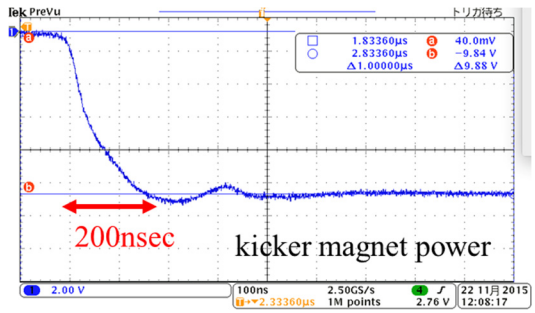

Figure 1: Abort kicker magnet power.

ABORT TRIGGER

The abort trigger system collects several types of abort trigger requests as shown in Fig. 2. First type is direct trigger from hardware components such as RF, vacuum, magnet and monitor. For example, the RF group monitors the cavity voltage, klystron power, synchrotron oscillation phase and so on. The vacuum group monitors the vacuum pressure and temperature of the chamber in the ring. The magnet group uses the comparator current of power supply.

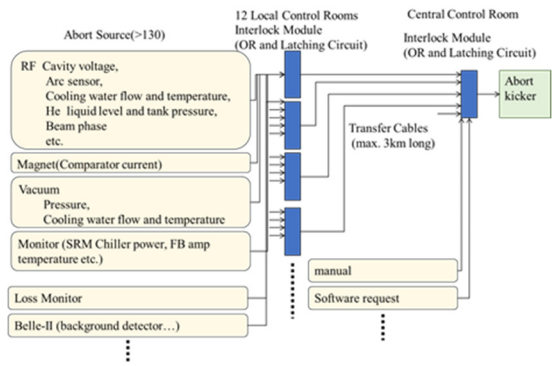

Figure 2: Abort trigger flow.

The second trigger type is as follows. Beam loss monitor is the main abort trigger to protect the hardware of the accelerator and detector [7]. We are using the ion chambers (ICs) and PIN photo-diodes (PINs) as beam loss monitor sensor. ICs are installed in various places in the tunnel to detect beam loss in a wide area, and PINs are installed mainly in the downstream of the collimator where the aperture is narrow.

† hitomi.ikeda@kek.jp

ISBN: 978-3-95450-227-1 ISSN: 2673-5490 doi:10.18429/JACoW-IPAC2022-MOPOMS050

RIGOROUS APPROACH FOR CALCULATION OF RADIATION OF A CHARGED PARTICLE BUNCH EXITING AN OPEN-ENDED DIELECTRICALLY LOADED WAVEGUIDE*

S. N. Galyamin†, St. Petersburg State University, St. Petersburg, Russia
S. S. Baturin, ITMO University, St. Petersburg, Russia

Abstract

First, recent results on radiation of a Cherenkov mode at the open end of a dielectric-lined circular waveguide (including a three-layer case) are presented. Second, rigorous solution is presented for the case of a charged particle bunch exiting the open end of a waveguide with unifiorm dielectric filling.

INTRODUCTION

Among prospective applications of dielectric-filled waveguides and Cherenkov effect one can mention dielectric wakefield acceleration [1–3], bunch manipulation [4–6] and beam-driven radiation sources [7–9]. Mentioned cases typically involve interaction of both EM waves and charged particle bunches with an open end of certain open-ended waveguide structure loaded with dielectric. Convenient rigorous approach for the circular waveguide geometry has been presented recently [10, 11] (internal excitation in the form of a slow waveguide mode has been used). However, problems with more complicated layered filling [9] and excitation in the form of a charged particle bunch require similar analytical solution. These are main topics of the present paper.

OPEN-ENDED WAVEGUIDE WITH DIELECTRIC LINING

First, we briefly discuss a two-layer open-ended waveguide with PEC walls excited by single waveguide mode (details can be learned from [11]), see Fig. 1. A φ-symmetric TM problem is considered in the harmonic regime with time dependence in the form $H_\varphi(\rho,z,t) = H_{\omega\varphi}(\rho,z)\exp(-i\omega t)$. Single symmetrical TM_{0l} mode is incident on the open end while the reflected field inside the waveguide $H^{(r)}_{\omega\varphi}$ is decomposed into a series of such modes propagating in the opposite direction (z-dependence for the incident mode is $\sim\exp(ik_{zl}z)$) with unknown "reflection coefficients" $\{M_m\}$ that should be determined:

$$H^{(r)}_{\omega\varphi} = \sum_{m=1}^{\infty} M_m e^{-ik_{zm}z} \times \begin{cases} J_1(\rho\sigma_m)/\sigma_m & \text{for } \rho < b, \\ \left[J_1(\rho s_m)Y_0(as_m) - Y_1(\rho s_m)J_0(as_m)\right] & \\ \times J_1(b\sigma_m)/\left[\sigma_m\psi_0(s_m)\right] & \text{for } b<\rho<a, \end{cases} \quad (1)$$

where J_ν and Y_ν are Bessel and Neumann functions, transverse wave numbers σ_m and s_m are determined by dispersion equation (Eq. (4) in [11]),

$$\psi_0(s_m) = J_1(bs_m)Y_0(as_m) - J_0(as_m)Y_1(bs_m), \quad (2)$$

longitudinal wave numbers $k_{zm} = \sqrt{k_0^2 - \sigma_m^2} = \sqrt{k_0^2\varepsilon - s_m^2}$, $\mathrm{Im}k_{zm} > 0$, $k_0 = \omega/c + i\delta$ ($\delta \to 0$ is responsible for small dissipation), c is the light speed in vacuum.

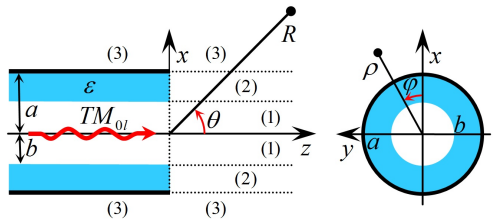

Figure 1: Two-layer problem and main notations.

After a series of calculations involving field matching, deriving Wiener-Hopf equation, factorization (see [11] for details) we arrive at the following infinite linear system:

$$\sum_{m=1}^{\infty} W_{pm}M_m = M^{(i)}w_p, \quad p = 1,2,\ldots, \quad (3)$$

$$W_{pm} = \left(k_{zm}\varepsilon^{-1} + \alpha_p\right)\eta_m(\alpha_p) - \frac{\zeta_m(\alpha_p)}{k_{zm} - \alpha_p} + u_p \times \sum_{q=1}^{\infty}\left[\left(\frac{k_{zm}}{\varepsilon} - \alpha_q\right)\eta_m(\alpha_q) - \frac{\zeta_m(\alpha_q)}{k_{zm} + \alpha_q}\right]v_{pq}, \quad (4)$$

$$w_p = \left(k_{zl}\varepsilon^{-1} - \alpha_p\right)\eta_l(\alpha_p) - \frac{\zeta_l(\alpha_p)}{k_{zl} + \alpha_p} + u_p \times \sum_{q=1}^{\infty}\left[\left(\frac{k_{zl}}{\varepsilon} + \alpha_q\right)\eta_l(\alpha_q) - \frac{\zeta_l(\alpha_q)}{k_{zl} - \alpha_q}\right]v_{pq}, \quad (5)$$

$$u_p = \kappa_+(\alpha_p)G_+(\alpha_p)J_1(j_{0p})a/(2ij_{0p}),$$

$$v_{pq} = \kappa_+(\alpha_q)G_+(\alpha_q)j_{0q}\left[a^2\alpha_q J_1(j_{0q})(\alpha_p + \alpha_q)\right]^{-1},$$

$M^{(i)}$ is amplitude constant for the incident mode, $G(\alpha) = \pi a\kappa J_0(a\kappa)H_0^{(1)}(a\kappa) = G_+(\alpha)G_-(\alpha)$ (subscripts $\pm$ mean that function is holomorphic and free of poles and zeros in areas $\mathrm{Im}\,\alpha > -\delta$ and $\mathrm{Im}\,\alpha < \delta$, correspondingly), $\kappa = \sqrt{k_0^2 - \alpha^2}$, $\kappa_\pm = \sqrt{k_0 \pm \alpha}$, $\alpha_q = \sqrt{k_0^2 - j_{0q}^2/a^2}$, $J_0(j_{0m}) = 0$, functions $\Pi(\alpha)$, $\eta_m(\alpha)$, $\zeta_m(\alpha)$ are defined in [11]. For finite p and $m \to +\infty$ we have $W_{pm}M_m = o(m^{-3/2})$, the series (3) converges and can be solved numerically.

For $z > 0$ the following representation holds:

$$H_{\omega\varphi} = \sum_{q=1}^{\infty}\Pi(-\alpha_q)\frac{\kappa_+(\alpha_q)G_+(\alpha_q)j_{0q}}{a^2b^{-1}\alpha_q J_1(j_{0q})}\frac{L_q^+(\rho,z)}{2}, \quad (6)$$

* Work supported by Russian Science Foundation, Grant No. 18-72-10137
† s.galyamin@spbu.ru

ISBN: 978-3-95450-227-1 ISSN: 2673-5490 doi:10.18429/JACoW-IPAC2022-MOPOMS052

6 MeV NOVEL HYBRID (STANDING WAVE - TRAVELING WAVE) PHOTO-CATHODE ELECTRON GUN FOR A THz SUPERRADIANT FEL

A. Nause*, A. Fridman, A. Weinberg, L. Feigin, Ariel University, Ariel, Israel
A. Fukasawa, J. Rosenzweig, University of California in Los Angeles, US
B. Spataro, INFN, Rome, Italy

Abstract

A novel 6 MeV hybrid photo injector was designed and commissioned at the Schlesinger center in Ariel University in Israel as an on-going collaboration with UCLA. This unique, new generation design provides a radically simpler approach to RF feeding of a gun/buncher system, leading to a much shorter beam via velocity bunching owed to an attached traveling wave section of the photo-injector. This design results in better performance in beam parameters, providing a high-quality electron beam, with energy of 6 MeV, emittance of less than 3μm, and a 150 fs pulse duration at up to 1 nC per pulse. The Hybrid gun is driven by a SLAC XK5 Klystron as the high-power RF source, and third harmonic of a fs level IR Laser amplifier (266 nm) to extract electrons from the Cathode. The unique e-gun will produce a bunched electron pulse to drive a THz FEL, which will operate at the super-radiance regime, and therefore requires extraordinary beam properties. It will also be used for MeV UED experiments in a separate line using a dogleg section. Here we describe the gun and presents experimental results from the gun and its sub-systems, including energy and charge measurements, compared with the design simulations.

HYBRID PHOTO-CATHODE GUN

A Hybrid S-band (2856 MHz) photo injector is in operation in Ariel University [1, 2], also seen in Fig. 1. It was designed by the PBPL (Particle Beam Physics Laboratory) group at UCLA [3], based on a lower-energy prototype [7]. Main purpose on the gun is to drive a 150 kW, ultra-fast THz-FEL, using a 90 cm Undulator, emitting super-radiantly at 1-3 THz [6]. In order for the electrons to emit coherently, the emitting electron bunch must be shorter than the wavelength of the emitted radiation (Fig. 2).

Figure 1: FEL beam line at the Schlesinger center in Ariel University

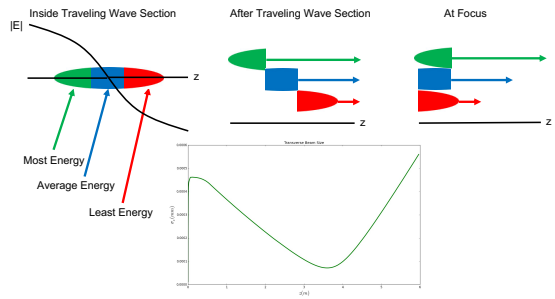

Figure 2: Conversion of applied velocity bunching by the traveling wave section of the gun, to a density bunching after a drift. Green line shows longitudinal compression of the e-bunch.

RF Cavity Design

The Hybrid cavity is an integrated structure consisting of a relatively low gradient initial standing wave (SW) gun cells (3.5) connected at the input coupler to even lower field, long traveling wave (TW) section (9 cells) with most of the RF power passing through the device and being directed to a load (another acceleration section can be added later). This novel design strongly mitigates RF reflections, as the SW section represents a small fraction (~10%) of the power usage, and the TW section is approximately impedance matched to the input waveguide. Thus there is no need for an RF circulator or coupler system to protect the klystron.

The RF coupling shown in Fig. 3 is accomplished in the fifth cell encountered by the beam, with the SW section electrically coupled to it on-axis. This mode of coupling is particularly fortuitous, as it is accompanied by a 90 deg phase shift in the accelerating field, resulting in strong velocity bunching effects on the beam that reverse the usual bunch lengthening induced after the gun exit in standard 1.6 cell photo-injectors.

Focusing solenoids are placed over the initial cells to control the beam, as transverse space-charge effects are more pronounced with low α_{RF} (the normalised vector potential of the accelerating field) designs [8]. Despite the need for focusing close to the cathode, the required solenoid fields are not high, peaking at 1.5 kG, thus making the solenoid implementation practical. This large Solenoid, with three separate sections (each with a different static magnetic field profile) is covering most of the gun cells as can be seen in Fig. 3.

* arieln@ariel.ac.il

ISBN: 978-3-95450-227-1 ISSN: 2673-5490 doi:10.18429/JACoW-IPAC2022-MOOPLGD2

SPS-II: A 4th GENERATION SYNCHROTRON LIGHT SOURCE IN SOUTHEAST ASIA

P. Klysubun†, P. Sudmuang, T. Pulampong, T. Chanwattana, S. Jummunt, P. Sunwong, S. Prawanta, A. Kwankasem, N. Juntong, T. Phimsen, S. Boonsuya, S. Srichan, O. Utke, K. Sittisard, P. Photongkam, Synchrotron Light Research Institute, Nakhon Ratchasima, Thailand

Abstract

Upon its completion, Siam Photon Source II (SPS-II) will be the first 4th generation synchrotron light source in Southeast Asia. The 3.0 GeV, 327.5 m storage ring based on the Double-Triple Bend Achromat lattice will have the natural emittance of 0.97 nm·rad. The storage ring includes 14 long and 14 short straight sections for insertion devices and machine subsystems. The beam injection will be performed by a 150 MeV linear accelerator and a full-energy concentric booster synchrotron sharing the same tunnel with the storage ring. In the first phase, there will be 7 insertion devices and 7 associated beamlines with the end stations for different techniques utilizing synchrotron radiation from 80 eV to 60 keV. High-energy and high-brightness radiation generated by the new light source will serve as one of the most powerful analytical tools in the region for advanced science and technology research.

INTRODUCTION

Siam Photon Source II (SPS-II), when completed, will be among the most important scientific research infrastructures in Southeast Asia. It will play a significant role in supporting Thailand, as well as other ASEAN countries, in the transition to research and innovation-driven economy. The facility will be available to synchrotron radiation users from within Thailand, from all the ASEAN countries, and from around the world. This new light source will strengthen scientific community in the region by providing high-energy and high-intensity synchrotron light for both academic and industrial research. The facility will be constructed at the Eastern Economic Corridor (EEC) area in the EECi (EEC of innovation) district in Rayong Province in order to provide support to the high-tech industry in the area. SPS-II will provide better photon beam characteristics compared to the existing Siam Photon Source (SPS) and will be globally competitive for the growing user community in the region.

SPS-II MACHINE OVERVIEW

Though it is a new machine, SPS-II has some constraints on its size due to the available area of its designated location and financial reasons. Medium size storage ring with the circumference below 400 m is sufficient to provide photon beam with emittance below 1.0 nm·rad while being able to accommodate more than 20 Insertion Device (ID) beamlines.

† pklysubun@slri.or.th

SPS-II accelerator complex consists of three main components as illustrated in Fig. 1: a 150 MeV injector linac, a 3 GeV booster synchrotron, and a 3 GeV electron storage ring. Electrons are supplied to the linac by a thermionic pulsed DC gun. The 3 GeV storage ring has a circumference of 327.5 m and the electron beam emittance of 0.97 nm·rad. The lattice is a Double Triple Bend Achromat (DTBA) lattice which was first proposed for the upgrade of Diamond Light Source [1]. The storage ring consists of 14 DTBA cells, resulting in 14 long and 14 short straight sections. Maximum stored beam current will be 300 mA [2].

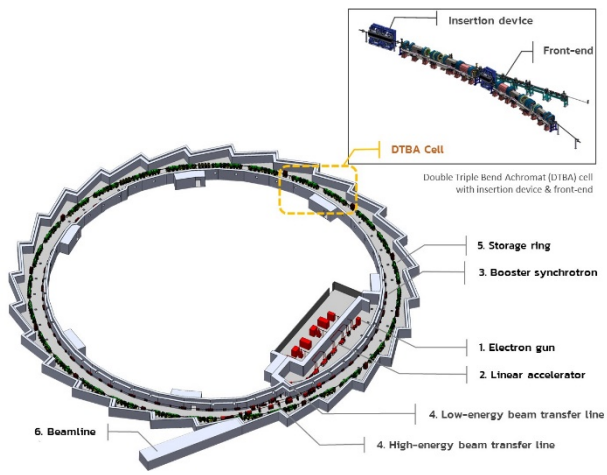

Figure 1: SPS-II accelerator complex.

In the process of designing SPS-II, we focus on three main aspects: performance, feasibility, and productivity. The DTBA lattice is adopted to achieve the beam emittance below 1.0 nm·rad, and to have an extra 3.10-m short straight section in the middle of DTBA cell in addition to the 5.02-m long straight section. As such, productivity or space usage reaches over 35%. The middle straight section can comfortably accommodate an undulator with the length of up to 2 m. To ensure manufacturing feasibility, requirements and specifications of the main machine components are kept moderate, for example, the required magnetic field and magnetic field gradient of the SPS-II magnets are modest and the magnets can be manufactured using available technologies.

The photon beam delivered by the much smaller electron beam of SPS-II compared to that of SPS provides higher brightness and coherence fraction. The new lattice cell offers twice the number of available straight sections for IDs per cell. Like most recent synchrotron light sources, the main radiation sources will be IDs, however, Infrared (IR) radiation can be extracted from SPS-II bending magnets.

ISBN: 978-3-95450-227-1 ISSN: 2673-5490 doi:10.18429/JACoW-IPAC2022-TUOXGD1

DESIGN AND CONSTRUCTION OF OPTICAL SYSTEM OF THE CORONAGRAPH FOR BEAM HALO OBSERVATION IN THE SUPERKEKB

G. Mitsuka*, T. Mitsuhashi, H. Ikeda, KEK, 1-1 Oho, Tsukuba, Ibaraki 305-0801, Japan

Abstract

We developed the coronagraph to measure beam halo in the SuperKEKB electron-positron collider. The coronagraph consists of three stages of optical systems: objective system, re-diffraction system, and relay system. As the coronagraph would be used 60 m downstream of the synchrotron radiation source point, an objective system with a long focal length was required. Because of the dimension of the diamond extraction mirror (20 mm (W) × 23 mm (H)) installed at 23.6 m downstream of the source point, the entrance pupil of the objective system was accordingly limited. To make a coronagraph achieve enough resolution in these constraints, we designed a reflective telephoto system based on the Gregorian telescope for the objective system. The focal length was 7028 mm, and the front principal plane was at the diamond mirror. The re-diffraction and relay systems were also designed based on a Kepler-type telescope. As a result of initial testing using the SuperKEKB electron and positron beams, the performance of the objective system had a diffraction-limited quality, and we achieved a contrast of six orders of magnitude. We present in this paper the early results of the measurements of beam halo at SuperKEKB.

DESIGN AND CONSTRUCTION OF GREGORIAN OBJECTIVE SYSTEM

Obtaining high contrast at the final stage in a coronagraph needs large transverse magnification at the first objective system. As shown in Fig. 1, the location of the coronagraph is 60 m downstream of the synchrotron radiation (SR) source point, and the entrance pupil of the objective system is limited to the aperture of the diamond mirror 20 mm (W) × 23 mm (H). For acquiring high transverse magnification in these conditions, we employ a telephoto system for the objective system. And to eliminate a chromatic aberration, this system adopts a reflective mirror system rather than a refractive lens system.

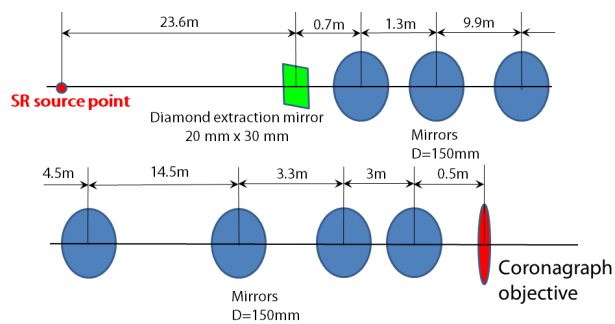

Figure 1: Geometry of the SR visible light optic axis.

One choice we consider here is which telescope system we use for the telephoto reflective system: Cassegranian or Gregorian. Our coronagraph chooses a Gregorian system (the top panel of Fig. 2) that uses a parabolic first mirror and an elliptical-concave second mirror (like a shallow parabolic). Making an elliptical-concave mirror is much easier than a hyperbaric-convex mirror employed in a Cassegranian system's secondary mirror.

The bottom panel of Fig. 2 shows the optical design of the objective system. The designed focal length is 7028 mm, the front principal plane is on the diamond mirror, and the distance between the front and rear principal planes is 24 608 mm. The first mirror is a parabolic concave mirror with a focal length of 1200 mm and the second mirror is a shallow elliptical mirror having a focal length of 205 mm.

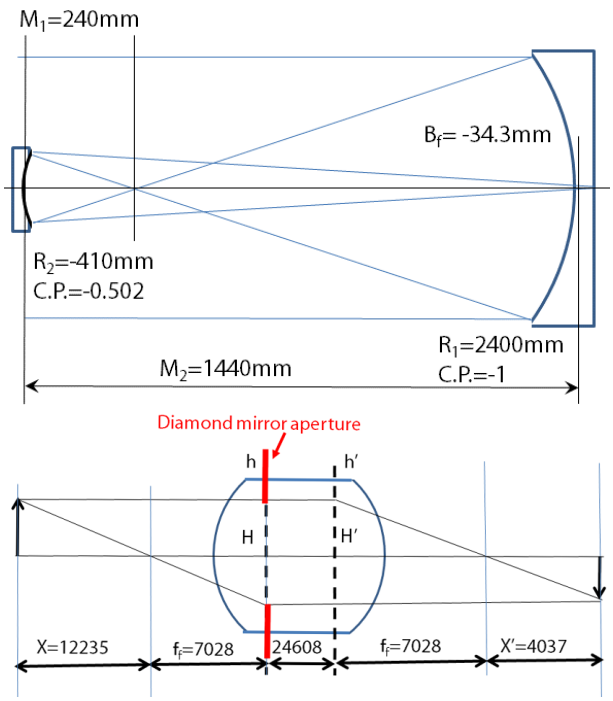

Figure 2: Top: A Gregorian objective system. Bottom: Conjugated system of the objective system.

Another concern in the optics design is scratching and digging on the surfaces of mirrors and lenses, which cause unwanted scattering noises [1]. Less number of lens surfaces in the focusing system reduces scattering noises. Therefore a well-polished singlet lens has been ordinally used in a coronagraph. We applied a special optical polishing to the second elliptical and optical flat mirrors to eliminate scattering sources such as scratch and dig. Note that the first parabolic mirror is made with a normal-grade optical polishing, since primarily the light intensity per area on the mirror

* gaku.mitsuka@kek.jp

ISBN: 978-3-95450-227-1 ISSN: 2673-5490 doi:10.18429/JACoW-IPAC2022-TUOXGD2

WIRELESS IoT IN PARTICLE ACCELERATORS: A PROOF OF CONCEPT WITH THE IoT RADIATION MONITOR AT CERN

Salvatore Danzeca, Alessandro Zimmaro, Tony Cass, Alessandro Masi, Rodrigo Sierra, CERN
CH-1211, Geneva 23, Switzerland

Abstract

The Internet of Things (IoT) is an ecosystem of web-enabled "smart devices" that integrates sensors and communication hardware to collect, send, and act on data acquired from the environment around them. In particle accelerators, IoT is not a new concept: systems and instruments have long been connected to the network to receive and to send data that are stored, analysed, and later used. What has been missing so far, is the IoT concept of "smart devices", and particularly of "wireless connectivity". Wireless technologies play an important role in the Internet of Things. Indeed, they allow to deploy of operational devices quickly and easily, and they significantly reduce infrastructure costs. This paper gives an overview of the main advantages of using LoRa, a particular IoT technology used to deploy wireless radiation monitors within the CERN particle accelerator complex.

INTRODUCTION

At CERN, measurements of the radiation fields and quantities related to damage to electronics equipment are carried out by the RadMon system. The RadMon devices allow to measure radiation levels in the accelerator complex and investigate if instantaneous failures of electronic systems are caused by radiation. As with other accelerator instruments, these devices have limited mobility and are subject to a fixed location, which is usually close to critical equipment in the beam lines or experimental caverns. Wireless IoT Radiation Monitors have been developed as the result of the growing demand to carry out radiation measurements wherever the cabled infrastructure is not available. Here we describe the technologies used for the project and the various advantages of their deployment in a particle accelerator environment. Although the focus is on radiation monitoring applications, the work is aimed at developing an IoT platform capable of integrating multiple and diverse sensors and applications. This approach opens up the way for the deployment of different and heterogeneous implementations and applications that would have been impractical so far. In the first section, the IoT and the RadMon concepts are discussed along with their use and impact in the context of the control of particle accelerators. The second section describes the requirements and the characteristics of a wireless IoT network for particle accelerators, as well as the technology used in this proof of concept.

Finally, the IoT platform developed for radiation monitoring is presented along with the challenges and the possibilities that can be exploited in the future.

IoT AND RADIATION MONITORING

IoT

The term IoT includes everything connected to the internet. It is a concept that covers devices, networks, services, and data. All these layers were defined in the 2014 Cisco "reference" model [1]. The seven layers defined in the reference model are not uncommon to particle accelerators; indeed, all the equipment, sensors, and devices are connected and well-integrated in what is usually called a "control system" [2]. One of the big differences between the two relies on the connectivity possibilities. Particle accelerators strongly rely on cabled networks and wired infrastructure, while the IoT concept gained great momentum mainly thanks to a new generation of wireless technologies. If implemented in a particle accelerator, this allows quick connectivity, easy installation, and virtually no cabling. This has a huge impact on a) availability: being easy to install when needed with small deadtime b) observability: giving the multiple positions that the devices can reach, and, obviously, c) cost.

RadMon

In this work, the radiation monitoring system for CERN electronics serves as a practical example of how to embrace IoT technology, highlighting its main requirements and capabilities. RadMon is a system capable of measuring the main quantities related to the radiation effects on electronics, such as the Total Ionizing Dose (TID), the Displacement Damage (DD) [3] the High Energy Hadron fluence (HEH), and the Thermal Neutron fluence (ThN). This device is used to monitor the radiation levels on the electronic systems in the accelerators, anticipate electronic degradation, benchmark simulations and help in the investigation into the cause of failures.

The RadMon system is fully integrated into the CERN infrastructure [3]. It requires two cables, for power and for communication with a Front-End Computer (FEC) which can manage up to 32 devices on same Fieldbus [4]. In operation, it's very common for users to request measurements in locations where RadMons are not installed. It is very difficult, even impossible, to plan proactively, because they respond to the need of tracking failures on specific equipment. For these operational cases, a wireless, battery-powered, standalone radiation monitor has been introduced. The challenges of these types of developments are a) wireless communication from a few hundred to a few km range with a data rate of ~1kB/h; b) low power electronics capable of running over batteries for at least one year; c) radiation tolerance up to at least 250 Gy and d) low cost.

ISBN: 978-3-95450-227-1 ISSN: 2673-5490 doi:10.18429/JACoW-IPAC2022-TUOXGD3

6D PHASE SPACE DIAGNOSTICS BASED ON ADAPTIVELY TUNED PHYSICS-INFORMED GENERATIVE CONVOLUTIONAL NEURAL NETWORKS

A. Scheinker*, Los Alamos National Laboratory, Los Alamos, USA
D. Filippetto, Lawrence Berkeley National Laboratory, Berkeley, USA
F. Cropp, University of California Los Angeles, Los Angeles, USA

Abstract

A physics-informed generative convolutional neural network (CNN)-based 6D phase space diagnostic is presented which generates all 15 unique 2D projections (x, y), (x, y'),...,(z, E) of a charged particle beam's 6D phase space (x, y, z, x', y', E). The CNN is trained by supervised learning over a wide range of input beam distributions, accelerator parameters, and the associated 6D beam phase spaces at multiple accelerator locations. The CNN is applied in an unsupervised adaptive manner without knowledge of the input beam distribution or accelerator parameters and is robust to their unknown time variation. Adaptive feedback automatically tunes the low-dimensional latent space of the encoder-decoder CNN to predict the 6D phase space based only on 2D (z, E) longitudinal phase space measurements from a device such as a transverse deflecting RF cavity (TCAV). This method has the potential to provide diagnostics beyond the existing state of the art at many accelerator facilities. Studies are presented for two very different accelerators: the 5-meter-long ultra-fast electron diffraction (UED) HiRES compact accelerator at LBNL and the kilometer long plasma wakefield accelerator FACET-II at SLAC.

INTRODUCTION

Particle accelerators are large complex systems with many coupled components. Accelerator beams are complex objects with dynamics governed by nonlinear collective effects such as space charge and coherent synchrotron radiation. Because of their complexity, particle accelerator controls and diagnostics can greatly benefit from advanced machine learning (ML) [1], and control theory techniques.

Supervised learning techniques are being applied at CERN for the reconstruction of magnet errors in the incredibly large (thousands of magnets) LHC lattice [2]. Bayesian methods have been developed for online accelerator tuning of the LCLS [3], Bayesian methods with safety constraints are being developed at the SwissFEL and the High-Intensity Proton Accelerator at PSI [4], and at SLAC Bayesian methods are being developed for the challenging problem of hysteresis [5] and surrogate models are being developed for the beam at the injector [6]. Convolutional neural networks (CNN) have been used to generate incredibly high resolution virtual diagnostics of the longitudinal phase space (LPS) of the electron beam in the EuXFEL [7]. A laser plasma wakefield accelerator has also been optimized by utilizing Gaussian processes at the Central Laser Facility [8].

A limitation of standard ML methods is the requirement of re-training whenever a system changes. Because accelerators are changing continuously and detailed beam measurements usually interrupt operations repetitive re-training is not a feasible solution. Recently, powerful model-independent feedback control methods, known as extremum seeking (ES), have been developed which can handle unknown and quickly time-varying nonlinear systems in which the direction of the controller's input is unknown and quickly time-varying [9, 10]. For example, it is possible to use ES for RF cavity resonance control based only on ambiguous reflected power measurements [11]. A limitation of model-independent feedback is the possibility of getting stuck in a local minimum.

Due to the complimentary strengths and weaknesses of ML and model-independent feedback, efforts are being made to combine the two fields via adaptive ML (AML) which provides the best of both worlds: an ability to learn directly from large complex data, while maintaining robustness to time variation and distribution shift. The first demonstration of the AML approach was the use of neural networks together with ES for automatic control of the time-varying longitudinal phase space distribution of the LCLS beam [12]. AML methods have also combined CNNs and ES to track time-varying input beam distributions at the HiRES UED [13], and preliminary results have shown an ability to adaptively tune the low-dimensional latent space of encoder-decoder CNNs to track all 15 unique 2D projections of beam's 6D phase space despite unknown and time-varying input beam distributions and accelerator and beam parametes [14].

AML FOR 6D DIAGNOSTICS

In this work we present simulation-based AML studies at the HiRES UED [15], for predicting all 15 unique 2D projections of a charged particle beam with unknown and time-varying input beam conditions at the photocathode, unknown beam charge and injector solenoid magnet strength, and demonstrate that this method has the capability to accurately predict beyond the span of the training set data.

Time-varying systems, or systems with distribution shift, are an open problem and an active area of research in the ML community [16–20]. In this work we tackle the problem of distribution shift by incorporating model-independent adaptive feedback directly within the architecture of an encoder-decoder CNN which takes beam distributions and parameters (charge and solenoid current) as inputs and generates

* ascheink@lanl.gov

ISBN: 978-3-95450-227-1 ISSN: 2673-5490 doi:10.18429/JACoW-IPAC2022-TUOXSP1

ORIGIN AND MITIGATION OF THE BEAM-INDUCED SURFACE MODIFICATIONS OF THE LHC BEAM SCREENS

V. Petit*, P. Chiggiato, M. Himmerlich, S. Marinoni, H. Neupert, M. Taborelli, L. Tavian
European Organization for Nuclear Research, CERN, Geneva, Switzerland

Abstract

All over Run 2, the LHC beam-induced heat load on the cryogenic system exhibited a wide scattering along the ring. Studies ascribed the heat source to electron cloud build-up, indicating an unexpected high Secondary Electron Yield (SEY) of the beam screen surface in some LHC regions. The inner copper surface of high and low heat load beam screens, extracted during the Long Shutdown 2, was analysed. On the low heat load ones, the surface was covered with the native Cu_2O oxide, while on the high heat load ones CuO dominated at surface, and it exhibited a very low carbon coverage. Such chemical modifications increase the SEY and inhibit a proper conditioning of the affected surfaces. Following this characterisation, the mechanisms for CuO build-up in the LHC beam pipe were investigated on a newly commissioned cryogenic system allowing electron irradiation, surface chemical characterisation by X-ray Photoelectron Spectroscopy and SEY measurements on samples held below 15 K. In parallel, curative solutions against the presence of CuO in the LHC beam screens were explored, which could be implemented in-situ to recover a proper conditioning and lower the beam-induced heat load.

INTRODUCTION

An unexpected high beam-induced heat load was measured in the beam screen cooling circuit of half of the eight LHC arcs all over Run 2 (2015-2018). This puzzling data was detected first after the Long Shutdown 1 (LS1), a period of maintenance and upgrade including the venting of the cryogenic beam vacuum system to air [1]. Surface analyses were performed on the copper layer of beam screens extracted from the accelerator during the LS2 (2019-2021). The measurements evidenced the presence of native Cu_2O oxide on the surface of the low heat load beam screens, while the high heat load ones were oxidized to non-native CuO oxide and showed an exceptionally low carbon coverage [2]. In addition, the Secondary Electron Yield (SEY) of the beam screens after extraction was found higher when CuO was present. Finally, the room temperature conditioning by electron irradiation of CuO-rich surfaces was observed to be moderate compared to the one of Cu_2O, but not completely inhibited, and CuO was observed to be partially reduced to Cu_2O [2]. This reduction could be hindered or slowed down in the operating conditions of the beam screens, namely between 5 and 20 K, leading to the survival of a high-SEY oxide in some LHC beam screens, to an intense electron cloud activity and to the related high beam-induced heat load. Here, the behaviour of CuO under electron irradiation in cryogenic conditions and the origin of its build-up in some LHC beam screens are assessed. In addition, possible techniques for in-situ CuO reduction are reviewed.

CONSEQUENCE AND ORIGIN OF CuO BUILD-UP IN THE LHC

The cryo-conditioning tests performed in this work were carried out on a new system enabling X-ray photoelectron spectroscopy (XPS), electron irradiation and SEY measurement (part still under commissioning) of samples below 15 K. Irradiation was performed by 250 eV electrons.

Cryo-conditioning of CuO

The fraction of CuO at the surface of beam screen samples was deduced from XPS measurements of the Cu $2p_{3/2}$ state [3]. CuO fraction evolution during electron irradiation at 250 eV, both at room temperature and 15 K, is shown in Fig. 1.

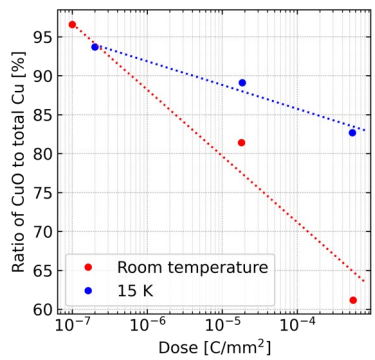

Figure 1: Effect of temperature on CuO reduction under electron irradiation at 250 eV (lines are guide to the eye).

CuO reduction is significantly hindered at 15 K, possibly because of the reduced diffusivity of Cu and O ions in the oxide layer at cryogenic temperature. Therefore, the build-up and the stability of this high-SEY oxide at cryogenic temperature together with the low content of carbon, which limits the graphitic coverage essential for SEY decrease [4, 5], could be responsible for the high beam-induced heat load occurring in some regions of the LHC arcs.

Origin of CuO build-up

Copper hydroxide $Cu(OH)_2$, which spontaneously grows on air-exposed copper surfaces [6], has been proposed as a precursor for CuO build-up in the LHC [2]. However, room temperature conditioning of airborne $Cu(OH)_2$ layers led to their conversion to Cu_2O, i.e. a reduction to Cu^+, which has a sufficiently low SEY [5]. Nevertheless, also in this case, temperature is expected to play a major role in elec-

*valentine.petit@cern.ch

ISBN: 978-3-95450-227-1 ISSN: 2673-5490 doi:10.18429/JACoW-IPAC2022-TUOXSP2

ANALYSIS OF LOW RRR SRF CAVITIES*

K. Howard†, Y.-K. Kim, University of Chicago, Chicago, IL, USA
D. Bafia, A. Grassellino, Fermi National Accelerator Laboratory, Batavia, IL, USA

Abstract

Recent findings in the superconducting radio-frequency (SRF) community have shown that introducing certain impurities into high-purity niobium can improve quality factors and accelerating gradients. Success has been found in nitrogen-doping, diffusion of the native oxide into the niobium surface, and thin films of alternate superconductors atop a niobium bulk cavity. We question why some impurities improve RF performance while others hinder it. The purpose of this study is to characterize the impurity profile of niobium with a low residual resistance ratio (RRR) and correlate these impurities with the RF performance of low RRR cavities so that the mechanism of recent impurity-based improvements can be better understood and improved upon. Additionally, we perform a low temperature bake on the low RRR cavity to evaluate how the intentional addition of oxygen to the RF layer affects performance. We have found that low RRR cavities experience low temperature-dependent BCS resistance behavior more prominently than their high RRR counterparts. The results of this study have the potential to unlock a new understanding on SRF materials.

INTRODUCTION

As we approach the theoretical limit of niobium for superconducting radio-frequency (SRF) cavities, the last decade has brought immense improvements in quality factor (Q_0) and accelerating gradients though intentionally added impurities into the niobium surface [1, 2]. Many SRF studies follow a "clean bulk dirty surface" technique to optimize the BCS resistance by adding extrinsic impurities to the surface layer of high purity niobium [3, 4]. Advancements have been made with nitrogen through N-doping, where cavities experience an anti Q_0 slope and record breaking Q_0's at mid fields [5–7]. Oxygen added through a low temperature bake (LTB) has also provided high Q_0's and mitigation of the high field Q_0 slope typically seen in electropolished (EP) niobium cavities [8, 9].

The success of intentionally added impurities to the niobium surface has drawn deeper questions about how these impurities affect cavity behavior, and has prompted an investigation of cavities with a low residual resistance ratio (RRR). Low purity niobium has been studied before in the context of cost reduction [10]; here we are looking through the lens of using the intrinsic impurities as a resource to optimize the BCS resistance. RRR and mean free path (mfp) have a direct relationship, so we might expect experience low BCS resistance behavior at low RRR, as seen in Fig. 1. We ask if the intrinsic impurities perform similar functions as extrinsic impurities which have been shown to improve performance.

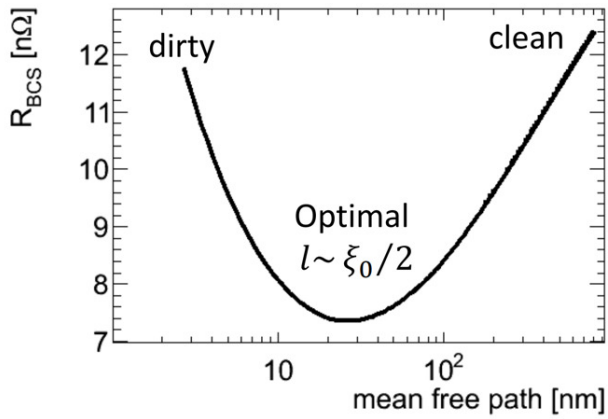

Figure 1: BCS resistance versus mean free path shows an optimization in BCS resistance for moderately dirty surface, adapted from [11].

In this study, we investigate a single-cell TESLA-shaped 1.3 GHz cavity with RRR 61 and primary impurity tantalum at weight percent 0.0193. First, the cavity receives EP treatment to give a uniform surface layer same as the bulk [12]. The testing involves a measurement of Q_0 versus accelerating gradient in the vertical test stand [2], as well as frequency versus temperature [13]. We compare the performance of this cavity with its high RRR counterpart in EP condition to understand how the intrinsic impurities affect the bulk and surface behavior of the cavity. Then, we perform a LTB at 120 °C for 48 hours and repeat the testing to evaluate how the addition of the surface oxide to the RF layer further affects performance.

RESULTS

Quality Factor

We measure the Q_0 at a given gradient by maintaining the cavity at its resonant frequency, pumping power in, and then measuring the reflected and transmitted power [14]. The Q_0 is defined as the ratio of the energy gain per RF period and dissipated power.

The Q_0 at 2 K is graphed in Fig. 2. The transition from EP to LTB condition in the low RRR cavity shows a slight increase in Q_0 at low gradients, as well as improved performance through higher gradients. All cavities' performance is similar at mid gradients. Oxygen improves performance of low RRR cavity but in a different way than we see in high RRR cavities, as the LTB treatment delays Q_0 slope in low

* This manuscript has been authored by Fermi Research Alliance, LLC under Contract No. DE-AC02-07CH11359 with the U.S. Department of Energy, Office of Science, Office of High Energy Physics. This work was supported by the University of Chicago.
† khoward99@uchicago.edu

ISBN: 978-3-95450-227-1 ISSN: 2673-5490 doi:10.18429/JACoW-IPAC2022-TUOXSP3

EVALUATION OF GEOMETRICAL PRECISION AND SURFACE ROUGHNESS QUALITY FOR THE ADDITIVELY MANUFACTURED RADIO FREQUENCY QUADRUPOLE PROTOTYPE*

T. Torims†, A. Ratkus, G. Pikurs, D. Krogere, Riga Technical University, Riga, Latvia
M. Vretenar, A. Cherif, CERN, Geneva, Switzerland
S. Gruber, E. Lopez, Fraunhofer IWS, Dresden, Germany
M. Pozzi, M. Foppa Pedretti, Rösler Italian S.R.L, Concorezzo, Italy
P. Wagenblast, M. Thielmann, TRUMPF GmbH, Ditzingen, Germany
M. Vedani, Politecnico di Milano, Italy
N. Delerue, IJCLab, Orsay, France
T. Otto, TalTech, Tallinn, Estonia

Abstract

A multidisciplinary collaboration within the I.FAST project teamed-up to develop additive manufacturing (AM) technology solutions for accelerators. The first prototype of an AM pure-copper Radio Frequency Quadrupole (RFQ) has been produced, corresponding to ¼ of a 4-vane RFQ. It was optimised for production with state-of-the-art laser powder bed fusion technology. Geometrical precision and roughness of the critical surfaces were measured. Although the obtained values were beyond standard RFQ specifications, these first results are promising and confirmed the feasibility of AM manufactured complex copper accelerator cavities. Therefore, further post-processing trials have been conducted with the sample RFQ to improve surface roughness. Algorithms for the AM technological processes have also been improved, allowing for higher geometrical precision. This resulted in the design of a full 4-vane RFQ prototype. At the time of the paper submission the full-size RFQ is being manufactured and will undergo through the stringent surface quality measurements. This paper is discussing novel technological developments, is providing an evaluation of the obtained surface roughness and geometrical precision as well as outlining the potential post-processing scenarios along with future tests plans.

RFQ BY ADDITIVE MANUFACTURING

The RFQ is a crucial accelerator component downstream the particle source, providing simultaneous and efficient focusing, bunching and acceleration of a particle beam before injection into the linear accelerator [1]. Conventionally it is manufactured from highly conductive materials and consists of four complex shape segments with modulated vanes. To ensure optimum beam optics and radio-frequency properties, all internal surfaces of the RFQ are designed with high-precision tolerances and fine surface roughness parameters. Consequently, the standard RFQ manufacturing routine is complex; each sequence is costly, time consuming and requires expensive technological operations. Among other things, this involves series of multiple high-precision machining operations followed by specialized brazing and material stress-release treatment [2, 3]. Thus, there is an opportunity to re-evaluate established manufacturing approaches and to consider other emerging technologies.

Additive Manufacturing (AM) is a natural candidate, as one of the enabling technologies that has reached the required maturity level to be applied within the accelerator community. The comprehensive study carried out by the I.FAST project confirms the opportunities provided by AM technology [4, 5]. Initial results of the survey have revealed that metal AM activities within the community started already in 2007 and since, the number of applications is growing exponentially. This is explained by the virtues of AM technology: it is accessible, has wide applications within aerospace, medical and automotive industries and is changing the technological paradigm and way of thinking within the engineering wing of the accelerator community. Indeed, AM is offering valuable opportunities, such as the capability to work with a wide range of materials and to provide new design options [6]. Proliferation of the AM has led to the standardisation of this technology. For instance, today the ISO 52900:2021 standard [7] provides for general terms and common language for the growing AM community. Subsequently, series of the standards are being compiled within the Guide to AM Standards [8].

Furthermore, it has been demonstrated [9] that AM can contribute to the manufacturing routines of the RFQ's, e.g., is enabling for design optimisation and improved general properties. The biggest advantage is that AM allows for the RFQ to be built in a single piece, thereby avoiding the complex technological operations, and permitting the design of more efficient internal cooling channels. Recent attempt to produce with AM the pure copper drift tube linac components, is showing that cavity parameters (e.g. quality factor Q and shunt impedance per unit length R_L) are of comparable values to the conventionally machined elements [10].

At the same time, it is important to note that the pure copper, applied for RFQs, is a challenging material for laser-based AM processes itself. It requires state-of-the-art equipment and expertise which is not yet self-evident

* This project has received funding from the European Union's Horizon 2020 Research and Innovation programme under grant agreement No 101004730 and is supported by the Latvian Council of Science under grant agreement VPP-IZM-CERN-2020/1-0002.
† toms.torims@rtu.lv

ISBN: 978-3-95450-227-1 ISSN: 2673-5490 doi:10.18429/JACoW-IPAC2022-TUIYGD1

THE STATUS OF THE ESS PROJECT

A. Jansson, European Spallation Source ERIC, Lund, Sweden
on behalf of the European Spallation Source ERIC (ESS)
and the ESS Accelerator Collaboration

Abstract

The European Spallation Source (ESS), currently under construction in Lund, Sweden, will be the world's most powerful linear accelerator driving a neutron spallation source, with an ultimate beam average power of 5 MW at 2.0 GeV. The LINAC accelerates a proton beam of 62.5 mA peak current at 4 % duty cycle (2.86 ms at 14 Hz). The accelerator uses a normal conducting front-end bringing the beam energy to 90 MeV, beyond that the acceleration up to 2 GeV is performed using superconducting structures. The accelerator is built by a European collaboration consisting of 23 European institutes delivering in-kind contributions of most hardware but also of services for installation and testing. More than half of the original 510 M€ for the accelerator budget being in form of in-kind contributions. This talk will give an overview of the status of the ESS accelerator and comment on the challenges the accelerator collaboration has encountered and how we together are addressing these challenges.

THE ESS PROJECT

The European Spallation Source is currently under construction in Lund, Sweden. When in full operation it will host some 800 experiment and 3000 scientists annually.

The ultimate goal is to build a 5 MW LINAC based long pulse (2.86 ms) neutron sourced operating at 14 Hz serving 22 instruments. However, due to budget constraints the accelerator power has been reduced from 5 MW to 2 MW, by reducing the energy from 2 GeV to 800 MeV.

The number of neutron instruments have also been reduced from 22 to 15, and some detectors have had their coverage reduced. The reductions in the accelerator and instrument scope have been made in such a way that it can be restored at a later stage.

The target station, on the other hand, is being built for the full 5 MW scope. The reduction in accelerator power and instrument scope is largely offset by a significant improvement in the moderator design [1], resulting in a neutron brightness at the level of the original 5 MW design, and meaning the facility is still expected to be world leading shortly after it becomes operational.

First beam on target is expected in 2025, with user operation of the first few instruments planned for 2026 and the full 2 MW LINAC and 15 instruments operational at the end of 2027.

Figure 1: Aerial photograph of European Spallation Source Site, taken in April 2022.

ISBN: 978-3-95450-227-1 ISSN: 2673-5490 doi:10.18429/JACoW-IPAC2022-TUIYGD2

THE PRESENT STATUS AND FUTURE PLAN WITH CHARGE STRIPPER RING AT RIKEN RIBF

H. Imao†, RIKEN Nishina Center for Accelerator-Based Science, Wako, Japan

Abstract

RIKEN RI Beam Factory (RIBF), providing the world's most intense heavy-ion beams more than 345 MeV/u, is a leading facility for generating in-flight RI beams. The RIBF has been steadily developing its performance. In particular, the beam intensity of uranium beams, which is important to produce in-flight fission RI beams, was drastically increased by a factor of 240 compared to 2008.

For further intensity upgrade of the uranium beams, a new acceleration scheme with charge stripper rings (CSRs) as a cost-effective way to enhance the charge stripping efficiency has been proposed. The CSR recycles beams other than the selected charge state. The CSR is being studied as a future plan, aiming at a 20-fold increase in the intensity of the uranium beams. We present some calculation results on the key design issues of a CSR.

INTRODUCTION

The RIKEN RI Beam Factory (RIBF) [1] is a leading facility for generating in-flight RI beams. The RIBF is a cyclotron-based heavy ion accelerator complex, operating since 2006. The RIBF uses three injectors (RILAC [2,3], RILAC2 [4], and AVF cyclotron [5]) and four ring cyclotrons (RRC, RIKEN ring cyclotron, K = 540 MeV [6]; fRC, fixed-frequency ring cyclotron, K = 700 MeV [7, 8]; IRC, intermediate-stage ring cyclotron, K = 980 MeV [9]; and SRC, superconducting ring cyclotron, K = 2600 MeV [10]), which can accelerate various heavy ions of up to 345 MeV/u or more by utilizing three different acceleration modes. In-flight RI beams produced from the primary heavy ion beam are separated using BigRIPS [11] and are applied in various experiments for nuclear physics and different applications.

For the acceleration of uranium (^{238}U) beams, which are exceptionally important for the production of rare RI beams by in-flight fission, two charge stripping processes are applied. The uranium beam intensity, which was 0.4 pnA in 2008, has been drastically enhanced to approximately 117 pnA in 2020. This is due to the continuous performance improvements of the 28-GHz super-conducting ion source [12–14], several innovations in the durability and quality of the charge strippers [15–20], the sophistication of the high-intensity beam operation, and steady improvements in other various accelerator components [21–25].

ACCELERATION SCHEME FOR ^{238}U AT RIBF

Figure 1 shows the acceleration scheme of uranium ions at RIBF. We use the He gas stripper and a rotating carbon-disk stripper in the acceleration scheme. U^{35+} ions originated from the superconducting ECR ion source is converted to U^{64+} with the stripping efficiency of ~20% at 10.8 MeV/u with the He stripper and then further converted to U^{86+} with the efficiency ~25% at the second stripper at 50.8 MeV/u. Both strippers solved lifetime problems of fixed carbon foil strippers for uranium accelerations. We briefly introduce the strippers in the followings.

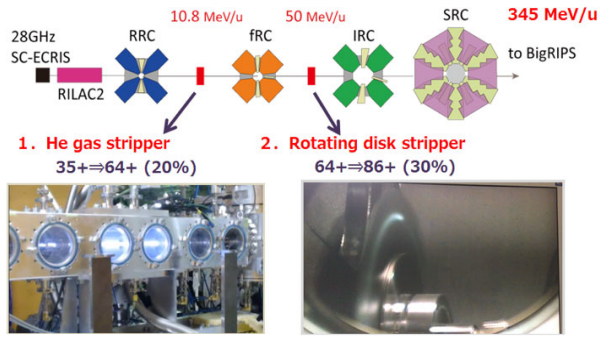

Figure 1: Acceleration scheme for ^{238}U at RIBF.

He Gas Stripper

Our group has developed a low-Z gas stripper to replace the traditional carbon-foil strippers [17–20]. The stripper is non-destructive and simultaneously provides uniform thickness and high charge state equilibrium of the low-Z gas. The high charge equilibrium is owing to the slow velocity of the 1-s electrons of low-Z gas. Such slow electrons are difficult to transfer to fast projectiles because of poor velocity matching so that the electron capture process is strongly suppressed.

One of the primary technical challenges in realizing the He gas stripper is gas confinement in a windowless vacuum because He gas is very diffusive. Figure 2 shows the actual design of the He gas stripper. The system consists of two 5-stage differential pumping systems, one on each side of the 50-cm target region. 26 pumps are used in the system. The stripper is designed to achieve vacuum reduction from the target pressure of 7 kPa to 10^{-5} Pa within a length of ~2 m while ensuring a 12-mm beam path. The He gas flow rate is about 300 m^3/day.

The stripper works well since 2012 and provide infinite lifetime for use.

Rotating Graphite Carbon Stripper

As the second stripper, we have developed rotating disk stripper [15, 16]. The module of the rotating stripper can provide the rotation speed up to ~1000 rpm. The disk diameter is 11 cm. It provides the irradiation area more

† imao@riken.jp

ISBN: 978-3-95450-227-1 ISSN: 2673-5490 doi:10.18429/JACoW-IPAC2022-TUIYGD3

FRIB COMMISSIONING AND EARLY OPERATIONS*

J. Wei†, H. Ao, B. Arend, S. Beher, G. Bollen, N. Bultman, F. Casagrande, W. Chang, Y. Choi, S. Cogan, C. Compton, M. Cortesi, J. Curtin, K. Davidson, X. Du, K. Elliott, B. Ewert, A. Facco[1], A. Fila, K. Fukushima, V. Ganni, A. Ganshyn, T. Ginter, T. Glasmacher, J. Guo, Y. Hao, W. Hartung, N. Hasan, M. Hausmann, K. Holland, H.-C. Hseuh, M. Ikegami, D. Jager, S. Jones, N. Joseph, T. Kanemura, S.-H. Kim, C. Knowles, P. Knudsen, T. Konomi, B. Kortum, E. Kwan, T. Lange, M. Larmann, T. Larter, K. Laturkar, R.E. Laxdal[2], J. LeTourneau, Z.-Y. Li, S. Lidia, G. Machicoane, C. Magsig, P. Manwiller, F. Marti, T. Maruta, E. Metzgar, S. Miller, Y. Momozaki[3], M. Mugerian, D. Morris, I. Nesterenko, C. Nguyen, P. Ostroumov, M. Patil, A. Plastun, J. Popielarski, L. Popielarski, M. Portillo, J. Priller, X. Rao, M. Reaume, H. Ren, K. Saito, B. M. Sherrill, M. K. Smith, M. Steiner, A. Stolz, O. Tarasov, B. Tousignant, R. Walker, X. Wang, J. Wenstrom, G. West, K. Witgen, M. Wright, T. Xu, Y. Xu, Y. Yamazaki, T. Zhang, Q. Zhao, S. Zhao,
Facility for Rare Isotope Beams, Michigan State University, East Lansing, Michigan, USA
M. Wiseman, Thomas Jefferson National Laboratory, Newport News, Virginia, USA
M. Kelly, Argonne National Laboratory, Argonne, Illinois, USA
K. Hosoyama, KEK, Tsukuba, Japan
S. Prestemon, Lawrence Berkeley National Laboratory, Berkeley, California, USA
[1] also at INFN - Laboratori Nazionali di Legnaro, Legnaro (Padova), Italy
[2] also at TRIUMF, Vancouver, British Columbia, Canada
[3] also at Argonne National Laboratory, Argonne, Illinois, USA

Abstract

This paper summarizes the FRIB driver linac commissioning and early operations experience. Strategic planning, operational envelope conformance, technical risk mitigation, and lessons learned are discussed.

INTRODUCTION

Technical construction for the Facility for Rare Isotope Beams (FRIB) was completed in January 2022, five months ahead of the baseline schedule established about 10 years ago [1]. Beam commissioning was done in seven phases starting in 2017 when the normal-conducting ion source and RFQ were commissioned. In April 2021, the driver linac commissioning was completed with acceleration of heavy ions to energies above 200 MeV/nucleon (MeV/u) using 324 superconducting radiofrequency resonators housed in 46 cryomodules. In preparation for high-power operations, a liquid lithium charge stripper was used to strip the primary beams [2], and multiple charge states were accelerated simultaneously [3]. By January 2022, the target and fragment separator commissioning was completed, with rare isotope (RIs) produced and identified [4]. The first user scientific experiment was done in May 2022.

Because of the large project scope (Fig. 1), 8-year technical construction schedule, and state-of-the-art performance goals, FRIB developed a staged beam commissioning strategy. Table 1 summarizes the beam commissioning runs, each lasting for up to two weeks, with specific strategic goals.

Table 1: Beam Commissioning Stages for the FRIB Accelerator Complex

Run	Area with beam	Beam energy (MeV/u); species	Date	Main goals
1	Front end	0.5; Ar, Kr	Jul 2017	Front end and civil integration
2	+ 3 cryomodules	~2; Ar, Kr	May 2018	Cryogenic integration
3	FE + LS1 + FS1	~20; Ar, Kr, Xe, U	Feb 2019	QWR and charge stripping validation
4	+ FS1 + LS2	~200; Ar, Kr, Xe	Mar 2020	2 K cryogenics and HWR validation
5	+ FS2 + LS3 + BDS	~200; Ar, Kr, Xe	Apr 2021	Driver linac validation
6	+ target & beam dump	RI (Se, etc.)	Dec 2021	Targetry and RI production demonstration
7	+ fragment separator	~200; Ar, Kr	Jan 2022	Readiness for user operations

*Work supported by the U.S. Department of Energy Office of Science under Cooperative Agreement DE-SC0000661, the State of Michigan, and Michigan State University.
†wei@frib.msu.edu

ISBN: 978-3-95450-227-1 ISSN: 2673-5490 doi:10.18429/JACoW-IPAC2022-TUOZGD1

NEED FOR PORTABLE ACCELERATORS IN CULTURAL HERITAGE

T. K. Charles*[1], University of Liverpool, Liverpool, UK
A. Castilla†[2], Lancaster University, Lancaster, UK
R. M. Bodenstein, Thomas Jefferson National Accelerator Facility, Newport News, VA, USA
[1]also at Cockcroft Institute, Daresbury, UK
[2]also at CERN, Geneva, Switzerland

Abstract

Ion Beam Accelerators (IBA) centres have provided researchers with powerful techniques to analyse objects of cultural significance in a non-destructive and non-invasive manner. However, in some cases it is not feasible to remove an object from the field or museum and transport it to the laboratory. In this contributed talk, we present as a manner of a short review, examples of the benefits provided from these techniques in the study of material culture and discuss the initial steps to consider when investigating the feasibility of a compact accelerator that can be taken to sites of cultural significance for PIXE analysis. In particular, we consider the application of a compact, robust 2 MeV proton accelerator that can be taken into the field to perform PIXE measurements on rock art. We detail the main challenges and considerations for such a device.

INTRODUCTION

Ion Beam Accelerators (IBA) and synchrotron light source facilities have proved their worth in examining items of cultural heritage. As an example, the non-destructive nature of Ion Beam Analysis and X-Ray Fluoresce has allowed researchers to identify the exchange networks of variscite ($AlPO_4{\cdot}4H_2O$) in Southern Europe during the Neolithic [1]. Variscite was then a highly valued funerary jewel, commonly found in tombs, and these studies lead to identifying social inequalities during this period [2]. Other IBA contributions include the revelation of hidden portraits through measuring elemental maps in, for example, Van Gogh's *Patch of grass* [3], Degas' *Portrait of a Woman* [4], and many others.

These examples illustrate the powerful accelerator techniques that can be used to reveal secrets of artworks and material culture. However, some immovable items cannot take advantage of these techniques. A portable proton accelerator would be needed to study frescos, rock art, elements of the built environment, some archaeologically sites, or even sensitive items in museums that curators would prefer to not risk transporting. Presently, the only way to analyse these immovable objective with particle accelerators is by taking small destructive samples.

In these proceedings we take a close look at the need for a portable accelerator for rock art. Whilst there are many clear examples of cultural heritage that could benefit from a portable accelerator, rock art is possibly the most challenging, requiring robustness for operating in remote areas, and a design with optimised efficiency and minimal footprint and weight. If these more stringent challenges can be met, then the accelerator could equally be used in the other cases.

CASE STUDY: ROCK ART

Rock art can be found in many countries around the world. In some cases it's tens of thousands of years old, and forms a rich part of shared cultural heritage [5]. Unfortunately, with time, rock art fades. Often researchers take photos of the rock art, upload them to an image processing software like Photoshop or similar, and then adjust the contrast in order to better see how the rock art originally looked. This process is called digital enhancement [6, 7]. For examples of digital enhancement, see [8–11]. The fact that digital enhancement is so effective, means we know the pigments are still present, but the contrast between the pigments and the rock substrate is so close, we cannot easily make the distinction with our eyes.

Measuring 2-D elemental maps, that would outline where the pigments are located, could allow us to build up an image of the rock art (similar to the XRF examples that revealed hidden portraits). The remaining rock art pigment may exist in trace amounts or obscured by dust, grime or graffiti.

In our IPAC21 paper [12], we outline some of the main challenges and possible solutions to these challenges for a portable 2 MeV RFQ accelerator with the specific application of rock art.

OPTIONS FOR A PORTABLE DEVICE

The main requirements for an accelerator for cultural heritage investigations is that the beam be non-destructive and the accelerator be portable. An external beam is required, meaning that the particle beam exits the vacuum of the accelerator and travels through air in the last few centimeters between the sample and a thin window (for example SiNx).

Particle Induced X-ray Emission (PIXE) is a non-invasive and non-destructive technique, that can determine the elemental compositions of samples [13]. The basic principle of PIXE is as follows: particles (often protons, typically 2-5 MeV) are fired at the object, ionising an electron from an inner shell. When an electron from a higher energy shell falls down to fill the vacancy, it emits a characteristic X-ray photon, which can be used to identify the elements in the sample.

* tessa.charles@liverpool.ac.uk
† a.castilla@cern.ch

ISBN: 978-3-95450-227-1 ISSN: 2673-5490 doi:10.18429/JACoW-IPAC2022-TUOZGD2

A COMPACT SYNCHROTRON FOR ADVANCED CANCER THERAPY WITH HELIUM AND PROTON BEAMS*

M.Vretenar†, M. E. Angoletta, G. Bisoffi[1], J. Borburgh, L. Bottura, K. Paļskis[2], R. Taylor, G. Tranquille, CERN, Geneva, Switzerland
E. Benedetto, M. Sapinski[3], SEEIIST Association, Geneva, Switzerland

Abstract

Recent years have seen an increased interest in the use of helium for radiation therapy of cancer. Helium ions can be more precisely delivered to the tumour than protons or carbon ions, presently the only beams licensed for treatment, with a biological effectiveness between the two. The accelerator required for helium is considerably smaller than a standard carbon ion synchrotron.

To exploit the potential of helium therapy and of other emerging particle therapy techniques, in the framework of the Next Ion Medical Machine Study (NIMMS) at CERN, the design of a compact synchrotron optimised for acceleration of proton and helium beams has been investigated. The synchrotron is based on a new magnet design, profits from a novel injector linac, and can provide both slow and fast extraction for conventional and FLASH therapy. Production of mini-beams, and operation with multiple ions for imaging and treatment are also considered.

This accelerator is intended to become the main element of a facility devoted to a parallel programme of cancer research and treatment with proton and helium beams, to both cure patients and contribute to the assessment of helium beams as a new tool to fight cancer.

CANCER TREATMENT WITH HELIUM

The recent re-emergence of interest in the clinical use of helium ions for cancer treatment is mainly based on the underlying physical properties and corresponding biological effects - intermediate between the clinically approved proton and carbon ion beams.

Helium ion beams exhibit lower range straggling compared to proton beams, resulting in sharper Bragg peak and distal fall-off. Along with a reduction in multiple Coulomb scattering resulting in a decreased lateral penumbra, they can provide physical beam conformality comparable to carbon ion beams. Additionally, helium ions undergo less nuclear fragmentation processes than carbon ions, resulting in greatly reduced fragmentation tail and less complex mixed radiation beam, which in turn provides less uncertainties in biological effect estimations. The resulting secondary particle spectrum also exhibits decreased neutron production compared to carbon ions. The resulting neutron biological dose might be even lower than in proton beams [1], greatly reducing neutron dose associated risks in paediatric patients.

With linear energy transfer (LET) in the range of 4 to 40 keV/µm, helium ion beams exhibit an increased relative biological effectiveness (RBE) compared to protons, while also not reaching "overkill region" in the distal Bragg peak like high LET carbon beams [1]. With an increase in LET values, helium ions also provide reduction in oxygen enhancement ratio (OER) compared to proton beams, opening up certain possibilities for hypoxic tumour treatment.

Thanks to these characteristics, helium ion beams have potential to increase clinical efficacy for treatment sites in close proximity to vital organs and to even greater extent – i.e., in paediatrics. Along with better performance in ion radiography applications, pathways for in-vivo range verification and possibilities with treatment modalities as FLASH and mini-beams [2, 3], helium ion beam therapy holds a promising innovation position in cancer treatment.

ACCELERATOR MAIN PARAMETERS

The ideal accelerator to bring helium ions at cancer treatment energy is a compact synchrotron at a maximum magnetic rigidity of 4.5 T/m, corresponding to 220 MeV/u for 4He ions with a penetration of 30 cm in water, sufficient to access all types of cancer under consideration. The synchrotron will allow for the acceleration of proton beams at the energies required for cancer treatment and above, for proton radiography.

The synchrotron can be the central element of a facility for cancer research and therapy as sketched in Fig. 1. A linear accelerator injects proton or helium beams in the synchrotron. Operating at higher duty cycle than required for synchrotron injection, it can send beam to a target for production of radioisotopes to be used for imaging or for cancer treatment with alpha-emitters [4]. The beams extracted from the synchrotron can go to the treatment rooms, one of which equipped with a rotating superconducting gantry of novel design [5], or to an experimental room.

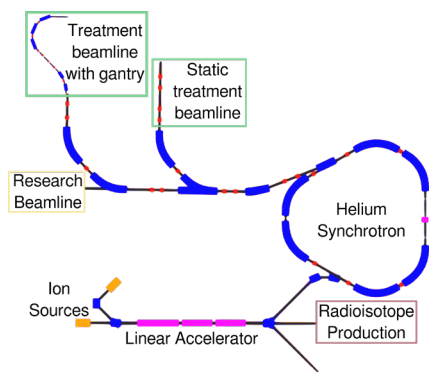

Figure 1: Layout of a compact cancer research and therapy facility with proton and helium beams.

* This study was partially supported by the European Union H2020 research and innovation programme under GA 101008548 (HITRIplus).
† Maurizio.vretenar@cern.ch
[1] on leave of absence from INFN-LNL, Legnaro, Italy
[2] permanent address: Riga Technical University, Riga, Latvia
[3] present address: PSI, Villigen, Switzerland

ISBN: 978-3-95450-227-1 ISSN: 2673-5490 doi:10.18429/JACoW-IPAC2022-TUIZSP1

STATUS OF THE e^+e^- COLLIDER PROJECTS IN ASIA AND EUROPE: CEPC AND FCC-ee

Xinchou Lou, IHEP, Beijing, China
F. Zimmermann, CERN, Geneva, Switzerland
M. Boscolo, INFN-LNF, Frascati, Italy

Abstract

Since the Higgs boson discovery at CERN, precision measurement of its properties has become the first priority in the field of High Energy Physics. Two laboratories, CERN from Europe and IHEP from China, are studying future large scale circular electron-positron colliders, namely FCC-ee and CEPC. Record luminosities are expected in the center of mass energy range from 90 to about 365 GeV. In this talk, the statuses of both projects are reviewed: Following the publication of the first CDR, FCC-ee and CEPC are entering the phase of consolidation and feasibility study. Special focus will be put on R&D plans, prototyping and key technologies.

SCIENCE MOTIVATION

The Higgs boson is a vital part of the Standard Model (SM). It is directly related to many mysteries that include the large hierarchy between the weak scale and the Planck scale, the nature of the electroweak phase transition, the origin of masses of fundamental fermions and the W, Z bosons, and the stability of vacuum. The Higgs can serve as an important portal to detect the dark matter and understand its nature. Precise measurements of the properties of the Higgs boson serve as probes of the underlying fundamental physics principles of the SM and beyond.

The discovery of the Higgs boson at the Large Hadron Collider (LHC) in July 2012 has created an excellent new opportunity for scientists to envision e^+e^- Higgs factories, by which millions of clean Higgs events and unprecedented high statistics Z, W bosons and top quark can be produced. At ~125 GeV, the Higgs boson mass makes it possible to design a Higgs factory based on the circular electron–positron collider with mature technology and high luminosity, and affordable power consumption.

TWIN PROPOSALS

Two future large circular e^+e^- colliders are being proposed, one on a greenfield site in China, the other linked to the existing CERN facilities. These are the Circular Electron Position Collider (CEPC) [1,2] and the Future Circular lepton Collider (FCC-ee) [3]. Both of these would serve as high-luminosity Higgs, precision electroweak and top factories. Either collider requires a roughly circular tunnel with a circumference of about 100 km. In a subsequent project stage, this same tunnel could later accommodate a high energy hadron collider, such as Super Proton-Proton Collider (SPPC) or FCC-hh, respectively.

Both CEPC and FCC-ee are conceived as double ring colliders, with 2 (or 4) interaction points (IPs), up to 2 radio-frequency (RF) system straights, and a tapering of the arc magnet strengths to match local energy. The two layouts are shown in Fig. 1. Both collider designs consider an asymmetric interaction region to limit SR of incoming beams towards detectors and to generate the required large crossing angle. Common use of RF systems for both beams at highest energy working points, starting from the ZH production mode. Each of the two machines is accompanied by a full-energy top-up booster ring situated in the same large tunnel.

FCC-ee

The FCC design efforts were launched and extended in response to the latest two Updates of the European Strategy for Particle Physics, in 2013 and 2020 [4, 5]. A comprehensive Conceptual Design Report (CDR) for the FCC was published in 2019 [3, 6, 7], reporting the physics cases, the design of the lepton and hadron colliders, along with the related technologies and infrastructures. The proposed FCC integrated project, consisting of FCC-ee followed by FCC-hh, is inspired by the successful past Large Electron Positron collider (LEP) and Large Hadron Collider (LHC) projects at CERN. It represents a comprehensive long-term programme maximising physics opportunities.

Following the 2020 European Strategy Update, in 2021 the CERN Council has launched the FCC Feasibility Study (FS), that will address not only the technical aspects of the accelerators, but also, and in particular, the feasibility of tunnel construction and technical infrastructures, and the possible financing of the proposed future facility. As requested by the European Strategy, the FCC Feasibility Study is organized as an international collaboration, with presently about 150 participating institutes plus 30 industrial companies.

The FCC shall be located in the Lake Geneva basin and be linked to the existing CERN facilities. The 2019 FCC CDR described an FCC design with a circumference of 97.75 km, 12 surface sites, and two primary collision points. In 2021, a placement optimisation resulted in a new circumference of about 91.1 km, and a configuration with only 8 surface sites, allowing for either 2 or 4 IPs. Re-optimization of the beam parameters is in progress, taking into account the new placement, the maximum number of 4 IPs, further beam dynamics studies, and a variety of machine errors.

The FCC-ee, as the first stage of the FCC integrated project, is planned to, at first, run on the Z pole, 91 GeV c.m., for 4 years, then on the W threshold, 160 GeV, for 2 years, later on the ZH production peak, 240 GeV c.m., for 3 years, and, after a full year of shutdown, at the $t\bar{t}$ threshold, 365 GeV, for another 5 years. Additional RF systems

ISBN: 978-3-95450-227-1 ISSN: 2673-5490 doi:10.18429/JACoW-IPAC2022-TUIZSP2

THE MUON COLLIDER

Daniel Schulte*, CERN, Meyrin, Switzerland
on behalf of the International Muon Collider Collaboration

Abstract

Muon colliders are considered nowadays in the landscape of future lepton colliders. Since the MAP project in USA, an important effort is being made in Europe with support from the international community to identify the neccesary R&D to advance towards a Conceptual Design Report in the next years. The paper will review the status of the technologies and accelerator designs and will present the R&D plans.

INTRODUCTION

Circular muon colliders have the potential to reach centre-of-mass energies in the multi-TeV range with high luminosity [1]. The concept has been developed in the past by the MAP collaboration mainly in the US [2]. Experimental verifications have also been carried out in the UK by the MICE collaboration [3] and an alternative muon production scheme (LEMMA) has been studied mainly by INFN [4].

Following the recommendation of the recent Update of the European Strategy for Particle Physics [5] an international collaboration [6] has been initiated by the European Large National Laboratories Directors Group (LDG) [7]. Following a request by CERN Council, guided by the LDG and with the help of the global community, the collaboration assessed the muon collider challenges and devised a Roadmap toward a muon collider. This includes a detailed workprogramme for the next five years and estimates of the required reources. Following the presentation of the Roadmap, CERN Council asked for an implementation plan. The collaboration also submitted white papers [8–11] to the ongoing strategy process in the US and a proposal for an EU cofunded Design Study.

The muon collider collaboration envisages to study a 10 TeV option, and also explore lower and higher energy options, e.g., a 3 TeV option as a step toward 10 TeV.

THE CONCEPT

MAP developed the concept shown in Fig. 1. The proton complex produces a short, high-intensity proton pulse that hits the target and produces pions. The decay channel guides the pions and collects the produced muons into a bunching and phase rotator system to form a muon beam. Several cooling stages then reduce the longitudinal and transverse emittance of the beam using a sequence of absorbers and RF cavities in a high magnetic field. A system of a linac and two recirculating linacs accelerate the beams to 60 GeV followed by one or more high-energy accelerator rings; e.g. one to 300 GeV and one to 1.5 TeV. In the 10 TeV collider an additional ring from 1.5 to 5 TeV follows. These rings can be either fast-pulsed synchrotrons or FFAs. Finally the beams

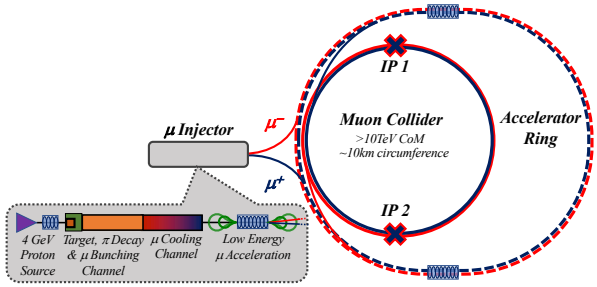

Figure 1: A conceptual scheme of the muon collider, courtesy M. Palmer.

are injected at full energy into the collider ring. Here, they will circulate to produce luminosity until they are decayed; alternatively they can be extracted once the beam current is strongly reduced. The exact energy stages of the acceleration system have to be developed.

LEMMA is an alternative scheme to produce a muon beam with a very small emittance. An injector complex produces a high-current positron beam. The positrons impact a target with an energy of 45 GeV, sufficient to produce muon pairs by annihilating with the electrons of the target. This scheme can produce small emittance muon beams. However, it is difficult to achieve a high muon beam current and hence competative luminosity. Novel ideas are required to overcome this limitation.

MOTIVATION

High-energy lepton colliders combine cutting edge discovery potential with precision measurements [8, 12]. Because leptons are point-like particles in contrast to protons, they can achieve comparable physics at lower centre-of-mass energies. The relative physics reach depends on the channels considered but a 10 to 14 TeV lepton collider would be comparable to a 100 TeV proton-proton collider.

The energy reach of circular electron-positron colliders is limited by synchrotron radiation. Linear colliders in contrast need to accelerate the beam in a single passage and collide it only once. CLIC, the highest energy lepton collider proposed during the update of the European Strategy for Particle Physics, is not fundamentally limited to 3 TeV. But linear collider cost and length scale approximately linearly with energy and power consumption roughly linearly with luminosity.

The large muon mass suppresses synchrotron radiation and enables the use of circular accelerator and collider rings. This reduces the required RF voltage and provides repeated collisions. However, the short muon lifetime of $\tau = 2.2$ s at rest (about $\tau\gamma \approx 104$ ms at 5 TeV) limits the number of turns in the accelerator and collider.

* daniel.schulte@cern.ch

ISBN: 978-3-95450-227-1 ISSN: 2673-5490 doi:10.18429/JACoW-IPAC2022-TUOZSP1

PROSPECTS FOR OPTICS MEASUREMENTS IN FCC-ee

J. Keintzel*, R. Tomás and F. Zimmermann, 1211 CERN, Geneva 23, Switzerland

Abstract

Within the framework of the Future Circular Collider Feasibility Study, the design of the electron-positron collider FCC-ee is optimised, as a possible future double collider ring, currently foreseen to start operation during the 2040s. With close to 100 km of circumference and strong synchrotron radiation damping at highest beam energy, adequate beam measurements are needed to control the optics at the desired level. Various possible techniques to measure the optics in FCC-ee are explored, including the option of turn-by-turn measurements in combination with an AC-dipole.

INTRODUCTION AND MOTIVATION

The future circular lepton collider, FCC-ee, is a synchrotron with 91 km circumference, which requires a new tunnel in the Lake Geneva basin and which will be connected to the existing CERN accelerator complex [1,2]. With a possible commissioning date around 2045, FCC-ee would allow for a smooth continuation of frontier particle-physics research after the end of the High Luminosity Large Hadron Collider (HL-LHC) program [3], expected around 2040.

The FCC-ee is designed for high precision physics experiments on the Z- pole, WW-threshold, HZ-production peak and for $t\bar{t}$ quark production, corresponding to beam energies of 45.6, 80, 120 and 182.5 GeV, respectively, with collisions in up to four interaction regions [4]. Although the beams are injected at collision energy (top-up injection), energy losses from e.g. synchrotron radiation (SR) need to be compensated. This is achieved through superconducting radiofrequency cavities. The combination of energy losses and localized RF sections leads to variations of the beam energies and the center-of-mass energies around the machine (further details in [5]). At the lower energy stages it is envisaged to measure the average beam energy by resonant depolarization of a few hundred transversely polarized low-intensity (10^{10}) pilot bunches. Once sufficient polarization (≈10 %) is achieved with wigglers, they are switched off and all nominal bunches (2.5×10^{11}) will be injected and brought to collision. Since misalignment and optics errors can limit the achievable polarization and can drastically limit the performance, they need to be controlled. In addition to precise alignments of elements and girders [6], beam-based measurements need to be performed to identify alignment and optics errors, to then apply dedicated corrections. One crucial design challenge is developing suitable and reliable measurement techniques, adapted to the FCC-ee. We study here the merits and limitation of various optics measurement techniques for the FCC-ee, and highlight pertinent experiences from existing storage rings facilities. Complementary beam tests for other design challenges are reported in [7].

* jacqueline.keintzel@cern.ch

BEAM POSITION MONITORS

Crucial devices for optics measurements are Beam Position Monitors (BPMs), which record the center-of-charge of particle beams. In storage rings such as the LHC, SuperKEKB or ESRF they are typically installed next to each quadrupole magnet. This approach is presently assumed in various optics tuning studies [8] and requires about 1800 BPMs for the FCC-ee. One of the most common types are so-called button BPMs. The alignment of their electrodes varies, for example, in the LHC they are aligned on the transverse axis. Due to strong emitted SR in SuperKEKB, the buttons are rotated by 45° in the transverse plane [10]. BPMs can be used to measure the centroid orbit in each turn for Turn-by-Turn (TbT) measurements, or by recording the average orbit over several turns, or both simultaneously. The BPM resolution depends on the chosen recording setting and also on the beam current. It is typically higher for recording the average orbit of high beam currents.

K-MODULATION

The average β-function in a quadrupole can be measured by the change of its strength and its effect on the transverse tune $Q_{x,y}$, assuming the working point is far away from strong resonances and the tune change is small. This method is typically applied to the final focus quadrupoles, allowing to propagate the measured values to the interaction point, and has successfully been used in various machines including the LHC [11] and SuperKEKB [12]. The main limitation is the accuracy of the tune measurement and fluctuations of the power supplies for the magnetic elements.

ORBIT RESPONSE MATRIX

For an Orbit Response Matrix (ORM) measurement approach, dipole kickers distort the beam orbit one after the other and the response is measured at BPMs. The required time for ORM increases with the size of a storage ring and is hence expected to be time consuming for the FCC-ee. Since the average is taken over several turns, the BPM resolution is good and e.g. for SuperKEKB in the order of a few µm [13]. However, presently the maximum orbit is limited to 10 to

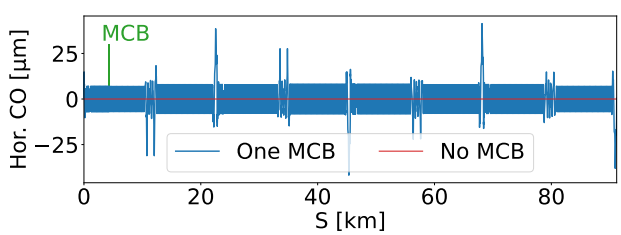

Figure 1: Horizontal closed orbit with one activated dipole kicker (MCB) (blue) and without (red) for the $t\bar{t}$-lattice.

ISBN: 978-3-95450-227-1 ISSN: 2673-5490 doi:10.18429/JACoW-IPAC2022-TUOZSP3

THE EUROPEAN ERL ROADMAP*

M. Klein, University of Liverpool, Liverpool, United Kingdom
A. Hutton, Jefferson Lab., Newport News, USA
B. Kuske, Helmholtz-Zentrum Berlin, Berlin, Germany

Abstract

Following the European Strategy process in 2019, five Roadmap Panels were set up to prepare the technologies needed for future accelerators and colliders: high-field magnets, SRF, muon colliders, plasma wakefield accelerators and Energy Recovery Linacs (ERLs). The ERL Roadmap Panel, consisting of ERL experts from around the world, first developed an overview of current and future ERLs. From this it was possible to carry out a gap analysis to see what R&D would be needed, from which the roadmap could be developed. The European ERL Roadmap [1] focused on three main aspects: 1) the continuation and development of facility programs for which no additional funds are needed, S-DALINAC in Darmstadt and MESA in Mainz; 2) technology development for room-temperature HOM damping and twin-axis SRF cavities; 3) the timely upgrade of bERLinPro for 100 mA current and the construction of PERLE at Orsay as a dedicated 10 MW power multi-turn facility. The roadmap entails a vision of a future energy frontier electron-positron and electron-hadron collider and describes a high-quality ERL program for 4.4 K SRF technology at high Q_0.

INTRODUCTION

Future HEP colliders will require revolutionary advances in technology for both accelerators and detectors, and complementary facilities will be required, as has been shown in the past decades. In addition, energy efficiency and other sustainability aspects will be important factors in the design of a new facility. ERLs, which recycle the kinetic energy of a used beam for accelerating a newly injected beam to minimize the power consumption, and avoid the emittance growth of storage rings, are set to become the technology of choice for the next generation of HEP colliders. This will require R&D to extrapolate the excellent results obtained in small facilities. The ERL Roadmap Panel was charged with developing a coherent plan, which is described in this paper.

COMPLETED FACILITIES

The landscape of past, existing and future ERLs is shown in Figure 1 [1]. Only those ERLs that still hold a record for at least one parameter have been retained.

ALICE [2] in Daresbury was the first European ERL. It operated successfully for a decade until 2019, when it was decommissioned to provide space for a medical facility.

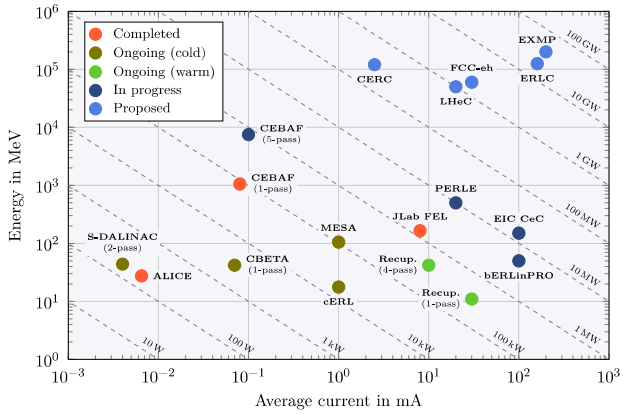

Figure 1: Landscape of past, present and proposed ERLs. of past, present, and proposed ERLs. The dashed lines are contours of constant beam power.

The Jefferson Lab FEL [3-6], which closed when it lost funding, still holds records for maximum beam current recirculated in a superconducting ERL (8.5 mA), and maximum beam power (1.3 MW). The maximum power into the building is 650 kW, underlining the energy efficiency of ERLs.

An experiment was successfully carried out at Jefferson Lab on CEBAF [7] to recirculate beam once around the facility, which at that time had 39 cryomodules, demonstrating that there were no unforeseen issues.

ONGOING ACTIVITIES

CBETA at Cornell was built as the first multi-pass ERL using an FFAG lattice for all four beams, both accelerating and decelerating [8]. All of the key performance indicators were successfully met, showing that this concept is viable for other facilities [9].

The Compact Energy-Recovery Linac (cERL) has been operating since 2013 at KEK as a test accelerator operating with a 1 mA average beam current and excellent beam quality [10], and is now being developed for industrial applications.

The Recuperator at BINP, Novosibirsk is a normal conducting ERL [11], and includes three FELs operating in the terahertz, far-, and mid-infrared spectral ranges. The facility holds the record for the highest bunch charge (1.5 nC), and several records for FEL output power at different wavelengths.

The S-DALINAC has been in operation in Darmstadt since 1991 [12]. Initially built as a twice-recirculating machine, but a new recirculation beam line was installed allowing for the operation as an ERL. In August 2017, once-recirculating ERL operation was demonstrated and twice recirculating ERL mode was achieved in 2021 [13].

* AH was supported by the U.S. Department of Energy, Office of Science, Office of Nuclear Physics under Contract No. DE-AC05-06OR23177

ISBN: 978-3-95450-227-1 ISSN: 2673-5490 doi:10.18429/JACoW-IPAC2022-TUPOST001

PARASITIC OPTIMIZATION OF THE TRANSFER BEAMLINE EFFICIENCY AT ELSA

S. Witt*, K. Desch, D. Elsner, D. Proft, Physics Institute, University of Bonn, Germany

Abstract

The 3.2 GeV electron accelerator ELSA in Bonn consists of three acceleration stages each interconnected by tunable transfer beamlines. The steering of the electron beam through the transfer line from linear accelerator to the Booster Synchrotron is currently adjusted by hand, which limits a systematic improvement of the transfer efficiency. An automated optimization using the "simulated annealing" technique has been developed and integrated into the control system to improve the situation. It allows for a continuous optimization without interfering with usual beamtime for experiments by utilizing the 6s off-time in between injections into the stretcher ring. In a simulation using the actual accelerator's settings as starting parameters, transmission rates have been increased significantly. The methods and results with the accelerator hardware are presented.

ELECTRON STRETCHER FACILITY ELSA

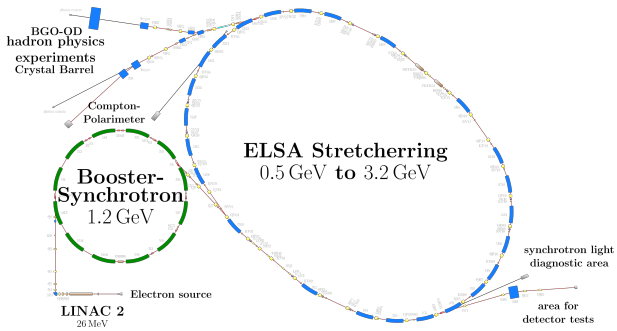

Figure 1: The Electron Stretcher Facility ELSA.

The electron stretcher facility ELSA in Bonn (Fig. 1) is a three stage electron accelerator capable of accelerating electrons to energies up to 3.2 GeV. The acceleration process is cyclical: The electron gun, linear accelerator LINAC2 and Booster Synchrotron are triggered with 50 Hz during the injection phase into the stretcher ring, which takes around 0.5 s. Then, those first two acceleration stages idle while the stretcher ring ramps up the electron energy and extracts the electrons to one of the experimentation sites. This phase typically takes 6 s, before the cycle starts over [1].

The transfer beamline between LINAC2 and the synchrotron (Fig. 2) guides the electron beam via 8 quadrupoles, 7 corrector magnets for both planes and 2 dipole magnets, all of which are controllable from the control system software, leading to a 24-dimensional parameter space. These parameters can be optimized to improve the transfer efficiency of the beamline.

* sebastian-witt@outlook.de

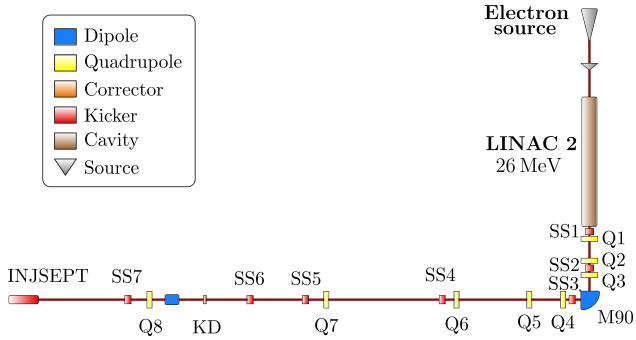

Figure 2: The transfer beamline between LINAC2 (right) and the Booster synchrotron (left).

OPTIMIZATION PROBLEM

Due to the high dimensionality of the problem, optimization of the transfer efficiency is a nontrivial problem. The interplay of different magnetic elements makes the electron transmisson rate into the synchrotron a non-convex target function featuring many local extrema. Due to the fact that the magnetic elements take up to 1 s to reach the desired magnetic field after a set command is issued, evaluations of this target function $y_i = f(x_i)$ are quite costly and need to be kept to a minimum. The optimization algorithm known as Simulated Annealing fits the problem [2], as it does not rely on gradient information or any knowledge of the underlying target function, and is designed to escape local extrema of non-convex target functions (see Fig. 3). The *iterative*

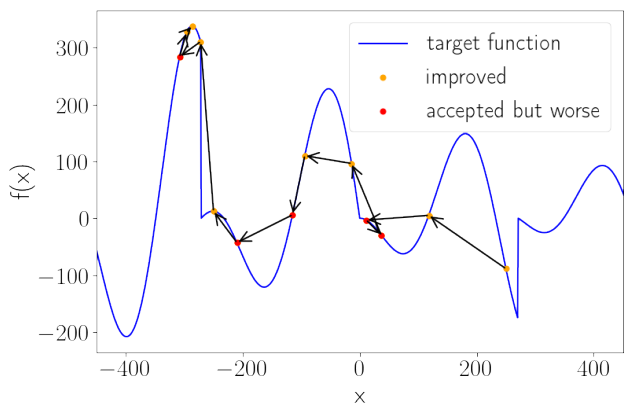

Figure 3: Example of Simulated Annealing on a one-dimensional non-convex target function $f(x)$.

algorithm (schematically depicted in Fig. 4) explores the parameter space by adding *random steps* Δx drawn from a uniform distribution to the current configuration x_n of magnet strengths before evaluating the target function (resulting transmission rate) and comparing this y_t to the previous iter-

ISBN: 978-3-95450-227-1 ISSN: 2673-5490 doi:10.18429/JACoW-IPAC2022-TUPOST002

UPGRADE OF THE 25 MW RF STATION FOR THE LINEAR ACCELERATOR LINAC2 AT ELSA

D. Proft*, K. Desch, D. Elsner, M. Switka, Physics Institute, University of Bonn, Germany

Abstract

At the Electron Stretcher Facility ELSA in Bonn the first acceleration stage consists of a 3 GHz traveling wave linear accelerator. It was powered by a 25 MW pulsed high power klystron amplifier, which had been in use for the last thirty years. After a major failure and due to the lack of spare part availability the RF station was rebuilt. In addition to a new klystron including its high voltage tank, the new setup also consists of major upgrades of the infrastructure, the pulse forming network and the safety interlocks to satisfy the contemporary requirements.

A new monitoring system consisting of multi-channel sampling ADCs allows for automatic pulse-by-pulse analysis of the klystron parameters and simultaneous evaluation of RF performance and stability.

In this contribution we will present the new RF station setup, which has successfully been operating since the beginning of 2021 as well as the new monitoring capabilities.

ELECTRON STRETCHER FACILITY

At the Electron Stretcher Facility ELSA (see Fig. 1) polarized or unpolarized electrons are accelerated to energies of up to 3.2 GeV within a three-staged accelerator scheme including a Linac, the Booster Synchrotron and the ELSA stretcher ring [1]. The first and second stage of the facility are synchronized to the mains frequency of 50 Hz and consist of either a source for polarized electrons or a thermionic gun, operated at 50 kV and a traveling wave Linac. The following Booster Synchrotron further accelerates the electrons and transfers them to the main storage ring at an energy of 1.2 GeV. After accumulating typically 30 mA in the stretcher ring, the electrons are accelerated to 3.2 GeV and then slowly extracted to either two experimental sites for hadron physics experiments (E1 and E2) or to a second beamline dedicated for detector testing (E3) at user controllable rates between 200 Hz and 625 MHz.

Linac Section

The S band Linac (LINAC2) is used to accelerate 1 µs long electron pulses with a charge of up to 100 nC to a central energy of 26 MeV with an energy spread of below 5 %. It is powered by a 12.5 MW RF station with a frequency of 2.9987 GHz.

As the transfer beamline to the booster synchrotron comprises a 90° deflection dipole (see Fig. 1, lower left), a slit system behind the magnet is used in the feedback loop of a PID controller to stabilize the central electron energy by slightly adjusting the RF power provided to the Linac.

* proft@physik.uni-bonn.de

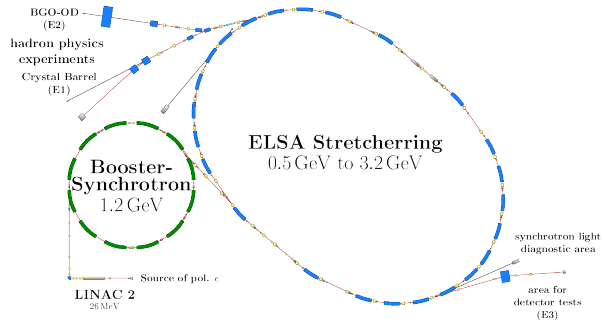

Figure 1: Sketch of the electron stretcher facility ELSA.

RF STATION UPGRADE

As the previously installed Linac klystron[1] showed degraded performance, major parts of the RF station were reconstructed in favor for a new type of klystron[2]. With the klystron a new high voltage tank, including a new pulse transformer, was installed.

Furthermore, major parts of the infrastructure (e.g. cooling system and its monitoring, SF6 gas handling in the waveguides, auxiliary power supplies with digital PLC interface) were also upgraded and extended to match the requirements. A new thyristor-based power supply for heating of the klystron's filament was developed in-house. It allows for stabilization of the heater current within 0.5 % and long term drifts smaller than 0.75 % at a peak output power of 1 kW.

Table 1: Modulator Specifications

Property	Value
PFN total capacity	650 nF
PFN impedance	4.3 Ω
peak (nominal) PFN voltage	30 kV (26.5 kV)
HV pulse duration	ca. 4 µs
RF pulse duration	ca. 3 µs

The existing modulator (for specs see Table 1), consisting of a high voltage power supply (HVPS) for charging of the pulse forming network's (PFN) capacitors to 30 kV, was largely reused with the new setup. The PFN's impedance and HV pulse duration were compatible. Nevertheless, a new tail clipper diode assembly for suppression of reflections from the klystron tank was installed into the PFN cabinet as replacement to the previously installed one that was located inside the tank but had to be disassembled due to space constraints.

[1] F2042E by Thomson-CSF, France
[2] TH2100D by Thales, France

ISBN: 978-3-95450-227-1 ISSN: 2673-5490 doi:10.18429/JACoW-IPAC2022-TUPOST005

RF VOLTAGE CALIBRATION USING PHASE SPACE TOMOGRAPHY IN THE CERN SPS

D. Quartullo*, S. Albright, H. Damerau, A. Lasheen,
G. Papotti, C. Zisou, CERN, Geneva, Switzerland

Abstract

Voltage calibration using longitudinal phase-space tomography is a purely beam-based technique to determine the effective RF voltage experienced by a bunch. It was applied in the SPS, separately to each of its six accelerating travelling wave structures. A low spread in voltage errors was obtained by carefully optimizing the number of acquired bunch profiles. The technique moreover provided the relative phases of the cavities, which allowed their alignment to be checked. Pairs of cavities were measured as well to validate the consistency of the single-cavity voltages. The beam measurements were repeated after several months to confirm the reproducibility of the results. Longitudinal beam dynamics simulations, including the full SPS impedance model, were performed as a benchmark. The aim was to verify that the effect of the cable transfer-function on the bunch profiles can be neglected, as well as collective effects and small errors in the accelerator parameters.

INTRODUCTION

Longitudinal phase-space tomography is used to reconstruct the bunch distribution in longitudinal phase-space from a set of measured bunch profiles as input [1–5]. The discrepance D gives the average of the absolute differences between measured and reconstructed profiles. The discrepance usually decreases during the iterative reconstruction process and converges to an equilibrium value $\widehat{D}$ after a sufficient number of iterations.

The actual RF voltage V_d acting on the beam and the phase position $\widehat{\varphi}_\mathrm{s}$ of the bucket center with respect to the acquisition trigger are difficult to measure with conventional techniques. The voltage V_d can be considerably different from the programmed one V_p, due to the limited precision of electrical voltage measurements and collective effects.

Longitudinal tomography can be used to determine V_d and $\widehat{\varphi}_\mathrm{s}$ [6, 7]. One approach is to perform tomographic reconstructions for $(V_\mathrm{rf}, \varphi_\mathrm{s})$ pairs forming a rectangular grid, then the pair giving the minimum $\widehat{D}$ determines the actual V_d and $\widehat{\varphi}_\mathrm{s}$. An alternative method uses a minimization algorithm which creates a path converging to the minimum $\widehat{D}$ in the $(V_\mathrm{rf}, \varphi_\mathrm{s})$ parameter space (Fig. 1, middle).

In this paper, tomography-based voltage calibrations are applied to the SPS fundamental-harmonic RF system. Firstly, voltage-calibration results derived from measurements taken in 2021 are reported. Then, the consistency and reliability of the voltage errors are verified by examining the synchrotron oscillations of the measured profiles, by applying calibrations to multiple cavities, and by using simulated bunch-profile data as input for tomography. Finally, preliminary results from voltage calibrations done in 2022 are reported.

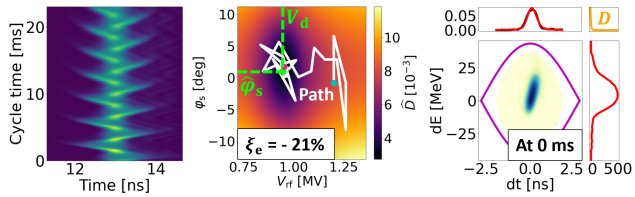

Figure 1: Left: example of bunch profiles measured in 2021 at SPS flat bottom. Only cavity 3 was active with V_p = 1.2 MV. Middle: corresponding voltage calibration. Right: phase-space reconstruction at injection. The measured (black) and reconstructed (red) bunch profiles overlap.

MEASUREMENTS SETUP

Beam measurements were performed at SPS injection energy during the first 23 ms (Fig. 1, left). A bunch with low intensity $N_\mathrm{p} < 5 \cdot 10^9$ p/b (protons per bunch) and smallest possible longitudinal emittance was generated by longitudinal shaving in the PSB and accelerated in the PS like a conventional single bunch for the LHC. The resulting bunch length at extraction from the PS was only about 1 ns.

Measurements were done in a single-harmonic RF system. Only one (or a subset) of the six accelerating RF cavities was active during a given cycle. Although the recorded bunch intensity was small, the Low Level RF (LLRF) One-Turn Delay Feedback (OTDFB) for beam-loading compensation was activated, since the set point of the OTDFB defines the voltage reference in the SPS [8].

Energy and phase mismatches between the PS and the SPS led to significant dipole oscillations (Fig. 1, left), which are crucial for tomography-based voltage calibrations. The beam-based LLRF loops were disabled to avoid damping dipole oscillations during measurements.

VOLTAGE CALIBRATIONS IN 2021

Two sets of measurements were taken in July and October. Five accelerator cycles were measured for each cavity to verify the reproducibility of results. The dependence of the relative voltage-error $\xi_\mathrm{e} = (V_\mathrm{d} - V_\mathrm{p})/V_\mathrm{p}$ on the number of synchrotron periods N_{T_s} used for voltage calibrations was investigated (Fig. 2). The measurement of ξ_e reached a convergence between 4 and 5 synchrotron periods, therefore only the voltage errors with $N_{T_\mathrm{s}} \in [4, 5]$ were considered.

Table 1 summarizes the voltage-calibration results. The average voltage errors vary between -21% and +3%, with spreads all within 1%. Comparing corresponding measure-

* danilo.quartullo@cern.ch

ISBN: 978-3-95450-227-1 ISSN: 2673-5490 doi:10.18429/JACoW-IPAC2022-TUPOST006

FREQUENCY-DEPENDENT RF VOLTAGE CALIBRATION USING LONGITUDINAL TOMOGRAPHY IN THE CERN PSB

D. Quartullo*, S. Albright, H. Damerau, CERN, Geneva, Switzerland

Abstract

Longitudinal phase-space tomography reconstructs the phase-space distribution from a set of bunch profiles and the accelerator parameters, which includes the RF voltage. The quality of the reconstruction depends on the accuracy to which these parameters are known. Therefore, it can be used for beam-based RF voltage calibration by analysing oscillations of a mismatched bunch. The actual RF voltage may be different from the programmed one due to uncertainties of the electrical gap voltage measurements and intensity effects. Tomography-based RF voltage calibration was systematically performed with low-intensity bunches in all four rings of the PS Booster (PSB) at injection and extraction energy. For each of the three RF cavities present in a given ring, the calibration was performed separately to extract the voltage errors while avoiding any influence of phase misalignments. The number of synchrotron oscillation periods available for the voltage calibration was constrained by the short duration of the PSB flat-bottom and top. Longitudinal beam dynamics simulations using the full PSB impedance model were performed to benchmark the results provided by the calibrations.

INTRODUCTION

Longitudinal tomography is a beam-based technique able to reconstruct the bunch distribution in longitudinal phase-space [1–4]. The main inputs are the measured bunch profiles, the output is the phase-space distribution whose projections best match the measured profiles. The discrepancy D represents the degree of matching between measured and reconstructed profiles. In a tomographic reconstruction, D typically decreases and reaches an asymptotic value $\widehat{D}$ after a sufficiently large number of iterations.

Tomography provides accurate results only when certain accelerator and beam parameters are known. While parameters like beam energy are normally known with high precision, the actual voltage V_d acting on the beam and the phase position $\widehat{\varphi}_\mathrm{s}$ of the bucket center with respect to the trigger are difficult to measure. In particular, V_d can be significantly different from the programmed voltage V_p, due to uncertainties in electrical voltage measurements and collective effects.

Tomography can be used to find V_d and $\widehat{\varphi}_\mathrm{s}$ [5–7] by determining the V_rf and φ_s values which minimize $\widehat{D}$. Two methods can be used, as shown in Fig.1. The first one computes $\widehat{D}$ for V_rf - φ_s pairs forming a rectangular grid to obtain the minimum $\widehat{D}$. The second method relies on a minimization algorithm which computes $\widehat{D}$ for selected V_rf - φ_s pairs and creates a path converging to the minimum $\widehat{D}$.

* danilo.quartullo@cern.ch

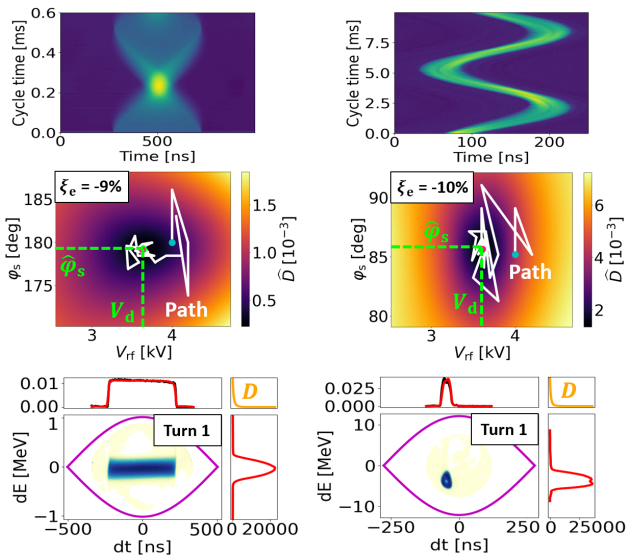

Figure 1: Top: bunch profiles measured with the S7 cavity at injection (left) and extraction (right) energy with V_p = 4 kV. Middle: voltage calibrations using as input the corresponding measured profiles shown above. Bottom: corresponding phase-space reconstructions at turn 1. The reconstructed (red) bunch profiles match well the measured (black) ones.

Bunch oscillations are needed for voltage calibration: if the bunch is perfectly matched, low discrepancy values are obtained with any voltage, since the longitudinal emittance is a free parameter.

The PSB consists of four superposed rings. Each ring is equipped with three independent RF cavities [8] in sectors 5 (S5), 7 (S7) and 13 (S13). In this contribution, tomography-based voltage calibration is applied to all the PSB RF cavities, at injection and extraction energies.

MEASUREMENTS SETUP

Beam measurements were performed at injection and extraction energies in each of the four PSB rings. The voltage at $h = 1$ in each of the cavities S5, S7 and S13 was measured separately in each ring for constant programmed voltages of 4 kV, 5 kV, 6 kV and 7.5 kV. For each combination of ring, cavity and programmed voltage, ten cycles were recorded. Low Level RF (LLRF) beam phase and radial loops were disabled to avoid damping bunch oscillations. The beam had low intensity to limit the influence of collective effects.

At flat-bottom, measurements started at injection and extended for the entire flat-bottom duration of 0.6 ms. At injection, the beam from Linac4 had a rectangular shape in the (dt, dE) phase space and was not matched to the RF

ISBN: 978-3-95450-227-1 ISSN: 2673-5490 doi:10.18429/JACoW-IPAC2022-TUPOST007

NEW GENERATION OF VERY LOW NOISE BEAM POSITION MEASUREMENT SYSTEM FOR THE LHC TRANSVERSE FEEDBACK

Daniel Valuch*, Accelerator Systems department, CERN, Geneva, Switzerland
Viera Stopjakova, UEF FEI, Slovak University of Technology, Bratislava, Slovakia

Abstract

Recent studies showed that the transverse feedback system noise floor in the Large Hadron Collider (LHC) must be reduced by at least factor of two in order to operate the machine with large beam-beam tune shift as foreseen in the High Luminosity (HL) LHC. Also, the future feedback system foreseen to suppress the LHC Crab Cavity noise relies on improved noise performance of the beam position measurement system. An upgrade program was launched to lower the LHC transverse feedback system noise floor during the LHC Long Shutdown II. A new generation, very low noise beam position measurement module was developed and tested with beam. Innovative methods in the RF receiver, digital signal processing, thorough optimization of every element in the signal chain from pickup to the kickers allowed to achieve a significant reduction of the system noise floor. This unprecedented noise performance opens also new possibilities for auxiliary instruments, using the position data from the transverse feedback. The paper presents the new system, notable implementation details and measured performance.

TRANSVERSE FEEDBACK IN LHC

The Large Hadron Collider (LHC) relies on a transverse feedback (TFB) to suppress coupled bunch instabilities and to damp injection oscillations conserving the injected beam emittance. Apart of these primary functions, the TFB in the LHC provides a large number of auxiliary functions, for example all kinds of beam excitation for abort and injection gap cleaning [1, 2], controlled transverse emittance blow-up for aperture and collimation measurements [3], or controlled transverse losses for special measurements [4].

During LHC Run I, the LHC TFB system started to provide very valuable bunch-by-bunch, turn-by-turn beam position data for diagnostics purposes. The data quickly became the second most important "commodity" delivered by the transverse feedback. A high performance computing system, called ADTObsBox was introduced [5] to collect and analyze these data in real time, allowing for example a real time detection of transverse instability onset, assisted tune measurements, collimator impedance measurements and many more. The beam position measurement quality is equally important also for this secondary application.

The beam position is sensed by four stripline type pickups in the arc around LHC point 4. Symmetrically at both sides of the former interaction point. The pickups are referenced as Q9 and Q7 (by the quadrupole magnets they belong to), Q8 and Q10 respectively. Signals of both pickup electrodes (referenced as electrode A and B) are transported to the surface. A and B signals are combined by a 180-degree, hybrid coupler to produce the analogue Σ and the delta Δ signals. These raw, impulse like signals are then feeding the Beam Position Measurement module (BeamPos), which downconverts and digitizes them. A normalized bunch position is calculated digitally by a field programmable gate array (FPGA). One data point per bunch per turn is sent over an optical link to Digital Signal Processing Unit where all feedback related calculations are performed. An analogue correction/excitation signal is sent back to the tunnel, amplified by tetrode amplifiers to a peak amplitude of up to 10 kV and fed to electric field kickers.

PERFORMANCE OF THE OLD SYSTEM

Though the TFB performance during the LHC Runs I (2009-2013) and II (2013-2018) was greatly sufficient for the LHC operation, recent studies showed that the TFB noise floor in the LHC must be reduced by at least factor of two in order to operate the machine with large beam-beam tune shift as foreseen in the High Luminosity (HL) LHC [6] and suppress the risk of loss of Landau damping by noise [7]. Improvement by factor of 4 is required to recover an emittance growth rate in the order of 2% per hour as in the present LHC. Also, the future feedback system foreseen to suppress the LHC Crab Cavity noise in HL-LHC [8] relies on improved noise performance of the upgraded TFB.

With the majority of the signal processing chain of the LHC TFB being digital, the beam position measurement subsystem is considered to define the noise performance of the whole LHC TFB system, therefore the effort to lower it focuses on improving the beam position measurement subsystem. The noise floor of the TFB system can be determined only indirectly: either beam based by measurement of transverse emittance blow-up [6], or by analysis of the beam position measurement hardware [9].

For latter, a complete numeric model of the receiver and the signal processing chain was constructed. The model was fed by a noiseless input signal corresponding to a full scale bunch position. Then a real BeamPos module in LHC was set to nominal operating conditions, but without beam and noise from the analogue to digital converters was measured. The signal was superimposed to the ideal position data and processed by the model. Distribution of the measured position was recorded.

Noise floor of the LHC TFB beam position measurement system used in the Run I/II was found to be 1.03-1.40 μm_{RMS}, depending on pickup, settings and operating conditions.

* daniel.valuch@cern.ch

ISBN: 978-3-95450-227-1 ISSN: 2673-5490 doi:10.18429/JACoW-IPAC2022-TUPOST008

DIGITAL LOW-LEVEL RF SYSTEM FOR THE CERN Linac3 ACCELERATOR

D. Valuch*, R. Alemany-Fernandez, Y. Brischetto, S.J. Faeroe, G. Piccinini, M. E. Soderen
CERN, Accelerator Systems Department, Geneva, Switzerland

Abstract

A major consolidation of the aging RF system of the CERN Linac3, the ion source for the whole CERN accelerator chain, started during the Long Shutdown II. The main changes were an upgrade of the analogue Low-Level RF system (LLRF) and replacement of the 350 kW tube amplifiers by a solid-state equivalent. The state-of-the-art digital LLRF system enabled new sophisticated features in field manipulations, significantly increased the operational flexibility and improved operational reliability and availability. The paper presents the new architecture, a low noise master clock generator, digital signal processing with direct sampling of the RF signals, pulse parameter measurement and cavity resonance control.

LINAC3 RF SYSTEM

Linac3, commissioned in 1994 is the ion source for the whole CERN accelerator chain. Seven different RF structures accelerate the beam: RFQ, Buncher, Cavity 1, Cavity 2, Cavity 3, Ramping and Debunching cavities. The Linac operates at a fundamental frequency of 101.28 MHz, with cavities 2 and 3 run at the second harmonic 202.56 MHz. Field in the accelerating structures was controlled by an analogue LLRF system, based on the Linac2 design, which became obsolete. The system provided no operational flexibility, it was very demanding to set up, or sensitive to environmental aspects. Spare parts for the aging system became difficult to obtain and maintain. Nevertheless, the analogue system was very robust. It is worth to mention that some of the LLRF boards removed during the upgrade campaign in the summer 2020 were marked "OK, 26.10.1977" and still operating properly.

The LLRF system for the Ramping cavity and the Debuncher was replaced in 2003 by a VME-based digital LLRF installed in a temporary movable rack [1, 2]. The main motivation was needed energy ramping capability by phase sweeping the field in these structures. The 350 kW tube power amplifiers for RFQ and Cavity 1 also became difficult to maintain and operate, so a consolidation project to replace the obsolete LLRF and power amplifiers was launched. The Linac3 uses its own, free running frequency reference and it is not frequency locked to the downstream LEIR accelerator [3].

FULLY DIGITAL LOW LEVEL RF SYSTEM

A fully digital LLRF system allows implementation of very sophisticated control algorithms and digital signal processing. With the measurement and observation capabilities, it provides a lot of operational flexibility which is needed in machines serving multiple beam users and dynamically changing the output beam parameters. An example of a newly added capacity is the active control of the momentum spread based on the measurements of beam injected into LEIR [4].

When the project started in 2017, it was clear the new LLRF system will be fully digital, however it was not yet clear what platform should be used. The VME LLRF technology was mature at CERN, with all resources available. The uTCA LLRF platform was only emerging at CERN and it was not guaranteed to be available within the expected project timeline. A conservative approach was adopted. The new, Linac3 digital LLRF was designed on VME platform.

RF Pulse Stability and Other Requirements

Due to the beam dynamics requirements in the RFQ and the IH structures (KONUS [5]), highly accurate physical parameters of the accelerating field are not a constraint, however high stability and reproducibility of the RF fields (phase and amplitude) are a requirement [6]. This high stability and reproducibility requirement is necessary over all time-scales. The stability required in the original design report [7] is 0.3° in phase and 0.3% in amplitude. The design report did not take into account how stable the future performance requirements might be for LEIR and LHC, these are listed in [6]. The updated performance is stricter for Cavity 1 and Cavity 2 amplitudes, however more relaxed on other parameters. In terms of other requirements, the new system must provide a pulse-by-pulse capability of RF phase and amplitude control. In terms of diagnostics the system should deliver a measurement of pulse RF parameters - one value per pulse, but also an on demand full rate acquisition of the executed RF pulse for diagnostics and accelerator physics purposes.

Direct RF Sampling and Quadrature Demodulation

The Linac3 operating frequencies, 101.28 MHz and the second harmonic 202.56 MHz, are compatible with full power bandwidth of modern, high speed analogue to digital converters. The new LLRF system was therefore designed to use direct RF sampling. The regulation bandwidth of the feedback loops is defined by the cavity bandwidth (tens of kHz), and it is negligible with respect to the operating RF frequency. An undersampling can also be employed to our advantage.

A direct quadrature demodulation can easily be obtained if the sampling frequency and the signal frequencies are locked in a defined ratio. It was desirable to use only one sampling

* daniel.valuch@cern.ch

ISBN: 978-3-95450-227-1 ISSN: 2673-5490 doi:10.18429/JACoW-IPAC2022-TUPOST009

ONLINE CORRECTION OF LASER FOCAL POSITION USING FPGA-BASED ML MODELS

J. Einstein-Curtis*, S.J. Coleman, N.M. Cook, J.P. Edelen, RadiaSoft LLC, Boulder, CO, USA
S. Barber, C. Berger, J. van Tilborg, Lawerence Berkeley National Lab, Berkeley, CA, USA

Abstract

Ultrafast lasers play an increasingly critical role in the generation, manipulation, and acceleration of electron beams for High Energy Physics applications. Laser plasma accelerators enable order of magnitude improvements in accelerating gradient and promise compact tunable GeV electron beam sources, while novel photocathode systems permit fundamental advances in electron beam manipulation for accelerator and radiation applications Advances in fast feedback systems are required to stabilize laser performance at kHz repetition rate operation against environmental fluctuations. A field programmable gate array (FPGA) based digital control system, coupled with responsive optics, can provide rapid and precise stabilization of ultrafast lasers. A collaboration between RadiaSoft and the Lawrence Berkeley National Laboratory BELLA Center to develop, test, and deploy these systems across a range of beamlines operating at >1 Hz repetition rate, including 1 kHz systems, was created.

INTRODUCTION

Laser plasma accelerators (LPAs) rely upon accurate control of ultrafast lasers, typically Ti:Sapph and Nd:Yag amplifier systems [1]. The BELLA Center at Lawerence Berkeley National Laboratory (LBNL) features several ultra-short pulse, high-energy beamlines to develop LPAs. These accelerators require highly repeatable, stable interaction points to generate high-quality electron beams, which necessitates a collection of active and passive controls to mitigate environmental, mechanical, and component variations.

Recent work has primarily focused on enhancing transverse beam stability [2]. This paper describes a a strategy to address focal position stability, leveraging a machine learning (ML) enhanced wavefront diagnostic in tandem with a Field Programmable Gate Array (FPGA) controller to correct focal position at a kHz-scale rate. By building a model of wavefront at the interaction point, it is possible to use a non-perturbative measurement to calculate the focal position.

FACILITY AND EQUIPMENT

The initial model was created for the BELLA HTU laser system, shown in Fig. 1. This beamline operates with 1 kHz seed pulses and a 1 Hz full-power pulse. A HASO FIRST Shack-Hartmann wavefront sensor was used as the ground-truth imaging device of the interaction and post-interaction region, with the pre-interaction region sensor a Thorlabs WFS20-7AR. A Xilinx Zynq ZCU104 FPGA evaluation kit was used for testing to provide flexibility during the prototype phase, including a variety of customizable I/O, well-supported manufacturer-provided software, and a variety of processing options in support of ML operations.

Table 1: Optimal lens movement vs focal shift and beam size change. Focus shift is per mm lens translation. Beam size change is change per mm lens translation.

	Shift	Size Change
Transmissive Amp3-in	2mm	x1.348
Transmissive Amp4-in	2mm	x1.046
Reflective Amp4-out	1mm	x1.002

FOCAL POSITION INVESTIGATIONS

To determine the optimal lenses to move for a focal shift, we looked at the magnitude of the shift at final focus and the (unwanted) increase in beam size throughout the optical chain. Table 1 summarizes these parameters for three different lenses in the telescope.

From these simulations we determined that the reflective Amp4-out is not ideal as a motorized correction optic for focal location because it is more weakly responsive, shifting the focus by only 1 mm per mm translation. Moreover, the off-axis reflective geometry introduces beam centroid kicks, even in response to relatively mild beam size variations. Ultimately, we determined the Amp4-in telescope is the best choice.

To verify our model, we measured the focal location vs lens separation at high power. Our measurement used a comparable method of capturing leakage from the final steering mirror thus measuring raw focal location without the need for further calibration or renormalization. The inset of Fig. 2 provides details of the measured focal position and radius of curvature taken from the wavefront sensor.

When comparing measurements to the simulation, we note that the focus shift per mm stage motion depends on the nominal Amp4-in lens separation. For a perfectly collimated beam entering the $-f_1/+f_2$ telescope, and for a perfectly collimated beam leaving the telescope (lens separation is f_2-f_1), the slope change is 2mm focus shift per 1mm change in lens separation.

However, for the situation where the lens separation is NOT equal to f_2-f_1, for example because the input beam has a divergence or the output beam is not perfectly collimated, this slope will have a different value.

By overlapping the experimental data (red circles) with the simulation (blue circles), we find a good agreement for

* joshec@radiasoft.net

ISBN: 978-3-95450-227-1 ISSN: 2673-5490 doi:10.18429/JACoW-IPAC2022-TUPOST011

SIMULATION STUDIES OF INTRA-TRAIN, BUNCH-BY-BUNCH FEEDBACK SYSTEMS AT THE INTERNATIONAL LINEAR COLLIDER

R. Ramjiawan[1,*] D.R. Bett[1], R. Bodenstein[2], P.N. Burrows, G.B. Christian[3], C. Perry,
John Adams Institute for Accelerator Science, University of Oxford, Oxford, United Kingdom
[1]also at CERN, Geneva, Switzerland
[2]also at JLab, Newport News, VA, USA
[3]also at DLS, Oxfordshire, UK

Abstract

The International Linear Collider (ILC) is a proposed electron-positron collider targeting collision energies from 250 GeV to 1 TeV. With design luminosities of order 10^{34} cm^{-2}s^{-1}, a beam-based, intra-train feedback system would be required near the Interaction Point (IP) to provide nanometre-level stabilisation of the beam overlap in the collisions. Here we present results from beam-tracking simulations of the 500 GeV ILC, including the impact of beam-trajectory imperfections on the luminosity, and the capability of the IP feedback system to compensate for them. Effects investigated include the position jitter introduced by the damping ring extraction kicker, short-range and long-range wakefields, and ground motion. The feedback system was shown to be able to correct for beam-beam offsets of up to 200 nm and stabilise the collision overlap to the nanometre level, within a few bunch crossings.

INTRODUCTION

The International Linear Collider [1] (ILC) is a proposed, next-generation, electron-positron collider, with an initial collision energy of 250 GeV and options for upgrades including stages at 500 GeV and 1 TeV [2]. The ILC could be used for precision tests of the properties of the Higgs boson [2]. The 500 GeV-stage parameters are given in Table 1. The electrons would be produced with a DC photo-cathode gun, accelerated in a 5 GeV injector linac and injected into a 3.2-km-long damping ring (DR). The bunches would be individually extracted from the DR to the Ring To Main Linac (RTML) using a fast extraction kicker. The beam would then be transferred to the Main Linac (ML) for acceleration to full energy and transferred to the Beam Delivery System (BDS) which would bring the beam to a focal point at the interaction point (IP).

The luminosity, $\mathscr{L}$, of a linear collider is given by [3]

$$\mathscr{L} = H_D \frac{N^2}{4\pi\sigma_x^*\sigma_y^*} n_b f, \quad (1)$$

where H_D is the luminosity enhancement from the focussing between opposing bunches, and the remaining terms are defined in Table 1. The strong electromagnetic fields at collision produce 'beamstrahlung' [4], which increases the energy spread of the beam and is characterised by the parameter, Υ, with $\langle\Upsilon\rangle \propto 1/(\sigma_x + \sigma_y)$. Therefore, to both maximise the luminosity and reduce beamstrahlung, the beam is designed to collide with $\sigma_x >> \sigma_y$.

Table 1: ILC Parameters for the 500 GeV Stage [2]

Parameter	Value
Repetition frequency (f)	5 Hz
Bunches per pulse (n_b)	1312
Particles per bunch (N)	2×10^{10}
Bunch separation	554 ns
Bunch length at IP	300 µm
Peak luminosity ($\mathscr{L}$)	1.8×10^{34} cm^{-2}s^{-1}
Horizontal beam size at IP (σ_x^*)	474 nm
Vertical beam size at IP (σ_y^*)	5.9 nm

An intra-train beam position feedback system [5] has been proposed for stabilising collisions at the IP; a schematic of the system is shown in Fig. 1. The deflection of an outgoing beam, caused by the misalignment of the two incoming beams at the IP, is measured with a stripline beam position monitor (BPM) [7] ~4 m downstream of the IP. A compensating angular deflection is applied via a kicker ~ 8 m upstream from the IP. If the offsets of the outgoing electron bunches are measured, the incoming positron bunches are corrected and vice versa, thus reducing the additional latency from signal propagation time. For bunch-by-bunch feedback, the system latency must be less than the 554 ns bunch separation. The design, construction and tests of a prototype bunch-by-bunch IP feedback system are presented in [8], demonstrating that the ILC IP feedback system latency, resolution and dynamic-range requirements were met.

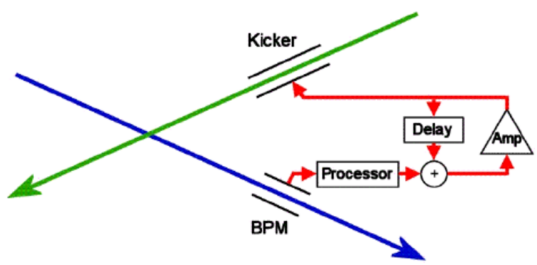

Figure 1: FONT IP feedback system layout [6].

As $\sigma_x >> \sigma_y$, here we focus on the more challenging vertical plane. The feedback system should operate over a ±200 nm range of relative vertical bunch position offsets

* rebecca.louise.ramjiawan@cern.ch

ISBN: 978-3-95450-227-1 ISSN: 2673-5490 doi:10.18429/JACoW-IPAC2022-TUPOST012

SIRIUS STORAGE RING RF PLANT IDENTIFICATION

D. Daminelli*, F. K. G. Hoshino, A. P. B. Lima,
Brazilian Synchrotron Light Laboratory, Campinas, Brazil
M. Souza, University of Campinas, Campinas, Brazil

Abstract

The design configuration of the Sirius Light Source RF System is based on two superconducting RF cavities and eight 65 kW solid-state amplifiers operating at 500 MHz. The current configuration, based on a 7-cell normal conducting PETRA cavity, was initially planned for commissioning and initial tests of the beamlines. A digital low-level RF (DLLRF) system based on ALBA topology has been operating since 2019. Sirius is currently operating in decay mode for beamline tests with 100 mA stored current. During the commissioning, several studies were carried out to increase the stored current with stable beam. This paper presents a study using parametric data-driven models to identify the Storage Ring RF plant, aiming to optimize the DLLRF PI control parameters.

INTRODUCTION

Sirius's current Storage Ring RF system is operating with a 7-cell normal conducting cavity driven by a 130 kW RF Plant consisted of two 65 kW solid state amplifiers (SSA). THe RF System is controlled by a digital low-level RF (DLLRF) [1] based on the ALBA's design to achieve 0.1 % amplitude and 0.1 ° phase stability under normal operating conditions [2, 3].

Until now, the DLLRF controller parameters were tuned with a pragmatic approach to ensure beam stability. In order to optimize these parameters, improving output disturbance rejection, and mitigate longitudinal instabilities [4], a study has been conducted to identify the RF plant and find a parametric polynomial model that can be used along with MATLAB's Control Toolbox [5] to fine tune the PI loop. The methods and results of this study are discussed in the following sections.

RF PLANT STRUCTURE

Figure 1 shows a block diagram from the Sirius Storage Ring RF System.

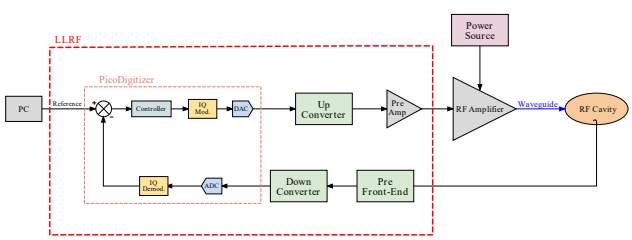

Figure 1: Sirius RF Plant block diagram.

The PicoDigitizer from Nutaq [6] houses the Virtex-6 SX315T FPGA and two FMC boards: a 16-channel 14-bit 125 MSPS ADC board and a 8-channel 16-bit 250 MSPS DAC board.

Regarding the many features available in LLRF, some were particularly useful for this study:

- IQ Digital Modulation/Demodulation
- PI Loops for Cavity Voltage Control in IQ (rectangular) or Polar loops
- Phase Shifters and Gain control on each DAC's outpus and ADC's Input
- Fast Data Logger (FDL) for fast data acquisition and post-mortem analysis
- Conditioning mode with a 10 Hz square-modulated RF Drive output.

LINEAR MODEL

System modelling and identification are very useful tools to extract information about a system from measured input-output data and to aid the design of high-performance controllers [7]. There are multiple ways of representing a system, but some are especially suitable for system identification, as they are based on well-established algorithms [8].

Parametric Polynomial Models

In this study, linear discrete representations fits well for this application. A general discrete model can be written as follows:

$$y(k) = \frac{B(q)}{A(q)F(q)}u(k) + \frac{C(q)}{A(q)D(q)}v(k), \qquad (1)$$

with q being the delay operator, that is $y(k)q^{-1} = y(k-1)$, $v(k)$ a white Gaussian noise and $A(q)$, $B(q)$, $C(q)$, $D(q)$, and $F(q)$ the following polynomials:

$$\begin{aligned} A(q) &= 1 - a_1 q^{-1} - \cdots - a_{n_y} q^{-n_y} \\ B(q) &= b_1 q^{-1} + \cdots + b_{n_u} q^{-n_u} \\ C(q) &= 1 + c_1 q^{-1} + \cdots + c_{n_v} q^{-n_v} \\ D(q) &= 1 + d_1 q^{-1} + \cdots + d_{n_d} q^{-n_d} \\ F(q) &= 1 + f_1 q^{-1} + \cdots + f_{f_v} q^{-f_v}. \end{aligned} \qquad (2)$$

From the generic model shown in (1) we can obtain simpler models useful for the identification of several types of systems. For this study, an Output Error model, shown in Eq. (3) was chosen to describe the RF Plant.

$$y(k) = \frac{B(q)}{F(q)}u(k) + v(k) \qquad (3)$$

* david.daminelli@cnpem.br

ISBN: 978-3-95450-227-1 ISSN: 2673-5490 doi:10.18429/JACoW-IPAC2022-TUPOST013

CONCEPT AND DEVELOPMENT OF 65 kW SOLID-STATE RF AMPLIFIERS FOR SIRIUS

M. H. Wallner*, R. H. A. Farias, A. P. B. Lima, CNPEM, 13083-100, Campinas, Brazil

Abstract

Sirius is a 4th generation synchrotron light source currently operating with 100 mA stored beam and one room temperature RF cavity driven by two 65 kW solid-state amplifiers (SSAs). After installation of the cryogenic plant, two superconducting (SC) RF cavities are planned to replace the room temperature cavity. Each SC cavity is going to be driven by a 250 kW RF signal at 500 MHz, resulting from the combination of four 65 kW RF SSAs. Due to the recent development of 900 W solid-state power amplifier modules, a new topology was proposed for the four amplifiers that still need to be constructed. For the amplifier's combining stage, a cavity combiner with 80 input ports was simulated. For the dividing stage, 8-way and 10-way power splitters were designed. The general scheme of the amplifier is presented, as well as simulation and measurement results.

INTRODUCTION

Sirius is a 4th generation synchrotron light source located in the city of Campinas, Brazil. It comprises a 350 MeV, 3 GHz linac, a 2 Hz booster and a 3 GeV, 500 MHz storage ring. It is currently able to store a stable 100 mA electron beam, accelerated by a room temperature 7-cell PETRA cavity. This cavity is driven by two solid state amplifiers, each one able to deliver up to 65 kW RF power. After the cryogenic plant installation, the PETRA cavity is expected to be superseded by two superconducting (SC) CESR B-cell cavities to enable the storage of higher beam currents. To achieve 350 mA, each cavity will require up to 250 kW at 500 MHz, so more RF amplifiers are necessary.

The Brazilian Synchrotron Light Laboratory (LNLS) was one of the first facilities of its kind to employ solid state technology on RF amplifiers, along with SOLEIL. LNLS' late 2nd generation synchrotron light source operated for 10 years with solid state amplifiers (SSAs) on its storage ring with positive results. Its benefits, like modularity, high MTBF and efficiency, absence of high DC voltages, among others, are well known. Therefore, solid state technology continues to be the choice for RF amplification at Sirius' storage ring.

The two 65 kW SSAs currently operating will also be employed for one of the SC cavities, along with other two amplifiers of the same topology that are being assembled and will be tested on the second semester of 2022. For the other SC cavity, a new solid-state power amplifier module has been developed in 2021 and has shown better efficiency, as well as higher gain and output power level. For several reasons, these amplifier modules would be incompatible with the current SSA topology, so an effort has been made to devise a new topology, which includes a different RF power splitting and combining scheme.

The following sections are dedicated to briefly present RF devices of the proposed RF amplifier, as well as studies to evaluate key parameters for future operation.

AMPLIFIER MODULE

The desgined amplifier module has been already mentioned in a previous conference, along with the performance of some prototypes [1]. It was able to output 900 W in the workbench reliably, but could not handle full reflected output power at the isolator due to poor thermal management of the RF termination, which was only rated for 800 W.

Therefore, an aluminum case with embedded copper tube was designed to assure better thermal dissipation. Thermal simulations were carried out to optimize the copper tube path and location. Minor changes on the RF and bias circuit were also made. Moreover, some room inside the case was left to house an eventual control board dedicated to gate bias control and data acquisition. Finally, a 1200 W RF termination was selected for the new version.

The modified aluminum cases will arrive soon and fine tuning of the RF parameters will be done on the workbench. After that, the production of a test batch will be launched. Fig. 1 presents a detailed 3D drawing of the assembled amplifier module.

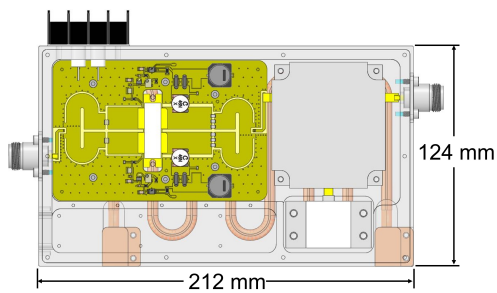

Figure 1: Top view of the amplifier module mechanical assembly CAD.

POWER DIVIDERS

8-Way Divider

Each amplifier module will be driven by one of the output ports of an 8-way RF power divider. It is built by cascading 2-way Wilkinson power dividers three times. It isolates output ports and prevents failing modules from impacting other modules' input power. This device was simulated in HFSS and a prototype was assembled and soldered in-house and is presented in Fig. 2. Main RF parameters are presented

* mark.wallner@cnpem.br

ISBN: 978-3-95450-227-1 ISSN: 2673-5490 doi:10.18429/JACoW-IPAC2022-TUPOST014

SIRIUS STORAGE RING RF SYSTEM STATUS UPDATE

A. P. B. Lima*, D. Daminelli, M. H. Wallner, F. K. G. Hoshino, I. C. Almeida, R. H. A Farias
Brazilian Synchrotron Light Laboratory, CNPEM-LNLS, Campinas, Brazil

Abstract

Sirius's nominal operation phase consists of two 500 MHz CESR-B type superconducting cavities, each being driven by four 65 kW solid-state amplifiers, and a passive superconducting third harmonic cavity. Currently a normal conducting 7-cell PETRA cavity is being used along with two 65 kW RF amplifiers and was recently able to achieve 100 mA stored current. The performance of the storage ring RF system and the updated installation plans update are presented and discussed.

INTRODUCTION

Sirius's storage ring RF system is currently operating with a 7-cell normal conducting cavity driven by a 130 kW RF plant comprised of two 65 kW solid-state amplifiers (SSA) and controlled by a digital low-level radio frequency (DLLRF) based on ALBA's platform [1]. Sirius has been operating in decay mode for beamline tests with 100 mA stored current [2].

The RF system for Sirius's storage ring will be comprised of two CESR-B type superconducting (SC) cavities in its final design configuration to provide the 3 MV gap voltage required for the operation with 350 mA storage current. The final RF design also contemplates the installation of a SC passive third harmonic cavity.

CURRENT SYSTEM STATUS

Sirius's RF system has been in operation for over two and a half years. Trips concerning the RF system are mostly related to the cavity pressure or temperature. The following subsections will discuss further aspects related to the system performance and operation at the present status.

Performance

Figure 1 shows the SSAs global efficiency and gain. Each SSA operates with about 55 kW output power at 100 mA stored beam current. At this operating point, the global efficiency is about 50% and the gain is around 51 dB. At maximum output power (65 kW) the amplifiers operate with efficiency around 60% as usual for a class AB amplifier.

The two SSAs have been operated for roughly 15 thousand hours with reliability close to 100% since the installation and commissioning of the Sirius RF system. Even though the SSAs are not being the cause of any trip of the RF system during operation, a considerable number of modules had to undergo some sort of maintenance, where 17.8% of the modules had to be repaired, most of them due to poor quality of one pi-filter in the gate bias circuit. These faults had no effective impact on the system and these filters are being preventively replaced during scheduled maintenances, as degradation of the module's current consumption is observed.

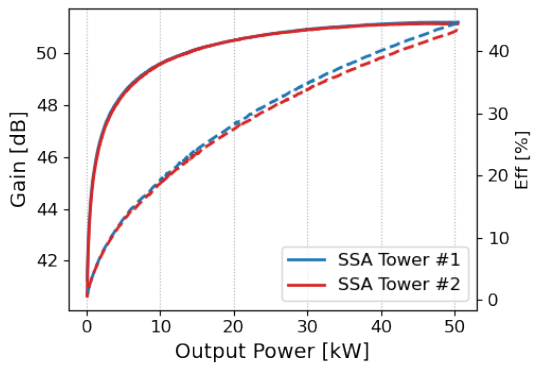

Figure 1: Sirius RF SSAs efficiency (dashed) and gain (solid).

Figure 2 shows the number of amplifier modules that have failed so far. To date, only 2 out of 264 transistors from the modules have failed during the conditioning phase of the SSAs before their installation in the machine.

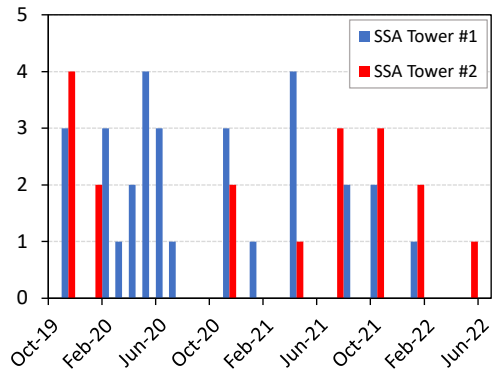

Figure 2: Repaired amplifier modules over the years.

Operation

Since the 7-cell cavity is in operation for a longer period than initially planned, some optimizations were made. This cavity has no HOM damping, but the operating temperature was adjusted to minimize the impact of these HOMs and guarantee the beam stability, supported by the longitudinal BbB system, designed to operate with a beam current up to 100 mA [3]. Despite the absence of HOM dampers, it is possible to accumulate about 85 mA of a stable beam without longitudinal BbB feedback.

Sirius is currently operating in decay mode with current starting at 100 mA during beamlines users run with bunch-by-bunch (BbB) and slow orbit feedback (SOFB) systems

* andre.lima@cnpem.br

ISBN: 978-3-95450-227-1 ISSN: 2673-5490 doi:10.18429/JACoW-IPAC2022-TUPOST015

COMMISSIONING AND FIRST RESULTS OF AN X-BAND LLRF SYSTEM FOR TEX TEST FACILITY AT LNF-INFN

L. Piersanti *, D. Alesini, M. Bellaveglia, S. Bini, B. Buonomo, F. Cardelli, C. Di Giulio, E. Di Pasquale, M. Diomede, L. Faillace, A. Falone, G. Franzini, A. Gallo, G. Giannetti, A. Liedl, D. Moriggi, S. Pioli, S. Quaglia, L. Sabbatini, M. Scampati, G. Scarselletta, A. Stella, S. Tocci, L. Zelinotti, INFN - Laboratori Nazionali di Frascati, Via Enrico Fermi 54, 00044, Frascati, Italy

Abstract

In the framework of LATINO project (Laboratory in Advanced Technologies for INnOvation) funded by Lazio regional government, the commissioning of the TEst stand for X-band (TEX) facility has started in 2021 at Frascati National Laboratories of INFN. Born as a collaboration with CERN to test high gradient accelerating structures, during 2022 TEX aims at feeding the first EuPRAXIA@SPARC_LAB X-band structure prototype. During 2021 the commissioning has been successfully carried out up to 48 MW. The power unit is driven by an X-band low level RF system, that employs a commercial S-band (2.856 GHz) Libera digital LLRF (manufactured by Instrumentation Technologies), with an up/down conversion stage and a reference generation and distribution system able to produce coherent frequencies for the American S-band and European X-band (11.994 GHz), both designed and realized at LNF. The performance of the system, with a particular focus on amplitude and phase resolution, together with klystron and driver amplifier jitter measurements, will be reviewed in this paper. Moreover, considerations on its suitability and main limitations in view of EuPRAXIA@SPARC_LAB project will be discussed.

INTRODUCTION

The TEX facility [1] is one of the pillars of the LATINO project [2], funded by Lazio regional government, that aims to provide companies and the scientific community with the advanced technologies and skills developed in the field of particle accelerators for research, medical and industrial applications. Its commissioning has started in November 2021 at INFN National Laboratories of Frascati with the Site Acceptance Test (SAT in the following) of the RF power unit [3]. During these preliminary tests also the LLRF system has been commissioned, showing some promising results, but also highlighting some critical aspects concerning, for instance, sample rate, front-end and back-end bandwidth, which are particularly important for a future LLRF system development for an X-band driven linac.

TEX TEST FACILITY

The TEX facility main goal is to test at high power X-band RF components at LNF. Waveguide devices and accelerating structures could be conditioned at this frequency in the facility, which is supplied by a VKX8311A 50 MW, 1.5 µs klystron from CPI LLC (USA), and a K400 450 kV solid state modulator from Scandinova (Sweden). The repetition rate will be at least 50 Hz. A new control room has been realized and equipped, and a concrete shielded bunker has been built to host the structures under test. A Memorandum of Understanding has been also signed with CERN, to profit from the well established experience on X-band technology acquired with the operation of the XBOX test stands. In fact, the test-facility will be also used to test and condition CLIC structures. TEX will be also an R&D and test facility for X-band RF components, LLRF systems, beam diagnostics, vacuum technologies and control system in view of INFN future accelerator EuPRAXIA@SPARC_LAB [4, 5] that will be built at LNF. This project foresees in fact the construction of a X-band linac booster up to 1 GeV, working with a target accelerating gradient of 60 MV/m.

A sketch of the TEX area is reported in Fig. 1, where the modulator cage, the bunker and the waveguide network CAD design is reported.

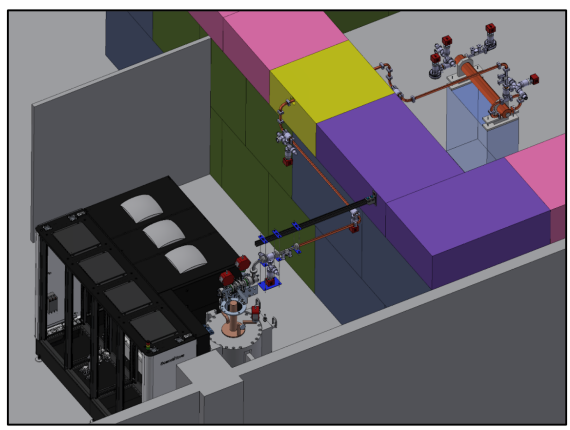

Figure 1: 3D CAD drawing of the TEX facility experimental area.

The SAT of the RF power unit took place in November 2021, once the building air conditioning and civil engineering works have been completed. The entire waveguide network is now in place up to the final RF splitter right before the accelerating structure input coupler (where two 25 MW RF loads have been connected in parallel for the high power tests instead). Using this RF layout, it was possible to reach 48 MW, with a pulse length of 150 ns at 50 Hz repetition rate during the SAT. In Fig.2 is shown the waveguide network outside (left) and inside (right) the bunker.

* luca.piersanti@lnf.infn.it

ISBN: 978-3-95450-227-1 ISSN: 2673-5490 doi:10.18429/JACoW-IPAC2022-TUPOST016

STATUS OF LLRF AND RESONANCE CONTROL DEDICATED ALGORITHMS EXTENSION FOR PolFEL

W. Jalmuzna, W. Cichalewski, A. Napieralski, P. Sekalski,
Lodz University of Technology, Lodz, Poland

Abstract

PolFEL (POLish Free Electron Laser) is the new superconducting-based facility, which is under construction in Poland. It will provide a continuous electron beam with energy up to 160 MeV, which will be converted to light pulses with wavelengths as short as 150 nm. CW (Continuous Wave) operation of the superconducting linear accelerator with narrow bandwidth and high electromagnetic field gradient (presumably above 30 MV/m for single structure) creates new challenges while dealing with RF field stability, the influence of mechanical de-tuning of resonating structures and must consider all limits induced by power amplifiers and cryo-system. The real-time control algorithm responsible for RF field, motor tuners, and piezo control must strictly interact with each other to provide the satisfactory performance of the whole facility. In addition, constant monitoring of such parameters as detuning, bandwidth, power margins of the amplifier, state of cavities must be done. The paper presents the status of implementation of PolFEL's LLRF Controller (extending GDR to other modes of operation as SEL, PLL) and Piezo Controller (both hardware and firmware layers).

INTRODUCTION

PolFEL (Polish Free Electron Laser) is the free electron laser facility, which is under construction in Poland. The main operation modes of its superconducting based linear accelerator will be Continuous Wave (CW) and Long Pulse. The accelerator itself will consist of 4 cryo-modules with 8 TESLA superconducting cavities in total and will provide continuous electron beam with energies from 120 MeV up to 160 MeV. The beam will be passed through VUV undulators to generate radiation with wave lengths staring at 0.3 mm down to 150 nm (50 nm for third harmonic) – the total photon pulse energy will reach 100 uJ with repetition rate of 100 kHz. After leaving undulators, the beam will be used for neutron generation or Compton scattering experiments. The estimated end of construction and commissioning of the whole facility is in 2023.

PolFEL will use relatively high accelerating electromagnetic field gradients (presumably above 30 MV/m for single structure). Work in such conditions requires either high input power (which exceeds limits achievable by existing high-power amplifiers and power distribution systems) or increase of input power coupling, which corresponds to Loaded Quality of the resonator and in the result narrows down system bandwidth to several Hertz. Under these circumstances any detuning of the resonating frequency of the cavity (either caused by microphonics or Lorentz Force) will have big influence on stability of the RF Accelerating field (up to the point where no operation is possible). Therefore, it must be compensated by interaction between cavity tuning system/algorithms based on piezo actuators and dedicated RF control algorithms with special functionality related to out of band operations.

The Department of Microelectronics and Computer Science, Lodz University of Technology, with all its experience gathered during work in such experiments as Flash, EuXFEL and ESS, is involved in design and development of several subsystems of the facility.

SCOPE OF WORK

As part of the work, dedicated hardware device for resonance control system will be designed and manufactured. It will be implemented in a form of standalone integrated 19" box and will contain at least 18 piezo drivers able to drive 16 piezo stacks (2 per superconducting cavity) in LINAC section and additional 2 stacks at RF-Gun cavity.

Resonance Control Hardware must be integrated with other uTCA based systems (especially LLRF) to provide consistent platform for algorithm execution and control system integrations. These will be achieved by using external communication links and special adapters on LLRF system side.

In addition to the hardware platform, the several control algorithms will be implemented. These are divided into two groups:

- Field Control Algorithms -The algorithms must ensure overall stability of the RF Accelerating Field parameters to deliver electron beam of required quality and provide additional information for other systems (i.e. resonance control) and operators to improve operation and prevent unexpected faults.
- Resonance Control Algorithms - The algorithms and hardware subsystems for piezo control must be able to compensate both Lorentz Force Detuning (LFD) and frequency deviations caused by environmental mechanical vibrations (microphonics). This can be achieved using such algorithms like online cavity parameters identification and adaptive noise compensation.

As stated before, both groups of the algorithms implemented must exchange data and closely interact with each other to make the operation with required field parameters possible.

RESONANCE CONTROLLER REQUIREMENTS

The superconductive cavities are mounted inside cryomodule using fixture equipped with motor tuner and two piezo stacks. In many applications one of the stacks is used

ISBN: 978-3-95450-227-1 ISSN: 2673-5490 doi:10.18429/JACoW-IPAC2022-TUPOST017

PEG CONTRIBUTION TO THE LLRF SYSTEM FOR SUPERCONDUCTING ELLIPTICAL CAVITIES OF ESS ACCELERATOR LINAC*

W. Cichalewski†, G. Jablonski, K. Klys, D. Makowski, A. Mielczarek,
A. Napieralski, P. Perek, P. Plewinski, TUL-DMCS, Lodz, Poland
A. Abramowicz, K. Czuba, M. Grzegrzolka, K. Oliwa, I. Rutkowski, W. Wierba
WUT-ISE, Warsaw, Poland
P. Bartoszek, K. Chmielewski, Z. Golebiewski, K. Kostrzewa, T. Kowalski, D. Rybka,
M. Sitek, J. Szewinski, Z. Wojciechowski, NCBJ, Swierk/Otwock, Poland
M. Jensen, A. Svensson, ESS, Lund, Sweden, A. Johansson, Lund University, Lund, Sweden

Abstract

The LLRF (Low-Level Radio Frequency) system optimizes energy transfer from the superconducting resonator to the accelerating beam. At ESS, one LLRF system regulates a single cavity. This digital system's hardware platform is the MTCA.4 standard. The system has been co-designed by ESS, Lund University, and the PEG (Polish Electronic Group) consortium. The PEG is also responsible for the system components design, evaluation, and production (like Local Oscillator Rear transition module, piezo tuner driver RTM, RTM carrier board, and others). The PEG delivers a hardware/software cavity simulator, an LLRF system test-stand, and provides necessary integration and installation services required for complete system preparation for the linac commissioning and operation phase. The paper summarizes the PEG work on the development and preparation of the LLRF systems for the ESS elliptical structures. The efforts concerning hardware and software components prototyping and evaluation are discussed. Moreover, we present the current status of the project, including components mass production, integration, and installation work.

INTRODUCTION - LLRF SYSTEMS FOR ESS ELLIPTICAL RESONATORS

The Low-Level Radio Frequency (LLRF) control system's primary goal is to provide optimal energy transfer from the cavity to the accelerated particles beam.

The ESS project foresees a single cavity regulation scheme (see Fig. 1). The presented diagram describes the system setup for spokes and elliptical cavities. But the general idea was the unification of different system types. The MTCA.4 [1] standard provides enough versatility by means of dedicated sub-modules configuration ability for given system kind. The set-up of the controller comprises of different hardware modules [3]. Some of them were designed and delivered by PEG (RTM carrier, LO-RTM, Piezo driver). The consortia members responsibility includes also LLRF system integration and installation at the ESS linac side. The elliptical cavity simulator and complete system loop test-stand enabled reliable verification of the LLRF system components and set-up.

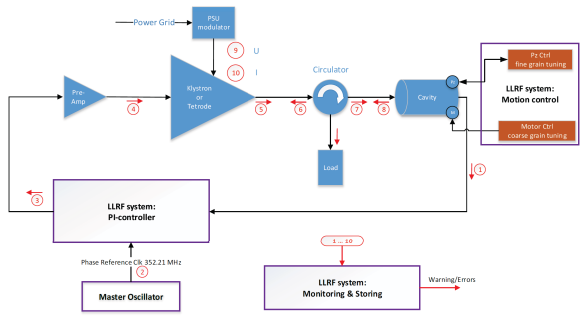

Figure 1: Overview of the LLRF system [2].

MTCA.4 HARDWARE MODULES DESIGNED BY PEG

RTM Carrier AMC Module

The RTM Carrier (Fig. 2) is low cost FPGA based MTCA.4 AMC module, dedicated for supporting LO RTM (Fig. 3) and Piezo RTM (Fig. 4) boards in the LLRF systems. Board is equipped in Artix-7 FPGA device, it has also 1GB of DDR3 memory and covers PCIe x2 and Low latency Links (direct board-to-board connections) on the MTCA backplane. In the LLRF system architecture, the RTM Carrier board provides minimal functionality that allows RTMs to operate. The general required functionality of the board is: communication with the RTM via ZONE 3, powering RTM devices, communication with the other devices using PCI-Express on the backplane, data processing in the FPGA, fulfilling all the other requirements for the AMC board defined in the MTCA.4 standard.

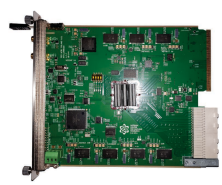

Figure 2: RTM Carrier AMC module.

* Work supported by Polish Ministry of Education and Science, agreement number 2021/WK/04
† wcichal@dmcs.pl

ISBN: 978-3-95450-227-1 ISSN: 2673-5490 doi:10.18429/JACoW-IPAC2022-TUPOST018

LONG PULSE OPERATION OF THE E-XFEL CRYOMODULE

W. Cichalewski*, TUL-DMCS, Lodz, Poland
J. Sekutowicz, DESY, Hamburg, Germany and NCBJ, Swierk, Poland

Abstract

The CW operation becomes more attractive mode of beam and RF operation, even for infrastructures initially developed as pulsed experiments. Compared to the short (single ms) pulse the CW or long pulse (LP) operation allows for a more relaxed bunch scheme and enables higher bunch quantities during the experiment run. The Long Pulse operation scenario is one of the possible EXFEL modes of work in the future. LLRF systems that work in CW (and LP) are in operation worldwide. Most of them are dedicated to single cavity control. The XFEL dedicated system is capable of multi-cavity cryomodules vector-sum operation. In such a configuration switching from short-pulse operation into long-pulse with the existing limitations from the allowed cryo heat load level, average input power per coupler (and others) can be extremely challenging. For this setup the support from the dynamic resonance control system is essential. This paper summarizes efforts towards the successful vector-sum operation of the X-FEL type cryomodule in the LP operation mode. Modifications to the original LLRF setup together with challenges of narrow bandwidth operation in moderate and high gradients are discussed.

INTRODUCTION

Current Low Level Radio Frequency (LLRF) control systems offer more and more versatility and flexibility that can cover a wide scope of applications to be realized by the same set-up.

The system designed and developed initially for accelerating field parameters regulation in short (millisecond scale) pulse operation fulfills CW operation requirements too.

One such example is the LLRF system of the EXFEL project. The facility is in operation since 2017. Although the design nominal operation parameters foresee up to around 1,4 ms pulses with a 10 Hz repetition rate the work on the CW and LPO upgrade possibilities started already in 2011. Over last years, different studies have taken place to determine the necessary modification for the controller system. At the same time, the work continued on system usage limitations determination and environment restrictions.

Majority of the CW and LPO work took place at the Cryo Module Test Bench (CMTB) facility at DESY (Hamburg, Germany). This facility operates single TESLA cavities cryo module that comprises 8 niobium structure. It can operate either the short pulse (using klystron) or CW/LPO (using an IOT prototype) in 2K temperature conditions.

* wcichal@dmcs.pl

LLRF SYSTEM STRUCTURE

The LLRF system of the DESY facilities (like FLASH or EXFEL) [1] is the controller capable of multi-cavity operation configuration. It optimizes the electro-magnetic field in 8 up to 32 resonators (4 cryomodules) strings. The implementation diagram with the simple proportional feedback loop configuration is summarized in Figure 1. The single

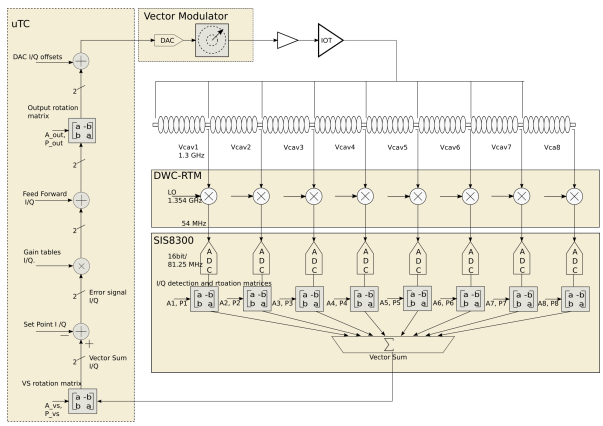

Figure 1: Overview of the LLRF system main RF control loop.

RF controller generates a command signal for all resonators simultaneously. Based on the vector sum information, the error signal reflects the difference between the desired pulse shape and the actual field in cavities. The system allows for different resonator impact adjustments using single rotation and scaling parameters configurations. The other control loop dedicated and more engaged during the CW and LPO operation is the one that provides fine frequency tuning of each cavity (see Figure 2).

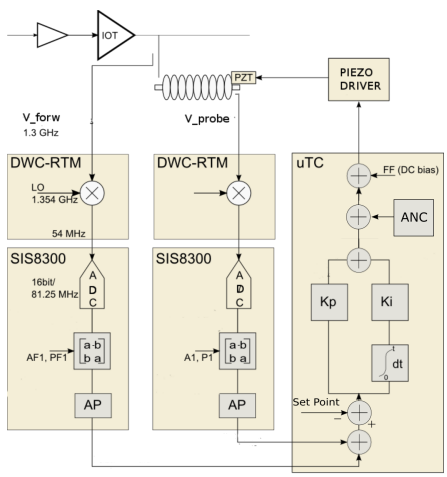

Figure 2: Overview of the cavity resonance control structure.

ISBN: 978-3-95450-227-1 ISSN: 2673-5490 doi:10.18429/JACoW-IPAC2022-TUPOST019

EVALUATION OF PIP-II MASTER OSCILLATOR COMPONENTS *

I. Rutkowski †, K. Czuba, A. Šerlat , Warsaw University of Technology, Warsaw, Poland
B. E. Chase, E. Cullerton, Fermi National Accelerator Laboratory/PIP-II, Batavia, Illinois, USA

Abstract

The Proton Improvement Plan-II (PIP-II) is a planned proton facility at Fermilab. The short- and long-term beam energy stabilization requirements necessitate using a high-quality Master Oscillator (MO). The consecutive sections of the Linac will operate at 162.5, 325, and 650 MHz. The phase relations between reference signals of harmonic frequencies should be kept constant, and the phase noise should be correlated in a wide bandwidth. The possibility of simultaneously meeting both requirements using popular frequency synthesis schemes is discussed. The ultra-low noise floor of the fundamental source is challenging for other devices in the phase reference distribution system. Therefore, the sensitivity to operating conditions, including impedance matching, input power level, and power supply voltage, must be considered. This paper presents a preliminary performance test of critical components selected for the PIP-II Master Oscillator system performed using a state-of-the-art phase noise analyzer.

INTRODUCTION

The Proton Improvement Plan II (PIP-II) is a plan of enhancement to the Fermi National Accelerator Laboratory (Fermilab) accelerator complex [1], the key component which is a 800 MeV superconducting radio-frequency linear accelerator made up of three consecutive sections operating at 162.5, 325, and 650 MHz. In addition, 1.3 GHz signal is needed to generate the high speed FPGA clock and a feedback for the phase reference line. The short- and long-term beam energy stabilization requirements necessitate using a high-quality Master Oscillator (MO). The reference generation will be combined with the distribution system to minimize the number of components. The MO will produce the lowest operating frequency, and harmonics will be generated at the beginning of a corresponding section.

The phase relations between reference signals of harmonic frequencies should be kept constant, and the phase noise should be correlated in a wide band (1 MHz or more). With these two aspects in mind, we will investigate the main classes of synthesizers:

- indirect digital,
- direct digital,
- direct analog.

An indirect digital synthesizer utilizes a Phase Lock Loop (PLL) with an integer or fractional frequency divider. The loop bandwidth is limited (typically below one hundred kHz) due to the high gain of a low phase noise VCO and insufficient phase margin. The phase relation is maintained constant by the loop.

A direct digital synthesizer (DDS) uses a numerically controlled oscillator feeding a digital-to-analog converter, both synchronized by the same clock. Without increasing the input clock internally (typically using an additional PLL), a DDS can not generate an output signal of a frequency higher than the reference. This limitation renders it unsuitable for this application.

The direct analog approach uses frequency dividers, mixers, and filters to produce and select the desired spectral component at the mixer's output. Within the band-pass, the device closely follows the PN of the reference, with the additional noise induced by the optional divider and the mixer.

In the direct methods, there is no loop guaranteeing the phase relations.

In all three aforementioned methods, the frequency ratio ($\frac{f_{out}}{f_{in}}$) can be fractional. If the allowed ratios are limited to natural values (in this application, this limitation is not prohibitive), other techniques can be employed. Non-linear elements like step recovery diodes generate a train of very fast pulses occurring one every cycle of the input signal. A notch filter selects the desired harmonic. The noise correlation bandwidth is determined by the filter (making it easy to obtain a wide bandwidth), but the phase relation is not guaranteed.

No architecture simultaneously fulfills both requirements. Since the phase can be stabilized with an auxiliary circuit, the harmonic generation technique was selected as it can provide the lowest residual noise.

Fermilab and Warsaw University of Technology (WUT) are collaborating on the design of the MO and the phase reference line for PIP-II. In the following sections, the measurement results of the proposed MO and frequency multipliers are presented. Unless otherwise noted, the measurements were performed at WUT in a Faraday cage using a Rhode & Schwarz FSWP phase noise analyzer. The jitter will be given as an integral in the 10 Hz to 1 MHz band.

MASTER OSCILLATOR

A vibration isolated narrow-band voltage controlled oscillator generating 10 MHz and 162.5 MHz output signals was custom-made by Wenzel for the linac. Figure 1 shows the measured phase noise spectra of both signals as well as the calculated spectrum of the 10 MHz signal perfectly

* The paper was prepared by Warsaw University of Technology and Fermi National Accelerator Laboratory/PIP-II, using the resources of Fermi National Accelerator Laboratory (Fermilab), a U.S. Department of Energy, Office of Science, HEP User Facility. Fermilab is managed by Fermi Research Alliance, LLC (FRA), acting under Contract No. DE-AC02-07CH11359.
Research was funded by POB HEP of Warsaw University of Technology within the Excellence Initiative: Research University (IDUB) programme.
† Igor.Rutkowski@pw.edu.pl

ISBN: 978-3-95450-227-1 ISSN: 2673-5490 doi:10.18429/JACoW-IPAC2022-TUPOST021

THE CERN SPS LOW LEVEL RF: THE BEAM-CONTROL

A. Spierer†, P. Baudrenghien, J. Egli, G. Hagmann, P. Kuzmanovic, I. Stachon, M. Suminski, T. Wlostowski, CERN, Geneva, Switzerland

Abstract

The Super Proton Synchrotron (SPS) Low Level RF (LLRF) has been completely upgraded during the CERN long shutdown (LS2, 2019-2020). The old NIM and VME based, mainly analog system has been replaced with modern digital electronics implemented on a MicroTCA platform. The architecture has also been reviewed, with synchronization between RF stations now resting on the White Rabbit (WR) deterministic link. This paper is the first of a series of three on the SPS LLRF upgrade. It covers the Beam-Control part, that is responsible for the generation of the RF reference frequency from a measurement of the magnetic field, and beam phase and radial position. It broadcasts this frequency word to the RF stations, via a White Rabbit network. The paper presents the architecture, gives details on the signal processing, firmware, hardware and software. Finally, results from the first year of beam commissioning are presented (2021).

OVERVIEW OF THE LLRF UPGRADE

The CERN LHC Injectors Upgrade (LIU) project plans doubling the proton intensity extracted from the Super Proton Synchrotron (SPS) for injection into the Large Hadron Collider (LHC), therefore requiring a major upgrade [1]. Also planned is the doubling of the Lead ion beam intensity in the LHC, using a slip-stacking scheme in the SPS [2]. The Beam-Control has been upgraded along with the 200 MHz Cavity-Controllers [3,4] and the high level RF system. The two additional RF cavities (now six in total) and the need to control them individually called for a new architecture. The transition from a mostly analog to a digital system allows for new RF manipulations and an improvement of the beams' characteristics. In addition, parts of the system were aging and were difficult to maintain.

After the long shutdown (January 2019 - March 2021), the SPS commissioning with beam started in mid-April 2021 and the first proton beam was accelerated to 450 GeV/c by mid-May. During the year proton beams were delivered to the following experiments: Fixed Target, AWAKE and HiRadMat. From October to December, tests were conducted with the SPS Lead ion beam and with low intensity protons extracted to the LHC transfer lines. The first quarter of 2022 was dedicated to beam intensity increase and fine tuning of the different beams for the start of physics.

ARCHITECTURE

The new architecture relies on the White Rabbit (WR) technology [5] to synchronize the RF generation in different nodes. As shown in Figure 1, the newly developed LLRF devices are all connected to the same WR network and reconstruct their clocks for sampling and signal processing from the WR data stream.

The Beam-Control computes and broadcasts an ethernet RF frame on the WR network. It contains Frequency Tuning Words (FTW, among which the instantaneous revolution frequency) that are inputs for the distributed Numerically Controlled Oscillators (RFNCO). To generate the RF synchronously in every node, we use the fixed latency feature of the WR streamers [5]. The RFNCO core also provides frequency and amplitude modulation signals used for ions Fixed Frequency Acceleration (FFA) [6].

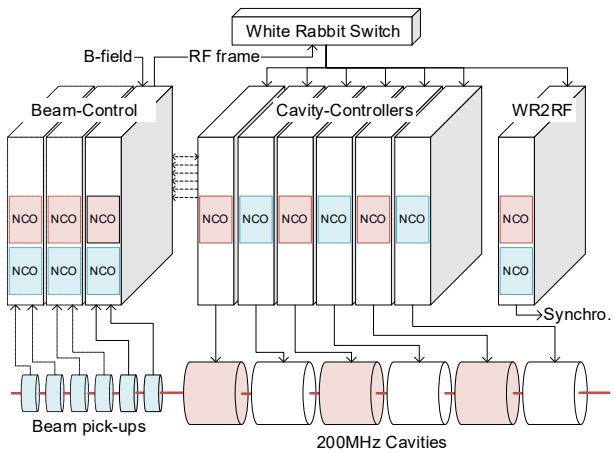

Figure 1: The SPS LLRF architecture.

The MicroTCA platform is used to host the Beam-Control and Cavity-Controllers' boards, providing controls and high bandwidth over PCIe for data acquisition.

THE BEAM-CONTROL SYSTEM

A Zynq System on Chip (SoC) is used to implement the digital signal processing and interfaces. The processing is balanced between the ARM CPU (turn by turn update) and the programmable logic for RF pre-processing (see Fig. 2).

The output of the Beam-Control is a set of FTWs and setpoints sent at the revolution frequency (~43 kHz). The FTW format allows for a 2 mHz resolution at 200 MHz.

Table 1: The WR RF Frame Content

Fields	Size in bits
FTW [main, on (FFA), program]	3*48
ΔFTW slip-stacking [group 1, 2]	2*32
Controls [modulation rate, resets]	1*16
Cavity setpoints [1..6][Amp., Phase]	6*32

For slip-stacking, a separate frequency ramp is provided for each of the two cavity groups (ΔFTW in Table 1), to let the two batches slip toward each other [6].

† arthur.spierer@cern.ch

ISBN: 978-3-95450-227-1 ISSN: 2673-5490 doi:10.18429/JACoW-IPAC2022-TUPOST022

THE CERN SPS LOW LEVEL RF: LEAD IONS ACCELERATION

P. Baudrenghien†, J. Egli, G. Hagmann, A. Spierer, T. Wlostowski, CERN, Geneva, Switzerland

Abstract

This paper is the third of a series of three on the Super Proton Synchrotron (SPS) Low Level RF (LLRF). Its focus is the upgrade concerned with the acceleration of Lead ions for injection into the LHC. Lead ions are far from relativistic at injection into the SPS. Therefore, the classic acceleration scheme at constant harmonic number (h=4620) does not work as the RF frequency swing does not fit within the cavity bandwidth. Fixed Frequency Acceleration (FFA) is therefore used. The upgraded LLRF uses a completely new implementation of the FFA, based on a Numerically Controlled Oscillator (NCO) implemented as an FPGA IP in the Controller of each cavity. In addition, the 2022 scheme for LHC ions filling calls for slip-stacking of two families of bunches, 100 ns spacing, to generate a 50 ns spacing after interleaving. The paper presents the key components for FFA and ions slip-stacking as implemented in the new system, together with successful first tests performed in Autumn 2021.

MOTIVATION

The LHC Injector Upgrade project (LIU) aims at the doubling of the total intensity of the Lead ion beam in the LHC with 50 ns bunch spacing [1]. The SPS injector (CPS) cannot provide the 50 ns spacing; the nominal scheme therefore calls for injection of several batches of 100 ns spaced bunches in the SPS and reduction of the bunch spacing to 50 ns using momentum slip-stacking in the SPS to interleave bunches from the several batches [2].

THE SPS LEAD ION CYCLE

The new SPS ion cycle for LHC filling was tested in November 2021. Figure 1 shows the cycle used: Momentum in red color (from 17 Z GeV/c to 450 Z GeV/c with a slip-stacking plateau at 300 Z GeV/c), DC beam current in yellow. The test cycle included the injection of two batches, each containing four bunches spaced by 100 ns. In 2022 the operational LHC filling cycle will include the injection of up to fourteen four-bunches batches from the CPS, with 150 ns gap between batches. The SPS flat bottom will therefore be much longer.

Fixed Frequency Acceleration

All SPS proton beams are accelerated with a fixed harmonic number h=4620. The bandwidth of the six 200 MHz accelerating cavities (Travelling Wave type) covers the required frequency range [3, 4]. With Lead ions, on the other hand, the required frequency variation exceeds the cavity bandwidth, if the harmonic number is kept constant. A solution was proposed in the late eighties and made operational, the Fixed Frequency Acceleration (FFA): Given that the beam fills less than half the circumference, and thanks to the small filling time of the cavities, we can apply 100% Amplitude Modulation (AM) during a turn with the RF ON during beam passage only. Frequency Modulation (FM) is applied in synchronism, with a fixed frequency chosen within the cavity bandwidth during the RF ON segment, and a variable frequency during the rest of the turn, adjusted to have a fixed 4620 RF periods during one revolution [5].

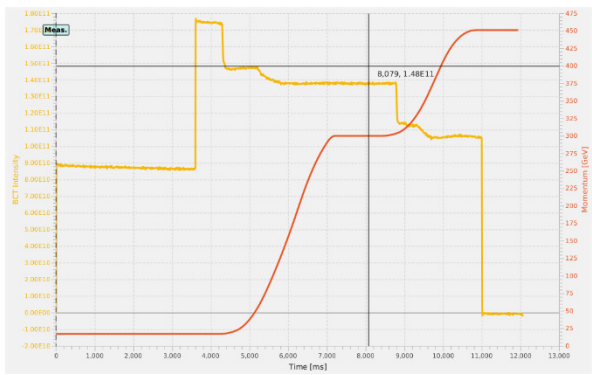

Figure 1: The SPS short ion cycle used in 2021 for setting-up momentum slip-stacking.

As explained in two companion papers [6, 7] the new LLRF architecture relies on the White Rabbit (WR) to keep the RF stations in synchronism [8]. The WR is a deterministic network, with fixed latency, distributing numerical data including Frequency Tuning Words (FTW) in our application, and providing a reset timing, at the start of each cycle. The clock of all digital electronics is recovered from the WR data stream [8, 9]. The RFNCO IP core is implemented in each station (see Fig. 2). Thanks to the WR architecture, different instances of the RFNCO will generate the exact same RF waveform at distant locations.

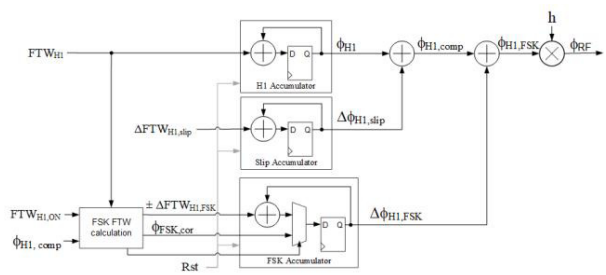

Figure 2: The RFNCO IP core.

The WR transmits the FTW_{H1} that corresponds to the revolution frequency, and the $FTW_{H1,ON}$ that encodes the RF ON frequency reduced to harmonic 1. It generates the instantaneous RF phase ϕ_{RF} (sawtooth), after multiplication by h=4620, and addition of a sawtooth $\Delta\phi_{H1,FSK}$ (for

† Philippe.Baudrenghien@cern.ch

ISBN: 978-3-95450-227-1 ISSN: 2673-5490 doi:10.18429/JACoW-IPAC2022-TUPOST023

THE CERN SPS LOW LEVEL RF: THE CAVITY-CONTROLLER

G. Hagmann†, P. Baudrenghien, J. Egli, A. Spierer, M. Suminski, and T. Wlostowski,
CERN, Geneva, Switzerland

Abstract

This paper is the second of a series of three on the Super Proton Synchrotron (SPS) Low Level RF (LLRF) upgrade. It covers the 200MHz Cavity-Controller part, that is responsible for the regulation of the accelerating field in a single SPS cavity. When the SPS is used as Large Hadron Collider (LHC) proton injector, the issue is the high beam loading that must be compensated to guarantee longitudinal stability and constant parameters over the bunch train. That calls for strong One-Turn Delay Feedback (OTFB) and Feed-Forward (FFWD). The SPS is also accelerating Lead ions (Pb). There the issue is Frequency-Modulation (FM) and Amplitude-Modulation (AM) over the turn (so called Fixed Frequency Acceleration - FFA) plus RF gymnastics for the new ions slip-stacking. The paper reviews the functional requirements, presents the block diagram, then gives details on the signal processing, firmware and hardware. Finally results from the first year of beam commissioning are presented (2021).

MOTIVATIONS NEW FUNCTIONALITIES

The SPS was restarted in April 2021 after a Long-Shutdown (LS2, 2019-2020) during which the LLRF system was upgraded to achieve the beam performance required for the SPS as High Luminosity LHC (HL-LHC) injector [1].

Bunch Intensity

For protons, the SPS bunch intensity will double during run 3 to reach 2.3e11 p+/bunch at extraction to the LHC [2, 3]. The new LLRF has improved the compensation of the beam loading to reduce the cavity impedance and prevent longitudinal coupled-bunch instabilities that have limited the bunch intensity to 1.4e11 p+/bunch in the SPS before LS2 [2].

For LHC high intensity beam and AWAKE single bunch beam, the RF voltage required, exceeds the average power of the amplifiers. Therefore, the LLRF now operates with 100% AM to exploit the maximum RF peak power.

Complete renovation of the FFWD and Longitudinal Damper (LD) was required to integrate the new architecture. The old FFWD implementation proved very noisy, and the old LD design did not effectively follow the change of optics resulting in the increase of synchrotron frequency.

Ions Slip-stacking

For ions, the target is a doubling of the LHC beam intensity with 50 ns bunch spacing [4]. The new LLRF must implement momentum slip-stacking to produce 50 ns spacing from two batches of bunches at 100 ns spacing [5]. Moreover, the One-Turn Delay Feedback (OTFB) is now operational for ions with FM and 100% AM over the turn.

Obsolescence

The upgrade of the entire SPS LLRF was motivated by: the critical obsolescence of the electronics where some modules were designed in the late 70's; the lack of LLRF control required to produce the new proton and ion beams; the installation of two additional 200 MHz travelling wave cavities.

ARCHITECTURE

Figure 2 shows the SPS LLRF architecture [1] based on the White-Rabbit network (WR) and on Numerically Controlled Oscillators (RFNCO) to synchronize all RF stations. The Beam-Control [6] computes the Frequency Tuning Word (FTW) for harmonic h=1 (revolution frequency) and sends it over WR to the Cavity-Controllers. The Cavity-Controllers (one instance per cavity) regulate the cavity field and reduce the beam loading by measuring the cavity voltage and the beam current to produce the correcting RF drive to the power amplifier.

RF Feedback

The RF feedback is the core of the Cavity-Controller. It contains two branches as shown in Fig. 1. The low-pass branch, switched on before injection, is a classic RF feedback regulating the cavity voltage with a 1 kHz bandwidth centered at the RF frequency.

The high pass branch is a One-Turn Delay Feedback with gain on the revolution frequency sidebands. It compensates the transient beam loading and prevents longitudinal instabilities linked to the impedance on the synchro-revolution sidebands. A triple comb filters is implemented [1] and operates at a fixed processing clock. The biquad structure of the comb filters and the loop delay both include a variable fractional delay tracking the changing revolution period during the acceleration.

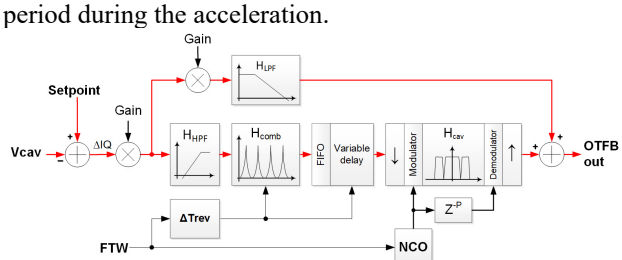

Figure 1: RF Feedback and One-Turn Delay Feedback.

As shown in Fig. 2, the cavity voltage (Vcav) cable and power amplifier introduce a delay and therefore a phase shift that varies with the RF frequency. The FIFO on the IQ demodulator local oscillator at ω_0 cancels this phase shift. As this delay is different amongst the cavities and because

† gregoire.hagmann@cern.ch

ISBN: 978-3-95450-227-1 ISSN: 2673-5490 doi:10.18429/JACoW-IPAC2022-TUPOST024

A NEW BEAM LOADING COMPENSATION AND BLOWUP CONTROL SYSTEM USING MULTI-HARMONIC DIGITAL FEEDBACK LOOPS IN THE CERN PROTON SYNCHROTRON BOOSTER

D. Barrientos*, J. Molendijk, M. Jaussi, S. Albright, M. E. Angoletta, A. Findlay
CERN, Geneva, Switzerland

Abstract

As part of the LHC Injectors Upgrade, the CERN Proton Synchrotron Booster (PSB) has been upgraded with new wide-band Finemet cavities and a renovated Low-Level Radio Frequency system with digital cavity controllers implemented in FPGAs. Each controller synchronously receives the computed revolution frequency, used to generate 16 harmonic references. These are then used to IQ demodulate the voltage gap and modulate the 16 RF drive signals each controlled through a Cartesian feedback loop (with individual voltage and phase control). The sum of these digital drive signals is then sent to the cavities. In addition, a configurable blow-up system providing a sinusoidal or custom noise pattern can be used to excite the beam. An embedded network analyzer allows studying the stability of the feedback loops of the individual harmonics. The 16 harmonic feedback loops have been successfully operated during 2021, allowing to reduce the beam induced voltage and control the longitudinal emittance of the beam. In this paper we present the system architecture as well as the performance of the complete cavity controller during operation in the PSB.

INTRODUCTION

The Low Level Radio Frequency (LLRF) system of the CERN Proton Synchrotron Booster (PSB) has been significantly upgraded during the Long Shutdown 2 (LS2) as part of the LHC Injectors Upgrade project [1]. In order to cope with the new wide-band Finemet™ cavities [2], the new LLRF system is capable of controlling the phase and amplitude of 16 harmonics of the revolution frequency, and includes extra functionalities not present in the previous system.

The LLRF system of the PSB has been conceived to be fully modular, meeting the accelerator architecture. This system belongs to a family of LLRF systems used to operate several machines at CERN [3]. An overview of the system architecture can also be found here [4].

The PSB consists of 4 superposed rings with 3 straight sections used for Radio Frequency (RF) cavities. The High Level Radio Frequency (HLRF) system provides a single RF drive and voltage gap monitor signal for each ring and straight section. The cavity controller feedback loops in the LLRF system have been designed to cope with these 12 systems individually.

As already shown in simulations [5] and during the previous beam tests [4], the induced voltage in the cavities would compromise the longitudinal stability of the beam. Thus, a precise system including individual phase and magnitude control of the voltage in the cavity is required.

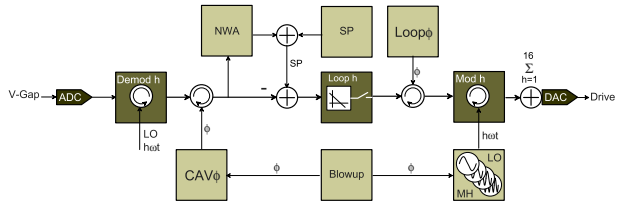

Figure 1: Building blocks of the multi-harmonic digital feedback system implemented in FPGA. Demodulator, feedback loop and modulator blocks are replicated 16 times.

SYSTEM ARCHITECTURE

Figure 1 shows an overview of the multi-harmonic digital feedback loops implemented in Field-Programmable Gate Arrays (FPGA). The voltage gap is digitized with a fixed frequency clock at about 122.7 MHz. This signal is digitally demodulated into 16 IQ pairs using a multi-harmonic source. For each harmonic, there is a cavity rotator allowing to individually control the cavity phasing. These are used to compensate different delays of the gap return cables of the different cavities. Moreover, it is used to set the phase of the RF signal in the cavities to be same in the 3 straight sections as perceived by the beam.

The setpoint (SP) of the feedback loop is set using a voltage function for each individual harmonic. The loop rotator allows using a phase function for each individual harmonic to insure loop stability. This rotator subtracts the cavity rotator phase in order to make both controls independent. The setpoint generation includes a limiter to avoid driving the cavities beyond their operating frequency range or setting a setpoint beyond the voltage acceptance limits. It also provides a mechanism to ramp the voltage up or down when an overflow condition is detected.

IQ values produced after the loop rotator arrive at the modulator, which applies a feed-forward compensation in gain and phase before up-modulating them using the corresponding harmonic local oscillator signal. All harmonics are then summed digitally and converted to the analog RF drive signal sent to the HLRF system.

Multi-harmonic Source

In order to increase the regulation bandwidth (decrease electronics delay), reduce cabling and optimize the resources usage, all harmonic feedback loops for the same cavity

* diego.barrientos@cern.ch

ISBN: 978-3-95450-227-1 ISSN: 2673-5490 doi:10.18429/JACoW-IPAC2022-TUPOST025

BEAM COMMISSIONING OF THE NEW DIGITAL LOW-LEVEL RF SYSTEM FOR CERN'S AD

M. E. Angoletta†, S. Albright, D. Barrientos, M. Jaussi, A. Findlay, A. Rey, M. Suminski
CERN, Geneva, Switzerland

Abstract

CERN's Antiproton Decelerator (AD) has been re-furbished and equipped with a new digital Low-Level RF (LLRF) system, successfully commissioned in 2021.

The new LLRF system routinely captures and decelerates more than 3E7 antiprotons from 3.5 GeV/c to 100 MeV/c in successive steps, interleaved with cooling periods. It implements the frequency program, beam phase/radial and cavity amplitude/phase feedback loops. An extraction synchronization loop allows transferring a bunch of antiprotons to the Extra Low ENergy Antiproton ring (ELENA). The LLRF parameters are controlled by a dedicated application and operational modes such as bunched beam cooling have been successfully deployed.

This paper gives an overview of the LLRF commissioning and challenges. Hints on future steps are also provided.

INTRODUCTION

CERN's Antiproton Decelerator (AD) has been re-furbished to provide reliable operation to the Extra Low ENergy Antiproton ring (ELENA), now its sole user. Upgrades included replacing the ferrite-based decelerating High-level RF (HLRF) system with one based on Finemet® alloy. A new Low-Level RF (LLRF) system was commissioned in 2021 to carry out beam and cavity loops.

Table 1 shows the momentum and revolution frequency values at each flat-top. Figure 1 shows the typical AD production cycle and its RF segments, i.e. cycle parts where the RF is active. The current cycle duration is 115 s.

Table 1: AD Flattop Momentum and Frequency Values

Flat-top	Momentum	Revolution frequency
FT1	3.57 GeV/c	1.589478 MHz
FT2	2 GeV/c	1.487728 MHz
FT3	300 MeV/c	500.465 kHz
FT4	100 MeV/c	174.155 kHz

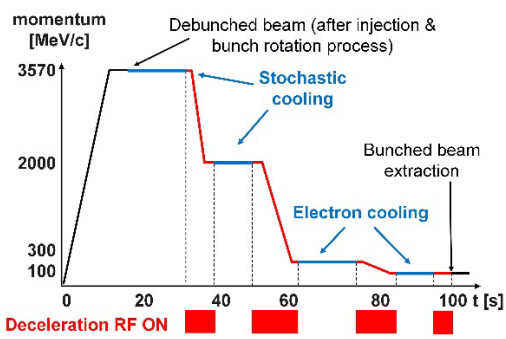

Figure 1: AD production cycle.

† maria.elena.angoletta@cern.ch

LLRF OVERVIEW

Layout

The AD LLRF belongs to the LLRF family operational in several CERN machines [1] and is a customised version of the ELENA LLRF [2]. Figure 2 shows a schematic view of the system and of its available functionalities. An initial description is available elsewhere [3]; here only previously un-mentioned features are outlined.

One Highland V346 waveform generators module, hosted in a separate VME crate and controlled by the AD LLRF, gives the reference to the AD extraction synchronisation loop. Harmonics of this signal provide timings to the AD extraction/ELENA injection kickers as well as the ELENA LLRF injection reference. The same module generates fixed trains at the flattops frequencies used by spectrum analysers for cooling setup. A remotely controlled programmable amplifier increases the signal level within the cycle for debunched beam data acquisition/analysis.

System Operation

The AD beam is decelerated in successive steps, called RF segments. The four segments now used in operation are shown in red in Figure 1; different segments can be used for test purposes. The beam is adiabatically bunched at the start of each segment and is debunched at its end. An exception is the last segment where an extraction synchronisation loop permits extracting a single bunch to ELENA. Beam phase/radial loops stabilise the beam and keep it in the centre of the pipe. A voltage/phase cavity loop maintains the desired voltage in the cavity. The sampling period of the digital loop is 12.5 µs thus allowing a satisfactory bandwidth of several kHz. Features such as deceleration harmonic number, voltage program and loop gains are defined and loaded onto the LLRF on a "per segment" basis. Other operational modes such as bunched beam cooling and bunch rotation at extraction are available.

LLRF BEAM COMMISSIONING

Overview

The AD LLRF commissioning planning included 13 working days in July 2021, interleaved with cooling commissioning periods. The cooling commissioning was longer than expected hence the overall AD LLRF commissioning overflowed into ELENA's one. Antiproton physics was started timely on August 24th, 2021 whilst setup activities continued for one more month.

Four weeks of beam commissioning were allocated to AD/ELENA in April 2022 to restart the machines after the winter shutdown. This second commissioning slot allowed us to deploy new features devised during the 2021 run.

ISBN: 978-3-95450-227-1 ISSN: 2673-5490 doi:10.18429/JACoW-IPAC2022-TUPOST027

MACHINE LEARNING-BASED TUNING OF CONTROL PARAMETERS FOR LLRF SYSTEM OF SUPERCONDUCTING CAVITIES

J. Diaz Cruz*, S. Biedron[1], S. Sosa, R. Pirayesh, University of New Mexico, Albuquerque, NM, USA
[1]also at Element Aero, Chicago, IL, USA

Abstract

The multiple systems involved in the operation of particle accelerators use diverse control systems to reach the desired operating point for the machine. Each system needs to tune several control parameters to achieve the required performance. Traditional Low-Level RF (LLRF) systems are implemented as proportional-integral (PI) feedback loops, whose gains need to be optimized. In this paper, we explore Machine Learning (ML) as a tool to improve a traditional LLRF controller by tuning its gains using a Neural Network (NN). We present the data production scheme and a control parameter optimization using a NN. The NN training is performed using the THETA supercomputer.

INTRODUCTION

The LLRF system is in charge of controlling the amplitude and phase of the electromagnetic field that drives superconducting RF (SRF) cavities. For facilities like the Linac Coherent Light Source II (LCLS-II), tight requirements for amplitude and phase are defined: 0.01% and 0.01 degrees, respectively [1]. The quality of the X-rays produced by this type of facilities depends on the quality of the electron beam.

LLRF systems wit a single source single cavity configuration, like the one for LCLS-II, use traditional PI loops for amplitude and phase control, having a total of 4 parameters to be tuned. Tuning these parameters takes into account quantities like the cavity gain and cavity bandwidth, the closed-loop bandwidth and latency, and the amplitude set-point. In this paper, we propose a ML-based tuning of the LLRF controller parameters, which uses a NN to calculate the optimal proportional and integral gains to minimize amplitude and phase errors. We also present a data production scheme based on simulations and an algorithm for stochastic optimization [2].

LLRF MODEL AND DATA PRODUCTION

Traditional LLRF controllers for particle accelerators are PI controllers like the one shown in Fig. 1. It usually consists of a couple of feedback loops: one for amplitude and one for phase. Therefore, the controller has 4 parameters: proportional and integral gains for amplitude and phase. Tuning this parameters is not a trivial task and can be time consuming for control room operators, specially when the accelerator has a large amount of SRF cavities (280 SRF cavities in the case of the LCLS-II). The tuning process can be automated based on control theory and the desired behaviour of the closed-loop, taking into account quantities like the cavity gain and cavity bandwidth, the closed-loop bandwidth and latency, and the amplitude set-point. However, this automation does not guarantee optimal parameters. Furthermore, drift in the system parameters would require to perform characterization of the cavity and the closed-loop system parameters multiple times.

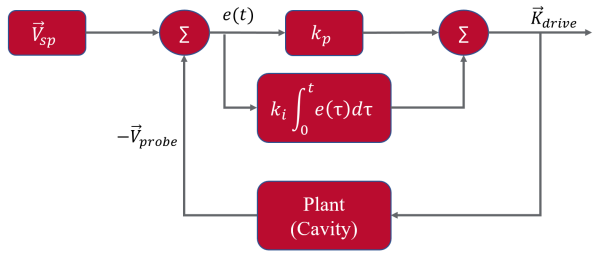

Figure 1: Simplified diagram of a traditional PI LLRF controller.

In this paper, we propose a tuning process to minimize the amplitude and phase stability errors, and a NN can be trained to learn this optimization. In the next subsections, we explain the cavity model and the simulations of the cavity field feedback loop.

Cavity Model

A multi-cell SRF cavity can me modeled as a group of RLC circuits (resonant circuits), each one corresponding to an eigenmode of the cavity. Figure 2 is the equivalent RLC circuit of each eigenmode. The differential equations that describe the electrodynamics of the systems are derived in [3] and result in the following set of equations:

$$V = Se^{j\theta}, \tag{1}$$

$$\frac{d\theta}{dt} = w_d, \tag{2}$$

$$\frac{dS}{dt} = -w_f S + w_f e^{-j\theta}(2K_g\sqrt{R_g} - R_b I), \tag{3}$$

where V is a representative measure of each mode's energy, with magnitude S and phase θ, w_d is the detuning frequency and w_f is the cavity bandwidth. K_g is the incident wave amplitude, which represents the power that drives the cavity, R_g is the coupling impedance of the beam, and I represents the beam current.

Using this model for simulations and data production, we have simulated a LLRF closed-loop under different setting points of RF power and electron beam current. Additionally, different levels of cavity frequency detuning and measurement noise can be applied to the simulations.

* jorgedc@unm.edu

ISBN: 978-3-95450-227-1 ISSN: 2673-5490 doi:10.18429/JACoW-IPAC2022-TUPOST029

SMALL TALK ON AT

P. Schnizer, W. S. Khail and J. Bengtsson
Helmholtz-Zentrum Berlin, BESSY, Berlin, Germany

Abstract

Tracy 3 — was implemented by the 3rd author by pursuing a first principles approach, aka Hamiltonian dynamics for an on-line model to guide the ALS and LBL comissioning in the early 1990s. With its origin as a Hamiltonian based pascal online model used 90 — it is the core of today's accelerator tool box. These Hamiltonians have not been changed. Software design has evolved since then: C++ and in particular its standardisation C++11 and C++2xa. In this paper we outline our strategy of modernisation of tracy: reorganisation of the beam dynamics library in cleanly designed modules, using well proven open-source libraries (GSL, armadillo) and so on. Furthermore, Python and Matlab Interfaces based on modern tools are being pursued. We report on the interface design, the status of modernisation. This project has been renamed to thor-scsi-lib and is available at Github. Collaboration's welcome.

INTRODUCTION

The Helmholtz Zentrum Berlin is looking into modernising and upgrading its own synchrotron light source BESSY II next to the one it operates on behalf of PTB, the light source MLS. These will now transit to a 4th and 3rd generation light source. In parallel the existing light sources BESSY II and MLS are constantly upgraded. These upgrades require proper tools for modelling these accelerators for predictable results.

Software concepts, introduced in the sixties (e.g. at Xerox Palo Alto with the development of Small Talk) are now being readily available in commonly spread languages: C++, in particular in its form of C++11 or Python. Furthermore interfacing between these languages simplify developing flexible user interfaces.

Tracy in its different implementations has been used to guide the control of the non-linear dynamics for robust design for predictable results for [1] ans the beam dynamics model – with related controls algorithms – was also used for on-line models for e.g. [2]. The beam performance predictions of Tracy gave sufficient confidence that MAX IV was proposed and funded [3]: a machine that has revolutionised the synchrotron light source landscape by introducing several paradigm shifts [4]. The code base of Tracy, however, was always adapted to the different project needs; essentially by a solo effort. Project dead lines prevented to modernise the code base and update it.

BESSY II is providing a digital twin with a "numerical engine" based on the Hamiltonian framework already provided by Tracy [5]. Given that the modernised software architecture & code base has a significantly changed interface the project name was changed to Thor Scsi. The code is available at `https://github.com/jbengtsson/thor-scsi-lib`. In this paper we outline the main changes that the code base underwent. .

FOUNDATIONS

Thor Scsi is based on the traces of Tracy 2 and Tracy 3. It is "self consistent": i.e. based on an Hamiltonian formulation and it is symplectic. The same Hamiltonian and integration method are used for tracking or computing the global properties of the lattice: e.g. linear optics, radiation effects and driving terms; engineering tolerances for a realistic lattice are consistent: e.g. the effects of magnetic roll angles studied in particle tracking will also effect the calculated vertical emittance. The charge of the tracked particles can be defined at compile time: it defaults to electrons. Mathematical details are given in [5].

UPGRADED CODE BASE

At the start of the refactoring the code base was still a result of the procedural programming paradigm. So the classes were redesigned. Each element can be seen similar to a LEGO block (see also Figure 1). Two coordinate systems are used: a left handed global coordinate system [5] and a left handed local one. Apart from the drift type, all elements are calculating in local coordinate space. These coordinate transformations are handled by implementing the Euclidean group in delegates of the classes "LocalGalilean" or ""LocalGalileanProt". The first transforms from global to local coordinates by a general rotation and translation, while the 2nd to the magnet's natural local coordinates, which generates the horizontal edge-focusing for dipole magnets.

The later one not only translated the global to local by location and translation but furthermore allows handling a non sector bend magnet . Thick lenses are implemented here as Drift-Kick-Drift sequences. Here the kick element uses a field interpolation object to obtain the strength of the magnetic field at the particle location. Thus the magnetic field representation is not limited to solely Taylor expansion or Beth's representation [6] but any 2D field representation (expansion to higher dimensions is considered to be a straightforward extension) .

At the current stage only part of the elements existing in Tracy have been ported to Thor Scsi, in particular: drift, marker, beam position monitor, magnetic multipole (dipole, quadrupole, sextupole), cavity. Radiation effects are delegated to registered objects: thus the user has full control for which elements radiation shall be computed. Tracking or global parameter computations are implemented propagating a state space object through the beamline elements: a phase space floating point vector for tracking, or a truncated

ISBN: 978-3-95450-227-1 ISSN: 2673-5490 doi:10.18429/JACoW-IPAC2022-TUPOST031

ONLINE OPTIMISATION OF THE TRANSFER LINE FROM UNILAC TOWARDS SIS18 AT GSI USING A GENETIC AUTOTUNE ALGORITHM

S. Reimann*[1], GSI, Darmstadt, Germany
[1]also at IAP, Frankfurt am Main, Germany

Abstract

Due to the complexity of GSI's accelerator facilities and it's upcoming expansion FAIR [1], various methods for optimising accelerator settings are currently being studied to increase efficiency and to minimise the need for manual intervention. Besides a necessary improvement of the accelerator models [2–5], a better reproducibility of settings and the development of feedback systems [6, 7], also heuristic methods are in the focus of the investigation [8–10]. This work presents the results, recently achieved in optimising the transfer line from UNILAC towards SIS18 (TK) using a genetic Autotune algorithm.

INTRODUCTION

The object of investigation was a 75 m long section of the transfer line from UNILAC to synchrotron SIS18 behind stripping and charge separation. Starting point was the beam transformer GTK3DT4, where the reference current I_0 for the optimization was measured. End point was the beam transformer GTK7DT3. The original intention was to optimize the entire beam transport up to the injection point of the SIS18, but the last two transformers GTK8DT7 and GTK9DT8 could not be used due to a technical defect.

The manual setup of the transfer line usually takes 1-2 hours. Since the SIS18 allows cycle times of < 1 s (in FAIR-booster mode 2.7 Hz operation is foreseen [1]) and different ion types and charge states can be requested from pulse to pulse, the transfer channel is designed for a corresponding repetition rate and all magnets can be pulsed with a frequency up to 10 Hz. The high repetition rate is an ideal condition for automatic optimisation procedures.

SIMULATION

A simulation was carried out to check the general feasibility and to find the optimal operating parameters for the genetic algorithm [11]. For the particle tracking the TK Lattice, measured and reconstructed by Y.El Hayek [12] (Fig. 1) was used. The standard deviation of fluctuations of the actual current of the power supplies were measured to 0.1% for quadrupoles and 0.04% for steerer magnets. These values were included in the simulation. The measuring accuracy of the transformers (0.3%) was also considered in order to represent the conditions of the real machine as close as possible. Several simulations were carried out to find the parameter set for the fastest possible convergence of the genetic algorithm. The fitness function to be minimized (1) represents the sum of the beam losses, measured via

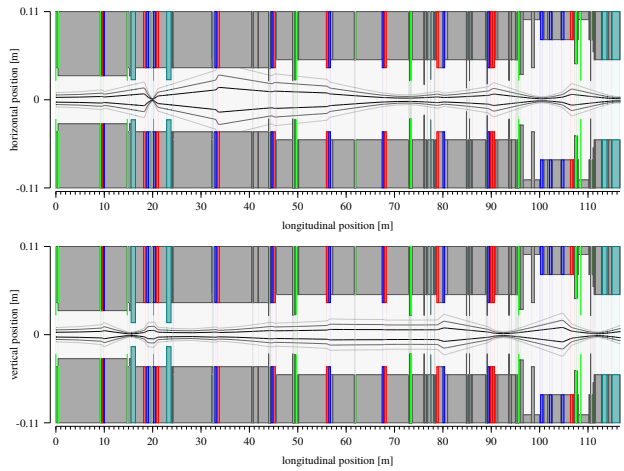

Figure 1: lattice of the transfer line (top = horizontal, bottom = vertical): blue elements are vertical focusing and red elements are horizontal focusing quadrupoles, cyan elements are bending dipoles.

four consecutive beam transformers with the transmission $\tau_i = \frac{I_i}{I_0}$ weighted with a factor w^i. Compared to the fitness function which directly evaluates the beam losses, the slightly modified version converges more reliably.

$$F = \sum_{i=0}^{4} w^i (1 - \tau_i) \tag{1}$$

For this work, the same implementation of a genetic algorithm was used as in [13]. All parameters were scanned [14]. The algorithm is quite robust against hyperparameter changes, as can be seen from the example of mutation probability (Fig. 2). The optimal parameters for the given transfer line are listed in Table 1.

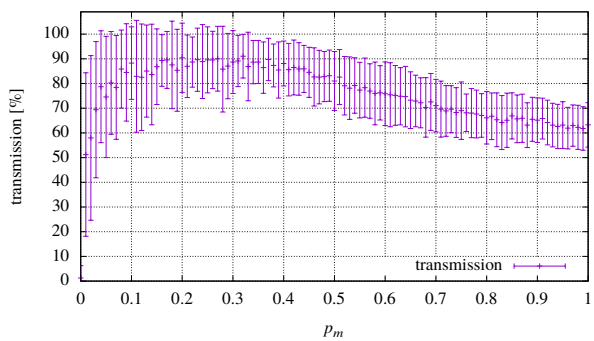

Figure 2: parameter scan of mutation probability p_m with respect to total transmission.

* s.reimann@gsi.de

ISBN: 978-3-95450-227-1 ISSN: 2673-5490 doi:10.18429/JACoW-IPAC2022-TUPOST032

SLS 2.0, THE UPGRADE OF THE SWISS LIGHT SOURCE

A. Streun*,[1], Paul Scherrer Institut, 5232 Villigen PSI, Switzerland
[1]on behalf of the SLS 2.0 project team

Abstract

The Swiss Light Source (SLS) will be upgraded by replacing the storage ring in the existing hall in 2023–24. The SLS lattice build from 12 triple-bend arcs operating at 2.4 GeV is replaced by a 12×7-BA lattice operating at 2.7 GeV to increase hard X-ray brightness by a factor 60. The layout is constrained by the existing tunnel to 288 m circumference, nevertheless a low emittance of 158 pm is realized using longitudinal gradient and reverse bends. Dynamic aperture is sufficient to start with classical injection based on a 4-kicker bump. An upgrade path for on-axis injection with fast kickers has been implemented. Small beam pipes of 18 mm inner diameter and corresponding reduction of magnet bores, and the use of permanent magnets for all bending magnets enables a densely packed lattice and contributes most to a reduction of total power consumption of the facility by 30%.

INTRODUCTION

The Swiss Light Source (SLS) started user operation in 2001. Today it is fully equipped with a set of 18 beam lines and delivers about 5000 h of user beam time per year at excellent availability (98.5% average 2012-21) and stability (<1 µm) rms at front ends). However, with the advent of modern diffraction limited storage rings (DLSR) of multi-bend achromat (MBA) type it became clear, that the SLS emittance of 5.0 nm at 2.4 GeV would no longer be competitive, and planning for an upgrade started in 2014. Project funding was secured by end of 2020, and the technical design report was published one year later [1]. Between fall 2023 and end of 2024 the existing storage ring will be exchanged by a new one providing much lower emittance of 158 pm at 2.7 GeV, to be installed in the existing tunnel with radial source point shifts limited to ±70 mm. The combination of lower emittance and higher beam energy provides a factor 60 increase of hard X-ray brightness (>10 keV), which will be further enhanced by means of new undulators of shorter period. Long period elliptic undulators on one side, and superbends of up to 5 T peak field on the other side, will support experiments spanning a photon energy range from 6 eV to 80 keV. Routine user operation will resume by mid 2025. In this report we will summarize the upgrade concept and highlight the most challenging issues.

LATTICE

The minimum emittance of a storage ring scales approximately inversely with the third power of circumference, thus the SLS is handicapped by its comparatively small circumference of 288 m. In order to get competitive emittance a new lattice cell was developed. It employs reverse bends (RB), which are realized by slightly shifting the horizontally focusing quadrupoles radially away from the storage ring center, and longitudinal gradient bends (LGB), which are realized in the most simple configuration as a sandwich of a pure dipole between two vertically focusing combined function magnets (VC) of lower field: in the periodic unit cell of an MBA the RB suppresses the dispersion at the LGB center, where the field is highest, in order to minimize quantum excitation, which is the source of emittance [2].

The transverse gradients in the RBs and VCs increase the horizontal damping partition and thus further reduce emittance on expense of higher energy spread. A regular 7-BA arc was found as best compromise between low emittance and feasibility in terms of technology and non-linear dynamics. A summary of the most important lattice parameters for SLS (without the FEMTO insertion for laser beam slicing and without undulators) and for SLS-2.0 is given in Table 1.

Table 1: SLS and SLS 2.0 Lattice Parameters (bare lattice → all undulators closed)

Parameter	Units	SLS	SLS-2.0
Circumference	[m]	288.0	
Beam energy	[GeV]	2.41	2.70
Hor. emittance	[pm]	5030	158 →131
Vert. emittance	[pm]	5–10	10
Energy spread	[10^{-3}]	0.88	1.15 →1.04
Radiation loss	[keV]	574	689 →900
Beam current	[mA]	400	
Beam lifetime	[h]	≈ 10	≈ 11

The alternative of a hybrid-MBA [3] as used for other projects, mainly for larger rings at higher energy, was investigated too. However for SLS a regular MBA was found to better fulfill the requirements on emittance reduction, available straight length and beam lifetime while still providing sufficient transverse dynamic aperture for off-axis injection.

In order to follow the footprint of the existing storage ring as close as possible, the 12 arcs are connected by 6 short, 3 medium and 3 long straight sections. Although the footprint thus has 3-fold symmetry and the linear beam optics as shown in Fig. 1 has no periodicity at all due to a high-beta optics in the injection straight, the (on-momentum) non-linear optics is tuned to 12-fold symmetry by adjusting the phase advance of all arcs to the same value irrespective of the type of the adjacent straights.

As a compromise between brightness and beam lifetime, the vertical emittance is set to about 10 pm by means of 22 skew quadrupoles per arc generating closed bumps of vertical dispersion while suppressing betatron coupling in the straight sections.

* andreas.streun@psi.ch

ISBN: 978-3-95450-227-1 ISSN: 2673-5490 doi:10.18429/JACoW-IPAC2022-TUPOST033

A PYTHON FRAMEWORK FOR HIGH-LEVEL APPLICATIONS IN ACCELERATOR OPERATIONS

J. Chrin, V. Erçağlar, T. Schietinger, Paul Scherrer Institut, 5232 Villigen PSI, Switzerland

Abstract

A Python graphical framework providing reusable components to facilitate the development of accelerator applications, that meet the basic requirements of experts and operators alike, is presented. Such a collective approach serves to bridge the gap between the expert developer and the operational team, resulting in applications that are inherently cohesive, durable and easily navigable. The operational advantages and underlying principles are exemplified in a reference application that provides executable examples of customary practices, and further highlights a number of composite and control system-enabled widgets.

PERSPECTIVE AND MOTIVATION

The development of high-level applications crosses the domain of several groups, each possessing a distinctive skill set and ambition. Typically the 'expert' application is developed by the scientist, engineer, whose primary interest is in providing an interface that details the hardware capabilities of the system. The 'operator' application on the other hand may require only a condensed view and one that offers automated procedures geared towards the everyday operation of the accelerator. Other, beam dynamics, applications will undertake specific measurements crucial to the optimization of the accelerator, and may further require interaction with accelerator models, message reporting capability, and the means to store and retrieve data resulting from their analyses. Many such measurements and procedures are first deployed by the expert in the commissioning phase of the accelerator before ultimately being delegated to machine operators once routine operation is established. The diversity of developers, however, inevitably leads to a variety of frameworks and appearances, with some duplication in that similar functionalities are instigated in different manners and with a non-uniform behaviour. These subtle details of cross-domain application development are acknowledged to add to the tasks and challenges faced by the operator [1, 2].

This inadvertent disparity between applications, however, can be alleviated by supplying a controlled, coordinated, and configurable graphical interface wherein common functionality is provided through predetermined inputs with well defined responses. Applications then become inherently homogeneous, and developers are further relieved of implementing peripheral tasks, releasing time to prioritize their particular area of interest.

In the following, a Python graphical framework is described that provides a base class that can be inherited by the application developer, and adapted to specific needs. The focus is on the components and methodology that constitute the framework, rather than any specific application that is built upon the infrastructure, as applied within the context of SwissFEL and the Swiss Light Source (SLS).

A PYTHON GRAPHICAL FRAMEWORK

The Python programming is presently enjoying a high profile within the accelerator community being the preferred language for application development at facilities of various size [3, 4]. While scripting is regarded as gratifyingly intuitive and powerful, our applications are inherently graphical and this in itself adds a new level of complexity. To this end, PyQt, a Python graphical user interface (GUI) module that connects to the Qt C++ framework [5, 6], is the prevailing choice. Significantly, in this work, Qt modules are imported through the QtPy abstraction layer [7] allowing our framework to be used effortlessly across Qt versions.

The Qt library provides much functionality, with numerous classes. Its specific application domain of windows, widgets, layouts, colours, shapes, and more, however, presents the developer with expansive possibilities to interrogate and discern before converging on a finely-tuned appearance. Furthermore, and rather critically, any complex physics analysis, or any other resource intensive operation having a long running time, needs to be delegated to a separate thread. Here, Qt's dedicated thread support is a fitting option given that our applications interact with other components of the Qt library. In this way, the main thread remains responsive at all times, widgets with read backs continue to be updated, and user interaction, where permitted, is not interrupted. Such considerations are a prerequisite in gaining a satisfactory user experience. Once these challenges are overcome, the programmed solutions may be presented to the developer in a reusable form.

Apps4Ops: A Characteristic Style

The GUI implementation class follows Qt's customary 'main-window-style' approach that offers predefined options for user input in the form of a menu bar, toolbar, status bar, a central widget, and dock windows. The adoption of such a ready-made, integrated approach, at the outset, is an important factor in achieving a polished, intelligible, and navigable user interface. The static visualization of data is accomplished through the comprehensive Matplotlib library [8, 9]. For the display of continuous, real-time data, however, the PyQtGraph [10] library, based on Qt's GraphicsView framework, is preferred for its speedier response time. The principle components that constitute the framework, and other practicalities that play a part in achieving the desired homogeneity among applications, coupled with an optimized user experience, are elaborated.

ISBN: 978-3-95450-227-1 ISSN: 2673-5490 doi:10.18429/JACoW-IPAC2022-TUPOST035

BOLINA, A SUITE FOR HIGH LEVEL BEAM OPTIMIZATION: FIRST EXPERIMENTAL RESULTS ON THE ADIGE INJECTION BEAMLINE OF SPES

V. Martinelli, L. Bellan, D. Bortolato, M. Comunian, E. Fagotti,
P. Francescon, A. Galatà, D. Marcato, G. Savarese,
INFN Laboratori Nazionali di Legnaro, Legnaro, Italy

Abstract

A high-level software BOLINA (Beam Orbit for LINear Accelerators) has been designed to fully characterise and automatically correct the ion beams trajectory, to help operators during the beam transport with an easily scalable suite for LINACs. Currently, the high-level software, interfaced with an EPICS control system, acts on accelerator devices to preserve the beam quality, including beam-based alignment and, if needed, dispersion-free steering software. The suite has been developed to satisfy and commutate the software easily on different machines, using interceptive/not interceptive diagnostics. The software was designed for ELI-np and now is under test at Legnaro National Laboratories of INFN using the installed accelerators complex. BOLINA has been successfully tested on the Adige Injector 1+ beamline of the SPES Project, where the system response matrix is measured on interceptive beam diagnostic by varying both electrostatic and magnetic steerers. This paper describes results and strategies to reduce trajectory residuals close to the diagnostic resolutions and their effectiveness to prepare the commissioning of LINACs.

INTRODUCTION

The study of beam dynamics under ideal conditions is fundamental and the first step to designing particle accelerators. Deviation from the ideal trajectory causes emittance growth and beam degradations or losses. In a real accelerator many fields and misalignment errors of unknown location and magnitude must be expected. Some uncertainties include diagnostic offsets produced both by mechanical displacements and by biases in the electronics readout, others by misalignment of the magnetic centre of the quadrupole or by the electromagnetic centre of accelerating structures. Many other such errors can cause unexpected beam trajectories that degrade the beam quality and force operators to correct it using steering magnets. Especially for user facilities, to speed up the machine set-up, it is fundamental to have a fast online correction suite.

The BOLINA (Beam Orbit for LINear accelerators) software, designed to help accelerator operators, provide simultaneous optimization of the orbit, finding the trajectory that maximises the beam transport and preserve the emittance to reach the accelerator's nominal parameters. For guarantees the flatness of the orbit, consisting of the simultaneous zeroing of the beam position monitor offset readings, the one-to-one correction algorithm is used. The renowned algorithm [1, 2] in BOLINA is used by minimising a X^2 in Eq. (1)

$$\chi^2 = | \overrightarrow{b_m} + \boldsymbol{R}\ \vec{\theta} |^2 \quad (1)$$

knowing the beam position offset $\overrightarrow{b_m}$ on the diagnostics and the response matrix previously measured by varying the steerer sets $\vec{\theta}$.

The most interesting part of the BOLINA diagnostic and correction suites is the machine independency. This high-level software is meant to be interfaced with the EPICS control system and to manage accelerator devices to allow beam diagnostic measurements.

BOLINA routines are written in Python: it is fully machine-independent and can be automatic re-used for any type of accelerators by changing just the layout file.

Thanks to its characteristics, it has been possible to test and develop rapidly the BOLINA correction suite for ADIGE Injector 1+ beamline [3].

INTEGRATION WITH THE CONTROL SYSTEM

The EPICS [4] IOC of BOLINA is divided into different databases. The database defines the functionality of the IOC: which process data it provides, how the data is handled and stored. The database can contain any number of records, each of which belongs to a specific record type. For BOLINA we use five different databases, shown in Fig. 1 one for each type of record.

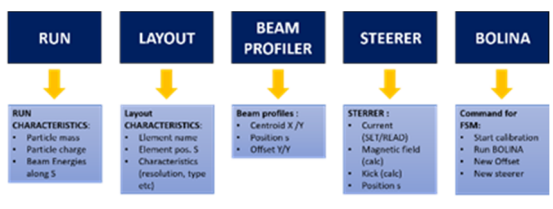

Figure 1: The BOLINA IOC flowchart: dark blue boxes represent the different databases, in light blue the corresponding records and their characteristics.

The RUN database contains all the information of the source and of the beam line characteristics, this is useful to save data in an appropriate way, remembering the beam dynamics characteristics of the specific run like the beam charge, the particle charge, and the beam energy along the beamline. This is used to archive data and remember which accelerator and which beam belongs to it. This allows reuse, saving the calibration file, previous beam response

ISBN: 978-3-95450-227-1 ISSN: 2673-5490 doi:10.18429/JACoW-IPAC2022-TUPOST037

RECONSTRUCTION OF TRANSVERSE PHASE SPACE FROM TRANSVERSE FEEDBACK DATA FOR REAL TIME EXTRACTION OF VITAL LHC MACHINE PARAMETERS

G. Kotzian*, M. Söderén, P. S. Solvang, D. Valuch,
Accelerator Systems department, CERN, Geneva, Switzerland
V. Stopjakova, UEF FEI, Slovak University of Technology, Bratislava, Slovakia

Abstract

The LHC transverse feedback system (ADT) provides bunch by bunch, turn by turn, normalized and digitized beam position signals from four pick-ups per plane and for each beam. Together with already existing powerful computer-based observation systems, this data can be used to reconstruct in real-time the transverse phase space coordinates of the centre-of-charges, for each individual bunch. Such information is extremely valuable for machine operation, or transverse instability diagnostics.

This paper aims on discussing and evaluating methods of combining four position signals for such analysis in the presence of noise and with active transverse feedback. Comparisons are made based on the extraction of vital parameters like the fractional tune or transverse activity. Analytical and numerical results are further benchmarked against real beam data.

TRANSVERSE FEEDBACK AND ADTOBSBOX

During the LHC Long Shutdown II the LHC transverse feedback system (ADT) [1] was subject to an upgrade of its Beam Position Monitor (BPM) hardware, aiming for an improvement of the system's noise floor [2]. New low-noise beam position hardware is now available for LHC Run III, providing independent processing of 16 dedicated pick-ups. This allows for a total of four beam position streams per plane and per beam, representing the transverse centre-of-charges of each individual bunch.

This data is available in real-time to the LHC Transverse Feedback system for damping and stabilizing the beam, as well as to the computer-based observation system ADTObsBox [3]. The ADTObsBox is capable of recording and processing all digital data streams from the available pick-ups at full data rate (bunch-by-bunch or 40 Msps, with 16 bit resolution), for instance, to combine the data in real-time and extracting valuable metrics of the ADT performance (e.g. transverse activity) or the beam itself (bunch-by-bunch fractional tune).

One considerably useful representation of transverse motion is the use of phase space coordinates, readily described in Ref. [4] as an analytic signal $x[n]$, expressed as,

$$x[n] = y[n] + jy'[n]. \tag{1}$$

Here, the transverse normalized phase space coordinates $y[n]$ and $y'[n]$ represent normalized position data respectively the corresponding normalized slope values at turn index n.

From the notation in Eq. (1) we can immediately derive a measure of transverse beam activity, denoted by $A[n]$, as the modulus – or amplitude – of the complex vector,

$$A[n] = \text{abs}\,\{x[n]\}\,. \tag{2}$$

If $A[n]$ decreases over time then the transverse activity is considered to be damped, whereas growing values provide an indication of transverse instability.

Equivalently, the fractional tune, $Q[n]$, follows from phase space data by observing the phase component $\varphi[n] = \arg\{x[n]\}$ of Eq. (1), specifically, the relative phase advance between consecutive turns, described as,

$$Q[n] = \frac{1}{2\pi}\arg\left\{\frac{x[n-1]}{x[n]}\right\} = \frac{1}{2\pi}\left(\varphi[n-1] - \varphi[n]\right). \tag{3}$$

For the analytic evaluation, we implicitly assume that the beam is centred in the pick-ups and we observe betatron oscillations, i.e. $(y)^2 + (y')^2 = \text{const}$. Furthermore, for our assessment, we shall use a damped, complex-valued harmonic oscillator as beam model, which provides for the k^{th} beam position monitor at the n^{th} turn the phase space coordinates as follows,

$$x_k[n] = A_0 e^{-j\phi_k}\left(\alpha \cdot e^{-j\omega_0}\right)^n. \tag{4}$$

Here, A_0 and ϕ_k are initial conditions, α accounts for an amplitude decay and $\omega_0 = 2\pi Q_f$ represents the angular frequency at the fractional betatron tune Q_f.

PHASE SPACE RECONSTRUCTION

In order to satisfy Eq. (1), and by acknowledging that the ADT Beam Position Monitors readily provide normalized readings, we are looking for indirect methods to obtain slope samples from beam position measurements.

In the following, we evaluate two methods for combining beam position data of four LHC pick-ups, identified as a *spatial* and a *temporal phase shift* in Ref. [5]. The first combines the information of several beam position monitors based on their longitudinal distribution in the accelerator, the later relies on processing the history of recorded beam position data using filter kernels.

* gerd.kotzian@cern.ch

ISBN: 978-3-95450-227-1 ISSN: 2673-5490 doi:10.18429/JACoW-IPAC2022-TUPOST040

AUTOMATED INTENSITY OPTIMISATION USING REINFORCEMENT LEARNING AT LEIR

N. Madysa*, V. Kain†, CERN, Geneva, Switzerland
R. Alemany Fernandez, N. Biancacci, B. Goddard, F. M. Velotti, CERN, Geneva, Switzerland

Abstract

High intensities in the Low Energy Ion Ring (LEIR) at CERN are achieved by stacking several multi-turn injections from the pre-accelerator Linac3. Up to seven consecutive 200 µs long, 200 ms spaced pulses are injected from Linac3 into LEIR. Two inclined septa, one magnetic and one electrostatic, combined with a collapsing horizontal orbit bump allows a 6-D phase space painting via a linearly ramped mean momentum along the Linac3 pulse and injection at high dispersion. The already circulating beam is cooled and dragged longitudinally via electron cooling (e-cooling) into a stacking momentum to free space for the following injections. For optimal intensity accumulation, the electron energy and trajectory need to match the ion energy and orbit at the e-cooler section.

In this paper, a reinforcement learning (RL) agent is trained to adjust various e-cooler and Linac3 parameters to maximise the intensity at the end of the injection plateau. Variational Auto-Encoders (VAE) are used to compress longitudinal Schottky spectra into a compact latent space representation as state input for the RL agent. The RL agent is pre-trained on a surrogate model of the LEIR e-cooling dynamics, which in turn is learned from the data collected for the training of the VAE. The performance of the VAE, the surrogate model, and the RL agent is investigated in this paper. An overview of planned tests in the upcoming LEIR runs is given.

INTRODUCTION

LEIR [1, sec. 4] is an ion synchrotron equipped with an e-cooler. It is situated in the CERN accelerator chain between Linac3 and the Proton Synchrotron (PS).

In nominal operation mode, it receives ions from Linac3 at 4.2 MeV per nucleon in seven consecutive pulses per cycle. The pulses have a spacing of 200 ms and are 200 µs long. They are injected into LEIR via 6-D phase space painting with a collapsing horizontal bump and a momentum sweep. The latter is achieved with the debunching and the ramping radio-frequency (RF) cavity at the exit of Linac3.

While circulating, each pulse is cooled and longitudinally dragged by the e-cooler and stacked in a narrow phase space volume to make space for the next pulse. Once all pulses are injected, the beam is dragged back to nominal momentum, captured into bunches and accelerated to the nominal target beam rigidity. (For lead ions, this target corresponds to an energy of 72.2 MeV per nucleon.) It is then finally ejected into the transfer line towards the PS.

* nico.madysa@cern.ch
† verena.kain@cern.ch

Ten parameters have been identified as crucial for this process: the start and end phase of the ramping and the debunching RF cavity; the electron gun voltage at the start and end of e-cooling; as well as the orbit positions (x, y) and angles (x', y') at the e-cooler, controlled by orthogonal orbit bumps.

These parameters $\vec{p}$ require frequent adjustment to ensure that LEIR maintains its beam intensity in the ring after RF capture ($I_{\mathrm{R,cap}}$) above the nominal target $I^{\mathrm{nom}}_{\mathrm{R,cap}} = 10 \times 10^{10}$ charges. Since LEIR entered operation in 2005, these parameters have been optimised manually by the operations team. This is time consuming and often based on trial and error. Instead, we propose an automatic system based on machine learning that maximises beam intensity in a fast and deterministic manner.

Data acquisition at LEIR takes several seconds per machine interaction. This precludes approaches that require many evaluations of the loss function, particularly gradient-based optimisation and model-free RL. Instead, we present an approach based on a *surrogate* model. Using a limited amount of data, we use supervised learning to train a model of LEIR's injection process and its dynamics at flat bottom, then optimise this surrogate numerically and via RL.

DATA TAKING

Two runs of data were taken at the end of 2021 under nearly identical machine conditions. Run 1 occurred on November 8 and took 4293 samples over 15.5 h, Run 2 on November 13 and took 4414 samples over 18 h.

Each sample recorded the following features:

- the parameters before ($\vec{p}_{n-1}$) and after the change ($\vec{p}_n$);
- the change itself, $\Delta\vec{p}_n := \vec{p}_n - \vec{p}_{n-1}$;
- the longitudinal Schottky spectrum after the change;
- the beam intensity after Linac3 and in the LEIR ring.

For both runs, the machine was first set up to the same parameters, which had been found by manual optimisation. This was recorded as the first sample. Then, for the rest of the run, parameter settings were sampled from a uniform distribution. They were applied to the machine and a new sample was recorded.

Samples were discarded if their settings violated safety limits. If the Linac3 intensity dropped below a certain threshold due to temporary faults, recording was temporarily suspended until it returned to expected levels.

During Run 1, parameters were sampled from a comparatively narrow distribution around the optimum; for Run 2, the distribution was widened and almost all samples had a very low intensity. This ensured that the data set contained a comparable amount of high- and low-intensity samples.

ISBN: 978-3-95450-227-1 ISSN: 2673-5490 doi:10.18429/JACoW-IPAC2022-TUPOST041

EXPERIENCE WITH COMPUTER-AIDED OPTIMIZATIONS IN LINAC4 AND PSB AT CERN

P. K. Skowroński, I. Vojsković[1] and M.A. Fraser, CERN, Geneva, Switzerland
[1]also at Chalmers University of Technology, Gothenburg, Sweden

Abstract

Currently, accelerator optimizations are routinely performed with the help of computer algorithms that allow to fully automatize these tasks. However, their efficiency, speed, and implementation time largely vary among them. In LINAC4, a few optimization tasks were targeted using different algorithms found by conducting a comparative analysis. We present the problems for which computer algorithms were used and the results of our comparative study.

INTRODUCTION

Numerical methods in accelerator performance optimization have become a standard. A dedicated framework, called GeOFF [1], has been developed at CERN to facilitate the exploitation of optimizing algorithms. This generic optimization framework acts as a high-level interface between the CERN accelerator control system and different algorithms, such that only the problem-specific code needs to be developed. Another advantage is the possibility to choose from a wide range of different conventional optimizers, and, if needed, switch between them. In this article we describe the tools and the achieved results for LINAC4 and for the PSB extraction recombination line.

In 2020 LINAC4 replaced LINAC2 as the Proton Synchrotron Booster (PSB) injector. It accelerates negative hydrogen ions (H^-) to the kinetic energy of 160 MeV [2]. It is a normal conducting linear accelerator operating at a frequency of 352 MHz. The linac was constructed and commissioned in stages between 2013 and 2016 [3–6]. Reliability runs took place in 2017 and 2018 [7, 8]. The commissioning of the transfer line connecting it to the PSB took place in 2019 and of the charge exchange injection in 2020 [9].

The PSB is a synchrotron made of four superimposed rings. At injection, each (H^-) beam pulse is vertically distributed over the rings, and at ejection the proton bunches are recombined vertically to follow the same trajectory when sent to the PS or the ISOLDE experimental facility.

For the problems described in this document, it was not practical to build a model through simulation, nor was it efficient to employ full-scale approximation using, e.g., neural networks. Some of the optimized quantities depend on factors that cannot easily be controlled and eventually change with time, making it difficult to model these phenomena reliably. Alternatively, the model could be learned from accelerator data. However, this approach would require extensive beam time. Therefore, for the studies presented here, we opted for efficient algorithms for handling cases with limited data, like numerical optimizers and linear correction via Singular Value Decomposition (SVD) [10, 11].

MACHINE SAFETY

Computer-driven optimizations must be carefully programmed because, in most cases, the beams have destructive potential. An algorithm may decide to test settings corresponding to significant beam losses, which could lead to accelerator failure. Particle accelerators such as LINAC4 and the PSB are protected with multiple interlock systems, but one cannot afford to rely solely on them when running an optimization algorithm. Instead, the allowed parameter ranges and step sizes must be set such that any increase in beam losses stays within the acceptable ranges, and the penalty for the beam loss is significantly higher than the other terms in the objective function. It should be ensured that losing the beam is not a way to find an optimum value.

Because of the aforementioned safety considerations and the importance of the speed in finding an optimum, we concentrated on Derivative-Free Optimization (DFO) methods that use a deterministic approach and discarded Bayesian optimizers for initial tests. There exist different machine-specific limits for the elements in the accelerators. Suppose the parameter space breaches one of the element's machine-specific limits. If an out of range settings is attempted then, in the best case, an exception is thrown halting the program or the device stops with a fault. To ensure that this does not happen, the program changes a given parameter scale s_{max} to be within the allowed range $s_{max} = |c - s_0|$, where c is the machine constraint and s_0 initial condition for this parameter. Every parameter has its own s_{max}. The same applies for s_{min}. As a result, the relative parameter change will be smaller than it initially would be, but inconsequential for the algorithm's performance.

DERIVATIVE-FREE ALGORITHMS

For the studies presented here, we focused on a branch of DFOs called model-based methods. Here a surrogate model of the objective function is constructed, defining the next iteration by seeking to minimize this model inside a trust region. One such method is COBYLA [12] and it employs linear approximations of the objective and constraint functions. The approximations are formed by linear interpolation at $n + 1$ points in the space of the parameters and are regarded as vertices of a simplex. The model is equivalent to a 1st-order Taylor expansion and at each step its accuracy is improved asymptotically. By extending this to a 2nd-order Taylor expansion, the trust-region minimization can now take curvature into account. An example of such an algorithm is BOBYQA [13]. However, the quadratic model comes at the price of making the model construction and the trust-region minimization more difficult.

ISBN: 978-3-95450-227-1 ISSN: 2673-5490 doi:10.18429/JACoW-IPAC2022-TUPOST042

TOWARDS THE AUTOMATIC SETUP OF LONGITUDINAL EMITTANCE BLOW-UP IN THE CERN SPS

N. Bruchon*, I. Karpov, N. Madysa, G. Papotti, D. Quartullo, C. Zisou[1],
CERN, 1211 Geneva, Switzerland
[1]also at Aristotle University of Thessaloniki, 54124 Thessaloniki, Greece

Abstract

Controlled longitudinal emittance blow-up in the CERN SPS is necessary to stabilize high-intensity beams for the High-Luminosity LHC (HL-LHC) by increasing the synchrotron frequency spread. The process consists of injecting bandwidth-limited noise into the main RF phase loop to diffuse particles in the core of the bunch. The setting up of the noise parameters, such as frequency band and amplitude, is a non-trivial and time-consuming procedure that has been performed manually so far. In this preliminary study, several optimization methods are investigated to set up the noise parameters automatically. We apply the CERN Common Optimization Interfaces as a generic framework for the optimization algorithm. Single-bunch profiles generated with the BLonD simulation code have been used to investigate the optimization algorithms offline. Furthermore, analysis has been carried out on measured bunch profiles in the SPS to define the problem constraints and properly formulate the objective function.

INTRODUCTION

Ensuring the longitudinal stability of high-intensity LHC-type beams in the CERN SPS is mandatory. This is achieved by using the fourth harmonic RF system in combination with controlled longitudinal emittance blow-up. Both techniques enhance Landau damping by increasing the synchrotron frequency spread within the bunch [1, 2].

For the controlled longitudinal blow-up, bandwidth-limited phase noise is injected into the beam phase loop locking the bunch phases to the main RF system operating at 200 MHz. The noise generation is critical: it requires a band-limited excitation spectrum (pink noise) which follows the variation of the small-amplitude synchrotron frequency f_{s0} during the acceleration ramp [3]. The input parameters for the noise generation algorithm are the low and high cutoff frequencies (normalized with respect to f_{s0}) that define the excitation band, f_{low} and f_{high} respectively, and the desired amplitude, a, of the noise. The frequencies f_{low} and f_{high} are ideally chosen to target the core of the bunch without affecting the tails. Beam stability can be reached by finding the optimal values of these three settings during the time the blow-up is active.

Adjusting the blow-up settings was done manually in the past, and it needed to be reviewed when significant changes in beam parameters occurred, e.g. increased bunch intensity. Therefore, a study of the feasibility of applying automatic optimization methods to provide longitudinal stabilization of the beam was performed.

For this purpose, the search for proper noise settings is defined as an optimization problem integrated into the CERN Machine Learning (ML) project [4]. This activity aims at bringing numerical optimization, machine learning, and reinforcement learning into day-to-day operation at the CERN accelerator complex. In addition, we propose an objective function based on the width at different heights of the longitudinal bunch profile, as a means to quantify its shape.

In this paper, after briefly presenting the generic optimization tool employed, the implementation of an automatic procedure to optimize the longitudinal emittance blow-up in the CERN SPS is described. The novel objective function is applied, and results from offline and online optimization runs are shown and analyzed.

GENERIC OPTIMIZATION TOOLS AT CERN

Optimization is fundamental to improve the performance of the accelerator facilities [5]. From this wide experience, a tool for generic optimization has been developed.

The Common Optimization Interfaces (COI) aims at unifying multiple approaches into a single generic optimization application supported by a graphical user interface, the Generic Optimization Frontend and Framework (GeOFF). COI is the software running numerical optimization and reinforcement learning on CERN accelerators facilities. Currently, several algorithms are already implemented in the application, e.g. Bound Optimization BY Quadratic Approximation (BOBYQA) [6], Constrained Optimization BY Linear Approximation (COBYLA) [7], Nelder Mead [8], and Powell's conjugate direct method [9].

Ideally, the COI can manage every optimization problem encapsulated in an appropriate structure, as described in [4]. This means that it is sufficient to properly formulate the problem, and COI dynamically selects this implementation of classical single-objective optimization, reinforcement learning, or both, depending on the supported approaches.

LONGITUDINAL BLOW-UP CONTROL

The goal is to ensure the desired bunch emittance and distribution at the SPS flat-top, by exciting the core of the bunch with a band-limited noise, without exciting the bunch tails. Often, the settings are kept constant for the entire duration of the noise injection for simplicity, while in principle they could be defined by time-dependent functions.

* niky.bruchon@cern.ch

ISBN: 978-3-95450-227-1 ISSN: 2673-5490 doi:10.18429/JACoW-IPAC2022-TUPOST043

A NOVEL METHOD FOR DETECTING UNIDENTIFIED FALLING OBJECT LOSS PATTERNS IN THE LHC

L. Coyle*, CERN, Geneva, Switzerland
A. Lechner, D. Mirarchi, M. Solfaroli Camillocci, J. Wenninger, CERN, Geneva, Switzerland
F. Blanc, D. Di Croce, T. Pieloni, EPFL, Lausanne, Switzerland

Abstract

Understanding and mitigating particle losses in the Large Hadron Collider (LHC) is essential for both machine safety and efficient operation. Abnormal loss distributions are telltale signs of abnormal beam behaviour or incorrect machine configuration. By leveraging the advancements made in the field of Machine Learning, a novel data-driven method of detecting anomalous loss distributions during machine operation has been developed. A neural network anomaly detection model was trained to detect Unidentified Falling Object events using stable beam, Beam Loss Monitor (BLM) data acquired during the operation of the LHC. Data-driven models, such as the one presented, could lead to significant improvements in the autonomous labelling of abnormal loss distributions, ultimately bolstering the ever ongoing effort toward improving the understanding and mitigation of these events.

INTRODUCTION

To monitor particle losses, the LHC is equipped with over 3000 BLMs placed along the circumference of the machine, see Fig. 1. This vast BLM array provides a very detailed account of the amount, the location and time evolution of particle losses occurring in the LHC at any given moment. The LHC BLM system provides data on many different time scales called Running Sum (RS), ranging from 40 μs to 1.9 s.

Figure 1: BLMs on the LHC

The spatial distribution of particle losses across the LHC is referred to as a loss map. These loss maps provide key information to identify loss mechanisms, but also to ensure a proper alignment of the LHC collimators. They are monitored throughout machine operation and are heavily relied upon throughout the commissioning phase for the setup of the machine protection related accelerator components.

This paper will focus on a specific type of particle loss event referred to as an Unidentified Falling Object (UFO) [1, 2].

Unidentified Falling Objects

UFOs are a very fast and localized loss events caused by micrometer sized dust particles which interact with the particle beams. UFOs have been the cause of many beam dumps in the past and as such, a detection algorithm named UFO-Buster was developed to monitor these events, including those that remain below the dump threshold of the BLM system [1, 3]. A loss map with a UFO event is presented in Fig. 2.

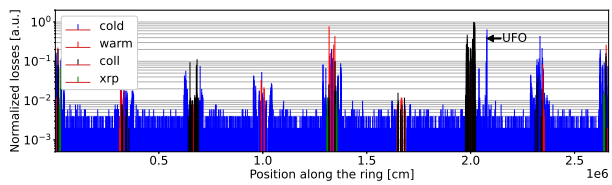

Figure 2: An example loss map with a UFO event indicated, fill 6648 on 2018-05-06 at 20:01:23

UFO BUSTER

Algorithm Description

The UFO-Buster continually monitors the BLM signals and when a series of criteria are met, the event is labeled as UFO candidate and is added to a UFO event database. The main criteria is that 2 BLMs within a distance of 40 m must exceed a dose rate threshold, usually set to $1\times10^{-4} Gy/s$, and that the event duration must be on the millisecond timescale, see [1] for details.

UFO Dataset

The UFO-Buster's UFO assignments are used to create a dataset of known UFO events on which to train the model in a supervised manner. For this study, only UFOs occurring in the arc sections of the LHC, during the stable beam mode of physics runs in 2018 were considered. In total 744 UFO events were used with each of these UFO containing loss maps consisting of 3595 individual BLMs, resulting in an initial dataset of shape 744×3595.

MACHINE LEARNING MODELLING

The objective is to create a machine learning model capable of identifying UFOs within operational loss maps, using

* loic.thomas.coyle@cern.ch

ISBN: 978-3-95450-227-1 ISSN: 2673-5490 doi:10.18429/JACoW-IPAC2022-TUPOST044

FORTUNE TELLING OR PHYSICS PREDICTION? DEEP LEARNING FOR ON-LINE KICKER TEMPERATURE FORECASTING

F. M. Velotti, * M.J. Barnes, B. Goddard, I. Revuelta
CERN, Geneva, Switzerland

Abstract

The injection kicker system MKP of the Super Proton Synchrotron SPS at CERN is composed of 4 kicker tanks. The MKP-L tank provides additional kick needed to inject 26 GeV Large Hadron Collider LHC 25 ns type beams. This device has been a limiting factor for operation with high intensity, due to the magnet's broadband beam coupling impedance and consequent beam induced heating. To optimise the usage of the SPS and avoid idle (kicker cooling) time, studies were conducted to develop a recurrent deep learning model that could predict the measured temperature evolution of the MKP-L, using the beam conditions and temperature history as input. In a second stage, the ferrite temperature is also estimated putting together the external temperature predictions from accurate thermo-mechanical simulations of the kicker magnet. In this paper, the methodology is described and details of the neural network architecture used, together with the implementation of an ad-hoc loss function, are given. The results applied to the SPS 2021 operational data are presented.

INTRODUCTION

The restart in 2021 after the Long Shutdown (LS) 2 of the CERN accelerator complex was the first year where all the upgrades of the LHC Injector Upgrade (LIU) project were deployed with the goal of achieving the High Luminosity (HL) LHC brightness requirements [1, 2]. The brightness increase is achieved by doubling the intensity per bunch of the beams and reducing the transverse emittances [3].

The SPS injection system comprises a septum system, MSI, and a kicker system, MKP. The kicker system is composed of four tanks, The first three are used to inject 14 GeV beams, and the last one, the so-called MKP-L, aids to inject the 26 GeV beam for LHC physics.

The MKP-L is one of the main limiting systems to the maximum storable beam intensity in the SPS. Due to beam induced heating via broadband coupling impedance, the MKP-L temperature rises at a rate much higher than all other MKP kickers, risking the ferrite to reach the Curie temperature and inducing significant out-gassing. This translates in reduced availability of the system, as machine operation has to stop to restore safe conditions. Such stops are in the order of many hours due to the large thermal inertia of the MKP-L kicker modules.

In order to optimise the machine time and to avoid idle time, we propose a data-driven model to estimate the MKP-L temperature readings starting from beam parameters and expected operational scenarios. The limitation of such an approach are the temperature probe locations, as they are not on the ferrite directly. In this paper we summarise the purely data-driven model and its application. We present the thermo-mechanical simulation studies that aim to model the full heat transfer from the beam induced power deposition in the ferrite, and finally we give an overview on how to combine the two approaches using PINN.

* francesco.maria.velotti@cern.ch

Brief Physical Model Description

The MKP-L showed a factor of three to four larger temperature increase with high intensity beam operation than the other MKP kickers [4]. This is due to the large real longitudinal beam impedance of the MKP-L. The beam induced power loss can be written as:

$$\Delta W = (f_0 e I_b N_b)^2 \sum_{k=-\infty}^{\infty} (|\Lambda(k\omega_0)|^2 \Re\left[Z_{\|}(k\omega_0)\right]) \quad (1)$$

where f_0 is the revolution frequency, $I_b N_b$ is total number of particles in the accelerator, $\Lambda(k\omega_0)$ is the normalised beam spectrum and $\Re\left[Z_{\|}(k\omega_0)\right]$ is the real part of the longitudinal impedance of the kicker. From simple considerations, the temperature variation due to ΔW power loss is [5]:

$$\frac{d}{dt}T = \frac{\Delta W}{F_{cool} C_{th}} \quad (2)$$

where C_{th} is the thermal capacitance and F_{cool} is the cooling factor. In order to extend the calculation to a different location in a kicker module, one considers a simplified model of the heat propagation:

$$\frac{\partial T}{\partial t} = \frac{k}{\rho C_p}\frac{\partial^2 T}{\partial x^2} + \frac{\Delta W(x,t)}{\rho C_p} \quad (3)$$

where k is the thermal conductivity, ρ is the density of the material and C_p is the specific heat capacity. Solving Eq. (1) and Eq.(3), one can compare data from the temperature probe, as measured in the SPS, with expected temperature of the same location in the MKP-L module.

LONG SHORT TERM MEMORY MODEL FOR TEMPERATURE PREDICTIONS

Deep neural networks are not designed to deal with time-series, where causality imposes well determined constraints. To solve this problem, the proposed architecture was the so-called recurrent neural network (RNN [6]) which exploits recursion to deal with sequences with time dependence. Due to practical issues [7], pure RNN are not very common anymore and they have been replaced with Long Short Term Memory (LSTM) networks [8].

ISBN: 978-3-95450-227-1 ISSN: 2673-5490 doi:10.18429/JACoW-IPAC2022-TUPOST045

OVERVIEW OF THE MACHINE LEARNING AND NUMERICAL OPTIMISER APPLICATIONS ON BEAM TRANSFER SYSTEMS FOR LHC AND ITS INJECTORS

F. M. Velotti, * M.J. Barnes, E. Carlier, Y. Dutheil, M.A. Fraser,
B. Goddard, N. Magnin, R. Ramjiawan, E. Renner, P. Van Trappen, E. Waagaard
CERN, Geneva, Switzerland

Abstract

Machine learning and numerical optimisation algorithms are getting more and more popular in the accelerator physics community and, thanks to the computing power available, their application in daily operation more likely. In the CERN accelerator complex, and specifically on the beam transfer systems, many promising numerical tools have been put in place in the last years. Some of the state-of-the-art machine learning models have been explored and used to solve problems that were never fully addressed in the past. In this paper, the most recent results of application of machine learning and numerical optimisation for injection, extraction and transfer of beam from machine and to experimental areas are presented. An overview of the possible next steps and shortcomings is finally discussed.

INTRODUCTION

The CERN accelerator complex went through a large refactoring over the last few years with the LHC Injector Upgrade project. All the accelerators are now capable of providing better beam brightness, which has the final goal of feeding High-Luminosity LHC (HL-LHC). Nevertheless, all the experiments linked to the different injectors will also benefit from the increase in performance.

Transfer lines, injection and extraction systems have been a core part of the machine renovations, not only with new hardware but also with new analysis methodologies and more thorough studies. One of the possible sources of performance boost is to move manual tuning and scanning of system parameters to numerical methods. This is highly relevant in cases where models are not available, where instrumentation is not adequate, as well as situations where the machine time is expensive or not always available.

In this context, numerical optimisers and machine learning algorithms can play a significant role to boost our system performance, improve stability and speed up commissioning and tuning. Taking as an example the impressive progress across the accelerators in the world, in this paper we summarise the effort ongoing to test and explore ML techniques on beam transfer systems and transfer lines in the CERN accelerator complex.

* francesco.maria.velotti@cern.ch

NUMERICAL OPTIMISERS APPLICATIONS

During recent years, many of the most common and powerful numerical algorithms are made available to simple implementation via the Python Package Index (PyPI). Thanks to the support of python in the CERN control system, the application of numerical methods directly to the accelerators is now streamlined. Also, thanks to the additional software layer put in place [1], we now have available a simplified manner to deploy solutions via numerical optimisations to problems which were addressed with lengthy manual scans.

Transfer Line Steering with BLMs

The Proton Synchrotron (PS) routinely delivers protons to the neutron Time-of-Flight (n_TOF) experiment via the FTN transfer line. From the same extraction channel, the PS provides anti-protons to the Anti-proton Decelerator (AD) after production via the proton-target interaction at the end of the so-called FTA line. Both transfer lines are equipped with almost no beam diagnostics for steering or beam size measurements, but beam loss monitors (BLM) are available along their lengths. To address both steering issues, derivative-free numerical optimisers are now applied to minimise the BLM readings. The main algorithm used for this type of minimisation is BOBYQA [2] as it was the one showing the best results in terms of convergence and machine time needed. Studies to assess the performance of different algorithms are ongoing.

Slow Extraction Losses Optimisation

The Super Proton Synchrotron (SPS) physics program is dominated by the North Area (NA) users, which are provided with a 400 GeV beam which is split among three primary targets. The protons provided to the NA are slowly extracted from the SPS using third-integer resonant slow extraction [3]. The main drawback of this technique are the beam induced losses at the electrostatic septum (so-called ZS), due to the direct interaction of primary protons with the anode wires. The main contribution to the approximately 3% proton lost at the ZS is the wires' alignment, as the projected size on the beam transverse coordinate increases in case of misalignment. In order to reduce to the minimum the effective thickness of the ZS, numerical optimisers have been shown to successfully reduce the time needed for this procedure [4]. This is now routinely applied and the time has also been significantly reduced using the BOBYQA algorithm: it went

ISBN: 978-3-95450-227-1 ISSN: 2673-5490 doi:10.18429/JACoW-IPAC2022-TUPOST046

MACHINE LEARNING APPLIED FOR THE CALIBRATION OF THE HARD X-RAY SINGLE-SHOT SPECTROMETER AT THE EUROPEAN XFEL

C. Grech*, M. Guetg, Deutsches-Elektronen Synchrotron, DESY, Hamburg, Germany
G. Geloni, EuXFEL, Schenefeld, Germany

Abstract

Single-crystal monochromators are used in free electron lasers for hard x-ray self-seeding, selecting a very narrow spectral range of the original SASE signal for further amplification. When rotating the crystal around the roll and pitch axes, one can exploit several symmetric and asymmetric reflections as established by Bragg's law. This work describes the implementation of a machine learning classifier to identify the crystal indices corresponding to a given reflection, and eventually calculate the difference between the photon energy as measured by a single-shot spectrometer and the actual one. The image processing techniques to extract the properties of the crystal reflection are described, as well as how this information is used to calibrate two spectrometer parameters.

INTRODUCTION

Hard X-Ray Self-Seeding (HXRSS) is based on the principle of using crystal monochromators to narrow down the spectral range of self-amplified spontaneous emission (SASE) free electron lasers (FELs) whilst increasing the peak spectral brightness [1, 2]. In its simplest configuration, a self-seeded XFEL consists of an input undulator and an output undulator separated by a single crystal monochromator. In order to ease heat loading effects at high repetition rate and low photon energies, at the European XFEL (EuXFEL) we installed two cascaded HXRSS systems at the SASE2 undulator line, as shown in Figure 1.

HXRSS can only be achieved when the incident beam hits the crystal at the Bragg angle corresponding to the seed frequency for a specific reflection. Thus, the seeded XFEL output is reliant on the diffraction process in the crystal, which highly depends on the crystal orientation with respect to the incident beam direction. The crystal orientation can be controlled in pitch and roll by means of dedicated stages, where the pitch angle θ_p can move in the range $30^\circ \leq \theta_p \leq 120^\circ$. The yaw plane controlled by θ_y is kept constant and unchanged throughout operation. Figure 1 shows the crystal rotational convention considered in this work. The pitch rotation axis is orthogonal to the beam incident direction and parallel to the floor, while the roll rotation axis has an axis lying parallel to the beam incident direction when $\theta_p = 0^\circ$.

The HIgh REsolution hard X-ray single-shot (HIREX) spectrometer installed at the SASE2 undulator beamline of the European XFEL is employed to measure the spectrum

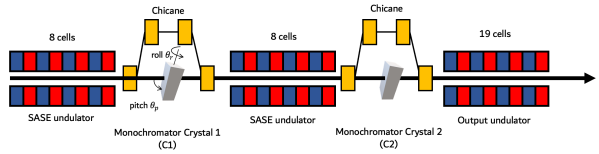

Figure 1: EuXFEL's SASE2 undulator two-crystal hard x-ray self-seeding scheme.

of individual photon pulses. The spectrometer is based on diamond gratings, bent crystals, and a MHz-repetition-rate strip Gotthard detector [3]. An X-ray Gas Monitor (XGM) detector provides a complementary measure of the total x-ray pulse energy, without spectral information. The pySpectrometer photon diagnostic software developed for the European XFEL [4] is used to monitor the measured spectrum, as well as control the calibration of the HIREX spectrometer. Two spectrometer calibration parameters can be controlled through this diagnostic tool: the reference energy and the pixel calibration. The reference energy parameter E_0 provides an absolute energy value, as a reference for the measured spectrum. It does not necessarily correspond to the seeding energy. The second parameter, the pixel calibration, is defined as the change in energy corresponding to a displacement of one pixel, with respect to the pitch angle.

Identifying the actual photon energy to obtain the desired crystal reflection can be arduous. In fact, there often are many neighbouring (in terms of pitch angle and photon energy) reflections, and it can be difficult to identify the actual one based on visual inspection. Machine Learning (ML) methods applied to particle accelerator controls are becoming more common, with the focus being on the efficient use of large amounts of sensor data. In this paper, we propose and demonstrate a machine learning technique, which can be applied at any XFEL facility utilising a monochromator crystal setup to identify crystal reflections, and as a result to identify the operational absolute photon energy. In this study, data obtained at the EuXFEL over two years of HXRSS commissioning and operation is considered, with photon energies ranging from 6 keV to 18 keV. A measurement model is developed based on Bragg's law, and is used to train a classifier that can identify the crystal reflection. Crystal pitch angle and photon energy scans in the form of an image are obtained from the spectrometer, fed to the model and all reflections present in the image are identified. In the end, this information is used to update the two spectrometer calibration parameters. Figure 2 summarizes the complete process from obtaining the image to determining the calibra-

* christian.grech@desy.de

ISBN: 978-3-95450-227-1 ISSN: 2673-5490 doi:10.18429/JACoW-IPAC2022-TUPOST048

DEVELOPMENT OF A VIRTUAL DIAGNOSTIC FOR ESTIMATING KEY BEAM DESCRIPTORS

K. R. L. Baker*, I. D. Finch, S. Lawrie, A. Saoulis,
ISIS Neutron and Muon Source, Rutherford Appleton Laboratory, U.K.
S. Basak, J. Cha, J. Thiyagalingam
Scientific Machine Learning, Rutherford Appleton Laboratory, U.K.

Abstract

Real-time beam descriptive data such as emittance, envelope and loss, are central to accelerator operations, including online diagnostics, maintenance and beam quality control. However, these cannot always be obtained without disrupting user runs. Physics-based simulations, such as particle tracking codes, can be leveraged to provide estimates of these beam descriptors. However, such simulation-based methods are computationally intensive requiring access to high performance computing facilities, and hence, they are often non-realistic for real-time purposes. The proposed work explores the feasibility of using machine learning to replace these simulations with fast-executing inference models based on surrogate modelling. The approach is intended to provide the operators with estimates of key beam properties in real time. Bayesian optimisation is used to generate a synthetic dataset to ensure the input space is efficiently sampled and representative of operating conditions. This is used to train a surrogate model to predict beam envelope, emittance and loss. The methodology is applied to the ISIS MEBT as a case study to evaluate the performance of the surrogate model.

INTRODUCTION

An ultimate goal at accelerator facilities is to produce a high quality, efficient and reliable beam. However, due to the quantity and complexity of the systems involved, significant operator intervention is required to maximise these objectives. If key beam descriptors such as the envelope, emittance, bunch length and beam loss levels are known, it is easier for operators to identify and rectify the cause of a problem to restore the machine back to optimum performance levels. In reality, accessing these descriptors can be difficult for a variety of reasons. The measurements may be physically impossible to take, require disruptive measurements to the beam which would result in user down-time or there may be limited space available for the necessary diagnostic equipment.

Physics simulations can be used to estimate these beam parameters given a set of control parameters. Their dependence on fast Fourier transforms (FFTs) makes them impractical for use in real-time applications as a single simulation can take on the order of days to complete.

A possible solution is to make use of data-driven techniques such as machine learning to replicate these expensive calculations at much shorter timescales. These models can then be linked into control systems to produce real-time estimates for key beam descriptors to allow operators to diagnose and respond to problems more accurately.

For the purpose of this study, we take the new Medium Energy Beam Transport (MEBT), to be installed in the ISIS linear accelerator [1] as part of an ongoing upgrade [2] ,as a case study. As ISIS has evolved organically over time [3], the physical space available for the MEBT is limited; even more so for additional diagnostic equipment. It is therefore an ideal candidate to test the practicality of a surrogate model.

DATA GENERATION

For a virtual diagnostic to be useful, the input space used to train the machine learning model must be comparable to that seen during operation. We therefore define the controllable parameters in the MEBT (cavity and quadrupole strengths) as Gaussian variables from which we can sample to generate the input space. The mean of each Gaussian is the optimum setting found during the MEBT's design phase, while the standard deviation is calculated using a minimum and maximum operating range that is assumed to represent 95% of the data.

Parameters over which the machine operators have no control, such as the incoming beam position, emittance and beam current are defined as uniform random variables that can take any value between a given maximum and minimum. Combining both sets of inputs results in 17 different input features for the machine learning model.

Randomly combining accelerator machine settings will inevitably lead to unfavourable combinations which lead to losses well above the permitted operational levels. To circumvent this issue we intelligently sample the input space using a Bayesian optimisation to select combinations of inputs that would result in low losses that reflect expected operating conditions more accurately. As running each new set of inputs selected by the Bayesian optimisation loop is embarrassingly parallel, we were able to generate a data set of 2136 simulations using the lume-astra [4] Python interface to Astra [5] by utilising multiple CPUs

DATA PROCESSING

Each simulation used a different combination of 17 scalar input parameters and produces spatial 200 length arrays of the emittance (ϵ_{xyz}), transverse envelope (σ_{xy}), bunch length (σ_z), longitudinal energy spread (ΔE) and loss along the length of the MEBT.

* k.baker@stfc.ac.uk

ISBN: 978-3-95450-227-1 ISSN: 2673-5490 doi:10.18429/JACoW-IPAC2022-TUPOST049

SIMULATION STUDY FOR AN INVERSE DESIGNED NARROWBAND THz RADIATOR FOR ULTRARELATIVISTIC ELECTRONS

G. Yadav*, C. P. Welsch, Cockcroft Institute and University of Liverpool, UK
B. Hermann, Paul Scherrer Institut, 5232 Villigen, PSI, Switzerland,
Institute of Applied Physics, University of Bern, 3012 Bern, Switzerland,
Galatea Laboratory, Ecole Polytechnique Fédérale de Lausanne (EPFL), 2000 Neuchâtel, Switzerland
U. Haeusler, Department Physik, Friedrich-Alexander-Universität Erlangen-Nürnberg (FAU),
91058 Erlangen, Germany
A. Kirchner, P. Hommelhoff, Department Physik, Friedrich-Alexander-Universität
Erlangen-Nürnberg (FAU), 91058 Erlangen, Germany
T. Feurer, Institute of Applied Physics, University of Bern, 3012 Bern, Switzerland
R. Ischebeck, Paul Scherrer Institut, 5232 Villigen, PSI, Switzerland

Abstract

THz radiation has many applications, including medical physics, pump-probe experiments, communications, and security systems. Dielectric grating structures can be used to generate cost-effective THz radiation, synchronous to a relativistic beam based on the Smith-Purcell effect. We present a 3D simulation study for the THz radiation emitted from an inverse-designed grating structure after a 3 GeV electron bunch traverses through it. Our farfield simulation results show a narrowband emission spectrum centred around 881 µm, close to the designed value of 900 µm. The grating structure was experimentally tested at the SwissFEL facility, and our simulated spectrum shows good agreement with the observed one.

INTRODUCTION

THz radiation sources are extremely useful in electron acceleration [1–3], wireless communication [4], material and biomedical sciences [5, 6]. The wavelength of this radiation lies between the microwave and infrared regime of the electromagnetic spectrum. Several methods such as optical rectification [7, 8], vacuum tubes and integrated circuits [9, 10] have been used to generate THz radiation. Among these, the Smith-Purcell effect is a cost-effective and compact alternative [11]. Being a precursor of a free electron laser (FEL), this effect is the radiation of light when charged particles pass along periodic metallic or dielectric grating structures. For an electron bunch with relativistic velocity ratio β, the wavelength λ and direction of emitted radiation θ is related to the grating periodicity a by the following Smith-Purcell equation

$$\lambda = \frac{a}{n}\left(\frac{1}{\beta} - \cos\theta\right), \qquad (1)$$

where n is the order of the harmonic mode.

Recent advances in computational optimization have paved the way for designing the optical structures algorithmically, purely based on the desired performance and thus skipping the hardships of brute force optimization. Inverse design is such an approach which can be used to devise photonic structures by searching a much broader space of fabricable devices.

Here we present the 3D simulation study of the THz radiation from such a structure designed using the inverse design algorithm [12] and present the comparison with the experimental observation. The structure which we used for investigating the THz radiation was designed using the inverse design method. The optimization process was performed for a single unit cell in a 2D finite-differences frequency-domain simulation (FDFD). Periodic boundary conditions were applied in the direction of electron bunch propagation and to imitate free space, perfectly matched layers were used. The design was aimed for narrowband THz radiation from ultrarelativistic electrons. In contrast to the conventional metallic gratings for Smith-Purcell radiation, a dielectric structure was used as it has a 1-2 order of magnitude higher damage threshold than metals [15]. The 3D version of the optimized structure is shown in the Fig. 1. The structure was scaled to have a length of 45 mm and a height of 6 mm and fabricated by a 3D printer using stereolithography (SLA) technique. For the dielectric material, Formlabs high tem-

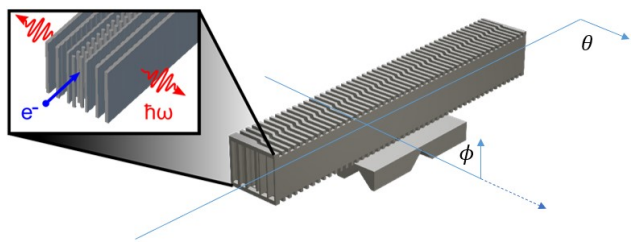

Figure 1: The dielectric grating structure optimized by inverse design approach (top view). Full 3D structure with the base which was experimentally tested in the SwissFEL [13] laboratory and used in 3D time domain simulation. The electron bunch travelled along the grating periodicity direction and the THz radiation was obtained in its perpendicular direction (inset) [14].

* gyanendra.yadav@liverpool.ac.uk

ISBN: 978-3-95450-227-1 ISSN: 2673-5490 doi:10.18429/JACoW-IPAC2022-TUPOST050

LIVERPOOL CENTRE FOR DOCTORAL TRAINING FOR INNOVATION IN DATA INTENSIVE SCIENCE*

C. P. Welsch†, University of Liverpool/Cockcroft Institute, UK

Abstract

The Liverpool center for doctoral training for innovation in data intensive science (LIV.INNO) is an inclusive hub for training three cohorts of students in data intensive science. Starting in October 2022, each year will train about 12 PhD students in applying data skills to address cutting edge research challenges across astrophysics, nuclear, theoretical and particle physics, as well as accelerator science. This framework is expected to provide an ideal basis for driving science and innovation, as well as boosting the employability of the LIV.INNO PhD students.

This paper gives examples of the accelerator science R&D projects in the center. It includes details about research into the optimization of 3D imaging techniques and the characterization of photocathodes for accelerator applications.

INTRODUCTION

Analysis and manipulation of Big Data has long been a specialty of researchers in STFC-funded research areas. The new Center for Doctoral Training (CDT) LIV.INNO will provide training for three cohorts of PhD students through an interdisciplinary approach [1]. At the University of Liverpool (ULIV) and Liverpool John Moores University (LJMU), we have an outstanding track record in the design, construction and operation of scientific instruments and the science they enable. This had led to strong links with many research laboratories and industry partners. The CDT will capitalize on the wider research and training activities at both partner universities where data science is an identified priority research theme. Amongst others, the CDT will benefit from a range of existing initiatives, such as the Virtual Engineering Centre (VEC), the strategic partnership between UoL and STFC Daresbury, as well as the new £12M Digital Innovation Facility (DIF) .

Liverpool researchers have an excellent track record in delivering science for STFC: At UoL the accelerator science group based at the Cockcroft Institute, particle physics and nuclear physics groups have the highest rate of STFC funding per academic in the UK, attracting more than £70M of funding from STFC over the past decade. Our Physics department has designed, built and contributed detectors to many particle and nuclear physics experiments, including ATLAS, LHCb and ALICE at the LHC, g-2, T2K, SNO+, proto-DUNE, LZ, AGATA, NuSTAR, AWAKE, HLLHC and R3B. The data analysis on these detectors and many running experiments and those that have recently completed data taking is aided by more than 100 PhD students. The very large data volumes from these experiments has given staff and PhD students expertise in data handling, data reduction techniques and the management of systematic uncertainties in these very large-scale analysis tasks. We have also developed code to run on non-traditional processor architectures, the integrated data acquisition, trigger and data compression required for readout systems and simulation of all of the expected and some of the possible physics processes the detectors will be sensitive to. Research will be complemented by the strong involvement of our Mathematics and Computer Science departments which contribute additional skills and important links with external partners. The 14-strong STFC-supported Theoretical Physics group in MS access national high-performance computing (HPC) facilities such as DiRAC to perform lattice field theory simulations for particle, nuclear and condensed matter physics, and employ machine learning techniques for complex problems such as the classification of string theory vacua.

We are very experienced as coordinator of large-scale postgraduate training initiatives, having coordinated training networks worth more than 20M€ for almost 100 Marie Curie Fellows across physics, engineering and life sciences. We have also hosted THE very successful STFC CDT LIV.DAT with LJMU between 2017 and 2020 with around 40 PhD students trained in recent years [2]. These initiatives have driven inclusivity and equality of opportunity: In our OMA network [3], 47% of the Fellows were female, in our CDT LIV.DAT, our students acted as ambassadors for the national IOP Bell Burnell fund to improve diversity in physics [4], and the LIV.INNO Director was one out of only five (and the only male) invited representatives within the 2021 UK country delegation at the International Conference on Women in Physics (ICWIP) where he presented Liverpool EDI initiatives [5] and an update on progress made in the UK [6].

The Astrophysics Research Institute (ARI) of LJMU consists of 55 academic, technical, admin and research staff and more than 40 research students. ARI carries out fundamental research across a wide area of the STFC priority astronomy areas: galaxy evolution, numerical simulations of galaxy formation, star formation and stellar evolution, time domain astrophysics and astronomical instrumentation. ARI research connects well to Big Data, e.g. execution and analysis of massively-parallel numerical simulations of cosmic structure formation, and in time-domain astrophysics covering gamma-ray bursts, super luminous supernovae, and potential electromagnetic counterparts to gravitational wave sources. Central to the ARI's time domain activities is the Liverpool Telescope, the world's largest fully robotic telescope, located on La Palma in the Canary Islands, owned and operated by LJMU and nationally funded by STFC.

* This project has received funding from STFC.
† c.p.welsch@liverpool.ac.uk

ISBN: 978-3-95450-227-1 ISSN: 2673-5490 doi:10.18429/JACoW-IPAC2022-TUPOST051

USING DATA INTENSIVE SCIENCE FOR ACCELERATOR OPTIMIZATION*

C. P. Welsch†, University of Liverpool/Cockcroft Institute, UK

Abstract

Particle accelerators and light sources are some of the largest, most data intensive, and most complex scientific systems. The connections and relations between machine subsystems are complicated and often nonlinear with system dynamics involving large parameter spaces that evolve over multiple relevant time scales and accelerator systems. In 2017, the Liverpool Centre for Doctoral Training in Data Intensive Science (LIV.DAT) was established. With almost 40 PhD students, the centre is now established as an international hub for training PhD students in data intensive science. This paper presents results from studies carried out in LIV.DAT into novel high gradient accelerators with a focus on the data science techniques that were used. This includes studies into inverse-designed narrowband THz radiators for ultra-relativistic electrons, simulation of the transverse asymmetry and inhomogeneity on seeded self-modulation of beams in plasma, as well as studies into the physical aspects of collinear laser injection in Trojan Horse laser plasma experiments.

INTRODUCTION

In 2017 LIV.DAT, the Liverpool Centre for Doctoral Training in Data intensive science was established. LIV.DAT has quickly established itself as a center of excellence in data science, across a significant part of STFC research, including nuclear, particle and astrophysics, as well as accelerator science. The center also acts as a model for training cohorts of student in Data Intensive Science and currently trains 36 PhD students [1].

Recent years have witnessed a dramatic increase of data in many fields of science and engineering, due to the advancement of sensors, mobile devices, biotechnology, digital communication and internet applications. Very little targeted training is provided internationally to address a growing skills gap in this area. LIV.DAT provides a comprehensive training program to its students to close this skills gap through a cutting-edge research program.

SELECTED RESEARCH RESULTS

The focus of the LIV.DAT center is on addressing cutting-edge research challenges by using state-of-the-art data science techniques across three scientific work packages:

- Monte Carlo (MC) methods as tools to address a wide range of physics problems, from the dynamic behaviour of galaxies, cross sections in specific particle interactions to dose delivery planning in ion beam therapy;
- High Performance Computing (HPC) and Machine Learning (ML) using computing clusters to simulate cutting edge physics and engineering problems that cannot be dealt with on desktop computers;
- Data Analysis across the entire spectrum of physics research.

All three work packages are highly relevant for accelerator science R&D. In the following, selected research highlights from studies that are presented at this year's IPAC conference are given.

Inverse-Designed Narrowband THz Radiators for Ultra-relativistic Electrons

THz radiation sources are extremely useful for a wide range of applications and a number of methods [2-4] have been used to generate this radiation with lies between the microwave and infrared spectrum. Amongst these methods, the Smith Purcell effect has proven to provide a cost effective and compact solution [5].

Recent advances in computational design and optimization have paved the way for designing the underpinning optical structures algorithmically and thus allowing computer-guided structure optimization. LIV.DAT student Gyanendra Yadav has successfully carried out 3D-simulation studies into the generation of THz radiation from structures designed using the inverse function algorithm [6]. These have formed an important contribution to experiments demonstrating the capabilities of such radiators [7].

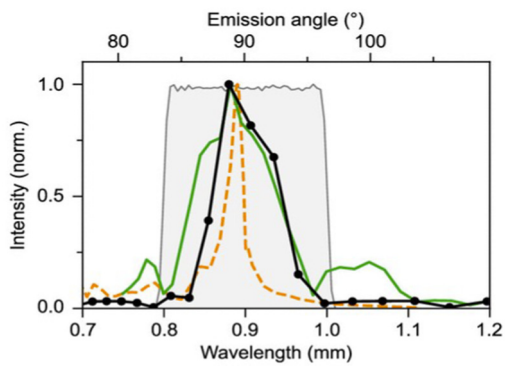

Figure 1: Measured and simulated emission spectrum. The black curve shows experimental data, whilst the orange and green curves show results from frequency domain and time domain simulations, respectively [7].

Full 3D time domain simulations for obtaining the resulting THz radiation spectrum were performed in the established simulation code CST Studio [8]. Figure 1 shows the resulting electromagnetic spectrum as obtained in CST Studio in direct comparison with experimental data and frequency domain simulations. It can be seen that an

* This work was supported by STFC under grant agreement ST/P006752/1.
† c.p.welsch@liverpool.ac.uk

ISBN: 978-3-95450-227-1 ISSN: 2673-5490 doi:10.18429/JACoW-IPAC2022-TUPOST053

BEAM TUNING AT THE FRIB FRONT END USING MACHINE LEARNING*

Kilean Hwang†, Tomofumi Maruta, Alexander Plastun, Kei Fukushima, Tong Zhang, Qiang Zhao, Peter Ostroumov, Samuel Nash
Facility for Rare Isotope Beams, Michigan State University, East Lansing, Michigan, USA

Abstract

The Facility for Rare Isotope Beams (FRIB) at Michigan State University produced and identified the first rare isotopes demonstrating the key performance parameter and completion of the project. An important next step toward FRIB user operation includes fast tuning of the Front End (FE) decision parameters to maintain optimal beam optics. The FE consists of the ion source, charge selection system, LEBT, RFQ, and MEBT. The strong coupling of many ion source parameters, strong space-charge effects in multi-component ion beams, and a not well-known neutralization factor in the beamline from the ion source to the charge selection system make the FE modeling difficult. In this paper, we present our first effort toward the Machine Learning (ML) application for automatic control of the beam exiting the FE.

INTRODUCTION

FRIB houses a powerful heavy-ion linear accelerator to produce wide spectrum of rare isotope species of variety of charge states [1–3]. Such an unprecedented capability requires a frequent switch of primary beam ion species followed by optics tuning in FE. Therefore, fast FE beam optics tunning as well as maintaining the beam quality is crucial for the mission. We have been successfully utilizing the NelderMead [4] – a simplex method – for automated fast tuning of FE upon initialization of the beam commissioning. This optimization algorithm decides the next optimal decision parameters to be evaluated based only on a few data points that form a simplex over the decision parameter domain. If we can exploit all the data points we visited since the start of the optimization, we may get more sample-efficient[1] decision. Furthermore, if the all the historical (or archived) data from past operations is somewhat consistent[2], we may able to exploit it to enhance the sample efficiency even more. In this regard, we develop and test the prior-mean-assisted Bayesian optimization (pmBO) where the prior model is trained over the historical (or archived) data. We are also creating surrogate models of physics simulation of FE for fast and large data collection purposes so as to realize the application of pmBO for FE tuning.

PRIOR MEAN ASSISTED BAYESIAN OPTIMIZATION

The ML methods for the online beam tuning that are reported until today may be in largely two categories: reinforcement learning (RL) and surrogate model assisted optimization (SMAO) [5–7]. The Bayesian optimization (BO) belongs to the latter category. In general, compared to RL, SMAO is more sample efficient but less robust to the machine drift, and heavier in numerical complexity [8]. Furthermore, SMAO is, generally, not suitable for continuously tunning due to the assumption of static problems and the numerical complexity[3]. Nevertheless, we find SMAO, (especially BO) is a good fit for our purpose due to the ability to incorporate the historical (or archived) data naturally in terms of the prior model as well as the sample efficiency. And the numerical complexity problem can be relieved if optimization converges in a few steps thanks to the good prior model. Finally, once the optimization converged, we can use either a pre-trained (off-policy, offline) RL or traditional control algorithms like the Extremum-Seeking for continuous tunning for adaption to the machine drift [9].

In this section, we present how we model the data reflecting the effect of the machine drift, and exploit the data for optimization on two test problems: Rosenbrock and Rastrigin functions:

$$\begin{aligned}\mathfrak{Rosen}\left(x_1, x_2, \ldots, x_d\right) &= \sum_{i=1}^{d-1}\left(x_{i+1} - x_i^2\right)^2 + \frac{(1-x_i)^2}{100} \\ \mathfrak{Rastr}\left(x_1, x_2, \ldots, x_d\right) &= \sum_{i=1}^{d-1}\frac{x_i^2 - \cos\left(2\pi x_i\right)}{d} - 1 \end{aligned} \quad (1)$$

These are commonly used objective functions for benchmarking optimization algorithms. Figure 1 shows them for the 2-dimensional case.

Historical Data Model

We assume that the system dynamics in terms of the objective $f(\cdot)$ of interest is fully describable by the decision parameters $\boldsymbol{x}_{decision}$, and known $\boldsymbol{x}_{known}$ and unknown $\boldsymbol{x}_{unknown}$ environmental parameters except for small noises $\epsilon \sim \mathcal{N}(0, 0.01)$:

$$y = f\left(\boldsymbol{x}_{decision}; \boldsymbol{x}_{known}, \boldsymbol{x}_{unknown}\right) + \epsilon \quad (2)$$

* Work supported by the Director of the Office of Science of the US Department of Energy under Cooperative Agreement DE-SC0000661, the State of Michigan and Michigan State University
† hwang@frib.msu.edu
[1] By "sample efficiency", we mean a faster optimization in terms of the number of objective evaluations. This does not necessarily mean a faster optimization in terms of the wall clock.
[2] Here we mean the consistency of historical (or archived) data in a sense that the present machine status in terms of the relationship between the decision parameters and the objective of interest is not very far from most of the past machine statues (due to machine drift) when the data was collected.
[3] It involves with the surrogate model training and optimization over the surrogate model or an acquisition function that is a function of the surrogate model.

ISBN: 978-3-95450-227-1 ISSN: 2673-5490 doi:10.18429/JACoW-IPAC2022-TUPOST054

EXPERIMENT OF BAYESIAN OPTIMIZATION FOR TRAJECTORY ALIGNMENT AT LOW ENERGY RHIC ELECTRON COOLER*

Y. Gao[1,†], K. A. Brown[1], X. Gu[1], J. Morris[1], S. Seletskiy[1]
W. Lin[2,‡], G. H. Hoffstaetter[1,2], J. A. Crittenden[2]
[1]Collider-Accelerator Department, Brookhaven National Laboratory, Upton, NY, USA
[2]CLASSE, Cornell University, Ithaca, NY, USA

Abstract

As the world's first electron cooler that uses radio frequency (rf) accelerated electron bunches, the low energy RHIC electron cooling (LEReC) system is a nonmagnetized cooler of ion beams in RHIC at Brookhaven National Laboratory. Beam dynamics in LEReC are different from the more conventional electron coolers due to the bunching of the electron beam. To ensure an efficient cooling performance at LEReC, many parameters need to be monitored and fine-tuned. The alignment of the electron and ion trajectories in the LEReC cooling sections is one of the most critical parameters. This work explores using a machine learning (ML) method - Bayesian Optimization (BO) to optimize the trajectories' alignment. Experimental results demonstrate that ML methods such as BO can perform control tasks efficiently in the RHIC controls system.

INTRODUCTION

The Low Energy RHIC electron Cooler (LEReC) is commissioned by the Collider-Accelerator Department (C-AD) at Brookhaven National Laboratory (BNL) to increase the collision rate [1] at the Relativistic Heavy Ion Collider (RHIC). During 2020 and 2021 runs, LEReC has proven to be successful in increasing the ion luminosity at RHIC.

Figure 1 shows the layout of the LEReC system at BNL. Electrons are generated by the gun and accelerated to 1.6 - 2 MeV by the superconducting rf cavity to match the energy of ions in RHIC. The electron bunches have a frequency of 704 MHz, and they are grouped into 30 - 36 macro-bunches with a frequency of 9 MHz. The accelerated electron bunches then travel through the transport line to interact with the ions in two cooling sections (CS) in the "Yellow" and "Blue" RHIC ring, each 20 meters long, connected by a 180-degree bend. Thus, ions in both rings of the collider can be cooled simultaneously. After interacting with the ions, the electrons are extracted from the Blue CS and discarded in the beam dump.

In the two cooling sections, ions experience a cooling force from the co-traveling electrons due to Coulomb interaction. As a result, the energy spread of the ion beam is reduced, and its phase-space density is increased [2, 3]. One of the key factors affecting the magnitude of the cooling force, hence affecting the cooling performance, is the relative angle of the electron beam trajectory with respect to the ion beam.

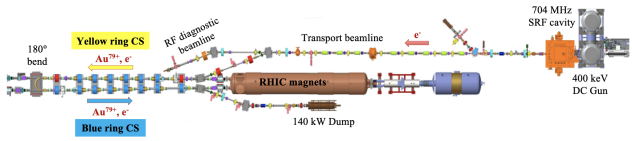

Figure 1: LEReC system layout (not to scale).

In this work, we use a machine learning (ML) method called Bayesian optimization (BO) to optimize the electron-ion trajectory alignment by matching the electron and ion positions observed at all of the beam position monitors (BPMs) in the cooling sections.

Bayesian optimization (BO) is a powerful tool for finding the optimum of an expensive objective function f with as few samples as possible. It contains two important components: a surrogate model, which learns and then predicts the behavior of the objective function, and an acquisition function, which determines quantitatively which inputs are most likely to generate optimal output. Bayesian optimization is applied in various fields, including finance, engineering, environmental science, and robotics. A basic BO background and some of its applications are detailed in [4].

To perform trajectory optimization at LEReC, preliminary simulation studies were conducted using both BO and another ML method called Q-Learning on the LEReC system simulator [5]. After obtaining satisfactory results from the simulation studies, we present in this paper the experimental results from testing the BO method on the real LEReC system. A more detailed description of the experiment, including simulation studies and BO algorithm structures, can be found in [6].

EXPERIMENTAL RESULTS

Preliminaries

Due to its high magnetic rigidity, the ion beam has a straight trajectory in the LEReC cooling sections. The lower-rigidity electron trajectory is controlled by 8 pairs of horizontal/vertical correctors and is monitored by 8 BPMs in each cooling section. Currently, there is an orbit correction program in place to manipulate correctors based on the BPM feedback, so electrons always stay at desired positions throughout the cooling sections. After calibration, the straight ion trajectory is kept at the center of the cooling

* Work supported by Brookhaven Science Associates, LLC under Contract No. DE-SC0012704 with the U.S. Department of Energy, and by the U.S. National Science Foundation under Award PHY-1549132.
† ygao@bnl.gov
‡ wl674@cornell.edu

ISBN: 978-3-95450-227-1 ISSN: 2673-5490 doi:10.18429/JACoW-IPAC2022-TUPOST055

TOWARD MACHINE LEARNING-BASED ADAPTIVE CONTROL AND GLOBAL FEEDBACK FOR COMPACT ACCELERATORS*

F. Cropp†, P. Musumeci
Department of Physics and Astronomy, University of California Los Angeles,
Los Angeles, CA 90095, USA
A. Scheinker
Applied Electrodynamics Group, Los Alamos National Laboratory,
Los Alamos, NM 87545, USA
D. Filippetto, A. Gilardi, S. Paiagua, D. Wang
Lawrence Berkeley National Laboratory, Berkeley, CA 94720, USA

Abstract

The HiRES beamline at Lawrence Berkeley National Laboratory (USA) is a state-of-the-art compact accelerator providing ultrafast relativistic electron pulses at MHz repetition rates, for applications in ultrafast science and for particle accelerator science and technology R&D. Using HiRES as testbed, we seek to apply recent developments in machine learning and computational techniques for machine learning-based adaptive control, and eventually, a full control system based on global feedback. The ultimate goal is to demonstrate the benefits of such a suite of controls to UED, including increased temporal and spatial resolution. Concrete steps toward these goals are presented, including automatic, model-independent tuning for accelerators, and energy virtual diagnostics with direct application to improving UED temporal resolution.

INTRODUCTION

Because of the complexity of accelerators and their natural parameter movement, both in the short and long term (hereafter, jitter and drift, respectively), accelerators could see major improvement from machine learning (ML). The application of ML has been shown to solve or mitigate a plethora of accelerator control and diagnostic problems, for example, for navigating efficiently the multi-dimensional parameter space to find control set points [1, 2], for inverting a large parameter space to make a parasitic diagnostic [3, 4], or for non-destructive virtual diagnostics [5, 6]. Further, ultrafast electron diffraction (UED) has benefited from ML-based static models and virtual diagnostics [7, 8]. The advantages of static ML models are incontrovertible, but they have limits. For example, it is an open question as to how an optimal ML-based control system should treat a system when parameter drift brings a the state of the machine outside the training set [9]. At HiRES [10], a state-of-the-art MHz-class UED facility with short, high 6-D brightness beams, a model-independent optimization method is detailed for dealing with this case. Further work is shown to apply time of arrival virtual diagnostics to increase the short- and long-term stability of the already-state-of-the-art stability at HiRES to the 10^{-4} level and below. Such work will make up the building blocks of an adaptive control and global feedback system, with application to UED measurements.

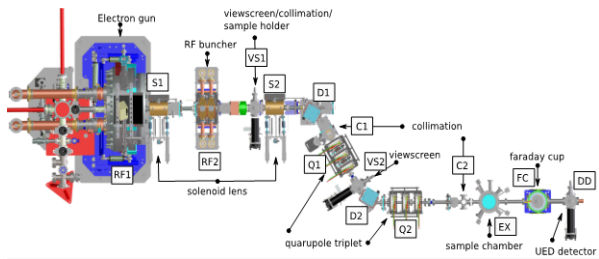

Figure 1: The HiRES beamline, from [10].

INITIAL EXPERIMENTAL TESTS OF ML-ENHANCED OPERATIONS

The ultimate goal is to demonstrate the benefits of such a suite of controls to UED, including increased temporal and spatial resolution. The inital experimental results, showcasing the potential for enhanced stability and autonomous operations, are shown.

Adaptive Control

Extremum seeking (ES) [11–13] is a powerful, model-independent optimization routine that can be applied to optimize quickly and control particle accelerators. It has myriad uses for particle accelerators, including optimizing an electron beam via automatic tuning of accelerator parameters [14] to tuning the latent space of a convolutional neural network-based digital twin of the accelerator to make it more robust to drifting parameters [9]. This work seeks to combine these approaches to build a tool for adaptive, on-line control of accelerators.

Often, when operating an accelerator, it is necessary to change modes of operation. At HiRES, ES was demonstrated to be able to follow a moving cost function. In this example,

* This work was supported by the DOE Office of Science Graduate Student Research (SCGSR) program, by the DOE Office of Basic Energy Sciences under Contract No. DE-AC02-05CH11231, by the DOE Office of Science, Office of High Energy Physics under contract number 89233218CNA000001 and DE-AC02-05CH11231 and by the NSF under Grant No. PHY-1549132.
† ericcropp@physics.ucla.edu

ISBN: 978-3-95450-227-1 ISSN: 2673-5490 doi:10.18429/JACoW-IPAC2022-TUPOST056

MULTI-OBJECTIVE BAYESIAN OPTIMIZATION AT SLAC MeV-UED *

Fuhao Ji†, Auralee Edelen, Joel England‡, Xiaozhe Shen, Sara Miskovich, Ryan Roussel, Stephen Wheathersby, Duan Luo, Mianzhen Mo, Patrick Kramer, Christopher Mayes, Xijie Wang, Alexander Reid, Michael Minitti,
SLAC National Accelerator Laboratory, Menlo Park, CA, USA

Abstract

SLAC MeV-UED, part of the LCLS user facility, is a powerful "electron camera" for the study of ultrafast molecular structural dynamics and the coupling of electronic and atomic motions in a variety of material and chemical systems. The growing demand of scientific applications calls for rapid switching between different beamline configurations for delivering electron beams meeting specific user run requirements, necessitating fast online tuning strategies to reduce set up time. Here, we utilize multi-objective Bayesian optimization(MOBO) for fast searching the parameter space efficiently in a serialized manner, and mapping out the Pareto Front which gives the trade-offs between key beam parameters, i.e., spot size, q-resolution, pulse length, pulse charge, etc. Algorithm, model deployment and first test results are presented.

INTRODUCTION

Machine learning(ML) and artificial intelligence(AI) have revolutionized many computational and real world tasks in recent years, from autonomous driving, protein folding prediction [1] to fusion reactor control [2]. Speeding up and aiding online optimizations of complex particle accelerators is one of the key areas where AI/ML can make substantial contributions [4–10]. At MeV-UED [3], the growing demand of scientific applications calls for highly automated and rapid switch between different machine configurations for delivering electron beams meeting specific user run requirements, necessitating fast online tuning strategies to reduce set up time. At mean time, rapid R&D activities are undergoing for enabling future science applications, which pose additional challenges for beam tuning and optimizations.

We utilize AI/ML based techniques for speeding up online beam tuning at MeV-UED. In particular, the recently introduced Multi-Objective Bayesian Optimization(MOBO) scheme [8] was used for searching the parameter space efficiently in a serialized manner, and mapping out the Pareto Front which gives the trade-offs between key beam parameters, i.e., spot size, q-resolution, pulse length, pulse charge, etc. This method uses a set of Gaussian Process(GP) surrogate models, along with a multi-objective acquisition function, to reduce the number of observations needed to converge by at least an order of magnitude over current methods, i. e., Multi-Object Genetic Optimization (MOGA), and is thus a critical step toward online multi-objective optimization on real accelerator systems.

MULTI-OBJECTIVE BAYESIAN OPTIMIZATION

The goal of multi-objective optimization is to search the input parameter space and minimize(for simplicity, here we discuss the minimization case) the vector objective function $\mathbf{f}(\mathbf{x}) = \{f_1(\mathbf{x}), f_2(\mathbf{x}), ..., f_M(\mathbf{x})\}$. Usually, there is no single solution $\mathbf{x}^*$ that simultaneously minimizes all objectives. Instead, objective vectors are compared using Pareto domination: an objective vector $\mathbf{f}(\mathbf{x})$ dominates another vector $\mathbf{f}(\mathbf{x}')$ if $f_m(\mathbf{x}) \leq f_m(\mathbf{x}')$ for all $m = 1, ..., M$ and there exists at least one n such that $f_n(\mathbf{x}) < f_n(\mathbf{x}')$. The Pareto Front (PF) $\mathcal{P}$ is the set of non-dominated objective vectors which gives the optimal trade-offs between objectives. Thus the goal of a Pareto optimization algorithm is to identify the PF within a pre-specified budget of function evaluations. Hypervolume(HV) is an often used metric to evaluate the quality of a PF, the HV quantifies the hypervolume(area in the 2 objective case) of the set of points dominated by $\mathcal{P}$ intersected with a region of interest in objective space bounded below by a reference point $\mathbf{r}$ (see Figure 1). MOBO attempt to maximize HV during the optimization process. Given a set of N observations:$D_N = \{(\mathbf{x}_1, \mathbf{y}_1), (\mathbf{x}_2, \mathbf{y}_2), ..., (\mathbf{x}_N, \mathbf{y}_N)\}$, each objective is modeled as an independent GP surrogate model:

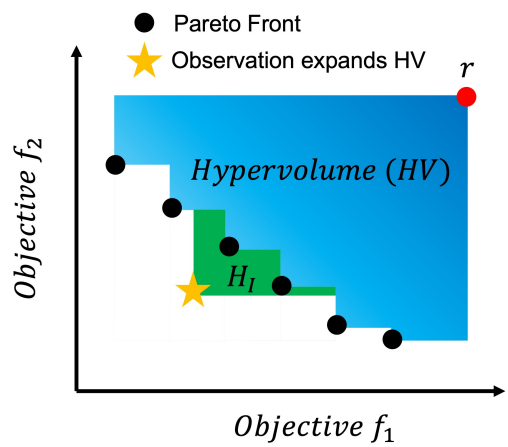

Figure 1: Multi-objective optimization, Pareto Front is formed by non-dominated vectors in the objective space, the optimizer attempts to maximize Hypervolume(HV) during the optimization process.

* Work supported by U.S. Department of Energy Office of Science, Basic Energy Sciences under Contract No. DE-AC02-76SF00515
† fuhaoji@slac.stanford.edu
‡ england@slac.stanford.edu

ISBN: 978-3-95450-227-1 ISSN: 2673-5490 doi:10.18429/JACoW-IPAC2022-TUPOST058

BADGER: THE MISSING OPTIMIZER IN ACR*

Z. Zhang†, A. Edelen, C. Mayes, J. Garrahan, J. Shtalenkova, R. Roussel, S. Miskovich, D. Ratner
SLAC National Accelerator Laboratory, 94025 Menlo Park, USA
M. Boese, S. Tomin
Deutsches Elektronen-Synchrotron, 22607 Hamburg, Germany
G. Wang, Y. Hidaka
Brookhaven National Laboratory, 11973 Upton, USA

Abstract

Online optimization is crucial during accelerator operations to achieve satisfying machine performance. Optimization algorithms such as Nelder-Mead simplex, Gaussian process (GP), and robust conjugate direction search (RCDS) have been widely used in accelerator online optimization scenarios. The usual way of doing online optimization in accelerator control rooms (ACR) is to write a script that connects the algorithm to the problem. This approach would accrue code fragments that are difficult to maintain and reuse, plus the optimization progress can not be easily monitored and controlled. In this study, we propose an optimization platform named Badger to tackle the obstacles in ACR online optimizations. The design philosophies and features of Badger would be introduced and discussed.

INTRODUCTION

Modern large-scale accelerator facilities become more and more complicated, in consequence, the performance of the accelerators in operation usually differs from the design. Online optimization during operation is the key to bridging the gap between the designed properties and the ones in action, to achieve satisfying machine performance [1–7]. One obstacle to applying various algorithms in machine tuning tasks is that different algorithms usually work in different ways, the users have to write wrapper code to adapt the algorithms to their cases. This approach is not ideal since the number of the wrapper scripts would increase with time, and consequently makes it hard to manage and reuse these machine tuning-related scripts. Another drawback of creating a wrapper script for every new machine tuning task is code redundancy. For example, a large chunk of similar optimization progress visualization code needs to be written again and again – it is essential to see the optimization progress on the fly, although the visualization code itself is trivial and distracting.

The issues described above can be solved by employing an optimization framework that has a wide range of built-in algorithms, provides a straightforward way to create a custom optimization problem, and can monitor the optimization progress in some way. Xopt [8], Ocelot optimizer [9], and Teeport [10] are good candidates of optimizers that can be applied in online optimization scenario. However, more considerations must be taken in the accelerator control rooms (ACR), to boost the efficiency of the machine tuning tasks in daily operations: 1) The tasks are usually repeated hundreds of thousands of times, so rerunning a task should be as easy as possible, 2) optimization data for all history runs should be archived and logged properly, for future references, 3) optimizations are required to be strictly safe – no violations on variable hard boundaries would be tolerated, and 4) the optimization progress must be monitorable and controllable – the operators should be able to pause/resume/terminate a task according to the situation. We developed Badger – an online optimization framework that was designed with ACR usage in mind – that accounts for all the requirements above. Badger has been tested and verified to work in ACR of SLAC, DESY, and BNL.

CONCEPTS

Badger abstracts an optimization run as an optimization algorithm interacts with an environment, by following some pre-defined rules. As visualized in Figure 1, within an optimization routine, the environment is controlled by the algorithm and tunes/observes the control system/machine through an interface, while the users control/monitor the optimization flow through a graphical user interface (GUI) or a command-line interface (CLI).

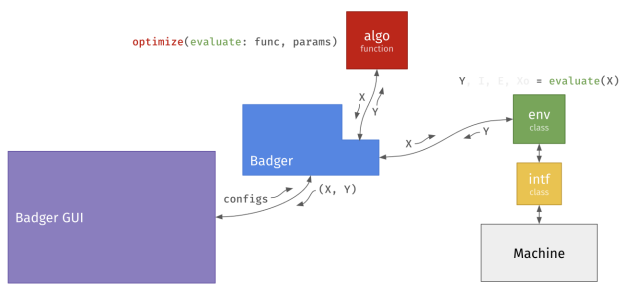

Figure 1: The architecture of Badger. The algorithm accepts an `evaluate` function provided by Badger as an argument, while the `evaluate` function sends trail solutions to be evaluated to the environment. Environment talks to the machine through an optional interface, to get or set the process variable (PV) values. The data flow during the optimization goes through the Badger core (shape in blue) and the optimization progress can be monitored/controlled by the Badger GUI or CLI (not shown in the plot).

* This work was supported by the U.S. Department of Energy, under DOE Contract No. DE-AC02-76SF00515 and the Office of Science, Office of Basic Energy Sciences.
† zhezhang@slac.stanford.edu

ISBN: 978-3-95450-227-1 ISSN: 2673-5490 doi:10.18429/JACoW-IPAC2022-TUPOST059

PyEmittance: A GENERAL PYTHON PACKAGE FOR PARTICLE BEAM EMITTANCE MEASUREMENTS WITH ADAPTIVE QUADRUPOLE SCANS*

S. A. Miskovich†, A. Edelen, C. Mayes
SLAC National Accelerator Laboratory, Menlo Park, California, CA 94025 USA

Abstract

The emittance of a particle beam is a critically important parameter for many particle accelerator applications. Its measurements guide the initial tuning of an accelerator and are typically done using quadrupole or wire scans. Quadrupole scans are time-intensive, and it can be difficult to determine scan values that provide a good emittance measurement. To address this issue, we describe an adaptive quadrupole scan method that automates the determination of the scan range. With a given initial set of scanning values, our method adapts the range to capture the waist of the beam, and returns the Twiss parameters and a measure of the beam matching at the measurement screen. With the added capability to repeat beam size measurements when needed, this method provides a reliable measurement of the emittance even with sub-optimal initial conditions. To efficiently integrate these measurements into Python-based machine learning optimizations, the method was developed into a Python package, `PyEmittance`, at the SLAC National Accelerator Laboratory. We present the experimental tests of `PyEmittance` as performed at the Linac Coherent Light Source (LCLS) and the Facility for Advanced Accelerator Experimental Test (FACET-II).

INTRODUCTION

Emittance is a conserved property of a particle beam that characterizes its volume or area in the position-momentum phase space of the particles. A low emittance is desired for ensuring that the entire beam is transported with minimal losses, and is crucial the performance of X-ray free-electron lasers (FELs). The transverse beam emittance ϵ represents the area of the beam in the transverse planes defined by the positions and momenta, x and p_x in the horizontal plane, and y and p_y in the vertical plane. In the following, all references to the emittance indicate the transverse emittance.

The emittance is often measured using a single quadrupole scan with invasive wire or screen beam size measurements [1]. The quadrupole strength is varied over some range, and the consequent change in beam size is measured at a downstream wire (or screen). The range over which the scan is performed is typically selected by trial and error, and requires adjustment when upstream beam line elements are changed. For applications requiring efficient and robust emittance measurements, such as automated tuning algorithms or machine learning (ML) based optimizations, this process is inefficient and limiting. Additionally, the current MATLAB-based emittance measurement software at SLAC National Accelerator Laboratory (SLAC) is difficult to integrate with modern ML software being run and deployed on the machine.

In this paper, we present `PyEmittance`, a new Python package that provides general beam emittance measurements with adaptive quadrupole scans [2]. We show the benefit of the adaptive measurements method when robustness and automation are crucial, and present the test measurements performed at SLAC, at the Linac Coherent Light Source (LCLS) and the Facility for Advanced Accelerator Experimental Test (FACET-II).

IMPLEMENTATION

While `PyEmittance` can be used as an out-of-the-box emittance calculator given a data set of quadrupole strengths and corresponding beam sizes, the data acquisition and adaptive scanning available in the package are useful in cases where hand-tuning of the quadrupole scanning range is unavailable, or when efficient and robust measurements are needed. The package has optional functions that can be performed ahead of calculating the emittance for a flexible way of obtaining a robust emittance measurement. The general method to run a measurement follows the steps below:

1. Select initial scan of 3+ points within some predefined quadrupole range (can be random or specified by the user) and acquire transverse beam sizes for each initial scan point.

2. Given the data collected, calculate a new adapted scanning range to better capture the beam waist. Acquire new beam size measurements within the adapted range (the number of points measured is specified by the user).

3. Check the symmetry of the obtained curve, and if needed, acquire new beam sizes to evenly sample on each side of the minimum.

4. Remove any points beyond the turning point(s) of the curve to maintain a concave curve. If the number of points is now below the number specified, add points within the final range.

5. Finally, calculate the emittance and the match.

* Work supported by the U.S. Department of Energy, under DOE Contract No. DE-AC02-76SF00515 and the Office of Science, Office of Basic Energy Sciences.
† smiskov@slac.stanford.edu

ISBN: 978-3-95450-227-1 ISSN: 2673-5490 doi:10.18429/JACoW-IPAC2022-TUPOPT005

STATUS OF THE SUPERCONDUCTING SOFT X-RAY FREE-ELECTRON LASER USER FACILITY FLASH

M. Vogt*, Ch. Gerth, K. Honkavaara, M. Kuhlmann, J. Roensch-Schulenburg,
L. Schaper, S. Schreiber, R. Treusch, J. Zemella,
Deutsches Elektronen-Synchrotron DESY, Germany†

Abstract

The XUV and soft X-ray free-electron laser FLASH at DESY is capable of operating two undulator beamlines simultaneously with up to several thousand bunches per second. It is driven by a normal conducting RF photo-cathode gun and a superconducting L-band linac. FLASH is currently undergoing a substantial refurbishment and upgrade program (FLASH2020+). The first 9-months installation shutdown started in November 2021. Here we report on the operation in 2021 and present main upgrades during the ongoing shutdown.

THE FLASH FACILITY

The superconducting XUV and soft X-ray FEL (free-electron laser) facility FLASH at DESY [1–5] can provide up to 500 bunches per train at 10 trains per second. Each train is typically divided into two sub-trains for the two beamlines with a variable transition time to cover the rise time of the extraction kickers and the adaption between the RF flat tops for the sub-trains. The bunches are generated in a normal conducting 1.3 GHz RF-photo-cathode gun using a Cs_2Te cathode and 3 independent injector lasers [6, 7] capable of producing bursts of UV pulses with up to 1 MHz[1]. Laser 1 and 2 generate equally spaced pulses with a duration of 4.5 ps and 6.5 ps (rms) respectively, while laser 3 can generate arbitrary pulse patters within a 1 MHz raster and rms pulse durations from 0.8 ps to 1.6 ps. Each laser has an independent attenuation system. Laser 1 and 2 share a common BSA (beam shaping aperture) optimized to produce beam spots on the cathode suited for medium to high bunch charges, while laser 3 has an independent BSA adapted (reduced bore diameters) in particular to low charges. Therefore the bunch charges and temporal patterns for the two beamlines can be chosen rather independently, while keeping the space charge effects in the injector to a large extent comparable.

FLASH uses seven TESLA-type superconducting 1.3 GHz RF-modules with 8 cavities with 9 cells each for beam acceleration. Bunch compression is realized in two stages: A first RF-module plus a 3rd harmonic linearizer followed by the first C-type dipole chicane operated at 146 MeV; and two more superconducting RF-modules followed by the 2nd S-type dipole chicane operated at 450 MeV. The following 4 RF-modules constitute the main linac and allow acceleration up to 1250 MeV and under certain conditions deceleration down to 380 MeV. All RF stations are equipped with versatile LLRF (low level RF) controllers suited for long pulse operation and capable of generating distinct RF flat tops for the two sub-trains allocated for the two undulator beamlines. The flexible laser- and LLRF systems generate a great amount of freedom to meet the different needs of independent experiments at the two undulator beamlines.

Table 1: FLASH 2021 Operational Parameters

Parameter (e^-,γ)		**FLASH1**	**FLASH2**
beam energy	GeV	0.38 – 1.25	
bunch charge	pC	20 – 1000	
$\varepsilon^{1\sigma}_{\perp,n}$ (inj)	µm	0.5 – 1.0	
bunches/sec.		1 – 5000	
undul. gap		fixed	variable
undul. period	mm	27.3	31.4
photon pulse energy	µJ	1 – 500	1 – 1000
photon wavelength	nm	4.2 – 51	4 – 90
spectr. width (FWHM)	%	0.7 – 2	0.5 – 2
pulse duration (FWHM)	fs	< 30 – 200	
photons/pulse		10^{11} – 10^{14}	
average brilliance	(∗)	10^{17} – 10^{21}	
peak brilliance	(∗)	10^{28} – 10^{34}	

(∗): s^{-1} $mrad^{-1}$ mm^{-1} /0.1%bw

The sub-trains for the two beamlines are separated with a kicker/septum scheme consisting of 3 vertical flat top kickers and a horizontal Lambertson (DC) septum. The extraction beamline into FLASH2 contains a DC dipole to potentially send beam into a 3rd beamline (FLASH3) that houses the FLASHForward plasma wakefield acceleration experiment [8, 9]. For the time being FLASH2 and FLASH3 can only be operated exclusively. FLASH1 has six 4.55 m long fixed gap undulators while FLASH2 has twelve 2.39 m long variable gap undulators. Both undulator beamlines are dedicated SASE (self-amplified spontaneous emission) FELs. FLASH1 also houses a seeding experiment Xseed [10] in preparation of the seeding beamline to be built for the FLASH2020+ upgrade project [11–13]. In addition FLASH1 contains a THz undulator that uses the spent e^-–beam from the FEL to generate THz radiation for pump-probe experiments. Both beamlines contain transverse deflecting RF structures for longitudinal diagnostics: An S-band structure (LOLA) [14] located *upstream* of the main-undulators (downstream of Xseed) in FLASH1; and two variable polarization X-band structures (PolariX) [15–17]

* vogtm@mail.desy.de
† for the FLASH team
[1] up to 3 MHz is possible in 5 Hz operation. And the 3 inj. lasers could be interleaved and sent to one beamline

ISBN: 978-3-95450-227-1 ISSN: 2673-5490 doi:10.18429/JACoW-IPAC2022-TUPOPT006

THE NEW FLASH1 BEAMLINE FOR THE FLASH2020+ PROJECT

Mathias Vogt*, Johann Zemella,
Deutsches Elektronen-Synchrotron DESY, Germany

Abstract

The 2nd stage of the FLASH2020+ project will be an upgrade of the FLASH1 beamline, downstream of the injector/linac section FLASH0 which is currently being upgraded. The currently existing beamline drives the original planar fixed gap SASE undulators from the TTF-2 setup, a THz undulator that uses the spent electron beam and deflects the e-beam into a dump beamline capable of safely dumping several thousand bunches per second. The updated beamline has been designed for EEHG seeding with 2 modulators, 3 chicanes, and a helical Apple-III undulator beamline as seeding radiator, followed by a transverse deflecting (S-band) structure for longitudinal diagnostics. The separation of the electron beam from the FEL beam will be moved upstream w.r.t. the old design to create more space for the photon diagnostics and will be achieved by a 5deg double-bend-almost-achromat. To allow enable high power THz radiation output from a moderately compressed seeding beam, a post compressor will be installed. The capability of dumping the the long bunch trains safely may and will not be compromised by the design. This article describes the beamline concept and some details on the part downstream of the radiator.

INTRODUCTION

FLASH the, Free-electron LASer in Hamburg [1, 2], is currently undergoing a substantial upgrade and refurbishment project, FLASH2020+ [3, 4]. Flash consists of four functionally distinct sections: the common part (injector, linac), called FLASH0, the two independent undulator beamlines FLASH1 & FLASH2, and the experimental beamline FLASH3. The superconducting linac supplies sufficiently long RF pulses (flat top for beam operation up to 800 µs), to serve both, FLASH1 and FLASH2, with sub-trains of up to several hundred bunches at every RF-pulse. The pulse repetition frequency is 10 Hz.

While FLASH0 upgraded and refurbished in the current shutdown [2], FLASH1 will be basically completely rebuilt in 2024/25.

Conceptual Overview of the Beamline

So far FLASH1/2 are plain SASE (Self-Amplified Spontaneous Emission) FELs (Free-Electron Lasers). The new FLASH1 beamline, however will be optimized for high repetition rate HGHG (High Gain Harmonic Generation) and EEHG (Echo-Enabled Harmonic Generation) external seeding [3] within the project. SASE is an extremely powerful FEL mechanism, but external seeding enhances the control over properties of the produced FEL radiation, i.p. the longitudinal coherence, substantially [3]. Seeding, i.p. EEHG, is a delicate two-stage process: The bunch, with incoming PSD (phase space distribution) Ψ_0 and reference energy E_0, is overlaid in the first undulator (modulator UM1) with the first seed laser beam (L1). Overlaid means transverse overlap for a finite distance (undulator length) ($\rightarrow x, x', y, y'$), temporal overlap, and that the energy of the seeded slice is in resonance with the laser beam L1 in undulator UM1. Then the energy modulation from L1 and UM1 is strongly oversheared in the first magnetic chicane (**CH1**), and the bunch is overlaid in the second undulator (modulator UM2) with the second seed laser beam (L2). The conditions on overlay are just the same as in UM1. In addition the distance between the two modulation stages (M1,M2) should be as short as possible, so that the delicate over-sheared PSD from M1 is not distorted by spurious dispersion, intra-beam scattering, etc. Finally the modulated, over-sheared, and re-modulated PSD is moderately sheared in the second magnetic chicane (**CH2**) to enhance the higher order Fourier harmonics of the charge density that will seed the FEL process in the radiator. In order to make the above, highly intricate procedure operationally feasible, the beamline needs a sophisticated design and advanced high-quality hardware.

In addition FLASH1 has a long wavelength electromagnetic undulator which uses the spent e^--beam for the generation of THz radiation for highly synchronized pump-probe experiments. However, high THz pulse energy requires that a significant fraction of the bunch is concentrated in a structure smaller than the wavelength of the radiation. This is typically achieved by a spike-like longitudinal structure. The moderately compressed and highly linear seeding bunch does not such features. Hence a post-compressor chicane was designed to located downstream between FEL radiator and THz undulator. Finally the beam is vertically bent into the dump beamline capable of safely disposing of 100 kW beam power.

Here we give an overview of the FLASH1 beamline with emphasis on the "non-photon" sections, namely the collimation and matching section, the chicanes, the longitudinal diagnostics and the THz and dump beamline. The "photon-related" sections of the beamline, namely the modulators and the radiator will be described in greater detail in [5].

BEAMLINE DETAILS

The beamline is split into several functional sections as is shown in FIg. 1

The 1st collimator is located downstream of the last accelerating module. FLASH1 has a 2nd collimator close to the start of the in-coupling chicane (**InC**) in FL1MOD1. The optics has been optimized so that almost all transverse

* vogtm@mail.desy.de

ISBN: 978-3-95450-227-1 ISSN: 2673-5490 doi:10.18429/JACoW-IPAC2022-TUPOPT008

AN OVERVIEW OF THE T20 BEAMLINE FOR THE LUXE EXPERIMENT AT THE EUROPEAN XFEL

S. D. Walker*, N. Golubeva
Deutsches Elektronen-Synchrotron (DESY), Hamburg, Germany

Abstract

The Laser Und XFEL Experiment (LUXE) at the EuXFEL aims to explore hitherto unprobed regions of quantum electrodynamics characterised by both high-energy and high-intensity. This will be accomplished by leveraging the electron beam provided by the EuXFEL and an intensely-focused laser to study electron-photon and photon-photon interactions. The LUXE experiment will be placed in the empty XTD20 tunnel and to this end a new beamline, T20, will need to be installed to deliver one bunch per bunch train to LUXE. The T20 beamline feature a total bend angle of 6.7°, which, combined with the very short bunches provided by the EuXFEL raises concerns regarding the deleterious impact of coherent synchrotron radiation (CSR) on the bunch emittances. As the LUXE experiment has specific beam size requirements at its IP, these effects and the limits on the focus must be characterised. In this paper the T20 beamline design and its final focus are outlined. Furthermore, the impact of collective effects on the beam quality at the LUXE IP are discussed, and finally a means to mitigate the impact of these effects and improve the beam quality at the LUXE IP is shown.

INTRODUCTION

The European X-Ray Free Electron Laser (EuXFEL) [1] in Hamburg, Germany, is a 3.1 km-long multi-user facility capable of providing hard and soft x-rays to various experiments and has been operating successfully since 2018. To maximise the number of operable experiments using the electron beam, the main accelerating linac branches into two beamlines at the 2 km mark, to a hard x-ray undulator to the left (SASE2), and to hard and soft x-ray undulators straight ahead from the main linac (SASE1 and SASE3, respectively). Further installations of undulators are planned in the future, firstly hard x-ray undulators in the left branch after SASE2 [2], and then construction of an entire new branch to the right in 2029 (requiring a new tunnel to be drilled). However, as a small section ($\approx$ 50 m) of this new tunnel has already been dug, there is a period of opportunity before 2029 where this tunnel section (called XTD20) may house an experiment which uses the high-quality electron beam provided by the EuXFEL for novel particle physics searches. This is how the LUXE experiment [3] fits into the broader EuXFEL programme.

The LUXE experiment will operate parasitically off the main XFEL linac in the XTD20 tunnel, taking one electron bunch per bunch train (out of 2700 bunches per train) and collide it with an intensely-focused laser. As the future installation of undulators in a whole new branch from the linac has long been planned, the beamline arc, called T20, which transfers the beamline to the XTD20 tunnel has already undergone considerable development during the main EuXFEL design process [4–6].

The extreme bunch conditions at the EuXFEL present challenges at LUXE. Specifically, the electron bunches at the end of the linac will generally be very short ($\sigma_z \approx 5\,\mu$m) due to requirements in the downstream undulators. At these short bunch lengths and high energies (14 GeV to 17.5 GeV) the bunch will radiate partially coherently in all typical EuXFEL bending magnets likely to be used in any T20 arc design [7]. Furthermore, the overtaking criterion, shown in Eqn. 1, is satisfied in these same magnets at these bunch lengths, meaning that steady state CSR fields will dominate and that the projected and slice emittances are liable to be diluted due to these self-fields.

$$L_s = \frac{R\varphi^3}{24} > \sigma_z \tag{1}$$

In this paper, recent developments in the T20 beamline design and its use for LUXE are presented and discussed. Specifically, this involves integrating the arc into the current switchyard design and the design of the final focus system, as well as beam dynamics simulations featuring full collective effects, with particular focus on the impact of CSR on the focus spot size. Finally, an alternative compression scheme in the main linac is discussed as a means to achieve the required focus at the LUXE IP.

T20 BEAMLINE AND FINAL FOCUS SYSTEM FOR LUXE

The Switchyard

The switchyard featuring both T20 and LUXE and its relation to the other beamlines is shown in Fig. 1. The extraction system will employ a Lambertson septum-kicker pair to extract the beam from the main linac. Although only one bunch per train will be used by the LUXE experiment, the rise time of the extraction kicker, at 2 µs, mandates that an additional ten bunches must be dumped upstream of the switchyard.

The Final Focus

The final focus system for LUXE will use four quadrupoles making up the inner triplet and two quadrupoles for the matching section. The vertical and horizontal dispersions are brought to zero at the end of the arc and before the matching section. Two possible focuses are considered assuming

* stuart.walker@desy.de

ISBN: 978-3-95450-227-1 ISSN: 2673-5490 doi:10.18429/JACoW-IPAC2022-TUPOPT010

VIRTUAL COMMISSIONING OF THE EUROPEAN XFEL FOR ADVANCED USER EXPERIMENTS AT PHOTON ENERGIES BEYOND 25 keV USING LOW-EMITTANCE ELECTRON BEAMS

Y. Chen*, F. Brinker, W. Decking, M. Scholz, L. Winkelmann, Z.-H. Zhu†
Deutsches Elektronen-Synchrotron DESY, Notkestr. 85, 22607 Hamburg, Germany

Abstract

Growing interests in ultra-hard X-rays are pushing forward the frontier of commissioning the European X-ray Free-Electron Laser (XFEL) for routine operation towards the sub-ångström regime, where a photon energy of 25 keV (0.5 Å) and above is desired. Such X-rays allow for larger penetration depths and enable the investigation of materials in highly absorbing environments. Delivering the requested X-rays to user experiments is of crucial importance for the XFEL development. Unique capabilities of the European XFEL are formed by combining a high energy linac and the long variable-gap undulator systems for generating intense X-rays at 25 keV and pushing the limit even further to 30 keV. However, the FEL performance relies on achievable electron bunch qualities. Low-emittance electron bunch production, and the associated start-to-end modelling of beam physics thus becomes a prerequisite to dig into the XFEL potentials. Here, we present the obtained simulation results from a virtual commissioning of the XFEL for the user experiments at 25 keV and beyond, including the optimized electron bunch qualities and corresponding FEL lasing performance. Experimental results at 30 keV from the first test run are presented.

INTRODUCTION

Linear accelerator based self-amplification spontaneous emission (SASE) free-electron lasers (FEL) produce extremely short, brilliant and coherent X-ray pulses [1–7]. This made it possible using the X-rays to probe distances at the atomic scale and explore the dynamics of atomic and molecular process on their natural length and time scale. The XFEL has greatly set forward the frontiers of resolving the structure of matters with X-rays over the last decade.

The XFELs capable of operating at short wavelengths of 0.10 nm to 0.01 nm, that is, at high photon energies of about 12.40 keV to 123.98 keV, can provide the so-called hard X-rays in the sub-ångström regime. These hard X-rays are of significant importance to temporally and spatially-resolved analysis and reconstruction of materials with various degrees of crystallinity. Harder X-rays above 12.40 keV are more beneficial to characterizing semi and noncrystalline materials, observing structural in-situ phase transitions, acquiring structural information, reconstructing material spatial distributions, etc.

At the European X-ray Free-Electron Laser (EuXFEL) [2], hard X-ray pulses have been delivered for routine user experiments since 2017. At a nominal electron beam energy of 14 GeV, stable, high-intensity SASE performance is achieved at photon energies up to 14 keV in routine user runs [8–10], while in test runs, good lasing signals towards 25 keV have been achieved with only limited tuning time. The actual lasing capability of the European XFEL in an even deeper sub-ångström emission regime is not yet demonstrated, although relevant theoretical studies have been carried out in [11, 12] under specific working modes and conditions.

SIMULATION

Here we present the obtained results from a virtual commissioning of the EuXFEL by start-to-end beam physics simulations and SASE optimization at high photon energies of 25 keV and above. Table 1 shows typical machine operation parameters which are employed correspondingly in the follow-up numerical studies. The codes OCELOT [13] and GENESIS [14] are used. The EuXFEL photoinjector [15] is optimized in the simulations taking into account the collective effects as studied in detail in [16]. The close-to cathode beam dynamics is carefully considered using the 3D approach as reported in [17].

Table 1: Machine Operation Parameters

Parameter	Value	Unit
Bunch charge	250	pC
Bunch shaping aperture [a]	1.0	mm
Cathode laser pulse shape	Gauss	n/a
Cathode laser pulse length[b]	3.0	ps
Cathode accelerating gradient	56.7	MV/m
Beam energy at BC0[c]	130	MeV
Beam energy at BC1	700	MeV
Beam energy at BC2	2400	MeV
Beam energy downstream L3[d]	16300	MeV
R56 at BC0	-50	mm
R56 at BC1	-50	mm
R56 at BC2	-30	mm
Undulator period[e]	4	cm
Undulator length	175	m

[a] in diameter
[b] root mean square value
[c] BCi stands for the i-th bunch compression stage, see Fig.1.
[d] L3 stands for the main linac, see Fig.1.
[e] for the undulators in SASE1 and SASE2 beamlines, see Fig. 1.

Figure 2 shows the slice emittance of an optimized electron bunch at the injector exit (i.e. in section I1 as shown in Fig. 1). This is done by scanning the phase of the gun

* ye.lining.chen@desy.de
† on leave from SINAP, Shanghai, China

ISBN: 978-3-95450-227-1 ISSN: 2673-5490 doi:10.18429/JACoW-IPAC2022-TUPOPT011

START TO END SIMULATION STUDY FOR OSCILLATOR-AMPLIFIER FREE-ELECTRON LASER

H. Sun, Z. Zhu, C. Feng*, B. Liu †
Shanghai Institute of Applied Physics, Chinese Academy of Sciences, Shanghai 201800, China
University of Chinese Academy of Sciences, Beijing 100049, China
Shanghai Advanced Research Institute, Chinese Academy of Science, Shanghai, 201210, China

Abstract

External seeding techniques like high-gain harmonic generation (HGHG) and echo-enabled harmonic generation (EEHG) have been proposed and proven to be able to generate fully coherent radiation in the EUV and X-ray range. A big challenge is to combine the advantages of seeding schemes with high repetition rates. For seeding at a high repetition rate, an optical resonator scheme has been introduced to recirculate the radiation in the modulator to seed the high repetition rate electron bunches. Earlier studies have shown that a resonator-like modulator combined with an amplifier in high gain harmonic generation (HGHG) configuration can be used to generate radiation whose wavelength can reach the water window region. This scheme overcomes the limitation of requiring high repetition rate seed laser systems. In this contribution, we present start-to-end simulation results of this oscillator-amplifier FEL scheme.

INTRODUCTION

For over ten years, SASE FELs [1] have been delivering radiation to users in XUV and X-ray wavelength range. However, SASE suffers from poor longitudinal coherence and large shot-to-shot fluctuations due to the stochastic behavior of the start-up process. To overcome these limitations, several external seeding techniques like high-gain harmonic generation (HGHG) [2] and echo-enabled harmonic generation (EEHG) [3, 4] have been proposed and proven to be able to generate fully coherent radiation in the EUV and X-ray range. The continuous wave (CW) machines with superconducting accelerator technology can deliver a million pulses per second. However, the repetition rate of current laser systems with sufficient power to modulate the electron beam is limited to the kilohertz range.

For seeding at a high repetition rate, an optical resonator scheme has been introduced to recirculate the radiation in the modulator to seed the high repetition rate electron bunches. Earlier studies have shown that a resonator-like modulator combined with an amplifier in an HGHG configuration can be used to generate radiation whose wavelength can reach the water window region [5, 6]. This scheme overcomes the limitation of requiring high repetition rate seed laser systems. The usage of the oscillator-amplifier setup for a seeded FEL is a promising approach to reach short wavelengths at the high repetition rates based on superconducting linear accelerators. In this contribution, start-to-end simulation with a more realistic electron beam is conducted for this scheme.

THE LAYOUT

High-Gain Harmonic Generation has been proposed and proven to be able to generate fully coherent radiation in a single pass. In this process, the electron beam achieves an energy modulation in a modulator. The energy modulation is converted into a density modulation in a dispersive section. Finally, the electron beam which has sufficient bunching in the desired harmonic of the seed laser will generate fully coherent FEL radiation in the amplifier.

The layout of oscillator-based HGHG is shown in Fig. 1. Different from a regular single-pass HGHG, this scheme has an optical cavity which consists of simple transportation mirrors and focusing mirrors. In addition, the intra-cavity modulator is longer to achieve higher gain and compensate the losses in the cavity. The power of the radiation is amplified by its interaction with the electron bunch in the intra-cavity modulator, and the optical field is stored in the cavity to seed the next electron bunch. The modulated electron beam is guided to the following dispersion section to achieve sufficient bunching in the desired harmonic of the seed laser. Finally, it generates radiation at a harmonic of the modulator wavelength in the amplifier.

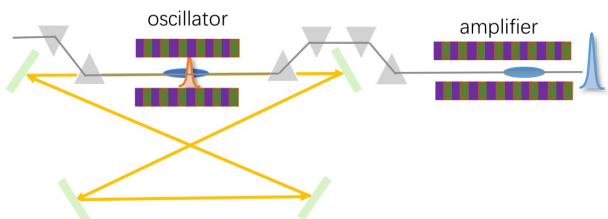

Figure 1: A possible design for the implementation of an HGHG seeded Oscillator-Amplifier.

SIMULATIONS

Start-to-end simulation is carried out for this oscillator-amplifier scheme. ASTRA is used to track the particles from the gun to the end of the injector, which considers longitudinal space charge and microbunching instability effects. ELEGANT is utilized to track the particles in the linac and bunch compressors, which considers the coherent

* fengchao@zjlab.org.cn
† liubo@zjlab.org.cn

ISBN: 978-3-95450-227-1 ISSN: 2673-5490 doi:10.18429/JACoW-IPAC2022-TUPOPT013

TWIN DELAYED DEEP DETERMINISTIC POLICY GRADIENT FOR FREE-ELECTRON LASER ONLINE OPTIMIZATION

M. Cai[1,2], Z. H. Zhu[1,2], K. Q. Zhang [3*], C. Feng[1,2,3†], L. J. Tu[1,2], D. Gu [3], Z. T. Zhao[1,2,3]
[1]Shanghai Institute of Applied Physics, Chinese Academy of Sciences, Shanghai, China
[2]University of Chinese Academy of Sciences, Beijing, China
[3]Shanghai Advanced Research Institute, Chinese Academy of Sciences, Shanghai, China

Abstract

X-ray free-electron lasers (FEL) have contributed to many frontier applications of nanoscale science which benefit from its extraordinary properties. During FEL commissioning, the beam status optimization especially orbits correction is particularly significant for FEL amplification. For example, the deviation between beam orbit and the magnetic center of undulator can affect the interaction between the electron beam and the FEL pulse. Usually, FEL commissioning requires a lot of efforts for multi-dimensional parameters optimization in a time-varying system. Therefore, advanced algorithms are needed to facilitate the commissioning procedure. In this paper, we propose an online method to optimize the FEL power and transverse coherence by using a twin delayed deep deterministic policy gradient (TD3) algorithm. The algorithm exhibits more stable learning convergence and improves learning performance because the overestimation bias of policy gradient methods is suppressed.

INTRODUCTION

X-ray free-electron lasers (FEL) open new chapters to various frontiers of scientific applications in biology, chemistry, and material science for its abilities to generate femtosecond and nanoscale pulses with gigawatt peak power and tunable wavelength down to less than 0.1 nm [1–3]. In recent years, several FEL facilities worldwide are constructed and operated successfully, which indicates a new era of X-ray science. To ensure the stable operation of FEL facilities, a robust and collimated beam orbit is generally required to achieve precise overlaps between the electron beam and radiation. The deviation between the beam orbit and the center of magnetic elements can induce a significant decrease in the peak power and transverse coherence of FEL radiation [4].

For a traditional FEL commissioning, beam orbit alignment can be roughly achieved by adjusting the current of correctors. However, the precise beam orbit alignment is usually difficult to be implemented and the beam orbit can change with the variation of beam status. Moreover, the effect of beam orbit alignment will also rely on the beam orbit stability. Therefore, manual beam orbit alignment and optimization require a lot of efforts in the accelerators which is a time-varying dynamics system of multi-dimensional parameters [5, 6]. In recent years, deep reinforcement learning (DRL) methods have been adopted in the commissioning and optimization of FEL facilities since they can work at different operating points and do not require labeled datasets compared to supervised learning methods [7, 8].

This work proposes an online optimization method in FEL based on a model-free off-policy actor-critic algorithm tailored to Markov decision processes. The modified DRL method can achieve good convergence and reduce overestimation by improving policy gradient approaches. Due to practical restrictions such as radiation safety and the potential for damage to the hardware of facility from erroneous online state, optimization with previous FEL simulation is usually the preferred solution. In this paper, we assess the algorithm in a simulated FEL environment firstly, and the simulation results of two methods are compared.

TWIN DELAYED DEEP DETERMINISTIC POLICY GRADIENT

As a subfield of machine learning, reinforcement learning (RL) has advantages in solving control tasks that conform to Markov decision processes [9]. In tasks with sufficient nonlinearity, complexity and time-varying systems like the FEL tuning process, RL is a more appropriate consideration than traditional control methods.

Reinforcement learning aims to find the optimal policy π_φ, with parameters φ, by maximizing the discounted sum of rewards $R_t = \sum_{i=t}^{T} \gamma^{i-t} r(s_i, a_i)$, where γ is a discount factor. The action-value function describes the expected return after taking an action in state s_t following policy π:

$$Q^\pi(s_t, a_t) = E_{s_i \sim E, a_i \sim \pi}[R_t | s_t, a_t]$$

The function can be estimated recursively through Bellman equation:

$$Q^{\pi_\varphi}(s_t, a_t) = E_{s_{t+1} \sim E}[r(s_t, a_t) + \gamma Q^{\pi_\varphi}(s_{t+1}, \pi_\varphi(s_{t+1}))]$$

A neural network function approximator parameterized by θ^Q can be trained by minimizing the loss:

$$L(\theta^Q) = E_{s_t \sim E, a_t \sim \pi_{\varphi_i}}[(Q(s_t, a_t | \theta^Q) - y_t)^2]$$

where $y_t = r(s_t, a_t) + \gamma Q(s_{t+1}, \pi_\varphi(s_{t+1}) | \theta^Q)$.

Deep Deterministic Policy Gradient (DDPG) is a model-free Q-Learning method in continuous action space [10] by combining Deep Q-network [11] and Deterministic Policy Gradient [12]. However, the performance of the Q-learning algorithm is known to be influenced by the systematic overestimation of values because of the output prediction noise [13].

* zhangkaiqing@zjlab.org.cn
† fengchao@zjlab.org.cn

ISBN: 978-3-95450-227-1 ISSN: 2673-5490 doi:10.18429/JACoW-IPAC2022-TUPOPT014

THE STATUS OF THE SASE3 VARIABLE POLARIZATION PROJECT AT THE EUROPEAN XFEL

S. Karabekyan†, S. Abeghyan, M. Bagha-Shanjani, S. Casalbuoni, W. Freund, U. Englisch, G. Geloni, J. Grünert, S. Hauf, C. Holz, D. La Civita, J. Laksman, D. Mamchyk, M. Planas, F. Preisskorn, S. Serkez, H. Sinn, M. Wuenschel, M. Yakopov, C. Youngman
European XFEL GmbH, Schenefeld, Germany
P. Altmann, A. Block, W. Decking, L. Froehlich, O. Hensler, T. Ladwig, D. Lenz, D. Lipka, R. Mattusch, N. Mildner, E. Negodin, J. Prenting, F. Saretzki, M. Schloesser, F. Schmidt-Foehre, E. A. Schneidmiller, M. Scholz, D. Thoden, T. Wamsat, T. Wilksen, T. Wohlenberg, M. V. Yurkov
DESY, Hamburg, Germany
J. Bahrdt, Helmholtz-Zentrum Berlin für Materialien und Energie, Berlin, Germany
Y. Li, Institute of High Energy Physics, CAS, Beijing, P. R. China
Dong-Eon, Kim, Pohang Accelerator Laboratory, Pohang, Korea
M. Bruegger, M. Calvi, S. Danner, R. Ganter, L. Huber, A. Keller, C. Kittel, X. Liang, S. Reiche, M. Schmidt, T. Schmidt, K. Zhang, Paul Scherrer Institute, Villigen, Switzerland

Abstract

The undulator systems at the European XFEL consist of two hard X-ray systems, SASE1 and SASE2, and one soft X-ray system, SASE3. All three systems are equipped with planar undulators using permanent neodymium magnets. These systems allow the generation of linearly polarized radiation in the horizontal plane [1]. In order to generate variable polarization radiation in the soft X-ray range, an afterburner is currently being implemented behind the SASE3 planar undulator system. It consists of four APPLE-X [2, 3] helical undulators UE90. The project, called SASE 3 Variable Polarization, is close to being put into operation. All four helical undulators have been installed in the tunnel during the 2021-2022 winter shutdown. This paper describes the status of the project and the steps toward its commissioning. It also presents lessons learned during the implementation of the project.

CHARACTERISTICS OF THE HELICAL AFTERBURNER

The basic principle of the project is the possibility of using planar undulators to generate a micro-bunched electron beam. This beam is then directed to a system of helical undulators, which generate a laser emission of the desired polarization. Based on this, the technical characteristics of the helical undulators were calculated so that the energy spectrum of photons generated by the helical undulators overlapped the energy spectrum generated by the planar undulators. Simulation spectra of the photons generated by the helical undulator and comparison with the spectrum generated by the planar undulators for different energies of the electron beam are presented in detail in [4]. After the magnetic measurements, the boundary values of the K parameters of the undulators were determined. These values for different types of polarization are presented in Table 1. It also shows the photon energy ranges generated by the UE-90 undulator by varying only the gap for linear horizontal (LH), linear vertical (LV), circular clockwise (C+), circular anticlockwise (C-), and 45° linear polarization modes. It should be mentioned that the maximum photon energy for the SASE3 beamline transport system is 3 keV.

Table 1: K Values and Generated Photon Energies

Polarization mode	LH/LV/C+/C-	Linear 45°/135°
K-Range	9.40 − 3.37	6.62 − 2.36
Photon Energy Range [keV]		
@8.5 GeV	0.169 − 1.141	0.332 − 2.012
@11.5 GeV	0.309 − 2.088	0.608 − 3.684
@14 GeV	0.457 − 3.095	0.902 − 5.459
@16.5 GeV	0.635 − 4.299	1.252 − 7.583
@17.5 GeV	0.715 − 4.835	1.409 − 8.530

Magnetic Measurements

Magnetic measurements of the undulator were performed using a Self-Aligned Field Analyzer with Laser Instrumentation (SAFALI) system designed and provided by Paul Scherrer Institute (PSI). The magnetic field was measured using a Senis 3-Axis Hall Probe I3C-03D. Two robots mounted on either side of the undulator were used to shim the magnets. These robots allowed shimming the magnets of both upper and lower magnetic structures. More details about the program and the results of magnetic measurements for UE90 undulators presented in [5].

FINDINGS AND CORRECTIONS

Initial measurements and calibration of the undulator were performed for the LH polarization mode. A strong, unexpected change in the magnetic field integrals was observed during the measurements in LV1 mode.

†suren.karabekyan@xfel.eu

ISBN: 978-3-95450-227-1 ISSN: 2673-5490 doi:10.18429/JACoW-IPAC2022-TUPOPT016

STATUS OF THE THz@PITZ PROJECT – THE PROOF-OF-PRINCIPLE EXPERIMENT ON A THz SASE FEL AT THE PITZ FACILITY*

T. Weilbach, P. Boonpornprasert, G. Georgiev, G. Koss, M. Krasilnikov, X. Li,
A. Lueangaramwong, F. Mueller, A. Oppelt, S. Philipp, F. Stephan, DESY, Zeuthen, Germany

Abstract

In order to allow THz pump–X-ray probe experiments at full bunch repetition rate for users at the European XFEL, the Photo Injector Test Facility at DESY in Zeuthen (PITZ) is building a prototype of an accelerator-based THz source. The goal is to generate THz SASE FEL radiation with a mJ energy level per bunch using an LCLS-I undulator driven by the electron beam from PITZ. Therefore, the existing PITZ beam line is extended into a tunnel annex downstream of the existing accelerator tunnel.

The final design of the beam line extension consists of a bunch compressor, a collimation system and a beam dump in the PITZ tunnel. In the tunnel annex one LCLS-I undulator is installed for the production of the THz radiation with a quadrupole triplet in front of it for matching the beam parameters for the FEL process. Behind the undulator two screen stations couple out the THz radiation, for measurements like bunch compression, pulse energy or spatial and transverse distribution. A dipole separates the electron from the THz beam and a quadrupole doublet transports the electron beam to the beam dump. The installation progress will be presented.

INTRODUCTION

The European XFEL plans to expand the wavelength range for pump-probe experiments into the THz-regime for probing the samples. Therefore different options for the THz generation were studied [1, 2]. For the accelerator based source the installations for a proof-of-principle experiment at the Photo Injector Test Facility at DESY in Zeuthen (PITZ) are nearly finished. Here the THz radiation is produced using a Self-Amplified Spontaneous Emission (SASE) FEL in an LCLS-I undulator [3], driven by the electron bunches from the PITZ accelerator. Start-to-End simulations for this setup, i.e. beam energies of 16 to 22 MeV/c and a peak current of 200 A (i.e. 4 nC bunch charge), yielded a THz pulse energy of about 0.5 mJ at a wavelength of 100 µm [4, 5].

A schematic overview of the current PITZ beam line as well as the extension (red dashed box) currently under installation, is shown in the top part of Fig. 1. The electrons are generated in the gun, accelerated up to ≈ 7 MeV/c, before further acceleration by the booster to the final energy of ≈ 22 MeV/c takes place. The different diagnostic devices, e.g. HEDA1, EMSY and TDS, allow for a measurement of the six dimensional phase space of the electron beam and therefore to characterize the photo-injector performance.

* This work was supported by the European XFEL research and development program.

BEAM LINE DESIGN

For the THz@PITZ project the PITZ beam line had to be modified and also had to be extended into a second tunnel. A bunch compression chicane was added to the beam line in tunnel 1 allowing the generation of THz radiation with lower bunch charges than the planed 4 nC by maintaining the peak current of the electron beam through longitudinal compression [6]. In addition to that, it enables the investigation of seeding methods for the THz generation [7]. Two quadrupole triplets, one in each tunnel, were added for the matching of the electron beam into the undulator. Additionally, a collimator system reduces the number of halo particles and dark current before the beam enters tunnel 2. This should reduce the beam loss in the undulator significantly.

The beam line in tunnel 2, where the undulator is installed, starts with a dipole magnet, which is used as a switchyard to serve a second beam line in the future [8]. In addition to the matching quadrupole triplet, two additional quadrupole magnets and a dipole for the deflection of the beam to the high power beam dump are installed. The beam dump in the straight section will only be used to set up the beam or for moderate to average power operation. In total, five new BPMs were installed to measure beam position and charge. These are located in the chicane, in front of the wall as well as in front and behind the undulator. The last one is located in front of the new beam dump in tunnel 1 to ensure beam transportation to the dump.

In total three screen stations for THz diagnostics, one in front of and two behind the undulator, are installed. The first one is used for bunch compression measurements when the bunch compression chicane is used. In addition it can be used for coupling in seeding radiation for future seeding experiments and it will be used to calibrate the positions of the THz mirrors behind the undulator. The two screen stations behind the undulator are equipped with mirrors to deflect the THz radiation vertically to a view port where it is coupled out of the vacuum system and guided to the THz diagnostic table. The THz diagnostic setup is used to measure the total pulse energy, the polarization as well as the transverse and spectral distribution with a pyro detector, a Michelson interferometer set-up and a THz camera. + A detailed 3d-model of the design of the beam line extension is shown in Fig. 1 (bottom).

INSTALLATION PROGRESS

During the installation of the beam line in both tunnels, additional infrastructure work was carried out in parallel. This included power, pressured air and gas supply in both tunnels as well as cable pulling for the new beam line ele-

ISBN: 978-3-95450-227-1 ISSN: 2673-5490 doi:10.18429/JACoW-IPAC2022-TUPOPT017

START-TO-END SIMULATIONS FOR BUNCH COMPRESSOR AND THz SASE FEL AT PITZ*

A. Lueangaramwong†, X. Li, P. Boonpornprasert,
M. Krasilnikov, F. Stephan, DESY Zeuthen, Zeuthen, Germany

Abstract

The magnetic bunch compressor was designed as part of a THz accelerator source being developed at the Photo Injector Test facility at DESY in Zeuthen (PITZ) as a prototype for pump-probe experiments at the European XFEL. As an electron bunch is compressed to achieve higher bunch currents for the THz source, the beam dynamics in the bunch compressor was studied by numerical simulations. A start-to-end simulation optimizer including coherent synchrotron radiation (CSR) effects has been developed by combining the use of ASTRA, OCELOT, and GENESIS to support the design of the THz source prototype. In this paper, we present simulation results to explore the possibility of improving the performance of the THz FEL at PITZ by using the developed bunch compressor.

INTRODUCTION

An accelerator-based THz source prototype for pump-probe experiments at the European XFEL is in the final stage of installation at the Photo Injector Test Facility at DESY in Zeuthen (PITZ). The electron beam from the RF gun is further accelerated to a beam momentum of ~17 MeV/c by the CDS booster cavity. In order to achieve a THz Self-amplified spontaneous emission (SASE) free electron laser (FEL) with pulse energy in the mJ-range, highly space-charge-dominated electron beams such as 4 nC beams with a bunch current of about 160-200 A are set as a nominal setting [1–3] with a challenge in beam transport and matching to the undulator. Alternatively, relatively-lower-charge beams such as 1.5-2.5 nC beams with an average bunch current near 200 A are considered as an option when using a bunch compressor [4]. In this option, the lower-charge beams may also provide experimental benefits such as less challenges in beam transport and matching, etc.

The bunch compressor using a magnetic chicane has been foreseen and assigned as a part of the prototype for various applications such as the SASE FEL, seeded FEL, superradiant radiation, etc [4, 5]. The chicane consists of four rectangular dipole magnets with identical strength and length. Due to limited available space in the PITZ tunnel, this chicane has a vertical bending plane with an angle of 19 degrees in order to make a vertical clearance above the original PITZ beamline components. These dipole magnets are obsoleted from the HERA beamline [6]. While the magnetic field of the dipole magnet is yet to be measured, the effective length of each dipole of 0.327 m is estimated from the magnetic field simulation via the program CST Studio Suite [7]. Therefore, R_{56} of this chicane is 0.215 m.

We study the bunch compressor option at PITZ by simulating the beam dynamics and SASE FEL. A start-to-end simulation optimizer has been developed by combining the use of the programs ASTRA [8], OCELOT [9], and GENESIS 1.3 [10] to support our test experiments on the THz source prototype. Note that coherent synchrotron radiation (CSR) effects influencing the performance of the bunch compression was discussed in [4]. In this paper, we report simulation results such as optimized FEL pulse energy with booster phases as a beam-energy-chirp tuning knob, while discussing possible beam transports using available quadrupole magnets.

START-TO-END BEAM DYNAMIC SIMULATION

The start-to-end beam dynamic simulation [4] was previously developed with a combination of the programs ASTRA [8], OCELOT [9], and IMPACT-t [11]. ASTRA is firstly used to track the electron from the cathode to the booster, and then OCELOT and IMPACT-t are set up to investigate the bunch compression performance including CSR effects. While the CSR simulation with OCELOT is benchmarked with IMPACT-t, IMPACT-t is replaced by OCELOT for faster optimization in the investigation of beam transport and FEL performance. The FEL performance parameters such as saturation length and pulse energy are estimated by both the program GENESIS and a semi-analytical calculation of M. Xie's solutions in the framework of the one-dimensional model [12, 13] implemented to OCELOT evaluation functions. In this semi-analytical calculation, when the electron bunch is much longer than the FEL cooperation length (~400 μm), the electron bunch is sliced and the SASE power growth of each slice is estimated.

SIMULATION OF BEAM TRANSPORT AND MATCHING IN CHICANE

Since several quadrupole magnets prior to the chicane at PITZ are installed [14], it is possible to transport the beam with constraints. In this study, the first constraint is described by a following mathematical condition at the middle z-position of the chicane with the Courant–Snyder (CS) parameters,

$$\alpha_x = \alpha_y = 0. \quad (1)$$

This condition is applied to all cases in a scan of bunch charge and booster phase. Note that other constraints can also be

* Work supported by the European XFEL Gmbh
† anusorn.lueangaramwong@desy.de

ISBN: 978-3-95450-227-1 ISSN: 2673-5490 doi:10.18429/JACoW-IPAC2022-TUPOPT018

FERMI 2.0 UPGRADE STRATEGY

L. Giannessi, E. Allaria, L. Badano, F. Bencivenga, C. Callegari, F. Capotondi, D. Castronovo, P. Cinquegrana, M. Coreno, M. B. Danailov, A. Demidovich, G. De Ninno, P. Del Giusto, S. Di Mitri, B. Diviacco, W. M. Fawley, M. Ferianis, G. Gaio, F. Gelmetti, G. Kurdi, M. Lonza, M. Malvestuto, M. Manfredda, C. Masciovecchio, I. Nikolov, G. Penco, K. C. Prince, E. Principi, P. R. Rebernik, C. Scafuri, N. Shafqat, P. Sigalotti, A. Simoncig, S. Spampinati, C. Spezzani, L. Sturari, M. Trovò, M. Veronese, R. Visintini, M. Zangrando
Elettra-Sincrotrone Trieste S.C.p.A, Basovizza, Italy
T. Tanaka, RIKEN SPring-8 Center, Hyogo, Japan
G. Penn, Lawrence Berkeley National Laboratory, USA
G. Perosa, F. Sottocorona, Università degli Studi di Trieste, Trieste, Italy

Abstract

FERMI is undergoing a series of upgrades to keep the facility in a world-leading position. The ultimate goal of the development plan consists in extending the facility spectral range to cover the water window and above, and to reduce the minimum pulse duration below the characteristic lifetime of core hole electrons of light elements. We present here the main elements of this upgrade strategy.

INTRODUCTION

The upgrade involves deep modifications of the linac and of the two FERMI FELs with the ambition of extending the FEL performances and the control of the light produced to include the K-edges of N and O, the L_{23}-edges of elements of the third period, and early elements of the fourth period (Sc to Cr). One of the main requisites of this upgrade is the preservation of the uniqueness of FERMI: the possibility to control the properties of the radiation by seeding the FEL with an external laser system. Through the control of the microbunching formation in the electron beam the seed allows amplification of almost Fourier transform-limited pulses [1–3], to synchronize the FEL pulses with unprecedented precision to an external laser [4] and to control many pulse properties, such as phase and coherence [5,6]. The extended photon energy range will allow resonant experiments (XANES, XMCD, SAXS, CDI,…) exploiting several important edges (life-time in the range of few fs), larger wave-vector (non-linear optics), ultrafast chemistry (conical intersections, lifetime 0.5 – 10 fs) [7]. Presently, the spectral range up to 310 eV is covered by the two FELs: FEL-1 and FEL-2; the first provides photons in the range 20-65 eV, the second in the range 65-310 eV. In view of the upgrade, the photon energy distribution between the two FELs has to be adapted to the upgraded scenario, with FEL-1 still covering the low photon energy range, but extended to reach a photon energy of 100 eV (see C. Spezzani *et al.*, these proceedings), and FEL-2 dedicated to the high energy range, from 100 eV to about 550 eV.

FEL-2 UPGRADE

To extend the FEL-2 spectral range to the oxygen K-edge, two options were considered, either by using EEHG directly, or with a cascade employing both EEHG and HGHG techniques in the "fresh-bunch" injection technique now used on FEL-2. The implementation of the first solution, EEHG, requires a first large dispersion chicane of up to 15 mm for optimized EEHG operation. This makes the scheme prone to a number of effects which may result in a degradation of the FEL spectral purity and of the FEL gain in the final radiator [8, 9]. The large chicane is indeed an amplifier of microbunching instability (MBI). A second issue is the emission of incoherent synchrotron radiation (ISR) and the intra-beam scattering (IBS) along the chicane. These two effects are the source of mixing of the filamented phase space that produces the high harmonic bunching in EEHG after the second chicane, a factor reducing the bunching at the entrance of the amplifier.

All these effects would be mitigated in a scheme where the chicanes have a lower dispersion. This is the reason why we considered the second option, where the EEHG generates a seed that is then used in fresh-bunch to seed a second HGHG stage, similar to what is done in the present FEL-2 configuration. The present double-stage HGHG with fresh-bunch scheme can be upgraded by converting the first stage to an EEHG configuration aimed at reaching harmonics of the order of 30. The second stage would then up-convert the output of the first stage to harmonics of the order 120-130 as required.

This configuration needs a much lower dispersion, of the order of 4-5 mm, which is only a factor two larger than the one used in the FERMI EEHG experiment. We analysed the four different configurations of seeded FELs shown in Fig. 1 and selected the most promising one with the aim of extending the seed coherence to the highest harmonic orders.

The explicit dependence of the pulse peak power on the various parameters and for linear polarization is shown in the plots represented in Fig. 2. Table 1 lists the parameters used in the calculations.

ISBN: 978-3-95450-227-1 ISSN: 2673-5490 doi:10.18429/JACoW-IPAC2022-TUPOPT019

FERMI FEL-1 UPGRADE TO EEHG

C. Spezzani, E. Allaria, L. Badano, D. Castronovo, P. Cinquegrana, M. B. Danailov, R. De Monte, G. De Ninno, P. Delgiusto, A. Demidovich, S. Di Mitri, B. Diviacco, M. Ferianis, G. Gaio, F. Gelmetti, L. Giannessi, G. Kurdi, M. Lonza, C. Masciovecchio, I. Nikolov, G. Penco, P. Rebernik Ribic, C. Scafuri, N. Shafqat, P. Sigalotti, S. Spampinati, L. Sturari, M. Trovo, M. Veronese, R. Visintini, Elettra-Sincrotrone Trieste S.C.p.A., Basovizza, Italy
G. Perosa, F. Sottocorona, Università degli Studi di Trieste, Trieste, Italy

Abstract

In order to extend the FERMI FEL spectral range over the whole water window, we are developing an upgrade strategy that is based on the implementation of the Echo Enabled Harmonic Generation scheme.

The strategy is structured as follows: during a first phase, the single cascade FEL-1 branch will be adapted to operate either in EEHG or in HGHG. This upgrade can be achieved with relatively low cost and impact on FERMI operations and will extend the spectral range, and improve spectral quality and flexibility of FEL-1. Furthermore, it will provide a versatile test bench opening the possibility to explore in detail the EEHG scheme potentialities in the operation of the facility. This will contribute to identify and address the possible issues related to the second and more critical phase of the upgrade project: the upgrade of FEL-2. These two phases will proceed in parallel to an upgrade of the LINAC where we will increase the maximum energy of operation. Solutions aiming at a peak beam energy of 1.8 and 2.0 GeV are under study.

In this contribution, we will focus on the upgrade of the FEL-1 branch that has already started and is foreseen to provide light to users with the new configuration by spring 2023.

INTRODUCTION

The FERMI Free Electron Laser (FEL) facility is in operation since 2010 and provides to the user community ultrashort coherent pulses in the VUV- XUV range (100 – 4 nm) [1]. It works in the so-called High Gain Harmonic Generation (HGHG) scheme making use of a tunable external UV laser to create the needed bunching at high harmonic order. FERMI offers two FEL amplifier lines operating in single (FEL-1) and double (FEL-2) cascade mode. This layout permits to cover the above-mentioned wavelength range with nearly transform limited XUV pulse and GW peak power at a repetition rate of 50 Hz.

The main limitation of the HGHG technique is related to the reduction of the ratio between bunching at a given harmonic and energy spread as the harmonic order increases. On FEL-1, efficient bunching for harmonic amplification can be created up to approximately harmonic 15 in single cascade. This is the limiting factor for achieving shorter wavelengths on this FEL line.

EEHG has been successfully tested at FERMI in 2018 [2]: implementing a temporary modification of the FEL-2 layout, we have demonstrated high gain lasing in EEHG mode up to harmonic 45 in a single cascade.

The need to increase the photon energy of FEL-2 by a factor of 2 with respect to the current limit requires a significant change in the FEL-2 layout and a change in the undulator parameters. This may affect the FEL-2 capability to be operated in a wavelength range extended from 20 nm to 2 nm. As a result, the FEL-2 upgrade is planned in parallel with an upgrade of FEL-1, such that the 20 – 10 nm can be also covered by FEL-1.

The upgrade of FEL-1 is realized with relatively modest impact on the original layout. It has been scheduled early in time with respect to the one of FEL-2 also to contribute to form our experience in running an EEHG seeded FEL for users and to provide additional studies of EEHG at very high harmonics, which will help in steering the design of FEL-2 in the technical definition of the final FEL upgrade.

Echo-enabled harmonic generation (EEHG) was first proposed by G. Stupakov [3] as a means to overcome the limitations of the standard HGHG scheme, posed by incoherent energy spread, in reaching extremely high harmonic numbers (e.g., n>100) for generation of soft X-ray radiation when starting from the radiation from an external, ultraviolet seed laser.

Figure 1: A sketch of the EEHG configuration.

Unlike the standard HGHG scheme that for high harmonic number n has the coherent bunching fraction b_n decaying exponentially as n^2, EEHG when properly tuned leads b_n decaying only as $n^{1/3}$ in the absence of other effects such as incoherent intrabeam scattering. Figure 1 illustrates schematically the EEHG approach. At the beginning, a seed laser (seed-1) at wavelength λ_1 together with a short modulator induces a moderate, coherent energy modulation on the input electron beam. The dispersive section that follows is sufficiently strong such that $R_{56}\frac{\sigma_\gamma}{\gamma} \gg \lambda_1$, thus shearing the longitudinal phase space and, at a given phase, leading to multiple, alternating bands of large and small density as a function of the energy. The first part of the EEHG configuration is devoted to the generation of this energy modulated beam distribution. The

ISBN: 978-3-95450-227-1 ISSN: 2673-5490 doi:10.18429/JACoW-IPAC2022-TUPOPT023

UNDULATOR TAPERING STUDIES OF AN ECHO-ENABLED HARMONIC GENERATION BASED FREE-ELECTRON LASER

F. Pannek*, W. Hillert, University of Hamburg, Hamburg, Germany
S. Ackermann, E. Ferrari, L. Schaper, Deutsches Elektronen-Synchrotron DESY, Hamburg, Germany

Abstract

The free-electron laser (FEL) user facility FLASH at DESY is currently undergoing an upgrade which involves the transformation of one of its beamlines to allow for external seeding via so-called Echo-Enabled Harmonic Generation (EEHG). With this seeding technique it will be possible to provide stable, longitudinal coherent and intense radiation in the XUV and soft X-ray regime at high repetition rate. To ensure an efficient FEL amplification process, sustainable energy exchange between the electrons and the electromagnetic field in the undulator is mandatory. Adequate adjustment of the undulator strength along the beamline allows to compensate for electron energy loss and to preserve the resonance condition. The impact of this undulator tapering on the temporal and spectral characteristics of the EEHG FEL radiation at 4 nm is investigated by means of numerical simulations performed with the FEL code GENESIS1.3, version 4. Different tapering methods are examined and it is shown that specific tapering of the undulator strength allows to exceed the FEL saturation power while maintaining a clear temporal and spectral shape of the FEL pulse.

INTRODUCTION

In the Echo-Enabled Harmonic Generation (EEHG) seeding scheme [1] density modulations at high harmonics of the seed laser wavelength are imprinted on an electron bunch before it is injected into a subsequent undulator radiator for free-electron laser (FEL) emission. Due to the pre-bunched electron beam the amplification in the radiator develops fast. A long radiator section makes it crucial to adjust the undulator strength of the individual radiator modules along the beamline to exceed the saturation power of the FEL [2, 3].

In the following, different undulator tapering methods and their effect on the spectro-temporal characteristics of the FEL radiation are studied for an EEHG based FEL at 4 nm. For this, numerical simulations with the FEL code GENESIS1.3, v4 [4, 5] are carried out within the parameter range of the future FLASH2020+ upgrade [6] of the FEL user facility FLASH at DESY [7–9].

EEHG SETUP

The longitudinal phase space distribution of the electron bunch is manipulated in two undulators, so-called modulators, where the electrons interact with a seed laser and are modulated in energy. The resulting energy modulation amplitudes A_1 and A_2 are expressed as a multiple of the rms beam energy spread σ_E. Each modulator is followed by a chicane to create longitudinal dispersion $R_{56,1}$ and $R_{56,2}$. Parameters used in the simulations are listed in Table 1. The current distribution as well as the power profiles of the two seed lasers are Gaussian, where τ is the full width at half maximum. Proper adjustment of the EEHG setup results in a peak bunching of about 5 % at the entrance of the radiator, as shown in Fig. 1. Note that the energy spread in the area with high bunching increases up to 635 keV.

Table 1: Simulation Parameters for EEHG at 4 nm

Electron Beam		Seed Lasers		EEHG	
E	1.35 GeV	λ_1	300 nm	A_1	5
σ_E	150 keV	λ_2	300 nm	A_2	3
I_p	500 A	τ_1	150 fs	$R_{56,1}$	7.05 mm
ε_n	0.6 mm mrad	τ_2	50 fs	$R_{56,2}$	81.25 µm
τ_e	314 fs				

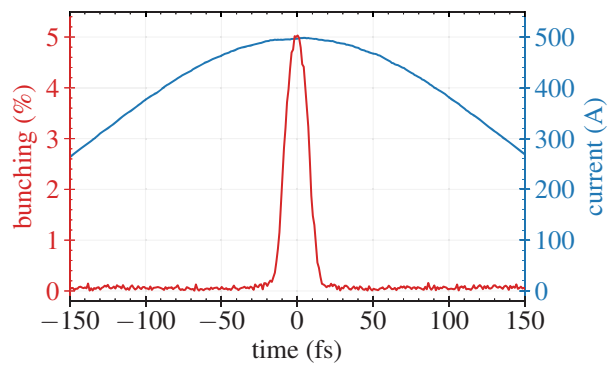

Figure 1: Bunching at 4 nm and current profile (calculated within 300 nm slices) before entering the radiator.

UNDULATOR TAPERING

The radiator beamline is made up of 11 helical undulator modules of $L_\mathrm{u} = 2.508$ m length with a $\lambda_\mathrm{u} = 33$ mm period length. Quadrupoles located between the modules are used for proper matching, resulting in an average rms transverse electron beam size of $\sigma_{x,y} = 45.5$ µm along the radiator. The undulator strength $K = K_\mathrm{rms}$ is set to a constant value along each individual module. The undulator strength K_r derived from the FEL resonant condition for a resonant wavelength of $\lambda_\mathrm{r} = 4$ nm serves as reference:

$$\lambda_\mathrm{r} = \frac{\lambda_\mathrm{u}}{2\gamma_\mathrm{r}^2}\left(1 + K_\mathrm{r}^2\right), \tag{1}$$

where the initial electron energy is given by the Lorentz factor γ_r.

* fabian.pannek@desy.de

ISBN: 978-3-95450-227-1 ISSN: 2673-5490 doi:10.18429/JACoW-IPAC2022-TUPOPT024

RECENT DEVELOPMENTS AT SOLARIS NATIONAL SYNCHROTRON RADIATION CENTRE

A. I. Wawrzyniak †, P. Andryszczak, G. Cios, K.Guła, G.W. Kowalski,A. M. Marendziak, A. Maximenko, R. Panaś, T. Sobol, M. Szczepaniak, J. Wiechecki, M. Wiśniowski, , M. Zając
SOLARIS NSRC, Krakow, Poland
A. Curcio, CLPU, Salamanca, Spain
H. Lichtenberg, Hochschule Niederrhein University of Applied Sciences, Krefeld, Germany

Abstract

SOLARIS National Synchrotron Radiation Centre is under constant development of the research infrastructure. In 2018 first users were welcomed at three different experimental stations. Up to now 5 end stations are available at SOLARIS for experiments at 4 beamlines, and 4 new beamlines are under construction. In 2021 new front end for POLYX beamline was installed and degassed. Moreover, ASTRA beamline components were installed and first commissioning stage has stared. Additionally, a plasma cleaning station has been designed, built and is currently tested. Apart of the beamlines, upgrades to the linac and storage ring operation have been done. During the COVID-19 pandemic the software for remote injection process was developed and is used on daily basis. The transverse beam emittance measurement on the visible light beamline LUMOS was implemented and gives results that are complementary to the Pinhole beamline. Within this presentation the overview of the recent developments with insight to the details to be presented.

INTRODUCTION

SOLARIS National Synchrotron Radiation Centre is operating in Krakow, Poland since 2015. It consists of 600 MeV injector with thermionic RF gun and 1.5 GeV storage ring of 96 m circumference with 6 nm rad emittance [1-2]. The facility was built with tight cooperation with MAXIV Laboratory in Sweden. Nowadays SOLARIS is under constant development of the research infrastructure. In 2018 first users were welcomed at three different experimental stations. Up to now 5 end stations are available at SOLARIS for experiments at 4 beamlines, and 4 new beamlines are under construction. Moreover in 2022 the experimental hall extension works has just stared, which will allow for long beamlines accommodation.

NEW INSTALLATIONS

ASTRA Beamline

ASTRA is a compact bending magnet beamline designed for X-ray absorption spectroscopy measurements in the tender and hard X-ray range (1 – 15 keV). The beamline has no windows between the source point and the monochromator in order to minimize absorption of low energy photons [3]. The project is an international collaboration of Niederrhein University of Applied Sciences (Germany), the Synchrotron Light Research Institute (SLRI, Thailand), Bonn University (Germany) and SOLARIS. In the first half of 2020 the front end section of the beamline was installed (Fig. 1a). The main degassing process of the front end components was finished in June 2020 and the pressure level with the photon beam at 300 mA electron current in the storage ring was below 9.7e-9 mbar. In 2021 the main beamline components downstream from SOLARIS´ radiation shield wall were installed (Fig. 1b). A diagnostic module with a fluorescence screen and a wire-type X-ray beam position monitor is used to visualize and determine the white beam's position and profile. A compact differential ion pump maintains the pressure difference of 4–5 orders of magnitude between the diagnostic module (base pressure 1.0e-9 mbar) and the fixed exit beam Lemmonier type double crystal monochromator (1.0e-5 mbar). The high vacuum operating pressure of the monochromator allows to quickly exchange crystal pairs in order to cover the target energy range.

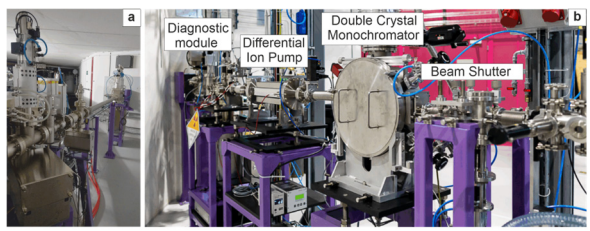

Figure 1: (a) Front end section, (b) main beamline components downstream the radiation shield wall.

In Autumn 2021, the first EXAFS spectra at the beamline were measured in transmission. During commissioning in January 2022, key performance parameters such as energy resolution (e.g. for InSb(111) at the sulfur K edge: $\Delta E/E = 7.0e\text{-}4$), photon flux (1.0e10 ph/s/0.1 A) and spatial stability of the monochromatic beam were evaluated. After recording XAS spectra of various reference compounds over the full energy range, experiments were carried out in cooperation with "friendly users" at different absorption edges, e.g. Mg, Al, Si, P, S, Cl, Fe, Ni, Zn, Sb and U in transmission mode. The obtained high-quality data shows the outstanding potential of this new beamline for academic and industrial research. The beamline was opened for the spring 2022 call for proposals and received a large interest from both Polish and international users. Within the EU project SYLINDA a compact vacuum X-ray spectrometer for high energy resolution fluorescence detection was recently added to the beamline, and the beamline staff performs its commissioning. Implementation of fluorescence and surface-sensitive total electron yield

† adriana.wawrzyniak@uj.edu.pl

ISBN: 978-3-95450-227-1 ISSN: 2673-5490 doi:10.18429/JACoW-IPAC2022-TUPOPT025

CONCEPT OF ELECTRON BEAM DIAGNOSTICS FOR PolFEL*

P. Czuma, R. Kwiatkowski, M. Krakowiak, P. Krawczyk, S. Mianowski, R. Nietubyć, M. Staszczak, J. Szewiński, M. Terka, M. Wójtowicz, National Centre For Nuclear Research, Otwock, Poland
Q. I. Wawrzyniak†, G.W. Kowalski, R. Panaś, A. Marendziak
SOLARIS National Synchrotron Radiation Centre, Krakow, Poland
A. Curcio, Centro De Láseres Pulsados, Salamanca, Spain
K. Łasocha, Institute of Physics, Jagiellonian University, Krakow, Poland

Abstract

PolFEL - Polish Free Electron Laser will be driven by a continuous wave superconducting accelerator consisting of low emittance superconducting RF electron gun, four accelerating cryomodules, bunch compressors, beam optics components and diagnostic elements. The accelerator will split in three branches leading to undulators producing VUV, IR and THz radiation, respectively. Two accelerating cryomodules will be installed before a dogleg directing electron bunches towards IR and THz branches. Additional two cryomodules will be placed in the VUV branch accelerating electron bunches up to 185 MeV at 50 kHz repetition rate. Moreover, the electron beam after passing the VUV undulator will be directed to the Inverse Compton Scattering process for high energy photons experiments in a dedicated station. In order to measure and optimise the electron beam parameters along the entire accelerator the main diagnostics components like BPMs, charge monitors, YAG screens, coherent diffraction radiation (CDR) monitors and beam loss monitors are foreseen. Within this presentation the concept of the electron beam diagnostics will be discussed.

INTRODUCTION

The Polish Free Electron Laser, PolFEL, proposed in 2009, and accepted for the Polish Roadmap for Research Infrastructures, is to be constructed in two phases. First phase is designed with lower electron energy and second – with more accelerating sections and maximum electron energy up to about 600MeV. The electron beam will be generated in the all superconducting gun (ASG) and accelerated in TESLA cavities, housed in HZDR/RI-like cryomodules. After passing through two cryomodules (with two RF-cavities each), electrons will be directed to THz and IR undulators or, after going through bunch compressors, further accelerated by remaining two cryomodules. The fast electrons will go to VUV undulators and then into electron experimental stations, e.g. Inverse Compton Scattering experiments and neutron generation station. The undulators will be made of permanent magnets, for VUV, IR and THz branches. The layout of the PolFEL is presented in Fig. 1.

The features, which make PolFEL a unique facility is the use of both superconducting gun technology and superconducting cavities, which make possible to operate in continuous wave regime and low emittance. The SRF gun provides important advantages compared to hot injectors: operation in CW mode and significant reduction of RF power dissipation [1], although it still remains immature.

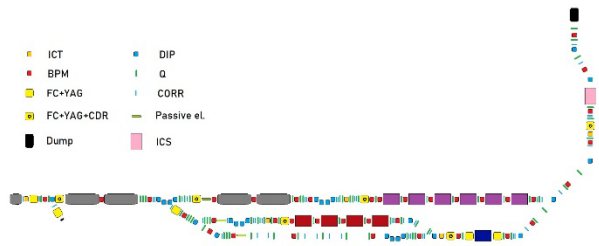

Figure 1: The layout of PolFEL facility with diagnostics components distribution.

The most important parameters of PolFEL electron accelerator are listed in Table 1 [2, 3].

Table 1: The Parameters of Polfel Electron Beam (Maximal Values, Continuous Wave Mode)

Parameter	Gun	VUV	IR	THZ
Bunch charge [pC]	250	100	250	250
Rep. rate [kHz]	50	50	50	50
Bunch length [ps]	10	0.4	1.2	1.2
Beam energy [MeV]	4	154	79	79
Beam current [μA]	12.5	5	12.5	12.5
Beam power [W]	50	770	988	988
Sliced emittance [um*rad]	0.2-1.0	<0.5	1.4	1.4

DIAGNOSTIC INSTRUMENTS

Beam Position Monitors

For the whole PolFEL linac 40 Beam Position Monitors (BPMs) are required in order to trace the beam position in the horizontal (X) and vertical (Y) planes as an input for a trajectory feedback system. Based on the resolution requirements that were set up to 10 μm along the linac, button BPMs similar to the ones used in European XFEL machine will be used in the warm sections.

If better resolution will be required especially in the undulator sections, the cavity BPMs with the resolution <1 μm are to be considered as an option or future upgrade.

* Work supported by the European Regional Development Fund in the framework of the Smart Growth Operational Programme and Regional Operational Programme for Mazowieckie Voivodeship.
† adriana.wawrzyniak@uj.edu.pl

ISBN: 978-3-95450-227-1 ISSN: 2673-5490 doi:10.18429/JACoW-IPAC2022-TUPOPT026

DESIGN AND STATUS OF FAST ORBIT FEEDBACK SYSTEM AT SOLARIS

G. W. Kowalski*, K. Guła, R. Panaś, A. I. Wawrzyniak, J. Wiechecki
National Synchrotron Radiation Centre SOLARIS, Kraków, Poland

Abstract

SOLARIS storage ring has been built with basic set of diagnostic and feedback systems. FOFB system, as much more advanced and not as critical for startup was envisioned as later addition to the design. Now, we are in the process of implementing this addition. The system's workhorse is Instrumentation Technologies Libera Brilliance+ with its Fast Acquisition data path and customizable FPGA modules. Feedback algorithm running in hardware provides fast calculations and direct communication with fast power supplies. The hardware installation is almost finished with configuration and software works running in parallel. First measurements of response matrix and proof-of-concept tests were performed.

DESIGN OF SOLARIS DOUBLE-BEND ACHROMAT (DBA) MAGNET CELLS

The SOLARIS storage ring consists of 12 double bend achromat (DBA) cells (Fog. 1). Conceptually, the magnet design is identical to MAX IV 1.5 GeV storage ring. All magnet elements are machined out of one solid block of iron, about 4.5 m long. The magnet design is optimized for 1.5 GeV beam energy, but since SOLARIS injector currently operates at 0.5 GeV it has been evaluated for that energy as well [1].

DESIGN OF SOLARIS ORBIT FEEDBACK SYSTEMS

Slow Orbit Feedback (SOFB)

The Slow Orbit Feedback system is used for initial beam positioning and maintaining a stable orbit. This system uses 36 beam position monitors (BPMs) (3 per DBA cell) and 72 corrector magnets (3 per plane per DBA cell) [2]. The SOFB correctors are much stronger than the FOFB ones, with current range of $\pm$11.5 A. This allows for correction of larger beam displacement, but comes at the cost of increased current rise time and thus reduced correction frequency. During standard user operation the SOFB system runs with a frequency of 0.25 Hz or 0.33 Hz, with theoretical maximum of 1 Hz. Software-wise, there are currently two applications used interchangeably: the Matlab MML-based solution [3] and a TangoFeedback based application integrated into the control system [4].

Fast Orbit Feedback (FOFB)

The Fast Orbit Feedback application is a system used for the stabilization of the electron beam and is thought to achieve a stable photon beam for users. It consists of several subsystems that together actively monitor and stabilize the beam position. The main reference is an ideal orbit (so-called golden orbit) which is implemented into the control system and used as a reference for all calculations. The orbit position is established in real-time via BPMs. The BPMs used by the FOFB system are the same ones used by SOFB. The orbit correction uses 24 dual-plane corrector magnets for fast positioning around the storage ring. Once the deviation of the electron beam from its golden orbit is detected, the control signal calculated from the orbit correction bumps magnets towards the setpoint. Each value is unique for each of the magnets and depends on its location around the storage ring and displacement measured at that point. The heart of the system is Libera Brilliance+ (LB+) instruments used for the calculation of the electron position. The closed-loop control follows in several stages: beam position measurements, orbit data concentration from several LB+ instruments into the single orbit data packet, interlock status check, orbit correction calculation, and streaming of the magnet data to the serial output module of LB+.

FOFB COMPONENTS OVERVIEW

BPM Pickups

The SOLARIS storage ring uses 36 quarter wave diagonal button pickups, 3 per DBA cell. There are two types of sensor heads arrangement: type I used at both ends of DBA cell is aligned directly along diagonal coordinates, and type II used at the centre of DBA with heads aligned along vertical axis [3].

Libera Brilliance+ Instruments

Libera Brilliance+ is a high precision beam position measurement device from Instrumentation Technologies. Single instrument can support up to 4 BPM modules and provides different data paths for different purposes, all of which can be accessed simultaneously. Out-of-the-box support for MRF's digital timing protocol greatly simplifies control, triggering and synchronization. The optional GDX and SER modules provide a framework for orbit feedback applications running entirely inside the device.

Itest Fast Power Supplies

Itest BE5495 power supplies are magnet power supply modules specifically designed for Fast Orbit Feedback applications. The available current range is $\pm$2 A with 10 kHz setpoint change frequency. The modules support communication over Ethernet and RS485 serial link, and are mounted in Itest BN210 chassis.

* g.kowalski@uj.edu.pl

ISBN: 978-3-95450-227-1 ISSN: 2673-5490 doi:10.18429/JACoW-IPAC2022-TUPOPT027

NUMERICAL SIMULATION OF A SUPERRADIANT THz SOURCE AT THE PITZ FACILITY

N. Chaisueb*[1,2], P. Boonpornprasert[3], M. Krasilnikov[3], X-K. Li[3],
A. Lueangaramwong[3], S. Rimjaem[1,4]
[1]PCELL, PBP, Faculty of Science, Chiang Mai University, Chiang Mai, Thailand
[2]also at Ph. D. Program in Physics, Chiang Mai University, Chiang Mai, Thailand
[3]DESY, Platanenallee 6, Zeuthen, Germany
[4]also at ThEP Center, MHESI, Bangkok, Thailand

Abstract

An accelerator-based THz source is under development at the Photo Injector Test Facility at DESY in Zeuthen (PITZ). The facility can produce high brightness electron beams with high charge and small emittance. Currently, a study on development of a tunable high-power THz SASE FEL for supporting THz-pump, X-ray-probe experiments at the European XFEL is underway. An LCLS-I undulator, a magnetic chicane bunch compressor, and THz pulse diagnostics have been installed downstream the previously existing setup of the PITZ beamline. Additional to the SASE FEL, a possibility to generate superradiant THz undulator radiation from short electron bunches is under investigation, which is the focus in this study. Numerical simulations of the superradiant THz radiation by using sub-picosecond electron bunches with energy of 6 - 22 MeV and bunch charge up to 2 nC produced from the PITZ accelerator are performed. The results show that the radiation with a spectral range of 0.5 to 9 THz and a pulse energy in the order of sub-μJ can be obtained. The results from this study can be used as a benchmark for the future development.

INTRODUCTION

The PITZ facility can produce high brightness electron beam with small emittance by using a photocathode RF gun [1]. The photocathode laser system can generate various temporal pulse shapes including flattop, Gaussian, and 3D (ellipsoidal) profiles [2]. The electron bunches have a beam energy up to 22 MeV and a bunch charges up to 4 nC. The transverse emittance is around 1 - 10 mm.mrad and the energy spread is about 0.5%. The peak current of the present beamline can be adjusted up to 200 A.

The PITZ facility develops the RF electron guns for FLASH and the European XFEL [3, 4]. Thus, characteristics of the electron beam produced from the RF electron guns at PITZ and the European XFEL are identical. The European XFEL has planned to perform pump-probe experiments by using x-ray and THz pulses. The PITZ accelerator is suitable to be used to develop a prototype for a high power tunable THz source for this experiment because the THz radiation generated at PITZ will have the same pulse train structure and is synchronized with the x-ray pulses at the European XFEL [5]. The THz pump and X-ray probe experiment requires THz pulses with μJ - mJ pulse energies. Frequency of the emitted radiation covers the range of 0.1 - 30 THz, which is equivalent to a wavelength range of 3 mm - 10 μm [6]. There are four options to produce THz pulses at PITZ, including SASE FEL, seeded FEL, coherent transition radiation and superradiant FEL. This paper focuses on the superradiant or coherent undulator radiation technique. It requires ultra-short and high-charged electron bunches. When the electron bunch length is equal to or shorter than the radiation wavelength, the radiation emitted from different undulator poles overlaps and interferes constructively. This leads to coherent radiation pulse with intensity proportional to number of electron squared. Therefore, the possibility to generate the superradiant THz FEL from high brightness electron bunches produced at PITZ was investigated.

The basic setup of the accelerator and beamline at the PITZ facility consists of a photocathode RF gun, a booster cavity, and several electron beam diagnostics. To develop the beamline to be an intense THz source, a chicane bunch compressor, an LCLS-I undulator magnet, and THz pulse diagnostics have been inserted at the end of the previously existing setup. The LCLS-I undulator magnet, which is a planar permanent undulator magnet with a period length of 30 mm and an undulator parameter of 3.58, will be used as a radiation source. Specifications of the LCLS-I undulator magnet are shown in Table 1. The vacuum chamber of the undulator magnet is rather small. This significantly affects to electron beam dynamics and generation of the THz radiation.

Table 1: Specification of the LCLS-I Undulator Used at the PITZ Facility

Specifications	Value
Type	Planar
Period length (mm)	30
Number of periods	113
Total length (m)	3.42
Peak magnetic field (T)	1.28
Undulator parameter (K)	3.58
Vacuum chamber size (mm)	11×5

* natthawut_chai@cmu.ac.th

ISBN: 978-3-95450-227-1 ISSN: 2673-5490 doi:10.18429/JACoW-IPAC2022-TUPOPT028

THz UNDULATOR RADIATION BASED ON SUPER-RADIANT TECHNIQUE AT CHIANG MAI UNIVERSITY

E. Kongmon [*,2], N. Chaisueb[1,3], S. Rimjaem[1,4]
[1]PCELL, PBP, Faculty of Science, Chiang Mai University, Chiang Mai, Thailand
[2]Ph. D. Program in Applied Physics (Int'l program), Chiang Mai University, Chiang Mai, Thailand
[3]Ph. D. Program in Physics (Int'l program), Chiang Mai University, Chiang Mai, Thailand
[4]ThEP Center, MHESI, Bangkok, Thailand

Abstract

A linear accelerator system at the PBP-CMU Electron Linac Laboratory is used as an electron source for generating coherent THz radiation and MIR-FEL. To achieve high power THz radiation, the super-radiant technique using pre-bunched electrons and undulator magnet is utilized. In this study, we investigate the generation of such radiation with comparable properties as the FEL. The beamline composes of a 180° magnetic bunch compressor, a 2 m-electromagnet undulator, quadrupole magnets and diagnostic devices. This work includes the undulator design and investigation on properties of electron beam and THz radiation. Based-on the results of beam dynamic study, the optimized electron beams have an energy in a range of 10-16 MeV, a bunch charge of 100 pC, and a bunch length of 300 fs. The radiation with frequency covering from 0.5 to 3 THz yields a peak power of 5.21 MW at 1.15 THz. This information was used as an initial parameter for undulator design by using the CST-EM Studio software. It has 19.5 periods with a period length of 100 mm. The design results show that the maximum magnetic field is 0.2317 T. The results of this study are used as the guidline for construction of the undulator and the THz-FEL beamline.

INTRODUCTION

Terahertz (THz) radiation occupies the frequency gap between microwave and infrared in the electromagnetic spectrum with the frequency in the range from 0.3 to 10 THz (100 - 1000 μm) [1]. With the dominant feature of the THz radiation having low photon energy, it is non-ionizing radiation that does not cause damage on living tissues. Furthermore, it can penetrate non-conducting materials i.e. plastic and wood and can be absorbed by water [2]. It thus has been used in many areas such as the semiconductor industry, biological science, quality control of food, medical imaging, security, environmental science, etc. [3, 4].

The aim of this study is to design and develope the system to generate coherent THz undulator radiation at the PBP-CMU Electron Linac Laboratory (PCELL), of the Plasma and Beam Physics (PBP) Research Facility, Chiang Mai University (CMU) in Thailand. The energy of electron beam produced from our accelerator can be adjusted from 5 to 30 MeV. In our work, we chose the electron energy in a range of 5 to 16 MeV.

In this paper, we present the approach to design the electromagnet undulator for generating THz radiation using the super-radiant technique. This THz source will be utilized for a variety of purposes, including THz spectroscopy and pump-probe experiments.

The THz radiation can be emitted as a synchrotron radiation when electrons traveling in a sinusoidal magnetic field through an undulator magnet. The frequency of the radiation is determined by the electron energy and the strength of the undulator magnetic field (K-parameters) as Eq. (1) [5].

$$\lambda_r = \frac{\lambda_u}{2n\gamma^2}\left(1 + \frac{K^2}{2} + \gamma^2\theta^2\right), \quad (1)$$

where n is the harmonic number, γ is the Lorentz's factor and θ is the radiation observation angle. In this research, we consider only the fundamental frequency, thus the harmonics number is unity (n = 1) and we observe only on-axis of the radiation ($\theta = 0$).

The undulator parameter K is defined as a function of undulator magnetic field intensity (B_0) and undulator period length (λ_u) as using $K = 0.934B_0[T]\lambda_u[cm]$. According to Eq. (1), the radiation in the THz domain was calculated by taking into account the electron energy and the undulator period length. The relationship between these variables is plotted in Fig. 1 for the undulator period length of 100 mm, which was already optimized by compomizing between available space in the accelerator hall and the aimed radiation wavelength.

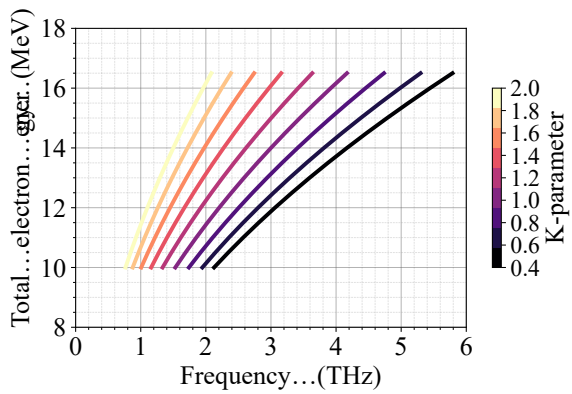

Figure 1: The relation between electron energy and radiation frequency as a function of radiation frequency for different undulator parameters (K), where the undulator period length is equal to 100 mm.

* Ekkachai_kong@cmu.ac.th

ISBN: 978-3-95450-227-1 ISSN: 2673-5490 doi:10.18429/JACoW-IPAC2022-TUPOPT029

INFRARED FREE-ELECTRON LASER PROJECT IN THAILAND

S. Rimjaem*,[1], P. Apiwattanakul, N. Chaisueb, P. Jaikaew, W. Jaikla, N. Kangrang, P. Kitisri, K. Kongmali, E. Kongmon, P. Nanthanasit, S. Pakluea, M. W. Rhodes[1], J. Saisut[1], S. Sukara, K. Techakaew, C. Thongbai[1], P. Wongkhammoon, PCELL, PBP, Faculty of Science, Chiang Mai University, Chiang Mai, Thailand
M. Jitevisate[1], School of Physics, Institute of Science, Suranaree University of Technology, Nakhon Ratchasima, Thailand
[1]also at ThEP Center, MHESI, Bangkok, Thailand

Abstract

The infrared free-electron laser (IR FEL) project is established at Chiang Mai University (CMU) in Thailand with the aim to provide experimental stations for users utilizing accelerator-based coherent terahertz (THz) and mid-infrared (MIR) radiation. Main components of the accelerator system include a thermionic radio-frequency (RF) gun, an alpha magnet as a bunch compressor and energy filter, a travelling-wave RF linear accelerator (TW RF linac), a THz transition radiation (THz TR) station, two magnetic bunch compressors and beamlines for MIR/THz FEL. The system commissioning is ongoing to produce the beams with proper properties. Simulation results suggest that the oscillator MIR FEL with wavelengths of 9.5-16.6 μm and pulse energies of 0.15-0.4 μJ can be produced from 60-pC electron bunches with energy of 20-25 MeV. The super-radiant THz FEL with frequencies of 1-3 THz and 700 kW peak power can be generated from 10-16 MeV electron bunches with a charge of 50 pC and a length of 200-300 fs. Furthermore, the coherent THz TR with a spectral range of 0.3-2.5 THz and a pulse power of up to 1.5 MW can be obtained. The MIR/THz FEL will be used for pump-probe experiments, while the THz TR will be used in Fourier transform infrared (FTIR) and time-domain spectroscopy (TDS).

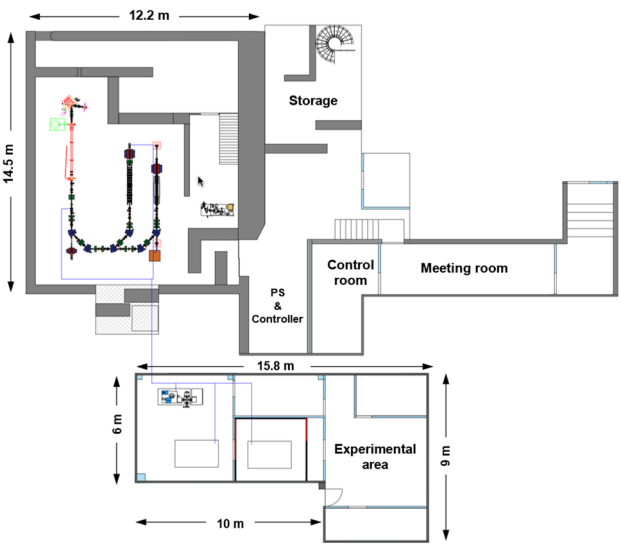

Figure 1: A layout of the IR FEL facility at PCELL consisting of areas for accelerator and experimental stations.

*sakhorn.rimjaem@cmu.ac.th

INTRODUCTION

Ultrashort electron and photon pulses, especially in the femtosecond time scale, have become important tools for various applications in life science and materials science [1]. Accessibility to such short pulses is being offered at the PBP-CMU Linac Laboratory (PCELL) of the Plasma and Beam Physics (PBP) Research Facility, Chiang Mai University (CMU). At PCELL, we are especially interested in using ultrashort electron pulses to produce coherent THz radiation, MIR radiation and X-ray.

The establishment of the infrared free-electron laser (IR FEL) facility at PCELL includes the development of accelerator system, stations and beamlines for generating THz transition radiation (THz TR), MIR FEL, THz FEL, short-pulsed electron and X-ray as well as advanced experimental stations including FTIR spectroscopy, THz TDS and pump-probe experiments. This facility will be the first facility of its kind in Thailand and South-East Asia. The layout of the whole facility, including areas for the accelerator and the experiments is presented in Fig. 1. All buildings and infrastructure for both areas are already available and ready for installation of new accelerator components and experimental setups.

ACCELERATOR AND BEAMLINES

The accelerator system consists of a thermionic RF gun for producing electron beam with maximum kinetic energy of ~2 MeV, an alpha magnet for bunch compression and energy filtering, a TW linac for further accelerating the beam to reach energy in a range of 10 - 25 MeV. Two magnetic bunch compressors for MIR-FEL and THz-FEL beamlines are installed downstream the linac.

The advantage of PCELL facility comes from the original design of our electron accelerator system, which was constructed to produce electron beams with ultra-short bunch length in scale of femtosecond [2]. The electron beam with a bunch length as short as 180 fs was experimentally obtained [3]. Figure 2 shows the present setup of the accelerator system, radiation station and beamlines in the radiation shielding accelerator hall. Installation of beamline components is underway and it is expected to be completed in 2023. There are two stations for generating THz TR and short-pulsed electron/X-ray, and two beamlines for generating MIR and THz FEL.

ISBN: 978-3-95450-227-1 ISSN: 2673-5490 doi:10.18429/JACoW-IPAC2022-TUPOPT030

DESIGN AND SIMULATION OF THE MIR-FEL GENERATION SYSTEM AT CHIANG MAI UNIVERSITY

S. Sukara*[1], S. Rimjaem†[2], K. Kongmali[1]
PCELL, PBP, Faculty of Science, Chiang Mai University, Chiang Mai, Thailand
H. Ohgaki, Institute of Advanced Energy, Kyoto University, Kyoto, Japan
[1]also at Ph. D. Program in Physics (Intl. Program), Chiang Mai University, Chiang Mai, Thailand
[2]also at ThEP Center, MHESI, Bangkok, Thailand

Abstract

At the PBP-CMU Electron Linac Laboratory, the system to generate MIR-FEL using the electron linac has been developed. In this contribution, the design and simulation results of the MIR-FEL generation system are presented. The system is designed as the oscillator-FEL type consisting of two mirrors and a 1.6-m permanent planar undulator. The middle of the undulator is determined as the laser beam waist position. Both two mirrors are the concave gold-coated copper mirrors placing upstream and downstream the optical cavity, which has a total length of 5.41 m. The FEL is designed to coupling out at a hole with diameter of 2 mm on the upstream mirror. The optical cavity is optimized to obtain high FEL gain and high FEL power using GENESIS 1.3 simulation code. The electron beam with energy of 25 MeV is used in the consideration. As a result, the MIR-FEL with central wavelength of 13.01 μm is obtained. The optimum upstream and downstream mirror curvatures are 3.091 m and 2.612 m, respectively, which give the Rayleigh length of 0.631 m. This optical cavity yields the power coupling ratio of 1:1000 and the FEL gain of up to 40%. The extracted MIR-FEL peak power in 100 kW scale is obtained at the coupling hole. The construction of the practical MIR-FEL system is conducted based on the results from this study.

INTRODUCTION

At the Plasma and Beam Physics Research Facility, Faculty of Science, Chiang Mai University (PBP-CMU), the research team of the PBP-CMU Electron Linac Laboratory (PCELL) has developed an electron linear accelerator system (linac) to produce ultra-short electron bunches. The system has been upgraded to have a potential to accelerate electron beam with a kinetic energy of up to 25 MeV [1]. With this electron beam, we aim to produce free electron laser (FEL) in mid-infrared (MIR) and terahertz (THz) regimes using two undulator systems. The radiation generation system is separate into two sections; one for the MIR-FEL generation and the other is for the THz-FEL generation. The top-view layout of this system is illustrated in Fig. 1.

In this study, the MIR-FEL section is designed. In this section, there is a Halbach-type permanent magnet undulator with a length of 1.6 m [2] obtained from KU-FEL facility, Kyoto University, Japan, in 2018. It was used to generate the first MIR-FEL at the KU-FEL facility in 2007 using 25 MeV electron beam [3]. Then, this undulator was transferred to PCELL with the aim to generate the first MIR-FEL in South-East Asia region. The MIR-FEL generation at PCELL is designed as an oscillator type consisting of two concave mirrors at two ends of the MIR-FEL section. This paper presents the design of the optical cavity and optimization of the mirror curvatures to obtain high MIR-FEL output power and large FEL gain using a computer simulation. The FEL simulation code named GENESIS 1.3 [4] with the modified version from KU-FEL facility [5] is used for estimating the MIR-FEL power evolution in multi-round trips. The time-independent mode was applied assuming that the electron beam current in the longitudinal axis has a uniform and continuous distribution.

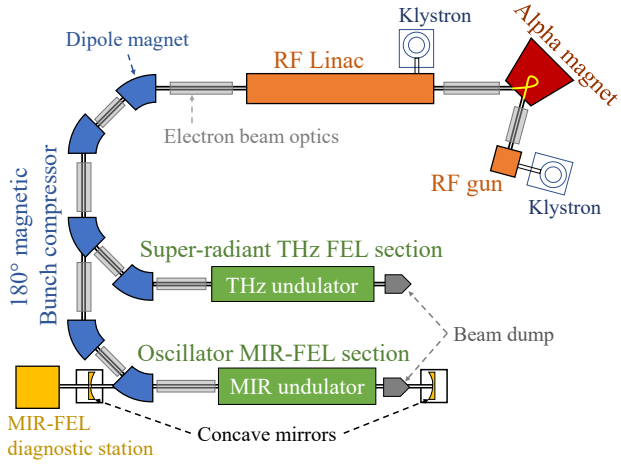

Figure 1: Layout of the accelerator system together with the MIR- and THz-FEL generation system at PCELL.

DESIGN OF MIR-FEL GENERATION SYSTEM

Figure 2 presents the layout and positions of the optical mirrors and the 1.6-m undulator for the MIR-FEL system at PCELL. The middle of the undulator is determined as the laser waist position where the laser beam has the smallest transverse size. The total length of the optical cavity is 5.405 m that contains 102 FEL pulses with repetition rate of 2,856 MHz. Both two concave mirrors are gold-coated copper mirror that have the reflectivity of 99%. At the center of the upstream mirror, there is a hole with diameter of

* Supasin.cmu@gmail.com
† Sakhorn.rimjaem@cmu.ac.th

ISBN: 978-3-95450-227-1 ISSN: 2673-5490 doi:10.18429/JACoW-IPAC2022-TUPOPT032

SIMULATING BEAM TRANSPORT WITH PERMANENT MAGNET CHICANE FOR THz FEL

A. Fisher*, Y. Park, M. Lenz, A. Ody, P. Musumeci†, UCLA, Los Angeles, USA
R. Agustsson, T. Hodgetts, A. Murokh, RadiaBeam Technologies, Santa Monica, USA

Abstract

Free electron lasers are an attractive option for high average and peak power radiation in the THz gap, a region of the electromagnetic spectrum where radiation sources are scarce, as the required beam and undulator parameters are readily achievable with current technology. However, slippage effects require the FEL to be driven with relatively long and low current electron bunches, limiting amplification gain and output power. Previous work demonstrated that a waveguide could be used to match the radiation and e-beam velocities in a meter-long strongly-tapered helical undulator, resulting in 10% energy extraction from an ultrashort 200 pC, 5.5 MeV electron beam. We present simulations for a follow-up experiment targeting higher frequencies with improvements to the e-beam transport including a permanent magnet chicane for strong beam compression. FEL simulations show >20% extraction efficiency from a 125 pC, 7.4 MeV electron beam at 0.32 THz.

INTRODUCTION

Compact and efficient high average and peak power radiation sources are in high demand for scientific and industrial applications including time-domain spectroscopy, high field resonant and non-resonant excitation of solid state systems, and THz-based imaging for medical and security [1, 2]. Free Electron Lasers (FELs) use the ponderomotive interaction between an electromagnetic wave and a relativistic electron beam copropagating in a magnetic undulator and are an attractive source in the 0.1-10 THz range as the necessary undulator and beam parameters are easily achievable [3, 4]. Addition advantages include high peak power and repetition rates limited only by the electron beam provided. FEL facilities have already played an important role in the development of THz science [5–10], with more facilities coming online [11–13] and being planned for the future [14–16].

Our previous experiment [17] showed that by using a waveguide to contain diffraction and match group velocities, a 10% extraction efficiency could be achieved from an ultrashort 200 pC, 5.5 MeV beam. After reviewing the zero-slippage conditions in a waveguide FEL, we investigate a proposed follow-up experiment to double the frequency of THz produced. We discuss improvements to the beamline, a design for a tunable permanent magnet chicane, and the consequences of increasing the resonant frequency. Start to end simulations are presented for the electron beam transport and FEL interaction.

* afisher000@g.ucla.edu
† musumeci@physics.ucla.edu

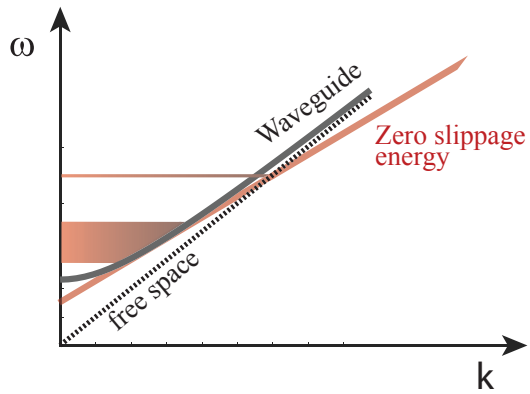

Figure 1: Dispersion diagram for a waveguide FEL. Electrons (red) in free space can only be resonant at a single frequency, whereas a waveguide allows interaction over a large bandwidth.

ZERO-SLIPPAGE RESONANCE

The zero-slippage FEL interaction requires satisfying the traditional FEL phase resonance condition, $(k_z + k_u) = \frac{\omega}{\beta_z c}$ and the group-velocity or zero-slippage condition, $\frac{c^2 k_z}{\omega} = \beta_z c$. In these expressions, the longitudinal wavevector k_z and radiation frequency ω are connected by the waveguide dispersion relation $\omega^2/c^2 = k_z^2 + k_\perp^2$ where $k_\perp = 1.8412/R$ for the TE11 circular waveguide mode [18], R is the waveguide radius, $k_u = 2\pi/\lambda_u$ where λ_u is the undulator period, and $c\beta_z$ is the longitudinal beam velocity in the undulator. Figure 1 illustrates the large bandwidth interaction when the phase velocity (point) and group velocity (slope) are adequately matched.

It can be shown from these conditions that the resonant frequency at zero-slippage is given by $2\pi f_{zs} = ck_u\beta_{z0}\gamma_{z0}^2$ where $\gamma_{z0} = \gamma_0/\sqrt{1+K^2}$. For relativistic beams, $\gamma_0 = \frac{k_\perp}{k_u}\sqrt{1+K^2}$ and we see that for given waveguide and undulator parameters, the resonant beam energy is uniquely determined.

To maintain resonance with the decelerating electrons, the magnetic field strength must be strongly tapered along the undulator to enhance the stimulated superradiant radiation emission (TESSA) of the electrons [19].

A final consequence of the zero-slippage conditions is that the ratio of the helical beam trajectory radius to the waveguide radius is $\frac{r_{max}}{R} = \frac{1}{1.8412}\frac{K}{\sqrt{1+K^2}} \leq 0.543$ with an upper bound independent of frequency.

ISBN: 978-3-95450-227-1 ISSN: 2673-5490 doi:10.18429/JACoW-IPAC2022-TUPOPT034

MODELLING OF X-RAY VOLUME EXCITATION OF THE XLO GAIN MEDIUM USING FLASH

P. Manwani*, N. Majernik, B. Naranjo, J. B. Rosenzweig, UCLA, Los Angeles, CA, USA
E. Galtier, A. Halavanau, C. Pellegrini, SLAC, Menlo Park, CA, USA

Abstract

Plasma dynamics and crater formation of laser excited volumes in solids is a complex process due to thermalization, shockwave formation, varying absorption mechanisms, and a wide range of relevant physics timescales. The properties and interaction of such laser-matter systems can be modeled using an equation of state and opacity based multi-temperature treatment of plasma using a radiation hydrodynamics code. Here, we use FLASH, an adaptive mesh radiation-hydrodynamics code, to simulate the plasma expansion following after the initial energy deposition and thermalization of the column, to benchmark the results of experiments undertaken at UCLA on optical laser ablation. These computational results help develop a quantitative understanding of the material excitation process and enable the optimization of the gain medium delivery system for the x-ray laser oscillator project [1].

INTRODUCTION

The x-ray laser oscillator, termed XLO [1], is a project at the Stanford Linear Accelerator Facility (SLAC) to induce population inversion of the electrons in copper using an x-ray free electron laser (XFEL) to deliver pump pulses to enable stimulated emission in the at the K_α line of the gain medium. The proposed gain medium is a liquid jet of copper sulphate or a solid copper foil. This gain medium needs to be rapidly replaced so each subsequent pulse, spaced at ~30 ns, has fresh material [2, 3]. The required speed of the target depends on the crater geometry left by the x-ray pulse and simulations using FLASH (adaptive mesh hydrodynamic code solver) [4, 5] will be used to understand the laser plasma interaction and resulting ablation. We use this code to study the plasma evolution as particle-in-cell codes are computationally intensive at these densities. The FLASH code supports a tabulated equation of state (EOS) and opacity based multi-temperature model for plasmas. This is important as the thermodynamic properties of materials at high temperatures and pressure cannot be modelled using a power law. Specifically, we use the tabulated EOS and radiative opacity from the PROPACEOS [6] database that calculates the ionization using the Saha model [7] which yields the ionization degree of a plasma at a equilibrium temperature. There are two kinds of interaction regimes that we want to investigate using this code: optical and x-ray ablation. FLASH has capabilities to model both types of interactions, albeit with some assumptions on the initial conditions; these will be described below. Experiments were performed to optically ablate copper foils to benchmark the FLASH simulations and these results are presented in the context of the XLO project.

OPTICAL ABLATION

During the development of the sample delivery system, it is challenging to get access to XFEL pulses for iterative testing. Instead, we turn to the use of an optical laser to approximate certain aspects of the laser-target interaction. Two elements in particular are of the greatest interest for target development: characterizing the longitudinal oscillations caused by the ablation of the target and the longevity of the target as more and more damage is done. The constraints on the allowed oscillation (<30 μm) and target lifetime (~hours) are discussed in [3].

Since the optical laser cannot be focused as tightly as an x-ray pulse (10s of μm vs 100s of nm) and since the interaction is largely at the surface, rather than a volume interaction, the expected impulse from the optical laser is a worst case scenario. Using a Nd:YAG laser (max energy, 500 mJ/pulse) and a short focal length lens (100 mm), the energy of the laser pulse was reduced until the focused beam was barely able to create a hole through the 25 μm thick foil. Then, the spatial profile of the focus was measured using a CCD, the temporal profile was measured with a fast photodiode, and the energy was recorded using a pyroelectric laser energy meter. These measured parameters informed the simulation settings, detailed in Table 1. The ablated foils were imaged using a scanning electron microscope (SEM) with the results are shown in Fig. 1. These benchmarked, optical laser simulations will be compared to simulations of the XFEL-target interaction to confirm that the impulse and crater size of the optical case are, indeed, representative of a worst case scenario. Finally, the target will be exposed to a series of optical laser shots; if the target satisfies both the longevity and oscillation requirements (characterized by laser Doppler vibrometry) we may be confident that it will perform well when installed on an XFEL beamline.

Table 1: Laser Parameters

Parameter	Value	Unit
Laser energy, E_l	77	mJ
Laser wavelenth, λ_l	1064	nm
Pulse duration (FWHM)	20	ns
Beam diameter (before lens)	6	mm
Focal length (lens)	100	mm
Beam waist ($1/e^2$)	35	μm

* pkmanwani@gmail.com

ISBN: 978-3-95450-227-1 ISSN: 2673-5490 doi:10.18429/JACoW-IPAC2022-TUPOPT035

INTRODUCTION OF WESTWOOD LINEAR ACCELERATOR TEST FACILITY IN UNIVERSITY OF CALIFORNIA LOS ANGELES

Y. Sakai, O. Camacho, P. Manwani, G. Lawler, N. Majernik, G. Andonian, B. Naranjo, O. Williams, A. Fukasawa, J. Rosenzweig
University of California at Los Angeles, Los Angeles, California 90095, USA

Abstract

An electron linear accelerator test facility located on UCLA's southwest campus in Westwood, SAMURAI, is presently being constructed. A RF-based accelerator consists of a compact, 3 MeV S-band hybrid gun capable of velocity bunching to bunch lengths in the 100s fs range with 100s pC of charge. This beam is accelerated by an 1.5 m S-band linac with a peak output energy of 30 MeV which can be directed to either a secondary beamline or remain on the main beamline for final acceleration by a SLAC 3 m S-band linac to an energy of 80 MeV. Further acceleration by advanced boosters such as a cryo-cooled C-band structure or numerous optical or wakefield methods is under active investigation. In combination with a 3 TW Ti:Sapphire laser, initial proof of principle experiments will be conducted on topics including the ultra-compact x-ray free-electron laser, advanced dielectric wakefield acceleration, bi-harmonic nonlinear inverse Compton scattering, and various radiation detectors. Furthermore, development of a tertiary beamline based on an ultra low emittance, cryo-cooled gun will eventually enable two-beam experiments, expanding the facility's unique experimental capabilities.

INTRODUCTION

Owing to the establishment of basic beam physics research and experience through the high energy beam experiments, demand for compact lower to medium energy electron linear accelerators has been increased these days in a wide range of communities. Significant interest can be seen for radiation productions in the photon energy of THz, Extreme UltraViolet (EUV), soft X-ray, hard X-ray to the MeV Gamma-ray regime which requires different electron beam parameters depending on the required radiation's characteristics. These are spectral brightness, polarization, coherency, and ultimate discrepancy between each purpose may be total intensity per pulse or average flux. As nature of university laboratory focusing on feasibility studies, including optimization of interaction point, beam manipulation and unique detection system, we are looking for following list of a examples of pulsed photon production and related topics capable by a method of Dielectric WakeField Acceleration (DWFA) [1], Ultra Compact Free Electron Laser (UCFEL) [2], nonlinear Inverse Compton Scattering (ICS) [3] utilizing a University laboratory scale compact electron linac:

- THz-DWA
  - ♦Non destructive material, pump probe, imaging of a Molecular - Plasmonics
  - ♦Low energy e-beam manipulation
- EUV-UCFEL(Coherent 13.5nm, $\Delta E/E < 10^{-3}$)
  - ♦Metrology for such as precision mask manufacturing for lithography (< resolution 5 nm)
  - ♦R & D and calibration of multilayer optics
- Soft X-ray-UCFEL (with compact tunable undulator)
  - ♦Contrast imaging of a nanoscale structure of biological samples (> 1 μm thickness) through water window ($h\nu$ = 2.3 - 4.4 nm)
  - ♦Photoemission spectroscopy for low Z material
  - ♦Polarization sensitive soft x-ray microscopy
- Hard X-ray ICS
  - ♦Data collection for photon activation with nano particle
  - ♦Energy dependent radiography of high Z material
  - ♦Crystal optics R & D including polarization aspect
- Gamma-ray ICS
  - ♦Polarization sensitive Nuclear photonics [4]
  - ♦High energy gamma detector [5]

In this regard, electron linac based on S-band RF cavities at average energy of 80 MeV is under construction as a basic infrastructure to expand these studies in Westwood, Los Angeles. In addition, initial infrastructure of 3TW Ti: Sapphire laser (Coherent Inc., Model: Astrella, Hydra) allows us to enhance e-beam manipulation studies via Inverse Free Electron Laser(IFEL) [6] or Laser Plasma Wakefield Acceleration covering laboratory astrophysics such as space plasma simulator [7].

In the context of optimization of beam interaction points, realization of high gradient and low emittance cryo-temperature C-band gun is under rigorous investigation. A peak surface field at the cathode 240 MV/m, twice as high as conventional field, could have a potential to lower emittance down to 50 nm rad regime by suppressing beam expansion, due to space charge force, which inversely proportional to beam kinetic energy ~$1/\gamma^2$ [8].

OVERVIEW OF THE TEST FACILITY

As shown in the schematic diagram of Fig. 1, the main beam line starts as a Beam Line East (BL-E) from South toward North. A S-band Hybrid gun [9] composed of

* Work supported by U.S. DOE: DE-SC0009914, U.S. DOD: DARPA GRIT 20204571, U.S. DOE: DE-SC0020409-Cryo RF

† email address yusuke@physics.ucla.edu
rosen@physics.ucla.edu

ISBN: 978-3-95450-227-1 ISSN: 2673-5490 doi:10.18429/JACoW-IPAC2022-TUPOPT036

TWO AND MULTIPLE BUNCHES WITH THE LCLS COPPER LINAC*

F.-J. Decker†, W. Colocho, A. Halavanau, A.A. Lutman, J.P. MacArthur, G. Marcus, R.A. Margraf, J.C. Sheppard, J. Turner, S. Vetter, SLAC, Menlo Park, CA, USA

Abstract

Two, four, and even eight bunches were accelerated through the copper linac. Two and four bunches were delivered successfully to photon experiments in both the hard (HXR) and soft (SXR) LCLS x-ray lines. In this paper we will concentrate on the more challenging issues, such as: the BPM deconvolution for both bunches, RF kicks at longer separations, tuning challenges, bridging the communications gap between the photon and electron side, the lower bunch charges for the eight bunch case, and rapid timing scans over several ns. We will describe some of the developed solutions and plans for the rest.

INTRODUCTUION

Two bunch running is now quite well established, only longer time separation of 220 ns and beyond are more problematic. For a general reference, see [1].

FOUR AND EIGHT BUNCHES

Eight bunches, 0.7 ns apart were accelerated in the LCLS copper linac and brought onto the dump screen (Fig. 1). The differences are quite obvious and come from the different intensities from the laser pulses onto the gun cathode.

Multi-Bunch Generation

The Multi-Pulse Pulse-Stacker (MPPS, see Fig. 2 in [2]) splits, delays and combines light pulses of two laser (Coh1, Coh2) into four pulses each. In Figure 1 the order is: Coh1 B1+B2+B3+B4 then Coh2 B1+B2+B3+B4. Bunches 3 and 4 from each laser have lower intensity and Coh1 was lower than Coh2. Lower charge bunches get off the cathode faster and in the end get compressed more. The charges were quite far away from equal (12.5% each). The deviations from that number in percent were: -6, +7, -29, -26, +22, +40, -6, -2, making the 6th bunch about twice as intense as the 3rd one. The average charge of 60 pC was about a third of the typical intensity.

Charge Sensitivity

Even though the phase change due to charge is quite small the effect on peak current and therefore CSR kick is large, see Fig. 2 and 3. Besides the initial difference in charges which were caused by a not ideal 50/50 splits, it was recently found that some of the mirrors for the delayed bunches were clamped so hard that the mirrors deformed and caused the delayed laser pulses to a more elliptical than round shape and therefore causing some intensity loss due to apertures. For two bunches a charge difference can be used for tuning.

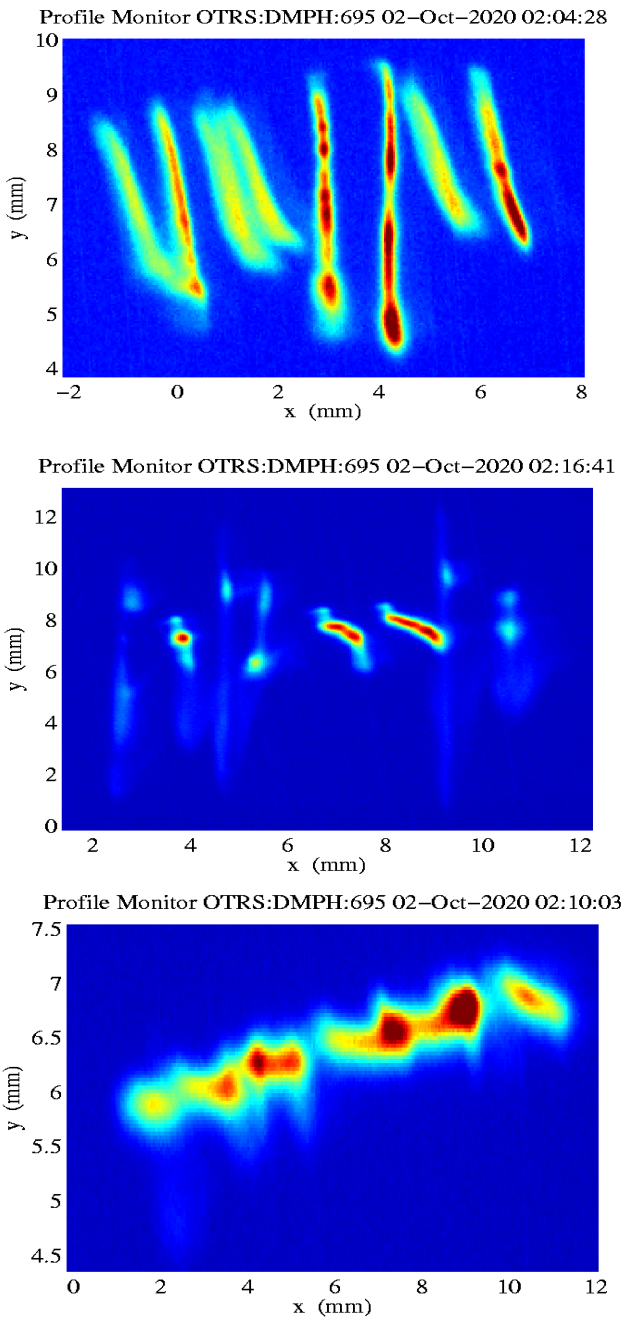

Figure 1: Eight bunches 0.7 ns apart on the OTR dump screen. The time resolving transverse cavity XTCAV was detuned in temperature so the eight bunches don't overlap in time (horizontal). The vertical dimension is proportional to energy. All bunches are over-compressed (top), while for the middle the compression was reduced (-32° to -30°), so bunches B2, B5 and B6 were under-compressed. At the bottom (at -29° in L2 phase) all are under-compressed. The energy slope along the bunches of about +2% is real. It was not corrected at the time.

*Work supported by U.S. Department of Energy, Contract DE-AC02-76SF00515.
† Decker@SLAC.Stanford.edu

ISBN: 978-3-95450-227-1 ISSN: 2673-5490 doi:10.18429/JACoW-IPAC2022-TUPOPT037

LCLS MULTI-BUNCH IMPROVEMENT PLAN: FIRST RESULTS

A. Romero, A. Halavanau, A. Krasnykh, A. A. Lutman, T. Beukers, J. Hugyik, A. Le, K. Luchini, E. Jongewaard, A. Sy, A. Ibrahimov, L. Borzenets, M. M. Petree, A. Benwell, A. Marinelli, F. J. Decker
SLAC National Accelerator Laboratory, Stanford University, Menlo Park CA, USA

Abstract

LCLS copper linac primarily operates in a single bunch mode with a repetition rate of 120 Hz. Presently, several in-house projects and LCLS user experiments require double- and multi-pulse trains of X-rays, with inter-pulse delay spanning between 0.35 and 220 ns. We discuss beam control improvements to the copper linac using ultra-fast stripline kicker, as well as additional photon diagnostics. We especially focus on a case of double-pulse mode, with 220 ns separation.

INTRODUCTION

LCLS has been offering ns-spaced hard x-ray (HXR) pulse trains to users for a several years [1]. The multi-bunch performance of the LCLS copper linac has been largely impaired by variations of RF phases in different klystrons, accelerating sections' misalignment [2], and, as a result, differences in the HXR undulator trajectories. Recently we have proposed to improve the performance of the LCLS multi-bunch mode by introducing ultra-fast e-beam TEM stripline kickers in the linac beamline. The choice of kicker technology was dictated by the minimum attainable pulse separation with the current state-of-the art electronics, and possible extension in the future to 8 or more pulses in a train. We designed and built two 0.3 m stripline structures, and installed them into the LCLS LI21-9 section. The details of the stripline design have been provided in [3]. The beamline installation model is presented in Fig. 1.

To energize the striplines, we designed and built a versatile system, with broadband high power solid-state amplifiers for the multi-bunch mode, and state-of-the-art solid state pulsers (based on drift step-recovery diodes (DSRD)) for the two-bunch mode. The amplifiers have been procured from the R&K company, and can output up to 1 kW of RF power in CW mode, and with 10 kHz - 300 MHz bandwidth. The feasibility and early design of the high-voltage pulsers based on DSRD technology has been presented in Ref. [4]. We have built two pulser units corresponding to the principal schematics in Fig. 2, D in Ref. [4], with the maximum attainable voltage of ± 5 kV.

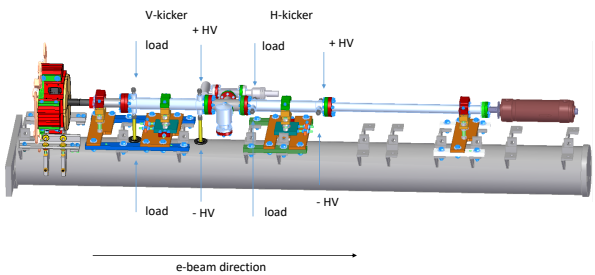

Figure 1: CAD model of the LCLS copper linac LI21-9 section installation.

FIRST EXPERIMENTAL RESULTS

We have commissioned the first two stripline kickers (X and Y) in LI21-9 section of the LCLS copper linac. The kickers were first energized with the strongest 7 kV pulse to verify no arcing or breakdown was occurring. We then proceeded with energizing the stripline structures together with the e-beam, and observing the corresponding trajectory responses.

Figure 2 shows e-beam X deflection as a function of time of arrival at the stripline structure, which has been powered with an RF waveform, generated with an arbitrary waveform generator (AWG) procured from Tabor Electronics and high power R&K amplifiers. The AWG clock was externally synchronized with a custom in-house built frequency multiplier which generated 1.428 GHz signal multiplying 119 MHz master oscillator clock by 12. We see that despite a quite "unconventional" application of the amplifiers in the pulsed mode, the e-beam transverse jitter remains the same across the waveform. Due to the full waveform tunability, we were later able to control pulse trains with the separations as small as 2 ns, and enhance x-ray intensity delivery in the multi-pulse user experiment.

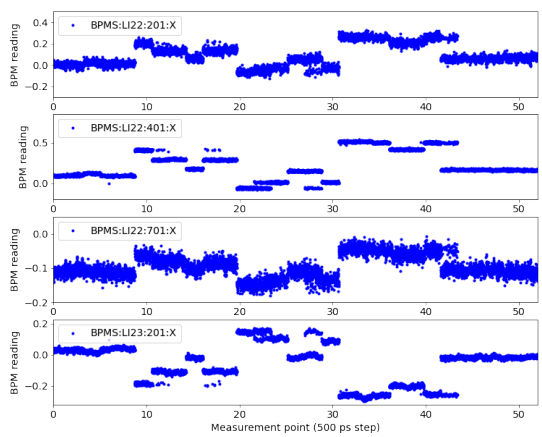

Figure 2: Scanning e-beam time of arrival through an arbitrary waveform generated by a pair of two solid-state amplifiers.

ISBN: 978-3-95450-227-1 ISSN: 2673-5490 doi:10.18429/JACoW-IPAC2022-TUPOPT038

FAST-GREENS: A HIGH EFFICIENCY FREE ELECTRON LASER DRIVEN BY SUPERCONDUCTING RF ACCELERATOR

P. Musumeci, A. Fisher, P. Denham, J. Jin, Y. Park,
Department of Physics and Astronomy, University of California Los Angeles, CA 90095, USA
R. Agustsson, L. Amoudry, T. Hodgetts, M. Ruelas, A. Murokh,
RadiaBeam Technologies, Santa Monica, CA 90404, USA
A. Lumpkin, A. Zholents, Argonne National Laboratory, Lemont, IL 60439, USA
D. Broemmelsiek, S. Nagaitsev, J. Ruan, J. Santucci, G. Stancari, A. Valishev,
Fermilab National Laboratory, Batavia, IL 60510, USA
J. Edelen, C. Hall and D. Bruhwiler, RadiaSoft, Boulder, CO 80301, USA

Abstract

In this paper we'll describe the status of the FAST-GREENS experimental program where a 4 meter long strongly tapered helical undulator with a seeded prebuncher is used in the high gain TESSA regime to convert a significant fraction (up to 10%) of energy from the 220 MeV electron beam from the FAST linac to coherent 515 nm radiation. We'll also discuss the longer term plans for the setup where by embedding the undulator in an optical cavity matched with the high repetition rate from the superconducting accelerator (3 MHz or 9 MHz), a very high average power laser source can be obtained. Eventually, the laser pulses can be redirected onto the relativistic electrons to generate by inverse compton scattering a very high flux of circularly polarized gamma rays for polarized positron production.

INTRODUCTION

Improving the conversion efficiency of relativistic electron beam power into coherent short wavelength radiation is at the center of both scientific and industrial interests as it would enable light sources to reap the benefits of 100 years development in charged particle accelerator technology on how to be extremely efficient in terms of wall-plug energy usage. In the X-ray it would facilitate ultrahigh intensity X-ray laser pulses for single shot coherent imaging and Schwinger-field physics exploration, in the EUV it would meet the demands of fast throughput material processing (EUV-lithography) and at visible wavelengths it would enable high efficiency, high average and peak power lasers. It is helpful to note here how state-of-the-art X-ray sources based on the Free Electron Laser principle take advantage of only a minimal fraction ($< 0.1\%$) of the available power stored in the beam and most of it is is simply wasted on the beam dump.

The TESSA program aims at fundamentally addressing this current limitation in electron-based coherent radiation generation by exploiting a deeper understanding of the interaction of relativistic electrons with the electromagnetic field in tapered undulator systems, leveraging the progress in high brightness beam generation and control.

The physical concept behind our approach is the so-called Tapering-Enhanced-Stimulated-Spontaneous-Amplification regime of FELs where high intensity seed and pre-bunched electron beams are used in combination with strongly tapered undulators to sustain high gradient deceleration over extended distances and convert a large fraction of the beam energy into coherent radiation [1]. The main advantages of this coupling scheme are the absence of nearby boundary or media (i.e. this is a vacuum plane-wave interaction), so that there are basically no mechanisms for the energy to flow out of the particle-field system. In TESSA, the initial conditions for the system allow for particle deceleration at a very high average energy exchange rates (typically in excess of 10 MV/m) larger than in any known FEL, in order to beat the onset of sideband instabilities which have been known for decades to set the limit on tapered FEL energy exchange [2]. Previous experiments based on the TESSA concept [3] demonstrated efficiencies as high as 30% in the far-infrared. Nevertheless, they were carried out in a very low gain amplification regime resulting in a strong background signal from the seed laser which precluded obtaining direct measurements of the transverse and spectral profiles of the amplified radiation. A recent application of the TESSA concept in the THz regime demonstrated 10% conversion efficiency in 1 m long tapered helical undulator at 160 GHz [4].

Scientific and Technical Goals

The TESSA initiative at FAST is an FEL experiment aimed at demonstrating high extraction efficiency lasing (10% e-beam to light conversion) in a strongly tapered seeded regime in the visible range of the electromagnetic spectrum (initial tuning at 515 nm) with two stated scientific goals:

- The demonstration of single pass record high energy extraction efficiency from a relativistic electron beam in the visible region of the electromagnetic spectrum.
- The first experimental measurements of spectral and transverse profile characteristics of the radiation amplified in the TESSA regime of operation.

Both of these goals would represent significant breakthroughs for the development of future high efficiency light sources.

ISBN: 978-3-95450-227-1 ISSN: 2673-5490 doi:10.18429/JACoW-IPAC2022-TUPOPT039

CHARACTERIZATION OF DIAMOND WITH BURIED BORON-DOPED LAYER DEVELOPED FOR Q-SWITCHING AN X-RAY OPTICAL CAVITY*

R. A. Margraf† [1], J. Krzywinski, T. Sato, J. P. MacArthur, D. Zhu, M. L. Ng, A. Halavanau, R. Robles[1], A. Robert[2], Z. Huang[1], G. Marcus, SLAC, Menlo Park, USA
M. D. Ynsa, Center for Micro Analysis of Materials, Autónoma, Madrid, Spain
F. Ke, Stanford University, Stanford, USA
S.-K. Mo, Y. Zhong[1], Lawrence Berkeley National Laboratory, Berkeley, USA
P. Pradhan, Argonne National Laboratory, Lemont, USA
[1]also at Stanford University, Stanford, USA, [2]also at MAX IV, Lund, Sweden

Abstract

X-ray Free-Electron Laser Oscillators (XFELOs) and X-ray Regenerative Amplifier FELs (XRAFELs) are currently in development to improve longitudinal coherence and spectral brightness of XFELs [1]. These schemes lase an electron beam in an undulator within an optical cavity to produce X-rays. X-rays circulate in the cavity and interact with fresh electron bunches to seed the FEL process over multiple passes, producing progressively brighter and more spectrally pure X-rays. Typically, the optical cavities used are composed of Bragg-reflecting mirrors to provide high reflectivity and spectral filtering. This high reflectivity necessitates special techniques to out-couple X-rays from the cavity to deliver them to users. One method involves "Q-switching" the cavity by actively modifying the reflectivity of one Bragg-reflecting crystal. To control the crystal lattice constant and thus reflectivity, we use an infrared (IR) laser to heat a buried boron layer in a diamond crystal. Here, we build on earlier work [2] and present the current status of our Q-switching diamond, including implantation with 9 MeV boron ions, annealing and characterization.

INTRODUCTION

In Q-switching an optical cavity, as described in [2], an IR laser heats a region of a Bragg-reflecting mirror, actively modifying its reflectivity, and enabling out-coupling of X-rays. A crystal used for this purpose must have a uniform rocking curve (less than the rocking curve width of 8 µrad for 9.831 keV X-rays reflecting off diamond 400 planes) over a region the size of the X-ray beam ~40 µm. The crystal must also absorb IR light strongly. Diamond has thermal dissipation properties which make it ideal for use in in a cavity-based XFEL. A buried boron layer can be implanted to increase the IR absorption of diamond for Q-switching.

IMPLANTATION AND ANNEALING

A high-temperature-high pressure (HPHT) diamond, described in [2] was implanted as described in [3] with 9 MeV boron ions using the microbeam line at the Center for Micro Analysis of Materials (CMAM) at the Autonomous University of Madrid. 200 x 200 µm areas were implanted with fluences of 5×10^{15}, 1×10^{16},1.5×10^{16} 2×10^{16} and 2.5×10^{16} ions/cm^2 by scanning a focused beam of boron ions in a spiral rastering pattern.

Following implantation, five high-temperature in-vacuum annealings at 900, 950,1150, 1300, and 1450 °C were performed to heal implantation damage. 900 and 950 °C annealings were performed in a UHV chamber heated by a filament under 2.7×10^{-8} mbar or better vacuum. The filament was heated to the target temperature, then annealed for 1 hr. The 1150, 1300, and 1450 °C annealings were performed in a Red Devil G vacuum furnace manufactured by R. D. Webb Company Inc under 1×10^{-4} mbar or better vacuum, similar to [4]. The furnace was ramped up at 2 °C/min, annealed for 3 hr, then ramped down at 3 °C/min to 700 °C and cooled.

During this process, we did see some graphitization, as shown in Fig. 1, but not on our regions of interest.

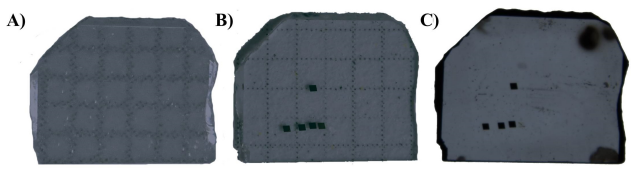

Figure 1: 1x images of HPHT diamond. A) Pre-implantation, B) Post-implantation, Post 1450 °C annealing.

CHARACTERIZATION

We performed several measurements to characterize healing in the boron-implanted regions.

IR Transmittance

To show implantation increases IR absorption, we measured IR transmittance. A Thorlabs CPS780S laser diode beam was expanded, collimated and transmitted through our sample. A Thorlabs FL780-10 780 nm filter selected the signal wavelength before a Mako G-319C POE camera.

The post 1450 °C annealing case is shown in Fig. 2. The IR transmittance of un-implanted diamond and the region of lowest doping is similar, 66 - 69 %, and the more highly doped regions transmit less IR light, 15 - 26 %. To account for variation in transmittance across the diamond, we also

* This work was supported by the Department of Energy, Laboratory Directed Research and Development program at SLAC National Accelerator Laboratory, under contract DE-AC02-76SF00515.
† rmargraf@stanford.edu

ISBN: 978-3-95450-227-1 ISSN: 2673-5490 doi:10.18429/JACoW-IPAC2022-TUPOPT044

HIGH-POWER ATTOSECOND PULSES VIA CASCADED AMPLIFICATION*

P. L. Franz†, Z. Guo, R. Robles, Stanford University, Stanford, CA, USA
D. K. Bohler, D. Cesar, X. Cheng, T. Driver, J. P. Duris, A. Kamalov, S. Li, R. Obaid, N. S. Sudar, A. L. Wang, Z. Zhang, J. P. Cryan, A. Marinelli, SLAC National Accelerator Laboratory, Menlo Park, CA, USA

Abstract

The timescale for electron motion in molecular systems is on the order of hundreds of attoseconds, and thus the time-resolved study of electronic dynamics requires a source of sub-femtosecond x-ray pulses. Here we report the experimental generation of sub-femtosecond duration soft x-ray free electron laser (XFEL) pulses with hundreds of microjoules of energy using fresh-slice amplification in two cascaded stages at the Linac Coherent Light Source. In the first stage, an enhanced self-amplified spontaneous emission (ESASE) pulse is generated using laser-shaping of the electron beam at the photocathode. The electron bunch is then delayed relative to the pulse by a magnetic chicane, allowing the radiation to slip onto a fresh slice of the bunch, which amplifies the ESASE pulse in the second cascade stage. Angular streaking will be used to characterize the experimental pulse durations.

INTRODUCTION

Valence electronic motion in molecular systems is on the order of hundreds of attoseconds. Consequently, the time-resolved study of electron dynamics requires a source of sub-femtosecond pulses.

The X-Ray Laser-Enhanced Attosecond Pulse Generation (XLEAP) collaboration is an ongoing project for the development of attosecond capabilities at the Linac Coherent Light Source (LCLS). The XLEAP project has previously demonstrated the generation of isolated soft x-ray attosecond pulses with pulse energy millions of times larger than any other source of isolated attosecond soft x-ray pulses, with a median pulse energy of 10 μJ and median pulse duration of 280 as [1]. Here we report recent development of a high power attosecond mode via cascaded amplification of the x-ray pulse. We experimentally demonstrate generation of sub-femtosecond duration soft x-ray free electron laser pulses with hundreds of microjoules of energy.

CASCADED AMPLIFICATION

A density perturbation is introduced in the electron beam by laser pulse stacking at the photocathode [2]. The perturbation is amplified to a high current spike by acceleration and beam compression in downstream wigglers and a magnetic chicane. In the first cascade stage, the undulator taper is matched to the chirp of the electron beam at the current spike to produce the initial enhanced self-amplified spontaneous emission (ESASE) [3] pulse. The bunch is then delayed relative to the pulse by a second magnetic chicane, allowing the radiation to slip pass the initial lasing region to be overlapped with a fresh slice of the bunch and be amplified in the second cascade stage (Fig. 1).

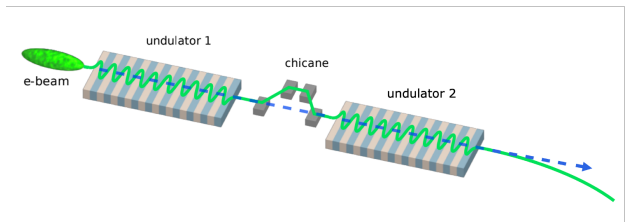

Figure 1: Schematic of the two-stage cascade.

PRELIMINARY RESULTS

The XLEAP project has experimentally demonstrated the generation of soft x-ray pulses with hundreds of microjoules of energy using cascaded amplification in two FEL stages at LCLS, the highest energy shots having over 300 μJ of pulse energy. These higher energy pulses also have sufficient bandwidth to have sub-femtosecond duration near the fourier transform limit (Fig. 2). Previous XLEAP configurations have been within a factor of 2 of the fourier transform limit [1].

In the electron beam phase space, energy loss from reamplification in the second stage is seen as the lasing spike in the head of the beam (Fig. 3). The ESASE pulse is initially lased at the current spike near the center of the beam, and is then slipped ahead to the fresh, non-chirped head of the beam. Energy loss from lasing in the head is visible for the higher energy shots, indicating that amplification of the ESASE pulse is taking place.

CONCLUSION

The preliminary results suggest we can deliver a high power, sub-femtosecond duration soft x-ray mode at LCLS. This set-up is scalable to the upcoming high repetition rate at LCLS-II. Future work will use angular streaking [4] of the experimental soft x-ray pulses to reconstruct the temporal profile of the x-ray pulses and characterize peak power. Additionally, the broadening of bandwidth with pulse energy is characteristic of superradiant lasing (Fig. 4). It is

* This work was supported by US Department of Energy Contracts No. DE-AC02-76SF00515.
† FRANZPL@STANFORD.EDU

ISBN: 978-3-95450-227-1 ISSN: 2673-5490 doi:10.18429/JACoW-IPAC2022-TUPOPT046

ELECTRON TRANSPORT FOR THE LCLS-II-HE LOW EMITTANCE INJECTOR*

Y. Nosochkov†, C. Adolphsen, R. Coy, C. Mayes, T. Raubenheimer, M. Woodley,
SLAC, Menlo Park, CA, USA

Abstract

The Low Emittance Injector (LEI) is a recent addition to the LCLS-II High Energy (LCLS-II-HE) Project under design at SLAC National Accelerator Laboratory. It will provide a second beam source capable of producing a low emittance electron beam that increases the XFEL photon energy reach to 20 keV. The LEI will include an SRF electron gun, a buncher system, a 1.3 GHz cryomodule, and a beam transport system with a connection to the LCLS-II beamline and a stand-alone diagnostic line. The LEI transport beamlines and diagnostic are discussed.

INTRODUCTION

The Low Emittance Injector (LEI) [1] is a recent addition to the LCLS-II High Energy (LCLS-II-HE) Project [2]. It will (1) improve the beam brightness to increase the XFEL photon energy reach to 20 keV and (2) provide a second injector for higher LCLS-II availability. The goal is to achieve the LEI transverse beam emittance of 0.1 mm-mrad at 100 MeV energy and 100 pC bunch charge. The LEI will include a state-of-the-art SRF electron gun, a buncher system, an 8-cavity 1.3 GHz cryomodule (CM00), and a beam transport system with a dogleg connection to the LCLS-II beamline and a stand-alone diagnostic line. The LEI will be installed in a separate tunnel parallel to the LCLS-II injector tunnel – see plan view in Fig. 1, where the LEI is at the top of the figure and the LCLS-II injector is at the bottom. The LEI beam can be either (1) delivered to the LCLS-II beamline for further transport to undulators or (2) sent into a straight-ahead diagnostic line for stand-alone operation.

This paper primarily describes the LEI beam transport and diagnostic systems downstream of the CM00 cryomodule. The aforementioned transport include: (1) a matching section downstream of the cryomodule, (2) an achromatic dogleg connection from the LEI to the LCLS-II beamline, and (3) a diagnostic line that supports measurements of bunch emittance, energy, charge, spatial profile, and beam halo and dark current. As a future upgrade, a horizontal RF deflecting cavity (TCAV) [3] and RF cavity BPMs are proposed to be added in the reserved spaces which will enable measurements of bunch length, slice energy spread, and vertical slice emittance. For a cost-effective design, the beamlines are made as compact as possible based on the existing magnets and devices or existing designs at SLAC. The location of the LEI connection to the LCLS-II is carefully selected; it does not require any modification to the existing LCLS-II beamline components, and the LCLS-II beam can operate normally when the LEI is in stand-alone operation.

LEI MAIN BEAMLINE

Figure 1 shows the layout of the LEI and LCLS-II injector tunnels and the beamline components. The initial design is based on 6-m distance between the LEI and LCLS-II injector lines, however there is a plan to increase the separation. The latter will not affect the present design except lengthening the dogleg.

The LEI main beamline transports the beam to the LCLS-II. It starts at the SRF gun followed by a buncher system, an 8-cavity 1.3 GHz cryomodule (CM00), an optics matching section, and a dogleg which connects the LEI to the LCLS-II injector beamline. The LEI and LCLS-II are merged in the free area of the LCLS-II Laser Heater (LH) where the LEI optics match is done using six downstream LH quadrupoles.

When the LEI beam is delivered to the LCLS-II, the beam from the LCLS-II injector must be turned off. Alternatively, the LEI beam can be directed to the LEI diagnostic line for beam measurements in stand-alone operation. In this case, the dogleg dipoles are turned off, and the beam from the LCLS-II injector can operate normally.

The matching section downstream of the CM00 consists of four quadrupoles. It accommodates vacuum components, a beam halo and dark current collimator, and reserves space for a future horizontal RF deflector. The four quadrupoles along with an upstream CM00 quadrupole are sufficient for match to the downstream dogleg optics including scenario where the incoming lattice functions are altered due to upstream errors or design updates. Steering correctors and BPMs are included for orbit correction.

The dogleg section creates a 35° horizontal angle to direct the LEI beam towards the LCLS-II beamline. The bending is performed by two pairs of 17.5° horizontal dipoles located at the beginning and end of the dogleg. The four dipoles and eight quadrupoles are positioned symmetrically relative to the dogleg center. Optics functions in the dogleg and the upstream matching section are shown in Fig. 2 calculated using MAD8 [4].

The dogleg is designed to cancel both linear and second order dispersion in order to suppress the chromatic emittance growth; the emittance preservation was confirmed in tracking simulations. The linear dispersion is cancelled using a double-bend achromat (DBA) cell at each end of the dogleg. The second order dispersion (see Fig. 2) is cancelled by constraining the horizontal phase advance between the DBA centers to 2π. Quadrupoles are powered symmetrically, yielding symmetric beta functions, which were minimized. Each dogleg quadrupole has a BPM and a steering corrector next to it for orbit correction.

* Work supported by the Department of Energy Contract DE-AC02-76SF00515.
† yuri@slac.stanford.edu

ISBN: 978-3-95450-227-1 ISSN: 2673-5490 doi:10.18429/JACoW-IPAC2022-TUPOPT047

PROGRESS REPORT ON POPULATION INVERSION X-RAY LASER OSCILLATOR AT LCLS

A. Halavanau, F. Fuller, R. Robles, R. Margraf, A. Aquila, M. Liang, R. Alonso-Mori,
R. H. Paul, A. A. Lutman, F.-J. Decker, C. Pellegrini
SLAC National Accelerator Laboratory, Stanford University, Menlo Park CA 94025, USA
P. Manwani, N. Majernik, J. B. Rosenzweig
University of California, Los Angeles, CA, 90095, USA
N. Welke, R. Ash, U. Bergmann
University of Wisconsin, Madison, WI, 53706, USA
Š. Krušič, M. Žitnik
Jozef Stefan Institute, Ljubljana, Slovenia
A. Benediktovitch, N. Rohringer
University of Hamburg, CFEL/DESY, Germany

Abstract

We report the progress in the design and construction of a population inversion x-ray laser oscillator (XLO) using LCLS as an x-ray laser pump, being developed by a SLAC, CFEL, University of Hamburg (Germany), University of Wisconsin, Josef Stefan Institute (Slovenia) and UCLA collaboration. In this proceeding, we will present the latest XLO design and numerical simulations substantiated by our first experimental results. In our next experimental step XLO will be tested on the Coherent X-ray Imaging (CXI) end-station at LCLS as a two pass Regenerative Amplifier op-erating at the Copper K_α photon energy of 8048 eV. When built, XLO will generate fully coherent transform limited pulses with about 50 meV FWHM bandwidth. We expect the XLO will pave the way for new user experiments, e.g. in inelastic x-ray scattering, parametric down conversion, quantum science, x-ray interferometry, and external hard x-ray XFEL seeding.

INTRODUCTION

A population inversion X-ray laser oscillator, XLO, pumped by an X-ray FEL like LCLS at SLAC, will provide high intensity, transform limited pulses, opening-up new experimental possibilities in the exploration of atomic and molecular systems at the angstrom/femtosecond space and time scale, interferometry, X-ray quantum science and more. We discuss in this paper several experimental and simulation steps that the XLO collaboration is taking to realize the oscillator. Our present efforts are mainly addressed to a precise determination of the extent of the damage done by the X-ray pump pulse to the gain medium, the development of a solid copper, high speed, gain medium target that would provide fresh copper material to the pumping pulses, repetition of the amplified spontaneous emission (ASE) [1–4] gain measurement with and without external seeding, optical cavity alignment using Si crystals, advanced 3D numerical simulations. In addition, we are working to generate from LCLS the train of pump pulses separated by about 30 ns needed to operate the oscillator. As a first step toward the realization of XLO we will have a two-pulse pump regenerative amplifier.

FAST MOVING SOLID TARGET

In our initial work on XLO we considered using a high-speed jet of a copper nitrate solution as the pump pulse target [5]. Preliminary experiments with the liquid jet have shown that at extreme x-ray power densities the liquid ma-terial undergoes through a process of violent expansion on tens of nanoseconds time scale [6, 7]. This fact prevents the use of simple liquid jet systems in the XLO-like experiments. While an ultra-fast liquid jet is technologically possible, it requires a substantial development and installation effort, and is outside of the scope of our project.

We therefore considered using a fast spinning solid target. There are several advantages of solid w.r.t liquid target. First, a larger, about 10 times, density of copper atoms allows to reduce pump pulse requirements from several mJ, as in the original proposal, to tens of µJ. The reduced pulse intensity is much easier to be achieved at the XFEL, and it drastically reduces the heat load on the cavity in-coupling crystal; see Ref. [1, 5]. The target thickness has been optimized in the state-of-the-art simulation XLO-SIM toolbox that will be described in detail elsewhere [8]. The optimum target width was found to be 25 µm; see Fig. 1. We refer the reader to Refs. [9, 10] for a detailed description of the target assembly and XFEL induced damage.

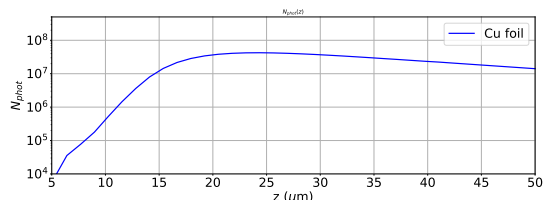

Figure 1: Simulated number of photons after the first pass in the XLO.

ISBN: 978-3-95450-227-1 ISSN: 2673-5490 doi:10.18429/JACoW-IPAC2022-TUPOPT048

bERLinPro BECOMES SEALab: STATUS AND PERSPECTIVE OF THE ENERGY RECOVERY LINAC AT HZB*

A. Neumann†, B. Alberdi[1], T. Birke, P. Echevarria, D. Eichel, F. Falkenstern, R. Fleischhauer, A. Frahm, F. Goebel, A. Heugel, F. Hoffmann, H. Huck, J.-G. Hwang, T. Kamps[1], S. Klauke, G. Klemz, J. Knobloch[2], J. Kolbe, J. Kuehn, B.C. Kuske, J. Kuszynski, S. Mistry, N. Ohm, H. Ploetz, S. Rotterdam, O. Schappeit, G. Schindhelm, C. Schröder, M. Schuster, H. Stein, E. Suljoti, Y. Tamashevich, M. Tannert, J. Ullrich, A. Ushakov, J. Voelker, C. Wang[2],
Helmholtz-Zentrum Berlin, Berlin, Germany
[1]also at Humboldt-Universität zu Berlin, Germany
[2]also at Universität Siegen, Germany

Abstract

Since end of the year 2020 the energy recovery linac (ERL) project bERLinPro of Helmholtz-Zentrum Berlin (HZB) has been officially completed. But what is the status of this facility, the next scientific goals in the framework of accelerator physics at HZB, what are the perspectives? To reflect the continuation of this endeavor and the broadening of applications of this machine from high current SRF based energy recovery concept up to an ultrafast electron diffraction (UED) facility producing shortest electron pulses, the facility is now named Sealab, Superconducting RF Electron Accelerator Laboratory. In this contribution, an overview of lessons learned so far, the status of the machine, the coming set up and commissioning steps with an outlook to midterm and future applications will be given. In summary, Sealab will expand, including the ERL application, and become a general accelerator physics and technology test machine to employ UED as a first study case and will also be an ideal testbed to investigate new control schemes based on digital twins or machine learning methods.

STATUS OF THE BERLINPRO PROJECT

In end of 2020 the ERL facility bERLinPro [1] accomplished the project phase by finalizing the building, setup of all technical infrastructure and installation of all major components of the warm machine. In summer 2021 also the final part of the beamline vacuum system with the recirculator was closed and assembled under ISO5 cleanroom conditons (see Fig. 1), as all of the machine to allow to preserve the high level particulate free environment for proper operation of the SRF cavity systems of photo-injector, booster module of the injector line and any future linac installation in the main recirculator. Currently, the facility is in its final assembly and commissioning phase for diagnostics, cryo-plant, SRF modules and photo-cathode laser system. Growing of high quantum-efficiency photo-cathodes and research in improved recipes is being continued and presented here [2]. After being operated in a dedicated laboratory [3, 4], the SRF photo-injector underwent a refurbishment program [5, 6] to recover the cavities and improve the installations and assembly routines. The focus is currently on finalizing the cryo-module and produce first beam from the photo-injector only, followed-up by the booster installation, for which the high power coupler processing is close to be accomplished [7]. Figure 2 displays an overview of the whole accelerator, whereas Table 1 summarizes the main parameters of the high current ERL and variable current injector setup implementing the two cathode laser systems at 50 and 1300 MHz [8].

Table 1: bERLinPro/SEALab Parameters

Parameter	ERL	Injector/UED
Beam energy (MeV)	50	6.5-10/2
I_{avg} (mA)	100	6-10/0.0025
Laser freq. (MHz)	1300	50, 1300
RF freq. (MHz)	1300	1300
ϵ_{norm} (mm mrad)	1 (0.6)	0.6/0.03
σ_t (ps)	2 (0.1)	0.02-2
Bunch charge (pC)	77	0.05-400

Figure 1: A view on the vacuum system of the bERLinPro accelerator.

* Work supported by German Bundesministerium für Bildung und Forschung, Land Berlin, and grants of Helmholtz Association
† axel.neumann@helmholtz-berlin.de

ISBN: 978-3-95450-227-1 ISSN: 2673-5490 doi:10.18429/JACoW-IPAC2022-TUPOPT050

INVESTIGATION OF POLARIZATION DEPENDENT THOMSON SCATTERING IN AN ENERGY-RECOVERING LINEAR ACCELERATOR ON THE EXAMPLE OF MESA*

C. L. Lorey, Institut für Kernphysik, JGU, Mainz, Germany
A. Meseck[1], Institut für Kernphysik, JGU, Mainz, Germany
[1]also at Helmholtz Zentrum, Berlin, Germany

Abstract

At the Johannes Gutenberg University (JGU) in Mainz, a new accelerator is currently under construction in order to deliver electron beams of up to 155 MeV to two experiments. The Mainz Energy-recovering Superconducting Accelerator (MESA) will offer two modes of operation, one of which is an energy-recovering (ER) mode. As an ERL, MESA, with it's high brightness electron beam, is a promising accelerator for supplying a Thomson back scattering based Gamma source. Furthermore, at MESA, the polarization of the electron beam can be set by the injector. The aim of this work is to provide a concept and comprehensive analysis of the merit and practical feasibility of a Thomson backscattering source at MESA under consideration of beam polarization and transversal effects. In this paper, an overview and results of our semi analytical approach to calculate various Thomson back scattering light source scenarios at MESA will be given. Furthermore we will discuss the benefits of using polarized electrons in combination with a polarized laser beam.

INTRODUCTION

The Mainz Energy-recovering Superconducting Accelerator (MESA) at the Institute for Nuclear Physics (KPH) of the JGU Mainz is being built for two modes of operation for two respective experiments. In the external beam (EB) mode, in which an electron beam of 150 µA current will be accelerated to an energy of 155 MeV, the accelerated particle bunches will be dumped after interaction with the target. In the energy-recovery (ER) mode, a beam current of 1-10 mA will be accelerated to an energy of 105 MeV. After the experiment, the spent electron bunches re-enter the accelerating cavities with a phase shift of 180° with respect to the RF field. Now synchronized to the cavity RF in deceleration phase, the electrons transfer the energy back to the RF field, allowing for an elegant way to recover the energy stored within the electron bunches before dumping the beam. The acceleration takes place in two superconducting MESA Enhanced Elbe Cryomodule (MEEC) cavities, a modified version of ELBE style cryomodules. Each pass through a cryomodule increases the electron energy by 25 MeV. [1]
In the MESA injection system [2], the electron beam spin polarization can be set via 2 solenoids and 2 Wien filters in both ER and EB mode, albeit at a lower beam current of 150 µA instead of 10 mA (numbers are potentially subject to change in development). [3] It is known that the spin polarization of both photon and electron beam affects the scattering cross section and energy spectrum both [4]. Ways to potentially make use of the polarization dependent properties are to be explored.
Implementation via dedicated Thomson scattering arc into the MESA layout was discussed in last year's IPAC paper [5] and will omitted from this year's. Due to the low impact on the electron beam, another option is to implement a Thomson scattering experiment parasitically into an existing MESA beam line. In this scenario, the Thomson scattering experiment can only be conducted during another MESA mode activity, but the necessary changes to the overall MESA layout would be reduced.
This report is structured as follows:
Sections 1, polarized Thomson scattering with recoil, summarizes the mathematical foundation of our calculations and introduces the aspect of polarization. In section 2, the results of our calculations for an example scenario are discussed. Lastly, section 3 gives a brief outlook on future tasks.

POLARIZED THOMSON SCATTERING WITH RECOIL

The term Thomson scattering, or Thomson back scattering, is used to describe the process in which photons scatter quasi-elastically on free electrons. It is the low incidence photon energy limit of Compton scattering. While in literature we find definitions in which the recoil experienced by the electron is zero, others are writing about a process in which the recoil is merely low. In this release, we are following the latter. As we are expecting relativistic electrons, our calculations are taking place in Lorentz boosted reference frames using four-vector algebra. The Lorentz factor γ^* of the boosted system is defined by the relation between the overall energy contained in the laboratory frame E_{lab} to that contained in the center of mass frame E_{cm}:

$$\gamma_{cm} = \gamma^* = \frac{E_{lab}}{E_{cm}} = \frac{E_e + h\nu}{m_e c^2 \sqrt{1+\Delta}} \simeq \frac{\gamma}{\sqrt{1+\Delta}} \qquad (1)$$

While E_{lab} is the sum of the initial electron E_e and photon energy $h\nu$, E_{cm} can be expressed for unpolarized beams via relativistic recoil factor $\Delta \equiv \frac{2h\nu\gamma}{E_0} + \frac{2\hbar c^2}{E_0^2}(k_x P_x + k_y P_y + k_z P_z)$ where k_i & P_i $(i = (x, y, z))$ are the photon respectively electron momenta in 3D and E_0 is the electron rest energy.
Transforming the reference frame and with it each four-

* Work supported by RTG 2128 AccelencE

ISBN: 978-3-95450-227-1 ISSN: 2673-5490 doi:10.18429/JACoW-IPAC2022-TUPOPT051

RECONSTRUCTION AND BEAM-TRANSPORT STUDY OF THE cERL DUMP LINE FOR HIGH-POWER IR-FEL OPERATION

N. Nakamura†, Y. Tanimoto, N. Higashi, K. Harada, M. Shimada, T. Uchiyama, T. Nogami, A. Ueda, S. Nagahashi, T. Obina, R. Takai, H. Sagehashi, K. Nigorikawa, O. Tanaka, R. Kato, H. Sakai, High Energy Accelerator Research Organization, Tsukuba, Japan

Abstract

Infrared (IR) SASE-FEL emission was successfully generated for macro pulses of about 1 μs with the maximum repetition rate of 5 Hz at the cERL. In the future, high-power FEL operation will be planned to increase electron bunches drastically with energy recovery. Therefore, the dump line was redesigned and reconstructed to increase the momentum acceptance and to improve the magnet system for avoiding serious beam loss in the high power FEL operation. Furthermore, the first beam-transport study was performed by transporting the beam directly from the injector to the beam dump through the reconstructed dump line. In this paper, we present the reconstructed dump line and the beam-transport study. The new dump line can be a model for dump lines of high-power ERL-FELs.

INTRODUCTION

A significant FEL pulse energy was generated at the cERL IR-FEL [1] in Burst mode where a macro pulse of about 1 μs is repeated at the maximum frequency of 5 Hz. In the next step, high-power FEL operation in CW mode should be carried out with energy recovery by increasing electron bunches drastically. However, momentum spread of the electron beam increases due to the FEL emission and the space charge effects and may cause serious beam loss by exceeding the momentum acceptance of the cERL downstream of the FEL. Therefore, we reconstructed the dump line in Autumn 2020 to greatly increase the momentum acceptance and to improve the magnet system for more flexible beam control. Then we carried out the beam-transport study of the new dump line in March 2021 by injecting the beam directly from the injector without passing the recirculation loop.

MOMENTUM ACCEPTANCE

Beam loss must be efficiently suppressed in the high-power FEL operation at the cERL [2] in terms of radiation safety and machine protection, because the beam current is much increased in CW mode as compared that in Burst mode. The electron beam can have large momentum spread due to the FEL emission and the longitudinal space charge effects and cause significant beam loss at the dispersion sections by exceeding the apertures of the beam ducts. To avoid it, the momentum acceptance downstream of the FEL must be sufficiently large compared to the momentum spread of the electron beam. The main dispersion sections downstream of the FEL are the 2nd arc and the dump line as shown in Fig. 1. In the FEL operation, we have so far used Burst mode, where the electron beam is dumped without energy recovery at the movable dump before the dump line. In the high-power FEL operation, the high-current beam is decelerated in the main linac for energy recovery and transported to the beam dump through the dump line.

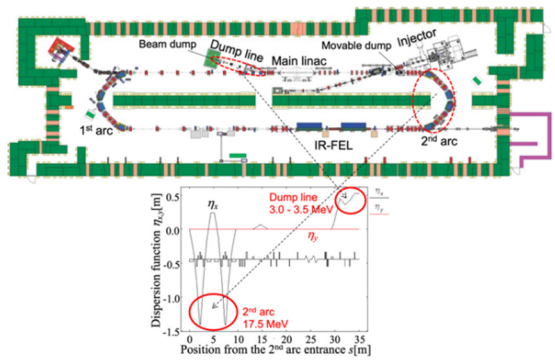

Figure 1: Layout of the cERL including the two dispersive sections, the 2nd arc and dump line, downstream of the IR-FEL with the dispersion functions.

The momentum acceptance is defined with the maximum dispersion function $\eta_{x,\,max}$ and the beam-duct aperture A_x in the dispersion section by the following equation.

$$\left(\frac{\Delta p}{p}\right)_{MA} = \frac{A_x}{\eta_{x,max}} \quad (1)$$

In Eq. (1), the effect of the betatron beam size is neglected for simplicity.

In the cERL, two beams with different momenta pass for energy recovery between the exit of the injector and the entrance of the dump line. In the injection and dump chicanes, the lower-momentum beam is deflected by 16 degrees for injection and dump and the higher-momentum beam makes closed bump orbits. The ratio of the lower and higher momenta must be less than 1/5 in order that the higher-momentum beam does not hit the beam ducts in the injection and dump chicanes. Therefore, the beam energy at the dump line must be 3.5 MeV or lower when the beam energy in the recirculation loop including the FEL and the 2nd arc is set to 17.5 MeV. Table 1 shows the parameters of the two dispersion sections downstream of the IR-FEL, the 2nd arc and the dump line before and after the reconstruction. The values within parentheses in the table are the momentum acceptances of the dump line normalized by the momentum at the 2nd arc for comparing the momentum acceptances of the different momenta. The normalized momentum acceptance before the

† noro.nakamura@kek.jp.

ISBN: 978-3-95450-227-1 ISSN: 2673-5490 doi:10.18429/JACoW-IPAC2022-TUPOPT052

PROPOSAL FOR NON-DESTRUCTIVE ELECTRON BEAM DIAGNOSTIC WITH LASER-COMPTON BACKSCATTERING AT THE S-DALINAC *

M. Meier†, M. Arnold, J. Enders and N. Pietralla
Technische Universität Darmstadt, Department of Physics,
Institute for Nuclear Physics, Schlossgartenstr. Darmstadt, Germany

Abstract

To recover a large fraction of energy from the accelerator process in an energy-recovery linac, experiments, secondary-beam production, and beam diagnostics must be non-destructive and/or, hence, feature a low interaction probability with the very intense electron-beam. Laser-Compton backscattering can provide a quasi-monochromatic highly polarized X-ray to γ-ray beam without strongly affecting the electron beam due to the small recoil and the small Compton cross-section. Highest energies of the scattered photons are obtained for photon-scattering angles of 180°, i. e., backscattering. A project at TU Darmstadt foresees to synchronize a highly repetitive high-power laser with the Superconducting DArmstadt electron LINear ACcelerator S-DALINAC, capable of running in energy recovery mode to realize a laser-Compton backscattering source with photon beam energy up to 180 keV. The source will be first used as a diagnostic tool for determining and monitoring key electron-parameters, in particular energy and the energy spread at the S-DALINAC operation. Results are foreseen to be used for optimizing the design of laser-Compton backscattering sources at energy-recovery linacs.

INTRODUCTION

Bright, monochromatic and tunable X-Ray to γ-ray sources of very small spot size are necessary for a wide range of applications from diffraction and spectroscopy in material and radiography and tomography biomedical science [1, 2] to photo nuclear reactions [3] like nuclear resonance fluorescence or photo fission [4]. Photon beams with energies in the range from 1 keV to 200 keV are mostly generated in synchrotrons with undulators. These facilities usually have the disadvantage that they are very large and would require electrons in the high GeV range for higher photon energies. For these cases, more and more Compton backscattering sources have become increasingly interesting [5]. By combining small storage rings and novel laser systems, the size of laser-Compton backscattering (LCB) sources can be reduced to less than 100 m^2 [6]. But also with conventional accelerators photon energies far above 1 MeV can be generated. Here the inverse Compton effect is used, where a photon, at an angle of 180°, is scattered by a relativistic electron, thereby gaining energy. The photons get Lorentz boosted in the direction of electrons, giving the characteristic radiation cone, with an opening angle proportional to $1/\gamma$ and the typical maximum energy in head-on geometry [7] of $E_\gamma = 4\gamma^2 E_L$ with the laser photon energy E_L starting from infrared up to ultraviolet and the Lorentz factor $\gamma = E_e/m_e c^2$, where c is the speed of light and m_e is the rest mass of the electron. Thus, it takes electrons with an energy of approx. 240 MeV to scatter laser photons in the infrared region to produce photons with an energy greater than 1 MeV. In most cases, due to the use of lasers, the energy of the incident photon is much less than the rest energy of the electron, making the recoil of the electrons negligible. Also, the effective cross section of the scattering is very small, which keeps the probability of multiple scattering low. Therefore LCB is perfect suited as in beam experiment at energy-recovery linacs (ERL) [7]. ERL-based LCB sources are expected to feature higher brightness from high duty factor and increased beam currents with low emittance and energy spread. Another useful aspect of LCB is the ability to monitor the electron beam non-destructively in its energy and energy spread [8–10].

This contribution focuses on the proposed design, feasibility, and investigation of an LCB source at the thrice-recirculating S-DALINAC, with the possibility to operate as ERL [11].

COMPTON BACKSCATTERING

Compton backscattering occurs when a photon with energy E_L hits a relativistically moving electron with energy E_e and is backscattered. Energy is transferred from the electron to the photon. The recoil factor $X = (4E_eE_L)/(m_e^2)$ [12] indicates how strong the energy loss and thus the influence on the electrons is. The energy of the scattered photons E'_L can be calculated by [13]

$$E'_L = \frac{(1-\beta\cos(\theta_i))E_L}{(1-\beta\cos(\theta_s)) + (1-\cos(\theta_r))\frac{E_L}{E_e}} \qquad (1)$$

for electrons with $\beta = v/c$, v the average speed of the electrons, c the speed of light, θ_i the angle between the incident photons and electrons, θ_s the scattering angle of the scattered photons and the electron beam axis and $\theta_r = \theta_i - \theta_s$ the reflecting angle between incident and scattered photons. From eq. (1) it can be concluded that the desired photon energy can be achieved by adjusting both the original electron and photon energy. However, this can also be achieved in a small ranges by an angle-dependent positioning of the target or detector to the beam axis of the scattered photons, a variation of θ_r. The highest photon energy can be achieved

* Work supported in part by the state of Hesse within the research cluster ELEMENTS (project ID 500/10.006) and the LOEWE research cluster Nuclear Photonics and by DFG through GRK 2128 "Accelence" and Inst163/308-1 FUGG.
† m.meier@ikp.tu-darmstadt.de

ISBN: 978-3-95450-227-1 ISSN: 2673-5490 doi:10.18429/JACoW-IPAC2022-TUPOPT053

STUDY OF BUNCH LENGTH MEASUREMENT BY FORWARD COHERENT SMITH-PURCELL RADIATION

H.Yamada†, F. Hinode, S. Kashiwagi, T. Muto, S. Miura, K. Nanbu, K. Kanomata,
I. Nagasawa, H. Saito, K. Shibata, K. Takahashi and H. Hama,
Research Center for Electron Photon Science, Tohoku University, 982-0826 Sendai, Japan

Abstract

A bunch length monitor with non-destructive and single-shot capabilities using the Coherent Smith-Purcell Radiation (CSPR) is under development at the Research Center for Electron Photon Science, Tohoku University. Since the angular distribution of CSPR reflects the longitudinal bunch length, it is expected that measurements of the peak position of the emission angle can be used to discriminate changes in the bunch length, which making it possible to monitor relative bunch length fluctuations. A concept of the monitoring system and the status of preliminary measurements for development are presented.

INTRODUCTION

So far, the attempts for a bunch length measurement using the coherent radiation have been studied by many researchers, with the radiation sources including the Smith-Purcell Radiation (SPR) [1-4]. For reliable bunch shape measurement with CSPR, it is necessary to know a grating factor accurately. The grating factor is a complicated function that depends on the grating geometry and the radiation angles, which is generally obtained only numerically, and the obtained results depend on the model used and are not clear so much [5]. Apart from the absolute bunch shape measurement, non-destructive and single-shot measurement would be useful for beam control in accelerators, even if it could only monitor relative fluctuations of the overall bunch length. Such application may be found in next-generation plasma-based accelerators, which can produce ultra-short bunch with the fs level but tend to be less stable from shot-to-shot [6]. It is expected that such monitor can be realized by adopting SPR. It is also worth noting that, in CSPR spectrum measurement, a compact measurement system can be constructed, because a separate spectrometer is not required unlike other radiation such as transition radiation. We aim to study experimentally whether such application of CSPR is possible at a test accelerator, t-ACTS, which can stably generate a short bunch beam less than 100 fs in average by applying the velocity bunching to a multi-bunch beam from a thermionic RF-gun. In the following, we describe the concept for monitoring the relative bunch length variation and then present the status of preliminary measurements for the development.

BUNCH LENGTH VARIATION MONITOR

Smith-Purcell Radiation

SPR is obtained when electrons pass over a metal surface with a periodic structure [7] and has a characteristic relationship between the radiation wavelength λ_m and the polar observation angle θ;

$$\lambda_m = \frac{d}{m}\left(\frac{1}{\beta} - \cos\theta\right) \quad (1)$$

where β is v/c, d is the period length of the periodic structure, and m is the order of the radiation. In the Surface Current (SC) model [8] the energy dI emitted per unit solid angle $d\Omega$ by a single electron passing at a distance h above the grating is given by

$$\left(\frac{dI}{d\Omega}\right)_1 = 2\pi q^2 \frac{Z}{d^2}\frac{m^2\beta^3}{(1-\beta\cos\theta)^3} R^2 \exp\left(-\frac{2h}{\lambda_e}\right), \quad (2)$$

where Z is the length of the grating, q is the electron charge and R^2 is the grating factor. The quantity λ_e in Eq. (2) is "evanescent wavelength" and defined with the azimuthal angle ϕ by

$$\lambda_e \equiv \left(\frac{4\pi}{\gamma\beta\lambda_n}\sqrt{1+\gamma^2\beta^2\sin^2\theta\sin^2\phi}\right)^{-1}. \quad (3)$$

Bunch Length Variation Monitor Using CSPR

Since the emission angle of SPR has a dispersion relation as shown in Eq. (1), the change in bunch length can be observed as the difference in peak position in the angular distribution of CSPR intensity. Figure 1 (a) shows an example of the angular distribution for the various bunch lengths calculated based on the SC model, with d = 600 μm, h = 500 μm, and beam energy and charge of 20 MeV and 10pC, respectively. The grating period affects not only the radiation intensity but also the shape of angular distribution through the grating factor, so it must be determined in consideration of actual experimental conditions. The 600 μm period in this preliminary measurement was determined by two points: the magnitude of the change in peak angle when the bunch length was changed, and the limitation of the angular range for detecting radiation in the current setting. The single-shot measurement can be realized by placing multiple detectors on the circumference with different

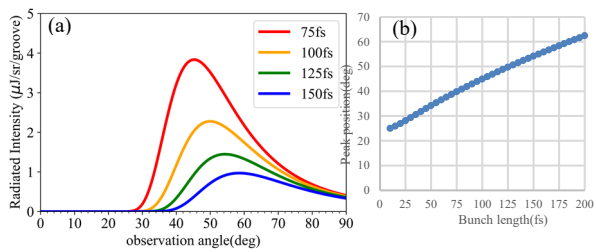

Figure 1: Calculated angular distribution of SPR for various bunch length; 75fs, 100fs, 125fs, and 150fs(a) and dependence of the bunch length on the peak position of emission angle of CSPR (b).

† yamada@lns.tohoku.ac.jp

ISBN: 978-3-95450-227-1 ISSN: 2673-5490 doi:10.18429/JACoW-IPAC2022-TUPOPT054

GENERATION OF COHERENT THz TRANSITION RADIATION FOR TIME DOMAIN SPECTROSCOPY AT THE PBP-CMU ELECTRON LINAC LABORATORY

S. Pakluea[1,*], J. Saisut[2], C. Thongbai[2], S. Rimjaem[2,†], PCELL, PBP, Faculty of Science, Chiang Mai University, Chiang Mai, Thailand
M. Jitvisate[2], School of Physics, Institute of Science, Suranaree University of Technology, Nakhon Ratchasima, Thailand
[1]also at Ph. D. Program in Physics (International Program), Chiang Mai University, Chiang Mai, Thailand
[2]also at ThEP Center, MHESI, Bangkok, Thailand

Abstract

The accelerator system at the PBP-CMU Electron Linac Laboratory (PCELL) of the Plasma and Beam Physics (PBP) Research Facility is used to generate terahertz (THz) coherent transition radiation (CTR). Due to broad spectrum, it can be used as a light source for THz time-domain spectroscopy (TDS) to measure both the intensity and phase of the THz signal. This contribution presents the generation of THz-TR produced from 10 – 25 MeV electron beams. Compressed electron bunches with a length in femtosecond scale are used to generate the THz-TR employing a 45°-tilted aluminum (Al) foil as a radiator. The radiation properties including angular distribution and radiation spectrum are measured at the TR station in the accelerator hall and at the TDS station in the experimental area. The radiation spectral range covering up to 2.3 THz with a peak power of 0.5 – 1.25 MW is expected. The collection efficiency and influence of optical components on the radiation properties were studied. The results show that the considered effects have a significant impact on the TR properties. Results from this work will be used in the TR characterization that is needed to be interpreted carefully.

INTRODUCTION

THz radiation is an electromagnetic wave with a frequency range of $(0.3 - 3) \times 10^{12}$ Hz. This frequency range corresponds to rotational and vibration modes of many molecules. Therefore, it can be used to study, e.g., characteristics of intermolecular bonds by using THz spectroscopic technique [1–4]. One of the most promising sources for THz spectroscopy is linac-based coherent THz radiation from ultrashort electron bunches [5–9]. With an electron bunch as short as femtosecond scale, the radiation emitted from all electrons in the bunch add up coherently and has high intensity, which is proportional to the number of electrons in the bunch squared. The shorter electron bunches provide the broader THz radiation spectrum with higher radiation intensity. At PCELL, CTR has been generated from electron bunches with a length of about 200 fs [10–13]. The features of intense, coherent and broadband spectral range of THz-TR leads to the interest on using it as a light source for THz-TDS, which has the advantage to measure both the intensity and phase of electric fields from THz radiation. This allows us to determine not only the absorbance of the sample, but the complex refractive index [14]. The design and development of the THz-TDS system at PCELL require several aspects, which are generation and characterization of THz-TR, transportation of the THz-TR from the radiation station in the accelerator hall to the application room where the TDS system will be located. In this study, we report the characterization of the CTR produced from short electron bunches with an average energy in a range of 10 – 25 MeV. The radiation properties including radiation spectrum and angular distribution are investigated. Furthermore, we evaluated some effects that affect the transmission efficiency in the Michelson interferometer for radiation spectrum measurement.

METHODOLOGY

At our facility, a train of electron bunches is generated from a thermionic cathode radio-frequency (RF) electron gun with a maximum kinetic energy of about 2 – 2.5 MeV. The electron bunches are then accelerated by an RF linear accelerator (linac) to reach kinetic energy of about 8 – 25 MeV. The electron bunches are compressed to have a bunch length of 100 – 300 fs at the CTR experimental station downstream the linac by using an alpha magnet and velocity bunching process in the linac. At the CTR station, an Al foil with a thickness of 25 μm and a diameter of 24 mm is used as a radiator by placing it 45° with respect to the electron beam direction. The backward TR is emitted at the radiator surface and is collimated by a goal-coated parabolic mirror placing at its focal point in the vacuum chamber below the center of the radiator. The collimated radiation is then guided to pass through a high density polyethylene (HDPE) window as shown in Fig. 1. The radiation then enters the measuring system. The HDPE window has a diameter of 32 mm and a thickness of 1.25 mm. The radiation spectrum is measured using the Michelson interferometer. The CTR with a spectral range of upto 2.3 THz and a peak power of 0.5 - 1.25 MW is expected.

* siriwan_pakluea@cmu.ac.th
† sakhorn.rimjaem@cmu.ac.th

ISBN: 978-3-95450-227-1 ISSN: 2673-5490 doi:10.18429/JACoW-IPAC2022-TUPOPT057

USING SURROGATE MODELS TO ASSIST ACCELERATOR TUNING AT ISIS

A. A. Saoulis*, K. R. L Baker, H. V. Cavanagh, R. E. Williamson,
ISIS Neutron and Muon Source, Rutherford Appleton Laboratory, U.K.
S. Basak, J. Cha, J. Thiyagalingam,
Scientific Machine Learning, Rutherford Appleton Laboratory, U.K.

Abstract

High intensity hadron accelerator performance is often dominated by the need to minimise and control beam losses. Operator efforts to tune the machine during live operation are often restricted to local parameter space searches, while existing physics-based simulations are generally too computationally expensive to aid tuning in real-time. To this end, Machine Learning-based surrogate models can be trained on data produced by physics-based simulations, and serve to produce fast, accurate predictions of key beam properties, such as beam phase and bunch shape over time. These models can be used as a virtual diagnostic tool to explore the parameter space of the accelerator in real-time, without making changes on the live machine. At the ISIS Neutron and Muon source, major beam losses in the synchrotron are caused by injection and longitudinal trapping processes, as well as high intensity effects. This paper describes the training and inference performance of a neural network surrogate model of the longitudinal beam dynamics in the ISIS synchrotron, from injection at 70 MeV to 800 MeV extraction, and evaluates the model's ability to assist accelerator tuning.

INTRODUCTION

Machine learning (ML) has emerged as a valuable tool across many sub-disciplines within accelerator physics. Recent work has demonstrated its potential in control [1–3], tuning and optimisation [4–7], and virtual diagnostics [8–10]. Several of these recent advances rely on ML-based surrogate models [11, 12], which can offer an accurate substitute for traditional physics-based simulations with several orders of magnitude reduction in computation time. This paper will focus on training a parameter-to-image convolutional neural network (CNN) that takes the initial beam parameters and machine settings as input to reconstruct simulation-generated images representing key beam properties in the ISIS synchrotron.

At the ISIS Neutron and Muon source up to 3×10^{13} protons per pulse are accelerated from 70 MeV to 800 MeV by a 50 Hz rapid cycling synchrotron [13]. The majority of beam losses at the facility occur in the synchrotron, due to injection and longitudinal trapping processes as well as high intensity effects. Since operators must rely on feedback from the live machine during tuning, they are restricted to making small, incremental changes to ensure important operational constraints such as low loss are always satisfied. This approach can be time-consuming for operators, and such a restricted parameter space search is likely to yield sub-optimal local minima for a given optimisation problem.

A method for searching the parameter space without such constraints is clearly desirable, and physics-based simulations can be leveraged to address this. However, since these simulations are generally too computationally expensive to aid tuning in real-time, fast-executing surrogate models may offer an alternative that allows for real-time use in the control room to aid machine tuning.

Modelling the ISIS Synchrotron

The accelerator physics group at ISIS has developed a C++ turn-by-turn physics-based simulation of the longitudinal dynamics of the ISIS synchrotron [14]. The simulation takes in a wide range of inputs that define properties of the injected beam as well as how the RF settings vary over the 10 ms injection cycle, and outputs several bunch properties at each turn, including longitudinal bunch charge distribution and emittances.

One key measurement that is frequently used as a diagnostic during tuning is an image representing the evolution of the longitudinal charge density of a bunch in the synchrotron over time, see Fig. 1. Each row represents the longitudinal charge distribution of the bunch at a particular turn. This is referred to as a "waterfall plot" by ISIS operators, and can be used to quickly diagnose the state of the synchrotron by identifying common unstable modes such as oscillations in the mean phase and root mean square bunch length. The CNN models explored in this paper were trained to reconstruct these waterfall plots from simulation data.

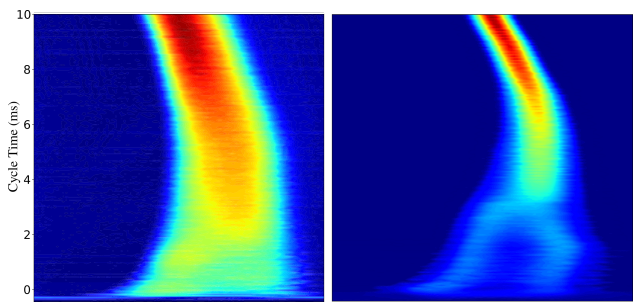

Figure 1: Left: Waterfall plot acquisition from a single beam position monitor in the ISIS synchrotron. Right: Simulation-generated waterfall plot. The bunch charge distribution evolves from injection at the bottom of the plot to extraction at the top over the 10 ms acceleration cycle.

* alex.saoulis@stfc.ac.uk

ISBN: 978-3-95450-227-1 ISSN: 2673-5490 doi:10.18429/JACoW-IPAC2022-TUPOPT058

A MACHINE LEARNING APPROACH TO ELECTRON ORBIT CONTROL AT THE 1.5 GeV SYNCHROTRON LIGHT SOURCE DELTA

D. Schirmer*
Center for Synchrotron Radiation (DELTA), TU Dortmund University, Germany

Abstract

Machine learning (ML) methods have found their application in a wide range of particle accelerator control tasks. Among other possible use cases, neural networks (NNs) can also be utilized for automated beam position control (orbit correction). ML studies on this topic, which were initially based on simulations, were successfully transferred to real accelerator operation at the 1.5–GeV electron storage ring of the DELTA accelerator facility. For this purpose, classical fully connected multi-layer feed-forward NNs were trained by supervised learning on measured orbit data to apply local and global beam position corrections. The supervised NN training was carried out with various conjugate gradient backpropagation learning algorithms. Afterwards, the ML-based orbit correction performance was compared with a conventional, numerical-based computing method. Here, the ML-based approach showed a competitive orbit correction quality in a fewer number of correction steps.

INTRODUCTION

Stable electron orbit control is an important task especially for modern synchrotron light sources. For this purpose, singular value decomposition (SVD) of the orbit response matrix is a standard numerical tool at storage rings worldwide. An alternative concept applies machine learning techniques as an heuristic method, inspired by the pioneering work done at NSLS/BNL [1]. Since 2018, machine learning (ML) based orbit correction (OC) methods have extensively been studied and applied at DELTA [2–5], a 1.5–GeV electron storage ring operated as a synchrotron light source [6] and a new facility for ultrashort pulses in the VUV and THz regime [7, 8].

MACHINE OPERATION

The OC hardware setup of the DELTA storage ring consists of 54 beam position monitors (BPMs) which determine the position in both orbit planes simultaneously as well as 30 horizontal and 26 vertical corrector magnets (steerers) [9]. The ML methods, which were successfully tested by means of simulations on a DELTA storage ring OC model, were applied to the real storage ring.

ML-Data Acquisition

Compared to the uncoupled case in previous real machine studies [3], now a dedicated data acquisition script randomly varies all steerer strengths in both planes at once within intervals from typically ±200 mA up to ±500 mA. The interval limits are a compromise between risk of beam losses and minimizing relative measurement errors due to the limited steerer strength resolution of 2.4 mA. After each perturbation, the steerer strength changes and the emerging closed orbit differences in both planes are measured, error-cleaned (e.g., deleting of hardware and software related readout errors) and recorded. The data pool noise level was estimated to approximately 2% caused by the combined error of BPM and steerer strength readback accuracies, mainly dominated by the limited steerer strength granularity.

Weighted Beam Position Monitors

To increase the impact of orbit deviations at more important storage ring positions (e.g., synchrotron radiation source points or the injection region) each BPM can be assigned with an individual weight factor. With $\tilde{w}^{\mathrm{BPM}}_{x,z}$ as a diagonal matrix of BPM weight factors, the weighted closed-orbit error $\chi^{w}_{x,z}$ can be evaluated as a scalar quantity for both planes (x, z) by

$$\chi^{w}_{x,z} = \left\| \tilde{w}^{\mathrm{BPM}}_{x,z} \cdot (\overrightarrow{\Delta d}_{x,z} + \tilde{R}_{x,z} \cdot \overrightarrow{\Delta I}_{x,z}) \right\|_2 . \qquad (1)$$

The goal for an orbit correction algorithm is to minimize the residual closed-orbit error $\chi^{w}_{x,z}$ for arbitrary orbit deviations $\overrightarrow{\Delta d}_{x,z}$ with respect to any desired reference orbit. The product of the response matrix $\tilde{R}_{x,z}$ and the steerer strength changes $\overrightarrow{\Delta I}_{x,z}$ in Eq. 1 can be determined by means of a reverse NN (see Fig. 1). It can also be trained with the experimental data patterns, but now each squared network error $e^2_{pj} = (o^{\mathrm{BPM}}_{pj} - t^{\mathrm{BPM}}_{pj})^2$ must be weighted by an individual BPM weight factor w^{BPM}_{pj} as follows:

$$E^{R}_{\mathrm{mse}} = \frac{1}{P} \sum_{p=1}^{P} \frac{1}{N} \sum_{j=1}^{N} w^{\mathrm{BPM}}_{pj} (o^{\mathrm{BPM}}_{pj} - t^{\mathrm{BPM}}_{pj})^2 . \qquad (2)$$

The reverse mean squared NN error E^{R}_{mse} sums up the squared differences between all numbers of neurons N at the NN target t and output o for a specific quantity of data patterns P. Thus, the reverse trained NN, as a representation of the orbit response matrix $\tilde{R}_{x,z}$, is able to determine orbit deviations $\overrightarrow{\Delta d}_{x,z}$ at all BPMs for given steerer strength changes $\overrightarrow{\Delta I}_{x,z}$. Afterwards, the weighted orbit error $\chi^{w}_{x,z}$ in Eq. 1 can be minimized using a numerical optimizer, e.g., the BFGS Quasi-Newton method [10]. In addition, the optimizer itself has also been replaced by a pre-trained NN. For this purpose, the optimizer has to pre-calculate the optimum $\chi^{w}_{x,z}$-values for all measured orbit deviations $\overrightarrow{\Delta d}_{x,z}$. These data pairs again serve as labeled input/target data to train a dedicated NN as an optimizer substitute.

* detlev.schirmer@tu-dortmund.de

ISBN: 978-3-95450-227-1 ISSN: 2673-5490 doi:10.18429/JACoW-IPAC2022-TUPOPT059

MACHINE LEARNING METHODS FOR CHROMATICITY CONTROL AT THE 1.5 GeV SYNCHROTRON LIGHT SOURCE DELTA

D. Schirmer*, A. Althaus, T. Schüngel
Center for Synchrotron Radiation (DELTA), TU Dortmund University, Germany

Abstract

In the past, the chromaticity values at the DELTA electron storage ring were manually adjusted using 15 individual sextupole power supply circuits, which are combined into 7 magnet families. To automate and optimize the time-consuming setting process, various machine learning approaches were investigated. For this purpose, simulations were first performed using a storage ring model and the performance of different neural networks based models was compared. Subsequently, the neural networks were trained with experimental data and successfully implemented for chromaticity correction in real accelerator operation.

INTRODUCTION

DELTA is a 1.5–GeV electron storage ring facility operated by the TU Dortmund University as a synchrotron light source [1] and as a facility for ultrashort pulses in the VUV and THz regime [2, 3].

In recent years, different machine learning (ML) based projects have been investigated to support automated monitoring and operation of the DELTA electron storage ring facility [4]. This includes self-regulating global and local orbit correction of the stored electron beam [5, 6] and a betatron tune feedback [7]. In addition, a ML-based electron transfer rate (injection) optimization is in preparation [8].

So far, the storage ring chromaticity values have been adjusted empirically based on experience. The setting of desired target values can only be achieved by time-consuming trial and error. For this reason, ML-based algorithms for automated chromaticity adjustment were investigated, very similar to the already implemented ML-based betatron tunes control [7].

In previous studies, the workflow was successfully simulated on a storage ring model. Therefore, the correlation between sextupole magnet strength changes and the related chromaticity shifts was investigated. In this case, the magnets were grouped via software in four horizontal and three vertical focusing families. Here, clear correlations were identified during training of conventional 3-layered feed-forward neural networks (NNs), without any over- or underfitting issues. Afterwards, the trained NN-based models were able to match the chromaticity to any desired value in the simulated storage ring. Some results are summarized in [4] and [8].

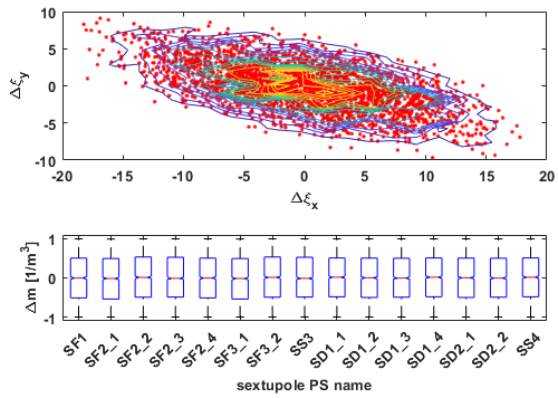

Figure 1: Distribution of 3000 chromaticity shifts (top) invoked by uniformly randomized strength variations of 15 independent sextupole power supplies (PS) circuits (bottom). The data are obtained by AT optics simulations based on a DELTA storage ring lattice model.

ML-BASED SIMULATED CHROMATICITY CONTROL

To increase the degree of freedom for automated chromaticity control, we repeated the pre-studies, but now utilizing all 15 sextupole PS circuits individually. A detailed lattice model of the DELTA storage ring served as the basis for x,y-coupled optics and chromaticity (ξ_x, ξ_y) computations within the Accelerator Toolbox (AT) framework [9, 10]. To acquire suitable ML training data, the sextupole strengths were randomly varied for all 15 PS individually and for each strength change setting, the associated chromaticity shifts were calculated. Fig. 1 visualizes the corresponding AT simulation results.

These labelled data pairs (strength variations and chromaticity shifts) were used for supervised training of multilayered NNs. The NNs serve as surrogate models for the chromaticity determination, which afterwards are applied to automatically adjust and control the chromaticity values.

Fig. 2 illustrates a sample application for a simulated chromaticity matching run performed with a 3-layered NN which has been trained by scaled conjugate gradient (scg) back-propagation [11] applying the data depicted in Fig. 1. The natural chromaticity ($\xi_x = -21$, $\xi_y = -8$) which occurs with all sextupoles switched off (0. iteration) can be adjusted to full chromaticity compensated values (4. iteration, $\xi_x = \xi_y = 0$) by the ML-based control loop. The step size (number of iterations) depends mainly on the granularity ($\Delta\xi_{x,y}$) of

* detlev.schirmer@tu-dortmund.de

ISBN: 978-3-95450-227-1 ISSN: 2673-5490 doi:10.18429/JACoW-IPAC2022-TUPOPT060

EPICS-BASED TELEGRAM INTEGRATION FOR CONTROL AND ALARM HANDLING AT TEX FACILITY

D. Moriggi*, S. Pioli, F. Cardelli, C. Di Giulio, P. Ciuffetti
INFN - Laboratori Nazionali di Frascati, Italy

Abstract

TeXbot is a Telegram bot developed in python language used to notify in asynchronous way event in TEX (TEst stand for X-band) facility at Frascati National Laboratories. The application has been realized making use of framework such as telepot and pysmlib, to interface with Telegram and with EPICS environment respectively.

The bot make able the user to subscribe to multiple topic in order to be automatically notified in case of different set up of the machine or when an interlock occurs on a single component. Furthermore the user can request accurate information about subsystem of the accelerator by simply make use of special commands and token in Telegram app.

INTRODUCTION

In any industrial context it is present the need to have information delivered in the fastest way as possible.

In this environment the Telegram TeXbot solution can be deployed, since it can control and handle alarm when a subsystem goes in an interlock state or certain event occurs to the system.

The bot is developed at National Laboratory of Frascati and running at TEX (EuPRAXIA TEst stand for X-band) facility and is capable of sending automatic live messages through Telegram app displaying information on particle accelerator system state.

The final user can start joining private chat and once inserted the correct password can initiate conversation with bot asking for precise information about the TEX facility. Through text recognition the bot can answer by sending information directly or can eventually submit different kind of menu used to let user choose the appropriate content.

Moreover the consumer can handle subscription to specific categories in order to receive accurate notifications on certain devices in real-time, or also ask for the chart representing the history for a particular component in a given time span.

FRAMEWORK

This system is realized thanks to the integration of multiple framework each devoted to a different type of functionalities. The first to be mentioned is Telepot [1], a Python repository downloadable from pip, the packet manager for Python, that encapsulate Telegram API (Application Program Interface) [2] making able to build up and control the bot.

The second Python library used to create state machine capable of handling events during system operations and making able the bot to communicate with EPICS is pysmlib [3], which is built on top of PyEpics and therefore guarantees a perfect integration with EPICS Channel Access.

The last is flask [4] used to realize the back-end component responsible to make available API to retrieve and manipulate data coming from the EPIC S Archiver Appliance [5, 6] used to store data of the TEX facility.

ARCHITECTURE

The main four components that constitute the overall architecture are shown in Fig. 1 and it will be described in the following:

- the EPICS Channel Access
- TeXbot, the Telegram bot
- Flask back-end for retrieval
- EPICS Archiver Appliance

The first fundamental requirement for this kind of setup is the need of EPICS CA (Channel Access), that once a connection it's established with it, make the system able to retrieve live information on PVs (Process Variables) of the TEX facility.

Then obviously comes the TeXbot that could be thought and refer to it as a listener in the framework, because it is distributed in reading-mode respect to data, interrogating the CA and sending raw information to Telegram user.

Another component is represented by the back-end service that behave in its own container and it is responsible to exposes APIs used to retrieve manipulated information coming not only from live data, but even from the archived ones.

The last independent service that runs in its dedicated container is the EPICS Archiver Appliance, which is devoted to handle a layered data storage by saving information in three different area depending on its date of acquisition.

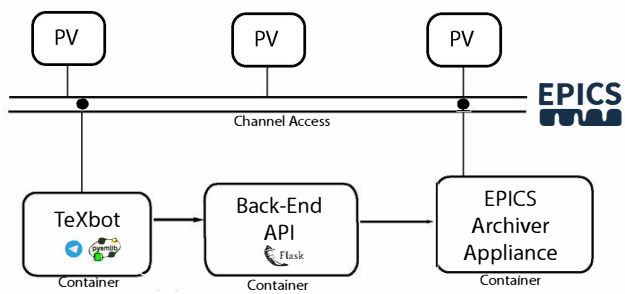

Figure 1: Architecture.

* daniele.moriggi@lnf.infn.it

ISBN: 978-3-95450-227-1 ISSN: 2673-5490 doi:10.18429/JACoW-IPAC2022-TUPOPT061

STATUS AND COMMISSIONING OF THE FIRST X-BAND RF SOURCE OF THE TEX FACILITY

F. Cardelli*, D. Alesini, M. Bellaveglia, S. Bini, B. Buonomo, G. Catuscelli, M. Ceccarelli, R. Ceccarelli, A. Cecchinelli, R. Clementi, C. Di Giulio, E. Di Pasquale, A. Falone, G. Franzini, A. Gallo, A. Liedl, D. Moriggi, G. Piermarini, L. Piersanti, S. Pioli, S. Quaglia, L. A. Rossi, L. Sabbatini, G. Scarselletta, M. Scampati, S. Strabioli, S. Tocci, R. Zarlenga
INFN - Laboratori Nazionali di Frascati, via Enrico Fermi 54, Frascati, Italy

Abstract

In 2021 started the commissioning of the TEX (TEst stand for X-band) facility at the Frascati National laboratories of INFN. This facility has been founded in the framework of the LATINO (Laboratory in Advanced Technologies for INnOvation) project. The current facility layout includes a high power X-band (11.994 GHz) Radiofrequency (RF) source, realized in collaboration with CERN, which will be used for validation and development of the X-band RF high gradient technology in view of the EuPRAXIA@SPARC_LAB project. The RF source is based on a CPI VKX8311 Klystron and a solid state ScandiNova k400 modulator to generate a maximum RF output power of 50 MW at 50 Hz, that will be mainly used for accelerating structure conditioning and waveguide components testing. In this paper the layout, the installation, commissioning and stability measurements of this source are described in detail. The test stand will be soon operative and ready to test the first X-band accelerating structure prototype.

INTRODUCTION

The X-band (11.994 GHz) was chosen as the basic RF technology for the realization of the booster of the EuPRAXIA@SPARC_LAB Linac [1, 2]. This project aims at constructing a free electron laser source based on a normal conducting RF Linac and a plasma acceleration module to generate a high brightness 1 GeV electron beam. The X-band is at present the most advanced RF technology, with demonstrated capability of providing accelerating gradients up to 100 MV/m and beyond. Achieving top level performances requires great expertise in the RF design, fabrication techniques and conditioning procedures. For this reason, as part of the preparatory activities related to the EuPRAXIA@SPARC_LAB project, a high-power test stand for X-band (TEX) has been commissioned at INFN Frascati National Laboratory. The purpose of this source is mainly to test and condition RF devices and high gradient accelerating structures but it will also allow R&D activities on LLRF systems, beam diagnostics, vacuum and control system. Its design has been done in collaboration with CERN and so the facility will be also used to test and condition structures for the CLIC project.

Through the LATINO project [3], it will be also accessible to external users, including national and international laboratories and companies. This is a project funded by the government of "Regione Lazio" aimed at promoting and increasing the technology transfer between research centres of excellence and the surrounding economic framework. In November 2021 started the commissioning of the TEX RF source with the site acceptance test of the modulator and the commissioning of the LLRF and Control system. The TEX Layout and the main results obtained during these preliminary tests are shown below.

TEX FACILITY LAYOUT

TEX is located at the building 7 of the Frascati national laboratory of INFN, that has been completely refurbished. As reported in [4], the TEX facility includes a control room, a rack room, the X-band source cage and a concrete bunker in which the RF devices and high gradient structures to be tested will be installed. The rack room hosts all the ion pumps controllers, the rack of the EPICS control system and the LLRF system.

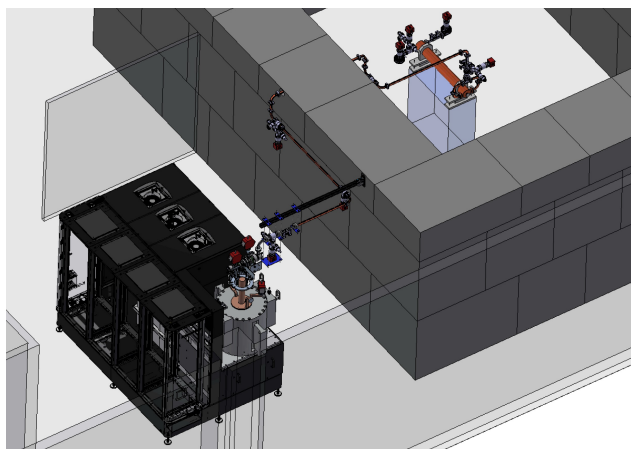

Figure 1: TEX RF Source layout.

The TEX RF power source layout is based on a Solid State Scandinova K400 modulator and a VKX8311A Klystron which was given to us by CERN on permanent loan. A sketch of the current TEX layout is reported in Fig. 1. At full specifications it will be able to produce RF pulses of 50 MW long 1.5 μs with a rep rate of 50 Hz. Table 1 shows the main parameters of the RF Source.

The pulsed modulator (Fig. 2) is capable to reach 430 kV with a maximum average power of 50 kW. The RF pulse at the klystron input is preamplified by a solid state drive

* fabio.cardelli@lnf.infn.it

ISBN: 978-3-95450-227-1 ISSN: 2673-5490 doi:10.18429/JACoW-IPAC2022-TUPOPT062

A DATA-DRIVEN ANOMALY DETECTION ON SRF CAVITIES AT THE EUROPEAN XFEL

A. Sulc*, A. Eichler, T. Wilksen, DESY, Hamburg, Germany

Abstract

The European XFEL is currently operating with hundreds of superconducting radio frequency cavities. To be able to minimize the downtimes, prevention of failures on the SRF cavities is crucial. In this paper, we propose an anomaly detection approach based on a neural network model to predict occurrences of breakdowns on the SRF cavities based on a model trained on historical data. We used our existing anomaly detection infrastructure to get a subset of the stored data labeled as faulty. We experimented with different training losses to maximally profit from the available data and trained a recurrent neural network that can predict a failure from a series of pulses. The proposed model is using a tailored architecture with recurrent neural units and takes into account the sequential nature of the problem which can generalize and predict a variety of failures that we have been experiencing in operation.

INTRODUCTION

The superconducting radio-frequency (SRF) cavities are responsible for accelerating beams which are used in the European X-ray Free Electron Laser (EuXFEL) to obtain extremely brilliant X-ray photon light.

Particle accelerators use the cavity resonators operating in radio-frequency spectra to accelerate particles by synchronization with their frequency. The cavities accelerate and energize particles by the induced alternating electric field.

For superconductivity, it is necessary to maintain the cavities cooled to very low temperatures, usually near absolute zero, with a cryogenic system. The cryogenic system maintains the temperature to preserve the superconductivity. The superconductivity minimizes the losses through the wall to a minimum and thus almost all RF power can be transmitted to the passing beam.

EuXFEL is currently operating 784 SRF cavities and it is necessary to use automated algorithms to prevent failures. One kind of failure we are particularly interested in are quenches. A quench is when cavity walls lose their superconductivity due to temperature breakdown. It leads to a loss of superconductivity and energy is dissipated through the cavity walls (the surrounding helium bath is heated up) thus the quality factor decreases, i.e. efficiency decreases. Although the quench limits are experimentally tested and set in the firmware to hard limits, there are numerous situations where the cavity can quench due to e.g. degradation which lowers quench limits.

EuXFEL SRF cavities are operating in pulsed mode, therefore we have available a sequence of waveforms with a fixed length. The current quench detection system at EuXFEL is observing the quality factor [1]. It is one of the classic methods for the detection and prevention of such quenches. In [2] an online approach for quench detection based on the calculation of detuning and bandwidth on superconducting cavities is presented which is specially tailored to continuous wave operation. A model-based approach for anomaly detection on cavities is shown in [3]. In [4, 5] the parity space method is used to detect anomalies on SRF cavities. Recently data-driven machine learning approaches [6, 7] are used for cavity breakdown prediction on cavities.

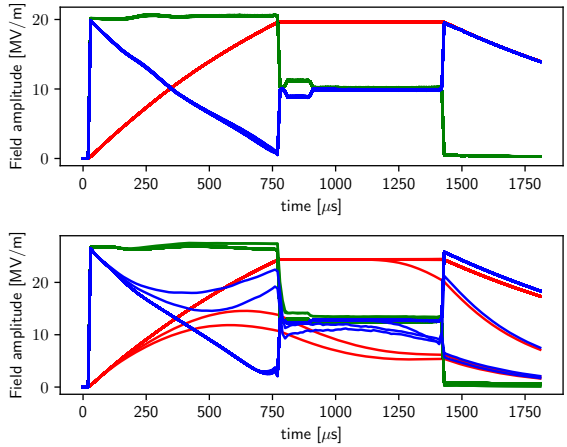

Figure 1: Two examples of amplitudes of healthly (top) and quenching amplitudes (bottom). Probe **p**, forward **f** and **r** signals are depicted red, green, and blue respectively.

Our currently deployed quench detection server [1] provides a daily overview of probable quenches. Recently, EuXFEL created a dataset of events that are probable faults. The availability of such a labeled dataset allowed us to experiment with data-driven machine learning models. This paper presents a study of data-driven anomaly detection to detect faults on RF cavities tailored to the case of EuXFEL. We demonstrate that vanilla data-driven machine learning methods can be trained to predict potential failures with very limited access to training data labeled as faulty.

The structure of this paper is the following: First, we describe the procedure of preprocessing data. Then, we present details of the proposed architecture used for the prediction of faults. Lastly, we show the results of our approach on a test set using different data-driven approaches.

METHOD

Notation

At a time moment t we observe a pulse which consists of three types of complex-valued waveforms: probe **p**, forward **f**, reflected **r**, see Fig. 1. Each event consists of a series of

* antonin.sulc@desy.de

ISBN: 978-3-95450-227-1 ISSN: 2673-5490 doi:10.18429/JACoW-IPAC2022-TUPOPT063

Vsystem TO EPICS CONTROL SYSTEM TRANSITION AT THE ISIS ACCELERATORS

I. D. Finch*, B. R. Aljamal, K. R. L. Baker, R. Brodie, J. L. Fernandez-Hernando, G. Howells, M. Leputa, S. A. Medley, A. Saoulis, STFC/RAL/ISIS, Chilton, Didcot, Oxon., United Kingdom
A. Kurup, Imperial College of Science and Technology, London, United Kingdom

Abstract

The ISIS Neutron and Muon Source at Rutherford Appleton Laboratory is a pulsed source used for research in material and life sciences. A linac and synchrotron accelerate protons to produce neutrons in two spallation targets. The accelerators are currently operated using commercial Vsystem control software. A transition to the EPICS control system is underway, with the end goal of a containerised system preferring the pvAccess protocol. We report the progress of this transition, which is being done without disrupting ISIS operations. We describe a bidirectional interface between Vsystem and EPICS that enables the two control systems to co-exist and interact. This allows us to decouple the transition of controls UI from the associated hardware. Automated conversion of the binary-format Vsystem control screens has been developed that replicates the current interface in EPICS, allowing minimal retraining of operators. We also outline the development of EPICS interfaces to standard and unique-to-ISIS hardware, reuse of and managing continuity of existing long-term data archiving, the development of EPICS interfaces to standard and unique-to-ISIS hardware, and migration of alerts.

INTRODUCTION

The accelerators at the ISIS Neutron and Muon Source [1, 2] at Rutherford Appleton Laboratory currently operates using Vsystem [3] commercial control system software. A transition to the open source EPICS control system [4] is in progress. (Note that ISIS Experiment Controls has already transitioned to the use of EPICS [5].) One of the requirements of this transition is that operations must not be interrupted. For this reason the two control systems will be run in parallel during the transition.

There are a variety of different ways to configure an EPICS control system and so a number of high-level decisions had to be made before beginning the transition work. Some of the decisions driving the ISIS accelerator controls transition are:

- to prefer pvAccess [6] over Channel Access
- to prefer IOCs (or equivalents) in containers on centrally managed servers
- to deploy Phoebus [7] for user interaction

Other decisions have been deferred, these include:

- selection of technology for long-term archiving of PVs
- selection of alarm handler software

* ivan.finch@stfc.ac.uk

PVECHO - VSYSTEM/EPICS BRIDGE

To allow the simultaneous use of Vsystem and EPICS during the transition period software called PVEcho [8] has been developed to act as a bridge between the two control systems. PVEcho allows changes in the channels or process variables (PVs) of one control software system to be reflected immediately in the other. PVEcho is divided into two parts – v2e and e2v – depending on whether the underlying hardware interface is managed by Vsystem or EPICS respectively. In light of the decision to prefer pvAccess, PVEcho only fully supports this EPICS protocol.

If the hardware interface is managed by Vsystem then v2e creates a set of EPICS process variables which mimic the Vsystem channels, reflecting the changes in those channels and if modified via EPICS propagating the change to Vsystem. This allows Phoebus screens to be deployed to control and monitor hardware for which Vsystem interfaces exist without needing to move the associated hardware interfaces immediately to EPICS IOCs.

If the hardware interface is managed by EPICS then e2v similarly acts as a bridge to propagate values to Vsystem channels and to propagate any changes to those Vsystem channels back to the matching EPICS PV. Thus hardware interfaces may be moved to EPICS without requiring all associated Vsystem control screens or scripts to be ported at the same time.

This approach allows the two major areas of the transition work – transition of hardware interfaces and transition of control screens (and scripts) – to be decoupled.

CONVERSION OF CONTROL SCREENS

ISIS operations are managed from a Main Control Room (MCR) which is staffed at all times. The MCR crew are the principal users of the control system, using the alarm system and control screens to interact with hardware across the accelerators and targets. The control screens are also used by machine physicists during setup of ISIS before a user run, tuning of the machine during the run, and for studies of the properties of the machine. Equipment owners access the control screens during commissioning of their equipment and for routine inspection and monitoring during operation.

There are more than 800 Vsystem control screens accessible through the ISIS control system. Transitioning these screens to Phoebus represents a very significant conversion effort. The initial plan was for this to be done manually by contractors. However, a technical alternative was developed.

The Vsystem control screens are created and run by Vdraw [9] and are stored in binary encoded files. Software writ-

ISBN: 978-3-95450-227-1 ISSN: 2673-5490 doi:10.18429/JACoW-IPAC2022-TUPOPT064

ONLINE OPTIMIZATION OF NSLS-II DYNAMIC APERTURE AND INJECTION TRANSIENT*

X. Yang†, G. Wang, V. Smaluk, L. H. Yu, T. Shaftan, Y. Li, F. Plassard, S. Buda, Y. Hidaka, D. Durfee, Y. Tian, Y. Hu, K. Ha, A. Derbenev, B. Bacha, C. Danneil, D. Padrazo
National Synchrotron Light Source II, Brookhaven National Laboratory, Upton, NY, USA

Abstract

The goal of the NSLS-II online optimization project is to improve the beam quality for the user experiments. To increase the beam lifetime and injection efficiency, we have developed a model-independent online optimization of nonlinear beam dynamics using advanced algorithms, such as Robust Conjugate-Gradient Algorithm (RCDS). The optimization objective is the injection efficiency and optimization variables are the sextupole magnet strengths. Using the online optimization technique, we increased the NSLS-II dynamic aperture and reduced the amplitude-dependent tune shift. Recently, the sextupole optimization was successfully applied to double the injection efficiency up to above 90% for the high-chromaticity lattice being developed to improve the beam stability and to increase the single-bunch beam intensity. Minimizing the beam perturbation during injection is the second objective in this project, realized by online optimization of the injection kickers. To optimize the full set of kicker parameters, including the trigger timing, amplitude, and pulse width, we upgraded all kicker power supplies with the capability of tunable waveform width. As a result, we have reduced the injection transient by a factor of 29, down to the limit of 60 μm.

INTRODUCTION

The Facility Improvement Project "Methods of online optimization of NSLS-II storage ring concurrent with user operations" was dedicated to developing a set of software tools for online optimization of beam dynamics and minimization of the injection transients. The online optimization approach is based on the use of the measured beam and machine parameters to evaluate performance functions, which are optimized using advanced algorithms designed to work reliably in noisy environments.

In the frameworks of this project, we planned to explore and improve the performance of the optimization algorithms. We use beam-based model-independent online methods to improve the injection efficiency and beam lifetime by direct optimization of sextupoles. For the minimization of the injection transients [1-4], the specific plan was to optimize the matching of Storage Ring (SR) injection kickers [5-7].

We expect the NSLS-II user community to benefit from the reduced top-off injection frequency, improved beam stability, and transparent injection. Since nonlinear beam dynamics is a subject of high scientific interest, we believe the results of this project will be beneficial not only for NSLS-II but also for other present and future light sources.

* This manuscript has been authored by Brookhaven Science Associates, LLC under Contract No. DE-SC0012704 with the U.S. DOE
† xiyang@bnl.gov

STUDY RESULTS

Optimization of Sextupoles to Increase DA

To test the RCDS optimization algorithm [8], we loaded the high chromaticity 7 lattice. The injection efficiency was decreased to around 20%. The RCDS online optimization of sextupoles recovered the injection efficiency up to 90% at the second iteration. In this experiment, we found two to three iterations were adequate to achieve the optimal solution. Extra iterations were not so effective, the injection efficiency went from mild improvement to no improvement at all. The evolution of the power supply currents of the NSLS-II sextupole families is shown in the right plot of Fig. 1.

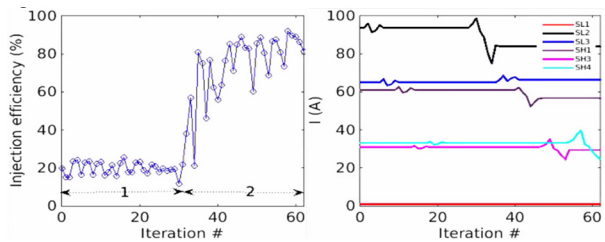

Figure 1: Two iterations of the RCDS online optimization of sextupoles for the high chromaticity 7 lattice: injection efficiency (left) and the sextupole settings (right).

We characterized the dynamic aperture (DA) for the NSLS-II operational lattice. We injected a beam of 2 mA current in 50 bunches, which were well aligned on the flat top of the pinger pulse. Then, we gradually increased the pinger voltage and recorded the beam current measured by the DCCT. Figure 2 shows the horizontal (left) and vertical (right) DA before (red) and after (blue) RCDS online optimization. We have achieved a more than 20% increase in the horizontal DA with no change in the vertical DA. We also analysed the measured betatron tune shift with amplitude and observed a reduction of the horizontal tune shift with amplitude by a factor of two.

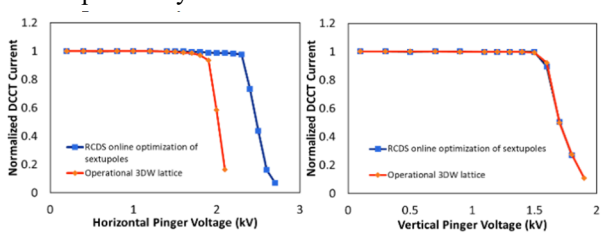

Figure 2: Horizontal (left) and vertical (right) DA before (red) and after (blue) sextupole optimization in the 3DW lattice.

We successfully applied the sextupole optimization to the lattice with high chromaticity, +7, in both horizontal

ISBN: 978-3-95450-227-1 ISSN: 2673-5490 doi:10.18429/JACoW-IPAC2022-TUPOPT065

DISPERSION-FREE STEERING BEAM BASED ALIGNMENT AT SwissFEL

Eugenio Ferrari*, Marco Calvi, Romain Ganter, Christoph Kittel[1], Eduard Prat, Sven Reiche, Thomas Schietinger, Paul Scherrer Institut, CH-5232 Villigen PSI, Switzerland
[1]also at Faculty of ICT, University of Malta, Msida MSD 2080, Malta

Abstract

Micron-level alignment of the undulator line is required for successful operation of linear accelerator based high gain free electron lasers to produce powerful radiation at X-rays' wavelengths. Such precision in the straightness of the trajectory allows for an optimal transverse superposition between the electrons and the photon beam. This is extremely challenging and can only be achieved via beam-based techniques. In this paper we will report on the dispersion-free steering approach implemented at SwissFEL, that helped achieving improved performance for both the hard and soft X-ray beamlines.

INTRODUCTION

SwissFEL [1] is a free-electron laser (FEL) user facility, based on the SASE principle, delivering ultrashort photon pulses in the X-ray regime. For a schematic representation of the facility, see Fig. 1. The electrons needed for FEL production are generated in a normal conducting photocathode gun and accelerated through a normal conducting linac. The gun and booster sections, before the first bunch compressor, employ S-band technology. All the other accelerating cavities, divided for convenience into 4 linacs, are at C-band frequency. Two magnetic chicanes are used to compress the pulse duration. An X-band harmonic cavity is also installed and used to linearise the phase space before compression.

Two different photoinjector lasers are used to generate two electron bunches with temporal separation of 28 ns. This allows parallel operation of two distinct FEL beamlines. The electrons of bunch 1 are accelerated to the required energy and injected in the Aramis undulator, for hard-X-ray generation in the 2–12 keV photon energy range. The typical electron beam energies are 3–6 GeV, depending on the requirement of the specific user experiment. Bunch 2 electrons are extracted after Linac 2, using a combination of resonant kicker and septum, and they are injected at 3 GeV in the Athos branch for soft-X-ray production. The photon energy range of the second beamline is 0.25–1.9 keV. Both beamlines can operate in parallel at a full repetition rate of 100 Hz.

The Aramis undulator [1] consists of 13 in-vacuum variable-gap modules, each 4 m-long, interleaved with 0.75 m break sections containing a sub-μm resolution BPM, a quadrupole magnet and a phase shifter. Athos [2] on the other hand consists of 16 out-of-vacuum Apple-X modules of 2 m length with break lengths of 0.8 m, housing a CHIC-chicane instead of the phase shifter [3]. Each quadrupole/BPM pair is mounted on a remotely controlled plate with travel range of 1 mm in the horizontal and vertical planes for alignment purposes in both the Aramis and Athos undulator beamlines. The BPM offsets relative to the centre of the quadrupoles can be corrected via software. The undulator modules can also be remotely aligned, in the horizontal and vertical plane, both in offset and angle.

To achieve best lasing performance in a reproducible way, the alignment of the quadrupole magnets is critical. The electron and photon beams must be transversally superimposed inside the undulator for efficient FEL amplification. The maximum allowed transverse misalignments should be better than 10 μm. Such extreme tolerances are not achievable using traditional alignment techniques (tunnel survey), hence it is necessary to implement beam-based alignment (BBA) techniques.

PROCEDURE

Originally developed for the LCLS [4] and successfully demonstrated at PAL [5] and EuXFEL [6], the dispersion-free steering BBA is a procedure that allows finding a straight electron beam trajectory along the undulator line. The straightness of the trajectory inside each of the undulator module relies instead on the correct compensation of first and second field integrals, corrected using dedicated coils set according to feed-forward tables. The procedure allows the reconstruction of the position of the quadrupoles with respect to a straight line as well as the offsets of the BPMs by measuring and minimising the dispersion along the beamline. It is based on measuring the electron beam trajectories for widely different energies in order to distinguish between magnetic kicks, caused by quadrupole offsets or other spurious kicks, which scale linearly with energy, and BPM offsets, which are energy independent [4, 5]. Critical for the success of the procedure is that the transport optics till the entrance of the beamline stays constant when changing energy, while nothing must be changed in the undulator beamline.

In the case of SwissFEL, for such wide energy changes we follow different strategies depending on the beamline. In the case of Aramis, we put off timing the RF of successive accelerating cavities in Linac 3, see Fig. 1, such that the beam energy is varied from 5.9 GeV to 3 GeV. We usually consider four energy steps, equally spaced in inverse electron beam energy, such that the strength of the quadrupole magnets varies by the same amount (while staying at the same current). In the case of Athos, we change the acceleration settings of Linac 2, see Fig. 1, while compensating the

* eugenio.ferrari@psi.ch

ISBN: 978-3-95450-227-1 ISSN: 2673-5490 doi:10.18429/JACoW-IPAC2022-TUPOPT066

KEK LUCX FACILITY LASER-TO-RF&RF-TO-RF STABILITY STUDY AND OPTIMIZATION

K. Popov†, The Graduate University for Advanced Studies (SOKENDAI), Shonan Village, Hayama, Kanagawa 240-0193, Japan
A. Aryshev, N. Terunuma, J. Urakawa, High Energy Accelerator Research Organization (KEK), 1-1 Oho, Tsukuba, Ibaraki 305-0801, Japan

Abstract

The KEK LUCX facility is a linear accelerator devoted to the beam instrumentation R&Ds for present and future accelerator systems and colliders. Also, it is used for the development of a compact and intense source of monochromatic X-rays based on the Compton backscattering phenomena and for development of cost-effective LLRF feedback systems. We aim to achieve RF-gun Laser-to-RF&RF-to-RF phase stability of 0.35°(RMS) and amplitude stability of 0.07%(RMS) with implementation of the Digital LLRF feedback based on commercially available FPGA board and digital trigger system.

As the first step to achieve that level of stability, present RF phase and amplitude jitters were measured using time- and frequency-domain techniques. After that, jitter influence on beam parameters after RF-gun and main solenoid magnet was simulated with ASTRA tracking code and results were cross-checked during LUCX facility beam operation. Finally, a stable digital trigger system and digital LLRF phase monitor based on SINAP EVG&EVR and STEMlab 125-14 modules were implemented.

This report demonstrates the results of Laser-to-RF&RF-to-RF phase and amplitude jitter measurements cross-checked with ASTRA simulation and real beam parameters measurements.

INTRODUCTION

The KEK LUCX facility [1] (Fig. 1) is the compact linear accelerator employing an Nd:YAG laser system to generate a multi-bunch electron beam of a Cs:Te photocathode and accelerate it in a 3.6-cell S-band (2856 MHz) standing wave RF-gun and 12-cell S-band standing wave booster. The beamline electron optics includes a solenoid, quadrupole, steering and bending magnets. Beam diagnostics include Inductive Current Transformers (ICTs), button type Beam Position Monitors (BPMs) and ceramic luminophore screen (DMQ), YAG and OTR screens. With the help of Nd:YAG laser it is possible to generate a nC bunches of the picosecond duration. The development of a compact and intense source of monochromatic X-rays based on the Compton backscattering [2] at the KEK LUCX facility faces a few technical challenges affecting the stability of X-ray photon flux characteristics due to Laser-to-RF, RF-to-RF phase and amplitude jitter. Therefore it was decided to develop a new LLRF feedback system for S-band RF-gun and 12-cell accelerating structure to achieve 300 fs phase stability of the accelerating field 2856 MHz using cost-effective and commercially available FPGA boards [3]. The realistic way to stabilize RF and timing systems to the abovementioned level is to employ a digital trigger/gate/delay generators, digital Low-Level RF (LLRF) and digital feedback systems.

The common trigger/timing distribution systems are semi-analogue solution, which are based on the NIM Linear Synchronization modules fed by a Signal Generator Continuous Wave and analogue NIM FANOUTs, gate generators, NIM/TTL or TTL/NIM level converters with digital CAMAC/VME time delay modules. Many of the LLRF distribution systems are still based on NIM frequency dividers/multipliers, power dividers, RF amplifiers and attenuators modules with semi-analogue feedback modules of a different architectures (I/Q demodulators, CPU, FPGA [4] with implemented PID controllers, I/Q modulator) based on different standards (VME, microTCA, etc). Moreover, all three subsystems should be phase-locked on each other.

It was decided to follow the cutting-edge approach to achieve extremely low Laser-to-RF and RF-to-RF phase jitter of a 300 fs (RMS) of 2856 MHz at KEK LUCX. It is based on a digital multichannel programmable trigger/delay/gate generator as a stand-alone module (Highland Technology [5], Berkley Nucleonics [6] or SINAP EVG&EVR [7]), as well as utilizing the optical fibers for LLRF distribution instead of coaxial RF cables. Furthermore, modern cost-effective feedback systems can be based on RedPitaya FPGA boards (for example STEMlab 125-14 [3]) which can sample the down-converted from 2856 MHz to 10 MHz signals. These feedback systems have 2 ADC input and 2 DAC output channels for RF pulses from RF-gun and 12-cell booster and a separated input channel for a trigger signal and external synchronized RF clock.

STABILITY MEASUREMENT TECHNIQUES

It was necessary to measure KEK LUCX facility RF phase&amplitude stability as initial step of the timing and feedback systems upgrade, thereafter simulate its jitter influence on the beam characteristics along beamline, especially at Compton Interaction Point (IP). The Tektronix DPO 7354 oscilloscope with DPX option [8] was used to measure Laser-to-RF and RF-to-RF phase&amplitude stability. The "interpolation" measurement mode with 40 GSa/s sampling rate and 250 fs/point resolution was set during these measurements. The display horizontal scale was equal to 62.5 ps.

† popovkon@post.kek.jp.

ISBN: 978-3-95450-227-1 ISSN: 2673-5490 doi:10.18429/JACoW-IPAC2022-TUPOPT067

DEVELOPMENT OF A TRIGGER DISTRIBUTION SYSTEM BASED ON MicroTCA.4

H. Maesaka[†, 1], T. Inagaki[1], RIKEN SPring-8 Center, Sayo, Hyogo, Japan
N. Hosoda[2], E. Iwai[2], T. Ohshima[2], JASRI, Sayo, Hyogo, Japan
[1]also at JASRI, Sayo, Hyogo, Japan
[2]also at RIKEN SPring-8 Center, Sayo, Hyogo, Japan

Abstract

We designed a trigger timing distribution system for MicroTCA.4-based (MTCA.4) electronics and developed a new advanced mezzanine card (AMC) and a level converter module for this purpose. A trigger signal is transmitted through a high-speed serial data stream in an optical fiber. This AMC has five optical transceivers, one for receiving trigger signals from upstream and four for fanouts to downstream. A master AMC distributes trigger timing signals, trigger counts, and event data and slave modules generate trigger output signals with appropriate delays according to the received event data and the local setting for each output channel. The trigger timing of each output can be precisely adjusted with the interval of 509 MHz or 238 MHz clocks. The timing can also be fine-tuned by ~80 ps tap delay. The timing jitter was measured to be approximately 40 ps std., which is significantly smaller than the clock period of the reference clock and sufficient for most applications. The developed trigger system has been utilized in SPring-8, SACLA, and NewSUBARU, and various accelerator components are synchronously operated with sufficient timing accuracy.

INTRODUCTION

A particle accelerator has many components that need precise synchronization among them, such as electron and ion sources, pulsed rf sources, pulsed power supplies, beam diagnostics, etc. The control sequence of these components is getting complex and the data amount is also increasing thanks to the evolution of control and data acquisition electronics. MicroTCA.4 (MTCA.4) [1] is one of the electronics platforms to process large-volume data and it is employed in many accelerator facilities.

In the third-generation light source, SPring-8, for example, the electron beam injector was switched from the combination of linac and booster synchrotron to the linac of the x-ray free-electron laser (XFEL), SACLA [2]. To inject an electron beam in parallel with XFEL operation, the accelerator components must be controlled shot-to-shot by an intelligent triggering system. Therefore, we developed a trigger signal distribution system based on MTCA.4 to synchronize the accelerator components and generate flexible trigger signals for complex operation sequences.

This trigger system was installed into SPring-8, SACLA, and NewSUBARU [3]. The new 3 GeV light source "NanoTerasu" in Tohoku, Japan [4], also employed this trigger system. In this article, we describe the design and performance of the trigger signal distribution system.

DESIGN

Requirements

Since the distance between accelerator components can be in kilometer order, it is hard to transmit high-speed signals through a long metal cable. Therefore, the trigger signal should be distributed by fiber optical links. More than 10 trigger outputs are necessary on the front panel, backplane, and Zone 3. Some signal inputs are also needed for trigger inputs and some other controls. The trigger signal must be synchronized to the acceleration rf frequency of 509 MHz or 238 MHz used in SPring-8, SACLA, NewSUBARU, etc.

Since most of the accelerator components are also synchronized to the power line frequency of 50 or 60 Hz, the trigger signal should be generated with this repetition rate. We call this as a master trigger. The timing of the trigger signal from each output channel should be precisely delayed for up to 20 ms (period of 50 Hz) from the master trigger. The resolution of the timing control should be 0.1 ns level and the jitter should be well below 0.1 ns std. for precise timing adjustment within the acceleration rf period. The trigger output should be turned on or off shot-to-thot according to a given output pattern.

Some frequency-divided signals from the acceleration rf clock are also demanded, such as a revolution clock of a storage ring, for example. Some asynchronous triggers unrelated to the accelerator repetition rate are also needed. By generating an asynchronous trigger from an alarm signal, we can take data from various components at this alarm, which can be useful for postmortem analysis.

Since each accelerator component requires a different trigger input level, the trigger system should deliver appropriate levels of trigger signals. Some components may accept only single-ended signals and some may need differential signals. Since an MTCA.4 board is difficult to generate various output levels and cope with various connector types, an additional interface module is needed.

Trigger Signal Distribution

Based on the requirements described above, we considered the concept of the trigger system. The schematic diagram of the trigger distribution network is shown in Fig. 1. The trigger signal is generated and distributed by a newly developed MTCA.4 advanced mezzanine card (AMC). The master module of the trigger AMC receives an external master trigger signal (60 Hz maximum) and the trigger signal is embedded in a high-speed serial data stream and transferred by optical fibers. The trigger AMC was

ISBN: 978-3-95450-227-1 ISSN: 2673-5490 doi:10.18429/JACoW-IPAC2022-TUPOPT068

TRANSVERSE AND LONGITUDINAL MODULATION OF PHOTOINJECTION PULSES AT FLUTE

M. Nabinger*†, C. Sax*, M. J. Nasse, J. Schäfer, C. Widmann, C. Xu, A.-S. Müller
Karlsruhe Institute of Technology, Karlsruhe, Germany

Abstract

To generate the electrons to be accelerated, a photoinjection laser is used at the linac-based test facility FLUTE (Ferninfrarot Linac- Und Test Experiment) at the Karlsruhe Institute of Technology (KIT). The properties of the laser pulse, such as intensity, laser spot size or temporal profile, are the first parameters to influence the characteristics of the electron bunches. In order to control the initial parameters of the electrons in the most flexible way possible, the laser optics at FLUTE are therefore supplemented by additional setups that allow transverse and longitudinal laser pulse shaping by using spatial light modulators (SLMs). In the future, the control of the SLMs will be integrated into a machine learning (ML) supported feedback system for the optimization of the electron bunch properties. In this contribution, the first test experiments and results on laser pulse shaping at FLUTE on the way to this project are presented.

INTRODUCTION

Modern and future accelerator projects require electron beams with an exceptional combination of high brightness and low emittance. As a consequence, in recent years there has been a strong interest in the improvement of RF photoinjectors [1–3]. Of particular interest is the tailoring of the photoinjection pulse properties [4]. Arbitrary shaping of the drive laser pulse in both transverse and longitudinal directions provides a powerful tool to significantly influence and control the electron bunch characteristics.

Among the most promising devices for realizing individual pulse shaping are liquid crystal SLMs, pixel-based electro-optical components that allow a modulation in phase and/or intensity of the incident light. The working principle of the phase-only modulating SLMs, which are used in this work, is shown in Fig. 1. The birefringent liquid crystal molecules (LCM) are embedded in several cells/pixels between pairs of electrodes on a silicon substrate, protected by a glass layer on top. In such a setup - also known as liquid crystals on silicon (LCoS) - the orientation of the LCM can be changed by applying a voltage to the cell, which leads to a change of the effective refractive index seen by the incident light wave. As a result, the phase of the reflected wave can be modulated for every pixel independently.

In order to create arbitrary images, the voltages corresponding to the phase shift for each single pixel in the array must be controlled entirely. This is achievable by computing and applying a 2D phase distribution or *phase mask*, also known as a computer generated hologram (CGH). For the calculation of a CGH, several algorithms can be used, for instance the Gerchberg-Saxton (GS) algorithm, which is based on inverse Fourier transforms.

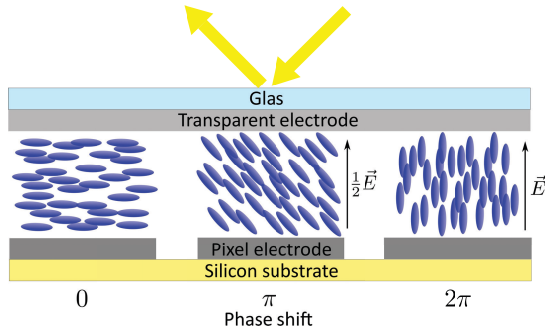

Figure 1: Working principle of an SLM with embedded LCM. By applying a voltage, the orientation of the LCM can be changed and thus the phase of the incident light can be modulated.

At the linac-based test facility FLUTE at KIT, a 800 nm Ti:Sa laser with 35 fs bandwith-limited pulse length is used for photoinjection. The copper photocathode requires a conversion of the wavelength to 266 nm by third harmonic generation. Such nonlinear processes and also the subsequent relatively complex beam path with many optical elements are difficult to take into account in the conventional calculation of CGHs. This leads to distortions of the final image on the photocathode. Hence, a simple application of the GS algorithm is insufficient. Therefore, first approaches to ML-assisted control of pulse modulation by SLMs have been introduced [5, 6]. Recently, promising attempts have been investigated and further developed at FLUTE [7].

In this paper, we present two test setups and the achieved results for transverse and longitudinal pulse shaping using a LCoS-SLM at FLUTE at KIT. Here, a commercially available Hamamatsu LCoS-SLM X13138-02 optimized for a wavelength range of 800 nm ± 50 nm with a resolution of 1024×1272 pixels was used. In addition, a first integration of an SLM into the photoinjection path of FLUTE was realized. We present the first transversely modulated photoinjection pulses at FLUTE and the resulting double electron beam.

PULSE SHAPING TEST SETUPS

Transverse Modulation

As schematically shown in Fig. 2a, the transversal test setup was realized by using a widened linearly polarized red alignment laser of 638 nm wavelength to allow simple initial optimization of the CGH calculations. Despite the wavelength mismatch in terms of optimal use, the SLM

* Both authors have contributed equally.
† matthias.nabinger@kit.edu

ISBN: 978-3-95450-227-1 ISSN: 2673-5490 doi:10.18429/JACoW-IPAC2022-TUPOPT069

PREPARATION AND CHARACTERIZATION OF BTO-BFO MULTIFERROIC CERAMICS AS ELECTRICAL CONTROLLABLE FAST PHASE SHIFTING COMPONENT

N.W. Martirosyan† [1, 2], A.H. Grigoryan[1], R.H. Ghazaryan[2], G.S. Karoyan[2], K.G. Kirakosyan[2]
M.M. Mkrtchyan[2], A.A. Sargsyan[1], V.V. Sahakyan[1], T.V. Vandunts[2]
[1] Center for the Advancement of Natural Discoveries using Light Emission, 0040 Yerevan, Armenia
[2] National Polytechnic University of Armenia, 0009 Yerevan, Armenia

Abstract

A rich variety of dielectric, optical, acoustic/piezoelectric, ferromagnetic properties of ferroelectric and multiferroic composite materials open a new perspective for the development of modern accelerators with new type of electron acceleration and control system. A Self-propagating High-temperature Synthesis (SHS) technology for obtaining ceramic materials, based on (1-x)$BiFeO_3$–x$BaTiO_3$ compositions with various dopant (MgO, MnO, etc.) to get electrically controlled phase tuning and amplitude modulating ultrafast devices has been developed.

The general parameters of the SHS process (temperature and propagation velocity of the combustion front) are measured. The dependences of microstructure (grain size, density, and porosity), as well as electro physical properties of the prepared samples on compaction and sintering thermodynamic variables, such as the pressing pressure and duration, sintering temperature, sintering duration and atmosphere, heating and cooling rates, are experimentally investigated.

INTRODUCTION

Perovskite ferroelectrics and multiferroics are multifunctional materials characterized by a rich variety of properties, such as dielectric, optical, acoustic/piezoelectric, ferromagnetic, etc. These properties may be controlled by external stimuli like electric and/or magnetic fields, temperature and mechanical stress. Nevertheless, multiferroics are the best when it comes to multifunctionality. They combine ferroelectric, ferromagnetic and piezoelectric, etc. properties.

The dielectric permittivity of BSTO and BFO-BTO can be altered very rapidly by an applied bias voltage pulse that make them extremely attractive for high-energy accelerator applications as fast switchers and high-power controlling tuners [1-4].

Since multiferroics combine magnetic and electric properties in the same phase and can present a coupling between the magnetic and electric properties (the induction of a magnetization by an electric field), they provide a new perspective for devices design and can be used to construct new RF phase rotator/shifter (phase and amplitude modulator) based on the simultaneously change of dielectric and magnetic penetration in ferroelectric under the impact of external field [5-7].

$Ba_{1-x}Sr_xTiO_3$ and (1-x)$BiFeO_3$–x$BaTiO_3$ compositions with MgO and MnO_2 dopant fully satisfy the requirements for a fast electrically-controlled tuner for Brookhaven National Laboratory (BNL) and for high-power fast RF phase shifters to be used for the spallation neutron source (SNS) vector modulation applications. The research and previous calculation of properties of $Ba_{1-x}Sr_xTiO_3$ carried out by A. Kanareykin, E. Nenasheva, et al., show that these materials can be used as key elements of the tunable and switching accelerator components, providing the dielectric constant of the material in the range of 400-500, loss tangent less than (2-5)×10^{-3} at 10 GHz and the tunability factor (defined as a ratio of the dielectric constant at zero biasing field to that at a specific applied electric field) in the range of 1.15-1.20 at a 5 V/μm (50 kV/cm) biasing field [8]. In this work [1-y][(1-x)$BiFeO_3$–x$BaTiO_3$]-yMn solid solutions are suggested which are multiferroic. Both dielectric and magnetic permeabilities of [1-y][(1-x)$BiFeO_3$–x$BaTiO_3$]-yMn solid solutions can be controlled by an electric field [9,10]. Till now ferroelectric perovskites were used to solve the aforementioned problems, thus, [1-y][(1-x)$BiFeO_3$–x$BaTiO_3$]-yMn multiferroic compositions open new perspective and are the most promising materials for accelerator applications as typical representatives of ferroelectric solid solutions.

In this paper self-propagating high-temperature synthesis (SHS) technologies for obtaining high-quality ceramic materials based on (1-x)$BiFeO_3$–x$BaTiO_3$ compositions with various dopants (MgO, MnO, etc.) are presented which will be used for getting electrically controlled phase tuning and amplitude modulating ultrafast facilities. These tools can be used in accelerator technologies, particularly at AREAL linear accelerator, which is currently operating at CANDLE Synchrotron Research Institute, for adjusting the 3 GHz wave phase and amplitude used at the accelerating structures [11, 12].

EXPERIMENTS AND PROPERTES INVESTIGATION

The powders of Mn-doped (1-x)$BiFeO_3$–x$BaTiO_3$ complex oxide have been produced by SHS from powder mixtures of Bismuth oxide, Bi_2O_3, (99.975% purity), Iron oxide, Fe_2O_3, (99.5% purity), Manganese dioxide, MnO_2, (99.9% purity), Barium peroxide, BaO_2, (99.9% purity), Titanium oxide,TiO_2, (99.5% purity), Titanium, Ti, (99.9% purity) and Iron, Fe, (99.9% purity). Materials were synthesized according to the following chemical scheme:

† marnorw@yahoo.com

ISBN: 978-3-95450-227-1 ISSN: 2673-5490 doi:10.18429/JACoW-IPAC2022-TUPOPT070

SURROGATE MODELLING OF THE FLUTE LOW-ENERGY SECTION

C. Xu*, E. Bründermann, A.-S. Müller, J. Schäfer, and A. Santamaria Garcia
Karlsruhe Institute of Technology (KIT), Karlsruhe, Germany

Abstract

Numerical beam dynamics simulations are essential tools in the study and design of particle accelerators, but they can be prohibitively slow for online prediction during operation or for systematic evaluations of new parameter settings. Machine learning-based surrogate models of the accelerator provide much faster predictions of the beam properties and can serve as a virtual diagnostic or to augment data for reinforcement learning training. In this paper, we present the first results on training a surrogate model for the low-energy section at the Ferninfrarot Linac- und Test-Experiment (FLUTE).

INTRODUCTION

Compared to single beam dynamics, collective effects are computationally more expensive to calculate. For example, a detailed space charge particle tracking simulation often takes minutes to run and thus makes parameter optimization or training of machine learning algorithms on simulation data very time consuming or even infeasible. A surrogate model can be used to provide rapid evaluations and replace the time-consuming simulations by approximating the outputs. Common methods to build a surrogate model include Gaussian process regression, random forests, and deep neural networks (NN) [1–3]. In addition, surrogate models could be used as virtual diagnostics, predicting valuable information of the beam in a non-destructive way, e.g. the longitudinal phase space of the electron bunches [4, 5]. In this paper, we present the development of a neural network surrogate model of the low-energy section at the Ferninfrarot Linac- und Test-Experiment (FLUTE). We describe the training process and compare the NN-predicted bunch properties to both simulations and measurement data. Finally, we discuss applications of the surrogate model as an online virtual diagnostic and as a training environment for other algorithms.

TRAINING THE SURROGATE MODEL

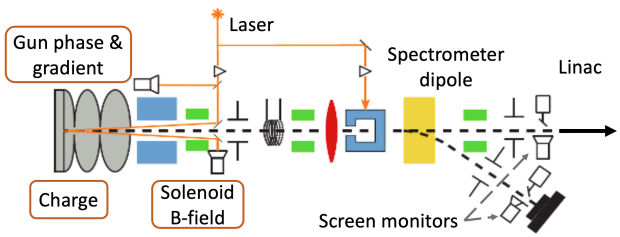

Figure 1: Schematic layout of FLUTE low-energy section with the inputs to the surrogate model marked with an orange box. Figure adapted from [6].

* chenran.xu@kit.edu

Figure 1 shows the schematic layout of the low-energy section of the the KIT linac-based test facility, FLUTE [7]. The electrons are generated at the RF photoinjector and accelerated up to 7 MeV. The input layer of the surrogate model NN consists of 4 neurons representing the bunch charge, the RF gun phase, the RF gun maximal gradient, and the solenoid magnetic field. The output layer returns 6 scalar values representing the bunch properties, namely the transverse beam size σ_x, bunch length σ_z, mean energy E, relative energy spread σ_E, normalized transverse emittance ϵ_x, and percentage of the remaining particles. These bunch properties can also be measured using the diagnostic devices [8], so that the model can be further retrained and fine-tuned to match the measurement results.

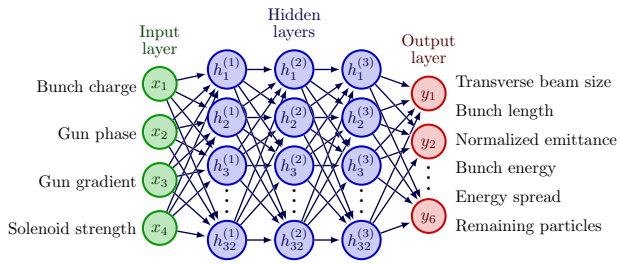

Figure 2: Architecture of the fully connected neural network. The 4 machine parameters are fed into the neural network with 3 hidden layers, each with 32 neurons.

Table 1: Input parameter range used to generate training data

Input Parameters	Range	Unit
Charge	1 to 30	pC
Gun phase	175 to 235	deg
Gun max. gradient	50 to 100	MV/m
Solenoid B-field	0.08 to 0.2	T

We use a fully connected feed-forward NN with 3 hidden layers, as shown in Fig. 2, each layer with 32 neurons and the hyperbolic tangent function (tanh) as the activation function. The size of the network is chosen to sufficiently approximate the transfer map from photocathode to linac, but not too large so that it fully memorizes the dataset. In such a case, the network will not be able to generalize to unseen scenarios. The NN is implemented using the open-source library pyTorch [9]. The training data consists of 10^4 samples randomly selected from the parameter space listed in Table 1. For each parameter setting, the bunch properties are obtained via an ASTRA tracking simulation. The NN training parameters are summarized in Table 2. The input and output parameters are min-max normalized, mapped to [0,1] intervals, to speed up the training process. The output

ISBN: 978-3-95450-227-1 ISSN: 2673-5490 doi:10.18429/JACoW-IPAC2022-TUPOTK002

RESULTS OF THE RF POWER TESTS OF THE ESS CRYOMODULES TESTED AT CEA

O. Piquet, C. Arcambal, P. Bosland, S. Berry, A. Bouygues, E. Cenni, G. Devanz, T. Hamelin, C. Madec, C. Mayri, P. Sahuquet, Q. Bertrand, CEA, Gif sur Yvette, France
P. Pierini, ESS, Lund, Sweden
D. Sertore, INFN, Milano, Italy
M. Ellis, STFC, Daresbury, United Kingdom

Abstract

Eight of the medium and high beta cryomodules delivered to ESS by CEA are tested at CEA before delivery; the two medium and high beta prototypes and the three first of each type of the series. The goal of these tests is to validate the assembly and the performances on few cryomodules before the next cryomodules of the series are delivered to ESS. This paper summarizes the general results obtained during the tests at 2 K and at high RF power, Pmax = 1.1 MW. The cavities reach the ESS requirements, Eacc = 16.7 MV/m (Medium beta) and 19.9 MV/m (High beta) with an efficient compensation of the Lorentz detuning by the piezo tuner over the full RF pulse length of 3.6 ms at 14 Hz. After the successful tests at CEA, the first cryomodules have been shipped to ESS where the final acceptance test are performed.

INTRODUCTION

In the framework of its In Kind contribution for the construction of the ESS accelerator [1, 2], CEA developed a stand to perform the tests of the elliptical ESS cryomodules at high RF power (Fig. 1). The goal of these tests is to validate the quality of the assembly and the performances of few cryomodules before the next cryomodules of the series are delivered to ESS and tested there [3, 4].

We have already tested seven cryomodules over eight scheduled; the 2 medium and high beta prototypes (CM00 and CM30), 3 medium beta cryomodules of the series (CM01, CM03 and CM05) and the 2 first high beta (CM31 and CM32).

Previous papers have already presented test results obtained on the medium beta cryomodule demonstrator CM00 [5]. This paper presents a summary of the results we have obtained during the tests of the seven cryomodules.

THE TEST STAND

The test stand is about 100 m from the cryomodule assembly hall. It is equipped with a liquefier that can deliver 90 l/h of 4 K LHe at 1.1 bar to the 2000 l Dewar close to the cryomodule. The cryomodule is equipped with an internal Hampson heat exchanger (HX) that is well adapted to the supercritical helium fluid used at ESS, but is not adapted for diphasic helium at 1 bar containing a too high rate of bubbles. This caused some difficulties in the first tests performed on the prototype CM00. We fixed this issue adding a small phase separator to remove part of the GHe generated in the last 10 meters of cryogenic line between the Dewar and the cryomodule. This small phase separator allows the HX to run and we obtain an easy regulation of the 2 K LHe level above the cavities.

The thermal shield is cooled at 80 K with LN2. This is a second difference with the ESS nominal cryogenic conditions where the liquefier delivers 40 K GHe at 20 bars to cool the thermal shield.

The RF power source is a 704 MHz klystron with a home-made modulator. It can generate 1.1 MW RF pulses of 3.6 ms length at 14 Hz. The RF distribution line (Fig. 1) is equipped with an RF switch that can send the RF power in one of the two branches at the entrance of the test stand. Each branch is equipped with a power divider that can distribute the power in one cavity or two cavities. We can test one cavity at a time, or two maximum together. Test with the four cavities running altogether is not possible at CEA.

The cryogenic and tuners control/command system is based on Muscade/Anibus. The RF control/command system is based on EPICS.

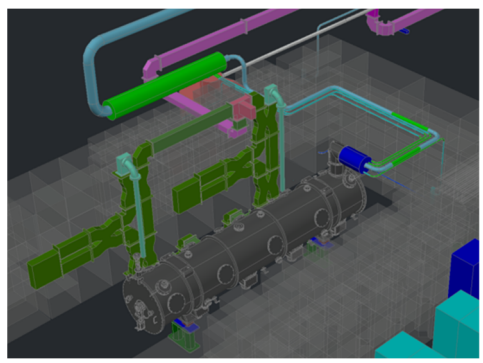

Figure 1: Test stand of ESS cryomodule at CEA.

RF POWER TESTS AT 2 K

The duration of each test was about 3 months for the first cryomodules. This duration is now reduced to about five weeks; two weeks for the installation in the test stand, cavity vacuum pumping and coupler conditioning at room temperature and three weeks for the test at cold.

We systematically perform the RF conditioning of the power couplers at room temperature before cooling down the cavities. The power couplers are conditioned in about 4 h to 7 h. This short duration can be reached thanks to the high pumping speed group, roughly 60 L/h that allows to recover quickly acceptable pressure when high degassing occurs during RF conditioning (Fig. 2).

ISBN: 978-3-95450-227-1 ISSN: 2673-5490 doi:10.18429/JACoW-IPAC2022-TUPOTK003

HIGH POWER RF CONDITIONING OF THE ESS RFQ

O. Piquet, M. Baudrier, A.C. Chauveau, M.J. Desmons, P. Hamel
CEA-IRFU, University Paris-Saclay, Gif-sur-Yvette, France
E. Trachanas, B. Jones, D. Noll, A.G. Sosa, R. Zeng
European Spallation Source ERIC (ESS), Lund, Sweden

Abstract

The 352.21 MHz Radio Frequency Quadrupole (RFQ) for the European Spallation Source ERIC (ESS) has been delivered by the end of 2019 by CEA/IRFU. The RFQ is designed to accelerate a 70 mA proton beam from 75 keV up to 3.62 MeV. It consists of a 4-vane resonant cavity with a total length of 4.6 m. Two coaxial power loop couplers feed the RFQ with the 1.4 MW of RF power required for beam operation. This paper first presents the main systems required for the RFQ conditioning. Then it summarizes the main steps and results of this high power RF conditioning completed at ESS from June 9 to July 29, 2021 in order to achieve the nominal field for a pulse length of 3.2 ms at the repetition rate of 14 Hz.

INTRODUCTION

CEA/IRFU was in charge of the RFQ design [1], manufacturing [2], installation [3], and conditioning at ESS (Lund). An important step towards beam commissioning is the high power conditioning in order to achieve the nominal field for the proton acceleration. During this procedure where the power, width and repetition rate of the RF pulses sent to the cavity are increased gradually, confined gasses and water are released from the cavity surface and electrical sparks and discharges even out surface imperfections. The high power conditioning of RFQ (Fig. 1), was realized in 7 weeks following a period of extensive tests in the overall system chain.

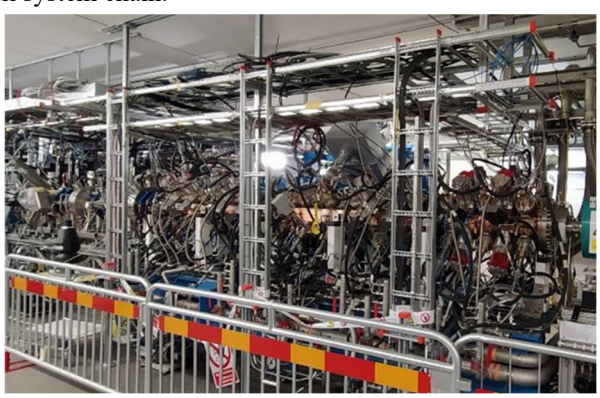

Figure 1: ESS RFQ.

RFQ ANCILLARY SYSTEMS

RF System

The RF power system for the RFQ is comprised of the 660 kVA modulator (115kV/100A amplitude, 3.5 ms width and 14 Hz repetition rate), the klystron, and the RF distribution system. RF produced by the klystron is guided through waveguides (in addition to a power split towards a dummy load) to the symmetrically placed coaxial cavity couplers. The forward power requirements for operation are expected to be 1.4 MW (729 kW for cavity plus 225 kW beam loading and 30% margin for LLRF feedback evaluated during the bead-pull measurement campaign in December 2019 [3].

Low Level RF System

The Low Level RF system monitors and adjusts the amplitude and phase of the cavity. Stable operating frequency is achieved by tandem operation of LLRF and RFQ water system by regulation of the temperature in the 4 cooling loops. During RFQ conditioning, a feedback control loop adjusts the frequency of the provided RF power to compensate for cavity detuning during heating. Although in normal operations LLRF systems measures the detuning of the cavity and adjusts the water temperature to regulate cavity resonant frequency.

Vacuum System

In order to achieve nominal vacuum level (7 10^{-8} mbar) during beam operation, 10 turbo pumps are installed at the RFQ. Two cold-cathode gauges are installed at the beginning and the end of the cavity body and two at the couplers for monitoring the cavity vacuum levels during conditioning process.

Local Protection System

Local protection system (RF-LPS) is structured as a multistate machine to manage interlocks in the entire system chain with different response times: a slow interlock module with interlock times of some milliseconds and a fast interlock module with response times less than 20 microseconds. There are multiple interlock conditions that can lead to the shut-off of the RF power.

During conditioning the forward power from the klystron was limited to 800 kW or 400 kW for each arm feeding the two couplers. Electric breakdowns or sparks lead to significant power reflections monitored by the reflected power interlock. Because of the high reflection during the filling time of the cavity and at the end of the RF pulse this area is masked out and excluded from the interlock monitoring. Moreover electric field breakdown inside the cavity leads to a drop of the field with a speed faster than the usual field decay time. The RF decay interlock detects this slope with the pickup used by the LLRF and switch off the RF power.

ISBN: 978-3-95450-227-1 ISSN: 2673-5490 doi:10.18429/JACoW-IPAC2022-TUPOTK004

TIME RESOLVED FIELD EMISSION DETECTION DURING ESS CRYOMODULE TESTS

Enrico Cenni†, Matthieu Baudrier, Guillaume Devanz, Luc Maurice, Olivier Piquet
CEA Université Paris-Saclay, Gif-sur-Yvette, France

Abstract

At CEA-Saclay we are currently testing the European Spallation Source (ESS) high beta cryomodules (CM). Each cryomodule is equipped with four superconducting elliptical cavities with their ancillaries (fundamental power couplers (FPC), frequency tuners and magnetic shields). The cavity is designed to accelerate protons with relativistic speed about beta=0.86 and operate at an accelerating field of 19.9MV/m. During cryomodule test, operational parameters are inspected by powering up one cavity at the time. A dedicated gamma ray detection system has been designed and installed around the cryomodule in order to have a more precise insight into field emission phenomenon occurring during cryomodule operation. Recently we were able to obtain time resolved data concerning radiation emerging from the cavities due to field emission.

INTRODUCTION

In addition to the production of the 30 medium and high beta cryomodules of the European Spallation Source (ESS) LINAC, CEA performs the high RF power tests of two prototype CMs and of the three first CMs of each type assembled in Saclay. CEA currently tested two CM prototypes [1] and three from the medium beta section series, which will be re-tested at ESS test stand. Part of the testing operation consists in assessing the dose rate around the CM during operation [2]. At CEA we keep developing detectors, simulation codes and analysis tools in order to better understand field emission phenomena during CM testing and detect possible source of contamination on the cavity surface.

We present here the most recent application of plastic scintillator for gamma detection during the first two high beta series cryomodule tests (*i.e.* CM31 and CM32). The four cavities installed in the cryomodule were manufactured and prepared by Research Instrument under the supervision of UKRI Daresbury. The string assembly was carried out at CEA Saclay by a subcontractor, while the power test was performed by CEA staff [3].

EXPERIMENTAL SET UP

In Saclay we are equipped with a 704 MHz cryomodule test stand where it is possible to assess their performance by operating close to working conditions. A first set up has been described in previous publications [4,5], here we will focus on the newly designed gamma detection system developed at CEA.

Cavities and Cryomodule

The cryomodule accommodates four high beta cavity manufactured with fine grain high purity niobium [6]. In Table 1 are summarized the most significant cavity RF parameters.

Table 1: Design Parameters for High Beta Cavities [6]

Design parameters	Value
Geometrical beta - β_{geom}	0.86
Nominal gradient E_{acc} [MV/m]	19.9
Q_0 at nominal gradient	$>5x10^9$
G [Ω]	241
R/Q [Ω]	435
E_{pk}/E_{acc}	2.2
B_{pk}/E_{acc} [mT/(MV/m)]	4.3
E_{pk}@nominal E_{acc} [MV/m]	43.8
B_{pk}@nominal E_{acc} [mT]	85.6

Gamma and Neutron Diagnostic Systems

Part of the testing activities consist of radiation dose profile measurements with respect to cavities voltage, RF pulse structure and cavity position.

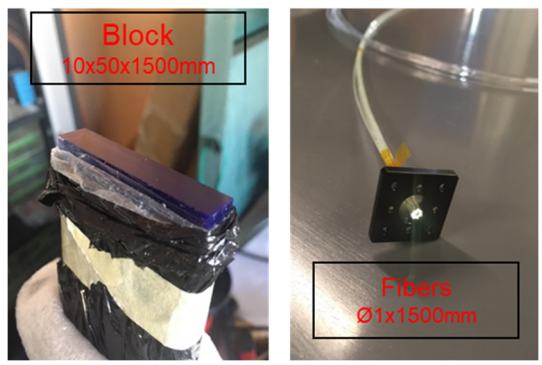

Figure 1: Plastic scintillators, block (left) and fibres bundle (right).

The current set up consist of two NaI(Tl) scintillators connected to a photo multiplier and a multichannel analyser and eight Geiger-Muller (GM) counters (LB6500-H10 connected to a LB5340 data logger). The power tests are performed mostly one cavity at the time. Six G-M are placed around the vacuum vessel close to the powered cavity, while the remaining two are always fixed at the cryomodule ends. On Figures 2 and 3 are shown their location when cavity #2 is powered, GM1 to GM6 are for low dose rate while GM7 and GM8 are for high dose rate. A neutron detector (LB6411) is installed close to the bunker wall

†enrico.cenni@cea.fr

ISBN: 978-3-95450-227-1 ISSN: 2673-5490 doi:10.18429/JACoW-IPAC2022-TUPOTK005

MITIGATION OF PARASITIC LOSSES IN THE QUADRUPOLE RESONATOR ENABLING DIRECT MEASUREMENTS OF LOW RESIDUAL RESISTANCES OF SRF SAMPLES

S. Keckert*, R. Kleindienst, J. Knobloch[1], F. Kramer, O. Kugeler, D. Tikhonov,
Helmholtz-Zentrum Berlin, Berlin, Germany
[1]also at Universität Siegen, Siegen, Germany
W. Ackermann, H. De Gersem, Technische Universität Darmstadt, Darmstadt, Germany
M. Wenskat, Universität Hamburg, Hamburg, Germany
X. Jiang, A. O. Sezgin, M. Vogel, Universität Siegen, Siegen, Germany

Abstract

The quadrupole resonator (QPR) is a dedicated sample-test cavity for the RF characterization of superconducting samples in a wide temperature, RF field and frequency range. Its main purpose are high resolution measurements of the surface resistance with direct access to the residual resistance thanks to the low frequency of the first operating quadrupole mode. Besides the wellknown high resolution of the QPR, a bias of measurement data towards higher values has been observed, especially at higher harmonic quadrupole modes. Numerical studies show that this can be explained by parasitic RF losses on the adapter flange used to mount samples into the QPR. Coating several micrometer of niobium on those surfaces of the stainless steel flange that are exposed to the RF fields significantly reduced this bias, enabling a direct measurement of a residual resistance smaller than 5 nΩ at 2 K and 413 MHz.

INTRODUCTION

This contribution addresses the key results of our study on parasitic losses in the QPR and their mitigation. For a comprehensive discussion and further details see [1].

The surface resistance of superconducting radio frequency (SRF) cavities is commonly approximated by

$$R_S = R_{BCS} + R_{res} = \frac{af^2}{T} \exp\left(-\frac{\Delta}{k_B T}\right) + R_{res} \qquad (1)$$

with intrinsic BCS resistance (R_{BCS}) and a residual resistance (R_{res}). R_{BCS} depends on a material parameter (a) and the superconducting energy gap (Δ), the contributions to R_{res} are less well understood and are still under investigation. Hence, for R&D on materials, coatings or surface treatments aiming at application in SRF cavities, precision measurements of the surface resistance are required.

The QPR provides high resolution measurements in a wide parameter space of temperature and RF field at three different frequencies [2–5]. With a first operating quadrupole mode at about 415 MHz, R_{BCS} at 2 K is typically smaller than 2 nΩ, enabling direct measurements of R_{res}. Operational experience indicates a bias of measurement data towards a systematically overestimated R_S, limiting the accuracy at low R_S and hence especially impacting R_{res} [6–8].

* sebastian.keckert@helmholtz-berlin.de

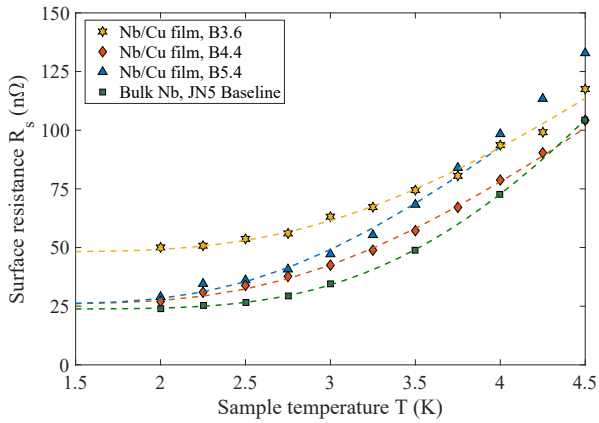

Figure 1: Representative measurement results of different niobium on copper films as well as for a bulk Nb sample at 415 MHz. The BCS resistance is fitted using Eq. (1).

As an example, Fig. 1 shows a series of measurements of R_S vs. temperature for different Nb on copper films as well as for a bulk Nb sample (JN5). The results show that at the first quadrupole mode ($f \approx 415$ MHz), R_{res} is larger than 20 nΩ, even for the bulk niobium sample.

A calorimetric compensation technique is used to derive the sample's R_S at the actively stabilized temperature of interest. Comparing the levels of DC heater power that are required in thermal equilibrium either with or without applied RF field, directly gives the RF dissipated power and hence R_S according to

$$R_S = \frac{2P_{diss}}{\int_{sample} ||H||^2 \, dS} = 2c\frac{\Delta P_{DC}}{P_t Q_t} \qquad (2)$$

with transmitted power P_t, pickup coupling Q_t and calibration constant c. It is important to keep in mind, that any heating occurring in the thermal system of the sample assembly will be interpreted as R_S of the sample.

We will see that the observed behavior of biased R_{res} is dominated by parasitic losses on the normal conducting sample adapter flange. Coating this flange with niobium reduced this bias at the first quadrupole mode by more than 10 nΩ. At 1.3 GHz this improvment is even larger where due to a reduced damping in the coaxial gap a measurement of R_{res} hitherto was impossible.

ISBN: 978-3-95450-227-1 ISSN: 2673-5490 doi:10.18429/JACoW-IPAC2022-TUPOTK006

SYSTEMATIC INVESTIGATION OF FLUX TRAPPING DYNAMICS IN NIOBIUM SAMPLES

F. Kramer*, S. Keckert, O. Kugeler, J. Knobloch[1], Helmholtz-Zentrum Berlin, Berlin, Germany
[1]also at Universität Siegen, Siegen, Germany

Abstract

Trapped magnetic flux in superconducting cavities can significantly increase surface resistance, and, thereby, limits the cavities' performance. To reduce trapped flux in cavities, a better understanding of the fundamental mechanism of flux trapping is vital. We develop a new experimental design: measuring magnetic flux density at 15 points just above a niobium sheet of dimensions (100 x 60 x 3) mm with a time resolution of up to 2 ms and a flux resolution better than 0.5 µT. This setup allows us to control the temperature gradient and cooldown rate, both independently of each other, as well as the magnitude and direction of an external magnetic field. We present data gathered on a large-grain sample as well as on a fine-grain sample. Our data suggests that not only the temperature gradient but also the cooldown rate affects trapped flux. Additionally, we detect a non-trivial relationship between trapped flux and magnitude of applied field.

INTRODUCTION

Rising demands on modern accelerators can in many cases only be met with superconducting cavities. This is especially true of accelerators intended to operate in continuous wave (CW) mode. Nonetheless, when operating superconducting cavities in the radio frequency (RF) range losses occur. These losses stem from non-vanishing surface resistance of superconductors in RF fields. A significant part of the surface resistance is caused by trapped flux: A perfect superconductor expels all magnetic flux when it transitions from normal conductivity to superconductivity. In contrast, real-life superconductors are not perfect, they trap magnetic flux lines. These lines oscillate in an RF field generating losses [1]. Since these cavities are operated at a temperature around 2 K, and 1 W of dissipated power requires close to 1 kW of wall plug power, the cryoplants needed to cool these cavities are a major cost driver for SRF accelerators, which is why reducing surface resistance is crucial. This permits the construction of larger machines, and reduces costs of smaller ones.

The approach to reducing trapped flux presented in this paper is to get a better understanding of the fundamental mechanism of flux trapping before trying to minimize it. To this end, we have built an experiment to measure trapped flux in samples instead of cavities [2]. This allows us to independently control the parameters which might have an influence on trapped flux (temperature gradient, cooldown rate, magnetic field). It also increases the number of possible thermal cycles drastically (~300/day instead of ~1/day). Since the samples are large flat sheets, the geometric effects that arise from demagnetisation are readily separated from effects due to the material's properties. .

First, the setup will be presented in more detail. Then, experimental data will be presented, where the parameters mentioned above (temperature gradient, cooldown rate, magnetic field) are investigated.

EXPERIMENTAL SETUP

Trapped flux in the SRF context is typically investigated using cavities [3–6]. However, experiments with cavities are costly and time consuming. Most importantly, the cavity's geometry complicates the control of cooldown parameters. It also affects how flux is trapped [7, 8]. The new setup remedies these problems:

The sample is a flat sheet of dimensions (100 x 60 x 3) mm. It is carefully clamped in between two copper blocks at the top, and bottom (Fig. 1a). These blocks can be heated with two independent heaters. Purpose of the blocks is to have the electric heaters as far away from the sample as feasible, so magnetic field created by the heaters does not reach the sample. The temperature of the sample is monitored with up to eight Cernox sensors that are glued directly on the sample (not shown in Fig. 1a). On the back side of the sample a PCB with 15 AMR sensor [9] groups is mounted barely touching the sample. In each group, three AMR single axis sensors are combined to measure the full magnetic field vector. To measure the trapped flux as closely to the sample as possible the PCB is designed such that the center of the sensor groups have a distance of only 2.3 mm to the sample. All AMR sensors are calibrated to three Fluxgate sensors. The horizontal component of the magnetic field is controlled with two Helmholtz-coils, and the vertical component is created with a solenoid wrapped around the cryostat (Fig. 1b). Since the cryostat is not shielded the earth magnetic field is compensated with the coils as well.

The magnetic field sensors can be recorded with a time resolution of up to 2 ms with a multi-channel readout system [10]. This allows us to record the dynamics during the cooldown with a very high resolution. The Cernox sensors are wired in a way that allows us to record them with this system as well. This reduces the minimal readout time from 500 ms (Lake Shore [11]), to 10 ms (reducing the readout time further creates a lot of noise). This is vital for fast cooldowns (< 1 s).

Measurement Procedure

The setup is cooled with helium gas. To achieve this the setup is mounted above a liquid helium bath. By evaporating

* f.kramer@helmholtz-berlin.de

ISBN: 978-3-95450-227-1 ISSN: 2673-5490 doi:10.18429/JACoW-IPAC2022-TUPOTK008

CAVITY DESIGNS FOR THE CH3 TO CH11 AND BELLOW TUNER INVESTIGATION OF THE SUPERCONDUCTING HEAVY ION ACCELERATOR HELIAC*

T. Conrad†, M. Busch, H. Podlech[1], M. Schwarz, IAP, Frankfurt am Main, Germany
K. Aulenbacher[2, 3], W. Barth[3], M. Basten[2], F. Dziuba[3], V. Gettmann[2], M. Heilmann, T. Kuerzeder[2], S. Lauber[2], J. List[3], M. Miski-Oglu[2], A. Rubin, A. Schnase, S. Yaramyshev[2],
GSI, Darmstadt, Germany
[1]also at HFHF, Frankfurt am Main, Germany
[2]also at HIM, Mainz, Germany
[3]also at IKP, Mainz, Germany

Abstract

New CH-DTL cavities designs of the planned Helmholtz Linear Accelerator (HELIAC) are developed in collaboration of HIM, GSI and IAP Frankfurt. The linac, operated in cw-mode with a final energy of 7.3 MeV/u, is intended for various experiments, in particular with heavy ions at energies close to the Coulomb barrier for research on SHE. Twelve sc CH cavities are foreseen, divided into four different cryostats. Each cavity will be equipped with dynamic bellow tuner. After successful beam tests with CH0, CH3 to CH11 are being designed. Based on the experience gained so far, optimizations will be made, which will lead to both an increase in performance in terms of reducing the peak fields limiting superconductivity and a reduction in manufacturing costs and time. In order to optimize manufacturing, attention was paid to design many parts of the cavity, such as lids, spokes, tuner and helium shell, with the same geometrical dimensions. In addition, a tuner test rig was developed, which will be used to investigate the mechanical properties of the bellow tuner. For this purpose, different simulations were made in order to realize conditions as close as possible to reality in the test bench.

INTRODUCTION

The HELIAC at GSI in collaboration between IAP, GSI and HIM is a superconducting cw-operated Linac to be built. Since UNILAC, which is currently being upgraded as part of the FAIR project, will no longer be suitable for superheavy element (SHE) synthesis experiments, HELIAC will replace it for these experiments [1]. For this purpose, a demonstrator cavity CH0 has already been designed, built and successfully tested [2]. After this two identical cavities CH1 and CH2 were designed, built and also successfully characterized in a cold test [3]. Through various experiments at GSI,HIM [2, 4-8] and IAP [9-17] as well as different adaptations and investigations of the CH cavity design, different experiences could be gained. The entire HELIAC will consist of a total of four cryomodules, each containing three superconducting CH cavities, one solenoid and two superconducting bunchers.

In august 2018 the design of nine 216.816 MHz sc CH-cavities (CH3 to CH11) for the HELIAC has started [18]. The design of these nine cavities is based on the design of the CH1 and CH2 cavities [3]. During this design process, various adjustments were made to the design. A modular cavity design for superconducting CH cavities was developed at IAP, which simplifies manufacturing and thus reduces both production costs and time. In addition to the design cavities, a bellow tuner test bench was designed, which will be used to test the mechanical properties of the bellow tuners made of niobium.

CAVITY DESIGN

The basic design of the nine 216.816 MHz sc CH cavities is the same for all cavities (see Fig. 1). They differ only in some parameters like the number of gaps, the gap lengths, the radius and the total length. All cavities are designed to incorporate two static tuners for frequency adjustment during manufacture and two dynamic bellow tuners for frequency adjustment during operation.

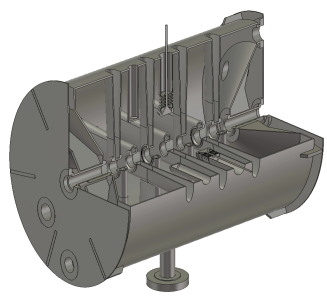

Figure 1: Layout of CH-cavity CH4 without helium vessel. The basic design of all cavities is the same except for the number of gaps, the gap lengths, the radius and the length.

The radius of the individual cavities increases steadily from CH3 to CH11, since the increasing beta causes the gap mean distances to increase from cavity to cavity and thus the capacity on the beam axis decreases. The total length of

* Work supported by the Federal Ministry of Education and Research (BMBF, contract no. 05P21RFRB2)
† conrad@iap.uni-frankfurt.de

ISBN: 978-3-95450-227-1 ISSN: 2673-5490 doi:10.18429/JACoW-IPAC2022-TUPOTK009

DEVELOPMENT OF SUPERCONDUCTING CH CAVITY PREPARATION AT IAP*

P. Mueller[1†], K. Aulenbacher[2,3], W. Barth[2,3], M. Basten[2,3], F. Dziuba[2], V. Gettmann[2,3], T. Kürzeder[2,3], M. Miski-Oglu[2,3], H. Podlech[1,4]

[1]IAP, Goethe University, Frankfurt, Germany
[2]HIM, Helmholtz Institute Mainz, Mainz, Germany
[3]GSI, Helmholtzzentrum für Schwerionenforschung, Mainz, Germany
[4]HFHF, Helmholtz Research Academy Hesse for FAIR, Frankfurt, Germany

Abstract

Goethe University (GU), Gesellschaft für Schwerionenforschung (GSI) and Helmholtz Institut Mainz (HIM) work in collaboration on the Helmholtz Linear Accelerator (HELIAC). A new superconducting (sc) continous wave (cw) high intensity heavy ion linear accelerator (Linac) will provide ion beams with maximum duty factor up to beam energies of 7.3 MeV/u. The acceleration voltage will be provided by sc Crossbar-H-mode (CH) cavities, developed of Institute for Applied Physics (IAP) at GU. Cavity preparation is researched and optimized towards widely used elliptical multicell cavities. A standardized preparation protocol for CH cavities is researched in collaboration between GU, GSI and HIM on a 360 MHz 19 gap CH prototype. Compared to baseline measurements, a 120°C 48 hour bake produced higher maximum gradient, decreased intrinsic quality factor and a shorter cavity conditioning phase. As a critical preparation step, High Pressure Rinsing (HPR) with ultra pure water will be performed at HIM and is currently in preparation. HPR cycles were successfully tested on a CH dummy with a new nozzle layout that is optimized towards CH cavity geometry.

BASELINE MEASUREMENTS

Coupler Re-Design

Cavity preparation is performed on a 360 MHz 19 gap CH prototype. The cavity was stored for over ten years with inserted nitrogen gas. After first examination, the cavity had a different coupler installed than in past measurement. A new coupler for an expected intrinsic quality factor of 7×10^8 [1] was necessary for the following cold tests at 4K. Therefore, dummy couplers of different coupling strength were build and measured in the clean room at Frankfurt university. Simulations and measurements at room temperature resulted in an intrinsic quality factor of $Q_0 = 4300$. Stem length differs in 1.5 mm increments and three different coupler head pieces were build, see Fig. 1. An ideal coupling strength was found for a dummy coupler length of 128.5 mm with a quality factor of 3.16×10^8. Confirmation measurement of the final coupler of 128.3 mm length resulted in a quality factor of 2.97×10^8.

Figure 1: Dummy parts on the right were tested to achieve critical coupling strength at room temperature. Center dummy components are of similar dimensions to the previously installed coupler on the left and were used to determine the required length adjustment.

Cold Test

Cold tests at 4K were performed with the newly installed coupler. RF parameter results of all referenced tests in this proceeding are summarized in Table 1. An intrinsic quality factor of $Q_0 = 10^9$ and coupling strength $\beta = 2.6$ were measured during low level tests. This put the quality factor of the new coupler to 3.69×10^8 which varies from room temperature measurements. The coupler reacts very sensitive to small displacements. Cooldown to 4 Kelvin from room temperature could have led to displacement by thermal shrinkage. Subsequent power test showed a diminished maximum electrical field compared to 2007 measurements, with a drop from 8 MV/m to 3 MV/m. Intrinsic quality factor decreases at an electric field of $E = 3\,\mathrm{MV/m}$ with the onset of field emission. Analysis via Fowler-Nordheim equation delivers an amplification coefficient greater than $\beta = 3500$ compared to 2007's $\beta = 240$. This increase suggests an accidental insertion of particles. Possible causes are a short ventilation of the cavity during the prolonged storage time period or the dummy coupler tests and installation.

* Work supported by BMBF Contr. Nr. 05P21RFRB2, HGS-HIRe and HFHF
† P.Mueller@iap.uni-frankfurt.de

ISBN: 978-3-95450-227-1 ISSN: 2673-5490 doi:10.18429/JACoW-IPAC2022-TUPOTK010

NITRIC ACID SOAKING AFTER IMPERFECT FURNACE TREATMENTS

R. Ghanbari†, M. Wenskat, C. Bate, W. Hillert,
Institute of Experimental Physics, University of Hamburg, Hamburg, Germany
A. Dangwal Pandey, Deutsches Elektronen-Synchrotron, Hamburg, Germany

Abstract

Annealings of niobium cavities in UHV or nitrogen atmospheres are crucial for the performance in the later cryogenic tests and operation. Recovery methods for imperfect annealing conditions have been discussed, and a more recent proposal, the so-called "nitric acid soak" has been studied here in detail. It shows surprising recovery potential, albeit the unclear origin of this improvement. We present our investigation on the several potential origins. For this, we used SEM, SIMS and XPS measurements of niobium samples to study the surface morphology and contaminations. We can reject the favored hypothesis on the origin of the improvement, and propose an alternative origin.

INTRODUCTION

As niobium (Nb) cavities are a key technology of linear collider, the properties of the inner surface play a crucial role to increase cryogenic performance of cavities [1, 2]. In such manner, different annealing treatments in UHV or nitrogen (N_2) atmosphere have been done on the surface of niobium [3-5] and different recipes have been presented to improve reproducibly of cavities [6, 7]. To reduce the impact of a pollution within the furnace, the usage of niobium caps during the anneal is now an established method [8, 9]. Moreover, Jefferson Lab reported using nitric acid (HNO_3) soak as an effective recovery method, even though the origin of the improvement is not clear yet [10]. Previous reports show that sulfur (S), titanium (Ti) and tin (Sn) contaminations are detrimental to the cavity performance [6, 11]. Nitric acid soak was already utilized to recover cavities which are polluted with indium (In) contamination [12]. The advantages of nitric acid are, that it does not dissolve the protective niobium pentoxide layer and is able to dissolve many metal contaminations [13]; hence this acid is a preferred candidate for a recovery of a Nb surface.

At DESY, we struggle with cavity deterioration after annealing procedures in sub-optimal atmospheres, causing formation of Nb carbides on the surface of cavities [3, 9]. Therefore, nitric acid soak as a recovery method is a potential interesting approach. This paper is organised as follows. We devote next sections to a discussion on hypotheses as possible origins of the cavity-performance improvement, our approach and, finally, the structural properties of Nb surface before and after using nitric acid soak, through SEM (scanning electron microscope), SIMS (Secondary-ion mass spectrometry) and XPS (X-ray photoelectron spectroscopy). Then we briefly report results of our study in the concluding section.

† rezvan.ghanbari@desy.de

ORIGIN OF THE IMPROVEMENT

In order to plan our study of the nitric-acid-soak effect on cavity performance, we discuss possible origins of the improvement. To this end, Nb carbides and metal contaminations are suggested as recommended nominees to deteriorate cavity performance during furnace treatment which are supposed to be removed by nitic acid soak [14, 15]. We also propose dissolving interstitial carbon as another possible origin based upon results in a preceding report [16]. Detail of hypotheses are given in the subsequent paragraphs.

Dissolving Niobium Carbides

As nitrogen infusion exhibit improvements of the performance for the Superconducting Radio Frequency (SRF) cavities, DESY tried to establish an appropriate nitrogen infusion recipe in an imperfect furnace [9]. Niobium carbide formation, star-shaped β-Nb_2C structures, were founded as the cause for the performance deterioration [8, 9]. Nb carbides are not only the origin of increased losses, but also cause the cavity to quench [9, 17]. Dissolving niobium carbides during nitric acid soak is the favoured assumption for the origin of the improvement. For this, we have studied sample surface with SEM before and after a nitric acid soak.

Dissolving Interstitial Carbon

SIMS results of a recent study, illustrate significant reduction of interstitial carbon concentration for nitric-acid-soaked samples [16]. A mechanism which can cause such a dissolution of interstitial carbon was not identified. To investigate this new hypothesis, we compared the carbon concentration before and after the nitric acid soak using SIMS.

Dissolving Metal Contaminations

Besides hydrocarbons and metallic contaminations in the furnace environment are detrimental to the performance of SRF cavities [6]. As Sn contamination is a considerable issue for Jefferson-Lab cavities after exposure to the furnace with and without caps [15], we have scanned our samples using XPS for such a contamination and plan a nitric acid soak for samples which showed such a contamination.

In the following section, we present the details of our samples used for this study.

OUR APPROACH

First, we identified 4 samples which are contaminated with Nb carbides from previous annealing studies (samples #1-4, see Table 1) to test the first assumption. To control

ISBN: 978-3-95450-227-1 ISSN: 2673-5490 doi:10.18429/JACoW-IPAC2022-TUPOTK011

COMMISSIONING OF A NEW MAGNETOMETRIC MAPPING SYSTEM FOR SRF CAVITY PERFORMANCE TESTS*

J. C. Wolff†, J. Eschke, A. Goessel, D. Reschke, L. Steder, L. Trelle
Deutsches Elektronen-Synchrotron (DESY), Notkestraße 85, D-22607 Hamburg, Germany
W. C. A. Hillert
University of Hamburg, Luruper Chaussee 149, D-22761 Hamburg, Germany

Abstract

Magnetic flux trapped in the niobium bulk material of superconducting radio frequency (SRF) cavities degrades their quality factor and the accelerating gradient. The sensitivity for flux trapping is mainly determined by the treatment and the geometry of the cavity as well as the niobium grain size and orientation. To potentially improve the flux expulsion characteristics of SRF cavities and hence the efficiency of future accelerator facilities, further studies of the trapping behavior are essential. For this purpose a magnetometric mapping system to monitor the magnetic flux along the outer cavity surface of 1.3 GHz TESLA-Type single-cell SRF cavities has been developed and is currently in the commissioning phase at DESY. Contrary to similar approaches, this system digitizes the sensor signals already inside of the cryostat to extensively reduce the number of required cable feedthroughs. Furthermore, the signal-to-noise ratio (SNR) and consequently the measuring sensitivity can be enhanced by shorter analog signal lines, less thermal noise and the μ-metal shielding of the cryostat. In this contribution test results gained by a prototype of the mapping system are presented.

INTRODUCTION

Based on the first magnetometric-mapping approach at Helmholtz-Zentrum Berlin (HZB) [1, 2] a system using Anisotropic MagnetoResistive (AMR) sensors of type Sensitec AFF755B [3] has been developed at DESY to study the flux expulsion characteristics of 1.3 GHz TESLA-Type single-cell cavities. A prototype of this system already underwent a successful perfomance test described in [4] to evaluate the system capabilities, detect potential weak spots and find options for improvements. Before the production of the final card sets, the prototype was used again to study the flux expulsion characteristics of the test cavity 1DE9 after three hour ultra high vacuum (UHV) 300 °C mid-T furnace treatment because of the impact on the cavity's sensitivity to trapped magnetic flux S. Here, S is given by:

$$S = \frac{\Delta R_s}{B_{trap}} \tag{1}$$

where ΔR_s depicts the increase of the surface resistance R_s per unit of trapped magnetic flux B_{trap} [5]. Contrary to the in-situ mid-T bake treatment of Fermi National Accelerator Laboratory (FNAL) [6] based on the work of Palmer et al. [7, 8], the by High Energy Accelerator Research Organisation (KEK) introduced and here used modification [5] mid-T furnace baking exposes the inner cavity surface to air after the furnace treatment. Both procedures showed unprecedented high intrinsic quality factors Q_0 of up to $5 \cdot 10^{10}$ at 2 K and quench fields between 20 – 37 MV/m [5, 6, 9]. Furthermore, the anti-Q-slope phenomenon appeared in all tests which is usually observed at cavities treated by nitrogen-doping [5, 6, 9]. Indeed, an increased S was observed at FNAL and KEK [5, 6].

The measurement setup (except the test cavity) used for the studies at DESY and shown in Fig. 1 as well as the sensor calibration procedure and the analog-to-digital converter settings are identical to the former system performance test described in [4].

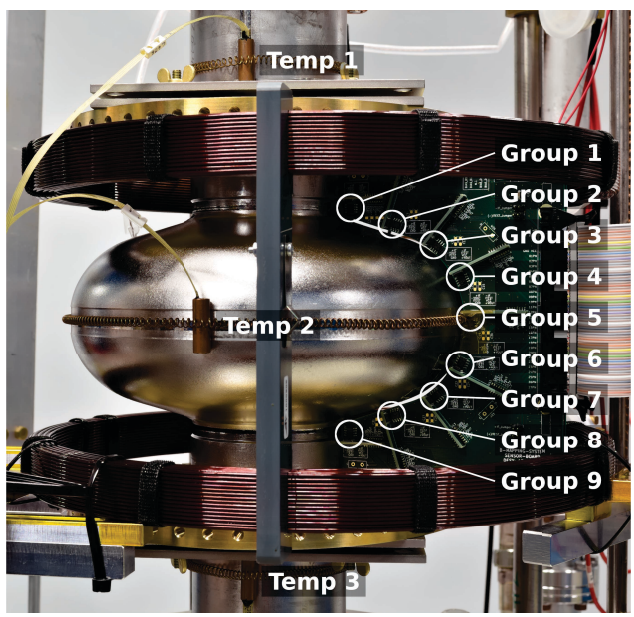

Figure 1: Test setup: Cavity 1DE9 made of fine grain material (after mid-T furnace treatment) equipped with a single sensor board. To monitor the T_c transition at the outer cavity surface three Lake Shore Cryotronics CERNOX CX1030 thermocouples are used. The setup is surrounded by a Helmholtz coil (HC) to apply a defined magnetic flux. Since the HC radius is too small to be centred around the cavity for the given setup, it was mounted with an offset of 29 mm.

* This work was supported by the Helmholtz Association within the topic Accelerator Research and Development (ARD) of the Matter and Technologies (MT) Program.
† Jonas.Wolff@desy.de

ISBN: 978-3-95450-227-1 ISSN: 2673-5490 doi:10.18429/JACoW-IPAC2022-TUPOTK012

NITROGEN INFUSION SAMPLE R&D AT DESY

C. Bate*[1], A. Ermakov, D. Reschke, J. Schaffran, W. Hillert[1], M. Wenskat[1],
DESY, 22607 Hamburg, Germany
[1]also at University of Hamburg, 20146 Hamburg, Germany

Abstract

Many accelerator projects such as the ILC would benefit from cavities with reduced surface resistance (high Q-values) while maintaining a high accelerating gradient. A possible way to meet the requirements is the so-called nitrogen-infusion procedure on niobium cavities. However, a fundamental understanding and a theoretical model of this method are still missing. One important parameter is the residual resistance ratio (RRR) which is related to the impurity content of the material. We report the investigated RRR on samples in a wide temperature range in a vacuum and under a nitrogen atmosphere. This comparison made it possible to make statements about the differences in the concentration of nitrogen by varying the temperature. The samples are pure cavity-grade niobium and treated in the same manner as cavities. For this purpose, a small furnace dedicated to sample treatment was set up to change and explore the parameter space of the infusion recipe. Care was taken to achieve the highest level of purity possible in the furnace and in a pressure range of $1 \cdot 10^{-8}$ mbar in order to meet the high requirements of nitrogen infusion.

NITROGEN INFUSION ON SAMPLES

In [1] a recipe was reported that drastically improved the performance in quality factor and accelerating gradient of superconducting 1.3 GHz TESLA-type cavities. The formula calls for a three-hour heat treatment at 800°C under vacuum, followed by a ramp down to and hold at 120°C. A partial pressure of nitrogen ($3.3 \cdot 10^{-2}$ mbar) is provided during the 48-hour hold at 120°C. The latest cavity treatment recipes ([1–4]) have shown that we are far away from the possible theoretical limit of achievable SRF performance, many areas of the possible parameter space of cavity treatments are still unexplored. Therefore, excessive sample studies were performed in a dedicated vacuum oven also allowing for nitrogen-infusion investigations. At room temperature, the pump system saturates at an end pressure of $p < 5 \cdot 10^{-8}$ mbar. The RRR value is an interesting parameter that should be examined in more detail for correlation with the cavity performance, since it is also directly related to the mean free path [5]. In this study, the RRR value is examined when the temperature of the nitrogen infusion is varied.

RESIDUAL RESISTIVITY RATIO - RRR

The electrical resistivity following from the Mathiessen rule [6] for metals at low temperatures can be written as the sum of

$$\rho = \rho_{res} + \rho_{ph}(T), \tag{1}$$

where ρ_{res} describes the residual resistivity at $T = 0$ K that is predominantly evoked due to electron-impurity scattering and scattering on lattice defects while ρ_{ph} is caused by the temperature dependent electron-phonon scattering. The residual resistivity scales linearly with the impurity concentration C_i as $\rho_{res} = \sum \frac{\Delta\rho_i}{\Delta C_i} C_i$ and hence Eq. (1) can be written as

$$\rho = \sum \frac{\Delta\rho_i}{\Delta C_i} C_i + \rho_{ph}(T), \tag{2}$$

with $\frac{\Delta\rho_i}{\Delta C_i}$ being the resistance coefficients. The coefficients for some important impurities are given in Table 1. The RRR is defined as the ratio of the electrical resistance at room temperature to the residual one at 4.2 K

$$\mathrm{RRR} = \frac{\rho(295\,\mathrm{K})}{\rho(4.2\,\mathrm{K})}. \tag{3}$$

However, since the critical temperature of niobium is with $T_c = 9.2$ K, above the temperature of liquid helium, the value of $\rho(T_c = 9.2\,\mathrm{K})$ is used or extrapolated down to $\rho(4.2\,\mathrm{K})$. The RRR value is sensitive to changes in surface impurities due to diffusion during heat treatments in vacuum conditions or under certain gas atmospheres and after chemical surface treatments. The extent to which the nitrogen treatment changes the RRR value was therefore investigated on niobium samples.

Table 1: Resistance Coefficients for Different Elements [7] Determined by Resistance Measurements on Niobium Intentionally Contaminated by Impurities

Element	O	N	C	Ta	Zr
$\frac{\Delta\rho_i}{\Delta C_i}\left(10^{-11}\,\frac{\Omega\mathrm{m}}{wt.ppm}\right)$	2.64	3.49	3.33	0.12	0.6

RRR 4-PT CONTACT METHOD

Small fine grain (50 μm grain size on average) niobium samples cut from cavity material, to a size of (2.88 x 3 x 42) mm, were used. To evaluate the effect of nitrogen infusion on sample RRR values, a 4-point-contact approach was chosen. The sample holder is shown in Fig. 1. The sample is immersed in liquid helium for the warm-up and cool-down procedures. Since $\rho = U/I$ it follows by Eq. (3) that the RRR at T_c is determined by

$$RRR_{9.2\,\mathrm{K}} = \frac{U(295\,\mathrm{K})}{U(T_c \approx 9.2\,\mathrm{K})}. \tag{4}$$

A Keithley Digital-Multimeter is used to measure the voltage, which has an accuracy of about 1 nV and a magnitude of about 2 mV thanks to the use of a pre-amplifier and a

* christopher.bate@desy.de

ISBN: 978-3-95450-227-1 ISSN: 2673-5490 doi:10.18429/JACoW-IPAC2022-TUPOTK013

PEALD SIS STUDIES FOR SRF CAVITIES

I. González Díaz-Palacio[1], R. H. Blick[1], W. C. A. Hillert[2], A. Jeromin[3], T. F. Keller[1,3], N. Krupka[3], A. Stierle[1,3], M. Wenskat[2], R. Zierold[1]

[1]Institute of Nanostructures and Solid State Physics, Universität Hamburg, Germany
[2]Institute of Experimental Physics, Universität Hamburg, Germany
[3]DESY, Hamburg, Germany

Abstract

Recent technological advances and material treatments have pushed Nb superconducting radio frequency (SRF) cavities to their maximum RF performance. A novel approach for overcoming this limitation is the coating of multilayers by PEALD (plasma-enhanced atomic layer deposition) onto the interior surface of a cavity. Specifically, SIS (superconductor-insulator-superconductor) multilayers provide magnetic screening of the bulk Nb cavity, increase the field at which the vortex penetration starts, and lead as a consequence to higher quality factors of the cavity. Note, ALD is closely related to chemical vapor deposition and bases on sequential self-limiting gas-solid surface reactions facilitating conformal coatings with sub-nm precision even on complex substrates such as the interior of a cavity. As a preliminary study for potential SIS SRF cavities, we investigated AlN-NbTiN multilayers grown by PEALD in a supercycle approach. Different compositions and post-deposition thermal treatments have been investigated with respect to their superconducting properties, stoichiometry, and crystallinity.

INTRODUCTION

Over the past decades, bulk niobium has been the material of choice for SRF cavities, since it satisfies the requirement of having a high critical temperature (TcNb=9.2 K) and high lower critical field (Bc1Nb=170 mT), being widely investigated [1]. Different surface treatments have continuously improved the RF performance pushing up the accelerating field into the intrinsic material limit (B0≃200 mT; Eacc≃50 MV/m) [2]. This field limitation for SRF cavities is established by the superheating field Bs corresponding to the maximum magnetic field that the superconductor can withstand before the Meissner state becomes unstable and vortices penetrate at the superconductor surface defects which, at the low operating temperature, would develop a flux avalanche and cavity deterioration [3,4]. Thus, alternative superconductors with higher vortex penetration fields are needed in order to achieve higher acceleration gradients.

In this framework, an alternative approach proposed by A. Gurevich [5] may allow for applying higher accelerating fields while preventing vortex dissipation and revealing low RF surface resistance at the same time. This idea bases on the formation of alternating thin superconducting and insulating layers (SIS multilayers, see Fig.1) onto the inner surface of an SRF cavity (see Figure 1). Due to the strong increase of the first flux penetration in a thin film (where $d<<\lambda$), type II superconductors with $T_c > T_c^{Nb}$, and consequently lower surface resistance, can be used without being limited by their lower B_{c1}^{bulk}. Moreover, the SIS layers provide a significant magnetic shielding of the bulk cavity, block the propagation of local vortices and prevent avalanches which would cause a quench. Therefore, SIS structures improve the SRF cavity performance and can lead to an increase in the accelerating field and the RF performance. Specifically, A. Gurevich calculated this enhancement assuming a 50 nm of Nb_3Sn deposited on a Nb bulk cavity with an insulating interlayer would push up the field from B_0≈180 mT to B_0≈280 mT, and triple the quality factor Q.

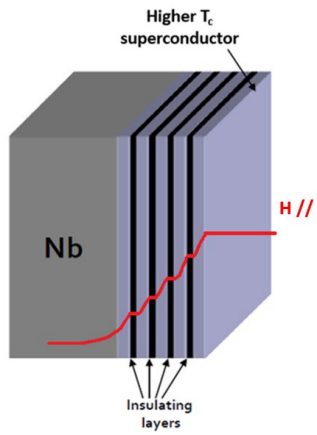

Figure 1: SIS multilayers for SRF cavities concept. The magnetic field is attenuated by the multilayers, leading to a reduction to a value that is lower than Bc1bulk for a bulk Nb cavity.

In addition, the use of other superconductors with lower BCS resistance, such as Nb3Sn, NbN or NbTiN, [6] offers the possibility of increasing the operating temperature to 4.2 K, resulting in a significant cryogenic cost reduction.

Good superconductors for SIS multilayer SRF applications need to have higher Tc, larger Δ, and lower normal conducting resistivity than bulk Nb. Some of the compounds which satisfy the aforementioned requirements are A15-compounds (such as Nb3Sn, Nb3Al, and V3Si) and Nb B1-compounds (such as NbN and NbTiN). In particular, our studies are based on previous results on binary and ternary Nb nitrides, since both present high Tc (T_c^{NbN}=17.3 K and T_c^{NbTiN}=17.8 K) [6]. However, the binary NbN cubic δ-phase (phase of interest) is metastable at room temperature, and has a very high normal conducting resistivity,

ISBN: 978-3-95450-227-1 ISSN: 2673-5490 doi:10.18429/JACoW-IPAC2022-TUPOTK014

REFURBISHMENT OF SRF CAVITIES AND HOM ANTENNA COATING STUDIES FOR THE MAINZ ENERGY-RECOVERING SUPERCONDUCTING ACCELERATOR (MESA)*

P. S. Plattner†, F. Hug, T. Stengler
(KPH) Fachbereich Physik Institut für Kernphysik, Mainz, Germany

Abstract

The commercial available cryomodules of the ELBE/Rossendorf-type, produced by Research Instruments (RI), found use in various superconducting accelerators. Requirements for the cryomodules changed in the last two decades. In particular, this was the case for the Mainz Energy-Recovering Superconducting Accelerator (MESA), so the so-called MESA Enhanced Elbe-type Cryomodule (MEEC) was produced by RI to fulfil the specific requirements for MESA. In addition, an ELBE-type cryomodule from the decommissioned Accelerator and Light In Combined Experiments (ALICE) from Daresbury, United Kingdom[1], was gifted to us. The ALICE module needs a refurbishment to fulfill the requirements for MESA. Therefore, the investigation of a possible use as a spare cryomodule started as well as a study for using coated HOM antennas. This includes a clean room treatment with a high pressure rinse (HPR). The existing clean room structure at the Helmholtz Institut Mainz (HIM) will be used for this purpose. Through corona regulations it was not possible to perform a HPR with the ALICE cavities till now, but an injector cavity from the S-DALINAC could be refurbished successfully in 2021.

INTRODUCTION

Currently, a cryomodule of ALICE [1] is under refurbishment at the Institut für Kernphysik at the Johannes Gutenberg-Universität Mainz. This Module contains two 1.3 GHz TESLA/XFEL-type cavities like the MESA MEEC [2] modules. It is planned to test Higher Order Mode (HOM) antennas with a coating of better superconductors, like Nb_3Sn and NbTiN at a later stage. With further modification, the ALICE module will finally become a spare cryomodule for MESA. These modifications include an upgrade of the tuner, HOM antennas and Helium port. It is expected that coated HOM antennas allow better damping of HOMs and thus enable the transport of more beam current.

MESA Layout

Figure 1 shows the lattice of MESA [3]. The injector includes the Small Thermalised Electron Source at Mainz (STEAM), MESA Low Energy Beam Apparatus (MELBA) and MilliAMpere BOoster (MAMBO) and accelerates the polarised and unpolarised electrons up to an energy of 5 MeV. The two superconducting cryomodules drive the main accelerator and provide an energy gain of 100 MeV for MAGIX in the energy-recovering (ER) mode and 150 MeV for the P2 and BDX in the beam dump mode. Table 1 compares the key parameters of ALICE and MESA. The cryomodules are similar as they are both based on the ELBE/Rossendorf design [4]. Since MESA is planned to run in the ER mode with a factor of 100 higher beam currents, it is necessary to refurbish the ALICE module and modify it for the use in MESA.

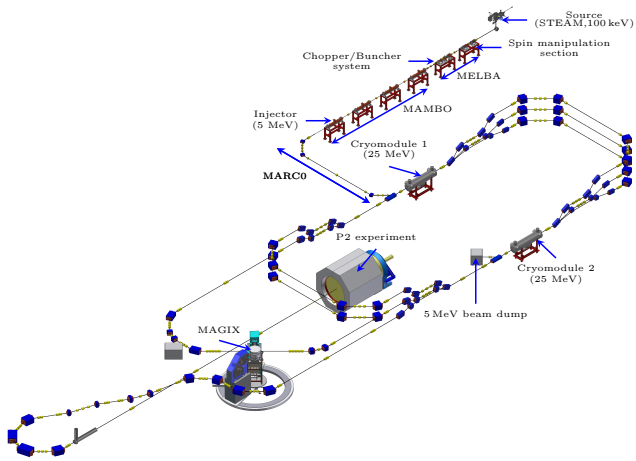

Figure 1: MESA lattice with a normal conducting injector and superconducting main accelerator. Two superconducting cryomodules prepare the electron beam for the experiments by MESA.

Table 1: Comparison of the Key Parameters of ALICE and MESA

Parameter	MESA	ALICE
Q_0	1.25×10^{10}	5×10^9
Field gradient	12.5 MV m^{-1}	12.9 MV m^{-1}
Beam current (ERL)	1(10) mA	13 µA
RF Frequency	1.3 GHz	1.3 GHz
Cavities	9-cell XFEL/TESLA	9-cell XFEL/TESLA

REFURBISHMENT OF SRF CAVITIES

Clean Room Infrastructure at HIM

For the clean room treatment of the Niobium cavities the existing clean room infrastructure at HIM is used. It contains

* The work received funding by BMBF through 05H21UMRB1.
† pplattne@uni-mainz.de
[1] We would like to thank the Daresbury Laboratory for their generous gift.

ISBN: 978-3-95450-227-1 ISSN: 2673-5490 doi:10.18429/JACoW-IPAC2022-TUPOTK015

HOM COUPLER DESIGN AND OPTIMIZATION FOR THE FCC-ee W WORKING POINT

S. Udongwo*, University of Rostock, Rostock, Germany
S. Gorgi Zadeh, CERN, Geneva, Switzerland
R. Calaga, CERN, Geneva, Switzerland
U. van Rienen, University of Rostock, Rostock, Germany

Abstract

A 2-cell 400 MHz superconducting radio-frequency cavity with improved damping has been designed as an alternative to the baseline 4-cell cavity for the **W** working point of the future circular lepton collider (FCC-ee). For this cavity, the longitudinal higher-order modes' (HOMs) impedance stay under the beam stability threshold value. This paper, therefore, focuses on the design of the HOM couplers for the purpose of damping the high-impedance transverse HOMs. The resulting impedance of the HOM-damped cavity is then calculated and compared with the impedance limit set by synchrotron radiation.

INTRODUCTION

The Future Circular electron-positron Collider (FCC-ee) is planned to operate with beam energies from 45.6 to 182.5 GeV and beam currents from 5.4 to 1390 mA [1]. The purpose is to study the properties of the **Z**-, **W**- and **H**iggs boson and the top and anti-top ($\mathbf{t\bar{t}}$) quarks. The beam current of 147 mA of the **W** working point requires particular care to strongly damp the HOMs excited by the beam. A 2-cell superconducting radiofrequency (SRF) elliptical cavity has been designed for the **W** working point of the FCC-ee [2]. The geometric dimensions of the cavity are given in Table 1. Figure 1 shows the longitudinal and transverse impedance plots of the cavity. It can be seen that the frequency of two high impedance modes, the TE_{111} and TM_{110} modes, 487 MHz and 520 MHz, respectively, are below the TE_{11} cut-off frequency of the beampipe to which they can couple. The $R/Q_\perp$ of the modes are 15.46 Ω and 26.35 Ω, respectively. The LHC hook-type HOM coupler design is thus adopted [3] for the damping of these two modes. This coupler is particularly designed for the strong damping of the modes in the first dipole passband. The general requirements of such HOM couplers are to extract as much energy as possible from the potentially parasitic modes while rejecting the fundamental mode (FM).

Table 1: Geometric Dimensions of the Designed Cavity (C_{3794}), The Parameters Correspond to the Common Definition used for Parametrizing an Elliptical Cavity [2]

All dimensions in mm except stated otherwise.

A	B	a	b	R_i	L	R_{eq}	α [°]
73.52	131.75	106.25	118.7	150	187	369.63	107.23

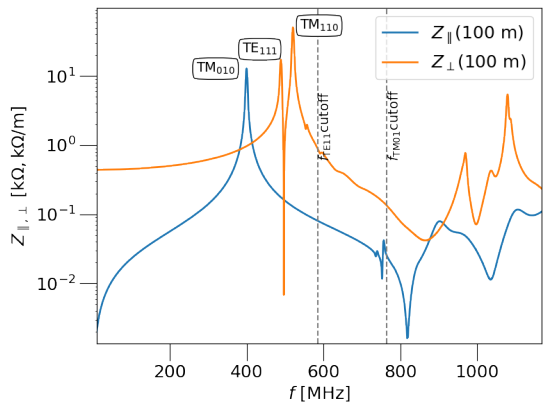

Figure 1: Longitudinal and transverse wakefield impedance plot for the designed cavity (simulated wakelength = 100 m).

HOOK-TYPE HOM COUPLER

The design methodology of the hook coupler in [3] follows the analysis of an approximate lumped element circuit model followed by a conversion to a 3D geometric model. This type of coupler has been developed from such a circuit model first and then translated to a 3D equivalent geometry as shown in Fig. 2 [3, 4].

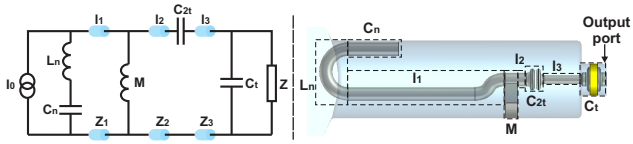

Figure 2: Lumped element circuit model and CST Studio Suite® 3D model.

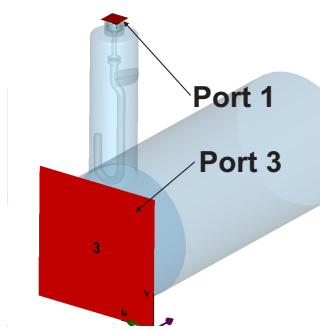

Figure 3: The excited ports (red) of the hook-type coupler.

* sosoho-abasi.udongwo2@uni-rostock.de

ISBN: 978-3-95450-227-1 ISSN: 2673-5490 doi:10.18429/JACoW-IPAC2022-TUPOTK016

HiPIMS-COATED NOVEL S(I)S MULTILAYERS FOR SRF CAVITIES

A.Ö. Sezgin[1], I. Gonzales Diaz-Palacio[3], X. Jiang[1], S. Keckert[4], J. Knobloch[4,5], O. Kugeler[4], R. Ries[2], E. Seiler[2], D. Tikhonov[4], M. Vogel[1], R. Zierold[3]
[1]Institute of Materials Engineering, University of Siegen, Siegen, Germany
[2]Institute of Electrical Engineering SAS, Bratislava, Slovakia
[3]Center for Hybrid Nanostructures (CHyN), University of Hamburg, Hamburg, Germany
[4]Helmholtz-Zentrum Berlin für Materialen und Energie GmbH, Berlin, Germany
[5]Department of Physics, University of Siegen, Siegen, Germany

Abstract

Pushing beyond the existing bulk niobium SRF cavities is indispensable along the path towards obtaining more sustainable next generation compact particle accelerators. One of the promising candidates to push the limits of the bulk niobium is thin film-based multilayer structures in the form of superconductor-insulator-superconductor (SIS). In this work, S(I)S multilayer structures were coated by high power impulse magnetron sputtering (HiPIMS), having industrial upscaling potential along with providing higher quality films with respect to conventional magnetron sputtering techniques (e.g., DCMS), combined with (PE)-ALD techniques for deposition of the *ex-situ* insulating layers. On the path towards formulating optimized recipes for these materials to be coated on the inner walls of (S)RF cavities, the research focuses on innovating the best performing S(I)S multilayer structures consisting of alternating superconducting thin films (e.g., NbN) with insulating layers of metal nitrides (e.g., AlN) and/or metal oxides (e.g., Al_xO_y) on niobium layers/substrates (i.e., Nb/AlN/NbN) in comparison to the so-called SS multilayer structures (i.e., Nb/NbN). This contribution presents the initial materials and superconducting and RF characterization results of the aforementioned multilayer systems on flat samples.

INTRODUCTION

The next generation compact particle accelerators require higher performances with reduced infrastructural and operational costs. In order to realize these goals, innovative solutions are needed to overcome the theoretical field limit along with the technological challenges set by the existing bulk niobium superconducting radio-frequency (SRF) cavity technology, which has been the leading accelerator technology for both high-energy and high-luminosity accelerator applications so far [1].

One of the promising candidates to push the limits of the bulk niobium is coating (S)RF cavities with alternating thin film-based multilayer structures in the form superconductor-insulator-superconductor (SIS).

According to the theory related to *the alternating multilayer structures* proposed by A. Gurevich [2], especially for bulk niobium cavities, the simplest alternating multilayer structures (SIS), made of superconductive thin films with thicknesses less than the London penetration depth of the cavity wall material, are expected to enhance not only the quality factor (Q_0) with lower surface resistance R_s , but also the vortex penetration field by means of the insulating layers, leading to sustain the Meissner state at higher accelerating gradients (E_{acc}), by delaying the RF vortex dissipation, and the related strong RF dissipation beyond the thermodynamic critical field of Nb (B_c (Nb)) so as to take advantage of higher T_c superconductors (e.g., B_1 and A_{15} compounds such as NbN and Nb_3Sn, respectively) without being penalized by their relatively small lower critical field (B_{c1}) with respect to the B_{c1} of Nb (200mT).

Theoretically, the SIS structure is a stronger candidate to increase the theoretical field limit as well as the onset of the vortex penetration thanks to the presence of the insulating layer, provided that the optimum layer thicknesses and material combinations are realised, as compared to the SS bilayer structure without any insulating layer; yet, the SS bilayers are also worth studying as being a simpler structure with promising RF performance of the SRF cavities by enhancing the onset of the vortex penetration to some extent owing to the SS boundary [3].

The emergence of the novel scalable sputtering technologies such as high-power impulse magnetron sputtering (HiPIMS) has provided the SRF community another tool to improve the quality of the deposited films by providing denser microstructures, more uniform morphologies, and homogenous crystalline phases in the recent years. Owing to its higher peak power magnitudes applied to the sputtering cathode in pulsed modes at certain duty cycles, HiPIMS technique yields highly ionized denser plasmas, as compared to conventional physical vapor deposition techniques, allowing more effective control of the kinetic energy of the sputtered species with high ionization fraction, arriving onto the substrate surface, by tuning the deposition parameters (i.e., substrate bias) [4].

Aside from HiPIMS, atomic layer deposition (ALD) has also drawn interest from the SRF community recently, especially for depositing insulating layers in multilayer structures [5].

The first investigations of the novel parameter space for HiPIMS-coated S(I)S structures, incorporating also (PE)-ALD-coated insulating layers as well as the further developments of the previously studied SIS structures, based on the QPR sample tests, are detailed in this paper.

ISBN: 978-3-95450-227-1 ISSN: 2673-5490 doi:10.18429/JACoW-IPAC2022-TUPOTK018

COMBINED IN-SITU QEXAFS AND XRD INVESTIGATIONS ON Nb-TREATMENTS IN N_2 GAS ATMOSPHERES AT ELEVATED TEMPERATURES*

P. Rothweiler†, F. Eckelt, L. Voss, S. Paripsa, D. Lützenkirchen-Hecht††,
University of Wuppertal, Wuppertal, Germany

Abstract

Thin polycrystalline Nb metal foils were treated in N_2 gas atmospheres at elevated temperatures of 900 °C up to 1200 °C. A combination of transmission mode Quick X-ray absorption spectroscopy (QEXAFS) at the Nb-K-edge and X-ray diffraction (XRD) used in parallel were used to investigate changes in the atomic short and long-range structure of the bulk Nb-material in-situ. A dedicated high-vacuum heating cell with a base pressure of 10^{-6} mbar was used to perform the heat treatments under a vacuum and nitrogen gas atmosphere. The treatments typically included (i) a preheating at 900 °C under high-vacuum, (ii) treatment in 3 mbar nitrogen gas at the desired temperature, and (iii) cooling down to room temperature under vacuum conditions. The QEXAFS and XRD data were collected in parallel during the entire process with a time resolution of 4 s. While the samples treated at 900 °C show the typical N-uptake to the octahedral interstitial sites, the samples treated at higher temperatures show the growth of distinct niobium nitride phases.

INTRODUCTION

Nowadays almost all Nb-cavities used for particle accelerators are treated in N_2-atmospheres to improve their performance, in particular Q-factor, accelerating gradient, superconductivity, etc. Therefore, several different treatment recipes like the Nb-doping [1], Nb-infusion [2] or mid-T-bake [3] have been worked out, variating the treatment temperature duration and used gas pressures. Recent studies on the N-doping have shown that the N-atoms are likely to occupy the interstitial octahedral sites of the Nb unit cells [4]. Additional to this effect Nb is known to tend to build up Nitrides with growing temperatures. This is crucial information to treat the cavities in the way wanted. In the presented work thin Nb metal foils are treated in N_2-atmospheres at temperatures between 900 and 1200 °C, investigated by using in-situ EXAFS and XRD measurements. In the following, the first prom-ising results of the ongoing studies will be presented.

EXPERIMENTAL DETAILS

The EXAFS and XRD measurements were performed in a dedicated high-temperature vacuum cell (Fig. 1) [5]. The cell features a ceramic heating plate allowing tem-peratures up to 1200 °C (heating rate ~350 °C/min), an oil-free turbo-molecular pump (base pressure 10^{-6} mbar), and a combination of fine leak and magnetic valves to control the treatment process. The main chamber has two air-cooled Kapton windows and a ZnSe-window for infra-red-temperature measurements. Additionally, there are two thermocouples inside the cell. The experiments were performed at Beamline P64, PETRA III at Desy [6], for the XRD measurements a Pilatus 100K pixel detector was used.

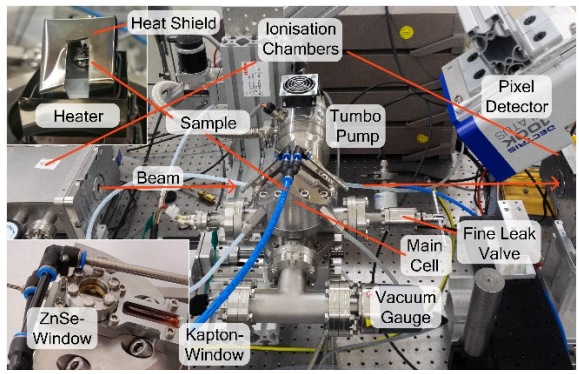

Figure 1: Photography of high-temperature vacuum cell [6] at P64 PETRA III at Desy mounted on the beamlines diffractometer and the Pilatus 100K pixel detector in the upper right-hand corner. The inset in the upper left-hand corner shows an Nb-metal-foil in the sample holder underneath the heat shield., the inset below shows the cell's air-cooled ZnSe- and Kapton windows.

The treatments (Fig. 2) typically consist of a preheating phase in a vacuum at a temperature of 900 °C for 60 min (if not mentioned differently in the following, temperatures are measured at the heater), followed by the treatment in a 3 mbar N_2-atmosphere at a dedicated temperature. After this, the cooldown is performed under vacuum conditions.

* Work supported by the German Federal Ministry for Education and Research (BMBF) under Grant No. 05H18PXRB1.
† rothweile@uni-wuppertal.de †† dirklh@uni-wuppertal.de

ISBN: 978-3-95450-227-1 ISSN: 2673-5490 doi:10.18429/JACoW-IPAC2022-TUPOTK020

STATUS OF LASA-INFN R&D ACTIVITY ON PIP-II LOW-BETA PROTOTYPES

M.Bertucci*, A. Bosotti, A. D'Ambros, E. Del Core, A. T. Grimaldi, P. Michelato, L. Monaco, C. Pagani[1], R. Paparella, D. Sertore, INFN LASA, Segrate (MI), Italy
A. Gresele, Zanon Research & Innovation, Schio (VI), Italy
[1]also at Università degli Studi di Milano, Milano (MI), Italy

Abstract

INFN LASA is developing some PIP-II $\beta = 0.61$ cavity prototypes so to setup a high-Q recipe allowing to reach the PIP-II performance target in view of the series production. A single cell cavity was treated with a baseline recipe, whereas a multicell cavity underwent a mid-T bake step as final surface treatment. Both cavities were then tested at the LASA vertical experimental facility. The test results are here reported and discussed. Basing on the satisfactory results so far obtained, a strategy for the qualification and upgrade of the LASA vertical test facility is outlined.

INTRODUCTION

INFN LASA is appointed to build 40 650 MHz $\beta = 0.61$ superconducting cavities that will constitute the low-beta (LB) section of the PIP-II Linac. Specifications for operation in the machine are $E_{acc} = 16.9\,\mathrm{MV\,m^{-1}}$ with a $Q_0 \geq 2.4 \cdot 10^{10}$. Given such challenging target, the treatment recipe has been based on Electropolishing (EP) as main surface removal treatment. The bulk EP will be the starting point of a so-called "high-Q" surface recipe.

The definition of the whole treatment sequence is under way. In parallel with the activities carried out at FNAL [1], INFN-LASA is conducting an analogous R&D effort, on single and multi-cell cavity prototypes, manufactured at the company Zanon Research & Innovation Srl. Some of the cavities were shared with FNAL, in sake of a joint effort on many technical issues that need to be addressed. The final goal is the definition of the specifications for the fabrication of the forthcoming cavity series production.

PROTOTYPES TREATMENT VALIDATION STRATEGY

The first phase of the treatment optimization activity consisted on the setup of the Electropolishing plant operating at the company Zanon Research & Innovation Srl. The facility is the same employed in the series production of XFEL [2] and LCLS-II [3] 1.3 GHz superconducting cavities. Due to the different size and geometry of PIP-II LB cavities, the treatment parameters were finely tuned by several short EP trials carried out on the single-cell prototype B61S-EZ-002 so to optimize smoothness, removal rate and iris/equator removal ratio [4]. Pivotal was the installation of Aluminum cathode enlargements in correspondence of the cells, which noticeably increased the current density at the equators.

* michele.bertucci@mi.infn.it

Afterwards, the activity proceeded with the definition of a baseline treatment recipe, which served as a reference for the forthcoming treatments. Among the various recipes which are nowadays available, the so-called mid-T bake [5] and the 2/0 nitrogen doping [6] were chosen as possible candidates, since they guarantee high-Q operation at a medium accelerating field. The aforementioned recipes are discussed here in the specific case of the PIP-II 650 MHz LB cavity.

The Baseline Recipe

The baseline recipe was applied on the single cell cavity B61S-EZ-002. The treatment steps went along the same lines of the XFEL 1.3 GHz cavity production, in the "final EP" scheme. At first, a bulk EP of 150 µm removed the damaged layer on the inner RF surface. Then, the cavity was heat treated at 800 °C for 2 hours to degas the hydrogen adsorbed by the Niobium during the fabrication and the surface treatment. After this, the cavity proceeded with a 25 µm final EP. Differently to XFEL, the "cold" EP regime was adopted. In this variant, a lower acid temperature (around 8 °C) is used so to yield a lower average temperature on cavity surface (around 12 °C). Cold EP allows to obtain a smoother surface and a more uniform removal over the cavity [7], therefore limiting non-linear losses increasing power dissipation at higher fields [8]. Eventually, the baseline recipe ended with the low temperature baking (48 hours at 120 °C in UHV conditions), whose goal is to get rid of the high-field Q-slope.

The Nitrogen Doping Recipe

Nitrogen doping allows to obtain high Q values at medium accelerating fields, and it has been applied with success during the LCLS-II cavity production. Anyway, some issues emerged in the case of 650 GHz LB cavities [1]. The anti-Q slope typical of 1.3 GHz cavities is absent even though a decrease in BCS surface resistance is evident. On the other side, an increase in residual resistance was also noticed, due to an increase in trapped flux sensitivity. A $T > 900\,^{\circ}\mathrm{C}$ annealing is needed to recover the magnetic flux properties of the material. This in turn may affect the mechanical stability of the cavity. The impact of these issues on the cavity operation in the cryomodule is under investigation.

The first trials of doping performed by FNAL confirmed that nitrogen doping recipe enables higher Q operation w.r.t. baseline treatments. INFN-LASA will apply the same recipe on the B61S-EZ-003 single cell cavity. After a bulk EP treatment of 150 µm, the cavity will be annealed in UHV at

ISBN: 978-3-95450-227-1 ISSN: 2673-5490 doi:10.18429/JACoW-IPAC2022-TUPOTK021

RECENT UPDATE ON ESS MEDIUM BETA CAVITIES AT INFN LASA

D. Sertore*, M. Bertucci, M. Bonezzi, A. Bosotti, D. Cardelli, A. D'Ambros, A. T. Grimaldi, L. Monaco, R. Paparella, M. Zaggia, INFN Milano - LASA, Segrate, Italy
C. Pagani[1], Università degli Studi di Milano, Segrate, Italy
[1]also at INFN Milano - LASA, Segrate, Italy

Abstract

The INFN LASA contribution to the European Spallation Source ERIC (European Research Infrastructure Consortium) Superconducting Linac is focused on supplying 36 cavities for the Medium Beta section of the proton accelerator. Twenty eight cavities have been fully qualified and delivered to CEA for integration into the cryomodules. We present the status of the activities dedicated to completing our contribution both by applying alternative surface treatments with respect to the series vertical BCP and by procuring new cavities.

INTRODUCTION

The European Spallation Source (ESS) ERIC will be, once in operation, the most intense neutron source in the world [1]. ESS make use of a superconducting linac section to accelerate a 62.5 mA proton beam to an energy of 2 GeV. This powerful beam will then be delivered to a target station for producing a neutron beam by the spallation process [2].

The 5 MW beam will be pulsed at 14 Hz with each pulse being 2.86 ms long. This long pulse operation is a real challenge and, to achieve this and save in cost, superconducting cavities are required and they need to operated at high accelerating gradient.

INFN Milano - LASA contributes, as part of the Italian In-Kind contribution, to the Medium Beta ($\beta = 0.67$) Section of the ESS Superconducting Linac with thirty-six cavities that will boost the proton beam energy from 216 MeV up to 571 MeV [3, 4]. Table 1 reports the key parameters of the INFN MB cavities. Ref. [5] reports a discussion on the rationale for the cavity electromagnetic and mechanical parameters selection and the path towards the final design of the resonator.

In this paper, we briefly present the status of the project and then we will report on the results of the cavities tested so far. A dedicated section is reserved for discussing ongoing activities related to the qualification of the last batch of cavities needed to complete our contribution.

PROJECT STATUS

The ESS Medium Beta cavity production is now in a well advanced phase.

The description of the production process and of the related Quality Assurance (QA) and Quality Control (QC) steps have been already presented in previous papers (see [6] for the most recent update).

Table 1: ESS Medium Beta Cavities Main Parameters

Parameter	Value
R_{iris}	50 mm
Geometrical β	0.67
π-mode Frequency	704.42 MHz
Acc. length	0.855 m
Cell-to-cell coupling k	1.55 %
π-5π/6 mode sep.	0.70 MHz
Geometrical factor G	198.8 Ω
Optimum beta, β_{opt}	0.705
Max R/Q at β_{opt}	374 Ω
E_{acc} at β_{opt}	16.7 MV/m
E_{peak}/E_{acc}	2.55
E_{peak}	42.6 MV/m
B_{peak}/E_{acc}	4.95 $\frac{mT}{MV/m}$
Q_0 at nominal gradient	>5×10^9
Q_{ext}	7.8×10^5

Here, we only remind that the production of the cavities is divided, also for QC, in five Acceptance Levels (AL) namely:

- AL1: Cavity after Electron Beam welding
- AL2: Cavity Bu˙ered Chemical Polished and RF tuned
- AL3: Cavity integrated and ready for Vertical Test
- AL4: Cavity successfully tested in cryogenic operation
- AL5: Cavity delivered to CEA for integration into cryomodule

Twenty eight cavities have successfully reached the final step AL5 and are now integrated at CEA in the cryomodule named CM01 to CM07, hosting four cavities each.

In Fig. 1, we report the result of the qualification test i.e. the quality factor (Q_0) versus the accelerating gradient (E_{acc}) measured at 2 K at the AMTF facility in DESY [7].

All the qualified cavities have a very high Q_0 in the region of 2×10^{10} at low accelerating field. Even at the reference ESS goal gradient of 16.7 MV/m, the quality factor is well above 1×10^{10} With respect to the ESS Reference Power (ERP), the performance of the Medium Beta cavities allow operation between one half and one fourth of the foreseen nominal cryogenic power.

Figure 2 reports the measured X-ray level reached during the previous mentioned test versus the accelerating field for the detector placed below the cavity. A second detector is placed on top of the cryostat during operation [8]: this

* daniele.sertore@mi.infn.it

ISBN: 978-3-95450-227-1 ISSN: 2673-5490 doi:10.18429/JACoW-IPAC2022-TUPOTK022

INFN-LASA FOR THE FERMILAB PIP-II

R. Paparella*, M. Bertucci, M. Bonezzi, A. Bosotti, D. Cardelli, A. D'Ambros, E. Del Core, A. T. Grimaldi, L. Monaco, D. Sertore, G. M. Zaggia, INFN Milano LASA, Segrate, Italy
C. Pagani, Università degli Studi di Milano and INFN Milano LASA, Segrate, Italy

Abstract

The status of INFN LASA contribution to the PIP-II project at Fermilab is reported in this paper. Experimental results and ongoing activities on prototypes are summarized together with the development of related testing infrastructures. The series production of the 38 INFN LASA designed, 5-cell cavities with beta 0.61 for the LB650 section of the PIP-II linac recently commenced, the status of major procurements and associated activities is here below conveyed. All cavities will be produced and surface treated in industry to reach the unprecedented performances required, qualified through vertical cold test at state-of-the art infrastructures and delivered as linac-ready at the string assembly site.

INFN LASA CONTRIBUTION

The Fermilab Proton Improvement Plan II (PIP-II) Linac [1, 2] is designed to deliver a 1.2 MW H^- beam upgradable to multi-MW to enable LBNF and DUNE neutrino physics projects. The 800 MeV beam will be injected into the upgraded Booster Ring via a linac-to-booster transfer line and it will then proceed to the Main Injector Ring.

The PIP-II linac features a flexible time structure for its 0.55 ms, 2 mA beam pulse in order to satisfy different experimental needs, with radiofrequency (RF) repetition rate of 20 Hz pulsed but with components capable of supporting continuous-wave (CW) operations.

A key section of the linac is the 650 MHz superconducting part with geometric beta factor of 0.61 (LB650) that currently encloses 36 five-cell elliptical cavities in 9 cryomodules, accelerating beam from 177 MeV to 516 MeV. Target cavity accelerating gradient is set at 16.9 MV/m with a quality factor higher than 2.4 10^{10}, an unprecedented working point for this type of resonators.

INFN LASA firstly provided a novel electromagnetic and mechanical design for the LB650 cavities [3], fully compatible to the performances and technical interfaces posed by the project as well with beam pipes and flanges, power coupler, helium tank, tuner.

On December 4th, 2018, the U.S. Department of Energy (DOE) and Italy's Ministry of Education, Universities and Research (MIUR) signed an agreement to collaborate on the development and production of technical components for PIP-II [4]. Following this milestone, on June 28th, 2021, INFN president, A. Zoccoli, officially signed the finalized INFN PIP-II Project Planning Document (PPD) [5].

INFN in-kind contribution will cover the needs of the LB650 section of the linac, namely:

- Grand total of 40 SC cavities (36 plus 2 spares, and 2 initial prototypes) delivered as ready for string assembly, equipping a total of 9 cryomodules.
- Qualification via vertical cold-tests provided by INFN either through the LASA test stand or through a qualified cold-testing partner infrastructure.
- Dual Acceptance Review, initially on INFN responsibility upon cold qualification and later under project responsibility at the string assembly site.
- Compliance to the PIP-II Technical Review Plan, the procedure issued by DOE and Fermilab in order to meet PIP-II technical, schedule and budget commitments.

* rocco.paparella@mi.infn.it

PIP-II LB650 CHALLENGES

A successful cavity design is the result of an interplay of multiple state-of-the-art competences existing at INFN-LASA in electromagnetic, mechanical and technical domains [6].

PIP-II LB650 cavities are themselves among the key scientifical challenges of the whole project, requiring:

- An unprecedented quality factor for these resonators, e. g. more than four times higher than that of ESS cavities at a similar gradient.
- The proper surface treatment recipe, based in Electro-Polishing etching (EP), must be developed and qualified on these low-beta resonators.
- Assessment of High-Order Modes (HOMs) risks so that neither instabilities nor additional cryogenic losses pose critical issues.
- Deep understanding of Lorentz Force detuning, pressure sensitivity and mechanical leading parameters as rigidities, yield limits, stresses [7]. PIP-II operational scenario is an uncharted territory in terms of cavity detuning control, especially in view of foreseen pulsed operation of these high loaded-Q cavities.
- Potential mutual compliancy to both European pressure vessel directives (PED) and U.S. codes (ASME) shall be resolved.

PROTOTYPES AND OTHER PRE-PRODUCTION ACTIVITIES

In total, seven PIP-II LB650 prototype cavities have been produced counting both single and multi-cell, and three of them are shared with Fermilab since early 2020 for a joint development effort (Fig. 1).

The actual status and perspectives of each of these prototype cavities is resumed here below, more insights are instead reported in M. Bertucci at al. at this conference [8].

B61S-EZ-001 Single-Cell

- High-Q recipe at FNAL [9]: *160 μm bulk EP + 900°C heat treatment (HT) for 3 hours +2/0 N-Doping at 800°C + final EP.*

ISBN: 978-3-95450-227-1 ISSN: 2673-5490 doi:10.18429/JACoW-IPAC2022-TUPOTK023

STUDY ON COMMERCIAL DIODES AS THERMOMETERS AT LOW TEMPERATURE FOR TEMPERATURE MAPPING SYSTEM OF Nb_3Sn SUPERCONDUCTING RADIOFREQUENCY CAVITIES

R. Wanison[†, 1, 3], K. Takahashi[2], K. Umemori[1,2], T. Yamada[1]
[1]High Energy Accelerator Research Organization (KEK), Tsukuba, Japan
[2]Graduate University for Advanced Studies (SOKENDAI), Tsukuba, Japan
[3]Department of Mechanical Engineering, Chiang Mai University, Chiang Mai, Thailand

Abstract

Nb_3Sn Superconducting radiofrequency (SRF) cavities has been researched and developed at Center for Applied Superconducting Accelerator (CASA), KEK. One of effective tools for research on the performance of SRF cavities is a temperature mapping (T-map) system for detecting small increases in temperature. It is a thermometer array positioned precisely on an outer surface of cavity wall. Thermometer should cover at least from the range of typical operating temperature of 4 K to the transition temperature of 18 K, for the Nb_3Sn SRF cavities. Therefore, carbon resistor can not be used as a cheap thermometer due to low sensitivity at this temperature range. In this proceeding, we report the results of the test for various commercially available diodes as a thermometer for T-map system. The sensitivity, stability and the repeatability are measured, cooled by a GM cryocooler.

INTRODUCTION

The key parameter of a superconducting radio frequency (SRF) cavity are quality (Q) factor and accelerating gradient. One of effective method to investigate the performance of SRF cavity is a temperature mapping (T-map) system for detecting small increases in temperature while operating SRF cavity [1, 2]. The T-map system consists of thermometer arrays positioned precisely on external surface of a cavity wall. The number of thermometers used in ranges from hundreds to thousands. There are commercially available thermometers with high accuracy and long-term stability. The price is, however, costly to use for the T-map system. Previously, the T-map system has been researched and developed by using resistor as a thermometer for low temperature. Many articles have been published describing their properties, such as resistance *R* and temperature *T* (R-T curve) data [3, 4]. One of the advantages of a resistance thermometer is that they can use a current-reversal technique to cancel the effects of thermal electromotive force (thermal EMF). Nevertheless, the disadvantage is the small change of resistance with temperature. It was found that the resistance thermometer has a good accuracy and reproducibility at temperature below 4 K [5]. In contrast, the use of a diode as thermometer makes wider operating temperature. The advantage of diode is that they have high sensitivity thermometer over the 1 K to 500 K temperature range [6].

Center for Applied Superconducting Accelerator (CASA) at KEK has researched and developed next generation of surface material for SRF cavities, that is Nb_3Sn. Owing to a higher critical temperature (T_c) of Nb_3Sn (~18 K) comparing to Nb (~9 K), Nb_3Sn has allowed it to achieve higher Q factor than Nb in an operating temperature of ~4 K.

In this research, therefore, we focus on experimentally investigate the behaviour of commercially available diode as a cheap thermometer for low temperature use. The scope of this research is to examine sensitivity, stability and repeatability of many types of commercially available diodes from 2.7 K to 77 K cooled by a GM cryocooler.

EXPERIMENTAL SETUP

The experimental set up is shown in Figure 1. It consisted of a GM cryocooler inside the cryostat to maintain the operating temperature from 2.7 K to 77 K, and a test section for installing diode sensors. As described later, commercially available diodes were installed to the test section. The stainless steel plate (3mm-SUS), with a dimension of 120×120 mm, and 3 mm in thickness, was inserted between 2nd stage of a cryocooler and the test section for thermal barrier, and thermal stability.

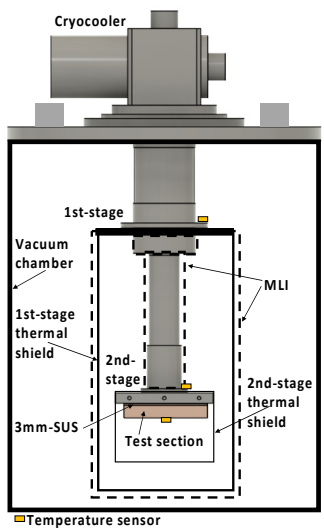

Figure 1: The experimental set up.

Test Section

The test section is shown in Figure 2. It has a dimension of 120×120 mm, and 20 mm in thickness, made by copper. It was designed for installing of nine diodes. There were different sizes of holes for several types of the diodes, and area for calibrated temperature sensor (DT-670 Silicon

† ramnarong.wanison@cmu.ac.th

ISBN: 978-3-95450-227-1 ISSN: 2673-5490 doi:10.18429/JACoW-IPAC2022-TUPOTK024

MULTIPACTING SIMULATION ON HALF-WAVE RESONATOR FOR 200 MeV ENERGY UPGRADE OF KOMAC PROTON LINAC*

J.J. Dang†, H.S. Kim, H.-J. Kwon, S. Lee,
Korea Multi-purpose Accelerator Complex,
Korea Atomic Energy Research Institute, Gyeongju, Korea

Abstract

A superconducting radio frequency cavity has been developed for proton beam energy upgrade from 100 MeV to more than 200 MeV at KOrea Multi-purpose Accelerator Complex (KOMAC). The half-wave resonator (HWR) is designed for the SRF linac. 350 MHz, beta = 0.56 HWR is designed to provide 3.6 MV accelerating voltage. After the electromagnetic design study and the electromagnetic – mechanical coupled analysis, an analysis on a multipacting (MP) of the HWR was carried out. The MP simulation was performed by using the CST Particle Studio. To understand a feature of the MP occurrence in the HWR, a particle-in-cell (PIC) simulation was conducted while changing various conditions such as an RF amplitude, an RF phase, and a primary electron emission surface.

INTRODUCTION

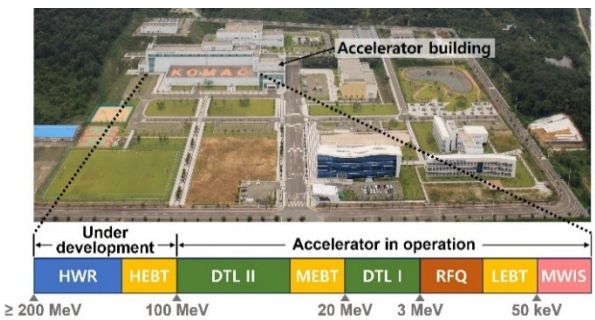

Figure 1: Layout of the 100 MeV proton linac at KOMAC and upgrade plan.

The linac at KOMAC has provided a 100 MeV beam for the proton irradiation research since 2013. Although the proton linac is stably operated, the upgrade of the linac is continuously requested to expand the application field including a spallation neutron source. Various proposals for enhancing the performance of the proton accelerator are discussed, and basic research is conducted. One such basic study is the study on the superconducting RF (SRF) linac that accelerate the 100 MeV proton beam as shown in Fig. 1. The RF design study and electromagnetic (EM) - mechanical coupled analysis on the HWR were conducted and presented [1]. The driving RF frequency of the HWR is 350 MHz which is RF frequency of the 100 MeV linac. The optimum beta and the accelerating voltage of the cavity are 0.56 and 3.6 MV. The HWR is depicted in Figure 2., and it consists of an inner conductor, an outer conductor, short plates connecting conductors, and ports for a RF power coupler, beam transport, and rinsing.

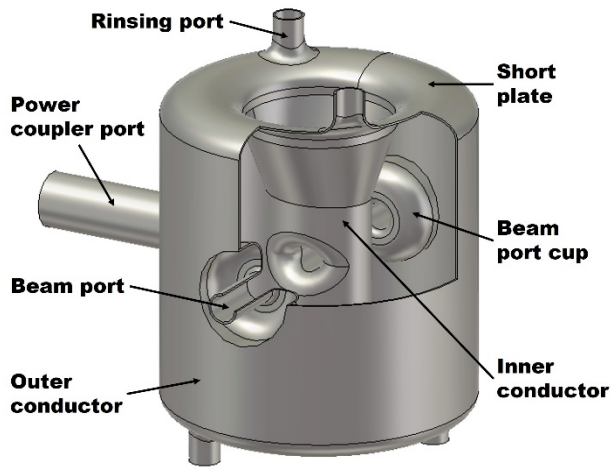

Figure 2: Cutaway drawing of the HWR designed by KOMAC.

After EM and mechanical analysis, the multipacting simulation was carried out using this design. The MP is a phenomenon that is an exponential growth of the electron by a secondary electron emitted at the surface impacted by an electron accelerated by the RF field. The MP causes problems such as unnecessary RF power consumption and limiting accelerating voltage. In the SRF cavity, the MP leads to additional heat load on the cavity surface, even causes loss of superconductivity [2]. Therefore, the characterization of the MP is required to improve cavity design or perform cavity processing. Thus, the MP simulation was conducted, and the simulation set up and result are presented in this paper.

MULTIPACTING SIMULATION MODEL AND SET UP

Simulation Tool

The MP simulation was conducted using the CST Studio Suite [3] because the CST provides integrated system for the analysis on the RF field and the particle behavior. Also, the CST material library supports an advanced secondary electron emission model called as Furman-Pivi model [4]. The CST includes the particle-in-cell (PIC) solver and tracking solver for particle simulation. In this study, the particle-in-cell (PIC) solver was utilized for the MP simulation. Although requires more computing resource and computational time compared to the TRK solver, it provides detailed data such as the number of electrons over

* This work was supported through KOMAC operation fund of KAERI by the National Research Foundation of Korea (NRF) grant funded by the Korea government (MSIT) (KAERI-524320-22).
† jjdang@kaeri.re.kr

ISBN: 978-3-95450-227-1 ISSN: 2673-5490 doi:10.18429/JACoW-IPAC2022-TUPOTK025

DESIGN STUDY OF THE THIRD HARMONIC SUPERCONDUCTING CAVITY FOR A BUNCH LENGTHENING

J. Yoon[1,2], E. S. Kim*[1], J. Han[2], H. S. Park[2], E. Kako[3]
[1]Dept. of Accelerator Science, Korea University, Sejong, South Korea
[2]Kiswire Advanced Technology Ltd, Daejeon, South Korea
[3]High Energy Accelerator Research Organization (KEK), Tsukuba, Japan

Abstract

The bunch lengthening by the 3rd harmonic cavity reduces the electron collisions in a bunch and increases the Touschek lifetime of a storage ring. We performed the multi-physics simulations including the electromagnetic, thermal, and mechanical analysis of the cavity. In the electromagnetic simulation, the geometry is optimized for the required performance of the cavity. The elliptical double-cell geometry is selected to increase the accelerating voltage and reduce the power losses of the cavity. Thermal/mechanical analyses were performed to check the deformation of the thermal and pressure contraction. The prototype cavity does not require the power coupler as it is a passive type. The conceptual design and copper prototype of the 3rd harmonic cavity will be described in this paper. Based on this design, the fabrication of Niobium cavity is in progress.

DESIGN REQUIREMENTS

The design requirements of the cavity are shown in Table 1. The resonant frequency (f_{res}) of the 3rd harmonic cavity is 1499.631 MHz as the frequency of the main cavity is 499.877 MHz. The main features are a passive type and superconductor. In the case of a passive cavity, it can be operated without a power coupler.

Table 1: Design Requirements of the 3rd Harmonic SRF Cavity

Parameter	Value
f_{res}	1499.631 MHz
Type	Passive, Superconductor
RF voltage	800 kV
$(R/Q)_{\text{per cell}}$	90 Ω

The shunt impedance divided by the unloaded quality factor (R/Q) is calculated by Eq. (1) [1]. Since the beam current and accelerating voltage of the cavity are 400 mA and 800 kV, the R/Q and δf (detuning frequency) is calculated as 90 Ω and 69.5 kHz.

$$V = I_b \left(\frac{R}{Q}\right)_{\text{per cell}} \frac{f_0}{\delta f} \quad (1)$$

* eskim1@korea.ac.kr

ELECTROMAGNETIC DESIGN

Basic Geometry and Parameter Sweeping

The basic geometry of the 3rd harmonic superconducting cavity (HSC) is adopted as an elliptical cavity. The 3rd HSC has relatively low accelerating voltages and gradients. Therefore, we chose the low loss geometry to minimize the power loss of the cavity [2].

Figure 1 shows variations of the shunt impedance divided by unloaded quality factor due to the changes in the bore radius. If the bore radius changes, the diameter of the cavity also changed for the target resonant frequency. Therefore, the horizontal axis is expressed as a ratio of radius and diameter. We can reach the R/Q to 90 Ω by the adjustment of a ratio of the cavity. However, the strength of higher-order modes (HOM) are not negligible [3]. Therefore, we will suppress it with HOM absorbers and design progress is ongoing.

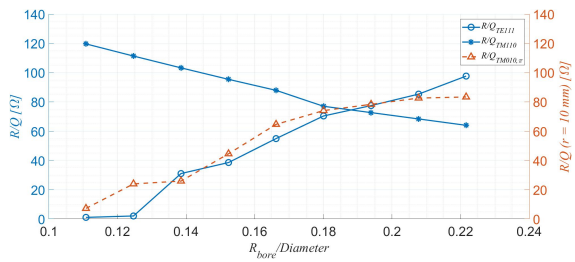

Figure 1: R/Q variations due to the bore diameter.

Number of Cells

Figure 2 shows the geometry of the cavities, and the main parameters are listed in Table 2. The double-cell geometry can reach the required accelerating voltage at lower accelerating gradient. This geometry has also a lower strength of the surface magnetic field compared to the single cell.

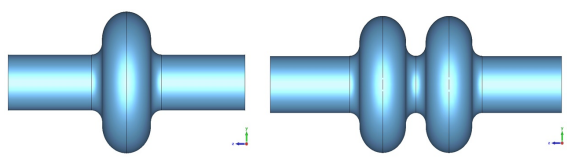

Figure 2: Geometry of the cavity: (left) Single-cell and (right) Double-cell.

Lorentz Force Detuning

The electromagnetic field induces the surface current on the wall of the cavity. For this reason, the Lorentz pressure

ISBN: 978-3-95450-227-1 ISSN: 2673-5490 doi:10.18429/JACoW-IPAC2022-TUPOTK026

ESS ELLIPTICAL CRYOMODULES TESTS AT LUND TEST STAND*

C. G. Maiano*, E. Asensi, N. Elias, P. Goudket, W. Hees, P. Pierini, L. Sagliano, F. Schlander, M. Wang, European Spallation Source, Lund, Sweden,
D. Bocian, W. Gaj, P. Halczynski, M. Sienkiewicz, F. D. Skalka, J. Swierblewski, K. M Wartak, M. Wartak, IFJ PAN, Kraków

Abstract

We present an overview and description of the elliptical cryomodules test activities at Lund Test Stand 2. During 2021 the test facility was commissioned with one prototype, and four series medium beta modules have now been successfully tested at ESS in Lund. This activity allowed the joint ESS and IFJ PAN team to develop all the procedures and the necessary automated tools for the different phases of the site acceptance test campaign (e.g. incoming inspections, coupler conditioning, cooldown strategies, tuning to resonance and electromagnetic/cryogenic performance verification). During the initial test period techniques for diagnostics of limiting mechanisms have been developed and improved up to a consolidated and mature state for the rest of the test campaign. Tests results and the initial statistics is presented and commented.

INTRODUCTION

Cryomodules and cavities for the ESS linac [1] are in-kind contribution by several of the project partners (CEA, STFC, INFN, IJCLAB). The Lund Test Stand, TS2, is dedicated to medium and high beta elliptical cryomodules site acceptance tests, SAT. TS2 operation is made possible with the long-term presence of the IFJ PAN at Lund team for the whole duration of the elliptical cryomodule test activities. ESS and IFJ PAN act as a single team for everyday operation from cryomodule transport [2], incoming inspection, to definition and execution of tests protocols and finally to the preparation for installation in the ESS tunnel.

CRYOMODULE DOCUMENTATION

The design and individual component documentation packages, as received by the in-kind partners, are stored in the ESS central engineering documentation management system (CHESS), for the long-term maintenance needs of the facility. These include quality documentation and calibration data for instrumentation. The received documentation is further extended during the TS2 workflow, to document the ESS SAT activities for the component acceptance.

CRYOMODULE TEST CYCLE

The cryomodule testing workflow is split in phases and at each phase a number of test reports are produced. Phases and the flow of testing phases are illustrated in Fig. 1. Incoming inspections include: mechanical, electrical, vacuum and cavity frequencies surveys.

#	Phase	Areas	
		From	To
1	Cryomodule reception	G02-CXL	CM-IRA
2	Cryomodule preparation	CM-IRA	
3	Cryomodule installation	CM-IRA	Bunker
4	Cryomodule Warm Validation	TS2 Bunker	
5	Cryomodule Cold Validation		
6	Cryomodule Warm-up		
7	Cryomodule Disconnection	Bunker	CM-IRA
8	Cryomodule Preparation for Dispatch	CM-IRA	G02-CXL
9	Cryomodule Dispatch	G02-CXL	HLB Hall or Storage

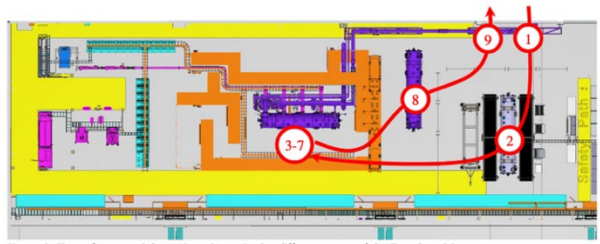

Figure 1: Phases of the TS2 cryomodule test activities.

SRF Incoming Reception and Cavity Data

Cavity data is collected from in-kind partners during the follow-up of the component handover, from fabrication at vendors, installation in the modules, and to the shipment to ESS. This data is collected and consolidated in the ESS cavity database, ESSCDB[3]. The ESCSDB is used after the module reception to store all incoming and verification measurements. This allows to follow cavities history, collect in-kind calibration coefficients (e.g. the field calibration constant k_t and the transmitted power antenna quality factor Q_t from vertical tests), create incoming reports and manage cryomodules configurations. The reports are constantly used in the receiving station and in the control room during tests to cross check the measured performance with the experience reported during the activities at the in-kind partners laboratories. Figure 2 shows an example.

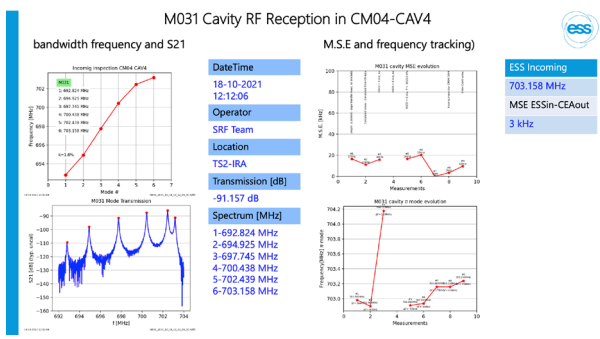

Figure 2: The ESSCDB allows to summarize the main cavity data (bandwidth, frequency evolution and deviations).

* Cecilia.maiano@ess.eu

ISBN: 978-3-95450-227-1 ISSN: 2673-5490 doi:10.18429/JACoW-IPAC2022-TUPOTK027

FIELD EMISSION MEASUREMENTS AT LUND TEST STAND

C.G. Maiano*, N. Elias, E. Laface, P. Pierini, L. Sagliano, M. Wang
European Spallation Source ERIC, Lund, Sweden
E. Cenni, CEA-IRFU, Gif-sur-Yvette, Paris France

Abstract

We present here a description of field emission (FE) measurements set-up developed for elliptical cryomodules test activities at Lund Test Stand 2. A test campaign of field emission measurements has been developed and optimized during cryomodules tests. The scintillator detectors (and their respective shields), chosen for these measurements, have been characterized and optimized. The field emission application has been developed and integrated in the cryomodules tests operator interface. The Initial test results are presented and commented.

INTRODUCTION

The Test Stand 2 (TS2) at ESS in Lund, Sweden, is dedicated to medium and high beta supeconducting cryomodules (CMs) site acceptance test (SAT). During 2021 the test facility was fully commissioned with one prototype module. Between 2021 and first half of 2022 four medium beta modules of the series were successfully tested. The Field Emission (FE) measurements were set-up during the first CM test in order to develop the methodology to assess onset of field emission during module tests. Only partial data is thus available for this first module, CM01.

The goals of the measurements are:

- to quantify the field emission energy endpoint and to collect the count rate increase vs accelerating gradient, E_{acc}, to make an assessment where the field emission starts;
- to compare measurements taken during CMs tests with the results from Vertical Tests (VT)[1];
- to build an overview of FE spatial distribution with the goal of quantifying the emitted radiation with respect to the direction of the beam-line.

MEASUREMENTS SET-UP

To perform FE measurements, scintillators detectors (NaI(Tl) crystals) were chosen [2]. Two GAMMA-RAD 5 gamma rays spectrometers from Amptek (3 x 3 inches scintillators provided with photomultiplier PMT) were chosen as a single, integrated and portable module. The energy resolution of the detectors is less than 7% on the ^{133}Cs line at 662 keV.

A dedicated shielding has been designed and realized to be able to detect potential high x-rays count rate (Fig. 1).

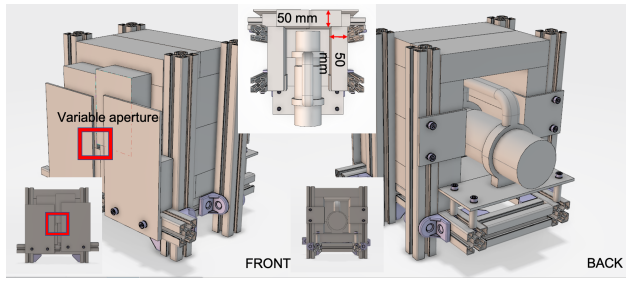

Figure 1: Detectors shielding of varnished bricks and supports. On the left the frontal side is shown; on the right the back side is shown. The thickness is 50 mm thick. The top view is shown in the middle, where the shielding roof has been removed to show detector position.

The lead shielding is 50 mm thick and covers frontally and laterally the detectors. The shielding has a window aperture of 10 x 10 mm. In the measurements presented in this paper the shielding was closed to avoid detector saturation. Dedicated measurements of the detector dead time vs. front aperture will be performed during the testing of the next modules. The two detectors have been calibrated with ^{137}Cs

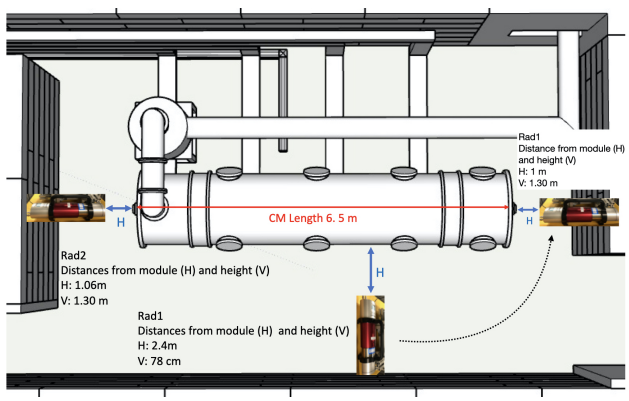

Figure 2: Overview of test stand 2 bunker. The detector 2 was placed along the longitudinal axes of the cryomodule; the detector 1 was used in two configurations: one orthogonal to the symmetry axes of the module and the another on the opposite side with respect to detector 2.

(661 keV) and ^{60}Co (1173 and 1332 keV plus the sum peak at 2505 keV) and no additional source above 3 MeV is available. This implies that the measurements at 8 MeV, that is our activation threshold, is evaluated with extrapolation from the calibration with a certain error.

The detectors were placed according to the Fig. 2.

* cecilia.maiano@ess.eu

ISBN: 978-3-95450-227-1 ISSN: 2673-5490 doi:10.18429/JACoW-IPAC2022-TUPOTK028

TUNING OF SUPERCONDUCTING CAVITIES USING THE FFT OF TRANSMITTED POWER

E. Laface*, C. G. Maiano, P. Pierini, M. Wang, European Spallation Source ERIC, Lund, Sweden

Abstract

We implemented a method to tune the ESS superconducting cavities based on the spectral analysis of the high resolution data available from the Low Level RF system (LLRF) for the transmitted power, without the need of connecting a network analyzer or any other dedicated instrumentation along the RF chain. A frequency peak up to 4 MHz off from the resonating frequency can be detected and used to control the stepper motor of the tuner until the cavity is stretched to the proper length to reach the correct operation frequency. Experience of its use at the ESS Test Stand 2 (TS2) facility at Lund during cryomodule acceptance testing is presented.

INTRODUCTION

The European Spallation Source superconducting linac is composed by 36 elliptical cavities with geometric β of 0.67 and 84 elliptical cavities with geometric β of 0.86. The cavities are assembled in groups of 4 per each cryogenic module as described in [1,2] and operate at the frequency of 704.42 MHz, accelerating the proton beam from 216 MeV up to the 2 GeV.

Superconducting cavities are fabricated with a lower frequency than the operational one and, once cooled down in a bath of helium at 2.0 K, the thermal contraction brings them close to the goal frequency, but not with the needed accuracy imposed by the small cavity bandwidth. The final adjustment needs to be done with a tuner that stretches the cavity through the action of a step motor. In order to follow the tuning process, one of the standard techniques consists in monitoring the S21 cavity transmission with a Vector Network Analyzer (VNA). The use of VNA S21 requires either to modify the high power RF wave-guide distribution system (RFDS) inserting matched transitions and disconnecting the pickup cables, or to inject the signals from the strongly attenuated ports in the directional couplers of the RFDS, with additional amplifier stages. Both methods introduce risks in the linac installation (RFDS leaks, missing cable re-connections) and is time consuming.

In all modern LLRF systems the cavity pick up (PU) for the transmitted signal is available with a high sampling rate (~10 mega samples per second) along the pulse. Its analysis in the spectral domain provides sufficient accuracy to identify the narrow cavity resonance in the noisy pattern of the highly detuned (~200 band widths) system. The pulsed klystron power, which has a carrier frequency of 704.42 MHz, has Fourier components that fall into the cavity resonance, and these appear with a clear signature peak in the spectral analysis of the transmitted signal. A similar approach was used to tune the 1.3 GHz SRF cavities at the European XFEL, DASY, Hambourg, Germany [3].

THE FFT TECHNIQUE FOR TUNING

The technique is illustrated in Fig. 1, where the FFT of the transmitted power signal is shown at three different positions during the motion of the tuner. The signature peak of the detuned frequency in the upper plot is shifted of 45 kHz with respect to the 704.42 MHz design frequency, and in the lower plots it moves towards the klystron frequency due to the tuner motion.

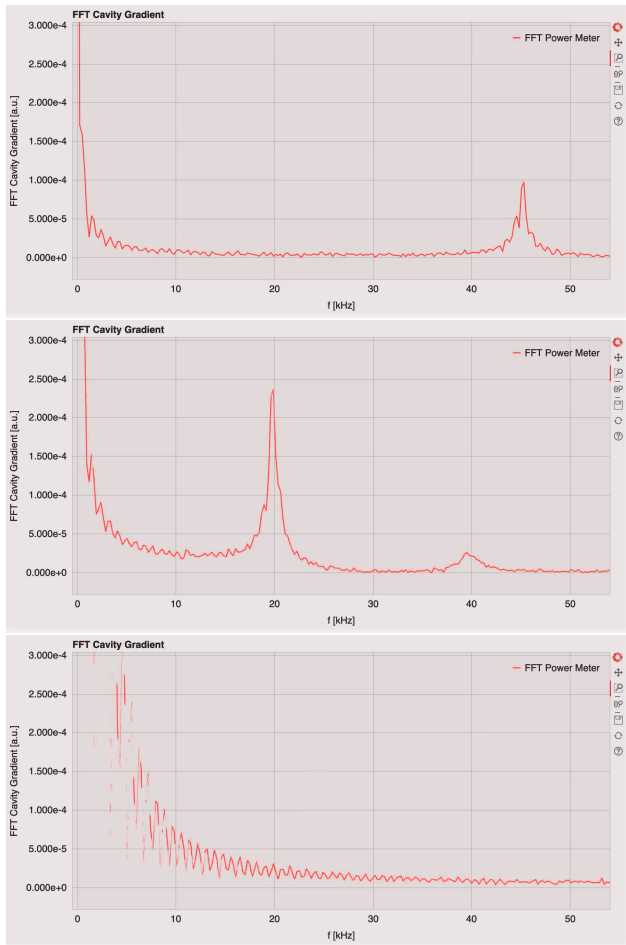

Figure 1: Fast Fourier Transform of the transmitted power in three moments of the tuning process for the 3rd cavity in the cryomodule CM01. The peak moves toward the zero (carrier RF frequency) when the cavity is approaching the driver frequency of the klystron, and in the last step it is no longer visible.

The method has been initially implemented at the ESS TS2 as a high level application that acquires (here at 1 Hz)

* emanuele.laface@ess.eu

ISBN: 978-3-95450-227-1 ISSN: 2673-5490 doi:10.18429/JACoW-IPAC2022-TUPOTK029

OPEN XAL STATUS REPORT 2022

A. Zhukov*, A. Hoover, A. Shishlo, ORNL, Oak Ridge, Tennessee, USA
J. F. Esteban Müller, E. Laface, Y. Levinsen, N. Milas,
European Spallation Source ERIC, Lund, Sweden

Abstract

The Open XAL accelerator physics software platform has been developed through international collaboration among several facilities since 2010. The goal of the collaboration is to establish Open XAL as a multi-purpose software platform supporting a broad range of tool and application development in accelerator physics and high-level control (Open XAL also ships with a suite of general-purpose accelerator applications). This paper discusses progress in beam dynamics simulation and updated application framework along with new generic accelerator physics applications. We present the status of the project at each participating facility and a roadmap for continued development.

SNS STATUS

The Spallation Neutron Source (SNS) continues to use Open XAL as the main control room accelerator physics tool. The SNS switched to the latest Java 17 LTE release in Control Room. Several new features were implemented for linac tuning and emittance measurements in the ring.

Scaling Magnets in Superconducting Linac

One routine operational task in the SNS is to rescale the magnetic fields in the ring and transport lines after changing the final beam energy in the linac. Until recently, this task was performed with the Open XAL Energy Manager application. Since Energy Manager has a complicated logic and interface, it has been replaced by an addition to the Superconducting Linac (SCL) Tuner Wizard. The new addition to SCL Wizard measures the final beam energy in the linac and rescales the downstream magnetic fields accordingly. A screenshot of the magnet scaling addition is shown in Fig. 1. On the left panel, there are new buttons for initialization and setting new values, and a list of all beam transport lines after the SCL. The user can also choose particular beam lines and magnets for scaling. The red color is a warning sign that some of the power supplies in the sequence will not be able to set the calculated field.

Cavity Failure Test in SCL

The Cavity Failure Test addition to the SCL Tuner Wizard application (Fig. 2) demonstrates an automated retuning procedure of the SCL in the case of the failure of one of the SCL cavities. Before starting this part of the SCL Wizard,

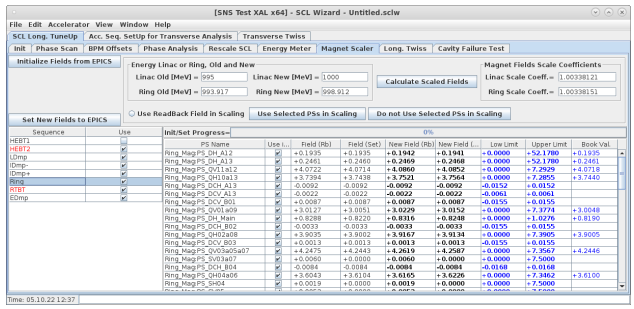

Figure 1: Magnet scaling part of the SCL Tuner Wizard Open XAL application.

the user should define which cavity should be monitored, save and prepare Amplitude Feed Forward waveforms for the downstream cavities that will be used in the correction, and define the goal for a detuning parameter for the failing cavity. The algorithm and successful results of using this test are described in [1]. The Cavity Failure Test addition is not intended to be used during SNS production: this type of cavity failure is not critical to the SNS availability metrics and is handled by operators with thorough documentation of the circumstances of the event.

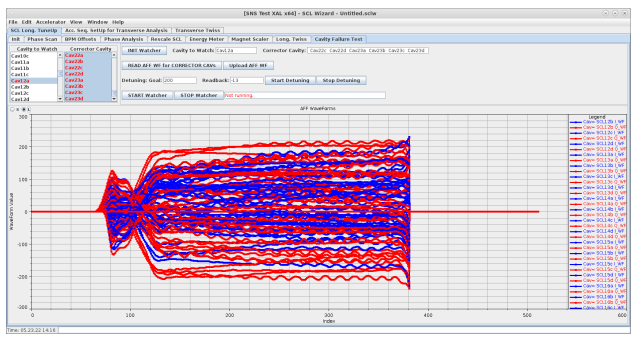

Figure 2: Cavity Failure Test Addition to SCL Tuner Wizard.

4D Emittance Measurement in SNS Ring

A critical component of efforts to produce an approximately self-consistent beam [2] in the SNS ring is to measure the four-dimensional (4D) beam emittance [3] during accumulation. The 4D emittance can be reconstructed from at least four horizontal, vertical, and diagonal wire-scanner measurements with different transfer matrices connecting the wire-scanner and reconstruction locations [4]. An Open XAL application has been developed to carry out this measurement using four wire-scanners in the ring-target beam transport (RTBT) section of the SNS.

* zhukovap@ornl.gov

ISBN: 978-3-95450-227-1 ISSN: 2673-5490 doi:10.18429/JACoW-IPAC2022-TUPOTK030

X-RAYS ENERGY MEASUREMENTS DURING THE RFQ CONDITIONING AT THE EUROPEAN SPALLATION SOURCE

E. Laface*, C. G. Maiano, R. Zeng, European Spallation Source ERIC, Lund, Sweden
O. Piquet, CEA Paris-Saclay - DRF/Irfu/DACM, France

Abstract

The Radio Frequency Quadrupole (RFQ) was conditioned at the European Spallation Source during spring 2021. We used part of the conditioning time to estimate the accelerating potential within the RFQ analyzing the x-rays bremsstrahlung radiation emitted by the electrons released and accelerated in the RFQ. The results of these measurements are in good agreement with the theoretical prediction.

INTRODUCTION

The Radio Frequency Quadrupole, [1] section 3.2 and [2], is an accelerating, focusing and bunching structure located after the Ion Source and Low Energy Beam Transport at the European Spallation Source in Lund, Sweden. This structure has the goal of accelerating the 62.5 mA of proton beam from 75 keV to 3.6 MeV at a frequency of 352.21 MHz with a repetition rate of 14 Hz for a pulse of 2.86 ms. In order to achieve this goal, the RFQ needs several weeks (in our case eight) of conditioning, where the power, the repetition rate and the length of the pulse are gradually increased up to the nominal level. The conditioning phase removes the residual contaminants deposited on the surface, as well as surface imperfections, making the device stable in terms of operations.

A side effect of the RFQ powering is that some electrons are generated and accelerated within the RFQ itself and, when those electrons hit the surface they release the energy as x-rays that can be measured outside the RFQ structure. The distribution of energies among the electrons follows the spectrum of bremsstrahlung, and in particular the maximum reachable energy (the asymptotic behaviour) is expected to be the potential produced withing the RFQ. This gives a method to measure the potential produced in the RFQ for each applied power [3–5].

THE X-RAYS DETECTOR

The x-rays measurements were performed using CdTe detector from Amptek: Model XR-100-CdTe is a high performance x-rays detector, pre-amplifier, and cooler system using a $5 \times 5 \times 1$ mm^3 Cadmium Telluride (CdTe) diode detector mounted on a two-stage thermoelectric cooler. Cadmium Telluride (CdTe) crystal is the sensor material for direct conversion of the x-rays radiation [6]. This high-Z semiconductor material (Cd with Z=48, Te with Z=52) provides excellent stopping power and thus high efficiency in the desired energy range (see Fig. 1).

* emanuele.laface@ess.eu

The detector and Digital Pulse processor, (Fig. 2) were installed on a flange outside the fourth slot of the fifth RFQ module at a distance of 3.03 m from the beginning of the RFQ (Fig. 3).

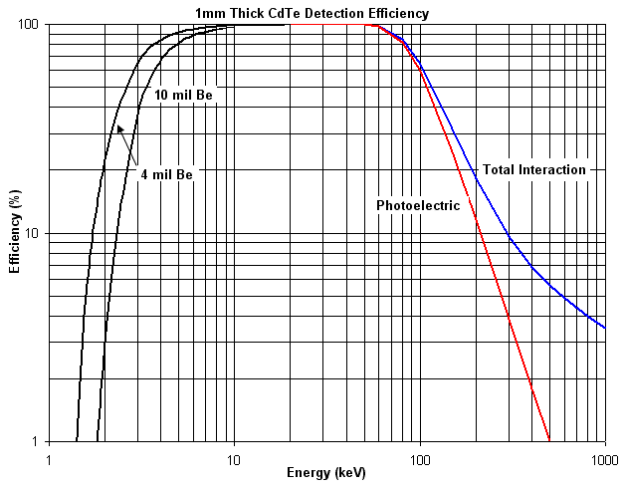

Figure 1: Detector efficiency (1 mm thick crystal).

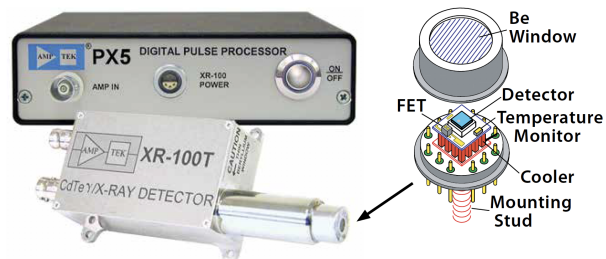

Figure 2: Detector.

After some tests of setup it was decided to avoid the use of a shielding liner for the installation of the x-ray detector because the copper of the RFQ and the stainless steel of the flange was sufficient to shield the low energy x-rays avoiding the saturation of the detector.

Calibration

Before starting to acquire the measurements we did a calibration of the detector, using isotopes with lines in the energy region of interest, which is from 0 to 120 keV. The selected sources for the calibration were:

- ^{241}Am with lines at 13.81, 17.70, 20.70, 26.34 and 59.54 keV as in Fig. 4

ISBN: 978-3-95450-227-1 ISSN: 2673-5490 doi:10.18429/JACoW-IPAC2022-TUPOTK031

A FIRST 6 GHz CAVITY DEPOSITION WITH B1 SUPERCONDUCTING THIN FILM AT ASTeC *

A. Hannah†, R. Valizadeh, O.B. Malyshev, STFC/DL, Daresbury, Warrington, UK
V.R. Dhanak, The University of Liverpool, Liverpool, UK
G. Stenning, STFC/RAL, Didcot, UK
V. A. Garcia Diaz, E. Chyhyrynets, C. Pira, INFN/LNL, Legnaro, Padova, Italy

Abstract

Nb_3Sn, NbTiN and NbN are superconductors with critical temperatures of 18.3, 12.6-17 and 11.6-17.5 K, respectively, these are higher than that of Nb at 9.3 K. Hence, at 4 K, they have an RF resistance, an order of magnitude lower than that of Nb, which leads to quality factors above those of Nb. In recent years, there has been an extensive effort converting Nb cavities into Nb_3Sn. Alloying the top inner layer of the cavity using Sn diffusion at a high temperature has had some degree of success, however, the reproducibility remains a major hindering and limiting factor.

In this study, we report on the PVD deposition of NbTiN inside a 6 GHz cavity, using an external magnetic coil configuration. The deposition is done at an elevated temperature of about 650 °C.

We report on the superconducting properties, film structure and its stoichiometry and surface chemical state. The films have been characterised with SEM, XRD, XPS, EDS and SQUID magnetometer.

INTRODUCTION

500 MHz Copper cavities coated with a thin Nb film (1.5 to 5 µm), have been operational since 1980 in various particle accelerators [1]. However, their performance has only matched those of bulk Nb cavities at moderate accelerating gradient of up to 8.6 MV/m. In the past two decades, due to advancement in thin film deposition technology and better understanding of surface preparation, there has been a coordinated effort by the SRF community to push the performance of thin film, SRF cavities to a level that can compete with bulk Nb, at high-accelerating gradients of up to 20 MV/m.

Furthermore, this advancement allowed materials with a critical temperature (T_c) higher than Nb, to be synthesised on copper substrates, with superconducting properties matching their respective bulk materials.

Using materials with T_c higher than for Nb, such as NbN, Nb_3Sn, NbTiN, MgB_2, etc., as well as multilayer structures, allows us to reach parameters that are unreachable for existing RF cavities:

- Increasing the quality factor Q, reduces the heat produced, and, hence, the electricity consumption of the cryogenic system during the RF cavity operation.
- Using high T_c superconducting materials allows to operate RF cavities at 4.2 K instead of 1.9 K, used for the high-performance Nb cavities, more than doubling the efficiency of the cryogenic system.
- Increasing the cost-effective acceleration field E (at present the minimum cost is achieved at just over 30 MV/m) will result in massive saving in the infrastructure (tunnel, LHe supply and He recovery lines, electric cables, controllers, cryostats, pumps, etc), for example 20% increase in the acceleration field allows 20% reduction in the acceleration line (compare: a 4-km long tunnel for EU-XFEL instead of a 5-km long one, or 50-km long tunnel for ILC instead of 60-km).

This improvement goes by a few routes.

Other alloy forms of Nb, known as A15, such as Nb_3Sn or Nb_3Al, with a higher T_c, a potentially higher critical field H_{c2}, leading to potentially significant cryogenics cost reduction if the cavity operation temperature is 4.2 K or higher. Single crystal, high quality films have been achieved on a single crystal MgO [2, 3], sapphire and single crystal copper substrates, but more effort is needed for translating these remarkable results onto real 3D geometry cavity.

Multilayer film of Superconductor/Insulator/Superconductor (SIS) should provide a much higher E_a than a single layer film [4].

Currently, thin film SRF cavity production is based on PVD processes, where sputtering is the preferred method due to its ease of scalability, moderate conformability and above all its ability to control the film morphology and microstructures. The SRF thin film synthesis by sputtering process owes much of its success to being a single element thin film (mostly Nb). Synthesis of an alloy SRF thin film on a 3D geometry such as cavity is much more challenging.

At ASTeC (UKRI/STFC Daresbury Laboratory), alloy-superconducting material such as Nb_3Ge, Nb_3Sn, V_3Si, NbTi, NbTiN and NbN have been successfully synthesized on various flat substrates either using alloy target or by co-sputtering, i.e., by sputtering simultaneously two constituents on a temperature-controlled substrate. In co-sputtering, the achieved composition is dependent on the relative positions of the target and the substrate. The perfect stoichiometry can then be obtained by manipulating these positions. However, the control of the stoichiometry may be

* Work supported by the IFAST collaboration which has received funding from the European Union's Horizon 2020 Research and Innovation programme under Grant Agreement No 101004730.
† adrian.hannah@stfc.ac.uk

ISBN: 978-3-95450-227-1 ISSN: 2673-5490 doi:10.18429/JACoW-IPAC2022-TUPOTK033

FIRST RF MEASUREMENTS OF PLANAR SRF THIN FILMS WITH A HIGH THROUGHPUT TEST FACILITY AT DARESBURY LABORATORY*

D. Seal[1,2] †, T. Sian[1,2], O.B. Malyshev[2,3], H. Marks[1,2], R. Valizadeh[2,3], P. Goudket[2,3,4], G. Burt[1,2]
[1]Engineering Department, Lancaster University, Lancaster, UK
[2]Cockcroft Institute, UKRI/STFC Daresbury Laboratory, Daresbury, Warrington, UK
[3]ASTeC, UKRI/STFC Daresbury Laboratory, Daresbury, Warrington, UK
[4]Now at European Spallation Source, Lund, Sweden

Abstract

The research on superconducting thin films for future radio frequency (RF) cavities requires measuring the RF properties of these films. However, coating and testing thin films on full-sized cavities is both challenging and time-consuming. As a result, films are typically deposited on small, flat samples and characterised using a test cavity. At Daresbury Laboratory, a facility for testing 10 cm diameter samples has recently been commissioned. The cavity uses RF chokes to allow physical and thermal separation between itself and the sample under test. The facility allows for surface resistance measurements at a resonant frequency of 7.8 GHz, at temperatures down to 4 K, maximum RF power of 1 W and peak magnetic fields of a few mT. The main advantage of this system is the simple sample mounting procedure due to no physical welding between the sample and test cavity. This allows for a fast turnaround time of two to three days between samples. As such, this system can be used to quickly identify which samples are performing well under RF and should require further testing at higher gradient. Details of recent upgrades to this facility, together with measurements of both bulk niobium and thin film samples, will be presented.

INTRODUCTION

Bulk niobium superconducting radio frequency (SRF) cavities are close to reaching their theoretical performance limits in terms of accelerating gradients and Q factors. As a result, there is a push to develop cavities using materials beyond Nb. These include, but are not limited to, Nb_3Sn, NbN, NbTiN, MgB_2. The materials are deposited as thin films, typically on copper cavities. The main reasons for this are: Cu is cheaper than Nb, it is more easily machinable and it benefits from a higher thermal conductivity.

The performance of thin films is usually studied on small, planar substrates. The main advantage over full cavity depositions is that small samples are much cheaper to produce and easier to deposit on. Also, some of the new materials being investigated are not yet developed enough to deposit on cavities. Having planar samples also allows for easier measurements under DC conditions and surface analysis techniques.

In order to study the performance of planar samples under RF conditions, a facility at Daresbury Laboratory has been developed over the past few years. This system allows us to measure the surface resistance, R_S, of small samples under RF conditions. The main advantage of this facility, compared with other RF testing facilities around the world [1], is the ability to test samples with a short two to three day turnaround time. This would importantly allow for the rate of sample characterisation to keep up with sample production.

The ultimate goal will be to follow up the sample tests with additional measurements using other facilities at Daresbury Laboratory. Future modifications to a magnetic field penetration facility on site [2] will allow testing of the same samples under DC conditions in order to obtain measurements of critical magnetic fields and relate the DC and RF superconducting properties. This, combined with surface analysis, will help identify the best performing thin films that will be worth up-scaling to full cavity tests.

This paper reports on the current status of the facility as well as sample measurements to demonstrate its capabilities.

FACILITY OVERVIEW

The test cavity used for studying the RF properties of planar samples, was first reported in [3]. The cavity itself is a bulk-Nb half cell (~ 31 mm diameter) surrounded by three quarter-wavelength chokes. The entire structure is 104 mm in diameter and 12 mm thick, shown in Fig. 1.

The cavity is mounted to an oxygen-free high conductivity (OFHC) Cu plate in a liquid helium (LHe) free cryostat cooled by a Gifford-McMahon cryocooler. This plate is able to reach a base temperature of 3.5 to 4 K. Details of this cryogenic facility can be found in [4]. A previous setup for this cavity used a LHe cryostat [5]. However, with a sample testing time of 2 weeks, this was considered to be too long, despite achieving lower base temperatures of 2.5 K. The LHe-free cryostat instead allows for a much faster sample testing time of just 2-3 days, not to mention the environmentally sustainable benefits from not using LHe supplies.

The choke structures allow for a small vacuum gap between the sample and cavity whilst minimising RF leakage. A 1 mm spacer made from G-10 is used to maintain this gap, allowing the two to be thermally and physically isolated. Therefore no welding is required between the sample and cavity. This is another reason why the system allows for easy sample changeover and short testing times.

* This work has been supported by: the IFAST collaboration which has received funding from the European Union's Horizon 2020 Research and Innovation programme under Grant Agreement No 101004730.
† daniel.seal@cockcroft.ac.uk

ISBN: 978-3-95450-227-1 ISSN: 2673-5490 doi:10.18429/JACoW-IPAC2022-TUPOTK034

EVALUATING THE EFFECTS OF NITROGEN DOPING AND OXYGEN DOPING ON SRF CAVITY PERFORMANCE*

H. Hu†, Y.-K. Kim, University of Chicago, Chicago, IL, USA
D. Bafia, Fermi National Accelerator Laboratory, Batavia, IL, USA

Abstract

Superconducting radiofrequency (SRF) cavities are resonators with extremely low surface resistance that enable accelerating cavities to have extremely high quality factors (Q_0). High Q_0 decreases the capital required to keep the accelerators cold by reducing power loss. The performance of SRF cavities is largely governed by the surface composition of the first 100 nm of the cavity surface. Impurities such as oxygen and nitrogen have been observed to yield high Q_0, but their precise roles are still being studied. Here, we compare the performance of cavities doped with nitrogen and oxygen in terms of surface composition and heating behavior with field. A simulation of the diffusion of oxygen into the bulk of the cavity was built using COMSOL Multiphysics software. Simulated results were compared to the actual surface composition of the cavities as determined from secondary ion mass spectrometry analysis. Understanding how these impurities affects performance allows us to have further insight into the underlying mechanisms that enable these surface treatments to yield high Q_0.

INTRODUCTION

The role of impurities in Nb is critical in SRF cavity performance. Nitrogen doped cavities have displayed high quality factors (Q_0) of $> 4 \times 10^{10}$ and high accelerating gradients (E_{acc}) of > 38 MV/m [1]. Recent work has shown that low temperature baking (LTB), which relies on diffusion of oxygen from the native oxide, mitigates high field Q-slope (HFQS) and improves Q_0 at high E_{acc} [2]. Motivated by these studies on LTB, we conduct initial studies on a new treatment technique called oxygen doping, also referred to as oxygen alloying, which achieves doping-like performance but without any extrinsic impurities [3]. Oxygen doping diffuses oxygen from the native oxide following Fick's second law to achieve a uniform concentration of impurities in the first 100 nm of the surface [3]. Solutions to this diffusion process have been analytically obtained in Refs. [4, 5]. We take an alternative approach by simulating the diffusion process of oxygen into niobium. With this simulation, we can associate cavity performance with an impurity profile such that the oxygen doping treatment can be fine tuned for the desired performance.

This work presents an initial study evaluating and understanding the precise roles of oxygen and nitrogen in enabling high Q_0. We find that even in the absence of nitrogen, we can achieve doped-like anti-Q slope performance, as well as high Q_0 and E_{acc}. The biggest discrepancy seems to lie in the turning on of additional loss mechanisms at higher fields, driving both higher resistance as well as causing significant heating within the cavity. Further work is required to optimize this treatment and understand the causes of these high field losses. Initial data supports that oxygen doping a promising treatment comparable to nitrogen doping.

EXPERIMENTAL METHOD

One single cell, TESLA shaped Nb cavity with resonant frequency of 1.3 GHz was first baselined with an 800°C degas and 40 µm electropolishing (EP) removal [2]. The cavity was then treated with subsequent steps of baking and chemical processing. First, the cavity was *in-situ* baked at 200°C to diffuse oxygen from the native niobium oxide into the bulk. Next, the cavity underwent two rounds of HF rinsing to strip the oxide, leaving the Nb metal untouched. Following each HF rinse, the cavity was exposed to air to allow a new, undepleted Nb_2O_5 layer to form [6]. The regrowth process consumes about 2 µm of Nb but otherwise, the impurity profile of the rf layer is unaffected [6]. After each treatment, the cavity was tested to find Q_0 vs. E_{acc} at both 2 K and low T (< 1.5 K) in continuous wave (CW) operation to determine the decomposition of surface resistance into BCS and residual resistances [7]. Before testing, the cavity was evacuated and assembled with resistance temperature detectors (RTDs), flux gates at the equator, and Helmholtz coils. The cavity was cooled to 4.2 K with the fast cool down protocol to minimize the possibility of trapping magnetic flux [2].

In addition to Q_0 and E_{acc}, we also investigated how the cavity heated with increasing fields using thermometry mapping (TMAP) [8]. 576 carbon RTDs were installed on the outside of the cavity during assembly. The temperature at each RTD was recorded periodically during CW testing. In parallel with cavity testing, we also treated cavity cutouts of 1 cm in diameter to the same treatments as the single cell cavity. These samples were analyzed with time of flight secondary ion mass spectrometry (TOF-SIMS) to associate performance with surface composition [9].

RESULTS AND DISCUSSION

We compare the performance for each of our three treatment steps with that of a nitrogen doped single cell cavity that was treated with 2/0 + 5 µm EP nitrogen doping [1]. Data for the nitrogen doped cavity is from Ref. [8].

* Work supported by the Fermi National Accelerator Laboratory, managed and operated by Fermi Research Alliance, LLC under Contract No. DE-AC02-07CH11359 with the U.S. Department of Energy; the University of Chicago.
† hannahhu@uchicago.edu

ISBN: 978-3-95450-227-1 ISSN: 2673-5490 doi:10.18429/JACoW-IPAC2022-TUPOTK035

CVD Nb_3Sn-ON-COPPER SRF ACCELERATOR CAVITIES *

G. Gaitan†, P. Koufalis, M. Liepe, Cornell University, 14853 Ithaca, NY, USA
S. R. McNeal, V. Arrieta, Ultramet, 91331 Pacoima, CA, USA

Abstract

Nb_3Sn is the most promising alternative material for achieving superior performance in Superconducting Radio-Frequency (SRF) cavities, compared to conventional bulk Nb cavities now used in accelerators. Chemical vapor deposition (CVD) is an alternative to the vapor diffusion-based Nb_3Sn growth technique predominantly used on bulk niobium cavities now and may enable reaching superior RF performance at reduced cost. In collaboration with Cornell, Ultramet has developed CVD process capabilities and reactor designs to coat copper SRF cavities with thick and thin films of Nb and Nb_3Sn. In this paper, we present our latest research efforts on CVD Nb_3Sn-on-copper SRF cavities, including RF performance test results from two 1.3 GHz SRF cavities coated by Ultramet.

INTRODUCTION

Nb_3Sn is the most promising material for next-generation SRF cavities, as it can reach a T_c as high as 18 K and has the potential to double the gradients achieved by Nb [1]. Achieving higher operating gradients would decrease overall length and cost, while a high T_c would lead to an important reduction in cryogenic costs.

A vapor diffusion-based growth process for Nb_3Sn has given the best RF results from current growth methods [2], but it still performs well below the ultimate predicted limit of this material. Defects and surface roughness are limiting factors of these films so exploring alternative Nb_3Sn growth methods is important for improving performance beyond current limits.

The SRF Group at Cornell tested two 1.3 GHz single-cell SRF cavities. They are comprised of copper substrates with thin-film interior surface coatings of niobium interlayer/CTE(coefficient thermal expansion)-bridge and Nb_3Sn formed via chemical vapor deposition (CVD). The coating was performed by industry partner Ultramet using unique CVD precursor materials developed by researchers at Florida State University.

The copper cavity substrates were fabricated by Niowave (welded) and Bailey Tool (seamless). The high thermal conducting copper substrates were used to promote efficient heat dissipation for added thermal stability [3] and reduce per-cavity Nb requirements. Detailed RF performance test results are presented for the two cavities identified as SN 38-39 (welded) and SN 4 (seamless).

OBSERVATIONS FOR THE CVD COATING

Ultramet was able to achieve Nb_3Sn coatings on coupons ($\approx .75$ " $\times .75$ ") with a Sn content of 24 – 25% using the processing developed during this project. However, scaling up the Nb_3Sn CVD process to obtain coatings with a consistent 24 – 25% Sn content over large surface areas (e.g.: ILC cavities) has been found to be challenging. This is reflected in the RF test results presented below.

Both cavities had some degree of substrate surface texture/terrain issues/distress that might explain the low quality factors discussed below. This also encourages further copper cavity substrate manufacturing process and conditioning process development. Annealing at high temperatures might improve the surface structure, but the low melting point of copper makes that difficult. The Nb_3Sn coating had a crack in the beam tube section of SN 38-39. When Ultramet performed Nb_3Sn coatings directly on bare copper cavities (no CVD Nb interlayer) early in the project, there were no cracks in the Nb_3Sn coating. This might be explained by a much thicker coating of Nb_3Sn of $\approx$ 50-100 μm initially, versus the current thickness, 13-25 μm of Nb_3Sn on the surface. This crack might suggest the CVD Nb interlayer was too thin in the latest coating in that particular section, which is an issue that can be fixed with more process development. The CVD Nb interlayer was intended to function as a CTE-bridge to relieve stress between coating and substrate.

An optimized copper-Nb_3Sn ILC cavity (even with a thin CVD Nb interlayer) would reduce the per-cavity Nb raw material requirements by over 90% as compared to bulk Nb cavities.

Figure 1: SN 38-39 cavity on the RF testing insert under vacuum.

* This work was supported by the DOE SBIR award DE-SC0017902 to Ultramet and by U.S. National Science Foundation under Award PHY-1549132, the Center for Bright Beams
† gg465@cornell.edu

ISBN: 978-3-95450-227-1 ISSN: 2673-5490 doi:10.18429/JACoW-IPAC2022-TUPOTK036

STUDY OF CHEMICAL TREATMENTS TO OPTIMIZE NIOBIUM-3 TIN GROWTH IN THE NUCLEATION PHASE *

L. Shpani†, S. Arnold, G. Gaitan, M. Liepe, Z. Sun,
Cornell Laboratory for Accelerator-Based ScienceS and Education (CLASSE), Ithaca, NY, USA
T. Arias, M. Kelley, N. Sitaraman, Cornell University, Ithaca, NY, USA

Abstract

Niobium-3 tin (Nb_3Sn) is a high-potential material for next-generation Superconducting Radiofrequency (SRF) cavities in particle accelerators. The most promising growth method to date is based on vapor diffusion of tin into a niobium substrate with nucleating agent tin chloride ($SnCl_2$). Still, the current vapor diffusion recipe has significant room for realizing further performance improvement. We are investigating how different chemical treatments on the niobium substrate before coating influence the growth of a smooth and uniform Nb_3Sn layer. More specifically, this study focuses on the interaction between the $SnCl_2$ nucleating agent and the niobium surface oxides. In this paper, we present preliminary results of the comparison of the effect of different chemical treatments (with different pH values) on the tin droplet distribution on niobium after the nucleation stage of coating.

INTRODUCTION

Niobium-3 tin is a promising material for next-generation SRF cavities, due to its higher critical temperature and higher superheating field in comparison to other SRF materials. Many labs, including Cornell, Fermi Lab, Jefferson Lab, and KEK have continuing research and development projects focusing on improving Nb_3Sn growth. [1–9] The most promising growth method to date is based on vapor diffusion of tin into a niobium substrate with nucleating agent of tin chloride. The oxide layer of Nb_2O_5 on the surface of niobium plays an important role in the binding of the nucleating agent ($SnCl_2$) [2, 7, 10], and this research focuses precisely on optimizing the oxide layer to get a more uniform distribution of tin after the nucleation step.

Previous studies have shown Nb_2O_5 to be a very active catalyst for many processes as a result of its surface acidity and molecular binding sites [11, 12] . Different Nb_2O_5 surface structures and acidities have been shown to have varying abilities to bind to other molecules, making some structures better suited for our nucleation process. There are many ways to adjust the surface acidity, including water, solvent mixes, and surfactants. Temperature treatments can be used to modify the structure of the binding sites, with a higher temperature treatment leading to lower surface acidities.

In this study, we used varying solvent mixes to vary the surface acidity before nucleation, and changed the nucleation temperature to observe its influence on the binding of $SnCl_2$ onto our Nb_2O_5 surface. The ideal chemical treatment will yield a uniform and dense tin droplet distribution. After the nucleation step, we expect to see tin droplets in the nucleation sites, as well as a very thin Sn-Nb film. [7]

* Work supported by the National Science Foundation under Grant No. PHY-1549132, the Center for Bright Beams
† ls936@cornell.edu

PREPARATION OF SAMPLES

Pre-Coating Chemical Treatments

All samples were electropolished and anodized before the chemical treatments. The list of treatments and their corresponding pH value is shown in Table 1, with sample −1 being the non-treated sample.

Table 1: Summary of Chemical Treatments

Sample #	Chemical Treatment	pH
-1	-	
0	H_2O	
1	H_2O_2	4.7
2	$NaOH$	11
3	$NaOH$	9
4	NHO_3	3
5	NHO_3	5
6	HCl	5
7	HCl	3

Figure 1: Samples after chemical treatments, before coating.

Samples 0 through 8 are shown in Fig.1 starting from the top left, after the chemical treatments and before the coating. Note that they are all slightly different colors, due to the different chemical treatments.

ISBN: 978-3-95450-227-1 ISSN: 2673-5490 doi:10.18429/JACoW-IPAC2022-TUPOTK037

STATUS UPDATE ON CORNELL'S SRF COMPACT CONDUCTION COOLED CRYOMODULE*

N.A. Stilin†, A. Holic, M. Liepe, T. O'Connell, J. Sears, V.D. Shemelin and J. Turco
Cornell Laboratory for Accelerator-Based ScienceS and Education (CLASSE)
Ithaca, NY 14853, USA

Abstract

A new frontier in Superconducting RF (SRF) development is increasing the accessibility of SRF technology to small-scale accelerator operations which are used in various industrial or research applications. This is made possible by using commercial cryocoolers as a cooling source, which removes the need for expensive liquid cryogenics and their supporting infrastructure. In addition, the use of Nb_3Sn-coated cavities allows for efficient operation at 4.2 K. Cornell University is currently developing a new cryomodule based on a conduction cooling scheme. This cryomodule will use two pulse tube cryocoolers in place of liquid cryogenics in order to cool the system. A new 1.3 GHz cavity has been designed with a set of four niobium rings welded at the equator and irises which allow for a direct thermal link between the cavity and cryocooler cold heads. The cavity will use two coaxial RF input couplers capable of delivering up to 100 kW total RF power for high-current beam operation. This coupler design was modified from the Cornell ERL injector couplers, including simplifications such as removing the cold RF window and most outer bellows, while retaining inner bellows for adjustable coupling.

INTRODUCTION

Reports from the U.S. DOE and national labs indicate that small-scale accelerators producing beams of a few MeV can be used for important applications in various fields such as medicine, environmental progress, national security and more [1, 2]. Although these operations would benefit from the vastly improved efficiency of SRF technology, the complexity and cost of the required liquid helium infrastructure quickly becomes prohibitive. However, the combination of current cryocooler technology and Nb_3Sn-coated cavities has opened a new path to utilizing SRF technology. Today's cryocoolers are capable of removing a couple watts of heat at 4 K [3], while steady improvements to Nb_3Sn coatings have produced cavities which operate reliably and efficiently at 4.2 K with accelerating fields relevant to the applications mentioned [4–10]. Therefore, demonstrating that Nb_3Sn cavities can successfully operate while being cooled with cryocoolers in place of liquid helium will represent a major step forward in making SRF technology accessible to small-scale industry applications.

Previous studies conducted at Cornell demonstrated the feasibility of this concept. These studies achieved the first-ever demonstration of a conduction-cooled SRF cavity operating continuously at 10 MV/m [11]. In addition, it was found that if the cryocooler is allowed to cool the system down freely, significant thermal gradients will be created across the cavity, leading to poor performance [12]. Therefore, controlling the cooldown is a requirement when using crycoolers for SRF applications. These studies also showed that placing heaters on the cavity irises provided the most precise and repeatable control of thermal gradients during cooldown [12]. We would like to acknowledge that important progress has also been made at Fermilab [13] and Jefferson Lab [14], in which different implementations of conduction cooling assemblies were examined.

Cornell is now designing a new compact cryomodule which will use two cryocoolers in place of liquid cryogenics. The system will have a single-cell 1.3 GHz Nb_3Sn-coated cavity powered by two coaxial couplers. The couplers will deliver a total of 100 kW RF power to a 100 mA beam with the cavity operating at 10 MV/m; see Table 1.

Table 1: Cryomodule Operating Specifications

Property	Value	Units
Frequency	1.3	GHz
Energy Gain	1	MeV
Max Current	100	mA
Max Power	100	kW

ACCELERATING CAVITY

The SRF cavity used in our cryomodule is based on the design for the 1.3 GHz 2-cell injector cavities from Cornell's ERL [15]. For the new cryomodule, the cavity has been modified to a single-cell design (see Fig. 1) and will be coated with Nb_3Sn to enable efficient 4.2 K operation. The primary additions to the cavity design are the Nb thermal intercept rings located outside of the cavity equator and irises. The equator ring design is inspired by Fermilab's study on a 650 MHz cavity [13]. The equator rings extract the cavity's primary heat load, while the newly-designed iris rings extract smaller heat loads and serve as mounting locations for heaters. All four rings can be seen attached to the cavity in the bottom-right image of Figure 1.

Thermal modelling was performed in Ansys to study the effectiveness of this design. This modelling includes the full beam line extending out to the vacuum vessel walls at

* This work was supported by U.S. DOE award DE-SC0021038 "Next Steps in the Development of Turn-Key SRF Technology," which supports the full development of a conduction cooling based cryomodule.
† nas97@cornell.edu

ISBN: 978-3-95450-227-1 ISSN: 2673-5490 doi:10.18429/JACoW-IPAC2022-TUPOTK038

NEXT GENERATION SRF CAVITIES AT CORNELL UNIVERSITY*

N. Verboncoeur†, R. D. Porter, M. Liepe, L. Shpani,
Cornell Laboratory for Accelerator Based Sciences and Education, Ithaca, NY, USA

Abstract

Our goal is to develop new materials and protocols for the growth and preparation of thin-film and layered superconductors for next generation SRF cavities with higher performance for future accelerators. We are working primarily with Nb_3Sn to achieve this goal, as well as other materials which aim to optimize the RF field penetration layer of the cavity. This contribution gives an update on our most recent Nb_3Sn simulations and cavity test results. A deeper insight into RF loss distribution and dynamics during cavity testing is gained using a new global high-speed temperature mapping system (T-Map).

INTRODUCTION

Nb_3Sn is well acknowledged as a promising material for the improvement of superconducting radio-frequency (SRF) cavity performance [1]. Its critical temperature of 18 K is nearly double that of Nb's, which is only 9.2 K, making for lower losses during operation. Additionally, the superheating field of Nb_3Sn is ~425 mT compared to ~220 mT for pure Nb [2], meaning that much higher accelerating gradients are achievable with the theoretical potential to reach 90 MV/m [3, 4]. Improvements to the SRF community's understanding of Nb_3Sn and how to optimize it's usage continues to be a priority for the SRF community. Many labs, including Cornell, Fermi Lab, Jefferson Lab, and KEK have continuing research and development projects focusing on Nb_3Sn [5–7].

Our goal is to develop new protocols for the growth and preparation of thin-film and layered superconductors for next generation SRF cavities with higher performance for future accelerators. We present here our latest work on Nb_3Sn cavities produced using a vapor diffusion based coating process. Achieving higher accelerating gradients and/or a lower RF dissipation would have a ripple effect of advancements in other fields from fundamental particle physics to medical accelerators to food sterilization.

THE CORNELL HIGH SPEED GLOBAL TEMPERATURE MAPPING SYSTEM

Cornell uses the a high-speed global temperature mapping system (T-Map) to see in real time what temperature fluctuations are occurring on the surface of a cavity during RF testing. This system uses over 600 Allen-Bradley carbon resistors to monitor local temperatures at a resolution on the order of 100 μK at helium bath temperatures of 2 K. The high-speed DAQ electronics developed for this system are able to read all of the sensors simultaneously at a maximum sample rate of 50k samples/s [8, 9].

The T-Map is used to take short exposure snapshots and dynamic long exposures of heating events that the cavity experiences during RF testing. These can capture when a cavity ceases superconductivity (quenches), giving us insight into where and why the cavity is heating up. We are interested in better understanding quench mechanisms so that they can be resolved and higher fields achieved. Nb_3Sn cavity performance is still well below the theoretical limit. An example of such a quench is shown in Fig. 1, where the initial limiting mechanism is multipacting.

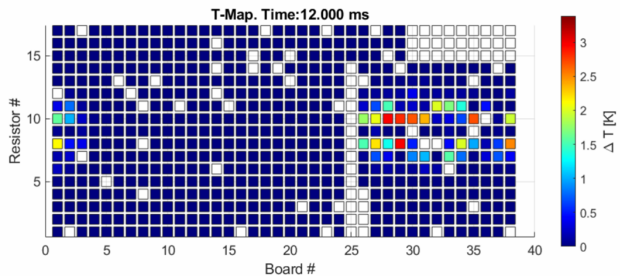

Figure 1: Example of a suspected multipactor quench captured on the T-Map.

Later in the same test, the same cavity that produced the multipacting in Fig. 1 changed to a quench caused by a defect on the RF surface of the cavity as seen in Fig. 2 caused by a defect on the RF surface of the cavity. We were interested in better understanding what the T-Map was seeing, so we turned to simulations to see if we could create a reliable model.

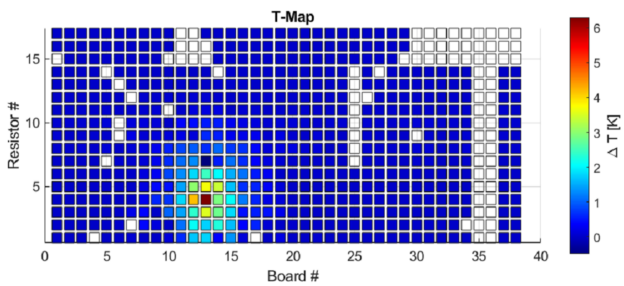

Figure 2: Example of a quench due to a surface defect captured on the T-Map.

THERMAL SIMULATIONS

In order to better understand the quench mechanisms shown by T-Map studies, thermal models of the Nb_3Sn film and Nb substrate were done using a simulation of a Nb_3Sn–Nb substrate – Nb_3Sn layered surface, as shown in

* Work supported by U.S. DOE grant No. DE-SC0008431
† nmv39@cornell.edu

ISBN: 978-3-95450-227-1 ISSN: 2673-5490 doi:10.18429/JACoW-IPAC2022-TUPOTK040

DESIGN OF THE ELECTRON ION COLLIDER ELECTRON STORAGE RING SRF CAVITY*

J. Guo†, E. Daly, J. Henry, J. Matalevich, G.-T. Park, R. A. Rimmer, H. Wang, S. Wang
JLAB, Newport News, VA, USA
D. Holmes, K.S. Smith, W. Xu, A. Zaltsman, BNL, Upton, NY, USA

Abstract

The Electron Ion Collider (EIC) under construction at Brookhaven National Laboratory is a high luminosity collider as the next major research facility for the nuclear physics community. Among the numerous RF subsystems in the EIC, the electron storage ring (ESR) fundamental RF cavities system is one of the most challenging. This system will handle a high beam current of up to 2.5 A and replenish up to 10 MW of beam power losses from synchrotron radiation (SR) and high-order modes (HOM). Variable coupling is required in the cavities due to the wide range of required total RF voltage and beam current combinations. In this paper, we will present the status of the design and future plans.

EIC ESR CAVITY DESIGN

EIC ESR is a high current electron storage ring required to operate at various beam energy (5-18GeV) and beam current (0.23-2.5A average, with one abort gap) [1, 2]. Up to 10 MW of beam power will be provided by 17-18 SRF elliptical cavities of 591 MHz, installed in single phase. The required total cavity voltage and beam current ratio for different operation energies results in the wide range of cavity Qext (factor of ~15) if optimal coupling/detuning is desired. Even if we allow some reflected RF power for the low energy operations when extra RF power is available, a factor of 6-10 variation in the Qext is still needed for the conventional operation with all cavities in the same focusing phase.

One possibility is to operate some cavities in reversed or defocusing phase (RPO). For low energy operations, this configuration can increase the single cavity voltage while keeping the vector sum of voltage the same. Transient beamloading induced by the abort gap for low energy/high current operations can also be mitigated, in combination of a low R/Q design. This concept has been demonstrated at SuperKEKB [3], although long term operation risks need to be studied further. With RPO, it's possible to operate the ESR cavities at fixed Qext of ~3.5×10^5, as shown in Table 1. We design the cavity with two coax fundamental power couplers (FPCs) using pringle shaped tips and nominal Qext of 3.5×10^5 per cavity, and use external stub tuners to adjust Qext as needed.

The baseline of the cryomodule design contains a single symmetric cavity, with beampipes tapered to 75 mm radius to match the largest available gate valve possible to fit in the space available for the ESR. Two single-cavity cryomodules will be arranged in one straight between two quadrupole magnets. The possibility to integrate two cavities in a single cryomodule is still under study, which may provide further space and cost savings.

The ESR cavity started with a symmetric design by F. Marhasuser, which is currently the baseline in the EIC CDR [1]. Recently we proposed an asymmetric design. On one side of the beampipe it has the same 137 mm radius as the symmetric design and tapers to 75 mm, and a 75 mm radius beampipe on the other side without tapering. Figure 1 compares the geometry of the two designs. The asymmetric design has similar figure of merits as the symmetric design, as shown in Table 2. The opened up 137 mm radius beampipe helps to lower the fundamental mode R/Q as well as to damp HOMs in both designs. However, the asymmetric design is obviously more compact longitudinally; it also provides more room for the coupler, which will determine the transverse size of the cryomodule.

Each ESR cavity will use two beamline absorbers (BLAs) to damp the HOM. The BLA is assumed to be a cylindrical warm SiC absorber SC35 from CoorsTek, using the shrink-fit fabrication technique, similar to the BLA used by APS-Upgrade but in a larger radius [4, 5]. In the asymmetric design, the 75 mm radius BLA is about half the length of the 137 mm BLA and provides similar or better attenuation. Figure 2 shows the CST model of an asymmetric version of the cavity with FPCs include the doorknob transitions, Qext tuning stubs, and BLAs.

The maximum voltage of each ESR cavity is 4 MV, and the gradient is 15.8 MV/m, which is reasonable for a high current SRF cavity.

Table 1: Estimate of ESR Cavity Power and Qext for Different Operation Cases, Assuming 18 Cavities in Total

Beam energy		18GeV	10GeV	5GeV
Beam current (A, exc gap)		0.271	2.841	2.841
Beam current (A, average)		0.25	2.616	2.616
Beam power/cav (kW)		501.3	597	189.8
V total (MV)		61.5	21.7	9.84
All Focusing	Vcav (MV)	3.42	1.21	0.55
	Qext per cav	3.2E5	3.3E4	2.4E5
	Pfwd/FPC, kW	311.7	373.1	392.7
RPO, Focus Cav	Vcav (MV)		3.73	3.9
	Qext		3.5E5	3.5E5
	Pfwd/FPC(kW)		373.8	161.8
RPO, Defocus Cav	Vcav (MV)		3.9	3.65
	Qext		3.5E5	3.5E5
	Pfwd/FPC, kW		373.1	151.6
	# of def cav		6	8

Margins added for beam current (higher than nominal)
Beam power includes SR and HOM losses

* Authored by Jefferson Science Associates, LLC under U.S. DOE Contract No. DE-AC05-06OR23177, with additional support from U.S. DOE Award Number DE-SC-0019287

†jguo@jlab.org

ISBN: 978-3-95450-227-1 ISSN: 2673-5490 doi:10.18429/JACoW-IPAC2022-TUPOTK042

CHALLENGES TO RELIABLE PRODUCTION NITROGEN DOPING OF Nb FOR SRF ACCELERATING CAVITIES*

C. E. Reece†,1, J. W. Angle[2], E. M. Lechner[1], A. D. Palczewski[1], F. A. Stevie[3], M. J. Kelley[1,2]
[1] Thomas Jefferson National Accelerator Facility, Newport News, VA, USA
[2] Virginia Polytechnic Institute and State University, Blacksburg, VA, USA
[3] Analytical Instrumentation Facility, North Carolina State University, Raleigh, NC, USA

Abstract

Over the last several years, alloying of the surface layer of niobium SRF cavities has been demonstrated to beneficially lower the superconducting RF surface resistance. Nitrogen, titanium, and oxygen have all been demonstrated as effective alloying agents, occupying interstitial sites in the niobium lattice within the RF penetration depth and even deeper, when allowed to thermally diffuse into the surface at appropriate temperatures. The use of nitrogen for this function has been often termed "nitrogen doping" and is being applied in the LCLS-II and LCLS-II HE projects. We report characterization studies of the distribution of nitrogen into the exposed niobium surface and how such distribution is affected by the quality of the vacuum furnace environment in which the doping takes place, and the complexity of nitride crystal growth on different grain orientations of surface niobium. Using state-of-the-art quantification methods by dynamic secondary ion mass spectrometry (SIMS) depth profiling in niobium, we identify several phenomena involving furnace-sourced contamination. We also highlight a potential issue with N_2 flow constraints from the flange "caps" used during heat treatments.

INTRODUCTION

The thermal diffusion of interstitial nitrogen into the surface of Nb has been demonstrated to yield reduced rf surface resistance under conditions that are very useful for CW SRF accelerator applications. This alloying of the Nb lattice, commonly called "nitrogen doping", reduces the electron mean free path within the rf penetration depth and is also strongly suspected of inhibiting the formation of lossy hydrides at low temperatures.

The common process for introducing nitrogen into the niobium surface is via provision of low-pressure N_2 gas at 800 °C into a vacuum furnace at the end of a hydrogen degassing run. Several exposure-time (min)/subsequent anneal-time (min) process combinations have been tried, the most common of which are 2/6, 2/0, and 3/60. The first was chosen for use in LCLS-II [1], the second for LCLS-II HE [2]; the third has seen limited use, but yielded the best performing 9-cell cavities to date (see Fig. 1).

While the basic process has proved stable enough for major project exploitation, variations in performance obtained by different cavity processors motivated research into the sources of process vulnerabilities. We report here the fruit of this research.

* Work supported by U.S. DOE contract DE-AC05-06OR23177.
† reece@jlab.org

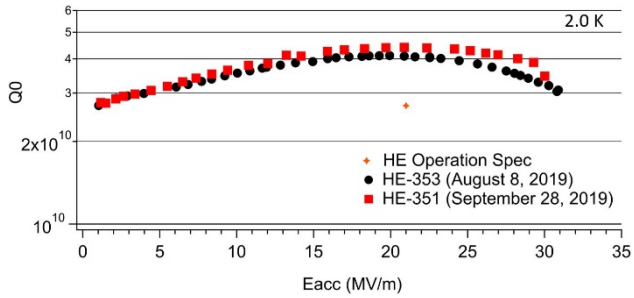

Figure 1: Best-performing N-doped 9-cell cavities to date. Cavities were fabricated by Zanon, with all chemistry, 3/60 doping, 10 µm EP, cleanroom work, and testing performed at Jefferson Lab.

A key feature of this nitrogen doping process is that the desirable interstitial nitrogen is largely mediated by the growth of crystalline nitrides on the niobium surface. The details of the near surface growth dynamics of these nitrides is complex—depending on Nb grain orientation, grain boundary angles, and also surface contamination.

To first order, the standard process removes the nitrides decorating the niobium surface via a shallow electropolish. This presents one of the process optimization challenges: how much material to remove to leave "good" quality surface while still leaving behind sufficient Nb with beneficial interstitial N content. The projects made empirical choices that meet project requirements. Analysis of comparably treated samples, however, reveals complexities that contribute to performance variabilities.

Another open question has been the source of performance differences when nominally the same process is applied at different institutions. We would like to understand the source of performance variability that results from use of different vacuum furnaces. The designs of furnaces in use vary considerably. We examined differences in residual surface contamination found on samples and correlated that with resultant nitrogen concentration profiles. The results highlight the need for minimized carbon sources and well-designed "caps" to intercept evaporative metals, particularly those that derive from prior use of the furnace with other materials.

This research has been enabled by two parallel developments, the establishment of high-quality standard samples with appropriate grain size and surface flatness to enable high-quality dynamic SIMS measurements including implant standards, and the refinement of state-of-the-art dynamic SIMS characterization techniques via the PhD work of Jonathan Angle at Virginia Tech [3].

ISBN: 978-3-95450-227-1 ISSN: 2673-5490 doi:10.18429/JACoW-IPAC2022-TUPOTK044

PRELIMINARY RESULTS OF MAGNETIC AND TEMPERATURE MAP SYSTEM FOR 3 GHz SUPERCONDUCTING RADIO FREQUENCY CAVITIES*

I. Parajuli†, B. Khanal, G. Ciovati[1], J. Delayen and A. Gurevich, Old Dominion University, Norfolk, USA
[1]also at Jefferson Lab, Newport News, USA

Abstract

Superconducting radio frequency (SRF) cavities are fundamental building blocks of modern particle accelerators. When we cool these cavities at cryogenic temperature ~2 – 4 K, we can get optimum performance by minimizing RF losses on the inner cavity surface. However, temperature-independent residual losses in SRF cavities cannot be prevented entirely. One of the leading sources of residual losses in SRF cavities is trapped magnetic flux. The flux trapping mechanism depends on different surface preparations and cool-down conditions. We have designed, developed, and commissioned a combined magnetic (B) and temperature (T) mapping system using anisotropic magneto-resistance (AMR) sensors and carbon resistors to study the flux trap mechanism in 3 GHz single-cell niobium cavities. In this contribution, we present the preliminary results of the newly commissioned B & T mapping system.

INTRODUCTION

Niobium (Nb) is an elemental superconductor used to fabricate cavities, the fundamental building block of modern particle accelerators. Superconducting radio frequency (SRF) cavities are resonators, which can be excited by the rf field to get the maximum electric field along their axis. SRF cavities operate at cryogenic temperatures 2-4 K to reduce the temperature-dependent, BCS surface resistance. However, the temperature-independent residual resistance provides a lower limit to the quality factor, Q_0, of the SRF cavities. There are several contributors to the residual losses [1, 2], a major one being the magnetic flux trapped on the cavity surface. To understand the mechanism of trapped flux on the cavity surface, diagnostic tools are in high demand.

We have designed, developed, and commissioned a combined magnetic and temperature map (B&T map) system using anisotropic magneto-resistance sensors (AMR) and carbon resistors to study the flux trap mechanism in 3 GHz single-cell niobium cavities. This contribution presents the preliminary results of the newly commissioned B & T mapping system.

* Work supported by NSF Grant 100614-010. Jlab work is supported by Jefferson Science Associates, LLC under U.S. DOE Contract No. DE-AC05-06OR23177.
† ipara001@odu.edu

EXPERIMENTAL SETUP AND PROCEDURE

Thermometry System

The temperature map system was designed based on the system originally developed at Cornell University for 1.5 GHz cavities [3] and adopted at Jefferson Lab for 1.3 GHz and 1.5 GHz cavities [3, 4]. There are 88 Allen-Bradley carbon resistors (100 Ω) in the T-map system, which are used as resistance-temperature devices (RTD). Their sensitivity is ~10 Ω/mK at 2 K. Details about the fabrication of the thermometer can be found in [3, 4]. Eight printed circuit boards (PCB) of G10 material are designed and machined to place the 11 thermometers in contact with the cavity surface. Figure 1 shows a picture of a thermometer board. The spacing between each thermometer is ~1 mm. The thermometers were excited by ~5 μA current at 2 K so that the typical voltage drop across 7 kΩ resistors is ~35 mV.

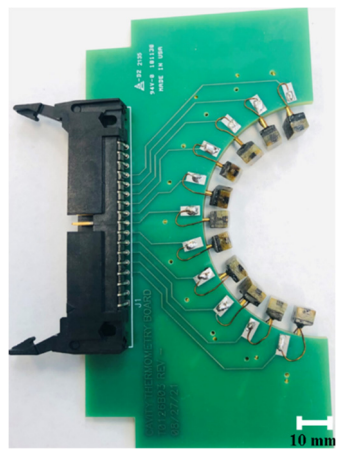

Figure 1: Complete thermometry board.

The SCXITM system from National Instrument was used to measure the voltage across 88 thermometers. Four SCXI-1102 modules are connected to a single SCXI-1001 chassis. Each SCXI-1102 module is capable of multiplexing 32 differential inputs. A Keithley 2400 source meter was used to provide the excitation voltage to the thermometers. The helium bath temperature was measured as the average of the temperature measured with four calibrated Cernox sensors and a Lakeshore 218 temperature monitor.

Magnetometry System

Figure 2 shows the schematic diagram of a magnetic field sensor assembly. It consists of two AMR sensors [5-

ISBN: 978-3-95450-227-1 ISSN: 2673-5490 doi:10.18429/JACoW-IPAC2022-TUPOTK045

MAGNETIC FIELD MAPPING OF 1.3 GHz SUPERCONDUCTING RADIO FREQUENCY NIOBIUM CAVITIES*

I. Parajuli†, G. Ciovati[1], J. Delayen, A. Gurevich, Old Dominion University, Norfolk, USA
[1]also at Jefferson Lab, Newport News, USA

Abstract

Niobium is the material of choice for building superconducting radiofrequency (SRF) cavities, which are fundamental building blocks of modern particle accelerators. These cavities require a cryogenic cool-down to 2 – 4 K for optimum performance minimizing RF losses on the inner cavity surface. However, temperature-independent residual losses in SRF cavities cannot be prevented entirely. One of the significant contributors to residual losses is trapped magnetic flux. The flux trapping mechanism depends on different factors, such as surface preparations and cool-down conditions. We have developed a diagnostic tool: a magnetic field scanning system (MFSS) using Hall probes and anisotropic magneto-resistance sensors to study the spatial distribution of trapped flux in 1.3 GHz single-cell cavities. The first results from this newly commissioned system revealed that the trapped flux on the cavity surface might redistribute with increasing RF power. The MFSS was also able of capturing significant magnetic field enhancement at specific cavity locations after a quench.

INTRODUCTION

Superconducting radio frequency (SRF) cavities are fundamental building blocks of modern particle accelerators. Niobium (Nb) is an elemental superconductor that is most commonly used to build SRF cavities, which operate at liquid helium temperature, 2-4 K. By operating them at such low temperatures the surface resistance due to quasiparticle oscillation under an RF field can be significantly reduced. However, temperature-independent surface resistance referred to as residual resistance is also present, limiting the maximum achievable quality factor, Q_0, of SRF cavities. There are several contributors to the residual losses [1, 2]. A significant one is magnetic flux trapped on the cavity surface. To understand the contribution of trapped flux on residual resistance a diagnostic tool is in high demand. We have designed, developed, and commissioned a magnetic field scanning system (MFSS) that can be used to study trapped flux in SRF cavities. MFSS was developed to use two types of magnetic field sensors: a) Hall probes and b) Anisotropic magnetoresistive (AMR) sensors. Details about the AMR sensor can be found in references [3-10]. The choice of sensors in the MFSS setup is discussed in Ref. [11]. In this contribution, we will discuss the initial results of the newly commissioned MFSS.

* Work supported by NSF Grant 100614-010. Jlab work is supported by Jefferson Science Associates, LLC under U.S. DOE Contract No. DE-AC05-06OR23177.
† ipara001@odu.edu.

EXPERIMENTAL SETUP AND PROCEDURE

Figure 1(a) shows the experimental setup of MFSS. It consists of two brackets supported by a rotating gear system. The gear system is driven by a stepper motor connected to a rotary feedthrough outside the cryostat and allows moving the brackets one full turn in either direction around the cavity. Limit switches are installed to determine the initial and final positions. The angular resolution of the system is 6.8×10^{-3} degrees, corresponding to 13 µm. The initial design of the MFSS made use of a cryogenic stepper motor on each bracket to allow moving the sensors along the cavity contour in the vertical direction [12]. However, the movement of the sensors below ~100 K was unreliable, and we opted for a fixed number of sensors in each bracket. One bracket holds eight Hall probes (HPs) as shown in Fig. 1(c), such that they can measure the radial magnetic field

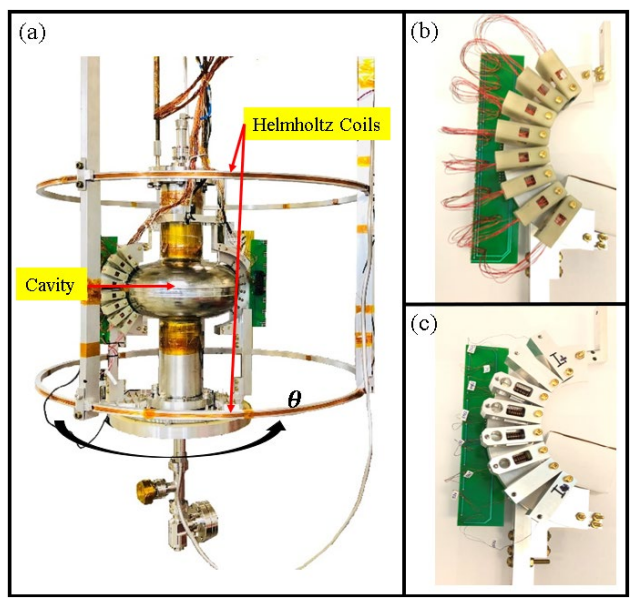

Figure 1: MFSS setup assembled on a 1.3 GHz niobium cavity along with Helmholtz coils (a), AMR sensors attached on a bracket (b), and Hall probes attached on another bracket (c).

on the cavity surface. The other bracket consists of sixteen AMR sensors as shown in Fig. 1(b). Out of sixteen AMR sensors, eight AMR sensors can detect the tangential component of the magnetic field (AMRt), and the remaining eight can measure the radial component of the magnetic field on the cavity surface (AMRr). Each AMRr sensor is ~3 mm away from the corresponding AMRt sensor. The sensors are located in the high RF magnetic field region of the cavity, with sensor No. 1 being the farthest below the

ISBN: 978-3-95450-227-1 ISSN: 2673-5490 doi:10.18429/JACoW-IPAC2022-TUPOTK048

OPTIMIZATION OF A 600 MHz TWO-CELL SLOTTED WAVEGUIDE ELLIPTICAL CAVITY FOR FCC-ee

S. Gorgi Zadeh*, F. Peauger. I. Syratchev, O. Brunner, CERN, Geneva, Switzerland

Abstract

The radio-frequency (RF) system of the future circular lepton collider (FCC-ee) must cope with different machine parameters ranging from Ampere-class operation required for the Z-peak working point to the high-gradient operation for the $t\bar{t}$ threshold. The Superconducting Slotted Waveguide Elliptical cavity (SWELL) concept was recently proposed as an alternative to the challenging RF baseline design of the FCC-ee. In this paper, random optimization methods are used to minimize the peak surface magnetic field and the maximum longitudinal impedance of the higher order modes (HOM) of a two-cell 600 MHz SWELL cavity. In the next step, the waveguide slots are optimized to first have a smooth transition from the cavity to the slots to avoid large peak surface fields and second to achieve high transmission at dipole mode frequencies and low transmission at fundamental mode frequency while keeping the design compact.

INTRODUCTION

The strong wakefield effects in the radio frequency (RF) cavities of the Future Circular lepton Collider (FCC-ee) at the Z and W working points are one of the many problems facing the RF design of FCC-ee [1, 2]. A Superconducting Slotted Waveguide Elliptical cavity (SWELL) with two cells and four slots at 600 MHz is proposed in [3] as a possible efficient alternative for the baseline design of FCC-ee described in [4]. The SWELL geometry consists of four quadrants separated by narrow waveguide (WG) slots that provide strong damping of transversal higher-order modes (HOM). The SWELL cavity has several advantages compared to the standard elliptical cavities such as: heavy transversal mode damping via WG slots, easier access to the cavity surface for niobium coating, no welded joints at high magnetic field zones of the cavity, and a robust shape against microphonics. The SWELL design has very weak interaction with transverse-magnetic (TM) monopole modes, i.e., the fundamental mode (FM) and the monopole HOMs which can have a large longitudinal impedance. This paper aims to optimize the design of the SWELL cavity to untrap the longitudinal HOMs (thus eliminating the need for additional HOM couplers), minimize the peak surface magnetic field, and have strong damping of the dipole modes via WG slots.

ELLIPTICAL CAVITY OPTIMIZATION

The elliptical cavity forms the basis of the SWELL cavity and must be designed first. Parametrization of a two-cell elliptical cavity is shown in Fig. 1. The two cells are assumed to be identical and the inner and outer half-cells can have different shapes. Since the WG slots of the SWELL do not damp the longitudinal HOMs, we try to minimize the peak of the real part of the longitudinal impedance of the HOMs ($\Re(Z_{\parallel, f>f_{\mathrm{FM}}})$) when designing the elliptical cavity. Low $\max(\Re(Z_{\parallel, f>f_{\mathrm{FM}}}))$ normally degrades the normalized magnetic field on the cavity surface ($B_{\mathrm{pk}}/E_{\mathrm{acc}}$). Maintaining a low surface electromagnetic (EM) field is another critical design parameter, as surface fields are expected to enhance in the next step when WG slots are connected to the cavity. Thus, the following problem is formulated for the optimization of the elliptical cavity:

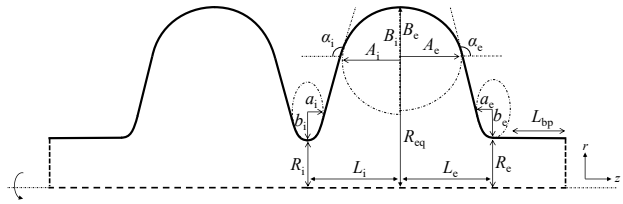

Figure 1: Parametrization of a two-cell elliptical cavity. In the simulations L_{bp} is assumed to be $4L_{\mathrm{i}}$.

$$\begin{aligned} \underset{\substack{R_{\mathrm{i}}, A_{\mathrm{i}}, B_{\mathrm{i}}, a_{\mathrm{i}}, b_{\mathrm{i}} \\ R_{\mathrm{e}}, A_{\mathrm{e}}, B_{\mathrm{e}}, a_{\mathrm{e}}, b_{\mathrm{e}}}}{\text{minimize}} \quad & \left(B_{\mathrm{pk}}/E_{\mathrm{acc}}, \max(\Re(Z_{\parallel, f>f_{\mathrm{FM}}}))\right) \\ \text{subject to} \quad & f_{\mathrm{FM}} = 600.00\ \mathrm{MHz}\ ,\ 130^\circ \geq \alpha_{\mathrm{i}} \& \alpha_{\mathrm{e}} \geq 90^\circ. \end{aligned} \tag{1}$$

The FM frequency (f_{FM}) is set fixed and wall angles are maintained in an acceptable range as constraints. Ten geometric parameters can be varied in the optimization problem. L_{i} and L_{e} are fixed at a quarter of the wavelength of the FM, and R_{eq} is used to tune f_{FM}. The geometric constraints in the optimization problem is given in Table 1.

Table 1: Lower Bound (LB) and Upper Bound (UB) of the Optimization Parameters

	(R_{i})	(R_{e})	(A_{i}, A_{e}, B_{i}, B_{e})	(a_{i}, a_{e}, b_{i}, b_{e})
LB [mm]	85	100	50	20
UB [mm]	105	105	110	80

To find a Pareto front between the two objective functions of Eq. (1), we used the genetic algorithm (GA) method as implemented in MATLAB's global optimization toolbox [5]. For each individual (candidate solution) of GA, a 1D optimization problem on R_{eq} was first solved to tune f_{FM} to 600 MHz, then an eigenvalue problem was solved with SLANS [6] to calculate f_{FM} and $B_{\mathrm{pk}}/E_{\mathrm{acc}}$, and a wakefield simulation was done with ABCI [7] to obtain $\max(\Re(Z_{\parallel, f>f_{\mathrm{FM}}}))$. The resulting Pareto front is shown in Fig. 2. In the next step, Monte-Carlo (MC) method was applied in the neighborhood of the selected geometry from the GA method (shown by

* shahnam.gorgi.zadeh@cern.ch

ISBN: 978-3-95450-227-1 ISSN: 2673-5490 doi:10.18429/JACoW-IPAC2022-TUPOTK049

UPGRADE OF ELSA'S BOOSTER SYNCHROTRON RF WITH A SOLID STATE POWER AMPLIFIER

M. Switka*, K. Desch, D. Elsner, F. Frommberger, P. Hänisch
Physics Institute, University of Bonn, Germany

Abstract

The 1.6 GeV booster synchrotron of the ELSA facility at the University of Bonn uses a DESY-type RF resonator which has been driven by a conventional klystron amplifier since its early days in 1967. The setup was modified to serve the ELSA stretcher ring as booster synchrotron in 1987, but the RF infrastructure was barely altered. As repairs of the reliable, but antiquated RF source became foreseeingly impossible due to the lack of spare part availability, the replacement of the klystron amplifier chain in favour of a state-of-the-art solid state amplifier was carried out. We describe the replacement and the operation experience with the new RF power amplifier.

INTRODUCTION

From 1967 to 1987 today's *booster* synchrotron of the ELSA facility was operated as 2.5 GeV machine serving nuclear physics experiments [1]. The RF system consisted of two 500 MHz DESY-type resonators powered by a single 40 kW CW klystron of type *F 2008* or *KAP 1216A*[1]. The RF was guided through $3\frac{1}{8}$" and *43-98* rigid coaxial lines towards both operating resonators through a "T-junction" splitter, before which the line impedance was pre-matched from 50 Ω to 25 Ω. In front of the cavity in each branch the RF was coupled via a *door-knob coupler* into a *WR*1800 waveguide, in which a 11 dB water-cooled ferrite isolator with insertion loss < 0.4 dB protected the source from reflections, e.g. when the beam loading changed with beam current or impedance mismatching occurred from cavity detuning.

Serving as 1.2 GeV injector for the ELSA storage ring [2], the synchrotron has been operated with a single cavity, fed through the original klystron and power transmission setup with decommissioned "T-junction". The original analogue low-level RF (LLRF) system remained operational, but the RF magnitude feed-forward generator was upgraded from analogue circuitry to a microcontroller-based version in 2011 [3]. A replacement of the klystron amplifier was recently carried out and first beam was accelerated using the new solid-state power amplifier in February 2022.

BOOSTER OPERATION SCHEME

The synchrotron is a strong focusing combined-function machine operating at a 50 Hz cycle. The magnetic guiding field is produced by a power supply combining AC and DC currents at a ratio of $I_{AC}/I_{DC} = 1.0689$. To increase the dynamic aperture at injection, the RF power is switched on with delay, allowing the orbit to drift away from the injection septum with increasing bending field. At the zero-crossing and at the peak field two trigger signals $t(B = 0)$ and $t(B_{max})$ are generated. The derivative of the magnetic field $\dot{B}$ is measured through a pick-up coil.

The required acceleration voltage U_{acc} corresponds to the increasing guiding field ($\propto \dot{B}$), the losses due to the emission of synchrotron radiation ($\propto B^4$) and beam loading:

$$U_{acc} = c_0 + c_{\dot{B}}\dot{B} + c_{B^4}B^4 + U_{bl} \,, \tag{1}$$

where c_0, $c_{\dot{B}}$ and c_{B^4} are machine-specific coefficients and U_{bl} is the induced beam load voltage. The operation scheme is visualized in Fig. 1 for different selectable extraction energies.

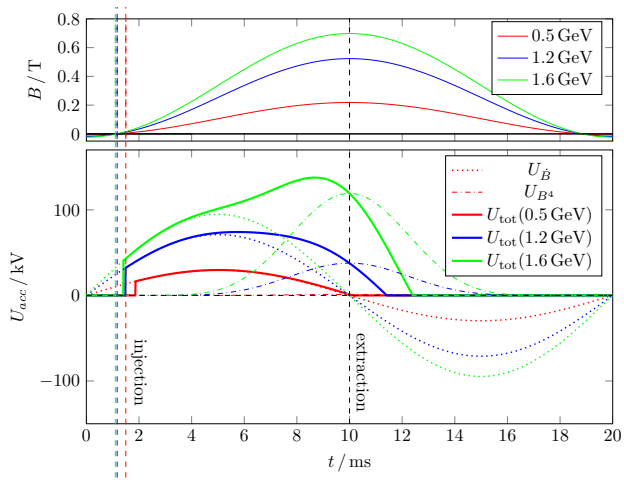

Figure 1: Magnetic guiding field (top) and corresponding feed-forward signal for the RF amplitude (bottom) for different extraction energies and negligible beam loading. The RF power remains switched off at injection and after extraction.

To accelerate $I_{beam} = 15$ mA to 1.2 GeV at an overvoltage factor of $q = U_{cav}/U_{acc} = 1.4$, amplifier RF power

$$P_{amp} = \frac{U_{cav}^2}{2R_s} + U_{acc} \cdot I_{beam} + P_{loss} \tag{2}$$

of ~ 1.7 kW peak is required for ideal booster operation. Therein, the cavity's shunt impedance is R_S =9 MΩ and we assume an ideal coupling coefficient of $\kappa \sim 1$, resulting in a loaded shunt impedance of $R_{SL} \approx R_S/2$. The power loss due to the 15 m long transmission line (including the ferrite isolator) is $P_{loss} < 0.5$ dB. For low current applications (e.g. serving the detector test community), nano-ampere beam currents are injected into the storage ring, which is achieved

* switka@physik.uni-bonn.de
[1] Thomson-CSF, France

ISBN: 978-3-95450-227-1 ISSN: 2673-5490 doi:10.18429/JACoW-IPAC2022-TUPOTK050

DEVELOPMENT OF Zynq SoC-BASED EPICS IOC FOR KOMAC REMOTE CONTROL SYSTEM*

Y.G. Song†, S.Y. Cho, J.H. Kim, S.P. Yun,
Korea Multi-purpose Accelerator Complex, Korea Atomic Energy Research Institute, Korea

Abstract

The KOMAC proton accelerator consists of a 100 MeV linear accelerator and beam lines for beam services. Devices of various form factors are used as control systems in accelerator control systems and beam diagnosis systems. With the recent upgrade of the control system, a Zynq-based control system has been developed that enables the latest technology and low cost. The Zynq-based DAQ system was developed by adopting Digilent's Zybo z7 series board and AD7605 analog-to-digital data acquisition system. The Zybo z7 is an embedded software and digital circuit development board built around the Xilinx Zynq-7000 family. The Zynq is based on Xilinx All Programmable System-on-Chip (AP SoC) architecture, which tightly integrates a dual-core ARM Cortex-A9 processor with Xilinx7-series Field Programmable Gate Array (FPGA) logic. The AD7605 is a 4-channel and 16bit ADC with 300 kSPS on all channels. The Zynq SoC-based DAQ system will be used for beam feedback control and RF signal monitoring at KOMAC. This paper introduces the development of configurations for the development of Zynq-based control systems, programmable Logic (PL) builds, and Linux and EPICS porting.

INTRODUCTION

The KOMAC linac and multi-beam lines were designed to provide users with a proton beam under various beam conditions. Representative specifications of the KOMAC linac are maximum beam energy of 100 MeV, and peak beam current of 20 mA, and the adjustable repetition rate is up to 120 Hz. The KOMAC has four beam extraction points at 20 and 10 MeV for proton beam utilization [1].

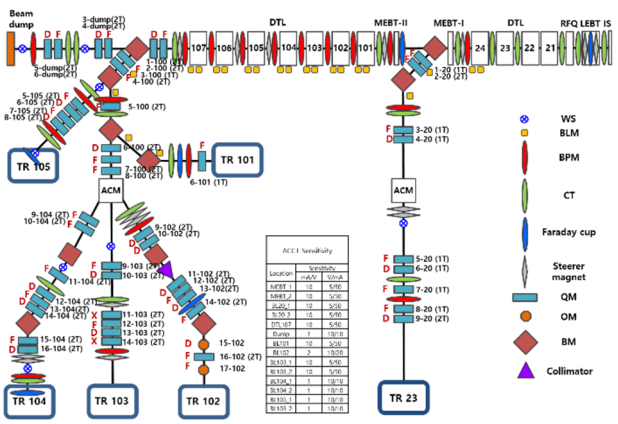

Figure 1: Beam Diagnostic Layout installed on 100 MeV Linac and beam lines.

The accelerated proton beam from the linac is transmitted to the target room via the beam lines. Figure 1 illustrates the beam diagnostic systems located on the Linac and beamlines. Various diagnostic equipment for beam diagnosis are used in linear accelerators and beam lines. The control system processes beam signals from the 100-MeV linac and beam lines and support remote access. Then the beam waveform and beam parameters are visualized in real time. The beam diagnostic equipment in the target compartment was also equipped with a Beam Position Monitor (BPM) and an AC Current Transformer (ACCT). Figure 2 shows the equipment of the radiation testing facilities.

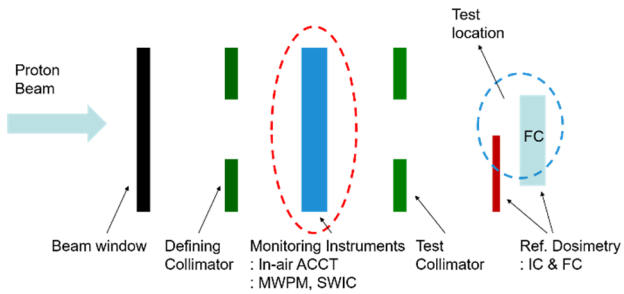

Figure 2: Equipment in radiation impact testing facilities.

When irradiating beams in irradiation test facilities, AC current transformer and faraday cup are used as beam diagnostic equipment to measure beam current. The beam user is required to monitor the accumulated amount of irradiation in real time. The configuration diagram of the system for integrated control of these devices is shown in the Fig. 3 [2].

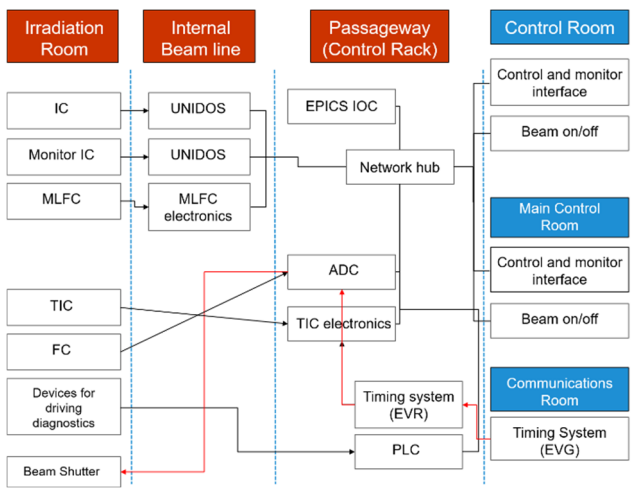

Figure 3: Integrated control interface for target room.

* Work supported through KOMAC operation fund of KAERI by the Korea government (MSIT) (No. 524320-22)
† ygsong@kaeri.re.kr

ISBN: 978-3-95450-227-1 ISSN: 2673-5490 doi:10.18429/JACoW-IPAC2022-TUPOTK051

DESIGN STUDIES ON A HIGH-POWER WIDE-BAND RF COMBINER FOR CONSOLIDATION OF THE DRIVER AMPLIFIER OF THE J-PARC RCS

H. Okita*, F. Tamura, M. Yamamoto, M. Nomura, T. Shimada, M. Yoshii, C. Ohmori, Y. Sugiyama, K. Hasegawa, K. Hara, J-PARC Center, JAEA & KEK, Tokai-mura, Japan
M. M. Paoluzzi, CERN, Geneve, Switzerland

Abstract

A power upgrade of the existing 8-kW solid-state driver amplifier is required for the acceleration of high intensity proton beams on the J-PARC 3-GeV Rapid Cycling Synchrotron. The development of a 25-kW amplifier with gallium nitride (GaN) HEMTs, based on 6.4-kW modules is ongoing. The combiner is a key component to achieve such a high output power over the wide bandwidth required for multi-harmonic RF operation. This paper presents the preliminary design of the combiner. The circuit simulation setup and results, including the realistic magnetic core characteristics and frequency response of the cable, are reported.

INTRODUCTION

In the J-PARC 3-GeV Rapid Cycling Synchrotron (RCS), the consolidation of the amplifier chain of the RF system is desired [1]. The solid state amplifier is one of the important components of the amplifier chain. The output power and bandwidth of the existing solid state amplifier are 8 kW and 450 kHz–5.1 MHz, respectively. For the high power beam acceleration, improvements in both the output power and bandwidth are desired.

The development of the 25-kW amplifier with gallium nitride (GaN) HEMTs is ongoing. The target bandwidth is 100 kHz–10 MHz. The 25-kW amplifier consists of four 6.4-kW amplifier modules and one 25-kW combiner as shown in Fig. 1. In the current design, the bandwidth of the 6.4-kW amplifier module sufficiently covers our requirements. Hence, the realization of the high power combiner with the target bandwidth is the key of the development of the amplifier.

Transmission line transformers (TLTs) are the primary component of the 25-kW combiner. TLTs have wide bandwidths and high transmission efficiencies. A typical TLT consists of magnetic cores and transmission lines. To realize a wide bandwidth, it is necessary to design TLTs with a short cable length and a large number of winding turns.

Beyond 1 kW, the TLT design is challenging. Since high power coaxial cables are generally thick and stiff, the cable length and winding turn of the coil are inevitably longer and fewer. Furthermore, the power loss in the magnetic core should also be taken into account. We develop the TLT model using the electric circuit simulator, which can evaluate the bandwidth and power loss in the core considering the actual cable characteristics and complex permeability. A preliminary design of the 25-kW combiner is presented.

* hidefumi.okita@j-parc.jp

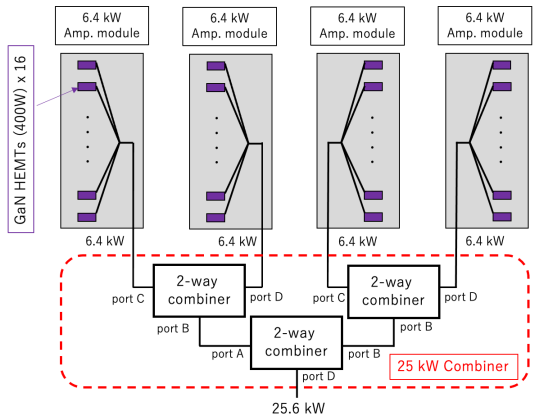

Figure 1: The configuration of 25-kW GaN amplifier.

OVERVIEW OF THE 25 KW COMBINER

The 25-kW combiner consists of three 2-way combiners as shown in Fig. 1. The 2-way combiner has four ports and consists of six TLTs as shown in Fig. 2. When P_A and P_B are input to ports A and B, ports C and D output $1/2(\sqrt{P_A}-\sqrt{P_B})^2$ and $1/2(\sqrt{P_A}+\sqrt{P_B})^2$, respectively. When P_C and P_D are input to ports C and D, ports A and B output $1/2(\sqrt{P_C}-\sqrt{P_D})^2$ and $1/2(\sqrt{P_C}+\sqrt{P_D})^2$, respectively.

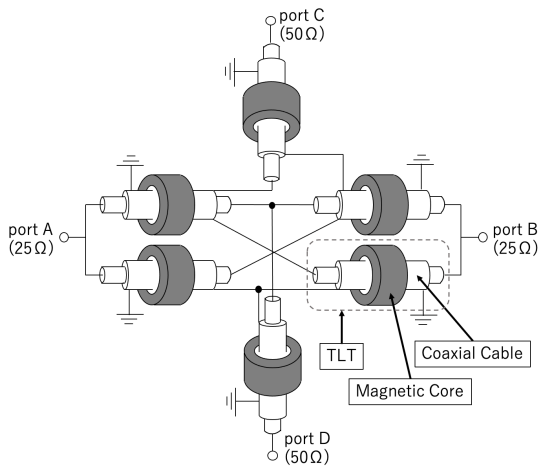

Figure 2: The configuration of the 2-way combiner [2].

The bandwidth of the 25-kW combiner depends on the TLT design. The cable attenuation due to the skin effect degrades the high frequency response. Cables with a low attenuation and short length should be employed. The isolation of the TLTs is associated with the low frequency response.

ISBN: 978-3-95450-227-1 ISSN: 2673-5490 doi:10.18429/JACoW-IPAC2022-TUPOTK052

INFLUENCE OF A POSITIVE GRID BIASING ON RF SYSTEM IN J-PARC RCS

M. Yamamoto*, M. Nomura, H. Okita, T. Shimada, F. Tamura
Japan Atomic Energy Agency, Tokai, Ibaraki 319-1195, JAPAN
K. Hara, K. Hasegawa, C. Ohmori, Y. Sugiyama, M. Yoshii
KEK, Tsukuba, Ibaraki 305-0801, JAPAN

Abstract

In order to accelerate a high intensity beam in the RCS, a large amplitude of the rf current is provided by a tube amplifier to compensate a heavy beam loading. Tetrode vacuum tubes are used in the RCS, and the control grid voltage enters into a positive region to feed such a large rf current. The positive grid biasing affects the waveform of the control grid voltage; it is deformed due to the induced control grid current under the condition of the multi-harmonic rf driving. Furthermore, the DC bias voltage drop on the control grid is observed because of the exceeding the ability for the control grid power supply. We describe the influence of the positive grid biasing in the RCS.

INTRODUCTION

The Japan Proton Accelerator Research Complex (J-PARC) Rapid Cycling Synchrotron (RCS) has been conducting beam commissioning to minimize beam loss at the design beam power of 1 MW [1]. One of the most important issues for stable beam acceleration is compensating the heavy beam loading at the rf system. A beam loading compensation system based on the rf feedback method has been successfully commissioned [2, 3].

A final-stage amplifier with tetrode vacuum tubes provides a large amplitude of the anode current into the rf cavity to compensate the heavy beam loading at the high intensity beam acceleration. The acceleration voltage pattern generated by a low-level rf system is amplified by a solid-state amplifier and fed into the control grid of the tube. The large amplitude of the anode current is driven by the large amplitude of the control grid voltage. The operation point of the tube in the RCS is set as the anode voltage of 12 kV and the control grid DC bias voltage is around −350 V, while the amplitude of the control grid driving voltage is often larger than 350 V. Thus, the positive grid biasing happens during the acceleration.

A part of the anode current flows into the control grid under the condition of the positive grid biasing and it is added to the current for the acceleration voltage pattern provided by the solid-state amplifier. Two tetrode vacuum tubes are installed in the final-stage amplifier to drive the cavity in a push-pull mode, and the acceleration voltage pattern is divided by a power splitter and fed into each control grid. The waveform of the voltage is in counterphase on each control grid and the shape is symmetric without positive grid biasing. However, the symmetricity is broken because the current provided by positive grid biasing is not in counterphase on each control grid in the RCS. This is one of the influences of positive grid biasing.

Furthermore, the current flow into the control grid caused by positive grid biasing is added to the current to sustain a DC bias voltage of around −350 V. Although the voltage is provided by a control grid power supply under the control of the constant voltage mode, the DC bias voltage can not be sustained when the positive grid biasing exceeds the capability of the control grid power supply. In such a case, the sudden drop of the DC bias voltage is observed leading to a further increase in the output power of the solid-state amplifier.

We describe the influence of the positive grid biasing on the RCS rf system.

POSITIVE GRID BIASING

Control Grid Circuit

Figure 1 shows the schematic view of the control grid circuit in the final-state amplifier. First, the acceleration voltage pattern signal amplified by the solid state amplifier is divided by the power splitter. The power splitter is fabricated as the waveforms on the two output ports are in the counterphase to drive the cavity in the push-pull mode.

After that, a bridged-T type all-pass network is applied to the control grid circuit as shown in Fig. 1. The impedance seen from the input side of this network always becomes 50 Ω over any frequency, if the following conditions are satisfied:

$$L = \frac{1}{2}RC_{\mathrm{cg}} \quad (1)$$

$$C = \frac{1}{4}C_{\mathrm{cg}}\ , \quad (2)$$

where C_{cg} is a capacitance of the control grid. The control grid voltage has low-pass characteristics and the upper cut-off frequency is $2/RC_{\mathrm{cg}}$. The RCS uses Thales TH589 tetrode and its C_{cg} is around 1.3 nF. In this case, the cut-off frequency becomes 4.9 MHz when R is 50 Ω.

The control grid DC bias voltage is provided by two control grid power supplies connected to the all-pass network as shown in Fig. 1.

Asymmetric Voltage

Figure 2 shows that the measured control grid voltage and current at the 1-MW beam acceleration. The upper graph

* masanobu.yamamoto@j-parc.jp

ISBN: 978-3-95450-227-1 ISSN: 2673-5490 doi:10.18429/JACoW-IPAC2022-TUPOTK053

DESIGN PROGRESS OF HIGH EFFICIENCY KLYSTRON FOR CEPC LINAC *

Z. D. Zhang[1], Z. S. Zhou[1†], O. Z. Xiao, M. Iqbal, S. C. Wang, S. Zhang[1], D. Dong, G. X. Pei[1], Y. L. Chi, Institute of High Energy Physics, Beijing, China
[1]also at University of Chinese Academy of Sciences, Beijing, China

Abstract

The injector linear accelerator (LINAC) for the CEPC requires a higher efficiency klystron with 80 MW output power than S band 65 MW pulsed klystron currently operating in LINAC of BEPCII to reduce energy consumption and cost. The efficiency is expected to improve from the currently observed 42% to more than 55% and output power will be improved from 65MW to more than 80 MW with same operation voltage. In this paper, BAC bunching method is applied for klystron efficiency improvement. The optimization of the gun and solenoid parameters is completed with 2-D code DGUN and then 3-D code CST. The preliminary design of the cavity parameters is also completed in 1-D disk model based AJDISK code and then further checked by 2-D code EMSYS. Finally, new klystron prototype will be fabricated in Chinese company after design parameters are determined.

INTRODUCTION

After the discovery of the Higgs particle at Large Hadron Collider (LHC) in 2012, a 240 GeV Circular Electron Positron Collider (CEPC) was proposed at institute of high energy physics (IHEP), China [1]. The design of CEPC RF source system includes CW klystron for CEPC collider and pulsed klystron for CEPC LINAC. In order to reduce the energy consumption and cost, the main goal of the klystron design is efficiency improvement. Several methods have been proposed to increase the efficiency of a klystron. These methods can be divided into two main categories: The first kind is a multi-beam klystron (MBK) which has several low perveance beam-lets because lower perveance usually corresponding to higher efficiency [2]. Each beam-let carries a small amount of current, but the total current can be large. The other kind focuses on novel bunching mechanisms. Based on this idea, the core oscillation method [3], bunching-alignment-collection (BAC) [4], and core stabilization method (CSM) [5] are proposed.

The RF power source system of CEPC LINAC includes 75 sets of pulsed klystron operating at a frequency of 2860 MHz. The power of these klystron are excepted to be 80MW so that the gradient of the accelerating structure will be 22 MV/m as shown in Fig. 1 [1]. Based on the existing S band 65 MW klystron currently applied in the BEPCII LINAC injector, the BAC method will be adopted to increase the klystron efficiency from 42% to 55% to meet the CEPC power requirement. Table 1 compares the parameters of the klystron operating in BEPCII and the proposed BAC-based klystron. The output power will be improved from 65 MW to 80 MW with the same beam power.

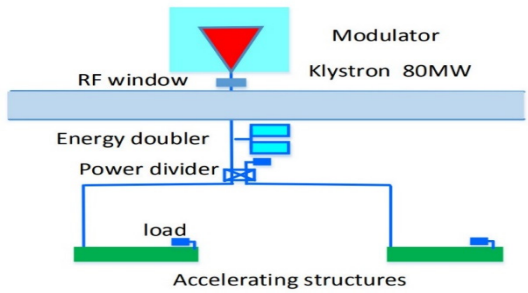

Figure 1: Accelerating structure of CEPC LINAC.

Table 1: Klystron Parameters

Parameters	Original	BAC-based
Operating frequency	2856 MHz	2856 MHz
Output power	65 MW	80 MW
RF pulsed width	4 μs	4 μs
Beam voltage	350 kV	350 kV
Beam current	414 A	414 A
Beam perveance	2.0 μP	2.0 μP
Efficiency	42%	55%

BAC METHOD

The BAC method consists of 3 stages: traditional bunching, alignment velocity spread of electrons and collecting outside electrons [6]. Compared with COM bunching mechanism, BAC method can shorten the length of klystron besides improving efficiency. The present BEPCII S band 6 5MW klystron has 6 cavities in its interaction section. In order to apply BAC method, we insert 4 additional cavities including 2 second harmonic cavities between the 4th and 5th cavity of the original klystron. Various codes, such as AJDISK [7], EMSYS, MAGIC, KLYC and CST, can be used for klystron dynamic simulation. The 1-D code AJDISK is suitable for the preliminary optimization of the interaction section parameters. Based on AJDISK, a 1-D automatic optimization code via NSGA-II was developed at IHEP. With this code, the length of the drift tube between the cavities and the cavity characteristic parameters such as frequency, R/Q and coupling coefficient are optimized to obtain a maximal efficiency. And then these parameters are further checked by 2-D code EMSYS combined with the parameters of gun and solenoid.

Figure 2 shows the 1-D AJDISK simulation result of the original klystron and the proposed BAC-based klystron. With the help of the four new cavities, the process of the electron core oscillation and the process of collecting 'particle-outsiders' is accelerated. Therefore, compared with

* Work supported by Yifang Wang's Science Studio of the Ten Thousand Talents Project
† Corresponding author: zhouzs@ihep.ac.cn

ISBN: 978-3-95450-227-1 ISSN: 2673-5490 doi:10.18429/JACoW-IPAC2022-TUPOTK054

SOLID STATE AMPLIFIERS FOR BEAM TEST SYSTEM OF PAPS AT IHEP*

O. Z. Xiao†, Y. L. Chi, N. Gan, X. P. Li, Z. D. Zhang
Institute of High Energy Physics, Chinese Academy of Sciences, Beijing 100049, China

Abstract

Solid state amplifiers are being increasingly used as RF power sources in accelerators around the world. Two solid state amplifiers with different output power and frequency have been applied in beam test system of PAPS at IHEP. A 10kW solid state amplifier operating at 1.3 GHz is used to feed a normal conducting buncher. A 650 MHz solid state amplifier with the output power of 150 kW is used to feed two 2-cell superconducting cavities. So far, the debugging and acceptance test of solid state amplifiers have been finished. During the beam test system commissioning and operation, all solid state amplifiers operate stably. In this paper, the specifications and high power test results of solid state amplifiers are presented.

INTRODUCTION

The beam test system for platform of advanced photon source technology R&D (PAPS) is used to test key technologies of 650 MHz superconducting radio frequency (SRF) system, which is mainly composed of a photocathode DC-Gun, a 1.3 GHz buncher, two 650 MHz 2-cell superconducting cavities in a crymodule and a beam dump. According to the physical design requirements, the buncher and two superconducting cavities require RF power of 10kW and 150kW respectively. With the progress of transistor technology, the output power and efficiency of a single transistor has been greatly improved. The high power can be obtained by combination of numerous transistors. Up to date, the power capability of solid state amplifier (SSA) can extend from a few kW to several hundred kW, and the operating frequency from less than 100 MHz to above 1 GHz [1-6]. Compared with vacuum electronic tube, there are many advantages for SSA such as high reliability for redundancy design, high flexibility for module design, high stability, absence of warm-up time and reasonable efficiency [7]. So the SSA is a priority RF power source for beam test system of PAPS. In this paper, the specifications and high power test results of solid state amplifiers are presented.

650 MHz/150 kW SSA

The 650 MHz solid state amplifier with the output power of 150 kW is used to feed two 2-cell superconducting cavities, which is manufactured by Beijing BBEF Science & Technology Co., Ltd (BBEF) in China. It consists of a control cabinet and four power amplifier towers, as shown in Fig. 1. Each tower can produce RF power of more than 45 kW by combining 64 power modules. The single power module must include circulator and absorbing load to ensure isolation between modules and withstand the full reflection power. The status data of every power module such as voltage, current and temperature are monitored. Also, interlock is necessary for external faults like low water flow rate and over excitation. The mean time between failures (MTBF) should be larger than 20,000 hours, and less than 5% of the power modules fail per year. The failure of 2 power modules for each tower can still run. After combining the power of four power amplifier towers, the maximum power can achieve more than 150 kW. The output port is standard WR1500 waveguide. In June 2021, the acceptance test of 650 MHz SSA was completed. Figure 2 shows the relation between input power and output power. The maximum output power reach 159 kW with less than 1dB compression. The 1dB bandwidth is larger than 2 MHz and the total efficiency is about 42%. Figure 3 shows that the harmonic power is less than -50 dBc. Figure 4 indicates that the amplitude and phase stability is less than 0.2% and 0.15° respectively. The high power test results of 650 MHz SSA are summarized in Table 1. All performance indicators meet the requirement of beam test system.

Figure 1: 650 MHz/150 kW SSA.

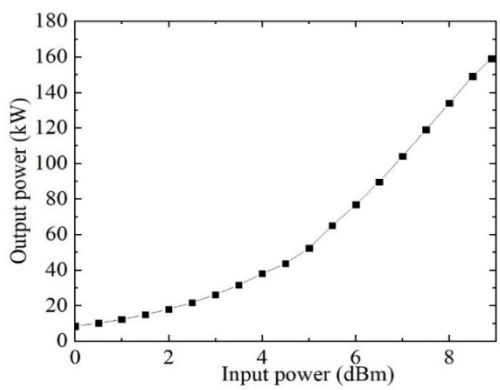

Figure 2: Transfer curve.

* Work supported by Beam Test System of PAPS.
† xiaooz@ihep.ac.cn

ISBN: 978-3-95450-227-1 ISSN: 2673-5490 doi:10.18429/JACoW-IPAC2022-TUPOTK055

ONE YEAR OF OPERATION OF THE NEW WIDEBAND RF SYSTEM OF THE PROTON SYNCHROTRON BOOSTER

G. Gnemmi*, M. Paoluzzi, S. Energico, M. Haase, C. Rossi, CERN, Geneva, Switzerland

Abstract

Within the LHC Injectors Upgrade project, the PS Booster (PSB) has been upgraded. Both the injection (160 MeV) and extraction (2 GeV) energies have been increased, bringing also changes in the injection beam revolution frequency, the maximum revolution frequency, and the beam intensity. To meet the requirements of the High Luminosity LHC a new RF system has been designed, based on the wideband frequency characteristics of Finemet®Magnetic Alloy and solid-state amplifiers. The wideband frequency response (1 MHz to 18 MHz) covers all the required frequency schemes in the PSB, allowing multi-harmonics operation. The system is based on a cellular configuration in which each cell provides a fraction of the total RF voltage. The new RF system has been installed in 3 locations replacing the old systems. The installation has been performed during 2019/2020, while the commissioning started later in 2020 and relevant results for the physics have been already observed. This paper describes the new RF chain, the results achieved and the issues that occurred during this year of operation, together with the changes made to the system to improve performance and reliability.

INTRODUCTION

The new RF system is based on a cellular configuration in which each cell provides a fraction of the total RF voltage, up to a peak voltage of approximately 700 V per cell across a frequency range from a few hundred kHz up to 20 MHz. Each cell is built around a vacuum chamber with a ceramic gap at its center and two Finemet disks, one on each side. A solid state amplifier is driving the two sides of the gap with opposite phase signals. To prevent overheating, the cells are water-cooled. Three new RF systems have been installed in the PSB tunnel in sections 5L1, 7L1 and 13L1. Each RF system is composed of 4 cavities, corresponding to the 4 vertically stacked rings of the PSB. Each cavity is equipped with 12 cells arranged in two groups of 6. The voltage requirements in each ring are: 8 kV for acceleration at the beam revolution frequency at *h1* (from 1 to 1.8 MHz), 8 kV for bunch shaping at *h2* and 4 kV for blow-up at *h10* [1]. The cavities installed in the 3 sections provide the required voltage.

SYSTEM DESCRIPTION

The new amplification chain, shown schematically in Fig. 1, is located partly outside the ring and partly in the tunnel.

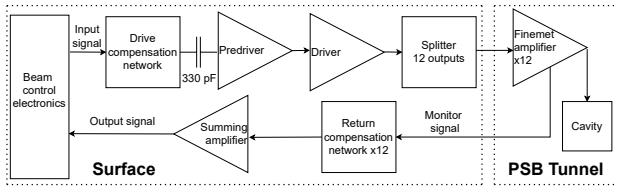

Figure 1: Block diagram of the new RF system for one ring.

The amplification chain begins on the surface where the RF input signal, provided externally by the beam control electronics, is fed through a passive compensation circuit to offset the frequency-dependent attenuation caused by the long cables from the surface to the ring. Subsequently, the signal passes through a 330 pF series capacitor which, together with the pre-driver input impedance, forms a high-pass filter compensating the low-pass response of the Finemet amplifier. Then the signal is fed into two amplifiers in sequence, gaining up to this node ~23 dB at the reference frequency of 1 MHz. Subsequently, the signal is driven through a splitter that partitions it onto 16 outputs; 12 of them are used to feed the 12 Finemet amplifiers composing a cavity. Due to the splitting, each of the outputs provides a signal attenuated of ~12 dB in the entire frequency spectrum of interest.

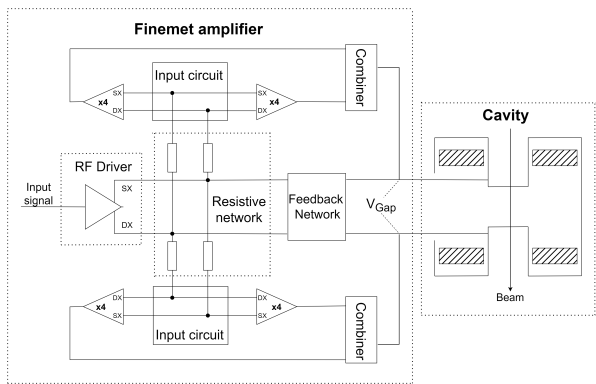

Figure 2: Block diagram of main components of a Finemet amplifier.

The signals from the splitter are fed into the Finemet amplifiers. Figure 2 shows a schematic of the push-pull amplifier, outlining its main components: the RF driver, the dampening resistive network, the two differential halves, each with an input circuit and 8 power MOSFETs and the combiner. The RF driver acts as a high impedance push-pull stage composed of a VRF151G dual power MOSFETs, driving in parallel the gates of all the 16 power MOSFETs in the final stages; eight of these modules are combined together, the same for the other eight and driven in anti-phase to obtain a differential output. Additionally, a radiation compensation

* giulia.gnemmi@cern.ch

ISBN: 978-3-95450-227-1 ISSN: 2673-5490 doi:10.18429/JACoW-IPAC2022-TUPOTK057

INNOVATIVE MAGNETRON POWER SOURCES FOR SUPERCONDUCTING RF (SRF) ACCELERATORS*

M. Neubauer, M. Popovic, R. Johnson, R. Lentz, M. Neubauer, T. Wynn
Muons, Inc., Batavia, IL 60510 USA
R. Rimmer, H. Wang
Thomas Jefferson National Accelerator Facility, Newport News, VA 23606 USA

Abstract

A magnetron suitable for 1497 MHz klystron replacements at Jefferson Lab will be constructed and tested with our novel patented subcritical voltage operation methods to drive an SRF cavity. The critical areas of magnetron manufacturing and design affecting life-cycle costs that will be modeled for improvement include: Qext, filaments, magnetic field, vane design, and novel control of outgassing. The most immediate benefit of this project is to make SRF accelerator projects more affordable for NP and other users of SRF Linacs. One of the most attractive commercial applications for SRF accelerators is to drive subcritical nuclear reactors to burn Light Water Reactor Spent Nuclear Fuel (LWR SNF). A 1 GeV proton beam hitting an internal uranium spallation neutron target can produce over 30 neutrons for each incident proton to allow the reactor to operate far below criticality to generate electricity or process heat while reducing high-level waste disposal costs. This commercial application has the additional attribute of addressing climate change.

INTRODUCTION

The construction, replacement, and operating costs for klystron power sources now used for superconducting RF (SRF) accelerators are high. In their most cost-effective configuration, one high-power klystron drives several SRF cavities that have separate requirements for phase and amplitude control, requiring additional phase and amplitude control devices for each cavity. Magnetron RF power sources for single cavities can cost much less and operate at much higher efficiency than klystrons, but they do not have the phase and amplitude control or lifetime needed to drive SRF cavities for NP particle accelerators.

Starting in 2021, Muons Inc. (MUONS) has been working with Richardson Electronics (RELL), a supplier of many commercial vacuum tubes, including magnetrons used for industrial applications. The RELL production-line approach to manufacturing quantities of tubes according to MUONS designs and specifications has started and has already been applied to the first prototype of the 1497 MHz, 15 kW tube (built under STTR grant DE-SC0013203) that can be the basis for a plan to replace CEBAF klystrons. The payback time for the replacement in power savings alone has been estimated to be about 5 years. In the next months, the prototype will be power tested at RELL and shipped to JLab for tests. Figure 1 shows the prototype 1497 MHz magnetron in the bakeout oven at RELL.

* Work supported by under DOE NP STTR DE-SC0022484
† mike@muonsinc.com

Figure 1: The prototype 1497 MHz magnetron in the bakeout oven at RELL, showing the ion pump used for conditioning.

In order to properly compensate for microphonic and Lorenz detuning of SRF cavities, injection locked magnetron techniques will need to be developed. MUONS has numerical simulation models and experimental demonstrations at 2.45 GHz that have generated patents and predictions of a broader range of power control, better phase stability, higher efficiency, and longer tube lifetime with subcritical anode voltage operation. One patent, for example, describes the operation of a pulsed magnetron that does not require an expensive HV modulator.

TECHNICAL APPROACH

One purpose of this proposed project is to bring on board a manufacturing partner, Richardson Electronics, and incorporate and study various techniques that will enhance the magnetron operation for NP applications:

- Further investigate operating in sub-critical conditions with injection locking signals
- Minimize the life-cycle costs
- Novel surface coatings to eliminate outgassing from the iron polepieces
- Model injection-locking magnetron design variables which may improve injection-locking gain, for example: Qext and number of vanes.
- Filament voltage control to minimize thermal proficle due to return electrons
- Permanent magnet design to replace solenoid field while keeping the trim coil for amplitude modulation

Several areas are described below, along with design elements for optimization the life-cycle costs of refurbishing.

ISBN: 978-3-95450-227-1 ISSN: 2673-5490 doi:10.18429/JACoW-IPAC2022-TUPOTK058

DEVELOPMENT AND TESTING OF HIGH POWER CW 1497 MHz MAGNETRON*

M. Popovic[1†], T. Blassick[2], M.A. Cummings[1], A. Dudas[1], R. P. Johnson[1], K. Jordan[3], R. Lentz[1], M. Neubauer[1], R. Rimmer[3], H. Wang[3], J. Wessel[2], T. Wynn[1]
[1]Muons, Inc., Batavia, IL 60510 USA
[2]Richardson Electronics Ltd., LaFox, IL 60147 USA
[3]Thomas Jefferson National Accelerator Facility, Newport News, VA 23606 USA

Abstract

We have designed, built, and tested a new magnetron tube that generates RF power at 1497 MHz. In the tests so far, the tube has produced CW 9 kW RF power, where the measured power is limited by the test equipment. The final goal is to use it to power superconducting (SC) cavities.

INRODUCTION

This tube was designed under DOE NP STTR that Mike Neubauer directed as the PI. The design itself was primarily the work of Alan Dudas working with our advisors from California Tube Laboratory (CTL), Tony Wynn and Ron Lentz. The tube, shown in Figure 1, was constructed by companies in California, but final repairs, reassembly, and testing were done at Richardson Electronics (RELL) in Illinois.

Figure 1: Tube at RELL ready to be baked.

DESIGN

This tube is like a 75 kW CW 915 MHz tube designed and built by CTL. The water-cooled tube has 10 strapped cavities. Power is extracted using a three-legged antenna that is enclosed in a ceramic dome. The cathode stalk has a 2 liter/s ion pump and connectors for high voltage and filament power input. These elements are shown in Figures 2a and 2b.

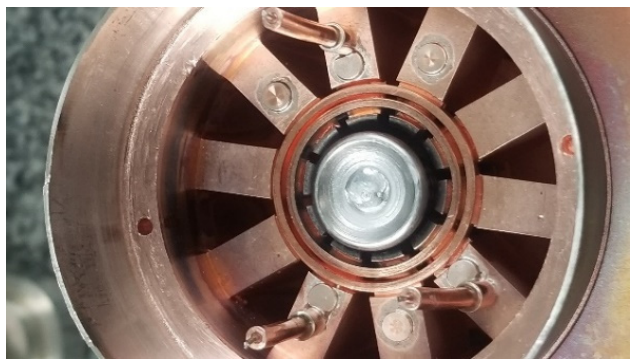

Figure 2a: Picture showing 10 cavities, straps, and antenna posts attached to the vanes of the anode body.

Figure 2b: Antenna attached to anode body.

The design process involved special consideration regarding heat distribution and removal. The biggest concern with heat dissipation was related to the cathode stalk. After assembling the filament, the temperature of the helical filament was measured in a Bell jar for several different currents. The conclusion was that 75 amps and around 8 volts will create conditions for large electron emission.

* Work supported by DOE NP STTR DE-SC0013203 and Muons Inc. and Jefferson Lab CRADA JSA 2016S004
† popovic@muonsinc.com

ISBN: 978-3-95450-227-1 ISSN: 2673-5490 doi:10.18429/JACoW-IPAC2022-TUPOTK059

MODELING O AND N ALLOYING IN Nb FOR SRF APPLICATIONS*

E.M. Lechner†,1, J.W. Angle[2], A.D. Palczewski[1], F. A. Stevie[3], M. J. Kelley[1,2], and C. E. Reece[1]
[1] Thomas Jefferson National Accelerator Facility, Newport News, VA, USA
[2] Virginia Polytechnic Institute and State University, Blacksburg, VA, USA
[3] Analytical Instrumentation Facility, North Carolina State University, Raleigh, NC, USA

Abstract

Impurity alloying Nb has ushered in highly efficient superconducting radio frequency cavities. Modeling impurity diffusion profiles for superconducting radio frequency (SRF) applications will be crucial for developing next generation accelerators and engaging with modern theories to enhance performance. Here we describe modeling of oxygen and nitrogen alloying in Nb.

INTRODUCTION

Superconducting radio frequency cavities are the building blocks of contemporary particle accelerators. Major particle accelerators utilize SRF technology to facilitate fundamental research. In Nb SRF cavities, trace impurities can have tremendous impact. With quality factors, Qo, exceeding the previous state of the art by 2-4, LCLS-II and LCLS-II HE [1, 2] will employ nitrogen-alloyed Nb for their continuous wave accelerators. A goal remains to develop impurity diffusion models to tune interstitials optimally to modify Q_0 and E_{acc} for an intended application. This work requires the use of secondary ion mass spectrometry (SIMS). The high depth resolution and ability to quantify trace impurities makes SIMS the premier tool for testing diffusion models and parameter determination using the measured impurity depth profiles.

While Nb approaches its intrinsic limits, an opportunity presents itself to explore its ultimate limits via impurity management and nanostructuring [3-9] to reduce the surface resistance and increase the accelerating gradient. An important vector of RF surface resistance modification is electron mean free path tuning via alloying using various impurities [10-16]. Impurities greatly affect sensitivity to trapped flux [17-20] and a normal-conducting hydride precipitate blocking effect [21-24] which constitutes another vector of RF surface resistance optimization which must be carefully considered in managing impurities. Thorough exploration of these topics will optimize SRF properties for Nb and the lessons learned may be applicable to future materials [25, 26] in an effort to reduce the footprint and capital cost of future accelerators.

EXPERIMENTAL

SIMS measurements were made using a CAMECA 7f Geo magnetic sector SIMS instrument on Nb samples as described elsewhere [27]. The primary ion beam, made of Cs^+, is accelerated using a potential of 5 kV and sample potential of -3 kV for an impact energy of 8 keV. The Cs^+ ion beam was rastered over an area of 150 × 150 μm^2 with the collected data coming from a 63 × 63 μm^2 area in the center of the larger raster. Quantitation of the SIMS oxygen depth profiles was made using an implant standard to convert the ion signal to impurity concentration [28, 29]. Here, we used an O implant standard dosed with O at 2×10^{15} atoms/cm^2 at 180 keV by Leonard Kroko Inc to quantify the O composition of the RF penetration layer and beyond by detecting $^{16}O^-$ in conjunction with a $^{93}Nb^-$ reference signal.

NITROGEN ALLOYING

Alloying a Nb SRF cavity with N involves vacuum heat treating the cavity at 800 °C for 3 hours for H degas, exposure to N at 800 °C and a post-alloy anneal as shown in Fig. 1. After heat treatment, the cavity is electropolished 5-7 μm to remove lossy phases on the surface. Gonnella *et al.* [30, 31] showed that a diffusion model [32] fit their SIMS data reasonably well at depths greater than 10 μm, but was incapable of reproducing a depletion of interstitial N near the surface. No further modeling was pursued.

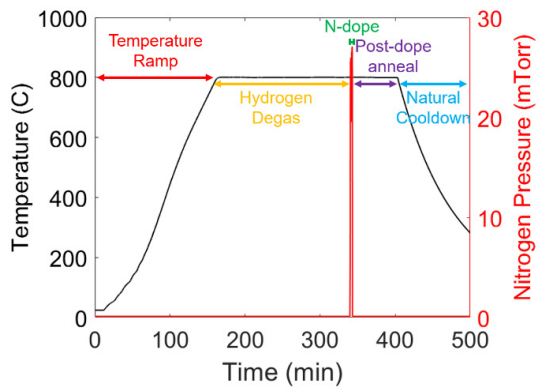

Figure 1: Furnace temperature and pressure profile relevant for N-alloying of Nb SRF cavities.

The N diffusion model of [32] accounts for a two-phase system consisting of a growing nitride layer on the surface and interstitial N migrating toward the bulk. Given nitrides populate the surface in such doping schemes for SRF [13], such a diffusion model may be a good starting point, however several convenient approximations are voluntarily forfeited when the alloying is chosen to be performed during a short time compared to the annealing process and furnace cooldown. These facts require that a model of N alloying relevant for SRF cavities must incorporate the following: 1. A sink term describing the depletion of N near the surface. 2. An annealing step. 3. Accurate understanding of N uptake. 4. Accurate understanding of the N diffusion coefficient.

*Work supported by U.S. DOE contract DE-AC05-06OR23177.
† lechner@jlab.org

ISBN: 978-3-95450-227-1 ISSN: 2673-5490 doi:10.18429/JACoW-IPAC2022-TUPOTK060

SIMULATIONS OF MISCUT EFFECTS ON THE EFFICIENCY OF A CRYSTAL COLLIMATION SYSTEM*

M. D'Andrea†, D. Mirarchi, S. Redaelli,
CERN, European Organization for Nuclear Research, CH-1211 Geneva 23, Switzerland

Abstract

The concept of crystal collimation relies on the use of bent crystals which can coherently deflect high-energy halo particles at angles orders of magnitude larger than what is obtained from scattering with conventional materials. Crystal collimation is studied to further improve the collimation efficiency at the High Luminosity Large Hadron Collider (HL-LHC). In order to reproduce the main experimental results of crystal collimation tests and to predict the performance of such a system, a simulation routine capable of modeling interactions of beam particles with crystal collimators was developed and recently integrated into the latest release of the single-particle tracking code SixTrack. A new treatment of the miscut angle, i.e. the angle between crystalline planes and crystal edges, was implemented to study the effects of this manufacturing imperfection on the efficiency of a crystal collimation system. In this paper, the updated miscut angle model is described and simulation results on the cleaning efficiency are presented, using configurations tested during Run 2 of the LHC as a case study.

INTRODUCTION

Crystal collimation is an advanced collimation technique that exploits the peculiar properties of materials with highly ordered atomic structure. Depending on their impact angle, charged particles can get trapped in the potential well generated by neighboring crystalline planes, oscillating in relatively empty space and traversing the crystal for its full length with reduced probability of inelastic interactions. This process, called *crystal channeling*, allows a bent crystal to steer charged particles with necessary impact conditions [1, 2].

This concept has been studied at CERN as a way to improve the collimation performance of the LHC by steering beam halo particles onto a single absorber [3–5]. Since 2016, a complete test stand composed of four single-sided crystal collimators (two per each circulating beam, one on the horizontal plane and one on the vertical plane) has been installed in the LHC betatron collimation system [6–8]. A standard secondary collimator with jaws made of carbon fiber composite (CFC) can be used to safely intercept and dispose of channeled halo particles for heavy ion beams with a total stored energy up to 20 MJ, while only low-intensity proton beams are sustainable with the current setup [9]. An extensive test campaign conducted during Run 2 of the LHC (2015-2018) demonstrated the improved cleaning provided by crystal collimation of 6.37 Z TeV Pb ion beams [4, 5], leading to the integration of this technology in the HL-LHC baseline. Crystal collimation is planned to be used in operation with Pb ion beams already in Run 3 (2022-2025) [10, 11].

To reproduce key experimental results and predict the performance of a crystal collimation system, a dedicated simulation routine was developed and recently integrated in the latest version of SixTrack [12–15], a single-particle tracking code widely used at CERN for simulating beam dynamics in circular accelerators. This code performs a symplectic and fully chromatic tracking of protons and ions [16–18] through a magnetic lattice which includes all machine elements affecting the beam dynamics (such as magnets, RF cavities, etc.). A specific version of SixTrack, which can treat interactions of beam particles with the constituting material of machine elements [19, 20], is used for collimation studies to predict the distribution of losses in the accelerator ring. A dedicated routine models coherent interactions between charged particles and bent crystal collimators via a Monte-Carlo simulation [21–24], which was extensively benchmarked against experimental data [3, 4, 24–27]. Only simulations with proton beams are supported by this routine.

DEFINITION OF MISCUT ANGLE AND UPDATED GEOMETRICAL MODEL

Crystal collimation simulations for LHC consider perfectly cut crystals, with planes aligned to the lateral surface facing the beam. In reality however, a non-zero angle, called *miscut angle*, is unavoidable and causes a series of edge effects that can hinder the performance of a crystal collimation system. In particular, channeled particles travel inside the crystal for different lengths depending on their impact parameter, i.e. the distance between the impact point and the lateral side (x_{cry} in Fig. 1, while s_{cry} is the longitudinal direction tangent to the curvature of the crystal), and acquire different deflections. This is particularly relevant for the

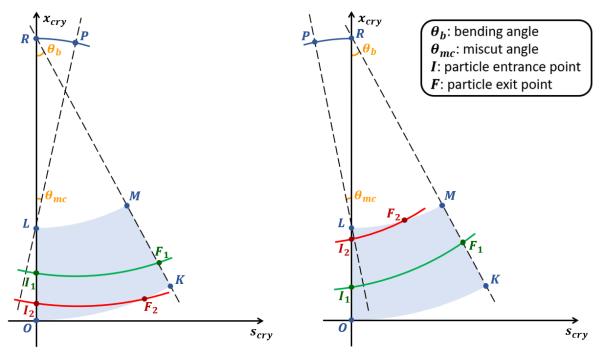

Figure 1: Geometrical model for negative (left) and positive (right) miscut in the reference frame of the bent crystal.

* Work supported by the HL-LHC Project
† marco.dandrea@cern.ch

ISBN: 978-3-95450-227-1 ISSN: 2673-5490 doi:10.18429/JACoW-IPAC2022-TUPOTK061

PROSPECTS TO APPLY MACHINE LEARNING TO OPTIMIZE THE OPERATION OF THE CRYSTAL COLLIMATION SYSTEM AT THE LHC*

M. D'Andrea†, G. Azzopardi, M. Di Castro, E. Matheson,
D. Mirarchi, S. Redaelli, G. Ricci[1], G. Valentino[2],
CERN, European Organization for Nuclear Research, CH-1211 Geneva 23, Switzerland
[1] also at Università degli Studi di Roma "La Sapienza", Roma, 00185 RM, Italy
[2]also at University of Malta, Msida, MSD 2080, Malta

Abstract

Crystal collimation relies on the use of bent crystals to coherently deflect halo particles onto dedicated collimator absorbers. This scheme is planned to be used at the LHC to improve the betatron cleaning efficiency with high-intensity ion beams. Only particles with impinging angles below 2.5 μrad relative to the crystalline planes can be efficiently channeled at the LHC nominal top energy of 7 Z TeV. For this reason, crystals must be kept in optimal alignment with respect to the circulating beam envelope to maximize the efficiency of the channeling process. Given the small angular acceptance, achieving optimal channeling conditions is particularly challenging. Furthermore, the different phases of the LHC operational cycle involve important dynamic changes of the local orbit and optics, requiring an optimized control of position and angle of the crystals relative to the beam. To this end, the possibility to apply machine learning to the alignment of the crystals, in a dedicated setup and in standard operation, is considered. In this paper, possible solutions for automatic adaptation to the changing beam parameters are highlighted and plans for the LHC ion runs starting in 2022 are discussed.

INTRODUCTION

In the context of the intensity upgrade foreseen by the High-Luminosity LHC (HL-LHC) Project [1, 2], collisions with high-intensity ion beams close to the HL-LHC baseline will be delivered already during Run 3 of the LHC [3], starting in 2022. An upgrade of the collimation system is crucial to ensure high-efficiency operation in these demanding conditions, since losses generated by high-intensity ion beams were already close to the quench limits of the superconducting magnets in Run 2 [4–6].

Crystal collimation is an innovative collimation technique that has been extensively studied over the course of Run 2 as a way to improve the cleaning efficiency of the LHC collimation system [7–13]. This concept exploits the property of materials with highly ordered atomic structure to capture charged particles with suitable impact conditions in the potential well generated by neighbouring crystalline planes, a process called *crystal channeling*. Bent crystals can thus be used to efficiently steer beam halo particles by forcing them to follow the curvature of the crystal itself. Since channeled particles oscillate in the relatively empty space between crystalline planes, inelastic interactions with the constituting atoms of the crystal are greatly suppressed, reducing the production of off-momentum particles. After the promising results obtained in first beam tests during Run 2 [14–18], it is planned to use crystal collimation in Run 3 for operation with ion beams, for which a standard secondary collimator can be safely used to intercept the channeled halo [19].

Achieving and maintaining optimal channeling conditions is a crucial element of the setup of a crystal-based collimation system. Only particles whose incident direction is close enough to the direction of the crystalline planes can be caught in the potential well and be efficiently channeled. This process defines an acceptance angle for the channeling phenomenon, which is heavily dependent on the particle energy and changes during dynamical phases of LHC operation, reaching values as low as about 2.5 μrad for energies close to 7 Z TeV. The crystal goniometer assembly is equipped with a high-resolution goniometer with a piezo actuator [20–22] to align its orientation to the beam halo. However, even when achieved, optimal channeling conditions can be easily lost in case of changes in beam dynamics, if the crystal orientation is not promptly and precisely adjusted.

CHALLENGES FOR THE OPERATION OF CRYSTAL COLLIMATORS

The optimal channeling orientation can be identified using Beam Loss Monitors (BLMs) [23, 24] that are ionization chambers placed around the ring to detect secondary showers produced by the interactions of beam particles with machine equipment. In total, around 3500 of these monitors are installed in the LHC. By monitoring losses at the crystal location while it is slowly rotated (a procedure called *angular scan*), a characteristic pattern can be measured when different coherent interactions of beam particles with the crystalline planes become dominant. As can be seen in the top frame of Fig. 1, the optimal channeling orientation corresponds to a minimum in the loss pattern observed at the crystal location during the scan, called *channeling well* (2), due to the decreased probability of inelastic interactions. Given the limited angular range of the region of interest (only a few tens of μrad) and the relatively low reduction factor of local losses for raw data, identifying the optimal channeling orientation online is particularly challenging. Correspondingly, an increase of losses at the location of the secondary collimator used to intercept the channeled halo

* Work supported by the HL-LHC Project
† marco.dandrea@cern.ch

ISBN: 978-3-95450-227-1 ISSN: 2673-5490 doi:10.18429/JACoW-IPAC2022-TUPOTK062

SETTINGS FOR IMPROVED BETATRON COLLIMATION IN THE FIRST RUN OF THE HIGH LUMINOSITY LHC*

B. Lindstrom, A. Abramov, R. Bruce, R. De Maria, P. Hermes, J. Molson, S. Redaelli, F. Van der Veken, CERN, Geneva, Switzerland

Abstract

The current betatron collimation system in the LHC is not optimized to absorb off-momentum particles scattered out from the primary collimators. The highest losses are concentrated in the downstream dispersion suppressor (DS). Given the increased beam intensity in the High Luminosity LHC (HL-LHC), there is concern that these losses could risk quenching the superconducting DS magnets. Consequently, a dedicated upgrade of the DS has been studied. However, at this stage, the deployment for the startup of the HL-LHC is uncertain due to delays in the availability of high-field magnets needed to integrate new collimators into the DS. In this paper, we describe the expected collimation setup for the first run of the HL-LHC and explore various techniques to improve the collimation cleaning. These include exploiting the asymmetric response of the two jaws of each primary collimator and adjusting the locally generated dispersion in the collimation insertion.

INTRODUCTION

An efficient control of beam losses is essential in the Large Hadron Collider (LHC) to ensure efficient operation and avoid quenches of the superconducting magnets [1, 2]. For this purpose, two dedicated cleaning insertion regions (IRs) exist in the LHC lattice, the momentum cleaning in IR3 and the betatron cleaning in IR7. In these insertions, a well-defined transverse hierarchy of collimators is deployed to diffuse and absorb the energy carried by the beam halo, before they impact on the superconducting magnets [3–5]. Nevertheless, there is inevitably some leakage of particles from the collimators. The fraction of particles lost in the aperture defines the cleaning efficiency. The majority of leaked particles have large momentum offsets and are immediately lost in the dispersion suppressor (DS), where the first dispersion peaks occur downstream of the IR.

The High Luminosity LHC (HL-LHC) project [6] aims to increase the bunch population from the LHC nominal value of 1.15×10^{11} to 2.3×10^{11} protons. The expected increase of losses in the IR7 DS might induce quenches in the superconducting dipole magnets located there [2]. Thus, it was foreseen to replace one of the main dipole magnets (8.33 T, 14.3 m) by two 11 T dipoles of 5.5 m each, opening up space for a new collimator, TCLD [7]. Their deployment, foreseen for Run 3 (2022-2025) [8], is postponed due to delays in the 11 T dipole production. Their availability for Run 4 (2029-2032) [9], the first run of HL-LHC, is under evaluation. In Run 3, proton intensities reach a maximum of 80 % of the HL-LHC target [10]. For ion beams, the absence of the TCLDs is mitigated by crystal collimators [11–13].

This paper introduces the Run 4 proton baseline scenario. Due to the uncertainty of the TCLD installation, as well as other changes to the operational scenario [14], alternative improvements to the cleaning performance must be explored [15]. In view of this, the effect of increased single pass dispersion and asymmetric collimator jaws is analyzed.

BASELINE SCENARIO

The Run 4 optics and collimation settings are detailed in [14,15]. A normalized emittance of 2.5 µm rad and a beam energy of 7 TeV are assumed. Due to impedance concerns with the larger bunch population, it was decided to retract the IR7 primary collimators (TCP) by 1.8 σ (σ is the RMS beam size), together with a 1σ retraction of the IR6/7 secondary collimators (TCS), IR7 absorbers (TCLA) and IR1/5 tertiary collimators (TCT) compared to the nominal settings for 15 cm β^* [2]. The design report settings are referred to as "tight settings", while the new proposal is called "relaxed settings". A summary of key settings can be found in Table 1, where the number in the collimator name refers to the IR in which they are located. Note that the TCL/TCT settings in units of σ depend on the β^*.

Table 1: Comparison of some optics parameters and collimator settings between Run 4 [15] (relaxed) and the nominal HL-LHC design [6].

Parameter	Run 4	Design
β^*_{min} [cm]	20	15
bunch population [10^{11} p^+]	2.3	2.3
TCP7 [σ]	8.5	6.7
TCS7 [σ]	10.1	9.1
TCLA7 [σ]	13.7	12.7
TCDQ6 [σ]	11.1	10.1
TCS6 [σ]	11.1	10.1
TCT1/5 [σ] (for β^*_{min})	13.2	10.4
TCL1/5 [σ] (for β^*_{min})	16.4	14.2

Particle losses are simulated in SixTrack [16, 17] coupled to FLUKA [18–21], using optics version HLLHCV1.5 [22]. Losses on the accelerator aperture are binned over the length of the accelerator, in 10 cm long bins. The energy lost into the aperture is normalized to the total energy lost in the collimators, as well as the bin length. Losses are referred to as horizontal or vertical depending on whether their primary impacts are on the horizontal or vertical primary collimators.

A set of simulated loss maps, zoomed into the IR7 region, is shown in Fig. 1, for the β^*=20 cm settings in Table 1: (a)

* Work supported by the High Luminosity LHC project

ISBN: 978-3-95450-227-1 ISSN: 2673-5490 doi:10.18429/JACoW-IPAC2022-TUPOTK063

CERN LINAC4 CHOPPER DUMP: OPERATIONAL EXPERIENCE AND FUTURE UPGRADES

C. J. Sharp*, R. Franqueira Ximenes†, M. Calviani‡, D. Grenier, C. Y. Mucher, E Grenier-Boley, C. Torregrosa, J. R. Hunt, L. S. Esposito, G. Costa, P. Andreu Muñoz, A. M. Krainer,
European Organization for Nuclear Research (CERN), CH-1211 Geneva, Switzerland

Abstract

The Chopper Dump in the Linac4 accelerator at CERN is a beam-intercepting device responsible for the absorption of the 3 MeV H^- ion beam produced by the Linac4 source and deflected upstream by an electromagnetic chopper. It allows a portion of the beam, which would otherwise fall into the unstable region of the radiofrequency buckets in the Proton Synchrotron Booster, to be dumped at low energy with minimal induced radiation. It may also be used to absorb the entire beam. With peak currents of 25 to 45 mA and shallow penetration, this results in large deposited energy densities, thermal gradients and mechanical stresses. Additional constraints arise from geometric integration, vacuum and radiation protection requirements. Material selection, beam-matter interaction studies and thermo-structural analyses are important aspects of the design process. The Chopper Dump underwent modification in 2019 following observed material degradation in the original version of the device. The experience gained, modifications made and observations noted since then are detailed herein. Against this background, the design and analysis of an upgraded device, intended to cope with future operational conditions, is outlined and discussed.

INTRODUCTION

Chopping of the 3 MeV H^- beam in CERN's Linac4 accelerator allows bunches that would fall into the unstable region of the radiofrequency buckets of the PS booster to be dumped at low energy [1]. A chopping system consisting of electrostatic plates and quadrupole magnets is used to deflect particles vertically onto a conical dump in the medium energy beam transport (MEBT) line. Chopping at low energy minimises the required chopping element strength and induced radiation, but results in more demanding low-penetration conditions for the absorbing surface. The dump must absorb the entire beam when required and dissipate the resulting heat so as not to exceed material limits on temperature or stress. Additional challenges in the design arise from tight geometric constraints, vacuum and radiation protection.

Material degradation in a previous version of the dump prompted installation of a modified version during 2019 [2]. This has operated successfully at 25 mA peak dumped current but is predicted not to withstand future conditions up to 45 mA. Activation due to ^{65}Zn production also restricts long term use. A project to consolidate the dump is ongoing.

* calum.james.sharp@cern.ch
† rui.franqueira.ximenes@cern.ch
‡ marco.calviani@cern.ch

OPERATIONAL EXPERIENCE

Nickel-Coated Device

The original dump, first operated in 2013, consisted of a GlidCop® AL-60 core (Fig. 1a) – a dispersion-strengthened copper-based metal-matrix composite desired for its high thermal conductivity and good mechanical properties – with the internal surface coated in nickel to reduce activation [3].

Observed Degradation

In 2019, material degradation in the form of delamination and local melting of the nickel was observed (Fig. 1b), a concern for device integrity and potential introduction of debris in the beamline. Subsequent analysis concluded that the degradation was a result of a loss of local heat conduction due to subsurface cracks or voids in the coating, potentially caused by plastic deformation and low-cycle fatigue during the pulse-cooldown cycle [2]. Hydrogen implantation and blistering was identified as another possible cause.

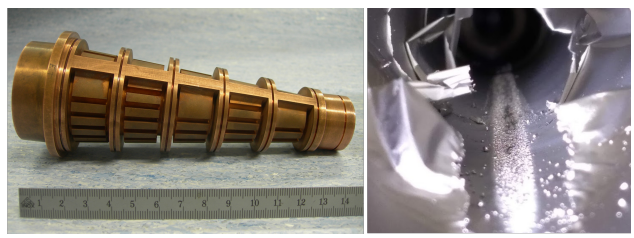

Figure 1: (a) GlidCop® core, (b) damaged Ni coating [2].

Modifications

A modified version of the dump with the nickel coating removed (except for a small region at the aperture) was installed in August of that year. With the beam impinging directly on the GlidCop® substrate, this provides better heat conduction and increased resilience owing to the material's superior thermo-mechanical properties. Device activation is increased but acceptable in the short term.

Operation and Subsequent Inspection

The modified device has operated during Linac4 commissioning and the start of Run 3 during 2019-2022. An inspection in the 2021 year-end technical stop observed no sign of melting or delamination problems as experienced in the previous device. Some minor changes were noted, however are not thought to have a significant impact on continued operation in 2022. These included discolouration (darkening) approximately in the region of beam impact (Fig. 2) thought to be caused by migration of intrinsic carbon to the

ISBN: 978-3-95450-227-1 ISSN: 2673-5490 doi:10.18429/JACoW-IPAC2022-TUPOTK064

HL-LHC CRAB CAVITY HOM COUPLERS: CHALLENGES AND RESULTS*

J. Mitchell†, R. Calaga, E. Montesinos, CERN, Geneva, Switzerland

Abstract

To compensate for the detrimental effect of the crossing angle on luminosity production in the High Luminosity Large Hadron Collider's (HL-LHC) interaction regions, superconducting crab cavities (vertical and horizontal) will be installed at the two interaction regions of the ATLAS and CMS experiments. Both cavity designs use multiple Higher Order Mode (HOM) couplers to reduce beam instabilities and heat loads caused by the very high proton current in the HL-LHC. The conceptual RF designs of the HOM couplers are firstly presented, evaluating HOM damping requirements, fundamental mode rejection and dynamic heat load constraints. A special focus is given to the coupler's characteristic impedance (Z_0), to improve the robustness during transport and operation. Following this, RF measurements of the HOM couplers before installation and when installed on the superconducting cavities are detailed, analysing deviations from the simulated case.

INTRODUCTION

The 'dressed' Double Quarter Wave (DQW) [1,2] and Radio Frequency Dipole (RFD) [3,4] crab cavities are shown in Fig. 1, highlighting the Higher Order Mode (HOM) couplers used in each case.

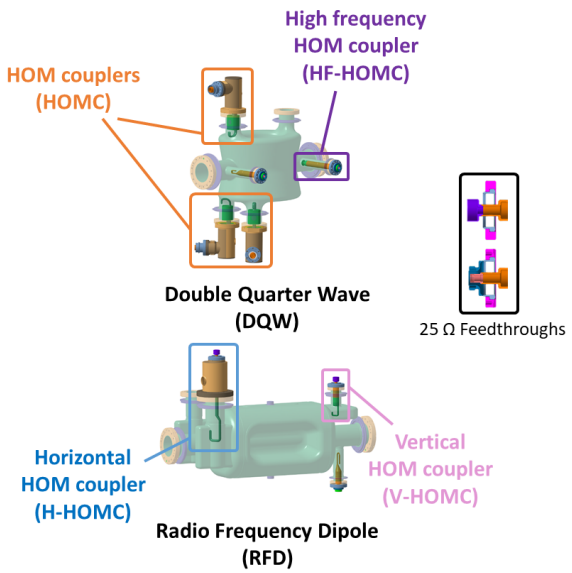

Figure 1: Double Quarter Wave (DQW) and Radio Frequency Dipole (RFD) 'dressed' crab cavities, highlighting the HOM couplers and feedthroughs.

The DQW cavity uses three on-cell, coaxial, superconducting HOM couplers [2] to damp the HOMs, whist providing a stop-band at the cavity's fundamental mode frequency of 400 MHz. In addition to the three on-cell couplers, a beampipe coupler is used to damp two horizontally polarised transverse modes, for which there is a field node at the position of the three other HOM couplers.

The RFD crab cavity uses a Vertical and Horizontal HOM Coupler (V-HOMC and H-HOMC) [5] to damp high impedance transverse HOMs in the respective planes. The H-HOMC is also used to damp modes with a large longitudinal impedance. In order to minimise fundamental mode leakage, the two couplers are mounted on waveguide 'stubs' with cut-off frequencies above 400 MHz. An additional band-stop ladder filter is incorporated into the H-HOMC's geometry to provide further rejection.

TRANSPORT CONSIDERATIONS AND CHANGING Z_0 FROM 50 TO 25 Ω

Both cavity designs, ancillaries and RF feedthroughs will be manufactured and assembled in several locations across Europe, the United States and Canada. During the prototyping phase, the RF feedthroughs (Fig. 1) were identified as a potential risk in the final cryomodule transport to CERN. With a characteristic impedance of 50 Ω, the inner conductor at the Alumina (Al_2O_3) [6] window has a diameter of only 3 mm. The forces associated with air, sea and road transport [7] impose stresses which put the feedthroughs at risk of deformation and fracture - resulting in an unusable cryomodule.

To improve the robustness of the feedthroughs, the characteristic impedance of the HOM couplers was changed from 50 to 25 Ω, in order to increase the inner conductor diameter at the window to 14 mm (when optimised for the full bandwidth). Simulations showed that changing the CERN feedthrough design to the new characteristic impedance increased the ultimate tensile stress by a factor of 4. To test the hypothesis, feedthroughs with inner diameters of 6 and 14 mm were manufactured (3 mm, i.e. 50 ohms, was simply too small to manufacture). Physical drop tests of HOM coupler assemblies showed that the feedthroughs with the larger diameter could sustain a drop of at least 2 times that of the 6 mm versions [8], validating the principle.

SIMULATIONS

The simulated impedance spectra for the two cavities, with HOM couplers adapted and tuned for the new characteristic impedance, are shown in Fig. 2. The imposed limits were 200 kΩ and 1 MΩ/m for the longitudinal and transverse modes respectively. In addition to the improved struc-

* Research supported by the HL-LHC project.
† james.mitchell@cern.ch

ISBN: 978-3-95450-227-1 ISSN: 2673-5490 doi:10.18429/JACoW-IPAC2022-TUPOTK065

DESIGN OF A PASSIVE SUPERCONDUCTING HARMONIC CAVITY FOR HALF STORAGE RING

Y. Wei*, J. Pang, B. Du, D. Jia, S. Zhang and G. Feng†, National Synchrotron Radiation Laboratory, University of Science and Technology of China, Hefei, China
H. D. Zhang, C. P. Welsch, Cockcroft Institute and University of Liverpool, Daresbury, UK

Abstract

Higher harmonic cavities, also known as Landau cavities, have been proposed to improve beam lifetime and provide Landau damping by lengthening the bunch without energy spread for stable operations of present and future low-emittance storage rings. This contribution presents design of a passive superconducting 3rd-harmonic cavity (super-3HC) for the planned Hefei Advanced Light Facility (HALF) at University of Science and Technology of China. It is designed to provide 0.43 MV at 1499.4 MHz for the nominal 2.2 GeV, 350 mA electron beam, and 1.44 MV main RF voltage in storage ring. Through optimizations it has a low R/Q < 45 Ω, which has potential to achieve a good bunch lengthening. Higher-order-modes are strongly damped using a pair of room-temperature silicon carbide (SiC) rings to meet the requirement of beam instabilities. In addition, preliminary engineering design for the super-3HC cryomodule is also described in this contribution.

INTRODUCTION

Hefei Advanced Light Facility (HALF) [1] is a soft X-ray and Vacuum Ultra-Violet (VUV) fourth-generation diffraction-limited light source which is planned to be constructed by National Synchrotron Radiation Laboratory (NSRL), University of Science and Technology of China (USTC). The HALF storage ring employs modified hybrid 6BA lattice as the baseline lattice to generate a beam with 85 pm·rad emittance, 350 mA current and 2.2 GeV energy [2]. The storage ring parameters are listed in Table 1.

Table 1: HALF Storage Ring Parameters

Parameters	Symbol	Value
Energy reference particle	E_0 [GeV]	2.2
Average current	I_0 [mA]	350
Harmonic number	h	800
Circumference	C [m]	~480
Energy spread	σ_p	0.00062
Nature emittance	ε_e	85 pm·rad
Momentum compaction	α	0.00009
Energy loss per turn (1st Term)	U_{s1} [MeV]	~0.4
Energy loss per turn (2nd Term)	U_{s2} [MeV]	~0.6

PHYSICAL REQUIREMENTS

In order to suppress the emittance diluting caused by the intrabeam scattering effect and increase the beam Touschek lifetime in storage ring, a passive superconducting 3rd-harmonic cavity (super-3HC) is employed to lengthen the beam bunches. Then the HALF storage ring has double RF systems: the main one and harmonic one. In such a storage ring, the voltage V(τ) seen by an electron in the beam with arrival time τ is

$$V(\tau) = V_1 \cos(2\pi f_{\mathrm{rf}}\tau + \phi_1) + V_{\mathrm{m}} \cos(3 \times 2\pi f_{\mathrm{rf}}\tau + \phi_{\mathrm{m}}), \quad (1)$$

where V_1 and V_{m} are the voltage amplitude of the main and harmonic RF cavities, respectively, f_{rf} is the frequency of the main RF cavity, ϕ_1 and ϕ_{m} are the phases of the synchronous particle in the main and harmonic RF cavities, respectively.

To compensate for the energy loss per turn $U_s = eV_s$, it is required that $V(0) = V_s$ for the synchronous particle. The longitudinal dynamics in the double RF systems described by Eq. (1) has been comprehensively discussed, together with optimal conditions for bunch lengthening [3]. Thus we obtain the optimum parameters for HALF double RF systems consisting of a single main superconducting cavity and a single super-3HC, as shown in Table 2.

Table 2: HALF Storage Ring Double RF Systems

RF System Parameters	Symbol	1st Term	2nd Term
Energy loss per turn	U_s [MeV]	~0.4	~0.6
Main frequency	f_{rf} [MHz]	499.8	499.8
Harmonic frequency	$3f_{rf}$ [MHz]	1499.4	1499.4
Main voltage	V_1 [MV]	1.20	1.44
Harmonic voltage	V_m [MV]	0.374	0.43
Main phase	ϕ_1 [°]	70.53	65.37
Harmonic phase	ϕ_m [°]	90.0038	90.0044
Main quality factor	Q_1	1E9	1E9
Harmonic quality factor	Q_m	2E8	2E8
Harmonic detuning angle	ψ_m[°]	89.9962	89.9956
Bunch lengthening factor	σ_{tm}/σ_{t0}	5.7	5.9
Tousheck life time ratio	$R_{Touschek}$	6.1	6.2

*wylong@ustc.edu.cn
†fenggy@ustc.edu.cn

ISBN: 978-3-95450-227-1 ISSN: 2673-5490 doi:10.18429/JACoW-IPAC2022-TUPOMS001

CONCEPTUAL DESIGN OF A FUTURE AUSTRALIAN LIGHT SOURCE

R. T. Dowd*, M. Atkinson, R. Auchettl, J. W. Chi, Y-R, Tan, D. Zhu, K. Zingre,
Australian Synchrotron ANSTO, Melbourne, Australia

Abstract

ANSTO currently operates the Australian Synchrotron, a 3 GeV, 3rd generation light source that begun user operations in 2007. The Australian synchrotron is now halfway through its expected life span and we have begun planning the next light source facility that will eventually replace it. This paper describes the conceptual design of an entirely new light source facility for Australia, which makes use of the latest advances in compact acceleration technology and 4th generation lattices.

INTRODUCTION

The Australian Synchrotron light source was commissioned in 2006 and begun operations in 2007. It was designed and delivered to be a world-class synchrotron radiation facility that could meet the needs of 95% of the Australian user community. Since then it has performed with world-leading reliability, has achieved record coupling control [1] and is currently undergoing an expansion of its beamline suite to continue to service the Australian user community. The Australian Synchrotron is halfway into its expected 30 year lifetime and it is now the appropriate time to consider how best to service the Australian Synchrotron user community beyond the 15 year horizon.

OVERVIEW OF EXISTING FACILITY

The Australian Synchrotron Light Source is a 3rd Generation Light source facility (Figure 1. It operates a 200 mA, 3 GeV electron beam producing synchrotron radiation for a suite of beamlines. It has 14 fold symmetry and currently services 10 beamlines, with another 8 being currently built.

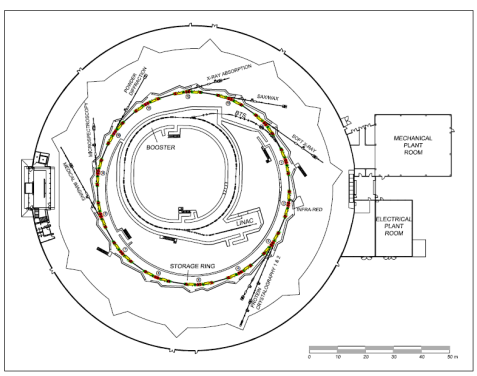

Figure 1: Layout of the Australian Synchrotron light source.

It uses a full energy injector system comprising of a 100 MeV linac and 3 GeV booster synchrotron to inject beam into its storage ring. The full energy injector allows for 'top-up' mode operation of the storage ring, which requires frequent, small injections of beam to keep the storage ring current within a few percent of maximum at all times. The Australian Synchrotron's accelerator systems were installed and commissioned between 2005 and 2006, with first light in July 2006. It entered into full user operations in July 2007. Since then, it has delivered approximately 5000 hours of user beam per year and maintained a world-leading reliability of ~ 99%.

UPGRADE VS NEW FACILITY

The Going into the Future, a new or upgraded facility will still need to provide for 95% of Australia's diverse user community as it will be the only light source facility within thousands of kilometres. This necessitates a design in which a wide range of X-ray energies can be utilised, ensuring a broad range of synchrotron based techniques are catered for. It also makes a reduction of dark time during any upgrades a priority.

A study into an upgraded lattice utilising the existing 216 metre storage ring [2] which we have labelled AS-U. This lattice was severely constrained by the available space, resulting in a design that would have considerable design challenges while still delivering an emittace that would place it at the tail end of what is achievable by 4th generation light sources. Therefore we have embarked on a design study of a new facility, allowing for a larger ring, new injector and possibility of an associated FEL facility.

NEW LIGHT SOURCE DESIGN

One of the main constraints in upgrading the existing Australian Synchrotron was the small circumference of the storage ring (216m) which limited achievable emittance and pushed up the RF requirements. Lowering the beam energy to alleviate this is not compatible with user requirements for good flux at high photon energies. Therefore we are now considering a larger ring design on a new or 'greenfield' site. One of the features of ultra-low emittance lattices is that they have smaller dynamic apertures, requiring injection of low emittance beams, ideally from a linear accelerator, for efficient capture. With the increasing use of higher gradient accelerating technologies and in line with current local research programs in compact accelerator technology, we have decided to use an X-band linear accelerator as a full energy injector for the new storage ring. The new facility will therefore be close in layout to MAX IV Light source arrangement, with the linac injecting into the storage ring from the outside of the ring (Figure 2). Using CLIC X-band RF technology with accelerating gradients of around 70 MV/m will allows

* rohan.dowd@ansto.gov.au

ISBN: 978-3-95450-227-1 ISSN: 2673-5490 doi:10.18429/JACoW-IPAC2022-TUPOMS002

STATUS OF SIRIUS OPERATION

L. Liu†, M. B. Alves, F. H. de Sá, R. H. A. Farias, S. R. Marques, A. C. S. Oliveira, X. R. Resende, R. M. Seraphim, H. Westfahl Jr
Brazilian Synchrotron Light Laboratory (LNLS/CNPEM), Campinas, Brazil

Abstract

SIRIUS is a Synchrotron Light Source Facility based on a 3 GeV electron storage ring with 518 m circumference and 250 pm.rad emittance. The facility was built and is operated by the Brazilian Synchrotron Light Laboratory (LNLS), located in the CNPEM campus, in Campinas, Brazil. The accelerator commissioning and operation has been split into 2 phases: Phase0, corresponding to the initial accelerator commissioning with 6 beamlines, has been completed, and the project is now in preparation for Phase1, with full accelerator design performance and 14 beamlines in operation. We report on the status of SIRIUS last year operation and ongoing activities towards achieving completion of Phase1.

INTRODUCTION

SIRIUS is the new Brazilian synchrotron light source based on a 3 GeV electron storage ring, comprising a 20-cell 5BA magnetic lattice with 250 pm.rad emittance. It is one of the three 4th generation storage-ring-based light sources in operation worldwide. The new facility can house up to 40 beamlines based on insertion devices or low field (0.6 T) and high-field (3.2 T) bending magnets of the lattice, covering an energy range from infrared to hard x-rays.

The project commissioning is planned to take place in 2 Phases: Phase0 with 100 mA and 6 beamlines, and Phase1 with full accelerator performance at 350 mA in top-up mode, conclusion of 14 beamlines, high performance insertion devices, support labs, and computing infrastructure. Phase0 has been completed by the end of 2021 and the project is now preparing to complete Phase1 by mid 2024. All facility instruments were optimized for cutting-edge experiments in agriculture, environmental science, health, and energy experiments, spanning diverse scientific programs strategic for Latin American science and technology.

In this report, we present the SIRIUS current operation status, and the preparation for achieving Phase1 parameters.

PRESENT PERFORMANCE

Presently, the SIRIUS storage ring is operating regularly, delivering beam for users shifts, for machine studies and subsystem tests. In 2022, 3408 hours are scheduled for user's shifts, 1272 hours for machine studies and subsystem tests with beam, and 1944 hours for installations and maintenance with access to the accelerators tunnel. The remaining hours are shared between machine recovery from longer stops, special tests and shutdown period.

There are presently six beamlines in operation in science commissioning mode. Five beamlines are based on adjustable phase (APU) commissioning undulators, and one beamline is from a dipole source.

For user's shifts, the SIRIUS storage ring is running with 100 mA in current decay mode with 2 injections per day, in uniform filling pattern mode with 864 bunches.

The stored current is presently limited by the RF system, consisting of a 500 MHz room temperature Petra 7-cell RF cavity, without HOM dampers, driven by 2x65 kW solid state amplifier towers. This cavity is temporarily being used while the final system is not available. The stored current was achieved after a careful work of temperature tunning of the Petra7 cavity. The final RF system will comprise 2 superconducting 500 MHz cavities driven by total power of 8x65 kW, and a superconducting passive third harmonic cavity.

Figure 1 shows the machine reliability, defined as the delivered beam time to the experiments within programmed time, over the last 13 months. The overall reliability in this period is 94.7%. During this period, the mean time between failures (MTBF) was 38 hours and the mean time duration of each failure was about 2 hours. There were 23 beam interruptions, with a concentration in the beginning of 2021.

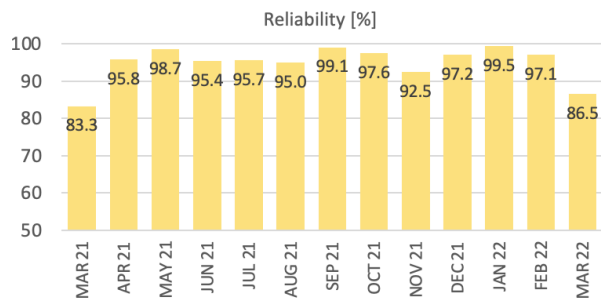

Figure 1: Machine reliability from March 2021 to March 2022.

The storage ring linear optics is close to design after correction using the LOCO algorithm applied to the machine with orbit corrected after calibration of BPM offsets with BBA. Presently, BBA and LOCO calibrations are routinely performed to check for machine conditions after maintenance periods. Optics symmetry is restored using both quadrupole family strength adjustments and individual quadrupole trim coil adjustments, as can be seen in Figure 2, where the measured betatron function at BPMs using the principal component analysis (PCA) in shown. The beta-beat at BPMs is corrected to 2.2% rms and 1.8% rms respectively, in the horizontal and vertical planes.

The measured beam lifetime at 100 mA is 17 h for 3% emittance ratio and for uniform filling. It is limited by the Touschek scattering effect. An experiment to measure the contribution of each effect to the total lifetime using 2

† liu@lnls.br

ISBN: 978-3-95450-227-1 ISSN: 2673-5490 doi:10.18429/JACoW-IPAC2022-TUPOMS003

CLS OPERATIONAL STATUS AND FUTURE OPERATIONAL PLANS*

M. J. Boland †[1], F. Le Pimpec, Canadian Light Source, Saskatoon, Canada
[1]also at University of Saskatchewan, Department of Physics and Engineering Physics, Saskatoon, Canada

Abstract

The Canadian Light Source (CLS) has been in operation for users since 2005 and recently commissioned its 22nd photon beamline. In 2021 the CLS implemented and commenced top-up operations at 220 mA. This new mode, for CLS, has been extremely well received by our scientific users. The storage ring is still RF power limited and require a second RF cavity to move towards realising the design goal of 500 mA. The 250 MeV electron injector complex for the CLS booster synchrotron ring dates back to the original linac from 1962 and the Saskatchewan Accelerator Laboratory and is in needs of an upgrade. This paper will give an overview of the present status of the accelerator systems for user operations and the operational improvement plans for a second RF cavity in the storage ring and a new linac.

INTRODUCTION

The CLS [1] has been in operation since 2005 but is only now starting to realise some of the design goals for the machine (Fig. 1). The primary goal has been the completion of the 22 beamlines [2], the last of which was completed in 2021. Also realised in 2021 is Top-Up Mode (Fig. 2), which has drastically improved the performance of the machine and provide a better quality beam for our users. Yet the facility to be able to stay competitive need to operate with at least 220 mA of current in any given configuration of the insertion devices installed in 9 straights of 12. The machine is powered by one Superconducting RF cavity and a second one is needed to reach higher beam currents due to power limits. Yet the machine has been designed for a 500 mA of operation and getting more RF power from new type of RF power system like Solid State amplifier will definitely be a game changer in terms of performance and reliability.

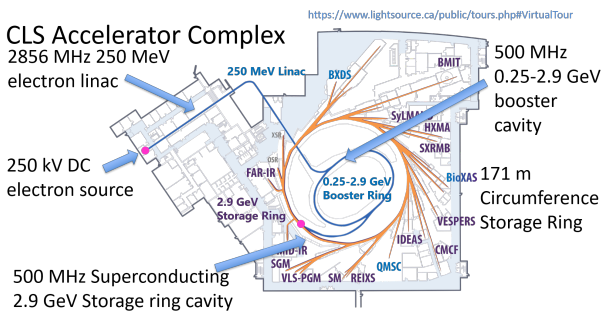

Figure 1: CLS accelerator complex overview.

PRESENT STATUS OF OPERATIONS

The CLS injector [3] makes use of the repurposed linac from the Saskatchewan Accelerator Laboratory which was established in 1964. Some improvements have been made to increase the performance of the linac over the years. For example two of the last three original 5 m long 2856 MHz Varian accelerating structures from 1964 have been replaced by two 3 m long 2856 MHz SLAC structures. The original structures were suffering from corrosion, vacuum leaks and water leaks, requiring regular RF reconditioning to reach full power. The space created by using shorter SLAC structures allowed for the installation of additional diagnostics, including YAG screens and cameras, FCTs and cavity BPMs in between each of the new structures.

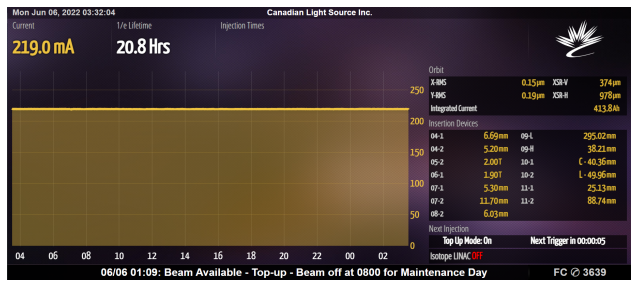

Figure 2: Typical 24 hours of user top-up mode.

One of the statistic that is of utmost importance for a research infrastructure which duty is to be a production facility of science is the up-time of its tools. All facilities aim to have an up-time or availability to be 100% meaning that all scheduled time for the photon user community is delivered. CLS aimed at delivering up to 4200 hrs of user beam with an uptime above 95%. The integrated hours planned and delivered up to June 2022 for this year is shown in Fig. 3.

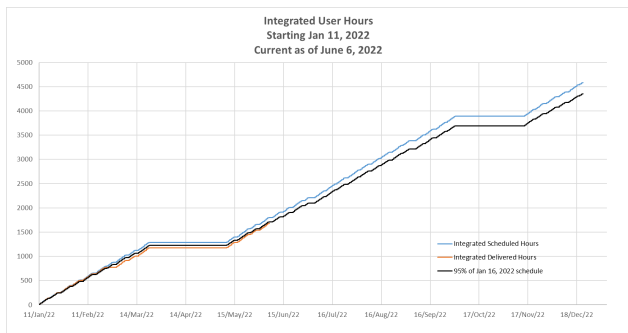

Figure 3: User beam availability and integrated beam delivered for 2022.

* Work supported by the CLS Accelerator Operations and Development Department.
† mark.boland@lightsource.ca

ISBN: 978-3-95450-227-1 ISSN: 2673-5490 doi:10.18429/JACoW-IPAC2022-TUPOMS004

TDR BASELINE LATTICE FOR THE UPGRADE OF SOLEIL

A. Loulergue*, O. R. Blanco-Garcia, P. Brunelle, W. Foosang, A. Gamelin, A. Nadji, L. S. Nadolski, R. Nagaoka, R. Ollier, M.-A. Tordeux, Synchrotron SOLEIL, Saint Aubin, France

Abstract

Previous CDR studies for the SOLEIL Upgrade project have converged towards a lattice alternating 7BA and 4BA HOA type cells providing a low natural horizontal emittance value in the 80 pm.rad range at an energy of 2.75 GeV. This lattice adapts to the current tunnel geometry as well as to preserve as much as possible the present beamline positions. The TDR lattice is an evolution of the CDR one including longer short straight sections, better relative magnet positioning, and the replacement quadrupole triplets by quadruplets for improving flexibility of optics matching in straight section. The SOLEIL upgrade TDR lattice is then composed of 20 HOA cells with a two-fold symmetry, and provides 20 straight sections having four different lengths of 3.0, 4.2, 8.0, and 8.2 m. This paper reports the linear and the non-linear beam dynamic optimization based on intense MOGA investigations, mainly to improve the energy acceptance required to keep a large enough Touschek beam lifetime. Some future directions for performance improvement are discussed.

INTRODUCTION

SOLEIL is the French third generation light source routinely operated for external users since 2008 with a low electron beam emittance of 4 nm·rad at an energy of 2.75 GeV in high intensity (500 mA, multibunch) and temporal structure (e.g. 8 bunches) modes [1,2]. After 15 years of successful operation, a series of feasibility studies were initiated for a possible upgrade of the storage ring with a significantly lower emittance. The approach taken is to employ all useful methods to reduce the emittance while respecting the geometric constraints such as the circumference of the ring and the available straight sections, in order to limit the impact on the existing beamlines and the building costs.

LATTICE LAYOUT

The current lattice of the SOLEIL storage ring is composed of 16 modified two-bend achromat cells, 8 of which have short straight sections between the dipoles, altogether giving a total of 24 straight sections covering up to 46% of the 354.1 meter long circumference [3] with 3 different lengths: 4×12, 12×7, and 8×3.8 m. This compact lattice provides a natural horizontal emittance of 4 nm.rad at an energy of 2.75 GeV.

Alternating 7BA and 4BA cells was then identified during the Conceptual Designe Report phase (CDR) [4,5] as the natural solution to best fit the current beamline (BL) positioning and leave the tunnel shielding wall unchanged [3, 4]. The TDR reference lattice is then composed of 20 HOA cells alternating 7BA and 4BA cells (Fig. 1), giving a natural horizontal emittance of 84 pm.rad at an energy of 2.75 GeV. In addition, the optical β-functions are focused down to low values (~1.5 m) in the short and medium sections for insertion devices (ID). The main comparison parameters are listed in Table 1.

Table 1: Main Lattice Parameters

	Actual	Upgrade
Emittance (2.75 GeV)	4 nm.rad	84 pm.rad
Circumference	354.1 m	353.5 m
Straight section number	24	20
Long straight length	12 m	8.00 / 8.35 m
Medium straight length	7 m	4.20 m
Short straight length	3.8 m	3.00 m
Straight sec. length ratio	46 %	25 %
Betatron tunes	18.16 10.23	54.2 18.3
Mom. comp. factor	$4.4\ 10^{-4}$	$1.05\ 10^{-4}$
RMS energy spread	0.1 %	0.091 %
Energy loss per turn w/o IDs	917 keV	458 keV
Damping times (ms)	3.3/3.3/6.6	7.7 /14.4 /12.2
RMS Nat. bunch length	15.17 ps	8.5 ps
RF Voltage	2.8 MV	1.8 MV

EVOLUTIONS FROM THE CDR

The first evolution was to change the matching sections from triplet to quadruplet of quadrupoles and to significantly rearrange their implantation for a much better mechanical integration of magnets, BPMs and crotches. In addition, all these quadrupoles became pure permanent magnets. The TDR lattice is then fully based on permanent magnets for all dipolar and quadrupolar main fields. Other magnets (sextupoles and octupoles) are naturally kept electromagnetic. To preserve optics tuning capabilities, 196 auxiliary thin air-cooled quadrupolar electromagnets were added along the arc cells. Added to the quadrupolar fields available in all the octupoles leading to a total of 412 quadrupolar correctors. In parallel, the nominal working point was shift away from the coupling resonance (Fig. 2). In terms of risk analysis, a coupling value of 30% with white noise excitation was finally preferred to the non-linear dissonance condition during injection process.

In addition to the ID beamlines, the ring must provide high magnetic fields for BLs on dipoles even if their number and location are not yet completely decided. To be more flexible, the second evolution was to split the 76

*alexandre.loulergue@synchrotron-soleil.fr

ISBN: 978-3-95450-227-1 ISSN: 2673-5490 doi:10.18429/JACoW-IPAC2022-TUPOMS005

SOLEIL MACHINE STATUS AND UPGRADE

L. S. Nadolski*, G. Abeille, Y.-M. Abiven, N. Béchu, F. Bouvet, P. Brunelle, M.-E. Couprie, X. Delétoille, S. Ducourtieux, S. Duigou, A. Gamelin, C. Herbeaux, N. Hubert, M. Labat, J.-F. Lamarre, V. Le Roux, A. Lestrade, A. Loulergue, O. Marcouillé, F. Marteau, A. Nadji, R. Nagaoka, M. Nouna, Y. Rahier, F. Ribeiro, G. Schaguene, K. Tavakoli, M.-A. Tordeux,
Synchrotron SOLEIL, L'Orme des Merisiers Saint-Aubin, BP 48 Gif-sur-Yvette Cedex, France

Abstract

SOLEIL is both a 2.75 GeV third generation synchrotron light source and a research laboratory at the forefront of experimental techniques dedicated to matter analysis down to the atomic scale, as well as a service platform open to all scientific and industrial communities. We present the performance of the accelerators delivering extremely stable photon beams to 29 beamlines. We report on the commissioning of a superbend magnet replacing a standard 1.71 T dipole with a 2.84 T narrow peak permanent magnet-based dipole. It required local modification of the lattice to compensate linear and nonlinear optics distortions introduced by the new magnet field. The latest measurements made with a Multipole Injection Kicker are also reported. Work on the NEG test bench and its dedicated front-end for a 10 mm inner diameter vacuum pipe and other major R&D areas are also addressed in the frame of the SOLEIL upgrade.

ACCELERATOR PERFORMANCE

Since January 2008, the synchrotron SOLEIL [1, 2] has been providing external users with high stability, high flux and high brightness photon beams. Among the 29 beamlines (BLs), 20 are on insertion devices (IDs), 9 on bending magnets including 2 IR beamlines: 27 diverse IDs are daily operated (gap/phase) by the users (2 in-vacuum in-vacuum cryogenic permanent magnet undulators (CPMUs), 6 in-vacuum undulators (IVUs), 13 Apple-II type undulators, 4 electromagnetics IDs, and 2 wigglers). The overall facility has been performing at a high level during the year 2021: 4935 hours (including 32 h of radiation safety tests) with a beam availability of 98.4 % and a record meantime between failure (MTBF) of 109 hours. All five operation modes were delivered in top-up mode of injection (availability: 99.7 %; MTBF: 25h) keeping the current within ±0.5% of its nominal value for the uniform and hybrid mode with a distribution given by Fig. 1. The year 2021 showed a significant increase of machine dedicated time (1431 h) to commission several innovative systems as described in the following section.

MAIN ACHIEVEMENTS

Lattice Modification for the ROCK BL Superbend

The storage ring (SR) lattice features a one-fold symmetry based on a modified double-bend achromat structure [3] allowing the space for 24 straight sections (see Table 1). One of the long straight sections, SDL13, hosts two canted

Table 1: Storage Ring Main Parameters

Parameters	Values
Energy	2.75 GeV
Circumference	354.097 m
Natural chromaticities (H/V)	-53/-19
Natural Emittance	4.0 nm · rad
Number of Cells/Symmetry	16/1
Tunes (H/V)	18.155 / 10.229
RF frequency (harmonic number)	352.197 MHz (416)
Total RF Voltage	2.8 MV

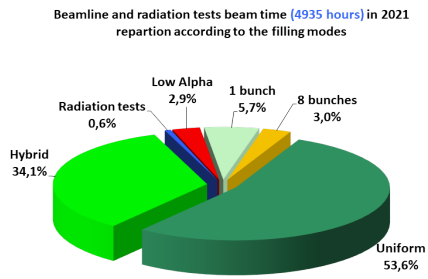

Figure 1: Filling pattern distribution during the year 2021.

BLs accommodating a double beta waist in the vertical plane for the simultaneous closure of the two 2 m long CPMUs at 5.5 mm minimum gap [4, 5].

Since August 2021, another major modification of the lattice has been introduced: the nominal 1.71 T dipole source of the ROCK beamline was replaced with a superbend, an permanent magnet 2.84 T dipole developed in-house (Fig. 2). A full week was necessary to complete its commissioning and the campaign of radiation safety test in order to qualify the storage ring and all beamlines with the superbend. The first photon beam was recorded by the ROCK beamline on August 27, 2021; two days later a flux increase by a factor 7.4 was measured at a photon energy of 40 keV as predicted. The additional focusing of the superbend was locally compensated using LOCO [6] and the strong chromatic contribution of the high field sextupolar component was first corrected globally before further MOGA-based [7] sextupole optimization enabling to recover most of the dynamic aperture and then a better injection rate. The latest performance results in an average total beam lifetime of 12 hours at 500 mA with an injection efficiency closed to 86 % for the bare lattice.

* laurent.nadolski@synchrotron-soleil.fr

ISBN: 978-3-95450-227-1 ISSN: 2673-5490 doi:10.18429/JACoW-IPAC2022-TUPOMS006

FILO: A NEW APPLICATION TO CORRECT OPTICS IN THE ESRF-EBS STORAGE RING

S.M. Liuzzo, N. Carmignani, L.R. Carver, L. Farvacque,
L. Hoummi, T. Perron, B. Roche, B. Vedder, S. White
ESRF, Grenoble, France

Abstract

A new optics correction application (Fit and Improvement of Linear Optics, FILO) was designed and set in place for the ESRF-EBS storage ring. The widely used software LOCO is not available at ESRF and despite a few trials to set it in operation, it has been decided to write a new code. The application is flexible, may be used via the control system simulators and is adapted to a user friendly operation thanks to a wizard mode. Some features of LOCO are copied over, some others are yet to be implemented. The measurement of on and off-energy response matrices using slow or fast steerers is integrated in the same application. Results obtained with this application are presented together with an overview of the future developments.

INTRODUCTION

Optics correction are necessary at synchrotron radiation storage rings (SR) to reach and maintain the user service mode (USM) properties in terms of beam equilibrium emittance, coupling and lifetime. The data necessary to perform optics corrections are either BPM turn by turn data [1] or orbit response matrix and dispersion [2]. We describe in this paper the matlab [3] application set up at ESRF to perform the second kind of measurements. Experimental results of ESRF-EBS optics correction and measurements can be found in [4, 5].

OPTICS CORRECTIONS FOR EBS

The optics of the ESRF-EBS storage ring are corrected routinely upon each restart of the accelerators. These corrections are not necessary during user operation, but only after interventions on the magnets. Usually simply restoring orbit and tunes is sufficient to recover the expected operational performances in terms of beta-beating and coupling. Optics corrections are intended here as the adjustment of normal and skew quadrupole strengths based on the measurement of: 1) a partial orbit response matrix (*ORM* see Eq. (1) with $x_{h,v}$ the orbit at the usable BPMs and $\theta_{H,V}$ the steerers strengths) and 2) the response of beam in the horizontal and vertical plane to a shift of RF frequency (see Eq. (1)).

$$ORM_{(h,v),(H,V)} = \frac{\Delta x_{h,v}}{\Delta \theta_{H,V}}, \quad \eta_{h,v} = \frac{\Delta x_{h,v}}{\Delta f_{RF}} \tag{1}$$

The signals to be corrected to their theoretical values are described by the vectors $D_{n,s}$ in Eq. (2) and (3) where the subscripts n and s refer to normal or skew, the weights w_η and w_t define a different scaling for the dispersion and tunes.

$$D_n = [ORM_{h,H}, ORM_{v,V}, w_\eta \eta_h, w_t \nu_h, w_t \nu_v] \tag{2}$$

$$D_s = [ORM_{h,V}, ORM_{v,H}, w_\eta \eta_v] \tag{3}$$

$J_{n,s}$ in Eq. (4) is the derivative of $D_{n,s}$ for a given error.

$$J_{n,s} = \frac{\Delta D_{n,s}}{\Delta V_{n,s}} \tag{4}$$

The computation of $J_{n,s}$ is performed numerically based on the lattice model. The quantities $V_{n,s}$ refer to any variable that the user wants to use to fit the lattice model such to reproduce the measurements. This usually include the normal and skew quadrupole correctors gradients, beam position monitors scale and rotation errors, steerers gains and tilts. The fit is performed using an singular value decomposition pseudo-inversion in order to compute the values of $V^{cor}_{n,s}$ that would yield a vector $D_{n,s}$ as close as possible to the measured one $D^{measured}_{n,s}$.

$$V^{cor}_{n,s} = J^{-1}_{n,s}(D^{measured}_{n,s} - D^{model}_{n,s}) \tag{5}$$

The values of the fitted variables (sometimes assumed as measured lattice errors) are included in the optics model to create a *fitted optics* model. This model is then used to compute the skew and normal quadrupole corrections in two possible ways:

- applying the fitted normal and skew quadrupole errors to the lattice, or,
- in the general case of correction locations not strictly identical to the errors fit locations, computing the normal and skew quadrupole resonant driving terms (RDTs) and correcting them as described in [6].

MEASUREMENT

The procedure to perform optics correction is the following:

1. measure initial emittances
2. measure an orbit response matrix with a given subset of steerers and BPMs
3. measure the frequency response at the same BPMs
4. select a series of variables to fit the measured quantities
5. prepare $J_{n,s}$ (see later sections)
6. construct a fitted lattice model
7. compute normal and skew quadrupole corrections
8. plot expected results for inspection by the user
9. apply correction
10. measure the final emittances and dispersion

ISBN: 978-3-95450-227-1 ISSN: 2673-5490 doi:10.18429/JACoW-IPAC2022-TUPOMS007

A LONG BOOSTER OPTION FOR THE ESRF-EBS 6 GeV STORAGE RING

S. Liuzzo, N. Carmignani, L.R. Carver, L. Hoummi, T. Perron, S. White
ESRF, Grenoble, France

Abstract

Despite the several fruitful upgrades undergone, the present injector complex of the ESRF-EBS has a rather large horizontal natural emittance at extraction of > 60 nm rad. Several light sources [1–3] have adopted booster injectors fitting in the same tunnel as the main SR. The study of such an injector is shown in this paper for the ESRF-EBS. The proposed solution is based on a DBA lattice structure with five quadrupole families and two sextupole families. The possibility to install this long booster on the internal wall of the ESRF storage ring tunnel is assessed and the adequate distances are analyzed. The possibility to keep the existing injector is also considered in order to use this additional ring as an accumulator ring. Injection and extraction schemes are described.

INTRODUCTION

After the successful upgrade of the ESRF-EBS storage ring (SR) lattice to HMBA [4] injection efficiency is below the design, reaching at most 85% in User Service Mode (USM) while the simulations predicted up to 95% injection efficiency [5]. The simulations assumed a smaller injected beam in the storage ring and larger errors than those observed in the SR. Also the measured dynamic aperture of the EBS SR is about 1 mm less than the expected one (see [4]). Moreover future upgrades will potentially have a detrimental impact on injection efficiency, such as the possibility to reduce insertion devices minimum gaps below 6 mm. For these reasons several options have been studied to upgrade the injectors of the ESRF storage ring and in particular the full energy booster, toward a lower injected beam horizontal emittance [6–8]. In this paper we study only one of the options considered: a long booster fitting the same tunnel of the storage ring. This option is not easily feasible due to the limited space in the tunnel, but it is studied in order to compare performances.

LATTICE

The double bend achromatic (DBA) lattice has been simplified and scaled to the appropriate length. Considering a common RF frequency with the main storage ring, the length is defined by the harmonic number of the storage ring minus a given value. For the lattice presented here, the main SR harmonic number is 992 and the booster harmonic number is set to 979. This value is chosen as it gives a distance between the storage ring beam and the booster beam of 1.76 m, fitting within the minimum total available distance of about 1.90 m and leaving 14 cm from the wall to be occupied by the magnet's yokes. Even if this space seems limited, ramped magnets have a smaller profile that standard magnet (imagine for example septa dipoles). Considering the SR magnets, about 1 m free space remain between booster and SR. Further investigation will define the optimal value of the harmonic number of the booster to allow maximum flexibility for the main SR filling patterns. The option to install the booster at a different vertical height is also envisaged, but not studied in the present document. The possibility to place the booster on top of the existing storage ring is discarded for geometry and maintenance issues.

Table 1: ESRF-EBS Long DBA Booster Magnet Gradients Required at 6 GeV

	L	KL	$KB\rho$
B	3.5 m	98.1748 mrad	0.5614 T
QF1	0.6 m	0.3822 1/m	12.7489 T/m
QD2	0.6 m	-0.3992 1/m	-13.3172 T/m
QD3	0.6 m	-0.3065 1/m	-10.2232 T/m
QF4	0.6 m	0.3121 1/m	10.4108 T/m
SF2	0.2 m	0.7034 1/m^2	70.3909 T/m^2
SD2	0.4 m	-2.5523 1/m^2	-127.7056 T/m^2

The optics for one cell of the proposed ESRF-EBS long booster are shown in Fig. 1.

Compared to classic DBA cells [9] there are only two sextupole families and the defocusing sextupole and quadrupole in the center of the cell are swapped, to allow for larger separation and increased beta functions at the sextupoles. The straight sections are kept, but may be shortened if needed. The ring is composed of 32 cells, corresponding to the main SR cells. The maximum magnet gradients presented in Table 1 are easily achievable. The relevant parameters at 6 GeV are available in Table 2, in particular producing an equilibrium emittance of 6.2 nm rad.

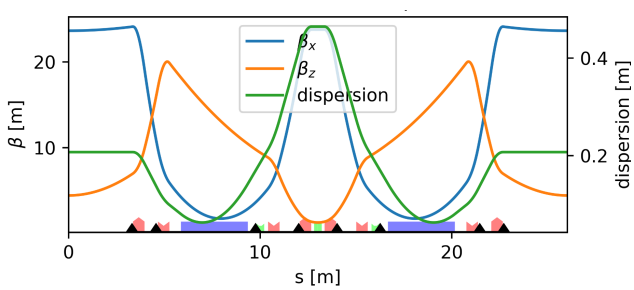

Figure 1: Magnets layout for a 32 cells DBA booster injector. Only two sextupole families will be required.

A total of seven synchronous ramped power supplies are needed for: one dipole family, four quadrupole families and two sextupole families. The magnets lengths are as much

ISBN: 978-3-95450-227-1 ISSN: 2673-5490 doi:10.18429/JACoW-IPAC2022-TUPOMS008

LIFETIME CORRECTION USING FAST-OFF-ENERGY RESPONSE MATRIX MEASUREMENTS

S.M. Liuzzo, N. Carmignani, L.R. Carver, L. Hoummi, T. Perron, B. Roche, S. White
ESRF, Grenoble, France

Abstract

Following the measurements done at MAX-IV [1], we try to exploit for the ESRF-EBS Storage Ring (SR) off-energy response matrix measurement for the optimization of Touschek lifetime. The measurements performed with fast AC steerers on- and off-energy are analyzed and fitted producing an effective model including quadrupole and sextupole errors. Several alternatives to extrapolate sextupoles strengths for correction are compared in terms of lifetime. For the time being none of the corrections could produce better lifetime than the existing empirically optimized set of sextupoles.

INTRODUCTION

The ESRF-EBS SR Touschek lifetime is optimized routinely using an empirical approach [2]. In the recent paper by Olsson et al. [1] it was shown that it is possible based on on- and off-energy orbit response matrix measurements to determine a set of sextupoles able to improve the lifetime, by correcting the off-energy optics of the SR.

Having seen the promising results presented, the Nonlinear optics from off-Energy Closed Orbit (NOECO) technique shown in [1] is applied to the EBS SR. This paper reports about the initial simulations and the preliminary results obtained during the first two dedicated experimental shifts.

NOECO CORRECTION

The NOECO correction exploits the dependence on sextupole strengths of the off-energy orbit response matrix. A set of normal sextupole correctors $K_{\text{sext}}^{\text{cor}}$ is computed based on two off-energy orbit response matrices (ORM) and dispersion (η_h) measurements by solving the following system of equations using a SVD pseudo-inverse:

$$V = \frac{(ORM, \alpha_\eta\, \eta_h)_{+\delta} - (ORM, \alpha_\eta\, \eta_h)_{-\delta}}{\partial \delta} \quad (1)$$

$$V_{\text{measured}} - V_{\text{model}} = \frac{\partial V}{\partial K_{\text{sext}}} K_{\text{sext}}^{\text{cor}} \quad (2)$$

where V is a vector including the variation of all the ORM elements and horizontal dispersion with respect to an energy deviation δ and α_η is a weight to determine the relative balance among ORM and η_h correction (initially set to give similar amplitude to the dispersion response compared to the ORM and then empirically tuned). Only the diagonal blocks (horizontal response to an horizontal steerer and vertical response to a vertical steerer) of the ORM are used. The Jacobian $\partial V / \partial K_{\text{sext}}$ is computed numerically using the Matlab [3] version of Accelerator Toolbox (AT) [4]. In the analysis all the BPMs are considered equal and no weight factor is used. For the details of the correction we refer to the original paper.

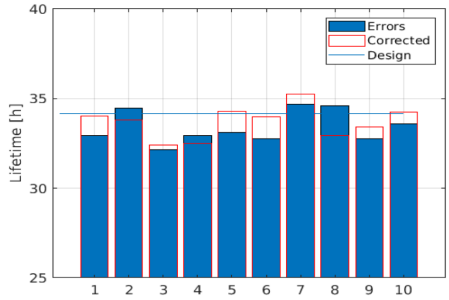

Figure 1: Lifetime before and after NOECO correction for 10 simulated lattices including errors and corrections with identical α_η and number of singular values. Three seeds out of ten require ad-hoc tuning of α_η and number of singular values in order to improve the lifetime.

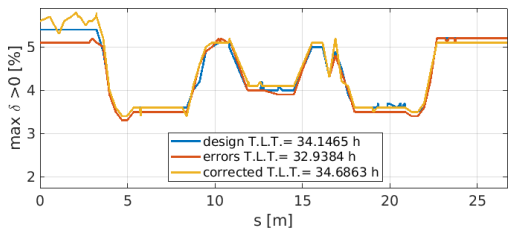

Figure 2: Local momentum acceptance for the first cell of the EBS SR for the design lattice without errors, a lattice with errors and the same lattice with sextupole corrections computed using NOECO.

SIMULATIONS

Simulations of the NOECO correction were done in AT using lattices with realistic errors and corrections based on a commissioning-like simulation loop [5]. For most of the seeds considered the computed lifetime improved after NOECO correction, as shown in Fig. 1. With a change of the singular values or of the weights α_η, seeds 2, 4 and 8 had their simulated lifetime improved compared to the one without NOECO sextupole correction. The local momentum acceptance for the first cell of the SR is compared in Fig. 2 before and after correction to the one without any errors. The NOECO correction effectively restores the ideal momentum acceptance. The injection efficiencies contextually computed for each seed do not show significant variations (<1%). The sextupole errors present in these lattices are taken from a random Gaussian with standard deviation of 0.35% of the main sextupole field as defined by the magnet

ISBN: 978-3-95450-227-1 ISSN: 2673-5490 doi:10.18429/JACoW-IPAC2022-TUPOMS009

FIRST YEAR OF OPERATION OF THE ESRF-EBS LIGHT SOURCE

J-L Revol, C. Benabderrahmane, P. Borowiec, E Buratin, N. Carmignani, L. Carver, A. D'Elia, M.Dubrulle, F. Ewald, A Franchi, G. Gautier, L. Hardy, L. Hoummi, J. Jacob, G. Le Bec, L. Jolly, I. Leconte, S. M. Liuzzo, M. Morati, T. Perron, Q. Qin, B. Roche, K. B. Scheidt, V. Serrière, R. Versteegen, S. White, European Synchrotron Radiation Facility, Grenoble, France

Abstract

The European Synchrotron Radiation Facility - Extremely Brilliant Source (ESRF-EBS) is a facility upgrade allowing its scientific users to take advantage of the first high-energy 4th generation storage ring light source.

In December 2018, after 30 years of operation, the beam stopped for a 12-month shutdown to dismantle the old storage ring and to install the new X-ray source. On 25th August 2020, the user programme restarted with beam parameters very close to nominal values.

This paper reports on the present operation performance of the source, highlighting the ongoing and planned developments.

INTRODUCTION

The ESRF, located in Grenoble France, is a facility supported and shared by 22 partner nations. This light source, in operation since 1994 [1 - 3], has been delivering 5500 hours of beam time per year on up to 42 beamlines. The chain of accelerators consists of a 200 MeV linac, a 4 Hz full-energy booster synchrotron and a 6 GeV storage ring (SR) 844 m in circumference. A large variety of insertion devices (in-air, in-vacuum and cryo-in-vacuum undulators, as well as wigglers) are installed along the 28 available straight sections. Bending-magnet radiation, now produced by short bends and wigglers, is used by 12 beamlines.

Since 2009, the ESRF has embarked on an upgrade programme of its infrastructure, beamlines and accelerators. The second phase (2015-2022), saw the design and the installation of a new storage ring based on a hybrid multibend achromat (HMBA) replacing the double-bend lattice [4 - 7]. Reducing the horizontal emittance from 4 nm rad down to 133 pm rad (Table 1) allows a dramatic increase in brilliance and coherence.

Started in 2015, the project was conducted in four years for the design, procurement and assembly. The down time for the installation was slightly less than one year. After 6 months of commissioning, the beam was back for the users on 25th August 2020, the target date [8 - 13].

Table 1: Main Parameters of the Old and New SR

	Units	ESRF	ESRF-EBS
Energy	*GeV*	6	6
Circumference	*m*	844.4	844
Lattice		DBA	HMBA
Current	*mA*	200	200
Lifetime	*h*	50	23
Emittance H	*pm rad*	4000	133
Emittance V	*pm rad*	4	10*

(*) Vertical emittance increased from 1 to 10 pm rad.

USER-MODE OPERATION

Despite the restrictions due to the Covid-19 pandemic, most beamlines were able to take beam on August 2020. The main beam parameters, chiefly beam intensity, lifetime and emittances, were already reached [9]. Since that date, the beam was continuously delivered to the users. During the second and third confinements in France, USM delivery was reduced to three and four days/week, respectively.

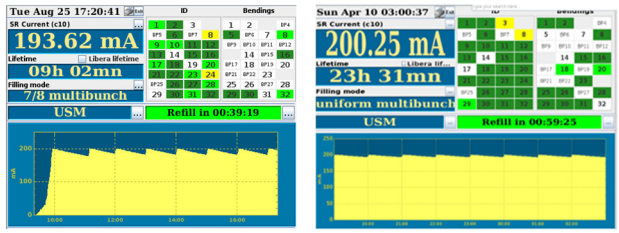

Figure 1: First USM Day on 25th August 2020 and delivery in April 2022.

Beam Lifetime

Even though a vertical emittance of about 1 pm rad could be achieved after coupling correction, the electron beam is voluntarily blown up vertically in order to reach an operational lifetime. Tests performed with the most sensitive beamlines indicated that 10 pm rad was an acceptable vertical emittance. Vacuum conditioning and optics tuning [14] led to a stable operational lifetime longer than 20 hours with the emittance artificially kept at 10 pm rad by a dedicated feedback loop (see Fig. 1).

Most of the electron beam losses are localized at the two shielded collimators for radioprotection safety and to protect insertion devices from demagnetisation [15]. The efficiency of the relocation is around 50% instead of the planned 80%. The closure of the collimators is tuned so as to reduce losses on the undulators as much as possible, with a maximum accepted reduction of the total beam lifetime of 8%, with ID gap open. Beam loss references just after the insertion devices were taken in 2018. The objective is to maintain the same level of losses with undulators closed.

Beam Stability and Top-up

Despite the reduction of the horizontal emittance, the beam stability fulfils today the beamline requirement. Associated to the slow orbit correction, a fast orbit feedback stabilizes the orbit up to 100 Hz motion to a residual motion of 0.8% and 2.8% of the horizontal and vertical beam size. A task force has been established to monitor and further improve the beam orbit against different sources of perturbation. Those occurring during top-up injections are disturbing and even preventing some beamlines from acquiring data during these (short) periods. Off-axis injection

ISBN: 978-3-95450-227-1 ISSN: 2673-5490 doi:10.18429/JACoW-IPAC2022-TUPOMS010

BESSY III STATUS REPORT AND LATTICE DESIGN PROCESS

P. Goslawski*, M. Abo-Bakr, M. Arlandoo, J. Bengtsson, K. Holldack,
A. Jankowiak, B. Kuske, A. Meseck, M. Titze, M. Sauerborn, J. Viefhaus, J. Völker
Helmoltz-Zentrum Berlin, BESSY, Berlin, Germany

Abstract

Since 2020 a detailed discussion about a BESSY II successor is ongoing at Helmholtz Center Berlin (HZB) and its user community in order to define the science and layout of the new facility. Still free locations close to BESSY II have triggered a discussion about a greenfield project, but in-house upgrade solutions have also been investigated. As a special boundary condition, BESSY III has to meet the requirement of the Physikalische Technische Bundesanstalt (PTB) for radiation sources for metrology applications and bending magnet sources for tender X-rays. A Conceptional Design Report is in preparation. Here, we give a status report including a first parameter space, technical specifications and a first candidate for the linear lattice.

THE BESSY III REQUIREMENTS & OBJECTIVES

A first sketch of the upgrade discussion of BESSY II with its user community and the envisaged parameter space has been given in [1] and is briefly summarized in Table 1. The main objectives and also largest changes compared to BESSY II are the increase of energy up to 2.5 GeV and the decrease of emittance down to 100 pm rad, motivated by the science case request for diffraction limited radiation with adjustable polarisation up to 1 keV photon energy from the 1st undulator harmonics.

Table 1: Main Parameters of BESSY II and BESSY III

Parameter	BESSY II	BESSY III
Energy	1.7 GeV	2.5 GeV
Circumference	240 m	~ 350 m
# of straights	16 with 5.0 m	≥ 16 with 5.6 m
Emittance ϵ_0	5 nm rad	100 pm rad
$\beta_{x,y}$ in straights	(1.2, 1.2) m	< (3, 3) m
mom. comp. α_p	7.0e-4	> 1.0e-4

Further demands on the lattice are under discussion. For example, small $\beta_{x,y}$ functions of < 3 m in straights and the operation of round beam in order to match the electron beam and photon beam phase space within the undulators. And the momentum compaction α_p was chosen to be $>1.0 \times 10^{-4}$ in order to achieve reasonable bunch length and lifetime and not be dominated by collective effects. Owing to capacity reasons, at least one bending magnet source within the sector is also needed to deliver radiation in the soft-to-tender range, e.g., 1 keV to 10 keV.

The developments on "TRIBs / Two orbit operation" over the last years at BESSY II [2, 3] motivate the task to study such beam optics and operation scheme for BESSY III and investigate the impact on the achievable parameters compared to a standard user mode with one orbit [4].

Due to the long standing partnership since BESSY I (1981) with the PTB, Germany's national institute for standards & metrology, an absolutely mandatory demand on the BESSY III facility is to provide a radiation source, usable as primary radiation standard, i.e., an absolute, predictable and traceable radiation source for metrology purposes. For that the deflecting, magnetic field around the source point has to be known to highest precision and be accessible for a NMR probe measurement. As the measurement sensor itself has certain spatial dimensions of (10 x 10 x 10) mm^3 volume, a purely homogeneous magnet field is required at least for this volume or along the orbit of the electron beam. This is best realized with a purely homogeneous dipole magnet, which has to be included in the lattice. A combined function bend with gradient, i.e., changing magnetic field in the horizontal plane, which is often used in the mulitbend-achromat (MBA) unit cell, is therefore not a good choice. The request for the **homogeneous metrology bend** strongly influenced our lattice design process towards a first baseline lattice, which will be mainly discussed in this contribution.

THE BESSY III LATTICE DESIGN APPROACH

The development process towards a first baseline lattice for BESSY III could be broken down into three steps, which will be explained in the following.

- First tries, technical limitations & the choice for a Higher Order Achromat (HOA),
- 1st milestone lattice: "Simplest HOA" with only two chromatic sextupole families and integer tunes,
- 2nd milestone lattice: first non-linear optimization.

First Tries, Technical Limitations & HOA

First lattice attempts like a 16-period 9MBA based on the ALS-U design or a 18-period 5MBA resulted in very ambitious magnetic specifications, which have triggered a discussion about the hardware limits and technical realization. Within the CDR phase, the decision has been made to follow a more conservative ansatz and rely on already existing magnet technology, e.g., conventional state-of-the-art iron yoke electromagnet technology for multipoles. The CDR magnet specifications have not been driven to technical limits, and are listed in Table 2. Sticking to the technical limits and keeping the circumference of ~350 m a 6MBA compared to 7- or 8MBA seems to be the best solution in respect to emittance and the momentum compaction factor. The 5MBA does not allow to implement a HOA with strong

* paul.goslawski@helmholtz-berlin.de

ISBN: 978-3-95450-227-1 ISSN: 2673-5490 doi:10.18429/JACoW-IPAC2022-TUPOMS011

PROGRESS TOWARDS EEHG SEEDING AT THE DELTA STORAGE RING*

B. Büsing†, A. Held, H. Kaiser, S. Khan, C. Mai, A. Radha Krishnan,
Zentrum für Synchrotronstrahlung (DELTA), TU Dortmund, 44227 Dortmund, Germany

Abstract

Seeding of free-electron lasers (FELs) with external laser pulses triggers the microbunching process such that the spectrotemporal properties of coherently emitted FEL radiation are under better control compared to self-amplified spontaneous emission. High-gain harmonic generation (HGHG) based on the interaction of electrons with a single laser pulse is routinely applied at a few FELs, and echo-enabled harmonic generation (EEHG) with a twofold laser-electron interaction has been demonstrated. Both schemes can be adopted in storage rings for the coherent emission of ultrashort radiation pulses. Coherent harmonic generation (CHG) is the counterpart to HGHG without FEL gain. It has been employed at several storage rings and presently provides ultrashort pulses in the vacuum ultraviolet regime at the 1.5-GeV electron storage ring DELTA operated by the TU Dortmund University. EEHG, which allows to reach higher harmonics of the seed wavelength, has not yet been implemented at any storage ring but is pursued at DELTA as an upgrade plan. The paper presents the layout of the envisaged EEHG facility, and it reviews simulation studies and the technical progress towards EEHG seeding at DELTA.

ECHO-ENABLED HARMONIC GENERATION (EEHG)

Based on a twofold laser-electron interaction, the seeding scheme echo-enabled harmonic generation (EEHG) [1] is a promising method to provide ultrashort radiation pulses in the femtosecond regime of wavelengths in the extreme vacuum ultraviolet at storage rings. Co-propagating laser pulses and electron bunches in two undulators (modulators) tuned to the laser wavelength lead to energy modulations, which are converted by dispersive chicanes after the modulators into a complex density modulation, so-called microbunches.

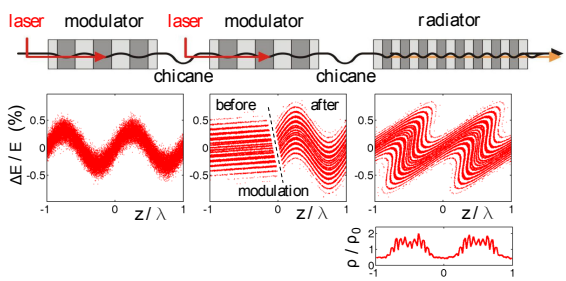

Figure 1: Magnetic setup for EEHG, corresponding longitudinal phase space distributions and the final longitudinal electron density.

Here, the first chicane is strong and forms thin stripes in the longitudinal phase space, while the second weaker chicane generates the microbunches. These michrobunches lead to coherent emission of radiation in the successive radiator tuned to a harmonic of the laser wavelength. The scheme is depicted in Fig. 1.

EEHG AT DELTA

Currently the short-pulse facility at DELTA, a 1.5-GeV storage ring operated by the TU Dortmund University, is based on the coherent harmonic generation scheme (CHG) [2, 3] where only one laser-electron interaction takes place. Modulator, chicane and radiator are realized within a single undulator U250 as shown in Fig. 2 (top). A Ti:sapphire laser system enables seeding with 800 nm laser pulses or their second harmonic.

Storage Ring Optics

To implement EEHG, the short-pulse facility needs to be remodeled to create a long straight section where all components can be arranged directly in one straight section, see Fig. 2 (bottom). The magnet positions were determined by several boundary conditions regarding the beta functions in the modulators to match the laser and electron bunch size, an achromatic straight section to not disturb the longitudinal phase space and to keep the optical functions outside the modified section unchanged as to not influence the other beamlines [4]. To fulfill all the requirements, simulations of the optics of the present and future ring were performed with the simulation code *elegant* [5]. The resulting main parameters of present and future ring are listed in Table 1 and Fig. 3 shows the beta functions of the two setups. Simulations of the dynamic aperture have also been performed [6].

Table 1: Main Parameters of the DELTA Storage Ring

Parameter	Present	EEHG
electron beam energy	1.5 GeV	1.5 GeV
circumference	115.20 m	115.21 m
hor. tune	9.19	8.59
vert. tune	3.28	3.55
mom. comp. factor	$4.9 \cdot 10^{-3}$	$4.7 \cdot 10^{-3}$
rel. energy spread	$7 \cdot 10^{-4}$	$7 \cdot 10^{-4}$
hor. emittance	16 nm rad	22 nm rad
max. hor. beta function	45 m	22 m
max. vert. beta function	51 m	25 m

MAGNETS

The quadrupole magnets as well as the girders and power supplies of the present setup will be reused. The 10° dipoles

* Work supported by the BMBF under contract 05K16PEB and 05K19PEB, Forschungszentrum Jülich and by the Federal State NRW
† benedikt.buesing@tu-dortmund.de

ISBN: 978-3-95450-227-1 ISSN: 2673-5490 doi:10.18429/JACoW-IPAC2022-TUPOMS012

INVESTIGATION OF SPECTRO-TEMPORAL PROPERTIES OF CHG RADIATION AT DELTA*

A. Radha Krishnan† , B. Büsing, A. Held, H. Kaiser, S. Khan, C. Mai, Z. Usfoor, V. Vijayan
Center for Synchrotron Radiation (DELTA), TU Dortmund, Dortmund, Germany

Abstract

At the synchrotron light source DELTA operated by the TU Dortmund University, the short-pulse facility employs the seeding scheme coherent harmonic generation (CHG) and provides ultrashort pulses in the vacuum ultraviolet and terahertz regime. Here, the interaction of laser pulses with the stored electron bunches results in a modulation of the longitudinal electron density which gives rise to coherent emission at harmonics of the laser wavelength. The spectral and temporal properties of such coherent short pulses can be manipulated by the seed laser and magnetic chicane properties. CHG spectra at several harmonics of the 800 nm seed laser were recorded using an image-intensified CCD (iCCD) camera and a newly installed XUV spectrometer. Numerical simulations to calculate the spectral phase properties of the seed laser from the observed spectra were carried out.

INTRODUCTION

Synchrotron radiation is a vital tool in studying the properties of matter in a variety of experiments, thanks to its characteristics such as high intensity, collimation and tunable wavelength. However, the minimum pulse length is limited by the electron bunch length which is in the order of several tens of picoseconds. These pulses lack the temporal resolution to probe the atomic processes taking place on the sub-picosecond scale. On the other hand, conventional mode-locked lasers can produce light pulses in the femtosecond regime but are usually of long-wavelengths. Coherent harmonic generation (CHG) [1] is a technique that combines the advantages of these two radiation sources to produce coherent femtosecond light pulses of short wavelength.

CHG is similar to the high-gain harmonic-generation seeding scheme used for free-electron lasers (FEL), but without the FEL gain in conventional storage rings [2–4]. As depicted in Fig. 1, CHG is based on a laser-electron interaction in an undulator that is tuned to the seed laser wavelength (modulator). This results in a sinusoidal modulation of the electron energy, which is transformed into a density modulation (microbunches) via a magnetic chicane. In a subsequent undulator (radiator), the microbunches produce coherent emission at harmonics of the laser wavelength. Since the laser pulse only modulates a very short slice of the electron bunch, the resulting coherently emitted pulse will also have a pulse length comparable to that of the laser pulse.

The power of the CHG radiation at the n^{th} harmonic of the laser wavelength λ is given by

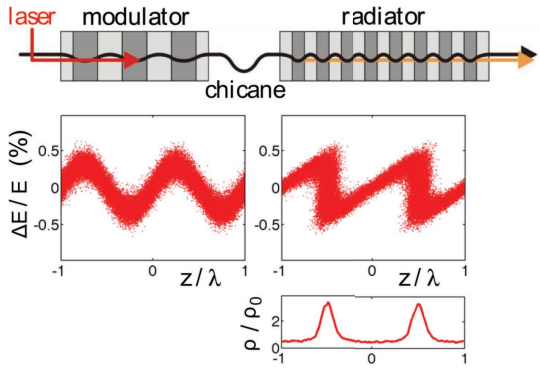

Figure 1: Magnetic setup for CHG, corresponding longitudinal phase space distributions and final longitudinal electron density.

$$P_n(\lambda) \sim N_e^2 b_n^2(\lambda) \tag{1}$$

where b_n is the bunching factor and N_e is the number of modulated electrons. For the CHG scheme, the bunching factor is given by [5],

$$b_n = |J_n(nAB)| e^{-\frac{n^2 B^2}{2}} \tag{2}$$

where $A = \Delta E_{\max}/\sigma_E$ is the relative energy modulation amplitude and $B = R_{56} k \sigma_E / E_0$ is the dimensionless chicane parameter. Here R_{56} is the matrix element of the chicane describing its longitudinal dispersion, E_0 is the nominal beam energy, σ_E is the rms energy spread and $k = 2\pi/\lambda$. When seeded with a laser pulse, the energy modulation amplitude A follows the pulse shape of the laser. Due to this non-uniform energy modulation, the chicane parameter influences the pulse shape of the CHG radiation. As can be seen in Fig. 2, at an R_{56} of 45 μm (green line) where the bunching is maximized, the resulting CHG radiation will be a single bell-shaped pulse. For stronger chicanes, e.g. 100 μm (red line), microbunching occurs for the electrons with a lower energy modulation at the head and tail of the modulated slice, while the electrons at the centre with maximum energy modulation are overbunched. Consequently, this results in separate pulses originating from different longitudinal positions. This allows one to manipulate the CHG pulse shape by tuning the laser and chicane properties, as demonstrated in the case for FERMI [6].

The spectral content of the CHG pulses does not only depend on R_{56}, but also on the wavelength distribution along the seed pulse. A laser pulse can be expressed in the frequency domain in terms of spectral amplitude $\tilde{E}(\omega)$ and spectral phase $\phi(\omega)$

* Work supported by BMBF (05K16PEA, 05K19PEB), DFG (INST 212/236-1 FUGG) and the federal state of NRW.
† arjun.krishnan@tu-dortmund.de

ISBN: 978-3-95450-227-1 ISSN: 2673-5490 doi:10.18429/JACoW-IPAC2022-TUPOMS013

NOVEL HIGH REPETITION RATE CW SRF LINAC-BASED MULTISPECTRAL PHOTON SOURCE

P. Evtushenko†, Helmholtz-Zentrum Dresden-Rossendorf
Institute or Radiation Physics, Dresden, Germany

Abstract

We discuss a design of a CW SRF linac-based photon facility for the generation of MIR-THz and VUV pulses at high repetition rates of up to 1 MHz. The MIR-THz sources would cover the frequency range from 0.1 to 30 THz with the pulse energies of a few 100 µJ. The use of the CW SRF linac and the radiation source architecture will allow for high flexibility in the pulse repetition rate. Conventional superradiant THz sources, driven by electron bunches shorter than the radiation wavelength, would cover the wavelength range from 0.1 THz to about 2.5 THz. A different approach is developed to extend the operation of the superradiant undulators well beyond the few THz. For this, a longitudinally modulated electron bunch would be used to achieve significant bunching factors at higher frequencies. The proposed VUV FEL would use the HGHG FEL scheme. It will allow the construction of a unique, fully coherent, high repetition rate source operated with about 30 µJ pulse energy at the first harmonic in the design wavelength range. An FEL oscillator, operating at a wavelength 3-5 times longer than the HGHG system, can generate the seed required for the high repetition rate HGHG scheme.

HIGH-FIELD MIR-THZ SOURCE

The Radiation Source ELBE at Helmholtz-Zentrum Dresden-Rossendorf (HZDR) is a user facility based on a 1 mA - 40 MeV CW SRF LINAC. ELBE operates several high-repetition-rate IR and THz sources. Two FEL oscillators operating with a 13 MHz pulse repetition rate cover wavelength range from 5 through 250 µm and can deliver pulse energy of a few µJ. A superradiant undulator delivers 0.3 – 2.5 THz pulses at a few 100 kHz and pulse energy of a few µJ and operates simultaneously with a single-cycle coherent diffraction radiation source, which provides pulse energies of a few 100 nJ. There is a strong interest from the IR FEL and THz user community for pulse energies up to 1000 µJ! Another critical parameter of the required MIR-THz pulses is it's electrical field, which needs to reach a few MV/cm level. To achieve the required high pulse energies, a design of a new facility is under development.

One part of the new facility concept is a conventional superradiant undulator driven by a strongly compressed bunch. It is planned to operate the new facility with the bunch charge of 1 nC. It is also planned to use a second-order bunch compressor to remove the 2nd order RF curvature imprinted by the 1.3 GHz LINAC. In this case, micro-bunching instability estimations suggest that it will be possible to compress the bunch to about 200 fs (RMS). This will allow to increase the pulse energy to about 100 µJ, but only in the frequency range up to about 2 THz [1]. For the frequency range from 1.5 through 30 THz a different concept is being developed. Here instead of a strong bunch, compression longitudinal beam density modulation will be used. The scheme is inspired (naturally) by the FEL interaction process. The proposed scheme will operate similarly to HGHG FEL radiating at the first harmonic or an optical klystron. First, the beam energy will be modulated by a photon beam copropagating with the electron beam in an undulator-modulator. The energy modulation will be converted to a density modulation in a dispersive section. The modulation will be done at the wavelength of the desired radiation. We plan to operate such a source in the wavelength range from 10 µm through 250 µm. HGHG FEL theory shows that to maximize the beam bunching factor, the amplitude of the energy modulation needs to be comparable with the slice energy spread. Linear, 1D micro-bunching instability theory predicts allows estimating the growth of the slice energy spread to ~ 50 keV for the 1 nC bunch when it is accelerated to 50 MeV. For the concept robustness we assume that the energy modulation amplitude up to 200 keV might be necessary. An assumption of 1 m long modulator-undulator leads to the required amplitude of the modulating optical (MIR-THz) pulses of 40 MV/m with the pulse length of a few ps.

We argue that such modulating photon pulses in the wavelength range from 10 µm through 250 µm, with the requirements of (a) complete wavelength tunability and (b) repetition rate of up to 1 MHz, can be generated only by an FEL. Moreover, we intend to use the intracavity optical pulse of an FEL oscillator to relax the electron beam requirements. FEL modelling based on the set of J. Dattoli's analytical formulas [2], aided by empirical correction factors introduced by S. Benson, shows that for any wavelength in the required range, the intra-cavity pulse can provide electrical fields of at least five times higher than the required one. For such modelling we assume (a) the use of an undulator with period of 100 mm and 40 periods, (b) electron beam parameters as presently used at ELBE: bunch charge of 77 pC, the RMS pulse length of 0.5 ps, the longitudinal emittance of 50 keV-ps, and transverse normalized emittance in both planes of 10 mm-mrad, and (c) an optical resonator with Rayleigh length of 1 m. We are considering implementing such an optical resonator as a ring resonator. Two undulators would be installed on the ring-resonator; one for the FEL generation and another for the high bunch charge beam energy modulation. A somewhat more detailed description of the proposed system layout can be found in [3].

† email: P.Evtushenko@hzdr.de

ISBN: 978-3-95450-227-1 ISSN: 2673-5490 doi:10.18429/JACoW-IPAC2022-TUPOMS014

PETRA IV STORAGE RING DESIGN

I. Agapov*, S. Antipov, R. Bartolini, R. Brinkmann, Y.-C. Chae, D. Einfeld,
T. Hellert, M. Hüening, M. Jebramcik, J. Keil, C. Li, R. Wanzenberg
Deutsches Elektronen-Synchrotron DESY, Hamburg, Germany

Abstract

PETRA IV [1–5] will be a diffraction-limited 6 GeV synchrotron light source with an emittance of 20 pm rad at DESY Hamburg. The TDR phase is nearing completion, and the lattice design is being finalised. The lattice will be based on the six-bend achromat cell with extensive use of damping wigglers. The key challenges of the lattice design are finding the balance between emittance minimisation and non-linear beam dynamics performance, and adapting the lattice to a collider-type tunnel geometry of the PETRA facility, with the long straight sections and low degree of superperiodicity. We present the lattice design and the beam physics aspects, focusing on the beam dynamics performance and optimisation.

OVERVIEW

Lattice Design Goals and Constraints

The next generation of photon science experiments would greatly benefit from hard x-ray (10-50 keV) photon beams with a high degree of transverse coherence and brightness levels in excess of 10^{22} phot./mm/mrad/0.1%BW. These unprecedented levels of brightness and coherence are achieved by using improved undulator technologies such as cryogenic in-vacuum or superconducting devices, but first of all, by generating electron beams of extremely low (tens of pm rad) emittance. These levels are achievable in a 6 GeV synchrotron of 2.3 km circumference such as PETRA by employing the multi-bend achromat (MBA) lattices [6]. While theoretically very low emittances (in the pm range) are possible, the design parameters are set taking realistic constraints into account, that will be discussed further. Taking these constraints into account, the goals were set to deliver emittances of below 30 pm rad and beam currents of up to 200 mA. In PETRA IV, similar to PETRA III [7], only part of the lattice can be equipped with insertion devices. PETRA IV will feature a new experimental hall with additional beamlines significantly increasing the total space available for insertion devices (see Fig. 1). Outside of the experimental halls, i.e. for about half of the circumference, the machine should follow the existing tunnel. The tunnel has a width of only about 3.1 m, which together with the need for cables, escape routes, and other infrastructure elements, constrains the machine geometry transversely to an envelope of about 10 cm. PETRA III was designed to make most use of the limited number of ID straights. This was achieved by, first, having a short DBA ([8]) cell of ca. 23 m length that has sextupoles removed, with the chromaticity correction distributed to the FODO cells of the rest of the ring; and second, by extensively exploiting the so-called canting, i.e. operating two insertion devices in one straight, with a corrector magnet used to introduce an angle (of 1 mrad, 5 mrad, or 20 mrad depending on location) in the electron trajectory between two devices, thus separating the radiation cones and allowing multiple beam-lines per insertion straight section. While preserving the whole arrangement of source points is impossible when no significant emittance deterioration is allowed, many beam-lines can be kept, significantly simplifying the logistics when a ca. 23 m cell is adopted. For those several beam-lines that feature a 20 mrad canting angle, the dispersion generated in the straight is such that the influence of insertion devices on emittance is prohibitively strong. Canting angles larger than ca. 5 mrad are not compatible with the low emittance ring design. Only moderate technological advances wrt. e.g. achievable magnet gradients are permissible to allow project implementation in the nearest future with minimal R&D effort on magnet technology.

Key Challenges

The design objective of the PETRA IV lattice is to maximize the brightness delivered by a portfolio of insertion devices. As with all low-emittance ring designs, there is a number of trade-offs to be considered: The most significant technical limitation in the low emittance ring design is the maximum achievable quadrupole and sextupole strength. Without this limit (and neglecting any nonlinear dynamics limitations) the natural emittance can be made almost arbitrarily small. The maximum gradient is limited by the field saturation limits of commonly available magnetic materials. The field gradients can be further increased by reducing the bore radius. With decreased bore radius the implementation of the vacuum system becomes challenging and the effect of impedance increases. These considerations lead to limiting the maximum achievable magnet strength to about 115 T/m and the minimum bore radius to about 9 mm. Another important factor is the relative length of insertion devices with respect to the ring circumference (filling factor). Since the emittance is generated in the arcs, its minimization could be achieved by reducing the filling factor, while for maximizing the experimental throughput larger filling factor would be beneficial. In practice, ID straight section length of approx. 5 m for a cell length of approx. 23–25 m is the best compromise for PETRA IV. Further, emittance can be minimized by either extensively exploiting damping wigglers, or creating lattices with a large partition shift (i.e. shifting the damping from the longitudinal to the transverse plane). Both approaches can at the same time lead to increased beam energy spread. The energy spread is detrimental to the brilliance. The exact effect depends on parameters of the

* ilya.agapov@desy.de

ISBN: 978-3-95450-227-1 ISSN: 2673-5490 doi:10.18429/JACoW-IPAC2022-TUPOMS015

PROPOSAL OF A GIRDER REALIGNMENT TEST IN PETRA III

M. Schaumann*, I. Agapov, R. Bartolini, M. Bieler, R. Böspflug, D. Einfeld,
M. Hoffmann, J. Keil, L. Liao, G. Priebe, M. Schlösser, R. Wanzenberg
Deutsches Elektronen-Synchrotron DESY, Notkestr. 85, 22607 Hamburg, Germany

Abstract

PETRA IV can benefit from the fine control of the girders that carry the storage ring elements to achieve the design beam performance. Based on the corrector magnet strength pattern it is desired to realign girders to stay within the alignment tolerances. In the current PETRA III configuration, the girders in the Max von Laue Hall are equipped for remote alignment, however, those have not been moved since their initial installation and the alignment system is currently not connected to the control system. In preparation for PETRA IV, a movement test of one of the PETRA III girders should confirm the ability to safely and precisely remote control the equipment based on an optics model that describes the effect of the girder movement on the orbit. This paper studies the feasibility of this test and prepares an initial mock-up experiment to be performed on a spare girder.

INTRODUCTION

The PETRA III storage ring at DESY [1] is currently one of the world's brightest synchrotron light facilities in the hard X-ray range. It is planned to be upgraded to PETRA IV [2,3], which will be operated with an ultra-low emittance providing diffraction-limited hard X-ray beams with more than two orders of magnitude increase in brightness and coherence compared to its precursor. Owing to the lower emittance, PETRA IV will have a factor of two lower alignment and aperture tolerances with respect to PETRA III. Nevertheless, PETRA IV should be build within and extend the existing infrastructure of PETRA III, where the buildings are based on tunnels and halls from different construction periods.

Investigations at PETRA III related to long-term orbit stability and its correlation to environment parameters, including the tunnel temperature and the mechanical movement of different tunnel segments with respect to each other, revealed that without countermeasures the expected ground motion could potentially impact the machine performance of PETRA IV [1, 4, 5].

Similar to other light sources, the storage ring elements in the lattice of PETRA IV will be placed on girders that mechanically connect and carry a group of elements, such that those can be assembled, transported and aligned as a unit. In order to counteract the misalignment introduced by ground motion and temperature effects, the girders will feature a remote controlled alignment system. Based on the corrector strength patterns and a response matrix, alignment corrections will be applied to individual girders and so provide an alignment stability within the required tolerances [6].

Girder re-alignment based on corrector current data has been successfully performed in other machines [7]. The reconstruction however depends on the actual machine and its properties, like optics, phase advances and arrangement of girders. Therefore, the procedure and model have to be proven individually for each machine.

In PETRA III the Max von Laue Hall (MvL) is equipped with girders that have a remote controllable alignment system (see Fig. 1). However, here the girders are not moved during beam operation, the system has only been used during the initial installation of the elements in the tunnel in 2009. Thanks to the large tolerances, potential movements or drifts are well compensated by the orbit correction system.

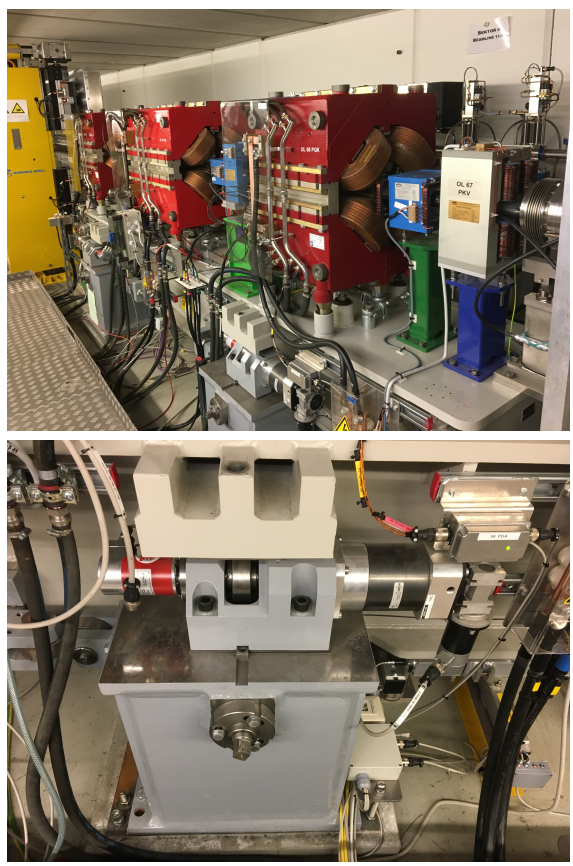

Figure 1: Top: View of a girder installed in the PETRA III tunnel downstream of an undulator (yellow element on the left), carrying three quadrupole magnets. Bottom: Zoom of the motor and encoders installed on the cam-based alignment system connecting the supporting feet to the girder table.

* michaela.schaumann@desy.de

ISBN: 978-3-95450-227-1 ISSN: 2673-5490 doi:10.18429/JACoW-IPAC2022-TUPOMS016

A PIPELINE FOR ORCHESTRATING MACHINE LEARNING AND CONTROLS APPLICATIONS

I. Agapov*, M. Böse, L. Malina
Deutsches Elektronen-Synchrotron DESY, Notkestr. 85, 22607 Hamburg, Germany

Abstract

Machine learning and artificial intelligence are becoming widespread paradigms in control of complex processes. Operation of accelerator facilities is not an exception, with a number of advances having happened over the last years. In the domain of intelligent control of accelerator facilities, the research has mostly been focused on feasibility demonstration of ML-based agents, or application of ML-based agents to a well-defined problem such as parameter tuning. The main challenge on the way to a more holistic AI-based operation, in our opinion, is of engineering nature and is related to the need for significant reduction of the amount of human intervention. The areas where such intervention is still significant are: training and tuning of ML models; scheduling and orchestrating of multiple intelligent agents; data stream handling; configuration management; and software testing and verification requiring advanced simulation environment. We have developed a software framework which attempts to address all these issues. The design and implementation of this system will be presented, together with application examples for the PETRA III storage ring.

RATIONALE

One of the promises of AI technology for research facilities is the increased automation of operation. A significant progress has been achieved in recent years in understanding the potential of AI and ML for accelerator operation. A usual common feature of the developed ML solutions is the increased complexity of the software and the algorithms: so, a Neural Network (NN)-based controls approach usually requires a more complex software stack, model storage, model tuning and re-training. In our previous work [1] we realized that being a more powerful representation in control problems, NNs can be prohibitively complex compared to more simple linear control approaches, as the results have to be constantly interpreted and evaluated, and the software stack common in data science becomes unsatisfactory for robust on-line applications. Significant human intervention was always required, making the operation not more but less autonomous. Based on this experience we started developing a software framework that would help address these issues. The framework allows execution and communication of services, each responsible for a certain subset of tasks necessary for intelligent control and operation.

Services with well-defined functionality and interfaces. All operations are performed by *services*. A *service* performs well-defined action such as orbit correction, retraining a model etc. Each *service* has a well-defined API, with standard operations being starting, stopping, and re-configuring. An arbitrary number of *services* can be running, any functionality can be implemented as soon as the API is adhered to, and automatic *service* discovery is allowed.

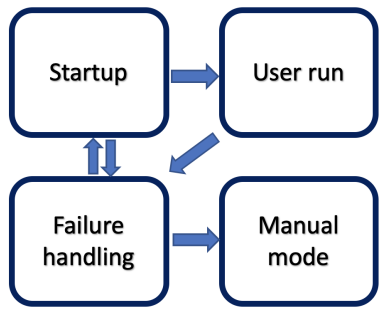

Figure 1: Basic states for autonomous operation.

Distributed deployment and communication bus. All *services* have access to a common communication bus, and are able to send and receive messages. A message header contains information such as the addressed service (or broadcast) and the body contains an arbitrary set of instructions and data in the form of a dictionary. *Services* can run anywhere on the network, and the system can be transparently scaled up by deploying certain *services* on an HPC cluster.

Decentralized architecture While the software does not impose any constraints on the kind of *services* that are being run, the design is geared towards the needs of autonomous operation, based on the following paradigm (see Fig. 1): there are a number of *services* related to machine startup, that can include: health checks of various subsystems, first-turn steering and trajectory correction, orbit correction, optic correction, accumulation (top-up). A supervision *service* monitors the machine startup and decides if the startup has been accomplished successfully, in which case transition into the "use run" mode can be performed, otherwise failure handling is activated, which can either attempt to resolve the issue autonomously or transition into manual mode. In the user mode a number of monitoring and slow correction *services* are active. A user run can either end normally or in a failure. A failure resolution can be attempted in an autonomous mode, or manual control can be initiated. Failure handling is one of the most important aspects of autonomous operation, with research activities ongoing.

Digital twin: simulation mode. The software follows the methodology of OCELOT [2,3] where the so-called *MachineAdaptors* are used to encapsulate the control systems

* ilya.agapov@desy.de

ISBN: 978-3-95450-227-1 ISSN: 2673-5490 doi:10.18429/JACoW-IPAC2022-TUPOMS018

ERROR ANALYSIS AND COMMISSIONING SIMULATION FOR THE PETRA-IV STORAGE RING

T. Hellert*, I. Agapov, S. A. Antipov, R. Bartolini, R. Brinkmann, Y. Chae, D. Einfeld, M. Jebramcik, J. Keil, DESY, Hamburg, Germany

Abstract

The upgrade of the PETRA-III storage ring into a diffraction limited synchrotron radiation source is nearing the end of its detailed technical design phase. We present a preliminary commissioning simulation for PETRA-IV demonstrating that the final corrected machines meet the performance design goals.

INTRODUCTION

The PETRA-IV project [1] for upgrading the 2.3-km 6-GeV PETRA III storage ring to a diffraction-limited synchrotron radiation source is nearing the end of its detailed technical design phase.

Alignment errors and multipole errors in magnets are usual sources of machine imperfection. While the allowed multipole errors are not dissimilar to what has been specified and achieved at many accelerator facilities, i.e. at the $5 \cdot 10^{-4}$ level, the sensitivity to alignment is significantly increased due to the combined strong nonlinearities and focusing. This places emphasis on the need for realistic modeling of the relevant errors, the development of efficient beam orbit/optics correction schemes, with the goal to establish feasible error tolerance specifications and ensure rapid commissioning.

In this paper we present a preliminary commissioning simulation and performance results of a statistical ensemble of corrected machines for the current baseline error assumptions. This procedure follows the standard approach used in MBA simulated lattice commissioning [2–4].

SIMULATION SETUP AND ERRORS

The storage ring has a geometry inherited from the HEP programme of PETRA in the 1970s, which is unusual for a synchrotron radiation facility. It has eight arcs, four straight sections of approx. 108 m length, and four straight sections of approx 64 m length. Each arc is composed of nine hybrid six-bend achromat (H6BA) cells, of which a schematic can be seen in Figure 1. A selection of lattice parameters can be found in Table 1. A total of 643 CMs in both planes, 288 skew quadrupole correctors and 786 BPMs all suitable for turn-by-turn evaluations are available.

RMS machine-errors are assigned according to the values reported in Table 2, with each error source following a Gaussian distribution truncated at $\pm 2\sigma$.

Performance of the uncorrected lattice: To start to gain some insight into the lattice performance we studied the particle dynamics in the presence of all the errors included in our model (misalignments, calibration errors, etc.) but before any correction to the orbit or linear optics. This provides an interesting way to draw comparisons with other machines [2–4]. The study scaled all the errors from Table 2 by the same multiplicative scaling factor; thus, an error scaling factor of 1 corresponds to the nominal errors.

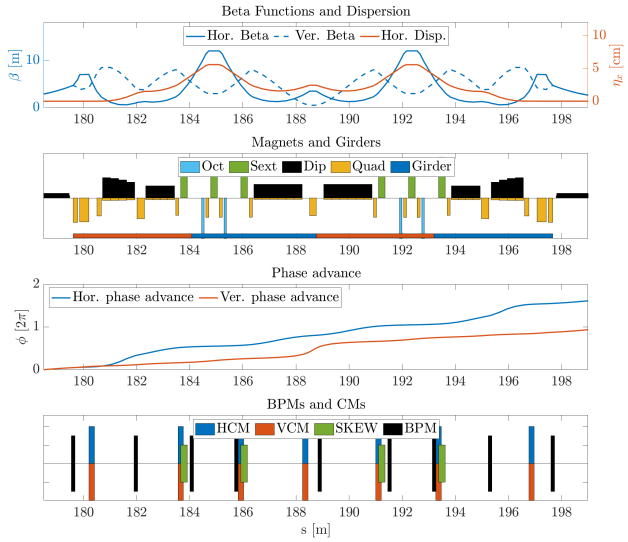

Figure 1: Lattice and magnet layout within one cell. Shown are (from top to bottom): the betatron and the dispersion functions, the the distribution of magnets and girders, the phase advance and the distribution of skew quadrupole and dipole corrector magnets and BPMs for orbit correction.

Table 1: Selected Lattice Parameters

Parameter	Value
Tunes ν_x/ν_y	135.18 / 86.27
Natural chromaticity ζ_x/ζ_y	-232 / -155
Corrected chromaticity ζ_x/ζ_y	6 / 6
Momentum compaction factor α_C	3.3 10^{-5}
Standard ID space	4.9 m
$\beta_{x,y}$ at ID, standard cell	2.2 m, 2.2 m
$\beta_{x,y}$ at ID, flagship IDs	4 m, 4 m
Nat. hor. emittance ε_x with IDs, zero current	19 pm rad

Table 2: Magnet and BPM Errors. Distributions applied in simulations are truncated 2σ Gaussians.

Error Type	rms value	Error Type	rms value
Girder rolls	200 µrad	BPM offset	30 µm
Girder trans. offset	100 µm	BPM roll	0.4 mrad
Magnet trans. offset	30 µm	BPM noise (TbT)	20 µm
Magnet rolls	200 µrad	BPM noise (CO)	0.1 µm
Quad. calibration	0.5E-3	BPM calibration	2 %
Dip./Sext. calibration	1E-3	CM calibration	2 %

* thorsten.hellert@desy.de

ISBN: 978-3-95450-227-1 ISSN: 2673-5490 doi:10.18429/JACoW-IPAC2022-TUPOMS019

COLLIMATION STRATEGY FOR THE LOW-EMITTANCE PETRA IV STORAGE RING

M. A. Jebramcik*, I. Agapov, S. A. Antipov, R. Bartolini, R. Brinkmann, D. Einfeld, T. Hellert, J. Keil, Deutsches Elektronen-Synchrotron (DESY), 22607 Hamburg, Germany

Abstract

The beam-intensity losses in the proposed PETRA IV electron storage ring that will replace DESY's synchrotron light source PETRA III will be dominated by the Touschek effect due to the high bunch density. The beam lifetime will only be in the range of 5 h in the timing mode (80 high-intensity bunches) leading to a maximum power loss of 170 mW along the storage ring (excluding injection losses). To avoid the demagnetization of the permanent-magnet undulators and combined-function magnets, this radiation-sensitive hardware has to be shielded against losses as well as possible. Such shielding elongates the lifetime of the hardware and consequently reduces the time and the resources that are spent on maintenance once PETRA IV is operational. This contribution presents options for collimator locations, e.g., at the dispersion bump in the achromat cell, to reduce the exposure to losses from the Touschek effect and the injection process. This contribution also quantifies the risk of damaging the installed collimation system in case of hardware failure, e.g., RF cavity or quadrupole failure, since the beam with an emittance of 20 pm could damage collimators if there is no emittance blow-up.

LOSS MECHANISMS IN PETRA IV

The Touschek effect is the major mechanism leading to losses in PETRA IV [1, 2]. Reason for this is the small beam size and large bunch current. Assuming some pessimistic 5 % beta-beating along the machine, a beam lifetime of roughly $\tau = 5$ h in the so-called Timing mode (80 high-current bunches with 1 mA bunch current each) and $\tau = 30$ h in the Brightness mode (200 mA distributed on 1600 bunches) is expected. It is therefore crucial to investigate the loss locations of these off-energy particles since the residual-gas scattering lifetime is envisaged to be at least $\tau = 50$ h [3] and is therefore of minor interest. The reduced beam lifetime implies that a power loss in the 170 mW range (Timing mode) will be constantly distributed along the aperture and may cause the demagnetization of permanent magnets within the combined-function dipoles (DLs), undulators and wigglers [4]. It is important to identify locations for potential collimators to intercept these particles before impacting these sensible magnets.

TOUSCHEK-EFFECT LOSSES

Although the dose that determines the risk of inflicting damage onto sensitive hardware has not been estimated yet, it is important to intercept most Touschek-effect losses to elongate the hardware lifetime substantially in any case.

Potential collimator locations

The ESRF-EBS project uses collimators (scrapers) located at the dispersion bump in the achromat cell to intercept off-energy particles [5]. This strategy is also a potential option for PETRA IV. PETRA IV's hybrid six-bend achromat (H6BA) cells feature a peak dispersion of $D_x = 55$ mm and $D_x = 48$ mm at the location of the potential collimator (approximately 20 cm active material). The optics function and the respective collimator location is shown in Fig. 1. It is worth mentioning that only a handful of collimators are required in PETRA IV and these will be placed in the last cell of the octants that feature the damping wigglers with long straight section following the collimators. This way, the collimation does not take place in the arcs featuring the regular undulators, and it is avoided that these are interacting with a potential shower.

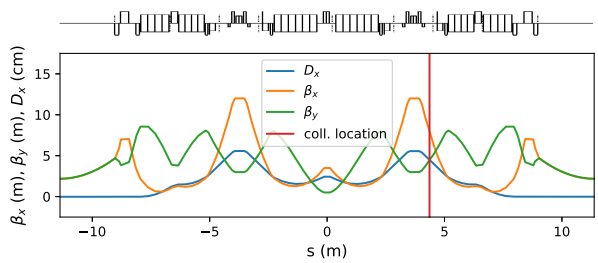

Figure 1: Placement of the collimator within the H6BA cell of PETRA IV. The collimator is located on the falling flank of the dispersion function in the second dispersion bump.

An alternative for collimators in the achromat cells is the introduction of artificial dispersion bumps in the long straight sections for the cost of a larger emittance due to its contributions to the radiation integrals of PETRA IV. Since most of the long straight section feature two ~10 m long drifts for accommodating undulators for flagship beam-lines while not all of these slots are occupied, a design idea could be creating the artificial dispersion bumps in multiple of these unoccupied undulators slots. A test has shown that the increase in terms of the emittance for two such of these bumps is in the range of $\Delta\epsilon_x \approx 1.5$ pm for $D_x = 40$ mm in the center of the artificial dispersion bumps. Hence, an increase of $\Delta\epsilon_x \approx 1.5$ pm is already a 7.5 % emittance increase. This is the reason this design choice is not envisaged and may only be considered if the there is no other effective way of intercepting off-energy particles after the PETRA IV accelerator layout has been finalized.

* marc.andre.jebramcik@desy.de

ISBN: 978-3-95450-227-1 ISSN: 2673-5490 doi:10.18429/JACoW-IPAC2022-TUPOMS020

LONG-TERM ORBIT STABILITY IN THE PETRA III STORAGE RING

L. Liao*, M. Schaumann, M. Bieler, J. Keil, C. Li, R. Wanzenberg,
Deutsches Elektronen-Synchrotron DESY, Notkestr. 85, 22607 Hamburg, Germany

Abstract

The study of long-term orbit stability in the PETRA III light source plays an important role for the design of its upgrade to PETRA IV. The PETRA III tunnel is made of individual segments that move against each other. Here, the long-term drifts of the tunnel ground that are mostly introduced by temperature variations, are of the highest concern for the PETRA IV alignment tolerances and orbit stability. This paper studies the evolution of the beam orbit and corrector magnet currents over several years and correlates tunnel movement to RMS orbit drifts.

INTRODUCTION

The third-generation light source PETRA III in Hamburg is operated since 2009. An overview of its tunnel layout is shown in Fig. 1. The naming convention to identify locations in the storage ring follows geographic directions. As indicated in Fig. 1, PETRA III provides synchrotron light in the hard X-ray range to its users in the three experimental halls, the so-called *Paul P. Ewald Hall* (Ewald Hall) in the North, the *Max von Laue Hall* (Laue Hall) in the North-East and the *Ada Yonath Hall* (Yonath Hall) in the East.

The storage ring tunnel was build from individual tunnel segments in 1976 to host the electron-positron collider PETRA I. It is constructed of 82 segments [1] with varying length: the major part (57 segments) are 24 m long, the shortest segment measures only 10.4 m, and the three experimental halls build the longest segments with up to 286.0 m (Laue Hall).

Natural ground motion and temperature effects lead to tunnel movements that are not only visible on the particle beam orbit during operation, but that are large enough to create cracks in the wall at every point where tunnel segments connect to each other or to the experimental halls. The movement of these tunnel segments is transferred to the girders and support feet, on which the magnets and other beamline equipment are installed. Therefore, this movement contributes to the misalignment error and, as seen as well in other storage rings [2, 3], this will affect the long-term orbit stability.

For the upgrade to the ultra-low-emittance storage ring PETRA IV [4, 5] it is again foreseen to reuse parts of the existing tunnel. Because of the smaller alignment tolerances, it is important to study the long-term orbit stability of PETRA III in the scope of the risk management strategy for PETRA IV.

* Lang.Liao@desy.de

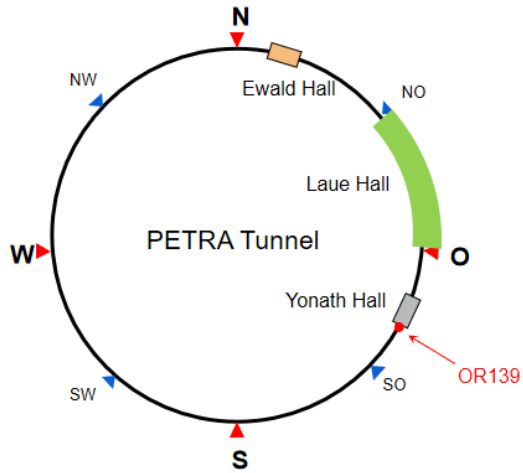

Figure 1: Overview of the PETRA III tunnel layout. Location OR139 (139 m right of East hall) is highlighted (red) as the location of the tunnel motion measurement presented in Fig. 2.

TUNNEL MOVEMENT

The relative movement between two adjacent tunnel segments is monitored in ten locations around the tunnel. These mechanical measurement devices provide data in three dimensions, however only in form of a point like position information. This means that possible tilts or rotations of the tunnel segments to each other remain invisible. The detailed study of the tunnel motion, including the analysis of this mechanical position data and its correlation to environment parameters is presented in Ref. [6].

As an example, Fig. 2 shows the evolution of the longitudinal (in beam direction) and horizontal (radially pointing towards the outside of the ring) position change between the Yonath Hall and the tunnel segment connecting to it on the downstream end (labelled *OR139*, indicating the position 139 m to the right of the East (*Ost* in German) symmetry point, see also Fig. 1). The data over 1.5 years clearly shows a periodic pattern that can be correlated to the temperature changes induced by the normal-conducting magnet cycles, but also to the seasonal change of the outside temperature [6]. The longer the tunnel has time to cool down after switching off the magnets, the larger the floor offset becomes. This effect is especially evident in the longitudinal plane (orange line), where during winter shutdowns tunnel movements in the order of a few millimetres have been observed. Figure 2 highlights the period of the winter (orange shade) and summer (green shade) shutdowns that are the longest cool down periods. But also the shorter service weeks, that usually

ISBN: 978-3-95450-227-1 ISSN: 2673-5490 doi:10.18429/JACoW-IPAC2022-TUPOMS021

PETRA III OPERATIONAL PERFORMANCE AND AVAILABILITY

Rainer Wanzenberg*, Michael Bieler, Joachim Keil,
Lang Liao, Gajendra Kumar Sahoo, Michaela Schaumann
Deutsches Elektronen-Synchrotron DESY, Hamburg, Germany

Abstract

At DESY the Synchrotron Light Source PETRA III offers scientists outstanding opportunities for experiments with hard X-rays of exceptionally high brilliance since 2009. The light source is operated mainly in two operation modes with 480 and 40 bunches at a beam energy of 6 GeV. With the completion of the last milestone of the extension project in summer 2021, which brought the new dipole beamline P66 into operation, 2022 is the first year where almost 5000 hours of user run time could be scheduled. This paper will review the statistics of availability and failures over the years and provides a detailed description of the operation in 2021. Additionally, an outlook for the next runs is given.

INTRODUCTION

The Synchrotron Light Source PETRA III is one of the core facilities at DESY offering each year more than 2000 users outstanding opportunities for experiments with hard X-rays of exceptionally high brilliance. In the seventies PETRA was originally built as an $e^- - e^+$ collider, which was later used as a pre-accelerator for the HERA lepton-hadron collider. After the end of the HERA collider physics program in 2007 the PETRA ring was converted into a dedicated 3rd generation synchrotron radiation facility, called PETRA III [1].

Beam operation started in 2009 [2] and 14 beamlines in the Max von Laue hall are operational since 2011. Because of the high demand for additional beamlines, the lattice of the ring was redesigned to accommodate additional beamlines in the framework of the PETRA III extension project. In 2014 two tunnel sections of about 80 m each in the North and the East of the PETRA ring were completely reconstructed and new experimental halls were build. The storage ring was recommissioned in 2015 [3]. The present layout of PETRA III is shown in Fig. 1, including the experimental halls of the extension project: Paul P. Ewald in the North and Ada Yonath in the East. Presently, 25 beamlines are operational. The operational parameters are summarized in Table 1. In total 80 m of wigglers are installed in the straight sections in the West and the North to achieve the horizontal emittance of 1.3 nm.

In the framework of the PETRA IV project, it is foreseen to upgrade the existing synchrotron radiation source PETRA III to a synchrotron radiation source with an ultra-low emittance, based on a multi-bend achromat, which was pioneered at MAX IV [4] and ESRF-EBS [5, 6]. Unique new experiments and scientific opportunities will be made possible. The project includes the construction of a new experimental building in the West of the PETRA ring. The conceptual design report was published in 2019 [7]. Presently, the project team is preparing a technical design report [8].

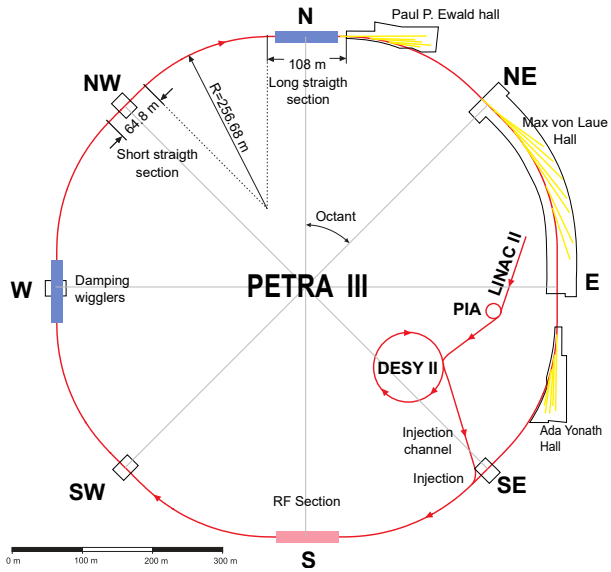

Figure 1: Layout of PETRA III.

Table 1: PETRA III Parameters

Parameter	PETRA III	
Energy /GeV	6	
Circumference /m	2304.0	
Total current /mA	120	100
Number of bunches	480	40
Bunch Population /10^{10}	0.5	12.0
Emittance (horz. /vert.) /nm	1.3 / 0.01	

INSTALLATION OF A NEW DIPOLE BEAMLINE

During the winter shut-down 2020–2021 and in the summer shut-down 2021, a new beamline P66 was successfully installed close to the Paul P. Ewald hall in the North East of the PETRA ring, see Fig. 2. The beamline P66 is the first dipole beamline of the PETRA III facility, dedicated to VUV luminescence and reflection spectroscopy experiments. Thanks to essential efforts of all technical groups, all shut-down activities could be finished within the schedule. First synchrotron light from the dipole was guided to the absorber of the beamline on 30 July 2021. A mirror reflects the light then from the accelerator level upwards to the experimental hutch, which is located in building 47k on top

* Rainer.Wanzenberg@desy.de

ISBN: 978-3-95450-227-1 ISSN: 2673-5490 doi:10.18429/JACoW-IPAC2022-TUPOMS022

COOLING CHALLENGES IN A NEG-COATED VACUUM CHAMBER OF A LIGHT SOURCE

S. Talebi Motlagh†,1,2, A. Danaeifard[1], J. Rahighi[1], F. Saeidi[1], F. Zamani[2]
[1]Iranian Light Source Facility Institute for Research in Fundamental Sciences (IPM), Tehran, Iran
[2]University of Kashan, Kashan, Iran

Abstract

In a Light Source, unused synchrotron radiation is being distributed along the walls of the chambers. Due to the small conductance of the chambers, vacuum pumping will be based on the distributed concept, and then non-evaporable getter (NEG) coating is extensively used. The vacuum chambers are made of copper alloys tube, and cooling circuits are welded to the chamber to remove the heat load from the radiation generated. Filler metal creates a brazed joint between the water-cooling pipe and the vacuum chamber body. The thermal conductivity of the fillers is less than the vacuum chamber body. On the other hand, the velocity of the water in the cooling pipe is a critical parameter in thermal calculations that must be taken into account. So, in this paper, we study and investigate the effects of the filler metal and the cooling water velocity on cooling the NEG-coated chambers.

INTRODUCTION

The ILSF storage ring lattice is based on 20 five-bent achromats; Each achromat contains three unit cells and two matching cells. The unit cells have a 3.9° bending magnet, while the matching cells deflect the beam 3.15° [1]. The radiation of these five dipole magnets is uniform in the horizontal direction (plane of the storage ring), while in the vertical direction, it follows a narrow Gaussian profile.

The irradiate power and the radiation power density on the vacuum surface are simulated by Synrad+ software [2]. It is assumed that the chamber body will absorb all the radiation, and no reflection would happen. Hence, the facets' sticking factor has been considered equal to 1. The cooling of this chamber and its challenge will be studied in the present work.

The commonly used thermal absorber design criteria are [3]:

1. The maximum cooling wall temperature T_{Max}^{CW} should be lower than water boiling temperature $T_{boiling}$ at the pressure of the water in the cooling tubes
2. The maximum temperature of the chamber T_{Max}^{Ch} must be significantly lower than the melting point of the copper and the brazing temperature.
3. The maximum temperature rise in the chamber should be less than 300°C for Glidcop and 150°C for oxygen-free high thermal conductivity (OFHC) copper, which are also used at APS [4].

THEORY

The total radiative power of all the bending magnets in a ring is determined by the electron's energy $E\ [GeV]$, the bending magnet's field $B\ [T]$, and the electron beam current $I_b[mA]$, as the following equation [5]:

$$P_{total}[kW] = 26.6E^3[GeV]I_b[A]B[T] \quad (1)$$

Correspondingly, the power density on the beam axis can be obtained as follows:

$$\frac{dP}{d\Omega}\left[\frac{W}{mrad^2}\right]|_{\psi=0} = 5.44E^4[GeV]I_b[A]B[T] \quad (2)$$

Since the magnitude of the magnetic field in the dipoles of the ILSF storage ring is about $B = 0.567\ T$ according to Eq. (2), at a current of 400 mA and an energy of 3 GeV, the total output power due to synchrotron radiation will be 162.95 kW. It means that for 100 dipole magnets in the ring, each bend chamber wall receives 1.05 kW radiation power.

A maximum value of 8.35 W/mm^2 for the power density has been obtained analytically.

Most of the power will be distributed along the water-cooled vacuum chambers. So, a cooling circuit channel is welded to each chamber to remove the heat load from the radiation generated as seen in Fig. 1. In this research, a simple model of a curved vacuum chamber in a dipole without photon extraction is studied to investigate the thermal effects, as seen in Fig. 2. Although the electrons travel parallel with the chamber in a curved path but the radiant photons go in a straight line. So, significant radiation collisions will be happen along the second half of the chamber. Therefore, the initial part of the chamber will have an ambient temperature, while the final part will be warm due to the radiation, as discussed here.

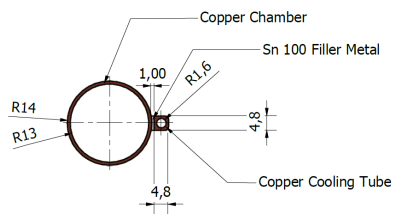

Figure 1: The ILSF chamber cross-section view.

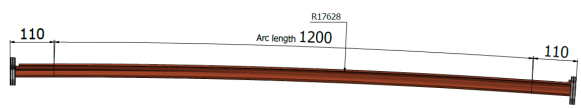

Figure 2: Simple model of the vacuum chamber in a dipole without photon extraction.

† s.talebimotlagh@ipm.ir

ISBN: 978-3-95450-227-1 ISSN: 2673-5490 doi:10.18429/JACoW-IPAC2022-TUPOMS023

THE ELETTRA 2.0 PROJECT

E. Karantzoulis†, A. Fabris, S. Krecic, Elettra – Sincrotrone Trieste, Trieste, Italy

Abstract

The project status of the future Italian 2.4 GeV fourth generation light source Elettra 2.0 that will replace the third-generation light source Elettra is presented. Elettra 2.0 will be the ultra-low emittance light source that will provide ultra-high brilliance and coherence and at the same time aims to provide very short pulses for time resolved experiments.

INTRODUCTION

Located on the outskirts of Trieste, Italy, Elettra operates for users since 1994 being the first third generation light source for soft X-rays in Europe. During those 27 years, many improvements were made in order to keep the machine updated and therefore competitive with the other more recent and modern light sources already designed to operate in top-up. Following the successful set in operation of the full energy injector in 2008, after 14 years of energy ramping, Elettra established top-up operations [1] in spring 2010, although not originally designed for it. Operating in top-up proved to be, and still is, very beneficial for the machine [2].

Although Elettra performs very well and is serving the user community with excellent results, in order to keep the light source competitive for synchrotron research and enable new science and new technology developments, after 28 years of operation the diffraction limited storage ring Elettra 2.0 is going to replace Elettra.

ELETTRA STATUS

Elettra operates 24 hours/day, seven days a week delivering more than 5000 hours/year of synchrotron light from infrared (IR) to hard x-rays to 28 beam lines. Ten of them are served by bending magnets. Two beam-lines use light from a superconducting 49-pole, 64-mm period, 3.5 T wiggler.

Many types of insertion devices are installed such as planar, polarizing, electromagnetic, superconducting including canted APPLE II type undulators occupying all the eleven available long straights while the dispersive short straights are also used for short insertion devices such as the 1 m long double APU (Adjustable Phase Undulator) device serving the TwinMic beam line.

The machine consists of a 100-MeV linac, a 2.5 GeV booster and a 2.0/2.4 GeV storage ring. For about 75% of user-dedicated time Elettra operates at 2 GeV while for the remaining 25% it operates at 2.4 GeV, being the only facility to operate at two energies (both in top-up). The main operating modes are multi-bunch with a dark gap of 42 ns and hybrid i.e. multi-bunch with one (for time resolved experiments) or two single bunches (distant 40 ns in a dark gap of 120 ns for pump and probe experiments). In 2021, hybrid mode user beam time amounted to 30 % of the total user beam time. The operating intensities are 310 mA at 2 GeV and 160 mA at 2.4 GeV with 5 mA single bunch(es) added when in hybrid mode.

The total availability, i.e. including the power outages, is 97% and the Mean Time between Failures (MTBF) is higher than 75 hours. The mean maximum time between failures is currently at about 321 hours with peaks at 451 hours. The top-up availability to the total user scheduled time for 2021 was 99 %.

ELETTRA 2.0: OVERVIEW

Already since 2014 discussions with beamline responsibles, users and partners started in order to define the requirements of the new machine described in a series of papers [3-9] resulting to a preliminary but otherwise complete Conceptual Design Report (CDR) [8]. Since 2017 a series of workshops with the users and partners established some new and final requirements. Thus, it has been decided to operate mainly at 2.4 GeV while letting open the possibility to operate for some time and for a limited percentage of user time also at 2 GeV. It has also been requested to let open the possibility of creating short pulses as small as 0.5-1 ps (fwhm) for time resolved experiments using vertically deflecting (crab) cavities that are planned to be installed in section 2 of the ring. All other long straight sections will be occupied by insertion devices with the exception of the injection straight (section 12). It has been also requested to increase the intensity to 400 mA, the available slots for insertion devices and to install super-bends and in vacuum undulators. The constraints were to keep the same circumference, to keep the present injection scheme and to minimize the dark time to 18 months.

The Elettra 2.0 project was approved by the Italian Government in 2019 and according to the current schedule the new machine will start serving the users at the end of 2026. Since some of the original requirements, as appeared in the CDR, have changed, based on the new revised requirements an enhanced version of our S6BA (symmetric six bend achromat) was produced namely S6BA-E (symmetric six bend achromat-enhanced), see Fig. 1, by using longitudinal gradient (LG) dipoles (Fig. 2) and reverse bends. Although most of the CDR part is still valid, a new Technical Design Report (TDR) was produced and is available since June 2021 [10].

ELETTRA 2.0: CHARACTERISTICS

The enhanced symmetric six bend achromat (S6BA-E) lattice (Fig. 1) has a total length equal to that of the present Elettra, i.e. 259.2 m and is made of 24 symmetric arcs, 12 long straights and 12 short straights sections, it has a 12-fold symmetry and is invariant under relative position shifts between them. Thus, the short straight sections in the

†emanuel.karantzoulis@elettra.eu (2022)

ISBN: 978-3-95450-227-1 ISSN: 2673-5490 doi:10.18429/JACoW-IPAC2022-TUPOMS024

SENSITIVITY OF EEHG SIMULATIONS TO DYNAMIC BEAM PARAMETERS

D. Samoilenko*, W. Hillert, F. Pannek
University of Hamburg, 20148 Hamburg, Germany
S. Ackermann, E. Ferrari, N. Mirian, P. Niknejadi, G. Paraskaki, L. Schaper
Deutsches Elektronen-Synchrotron DESY, 22607 Hamburg, Germany
F. Curbis, M. Pop, S. Werin, Lund University & MAX IV Laboratory, 22363 Lund, Sweden

Abstract

Currently, the Free electron laser user facility FLASH at DESY is undergoing a significant upgrade involving the complete transformation of one of its beamlines to allow external seeding. With the Echo-Enabled Harmonic Generation (EEHG) seeding method, we aim for the generation of fully coherent XUV and soft X-ray pulses at wavelengths down to 4 nm. The generated FEL radiation is sensitive to various electron beam properties, e.g., its energy profile imprinted either deliberately or by collective effects such as Coherent Synchrotron Radiation (CSR). In dedicated particle tracking simulations, one usually makes certain assumptions concerning the beam properties and the collective effects to simplify implementation and analysis. Here, we estimate the influence of some of the common assumptions made in EEHG simulations on the properties of the output FEL radiation, using the example of FLASH and its proposed seeding beamline. We conclude that the inherent properties of the FLASH1 beam, namely the negatively chirped energy profile, has dominant effect on the spectral intensity profile of the radiators output compare to that of the CSR induced chirp.

INTRODUCTION

Echo-Enabled Harmonic Generation (EEHG) [1] is an external seeding technique for Free Electron Lasers (FEL). In comparison with the classical Self Amplified Spontaneous Emission (SASE) scheme, seeding techniques offer temporally coherent, narrow-bandwidth FEL radiation with much better shot-to-shot stability [2]. In comparison with other seeding schemes, EEHG provides higher conversion efficiency at high harmonics of the seed laser wavelength and more robustness with respect to the initial beam quality [3]. FLASH2020+ [4] is a major upgrade of the existing FLASH (Free electron LASer in Hamburg) facility, which includes the reconstruction of the FLASH1 beamline to allow external seeding. The EEHG option in FLASH1 beamline will be used to generate soft X-ray radiation with wavelengths down to 4 nm. The realization of EEHG is more challenging at shorter wavelengths because of the precise phase space transformations in the dedicated seeding section of the beamline at higher harmonics. The essential components of the seeding section are the two modulators and the two magnetic chicanes, as depicted in Fig 1. Each component induces specific longitudinal energy correlations, which have to be carefully chosen and transported through the beamline. Any deviations from the design beam parameters at each point of the beamline could have a detrimental effect on the performance of EEHG-based FEL. Therefore, it is crucial to investigate this section's dynamic beam parameters in detail. Particle tracking simulations are a widely used tool for investigating beam dynamics, which can help anticipate detrimental effects and indicate ways of mitigating them. At the same time, the accuracy of the simulations in each particular case is restricted by the underlying approximations and assumptions. Some of these assumptions are related to the functionality of the simulation code. For example, in EEHG simulations performed with `Genesis 1.3` [5] the effect of Coherent Synchrotron Radiation (CSR) in the chicanes is not taken into account, even though it can have a noticeable effect on the electron beam parameters [6]. Other assumptions are made deliberately by the user to make the implementation or interpretation of the simulations more straightforward. For example, while tracking the electron beam through the EEHG seeding section with `elegant` [7], one can neglect the initial electron beam energy chirp. The effect of the initial electron beam energy modulations on EEHG itself is well studied elsewhere (see, e.g., [8]), but an interplay between the initial chirp and the modulations induced by the CSR might be possible. In this work, we use the example of the future EEHG beamline at FLASH to see how the assumptions mentioned above can change the properties of the output FEL radiation.

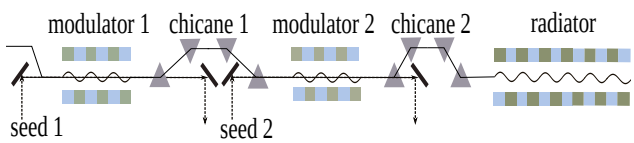

Figure 1: Schematic of the simulated setup.

METHODS

The simulations are performed in two steps. First, we start at the entrance of the first EEHG modulator, where the electron distribution is generated by `elegant` according to the beam parameters specified in Table 1. Two ideal matched initial electron beam distributions are considered: in one, the energy chirp is 0 MeV/ps (no chirp), and in the other −15 MeV/ps, which is the expected value for 4 nm working

* dmitrii.samoilenko@desy.de

ISBN: 978-3-95450-227-1 ISSN: 2673-5490 doi:10.18429/JACoW-IPAC2022-TUPOMS027

ALBA II ACCELERATOR UPGRADE PROJECT

F. Pérez, I. Bellafont, G. Benedetti, J. Campmany, M. Carlà, J. Casas, C. Colldelram, F. Fernández, J.C. Giraldo, T.F. Günzel, U. Iriso, J. Marcos, Z. Martí, V. Massana, R. Muñoz, M. Pont, L. Ribó, P. Solans, L. Torino, ALBA Synchrotron, CELLS, Barcelona, Spain

Abstract

ALBA is working on the upgrade project that shall transform the actual storage ring, in operation since 2012, into a 4th generation light source, in which the soft X-rays part of the spectrum shall be diffraction limited. The project has been officially launched in 2021 and a White Paper presenting the main concepts of the upgrade will be published in 2022. The storage ring upgrade is based on a 6BA lattice which has to comply with several constraints imposed by the decision of maintaining the same circumference (269 m), the same number of cells (16), the same beam energy (3 GeV), and as many of the source points as possible unperturbed. The lattice optimization has achieved an emittance of 140 pm rad, which is a factor 30 smaller than that of the existing ring, but with a cells compactness that presents technological challenges for the magnets, vacuum, diagnostics, RF systems and injection elements designs that are being investigated through an intensive R&D program.

INTRODUCTION

The main goal of the accelerator upgrade for ALBA II is the transformation of ALBA into a diffraction limited storage ring, which implies the reduction of the emittance by at least a factor of twenty.

The upgrade has been conceived as a cost and time effective process, to be realized before the end of the decade and profiting at maximum from the existing infrastructures, in particular the building which is now hosting the facility. It has been decided that the storage ring (SR) upgrade will be done without any major modification of the shielding tunnel. Furthermore, the requirement of maintaining the Insertion Devices (IDs) as close as possible to their present position will preserve them operative for ALBA II and will imply minor modifications to the beamlines.

Another important decision has been the determination of the beam energy of ALBA II, which will be maintained at 3GeV, after having considered several factors. First, the circumference of the SR is constrained to be about 270 m in order to reuse the tunnel; and since we want to preserve also the IDs position, a sixteen-cell geometry is imposed. With these constraints the length of the arcs is too short for obtaining a substantial reduction of the beam emittance at higher beam energies, also considering that the emittance scales with the square of the energy. Another consideration is related to the injector: increasing the energy of the SR would require replacing the whole booster, which increases the cost of the project and lengthens its realization.

LATTICE

In order to fit these goals and constrains, an extremely optimized lattice design based on a six bend achromat (6BA) has been conceived [1], whose main parameters are listed and compared with the ones from ALBA in Table 1.

Table 1: List of ALBA and ALBA II Parameters

Parameter	ALBA	ALBA II
Emittance, pm rad	4600	140
Circumference, m	268.8	268.8
Energy, GeV	3.0	3.0
Number of Cells	16	16
Number of straights	4 / 12 / 8	16
Straight ratio, %	36	24
Tunes (hor, ver)	(18.16, 8.36)	(43.68, 11.67)
Mom. Comp. Factor	8.9e-4	0.8e-4
Beam current, mA	250	300
Energy loss/turn, keV	1023	845
Nat. bunch length, ps	15	6

The choice of a 6BA is the result of an optimization work, performed with a tracking code developed on purpose [2], aiming to balance the demand for both, a low emittance and a large as possible dynamic aperture and momentum acceptance, maintaining a limit to the maximum quadrupolar and sextupolar fieds in the magnets; together with the geometrical constrains due to the available space, and the fixed position of the insertion devices.

The new 6BA optics allows for a reduction of the horizontal natural emittance by about a factor 30, while keeping the current ALBA cell length. The overall ring symmetry is preserved: the lattice is composed by 16 cells organized in 4 quadrants.

All arcs have the same low-emittance lattice, but four straight sections have high-betas, see Figure 1. One of them is required for the injection, two more are for RF cavities and one is available for an ID.

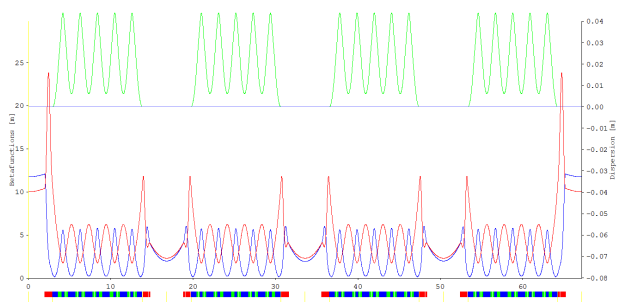

Figure 1: Dispersion (top) and β-functions (bottom) along a quadrant of the 6BA ALBA-II lattice.

ISBN: 978-3-95450-227-1 ISSN: 2673-5490 doi:10.18429/JACoW-IPAC2022-TUPOMS028

3HC – THIRD HARMONIC NORMAL CONDUCTING ACTIVE CAVITY COLLABORATION BETWEEN HZB, DESY AND ALBA*

F. Perez, J. Ocampo, A. Salom, P. Solans, ALBA Synchrotron, CELLS, Barcelona, Spain
M. Ebert, R. Onken, P. Hülsmann, DESY, Hamburg, Germany
W. Müller, TEMF, Darmstadt, Germany
W. Anders, V. Duerr, T. Loewner, A.N. Matveenko, M. Ries, L. Shi, Y. Tamashevich, A. Tsakanian
HZB, Berlin, Germany

Abstract

A collaboration agreement between the HZB, DESY and ALBA institutions was signed on 2021 in order to test the 3rd harmonic normal conducting, HOM damped, active cavity designed and prototyped by ALBA [1]. The test will involve low power characterization of the fundamental mode, bead pull measurements to fully determine the HOM characteristics, a full high power conditioning to validate the power capability of the cavity, and finally, the installation of the cavity in the BESSY II storage ring in order to test the cavity in real conditions with beam. In this paper the low power, bead pull and conditioning results will be presented. The cavity has been installed at BESSY II on May 2022 to be tested after the summer shutdown.

INTRODUCTION

The interest of the three parties of the collaboration on harmonic cavities is motivated mainly by the 4th generation upgrade projects that are under development by each of the parties, i.e. ALBA II [2], Petra IV [3], MLS II and BESSY III [4].

ALBA has designed and built a prototype of a 3rd harmonic normal conducting, HOM damped, active cavity [1], and the goal of the collaboration is to fully test this cavity in order to validate its performance, with the final goal of installing it at the BESSY II ring to be actively tested with beam.

The cavity is active, so it is part of a whole 1.5 GHz RF system, which is composed by different parts provided by the different members of the collaboration:

- 1.5 GHz cavity prototype – by ALBA
- 15 kW solid state amplifier – by HZB
- Waveguide system – by DESY
- Digital LLRF – by ALBA
- Controls – by HZB

CAVITY

The cavity is a down-scaled version at 1.5 GHz, of the 500 MHz HOM damped normal conducting cavity installed in ALBA, which was based on the EU-design developed at BESSY [5].

With the main difference that the damping mechanism of the HOMs at the end of the dampers it is not an in-vacuum ferrite absorber, but a broad band antenna which couple the power to an external load, so called *TransDampers*, see Figure 1.

Detailed information of the cavity design can be found at [6], and of the prototype construction† and acceptance test at [1].

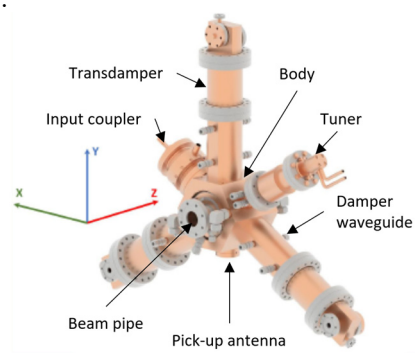

Figure 1: 1.5 GHz cavity, HOM damped with Ridged Circular waveguide and *TransDampers*.

E-M SIMULATIONS

At the design stage, electromagnetic simulations of the fundamental and of the HOMs were performed, but with the final design which was used for the construction of the prototype, the simulations have been repeated within the collaboration, together with the Institut für Teilchenbeschleunigung und Elektromagnetische Felder (TEMF).

After simulating the modes, at the moment of its identification, it was realised that due to the small cavity body of a 1.5 GHz cavity the HOM couplers attached to it are relatively large, resulting in disturbed higher modes which cannot be classified into TM- and TE-types. Only mixed forms appear, which can be called HEM modes (Hybrid Electromagnetic modes).

The electrical axis and beam axis of the cavity does no longer coincide, and sometimes the electrical axes are also skewed. This is mainly due to the fact that the three HOM couplers are distributed asymmetrically in longitudinal direction. In addition, each mode splits up to a passband of four coupled modes, due to the three HOM dampers plus the cavity body. Thus, a tremendous number of modes are formed, with most of the modes being irrelevant to particle dynamics.

The aforementioned phenomena lead to the following consequences: the undisturbed, non-attenuated cavity cannot be compared to the attenuated cavity at all; and the

* Collaboration agreement RCN-CIN202100124, BOE Resolution 8506 of May 14th, 2021. Published in May 21st, 2021.

† The prototype construction was co-funded by the European Regional Development Fund (ERDF) within the Framework of the Smart Growth Operative Programme 2014-2020.

ISBN: 978-3-95450-227-1 ISSN: 2673-5490 doi:10.18429/JACoW-IPAC2022-TUPOMS029

STATUS OF THE PETRA IV MACHINE PROJECT

R. Bartolini, I. Agapov, A. Aloev, R. Bacher, R. Böspflug, H-J. Eckoldt, D. Einfeld, J. Hauser, M. Hüning, P. Hülsmann, N. Koldrack, B. Krause, C. Kula, L Lilje, G. Loisch, R. Onken, A. Petrov, J. Prenting, S. Pfeiffer, H. Schlarb, M. Thede, M. Tischer,
DESY, Notkestraße 85, 22607, Hamburg, Germany

Abstract

DESY is planning the upgrade of PETRA III to a fourth-generation light source, providing high brightness, quasi diffraction limited hard X-ray photons. The project is underpinned by the construction of a new storage ring PETRA IV, based on a 20 pm accelerator lattice using a hybrid 6-bend achromat concept. We review here the status of the machine project, the latest development in the different technical subsystems, the status of the engineering integration and the plans for the implementation of the new ring in the existing PETRA III tunnel.

PROJECT OVERVIEW

The PETRA IV machine project aims at the construction of an ultra-low emittance storage ring delivering operating at 6GeV with a 20 pm emittance, to be installed in the existing 2.3 km PETRAIII tunnel. Significant changes to the machine concept were made since the CDR [1]. The PETRA IV complex will reuse the existing LINAC-II (450 MeV) and the PIA accumulator ring. A new low emittance booster DESY-IV, will replace the existing DESY-II booster. The storage ring will follow the geometry of the old PETRA collider with 8 octants made of arcs, each hosting nine H6BA cells, connected by long straight section as shown in Fig. 1.

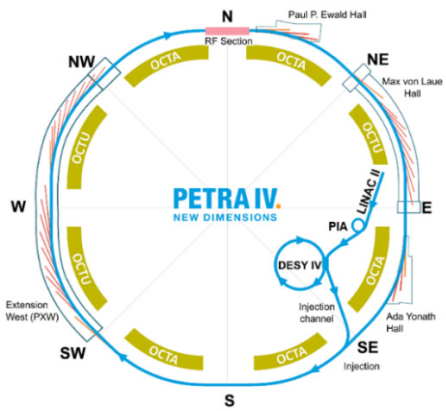

Figure 1: Layout of the PETRA IV accelerators and the experimental Halls.

Given the constraints on the DESY campus, only three octants can host beamlines (OCTU). The facility will reuse the PIII experimental halls and will build a new experimental hall covering two octants of the ring in the West. The remaining octants (OCTA) will host Damping Wiggler for the control of the emittance. The design operational parameters of the storage ring are reported in Table 1. The present timeline assume that, in funding will be available by mid-20204, the PETRA III shutdown will starting in January 2027, and with two years dark period, the machine operation can restart in January 2029.

Table 1: PETRA IV Main Parameters

Energy	6 GeV
Emittance (with DW)	20 pm
Rel. energy spread (with DW)	$9.0 \cdot 10^{-4}$
Loss per turn	4.19 MeV/turn
Momentum compaction	$3.3 \cdot 10^{-5}$
β_x, β_y, (at IDs)	2.2m; 2.2m
RF voltage (main, 3HC)	8 MV, 2.4 MV

LATTICE

The H6BA lattice is a modification of the H7BA developed for the ESRF-EBS. The main improvement consists in the replacement of the quadrupole doublet in the undulator straight section, with a triplet allowing a better control of the optics function for matching the electrons and the photons phase space. Dispersion bumps are generated to locate the chromatic sextupole families. The central part of the H7BA section is simplified to two quadrupole gradients with a phase advance of π in both planes, unlike (3π, π) in (H, V) as in H7BA. This sextupole pairing allow a very effective chromatic correction. Figure 2 shows the optics function in the H6BA cell.

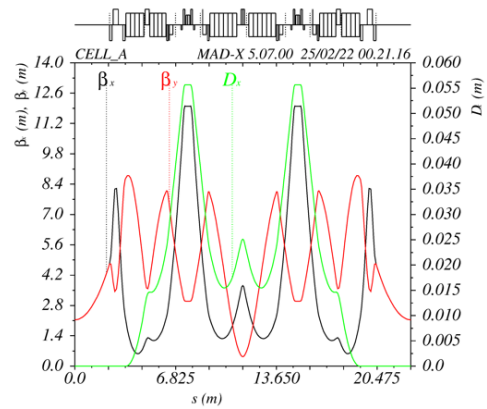

Figure 2: H6BA optics functions and layout from MAD-X.

The cell design is relaxed to provide an emittance of 43 pm. The target emittance of 20 pm is achieved by using damping wiggler in the straight section of the five octants that will not host beamlines. Details of the beam dynamics optimisation are reported in a companion paper [2].

MAGNETS

The H6BA cell consists of 6 dipoles, two of which are combined longitudinal and transverse gradient dipoles

ISBN: 978-3-95450-227-1 ISSN: 2673-5490 doi:10.18429/JACoW-IPAC2022-TUPOMS030

EVENT TREE MODEL FOR SAFETY RELIABILITY ANALYSIS OF HIGH ENERGY ELECTRON 1.2 GeV RADIATION MONITORING SYSTEM DESIGN*

P. Aim-O†, N.S. Pamungkas[1], M. Sophon, N. Sumano, P. Kulthanasomboon,
S. Ruengpoonwittaya, K. Manasatitpong, A. Thongwat
Synchrotron Light Research Institute, Nakhon Ratchasima, Thailand
[1]Chulalongkorn University, Bangkok, Thailand

Abstract

The SPS Radiation Monitoring System II (SPSRMS-II) has been designed to measure the ionizing radiation which is generated from the high-energy electron 1.2 GeV. SPSRMS-II design shall be performed to assure an adequate performance system to prevent the radiation exposure of workers and the public in the synchrotron facility. The research purpose is to evaluate the frequency of failure of real-time radiation monitoring system design that might be happened from the abnormal case which is unable to transfer the important radiation dose continuously. An Event Tree Analysis (ETA) had been approached to evaluate the safety reliability of the SPSRMS-II which is a method of deducing possibilities and outcomes in chronological order. The chance of unfavourable consequences that can cause harm and result from the chosen initiating event has been determined using this method. The scenario results showed that reliability was increased from 99.9197%±19.5921% to 99.9217%±19.5928% (95% confidential level) after adding redundancy in all the devices. The reliability assessment results of SPSRMS-II are presented.

INTRODUCTION

High electron energy 1.2 GeV provides radiation from infrared (IR) to low-energy X-rays for various user programs. It comprises a 40-MeV linac, a 1.2 GeV booster, a 1.2 GeV storage ring, and a transport line connecting the booster and the storage ring [1]. The bremsstrahlung of runaway electrons driven by a strong electric field in the environment produces X-rays, gamma-rays, and neutron radiation in a synchrotron facility [2]. For detecting and measuring radiation, a range of equipment are determined.

For each hazard scenario, a Safety Instrumented Function (SIF) is developed to first recognize the need and then act to get the system to a safe state. The level of risk reduction that a SIF is required to provide is defined by the Safety Integrity Level (SIL). SIF provides SIL, which represents the degree of risk reduction. The appropriate SIL is critical for ensuring the desired level of safety while designing a SIF [3]. A higher SIL level typically means a more sophisticated system with greater installation and maintenance expenses [4]. However, the study of SIF and SIL for high-energy electron facilities was very limited. Researchers have recently proposed the ETA technique as one of the quantitative risk management techniques; however, practical applications of ETA to the risk management of high-energy electrons of 1.2 GeV in this study remain limited.

This study will undertake a preliminary investigation of the linked instrument in radiation detection and measurements and safety reliability analysis of high-energy electron 1.2 GeV radiation monitoring system design using the event tree model to evaluate the frequency of failure per year, the probability of failure, and the reliability. The results of this study provide physical insight into the complex system of radiation monitoring of the proposed design.

METHODOLOGY

Risk Analysis

A checklist technique can be used to verify what the most potential risk is. The historical data was used to evaluate it at the beginning stage.

Mean Time to Failure (MTTF)

Mean Time to Failure (MTTF) measures the reliability of non-repairable items and equals the meantime expected until the first failure of a component, assembly, or system. First, the total work of the instrument was calculated using Eq. (1) follows [5]:

$$\text{Total work} = \text{Total workday} \times \text{Total work hour} \quad (1)$$

After that, Eq. (2) was used to calculate MTTF.

$$\text{MTTF} = \text{Total work} / \text{Total unit of instrument(s)} \quad (2)$$

Failure Rate

In the calculations of reliability engineering, the failure rate (λ; Lambda) is considered to represent the expected failure intensity assuming the component is fully operational in its initial condition. The formula [Eq. (3)] is given for repairable and non-repairable systems respectively as follows [5]:

$$\text{Failure rate per unit } (\lambda) = 1 / \text{MTTF} \quad (3)$$

Reliability

The reliability of a system follows an exponential failure law, which indicates that as the period considered for reliability calculations passes, the reliability of the system decreases. Eq. (4) was used to calculate the reliability [5].

$$\text{Reliability } (R(t)_1) = e^{-\lambda t} \quad (4)$$

Then, the failure probability of the unit instrument was calculated using Eq. (5) [5].

*Work supported by Synchrotron Light Research Institute
†pawitra@slri.ot.th

ISBN: 978-3-95450-227-1 ISSN: 2673-5490 doi:10.18429/JACoW-IPAC2022-TUPOMS031

FILL PATTERN FOR REDUCING TRANSIENT BEAM LOADING AND ION-TRAPPING IN THE DIAMOND-II STORAGE RING

T. Olsson* H.-C. Chao, Diamond Light Source, Oxfordshire, UK

Abstract

The Diamond-II upgrade will replace the existing Diamond storage ring with a multibend achromat lattice providing higher brightness to the users by reducing the emittance and increasing the beam energy. The new storage ring will require a harmonic cavity that lengthens the bunches to increase the Touschek lifetime as well as mitigate instabilities and suppress the emittance blow up from intrabeam scattering. It is expected that the ring will have to operate with gaps in the fill pattern for ion-clearing, but that will lead to transient beam loading resulting in reduced bunch lengthening. The length and occurrence of the gaps therefore have to be determined as a trade-off between the requirements for transient beam loading and ion-trapping. This paper presents simulations of both effects for the Diamond-II storage ring to find an optimal fill pattern.

INTRODUCTION

An upgrade is planned of the Diamond Light Source to replace the existing storage ring with a multibend achromat lattice which provides higher brightness for the users by reducing the emittance and increasing the beam energy [1, 2]. The new Diamond-II storage ring is planned to operate with a passive harmonic cavity to increase the Touschek lifetime, reduce intrabeam scattering and mitigate instabilities by lengthening the electron bunches. The existing Diamond storage ring is mostly operated with a fill pattern with 900 bunches, resulting in a single gap of 74 ns for ion-clearing. It is anticipated gaps will also be required in the fill pattern for the new ring to avoid ion instabilities. Gaps however give rise to transient beam loading which when operating with a harmonic cavity results in a variation of the phase and bunch length over the bunch train as well as a reduced average bunch lengthening [3]. Previous studies for Diamond-II have shown that a similar fill pattern as the one currently operated will give rise to significant transient beam loading [4] and a new fill pattern which gives larger bunch lengthening is therefore required. This paper presents simulations of the transient beam loading and ion instabilities for the Diamond-II storage ring for different gap configurations. The purpose is to find the optimal fill pattern when considering the requirements of both effects as well as the best approach to minimise the impact on the bunch lengthening in case of issues with ion instabilities during commissioning.

This paper focuses on the fill pattern for the standard mode, but the existing storage ring is also operated for a couple of weeks per year in a hybrid mode with a 3 nC bunch in the middle of a longer gap for timing users. A hybrid mode is also under study for the Diamond-II storage ring, but depending on the gap length required by the users it will give rise to significant transient beam loading. For this mode other options for increasing the lifetime may need to be considered, such as increasing the vertical emittance or operating at lower currents. More details about the hybrid mode can be found in [1].

* teresia.olsson@diamond.ac.uk

MACHINE AND CAVITY PARAMETERS

The machine parameters used in the simulations can be seen in Table 1. Closing all the insertion devices (IDs) reduces the equilibrium emittance [1, 5], resulting in a reduction of the horizontal emittance whereas the vertical emittance is planned to be kept at 8 pm rad with an emittance feedback. In these simulations it has been assumed that this is achieved by betatron coupling, but a new emittance feedback based on excitation at a synchrotron sideband is currently under development [6]. The effect of intrabeam scattering on the emittance has not been included. The IDs also have a significant impact on the damping times.

Table 1: Machine Parameters for the Diamond-II Storage Ring with Open and Closed Insertion Devices

	Open IDs	Closed IDs
Energy [GeV]	3.5	
Circumference [m]	560.561	
Harmonic number	934	
RF frequency [MHz]	499.511	
Tune (h/v)	54.15/20.27	
Chromaticity (h/v)	2.0/2.3	
Momentum compaction	$1.04 \cdot 10^{-4}$	
Nominal current [mA]	300	
RF voltage [MV]	1.42	2.53
Emittance (h/v) [pm rad]	153.7/8	113/8
Energy spread [%]	0.094	0.11
Energy loss/turn [MeV]	0.723	1.68
Damp. time (h/v/l) [ms]	9.7/18.1/16.0	5.7/7.8/4.8

The ring will operate with eight active normal conducting main cavities and one passive superconducting third order harmonic cavity [1]. Table 2 shows the parameters used for the cavities. The main cavities correspond to the EU HOM-damped cavities already under test in the existing Diamond storage ring [7] whereas the harmonic cavity is based on the CEA Super-3HC cavity used at SLS and Elettra [8]. As can be noted, the total R/Q of the main cavities is higher than for the harmonic cavity and they therefore dominate the transient beam loading.

ISBN: 978-3-95450-227-1 ISSN: 2673-5490 doi:10.18429/JACoW-IPAC2022-TUPOMS032

PERFORMANCE OF THE DIAMOND-II STORAGE RING COLLIMATORS

H. Ghasem, J. Kallestrup, I.P.S. Martin, Diamond Light Source, Oxfordshire, UK

Abstract

Particle losses in a storage ring are unavoidable and it is very important to capture them and protect the machine from any possible damage. For this purpose, 6 collimators have been introduced in the Diamond-II storage ring lattice. This paper describes the main layout of the collimators with their corresponding impact and performance.

INTRODUCTION

There are many sources of particle loss in storage rings. The lost particles may hit the vacuum chamber affecting the pressure profile or cause damage to diagnostic instruments or in-vacuum insertion devices. As such, it is essential to provide a means to collect them and ensure machine protection. In this paper, we present investigations into the performance of the collimators for the various loss mechanisms.

LAYOUT OF COLLIMATORS

Many different locations and numbers have been investigated for the collimators and finally a 6-collimator scheme has been selected for the Diamond-II storage ring [1, 2], 3 horizontal and 3 vertical. The general layout of the ring including the collimators is displayed in Fig. 1. The blue and red lines indicate which are the horizontal and vertical collimators respectively.

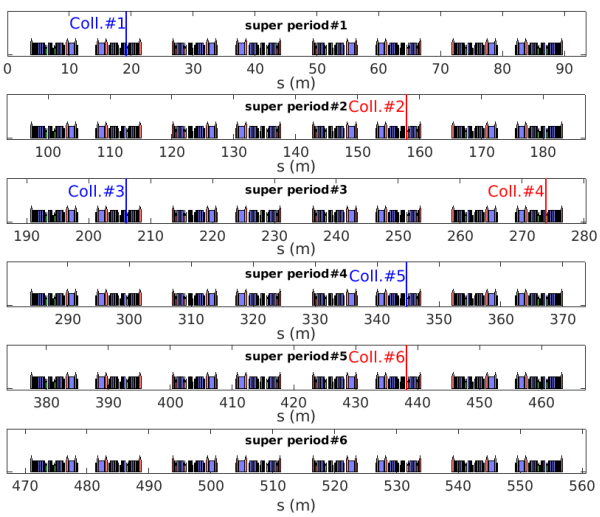

Figure 1: General layout of the collimators in the Diamond-II storage ring.

All the collimators are placed in the downstream half of the dispersion bumps following the mid-straights. Optics at this point are favourable for collimation as the dispersion and beta-functions are relatively large, meaning the oscillation amplitudes for both on and off-momentum particles will also be large. This location is also relatively free from engineering restrictions making it an obvious choice.

LATTICE PERFORMANCE

Inserting collimators into the ring will affect many accelerator parameters such as the dynamic and momentum apertures, injection efficiency (IE) and lifetime. A study of different values of horizontal and vertical collimator gaps has been carried out to determine the optimum compromise between machine protection and machine performance. All the plots in the lattice and collimator performance sections are the average over 20 seeds of errors and the ELEGANT [3] is employed for the calculations. The average dynamic aperture (DA) is displayed in Fig. 2. As expected, closing the collimator gaps leads to reduction in the DA. The top plot in Fig. 2 reveals that keeping the half gap of the vertical collimators (VGAP) at ±1.5 mm and closing the half gap of the horizontal collimators (HGAP) leads to shrinkage mainly in the horizontal DA, while keeping HGAP at = ±3.5 mm and closing VGAP results to more drastic situation with smaller DA in both planes (bottom plot).

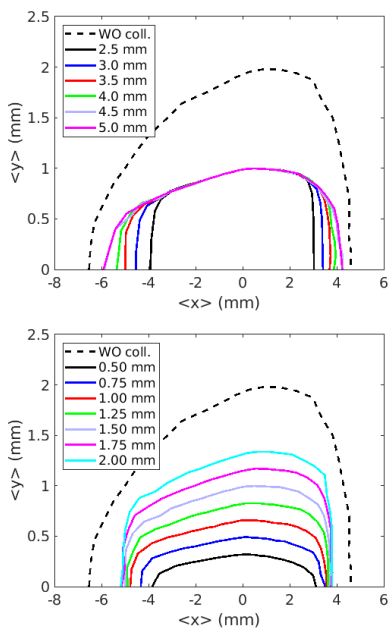

Figure 2: Mean dynamic aperture at the centre of the long straight section for various gaps of horizontal (top) and vertical (bottom) collimators. VGAP in the top plot is set to ±1.5 mm while HGAP in the bottom plot is kept at ±3.5 mm.

The mean momentum aperture (MA) for one super period is shown in Fig. 3 for various HGAPs and VGAPs. All momentum aperture curves overlap for the cases of high HGAPs and VGAPs, while a significant decrease in MA is

ISBN: 978-3-95450-227-1 ISSN: 2673-5490 doi:10.18429/JACoW-IPAC2022-TUPOMS033

DIAMOND-II STORAGE RING DEVELOPMENTS AND PERFORMANCE STUDIES

I.P.S. Martin, H.-C. Chao, R.T. Fielder, H. Ghasem, J. Kallestrup, T. Olsson, B. Singh, S. Wang,
Diamond Light Source, Oxfordshire, U.K.

Abstract

The Diamond-II project includes a replacement of the existing double-bend achromat storage ring with a modified hybrid 6-bend achromat, doubling the number of straight sections and increasing the photon beam brightness by up to two orders of magnitude. The design and performance characterisation of the new storage ring has continued to progress, including a switch to an aperture-sharing injection scheme, freezing the magnet layout, studying the impact of IDs, developing a commissioning procedure and investigating collective effects. In this paper we present an overview of these studies, including final performance estimates.

INTRODUCTION

The lattice design for the Diamond-II storage ring remains largely unchanged since the work presented in [1], with the majority of effort focussed on developing the engineering design and characterising the performance of the lattice under realistic conditions [2]. This paper presents an overview of these studies. For reference, a plot of the Twiss parameters for a single cell spanning long, mid and standard straights is shown in Fig. 1 and a summary of the main lattice parameters for the nominal optics is given in Table 1.

DIAMOND-II STORAGE RING

Lattice Modifications

Although the magnet layout and nominal optics remains unchanged, minor modifications have been made to accommodate the evolving engineering design. The largest change has occurred on the mid-to-long straight (ML) and mid-to-standard straight (MS) girders to create space for the collimators. This has involved small shifts in the BPM locations and relocating one of the fast corrector magnets from between the DQ and DL dipoles to be inside the dispersion bump.

Six collimators have been added to the lattice to provide machine protection against lifetime and injection losses, in addition to the beam-dumps occurring due to RF switch-off. The collimators have been located at the downstream half of the MS and ML girders where the dispersion and beta-functions are large, with a total of three collimators in each plane. Optimal gaps of ±3.5 mm horizontally and ±1.5 mm vertically were arrived at after an extensive investigation into the collection efficiency and the impact on lifetime and injection. Details of these studies can be found in [3].

A review of the magnet strength limits has been conducted, the purpose of which was to ensure there is sufficient tuning range to allow for future changes to the machine optics and nonlinear optimisation. These studies included:

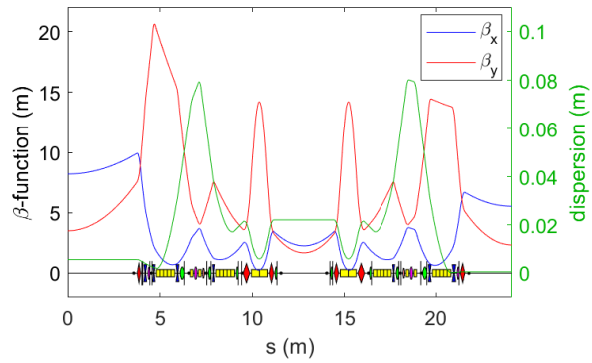

Figure 1: Twiss parameters for one M-H6BA cell including long, mid and standard straight sections.

Table 1: Summary of Diamond-II Lattice Parameters

Parameter	**Bare Lattice**
Circumference (m)	561.561
Tot. Bending Angle (deg)	388.8
Betatron Tunes	[54.15, 20.27]
Nat. Chromaticity	[-67.6, -88.5]
Mom. Comp. Factor	1.04×10^{-4}

Parameter	**Bare Lattice**	**IDs Closed**
Nat. Emittance (pm.rad)	161.7	121.0
Nat. En. Spread (%)	0.094	0.110
RF Voltage (MV)	1.4	2.5
Nat. Bunch Length (ps)	12.5	11.7
En. Loss per Turn (MeV)	0.72	1.68
τ_x (ms)	9.7	5.7
τ_y (ms)	18.1	7.8
τ_E (ms)	16.0	4.8

- scanning the fractional tune within Qx = 54 to 55 and Qy = 20 to 21, maintaining the '-I' and cell phase advance constraints;
- stepping the horizontal integer tune from 54.2 to 62.2;
- increasing the chromaticity in integer steps from [+2, +2] to [+10, +10] at fixed tune point;
- running MOGA optimisations with a variety of constraints and variable parameters.

Two alternative operating modes using the nominal lattice hardware were found during this study, one with reduced beta-functions at the IDs to improve the phase-space matching to the photon beams, the other with smaller natural emittance [4]. These have smaller dynamic aperture and lifetimes than the baseline lattice and are under consideration for a future 'brightness' upgrade.

ISBN: 978-3-95450-227-1 ISSN: 2673-5490 doi:10.18429/JACoW-IPAC2022-TUPOMS034

TUNABILITY AND ALTERNATIVE OPTICS FOR THE DIAMOND-II STORAGE RING

H. Ghasem, I.P.S. Martin, B. Singh, Diamond Light Source, Oxfordshire, UK

Abstract

When defining the magnet specifications, a key consideration is that the hardware should be flexible enough to allow some contingency for future tuning requirements or for alternative lattice solutions to be implemented. To define the required tunability of the magnets, we have investigated two lattice solutions for the Diamond-II storage ring upgrade, one with reduced beta functions at the straight sections for improved matching to the photon beam and one with an ultra-low emittance of 87 pm with IDs. In this paper, the linear and nonlinear beam dynamic issues as well as the photon beam brightness for these two options will be presented and discussed.

INTRODUCTION

In order to define the required tuning ranges and specifications for the different magnet types a number of investigations have been carried out. These include:

- Scanning the fractional tune point within the cell Q_x = 54 to 55 and Q_y = 20 to 21 whilst maintaining the phase advance constraints and nominal chromaticity.
- Keeping the fractional tune point constant but stepping the horizontal tune in integer units from 54.2 to 62.2, maintaining the phase advance constraints and nominal chromaticity.
- Increasing the chromaticity in integer steps from [+2, +2] to [+10, +10] at fixed tune point.
- Running MOGA optimisations with a variety of constraints and variable parameters, including adjusting the Twiss parameters at the sextupole or ID locations, altering the phase advance constraints and reconfiguring the sextupole families and allowing the chromaticity to vary.

The results of these investigations were used to develop the individual magnet designs, including altering the magnet lengths to either free-up space or keep peak gradients within practical limits.

An important principle when considering alternative optics is that the reference trajectory for the electron beam must remain fixed to avoid shifting the beamline source-points or altering which parts of the vacuum chamber are illuminated by synchrotron radiation. The consequence of this is that, if different optics were to be implemented at a later stage that involved changing the gradients in the anti-bends, the transverse offsets of the anti-bend (AB) magnets would need to be adjusted in proportion to the change in gradient to keep the bend angle constant. The OPA [1] and ELEGANT [2] codes have been employed for the optimizations. The final magnet strength limits adopted for the magnet specifications and imposed on the lattice tuning studies are given in Table 1.

Table 1: Magnet Strength Limits Used for Magnet Designs and During Lattice Optimisation Studies

Magnet	Parameter	Max. Value
Quadrupole	Gradient (T/m)	90
Anti-bend (high-gradient)	Gradient (T/m)	80
	Offset range (mm)	2.5 to 3.6
Anti-bend (low-gradient)	Gradient (T/m)	60
	Offset range (mm)	3.4 to 7.8
Skew-quadrupole	Gradient (T/m)	2.0
Sext. (narrow bore)	Gradient (T/m^2)	5000
Sext. (wide bore)	Gradient (T/m^2)	3500
Octupole	Gradient (T/m^3)	70000
Hor./Ver. corr.	Bend angle (mrad)	1.0
Hor./Ver. fast corr.	Bend angle (mrad)	0.02

LINEAR BEAM DYNAMICS

An illustration of the tunability of the lattice is given by the two alternative solutions shown in Fig. 1.

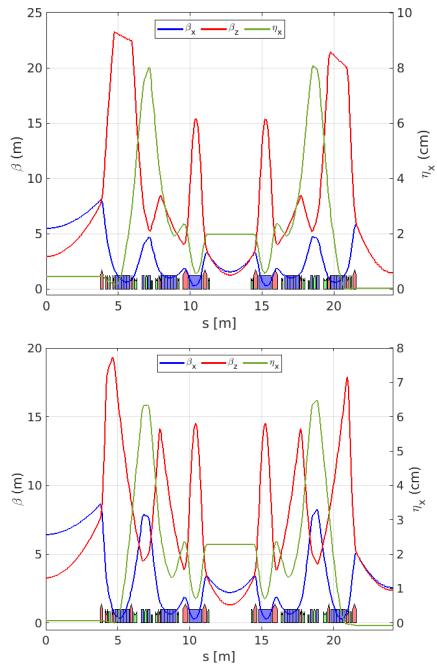

Figure 1: Optical functions in a unit cell, low beta (top) and low emittance (bottom) optics.

The first of these (referred to as the low beta solution) shows an optimisation where the beta functions at the ID source points have been reduced to give a better matching of the electron beam phase space to the intrinsic photon beam size and divergence, thereby increasing the brightness. In the second solution (referred to as the low emittance solution) the horizontal tune point has been further

ISBN: 978-3-95450-227-1 ISSN: 2673-5490 doi:10.18429/JACoW-IPAC2022-TUPOMS035

EMITTANCE FEEDBACK FOR THE DIAMOND-II STORAGE RING USING RESONANT EXCITATION

S. Preston*, T. Olsson, B. Singh, Diamond Light Source, Oxfordshire, UK

Abstract

In the Diamond Light Source storage ring, the vertical emittance is kept at 8 pm rad during operation to maintain the source brightness for the users. This is achieved by a feedback which modifies the skew quadrupole strengths, but has disadvantages such as the introduction of betatron coupling and vertical dispersion. For the proposed Diamond-II upgrade, the storage ring will have a much smaller horizontal emittance, meaning a significantly larger coupling would be required to reach the target vertical emittance, negatively affecting the off-axis injection process. To solve this problem, a feedback using the transverse multibunch feedback striplines to drive the beam at a synchrotron sideband is planned. By driving the beam resonantly in this way, the emittance can be increased without modification of the optics. This paper describes simulations of the effects of linear and non-linear optics on the excitation as well as the impact of the machine impedance for the Diamond-II storage ring.

INTRODUCTION

In synchrotron light storage rings, the emittance of the beam must be controlled during operations to stabilise the source brightness and lifetime for users as conditions vary due to long-term drifts and insertion device (ID) gap movement. At the existing Diamond storage ring, the vertical emittance is kept at 8 pm rad by a feedback which modifies the skew quadrupole strengths [1], but this introduces betatron coupling and vertical dispersion. An upgrade of the ring is planned [2] to significantly reduce the horizontal emittance, meaning the new Diamond-II storage ring will require a larger coupling to reach the same vertical emittance, affecting the off-axis injection. Studies at BESSY II and MAX IV [3–6] have shown that the emittance can be blown up by driving the beam at a synchrotron sideband. The purpose of those studies was to increase the emittance of a single bunch to provide light for timing users while operating with a multi-bunch fill pattern [7], but at Diamond the same method is planned to be used for an emittance feedback acting on all bunches without affecting the optics. The emittance will be measured using the existing pinhole cameras and then the feedback will adjust the gain of an excitation from the multi-bunch feedback striplines, to keep the emittance at the target value. The vertical emittance will first be corrected to a few pm rad using LOCO [8] and then increased to 8 pm rad with the emittance feedback. This paper presents simulations of the effect of linear and non-linear optics as well as impedance on the optimal excitation frequency for the Diamond-II storage ring.

* shaun.preston@diamond.ac.uk

SIMULATION SETUP

Simulations were performed in Elegant [9, 10] including broadband impedance given by the sum of the resistive-wall and geometric contributions [11]. A bunch of 1,000 particles was tracked to equilibrium using a one-turn map including radiation damping, quantum excitation and non-linear optics terms (second and third order chromaticity, and amplitude-dependent tune shifts). The bunch was excited vertically using a zero-length kicker with a sinusoidal kick angle given by

$$\theta = A\cos(2\pi f t) \tag{1}$$

where A is the maximum kick angle, f the excitation frequency and t the arrival time at the kicker.

SIDEBAND DISTORTION

Figure 1 shows the beam oscillation and size as a function of excitation frequency. The symmetry of the synchrotron sidebands is broken by the impedance and non-linear terms. The impedance widens and shifts them closer to the tune while the non-linear terms narrow the lower sidebands.

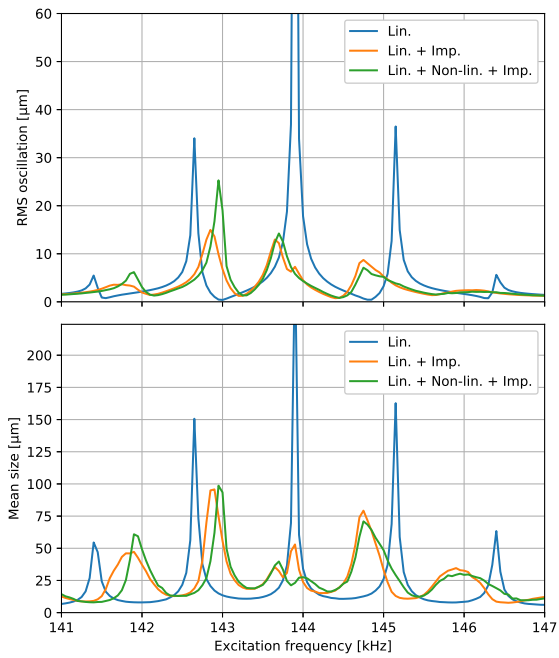

Figure 1: Beam oscillation and size as a function of excitation frequency due to linear chromaticity, non-linear terms and impedance at nominal bunch current 0.32 mA and vertical chromaticity 2.33 for a kick angle of 50 nrad. Black lines mark the nominal positions of the vertical betatron tune (solid) and synchrotron sidebands (dashed).

ISBN: 978-3-95450-227-1 ISSN: 2673-5490 doi:10.18429/JACoW-IPAC2022-TUPOMS036

COMMISSIONING OF THE LOWER EMITTANCE LATTICE AT SPEAR3*

K. Tian†, J. Corbett, S. Gierman, X. Huang, J. Kim, J. Langton, N. Parry, J. A. Safranek, J. J. Sebek, M. Song, Z. Zhang
SLAC National Accelerator Laboratory, Menlo Park, California, USA

Abstract

SPEAR3, commissioned in 2004, is a third-generation light source at the SLAC National Accelerator Laboratory. The low emittance lattice with an emittance of 10 nm had been operated for over a decade until the recent commissioning of a lower emittance lattice with the 7 nm emittance. The new lattice, with additional flexibility to adjust the sextupoles, has pushed toward the design limit of double-bend achromat lattice in SPEAR3. In this paper, we will elaborate on our commissioning experience for the new lattice in SPEAR3.

INTRODUCTION

By adopting a compact double-bend achromat (DBA) lattice design, SPEAR3 is efficient in achieving low emittance. However, with the growing number of next generation synchrotron radiation light sources under construction, there is a strong desire to push the limit of the lattice to lower emittance to benefit high brightness user experiments. Lower emittance lattice development efforts started in 2011. As a result, two lattice options, 6 nm lattice and 7 nm lattice, were developed [1]. Several hardware upgrades were identified to pave a pathway to user operation of the lower emittance lattice. First, the pulser of the second injection kicker, K2, was required to be upgraded to provide a stronger kick. This was completed in summer 2014. In the same year, new sextupole power supplies were added to break up the standard cell sextupoles from two large strings power supplies to eight smaller groups. The additional degrees of freedom allow simultaneous optimization of dynamic aperture and momentum aperture. The injection septum upgrade [2], which was completed in summer 2019, was essential to the operation of the lower emittance lattice. The new septum wall thickness was reduced from 5.4mm to 2.5 mm to provide efficient injection with the smaller dynamic aperture in the new lattice. The last hardware upgrade was the beam dump modification to address the radiation safety requirement. Following the installation of the beam dump in April 2021, SPEAR3 has started user beam operation in 7 nm lattice with highly reliable performance.

LATTICE OPTIONS

SPEAR3 has a race-track layout with 14 standard DBA cells and 4 matching DBA cells. The standard DBA cells need to be matched to the four matching cells of the two long straight sections. Based on the results of a global scan of the SPEAR3 standard DBA cell performance, it was determined to increase the horizontal tune by one unit to achieve emittance reduction. After explorations of the working point and phase advances of the matching cells, two lower emittance lattices were developed as upgrade options: 7 nm lattice and 6 nm lattice [1]. Selected parameters of these lattices, such as betatron tunes, emittance, effective emittance, horizontal/vertical beta functions at the ID straights, and the horizontal dispersion at the ID, are listed in Table 1. The parameters of the previous 10 nm lattice are listed for comparison.

Table 1: Lattice Parameters

	10 nm	**7 nm**	**6 nm**
ν_x, ν_y	14.106,6.177	15.10,6.16	15.32,6.18
ϵ_x (nm), w/IDs	9.6	6.7	6.1
$\epsilon_{x,eff}$ (nm)	10.1	7.2	6.7
$\beta_{x,ID}$ (m)	8.85	8.96	9.46
$\beta_{y,ID}$ (m)	4.86	5.29	5.24
$D_{x,ID}$ (m)	0.10	0.11	0.12

The lower emittance lattices boost the beam brightness significantly from the 10 nm lattice. Their effective emittances are 7.2 nm and 6.7 nm, respectively. Considering other factors such as the increased horizontal beta function in the 6 nm lattice, the two lattices offer comparable performance for most user experiments in SPEAR3. However, the 6 nm lattice is more challenging in terms of nonlinear beam dynamics, which is critical for efficient beam injection to the storage ring. Therefore, the 7 nm lattice was developed as the working option to serve as the initial operation lattice after the required hardware upgrades.

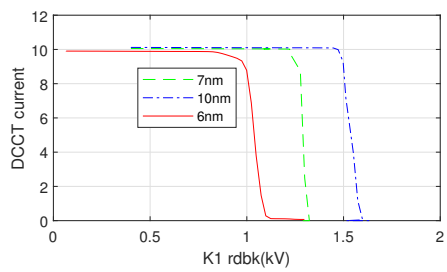

Figure 1: Dynamic aperture of different lattices.

During the development of the 7 nm and 6 nm lattices, various online optimization methods have been used to increase the dynamic aperture [3-5]. We believe that, after extensive nonlinear optimizations, we have explored the full potential of these two lattices. We compare the optimized dynamic

* Work supported by U.S. Department of Energy under Contract No. DE-AC02-76SF00515
† ktian@slac.stanford.edu

ISBN: 978-3-95450-227-1 ISSN: 2673-5490 doi:10.18429/JACoW-IPAC2022-TUPOMS037

RCDS-S: AN OPTIMIZATION METHOD TO COMPENSATE ACCELERATOR PERFORMANCE DRIFTS*

Z. Zhang, M. Song[1], X. Huang†, SLAC National Accelerator Laboratory, Menlo Park, CA, USA
[1]also at Department of Physics, Illinois Institute of Technology, Chicago, IL, USA

Abstract

We propose an optimization algorithm, Safe Robust Conjugate Direction Search (RCDS-S), which can perform accelerator tuning while keeping the machine performance within a designated safe envelope. The algorithm builds probability models of the objective function using Lipschitz continuity of the function as well as characteristics of the drifts and applies to the selection of trial solutions to ensure the machine operates safely during tuning. The algorithm can run during normal user operation constantly, or periodically, to compensate the performance drifts. Simulation and online tests have been done to validate the performance of the algorithm.

INTRODUCTION

Online optimization is an effective approach to find accelerator settings with high performance. Efficient optimization algorithms are key to online optimization. Popular optimization algorithms for online accelerator applications include Nelder-Mead simplex [1], robust conjugate direction search (RCDS) [2], particle swarm [3], and Bayesian optimization [4]. During an optimization run, as the algorithm gradually discovers machine settings with high performance, it can also produce solutions with poor performance, which cannot be tolerated for normal user operation. Therefore, online optimization is usually performed during dedicated machine development or study shifts. However, in many cases, an ideal machine setting will not maintain the high performance during the long period of user operation. Small variations in the accelerator components, caused by or coupled with variations of the surrounding environment, can cause the machine performance to drift with time.

In this study, we propose a safe tuning method that can be used during user operation. The new algorithm is called safe robust conjugate direction search (RCDS-S). It employs iterative one-dimensional (1-D) optimization over a conjugate direction set in a similar manner as the RCDS method. However, its 1-D optimization is done by a more prudent and informed fashion, which employs a probability model of the objective function to assess the risk of exceeding a safety threshold by the trial solution.

THE RCDS-S METHOD

Our goal of the study is to develop an optimization method that can be used to optimize accelerator performance during user operation by keeping the performance above a certain threshold. Such a method could be termed "safe" optimization algorithm. A safe optimization algorithm could be used to compensate the performance drift with time, as it can run in the background continuously, periodically, or as needed.

In the following, we first discuss the uncertainty of the objective function as it is probed. By constructing a probability model of the uncertainty and using it to guide the selection of new trial solutions, we devised a safe 1-D optimization method. Combining this safe 1-D optimization method and the conjugate direction search method, we arrived at the new algorithm, RCDS-S.

Modeling Uncertainty of Objective Function

In this study, we assume the optimization problem to be a minimization problem, with measurement error (noise) and time-dependent error (systematic drift). Firstly the gradient of the objective function has to be limited for a safety setting. We assume the objective function to be L-Lipschitz continuous, which means for any $\mathbf{x}, \mathbf{x_0} \in \mathbf{D}$, where $\mathbf{D}$ is the domain of the function, we have,

$$\|f(\mathbf{x}) - f(\mathbf{x_0})\| \leq L \cdot \|\mathbf{x} - \mathbf{x_0}\| .$$

On the other hand, without further information about the specific optimization problem, the drift can be modeled as a random walk process. Under this assumption, the uncertainty of the measurement becomes a time varying random variable,

$$y = f(\mathbf{x}) + \epsilon(t),$$

where $\epsilon(t) \sim N(0, \sigma_n^2 + t\sigma_d^2)$. Here σ_n is the noise level, σ_d^2 represents the increase of the variance within a unit time interval, and t the time elapsed from a reference point.

Given the safety threshold h, to guarantee $y \leq h$ we have:

$$\hat{\epsilon} \leq \frac{h - E_{\max}}{\sqrt{2\sigma_n^2 + t \cdot \sigma_d^2}}, \tag{1}$$

here $E_{\max}$ is the maximum expected value of objective y at point $\mathbf{x}$ which satisfies $E_{\max}(\mathbf{x}) = y_0 + L \cdot \|\mathbf{x} - \mathbf{x_0}\|$, and $\hat{\epsilon} \sim N(0, 1)$.

1D Safety Exploration

For a 1D problem, given a few observations, the safety probability of each candidate can be computed with Eq. (1). The idea is that each observation would provide safety information for all the other candidates along the direction, based on the relative measurement time and position with regard to the candidate of interest, and the final safety probability of one candidate can be determined by combining the safety information from all the observations. One example safety

* Work supported under DOE Contract No. DE-AC02-76SF00515
† xiahuang@slac.stanford.edu

ISBN: 978-3-95450-227-1 ISSN: 2673-5490 doi:10.18429/JACoW-IPAC2022-TUPOMS038

RFQ NEWGAIN: RF AND THERMOMECHANICAL DESIGN*

P. Hamel†, N. Sellami, M. Desmons, O. Piquet, B. Prevet, CEA-IRFU, 91191 Gif-sur-Yvette, France

Abstract

A new injector called NEWGAIN will be added to the SPIRAL2 Linear Accelerator (LINAC) [1], in parallel with the existing one. It will be mainly composed of an ion source and a Radio Frequency Quadrupole (RFQ) connected to the superconductive LINAC of SPIRAL2. The new RFQ will accelerate at 88.05 MHz particles with charge-over-mass ratio (Q/A) between 1/3 and 1/7, from 10 keV/u up to 590 keV/u. It consists of a 4-vane resonant cavity with a total length of 7 m. It is a CW machine that has to show stable operation, provide the request availability, have the minimum losses in order to provide the highest current to the superconductive LINAC and show the best quality/cost ratio. This paper will present the preliminary RF design and the thermomechanical study for this RFQ.

INTRODUCTION

The purpose of the NEWGAIN project is to develop a new injector, consisting of an ion source (type: superconductive ECR) and a RFQ (A/q = 7), for the SPIRAL2 LINAC. It will enable GANIL to provide ion beams of worldwide highest intensities (from proton to uranium), thus opening up unprecedented opportunities for nuclear structure and reaction studies at the extremes of the chart of nuclides from N=Z nuclei at the proton dripline to super-heavy species, including the discovery of new elements, and the production of radioisotopes. It also makes it possible to extend the use of SPIRAL2 beams to interdisciplinary research as well as applications.

The NEWGAIN RFQ cavity RF is very close to the SPIRAL2 RFQ cavity, currently operating in GANIL as they both operate at the same frequency. The choice is made to assemble the cavity mechanically, the same as SPIRAL2, in order to skip the complex process of brazing of such large cavity sections. The RF design and thermomechanical study follow the procedure developed at CEA and presented in [2].

RF DESIGN

Beam Dynamic Specifications

The modulations of the RFQ vanes have been optimized using the TOUTATIS solver. At the end of this optimization, the Kilpatrick limit remains below 1.6 and the vane voltage is constant, at 70 kV, along the RFQ. The RFQ length, about 7 m, ensures a frequency distance of about 1 MHz between the accelerator mode and neighboring dipole modes which have to be avoided. This will guarantee stability during the operation.

Transmisson Line Model (TLM)

From a microwave point-of-view, a RFQ is merely a waveguide-based circuit, consisting of small 3D devices at the end regions, connected by multiple segments of waveguide with constant cross-section. Thus, this RF circuit is modeled as a transmission line model composed of capacitances and inductances as illustrated in Fig. 1:

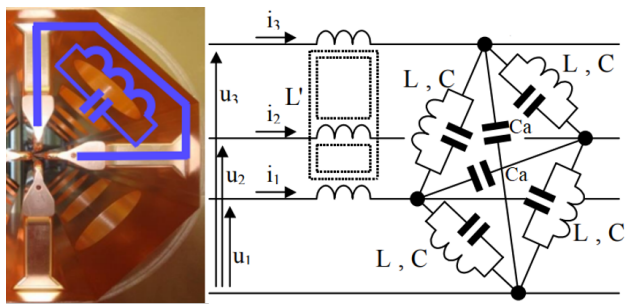

Figure 1: TLM. Left: electrical circuit corresponding to the geometry. Right: 4-wire line equivalent circuit.

Cross-section Design

The final RFQ will be made of seven 1-m long sections. Since the vane voltage has to be constant along the RFQ, the cutoff frequency of the cross-section has to be also constant. For an easier manufacturing process, the radius of the cavity has been set constant. Thus, the inductance, proportional to the surface cross-section, will also be constant. From these considerations, the capacitance has also to be constant. Despite the vane radius and the mean distance of the vane to the axis being constant along the RFQ, the sine shape of the modulation implies a modification of the vane from cell to cell, to adjust the capacitance. One geometrical parameter, called J1, has been selected for profile tuning taking into account ease of machining: this parameter is adjusted piecewise linearly to best fit the required voltage profile at a lower cost. The geometry cross-section and the J1 position are illustrated in Fig. 2:

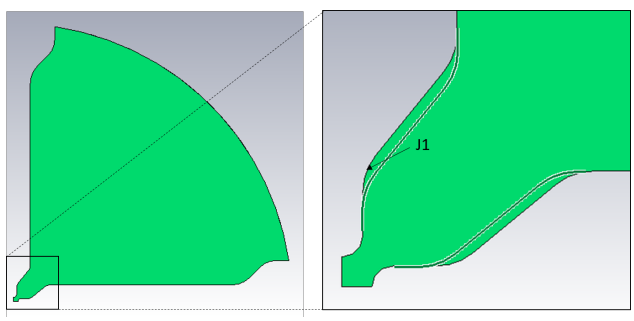

Figure 2: Cross-section geometry.

* Work supported by Agence Nationale de la Recherche (ANR)
† pierrick.hamel@cea.fr

ISBN: 978-3-95450-227-1 ISSN: 2673-5490 doi:10.18429/JACoW-IPAC2022-TUPOMS040

CHARACTERIZATION OF HIGHER-ORDER-MODES (HOM) IN THOMX STORAGE RING RF CAVITY

M. El Khaldi, JN. Cayla, H. Monard, Université Paris-Saclay, CNRS/IN2P3, IJCLab, Orsay, France
M. Diop, F. Ribeiro, SOLEIL, Gif-sur-Yvette, France

Abstract

The RF system of the ThomX storage ring consists in a 500 MHz single cell copper cavity of the ELETTRA type, powered with a 50 kW CW solid state amplifier, and the associated Low-Level RF feedback and control loops. The low operating energy of 50-100 MeV makes the impedances of the cavity higher order modes (HOMs) particularly critical for the beam stability. Their parasitic effects on the beam can be cured by HOM frequency shifting techniques, based on a fine temperature tuning and a dedicated adjustable plunger. A cavity temperature stability of ± 0.1 °C within a range from 30 up to 70 °C is achieved by a precise control of its water-cooling temperature. On the other hand, the tuning of the cavity fundamental mode is achieved by changing its axial length by means of a mechanical tuner. In order to insure a fine control of the HOM frequencies, a good knowledge of their characteristics is mandatory. The main parameters of the fundamental and of the HOMs up to 2.2 GHz versus temperature have been measured at low power using a vector network analyzer (VNA).

INTRODUCTION

ThomX is a Compton source project in the range of the hard X rays (45/90 keV). The machine is composed of a 50/70 MeV injector LINAC and a storage ring where an electron bunch collides with a laser pulse accumulated in a Fabry-Perot resonator. The final goal is to provide an X-ray average flux of 10^{12} – 10^{13} ph/s. The emitted flux will be characterized and used for experiments by a dedicated X-ray line [1]. Different users are partners in the ThomX project [2], especially in the area of medical science [3] and cultural heritage [4]. Their main goal is the transfer of experimental techniques currently developed on large synchrotron rings to more compact and flexible machines. ThomX is a demonstrator built on the Paris-Saclay university campus. The THOMX LINAC is presently under commissioning (Phase 1: 100 pC, 50 MeV at 10 Hz).

The RF system for the ThomX storage ring is described in [5]. It consists in a 500 MHz single cell cavity of the ELETTRA type, powered with a 50 kW CW solid state power amplifier (SSPA), and the associated Low-Level RF feedback and longitudinal and transverse feedbacks.

When a bunch traverses a high Q resonator like a RF cavity, it excites its higher order modes (HOMs). The induced long-term electromagnetic wakefields act back on the bunch over many revolutions and therefore can cause beam instabilities resulting in degradation of the beam quality or even beam losses.

In a low energy ring like ThomX, the natural damping time is so weak (~ 1 s) that a stationary stable condition can never be reached during the beam storage time, which is as short as 20 ms. On the other hand, it is sufficient to maintain the instability growth time larger than the beam storage time in order to keep at tolerable level the effect on the beam. That requires very strong attenuation of the cavity HOM impedances, typically by a few 10^3.

There are essentially two methods of coping with such HOM impedances, either a strong de-Qing of the HOM resonances [6, 7] or a tuning of their frequencies away from the beam spectral lines to prevent resonant excitations [8]. With the former it is difficult to reach attenuation factors larger than a few 10^2 over a wide frequency range. The latter, which consists in controlling the HOM frequencies, is better suited to a small circumference machine like ThomX, where the beam spectral lines spacing i.e. revolution frequency f_{rev} =16.67 MHz is very large as compared to the HOMs bandwidth.

That led us to choose the ELETTRA type cavity which allows applying this technique in combining three tuning means. The HOM frequencies are precisely controlled by proper setting of the cavity water cooling temperature within a range from 30 up to 70 °C with a stability of ± 0.1 °C, while the fundamental frequency is recovered by means of a mechanical tuner which changes the cavity length. Besides, a movable plunger (HOMFS) provides another degree of freedom for tuning the HOM frequencies.

In order to insure a fine control of the HOM frequencies, a good knowledge of their characteristics is mandatory. The main parameters of the fundamental and of the HOMs up to 2.2 GHz versus temperature have been measured at low power using a vector network analyzer (VNA).

As it will be hard to cope with all these modes only by applying the tuning technique, one relies on the longitudinal and transverse feedbacks in order to bring additional damping.

RF CAVITY

One 500 MHz single cell cavity of the ELETTRA type, powered with a 50 kW CW SSPA, will provide the required RF voltage of 500 kV. It is made out of OFHC copper and equipped with 8 equatorial connecting ports: 3 large ones for the input power coupler, the pumping system, the plunger tuner and 5 smaller ones for vacuum and RF monitoring and temperature monitoring sensors. It is water cooled by means of copper pipes, brazed on its external wall surface. Its temperature can be set within a range from 30 up to 70 °C with a stability of ± 0.1 °C by re-circulating the cooling water through an appropriate heat exchanger (cooling rack), The cavity cut-off tube (Ø 100 mm) will be connected to the octagonal shaped vacuum chamber by means of two 30 cm long tapers, made of 316 L stainless steel and bellows. The cavity assembly is shown in Fig. 1.

ISBN: 978-3-95450-227-1 ISSN: 2673-5490 doi:10.18429/JACoW-IPAC2022-TUPOMS041

HIGH POWER RF-CAVITY DEVELOPMENT FOR THE HBS-DRIVER LINAC

M. Basten * [1,2], K. Aulenbacher [1,2,3], W. Barth[1,2,3], C. Burandt[1,2], F. Dziuba[1,2,3], V. Gettmann[1,2], T. Gutberlet[4], T. Kürzeder[1,2], S. Lauber [1,2,3], J. List[1,2,3], M. Miski-Oglu[1,2], H. Podlech[5,6], M. Vossberg[1], S. Yaramyshev[1,2]

[1] GSI Helmholtzzentrum für Schwerionenforschung GmbH, Darmstadt, Germany
[2] HIM Helmholtz Institute Mainz, Mainz, Germany
[3] KPH Johannes Gutenberg-University Mainz, Mainz, Germany
[4] JCNS Forschungszentrum Jülich GmbH, Jülich, Germany
[5] IAP Institut für Angewandte Physik, Frankfurt am Main, Germany
[6] Helmholtz Research Academy Hesse for FAIR HFHF, Frankfurt am Main, Germany

Abstract

Neutron research in Europe is mainly based on various nuclear reactors that will be successively decommissioned over the next years. This means that despite the commissioning of the European Spallation Source ESS, many neutron research centres, especially in the medium flux regime, will disappear. In response to this situation, the Jülich Centre for Neutron Science (JCNS) has begun the development of a scalable, compact, accelerator-based High Brilliance neutron Source (HBS). A total of three different neutron target stations are planned, which can be operated with a 100 mA proton beam of up to 70 MeV and a duty cycle of up to 6 %. The driver Linac consists of an Electron Cyclotron Resonance (ECR) ion source followed by a LEBT section, a 2.5 MeV double Radio-Frequency Quadrupole (RFQ) and 35 normal conducting (NC) Crossbar H-Mode (CH) cavities. The development of the cavities is carried out by the Institute for Applied Physics (IAP) at the Goethe University Frankfurt am Main. Due to the high beam current, all cavities as well as the associated tuners and couplers have to be optimised for operation under high thermal load to ensure safe operation. In collaboration with the GSI Centre for Heavy Ion Research as the ideal test facility for high power tests, two cavities and the associated hardware are being designed and will be tested. The design and latest status of both cavities will be presented in this paper.

INTRODUCTION

RF cavities that are operated with high duty cycles or with high beam currents must, on the one hand, have an efficient cooling concept that limits the maximum temperature within the cavities. On the other hand, corresponding tuners must be able to compensate for the frequency change caused by the heating of the cavity and the RF power couplers must be optimised accordingly to ensure stable long-term operation. The GSI Centre for Heavy Ion Research has a long history of developing and operating various types of RF resonators, making it an ideal test facility for both cavities and the associated infrastructure. In collaboration with JCNS and with strong support by the HBS Innovationspool Project, two NC cavities together with the associated tuners and power couplers have been optimised for operation in continuous wave (CW) mode. These cavities will be used as prototypes for the HBS project [1–3] as well as for a new CW operated HElmholtz LInear ACcelerator (HELIAC) [4–8] which is currently under development at GSI and Helmholtz-Institute Mainz (HIM) [9, 10]. HELIAC will continue to enable experiments with long pulses and high repetition rates previously provided by the UNIversal Linear ACcelerator (UNILAC), which will in future provide high-intensity short-pulse beams for the Facility for Antiproton and Ion Research (FAIR) [11–18]. The HELIAC itself comprises a NC injector based on an ECR ion source, an RFQ and two Interdigital H-Mode (IH) cavities [19] followed by four cryomodules with superconducting (SC) CH-type cavities [5, 20, 21]. Together, they allow for an acceleration of heavy ions ($A/Z \leq 6$) to variable output energies ranging from 3.5 MeV/u to 7.3 MeV/u, with an energy spread less than ±3 keV/u. The overall parameters of the HELIAC are shown in Table 1.

Table 1: Design Parameters of the HELIAC

Mass/charge	≤6
Max. beam current	1 mA
Repetition rate	continuous wave
Output energy	3.5 – 7.3 MeV/u
Output energy spread	±3 keV/u
Frequency NC injector	108.408 MHz
Frequency SC accelerator	216.816 MHz

Both NC injector DTL cavities are based on the concept of Alternating Phase Focusing (APF), which applies synchronous phase changes between negative and positive phases to provide for successive transversal and longitudinal focusing during the acceleration [22]. This allows long accelerating sections with full transmission without the need for additional magnetic focusing elements.

* m.basten@gsi.de

ISBN: 978-3-95450-227-1 ISSN: 2673-5490 doi:10.18429/JACoW-IPAC2022-TUPOMS042

CAVITY R&D FOR HBS ACCELERATOR

N. F. Petry*, K. Kümpel, M. Schwarz, S. Lamprecht, O. Meusel, H. Podlech[1],
IAP, Goethe University Frankfurt, Frankfurt am Main, Germany
[1]also at Helmholtz Research Academy Hesse for FAIR, Frankfurt am Main, Germany

Abstract

The demand for neutrons of various types for research is growing day by day worldwide. To meet the growing demand the Jülich High Brilliance Neutron Source (HBS) is in development. It is based on a high power linear proton accelerator with an end energy of 70 MeV and a proton beam current of 100 mA. After the injector and the MEBT is the main part of the accelerator, which consists of about 36 CH-type cavities. The design of the CH-type cavities will be optimized in terms of required power, required cooling and reliability and the recent results will be presented in this paper.

HBS

The High Brilliance Neutron Source (HBS) as a project was first presented and published in 2015/2016 [1] [2]. The goal is to have a source which relies on a proton linear accelerator with a high current to achieve the level of existing medium to high flux neutron sources in terms of neutron brilliance and flux. To reach that goal, the following specification need to be fulfilled by the linear accelerator, summarized in Table 1.

Table 1: HBS Top-Level Requirements [3]

Parameter	Specifications
Final energy	70 MeV
Peak beam current	100 mA
Particle type	Protons
Peak beam power	7 MW
Average beam power	952 kW
Beam duty factor	13.6 %
RF duty factor	15.3 %
Pulse length	208/833/2000 s
Repetition rate	96/24/48 Hz

After the requirements are set the technology for acceleration needs to be specified. In general the shunt impedance is higher for drift tube structures used for acceleration at lower energies. For example are very efficient H-mode drift tube cavities available at low energies. Above 100 MeV superconducting cavities become the better choice in comparison to normal conducting cavities. Because of the inefficiency of normal conducting structures at high energies, this is also valid for accelerators with a low duty cycle. More general, normal conducting cavities are better suited for high currents at low energies and a low duty cycle. The opposite is true for superconducting cavities. Both technologies have

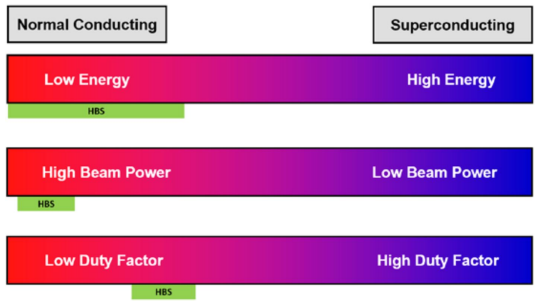

Figure 1: Classification of HBS into three different categories regarding superconducting and normal conducting.

their down and upsides. Superconducting structures need a complex cooling system with an onsite helium infrastructure and R&D of those structures binds a lot of resources for simulations and prototyping. Furthermore they are very sensible to impurities, contamination, etc. While having an accelerator with a high beam current of 100 mA the required RF-power is mainly driven by the required beam power. This even applies for normal conducting structures. Looking at a superconducting cavity, which in case of HBS provides 2.5 MeV, a RF-power of about 250 kW plus an safety margin is needed [4]. In comparison a normal conducting structure will require about 100 kW more RF-power. After looking at the pros and cons and having the rough time schedule in mind, the decision falls on normal conducting cavities.

CH TYPE CAVITIES

The 176.1 MHz linac should be as efficient as possible while being as modular as possible, easy to maintain and

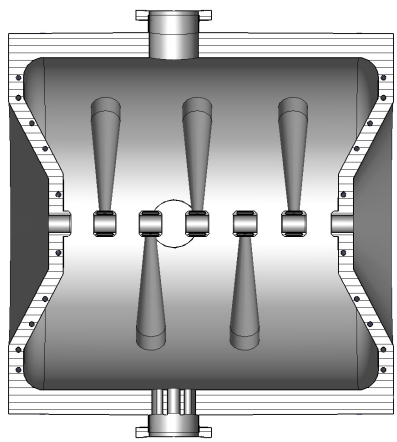

Figure 2: Side view of cross section of the used design for the HBS CH cavities.

* petry@iap.uni-frankfurt.de

ISBN: 978-3-95450-227-1 ISSN: 2673-5490 doi:10.18429/JACoW-IPAC2022-TUPOMS043

HIGH POWER TESTS OF A NEW 4-ROD RFQ WITH FOCUS ON MECHANICAL VIBRATIONS

S. Wagner*, D. Koser, K. Kümpel, H. Podlech[1]
Institut für angewandte Physik (IAP), Goethe-University Frankfurt am Main, Germany
K. Bahrke-Rhein, SAM at TU Darmstadt, Germany
M. Basten[2], GSI Darmstadt, Germany
[1]also at Helmholtz Research Academy for FAIR (HFHF), Frankfurt, Germany
[2]also at Helmholtz-Institut Mainz (HIM), Mainz, Germany

Abstract

Because of strong mechanical vibrations of the electrodes and its sensitivity to changes of thermal load, the operational stability of the existing 4-rod RFQ at the High Charge State Injector (HLI) at the GSI Helmholtz Centre for Heavy Ion Research in Darmstadt, Germany, could not be ensured for all planned operating states. To resolve this issue and ensure stable injection into the HLI, a new RFQ-prototype, optimized in terms of vibration suppression and cooling efficiency, was designed at the Institute of Applied Physics (IAP) of Goethe University Frankfurt. To test the performance of this prototype and demonstrate the operational stability in terms of mechanical vibration as well as thermal load, high power tests with more than 25 kW/m were performed at GSI. After initial conditioning, detailed vibrational measurements during high power RF operation using a laser Doppler vibrometer were performed, which were then compared to previously conducted simulations using ANSYS. Ultimately, the ability for stable operation up to high power levels with an efficient vibration suppression and moderate heating have clearly been demonstrated.

INTRODUCTION

To meet the increasing requirements in terms of beam quality and RF duty cycle for the planned HLI upgrade program, a new 4-rod RFQ has been commissioned and integrated into the High Charge State Injector (HLI) at GSI in 2010 [1]. To achieve the HLI operating frequency of 108 MHz and reduce the RF power dissipation to less than 60 kW, as provided by the designated power amplifier at that time, this RFQ design features a large stem distance of 173 mm as well as a thin profile of the RFQ electrode rods to reduce capacitance. These structural properties favor increased mechanical vibrations of the electrodes; especially at the levitating electrode overhangs and the inter-stem sections [2]. The electrode vibrations periodically alter the overall capacitance of the RF structure, resulting in an impedance mismatch, which leads to modulated power reflections. This poses significant problems for the tuning of the RF frequency by the plunger tuner [3]. To identify the problematic vibration modes of the existing HLI-RFQ, comprehensive structural-mechanical simulations as well as vibration measurements using a laser Doppler vibrometer were conducted. Based on this analysis a newly revised 4-rod RFQ prototype with 6 stems was designed and tested at high average power levels (>25 kW/m) at GSI. Here we present the mechanical vibration measurements during high power operation together with a comparison to simulations using CST Studio Suite [4] and ANSYS [5].

MODAL ANALYSIS

One of the defining properties of mechanical oscillation is the eigenfrequency of the observed mode. If the frequency of the mode corresponds to a multiple of the frequency of excitation, amplified harmonics can arise.

Numerical Simulations

With specialized simulation software, like the ANSYS-program package, it is possible to simulate the behavior of a rigid body under the influence of an applied force. For the here presented results, two different methods of simulation have been performed. First, a harmonic simulation, in which a harmonic load is applied, and second a transient simulation in which it is possible to define force-pulses and analyze the response of the object [6]. Even though the harmonic simulation does not yield good quantitative results for the performed experiment, it is a good method to determine the dominant modes of the structure, which are shown in Fig. 1.

To make assumptions regarding the amplitudes of existing oscillations, a much more time-consuming transient simulation is needed. Here it is possible to define the duration, orientation, and amount of an applied force. Using the square relation between the Lorentz force acting on the electrodes (F_L) and the power inside the cavity (P_C) it is possible to tune the simulated force to a corresponding one which existed during experimental measurements.

The simulated velocity and displacement of an inter-stem section is presented in Fig. 2. The strong visible displacement to negative magnitudes is due to restrictions in implementing the force: In reality, due to the very high frequency utilized in the cavity, the electric field would quickly oscillate for every position on the electrode. The corresponding force would therefore change between its maximal value and zero approximately every 10 ns. This is nearly impossible to implement into the software. The way the force was implemented is as a constant applied force with a pulse duration of 6.5 ms, which is applied evenly to the whole electrode and therefore resulting in a stable position in negative displacements, around which the electrode oscillates. The simulated results regarding vibration velocity and displacement are shown in Fig. 2.

*s.wagner@iap.uni-frankfurt.de

ISBN: 978-3-95450-227-1 ISSN: 2673-5490 doi:10.18429/JACoW-IPAC2022-TUPOMS044

DIELECTRIC LOADED THz WAVEGUIDE EXPERIMENTALLY OPTIMIZED BY DISPERSION MEASUREMENTS

M. Kellermeier*, R. W. Assmann[1], K. Floettmann, F. Lemery
Deutsches Elektronen-Synchrotron DESY, Germany
W. Hillert, Universität Hamburg, Hamburg, Germany
[1]also at Istituto Nazionale di Fisica Nucleare, Frascati, Italy

Abstract

Emerging high power THz sources pave the road for THz-driven acceleration of ultra-short bunches, and enable their manipulation for diagnostic purposes. Due to the small feature sizes of THz-guiding devices new methods are necessary for their electromagnetic characterization. A new technique has recently been developed which characterizes THz waveguides with respect to their dispersion relations and attenuation. Here, the method is applied to circular waveguides, partially filled with polymer capillaries of different thicknesses, to find a suitable size for THz driven streaking at 287 GHz. Further, rough 3d-printed metallic waveguides are measured to study the effect of roughness on attenuation and phase constant. In general, additive manufacturing techniques show promise for advanced integrated designs of THz driven structures.

INTRODUCTION

In recent years, there has been growing interest in Terahertz (THz) radiation as driving source for particle accelerators [1–5] due to the availability of emerging laser-based high-power sources [6, 7] and promises in supporting higher field gradients than conventional RF-driven structures. Beyond acceleration, THz driven structures are also studied for beam manipulation, for instance, as transverse deflecting structures [8–12] to measure the bunch length with high resolution. One potential design is based on dielectric loaded waveguides which profit from higher streaking voltage and reduced non-linearities of the field distribution [13, 14]. Due to the small feature size on mm-scale, established characterization methods from radio-frequency structures are difficult to apply. Laser-based techniques partially take over, for instance, in measuring waveguide dispersion [15]. Alternatively, a new RF-based approach has been proposed by the authors to characterize THz structures by their dispersion [16]. The method does not rely on the integrated phase shift, but is able to provide local information within the waveguide.

In the present work, the inner radius of a dielectric loaded waveguide, formed by inserting a polymer capillary in a circular metallic waveguide, is adjusted to match synchronous phase velocity, $v_{ph} = c$, to the design frequency of 287 GHz. The design frequency is based on a THz generation setup located at the REGAE facility [13, 17] at DESY. Frequency tunability of the THz source restricts the waveguide's phase synchronous mode to 286 GHz to 288 GHz.

Further, the dispersion of pure metallic waveguides fabricated by selective laser melting (SLM) is measured. Due to the rough surface the diameter of the cross-section can only be estimated by microscopy. The measured dispersion allows to determine an effective diameter due to the electromagnetic response.

The first chapter briefly recapitulates the experimental setup and the analysis method. In the second chapter, measurements on a metallic waveguide equipped with polymer capillaries are presented. Aiming for a specific design frequency at which the mode propagates synchronously with a potential bunch, the optimal capillary loading is determined. Afterwards, experiments on 3D printed, pure metallic waveguides are shown. Finally, an outlook is given towards an accelerator-based experiment.

EXPERIMENTAL SETUP AND NETWORK MODEL

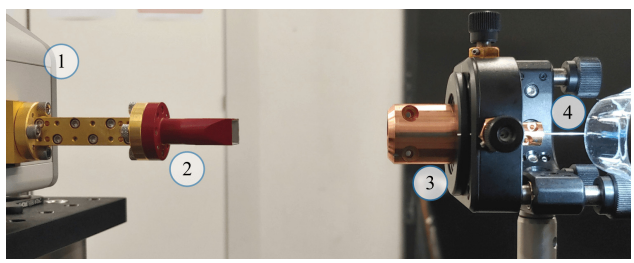

Figure 1: Experimental setup. (1) Extender waveguide port (2) Horn antenna (3) Integrated horn-waveguide structure (4) Movable obstacle. Reproduced from Ref. [16]

The main part of the experimental setup is shown in Fig. 1. Scattering parameters are measured via a Rohde & Schwarz ZVA67 vector network analyzer (not shown) to which a frequency extender ZC330 is connected, spanning the band from 220 GHz to 330 GHz. A pyramidal horn antenna is attached to the waveguide port of the extender. The waveguide under test, which is monolithically integrated with its conical horn coupler, is mounted in a distance of about 7 cm. A reflecting obstacle is placed inside the waveguide from the other side. The obstacle is mounted on a linear translation stage to scan the reflection position in sub-wavelength steps. The position sweep shifts the phase of S_{11} of the device under test. Multiple reflections between the reference port and the test device distort the S-parameter $S_{11}^{(m)}$ measured

* max.kellermeier@desy.de

ISBN: 978-3-95450-227-1 ISSN: 2673-5490 doi:10.18429/JACoW-IPAC2022-TUPOMS045

DESIGN VALIDATION OF HIGH CURRENT INJECTOR FACILITY AT IUAC DELHI

R. V. Hariwal*, Rajeev Ahuja, Pradip Barua, Radhakishan Gurjar, Sanjay Kumar Kedia
Ashok Kothari, Ajith Kumar, Mukesh Kumar, Prem Kumar, Raj Kumar, Rajesh Kumar
Sarvesh Kumar, Sugam Kumar, Singh Kundan, Plankudy S. Lakshmy, Kedar Mal
A. Malyadri, Yadhuvansh Mathur, Rajeev Mehta, Deepak Kumar Munda, U. Naik, U. Rao
Gerard Oscar Rodrigues, Cholakka Parambath Safvan, Abhijit Sarkar, Chandrapal Shakya
Parmanand Singh, Somasundara Kumar Sonti, Subhash Kumar Suman, Thomas Varughese
Sankar Raja Venkataramanan, Veera Venkata Satyanarayana Venna, Jimson Zacharias
Inter University Accelerator Centre, New Delhi, India

Abstract

High Current Injector (HCI) is an upcoming heavy ion accelerator facility at Inter University Accelerator Centre (IUAC), New Delhi, INDIA and it will serve as an alternative injector to the existing Superconducting Linear accelerator(SC-Linac). HCI is designed to achieve the maximum energy gain of 1.8 MeV/u for the ions, including the Noble gasses and metallic ions, having $A/q \leq 6$. It consists of an 18 GHz high temperature superconducting electron cyclotron resonance ion source, multi-harmonic buncher, Radio Frequency Quadrupole (RFQ), spiral buncher and six interdigital H-mode Drift Tube Linac (IH DTL) cavities operating at 97 Mhz resonant frequency. The RFQ accelerates the ions from 8keV/u to 180keV/u energy and the six DTL cavities are used to achieve the maximum energy gain of 1.8 MeV/u. Recently, the bunched beam of N^{5+} was successfully accelerated through RFQ and six IH-DTL cavities and we achieved the designed energy goal, which is an important milestone of this project. These results validated the design parameters of all RF cavities, accelerating to achieve the designed energy goal of 1.8MeV/u. Here, present status and future plans of the project shall be presented.

INTRODUCTION

HCI was envisaged to meet the requirement of higher beam intensity (tens of eμA) and provide almost all the ions from the periodic table including the Nobel and metallic ions to the existing beam time user [1-3]. Higher beam current intensity endorse the scientist to probe the low cross-section reactions processes. There is another possibility to produce the higher charge state from HCI and allowing higher energetic charged particle beams for the injection into SC-Linac. This project has been started early in 2005-06 including the design of a compact HCI building, beam optics, layout, prototyping of its major beam line components, indigenous development of RF cavities and their control systems. In this context, the low level RF and beam test of the individual RF components, installed in the beam line, have been carried out to check their performances and functionalities time to time. The commissioning of HCI up to first achromatic bending magnet was completed in the mid of 2019-20 in Beam Hall III at IUAC Delhi and it was kept ready for the beam acceleration and design validation of its energy gain. A control room was also established to keep an eye on all the parameters of individual system during the first beam test. After the installation of all beam line components up to the first achromatic analyser bending magnet, N^{5+} (A/q=2.8) beam was successfully accelerated and the first major milestone of this project was achieved in the year of 2021 in spite of having Covid-19 pandemic spread worldwide. In order to validate the designed energy gain from each of the RF cavities, N^{5+} beam was accelerated through all individual cavities one by one and the output energy gain was verified by applying the required analysing magnetic field. In this paper, the HCI design goals, major components, layout, beam test results, cavities performances during test, present status and future projections shall be discussed.

HCI DESIGN GOALS AND MAJOR COMPONENTS

HCI consists of mainly an 18 Ghz High Temperature Superconducting Electron Cyclotron Resonance Ion Source (HTSC-ECRIS), Multi-harmonic Buncher (MHB), 48.5 Mhz Radio Frequency Quadrupole (RFQ), 48.5 Mhz Spiral Buncher and six interdigital H-mode Drift Tube Linear Accelerator (IH-DTL) cavities operating at 97 Mhz resonant frequency along with the other beam line components like dipole and quadrupole magnets and associated beam diagnostic devices [4]. The final design plan and its 3D layout based on the calculated beam optics is shown in Fig. 1 and its major components are discussed here.

HTSC-ECR Ion Source

18 Ghz HTSC-ECRIS is one of its own kind of ion source covering almost all the ions from the periodic table up to U^{238}. It was developed with the collaboration of PANTECHNIK, France and IUAC Delhi, INDIA and known as a PKDELIS [5]. It produces the large amounts of highly charged positive ions and currents higher than those available from the existing Pelletron accelerator at IUAC. In the ECRIS, the plasma potential plays an important role in the optimization of longitudinal focussing and transportation of the beam through the HCI beam line.

* hariwal@gmail.com

ISBN: 978-3-95450-227-1 ISSN: 2673-5490 doi:10.18429/JACoW-IPAC2022-TUPOMS046

FABRICATION AND LOW-POWER TEST OF DISK-AND-WASHER CAVITY FOR MUON ACCELERATION

Y. Takeuchi*, J. Tojo, Kyushu University, Fukuoka, Japan
Y. Nakazawa, Ibaraki University, Ibaraki, Japan
Y. Kondo, R. Kitamura, T. Morishita, JAEA, Ibaraki, Japan
E. Cicek, H. Ego, K. Futatsukawa, N. Kawamura, M. Otani,
T. Yamazaki, M. Yoshida, T. Mibe, N. Saito, KEK, Ibaraki, Japan
Y. Iwashita, Kyoto University, Osaka, Japan
U. Sue, K. Sumi, M. Yotsuzuka, Nagoya University, Nagoya, Japan
H. Yasuda, University of Tokyo, Tokyo, Japan

Abstract

The muon g-2/EDM experiment is under preparation at Japan Proton Accelerator Research Complex (J-PARC), and the muon linear accelerator for the experiment is being developed. A Disk-and-Washer (DAW) cavity will be used for the medium-velocity part of the accelerator, and muons will be accelerated from $v/c = \beta = 0.3$ to 0.7 with the operating frequency of 1.296 GHz. Machining, brazing, and low-power measurements of a prototype cell reflecting the design of the first tank of DAW were performed to identify fabrication problems. Several problems were identified, such as displacement of washers during brazing, and some measures will be taken in the actual tank fabrication. In this paper, the results of the prototype cell fabrication will be reported.

INTRODUCTION

At Japan Proton Accelerator Research Complex (J-PARC), an experiment using muons accelerated by a linac is planned to measure the anomalous magnetic moment of muons and to search for the electric dipole moment [1]. A 1296 MHz disk and washer (DAW) cavity is being developed for use in the medium-velocity section of the muon linac [2]. DAW cavity is a type of coupled cavity linac (CCL) consisting of disks, washers, and supporting stems. DAW CCL has many advantages, such as high shunt impedance and high coupling between the accelerating and coupling cells, but has the disadvantage that many adjacent modes are difficult to analyze. For this reason, there are only a few cases where it is actually employed [3]. However, recent improvements in computational capabilities have made it possible to design cavities including stems that fully account for 3D electromagnetic fields. The muon DAW consists of three modules with four or five tanks per module, and each tank has 11 acceleration gaps. The tanks are connected to each other by bridge couplers (bc), and each bc is equipped with an electromagnetic quadrupole doublet for focusing. Each module is driven by a 2.5 MW L-band klystron. The configuration of the muon DAW is shown in Fig. 1.

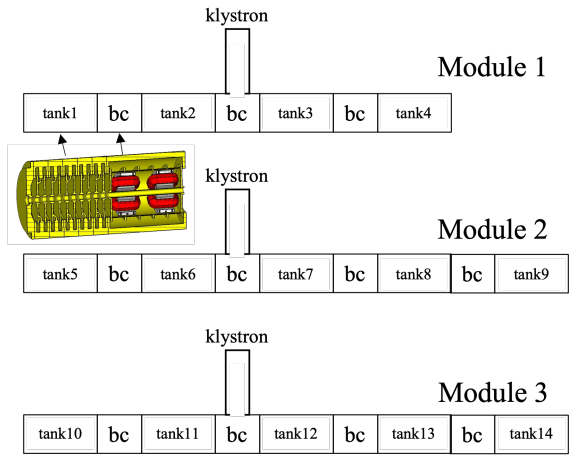

Figure 1: The configuration of the muon DAW. Schematic of the entire accelerator and 3D model of the 1st tank with bc is shown.

PROTOTYPE CELL FABRICATION

The cavity shape has been carefully studied using the CST MW studio [4], and fabrication of the cavity was begun in 2021. Prior to the first tank, a prototype cell was fabricated, and several tests were conducted to identify problems in the fabrication process and to study countermeasures. Configuration of the prototype cell is shown in Fig. 2.

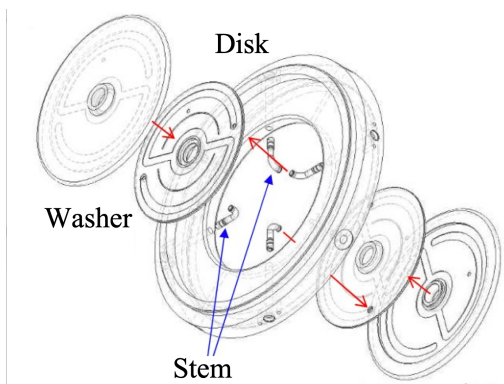

Figure 2: Configuration of prototype cell.

* takeuchi@epp.phys.kyushu-u.ac.jp

ISBN: 978-3-95450-227-1 ISSN: 2673-5490 doi:10.18429/JACoW-IPAC2022-TUPOMS049

DIGITAL LLRF FOR THE CANADIAN LIGHT SOURCE

P. Solans, A. Salom, F. Perez, ALBA Synchrotron, CELLS, Barcelona, Spain
D. Beauregard, C. Boyle, J. M. Patel, H. Shaker, J. Stampe, CLS, Saskatoon, Canada

Abstract

The Canadian Light Source, at the University of Saskatchewan, is a 3rd generation synchrotron light source located in the city of Saskatoon, Canada. The facility comprises a 250 MeV LINAC, a full energy booster and a 2.9 GeV storage ring. The radiofrequency system in the booster consist of two 5-cell cavities feed with a single SSPA. The analogue LLRF for the booster has been recently replaced by a digital LLRF based in the ALBA design with a Picodigitizer, a stand-alone commercial solution provided by Nutaq. Also, the firmware of the new DLLRF is configurable to allow operation with a superconducting cavity feed with one amplifier, thus providing the possibility to replace the CLS SR LLRF as well. The main hardware components, the basic firmware functionalities and the commissioning measurements of the new DLLRF for the CLS booster will be presented in this paper.

INTRODUCTION

The CLS was first funded in the University of Saskatchewan in 1999. After a short period of construction and commissioning, operation for users started in 2005. The SR is a 2.9 GeV machine of 170.88 m long. It consists of 12 double bend achromat (DBA) cells. A 500 MHz radiofrequency system restores the energy of the electrons by means of a CESR-B superconducting cavity feed with a 300 kW klystron. [1,2].

The CLS booster is a full energy synchrotron of 102 m length. The lattice consists of a modified 28-fold supersymmetric FODO lattice that provides the required space to install the two DORIS-type 5-cell cavities in one straight section [3]. A beam up to 10 mA is captured from the LINAC and accelerated to nominal energy with a repetition rate of 1 Hz.

A single SSPA able to provide up to 100 kW feeds the two cavities of the booster. After a high power isolation circulator, the power is split in two branches with a magic-T. The cavities were first installed at the proper distance to assure the right phase difference between them. Nevertheless, a phase shifter at each branch is used to assure this condition, since the phase in the cavities cannot be controlled individually with the LLRF.

In order to replace the analogue control system in the CLS booster, a new DLLRF has been developed based in the ALBA design which was implemented at SIRIUS [4] and modified in order to be able to drive two 5-cell cavities with two plunger each feed by a single SSPA.

Also, the ALBA DLLRF design has been modified to meet the CLS SR requirements, i.e., to be able to drive one or two superconducting cavities with one or two amplifiers. This will allow to install the new DLLRF in the SR also.

HARDWARE

The main DLLRF components are:

- Picodigitizer: FPGA mother board + FMC boards for ADCs and DACs + mezzanine Mestor with digital GPIO bus.
- Front Ends: RF signals down-conversion, RF drives up-conversion and LO generation with MO reference.
- Digital Patch Panel: Connectors and voltage level conversion between DLLRF and RF plants sub-systems.
- Level translator: CLS designed hardware for extra voltage conversion and electrical isolation.
- Power Supply Unit: Supplies for the active components of the DLLRF.

All DLLRF hardware components, except for the PSU, have been allocated inside an EMI rack (see Fig. 1).

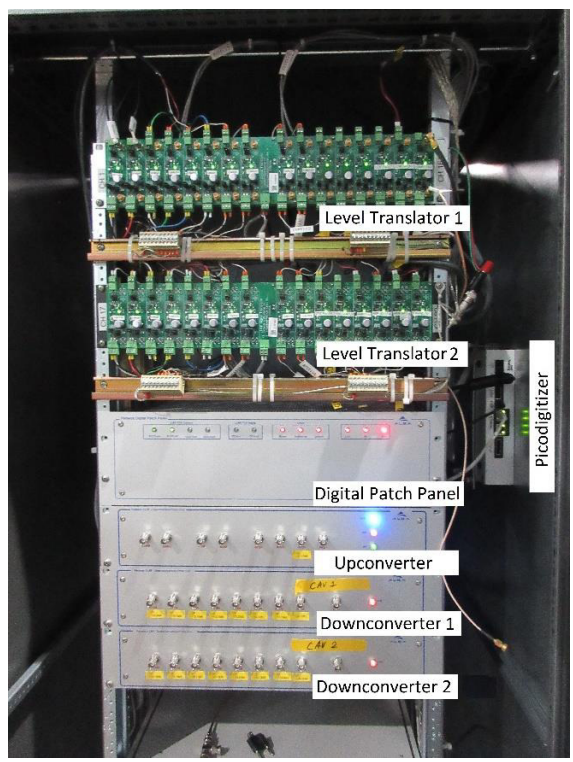

Figure 1: DLLRF components inside the EMI rack.

Picodigitizer

It is a stand-alone board solution provided by Nutaq, that contains a Virtex-6 SX315T FPGA and two FMC boards, one with 16 ADCs channels of 14 bits capable to operate up to 125 MHz and another with 8 DACs of 16 bits up to 250 MSPS. The resolution of the ADCs is better than 0.06 % rms in amplitude and 0.04 º rms in phase. The SNR is better than 70 dB [5].

ISBN: 978-3-95450-227-1 ISSN: 2673-5490 doi:10.18429/JACoW-IPAC2022-TUPOMS051

PROTOTYPE FABRICATION OF AN ACTIVE NORMAL CONDUCTING THIRD HARMONIC CAVITY FOR THE ALBA STORAGE RING*

J. R. Ocampo, J. M. Álvarez, B. Bravo, F. Pérez, A. Salom, P. Solans, ALBA Synchrotron, CELLS, Barcelona, Spain

Abstract

ALBA has designed a normal conducting active 1.5 GHz HOM damped cavity for the active third harmonic RF system for the ALBA Storage Ring (SR), which also will serve for the upgraded ALBA II. The third harmonic cavity at ALBA will be used to increase the bunch length in order to improve the beam lifetime and increase the beam stability thresholds. A prototype has been constructed by the company AVS in collaboration with VITZRO TECH. This paper presents the design of the cavity, the constructed prototype, the Acceptance Tests measurements, and future plans.

INTRODUCTION

ALBA has designed a prototype of a 1.5 GHz normal conducting HOM damped cavity, based on the 500 MHz EU damped cavity design [1]. In addition to scaling down the dimensions to adapt to the higher resonant frequency, the HOM absorbers have been replaced by transitions to coaxial N-type connectors named Transdampers. This design allows extracting the power of HOMs excited by the beam to external loads, eliminating the need for complicated ferrite absorbers [2].

The cavity has been manufactured in collaboration between the Spanish company AVS and the South-Korean company VITZRO TECH.

CAVITY COMPONENTS

The main part of the cavity comprises the resonant cavity body, the waveguide sections of the three HOM dampers, the beam pipe ports as well as ports for the rest of components: Transdampers, pick-up antenna, tuner and input coupler, see Fig. 1.

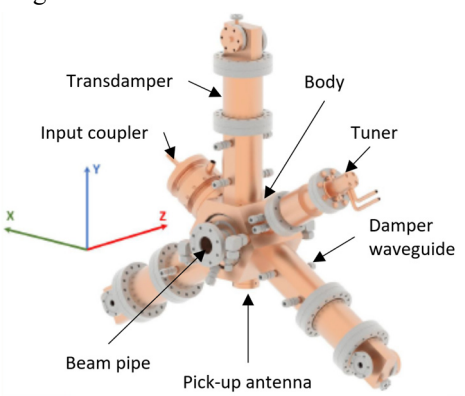

Figure 1: Components of the 1.5 GHz cavity.

* This project is co-funded by the European Regional Development Fund (ERDF) within the Framework of the Smart Growth Operative Programme 2014-2020.

Body and Damper Waveguides

The cavity is a pillbox-type resonator with nose cones [3]. In order to damp HOM excited by the beam into the cavity, three circular ridged waveguides with a cut-off frequency of 1.72 GHz are brazed into the body in such a way that there are no discontinuities in the copper to avoid overheating in the base of the dampers, see Fig. 2, as experienced with the 500 MHz original design [4].

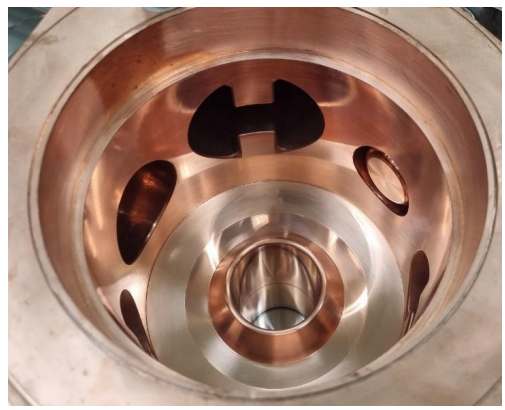

Figure 2: Inner view of the cavity body. Courtesy of VITZTRO TECH.

After manufacturing all components of the cavity, the resonant frequency was adjusted by shortening the length of the nose cones, as the resonant frequency of the cavity has a strong linear dependency on this dimension. The length of the nose cones is controlled by the radius of the roundness at the end of the nose cone. Figure 3 shows the simulated and measured values during the adjustment of the resonant frequency.

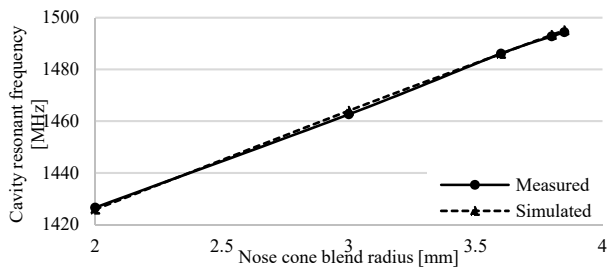

Figure 3: Simulated and measured resonant frequencies during adjustment. Data courtesy of VITZRO TECH.

Transdampers

The Transdampers take the HOM power extracted by the damper arms out of the cavity. They are made out of two components: a transition from circular ridged waveguide to rectangular waveguide and a wideband transition from rectangular waveguide to coaxial [3]. Finally, a commercial

ISBN: 978-3-95450-227-1 ISSN: 2673-5490 doi:10.18429/JACoW-IPAC2022-TUPOMS052

CONSIDERATONS FROM DEPLOYING, COMMISSIONING, AND MAINTAINING THE CONTROL SYSTEM FOR LCLS-II UNDULATORS*

M. A. Montironi†, C. Andrews, G. Marcus, H.-D. Nuhn
SLAC National Accelerator Laboratory, Menlo Park, USA

Abstract

Two new undulator lines have been installed as part of the Linac Coherent Light Source upgrade (LCLS-II) at SLAC National Accelerator Laboratory. One undulator line, composed of 21 horizontally polarizing undulator segments, is dedicated to producing Soft X-Rays (SXR). The other line, composed of 32 vertically polarizing undulator segments, is dedicated to producing Hard X-Rays (HXR). The devices were installed, and the control system was deployed in 2019. Commissioning culminated with the achievement of first light from the HXR undulator in the Summer of 2020 and from the SXR undulator in the Fall of 2020. Since then, both undulator lines have been successfully providing x-rays to user experiments with very limited downtime. In this paper, we first describe the strategies utilized to simplify the deployment, commissioning, and maintenance of the control system. Such strategies include scripts for automated components calibration and monitoring, a modular software structure, and debugging manuals for accelerator operators. Then, we discuss lessons learned which could be applicable to similar projects in the future.

INTRODUCTION

Two new undulator lines have been installed as part of the Linac Coherent Light Source upgrade (LCLS-II) at SLAC National Accelerator Laboratory. One undulator line, composed of 21 horizontally polarizing undulator segments, is dedicated to producing Soft X-Rays (SXR). The other line, composed of 32 vertically polarizing undulator segments, is dedicated to producing Hard X-Rays (HXR). Details of the motion control system design and implementation are discussed in [1] and [2] and a brief overview is provided in the next section. Devices installation, deployment of the control system, and functional checkout commenced in the Summer of 2019 and was completed in the Spring of 2020. Commissioning culminated with the achievement of first light from the HXR undulator in the Summer of 2020 and from the SXR undulator in the Fall of 2020. Since then, both undulator lines have been successfully providing x-rays to user experiments with very limited downtime. In this paper, we focus on the undulators motion control and first describe the strategies utilized to simplify the deployment, commissioning, and maintenance of the control system. Then, we discuss lessons learned which could be applicable to similar projects in the future.

* Work supported by Department of Energy, Office of Basic Energy Sciences, contract DE-AC02-76SF00515
† alexmon@slac.stanford.edu

UNDULATOR LINE ARCHITECTURE

The LCLS-II undulator lines are organized in a repetition of identical segments called cells. Each cell being composed of an undulator segment and of an interspace break. The interspace supports a quadrupole magnet, vacuum components, beam diagnostic components and a phase shifter. An SXR undulator cell is shown in Fig. 1 with the main functional components numbered. The undulator segment (1) is positioned upstream of the interspace pedestal and plate (2). The BPM, quadrupole magnet, and vacuum components (3) are mounted on the interspace plate together with a phase shifter (4).

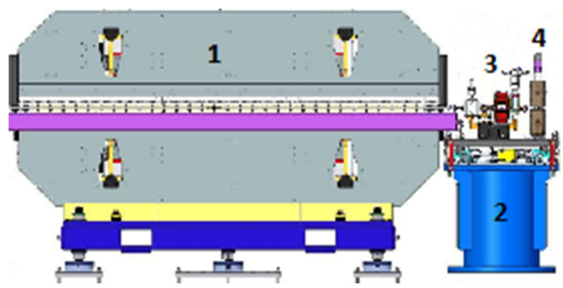

Figure 1: SXR undulator cell with main functional components numbered.

An HXR undulator cell is shown in Fig. 2 with the main functional components numbered. The undulator segment (1) is mounted on the same girder as the downstream interspace plate (2). This plate supports a quadrupole magnet, a BPM, a phase shifter, and vacuum components (3).

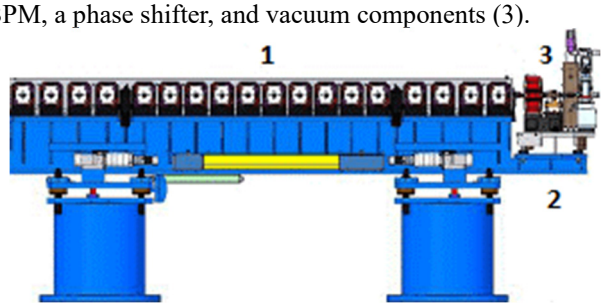

Figure 2: HXR undulator cell with main functional components numbered.

For each cell, the undulator motion control system provides users with the ability to set and read back the undulator segment gap and K value, and the relative position of the segment magnetic axis with respect to beam path. It also allows to change the pointing of the undulator line through a system of cam movers [3]. The phase shifter motion control system allows to monitor and set the phase

ISBN: 978-3-95450-227-1 ISSN: 2673-5490 doi:10.18429/JACoW-IPAC2022-TUPOMS053

START-TO-END SIMULATIONS OF THE LCLS-II HE FREE ELECTRON LASER

D. Cesar*, G. Marcus, H.D. Nuhn, T. Raubenheimer, SLAC, Menlo Park, USA
J. Qiang, LBNL, Berkeley, USA

Abstract

In this proceeding we present start-to-end simulations of the LCLS-II-HE free electron laser. The HE project will extend the LCLS-II superconducting radio-frequency (SRF) linac from 4 GeV to 8 GeV in order to produce hard x-rays from the eponymous hard x-ray undulators (26 mm period). At the same time, soft x-ray performance is preserved (and extended into the tender regime) by using longer period undulators (56 mm period) than were originally built for LCLS-II (39 mm period). Here we use high-fidelity numerical particle simulations to study the performance of several SASE beamline configurations, and compare the resulting x-ray energy, power, duration, and transverse properties. Using the LCLS-II normal-conducting gun, we find that the x-ray pulse energy drops off rapidly above 15 keV, while using the lower emittance beam from a proposed SRF gun, we improve the cutoff to 20 keV.

LCLS-II HE

The next generation of free electron laser (FEL) facilities [1–3] is being built with superconducting radio-frequency (SRF) accelerators which can deliver beam at MHz repetition rates in order to simultaneously provide both high average and high peak power x-ray pulses. The LCLS-II HE project [4] plans to extend the operation of the LCLS-II facility from 4 GeV to 8 GeV by installing a new (SRF) linac downstream of the bunch compression and before the beam switchyard which delivers beam to the undulators. The SRF linac can be fed by two injectors: the LCLS-II very high frequency (VHF) injector; and a new (planned) superconducting, low emittance injector (LEI) [5, 6]. After being accelerated to 8 GeV the beam(s) can then be distributed to either hard or soft x-ray undulators, as shown in Fig. 1.

Doubling the beam energy will boost the resonant photon energy by a factor of four, allowing the 26 mm period hard x-ray undulators to produce first-harmonic photons out to 20 keV. At such small wavelengths 3D effects [7] greatly impact the gain length, and so the new low emittance injector is being designed to deliver (rms) emittances as low as 0.1 um. Simulations show that this lower emittance dramatically improves the yield above 15 keV and allows us to take full advantage of the 8 GeV beam.

At the same time, the existing 39 mm ($K_{max} \approx 5.4$) period LCLS-II soft x-ray undulators will be unable to produce photon energies below 1 keV when the electron beam energy is 8 GeV. In order to reach the often requested C (285 eV), N (400 eV), and O (532 eV) k-edges the HE project currently plans to replace the existing 39 mm period soft x-ray undulators with longer, 56 mm period undulators ($K_{max} \approx 9.2$) (rather than build a 4 GeV extraction line). Increasing the undulator period from 39 mm to 56 mm allows the 8 GeV beam to be resonant with lower photon energies, but it also increases the physical gain length. For fixed photon energy, beam current, emittance, and focusing lattice, the Pierce parameter, $\rho \propto \frac{1}{\gamma}\left(\frac{K\lambda_u}{\sigma_r}\right)^{2/3}$, increases by only 10% from 4 to 8 GeV, while the 1D gain length $L_g \propto \lambda_u/\rho$ increases by more than 30% [7]. The HE program plans to add extra undulator segments to make up the difference (one design under study is shown in Fig 1).

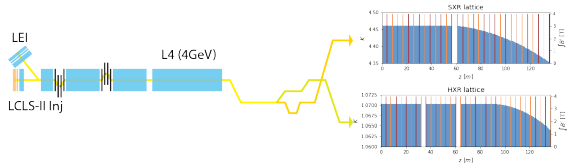

Figure 1: Cartoon of the LCLS-II HE facility (excluding the normal conducting, "copper" accelerator). Two injectors (the LCLS-II VHF gun and a new low emittance injector (LEI)) can feed an 8 GeV linac. A beam switchyard delivers these beams to the HXR line (bottom) or the SXR line (top).

START TO END SIMULATIONS

High fidelity numerical particle simulations have an established history of use for modeling and optimizing facility design. Here we use the IMPACT suite for the accelerator [8, 9], and then we use GENESIS [10] to model the FEL lasing process. The IMPACT codes include, where necessary, the effects of shot noise, 3D space charge, RF and resistive wall wakefields, coherent synchrotron radiation (CSR), and intra-beam scattering; while GENESIS models the FEL instability slice-wise, in the slowly varying envelope approximation. This approach has been benchmarked at LCLS [11] and was used extensively during the development of LCLS-II [12, 13].

Electron Beam

In Fig. 2 we show three sample electron beams delivered to the HXR undulator: 20 pC and 100 pC beams from the LCLS-II VHF injector, as well as a 100 pC beam from a low emittance injector. The (core) beam quality is summarized in Table 1. The low emittance injector has the best beam quality, while the 20 pC has the worst. However, the 20 pC beam still has use in reducing the average electron beam power and also creates for creating a shorter FEL pulse (20 fs vs 40 fs) that is less sensitive to 3D effects than the

* dcesar@slac.stanford.edu

ISBN: 978-3-95450-227-1 ISSN: 2673-5490 doi:10.18429/JACoW-IPAC2022-TUPOMS054

DATA AUGMENTATION FOR BREAKDOWN PREDICTION IN CLIC RF CAVITIES

H. S. Bovbjerg *[1,2], C. Obermair[1,3], A. Apollonio[1], T. Cartier-Michaud[1], W. Millar[1], Z.H. Tan[2], M. Shen[2], D. Wollmann[1]
[1]CERN, Geneva, Switzerland [2]Aalborg University, Aalborg, Denmark [3]TU Graz, Graz, Austria

Abstract

One of the primary limitations on the achievable accelerating gradient in normal-conducting accelerator cavities is the occurrence of vacuum arcs, also known as RF breakdowns. A recent study on experimental data from the CLIC XBOX2 test stand at CERN proposes the use of supervised machine learning methods for predicting RF breakdowns. As RF breakdowns occur relatively infrequently during operation, the majority of the data was instead comprised of non-breakdown pulses. This phenomenon is known in the field of machine learning as class imbalance and is problematic for the training of the models. This paper proposes the use of data augmentation methods to generate synthetic data to counteract this problem. Different data augmentation methods like random transformations and pattern mixing are applied to the experimental data from the XBOX2 test stand, and their efficiency is compared.

INTRODUCTION

The RF cavities of the Compact LInear Collider (CLIC) are designed to operate at a gradient of ~100 MV/m [1]. One of the primary limitations on the achievable gradient in normal conducting RF cavities is the occurrence of RF breakdowns, which can degrade a passing beam and potentially result in damage to the cavity surface [2–4]. In order to minimize the impact of breakdowns during the cavity commissioning and operation, CERN's CLIC test stands [5] employ an automatic conditioning algorithm [6, 7]. The algorithm monitors how frequently breakdowns occur during operation and dynamically adjusts the gradient based on a preset breakdown-rate threshold [8]. In this approach, the handling of breakdowns is therefore purely reactive, thus breakdowns cannot be prevented beforehand.

In a recent study, a deep learning approach was proposed with the goal of (1) performing data-driven breakdown investigation and (2) studying the possibility of adopting a predictive conditioning algorithm. The study was based on historical data of the CERN XBOX2 test stand, consisting of 124 505 healthy RF pulses and 479 breakdown events [9].

Previously, it has been noted that breakdowns occur predominantly in groups as opposed to isolated, single events. This observation has led to the classification of breakdown events as either *primary breakdowns*, which are purely stochastic, and *followup breakdowns*, which are thought to be a consequence of the previous breakdown [10]. Using the XBOX2 data, neural networks were able to predict the occurrence of followup breakdowns. However, the prediction accuracy varied depending on different data used for the prediction, e.g. for different adopted parameters for cavity powering. This variation indicates that the models were not able to generalize well to unseen data [11]. Specifically, the bad generalization is due to the low number of breakdown events compared to the number of healthy events, i.e. the so-called high *class imbalance*. We therefore investigated the use of time series data augmentation methods for improving the generalization capabilities of CLIC breakdown prediction. The basic principle of these methods involves generating synthetic patterns that resemble real data to better represent the underlying distribution of the underrepresented class in the data set. This is an established practice for image recognition tasks [11–13] and is also used for speech and audio [14, 15].

The paper is structured as follows: first, a summary of the prior work is given, including a description of the data and model used in our study. Next, an overview of the augmentation methods used in this paper is presented. Finally, the conducted experiments are described, and their results are discussed.

PRIOR WORK

This section summarizes the prior work which this work builds upon, including a description of the data set used in the study, and a description of the RF breakdown prediction models used.

XBOX2 Data Set

The XBOX2 test stand is one of three experiments used to test the prototype 12GHz RF components for the CLIC project at CERN. Fundamentally, the test stand is composed of a 50 MW klystron, pulse compressor, and high-power RF load. A more detailed description of the setup is available elsewhere [7, 9].

In 2018 this test stand produced 90 GB of data during an operational period of six months, consisting of so-called trend and event data [9]. The trend data contains 30 different scalar values such as temperatures and pressures measured at different locations in the test-stand. The event data consists of time-series measurements of the RF signals at different locations in the waveguide network and the current detected by two Faraday cups. A summary of the data is given in Fig. 1. Here, two features of the forward travelling wave signal F2 (see fig. 2), namely the maximum (blue) and the pulse width (green), are shown with respect to the RF cavity pulses. Additionally, the cumulative breakdown count (red)

* holger.severin.bovbjerg@cern.ch

ISBN: 978-3-95450-227-1 ISSN: 2673-5490 doi:10.18429/JACoW-IPAC2022-TUPOMS055

A MODERNIZED ARCHITECTURE FOR THE POST MORTEM SYSTEM AT CERN

J.F. Barth, F. Bogyai, J.C. Garnier, M.L. Majewski, A. Mnich, M.P. Pocwierz, T.M. Ribeiro, R. Selvek, R. Simpson, A. Stanisz, D. Wollmann, M. Zerlauth
CERN, Geneva, Switzerland

Abstract

The control system of the accelerators at CERN stores and analyzes more than 200 million dumps of high resolution data recordings every year in the Post Mortem (PM) system. A continuous increase in the complexity of the Large Hadron Collider's (LHC) systems and the desire to collect more accurate data requires continuous improvement of the PM system. Recently, the PM system has been modernized ahead of the third operational Run of the LHC. The upgraded system implements well known data engineering principles such as horizontal scaling, stateless services and readiness for extensions. This paper recalls the purpose of the PM service and its current use cases. It presents its modernized architecture, reviews the current performance and limitations of the system, and draws perspectives for the next steps in its evolution.

INTRODUCTION

The particle beams and the magnet circuits of the LHC store unprecedented amounts of energy. An uncontrolled release of this energy would cause significant damage to the accelerator complex, requiring extensive repairs which considerably reduce the available time of the accelerator to produce physics [1].

Therefore, it is imperative to verify the correct behavior of the accelerator's many control and protection systems after each beam dump. Furthermore, it is important to understand the origin of the termination of a physics fill (beam dump) and the conditions under which the event occurred to decide whether the next beam injection is safe or whether a device is behaving faulty. Since 2008, the PM system has stored and used data recorded at the moment of a beam dump by thousands of devices installed in the LHC to reliably provide diagnostic assistance, verify device behavior, explain unexpected events, and ultimately guarantee the safe and efficient operation of the LHC [2]. In addition to providing machine protection, PM also aides with monitoring and tuning of the Super-Proton-Synchroton (SPS) for performance optimisation.

During CERN's recent Long Shutdown 2 (LS2) from 2018 to 2022, the PM system underwent substantial upgrades in areas of data collection, storage, and access, to address the drawbacks identified in the previous architecture [3]. The first section of this paper explains the current use cases of the system. The second section outlines the modernized architecture, giving detailed explanation of data collection, data storage, data access, event building, data analysis, and the data model. Finally, the limitations of the new system are highlighted and the vision for the future is discussed.

USE CASES

The PM system needs to be able to reliably collect, store, analyze, expose and persist large amounts of data arriving as a discontinuous stream with load peaks both for storing and retrieving data during events between quiet hours. Table 1 summarises the different PM use cases.

Deterministic Time Constraints

For deterministic time constraint use cases, the data sent to the PM system must be analyzed within an exact time frame to provide operators with critical in-time information. During SPS Quality Checks (SPSQC), operators need to monitor and tune certain accelerator parameters for each successive cycle of the accelerator to improve the overall performance. A cycle has a minimum length of 10 seconds in which the the beam is injected, accelerated, and extracted. This means that PM must reliably collect, store, and analyze a high volume of data within 10 seconds. Other CERN applications of deterministic time constraint use cases are the Injection Quality Checks (IQC) for checking the quality of beam injections into the LHC [4], and Extraction Post Operational Checks (XPOC) for checking that a beam extraction occurred under nominal conditions [5].

Non-Deterministic Time Constraints

For non-deterministic time constraints, the data collection, storage, and analysis do not have to be complete in a strict time frame. There are two main use cases that are not bound by deterministic time constraints. Global Event Analysis for analysing events affecting all device domains in the LHC and Global Powering Analysis for analysing events affecting magnet powering devices such as Quench Protection Systems (QPS) [6] and power converters in the LHC.

Table 1: PM Use Cases

Use Case	Type
Global Event Analysis	Non-deterministic
Powering Event Analysis	Non-deterministic
SPSQC	Deterministic
IQC	Deterministic
XPOC	Deterministic

ISBN: 978-3-95450-227-1 ISSN: 2673-5490 doi:10.18429/JACoW-IPAC2022-TUPOMS057

DESIGN STUDY OF HOM COUPLERS FOR THE C-BAND ACCELERATING STRUCTURE

D. Kim†, E. I. Simakov, Los Alamos National Laboratory, Los Alamos, USA
Z. Li, SLAC National Accelerator Laboratory, Menlo Park, USA
S. G. Biedron, University of New Mexico, Albuquerque, USA

Abstract

A cold copper distributed coupling accelerator, with a high accelerating gradient at cryogenic temperatures (~77 K), is proposed as a baseline structure for the next generation of linear colliders. This novel technology improves accelerator performance and allows more degrees of freedom for optimization of individual cavities. It has been suggested that C-band accelerating structures at 5.712 GHz may allow to maintain high efficiency, achieve high accelerating gradient, and have suitable beam dynamics with wakefield damping and detuning of the cavities. The optimization of the cavity shape was performed, and we computed quality factor, shunt impedance, and beam kick factor for each of the proposed cavity geometries using CST Microwave Studio. Next, we proposed a configuration for higher order mode (HOM) suppression that includes waveguide slots running parallel to the axis of the accelerator. This paper reports details of the parametric study of performance of the HOM suppression waveguide, and the dependence of HOM Q-factors and kick factors on the cavity's and HOM waveguide's geometries.

INTRODUCTION

In the higher energy physics accelerator community, developing multi-TeV scale e^+e^- linear colliders is considered to be one of the major goals [1-3]. High-gradient C-band cryo-cooled normal-conducting radio-frequency (NCRF) cavities are highly promising for this application. The new concept for RF power coupling to the accelerating cavities was recently proposed and is called the disbributing coupling where the RF power is delivered directly to each cell of the structure from a parallel feeding waveguide. This novel system allows to increase RF efficiency and the achievable accelerating gradient. In addition, each single resonator can now be optimized to deliver maximum energy to the beam. Operating copper accelerators at cryogenic temperatures (~77 K) increase shunt impedance and reduces breakdown rates.

As a preliminary study of the advanced NCRF structures, we simulated several C-band accelerating cavities and computed Q-factors and wavefield kick factors for the TM monopole and dipole modes using CST Microwave Studio [4]. Next, we designed waveguide damping slots and HOM damping features for wakefield suppression and simulated the reduction of Q-factors due to damping.

† dskim84@lanl.gov

CALCULATION FOR Q-FACTORS AND KICK FACTORS

Seven different cavity geometries were optimized by SLAC and were simulated using eigenmode solver in CST Microwave Studio. The cavity geometries are shown in Fig. 1. In the CST simulation, periodic boundary condition was adopted along the longitudinal direction of each cell. Symmetry boundary conditions were used to calculate different monopole and dipole modes. A size of the mesh for the structure was 18 cells per wavelength. For each mode between 5 and 20 GHz, we calculated correct phase advance, the Q-factors, and the kick factors. Here, the phase advance (φ) can be expressed as

$$\varphi\,(rad) = \frac{\omega \times L_{cav}}{c}. \quad (1)$$

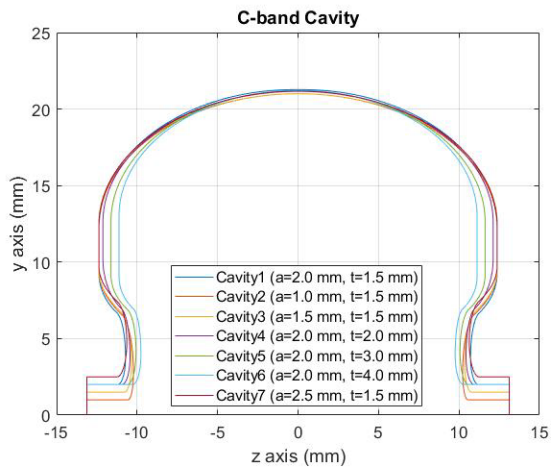

Figure 1: 7 different cavity geometries. a and t indicate the iris radius and iris thickness, respectively.

Figure 2 illustrates the electric field patterns in two different modes in cavity 1. As shown in Fig. 1(a), the fundamental working mode (TM_{010}) with a Q-factor of 13,000 was found at 5.712 GHz. Figure 1(b) shows the electric field magnitude in the first dipole mode (TM_{110}) with a Q-factor of 17,000 at 9.247 GHz.

The results of computation of the Q-factors and kick/loss factors for longitudinal and transverse wakefields are shown in Fig. 3. For monopole mode, ohmic wall losses (Q_0) and longitudinal kick factors from each cavity are shown in Fig. 3(a). The highest quality factor was about 23,000 for the mode at 14.84 GHz. The peak value of the longitudinal loss was about 100 V/pC/m at the fundamental mode. With a small offset as 0.4 mm in x axis, dipole mode's Q_0 and transverse kick factors were

ISBN: 978-3-95450-227-1 ISSN: 2673-5490 doi:10.18429/JACoW-IPAC2022-TUPOMS058

C-BAND HIGH GRADIENT TESTING OF THE BENCHMARK a/λ=0.105 CAVITY*

E.I. Simakov†, D. Gorelov, M. Middendorf, T. Tajima, MD R.A. Zuboraj,
Los Alamos National Laboratory, Los Alamos, NM, U.S.A
S.G. Biedron, University of New Mexico, Albuquerque, NM, U.S.A.

Abstract

This paper reports the design and status of high gradient testing of the benchmark C-band three-cell radio-frequency (RF) cavity. Modern applications such as X-ray sources require accelerators with optimized cost of construction and operation, naturally calling for high-gradient acceleration. At Los Alamos National Laboratory (LANL) we commissioned a C-band Engineering Research Facility of New Mexico (CERF-NM) powered by a 50 MW, 5.712 GHz Canon klystron. The test stand is capable of conditioning accelerating cavities for operation at surface electric fields in excess of 300 MV/m. CERF-NM is the first high gradient C-band test facility in the United States. An important milestone for this test stand is demonstration of conditioning and high gradient testing of the most basic high gradient RF cavity of geometry that has been extensively studied at other frequencies, such as X-band. The cavity is the three-cell structure with the highest gradient in the central cell and two coupling cells, and the ratio of the radius of the coupling iris to the wavelength a/λ=0.105. This paper reports current conditioning status, achieved gradients, and other characteristics measured during the high-power operation of this cavity.

INTRODUCTION

High gradient C-band (5.712 GHz) accelerator structure research is ongoing at Los Alamos National Laboratory (LANL) motivated by a number of LANL-specific mission needs. LANL has proposed a high gradient C-band upgrade to Los Alamos Neutron Science Center (LANSCE) proton linac to increase the final energy of the proton beam to 3 GeV. Material science research at LANL may benefit from a powerful directional high-repetition-rate X-ray source of 43 keV photons that may be produced by a 42 MeV electron beam through Inverse Compton Scattering (ICS). Achieving high gradient in normal-conducting radio-frequency (NCRF) copper-based accelerator structures requires understanding of copper alloys behavior under extreme electromagnetic fields and at its core is the material science problem which LANL is perfectly positioned to address leveraging its extensive expertise in material science and metallurgy [1].

We have recently commissioned the C-band Engineering Research Facility of New Mexico (CERF-NM) [2]. The CERF-NM is built around a 50 MW 5.712 GHz Canon klystron that produces 50 MW pulses with the pulse length between 300 ns and 1 microsecond, repetition rate up to 200 Hz, and is tunable within the frequency band of 5.707 GHz to 5.717 GHz. The RF power from the klystron is coupled into WR187 rectangular waveguide. The power is split into two halves by a magic tee that is installed at the klystron's output and protects the klystron from excess reflected power that may come from the device-under-test. The WR187 waveguide brings power into a 3 foot by 4 foot lead box that provides radiation protection to equipment and operators. The lead box is radiologically certified for dark currents with electron energy up to 5 MeV and average current up to 10 μA.

Many cavities that we plan to test at CERF-NM are to be coupled on axis to reduce peak surface magnetic fields. Thus, the mode launchers were designed and fabricated for the test stand. The mode launchers convert the TE_{10} mode of the rectangular WR187 waveguide into the TM_{01} mode of the cylindrical waveguide for the on-axis coupling. Four mode launchers were fabricated and conditioned up to the maximum input power of 10 MW. For more details on the mode-launcher design, fabrication, and testing see ref. [3].

One of the first cavity tests to be performed at CERF-NM aimed to establish the benchmark for high gradient performance at C-band. For this test we designed and fabricated a three-cell test structure with the ratio of the iris radius, a, to the wavelength, λ, of a/λ=0.105. The structure was a direct scale of the similar test structures fabricated and tested by other institutions at the frequencies of X-band and S-band [4,5]. This exact cavity shape is most commonly used to make comparison between high gradient performance of cavities fabricated of different alloys and by different fabrication methods. Testing the cavity of this most common shape at the frequency of 5.712 GHz allows us to eliminate the effects of specific cavity geometry on the high gradient performance and compare high gradient performance of C-band structures to that of the higher frequency structures (X-band) and lower frequency structures (S-band).

This paper summarizes the design parameters of the a/λ=0.105 test cavity, describes the results of fabrication and cold-testing of the two copper cavities, and reports the initial results of the high gradient testing of the first cavity and achieved peak surface fields.

DESIGN OF THE a/λ=0.105 BENCHMARK CAVITY

The scaling and design of the test cavity was performed with the CST Microwave Studio [6]. Distribution of the magnitude of the electric field in the three-cell structure is shown in Fig. 1 (top). The maximum electric field in the two coupler cells was approximately two times smaller

*This work was supported by Los Alamos National Laboratory's Laboratory Directed Research and Development (LDRD) Program.
† smirnova@lanl.gov

ISBN: 978-3-95450-227-1 ISSN: 2673-5490 doi:10.18429/JACoW-IPAC2022-TUPOMS060

HIGH GRADIENT CONDITIONING AND PERFORMANCE OF C-BAND β=0.5 PROTON NORMAL- CONDUCTING COPPER AND COPPER-SILVER RADIO-FREQUENCY ACCELERATING CAVITIES

M. Zuboraj*, R. Fleming, D. Gorelov, M. Middendorf and E. I. Simakov
Los Alamos National Laboratory, Los Alamos, NM, USA
M. Schneider*, V. Dolgashev, E. Jevarjian, E. Snively, J. W. Lewellen, S. G. Tantawi, and E. Nanni
SLAC National Accelerator Laboratory, Menlo Park, CA, USA
S. Baryshev, Department of Electrical and Computer Engineering, Michigan State University, East Lansing, MI, USA

Abstract

This paper reports the results of high gradient testing of the two C-band (5.712 GHz) normal conducting β=0.5 accelerating cavities. The first cavity was made of copper and the second was made of copper-silver alloy with 0.085% silver concentration. The tests were conducted at the C-Band Engineering Research Facility of New Mexico (CERF-NM) located at Los Alamos National Laboratory. Both cavities achieved gradients more than 200 MeV/m and surface electric fields more than 300 MV/m. The breakdown rates were mapped as functions of peak surface fields. The gradients and peak surface fields observed in the copper-silver cavity were about 20% higher than those in the pure copper cavity with the same breakdown rate. It was concluded that the dominant breakdown mechanism in these cavities was not the pulse heating but the breakdown due to very high surface electric fields.

INTRODUCTION

Accelerators are essential for numerous applications in National Security (NNSA, DoD), medicine, discovery science and industry. These applications require accelerators with optimized cost of construction and operation, naturally calling for high-gradient acceleration. At Los Alamos National Laboratory (LANL), we started a new project with the major goal to use a multi-disciplinary approach that includes accelerator design, molecular dynamics simulations, and advanced manufacturing of metals to develop high-gradient, high-efficiency radio-frequency (RF) structures for both compact and facility-size accelerator systems [1]. Recently, we commissioned a high gradient test stand called C-band Engineering Research Facility of New Mexico (CERF-NM) that allows high gradient testing of C-band accelerating structures [2]. As a part of a collaboration with Stanford Linear Accelerator Center (SLAC) National Accelerator Laboratory, LANL has completed testing two high gradient C-band accelerator cavities designed for operation with the proton beam traveling at half of the speed of light (β=0.5). These cavities are part of research on a compact accelerator-based beam delivery system that will deliver protons to medical accelerators used for cancer therapy. The benefit of using protons over X-ray photons for cancer treatment is that the particle beams are more precise and target-oriented and cause less damage to neighboring healthy tissues compared to photon-based therapy. However, delivering hadron beams such as protons or light ions require accelerators on gantries that are larger and more expensive than conventional radiation therapy machines and gantries. The particle beams also have slow energy scanning rates, which increases the overall treatment time and makes the success of treatment susceptible to patient motion. In addition, the full potential of these machines is compromised because the slow methods used to adjust beam energies, also introduce additional energy and momentum spread in the beam. SLAC goal is to enable 3D scanning over a tumor volume of up to 4 liters in both transverse and longitudinal dimensions [3]. The cavities that are described in this paper are used to adjust the energy of the proton beam for longitudinal variation in dose deposition. They are designed for optimal operation with 150 MeV protons with a radial port for coupling power and no on-axis coupling. Each accelerating cell in the linac will be individually powered so that the phase can be adjusted for the beam energy and vary rapidly and dynamically. This allows the linac to maintain its efficiency whether accelerating or decelerating the beam within a range of at least 50 MV/m.

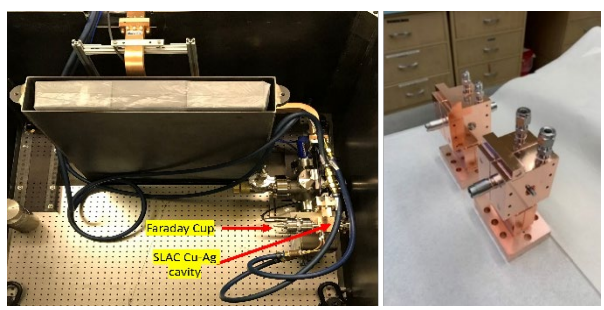

Figure 1: A photograph of the two β=0.5 accelerator cavities fabricated at SLAC (right). A photograph of the copper cavity installed on the test stand for high gradient testing (left)

HIGH GRADIENT TESTING SYSTEM (CERF-NM)

CERF-NM, is powered by a Canon klystron capable of producing peak power of 50MW with operating pulse length up to 1 μs at a maximum repetition rate of 200 Hz.

*Both Authors Contributed Equally

ISBN: 978-3-95450-227-1 ISSN: 2673-5490 doi:10.18429/JACoW-IPAC2022-TUPOMS061

RF SYSTEM DESIGN FOR ELETTRA 2.0

C. Pasotti†, M. Bocciai, L. Bortolossi, M. Rinaldi, Elettra Sincrotrone Trieste, 34149, Italy

Abstract

The Elettra 2.0 low emittance light source project aims to a substantial increase of the brilliance and coherence fraction of the source improving, at the same time, the storage ring stability and reliability. The Radio Frequency (RF) system plays a pivotal role in the beam quality, stability and reliability for the user operation.

This paper will cover the design and the implemented strategy to meet these features for the Elettra 2.0 RF system. Starting point of the new RF design is the final choice of the RF frequency, 500 MHz, and the available room, 1260 mm, to install the accelerating cavities.

Thanks to the 500 MHz frequency choice, some components of the new RF system for Elettra 2.0 are already installed and set into operation in the current Elettra storage ring. Their features and performance's optimization can therefore start well in advance with respect to the foreseen operation the new Elettra 2.0 storage ring.

INTRODUCTION

The preliminary design of the RF system for the Elettra 2.0 presented in [1] has continued to grow according to the following guidelines.

- The stated RF frequency is 500 MHz.
- Normal conducting accelerating cavities.
- RF power source based on solid state transistors.

The Elettra 2.0 RF system main parameters are listed in Table 1.

Table 1: Elettra 2.0 Main Specification

Storage Ring Parameters	
Energy (GeV)	2.4
Current (mA)	400
Momentum Compaction	$1.2\ 10^{-4}$
RF Frequency (MHz)	499.654
Harmonic Number	432
Energy Spread	$1.0\ 10^{-3}$
Energy Losses, maximum (keV)	670
Beam Power (kW)	268
Accelerating Voltage total (MV)	2.0

Considering the guidelines and the required beam power the number of cavities and RF power amplifiers has been set. Four independent and equivalent RF plants fulfil the Elettra 2.0 parameters that means four amplifiers and four cavities. The possibility to add a fifth RF plant to increase the total available RF power is kept ready. This backup plan foresees the re-use the one of the two Elettra IOT transmitters, the spare cavity and the spare RF passive components with a minimal impact on the planned budget but it is conditionally subordinated to identify a free room to host the fifth cavity into the crowded Elettra 2.0 storage ring. Therefore the four Elettra RF plant are under revamping to match the Elettra 2.0 parameters.

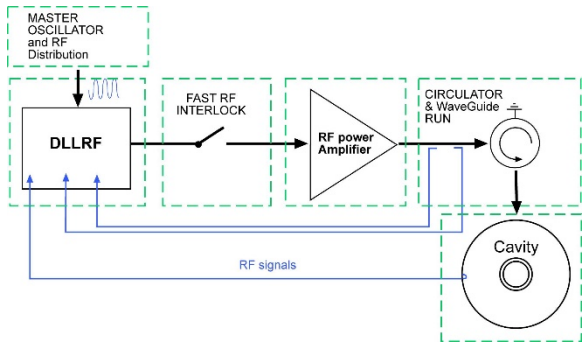

Figure 1: Schematic blocks of the RF plant.

Each RF plant can be subdivided in blocks as shown with green dashed squares in Fig. 1. All these blocks will be upgraded but the accelerating cavity. The existing "*Elettra type*" cavity that matches the available short straight section room is re-used achieving a good compromise between the cost saving and the attainable performances. The amplifier and the RF power run and passive high RF power components must be brand new due to the RF power increase. The Digital Low Lever RF and the dedicated local fast interlock are going to be designed according to the state of the art of the digital electronic.

The master oscillator and the low power RF signal distribution that have never suffered from any fault during more than 28 years of operations of Elettra will also be recycled contributing to the green economy.

The confirmation of the 500 MHz as a RF frequency has cleared the path for the procurement of the high RF power passive components such as high power circulators, loads, wave guides and, mainly, of the RF power amplifiers. The Elettra 2.0 project has given the chance to move towards the solid state technology using RF power transistors that now easily achieves more than 100 kW of output power at 500 MHz in a quite compact room. The contracts for the high RF power components are running now even if slowed down a little due to the raw materials shortage on the market and difficulty in obtaining new component. However this delay is not yet on the critical path.

The Booster RF plant, a 2.5 GeV ring used together with a 100 MeV Linac as the injector of the Elettra machine, is qualified also for the Elettra 2.0 project. A proposal to raise the available Booster RF power is under discussion. Today the RF power available for the Booster is 18 kW. The second 80 kW Inductive Output Tube (IOT) transmitter dismantled from the storage can be installed in the Booster RF plant allowing the Booster natural bunch length decreasing of 30% and thus predisposing the beam quality foreseen in the new Elettra 2.0 ring. This solution is almost free of

† cristina.pasotti@elettra.eu

ISBN: 978-3-95450-227-1 ISSN: 2673-5490 doi:10.18429/JACoW-IPAC2022-TUPOMS062

OVERALL PERFORMANCE OF 26 POWER STATIONS AT 400 kW - 352 MHz

C. Pasotti*, A. Cuttin, Elettra Sincrotrone Trieste S.C.p.A., Trieste, Italy

Abstract

The spoke cavities section of the European Spallation Source (ESS) linac will be powered by 26 Radio Frequency Power Stations (RFPSs). Each RFPS delivers 400 kW of Radio Frequency (RF) power at 352.21 MHz in pulsed mode at a repetition rate up to 14 Hz and a 5 % duty cycle, thanks to a twin tetrodes RF power sources integration. This equipment belongs to the Italian In-Kind Contributions (IKCs) to ESS. Elettra Sincrotrone Trieste S.C.p.A (Elettra) is responsible for the development, manufacturing and commissioning of the RFPSs and is managing the RFPS manufacturing contract awarded to European Science Solutions s.r.l (ESS-It). So far, 24 units have been delivered and, by mid 2022, the entire contribution, plus a complete spare unit, will be delivered to ESS. The overall performance of the RFPSs, the lessons learned, and the optimizations adopted along the manufacturing process and the difficulties that the COVID-19 pandemic has posed along the way are presented in this contribution.

INTRODUCTION

The European Spallation Source (ESS) project has the objective of generating neutrons by spallation reaction of protons on a tungsten rotating target at an average beam power of 5 MW. It is carried out by more than 20 European partner laboratories, and hosted by Sweden and Denmark [1]. As a founding member of ESS European Research Infrastructure Consortium, Italy participates to the project as an In-Kind (IK) partner.

Within this framework, the Radio Frequency Power Stations (RFPSs), provided by European Science Solutions s.r.l (ESS-It) with the supervision of Elettra Sincrotrone Trieste S.C.p.A (Elettra), represent one of the Italian In-Kind Contributions (IKCs) to ESS [2]. They will power 26 spoke cavities, installed in the first segment of the superconducting section of the proton linac.

After nearly two years of manufacturing and testing, mainly carried out during the COVID-19 pandemic with an innovative approach [3], the main results of 26 Factory Acceptance Tests (FATs), out of 27, are presented, providing new insights about this IKC. As of the date of writing, 24 RFPS units have already been delivered to ESS, with only the last batch to be shipped.

The manuscript is organized as follows: the next section offers an overview of the RFPS and its sub-systems; then, the FAT protocol is detailed in its main steps. After that, the RFPS performance is presented in terms of Radio Frequency (RF) key parameters, resulting from FAT measurements; finally the results are discussed and next steps proposed.

* cristina.pasotti@elettra.eu

Figure 1: FAT setup. The six-racks RFPS is shown with the middle covers removed, revealing the twin cavities configuration. On the far left, the rack of the required instruments.

RFPS OVERVIEW

With a very compact design, the RFPS achieves 400 kW of peak power at 352.21 MHz, with a pulse length up to 3.5 ms and a repetition rate up to 14 Hz [4].

It consists of two identical branches, each one having a Solid State Driver (SSD) (KDP10000) followed by a tetrode-cavity Power Amplifier (PA) (Thales TH595A and TH18595A). The two branches are fed by a single RF distribution module, which provides amplitude adjustment on one arm, and phase adjustment on the other. The signals are then added together by means of a 3 dB hybrid combiner.

The RFPS features an original Supervisory Control System (SCS) that combines standard Programmable Logic Controller (PLC) equipment with specifically designed Field Programmable Gate Array (FPGA) boards for handling the interlocks in a fast way (in the order of 1×10^{-6} s with respect to 1×10^{-3} s specified for the tetrode).

In Fig. 1, a RFPS can be seen in the typical FAT setup. From left to right, the first rack holds the SSDs, the RF distribution module, the Human Machine Interface (HMI) and the main PLC module of the SCS. The second rack is dedicated to 4 screen and control grid Power Supplies (PSs), and Alternate Current (AC) distribution. In the middle, the twin TH18595A cavities are placed, together with their ancillary equipment. The fifth and sixth rack contain the High Voltage (HV) PS, supplying the anodic voltage to both tetrodes. It features a switching power converter, a capacitor bank, a solid state series switch. and a FPGA module of the SCS.

FAT OVERVIEW

The FAT process is conceived in a way that allows to individually test the RFPS sub-systems, and, at the same time, to avoid useless downtime between subsequent steps. The test sequence is such that the machine is progressively put into

ISBN: 978-3-95450-227-1 ISSN: 2673-5490 doi:10.18429/JACoW-IPAC2022-WEIXGD1

EIC BEAM DYNAMICS CHALLENGES*

D. Xu†, E. C. Aschenauer, G. Bassi, J. Beebe-Wang, J. S. Berg, W. Bergan, M. Blaskiewicz, A. Blednykh, J. M. Brennan, S. Brooks, K. A. Brown, Z. Conway, K. A. Drees, A. V. Fedotov, W. Fischer, C. Folz, D. Gassner, X. Gu, R. Gupta, Y. Hao, C. Hetzel, D. Holmes, H. Huang, J. Kewisch, Y. Li, C. Liu, H. Lovelace III, Y. Luo, G. Mahler, D. Marx, F. Meot, M. Minty, C. Montag, S. Nayak, R. B. Palmer, B. Parker, S. Peggs, B. Podobedov, V. Ptitsyn, V. H. Ranjbar, G. Robert-Demolaize, M. Sangroula, S. Seletskiy, K. S. Smith, S. Tepikian, R. Than, P. Thieberger, N. Tsoupas, J. Tuozzolo, S. Verdu-Andres, E. Wang, D. Weiss, F. J. Willeke, H. Witte, Q. Wu, W. Xu, A. Zaltsman
Brookhaven National Laboratory, Upton, NY 11973, USA
S. Benson, B.R.P. Gamage, J. Grames, T. Michalski, E. Nissen, J. Preble, R. Rimmer, T. Satogata, A. Seryi, M. Wiseman, W. Wittmer
TJNAF, Newport News, VA 23606, USA
V. Morozov, F. Lin, Oak Ridge National Laboratory, Oak Ridge, TN 37831, USA
E. Gianfelice-Wendt, Fermi National Accelerator Laboratory, Batavia, IL 60510, USA
Y. Cai, Y. Nosochkov, G. Stupakov, M. Sullivan, SLAC, Menlo Park, CA 94025, USA
J. Qiang, Lawrence Berkeley National Laboratory, Berkeley, CA 94720, USA
G. Hoffstaetter, D. Sagan, M. Signorelli, J. Unger, Cornell University, Ithaca, NY 14850, USA

Abstract

The Electron Ion Collider (EIC) under construction at Brookhaven National Laboratory aims to produce luminosities of up to 10^{34} cm^{-2}s^{-1} . The machine will operate over a broad range of collision energies with highly polarized beams. The coexistence of highly radiative electrons and nonradiative ions produces a host of unique effects. In order to maximize the luminosity, the beam-beam collision parameters are pushed to limits achieved only in collisions with equal species. Moreover, collisions occur with a 25 mrad crossing angle; the resulting luminosity reduction is compensated to lowest order by crabbing both beams by means of transverse RF oscillators. Keeping the beams stable under these conditions is challenging. The average polarization of electron and light ion beams must be 70%. Beams therefore must be injected fully polarized and polarization must be well preserved during beam acceleration and collision. Electron beam currents are up to 2.5 A, which is associated with a number of collective effects that need to be controlled. Hadron beam currents of 1 A are effected by the electron cloud effect, which will be suppressed by low secondary electron-emission yield (SEY) vacuum chamber coating. Strong hadron cooling will reduce and stabilize the hadron beam emittance and will boost the luminosity by a factor of three. These are some of the accelerator science challenges and the corresponding cures and resolutions that are described in this report.

* Work supported by Brookhaven Science Associates, LLC under Contract No. DE-AC02-98CH10886 with the U.S. Department of Energy.
† dxu@bnl.gov

INTRODUCTION

EIC, an ultimate electron microscope to be built at Brookhaven National Laboratory, provides the capability to look inside the nucleon. The EIC enables the study of the contribution of quarks and gluons to nucleon spin and mass. To answer this question, achieving high luminosity from polarized beams with variable center-of-mass energy is essential [1].

The center-of-mass energy in electron-proton collisions ranges from 29 to 141 GeV, accomplished by colliding 5 – 18 GeV electrons with 41 – 275 GeV ions. The peak luminosity is 10^{34} cm^{-2}s^{-1}, which will be achieved by colliding 10 GeV electrons with 275 GeV protons. Two IRs are considered in EIC. The first one is designed at IR6, and the second one is reserved at IR8 for future upgrade.

Figure 1 presents the schematic diagram of the EIC layout. Ion beams from protons to uranium will be accelerated to desired energy and stored in the Hadron Storage Ring (HSR), which will use existing RHIC complex. Strong Hadron Cooling will be used to maintain the required emittance of the flat hadron beam. An Energy Recovery LINAC (ERL) is being designed to provide electron beams for cooling. The Electron Storage Ring (ESR), which will be installed in the existing RHIC accelerator tunnel, will operate at three fixed energies. The polarized electrons will be injected from the Rapid Cycling Synchrotron (RCS) [2].

LUMINOSITY

In EIC, electron and hadron beams will cross with a horizontal angle of 25 mrad to avoid parasitic collisions. Crab cavities tilt the ion and electron bunches in the $z - x$ plane by half the crossing angle to compensate for the geometric luminosity loss, as shown in Fig. 2. Table 1 lists the key

ISBN: 978-3-95450-227-1 ISSN: 2673-5490 doi:10.18429/JACoW-IPAC2022-WEOXGD1

STUDIES AND MITIGATION OF COLLECTIVE EFFECTS IN FCC-ee*

M. Migliorati†[1], C. Antuono[2], E. Carideo[1,2], University of Rome La Sapienza, Rome, Italy
M. Behtouei, B. Spataro, M. Zobov, INFN - LNF, Frascati, Italy
Y. Zhang, Institute of High Energy Physics, Beijing, China
[1]also at INFN - Roma1, Rome, Italy, [2]also at CERN, Geneva, Switzerland

Abstract

In order to achieve a high luminosity in the future electron-positron circular collider (FCC-ee) very intense multi-bunch colliding beams should have nanometer scale transverse beam sizes at the collision points. For this purpose the emittances of the colliding beams are chosen to be very small, comparable to those of the modern synchrotron light sources, while the stored beam currents should be close to the best values achieved in the last generation of particle factories. In order to preserve beam quality and to avoid collider performance degradation, a careful study of the collective effects and techniques for their mitigation is required. The current status of these studies is discussed in the paper.

INTRODUCTION

The Future Circular Collider (FCC) is a challenging project that includes, in a single tunnel of about 100 km, both hadron [1] (FCC-hh) and electron-positron [2] (FCC-ee) colliders in the CERN area. The electron-positron machine will operate in four different stages corresponding to four energies, 45.6 , 80, 120 and 182.5 GeV, which will allow to study the properties of the Higgs, W and Z bosons, and top quark pair production thresholds with unprecedented precision.

In this paper we focus our study on the collective effects and instabilities of the lowest energy machine. The parameter list which we refer to, and shown in Table 1, has been updated with respect to that of the conceptual design report [2] (CDR). Therefore, previously evaluated impedances and related instabilities [3–6], as well as electron cloud and other effects [7–9], need to be reviewed.

The combined effect of beam-beam interaction and beam coupling impedance, which has a strong impact on the stability of the colliding beams, is particularly important for this machine. The beam-beam interaction alone has already given rise to new effects, such as beamstrahlung [10], coherent X-Z instability [11] and 3D flip-flop [12]. The beam dynamics becomes even more complex when also the wakefield effects are included [13–16]. Indeed, the combination of the beam-beam interaction with the longitudinal impedance reinforces the X-Z coherent beam-beam instability reducing and shifting the stable tune areas. In ref. [15], in order to find a stable tune area with the original CDR parameters, two mitigation techniques, that is the use of the harmonic cavities and an increase of the lattice momentum compaction factor, have been proposed. The updated parameter list has now a lattice with a momentum compaction factor twice that of the CDR. Additionally, another relevant change with respect to the CDR is the possibility of using 4 interaction points (4 IPs) instead of 2 IPs, as requested by particle physicists.

Table 1: Parameter List of the Z Machine with 4 IPs

Parameter	Value
Circumference (km)	91.174
Beam energy (GeV)	45.6
Bunch population (10^{11})	2.53
Bunches per beam	9600
RF frequency (MHz)	400
RF Voltage (GV)	0.12
Energy loss per turn (GeV)	0.0391
Longitudinal damping time (turns)	1167
Momentum compaction factor 10^{-6}	28.5
Horizontal tune/IP	55.563
Vertical tune/IP	55.600
Synchrotron tune	0.0370
Horizontal emittance (nm)	0.71
Verical emittance (pm)	1.42
Bunch length (mm) (SR/BS)*	4.37/14.5
Energy spread (%) (SR/BS)*	0.039/0.130
Piwinski angle (SR/BS)*	6.35/21.1
ξ_x/ξ_y	0.004/0.152
Horizontal β^* (m)	0.15
Vertical β^* (mm)	0.8
Luminosity/IP (10^{34}/cm^{2}s)	181

*SR: synchrotron radiation, BS: beamstrahlung

IMPEDANCE MODEL

Since FCC-ee is an evolving project, the machine impedance model is undergoing constant changes. Indeed, for several devices, as, for example, the collimators and injection kickers, a design has not been defined yet. Additionally, for some other devices, refined models for the determination of the coupling impedance are in progress. As a consequence, we report here the latest evaluation of some important contributions that already demonstrates how this machine can become critical due to collective effects.

The resistive wall represents the most important impedance source of FCC-ee [3]. For its evaluation we have considered a circular beam vacuum chamber with a radius of 35 mm and with two small lateral winglets necessary to place synchrotron radiation absorbers and to attach

* Work partially supported by the European Union's Horizon 2020 research and innovation programme under grant No 951754 - FCCIS Project, by the National Natural Science Foundation of China, Grant No. 11775238, and by INFN National committee V through the ARYA project
† mauro.migliorati@uniroma1.it

ISBN: 978-3-95450-227-1 ISSN: 2673-5490 doi:10.18429/JACoW-IPAC2022-WEOXGD2

ELECTRON ACCELERATOR LATTICE DESIGN FOR LHeC WITH PERMANENT MAGNETS*

D. Trbojevic†, S. Brooks, S. J. Berg, BNL, Upton, NY, 11973, USA
G. Hoffstaetter, Cornell University – CLASSE, Ithaca, New York, USA
A. Bogacz, JLAB, Newport News, Virginia, USA

Abstract

We present a new 'green energy' approach to the 60 GeV electron Energy Recovery Linac (ERL) of LHeC using a single beam line made of combined function permanent magnets, using a Fixed Field Accelerator (FFA) design with very strong linear gradients. We are basing our design on recent successful commissioning results of the Cornell University and Brookhaven National Laboratory ERL Test Accelerator "CBETA" in 2019-20 [1-6].

INTRODUCTION

- Future Electron Ion Colliders (EICs) could be 'green energy colliders' as Energy Recovery Superconducting Linacs (ERLs) can be used to make energy fully recovered.
- Electron beam is brought back to the linac by a single permanent magnet beam line without requiring electric power, reducing the estimated wall power of 100 MW in the present LHeC design to a negligible power for arcs.
- The single beam line transports all electron energies at once using the Fixed Field Alternating Gradient (FFA) principle with very strong focusing.
- The design is based on experience from the successful commissioning of the **C**ornell University and **B**rookhaven National Laboratory **E**nergy Recovery **T**est **A**ccelerator – '**CBETA**'.
- The green EIC of the CERN Large Hadron Collider - LHeC is presented, as well as an alternative design for the PERLE ERL.
- The FFA non-linear gradient design is a racetrack shape, where, as in CBETA, the arcs are matched by an adiabatic transition to the two straight sections. • Two 8.57 GeV superconducting linacs, replaced the 10 GeV linacs in the previous design, are placed on both sides of the Interaction Region (IR) to reduce the power of synchrotron radiation loss significantly.

PREVIOUS CBETA EXPERIENCE

The Energy Recovery Linac CBETA built with a single permanent magnet beam line was successfully commissioned in 2019-2020 showing a perfect transport of electrons passing 4 times in acceleration and three with energy recovery with an energy range between 42 to 150 MeV. One of the major new achievements during the commissioning was full energy recovery and proof of principle for the FFA large momentum transport and arc to straight adiabatic orbit merging achieved for the first time in the history of fixed field accelerators. The same principle is proposed for the LHeC lattice. We are basing our confidence in this proposal on the previous FFA experimental confirmation and on the well-established new permanent magnet technology in CBETA.

PRESENT AND PROPOSED LHEC

The LHeC design assumed two superconducting linear accelerators, each being capable of an acceleration of 10 GeV, and three accelerating and three decelerating passages through both linacs for the electron beam with a racetrack layout with a maximum electron beam energy of 60 GeV. This proposal replaces the three arcs for accelerating and decelerating electron passes, with a single line FFA arc. The two 10 GeV linacs are replaced with two 51.72 GeV linacs but at the same side of the racetrack with interaction region. This reduces the synchrotron radiation loss in the arcs as the maximum electron energy in the arcs is reduced from 60 GeV to 51.72 GeV. The 60 GeV beam is brought into collision with one of the LHC hadron beams. The racetrack shaped electron accelerator can therefore lie tangentially to the existing LHC machine as shown in Fig. 1 [7].

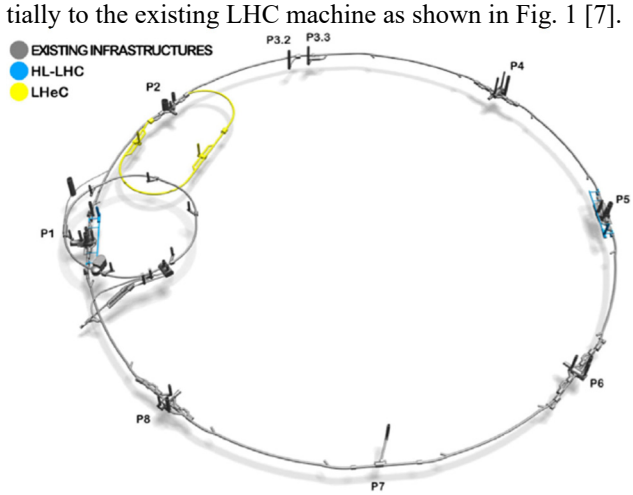

Figure 1: Proposed layout of the LHeC at CERN [7].

The initial goal of the LHeC assumes a total wall plug power consumption of 100 MW for the electron beam. This proposal significantly reduces the wall plug power using the permanent magnets reducing the total installation cost as the three arcs are replaced with one. The updated LHeC design has a peak current from the source of 20 mA and total currents within the SRF cavities of more than 120 mA with accelerating 3 × 20 mA and decelerating 3 × 20 mA. A comparison between the previous LHeC design and this proposal is shown in Figs. 2 and 3.

*This manuscript has been authored by employees of Brookhaven Science Associates, LLC under Contract No. DE-SC0012704 with the U.S. Department of Energy. †dejan@bnl.gov

ISBN: 978-3-95450-227-1 ISSN: 2673-5490 doi:10.18429/JACoW-IPAC2022-WEOXGD3

AN ALTERNATIVE DESIGN FOR BEPCII UPGRADE

H. Geng[1], J. Xing[1], Y. Zhang[1,2], C. Yu*[1,2]
[1]Key Laboratory of Particle Acceleration Physics and Technology,
Institute of High Energy Physics, Chinese Academy of Sciences, Beijing, China
[2]University of Chinese Academy of Sciences, Beijing, China

Abstract

The Beijing Electron Positron Collider II (BEPCII) has achieved a series of achievements in high energy physics study. Along with the deepening of the research, more important physcis is expected in higher energy region (> 2.1 GeV). As the upper limit of BEPCII design energy is 2.1 GeV, an urgent upgrade is required.

To achieve a higher luminosity at higher energy, the number of RF cavities is expected to be doubled. In this paper, an alternative lattice design for the upgrade of BEPCII is studied. The survey of the RF region is modified in contrast to the baseline design to accommodate two RF cavities in each ring. The dynamic aperture tracking result show that the lattice could meet the injection requirement of BEPCII beam with reasonable margin.

INTRODUCTION

The Beijing Electron Positron Collider II (BEPCII) [1] is a two-ring eletron positron collider running in the tau-charm energy region. The upper limit of designed beam energy of BEPCII is 2.1 GeV, with an optimized performance at 1.89 GeV. The commissioning of BEPCII started at 2007, and since then, a series of achievements has been achieved in high energy physics study. Along with the deepening of the research, more important physcis is expected in higher energy region (> 2.1 GeV) [2]. An urgent upgrade is required for BEPCII to ensure the competitive advantage in high energy physics study.

To improve the performance at higher energy, BEPCII is expected to upgrade the RF system from one-cavity to two-cavity per ring, so as to dramatically boost the cavity voltage. The arrangement of elements in BEPCII is very compact, so finding enough space for the extra cavity in each ring is not trivial. In this paper, we show one novel layout that successfully provides enough space for two cavites in each ring by shifting the north crossing point to the east by 8 meters in contrast to the baseline design to accommodate two RF cavities in each ring [3]. The lattice design and the dynamic aperture tracking result in the new layout will be shown.

PARAMETER DESIGN

To minimize technical crisis and avoid heavy workload, BEPCII has chosen the classic scheme, which is maintaining the small Pinwinski angle, and raising the beam current and cavity voltage at the same time to achieve a much higher luminosity at higher beam energy.

Table 1: The designed parameters and the comparison with the present BEPCII operation parameters at the energy of 2.35 GeV

	BEPCII	BEPCII-U
RF voltage [MV]	1.6	3.3
β_{y*} [cm]	1.5	1.35
bunch current (mA)	7.1	7.5
bunch number	56	120
SR power (kW)	110	250
$\xi_{y,lum}$	0.029	0.036
ϵ_x [nm·rad]	147	152
coupling %	0.53	0.35
bucket height	0.0069	0.011
$\sigma_{z,0}$ [cm]	1.54	1.04
σ_z [cm]	*1.10=1.69	1.3
Lum$[10^{32}cm^{-2}s^{-1}]$	3.5	11

When optimizing the parameters, the synchrotron radiation power is restricted to 250 kW, the bunch number is limited to 120, the bunch current is kept as low as possible for each cavity voltage. Also, for each cavity voltage, the vertical β function at the IP β_y^* is chosen according to the bunch length, then the coupling of emittances is then chosen according to the beam beam parameter ξ_{y0}.

The designed parameters and the comparison with the present BEPCII operation parameters at the energy of 2.35 GeV are shown is Table 1.

MODIFICATION OF THE RF REGION

Current layout of the RF region is shown in Fig. 1 We can see from Fig. 1 that the north crossing point is in the middle of the hall with higher roofing, the two RF cavities which are currently in running in BEPCII are placed at the two ends of the hall. Away from the hall, is the normal tunnel with a height of 3.5 m. The total length of the straight section at RF region is about 20 m.

According to design of present BEPCII RF cavities [4], the height of the RF cavity is 2.75 m, the inner conductor of the coupler is installed upright with a length of about 1 m. To ensure the coupler can be maintained and replaced online, an extra height of 1m is needed for pulling out the inner conductor. Thus, the requirement of tunnel height for installing RF cavities is > 3.75 m. The tunnel height of

* yuch@ihep.ac.cn

ISBN: 978-3-95450-227-1 ISSN: 2673-5490 doi:10.18429/JACoW-IPAC2022-WEIXSP1

TOWARDS HIGH-REPETITION RATE PETAWATT LASER EXPERIMENTS WITH CRYOGENIC JETS USING A MECHANICAL CHOPPER SYSTEM

M. Rehwald*[1], S. Assenbaum[1], C. Bernert[1], U. Schramm[1], K. Zeil
Helmholtz-Zentrum Dresden - Rossendorf, Institute of Radiation Physics,
Bautzner Landstr. 400, 01328 Dresden, Germany
S. Göde, European XFEL GmbH, Holzkoppel 4, 22869 Schenefeld, Germany
C. B. Curry[2], M. Gauthier, S. H. Glenzer, C. Schoenwaelder[3], F. Treffert[4]
High Energy Density Science Division, SLAC National Accelerator Laboratory, Menlo Park, California 94025, USA
[1] also at Technische Universität Dresden, 01062 Dresden, Germany
[2] also at University of Alberta, Edmonton, Alberta T6G 1H9, Canada
[3] also at Friedrich-Alexander Universität Erlangen-Nürnberg, 91054 Erlangen, Germany
[4] also at Technische Universität Darmstadt, 64289 Darmstadt, Germany

Abstract

Laser-plasma based ion accelerators require suitable high-repetition rate target systems that enable systematic studies at controlled plasma conditions and application-relevant particle flux. Self-refreshing, micrometer-sized cryogenic jets have proven to be an ideal target platform. Yet, operation of such systems in the harsh environmental conditions of high power laser induced plasma experiments have turned out to be challenging. Here we report on recent experiments deploying a cryogenic hydrogen jet as a source of pure proton beams generated with the PW-class ultrashort pulse laser DRACO. Damage to the jet target system during application of full energy laser shots was prevented by implementation of a mechanical chopper system interrupting the direct line of sight between the laser plasma interaction zone and the jet source.

INTRODUCTION

Laser-driven particle sources have been studied extensively over the last two decades[1]. The interest originates from unique beam properties that are useful for a number of applications ranging from ultrafast electromagnetic field probes [2, 3] and high flux neutron converter for material radiography [4] through isochoric heating of warm dense matter [5] and inertial confinement fusion [6] to injection sources for conventional accelerator structures [7] and medical applications [8–10]. Ongoing research in this field aims for the realization of a sufficiently high repetition rate which is needed to achieve application-relevant particle yields. Therefore target systems are required that are suitable for the challenges arising from the high laser shot rates. This includes target insertion and alignment as well as mitigation of debris produced by the evaporation of the target material during the shot potentially causing coating and damage of sensitive optical components. Recently developed renewable cryogenic jets allow for debris-free operation and rapid injection of fresh targets [11, 12]. No debris is produced as the material is gaseous at ambient temperatures and removed by the vacuum pumps.

The target system has to withstand the harsh environment of the high-power laser plasma interaction. When the laser pulse hits the target, energy is transferred to target electrons which can be accelerated to relativistic energies. This results in broad emission of radiation as the electrons recirculate inside the target and further interact with the laser light. The most energetic electrons are emitted from the target, building up charge separation fields, that lead to the acceleration of ions. The charge imbalance in the interaction region drives return currents in the target assembly, and the radiation pressure from the high intensity laser launches spherical shock waves which have a component along the jet axis. These combined effects of energy dissipation into vacuum (radiation, charged particles) or within the bulk of the target may not only cause problems with electronic systems (motors, diagnostics etc..) but can also damage the jet target system itself (the nozzle aperture in particular).

At laser powers in the 100 TW range, cryogenic hydrogen jet targets were successfully implemented and operated in a number of experiments [13–15]. Damage was mainly prevented by focusing the laser at a sufficient distance from the target source. This comes at the cost of increased shot-to-shot fluctuations due to the pointing jitter of the flowing jet. Extending the scope of applications of laser-driven beams demands higher particle energies that can only be realized with petawatt-class laser systems. This intuitively worsens the potential for damage. Besides further increasing the distance between target source and interaction point which would substantially decrease the hit rate, replacing the damaged part after every shot was the second option until now. Clearly, both options are incompatible with systematic studies with high repetition rates and therefore more advanced methods are needed.

In this paper, we report on implementation and demonstration of two new methods to shield the target system from damage caused by the high-power laser plasma interaction. First, the solid jet between the interaction point and the tar-

* m.rehwald@hzdr.de

ISBN: 978-3-95450-227-1 ISSN: 2673-5490 doi:10.18429/JACoW-IPAC2022-WEOXSP1

PROPOSAL FOR A COMPACT NEUTRON GENERATOR BASED ON A NEGATIVE DEUTERIUM ION BEAM

Kouichi Jimbo†, Toshiyuki Shirai
National Institutes for Quantum Science and Technology,
Accelerator and Medical Physics, Chiba, 263-8555, Japan
Ka-Ngo Leung, Karl van Bibber
Department of Nuclear Engineering, University of California Berkeley,
Berkeley, CA, USA

Abstract

Interest in high intensity generators of neutrons for basic and applied science has been growing, and thus the demand for an economical neutron generator has been growing. A major driver for the development of high intensity neutron generators are studies of neutron disturbance in integrated circuits, for which a compact generator that can be easily accommodated in an ordinary size lab would be highly desirable. We have investigated possible designs for neutron generators based on the D-D fusion reaction, which produce direction dependent mono-energetic neutrons with carry-off energy larger than 2.45 MeV. Specifically, we find a negative deuterium ion beam most attractive for this application, and plan to construct such a system with a negative deuterium ion beam of 200 keV energy and 100 mA current as a prototype of this concept.

INTRODUCTION

The National Institute for Quantum Science and Technology (QST, Chiba) hosted a long-standing program of neutron irradiation of biological specimens under pathogen-free background conditions, the Neutron exposure Accelerator System for Biological Effect Experiment (NASBEE). Neutrons were produced by 4 MeV positive hydrogen and deuterium ion beams striking on a beryllium target through the ^{9}Be(p,n) and ^{9}Be(d,n) reactions [1]. Unfortunately, due to the large size of the neutron generating system, and its high operational cost, its operation had to be terminated.

Similarly, there is an unmet need of widely available neutrons for radiation effect studies on integrated circuits. Such studies are imperative, particularly for electronics in space and high-altitude flight, as cosmic rays collide with nuclei in the atmosphere, producing approximately ten neutrons per cm^2 per hour. These cosmic rays create secondary neutrons of 1 MeV or higher [2]. These neutrons undergo scattering in integrated circuits and cause soft errors in them, also known as single-event upsets. Soft errors are a phenomenon by which one or more bits within the data on the semiconductor device have their values reversed. A soft error does not damage the semiconductor device itself. Given the large and growing number of high-altitude aircrafts and satellites being deployed, there is a great need for chip testing and certification capacity, particularly with fast neutrons, but below 3 MeV. This need also points to the necessity of new types of neutron generators [3].

In Japan, accelerator driven neutron generators based on the ^{9}Be(p,n) reaction are commonly used; these involve the acceleration of protons to ~10 MeV directed onto a beryllium target. There are currently many neutron generators of this kind are available [4]. However, the requirement of an ion source and an accelerator makes this design very large and very expensive. Furthermore, the target area becomes highly activated due to the high neutron flux emitted at all angles, not just those neutrons impinging on the sample of interest. The maintenance expenses likewise are not small.

The two examples above, from the biomedical and semiconductor sectors, are indicative of the general demand for commercial neutron applications, and which are increasing over all energy ranges. Thus we would like to develop a compact neutron generator with its power supply system, that could be affordably acquired, and occupy an ordinary size laboratory room of a university or a private company.

D-D REACTION BASED NEUTRON GENERATORS

Neutron generators based on the D-D fusion reaction, and isotopically producing neutrons of carry off energies larger 2.45 MeV (zero deuterium ion incident kinetic energy) have a long and successful history. The mono-energic energy-angle distribution changes only as a function of incident deuterium ion energy. One design of a deuterium ion source-driven neutron generator, based on a self-loading target [5], has been developed and utilized for a broad range of basic and applied science interests (geochronology, medical isotope studies, nuclear data for reactor design, etc.) at the Nuclear Engineering Department of University of California Berkeley.

The near mono-energetic neutrons with an energy of approximately 2.8 MeV at zero degrees with respect to the deuterium ion beam direction was obtained. The basic concept for this particular device, the High Flux Neutron Generator (HFNG) owes to K.-N. Leung, with elaborations and upgrades being carried out largely by students and postdocs [6,7].

In the HFNG, positive deuterium ions are accelerated up to 125 keV after extraction from the high atomic ratio RF-driven plasma ion source. The symmetric planar water-cooled (cathode) target is positioned in between two opposing plasma ion sources, 10 cm away on each side

† kouichi.jimbo@qst.go.jp

ISBN: 978-3-95450-227-1 ISSN: 2673-5490 doi:10.18429/JACoW-IPAC2022-WEOXSP2

ALL OPTICAL CHARACTERIZATION OF A DUAL GRATING ACCELERATOR STRUCTURE

S. Crisp*, A. Ody, P. Musumeci
UCLA, Los Angeles, USA

Abstract

Dielectric laser accelerators have thus far relied on custom nanofabrication of structures. Moving toward MeV scale energy gain requires longer structures which, when made of 2 gratings, are difficult to bond with nm level precision. The efficiency of dual grating structures depends highly on both offset and gap, which has thus far only been measurable by observed transmission and modulation of electrons. We present a structure constructed of commercially available gratings which allow for full flexibility in gap and offset. This structure is then optically characterized, matching diffraction order intensities to simulation results.

INTRODUCTION

The Accelerator on a Chip International Program (ACHIP) seeks to use dielectric laser accelerators (DLAs) to shrink accelerators to the sub-millimeter scale. The nonrelativistic regime has had success in obtaining net acceleration and attosecond bunching using nanofabricated pillar based structures made from B:Si [1, 2]. Fused silica has a high damage threshold for femtosecond-class laser pulses, allowing for GV/m gradients as demonstrated in the relativistic regime [3–5]. These relativistic structures are dual grating structures, meaning they are simple to fabricate in addition to having built-in filtering – electrons that do not get accelerated simply hit the glass, and do not obfuscate a modulation signal.

The ability of the structure to convert input laser intensity into acceleration, known as the structure factor, depends critically on the gap size and relative offset of the gratings. Prior structures have been made by bonding two gratings together[6], which has made characterizing them without the use of an electron beam difficult. Up to now, the only way to probe gap size was to measure transmission with an electron beam and infer offset from structure factor. As the DLA effort drives toward higher interaction lengths and therefore longer structures, characterizing the structures outside of using an electron beam is useful to conserve beam time and compensate for resulting dynamic effects [7, 8].

In this paper, we discuss the optical characterization of a dielectric structure made of 2 independently mounted gratings. Measurements are compared to simulation of the relative weight of the +-1 diffraction lobes off a dual grating structure. The diffraction measurement can be performed in air, with the use of only a small laser diode. In addition, it can also be done in-situ, with the structure installed on the beamline, in order to fine-tune the relative offset of the gratings during a beam-on DLA run.

* sophiecrisp@physics.ucla.edu

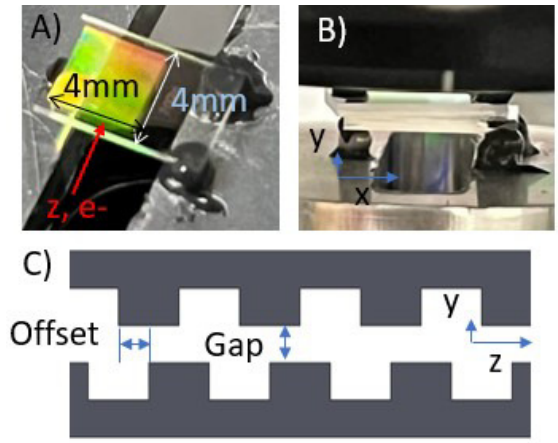

Figure 1: A) The 4 mmx4 mm grating is inset on 5 mmx8 mm x0.625 mm piece of fused silica. The future electron direction is denoted by the z direction, and is perpendicular to the grating direction. This is mounted using an aluminum filled epoxy on three points, one in the center of the grating side, and 2 on the edges away from the grating. This creates a flat plane and minimizes glass warping as the epoxy dries. Holes below and to the sides of the lower grating allow the first diffraction orders to be measured. B) Head on view of the assembled grating structure. C) A schematic defining the relative offset as the distance between opposing grating teeth and gap as the absolute distance between the two gratings.

ASSEMBLY

The DLA structures are constructed using two commercially available gratings, shown in Fig. 1. These gratings have 800 nm periodicity, allowing them to be driven by a 780 nm laser. In order to have full flexibility in grating mounting, a number of motorized and manually controlled degrees of freedom are implemented, as described in Table 1. Simulations indicate that at gaps larger than 800 nm, the structure factor of a DLA is greatly reduced. This scale requires the use of a piezo motor assembly for gap and angle control.

The upper grating sits in a 2-D translation mount, which is itself mounted in a kinematic mount. This allows coarse control of x, x', and z', and fine control of the offset, z. The lower grating sits atop a 3 piezo motor assembly. This is mounted on a vertical translation stage, which is itself attached to a rotation stage. This combination allows fine and coarse control of the gap, y, as well as fine control of every angle, x', y', and z'. The only dimension not finely controlled via motor is x; this is set by a finely threaded

ISBN: 978-3-95450-227-1 ISSN: 2673-5490 doi:10.18429/JACoW-IPAC2022-WEOXSP3

mm-WAVE STRUCTURE DEVELOPMENT FOR HIGH GRADIENT ACCELERATION*

E. C. Snively†, A. Gabriel, M. A. K. Othman, A. Sy, E. A. Nanni,
SLAC National Accelerator Laboratory, Menlo Park, U. S. A.

Abstract

We report on the design of high shunt impedance accelerator structures operating near 100 GHz. Simulations of the cavity geometry and RF coupling are performed in ANSYS-HFSS and using SLAC's parallel electromagnetic code suite ACE3P. We present experimental results for structures fabricated from copper, niobium, and copper plated with NbTiNi. We report on techniques for tuning these high frequency structures. A mm-wave accelerator cavity enables not only a high achievable gradient due to higher breakdown thresholds, but also reduced fill times which decrease pulsed heating and allow for higher repetition rates.

INTRODUCTION

Accelerators operating in the mm-wave regime offer an attractive opportunity to reach accelerating gradients of hundreds of MeV/m and repetition rates exceeding 1 kHz. Recent research exploring the high gradient performance and breakdown statistics of mm-wave structures has demonstrated gradients up to 225 MeV/m [1,2]. The cavity geometry in this case was designed to match X-band cavities used in previous experiments, allowing direct comparison of the breakdown statistics collected in both frequency regimes [3,4]. The research presented here builds on this foundation of high-power mm-wave tests with measurements of cavities matching the first-generation geometry, along with a second-generation cavity geometry for higher shunt impedance. The challenge of extending the mm-wave structure is met with a side-coupled cell design for a distributed power coupling manifold [5]. Tuning techniques adapted for the mm-wave regime are tested with first-generation cavities.

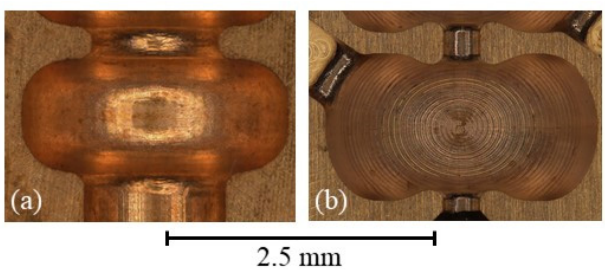

Figure 1: (a) Microscope image of a "first-generation" mm-wave cavity (110 GHz) with power coupling on-axis. (b) Microscope image of a "second-generation" cavity (94 GHz) with re-entrant nose cones and side power coupling.

* Work supported by U.S. Department of Energy Contract No. DE-AC02-76SF00515, SLAC LDRD project 21-014 and Internal Agency Agreement 21-0007-IA (MIPR HR0011150657).

† esnively@slac.stanford.edu

ACCELERATOR DESIGN

A key difference between the first-gen and second-gen cavity design is the approach to power coupling. Figure 1 shows microscope images of fabricated cavities of each type. Both structures are π-mode standing wave cavities resonant near 100 GHz. The first-gen cavity has large iris apertures which facilitate power coupling on-axis; the second-gen cavity has a side-coupled power feed and small iris apertures (330 μm) with reentrant nose cones. Measurements taken with a Vector Network Analyzer (VNA) to characterize the first-gen structures must rely on coaxial probes aligned within the beam pipe. Measurements of the second-gen structure use WR-10 waveguide connections routed to each cavity as shown in Fig. 2a. The re-entrant nose cones and small iris apertures enable a high shunt impedance, around 440 MΩ/m, while significantly reducing coupling between cells as shown in the HFSS simulations of the field profiles in Figure 2.

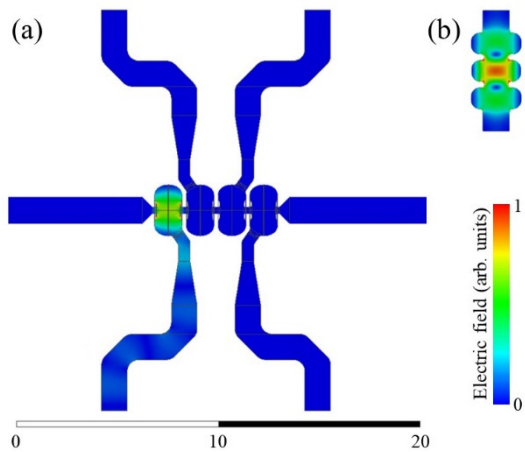

Figure 2: (a) HFSS simulation of the 4-cell side-coupled second-gen prototype with power driven at 93.9 GHz into the first cell. (b) HFSS simulation of the 3-cell first-gen design with peak field intensity localized in the central cell.

The length-scale of mm-wave structure fabrication pushes the limits of conventional machining technology. To test the feasibility of fabricating the second-gen cavity geometry with features like the side-coupled waveguide feeds and re-entrant nose cones, the four-cell prototype geometry shown in Fig. 2a was designed. Machining tolerances for the re-entrant nose cone feature were informed by the results of a mm-wave cavity design study for a beam driven power extractor [6]. The waveguide routing of the 4-cell second-gen cavity prototype allows for the characterization of each cell individually, without the added complexity of a power distribution manifold that would require

ISBN: 978-3-95450-227-1 ISSN: 2673-5490 doi:10.18429/JACoW-IPAC2022-WEIYGD1

ACHIEVEMENTS AND PERFORMANCE PROSPECTS OF THE UPGRADED LHC INJECTORS

V. Kain*, S. Albright, R. Alemany, M.E. Angoletta, F. Antoniou, T. Argyropoulos, F. Asvesta, B. Balhan, M. Barnes, D. Barrientos, H. Bartosik, P. Baudrenghien, G. Bellodi, N. Biancacci, A. Boccardi, J. Borburgh, C. Bracco, E. Carlier, J. Coupard, D. Cotte, H. Damerau, A. Findlay, M. Fraser, A. Funken, G.P. Di Giovanni, B. Goddard, G. Hagmann, K. Hanke, A. Huschauer, M. Jaussi, I. Karpov, T. Koevener, D. Kuchler, J.-B. Lallement, A. Lasheen, T. Levens, K. Li, A. Lombardi, N. Madysa, E. Mahner, M. Meddahi, L. Mether, B. Mikulec, J. Molendijk, E. Montesinos, D. Nisbet, F.-X. Nuiry, G. Papotti, K. Paraschou, F. Pedrosa, T. Prebibaj, S. Prodon, D. Quartullo, E. Renner, F. Roncarolo, G. Rumolo, B. Salvant, M. Schenk, R. Scrivens, E. Shaposhnikova, P. Skowronski, A. Spierer, F. Tecker, D. Valuch, F. Velotti, R. Wegner, C. Zannini
CERN, Geneva, Switzerland

Abstract

To provide HL-LHC performance, the CERN LHC injector chain underwent a major upgrade during an almost 2-year-long shutdown. In the first half of 2021 the injectors were gradually re-started with the aim to reach at least pre-shutdown parameters for LHC as well as for fixed target beams. The strategy of the commissioning across the complex, a summary of the many challenges and finally the achievements will be presented. Several lessons were learned and have been integrated to define the strategy for the performance ramp-up over the coming years. Remaining limitations and prospects for LHC beam parameters at the exit of the LHC injector chain in the years to come will be discussed. Finally, the emerging need for improved operability of the CERN complex will be addressed, with a description of the first efforts to meet the availability and flexibility requirements of the HL-LHC era while at the same time maximizing fixed target physics output.

SCOPE OF THE LHC INJECTORS UPGRADE

The LHC Injectors Upgrade (LIU) project aimed at increasing the intensity and brightness in the injectors to match the HL-LHC requirements [1] for both lead (Pb) ions and protons (shown in Fig.1). This goal required a series of major upgrades in all accelerators of the LHC injector chains, which are detailed in [2, 3]. The main items will be briefly summarised in the following.

To double the brightness reach of the PSB, the 50 MeV proton linac, was replaced by the 160 MeV Linac4 accelerating H^- and requiring a charge exchange injection into the four rings of the PSB. The higher PSB extraction energy required an increase of the PSB magnetic fields as well as the replacement of its main power supply and RF systems.

In the PS, the next accelerator in the chain, the injection energy increase to 2 GeV (in combination with optimized longitudinal beam parameters at the PSB-PS transfer) was needed in order to maintain the same space charge tune spread with double the beam brightness.

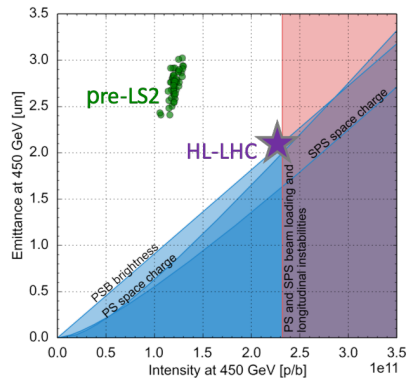

Figure 1: This plot shows the required emittance and bunch intensity for protons at the end of the injector chain. It corresponds to 2.3×10^{11} protons per bunch in 2.1 μm emittance. These parameters have to be achieved for 288 bunches of 25 ns spacing. The measured performance before Long Shutdown 2 (LS2), before the LIU upgrades were installed, are shown in green. The parameter limitations of the different machines after the upgrade are indicated with the shaded regions.

Also in the PS, longitudinal feedback, reduction of the impedance of the 10 MHz RF system and implementation of multi-harmonic feedback systems on the high frequency RF systems were required to increase the threshold of the longitudinal coupled bunch instabilities that previously limited LHC beams.

In the SPS, the 200 MHz RF power was increased by adding two new 200 MHz power plants, changing to a pulsed operation mode and rearranging the 200 MHz cavities to reduce their impedance and the beam loading effect with LHC-type beams. A reduction of the cavity High Order Modes (HOM) was achieved through the installation of specially designed couplers. A new low-level RF (LLRF) system for the 200 MHz RF system was also implemented to

* Verena.Kain@cern.ch

ISBN: 978-3-95450-227-1 ISSN: 2673-5490 doi:10.18429/JACoW-IPAC2022-WEOYGD1

RECENT RESULTS OF BEAM LOSS MITIGATION AND EXTREMELY LOW BEAM LOSS OPERATION OF J-PARC RCS

P. K. Saha*, K. Okabe, T. Nakanoya, Y. Shobuda, H. Harada,
F. Tamura, H. Okita, M. Yoshimoto
J-PARC Center, JAEA and KEK Joint Project, Tokai-mura, Naka-gun, Ibaraki-ken, Japan
Hideaki Hotchi, KEK, Tokai, Ibaraki-ken, Japan

Abstract

In the 3-GeV RCS (Rapid Cycling Synchrotron) at J-PARC (Japan Proton Accelerator Research Complex), multi-turn H^- charge-exchange injection is performed by using a thin stripped foil. The residual radiation at the injection area caused by the uncontrolled beam loss occurred by foil scattering of the circulating beam is a serious issue for regular maintenance works. In addition, the beam loss at the collimator section and its downstream caused for a large emittance beam also should be reduced, especially at high intensity operation. For that purpose we have minimized injection beam size and implemented a smaller size stripper foil. The circulating beam hitting rate is reduced by using a smaller foil, while an optimized vertical angle of the smaller injection beam for vertical transverse painting also gave a reduction of the circulating beam emittances and resulted a further significant beam loss mitigation at the collimator section and its downstream. As a result, the residual radiation after user operation at 700 kW beam power was also measured to be significantly reduced.

INTRODUCTION

The 3-GeV RCS at J-PARC delivers high intensity proton beam to both MLF (Materials and Life Science Experimental Facility) and the MR (30-GeV Main Ring Synchrotron) [1]. The injection beam energy is 400 MeV, which is accelerated to 3 GeV at repetition rate of 25 Hz and simultaneously delivered to the MLF and MR. The designed beam power is 1 MW (8.33×10^{13} protons/pulse), while at the latest it is 800 kW to the MLF and nearly 800 kW equivalent beam power to the MR. As more than 90 % of the beam is delivered to the MLF, a beam loss reduction in the RCS for operation to the MLF is highly important.

Due to multi-turn (307 turns in 0.5 ms) charge-exchange injection of H^- performed by using a stripper foil, the foil scattering beam losses of the circulating beam is the dominant uncontrolled beam loss and high residual radiation sources at injection area. Figure 1 shows a layout of the RCS injection area and a schematic view of the transverse painting (TP) process performed at injection. The TP at injection is adopted to produce a wider beam profile required by MLF to minimize beam density on the neutron production target as well as to reduce circulating beam hitting rate on the foil by large betatron oscillation occurred by varying horizontal closed orbit with 4 horizontal painting magnets (PBH1-4) and varying vertical angle of the injection beam by using two vertical painting magnets (PBV1,2) placed at the injection beam transport (BT) [2, 3]. The average foil hits of the circulating beam at a painting area of 200 π mm mrad for the MLF can be kept to only 7 , but similar to other facilities the residual radiation at the injection area caused by the foil scattering beam losses is very high even at a lower beam power [4–7]. The foil thickness is 333 $\mu g/cm^2$ to achieve a stripping efficiency of 99.7 %, while the un-stripped beams are further stripped to protons by secondary foils and disposed at the injection beam dump (I-Dump) [8]. Due to nonlinear nature of the space charge (SC) effect, the beam loss at high-intensity also increases non-linearly, especially at the collimator section and affects the downstream 1st arc section. The beam loss reduction at the collimator section is also highly important for stable operation at 1 MW beam power in a near future. In this research we have succeeded to reduce both uncontrolled beam losses at the injection area caused by the foil scattering of the circulating beam as well as the beam losses caused by the beam halos at the collimator section and its downstream.

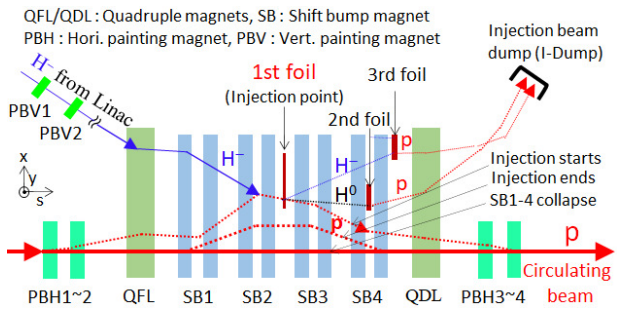

Figure 1: Layout of the RCS injection area and a schematic view of the TP process at injection. The PBH1-4 and PBV1-2 are used for horizontal and vertical painting, respectively.

PRESENT APPROACH AND NUMERICAL SIMULATION RESULTS

Figure 2 shows a schematic view of our present approach. We minimized vertical size of the injection beam at the 1st stripper foil by manipulating its vertical twiss parameter (β_y) to reduce vertical size of the foil. The foil hitting rate of the circulating beam and the corresponding beam losses caused by the foil scattering can be thus reduced. A smaller vertical size of the injection beam allows us to reduce both sides of the vertical foil instead of a single side if done for the

* saha.pranab@j-parc.jp

ISBN: 978-3-95450-227-1 ISSN: 2673-5490 doi:10.18429/JACoW-IPAC2022-WEOYGD3

ISOCHRONOUS MODE OF THE EXPERIMENTAL STORAGE RING (ESR) AT GSI

S. Litvinov, R. Hess, B. Lorentz, M.Steck
GSI, Darmstadt, Germany

Abstract

The isochronous optics of the ESR is a unique ion-optical setting in which the particles within a finite momentum acceptance circulate at constant frequency. It is used for direct mass measurements of short-lived exotic nuclei by a Time-of-Flight method. Besides the mass spectrometry, the isochronous ESR has been used as an instrument for the search of short lived isomers stored in the ring, which was performed in 2021 for the first time. Introduction to the isochronous mode of the ESR, recent machine experiments with the new LSA control system will be presented here. Possible improvements of the isochronous optics at the ESR and perspectives of the isochronous mode at CR, FAIR will be outlined.

INTRODUCTION

The stable primary beams are accelerated by the linear accelerator UNILAC to an energy of 11.4 MeV/u and then by the synchrotron SIS18 to energies 100–1000 MeV/u at the facility GSI [1]. They impinge on a thick (1-8) g/cm^2 production targets and then secondary beams of several hundred MeV/u are produced via fission or fragmentation and separated in flight either by the FRagment Separator (FRS) [2] or in the straight transfer line from the SIS18, injected and stored in the Experimental Storage Ring (ESR) [3] (see Fig. 1).

The ESR is a unique instrument for the physics experiments with highly charged ions. The ESR is operated for accumulation, storage, cooling and deceleration of heavy ion beams in the energy range from 4–400 MeV/u. The decelerated beams can be used for in ring experiments or can be fast extracted either to the low energy CRYRING [4] (with extraction energy of 10 MeV/u) or to the Heavy Ion TRAP facility (HITRAP) [5] with the extraction energy of 4 MeV/u. It is a symmetric ring with two arcs and two straight sections and a circumference of 108.36 meters. The ESR consists of 6 dipole magnets (deflection angle is 60°) and 10 quadrupole families (20 quadrupoles in total). For the second-order corrections 8 sextupole magnets are installed in the arcs. Each dipole magnet is equipped with 17 special correction coils (102 in total) which smooth the radial magnetic field in the good field region of ±110 mm of the dipole.

The ESR can be operated at a maximum magnetic rigidity of 10 Tm. For reducing transverse and longitudinal emittances of the stored ion beams, the ESR is equipped with the electron cooler which is installed in one of straight sections of the ring. In another straight section the internal gas-jet target and TOF detector are installed (see Fig. 1). The relative change of revolution time T (or revolution frequency *f*)

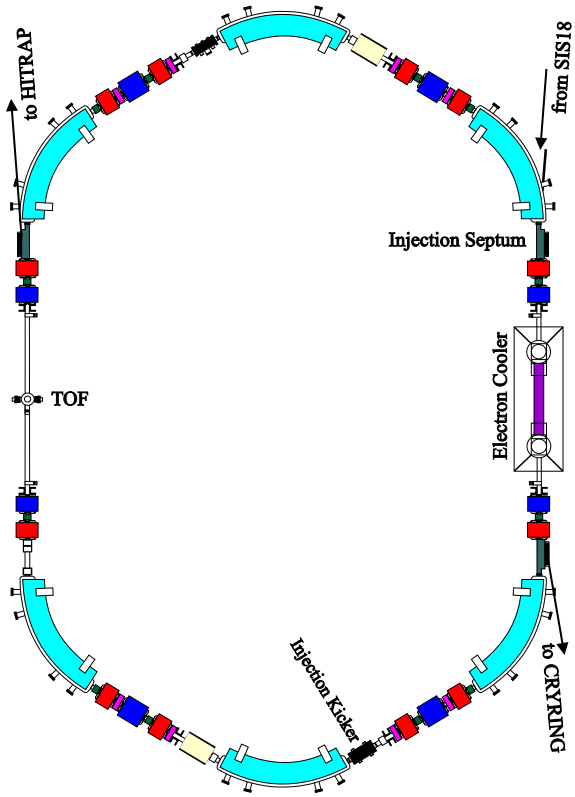

Figure 1: Layout of the Experimental Storage Ring (ESR). Dipoles, focusing, defocusing quadrupoles and sextupoles are marked by light blue, red, blue and pink colors correspondingly. Positions of the electron-cooler and the TOF detector are indicated in the straight sections.

due to different mass-to-charge ratio m/q and velocity v of the stored ions circulating in the ring can be written:

$$-\frac{\Delta f}{f} = \frac{\Delta T}{T} = \frac{1}{\gamma_t^2} \cdot \frac{\Delta(m/q)}{(m/q)} + \left(\frac{\gamma^2}{\gamma_t^2} - 1\right)\frac{\Delta v}{v}, \quad (1)$$

where γ is the relativistic Lorentz factor and γ_t is the transition energy of the ring. If the second term in Eq. (1) becomes negligible, then the revolution time defines m/q.

To achieve this condition, two complimentary methods are developed and successfully used in the ESR. In the Schottky Mass Spectrometry (SMS) [6] the velocity spread is reduced by the electron cooler to about 10^{-7} depending on the intensity. Thus, the disturbing second term in Eq. (1) gets eliminated. The revolution frequencies are measured by Schottky pick-ups installed in the other straight section of the ESR. The disadvantage of this technique is that the electron cooling takes at least a few seconds thus limiting the accessible nuclides.

ISBN: 978-3-95450-227-1 ISSN: 2673-5490 doi:10.18429/JACoW-IPAC2022-WEIYSP1

NEW DESIGNS OF SHORT-PERIOD UNDULATORS FOR PRODUCING HIGH-BRIGHTNESS RADIATION IN SYNCHROTRON LIGHT SOURCES

E. Wallen *, Lawrence Berkeley National Laboratory, Berkeley, California, USA

Abstract

We review modern state-of-the-art and new concepts of undulators planned for new generation light sources. Both superconducting and permanent-magnet-based insertion devices feature unique solutions to reach high precisely tunable fields in the period range of 10-18 mm, 2-4 meters in length and with the ID gaps of less than 5 mm. The same quest for small gaps and shortest possible period length exists also for elliptically polarizing undulators. A review of new designs in Europe, Asia and Americas will be in the focus of this presentation.

INTRODUCTION

Today's state of the art light sources, such as 3rd generation synchrotron radiation storage rings, diffraction limited storage rings, and linear accelerator free electron lasers are all using undulators for the production of high brightness synchrotron radiation.

In order to push the photon energy spectrum to higher photon energies, without increasing the energy of the accelerator electron beam, the period length should be as short as possible.

For short wavelength planar polarization, in-vacuum undulators is the main workhorse at light sources. For elliptically polarized light, small gap elliptically polarizing undulators are installed around a thin extruded aluminum vacuum chamber. The most common elliptically polarizing undulator type is the APPLE II type.

A recent development is that the new diffraction limited storage rings, as well as free electron lasers, allow the installation of round small diameter vacuum chambers, which opens up possibilities for new undulator concepts.

The intention with this presentation is to give an overview of the development of short period undulators, both planar and elliptically polarizing.

IN-VACUUM UNDULATORS

After the first proposal to build and install an in-vacuum undulator at KEK in Japan [1], there has been a tremendous evolution of the in-vacuum technology. The main initial driver of the development of in-vacuum undulators was SPring8 in Japan [2,3]. Other laboratories have followed and in-vacuum undulators have been further developed at, for example, the ESRF in France [4] and PSI in Switzerland [5]. For example, the 100 m long rows of in-vacuum undulators at the SACLA FEL is an impressive achievement [6]. The SwissFEL has a comparable installation of in-vacuum undulators at the ARAMIS beamline [5].

The in-vacuum undulator technology is fully mature and industrial partners can deliver complete undulator systems with individual undulator lengths of 5 m or more. The grade of magnet material used in the hybrid type magnet structure stands the elevated temperatures during the initial vacuum bake-out after installation and vacuum problems are rare. Mechanical problems are also rare [7]. The main problem with in-vacuum undulators is that, being close to the smallest aperture in the accelerator, they may be exposed to demagnetization, showing reduced radiation properties and changing multipole contents [8]. The maximum field strength is limited by the maximum remanence of the rare earth alloys used. Some enhancement of the field is obtained by carefully surround the poles, which are made of soft magnetic material, with permanent magnet material.

CRYOGENICALLY COOLED IN-VACUUM UNDULATORS

The shortcomings of the in-vacuum undulator, with sensitivity to radiation induced demagnetization and the limit put by rare earth materials at room temperature, were addressed by suggesting to cool the magnet rows down to cryogenic temperatures and that make use of the increased remanence and intrinsic coercivity of the magnet material at low temperatures [9].

In principle, the change from running cooling water to keep the in-vacuum undulator at room temperature, to instead run a cryogenic fluid or install cryocoolers to keep the magnet rows at cryogenic temperatures, is minor. In practice, however, it is rather complicated. Finding solutions to the problems given by the various thermal expansion rates of the mechanical supports structure, the magnet material properties that change with temperature, and the necessity of carrying out magnetic measurement in-situ under vacuum in the undulator have been challenging.

By a major effort carried out at several laboratories [10–16], the challenges have been overcome and the cryogenically cooled undulator technology is now a mature technology and it is possible to order cryogenically cooled undulators from industry. The maximum length is however limited to about 4 m.

SUPERCONDUCTING UNDULATORS

Superconducting wavelength shifters and wigglers have with success been used at synchrotron light sources for decades and the experience from these application regarding cryostats, cryocoolers, heat loads, winding techniques, and current leads was valuable for the development of superconducting undulators.

* ejwallen@lbl.gov

ISBN: 978-3-95450-227-1 ISSN: 2673-5490 doi:10.18429/JACoW-IPAC2022-WEOYSP1

EXPERIMENTS WITH UNDULATOR RADIATION, EMITTED BY A SINGLE ELECTRON*

I. Lobach†, Argonne National Laboratory, Lemont, IL, USA
S. Nagaitsev[1], A. Romanov, A. Shemyakin, G. Stancari, Fermilab, Batavia, IL, USA
[1]also at The University of Chicago, Chicago, IL, USA

Abstract

We study a single electron, circulating in the Fermilab IOTA storage ring and interacting with an undulator through single and multi-photon emissions. The focus of this research is on single-photon and two-photon undulator emissions. We begin by using one Single Photon Avalanche Diode (SPAD) detector to detect the undulator radiation photons and search for possible deviations from the expected Poissonian photon statistics. Then, we go on to use a two-photon interferometer consisting of two SPAD detectors separated by a beam splitter. This allows to test if there is any correlation in the detected photon pairs. In addition, the photocount arrival times can be used to track the longitudinal motion of a single electron and to compare it with simulations. This allowed us to determine several dynamical parameters of the storage ring such as the rf cavity phase jitter and the dependence of the synchrotron motion period on amplitude.

INTRODUCTION

In our previous experiments [1–3] with an electron bunch we showed that turn-to-turn fluctuations $\mathrm{var}(\mathcal{N})$ of the number of detected undulator radiation photons per turn $\mathcal{N}$ have two contributions: (1) a Poissonian contribution equal to $\langle\mathcal{N}\rangle$, due to the discrete quantum nature of light, and (2) a collective contribution $\propto \langle\mathcal{N}\rangle^2$, related to the interference between the fields generated by the electrons in the bunch. In this paper, we get rid of the collective contribution by considering a single electron circulating in the Integrable Optics Test Accelerator (IOTA) storage ring at Fermilab in order to thoroughly study the quantum fluctuations and verify that they follow the Poissonian photostatistics $\mathrm{var}(\mathcal{N}) = \langle\mathcal{N}\rangle$, predicted by [4–7]. This research is motivated by the surprising observation of sub-Poissonian photostatistics ($\mathrm{var}(\mathcal{N}) < \langle\mathcal{N}\rangle$) in synchrotron radiation reported in Ref. [8] in a similar experiment setting. In addition, we will use the recorded detection times to study the synchrotron motion of a single electron in IOTA [9], similar to previous experiments in Novosibirsk [10, 11].

APPARATUS

In our experiment, a single electron circulated in IOTA with a revolution period of 133 ns and an energy of 96.4 MeV. The undulator parameter is $K_\mathrm{u} = 1.0$ with the number of periods $N_\mathrm{u} = 10.5$ and the period length $\lambda_\mathrm{u} = 5.5$ cm. The wavelength of the fundamental was $\lambda_1 = \lambda_\mathrm{u}(1 + K_\mathrm{u}^2/2)/(2\gamma^2) = 1.16\,\mu$m, where $\gamma = 188.6$ is the Lorentz factor. The second harmonic was in the visible wavelength range. We used a Single Photon Avalanche Diode (SPAD) [12] as a detector, which was mostly sensitive to the visible light with detection efficiency of up to 65 %. We also used two edge-pass filters to only collect the radiation between 550 nm and 800 nm. The radiation was focused on the sensitive area of the detector ($\varnothing 180\,\mu$m) by a single focusing lens with a focal distance of 180 mm, see Figs. 1(a),(b). The radiation was collected in a large angle $> 1/\gamma$. The SPAD detector produced a 10-ns-long TTL pulse at each detection event. Its dead time (20 ns) was shorter than the IOTA revolution period (133 ns). Our data acquisition system (Fig. 1(c)) allowed us to record the revolution number and the arrival time relative to the IOTA revolution marker for each detection event for as long as 1 minute at a time.

PHOTOSTATISTICS MEASUREMENTS

In the optimal focusing, the measured photocount rate was 24.7 kHz, or one photocount per 304 revolutions in IOTA (on average). The dark count rate of the SPAD detector was 108 Hz. In addition, we used a 5-ns-long gate around the expected detection arrival time, which allowed us to reduce the effective dark count rate to 4.0 Hz.

Before any analysis of the photostatistics, it was important to realize that the SPAD detector is binary. It produces the same type of pulses (TTL, 10-ns-long) no matter how many photons are detected per one pass. The collected turn-by-turn data can be represented as a sequence of zeros and ones only. Therefore, we had to alter our original expectation of Poissonian photostatistics to a sequence of Bernoulli trials, i.e., there is a probability p of a detection at every revolution, and a probability $(1 - p)$ of no detection. In our case, $p = (3.29 \pm 0.02) \times 10^{-3}$. Figure 2 illustrates the comparison between the expectation (for a sequence of Bernoulli trials) and the measurement for (a) the distribution of interarrival times and for (b) the distribution of the number of photocounts in a certain time window. In both cases, the χ^2 goodness-of-fit test [13, p. 637] results in a P-value [13, p. 140] above the conventional 0.05 threshold. This means that the null hypothesis (exponential or binomial distribution, respectively) cannot be rejected.

We have also carried out some measurements with an upgraded setup consisting of two SPAD detectors separated by a beam splitter [14]. In this case, the photon number

* The work is supported by the U.S. Department of Energy, Office of Science, Office of Basic Energy Sciences, under Contract No. DE-AC02-06CH11357.
† ilobach@anl.gov

ISBN: 978-3-95450-227-1 ISSN: 2673-5490 doi:10.18429/JACoW-IPAC2022-WEOYSP2

FIRST ELECTRON BEAM OF THE THOMX PROJECT*

C. Bruni†, M. Alkadi, J. N. Cayla, I. Chaikovska, S. Chancé, V. Chaumat, O. Dalifard, N. Delerue, K. Dupraz, M. El Khaldi, N. ElKamchi, E. Ergenlik, P. Gauron, A. Gonnin, E. Goutierre, H. Guler, M. Jacquet, V. Kubytskyi, P. Lepercq, F. Letellier-Cohen, J. C. Marrucho, B. Mercier, E. Mistretta, H. Monard, A. Moutardier, M. Omeich, V. Soskov, F. Wicek
Université Paris-Saclay, CNRS/IN2P3, IJCLab, 91405, Orsay, France,
on behalf of the ThomX collaboration [1].

Abstract

The ThomX accelerator beam commissioning phase is now ongoing. The 50 MeV electron accelerator complex consists of a 50 MeV linear accelerator and a pulsed mode ring. It is dedicated to the production of X-rays by Compton backscattering. The performance of the beam at the interaction point is demanding in terms of emittance, charge, energy spread and transverse size. The choice of an undamped ring in pulsed mode also stresses the performance of the beam from the linear accelerator. Thus, commissioning includes a beam based alignment and a simulation/experimental matching procedure to reach the X-ray beam requirements. We will present the first 50 MeV electron beam obtained with ThomX and its characteristics.

THOMX ACCELERATOR DESCRIPTION

ThomX [2–4] is a compact Compton scattering source hosted in the Paris-Saclay scientific university campus (Orsay, France). The goal is to demonstrate the production of hard X-rays (45 keV) with a flux of 10^{11}-10^{13} ph/s. The ThomX accelerator complex is composed of a linear accelerator combined with a 50 MeV electron ring. The ThomX linear accelerator is composed of two main warm RF components: the RF gun and the accelerating section that boosts the electrons to the final energy for the ring injection. ThomX RF gun has mainly the same design as the CTF3 model [5, 6] with a nominal RF field amplitude to be reached of 80 MV/m. The accelerating section is lent by Synchrotron SOLEIL. To achieve a final energy of 50 MeV, the energy gain in the section must be 45 MeV [7].

The compactness of the ring allows a high repetition rate of the electron bunch at the Compton interaction point to maximize the X-ray flux. Due to the short Touschek lifetime at this low energy, the ring does not operated in a damped mode, but in a pulsed mode [8]. In such a case, a single electron bunch is injected in the ring every 20 ms. Then, Radiation damping is negligible during the storage time as it is in the order of 1 second. The 20 ms cycle has been chosen to prevent the electron beam degradation due to the Compton collisions that produce the x-rays, and collective effects as Intrabeam scattering [9].

Since the quality of the X-ray production is mostly determined by the electron beam characteristics [10–12], the lack of radiation damping in the ring makes a high quality electron beam essential at the exit of the linac. In fact, the emittance at the interaction point will be dominated by the one achieved by the linac and the transfer line. So the characteristic of the beam coming from the linac should avoid emittance degradation in the transfer line due to collective and chromatic effects. The electron beam properties at the exit of the transfer line strongly dominate the subsequent particle dynamics in the ring and the ultimate machine performances at the interaction point. So, a dedicated tuning of the linac is necessary.

During May 2021, Phase I authorization from the French Nuclear Safety Authority was given. It implies that the beam parameters be limited to 100 pC, 50 MeV, and 10 Hz of repetition rate of the RF source and a limitation on the linac straight section with the impossibilities to send the electron beam into the transfer line and then the ring. The paper first presents the conditioning stage of the linac RF cavities, then the first beam established in 3 days at 37 MeV, and finally the characterisation and optimisation stages that are currently underway.

FIRST ELECTRON BEAM

Different working points have been prepared for 100 pC, 500 pC, and 1 nC. The beam parameters are summarized in Table 1. The first commissioning phase allowed us to accelerate up to 100 pC maximal charge with an expected emittance value of 2 π mm mrad according to a rms spot size of 0.3 mm.

Table 1: Summary of the Linac Performances

Charge (nC)	1	0.5	0.1
rms Laser transverse size (mm)	0.5	0.4	0.3
Energy spread at linac output (%)	0.25	0.25	0.25
Normalised Emittance linac output (π mm mrad)	4.4	3	1.5

Following authorization from the French Nuclear Safety Authority (ASN) for the first phase (100 pC, 50 MeV at 10 Hz), the RF conditioning of the ThomX linac was carried out from July to October 2021 in several phases. RF cavities should be conditioned by applying progressive RF power to the system. Up to 9 MW RF power at 10 Hz, LIL section was conditioned in two days in June 2021 as it was in use

* Work supported by the French "Agence Nationale de la Recherche" as part of the program "investing in the future" under reference ANR-10-EQPX-51 and by grants from Région Ile-de-France
† christelle.bruni@ijclab.in2p3.fr

ISBN: 978-3-95450-227-1 ISSN: 2673-5490 doi:10.18429/JACoW-IPAC2022-WEOYSP3

OPERATION EXPERIENCE WITH SESAME RF SYSTEM

D. Foudeh, N. Sawai, A. Kurdi, SESAME Synchrotron, Allan, Jordan

Abstract

SESAME RF system has been in operation for five years during which the operational beam current has been increased from 100 mA to 300 mA. The higher operational beam current with the need to have longer beam lifetime to reduce number of injections per day, required higher forward RF power, on the other hand; more attention needed to be paid to monitor and tackle the current driven High Order Modes and to respect the limitation on the forward RF power coming from the solid-state amplifiers. In this paper we describe the RF system and report on the challenges we faced in addition to the operational experience we had with the RF system.

INTRODUCTION

SESAME is an international third-generation light source that has been hosting users since Jul.2018. The storage ring (Table 1) is filled with current that reached 300 mA in the last year, at 1Hz repetition rate using 800MeV injector, then its energy is ramped up to 2.5 GeV. Due to the long beam lifetime, around 24h at 300 mA, one injection per day is sufficient for users.

Table 1: Operational Main RF Parameters

parameter	unit	value
Circumference	m	133.2
RF	MHz	499.671
Energy	GeV	2.5
Current	mA	300
Filled buckets		≈198
Harmonic number h.		222
Energy Losses per turn	keV	603
Momentum compaction factor		0.00828
No of cavities		4
RF Voltage	MV	1.8

SESAME storage ring RF system is composed of four identical plants where each has one Elettra cavity powered by 80kW solid state amplifier (SSA) through WR1800 waveguide (Fig.1). The RF plant is controlled via digital low level RF (D-LLRF) system from DIMTEL. The RF system had been installed and commissioned in 2016 while the first beam stored beginning of 2017 [1].

Figure 1: Top view for 4x80 kW RF plants.

MASTER OSCILLATOR

In the commissioning period of the machine there was a frequent need to change the master oscillator (MO) frequency which was unfortunately causing a trip in the RF system even with steps of tens of hertz. It appeared that MO was losing its phase at the frequency change leaving the D-LLRF with no reference signal, consequently creating a high reflected power tripping the RF system. Figure 2 shows the amplitude and phase of RF signals relative to the reference channel, where forward and reflected jumps are associated with the frequency change at about 106 µs into the record, resulting in an interlock trip at 110 µs [2].

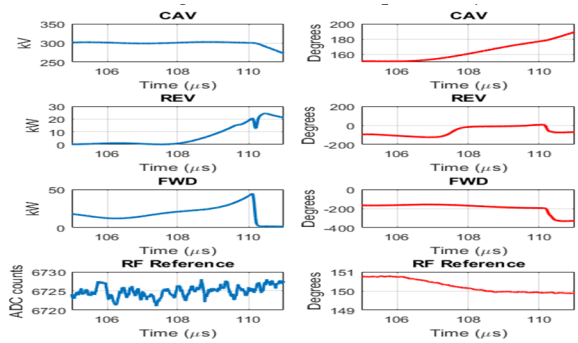

Figure 2: Post-mortem showing FWD phase change.

To avoid this situation; a temporary setup had been implemented to change frequency via FM DC-coupled modulation which preserves phase continuity. This setup required a frequency counter to keep measuring the MO frequency. Later, the old MO was replaced by a new phase-coherent signal generator model HS9001B manufactured by Holzworth which is free of phase glitch regardless to the step size of frequency change with about -10 dB phase noise improvement.

80 KW SOLID STATE AMPLIFIER

The 80 kW SSA is composed of 160x550 W RF modules whose outputs are combined using a set of coaxial combiners arranged in (8x10x2x1) scheme. Similarly, the driving signal is buffered by another 5 modules and then split into 1x5x4x8 scheme. Operational voltage of modules ranges from 46 to 50 VDC which is chosen as the default operational DC voltage. The power supplies are assembled in 5 groups, installed on the top of SSA cabinet, each has 16x2kW power supply modules. The SSA showed high reliability during machine operation, only 30 out of 660 RF modules had transistors repaired and one 2 kW power supply was found defected out of 340 rectifiers. Due to the proven performance of SSA, an in-house 4 kW SSA was assembled from the spare modules to be used for booster RF plant. The new amplifier replaced the old 2 kW commercial TV amplifier.

ISBN: 978-3-95450-227-1 ISSN: 2673-5490 doi:10.18429/JACoW-IPAC2022-WEOZGD1

DESIGN OF AN LPA-BASED FIRST-STAGE INJECTOR FOR A SYNCHROTRON LIGHT SOURCE

Xueyan Shi[1,2,*], Haisheng Xu[1,†]
[1]Institute of High Energy Physics, Chinese Academy of Sciences, Beijing, China
[2]University of Chinese Academy of Sciences, Beijing, China

Abstract

Study of plasma-based acceleration has been a frontier of accelerator community for decades. The beam quality obtained from a laser-plasma accelerator (LPA) becomes higher and higher. Nowadays, the combination of LPAs and the conventional RF accelerators attracts quite some research interests. One of the interesting directions to go is to replace the LINAC of a synchrotron light source by an LPA. However, there are still challenges, e.g., the energy stability of the electron bunches, to be solved. In this paper, we present a preliminary physical design of a 500 MeV LPA-based first-stage injector for a synchrotron light source. Preliminary study for suppressing the energy deviation of the electron bunches generated by LPA is also presented.

INTRODUCTION

Laser-plasma accelerator (LPA) has become an important direction in future particle accelerators because of the high accelerating gradient. In the past years, there were many researches for improving the beam quality of LPAs, such as the beam energy [1], energy stability [2] and bunch charge. The future LPAs are expected to be used in many applications, such as FELs, light sources, and colliders. We are interested in the application of LPAs in synchrotron light sources.

Synchrotron light sources have been widely used in different fields. As far as we know, most of the existing synchrotron light sources consist of LINACs, booster synchrotrons, and storage rings. The LINACs and boosters are usually called the "injectors" of the storage rings, which are used to generate electron bunches and to accelerate electron bunches to the desired energy of the storage rings. It would be very interesting if the injectors of storage rings can be replaced by LPAs because it would reduce the size of the injector significantly. However, it requires several GeV level beam energy and very good stability to the LPA. Therefore, we believe that it's reasonable to consider using an LPA to replace the injector of booster (LINAC) as the starting point, saying, lower expectation at the beginning.

However, the few percent level central energy jitter and energy spread of electron bunches generated by LPAs (e.g., approximately 2.4% central energy jitter and 4% energy spread presented in [2]) are still not small enough for injection into the booster (a typical value of energy acceptance ±3%). Several schemes [3–6], therefore, were proposed to suppress the energy spread of electron bunches, such as the passive plasma dechirper which can reduce the energy spread but not the central energy deviation. One of the most promising approaches is to combine a chicane with an active dechirper [7, 8], this scheme, in principle, can reduce not only the energy spread but also the central energy jitter of electron bunches. The principle is to add a nearly linear negative energy chirp (energy-position correlation, the energy of particles decrease from bunch head to tail) to the bunch by a chicane with positive R_{56} (high energy particles will run to the head and the lows will run to the tail), then use the longitudinal wakefield generated by the dechirper to compensate the chirp, so as to reduce the energy deviation. On this basis, in order to meet the demands of synchrotron light sources, we wonder whether the scheme works if we keep increasing the charge of the injected electron bunch.

We found that there are three main challenges: (1) the severe beam loading effect will destroy the linearity of longitudinal wakefield E_z in the active plasma dechirper (APD) which works in the nonlinear regime; (2) the bunch length is subjected to the plasma wavelength of APD, which in turn is limited by the increasing laser peak power; (3) the chromatic effect in the quadrupoles makes it difficult to focus the RMS beam size within the radius of the plasma bubble.

Here we present the preliminary design of a beamline starting from a LPA, followed by a triplet, a magnetic chicane, and an APD, showed in Fig. 1. The rest of this manuscript is arranged as follows: Section II gave the typical parameters of an electron bunch, which was used as the initial bunch in the following design and simulations, generated by an LPA. Then, the considerations in the selection of the main parameters were described in Section III, followed by the basic design of the Twiss parameters of the beamline in Section IV. Section V showed the main simulations results in the APD. Conclusions and discussions were given in Section VI.

Figure 1: Elements from left to right: laser plasma accelerator, triplet, chicane and active plasma dechirper.

ELECTRON BUNCH FROM AN LPA

Since it's a very big topic to study how to generate high quality electron bunches in a LPA, we didn't really go into details of this topic. We just assume that the LPA can provide the initial electron beams we used which are not from the LPA simulations but generated by MATLAB according to a set of LPA beam parameters [4, 9]. The main parameters of

* shixueyan@ihep.ac.cn
† xuhs@ihep.ac.cn

ISBN: 978-3-95450-227-1 ISSN: 2673-5490 doi:10.18429/JACoW-IPAC2022-WEINGD1

INDUSTRY AND ACCELERATOR SCIENCE, TECHNOLOGY, AND ENGINEERING – THE NEED TO INTEGRATE (BUILDING BRIDGES)

R. Geometrante, Kyma SpA, Trieste, Italy
S. Biedron, Element Aero and the Center for Bright Beams, USA
E. Braidotti, CaenELS, Trieste, Italy
H. Priem, VDL-ETG, Eindhoven, The Netherlands
J. C. Rugsancharoenphol, Federation of Thai Industries (FTI), Thailand
S. Sheehy, University of Melbourne, Australia
M. Vretenar, CERN, Geneva, Switzerland

Abstract

Finally, after two years of many virtual-only events, IPAC22, the International Particle Accelerator Conference 2022, could be held in person in Bangkok, Thailand, from June 12-17, 2022.

Following up on the conclusions reached in the Industrial Session of IPAC21, remotely hosted by the Laboratório Nacional de Luz Síncrotron (LNLS) in Campinas, Brazil, the industrial session of IPAC22 had the opportunity to renew the discussions along with new ideas and opportunities. At IPAC22 (Fig. 1), an innovative and integrated approach was adopted, and new impactful strategies were discussed and proposed to foster a true and realistic as well as effective and global accelerator ecosystem/network.

One key point of the session was that the collaborative and fertile environment between industry and research laboratories will continue to be crucial for the successful development and implementation of the technologies required in the next years. These collaborations and associated technological developments will have to satisfy and allow the progress foreseen in exponentially growing markets such as those of particle accelerators.

The session also discussed the importance of universities for basic and more advanced technology insertions into the labs and industry as well as for the workforce pipeline. Further, we also discussed the importance of interactions with governments and not-for-profits, e.g. professional societies, consortiums.

Enhanced across the board collaboration will be beneficial both for industry and for advancing the science, technology and engineering (STE): when well-integrated, accelerators help solve global problems, as proven in solving societal puzzles such as in developing the COVID vaccines, and the industry can grow, this brings in more tax income, more budgets for STE, more applications, etc. in a virtuous circle.

During the Industrial Session of IPAC22, much was discussed considering the different points of industry, laboratories, universities, and other collaborating entities. The aim was to generate and compile novel ideas and concrete actions on how best to implement and apply strategies that would help the integration and co-innovation between industry and collaborators for STE, with the purpose of building a global, collaborative accelerator economy: making accelerator-based research sustainable over the long-term, increasing at the same time the benefits of particle accelerators for society are the main challenges to the accelerator community in the century after next.

INTRODUCTION

Particle accelerators are at a crucial moment in their evolution. In this critical phase, innovation is drastically needed, to overcome the limitations in, for instance, the sustainability of large accelerator for fundamental research and in the integration of advanced data science and control for remotely-stationed medical accelerators, as well as to foster the ongoing transition of accelerator technologies towards STE and society.

Traditionally, innovation for particle accelerators and their peripherals takes place in scientific laboratories, possibly supported by a network of universities, and then either remains in the domain of the laboratory or is "transferred" to industry. This scheme worked quite well in the past but is now showing its limitations because on the one hand the breadth and complexity of new technologies feeding into new accelerators is beyond the capabilities of a single laboratory or national network, and on the other hand because the risk and costs of transforming ideas into "products" is often beyond what can be afforded by the shrinking budgets of public research institutions.

Times have changed: the particle accelerator community is entering the age of open innovation where ideas and know-how have to be shared between scientific institutions and companies, to improve high technology products and to identify new products and markets.

Creation of an innovation ecosystem based on community, trust, openness, creativity, connection is needed, with the long-term goal to create a common language and a common working ground between academia and industry, and to favor exchanges – in both directions.

Of course, to achieve these goals we must face many challenges. Administrative issues (on both sides!), rigid corporate culture in large companies, agreement on sharing of responsibilities and risks, IP management, keeping competition for series production, are among the many obstacles to overcome to create a real academia-industry innovation ecosystem. But for each of these problems there are solutions, and all problems can be solved if there is mutual trust and if we overcome the traditional mentality of industry as "supplier", and instead we go towards considering industry as a "co-innovator".

ISBN: 978-3-95450-227-1 ISSN: 2673-5490 doi:10.18429/JACoW-IPAC2022-WEIZSP2

TRAPPING OF NEUTRAL MOLECULES BY THE ELECTROMAGNETIC BEAM FIELD*

G. Franchetti[1], GSI, Darmstadt, Germany
F. Zimmermann, CERN, Geneva, Switzerland
[1]also at HFHF, Frankfurt, Germany

Abstract

Trapping phenomena are common in physics and are of relevance for the accelerators. We discuss the phenomenon of neutral molecule trapping into the beam electromagnetic potential and highlight the potential influence on the vacuum density. The effect of molecule agglomerates is discussed for high energy accelerators.

INTRODUCTION

At large accelerator laboratories, such as GSI [1], CERN [2], or BNL [3], the vacuum pressure in the beam pipe of storage rings ranges from 10^{-8} to 10^{-10} Pa. In cryogenic rings [4], the vacuum pressure p may reach a level of 10^{-13} Pa or less, at a low temperature T. A low vacuum pressure ensures a low density of atoms and molecules, according to $n = p/(k_b T)$, with k_b the Boltzmann constant. The residual gas density n is a key quantity defining the "beam lifetime". In fact, the presence of neutral vacuum molecules in accelerator beam pipes lead to occasional collisions between beam particles and vacuum molecules, which may create several undesirable effects, ranging from the emission of beamstrahlung photons by beam electrons or positrons, over the stripping of electrons from partially stripped heavy-ion beam particles, to the fragmentation of the neutral molecule itself. The consequences of the beam-gas collisions may vary between a mild drop in the beam lifetime to a nearly catastrophic phenomenon, as in the case of a dynamical vacuum instability [5]. More generally, the presence of ionized gas molecules or liberated electrons inside the accelerator beam pipe can have undesired consequences, such as the creation of an electron cloud [6–10].

In this paper, we present a study of the dynamics of neutral molecules under the effect of the beam electromagnetic fields. We discuss a possible accumulation of neutral molecules in the vicinity of the beam [11], with potential negative impact on the beam lifetime.

DYNAMICS OF NEUTRAL MOLECULES AND APPROXIMATIONS

At first sight, neutral particles are not affected by an electromagnetic field unlike particles carrying an electric charge. However, the situation can be different for neutral molecules which may exhibit a non-homogeneous charge distribution. To first order, this charge distribution $\rho(\vec{r})$ is characterized by its electric dipole moment $\vec{p} = \int \vec{r}\rho_M(\vec{r})dv$. A similar discussion applies to the intrinsic magnetic field of a molecule, which may be characterized by a magnetic dipole moment $\vec{\mu}$.

In general, the geometry of a molecule is not rigid, but exhibits an equilibrium configuration of its elementary particles subject to internal restoring forces, which, for example, give rise to natural vibration states of the molecule around an equilibrium mechanical geometry. The frequency of these internal oscillations is high and, therefore, we consider the geometry as rigid to a good approximation.

The effect of a homogeneous electric or magnetic field on a molecule with a dipole moment is to inflict a torque. If the field is not homogeneous a net force on the center of mass will also arise. These forces and torques are as follows [12]:

$$\begin{cases} \vec{\tau} = \vec{p} \times \vec{E} + \vec{\mu} \times \vec{B} \\ \vec{F}_{\rm cm} = (\vec{p} \cdot \nabla)\vec{E} + (\vec{\mu} \cdot \nabla)\vec{B} \end{cases} \quad (1)$$

We observe that in both cases the torque in Eq. (1) disappears when the dipole moment has either the same or the opposite direction of the corresponding field. A stability analysis shows that the dipole moment dynamics is stable only if the dipole moment has the same direction as the field. Clearly, it is difficult that a molecule may simultaneously have $\vec{p}$ and $\vec{\mu}$ aligned with $\vec{E}$ and $\vec{B}$. However, in our study we consider only molecules equipped either with an electric dipole moment (EDM) or with a magnetic dipole moment (MDM). For example, in the case of an EDM molecule, the equation of angular motion of $\vec{p}$ is

$$\frac{d^2\theta}{dt^2}\hat{n} = \omega_E^2 \hat{p} \times \hat{E} \ , \quad (2)$$

where $\hat{p}$ and $\hat{E}$ designate unit vectors in the direction of $\vec{p}$ and $\vec{E}$, respectively, and $\hat{n}$ is the unit vector orthogonal to $\hat{p}$ and $\hat{E}$. The angle θ is the angle between $\vec{p}$ and $\vec{E}$. The quantity $\omega_E = \sqrt{pE/I_i}$, characterizes the oscillation frequency of $\hat{p}$ around the equilibrium direction $\hat{E}$, and similarly, for MDM molecules we find $\omega_B = \sqrt{\mu B/I_i}$. We denote with I_i the moment of inertia of the molecule, which for a bi-atomic molecule is $I_i = \frac{1}{2}mL^2$, with L a characteristic length of the molecule and m an atom mass. The solution of Eq. (2) for small θ is a harmonic oscillations of θ around the equilibrium direction ($\theta = 0$) with the characteristic angular frequency ω_E. This frequency of oscillation is typically fast. For example, in a molecule of H_2O the electric dipole moment is $p = 1.87$ D, being D the unit of Debye, 1D = 0.2082 eÅ. An equivalent bi-atomic molecule, i.e. with equal dipole moment and the equal momentum of inertia, will have size $L = 0.65$ Å, hence we

* This work was supported, in part, by the European Union's Horizon 2020 Research and Innovation Programme under grant agreement No. 101004730 (I.FAST).

ISBN: 978-3-95450-227-1 ISSN: 2673-5490 doi:10.18429/JACoW-IPAC2022-WEOZSP1

LONGITUDINAL BUNCH SHAPING USING AN X-BAND TRANSVERSE DEFLECTING CAVITY POWERED BY WAKEFIELD POWER EXTRACTOR AT ARGONNE WAKEFIELD ACCELERATOR FACILITY*

Seong-Yeol Kim†, John Power, Gongxiaohui Chen, Scott Doran, Wanming Liu, Eric Wisniewski
Argonne National Laboratory, Lemont, IL 60439, USA
Chunguang Jing‡, Alexis Bibian, Ernest William Knight, Sergey Kuzikov
Euclid Techlabs, Bolingbrook, IL 60440, USA
Philippe Piot, Northern Illinois University, DeKalb, IL 60115, USA

Abstract

Longitudinal bunch shaping using transverse deflecting cavities (TDC) was recently proposed [Gwanghui Ha *et al., Phys. Rev. Accel. Beams* **23**, 072803, 2020]. This configuration is well suited for shaping the current profile of high-charge bunches since it does not use dipole magnets, and therefore, is not prone to deleterious effects arising from coherent synchrotron radiation. An intercepting mask located downstream of the first TDC, which introduce a spatiotemporal correlation, transversely shape the beam. Downstream of the second TDC, upon removal of the cross-plane correlation, the bunch is temporally shaped. In this paper, we investigate longitudinal bunch shaping with an X-band TDC powered by an X-band, short-pulse wakefield Power Extraction and Transfer Structure (PETS), where the wakefield from the drive beam propagating through the PETS is the power source. We describe the RF designs of the X-band TDC and the configuration of the overall shaping system. Finally, we explore via beam-dynamics simulations the performances of the proposed shaper and its possible application to various bunch shapes relevant to beam-driven acceleration and coherent radiation generation.

INTRODUCTION

Longitudinal bunch shaping demonstration has been actively investigated to achieve high-gradient accelerating field through structure or plasma-based accelerators and to improve the acceleration efficiency of the witness beam through those advanced accelerators. In particular, experimental demonstrations have been carried out to generate the electron beam where the longitudinal distribution is triangle, thus being used as a drive source in the wakefield accelerator, increasing the transformer ratio of the wakefield to be larger than 2 [1–3]. In order to increase the transformer ratio and high-gradient at the same time, drive beam charge should be increased further given that the beam energy is fixed [4].

For the manipulation of high-charge beam, we can consider well-developed beam manipulation techniques such as emittance exchange beamline [5–7], shaping of the laser [8], and energy-correlation-based shaping method [9–11]. However, those methods have limitations for the high-charge beam manipulation due to i) coherent synchrotron radiation (CSR) and ii) space charge force.

To overcome the limitations on the beam manipulation with high-charge beam, use of transverse-deflecting cavity (TDC) arises an alternative solution [12–15]. The TDC-based beamline is straight line; we do not need to consider the effects of the CSR. In addition, this shaping method is used where the beam to be shaped is relativistic. Therefore, we do not significantly consider the space charge effects.

In this paper, we will show the X-band TDC powered by Power Extractor and Transfer Structure (PETS) installed at the Argonne Wakefield Accelerator (AWA) facility. X-band TDC-based longitudinal bunch shaping system will also be shown. In addition, the bunch shaping results with mask, obtained by the particle tracking results, will be presented.

TDC-BASED SHAPING SYSTEM

A schematic view of the TDC-based shaping system is shown in Fig. 1. Note that this shaping method is based on

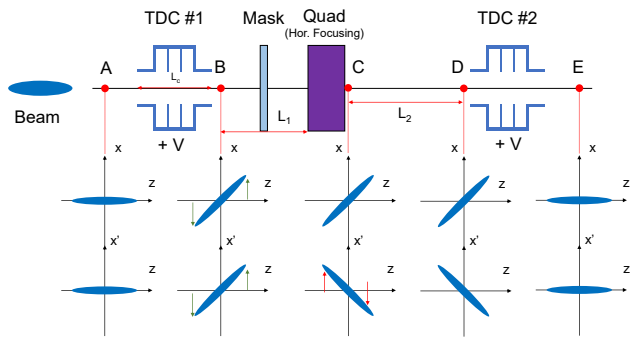

Figure 1: Schematic vewi of the TDC shaping system. Beam propagates from left to right. At different positions from *A* to *E*, electron beam phase spaces are shown.

preceding studies reported in Refs [12, 15]. It consists of two TDCs. In between TDCs, mask and quadrupole magnet are installed. From the position *A* to *E*, slice distribution $(z - x)$ and $(z - x')$ are shown. From *A*, as the beam propagates through the TDC, the beam is kicked in longitudinal plane, and *z*-slice information is projected into $(x - y)$ plane. Then, using the mask, the longitudinal distribution is tailored. The quadrupole magnet installed inside the system is to rotate the horizontal divergence, changing the angle of $(z - x')$

* Work supported by DoE SBIR Grant DE-SC0021733
† seongyeol.kim@anl.gov
‡ jingchg@anl.gov

ISBN: 978-3-95450-227-1 ISSN: 2673-5490 doi:10.18429/JACoW-IPAC2022-WEOZSP2

SUPPRESSION OF CRAB CAVITY NOISE INDUCED EMITTANCE GROWTH BY TRANSVERSE BEAM COUPLING IMPEDANCE*

N. Triantafyllou†, CERN, Geneva, Switzerland and also at University of Liverpool, Liverpool, UK
F. Antoniou, H. Bartosik, P. Baudrenghien, X. Buffat, R. Calaga, Y. Papaphilippou,
CERN, Geneva, Switzerland
T. Mastoridis, California Polytechnic State University, San Luis Obispo, US
A. Wolski, University of Liverpool, Liverpool, UK

Abstract

Crab cavities are a key component of the High Luminosity LHC (HL-LHC) upgrade, as they aim to mitigate the luminosity reduction induced by the crossing angle. Two superconducting crab cavities (CCs) were installed in the Super Proton Synchrotron (SPS) at CERN in 2018 to demonstrate their operation in a proton machine for the first time. An important point to consider is the transverse emittance growth induced by noise in the CC RF system. During a first experimental campaign in 2018, the measured emittance growth was found to be a factor of 4 lower than predicted by analytical models. In this paper, the effects of transverse beam coupling impedance on emittance growth driven by CC RF noise are presented and the results of the second experimental campaign, which took place in the SPS in 2022, are discussed.

INTRODUCTION

Crab cavities (CC's) are key components for achieving the luminosity goals in HL-LHC, in particular to optimize the luminous region in the detectors [1]. Transverse emittance growth due to noise in the CC RF system [1]is a concern, as it degrades luminosity [3]. In order to define the specifications for acceptable noise levels for the design of the HL-LHC CC RF system, an analytical formula predicting the transverse emittance growth caused by such noise has been derived and validated through HEADTAIL simulations [4]. However, to gain confidence in the validity of the theoretical model benchmark against experimental data was deemed necessary.

During a dedicated experiment that took place in the SPS in 2018 with the prototype CCs, the measured emittance growth was found to be a factor four (on average) lower than expected from the theory [5]. The reason for this discrepancy remained unresolved for some time, as detailed studies excluded the possibility that the discrepancy is a result of some error in the analysis of the experimental data or the actual level of noise in the CCs.

It was recently found that the transverse beam coupling impedance, which is not included in the above mentioned theory, may impact the noise-induced emittance growth and may therefore explain the experimental observations. In particular, PyHEADTAIL [6] simulations including the accurate SPS impedance model [7] demonstrated that the noise-induced emittance growth is suppressed by about a factor four for the experimental machine conditions [5]. In this paper, the damping mechanism from the transverse impedance is discussed and the measurements that took place in 2022 in the SPS aiming to validate the impedance as the source of the discrepancy are presented.

EMITTANCE GROWTH FROM CRAB CAVITY NOISE AND SUPPRESSION FROM BEAM COUPLING IMPEDANCE

Amplitude and phase noise in the CCs result in emittance growth through decoherence. The noise generates momentum kicks which drive betatron oscillations of the particles. If the noise spectrum overlaps with the betatron tune distribution, the betatron oscillations can reach large amplitudes which translate the oscillations to emittance growth [4, 8].

The impact of CC amplitude and phase noise to bunch motion can be different. In particular, the momentum kicks from amplitude noise are out of phase by 90° from the phase noise kicks [4]. Given that in its usual operational mode the CC RF wave has its zero crossing at the longitudinal bunch center, amplitude noise kicks the head and the tail of the bunch in opposite transverse directions, resulting in intra-bunch (head-tail) oscillations. On the other hand, the phase noise induces mostly a centroid shift of the bunch, corresponding to a dipole mode, in which the transverse oscillations at each point along the bunch are in phase.

Emittance growth suppression mechanism

PyHEADTAIL simulations including the SPS impedance model [7] revealed that decoherence of the dipole oscillations and thus the phase-noise-induced emittance growth is suppressed once the coherent betatron tune is shifted outside of the incoherent tune spectrum. A similar effect of decoherence suppression was studied in the past [9–12] in the context of beam-beam modes. It was shown that when the coherent tune is outside the incoherent spectrum only part of the energy from the noise kick drives incoherent motion, resulting in irreversible emittance growth, while the rest of the energy from the noise kick is absorbed by the coherent mode, which can be damped. By separating the coherent and incoherent tunes, transverse impedance leads to an effective suppression of phase-noise-induced emittance

* Work supported by the HL-LHC project and partially by the U.S. Department of Energy, Office of Science, Office of High Energy Physics, under Award Number DE-SC-0019287
† natalia.triantafyllou@cern.ch
[1] Past studies with CC RF noise performed in KEKB with leptons can be found in Ref. [2].

ISBN: 978-3-95450-227-1 ISSN: 2673-5490 doi:10.18429/JACoW-IPAC2022-WEOZSP3

MEASUREMENTS OF RADIATION FIELDS FROM A CERAMIC BREAK

Y. Shobuda, T. Toyama, M. Yoshimoto, S. Hatakeyama
J-PARC Center, JAEA/KEK, Ibaraki, Japan

Abstract

Ceramic breaks are used in synchrotrons for many purposes. For example, they are inserted between the Multi-Wire Profile Monitor (MWPM) on the injection line at the Rapid Cycling Synchrotron (RCS) in J-PARC to completely prevent the wall currents accompanying beams from affecting the MWPM. On the other hand, from the viewpoint of suppressing beam impedances and the radiation fields from the ceramic breaks, it would be preferable that the inner surface of the ceramic break is coated with Titanium Nitride (TiN), or covered over capacitors. In this report, we measure the radiation fields from the ceramic break with and without capacitors as well as the beam profile and investigate the effect of the ceramic breaks on the measurements.

INTRODUCTION

The RCS in J-PARC [1] has been realizing the high-intensity beams [2–4] by accumulating H^- injection beams from the LINAC. During the injection painting process [5], the H^- beams are transformed into the proton beams after being hit on the foil at the injection point. When two bunched beams, each containing 4.15×10^{13} particles per bunch, are accelerated from 400 MeV to 3 GeV at a repetition rate of 25 Hz, a 1 MW beam can be performed at the RCS.

Precise adjustment of the injection beams on the phase space area during the painting process is important to realize the high intensity beams with low beam loss rate. Hence, seven MWPMs [6] are installed, where MWPM1 is on the injection line to the RCS, MWPM2-5 are on the merging area in the RCS, and MWPM6-7 are on the dump line to measure the unstripped H^- beams. Based on the design concept of RCS, MWPM1 is sandwiched by two ceramic breaks to completely prevent the wall currents with H^- beams from interfering with the measurements with MWPM1 (see Fig. 1).

On the other hand, suppressing beam coupling impedances [7, 8] is a critical issue to accomplish high intensity beams. Since the impedance of ceramic breaks is closely related to the radiations from the ceramic break [9–13], covering capacitors on the ceramic breaks is an effective way to suppress both the impedance and radiations from the ceramic breaks. Therefore, it is important to directly measure the radiations from several types of ceramic break, and investigate the effects of ceramic breaks on the monitors.

The MWPM1 and the ceramic breaks next to it are good tools because the residual dose around there is kept below at most ten micro-sievert per hour even after 4 hours of 830 kW beam operation stop of the RCS. In this report, we measure the radiations from 15 mm long ceramic break with 101 mm inner and 111 mm outer radii beside MWPM1 by which the transverse beam profile is measured under several conditions, after test-measuring the magnetic field in the electromagnetic anechoic chamber in JAXA [14].

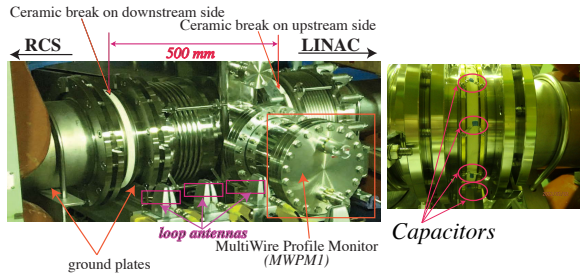

Figure 1: MWPM1 and the ceramic breaks without (left) and with capacitors (right).

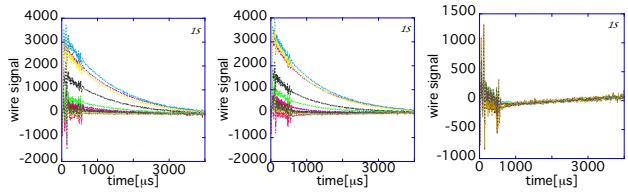

Figure 2: Signals if the ceramic break is covered by capacitors (left), or by Al with (center) and without beams (right).

MEASUREMENTS OF THE TRANSVERSE BEAM PROFILE

MWPM1 consisting of 27 wires measures the transverse beam profile in u and v axes, which are tilted 45° from the horizontal and vertical axes. Each wire moves 0.1 mm/s filling the intervals of respective wires, while 100 LINAC beams pass there with a 1 Hz repetition rate [6]. The integration of respective wire signals over 4 ms after being excited by a hit of the beam provides the beam density at the wire positions, so that a smooth bunch distribution is obtained after 100 LINAC beam shots.

Here, let us cover the ceramic break on the downstream side by twelve 1μF capacitors [15] with 2 MHz resonant frequency or by Aluminum (Al) sheet to investigate the effects on the beam profiles. The measured 27 wire signals are shown in Fig. 2. We can identify the noise from 0 to 0.7 ms in both cases (left/center). Though the capacitors are expected to suppress the low-frequency components of currents, high-frequency components contribute to the noise. This is a systematic error by the trapezoid bump magnets [16] at the injection area on the RCS rather than the wall currents with beams because it is excited even in the case without beams (see the right). As a result, it can be eliminated in principle to produce the smooth beam profiles.

ISBN: 978-3-95450-227-1 ISSN: 2673-5490 doi:10.18429/JACoW-IPAC2022-WEOZSP4

FULL COUPLING STUDIES AT ALBA

Z.Martí*, G.Benedetti, M.Carlà, U.Iriso, and L.Torino
ALBA-CELLS Synchrotron, Cerdanyola del Vallès, Spain

Abstract

As other low emittance machine upgrades ALBA-II proposal considers operating in full coupling. In such configuration the horizontal emittance is further reduced while the lifetime is increased at the price of working close to equal fractional tunes. This mode of operation has not been adopted by any existing light source to date, and it presents a few disadvantages, like the optics degradation, injection efficiency reduction and beam size stability. In this paper the above mentioned difficulties are studied for the present ALBA storage ring in full coupling conditions.

INTRODUCTION

To ensure a proper beam lifetime, several future low emittance light sources designs [1–4] rely on the ability to operate on or next to the coupling resonance $Q_x = Q_y + n$, where $Q_{x,y}$ are the horizontal and vertical tunes and n is an integer. Such constraint on the working point is not used on the operation of existing light sources, which has triggered several studies in such working conditions [5–7]. The injection schemes, the physical apertures aspect ratio and the non-linear strength of future low emittance light sources differ substantially from present machines. The experience in present light sources in full coupling can not be extrapolated directly, however achieving a good agreement with simulations is a first step towards relaying on this type of operation.

Working in full coupling changes the constraints given by the collective effects. Up to now, for the ALBA case we have found that such changes are mostly beneficial.

Other groups [8, 9] have studied the possibility to generate the same full coupling effects in terms of lifetime gain and horizontal emittance reduction without the considerable optics design constraint of the coupling resonance condition. In that case an AC skew quadrupolar field excited at a $Q_x - Q_y$ frequency is used. Some first tests have been performed in the present ALBA machine in order to check our understanding of such technique and in the future this possibility will be further explored for the ALBA-II design.

None of the above is used in present light-sources, instead, in the case of the EBS, a vertical dipolar white noise excitation has been successfully used in operation [10].

LATTICE CONFIGURATIONS

Full coupling operation of future low emittance lattices requires an optimization of the coupling strength $|C_0|$ [11]. On one side, a larger C_0 implies a wider coupling resonance, and so a more stable machine operation (against power supply noise, insertion device errors, etc). On the other hand, near the resonance a high coupling strength produces an optics distortion which potentially translates to worse dynamical aperture and injection efficiency.

Our simulations for ALBA-II indicate that the optics correction near the coupling resonance requires also tuning the skew quadrupole correctors. Therefore, the distribution of the skew quadrupole strengths should be a key issue. In this first work we have not studied that in detail.

When setting up the full coupling lattice, the optics was first corrected with LOCO [12] without applying any skew quadupole change. Based on that same normal quadrupole settings, the measurements described in the next sections have been carried out for three different skew quadupole configurations:

- corrected: LOCO based skew quadrupoles (applied after two iterations);
- not corrected: no skew quadrupoles applied with;
- anti corrected: LOCO based skew quadrupoles applied with opposite polarity.

Each of the configurations was later analyzed with a LOCO measurement. Here the coupling strength has been calculated using the analytical formula described in [11]. The optics degradation in terms of beta beating is between 2.5% and 5.7% which we think should have no major effects on the measurements.

COUPLING MEASUREMENT

The global coupling in a ring is typically defined as the emittance ratio $k = \epsilon_y/\epsilon_x$ which in this case is measured in two different methods:

- from the emittance ratio at the pinhole locations;
- from the turn by turn (TbT) action transfer ratio at the beam position monitors (BPM).

The first method consists in calculating the emittance from the measured beam sizes $\sigma_{x,y}$ at the pinhole cameras, the modelled optical functions (obtained via a LOCO measurement) $\beta_{x,y}$ and $\eta_{x,y}$ and the modelled energy spread σ_δ:

$$\epsilon_{x,y} = \frac{\sigma_{x,y}^2 - (\sigma_\delta \eta_{x,y})^2}{\beta_{x,y}}. \quad (1)$$

The second method is described in [13]. In this case the TbT BPM readings after a pinger kick are analyzed via Fourier decomposition. The two main spectral lines (the horizontal and vertical tunes, as here we assume no other relevant lines) amplitudes a_1 and a_2 determine the action transfer. The amplitude squared a^2 (proportional to the action) along the turns n can be expressed as:

$$a^2 = a_1^2 + a_2^2 + 2a_1a_2\cos\left((Q_1 - Q_2)2\pi n + \mu_1 - \mu_2\right), \quad (2)$$

* zeus@cells.es

ISBN: 978-3-95450-227-1 ISSN: 2673-5490 doi:10.18429/JACoW-IPAC2022-WEPOST001

RADIATION LOAD STUDIES FOR SUPERCONDUCTING MAGNETS IN A 10 TeV MUON COLLIDER

D. Calzolari*, B. Humann, C. Carli, A. Lechner, G. Lerner, F. Salvat-Pujol, D. Schulte, K. Skoufaris
CERN, Geneva, Switzerland

Abstract

Among the various future lepton colliders under study, muon colliders offer the prospect of reaching the highest collision energies. Despite the promising potential of a multi-TeV muon collider, the short lifetime of muons poses a severe technological challenge for the collider design. In particular, the copious production of decay electrons and positrons along the collider ring requires the integration of continuous radiation absorbers inside superconducting magnets. The absorbers are needed to avoid quenches, reduce the heat dissipation in the cold mass and prevent magnet failures due to long-term radiation damage. In this paper, we present FLUKA shower simulations assessing the shielding requirements for high-field magnets of a 10 TeV muon collider. We quantify in particular the role of synchrotron photon emission by decay electrons and positrons, which helps in dispersing the energy carried by the decay products. For comparison, selected results for a 3 TeV muon collider are also presented.

INTRODUCTION

Circular muon colliders offer the prospect of reaching significantly higher center-of-mass energies than electron-positron colliders, since the latter option is limited by the synchrotron radiation emission. The design of muon colliders is, however, less mature and involves various technical challenges [1]. The recently formed International Muon Collider Collaboration [2] aims to address key design questions for a multi-TeV collider, with a center-of-mass energy $\sqrt{s}$ of 10 TeV or even higher. Despite the Lorentz boost, multi-TeV muons still have a relatively short mean lifetime in the laboratory frame 0.1 s for $\sqrt{s}$=10 TeV and hence they rapidly decay while circulating in the collider ring. The decay electrons and positrons carry on average around one third of the muon energy, while the rest escapes in the form of neutrinos. Contrary to e^-/e^+ colliders, where the heat load is from synchrotron radiation from the primary beam, in the muon collider case it is arising from secondary particles generated by the decay. The resulting power dissipated by those amounts to several 100 W per meter [2]. This poses a significant challenge for the collider design due to the instantaneous heat deposition and cumulative radiation damage in the collider equipment. To sustain the radiation load, superconducting magnets need to be protected with a continuous absorber. The absorber must fulfil different purposes, as preventing beam-induced quenches, reducing the thermal load to the cryogenic system, and avoiding magnet failures due to the cumulative dose in insulators and atomic displacements in superconductors [3].

Radiation load studies for muon collider magnets have been previously carried out in the scope of the US Muon Accelerator Program (MAP) [4]. These studies [5–10] focused, however, on lower center-of-mass energies $\sqrt{s}$=0.125-4 TeV. In this paper, we present a first generic shielding assessment for the arc magnets of a higher-energy collider with a center-of-mass energy of $\sqrt{s}$=10 TeV. For comparison, we also show results for a $\sqrt{s}$=3 TeV machine. The studies were carried out with the FLUKA particle shower code [11–13], which is the standard code at CERN for accelerator shielding applications. The beam parameters considered in this paper (see Table 1) have been scaled from the design parameters previously adopted by the MAP collaboration. The collider design foresees two counter-rotating muon bunches of opposite charge, which share the same vacuum chamber. To reach the desired design luminosity, new bunches need to be injected multiple times per second. We assume that bunches are injected with a frequency of 5 Hz and that all injected muons decay in the collider ring. This assumption is justified since the luminosity burn-off in the collision point is small compared to the number of decays. We also neglect possible beam halo losses on the aperture.

SIMULATION MODEL

To derive general conclusions, we do not consider a specific arc lattice, but we model a generic string of dipoles, with magnetic fields of 7 T and 10.4 T for the 3 TeV and 10 TeV machines, respectively. The power dissipated by decay electrons and positrons per unit length is comparable in both colliders (about 500 W/m) due to the different ring circumferences. Previous shielding studies for muon colliders considered different magnet design options, including open mid-plane dipoles, where the decay products impact on an absorber located at a larger radius than the coils [5–7]. This design has some advantages in terms of heat load management, but adds some complexity to the magnet design.

Table 1: Parameters

	$\sqrt{s}$=3 TeV	$\sqrt{s}$=10 TeV
Beam energy	1.5 TeV	5 TeV
Bunch intensity	2.2×10^{12}	1.8×10^{12}
Number of bunches	1	1
Injection frequency	5 Hz	5 Hz
Circumference	4.5 km	10 km
Arc dipole strength	7 T	10.4 T
Power lost in e^+/e^- per beam	400 W/m	500 W/m

* daniele.calzolari@cern.ch

ISBN: 978-3-95450-227-1 ISSN: 2673-5490 doi:10.18429/JACoW-IPAC2022-WEPOST002

SYNCHROTRON RADIATION IMPACT ON THE FCC-ee ARCS

B. Humann*[1], F. Cerutti, R. Kersevan, CERN, Geneva, Switzerland
[1]also at TU Wien, Vienna, Austria

Abstract

Synchrotron radiation (SR) emitted by electron and positron beams represents a major loss source in high energy circular colliders, such as the lepton version of the Future Circular Collider (FCC-ee) at CERN. In particular, for the operation mode at 182.5 GeV (above the top pair threshold), its spectrum makes it penetrate well beyond the vacuum chamber walls. In order to optimize its containment, dedicated absorbers are envisaged. In this contribution we report the energy deposition studies performed with FLUKA to assess heat load, time-integrated dose and particle fluence distribution in the machine components and the surrounding environment. Different choices for the absorber material were considered and shielding options for electronics were investigated. Furthermore, possible positions for the booster ring were reviewed from the radiation exposure point of view.

INTRODUCTION

The lepton machine of Future Circular Collider (FCC-ee) is one option for a future accelerator at CERN. With a circumference of around 91 km, it is meant to collide electrons and positrons at four different energies ranging from 45.6 GeV (Z mode) to 182.5 GeV (ttbar mode) [1]. In a lepton machine, synchrotron radiation (SR) is a major source of beam energy loss impacting the accelerator. Therefore, it is necessary to assess its effects on the magnets and the tunnel environment. These studies are performed with FLUKA [2–4], a Monte Carlo particle transport and interaction code, with which the energy deposition caused by the SR in the FCC-ee collider arcs was simulated.

SR is electromagnetic radiation emitted tangentially by charged particles that follow a curved trajectory. The energy loss per turn, ΔE, is given as

$$\Delta E = \frac{e^2}{3\varepsilon_0 (m_0 c^2)^4} \frac{E^4}{\rho}, \quad (1)$$

indicating the high impact of SR in electron and positron colliders due to the small rest mass, m_0, of these particles. In Eq. 1, e is the elementary electric charge, ε_0 the vacuum permittivity, E the energy of the circulating particles and ρ is the bending radius, equal to 10.76 km for the FCC-ee machine [5]. This leads to $\Delta E_{182.5\,\mathrm{GeV}} = 9.2\,\mathrm{GeV/turn}$ and $\Delta E_{45.6\,\mathrm{GeV}} = 0.036\,\mathrm{GeV/turn}$. The critical energy E_C is defined as splitting the emitted photon spectrum in two equal parts in terms of integrated power [6]. Its expression

$$E_C = \frac{3}{2}\hbar c \frac{\gamma^3}{\rho} \approx 2.21 \cdot 10^{-6} \frac{E^3[GeV]}{\rho[km]}[MeV] \quad (2)$$

yields $E_C^{182.5\,\mathrm{GeV}} = 1.25\,\mathrm{MeV}$, being γ the relativistic Lorentz factor. For the operation mode at 45.6 GeV, where the energy is a factor 4 lower, the critical energy is $E_C^{45.6\,\mathrm{GeV}} = 19\,\mathrm{keV}$. Figure 1 shows the SR photon spectra for the two extreme energies of colliding beams in FCC-ee, emphasising the very different penetration capacity of the emitted radiation, which in the Z mode is fully absorbed by the vacuum chamber walls.

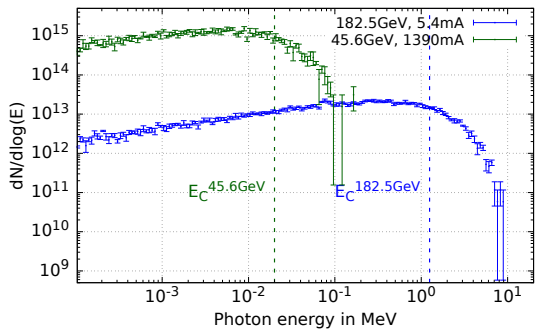

Figure 1: SR spectra for the 45.6 GeV and 182.5 GeV FCC-ee operation modes, as generated by FLUKA. Their integral gives the amount of photons emitted by the electron/positron beam over 1 cm.

By design, the SR power shall be constant for all operation modes and amount to 50 MW per beam. This implies a current of 5.4 mA for the highest operation energy and 1390 mA for the lowest one.

SIMULATION SETUP

For this study, a representative 140 m long periodic cell of the FCC-ee arc was simulated, as displayed in Fig. 2. It consists of 5 dipoles (MB), 5 quadrupoles (MQ) and 4 sextupoles (MS), that are held at room temperature. Two dipoles have a length of 21 m and the other three are 24 m long. The MQs have a length of 3 m and the MSs, that are placed in pairs before the first two MQs (according to the clockwise direction), have a length of 1.3 m. The MB and MQ geometries are based on the technical drawings of the already existing prototypes [1], while the MS model was extracted from an early stage sketch.

Three different SR shielding options are investigated. The main focus is on the shielding performed with dedicated photon absorbers. In total, 25 absorbers per beam with a length of 30 cm each are placed every 5-6 m inside the MB and MQ vacuum chamber, in order to prevent the latter from being directly impacted by the SR. They are made of a CuCrZr alloy, which has good absorption and mechanical properties. In the following, they are referred to as "copper absorbers". As an alternative, absorbers made out of a tungsten alloy

* barbara.humann@cern.ch

ISBN: 978-3-95450-227-1 ISSN: 2673-5490 doi:10.18429/JACoW-IPAC2022-WEPOST003

IMPLICATIONS OF THE UPGRADE II OF LHCb ON THE LHC INSERTION REGION 8: FROM ENERGY DEPOSITION STUDIES TO MITIGATION STRATEGIES

A. Ciccotelli[1]*, F. Cerutti, F. Butin, L. S. Esposito, B. Humann[2]
M. Wehrle, CERN, Geneva, Switzerland
R. B. Appleby, University of Manchester, Manchester, United Kingdom
[1]also at University of Manchester, Manchester, United Kingdom
[2]also at Wien University of Technology, Vienna, Austria

Abstract

Starting from LHC Run 3, a first upgrade of the LHCb experiment (Upgrade I) will enable operation with a significantly increased instantaneous luminosity in the LHC Insertion Region 8 (IR8), up to $2 \cdot 10^{33}\,\mathrm{cm^{-2}\,s^{-1}}$. Moreover, the proposed second upgrade of the LHCb experiment (Upgrade II) aims at increasing it by an extra factor 7.5 (up to $1.5 \cdot 10^{34}\,\mathrm{cm^{-2}\,s^{-1}}$, as of Run 5) and collecting an integrated luminosity of $400\,\mathrm{fb^{-1}}$ by the end of Run 6. Such an ambitious goal poses challenges not only for the detector but also for the accelerator components. Monte Carlo simulations represent a valuable tool to predict the implications of the radiation impact on the machine, especially for future operational scenarios. A detailed IR8 model implemented by means of the FLUKA code is presented in this study. With such a model, we calculated the power density and dose distributions in the superconducting coils of the LHC final focusing quadrupoles (Q1-Q3) and separation dipole (D1) and we highlight a few critical issues calling for mitigation measures. Our study addresses also the recombination dipole (D2) and the suitability of the present TANB absorber, as well as the proton losses in the Dispersion Suppressor and their implications.

INTRODUCTION

The High Luminosity LHC (HL-LHC) is meant to extend the physics discovery potential of the LHC experiments in the next two decades, reaching a proton–proton integrated luminosity of 3000 to $4000\,\mathrm{fb^{-1}}$ in the ATLAS and CMS detectors [1]. The LHCb experiment, placed in the Insertion Region 8 (IR8), was originally designed to operate at a lower luminosity ($2 \cdot 10^{32}\,\mathrm{cm^{-2}\,s^{-1}}$) with respect to the two general purpose LHC experiments and looks to explore complementary physics to ATLAS and CMS [2]. The LHCb detector is a single arm forward detector placed close to the vacuum chamber. The LHCb maximum luminosity was limited on purpose to guarantee the primary vertex detection. Recently, a first upgrade (LHCb Upgrade I) has been implemented during the Long Shutdown 2 (LS2 from December 2018 to mid-2022) enabling operation with a significantly increased instantaneous luminosity of up to $2 \cdot 10^{33}\,\mathrm{cm^{-2}\,s^{-1}}$. Nevertheless, the Upgrade I does not fulfil the ultimate precision goals for many key observables, as described in [3], and therefore, a second upgrade of the LHCb experiment (Upgrade II), proposed for installation in LS4, aims to reach a 7.5 times higher instantaneous luminosity ($1.5 \cdot 10^{34}\,\mathrm{cm^{-2}\,s^{-1}}$) to collect an integrated luminosity of $400\,\mathrm{fb^{-1}}$ by the end of the HL-LHC era. Such an ambitious goal poses challenges not only for the detector but also from the point of view of the sustainability and safety of the LHC. The key points are related to the absence of the protection elements installed instead in IR1 (ATLAS) and IR5 (CMS), and considered so far unnecessary in IR8 due to the lower peak luminosity, e.g. TAS and TAN absorbers and TCL collimators [4]. The objective of this study is to provide an overview of the main challenges associated to the Upgrade II, concerning the potential radiation induced degradation of LHC magnets, the possibility to operate the superconducting ones without recurrent occurrence of quenches (i.e. transition to the normal conducting state due to radiation heat), and the increased heat load on the cryogenic system. Consequent mitigation measures are introduced.

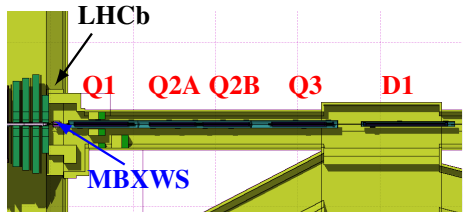

Figure 1: 3D top view of the FLUKA geometry including the muon detector of the LHCb detector (on the left) and the LHC final focusing triplet quadrupoles (Q1-Q2A-Q2B-Q3) and separation dipole (D1). The short warm dipole compensator (MBXWS) is also indicated.

THE FLUKA MODEL OF IR8

A detailed IR8 model implemented by means of the FLUKA code [5–7] is used in this study. The accelerator section has been assembled using a dedicated Python-based tool, called Linebuilder [8]. In addition to the lattice elements, the model of IR8 features the detector, the experimental cavern and the LHC tunnel, including service tunnels and alcoves. Figure 1 shows the geometry layout on the right side of the Interaction Point 8 (IP8). The presence of the LHCb dipole produces a deflection of the circulating beam on the horizontal plane. This magnet is designed to operate with two

* alessia.ciccotelli@cern.ch

ISBN: 978-3-95450-227-1 ISSN: 2673-5490 doi:10.18429/JACoW-IPAC2022-WEPOST007

CENTRE-OF-MASS ENERGY IN FCC-ee

J. Keintzel*, A. Blondel, D. Shatilov†, T.H.B. Persson, R. Tomás, F. Zimmermann
CERN, Geneva 23, Switzerland

Abstract

The Future Circular electron-positron Collider (FCC-ee) is designed for high precision particle physics experiments. This demands a precise knowledge of the beam energies, obtained by resonant depolarization, and from which the center-of-mass energy and possible boosts at all interaction points are then determined. At the highest beam energy mode of 182.5 GeV, the energy loss due to synchrotron radiation is about 10 GeV per revolution. Hence, not only the location of the RF cavities, but also a precise control of the optics and understanding of beam dynamics, are crucial. In the studies presented here, different possible locations of the RF-cavities are considered, when calculating the beam energies over the machine circumference, including energy losses from crossing angles, a non-homogeneous dipole distribution, and an estimate of the beamstrahlung effect at the collision point.

INTRODUCTION

The Large Hadron Collider (LHC) [1] with 27 km circumference is presently the world's largest particle collider and has reached an instantaneous luminosity of about 2×10^{34} cm^{-2}s^{-1}. Its luminosity upgrade, the High Luminosity LHC (HL-LHC) [2] aiming at levelling the luminosity around 5×10^{34} cm^{-2}s^{-1}, will be commissioned in 2029 and is planned to be operating until the 2040s.

Following on from the HL-LHC, a sequence of one possible future lepton and one hadron collider is studied within the framework of the Future Circular Collider (FCC) Feasibility Study, launched by CERN Council in 2021. The FCC integrated project [3] foresees first the construction of an approximately 100 km tunnel incorporating the lepton collider FCC-ee [4]. In a second stage this is followed by a hadron collider, FCC-hh [5]. The FCC-ee is an electroweak, Higgs and top factory, and is set to operate at four distinct energy stages of 45.6, 80, 120 and 170-185.5 GeV, allowing for precision measurements of the Z-, W-, and Higgs-bosons, and the top quark, respectively.

One major change with respect to the CDR design with 12 insertion regions and 2 interaction points (IPs), is that the present baseline features a 4-fold symmetry and 4-fold super-periodicity, and foresees only 8 insertion regions and surface sites (PA, PB, PD, PF, PG, PH, PJ, PL) connected by arcs, with 4 IPs (PA, PD, PG, PJ), and a total circumference of 91 km [6]. A schematic layout of the current FCC-ee layout is shown in Fig. 1. The lepton bunches are injected from the booster at nominal energy into the main rings (top-up injection). RF-cavities are installed in the collider straight sections without an IP, and are compensating for all energy losses, primarily from synchrotron radiation (SR), but also from beamstrahlung and others. For example, at the top-energy about 5 % of the beam energy is lost within one revolution due to SR. Recent preliminary civil engineering studies [7] suggest that PH and PL are the most favorable ones for hosting an RF-system, with PF possibly another, more difficult option. For the data taking around the Z-pole and the W-pair threshold, only one RF-section is used, providing almost equal centre-of-mass (ECM) energies in all interaction points. At $\mathrm{t\bar{t}}$ threshold, two RF-sections are necessary, and thus different RF configurations are considered in this work.

Since the FCC-ee is designed for high-precision physics experiments, the exact knowledge of the ECM and the collision energy boost at all interaction points is demanded. Various factors impact the ECM, such as the placement and number of the RF-sections, energy losses, non-zero dispersion, chromatic β-functions, optics errors, orbit offsets, or beam-beam effects [8]. First results of the ECM and the boosts at all interaction points for the newest FCC-ee lattices are presented here, taking into account SR and beamstrahlung losses. Other contributions are not considered and will need to be evaluated carefully in future studies.

The simulations presented in the following are performed for the Z- and the $\mathrm{t\bar{t}}$-lattices. At $\mathrm{t\bar{t}}$ the beam energy is about 3 times higher than for the initial stage, implying a significant energy loss per turn due to SR. Operation with transversely polarised pilot bunches for precise (10-100 keV) beam energy calibration, using the technique of resonant depolarisation, is envisaged for Z-pole and W-pair operation. At

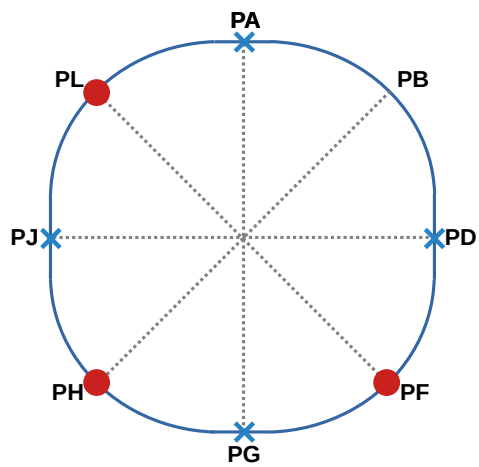

Figure 1: Schematic FCC-ee layout with eight insertion regions. The four IPs are marked with a blue cross. Points suitable to host a RF-system are marked with a red dot.

* jacqueline.keintzel@cern.ch
† on leave from BINP, Novosibirsk, Russia

ISBN: 978-3-95450-227-1 ISSN: 2673-5490 doi:10.18429/JACoW-IPAC2022-WEPOST008

OPTICS CORRECTION STRATEGY FOR RUN 3 OF THE LHC

T. Persson, F. Carlier, A. Costa Ojeda, J. Dilly, H. García Morales, V. Ferrentino, E. Fol, M. Hofer, E.J Høydalsvik, J. Keintzel, M. Le Garrec, E.H. Maclean, L. Malina, F. Soubelet, R. Tomás, L. Van Riesen-Haupt and A. Wegscheider, CERN, Geneva, Switzerland
J. Cardona, Universidad Nacional de Colombia

Abstract

After more than 3 years of shutdown the LHC is again operational in 2022. Experience from the previous Long Shutdown (LS) has shown that the local errors in the triplet quadrupoles changed significantly between Run 1 and Run 2, and first measurements in 2022 unveil further changes. In the LHC, feed-down from the Interaction Region (IR) non-linear corrections to linear errors requires an iterative approach between the two types of corrections. In this article we describe the key measurements and corrections performed in 2021 and 2022 until the write-up of this report.

INTRODUCTION

The Run 3 presents a new set of challenges for the optics commissioning. Run 2 was started with a moderate β^* of 80 cm and it was then reduced in yearly steps [1, 2]. This gave time to optimize the corrections iteratively as well as focusing on the linear optics in the first 2 years, shifting the focus to the nonlinear IR contributions in the rest of the run. Another challenge is the increase of the range in the operational β^* for physics [3], requiring accurate corrections for a larger number of optics. Run 3 optics features the largest telescopic squeeze factor [4] used in operation so far, implying the largest arc β functions and the consequent enhancement of arc optics errors. The Run 3 energy has been increased from 6.5 TeV in Run 2 to 6.8 TeV which could have some consequences for the magnetic field quality.

In 2021 a dedicated beam test took place at injection energy. This period allowed to measure and correct the optics at injection. In this article we outline the linear measurements at injection and give a snapshot of the status of the LHC commissioning to date. A full picture is unfortunately not available since the LHC commissioning is still ongoing.

INJECTION

The first measurement of the injection optics, during the beam test, revealed a surprisingly large β-beating compared to what was measured in Run 2. This triggered some investigations and the optics error was localised using the Segment-by-Segment (SbS) technique [5] to come from the RQTL7.R3 quadrupole. Its Beam 1 and Beam 2 powering was swapped as also found in 2008 [5]. This swap was accidentally re-introduced during the Long Shutdown 2. A change on the software side fixed the issue within hours restoring global β-beating to the same level as in Run 2. A global optics correction reduced peak β-beating to about 10% which is well within the requirements for machine protection. The measured β-beating before and after correction is shown in Fig. 1.

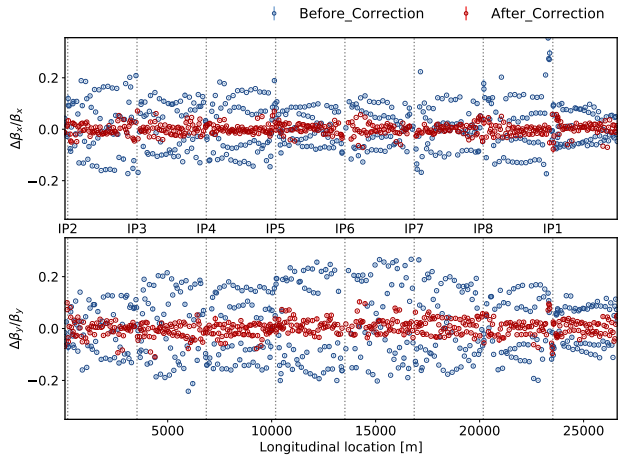

Figure 1: β-beating at injection before and after global corrections for the LHC Beam 1 in the 2021 beam test.

The optics was also re-measured in 2022 with the same global corrections and even though a small degradation of a few percent was observed in the peak β-beating it was still acceptable for operation.

FIRST OPTICS MEASUREMENTS AT 6.8 TEV

In order to determine the Interaction Region local corrections the optics was squeezed down to β^* = 30 cm without any optics corrections. This is the smallest β^* ever reached in the LHC without triplet corrections. The measurement revealed a peak β-beating of around 150% which is also the highest ever measured in the LHC. The usual procedure to compute local IR corrections was followed. It consists of taking turn-by-turn data with the AC-dipole [6] and performing K-modulation for the most inner quadrupole (Q1) left and right of IP1 and IP5 [7]. The local corrections calculated in Run 2 were all based on the SbS technique [5, 8]. In Run 3 two additional methods based on Action-Phase-Jump (APJ) [9–12] and Machine Learning (ML) [13–15] were used. The SbS and APJ techniques are using both the AC-dipole turn-by-turn data and the results from the K-modulation while the ML currently only uses the Turn-by-Turn (TbT) data. The three different methods performed well but the ML was less local in the correction and therefore the choice was then between the SbS and APJ. Even though the corrections are different in strength, see Tab. 1, they had almost identical impact on both the phase and the

ISBN: 978-3-95450-227-1 ISSN: 2673-5490 doi:10.18429/JACoW-IPAC2022-WEPOST009

MUON COLLIDER BASED ON GAMMA FACTORY, FCC-ee AND PLASMA TARGET *

J. Farmer, A. Latina, F. Zimmermann†, CERN, Meyrin, Switzerland
A.P. Blondel, U. Geneva, Geneva, Switzerland
M. Antonelli, M. Boscolo, INFN-LNF, Frascati, Italy

Abstract

The LEMMA-type muon collider generates muon pairs by the annihilation of 45 GeV positrons with electrons at rest. Due to the small cross section, an extremely high rate of positrons is required, which could be achieved by a "Gamma factory" based on the LHC. Other challenges with the LEMMA-type muon production scheme include the emittance preservation of muons and muon-generating positrons upon multiple traversals through a target, and the merging of many separate muon bunchlets. These two challenges may potentially be overcome by (1) operating the FCC-ee booster with a barrier bucket and induction acceleration, so that all positrons of a production cycle are merged into one single superbunch, instead of storing ~10,000 separate bunches; and (2) sending the positron superbunch into a plasma target. During the passage of the positron superbunch, the electron density is enhanced more than 1000-fold without any increase in the density of nuclei, so that beamstrahlung and Coulomb scattering are essentially absent. We investigate prospects and difficulties of this approach, including emittance growth due to filamentation in the nonlinear plasma channel and due to positron self-modulation.

INTRODUCTION

The LEMMA scheme for a muon collider is based on the annihilation of positrons with electrons at rest [1]. The cross section for continuum muon pair production $e^+e^- \to \mu^+\mu^-$ has a maximum value of about 1 μb at a centre-of-mass energy of ~0.230 GeV, which corresponds to a e^+ beam energy of about 45 GeV, exactly as required for the FCC-ee operating at TeraZ factory and provided by the FCC-ee full-energy booster [2, 3].

MUON PRODUCTION BASED ON FCC-ee

Challenges with the LEMMA-type muon production scheme relate to the emittance preservation of muons and muon-generating positrons upon multiple traversals through a target, and the merging of many separate muon bunchlets, due to production by many separate e^+ bunches and numerous e^+ bunch passages [4].

These challenges may potentially be overcome by:

(1) Operating the FCC-ee booster with a barrier bucket and induction acceleration, so that all positrons of a cycle are merged into one single superbunch, instead of ~ 10,000 separate bunches.

(2) Sending the positron superbunch from the booster into a plasma target, where, during the passage of the e^+ superbunch, the electron density is enhanced more than 1000 fold without any significant density of nuclei, hence beamstrahlung and Coulomb scattering essentially absent.

POSITRON SUPERBUNCH

As described in the FCC-ee Conceptual Design Report [2], the FCC-ee booster can accelerate 3.5×10^{14} positrons every 50 s. Using the much more powerful Gamma Factory e^+ source, with a rate of 10^{16}–10^{17} e^+ s^{-1} [5], provided by laser excitation of partially stripped heavy-ion beams in the LHC or FCC-hh, and injecting into the booster during one or a few seconds, of order 10^{17} e^+ can be accumulated, at the booster injection energy of ~20 GeV. The positrons can be captured into a single barrier RF bucket, with a final length of ~ 5 m, where the longitudinal density would be about 1000 times higher than the peak bunch density in the collider ring (without collision). The stability of this beam configuration would need to be examined, e.g., with regard to microwave and TMCI thresholds.

Accelerating the long superbunch containing 10^{17} e^+ by 25 GeV requires a total energy of 0.4 GJ, or, if accelerated over 2 s, about 200 MW of RF power. This translates into an induction acceleration voltage of ~2 MV per turn, which is three orders of magnitude higher than the induction voltage of the KEK digital accelerator [6], but about 10 times lower than the induction RF voltage produced at the LANL DARHT-II [7], at much higher or lower repetition rate, respectively. On the ramp and at top energy, the full bunch length l_b can conceivably be compressed to the assumed $l_b \approx 5$ m, by squeezing the gap of the barrier bucket (which requires substantially more voltage for the barrier RF system) – also see [6, 8]. Tentative parameters of the e^+ superbunch are compiled in Table 1. We assume that the booster ring runs near the coupling resonance so that the emittance is shared between the two transverse planes. The matched beta function inside a plasma of e^- density n_e is estimated as $\beta_{x,y} \approx (\gamma/(2\pi n_e r_e))^{1/2}$. For a typical initial plasma e^- density of $n_e = 10^{23}$ m^{-3}, this leads to an initial matched beta of 7 mm, decreasing to 0.2 mm, as a result of e^- accumulation. The e^- oscillation wavelength $\lambda_p \approx \sqrt{2\pi/(r_e n_{e^+})}$ is ~5 μm.

PLASMA TARGET RESPONSE

As the 45 GeV e^+ beam enters the plasma, the plasma electrons will move to compensate the beam charge. However, the charge density of the e^+ beam is extremely high,

* Work supported by the European Union's Horizon 2020 Research and Innovation programme under Grant Agreement No. 101004730 (iFAST).
† frank.zimmermann@cern.ch

ISBN: 978-3-95450-227-1 ISSN: 2673-5490 doi:10.18429/JACoW-IPAC2022-WEPOST010

CONTROLLING e^+/e^- CIRCULAR COLLIDER BUNCH INTENSITY BY LASER COMPTON SCATTERING*

F. Zimmermann†, European Organization for Nuclear Research (CERN), Meyrin, Switzerland
T.O. Raubenheimer, SLAC National Accelerator Laboratory, Menlo Park, CA, U.S.A.

Abstract

In the future circular electron-positron collider "FCC-ee", the intensity of colliding bunches must be tightly controlled, with a maximum charge imbalance between collision partner bunches of less than 3–5%. Laser Compton back scattering could be used to adjust and fine-tune the bunch intensity. We discuss a possible implementation and suitable laser parameters.

INTRODUCTION

In the future circular electron-positron collider FCC-ee, the intensity of colliding bunches must be tightly controlled, through frequent top-up injections, with a maximum charge imbalance between collision partner bunches of less than 5% on the Z pole and less than 3% at the other collision energies [1–3]. If the charge imbalance exceeds this tolerance, due to the strong effect of beamstrahlung on the bunch length, a "flip-flop" effect [4] results, with the more intense bunch shrunk and the weaker bunch blown up. This is the reason why, when filling the machine from zero, a "bootstrapping" injection scheme [3] is proposed with alternate injections of small portions of the design intensity into the RF buckets accommodating a colliding pair of electrons and positrons.

In this paper, we consider the possible use of laser Compton back scattering to adjust and fine-tune the bunch intensity, in one or both collider rings, between subsequent top-up injections. The laser of the Compton polarimeter [5] could be used for this purpose, provided that its laser power is increased to a sufficiently high value.

The same approach could be applied with a dedicated laser in the full-energy booster (which alternatingly serves as injector to both collider rings), in order to pre-adjust the bunch intensity to the instantaneous needs of the collider, prior to each beam extraction from the booster and top-up injection in the collider. This could be particularly interesting if the pre-injector linac operates in a multi-bunch mode, which may require precise intensity adjustments downstream, before top-up injection, to accord with the respective intensity pattern of the collider at that moment in time.

Finally, the laser Compton back scattering could also be used, as a last resort, to remove single bunch pairs from the stored fill pattern in the collider, after experiencing a beam-beam flip-flop effect, so as to make space for injecting a fresh pair of bunches, restarting at zero bunch current.

* Work partially supported by the European Union's H2020 Framework Programme under grant agreement no. 951754 (FCCIS).
† frank.zimmermann@cern.ch

BEAM PARAMETERS

We consider FCC-ee Z pole operation where the beam size is largest, the beam energy lowest, and the number of bunches the highest. In several respects, this represents the most difficult case.

At a beam energy of 45.6 GeV the geometric emittances, according to the FCC Conceptual Design Report [1], are $\varepsilon_x = 0.27$ nm, and $\varepsilon_y = 1$ pm. With local beta functions of $\beta_x^{\rm CP} = 140$ m and $\beta_y^{\rm CP} = 30$ m at the polarimeter [6], we obtain the rms beam sizes $\sigma_x^{\rm CP} \approx 200$ μm and $\sigma_y^{\rm CP} \approx 5$ μm. The vertical beam size considered in an earlier study [5] was about 5 times larger.

Other beam energies of interest relate to the FCC-ee operation at the WW threshold (80 GeV), or at the ZH production peak (120 GeV), and the $\bar{\rm t}$t running (182.5 GeV).

LASER PARAMETERS

The laser pulse length is not critical for our application, as long as the trajectory of electrons or positrons overlaps with the path of the full laser pulse. A pulse duration of order 1 ns or higher would be acceptable. Long pulse lengths imply a lower instantaneous peak power and may, thereby, avoid damage to optical mirrors and other components.

A Ti:sapphire J-class kHz laser system is ready to be built today [7–9]. Specifically, we consider a laser system operating with 1 J pulses at 3 kHz (the revolution frequency), with an average power of 3 kW, which translates to the same average laser power as for LBNL's k-BELLA initiative (3 J at 1 kHz) [10]. A wavelength of 800 nm, obtainable from a Ti:sapphire laser, corresponds to a photon energy of 1.5 eV. We note that, instead, previously [5] considered a laser wavelength λ of 532 nm, as could be provided by a frequency-doubled Nd:YAG laser. As an encouraging example, in 2021, a 1 J laser with 1 kHz repetition rate at $\lambda = 515$ nm was demonstrated by frequency doubling temporally shaped square 2 ns pulses from a cryogenically cooled Yb:YAG laser in LBO crystals [11].

While a laser system like k-BELLA's appears sufficient for an application targeting single or few bunches, we were informed that LLNL is in the process of developing extremely high average-power laser concepts with Tm-based materials [12]. Such a Tm:YLF laser, operating at a wavelength of 2 μm, could potentially provide much higher energy, photon intensity, and average power, which would render the proposed technique more flexible, and which would, in particular, allow the intensity of many bunches to be controlled simultaneously.

ISBN: 978-3-95450-227-1 ISSN: 2673-5490 doi:10.18429/JACoW-IPAC2022-WEPOST011

STUDIES ON TOP-UP INJECTION INTO THE FCC-ee COLLIDER RING

P. J. Hunchak[1*], M. J. Boland[1], Canadian Light Source, Saskatoon, Canada
[1]also at University of Saskatchewan, Saskatoon, Canada
W. Bartmann, Y. Dutheil, M. Hofer, R. Ramjiawan, F. Zimmermann, CERN, Meyrin, Switzerland
M. Aiba, Paul Scherrer Institute, Villigen, Switzerland

Abstract

In order to maximize the luminosity production time in the FCC-ee, top-up injection will be employed. The positron and electron beams will be accelerated to the collision energy in the booster ring before being injected with either a small transverse or longitudinal separation to the stored beam. Using this scheme essentially keeps the beam current constant and, apart from a brief period during the injection process, collision data can be continuously acquired. Two top-up injection schemes, each with on- and off-momentum sub-schemes, viable for FCC-ee have been identified in the past and are studied in further detail to find a suitable design for each of the four operation modes of the FCC-ee. In this paper, injection straight optics, initial injection tracking studies and the effect on the stored beam are presented. Additionally, a basic proxy error lattice is introduced as a first step to studying injection into an imperfect machine.

INTRODUCTION

The Future Circular Collider (FCC) study includes focus on a high energy and high brightness electron-positron collider (FCC-ee) to serve the international scientific community through the 21st century. Part of this proposed project is reaching unprecedented luminosity in an electron-positron collider. The FCC-ee design luminosity is to be more than 10,000 times greater than what was achieved at the Large Electron Positron collider (LEP), the previous highest energy electron-positron collider, when operating with a beam energy of 45.6 GeV [1].

Within the FCC-ee study there are four different working points for energy of the collisions, initially in the Z-pole energy range and moving through increasing operation energies to the $t\bar{t}$ threshold [1]. Some basic parameters of the four operation modes of the proposed machine are shown in Table 1. First studies, presented in the following, focus on operation in Z-mode (45.6 GeV beam energy) due to the importance of machine protection with its high, 20 MJ stored beam energy.

In order to maximize the luminosity of the FCC-ee top-up injection is required to maintain the beam current and allow for continuous, full-energy collisions [2]. LEP used fill and ramp injection which provides lower integrated luminosity due to the decay of the colliding beam current and lost collision time during injection and ramping of the ring. When using top-up injection beams are accelerated to collision energy in a booster ring before being injected into the collider ring. This allows the collider to stay in almost constantly in collision mode. Top-up injection has been successful in the colliders at both KEKB and SLAC and the integrated luminosity gain was as much as 50% [3]. Top-up is also a mainstay for modern lightsources.

Table 1: Selection of FCC-ee parameters for the four operation modes. From Table 1 in Ref. [1].

	Z	WW	ZH	$t\bar{t}$
Beam Energy (GeV)	45.6	80	120	175/182.5
Beam Current (mA)	1390	147	29	6.4/5.4
Horizontal Emit. ϵ_x (nm · rad)	0.27	0.84	0.63	1.34/1.46
Vertical Emit. ϵ_y (pm · rad)	1.0	1.7	1.3	2.7/2.9
Luminosity/IP (10^{34}cm^2 s)	230	28	8.5	1.8/1.55

Top-Up Injection Schemes for FCC-ee

Two viable top-up injection schemes have been identified for the FCC-ee: conventional orbit bump injection and multipole kicker injection (MKI) [2]. In the former, dipole kickers are used to introduce a bump in the orbit of the stored beam which brings it closer to the injection septum and reduces the separation of the stored and injected beams. Both beams are then bent back towards the design orbit within one turn, where the injected beam undergoes betatron oscillations until synchrotron radiation causes it to damp and join the stored beam.

In multipole kicker injection a specially designed magnet with a low-field region on-axis and significant off-axis field minimizes the disturbance of the stored beam while providing the kick required to store the injected beam which then damps to join the stored beam [4–6]. Though the stored beam passes through the low-field region of the MKI magnet, it is affected due to the finite width of the zero-field region. By introducing a compensation kicker upstream of the MKI magnet the emittance blow-up can be minimized. An MKI design for FCC-ee has been proposed previously, and studies of the feasibility of the injection hardware for each mode, including the injection septa and kickers are ongoing [2, 7].

Each of the two viable injection schemes also has an off-momentum option, where the injected beam has a fractional difference in energy compared to the stored beam. The injected beam is stored directly on a dispersive orbit to separate it from the stored beam. Damping occurs in the longitudinal

* patrick.hunchak@usask.ca

ISBN: 978-3-95450-227-1 ISSN: 2673-5490 doi:10.18429/JACoW-IPAC2022-WEPOST012

FEASIBILITY OF SLOW-EXTRACTED HIGH-ENERGY IONS FROM THE CERN PROTON SYNCHROTRON FOR CHARM

M.A. Fraser*, R. Garcia Alia, P.A. Arrutia Sota, K. Bilko, N. Charitonidis, S. Danzeca, M. Delrieux, M. Duraffourg, N. Emriskova, L.S. Esposito, A. Guerrero, O. Hans, G. Imesch, E.P. Johnson, G. Lerner, G. Pezzullo, I. Ortega, D. Prelipcean, F. Ravotti, F. Roncarolo, A. Waets, CERN, Geneva, Switzerland

Abstract

The CERN High Energy Accelerator Mixed-field (CHARM) High-energy Ions for Micro Electronics Reliability Assurance (CHIMERA) working group is investigating the feasibility of delivering high energy ion beams to the CHARM facility for the study of radiation effects to electronics components engineered to operate in harsh radiation environments, such as space or high-energy accelerators. The Proton Synchrotron (PS) has the potential of delivering the required high energy and high-Z (in this case, Pb) ions for radiation tests over the relevant range of Linear Energy Transfer (LET) of $\sim 10-40$ MeV cm^2 mg^{-1} with a >1 mm penetration depth in silicon, specifically for Single Event Effect (SEE) tests. This contribution summarises the working group's progress in demonstrating the feasibility of variable energy slow extraction and over a wide range of intensities. The results of a dedicated 5.4 GeV/u Pb ion beam test are reported to understand the performance limitations of the beam instrumentation systems needed to characterise the beam in CHARM.

INTRODUCTION TO CHIMERA

The CHIMERA working group at CERN is studying the feasibility of exploiting the PS to provide Very High Energy (VHE), > 100 MeV/u heavy ion beams for space applications, such as the qualification of active semiconductor components and boards. Lead ions are available for exploitation in the CERN accelerator complex within the framework of the LHC heavy ion programme [1]. Combined with the recent renovation of the East Area during Long Shutdown 2 (LS2) [2], the CHARM facility offers a unique opportunity to increase the limited availability and accessibility of beam time in Europe required for breakthrough research and innovation in the field. The CHIMERA activity falls inside the scope of the collaboration between CERN and the European Space Agency (ESA) who are supporting the study. A proposal has also been recently submitted to the European Union's HORIZON programme call "Strategic autonomy in developing, deploying and using global space-based infrastructures, services, applications and data 2021" under the name High-Energy Accelerators for Radiation Testing and Shielding (HEARTS) [3]. The objective of the proposal is to facilitate 2 – 3 weeks of heavy ion beam time annually as of 2023, for both CERN internal users, and external academic and industrial users.

* mfraser@cern.ch

The focus of the working group last year was demonstrating the feasibility of variable energy operation of both the slow extraction system in the PS and the network of transfer lines that transport the beam to the CHARM facility. In parallel, other studies also continued to understand the performance of instrumentation to characterise the ion beam in CHARM, to control the intensity in the transfer line with a collimation system and FLUKA [4, 5] studies to understand pollution from fragmentation of the beam as it passes material on the beam line, such as interceptive beam instrumentation devices and vacuum windows.

VHE HEAVY ION BEAM REQUIREMENTS

The PS is capable of delivering slow extracted VHE heavy ion beams suitable for mimicking the effects of galactic cosmic rays with a kinetic energy range of $\sim 70-5400$ MeV/u in spills of a few 100 ms in length. Due to the non-linear variation of the LET as a function of range in silicon, the lower end of the PS's energy range is most attractive for Pb ($\lesssim 1000$ MeV/u), see Fig. 1.

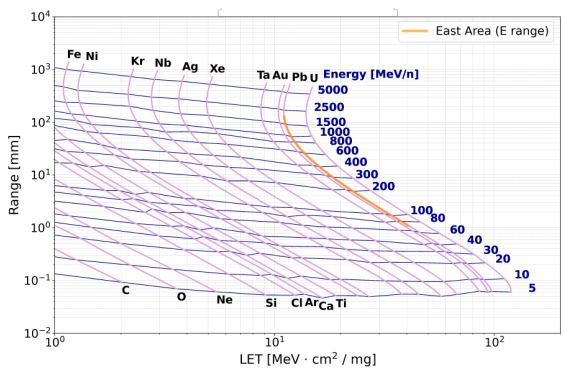

Figure 1: Range in silicon vs. LET for different heavy ions and the energy range of Pb available at the East Area [6].

The beam specification is summarised in Table 1, highlighting the main challenges at the PS including (i) guaranteeing the wide-range of beam energy and LET, (ii) providing reproducible spills at the relatively low beam intensities required to respect SEE testing standards and (iii) delivering a uniform beam distribution over a range of different test devices.

SLOW EXTRACTION AND BEAM TRANSFER DEVELOPMENTS

Building on the experience of first slow extraction tests of ions to the East Area before LS2 [7–9], regular machine

ISBN: 978-3-95450-227-1 ISSN: 2673-5490 doi:10.18429/JACoW-IPAC2022-WEPOST013

EXPLOITATION OF CRYSTAL SHADOWING VIA MULTI-CRYSTAL ARRAY, OPTIMISERS AND REINFORCEMENT LEARNING

F. M. Velotti,* M. Di Castro, L. S. Esposito, M. A. Fraser, S. Gilardoni,
B. Goddard, V. Kain, E. Matheson, CERN, Geneva, Switzerland

Abstract

The CERN Super Proton Synchrotron (SPS) routinely delivers proton and heavy ion beams to the North experimental Area (NA) in the form of 4.8 s spills. To produce such a long flux of particles, resonant third integer slow extraction is used, which, by design, foresees primary beam lost on the electrostatic septum wires to separate circulating from extracted beam. Shadowing with thin bent crystal has been proposed and successfully tested in the SPS, as detailed in [1]. In 2021, a thin crystal was used for physics production showing results compatible with what measured during early testing. In this paper, the results from the 2021 physics run are presented also comparing particle losses at extraction with previous operational years. The setting up of the crystal using numerical optimisers is detailed, with possible implementation of reinforcement learning (RL) agents to improve the setting up time. Finally, the full exploitation of crystal shadowing via multi-array crystals is discussed, together with the performance reach in the SPS.

INTRODUCTION

The CERN-SPS delivers approximately 3.5×10^{13} p every 15 s to serve a large number of fixed target experiments in the NA. Particles are extracted via resonant third-integer slow extraction. For most of these experiments, the integrated protons delivered along the year is a fundamental figure of merit. As documented in [1], the main limiting factor to the number of particles that can be extracted from the SPS Long Straight Section (LSS) 2 is limited by the electrostatic septum (ZS) activation. The losses are unavoidable for classic third-integer slow extraction as the concept relies on separation between circulating and extracted beam via a thin septum blade which directly sees the primary beam.

To reduce the number of particles impinging on the ZS wires, in [1, 2] was proposed the exploitation of silicon bent crystals [3, 4]. Thanks to this technique, loss reduction up to about 45% was measured in the SPS and up to four times is expected, with better exploitation of machine non-linearities and a thicker crystal (non-local crystal shadowing [1]).

In this paper, the results from a full year of experience with the crystal for septum shadowing and the methodology used to efficiently align it are presented. Also, we propose a manner to further reduce losses during slow extraction using Multiple Volume Reflection Array (MVRA [5]) crystals.

CRYSTAL SHADOWING IN DAILY OPERATION

The tests carried out in 2018 in the SPS showed that the crystal installed in LSS2 could reduce the beam induced losses on the ZS by about 20% when operating in volume reflection (VR) and up to 45% in channelling.

The main concerns about the channelling regime was the beam stability and the possibility to transport the beam to the NA targets. The first was addressed testing channelling stability during the first part of the physics run. It was possible to maintain this regime for weeks without the need to re-align the crystal. This was possible only for extracted intensities lower than 1×10^{13} p, due to the losses arising from losing the channelled beamlet along the transfer line to the targets. Attempts to adjust the transfer line optics and steer the beamlet together with the main beam were made, as proposed in [6], but measured losses remained unacceptable for daily operation. The impossibility of transporting the channelled beamlet through the transfer line is believed to be related to the inconsistencies observed in the transport line optics, which still remains unsolved.

The transport of VR beamlet is a much simpler task as the deflection angle is only 15 µrad. It was decided to use VR in operation for the full physics year, as the loss reduction was measured to be about 20%. Figure 1 shows the losses as a function of time starting from 2018 (no crystal in the SPS during operation), through 2021 (crystal in VR) to the first month of operation in 2022 (crystal still in VR). The large loss reduction achieved is a combination of the crystal operating in VR and the new ZS, which was exchanged before 2021[1]. The lower loss regime visible between July and August 2021 was thanks to the crystal in channelling.

Crystal Alignment

To align the crystal to the beam separatrix takes in the order of 150 machine cycles as accurate position and angle scans are needed to find channelling or VR and shadowing. For the SPS, this corresponds to a downtime for the physics users of more than 1 h due to unstable beam conditions. In order to speed up the setting up time, numerical optimisers were used. The very accurate tracking model available [1] was used to fit a deep neural network-based surrogate model, Fig. 2. Such a model is a fully connected neural network composed of 3 layers and 256 neurons per layer, with hyperbolic tangent as activation function.

In this manner, numerical optimisers were tested and the most performant chosen for machine operation. The algorithms tested are summarised in Fig. 3. Their performance

* francesco.maria.velotti@cern.ch

[1] The ZS assembly was exchanged with a new one where the wire support were chosen as the straightest among those available.

ISBN: 978-3-95450-227-1 ISSN: 2673-5490 doi:10.18429/JACoW-IPAC2022-WEPOST014

STUDIES ON PRE-COMPUTATION OF SPS-to-LHC TRANSFER LINE CORRECTIONS

C. Bracco*, F. M. Velotti, CERN, Geneva, Switzerland

Abstract

The injection process in the LHC gives a non-negligible contribution to the turnaround time between two consecutive physics fills. Mainly due to orbit drifts in the SPS, the steering of the SPS-to-LHC transfer lines has to be regularly performed in view of minimising injection oscillations and losses, which otherwise would trigger beam dumps. Moreover, for machine protection purposes, a maximum of twelve bunches has to be injected after any TL steering to validate the actual applied corrections. This implied at several occasions the need to interrupt a fill to steer the lines and introduced a further delay between fills. Studies are performed to evaluate the option of pre-calculating the required TL corrections based on SPS orbit measurements during the LHC magnet ramp down and the reconstruction of the beam position and angle at the SPS extraction point.

INTRODUCTION

The transfer of 450 GeV proton beams from the Super Proton Synchrotron (SPS) to the Large Hadron Collider (LHC) occurs through two ~3 km long transfer lines (TI2 for Beam 1 and TI8 for Beam 2, Fig. 1). Two conventional fast extraction systems [1] are installed in Long Straight Sections 6 (LSS6) and 4 (LSS4) of the SPS [2] to convey the beams respectively to TI2 and TI8. The circulating beam is extracted towards the lines by means of horizontal closed orbit bumpers, fast pulsed kickers (MKE) and DC magnetic septa (MSE and MST). Similarly, the injection in the LHC [3] is obtained by deflecting the beams from the transfer lines onto the closed orbit, with fast kickers (MKI) and septa (MSI), which are installed in straight section 2 (IR2) for Beam 1 and 8 (IR8) for Beam 2.

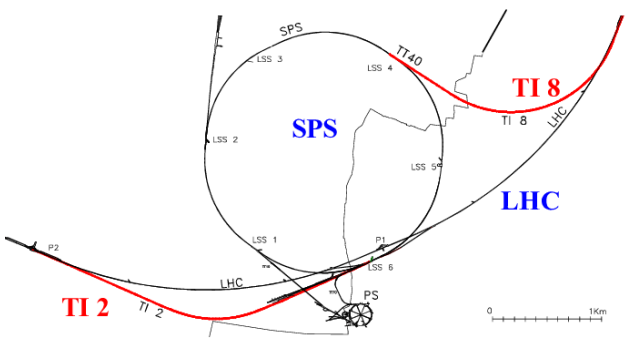

Figure 1: Layout of the transfer lines connecting the SPS extraction to the LHC injection points.

The LHC filling process consists in transferring up to 288 bunches of at least $1.2 \cdot 10^{11}$ protons each, corresponding to a stored energy of 2.5 MJ and, after the injectors upgrade [4], up to 4.8 MJ per injection can be achieved. A system of six collimators (TCDI) [5], placed at a relative phase advance of 60°, is installed towards the end of each transfer line to protect the LHC aperture from particles injected with dangerously large amplitudes (>5 σ). These collimators consist of two carbon-based jaws which are centered with respect to a reference trajectory that allows to minimize the injection oscillations into the LHC and is defined during the commissioning period.

TRANSFER LINE STEERING

A good control of the parameters at the LHC injection points, in terms of optics, position and angle, is crucial for luminosity performance and machine protection reasons. A periodic steering of the transfer lines, onto the pre-defined references, has to be carried out to keep the injection oscillations below 1 mm (peak-to-peak) and minimise the losses at the TCDIs. Small losses at these collimators create showers which can trigger the sensitive beam loss monitors (BLM) installed at the nearby LHC magnets and cause beam aborts during the fill [6]. Despite several mitigation measures (shielding, electronic filters and temporary BLM inhibition) were put in place to avoid these unnecessary dumps, a regular correction of the lines has to be performed to compensate for unavoidable trajectory drifts and keep them below 0.5 σ at the TCDIs (350 µm in average). An r.m.s. trajectory of 350 µm is considered as the target for the studies presented in the following. Each trajectory steering has to be validated by injecting maximum 12 bunches of $1.2 \cdot 10^{11}$ protons, which is considered as a safe beam, to verify that the correction algorithm worked properly and the correctors pulse at the right current. This procedure might require more iterations and thus several low intensity injections while the nominal LHC filling schemes foresee only one 12-bunch train. A dedicated steering time has to be accounted for and this can delay the turnaround [7] between two consecutive physics fills and thus impact the integrated luminosity. The drift of the SPS orbit is considered as the main source of the observed trajectory deviations [8]. The possibility of pre-computing the needed transfer line corrections, based on the orbit measured in the SPS during the ramp-down of the LHC magnets, is analysed in this paper. This would allow to use the only 12-bunch train to validate the applied corrections and continue filling the machine with a non negligible gain in physics time.

THE MODEL

The studies presented in the following are purely theoretical and focus on the steering in the horizontal plane for

* chiara.bracco@cern.ch

ISBN: 978-3-95450-227-1 ISSN: 2673-5490 doi:10.18429/JACoW-IPAC2022-WEPOST015

IMPLEMENTATION OF A TUNE SWEEP SLOW EXTRACTION WITH CONSTANT OPTICS AT MedAustron

P. A. Arrutia Sota*[1,2], P. N. Burrows[2], A. De Franco[3], M. A. Fraser[1], B. Goddard[1], V. Kain[1], F. Kuehteubl[4], M. T. F. Pivi[4], D. Prokopovich[4], and F. M. Velotti[4]

[1]CERN, Geneva, Switzerland
[2]University of Oxford, Oxford, UK
[3]National Institutes for Quantum Science and Technology, Japan
[4]MedAustron GmbH, Wiener Neustadt, Austria

Abstract

Conventional slow extraction driven by a tune sweep perturbs the optics and changes the presentation of the beam separatrix to the extraction septum during the spill. The constant optics slow extraction (COSE) technique, recently developed and deployed operationally at the CERN Super Proton Synchrotron to reduce beam loss on the extraction septum, was implemented at MedAustron to facilitate extraction with a tune sweep of operational beam quality. COSE fixes the optics of the extracted beam by scaling all machine settings with the beam rigidity following the extracted beam's momentum. In this contribution the implementation of the COSE extraction technique is described before it is compared to the conventional tune sweep and operational betatron core driven cases using both simulations and recent measurements.

INTRODUCTION

The MedAustron synchrotron employs a betatron core driven slow extraction to perform nominal operation. Another common slow extraction technique relies on ramping up (or down) some or all quadrupoles in the machine to vary betatron tune of the circulating beam towards the resonance. Implementing a tune sweep based method in MedAustron is interesting academically [1], as the machine was not designed to operate in such a way. Furthermore, MedAustron has contemplated performing bunched multi-energy extraction in order to speed up operation, which cannot be performed with the betatron core.

CONSTANT OPTICS SLOW EXTRACTION

There are certain issues with conventional tune sweep. As the tune is swept the radial position of the on-resonance separatrix moves along the dispersion vector due to the changing extracted momentum, rendering ineffective the superposition of separatrices achieved via the Hardt condition. Moreover, particles with different momenta 'see' different optics at extraction, due to the fact that they have different magnetic rigidities. These effects can be partially compensated with a dynamic extraction bump, but it complicates operation.

A solution to this can be achieved with COSE [2], where the whole machine's beam rigidity $B\rho$ (or reference momentum $p_{\mathrm{ref}} = q \cdot B\rho$, where q is the particle's electric charge) is scaled synchronously with the tune sweep. All magnets in the lattice must follow the same ramp from their respective $B_{n,\mathrm{start}}$ to $B_{n,\mathrm{end}}$ for COSE to be performed successfully, where B_n represents the n-th order multipole of the magnetic field. In order to determine magnet field strength sweep, it is sufficient to enforce a constant optics as follows,

$$k_{n,\mathrm{start}} = q\frac{B_{n,\mathrm{start}}}{p_{\mathrm{start}}} = q\frac{B_{n,\mathrm{end}}}{p_{\mathrm{end}}} = k_{n,\mathrm{end}}. \quad (1)$$

Since $p_{\mathrm{end}} = (1 + \Delta p/p)p_{\mathrm{start}}$, one can write,

$$\frac{B_{n,\mathrm{end}}}{B_{n,\mathrm{start}}} = (1 + \Delta p/p), \quad (2)$$

illustrating that the magnetic strengths must be scaled by the same relative change in momentum.

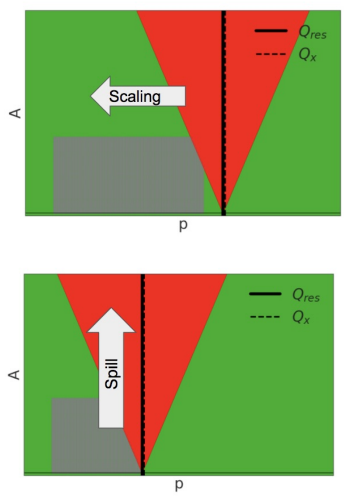

Figure 1: Steinbach diagram illustration of COSE.

An interesting way of conceptualising COSE is as the betatron core extraction in a different frame of reference. A particle with longitudinal momentum p has a tune distance

$$\delta Q = Q'_x\frac{\Delta p}{p} = Q'_x\frac{p - p_{\mathrm{ref}}}{p_{\mathrm{ref}}}. \quad (3)$$

* pablo.andreas.arrutia.sota@cern.ch

ISBN: 978-3-95450-227-1 ISSN: 2673-5490 doi:10.18429/JACoW-IPAC2022-WEPOST016

DEVELOPMENT OF COLLIMATION SIMULATIONS FOR THE FCC-ee*

A. Abramov[1†], R. Bruce[1], F. Carlier[1,2], M. Hofer[1], G. Iadarola[1], L. J. Nevay[1,3], T. Pieloni[2], M. Rakic[2], S. Redaelli[1], S. M. White[4],
[1]CERN, 1211 Meyrin, Switzerland
[2]EPFL, Lausanne, Switzerland
[3]JAI RHUL, Egham TW20 0EX, UK
[4]ESRF, Grenoble, Grenoble, France

Abstract

A collimation system is under study for the FCC-ee to protect the machine from the multi-MJ electron and positron beams and limit the backgrounds to the detectors. One of the key aspects of the collimation system design is the setup of simulation studies combining particle tracking and scattering in the collimators. The tracking must include effects important for electron beam single-particle dynamics in the FCC-ee, such as synchrotron radiation. For collimation, an aperture model and particle-matter interactions for electrons are required. There are currently no established simulation frameworks that include all the required features. The latest developments of an integrated framework for multi-turn collimation studies in the FCC-ee are presented. The framework is based on an interface between tracking codes, pyAT and Xtrack, and a particle-matter interaction code, BDSIM, based on Geant4. Promising alternative simulation codes and frameworks are also discussed. The challenges are outlined, and the first results are presented, including preliminary loss maps for the FCC-ee.

INTRODUCTION

The lepton Future Circular Collider (FCC-ee) is a design study for a future 97.5 km-long electron-positron collider with 4 operating modes at beam energies in the range 45.6–182.5 GeV, which would be part of the CERN accelerator complex [1]. In order to maximise the discovery potential and the luminosity, parameters such as the centre-of-mass energy for collisions, the stored beam energy, and the total synchrotron radiation power will be pushed beyond past and present lepton colliders. The stored beam energy reaches up to 20.7 MJ for the 45.6 GeV operation mode, which is comparable with the stored beam energy during Large Hadron Collider (LHC) operation with heavy-ion beams [2]. This is a new regime for lepton machines, in which beam losses could risk to damage equipment or quench any of the superconducting elements. A collimation system is therefore being designed for the FCC-ee [3, 4], not only to control detector backgrounds from synchrotron radiation (SR), but also to protect the collider from beam losses during both normal operation and failure scenarios.

Simulations are important tools for the collimation system design. Collimation tracking studies are the first step in determining the performance, where a distribution of particles corresponding to a selected beam loss scenario is tracked in a machine model with the collimators and the mechanical apertures included. For machines where beam losses can exceed the limits for safe operations, like the LHC, FCC-hh, and FCC-ee, it is important to track the particles out-scattered from the collimators. The requirements for collimation simulations are hence accurate and efficient tracking in the magnetic lattice, modelling of the scattering in the collimators, and accurate aperture loss recording. For lepton beams, synchrotron radiation (SR) must be supported in the particle tracking. In addition, due to the significant SR energy loss, the magnet strengths in the FCC-ee are adjusted to follow the beam energy around the ring (called optics tapering). This is essential for maintaining a centered closed orbit and must be included in the simulations. The goal of this study is to develop and benchmark a simulation framework that fits all the requirements for collimation simulations in the FCC-ee. The FCC-ee is a novel study in many aspects, also for optics design, model preparation, and particle tracking [5]. In the early design stages, it is necessary to consider and explore different software tools and pick the most appropriate ones for the studies. Tests and benchmarks are essential to ensure reliable and reproducible results, so the aim is to achieve adequate agreement between at least two software frameworks for each aspect of the studies.

SOFTWARE TOOLS

Different software tools were considered for FCC-ee collimation, including MAD-X [6], Merlin++ [7], pyAT [8], SixTrack [9], and Xtrack [10]. For the LHC, the most common software for collimation simulations is SixTrack in combination with a scattering routine for collimator interactions [11, 12], which can be built-in [13] or a coupling to FLUKA [14, 15]. In the SixTrack-FLUKA coupling framework [16–18], SixTrack performs tracking in the magnetic lattice and FLUKA simulates the physics interactions in 3D geometry models of collimators. While lepton beams can be defined and tracked in the SixTrack-FLUKA coupling, SR is not supported, which makes this framework less suitable for FCC-ee studies. In the current work it is used for benchmarks in an artificial configuration without radiation and tapering. Following evaluation and initial testing, a coupling between a particle tracking code and a Monte Carlo physical interaction code was selected also for FCC-ee. For the tracking, pyAT and Xtrack were chosen for further testing and develop-

* This work is partially supported by the Swiss Accelerator Research and Technology (www.CHART.ch) program.
† andrey.abramov@cern.ch

ISBN: 978-3-95450-227-1 ISSN: 2673-5490 doi:10.18429/JACoW-IPAC2022-WEPOST017

DESIGN OF A COLLIMATION SECTION FOR THE FCC-ee*

M. Hofer†, A. Abramov, R. Bruce, K. Oide, F. Zimmermann, CERN, 1211 Geneva, Switzerland
M. Moudgalya, T. Pieloni, EPFL, 1015 Lausanne, Switzerland

Abstract

The design parameters of the FCC-ee foresee operation with a total stored energy of up to about 20 MJ per beam, exceeding those of previous lepton colliders by almost two orders of magnitude. Given the inherent damage potential, a halo collimation system is studied to limit backgrounds and protect the machine hardware, in particular superconducting equipment such as the final focus quadrupoles, from sudden losses. The different constraints that led to dedicating one straight section to collimation will be outlined. In addition, a preliminary layout and optics for a collimation insertion are presented.

INTRODUCTION

The first stage of the Future Circular Collider (FCC) integrated program, the FCC-ee [1], is a proposed double-ring e^+e^- collider with a circumference of about 91 km. Four operation modes are foreseen, with beam energies of 45.6 GeV, 80 GeV, 120 GeV, and 182.5 GeV, referred to as Z, WW, ZH, and $t\bar{t}$ running. At 45.6 GeV, the beam current reaches 1.4 A, whereas only 6.4 mA are stored at 182.5 GeV.

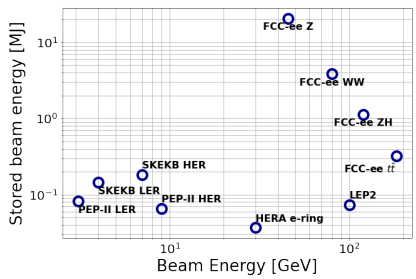

Figure 1: Comparison of stored beam energy between FCC-ee, LEP2, PEP-II, HERA, and SuperKEKB.

In Fig. 1, the stored beam energy for the different FCC-ee modes is compared to other lepton colliders [2–5]. The stored beam energy of about 20 MJ per beam at the Z-operation mode exceeds those of present and past e^+e^- colliders by about two orders of magnitude. The energy stored in either FCC-ee beam is still a factor ~ 20 lower than the energy contained in each of the two proton beams of the Large Hadron Collider (LHC), which is being successfully handled by a multi-stage collimation system. The stored beam energy of the FCC-ee is similar to the one expected for lead ion operation at the High Luminosity LHC [6,7]. Given the damage potential in case of beam loss, as is illustrated by incidents at SuperKEKB [8], a dedicated two-stage halo collimation system will be installed in the FCC-ee, profiting from the experience of the LHC collimation design. The purposes of the FCC-ee collimation are to limit the detector background and to protect sensitive equipment from beam loss induced damage or quench, e.g., the superconducting final-focus quadrupoles.

FCC-ee DESIGN

Since the publication of the FCC-ee conceptual design report [1], the design has undergone several changes. Those with implications on collimation are most notably, the circumference reduction from 98 km to 91 km motivated by a more favourable placement of the surface sites [9]. While the previous tunnel layout featured only a left/right symmetry, the new layout features a four-fold periodicity, a configuration providing the option to have either two or four interaction points (IP). Figure 2 shows the new 4-IP layout.

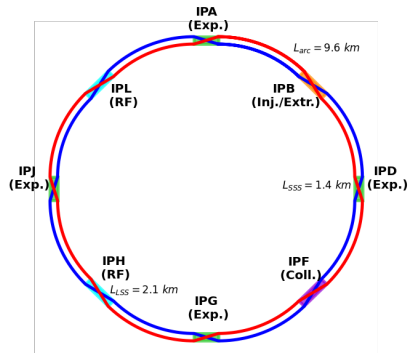

Figure 2: Assumed layout of the FCC-ee.

A final decision on the actual number of IPs will be taken at a much later moment in time. Here, we consider only the optics with 4 IPs and, correspondingly, 4 low-beta insertions. Two arc optics configurations will be used in FCC-ee, one for the two lower energy operation modes Z and WW, and another for the modes ZH and $t\bar{t}$. This change is necessary to achieve the target horizontal emittance at the higher energy modes, while keeping a large momentum compaction α_p at the low energy modes [10]. For the most recent layout [11], the phase advance over the FODO cell will be 90°/90° in all cases, with a variable cell length. In the lower energy modes, the cell will be twice as long compared to the high energy modes. The different arc layouts and the resulting optics are illustrated in Fig. 3.

The studies reported in the following focus on the Z and $t\bar{t}$ modes of operation, which correspond to the highest beam current and the largest energy loss from synchrotron radiation, respectively.

APERTURE MODEL

The collimation design requires a detailed aperture model around the ring, allowing to identify loss locations and bot-

* This work is partially supported by the Swiss Accelerator Research and Technology (www.CHART.ch) program.
† michael.hofer@cern.ch

ISBN: 978-3-95450-227-1 ISSN: 2673-5490 doi:10.18429/JACoW-IPAC2022-WEPOST018

POWER DEPOSITION STUDIES FOR CRYSTAL-BASED HEAVY ION COLLIMATION IN THE LHC*

J.B. Potoine[1,2], R. Bruce[1], R. Cai[1,3], L.S. Esposito[1], P. Hermes[1], A. Lechner[1], S. Redaelli[1], A. Waets[1], Frédéric Wrobel[2]
[1] CERN, Geneva, Switzerland
[2] University of Montpellier, Montpellier, France
[3] École Polytechnique Fédérale de Lausanne, Lausanne, Switzerland

Abstract

The LHC heavy-ion program with $^{208}Pb^{82+}$ beams is foreseen to benefit from a significant intensity upgrade in 2022. A performance limitation may arise from ion fragments scattered out of the collimators in the betatron cleaning insertion, which risk quenching superconducting magnets during periods of short beam lifetime. In order to mitigate this risk, an alternative collimation technique, relying on bent crystals as primary collimators, will be used in future heavy-ion runs. In this paper, we study the power deposition in superconducting magnets by means of FLUKA shower simulations, comparing the standard collimation system against the crystal-based one. The studies focus on the dispersion suppressor regions downstream of the betatron cleaning insertion, where the ion fragment losses are the highest. Based on these studies, we quantify the expected quench margin expected in future runs with $^{208}Pb^{82+}$ beams.

INTRODUCTION

Within the scope of its heavy-ion physics program, the Large Hadron Collider (LHC) will store and collide fully stripped $^{208}Pb^{82+}$ beams with energies up to 7 Z TeV and beam intensities up to 2.23×10^{11} ions [1, 2]. In case of beam losses, even a small fraction of this energy can perturb the accelerator performance by leading to magnet quenches, a phenomenon during which a superconducting (SC) magnets transit from SC to normal-conducting state due to the heat deposited by particle showers. While the stored beam energy in the high-luminosity (HL) era [3] is expected to reach 20 MJ [2] for heavy ions, only a few 10 mW/cm^3 of energy deposited in SC coils is enough to quench a magnet [4, 5]. Therefore the multistage betatron and momentum collimation systems of the LHC are essential to protect the machine against unavoidable beam losses [6].

Collimators are the closest elements to the circulating beam and represent the last line of defense against potential damage in case of accidental beam losses. They are also essential for preventing beam-induced quenches, which would limit the integrated luminosity due to the lengthy recovery of cryogenic conditions. The design goal is that no quenches occur in case of a beam lifetime drop to 0.2 h over a period of ten seconds [3], which translates into a maximum allowed halo loss rate of 3.64×10^8 ions/s in the HL era. However, the betatron collimation system, located in the insertion region 7 (IR7), exhibits a reduced cleaning efficiency for $^{208}Pb^{82+}$ ions compared to protons due to ion fragments scattered out of the collimators. Extrapolating from previous simulations [7] and experimental studies [8, 9], those fragments risk to induce magnet quenches during HL operation if the lifetime drops to the design value. The most exposed cold magnets are located in the dispersion suppressors (DS) and arcs downstream of IR7 [7–10]. Novel collimation measures had to be developed accordingly to avoid such quenches [3].

As a primary solution to reduce the risk of halo-induced quenches in heavy-ion operation, it is considered to substitute a dipole in the DS with shorter, but higher field magnets (11 T), creating space for an additional collimator [3]. Presently, the installation of this assembly is, however, postponed. As an alternative solution, a crystal-based collimation setup will be used featuring bent crystals of a few millimeters length [11–13]. Making use of the electromagnetic potential in their crystalline structures, bent crystals will deflect halo particles through their atomic planes. This phenomenon called channeling can deviate incoming particles at large angles of up to tens of řad onto an downstream absorber, as illustrated in Fig. 1. Due to the reduced probability of hadronic fragmentation and electromagnetic dissociation in the crystal and due to the large impact parameter on the channeled beam absorber, the crystal-based system reduces the fragment leakage to the DS and arc. So far the crystal-based collimation setup has only been used during dedicated tests [11–13] and in low-energy proton physics runs [14], but will be employed in regular heavy-ion operation from 2022.

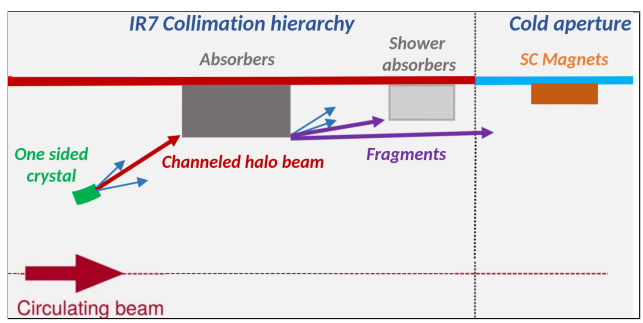

Figure 1: Principle of a crystal-based collimation setup, deflecting the primary beam halo onto an absorber. In reality, many more collimators are used (not shown for simplicity). Figure inspired by Ref. [3]

* Research supported by the HL-LHC project.

ISBN: 978-3-95450-227-1 ISSN: 2673-5490 doi:10.18429/JACoW-IPAC2022-WEPOST019

BENCHMARKS OF ENERGY DEPOSITION STUDIES FOR HEAVY-ION COLLIMATION LOSSES AT THE LHC*

J.B. Potoine[1,2], R. Bruce[1], R. Cai[1,3], P. Hermes[1], A. Lechner[1],
S. Redaelli[1], A. Waets[1], Frédéric Wrobel[2]
[1]CERN, Geneva, Switzerland
[2]University of Montpellier, Montpellier, France
[3]École Polytechnique Fédérale de Lausanne, Lausanne, Switzerland

Abstract

During some periods in its second physics run (2015-2018), the LHC has been operated with $^{208}Pb^{82+}$ ion beams at an energy of 6.37 *Z*TeV. The LHC is equipped with a betatron collimation system, which intercepts the transverse beam halo and protects sensitive equipment such as superconducting magnets against beam losses. However, hadronic fragmentation and electromagnetic dissociation of heavy ions in collimators generate off-rigidity particles, which can be lost in the downstream dispersion suppressor, putting the magnets at risk to quench. An accurate modelling of the beam-induced energy deposition in the collimation system and superconducting magnets is important for quantifying possible performance limitations arising from magnet quenches. In this paper, we compare FLUKA shower simulations against beam loss monitor measurements recorded during the 2018 $^{208}Pb^{82+}$ run. In particular, we investigate fast beam loss events, which led to recurring beam aborts in 2018 operation. Based on these studies, we assess the ability of the simulation model to reproduce the observed loss patterns in the collimation and dispersion suppressor region.

INTRODUCTION

Complementing its rich proton physics programme, the Large Hadron Collider (LHC) at CERN also stores and collides fully stripped heavy ion beams ($^{208}Pb^{82+}$) [1]. Heavy-ion operation typically takes place in the last few weeks before the regular winter shutdowns. In the second LHC physics run (2015-2018), a heavy ion energy of 6.37 *Z*TeV and a beam intensity of 1.54×10^{11} Pb ions (733 bunches) was achieved. While the LHC has been designed to store 3.8 MJ per Pb ion beam, it significantly surpassed this value during Run 2 (12.9 MJ) because of the higher-than-nominal intensity [2]. The stored energy is expected to reach an even higher value of 20-20.5 MJ in future runs due to a further increase of the ion energy (6.8-7 *Z*TeV) and beam intensity (2.23×10^{11} Pb ions, 1240 bunches) [2]. In case of beam losses, even a small fraction of the stored beam energy can perturb the LHC performance by leading to superconducting (SC) magnet quenches, a phenomenon during which a SC magnet transits from SC to normal-conducting state due to the heat deposited by particle showers. Therefore, the LHC is equipped with multistage betatron and momentum collimation systems, which are indispensable for protecting the magnets against unavoidable beam halo losses [3].

The collimation systems are organized in well defined hierarchies of more than 100 collimators, which are placed at different transverse positions from the beam. The beam-intercepting components of collimators, called jaws, accommodate blocks most commonly of carbon-fiber composite (CFC), Inermet-180 (tungsten alloy), or MoGR (from 2022) [3, 4]. Each collimator is composed of two jaws. Most of the collimators are located in two insertion regions (IRs), IR7 for betatron cleaning and IR3 for off-momentum cleaning. Operational experience showed that betatron losses dominate over momentum ones. The betatron collimation system exhibits a reduced cleaning efficiency in Pb runs compared to proton runs due to the leakage of secondary fragments to downstream dispersion suppressor (DS) magnets [5]. These secondary ions are the result of hadronic fragmentation and electromagnetic dissociation in collimator blocks, mainly in the primary collimators, which are the first collimators intercepting beam halo particles in the collimation hierarchy. Due to the large dispersion function in the DS, the fragments are lost in distinct lattice cells depending on their magnetic rigidity. Once the Pb ion energy and intensity increases in the future runs, these fragments risk to induce magnet quenches in case the beam lifetime drops to the design value of 0.2 h [4].

Numerical simulations are indispensable for understanding and predicting the power deposition in coils of DS magnets. In order to assess performance limitations and quench margins, an advanced simulation chain has been developed at CERN for studying collimation losses [6, 7]. The simulation chain couples the particle tracking code SixTrack [8, 9] with the Monte Carlo code FLUKA [10–12]. An initial

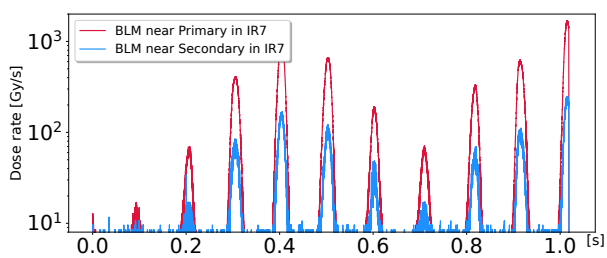

Figure 1: Time profiles of a fast beam loss event measured with BLMs in Run 2 heavy ion operation (28/11/2018). The BLMs were located in the IR7 collimation insertion.

* Research supported by the HL-LHC project.

ISBN: 978-3-95450-227-1 ISSN: 2673-5490 doi:10.18429/JACoW-IPAC2022-WEPOST020

EIC HADRON SPIN ROTATORS*

V. Ptitsyn, J. S. Berg, Brookhaven National Laboratory, Upton, USA

Abstract

The Electron-Ion Collider in BNL will collide polarized electrons with polarized protons or polarized ^{3}He ions. Spin rotators will be used to create the longitudinal beam polarization at a location of the EIC experimental detector. Helical spin rotators utilized for polarized proton operation in present RHIC will be reused in the EIC Hadron Storage Ring. However, due to a significant difference of EIC and RHIC interaction region layouts, the EIC spin rotator arrangement has several challenges. Turning on the EIC spin rotators may lead to a significant spin tune shift. To prevent beam depolarization during the spin rotator turn-on, Siberian Snakes have to be tuned simultaneously with rotators. The EIC spin rotators must be able to operate in a wide energy range for polarized protons and polarized ^{3}He ions. The paper presents the challenges of spin rotator usage in the EIC and remedies assuring the successful operation with the rotators.

INTRODUCTION

The scientists and engineers of Brookhaven National Laboratory (BNL) and Tomas Jefferson National Accelerator Laboratory (TJNAF) are continuing design developments of Electron-Ion Collider (EIC) which shall be built in BNL. Essential feature of this collider is the use of highly polarized beams of electrons, protons and ^{3}He ions. Spin rotators are used in both electron storage ring (ESR) and hadron storage ring (HSR) of the EIC to produce longitudinal beam polarization orientation in the collision point where an experimental detector is located. In this paper we revise how the spin rotators in the HSR are used for controlling polarization direction of polarized protons and polarized ^{3}He ions. The EIC HSR will re-use much of the hardware of existing RHIC rings [1]. This includes the RHIC spin rotators which have been very successfully used over many years in RHIC polarized protons runs. The Siberian Snakes used in RHIC for proton beam polarization preservation on acceleration ramp and at the store, will be also re-used in the HSR, but the number of the Snakes in the storage ring will be increased to six [2]. Both Siberian Snakes and spin rotators have a similar basic structure, based on a sequence of four helical dipole magnets [3, 4]. The magnets of Siberian Snakes can be tuned, if needed, to select an appropriate orientation of Snake axis, which allows adjusting the spin tune. By adjusting helical magnets of the spin rotator one can convert the vertical spin to arbitrary direction in the horizontal plane (with some limits discussed later in this paper). This is needed since in both RHIC and HSR the lattice contains bending magnets between rotators and the interaction point, giving requirements for polarization orientation after rotator varying with the beam energy.

SPIN ROTATOR LAYOUT IN HSR

The layout of the EIC interaction region differ drastically from the RHIC IR layout. The EIC IR is more complex than the RHIC one. It must provide collisions of electrons and hadrons in wide beam energy range, integrating forward acceptance detector elements into accelerator structure, arranging fast beam separation and crab-crossing scheme, and managing electron synchrotron radiation. The positioning of spin rotators in the EIC HSR is also very different from RHIC.

The Figure 1 shows the schematics of RHIC IR with the rotators. Each rotator consists of four helical dipole modules, with each module being one helical period long. The letters L and R in Fig. 1 denote the helical magnet helicity (left-handed or right-handed). And plus and minus signs characterize the sign of horizontal magnetic field at the entrance of each helical magnet. The first and last rotator magnets have the same field (B_1), and second and third magnets have the same field (B_2). The rotators are located at 60 meters distance and 3.7 mrad bending angle from the RHIC interaction point. It is important to note that the net bending between the spin rotators in RHIC is zero and, therefore, the second rotator just realizes inverse spin transformation as compared with first rotator. The spin transformation from the entrance of first rotator to the exit of the second one is unit transformation. Hence, the RHIC rotator system is completely spin transparent.

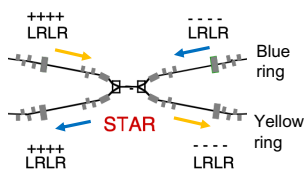

Figure 1: The spin rotators in the RHIC interaction region. There is a pair rotators in both Blue and Yellow rings of RHIC.

The Figure 2 shows the schematics of the EIC IR with HSR spin rotators. The vicinity of the interaction point is crowded with magnets, detector elements and crab-cavities. Thus, the spin rotators have to be pushed further away from the IP, both in terms of distance and bending angles. Also, the spin rotators in the HSR can not be placed symmetrically with respect to the IP. The Table 1 summarizes the location information for the RHIC and HSR spin rotators. The sign of bending angle is defined following the beam trajectory. One can note that there is a considerable left-right asymmetry in bending angle distances of HSR rotators. As a

* Work supported by Brookhaven Science Associates, LLC under Contract No. DE-SC0012704 with the U.S. Department of Energy.

ISBN: 978-3-95450-227-1 ISSN: 2673-5490 doi:10.18429/JACoW-IPAC2022-WEPOST021

THEORETICAL STUDY OF LASER ENERGY ABSORPTION TOWARDS ENERGETIC PROTON AND ELECTRON SOURCES

I. M. Vladisavlevici*[1,2], D. Vizman[2], E. d'Humières[1]
[1]University of Bordeaux – CNRS – CEA, CELIA, Talence, France
[2]West University of Timisoara, Faculty of Physics, Timisoara, Romania

Abstract

Our main goal is to describe and model the energy transfer from laser to particles, in the transparent regime of laser-plasma interaction in the ultra-high intensity regime, and using the results obtained to optimize laser ion acceleration. We investigate the case of an ultra high intensity (10^{22} W/cm^2) ultra short (20 fs) laser pulse interacting with a near-critical density plasma made of electrons and protons of density 5 n_c (where $n_c = 1.1 \cdot 10^{21}$cm^{-3} is the critical density for a laser wavelength of $\lambda = 1\,\mu$m). Through 2D particle-in-cell (PIC) simulations, we study the optimal target thickness for the maximum conversion efficiency of the laser energy to particles. Theoretical modelling of the predominant laser-plasma interaction mechanisms predicts the particle energy and conversion efficiency optimization. Our studies led to an optimization of the target thickness for maximizing electron and proton acceleration.

INTRODUCTION

At the interaction of an ultra-high intensity laser pulse ($I \geq 10^{18}$ W/cm^2) with a plasma, the laser energy is transferred to the plasma constituents which are accelerated up to relativistic velocities for electrons. This energy transfer depends on the initial target and laser parameters [1–3], as well as on the interaction regime [4]. The absorption of laser energy determines the characteristics of the accelerated particles. There are multiple optimization models for maximizing the absorption of energy and the particles energies, depending on the interaction regime [5–8].

In this paper we analyse the case of an ultra-high intensity ultra-short laser pulse interacting with a near critical density target. We want to optimize the transfer of the laser energy to the particles and using the results obtained, to maximize the energy of the accelerated particles. In the first section is described the 2D particle-in-cell (PIC) simulation setup. In section 2 we report a dependence of the laser energy transfer on the target density. Section 3 presents the results on the optimization of the target thickness for maximizing electron and proton acceleration, which are in good agreement with the theoretical predictions. Finally, the main conclusions and perspectives are summarized in Section 4.

SIMULATION SETUP

The 2D PIC simulation setup consists of an ultra high intensity laser pulse interacting with a plasma (the target is considered fully ionized) as shown in Fig. 1. We consider a Gaussian laser profile, linearly polarized. The laser intensity is $I = 10^{22}$ W/cm^2 corresponding to a normalized field amplitude of $a_0 = 85$, where $a_0 = 0.85\sqrt{I_{W/cm^2}/10^{18} W/cm^2}\,\lambda_{\mu m}$. The laser wavelength is $\lambda = 1\,\mu$m and the laser transversal width is 25 µm. The pulse duration is 20 fs.

The plasma is made of electrons and protons and the initial proton and electron densities are equal $n_{i0} = n_{e0}$. The density has a uniform profile and the initial density is $n_{e0} = 5\,n_c$, where $n_c = 1.1 \cdot 10^{21}$cm^{-3} is the critical density for $\lambda = 1\,\mu$m. The target transversal width L_y is 30 µm and the target thickness L_x increases from 5 µm to 50 µm.

The simulation box size is 60 × 120 µm divided in 3840 × 7680 cells and the number of particles in each cell is 30 for each particle species. The simulations are performed with SMILEI [9] on the Curta machine of MCIA computing facility [10].

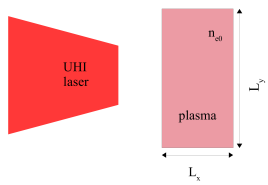

Figure 1: 2D PIC simulation setup: an ultra high intensity laser pulse irradiating a fully ionized target.

RESULTS ON ENERGY ABSORPTION

Fig. 2 shows the temporal evolution of the total energy in the simulations box. The initial electromagnetic laser energy is transferred to the plasma and is converted into 3 coefficients: A - the absorption coefficient representing the sum of the total kinetic energy of the particles and the radiation emitted by the electrons (see inset in Fig. 2) divided by the initial laser energy; R - the reflection coefficient representing the energy of the part of the laser which is reflected by the plasma and T - the transmission coefficient representing the energy of the part of the laser which passes through the target, both divided by the initial laser energy. The emission of radiation by electrons is simulated by two models: the continuous Landau-Lifshitz model ε_{rad} for low energy photons and a stochastic Monte Carlo model for the high energy photons [11].

Our goal is to maximize the absorption coefficient, by minimizing the other coefficients.

* iuliana.vladisavlevici94@e-uvt.ro

ISBN: 978-3-95450-227-1 ISSN: 2673-5490 doi:10.18429/JACoW-IPAC2022-WEPOST023

DESIGN OF A VERY LOW ENERGY BEAMLINE FOR NA61/SHINE

C. A. Mussolini*[1,2,3], P. N. Burrows[1,2], N. Charitonidis[3], Y. Nagai[4], E. D. Zimmerman[5]
[1]John Adams Institute for Accelerator Science, Oxford, United Kingdom
[2]St. John's College, University of Oxford, Oxford, United Kingdom
[3]CERN, Geneva, Switzerland
[4]Eötvös Loránd University, Budapest, Hungary
[5]University of Colorado, Boulder, USA

Abstract

A new, low-energy branch is being designed for the H2 beamline at the CERN North Experimental Area. This new low-energy branch would extend the capabilities of the current infrastructure enabling the study of particles in the low, 1–13 GeV/c, momentum range. The first experiment to profit from this new line will be NA61/SHINE (SPS Heavy Ion and Neutrino Experiment), a multi-purpose experiment studying hadron production in hadron-proton, hadron-nucleus and nucleus-nucleus collisions at the SPS. However, other future fixed target experiments or test-beam experiments installed in the downstream zones could also benefit from the low-energy particles provided. The proposed layout and expected performance of this line, along with estimates of particle rates, and considerations on the technical implementation of the beamline are presented in this contribution. A description on the instrumentation, which will enable particle-by-particle tagging, crucial for the experiments scope, is also discussed.

INTRODUCTION

Various neutrino experiments across the globe have shown significant interest in comprehensive hadron production measurements, especially in the low momentum regime, between 1–13 GeV/c. This demand has arisen due to the comparatively large uncertainties on the cross sections in these energy ranges which in turn has led to significant uncertainties in neutrino flux predictions [1]. To meet these requests, studies for the development on a new, custom made low-energy beamline has been underway for the past two years. This beamline would be housed in North Experimental Area [2] at CERN and would be serving the NA61/SHINE experiment [3] as a first user. NA61/SHINE is a fixed target experiment with the aims of: a) advancing the understanding of onset of deconfinement and the search for the critical point of strongly interacting matter [4] and b) obtaining precise hadron production measurements for improving calculations of neutrino beam flux in long-baseline neutrino oscillation experiments [5]. Additionally, the new line will enable a new range of measurements that today are not achievable with the current infrastructure. The new branch would be designed as an insertion to the H2 line by including a target to produce low-energy particles, which would be subsequently captured, momentum selected and transported downstream.

The development of this beamline will also expand the experimental capabilities of the CERN's North Area (NA), currently allowing the delivery of beams a with minimum momentum of ~30 GeV/c to all experiments, including NA61/SHINE. This is due to two reasons. Firstly, the H2 beamline, originally designed in the 1970s, was optimised for very high energy (300 GeV/c) beams. The power supplies used are therefore incapable of stably providing the currents required to operate at low energies. Additionally, secondary beams in the H2 line are produced at a primary target, T2 [6], which is located 600 meters upstream of the NA61/SHINE experiment. It is obvious that a large majority of the low energy (1–13 GeV/c particles) produced at T2 would decay before reaching the experimental detectors. Therefore the only way to tackle these issues is via the construction of a wholly new tertiary branch of the H2 line, where the tertiary, low-energy particles are produced closer to the experiment, inside the surface hall.

TRANSVERSE OPTICS

The beamline, shown in Fig. 1, consists of a target where the secondary, low-energy particles are produced [7]. Downstream, a high-acceptance quadrupole doublet, consisting of two large-aperture quadrupoles with opposite polarities, captures and maximises the number of accepted particles. The beam is then focused in the middle of a four-bend achromat, to momentum select the particles. Just before the experiment, a quadruplet focuses the beam onto the NA61/SHINE target, located just before the experiment's Time Projection Chamber (TPC). In the current layout envisaged, only components currently available at CERN, with well know properties, dimensions and performances, have been employed. The quadrupoles are large aperture 'QPL' magnets, while the dipoles are 'MBPL' type magnets [8].

The newly developed optics have an intrinsic momentum resolution better than 2%, however, momentum bites as low as 1% can be reached at the cost of particle rate. Figure 2, obtained using MAD-X PTC [9], shows the betatron oscillations of particles transported by the beamline for a beam with nominal momentum of 13 GeV/c. It is important to note the focusing of the beam in both the horizontal and vertical planes at the NA61/SHINE target, a critical parameter for the experiment.

These optics have been developed using a novel multi-parameter optimisation technique which requires scanning

* carlo.mussolini@cern.ch

ISBN: 978-3-95450-227-1 ISSN: 2673-5490 doi:10.18429/JACoW-IPAC2022-WEPOST024

PHYSICS BEYOND COLLIDERS: THE CONVENTIONAL BEAMS WORKING GROUP

C. A. Mussolini*[1,2], D. Banerjee, A. Baratto Roldan, J. Bernhard, M. Brugger, N. Charitonidis, G. D'Alessandro, L. Gatignon[3], F. Metzger[4], R. Murphy[1,5], E. Parozzi[6], S. Schuh-Erhard, F. Stummer[1,5], CERN, Meyrin, Switzerland
M. Van Dijk, EPFL Lausanne, Lausanne, Switzerland
A. Gerbershagen, PARTREC, UMCG, University of Groningen, Groningen, Netherlands
[1]also at John Adams Institute, United Kingdom
[2]also at University of Oxford, Oxford, United Kingdom
[3]also at Lancaster University, Lancaster, United Kingdom
[4]also at Helmholtz-Institut für Strahlen- und Kernphysik, Rheinische Friedrich-Wilhelms-Universität Bonn, Bonn, Germany
[5]also at Royal Holloway University of London, Egham, United Kingdom
[6]also at Universitá degli Studi di Milano Bicocca, Milano, Italy

Abstract

The Physics Beyond Colliders initiative aims to exploit the full scientific potential of the CERN accelerator complex and its scientific infrastructure for particle physics studies, complementary to current and future collider experiments [1]. Several experiments have been proposed to fully utilize and further advance the beam options for the existing fixed target experiments present in the North and East Experimental Areas of the CERN SPS and PS accelerators. We report on progress with the RF-separated beam option for the AMBER experiment, following a recent workshop on this topic. In addition we cover the status of studies for ion beams for the NA60+ experiment, as well as of those for high intensity beams for Kaon physics and feebly interacting particle searches. With first beams available in 2021 after a CERN-wide long shutdown, several muon beam options were already tested for the NA64mu, MUonE and AMBER experiments.

INTRODUCTION

The Physics Beyond Colliders (PBC) initiative is subdivided into several working groups, each with its independent, yet complementary goal. The Conventional Beams Working Group (CBWG) is a working group in the accelerators and technology sector, with the task of focusing on studies for fixed-target experiments using beams from the Super Proton Synchrotron (SPS) and the Proton Synchrotron (PS). The experiments served by the SPS are located in the two experimental halls EHN1 and EHN2, as well as in the experimental cavern ECN3 in the North Area (NA).

EHN1

EHN1 hosts currently both the NA61/SHINE and NA64e experiments.

NA60+

The NA60+ experiment plans to receive a beam of 10^7 lead ions per 10 s long spill at momenta of 30 – 158 A GeV/c. Operating for several weeks a year, the collaboration envisages to study the production of muon pairs and open charm final states. A new proposal of placing the detector in the H8 beam has been examined [2]. A more compact detector, additional shielding , installation of beam instrumentation, a modification of the zone access, and new beam optics have been developed by BE-EA, to be tested in 2022. A Letter of Intent by the collaboration is in preparation and expected soon.

NA61++

The NA61/SHINE collaboration is focusing on studies on the onset of deconfinement and on various neutrino-relevant cross section measurements. Its intended successor, NA61++, aims at continuing measurements with ion and hadron beams as before, but with 10 times higher beam intensity. Radiation measurements and simulations have been performed and it has been shown that for higher intensities, the shielding around the new PSD calorimeter has to be significantly reinforced. Furthermore, NA61++ intends several detector upgrades, which have been partly completed during the CERN Long Stop 2 and the annual shutdowns. For the NA61++ neutrino program, a new, low-energy branch is being designed. This new branch would extend the capabilities of the current infrastructure enabling the study of particles in the 1 – 13 GeV/c momentum range. Such a beamline will enable having measurements requested by several neutrino experiments, such as T2K, Hyper-K, DUNE, and others [3].

NA64e

The NA64 experiment is searching for sub-GeV dark matter candidates with the help of secondary electron beams in the H4 beam line [4], relying on synchrotron radiation tagging and tracking, as well as calorimetry to eliminate

* carlo.mussolini@cern.ch

ISBN: 978-3-95450-227-1 ISSN: 2673-5490 doi:10.18429/JACoW-IPAC2022-WEPOST025

A HIGH POWER PROTOTYPE OF A HARMONIC KICKER CAVITY

Gunn Tae Park, Gregory Grose, Jiquan Guo, Adam O'Brien, Sarah Overstreet, Robert Rimmer, Scott Williams, and Haipeng Wang, Jefferson Lab, Newport News, VA 23606, USA

Abstract

In this paper, we report the progress on a harmonic kicker development as an injection device for the Rapid Cycling Synchrotron (RCS) of the Electron-Ion Collider (EIC). A harmonic kicker, a beam exchange device that can deflect the beam at an ultra-fast time scale (a few ns), has been developed in Jefferson Lab [1], [2]. The high power prototype that can deliver more than a 100 kV kick at 7 kW was recently fabricated and will be tested with a beam at Upgraded Injector Test Facility (UITF) in Jefferson Lab.

INTRODUCTION

A harmonic kicker is a normal conducting RF device that delivers a deflecting kick on incoming bunches selectively over an ultra-fast time scale (~ ns). This becomes possible with an elaborate combination of five harmonic modes (see Fig. 1), which can be straightforwardly accommodated in a co-axial structure of the quarter wave resonator (QWR). Its first prototype was developed based on 95.2 MHz with a potential application as a beam exchange device to the Circulator Cooler Ring (CCR) of the Jefferson Lab Electron Ion Collider (JLEIC) [3].

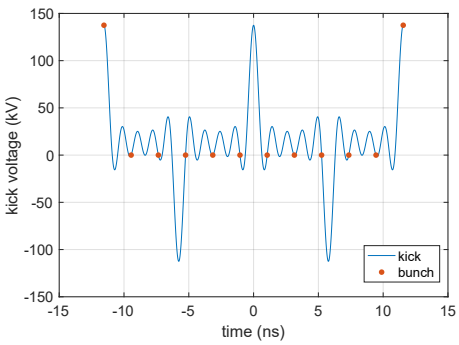

Figure 1: The temporal harmonic kick profile. The red dots correspond to the bunches at 476.3 MHz.

The upcoming second prototype (see Table 1 for the figures of merit), based on 86.6 MHz, is vacuum tight and prepared for the high power operation with the thermal analysis and cooling scheme applied, as well as for high current operation with its beam-coupling impedance checked [4]. This prototype can be beam-tested demonstrating its capability to selectively deflect the beam on MHz time scale. We plan the beam test at the UITF in Jefferson Lab. A successful test outcome would solidify the feasibility of the cavity as a beam injection device in the RCS of the EIC [5], [6], which is a recently found application of the kicker. In the RCS (as per a default 4-bunch scheme), a pair of a harmonic kickers—one with 147.8 MHz plus its third harmonic and the other with 2nd harmonic—can generate a sharp kick on injected bunches at a multiple of $f_{\mathrm{kick}} = 73.9$ MHz, while not affecting passing bunches at $f_{\mathrm{bunch}} = 591$ MHz (For more details, see [7]).

For a successful aforementioned operation, building and stably maintaining the designed kick profile (Fig. 1) in the real cavity is of critical importance. This is in turn achieved by the precise tuning of the frequencies, amplitudes, phases of all the harmonic modes. Thus during the fabrication of the cavity, special efforts were made to avoid geometry deformation on frequency-sensitive region of the cavity (for accurate frequency control), for precise insertion/alignment of tuning plungers (frequency) and power coupler antenna (for phase and amplitude via RF coupling β's and also frequency) so that the deviation in those RF parameters during operation is well-within tolerance limit of the amplifier and control system (the LLRF and tuning system).

Table 1: The Figures of Merit for a Harmonic Kicker Cavity (f : Freq. of Harmonic Modes, R/Q_0 : Shunt Resistance Over Quality Factor, P_{wall} : Wall Loss, β : RF Coupling Constant, G : Geometry Factor, V_{k} : Kick Voltage, The Numbers are for the High Power Operation as Originally Intended)

Parameter	1st	2nd	3rd	4th	5th
f (MHz)	86.6	259.8	433	606.2	779.4
R/Q_0 (Ω)	241	76	41	25	14
P_{wall} (W)	0.47	0.83	1.19	1.69	2.66
β	0.74	1.21	1.22	1.20	1.25
G (Ω)	15	43	77	107	133
V_{k} (kV)	-25	-25	-25	-25	-25

FABRICATION OF THE KICKER CAVITY

The kicker cavity parts were made of OFC (Oxygen free copper) and fabricated along two sub-assembly lines. One is an outer tube-line, where the parts were joined mostly by brazing, and the other is inner conductor-line, where the parts were machined and electron beam welded. In Figs. 2 and 3, two sub-assemebly groups are shown. The outer tube group in Fig. 2 is made from 4 mm thick OFC tube with multiple ports brazed into. Brazing was done in a high vacuum furnace (see Fig. 2a) at 1035° (for 30 minutes) with a standard filler alloy 65Cu/35Ag. During the braze, the deformation of the cavity occurred despite the rounding clamps and other fixtures, around the port joints in particular. Consequently, the multiple repair brazes of the ports with the filler alloys at lower melting temperatures were inevitable (see Fig. 2b). The outer tube after going through many brazing cycles soft-

ISBN: 978-3-95450-227-1 ISSN: 2673-5490 doi:10.18429/JACoW-IPAC2022-WEPOST026

CONCEPTUAL DESIGN OF THE FCC-ee BEAM DUMPING SYSTEM

A. M. Krainer*, W. Bartmann, M. Calviani, Y. Dutheil, A. Lechner, A. Perillo-Marcone, B. Andreu-Muñoz, F.-X. Nuiry, R. Ramjiawan[1], CERN, Geneva, Switzerland
[1]also at John Adams Institute, Oxford, UK

Abstract

The Future Circular electron-positron Collider (FCC-ee) will feature stored beam energies of up to 18 MJ. This is a factor 100 higher than any current or past lepton collider. A safe and reliable disposal of the beam onto a beam dump block is therefore critical for operation. To ensure the survival of the dump core blocks, transversal dilution of the beam is necessary. To reduce the complexity of the system and guarantee high system availability, an optimized, semi-passive beam dumping system has been designed. The main dump absorber design has been optimized following recent studies for high energy dump block materials for the LHC High Luminosity upgrade. First simulations regarding the radiation environment of the dumping system have been carried out, allowing the definition of preliminary constraints for the integration with respect to radiation sensitive equipment. The performance of the system has been evaluated using Monte-Carlo simulations as well as thermo-mechanical Finite-Element-Analysis to investigate potential material failure and assess safety margins. An experiment at the CERN HiRadMat facility has been carried out and preliminary results show good agreement with simulations.

INTRODUCTION

To ensure operation of the FCC-ee, beam disposal needs to be done in a safe and controlled way within one turn of the beam following a dump trigger event. The nominal operation foresees on average 2 beam dumps per day, as outlined in the FCC-ee Conceptual Design Report [1]. Depending on the operation mode, stored beam energies range from 0.3 MJ up to 18 MJ (see Table 1). To ensure the survival of the beam dump core, the beam has to be diluted. In previous studies a dilution system, similar to the one currently used for the LHC, was assumed [2]. There, dilution is achieved by using dedicated pulsed kicker magnets, followed by ~ 700 m of drift space before the dump block [3]. This dilution system works very well, but also introduces actively driven components and therefore a potential risk of dilution failure. To ensure high availability of the system and also minimizing the number of potential points of failure, a new semi-passive beam dumping system has been designed, using a defocusing triplet structure and passive beam diluters (spoilers). Particle transport simulations have been executed using the FLUKA Monte Carlo code [4–6], as well as finite element analysis, using the LS-DYNA [7, 8] explicit mechanical solver, 2-way coupled with an iterative thermal solver. In this paper the performance of this system is shown for Z pole operation, which is the most challenging due to the stored energy[1].

* alexander.krainer@cern.ch

Table 1: Parameters for different beam energies and physics modes [9]

	Z	WW	ZH	$t\bar{t}$
Beam Energy [GeV]	45.6	80	120	182.5
Bunches / beam	12000	880	272	40
Bunch population [10^{11}]	2.02	2.91	1.86	2.37
Stored beam energy [MJ]	17.7	3.28	0.97	0.28

EXTRACTION LINE LAYOUT

The extraction line is located in one of the short (~ 1.4 km long) straight sections. Since the extraction line is shorter than the full length of the straight section, flexibility for placement of other components is ensured. In Fig. 1 a schematic overview of the extraction system is shown, whereas a detailed description of this system is given in [10]. The overall length of the system is mainly defined by the chosen deflection angle of ~ 7 mrad and the resulting lateral separation between the main ring and the beam dump.

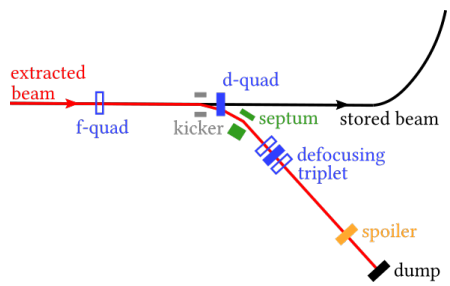

Figure 1: Schematic overview of the FCC-ee extraction system [10].

DILUTION SYSTEM

The full semi-passive dilution concept is described in [10]. Dilution of the beam is achieved in 2 steps. First the extracted beam is blown up by a defocusing magnetic triplet structure and ~ 600 m of drift space to increase the transversal beam spot size from $\sigma_x \times \sigma_y = 0.5\,\text{mm} \times 0.024\,\text{mm}$ at the triplet, to $\sigma_x \times \sigma_y = 11.3\,\text{mm} \times 1.2\,\text{mm}$ at the first spoiler. Secondly, three consecutive spoilers, made of isostatic graphite, are placed in the beam path to create dilution by multiple-Coulomb interactions. After another 70 m of drift space the beam spot size at the front of the beam dump is $\sigma_x \times \sigma_y = 21\,\text{mm} \times 11\,\text{mm}$. The full beam is then absorbed by the beam dump block.

ISBN: 978-3-95450-227-1 ISSN: 2673-5490 doi:10.18429/JACoW-IPAC2022-WEPOST029

FIRST START-TO-END SIMULATIONS OF THE 6 GeV LASER-PLASMA INJECTOR AT DESY

S. A. Antipov*, I. Agapov, R. Brinkmann, Á. Ferran Pousa, M. Jebramcik, A. Martinez de la Ossa, M. Thévenet, Deutsches Elektronen-Synchrotron DESY, 22607 Hamburg, Germany

Abstract

DESY is studying the feasibility of a 6 GeV laser-plasma injector for top-up operation of its future flagship synchrotron light source PETRA IV. A potential design of such an injector involves a single plasma stage, a beamline for beam capture and phase space manipulation, and a X-band rf energy compressor. Numerical tracking with realistic beam distributions shows that an energy variation below 0.1%, rms and a transverse emittance about 1 nm-rad, rms can be achieved under realistic timing, energy, and pointing jitters. PETRA IV injection efficiency studies performed with a conservative 5% beta-beating indicate negligible beam losses for the simulated beams during top-up. Provided the necessary progress on high-power lasers and plasma cells, the laser plasma injector could become a competitive alternative to the conventional injector chain.

INTRODUCTION

Using plasma as an accelerating medium has been attracting attention in the accelerator community for years, promising unmatched accelerating gradients and thus compact, energy-efficient acceleration [1]. Laser-plasma acceleration (LPA) in particular has shown significant progress, achieving (although in different setups) GeV energies [2], narrow energy spectrum [3], and low emittance [4]. Recently, the LUX LPA at DESY demonstrated a percent level of energy stability during a 24 hour long operation run [5].

This progress encourages considering an LPA as a possible injector for various applications. In a synchrotron light source, an LPA injector could be used to accumulate charge in the storage ring, significantly lowering the load on the conventional injector chain. The proposed injector is based on an active energy compensation scheme [6], utilizing an X-band rf cavity to compensate potential energy fluctuations of the LPA beam [7]. A low-energy demonstrator of the approach, based on the existing driving laser infrastructure [8] as well as already demonstrated plasma cell performance, is presently being designed at DESY [7].

LPA BEAM FOR TOP-UP INJECTION

PETRA IV is a future 6 GeV fourth generation light source [9]. In its Brightness operation mode it will store 1900 electron bunches of 1 nC each with a ~ 5 h lifetime. In its baseline scenario the machine will use an off-axis accumulation scheme to top up beam intensity as well as for the initial filling. In the off-axis accumulation mode one would have to top up about 100 pC at a 1 Hz repetition rate to compensate for beam losses (e.g. from Touschek effects) and keep the total charge in the ring constant, while also maintaining bunch-to-bunch charge fluctuations within 10%. To achieve an efficient off-axis injection the rms geometric emittance would have to be $\lesssim$ 1 nm and the rms relative energy spread and variation well below 1% [10].

A research on a suitable 6 GeV plasma cell parameters is currently under way at DESY. While it is in its early stage, preliminary numerical simulations show that with a single LPA stage driven by a ~ 20 J laser pulse could generate suitable beams. Figure 1 shows the LPA beam that has been obtained using a bayessian optimization [11] in the FBPIC particle-in-cell (PIC) code [12], taking into account the laser-plasma interaction, wakefields, beam loading, and a plasma density downramp [13]. The electron bunch at the exit of the plasma cell has a charge of 87 pC, a transverse emittance below 1 nm, rms divergence < 0.2 mrad, rms bunch length of 3 µm, and an rms momentum spread of 10^{-2} (Table 1). This LPA beam can then be captured and manipulated by a specially designed beamline.

BEAMLINE DESIGN

The injector beam line is based solely on proven conventional technology and pursues three main objectives: (a) capture the LPA electron beam with minimum chromatic emittance degradation; (b) improve its energy spread and stability to a sub-permille level; (c) match the optics functions to those at the injection point of PETRA IV (Table 1). Figure 2 (top) depicts a schematic view of the beamline and its linear lattice functions (bottom). First, the LPA beam is captured by a triplet of strong quadrupole mag-

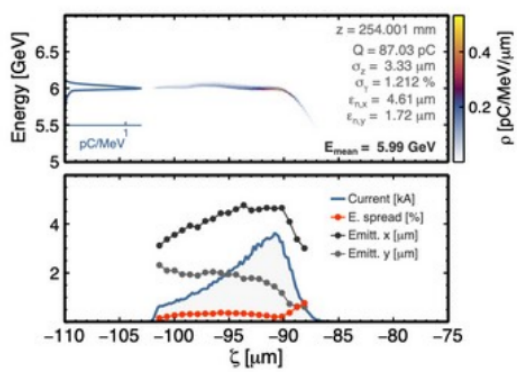

Figure 1: Estimated parameters of a potential LPA beam. Top – a longitudinal distribution of bunch energy spread; bottom – bunch current and normalized slice emittances. Results of an FBPIC [12] simulation; head is on the right.

* Sergey.Antipov@desy.de

ISBN: 978-3-95450-227-1 ISSN: 2673-5490 doi:10.18429/JACoW-IPAC2022-WEPOST030

MULTITASK OPTIMIZATION OF LASER-PLASMA ACCELERATORS USING SIMULATION CODES WITH DIFFERENT FIDELITIES

A. Ferran Pousa[1], S. Jalas[2], M. Kirchen[1], A. Martinez de la Ossa[1], M. Thévenet[1], S. Hudson[3], J. Larson[3], A. Huebl[4], J.-L. Vay[4], R. Lehe[4]
[1]Deutsches Elektronen-Synchrotron DESY, Notkestr. 85, Hamburg, Germany
[2]Department of Physics Universität Hamburg, Luruper Chaussee 149, Hamburg, Germany
[3]Argonne National Laboratory, Lemont, IL, USA
[4]Lawrence Berkeley National Laboratory, Berkeley, CA, USA

Abstract

When designing a laser-plasma acceleration experiment, one commonly explores the parameter space (plasma density, laser intensity, focal position, etc.) with simulations in order to find an optimal configuration that, for example, minimizes the energy spread or emittance of the accelerated beam. However, laser-plasma acceleration is typically modeled with full particle-in-cell (PIC) codes, which can be computationally expensive. Various reduced models can approximate beam behavior at a much lower computational cost. Although such models do not capture the full physics, they could still suggest promising sets of parameters to be simulated with a full PIC code and thereby speed up the overall design optimization.

In this work we automate such a workflow with a Bayesian multitask algorithm, where each task has a different fidelity. This algorithm learns from past simulation results from both full PIC codes and reduced PIC codes and dynamically chooses the next parameters to be simulated. We illustrate this workflow with a proof-of-concept optimization using the Wake-T and FBPIC codes. The libEnsemble library is used to orchestrate this workflow on a modern GPU-accelerated high-performance computing system.

INTRODUCTION

Laser-plasma accelerators (LPAs) are a promising acceleration technology that could have applications in high-energy physics, medicine, and materials science [1]. Many of these applications require finely tuning the different parameters of a given setup (e.g., plasma density, laser intensity, beam profile) in order to attain optimal performance (e.g., optimal beam quality). This *design optimization* is usually done by running a particle-in-cell (PIC) simulation for each prospective set of parameters in order to assess its corresponding performance (often quantified by a single objective function such as the final beam energy spread). Because these simulations are computationally expensive, however, one would like to make informed choices about which set of parameters to evaluate, so as to find the optimal configuration with as few simulations as possible.

One method to find these parameters is Bayesian optimization [2], whereby a Gaussian process model [3] of the objective function over the parameter space is progressively learned. At each iteration of this method, the model suggests the most promising set of parameters to be assessed by the simulation, and the simulation result is in turn used to update and refine the model. Importantly, the feasibility of Bayesian optimization for automated tuning of LPA setups has recently been demonstrated [4, 5].

A further step to reduce computational cost is to perform some of the simulations at a lower fidelity. Indeed, a number of *reduced* codes for laser-plasma acceleration have been developed that make different types of approximations. These approximations can result in dramatically faster simulations, at the cost of a potential loss of accuracy. Examples of these approximations include assuming cylindrical symmetry [6], averaging over the fast laser oscillations [7], or assuming the wakefield to be quasi-static [7, 8].

Here we show that incorporating lower-fidelity simulation output from reduced PIC codes into a Bayesian optimization method can reduce the overall computational cost of obtaining a high-fidelity solution by an order of magnitude. The combination of PIC codes with different fidelities into a single optimization is enabled by the multitask Bayesian optimization (MTBO) algorithm [9, 10], a special case of multifidelity optimization that operates with two levels of fidelity (i.e., two *tasks*): an inexpensive, low-fidelity model for broad parameter exploration and a computationally demanding, high-fidelity model for which only a reduced number of well-targeted simulations are performed. Incidentally, we note that other types of multifidelity algorithms have also been shown to perform well in a number of problems, including with multiobjective optimization [11].

MULTITASK BAYESIAN OPTIMIZATION

The MTBO algorithm [9, 10] builds a Gaussian process model [3] of the simulation output (a scalar that quantifies beam quality in our case) as a function of both the vector of design parameters x (e.g., plasma density, beam profile parameters) and the fidelity d. (We let $d = 1$ denote low-fidelity and $d = 2$ the high-fidelity, and we denote the respective simulation output at a given fidelity by $f_d(x)$.) Accordingly, the correlation kernel used inside the Gaussian process model depends on both the parameters x and the fidelity d and is assumed to be of the form $k((d, \mathbf{x}), (d', \mathbf{x}')) = B_{dd'}\kappa(x - x')$, where κ is typically a Mattérn kernel [3] and B is a 2×2 symmetric matrix. In practice, the coefficients of B (as well as the parameters of κ) are hyperparameters that are automatically determined by maximizing the marginal likelihood of the

ISBN: 978-3-95450-227-1 ISSN: 2673-5490 doi:10.18429/JACoW-IPAC2022-WEPOST031

RHIC POLARIZED PROTON OPERATION IN RUN 22*

V. Schoefer†, E.C.Aschenauer, D. Bruno, K.A. Drees, W. Fischer, C. J. Gardner, K. Hock, H. Huang, R. Hulsart, C. Liu, Y. Luo, I. Marneris, G. Marr, A. Marusic, F. Meot, K. Mernick, R. Michnoff, M. Minty, J. Morris, A. Poblaguev, V. Ptitsyn, V. Ranjbar, D. Raparia, G. Robert-Demolaize, J. Sandberg, W. B. Schmidke, F. Severino, T. Shrey, P. Thieberger, J. Tuozzolo, M. Valette, K. Yip, A. Zaltsman, A. Zelenski, K. Zeno, Brookhaven National Laboratory, Upton,NY, USA

Abstract

The Relativistic Heavy Ion Collider (RHIC) Run 22 physics program consisted of collisions with vertically polarized proton beams at a single collision point (the STAR detector). During initial startup of the collider, power outages damaged two of the coils in one of the RHIC helical dipole snake magnets used for polarization preservation in the Blue ring. That snake was reconfigured for use as a partial snake. We will outline some of the remediating measures taken to maximize polarization transmission in this configuration. These measures included changing the colliding beam energy from 255 GeV to 254.2 GeV to adjust the spin closed orbit at store and adjustment of the field in the other helical dipole in the Blue ring to improve injection spin matching. Later in the run, the primary motor generator for the AGS (the injector to RHIC) failed and a lower voltage backup had to be used, resulting in a period of lower polarization. Other efforts include detailed measurement of the stable spin direction at store and the commissioning of a machine protection relay system to prevent spurious firing of the RHIC abort kickers.

INTRODUCTION

The RHIC physics program in Run 22 required 16 weeks of colliding beam operations with 255 GeV polarized proton beams at one interaction point (the STAR detector). An additional sixteen days of collider operation were allotted for coherent electron cooling (CeC) experiments with gold beam which is discussed elsewhere in these proceedings [1].

The figures of merit for the STAR physics programs were LP_b^2 (for their forward physics) and LP_bP_y (for their mid-rapidity physics program), where L is the luminosity and P_b and P_y are the polarizations of the Blue and Yellow beams respectively. Each program required an integrated figure of merit of 120 pb^{-1}, which, assuming 55% average polarization in each beam, requires an integrated luminosity of about 400 pb^{-1}. It was also required that the instantaneous luminosity be leveled near a target value of $1.35 \times 10^{32} cm^{-2} s^{-1}$, which was accomplished using beta squeezes throughout the store. A nominal 8 hour store began at $\beta^* = 1.5$ m, squeezed to 1.2 m 3 hours into the store, and to 1.0 m at 6 hours into the store.

* Work supported by Brookhaven Science Associates, LLC under Contract No. DE-AC02-98CH10886 with the U.S. Department of Energy.
† schoefer@bnl.gov

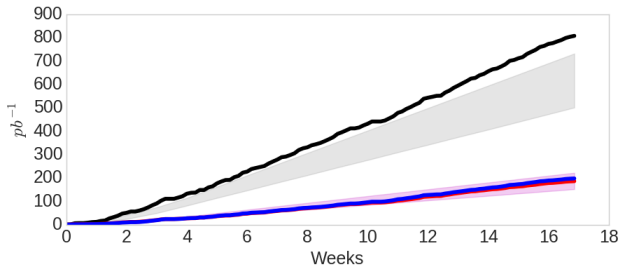

Figure 1: Integrated luminosity, L (black) and figures of merit LP_b^2 (blue) and LP_bP_y (red). Shaded regions show pre-run projections.

Delivered integrated luminosity and figures of merit are shown in Fig. 1.These delivered figures of merit correspond to total STAR-reported sampled figures of merit of 117.2 pb^{-1} (mid-rapidity) and 128 pb^{-1} (forward), which are97.7% and 107% of the respective targets.

HELICAL DIPOLE FAILURE

The primary method for preserving polarization during the RHIC acceleration ramp is a pair of helical dipole magnets (so-called Siberian snakes) in each ring. These snake magnets, placed opposite one another at 3 and 9 o'clock in the ring, each provide a full 180°spin rotation about an axis in the horizontal plane at ±45°to the beam direction. In this configuration depolarizing resonances are avoided since the design spin tune is fixed at 0.5 and the stable spin direcion aligned vertical at all energies [2].

Each RHIC snake consists of four helical modules (labeled #1-#4 in beamline order) [3]. In ordinary operation, the modules are wired in pairs, #1 with #4 and #2 with #3. In the first two weeks of beam operation, two coils in the Blue snake at 9 o'clock were damaged in two separate power outage incidents. After each incident, resistance measurements indicated that one of the coils had developed an open (coil #2 was damaged in the first incident and coil #4 in the second). Fortunately, the coils can be individually rewired from outside the cryostat. Wiring coils #1 and #3 in series, with coil #1 in the reversed polarity from normal operation, produces a "partial" snake, one that rotates the spin by $< 180°$ in one pass. In the modified configuration, the partial snake rotated the spin by 163° about an angle still in the horizontal plane, but at only −42° to the longitudinal axis.

ISBN: 978-3-95450-227-1 ISSN: 2673-5490 doi:10.18429/JACoW-IPAC2022-WEPOST032

STATUS REPORT OF THE 50 MeV LPA-BASED INJECTOR AT ATHENA FOR A COMPACT STORAGE RING*

E. Panofski†, C. Braun, J. Dirkwinkel, J. B. Gonzalez, L. Hübner, T. Hülsenbusch, L. Jeppe, M. Kirchen, A. R. Maier, P. Messner, J. Osterhoff, G. Palmer, A. Walker, P. Winkler,
Deutsches Elektronen Synchrotron, 22607 Hamburg, Germany
T. Eichner, S. Jalas, M. Schnepp, M. Trunk, C. Werle
University Hamburg, 20148 Hamburg, Germany
B. Härer, E. Bründermann, A.-S. Müller, A. Papash, C. Widmann
Karlsruhe Institute of Technology, 76131 Karlsruhe, Germany
M. C. Kaluza, A. Sävert, Helmholtz Institute Jena, 07743 Jena, Germany

Abstract

Laser-based plasma accelerators (LPA) have successfully demonstrated their capability to generate high-energy electron beams with intrinsically short bunch lengths and high peak currents at a setup with a small footprint. These properties make them attractive drivers for a broad range of different applications including injectors for RF-driven, ring-based light sources. In close collaboration the Deutsches Elektronen-Synchrotron (DESY), the Karlsruhe Institute of Technology (KIT) and the Helmholtz Institute Jena (HIJ) aim to develop a 50 MeV plasma injector and demonstrate the injection into a compact storage ring. This storage ring will be built within the project cSTART at KIT.

As part of the ATHENA (Accelerator Technology HElmholtz iNfrAstructure) project, DESY will design, setup and operate a 50 MeV plasma injector prototype for this endeavour. This contribution gives a status update of the 50 MeV LPA-based injector and presents a first layout of the prototype design at DESY in Hamburg.

INTRODUCTION

The development and operation of laser plasma accelerators have achieved significant milestones in the last years. The demonstration of generating and accelerating high energy [1], reproducible and stable [2], few-fs short [3] electron beams over several hours raises the hope to drive various applications with LPA-based facilities. In addition, a better understanding of injection processes and plasma effects [4] as well as the implementation of machine learning tools [5] pushes the achievable beam quality beyond well-known limits of this technology.

One innovative application of LPAs will be the usage as next generation of new driver-technology for storage rings and ring-based light sources. Beside a small footprint of the setup, the big potential of LPAs lies in their capability of generating electron beams with short bunch lengths and high peak currents. In particular, these features will allow to increase the current performance of synchrotron light sources. Physics on much shorter time scales can be investigated with the radiated photon beam. Further, the radiation spectrum can be extended far into the THz regime [6].

* Work supported by ATHENA, a project of the Helmholtz Association.
† eva.panofski@desy.de

Three German research institutes, DESY, KIT and HIJ, have started a collaboration for first proof-of-principle studies on an LPA-based plasma injector for the large acceptance, compact storage ring of the cSTART project at KIT. DESY is designing a 50 MeV plasma injector prototype, whose status will be reported in this contribution.

LASER-PLASMA INJECTOR PROJECT

The laser-plasma injector project is part of the ATHENA program [7]. Since 2018, ATHENA supports to build an R&D infrastructure platform in Germany to demonstrate the applicability of plasma-based accelerators in different fields. The application as an injector requires from the LPA a stable, reproducible, high quality electron beam with controlled transverse emittance and energy spread. Consequently, the accelerator design, available diagnostics and active feedback loops must be adapted for this purpose.

The injector prototype will be designed, setup and commissioned at DESY Hamburg. After successful demonstration of electron beams with injector-type quality, the facility will be used for injection into the large-acceptance, compact storage ring of the cSTART project at KIT [8-10]. Foreseen as an R&D facility the special lattice of the ring has been carefully optimized to handle an electron beam injected from an LPA with ultra-short bunch length, relatively large emittance and large energy spread compared to a beam accelerated by an RF system. An injection energy of 50 MeV has been chosen in order to enable the comparison of the performance of two injectors, FLUTE, a 50 MeV linear RF accelerator and the LPA injector [11]. Table 1 lists the key parameters of the storage ring [12].

Table 1: Parameters of the cSTART Lattice

Parameters	cSTART lattice
Circumference	43.2 m
Beam energy	50 MeV
Momentum acceptance	±5.5%
Momentum compaction	(-1 to +2)·10^{-2}
Dynamic aperture (horz./vert.)	15 mm/10 mm

The storage ring within the cSTART project is currently in procurement. The latest lattice design of the compact storage ring is displayed in Figure 1 [12].

ISBN: 978-3-95450-227-1 ISSN: 2673-5490 doi:10.18429/JACoW-IPAC2022-WEPOST034

MAGNETIC CHARACTERIZATION OF A SUPERCONDUCTING TRANSVERSE GRADIENT UNDULATOR FOR COMPACT LASER WAKEFIELD ACCELERATOR-DRIVEN FELs*

K. Damminsek†, A. Bernhard, A. W. Grau, H. J. Cha, M. Ning, S. C. Richter, R. Rossmanith, Y. Tong, A.-S. Müller, Karlsruhe Institute of Technology, Karlsruhe, Germany

Abstract

A transverse gradient undulator (TGU) is a key component compensating for the relatively large energy spread of Laser Wakefield Accelerator (LWFA)-generated electron beams for realizing a compact Free Electron Laser (FEL). A superconducting TGU with 40 periods has been fabricated at the Karlsruhe Institute of Technology (KIT). In this contribution, we report that the superconducting TGU has been commissioned with nominal operational parameters at an off-line test bench. An experimental set-up for mapping the magnetic field on a two-dimensional grid in the TGU gap has been employed for the magnetic characterization. We show the first preliminary results of these measurements showing the longitudinal quality, the transverse gradient and the transient behaviour of the superconducting TGU field.

INTRODUCTION

A superconducting transverse gradient undulator (TGU) demonstrator with 40 periods has been designed and constructed at the Karlsruhe Institute of Technology (KIT) [1] with the purpose of proving the technical feasibility of short-period and high-transverse gradient undulators as well as experimentally demonstrating the TGU's capability to generate narrow-bandwidth radiation in spite of a large energy spread of the electron beam. The TGU scheme has been discussed as a viable solution to enable Free Electron Lasers (FEL) driven by laser wakefield accelerators (LWFA) [2]. A schematic layout of a LWFA-driven TGU radiation source or FEL is shown in Fig. 1. It consists of a LWFA-based electron source, a dispersive beam transport line, for example a dogleg chicane, and the TGU. The design parameters of the superconducting TGU demonstrator under investigation here are listed in Table 1.

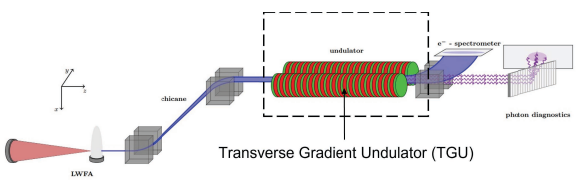

Figure 1: Schematic layout of a LWFA-based Transverse Gradient Undulator radiation source [3].

Table 1: Design parameters of the superconducting TGU demonstrator [4, 5]. E_0 denotes the nominal beam energy.

Parameter	Value	Unit
Relative energy acceptance ($\Delta E/E_0$)	±10	%
Period number (N_u)	40	
Period length	10.5	mm
Gap width (at $x(E_0)$)	2.40	mm
Magnetic flux density on axis $x(E_0)$	1.1	T
Undulator parameter (at $x(E_0)$)	1.10	
Transverse K gradient	150	m^{-1}
SC wire material	Nb-Ti	
Operating current	750	A

The TGU has been commissioned and investigated using its own cryostat, designed and manufactured by the company CRYOVAC, Germany. The cold mass is conduction-cooled employing a liquid-Helium thermosiphon scheme. The cool-down of the TGU to operating temperature (4.3 – 4.4 K) takes about 9 days [6].

MAGNETIC POWERING TEST

For the magnetic powering tests the two superconducting coils constituting the TGU were connected in series and powered through two pairs of high temperature superconductor (HTS) current feedthroughs with an ampacity of 600 A each, as schematically depicted in Fig. 2. Example TGU coil temperature recordings during the powering test are shown in Fig. 3.

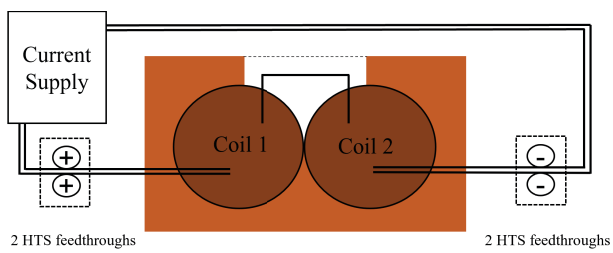

Figure 2: Circuit diagram of the TGU during the powering tests and magnetic measurements. The undulator coils are connected in series which allows to power the undulator coils through two parallel-connected pairs of 600 A-HTS feedthroughs up to the quench limit at 850 A.

In this example, the current is ramped with a ramping speed of 0.2 A s^{-1} from 0 to 700 A, leading to a temperature

* This work is supported by the Development and Promotion of Science and Technology Talents Project (DPST), Thailand) and by the Federal Ministry of Education and Research (BMBF), Germany, under grant No. 05K19VKA.
† kantaphon.damminsek@kit.edu

ISBN: 978-3-95450-227-1 ISSN: 2673-5490 doi:10.18429/JACoW-IPAC2022-WEPOST035

SPECTROSCOPIC MEASUREMENTS AS DIAGNOSTIC TOOL FOR PLASMA-FILLED CAPILLARIES*

S. Arjmand†,[1], University of Sapienza, Rome, Italy
[2]also at INFN, Laboratori Nazionali di Frascati, Frascati, Italy
M. P. Anania[2], A. Biagioni[2], G. Costa[2], L. Crincoli[2],
M. Ferrario[2], M. Del Franco[2], M. Galletti[2], V. Lollo[2], D. Pellegrini[2], R. Pompili[2]
D. Giulietti[3], Physics Department, University of Pisa, Pisa, Italy
A. Zigler[4], Racah Institute of Physics, Hebrew University of Jerusalem, Jerusalem, Israel

Abstract

The research concerns the study of the plasma sources for plasma-based accelerators (PBAs) at the SPARC_LAB test-facility (LNF-INFN). The interest in compact accelerators, overcoming the gigantism of the conventional radio-frequency (RF) accelerators, is growing in High Energy Physics. The plasma-based accelerating gradients can attain the GV/m scale. At the SPARC_LAB test-facility, a plasma device is under development. It consists of a capillary in which one or more inlets inject neutral gas (Hydrogen), ionized by a high-voltage (HV) discharge. Electron density has been measured as a function of time through the Stark broadening profiles of the Balmer line.

INTRODUCTION

The cutting-edge generation of accelerators based on plasma technology can force electron bunches to GeV energies within centimeter lengths [1, 2]. Such high accelerating gradients are produced by electron density modulations induced in the plasma by an intense and ultra-short laser pulse (Laser Wakefield Acceleration, LWFA) or a relativistic electron bunch (Particle Wakefile Acceleration, PWFA) [3–6]. The innovative acceleration technique proposed by Tajima and Dawson [7] in 1979 has prompted an expansive and rapidly extending field of research desiring to decrease the typical dimensions of the accelerating frames to the small-scale and invent futuristic miniaturized devices. This technique attains huge accelerating fields up to GV/m compared to the conventional radio-frequency (RF) technology limited to MV/m. The particle wakefield acceleration exploits the electric fields of a plasma wave compelled by a relativistic electron bunch used as a driver [8]. Such fields can be efficiently applied to a trailing bunch, the witness, which accumulates a part of the energy deposited by the driver. The experiment at the SPARC_LAB test-facility has been performed within the EuPRAXIA framework [9] by employing two bunches, a driver tracked by a witness (accelerated beam), propagating in a plasma confined in a 3 cm/long discharge capillary. Various methods are employed to generate the plasma from a neutral gas, such as Hydrogen, using a high-voltage (HV) discharge [2] or an ionizing laser pulse [10]. The plasma is dynamically formed shot-by-shot with a typical lifetime of a few tens of microseconds, its stability and reproducibility are essential features for the quality of the accelerated electron bunch. The plasma characteristics inside the gas-filled capillary depend on several parameters like its pressure and temperature, the applied voltage, the geometric of the capillary itself. The shape and the position of the gas injectors can influence the shot-to-shot stability and uniformity of the plasma. The features of the plasma inside and just outside the capillary are fundamental for preserving the electron bunch quality during the acceleration.

EXPERIMENTAL APPARATUS

The overall setup used to form and characterize the plasma behavior has shown in Fig. 1. The main component for plasma-based accelerators is a plasma-discharge capillary. It is a 3D-printed capillary tube, filled with Hydrogen by means of two injectors. Different diameters (1 and 2 mm) were tested.

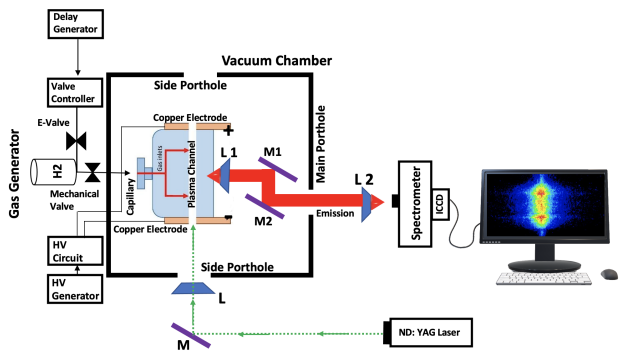

Figure 1: Scheme of the experimental set-up used at the SPARC_LAB test-facility to form and characterize plasma in a gas-filled capillary. An optical path is designed for guiding the plasma light into the spectrometer. L1, L2, represent lenses and M1, M2 indicate mirrors. The Copper electrodes have mounted on the capillary extremities. An Nd: YAG laser probe of 532 nm is used for the optical alignment.

We used capillaries with different geometries to oversee how the geometry can affect the plasma density distribution. Two gas inlets inject the Hydrogen gas inside the channel by

* Work supported by EU Commission in the Seventh Framework Program, Grant Agreement 312453-EuCARD-2, the European Union Horizon 2020 research, innovation program with the Grant Agreement No. 653782 (EuPRAXIA), and INFN with the GRANT73/PLADIP grant.
† sahar.arjmand@lnf.infn.it

ISBN: 978-3-95450-227-1 ISSN: 2673-5490 doi:10.18429/JACoW-IPAC2022-WEPOST039

MAPPING CHARGE CAPTURE AND ACCELERATION IN A PLASMA WAKEFIELD OF A PROTON BUNCH USING VARIABLE EMITTANCE ELECTRON BEAM INJECTION

E. Granados†, L. Verra[1], A.-M. Bachmann[1], E. Chevallay, S. Doebert, V. Fedosseev, F. Friebel, S. Gessner, E. Gschwendtner, S. Y. Kim[2, 3], S. Mazzoni, J. T. Moody[1], M. Turner
CERN, Geneva, Switzerland
[1]also at Max Planck Institute for Physics, 80805 Munich, Germany
[2]also at Department of Physics, UNIST Ulsan, Republic of Korea
[3]also at Argonne National Laboratory, Lemont, IL, USA

Abstract

In the Phase 2 of the AWAKE first experimental run (from May to November 2018), an electron beam was used to probe and test proton-driven wakefield acceleration in a rubidium plasma column. The witness electron bunches were produced using an RF-gun equipped with a Cs_2Te photocathode illuminated by a tailorable ultrafast ultraviolet (UV) laser pulse. The construction of the UV beam optical system enabled appropriate transverse beam shaping and control of its pulse duration, size, and position on the photocathode, as well as time delay with respect to the ionizing laser pulse that seeds the plasma wakefields in the proton bunches. Variable photocathode illumination provided the required flexibility to produce electron bunches with variable charge, emittance, and injection trajectory into the plasma column. In this work, we analyze the overall charge capture and shot-to-shot reproducibility of the proton-driven plasma wakefield accelerator with various UV illumination and electron bunch injection parameters.

INTRODUCTION

In the AWAKE experiment, an electron bunch is used to probe the proton-driven wakefield acceleration in plasma. During the initial experimental run in 2018, the first demonstration of electron beam acceleration was successfully achieved [1]. The experiments confirmed that the injected 19 MeV electron beam was in a 10 m long plasma cell, with a maximum energy gain of up to 2.0 GeV. The shot-to-shot performance of this accelerator was still not comparable to standard linac-based electron accelerators. With a view on improving parameters such as charge capture rate and overall acceleration efficiency, the AWAKE Run 2 experiment is currently being prepared. The goal is to achieve a charge capture efficiency and an energy gain of over 90%, while producing 10 GeV high charge electron beams [2].

To accomplish this goal the electron beam parameters at the plasma entrance must be accurately controlled, including: the pointing jitter, size, charge and emittance of the electron bunches. With the aim of understanding the sensitivity and limitations of AWAKE's experimental setup, we study here the influence of the several of those parameters on the overall charge capture and reliability measured during the first experimental run.

† eduardo.granados@cern.ch

In the AWAKE experiment, a 400 GeV proton beam is extracted from the CERN Super Proton Synchrotron (SPS) and utilized as a drive beam for wakefields in a plasma column to accelerate electrons. The plasma is generated in a 10 m long rubidium vapour source via the over-the-barrier ionization employing a high intensity laser field. In this scheme, an ultrafast infrared laser pulse (~100 fs) co-propagates with the SPS proton beam and initiates a self-modulation process at the front of the plasma column. As a consequence, the long SPS proton bunch (σ_z=12 cm) is heavily modulated into a train of longitudinal micro-bunches which in turn drive a periodic wakefield [3, 4], as shown in Fig. 1.

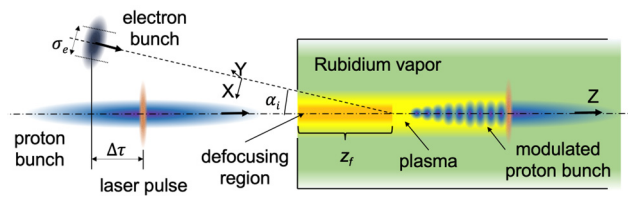

Figure 1: The oblique electron injection arrangement: an electron bunch of variable charge and size σe is injected into the plasma wakefields at an angle αi.

The injection of electrons into the wakefield is carried out at an angle and a distance z_f with respect to the plasma entrance. This is done to avoid the loss of electrons at the density transition region at the entrance of the plasma cell (defocusing region in Fig. 1). In this arrangement, the electrons approach the central axis in the region of constant plasma density and therefore get trapped into the established plasma wave.

The required injection angle α_i and radial offset of the electron beam at the orifice placed at the entrance of the plasma cell are small enough so the oblique injection does not require any hardware changes in the facility design, as compared to the on-axis injection. According to early theoretical models, the parameter space for good trapping is quite large when compared to the electron beam portrait [5, 6], so no fine-tuning of the injection angle or focus point is required for the best performance.

In this paper, we further present experimental results regarding the electron acceleration performance by varying some of the main electron beam parameters, including position, angle, size, emittance and charge. The goal is not to

ISBN: 978-3-95450-227-1 ISSN: 2673-5490 doi:10.18429/JACoW-IPAC2022-WEPOST040

COMPARING METHODS OF RECOVERING GAMMA ENERGY DISTRIBUTIONS FROM PEDRO SPECTROMETER RESPONSES

M.H. Oruganti, B. Naranjo, J.B. Rosenzweig, UCLA, Los Angeles, CA, USA
M. Yadav, University of Liverpool, Liverpool, UK

INTRODUCTION

As high energy atomic and subatomic particles interact, they emit gamma radiation in a wide range of energies, all of which can be used to determine the nature of the original interacting particles. To calculate the energy levels of the photons emitted, the new pair spectrometer (PEDRO) channels the photons through several Beryllium nuclear fields; since the photons of interest will likely have energies between 10 MeV and 10 GeV, those photons will produce electron-positron pairs through the nuclear field interaction [1].

Under a magnetic field, the electrons and positrons bend in opposite directions (due to their opposite charges) and at different angles (due to their differences in energies). A series of spaced out cells measure the number of electrons or positrons that strike at that location, which has some relation to the energies associated with the photons that generated those electrons and positrons.

The goal of this paper is to compare several methods of reconstruction and determine which best predicts original energy distributions based on simulated spectra.

METHODS

When considering electron-positron pair production from photon interactions with nuclear fields, it is important to recognize the linear relationship between the energy distribution of photons and the spectrometer's response. This linear relationship can be modeled as follows:

$$\begin{bmatrix} \alpha_{1,1} & \alpha_{1,1} & \cdots & \alpha_{1,64} \\ \alpha_{2,1} & \alpha_{2,1} & \cdots & \alpha_{2,64} \\ \vdots & \vdots & \ddots & \vdots \\ \alpha_{128,1} & \alpha_{128,1} & \cdots & \alpha_{128,64} \end{bmatrix} \times \begin{bmatrix} x_1 \\ x_2 \\ \vdots \\ x_{64} \end{bmatrix} = \begin{bmatrix} y_1 \\ y_2 \\ \vdots \\ y_{128} \end{bmatrix} \quad (1)$$

In the above system of equations, and throughout the rest of this paper, the x-vector will refer to the original distribution of photons based on their energies. While the energy values will become more relevant when interpreting the model's output, the numerical values that split the energy distribution into logarithmic bins were chosen out of convenience. The y-vector will always refer to the electron-positron spectrum PEDRO outputs in response to the corresponding x-vector, or incoming photon energy distribution.

Possible Methods of Recovery

To determine the best method of recovering the x-vector given a y-vector, several methods of computation were explored and compared when applied to standardized test cases. The three methods included machine learning, combining the model with the Maximum Likelihood Estimation algorithm, and QR decomposition.

Machine Learning (ML) Using Eq. (1), training data was synthesized from creating arbitrary energy distribution (each bin containing a random number of photons between 0 and 1×10^{10}) and multiplying each x-vector by the matrix to generate the corresponding spectrum (or y-vector) that PEDRO would measure. To simulate real world noise from electrons being scattered during the pair production process, low-level noise vectors were calculated and added to the y-vectors.

Table 1 summarizes the model's architecture. The model used the Adam optimizer with a learning rate of 0.005 over 600 epochs. Mean Squared Error was chosen as the loss function for the model, which was constructed using Python's Keras library [2].

Table 1: A Summary of the ML Model to Predict Incoming Gamma Spectra Based on Positron-Electron Detection

Layer (type, bias, activation)	Output Shape	Param Num
dense (Dense, true, linear)	(None, 64)	64
dense1 (Dense, true, linear)	(None, 64)	64

Maximum Likelihood Estimation + Machine Learning (Hybrid) Maximum Likelihood Estimation (MLE) is an algorithm that, given an initial guess for the solution of an equation, iteratively converges to the nearest solution that is the most probable. It converts the issue of calculating the original energy distribution based on the PEDRO output from an analytical problem to a statistical one to estimate a series of parameters [3].

While the MLE algorithm does not require training like the ML model, it does require a guess that is sufficiently close to the true solution of Eq. (1). Given the utility of machine learning, it is possible to provide a customized guess for every y-vector: the ML model's guess. This combination serves as a hybrid approach to recovering the original energy distribution as opposed to pure ML or QR Decomposition (as will be seen in the next section).

QR Decomposition The software's goal was to effectively invert the response matrix R so given a PEDRO spectrum, the originating x-vector could be recovered. This method of recovery required no additional information beyond the matrix to be decomposed (in this case, R).

ISBN: 978-3-95450-227-1 ISSN: 2673-5490 doi:10.18429/JACoW-IPAC2022-WEPOST041

PHYSICAL ASPECTS OF COLLINEAR LASER INJECTION AT SLAC FACET-II E-310: TROJAN HORSE EXPERIMENT

M.Yadav[1,2,3*], B. Naranjo[1], C. Hansel[4], P. Manwani[1], J.B. Rosenzweig[1]
O. Apsimon[2,3], E. Kukstas[2,3], B. Hidding[5] and C. P. Welsch[2,3]
[1]University of California, Los Angeles, CA, USA
[2]University of Liverpool, Liverpool, L69 3BX, United Kingdom,
[3]Cockcroft Institute, Warrington, United Kingdom
[4]University of Colorado Boulder, USA, and
[5]University of Strathclyde, United Kingdom

ABSTRACT

We report on challenges and details of the E-310 experiment which aims to demonstrate low emittance beam production from a plasma photocathode using a collinear injection laser at FACET-II. We performed simulations of planned experiments using the Particle-in-Cell code OSIRIS and examined the mitigation of beam hosing and drive beam depletion. We simulated the generated X-ray betatron radiation and discuss planned radiation diagnostics for the experiment.

INTRODUCTION

The Facility for Advanced Experimental Tests II (FACET-II) [1] is a test facility at SLAC National Accelerator Laboratory primarily dedicated to research and development of advanced acceleration technologies. One of the experiments planned at FACET-II is the E-310, which aims to demonstrate the creation of ultra low emittance electron beams from a plasma photocathode. E-310 builds on the E-210 experiment at the original FACET facility which first demonstrated a plasma photocathode[2]. A Plasma photocathode works by mixing two species of gas inside a vacuum chamber: a low ionisation threshold (LIT) gas and a high ionisation threshold (HIT) gas. We plan to use hydrogen and helium, respectively. A laser pre-ionizes the LIT gas and forms a plasma channel through which the beam propagates, forming a blowout bubble[3]. The second laser is used to locally ionize the HIT gas within the blowout[4], which produces electrons in the bubble which are accelerated by the wake and form the witness beam. The E-210 experiment which demonstrated this principle but did not attempt to produce low emittance beams used to ionise a gas that has HIT. The laser is perpendicular to the beam propagation direction, while the planned E-310 experiment will use a collinear ionization laser. An overview on the underlying principles of the hybrid plasma wakefield acceleration scheme dubbed "Trojan Horse" acceleration is given. The concept of this experiment is based on laser-controlled release of electrons directly into a particle-beam-driven plasma blowout, paving the way for controlled, shapeable electron bunches with ultralow emittance and ultrahigh brightness. In collinear Trojan Horse, it is usually essential to have a delay between the electron beam and the injection laser to achieve a stable witness beam using a plasma photo cathode technique. The generated helium electrons would be affected by the transverse electric field of the drive beam, which imprints a substantial transverse momentum that either prevents trapping altogether, or is detrimental to the emittance. One of the benefits of Trojan horse injection is the ability to adjust the injection position with respect to the wakefields. This allows us to inject at the zero-crossing of the accelerating wakefield in order to minimise interaction with the transverse wakefield.

To achieve the research goals of FACET-II, sophisticated beam diagnostics are required. The utility of betatron radiation diagnostics has already been proven in inverse Compton scattering experiments [5]. The upcoming set of experiments at FACET-II requires simulation models and instruments for recovering single-shot double-differential angular-energy spectra of emitted photons covering a wide energy range, extending from tens of keV through to ten MeV, with an angular resolution on the order of 100 μrad. These spectra provide a unique window into the high field generation, beam-plasma and laser-plasma interactions.

PARTICLE-IN-CELL SIMULATIONS

Using the fully relativistic 3D particle-in-cell (PIC) simulation code OSIRIS [6], we ran simulations of the E-310 experiment. We ran these simulations using the parameters we expect to achieve at FACET-II. These parameters are summarized in Table 1. The HIT ionization laser focus was chosen to be in the bubble at a distance $6k_p^{-1}$ behind the drive beam which is the location of the zero crossing of the longitudinal field E_z. The cell size used was 5 m × 5 m × 2.5 m and 8 macro-particles per cell were used to model the drive beam and plasma. All simulations use a ponderomotive guiding center (PGC), in which the particles are pushed through the laser ponderomotive force and through the self consistent plasma fields.

Plots of the pre-ionized (hydrogen) plasma electron density and the density of electrons generated from the plasma photocathode are shown in Fig. 1. The plasma bubble as well as the generated witness beam are both clearly visible. The longitudinal electric field inside the bubble is shown in Fig. 2. This shows the peak accelerating field in the bubble of

* monika.yadav@liverpool.ac.uk

ISBN: 978-3-95450-227-1 ISSN: 2673-5490 doi:10.18429/JACoW-IPAC2022-WEPOST042

RADIATION DIAGNOSTICS FOR AWA AND FACET-II FLAT BEAMS IN PLASMA

M. Yadav[1,2,3*], P. Manwani[1], H. Ancelin[1], G. Andonian[1], O. Apsimon[2,3], C. Welsch[2,3], J. Rosenzweig[1]
[1]University of California, Los Angeles, CA, USA
[2]University of Liverpool, Liverpool, L69 3BX, United Kingdom, and
[3] Cockcroft Institute, Warrington, United Kingdom

Abstract

In electron beam facilities like FACET-II and Argonne Wakefield Accelerator facility (AWA), beams with highly asymmetric emittance are of interest because they are the preferred type of beam for linear colliders (LC). That is ultimately the motivation: building a plasma based LC. In the flat beam case, the blowout radius is no longer equal in the two transverse planes. Focusing is required to keep the particles within the tight apertures, and characterizing these accelerators shows the benefits of employing ultra low beam emittances. Beams with high charge and high emittance ratios in excess of 100:1 are available at AWA. If the focusing is not equal, then we will have different radiation signatures for the flat and symmetric beams in the plasma. We use QuickPIC and OSIRIS particle-in-cell codes to compare various scenarios including a weak blowout and a strong blowout. Further, we determine the radiation generated in the system by importing particle trajectories into a Liénard Weichert code. We discuss future steps towards full diagnostics of flat beams using radiation.

INTRODUCTION

When relativistic electrons oscillate transversely in a nonlinear plasma ion column they emit synchrotron radiation which is also known as betatron radiation [1]. With the advances of plasma and laser techniques, betatron radiation from plasma wakefield accelerators has brought these goals of imaging and beam profile reconstruction closer to being achieved, and also could serve as an important beam diagnostic tool. For an accelerator with a bunch of few-GeV energy, few-fs pulse duration, few-mm-rad emittance, and significant energy spread, methods like pepper pot [2] and quadruple scan [3] are less effective emittance diagnostic methods because they are statistical rather than single shot and are destructive. We need sophisticated methods to measure the emittance in Plasma WakeField Accelerators (PWFAs) because the plasma vacuum boundaries can change the transverse phase space and divergence of the beam [2]. In comparison to a round beam, a flat beam suppresses the beamstrahlung at the interaction point in a linear collider and also breaks the symmetry of betatron motion in x and y planes. Flat beam generation was experimentally demonstrated a decade earlier [4, 5] and was proposed as an alternative to damping rings in linear colliders. The generated flat beam at AWA has few nC charge, MeV energy and μm spot size. Similar scenarios will be explored at FACET-II. There are three main regimes of beam-based PWFA: the linear, quasi-nonlinear and non-linear (or blowout) regimes [6]. In the linear regime, plasma electrons are not completely removed from the center of the wake. In the blowout case, the strong electric fields of the beam force the plasma electrons outward, resulting in a pure ionic column. The scenario for the case of the axisymmetric beam has been studied extensively [7, 8]. However, we don't fully understand the physics behind flat beams, and there is not much information available in the literature. This leaves unanswered questions like asymmetric blowout, plasma based lenses, transverse correlation and associated radiation [9]. In this paper, we systematically investigate the betatron radiation effect in the flat beam case considering realistic beam and plasma parameters. Radiation from the 10 GeV FACET-II and 50 MeV AWA beam diagnostics are explored. Betatron radiation diagnostics for flat and round beams could be used to measure the emittance, spot size, and energy gained by the accelerated electron bunch within the plasma. Studies are being done to examine the transverse profile of the electron beam [10].

AWA FLAT BEAM

Numerical simulations of drive bunch acceleration are carried out with the three-dimensional (3D) quasi-static particle-in-cell (PIC) code QuickPIC and the full PIC code OSIRIS for the parameters shown in Table 1. For the purpose of beam profile and emittance reconstruction, the complete spatial distribution of the beam is needed [11]. Therefore, it is very effective to look at the spatial distribution of betatron photons, as the radiation pattern on the screen is axisymmetric for an axisymmetric electron bunch. Space charge particularly affects the defocusing forces over the length of the bunch and changes the achievable phase space density, which also has a great impact on the betatron motion of the particles. Emittance of the bunch could be significantly improved by optimizing the magnetic field parameters and the beam.

In order to eliminate the influence of the head erosion seen, an examination of the back 50% of the beam particles was employed as shown in Figure 1. Betatron radiation and the electron dynamics are inter-related; hence, we may be able to use betatron radiation to indirectly measure the evolution of the beam size creating asymmetric blowout shown in Fig. 2 or even beam profile inside the plasma chamber. There are several difficulties in the study and the application of betatron diagnostics for electron and proton wakefield

* monika.yadav@liverpool.ac.uk

ISBN: 978-3-95450-227-1 ISSN: 2673-5490 doi:10.18429/JACoW-IPAC2022-WEPOST043

AN EFFECTIVE-DENSITY MODEL FOR ACCELERATING FIELDS IN LASER-GRAPHENE INTERACTIONS

C. Bonţoiu*, Ö. Apsimon[1], E. Kukstas, C. Welsch[1], M. Yadav
University of Liverpool, Liverpool, UK
G. Xia[1], University of Manchester, MManchester, UK
J. Resta-López, University de Valencia, Valencia, Spain
A. Bonatto, Federal University of Health Sciences of Porto Alegre, Brazil
[1]also at Cockroft Institute, Daresbury, UK

Abstract

With the advancement of high-power UV laser technology, the use of nanostructures for particle acceleration attracts renewed interest due to its possibility of achieving TV/m accelerating gradients in solid state plasmas. Electron acceleration in ionized materials such as carbon nanotubes and graphene is currently considered as a potential alternative to the usual laser wakefield acceleration (LWFA) schemes. An evaluation of the suitability of a graphene target for LWFA can be carried out using an effective density model, thus replacing the need to model each layer. We present a 2D evaluation of the longitudinal electric field driven by a short UV laser pulse in a multi-layer graphene structure, showing that longitudinal fields of ~5 TV/m are achievable.

INTRODUCTION

Unlike LWFA in gases, which can be achieved with laser pulses in the IR range, at peak intensities of 10^{18}-10^{19} W/cm^2 [1], the equivalent mechanism in solid-state plasmas requires an UV laser pulse with peak intensity in the range 10^{20}-10^{21} W/cm^2, because charge densities in solids are 4–5 orders of magnitude higher than in gas targets. Graphene [2] can be grown in the form of 2D layers of Carbon atoms, stacked together with a controllable inter-layer gap of a few nm. Due to its unique optical [3] and electronic [4] properties graphene is used as a medium for applications such as high-harmonic generation [5] or terahertz radiation [6]. Moreover, when fully ionized by intense laser pulses, each graphene layer delivers plasma with an electron density of $\sim 10^{23}$ cm^{-3} and the tunability of the inter-layer gap implies that variable effective plasma densities of $\sim 10^{22}$ cm^{-3} can be obtained. This enables resonant propagation of sufficiently intense laser pulses with wavelengths of up to 300 nm, and also allows electrons to move easier along the inter-layer gaps. Realistic Particle-In-Cell (PIC) simulations rely the capability of using mesh cells a few times smaller than the layer thickness, 0.34 nm and this poses a significant numerical overhead. However, reasonably accurate estimates of the electric fields can be obtained using an *effective density* equivalent. However, one should note that this approximation prevents the possibility to realistically study transient plasma dynamics at a resolution smaller than the inter-layer gap. To build it from a *layered target* model, the total amount of unperturbed charge is kept constant and uniformly distributed in the bulk volume of the target. The concept of effective density was already applied for PIC simulations involving electron bunches colliding with carbon nanotubes [7]. We have used the PIConGPU code [8] to evaluate the dynamics and magnitude of the longitudinal electric field in laser-graphene interactions.

SIMULATION SETUP

The 2D model uses a 1.2 µm-wide and 1.5 µm-long target, as the *effective density* equivalent of 60 graphene layers, spaced by 20 nm-wide edge-to-edge gaps. The laser pulse is Gaussian, both transversely with an FWHM spot size 400 nm, and longitudinally with 1 fs FWHM pulse duration. It has a linear polarization within the $yx-$plane. The carbon plasma *effective density* is initialized as $n_0 = 1.94 \times 10^{21}$ cm^{-3} but rises to $6\,n_0 = 1.61 \times 10^{22}$ cm^{-3} as the target is virtually instantaneously ionized completely. The mesh cell size is limited to 0.25 nm with 1 macroparticle per mesh cell. Moving rightwards along the $y-$axis (longitudinal), the laser pulse interacts with the target for 16 fs which corresponds to 48 cycles, and travels 4.8 µm. Table 1 lists all important laser parameters. The simulation ignores lattice effects since the carbon atoms are generated uniformly across the target volume and there is no ionization threshold specific to graphene. Three ionization mechanisms (barrier suppression, tunneling and collisional) are enabled but they use atom ionization levels. Recombination is not considered but it can be ignored, given the short interaction time studied in this work (10 fs). For the same reason, the motion of the carbon ions, evaluated at a few nm, does not affect the overall results.

Table 1: Laser Parameters

Quantity	Value	Unit
wavelength: λ	100	nm
period: T_{laser}	0.334	fs
peak intensity: I_0	10^{21}	W/cm^2
spot size*: w_0	0.4	µm
focal point: y_0	0.25	µm
pulse energy: ΔE	8	mJ
pulse length§: Δt	3	fs

*FWHM, §9 cycles

* Cristian.Bontoiu@liverpool.ac.uk

ISBN: 978-3-95450-227-1 ISSN: 2673-5490 doi:10.18429/JACoW-IPAC2022-WEPOST045

SIMULATING ENHANCED FOCUSING EFFECTS OF ION MOTION IN ADIABATIC PLASMAS

D. Chow[1*], P. Manwani[1†], M. Yadav[1,2,3], C. Hansel[4], O. Apsimon[2,3], C. Welsch[2,3], J. Rosenzweig[1]
[1]University of California Los Angeles, Los Angeles, CA, United States
[2]University of Liverpool, Liverpool, L69 3BX, United Kingdom
[3] Cockcroft Institute, Warrington WA4 4AD, United Kingdom
[4]University of Colorado, Boulder, CO, United States

Abstract

The FACET-II facility offers the unique opportunity to study low emittance, GeV beams and their interactions with high density plasmas in plasma wakefield acceleration (PWFA) scenarios. One of the experiments relevant to PWFA research at FACET-II is the ion collapse experiment E-314, which aims to study how ion motion in a PWFA can produce dual-focused equilibrium. As nonlinear focusing effects due to nonuniform ion distributions have not been extensively studied; we explore the difficulties of inducing ion motion in an adiabatic plasma and examines the effect an ion column has on beam focusing. A case study is performed on a system containing a plasma lens and adiabatic PWFA. Ions in the lens section are assumed to be static, while simulations of an adiabatic matching section are modified to include the effects of ion column collapse and their nonlinear focusing fields. Using the parameters of the FACET-II beam, we find that a collapsed ion column amplifies the focusing power of a plasma without compromising emittance preservation. This led to a spot size 33% smaller than that of a simply matched beam.

INTRODUCTION

This paper investigates the potential for ion motion at the upcoming E-314 experiment at the Facility for Advanced Experimental Tests II (FACET-II). FACET-II has the capability to produce ultra-high brightness, 10 GeV beams using the linear accelerator at SLAC National Laboratory. The E-314 experiment seeks to induce ion motion in a plasma wakefield accelerator (PWFA) and examine the effects high density ion columns have on a drive beam. Ion motion arises when a long, dense beam passes by plasma ions and exerts inwardly directed Coulombic forces on them. If the beam is orders of magnitude denser than the plasma, the uniformly distributed ion column will collapse inwards, resulting in an extremely dense, nonuniform ion distribution [1]. Focusing fields from a collapsed ion column are significantly stronger than those from a uniform ion distribution; we exploit these strong fields to enhance the focusing effects of a PWFA.

There are two difficulties associated with ion motion: for ion motion to occur in a similar timescale as electron evolution, the phase advance given by Eq. (1) must

$$\Delta\phi = 2\pi\sigma_z\sqrt{\frac{r_e Z_i n_{b,0} m_e}{m_i}} \tag{1}$$

satisfy $\Delta\phi \geq 1$ for gentle ion motion to occur, and $\Delta\phi \geq \frac{\pi}{2}$ to ensure maximum collapse of the ion column [2]. The phase advance depends on the beam parameters σ_z and $n_{b,0}$, which are the longitudinal rms and core (peak) density of the beam respectively. Other terms such as atomic number (Z_i), ion mass (m_i), electron mass (m_e), and classical electron radius (r_e) are either dependent on the plasma or are physical constants. Achieving a $\Delta\phi \geq \frac{\pi}{2}$ generally requires the density of the beam core to be many orders of magnitude larger than the density of the surrounding plasma [1], and is the primary issue associated with the FACET-II beam. The second issue is that moving ions have the potential to induce large emittance growth and interfere with beam-plasma matching by scattering beam electrons during ion column collapse. Mathematically describing the beam and plasma parameters when $\Delta\phi > \frac{\pi}{2}$ is quite complicated and is explored in [3], however this paper will not address the theory of ion motion and will instead focus on ion motion in an experimentally achievable setting.

We propose using the FACET-II beam to induce ion motion in a long, high density plasma system. The main challenge is achieving a high enough $n_{b,0}$ to induce ion motion, as the unmodified FACET-II beam falls short by orders of magnitude. To remedy this, a focusing system comprising of quadrupoles, plasma lenses, and an adiabatic matching section was proposed to decrease beam spot size while incurring as little emittance growth as possible. An experimentally achievable combination of lenses and adiabatic matching sections are examined using the quasi-static particle-in-cell code QuickPIC to model beam and ion evolution. QuickPIC is our primary tool for determining if the focusing system produces the desired results.

DEVELOPMENT OF THE PLASMA LENS

The aim of the pre-focusing lens is to uniformly reduce the rms width of the beam (σ_r) before it enters a high density adiabatic focuser. The theory laid out in [4] provides an excellent reference for the expected behavior of an electron beam after traversing a plasma lens. Most notable are the equations below,

* drchow37@gmail.com
† pkmanwani@gmail.com

ISBN: 978-3-95450-227-1 ISSN: 2673-5490 doi:10.18429/JACoW-IPAC2022-WEPOST046

BEAM MATCHING IN AN ELLIPTICAL PLASMA BLOWOUT DRIVEN BY HIGHLY ASYMMETRIC FLAT BEAMS

P. Manwani*, H. Ancelin†, N. Majernik, M. Yadav, G. Andonian,
J. Rosenzweig, UCLA, Los Angeles, CA, USA
G. Ha, J. Power, Argonne National Lab, Lemont, IL, USA

Abstract

Particle beams with highly asymmetric emittance ratios, or flat beams, are employed at accelerator facilities such as the AWA and foreseen at FACET-II. Flat beams have been used to drive wakefields in dielectric structures and are an ideal candidate for high-gradient wakefields in plasmas. The high aspect ratio produces a blowout region that is elliptical in cross section and this asymmetry in the ion column structure creates asymmetric focusing in the two transverse planes. The ellipticity of the plasma blowout decreases as the normalized peak current increases, and gradually approaches an axisymmetric column. An appropriate matching condition for the beam envelope inside the elliptical blowout is introduced. Simulations are performed to investigate the ellipticity of the resultant wakefield based on the initial drive beam parameters, and are compared to analytical calculations. The parameter space for two cases at the AWA and FACET facilities, with requirements for plasma profile and achievable fields, is presented.

INTRODUCTION

Particle beams with highly asymmetric emittances can be created at facilities like AWA [1] and are proposed at FACET-II [2]. These beams reduce beamstrahhlung at the interaction point [3] and have possible applications in future particle colliders and advanced accelerators. Asymmetric beams can also drive stable wakefields that are both focusing and accelerating in a hollow plasma channel which makes them good candidates for positron acceleration [4]. Flat beams can be employed to drive asymmetric wakefields in a plasma accelerator and the blowout created by these beams is transversely elliptical [5] when the density perturbation to the plasma is not large. In this paper, we aim to study the beam dynamics of the particles in the elliptical blowout that is created by beams that have transversely asymmetric spot sizes with asymmetric emittances. The importance of the ellipsoid distributions comes from the uniformity of the ion distribution within the bubble (neglecting the extreme case of ion motion), since uniformly charged ellipsoids have well-behaved linear self fields [6]. The linear focusing forces provided by the ion column can be used to match the divergence of the beam [7], which results in no oscillations of the beam envelope. A mismatched beam will undergo characteristic beating due to betatron oscillations, which can lead to an enlarged phase space or emittance dilution. The ellipticities of the ion column depends on the asymmetry of the beam and decreases with an increase in the beam density of the beam with respect to the plasma. Larger normalized beam densities lead to stronger blowouts, which concomitantly reduce the higher order moments and the blowout tends to be more axisymmetric. It is important to understand the dynamics of asymmetric drive beams and the necessary conditions to match these beams in a plasma wakefield accelerator (PWFA). Simulations were performed using QuickPIC [8], a 3D quasi-static particle-in-cell code, to investigate the plasma structures and beam dynamics resulting from the flat beam plasma interaction. Practical considerations for developing nascent experiments at the AWA and FACET-II facilities are also discussed.

TRANSVERSE FOCUSING

The transverse fields in the elliptical blowout structure can be calculated analytically by approximating it as an infinitely long cylinder of ions, similar to the axisymmetric case but with an elliptical cross section and is given by:

$$E_{x,p} = \frac{en_0 b_p x}{\epsilon_0(a_p + b_p)} = \frac{en_0 x}{\epsilon_0(1+\alpha_p)} \tag{1}$$

$$E_{y,p} = \frac{en_0 a_p y}{\epsilon_0(a_p + b_p)} = \frac{en_0 \alpha_p y}{\epsilon_0(1+\alpha_p)} \tag{2}$$

where a_p and b_p are the elliptical cross section's semimajor and semiminor axes respectively, and the ellipticity α_p is defined as the ratio a_p/b_p.

The matched beta functions for the beam envelope can be calculated from the transverse focusing forces of the elliptical column:

$$k_{\beta,x} = \sqrt{\frac{1}{\gamma m_e c^2}\frac{eE_x}{x}} = \sqrt{\frac{n_0 e^2}{\gamma \epsilon_0 m_e c^2(1+\alpha_p)}} \tag{3}$$

$$k_{\beta,y} = \sqrt{\frac{1}{\gamma m_e c^2}\frac{eE_y}{y}} = \sqrt{\frac{n_0 \alpha_p e^2}{\gamma \epsilon_0 m_e c^2(1+\alpha_p)}} \tag{4}$$

The spot size of the beam is then given by $\sigma_{x,m} = \sqrt{\beta_x \epsilon_x}$ and $\sigma_{y,m} = \sqrt{\beta_y \epsilon_y}$. The ellipticity of the matched beam, $\alpha_{b,m}$, is then given by:

$$\alpha_{b,m} = \frac{\sigma_{x,m}}{\sigma_{y,m}} = \sqrt{\frac{\epsilon_x}{\epsilon_y}\frac{\beta_x}{\beta_y}} = \sqrt{\frac{\epsilon_x}{\epsilon_y}\frac{k_{\beta,y}}{k_{\beta,x}}} = \sqrt{\frac{\epsilon_x}{\epsilon_y}\sqrt{\alpha_{p,m}}} \tag{5}$$

The ellipticity equation shows that the emittance needed to match the beam envelope to the focusing forces needs to account for the ellipticity of the plasma column.

* pkmanwani@gmail.com
† havynancelin@g.ucla.edu

ISBN: 978-3-95450-227-1 ISSN: 2673-5490 doi:10.18429/JACoW-IPAC2022-WEPOST048

EXCITATION OF VERY HIGH GRADIENT PLASMA WAKEFIELDS FROM NANOMETER SCALE BEAMS

P. Manwani*, D. Chow, H. Ancelin, N. Majernik, G. Andonian, M. Yadav, J. B. Rosenzweig
UCLA, Los Angeles, CA, USA
R. Robles, Stanford University, Menlo Park, CA, USA

Abstract

The plasma based terawatt attosecond project at SLAC, termed PAX, offers near mega-Ampere beams that could be used to demonstrate plasma wakefield acceleration at very high gradients (TV/m). The beam has a large aspect ratio which allows it to be used at high densities since the longitudinal beam size is lower than the plasma skin depth. This beam can be focused using a permanent magnitude quadrupole (PMQ) triplet to further reduce its transverse size. Since the beam is extremely short compared to the plasma skin depth, it behaves like a delta-function perturbation to the plasma. This reduces the expected focusing effect of the ion column and simulations show that only the tail of the beam is notably focused and decelerated. This scenario is investigated with attendant experimental considerations discussed. The creation of the witness beam by the deceleration of the tail of the beam is also discussed.

INTRODUCTION

Plasma accelerators can create beams that have ultra high brightness in a relatively small physical footprint due to the achievable high gradients. The plasma based terawatt attosecond x-ray source project, termed PAX [1], proposes to use this promising technique to generate near mega-Ampere beams with attosecond duration which can, in turn, be used to generate few-cycle, coherent, tunable soft x-ray pulses with terawatt peak power. The beam is created using density downramp injection [2, 3] in a plasma wakefield accelerator (PWFA). These PWFA accelerated beams will be cable of driving x-ray free electron laser (XFEL) pulses which are an order of magnitude more powerful and with shorter temporal duration than current, state of the art XFELs. Additionaly, this mega-Ampere beam with its attendant bunch length, on the order of nanometers, can be used to drive wakefields in high density plasmas as the longitudinal size of the beam is very small compared to the plasma skin depth ($\sigma_z \ll k_p^{-1}$), where $k_p = \omega_p/c = \sqrt{e^2 n_0/m\epsilon_0}$. The beam has a high aspect ratio and is significantly larger in the transverse direction, which can subject it to the current filamentation instability (CFI) [4]. We describe a focusing lattice, downstream of the first plasma stage, using a defocusing triplet and a high gradient quadrupole triplet based on permanent magnet quadrupoles (PMQ) [5]. Subsequently, we used the longitudinal and transverse dimensions of the density spike associated with the focused PAX beam to simulate the beam plasma interaction of the beam with a plasma with a very high density of 10^{20} cm^{-3} having a skin depth (k_p^{-1}) of 0.53 μm. A schematic of the proposed layout is shown in Figure 1. The focusing of the PMQ triplet is simulated using Elegant [6]. The simulations of the second plasma stage were performed using QuickPIC [7], a three-dimensional quasi-static particle-in-cell (PIC) code.

Table 1: Table of Beam Parameters after the Chicane

Parameter	Value	Unit
Beam charge, Q	81.1	pC
Energy, E_b	3.3	GeV
σ_z	0.0135	μm
σ_x, σ_y	12.7, 4.8	μm
$\epsilon_{n,x}$, $\epsilon_{n,y}$	2.48, 0.22	μm-rad
β_x, β_y	0.41, 0.67	m
Energy spread	1.5	%

Table 2: Table of Parameters for the Simulation shown in Fig. 3

Parameter	Value	Unit
Beam		
Norm. beam density, n_b/n_0	10.3	-
Energy, E_b	3.3	GeV
σ_z	0.0135	μm
σ_x, σ_y	1.95, 1.19	μm
$\epsilon_{n,x}$, $\epsilon_{n,y}$	2.48, 0.22	μm-rad
β_x, β_y	8.51, 27.4	mm
Energy spread	1.5	%
Plasma		
Species	H^+	-
Density, n_0	1.0×10^{20}	cm^{-3}
Simulation		
Simulation window (x,y,z)	(12, 12, 3.5)	k_p^{-1}
Grid cells	$(512)^3$	-
Particles per cell	4	-
Timestep	2.5	ω_p^{-1}
Beam macroparticles	1.68×10^7	-

FOCUSING SYSTEM

A witness beam is created in the first plasma stage via density downramp injection and accelerated to an energy of 3.3 GeV with a large, approximately constant, linear chirp. After the first plasma stage, the diverging, chirped witness beam is focused using a quadrupole triplet and compressed using a four dipole chicane ($R_{56} = 27$ μm). This compressed beam has a current spike of 0.64 MA with a length of 23 nm

* pkmanwani@gmail.com

ISBN: 978-3-95450-227-1 ISSN: 2673-5490 doi:10.18429/JACoW-IPAC2022-WEPOST050

FURTHER MEASUREMENTS OF BEAM-BEAM INTERACTIONS IN A GEAR-CHANGING SYSTEM IN DESIREE*

E. Nissen†, Thomas Jefferson National Accelerator Facility, Newport News, VA, USA
A. Källberg, A. Simonsson, Stockholm University, Stockholm, Sweden

Abstract

In this work we detail experiments performed on a gear-changing system using the Double ElectroStatic Ion Ring ExpEriment (DESIREE). A gear-changing system is one where there are different harmonic numbers in each ring. This experiment used carbon and nitrogen beams in a 4 on 3 gear-changing arrangement, with the last bunch of each left off. The bunch length can be measured and synchrotron motion detected. We performed this measurement on three different values of carbon current, and present the differences in the bunch length frequency spectrum here. The frequency difference corresponds to twice the synchrotron frequencies.

INTRODUCTION

This work was performed as a part of a larger project called Direct Observations in DESIREE of Gear-changing Events (DODGE). This program has used the Double ElectroStatic Ion Ring ExpEriment (DESIREE) to demonstrate gear-changing in an operational accelerator [1][2]. Gear-changing is a type of collider synchronization method where the two rings of a collider each have a different harmonic number of bunches [3]. In the experiments shown here, we had one carbon beam with four bunches colliding with a nitrogen beam with three bunches moving at 4/3 the velocity of the carbon. DESIREE sends both bunches in the same direction, usually at the same velocity to study ionization reactions [4]. In our experiment the velocity difference leads to collisions in a moving reference frame. A diagram of DESIREE is shown in Fig 1.

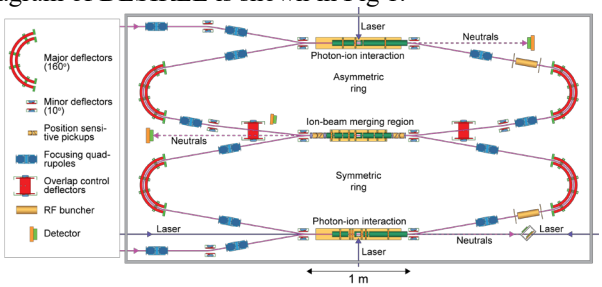

Figure 1: This is a schematic view of the DESIREE machine.

In this work we expand on previous experiments that were able to demonstrate a gear-changing system for over 37,500 turns (~1s) and were able to detect measurable longitudinal beam-beam interactions. The purpose of this experiment was to expand on those longitudinal beam-beam measurements by increasing the bunch charges of both beams. By then steadily increasing the charge of the carbon beams we can measure the change in the longitudinal synchrotron motion using bunch length oscillations.

THE EXPERIMENT

We measure these interactions by measuring the bunch lengths and how they evolve over time. This will give us a reading of twice the synchrotron frequency. We can take the evolution of the bunch lengths both with colliding beams, and baseline measurements with only one beam at a time. We then take the Fourier spectrum of each signal and compare them. The data was collected using the pickups at either end of the merger region. In order to measure the beam as it evolves, we use the missing bunch method. This leaves an empty bucket in each ring which creates a repeating pattern, giving us an evolving snapshot of the beam.

Earlier experiments used a curve fitting algorithm to match the BPM signals and extract the bunch lengths and positions. With higher currents, the shape of the bunches is often not well matched by a gaussian. For this work we instead applied a noise filter to the data and then calculated the moments of the distribution directly, treating the oscilloscope readings like a histogram.

We performed three sets of measurements; the plan was to keep the nitrogen current the same throughout the experiment while using three different carbon currents. We recorded 1156 carbon turns, and 1540 nitrogen turns. with collisions, and baselines with just the carbon and nitrogen beams as baselines. The beam parameters were chosen to show a carbon beam of 7, 14, and 21 nA, while the nitrogen beam was intended to keep steady value of 4 nA. The carbon beam was kept at an energy of 7.01 keV, and the nitrogen was kept at 14.3 keV.

EXPERIMENTAL RESULTS

The results of these measurements have shown clearer traces of longitudinal beam-beam interactions than were seen in previous work. This was due to a combination of larger beam currents and longer bunches, which made the uncertainties of the moments smaller.

Bunch Length Data

These higher currents have simplified the measurement of bunch length, and are able to visually show the differences between the bunch length frequency for collisions and for their baselines. This can be seen in Fig 2. In these cases, the data from one of the pickups is shown as a

This work was performed at the Swedish National Research Infrastructure, DESIREE (Swedish Research Council Contract No. 2017-00621).
† nissen@jlab.org

ISBN: 978-3-95450-227-1 ISSN: 2673-5490 doi:10.18429/JACoW-IPAC2022-WEPOST052

INFLUENCE OF PLASMA ELECTRODE APERTURE SIZE ON BEAM EMITTANCE FROM A MULTICUSP ION SOURCE

A.George*, S.Melanson, J.Munich, M.Dehnel, D-Pace, Nelson, Canada
N.G.R.Broderick, University of Auckland, New Zealand.

Abstract

D-Pace's TRIUMF-licensed multicusp filament ion source is capable of producing H^- beams up to 17.4 mA. In most cases the beam is transported to the entrance of an accelerator or a magnet for further applications. The emittance of the beam extracted from the ion source should be maintained as low as possible to reduce the beam losses to the walls of the transport pipes. The beam emittance from the ion source can be controlled by changing the aperture diameter of the plasma electrode. The current study deals with the range of H^- beam emittance that can be achieved from D-Pace's filament ion source, using plasma electrodes of different aperture sizes. The corresponding beam currents and the electron to ion ratios are also reported.

INTRODUCTION

Emittance is one of the most important quality parameters of an ion beam. A beam of very high emittance can suffer considerable loses during its propagation. The value of beam emittance is mostly determined by the initial focusing action at the plasma sheath which is the boundary layer between the quasi neutral plasma and the extraction region where mostly negative charges are present. The shape and location of the plasma sheath is determined by properties of the plasma, geometry of the electrodes around the plasma and electric potential on the electrodes. A picture of the plasma electrode assembly in the ion source is shown in Fig. 1.

The section view of D-Pace's TRIUMF-licensed multicusp filament ion source and extraction system is shown in Fig. 2 [1]. The ion source is capable of producing H^- beams up to 17.4 mA at an emittance of about 0.7 mm·mrad [2]. Plasma is sustained inside the plasma chamber of the ion source via thermionic emission from electrically heated Ta filaments. H^- ions are generated inside the plasma mostly through volume production methods [3]. As shown in the figure, the extraction system consists of the plasma electrode, the extraction electrode and the ground electrode. The plasma electrode and the extraction electrode are biased positive with respect to the plasma chamber for negative ion extraction. The co-extracted electrons are deflected on to the extraction electrode, before reaching the ground electrode, by the perpendicular magnetic field created by the magnets in the extraction electrode. Beam emittance is measured at about 368 mm downstream from plasma electrode, by D-Pace ES4 emittance scanner. This is an Allison-type emittance scanner which measures the beam intensity as a function of position (y) and angle (y′) simultaneously. Background electronic noise in the emittance data measurment is eliminated by discarding the beam intensity values below 4% of the maximum value. The Faraday cup is located at about 480 mm from the plasma electrode and can measure beam current (I_{FC}) with beam size up to 55 mm diameter.

* anand@d-pace.com

EXPERIMENTAL DETAILS

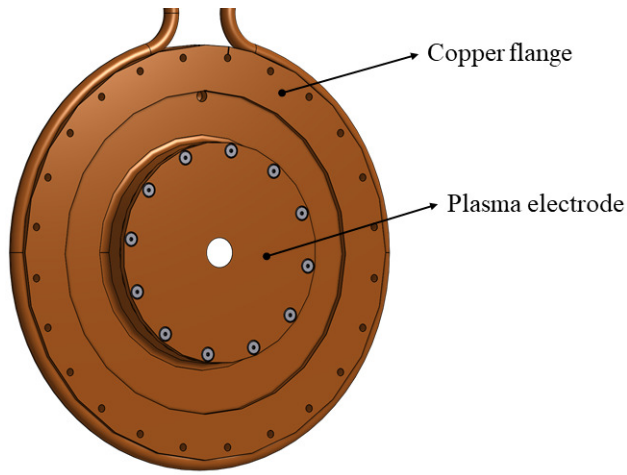

Figure 1: Picture of copper flange and plasma electrode. Ion beam is extracted through the aperture on the plasma electrode. 13.0 mm aperture is used for regular operations.

An experimental study was conducted in H_2 plasma to study the range of beam emittance values that could be obtained from D-Pace's filament ion source. Plasma electrodes of different aperture dimensions (8.0 mm, 11.5 mm, 13.0 mm and 16.0 mm) were used for this study. A picture of the plasma electrode and the copper flange is shown in Fig. 1. The ion beam is extracted through the aperture on the plasma electrode. The 13.0 mm aperture size is used for the regular experiments. The ion source had to be vented and opened before each experiment for replacing the plasma electrode.

H^- beam currents were measured at the Faraday cup for the different plasma electrodes and the results are shown in Fig. 3. The beam energy was fixed at 30 keV. The gas flow and electrode voltages were optimised for obtaining the maximum beam current at a fixed arc current. As can be seen from the graph, the beam current decreases as the size of the aperture decreases. I_{FC} decreases from 16 mA to about 9 mA, when the aperture size changes from 16 mm to 8 mm, for a fixed arc current. This result is expected as the effective plasma sheath emission area reduces as the aperture size decreases. This can be better understood with the help of IBSimu [4] simulations results shown in Fig. 4. The figure

ISBN: 978-3-95450-227-1 ISSN: 2673-5490 doi:10.18429/JACoW-IPAC2022-WEPOST053

EXTRACTION OF HIGH-CHARGE STATE ARGON AND α-PARTICLES FROM D-PACE PENNING ION SOURCE TEST STAND

N. Savard, J. Munich, M. Dehnel, D-Pace Inc, Nelson, Canada

Abstract

At the D-Pace Ion Source Test Facility (ISTF), we measure the extracted current of high-charge state ions from a hot cathode Penning ion source. Producing high-charge states of boron, arsenic, and phosphorous is of interest to the ion implantation community. Higher-charge states allow these doping agents to be accelerated to higher energies within the same accelerating electric fields. When used for doping silicon semiconductors, this allows for deeper implantation of the ions. We use helium and argon gas as a proxy (non-toxic gases) to determine whether the Penning ion source could be used for high-charge state production in ion implanters. The ability to reach charge states of greater than 4+ with argon and 1+ with helium leads to the possibility of producing high-charge state ions used in the ion implantation industry. This paper shows the extracted beam currents of Ar^{3+} - Ar^{6+} and α-ions for the hot cathode Penning ion source with variations in the confining magnetic field ($|\vec{B}|$ = 0.4 – 0.95 T), inlet gas flow (Q = 0.3 - 10 sccm), and arc discharge current (I_{arc} = 1 - 3 A).

INTRODUCTION

D-Pace Inc has developed a self-heated hot cathode Penning ion source for studying the production of α-particles as a function of operational parameters such as magnetic field strength, inlet gas flow, and arc current [1]. The purpose of this test stand is to determine how to optimize the ion source for α-particle production. It is believed that an optimized Penning ion source could be a potential replacement for Electron Cyclotron Resonance ion sources used to axially inject α-particles into medical cyclotrons; due to the existence of high-current α-particle producing Penning ion sources developed in the past [2]. However, Penning ion sources can also be used for producing high-charge state ions of other gases and metal vapors [3]. The production of high-charge state ions is especially beneficial to the ion implantation sector, as it allows ions to be accelerated to higher energies without increasing the size and cost of an accelerator [4]. Therefore, the Penning ion source could potentially be used for ion implanters looking to produce high-charge states of boron, arsenic, and phosphorous. As these are toxic elements, we use the inert gases of helium and argon as substitutes, with the assumption that the production of α-particles (ionization energy = 54.42 eV [5]) and charge-states higher than Ar^{4+} (ionization energy > 59.58 eV) would correlate to the production of high-charge state ions useful for ion implanters.

In this paper, we show how the extraction of α-particles from the ion source is correlated with each operational parameters: inlet gas flow, arc current, and magnetic field strength. In addition, similar experiments are performed using argon as the inlet gas, and the measurable currents for each high-charge state ion are shown. In addition, some comments are made on the experimental setup, and how the Penning ion source can be improved in the future to optimize high-charge state production.

EXPERIMENTAL SETUP

The general setup up of the Penning ion source test stand is shown in the disseration by Savard [1]. The simplified schematic of this test stand is shown in Fig. 1. This schematic presents the ion source within the pole gap of a C-Magnet, which produces a uniform magnetic field of 0.4 - 0.95 T. The ions are extracted by raising the ion source body up to 15 kV with respect to the grounded static puller and vacuum box walls. These extracted ions undergo a curved trajectory in the magnetic field, and are measured by a moving Faraday cup after undergoing a 180° turn.

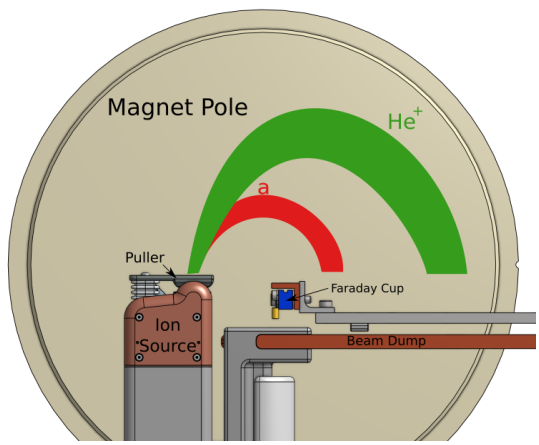

Figure 1: Simplified schematic of the experimental setup. Shown is the Penning ion source and the trajectories of the extracted ions (for helium operation) within the C-Magnet. A movable Faraday cup measures the current.

The Faraday cup is shielded by a grounded plate with a 62×2 mm slit. The measured current is fed through a load resistor (2.2 kΩ for helium), and the voltage across this resistor is measured by a NI USB-6001 data acquistion system. An example of the resultant peaks for a scan using helium is shown in Fig. 2. The upper estimate of current for each charge state is calculated by integrating the entire peak between their baselines, whereas the lower estimate is calculated by integrating over the full-width half-maximum of the peak. The appropriate peaks are found by converting the distance from the ion source extraction slit to the estimated

ISBN: 978-3-95450-227-1 ISSN: 2673-5490 doi:10.18429/JACoW-IPAC2022-WEPOPT001

NICA ION COLLIDER AND PLANS OF ITS FIRST OPERATIONS

E .Syresin†, O. Brovko, A. Butenko, A. Galimov, E. Gorbachev, V. Kekelidze, H. Khodzhibagiyan, S. Kostromin, V. Lebedev, I. Meshkov, A. Philippov, A. Sidorin, G. Trubnikov, A. Tuzikov
Joint Institute for Nuclear Research, Dubna, Russia

Abstract

The Nuclotron-based Ion Collider fAcility (NICA) is in assembling phase at JINR. The NICA goal is to provide colliding beams for studies of hot and dense strongly interacting baryonic matter and spin physics. The heavy ion injection complex of the NICA Collider consists of the following accelerators: a 3.2 MeV/u new heavy ion linac (HILAC) with RFQ and IH DTL sections, a new 600 MeV/u superconducting Booster synchrotron, and the upgraded Nuclotron - 3.9 GeV/n superconducting synchrotron. The heavy ion injection complex started operations with the first ion beams in beginning of 2022. Assembling of two Collider storage rings with two interaction points began in December 2021. The status of the NICA accelerator complex and plans for its first operation is discussed in the paper.

TWO STAGES OF NICA PROJECT

The NICA accelerator complex [1,2] is under assembling at JINR. Its commissioning is expected to start in 2023. The first phase of NICA experiments will be aimed on research of the mixed phase of baryonic matter, and the second phase - on the nature of the nucleon/particle spin. The NICA accelerator complex will operate in two modes: the Nuclotron ion beams extracted to a fixed target, and support of colliding ion beams in the Collider. The main elements of the NICA complex are the injection complex, the beam transfer lines and the Collider. The injection complex includes a set of ion sources, two linear accelerators, a new superconducting Booster and the superconducting upgraded synchrotron – Nuclotron. The Collider consists of two superconducting rings with two interaction points, which contain two detectors: the Multi-Purpose Detector and the Spin Physics Detector.

The project NICA will be performed in two stages. The stage I was complete at the end of March 2022. It involved construction and operation of the new heavy ion injection complex and the first fixed target experiments carried out in the Baryonic Matter at Nuclotron (BM@N) detector. The stage IIa is under implementation now. The construction of basic Collider systems is mainly finished, and the mounting of the Collider equipment for the basic configuration is started. The first colliding beam experiments are planned for the end of 2023. The stage IIb is related to formation of colliding beams with the design luminosity at operation of RF-3 cavities and the electron cooling system at the end of 2024.

†esyresin@jinr.ru

HEAVY ION INJECTION COMPLEX

The heavy ion linac HILAC constructed by the JINR-Bevatech collaboration has been operating since 2016. The efficiency of beam transport through the second and third IH sections is ~78%. The maximum ion beam current at the HILAC entrance during the first Booster runs corresponded to the design value of 10 mA. The current of 4 mA obtained at the HILAC exit is 3 times larger than the design value. The $^{4}He^{1+}$, $^{12}C^{4+}$ and $^{56}Fe^{14+}$ ions produced in the plasma and the laser ion sources were accelerated in HILAC and then injected into the Booster.

For the collider program the main project goal for the injection complex [1-3] (Fig.1) is accumulation of $2\cdot10^{9}$ $^{209}Bi^{35+}$ ions in the Booster with subsequent acceleration of heavy ions up to the energy of 578 MeV/n required for effective stripping which happens in Booster-to-Nuclotron transfers. Additionally, the electron cooling at 65 MeV/n helps to form the required beam emittances. The 211 m long Booster is located inside the yoke of the Synchrophasotron dipoles. All Booster dipoles and quadrupoles were fabricated and tested at JINR.

Figure 1: Booster ring inside Synchrophasotron yoke.

The first Booster run was carried out in November-December 2020. After the orbit correction and tuning of the injection system the intensity of the circulating $^{4}He^{1+}$ beam grew up to 7×10^{10} ions. The total charge of these ions in the beam is equal to the design charge of the beam required for the Collider: 2×10^{9} $^{209}Bi^{35+}$ ions.

During the first three runs the $^{4}He^{1+}$, $^{56}Fe^{14+}$ and $^{12}C^{4+}$ beams with the intensities of up to 4×10^{10}, 2.5×10^{8} and 2×10^{9}, respectively, were accelerated in the Booster.

The following main results of the second Booster run with $^{56}Fe^{14+}$ ion beams (Fig.2) were achieved: the beam injection efficiency with adiabatic capture at the 5th harmonic higher than 95%; acceleration up to the energy of 65 MeV/u with the efficiency of recapturing from the 1st to the 5th harmonic close to 100%; acceleration up to the energy of 578 MeV/u with dB/dt = 1.2 T/s; vacuum ion

ISBN: 978-3-95450-227-1 ISSN: 2673-5490 doi:10.18429/JACoW-IPAC2022-WEPOPT002

CONCEPTION OF HIGH INTENSIVE POLORIZED PROTON BEAM FORMATION IN NICA COLLIDER

E .Syresin†, A. Butenko, S. Kostromin, O. Kozlov, I. Meshkov, A. Sidorin, G. Trubnikov, A. Tuzikov, Joint Institute for Nuclear Research, Dubna, Russia
P. Zenkevich, Institute for Theoretical and Experimental Physics of National Research Centre "Kurchatov Institute", Moscow, Russia
N. Mityanina, Budker Institute for Nuclear Physics, Siberian Brunch of Russian Academy of Sciences, Novosibirsk, Russia
S. Kolokochikov, Y. Senichev, Institute for Nuclear Research, Russian Academy of Science, Moscow, Russia
Yu. Filatov, Moscow Institute of Physics and Technology (MIPT) State University, Dolgoprudny, Russia
A. Kondratenko, M. Kondratenko, Science and Technique Laboratory Zaryad, Novosibirsk, Russia

Abstract

NICA (Nuclotron-based Ion Collider fAcility) is a new accelerator complex being assembled at JINR to search for the mixed phase of baryonic matter and to investigate the nature of nucleon/particle spin. The polarized proton beams will be operated at the energy range of 5-12.6 GeV, the beam intensity in each ring of $2.2\cdot10^{13}$ and the luminosity of $1\cdot10^{32}$ $cm^{-2}\cdot s^{-1}$. The conception of formation of high intensive proton beams is discussed for two different schemes. In first scheme the protons are injected from Nuclotron to Collider at an energy of 2-2.5 GeV to provide the cooling and the storage at this energy and then they are accelerated up to energy of experiments. In the second scheme the cooling of protons is realized in one from accelerators of the injection chain and the protons are injected from Nuclotron to Collider at energy of experiments, where they are stored up required intensity.

INTRODUCTION

The accelerator facility of the NICA collider [1-3] has the following configuration for formation of polarized proton beams: the light ion linac LILAC, the acting superconducting synchrotron Nuclotron and two collider storage rings with two interaction points at the maximal energy E=13.5 GeV.

LUMINOSITY AND KEY PARAMETERS OF PROTON BEAMS

The main parameters of the NICA accelerator complex for the proton-proton collision mode are given in Table 1. The colliding beam luminosity [4] is determined by the beam stability conditions. The strongest limitations are the effects of the beam space charge — the so-called "Laslett effect" and "beam-beam effect". Both of them lead to shifts Δq and ξ in the frequencies of betatron oscillations of particles in the collider focusing system, bringing them closer to the frequencies of the nonlinear resonances. At luminosity simulations the total shift of the betatron frequency corresponds to $\Delta Q=\Delta q+2\xi=0.05$ for two IP, but the Luminosity is given for one IP (Fig. 1).

The longitudinal normalized rms emittance of a bunched beam is $\varepsilon_c=N_b\gamma_{exp}\beta_{exp}\sigma_s\sigma_p=0.27$ m. The rms momentum spread after the LILAC debuncher corresponds to $\sigma_p=10^{-3}$. On injection from LILAC into the Nuclotron, the beam occupies the orbit with the circumference $C_N=251.52$ m, which corresponds to the rms bunch length $\sigma_s=C_N/2\cdot3^{1/2}=74.4$ m.

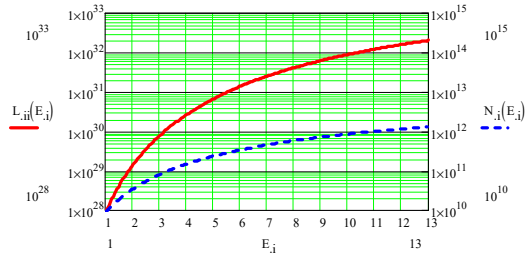

Figure 1: Dependence of the luminosity and the number of protons per bunch on the proton kinetic energy.

The normalized longitudinal emittance of the bunch in the Nuclotron is $\varepsilon_b=\gamma_{inj}\beta_{inj}\sigma_s\sigma_p=0.012$ m, where $\beta_{inj}=0.166$ at injection energy $E_{inj}=13$ MeV. The Nuclotron proton bunch intensity corresponds to $N_p=5\cdot10^{10}$, and the total intensity in the Collider ring is $N=2\cdot10^{13}$. As many as $N_{inj}=400$ injections from the Nuclotron to each Collider ring are required. Typical repetition injection time is $\tau_{rep}=3$ s. The total longitudinal emittance of all bunches at N_{inj} injections from the Nuclotron to each Collider ring corresponds to $\varepsilon_N=N_{inj}\gamma_{inj}\beta_{inj}\sigma_s\sigma_p=4.8$ m at the proton energy of 2.8 GeV. This value is a factor of 17.8 higher than the longitudinal emittance of the proton bunched beam in Collider experiments. The effective cooling system is obligatory to reduce the longitudinal emittance of the accumulated proton beam at the injection energy.

The Collider stochastic cooling could not be used for so intensive proton beams. The electron cooling can be

† esyresin@jinr.ru

ISBN: 978-3-95450-227-1 ISSN: 2673-5490 doi:10.18429/JACoW-IPAC2022-WEPOPT003

CHALLENGES OF LOW ENERGY HADRON COLLIDERS

E. Syresin†, A. Butenko, S. Kostromin, V. Lebedev, I. Meshkov, A. Philippov, A. Sidorin, G. Trubnikov, A. Tuzikov, Joint Institute for Nuclear Research, Dubna, Russia

Abstract

NICA (Nuclotron-based Ion Collider fAcility) collider complex [1-3] is under construction at JINR (Dubna, Russia). The initial configuration of the collider will support collisions of fully stripped heavy ions, ^{209}Bi, for a study of phase transition in the quark-gluon plasma in the energy range 1÷4.5 GeV/u per beam. Commissioning of the collider injection chain has been recently started. The complex includes two linacs, two Booster synchrotrons (Booster and Nuclotron to support the beam injection to the collider at the collision energy less than 3.9 GeV/u), and 2 collider rings with 503 m circumference. The design luminosity is ~10^{27} cm^{-2}·s^{-1} at 4.5 GeV/u. The heavy ions are generated in the ESIS-type ion source with intensity ~$5\cdot10^{8}$ per pulse. Then they are accelerated into the linac and Booster and directed to stripping target. Next, fully stripped ions are accelerated in Nuclotron and injected into Collider. Electron cooling at 65 MeV/u in Booster will be used to increase the beam phase space density. The electron and stochastic cooling are used in each of collider ring to support beam accumulation and to prevent emittance growth due to intrabeam scattering. Three RF systems are used for longitudinal phase space manipulations: RF-1 — barrier bucket RF for the beam accumulation, RF-2 makes initial bunching creating 22 bunches from a continuous beam, and RF-3 at the 66th revolution harmonic operating at the collisions.

An achievement of design luminosity requires overcoming many technological and beam physics problems which are shortly discussed in this paper.

INTRODUCTION

In the course of last 50 years the growth of beam energy was the major focus of hadron collider development. The next highest priority was maximizing the collider luminosity. To achieve maximum collision energy the protons and antiprotons were the particles of the choice. This road profoundly affected the development of the high energy physics and fundamentally changed our understanding of the world. However, recent developments in the nuclear physics have required a study of collisions of heavy ions in a range of relatedly small collision energy (< ~10 GeV/u) for a study of phase transitions in the quark-gluon plasma. The first attempt of such studies has been carried out at RHIC in the BNL [4]. The collider luminosity was relatively small since its operation was at the energy well below the design energy. It had two drawbacks: too large ring circumference which greatly reduced the cooling rates; and too small bending field which negatively affected the ring dynamic aperture and beam control. NICA collider complex is designed to address these challenges. It is currently under construction at JINR.

LUMINOSITY LIMITATIONS

The choice of main parameters was driven by the following considerations.

We account that: Eq. (1) the beam luminosity depends on the bunch population, N, and the beam emittance, ε, as $L \propto N^2/\varepsilon$; Eq. (2) the betatron tune shift is as $\Delta\nu \propto N/\varepsilon$. Then, excluding N one obtains that the luminosity is $L \propto \varepsilon\Delta\nu^2$. Typically, the betatron tune shifts are limited by a single particle stability to ~0.05, consequently the luminosity is proportional to the beam emittance. Thus, an increase of beam emittance to its limit is our first essential requirement.

An increase of beam emittance is limited by intrinsic non-linearity of the interaction region focusing. The edge field of quadrupoles creates non-linear kicks [5] in both transverse directions. For *x*-plane we have:

$$\Delta x = \frac{k}{12}(x^3 + 3xy^2)$$
$$\Delta P_x = -\frac{k}{4}((x^2 + y^2)P_x - 2xy \cdot P_y)$$

where k is the quadrupole gradient normalized to the magnetic rigidity, $P_x = dx/ds$, and $P_y = dy/ds$. The expression for *y*-plane is obtained by cycling permutation of x and y and by change of sign for k. In a thin lens approximation, the above equations yield the relative change of focusing strength for a particle passing through a quadrupole lens:

$$\frac{\partial\Phi}{\Phi} \approx \frac{x^2 + 3y^2}{4LF}, \quad (1)$$

where L is the quadrupole lens length, and $\Phi = 1/F$. In a low energy collider with collision optics in the interaction region (IR) the main non-linearity comes from the IR quadrupoles where local beta-functions are at least one order of magnitude larger than ones in the rest of the ring. Note that although formally this is a cubic nonlinearity it cannot be easily compensated by octupoles which make kicks proportional to $(x^2 - 3y^2)$. To make a rough approximation we assume that F is equal to the distance from the interaction point to the lens; and that the beta-function in the lens is: $\beta \approx F^2/\beta^*$, $F \gg \beta^*$. Here β^* is the interaction point (IP) beta-function. Then the betatron tune shift due to lens non-linearity at the aperture boundary is:

$$\delta\nu \approx F\varepsilon/\beta^{*2}. \quad (2)$$

Typically, the distance from IP to the IR quads, F, is set by the space required for the detector. In this case a reduction of the IP beta-function quadratically reduces the ring acceptance. Particle tracking in the real NICA optics shows

† esyresin@jinr.ru

ISBN: 978-3-95450-227-1 ISSN: 2673-5490 doi:10.18429/JACoW-IPAC2022-WEPOPT004

ACCELERATION AND CROSSING OF TRANSITION ENERGY INVESTIGATION USING AN RF STRUCTURE OF THE BARRIER BUCKET TYPE IN THE NICA ACCELERATOR COMPLEX

S. Kolokolchikov, Y. Senichev, A. Melnikov, Institute for Nuclear Research of the Russian Academy of Sciences, Moscow, Russia
E. Syresin, Joint Institute for Nuclear Research, Dubna, Russia

Abstract

During particle acceleration to the energy of experiment E_{exp} = 12.6 GeV (γ_{exp} = 14.4) in NICA collider there is a need for the crossing of transition energy E_{tr} = 5.709 GeV (γ_{tr} = 7.087). The slip-factor $\eta = \frac{1}{\gamma_{tr}^2} - \frac{1}{\gamma^2}$, which included in the equation of longitudinal motion, changes the sign, that leads to a loss of stability in the longitudinal plane when γ approaching to γ_{tr}. In order to minimize the reduction of the beam parameters, a rapid jump of transition energy is assumed during the time $t_{jump} \approx 10$ ms [1] with a simultaneous change of the polarity of the RF system to ensure the stability of the beam after the jump. RF structure based on "Barrier Bucket" a feature of the NICA collider accelerating system. A non-zero value of the field between the barriers, ensures the acceleration of the beam. This feature makes the system original.

In this paper, the main features of the dynamics of the longitudinal motion of the beam crossing through the transition energy are considered, taking into account its jump in the RF structure of the "Barrier Bucket" type. Due to the rapid jump of transition energy the time at which the particles are near the zero value of the first order slip-factor is significantly reduced. Obviously, in this case, the second order of the slip-factor begins to play a decisive role in the behaviour of particles inside the barrier bucket and completely determines the stability region near transition. In this case, when energy of particles crosses transition energy, focusing of the beam in the longitudinal plane disappears and the influence of the space charge becomes essential.

RAPID JUMP OF THE TRANSITION ENERGY

Jump Schemes

When the particle energy approaches the transition energy, it is assumed to make a rapid jump of the transition energy. This can be achieved by changing the field gradient in the focusing quadrupoles of the arcs, since for periodic structures $1/\gamma_{tr}^2 = \alpha_0 = 1/\nu_x^2$, where α_0 – first order of momentum compaction factor, ν_x – normalized frequency of betatron oscillations (tune) in the horizontal plane. The fast jump of transition energy is proposed to be equal to $2 \cdot \Delta\gamma_{tr} = 0.09$ (from $\gamma_{tr} = 7.087$ to $\gamma_{tr} - 2 \cdot \Delta\gamma_{tr} = 6.997$) [1]. With such a jump, the working point shifts the values from $\nu_x = 9.44$ and $\nu_y = 9.44$ to $\nu_x = 9.365$ and $\nu_y = 9.465$. The maximum change rate of transition energy is limited by the parameters of quadrupoles and their power systems $\dot{\gamma}_{tr} = \frac{d\gamma_{tr}}{dt} = 8.5s^{-1}$. Such a jump can be made during the time:

$$t_{jump} = T_0 \Delta n_{jump} = \frac{2 \cdot \Delta\gamma_{tr}}{\dot{\gamma}_{tr}} = 10.5ms, \qquad (1)$$

where $T_0 = 1.7\mu s$ – the time of one revolution period in the ring, $\Delta n_{jump} = 6226$ – the number of revolution periods during which a transition energy jump occurs.

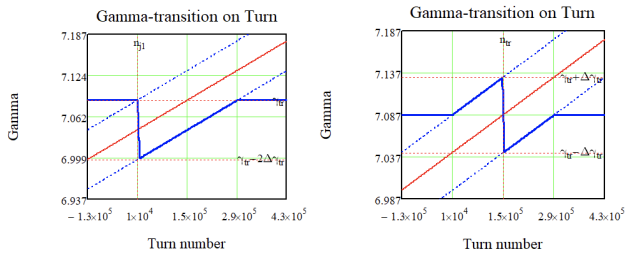

Figure 1: On the left – a schematic diagram of the transition energy γ_{tr} change during the jump and its recovery. On the right – another possible scheme. The blue solid line shows the transition energy γ_{tr}, the solid red line is the energy of particles γ. Blue dashed lines – γ of particles shifted by $\pm\Delta\gamma_{tr}$.

Figure 1 shows different schemes of the transition energy change γ_{tr} together with the beam energy γ at the moment of the jump and after it.

Dynamic Aperture

A change of the transition energy is possible due to a change in the tune of betatron tune in the x-plane, which is achieved by changing the gradient of the focusing lenses in the collider arcs. With the changed parameters of quadrupole lenses, the dynamic aperture was evaluated, it determines the stable area for movement of particles in the transverse plane. The corresponding calculations were carried out using OptiM and MADX programs.

The results shown on Figure 2 b indicate a working point at $\nu_x = 9.44$ and $\nu_y = 9.44$. For this working point is necessary to use octupole correctors to compensate nonlinear effects. If we assume the fact that it is necessary to reach the low frequency in the horizontal plane, with $\nu_x = 9.3627$ and in the vertical plane $\nu_y = 9.4541$ (see Figure 2 a). So thus, the transition energy is achieved $\gamma_{tr} - 2 \cdot \Delta\gamma_{tr} = 6.997$, the dynamic aperture in the horizontal plane disappears completely at these values of betatron tunes.

ISBN: 978-3-95450-227-1 ISSN: 2673-5490 doi:10.18429/JACoW-IPAC2022-WEPOPT005

INVESTIGATION OF POLARIZED PROTON SPIN COHERENCE TIME AT STORAGE RINGS

A. Melnikov*, A. Aksentyev[1], Y. Senichev,
Institute for Nuclear Research of the Russian Academy of Sciences, Moscow, Russia
E. Syresin, Joint Institute for Nuclear Research (JINR), Dubna, Russia
[1]also at National Research Nuclear University "MEPhI," Moscow, Russia

Abstract

The idea of the Electric Dipole Moment (EDM) search using the storage ring with polarized beam demands long Spin Coherence Time (SCT). It is the time during which the RMS spread of the orientation of spins of all particles in the bunch reaches one radian. Long SCT is needed to observe a coherent effect on polarization induced by the EDM. The possibility of getting a 1000 s SCT for deuterons has been shown experimentally at COoler SYnchrotron (COSY), accelerator at FZJ Jülich, Germany. Reaching high values of SCT for protons is more challenging due to a higher anomalous magnetic moment. Obtaining sufficient proton SCT is obligatory for planned EDM search experiments at COSY and the ProtoType EDM Ring (PTR). It has been shown that the second order momentum compaction factor (α_1) has to be optimized along with chromaticities ($\xi_{x,y}$) to get high SCT. Three families of sextupoles have to be used. The optimal values of chromaticities and α_1 are discussed. The racetrack option of PTR is investigated.

PRINCIPLES OF SCT OPTIMIZATION

To study the effects of spin decoherence one has to observe spin precession component orthogonal to the invariant axis. The in-plane spin precession is governed by the T-BMT equation and in a storage ring with magnetic bending the spin-tune is $\nu_s = G\gamma$, where G is anomalous magnetic moment. For non-reference particles the spin-tune is determined by the oscillation amplitudes in the phase space and lattice parameters such as chromaticities.

The first step in optimization of SCT, referring to [1], is turning on an RF cavity to suppress the first order spin-decoherence. It helps to increase SCT about three orders of magnitude.

In the presence of an RF cavity longitudinal motion is nonlinear in general case. The solution of nonlinear equations for the principle of synchronous acceleration gives the rise of equilibrium (average) energy level $\Delta\delta_{eq}$ [1]:

$$\Delta\delta_{eq} = \frac{\gamma_s^2}{\gamma_s^2\alpha_0 - 1}\left[\frac{\delta_m^2}{2}\left(\alpha_1 + \frac{3}{2}\frac{\beta_s^2}{\gamma_s^2} - \frac{\alpha_0}{\gamma_s^2} + \frac{1}{\gamma_s^4}\right) + \left(\frac{\Delta L}{L}\right)_\beta\right], \quad (1)$$

where betatron orbit lengthening term is:

$$\left(\frac{\Delta L}{L}\right)_\beta = -\frac{\pi}{L_0}\left[\epsilon_x\xi_x + \epsilon_y\xi_y\right]. \quad (2)$$

Here α_0 and α_1 is a first and second order momentum compaction factor. γ_s is a Lorentz factor and β_s is a relativistic beta factor for the synchronous particle. δ_m is an amplitude of synchrotron oscillations in $\frac{\Delta p}{p}$. $\xi_{x,y}$ are beam chromaticities and $\epsilon_{x,y}$ are the Courant-Snyder invariants.

The shift of equilibrium energy level for different values of α_1 is presented in Fig. 1. The calculations were done for the case of synchrotron motion without betatron oscillations.

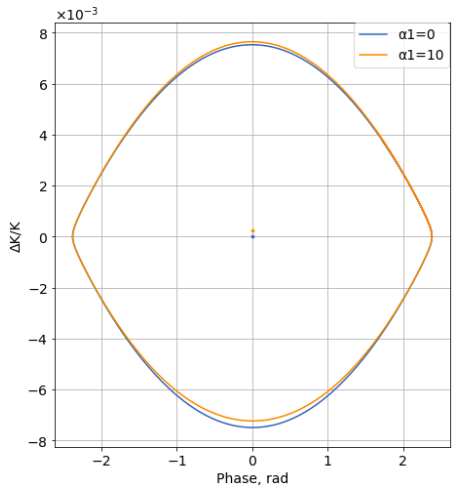

Figure 1: Phase trajectories in longitudinal plane for different values of α_1; $\xi_{x,y} = 0$. $\frac{\Delta K}{K}$ is a relative kinetic energy deviation.

From (1) and (2) it can be seen that ξ_x, ξ_y, α_1 have to be optimized to influence nonlinear longitudinal and spin motion. Three sextupole families need to be placed at points with different optical functions and dispersion to optimize these three parameters. Denoting the ansatz in Eq. (1) at δ_m^2 as κ, one can say that the sextupoles have to be tuned to zero ξ_x, ξ_y, κ to achieve long SCT. This comes from the fact that spin-tune deviation is determined by equilibrium energy level shift:

$$\Delta\nu_s = G\Delta\gamma_{eq}. \quad (3)$$

The investigation of this concept is presented below.

* alexei.a.melnikov@gmail.com

ISBN: 978-3-95450-227-1 ISSN: 2673-5490 doi:10.18429/JACoW-IPAC2022-WEPOPT006

INVESTIGATION OF SPIN-DECOHERENCE IN THE NICA STORAGE RING FOR THE FUTURE EDM-MEASUREMENT EXPERIMENT

A. E. Aksentev[1*], A. A. Melnikov, Y. V. Senichev,
Institute for Nuclear Research of the Russian Academy of Sciences, Moscow, Russia
V. P. Ladygin, E. M. Syresin, Joint Institute for Nuclear Research (JINR), Dubna, Russia
[1]also at National Research Nuclear University "MEPhI," Moscow, Russia

Abstract

A new experiment to measure electric dipole moments (EDMs) of elementary particles, based on the Frequency Domain method, has been proposed for implementation at the NICA facility (JINR, Russia). EDM experiments in general, being measurement-of-polarization experiments, require long spin-coherence times at around 1,000 seconds. The FD method involves a further complication (well paid off in orders of precision) of switching the polarity of the guiding field as part of its CW-CCW injection procedure. This latter procedure necessitates a calibration process, during which the beam polarization axis $\bar{n}$ changes its orientation from the radial (used for the measurement) to the vertical (used for the calibration) direction. If this change occurs adiabatically, the beam particles' spin-vectors follow the direction of the polarization axis — which undermines the calibration technique; however, concerns were raised as to whether violation of adiabaticity could damage spin-coherence. These concerns are addressed in the present investigation.

FREQUENCY DOMAIN METHOD

The proposed frequency domain method is a modification of the original "frozen spin" concept developed at Brookhaven National Laboratory [1–3].

The "frozen spin" family of EDM experiments has its foundation in the Thomas-Bargmann-Michel-Telegdi (T-BMT) spin precession described by the equation

$$\frac{\mathrm{d}\boldsymbol{S}}{\mathrm{d}t} = \boldsymbol{d}\times\boldsymbol{E} + \boldsymbol{\mu}\times\boldsymbol{B} = \boldsymbol{S}\times(\boldsymbol{\Omega}_{EDM}+\boldsymbol{\Omega}_{MDM}),$$

where $\boldsymbol{d}$, $\boldsymbol{\mu}$ are, respectively, the particle's electric and magnetic dipole moments, $\boldsymbol{\Omega}$'s are the corresponding spin-precession frequencies, and $\boldsymbol{S}$ is the precessing spin-vector.

In general, in order to utilize the T-BMT phenomenon for EDM-measurement in a "combined" storage ring, one introduces a radial electric field E_r. Then the accelerator's guiding field rotates the beam particles' spin-vectors via the magnetic dipole moment (MDM) at a frequency Ω_{MDM} in the horizontal plane, whereas E_r in the vertical plane with a frequency $\Omega_{EDM} \ll \Omega_{MDM}$ (see Fig. 1). One observes the vertical component of the beam polarization to oscillate:

$$P_v = P\frac{\Omega_{EDM}}{\Omega}\sin(\Omega\cdot t+\theta_0),$$
$$\Omega = \sqrt{\Omega_{EDM}^2+\Omega_{MDM}^2},$$

which we will call "the EDM-signature" signal.

The "frozen spin" method takes its name after the idea of "freezing" the MDM-precession, so that the spin precession plane turns completely vertical and the EDM-signature's amplitude is maximal. In theory, this also causes $P_v \approx P\cdot\Omega_{EDM}\cdot t$, so that one observes a slow linear buildup of vertical polarization at a rate proportional to the EDM. By measuring the amount of buildup ΔP_v per set time period T one can evaluate Ω_{EDM} and from that – the EDM itself. We may call it an "amplitude" (or "space domain") method, since the observable $P_v(T)$ is a realized fraction of the originating signal's amplitude, P (respectively, the magnitude of $\Delta\boldsymbol{P}_v$).

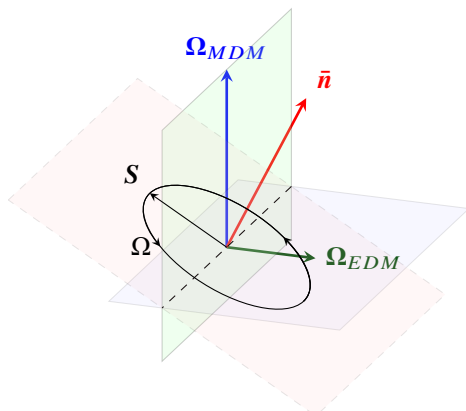

Figure 1: Thomas-BMT spin-precession. ($\boldsymbol{\Omega}_{EDM}$ has been extended by orders of magnitude for visual expediency).

However, E_r is only capable of reducing the *vertical* component of $\boldsymbol{\Omega}_{MDM}$. The radial component remains unaffected and is a major source of systematic errors. It also completely undermines any attempts at observing a *linear* polarization growth – unless Ω_r^{MDM} is made sufficiently small, which puts stringent conditions on the optical elements' installation precision.

Instead of trying to minimize the installation errors so as to purify the EDM-signature of *all* MDM contribution we could try to estimate the EDM from the signature signal's net frequency $\boldsymbol{\Omega} = \boldsymbol{\Omega}_{EDM} + \boldsymbol{\Omega}_{MDM}$. Since that frequency is a linear combination of both effects, two measurement cycles are required, in which the guiding field's polarity is reversed,

* a.aksentyev@inr.ru

ISBN: 978-3-95450-227-1 ISSN: 2673-5490 doi:10.18429/JACoW-IPAC2022-WEPOPT007

FIRST INTERACTION REGION LOCAL COUPLING CORRECTIONS IN THE LHC RUN 3*

F. Soubelet†, CERN, Geneva, Switzerland and University of Liverpool, Liverpool, UK
T.H.B. Persson, R. Tomás, CERN, Geneva, Switzerland
O. Apsimon, C.P. Welsch, University of Liverpool, Liverpool, UK

Abstract

The successful operation of large scale particle accelerators depends on the precise correction of unavoidable magnetic field or magnet alignment errors present in the machine. During the LHC Run 2, local linear coupling in the Interaction Regions (IRs) was shown to have a significant impact on the beam size, making its proper handling a necessity for Run 3 and the High Luminosity LHC (HL-LHC). A new approach to accurately minimise the local IR linear coupling based on correlated external variables such as the $|C^-|$ had been proposed, which relies on the application of a rigid waist shift in order to create an asymmetry in the IR optics. In this contribution, preliminary corrections from the 2021 beam test and the early 2022 commissioning are presented, as well as first results of the new method's experimental configuration tests in the LHC Run 3 commissioning.

INTRODUCTION

The approach to local coupling correction in the LHC has been to use the segment-by-segment technique [1] to calculate adequate powering of the MQSX magnets, the skew quadrupole correctors left and right of the Interaction Point (IP). The Interaction Region (IR) for point 1 is shown in Fig. 1, where the position of the dedicated correctors is highlighted in green.

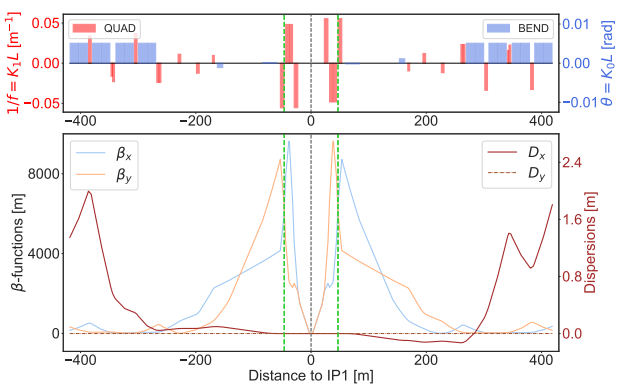

Figure 1: LHC IR1 for a round optics configuration at 7 TeV and $\beta^* = 25$ cm. The upper plot shows the machine layout with dipoles in blue and quadrupoles in red. The lower plot shows β and dispersion functions for both transverse planes. The vertical green lines highlight the location of the skew quadrupoles used for local coupling correction.

* This research is supported by the LIV.DAT Center for Doctoral Training, STFC and the European Organization for Nuclear Research.
† felix.soubelet@cern.ch

The coupling corrections calculated with the segment-by-segment technique are essential to reach low β^* with good optics control: at $\beta^* = 30$ cm the local errors compensated in Run 2 would contribute to the $|C^-|$ by the amount of 0.33 - too high for the arc correctors to handle. However, due to unfavorable phase advances in between Beam Position Monitors (BPMs) in the IRs, it is difficult to get a good measurement of the coupling Resonance Driving Terms (RDTs) in these regions. In turn, this means the method can hardly give a correction of coupling at the IP location, which is of importance to guarantee beam size and luminosity performance. A new method was developed which relies on breaking the symmetry of the IRs, and would allow to relate the coupling at IP to other external observables [2]. The first preliminary local coupling corrections of Run 3 and first implementation test of the new method in the LHC are presented in this paper.

SEGMENT-BY-SEGMENT CORRECTIONS

The segment-by-segment technique treats a segment of the accelerator as an independent line and propagates measured optics properties through this segment using the MAD-X code [3]. One then tries to find correction settings - powering changes of selected magnets - that would best reproduce the propagated optics. Thereby, inverting these settings and applying the inverted values in the machine corrects the measured errors.

In October 2021, a week of beam tests was done in the LHC at injection energy. From the measurements at 450 GeV a first set of local coupling corrections were calculated for each of the four main IRs using the segment-by-segment technique. Figure 2 shows the segment-by-segment results for the absolute value of the f_{1001} RDT in IR5, from the 12th BPM left to right of IP5. The vertical grey line indicates the location of the IP in the segment. Due to the skew quadrupole correctors in the IRs being single aperture magnets, one needs to find a single powering setting that works for both beams. As most of the error to be corrected derives from the triplets, which are also single aperture, this compromise is usually found. One can see that the determined correction in IR5 matches the propagated measurement within the tolerance of the error bars at the edges of the segment.

During the LHC Run 3 commissioning, local coupling corrections determined during the previous year beam test were trimmed in the machine from the start. After reaching the $\beta^* = 30$ cm optics, where the machine is more sensitive to local errors, a noticeable deviation around IP1 was observed

ISBN: 978-3-95450-227-1 ISSN: 2673-5490 doi:10.18429/JACoW-IPAC2022-WEPOPT008

SUPERVISED MACHINE LEARNING FOR LOCAL COUPLING SOURCES DETECTION IN THE LHC *

F. Soubelet†, CERN, 1211 Meyrin, Switzerland and University of Liverpool, Liverpool, UK
T.H.B. Persson, R. Tomás, CERN, 1211 Meyrin, Switzerland
O. Apsimon, C.P. Welsch, University of Liverpool, Liverpool, UK

Abstract

Local interaction region (IR) linear coupling in the LHC has been shown to have a negative impact on beam size and luminosity, making its accurate correction for Run 3 and beyond a necessity. In view of determining corrections, supervised machine learning has been applied to the detection of linear coupling sources, showing promising results in simulations. An evaluation of different applied models is given, followed by the presentation of further possible application concepts for linear coupling corrections using machine learning.

INTRODUCTION

Machine learning techniques have found their application in a wide range of particle accelerator control tasks in the past [1–7]. The precise knowledge of a coupling source's location and relative strength is valuable for further correction. While one can look at sudden jumps in the coupling Resonance Driving Terms (RDTs) f_{1001} and f_{1010} to deduce the presence of sources in between BPMs, such a method does not accurately pinpoint the location of a source, nor can it be used in locations with little instrumentation or unfavorable conditions. In the LHC, this approach is applicable for any source located in the arcs, but due to unfavorable phase advances between Beam Position Monitors (BPMs) in the Insertion Regions (IRs) and the necessity to have no strong sources between measuring BPMs, it is inappropriate for the detection of sources located within these regions. In this work, we explore the possibility of using supervised machine learning to detect betatron coupling sources in the LHC IRs.

SUPERVISED LEARNING FOR IR COUPLING SOURCES DETECTION

In order to perform a prediction of betatron coupling sources' locations, one first needs to compute the f_{1001} and f_{1010} RDTs. The strength and variations of the coupling RDTs throughout the machine is then used to estimate the location of coupling sources.

In terms of machine learning, this task can be defined as a regression problem that can be solved by training a model using measurements and corresponding solutions. Such a regression model requires a large data set in order to be able to generalize and produce reliable results. As from the real machine the location of sources is unknown, no real-world data is available for the training of machine learning models.

Data Set Generation

In order to create a training set, simulations are performed where random rotations around the s-axis are introduced into the MAD-X [8] quadrupoles, generating a skew quadrupolar component at the affected element and thus a source of coupling. It has to be noted though, that in the simulation of the training set we use tilt components to quadrupoles, given by the DPSI variable in MAD-X, which ignores the other potential sources such as feed-down from higher order magnets. While simulating the data, the introduced tilt components (DPSI values) are the input of the simulations and the produced coupling RDTs generated from the perturbed optics functions are the output. The data was generated for Beam 1 and 2 of the LHC, for the 2018 optics settings with $\beta^* = 30$ cm and using collision tunes ($Q_x = 0.31, Q_y = 0.32$). Figure 1 shows the reconstructed coupling RDTs for a given sample, calculated through the **C** matrix [9].

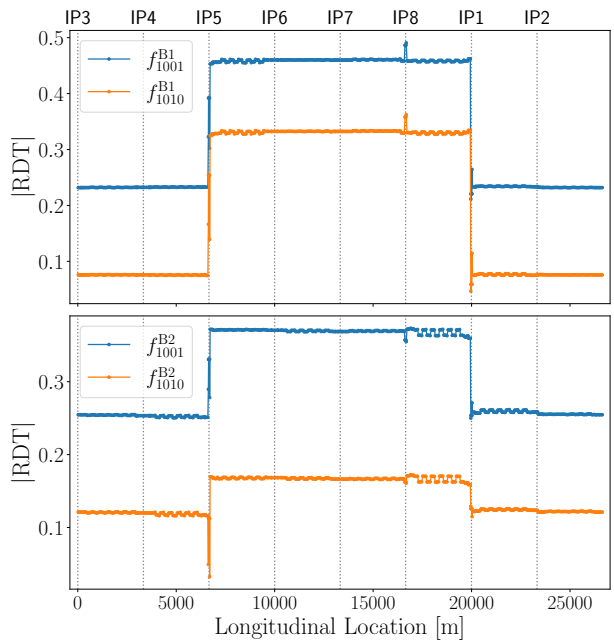

Figure 1: Coupling RDTs reconstructed for the LHC Beam 1 (top) and 2 (bottom) from the optics perturbed by the introduction of tilt errors to IR quadrupoles. Here a truncated Gaussian distribution with a standard deviation of 1 mrad was applied.

* This research is supported by the LIV.DAT Center for Doctoral Training, STFC and the European Organization for Nuclear Research.
† felix.soubelet@cern.ch

ISBN: 978-3-95450-227-1 ISSN: 2673-5490 doi:10.18429/JACoW-IPAC2022-WEPOPT009

OPERATIONAL SCENARIO OF FIRST HIGH LUMINOSITY LHC RUN

R. Tomás*, G. Arduini, P. Baudrenghien, O. Brüning, R. Bruce, X. Buffat, R. Calaga, F. Cerutti, R. De Maria, J. Dilly, I. Efthymiopoulos, M. Giovannozzi, P.D. Hermes, G. Iadarola, R. Jones, S. Kostoglou, B. Lindström, E.H. Maclean, E. Métral, N. Mounet, Y. Papaphilippou, T.H.B. Persson, T. Pugnat, S. Redaelli, G. Sterbini, H. Timko, F. Van der Veken, J. Wenninger, M. Zerlauth
CERN, Geneva, Switzerland

Abstract

A new scenario for the first operational run of the High Luminoisty LHC (HL–LHC) era (Run 4) has recently been developed to accommodate a period of performance ramp-up to achieve an annual integrated luminosity close to the nominal HL–LHC design target. The operational scenario in terms of beam parameters and machine settings, as well as the different phases to reach optimal performance, are described here along with the impact of potential delays to key hardware components.

PREVIOUS OPERATIONAL SCENARIOS

The HL–LHC operational scenario for Run 4 has been developed in [1], considering changes to the hardware configuration and new findings in beam dynamics with respect to the previous scenario presented in [2]. However, very recent changes to the schedule and potential delays in the installation of key hardware components are motivating its revision. This section presents the operational scenario as in [1] while the potential new scenarios are presented in the second section as reported in [3]. The key changes between [2] and [1] follow:

Postponing the installation of sextupoles (MS10) in the dispersion suppressor to after Run 4[1] It has been verified [4, 5] that beam lifetime due to Dynamic Aperture (DA) without these sextupoles is acceptable for optics with $\beta^* \geq 20$ cm in the two main experimental interaction points, IP1 & IP5, which is the current assumption for Run 4. Figures 1 and 2 show the DA at the start of collisions ($\beta^* = 1$ m) and at the end of the luminosity levelling ($\beta^* = 20$ cm), respectively. Note that at $\beta^* = 15$ cm these sextupoles are mandatory [6].

Reducing the scope of the secondary collimator upgrade, with not all being replaced with low-impedance collimators[1] **[7]** This decision is driven by cost considerations, with the drawback of a small increase of the machine impedance. The low-impedance collimators are Molybdenum coated Molybdenum Carbide-Graphite composite collimators.

Increasing in the primary collimator gap from 6.7 σ to 8.5 σ at top energy To ensure beam stability during the collision adjustment process [8], the impedance of the collimation system is reduced by increasing the collimator gaps. Some key collimator settings are shown in Table 1.

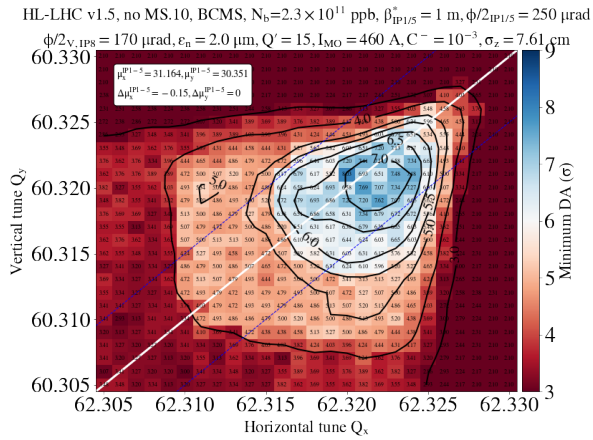

Figure 1: DA including beam-beam interactions at the end of the collision adjustment process versus horizontal and vertical tunes. An optimisation of the betatron phase between IP1 and 5 is applied as $\Delta\phi_x$=−0.15, $\Delta\phi_y$=0. A normalised emittance of 2 μm and bunch intensity of 2.3×10^{11} ppb are pessimistically considered to allow for brighter beams.

The increased gap has the advantage of reducing the halo density at the primary collimator.

Including Hollow Electron Lenses (HEL) in the HL–LHC baseline[1] [12] The HEL is an advanced tool for active control of the diffusion speed of halo particles, which will serve to mitigate losses from fast processes. Due to resources limitations the HEL will not be ready for Run 4.

Cancelling of the installation of 11 T dipoles in LS2 [10] Due to resources limitations Run 4 will happen without 11 T dipoles and associated new collimators in the IR7 dispersion suppressor [11].

The previous plan for the HL–LHC performance ramp-up allowed an integrated luminosity over 550 fb^{-1} at the end of Run 4. With 160 days of physics, the yearly integrated luminosity is expected to reach 240 fb^{-1}. In the first 1.5 years of Run 4, the bunch intensity is assumed to reproduce that of the Run 3, with minimum β^*=30 cm and full crossing angle of 450 μrad.

Figure 3 shows a schematic view of the Run 4 operational cycle including key beam parameters and expected luminosity. The abrupt jumps in bunch intensity and emittances during the collision adjustment process, just before

* rogelio.tomas@cern.ch

[1] System under review for the new Run 4 scenario

ISBN: 978-3-95450-227-1 ISSN: 2673-5490 doi:10.18429/JACoW-IPAC2022-WEPOPT010

PROGRESS ON ACTION PHASE JUMP FOR LHC LOCAL OPTICS CORRECTION

J. F. Cardona*, Y. Rodriguez[1], Universidad Nacional de Colombia, Bogotá, Colombia
H. García, R. Tomás, T. Persson, E. H. Maclean, M. Hofer, CERN, Geneva, Switzerland
[1]also at Universidad Antonio Nariño, Bogotá, Colombia

Abstract

The correction of the local optics at the Interaction Regions of the LHC is crucial to ensure a good performance of the machine. This is even more important for the future LHC upgrade, HL-LHC, where the optics is more sensitive to magnetic errors. For that reason, it is important to explore alternative techniques for local corrections. In this paper we evaluate the performance of Action Phase Jump method for optics correction in the LHC and the HL-LHC and explore ways to integrate this technique in regular operations.

INTRODUCTION

The quality of the beam in high luminosity experiments is highly dependent on the correction of linear magnetic errors at the Interaction Regions (IRs) where these experiments are located. In the past, Action and Phase Jump (APJ) analysis [1] has been used to estimate such corrections with results that are comparable to results provided by other techniques such as Segment by Segment (SbS) analysis [2]. For the first time at the LHC, corrections directly estimated with APJ have been used during the last Run (Run 3, 2022) showing very positive results, particularly for the IR where the ATLAS experiment is located. The first part of this paper describes the operational experience with APJ corrections and compares them to the corresponding SbS corrections.

The HL-LHC optics presents special challenges due to the small β functions at the Interaction Point (IP), expected to reach values as small as 15 cm. In the APJ technique, variables such as action and phase in the inter-triplet space depend on the β functions at the IP and therefore the accuracy with which these latter values are measured affect the performance of the APJ technique. Performance studies of the APJ technique applied to the HL-LHC are presented in the second part of this paper.

OPERATIONAL EXPERIENCE WITH APJ DURING RUN 3 OF THE LHC

The measurements used to estimate the corrections with APJ were taken when the beams were circulating with an energy of 6.8 TeV, all the linear corrections in the IRs were off, and the nominal values of β^* at IP1 and IP5 were 30 cm. To apply the APJ technique, TBT data is required. This data was generated by exciting both beams with the AC dipole and recording 6600 turns at all BPMs. This TBT data was preprocessed with averaging techniques [1, 3] and the action and phase plots were obtained around IR5 and IR1 as can be seen in Fig. 1. Average actions and phases in the arcs found in these plots are used to estimate the corrections in IRs. The actions and phases in the inter-triplet spaces are also necessary and they are estimated with the help of K-modulation data [4, 5]. During the measurements, K-modulation data was generated by changing the strengths of the quadrupoles closest to the IPs (Q1s) in IR1 and IR5 and recording the corresponding tunes changes. Once all the required data was available, corrections for IR1 and IR5 were estimated and applied in the machine a couple of days later. Significant reductions in the β-beating around the ring (from 150% to 20% [6]) and in the IPs were obtained as it can be seen in Table 1.

Corrections based on SbS were also estimated, applied, and their corresponding β^* measured as shown in Table 1. According to this Table, the values of β^* obtained from APJ corrections are close to the nominal values for IP1 while the values β^* corresponding to SbS corrections are closer to the nominal values for IP5. Therefore, a combination of both corrections is currently used for regular operations at the LHC.

APJ FOR THE HL-LHC

The effectiveness of the APJ correction for the HL-LHC and whether these corrections lead to a residual β-beating below the specified tolerances (less than 2% peak β beating in the IPs [7]) can be evaluated through simulated TBT data generated with different IR error distributions. Histograms of the residual peak β-beating after applying APJ corrections to 200 IR error distributions for the HL-LHC optics with β^* = 15 cm can be seen in Fig. 2 (simulations for HL-LHC optics with β^* = 30 cm can be found in [8]). The first histogram (red) is obtained assuming the β^* is known without any uncertainty. For that case, it can be seen that the peak β-beating is very low and only a couple of outliers exceed 2%. The β^* is expected to be one of the most critical measurement in the HL-LHC and it has been found that its accuracy will be around 4%. When this error is added to the previous simulations, there is a visible increase in the peak β-beating (green histogram) but still the number of outliers above 2% are moderate. At this point is should be mentioned that correction estimates done with APJ depend on w and β_w, the waist shift and the β function at the waist rather than the β^*. Therefore, to introduce the 4% error in β^*, a shift in w is added to reproduce this error for all 200 different magnetic error distributions.

Besides the uncertainties in the β^* already mentioned, the K-modulation technique has shown systematic unreliable

* jfcardona@unal.edu.co

ISBN: 978-3-95450-227-1 ISSN: 2673-5490 doi:10.18429/JACoW-IPAC2022-WEPOPT011

MODELLING FCC-ee USING MAD-X

L. van Riesen-Haupt*, T. Persson, R. Tomás and H. Burkhardt, CERN, Geneva, Switzerland

Abstract

We present the latest developments for simulating FCC-ee using CERN's MAD-X software. Along with updated benchmark studies, we describe how the latest MAD-X updates can facilitate the simulation of FCC-ee design features, including improvements in tapering and different options for implementing a tilted solenoid.

INTRODUCTION

The Future Circular Electron-Positron Collider (FCC-ee) [1] is a proposed new collider at the European Organization for Nuclear Research (CERN) for the era beyond the Large Hadron Collider (LHC). In order to design this machine and test its feasibility, it is important to ensure that the simulation tools used for this purpose provide reliable results.

In a previous publication [2], we presented studies that explore the simulation of more general optical properties obtained using CERN's Methodical Accelerator Design (MAD-X) [3] tool. An important feature in these studies was benchmarking the results to those obtained when using the Systematic Accelerator Design software (SAD) [4], which is designed for and thoroughly tested against the largest current lepton collider, Super KEK-B, located in Japan.

In this publication, we focus on the simulation of features that are more specific to the FCC-ee, including the computation of the beam emittance using tapered lattices and the effect of a tilted experimental solenoid. Again, benchmarking the results obtained using CERN tools against SAD plays a key role in these studies. Before presenting the new results we will provide a brief summary of previous work and put it in the context of this work.

Summary of Previous Results

In [2], it was established that for simulations without radiation, MAD-X and SAD compute identical optics to a relative precision of 10^{-6}. This is also true for off-momentum particles and the momentum detuning looks very similar for both codes. These results were obtained for FCC-ee lattices that did not include the tilted experimental solenoid.

MAD-X 5.6.00 was the first version to also include a tapering functionality [5]; this is a system in which the fields of the magnets around the ring are individually adjusted in order to compensate for the change in beam rigidity due to energy losses from synchrotron radiation. The MAD-X implementation is based on a similar scheme in SAD and in [2] we showed that the optical functions and tracking behaviour with radiation in tapered MAD-X lattices were very similar to those of SAD. The publication did not explore the emittances computed using MAD-X's EMIT module for these tapered lattices and the lattices did not include the tilted solenoid.

Table 1: Value of the five radiation integrals computed using MAD-X and SAD.

Integral	SAD	MAD-X
I_1	1.441818	1.441818
I_2	5.8860828×10^{-4}	5.8860839×10^{-4}
I_3	5.4659284×10^{-8}	5.4659304×10^{-8}
I_4	$-2.2581083 \times 10^{-10}$	$-2.2581086 \times 10^{-10}$
I_5	$5.2274385 \times 10^{-11}$	$5.2261809 \times 10^{-11}$

SYNCHROTRON RADIATION

Radiation Integrals

The radiation integrals are a set of simple optics integrals that can be computed from the accelerator's Twiss functions and bending radius and can help giving quick estimates of radiative properties such as energy loss per turn or equilibrium emittances [6]. Both MAD-X and SAD can compute the five commonly used radiation integrals. These were computed for the FCC-ee ZZ lattice version 213 [7] using MAD-X and SAD and the results are shown in Table 1.

From Table 1, it can be seen that there is a very good agreement between the two codes. Their values were also checked against integrals computed directly from the twiss files using python scripts. However, it should be pointed out that these integrals were computed for an on-momentum lattice in both cases. In SAD, the fourth radiation integral is momentum dependant and captures the fact that the bending radius depends on the local momentum of the beam. Some of this behaviour can be captured by the so-called I_8 integral as explained in [6]. To this end, the I_8 integral was added to MAD-X in version 5.06.00. This update also included the implementation of the I_6 integral, which captures the energy loss in the quadrupoles and is very relevant for colliders.

Emittance of Tapered Lattices

In the first iteration of the MAD-X tapering implementation, the EMIT module was not able to find a longitudinally stable orbit for the tapered FCC-ee lattices. To fix this, MAD-X version 5.07.00 introduced a minor change to the tapering that allows users to match the radio frequency cavity phase during the tapering process in order to achieve stability. This matching can be done using the MATCH module to constrain the p_t values to zero at the locations where the beam energy is equal to the reference energy.

This improvement makes it possible to determine the beam emittance using the matrix methods in MAD-X for tapered lattices and the results can be compared to those obtained from SAD. On top of SAD, the results can be compared to results obtained when computing the emittances

* leon.van.riesen-haupt@cern.ch

ISBN: 978-3-95450-227-1 ISSN: 2673-5490 doi:10.18429/JACoW-IPAC2022-WEPOPT012

MAD-X FOR FUTURE ACCELERATORS

T. Persson, H. Burkhardt R. De Maria, L. Deniau, T. Gläßle,
A. Latina, P. Skowronski, R. Tomás, L. Van Riesen-Haupt
CERN, Geneva, Switzerland
E. Høydalsvik,
Norwegian University of Science and Technology, Trondheim, Norway

Abstract

The development of MAD-X was started more than 20 years ago, and it still remains the main tool for single particle dynamics for both optics design, error studies as well as for operational model-based software at CERN. In this article, we outline some of the recent development of MAD-X and plans for the future. In particular, we focus on development of the TWISS module used to calculate optics functions in MAD-X which is based on first and second order matrices. These have traditionally been calculated as an expansion around the ideal orbit. In this paper we describe explicitly how an expansion around the closed orbit can be employed instead, in order to get more precise results. We also describe the latest development of the beam-beam long range wire compensator in MAD-X, an element that has been implemented using the aforementioned approach. Finally, we also present the newly implemented estimate of the C^-.

INTRODUCTION

MAD-X is a code that has been used for more than 20 years to perform optics and beam dynamic studies for a range of accelerators [1]. MAD-X is currently still in the center of many optics, aperture and emittances studies as well as a crucial part for various operational tools [2]. MAD-X itself is written in a combination of C, Fortran and C++. A relatively recent extension of MAD-X in the form of a Python interface called Cpymad has been made available and can be installed via pip [3]. There is also an internal interface to Polymorphic Tracking Code (PTC) [4] in MAD-X, which enables the user to utilise the two different physics engines while using the same sequence structure. This is very beneficial for cross-checks and to access features such as higher order normal forms, currently available through PTC.

In this article, we focus on recent MAD-X developments in terms of physics and functionalities. All the new features for each release, *e.g.* the recently implemented exact drift and the possibility to specify the number of particles directly in a beam-beam element can be found on the website under *Releases* [1].

EXPANSION

In the TWISS module, the closed orbit is first calculated and afterwards the optics is calculated for that orbit. This makes it possible to first find the closed orbit using the element transfer map and then calculate the first and second order transfer matrices based on the derivatives of the map. This is different from the previous approach in MAD-X where the matrices were calculated around the zero-orbit [5]. The previous method works well for small deviations, which is normally the case for machines such as the LHC, but in accelerators such as the FCC-ee, which is designed to operate with large crossing angles and momentum deviation, this approximation does not always hold. In order to overcome this, a Python code based on SymPy [6] has been developed in which one can input the exact equations and then the derivatives are calculated. There is a check to verify that the resulting matrix is symplectic and afterwards a Fortran code is generated in MAD-X format that can directly be included in the MAD-X source code. In the following sections we will show how this has been used for the exact drift and for Long Range Beam-Beam (LRBB) wire compensator.

EXACT DRIFT

The drift, when approximated, takes a simple form where the final position simply depends on the transverse momenta. In MAD-X the approximate drift has the following form:

$$x_f = x_i + l\,p_x\left(1 - \frac{p_t}{\beta_s}\right) \tag{1}$$

where l is the length of the drift, x_f is the final position, x_i is the position before the drift, p_x is the transverse normalised momenta, β_s is the relativistic factor for the reference particle and p_t is the energy deviation divided by the reference momenta P_s (see [5] for exact definitions). The drift when described exactly has interesting features such as introducing dependencies between planes. This can easily be seen by just observing the exact drift map:

$$x_f = x_i + l\frac{p_x}{\sqrt{\left(p_t^2 + \frac{2p_t}{\beta_s} + 1\right) - p_x^2 - p_y^2}}. \tag{2}$$

In Fig. 1 the deviations between the MAD-X expanded and PTC exact drifts and the new exact drift in MAD-X TWISS and PTC are shown. We can observe that there is a deviation in both the orbit and the β-function for the old method, while the new one follows within numerical precision the results from PTC. In order to activate the exact drift, one simply adds the keyword EXACT when calling TWISS. Even though this method requires more calculations, no measurable slowdown was observed when using it for the LHC lattice.

A recent related development on the analytical side [7] described the evolution of the W function in a drift considering the chromatic map shown in Eq. (1).

ISBN: 978-3-95450-227-1 ISSN: 2673-5490 doi:10.18429/JACoW-IPAC2022-WEPOPT013

EFFECT OF A SPURIOUS CLIQ FIRING ON THE CIRCULATING BEAM IN HL-LHC*

C. Hernalsteens, M. V. Basco, O. K. Tuormaa,
B. Lindstrom, E. Ravaioli, C. Wiesner, D. Wollmann
CERN, Geneva, Switzerland

Abstract

The High Luminosity LHC (HL-LHC) will reach a nominal, levelled luminosity of 5×10^{34} cm^{-1} s^{-2} and a stored energy of nearly 700 MJ in each of the two proton beams. The new large-aperture final focusing Nb_3Sn quadrupole magnets in IR1 and IR5, which are essential to achieve the luminosity target, will be protected using the novel Coupling Loss Induced Quench (CLIQ) system. A spurious discharge of a CLIQ unit will impact the circulating beam through higher order multipolar field components that develop rapidly over a few turns. This paper reports on dedicated beam tracking studies performed to evaluate the criticality of this failure on the HL-LHC beam. Simulations for different machine and optics configurations show that the beam losses reach a critical level after only five machine turns following the spurious CLIQ trigger, which is much faster than assumed in previous simulations that did not consider the higher order multipolar fields. Machine protection requirements using a dedicated interlock to mitigate this failure are discussed.

INTRODUCTION

The High Luminosity upgrade will increase the levelled luminosity of the CERN Large Hadron Collider (LHC) to 5×10^{34} cm^{-2} s^{-1} [1] by means of a higher beam brightness and using new equipment to reduce the β-function at the interaction points (IPs) (the so-called β^*) for the ATLAS and CMS experiments. The intensity increase means that the total stored beam energy will increase to 674 MJ for the nominal parameters for each of the two circulating beams [1]. This has a critical impact on machine protection systems of the LHC, which must ensure that the beams are extracted safely before uncontrolled beam losses would lead to equipment damage. In addition, the multi-stage collimation system of HL-LHC will feature a Hollow-Electron Lens (HEL) to reduce the beam halo population [2] by increasing the diffusion speed within the beam halo [3]. The halo population has a direct impact on the dynamics of the induced beam losses which in turn impacts the criticality of fast failures and requires detailed beam tracking studies to evaluate the evolution of beam losses [4].

The new equipment allowing to reduce the β^* down to 15 cm includes the large aperture superconducting final focusing quadrupole magnets (triplets). The active magnet protection of these magnets features the novel Coupling Loss Induced Quench (CLIQ) system [5]. The CLIQ magnet protection system will be used in the electrical circuit of the final focusing triplet quadrupoles around ATLAS (IP1) and CMS (IP5). Upon quench detection, the CLIQ discharge is activated, causing an additional and unbalanced current in the magnet poles, as compared to the nominal current. In the case of a spurious discharge of a CLIQ unit with circulating beams, the beam will be perturbed by the resulting multipolar magnetic field [6] at locations featuring very large β-functions and large amplitude of the crossing angle bump which increases the sensitivity to the field perturbation, as shown in Fig. 1. Initial studies of this failure case led to the modification of the CLIQ connection scheme so that the main field component became skew octupolar [7]. We report on beam tracking studies using the FailSim framework [8] which show that a spurious CLIQ discharge is the most critical fast failure identified for HL-LHC. The beam losses as a function of time are compared for different machine configurations to derive requirements on the interlock mechanism that needs to be developed to protect against such failure.

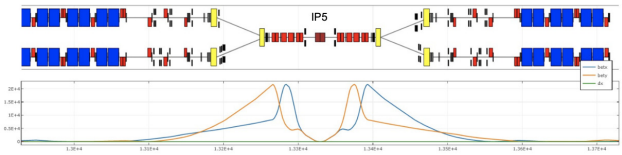

Figure 1: Horizontal (blue) and vertical (orange) β-functions around IP5. The β^* reaches 15 cm at the IP and over 20 km in the triplet region (shown as red boxes on both sides of the IP). Blue boxes represent main dipole magnets while yellow boxes represent the separation and recombination dipoles.

MACHINE, BEAM AND OPTICS MODELS

The nominal simulation setup uses the HL-LHC lattice V1.4 with the most critical optics configuration for round beams with $\beta^* = 15$ cm. We consider a full machine with 2736 bunches at top energy, as shown in Table 1. The baseline collimation scenario with the primary collimators (TCPs) cut set at 6.7 σ is compared with a collimation scheme with a TCP cut set at 8.5 σ[1]. The multipolar decomposition of the field components induced by the CLIQ discharge are reported in detail in [6]. The model of the transverse beam distribution is based on Run II beam scraping measurements performed to characterize the distribution and its halo up to the TCPs [9]. A fit on the measurement characterizes the transverse distribution as the sum of two Gaussian distributions which we extended to form the radial distribution over the 4D normalized transverse phase space

* Research supported by the HL-LHC project.

[1] For the relaxed collimation settings we use the HL-LHC lattice V1.5.

ISBN: 978-3-95450-227-1 ISSN: 2673-5490 doi:10.18429/JACoW-IPAC2022-WEPOPT014

THE EFFECT OF A PARTIALLY DEPLETED HALO ON THE CRITICALITY AND DETECTABILITY OF FAST FAILURES IN THE HL-LHC*

Cédric Hernalsteens, Meritxell Villén Basco, Christophe Lannoy, Oskari Kristian Tuormaa, Christoph Wiesner, Daniel Wollmann, CERN, Geneva, Switzerland

Abstract

In the High Luminosity LHC (HL-LHC) era, the bunch intensity will be increased to 2.2×10^{11} protons, which is almost twice the nominal LHC intensity. The stored energy in each of the two beams will increase to 674 MJ. The HL-LHC will feature beams whose transverse halos are partially depleted by means of a hollow electron lens. The reduced stored energy in the beam tails will significantly change the development of losses caused by failures. This paper reports on beam tracking simulations evaluating the effect of a partially depleted halo on the criticality and detection of failures originating from the superconducting magnet protection systems. In addition, the effect of the transverse damper operating as a coherent excitation system leading to orbit excursions on a beam with a partially depleted halo is discussed. The results in terms of time-dependent beam losses are presented. The margins between the failure onset, its detection, and the time to reach critical loss levels, are discussed. The results are extrapolated to failure cases of different origins that induce similar beam loss dynamics.

INTRODUCTION

The levelled luminosity of the CERN Large Hadron Collider (LHC) will be increased to 5×10^{34} cm^{-2} s^{-1} [1] following the High Luminosity upgrade. The higher bunch intensity will in turn increase the stored beam energy to 674 MJ for the nominal parameters for each of the two beams, see Table. 1. This will have an important impact on machine protection systems which must safely extract the beams before uncontrolled losses could induce damages to the machine equipment. The HL-LHC project also features an upgrade of the multi-stage collimation system to include a Hollow-Electron Lens (HEL) to reduce the transverse beam halo population [2]. This reduced beam halo density will impact the dynamics of the beam losses induced by fast failure scenarios [3]. Dedicated beam tracking simulations have been carried out to evaluate the criticality and detectability of occurrences of fast failures with depleted transverse beam halos [3, 4].

The following magnet protection system related scenarios are presented: the discharge of quench heater circuits with circulating beams, and the spurious discharge of a Coupling Loss Induced Quench (CLIQ) unit [5]. Next is the impact on the beam of a symmetric quench of one of the triplet magnets on the beam. An occurrence of such an event during Run II with fast propagation of the normal-conducting zone is taken as a typical case for such a failure mode and extrapolated to HL-LHC parameters [6]. Finally, the coherent excitation of the beam with the transverse damper is studied.

For all these cases, the time dynamics of the beam losses for these fast failure cases are simulated in detail to derive specifications for the interlock mechanisms to be developed to protect against such failures and machine protection requirements for the safe operation of HL-LHC with depleted transverse beam halos.

MODELING OF DEPLETED TRANSVERSE HALO

All simulations use the HL-LHC lattice V1.4 configured with the most critical optics settings for round beams, as shown in Tab. 1. The baseline collimation scenario with the primary collimators (TCPs) cut set at 6.7 σ is considered.

Table 1: Machine and Beam Parameters for the Squeezed HL-LHC Optics (as used in the simulations)

Parameter	HL-LHC
Energy	7 TeV
Stored beam energy	674 MJ
Bunch intensity (2736 bunches)	2.2×10^{11} p^+
Normalized emittance	2.5 µm
β^* at IP1-5	15 cm
Crossing angle at IP1-5	500 µrad
Primary collimator (TCP) cut	6.7 σ
HEL inner radius	4.7 σ

The model of the transverse beam distribution is based on Run II beam scraping measurements performed to characterize the distribution and its halo up to the primary collimators [7]. A fit on the measurement characterizes the transverse distribution as the sum of two weighted Gaussian distributions which have been extended to form the radial distribution over the 4D normalized transverse phase space. To account for the halo depletion induced by the HEL, this distribution function is modified by a decreasing exponential function within the HEL active radii - from the inner radius of the electron beam up to ρ_{TCP}, the radius at which the primary collimators are set - and then re-normalized. The halo depletion factor η represents the relative depletion in the halo. Here $\eta = 0$ implies a non-depleted halo. The resulting density projected on the horizontal displacement axis x is shown in Fig. 1 for different values of η. It should be noted that for a depleted halo the population is decreased at lower

* Research supported by the HL-LHC project.

ISBN: 978-3-95450-227-1 ISSN: 2673-5490 doi:10.18429/JACoW-IPAC2022-WEPOPT015

STUDY OF HYDRODYNAMIC-TUNNELLING EFFECTS INDUCED BY HIGH-ENERGY PROTON BEAMS IN GRAPHITE

C. Wiesner*, F. Carra, J. Don, I. Kolthoff, A. Lechner, R. Rasile, D. Wollmann
CERN, CH-1211 Geneva, Switzerland

Abstract

The design and assessment of machine-protection systems for existing and future high-energy accelerators comprises the study of accidental beam impact on machine elements. In case of a direct impact of a large number of high-energy particle bunches in one location, the damage range in the material is significantly increased due to an effect known as hydrodynamic tunnelling. The effect is caused by the beam-induced reduction of the material density along the beam trajectory, which allows subsequent bunches to penetrate deeper into the target. The assessment of the damage range requires the sequential coupling of an energy-deposition code, like FLUKA, and a hydrodynamic code, like Autodyn. The paper presents the simulations performed for the impact of the nominal LHC beam at 7 TeV on a graphite target. It describes the optimisation of the simulation setup and the required coupling workflow. The resulting energy deposition and the evolution of the target density are discussed.

INTRODUCTION

In order to evaluate the machine-protection systems for high-energy and high-intensity accelerators, the consequences of beyond-design failures (see page 445 in [1]) have to be considered. This includes the accidental, direct beam impact in one location. In this scenario, the damage range in the material can be dominated by an effect known as hydrodynamic tunnelling [2, 3]. The effect is caused by the beam-induced reduction of the material density along the beam axis, which allows subsequent bunches to penetrate deeper and deeper into the target. To take into account the changing material densities for the simulation, it is required to sequentially couple an energy-deposition code and a hydrodynamic code. In this generic study, the worst-case scenario of the direct impact of the full nominal Large Hadron Collider (LHC) proton beam at 7 TeV on a graphite target was simulated [4, 5]. The main aim of the study was to establish an efficient coupling workflow based on the FLUKA code [6–8] and the commercially available Autodyn code [9]. To facilitate future comparisons, similar beam parameters and the same equation of state as in a previous study (see Sec. 5.2. in [2], Sec. V in [10] and Chap. 8.3.2 in [11]), which was performed by coupling the codes FLUKA and BIG2 [12], were chosen.

* christoph.wiesner@cern.ch

SIMULATION SETUP AND PARAMETERS

Beam Parameters

For this study, the nominal LHC beam parameters [1] and a beam size of $\sigma = 0.5$ mm were used. The details of the LHC filling patterns were neglected and a constant bunch spacing of 25 ns was assumed. Table 1 summarizes the main beam parameters.

Table 1: Beam Parameters Used for the Simulations

Particle species	Protons
Beam Energy	7 TeV
Total number of bunches	2808
Protons per bunch	1.15×10^{11}
Bunch spacing	25 ns
Bunch length	0.5 ns
Filling scheme	None
rms beam size (sigma)	0.5 mm

Simulation Workflow

The simulation workflow for this study consisted of three main steps, which had to be performed in a loop:

1. Run the FLUKA simulation.
2. Import the energy-deposition map into Autodyn and perform the hydrodynamic simulation for a certain number of impacting bunches.
3. Update the target densities by interpolating the Autodyn results to the FLUKA regions and create the new FLUKA input file.

The general approach for the coupling simulations is discussed in [13]. For this study, an optimised coupling script [14] was used to update the target geometry of the FLUKA input file. The overall simulation cycle was stopped once it became evident that the propagation speed of the density depletion front in the target reached a near constant value, allowing to extrapolate the total penetration depth after the impact of all the bunches.

FLUKA Setup

The main target and FLUKA simulation parameters are summarised in Table 2. The target was modelled as a graphite cylinder with length of 10 m and a radius of 5 cm with axial symmetry. For the initial simulation step, a uniform target density of 2.28 g cm^{-3} was used. Therefore, no segmentation was required and the FLUKA model was implemented with a single region. However, for all subsequent

ISBN: 978-3-95450-227-1 ISSN: 2673-5490 doi:10.18429/JACoW-IPAC2022-WEPOPT016

BEAM-BASED RECONSTRUCTION OF THE SHIELDED QUENCH-HEATER FIELDS FOR THE LHC MAIN DIPOLES*

L. Richtmann†, L. Bortot, E. Ravaioli, C. Wiesner, D. Wollmann
CERN, CH-1211 Geneva, Switzerland

Abstract

Small orbit oscillations of the circulating particle beams have been observed immediately following quenches in the LHC's superconducting main dipole magnets. Magnetic fields generated during the discharge into the quench heaters were identified as the cause. Since the resulting, shielded field inside the beam screen cannot be measured in-situ, the time evolution of the field has to be reconstructed from the measured beam excursions.

In this paper, the field-reconstruction method using rotation in normalized phase space and the optimized fitting algorithm are described. The resulting rise times and magnetic field levels are presented for quench events that occurred during regular operation as well as for dedicated beam experiments. Finally, different approaches to model the shielding behavior of the beam screen are discussed.

INTRODUCTION AND MOTIVATION

The Large Hadron Collider (LHC) at CERN uses superconducting dipole magnets to guide the particles around their circular trajectory. The energy stored in each of the 8 main dipole circuits, comprising 154 magnets each, is around 1 GJ. Therefore, a sophisticated Quench Protection System (QPS) is installed to avoid damage in case of a resistive transition (quench) in one of the magnet coils [1–3].

An essential part of the QPS are the so-called quench heaters [4] that uniformly heat up the entire superconducting coil after the detection of a quench to avoid a local temperature hot spot. In case of a quench, a nominal current of 75 A [5, p. 174] is discharged through the quench heater strips that are attached to the outer part of each LHC dipole coil. To protect the superconducting coils from beam-induced heating and secondary particles, the beams travel inside a stainless-steel beam screen, which has a co-laminated copper layer with a nominal thickness of 75 µm [5, 6].

During Run 2 of the LHC (2015-2018), it was recognized that the magnetic field generated during the discharge of the quench heaters can cause oscillations of the circulating beam [7]. Although this effect is not considered critical for the current LHC operation, the fast development of the orbit perturbation has triggered detailed studies to understand its criticality for High Luminosity (HL)-LHC operation [7, 8].

Since the resulting field inside the beam screen cannot be measured in-situ, a method was developed to reconstruct it based on the measured beam excursions [9], which is a crucial input for any shielding model.

* This research was supported by the HL-LHC project.
† Lea.richtmann@aei.mpg.de

RECONSTRUCTION OF THE QUENCH-HEATER FIELD

BPM Measurements

In each of the two LHC rings, 516 Beam Position Monitors (BPM) are installed [5, ch. 13]. They measure the beam position averaged over all circulating bunches with a turn-by-turn resolution. Figure 1 shows the beam position measured by one BPM over 50 LHC turns after the firing of the quench heaters in one dipole magnet. The orbit deviation after the quench heater firing, taking effect at turn 14, can clearly be observed. Since the quench heaters produce a horizontal dipole field, the beam is displaced in the vertical plane [7, 8]. In contrast, a reduction of the main dipole field following the quench would displace the beam in the horizontal plane and would occur only on a time scale of tens of milliseconds.

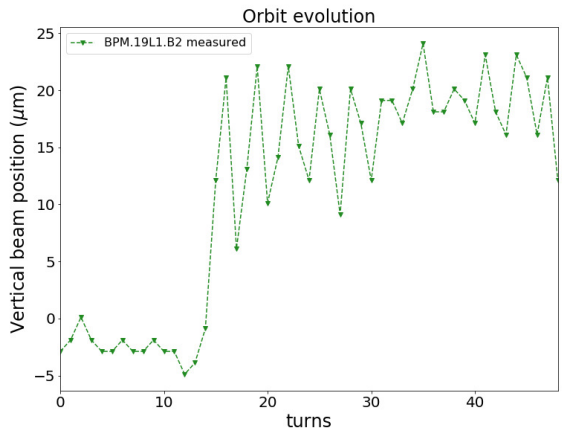

Figure 1: Example of the displacement of Beam 2 measured at one BPM after the firing of the quench heaters (timestamp: 2016-07-12 14:17:13, beam mode: collision, beam energy: 6.5 TeV, 1807 bunches per beam circulating). One LHC turn corresponds to a revolution time of 89 µs.

From the measured beam positions, one can then calculate the change of momentum or angle for each turn, which allows to reconstruct the magnetic field causing this change by using the method described in the following section.

Field-Reconstruction Method

For this method [9], it is assumed that the beam is kicked at one single location with a pure dipole field. However, no specific assumption on the time profile of the kick is made, such that this method can also be used for other cases.

In general, the envelope of a particle beam can be described by an ellipse in phase space [10], defined by the position y and the angle y'. By normalizing the position

ISBN: 978-3-95450-227-1 ISSN: 2673-5490 doi:10.18429/JACoW-IPAC2022-WEPOPT017

FIRST OPTICS DESIGN FOR A TRANSVERSE MONOCHROMATIC SCHEME FOR THE DIRECT S-CHANNEL HIGGS PRODUCTION AT FCC-ee COLLIDER

H. Jiang, HIT, Harbin, China and IJCLAB, Orsay, France
A. Faus-Golfe, IJCLAB, Orsay, France
F. Zimmermann, CERN, Geneva, Switzerland
K. Oide, KEK, Tsukuba, Japan
Z. Zhang, IHEP, Beijing, China and IJCLAB, Orsay, France

Abstract

The FCC-ee collider baseline foresees four different energy operation modes: Z, WW, H(ZH) and ttbar. An optional fifth mode, called s-channel Higgs production mode, could allow the measurement of the electron Yukawa coupling, in dedicated runs at 125 GeV centre-of-mass energy, provided that the centre-of-mass energy spread, can be reduced by at least an order of magnitude (5-10 MeV). The use of a special collision technique known as monochromatization scheme (mono-scheme) is one way to accomplish it. There are several methods to implement a monochromatization scheme. One method, named transverse monochromatization scheme, consists of introducing a dispersion function different from zero but of opposite sign for the two colliding beams at the Interaction Point (IP); Another one, named longitudinal monochromatization scheme, would make use of the correlation between the particle's longitudinal position and energy by means of RF cavities on each side of the IP. In this paper we will report about the first attempt to design a new optics to implement a transverse monochromatic scheme for the FCC-ee Higgs production totally compatible with the standard mode of operation without dispersion at the IP.

INTRODUCTION

The transverse monochromatization is a proposed way to reduce the centre-of-mass (CM) energy spread of FCC-ee [1] and then to increase the resolution in the CM energy with the natural energy spread, due to the synchrotron radiation (SR). For achieving the monochromatization schemes condition, opposite correlations between transverse position and energy have to be introduced. This requires a non-zero and opposite sign of dispersion function for the two beams, at the interaction point (IP). Monochromatization has been studied for 50 years [2-9], but has never used in any collider.

The FCC-ee collider consists of two horizontally separated rings for electrons and positrons, colliding with a crossing angle (30 mrad), so the horizontal dispersion at the IP can be generated independently with opposite signs. The non-zero dispersion functions are generated by changing the dipole configuration but keeping the crossing angle in the interaction region (IR).

In the following we will show first some analytical and parametric studies, second a first new design of the FCC-ee IR optics with a monochromatization scheme and finally a discussion of the issues to be solved in a future work.

THE PRINCIPLES OF MONOCHROMATIZATION

The standard collision scheme of a collider in comparison with the monochromatization colliding one is shown for comparison in Figure 1.

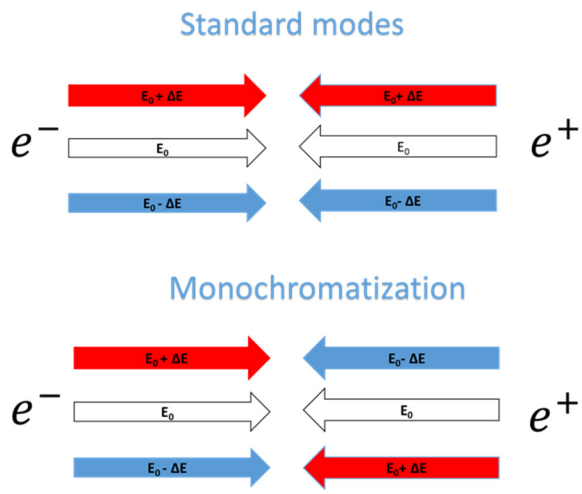

Figure 1: Schematic diagram of standard (Top) and monochromatization (Bottom) collision modes.

In the standard collision mode, the electron and positron beams have the same energy E_0 and energy spread ΔE (top part of Figure 1). In such a case the CM energy spread is given by:

$$\left(\frac{\delta w}{w}\right)_{standard} = \frac{\Delta E}{\sqrt{2}} \quad (1)$$

In the monochromatization collision mode, an IP dispersion of opposite sign for the two beams is introduced, so particles with energy ($E_0 + \Delta E$) will collide on average with particles of energy ($E_0 - \Delta E$) shown in the bottom part of Figure 1. In this configuration, the CM energy spread is reduced by the monochromatization (m.c.) factor λ, defined as [9]:

ISBN: 978-3-95450-227-1 ISSN: 2673-5490 doi:10.18429/JACoW-IPAC2022-WEPOPT019

RHIC BLUE SNAKE BLUES*

F. Méot†, E. Aschenauer, H. Huang, A. Marusic, V. Ptitsyn, V. Ranjbar,
G. Robert-Demolaize, V. Schoefer, Brookhaven National Laboratory, Upton, NY, USA

Abstract

Two helical full snakes are used in both Blue and Yellow rings of RHIC collider, in order to preserve beam polarization during acceleration to collision energy and polarization lifetime at store. A snake in RHIC is comprised of four 2.4 m long modules, powered by pair. During the startup of RHIC Run 22 in December 2021, two successive power dips have caused the 9 o'clock RHIC Blue ring snake to loose two of its four modules. In spite of this regrettable loss, it has been possible to maintain near 180° snake precession, by proper powering of the remaining two modules, as well as, by retuning the 3 o'clock sister snake, vertical spin precession axis around the ring and spin tune ½. Determining these new settings, in order to salvage polarization with the handicapped Blue snake pair, has required series of numerical simulations, a brief overview is given here.

INTRODUCTION

Two power supply dips at RHIC Run 22 startup in December 2021 caused RHIC Blue ring 9 o'clock snake to lose two of its four coils. Detailed spin dynamics simulations, using the OPERA field maps of the snakes, were undertaken to help determine new settings of RHIC Blue ring snake pair, accounting for the handicapped 9 o'clock snake [1]. Full polarization at store was eventually recovered, essentially as good as in earlier polarized proton RHIC runs, Fig. 1.

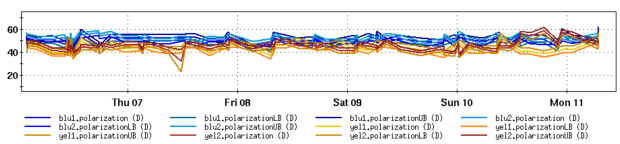

Figure 1: Sample polarization in Blue and Yellow rings during RHIC Run 22, over the period 4/6-11/2022.

RHIC snakes Blue and Yellow RHIC rings each house two helical snakes, Fig. 2 [2]. . A snake is a series of 4 right-handed helix modules (Fig. 3) with alternating field signs. A module is 2.4 m long, bore 10 cm (this matters regarding local closed orbit bump excursion), modules are spaced 0.212/0.448/0.212 m hence an overall length of 10.472 m.

Module currents are normally 100/-322/322/-100 Amp (R+R-R+R- series) and -100/322/-322/100 Amp (R-R+R-R+ series). The helical orbit requires centering along the snake, as part of the local closed orbit bump design during RHIC operation (Fig. 4 top row), with some tolerance as the magnetic field along the orbit, and thus spin motion, is

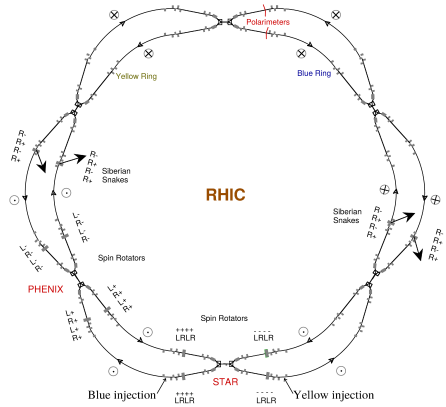

Figure 2: Location of snake series R+R-R+R- and R-R+R-R+ in Blue and Yellow rings, at 9 o'clock and 3 o'clock. Beam goes clockwise in Blue, counter-clockwise in Yellow.

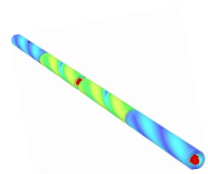

Figure 3: OPERA model of RHIC four helical module snake.

mostly independent of possible mis-centering (Fig. 4 top row, right),

Following the power supply dips, the 9 o'clock Blue snake was left with its sole coils 1 and 3, eventually operated in series in the 300^+ A region. Local closed orbit bump matching includes helix centering in this 2-coil R-0R+0 series (Fig. 4 bottom row).

Expected perturbation Given these new settings, RHIC Blue 9 o'clock snake is operated as ≈164° partial snake, a $\delta \approx 16°$ defect compared to full snake. This causes a $\delta/2 \approx 8°$ off-vertical tilt of the stable spin precession direction $\vec{n}_0(s)$ around a half of the ring - in particular $\vec{n}_0 = \left(\frac{\sqrt{2}}{2}\sin\frac{\delta}{2}, \frac{\sqrt{2}}{2}\sin\frac{\delta}{2}, \cos\frac{\delta}{2} \approx 1 - \frac{\delta^2}{8}\right)$ at 9 o'clock snake [1]. An additional adjustment of 3 o'clock snake to a similar value - as results from optimal settings, see below - doubles the defect. With vertical $\vec{n}_0$ at injection this would mean an expected polarization loss, other things being equal, of up to $1 - \cos 16° \approx 4\%$. To the first order in δ spin tune remains unchanged, $\nu_{sp} = 1/2$.

* Work supported by Brookhaven Science Associates, LLC under Contract No. DE-AC02-98CH10886 with the U.S. Department of Energy.
† fmeot@bnl.gov

ISBN: 978-3-95450-227-1 ISSN: 2673-5490 doi:10.18429/JACoW-IPAC2022-WEPOPT020

MODELING RHIC SPIN TILT AS LATTICE IMPERFECTIONS

V. H. Ranjbar*, F. Meot, E.C. Aschenauer, H. Huang, A. Marusic, V. Schoefer
Brookhaven National Laboratory, Upton, NY 11973, USA

Abstract

A tilt in the spin direction from the vertical has been observed for a number of years in the RHIC collider during store. This tilt has been extensively studied by scanning snake strengths, energies and orbital angles during the 2017 polarized proton run, and more recently during the 2022 polarized proton run. Using a spin transport model, we attempt to model this spin tilt by fitting all the relevant data.

INTRODUCTION

Since the 2013 polarized RHIC polarized proton run at 255 GeV a tilt in the spin at the location of Carbon target polarimeter has been observed. During the 2017 polarized RHIC [1]run we conducted several studies to better understand the cause of this tilt. These tests involved scanning the energy and snake settings and orbital angles at the snakes to observe the response of this spin tilt.

FITTING SINGLE IMPERFECTION SPIN RESONANCE

Our initial hypothesis was that possibly there might be some significant de-tuning of our snakes. That our snakes were not achieving the full 180 degree rotation about the ±45 degree angle relative to the beam trajectory. However other studies scanning the energy and snake settings at injection energy showed that deviations of the magnitude necessary to tilt the spin by the observed 15 degrees at 255 GeV would also perturb the spin tune and perturb the spin direction at injection energies as well. While there was some spin tilt at injection as we scanned the energy. The amount of spin tilt was too small to account for a systematic difference in the snakes even accounting for the energy difference. Additionally studies going on that year involving the spin tune and spin flipper didn't point to deviations in the performance of the snakes on the level to account for the observed spin tilt. Thus we believed that the source of the spin tilt was due to imperfection spin resonances, either due to a local or global source.

Using a simple spin transport model including snakes and single spin resonance we varied the phase and magnitude of an imperfection near the 255 GeV energy to see how well the introduction of such a perturbing spin resonance might explain the data. We modeled the snakes using the 2D spinor transport form:

$$\begin{aligned} e^{-i\frac{\mu}{2}(\cos\phi_s\sigma_1+\sin\phi_s\sigma_2)} &= \cos\frac{\mu}{2} - i(\sigma_1\cos\phi_s + \\ &\quad \sigma_2\sin\phi_s)\sin\frac{\mu}{/2} \\ &= T_s(\mu,\phi_s) \end{aligned} \quad (1)$$

where $\sigma_{1,2,2}$ are the 2x2 pauli spin matrices, μ is the angle of spin rotation and ϕ_s the angle of the axis relative to the direction of the beam about which the spin is rotated. Between the snakes the spin is transported using a solution to the Thomas-BMT equation for a single spin resonance:

$$\begin{aligned} &(\theta_f,\theta_i) = \\ &e^{-i\frac{K}{2}\theta_f\sigma_3}e^{\frac{i}{2}((K-G\gamma)\sigma_3+w_r\sigma_1-w_i\sigma_2)(\theta_f-\theta_i)}e^{i\frac{K}{2}\theta_i\sigma_3} \end{aligned} \quad (2)$$

Here K is the value of Gγ where the spin resonance is present, w_i and w_r the real and imaginary part of the spin resonance strength. The total spin transport once around the ring starting from the polarimeter where the tilt is measured now becomes:

$$\begin{aligned} &T = \\ &t(2\pi,\theta_s+\pi)T_s(\mu,-\phi_s)t(\theta_s+\pi,\theta_s)T_s(\mu,\phi_s)t(\theta_s,0) \end{aligned} \quad (3)$$

Here θ_s=2.04460321 rad is the location of the first blue snake relative to the polarimeter. From this one turn map the components of the closed orbit stable spin vector can be calculated using:

$$\begin{aligned} S_1 &= T^*_{1,1}T_{2,1} + T_{1,1}T^*_{2,1} \\ S_2 &= i(T^*_{1,1}T_{2,1} - T_{1,1}T^*_{2,1}) \\ S_3 &= |T_{1,1}|^2 - |T_{2,1}|^2 \end{aligned} \quad (4)$$

The angle relative to the vertical can then be estimated using $\theta = \arctan(S_3/S_1) - \pi$. Using this our best fits to the data for the first set of runs involving energy and snake scans yielded an imperfection at Gγ=486. This is relative to our nominal energy at 487. Including a 4 degree bump caused by the orbit through the snakes, we found an imperfection resonance strength with a total magnitude of about 0.07 with equal imaginary and real parts, could reproduce some (though not all) of the structure, as shown in Figures 1-5. However a later scan involving changing the orbital angle at the second snake (the one near 9 'oclock) showed that the best results involved using a single resonance K at Gγ of 487 with a magnitude of about 0.12 and real and imaginary strength of 0.01 and 0.12 respectively. In Figure 6 this fit is plotted along with the previous using K=486.

ANALYSIS AND FUTURE WORK

The use of this simple model does demonstrate that near 255 GeV modest imperfection resonances can produce tilts on the order observed. In some cases it does a decent job of capturing the tilt response, still a fully consistent picture alludes it. This suggests that a model with more complexity is required. This simple model has been extended to include multiple nearby spin resonances using an approach involving a magnus type of integrator which has been developed previously [2]. Perhaps more useful in the long run would

* vranjbar@bnl.gov

ISBN: 978-3-95450-227-1 ISSN: 2673-5490 doi:10.18429/JACoW-IPAC2022-WEPOPT021

A DISCHARGE PLASMA SOURCE DEVELOPMENT PLATFORM FOR ACCELERATORS: THE ADVANCE LAB AT DESY

J.M. Garland*, G. Loisch, R. D'Arcy, M. Dinter, S. Karstensen, S. Kottler, K. Ludwig, J. Osterhoff, A. Rahali, A. Schleiermacher, S. Wesch
Deutsches Elektronen-Synchrotron DESY, Germany

Abstract

Novel plasma-based accelerators, as well as advanced, high-gradient beam-manipulation techniques—for example passive or active plasma lenses—require reliable and well-characterized plasma sources, each optimized for their individual task. A very efficient and proven way of producing plasmas for these applications is by directly discharging an electrical current through a confined gas volume. To host the development of such discharge-based plasma sources for advanced accelerators, the ATHENA Discharge deVelopment ANd Characterization Experiment (ADVANCE) laboratory has been established at DESY. In this contribution we introduce the laboratory, give a summary of available infrastructure and diagnostics, as well as a brief overview of current and planned scientific goals.

INTRODUCTION

Plasma-wakefield accelerators could hold the key to revolutionising future particle accelerator facilities by significantly shrinking their footprint through the use of GV/m plasma-based accelerating stages [1–3]. In a typical discharge-ionised plasma source [4–6], a neutral gas confined within a solid structure is ionised by a high-voltage current pulse. Control of the spatial and temporal plasma profile can be realised by careful design of the structure confining the material, tuning of the current pulse properties and detailed knowledge of the evolution of the plasma. Figure 1 shows the geometry of a typical discharge plasma source used as an accelerating stage in a beam-driven plasma-wakefield experiment. In this mode, discharge plasma sources have several important applications in accelerator and photon science:

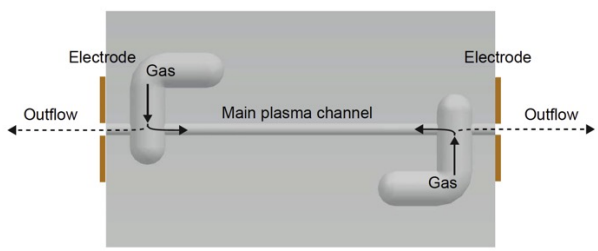

Figure 1: Schematic of a typical discharge plasma source used at DESY. The central channel and gas inlets (opposite ends of the main channel) have a circular cross-section and are milled from sapphire. The exits of the main channel are open to allow the passage of charged particles beams and lasers. Electrodes with the same diameter opening are placed around these exits.

- Accelerating stages, supporting GV/m accelerating gradients
- Waveguides, focusing EM radiation over multiple Rayleigh lengths
- Active plasma lenses (APL), producing radially uniform kT/m magnetic field gradients for charged particle focusing

The concept of accelerating and focusing charged particles using centimetre-scale plasma devices has already routinely demonstrated plasma acceleration, laser guiding and focusing of charged particles in APLs, all at repetition rates of 1 to 10 Hz [7–9]. However, this must be boosted into the multi-kHz continuous wave or MHz burst regime in a stable and reliable way in order to compete with the integrated-luminosity demands of the next generation of plasma-based photon science and particle physics facilities.

THE ADVANCE LAB

The ADVANCE (ATHENA Discharge plasma deVelopment ANd Characterization Experiments) lab was commissioned at DESY, Hamburg in order to facilitate the next steps in discharge plasma source development. The laboratory consists of several key features:

- Highly flexible vacuum chamber with modular outer panels, capable of hosting multiple plasma sources or long cells up to 1 m in length.
- Multiple, high repetition-rate high-voltage current pulse modulator systems
- Multiple plasma diagnostics including optical emission spectroscopy and two-color laser interferometry
- Auxiliary diagnostics such as synchronised, GHz-resolution signal readout and processing of current pulses and material temperature.
- A Ti:Sa laser with 1 kHz repetition rate, 35 fs, 3 mJ and an average power of 3 W
- On-site plasma source design and production.

Figure 2 shows a plasma source in operation at the ADVANCE lab. Multiple gas species can be used ranging from hydrogen to heavier gases such as argon. An ambient vacuum pressure of 1×10^{-7} mbar can be maintained without continuous gas flow and with continuous gas flow an ambient pressure of 1×10^{-3} mbar.

* jimmy.garland@desy.de

ISBN: 978-3-95450-227-1 ISSN: 2673-5490 doi:10.18429/JACoW-IPAC2022-WEPOPT023

A DESIGN OF ILC E-DRIVEN POSITRON SOURCE*

M. Kuriki†, H. Tajino, S. Konno, Z. Liptak, T. Takahashi, Hiroshima U. ADSE, Higashihirosima, Japan
M. Fukuda, T. Omori, Y. Seimiya, J. Urakawa, K. Yokoya, KEK, Tsukuba, Japan
S. Kashiwagi, Tohoku U. ELPH, Sendai, Japan

Abstract

ILC is an electron-positron linear collider based on Superconducting linear accelerator. Linear collider is the only solution to realize high energy electron-positron collision beyond the limit of synchrotron radiation energy loss by ring colliders. Beam current of injector of linear colliders is much larger than that of ring colliders because the beam is not reusable. Providing an enough amount of particles, especially positron is a technical issue. In this article, we present a design of electron driven positron source for ILC. After optimizations, the system design is established with an enough technical margin, e.g. avoiding potential damage on the production target.

INTRODUCTION

ILC is an e+e- linear collider with center of mass energy 250 GeV - 1000 TeV [1]. It employs Super-conducting accelerator to boost up the beam up to the designed energy. The beam is accelerated in a macro pulse with 1300 bunches by 5 Hz repetition. The bunch charge is 3.2 nC resulting the average beam current 21 A. This is a technical challenge, because the amount of positron per second is 40 times larger than that in SLC [2], which was the first linear collider.

The configuration of the positron source is schematically shown in Figure 1. The positron generated by electron beam is captured and boosted up to 5 GeV by two linacs. In the E-Driven ILC positron source, the drive beam energy is 3.0 GeV and the target is 16 mm thick W-Re alloy rotating with 5 m/s tangential speed. FC (Flux Concentrator) generates a strong magnetic field to compensate the transverse momentum. 36 1.3 m L-band Standing Wave (SW) cavities with 0.5 Tesla solenoid field are placed for positron capture. This section is called as the capture linac. At the downstream, a chicane is placed to removes electrons. The positron booster is composed from 2.0 m L-and and 2.0 m S-band Traveling Wave (TW) cavities. ECS (Energy Compression Section) is composed from 3.0 m L-band TW cavities with chicane.

In E-Driven ILC positron source, positrons are generated in a multi-bunch format as shown in Figure 2. One RF pulse contains 66 bunches with 80 ns gap. To generate 1312 bunches for positrons of one RF pulse in the main linac, this pulse is repeated 20 times in 64 ms to mitigate the potential damage on the production target. The number of positrons in one RF pulse is 20 times less than those in one RF pulse in the main linac, the instantaneous heat load on the target is also 20 times less [3].

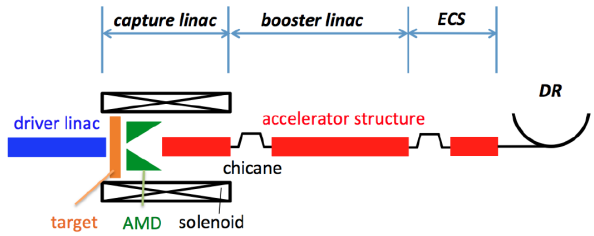

Figure 1: Configuration of E-Driven ILC positron source is schematically shown.

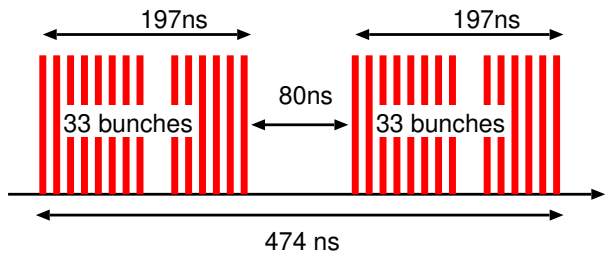

Figure 2: The beam structure in the positron source. Each mini-train contains 33 bunches.

A first simulation was performed by T. Omori [3] only for the capture linac. A simulation with the tracking down to DR (Damping Ring) was made by Y. Seimiya [4], but no beam loading effect was accounted. A new simulation with the beam-loading effect was done by Kuriki and Nagoshi [5, 6]. For those simulations, the peak energy deposition density on the target is kept less than 35 J/g [7], which is considered to be a practical limit of the safety operation.

To obtain uniform intensity positrons over the pulse, the transient variation of the acceleration field by the beam loading has to be compensated so that positrons are accelerated uniformly. Compensation for the transient beam loading by Phase Modulation (PM) on the input RF was proposed by Urakawa [8, 9]. The detail study of the compensation is discussed in Ref. [10, 11]. In this article, we present the electron driven ILC positron source accounting this effect.

SUBSYSTEMS

Electron Driver

3 GeV electron driver is composed from 2600 MHz (S-band) normal conducting TW cavity. The cavity is originally designed for ATF(Accelerator Test Facility) at KEK [12] in 2856 MHz and the parameters are scaled to 2600 MHz. 4 cavities are driven by two klystrons. Accounting 10 % power loss in RF wave guide, the input power to one cavity is 36 MW. The shunt impedance is 57.2 M/m with L=3.228 m and the attenuation τ is 0.57 resulting 0.91 s filling time. The beam loading compensation was performed by amplitude modulation (AM) [11]. The acceleration voltage per cavity

* Work supported by Grant-in-Aid for scientific research KAKENHI (B)
† mkuriki@hiroshima-u.ac.jp

ISBN: 978-3-95450-227-1 ISSN: 2673-5490 doi:10.18429/JACoW-IPAC2022-WEPOPT024

BEAM LOADING COMPENSATION OF STANDING WAVE LINAC WITH OFF-CREST ACCELERATION

M. Kuriki *, S. Konno, H. Tajino, Z. Liptak, T. Takahashi, Hiroshima U. ADSE, Higashihiroshima, Japan
S. Kashiwagi, Tohoku U. ELPH, Sendai, Japan
M. Fukuda, T. Omori, Y. Seimiya, J. Urakawa, K. Yokoya, KEK, Tsukuba, Japan

Abstract

In E-Driven positron source of ILC, the generated positron is captured by a standing wave cavity. Because the deceleration capture method is employed, the positron is off-crest over the linac. Because the beam-loading is expected to be more than 1A in a multi-bunch format, the compensation is essential to obtain uniform intensity over the pulse. A conventional method for the compensation controlling the timing doesn't work because RF and Beam induced field are in different phase. In this manuscript, we discuss the compensation with the off-crest acceleration case. A simple phase modulation on the input RF is a solution.

ILC is an e+e- linear collider with CME 250 GeV - 1000 TeV [1]. It employs Super-conducting accelerator (SCA) to boost up the beam up to the designed energy. The beam is accelerated in a macro pulse with 1300 bunches by 5 Hz repetition. The bunch charge is 3.2 nC resulting the average beam current 21 A. This is a technical challenge, because the amount of positron per second is more than 40 times larger than that in SLC [2].

INTRODUCTION

In the ILC positron source, the generated positron is captured in a RF bucket by a linac based on a standing wave (SW) linac with APS (Alternate Periodic Structure) cavity. The capture linac is composed from 36 1.3 m L-band APS cavities with 0.5 Tesla solenoid field.

In E-Driven ILC positron source, positrons are generated in a multi-bunch format as shown in Fig. 1. It contains 66 bunches with 80 ns gap. To generate 1312 bunches for positrons in one RF pulse in the main linac, the positron generation is repeated 20 times in 64 ms. Because the positron is generated over 64 ms, the instantaneous heat load on the target is much suppressed [3, 4].

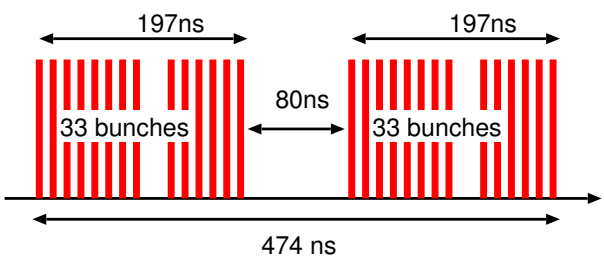

Figure 1: The beam structure in the positron source. Each mini-train contains 33 bunches. Each pulses contain 2 or 1 mini-trains.

* mkuriki@hiroshima-u.ac.jp

The generated positron has a large spread in both longitudinal and transverse momentum space. Capturing the positron in an RF bucket for further acceleration is the role of the capture linac. Deceleration capture was proposed by M. James et al. [5] for better capture efficiency. In this method, the positrons are placed on a deceleration phase initially and move to the acceleration phase by phase slipping.

This deceleration capture cause a difficulty on the beam loading compensation, because the cavity field induced by the beam (beam loading field) and the cavity field by RF (acceleration field) has a finite angle. Because the conventional theory of the compensation assumes the crest acceleration, the conventional method doesn't work in this case.

BEAM LOADING COMPENSATION WITH A STANDING WAVE LINAC

The acceleration voltage by a standing wave RF accelerator with the beam loading is

$$V(t) = \frac{2\sqrt{\beta PrL}}{1+\beta}\left(1-e^{-\frac{t}{\tau}}\right) - \frac{IrL}{1+\beta}\left(1-e^{-\frac{t-t_b}{\tau}}\right)e^{\imath\theta} \quad (1)$$

where β is coupling beta, P is input RF power, r is shunt impedance, L is structure length, $\tau = 2Q/\omega/(1+\beta)$, I is beam loading current, t_b is timing to start the beam acceleration, and θ is relative phase of the beam center to the RF. Here, we omit the RF oscillation term, $e^{\imath\omega t}$. If $\theta = 0$ and t_b is adjusted properly as $t_b = -\ln\left(\frac{I}{2}\sqrt{\frac{rL}{\beta P}}\right)$, $V(t)$ can be a constant.

If θ is a finite value, there is no solution in this framework. To compensate the voltage variation by the beam term, RF term should contain imaginary part, i.e. phase modulation (PM) is introduced. Figure 2 shows the phase diagram of the beam loading compensation with PM. V_{RF} is the amplitude of the asymptotic value of the cavity field by the input RF, ϕ is PM angle on the input RF, V_B is the asymptotic value of the beam loading voltage, θ is the beam phase, V_C is the cavity voltage when the beam acceleration is started. If the sum of $V_{RF}e^{\imath\phi}$ and $V_B e^{\imath\theta}$ is equal to V_C, the cavity field is kept as a constant at V_C.

$$V_{RF}e^{\imath\phi} + V_B e^{\imath\theta} = V_C \quad (2)$$

From this condition, ϕ is determined as

$$\phi = \sin^{-1}\left(-\frac{V_B}{V_{RF}}\sin\theta\right) \quad (3)$$

ISBN: 978-3-95450-227-1 ISSN: 2673-5490 doi:10.18429/JACoW-IPAC2022-WEPOPT025

FLAT BEAM GENERATION WITH THE PHASE SPACE ROTATION TECHNIQUE AT KEK-STF

M. Kuriki*, S. Aramoto, Z. Liptak, Hiroshima U. ADSE, Higashihiroshima, Japan
H. Hayano, X. Jin, Y. Seimiya, N. Yamamoto, Y. Yamamoto, KEK, Tsukuba, Japan
S. Kashiwagi, Tohoku U. ELPH, Sendai, Japan
K. Sakaue, U. of Tokyo, Tokyo, Japan
M. Washio, Waseda U., Tokyo, Japan

Abstract

Flat beam generation from angular momentum dominated beam with a phase-space rotation technique is an unique method to manipulate the phase-space distribution of beam. As an application, the asymmetric emittance beam generation for linear colliders is considered to compensate the Beamstrahlung effect at Interaction point. By using this technique, the asymmetric beam can be generated directly with the injector, instead of radiation damping with a damping ring. We present the result of a proof-of-principle experiment at KEK-STF.

INTRODUCTION

Electron Positron Collider is the only way to realize annihilation of elementary particles with controlled conditions with the current technology. Because there has been no any significant evidence of Super-symmetry in LHC experiments, the significance of detail studies of Higgs boson and searching inconsistency in the standard model with electron positron collider is maximized. ILC (International Linear Collider) [1] is an e+e- linear collider based on superconducting accelerator with center of mass energy from 250 to 1000 GeV. It would be constructed in Iwate, Japan, as the main project of High energy physics.

Luminosity L of linear colliders is

$$L = \frac{f n_b N^2}{4\pi \sigma_x \sigma_y}, \quad (1)$$

where f is repetition of pulse, n_b is number of bunches in a pulse, N is number of particles in a bunch, $\sigma_{x,y}$ is transverse beam size. In the linear collider, the beam after the collision is not recycled. If we employ a large current beam in linear colliders as same as in ring colliders, the required wall plug power is huge and such machine is unrealistic. One way to enhance the luminosity with a limited electricity is minimizing $\sigma_{x,y}$, but it causes a large energy spread by Beamstrahlung which is proportional to $(\sigma_x + \sigma_y)^{-2}$. A practical way to enhance the luminosity and suppress Beamstrahlung simultaneously is squeezing the beam in one of the transverse direction, e.g. $\sigma_x \gg \sigma_y$. For ILC, The beam size at interaction point, IP is 640 nm in horizontal direction and 5.7 nm in vertical direction. Emittances are 10 and 0.04 mm.mrad in horizontal and vertical directions, respectively [1]. This asymmetric emittance beam is made by radiation damping in a storage ring (damping ring) in the current design. The ring has to accommodate all bunches in one pulse, 1300 bunches and the circumference is 3 km.

We propose to generate the flat beam for ILC only with the injector by employing the emittance exchange technique and omitting the 3km storage ring. There are two methods as the phase-space rotation for the re-partitioning. One is RFBT (Round to Flat Beam Transformation) [2] generating a flat beam from an angular-momentum dominated beam produced by beam emission in a solenoid field. Another is TLEX (Transverse to Longitudinal Emittance eXchange) exchanging the phase-spaces between longitudinal and transverse directions by dipole mode cavity in a dispersive beam line [3]. These two techniques are experimentally demonstrated by P. Piot et al. [4] for RFBT and Y-E Sun et al. [5] for TLEX. The flat beam generation with RFBT and TLEX are explained in Ref. [6] for more detail. We propose the flat beam generation with the emittance exchange techniques, RFBT and TLEX as shown in Fig. 1. In the first part, the

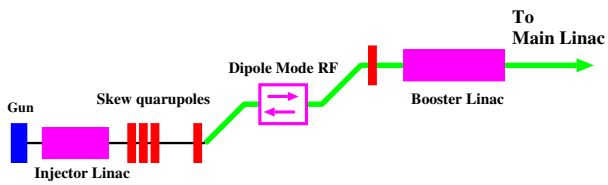

Figure 1: The injector design employing the emittance exchange techniques, RFBT and TLEX.

repartitioning between ε_x and ε_y by RFBT is performed. In the following section, TLEX exchanges ε_x and ε_z. The emittance budget is summarized in Table1. The first row is required emittance at IP for ILC. The second row is emittance at Gun when we employ only RFBT. In RFBT, the product of ε_x and ε_y is conserved. To make 10 mm.mrad and 0.04 mm.mrad only with RFBT, the emittance from Gun should be 0.6 mm.mrad in x and y directions. This small emittance cause several problems, e.g. emittance growth by space charge, a long bunch from gun due to the limited emission area, etc.

The third row shows the emittance at gun when we employ RFBT and TLEX as shown in Fig.1. If we employ RFBT and TLEX, the product of three emittance (x, y, and z) can be conserved and therefore, the initial ε_x and ε_y can be large to avoid the problem at the gun emission and the space charge emittance growth. The fourth row shows the

* mkuriki@hiroshima-u.ac.jp

ISBN: 978-3-95450-227-1 ISSN: 2673-5490 doi:10.18429/JACoW-IPAC2022-WEPOPT026

POSSIBILITIES FOR UPGRADING TO POLARIZED SuperKEKB

Z. J. Liptak*, Hiroshima University, Higashihiroshima, Japan

Abstract

The SuperKEKB accelerator is currently in operation in Tsukuba, Japan, with a planned long shutdown in 2026. Among the possible upgrades being considered during this period is the change to a polarized electron beam in the High Energy Ring. Such a change would require modifications in the source generation and transport, geometrical and lattice variations to provide spin rotation, and polarimetry. A Polarized SuperKEKB Working Group has been formed from members of the Belle II experiment and the SuperKEKB accelerator team to investigate the possibilities and challenges of these modifications. This talk lays out the goals of the proposed upgrade, considers the necessary changes to the existing accelerator and their feasibility and lays out the physics motivation behind such an effort.

INTRODUCTION

The SuperKEKB [1] accelerator began operation in 2016 at KEK in Tsukuba, Ibaraki, Japan, and has been providing electron-positron collisions for the Belle II experiment's full physics data taking operation since 2019. While the planned lifetime of the experiment is approximately 10 years, the KEK road map includes several long shutdowns for planned upgrades and maintenance.

At the moment, neither of SuperKEKB's beams are polarized; among the proposed upgrades during that time is the inclusion of spin polarization of the high-energy electron ring. This would open up new areas of measurement for Belle II with minimal changes necessary in the existing beam line.

The major improvements needed to produce a polarized beam are:

- Generation of a highly-polarized beam, and transport of polarized electrons from the electron source to the main storage ring
- Vertical spin preservation during storage in the main ring, and rotation to a longitudinal spin for collisions, followed by restoration to the vertical
- Precision polarimetry

A beam polarization working group, consisting of members of the SuperKEKB accelerator team and Belle II researchers, has been created to investigate possibilities for upgrading to a polarized electron beam and to determine and meet the challenges involved.

PHYSICS MOTIVATION

The weak mixing angle θ_W is a fundamental parameter of the Standard Model (SM), and precision measurements of neutral currents are considered one of the highest-priority avenues for discovery of physics beyond the SM. Any measurement finding a deviation of $\sin^2\theta_W$ from SM prediction would be a clear indication of new physics.

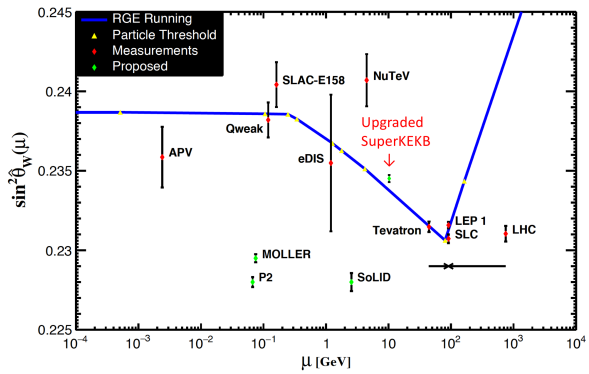

Figure 1: Scale dependence of $\sin^2\theta_W$ (giving the weak mixing angle) defined in the $\overline{MS}$ renormalization scheme. Adapted from reference [4] to include projected errors on proposed/upcoming experiments at particular energy scales, including that at an upgraded SuperKEKB that includes polarized electron beams.

The introduction of an electron beam spin-polarized above 70% would open a new avenue for measurement of weak neutral currents in a manner complementary to existing experiments.

In particular, a polarized beam would enable Belle II to measure the weak neutral vector coupling constants of the b and c quarks and muon with a substantial improvement in precision over past experiments [2, 3].

Figures 1 and 2 display the predicted precision of weak neutral vector current measurements with a data set of $20\,\text{ab}^{-1}$ taken with a polarized beam. In addition to precision, it can also be seen that Belle II's measurements would be in a parameter space of order 10 GeV, complementary to existing higher- and lower-energy range searches. Figure 3 shows the predicted resolving power for the vector couplings of the b and c quark compared to current SM predictions.

Furthermore, recent predictions also indicate that measurement of a chiral asymmetry in the process $e^+e^- \to \tau^+\tau^-$ at 1% precision would provide a measurement of the τ magnetic moment on the order of the current 4σ tension between the SM and experiment [5]. Such a measurement would be a new avenue at investigating anomalous lepton magnetic moments without the need to build a dedicated accelerator or experiment.

* zjl@hiroshima-u.ac.jp

ISBN: 978-3-95450-227-1 ISSN: 2673-5490 doi:10.18429/JACoW-IPAC2022-WEPOPT028

DESIGN UPDATE ON THE HSR INJECTION KICKER FOR THE EIC*

M. Sangroula†, C. Liaw, C. Liu, J. Sandberg, N. Tsoupas, B. Xiao
Brookhaven National Laboratory Upton, NY, USA
X. Sun, Argonne National Laboratory Argonne, IL, USA

Abstract

The Electron-Ion Collider (EIC), the next-generation nuclear science facility, is under the design at the Brookhaven National Laboratory. The present RHIC rings will be reconfigured as the Hadron Storage Ring (HSR) for the EIC. Design of a stripline injection kicker for the HSR for beams with the rigidity of ~ 81 T-m poses some technical challenges due to the expected shorter bunch spacing, heating due to higher peak current and the larger number of bunches, and the required higher pulsed voltage. Recently, we updated its mechanical design to optimize the characteristic and beam coupling impedances. In addition, we incorporated the impedance tuning capability by introducing the kicker aperture adjustment mechanism. Finally, we incorporated high voltage FID feedthroughs (FC26) to this kicker. This paper reports the design and optimization updates of the HSR injection kicker including the impedance tuning capability, optimization of both the characteristic and the beam coupling impedances, and finally the incorporation of a high voltage feedthrough design.

INTRODUCTION

The EIC [1–3], a next generation nuclear science facility, is under design and will be built at the Brookhaven National Laboratory. Design of a stripline injection kicker for the EIC Hadron Storage Ring poses some technical challenges due to expected shorter bunch spacing, heating due to higher peak current and larger number of bunches, and higher pulsed voltage required to operate this kicker. The basic information, design parameters, and initial geometry of this injection kicker can be found in [2, 4]. In summary, each kicker module is about a meter long structure having curved electrodes with a 59 mm (updated from 50 mm) gap between them. We may need up to 20 kicker modules to inject ~81 T-m hadron beam from the Alternating Gradient Synchroton (AGS) to the HSR. This article mainly focuses on the recent mechanical design updates and optimization of the kicker.

KICKER GEOMETRY UPDATE

The HSR kicker design is significantly matured, and almost ready for prototyping. Figure 1 compares its original design, [4] with the latest design. In comparison to its original design, we modified its cross-section to incorporate the impedance tuning capability. In addition, we reduced the total number of dielectric supports (from six to four) along with their length and width, and optimized the geometry of the tapered electrode to lower the impedance mismatch. Finally, we replaced the ideal coaxial feedthrough with a real design. We will present these mechanical design updates in the following sections.

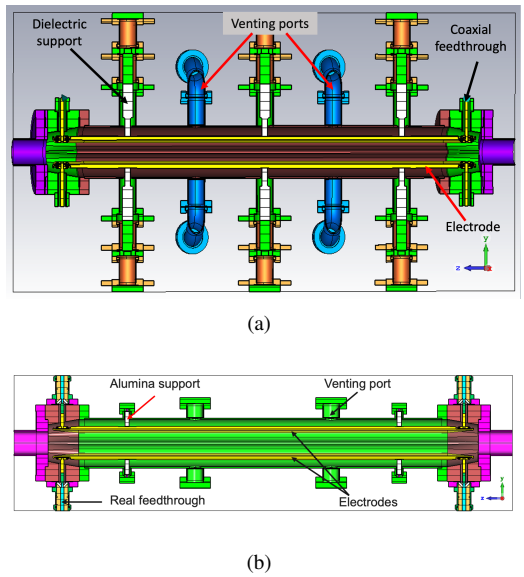

Figure 1: Top view of the EIC HSR horizontal kicker (a) in its initial geometry, and (b) with updated geometry.

IMPEDANCE TUNING CAPABILITY

The injection kicker is designed for a maximum of 25 ns full bunch length and the length of each stripline is ~3 ns. In order to produce a near constant amplitude kicking voltage along the entire length of a stripline, it is essential to minimize the characteristic impedance mismatch. The mismatch between the kicker and its connecting components such as: feedthroughs and cables introduces amplitude fluctuations due to the multiple power reflections between the feedthroughs and therefore causing beam emittance dilution. In practice, the actual impedance of a commercial 50 Ω cable or a feedthrough could vary from 48 Ω to 52 Ω. Based on this, we incorporated the impedance tuning capability, to properly match kicker's impedance with its connecting components, by adjusting the gap between the electrodes. The adjustment can be done by adding or removing shims on the alumina supports after the kicker is built.

To maintain the design requirement for the minimal gap between the electrodes of 50 mm, we ran CST [5] simulations to finalize the kicker's cross section. First, we increased the diameter of the kicker housing, at the fixed gap of 50 mm between the electrodes, until we get the maximum value of

* Work supported by Brookhaven Science Associates, LLC under Contract No. DE-SC0012704 with the U.S. Department of Energy
† msangroul@bnl.gov

ISBN: 978-3-95450-227-1 ISSN: 2673-5490 doi:10.18429/JACoW-IPAC2022-WEPOPT032

SUMMARY OF THE 3-YEAR BEAM ENERGY SCAN II OPERATION AT RHIC

C. Liu*, P. Adams, E. Beebe, S. Binello, I. Blackler, M. Blaskiewicz, D. Bruno, B. Coe, K.A. Brown, K.A. Drees, A.V. Fedotov, W. Fischer, C.J. Gardner, C. Giorgio, X. Gu, T. Hayes, K. Hock, H. Huang, R. Hulsart, T. Kanesue, D. Kayran, N. Kling, B. Lepore, Y. Luo, D. Maffei, G. Marr, A. Marusic, K. Mernick, R. Michnoff, M. Minty, J. Morris, C. Naylor, S. Nemesure, M. Okamura, I. Pinayev, S. Polizzo, D. Raparia, G. Robert-Demolaize, T. Roser, J. Sandberg, V. Schoefer, S. Seletskiy, F. Severino, T. Shrey, P. Thieberger, M. Valette, A. Zaltsman, K. Zeno, I. Zane, W. Zhang
Brookhaven National Lab, Upton, NY, USA

Abstract

Beam Energy Scan phase II (BES-II) operation in the Relativistic Heavy Ion Collider (RHIC), aiming to explore the phase transition between quark-gluon plasma (QGP) and hadronic gas, exceeded the goal of a four-fold increase in the average luminosity over the range of five gold beam energies (9.8, 7.3, 5.75, 4.59 and 3.85 GeV/nucleon) compared to those achieved during Beam Energy Scan phase I (BES-I). We will present the achievements in BES-II together with a summary of the measures taken to improve RHIC performance in the presence of several beam dynamics effects, and details on improvements made during the operation at 3.85 GeV/nucleon in 2021.

INTRODUCTION

BES-I [1–5] and BES-II [6, 7] explored the structure of the phase diagram by taking gold beam collision data at five energies: 9.8, 7.3, 5.75, 4.59 and 3.85 GeV/nucleon. BES-I operated from 2007 to 2014 at various energies for short periods of time, in order to provide preliminary data for the experiments, and to study the various beam dynamics effects that limit machine performance.

A plan for major hardware upgrades was put in place at the end of the BES-I, including for example electron cooling and 9 MHz RF cavities. These upgrades were used during BES-II from 2019 to 2021 at descending beam energies, with well-defined physics goals at each energy. The main goal was to provide enough experimental data by increasing the average luminosity by a factor of four. This goal was achieved, and in some cases exceeded, in part by improving the initial luminosity at the beginning of a store and by increasing the luminosity lifetime. The electron cooling system was used at the two lowest beam energies (4.59 and 3.85 GeV/nucleon). The luminosities achieved in BES-I and BES-II are presented in Fig. 1, and the primary beam parameters are summarized in Table 1.

The beam energy scans were challenging because the energies are well below the nominal energy range in RHIC – at or below gold beam injection energy of 9.8 GeV/nucleon. The challengings and counter-measures for BES-II operation have been summarised in a separate report [7]. We will present the operational conditions and improvements achieved during the last year BES-II operation at beam energy 3.85 GeV/nucleon.

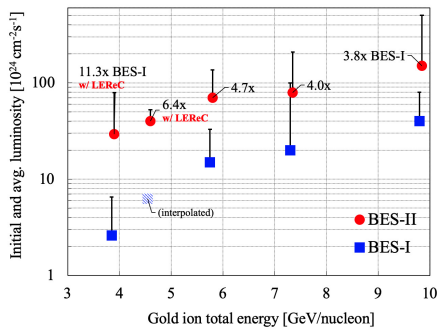

Figure 1: The initial and average luminosities at five gold beam energies achieved during BES-I and BES-II. Red dots and blue squares represent the average luminosity. A small horizontal bar marks the initial luminosity. The average luminosity at 4.59 GeV/nucleon during BES-I is interpolated based on data collected at 3.85 and 5.75 GeV/nucleon.

OPTIMIZING RHIC DURING ELECTRON COOLING

Three-dimensional electron cooling of colliding beams in both RHIC rings was realized for the first time [8] during BES-II. The electron cooling system was used at the two lowest beam energies (4.59 and 3.85 GeV/nucleon).

Early operations at 3.85 GeV/nucleon were performed with fractional tunes at 0.23. Tune space was explored with the goal of optimizing the average luminosity rather than enhancing just the cooling efficiency, and in particular to find better betatron tunes that enhance the ion beam lifetime in the presence of the high-current electron beam. Performance at 3.85 GeV/nucleon improved significantly when the fractional betatron tunes were lowered from 0.23 to 0.12. The single beam lifetime and the beam lifetime in collision were both improved, the injected bunch intensity was increased, and the initial collision rate was boosted by a factor of two.

* cliu1@bnl.gov; Work supported by Brookhaven Science Associates, LLC under Contract No. DE-AC02-98CH10886 with the U.S. Department of Energy.

ISBN: 978-3-95450-227-1 ISSN: 2673-5490 doi:10.18429/JACoW-IPAC2022-WEPOPT033

REPORT OF RHIC BEAM OPERATION IN 2021

C. Liu*, P. Adams, E. Beebe, S. Binello, I. Blackler, M. Blaskiewicz, D. Bruno, B. Coe, K.A. Brown, K.A. Drees, A.V. Fedotov, W. Fischer, C.J. Gardner, C. Giorgio, X. Gu, T. Hayes, K. Hock, H. Huang, R. Hulsart, T. Kanesue, D. Kayran, N. Kling, B. Lepore, Y. Luo, D. Maffei, G. Marr, A. Marusic, K. Mernick, R. Michnoff, M. Minty, J. Morris, C. Naylor, S. Nemesure, M. Okamura, I. Pinayev, S. Polizzo, D. Raparia, G. Robert-Demolaize, T. Roser, J. Sandberg, V. Schoefer, S. Seletskiy, F. Severino, T. Shrey, P. Thieberger, M. Valette, A. Zaltsman, K. Zeno, I. Zane, W. Zhang,
Brookhaven National Lab, Upton, NY, USA.

Abstract

The first priority of RHIC operation in 2021 was the Au+Au collisions at 3.85 GeV/nucleon, which is the lowest energy to complete the 3-year Beam Energy Scan II physics program, with RF-based electron cooling. In addition, RHIC also operated for several other physics programs including fixed target experiments, O+O at 100 GeV/nucleon, Au+Au at 8.65 GeV/nucleon, and d+Au at 100 GeV/nucleon. This report presents the operational experience and the results from RHIC operation in 2021. With Au+Au collisions at 3.85 GeV/nucleon reported in a separate report, this paper focuses on the operation conditions for the other programs mentioned above.

INTRODUCTION

RHIC [1] operation in 2021 ran from the end of January to the beginning of July for a total of 28 weeks including cool-down and warm-up of the superconducting magnets. Table 1 show the physics programs for RHIC operation in 2021. These programs were categorized in three tiers of priority, with the Au+Au collision at 3.85 GeV/nucleon beam energy [2,3] with cooling [4] as the top priority. There was a risk that not all parts of the program could be completed due to the difficulty of 3.85 GeV/nucleon operation. With the exceptional success of this top priority program, we were able to complete all proposed programs and an additional d+Au program. The goals of all the programs listed in Table 1 were either achieved or exceeded.

In addition to the physics programs, Coherent electron Cooling Proof of Principle experiment and accelerator physics beam studies continued in 2021. They alternated with the physics programs so the RHIC operations crew had to switch back and forth between different operational modes frequently which added complexity to operation. The switching involved mode switching (automated archiving and loading of machine settings), hardware changes (for example injection kicker and RF cavities termination), and cycling the magnets to establish stable machine conditions.

* cliu1@bnl.gov; Work supported by Brookhaven Science Associates, LLC under Contract No. DE-AC02-98CH10886 with the U.S. Department of Energy.

FIXED TARGET OPERATION

Fixed target experiments [5] were carried out at beam energies 3.85, 44.5, 70 and 100 GeV by scraping Au beam halo vertically at a gold foil installed in the beam pipe ~ 2 m upstream of the STAR detectors. Twelve bunches with moderate intensity (1.5E9 ions per bunch) were equally distributed in the yellow ring to avoid pile-up issue. The beams were brought close to the target by vertical orbit bumps of various amplitudes, and the bump amplitude was adjusted to maintain the rate.

Operation of 100 GeV FXT was challenging because the transverse beamsize is the smallest. An orbit bump of ~17 mm was established with maximum available strength on IR correctors. In addition, we had to introduce a few measures to dilute the beam emittance to obtain and maintain a stable collision rate. These measures are injection mismatch, applying single-turn kicks to individual bunches using tune meter kickers, introducing coupling to couple intrabeam scattering to the vertical plane, and applying continuous sinusoidal kicks to all bunches. With the maximum available orbit bump, the beam was still too small to generate collisions at first. The aforementioned measures were implemented to stimulate the growth of the beam size. The physics data taking only started when beam emittance in both planes grew to 7.5 mm mrad ~ 2 hours after beam was available (Fig. 1).

O+O COLLISIONS AT 100 GeV/NUCLEON

This was the first time in RHIC to run oxygen beams, produced by EBIS [6] using Alumina target, for collisions. The beam setup took 3 calendar days with the FXT programs running overnight. With much-reduced space charge and intrabeam scattering, beam lifetime was supreme. The store length was over 20 hours and 15 hours for the min-bias and central event data taking (Fig. 2). To reduce rms vertex length to 12 cm, beam was re-bucketed from 28 MHz to 197 MHz cavities and a crossing angle of 1.65 mrad was implemented. The experiment took 400 M min-bias events in 6 days, 200 M central events in 5 days and 100 M min-bias events with experimental solenoid reversed.

The luminosity and rms vertex length were recorded with various crossing angles. The dependence was not consistent with the prediction of analytic formula for Gaussian bunches.

ISBN: 978-3-95450-227-1 ISSN: 2673-5490 doi:10.18429/JACoW-IPAC2022-WEPOPT034

RECONFIGURATION OF RHIC STRAIGHT SECTIONS FOR THE EIC

C. Liu*, J.S. Berg, B. Bhandari, D. Bruno, C. Cullen, K.A. Drees, W. Fischer, X. Gu, R.C. Gupta, D. Holmes, R. Lambiase, H. Lovelace, F. Micolon, C. Montag, S. Peggs, V. Ptitsyn, G. Robert-Demolaize, R. Than, N. Tsoupas, J. Tuozzolo, M. Valette, S. Verdu-Andres, D. Weiss, D. Xu,
Brookhaven National Lab, Upton, NY, USA.
B.R.P. Gamage, T. Satogata, W. Wittmer,
Thomas Jefferson National Accelerator Facility, Newport News, VA, U.S.A.

Abstract

The Electron-Ion Collider (EIC) will be built in the existing Relativistic Heavy Ion Collider (RHIC) tunnel with the addition of electron acceleration and storage rings. The two RHIC rings will be reconfigured as a single Hadron Storage Ring (HSR) for accelerating and storing ion beams. The proton beam energy will be raised from 255 to 275 GeV to achieve the desired center-of-mass energy range: 20–140 GeV. It is also mandatory to operate the HSR with a constant revolution frequency over a large energy range (41–275 GeV for protons) to synchronize with the Electron Storage Ring (ESR). These and other requirements/challenges dictate modifications to RHIC accelerators. This report gives an overview of the modifications to the RHIC straight sections together with their individual challenges.

INTRODUCTION

The EIC [1], a discovery machine to be built at the Brookhaven National Laboratory, will collide electrons and various species of ions (protons to uranium ions) in a wide center-of-mass energy range (20–140 GeV). It is designed to provide luminosity of up to 10^{34} cm^{-2}s^{-1}, with high polarization (time-averaged polarization of ~ 70%) of both electron and light ion beams. One interaction region (IR) will be built within the scope of the project while maintaining the possibility of adding a second IR later. The electron injector, Rapid Cycling Synchrotron (RCS), and ESR will be added in the existing RHIC tunnels. Modifications will also be made to the RHIC accelerators to provide the required ion beams for collisions.

The HSR will be built on the basis of the two existing RHIC accelerators [2], however, with additional requirements. One requirement is that the path length of the HSR is adjustable such that the revolution frequency of ion bunches in a wide energy range (41–275 GeV for protons) can be matched exactly to that of the electron bunches. To achieve that, one needs to adjust the path length in two ways: by switching between an inner and an outer arc of the two RHIC accelerators (Fig. 1) to operate hadron beams at ~41 GeV and 100–275 GeV respectively, as well as by shifting the beam orbit radially off the center of the HSR to have the desirable path length for hadron beams in the energy range of 100–275 GeV [3]. The HSR will be operating at 3 times the RHIC beam current, 10 times shorter bunches and lower vertical beam emittance than RHIC. To achieve and maintain the required beam emittance, a coherent electron cooling device is planned to be installed at IR2. In addition, we need to remove the DX magnets (Fig. 1) to increase the proton beam energy from 255 to 275 GeV.

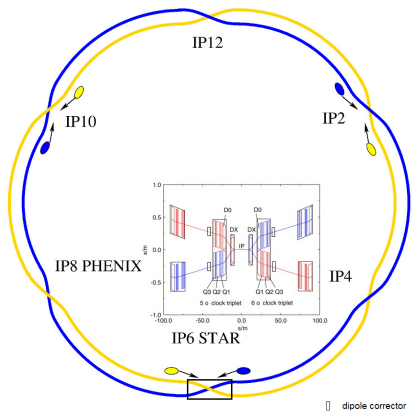

Figure 1: The schematic layout of RHIC with an expanded view of the STAR experimental area (IR6). The layout of the other straight sections in RHIC is similar to that at IR6. The path length of an outer arc is longer than that of an inner arc by 42 cm.

Figure 2 shows the schematics of the HSR. Hadron beams travel counterclockwise in the HSR, same as the beam does in the Yellow RHIC ring. Therefore, the HSR consists mostly of the Yellow RHIC arcs. The injection point in HSR moved from the current location in the Yellow ring at sector 5 to IR4 for adequate space for the kicker modules. The beam from the ATR (AGS to RHIC transfer line) will go over the HSR ring to merge into the Blue arc before reaching septum and kickers in IR4 [4]. The inclusion of the other two blue arcs will be explained in detail in the following section.

THE FUNCTIONALITY OF THE HSR STRAIGHT SECTIONS

Both RHIC and HSR comprise arcs that extend ~ $\pi/3$ angle and straight sections that connect the arcs. The straight sections host the final focusing triplets, warm spaces be-

* cliu1@bnl.gov; Work supported by Brookhaven Science Associates, LLC under Contract No. DE-SC0012704, and Jefferson Science Associates, LLC under Contract No. DE-AC05-06OR23177.

ISBN: 978-3-95450-227-1 ISSN: 2673-5490 doi:10.18429/JACoW-IPAC2022-WEPOPT035

OPTICS FOR STRONG HADRON COOLING IN EIC HSR-IR2

S. Peggs*, D. Xu, W.F. Bergan, D. Bruno, Y. Gao, D. Holmes, R. Lambiase, C. Liu, H. Lovelace III, G. Mahler, F. Micolon, V. Ptitsyn, G. Robert-Demolaize, Y. Than, J. Tuozzolo, E. Wang, D. Weiss, BNL, Upton, USA
S. Benson, T. Michalski, TJNAF, Newport News, USA

LAYOUT GEOMETRY

Strong Hadron Cooling (SHC) in the Hadron Storage Ring (HSR) [1] of the Electron-Ion Collider (EIC) uses microbunched electron cooling [2–9] to enable the highest luminosities. Figure 1 sketches the facility to be built in Insertion Region 2 (IR2) when the Relativistic Heavy Ion Collider (RHIC) is upgraded to become HSR. Electrons from an Energy Recovery Linac (ERL) co-move with hadrons as they pass through the Modulator straight (M). The imprint left by the hadrons on the electrons is amplified and then fed back to cool the hadrons as they co-move through the Kicker straight (K).

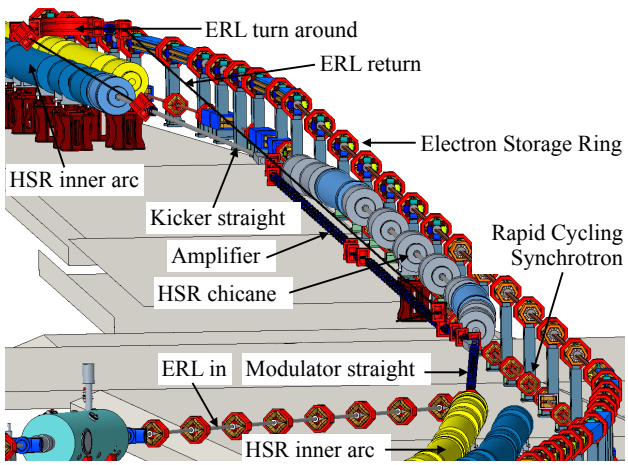

Figure 1: Hadrons and electrons co-move from bottom-right to top-left through the modulator and kicker straights. Electrons turn around and return to the ERL. IR2 is shared by two additional EIC accelerators – the Electron Storage Ring and the Rapid Cycling Synchrotron electron injector [10] – that do not participate in the cooling.

The "inner-arc-to-inner-arc" sequence shown in Fig. 2 is left-right symmetric in geometry and in optics [1]. RHIC magnets outside the IR-arc boundaries at quadrupoles Q10 (left and right) are unmoved, although they will be refurbished when RHIC becomes HSR.

COOLING RATES

Table 1 lists the primary optical parameters required and achieved in lattice HSR-220512a at two principal proton beam energies, 100 GeV and 275 GeV. Some intuition for their roles is gained by assuming that $\alpha_{x_0} = \alpha_{y_0} = D'_{x0} = D'_{y0} = 0$ at the K and M centers, and defining 3 cooling

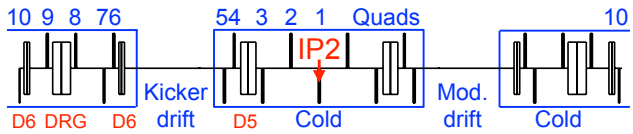

Figure 2: Left-right symmetric IR2 layout (to scale), with an isolated central cryostat and 4 warm-to-cold transitions. All quadrupoles are recycled from RHIC arcs with the same FODO cell spacing, except for doublets Q7-Q6 and Q5-Q4.

Table 1: Primary IR2 and ERL parameters. Subscript 0 and superscript star refer to the M and K straight centers and to the symmetry point IP2, respectively. Co-ordinate s advances from left to right.

Parameter	Unit	Proton energy [GeV]	
		100	275
Insertion Region 2			
Modulator/kicker length	m	39	39
Optics solution branch		JJ	DD
β_{x0}	m	40	40
α_{x0}		0	0
β_{y0}	m	~ 44	~ 60
α_{y0}		0	0
β^*_x	m	50	50
β^*_y	m	50	50
D_{x0} K & M	m	1.108	1.360
D'_{x0} slope at K		-0.0177	-0.0146
$\Delta\mu_x$ M-to-K phase adv.	rad	5.055	5.446
Chicane strength, $R_{56,h}$	mm	-6.35	-2.26
Energy Recovery Linac			
Electron energy	MeV	54.5	150
Charge	nC	1	1
Bunch length	mm	14	7
Peak Current	A	8.5	17
Average current	mA	100	100
Normalized emittance	μm	3	3
Slice rms $\Delta p/p$		$<1\times10^{-4}$	$<1\times10^{-4}$

coefficients [5, 11]

$$\begin{aligned} S_x &= (D_{x0}^2/\beta_{x0})\,\sin(\Delta\mu_x) \\ S_y &= (D_{y0}^2/\beta_{y0})\,\sin(\Delta\mu_y) \\ S_z &= R_{56}^h - S_x - S_y \end{aligned} \tag{1}$$

where the hadron chicane strength R_{56}^h follows the MADX sign convention. For *small* values of S the horizontal, vertical and longitudinal cooling rates are approximately

$$(\tau_x^{-1}, \tau_y^{-1}, \tau_z^{-1}) \approx C_\tau \cdot (S_x, S_y, S_z) \tag{2}$$

* peggs@bnl.gov

ISBN: 978-3-95450-227-1 ISSN: 2673-5490 doi:10.18429/JACoW-IPAC2022-WEPOPT036

DEPENDENCE OF BEAM SIZE GROWTH ON MACRO-PARTICLE'S INITIAL ACTIONS IN STRONG-STRONG BEAM-BEAM SIMULATION FOR THE ELECTRON-ION COLLIDER*

Y. Luo†, D. Xu, J. S. Berg, M. Blaskiewicz, W. Fischer, X. Gu, J. Kewisch, H. Lovelace III, C. Montag, S. Peggs, V. Ptitsyn, F. Willeke, Brookhaven National Laboratory, Upton, NY, USA
Y. Hao, Facility for Rare Isotope Beams, Michigan State University, East Lansing, MI, USA
J. Qiang, Lawrence Berkeley National Laboratory, Berkeley, CA, USA
G. Hoffstaetter, Cornell University, Ithaca, NY, USA
R. Gamage, H. Huang, V. Morozov, E. Nisson, T. Satogata,
Thomas Jefferson National Accelerator Facility, Newport News, VI, USA

Abstract

The Electron-Ion Collider (EIC) presently under construction at Brookhaven National Laboratory will collide polarized high energy electron beams with hadron beams with luminosities up to $1\times10^{34}\mathrm{cm}^{-2}\mathrm{s}^{-1}$ in the center mass energy range of 20-140 GeV. We simulated the planned electron-proton collision of flat beams with Particle-In-Cell (PIC) based Poisson solver in strong-strong beam-beam simulation. We observed a much larger proton emittance growth rate than that from weak-strong simulation. To understand the numerical noises further, we calculate the beam size growth rate of macro-particles as function of their initial longitudinal and transverse actions. This method is applied to both strong-strong and weak-strong simulations. The purpose of this study is to identify which group of macro-particles contributes most of the artificial emittance growth in strong-strong beam-beam simulation.

INTRODUCTION

The Electron-Ion Collider (EIC) presently under construction at Brookhaven National Laboratory will collide polarized high energy electron beams with hadron beams with luminosities up to $1 \times 10^{34}\mathrm{cm}^{-2}\mathrm{s}^{-1}$ in center mass energy range of 20-140 GeV [1]. We focus on the collision between 275 GeV protons and 10 GeV electrons since both protons and electrons reach their highest beam-beam parameters for this collision mode in the EIC. Table 1 lists the beam-beam related design parameters for this study.

Both strong-strong and weak-strong models are used for EIC beam-beam interaction simulation studies [2, 3]. For weak-strong model, the electron bunch is assumed rigid and the proton bunch is represented with macro-particles. The beam-beam kick to proton macro-particles are analytically calculated. For strong-strong model, both bunches are represented with macro-particles. Particle-in-cell (PIC) method and Fast Fourier Transformation (FFT) are used to solve 2-d Poisson equation on rectangle grids. The charge of each macro-particle is deposited onto nearest 9 grids and the beam-beam kick to each macro-particle is interpolated from the potentials on those nearest 9 grids.

Table 1: Beam-Beam Related Machine and Beam Parameters for Collision between 275 GeV Protons and 10 GeV Electrons

quantity	unit	proton	electron
Beam energy	GeV	275	10
Bunch intensity	10^{11}	0.668	1.72
(β_x^*, β_y^*) at IP	cm	(80, 7.2)	(55, 5.6)
Beam sizes at IP	μm	(95, 8.5)	
Bunch length	cm	6	0.7
Energy spread	10^{-4}	6.8	5.8
Transverse tunes		(0.228, 0.210)	(0.08, 0.06)
Longitudinal tune		0.01	0.069

Strong-strong simulation is subject to numerical noises due to limited macro-particles, transverse grids, longitudinal slices, and the algorithm itself. For the EIC beam-beam simulation, we observed a much larger proton emittance growth rate than that from weak-strong simulation. Through converging studies, the emittance growth rate from strong-strong simulation can be be reduced with increased macro-particle number.

To better understand the sources of numerical noises in the PIC based strong-strong simulation, we carried out extensive studies with the EIC design parameters. In this article, we will study the dependence of beam size growth rate on the longitudinal and transverse amplitudes of macro-particles. The goal of this study is to identify which group of macro-particles producing most of the artificial emittance growth in strong-strong simulation.

SIMULATION SETUP

In the strong-strong beam-beam simulation for this study, each bunch is represented by 0.5 million macro-particles. There is only one interaction point. For beam-beam interaction simulation, each bunch is split into longitudinal slices, 15 for the proton bunch, 5 for the electron bunch. Crab cavities are placed on both sides of IP with an exact $\pi/2$ phase advance in the horizontal plane. The ring transfer map is simply represented by a 6-d uncoupled one-turn transfer

* Work supportedh by Brookhaven Science Associates, LLC under Contract No. DE-SC0012704 with the U.S. Department of Energy.
† yluo@bnl.gov

ISBN: 978-3-95450-227-1 ISSN: 2673-5490 doi:10.18429/JACoW-IPAC2022-WEPOPT037

DYNAMIC APERTURE EVALUATION FOR EIC HADRON STORAGE RING WITH CRAB CAVITIES AND IR NONLINEAR MAGNETIC FIELD ERRORS*

Y. Luo†, X. Gu, J. S. Berg, W. Fischer, H. Lovelace III, C. Montag,
S. Peggs, V. Ptitsyn, H. Witte, D. Xu, Brookhaven National Laboratory, Upton, NY, USA
Y. Hao, Facility for Rare Isotope Beams, Michigan State University, East Lansing, MI, USA
J. Qiang, Lawrence Berkeley National Laboratory, Berkeley, CA, USA
V. Morozov, T. Satogata, Thomas Jefferson National Accelerator Facility, Newport News, VI, USA

Abstract

The Electron-Ion Collider (EIC) presently under construction at Brookhaven National Laboratory will collide polarized high energy electron beams with hadron beams with luminosities up to $1 \times 10^{34}\text{cm}^{-2}\text{s}^{-1}$ in the center mass energy range of 20-140 GeV. In this article, we evaluate the dynamic aperture for the Hadron Storage Ring (HSR) with symplectic element-by-element tracking. Crab cavities, nonlinear magnetic field errors, and weak-strong beam-beam interaction are included. We compared the dynamic aperture with crossing-angle collision to head-on collision and found the reason for the dynamic aperture reduction. We also studied the field error tolerances for IR magnets and for some particular magnets.

INTRODUCTION

The Electron-Ion Collider (EIC) presently under construction at Brookhaven National Laboratory will collide polarized high energy electron beams with hadron beams with luminosities up to $1 \times 10^{34}\text{cm}^{-2}\text{s}^{-1}$ in the center mass energy range of 20-140 GeV [1]. We focus on the collision mode involving 275 GeV protons and 10 GeV electrons since at this collision mode both protons and electrons reach their highest beam-beam parameters in EIC. Table 1 lists the beam-beam related design parameters for this study. In this article, we will evaluate the dynamic aperture calculation for the 275 GeV protons in the Hadron Storage Ring (HSR).

The HSR of EIC will re-use the existing RHIC arcs. Based on RHIC operational experience [2], simulated dynamic aperture in 10^6 turns with beam-beam interaction and IR nonlinear field errors should be larger than 5 σ with 3 $(dp/p_0)_{rms}$ to guarantee an acceptable beam lifetime at physics store. The beam-beam parameter for the proton beam in HSR is 0.012 which is comparable to RHIC, therefore we require the minimum dynamic aperture for HSR should be larger than 5 σ too.

SIMULATION SETUP

There are a few new features for HSR than RHIC [3]. First, EIC adopts a full crossing angle of 25 mrad at IP. To compensate the geometric luminosity loss due to the crossing angle, crab cavities are used to restore head-on collision. For EIC, local crabbing scheme is adopted. Ideally, crab cavities are placed on both sides of IP with a horizontal phase advance $\pi/2$ to IP.

To match the revolution frequency of Electron Storage Ring (ESR), HSR needs to be able to adjust its path length at various beam energies, which is achieved with radial shift orbit in arcs. The radial shift orbit is created with a field deviation from the nominal design value by $\Delta B/B_0$ to arc bending dipoles. Therefore, the on-momentum particle does not always have zero longitudinal coordinate $z = -c(t - t_0)$ in tracking code, where t_0 is the time flight on the reference orbit.

Based on the RHIC operational experience, IR magnetic field errors play an important role in dynamic aperture reduction. At the design phase of EIC, we will artificially assign magnetic field errors to all IR dipoles and quadruples within 160 m from IP to evaluate their impacts on the dynamic aperture of HSR.

Magnet field errors are defined as

$$(B_y L) + i(B_x L) = B(R_{ref})L\left[10^{-4}\sum_{n=0}^{N_{max}}(b_n + ia_n)\frac{(x+iy)^n}{R_{ref}^n}\right]. \quad (1)$$

Here L is the magnet length, R_{ref} is the reference radius where the magnetic field is measured, $B(R_{ref})$ is the main field at R_{ref}, b_n and a_n are the coefficients for normal and skew magnetic components.

Both systematic and random field errors can be assigned in the simulation. Here we focus on random field errors. In our study, we normally excluded the dipole and quadrupole

Table 1: Beam-beam Related Machine and Beam Parameters for Collision Between 275 GeV Protons and 10 GeV Electrons

quantity	unit	proton	electron
Beam energy	GeV	275	10
Bunch intensity	10^{11}	0.668	1.72
(β_x^*, β_y^*) at IP	cm	(80, 7.2)	(55, 5.6)
Beam sizes at IP	μm	(95, 8.5)	
Bunch length	cm	6	0.7
Energy spread	10^{-4}	6.8	5.8
Transverse tunes		(0.228, 0.210)	(0.08, 0.06)
Longitudinal tune		0.01	0.069

* Work supported by Brookhaven Science Associates, LLC under Contract No. DE-SC0012704 with the U.S. Department of Energy.
† yluo@bnl.gov

ISBN: 978-3-95450-227-1 ISSN: 2673-5490 doi:10.18429/JACoW-IPAC2022-WEPOPT038

SUMMARY OF NUMERICAL NOISE STUDIES FOR ELECTRON-ION COLLIDER STRONG-STRONG BEAM-BEAM SIMULATION *

Y. Luo†, D. Xu, J. S. Berg, M. Blaskiewicz, W. Fischer, X. Gu, J. Kewisch, H. Lovelace III, C. Montag, S. Peggs, V. Ptitsyn, F. Willeke, Brookhaven National Laboratory, Upton, NY USA
Y. Hao, Facility for Rare Isotope Beams, Michigan State University, East Lansing, MI USA
J. Qiang, Lawrence Berkeley National Laboratory, Berkeley, CA USA
G. Hoffstaetter, Cornell University, Ithaca, NY USA
R. Gamage, H. Huang, V. Morozov, E. Nisson, T. Satogata,
Thomas Jefferson National Accelerator Facility, Newport News, VI USA

Abstract

The Electron-Ion Collider (EIC) presently under construction at Brookhaven National Laboratory will collide polarized high energy electron beams with hadron beams with design luminosities up to $1\times10^{34}\mathrm{cm}^{-2}\mathrm{s}^{-1}$ in center mass energy range of 20-140 GeV. We studied the planned electron-proton collisions using a Particle-In-Cell (PIC) based Poisson solver in strong-strong beam-beam simulation. We observed a much larger proton emittance growth rate than in weak-strong simulation. To understand the numerical noise and its impact on strong-strong simulation results, we carried out extensive studies to identify all possible causes for artificial emittance growth and quantify their contributions. In this article, we summarize our study activities and findings. This work will help us better understand the simulated emittance growth and the limits of the PIC based strong-strong beam-beam simulation.

INTRODUCTION

The Electron-Ion Collider (EIC) presently under construction at Brookhaven National Laboratory will collide polarized high energy electron beams with hadron beams with design liminosities up to $1\times10^{34}\mathrm{cm}^{-2}\mathrm{s}^{-1}$ [1]. Both weak-strong and strong-strong models are used for the EIC beam-beam interaction simulation studies [2, 3]. For the weak-strong model, the electron bunch is assumed as a rigid 6-d Gaussian charge distribution. The proton bunch is represented with macro-particles. The beam-beam kick to proton macro-particles are calculated analytically. For the strong-strong model, each bunch is represented with typically 0.5 to 1 million macro-particles. Particle-in-cell (PIC) method and Fast Fourier Transformation (FFT) are used to solve 2-d Poisson equation on rectangle grids. The charge of each macro-particle is deposited onto nearest 9 grids and the beam-beam kick to each macro-particle is interpolated from the potentials on those 9 nearest grids.

In the following, we present simulation results for the collision between 275 GeV protons and 10 GeV electrons [4]. At this collision mode, the horizontal and vertical beam sizes are 95 μm and 8.5 μm at IP. The beam-beam parameter is 0.012 for the protons and 0.1 for the electrons, both reach their highest values in the EIC. We pay more attention on the proton bunch's emittance growth, especially in the vertical plane. We normally extrapolate beam size growth rate from a linear fitting in the tracking turns to %/hour. From strong-strong simulation, the simulated proton's vertical beam size growth rate is normally larger than 1000%/hour. However, from weak-strong simulation, it is less than 5%/hour.

Strong-strong simulation is subject to numerical noises due to limited macro-particle numbers, transverse grids, longitudinal slices, and the algorithm itself. To better understand the simulated growth rates and the numerical noises in the EIC strong-strong beam-beam simulation, we carried out extensive studies to identify all possible causes for the artificial emittance growth and quantify their contributions.

CONVERGING STUDY

Analytically, the numerical noise introduced artificial emittance growth rate in the strong-strong beam-beam simulation is inversely proportional to the number of macro-particles and proportional to the square of the beam-beam parameter. Figure 1 shows one example of simulated proton's vertical beam size growth rate versus the number of macro-particles of electron bunch. Increasing the macro-particles of electron bunch will reduce the simulated proton's emittance growth rate. If fitting the simulated growth rates with a function a/M_e^p, where M_e is the number of macro-particles of electron bunch, we found p is close 0.5 instead of 1 as predicted. We also found that fitting with a function $a/M_e + b$ can better match the simulation results. For the CDR design parameters, b is about 300%/hour.

Figure 2 shows the simulated proton beam size growth rates as function of proton's beam-beam parameter. In this study, we adjusted proton's beam-beam parameter by scaling down electron beam's bunch intensity while keeping the tunes of proton bunch center unchanged. The simulated proton's beam size growth rates can be fitted well with a function $a\times\xi_{bb}^q$, with q about 2.75 for both planes. With a lower beam-beam parameter about 0.008, we re-scanned the growth rate's dependence on the electron bunch's macro-particle number and obtained b between 50-100%/hour.

Sufficient number of longitudinal slices of electron bunch in strong-strong simulation is also important to reduce the

* Work supported by Brookhaven Science Associates, LLC under Contract No. DE-SC0012704 with the U.S. Department of Energy.
† yluo@bnl.gov

ISBN: 978-3-95450-227-1 ISSN: 2673-5490 doi:10.18429/JACoW-IPAC2022-WEPOPT039

FINE DECOUPLING TEST AND SIMULATION STUDY TO MAINTAIN A LARGE TRANSVERSE EMITTANCE RATIO IN HADRON STORAGE RINGS *

Y. Luo†, I. Blackler, M. Blaskiewicz, W. Fischer, A. Marusic, C. Montag, T. Shrey, D. Xu
Brookhaven National Laboratory, Upton, NY USA

Abstract

In previous and existing hadron storage rings, the horizontal and vertical emittances are normally the same or very close. For the Hadron Storage Ring (HSR) of the Electron-Ion Collider (EIC), the design proton transverse emittance ratio is 10:1. To maintain this large emittance ratio, we need to have an online fine decoupling system to prevent transverse emittance exchange. For this purpose, we carried out fine decoupling experiments in the Relativistic Heavy Ion Collider (RHIC) and reviewed its previous operational data. Analytical prediction and numerical simulation are preformed to estimate how small the global coupling coefficient should be to maintain a 10:1 emittance ratio.

INTRODUCTION

The Electron-Ion Collider (EIC) presently under construction at Brookhaven National Laboratory will collide polarized high energy electron beams with hadron beams, reaching luminosities up to $1\times10^{34}\mathrm{cm}^{-2}\mathrm{s}^{-1}$ in the center-of-mass energy range of 20-140 GeV. To achieve high luminosities, the EIC adopts crossing angle collision with more than 1000 bunches per ring, flat beams with small β^*s at the interaction point (IP), and strong hadron cooling [1].

For the collision between 275 GeV protons and 10 GeV electrons, the beam-beam parameters for both beams reach their highest values in EIC. The beam-beam parameters are 0.012 for protons and 0.1 for electrons. The beam sizes at interact point (IP) are (95 μm, 8.5 μm). The β^*s in the Hadron Storage Ring (HSR) are (80 cm, 7.2 cm). The un-normalized proton transverse emittances are (11.3 nm, 1.0 nm).

For previous or existing hadron colliders, the horizontal and vertical emittances are normally the same or close to each other. To achieve about a 10:1 emittance ratio in HSR, we will pre-cool the proton bunches at lower beam energies and employ strong hadron cooling at store energy to maintain this ratio. As we know, betatron coupling will mix transverse emittances. Therefore, fine decoupling is required in HSR to stop emittance transfer from the horizontal plane to the vertical plane. For HSR we may not have vertical cooling at store energy. If so, we also need to prevent any sizable emittance growth in the vertical plane.

The HSR of EIC will re-use the existing RHIC arcs. For RHIC, we developed a feedback system to continuously monitor and correct the global betatron coupling [2,3]. This system was proved robust and routinely operated at injection, on the energy ramp, and at store. For HSR, considering the large transverse emittance ratio, we need to make sure that current RHIC decoupling feedback is sufficient for HSR's fine decoupling requirement.

In the following, we will first present experimental results from previous years and in 2021 to demonstrate fine decoupling and possible 10:1 transverse emittance ratio in RHIC. Then we will analytically estimate the emittance exchange due to global coupling and its requirement for HSR. In the end, we will carry out multi-particle simulation to determine and verify the global decoupling requirement.

RESULTS FROM PREVIOUS YEARS

To demonstrate if we can achieve a large transverse emittance ratio in RHIC with current decoupling feedback, we performed several beam experiments in RHIC. The earliest one was done in 2017. In this experiment, we used Au (gold) ion beam. We filled the Yellow ring with nominal intensity bunches ($2x10^9$/bunch) for the first half of the bunch train and then half intensity bunches for the remainder. Intra-beam scattering (IBS) will generate longitudinal emittance growth and horizontal emittance growth through horizontal dispersion in the ring. IBS growth rate is related to bunch intensity and emittances. For RHIC, there is no vertical dispersion in the design lattice. We ramped Au ion bunches to 100 GeV/n and observed emittance growth for about 2 hours at store.

Figure 1 shows the emittance measurement data with Ion Profile Monitor (IPM). In the plot, there are two horizontal and two vertical emittance measurement data for Yellow ring at each time point, one for full bunch intensity and one for half bunch intensity. With global decoupling in Yellow ring, we observed a much slower vertical emittance growth than horizontal. After about 2 hours at store, the horizontal emittance reached double the vertical emittance. The vertical emittance increased slightly by 20-30% in 2 hours. At the end of experiment, we pushed the tune settings closer, from (0.2365, 0.2268) to (0.2340, 0.2291) in steps, we observed horizontal emittance transferred to vertical emittance.

A second experiment was done in 2018, where we focused on the minimum transverse tune split needed to stop the transverse emittance exchange. For this experiment, we also used Au ion beam at 100 GeV/n but with stochastic cooling. We deliberately switched off the horizontal stochastic cooling and kept the vertical plane cooling on. We adjusted the tune split by increasing the horizontal set tune to check at what

* Work supported by Brookhaven Science Associates, LLC under Contract No. DE-SC0012704 with the U.S. Department of Energy.
† yluo@bnl.gov

ISBN: 978-3-95450-227-1 ISSN: 2673-5490 doi:10.18429/JACoW-IPAC2022-WEPOPT040

NUMERICAL NOISE ERROR OF PARTICLE-IN-CELL POISSON SOLVER FOR A FLAT GAUSSIAN BUNCH*

Y. Luo†, J. S. Berg, M. Blaskiewicz, W. Fischer, X. Gu, H. Lovelace III, C. Montag, R. Palmer, S. Peggs, V. Ptitsyn, F. Willeke, D. Xu, Brookhaven National Laboratory, Upton, NY, USA
Y. Hao, Facility for Rare Isotope Beams, Michigan State University, East Lansing, MI, USA
J. Qiang, Lawrence Berkeley National Laboratory, Berkeley, CA, USA
H. Huang, V. Morozov, E. Nisson, T. Satogata,
Thomas Jefferson National Accelerator Facility, Newport News, VA, USA

Abstract

The Electron-Ion Collider (EIC) presently under construction at Brookhaven National Laboratory will collide polarized high energy electron beams with hadron beams with design luminosity up to $1 \times 10^{34}\text{cm}^{-2}\text{s}^{-1}$ in center mass energy range of 20-140 GeV. We simulated the planned electron-proton collision of flat beams with Particle-In-Cell (PIC) based Poisson solver in strong-strong beam-beam simulation. We observed a much larger proton emittance growth rate than that from weak-strong simulation. To better understand the emittance growth rate from the strong-strong simulation, we compare the beam-beam kicks between the PIC method and the analytical calculation and calculate the RMS variation in beam-beam kicks among 1000 sets of random Gaussian particle distributions. The impacts of macro-particle number, grid number, and bunch flatness are also studied.

INTRODUCTION

The Electron-Ion Collider (EIC) presently under construction at Brookhaven National Laboratory will collide polarized high energy electron beams with hadron beams with design luminosities up to $1 \times 10^{34}\text{cm}^{-2}\text{s}^{-1}$ in center mass energy range of 20-140 GeV [1]. We focus on the collision involving 275 GeV protons and 10 GeV electrons since both protons and electrons reach their highest beam-beam parameters for this collision mode in the EIC.

Both strong-strong and weak-strong models have been used for the EIC beam-beam simulation studies [2, 3]. For weak-strong model, electron bunch is assumed rigid and is represent by a 6-d Gaussian charge distribution. The beam-beam kick to protons are analytically calculated. For strong-strong model, both bunches are represented with typically 0.5-1 million macro-particles. Particle-in-cell (PIC) method and Fast Fourier Transformation (FFT) are used to solve 2-d Poisson equation on rectangle grids.

In the EIC beam-beam simulation studies, we observed a much larger proton emittance growth rate in strong-strong simulation than in weak-strong simulation. Strong-strong simulation is subject to numerical noises due to limited macro-particles, transverse grids, longitudinal slices, and the algorithm itself [4]. To understand the sources of numerical noises in the strong-strong simulation, in the following we will calculate RMS variations in beam-beam kicks for 1000 sets of 4-d Gaussian distributions. As we know, the emittance growth due to numerical noises is proportional to square of the beam-beam force's variation. Two kinds of beam flatness are used for comparison: a round beam and a flat beam.

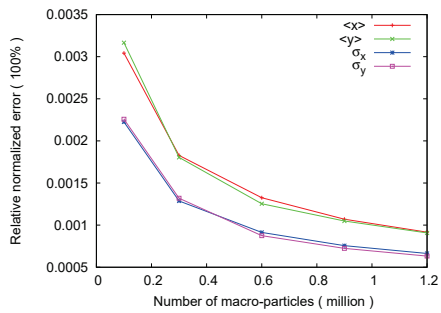

Figure 1: Relative RMS variations of <x>, <y>, and σ_x, σ_y as function of macro-particle number.

GAUSSIAN DISTRIBUTION ERRORS

First we study the statistical errors from a 4-d Gaussian particle distribution. We adopt the Gaussian distribution random number generator provided by GNU Scientific Library (GSL). Figure 1 shows the relative RMS variations in bunch center's position and beam sizes for 1000 sets of Gaussina distributions as function of the number of macro-particles. The relative error is normalized by the RMS beam size.

From the plot, the numerical error in the bunch center's position and RMS beam sizes decrease with increased macro-particles. For a typical 0.5 million macro-particles, the relative errors in the bunch center's position and beam sizes are about 0.1% - 0.2% of the RMS beam size. In our strong-strong simulation for the EIC, we observe about 0.2%-0.3% relative variations in turn-by-turn bunch center's position and transverse beam sizes.

* Work supported by Brookhaven Science Associates, LLC under Contract No. DE-SC0012704 with the U.S. Department of Energy.
† yluo@bnl.gov

ISBN: 978-3-95450-227-1 ISSN: 2673-5490 doi:10.18429/JACoW-IPAC2022-WEPOPT041

STRONG-STRONG SIMULATIONS OF COHERENT BEAM-BEAM EFFECTS IN THE EIC*

J. Qiang†, LBNL, Berkeley, California , U.S.A.
Y. Luo, C. Montag, D. Xu, F. Willeke, BNL, Long Island, New York, U.S.A.
Y. Hao, MSU, East Lansing, Michigan, U.S.A.

Abstract

The high luminosity electron ion collider (EIC) will provide great opportunities in nuclear physics study and is under active design. The coherent effects due to the beam-beam interaction of two colliding beams can cause beam size blow-up and degrade the luminosity in the EIC. In this paper, we report on the study of coherent beam-beam effects in the EIC design using self-consistent strong-strong simulations. These simulations show the coherent dipole and quadrupole mode instabilities in the tune working point scan and bunch intensity scan.

INTRODUCTION

The electron-ion collider (EIC) as a gluon microscope has been approved by the Department of Energy as the next major scientific facility that probes the detailed physics inside the nucleus with deep inelastic scattering using polarized high energy electron [1]. The EIC consists of two colliding rings, a hadron ring of 41-275 GeV and an electron storage ring of 5-18 GeV. The nominal design goal is to attain a peak luminosity of ~10^{34}/cm^2/s. The coherent instability driven by beam-beam interactions could cause beam size blow-up and degrade the peak luminosity [2-5]. Such an instability depends on the choice of transverse tune working points and beam bunch intensities as seen in the following strong-strong simulations.

COMPUTATION TOOL

The computational tool used in this study is a self-consistent strong-strong beam-beam code, BeamBeam3D [6,7]. The BeamBeam3D is a parallel three-dimensional particle-in-cell code to model beam-beam effects in high-energy ring colliders. This code includes a self-consistent calculation of the electromagnetic forces (beam-beam forces) from two colliding beams (i.e. strong-strong modeling), a linear and nonlinear high-order transfer map model for beam transport between collision points, a stochastic map to treat radiation damping, quantum excitation, a single map to account for chromaticity effects, a feedback model, an impedance model, and a Bremsstrahlung model. Here, the beam-beam forces can be from head-on collision, offset collision, and crossing angle collision. These forces are calculated by solving the Poisson equation using a shifted integrated Green function method, which can be computed very efficiently using an FFT-based algorithm on a uniform grid. For the crossing angle collision, the particles are transformed from the lab frame into a boosted Lorentz frame following the procedure described by Hirata [8] and by Leunissen et al. [9], where the beam-beam forces are calculated in the same way as the head-on collision. After the collision the particles are transformed back into the laboratory frame. The BeamBeam3D code can handle multiple bunches from each beam collision at multiple interaction points (IPs). The parallel implementation is done using a particle-field decomposition method to achieve a good load balance.

SIMULATION RESULTS

The nominal design parameters used in the simulations are given in the following table. These design parameters

Table 1: EIC Design Parameters

	electron	**proton**
Energy (GeV)	10	275
Tune	(0.08,0.06)	(0.228,0.21)
Particles (10^{11})	1.72	0.69
Emittance (nm)	(20,1.1)	(11.3,1.0)
β^* (cm)	(55,5.6)	(80,7.2)
Beam-beam para.	(0.088,0.1)	(0.01,0.012)
Chromaticity	(1,1)	(1,1)
Damp time (k turn)	(4,4,2)	
Crab freq. (MHz)	394	197

were chosen to produce ~10^{34}/cm^2/s peak luminosity for the collision of a 10 GeV electron bunch and a 275 GeV proton bunch with 25 mrad crossing angle [10]. Pairs of crab cavities are used on both sides of the collision point to correct the crossing angle for both colliding beams. The nominal beam-beam parameters for the electron beam are (0.088, 0.1), and (0.01, 0.012) for the proton beam. The large beam-beam parameters result in strong coherent beam-beam effects. Such effects can cause instability due to the collective dynamic interactions between the electron beam and the proton beam.

In the EIC design, the transverse tune working points have to be carefully selected. Figure 1 shows the proton beam and electron beam horizontal centroid evolution with different choice of electron beam horizontal and vertical tunes. In this scan, the proton beam tune working point is fixed. It is seen that for the electron horizontal tune between 0.1 and 0.14, both electron and proton beam centroid become unstable.

*Work supported by the Director of the Office of Science of the US Department of Energy under Contract no. DEAC02-05CH11231.
†jqiang@lbl.gov

ISBN: 978-3-95450-227-1 ISSN: 2673-5490 doi:10.18429/JACoW-IPAC2022-WEPOPT042

DESIGNING THE EIC ELECTRON STORAGE RING LATTICE FOR A WIDE ENERGY RANGE*

D. Marx†, J.S. Berg, J. Kewisch, Y. Li, C. Montag, V. Ptitsyn, S. Tepikian, F. Willeke, D. Xu, Brookhaven National Laboratory, Upton, NY, USA
G.H. Hoffstaetter, D. Sagan, M.G. Signorelli, J. Unger, Cornell University, Ithaca, NY, USA
V. Morozov, Oak Ridge National Laboratory, Oak Ridge, TN, USA
Y. Cai, Y. Nosochkov, SLAC, Menlo Park, CA, USA
B.R.P. Gamage, Thomas Jefferson National Accelerator Facility, Newport News, VA, USA

Abstract

The Electron-Ion Collider (EIC) will collide electrons with hadrons at center-of-mass energies up to 140 GeV (in the case of electron-proton collisions). A 3.8-kilometer electron storage ring is being designed, which will store electrons with a range of energies up to 18 GeV for collisions at one or two interaction points. At energies up to 10 GeV the arcs will be tuned to provide 60 degree phase advance per cell in both planes, whereas at top energy of 18 GeV a 90 degree phase advance per cell will be used, which largely compensates for the horizontal emittance increase with energy. The optics must be matched at three separate energies, and the different phase-advance requirements in both the arc cells and the straight sections make this challenging. Moreover, the spin rotators must fulfill requirements for polarization and spin matching at widely different energies while satisfying technical constraints. In this paper these challenges and proposed solutions are presented and discussed.

INTRODUCTION

The Electron-Ion Collider (EIC) [1, 2] is a new machine currently being designed that will collide polarized electrons with polarized hadrons (protons up to heavy ions) for the purpose of investigating the structure and properties of nucleons. It will be built at Brookhaven National Laboratory in the 3.8-kilometer tunnel that currently houses the Relativistic Heavy Ion Collider (RHIC) [3–5]. Two electron rings will be built in this tunnel: a rapid cycling synchrotron (RCS) [6] for accelerating electrons to collision energies and an electron storage ring (ESR) for colliding electrons with hadrons from a separate storage ring. Figure 1 shows a schematic of the EIC. Collisions will occur at a range of center-of-mass energies between 29 GeV and 140 GeV, providing luminosities up to $10^{34}\,\mathrm{cm}^{-2}\mathrm{s}^{-1}$. These luminosities are considerably greater than those achieved at HERA [5, 7], an electron/positron-proton collider that operated until 2007 at DESY, and, although the top center-of-mass energy will be less than HERA's 318 GeV, the EIC will be optimized for a much wider range of energies.

* Work supported by Brookhaven Science Associates, LLC, under Contract No. DE-SC0012704, by Jefferson Science Associates, LLC, under Contract No. DE-AC05-06OR23177, by UT-Battelle, LLC, under contract DE-AC05-00OR22725, and by SLAC under Contract No. DE-AC02-76SF00515 with the U.S. Department of Energy.
† dmarx@bnl.gov

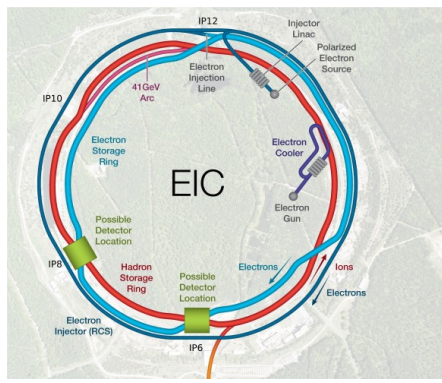

Figure 1: Schematic of EIC (not to scale).

The ESR lattice consists of six arcs with straight sections in between, labeled according to the numbers on a clock face. The baseline design for the EIC includes a single interaction point (IP), called IP6, where the beams will collide. A second IP and detector in the neighboring straight section, IP8, may be included in a future upgrade. Superconducting RF cavities will be installed at IP10, and the beam will be injected into the ring at IP12.

In order to achieve the desired range of center-of-mass energies, three values for the electron beam energy are considered: 5-6, 10, and 18 GeV. This introduces several challenges in the lattice design. As the horizontal equilibrium emittance increases with energy, this needs to be compensated to satisfy aperture requirements. Superbends in arc cells and changes to the arc phase advance are used to keep the horizontal emittance within an acceptable range. The nonlinear chromaticity correction scheme also needs to be altered for different energies, as the different arc phase advances call for different sextupole configurations.

One of the key requirements for the experimental program is a high level of longitudinal spin polarization. Beams are injected with vertical spin, which is the stable spin direction for the ring. On each side of the IPs, a solenoid-based spin rotator rotates the spin vector into or from the longitudinal direction. As the spin-rotation angles depend on energy, designing these spin rotators for operation at a wide range of energies is challenging.

Table 1 shows the main lattice parameters at different energies. In the following sections, the design challenges arising from the wide energy range are described.

ISBN: 978-3-95450-227-1 ISSN: 2673-5490 doi:10.18429/JACoW-IPAC2022-WEPOPT043

DYNAMIC APERTURE OF THE EIC ELECTRON STORAGE RING*

Y. Nosochkov†, Y. Cai, SLAC, Menlo Park, CA, USA
J. S. Berg, J. Kewisch, Y. Li, D. Marx, C. Montag, S. Tepikian, H. Witte,
Brookhaven National Laboratory, Upton, NY, USA
G. H. Hoffstaetter, J. Unger, Cornell University, Ithaca, NY, USA

Abstract

The Electron Ion Collider (EIC) is under design at Brookhaven National Laboratory. The EIC aims at providing high luminosity and high polarization collisions for a large range of beam energies. Dynamic aperture (DA) of the EIC Electron Storage Ring (ESR) must be sufficiently large in both transverse and momentum dimensions. The latter is a challenge due to low-beta optics in up to two interaction regions (IR). We have developed an advanced technique for efficient non-linear chromaticity compensation compatible with the different ESR lattice configurations at different energies. The solution for the most challenging lattice with two IRs at 18 GeV is presented. The lattice is then evaluated with magnet errors, where the error tolerances are determined for reaching the desired DA.

INTRODUCTION

The Electron Ion Collider (EIC) [1, 2] is under design at Brookhaven National Laboratory. The important goals are the high luminosity up to 10^{34} cm^{-2}s^{-1}, high average polarization, and a large range of beam energies in electron-hadron collisions. In this paper, we focus on the Electron Storage Ring (ESR) designed for beam energies from 5 to 18 GeV. Satisfying the EIC requirements results in a rather crowded ESR low-beta interaction region (IR) featuring strong final focus system, spectrometer magnets, crab cavities, and spin rotator sections [3] significantly constraining the IR optics. Emittance requirements also call for stronger focusing in the ESR arcs at top energy.

The ESR dynamic aperture (DA) must be sufficiently large both in transverse size and momentum range. This is a challenge due to high error sensitivity and large chromaticity characteristic of the IR final focus quadrupoles (FFQ) where beta functions are very high. In this paper, we consider the most difficult ESR configuration at 18 GeV with two low-beta IRs and strong arc focusing, where achieving the desired momentum range of $\delta = 1\%$ is extremely challenging. The proximity of the betatron tunes to integer values makes this task more difficult. In the course of the ESR study, we have developed an advanced technique for efficient non-linear chromaticity correction [4] which meets the design requirements for the different ESR optics at different energies. The lattice is then evaluated with magnet errors, where the error tolerances are determined for reaching the desired DA of 10σ without beam-beam effects.

* Work supported by the Department of Energy Contract DE-AC02-76SF00515, by Brookhaven Science Associates, LLC under Contract DE-SC0012704, and by the Ernest Courant Traineeship in Accelerator Science and Technology Award No. DE-SC0020375.
† yuri@slac.stanford.edu

CHROMATICITY CORRECTION

The ESR lattice functions at 18 GeV are shown in Fig.1, where the tune is $\nu_{x,y} = 52.12, 45.1$. The ring consists of six arcs made of 90° FODO cells and six straight sections labelled according to the clock. The two low-beta IRs (IR6 and IR8) have identical $\beta_x^* = 59$ cm, $\beta_y^* = 5.7$ cm at the interaction points (IP). The very large beta functions at the IR final focus quadrupoles make them the largest sources of linear chromaticity. The FFQs also create most of the ring non-linear chromaticity in the form of chromatic beta beating and higher order tune shift, which severely limit the momentum range. The beta beating is traditionally described by the Montague functions [5] or W-functions. Due to the complexity of the IRs which include crab cavities, spin rotator sections, and spectrometer dipoles, there is no suitable optics near the IP for a conventional local chromaticity correction based on -I non-interleaved sextupole pairs [6]. Hence, the chromaticity correction has to be carried out by sextupoles located farther away from the IPs in the arcs. The goal is to achieve the momentum range of $10\sigma_p = 1\%$ at 18 GeV.

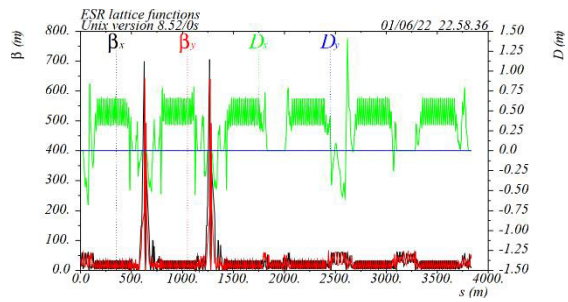

Figure 1: ESR lattice functions starting from IP4.

Semi-local Correction

Correction of the FFQ chromaticity is performed independently on each side of the IR using the adjacent arc sextupoles. Hence, this is a semi-local scheme. Since the non-linear chromatic tune shift is mostly driven by the large chromatic beta beating created in the FFQs, the main function of the arc sextupoles, in addition to correcting the linear chromaticity, is to cancel the FFQ beta beating by creating an opposite beta wave in phase with the FFQ.

We use a multi-family sextupole scheme where the sextupoles are placed in 16 periodic 90° cells of each arc next to F and D quadrupoles. In order to generate the net beta beating, sextupoles of the same family must be separated by 180° (two cells). This creates -I sextupole pairs where the sextupole non-linear geometric aberrations are cancelled [7]. A schematic of the semi-local scheme for one-

ISBN: 978-3-95450-227-1 ISSN: 2673-5490 doi:10.18429/JACoW-IPAC2022-WEPOPT044

ELECTRON-ION COLLIDER DESIGN STATUS*

C. Montag†, E. C. Aschenauer, G. Bassi, J. Beebe-Wang, J. S. Berg, M. Blaskiewicz, A. Blednykh, J. M. Brennan, S. Brooks, K. A. Brown, Z. Conway, K. A. Drees, A. V. Fedotov, W. Fischer, C. Folz, D. Gassner, X. Gu, R. Gupta, Y. Hao, C. Hetzel, D. Holmes, H. Huang, J. Jamilkowski, J. Kewisch, Y. Li, C. Liu, H. Lovelace III, Y. Luo, G. Mahler, D. Marx, F. Meot, M. Minty, S. Nayak, R. B. Palmer, B. Parker, S. Peggs, B. Podobedov, V. Ptitsyn, V. H. Ranjbar, G. Robert-Demolaize, M. Sangroula, S. Seletskiy, K. S. Smith, S. Tepikian, R. Than, P. Thieberger, N. Tsoupas, J. Tuozzolo, S. Verdu-Andres, E. Wang, D. Weiss, F. J. Willeke, H. Witte, Q. Wu, D. Xu, W. Xu, A. Zaltsman, Brookhaven National Laboratory, Upton, NY 11973, U.S.A., S. Benson, B.R.P. Gamage, J. Grames, T. Michalski, E. Nissen, J. Preble, R. Rimmer, T. Satogata, A. Seryi, M. Wiseman, W. Wittmer, TJNAF, Newport News, U.S.A., V. Morozov, F. Lin, Oak Ridge National Laboratory, E. Gianfelice-Wendt, Fermi National Accelerator Laboratory, Batavia, IL 60510, U.S.A., Y. Cai, Y. Nosochkov, G. Stupakov, M. Sullivan, SLAC, Menlo Park, CA 94025, U. S.A. G. Hoffstaetter, D. Sagan, M. Signorelli, J. Unger, Cornell University, Ithaca, NY 14850, U.S.A.

Abstract

The Electron-Ion Collider (EIC) is being designed for construction at Brookhaven National Laboratory. Activities have been focused on beam-beam simulations, polarization studies, and beam dynamics, as well as on maturing the layout and lattice design of the constituent accelerators and the interaction region. The latest design advances will be presented.

OVERVIEW

The Electron-Ion Collider (EIC) will be constructed at Brookhaven National Laboratory, utilizing the existing infrastructure and accelerator complex of the Relativistic Heavy Ion Collider (RHIC). The hadron storage ring (HSR) comprises arcs of the two superconducting RHIC storage rings. An electron storage ring (ESR) will be installed in the existing RHIC tunnel, where it will provide beam collisions with the HSR hadron beam in up to two interaction regions. Fully polarized electron bunches will be provided to the ESR by a rapid-cycling synchrotron (RCS) in the same tunnel. An interaction region with a crossing angle of 25 mrad has been designed that reaches a luminosity of 10^{34} cm^{-2} sec^{-1}. A second interaction region is feasible, but not within the EIC project scope. layout of the EIC complex. The highest luminosity of $1.0 \cdot 10^{34}$ cm^{-2} sec^{-1} is reached with 10 GeV electrons colliding with 275 GeV protons, which corresponds to a center-of-mass energy of 105 GeV. Higher center-of-mass energies are achieved by increasing the electron energy. To limit the total synchrotron radiation losses to 10 MW, the electron beam intensity has to be reduced accordingly, resulting in a corresponding reduction in luminosity.

ELECTRON PRE-INJECTOR

The EIC pre-injector provides 2×7 nC bunches within 2.5 µs. The LINAC will operate at 100 Hz to provide four pairs of bunches, with 10 msec spacing between pairs. A total of 8 bunches (4 pairs) will be provided at a repetition rate of 1 Hz. In the RCS, these will be merged to result in two 28 nC bunches. The polarized electron beam will be generated from a high voltage (HV) DC gun with a strained superlattice photocathode. The bunching section consisting of a 117.8 MHz pre-buncher, two of 591.1 MHz and a 2.856 GHz buncher will be used to compress the bunch length to 10 psec. Then eight of 2.856 GHz S-band normal conducting traveling wave plate LINACs boost the beam energy up to 400 MeV [1]. A dipole-solenoid spin rotator will be used for rotating the spin direction from longitudinal to vertical for injection into the RCS. The EIC HVDC polarized gun has achieved polarized electron beam with 7.5 nC bunch charge and 37.5 μA average current without QE decay [2].

RAPID-CYCLING SYNCHROTRON

A rapid-cycling synchrotron installed in the collider tunnel accelerates two bunches of polarized electrons every second to an energy of 5 to 18 GeV for injection into the ESR [3,4]. A dedicated design with high periodicity ensures that no depolarizing resonances are encountered during the entire energy ramp. This concept has been validated in extensive spin tracking studies, including realistic machine imperfections such as misalignments [5]. Optimization of the chromatic correction scheme resulted in sufficiently large

* Work supported under Contract No. DE-SC0012704, Contract No. DE-AC05-06OR23177, Contract No. DE-AC05-00OR22725, and Contract No. DE-AC02-76SF00515 with the U.S. Department of Energy.
† montag@bnl.gov

ISBN: 978-3-95450-227-1 ISSN: 2673-5490 doi:10.18429/JACoW-IPAC2022-WEPOPT045

TRANSVERSE ELECTRON BEAM TAILS AND BEAM LIFETIME IN THE EIC ELECTRON STORAGE RING *

Christoph Montag†, Brookhaven National Laboratory, Upton, NY 11973, U.S.A.

Abstract

While for most storage ring design activities it is sufficient to assume a Gaussian distribution of the beam particles, a more detailed prediction of the population in the transvese tails is necessary to predict the beam lifetime in a given aperture. Dominant processes that result in non-Gaussian distributions are the beam-beam interaction in a collider as well as beam-gas scattering. Simulations to determine the required apertures and vacuum levels in the EIC electron storage ring will be presented.

INTRODUCTION

When designing an electron storage ring and determining key parameters such as the minimum aperture or the vacuum pressure limit, an accurate model of the transverse electron distribution is often necessary because the beam-beam interaction as well as beam-gas scattering events result in an over-population of the transverse tails. This over-population occurs predominantly in the vertical plane due to the small vertical emittance, and it can severely limit the beam lifetime and detector background conditions if not taken into account during the machine design phase. In the following sections we describe simulation results for both beam-beam and beam-gas generated tails, determine the required vacuum pressure level for sufficient beam lifetime, and provide a simple fit to the transverse tail distribution to serve as input in simulation codes such as GEANT to study the detector background.

BEAM-BEAM TAILS

Non-Gaussian transverse tail distributions generated by the beam-beam interaction have been simulated using the method developed by D. Shatilov [1]. The vertical electron β-function at the interaction point of the EIC [2] approximately equals the proton bunch length, as shown in Table 1. As a result, the beam-beam kick experienced by the electrons is smeared out over a substantial amount of betatron phase advance, which leads to a net reduction of the effective beam-beam kick. It is therefore worthwhile studying the associated effect of collisions with long proton bunches on the transverse electron tails.

A number of tracking runs have been performed with the proton bunch divided into different numbers of slices, namely 1, 3, 9, and 19 slices. While the case with the proton bunch represented by a single slice corresponds to zero proton bunch length, the cases with multiple slices correspond to a non-zero bunch length. Collisions with a zero-length proton bunch result in a significant build-up of non-Gaussian tails in the vertical plane, as shown in Figure 1. When the proton bunch is represented by 3 or more slices, these vertical tails essentially disappear, and the transverse distribution remains approximately Gaussian. This behavior converges rapidly with the number of slices; in fact, no significant difference is observed between cases with 3, 9, or 19 slices. Based on these simulations we conclude that the beam-beam interaction will only have a minor effect on transverse tails in the EIC elecron storage ring.

Table 1: Simulation Parameters at 10 GeV

Parameter	Value
E [GeV]	10
τ_{parallel} [turns]	2500
σ_z [m]	0.01
α_x	0.0
β_x [m]	0.43
ϵ_x [m]	20×10^{-9}
α_y	0
β_y [m]	0.05
ϵ_y [m]	1.2×10^{-9}
Q_x	0.09
Q_y	0.07
Q_z	0.0537
ξ_x	0.073
σ_s	0.06
$\beta_{x,p}$ [m]	0.90
$\beta_{y,p}$ [m]	0.04
$\epsilon_{x,p}$ [m]	9.6×10^{-9}
$\epsilon_{y,p}$ [m]	1.5×10^{-9}
λ_{crab} [m]	1.52

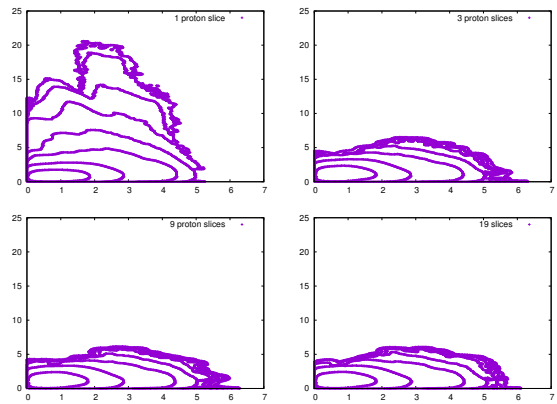

Figure 1: x - y distribution for different number of proton bunch slices.

* Work supported by Brookhaven Science Associates, LLC under Contract No. DE-SC0012704.
† montag@bnl.gov

ISBN: 978-3-95450-227-1 ISSN: 2673-5490 doi:10.18429/JACoW-IPAC2022-WEPOPT046

PREPARATION OF A PROTOTYPE PLASMA LENS AS AN OPTICAL MATCHING DEVICE FOR THE ILC e^+ SOURCE

M. Formela*, N. Hamann†, G. Moortgat-Pick[1], II. Institute of Theoretical Physics, University of Hamburg, Hamburg, Germany
K. Flöttmann, G. Loisch, Deutsches Elektronen-Synchrotron DESY, Hamburg, Germany
[1]also at Deutsches Elektronen-Synchrotron DESY, Hamburg, Germany

Abstract

In recent years, high-gradient, symmetric focusing with active plasma lenses has regained significant interest due to the potential advantages in compactness and beam dynamics compared to conventional focusing elements. One potential application is the optical matching of highly divergent positrons from the undulator-based ILC positron source into the downstream accelerating structures. A collaboration between University Hamburg and DESY Hamburg has been established to develop a prototype design for this application. Here, we discuss beam dynamics simulation results, preliminary parameters of the lens prototype, and the current status of the prototype design.

INTRODUCTION

At the International Linear Collider (ILC) electron and positron beams will be collided at up to 500 GeV centre-of-mass energies to enable, e.g., precision measurements of Higgs boson properties. The positron source is planned to be based on pair production of electrons and positrons by the interaction of high energy photons with a Titanium-target wheel rotating at high speed. Due to the large divergence of the produced positrons, an optical matching device (OMD) has to be placed as close as possible to the rotating target, to capture the largest possible amount of positrons. A high capture efficiency, also called yield, is essential to fulfill the luminosity requirements of the ILC physics programme.
Currently, the baseline option for this OMD is a quarter-wave transformer magnet. Despite a higher possible yield, flux concentrators cannot be applied at the ILC positron source due to the variation of their focusing field over the ILC's 1 ms long bunch trains. To increase the yield, it was proposed to use an active plasma lens (APL) as an OMD instead.

In an APL, a gas column is ionised to a plasma and a high-amplitude current pulse is directed through this plasma. A beam that travels co-axially through this plasma column experiences a radial force from the azimuthal magnetic fields induced by the lens' current. Compared to conventional focusing devices, this scheme features several advantages:

- fully symmetric focusing in both transverse planes
- high focusing gradients due to the close proximity of plasma current and beam
- focusing transverse to main direction of motion
- space charge mitigation by plasma electron motion
- reduced heat load on target due to minimal field outside of lens.

Nevertheless, the application as an OMD at the ILC positron source also poses several challenges on the plasma lens, which have not yet been tackled in APL research:

- MHz burst operation of plasma lens compared to the state-of-the-art few Hz operation
- high gas load on the downstream, close-by accelerating cavities.

A project has been initiated at the University Hamburg in collaboration with DESY Hamburg to explore the capabilities and limits of active plasma lenses for this application.

PARTICLE TRACKING SIMULATIONS

To explore the achievable positron yield and the operational parameters of the APL, particle tracking simulations have been performed using ASTRA [1]. A wide range of lens designs have been simulated, varying the total electric current I_0, the opening radius R_0, the exit radius R_1, the APL length L and the taper order n.

Figure 1 summarizes the results by showing the optimal achievable positron capture efficiency – the number of captured positrons relative to the total number – for every examined combination of electric current and taper order. It can be seen that a linear tapering ($n = 2$) is superior to weaker and stronger tapering in nearly every case, except for currents of 2 kA and below.

Results

A plasma lens design has been chosen to be the reference point for future prototype developments. Parameters for said design can be seen in Table 1. The simulated capture efficiency for this design lies at about **43 %** with 42917 total simulated positrons. Even though higher efficiencies can in simulation be achieved by assuming higher currents, the chosen set of parameters is considered a reasonable compromise between capture efficiency and technical feasibility.

The capture efficiency of this design proved to be stable in simulations for variances in the design parameters as can be seen in Table 2. In all cases single parameter errors of ±10 % lead to efficiency loss below −5.0 %.

* manuel.formela@desy.de
† niclas.hamann@desy.de

ISBN: 978-3-95450-227-1 ISSN: 2673-5490 doi:10.18429/JACoW-IPAC2022-WEPOPT047

BEAM OPTICS OF THE INJECTION/EXTRACTION AND BEAM TRANSFER IN THE ELECTRON RINGS OF THE EIC PROJECT*

Nicholaos Tsoupas†, Bijan Bhandari, Douglas Holmes, Chuyu Liu, Christoph Montag, Vadim Ptitsyn, Vahid Ranjbar, John Skaritka, Joseph Tuozzolo, Erdong Wang, and Ferdinand J. Willeke
Brookhaven National Laboratory Upton NY, 11973, USA

Abstract

The Electron-Ion Collider (EIC) project has been approved by the Department of Energy to be built at the site of Brookhaven National Laboratory (BNL). The goal of the project is the collision of energetic (many GeV/amu) ion species with electron bunches of energies up to 18 GeV. The electron accelerator of the EIC is comprised of a 400 MeV LINAC, and two electron rings, the Rapid Cycling Synchrotron (RCS) which accelerates the electron beam up to 18 GeV, and the Electron Storage Ring (ESR) which stores the electron beam for collisions with hadron beam, both to be built in the same tunnel as the Hadron Storage Ring (HSR). This paper discusses the layout and the beam optics of the beam injection/extraction into the electron rings and the beam optics of the transfer line from the RCS to the ESR.

INTRODUCTION

The EIC accelerator complex [1] will collide various ions species at energies up to 270 GeV/amu with electrons of energies 5, 10, and 18 GeV. The ions will be injected and accelerated to the final energy in the hadron accelerators [1] with the final acceleration stage, the Hadron Storage Ring (HSR) [2], and the electrons will be accelerated in the electron accelerators [1] which consists of a 400 MeV LINAC, the RCS ring which will accelerate the electrons up to 18 GeV and the ESR storage ring which will store the electron bunches for collisions with the hadrons. Fig. 1. The electron beam transfer from the 400 MeV LINAC to the ESR including the spin rotator is discussed in ref. [3]. In this paper we disuss the latest version of the beam optics of the injection/extraction in RCS and ESR and beam transfer form RCS to ESR. Specifically the following information will be provided regarding the EIC.

- Beam optic of RCS injection
- Beam optic of extraction from RCS
- Beam optics of transfer line form RCS to ESR
- Beam injection and extraction in ESR

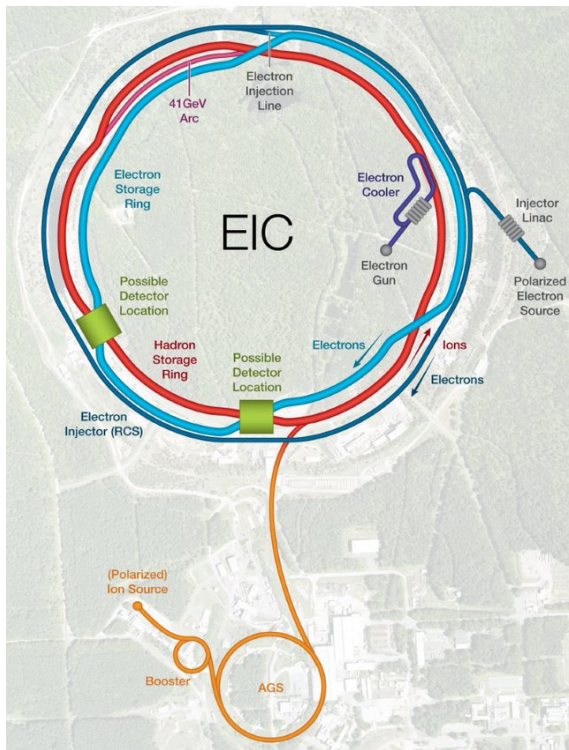

Figure 1: Schematic diagram of the EIC complex.

BEAM OPTICS OF RCS INJECTION

Following the Spin Rotator [3] the electron bunches are transported to the RCS for injection. This section describes the optics at injection into the RCS. To inject beam into the RCS, two sets of four bunches each are injected from the 400 MeV LINAC into the RCS at a frequency of 1 Hz. Each set is separated by 2 μsec, and the bunches in each set are separated by 1.6 nsec as shown in Fig. 2. This small separation (1.6 nsec) between the four consecutive bunches requires an injection RF-kicker which is described in [4]. An RF kicker is not strong enough to place the injected

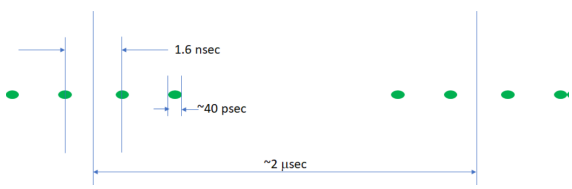

Figure 2: Bunch pattern at RCS injection.

bunch into the reference orbit without locally bumping the

* Work supported by Brookhaven Science Associates, LLC under Contract No. DE-SC0012704 with the US Department of Energy.
† tsoupas@bnl.gov

ISBN: 978-3-95450-227-1 ISSN: 2673-5490 doi:10.18429/JACoW-IPAC2022-WEPOPT049

BEAM-BEAM INTERACTION FOR TILTED STORAGE RINGS*

D. Xu†, Y. Luo, D. Holmes, C. Montag, F. Willeke, Brookhaven National Laboratory, Upton, NY, USA
Y. Hao, Michigan State University, East Lansing, MI, USA
J. Qiang, Lawrence Berkeley National Laboratory, Berkeley, CA, USA

Abstract

In the Electron-Ion Collider (EIC) design, to avoid vertical orbit bumps in the Electron Storage Ring (ESR) at some crossing points with Hadron Storage Ring (HSR) to preserve the electron polarization, we plan to tilt the ESR plane by 200 µrad with an axis connecting IP6 and IP8. In this article, we study the beam-beam interaction when two rings are not in the same plane. The Lorentz boost formula is derived and the required vertical crabbing strength is calculated to compensate the dynamic effect. The beam-beam simulations are performed to validate the theory.

INTRODUCTION

A large crossing angle in the interaction region (IR) is necessary for fast separation of two colliding beams in ring-ring type colliders to achieve high collision rates, IR background minimization, and overall detector component and IR magnet arrangements. Crab crossing is an effective way to restore the head-on collision for circular colliders [1]. The crab crossing scheme was first successfully implemented at KEKB-factory [2]. The crab cavities, which are key components in the crab crossing scheme, were also demonstrated for the hadron beam in CERN's Super Proton Synchrotron (SPS) recently [3]. Other dynamics effects about the crab cavities can be found in [4–6].

The Electron-Ion Collider (EIC) project adopts the local scheme to achieve the desired luminosity 10^{34} cm^{-2}s^{-1} [7], as shown in Fig. 1. In the local scheme, a pair of crab

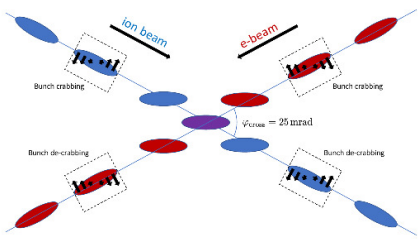

Figure 1: EIC local crabbing compensation scheme [7].

cavities are installed at both sides of the interaction point (IP). The upstream crab cavity tilts the beam in x - z plane, and the downstream crab cavity rotates the beam back. In the rest of the rings, both planes stay unaffected.

EIC rings consist of six arcs separated by six straight sections, which are labelled according to the hour markings of a clock from IR2 to IR12. A dedicated IR has been designed at 6 o'clock, and a potential second IR at 8 o'clock is reserved for future upgrade. To resolve the interference between rings, transfer lines, cooler ERS in IR2, the Electron Storage Ring (ESR) is proposed to be tilted by ~ 200 µrad to avoid vertical bends. Figure 2 illustrates the concept. The

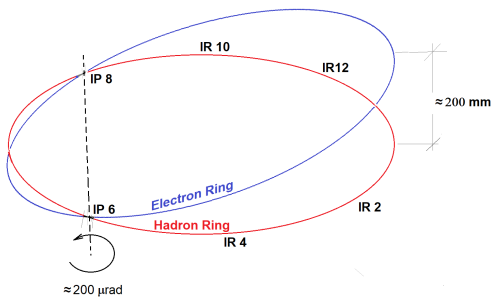

Figure 2: Schematic diagram of tilted ESR in EIC.

rotating axis goes through both interaction points: IP6 and IP8. Although the rotation angle is small, the longitudinal axis is changed, and the dynamic effect has to be studied.

This paper derives the Lorentz Boost formula for the tilted storage rings. The beam-beam simulation is also presented to demonstrate if the tilted scheme works or not. A summary is given at last.

LORENTZ BOOST

When two beams collide with a crossing angle, it is convenient to consider the beam-beam interaction in the boost frame [8], as shown in Fig. 3. Let $(\mathbf{E}_x, \mathbf{E}_y, \mathbf{E}_z)$ be the ba-

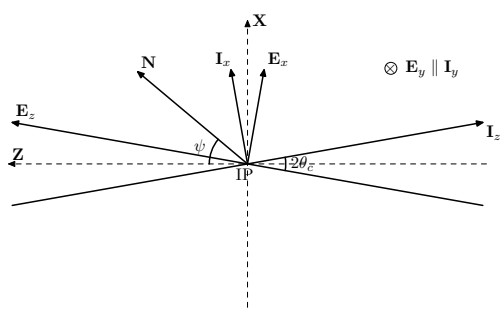

Figure 3: The boost frame for two beams colliding with a large crossing angle. **N** points from IP6 to IP8. θ_c = 12.5 mrad is the half crossing angle, and $\psi = \pi/6 + \theta_c$.

sis vectors for the Frenet-Serret frame of the electron ring, and the left-handed $(\mathbf{I}_x, \mathbf{I}_y, \mathbf{I}_z)$ for the ion ring. The vertical axes, $\mathbf{E}_y$ and $\mathbf{I}_y$, are parallel with each other before rotating the ESR frame. $(\mathbf{X}, \mathbf{Y}, \mathbf{Z})$ are the basis vectors of the boost

* Work supported by Brookhaven Science Associates, LLC under Contract No. DE-SC0012704 with the U.S. Department of Energy
† dxu@bnl.gov

ISBN: 978-3-95450-227-1 ISSN: 2673-5490 doi:10.18429/JACoW-IPAC2022-WEPOPT050

DETECTOR SOLENOID COMPENSATION IN THE EIC ELECTRON STORAGE RING*

D. Xu†, Y. Luo, J. Scott Berg, H. Lovelace III, S. Tepikian
Q. Wu, B. Xiao, J. Avronsart, H. Witte, M. Blaskiewicz, C. Montag, F. Willeke
Brookhaven National Laboratory, Upton, NY, USA
B. R. Gamage, Jefferson Lab, Newport News, VA, USA
V. Morozov, Oak Ridge National Lab, Oak Ridge, TN, USA
Y. Hao, Michigan State University, East Lansing, MI, USA

Abstract

The Electron-Ion Collider (EIC) uses crab cavities to restore the geometrical luminosity loss associated with the large crossing angle. Due to space limitations, the detector solenoid cannot be compensated locally. This paper presents the lattice design to compensate the detector solenoid effects without interfering with the crab cavities. Skew quadrupoles are employed to avoid additional crab cavities. The correction scheme is checked by beam-beam simulation.

INTRODUCTION

A large crossing angle in the interaction region (IR) is necessary for fast separation of two colliding beams in ring-ring type colliders to achieve high collision rates. Crab cavities, first proposed for linear colliders [1], can compensate for the geometrical luminosity loss induced by crossing angle. This idea was later expanded to include circular colliders [2].

The Electron Ion Collider (EIC) adopts the local crabbing scheme to achieve the desired luminosity [3], as shown in Fig. 1. In the local crabbing scheme, a pair of crab cavities

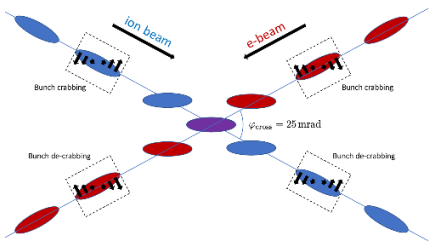

Figure 1: EIC local crabbing compensation scheme [3].

are installed at both sides of the IP. The upstream crab cavity tilts the beam in $x-z$ plane, and the downstream crab cavity rotates the beam back. In the rest of the rings, both planes stay unaffected.

In the ideal local crabbing scheme, the two crab cavities, located at the location with the betatron phase advance of $\pm\pi/2$ from IP, create desired crab "bump" between them. However, the detector solenoid, a 4 m long solenoid with an integrated strength of up to 12 T · m in EIC, would destroy the ideal configuration. Due to the IR space limitation, the anti-solenoid between the crab cavity and the detector solenoid, is not an option. Therefore, the vertical crabbing — the coupling of the vertical and longitudinal motion — is introduced, and has to be corrected in case of a significant luminosity loss.

This paper will first introduce the concept of crab dispersion. With the help of the crab dispersion, two methods are proposed to correct the vertical crabbing caused by the detector solenoid. The beam-beam simulations are performed to check the correction effect.

CRAB DISPERSION

The Hamiltonian of a thin crab cavity is

$$H = \left(\frac{x\lambda_x}{\Lambda_x} + \frac{y\lambda_y}{\Lambda_y}\right)\frac{\sin(k_c z)}{k_c} \tag{1}$$

where x, y, z are the horizontal, vertical, and longitudinal coordinates when a test particle pass through the thin crab cavity, $\lambda_{x,y}/\Lambda_{x,y}$ denoting the horizontal and vertical kick strength with $\Lambda_x = \sqrt{\beta_x^*\beta_{x,c}}, \Lambda_y = \sqrt{\beta_y^*\beta_{y,c}}$, and k_c the wave number. Here we use the lattice related parameters $\Lambda_{x,y}$ to normalize the crab cavity strength for simplicity.

Following the definition in [4], the crab dispersion is defined as the transverse dependence on longitudinal coordinate z,

$$\zeta = \left(\frac{\partial x}{\partial z}, \frac{\partial p_x}{\partial z}, \frac{\partial y}{\partial z}, \frac{\partial p_y}{\partial z}\right)^{\mathrm{T}} \tag{2}$$

Assuming the lattice is symmetrical around IP, the crab dispersion from the upstream and downstream crab cavities is,

$$\begin{aligned}\zeta_b &= \left(0, \lambda_{b,x}/\Lambda_x, 0, \lambda_{b,y}/\Lambda_y\right)^{\mathrm{T}}\\ \zeta_a &= \left(0, \lambda_{a,x}/\Lambda_x, 0, \lambda_{a,y}/\Lambda_y\right)^{\mathrm{T}}\end{aligned} \tag{3}$$

where the subscript "b" denotes before IP, and "a" denotes after IP. Projecting the crab dispersion back to IP, the crab dispersion before and after the collision is

$$\begin{aligned}\zeta_b^* &= \begin{bmatrix}\lambda_{b,x}\sin\Psi_x\\ \lambda_{b,x}\cos\Psi_x/\beta_x^*\\ \lambda_{b,y}\sin\Psi_y\\ \lambda_{b,y}\cos\Psi_y/\beta_y^*\end{bmatrix}\\ \zeta_a^* &= \begin{bmatrix}(\lambda_{b,x}-\lambda_{a,x})\sin\Psi_x\\ (\lambda_{b,x}+\lambda_{a,x})\cos\Psi_x/\beta_x^*\\ (\lambda_{b,y}-\lambda_{a,y})\sin\Psi_y\\ (\lambda_{b,y}+\lambda_{a,y})\cos\Psi_y/\beta_y^*\end{bmatrix}\end{aligned} \tag{4}$$

* Work supported by Brookhaven Science Associates, LLC under Contract No. DE-SC0012704 with the U.S. Department of Energy
† dxu@bnl.gov

ISBN: 978-3-95450-227-1 ISSN: 2673-5490 doi:10.18429/JACoW-IPAC2022-WEPOPT053

CHARACTERISATION OF COOLING IN THE MUON IONIZATION COOLING EXPERIMENT

C. Rogers*, STFC Rutherford Appleton Laboratory, Didcot, UK
and M. A. C. Cummings, Muons Inc, Batavia, USA

Abstract

A high-energy muon collider could be the most powerful and cost-effective collider approach in the multi-TeV regime, and a neutrino source based on decay of an intense muon beam would be ideal for measurement of neutrino oscillation parameters. Muon beams may be created through the decay of pions produced in the interaction of a proton beam with a target. The muons are subsequently accelerated and injected into a storage ring where they decay producing a beam of neutrinos, or collide with counter-rotating antimuons. Cooling of the muon beam would enable more muons to be accelerated resulting in a more intense neutrino source and higher collider luminosity. Ionization cooling is the novel technique by which it is proposed to cool the beam. The Muon Ionization Cooling Experiment collaboration has constructed a section of an ionization cooling cell and used it to provide the first demonstration of ionization cooling. Here the observation of ionization cooling is described. The results of the further analysis of the data are presented, including studies in different magnet configurations and with more detailed understanding of the detector systematic uncertainty.

THE NEED FOR MUON COOLING

The muon collider is an excellent prospect for the energy frontier [1], because:

- synchrotron radiation is suppressed due to the high muon mass, compared to electrons;
- muon recirculation through the detector leads to high luminosity, compared to linear colliders;
- muons are fundamental so have a much improved physics reach compared to protons at the same energy.

These characteristics can be used to make a collider that is:

- energy efficient;
- cost efficient; and
- compact.

Muons are produced by firing protons onto a pion production target, yielding a beam having large emittance. Achievement of high luminosity requires several orders of magnitude reduction in beam emittance. Muon ionization cooling [2] is the technique proposed to deliver this.

Muon ionization cooling may also be beneficial for a muon-based neutrino source [3]. In this case, muon cooling would enable more muons to be accelerated in a smaller aperture, improving the facility efficiency and performance.

Muon ionization cooling has been demonstrated by the Muon Ionization Cooling Experiment (MICE) [4]. Here we outline the current status of the data analysis.

EXPERIMENTAL APPARATUS

MICE was constructed at the Rutherford Appleton Laboratory in the UK [5]. A target was inserted into the proton synchrotron as the protons reached peak energy. Pions created in the target were transported through a series of focusing quadrupoles, momentum-selection dipoles, and a pion-decay solenoid which enabled selection of muon beams having different momentum, rate and pion contamination. A remotely operable beam diffuser just before the main cooling system enabled generation of different beam emittances. Samples were generated by accumulating particle-by-particle measurements.

Incident particles passed through a TOF station (TOF0), a pair of threshold Cherenkov counters and a further TOF station (TOF1), as shown in Fig. 1. The particle velocity was calculated by measuring the time-of-flight between TOF0 and TOF1. The rate was kept low enough that individual particles were reconstructed. As the transfer line had a relatively narrow momentum acceptance, pion and electron impurities could be rejected by studying the particle time-of-flight.

Scintillating fibre trackers upstream and downstream of the cooling apparatus, immersed in solenoid fields of several T, enabled measurement of the position and momentum of particles. Particles took a helical trajectory in the solenoid. The positions of the particles were measured in 5 stations in each tracker, enabling characterisation of the helix and hence inference of the particle momentum.

Several solenoid coils between the two trackers enabled focusing of the beam onto an absorber. In this paper lithium hydride (LiH) and liquid hydrogen absorbers are considered as well as the empty hydrogen absorber vessel and the case where no absorber was installed at all.

CONFIGURATIONS

Two solenoid configurations are studied here, with and without a polarity reversal at the absorber. When the solenoid polarity is not reversed at the absorber ('solenoid' mode), the beam develops canonical angular momentum as it passes through the absorber material. In a long channel this can be detrimental to the cooling performance. When the solenoid polarity is reversed at the absorber ('flip' mode), the coils near the absorber act in opposition so that higher

* chris.rogers@stfc.ac.uk

ISBN: 978-3-95450-227-1 ISSN: 2673-5490 doi:10.18429/JACoW-IPAC2022-WEPOPT054

TARGET STUDIES FOR THE FCC-ee POSITRON SOURCE

F. Alharthi*[1], L. Bandiera[3], I. Chaikovska[1], R. Chehab[1], J. Diefenbach[4], O. Khomyshyn[5], D. Klekots[5], W. Lauth[4], A. Mazzolari[3], V. Mytrochenko[6], S. Ogur[1], M. Romagnoni[3], P. Sievers[2], M. Soldani†[3], A.I. Sytov[3], A. Ushakov[1], S. Wallon[1], Y. Zhao[2]
[1]CNRS-IJCLab, Paris-Saclay U., Orsay, France
[2]CERN, Geneva, Switzerland
[3]INFN Ferrara, Ferrara, Italy
[4]Institute of Nuclear Physics, J. Gutenberg University Mainz, Mainz, Germany
[5]Taras Shevchenko National University of Kyiv, Kyiv, Ukraine
[6]NSC Kharkiv Institute of Physics and Technology, Kharkiv, Ukraine

Abstract

FCC-ee injector study foresees 3.5 nC electron and positron bunches with 200 Hz repetition and 2 bunches per linac pulse at 6 GeV extraction energy. Regarding the possible options of positron production, we retain both of the conventional amorphous target and the hybrid target options. The hybrid scheme uses an intense photon production by 6 GeV electrons impinging on a crystal oriented along a lattice axis. In such a way, it involves two targets: a crystal as a photon radiator and an amorphous target-converter. Therefore, to avoid early failure or damage of the target, the candidate materials for the crystal and conversion targets have started to be tested by using the intense electron beam at Mainzer Mikrotron in Germany by the end of 2021. By manipulating the beam intensity, focusing, and chopping, a Peak Energy Deposition Density in the tested targets could be achieved close to that generated by the electron/photon beam in the FCC-ee positron target. Radiation-damage studies of the crystal sample have been also performed allowing estimating the effect on the photon enhancement used in the hybrid positron source.

INTRODUCTION

The conceptual design of the Future Circular positron-electron Collider, the FCC-ee, has been continuously evolving [1]. The collective effects in the collider and the integration of the tunnel set boundaries have been studied, while the injectors were further optimized in order to meet and maintain the ~1.3 A stored beam at its Z-operation, which will collect physics for 5 years.

Amongst 4 operational stages to study Z, W, H bosons and $t\bar{t}$, Z-operation demands the highest e^- and e^+ charge flux, namely at the order of $10^{12} - 10^{13}$ particles per second for each species. Comparing this e^+ flux with the ever existing and designed colliders [2], the FCC-ee challenge would differ in terms of high linac repetition of 200 Hz with 2 bunches per RF pulse on the converter target.

The required bunch population is $\sim 3.5 \times 10^{10}$, therefore, the heat load as well as the Peak Energy Deposition Density (PEDD) need to be well addressed. On one side, the conventional target where a single amorphous target made of pure metals such as tungsten, tantalum, titanium, or the alloys such as W-Re26, TaW2.5 are retained as an option to be the standalone positron converter. On the other side, the hybrid target consisting of a thin crystal followed by a thicker amorphous target is promising [3]. However, the primary electron beam impinging on the crystal may deteriorate the crystal structure due to the important Coulomb scattering on the nuclei. Above some threshold nuclei can be dislodged from their sites [4]. A critical incident particle density (Fluence) may be determined; above such fluence the crystal structure is affected; that corresponds to the radiation damages on the crystal. Within this report, we will focus on the beam tests started in MAinzer MIkrotron (MAMI) to study the PEDD both on the amorphous and crystal targets and the effects of a high fluence, i.e. the total electron density on the targets. In case of the crystal target, the goal is to reach the fluence values close and even larger than those reached in the SLAC experiment [5]. The main results gathered in this experiment are presented hereafter.

THE FCC-ee PRE-INJECTOR AND POSITRON SOURCE

The FCC collaboration has submitted the conceptual design report in December 2018 [1]. The project design of the FCC-ee has been continuously evolving to overcome the technological difficulties as well as to ensure the realization of the best achievable lepton collider [6]. Further optimization of the extremely high luminosities led to an improvement of the injectors in comparison with the earlier design [7]. The linac operation is increased to 200 Hz with 2 bunches per RF pulse. Furthermore, 4 bunches per RF pulse consisting of 2 e^+ followed by 2 e^- bunches are needed during positron beam delivery to collider. The first 2 e^+ bunches will be put into the DR and the subsequent 2 e^- bunches will hit the positron converter and the generated positrons will be injected into the DR after acceleration to 1.54 GeV by a linac. The layout of the positron pre-injector and positron source is presented in Fig. 1. To ensure high reliability of the positron source, conventional and hybrid targets are currently under

* alharthi@ijclab.in2p3.fr
† mattiasoldani93@gmail.com

ISBN: 978-3-95450-227-1 ISSN: 2673-5490 doi:10.18429/JACoW-IPAC2022-WEPOPT055

LINAC3, LEIR AND PS PERFORMANCE WITH IONS IN 2021 AND PROSPECTS FOR 2022

S. Albright, R. Alemany Fernandez, D. Alves, M. E. Angoletta, D. Barrientos, H. Bartosik, G. Bellodi, S. Bertolo, N. Biancacci, D. Bodart, M. Bozzolan, H. Damerau, F. Di Lorenzo, A. Frassier, D. Gamba, A. Huschauer, S. Jensen, V. Kain, G. Kotzian, T. Koevener, D. Kuchler, A. Lasheen, G. Le Godec, T. Levens, N. Madysa, E. Mahner, O. Marqversen, C. Mastrostefano, P. D. Meruga, C. Mutin, M. O'Neil, G. Piccinini, R. Scrivens, P. Sandve Solvang, D. Valuch, F. Maria Velotti, R. Wegner, C. Wetton, M. Zampetakis,
CERN, Geneva, Switzerland

Abstract

CERN accelerators underwent a period of long shutdown from the end of 2018 to 2020. During this time frame, significant hardware and software upgrades have been put in place to increase the performance of both proton and ion accelerator chains in the High Luminosity LHC era. In the context of the CERN lead ion chain, 2021 has been mainly devoted to restore the injectors' performance and to successfully prove the slip-stacking technique in SPS. In this paper we summarise the key milestones of the ion beam commissioning and the achieved beam performance for the Linac 3 (including the source), LEIR and PS accelerators, together with an outlook on 2022 operation.

INTRODUCTION

In 2020 the CERN proton and ion accelerator chains restarted operation after a period of long shutdown in which beam equipment was upgraded within the LIU (LHC Injectors Upgrade) project [1]. Concerning the ion chain, the majority of the upgrade activities were performed in the Linac 3, equipped with new digital Low-Level RF (dLLRF) cavity controllers, and in SPS, were a significant RF power upgrade was put in place to meet the LIU project requirements with both protons and ions [2]. The SPS dLLRF was also upgraded [3] to be able to reduce the ion bunch spacing from 100 ns to 50 ns by means of the slip-stacking technique [4]. The main challenge of 2021 was therefore to re-establish the pre-shutdown performance across the LHC ion chain and establish the new slip-stacking technique in SPS. This work is structured as follows: in the next section we will cover the performance reached by the beam at the source and in Linac 3, we will then cover LEIR performance, and eventually PS performance up to the injection in SPS.

SOURCE AND LINAC 3

The GTS-LHC source profited of a dedicated testing period at the beginning of 2021 (from week 2 to week 13). This operation mode proved to be a valuable investment as the source setting improvements could be transferred directly to source operation, and a better understanding of the source could be obtained. One of the main achievements was installing a ceramic beak close to the crucible orifice as shown in Fig. 1 together with Molflow+ simulations [5]. This is done to avoid lead condensation [6] which can block the outlet and reduce the number of lead refills needed. Thanks to this modification, source fills lasted about 40 days on average (previously it was about 2 weeks [7]). On the other hand, with the new crucible design, there are no clear signs of performance degradation before the oven empties. For 2022 operation, it is therefore foreseen to implement a scheduled refill plan to minimise possible performance impact to the LHC.

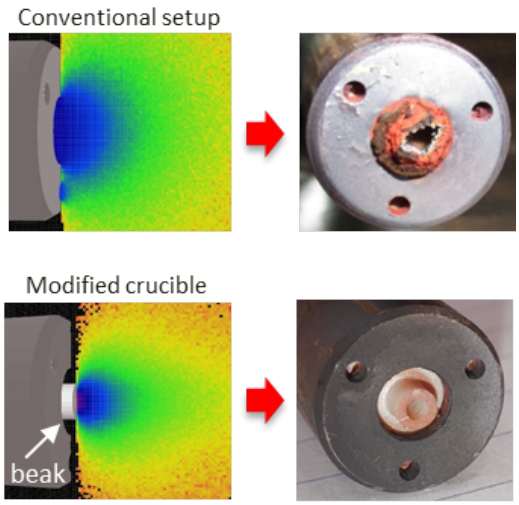

Figure 1: Modified source crucible to prevent lead oxides deposition and prolong the source fill duration. On the left, Molflow+ simulations of the lead extraction process without (top) and with (bottom) ceramic beak. On the right, typical corresponding status of the outer oven cover after source operation.

During the long shutdown important upgrades of the dLLRF were performed, mainly for the control of three cavities (buncher, ramping and debuncher). The main functionality of the dLLRF was systematically tested following dedicated procedures for hardware and beam commissioning [8, 9]. With respect to the past analog system, the new dLLRF allows for precision measurements of the RF signals even on systems where the previous analogue system remains in control. This is of particular importance in view of the Linac3-LEIR joint effort to improve the beam per-

ISBN: 978-3-95450-227-1 ISSN: 2673-5490 doi:10.18429/JACoW-IPAC2022-WEPOPT058

A RESPONSE MATRIX APPROACH TO SKEW-SEXTUPOLE CORRECTION IN THE LHC AT INJECTION

E. Waagaard[1], E.H. Maclean, CERN, Geneva, Switzerland
[1]also at Uppsala University, Uppsala, Sweden

Abstract

To date, no dedicated attempt has been made to correct the skew-sextupole (a_3) $3Q_y$ resonance in the LHC at injection. This topic has recently gained interest, following investigation of the emittance growth during the LHC energy ramp due to third-order islands. The LHC is equipped with skew-sextupole correctors in the experimental insertions, intended for local compensation at top energy, and with families of skew-sextupole magnets in the arcs, intended for chromatic-coupling correction (but not optimally placed for $3Q_y$ compensation). Simulation studies were performed to assess whether these correctors could compensate $3Q_y$ in the LHC at injection via a response matrix approach, based on values at the BPMs. Corrections for $3Q_y$ could be found within magnet powering limitations, but required significantly increased corrector strength compared to chromatic-coupling compensation.

a_3 CORRECTION SCHEME

Interest in $3Q_y$ resonance compensation at LHC injection (450 GeV) has arisen, due to potential influence of islands on emittance growth during the ramp [1] and on lifetime or emittance at flat-bottom in conjunction with e-cloud. Unfortunately, while two types of skew-sextupole (a_3) magnet are present in the LHC, the lattice was not designed with $3Q_y$ compensation at injection in mind.

In the arcs, several chromaticity sextupoles (*MS*) are rotated to provide skew-sextupoles (*MSS*) for chromatic-coupling correction. MSS are powered in series arc-by-arc, with 1 family (Arc34) broken and unusable, and are arranged in each arc to suppress their influence on $3Q_y$ [2]. The standard a_3 correction scheme uses MSS to minimize arc-by-arc a_3 errors in LHC main dipoles ('*MB*') weighted by optics functions, based upon magnetic measurements [2, 3]. It takes no account of additional sources (e.g. feed-down). Skew-sextupole strength ($[\mathrm{m}^{-3}]$) is defined for the LHC error model [4]

$$K_{n,skew} = -\frac{1}{B\rho}(n-1)!a_n = -\frac{1}{B\rho}\left.\frac{\partial^{n-1}B_x}{\partial x^{n-1}}\right|_{0,0,s} \quad (1)$$

with $n = 3$. MSS strengths from the standard correction are shown in Fig. 1. Beam-based minimization of chromatic-coupling has also been tested, with comparable order-of-magnitude strengths required [5, 6].

a_3 correctors (MCSSX) are also installed either side of the experimental insertions (IR[1,2,5,8]). MCSSX are intended for local correction of IR errors at top-energy [6, 7], and are not used at injection. Use is complicated by their location in the common insertions, meaning the beams cannot be controlled independently. Crossing and separation bumps also result in feed-down if used in operation.

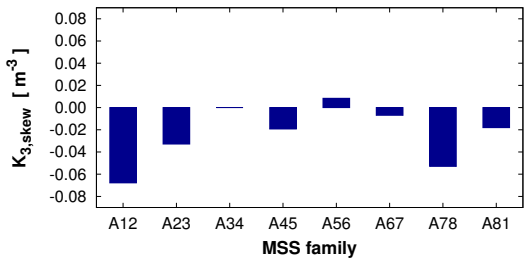

Figure 1: MSS strength for standard a_3 correction scheme.

Maximum MSS and MCSSX powering at 450 GeV are $K_{3,skew} = 6.19\,\mathrm{m}^{-3}$ and $K_{3,skew} = 1.5\,\mathrm{m}^{-3}$.

While neither MSS nor MCSSX were intended for $3Q_y$ compensation at 450 GeV, simulation-based studies were performed to test if they could in principle correct the $3Q_y$ resonance driving term (RDT) f_{0030} using a response matrix approach. Response matrix approaches for sextupole resonances have been employed at PSB [8] and Diamond [9]. Discussion of the simulations and results is given in [10]. An ideal LHC model with no errors was used to construct a response matrix $\mathbf{R}$ of $\mathrm{Re}[f_{0030}(s)]$ and $\mathrm{Im}[f_{0030}(s)]$ to the MSS and MCSSX,

$$\mathbf{R}\vec{\Delta k} = \vec{\Delta f} \quad (2)$$
$$\vec{\Delta f} = (\Delta f_{b1,\mathrm{Re}}, \Delta f_{b1,\mathrm{Im}}, ...\Delta f_{bm,\mathrm{Re}}, \Delta f_{bm,\mathrm{Im}})$$

where only BPM locations ($b1$...bm) are considered, reflecting operational scenarios where correction would be based on measured f_{0030} at BPMs. Models were generated in MAD-X and RDT values calculated via PTC.

Having determined $\mathbf{R}$ from the ideal model, simulations including various linear and nonlinear errors were performed. Modelled RDT values at BPMs ($\vec{f}$) were used to determine corrections via the pseudo-inverse of the response matrix $\mathbf{R}^+$ (calculated by SVD).

$$\vec{\Delta k} = -\mathbf{R}^+\vec{f} \quad (3)$$

$\vec{\Delta k}$ corrections were applied to the previous model, and RDTs re-calculated to test if the correction reduced $|f_{0030}|$. Only the Beam1 response was considered when using the MCSSX. Studies with MCSSX also only considered a flat-orbit (with crossing/separation bumps removed) to limit complications from feed-down.

f_{0030} CORRECTION RESULTS

The response matrix ('$\mathbf{R}$-matrix') approach was effective in simple test cases [10]: correctly identifying mispowered

ISBN: 978-3-95450-227-1 ISSN: 2673-5490 doi:10.18429/JACoW-IPAC2022-WEPOPT059

CORRECTIONS OF SYSTEMATIC NORMAL DECAPOLE FIELD ERRORS IN THE HL-LHC SEPARATION/RECOMBINATION DIPOLES*

J. Dilly†‡[1], F. F. Van der Veken, M. Giovannozzi, R. Tomás, CERN, Meyrin, Switzerland
[1]also at Humboldt University of Berlin, Berlin, Germany

Abstract

Magnetic measurements revealed that the new normal decapole (b_5) errors of the recombination dipoles (D2) for the HL-LHC could have a systematic component of up to 11 units. Based on previous studies, it was predicted that the current corrections would not be able to compensate this, thereby leading to a degradation of the dynamic aperture. On the other hand, the separation dipole D1 is expected to have a systematic b_5 component of 6 units to 7 units and its contribution to the resonance driving terms will partly compensate the effect of D2, due to the opposite field strength of the main component. Simulations were performed to address these concerns and to verify the compensation assumption, yet confirmed that the errors could only be partly compensated. In addition, various normal decapole resonance driving terms were examined as correction targets and the dependence of feed-down to amplitude detuning on this choice was discovered.

INTRODUCTION

During magnetic measurements it was found out that the b_5 values of the new D2 recombination dipoles (aka MBRD) in the High-Luminosity LHC (HL-LHC [1, 2]) might have a systematic b_5 component of up to 11 units [3]. Based on earlier studies, it was projected that the current correction scheme [4] will not be able to compensate these and that this will lead to a degradation of 0.5 σ to 1 σ in the Dynamic Aperture (DA) [1, 5]. In fact, contributions from D2 have not been incorporated into the correction scheme, as D2 is a dual aperture magnet, while the b_5 corrector is single aperture. Additionally, it is placed far away from the corrector package (CP, see Fig. 2 and [1]), leading to a large phase advance, lower β-function and different orbit. Hence it was uncertain, if the D2 inclusion would be beneficial to DA (see [5]). It was also investigated, whether the hitherto used Resonance Driving Term (RDT) f_{5000} was the optimal choice (see section "Closest Resonances"). Of further concern was the interplay between D2 and the other separation dipole, D1 (aka MBX). The new D1 is expected to have a systematic b_5 component of 6 units to 7 units [3]. Due to the opposite beam bending directions (see Fig. 2) in the two magnets, their contribution to the resonance driving terms will partly compensate. This is explored in section "Compensation". Tracking simulations have been run to estimate the influence of the measured errors and to explore for their correction. The setup is described in section "Simulation Setup" and their findings are presented in section "Results".

* this work has been supported by the HiLumi Project
† this work has been sponsored by the Wolfgang Gentner Programme of the German Federal Ministry of Education and Research
‡ joschua.dilly@cern.ch

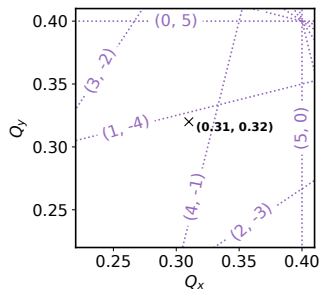

Figure 1: Tune diagram with HL-LHC collision working point and 5th order resonances.

CLOSEST RESONANCES

At collision energy, the HL-LHC has a design working point with fractional tunes of $Q_x = 0.31, Q_y = 0.32$. As seen in the tune diagram of Fig. 1, the closest normal decapole resonances are (1, -4), and (5, 0), which correspond to the RDTs f_{1004} and f_{5000}, respectively. With (1, -4) being the closest to the working point, one might assume that its influence might be the strongest and its correction the most beneficial. As the current implementation [6] on the other hand, chooses f_{5000} as correction target, its suitability was confirmed and the correction compared to targeting f_{1004}. The details are presented in the section "Results".

COMPENSATION

One part of the investigation was to check whether the D1 and D2 b_5 errors might compensate each other. The reasoning behind this is that D1 and D2 have opposite bending angles (see Fig. 2). In fact, they have an integrated dipole strength value K_1L of equal magnitude, but of opposite signs. For the used optics (see section "Simulation Setup") the b_5 of D2 needs to be about 3.1 times larger than the b_5 of D1 to cancel f_{5000} and 2.4 times larger to cancel f_{1004} in the RDT approximation used [4, 7]. The ratio of the estimated values of 6 units to 7 units for D1 and 11 units for D2, is about a factor 1.6 – 1.8 too low for total compensation, yet partial compensation has been observed and is described in section "Results".

SIMULATION SETUP

The DA studies were performed with AutoSix [8], a SixDesk [9] wrapper, on top of a HL-LHC V1.4 MAD-X [10] setup: The HL-LHC lattice was created from the de-

ISBN: 978-3-95450-227-1 ISSN: 2673-5490 doi:10.18429/JACoW-IPAC2022-WEPOPT060

CONTROLLING LANDAU DAMPING VIA FEED-DOWN FROM HIGH-ORDER CORRECTORS IN THE LHC AND HL-LHC*

J. Dilly†‡[1], E. H. Maclean, R. Tomás, CERN, Meyrin, Switzerland
[1]also at Humboldt University of Berlin, Berlin, Germany

Abstract

Amplitude detuning measurements in the LHC have shown that a significant amount of detuning is generated in Beam 1 via feed-down from decapole and dodecapole field errors in the triplets of the experiment insertion regions, while in Beam 2 this detuning is negligible. In this study, we investigate the cause of this behavior and we attempt to find corrections that use the feed-down from the nonlinear correctors in the insertion region for amplitude detuning.

INTRODUCTION

After correction of octupolar (b_4) errors, residual amplitude detuning in Beam 1 was measured during the LHC commissioning 2018, when the crossing orbit bumps were enabled [1, 2]. Further investigation [3] confirmed this finding and revealed the main contribution to be feed-down from high-order errors, i.e. decapole (b_5) and/or dodecapole (b_6) errors, to the octupole fields, due to the crossing schemes in the Interaction Point (IP) 5 and IP 1.

Throughout, b_n and a_n are used to name normal and skew relative field errors and K_n and J_n to indicate normal and skew field strengths. All field indices begin at $n = 1$ for dipole fields. The machine settings are given in Table 1, while the measurements are summarized in Table 2.

The magnitude of the amplitude detuning is comparable with the detuning which had been corrected with the octupole correctors. This amount of detuning is detrimental to the accuracy of the base-band tune (BBQ) measurement [4] and likely also to dynamic aperture and beam lifetime, which has only been tested and confirmed for lower β^* [4].

The harmful influence of b_5 and b_6 errors on dynamic aperture and beam lifetime in the upcoming High-Luminosity LHC (HL-LHC) has been shown in simulations and dedicated measurements, in which the b_6 errors were artificially increased to replicate the HL-LHC conditions [5–9].

In this paper, a correction option is explored to correct b_6 by targeting observed amplitude detuning from feed-down in the LHC by utilizing the feed-down to b_4 from the dodecapole correctors in the nonlinear corrector packages of the insertion regions (IRs).

* this work has been supported by the HiLumi Project
† this work has been sponsored by the Wolfgang Gentner Programme of the German Federal Ministry of Education and Research
‡ joschua.dilly@cern.ch

Table 1: Machine Settings used During Measurements

Tunes:		$Q_x = 0.31, Q_y = 0.32$
Optics:		$\beta^* = 30$ cm round optics
Comissioning		28 . 04 . 2018
Crossing:	IP-Plane	[IP1-V / IP2-V / IP5-H / IP8-H]
(half angles)	µrad	[160 / 200 / 160 / -250]
Separation:	IP-Plane	[IP1-H / IP2-H / IP5-V / IP8-V]
	mm	[-0.55 / 1.4 / 0.55 / 1.0]
MD3311		16 . 06 . 2018
Crossing:	IP5-H	160 µrad (half angle)
Separation:	IP5-V	0.55 mm
Offset:	IP5-V	−1.8 mm

AMPLITUDE DETUNING FROM FEED-DOWN

In thin lens approximation, as used for corrections calculated from simulations, multipole elements are split into single kicks at s_w surrounded by drift spaces, the kick strength being $K_n L_w$ - the integrated strength over the length L of element w. The β-function and orbit are then also approximated using the value at s_w.

The contribution to first order amplitude detuning from octupole fields of elements with integrated strength $K_4 L_w$ can be calculated [10] from

$$\frac{\partial Q_x}{\partial(2J_x)} = \frac{K_4 L_w}{32\pi}\beta_x^2(s_w) \quad (1)$$

$$\frac{\partial Q_x}{\partial(2J_y)} = \frac{\partial Q_y}{\partial(2J_x)} = -\frac{K_4 L_w}{16\pi}\beta_x(s_w)\beta_y(s_w) \quad (2)$$

$$\frac{\partial Q_y}{\partial(2J_y)} = \frac{K_4 L_w}{32\pi}\beta_y^2(s_w) \quad (3)$$

with the actions $J_{x,y}$. Including feed-down [11] due to the orbit x, y from normal and skew decapoles (K_5, J_5) and normal and skew dodecapoles ($K_6 L$, $J_6 L$) we get

$$K_4 L \mapsto K_4 L + x K_5 L + y J_5 L + \frac{1}{2}\left(x^2 - y^2\right) K_6 L + xy J_6 L \,. \quad (4)$$

In the following chapters the symbols

$$Q_{a,b} = \frac{\partial Q_a}{\partial(2J_b)}, \quad \text{and} \quad \tilde{\beta}_{a,b} = \begin{cases} \tilde{\beta}_{x,x} = \frac{\beta_x^2}{32\pi} \\ \tilde{\beta}_{x,y} = -\frac{\beta_x \beta_y}{16\pi} \\ \tilde{\beta}_{y,y} = \frac{\beta_y^2}{32\pi} \end{cases} \quad (5)$$

will be used.

ISBN: 978-3-95450-227-1 ISSN: 2673-5490 doi:10.18429/JACoW-IPAC2022-WEPOPT061

A FLEXIBLE NONLINEAR RESONANCE DRIVING TERM BASED CORRECTION ALGORITHM WITH FEED-DOWN

J. Dilly*†[1], R. Tomás, CERN, Meyrin, Switzerland
[1]also at Humboldt University of Berlin, Berlin, Germany

Abstract

The optics in the insertion regions of the LHC and its upgrade project the High Luminosity LHC are very sensitive to local magnetic errors, due to the extremely high beta-functions. In collision optics, the non-zero closed orbit in the same region leads to a "feed-down" of high-order errors to lower orders, causing additional effects detrimental to beam lifetime. An extension to the well-established method for correcting these errors by locally suppressing resonance driving terms has been undertaken, not only taking this feed-down into account, but also adding the possibility of utilizing it such that the powering of higher-order correctors will compensate for lower order errors. Existing correction schemes have also operated on the assumption of (anti-)symmetric beta-functions of the optics in the two rings. This assumption can fail for a multitude of reasons, such as inherently asymmetric optics and unevenly distributed errors. In this respect, an extension of this correction scheme has been developed, removing the need for symmetry by operating on the two separate optics of the beams simultaneously. Unlike earlier implementations, the resonance driving terms to be corrected can also be changed flexibly. The mathematical background as well as some implementation details of this new enhancement are presented.

INTRODUCTION

The sensitivity of accelerator beam optics to magnetic errors depends directly on the β-function, which is highest in the Insertion Regions (IR) around the Interaction Points (IP) with the lowest β^* (the value of the β-function at the location of the IP). Hence, correcting the non-linear magnetic errors in these regions has been of significant importance in optimizing the LHC machine performance [1–6]. Installation of stronger magnets in the IR and the decrease of β^* in operation in the High Luminosity upgrade of the LHC (HL-LHC) [7, 8], is foreseen to result in even tighter constraints on residual errors.

At the same time, the influence of feed-down has been observed and investigated in the IRs of the LHC as well, where the crossing-angle scheme of the collision optics creates a large orbit bump. For both, LHC and HL-LHC, the need to correct this feed-down has been established [2, 4–6, 9–12].

To estimate the powering of the corrector magnets, a local correction scheme based on the Resonance Driving Terms (RDTs) in the IRs has been utilized [13]. Up to now, the implementation of this scheme calculated the correction based on the input from a single optics, for either Beam 1 or Beam 2, and made use of symmetries between the beams to optimize the correction for both. Cases can occur in which this symmetry does not hold, e.g. through the introduction of feed-down, or the use of inherently asymmetric optics. An example of the latter are flat optics [14, 15], in which the β^* in the two transversal planes no longer has identical values. These optics allow for a more distributed radiation deposition in the LHC magnets as well as an increase in luminosity [15]. Their feasibility has been studied during machine developments in the LHC [16] and preliminary analysis regarding their influence on corrections and amplitude detuning has been conducted [17].

A new and flexible version of the correction principle has been implemented [18], taking both optics into account and hence not relying on symmetry assumptions, allowing to target RDTs freely, as well as including feed-down into the calculations. The implementation allows for the feed-down from higher orders to the RDT to be corrected, as well as using the feed-down from higher order corrector magnets to correct for lower order errors.

CORRECTOR PACKAGES

To compensate for errors locally, both sides of the LHC IRs hosting experiments (ATLAS in IR1, ALICE in IR2, CMS in IR5 and LHCb in IR8) are equipped with linear and non-linear corrector packages. As shown in the schematics for HL-LHC in Fig. 1, these packages are located within the common aperture region of the machines, between Q3 and the separation dipoles D1, and hence contain common magnets for the two beams. Any correction should therefore take the optics of both beams into account. In the experimental IRs of the LHC and in HL-LHC IR2 and IR8, nonlinear correctors for skew and normal sextupoles (a_3, b_3), skew and normal octupoles (a_4, b_4) and normal dodecapoles (b_6) are available. In IR1 and IR5 of HL-LHC on the other hand, the corrector package will be upgraded to also include skew and normal decapoles (a_4, b_5) as well as skew dodecapoles (a_6) and offer therefore a wider range of field errors to correct, to account for the increase in the β-function in this high-performance machine [8, 12, 19].

CORRECTION PRINCIPLE

The algorithm aims to minimize the RDT locally at the entrance of the IR, with some additional simplifications on the calculation of the RDT value (compared to e.g. [20]) as outlined in [13]:

* this work has been sponsored by the Wolfgang Gentner Programme of the German Federal Ministry of Education and Research
† joschua.dilly@cern.ch

ISBN: 978-3-95450-227-1 ISSN: 2673-5490 doi:10.18429/JACoW-IPAC2022-WEPOPT062

OPTIMISATION OF THE FCC-ee POSITRON SOURCE USING A HTS SOLENOID MATCHING DEVICE

Y. Zhao*, S. Doebert, A. Latina, CERN, Geneva, Switzerland
P. Martyshkin, BINP, Novosibirsk, Russia
I. Chaikovska, R. Chehab, S. Ogur, IJCLab, Orsay, France
B. Auchmann, P. Craievich, M. Duda, J. Kosse, R. Zennaro, PSI, Villigen, Switzerland

Abstract

In this paper, we present the simulation and optimisation of the FCC-ee positron source, where a high-temperature superconducting (HTS) solenoid is used as the matching device to collect positrons from the target. The "conventional" target scheme is used which simply consists of amorphous tungsten. The target is placed inside the bore of the HTS solenoid to improve the accepted positron yield at the entrance of the damping ring and the location of the target is optimised. The latest recommended baseline beam parameters are used and presented. An optimisation of the ideal positron yield using the analytic SC solenoid on-axis field is also performed and shows that the design of the HTS solenoid is optimal as far as the accepted positron yield is concerned.

INTRODUCTION

The matching device plays an important role in the FCC-ee positron source [1]. Positrons from the target are captured by the matching device with a strong magnetic field, followed by a capture linac that accelerates the positrons up to 200 MeV. The positrons are then accelerated by the injector linac to 1.54 GeV and matched to the damping ring (DR) acceptance at the DR entrance. The ratio between the number of positrons accepted by the DR and the number of primary electrons impinging on the target is defined as the "accepted" positron yield.

In our study, the FCC-ee positron source is simulated from the target to the injector linac. The "conventional" target scheme is assumed, which comprises a single amorphous tungsten target. Downstream of the target is the matching device. To increase the magnetic field at the target exit and improve the capture efficiency, a high-temperature superconducting (HTS) solenoid is used as the matching device, and the target is placed inside the bore of the HTS solenoid. The capture linac is composed of travelling wave (TW) or standing wave (SW) RF structures, surrounded by a normal conducting (NC) or superconducting (SC) solenoid that is assumed to provide a constant magnetic field. The injector linac is longitudinally simulated with an analytic calculation of the positron energy, while the transverse tracking is not considered. GEANT4 [2] is used to simulate the interactions between the primary electrons and the target. The target thickness is $5\,X_0$ (17.5 mm) [3], $X_0 = 3.5$ mm being the radiation length of the tungsten. Sampling with a Gaussian function is used to generate the initial distribution of electrons at the target entrance. RF-TRACK [4] is used to simulate the beam tracking in the matching device and capture linac. The schematic layout of the FCC-ee positron source assumed in this study is presented in Fig. 1.

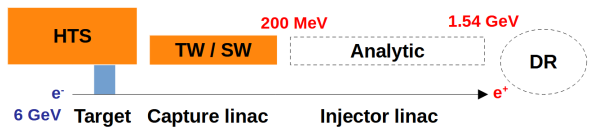

Figure 1: Schematic layout of FCC-ee positron source using the HTS solenoid as the matching device.

The latest recommended baseline primary electron beam parameters and positron beam parameters at the DR entrance, as well as the target parameters and energy depositions, are summarised in Table 1. The peak energy deposition density (PEDD) [1] and deposited power in the target are also presented, which are usually normalised by the accepted yield to achieve the required bunch charge at the DR entrance. A conservative normalised transverse emittance (~60 mm·mrad) is considered for the primary electrons. A smaller normalised transverse emittance (~15 mm·mrad) is also studied while the spot size is still the same (0.5 mm), and it is found that the impact on the results is negligible.

HTS SOLENOID

The HTS solenoid for the FCC-ee positron source is being designed and developed at the Paul Scherrer Institute (PSI) and the field map of the latest design [5] is used in our simulations. The solenoid is ~30 cm long including different parts such as the HTS coils, the radiation shield, the cryostat, etc. The outer diameter of the solenoid is assumed to be 46.5 cm, while the warm bore diameter is assumed to be 72 mm. Shielding material is assumed to be placed inside the warm bore surrounding the beam, with a thickness of 16–21 mm. Larger thickness of the shielding material than 21 mm would lead to more lost positrons and therefore reduce the accepted positron yield significantly.

The on-axis magnetic field of the HTS solenoid is displayed in Fig 2. The distance between the peak field and the solenoid exit position is designed to be ~100 mm. The full HTS solenoid field is presented by the dashed curve, while the effective field of the HTS solenoid that is used in the simulation is presented by the solid curve. In addition, a

* yongke.zhao@cern.ch

[1] Normalised PEDD is usually required to be < 35 J/g [6]

ISBN: 978-3-95450-227-1 ISSN: 2673-5490 doi:10.18429/JACoW-IPAC2022-WEPOPT063

THE FCCee PRE-INJECTOR COMPLEX

P. Craievich*, R. Zennaro, M. Schaer, N. Vallis, B. Auchmann, M. I. Besana, S. Bettoni, H. Braun, M. Duda, D. Hauenstein, E. Hohmann R. Ischebeck, P. Juranic, J. Kosse, G. L. Orlandi, M. Pedrozzi, J.-Y. Raguin, S. Reiche, S. Sanfilippo, Paul Scherrer Institut, Villigen PSI, Switzerland
Y. Zhao, A. Grudiev, W. Bartmann, M. Benedikt, T. Brezina, M. Calviani, S. Doebert, Y. Dutheil, O. Etisken[1], J. L. Grenard, B. Humann, A. Latina, A. Lechner, A. Marcone, H. Pommerenke, R. Ramjiawan, F. Zimmermann, CERN, Geneva, Switzerland,
I. Chaikovska, S. Ogur, F. Alharthi, IJCLab, Orsay, France
C. Milardi, A. De Santis , LNF-INFN, Frascati, Italy
K. Oide, Y. Enomoto, K. Furukawa, KEK, Japan
T. Raubenheimer, SLAC, Stanford, USA
[1]also at Kirikkale University, Kirikkale, Turkey

Abstract

The international FCC study group published in 2019 a Conceptual Design Report for an electron-positron collider with a centre-of-mass energy from 90 to 365 GeV with a beam currents of up to 1.4 A per beam. The high beam current of this collider create challenging requirements on the injection chain and all aspects of the linac need to be carefully reconsidered and revisited, including the injection time structure. The entire beam dynamics studies for the full linac, damping ring and transfer lines are major activities of the injector complex design. A key point is that any increase of positron production and capture efficiency reduces the cost and complexity of the driver linac, the heat and radiation load of the converter system, and increases the operational margin. In this paper we will give an overview of the status of the injector complex design and introduce the new layout that has been proposed by the study group working in the context of the CHART collaboration. In this framework, furthermore, we also present the preliminary studies of the FCC-ee positron source highlighting the main requirements and constraints.

INTRODUCTION

The FCC-ee injector complex must provide beam for top-up injection in the booster rings supporting a beam lifetime of about 18 minutes on Z pole and as low as 12 minutes at high energy. It must also allow for a filling from zero (alternating bootstrapping injection) within at most half an hour. For this purpose, the FCC-ee CDR [1] considers a 6 GeV linac, with at most 2 bunches per RF pulse, with a repetition rate up to 200 Hz. In this context, the FCC-ee Injector Study was created as a collaboration between PSI and CERN with some external partners, such as CNRS-IJCLab (Orsay), BINP (Novosibirsk), INFN-LNF (Frascati) and SuperKEKB (Tsukuba) as an observer. The project has two deliverables: the revision of the baseline FCC-ee injector design as published in the FCC-ee CDR [1] -including a cost estimate- and the proof of principle of the positron source through the PSI Positron Production (P^3 or P-cubed) experiment at PSI.

Table 1: Target Parameters for the Two Main Scenarios

	Baseline	**HE Linac**
Ring for injection	PBR	BR
Injection energy [GeV]	6	20
Bunch population 10^{10} (nC)	3.47 (5.55)	3.12 (5.0)
Repetition rate [Hz]	200	200
Number of bunches	2	2
Bunch spacing [ns]	15, 17.5, 20	15, 17.5, 20
Rms norm. emit. [mmmrad]	50, 50	50, 50
Rms bunch length [mm]	1	1
Rms energy spread [%]	0.1	0.1

MAIN PARAMETERS

Two possible scenarios have been identified for the injector complex. The first scenario remains the baseline, where the 6 GeV beams are injected into the existing Super Proton Synchrotron (SPS) ring or into a new pre-booster ring (PBR). In the second option, an additional high-energy (HE) linac would boost the energy from 6 GeV to 20 GeV and inject the beams directly into the main booster. The injector complex up to 6 GeV can be identical in the two scenarios. Table 1 lists the target parameters at the end of the injector complex for the two options. Another important specification is that the intensity of the electron and positron bunches have to vary randomly from 0 to 100 % depending on the intensity balance between the collider rings. Furthermore, the bunch-by-bunch stability for the injection has to be within 3 %.

Filling Scheme

The filling scheme of the colliders foresees 10 cycles for each species, designated to pre-compensate the charge loss due to collisions, and to always keep the charge imbalance within ±5 %. This operation mode is referred to as bootstrapping [2]. The times necessary for the accumulation and

* paolo.craievich@psi.ch

ISBN: 978-3-95450-227-1 ISSN: 2673-5490 doi:10.18429/JACoW-IPAC2022-WEPOPT064

SIMULATIONS AND MEASUREMENTS OF LUMINOSITY AT SuperKEKB

D. Zhou*, K. Ohmi, Y. Funakoshi, Y. Ohnishi, KEK, Tsukuba, Japan
Y. Zhang, IHEP, Beijing, China

Abstract

The interplay of beam-beam interaction, machine imperfections, and beam coupling impedance makes it difficult to predict the luminosity performance of SuperKEKB. Since 2020, the crab waist scheme was introduced to SuperKEKB to suppress beam-beam resonances. The coherent beam-beam head-tail instability and beam-beam driven synchro-betatron resonances due to large crossing angle can drive horizontal blowup, which cannot be suppressed by the crab waist. The longitudinal impedance modulates the synchrotron motion and therefore affects beam-beam instability. In this paper, we compare simulations and measurements of luminosity and discuss the challenges and direction toward developing a predictable luminosity simulation model for SuperKEKB.

INTRODUCTION

SuperKEKB [1] commissioning had three phases: Phase-1 [2, 3] (February - June 2016, without installations of the final focusing superconducting QCS magnets and roll-in of Belle II detector), Phase-2 [4] (February - July 2018, with QCS and Belle II, but without the Vertex detector), and Phase-3 [5] (from March 2019 until present with the full Belle II detector). Beam commissioning without collisions in Phase-1 achieved small vertical emittances less than 10 pm for both beams, which is essential for high luminosity. Machine tuning with collisions in Phase-2 confirmed the nano-beam collision scheme [6], i.e. collision with a large crossing angle and vertical beta function β_y^* at the interaction point (IP) much smaller than bunch length σ_z. However, without the crab waist (CW) the beam-beam (BB) driven vertical emittance blowup was severe, causing degradation of specific luminosity (Lsp) as bunch currents increased. This situation continued until April 2020 when the crab waist scheme [7] was adopted. The CW suppresses the beam blowup significantly and beam commissioning with CW has been successful [8], while luminosity performance has been worse than predictions of simulations.

OVERVIEW OF LUMINOSITY AND BEAM-BEAM EFFECTS AT SUPERKEKB

The specific luminosity $L_{sp} = L/(N_b I_{b+} I_{b-})$ for SuperKEKB with nano-beam collision scheme can be well approximated by

$$L_{sp} \approx \frac{e^{-\frac{\Delta^2}{2(\sigma_{y+}^{*2}+\sigma_{y-}^{*2})}}}{2\pi e^2 f \sqrt{\sigma_{y+}^{*2}+\sigma_{y-}^{*2}}\sqrt{\sigma_{z+}^2+\sigma_{z-}^2}\tan\frac{\theta_c}{2}} \quad (1)$$

Here N_b is the number of bunches, $I_{b\pm}$ is the bunch current, f is the revolution frequency, θ_c is the full crossing angle, $\sigma_{y\pm}^*$ and $\sigma_{z\pm}$ are the beam sizes at IP in the vertical and longitudinal directions, respectively. The quantity Δ indicates the relative vertical orbit offset of the colliding beams at IP. The incoherent BB tune shifts can be calculated from the BB kick [9], and are given by the approximate formulae

$$\xi_{x+}^i \approx \frac{r_e}{2\pi\gamma_+}\frac{N_-\beta_{x+}^*}{\sigma_{z-}^2\tan^2\frac{\theta_c}{2}+\sigma_{x-}^{*2}}, \quad (2)$$

$$\xi_{y+}^i \approx \frac{r_e}{2\pi\gamma_+}\frac{N_-\beta_{y+}^*}{\sigma_{y-}^*\sqrt{\sigma_{z-}^2\tan^2\frac{\theta_c}{2}+\sigma_{x-}^{*2}}} \quad (3)$$

for the positron beam. Exchanging the +/- by -/+ gives the formulae for the electron beam. Equations (1) to (3) are the basis of discussions on luminosity and BB effects in this paper.

Table 1: SuperKEKB machine parameters for β_y^*=2 mm on Jul.1, 2019 and β_y^*=1 mm on Apr. 5, 2022, respectively.

Parameters	2019.07.01		2022.04.05	
	LER	HER	LER	HER
I_b (mA)	0.51	0.51	0.71	0.57
ϵ_x (nm)	2.0	4.6	4.0	4.6
ϵ_y (pm)	40	40	30	35
β_x (mm)	80	80	80	60
β_y (mm)	2	2	1	1
σ_{z0} (mm)	4.6	5.0	4.6	5.1
ν_x	44.542	45.53	44.524	45.532
ν_y	46.605	43.583	46.589	43.572
ν_s	0.023	0.027	0.023	0.027
Crab waist ratio	0	0	80%	40%

Table 1 shows the typical machine parameters from operation without the CW (2019.07.01) and with the CW (2022.04.05). Using these parameters, the BB induced footprints of the LER beam are plotted in Fig. 1 with solid lines indicating the important resonances. The linear and chromatic coupling resonances $\nu_x - \nu_y + k\nu_s = N$ are driven by machine imperfections. The resonances at $\nu_x \pm n\nu_y = N$ are excited by BB interaction with a large crossing angle. The synchro-betatron resonances $2\nu_x - k\nu_s = N$ can be excited by both machine imperfections and BB interaction. Here the incoherent betatron and synchrotron tunes are used to describe the resonances. Transverse coupling impedances and BB effects can cause shifts of the incoherent betatron tunes, and potential-well distortion from longitudinal impedance

* dmzhou@post.kek.jp

ISBN: 978-3-95450-227-1 ISSN: 2673-5490 doi:10.18429/JACoW-IPAC2022-WEPOPT065

SIMULATIONS OF THE UPGRADED DRIVE-BEAM PHOTOINJECTOR AT THE ARGONNE WAKEFIELD ACCELERATOR

E. Frame[1*], S. Doran[2], S. Kim[2], X. Lu[1,2], P. Piot[1,2], J. G. Power[2], E. E. Wisniewski[2]
[1]Northern Illinois University, DeKalb, IL, USA
[2]Argonne National Laboratory, Lemont, IL, USA

Abstract

The Argonne Wakefield Accelerator (AWA) is planning to upgrade the photoinjector of its drive-beam accelerator. The main goal of the upgrade is to improve the beam brightness using a symmetrized RF-gun cavity and linac cavities. In the process, the photoinjector is reconfigured and some of the solenoid magnets will be redesigned. A challenging aspect of this optimization is that the injector should be able to produce bright low-charge (~ 1 nC) bunches while also being capable of operating with high-charge (~ 50 nC) bunches. This paper discusses the optimization of the beam dynamics for the low- and high-charge cases and explores the performances of the proposed configuration.

INTRODUCTION

At the Argonne Wakefield Accelerator (AWA), the drive-beam photoinjector is the backbone of the facility [1]. The photoinjector generates ≤ 70-MeV electron bunches in either a low-charge or high-charge regime. In the low-charge mode, single bunches with charge ≤ 1 nC are produced with an emphasis on forming low-emittance bunches to support various beam-dynamics experiments including beam-driven wakefield acceleration in THz structures. In the high-charge regime, bunches train comprising eight 50-nC bunches are produced and principally employed to excite fields in power extraction and transfer structures (PETS). These structures produce high-power (sub-GW), high-frequency (X-band and above) electromagnetic radiation to power high-frequency accelerating structures in the so-called two-beam acceleration (TBA) scheme [2, 3]. Over the last few years, AWA has increased its focus on developing methods to control bright beams [4]. Correspondingly, the AWA accelerator will be upgraded to enable the generation of low-emittance, low-charge electron beams.

LOW-ENERGY SECTION UPGRADE

The AWA drive-beam linac comprises a $1 + \frac{1}{2}$-cell 1.3-GHz RF gun surrounded by three solenoidal lenses, followed by a linac consisting of seven 1.3-GHz 7-cell standing-wave structures [1]. The low-energy section upgrade is primarily driven by the installation of a symmetrized RF gun to reduce the time-dependent kick produced by the sided input-power coupler. The kick is responsible for emittance growth and possible coupling as it occurs in a region with an axial magnetic field produced by solenoid lenses. In this report, we investigate possible configurations for one of the solenoid lenses (the "matching" solenoid located downstream of the RF gun) constrained by mechanical assembly and real-estate requirements and motivated by improving the beam brightness. Both the low- and high-charge regimes are explored and trade-off between the different designs are considered. In its current configuration, the "matching" solenoid installed immediately downstream of the RF gun has two iron plates fastened on each side to reduce the magnetic field fringe field while accommodating constraints that came from the beamline itself. However, these metallic plates generate a non-cylindrically symmetric magnetic field that negatively impacts the beam dynamics. The motivation behind the change in the solenoid design is to eliminate this field asymmetry and to possibly change the position of the solenoid. Two new solenoid designs were considered for this upgrade. One of the designs ("Design 1") is similar to the solenoid that is currently installed at AWA - the only difference being that the metal plates are removed. Due to the size of the bore, this solenoid is constrained to one position on the beamline (0.273 m downstream of the photocathode). The other design ("Design 2") has a larger bore which allows the position of the solenoid center to vary within $z_s \in [0.273, 0.330]$ m from the photocathode. The corresponding axial magnetic fields $B_z(r = 0, z)$ appear in Fig. 1(a).

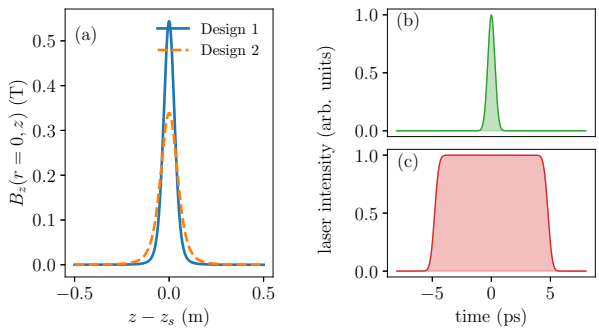

Figure 1: Comparison of the axial field produced by the two matching solenoid designs (a) and laser temporal profile for the Gaussian "1G" (b) and flat top "FT" (c) distributions.

SIMULATIONS & OPTIMIZATION

The goal of the optimization is to understand the trade-off between the transverse emittance $\varepsilon_\perp$ and rms energy spread σ_E. Given that AWA does not include any compression scheme, these two parameters are the most relevant to a number of applications often considered at AWA. Low-

* eframe@anl.gov

ISBN: 978-3-95450-227-1 ISSN: 2673-5490 doi:10.18429/JACoW-IPAC2022-WEPOTK001

STATUS OF THE NORMAL CONDUCTING LINAC AT THE EUROPEAN SPALLATION SOURCE

C. Plostinar*, C. Amstutz, S. Armanet, R. Baron, E. Bergman, A. Bhattacharyya, B. Bolling, W. Borg, S. Calic, M. Carroll, J. Cereijo Garcia, J. Christensson, J. Christie, H. Danared, C. Derrez, I. Kittelmann, E. Donegani, S. Ekström, M. Eriksson, M. Eshraqi, J. Esteban Müller, K. Falkland, A. Forsat, S. Gabourin, A. Garcia Sosa, A. Gorzawski, S. Grishin, P. Gustavsson, W. Hees, M. Jensen, B. Jones, S. Haghtalab, V. A. Harahap, H. Hassanzadegan, J. Jamroz, A. Jansson, M. Juni Ferreira, M. Kalafatic, H. Kocevar, S. Kövecses, E. Laface, B. Lagoguez, Y. Levinsen, M. Lindroos, A. Lundmark, M. Mansouri, C. Marrelli, C. Martins, J. Martins, S. Micic, N. Milas, R. Miyamoto, M. Mohammednezhad, R. Montano, M. Munoz, G. Mörk, D. Nicosia, B. Nilsson, D. Noll, A. Nordt, T. Olsson, N. Öst, L. Page, D. Paulic, S. Pavinato, S. Payandeh Azad, A. Petrushenko, J. Riegert, A. Rizzo, K. Rosengren, K. Rosquist, M. Serluca, T. Shea, A. Simelio, S. Slettebak, H. Spoelstra, A. Svensson, L. Svensson, R. Tarkeshian, L. Tchelidze, C. Thomas, E. Trachanas, P. van Velze, K. Vestin, R. Zeng, ESS, Lund, Sweden
A.C. Chauveau, P. Hamel, O. Piquet, CEA, Saclay, France
I. Bustinduy, A. Conde, D. Fernandez-Cañoto, N. Garmendia, P.J. Gonzalez, G. Harper, A. Kaftoosian, J. Martin, I. Mazkiaran, J.L. Munoz, A.R. Páramo, S. Varnasseri, A. Zugazaga, ESS-Bilbao, Bilbao, Spain
L. Antoniazzi, C. Baltador, L. Bellan, T. Bencivenga, M. Comunian, E. Fagotti, L. Ferrari, M. Giacchini, F. Grespan, P. Mereu, C. Mingioni, M. Montis, M. Nenni, L. Neri, E. Nicoletti, A. Palmieri, A. Pisent, D. Scarpa, INFN, Italy

Abstract

The construction of the European Spallation Source (ESS) accelerator is in full swing. Many key components have been delivered from our in-kind partners and installation, testing and commissioning is making remarkable progress. The first machine section to be commissioned with beam is the Normal Conducting Linac (NCL). When completed, a 14 Hz, 2.86 ms proton beam up to 62.5 mA will be transported from the Ion Source (IS), through the Low Energy Beam Transport (LEBT) line, the Radiofrequency Quadrupole (RFQ), the Medium Energy Beam Transport (MEBT) line and the five Drift Tube Linac (DTL) tanks up to 90 MeV where it will be injected in the first superconducting module of the machine [1]. This paper will highlight recent progress across the NCL, present briefly the first commissioning results and discuss the upcoming phases as well as challenges in delivering a machine capable of meeting the requirements for a next generation spallation neutron facility.

NCL DESCRIPTION

The world's most powerful linear accelerator is currently under construction in Lund, Sweden. At full completion, a 62.5 mA proton beam at 14 Hz and 2.86 ms will be accelerated up to 2 GeV. The resulting average beam power of 5 MW will be used to drive the production of spallation neutrons, enabling ESS to become a flagship research facility and to carry out world class science. While progress is being made across the board, from accelerator to target and neutron instruments [2], the NCL is the first section of the machine to transition from installation to integrated testing and commissioning with beam.

IS and LEBT

The NCL starts with a microwave discharge ion source producing a 75 keV proton beam that is further transported through the LEBT. The LEBT is a transport channel consisting primarily of two magnetic solenoids with steerers, an electrostatic chopping system, an iris, two repellers, a collimator and an extensive suite of diagnostics (Faraday Cup – FC, Beam Current Monitors – BCMs, Allison Scanner Emittance Measurement Unit – EMU, Beam Induced Fluorescence Non-Invasive Profile Monitor – NPM and a Doppler-shift spectroscopy system). The IS and the LEBT are in-kind contributions from INFN Catania in Italy.

RFQ

After the LEBT, a 4.6 m long, four-vane RFQ operating at 352.21 MHz, bunches and accelerates the beam up to 3.62 MeV. A BCM measures the beam current at the end of the RFQ. The RFQ is an in-kind contribution from CEA in France, while its RF system was provided by ESS-Bilbao in Spain.

MEBT

The subsequent MEBT is a transport line intended to match the beam to the DTL and consists of 11 quadrupoles with steerers, three buncher cavities, a fast chopping system, collimators and additional diagnostics to further characterise

* ciprian.plostinar@ess.eu

ISBN: 978-3-95450-227-1 ISSN: 2673-5490 doi:10.18429/JACoW-IPAC2022-WEPOTK002

INVESTIGATION, SIMULATION AND FIRST MEASUREMENTS OF A 2M LONG ELECTRON COLUMN TRAPPED IN A GABOR LENS DEVICE

K. I. Thoma*, M. Droba, O. Meusel, Goethe Universität Frankfurt am Main, Germany

Abstract

Various Gabor-Lenses (GL) were investigated at Goethe University. Confinements of sufficient electron densities ($n_e \sim 1 \cdot 10^{15}\,m^3$) were reached without any external source of electrons. Focusing of ion beams by low energy was demonstrated, long term stability and reproducibility were approved. Main differences compared to experiments and investigations of the pure non-neutral in Penning-Malmberg traps [1] are higher residual gas pressure and therefore higher collision rates, higher bulk temperatures, self-sustaining electron production process, much higher evaporation cooling rate. GL2000 is a new 2 m long device and was mainly designed for focusing of ion beams in energy ranges up to GeV but also for investigation of non-neutral plasma parameters. The confined electron column is much longer compared to previous constructed Lenses. This makes ion and hadron beam focussing much more efficient, in addition new physical phenomena can be expected and investigated. Simulation results of steady- and thermal equilibrium states with various external parameters and first measurements will be presented. The first operational tests show that it is possible to confine a two-meter long electron column.

INTRODUCTION

The Gabor-Lens (GL) [2], is an optical device used for focusing or defocusing of charged particle beams by a trapped electron column. Recently, an overview over a wide range of space charge lenses was given by Alexey Goncharov [3]. In a Gabor-Lens the radial confinement is provided by an axial magnetic field produced by coils. The longitudinal confinement is given by a potential well generated by a system of electrodes in axial direction. The electron cloud is created due to rest gas ionization inside the lens, it does not need any external source for the electron production, like other traps for example the Penning trap. The confined electron cloud fulfills plasma criteria for collective behaviour in many cases (Debye screening, number of particles in Debye-sphere, plasma frequency) it can be described as a non-neutral plasma [4]. Over recent years various GLs were systematically investigated at Goethe University. Confinement of sufficient electron density ($n_e \sim 1 \cdot 10^{15}\,m^{-3}$) was reached without any external source of electrons. Focusing of light and heavy ion beams by low energy was demonstrated, long term stability and reproducibility were approved. Thick aperture lenses were built and successfully tested [5]. Diagnostic methods based on optical detection, X-ray detection, RF-detection, rest gas monitor and spectrometer were developed and used for characterization of different non-neutral plasma states [6]. Experiments with GL as a focusing device and as an electron target for low energy ion beams were carried out to examine interactions between beam ions and electron cloud [7]. The confinement of an electron column in a toroidal configuration was also tested [8]. The radius r to length l ratio was subsequently changed from device to device. The focal length, chromatic aberrations of the lens as well as the charge exchange and charge recombination rates need to be investigated in the future.

The electron temperatures ranged typically from 10 eV to 1000 eV in these experiments, Debye lengths were calculated therefore between 1 mm and 10 cm with a typical cloud radius between 1-10 cm dependent on used external parameter settings (anode voltage, magnetic field, residual gas pressure).

MOTIVATION

With the new device GL2000, built in 2019, an aspect ratio of r/l = 0.0375 is realized. To our knowledge, this is the lowest aspect ratio with longest overall on-axis distance of about two meters designed to date. The focal length f of a Gabor-Lens is inversely proportional to its length [4].

$$\frac{1}{f} = k^2 \cdot L = \frac{q n_e}{4\varepsilon_0}\frac{L}{W_b}, \qquad (1)$$

where k is the focusing strength, L the length of the device and W_b in eV is the energy of the beam.

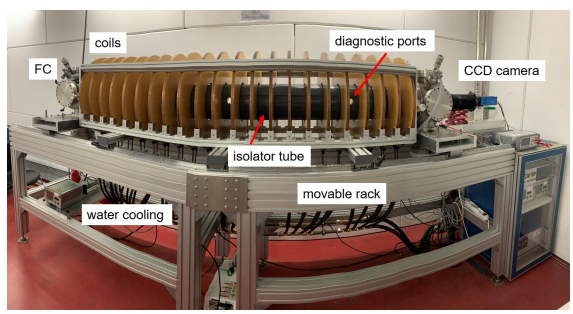

Figure 1: Setup of the experiment GL2000 in a concrete shielding.

For a given electron density $n_e \sim 1 \cdot 10^{15} m^{-3}$ GL2000 can be used for the focusing of ion beams with higher kinetic energy W_b compared to previous experiments. Further the focusing of relativistic (W_b in GeV range) highly charged ion beams can be studied and arrays of GL2000 applied as a final focus for fixed target experiments as discussed in NA61/Shine Collaboration at CERN [9]. It also enables

* thoma@iap.uni-frankfurt.de

ISBN: 978-3-95450-227-1 ISSN: 2673-5490 doi:10.18429/JACoW-IPAC2022-WEPOTK003

STATUS OF THE DEVELOPMENT OF THE ELECTRON LENS FOR SPACE CHARGE COMPENSATION AT GSI*

K. Schulte-Urlichs† [1,2], M. Droba[2], T. Dönges[2], O. Meusel[2], D. Ondreka[1], H. Podlech[2], P. Spiller[1], K. Thoma[1,2],
[1]GSI Helmholtzzentrum für Schwerionenforschung, Darmstadt, Germany
[2]Goethe-University Frankfurt, Frankfurt, Germany

Abstract

At GSI a prototype electron lens for space charge (SC) compensation is currently being designed and main components as the RF-modulated electron gun are already under commissioning. The goal of this project is the (partial) compensation of SC forces within the ion beam by an overlapping electron beam. This may help to increase the intensity of primary beams, especially in the FAIR facility and potentially all large synchrotrons operated at the SC limit. For an effective SC compensation, the generated electron beam needs to follow the transverse and longitudinal beam profile of the ion bunch structure. The requirements are maximum currents of 10 A and grid modulation to cover a broad frequency range from 400 kHz to 1 MHz. The RF-modulated electron gun was designed and manufactured in the scope of the ARIES collaboration and is currently being tested at the E-Lens Lab of Goethe University Frankfurt. A dedicated test bench was built for commissioning of the major e-lens components and diagnostics. In this contribution the overall set-up will be presented putting special emphasis on the beam dynamics and collector design as well as simulation results of the electron gun.

INTRODUCTION

The prototype electron lens for space charge compensation is being designed for the integration into the SIS18 and potentially the SIS100 synchrotron at GSI/FAIR. However, the SIS18 will serve as testbed to demonstrate the space charge compensation scheme and the electron lens with an interaction length of 3.36 m will be installed in one of the available drift sections [1]. The SIS18 ion beam has an elliptical cross section over the length of the interaction region and has to be transversally embedded into a homogeneous electron beam while the pulse needs to be exactly matched to the bunch form in order to avoid over-compensation of the bunch head and tail as presented in [2]. During acceleration of the ion beam the SC tune spread reaches its maximum. Therefore, the prototype electron lens shall support operation within the ramp leading to high requirements on frequency and bandwidth of the e-gun modulator.

A modulated electron gun was designed based on the parameters of the SIS18 and constructed in the scope of the ARIES collaboration WP16 [3]. In the course of this project, a test stand at Goethe-University Frankfurt was build to commission the gun. But it will also serve as test bench for further e-lens components as well as the diagnostics. In the following the status of test stand and the electron lens development with its underlying components will be presented.

ELECTRON LENS DESIGN AND BEAM DYNAMIC STUDIES

The space charge compensation (SCC) electron lens for SIS18 is currently designed at GSI and a 3D model of the actual, integrated layout is presented in Fig.1.

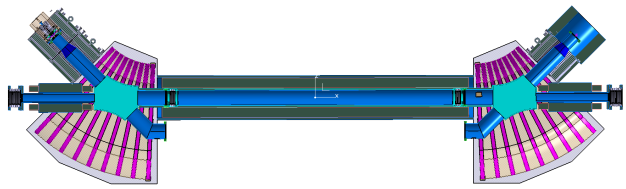

Figure 1: Preliminary 3D model of the SCC electron lens.

The layout of the magnetic system comprises two identical solenoids in the gun branch, two solenoids in the collector branch, two toroids, a main solenoid as well as two correction dipoles, all covered in an iron housing. It has been designed for a maximum longitudinal field of 0.6 T. As a result of the vertical field of the toroids two corrector dipoles are required to compensate the deflection of the ion beam. Due to lack of space in the synchrotron, the dipoles are integrated into the toroids but are positioned not to affect the electron trajectories.

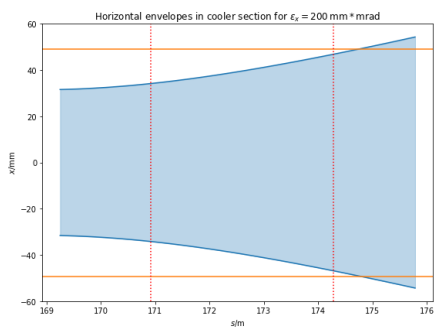

Figure 2: Calculated ion beam envelopes in the interaction section of the SCC electron lens. The red lines mark the interaction region, while the yellow lines represent the required horizontal size of the electron beam.

* Work supported from the European Union's Horizon 2020 Research and Innovation Program under Grant Agreement No 73087.
† k.schulte-urlichs@gsi.de

ISBN: 978-3-95450-227-1 ISSN: 2673-5490 doi:10.18429/JACoW-IPAC2022-WEPOTK004

STATUS AND UPGRADE PLAN OF THE MR RING RF SYSTEMS IN J-PARC

K. Hasegawa*, K. Hara, C. Ohmori, Y. Sugiyama, M. Yoshii, M. Nomura, H. Okita, T. Shimada, F. Tamura, M. Yamamoto, KEK and JAEA J-PARC, Tokai, Japan

Abstract

The J-PARC Main Ring (MR) is a high intensity proton accelerator and delivers 30 GeV proton beams for the long-base line neutrino experiment and the hadron experiments. At present, the beam intensity supplied to the neutrino experiment reached 520 kW with a cycle time of 2.48 s. Toward the design beam power of 750 kW and future goal of 1.3 MW, we chose shortening the MR operation cycle. Accelerating time is shortened in order to shorten the cycle, so a high accelerating voltage is required. Therefore, it is necessary to upgrade the RF systems. This RF upgrade expands the current nine RF systems to a total of thirteen. We are planning to fabricate four RF power sources and add four additional cavities that are recombined with existing cavities. The present status and upgrade plan of the MR RF systems are reported.

INTRODUCTION

The J-PARC facility is a high intensity proton accelerator and consists of a 400 MeV Linac, a 3 GeV rapid cycling synchrotron (RCS) and a 30 GeV main synchrotron (MR). In the MR, injected the proton beams from the RCS are accelerated from 3 GeV to 30 GeV and delivered to the neutrino experiment (T2K) in a fast extraction mode (FX) and to the hadron experimental facility in a slow extraction mode (SX). The current achieved beam power is 510 kW at 2.48-s cycle time in FX and 60 kW at 5.2-s cycle time in SX. In order to achieve the designed beam power of 750 kW and the future target power of 1.3 MW for the Hyper Kamiokande experiment (HK), high repetition cycle in MR was selected. It is planned to replace the main magnet power supplies. In this upgrade plan, the required accelerating voltage for the RF system is 510 kV or higher for the 750 kW and 600 kV or higher for the 1.3 MW. In order to achieve this required voltage, we have developed and mass-produced new magnetic alloy material core (FT3L), which has more than twice the impedance characteristics of the FT3M core that has been used since the beginning of operation [1, 2]. New 4-gap or 5-gap high accelerating field gradient cavities with FT3L cores were also developed [3] and we replaced all nine original 3-gap cavities with FT3M between 2014 and 2016. At present, the 9 RF systems, 7 systems for the acceleration and 2 systems for the 2^{nd} harmonic system, are operating without serious troubles.

MR RF SYSTEM CONFIGURATION

In operation after June 2022, when the magnet power supplies will be replaced, the operation cycle time will be reduced from 2.48 s to less than 1.36 s, and the accelerating time will be reduced from 1.4 s to 0.65 s. As a result, the required accelerating voltage will increase from 280 kV to 510 kV or higher. It is necessary to use all nine existing FT3L cavities as fundamental cavities for acceleration, and two new 2^{nd} harmonic RF systems are required. In addition, to achieve 1.3 MW, the cycle time and accelerating time will be 1.16 s and 0.58 s, respectively. And the required accelerating voltage will be 600 kV or higher. In this case, two more high accelerating field gradient system would be added for a total of 11 accelerating RF systems [4].

Upgrade of Anode Power Supplies

The anode power supply (APS) that supplies power to a final stage amplifier for driving a cavity consists of 15 inverter units and its current limit is 110 A. Figure 1 shows the measured peak anode current of the APS versus the number of circulating protons. The expected maximum number of circulating protons in a APS with 15 inverter units is 2×10^{14} protons per pulse (ppp) for a 5-gap cavity and 2.8×10^{14} ppp for a 4-gap cavity. At present, beam power of 520 kW in FX mode is now achieved with a 2.7×10^{14} ppp at 2.48-s cycle time. The design beam power of 750 kW can be reached at 2×10^{14} ppp for a 1.28-s cycle, which is below the current limit of the APS. However, to achieve 1.3 MW, 3.3×10^{14} ppp at 1.16-s cycle time is required, which exceeds the APS current limit of 110 A. This requires an increase in the output current capacity of the APS by adding inverter units. For a 4-gap cavity, this can be achieved with the APS with 19 inverters units by adding 4 inverter units (Fig. 2). However, 3 of 9 existing APS cannot add inverters due to the

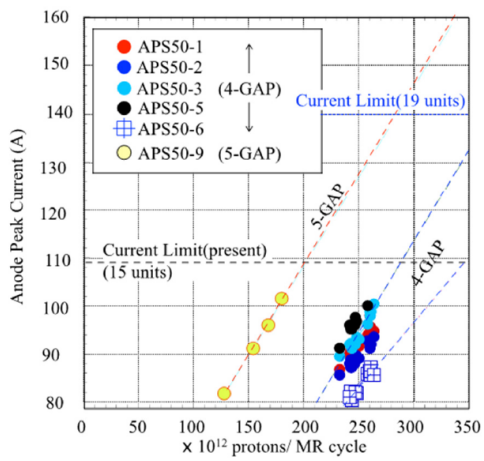

Figure 1: The measured peak anode current of the APS versus the number of circulating protons.

* katsushi.hasegawa@kek.jp

ISBN: 978-3-95450-227-1 ISSN: 2673-5490 doi:10.18429/JACoW-IPAC2022-WEPOTK005

ELECTROMAGNETIC ANALYSIS OF A CIRCULAR STORAGE RING FOR QUANTUM COMPUTING USING Vsim

S.I. Sosa*, S.G. Biedron[1,2], T. Bolin[2], Department of Electrical and Computing Engineering,
University of New Mexico, Albuquerque, NM 87131, USA
B. Huang, Department of Applied Mathematics and Statistics,
Stony Brook University, Stony Brook, NY 11794, USA
K. Brown[3], Collider Accelerator Department,
Brookhaven National Laboratory, Upton, NY, 11973, USA
[1] also at Department of Mechanical Engineering,
University of New Mexico, Albuquerque, NM 87131, USA
[2] also at Element Aero, Chicago, IL 60643, USA
[3] also at Department of Electrical and Computer Engineering,
Stony Brook University, Stony Brook, NY 11794, USA

Abstract

We discuss design considerations for a circular ion trap based on electromagnetic and particle beam simulations. This is a circular radiofrequency quadrupole (rfq) being designed for quantum information applications. The circular rfq should have good electromagnetic properties to accumulate and store the beam for prolonged times, while providing apertures for laser cooling and lower voltage electrodes to provide control over the beam. We use the electromagnetic and particle-in-cell software VSim, which uses finite difference time-domain and particle-in-cell methods, together with high performance computing tools

INTRODUCTION

Trapped ions are a useful research tool enabled by electromagnetic ion traps [1–3]. Ion traps are devices that use electromagnetic fields and lasers to control and manipulate individual or bunched ions [4]. In the same fashion, storage rings use electromagnetic fields to store beams of charged particles in a closed path. We are building upon the idea of using a compact circular storage ring for quantum computing applications [5]. The storage ring quantum computer (SRQC) is an ion trap concept in a rotating frame. This main difference from most conventional ion traps [1–3] allows to potentially store orders of magnitude more ions, which presents interesting possibilities for quantum information technologies. Together with the unprecedented number of ions that can be stored in a device like SRQC, and the possibility of storing multiple ion chains for parallel quantum computing, the use of ions as qubits allows for longer coherence times. Quantum decoherence is one of the main limitation of the current state of quantum technologies.

Ion Crystals for Quantum Computing

The dynamics of individual ions in the beam is driven by the trap produced fields and by Coulomb forces. For the SRQC application, the beam thermal energy needs to be sufficiently reduced to a level where internal and external quantum states of individual ions can be measured. Once an ion beam is stored in the SRQC, controlled laser pulses can be directed into the device for cooling via Doppler cooling [6]: ions absorb and re-emit photons of specific frequencies, resulting in a lower energy-state of the ion [4]. By sequentially cooling the beam below the Doppler limit, the thermal motion of the beam gets reduced and the Coulomb interaction becomes the dominant inter-ionic force. Ions arrange themselves into a crystalline beam state [7], where they oscillate around their equilibrium positions. If the crystalline beam is further cooled so that phonon modes can be measured, an Ion Coulomb Crystal (ICC) state can be formed. The SRQC concept is based on using the external and internal quantum states of ICC as qubits, where the internal modes are the hyperfine spin states and the external modes are the phonon modes of the ICC [5].

Because of the unprecedented number of ions[1] that can be potentially trapped in the SRQC, the controls engineering concerns need to be studied for SRQC from conception. We recently explored applications of Artificial Intelligence (AI) into the control of an ICC [8], in particular to determining the equilibrium positions of ions in a 1D ICC. We are exploring similar techniques for the accurate timing of laser pulses to the specific cooling needs of the ICC.

The use of a storage ring for trapping an ion crystalline beam was investigated before. The experiment, PAul Laser cooLing Accelerator System (PALLAS), stored beams of $^{24}Mg^{+}$, and cooled it enough to produce a crystalline beam [9]. For the SRQC, we aim at producing Ion Coulomb Crystals.

EM SIMULATIONS WITH VSIM

We use VSim [10, 11] for the electromagnetic analysis of an SRQC trap concept. The SRQC concept has two pairs of inner electrodes to tailor a quadrupolar electric field that

* salvadorsg@unm.edu

[1] Conventional ion traps usually manipulate a few dozen ions.

ISBN: 978-3-95450-227-1 ISSN: 2673-5490 doi:10.18429/JACoW-IPAC2022-WEPOTK006

PROTON BEAMLINE SIMULATIONS FOR THE HIGH INTENSITY MUON BEAMLINE AT PSI

M. Haj Tahar*, D. Kiselev, A. Knecht, D. Laube, D. Reggiani, J. Snuverink, V. Talanov
Paul Scherrer Institut, 5232 Villigen PSI, Switzerland

Abstract

The High Intensity Proton Accelerator (HIPA) cyclotron at the Paul Scherrer Institut (PSI) delivers 590 MeV CW proton beam with a maximum power of 1.42 MW. After extraction, the beam is transferred in a 120 m long channel towards two target stations (TgM and TgE) before depositing its remaining power at the spallation target SINQ for neutron production. As part of the High Intensity Muon Beamline (HIMB) feasibility study, which belongs to the IMPACT (Isotope and Muon Production using Advanced Cyclotron and Target technologies) initiative, the first of these targets will be replaced with a thicker one and its geometry optimized thereby specifically boosting the emission of surface muons. In order to assess the impact of the changes on the proton beamline, BDSIM/GEANT4 simulations were performed with the realistic technical design of the target insert, the collimation system was redesigned and the power depositions were benchmarked with MCNP6. In this paper, we discuss the major changes and challenges for HIMB as well as the key considerations in redesigning the optics of the high power beam in the vicinity of the target stations.

INTRODUCTION

The High Intensity Proton Accelerator (HIPA) complex at PSI is in operation since 1974, with several major upgrades enabling a maximum beam power of 1.42 MW [1]. To keep HIPA at the forefront of intensity frontier research, the IMPACT project [2] was recently proposed by the Paul Scherrer Institut (PSI), the University of Zurich (UZH), and the University hospital of Zurich (USZ). The project aims to construct two new target stations and beamlines at PSI. One of these target stations, the focus of the present paper, aims to increase the rate of surface muons by two orders of magnitude ($\sim 10^{10}\mu^+/s$), hence the name High Intensity Muon Beams (HIMB).

To achieve the goals for HIMB, the 5 mm Target M (TgM) [3] will be replaced with a newly designed Target H (TgH) such that the effective thickness of the target is increased to 20 mm, and its geometry as well as the connected beamlines optimized to enable two orders of magnitude increase in the rate of transmitted surface muons ($\sim 10^{10}\mu^+/s$) [2, 4]. As a consequence, the larger divergence induced by the thicker TgH shall lead to increased primary beam losses. Thus, the present paper discusses the main changes and challenges of replacing TgM with the thicker TgH from the point of view of the primary proton beamline.

* malek.haj-tahar@psi.ch

DESIGN CONSIDERATIONS

Owing to the complicated nature of the problem, which requires particle tracking simulations in electromagnetic fields, as well as the accurate simulation of the interaction processes between the high power beam and the beamline components, benchmarking the optics is a crucial task. For this reason, the Beam Delivery Simulation (BDSIM) is chosen as the reference program for all calculations [5]: BDSIM combines particle accelerator tracking routines with the standard high energy physics code GEANT4 [6]. The optics shall be benchmarked against TRANSPORT [7], MAD-X [8] and ZGOUBI [9] while the interaction processes shall be benchmarked against MCNP6 [10]. The latter will be discussed in the present paper. However, the interested reader is referred to the IMPACT Conceptual Design Report for further details [2]. Furthermore, to establish the validity of the developed simulation tools, an experimental campaign was performed to benchmark the existing MW-class beamline with various measurements [11].

The purpose of the transport channels is to transport the high power beam with minimum losses towards each target and to produce optimum matching conditions suitable for both the primary and the secondary beamlines.

Upstream of TgH the optics shall not experience any important change with the beam maintaining the same properties. The only exception to this is the addition of one vertical steerer magnet and the replacement of the existing one as illustrated in Fig. 1. This is justified as follows: TgH is surrounded by two capture solenoids producing a non negligible fringing field in the transverse X-direction. Such field component, if uncorrected, will alter the beam trajectory in the vertical plane. For flexibility reasons, the worst case scenario is treated in which both solenoids have the same polarity so that their stray fields add-up at TgH. In order to limit and compensate for the impact of the capture solenoids' stray fields on the proton beam, we proceed as follows:

1. Placing mirror plates adjacently to the solenoid entrances (from the viewpoint of the target) allows to reduce the fringing field extent, i.e., the field integral seen by the primary beam, by 30%. A mirror plate thickness of 40 mm is chosen to achieve this as a trade-off between the space constraint in the target region and the effectiveness of the plates to reduce the stray fields while being cooled.

2. A full cancellation of the impact that the remaining fringing field will have on the primary proton beam trajectory after the target, is possible by means of two vertical steering magnets. These are placed upstream of

ISBN: 978-3-95450-227-1 ISSN: 2673-5490 doi:10.18429/JACoW-IPAC2022-WEPOTK007

SIMULATING QUASI-INTEGRABLE OPTICS WITH SPACE CHARGE IN THE IBEX PAUL TRAP*

J. A. D. Flowerdew†, S. L. Sheehy[1], University of Oxford, Oxford, UK
D. J. Kelliher, S. Machida, STFC Rutherford Appleton Laboratory, Oxford, UK
[1]also at University of Melbourne, Victoria, Australia and ANSTO, Sydney, Australia

Abstract

The intensity frontier has called for new initiatives in hadron accelerator design in order to accommodate space charge dominated beams. Octupoles are often used to damp beam instabilities caused by space charge, however the insertion of octupole magnets leads to a nonintegrable lattice which reduces the area of stable particle motion. One proposed solution is Quasi-Integrable optics (QIO), where the octupoles are inserted between sections of a specific lattice insertion called a T-insert. An octupole with a strength that scales as $1/\beta^3(s)$ is applied in the drift region, where the horizontal and vertical beta functions are equal, to create a time independent octupole field. This leads to a lattice with a time-independent Hamiltonian which is robust to small perturbations. IBEX is a Paul trap which allows the transverse dynamics of a collection of trapped particles to be studied, mimicking the propagation through multiple quadrupole lattice periods, whilst remaining stationary in the laboratory frame. In order to test QIO at the IBEX experiment, it has recently undergone an upgrade to allow for the creation of octupole fields. We present our design of the IBEX experiment upgrade along with simulation results of our proposed experiment to test QIO with space charge.

INTRODUCTION

Space charge forces are the result of Couloumb interactions between charged particles in a beam. As higher intensity accelerators are being designed and built, resonances and instabilities caused by space charge can become the limiting factor in the intensities these machines can reach. Building test accelerators to study high intensity beams can be costly and, when carrying out beam loss studies, accelerator components can be activated and damaged. Therefore, simulations are a vital part of the accelerator design process, however they are computationally intensive when reproducing space charge forces over long timescales (tens of thousands of turns) and can never be a replacement for experimental verification.

These challenges led to the design and construction of linear Paul traps to investigate transverse beam dynamics more efficiently at Hiroshima University, Japan [1], Princeton University, US [2] and, most recently, the Intense Beams Experiment (IBEX), at the Rutherford Appleton Laboratories (RAL), UK [3]. IBEX is a table-top sized experiment that can replicate the transverse betatron motion in alternating gradient accelerators in a dispersion- and chromaticity-free environment.

This paper aims to simulate a lattice proposed by the theory of Nonlinear Integrable Optics (NIO) to damp coherent resonances created by space charge.

THE IBEX PAUL TRAP AND UPGRADE

The IBEX trap was recently upgraded to allow for the excitation of sextupole and octupole fields. The trap consists of two sections, an ionisation region (IR) and an experimental region (ER) as seen in Fig. 1. The design was adapted from the Hiroshima group's nonlinear trap [4]. Argon gas is introduced into the trap vessel and is ionised in the IR with an electron gun. Typically, a sinusoidal RF voltage is applied to the central rods with a maximum peak-to-peak of 300 V and frequency of 1 MHz. Voltages of the same form but opposite polarity are applied to the blue and red outlined rods in Fig. 1 to provide transverse confinement of the ions. Longitudinal confinement of the ions is achieved by applying a DC offset to the end caps and gate electrodes. Once the argon gas is ionised, the DC voltage on the gate is dropped to allow ions to pass into the experimental region.

Adjusting the peak voltage applied to the central rods is analogous to changing the quadrupole strength in an accelerator, which in turn changes the betatron tune in both the horizontal and vertical planes. Ions can be stored for around 1 s in IBEX, corresponding to 10^6 RF periods. Octupole and sextupole fields can be created by applying voltages to the plate electrodes in the ER. The DC voltage on the end caps is then dropped and the ions are directed onto a Micro-Channel Plate (MCP) detector. The number of ions stored in the trap is controlled by adjusting the length of time that the electron gun is on. This allows for a wide range of intensities to be studied within the trap. Due to the low energy of the ions (< 1 eV), high intensity beam loss studies can be carried out in the trap without damaging or activating components.

NONLINEAR INTEGRABLE OPTICS

Current synchrotrons and linacs utilize a system of alternating focusing and defocusing quadrupole magnets that are used to confine a beam of charged particles. The use of linear magnets leads to a Hamiltonian of the system that can be made time-independent and hence integrable. However, in reality these linear lattices are susceptible to perturbations such as magnet errors and space charge forces, and so components such as sextupoles and octupoles are often used to apply higher order corrections. In general, the addition of these nonlinear components creates a non-integrable system,

* Work supported by Royal Society grants
† jake.flowerdew@physics.ox.ac.uk

ISBN: 978-3-95450-227-1 ISSN: 2673-5490 doi:10.18429/JACoW-IPAC2022-WEPOTK008

FUTURE NEUTRINO BEAM STUDIES UNDER THE FRAMEWORK OF PHYSICS BEYOND COLLIDERS

E.G. Parozzi*[1,2,3], A. Baratto[1], J. Bernhard[1], M. Brugger [1], N. Charitonidis[1], A. Longhin[4,5], C. Mussolini[1,6], M. Pari[4,5], F. Pupilli[5], M. Perrin-Terrin[7], Y. Nagai[8], F. Terranova[2,3]
[1] CERN, Geneva, Switzerland
[2] INFN, Sezione di Milano-Bicocca, Milano, Italy
[3] Phys. Dep. Università di Milano-Bicocca, Milano, Italy
[4] Phys. Dep. Università di Padova, Padova, Italy
[5] INFN Sezione di Padova, Padova, Italy
[6] University of Oxford, [OX1 3RH] Oxford, United Kingdom
[7] Aix Marseille Univ, CNRS/IN2P3, CPPM, Marseille, France
[8] Eötvös Loránd University, Budapest, Hungary

Abstract

A Physics Beyond Colliders (PBC) initiative was recently established at CERN to exploit the full scientific potential of its accelerator complex and scientific infrastructure to tackle fundamental open questions in particle physics through experiments complementary to those in current and future colliders. This initiative brings together similar studies to optimize resources globally in order to reach a common goal and promote scientific development more efficiently. In this proceedings, we present the work performed by the Conventional Beam Working Group (CBWG) and specifically from the Neutrino Beams (NB) subgroup. The subgroup currently deals with two novel neutrino-tagged beams projects, ENUBET and NuTAG, as well as with a more conventional, low energy beamline dedicated to hadron cross-sections measurements with the NA61 experiment already installed in the H2 beamline of the CERN North Area. This contribution will detail the advances made with these three projects as well as their status and future plans.

ENUBET

The precision of the measurements of the various neutrino species cross-sections at the GeV scale is mainly limited by the knowledge of the initial flux, which in turn is affected by the uncertainties on hadro-production and particle propagation along the beamline [1]. This limitation leads to a precision of $O(5-10\%)$. Conventional neutrino beams are sources of muon neutrinos originating from pion or kaon decays, mixed with a small fraction of electron neutrinos produced by kaon and muon decays. [2] The ENUBET project (Enhanced NeUtrino BEams from kaon Tagging) aims to develop a facility that produces a beam of electron neutrinos originating from the decays of kaon mesons. The rate of K_{e3} ($K^+ \to \pi^0 e^+ \nu_e$) decay is tagged and monitored in a specially instrumented decay tunnel that tags all neutrinos on an event-by-event basis, in order to improve the precision of the neutrino cross-section measurements by an order of magnitude, reaching an overall precision of 1% [3]. The designed neutrino beam is a narrow-band beam with a short (~ 30 m) transfer line followed by a ~ 40 m long decay tunnel. Secondary kaons produced by the interaction of protons on target are focused, momentum selected and transported at the entrance of the decay tunnel. The electron neutrino flux is subsequently monitored observing the large-angle positrons produced by the decays with a longitudinally segmented calorimeter instrumenting the decay tunnel [4, 5].

Optics

A careful selection and transport of the secondary beam requires a systematic beamline optimization ([6]). Particle collimation, magnets apertures, and magnetic fields define the beamline phase space acceptance. The first order optics optimization has been performed using TRANSPORT [7] and the results have been validated using G4Beamline [8] and FLUKA [9, 10] to simulate re-interactions of stray particles and background inside the instrumented decay tunnel, called the tagger. ENUBET is currently pursuing two different beamline designs: a baseline layout as seen in Fig. 1 designed to transport kaons with an average momentum of 8.5 GeV and a ±20% momentum bite [1], and a "multi-momentum" beamline shown in Fig. 2 that transports secondary particles of 4, 6, and 8.5 GeV/c, with different layout and design, and the purpose to select more than one momentum, allowing the exploration of a larger phase-space of neutrino cross-section measurements, including the region of interest of T2K/HyperK [11, 12].

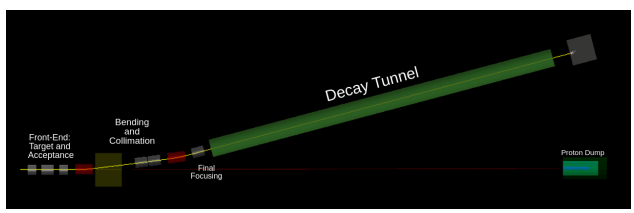

Figure 1: Baseline beamline layout in Genat4.

Both transfer lines have undergone systematic optimization processes, the baseline version using a framework based

* elisabetta.giulia.parozzi@cern.ch, on behalf of the ENUBET collaboration

ISBN: 978-3-95450-227-1 ISSN: 2673-5490 doi:10.18429/JACoW-IPAC2022-WEPOTK009

PROCESSES AND TOOLS TO MANAGE CERN PROGRAMMED STOPS APPLIED TO THE SECOND LONG SHUTDOWN OF THE ACCELERATOR COMPLEX

E. Vergara Fernandez, M. Pirozzi, M. Bernardini, A. Ansel, M. Barberan Marin, S. Chemli, J. Coupard, K. Foraz, D. Hay, J. M. Jimenez, D. J. Mcfarlane, F. Pedrosa, J.Ph. G. L. Tock, CERN, Geneva, Switzerland

Abstract

The preparation and follow-up of CERN accelerator complex programmed stops require clear processes and methodologies. The LHC and its Injectors were stopped in December 2018, to maintain, consolidate and upgrade the different equipment of the accelerator chain. During the Long Shutdown 2 (LS2), major projects were implemented such as the LHC Injectors upgrade and the LHC Dipoles Diodes consolidation. The installation of some equipment for the HL-LHC project took also place. This paper presents the application to the LS2 of the processes and tools to manage CERN programmed stops: it covers the preparation, implementation, and follow-up phases, as well as the KPIs, and the tools used to build a coherent schedule and to follow up and report the progress. The description of the methodology to create a linear schedule, as well as the construction of automatised broken lines and progress curves are detailed. It also describes the organizational set-up for the coordination of the works, the main activities, and the key milestones. The impact of COVID-19 on the long shutdown will be described, especially the strategy implemented to minimise its consequences.

INTRODUCTION

The CERN accelerator complex is compounded by a multidisciplinary set of systems and equipment. Due to the high-level technology required, the Large Hadron Collider (LHC) and its injectors chain (the LINAC 4, the Proton Synchrotron Booster [PSB], the Proton Synchrotron [PS], and the Super Proton Synchrotron [SPS]) have upgraded and consolidated several times during the so-called Programmed Stop periods to reach their current configuration.

A Programmed Stop is the time window where the conditions of the CERN accelerators are dedicated to standard maintenance and/or upgrades. The interventions vary from one programmed stop to another.

According to their duration, four different stops can be defined: Technical Stop (TS), if the duration goes from some hours to a few days; Year-End Technical Stop (YETS) and Extended YETS (EYETS), when the period includes the end of the year and lasts up to 4 months; Long Shutdown (LS), when major changes are implemented, requiring long intervention periods up to a few years.

Outside these periods, the accelerators are operational and exploit their functionality in the so-called Run period.

The execution of a structured and well-defined methodology is crucial to plan a huge number of activities meeting the highest safety and quality standards. We present the methodology followed and the specific tools implemented to coordinate the last Long Shutdown of the CERN accelerator complex (LS2) [1].

LS2 SCOPE

The LS2 [2] started in December 2018 with an initial duration of 2 years for the LHC and 1.5 years for the injectors; a major preparation effort began in 2016, 2 years ahead to optimise time and resources. The time window has been referred to as “the LS2 period”, as shown in Fig. 1.

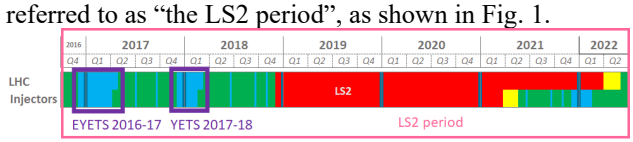

Figure 1: “LS2 period” timeline with the final durations.

The main objectives and challenges of the LS2 included:

- The LHC Injector Upgrade Project (LIU) [3] to increase the intensity and brightness of the injectors to match the LHC High Luminosity Project (HL-LHC) [4] requirements.
- Major maintenances and infrastructure consolidation activities.
- The Consolidation Project to increase the injector reliability and availability for the HL-LHC runs.
- Civil engineering works and beam equipment installation to anticipate the HL-LHC project.

Besides the LS2 original scope, new projects were added: LHC Diode Insulation and Superconducting MAgnet Consolidation (DISMAC) [5] project, SPS Fire Safety, SPS Access and Injectors De-cabling.

LS2 PROCESS: FROM PREPARATION TO EXECUTION

The LS2 management process is based on the previous experience [6] and the know-how of the Organisational, Scheduling and Support section (OSS). The applied methodology was designed to reduce the potential delays due to unexpected events with minimum contingency.

The Long-Term Schedule, the Master Schedule, and the Detailed Linear Planning are three scheduling levels with different granularity and information. While the Long-term schedule, defined a few years before each LS, provides a global overview of the CERN accelerators’ alternation between stops and beam run periods, for the entire accelerator’s lifecycle, as shown in Fig. 1.; the Master Schedule, defined about 2 years before the start, assigns the time dimension, according to the scope defined, as shown in Fig. 2; the Detailed Linear Planning, defined some months

ISBN: 978-3-95450-227-1 ISSN: 2673-5490 doi:10.18429/JACoW-IPAC2022-WEPOTK010

THE SECOND LONG SHUTDOWN OF THE LHC AND ITS INJECTORS: FEEDBACK FROM THE ACCELERATOR COORDINATION AND ENGINEERING GROUP

A. L. Perrot, F. Baltasar Dos Santos Pedrosa, M. Bernardini, S. Chemli, J. - P. Corso, J. Coupard, J. Etheridge, S. Grillot, J. M. Jimenez, K. Foraz, B. Nicquevert, S. Petit, J. - Ph. Tock, E. Vergara Fernandez, CERN, Geneva, Switzerland

Abstract

The operation of the Large Hadron Collider (LHC) at CERN started in September 2008. Every 5 or 6 years, Long Shutdowns (LS) are programmed to execute time-intensive ordinary and extra-ordinary maintenance of the LHC and its injectors. The second LS (LS2) started in December 2018 and was completed end of 2020 for the injectors and early 2022 for the LHC. A huge number of maintenance, consolidation and upgrade activities, especially the upgrade of the injectors complex, were performed with challenges at various levels, from technical, to organizational and managerial.

This paper presents the applied methodology put in place by the Accelerator Coordination & Engineering (EN-ACE) group, in charge of the technical coordination of the activities for the interventions and changes to the LHC and its injectors, to ensure that the installation activities are performed safely, meeting the required high level of quality, while optimizing the schedule. It highlights key points of success and lessons learnt in terms of general coordination, quality assurance, configuration and layout management, spatial integration, planning and scheduling, operational safety, logistics and worksite coordination.

INTRODUCTION

The Accelerator Coordination & Engineering group (ACE) is part of the CERN Engineering Department (EN). They coordinate and optimise the interventions and changes implementation all along the CERN accelerators life cycle. Their expertise cover the configuration & layout management, the spatial integration studies and maintenance of the related 3D-CAD scenes, the organisation and scheduling of the programmed stops, the management of the mid- and long-term schedules, the worksites follow-up, the management of LHC sites, the LHC electrical lock-outs and the operational safety advices. In addition, the ACE group hosts the Accelerator & Technology Sector (ATS) Quality Service, providing support throughout the sector (see Fig.1). The group's priorities are Safety, Quality, Scheduling and Organisation. It is structured to respond to the main requirements for an efficient management of the interventions during accelerators programmed stops.

This paper describes the methodology followed by the EN-ACE group to face the LS2 challenges. It reports key successes and lessons learnt for the future.

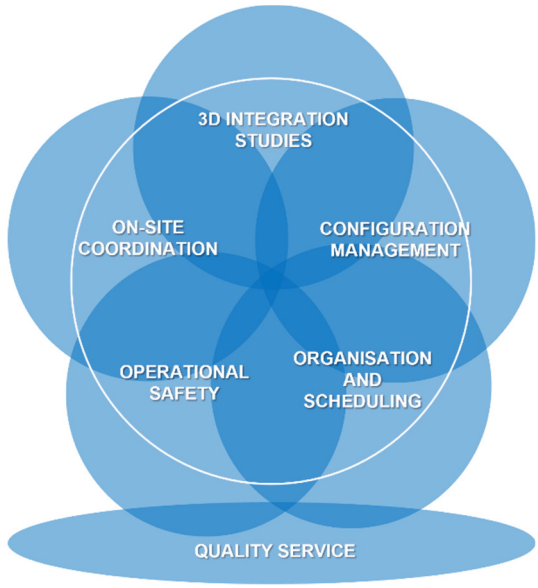

Figure 1: CERN EN-ACE areas of expertise.

METHODOLOGY

The preparation of the LS2 started in 2015, just at the end of the LS1 [1]. The methodology already implemented and recognised for its success during previous programmed stops [2, 3] was applied. From the early stage of the LS2 preparatory phase, strong links with the LS2 executive coordination team, with the main LS2 projects (LHC Injectors Upgrade (LIU), Consolidation, High Luminosity LHC (HL LHC) and Fire safety) and with the equipment owners were established. EN-ACE group members participated to the LS2 coordination team and also served as schedule officers for the main projects. They were giving regular status reports, identifying potential issues as early as possible. It allowed early warnings on difficulties and reactivity in solving them.

KEY POINTS OF SUCCESS

Safety

Safety is the highest priority at CERN and everybody is involved. The following points can be especially mentioned.

During the preparation phase, the Operational Safety Advisors (OSA) analysed the main activities with the relevant stakeholders to define the service to be provided in term of operational safety. This anticipation allowed placing dedicated contracts, to complement the existing team

ISBN: 978-3-95450-227-1 ISSN: 2673-5490 doi:10.18429/JACoW-IPAC2022-WEPOTK011

HIGH INTENSITY STUDIES IN THE CERN PROTON SYNCHROTRON BOOSTER

F. Asvesta*, S. Albright, F. Antoniou, H. Bartosik, C. Bracco, G. P. Di Giovanni,
E. Renner[1], G. Rumolo, P. Skowronski, C. Zannini
CERN, Geneva, Switzerland
[1] also at TU Wien, Vienna, Austria

Abstract

After the successful implementation of the LHC Injectors Upgrade (LIU) project, studies were conducted in the CERN Proton Synchrotron Booster (PSB) in order to assess the intensity reach with the increased beam brightness. The studies focused on the high intensity beams delivered to the PSB users, both at 1.4 and 2 GeV. In addition, possible intensity limitations in view of the Physics Beyond Colliders (PBC) Study were investigated. To this end, various machine configurations were tested including different resonance compensation schemes and chromaticity settings in correlation with the longitudinal parameters. This paper summarizes the results obtained since the machine recommissioning.

INTRODUCTION

During the beam commissioning period following the successful upgrades in the frame of the LIU project [1], the CERN PSB had to demonstrate an improved brightness for the LHC type beams [2], provide beam to high intensity users like ISOLDE [3] and n-TOF [4] and start exploring its intensity reach in the scope of the Physics Beyond Colliders (PBC) study [5, 6]. Limitations towards achieving the high intensities requested by the PSB users are imposed by the betatronic resonances and their interplay with the very strong space charge effects. To this end, extended resonance identification and compensation studies were conducted both before and after the implementation of the LIU project [7–9]. New resonance compensation schemes were developed that allowed reducing losses, however, remaining machine imperfections are still a cause of concern for intensities higher than 800×10^{10} protons per ring (ppr). Extended studies were conducted for ISOLDE trying to correlate losses to beam parameters such as the working point evolution and various mitigation measures were proposed and applied. A new instability was observed for the high intensity users accelerated up to the new extraction energy of 2 GeV, such as TOF. Initial studies revealed the intrabunch motion for this instability and techniques for curing it were applied, allowing normal operations.

RESONANCE COMPENSATION

Resonances up to 4$^{\text{th}}$ order have been identified in the CERN PSB through loss map studies during the first year of operation following the completion of the LIU upgrades.

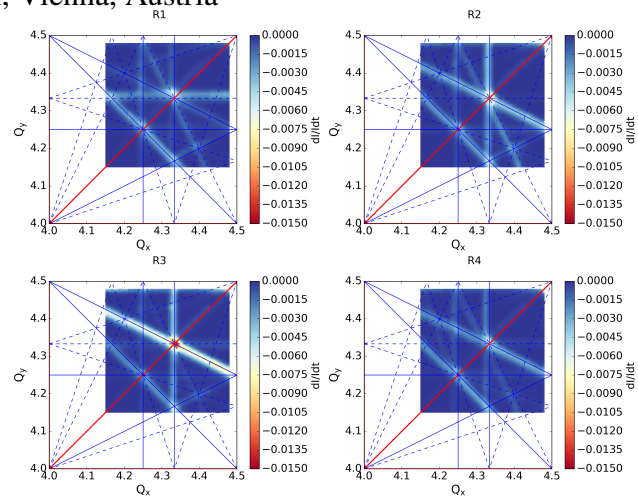

Figure 1: Loss maps resulting from dynamic tune scans in all four rings of the PSB. The tune space is color coded indicating the loss rate, calculated with a sample spacing of 1 ms. Resonance up to 4$^{\text{th}}$ order are plotted, normal in solid lines and skew in dashed. Non-systematic resonance lines are plotted in blue and the systematic in red.

The measurements are conducted using a flat cycle at injection energy, i.e. 160 MeV, in which the beam is stored for an extended period from 275 ms to 700 ms. The loss maps are produced using the dynamic tune scan technique, in which one of the tunes is kept constant throughout the cycle while the other one is varied. The procedure is repeated for all possible configurations, i.e. at first Q_x is kept constant while Q_y initially varies from max to min and then from min to max, and similarly for constant Q_y. The intensity is recorded during the tune change and resonances are revealed through induced losses. A beam with a small space charge tune shift of $\Delta Q_{x,y} = -0.035$ was used to increase the sensitivity of the measurements to machine driven resonances [10]. Figure 1 summarizes the results. All 3$^{\text{rd}}$ order (both normal and skew) and all 4$^{\text{th}}$ order (normal) resonances are excited in all rings. In ring 1 the 3$^{\text{rd}}$ order skew resonances appear stronger while in rings 2, 3 and 4 the normal components are dominant. It should be noted that it was the first time that such a behaviour was observed and the first time that any 4$^{\text{th}}$ order resonances were seen in loss maps in the PSB.

The resonances identified in Fig. 1 were individually compensated using the appropriate corrector magnets. The initial compensation values have been obtained by combining experimental and analytical techniques as discussed in [9]. However, the octupole correctors used for the compensation

* foteini.asvesta@cern.ch

ISBN: 978-3-95450-227-1 ISSN: 2673-5490 doi:10.18429/JACoW-IPAC2022-WEPOTK012

COMMISSIONING THE NEW LLRF SYSTEM OF THE CERN PS BOOSTER

S. Albright*, M. E. Angoletta, D. Barrientos, A. Findlay, M. Jaussi, J. Molendijk,
CERN, Geneva, Switzerland

Abstract

The Proton Synchrotron Booster (PSB) is the first synchrotron in the LHC injection chain and produces beams covering a large parameter space for the LHC and various fixed target experiments. Over Long Shutdown 2 (LS2), the Proton Synchrotron Booster was heavily upgraded as part of the LHC Injectors Upgrade (LIU) project. For the LLRF, the most significant changes are the new Finemet loaded cavities, the new injection mechanism, and the increased injection and extraction energies. The Finemet cavities provide exceptional flexibility, allowing an arbitrary distribution of voltage between harmonics, but at the cost of significant broadband impedance. The new injection mechanism allows bunch-to-bucket multi-turn injection, which significantly reduces the amount of beam loss at the start of the cycle. The longitudinal beam production schema for each beam-type was developed over LS2, and then modified during commissioning to suit the final operational configuration of the machine. This paper discusses the commissioning of the new LLRF, and the consequences of the LIU upgrades on the production of various beams.

INTRODUCTION

Over Long Shutdown 2 (LS2), the CERN PS Booster was heavily upgraded as part of the LHC Injectors Upgrade (LIU) project. The upgrades include a new Finemet based high-level RF system, which provide significant flexibility. To mitigate the effects of the higher cavity impedance, servoloops have been implemented in the Low-Level RF (LLRF) system to suppress the induced voltage, effectively reducing the impedance as seen by the beam.

Despite the impedance reduction provided by the servoloops, the impedance of the cavities at higher frequencies could still have an impact on the beam. Over LS2, new beam production schema were designed for each operational beam, which would utilise the flexibility of the new RF system. These beam production schema are discussed in [1], and they were implemented during beam commissioning in 2021.

NEW HARDWARE AND FUNCTIONALITY

New LLRF Carrier Boards

The PSB LLRF is implemented with Field Programmable Gate Arrays (FPGA) and Digital Signal Processors (DSP) on common carrier boards. For each Finemet cavity a dedicated carrier board is required to control the cavity and implement the servoloops. For each sector, the DSP requests the high-level RF amplifier to switch on, and aborts the cycle if the correct response is not received within a pre-defined timeout. One of the new DSPs receives the phase noise information and propagates it to the other boards for the controlled longitudinal emittance blow-up. Extensive diagnostics on voltage programs at each harmonic as well as detected and drive voltages are also available. A detailed description of the full LLRF system can be found in [2].

Servoloops

Due to the large bandwidth of the new Finemet cavities, significant induced voltage will occur over a large frequency range without feedback. This voltage would both limit the beam stability and significantly distort the driven RF voltage. Therefore, 16 cartesian feedback servoloops are used at revolution frequency harmonics to detect and suppress the induced voltage up to the maximum frequency allowed by the amplifiers (18.5 MHz).

At most harmonics, these servoloops act to force the detected voltage to remain as close to zero as possible. For specified harmonics, typically $h = 1$, $h = 2$ and $h = 10$, the servoloops control the detected voltage in amplitude and phase to follow the programmed values. A detailed description of the implementation and servoloops operation can be found in [3].

Phase noise

Controlled longitudinal emittance blow-up is a vital part of PSB operation both for longitudinal stability and to ensure the required longitudinal emittance at extraction. Prior to LS2, emittance blow-up was achieved with single-tone modulation of a high-harmonic RF system. Equivalent functionality to this has been maintained in the new RF system, however the use of bandwidth-limited phase noise is intended to be the primary operational method.

The suitability of phase noise for PSB operation was demonstrated in [4]. The LLRF system includes a noise buffer, which is populated with a given phase noise function to be applied to the beam. The noise is directly applied to the cavity drive signal in a way that is transparent to the beam phase loop.

Multi-Harmonic Operation

Since the beam in the PSB is space-charge dominated at the start of the cycle [1], it is beneficial to provide the lowest possible line density. Typically, two ($h = 1$ and $h = 2$) harmonics are operated in counter-phase (bunch lengthening mode), which gives a significant reduction in the line density. Thanks to the broadband impedance of the

* simon.albright@cern.ch

ISBN: 978-3-95450-227-1 ISSN: 2673-5490 doi:10.18429/JACoW-IPAC2022-WEPOTK013

DIRECT IMPEDANCE MEASUREMENT OF THE CERN PS BOOSTER FINEMET CAVITIES

S. Albright*, M. E. Angoletta, D. Barrientos, A. Findlay, M. Jaussi, J. Molendijk
CERN, Geneva, Switzerland

Abstract

Over CERN's Long Shutdown 2, the conventional ferrite-loaded cavities of the PS Booster were replaced with wide-band Finemet-loaded cavities. The Finemet cavities bring many operational advantages, but also represent a significant broadband impedance source. The impedance is mitigated by servo loops, which suppress the induced voltage, reducing the impedance as seen by the beam. Accurately including the impedance of the cavity and the effect of the servoloops in longitudinal tracking simulations is essential to predict the performance with beam.

This paper discusses the results of a measurement campaign, which is intended to give a direct measurement of the cavity impedance. Using the detected voltage and the measured beam profile, the cavity impedance can be inferred and used to improve beam dynamics modelling.

INTRODUCTION

The CERN PS Booster is the first synchrotron in the LHC proton injection chain. During Long Shutdown 2 (LS2), significant upgrades were implemented, which included replacing the ferrite-loaded cavities with Finemet-loaded cavities.

In each PSB ring, there are three nominally identical accelerating stations in sectors 5, 7 and 13. Each cavity is composed of 12 cells, which are assumed to have identical impedance. Each cell has a dedicated solid-state amplifier, which includes a fast feedback loop for impedance reduction. The amplifiers drive the two sides of the accelerating gap in anti-phase, causing it to act like a double $\lambda/4$-resonator.

In tracking simulations, an impedance model derived from S-parameter measurements was used. Figure 1 shows the absolute impedance from 0.5 MHz to 100 MHz [1]. The coloured bands in Fig. 1 indicate the frequency range of harmonics 1, 2 and 10, which are the ones most commonly used in operation. This study is focused on the impedance peak at approximately 19 MHz, indicated by the vertical red line in Fig. 1. In simulations, this peak was shown to cause longitudinal instabilities, potentially limiting the intensity reach [2].

The PSB provides beams covering a very large range of intensities with $O(10^9 \rightarrow 10^{13})$ protons per bunch and longitudinal emittances in the range from 0.3 eVs to 3.0 eVs. New beam production schemes, suited to the upgraded RF systems, were designed for the required PSB beam types [3]. During post-LS2 beam commissioning, it was found that the beam stability did not match predictions, therefore the production schemes were adapted [4]. The root causes

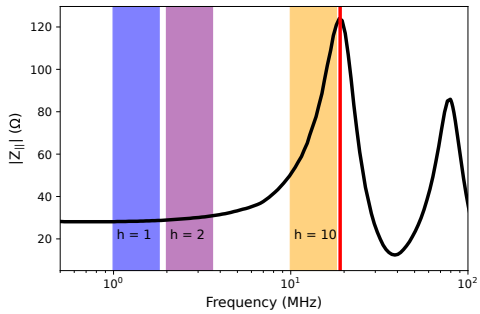

Figure 1: The absolute impedance of a single Finemet cell, the vertical red line is at 19 MHz and the coloured bands indicate the frequency spans of revolution harmonics 1, 2 and 10. Each cell is assumed to be identical in all cavities.

of the discrepancy are still under investigation, but possibly the impedance model applied in simulations is inaccurate. As the Finemet cavities are the dominant longitudinal impedance source, they were the first component to be studied, and this paper describes beam-based measurements of the cavity impedance.

Low Level RF (LLRF) servoloops suppress induced voltage for $h \leq 16$. When the frequency of a harmonic passes 20 MHz, the corresponding servoloop will open [5]. The resulting coupling impedance therefore depends on both the servoloop action and the open loop impedance. During commissioning in 2020, it was found that upgrades to the amplifiers were needed, which would also modify the open loop impedance [6]. For the results presented here, the cavities in sector 5 of all rings were therefore measured with beam in open loop, which includes two cavities with the original amplifiers (rings 1 and 2) and two with the upgraded amplifiers (rings 3 and 4). In the long term, all other sectors will also be measured in this way.

METHOD

Accelerator Configuration

To adequately identify the amplitude and location of the impedance peak, it is essential to maximise the beam power in the relevant frequency range. Therefore, a special beam was prepared to increase the beam power in the 10 MHz to 30 MHz range by adding extra RF voltage at the 10^{th} harmonic. Figure 2 gives the beam spectrum in this range with and without the $h = 10$ contribution, which shows the increased beam power at high frequency.

The voltage in all cells is summed and the result, referred to as the gap return signal, is used for measurements [5]. The

* simon.albright@cern.ch

ISBN: 978-3-95450-227-1 ISSN: 2673-5490 doi:10.18429/JACoW-IPAC2022-WEPOTK014

HADRON STORAGE RING 4 O'CLOCK INJECTION DESIGN AND OPTICS FOR THE ELECTRON-ION COLLIDER

H. Lovelace III*, J.S. Berg, B. Bhandari, D. Bruno, C. Cullen, A. Drees, W. Fischer, F. Micolon, X. Gu, R. Gupta, D. Holmes, R. Lambiase, C. Liu, C. Montag, S. Peggs, V. Ptitsyn, G. Robert-Demolaize, R. Than, N. Tsoupas, J. Tuozzolo, M. Valette, S. Verdu-Andres, D. Weiss
Brookhaven National Laboratory, Upton, NY, USA
T. Satogata, W. Wittmer, Thomas Jefferson National Accelerator Facility, Newport News, VA, USA

Abstract

The Hadron Storage Ring (HSR) of the Electron-Ion Collider (EIC) [1] will accelerate protons and heavy ions up to a proton energy of 275 GeV and Au^{+79} 110 GeV/u to collide with electrons of energies up to 18 GeV. To accomplish the acceleration process, the hadrons are pre-accelerated in the Alternating Gradient Synchrotron (AGS), extracted, and transferred to HSR for injection. The planned area for injection is the current Relativistic Heavy Ion Collider (RHIC) [2] 4 o'clock utility straight section (USS). To inject hadrons, a series of modifications must be made to the existing RHIC 4 o'clock straight section to accommodate 20 new 18 ns injection kickers [3] and a new injection septum, while providing sufficient space and proper beam conditions for polarimetry equipment. These modifications will be discussed in this paper.

INTRODUCTION

The EIC, to be built on the Brookhaven National Laboratory campus, will exceed the capabilities of previous collider beam accelerator facilities by providing center-of-mass energies ranging from 20 GeV to 140 GeV, collisions of both polarized protons and electrons, luminosities to 10^{34}, and a variety of ion species available for collisions with electron beams.

The pre-injector is a 400 MeV linear accelerator (LINAC) that injects into a Rapid Cycling Synchrotron (RCS). The RCS then ramps the polarized electron beam to an energy of 5 GeV, 10 GeV, or 18 GeV. The polarized electron beam is transferred to the ESR [4] at a frequency of 1 Hz. For polarized protons, the HSR pre-injector is the 200 MeV LINAC. The Electron Beam Ion Source (EBIS) will provide heavy ions and polarized He^{+3} for the HSR. The beam is transported through two accelerators, the AGS-booster and the AGS, to the HSR injection energy and extracted through a transfer line to the HSR. Modifications to each of the HSR straight sections will be needed [5]. The injection of the HSR is in the 4 o'clock USS. The beam will then travel counter clockwise around the ring to the cooling section of the 2 o'clock USS [6], the 12 [7] and 10 [8]o'clock switch yards, the 8 o'clock Interaction Region (IR) of another future experiment [9], which is not part of the current EIC scope, and then the 6 o'clock IR [10].

* hlovelace3@bnl.gov

4 O'CLOCK USS

The 4 o'clock USS from the Q10 slot to the Q4 slot magnetic lattice layout will not differ from RHIC.The D9 to D5 are optimized for dispersion matching and the doublets Q5 and Q4 designed for optics matching. The "D" designates a dipole magnet and "Q" a quadrupole. The RHIC triplet quadrupole magnets are preserved while 5 m warm dipoles are used to bend the hadron beam from the outer ring to the inner ring. The change of the position of the downstream warm dipole will cause a transverse shift of the triplet quadrupoles. Twenty injection kickers are located at the center of the 4 o'clock USS with an 8 m gap between the two groups of 10 kickers to allow for the ESR crossover. An injection septum and two warm quadrupoles are also proposed the injection system. Figure 1 is a schematic of the 4 o'clock USS.

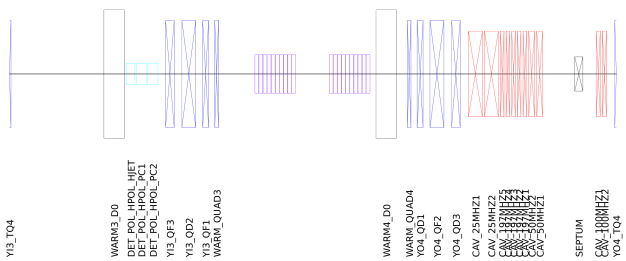

Figure 1: Magnetic lattice of the 4 o'clock USS from outer TQ4 to inner TQ4. The hadron beam travels from right to left.

The 4 o'clock USS contains the normal conduction copper radiofrequency (RF) cavities of the HSR in the same sector of the as the current RHIC cavities. In addition to the two 28 MHz cavities which will be tuned to a frequency of 24.6 MHz and 197.1 MHz cavities, two new RF systems will be added. The HSR will have two adiabatic bunch splittings from the injected 290 bunches to 580 and 1160. This will require the new RF systems of 49.3 MHz and 98.5 MHz.

The absolute polarimeter using a polarized hydrogen jet (H-jet) and two fast proton-carbon (pC) polarimeters will be located in the 4 o'clock USS. For He^+3 polarization measurements, forward taggers required to veto breakup of the He^+3 from the collisions of the H-jet. To separate the breakup products, protons, deuterons, and neutrons, a dipole downstream of the H-jet and allotted space for the taggers is necessary. This requirement is a driver for a 4 o'clock USS lattice configuration where the warm D0 dipole magnets positions

ISBN: 978-3-95450-227-1 ISSN: 2673-5490 doi:10.18429/JACoW-IPAC2022-WEPOTK015

THE ELECTRON-ION COLLIDER HADRON STORAGE RING 10 O'CLOCK SWITCHYARD DESIGN

H. Lovelace III*, J.S. Berg, B. Bhandari, D. Bruno, C. Cullen, A. Drees, W. Fischer, F. Micolon, X. Gu, R. Gupta, D. Holmes, R. Lambiase, C. Liu, C. Montag, S. Peggs, V. Ptitsyn, G. Robert-Demolaize, R. Than, J. Tuozzolo, M. Valette, S. Verdu-Andres, D. Weiss,
Brookhaven National Laboratory, Upton, NY, USA
T. Satogata, W. Wittmer,
Thomas Jefferson National Accelerator Facility, Newport News, VA, USA

Abstract

The Electron-Ion Collider (EIC) [1] Hadron Storage Ring (HSR) will be composed of the current Relativistic Heavy Ion Collider (RHIC) [2] yellow ring sextants with the exception of the 1 o'clock and the 11 o'clock arc. These two arcs use the existing blue ring inner (1 o'clock) and outer (11 o'clock) magnetic lattice for 275 GeV proton operation. The inner yellow 11 o'clock arc is used for 41 GeV energy operation. A switching magnet must be used to guide the hadron beam from the low and high energy arc respectively into the shared arc. This report provides the necessary lattice configuration, magnetic fields, and optics for the 10 o'clock utility straight section (USS) switchyard for both high and low energy while providing the necessary space allocations and beam specifications for accelerator systems such as an additional superconducting radiofrequency cavity and beam dump.

INTRODUCTION

The design of the EIC includes a newly designed electron storage ring (ESR) [3] capable of storing polarized electron beams with energy of 5, 10 or 18 GeV. A Rapid Cycling Synchrotron (RCS) will serve as the injector into the ESR. The RCS will ramp the electron beam from an energy of 400 MeV injection energy up to 18 GeV extraction. A 400 MeV linear accelerator will also be built as the pre-injector to the ESR. The HSR will have newly designed straight sections. The interaction point (IP) at the 6 o'clock location will have a 25 mrad full horizontal crossing angle. Injection will occur in the 4 o'clock USS [4], while the beam cooling systems will be in the 2 o'clock USS [5]. The 12 [6] and 10 o'clock USS will be the area for switching high and low configurations through the use of proposed normal conducting switching dipole magnets. We switch lines to create a shorter path length for the 41 GeV proton beam relative to the 100 and 275 GeV proton beams, so that orbit periods can be made the same at all energies to maintain synchronization with the electron bunches. We also radially shift the hadrons in the HSR arcs to increase or decrease the path length by applying a $\Delta B/B$ to the arc dipoles [7] to optimize the synchronization to the ESR. The 8 o'clock USS will be the location of another future experimental detector [8], which is not part of the current EIC scope.

* hlovelace3@bnl.gov

10 O'CLOCK USS

The 10 o'clock USS will be composed of RHIC insertion quadrupoles with the dispersion matching section D9, Q9, D8, Q8, Q7, D6, Q6, and D5 where "D" designates a dipole magnet and "Q" a quadrupole. The number indicates the slot position decreasing towards the midpoint of the USS. Within the dispersion matching section in the D7 slot of sector 9, a helical dipole snake for spin preservation. The Q5 and Q4 doublet and the Q3, Q2, and Q1 triplet are located in their appropriate slots and are used for β function matching. The TQ6, TQ5, and TQ4 trim quadrupoles are used for additional β function correction. There are four γ transition quadrupoles in slots 6 and 8 for the outer beam line or 5 and 7 for the inner beam line. The RHIC DX magnets, the final beam crossing before collision, will be removed. A 5.2 m superconducting 591 MHz cavity (SRF) will be placed in the 10 o'clock USS. The cavity is half the HSR ring away from the copper warm cavities in the 4 o'clock USS due to the SRF cavities of the ESR and RCS also being in the 10 o'clock region.

The HSR 4.7 m dump will be an internal dump inside the tunnel but outside the vacuum which is designed to handle the a beam current of up to 1 A for protons and 0.57 A for Au^{+79} with a 290 to 1160 bunch train of circulating hadrons. The dump location is approximately 5 m upstream of the CQT cryostat which houses the TQ4 quadrupole. The dump is separated from the from the vacuum chamber by a Ti alloy window and carbon-carbon blocks. The entire assembly is surrounded by marble slabs. It has been suggested that a different Ti alloy window, an additional vertical kicker to distribute the beam more efficiently on the window, or an in vacuum beam dump. The latter negating the need to use a Ti alloy window [9].

The five module abort kickers are located 24 m upstream from the beam dump. An estimate of 5 kW heat load per beam dump is absorbed by the abort kicker CMD10 ferrites. An upgraded cooling system from the RHIC kicker cooling system will be necessary for the HSR.

The power supply shunting scheme is preserved for the insertion quadrupoles in the 10 o'clock USS. The 10 o'clock USS houses the return for the quadrupole circuit. The quadrupole main bus is located in the 4 o'clock USS. The two sides of the 10 o'clock USS are independently powered. The quadrupole gradients in the USS can only be varied over a limited range due to limitations of the nested power supply

ISBN: 978-3-95450-227-1 ISSN: 2673-5490 doi:10.18429/JACoW-IPAC2022-WEPOTK016

STUDIES OF ECR PLASMAS AND MATERIALS MODIFICATION USING LOW ENERGY ION BEAM FACILITY AT IUAC

Puneeta Tripathi*, Shushant Kumar Singh, Pravin Kumar†
Inter-University Accelerator Centre, New Delhi, India

Abstract

The ECR ion sources are widely used to produce high intensity of highly charged positive ions. To increase their performance further, several techniques are employed. The addition of a lighter gas into the main plasma (so called gas mixing) shows a substantial effect on the charge state distribution of highly charged ions. Although many theoretical models were used to explain this gas mixing effect, yet it is not fully understood. The low energy ion beam facility (LEIBF) at Inter-University Accelerator Centre (IUAC), New Delhi, India, which comprises of a 10 GHz all-permanent magnet NANOGAN ECR ion source placed on a high voltage platform (400kV) has been used to develop several plasmas for the physical understanding of ions production and their confinement in a strong magnetic field. Further, the LEIBF allows us to extract ion beams from the plasma in the energy range of a few keV to tens of MeV for novel ion-matter interaction experiments. In this paper, the charge state distribution studies (relevant to gas mixing effect) of various atomic species at optimized ion source tuning parameters along with some interesting results on materials modification using ion beams is presented.

INTRODUCTION

The Electron Cyclotron Resonance ion sources (ECRISs) [1] are most suitable for producing high intensity of multiply charged ions and therefore, preferred as an injector in high energy particle accelerators. In fact there exists some ECRIS based implanter/low energy facilities for conducting research in materials science, atomic and molecular physics [2–4]. A cylindrical vacuum chamber consisting of multi-pole magnets around it and two solenoids at its ends, RF power injector and gas feed systems are essential components of ECRIS. The electrons gyrating in a magnetic field gain energy from the input RF wave via ECR and the plasma is formed by the step-by-step electron impact ionization. In the past few decades, a significant progress has been made to enhance the performance, mainly with the better understanding of of plasma and advancement in the magnetic field technology for its confinement. With the frozen design of the source, some additional techniques are also employed to further increase the intensity of highly charged ions. [5].

The gas mixing technique has been found to be very effective to boost the intensity of the highly charged ions in many folds (3-4 times) [6]. In most studies of gas mixing effect, He gas is chosen for lighter masses (such as O, N, Ne etc.), whereas O and N are used for heavier masses (Xe, Ar, Kr) [3, 7–12]. However, till now, there is no empirical rule for selecting a suitable gas for mixing purposes in a specific system. The gas mixing effect is mainly explained by the ion cooling model [13] and lowering a plasma potential [14]. These two processes decrease the ion temperature resulting a longer confinement time. However, a numerical simulation performed by Mironov et al. [15] showed that the ion temperature (T_i) actually increases in parallel with the potential dip ($\Delta\phi$), however $\Delta\phi/\mathrm{T}_i$ is always higher, following the overall ion confinement. Further, low frequency noise observed in the plasma due to instabilities and parametric decay of high frequency wave affect the ion dynamics by the process of selective ion heating [10, 16]. Due to the limited database of gas mixing experiments; it is very difficult to understand the ion behavior in the plasma and a consistent generalised model still needs to be established.

In present studies, we have recorded the charge state distributions (CSD) of Carbon (C) and Oxygen (O) in pure and Helium (He) mixed (at different %) CO_2 ECR plasma and touched upon various aspects of ion behaviour. Further, the extracted and analysed ion beams from ECR plasma are used for ion-matter interactions studies.

FACILITY DESCRIPTION

The Low Energy Ion Beam Facility (LEIBF) at IUAC, New Delhi, India [17] is a compact accelerator that has been functioning continuously for more than two decades, providing ion beams of energy ranging from tens of keV to a few MeV for diverse materials science and atomic molecular physics experiments. The schematic of the facility is shown in Fig. 1. The LEIBF consists of mainly a 10 GHz all-permanent-magnet ECR ion source, RF power and gas feed systems, efficient ion extraction system and an Einzel lens. All these components along with electronics and vacuum pumps are placed on a high voltage platform (V_{max} = 400 kV). These are powered by using an isolation transformer (10KVA) and controlled by the fibre-optic communication. The ions extracted from the plasma are further accelerated using a general purpose tube (GPT) having electrostatic field gradient. The pre-analysis section of LEIBF consists of electromagnetic lenses, a Faraday cup, a beam profile monitor and a double slit. For the analysis of ion beam in energy and momentum, a large analyser-cum-switching dipole magnet (B_{max} = 1.4 T) is used. For experiments, three beam lines at 75°, 90° and 105° equipped with proper beam line components, are available. The ions extracted from the plasma are transported to experimental chamber at the end of each beam line by focusing and steering those using electromagnetic lenses. All ion source and beam line

* punitatripathi1@gmail.com
† vishakhapk@gmail.com

ISBN: 978-3-95450-227-1 ISSN: 2673-5490 doi:10.18429/JACoW-IPAC2022-WEPOTK017

AN EFFICIENT H^-/ D^- EXTRACTION IN NEUTRAL BEAM INJECTION (NBI) ION SOURCES

V. Variale†, Istituto Nazionale Fisica Nucleare, Bari, Italy
M. Cavenago, Istituto Nazionale Fisica Nucleare-LNL, Legnaro (PD), Italy

Abstract

The negative ion source development has reached performances close to those required by the ITER project; see for example the test facilities ELISE and SPIDER [1,2,3]. The main residual problem seems to be the great amount of co-extracted electrons in the top part of the source. The introduction of a magnetic filter to remove the electrons from the extraction zone of the source causes **E**x**B** particle drifts (or shifts) which move both ions and electrons towards the top (or bottom depending on the B direction); in the top part, the electron concentration and extracted current increase and that limits the extracted ion number. In this contribution, as a possible solution, the application of a Planar Ion Funnel (PIF) extraction electric field configuration [4] on the source exit is proposed. The electric field line shape of PIF configuration, not only should change the relative directions between the magnetic filter **B** and the extraction electric field **E** in such a way to prevents the **E**x**B** electrons (e^-) drifts toward the source extraction, but also should give a more efficient H^-/D^- extraction. Preliminary simulations of D^- and e^- trajectories are presented to confirm the efficiency of the PIF ion extraction system.

INTRODUCTION

The world project for the nuclear fusion power production, ITER, is in construction at Cadarache, France. It will use Neutral Beam Injections (NBI) to reach the plasma temperature needed for nuclear fusion ignition. ITER should have two NBI with negative ion sources D^- (H^-) capable of provide ion currents of 40 A at 1 MeV (or 46 A at 0.87 MeV for H^-). To develop suitable ion sources a facility with large ion extraction, ELISE, has been realized at IPP Garching [1]. For efficient negative ions extraction (D^- /H^-) it is very important to avoid, or at least limit as most as possible, the e^- co-extraction. In ELISE a magnetic filter (B_F) field on the ion source extraction region is used for that purpose. B_F is produced, essentially, by applying an electric current flowing vertically on the Plasma Grid (PG), the grided plate from which the negative ions are extracted [5]. To further improve the ion extraction, a proper polarization is given also on PG and/or on a Biased Plate (BP) which is present in the source before PG. In ref. [3], however, experimental test carried out on the ELISE facility presented results where the number of electrons co-extracted with the H-/D- from the top part of the source is significantly bigger than that co-extracted from the bottom part. That important asymmetry caused of reducing the extracted ion current to avoid discharge in the extraction region. It seems that one of the main limitations to reach the ITER source performance be due to this asymmetry [1,2]. The top/bottom asymmetry can be ascribed to the presence of perpendicular electric (the source polarization) and magnetic (the filter) fields which causes the **E**x**B** particle drifts in the source extraction region. The reducing the vertical plasma drift, then, should be a very promising action for symmetrizing the top/bottom electrons co-extraction. In ref. [2] different techniques have been tried to modify **E** and **B** field lines to reduces the top/bottom asymmetry. To modify the electrostatic potential close to the PG some potential rods have been proposed and tested in ELISE [1]. The potential rods are water-cooled vertical plates made of nickel-coated copper placed in between the aperture groups. The rods shift the PG potential and the plasma potential close to the PG upwards by a few volts. The total co-extracted electron current and the top/bottom ratio are reduced to smaller values. The effect of the rods, however, is not sufficient for fully symmetrizing the co-extracted electrons in deuterium at high P_{RF}. Alternative methods to the potential rods have been also investigated to obtain better results. For example, different polarization of BP with respect to PG and source have been tried but with still unsatisfactory results [3].

To better understand the asymmetric top/bottom e^- extraction in the ITER type sources, a study of the charged particle trajectories in the source extraction region has been carried out by using SIMION code [5]. In those simulations has been assumed that the whole extraction region is placed in the source plasma sheet in front of PG. The plasma sheet depth is given by $d=\lambda_D(V_{app}/kT_e)$ (in our conditions few mm) with λ_D the Debye length [2]. Charged particles starting from that region feel the extraction electric field (with reduced 'self-shielding plasma effect') and then SIMION simulation (with no plasma effect) can be used to follow the ion and electron trajectories during their extraction. The simulation results presented in ref. [5] show as electron **E**x**B** drifts can be reduced by the polarization of BP and PG in such a way that the extracting field in the region before PG could be reduced. A similar effect can be obtained by using the Planar Ion Funnel (PIF) electrode configuration proposed as ion extraction system for the sources in mass spectrometer applications [6]. In this paper the **E**x**B** particle drifts simulation with PIF electrode configuration applied to a scaled SIMION model of MaMuG type source extraction system is presented, and the results discussed.

† vincenzo.variale@ba.infn.it

ISBN: 978-3-95450-227-1 ISSN: 2673-5490 doi:10.18429/JACoW-IPAC2022-WEPOTK018

SIMULATION OF HEAVY-ION BEAM LOSSES WITH CRYSTAL COLLIMATION*

R. Cai† [1], R. Bruce, M. D'Andrea, L. S. Esposito, P. D. Hermes, A. Lechner, D. Mirarchi, J. B. Potoine[2], S. Redaelli, F. Salvat Pujol, P. Schoofs, CERN, Geneva, Switzerland,
M. Seidel[3], Paul Scherrer Institut (PSI), Villigen, Switzerland
[1, 3]also at École Polytechnique Fédérale de Lausanne, Lausanne, Switzerland
[2]also at University of Montpellier, Montpellier, France

Abstract

With the higher stored energy envisioned for future heavy-ion runs in the LHC and the challenging fragmentation aspect of heavy-ion beams due to interaction with collimator material, the need arises for even more performing collimation systems. One promising solution is crystal channeling, which is used in the HL-LHC baseline and starts with Run III for heavy-ion collimation. To investigate an optimal configuration for the collimation system, a well-tested simulation setup is required. This work shows the simulations of channeling and other coherent effects in the SixTrack-FLUKA Coupling simulation framework and compares simulated loss patterns with data from previous beam tests.

INTRODUCTION

The Large Hadron Collider (LHC) [1] at CERN collides both proton and heavy-ion beams. Due to the high stored beam energies, beam losses could cause quenches of superconducting elements or even damage. In particular, to keep control of the continuous beam losses during operation due to diffusive effects, instabilities, collisions and other mechanisms that deviate particles from the nominal orbit, a multi-stage collimation system has been put into place [2–5], with the main betatron collimation system installed in the LHC insertion region 7 (IR7). Previous studies showed that the cleaning inefficiency is about two orders of magnitude worse for Pb ions than for protons [6–8]. Hence, heavy-ion collimation is more critical, even if the planned stored beam energy is about a factor 30 smaller than for protons.

To improve the ion collimation performance facing the imminent HL-LHC upgrades [9–11], where the stored beam energy will be increased from about 13 MJ to 20 MJ, an increase of a factor of three in cleaning efficiency would be needed. For this, the so-called crystal collimation [12, 13] will be used starting from 2022. This method exploits the electromagnetic potential in the crystalline structure of a bent silicon crystal to guide the incoming particles. This mechanism is called crystal channeling [14, 15] and it occurs when particles enter the crystal with an incident angle below the so-called critical angle [13]. For channeled particles a bent crystal acts as an ideal septum by deflecting channeled particles onto a downstream absorber [16] with an equivalent field strength of hundreds of Tesla, while circulating particles passing close to it are not affected.

After numerous studies, four strip crystal collimators have been installed in the LHC, one per beam per plane. The specifications of the crystals are shown in [17, 18].

Crystal collimation has been demonstrated to work also for protons with low-intensity beams [19]. However, the present standard collimators cannot be used as absorbers with LHC's high-intensity proton beams, which is why this technique is presently not considered for operational use.

Simulations are crucial in understanding, mitigating and optimizing critical collimation losses. Previously, a complete simulation framework for heavy-ion collimation using crystals including standard interactions with other collimators and a precise 6D tracking did not exist, thus heavy-ion crystal collimation could not be studied systematically. This paper presents an extension of the existing simulation framework for standard ion collimation studies to include crystals, as well as benchmarks and simulation results on proton and heavy-ion crystal collimation including full coverage of multi-turn effects.

SIMULATION FRAMEWORK

The newly built simulation framework relies on the existing SixTrack-FLUKA coupling [20–22], which is the standard tool for simulating ion collimation [7, 23]. This package provides a framework for active information exchange between SixTrack [24] and FLUKA [25–28]. SixTrack is a 6D symplectic particle tracking code, whereas FLUKA is a general-purpose Monte Carlo code. SixTrack is used for the tracking in the magnetic lattice, while FLUKA simulates the particle-matter interactions in collimators [20, 21].

A crystal routine has been developed and been recently integrated in FLUKA [29–31]. Building on that, the SixTrack-FLUKA coupling has been updated to include crystal collimators, carrying a special flag and several crystal-specific parameters in the inputs to activate the crystal physics routine. Geometry models of the LHC crystals which follow closely the real curved geometries have been implemented. Auxiliary components such as the holders have not been implemented, as they are much smaller than conventional collimator supporting systems and their contribution is likely small for tracking purposes since particles are not expected to impact on them. The properties of the crystal lattice have been defined according to the most recent X-ray and hadronic

* Research supported by the HL–LHC project
† rongrong.cai@cern.ch

ISBN: 978-3-95450-227-1 ISSN: 2673-5490 doi:10.18429/JACoW-IPAC2022-WEPOTK019

STATUS OF THE LASER ION SOURCE UPGRADE (LION2) AT BNL*

T. Kanesue†, B. Coe, S. Ikeda, S. Kondrashev, CJ. Liaw, M. Okamura, R. Olsen, T. Rodowicz, R. Schoepfer, L. Smart, D. Weiss, Y. Zhang, Brookhaven National Laboratory, Upton, NY, USA
A. Cannavò, Nuclear Physics Institute of CAS, Prague, Czech Republic

Abstract

A laser ion source (LION) at Brookhaven National Laboratory (BNL) has been operational since 2014 to provide low charge state heavy ions of various species for Relativistic Heavy Ion Collider (RHIC) and NASA Space Radiation Laboratory (NSRL). Pulsed ion beams (100~300 μs) with beam current ranging from 100 μA to 1 mA from any solid-state targets can be supplied without memory effect of previous beams at pulse-by-pulse basis. LION is an essential device for the operation of a galactic cosmic ray simulator at NSRL together with high-performance beams for RHIC. Because the importance of LION has been widely recognized, an upgraded version of LION, which is called LION2, is being developed for improved performance and reliability. The design and status of the LION2 will be shown.

INTRODUCTION

LION is a laser ablation ion source which utilizes a nanosecond laser to generate ions from any solid-state materials. The heavy ion source has provided various heavy ions with fast switching capability since 2014. LION generates singly charged ions for further ionization by an electron beam ion source called RHIC-EBIS. RHIC-EBIS works as charge breeder and highly charged heavy ions are further accelerated by the following RFQ and IH linac [1]. LION has two independent lasers and target systems to provide different beams for RHIC and NSRL at the same time. For NSRL, LION can switch ion species in as fast as a few seconds by switching target position. For galactic cosmic ray (GCR) study at NSRL target room, ion species are switched within 1 min to simulate GCR exposure [2]. This switching time is not limited by LION.

Demands of various heavy ion species has been growing significantly since the beginning of LION operation. When LION operation was started in 2014, there was only one laser line and target system for NSRL. This was the first operational laser ion source to provide stable heavy ions for user facility for months. LION demonstrated excellent beam performance and reliability, and the second laser line and target system for RHIC was developed and installed in 2015. The number of ion species prepared in a vacuum chamber has been increased from 5 in early times to currently around 10 for NSRL in addition to 1 or 2 species for RHIC. NSRL beam time was originally only daytime during weekdays. Recently, NSRL uses beams until night from Monday to Saturday. Occasionally beams are used even overnight and Sundays. A GCR simulator mode has been implemented since 2016 which requires much more frequent species change. With this mode, LION species for NSRL changes as much as over 100 times per day. In addition, some RHIC operation for low energy collider experiments requires much more frequent beam injection into RHIC at every 30 minutes compared to more than 10 hours for nominal 100 GeV/u beam energy.

LION2

LION2 will replace the entire LION1 except for target systems to provide better beam performance, operational capability, and maintainability. We aim to install LION2 during summer shutdown in 2023, which is the next year after the installation of the Extended-EBIS (July 2022 to the end of 2022), which will replace the existing RHIC-EBIS [3]. Figure 1 shows the location of LION2 in RHIC-EBIS pre-injector. LION2 design follows the basic design of LION1. It consists of lasers, a target chamber, target systems, a solenoid magnet to guide laser produced plasma, and an extraction chamber. We will use the same target systems as LION1. One is a two-dimensional linear stage (xy

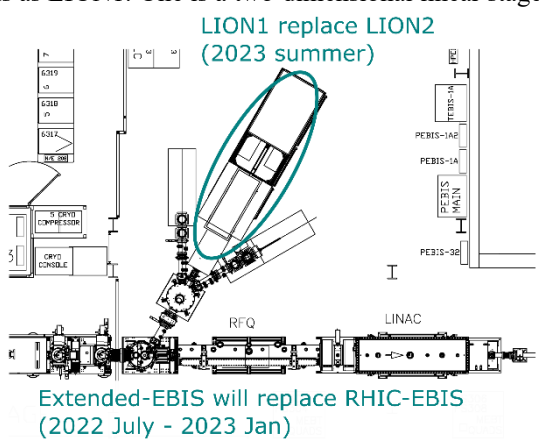

Figure 1: Future of BNL heavy ion pre-injector.

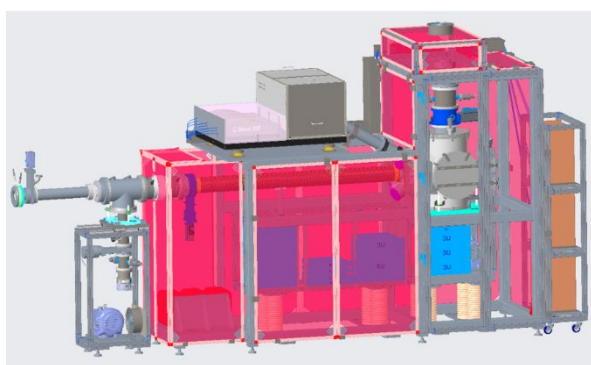

Figure 2: Future of BNL heavy ion pre-injector.

* Work supported by Brookhaven Science Associates, LLC under Contract No. DE-SC0012704 with the U.S. Department of Energy, and by the National Aeronautics and Space Administration
† tkanesue@bnl.gov

ISBN: 978-3-95450-227-1 ISSN: 2673-5490 doi:10.18429/JACoW-IPAC2022-WEPOTK020

SLANTED BEAM EXTRACTION ON LASER ION SOURCE*

M. Okamura†, T. Kanesue, S. Ikeda, S. Kondrashev
Brookhaven National Laboratory, Upton, NY, USA
A. Cannavò, Nuclear Physics Institute of CAS, Prague, Czech Republic

Abstract

We experimentally verify how performance is achieved when the direction of the extraction field is at an angle to the direction of motion of the plasma in a laser ion source. If the extraction field can be slanted without degradation of the ion source performance, it is considered to be able to shield neutral vapours and debris generated simultaneously with the plasma, which will be advantageous for the long-term operation of the laser ion source. Also, the layout of the laser ion source can be more flexible, since the long plasma drift section occupies a space at the very highly populated equipment area. The effect of the angle of the extraction surface on the beam current is greater than a simple angular reduction in the extraction area. However, an angle of up to about 25 degrees is acceptable in practical use.

INTRODUCTION

The laser ion source is a pulsed ion source capable of delivering a high current beam with low emittance. The laser beam is irradiated onto the surface of a solid target to generate an ablation plasma. This plasma is directed perpendicular to the target surface. At the same time, it diverges isotropically. The pulse length of the ion beam is determined by the time it takes for this expanded plasma to pass through the beam extraction electrodes of the ion source. Therefore, to obtain a long pulse, the plasma must be flown over a long distance. Also, flying over a longer distance means that the plasma has a longer time to expand isotropically, and thus the density of the plasma reaching the extraction zone becomes thinner. To mitigate this degradation of the plasma density, modern laser-ion sources use a long solenoid with a weak magnetic field[1]. Therefore, the solenoid occupies a large space of the laser-ion source.

Since 2014, at Brookhaven National Laboratory, we have been using a laser-ion source to generate ions at the beginning of the Hadron Accelerator Facility. This device is called LION. The solenoid of the LION that generates a few tens of gauss magnetic fields is 3 meters long. The distance used for this long expansion results in a pulse width of several hundred microseconds for the beam delivered to the EBIS charge breeder in the succeeding stage[2]. The solenoid magnetic field suppresses the isotropic expansion and can deliver beams in the submilliampere class.

Modern laser-ion sources require a large straight space at the front end of the real accelerator chain because the long solenoid limits the layout. Therefore, in this study, the solenoids were placed at an angle from the beam direction and experimentally verified that the performance of the source is not compromised. Normally, the plasma moves with constant velocity from the laser target to the extraction section at a velocity of several to several hundred electron volts, and the extraction voltage is applied without changing the direction of travel. However, when an angled extraction field is applied to the plasma velocity, the effect on emittance is expected to be limited if the extraction voltage is clearly greater than the plasma's flight velocity. A further complication is the solenoid magnetic field. It is usually weak, a few hundred gauss at most, so its contribution to emittance increase is almost negligible, but if it is angled, experimental verification is required.

EXPERIMENTAL SETUP

The laser was a Thales SAGA 230 and was set to produce mainly single charge state. The targets used were aluminium and tantalum. The laser power densities were estimated as 4.2E8 W/cm2 and 5.0E8 W/cm2 respectively and incident angle of the laser path was 30 degree. The laser parameters are summarized in Table 1. To obtain table beam, three hundred laser shots were applied before taking the data and possible impurities were minimized. Geometric information for the solenoid is listed in Table 2. The beam current measurement was done by a Faraday cup with a -3.5 kV bias mesh that represents an ion extraction electric field. Figure 1 shows how the Faraday cup was mounted. The cup was supported by a rotatable rod and can be swung without changing the aperture position. The cup was placed 103 mm downstream of the solenoid edge. The entire setup photo is shown in Fig. 2.

Table 1: Laser Parameters

Wavelength	1064 nm
Pulse width	6 ns
Energy for aluminium	550 mJ
Energy for tantalum	760 mJ

Table 2: Solenoid Geometries

Vacuum pipe ID	102 mm
Solenoid ID	114 mm
Number of layers	9
Length	1980 mm
Wire diameter	2 mm
From Target to entrance	312 mm
To FC from exit	103 mm

* Work supported by NASA and US DOE
† okamura@bnl.gov

ISBN: 978-3-95450-227-1 ISSN: 2673-5490 doi:10.18429/JACoW-IPAC2022-WEPOTK021

IMPROVEMENT OF SPILL QUALITY FOR SLOWLY EXTRACTED IONS AT GSI-SIS18 VIA TRANSVERSE EMITTANCE EXCHANGE

J. Yang*,[1], P. Forck, T. Giacomini, P. Niedermayer[1], R. Singh, S. Sorge,
GSI Helmholtzzentrum für Schwerionenforschung GmbH, Darmstadt, Germany
[1] also at Goethe Universität, Frankfurt am Main, Germany

Abstract

The temporal beam stabilization of slowly extracted beams from the synchrotron within several seconds is crucial for fulfilling the demands of fix-target experiments. Results from previous investigations suggest that the transit time spread can be increased by reducing the beam emittance in the plane of extraction. Increased transit time spread is known to cut-off high frequency noise introduced by magnet power supplies. A pilot experiment was performed at SIS18 at GSI to introduce transverse emittance exchange, resulting in the circulating beam's smaller horizontal beam size. The improvement of the spill micro structure is reported in this contribution.

INTRODUCTION

The quality of slowly extracted beams from GSI synchrotron SIS18 within 100 µs scale is required by fixed target experiments. The basic procedure of slow extraction consists of exciting the resonance and feeding the resonance [1]. Sextupoles are used for the excitation of the third-order resonance, leading to the formation of a triangular phase space area of stable betatron motion in the extraction plane. Its boundary is defined by separatrix [2, 3].

This contribution focuses on the slow extraction in the heavy-ion synchrotron SIS18 at GSI, which has a circumference of 216.72 m and a beam rigidity up to 18 Tm. Tune swept slow extraction is regularly performed in SIS18. The resonance is fed by executing the tune sweep by increasing the strength of two fast quadrupoles. The extracted beam, referred to as a spill, has a temporal variation on time scales of micro to milli seconds which is caused by the power supply ripples. It is called in the following spill micro structure. The mitigation of the spill micro structure is of high importance for fixed target experiments at GSI.

Previous investigations suggest that the horizontal beam size (emittance) influences the spill micro structure and decreasing the horizontal emittance would result in an improvement in spill quality. Thus, methods that reduce the beam size may result in an improvement of the spill micro structure [4]. There are several possibilities of reducing emittance, 1) less number of injected turns, 2) beam cooling using the electron cooler. However, less number of injected turns reduces the intensity and electron cooling needs time. Transverse emittance exchange allows a fast emittance exchange without reduction of intensity. The disadvantage might be transmission losses in the beamline due to larger vertical beam size. Transverse emittance exchange [5] is executed by utilizing linear horizontal-vertical betatron coupling while Q_x is crossing the second integer coupling resonance in a short time. The resonance in SIS18 is defined by $Q_x = Q_y + 1$. The amount of the emittance exchange is determined by the interplane coupling strengths and the speed of moving the tune across the coupling resonance [5].

Previous observations of transverse emittance exchange at SIS18 are described in [6]. For this paper, the improvement of the spill micro structure is studied by performing slow extraction measurements with and without utilizing transverse emittance exchange and comparing the results.

EXPERIMENTS

The measurements were performed using an Ar^{18+} beam injected at $E = 8.49$ MeV/u in 11 revolutions by horizontal multi-turn injection resulting in a horizontal emittance significantly larger than the vertical emittance. Afterwards, the beam was accelerated to 300 MeV/u.

In the first step, the transverse emittance exchange was performed to reduce the horizontal beam size just before the start of the extraction process. This was done by utilizing linear horizontal-vertical betatron coupling during a tune crossing in a short time caused by residual skew quadrupolar components in the SIS18. In the second step, the slow extraction was performed. The vertical tune was kept constant at $Q_y = 3.24$ during both steps of the spill measurement.

The transverse emittance exchange was performed by moving a horizontal tune from 4.17 to 4.2995 within 40 ms resulting in horizontal emittance reduction and vertical emittance increase. The beam profiles were simultaneously measured by an Ionization Profile Monitor (IPM) installed in SIS18 [7]. The profile readout period is 10 ms. The emittances exchanged at the time of 660 ms after the begin of the cycle. As shown in Fig. 1, after emittance exchange, the horizontal beam size (1σ) shrunk from 4.90 mm to 3.10 mm while the vertical beam size (1σ) increased from 2.83 to 5.18 mm.

The slow extraction was performed by sweeping the horizontal tune in 1.5 s by changing the strength of two fast quadrupoles, which was varying as a third polynomial function of time. The set value of the tune changing range in the control panel was from 4.3275 to 4.3345. The maximum sextupole strength was $k_2L = 0.05$ m^{-2}.

Spill Characterization

The spills were measured with a plastic scintillator (BC400) installed inside the transfer line with up to several 10^6 particles per second. The detected signal was recorded

* Jia.Yang@gsi.de

ISBN: 978-3-95450-227-1 ISSN: 2673-5490 doi:10.18429/JACoW-IPAC2022-WEPOTK022

HORIZONTAL BEAM RESPONSE AT EXTRACTION CONDITIONS AT THE HEIDELBERG ION-BEAM THERAPY CENTRE

E. C. Cortés García*, E. Feldmeier, Th. Haberer,
Heidelberg Ion-Beam Therapy Centre (HIT), Department of Radiation Oncology,
Heidelberg University Hospital, Heidelberg, Germany

Abstract

The Heidelberg Ion-Beam Therapy Centre's synchrotron makes use of the sextupole driven RF-KO method near the third-order resonance in order to slowly extract the beam that is delivered to the patients. The horizontal beam response of a coasting beam was studied experimentally and with simulations at extraction conditions in order to deduce regions of interest for an optimal excitation signal spectrum. Two narrow frequency regions were found were the beam reacts coherently. With these information an RF signal was proposed for the resonant slow extraction.

INTRODUCTION

The Heidelberg Ion-Beam Therapy Centre is a state-of-the-art facility capable of delivering four ion species of proton, ^{4}He, ^{12}C and ^{16}O and is equipped with the first heavy ion gantry worldwide. After the beam has reached it's final nominal energy in the synchrotron, it is slowly extracted by means of the sextupole driven RF-KO method [1, 2]. The horizontal tune is brought near a third-order resonance and this is actively fed further by resonance sextupoles. Under these conditions the beam's horizontal emittance is slowly blowed up with an external EM field. To ensure that the the extracted particle count remains constant, several techniques were implemented [3].

In this contribution the experimental data of the horizontal beam response of a coasting beam under extraction conditions and a simulation of it are presented. For the design of excitation RF signals for the slow extraction the typical approach was based on direct phenomenological studies (measurements and simulation) of the spill [4–7]. The study of the BTF at extraction conditions can aid to the design of the spectrum of the RF signal, since it can directly unveil the areas in frequency-space where the beam reacts coherently.

BTF MEASUREMENT

In this section the BTF measurement of a coasting carbon-ion beam $^{12}C^{6+}$ with kinetic energy $E_{\mathrm{kin}} = 124.25\,\mathrm{MeV/u}$ is presented. The experimental setup for the measurement of the Beam Transfer Function (BTF) is shown in Fig. 1. Relevant parameters of the linear ion-beam optics can be found in Table 1. The tune values were infered from the BTF signal measured at extraction flattop with sextupole magnets off. The chromaticity of the machine was measured by introducing an offset on the end frequency of the accelerating cavity to produce a momentum offset and determining the tune

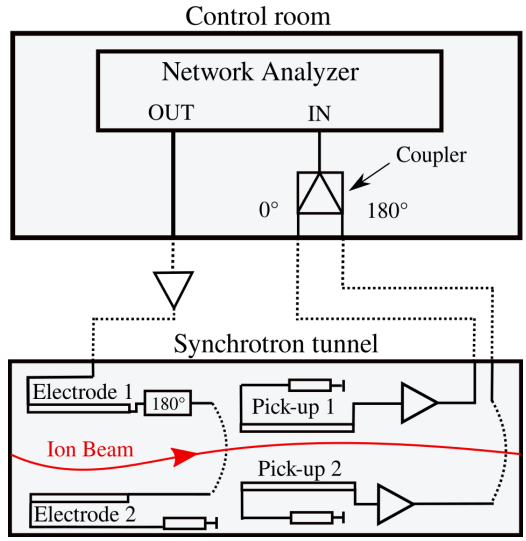

Figure 1: BTF experimental setup. The network analyzer (NA) generates an excitation signal and scans over a frequency span of interest. The response of the beam is then measured with two pick-up electrodes.

shift through the BTF measurement with sextupole magnets off. The value presented in Table 1 is meant to be the specific chromaticity of the machine, namely $\xi = \frac{\Delta Q}{Q} / \frac{\Delta p}{p}$. The slip factor was determined from the experimental value of the synchrotron frequency f_S. The momentum-spread was infered from the width of the Schottky pick-up signal of the second harmonic of the revolution frequency.

Table 1: Ion Optical and Beam Parameters of the HIT Synchrotron (The Momentum Spread is at FWHM)

Parameter	Symbol	Nom. Value	Meas. Value
Hor. tune	Q_x	1.67895	1.6795(1)
Ver. tune	Q_y	1.755	1.720(6)
Slip-factor	$\lvert\eta\rvert$	0.4766	0.44(2)
Hor. chroma.	ξ_x	-0.66	-0.72(6)
Mom. spread	σ_δ	-	$1.2{\cdot}10^{-3}$

After the beam has arrived to the nominal flattop energy, it is debunched and the tune is brought near the third order the resonance. Simultaneously the sextupoles are excited to the nominal strength for extraction, this corresponds for the resonance sextupoles to a strength of $k' = 0.9\,\mathrm{m}^{-3}$. This process lasts approx. 500 ms to ensure adiabaticity and that the

* Cristopher.CortesGarcia@med.uni-heidelberg.de

ISBN: 978-3-95450-227-1 ISSN: 2673-5490 doi:10.18429/JACoW-IPAC2022-WEPOTK023

SIMULATION STUDY OF FAST EXTRACTION IN THE ABSENCE OF ONE SEPTUM MAGNET FOR J-PARC MAIN RING

S. Iwata†, K. Ishii, Y. Sato, S. Igarashi, T. Shibata, T. Sugimoto, T. Yasui, H. Matsumoto, N. Matsumoto, KEK, Ibaraki, Japan

Abstract

At J-PARC main ring (MR), the two fast extracting beamlines to the neutrino facility and to the abort dump have a symmetrical layout of 6 septum magnets each, a total of 12. Since there are many magnets, it is necessary to be careful about failure. It is important to consider how to continue beam supply even if one of the septum magnets is missing. From July 2021, upgrade works of the FX septum magnets commenced with an aim of increasing the beam power of MR to 1.3 MW from 500 kW. We simulated the beam extraction without one of the septum magnets under the conditions of the new geometry of septum magnets and the new aperture. We found that the beam can be extracted by increasing the current of the surrounding septum magnets and compensating for the output.

INTRODUCTION

J-PARC MR plays a role in supplying high-intensity proton beams in the T2K Neutrino experiment. It is planned to achieve an output of 1.3 MW by shortening the repetition cycle to 1.16 s and increasing the number of particles by up to 3.3 $\times 10^{14}$ [1]. Fast extraction (FX) magnets have been replaced with equipment corresponding to this early repetition cycle since 2021. Figure 1 shows the FX section magnets picture and layout. The Neutrino beamline is at the inside of the ring, the Abort is at the outside, and the circulating beamline is at the center. From the upstream, five kicker magnets, two low magnetic field septum magnets, and four high magnetic field septum magnets are aligned. Two low field magnets (FX-EDDY1 and FX-EDDY2) and three high field magnets (SM30, 31, 32) were replaced in period from July 2021 to May 2022. The most downstream high field magnet (SM33) reuses the septum magnets that have been used.

An EDDY type septum magnet is used as a low magnetic field magnet of about 0.3 T. In the 1 Hz operation, heat generation of the coil is an issue. The EDDY type magnets are pulse-excited, which eliminates the problem of heat generation. The maximum magnetic field has also improved to be about double. Owing to this higher magnetic field, even if one of the EDDY magnets is rendered inoperable, the beam operation can be continued.

Four high magnetic field septum magnets produce magnetic fields above 1 T. The 1 Hz operation also makes the heat generated by the coil severe even in the high field magnet; furthermore, the heat generated by the eddy current that loops between the circulating and extracting vacuum ducts becomes a problem. We introduced ceramic ducts to overcome this problem of loop current. We are also considering expanding the aperture of quadrupole magnets between the septum magnets to reduce beam loss. QFR154 only needs an expansion of the duct aperture; however, QDT155 needs an expansion of the magnet aperture, and the QDT155 magnet will be longer in the future. In anticipation of this, the length of the septum magnet was shortened and optimized, and SM30, SM31, and SM32 were renewed. The power supplies of the high field septum magnets are reused, with each capable of providing an output of 4.5 kA-300 V. The margins of the SM30 and SM31 are about 10% in combination with the magnets, and SM32 and SM33 are about 50%.

The orbit calculation and the aperture of the FX section are described in reference [2]. The beam envelopes are

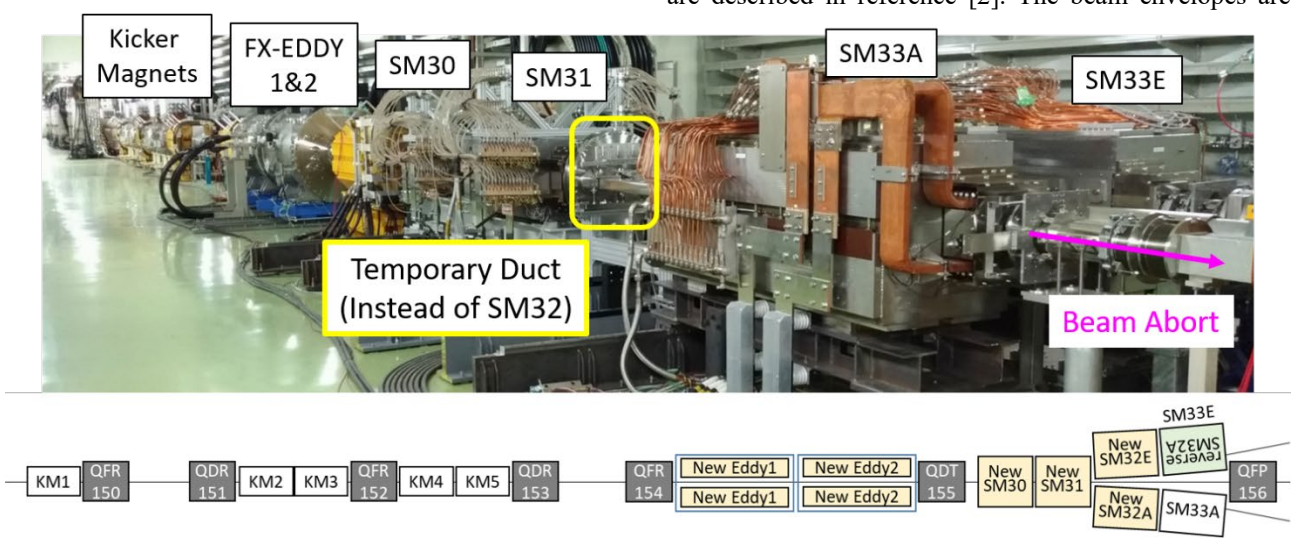

Figure 1: The layout of the FX magnets at J-PARC MR.

† soma.iwata@kek.jp

ISBN: 978-3-95450-227-1 ISSN: 2673-5490 doi:10.18429/JACoW-IPAC2022-WEPOTK024

UPGRADE OF SEPTUM MAGNETS FOR FAST EXTRACTION IN J-PARC MAIN RING

S. Iwata†, K. Ishii, T. Shibata, T. Sugimoto, H. Matsumoto, N. Matsumoto, M. Uota, Y. Sato,
KEK, Ibaraki, Japan

Abstract

We aim to supply a high-power proton beam of 1.3 MW to the neutrino facility from J-PARC Main Ring (MR) by shortening the repetition cycle to 1.16 s from 2.48 s and increasing the number of particles by 1.3 times. The six septum magnets for fast extraction (FX) need to be replaced to reduce the heat that is generated as a result of shortening the repetition cycle. The replacement of the septum magnets began in July 2021 and was completed at the end of May 2022. The beam commissioning starts in June 2022. We report the details of the replacement work and operation test of the new septum magnets. We found defects in the magnetic coil of the septum (SM32) in August 2021. We decided to postpone its installation to around September 2022 and produce new magnet coils for the SM32. The beam extraction in June 2022 will be performed using a temporary vacuum duct instead of the SM32 magnet, and the extraction beam orbit will be maintained by increasing the magnetic field of the other five septum magnets.

INTRODUCTION

J-PARC MR contributes to the T2K long baseline neutrino experiment by supplying a high-intensity proton beam. The construction of Hyper-Kamiokande is underway on the neutrino detector side, and J-PARC MR on the beam supply side is also updating the equipment to increase the output beam power. An upgrade plan is in progress, which will increase the number of particles and shorten the repetition cycle, and we plan to achieve a MR output of 1.3 MW. The design values of the MR upgrade plan are 1.16 s cycle and 3.3×10^{14} protons per pulse [1].

Figure 1 shows the layout of the septum magnets in the J-PARC MR FX section in 2022. The FX section plays the role of beam extraction to the neutrino target and to the beam abort and is realized by providing beam lines on both sides. The details of the updated plan are described in Reference [2]. From the upstream, two EDDY current type septum magnets of about 0.3 T (as low magnetic field magnets) are connected in series with four high magnetic field septum magnets (SM30, SM31, SM32, SM33) of about 1 T. The low magnetic field septum was switched to the pulse excitation type of EDDY septum due to the heat generation problems observed during operation at 1 Hz. We manufactured new magnets for SM30, SM31 and SM32 and introduced ceramic ducts. The flanges of the circulating and the extracting ducts at the up and down streams of SM30 and SM31 and the upstream of SM32 are difficult to separate, so one large flange was welded. If the ducts and flange are all made of metal, a generating eddy current on the ducts by the excitation passes through each other. The large eddy current passes through the ducts as a large loop, resulting in the generation of heat. The loop current on the duct is expected to be several kA, and the heat generation is several tens of kW, which is unacceptable without cooling. We decided to simply use ceramic ducts instead of having a cooling structure in the vacuum ducts. Additionally, we have a plan to manufacture a large aperture QDT (one type of quadrupole magnet in the MR) magnet to expand the beam aperture in the future, and we have shortened the magnet length of the high magnetic field septum to secure the new QDT magnet length.

Two of the power supplies for the EDDY magnets needed to be replaced because of the change to pulse excitation. The EDDY magnet can generate about twice the required magnet field and continue the beam operation even if one unit becomes inoperable. As for the high field septum magnets, their power supplies are reused. The four high magnetic field power supplies are capable of outputting 4.5kA-300V and were manufactured as power supplies that apply with the initial design value of MR 50 GeV acceleration. The MR is currently accelerating to 30 GeV, and

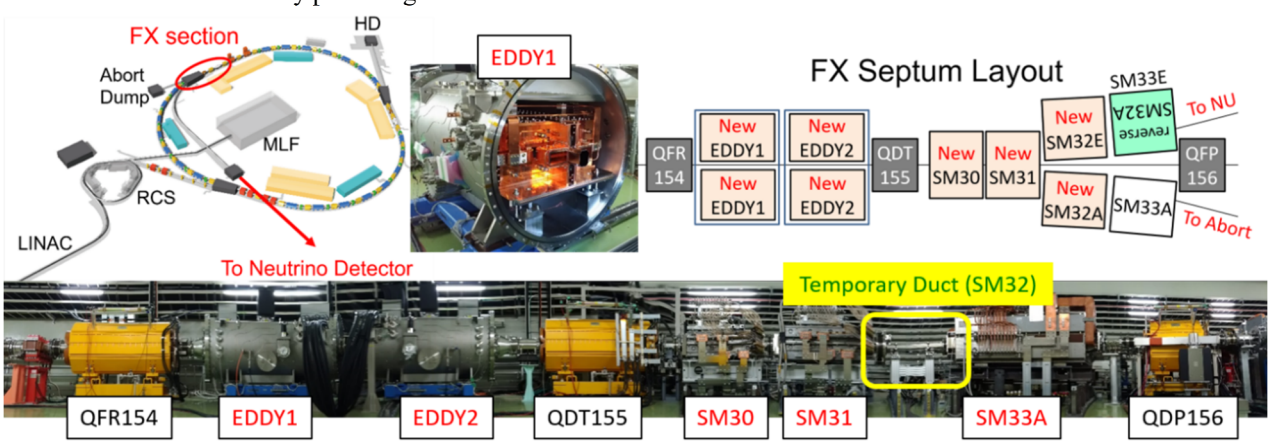

Figure 1: Pictures and schematic layout of the fast extraction septum magnets.

† soma.iwata@kek.jp

ISBN: 978-3-95450-227-1 ISSN: 2673-5490 doi:10.18429/JACoW-IPAC2022-WEPOTK025

CONCEPTS AND CONSIDERATIONS FOR FCC-ee TOP-UP INJECTION STRATEGIES

R. Ramjiawan*, W. Bartmann, Y. Dutheil, M. Hofer
CERN, Geneva, Switzerland
P.J. Hunchak, University of Saskatchewan, Saskatoon, Canada
M. Aiba, PSI, Villigen, Switzerland

Abstract

The Future Circular electron-positron Collider (FCC-ee) is proposed to operate in four modes, with beam energies from 45.6 GeV (Z-pole) to 182.5 GeV ($t\bar{t}$ production) and luminosities up to 4.6×10^{36} cm^{2}s^{-1}. At the highest energies the beam lifetime would be less than one hour, meaning that top-up injection will be crucial to maximise the integrated luminosity. Two top-up injection strategies are considered here: conventional injection, employing a closed orbit bump and septum, and multipole-kicker injection, with a pulsed multipole magnet and septum. On-axis and off-axis injections are considered for both. We present a comparison of these injection strategies taking into account aspects such as spatial constraints, machine protection, disturbance to the stored beam and injection efficiency. We overview potential kicker and septum technologies for each.

INTRODUCTION

The FCC-ee

The FCC-ee [1] is a proposed, high-luminosity, circular lepton collider; the parameters for the FCC-ee at lowest and highest energy are given in Table 1. The short lifetime of the beam requires it to be continuously topped up, where this top-up process is planned via a separate, full-energy booster ring, located in the same tunnel as the collider ring.

Table 1: FCC-ee parameters [1] for Z- and $t\bar{t}$-operation. The beam lifetime is given as that from radiative Bhabha scattering/beamstrahlung, and the quoted energy spread includes effects of beamstrahlung.

Parameter	Unit	Z	$t\bar{t}$
Beam energy	GeV	45.6	182.5
Beam lifetime	min	68/>200	39/18
Beam current	mA	1390	5.4
# bunches/beam		16 640	48
Magnetic rigidity	Tm	152.1	608.7
Emittance (x/y)	nm/pm	0.27/1.0	1.46/2.9
Energy spread	%	0.132	0.192

Injection Into the Collider

In these proceedings we consider two methods of top-up injection: conventional bump injection and multipole kicker injection (MKI) [2]. For beam tracking studies of these two methods see [3]. Conventional bump injection, depicted in Fig. 1(a), uses a dynamic π-orbit-bump created with dipole kickers, to bring the beam close to the septum blade. MKI (Fig. 1(b)) incorporates a 'multipole' kicker providing a kick to the injected bunch, which passes off-axis, and a field-free region on-axis for the stored beam.

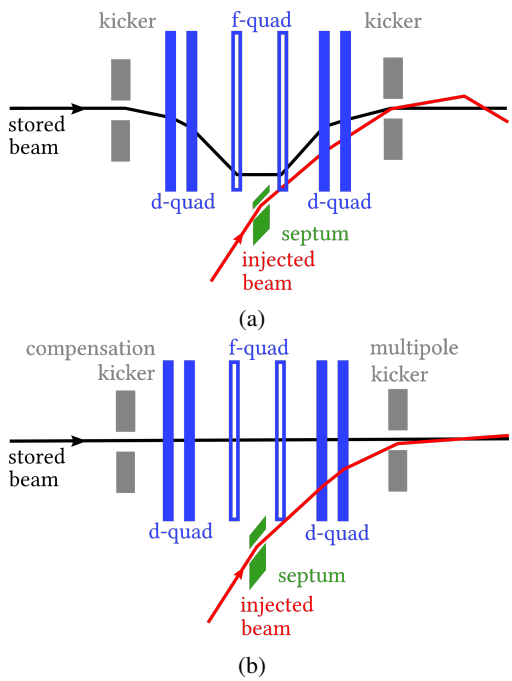

Figure 1: Schematic of (a) conventional bump injection and (b) multipole kicker injection.

As specified by Liouville's theorem [4], the density of the particles in phase-space stays constant while under conservative forces, hence you cannot inject particles into the phase-space of the stored bunches. Instead, beams are injected with a separation from the stored beams and merge via synchrotron radiation damping. For *off-axis* injection, bunches are injected with a separation from the stored beam in betatron phase (transverse offset). For *on-axis* injection, bunches are injected with a separation in synchrotron phase (momentum offset) onto the off-momentum closed orbit, thus requiring a non-zero dispersion at the septum (Fig. 2(b)). A large β_x-value at the septum reduces the impact of the septum width as it would be smaller compared with the beam size.

* rebecca.louise.ramjiawan@cern.ch

ISBN: 978-3-95450-227-1 ISSN: 2673-5490 doi:10.18429/JACoW-IPAC2022-WEPOTK026

COMMISSIONING OF THE ELENA ELECTROSTATIC TRANSFER LINES FOR THE ANTIMATTER FACILITY AT CERN

Y. Dutheil*, W. Bartmann, C. Carli, M.A. Fraser , D. Gamba, L. Ponce
CERN, Geneva, Switzerland

Abstract

ELENA is a small synchrotron ring that decelerates antiprotons down to a kinetic energy of 100 keV. With an experimental complex capable of housing up to 9 different experiments operating simultaneously, the transfer line design needed to be highly flexible. The low energy of the beam transported allowed the exploitation of electrostatic devices instead of magnets, to simplify design, production and operation.

This contribution presents the systematic characterisation of the beam optics at the different experimental handover locations during beam commissioning using H- ions from an external source, as well as the performance of the lines in operation with antiprotons. Finally, the effect of stray fields created by the experimental setup will be presented and compared with the first measurements.

INTRODUCTION

The Extra Low ENergy Antiproton storage ring (ELENA) [1] is the latest deceleration stage of the CERN antimatter factory. It decelerates antiprotons extracted from the Antiproton Decelerator (AD) from a kinetic energy of 5.3 MeV down to 100 keV. Such a low energy was motivated by the prospect of increasing the efficiency and physics opportunities of the antiproton facility [1]. However, it poses unique challenges to transport and control a beam at very low energy for instance due to potential stray fields.

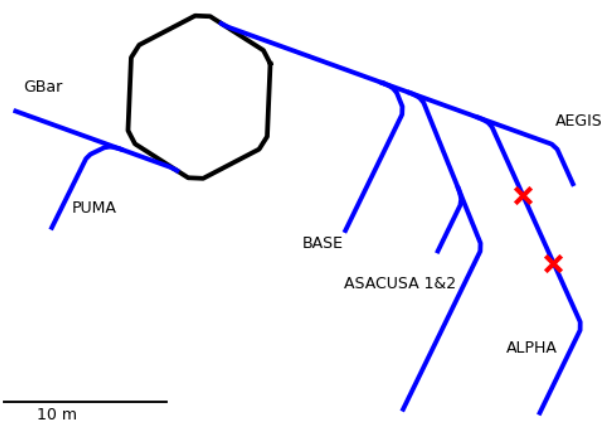

Figure 1: Layout of the ELENA experimental complex with the ring in black and extraction lines in blue. Locations of the 7 currently installed experiments are labelled and 2 red markers show vertical lines where experiments are not yet installed.

The extra low energy of the beams extracted from the ring made the use of electrostatic devices desirable. Figure 1 shows the extent of the extraction lines over the two sides of the ELENA ring. Totalling approximately 125 m of beam lines, they use 3 different types of electrostatic devices.

The first type of elements is a fast electrostatic deflector with a unique angle of 12.6° and using 400 mm long non-parallel but flat electrodes. Able to pulse (rise and fall) within less than 1 µs, it is used to deflect one or multiple bunches without affecting other bunches and it is also used in the ring to extract the circulating bunches. A total of 9 such elements are installed.

To accommodate the sharp turns between lines a second design uses a constant electrostatic field with quasi-spherical electrodes of varied angles and lengths, from 33° to 77°. There are 14 of such deflectors, including 2 of the largest angle to achieve a right angle for the branching towards the 2 vertical lines.

The third type of element is a quadrupole doublet assembly around a pair of dipole correctors, all within a single 390 mm long tank. Each quadrupole has an aperture of 60 mm and can provide an integrated quadrupole strength of up to 7.3 m^{-1}. The dipole correctors are composed of pairs of flat plates 37 mm long and may impart deflections of up to 0.57° to the beam. There are a total of 54 such assemblies installed in the beam lines to control and correct the shape and trajectory of the beam.

In total, there are 239 electrostatic elements in the ELENA extraction lines and twice that number of high voltage cables since positive and negative plates are connected to different power supplies. Each of the deflectors is connected to its own pair of power supplies while the 108 quadrupoles are connected to 75 pairs of power supplies. Such a large number of elements and limited experimental knowledge on the optical effect of such electrostatic devices makes commissioning with beam paramount to certify the performance of the lines.

BEAM COMMISSIONING

In preparation of the start of physics operation in the ELENA complex scheduled for the summer of 2021, a systematic commissioning of every extraction line was started in 2020. Using the H^- ion source [2], the beam dynamics in the extraction lines could be characterised and every element tested in advance of the scheduled start of the antiproton run. The ion source also permits a higher repetition rate of one cycle every less than 15 s compared to the antiproton repetition rate constrained by the AD cycle length of about 120 s.

* yann.dutheil@cern.ch

ISBN: 978-3-95450-227-1 ISSN: 2673-5490 doi:10.18429/JACoW-IPAC2022-WEPOTK028

IMPLEMENTATION OF RF CHANNELING AT THE CERN PS FOR SPILL QUALITY IMPROVEMENTS

P. A. Arrutia Sota *[1,2], P. N. Burrows[2], H. Damerau[1], M.A. Fraser[1], M. Vadai[1], and F.M. Velotti[1]

[1]CERN, Geneva, Switzerland
[2]University of Oxford, Oxford, UK

Abstract

Resonant slow extraction from synchrotrons aims at providing constant intensity spills over timescales much longer than the revolution period of the machine. However, the extracted intensity is undesirably modulated by noise on the machine's power converters with a frequency range of between 50 Hz and a few kHz. The impact of power converter noise can be suppressed by exploiting a Radio Frequency (RF) technique known as empty bucket channelling, which increases the speed at which particles cross the tune resonance boundary. In this contribution the implementation of empty bucket channelling in the CERN Proton Synchrotron (PS) is described via simulation and measurement. The technique was tested with both a resonant RF cavity and an inductive Finemet® cavity, which can produce non-sinusoidal waveforms, to significantly reduce the low frequency noise observed on the extracted spill.

INTRODUCTION

The CERN PS provides spills of 300 -400 ms to the East Area via third-integer resonant slow extraction. The extraction is performed by ramping all magnets in the lattice, driving the horizontal betatron tune Q_x of the beam into the resonant tune $Q_x = \frac{19}{3}$ in a controlled fashion. The tune is ramped linearly, but undesired power converter noise at low frequencies (50 ,100 ,250 Hz...) modulates this ramp. This compromises the uniformity of the extracted intensity. To first approximation, the extracted spill $I = \frac{dn}{dt}$ can be expressed as,

$$I = \frac{dn}{dt} = \rho \frac{dQ_x}{dt} = \rho[\dot{Q}_0 + \sum_i 2\pi f_i a_i \sin(2\pi f_i t + \phi_i)], \quad (1)$$

where $\rho = \frac{dn}{dQ_x}$ is the distribution of tunes in the ring, $\dot{Q}_0$ is the average tune speed across the boundary between stable and unstable betatron motion (separatrix) and a_i, f_i, ϕ_i are the i-th ripple amplitude, frequency and phase, respectively. The goal is to minimise the impact of the oscillatory terms in the sum above.

In order to quantify the quality of a given spill, we define the duty factor $\mathcal{F}_T$ as the ratio of DC power to total power in a time window of length T:

$$\mathcal{F}_T = \frac{\langle I \rangle_T^2}{\langle I^2 \rangle_T} \leq 1,$$

which can be expressed in terms of the tune by substituting I for Eq. 1 to obtain,

$$\mathcal{F} = \frac{1}{1+x}, \; x = \frac{\frac{1}{2}\sum_i (2\pi f_i)^2 a_i^2}{\dot{Q}_0{}^2}.$$

We can make x small by increasing $\dot{Q}_0$. However, if this was done by increasing the magnetic ramp speed, the spill would become shorter in time. This approach is incompatible with experimental constraints. In 1981, a technique known as empty bucket channelling [1] was developed that utilises an RF cavity to provide large $\dot{Q}_0$ near the resonance, while leaving the extraction time unaffected. In this contribution we explore this manipulation via simulation and experiment.

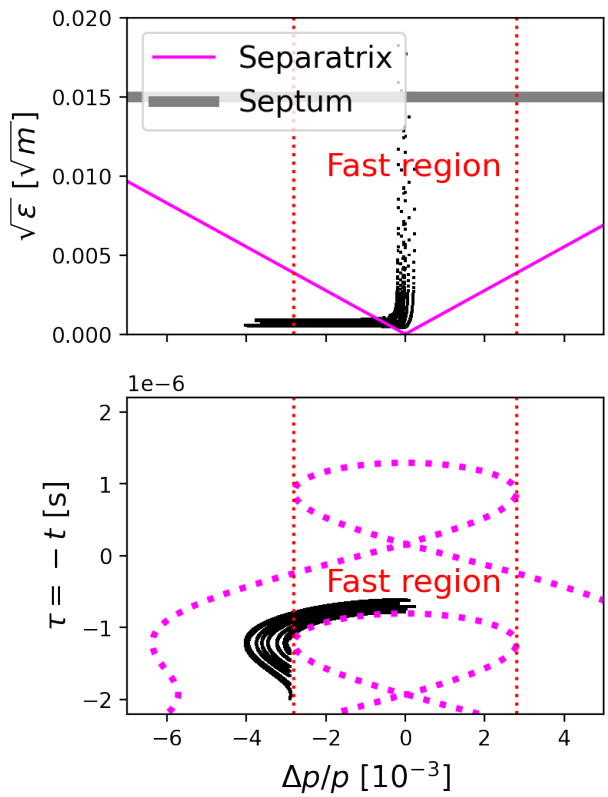

Figure 1: Illustration of the empty bucket channelling technique. Particles cross the resonance separatrix (top) while channelling between consecutive buckets (bottom).

* pablo.andreas.arrutia.sota@cern.ch

ISBN: 978-3-95450-227-1 ISSN: 2673-5490 doi:10.18429/JACoW-IPAC2022-WEPOTK029

ADVANCES IN LOW ENERGY ANTIMATTER BEAM GENERATION AND MANIPULATION *

C. P. Welsch†, University of Liverpool/Cockcroft Institute, UK

Abstract

The Accelerators Validating Antimatter physics (AVA) project has enabled an interdisciplinary and cross-sector R&D program on low energy antimatter research. The network comprises 13 universities, 9 national and international research centers and 13 partners from industry. Between 2016 and 2021, AVA has successfully trained 16 early-stage researchers that were based at universities, research centers and companies across Europe where they carried out cutting edge research into low energy antimatter physics and related technologies. This paper presents several research highlights that originated within or on the basis of AVA: Results from studies into carbon nanotubes as field emitters for cold electron beams with superior beam quality, the design of a low energy negative ion injection beamline for experiments with antiprotonic atoms, and studies into realistic simulations of antiproton deceleration in foil degraders.

INTRODUCTION

The project Accelerators Validating Antimatter physics (AVA) has enabled an interdisciplinary and cross-sector R&D program on antimatter research at the AD and the future FLAIR facility in Germany [1]. The network comprises 13 universities, 9 national and international research centers and 13 partners from industry. During the project duration it has successfully trained 16 early-stage researchers that were based at universities, research centers and companies across Europe where they carried out cutting edge research into low energy antimatter physics and related technologies.

Each Fellow also benefited from a comprehensive training program. In addition to research-based training at their host institution, they received a wider network-based training, including scientific schools, workshops, as well as training in complementary skills, enhancing their future employability. In the following section examples of research results in or on the basis of the AVA project that are presented at this year's IPAC conference are given, along with a summary of the scientific events that have been organized by the AVA consortium to date.

RESEARCH OUTCOMES

The AVA partners carried out a closely connected R&D program that span across three scientific work packages:

- **Facility Design and Optimization**;
- Design, development and testing of novel **Beam Diagnostics**;
- Design of novel low energy **Antimatter Experiments**.

The research within AVA has already led to a number of high impact physics results: This includes the measurement of ultralow heating rates of a single antiproton in a cryogenic Penning trap [2], the production of long-lived positronium via laser excitation in magnetic and electric fields [3], and the measurement of sympathetic cooling of protons and antiprotons with a common endcap Penning trap [4]. The following sections summarize accelerator-related research results from selected projects.

Stability and Lifetime Studies of Carbon Nanotubes for Electron Cooling in ELENA

The Extra Low ENergy Antiproton (ELENA) ring at CERN [5] will provide cooled, high quality beams of antiprotons with kinetic energies of 100 keV at intensities exceeding those achieved at the Antimatter Decelerator by a factor, depending on the experiment, of between ten to one hundred. The aim of studies by AVA Fellow Bruno Galante was to identify new ways to produce a mono-energetic and relatively intense electron beam. Based at CERN, he carried out optimization studies into the electron gun of the ELENA cooler with a focus on using a cold cathode based on carbon nanotubes (CNTs).

A cold cathode has good potential to bring a number of benefits in terms of the achievable electron beam energy and the overall simplicity of the gun itself. CNTs can emit relatively high currents while being mechanically stable and chemically inert [6, 7]. A honeycomb-like array was studied in detail [8] and CNT samples were characterized in terms of their stability, lifetime and overall performance during current switching.

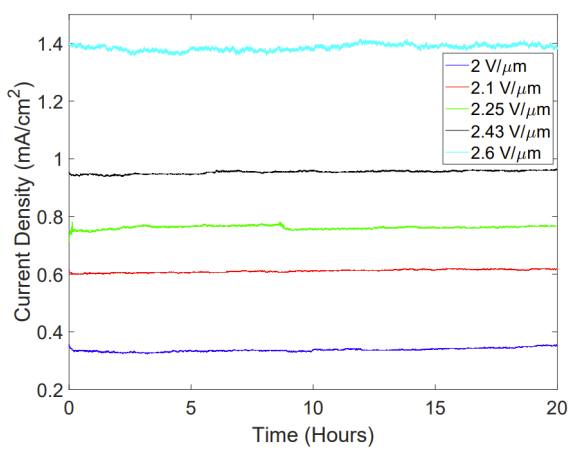

Figure 1: Current density as a function of time (hours) and electric field (V/μm). Five different measurements of 20 hours each at five different applied electric fields [8].

* This project has received funding from the European Union's Horizon 2020 research and innovation programme under the Marie Skłodowska-Curie grant agreement No 721559.
† c.p.welsch@liverpool.ac.uk

ISBN: 978-3-95450-227-1 ISSN: 2673-5490 doi:10.18429/JACoW-IPAC2022-WEPOTK030

MODELLING GROWTH AND ASYMMETRY IN SEEDED SELF-MODULATION OF ELLIPTICAL BEAMS IN PLASMA

A. Perera*, O. Apsimon, C.P. Welsch
University of Liverpool, Liverpool, UK and the Cockcroft Institute, Warrington, Cheshire, UK

Abstract

The seeded self-modulation (SSM) of long particle bunches for the generation of gigavolts-per-meter wakefields that can accelerate witness electron beams was first shown using the SPS beam as a driver by the AWAKE experiment. The stability of the produced microbunch trains over tens or hundreds of meters is crucial for extrapolating this scheme as proposed for use in several high energy plasma-based linear colliders. However, aside from the competing hosing instability, which has been shown to be suppressible by SSM when that process saturates, few works have examined other effects of transverse asymmetry in this process. Here, we use analytical modelling and 3D particle-in-cell simulations with *QuickPIC* to characterise the impact on the SSM growth process due to transverse asymmetry in the beam. A metric is constructed for asymmetry in simulation results, showing that the initial azimuthal complexity changes only slightly during SSM growth. Further, we show quantitative agreement between simulations and analytical predictions for the scaling of the reduction SSM growth rate with unequal aspect ratio of the initial beam profile. These results serve to inform planning and tolerances for both AWAKE and other SSM-based novel acceleration methods in the future.

INTRODUCTION

Proton-driven plasma wakefield acceleration (PDPWFA), has been proposed to overcome the problem of energy depletion of drivers in previous experiments, with the view of application towards a new generation of plasma-wakefield-based colliders for high energy physics research. However, current high-energy-content bunches, such as those of the Super Proton Synchrotron (SPS) used in AWAKE are too long by two orders of magnitude to efficiently drive a wakefield in plasma of suitable density . Therefore, the concept relies on the self-modulation of the long proton bunch in plasma due to an initial weak 'seed' wakefield driven by the unmodulated bunch which causes the bunch to compress and diverge at periodic intervals along its length. The resulting train of shorter micro-bunches, if formed so that they are positioned correctly within the wakefield [1], can then resonantly excite much stronger accelerating gradients in the plasma to accelerate a witness beam [2].

Seeding the self-modulation process requires an initial wakefield with a sufficiently strong longitudinal component at the plasma wavelength, $\lambda_p = 2\pi c\sqrt{\frac{m_e\epsilon_0}{n_p e^2}}$, where n_p is the plasma density, ϵ_0 is the permittivity of free space, c is the speed of light, and m_e and e are the electron mass and charge, respectively. This may be achieved by a smaller preceding bunch as proposed in AWAKE Run 2 [3] or by ionising the plasma with a co-propagating laser pulse placed at the midpoint of the Gaussian proton beam to create a discontinuity in beam longitudinal profile as seen by the plasma [4]. Such seeding is required to control the initial phase of the modulation process along the longitudinal beam profile, to ensure an efficient resultant microbunch arrangement upon saturation of the SSM growth [5].

It has been shown by numerical investigations in previous works that the seeded self-modulation (SSM) process may be sensitive to beam parameters such as emittance and radial spot size [6]. However, such works have almost consistently considered only transversely round bunches. Previously, it was shown that even slightly unequal aspect ratio of the driving beam leads to strong asymmetric profiles of the resultant microbunches [7] which is reflected in the transverse profiles of the resultant wakefields [8]. More recently, [9] has demonstrated the variation of the event-to-event aspect ratio of the SPS beam by as much as 15%. Here we present a metric constructed to represent the asymmetry of the beam transverse profile beyond parameterisation with only root-mean-square sizes. The examination of its evolution during the SSM growth is used to justify the model we derived in [10]. Finally a method for extracting a parametric dependence of the initial aspect ratio of the drive beam from simulations of the SSM process is outlined and used to verify the scaling of the model in [10] with initial aspect ratio.

SIMULATION SET-UP

Simulations were carried out using the 3D quasi-static particle-in-cell (PIC) code *QuickPIC* [11]. We use a uniform plasma density, $n_p = 7 \times 10^{-14}\,\mathrm{cm}^{-3}$, corresponding to a plasma skin-depth of $c/\omega_p = k_p^{-1} = 200\,\mu\mathrm{m}$, on a grid of $1024 \times 1024 \times 4096$ cells, spanning a volume of $12 \times 12 \times 130\,(c/\omega_p)^3$ in x, y, and ξ with 4 particles per cell. Here ξ is a co-moving coordinate along the length of the beam, defined in terms of the propagation length, s, and longitudinal coordinate in the lab frame, z, as $\xi = s - z$. The long proton bunches were initialized with parameters similar to the SPS bunches arriving at AWAKE, as transversely bi-Gaussian beams with root-mean-square radius $\sigma_r = 1.0$, Lorentz factor $\gamma_b = 427$ and equal x and y rms emittances of 3.5 mm mrad, but neglecting the 0.035% momentum spread. The self-modulation seed was achieved by using a sharp longitudinal density step up to the maximum density in the beam profile at $\xi = 0$, placed $2\,c/\omega_p$ from the front edge of the simulation window. Since we are interested in the general behaviour of elliptical SSM, and since the longitudinal

* aravinda.perera@liverpool.ac.uk

ISBN: 978-3-95450-227-1 ISSN: 2673-5490 doi:10.18429/JACoW-IPAC2022-WEPOTK031

LOW-ENERGY NEGATIVE ION INJECTION BEAMLINE FOR EXPERIMENTS WITH ANTIPROTONIC ATOMS AT AEgIS

V. Rodin*, A. Farricker, C. P. Welsch,
University of Liverpool, UK and The Cockcroft Institute, Daresbury, UK
M. Doser, G. Khatri
CERN, Geneva, Switzerland
G. Cerchiari,
Institut für Experimentalphysik, Innsbruck, Austria
G. Kornakov†
Warsaw University of Technology, Warsaw, Poland

Abstract

The interaction of low-energy antiprotons with nuclear targets provides fundamental knowledge about proton and neutron densities of many nuclei through the capture process, cascade on lower electron orbits, and annihilation with the nucleon. The expelled electrons produce X-rays and with the recoil particles after annihilation, thus, a sufficient amount of information can be obtained about this interaction. However, all previous experiments were done via formation of antiprotonic atoms in solid or gaseous targets. Therefore, annihilation occurs prior to reaching the S or P orbital levels and precise measurements are missing. Recently, the AEgIS collaboration [1] proposed a conceptually new experimental scheme. The creation of cold antiprotonic atoms in a vacuum guarantees the absence of the Stark effect. And with sub-ns timing and synchronization, previous experimental obstacles would be resolved. This will allow atomic properties, evolution, and fragmentation processes to be studied with improved precision and extended lifetimes. In this paper, an overview of the experimental scheme is given, along with details on the negative ion injection beamline in the AEgIS experiment.

INTRODUCTION

Novel approaches to study bound systems containing antiprotons such as light anti-nuclei, protonium, and other atoms or ions, where one of the orbital electrons is replaced by an antiproton will create new opportunities for studies into fundamental processes in nuclear and atomic physics.

Antiprotonic atoms may become a “swiss knife" that will uncover various properties of different nuclei, stable and radioactive isotopes, in a more precise way. Two of the well-known applications of such atoms, are the identification of neutron and proton densities on the surface of the nucleus, and the estimation of the neutron skin thicknesses for neutron-rich atoms [2]. The annihilation of antiprotons is most likely followed by meson emission, with the dominating process being pion production.

The reconstruction of annihilation inside antiprotonic atoms confined in a trap, paves the way for event-by-event detection of the emitted X-rays along with the determination of the charge multiplicity of the annihilation, We are able to resolve antiproton annihilations on protons (secondary pion charge = 0) from those on neutrons (secondary pion charge = −1) as long as all secondaries resulting from the annihilation are identified correctly.

In some cases, a final nucleus ${}^{A-1}_{Z-1}X$ or ${}^{A-1}_{Z}X$ may have a recoil energy that is low enough to remain trapped inside a particle trap. These fragments will help further understand the interaction between an antiparticle and an initial atomic nucleus.

Additionally, investigations into antiprotonic systems will allow a wide range of exotic physics topics covered in the recent reviews about existing and approachable in the near term experiments with an antimatter to be investigated [3–5].

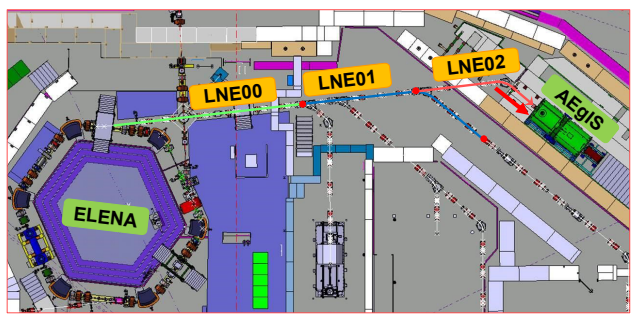

Figure 1: Top view CAD model of part of the AD hall with ELENA and the AEgIS experiment highlighted. Antiproton transfer is done via three electrostatic sections (LNE).

Low energy operation will improve atom formation and the trapping efficiency of antiprotons that is required for the proposed studies. Thus, the ELENA ring [6] in CERN’s Antimatter Factory remains the only facility capable of providing low energy (100) antiproton bunches, which are further slowed down to trappable energies (<5 keV) using drift tubes, an RFQ or moderating foils.

AEgIS is one of the experiments located in AD hall [1], performing studies into the formation of $\bar{H}$ and, primarily, gravity experiments with cold antimatter. The CAD model

* volodymyr.rodin@liverpool.ac.uk
† Research was funded by Warsaw University of Technology within the Excellence Initiative: Research University (IDUB) programme

ISBN: 978-3-95450-227-1 ISSN: 2673-5490 doi:10.18429/JACoW-IPAC2022-WEPOTK032

FAST ELECTROMAGNETIC MODELS OF EXISTING BEAMLINE SIMULATIONS

S. Padden*[1,2], P. Pusa[2], C. P. Welsch[1,2], V. Rodin[1,2,3], E. Kukstas[1,2]
[1]The Cockroft Institute, Daresbury, United Kingdom
[2]University Of Liverpool, Liverpool, United Kingdom
[3]CERN, Geneva, Switzerland

Abstract

The AD-ELENA complex decelerates antiprotons to energies of 100 keV before transport to experiments through electrostatic transfer lines. Transfer line optics are traditionally designed from a lattice based approach and are unaffected by external effects. Presented is a method of rapidly prototyping MAD-X simulations into G4Beamline models which propagate particles via electromagnetic fields rather than idealised optical lattice parameters. The transfer line to the ALPHA experiment is simulated in this approach. Due to the presence of fringe fields disagreement is found between the two models. Using an error minimisation technique, revised quadrupole strengths are found which improve agreement by 30% without any manual adjustment.

INTRODUCTION

The AD-ELENA (Antiproton Decelerator - Extra Low ENergy Antiproton) complex decelerates anti-protons ($\bar{p}$) down from 5.3 MeV to energies of 100 keV. After deceleration $\bar{p}$ are then transferred to and subsequently trapped by experiments, however experiments require energies in the sub 10 keV range to trap $\bar{p}$ efficiently. To achieve this, experiments routinely use destructive degrader foils which significantly impact the number of available $\bar{p}$ in the traps. Work is ongoing to model degrader foils using density functional theory in combination with molecular dynamics [1] to fine-tune foil degrader thickness, maximising the number of $\bar{p}$ available for trapping. In the process of this modelling it is important to have accurate simulations of the beam profile at the point of handover between ELENA transfer lines and experimental setups, as such the electrostatic transfer line which carries $\bar{p}$ from ELENA to ALPHA (Antihydrogen Laser PHysics Apparatus) is simulated in G4Beamline [2]. Previous work has shown the approaches used in modelling the electrostatic optics as well as the static bending elements within the beam to be effective [3].

Presented in this work is a new method of rapidly prototyping realistic simulations from existing MAD-X [4] models which use lattice based structures, into one which models a voxelised world space whereby electromagnetic fields determine the motion of particles. Electromagnetic fields are generated by realistically modelled structures, with quadrupole field gradients calculated directly from integrated field strengths returned from MAD-X. Whilst current work focuses on the ALPHA transfer line, with some user modification the method presented is extensible for any transfer line that uses repeated optical structures.

By utilising Enge style functions to model fringe fields [5], quadrupoles are modelled in a more realistic manner. The impact of these is seen as an increase in the quadrupole's effective length in G4Beamline simulations, causing a discrepancy between the beta values returned by MAD-X and those from G4Beamline. Similarly with sufficient modelling, the impact of any stray fields can be included and suitably accounted for [6].

The effects of fringe fields are reduced by development of a beta matching minimisation algorithm, resulting in significantly greater agreement between the two models.

TRANSFER LINE MODELLING

A number of transfer lines exist after ejection from ELENA. Extraction from ELENA is handled by a small kick fast deflector, similarly these are used for the shifting between beamlines. A number of static deflectors handle larger bends and are often situated directly after a fast deflector to produce a larger bend than the fast deflector could handle alone.

Optical Structures

Optical structures are built in a modular fashion, with each FODO cell (A repeated optical structure consisting of focusing and defocusing quadrupoles with drift spaces) consisting of 2 quadrupoles, and 2 corrector magnets sat in the space between each quadrupole. Although the geometrical structure of each FODO cell is identical to another, the electrostatic quadrupoles can be fine-tuned to aid in the focusing of the beam.

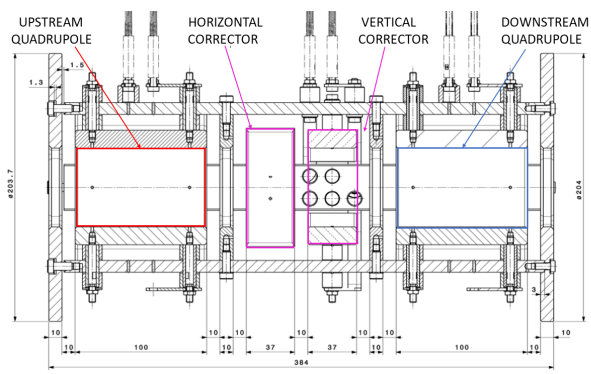

Figure 1: Schematic of a modular FODO cell utilised in the transfer lines.

* Spadden@liverpool.ac.uk

ISBN: 978-3-95450-227-1 ISSN: 2673-5490 doi:10.18429/JACoW-IPAC2022-WEPOTK033

LAYOUTS FOR FEASIBILITY STUDIES OF FIXED-TARGET EXPERIMENTS AT THE LHC

P. D. Hermes*, K. Dewhurst, A. Fomin, D. Mirarchi, S. Redaelli
European Organization for Nuclear Research (CERN), Geneva, Switzerland

Abstract

The Physics Beyond Colliders (PBC) study investigates means of exploiting the potential of the CERN accelerator complex to complement the laboratory's scientific programme at the main Large Hadron Collider (LHC) experiments. The LHC fixed-target (FT) working group studies new experiments at beam energies up to 7 TeV. One of the proposed experiments is based on a bent crystal, part of the collimation hierarchy, to extract secondary halo particles and steer them onto a target. A second bent crystal immediately downstream of the target is used to study electric and magnetic dipole moments of short-lived baryons. The possibility to install a test stand in the LHC off-momentum collimation Insertion Region (IR3) to demonstrate the feasibility and performance of this challenging scheme is currently under investigation. The integration of a spectrometer magnet into the present layout is particularly critical. In this contribution, we study a possible test setup which could be used in LHC Run 3.

INTRODUCTION

The CERN Large Hadron Collider (LHC) is the world's largest collider, designed to accelerate protons to energies of up to 7 TeV [1]. The Physics Beyond Colliders (PBC) study explores the opportunities offered by the CERN accelerator complex, including the LHC and its High Luminosity upgrade HL-LHC [2], to complement the goals of the main experiments of the laboratory's collider programme. The LHC fixed-target (FT) working group addressed gas-target and in-beam fixed-target experiments [3–5]. Different possible implementations in various regions of the LHC are currently under investigation for in-beam targets based on bent-crystals: the LHC momentum collimation region IR3 [6] or IR8, housing the LHCb experiment [7] are considered for the so-called double-crystal setup [8–13], while IR2, hosting the ALICE experiment [14, 15], is considered for conventional targets [16]. The integration of a proof-of-principle setup in IR3 is considered for beam tests at the LHC to collect important information for the validation of the layouts and their performance and to demonstrate the feasibility of these implementations.

Figure 1 illustrates the considered concept for the integration of the FT setup compatibly with the collimation hierarchy. It relies on planar channelling in bent crystals: charged particles channelled between the crystalline planes are forced to follow the geometrical bending of the crystal [17]. A first crystal (CRY1) intercepts particles in the secondary beam halo (produced by the betatron collimators in IR7 [6]) to create sufficient separation between channelled protons and the main beam, such that they hit a solid target, e.g. made of tungsten, located downstream at a safe transverse distance. The double-crystal setup involves a second crystal (CRY2) immediately adjacent to the target, to study the electric and magnetic dipole moments of short-lived baryons like the Λ_c^+, see [5] and references therein. One or multiple collimators are needed to intercept and safely absorb the channelled halo. A test has demonstrated the principle of the double-channelling setup with protons in the CERN SPS at 270 GeV [18]. Experimental data for higher beam energies has to be gathered, in particular to demonstrate the feasibility of this scheme in the specific LHC beam conditions. CRY1 in the IR3 layout is similar to the crystals used at the LHC for crystal collimation [19, 20] while CRY2 needs to provide a larger bending angle of 5 mrad [21, 22].

GOALS OF LHC BEAM TESTS

Given the complexity of the double-crystal setup in the LHC, crucial information could be gathered by a test under realistic conditions with beam in the LHC in the Run 3 at the planned operating energy of 6.8 TeV. Various high-priority goals are identified. The performance of the large-bending crystal shall be assessed in the energy range relevant for the LHC experiments. The baryon energy of interest is in the order of 1-2 TeV. This range is only accessible at the LHC, and the proposed setup shall enable the characterization at even larger beam energies.

The achievable performance in terms of protons on target is estimated with complex simulations of the multi-turn dynamics of the LHC beam halo, in presence of the tight betatron collimation hierarchy. A validation of these simulations shall be carried out to provide a solid experimental benchmark. This will provide important input for the specification of operational scenarios and performance estimates that critically depend on simulations and are potentially affected by unknown machine imperfections.

Various operational challenges, e.g., the alignment strategy of CRY2, to establish reference positions with respect to the circulating beam and the split halo produced by CRY1, are to be assessed experimentally before relying on this scheme. One crucial aspect to be studied with beam is the possibility of aligning the CRY2 using the main proton beam at low intensity and then to set it to achieve double-channelling reliably at the LHC energies, with adequate efficiencies. Other operational challenges that can be addressed involve the setup of orbit and optics changes that are studied on paper to optimize the performance.

* pascal.hermes@cern.ch

ISBN: 978-3-95450-227-1 ISSN: 2673-5490 doi:10.18429/JACoW-IPAC2022-WEPOTK034

LHC BEAM COLLIMATION DURING EXTENDED BETA*-LEVELLING IN RUN 3

F.F. Van der Veken*, R. Bruce, M. Hostettler, D. Mirarchi, S. Redaelli, CERN, Meyrin, Switzerland

Abstract

During the third operational Run of the Large Hadron Collider at CERN, starting in 2022, the bunch population will be increased to unprecedented levels requiring to deploy β^*-levelling of the luminosity over a wide range of values to cope with the limitations imposed by event pile-up at the experiments and heat load on the triplets induced by collision debris. During this levelling, both beam optics and orbit change in various areas of the ring, in particular around the high-luminosity experiments, where several collimators are installed. This requires adapting the collimation system settings adequately, in particular for the tertiary collimators (TCTs) that protect the inner triplet magnets. To this end, two strategies are considered: keeping collimators at fixed physical openings while shifting their centres following the beam orbit, or varying also the collimator openings. The latter strategy is planned when the larger optics range will be deployed. In this paper, we investigate several loss scenarios at the TCTs in different steps of the levelling, and present the proposed collimator settings during Run 3.

INTRODUCTION

In recent years, the performance of the Large Hadron Collider (LHC) at CERN [1] has been pushed to unprecedented levels [2]. In the present configuration, the maximum instantaneous luminosity is about $2 \cdot 10^{34}$ cm^{-2}s^{-1} limited by the cryogenic conditions at the triplet magnets around the high-luminosity experiments and by the number of collisions per beam crossing (pile-up). This limitation requires the use of a levelling scheme [3], where the collider is operated at a constant luminosity with a value below the achievable virtual maximum luminosity of $3.5 \cdot 10^{34}$ cm^{-2}s^{-1}. Luminosity levelling by changing the colliding β function, β^*, is envisaged. The first successful use of β^*-levelling at the LHC was done in 2018 after being verified in dedicated tests [4–6]. This was an important milestone for the upcoming high-luminosity upgrade for the LHC [7, 8], where β^*-levelling is essential.

For the third Run of the LHC (2022-2025), β^*-levelling will be a part of the operational cycle, with a range from $\beta^* = 60$ cm to 30 cm in the first year, and an extended levelling range from 120 cm to 30 cm in the following years [9]. The optics around the high-luminosity experiments, where the β^*-levelling is performed, will vary strongly as a function of the β^* value. Hence dedicated strategies need to be put in place for the settings of the jaw openings of the tertiary and physics debris collimators in the insertion regions (IRs), which are installed in these areas [10]. The rest of the collimation system is not affected by these local changes.

* frederik.van.der.veken@cern.ch

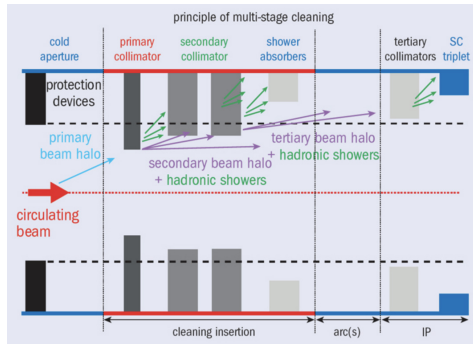

Figure 1: Hierarchy of the LHC collimation system.

COLLIMATION AROUND EXPERIMENTS

To protect the triplet magnets around the experimental insertions during collisions, the LHC collimation system includes collimators upstream of the interaction point (IP), made of a tungsten alloy and sitting as tertiary stage of the transverse betatron hierarchy, the so-called TCTs (see Fig. 1) [1, 10]. Their half-gap settings are defined at the smallest β^*, as this is the most constraining case for the triplet aperture. If the TCT settings at smallest β^* protect the triplets, they do so for all larger β^* in the range considered, so one could keep the same jaw opening in mm for the full β^*-range. These settings are reported in Table 1. Collimator half-gaps are expressed in RMS beam size units, defined as:

$$\sigma = \sqrt{\beta \epsilon_n / \beta_r \gamma_r}\,, \tag{1}$$

where β is the betatron function at the collimator, $\epsilon_n = 3.5\ \mu$m is the nominal normalised emittance, β_r is the relativistic speed, and γ_r is the relativistic Lorentz factor.

At the Run 3 collision energy of 6.8 TeV, the half-gaps of primary and secondary collimators of the betatron system are set to 5σ and 6.5σ, respectively. In order to respect the hierarchy, the TCT half-gap should hence be larger than this, including operational margins to account for imperfections studied in detail in [11]. The minimum TCT setting is further limited by the requirement to avoid damage in case of fast failures like asynchronous beam dumps: the TCTs should be shadowed by the dump protection collimator (TCDQ). This sets a tolerance on the phase advance between dump kickers and any TCT, which must be lower than 30°off the optimal (0°or 180°) [11, 12]. Accounting for the phase advance in the Run 3 optics and the available triplet magnet aperture, a TCT setting of 8.5 σ will be used at $\beta^* = 30$ cm.

The phase advance between the dump kickers (MKD) and the TCDQ can no longer be kept constant for a levelling range with initial β^* above 60 cm [13]. This changes the

ISBN: 978-3-95450-227-1 ISSN: 2673-5490 doi:10.18429/JACoW-IPAC2022-WEPOTK035

LAYOUT OF THE 12 O'CLOCK COLLIMATION STRAIGHT SECTION FOR THE EIC HADRON STORAGE RING*

G. Robert-Demolaize†, J. Scott Berg, B. Bhandari, A. Drees, D. Holmes, H. Lovelace III, S. Peggs, M. Valette, Brookhaven National Laboratory, Upton, NY, USA

Abstract

The design of the Electron-Ion Collider (EIC) Hadron Storage Ring (HSR) calls for using parts of both of the Relativistic Heavy Ion Collider (RHIC) Blue and Yellow rings. With the HSR having to circulate low (41 GeV/u) and high (100+ GeV/u) energy hadron beams while matching the time of flight in the Electron Storage Ring (ESR), it becomes necessary for the ring lattice to switch from an outer arc to an inner arc in order to accommodate the change in circumference. To do so, a switchyard is planned for installation in the HSR straight section at 12 o'clock with the other switchyard being placed in the straight section immediately downstream, 10 o'clock. The 12 o'clock area is simultaneously dedicated to the EIC 2-stage collimation system. The following reviews the layout constraints in the 12 o'clock straight section that come with installing such a switchyard, along with the implications on the linear optics for that straight section at all HSR rigidities. The space allocation, Twiss parameters and the mechanical requirements of the HSR betatron collimators that will be installed in this section are also discussed.

INTRODUCTION

The Electron-Ion Collider (EIC) [1–3] features two storage rings, one for electrons and one for hadrons. The Hadron Storage Ring (HSR) accommodates a broad range of energies in order to deliver collisions at center of mass energies from $\sqrt{s_{e-h}}$ = 20 GeV to 140 GeV. To enforce the synchronicity between electron (ESR) and hadron (HSR) rings, and since electrons are ultra-relativistic at their EIC energies, it becomes necessary to adjust the HSR circumference. Table 1 lists the required circumference changes, along with the equivalent radius changes, for HSR operations.

The ΔC for protons at 100-275 GeV, as well as for Au ions at 110 GeV/u, can be accommodated by dedicated Radial Shift schemes [4]. The operations at lower energies (protons at 41 GeV, Au at 40.7 GeV/u) require such a large change that it can only be achieved if one of the three outer arcs from the baseline HSR design is replaced by one of the inner arcs left over from RHIC, since the difference in arc length between inner and outer is around 900 mm. In the baseline design there are three outer HSR arcs, located between the "clock" markers 4-6, 8-10, and 10-12. Out of these three, only the 10-12 outer arc can have an alternate inner arc since the 6 o'clock and 8 o'clock areas are designed as hosts for experimental detectors. For low energy operations, the hadron beam is rerouted through this inner arc using two switchyards placed in the neighboring straight sections: 10 o'clock [5], and 12 o'clock.

Table 1: Primary hadron beam parameters and circumference changes for EIC operations over the range $\sqrt{s_{e-h}}$ = 20-140 GeV [1], including energy E, Lorentz factor γ_{rel}, velocity β, required circumference change ΔC, and the average radial offset $\langle \Delta R \rangle$. Protons pass through 3 inner and 3 outer arcs except at 41 GeV, when they pass through 4 inner and 2 outer arcs.

E_{tot} GeV(/u)	γ_{rel}	$1-\beta$ 10^{-3}	C m	ΔC mm	$\langle \Delta R \rangle$ mm
PROTONS					
41.0	43.70	0.2619	3832.92	-908.7	–
100	106.58	0.0440	3833.75	-73.4	-11.7
133	141.75	0.0249	3833.82	0.0	0.0
275	293.09	0.0058	3833.90	73.1	11.6
GOLD IONS					
40.7	43.70	0.2619	3832.92	-908.7	–
110	118.09	0.0359	3833.78	-42.1	-6.7

The 12 o'clock straight section is also planned as the location of the multi-staged HSR collimation system, on top of being the ESR injection region and having a crossover of the ESR ring as well. This has strong implications on the placement of the switchyard itself, which in turns affect the placement of the HSR collimators. Additionally, having two possible paths for the circulating hadron bunches implies that parts of the collimation system have to be duplicated to make sure that the multi-stage approach applies to all energies. The HSR linear optics of the 12 o'clock area are therefore adjusted by taking into account simultaneously the beam size requirements from the switchyard and the phase advance constraint from the collimation system.

MECHANICAL LAYOUT OF THE INNER/OUTER SWITCHYARD

The main difference between the RHIC and HSR layouts comes from the removal of the DX magnets that are the innermost bending dipoles placing the counter-rotating RHIC beams on their common colliding path. These dipoles cannot be used in the HSR due to mechanical (transverse aperture) and magnetic (attainable peak field at 275 GeV) limitations. As a consequence, the common section is removed and it is the D0 dipoles, the dipoles closest to the DX locations, that transport the beam from one side of the straight section to the other. With the 12 o'clock area having to allow for a switch between the inner and outer arcs on the downstream

* Work supported by the US Department of Energy under contract No. DE-SC0012704.
† grd@bnl.gov

ISBN: 978-3-95450-227-1 ISSN: 2673-5490 doi:10.18429/JACoW-IPAC2022-WEPOTK036

PROGRESS ON ELECTRON BEAM OPTIMIZATION FOR FLASH RADIOTHERAPY EXPERIMENT AT CHIANG MAI UNIVERSITY

K. Kongmali*[1], P. Apiwattanakul[2], N. Kangrang, S. Rimjaem†[3], J. Saisut[3], C. Thongbai[3]
PCELL, PBP, Faculty of Science, Chiang Mai University, Chiang Mai, Thailand
M. Jitevisate, School of Physics, Suranaree University of Technology,
Nakhon Ratchasima, Thailand
P. Lithanatudomg, Department of Biology, Faculty of Science, Chiang Mai University,
Chiang Mai, Thailand
[1]also at Ph. D. Program in Physics (International Program),
Chiang Mai University, Chiang Mai, Thailand
[2]also at Master Program in Physics, Chiang Mai University, Chiang Mai, Thailand
[3]also at ThEP Center, MHESI, Bangkok, Thailand

Abstract

At present, one of diseases that kills many people worldwide is cancer. The FLASH radiotherapy (RT) is a promising cancer treatment under study. It involves the fast delivery of RT at much higher dose rates than those currently used in clinical practice. The very short time of exposure leads to the destruction of the cancer cells, while the nearby normal cells are less damaged as compared with conventional RT. This work focuses on study of FLASH-RT experiment using electron beams produced from the accelerator system at the PBP-CMU Electron Linac Laboratory. The structure and properties of our electron pulses with microbunches in picosecond time scale and macropulses in microsecond time scale match well to FLASH-RT requirement. To optimize the condition for experiment, the electron beam simulations are performed by varying energy, charge and bunch length. The 25 MeV electrons energy before hitting the window for 50 and 100 pC bunch length have a bunch length of 1.16 and 1.97 ps. The transverse rms beam sizes of 50 pC and 100 pC bunch charges have the differences between ASTRA and GEANT4 from 7.90% to 34.0%. The optimized electron beam properties from this study will be used as the guideline for further simulation and experiment preparation.

INTRODUCTION

FLASH radiotherapy (RT) is the current trend option to treat the cancer cell. The concept of fast delivery of radiation or charged particle beam with high dose rate has high efficient capability to kill cancer cells, while the healthy cells nearby are unharmed. This kind of RT using electron beam has been developed in many facilities. In Armenia, there is the Advanced Research Electron Accelerator Laboratory (AREAL), which focuses on ultra-short electron beam pulses in energy range of 2 - 5 MeV. They study the effect of the dose rate in DNA by investigating the damage and repair process in vitro experiment [1, 2]. In Germany, there is the Helmholtz Institute Jena (HI Jena), which studied about the radio-biological effect when irradiating the electron beam on tumour cells. The electron pulses have energy in a range of 2 - 45 MeV [3, 4]. In 2016, they used the laser-based accelerator to produce electron pulses with ultra high dose rate. They compared the electron beam irradiation with high and low dose rate to study the effect in the normal cells [5].

The accelerator system at the PBP-CMU Electron Linac Laboratory (PCELL) has potential to produce electron beam with properties suitable for studying the RT with high dose rate. At our facility, electrons are generated from a thermionic cathode RF-gun. Then, they are accelerated through the gun cavities and travel to the alpha magnet. After exiting the alpha magnet, the electron bunches are accelerated in the RF-linac to reach maximum energy of up to 25 MeV. The electron beam properties including energy of 6 - 25 MeV, macropulse of 1 - 4 μs , microbunch of 0.3 - 1 ps, variable high current, and low emittance are well suit for FLASH-RT experiment. The experimental set up for the cell irradiation will be placed at the end of the beam dump as shown in Fig. 1. The computer simulations are used to study the dynamics of the electron beam. The aim of this work is to optimize the electron beam to reach the FLASH-RT conditions. The preliminary results from the simulations using ASTRA and GEANT4 program are presented in this work [6, 7].

METHODOLOGY

The research team at PCELL plans to study the FLASH-RT experiment by using electron beams with high dose rate ($\geq$ 40 Gy/s), which is defined for the FLASH-RT [8]. To reach the FLASH conditions, the electron beam has to be optimized. The electron beam dynamic simulation was performed by using a computer program ASTRA [6]. The space charge effects were included in this investigation. Electrons were generated in the RF-gun with 4 million macro-particles. The RF-wave separates the macroparticles into groups called microbunches. These electron bunches travel through the alpha magnet with a fixed gradient of 300 G/cm. The energy slit installed inside the vacuum chamber of the alpha magnet was used to choose the charge of electron bunch

* oom_b.pong2@hotmail.co.th
† sakhorn.rimjaem@cmu.ac.th

ISBN: 978-3-95450-227-1 ISSN: 2673-5490 doi:10.18429/JACoW-IPAC2022-WEPOTK037

RADIATION OF A PARTICLE MOVING ALONG A HELICAL TRAJECTORY IN A RESISTIVE-WALL CYLINDRICAL WAVEGUIDE*

M. I. Ivanyan†, B. Grigoryan, B. Sargsyan, A. Grigoryan[1], CANDLE SRI, Yerevan, Armenia,
K. Floettmann, F. Lemery, Deutsches Elektronen-Synchrotron, Hamburg, Germany
[1]also at Yerevan State University, 1 Alex Manoogyan, Yerevan, Armenia

Abstract

The radiation field of a particle moving on a helical trajectory in a cylindrical waveguide with resistive walls is calculated. The deformation of the energy spectrum of radiation as a result of the finite conductivity of the walls is investigated.

INTRODUCTION

The helical motion of a charged particle considered in this work simulates the operation of a helical undulator, which is widely used as a source of circularly polarized synchrotron radiation and FEL designs [1, 2]. Insertion of the helically moving particle in a cylindrical waveguide converts the radiation energy spectrum from continuous to discrete [3]. With an appropriate selection of parameters, it becomes possible to concentrate most of the radiation power at one frequency and, thereby, create a source of monochromatic radiation. In work [3], however, an ideal waveguide was used as a model. For a more accurate determination of the structure characteristics, it is necessary to consider the finite conductivity of the waveguide walls.

Usually the problem has been solved numerically, using simulation codes [1, 2, 4], or asymptotically [5-8]. An attempt of an analytical solution was made in [9]. Here the explicit expressions for the radiation fields are presented.

STATEMENT OF THE PROBLEM

Consider a relativistic point charge q with longitudinal velocity V and revolution frequency ω_0, moving along the helical trajectory in the resistive-wall cylindrical waveguide with inner radius b. The charge density ρ and current $\vec{j}$ are given in the forms:

$$\rho(r,\varphi,z,t) = q\,\frac{\delta(r-a)}{\sqrt{ra}}\delta(\varphi-\omega_0 t)\delta(z-Vt)$$
$$\vec{j}(r,\varphi,z,t) = (\omega_0 a\vec{e}_\varphi + V\vec{e}_z)\rho(r,\varphi,z,t) \qquad (1)$$

where $\vec{e}_\varphi$, $\vec{e}_z$ are unit vectors in the cylindrical coordinates r,φ,z and a orbit radius. The electromagnetic properties of a metal wall are determined by the dielectric $\varepsilon_1 = \varepsilon_0 + j\,\sigma/\omega$ and magnetic $\mu_1 = \mu_0$ (ε_0 and μ_0 are dielectric and magnetic permeability of vacuum) permeability of the wall material.

The search of a solution is performed in the form of a superposition of a particular solution $\vec{E}_n^0, \vec{H}_n^0$ of the inhomogeneous Maxwell equations and the general solution $\vec{E}_n^i, \vec{H}_n^i$ of the homogeneous Maxwell equations in the form of multipole expansions of TM and TE components of a point charged particle radiation fields:

$$\vec{E} = \sum_{n=1}^{\infty}\{\vec{E}_n^0 + \vec{E}_n^i\},\ \vec{H} = \sum_{n=1}^{\infty}\{\vec{H}_n^0 + \vec{H}_n^i\}, \qquad (2)$$

$$\vec{E}_n^0 = \vec{E}_n^{0,TM} + \vec{E}_n^{0,TE},\ \vec{H}_n^0 = \vec{H}_n^{0,TM} + \vec{H}_n^{0,TE}$$
$$\vec{E}_n^i = \vec{E}_n^{i,TM} + \vec{E}_n^{i,TE},\ \vec{H}_n^i = \vec{H}_n^{i,TM} + \vec{H}_n^{i,TE} \qquad (3)$$

The solutions are based on the vector functions containing the Bessel J_n and Hankel $H_n^{(1)}$ functions of the first kind:

$$\vec{e}_J = \{(\alpha r)^{-1} n\,J_n(\alpha r),\ j\,J_n'(\alpha r),\ 0\}\,exp(j\psi_n),$$
$$\vec{e}_H = \left\{(\alpha r)^{-1} n H_n^{(1)}(\alpha r),\ jH_n^{(1)'}(\alpha r),\ 0\right\}exp(j\psi_n),$$
$$\alpha = \begin{cases} \alpha_1 = \sqrt{\omega^2\varepsilon_1\mu_1 - k^2}, & in\ metal \\ \alpha_0 = \sqrt{\omega^2/c^2 - k^2}, & in\ vacuum \end{cases} \qquad (4)$$

In Eq. (4): α is the transverse wavenumber and $\psi_n = k(z-vt) + n(\varphi - \omega_0 t)$ is the phase factor with $k = (\omega - n\omega_0)/V$ being the longitudinal wavenumber.

PARTICULAR SOLUTION

As a particular solution of the inhomogeneous Maxwell equations, one takes the solution for the radiation of a particle moving along a helical trajectory in free space:

$$\vec{E}_n^0 = \vec{E}_n^{0,TM} + \vec{E}_n^{0,TE},\ \vec{H}_n^0 = \vec{H}_n^{0,TM} + \vec{H}_n^{0,TE} \qquad (5)$$

with

$$\vec{E}_n^{0,TM} = \begin{Bmatrix}\vec{E}_{H,n}^{0,TM}\\ \vec{E}_{J,n}^{0,TM}\end{Bmatrix} = \begin{cases} A_{H,n}^{0,TM}\,rot\,\vec{e}_H, & r > a \\ A_{J,n}^{0,TM}\,rot\,\vec{e}_J, & r < a \end{cases},$$

$$\vec{H}_n^{0,TM} = \begin{Bmatrix}\vec{H}_{H,n}^{0,TM}\\ \vec{H}_{J,n}^{0,TM}\end{Bmatrix} = \begin{cases} B_{H,n}^{0,TM}\,\vec{e}_H, & r > a \\ B_{J,n}^{0,TM}\,\vec{e}_I, & r < a \end{cases}$$

$$\vec{E}_n^{0,TE} = \begin{Bmatrix}\vec{E}_{H,n}^{0,TE}\\ \vec{E}_{J,n}^{0,TE}\end{Bmatrix} = \begin{cases} A_{H,n}^{0,TE}\,\vec{e}_H, & r > a \\ A_{J,n}^{0,TE}\,\vec{e}_J, & r < a \end{cases},$$

$$\vec{H}_n^{0,TE} = \begin{Bmatrix}\vec{H}_{H,n}^{0,TE}\\ \vec{H}_{J,n}^{0,TE}\end{Bmatrix} = \begin{cases} B_{H,n}^{0,TE}\,rot\,\vec{e}_H, & r > a \\ B_{J,n}^{0,TE}\,rot\,\vec{e}_J, & r < a \end{cases} \qquad (6)$$

Amplitudes $A_{H(J),n}^{0,TM(TE)}$, $B_{H(J),n}^{0,TM(TE)}$ remain undefined. To determine them, one should use the boundary conditions that establish a connection between the fields on both sides of the surface $r = a$ containing charges $\rho = q$ and currents

*The work was supported by the Science Committee of RA, in the frames of the research project № 21T-1C239.
† ivanian@asls.candle.am

ISBN: 978-3-95450-227-1 ISSN: 2673-5490 doi:10.18429/JACoW-IPAC2022-WEPOTK039

RADIATION OF A PARTICLE MOVING ALONG A HELICAL TRAJECTORY IN A SEMI-INFINITE CYLINDRICAL WAVEGUIDE*

M. I. Ivanyan†, A. Grigoryan[1], B. Grigoryan, V. Khachatryan, B. Sargsyan,
CANDLE SRI, Yerevan, Armenia
K. Floettmann, F. Lemery, Deutsches Elektronen-Synchrotron, Hamburg, Germany
[1]also at Yerevan State University, Yerevan, Armenia

Abstract

The radiation field of a particle which suddenly appears in an ideal waveguide and moves on a helical trajectory under the influence of external magnetic fields is calculated. The shape and character of the front of the propagating wave is determined.

INTRODUCTION

A combination of a waveguide and a helical undulator transforms the helical undulator radiation spectrum from continuous to discrete and thus improves the characteristics of its radiation significantly [1]. Usually, the stationary motion of a particle in an infinite rectangular [2-4] or circular [1, 5-9] waveguide is considered, which ignores the injection phenomenon, i.e. the instantaneous appearance of a particle at a certain point in the waveguide (some aspects of this problem are considered in [10-11]). In the present work, the problem of the stationary motion of a point particle with a charge varying with time and performing a helical motion in an infinite ideal cylindrical waveguide is considered. On this basis, the problem of a particle that suddenly appears at a certain moment of time and moves along a helical trajectory in the same waveguide is solved. In conclusion, a formula is derived that describes the gradual appearance of a bunch of charged particles, which simulates the process of its injection.

CHARGE VARYING IN TIME

Consider a relativistic point charge with longitudinal velocity V and charge $Q(t)$, with an arbitrary time dependence, moving in a homogeneous waveguide along a helical trajectory, with a revolution frequency ω_b. The waveguide is assumed to be circular with a radius b and has perfectly conducting walls. The charge density ρ and current $\vec{j}$ are given in the forms:

$$\rho(r,\varphi,z,t) = qQ(t)\,\frac{\delta(r-a)}{\sqrt{ra}}\,\delta(\varphi-\omega_b t)\delta(z-Vt)$$

$$\vec{j}(r,\varphi,z,t) = (\omega_b a\vec{e}_\varphi + V\vec{e}_z)\rho(r,\varphi,z,t) \qquad (1)$$

where $\vec{e}_\varphi$, $\vec{e}_z$ are unit vectors in cylindrical coordinates and a is the radius of the particle orbit. q is the elementary charge. The radiation field is determined from the wave equations:

$$\left\{\Delta - \frac{1}{c^2}\frac{\partial}{\partial t^2}\right\}\vec{E} = \mu_0\left\{\frac{\partial\vec{j}}{\partial t} + c^2\nabla\rho\right\}$$

$$\left\{\Delta - \frac{1}{c^2}\frac{\partial}{\partial t^2}\right\}\vec{H} = -rot\vec{j} \qquad (2)$$

with the magnetic permeability of vacuum μ_0.

In the time-frequency domain the electrical and magnetic fields are sought in the form of cylindrical mode compositions, which combine TM and TE harmonics:

$$\vec{E} = \sum_{n,m=1}^{\infty}\{\vec{E}_{nm}^{TM} + \vec{E}_{nm}^{TE}\} \qquad (3)$$

The longitudinal and transverse components of electric and magnetic harmonics are written in the form of expansion terms in Bessel functions of the first kind:

$$\tilde{E}_{nm_z}^{TM} = U_{nm}\psi_{nm}^{TM},$$

$$\psi_{nm}^{TM} = J_n\left(j_{nm}\frac{r}{b}\right)e^{jn(\varphi-\omega_0 t)}e^{jk(z-Vt)},$$

$$\tilde{H}_{nm_z}^{TE} = c\varepsilon_0 W_{nm}\psi_{nm}^{TE},$$

$$\psi_{nm}^{TE} = J_n\left(\nu_{nm}\frac{r}{b}\right)e^{jn(\varphi-\omega_0 t)}e^{jk(z-Vt)}$$

$$\vec{\mathcal{E}}_{nm}^{TM} = \{\mathcal{E}_{nm_r}^{TM}, \mathcal{E}_{nm_\varphi}^{TM}, 0\}, \qquad \vec{\mathcal{H}}_{nm}^{TE} = \{\mathcal{H}_{nm_r}^{TE}, \mathcal{H}_{nm_\varphi}^{TE}, 0\}$$

$$\vec{E}_{nm_t}^{TM} = A_{nm}\vec{\mathcal{E}}_{nm}^{TM}, \qquad \vec{H}_t^{TE} = D_{nm}\vec{\mathcal{H}}_{nm}^{TE}$$

$$\vec{H}_{nm_t}^{TM} = C_{nm}c\varepsilon_0[\vec{e}_z \times \vec{\mathcal{E}}_{nm}^{TM}]$$

$$\vec{E}_t^{TE} = -B_{nm}(c\varepsilon_0)^{-1}[\vec{e}_z \times \vec{\mathcal{H}}_{nm}^{TE}]$$

$$\vec{\mathcal{H}}_{nm}^{TE} = \{\mathcal{H}_{nm_r}^{TE}, \mathcal{H}_{nm_\varphi}^{TE}, 0\}$$

$$\vec{H}_t^{TE} = D_{nm}\vec{\mathcal{H}}_{nm}^{TE}$$

$$\mathcal{E}_{nm_r}^{TM} = \frac{\partial\,\psi_{nm}^{TM}}{\partial r}, \qquad \mathcal{E}_{nm_\varphi}^{TM} = j\frac{n}{r}\psi_{nm}^{TM}$$

$$\mathcal{H}_{nm_r}^{TE} = \frac{\partial\,\psi_{nm}^{TE}}{\partial r}, \qquad \mathcal{H}_{nm_\varphi}^{TE} = j\frac{n}{r}\,\psi_{nm}^{TE} \qquad (4)$$

where j_{nm} and ν_{nm} are the roots of the Bessel function and its derivative, respectively. The result of substituting (4) into (2) are second-order differential equations for the time-dependent amplitudes *U, A, B, W, C* and *D*:

$$f(g_X)X_{nm} + b^2(2j\omega X'_{nm} - X''_{nm}) = \mathrm{F}_X\big(jK_X Q(t) + R_X Q'(t)\big),$$
$$X = U,\ A,\ B,\ W,\ C,\ D \qquad (5)$$

with

$$f(g_X) = c^2(g_X^2 + b^2k^2) - b^2\omega^2 = b^2(\tilde{\omega}_N^2 - \omega^2),$$
$$\tilde{\omega}_N = \sqrt{c^2\,g_X^2/b^2 + k^2}, \qquad (6)$$

$g_X = j_{nm}$ for TM modes and $g_X = \nu_{nm}$ for TE modes.

*The work was supported by the Science Committee of RA, in the frames of the research project № 21T-1C239.
† ivanian@asls.candle.am

ISBN: 978-3-95450-227-1 ISSN: 2673-5490 doi:10.18429/JACoW-IPAC2022-WEPOTK040

SPIN-TRACKING SIMULATIONS IN A COSY MODEL USING Bmad

M. Vitz*,[1], Institut für Kernphysik 4, Forschungszentrum Jülich, Jülich, Germany
[1]also at III. Physikalisches Institut B, RWTH Aachen University, Aachen, Germany
on behalf of the JEDI Collaboration

Abstract

The matter-antimatter asymmetry in our Universe might be understood by investigating the EDM (Electric Dipole Moment) of elementary charged particles. A permanent EDM of a subatomic particle violates time reversal and parity symmetry at the same time and would be an indication for further CP violation than established in the Standard Model. The JEDI-Collaboration (Jülich Electric Dipole moment Investigations) in Jülich has performed a direct EDM measurement for deuterons with the so called precurser experiments at the storage ring COSY (COoler SYnchrotron). In order to understand the measured data and to disentangle an EDM signal from systematic effects, spin tracking simulations in an accurate simulation model of COSY are needed. Therefore a model of COSY was implemented using the software library Bmad. Systematic effects can be considered by including element misalignments, effective dipole shortening and steerer kicks. These effects rotate the invariant spin axis in addition to the EDM and have to be analyzed and understood. The most recent spin tracking results as well as the methods to find the invariant spin axis will be presented.

INTRODUCTION

In order to explain the matter-antimatter asymmetry in the Universe, $\mathscr{CP}$-violating processes beyond the ones already known are needed [1]. A non-vanishing EDM of a subatomic particle is a candidate for such a process, since it is a source of $\mathscr{P}$ and $\mathscr{T}$ violation leading to $\mathscr{CP}$ violation, assuming the $\mathscr{CPT}$-theorem holds. An EDM is similar to the MDM (Magnetic Dipole Moment) and is predicted by the SM. Its magnitude, however, is expected to be unobservably small with current techniques. Therefore, the measurement of an EDM at a higher magnitude would be an indication for further CP violation than explained by the SM. The so-called precurser experiments were carried out by the JEDI-Collaboration to perform an EDM measurement for deuterons at the storage ring COSY. A storage ring allows a direct measurement of an EDM, as the interaction of particle's spin with electromagnetic field results in spin rotations defined by EDM and MDM contribution [2, 3]. In order to separate systematic effects caused by misaligned elements, steerer contributions, unknown longitudinal fields, etc., from a potential EDM signal, spin tracking simulations in a simulation model of COSY are required [4]. The software tool used to study and benchmark the deuerton EDM effect in a simulation is the Fortran based library Bmad [5].

* m.vitz@fz-juelich.de

SPIN DYNAMICS IN STORAGE RINGS

The impact of electromagnetic fields in a storage ring on the spin $\vec{S}$ is described by the Thomas-BMT equation [2, 3]. Since COSY is a pure magnetic ring, ideally only magnetic fields $\vec{B}$, pointing in the vertical direction, act on the particle's spin. Therefore the Thomas-BMT equation is reduced to Eq. (1).

$$\frac{d\vec{S}}{dt} = (\vec{\Omega}_{MDM}+\vec{\Omega}_{EDM})\times\vec{S} = -\frac{q}{m}\left(G\vec{B} + \frac{\eta}{2}\vec{\beta}\times\vec{B}\right)\times\vec{S} \quad (1)$$

In Eq. (1), $\vec{\Omega}_{MDM}$ and $\vec{\Omega}_{EDM}$ indicate the angular frequency induced by the MDM and the EDM. The quantities q, m, G are the particle's electric charge, its mass and the gyromagnetic anomaly, while $\vec{\beta}$ denotes its velocity. The dimensionless proportionality factor η contains the EDM's magnitude. As shown by the Thomas-BMT equation, a permanent EDM rotates the spin vertically n_y, while the MDM rotates the spin horizontally n_x under the assumption of $\vec{\beta} \perp \vec{B}$ and $\vec{\beta}=(0, 0, \beta_z)^T$. For this reason, a characterization of the spin motion can be done using the invariant spin axis, the vector that is perpendicular to the spin's precession plane. Assuming no EDM contribution and an ideal ring, the invariant spin axis should always point in vertical direction n_y. However, in presence of an EDM, the invariant spin axis is tilted in the horizontal direction n_x by the angle ξ as indicated in Fig. 1. A theoretical prediction of ξ is given by Eq. (2).

$$\xi = \arctan\left(\frac{\eta\beta}{2G}\right) \quad (2)$$

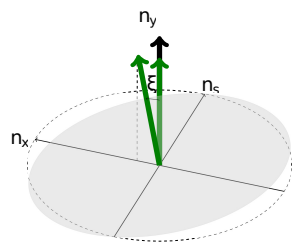

Figure 1: A permanent EDM of magnitude η tilts the invariant spin axis in horizontal direction n_x by the angle ξ. The longitudinal direction n_s is not affected by a permanent EDM.

SPIN-TRACKING SIMULATIONS

Invariant Spin Axis

In a simulation, the invariant spin axis can be studied directly by comparing the spin vectors of two successive turns

ISBN: 978-3-95450-227-1 ISSN: 2673-5490 doi:10.18429/JACoW-IPAC2022-WEPOTK043

MATCHING STUDIES BETWEEN THE CERN PSB AND PS USING TURN-BY-TURN BEAM PROFILE ACQUISITIONS WITH A RESIDUAL BEAM GAS IONISATION MONITOR

M.A. Fraser*, M.R. Coly, A. Guerrero, A. Huschauer, S. Jensen, S. Levasseur, F. Roncarolo, A. Rossi, H. Sandberg, J.W. Storey, CERN, Geneva, Switzerland

Abstract

In the framework of the LHC Injectors Upgrade (LIU) project, the Beam Gas Ionisation (BGI) profile monitors installed in the Proton Synchrotron (PS) were fitted with a gas injection system capable of boosting the signal rate high enough to capture single turn acquisitions immediately after injection. This contribution reports on the studies carried out during the beam commissioning of the BGI system in a turn-by-turn matching monitor mode for its eventual implementation in an optimisation framework to preserve emittance during transfer between the PS Booster and PS. The BGI commissioning included a benchmarking with data from a wire-grid secondary emission monitor (BSG) inserted into the circulating beam.

INTRODUCTION

The PS injection kinetic energy was increased from 1.4 to 2.0 GeV to reduce the degradative effects of space-charge as the beam brightness delivered by the Proton Synchronous Booster (PSB) is increased in preparation for the future high luminosity operation of the LHC [1]. The injection system, including the fast-pulsed kickers, septum and transfer line, was upgraded to cope with the increased beam rigidity and to remove the horizontal dispersion mismatch between the PSB and PS. The mismatch would have driven significant emittance growth as the longitudinal emittance (and momentum spread) of the beam is voluntarily increased to help alleviate space-charge effects [2].

The BGI profile monitor system deployed in the PS is capable of providing continuous, bunch-by-bunch and turn-by-turn measurements of the transverse beam profile [3]. Two instruments were installed in Straight Sections (SS) 82 and 84 of the PS for horizontal and vertical profile measurements, respectively. The system was exploited to study the turn-by-turn evolution of the beam envelope immediately after injection and to provide an operational tool to quantify and correct optical mismatch to prevent emittance dilution. Past studies of injection mismatch exploited wire-grids actuated into the circulating beam aperture [4, 5]. Although the wire-grid matching monitor system is well-established, the interaction of the circulating beam with the grid limits the number of turns that can circulate in the machine before it must be dumped to avoid damaging the wires. As a result, the time available for injection mismatch studies has been severely limited because inserting the wire-grids prevents operation of the CERN accelerator complex downstream of the PS. The BGI circumvents this limitation in almost all operational modes, except for parallel ion operation where the injection of gas was observed to degrade the ion lifetime.

* mfraser@cern.ch

TURN-BY-TURN ACQUISITION MODE

Measurement Conditions

The matching monitor studies were carried out with a relatively low intensity, single bunch LHC beam injected from the PSB containing $70-130\times10^{10}$ protons, compatible with the damage limit of the wire-grids, and with a longitudinal emittance of 2 eVs. The LHC cycle operates at a low chromaticity to combat the increased chromatic tune spread from the larger longitudinal emittance. The transverse feedback system is used to stabilise the beam against head-tail instabilities on the injection plateau, rather than relying on linear coupling as done in the past [6]. This paper only considers the horizontal plane because when the measurements were carried out only the horizontal BGI instrument in SS82 was available.

Beam Loss and Background Noise

The BGI profile monitor uses electric and magnetic fields to transport electrons from rest-gas ionisation to a Timepix3 [7] based detection system installed directly inside the beam vacuum. The beam profile is inferred from the transverse distribution of the detected electrons, which is disrupted when charged particles from other sources impinge the detector. The main source of background events stems from beam particles lost on the machine's aperture and the resulting secondary particle showers. The level of background noise is typically negligible throughout the PS cycle and can be filtered reasonably well online by discriminating on the energy of the pixel events alone. However, the beam loss intrinsic to and taking place during the injection process made the background rejection and data analysis more challenging when exploiting the BGI as an injection matching monitor.

Readout Rate Limitations

The readout rate (ionisation electrons per turn) of the front-end electronics was observed to saturate above the theoretical detector readout limit of 160 MHz or ~ 350 events per turn. Figure 1 shows the count rate of ionisation electrons as a function of the circulating beam intensity and gas pressure. The readout rate was also affected by the level of background events crowding the data acquisition system, which depends on the amount of beam lost during the injection process. A

ISBN: 978-3-95450-227-1 ISSN: 2673-5490 doi:10.18429/JACoW-IPAC2022-WEPOTK046

IMPROVED LONGITUDINAL PERFORMANCE OF THE LHC BEAM IN THE CERN PS

H. Damerau*, V. Desquiens, A. Huschauer, A. Jibar, A. Lasheen, B. Mikulec, M. Morvillo, C. Rossi, B. Woolley, CERN, Geneva, Switzerland

Abstract

At the end of the 2018 run the intensity target for the High-Luminosity LHC (HL-LHC) had just been reached at extraction from the Proton Synchrotron (PS). In the framework of the LHC Injectors Upgrade (LIU) project additional RF improvements have been implemented during the 2019/2020 long shutdown (LS2), mainly impacting the impedance of the 10 MHz, 40 MHz, and 80 MHz RF systems. With the upgraded injection energy of 2 GeV (kinetic), also the intermediate plateau energy for RF manipulations has been increased. Following a campaign of beam studies throughout the 2021 run, a bunch intensity of up to $2.9 \cdot 10^{11}$ p/b in trains of 72 bunches is achieved with the required longitudinal beam quality, surpassing the LIU target of $2.6 \cdot 10^{11}$ p/b. The threshold of longitudinal quadrupolar coupled-bunch instabilities is increased during acceleration, but they are again observed at the flat-top. While dipolar coupled-bunch oscillations are well damped by a dedicated feedback system, the quadrupolar modes are suppressed by operating a 40 MHz system as an active higher-harmonic Landau cavity. The main commissioning steps are outlined, together with the key contributions to the improved beam performance.

INTRODUCTION

Doubling the bunch intensity of the beam from the Proton Synchrotron (PS) for the High-Luminosity LHC (HL-LHC) to $N_b = 2.6 \cdot 10^{11}$ particles per bunch (p/b) at extraction, corresponding to a total beam intensity of $1.9 \cdot 10^{13}$ particles, has been a main objective of the LHC Injectors Upgrade (LIU) project [1]. To keep the bunch-by-bunch intensity spread acceptable for the LHC and to limit the beam loss at the PS-to-SPS transfer, the longitudinal beam quality has to be preserved at this increased intensity, i.e. 72-bunch batches (25 ns spacing) with a 4σ-bunch length below 4 ns and a longitudinal emittance below $\varepsilon_l = 0.35$ eVs. Already since the first long shutdown (LS1) substantial upgrades of all RF systems in the PS have been implemented and commissioned. Their combined improvements allowed to reach the LIU intensity for the first time in 2018, although yet with very large transverse emittances. The upgrade programme was completed during the 2019/2020 long shutdown (LS2), mainly impacting the impedances of the 10 MHz, 40 MHz, and 80 MHz RF systems. The longitudinal beam production scheme has moreover been adapted to the increase of the injection energy from $E_{kin} = 1.4$ GeV to 2 GeV, required to reduce space charge at flat-bottom for a higher transverse brightness [2]. Table 1 summarizes the main RF upgrades, focusing on changes during the LS2.

Table 1: Renovations and Upgrades of RF and Feedback Systems During the LS2

RF system	Upgrade	Remark
10 MHz	• New wide-band feedback amplifiers	• $\simeq$ 4 dB gain increase
	• 1-turn delay feedback, since 2014	• About 12 dB gain at $n \cdot f_{rev}$
40 MHz 80 MHz	• Improved wide-band feedback systems	• Shorter delay by airlines
	• Multi-harmonic feedback systems	• Up to 26 dB gain at $n \cdot f_{rev}$, new firmware
	• 40 MHz operation as Landau RF system at flat-top	
Wide-band	• Coupled-bunch feedback for dipole modes	• New firmware with internal diagnostics

CYCLE WITH INCREASED INJECTION ENERGY

The production scheme of the multi-bunch beams with 25 ns bunch spacing for the LHC is sketched in Fig. 1. The intermediate plateau, initially at $E_{kin} = 2.5$ GeV, is needed to triple-split each bunch from the RF harmonic, $h = 7$ at injection to $h = 21$ during acceleration. The RF system would not provide a sufficiently large bucket area for the start of acceleration at $h = 21$ (9.5 MHz) otherwise. Additionally, for the higher-brightness variant of LHC-type beams [3] based on batch compression, merging and triple splitting (BCMS), the higher plateau energy reduces space charge during the RF manipulation. Following acceleration of 18 bunches through transition energy they are split in four by two consecutive splittings at the flat-top, increasing the principal RF harmonic via $h = 42$ (20 MHz) to $h = 84$ (40 MHz). Each bunch injected from the PSB is hence split in twelve parts in the PS. A non-adiabatic bunch rotation with RF systems at 40 MHz and 80 MHz shortens the bunches to fit them into the 5 ns long buckets in the SPS.

With the increased injection energy, the intermediate plateau would have been too close to the flat-bottom. The space charge tune shift is favorably reduced proportional to $1/(\beta\gamma^2)$ at higher energy, $\beta = v/c$ being the relative particle velocity, v, with respect to the speed of light, c,

* heiko.damerau@cern.ch

ISBN: 978-3-95450-227-1 ISSN: 2673-5490 doi:10.18429/JACoW-IPAC2022-WEPOTK050

THE REPORT OF MACHINE STUDIES RELATED TO THE VERTICAL BEAM SIZE BLOW-UP IN SuperKEKB LER*

S. Terui†, T. Ishibashi, K. Ohmi, Y. Funakoshi, H. Fukuma, R. Ueki, Y. Ohnishi, M. Tobiyama
High Energy Accelerator Research Organization (KEK), Tsukuba, Japan
T. Nakamura, High Energy Accelerator Research Organization (KEK) J-PARC Center, Tokai, Japan

Abstract

In the Low Energy Ring (LER) for positrons in the SuperKEKB, a vertical beam size blow-up was observed when the bunch current was approximately 1 mA. If a beam size blow-up occurs, the design luminosity cannot be achieved. Therefore, beam size blow-ups must be prevented. According to calculations, the bunch current threshold of the Transverse Mode Coupling instability (TMCI) is 2 mA or more, and the observed value is 50% or smaller. Ordinary TMCI cannot explain this vertical beam size blow-up. This paper shows that the cause of the vertical beam size blow-up can be determined by analyzing factors such as beam oscillation. The study results showed that the vertical beam size blow-up in the LER was caused by a -1 mode instability.

INTRODUCTION

SuperKEKB is a high-luminosity electron-positron collider with asymmetric energies of 7 GeV (electron, High Energy Ring: HER) and 4 GeV (positron, Low Energy Ring: LER) [1]. SuperKEKB adopts a nanobeam scheme in which the vertical beta function (β_y^*) at the collision point is squeezed to the limit. The design value of β_y^* in the LER is 0.27 mm [2]. The minimum value of β_y^*= 0.8 mm was achieved in 2022. In the 2020c run (October 19, 2020–December 18, 2020), a vertical beam size blow-up was observed when the bunch current was increased. The vertical beam size blow-up subsided when the vertical collimator gap was widened, even under the same bunch current conditions [3]. This observation established that the instability causing the vertical beam size blow-up is related to the wake generated by the vertical collimator. The impedance of the collimator was calculated using GdfidL [4], assuming a bunch length of 6 mm. The following measurements were performed at β_y^*=1 mm in both the LER and HER, under the condition that the sum of the vertical beta function at the collimator location multiplied by the kick factor of the vertical collimator in the LER is approximately 31 × 10^{35} V/C, with fewer bunches (30 - 393) than the number of bunches under normal physics experiments (about 1600) to reduce the effect of multi-bunch instability and the synchrotron tune (ν_s) in the LER is 0.0227.

VERTICAL BEAM SIZE BLOW-UP IN THE LER DURING SINGLE-BEAM CONDITION

The beam sizes were measured using an X-ray beam size monitor [5]. Figure 1 shows the bunch current on the horizontal axis and vertical emittance on the vertical axis. The orange plots were measured with nominal settings of the Bunch-by-Bunch Feedback system (BBF) [6], which are set the same way as in normal physics experiments. The setting of the BBF for vertical oscillation during normal physics experiments is intended to dump the frequency of the 0 mode (vertical betatron tune: ν_y). The points circled by the black dashed line in Fig. 1 indicate that the vertical beam size blow-up occurs when the bunch current is about 0.9 mA or higher. The BBF and vertical beam size blow-up relationship will be explained later.

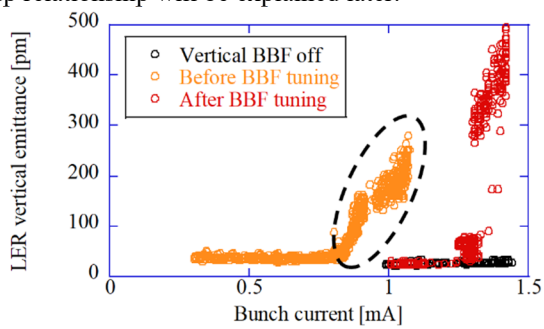

Figure 1: The LER vertical emittance before and after BBF tuning and BBF off versus bunch current.

To measure the tune, a pilot bunch is excited at varying frequencies near the betatron tune.The tune shift was calculated using PyHEADTAIL [7] and the Fast Fourier Transform (FFT) analysis of the vertical motion in the LER was conducted using the Bunch Oscillation Recorder (BOR) [8], as shown in Fig. 2. The orange and light blue dashed lines in Fig. 2 show the frequencies of the 0 mode and -1 mode ($\nu_y - \nu_s$), respectively, with the bunch current on the horizontal axis. ν_y at a bunch current of 0 mA is denoted as ν_{y0}. ν_{y0} is 0.5977 during the measurement in Fig. 2.

The measurement results showed different spectra in the oscillation of the pilot bunch and the non-pilot bunches. The FFT analysis of the pilot bunch revealed two high peaks. These two peaks, corresponding to the 0 mode in red and the -1 mode in blue, are plotted in Fig. 2. The tune shift of the measured value (red line) differs from the calculated value (orange dashed line) by approximately 20% in the slope. This difference may be due to an impedance source not yet included in the calculations.

The results of the FFT analysis for the non-pilot bunches showed no peaks at a low bunch current and only one high peak at a high bunch current. The frequency of the single peak point at the high bunch current for the non-pilot bunches is plotted in black in Fig. 2. This peak was found to have nearly the same frequency as that of the -1 mode for the pilot bunch. At low bunch currents, the peak of the

† sterui@mail.kek.jp

ISBN: 978-3-95450-227-1 ISSN: 2673-5490 doi:10.18429/JACoW-IPAC2022-WEPOTK051

BEAM INDUCED POWER LOSS ESTIMATION OF A MOVABLE SYNCHROTRON LIGHT EXTRACTION MIRROR FOR THE LHC

W. Andreazza, E. Bravin, F. Guillot-Vignot, M. Wendt*, CERN, Geneva, Switzerland

Abstract

Beam instruments based on synchrotron light are an important part of the beam monitoring diagnostics suite in the Large Hadron Collider (LHC) at CERN. In frame of the high luminosity upgrade (HL-LHC) additional synchrotron light diagnostics are demanded, too many to be covered by the present Beam Synchrotron-light Radiation Telescope (BSRT), which utilizes the light extraction mirror in a fixed position. Therefore, an additional synchrotron light diagnostics setup is under development, now with a movable mirror to extract the synchrotron light emitted solely by a superconducting LHC dipole magnet. With higher bunch intensities anticipated in the HL-LHC, the beam induced power losses, and therefore local heat dissipation, play a critical role in the design of the extraction mirror. This paper summarizes the estimation of the bunched-beam induced power losses based on numerical simulations and RF measurements on a prototype light extraction mirror.

INTRODUCTION

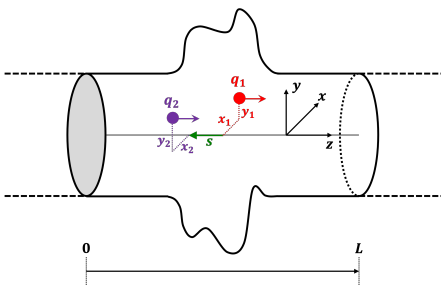

Figure 1: Definition of wakefields.

Any component or device, e.g. a beam manipulation device, a beam pickup or any other beam vacuum component that presents a discontinuity or change of geometry of the beam pipe of an accelerator alters the electromagnetic field of a leading source point charge q_1, and causes *wakefields* which acts on a trailing test point charge q_2, see also Fig. 1. The integration of the *Lorenz* force

$$\mathbf{F} = \frac{d\mathbf{p}}{dt} = q_2\,(\mathbf{E} + c\mathbf{e_z} \times \mathbf{B}) \tag{1}$$

over the relevant length L of the accelerator component leads to the *wake function* [1]

$$\mathbf{w}(x_1, y_1, z_1, s) = \frac{1}{q_1}\int_0^L dz\,[\mathbf{E}(x_2, y_2, z, t) + c\mathbf{e_z} \times \mathbf{B}(x_2, y_2, z, t)]_{t=(s+z)/c} \tag{2}$$

* manfred.wendt@cern.ch

The *Fourier* transformation of the wake function Eq. (2) is called *beam-coupling impedance*

$$Z_\parallel(x_1, y_1, x_2, y_2, \omega) = -\frac{1}{c}\int_{-\infty}^{+\infty} ds\, w_\parallel(x_1, y_1, x_2, y_2, s) e^{-j\omega s/c} \tag{3}$$

Eq. (3) is the definition for the longitudinal coupling impedance, because it is the real part of the longitudinal component $\Re[Z_\parallel(\omega)]$ that causes an energy loss, thus a beam induced power loss, and contributes to the so-called *RF heating* of an accelerator component.

The light extraction mirror of the Beam Synchrotron-light Radiation Telescope (BSRT) was a source of RF heating issues during Run 1 of the Large Hadron Collider (LHC) at CERN [2]. A successful overhaul of the BSRT light extraction mirror solved the RF heating problem, with no issue observed during LHC Run 2. For the high luminosity upgrade of the LHC (HL-LHC) the beam intensity will be doubled [3], and additional measurements based on synchrotron light are foreseen. Therefore, an additional synchrotron light monitor system, the BSRTM is under development, Fig. 2 shows a schematic view as it was used as geometric input for the numerical analysis. As of the new design, utilizing a movable mirror, and as of the anticipated higher beam intensity in the LHC, a prototype of the BRSTM light extraction mirror was build and installed during the long shutdown 2 of the LHC in 2021. This prototype tank is equipped with PT100 temperature sensors to monitor RF heating effects during LHC Run 3, which started in Spring of year 2022.

Before installation, the BSRTM prototype light extraction tank was analyzed applying a stretched-wire RF measurement method to estimate its beam-coupling impedance. This report summarizes the measurement results, along with a numerical analysis and the calculation of the related RF power losses based on the expected HL-LHC beam parameters.

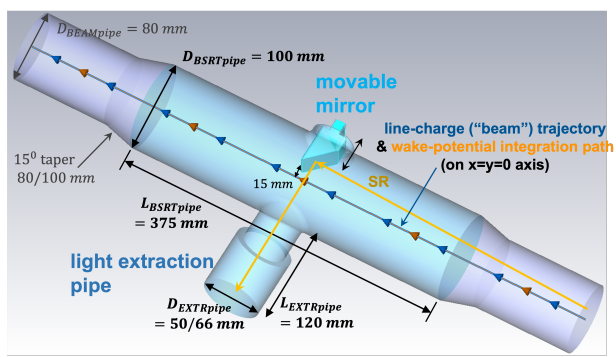

Figure 2: The LHC BSRTM synchrotron-light extraction mirror prototype.

ISBN: 978-3-95450-227-1 ISSN: 2673-5490 doi:10.18429/JACoW-IPAC2022-WEPOTK052

BEAM COUPLING IMPEDANCE STUDY AND ITS DATABASE OF SIAM PHOTON SOURCE STORAGE RING

N. Juntong*, T. Chanwattana, S. Jummunt, K. Kittimanapun, T. Pulampong, T. Phimsen, W. Promdee, Synchrotron Light Research Institute, Nakhon Ratchasima, Thailand

Abstract

Since the Siam Photon Source (SPS) had an electron beam energy upgraded from 1.0 GeV to 1.2 GeV in 2005, the storage ring impedance measurements were done once in 2007. Two insertion magnet devices have been installed in the SPS storage ring during June to August 2013. There are several vacuum components added to the storage ring; these affect the ring impedance. Quantitative understanding of instabilities requires detailed knowledge of the impedance of the ring. For this purpose, the development of an impedance database is a necessity, where the wake potentials of each vacuum component are kept and maintained in a standard format. The self-describing data sets (SDDS) file format will be utilized to record components wake potentials. The wake potentials of each vacuum component can be obtained from a particle tracking simulation; a CST particle studio program will be used in the simulation process. The wake potentials can also be included in a beam dynamic tracking program such as ELEGANT to observe beam behaviours with these instabilities and find a curing means. The study results will be presented.

INTRODUCTION

The SPS storage ring has 81.3 m circumference. It accommodates different types of vacuum components such as beam position monitor (BPM), bellows, pumping ports, vacuum beam ducts, and radio frequency cavity. Group and number of components are summarized in Table 1. These components affect the stored beam inside the ring in term of longitudinal and transverse instabilities. These instabilities caused by the wakefield, a scattered electromagnetic fields induced by electron beam itself.

Integration of wakefield over the path of electron bunch will get wake potentials. Taking Fourier transform of wake potentials divided by a bunch charge spectrum will give a beam induced impedance of that vacuum component. Wake potential is sum of electromagnetic force of wakefield inside vacuum component acting on a bunch charge travels in z direction [1] as

$$\vec{W}(s) = \frac{1}{Q}\int_{-\infty}^{\infty}(\vec{E} + c\vec{e}_z \times \vec{B})_{t=(z'+s)/c}dz' \qquad (1)$$

where Q is total charge of electron bunch, c is light velocity, $\vec{E}$, $\vec{B}$ is electric and magnetic fields of wakefield inside vacuum component, respectively.

Loss and kick factor can be calculated from wake potentials. Integration of wake potentials longitudinal component over bunch charge density will give a loss factor. With the same calculation on the transverse components will give a kick factor as

$$k_{\parallel} = \int_{-\infty}^{\infty}\rho(s)\cdot W_{\parallel}(s)ds \qquad (2)$$

$$k_{\perp}(s) = \frac{1}{Q}\int_{-\infty}^{\infty}\rho(s)\cdot W_{\perp}(s)ds \qquad (3)$$

where ρ is normalized bunch charge density, $W_{\parallel}$ and $W_{\perp}$ is a longitudinal and transverse components of wake potential, respectively.

Loss factor is a quantitative number of longitudinal effects to the beam of the wakefield. Longitudinal components can affect electron bunch such as the potential well bunch lengthening, bunch threshold current decreasing, and beam energy spread. In the same aspect, kick factor is a quantitative number to measure transverse effects to the beam of the transverse components of wakefield. It can cause a transverse beam instabilities or lead to a beam loss in a severe case.

Table 1: Vacuum Components in the SPS Storage Ring

Vacuum components	Number of components
BPM	26
Bellow	4
L42 bellow	12
L71 bellow	4
L72 bellow	4
VP1 upstream bellow	4
VP1 downstream bellow	4
VP1 pump port	4
Pump port - short	12
Short duct	8
L1000 duct	9
L1400 duct	12
Bump duct	3
RF cavity	1
Bending duct	8

WAKEFIELD SIMULATIONS

The wakefield and wake potentials of vacuum components can be obtained from electromagnetic field solvers in connection with particle tracking simulation. Wakefield module of CST Studio Suite ®will be used in the simulation process. The simulation will give wakefield, wake potentials, and impedances of the input geometry of each frequency in a study range. The longitudinal broadband impedance ($Z_{\parallel}/n$)

* nawin@slri.or.th

ISBN: 978-3-95450-227-1 ISSN: 2673-5490 doi:10.18429/JACoW-IPAC2022-WEPOTK053

SIMULATION OF BUNCH FORMATION FOR THE Mu2e EXPERIMENT

K. P. Harrig[1], E. Prebys[1], S. J. Werkema[2], V. Nagaslaev[2]
[1] University of California Davis Physics Dept., Davis, USA,
[2] Fermilab National Accelerator Laboratory, Batavia, USA

Abstract

The Fermilab Recycler is an 8 GeV storage ring composed of permanent magnets that was crucial to the success of the Fermilab Tevatron Collider program. It is currently being used to slip-stack protons for the high energy neutrino program and to re-bunch protons for use in the Muon g-2 and Mu2e experiments. For the latter applications, the Recycler re-bunches each 1.6 µs "batch" from the Fermilab Booster into four 2.5 MHz bunches. For the Mu2e experiment, it is crucial that beam more than 125 ns from the nominal bunch center be suppressed by at least a factor of 10^{-5}. While bunch formation is currently in operation for the g-2 experiment, this out of time requirement has not been met, and the reason is not understood. This work presents a simulation of bunch formation in the Recycler, in an effort to understand the reason for this excessive out of time beam and to search for a way to reduce it.

INTRODUCTION

The Mu2e experiment aims to observe conversion to an electron of a muon that has been captured by an aluminium nucleus. This process violates charged lepton favor number and is forbidden by the standard model. A conclusive result, null or otherwise, would shed light on beyond the standard model physics. The Mu2e collaboration aims to improve on the sensitivity of previous measurements of this process by four orders of magnitude. Specifically, the experiment will measure the ratio of the coherent neutrinoless conversion in the field of a nucleus of a negatively charged muon into an electron to the muon capture process.

$$R_{\mu e} = \frac{\mu^- + A(Z,N) \rightarrow e^- + A(Z,N)}{\mu^- + A(Z,N) \rightarrow \nu_\mu + A(Z,N)} \qquad (1)$$

The first search for a muon to electron conversion took place in 1955 [1]. However, more recent experiments placed a 90% CL limit on the process of 4.6×10^{-12}, and 7×10^{-13} [1]. A key component to the increase in sensitivity is the longitudinal structure of the proton beam shown in Fig. 1. Specifically, the experiment hopes to achieve $R_e = 6 \times 10^{-17}$ at 90% CL limit. The muons will be created via the decay of pions created by 800 GeV protons impinging on a tungsten target. The out-of-time protons will be eliminated using the extinction system located on the M4 beam line just before the tungsten target. The muons will then be captured on an aluminium nucleus and the resulting electrons will be detected [1]. A diagram of the accelerator complex is shown in Fig. 2. The proton pulses are ~ 250 ns wide and spaced 1.7 µs apart. Each pulse contains 39×10^6 protons. The experimental signature of the process will include a large background from muons decaying in the orbit of the nucleus before capture can occur.

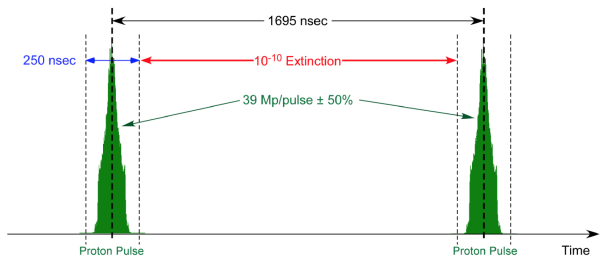

Figure 1: Longitudinal structure of the proton beam after exiting the delivery ring [2].

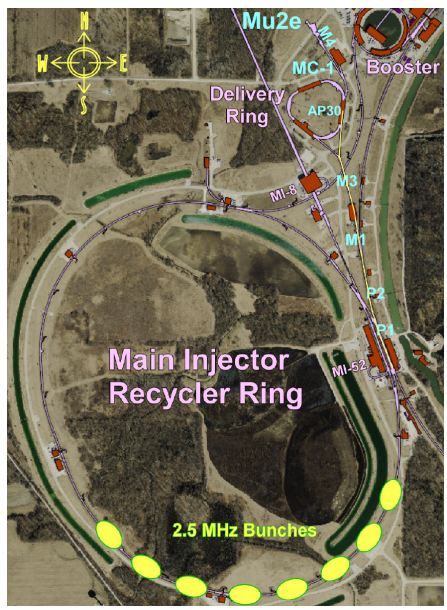

Figure 2: Fermilab accelerator complex.

EXTINCTION

The ratio of out of time protons to total number of protons in a pulse is defined as the extinction. The goal is to obtain a ratio of 10^{-10} by the time the protons reach the tungston production target. The extinction is in part accomplished with the formation of the bunches in the delivery ring.

At the delivery ring the extinction is at the 10^{-5} level. However, the extinction system depicted in Fig. 3 will be responsible for reducing the ratio another five orders of magnitude. The system will involve three collimators and two one meter long AC dipole magnets, that will be referred to as the AC Dipole. The tail collimator will remove the

ISBN: 978-3-95450-227-1 ISSN: 2673-5490 doi:10.18429/JACoW-IPAC2022-WEPOTK054

EXPERIMENTAL VERIFICATION OF DARHT AXIS 1 INJECTOR PIC SIMULATIONS*

A. F. Press†, M. A. Jaworski, D. C. Moir, S. Szustkowski
Los Alamos National Laboratory, Los Alamos, USA

Abstract

Validated particle in cell (PIC) simulations of the DARHT Axis 1 injector have the potential to reduce accelerator downtime, assist experimental data analysis and improve accelerator tunes. To realize these benefits, the simulations must be validated with experimental results. In this work, the particle in cell code Chicago is used to simulate the injector region of the dual-axis radiographic hydrodynamic test facility (DARHT) first axis. These simulations are validated against experiment using measured anode-cathode voltage, beam current at three positions, optical transition radiation and previously calculated emittance. Since all of these measurements contain some variation, the respective simulation parameters are varied to understand their effect. The resulting simulated beam current distributions can then be compared to the measured 2*RMS radius. This resulted in a reasonably well validated simulation model. Some inconstancy between simulated and measured results still exists, which future work will address.

EXPERIMENTAL AND SIMULATION SETUP

Figure 1 shows the DARHT Axis 1 injector geometry. Simulations are performed using the particle in cell code Chicago [1]. The anode magnet focuses the beam, while the bucking coil has the opposite polarization and is set to reduce the on-axis axial magnetic field to zero at the cathode face. The optical transition radiation (OTR) foil creates optical light proportional to the beam current density passing through it for a given beam energy. The foil is at a 50° angle, allowing the emitted light to be imaged using a gated CCD camera. The image is then corrected for angle and a background subtraction is performed. Figure 2 shows an example OTR image. An important factor in the OTR data is the width of the gate (10 ns, shown in Fig. 2) causing a small portion of the energy and current variation to be sampled. Only beam properties in the "flat-top" or steady state portion of the voltage and current pulse will be considered here. A range of beam profiles can be measured by changing the anode magnet field intensity. This results in a relationship between the anode magnet current and 2*RMS beam radius at a given axial position as shown in Fig. 3. A similar simulation geometry can be found in work performed by Plewa *et al.* [2], while detailed emitter region simulations can be found in work performed by Coleman *et al.*',[3].

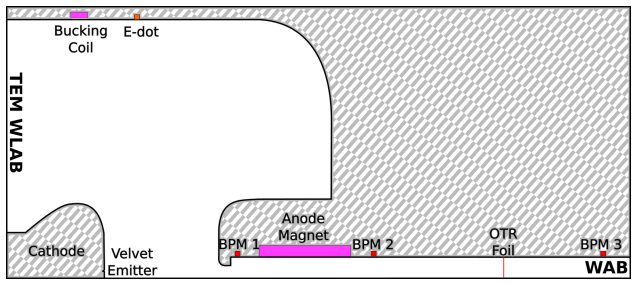

Figure 1: Geometry of the DARHT Axis 1 injector (not to scale). Far left vacuum boundary is a transverse electromagnetic launch and wave absorbing boundary (TEM WLAB). Far bottom right vacuum boundary is a wave absorbing boundary (WAB). The E-dot measures the cathode-anode voltage and was cross calibrated with permanent magnet spectrometer [4]. The anode-cathode gap is nominally 18 cm. BPM 1, 2 and 3 measure beam current at 24.5, 82.4 and 208.0 cm from the cathode face. The OTR measurement foil is located 163.0 cm from the cathode face. The velvet emitter is slightly recessed from the cathode face.

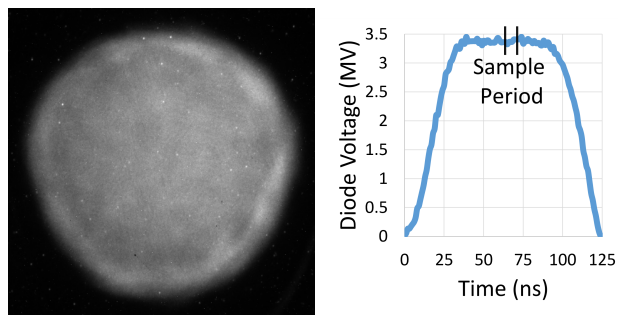

Figure 2: Left: OTR image taken 163 cm from the cathode face with an 186 A anode magnet current. Corrected for OTR foil angle. Right: Pulsed diode voltage showing flat-top and OTR sample period.

SIMULATION VALIDATION

There are several free parameters which need to be constrained in the simulation:

1. **Input voltage** is adjusted until the anode-cathode (diode) gap voltage is equal to that measured by the E-dot.

* This work is supported by the US Department of Energy through the Los Alamos National Laboratory. Los Alamos National Laboratory is operated by Triad National Security, LLC, for the National Nuclear Security Administration of the U.S. Department of Energy (Contract No. 89233218CNA000001).
† alexpress@lanl.gov

ISBN: 978-3-95450-227-1 ISSN: 2673-5490 doi:10.18429/JACoW-IPAC2022-WEPOTK055

BEAM LIFETIME MEASUREMENTS IN SIRIUS STORAGE RING

M. B. Alves*, F. H. de Sá, L. Liu, X. R. Resende
Brazilian Synchrotron Light Laboratory (LNLS), Campinas, Brazil

Abstract

SIRIUS is the new storage ring-based 4th generation synchrotron light source built and operated by the Brazilian Synchrotron Light Laboratory (LNLS) at the Brazilian Center for Research in Energy and Materials (CNPEM). In ultralow emittance storage rings such as SIRIUS, the dominant contribution to the beam lifetime is due to Touschek effect. We used the strategy of storing simultaneously two bunches with different currents to measure their Touschek lifetime independently of other contributions to the total lifetime, such as gas scattering. The measurements were carried out in different conditions of bunch current and RF voltage to compare the experimental results with those expected from theory and simulations for SIRIUS.

INTRODUCTION

Details about SIRIUS main parameters and current operation status can be found in [1–3].

Electrons in the same bunch can undergo Coulomb scattering in which part of the transverse momentum is transferred to the longitudinal. With this scattering, after energy exchange between electrons, the final energy deviations may exceed the acceptance of the ring, causing particle losses. This process is called Touschek effect and its loss rate for each bunch can be obtained by [4]:

$$\alpha_{\mathrm{t}} = \frac{1}{\tau_{\mathrm{t}}} = \frac{r_e^2 I_b}{8\pi\gamma^2}\int_0^{L_0}\frac{F(\tau_m, B_1, B_2)}{\tau_m \sigma_z \sigma_h}\mathrm{d}s, \qquad (1)$$

where r_e is the classical electron radius, I_b is the bunch current, γ the Lorentz factor, σ_z the bunch length, σ_h is related to transverse beam sizes, energy spread σ_δ and dispersion functions by $\sigma_h = \sqrt{\sigma_x^2\sigma_y^2 - (\sigma_\delta^2\eta_x\eta_y)^2}$. The parameter τ_m is related to the momentum acceptance by $\tau_m = \left(1-\gamma^{-2}\right)\delta_m^2 \approx \delta_m^2$. $F(\tau_m, B_1, B_2)$ is a functional of equilibrium parameters and lattice optics functions, parameterized in terms of $B_1(s)$ and $B_2(s)$ in an integral form that can be calculated numerically [4].

Other relevant contributions to the loss rate come from elastic and inelastic scattering between electrons and residual gas in the vacuum chamber, which depends mainly on vacuum pressure. In conditions in which quantum lifetime can be neglected, the total loss rate α_{total} is the sum of Touschek α_{t} and vacuum α_{v} contributions, such that $\mathrm{d}I/\mathrm{d}t = -\alpha_{\mathrm{total}} I = -\left(\alpha_{\mathrm{t}} + \alpha_{\mathrm{v}}\right) I$.

METHOD

The simple measurement of beam current decay provides the total beam lifetime and separating each contribution is typically complicated [5–12]. In order to measure each contribution independently, some strategies have been proposed to study the lifetime behavior in different operation conditions. In Ref. [13] the authors proposed a method of storing two bunches with different charge densities. In this setup, the two bunches densities experience the same pressure and, therefore, the same vacuum loss rate. Measuring the current decay of each bunch and applying the constraint of equal vacuum conditions for both, one should be able to extract the Touschek lifetime contribution. The original method proposed in [13] assumed that beam equilibrium parameters are independent of beam current, so the Touschek loss rate could be obtained algebraically from the total loss rates and current of each bunch as a function of time.

Touschek Lifetime Effective Model

For SIRIUS storage ring, beam equilibrium parameters are highly current-dependent given the small beam volume and large beam coupling impedances due to small vacuum chamber radius. Details about collective effects simulations and measurements for SIRIUS are discussed elsewhere [14].

The bunch-lengthening with single-bunch current, caused mainly by potential-well distortion induced by wakefields, can be included in the effective model of Touschek loss rate. Considering a linear approximation of this effect as $\sigma_z \approx \sigma_{z,0}\left(1+\mu_z I_b\right)$, where $\sigma_{z,0}$ is the bunch-length at zero-current, the Touschek loss rate can be factored as:

$$\alpha_{\mathrm{t}} = \bar{\alpha_{\mathrm{t}}}\frac{I_b}{1+\mu_z I_b}, \qquad (2)$$

where $\bar{\alpha_{\mathrm{t}}}$ is a normalized loss rate that should depend on zero-current equilibrium parameters and lattice optics.

However, other well-known current-dependent effects on beam parameters, such as intrabeam scattering (IBS) [15], are more involved to be captured with an effective model. For example, the functional $F(\tau_m, B_1, B_2)/\sigma_h$ in Eq. (1) generally has a non-trivial dependence on parameters $(\epsilon_x, \epsilon_y, \sigma_\delta)$ that are increased by IBS.

Fitting the Data

A possible approach to fit the loss rate is dividing the measured current decay data in small time segments and fit a linear decay to each one, although this process may be highly susceptible to data noise. In addition, the choice of the time span is not straightforward and may not attend both bunches data simultaneously due to the large difference in decay rates.

A fitting approach that is robust to noise relies on the solution of the differential equation by numerical integration.

* murilo.alves@lnls.br

ISBN: 978-3-95450-227-1 ISSN: 2673-5490 doi:10.18429/JACoW-IPAC2022-WEPOTK057

TOWARDS DIRECT DETECTION OF THE SHAPE OF CSR PULSES WITH FAST THz DETECTORS

J. L. Steinmann*, M. Brosi†, E. Bründermann, A. Mochihashi, P. Schreiber, A.-S. Müller
Karlsruhe Institute of Technology, Karlsruhe, Germany

Abstract

Coherent synchrotron radiation (CSR) is emitted when the emitting structure is equal to or smaller than the observed wavelength. Consequently, these pulses are very short and most detectors respond with their impulse response, regardless of the pulse length and shape. Here we present single-shot measurements performed at the Karlsruhe Research Accelerator (KARA) using a fast real-time oscilloscope and Schottky barrier detectors sensitive in the sub-THz range. The time response of this setup to CSR pulses emitted by electron bunches during the microbunching instability is shown to be sensitive to the shape of the electron bunch. Our results show how, in the future, the shape of electron bunches can be directly measured using a straightforward setup.

OVERVIEW

While incoherent radiation is independent of the electron distribution and the emitted optical power is therefore directly proportional to the bunch structure, coherent radiation, on the other hand, depends on the electron distribution, since the power for fully coherent radiation scales quadratically with the number of particles. In the past, our readout chain could not directly resolve the time structure of THz pulses but measured the total integrated pulse energy. Here we show for the first time direct time structure measurements of a short electron bunch suffering from the microbunching instability. During this instability, which was extensively studied in the past years [1], sub-structures on the bunch profile are created leading to a rich structure whose form factor extends up to several THz. With a commercial real-time oscilloscope and a fast sub-THz detector we were able to resolve some part of that structure.

SETUP AND CHARACTERIZATION

The optical measurement setup is quite simple as we used a single off-axis parabolic mirror to focus the synchrotron radiation at the KARA IR2 beamline onto the THz detector. The detector consists of a horn antenna coupling the radiation into a waveguide and onto a Schottky diode which rectifies the electric field pulse. Due to the filtering characteristic of the waveguide (WR2.2) and the diode itself, the detector is sensitive between 325 GHz to 500 GHz. Through a small hole in the parabolic mirror, some fraction of the optical light is transmitted and focused with an objective onto a photo diode detector sensitive in the visible range, thus measuring purely incoherent synchrotron radiation. This diode is specified with a rise time of 35 ps and a bandwidth of 10 GHz. The optical setup is shown in Fig. 1.

Each detector output is connected with a 1.2 m long RF cable to the 100 GHz, 256 GSa/s, 10-bit real-time oscilloscope. Apart from the oscilloscope, the equipment is not intended for this high frequency, which leads to some compromises that might affect the performance. The THz diode has a 2.92 mm K-connector where we connected a low-loss cable also with K-connectors to an K-to-V-Adapter and a V-to-1 mm-Adapter to the oscilloscope. The K connectors as well as the used Totoku Flexible Cable, TCF358, 1.2 m are specified only up to 40 GHz above which additional modes can propagate on the cable. The photo diode detector has an SMA connector but is limited to ~10 GHz bandwidth.

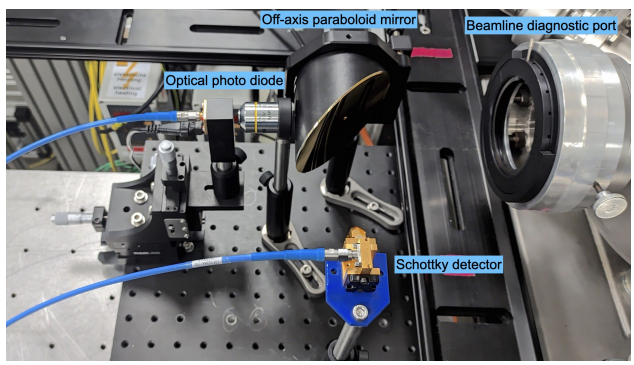

Figure 1: Optical setup: The radiation is coupled out via the diagnostic port of the IR2 beamline at KARA and focused with an off-axis parabolic mirror into the horn antenna of the THz detector. Through a hole in the mirror, visible light is guided through an objective onto a photo diode detector.

To characterize the THz detector setup and make sure we are not just seeing detector effects we measured a stable laser based THz source (TERA15-TX-FC) with a length of below 2 ps first, which is shorter than what our setup can resolve. Therefore, the impulse response of the system is probed. The photo diode detector was illuminated with incoherent synchrotron radiation in the visible range. To compensate for arrival time changes due to synchrotron oscillation, the pulses were aligned before averaging.

The measured detector outputs are shown in Fig. 2 (top). The THz detector shows a significantly lower standard deviation (compare the noise before the pulses) and a very stable pulse signal and corresponding readout. Though, small after-ringing and reflections are visible where not necessarily all of them have to come from the detector or the readout, as some are also visible in the THz time-domain spectroscopy

* steinmann@kit.edu
† now at MAX IV Laboratory, Lund

ISBN: 978-3-95450-227-1 ISSN: 2673-5490 doi:10.18429/JACoW-IPAC2022-WEPOTK058

EXPERIMENTAL STUDY OF THE TRANSVERSE MODE COUPLING INSTABILITY WITH SPACE-CHARGE AT THE CERN SPS

X. Buffat*, H. Bartosik, CERN, Geneva, Switzerland

Abstract

Past studies on the Transverse Mode Coupling Instability (TMCI) suggested that it can be suppressed in the presence of space-charge forces. Recent developments in this field show that for higher strength, space-charge forces lead to other types of instabilities. We investigate the characteristics of these instabilities by means of stability threshold measurements at the CERN SPS for various intensities, longitudinal and transverse emittances. These observations are compared to numerical tracking simulations.

INTRODUCTION

The Transverse Mode Coupling Instability (TMCI) often limits the maximum bunch intensity in synchrotrons [1]. While it is expected that weak space-charge forces can mitigate the TMCI [2], strong enough space-charge fields may give rise to new mode coupling instabilities [3, 4]. We present experimental studies aiming at demonstrating the existence of these instabilities and determine the dependence on the most relevant machine and beam parameters at the CERN SPS.

Instabilities with strong space-charge are predicted by linearised models which do not allow for quantitative comparison with experimental data, due to the lack of modelling for Landau damping caused by the tune spread driven by space-charge forces. We therefore use macroparticle tracking simulations for comparison with experimental data. The tracking through the lattice is performed using SixtrackLib [5] based on the thin lens optics of the SPS [6] featuring multipole errors in the dipoles and quadrupoles up to 7th order. Self-consistent space-charge field computations are preformed at discrete points around the machine using PyPIC [7]. Both lattice and space-charge computations are accelerated on GPU. The impact of the wake fields is computed with PyHEADTAIL [8] using the 2018 impedance model of the SPS [9]. The machine, beam and numerical parameters are listed in Tab. 1.

Table 1: Machine, Beam and Numerical Parameters

Energy [GeV]	26
Bunch intensity [10^{11} p/b]	1.5 to 2.4
Trans. norm. emit. [μm]	0.5 to 6
Long. emit. [eVs]	0.25 to 0.4
H/V tune	26.15 / 26.22
H/V chromaticity	3.0/2.0
H/V 2nd order chroma. [10^2]	2.8/1.2
H/V 3rd order chroma. [10^5]	-5.0/3.2
Synchrotron tune [10^{-4}]	4.2
RF Voltage (200MHz) [MV]	1
RF Voltage (800MHz) [MV]	0.1
Nb. turns	$1.3 \cdot 10^5$
Nb. macroparticles	10^6
Nb. slices for wake	500
Nb. slices for PIC	50
PIC grid size	128x128
Number of space-charge kicks	540

INSTABILITY THRESHOLD

A series of experiments were conducted at the SPS, during which a single bunch with different properties was injected and kept at flat bottom allowing for a monitoring of the evolution of the beam properties and assess in particular the transverse stability threshold. The experimental procedure consisted in varying the transverse emittances by approaching the integer tune and then the coupling resonance at the flat bottom of the PS, in order to obtain round beams yet maintaining the same intensity and longitudinal emittance. By doing so, the strength of the space-charge forces is varied keeping the strength of the wake fields constant. The operation was repeated for different intensities and longitudinal emittances, obtained with dedicated setup in the PSB.

We use the intensity transmission through the flat bottom of the SPS to characterise the stability of the beam. The experimental data as well as the results of simulations are shown in Fig. 1. The experimental data (dots) on the top plot corresponds to configurations featuring a measured longitudinal emittance of 0.3 eVs but varying intensities and transverse emittances. The simulations with space-charge (solid lines) are slightly pessimistic with respect to the observations, yet the dependence with the transverse emittance is well described. There is a significant uncertainty related to the longitudinal distribution, since it is measured at the PS flat top, before the phase-space rotation that occurs right before the injection into the SPS [10]. As discussed later, the instability may develop within tens to hundreds of turns following the injection into SPS, such that the longitudinal distribution is not yet fully matched. It is therefore expected that the simulations with 0.3 eVs are pessimistic. The agreement is significantly better with 0.4 eVs. The remaining differences may be attributed to the uncertainty on the measured transverse emittance ($\approx 20\%$).

* xavier.buffat@cern.ch

ISBN: 978-3-95450-227-1 ISSN: 2673-5490 doi:10.18429/JACoW-IPAC2022-WEPOTK059

SUPPRESSION OF EMITTANCE GROWTH BY A COLLECTIVE FORCE: VAN KAMPEN APPROACH

X. Buffat*, CERN, Geneva, Switzerland

Abstract

In hadron synchrotrons, external sources of noise affecting the beam results in emittance growth through the mechanism of decoherence. Active feedbacks are often used to suppress this emittance growth. In the presence of beam-beam interactions, it was shown that coherent modes of oscillations with frequencies shifted outside of the incoherent spectrum significantly enhances the efficiency of the emittance growth suppression by active feedbacks. We show that the same enhancement of the emittance growth suppression may be driven by a beam coupling impedance generating a real tune shift larger than the detuning.

INTRODUCTION

We aim at quantifying the emittance growth due to an external source of noise in the presence of a frequency spread and a collective force. In the next section we describe the mathematical model based on a perturbation of the linearised Vlasov equation and obtain a basis of functions representing the modes of oscillation of the beam. In the third section the problem is reduced to an initial condition problem by assuming that the noise can be represented by a superposition of individual kicks without interference. Thus, an initial condition corresponding to an offset beam is expressed in terms of modes of oscillation, such that the time evolution of the perturbation can be written explicitly. In the fourth section, an expression for the final emittance after decoherence is obtained by considering the limit of long time scale.

MODEL

In the following we use the action-angle variables J and θ relating to the transverse position x and momentum p_x:

$$x = \sqrt{2J}\cos(\theta) \quad (1)$$
$$p_x = \sqrt{2J}\sin(\theta). \quad (2)$$

The unperturbed distribution can then be written as

$$\Psi_0(J,\theta) = \frac{1}{2\pi} f_0(J). \quad (3)$$

The effective Hamiltonian of the lattice H_0 is the one of an oscillator featuring amplitude detuning as

$$\omega(J) \equiv \frac{\partial H_0}{\partial J}. \quad (4)$$

We add a collective force proportional to the average position of the bunch

$$F_c = -2\Delta\Omega_{ext}\langle x\rangle, \quad (5)$$

with $\Delta\Omega_{ext}$ the corresponding complex frequency shift. Thus we can write the Vlasov equation as:

$$\frac{\partial\Psi_1}{\partial t} + \frac{\partial\Psi_1}{\partial\theta}\omega(J) - \frac{\partial\Psi_0}{\partial J}\sqrt{2J}\sin(\theta)F_c = 0. \quad (6)$$

We will be looking for harmonic solutions with the form

$$\Psi_1(J,\theta,t) = \frac{1}{2\pi} g(J) e^{i(\theta-\Omega t)}. \quad (7)$$

The Vlasov equation becomes:

$$(\Omega-\omega)g = \frac{-1}{2}\Delta\Omega_{ext}\frac{df_0}{dJ}\sqrt{2J}\int dJ\sqrt{2J}g. \quad (8)$$

VAN KAMPEN MODES

Coherent Mode

A solution of Eq. (8), corresponding to a coherent mode of oscillation, can be expressed as:

$$g_c = \frac{-1}{2}\Delta\Omega_{ext}\frac{\sqrt{2J}\frac{df_0}{dJ}}{\Omega_c-\omega}, \quad (9)$$

choosing the mode frequency Ω_c such that:

$$\int dJ\sqrt{2J}g_c = 1. \quad (10)$$

This condition translates into the well known dispersion relation [1]:

$$\int dJ\frac{J\frac{df_0}{dJ}}{\Omega_c-\omega} = \frac{-1}{\Delta\Omega_{ext}} \quad (11)$$

Incoherent Spectrum

Following Van Kampen [2], we find another set of solutions in the realm of distribution functions:

$$g_k = \frac{-1}{2}\Delta\Omega_{ext}\left(\frac{\sqrt{2J}\frac{df_0}{dJ}}{\Omega_k-\omega}\right)_{\text{p.v.}} + \lambda_k\delta(J-k), \quad (12)$$

with $k\in[0,\infty[$. The notation $(\cdot)_{\text{p.v.}}$ indicates that the integration of the distribution function should be performed as a Cauchy principal value. As for the coherent mode, λ_k is chosen such that

$$\int dJ\sqrt{2J}g_k = 1. \quad (13)$$

This condition yields:

$$\lambda_k = \frac{1}{\sqrt{2k}}\left(1+\Delta\Omega_{ext}\,\text{p.v.}\int dJ\frac{J\frac{df_0}{dJ}}{\Omega_k-\omega}\right). \quad (14)$$

* xavier.buffat@cern.ch

ISBN: 978-3-95450-227-1 ISSN: 2673-5490 doi:10.18429/JACoW-IPAC2022-WEPOTK060

PROSPECTS OF ULTRAFAST ELECTRON DIFFRACTION EXPERIMENTS AT SEALab

B. Alberdi-Esuain *[1], J.-G. Hwang, T. Kamps[1], A. Neumann, J. Völker
Helmholtz-Zentrum Berlin für Materialien und Energie, 12489 Berlin, Germany
[1] also at Humboldt Universität zu Berlin, 10117 Berlin, Germany

Abstract

Ultrafast Electron Diffraction (UED) is a pump-probe experimental technique that aims to image the structural changes that happen in a target structure due to photo-excitation. Development of MeV UED capabilities is one of the main objectives at Sealab, a superconducting RF accelerator facility being commissioned in Helmholtz-Zentrum Berlin. In order to perform UED experiments, the optimization of temporal resolution is of the utmost importance. The composition of the SRF Photoinjector, currently the main beam-line in Sealab, offers superb flexibility to manipulate the longitudinal phase-space of the electron bunch. At the same time, the CW operation of the accelerator provides an enhanced beam stability compared to warm guns, together with a MHz repetition rate. This work aims to show the capacity of the SRF Photoinjector in Sealab to reach the required temporal resolution and explain the development and current status of the necessary tools to perform UED experiments at the facility.

INTRODUCTION

Over the last decade, cost-effective and compact Ultrafast Electron Diffraction (UED) machines have opened an era for examining an ultrafast structural dynamics associated with the diffraction of phase transformations and making and breaking of bonds in solids, chemical reactions, and rapid biological processes which was only allowed for the much larger Free Electron Lasers (FELs). Recent progress on semiconductor-based photocathodes have pushed thermal emittances down to few nanometer-radian at a femtocoulomb bunch charge, resulting in MeV-class electrons produced by a gun having the transverse coherency close to the hard X-rays. The strong scattering power of electrons enables observation of atomic and molecular structures at low intensity. The MeV-class beam energy increases penetration depth and accomplishes sufficient bunch charges at a short bunch length. These features enable the fine scanning of the structure at different time steps attained by adjusting the time-delay between pump and probe pulses. The remaining challenge of MeV-class UED accelerators is the generation of extremely short bunches with consummately reliable stability in terms of beam arrival time for achieving a high temporal resolution as well as sufficient lateral coherency. The SRF Photoinjector in Sealab is well suited for this purpose.

* benat.alberdi_esuain@helmholtz-berlin.de

SEALab

Superconducting Electron Accelerator Laboratory (Sealab) in Helmholtz-Zentrum Berlin is a test bench for beam dynamics, control and instrumentation R&D of high average current, ultrashort and high brightness beams. The main beam-line within the Sealab facility is a SRF Photoinjector. Offering user dedicated UED capabilities is among the goals of Sealab. A simplified sketch of the beam-line can be seen in Fig. 1. The laser system provides green light between 510 nm and 540 nm. The repetition rate of the laser system can reach 1.3 GHz. The laser spot size at the photocathode is limited in the lower side to 0.5 mm rms radius top-hat distribution. It has a minimum pulse length of 1.0 ps and a Gaussian longitudinal shape. The photocathode is located at the back-wall of a superconducting L-band (1.3 GHz) electron gun. Three more L-band superconducting booster cavities are located between the gun and the target station. All cavities operate in continuous wave (CW) mode.

Since the injectors of energy recovery linear accelerators (ERLs) produce intense electron beams of superior quality in 6-D phase space with an equivalent layout to the SRF Photoinjector, the approach presented here offers special scientific opportunities for these facilities. Given the capacity of superconducting injectors to operate with one bunch per RF cycle, this open the door for MHz repetition rate UED experiments, greatly increasing the signal to noise ratio.

METHODS

Different tasks are currently being undertaken with the goal of enabling high resolution UED capabilities in the SRF Photoinjector and develop the necessary tools for user operation. Amongst them are the study of time resolution optimization [1], the design of beam diagnostics systems for low intensity beams and short bunches [2], the development of a surrogate model of the SRF Photoinjector based on neural networks and the preparation of a proof of concept static diffraction experiment.

Time Resolution Optimization

The time resolution R_t in a UED experiment defines the capability of discerning minimum temporal extension of the structural dynamics. This quantity can be expressed by a square root of the sum of the quadrature of the different contributions,

$$R_t^2 = \sigma_{pump}^2 + \sigma_{probe}^2 + \tau_{jitter}^2 + \tau_{vm}^2,$$

ISBN: 978-3-95450-227-1 ISSN: 2673-5490 doi:10.18429/JACoW-IPAC2022-WEPOTK061

LATTICE DESIGN OF THE UVSOR-IV STORAGE RING

E. Salehi†, Y. Taira, UVSOR, Institute for Molecular Science, Okazaki, Japan
M. Fujimoto[1], L. Guo, NUSR, Nagoya University, Nagoya, Japan
M. Katoh[1], HSRC, Hiroshima University, Higashi-Hiroshima, Japan
[1]also at UVSOR, Institute for Molecular Science, Okazaki, Japan

Abstract

We are designing a storage ring lattice for the future plan of UVSOR. As a candidate, we have designed a storage ring of 1 GeV electron energy, which is higher than the present value, 750 MeV. The magnetic lattice is based on a compact double bend achromat cell, which consists of two bending magnets and four focusing magnets, all of which are of combined function. The circumference is 82.5 m. The emittance is 4 nm in the achromatic condition, which becomes lower in the non-achromatic condition. The lattice has moderately large dynamic aperture with four sextupole families. The lattice of 6-fold symmetry has six straight sections of 4 m long and six of 1.5 m long. Undulators can radiate nearly diffraction-limited light in VUV. If we install high field multipole wigglers at the short straight sections, they can provide high flux tender X-rays. We are expecting usage of a laser-based accelerator as the injector, which might be developed in the next decade. As an alternative plan, we have designed a traditional injector, which consists of a linear accelerator and a booster synchrotron that can be constructed inside of the storage ring.

INTRODUCTION

UVSOR is a low energy synchrotron light source, which had been operated since 1983. After two major upgrades [1-4], now it is called UVSOR-III. The circumference of the storage ring is 53 m and the electron beam energy 750 MeV. It has 8 straight sections and six of them are occupied with undulators of various kinds. One straight section is used for beam injection and another for RF acceleration. It has a moderately small emittance of about 17 nm and provides vacuum ultraviolet light of high brightness.

Nowadays, to meet the demand of diffraction limited light beam in the vacuum ultraviolet and x-ray range from scientific community, several synchrotron light sources, which have exceedingly small emittance less than 1nm, are under consideration, construction, or in operation [5-7]. In such a situation, we have started considering a future plan for UVSOR with an emittance smaller than at least a few nm to provide diffraction-limited light in the vacuum ultraviolet range. As the first step of the investigation, we have analyzed the present magnetic lattice of UVSOR based on tie diagram to explore the possibility to get a lower emittance with some minor changes in the configuration of magnets. We have found a few optics which has significantly (but not drastically) smaller emittance around 10 nm than the present value, 17 nm which may be useful for some special experiments [8]. To reach the low emittance around a few nm, we have started designing a totally new storage ring. The storage ring has a higher electron energy, 1 GeV and a larger circumference, 82.5m. The lattice consists of twelve double bend cells. Among twelve straight sections, two sections will be used for the injection and RF cavity, and ten sections will be used for insertion devices.

In this paper, we will describe the design of the new lattice for UVSOR-IV and the related beam dynamics studies.

LATTICE DESIGN

The lattice has been designed based on a compact double bend achromat cell (DBA), which consists of two bending magnets and four focusing magnets, all of which are combined function magnets. Two sextupole families are located in between two combined dipoles for the chromaticity correction and two harmonic sextupole families are also employed to correct the high order geometric aberrations. This lattice has twelve DBA cells with six long straight sections about 4 m and six short straight sections around 1.5 m long. These lengths are same as those of UVSOR-III. This may enable us to use the undulators at UVSOR_III in the new ring.

The lengths of the straight sections can be longer if the larger circumference is allowed.

It is noted that this lattice has a flexibility on the dispersion function at the straight sections, which enables to realize various operation modes such as of achromatic, lower emittance, or isochronous.

A tune survey was performed to find the linear optics with a low emittance and appropriate optical functions. ELEGANT [9] was used for the calculations. The emittance is around 4 nm in the achromatic condition, which becomes lower in the non-achromatic condition. Figure 1 shows the lattice functions in the achromatic condition. The major parameters are listed in Table 1 and are compared with those of UVSOR-III.

It is noticeable that if we occupy three of short straight sections with 2T multipole wigglers in symmetry, the energy loss due to the radiation in the wigglers enhances the damping effect and the emittance reduces to 3.7 nm. These wigglers can provides tender X-ray, which are hardly accessible at the present UVSOR-III.

† elham@ims.ac.jp

ISBN: 978-3-95450-227-1 ISSN: 2673-5490 doi:10.18429/JACoW-IPAC2022-WEPOTK062

INTRABUNCH MOTION WITH BOTH IMPEDANCE AND BEAM-BEAM USING THE CIRCULANT MATRIX APPROACH

E. Métral* and X. Buffat, CERN, Geneva, Switzerland

Abstract

In high-intensity high-brightness circular colliders such as the CERN LHC, coherent beam-beam effects and impedance cannot be treated independently. Coherent beam-beam dipole modes can couple with higher order head-tail modes and lead to the transverse mode coupling instability of colliding beams. This mechanism has been analysed in detail in the past through the eigenvalues, which describe the evolution of the beam oscillation mode-frequency shifts. In this contribution, the transverse mode coupling instability of colliding beams is studied using the eigenvectors, which describe the evolution of the intrabunch motion. As this instability exhibits several mode couplings and mode decouplings, the evolution of the intrabunch motion reveals quite some interesting features (such as a propagation of the traveling-wave not only from the head to the tail but also from the tail to the head and similar intrabunch signals for some mode coupling and mode decoupling), which are compared to past predictions in the presence of impedance only.

INTRODUCTION

A transverse mode coupling instability (TMCI) can be observed in the presence of impedance only [1], impedance and tune spread [2], impedance and beam-beam [3], electron cloud [4], impedance and space charge [5]. These instabilities are usually studied analytically with the linearized Vlasov equation, ending up with an eigenvalue system to solve, and in particular looking at the evolution of the eigenvalues as a function of the bunch intensity. However, in the presence of nonlinearities or when higher-order modes are involved, this becomes quite difficult, if not impossible, and the coupling between the modes cannot be directly measured (or simulated) anymore. Another important (and always accessible) observable is the intrabunch motion, which can be also computed analytically thanks to the eigenvectors. The case of an impedance only was already discussed in some detail in Refs. [6] [7], where it could be seen that the oscillation amplitude of the head of the bunch is significantly higher than the tail just above the TMCI intensity threshold. Increasing the intensity further beyond the threshold shifts the peak oscillation amplitude to the tail of the bunch. The purpose of this paper is twofold: first, study the intrabunch motion for the case of the CERN LHC with its transverse impedance only, using the circulant matrix approach [8] [9] and compare to previous studies [6] [7]; second, extend this type of analysis to the case where one beam-beam head-on interaction is added (see Table 1).

* Elias.Metral@cern.ch

Table 1: Machine, beam and numerical parameters for the studies with beam-beam (or impedance only)

Energy [TeV]	7
Bunch population [10^{11}]	1.2 (or scanned)
Bunch length [cm]	7.6
Rel. momentum spread [10^{-4}]	1.1
Trans. tune	0.31
Long. tune [10^{-3}]	2.1
Number of interaction points	1 (or 0)
Beam-beam model	Round, Gaussian and linearised
Number of slices	80
Number of rings	40
Slicing	Equidistant
Impedance / wake model	LHC 2022 flat top [11]

INTRABUNCH MOTION WITH IMPEDANCE ONLY

In the case of the transverse impedance only, the beam oscillation mode-frequency shifts as a function of the bunch intensity for the CERN LHC are depicted in Fig. 1, where it can be deduced that the TMCI intensity threshold appears at about 4.45×10^{11} protons. The evolution of the transverse intrabunch motion as a function of the bunch intensity is revealed in Fig. 2, where a similar behaviour as in previous studies [6] [7] can be observed. As predicted, we see first the signal mainly in the head with a signal in the tail growing with bunch intensity. We see, also as predicted, a fixed point (in the tail) at the start of the TMCI, which then disappears for higher bunch intensities. It is replaced by a traveling-wave with an amplitude growing from the head to the tail: it is worth stressing that when we mention "traveling-wave" here, we refer to the propagation of the maximum of the signal amplitude. After these careful checks, it can be concluded that the circulant matrix approach leads to the same results obtained in the past with the PyHEADTAIL macroparticle tracking code [10] [6] and the Vlasov formalism [7]. The combined effect of the impedance and beam-beam is discussed in the next section.

INTRABUNCH MOTION WITH BOTH IMPEDANCE AND BEAM-BEAM

In the case of both the transverse impedance and one beam-beam head-on interaction, the usual TMCI plots for the CERN LHC are depicted in Fig. 3, as a function of the beam-beam parameter. Considering round beams without crossing angle and neglecting the hourglass effect, the beam-

ISBN: 978-3-95450-227-1 ISSN: 2673-5490 doi:10.18429/JACoW-IPAC2022-WEPOTK063

A WIRELESS METHOD TO OBTAIN THE IMPEDANCE FROM SCATTERING PARAMETERS

C. Antuono* [1], C. Zannini, E. Métral,
CERN, European Organization for Nuclear Research, Meyrin, Switzerland
A. Mostacci, M. Migliorati Sapienza University of Rome, Rome, Italy
[1]also at Sapienza University of Rome, Rome, Italy

Abstract

The coaxial wire method is a common and appreciated choice to assess the beam coupling impedance of an accelerator element from scattering parameters. Nevertheless, the results obtained from wire measurements could be inaccurate due to the presence of the stretched conductive wire that artificially creates the conditions for the propagation of a Transverse ElectroMagnetic (TEM) mode.

The aim of this work is to establish a solid technique to obtain the beam coupling impedance from electromagnetic simulations, without modifications of the device under test. In this framework, we identified a new relation to get the resistive wall beam coupling impedance of a circular chamber directly from the scattering parameters and demonstrated that it reduces to the exact theoretical expression. Furthermore, a possible generalization of the method to arbitrary cross section geometries has been studied and validated with numerical simulations.

INTRODUCTION

The beam coupling impedance describes the electromagnetic interaction between the particle beam and the accelerating structure. Ideally, the beam coupling impedance of a device should be evaluated by exciting the device with the beam itself. However, in most cases, this solution is not possible, and one must resort to alternative methods to consider the effect of the beam.

A well-established technique is to simulate the beam by a current pulse flowing through a wire stretched along the beam axis, resulted in the development of the stretched Wire Method (WM) [1]. Nevertheless, the results obtained from wire measurements might not entirely represent the solution of our initial problem, because the presence of the stretched wire perturbs the EM boundary conditions. The most evident consequence of the presence of another conductive medium in the centre of the device under study is the artificial propagation of the TEM mode through the device, with zero cut-off frequency. The presence of a TEM mode among the solutions of the EM problem will have the undesired effect of causing additional losses. In this regard, the attention has been focused to possible approaches without modification of the Device Under Test (DUT). Wireless measurements have already been proposed in [2] and performed in [3] above the cut-off frequency of the device under test (DUT), where an approximated formula has been employed.

* chiara.antuono@cern.ch

An exact formula to obtain the longitudinal beam coupling impedance of the accelerator components is presented in this paper. The new formula, relating the longitudinal beam coupling impedance and the scattering parameters, has been analytically validated for a resistive circular chamber also below its cut-off frequency. Furthermore, a possible generalization to arbitrary chamber shapes above the cut-off frequency has been explored.

WIRELESS METHOD

The longitudinal beam coupling impedance is essentially related to the energy loss of the electromagnetic wave propagating in the structure and, therefore, is intrinsically linked to the transmission scattering parameter. Given these considerations and by analogy with the WM we looked for a Log-formula to express the beam coupling impedance by using the first propagating Transverse Magnetic (TM) mode in the DUT. The proposed relation to evaluate the impedance, without modifications of the DUT, has the following form:

$$Z = -K \cdot Z_{mode} \ln \frac{|S_{21DUT}|}{|S_{21REF}|}. \quad (1)$$

The Z_{mode} is the characteristic wave impedance of the TM propagating mode. The transmission scattering parameter S_{21DUT} refers to the 2-Port DUT, that is the chamber with finite electric conductive walls, while the S_{21REF} refers to the related reference structure, in this case, the chamber with Perfect Electric Conductive (PEC) walls. The term K is a possible constant to be determined in the analytical derivation.

Analytical Validation

The proposed formula has been analytically validated for the case of a circular resistive wall chamber of radius b, wall conductivity σ and length L, both below and above the cut-off frequency of the chamber. The longitudinal beam coupling impedance of the circular resistive chamber can be analytically calculated by using the following well-known equation [4]:

$$Z^{theory} = \frac{\zeta_s}{2\pi b} L, \quad (2)$$

where in the classical thick wall regime $\zeta_s = \zeta(1+j) = \sqrt{\frac{\omega\mu_0}{2\sigma}}(1+j)$, ω is the angular frequency and μ_0 the permeability of free space. In order to validate the proposed approach it has to be demonstrated that the formula of Eq. (1) reduces to the theoretical formula of Eq. (2). The analytical expression of the S_{21} of the resistive circular pipe

ISBN: 978-3-95450-227-1 ISSN: 2673-5490 doi:10.18429/JACoW-IPAC2022-WEPOTK064

GENERATING SUB-FEMTOSECOND ELECTRON BEAMS AT PLASMA WAKEFIELD ACCELERATORS

R. R. Robles*, C. Emma, R. Hessami, K. Larsen, A. Marinelli,
SLAC National Acccelerator Laboratory, CA, USA

Abstract

The Plasma-driven Attosecond X-ray source (PAX) project at FACET-II aims to produce attosecond EUV/soft x-ray pulses with milijoule-scale pulse energy via nearly coherent emission from pre-bunched electron beams. In the baseline approach [1, 2], a beam is generated using the density downramp injection scheme with a percent-per-micron chirp and 10^{-4} scale slice energy spread. Subsequent compression yields a current spike of just 100 as duration which can emit 10 nm light nearly coherently due to its strong pre-bunching. In this work, we report simulation studies of a scheme to generate similarly short beams without relying on plasma injection. Instead, we utilize a high-charge beam generated at an RF photocathode, with its tail acting as the witness bunch for the wake. The witness develops a percent-per-micron chirp in the plasma which is then compressible downstream. The final bunch length demonstrated here is as short as 100 nm, and is limited primarily by emittance effects. The configurations studied in this work are available for experimental testing at existing PWFA facilities such as FACET-II.

INTRODUCTION

There is significant recent interest in attosecond science due to the realization of attosecond x-ray pulse generation with high pulse energy at x-ray free-electron lasers (XFELs) [3]. Typical performance in this case for soft x-ray wavelengths is typically tens of microjoules per pulse and several hundred attosecond pulse durations. To push the pulse energy higher and the pulse duration shorter while still utilizing the relatively high efficiency of the FEL process, one requires higher electron beam brightness. It was proposed in [1] to take advantage of the high-quality beams projected to be generated by plasma wakefield accelerators to achieve this goal. This scheme is called the Plasma-driven Attosecond X-ray source (PAX). PAX combines two key concepts to generate mega-ampere class, sub-femtosecond electron beams. The first is the production of an initial beam with very low emittance and energy spread from advanced wakefield injection techniques - in this case, density downramp injection [4]. The plasma injected beam can naturally be produced with very high linear energy chirp on the order of a few %/μm due to the sawtooth nature of nonlinear plasma wakes. Such high chirps, when compressed in a magnetic chicane, lead to very short beams with minimal length limited to $R_{56}\sigma_\gamma$ where R_{56} is the momentum compaction of the chicane and σ_γ is slice energy spread of the original beam. In reality, chromatic and collective effects can conspire to limit the final pulse length to values larger than this minimum.

One of the key prerequisites of the PAX project as outlined in [1] is the demonstration of density downramp injection to achieve the high beam brightness. Before density downramp injection is available at FACET-II, it was also suggested that one could achieve a similar final beam profile by accelerating drive and witness bunches generated by an RF photoinjector together to produce a strongly chirped beam. In the present work we present yet another mechanism, in which a single bunch is accelerated through a standard RF accelerator such that it enters the plasma with a long tail. The tail then experiences the wake of the core of the bunch the same way as a separately generated witness bunch, and can similarly be compressed to ultrashort duration thereafter. We present simulation results based on the FACET-II facility indicating performance fitting for a stepping stone towards the plasma injected case [5].

BEAMLINE OVERVIEW

The simulation results presented below were all obtained using the Lucretia code [6]. The FACET-II beamline consists of a conventional RF photoinjector which injects the beam into the primary linac at roughly 135 MeV. From there the beam goes through three linac sections, L1, L2, and L3, arriving at the final energy 10 GeV. Between L1/L2 and L2/L3 there are four-dipole chicanes, BC11 and BC14, which facilitate compression of the beam. Finally, at the end of L3 immediately preceding the plasma portion of the beamline is a third bunch compressor, BC20, which employs a complicated set of optics to achieve anomalous compression.

The FACET-II injector can operate in single and dual bunch mode. In the present work we focus on the single bunch configuration, launching a 2 nC beam from the cathode with a 4 ps laser pulse length. The quality of the resulting beam is summarized in Fig. 1, as simulated in General Particle Tracer (GPT) [7].

From then on the beamline is optimized to achieve the highest possible peak current at the end of BC20. The longitudinal phase spaces and current profiles are shown after each bunch compressor in Fig. 2. By the time the beam has been compressed in BC14 there is a clear third-order curvature, which after subsequent acceleration and compression in BC20 transforms the beam into a highly nonlinear S-shaped longitudinal phase space. On either side of the >100 kA core are long regions of the beam with roughly flat phase space, low slice energy spread, and currents still largely exceeding 1 kA.

* riverr@stanford.edu

ISBN: 978-3-95450-227-1 ISSN: 2673-5490 doi:10.18429/JACoW-IPAC2022-WEPOTK065

REVISITING INTRABEAM SCATTERING FOR LAMINAR BEAMS

R. R. Robles*, Z. Huang, A. Marinelli, SLAC National Accelerator Laboratory, CA, USA

Abstract

Intrabeam scattering (IBS) is becoming an increasingly important effect in the design of high-brightness linear electron accelerators due to the ever-increasing transverse brightness of beams produced from radiofrequency photoinjectors. The existing theory describing the energy spread growth rate due to IBS was derived in the context of circular machines where the beam particles are frequently and randomly colliding, and therefore should only be applied to non-laminar, emittance dominated flow. This is not the case in the injector portion of a linear accelerator, where the beam is space-charge dominated and the flow is laminar. The different nature of the microscopic motion in the two cases demands a reevaluation of the applicability of IBS theory to the photoinjector. In this work, we present a simple analytic model for energy spread growth during perfectly laminar flow and show that it matches well to point-to-point multiparticle simulations. In this way we demonstrate that stochastic energy spread growth in laminar beams is more attributable to the initial random placement of the particles in the bunch rather than the traditional temperature rearrangement mechanism of IBS.

INTRODUCTION

The development of ever-brighter beam sources for linear accelerators demands precise understanding of the downstream mechanisms by which that brightness can be degraded. Of particular importance for the next generation of x-ray free-electron lasers (XFELs) is the preservation of the beam energy spread, which sets a threshold requirement for lasing in an XFEL [1, 2]. The best known way by which the energy spread can grow is the microbunching instability (μBI), which leads sufficiently cold beams to undergo space-charge amplification of initial shot noise [3]. Traditionally, μBI is suppressed with the use of a laser heater, and the minimal accepted input energy spread to mitigate μBI gain is much higher than that produced by the injector itself [4]. However, as more precise methods for controlling μBI gain are developed, the initial energy spread produced by the injector may become important.

This input energy spread is limited by yet another effect which has historically not attracted much attention in the field of linear accelerators: intrabeam scattering (IBS) [5–7]. IBS is generally thought of as the impact of stochastic, binary collisions on the beam dimensions. Because the beams produced by high-brightness beam sources are generally much colder longitudinally than transversely, IBS is thought to lead to a redistribution of thermal spread from the transverse emittance into the uncorrelated energy spread [8]. Theoretical models of this effect exist, but suffer from ambiguities from the evaluation of the Coulomb logarithm. Recently, there has been substantial interest in IBS for x-ray free-electron lasers due to the ever-increasing brightness of the beams they employ [9, 10].

Besides the difficulties making quantitative estimates resulting from the Coulomb log, there exists yet another reason to distrust the existing IBS theory in the context of linear accelerators. The picture of stochastic effects as being represented by constant and randomly distributed collisions does not make much sense in the injector portion of a linear accelerator where the beam flow is space-charge dominated and therefore quasi-laminar. This disparity between the relevant stochastic effects in injectors, and the existing models of IBS was found to have a notable impact on simulation comparisons with the theory in [11]. Indeed in this regime we expect effects which correspond more closely to the Boersch effect in electron microscopes [12]. Although there exists a theoretical description of the Boersch effect, it is best suited to the relatively low densities found in those systems, and is furthermore quite complicated [13]. With the extremely high beam densities found in XFELs, some simplifications can be found. As more machines are designed with ultra-high brightness beams in mind, a proper understanding of IBS in the context of XFELs is necessary.

In the rest of this paper we outline a simple numerical approach to evaluating slice energy spread growth induced by finite particle effects based on a simple scaling argument. We begin by laying out a basic first principles approach before deriving that the statistical width of the longitudinal space-charge field for a given three-dimensional charge distribution will in general scale with $N_e^{2/3}$, with N_e being the number of electrons in the bunch. With that fact established, the cumulative impact of the space-charge field width can be evaluated using Monte Carlo simulations with significantly fewer particles. Finally, we perform numerical benchmarks demonstrating the validity of the model, where for this paper we restrict ourselves to perfectly laminar flow scenarios. We outline in the conclusions how the method might be expanded to address more general accelerator scenarios.

THEORETICAL MODEL

General Approach

The theoretical model we propose is based on a first principles consideration of the statistics of the longitudinal space-charge field. A particle in the beam experiences an instantaneous rate of energy change given by

$$\frac{d\gamma_{\mathrm{IBS}}}{ds} = \frac{q}{mc^2}\delta E_z \tag{1}$$

where $\delta E_z \equiv E_z - \langle E_z \rangle$, with E_z being the longitudinal space-charge field in the lab frame and $\langle . \rangle$ indicating an ensemble average over the beam distribution function. Specifically,

* riverr@stanford.edu

ISBN: 978-3-95450-227-1 ISSN: 2673-5490 doi:10.18429/JACoW-IPAC2022-WEPOMS001

EFFECT OF BETATRON COUPLING ON TRANSVERSE MODE-COUPLING AND HEAD-TAIL INSTABILITIES

W. Foosang*, A. Gamelin, R. Nagaoka, Synchrotron SOLEIL, Gif-sur-Yvette, France

Abstract

In the context of SOLEIL Upgrade, the 4th generation storage ring project of SOLEIL, several methods are pursued to extend the beam lifetime and limit the emittance growth by reducing the Touschek effect and intra-beam scattering. Betatron coupling is one of the potential techniques to achieve this objective as it can increase the beam volume by transforming a flat beam into a round beam. However, the effect of the coupling on the collective effects is not fully comprehended, but some studies have shown an improvement in transverse instability thresholds. It was, therefore, crucial to investigate the impact of coupling on beam instability for SOLEIL Upgrade. This work presents numerical studies on the impact of coupling on the transverse mode-coupling and the head-tail instabilities. The results showed that coupling could be not only beneficial, but also detrimental.

INTRODUCTION

SOLEIL is moving towards a 4th generation light source in which beam emittance will be reduced below 100 pm rad [1–3]. In order to obtain this challenging emittance, the vacuum chamber radius needs to be reduced to about 6 mm - approximately half the size of the current one - to accommodate focusing magnets which are required to be as close to the beam as possible. This much smaller aperture will lead to stronger collective effects compared to the present SOLEIL ring. A consequence of the low-emittance design of the upgraded ring is the increased Touschek and intra-beam scattering rates due to the high electron density. For a betatron coupling corrected to 1%, the vertical emittance in the new ring can be as small as 0.8 pm.rad. The full parameter list of the SOLEIL Upgrade CDR lattice can be consulted in the conceptual design report [1].

Betatron coupling is one of the possible methods that can increase the beam volume, thus reducing the electron density, by going from a flat beam to a round beam. The main objective of employing this technique is to reduce the Touschek and intra-beam scattering rates. The smaller scattering rates given by a larger beam volume would extend the beam lifetime and limit the emittance growth. However, betatron coupling impacts several aspects of the beam dynamics and its effect on the collective effects has not been widely explored. Among a few papers on the topic, it has been observed that coupling could reduce instability threshold in some machines such as the CERN PS and SPS [4–6]. It is then of special interest to investigate this effect in the SOLEIL Upgrade case.

This article presents the effect of coupling on two single bunch transverse instabilities: the Transverse Mode-Coupling Instability (TMCI) and the Head-Tail Instabilty (HTI). All the simulations presented were done using the mbtrack2 tracking code [7].

* watanyu.foosang@synchrotron-soleil.fr

BETATRON COUPLING

Betatron coupling can transfer quantities related to betatron oscillation between the two transverse planes. The maximum coupling effect can be achieved when the ring is operated on the linear coupling resonance, which is when the fractional tune of the two transverse planes are equal, with a skew quadrupole component. This is the reason why the tunes were set at 54.2 and 18.2 in this study. The result of full coupling is an equipartition of beam qualities in both planes, this includes emittance and radiation damping times as shown in Fig 1. Note that Courant-Snyder invariant of a single particle is shown in the figure, not beam emittance. They are however interchangeable in case of multi-particle. It can be seen that the coupled Courant-Snyder invariant and the coupled damping time are the average of the non-coupled values. Here and throughout this work, the coupling was introduced by using a skew quadrupole with the integrated normalized strength $k_s l = 0.001\ \mathrm{m}^{-1}$.

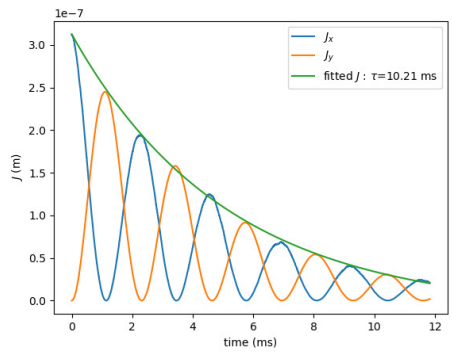

Figure 1: Courant-Snyder invariant of a single particle at full coupling. The non-coupled horizontal and vertical radiation damping times are 7.3 and 13.1 ms, respectively.

EFFECT ON HEAD-TAIL INSTABILITY

Head-tail instability (HTI) is a transverse single bunch instability commonly found in circular accelerators. It occurs in case of nonzero chromaticity and manifests itself in the form of local transverse coherence within a bunch, whose oscillation amplitude could, even though relatively slowly, constantly build up over beam revolutions around the ring. The rise time of HTI is inversely proportional to the transverse effective impedance. The coupling could affect this rise time as it can share the impedance from one plane to another. The plane that has a larger impedance will profit from

ISBN: 978-3-95450-227-1 ISSN: 2673-5490 doi:10.18429/JACoW-IPAC2022-WEPOMS003

BEAM DYNAMICS WITH A SUPERCONDUCTING HARMONIC CAVITY FOR THE SOLEIL UPGRADE

A. Gamelin*, W. Foosang, P. Marchand, R. Nagaoka, Synchrotron SOLEIL, Gif-sur-Yvette, France
N. Yamamoto, KEK, Ibaraki, Japan

Abstract

In 4th generation low emittance synchrotron light sources, harmonic cavities are critical components needed to reach the required performance. However, RF systems with harmonic cavities can be limited by their own set of instabilities. An instability dominated by the coupled-bunch mode $l = 1$ can prevent the RF system from reaching the flat potential condition, hence limiting the maximum bunch lengthening. Here we report how this instability impacts the performance of 3rd and 4th harmonic superconducting cavities for the SOLEIL Upgrade.

INTRODUCTION

The SOLEIL Upgrade project aims to replace the existing storage ring by a 4th generation light source [1–4]. In the framework of the project technical design report (TDR) phase, self-consistent longitudinal beam dynamics simulations are performed to compare different harmonic cavity (HC) technological options. So far, the proposed double RF system comprises:

- A fundamental RF system at 352 MHz, which will provide the required RF voltage and power to compensate for the energy lost by the electron beam and achieve a large enough longitudinal acceptance. It consists of four normal conducting (NC) cavities of the ESRF-EBS type [5, 6], each powered with a 200 kW solid state amplifier (SSA).

- A harmonic RF system, aimed at lengthening the electron bunches in order to preserve low emittance and ensure suitable lifetime. It consists of a cryomodule of the Super-3HC type, similar to that used in SLS and ELETTRA [7–13], which contains two superconducting (SC) passive cavities, tuned to the 3rd or 4th harmonic of SOLEIL (1.06 or 1.41 GHz).

This paper describes the beam dynamics with such a system and compares the respective performance in terms of bunch lengthening of the 3rd and 4th harmonic options for the main operation mode at 500 mA. The TDR lattice and its parameters are presented in [2]; the RF cavity parameters are listed in Table 1. This paper starts with the SC passive HC theory near the flat potential condition, then tracking simulation results are presented showing stable regime, instability regime and the impact of empty buckets in the bunch train.

* alexis.gamelin@synchrotron-soleil.fr

Table 1: Parameters for the RF Cavities

Parameters	MC	HC
Harmonic number m	1	3 or 4
Shunt impedance R (per cavity)	5 MΩ	4.5 GΩ
Unloaded quality factor Q	35 700	10^8
R/Q (per cavity)	140 Ω	45 Ω
Loaded quality factor	6 000	10^8
Cavity number	4	2

SC PASSIVE HC

Let us assume a RF system composed of two "ideal" cavities: a main cavity (MC) with a voltage V_1, a phase ϕ_1, an angular frequency ω_1 and a harmonic cavity (HC) of the m^{th} harmonic with a voltage V_2 and phase ϕ_2. The overall voltage V_{tot} provided by this system at time t is given by:

$$V_{tot}(t) = V_1 \cos(\omega_1 t + \phi_1) + V_2 \cos(m\omega_1 t + \phi_2) . \quad (1)$$

The condition to ensure energy balance for the synchronous particle is:

$$V_{tot}(0) = \frac{U_{loss}}{e} , \quad (2)$$

where U_{loss} corresponds to the energy loss per turn and e is the elementary charge. In such a system, one can adjust the bunch length by controlling the slope of the overall voltage at the synchronous phase, $\alpha_1 = \dot{V}_{tot}(0)$, and its derivative, $\alpha_2 = \ddot{V}_{tot}(0)$. Introducing ξ, as defined in [14]:

$$\xi = \frac{-mV_2 \sin(\phi_2)}{V_1 \sin(\phi_1)} . \quad (3)$$

The system is described by the following equations:

$$\cos(\phi_1) = \frac{U_{loss}}{eV_1} + \xi \frac{\sin(\phi_1)}{m \tan(\phi_2)} , \quad (4)$$

$$V_2 = -\xi \frac{V_1 \sin(\phi_1)}{m \sin(\phi_2)} , \quad (5)$$

$$\tan(\phi_2) = \xi m \tan(\phi_1) . \quad (6)$$

Expressing α_1 and α_2 as a function of ξ:

$$\alpha_1 = \xi\omega_1 \sin(\phi_1) \left(1 - \frac{1}{\xi}\right) , \quad (7)$$

$$\alpha_2 = -V_1{\omega_1}^2 \left[\cos(\phi_1) - \xi m \frac{\sin(\phi_1)}{\tan(\phi_2)}\right] . \quad (8)$$

One can see that the value $\xi = 1$ cancels both α_1 and α_2 and that going from $\xi \leq 1$ to $\xi \geq 1$ implies a change of sign

ISBN: 978-3-95450-227-1 ISSN: 2673-5490 doi:10.18429/JACoW-IPAC2022-WEPOMS004

INVESTIGATION OF RF HEATING FOR THE MULTIPOLE INJECTION KICKER INSTALLED AT SOLEIL

A. Gamelin*, P. Alexandre, R. Ben El Fekih, J. Da Silva Castro, M. El Ajjouri, A. Letresor, L. S. Nadolski, R. Ollier, S. Thoraud, Synchrotron SOLEIL, Gif-sur-Yvette, France
M. Sacko, S. Taurines, Avantis Concept, Saint-Cere, France

Abstract

During the commissioning of the new Multipole Injection Kicker (MIK) pulsed magnet at SOLEIL synchrotron, an anomalously high heating of the MIK chamber and flanges was found. To better manage the heat load, fans directed toward the MIK were added to improve the air-cooling flow. This allowed the nominal current to be reached in all operation modes while keeping reasonable temperatures on the MIK. Post-installation investigations subsequently showed that the initial estimate of the maximal heat load was in agreement with the measured temperature in several operation modes both with and without the additional fans. In this article, we present the complete study, starting from the impedance calculation to thermal simulations, and comparison with the measured data with beam.

MULTIPOLE INJECTION KICKER

Non-linear kicker magnets, such as the Multipole Injection Kicker (MIK), are key components for compact injection scheme of some 4th generation light sources [1, 2]. Non-linear kicker magnets are pulsed magnets characterized by an off axis field region where the injected beam is located and a field free region on the stored beam path. They are developing since their first use at KEK-PF [3] and BESSY II [4] as they allow for different types of on-axis and off-axis injections types in rings with small dynamic aperture [2]. The MIK provides a combined quadrupolar and octupolar pulsed field which allows for a near-transparent injection compared to the usual bump-based scheme using several kickers [1].

The MIK, designed and built by SOLEIL in collaboration with MAX IV, is composed of a racetrack chamber made of monocrystaline sapphire where grooves are precisely machined to hold copper conductors in the direction parallel to beam propagation, see Fig. 1. The inside of the chamber is coated with titanium to shield the beam from the sapphire body, allowing the image current to flow over the titanium layer and reducing the thermal load. But the coating thickness can not be too large as it induces a disturbance of the magnetic field and generates a pulsed quadrupolar component via eddy currents [5]. A compromise must therefore be found on the coating thickness to get a magnet with good performance with a contained thermal load.

A first prototype of the MIK was installed at MAX IV 3 GeV ring in 2017 where heating due to the 0.8 µm thin titanium coating was found to be an issue [1]. The problem was solved in 2019 when an improved chamber with a thicker coating of 3.5 µm was installed. The MIK is now routinely used for day to day operation at MAX IV with excellent performance [1].

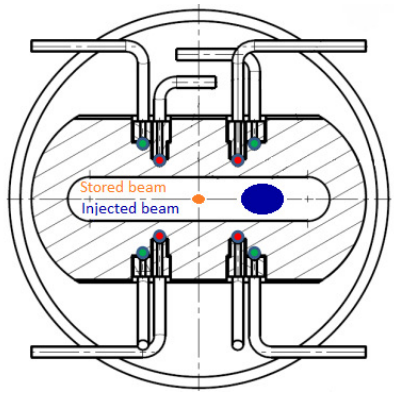

Figure 1: Cross section of the MIK showing the position of the copper conductors (red and green dots), the injected and stored beam.

Another MIK device was installed in the 2.75 GeV storage ring of SOLEIL in January 2021 and is being commissioned [6–8]. As the SOLEIL MIK also presents anomalously high temperatures, a post-installation investigation was initiated to review the RF heating estimate, the choice of the coating thickness and understand the observed high temperatures. This article describes the findings from this investigation and presents the different components: impedance calculations, temperature measurements with beam and thermal simulations.

IMPEDANCE CALCULATIONS

The impedance calculations shown here for the MIK chamber and flanges, the two elements where significant heating is observed, were performed prior to installation and are based on the MIK mechanical design that is described in detail in [9].

MIK Chamber

The MIK is composed of a single 33 cm long racetrack chamber with an inner aperture of 46.8 mm in horizontal and 7.8 mm in vertical plane. Its geometric (longitudinal) impedance is thus negligible compared to the resistive wall one produced by the titanium coating deposited on the sapphire body.

The coating thickness was measured at 3.5 µm using control pellets used during the deposit. The DC resistance of

* alexis.gamelin@synchrotron-soleil.fr

ISBN: 978-3-95450-227-1 ISSN: 2673-5490 doi:10.18429/JACoW-IPAC2022-WEPOMS005

SIMULATIONS OF THE MICRO-BUNCHING INSTABILITY FOR SOLEIL AND KARA USING TWO DIFFERENT VFP SOLVER CODES

M. Brosi*, P. Schreiber, A.-S. Müller, Karlsruhe Institute of Technology, Karlsruhe, Germany
C. Evain, E. Roussel, C. Szwajj, S. Bielawski, PhLAM - CERLA, CNRS/Lille University, France

Abstract

The longitudinal dynamics of a bunched electron beam is an important aspect in the study of existing and the development of new electron storage rings. The dynamics depend on different beam parameters as well as on the interaction of the beam with its surroundings. A well established method for calculating the resulting dynamics is to numerically solve the Vlasov-Fokker-Planck equation. Depending on the chosen parameters and the considered wakefields and impedances, different effects can be studied. One common application is the investigation of the longitudinal micro-wave and micro-bunching instabilities. The latter occurs for short electron bunches due to self-interaction with their own emitted coherent synchrotron radiation (CSR). In this contribution, two different VFP solvers are used to simulate the longitudinal dynamics with a focus on the micro-bunching instability at the SOLEIL synchrotron and the KIT storage ring KARA (Karlsruhe Research Accelerator).

INTRODUCTION

The longitudinal beam dynamics in a storage ring can be simulated based on the time evolution of the particle distribution in the longitudinal phase space (PS). The evolution of the system can be described by the Vlasov-Fokker-Planck (VFP) equation [1]. Various codes for the evaluation have been written with different methods focussing on different effects. A prominent use-case for the VFP equation, the micro-bunching instability, occurs for short electron bunches due to the self-interaction with the coherent synchrotron radiation (CSR). While it does not lead to beam-loss, it results in non-constant beam parameters. These fluctuations, especially in bunch length and energy spread, may affect the beam quality. At the same time, the increased emission of CSR in the long wavelengths can be utilized for experiments based on THz radiation. VFP solvers also play a vital role in the efforts towards control of this dynamic and providing the possibility for increased and more stable CSR emission or the possibility to suppress the instability [2, 3].

MICRO-BUNCHING INSTABILITY

The interaction of a bunch with its own CSR wakefield results above the instability threshold in substructures forming on the particle distribution in the longitudinal PS (see simulations in Fig. 1). Due to rotation in longitudinal PS these substructures cause continuous changes in the longitudinal bunch profile resulting in temporal fluctuations of the emitted CSR intensity and furthermore change the wakefield. Depending on beam parameters, this dynamic can manifest as the typical saw-tooth shaped bursts in emitted CSR intensity [4, 5]. While the occurrence of substructures is driven by the CSR wakefield, damping and diffusion lead to fillamentation of the structures and causes the bunch to lengthen and the structures to wash-out. This reduces the driving force allowing the bunch to further damp down and become short enough so that the resulting CSR wakefield supports the formation of substructures again. The presence of the micro-bunching instability has been observed at multiple light sources (e.g. [6–12]).

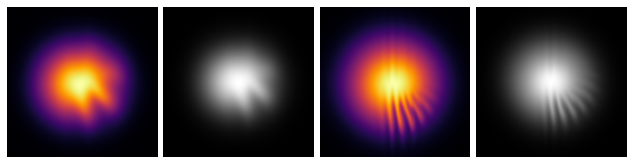

(a) Inovesa (b) PhLAM VFP (c) Inovesa (d) PhLAM VFP

Figure 1: Simulated charge density in the longitudinal PS. (a & b) at 0.26 mA for case **A**, (c & d) at 12 mA for case **C**.

VFP EQUATION & SOLVERS

The Vlasov-Fokker-Planck (VFP) equation describing the evolution of the particle density $\psi(z, E, t)$ with time t can be given by [1, 13, 14]

$$\frac{\partial \psi}{\partial \theta} + \frac{\partial H}{\partial p} \cdot \frac{\partial \psi}{\partial q} - \frac{\partial H}{\partial q} \cdot \frac{\partial \psi}{\partial p} = \beta_\mathrm{d} \frac{\partial}{\partial p} \left(p\psi + \frac{\partial \psi}{\partial p} \right) \quad (1)$$

with the Hamiltonian $H(q, p, t) = H_\mathrm{e}(q, p, t) + H_\mathrm{c}(q, t)$ consisting of the contribution by external fields and the perturbation by collective effects. The coordinates are given as $\theta = f_\mathrm{s} t$ time in synchrotron periods, $q = z/\sigma_{\mathrm{z},0}$ and $p = (E - E_0)/\sigma_{\delta,0}$ as normalised position and energy coordinates with natural bunch length $\sigma_{\mathrm{z},0}$ and energy spread $\sigma_{\delta,0}$. In the radiation damping and quantum diffusion term $\beta_\mathrm{d} = 1/(f_\mathrm{s}\tau_\mathrm{d})$ with the long. damping time τ_d.

The VFP solvers used in this contribution are based on the algorithm derived by Warnock and Ellison [1]. It operates on the charge density discretized in a grid. While the homogeneous solution represents a rotation in PS for the unperturbed case, the influence of diffusion and damping is incorporated as a particular solution.

PhLAM VFP Solver

The VFP solver developed at PhLAM [2, 15, 16] was modelled based on the aforementioned algorithm. The wake-functions for free space and the suppression by parallel plates [17, 18] are directly calculated based on the given input parameters. The necessary convolution of the bunch profile with the wake functions for the wakefield is performed in frequency domain. Therefore, the corresponding impedance is calculated once and multiplied at each time step with the

* miriam.brosi@kit.edu, miriam.brosi@maxiv.lu.se, now at MAX IV Laboratory, Lund

ISBN: 978-3-95450-227-1 ISSN: 2673-5490 doi:10.18429/JACoW-IPAC2022-WEPOMS006

SIMULATION OF THE EFFECT OF CORRUGATED STRUCTURES ON THE LONGITUDINAL BEAM DYNAMICS AT KARA

S. Maier*, M. Brosi†, A. Mochihashi, M. J. Nasse, P. Schreiber, M. Schwarz,
A.-S. Müller, Karlsruhe Institute of Technology, Karlsruhe, Germany

Abstract

Two parallel corrugated plates will be installed at the KIT storage ring KARA (KArlsruhe Research Accelerator). This impedance manipulation structure will be used to study and eventually control the beam dynamics and the emitted coherent synchrotron radiation (CSR). In this contribution, we present the influence of the parameters of the structure on its impedance and the results obtained with the Vlasov-Fokker-Planck solver Inovesa showing the impedance impact of different corrugated structures on the CSR power.

INTRODUCTION

In contrast to incoherent radiation, CSR scales quadratically with the number of particles and therefore enhances the photon flux by several orders of magnitudes. As the emission is coherent for wavelengths larger than the bunch length, high electron density and short bunches are necessary to extend CSR to higher frequencies and to increase the intensity of the radiation. In such short bunch regimes complex nonlinear phenomena can occur due to the interaction between the passing bunch and its emitted CSR. This results in dynamic instabilities and bunch deformations like the so-called microbunching instability [1]. This instability can cause longitudinal substructures on the bunches generating intense THz radiation.

At KIT, we are developing and designing a versatile impedance chamber for the KARA storage ring to study the microbunching instability by manipulating the wakefield and thereby affecting the longitudinal beam dynamics of the electrons. The additional impedance and the resulting wakefield change will be generated by two horizontal parallel plates with periodic rectangular corrugations. Although Bane *et al.* [2, 3] showed that narrow-band THz pulses can be generated by installing such structure into a linear accelerator, to our knowledge such a structure has never been installed into a storage ring, where the electrons pass the structure multiple times. In Fig. 1, a schematic drawing with the characteristic parameters periodic length L, corrugation depth h and corrugation width g, as well as the plate distance $2b$ is given. The theoretical longitudinal impedance $Z^{\parallel}$ for parallel corrugated plates is given by Ng *et al.* [4] under the assumptions $L \lesssim h \ll b$ as

$$\frac{Z^{\parallel}}{L} = \frac{Z_{\text{vac.}}}{\pi b^2}\left[\pi k_{\text{res}}\delta\left(k^2 - k_{\text{res}}^2\right) + i \cdot \text{P.V.}\left(\frac{k}{k^2 - k_{\text{res}}^2}\right)\right] \tag{1}$$

with the resonance wave number $k_{\text{res}} = \sqrt{\frac{2L}{bgh}}$, wave number

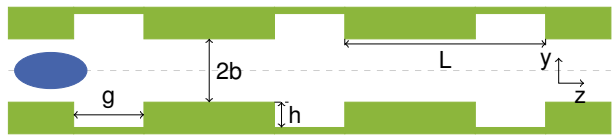

Figure 1: The corrugated plates in cross section with the relevant geometric parameters are shown. The electron bunch is indicated in blue.

$k = \frac{\omega}{c}$, the vacuum impedance $Z_{\text{vac.}}$, the δ-distribution, and principal value P.V.(x).

Previous impedance simulations with CST Studio [5] have shown how the parameters of the structure influence the impedance and that the results are in good agreement with the theoretical prediction [6]. The impedance can be described by the resonator model [7], which is characterized by the three parameters resonance frequency f_{res}, the shunt impedance Z_0, and the quality factor Q.

The resonance frequency of the investigated impedance is in the range between 50 GHz and 200 GHz, where a fraction of the CSR impedance is shielded by the beam pipe and therefore an additional impedance with Z_0=1 kΩ has a significant contribution to the total impedance of the KARA storage ring.

SIMULATION

For the beam dynamics simulations Inovesa [8], an in-house developed Vlasov-Fokker-Planck solver, is used, which describes the micro-bunching instability at the KARA storage ring [9] very well. For the results presented in this contribution, the settings were chosen so that they are comparable to the KARA short-bunch operation mode with synchrotron frequency $f_{\text{sync}} = 9.44\,\text{kHz}$ and the acceleration voltage $V_{\text{RF}} = 1.048\,\text{MV}$ at a beam energy of $E = 1.3\,\text{GeV}$.

For modeling the storage ring impedance the dominating CSR parallel plate impedance is used [10], which already has proven to govern the microbunching instability [9, 11] for KARA. The additional impedance of the corrugated plates is modelled by the resonator model with its parameters f_{res}, Z_0, Q. The impedance simulation for the corrugated structure has shown [6], that a quality factor $Q = 3$ and a shunt impedance $Z_0 = 1\,\text{k}\Omega$ are suitable for a structure length of 20 cm, which is the maximum space available along the beampipe in KARA. As long as it is not explicitly mentioned, these values are used for the Inovesa simulations.

Above the threshold current I_{thr} of the microbunching instability the first fluctuations of the CSR intensity occur. Therefore, the behaviour of the standard deviation (STD) of the CSR emission as function of the bunch current indicates

* sebastian.maier@kit.edu
† Now at MAX IV Laboratory, Lund, Sweden

ISBN: 978-3-95450-227-1 ISSN: 2673-5490 doi:10.18429/JACoW-IPAC2022-WEPOMS008

IMPACT OF BROADBAND IMPEDANCE ON LONGITUDINAL COUPLED-BUNCH INSTABILITY THRESHOLD*

I. Karpov† and E. Shaposhnikova, CERN, Geneva 23, Switzerland

Abstract

Coupled-bunch instabilities (CBI) and the loss of Landau damping (LLD) in the longitudinal plane can affect the performance of high-current synchrotrons. The former is driven by the narrowband impedance of resonant structures, while the latter is mainly determined by the broadband impedance of the entire accelerator and is a single-bunch effect. Therefore, the CBI and LLD thresholds are usually evaluated separately in order to define the corresponding critical impedance budget for given beam parameters. In this paper, we show that the CBI threshold in the presence of broadband impedance can be significantly lower than the one defined by only the narrowband impedance, especially if the LLD threshold is below the CBI threshold. In some cases, the beam becomes unstable even below the LLD threshold. This explains the low CBI threshold observed for the LHC-type beams in the CERN SPS. For HL-LHC, the broadband impedance may also significantly reduce the CBI threshold driven by higher-order modes of the crab cavities.

INTRODUCTION

A long-range wake-field induced by a beam due to a narrowband (NB) impedance in the ring may couple several bunches and, eventually, drive a coupled-bunch instability (CBI). This happens above a threshold beam intensity, which depends on beam and accelerator parameters. In absence of the synchrotron frequency spread inside the bunch (linear RF field) or other damping mechanisms (like synchrotron radiation damping) the threshold is zero. For this case, the growth rates of longitudinal CBI were first found by Sacherer [1] and analysed using different approaches (e.g. [2]).

For operation above the threshold intensity, a dedicated feedback system is required to keep the beam stable. Therefore the first mitigation step is usually to try and reduce (damp) the NB impedance below the critical (threshold) value. In the case of higher-order modes (HOM) in the RF resonators or other cavity-like structures, special couplers need to be designed and installed. This explains why the knowledge of the exact instability thresholds plays an important role, especially for the proton beams.

The CBI threshold can be accurately calculated using the approach developed in [3] and is based on solutions of the matrix equation derived by Lebedev [4] from the Vlasov equation. This matrix equation was also used recently, together with the method [5] suggested for analysis of single-bunch instability, to find the LLD threshold due to reactive impedance [6]. In particular, it was demonstrated that above transition energy, the threshold depends on the roll-off frequency of the inductive impedance, and it is zero for the constant $\mathrm{Im}Z/k$.

It is known that above the LLD threshold, a resistive component of the NB impedance can lead to CBI. For example, the CBI growth rates were affected when the broadband (BB) impedance was included in calculations [7]. Also, the growth rates of CBI driven by the low-frequency NB impedance in the presence of space charge impedance (without truncation in frequency) were recently derived [8]. In this paper, we use the Lebedev matrix equation to evaluate the CBI threshold taking into account two types of impedance sources. Then we present the results of self-consistent semi-analytical calculations with the code MELODY [9] and compare them with macro-particle tracking simulations using the code BLonD [10].

INSTABILITY THRESHOLD

The Lebedev equation [4] can be applied to evaluate beam stability for both single- and multi-bunch configurations. For the ring uniformly filled with L bunches it has a form

$$\tilde{\lambda}^l_{k'}(\Omega) = -\frac{\zeta}{h}\sum_{k=-\infty}^{\infty} G_{k'k}(\Omega)\,\frac{Z_k(\Omega)/k}{Z_0}\,\tilde{\lambda}^l_k(\Omega), \quad (1)$$

where $\tilde{\lambda}^l_k(\Omega)$ are the harmonics of the line-density perturbation for the frequency Ω with the coupled-bunch mode number l ($l = 0, 1, ..., L-1$), $k = f/f_0$, and $f_0 = \omega_0/(2\pi)$ is the revolution frequency, $Z_k(\Omega) = Z(k\omega_0 + \Omega)$ is the longitudinal impedance at frequency $k\omega_0 + \Omega$, and $Z_0 \approx 377\ \Omega$ is the impedance of free space. Note that $\tilde{\lambda}^l_k$ are non-zero only for $k = pL + l$, where $p = 0, \pm1, \pm2...$ We also introduced the dimensionless "intensity" parameter

$$\zeta = -\frac{qN_p\,h^2\,\omega_0\,Z_0}{V_0\cos\phi_{s0}}, \quad (2)$$

where q is the electrical charge, N_p is the number of particles per bunch, h is the harmonic number, V_0 is the RF voltage amplitude, and ϕ_{s0} is the synchronous phase.

The beam-transfer matrix elements $G_{k'k}$ in Eq. (1) are

$$G_{k'k}(\Omega) = -i\omega_{s0}^2\sum_{m=-\infty}^{\infty} m\int_0^{\mathcal{E}_{\max}}\frac{d\mathcal{F}(\mathcal{E})}{d\mathcal{E}}\,\frac{I_{mk}(\mathcal{E})I^*_{mk'}(\mathcal{E})}{\Omega - m\omega_s(\mathcal{E})}d\mathcal{E}, \quad (3)$$

with $f_{s0} = \omega_{s0}/2\pi$ being the frequency of small-amplitude synchrotron oscillations in a bare single-RF system, and

$$I_{mk}(\mathcal{E}) = \frac{1}{\pi}\int_0^{\pi} e^{i\frac{k}{h}\phi(\mathcal{E},\psi)}\cos m\psi\,d\psi, \quad (4)$$

* Work supported by the High Luminosity LHC project.
† ivan.karpov@cern.ch

ISBN: 978-3-95450-227-1 ISSN: 2673-5490 doi:10.18429/JACoW-IPAC2022-WEPOMS009

SIMULATION STUDIES OF LONGITUDINAL STABILITY FOR HIGH-INTENSITY LHC-TYPE BEAMS IN THE CERN SPS

D. Quartullo*, L. Intelisano, I. Karpov, G. Papotti, CERN, Geneva, Switzerland

Abstract

Beams in the SPS for the High Luminosity LHC (HL-LHC) must be stabilized in the longitudinal plane up to an intensity of $2.4{\cdot}10^{11}$ protons per bunch. The fourth harmonic RF system increases Landau damping, and controlled longitudinal emittance blow-up is applied to cope with coupled-bunch instabilities along the ramp and at flat-top. Longitudinal multi-bunch beam dynamics simulations of the SPS cycle were performed starting from realistic bunch distributions, as injected from the PS. The full SPS impedance model was included, as well as the effect of low-level RF (LLRF) feedback for beam-loading compensation. A realistic model of the beam-based LLRF loops was used for the particle tracking studies. Controlled longitudinal emittance blow-up was included by generating bandwidth-limited RF phase noise and by injecting it into the beam phase-loop input, exactly as in hardware. Due to the stringent constraints on particle losses and extracted bunch lengths, particular attention was paid to monitoring these parameters in the simulations, and to determining the best configuration for a stable acceleration of the beam.

INTRODUCTION

High-intensity proton beams in the SPS for the High Luminosity LHC (HL-LHC) require stabilization in the longitudinal plane to cope with coupled-bunch instabilities during the ramp and at the flat-top [1–3]. The voltage of the 200 MHz main RF system will be larger than the one currently used for LHC-type beams. A fourth-harmonic RF system is applied to increase the synchrotron frequency spread inside the bunch enhancing Landau damping [4]; bandwidth-limited RF phase noise blows up the longitudinal emittances of the distributions in a controlled way during the cycle [5–7].

The target injected bunch intensity for the four batches of 72 bunches is $N_\mathrm{p} = 2.4 \cdot 10^{11}$ p/b (protons per bunch). Stringent requirements on particle losses and extracted bunch lengths have to be fulfilled: the total losses along the cycle should be less than 5% of the injected intensity, while the extracted bunch lengths must be around 1.65 ns, with a maximum spread of 10%. Indeed, shorter bunches will be unstable in the SPS [2], while longer bunches will not fit into the 400 MHz RF buckets of the LHC.

Longitudinal beam dynamics simulations for present or HL-LHC beams in the SPS have been performed recently [2, 8, 9]. However, the previous studies at injection energy used simplified models of the Low Level RF (LLRF) beam-based loops and of the One-Turn Delay Feedback (OTDFB) for beam loading compensation [8, 9].

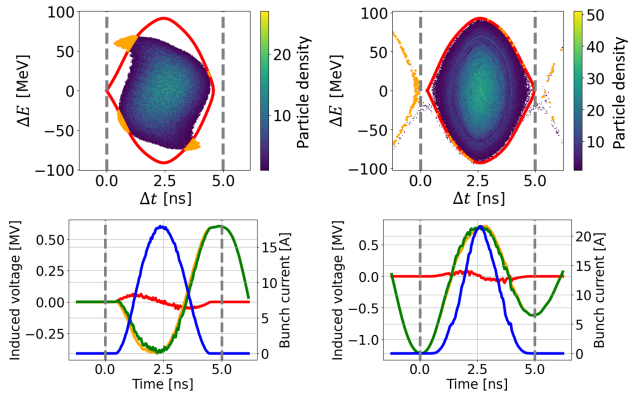

Figure 1: Top: distributions of bunch 1 at injection (left) and after 0.5 s (right). The particles marked in orange are outside the separatrix (red). Bottom: corresponding profiles (blue). The total induced voltage (green) is the sum of the induced voltage from the impedance model (orange) and the space-charge voltage (red). The grey lines mark the RF period.

In addition, tracking simulations along the ramp assumed constant longitudinal emittance [2].

This contribution presents refined simulations of HL-LHC beams in the SPS. One main goal of this study is to verify that the requirements mentioned above can be satisfied.

SIMULATIONS AT INJECTION ENERGY

For the studies at 26 GeV/c, one batch of 72 injected bunches with $N_\mathrm{p} = 2.4 \cdot 10^{11}$ p/b was tracked for 0.5 s using the CERN BLonD code [10]. The injected bunch distributions (Fig. 1, top left) were obtained by performing tracking simulations at PS flat-top [11, 12], including collective effects and assuming all the PS RF upgrades for the HL-LHC scenario. However, bunch-by-bunch emittance and intensity spreads were not considered. In simulations at SPS injection energy, the voltages of the 200 MHz and 800 MHz RF systems were respectively 4.5 MV and 0.45 MV. These voltages are currently applied to LHC-type beams at SPS flat-bottom.

The full SPS impedance model [2] was included in simulations, the space charge impedance had $\mathrm{Im}(Z)/n = -1\,\Omega$ [13]. The effect of the OTDFB was added by applying its transfer function [14, 15] to the longitudinal impedance of the 200 MHz and 800 MHz RF cavities (Fig. 2), using the nominal feedback gain of 26 dB. To resolve the notches of the OTDFB transfer function, the frequency resolution of the impedance was set to $\Delta f = f_0/50$, where f_0 is the revolution frequency. This corresponds to keeping in memory wake-fields extending for 50 turns.

An accurate model of the beam-based loops [16, 17] was adopted. The loop gains were set to the values presently in

* danilo.quartullo@cern.ch

ISBN: 978-3-95450-227-1 ISSN: 2673-5490 doi:10.18429/JACoW-IPAC2022-WEPOMS010

STUDIES OF TRANSVERSE COUPLED-BUNCH INSTABILITIES FROM RESISTIVE-WALL AND CAVITY HIGHER ORDER MODES FOR DIAMOND-II

S. Wang*, H.-C. Chao, R. Fielder, I.P.S. Martin, T. Olsson
Diamond Light Source, Oxfordshire, United Kingdom

Abstract

The transverse coupled-bunch instabilities from resistive-wall impedance and main cavity higher order modes (HOMs) are studied for the Diamond-II storage ring. The growth rates of all the coupled-bunch modes are calculated using both the results from tracking simulations and analytic formula, which show a good consistency. The instability threshold from the resistive-wall impedance is estimated and verified by simulation. The impact of the main cavity HOMs is studied in a similar way, and the results show instabilities from HOMs are much smaller than that from resistive-wall impedance.

INTRODUCTION

Diamond-II is an upgrade for the Diamond Light Source to provide higher brightness and more beamlines for the users. Some of the main parameters of the Diamond-II storage ring can be found in [1].

The coupled-bunch instability is one of the main sources of transverse collective instabilities in storage rings. It is important to know the instability threshold for a storage ring to maintain stable operation. Two sources of transverse coupled-bunch instability, the resistive-wall impedance and the transverse main cavity HOMs, are studied for the Diamond-II storage ring.

GROWTH RATE OF COUPLED-BUNCH MODES

The transverse motion of centroid of bunch n in an evenly filled beam affected by a dipolar long-range wake field is described by [2]

$$\ddot{y_n}(t) + \omega_\beta^2 y_n(t) = A \sum_k \sum_{m=0}^{M-1} W(-kC - \frac{m-n}{M}C) \times y_m(t - kT_0 - \frac{m-n}{M}T_0), \quad (1)$$

where ω_β is the betatron angular frequency, C is the circumference, T_0 is the revolution period, M is the number of bunches, W is the wake function, and A is some constant. The equation has M eigenvalues, each corresponding to a coupled-bunch mode with a certain phase difference between each bunch, the solution for mode μ can be expressed by:

$$y_n^{(\mu)}(t) = \mathrm{Re}(Be^{2\pi i\mu n/M} e^{-i\Omega_\mu t}), \quad (2)$$

where Ω_μ is the complex frequency of mode μ, and B is some constant. In the case of a small deviation from the betatron frequency, the complex frequency shift can be expressed by [2–4]:

$$\Delta\Omega_\mu = \frac{ecI_0}{4\pi E_0 \nu_\beta} \sum_p Z_{\perp,\mathrm{ELEGANT}}(\omega_p), \quad (3)$$

where c is the speed of light, I_0 the beam current, E_0/e the beam energy in eV, and $Z_{\perp,\mathrm{ELEGANT}}$ the lumped impedance in the ELEGANT convention, which is directly the Fourier transform of the wake function [5]. ν_β should be evaluated by $\nu_\beta = C/2\pi\bar{\beta}$, where $\bar{\beta}$ is already included in the impedance normalised by the local beta function. The impedance is evaluated at the frequencies:

$$\omega_p = (\mu + Mp + \nu_\beta)\omega_0,$$

where μ is the mode index (ranging from 0 to $M-1$), and ν_β is the betatron tune. The summation is made over the index p to get the total contribution to mode μ. The real part of the complex frequency shift gives the tune shift whereas the imaginary part gives the growth rate of the mode.

INSTABILITY FROM RESISTIVE-WALL IMPEDANCE

Due to the narrow vacuum chamber and in-vacuum IDs, it is expected that the resistive-wall impedance will cause the most significant transverse coupled-bunch instability. The vacuum vessel of the Diamond-II storage ring will be mostly composed of a NEG-coated copper circular pipe 10 mm in radius. For the simulations, a thickness of 1 µm has been assumed for the NEG coating with a conductivity of 10^5 S/m as a worst-case scenario. The long-range resistive-wall wake is generated for each element of the Diamond-II storage ring according to the chamber size and shape using the code ImpedanceWake2D [6] to include multilayered pipes with NEG coating. A lumped wake function is calculated by normalisation with the local beta function at each element:

$$W_\perp(t) = \frac{1}{\beta_{0x,y}} \sum_i \beta_{x,y,i} W_i(t), \quad (4)$$

where $\beta_{0x,y}$ represents the local horizontal or vertical beta function at the position where the lumped wake element is located. The step size of long-range resistive-wall wake function is taken to be half the bunch distance, and the wake function decreases monotonically as the time increases. It is estimated that after 1 turn the wake function decreases

* siwei.wang@diamond.ac.uk

ISBN: 978-3-95450-227-1 ISSN: 2673-5490 doi:10.18429/JACoW-IPAC2022-WEPOMS011

SINGLE BUNCH INSTABILITY STUDIES WITH A NEW IMPEDANCE DATABASE FOR DIAMOND-II

Richard Fielder†, Hung-Chun Chao, Siwei Wang, Diamond Light Source, Oxfordshire, UK

Abstract

We present an updated impedance database for the Diamond-II storage ring [1], along with an analysis of single bunch instabilities and thresholds based on particle tracking simulations using Elegant [2]. Various cases with different chromaticity, insertion device parameters and harmonic cavity settings were studied, and the effects on the microwave instability, bunch lengthening and phase shifts were simulated and compared with analytic formulae. Preliminary results show that the single-bunch instability thresholds are above requirements for a uniform fill, and with inclusion of a harmonic cavity the longitudinal and transverse instability thresholds can also satisfy requirements for a hybrid fill.

INTRODUCTION

Single bunch dynamics are an important consideration for synchrotron light sources, since they place limits on the maximum bunch charge and hence total beam current. The instability thresholds are strongly influenced by impedance, as well as other factors such as chromaticity.

Diamond-II is planned to operate with two different fill patterns. The standard fill will have all bunches with equal charge, with 5 gaps of 7 buckets for ion clearing, giving four trains of 180 bunches and one of 179. A hybrid fill pattern providing a single high-charge bunch in addition to the main bunch train will also be offered. The details of the hybrid fill are still under study, but the target is to offer the same 3 nC bunch charge as is currently available at Diamond. This gives requirements for the instability thresholds of at least 0.33 mA per bunch in standard fill and 1.6 mA in hybrid fill. These requirements are shown as black dash-dotted lines on the relevant figures. It is planned to operate at a nominal chromaticity of [2] for the horizontal and vertical planes respectively.

We previously reported [3] on the production of an impedance database for Diamond-II using an Accelerator Toolbox-like structure [4]. This has since been updated with more detail and updated designs for some components. We present here an overview of the updated impedance database and results of single bunch effects comparing analytic formulae and particle tracking.

IMPEDANCE DATABASE

There are 252 BPMs in the Diamond-II lattice. Some are integrated into the large dipole vessel assemblies, while the rest incorporate flanges, bellows and tapers in addition to the BPM block itself. One dipole vessel includes a mirror inserted horizontally for the visible light extraction system. The RF cavities remain the largest contributors to the longitudinal impedance.

Significant updated components include the collimators, three in each plane with a nominal gap of ±3.5 mm for the horizontal and ±1.5 mm for the vertical. Injection striplines and diagnostic screens have also been added. The contributions to the resistive wall impedance have also been updated, with the new values shown in Table 1.

Figure 1 shows the real and imaginary impedance in each plane calculated for a 3 mm sigma Gaussian bunch and weighted by the local beta function for each component, comparing the cases with IDs and collimators all fully open, and with IDs closed to minimum gaps and collimators at nominal gaps. The main contributions are highlighted separately for each plane, with the remaining components grouped as “other”.

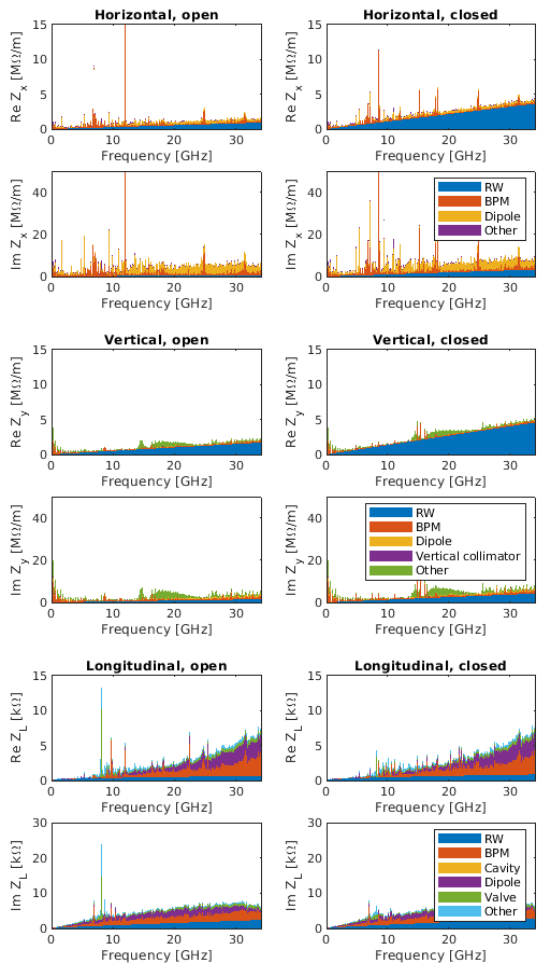

Figure 1: Real and imaginary impedance for Diamond-II with main contributions highlighted in each plane, with IDs and collimators open (left) and closed (right). Top: horizontal, middle: vertical, bottom: longitudinal.

† richard.fielder@diamond.ac.uk

ISBN: 978-3-95450-227-1 ISSN: 2673-5490 doi:10.18429/JACoW-IPAC2022-WEPOMS013

NEURAL NETWORK SOLVER FOR COHERENT SYNCHROTRON RADIATION WAKEFIELD CALCULATIONS IN ACCELERATOR-BASED CHARGED PARTICLE BEAMS *

A. L. Edelen[†‡], C. E. Mayes[‡], C. Emma, R. Roussel
SLAC National Accelerator Laboratory, Menlo Park, CA, USA

Abstract

Particle accelerators support a wide array of scientific, industrial, and medical applications. To meet the needs of these applications, accelerator physicists rely heavily on detailed simulations of the complicated particle beam dynamics through the accelerator. One of the most computationally expensive and difficult-to-model effects is the impact of Coherent Synchrotron Radiation (CSR). As a beam travels through a curved trajectory (e.g. due to a bending magnet), it emits radiation that in turn interacts with the rest of the beam. At each step through the trajectory, the electromagnetic field introduced by CSR (called the CSR wakefield) needs to computed and used when calculating the updates to the positions and momenta of every particle in the beam. CSR is one of the major drivers of growth in the beam emittance, which is a key metric of beam quality that is critical in many applications. The CSR wakefield is very computationally intensive to compute with traditional electromagnetic solvers, and this is a major limitation in accurately simulating accelerators. Here, we demonstrate a new approach for the CSR wakefield computation using a neural network solver structured in a way that is readily generalizable to new setups. We validate its performance by adding it to a standard beam tracking test problem and show a ten-fold speedup along with high accuracy.

INTRODUCTION AND MOTIVATION

Particle accelerators support a wide array of scientific, industrial, and medical applications. To meet the requirements of these applications, accelerator physicists rely heavily on detailed physics simulations of the particle beam dynamics through the accelerator, both for initial design of the accelerator and subsequent experiment planning (e.g. finding optimal accelerator settings for new experiments). One of the most important and difficult-to-model beam dynamics effects comes from the impact of Coherent Synchrotron Radiation (CSR) [1,2,3,4]. In simple terms, as a beam is transported through a curved trajectory, the particles in the beam emit radiation that in turn hits and adds momentum to other particles in the beam, as shown in Fig. 1. The CSR effect is a major driver of growth in the beam emittance, denoted ε, which is the overall beam size in position-momentum phase space and is a critical metric of beam quality in many applications. For example, ε has a large impact on the quality of light produced by free electron lasers (FELs) for scientists to interrogate biological, chemical, and material samples [5]. Figure 1c shows an example of the impact CSR has on an electron beam in the Linac Coherent Light Source (LCLS) [6], where ε is increased by a factor of 2 due to CSR. CSR also has a major effect on highly-compressed beams, such as those that will be generated by the FACET-II accelerator [7].

Simulations of accelerators are often conducted using "particle tracking" codes, which track the positions (x, y, z) and momenta (p_x, p_y, p_z) of particles in the beam (collectively, the 6D position-momentum phase space). As the beam travels through the accelerator, the phase space is iteratively updated based on forces from accelerator components (e.g. magnets for steering and focusing, rf cavities for accelerating) and any internal effects that the beam has on itself (e.g. CSR, self-fields due to beam charge, etc). To account for the CSR effect, the electromagnetic field introduced by CSR (i.e. the "CSR wakefield") needs to be computed at each tracking step. This is then used to calculate the induced change in momentum (called the CSR kick, or K_{CSR}) for every particle in the beam. The impact of CSR from all particles at all previous times in the beam trajectory must be taken into account, making this a very computationally intensive effect to simulate. A variety of methods are used for this [1], and most simplify the problem to reduce the computational complexity. The contribution from the beam charge density λ along z has the greatest impact on the beam, and as such the vast majority of simulation codes only include this 1D effect. 1D CSR is still computationally expensive to compute; for example, in cases we examined using the simulation code Bmad [8], inclusion of CSR slows down the simulation by a factor of 10.

Here we demonstrate a new approach for speeding up the CSR wakefield calculation by replacing the electromagnetic solver with a neural network (NN). The NN solver is constructed in a very general way, making it readily extensible for general use in accelerator simulations. We validate the NN solver's performance on a standard CSR benchmark problem. It is 10× faster to execute and shows good agreement with traditional solvers.

PROBLEM FORMULATION

In accelerator simulations, particles are "tracked" through accelerator components by updating their positions (x,y,z) and momenta (p_x,p_y, p_z) at each step δs through the component. In the 1D formulation of the CSR problem, the

* This work was supported by the U.S. Department of Energy, under DOE Contract No. DE-AC02-76SF00515 and the Office of Science, Office of Basic Energy Sciences.
† edelen@slac.stanford.edu
‡ Equal Contribution

ISBN: 978-3-95450-227-1 ISSN: 2673-5490 doi:10.18429/JACoW-IPAC2022-WEPOMS015

BASIC RELATIONS OF LASER-PLASMA INTERACTION IN THE 3D RELATIVISTIC, NON-LINEAR REGIME

D. F. G. Minenna*, L. Batista, E. Bargel, and P. A. P. Nghiem
CEA, IRFU, DACM, Université Paris-Saclay, Gif-sur-Yvette, France

Abstract

In the approximation where the plasma is considered as a fluid, basic relations are derived to describe the plasma wave driven by an ultra-intense laser pulse. A set of partial differential equations is obtained. It is then numerically solved to calculate the resulting 3D electric field structure that can be used as accelerating cavities for electrons. The laser strength parameter is varied to investigate regimes from weakly nonlinear up to total cavitation where all the initial electrons of the plasma are expelled.

INTRODUCTION

The high-gradient plasma-based acceleration is a growing research effort with world-wide ongoing experiences. This effort [1,2], that can be broken down into different configurations such as laser wakefield accelerator (LWFA), plasma beat wave accelerator (PBWA) or beam-driven plasma wakefield acceleration (PWFA), is of great interest because of the extremely large acceleration gradients achievable. When this technology will be mature, it is envisioned an important reduction of size and cost of future accelerators.

Plasma-based acceleration techniques have reached a maturity level which now makes it possible to envisage laser-plasma accelerators with strong requirements for high-quality beams [3]. Massive simulations to optimize the accelerating structure, i.e. the accelerating and focusing electric field profiles, will have to be considered, as for conventional radio-frequency accelerators. PIC (Particle-in-Cell) simulations depict the acceleration physics in the most realistic manner, but ask for significant computation time. They should be oriented beforehand by rough physics considerations, even when the latter are less precise and less realistic.

In this paper, we explore how far it is possible to progress in the way to characterize the accelerating structure without having to use PIC techniques. The fluid approximation is adopted, together with the Quasi-Static Approximation (QSA), and the unchanged laser amplitude approximation. Relativistic linear, then nonlinear regimes will be studied, in 1D then 2D configurations.

This paper is organized as follows: The first section recalls basic equations of the fluid system; the second section describes the linear regime; and the third section deals with the nonlinear regime.

* damien.minenna@cea.fr

STARTING EQUATIONS

The starting classical equations to be solved are, respectively, the continuity equation, the Lorentz Force equation, the electromagnetic wave equation and the Poisson equation

$$\frac{\partial n}{\partial t} + \nabla \cdot (n\mathbf{v}) = 0\,, \tag{1}$$

$$\frac{\mathrm{d}\gamma m\mathbf{v}}{\mathrm{d}t} = e\nabla\Phi + e\frac{\partial \mathbf{A}}{\partial t} - e\mathbf{v}\times(\nabla\times\mathbf{A})\,, \tag{2}$$

$$\Delta\mathbf{A} - \frac{1}{c^2}\frac{\partial^2\mathbf{A}}{\partial t^2} = \frac{en\mathbf{v}}{c^2\epsilon_0} - \frac{1}{c^2}\frac{\partial\nabla\Phi}{\partial t}\,, \tag{3}$$

$$\Delta\Phi = \frac{en}{\epsilon_0}\,, \tag{4}$$

with e, m the elementary charge and mass, $n = n_0 + \delta n$ the electron plasma density, $\mathbf{v}$ the electron velocity, Φ the scalar potential of the wakefield and ϵ_0 the permittivity of vacuum. Pressure terms are ignored. The Coulomb gauge $\nabla\cdot\mathbf{A} = 0$ is used, with $\mathbf{A}$ the vector potential associated with the laser field. In this paper, the normalized vector potential $\mathbf{a} = e\mathbf{A}/(mc)$ and the normalized scalar potential $\phi = e\Phi/(mc^2)$ are used. The QSA is used to the change of frame $t \to \tau$ and $z \to \xi + v_g t$, with z the longitudinal axis, $v_g = c\sqrt{1-\omega_{pe}^2/\omega_0^2}$ the laser group velocity, $k_{pe} = \omega_{pe}/v_g$, ω_{pe} the plasma frequency and ω_0 the laser frequency.

LINEAR REGIME

The fluid approach is one of the first theoretical approach used to describe the LWFA. The linear theory was developed independently by two teams [4,5] at the end of the 1980s. Both teams took advantage of the QSA to simplify the laser-plasma interaction. The wakefield (or its scalar potential) is then computed inside and after the laser pulse. The non-relativistic linear theory used in this section rests on [4].

The laser is assumed unperturbed, therefore, $\mathbf{A}$ is a known function in time and space. Since, in an underdense plasma, $\mathbf{A}$ varies rapidly in time compared to n, the time dynamics of A^2 is averaged to $1/2$ before applying the quasistatic approximation. The above dynamics equations are linearized at the first order, except for laser part of the velocity, which is taken to the second order (where occurs the ponderomotive force). Therefore, the motion equation becomes

$$\frac{\partial\mathbf{v}}{\partial t} = \frac{e\nabla\Phi}{m} - c^2\nabla\frac{a^2}{4}\,. \tag{5}$$

With a small rearrangement of the three above equations, it can be shown that the evolution of Φ behave as a forced harmonic oscillator

$$\frac{\partial^2\Phi}{\partial t^2} + \omega_{pe}^2\Phi = \frac{c^2 n_0 e a^2}{4\epsilon_0}\,. \tag{6}$$

ISBN: 978-3-95450-227-1 ISSN: 2673-5490 doi:10.18429/JACoW-IPAC2022-WEPOMS016

ON THE (APPARENT) PARADOX BETWEEN SPACE-CHARGE FORCES AND SPACE-CHARGE EFFECTS

P. A. P. Nghiem†, CEA/DRF/IRFU, Université Paris-Saclay, Gif-sur-Yvette, France

Abstract

With the advent of high-intensity linacs, space-charge forces are now well known as a major issue, causing undesirable effects on particle beam qualities like emittance growth or sudden losses. They should be stronger when there are more particles or when the latter are contained in a smaller volume. But a detailed examination of the beam along an accelerator show that space charge effects are weaker where the beam size is smaller. This article clarifies this paradox and revisits the recommendations on beam sizes in view of mitigating space charge effects.

INTRODUCTION

For high-intensity proton linacs, space charge is known as a major issue to be carefully addressed, at least in the sub-GeV energy range, as it contributes to distort the beam density profile, increasing the halo in the external parts of the beam, causing emittance growth and particle losses.

Space-charge forces are the integrated Coulomb forces of the whole beam on every witness particle within the beam. These forces are thus expected to be stronger when there are more charges or when they are closer to each other, i.e. the space occupied by them is smaller. However, when examining the equation governing the beam envelope along the accelerator, space charge effects appear to be weaker at places where the beam size is smaller.

The purpose of this paper is first to clarify the apparent paradox between space charge forces and space charge effects for a better understanding of beam behavior, and second to revisit the recommendations for mitigating harmful space charge effects when designing the beam, based on precise considerations of beam halo vs beam core.

SPACE-CHARGE FORCES

Let's consider the simplified case of an infinitely long cylinder of uniform positive charge density with a total radius R, moving at the same longitudinal speed v. According to Gauss' law, this produces an outward radial electric field, which acts as a defocusing field for the beam. At a given radius $r \leq R$, it is given by:

$$E_r(r) = \frac{Ir}{2\pi\varepsilon_0 v R^2} \tag{1}$$

where I is the beam intensity, and ε_0 the vacuum permittivity.

According to Ampere's law, an azimuthal magnetic field is also induced at the same position, focusing the beam:

$$B_\theta(r) = \frac{\mu_0 Ir}{2\pi R^2} \tag{2}$$

where μ_0 is the vacuum permeability.

A witness charge q at this position will be submitted to a radial force, which is called the space-charge force

$$F_{sc}(r) = q(E_r - vB_\theta) = \frac{qI}{2\pi\varepsilon_0 v\gamma^2}\frac{r}{R^2} \tag{3}$$

where γ is the Lorentz relativistic factor. This force is linear in r inside the beam for a uniform charge distribution, and is well stronger when the beam size R is smaller as expected.

SPACE-CHARGE EFFECTS

To see the effect of this space-charge force on an accelerator beam, let's look at the above charged cylinder which is now submitted in addition to focusing forces applied by various accelerator components surrounding the beam. These external forces are generally linear in r, characterized by the focusing coefficient k:

$$F_{ext}(r) = -kr. \tag{4}$$

By adopting the following notations for time derivatives and space derivatives along the longitudinal coordinate z:

$$\dot{r} = \frac{\partial r}{\partial t} \quad , \quad r' = \frac{\partial r}{\partial z} \quad , \qquad \ddot{r} = v^2\frac{\partial^2 r}{\partial z^2} \quad , \tag{5}$$

Newton Second law for a witness charge (rest mass m_0) is:

$$\gamma m_0 \ddot{r} = F_{ext} + F_{sc}. \tag{6}$$

The equation of motion for this charge can be deduced:

$$r'' + K_{ext}r - K_{sc}\frac{r}{R^2} = 0 \tag{7}$$

where

$$K_{ext} = \frac{k}{m_0 v^2 \gamma} \qquad (unit: \mathrm{m}^{-2}) \tag{8}$$

$$K_{sc} = \frac{qI}{2\pi\varepsilon_0 m_0 v^3 \gamma^3} \qquad (no\ unit). \tag{9}$$

K_{sc} is called the generalized perveance. For an arbitrary charge distribution but with elliptical symmetry, it is mentioned in [1] that Lapostolle and Sacherer independently shown that the equation of motion, Eq. (7) can be rewritten as

$$a_x'' + K_{ext,x}a_x - \frac{\varepsilon_x^2}{a_x^3} - \frac{K_{sc}}{2(a_x + a_y)} = 0 \tag{10}$$

$$a_y'' + K_{ext,y}a_y - \frac{\varepsilon_y^2}{a_y^3} - \frac{K_{sc}}{2(a_x + a_y)} = 0 \tag{11}$$

where x and y refer to the two transverse axes, a the rms beam size, ε the non-normalized beam emittance. These equations are called envelope equations.

† phu-anh-phi.nghiem@cea.fr

ISBN: 978-3-95450-227-1 ISSN: 2673-5490 doi:10.18429/JACoW-IPAC2022-WEPOMS017

SPACE CHARGE ANALYSIS FOR LOW ENERGY PHOTOINJECTOR

M. Carillo[1,4*], M. Behtouei[2], F. Bosco[1,4], O. Camacho[3], E. Chiadroni[1,4], L. Faillace[1,2], L. Ficcadenti[4], A. Fukasaway[3], L. Giuliano[1,4], A. Mostacci[1,4], M. Migliorati[1,4], B. Spataro[2], J. Rosenzweig[3], L. Palumbo[1,4]
[1]La Sapienza University of Rome, 00161 Rome, Italy
[2]INFN-LNF, 00044 Frascati, Italy
[3]UCLA, Los Angeles, 90095 California, USA
[4] INFN-Sez.Roma1, 00161 Roma, Italy

Abstract

Beam dynamics studies are performed in the context of a C-Band hybrid photo-injector project developed by a collaboration between UCLA/Sapienza/INFN-LNF/RadiaBeam [1, 2]. These studies aim to explain beam behaviour through the beam-slice evolution, using analytical and numerical approaches. An understanding of the emittance oscillations is obtained starting from the slice analysis, which allows correlation of the position of the emittance minima with the slope of the slices in the transverse phase space (TPS). At the end, a significant reduction in the normalized emittance is obtained by varying the transverse shape of the beam while assuming a longitudinal Gaussian distribution. Indeed, the emittance growth due to nonlinear space-charge fields has been found to occur immediately after moment of the beam emission from the cathode, giving insight into the optimum laser profile needed for minimizing the emittance.

INTRODUCTION

In the new generation of high-brightness beams [3] a fundamental role is played by the achievement of emittance compensation [4, 5]. This scenario includes the design of the Hybrid C-band photo-injector and the in-depth study of the dynamics of its output beam [6]. To do this, different approaches are exploited, such as beam slice analysis and the analytical study of the phenomena under consideration, including space charge fields.

BEAM SLICE ANALYSIS

Slice analysis has a key impact to understand beam dynamics and in the emittance compensation process. Starting from the definition of the beam rms emittance it is possible to separate four different components due to slice splitting [7]. In this analysis we will neglect the emittance terms due to the linear and non-linear contributions of the transverse offsets between the slices themselves because they give a negligible contribution to the total projected emittance [8].

The transverse rms emittance is defined starting from the second order moments according to the equation [9]:

$$\varepsilon_{rms}^2 = \sigma_x^2 \sigma_{p_x}^2 - \sigma_{x,px}^2. \tag{1}$$

Let us take a beam of N particles, divided into S slices, each one populated by a variable number of particles M_i. σ^2 moments can be written as function of sum of the slice second order moments:

$$\sigma_x^2 = \langle x^2 \rangle = \sum_{i=1}^{S} \sum_{j=1}^{M_i} \frac{x_j^2}{N} = \sum_{i=1}^{S} \frac{M_i}{N} \langle x^2 \rangle_i = \sum_{i=1}^{S} \frac{M_i}{N} \sigma_{x,i}^2 \tag{2}$$

where $\langle\rangle$ defines an ensemble average, and in the same way:

$$\sigma_{p_x}^2 \equiv \sum_{i=1}^{S} \frac{M_i}{N} \sigma_{p_x,i}^2 \,, \;\; \sigma_{xp_x} \equiv \sum_{i=1}^{S} \frac{M_i}{N} \sigma_{xp_x,i} \tag{3}$$

By replacing Eqs. (2), and (3) in to Eq. (1) the rms emittance becomes:

$$\begin{aligned} \varepsilon_{rms}^2 = & \sum_{i=j} \left(\sigma_{x,i}^2 \sigma_{p_x,i}^2 - \sigma_{xp_x,i}^2 \right) \\ & + \sum_{i \neq j} \frac{M_i M_j}{N^2} \left(\sigma_{x,i}^2 \sigma_{p_x,j}^2 - \sigma_{xp_x,i} \sigma_{xp_x,j} \right) \end{aligned} \tag{4}$$

where the first sum in the left-hand side is the emittance definition of $i-$th slice $\varepsilon_{rms_i}^2$, and the second one defines the correlated slices emittance expression, ε_{corr}^2. Since our goal is to optimize the emittance compensation process, a study on the double emittance oscillation at the gun exit [10] is performed. We assume, as initial conditions, the ones at the exit from the photoinjector and we study the evolution in a long drift.

Every single slice satisfies the envelope equation of a bunch in a free space, evolving under the effect of space charge force and emittance pressure, and each slice has different initial conditions $(\sigma_{0_i}, \sigma'_{0_i})$ but also different charge denisty λ_i and energy γ_i. The second order moment in Eq. (4) can be written as function in terms of of the envelope function σ and its derivative, with respect to the longitudinal position z, $\sigma' : \sigma_x = \sigma$, $\sigma_{xp_x} = \sigma\gamma\sigma'$ and $\sigma_{p_x} = \gamma\sigma'$. Assuming for simplicity, that each slice is populated by the same number of particles $M = S/N$, the correlated emittance term can be written as:

$$\varepsilon_{corr}^2 = \frac{1}{2S^2} \sum_{i \neq j} (\sigma_i \gamma_j \sigma'_j - \sigma_j \gamma_i \sigma'_i)^2. \tag{5}$$

Floettmann Model

In Floettmann emittance compensation analysis [11] using the slice model, it was demonstrated that to understand the emittance growth [12], it is well to know the orientation of

* martina.carillo@uniroma1.it

ISBN: 978-3-95450-227-1 ISSN: 2673-5490 doi:10.18429/JACoW-IPAC2022-WEPOMS018

MINIMUM EMITTANCE GROWTH DURING RF-PHASE SLIP

S. Koscielniak†, TRIUMF, Vancouver B.C. Canada

Abstract

This paper is concerned with finding operations consistent with the absolute minimum emittance growth. The system is an RF bucket containing a bunch of hadrons in a synchrotron; and the operation performed is to sweep the RF phase. As a result, the bunch centroid moves from one value of position and momentum to another. For given start and end points, we shall find the ideal RF phase-slip time-variation that minimizes emittance growth of the bunch.

INTRODUCTION

Customarily, emittance is the phase space area, at one moment in time, occupied by an ensemble. Single-particle "emittance" is the area swept out during an oscillation cycle. Both are conserved quantities in Hamiltonian dynamics. The bounding single-particle emittance can be identified as surrogate for the ensemble (bounding) emittance. Typically the ensemble is contained by longitudinal phase-focusing and a transverse focusing channel. In nonlinear systems, some processes may introduce voids into the phase space, such that the bounding emittance effectively increases, even though the detailed occupied area is preserved. This phenomenon, known as "emittance growth", has been studied extensively – particularly for the case of variation of the strength of focusing parameters [1], but much less so for the case that the centre of focusing moves (as occurs during an RF phase sweep).

The area swept out during a cycle is a surrogate for occupied area; and the former is proportional to the Hamiltonian, H, for that phase space orbit. Thus we can use changes of the bounding value of H to predict emittance growth. In general, an RF sweep changes H of both the centroid and a general particle trajectory. Thus to minimize emittance growth, we must minimize the differential change of Hamiltonian between general particle and centroid: ($\Delta H - \Delta H_c$). Subscript c denotes centroid. The minimization is performed with respect to variation (choice) of the RF-phase-sweep time law for given end points (final and initial) of the centroid coordinates. There is a minor complication: an arbitrary sweep may either increase or decrease the oscillation amplitude (i.e. Hamiltonian) depending on the oscillation phase at the moments the particle encountered the perturbation. So we must select those bounding trajectories for which $\Delta H>0$, and oscillation amplitude increases.

In general, the bunch centroid does not follow an arbitrary RF phase sweep. The choice of sweep is strongly constrained by the condition that the centroid be in equilibrium at the centre of the RF bucket at start and end of the sweep. If not satisfied, the bunch centroid circulates within the bucket and there is growth of the area swept out by the bunch; and eventually the area is filled due to "filamentation". The primary constraint is that the sweep be completed in an integer number, *n*, of synchrotron oscillations of the centroid. Nevertheless there is typically a small residual oscillation because the momentum offset caused by the RF sweep does not accrue enough phase slip of the bunch to catch up to the RF phase. The residual (which scales as $1/n^2$) may either be accepted, or zeroed by making a "fast" RF-phase jump at start or end of the sweep. "Fast" means completed in a small fraction of a synchrotron oscillation. A phase jump is the cause of a jump in H, but jump values are cancelled out when the difference ($\Delta H - \Delta H_c$) is formed.

Ideally, the difference ($\Delta H - \Delta H_c$) would be minimized with respect to the choice of the RF phase sweep, f(t), according to the calculus of variations, in the manner of the brachistochrone problem. However, we have not found a suitable variational principle; and so have resorted to trial and error in the choice of f(t). The trial functions are: (1) linear ramp, (2) ½-sinusoid, (3) bi-quadratic, (4) dual-sinusoid; and (5) cubic – all ramped between t=0 and t=T.

The steps in the procedure are: first, compute matching conditions for the centroid; second compute ($\Delta H - \Delta H_c$) for the trajectories as perturbed by the sweep f(t). The result is parametrized by the initial amplitude and number of synchrotron oscillations for the sweep. In one case alone, linear f(t), all quantities may be calculated exactly in terms of the Jacobi elliptic functions; and these results used to benchmark other methods. For other sweeps, we may introduce a simplified (and artificial) Hamiltonian that facilitates computation of ($\Delta H - \Delta H_c$) and retains the frequency dispersion of the pendulum oscillator, but adopts a harmonic potential well. Results from these analytic methods will be compared to those from particle tracking.

ANALYSIS

The equation of motion is that of a pendulum oscillator with a moving pivot point f(t):

$$x'(t) = p\,(t) \text{ and } p'(t) = -\omega^2 \sin\,(f\,(t) + x\,(t)). \quad (1)$$

The change of Hamiltonian is:

$$\Delta \mathrm{H} = \omega^2 \int_0^T f'(t) \sin\,(f\,(t) + x\,(t))\,dt. \quad (2)$$

The system is simplified by the transformations:

$$x(t) = \mathrm{x2}\,(t) - f\,(t)\ \&\ p(t) = \mathrm{p2}\,(t) - g\,(t). \quad (3)$$

Here $g(t)=df/dt$ is the momentum offset that will generate precisely the phase slip $f(t)$. The motion equations become:

$$\mathrm{x2}'(t) = \mathrm{p2}\,(t) \text{ and } \mathrm{p2}'(t) = f''(t) - \omega^2 \sin\,(\mathrm{x2}\,(t)) \quad (4)$$

$$\text{and } \Delta \mathrm{H} = \omega^2 \int_0^T g\,(t) \sin\,(\mathrm{x2}\,(t))\,dt. \quad (5)$$

The centroid matching conditions [2] are:

$$\Delta \mathrm{x2}_c = \int_0^T \mathrm{p2}_c\,dt = 0\ \&\ \Delta \mathrm{p2}_c = -\omega^2 \int_0^T \mathrm{x2}_c\,dt = 0;$$

and cannot be satisfied unless T is an integer number of synchrotron oscillation periods.

† shane@triumf.ca

ISBN: 978-3-95450-227-1 ISSN: 2673-5490 doi:10.18429/JACoW-IPAC2022-WEPOMS019

BEAM-BEAM RESONANCE WIDTHS IN THE HL-LHC, AND REDUCTION BY PHASING OF INTERACTION POINTS

Yi Lin Gao, University of Victoria, B.C., Canada
S. Koscielniak, TRIUMF, Vancouver, B.C., Canada

Abstract

Beam-beam interactions are a limiting factor in the planned high luminosity (HL) upgrade to the Large Hadron Collider (HL-LHC). Over the two main interaction regions of the LHC, a particle experiences two head-on and many long-range beam-beam interactions which drive betatron resonances in the system. Each resonance line in the space of horizontal and vertical tunes has a finite (non-zero) lock-on width. If particles' tunes fall within this width, they will eventually lock on to the resonance and be driven to large amplitude. We show that it is possible to reduce the resonance widths of a given order by using specific values of the phase advance between interaction points. This paper presents the derivation of resonance width for the weak-strong beam-beam effect, as an extension of A. Chao's width formulae for magnetic sextupoles. (A Lie-algebraic approach is used to combine the effect of the individual beam-beam impulses.) The paper then studies the lock-on width arising from two interaction regions containing 70 beam-beam impulses, and shows the cancellation of specific resonances by relative phasing of interaction points in the HL-LHC lattice.

INTRODUCTION

Beam-beam interactions drive betatron resonances and are a limiting factor for the HL-LHC. These resonances can occur when the vertical and horizontal betatron tunes are related by an integer equation. This is represented by straight lines (Fig. 1)in tune space:

$$m\nu_x + n\nu_y = q \tag{1}$$
$$m\mu_x + n\mu_y = 2\pi q\ , \tag{2}$$

where m, n, and q are integers, and ν, μ are tune and phase advances. Depending on the properties of the interaction(s) driving resonances, some of these lines can represent dangerous resonances with large lock-on widths. However, not all such lines represent an active resonance of the system and not all resonances are dangerous.

The model used in this paper is a 70 impulse Lie algebraic weak-strong model. The impulses are spread over two interaction regions (IR1 and IR5), including both head-on and long-range interactions. The separations and phasing for each bunch was calculated with MadX using the suggested HL-LHC lattice. The details can be found in Ref. [1]. The resonances of this model are analysed using a lock-on width formula. It is shown resonances of any order can be weakened or removed entirely by the relative phasing of interaction points.

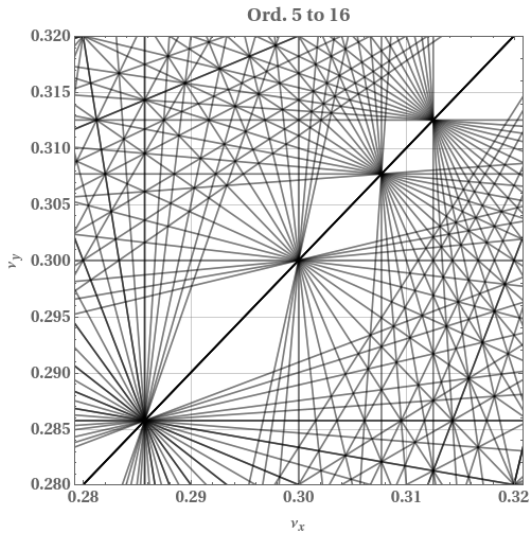

Figure 1: Potential resonance lines of order 5 to 16 near suggested working point (0.31,0.32)

RESONANCE WIDTH

The lock-on width of a one dimensional resonance line (Fig. 2) is defined as the range of tune oscillation amplitude (of a particle close to resonance) within which a particle will eventually lock-on to the precise resonance condition. A particle whose tune is inside the lock-on width will eventually land exactly on the resonant tune. The particle's motion then becomes co-periodic with the driving interaction; this allows the effects of the driving perturbation to accumulate.

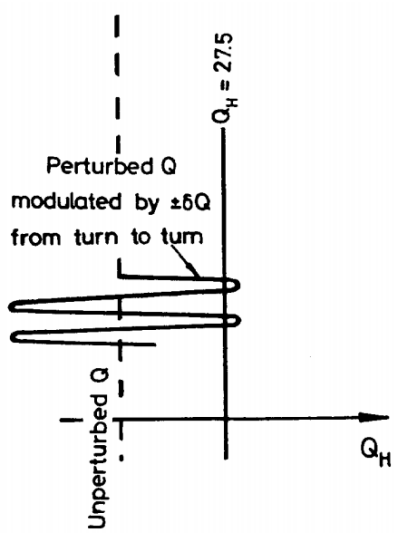

Figure 2: 1D Resonance width in tune space ($Q_H = \nu_x$), (Fig. 5 in Ref. [3])

ISBN: 978-3-95450-227-1 ISSN: 2673-5490 doi:10.18429/JACoW-IPAC2022-WEPOMS020

FAIR SIS100 LASER COOLING PILOT FACILITY

S. Klammes, Th. Kühl, P. Spiller, Th. Stöhlker*, D. Winters, GSI Darmstadt, Germany
M. Bussmann†, M. Siebold, U. Schramm‡, HZDR, Dresden, Germany
B. Langfeld, J. Gumm, Th. Walther§, TU Darmstadt, Germany
V. Hannen, K. Ueberholz, Ch. Weinheimer, WWU Münster, Germany
X. Ma, W.Q. Wen, IMP and CAS Lanzhou, China

Abstract

Ion beam cooling techniques are indispensable for generating high-quality ion beams and are, therefore, of great importance for accelerator research and fundamental physics experiments. For these reasons, ion beam cooling will play a major role in the accelerators of the Facility for Antiproton and Ion Research (FAIR), which is currently under construction in Darmstadt, Germany. The heavy-ion synchrotron SIS100 is the heart of FAIR and stores, accelerates and delivers high intensity ion beams at relativistic energies to the rest of the facility [1]. Since the highest charge states of heavy ions (*e.g.* $^{238}U^{92+}$) can only be produced by passing through a stripper foil at sufficiently high energies, the SIS100 accepts ion beams with a longitudinal momentum spread $\Delta p/p$ of the order of 10^{-3}. For experiments with extracted ion beams (*e.g.* for the generation of high energy density in matter) from the SIS100, it would be better to have a much lower value, *i.e.* $\Delta p/p \approx 10^{-6}$, which could be achieved by laser cooling of bunched heavy ion beams [2]. Therefore, a special working group was formed to develop and establish the SIS100 laser cooling pilot facility for FAIR [4]. This group consists of scientists and accelerator experts from GSI and the collaborating partner universities and research centers in Dresden-Rossendorf, Darmstadt, Jena, Münster, and Lanzhou (China) [5].

It will be world-wide unique and also the first time to demonstrate laser cooling of bunched ion beams in such a large and modern machine as the SIS100. The planned novel scheme of using three independent laser systems (cw and pulsed) to cool the intense heavy ion beams, which can have very high charge states (*e.g.* up to Xe^{51+}) at highly relativistic energies (γ up to 12), is therefore quite ambitious. But the expected improvement of the ion beam quality and especially the short ion pulses that could be created, offer unrivled possibilities for ion bunches extracted from the SIS100. Even without laser cooling, the bunch length in the SIS100 could already be as short as 50 ns, using the advanced bunch compression technique. Laser cooling could improve on that and first estimations show that bunch lengths down to about 10 ns, for cooling times of only a few seconds, could be achieved. The final longitudinal $\Delta p/p$ would then be on the level of $\approx 10^{-6}$ [3]. Such very cold and very short highly relativistic ion bunches could be used to generate high energy densities on a fixed target or serve a future secondary ion beam facility.

Laser cooling is based on the resonant absorption of laser photons (momentum & energy) in the longitudinal direction and the subsequent spontaneous random emission (fluorescence & ion recoil) by the ions, combined with a moderate bunching of the ion beam. Since the fluorescence emission occurs in a random direction, the recoil momenta average out to zero, leaving a net decelerating force on the ions. However, the ion beam must be cooled, not decelerated, which means it should "only" obtain a low $\Delta p/p$ value, keeping the ion revolution velocity in the accelerator constant (at $\beta \approx 1$). Therefore, a counteracting force to the laser force is required, which can be provided by an RF-bucket. This concept is thus also referred to as "bunched beam laser cooling".

The construction of the SIS100 tunnels is progressing well and a first important component for the laser cooling pilot facility (≈20 m underground) was already installed in January 2021. This component is part of the complete laser beamline, which will run from the SIS100 laser lab to the accelerator, crossing the gap between two tunnels (see 1). The complete laser beamline (length 25 m, diameter 20 cm) will be made out of stainless steel vacuum tubes. The vacuum has the advantage that laser light covering a very broad spectrum can be transported, ranging from the IR ($\lambda \approx \mu$m) down to the XUV range ($\lambda \approx$nm). GSI will provide the required infrastructure for the laser cooling pilot facility at FAIR, which includes a complete laser lab (180 m^2), a detector cave (45 m^2) in which special detector systems for x-ray measurements can be installed, the full laser beamline (including all components), special vacuum chambers for detectors and to couple the laser light in and out of the SIS100, scrapers for beam alignment (spatial overlap ≈25 m), control and data acquisition systems, etc. The Technical University of Darmstadt and the Helmholtz-Centre Dresden-Rossendorf contribute in total three laser systems, one cw and two pulsed systems. They can be operated either in the UV-range, at 257 nm with up to 250 mW (pulsed) and 600 mW (cw) of power, or in the visible range, at 514 nm with up to 23 W (pulsed) or 11 W (cw) of power. In the future, all three laser systems will be spatially, timely and spectrally overlapped to achieve a broad and a strong cooling force to address the full range of ion velocities [7]. For the detection of the strongly forward boosted fluorescence at the SIS100, the WWU Münster is currently developing and constructing an *in vacuo* xuv/soft x-ray detection system, which can be used as a fluorescence detector or as a spectrometer.

* also Jena University, Helmholtz-Institute Jena, Germany
† also CASUS, Görlitz, Germany
‡ also TU Dresden, Germany
§ also HFHF, Campus Darmstadt, Germany

ISBN: 978-3-95450-227-1 ISSN: 2673-5490 doi:10.18429/JACoW-IPAC2022-WEPOMS021

ENTROPY PRODUCTION AND EMITTANCE GROWTH DUE TO THE IMPERFECTION IN LONG PERIODICAL ACCELERATION CHAINS

M. Droba†, O. Meusel, H. Podlech[1], S. Reimann[2],
IAP, Goethe University, Frankfurt am Main, Germany
[1]also at Helmholtz Research Academy Hesse for FAIR(HFHF), Frankfurt am Main, Germany
[2] also at GSI Helmholtz Centre for Heavy Ion Research, Darmstadt, Germany

Abstract

Contemporary design of efficient linear accelerator is based on ideal periodical structures with an optimisation for perfect periodicity. However, practical realisation involves random errors in the structure (e.g. position of elements, off-sets, non-linearity of the fields etc.) which make prediction of emittance growth difficult. Error studies helps to understand critical points, but they are normally used at the end of the design process. The concept of beam entropy in very simple approximation (assumption of Ornstein-Uhlenbeck model) is used to evaluate emittance growth in perfect periodical chains. The analysis will be performed and differences in modern designs on some examples discussed. Focus will be laid on linac designs with short acceleration structures (RF-phase settings versus position error) and external transversal focusing magnets.

INTRODUCTION

Existing and planned linear accelerators cover wide range of parameters like energy, species, beam current, momentum spread, frequency, acceleration gradient, focusing elements etc. Therefore, it is hard to compare efficiency of such accelerator complex due to the individual goals and also to choose best design for future accelerators.

However, despite cost estimations and economic parameters, there is need for the best beam quality thus minimum emittance growth along the whole chain. Accelerator theory for beam motion in perfect periodical structures and design rules are already well known since many years, but there will be unavoidable imperfections in technical realisation.

The progress in solid state RF power technology opened new options in the DTLs design with relatively short H-mode cavities (number of gaps of about 6-15) and external focusing lenses. The development and the production of the new class high power solid-state amplifiers P>100 kW in a frequency range between 50-300 MHz are very attractive for application in proton and hadron linear accelerators. Additionally, a 6D beam handling along the acceleration chain could be active done by longitudinal phase plane control and steering through RF-phase settings individually in each cavity. In high space charge situation, there will be coupling between transversal and longitudinal planes hence control of RF-phase and transversal magnetic coupling will be coupled as well.

† email address: droba_m@yahoo.com, droba@iap.uni-frankfurt.de

THEORY

Commonly, the rms-emittance is used to evaluate the beam quality. It gives the luminosity for the experiments and represent the compactness of the whole phase space. The emittance along an accelerator chain growth, because of the Liouville's theorem, therefore, the emittance growth as a function of z is often a parameter to evaluate the performance of an accelerator.

In this paper, we express the rms-emittance by entropy of the beam plasma.

$$S = k_B \ln \varepsilon_{n,rms} + const.$$

Following the Ohrenstein-Uhlbeck entropy model [1, 2] it is possible to investigate the change of the beam entropy as a function of time. An assumption is made of the entropy production staying constant in time, which means constant impact on all periodic lengths along whole chain.

$$\frac{dS}{dt} = \frac{k_B}{\varepsilon_{n,rms}} \frac{d\varepsilon_{n,rms}}{dt} = k = const.$$

The solution can be rewritten in linear approximation $k/k_B \cdot t \ll 1$, which in proper design can be always applied,

$$\frac{1}{\varepsilon_{n,rms}} \approx 1 - \frac{k}{k_B} \cdot t.$$

The collection of the simulation results of some projects is depicted in Fig. 1.

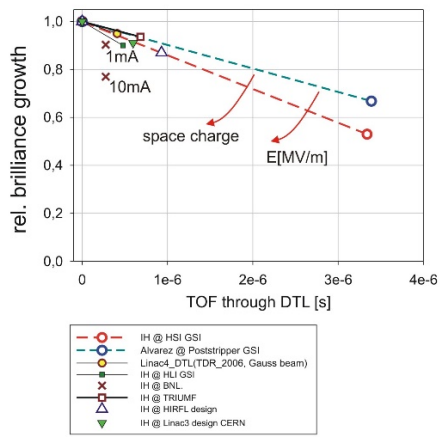

Figure 1: Comparison of the simulation results for various linear accelerators based on the theory [3].

ISBN: 978-3-95450-227-1 ISSN: 2673-5490 doi:10.18429/JACoW-IPAC2022-WEPOMS022

DETAILED ANALYSIS OF TRANSVERSE EMITTANCE OF THE FLUTE ELECTRON BUNCH

T. Schmelzer*, E. Bründermann, M.J. Nasse, R. Ruprecht, J. Schäfer, M. Schuh, N.J. Smale, P. Wesolowski and A.-S. Müller, Karlsruhe Institute of Technology, Karlsruhe, Germany

Abstract

The compact and versatile linear accelerator-based test facility FLUTE (Ferninfrarot Linac- Und Test-Experiment) is operated at KIT. Its primary goal is to serve as a platform for a variety of accelerator R&D studies like the generation of strong ultra-short terahertz pulses. The amplitude of the generated coherent THz pulses is proportional to the square number of particles in the bunch. With the transverse emittance a measure for the transverse particle density can be determined. It is therefore a vital parameter in the optimization for operation. In a systematic study, the transverse emittance of the electron beam was measured in the FLUTE injector. A detailed analysis considers different influences such as the bunch charge and compares this with particle tracking simulations carried out with ASTRA. In this contribution, the key findings of this analysis are discussed.

INTRODUCTION

The electron bunch at the Ferninfrarot Linac- und Test-Experiment (FLUTE) is generated with a photoinjector system [1]. A Ti:Sa laser system together with a 2.5 cell S-band cavity are used to accelerate the electron bunch up to 7 MeV bunch energy. In the first section, i.e., the low energy section, several diagnostic systems are installed to monitor the electron bunch parameters, which includes the bunch charge measured with an integrated current transformer (ICT) [2]. An experiment chamber in the low energy section allows to use the electron bunch for first experiments, e.g., the split-ring-resonator (SRR) experiment [3]. After the diagnostics a linear accelerator structure will be connected to increase the electron energy up to 41 MeV for short-bunch R&D. The characterization of the electron beam parameters is crucial for optimizing the beam for various experiments. One important parameter is the transverse bunch emittance, which can be measured at FLUTE via a quadrupole scan. For a detailed analysis the uncertainties from several parameters were measured and included in the simulations performed with ASTRA [4].

MEASUREMENTS

The transverse emittance was evaluated at the quadrupole position (1.45 m from the cathode surface), using the quadrupole scan technique described in [5]. Several bunch parameters influence the transverse emittance, such as the bunch energy and charge. Any parameter fluctuation during the quadrupole scan increases the uncertainty of the emittance result. For a detailed analysis the settings and fluctuations of the bunch parameters are needed and are listed in Table 1 together with the machine settings. The RF phase was adjusted to the highest energy gain at the beginning of the measurement.

Table 1: Emittance Measurement Settings

Property	Value	Unit
RF power input	10.345 ± 0.02	MW
RF phase[1]	0 ± 0.4	°
Laser pulse energy	24.5 ± 1.6	µJ
Laser spot width (rms)	0.21 ± 0.01	mm
Mean solenoid strength	151.6 ± 0.4	mT
Mean bunch energy	5.817 ± 0.003	MeV
Mean bunch charge	16.4 ± 1.5	pC

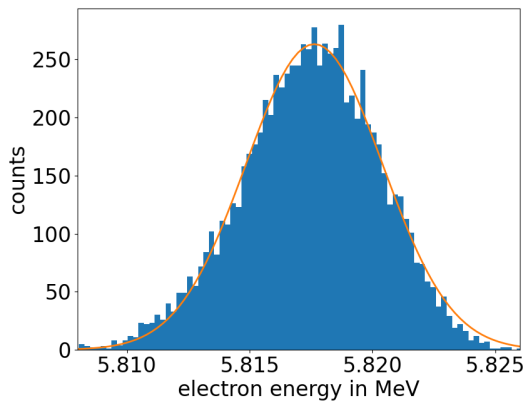

Figure 1: Fluctuation of mean bunch energy (data in counts in blue, Gaussian fit as solid line in orange).

At the low-energy spectrometer the bunch energy was measured for two hours using the profile monitor system, 2.86 m after the cathode [2]. The fluctuations of the mean bunch energy for the recorded 8000 shots are shown in Fig. 1. The slightly skewed Gaussian distribution is a result of the RF phase fluctuation and the used on-crest working point. Here, positive and negative phase fluctuations both result in a decrease of the mean bunch energy. Considering the uncertainty of one σ the bunch energy achieves a stability of 0.05%.

The bunch charge influences the transverse emittance due to space charge effects. During the quadrupole scan the bunch charge was monitored with the non-destructive measurement system Turbo-ICT from Bergoz [2]. With

* thiemo.schmelzer@kit.edu

[1] relative value; zero set to highest electron energy gain

ISBN: 978-3-95450-227-1 ISSN: 2673-5490 doi:10.18429/JACoW-IPAC2022-WEPOMS023

OPTIMIZATION STUDIES OF SIMULATED THz RADIATION AT FLUTE

C. Xu*, E. Bründermann, A. Santamaria Garcia, J. Schäfer, M. Schwarz, A.-S. Müller
Karlsruhe Institute of Technology (KIT), Karlsruhe, Germany

Abstract

The linac-based test facility FLUTE (Ferninfrarot Linac Und Test Experiment) at KIT will be used to study novel accelerator technology and provide intense THz pulses. In this paper, we present start-to-end simulation studies of FLUTE with different bunch charges. We employ a parallel Bayesian optimization algorithm for different bunch charges of FLUTE to find optimized accelerator settings for the generation of intense THz radiation.

INTRODUCTION

The accelerator test facility FLUTE [1] at KIT will be used to generate broadband THz radiation for various experiments. It will operate with a wide range of bunch charges from pC to nC, for which the radiation needs to be optimized. The electron bunch at FLUTE is first created at an RF photoinjector and accelerated up to 7 MeV. It then travels through a linac, which further accelerates the bunch up to 50 MeV. At the end, the bunch is compressed longitudinally via a bunch compressor with 4 dipole magnets down to the fs range, allowing the generation of intense THz pulses with coherent synchrotron radiation (CSR).

Spatial light modulators are being integrated into the photocathode laser system to have 3D control of the laser pulse and provide a tailored initial electron distribution for intense THz pulse generation [2, 3]. In previous studies, a genetic algorithm (GA) was employed in the parameter optimization to minimize the bunch length at 1 pC bunch charge [4]. Nevertheless, it is known that GA is prone to local optima and often requires more computation resources or multiple restarts to mitigate this problem [5]. In this paper, we implement a parallel variant of the Bayesian optimization (BO) [6], which is as efficient as GA and can globally optimize the given physical objective functions even with a large parameter space. We present the first optimization results using parallel Bayesian optimization (PBO) for minimum electron bunch length and maximum peak THz pulse E-field, both for low and high charge cases.

PARALLEL BAYESIAN OPTIMIZATION

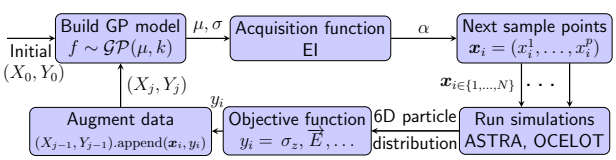

Figure 1: Workflow of the parallel Bayesian optimization algorithm. The boxes are calculations and the arrows are the input and output variables.

* chenran.xu@kit.edu

Bayesian optimization is widely used for global optimization of an unknown objective function $f(x)$. Figure 1 shows the BO algorithm workflow used in this paper. In each step, BO builds a statistical model, where the most widely used is a Gaussian process (GP), of the objective f. The GP model $\mathcal{GP}(\mu, k)$ predicts the mean $\mu(x)$ and uncertainty $\sigma(x)$ of the objective function value $y = f(x)$ at an unknown point $x = (x^1, \ldots, x^p)$, where p is the number of input parameters. The kernel function $k(x, x')$ describes the expected similarity between two data points. In this study, we choose the radial basis function (RBF) as kernel. Based on the GP model, an acquisition function α can be calculated to efficiently guide the optimization and choose the next point to sample x_i. Here we use the expected improvement (EI) [7] acquisition, which calculates the expected value of improvement of a point x over the best observed value so far f_{best}.

In the non-parallel version of BO, the next sample point is selected at the maximum of the acquisition $\alpha_{\text{EI}}(x)$. Since the objective is calculated through physics simulations, we can further increase the performance of BO by evaluating N multiple parameter settings in parallel, with N being the parallel capacity of available computing resources. For the parallel Bayesian optimization (PBO) implementation in this paper, we use a local penalization function to select batch sample points [6]. The i-th sample point x_i is chosen by maximizing the product of acquisition α and penalization function $\varphi_= \varphi_1 * \cdots * \varphi_{i-1}$, where $\varphi_{i-1} \in (0, 1]$ effectively penalizes the acquisition value of a point locally around a previous sample point in the parallel batch x_{i-1}. This allows an efficient sampling of the parameter space in a single optimization step j.

IMPLEMENTATION OF CSR OPTIMIZATION

Based on the knowledge of FLUTE, we choose the following 6 parameter as input for the PBO algorithm: phase and gradient of the photoinjector gun and linac RF field, solenoid magnetic field and the bunch compressor bending angle.

The total spectral intensity of the synchrotron radiation emitted by an electron bunch is

$$\frac{\mathrm{d}^2 I}{\mathrm{d}\omega \mathrm{d}\Omega} = [N_\mathrm{e} + N_\mathrm{e}(N_\mathrm{e} - 1)F(\omega)] \frac{\mathrm{d}^2 I_0}{\mathrm{d}\omega \mathrm{d}\Omega}, \qquad (1)$$

where N_e denotes the number of electrons in the bunch, $F(\omega)$ is the form factor, and $\mathrm{d}^2 I_0/\mathrm{d}\omega\mathrm{d}\Omega$ is the single particle spectral density. The first part is the incoherent radiation, scaling linearly with the electron number N_e. The second part is the coherent synchrotron radiation (CSR), which scales quadratically. Due to the large number of electrons in a bunch, the coherent radiation, where the form factor F is

ISBN: 978-3-95450-227-1 ISSN: 2673-5490 doi:10.18429/JACoW-IPAC2022-WEPOMS024

PRESENT STATUS OF THE INJECTOR AT THE COMPACT ERL AT KEK

O. A. Tanaka†, T. Miyajima, T. Tanikawa
High Energy Accelerator Research Organization (KEK), Tsukuba, Japan

Abstract

The Compact ERL at KEK is a test accelerator to develop ERL technologies and their possible applications. The first target of injector operation to demonstrate IR-FEL was to generate high bunch charge electron beams with low longitudinal emittance and short bunch length. In 2020, the injector was operated with the bunch charge of 60 pC, the DC gun voltage of 480 kV, the injector energy of 5 MeV and the bunch length of 2 ps rms, and the required beam quality for the IR-FEL has been achieved for a single-pass operation mode. The next target is to demonstrate IR-FEL generation for recirculation mode. The injector energy is decreased to 3.5 MeV due to a limitation of the energy ratio between injection and recirculation beams. Moreover, the DC gun voltage decreases to 390 kV due to the troubles of the DC gun. Therefore, control of the space charge effect is more important to design and optimize the beam transport condition of the injector. In this report, a strategy of the injector optimization together with its realization results and future prospects are summarized.

INTRODUCTION

The Compact Energy Recovery Linac (cERL) at KEK was originally built to operate high average beam current and beam quality [1]. The cERL consists of an injector using a photocathode DC electron gun, a superconducting accelerating cavity (main linac) with energy recovery operation, a recirculation loop, and a beam dump (see Fig. 1). In 2019 the cERL IR-FEL project was launched to meet a goal of developing high-power middle infrared lasers for high-efficiency laser processing using cERL [2]. Subsequently, the work on the injector optimization for successful production of the IR-FEL light was done [3], and the goal was achieved in a single-pass operation mode [4]. At that time the injector was operated with the bunch charge of 60 pC, the DC gun voltage of 480 kV, the injector energy of 5 MeV and the bunch length of 2 ps rms at the exit of the main linac.

The next target of the cERL operation for IR-FEL light generation is required to reproduce the previous result by an energy-recovery mode. To meet the new target, the injector energy was decreased to 3.5 MeV to allow energy recovery with an energy ratio of 1/5 (Einj = 3.5 MeV / Ecirc = 17.5 MeV). We also experienced some troubles with a DC gun. So the gun voltage was dropped to 390 kV. The beam performance is assured by the stable and high accelerating voltage supply of the DC gun. Once voltage drops, the space charge control at the injector becomes more challenging. Thus, our goal is to deliver the beam of proper quality to the exit of the main linac to assure both the FEL generation and the energy recovery. The layout of the cERL injector is shown in Fig. 2. Correspondent beam parameters are given in Table 1. The table also includes a comparison of machine parameters for two different operation modes: single-pass FEL and those with recirculation. More details on cERL injector optimization strategy and technique can be found in [3].

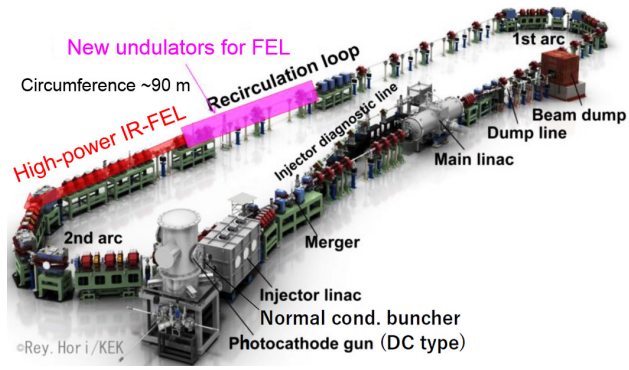

Figure 1: Schematic of the cERL.

Table 1: Design Parameters of the cERL

	Single-pass FEL	Recirculation mode
DC gun voltage	480 kV	390 kV
Repetition rate	1.3 GHz	1.3 GHz
Injector energy	5 MeV	3.5 MeV
Recirculation energy	17.5 MeV	17.5 MeV
Charge per bunch	60 pC	60 pC[1]
Rms bunch length[2]	2 ps	3.5 ps
Norm. rms transverse emittance[2]	< 3π mm mrad	< 3π mm mrad
Laser temporal distribution (FWHM)	40 ps single Gaussian	40 ps single Gaussian[3]

INJECTOR DESIGN

At the first step of the study we have optimized injector parameters using General Particle Tracer (GPT, [5]) with Multi-Objective Genetic Algorithm (MOGA, [6]). The target at the main linac exit is set up to a simultaneous minimization of a bunch length and a longitudinal emittance with an additional condition on a transverse emittance to be less than 3π mm mrad. For the required injection energy (3.5 MeV) and gun voltage (390 kV) the algorithm suggested a set of 13 variables including the currents of the 1st and the 2nd solenoids, the buncher's voltage and phase offset, the injector cavities' accelerating field, the 1st injector cavity's phase offset, and the straights of selected quadrupoles (see Fig. 2).

† olga@post.kek.jp

[1] 1 pC in operation.
[2] At the exit of the main linac.
[3] FWHM 40 ps single Gaussian and 3 ps rms single Gaussian in operation.

ISBN: 978-3-95450-227-1 ISSN: 2673-5490 doi:10.18429/JACoW-IPAC2022-WEPOMS025

INJECTOR DESIGN TOWARDS ERL-BASED EUV-FEL FOR LITHOGRAPHY

O. A. Tanaka†, N. Nakamura, T. Miyajima, T. Tanikawa, High Energy Accelerator Research Organization (KEK), Tsukuba, Japan

Abstract

A high-power EUV light source using ERL-based FEL can supply multiple semiconductor exposure devices. There are some requirements in the whole and its injector, in particular, and their examination and necessary development are being carried out. The requirement for the injector was to generate high bunch charge beams at a high-repetition rate. In this regard, a space charge effect should be treated carefully in the design of the injector. For FEL operation, not only short bunch length and small transverse emittance but also small longitudinal emittance are required. By using a multi-objective genetic algorithm, we are minimizing them at the exit of the injector to investigate the injector performance and its effect on the FEL generation. In this study, we describe the injector optimization strategies and possible options suited for the ERL-based EUV-FEL.

INTRODUCTION

An energy-recovery linac (ERL) based free-electron laser (FEL) as an extreme ultraviolet (EUV) light source has been designed using available technologies to demonstrate a generation of EUV power of more than 10 kW that supplies multiple semiconductor exposure devices [1, 2]. Figure 1 shows the schematic of the EUV light source using ERL-based FEL [1]. An electron beam is accelerated to 10.5 MeV at an exit of the injector section, and then to 800 MeV at an exit of the main linac. A final bunch compression is done using the 1st arc section to obtain a high peak current which will be required for SASE-FEL generation. After the bunch compression, the electron beam is sent to an undulator section to produce 13.5 nm EUV-FEL light. After the FEL generation the bunch is delivered to the 2nd arc section, and it will be decelerated by the main linac as energy recovery, and then disposed into a beam dump.

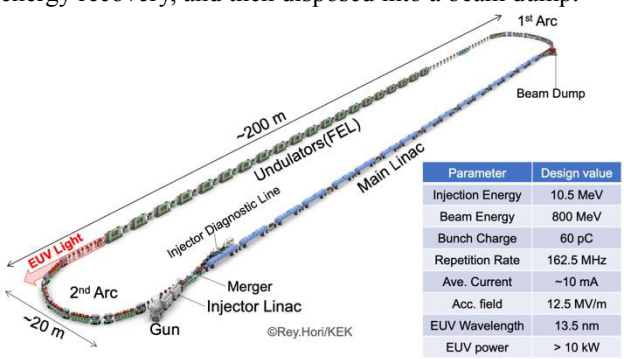

Parameter	Design value
Injection Energy	10.5 MeV
Beam Energy	800 MeV
Bunch Charge	60 pC
Repetition Rate	162.5 MHz
Ave. Current	~10 mA
Acc. field	12.5 MV/m
EUV Wavelength	13.5 nm
EUV power	> 10 kW

Figure 1: Design and specification of the ERL-based EUV-FEL light source for lithography.

With a bunch charge of 60 pC and a bunch repetition frequency of 162.5 MHz, the average current of the electron beam is about 10 mA. The disposed beam power is reduced from 8 MW to 100 kW by the energy recovery process. Proof-of-concept of the EUV-FEL using the ERL test machine at KEK (cERL) is given in Ref. [3, 4].

The goal of the injector design for the EUV-FEL is to deliver the beam with the proper quality at the injector exit [5]. The "proper beam quality" includes:

1. Bunch length is less than 3 ps;
2. Transverse emittance is less than 3 π mm mrad;
3. Longitudinal emittance is less than 10 keV ps.

In the previous work the injector has been optimized by a specific target: minimizing both the bunch length and the transverse emittance. This strategy gave an unreasonably large value of the longitudinal emittance (7.25 keV ps), while the transverse emittance was kept small enough (0.63 π mm mrad) at the injector exit. That resulted in the charge density relaxation at the FEL, and, consequently, in deficient FEL power.

In order to improve the beam quality, we have changed the designing strategy for the injector to minimize not only 1. and 2., but also 3. The discussion on how the new strategy affected the beam quality is given in the following.

In the present work we will give a comparison of 'old' and 'new' injector designs.

OPTIMIZATION METHOD

To clarify the optimization method used in this work, let us first introduce the layout of the EUV-FEL injector. As shown in Fig. 2, it consists of 3 sections: the injector section, the matching section, and the merger section. The injector section includes a 500 kV cERL-type DC electron gun to produce a stable electron beam, 2 solenoids to control the transverse beam size, a buncher cavity placed between 2 solenoids to compress the bunch length, and 2 superconducting cryomodules with 3 2-cell cavities each. Then the electron beam is reached to 10.5 MeV. The matching section includes 4 quadrupoles to match the injector optics to that of the recirculation loop. At last, the merger section consists of 3 bending magnets to guide the beam trajectory to the recirculation loop and 2 quadrupoles to facilitate the optics matching [6]. The matching point

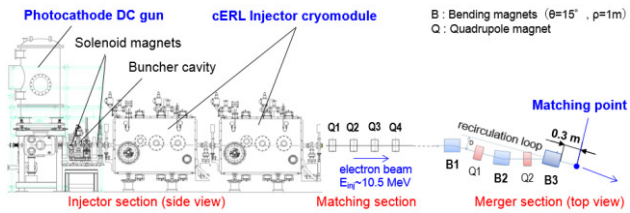

Figure 2: Schematic of the EUV-FEL injector.

† olga@post.kek.jp

ISBN: 978-3-95450-227-1 ISSN: 2673-5490 doi:10.18429/JACoW-IPAC2022-WEPOMS028

ELECTRON BEAM SHAPING TECHNIQUES USING OPTICAL STOCHASTIC COOLING*

A.J. Dick, P. Piot[1], Northern Illinois Center for Accelerator & Detector Development
Department of Physics, Northern Illinois University, DeKalb IL 60115, USA
[1] also at Argonne National Laboratory, Lemont, IL 60439, USA

Abstract

Optical Stochastic Cooling (OSC) has demonstrated its ability to reduce the three-dimensional phase-space emittance of an electron beam by applying a small corrective kick to the beam each turn. By modifying the shape and timing of these kicks we can produce specific longitudinal beam distributions. Two methods are introduced; single-pulse modulation, where the longitudinal profile of the OSC pulse is amplified by some function, as well as multiple-turn modulation, where the overall strength or phase is varied depending on the synchrotron oscillation phase. The shaping techniques are demonstrated using a model of OSC developed in the ELEGANT particle-tracking code program.

BACKGROUND

Optical Stochastic Cooling (OSC) is a beam cooling technique which uses a pair of undulators to correct the deviation in momentum of each particle [1, 2]. In the passive-OSC scheme, undulator radiation is focused directly from the pickup into the kicker undulator [3]. In the active-OSC scheme, the radiation is first amplified before being recombined with the particle beam. The amplification is typically performed uniformly (i.e. is constant along the bunch and on a turn-by-turn basis) to increase the cooling rate while reducing the emittance and increasing the beam lifetime by counteracting intra-beam scattering (IBS) effects. However, by modulating the amplification on a turn-by-turn basis or along the bunch and controlling the optical delay, OSC can be used to tailor the longitudinal phase space (LPS).

THEORY

There are two implementations enabling the OSC mechanism to be used to control the LPS distribution of an electron beam. One option is to implement a multiple-pass control of the corrective kick strength where the gain of the optical amplifier is dependent on some variable such as synchrotron oscillation phase. Another method is to control the temporal distribution of the laser amplifier so to apply a kick $\kappa(s)$ dependent on the bunch longitudinal coordinate.

The longitudinal OSC mechanism reduces each particle's deviation in momentum by a small fraction each pass, gradually reducing the energy spread and bunch length. A particle traces an ellipse in LPS (s,p) so a particle with high deviation in momentum and low spatial deviation $\phi = \pi/2$ later will have low momentum deviation and high spatial deviation. Unlike for the case of betatron motion, this varies relatively slowly and can be used as the independent variable in beam shaping techniques.

Multiple-Pass Control

Multiple-pass control uses time-dependent amplification of the undulator radiation to shape the longitudinal beam distribution. The main motivation for multiple-pass control is using this periodic behavior to reduce the longitudinal deviation of the beam in only one degree of freedom. That is, to reduce the momentum spread while leaving the bunch length unchanged (or vise versa depending on at what phase in the synchrotron period they are measured). This is achieved by applying the OSC kick at the same point every synchrotron period.

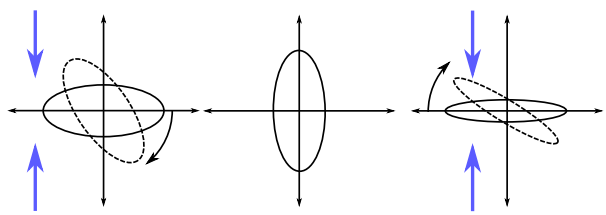

Figure 1: Synchrotron Phase

Figure 1 depicts this method implemented to "flatten" the beam LPS. The kick is applied and reduces the momentum spread. $\pi/2$ later, the beam has rotated so that what was the bunch length has converted into the momentum spread. The kick is turned off here so there is no reduction in the original bunch length. Finally, as the bunch rotates $\pi/2$ back to the minimum energy spread, the kick is turned back on thereby continuing to flatten the beam in one dimension only.

Single-Pass Control

The next tool for shaping electron beams with OSC is single-pass control of the amplification function. This relies on temporally shaping the amplification of the undulator radiation pulse. In traditional OSC, the pulse is amplified uniformly to reduce the phase-space emittance of the beam; see Fig. 2(a). This uniformly increases the electric field all particles in the bunch experience in the kicker. An amplification pulse with temporal (e.g. along s) dependence can be used to control specific slices within the bunch separately; Fig. 2(b). By applying a non-uniform amplification function

* This work is supported by U.S. Department of Energy under award No. DE-SC0013761 with Northern Illinois University and by the U.S. National Science Foundation under award PHY-1549132, the Center for Bright Beams. Fermilab is managed by the Fermi Research Alliance, LLC for the DOE under contract number DE-AC02-07CH11359.

ISBN: 978-3-95450-227-1 ISSN: 2673-5490 doi:10.18429/JACoW-IPAC2022-WEPOMS029

MODELING OF THE OPTICAL STOCHASTIC COOLING AT THE IOTA STORAGE RING USING ELEGANT

A. J. Dick, P. Piot[1], Northern Illinois Center for Accelerator & Detector Development
Department of Physics, Northern Illinois University, DeKalb IL, USA
J. Jarvis, Fermi National Accelerator Laboratory, Batvia, IL, USA
[1]also at Argonne National Laboratory, Lemont, IL, USA

Abstract

In support of the Optical Stochastic Cooling (OSC) experiment at IOTA, we implemented a high-fidelity model of OSC in the ELEGANT beam-dynamics program. The introduced element is applicable to any OSC configurations and models the main features of OSC including (*i*) the longitudinal time of flight OSC, (*ii*) the effects between the transverse motion of particles in the beam and the transverse distribution of undulator radiation, and (*iii*) the incoherent contributions of neighboring particles. Together these produce a highly accurate model of OSC and were benchmarked using the results from the IOTA OSC experiment.

BACKGROUND

Stochastic Cooling is a beam cooling technique which uses electromagnetic radiation produced by a beam in a storage ring at a specific location (the pickup) to provide a corrective kick to the beam at a point downstream (the kicker). Radiation with bandwidth $\delta\omega$ carries information on temporal slices with duration $\tau \sim 1/\delta\omega$ so that the kick corrects the mean properties of these slices. When applied over millions of turns, this corrective kick reduces the momentum spread of the stored beam. The ability for this method to correct a single particle is limited by the number of other particles in the sample slice which act as random fluctuations on the single-particle cooling force. Optical Stochastic Cooling (OSC) extends this principle to the optical range using undulator magnets for the pickup and kicker [1]. The use of optical radiation increases the bandwidth of the signal compared to conventional microwave stochastic cooling. This increased bandwidth ultimately results in a faster cooling.

An exact simulation of OSC would require use of a finite difference time-domain software to calculate the production and interaction of the undulator radiation with the beam. This would be too computationally prohibitive considering the stochastic nature and the number of turns required to cool the beam. Instead we have implemented a semi-analytical model of OSC in ELEGANT, a particle tracking software used to simulate storage rings and beam lines [2]. The model includes three main components: (i) the so-called transit-time OSC, (ii) effects of transverse beam size, and (iii) incoherent contributions of other particles in the sample slice.

MODEL

The model we have implemented considers two planar undulator elements as the pickup and kicker elements. The kicker element changes each particle's momentum depending on (*i*) the arrival time of each particle relative to its own radiation, (*ii*) the transverse motion of each particle from the pickup to kicker, and (*iii*) any incoherent kicks due to nearby particles (as determined by the system bandwidth).

Transit-Time OSC

Transit-time OSC introduces an energy-dependent delay between the pickup and kicker using a particle bypass [3]. Particles which deviate from the reference energy arrive in the kicker out of phase with their radiation produced at the pickup and receive a kick proportional to this delay. Considering only the longitudinal motion, the momentum kick experienced by the i-th nacroparticle is

$$\delta p_i/p = -\kappa \sin\left[\omega(t_i - t_0) + \psi\right], \tag{1}$$

where κ is the maximum kick strength, $\omega = 2\pi/\lambda$ (where λ is the fundamental wavelength of the undulator radiation) is the angular frequency, and ψ is a phase offset which accounts for optical delay. The difference $t_i - t_0$ is the difference between the time-of-flight of the i-th macroparticle and the mean time-of-flight of the bunch. Both κ and ψ are user-controlled parameters which can be modified on a turn-by-turn basis.

Transverse Effects

Undulator radiation produced in the pickup is emitted in a cone with $\theta = 1/\gamma$ and is imaged to the same point in the kicker undulator. A particle may arrive off-axis relative to its own radiation due to transverse motion between the pickup and kicker especially for larger transverse beam sizes. The far-field radiation of a single particle at the focusing lens is,

$$E_x(\rho, \phi) = \frac{\theta\left[J_0(\xi) + (\gamma\theta)^2 \cos(2\phi) J_2(\xi)\right]}{(1 + (\gamma\theta)^2)^4}, \tag{2}$$

where $\xi \equiv \rho k_0 \theta/(1 + (\gamma\theta)^2)$, J_0 and J_2 are Bessel functions of the first kind of $n = 0, 2$, $k_0 = 2\pi/\lambda$ is the wave number, γ is the Lorentz factor, and θ is the angle of the emitted radiation. The total field is found by integrating Eq. 2 from 0 to θ_m, the angular acceptance of the lens. The effects of transverse displacement at the kicker can be modeled by taking the strength of the off-axis field relative to the on-axis field $E_x(\Delta x, \Delta y)/E_x(0,0)$ and multiplying it by the nominal kick strength. Eq. 1 then becomes,

$$\delta p_i/p = -\kappa \sin\left[\omega(t_i - t_0) + \psi\right] \times \frac{E_x(\Delta x, \Delta y)}{E_x(0,0)} \tag{3}$$

ISBN: 978-3-95450-227-1 ISSN: 2673-5490 doi:10.18429/JACoW-IPAC2022-WEPOMS030

A PATH-LENGTH STABILITY EXPERIMENT FOR OPTICAL STOCHASTIC COOLING AT THE CORNELL ELECTRON STORAGE RING

S.J. Levenson*, M.B. Andorf, I.V. Bazarov, V. Khachatryan,
J.M. Maxson, D.L. Rubin and S.T. Wang, Cornell University, Ithaca, NY, USA

Abstract

To achieve sufficient particle delay with respect to the optical path in order to enable high gain amplification, the design of the Optical Stochastic Cooling (OSC) experiment in the Cornell Electron Storage Ring (CESR) places the pickup (PU) and kicker (KU) undulators approximately 80 m apart. The arrival times of particles and the light they produce in the PU must be synchronized to an accuracy of less than an optical wavelength, which for this experiment is 780 nm. To test this synchronization, a planned demonstration of the stability of the bypass in CESR is presented where, in lieu of undulators, an interference pattern formed with radiation from two dipoles flanking the bypass is used. In addition to demonstrating stability, the fringe visibility of the pattern is related to the cooling ranges, a critical parameter needed for OSC. We present progress on this stabilization experiment including the design of a second-order isochronous bypass, as well as optimizations of the Dynamic Aperture (DA) and injection efficiency.

INTRODUCTION

Optical stochastic cooling is a beam cooling technique based on the same principles as stochastic cooling with the radiation shifted from microwave to optical wavelengths to leverage the larger bandwidth supported by optical systems. First proposed in 1993 [1], this method starts with a particle emitting a wave-packet in a "pickup" undulator (PU), and receiving a corrective energy kick from the same wave-packet in a downstream "kicker" undulator (KU). When the particle bypass and light path are properly set, the arrival time of the reference particle is such that it receives no kick. Meanwhile, a generic particle having an energy offset or non-zero betatron coordinate will be delayed and receives an energy kick that is corrective. [2]. This paper addresses the status of the experiment at the Cornell Electron Storage Ring (CESR) at Cornell University [3–5].

For OSC at CESR, an arc-bypass has been designed and studied for an active OSC demonstration [3]. The arc-bypass uses the dipoles of the ring to delay the particle beam relative to the light. The advantage of this approach is a significantly larger delay than what can be achieved with a dog-leg chicane, enabling the use of a staged amplification scheme for high gain without sacrificing the systems cooling ranges. However, because the ring dipoles tend to have a larger bending angle, the particle transit time is more sensitive to magnetic field fluctuations. Moreover, the arc-bypass concept relies on mirrors in the optical transport which are susceptible to mechanical vibrations, introducing another source of transit-time jitter. As a step towards a high gain OSC demonstration in CESR, a path-stability demonstration is being pursued.

In this path length stability demonstration, optical radiation generated by two dipole magnets, B44W and B46E (as shown in Fig. 1), separated by a comparable distance as the PU and KU will be for the OSC experiment, will be interfered. The light path for this demonstration has been constructed and is detailed in [6]. By registering the intensity of interfered radiation field on a photodiode, the path-error can be measured and corrected with feedback. In our demonstration, we plan to use an Electro-Optic modulator (EOM) to correct the transit-time of the light path.

Figure 1: A conceptual overview of the experiment shown along the northern arc of the CESR ring. In the diagram, positrons circulate the ring clockwise, west to east. The light (yellow) from dipole B44W is propagated to the east where it is interfered with light from B46E. The diagram is not to scale.

INTERFERENCE OF FIELDS

A requirement for this stability experiment is good longitudinal interference visibility between the radiation of the two dipoles. Hence, the two radiation fields must be strongly correlated. This is achieved by minimizing the longitudinal mixing of the particles between the two radiation source points. For two points in an accelerator, longitudinal mixing is defined as the RMS deviation from the reference particle's path length between the two points. The relationship between longitudinal mixing (with first-order transport) and interference visibility has been discussed in [7]. For high visibility, the longitudinal mixing must be much less than the wavelength (λ_e) of the light, which for this experiment was chosen to be $\lambda_e = 780$ nm to be compatible with the Ti:sapphire gain medium.

The change in the longitudinal coordinate of a particle between two points is (ignoring the vertical coordinate) [8]:

$$\begin{aligned}\Delta s = {} & M_{51}(x+\eta\delta) + M_{52}(x'+\eta'\delta) + M_{56}\delta \\ & + \mathrm{T}_{512}(x+\eta\delta)(x'+\eta'\delta) + \mathrm{T}_{511}(x+\eta\delta)^2 \\ & + \mathrm{T}_{522}(x'+\eta'\delta)^2 + \mathrm{T}_{516}(x+\eta\delta)\delta \\ & + \mathrm{T}_{526}(x'+\eta'\delta)\delta + \mathrm{T}_{566}\delta^2\end{aligned} \tag{1}$$

* sjl354@cornell.edu

ISBN: 978-3-95450-227-1 ISSN: 2673-5490 doi:10.18429/JACoW-IPAC2022-WEPOMS031

LIGHT PATH CONSTRUCTION FOR AN OPTICAL STOCHASTIC COOLING STABILITY TEST AT THE CORNELL ELECTRON STORAGE RING

S.J. Levenson*, M.B. Andorf, I.V. Bazarov, D.C. Burke, J.M. Maxson, D.L. Rubin, S.T. Wang
Cornell University, Ithaca, NY, USA

Abstract

An experiment at the Cornell Electron Storage Ring (CESR) to test the optical path-length stability of a bypass suitable for Optical Stochastic Cooling (OSC) is being pursued. The approximately 80 m light path for this experiment has been assembled, and synchrotron light has been successfully propagated from both sources. A feedback system based on an Electro-Optic Modulator (EOM) to correct the path-error accumulated in both the light and particle path has been table-top tested. We present on the design and construction of the light optics for the OSC stability experiment at CESR.

INTRODUCTION

Optical Stochastic Cooling (OSC) [1] is a beam cooling technique. Based on the same principles as microwave stochastic cooling, OSC operates in the optical wavelength regime in order to take advantage of the large bandwidth, of the order of 100 THz, that an optical system can support. In the Cornell Electron Storage Ring (CESR) at Cornell University, an experimental program aimed at developing high gain OSC using an arc-bypass approach is under development [2–4]. As a stepping stone towards high gain OSC, Cornell is pursuing a path-length stabilization experiment based on the interference of synchrotron radiation produced by two dipoles at the start and end of the arc-bypass. The motivation, status and design of the beam optics are detailed in [5]. This paper focuses on the construction and initial commissioning of the light path to be used in the experiment.

LIGHT PATH DESIGN

The interference takes place between bend magnets B44W and the downstream B46E which are separated 71 meters along the nominal beam path. From each bend magnet, a portion of the synchrotron radiation is picked off from a 12.5 × 12.5 mm water-cooled beryllium (Be) mirror located 5.44 m from the source point. The mirrors are angled so that the bend radiation is directed perpendicularly through a viewport into an optics station. Interference is to be performed at the east station just downstream from B46E. The west station was designed with the purpose of aligning B44W's bend radiation along the light-path axis and collimating the radiation for the long transport to the east side.

To obtain an initial alignment of the light path, a HeNe laser was used. A pellicle beam splitter is used to join the HeNe path to B44W's. This same beam splitter also serves to direct a portion of the light to a substation used for co-aligning the HeNe light and radiation from B44W. This substation consists of two cameras separated by 0.5 m and another beam splitter so that radiation is incident on both cameras simultaneously. Two remotely controlled mirrors in the bend radiation path, prior to where it joins the HeNe path, are used so that the bend radiation can be made to spatially overlap the HeNe on both cameras.

A lens doublet is used for collimation. At the doublet, the radiation size is largely determined by the source divergence. Therefore, if the focusing is chosen so that $M_{22} = 0$, which occurs when $F_{\text{doublet}} = -L_{\text{source}}$ where F_{doublet} is the effective focal length of the lens doublet and L_{source} is the distance from the radiation source to the first lens of the doublet, we would expect a constant radiation size after the doublet. Taking into account the commercially available lens sizes and space constraints of the optics module, we selected $F_1 = -F_2 = 500$ mm. For $M_{22} = 0$, the doublet spacing, $l_d = 5.1$ cm. To account for the lenses having an error in the focal length on the order of 1%, the second lens in the doublet was placed on a controllable stage to make an adjustment of the effective focal length. The above argument is based on geometric optics and neglects diffraction. As a check, we used Synchrotron Radiation Workshop (SRW) [6] and confirmed the radiation becomes collimated to an approximately 6 mm RMS size without significant growth after the doublet.

After exiting the west station, the light path for B44W's transport is parallel to the beam trajectory before cutting across a chord along CESR's northern arc. This cut results in the optics path being approximately 20 cm shorter than the beam path. During OSC, part of this extra distance can be used to accommodate the use of a high gain amplifier. In addition to the storage ring, the CESR tunnel houses the synchrotron used for boosting the beam to the operational energy, nominally 6 GeV for CHESS but set to 3 GeV for this experiment. Two periscopes are used to raise and lower the light path over the synchrotron. The upper mirror of each periscope is on a remotely controlled, vertically oriented stage that can be used for rough adjustment of the light path-length. The light path is enclosed in 4" PVC pipe to protect against air drafts inside the tunnel.

Once on the east side, another substation holds the Electro-Optic Modulator (EOM) used for the path stabilization. A lens doublet chosen to behave as a reverse beam expander with 250 mm and 25.4 mm focal length lens are used to reduce the radiation to the 1 mm diameter aperture of the EOM.

* sjl354@cornell.edu

ISBN: 978-3-95450-227-1 ISSN: 2673-5490 doi:10.18429/JACoW-IPAC2022-WEPOMS032

SIMULATIONS OF COHERENT ELECTRON COOLING WITH ORBIT DEVIATION*

J. Ma†, G. Wang, V. N. Litvinenko[1], Brookhaven National Laboratory, Upton, New York, USA
[1]also at Stony Brook University, Stony Brook, New York, USA

Abstract

Coherent electron cooling (CeC) is a novel technique for rapidly cooling high-energy, high-intensity hadron beam. Plasma cascade amplifier (PCA) has been proposed for the CeC experiment in the Relativistic Heavy Ion Collider (RHIC) at Brookhaven National Laboratory (BNL). Cooling performance of PCA based CeC has been predicted in 3D start-to-end CeC simulations using code SPACE. The dependence of the PCA gain and the cooling rate on the electron beam's orbit deviation has been explored in the simulation studies.

INTRODUCTION

Strong hadron cooling (SHC) is essential to attain the luminosity required by the future Electron-Ion Collider (EIC) design. CeC [1-3] is a promising technique for the rapid cooling of high-energy high-intensity hadron beams in the EIC.

A CeC system consists of three main sections, the modulator, the amplifier, and the kicker. Several CeC schemes have been proposed with different implementations of the CeC amplifier. In this paper, we present simulation studies of the PCA-based CeC [4]. Working principle of PCA is the new plasma cascade instability (PCI) [5-6].

Figure 2 shows the layout of a PCA-based CeC system, where solenoids are used to modulate the transverse size of the electron beam and to excite the PCI.

Our simulation tool is the SPACE code [7], a parallel, relativistic, three-dimensional (3D), electromagnetic (EM) Particle-in-Cell (PIC) code, which has been used in the simulation studies for the mitigation effect by beam induced plasma [8], the modulation process in CeC [9-12], CeC with free electron laser (FEL) amplifier [13-16] and the CeC with PCA [17-18].

CEC WITHOUT ORBIT DEVIATION

The setup of the CeC system in the simulation study is based on the CeC experiment at BNL RHIC, which includes a 2.88-meter modulator, an 8-meter 4-cell PCA and a 3-meter kicker. The lengths of the PCA cells are 1.8 m, 2.2 m, 2.2 m, and 1.8 m. Table 1 lists two cases of electron beam parameters in simulations. The electron beam peak current and emittance are carefully chosen to excite the PCI in PCA, and therefore amplifier the density modulation introduced by ions in the modulator.

Table 1: Electron Beam Parameters

	Case 1	Case 2
Beam energy, γ	28.5	28.5
Peak current, A	50	75
Normalized KV emittance, mm mrad	6	7
RMS energy spread	2e-4	2e-4

A transverse Kapchinsky-Vladimirsky (KV) distribution has been applied to the electron beam in the simulations. Note that the KV emittance is 4 times of the traditionally defined root-mean-square (RMS) emittance.

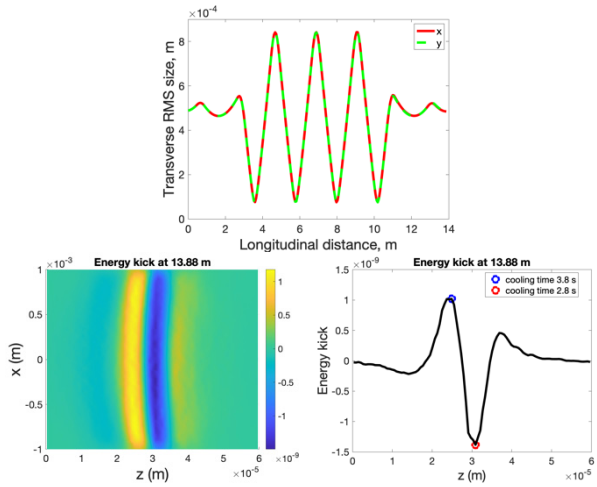

Figure 1: Evolution of transverse RMS beam size in a 4-cell-PCA based CeC system for electron beam peak current 50A (top), and the energy kick to ions in the kicker section for ions with various longitudinal and horizontal positions (bottom left) and for ions with zero horizontal position (bottom right).

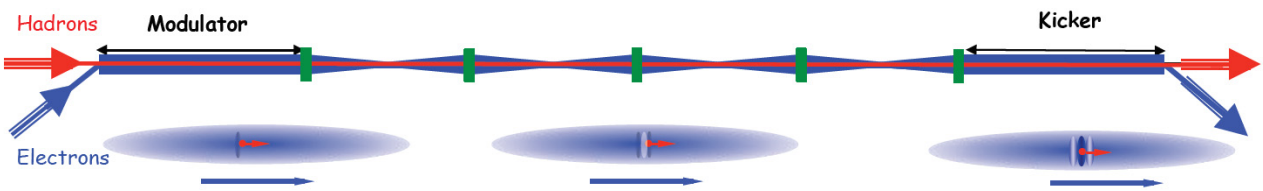

Figure 2: Schematic of a CeC system with the PCA.

* Work supported by Brookhaven Science Associates, LLC under Contract No. DE-SC0012704 with the U.S. Department of Energy.
† jma1@bnl.gov

ISBN: 978-3-95450-227-1 ISSN: 2673-5490 doi:10.18429/JACoW-IPAC2022-WEPOMS033

CETA-A CODE PACKAGE BEING DEVELOPED FOR COLLECTIVE EFFECT ANALYSIS AND SIMULATION IN ELECTRON STORAGE RINGS*

C. Li †,Y.-C. Chae, Deutsches Elektronen-Synchrotron, Hamburg, Germany

Abstract

The code Collective Effect Tool Analysis (CETA) is under development to study the collective effects in the electron storage ring. With the impedance either generated by itself or imported from an external file, CETA can calculate the loss and kick factors, the longitudinal equilibrium bunch length from a Haissinski solver, and the head-tail mode frequency shift from a Vlasov solver. Meanwhile, the code CETASim, which can track particles to study coupled-bunch instabilities caused by long-range wakefield, ion effects, transient beam loading effect, bunch-by-bunch feedback, etc., is also under development. In this paper, we describe the code status and give several simulation results from CETA and CETASim to show how these codes work.

INTRODUCTION

The design goal of the diffraction-limited storage ring is to have an ultralow emittance in combination with a high beam current, which naturally requires careful studies on both the single bunch and coupled bunch effects due to wakefield, beam-ion effet, transient beam loading, and the bunch-by-bunch feedbacks, etc. [1]. However, the numerical analysis of the beam instability is not straightforward due to the complexity of the intrabunch and interbunch beam dynamics characteristics. In the past decades, simulation codes such as Elegant [2], MBTrack [3], PyHeadTail [4], etc. are developed and are capable to cover various beam dynamics problems in this field. In this paper, we will introduce two codes recently developed, CETA and CETASim. The main purpose of CETA is to supply researchers quick and rough estimation of the influence from impedance to electron beam, meanwhile, CETASim is supposed to be a light version of the collective effect simulation code. In sections 2 and 3, simulation results obtained with different scenarios are given as demonstrations to show how CETA and CETASIm work. Plans for future studies are given in section 4.

RESULTS FROM CETA

Kick and Loss Factor

Figure 1 shows the kick and loss factors as a function of bunch length in Petra4, where 1 mA bunch current is assumed as the default setting. In the transverse direction, the resistive wall is one of the main impedance sources. Compared with the zero chromaticity results, at chromaticity 5, the kick factor due to the resistive wall is reduced roughly by a factor of two. However, the kicker factors of other elements are well suppressed by chromaticity 5. In the longitudinal direction, the resistive wall, the 3rd order harmonic cavity, and the kickers contribute most of the total loss factors.

Haisskinski Solver

The Haisskinski solver is used to study the bunch lengthening and longitudinal bunch shape distortion due to the longitudinal impedance. In CETA, the Haisskinski equation is numerically solved in a self-consistent way, where an iteration process is launched to ensure a convergent bunch density profile. Figure 2 shows the final bunch density profile where the resistive wall impedance is taken into account in a 40 ESRF-Cell type storage ring. Figure 3 shows the comparison of the bunch length obtained from CETA and Elegant simulation. The energy spread is assumed constant in the Haisskinski solver, it indicates that the prediction from the Haisskinski solver is not suitable anymore when the bunch current is beyond the longitudinal macro-wave-instability (MWI) threshold.

Vlasov Solver and TMCI

The Vlasov solver in CETA deals with the linearized Scaherer equations [1] in the frequency domain, in which the equilibrium beam profile is assumed as a Gaussian type and the perturbation is expressed in terms of Laguerre polynomials. Correspondingly, the perturbations in the real space is expressed by the Hermite polynomial. With a given transverse impedance, the interaction matrix M is established and solved numerically. Figure 4 shows the modes frequency shift comparison between results from the CETA Vlasov solver and Elegant tracking in the 40 ESRF-cell machine. The blue lines are the results from CETA. In Elegant simulation, only the vertical dipole impedance is considered, which ensures a fair comparison against CETA. The contour is the Fourier spectrum of the center oscillation from Elegant tracking. Both CETA and Elegant show that the $l = 0$ and $l = -1$ modes are coupled when the bunch charge reaches 1.6 nC.

RESULTS FROM CETA

The code CETASim is an upgraded version of the beam-ion simulation code developed in 2020 [5]. In the updated version, some new features are added to cover various coupled bunched motions due to the long-range wake. In bellow, we will give the beam-ion interaction in the transverse direction and the transient beam loading in the longitudinal direction Petra4 (lattice version 3.3).

Beam-Ion Effect

The updated version of CETASim is extended to cover multi-gas and multi-interaction points in the beam-ion sim-

* Work supported by the European Union's Horizon 2020 research and innovation program under grant agreement No. 871072
† li.chao@desy

ISBN: 978-3-95450-227-1 ISSN: 2673-5490 doi:10.18429/JACoW-IPAC2022-WEPOMS035

HARPY: A FAST, SIMPLE AND ACCURATE HARMONIC ANALYSIS WITH ERROR PROPAGATION

L. Malina, DESY, Hamburg, Germany

Abstract

Traditionally, in the accelerator physics field, accurate harmonic analysis has been performed by iteratively interpolating the result of Fast Fourier Transform (FFT) in the frequency domain. Such an approach becomes computationally demanding when relatively small effects are being studied, which is especially evident in the typical example of harmonic analysis of turn-by-turn beam position monitor data, i.e. many correlated but noisy signals. A new harmonic analysis algorithm, called Harpy, is about an order of magnitude faster than other methods, while often being also more accurate. Harpy combines standard techniques such as zero-padded FFT and noise-cleaning based on singular value decomposition. This combination also allows estimating errors of phases and amplitudes of beam-related harmonics calculated from cleaned data.

INTRODUCTION

In accelerator physics, accurate harmonic analysis is one of the critical numerical methods. Nowadays, the tighter tolerances shift the attention from the determination of frequencies, such as betatron or synchrotron frequency, to the measurement of phases of even smaller spectral lines. A good example and this paper's motivation is the beam optics measurement in storage rings. One of the ways to measure the beam optics in a storage ring is to analyse beam position monitor (BPM) orbit readings of coherently-excited beams recorded turn-by-turn (TBT) [1]. The calculations of the actual optical functions (for example, phase advances, β-functions and resonance driving terms) are the last steps in the analyses, which require frequencies, amplitudes and phases of the different spectral lines, commonly referred to as frequency spectra.

Traditionally, in the analysis process, TBT BPM data is first cleaned of noise using methods [2–4] based on Singular Value Decomposition (SVD). Then, frequency spectra of cleaned TBT data are computed for every BPM independently employing methods [5,6] based on frequency interpolation in the output of the Fast Fourier Transform (FFT). The computation is an iterative process, and in each iteration, the strongest signal in the FFT output is interpolated (i.e. found) and subtracted after Gram-Schmidt orthonormalisation. With typically hundreds of iterations the frequency analysis is computationally expensive. The phase accuracy of frequency-interpolation based methods [5,6] was found to be worse than FFT [7].

We presented an intermediate algorithm [8], which calculated the frequency spectra of the data decomposed by SVD and recomposed the BPM spectra in the frequency domain. As a result, it was more than an order of magnitude faster, which is essential for efficient beam operation, for example, in automatic coupling correction [9]. However, the accuracy issue remained unresolved for weak spectral lines.

The work presented here leverages modern open-source scientific libraries such as NumPy [10], SciPy [11] and pandas [12] used across various domains. Together with the current computational power, they allow for efficient high-level analyses, such as refined frequency analysis performing FFT only once, i.e. not in a number of iterations.

This paper describes Harpy, which combines SVD with zero-padded real FFT (RFFT) to clean the noise and compute frequency spectra efficiently, as shown in Figure 1. Such an approach addresses the performance issues (both speed and accuracy), makes the error propagation transparent, and allows for simpler use of windowing functions to trade frequency, phase, and amplitude accuracy.

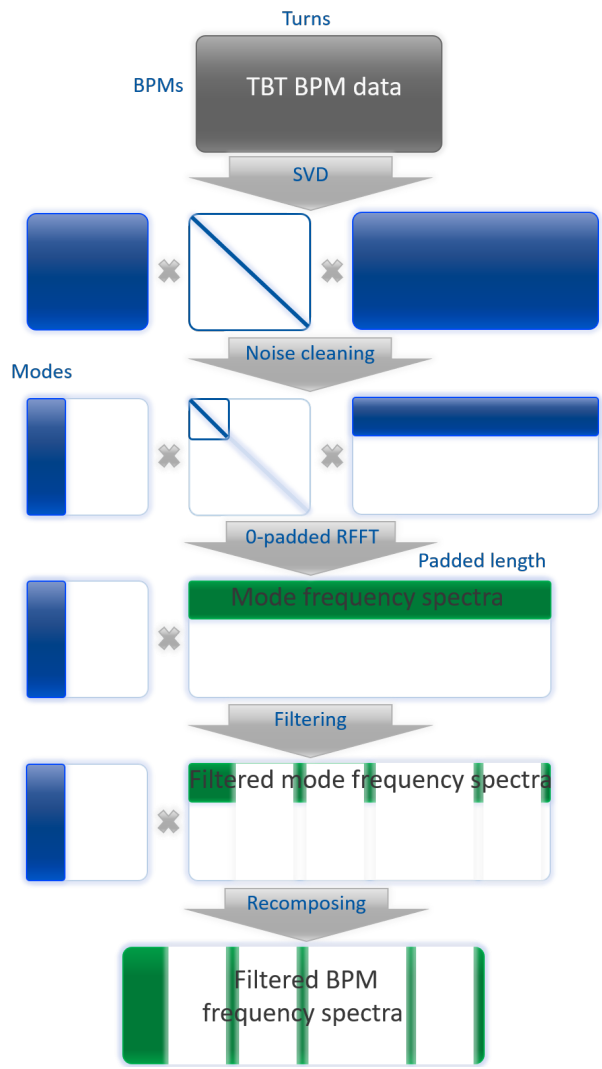

Figure 1: Schematic illustration of main Harpy principle.

ISBN: 978-3-95450-227-1 ISSN: 2673-5490 doi:10.18429/JACoW-IPAC2022-WEPOMS036

ACCELERATING LINEAR BEAM DYNAMICS SIMULATIONS FOR MACHINE LEARNING APPLICATIONS

O. Stein*, J. Kaiser, A. Eichler, I. Agapov
Deutsches Elektronen-Synchrotron DESY, Germany

Abstract

Machine learning has proven to be a powerful tool with many applications in the field of accelerator physics. Training machine learning models is a highly iterative process that requires large numbers of samples. However, beam time is often limited and many of the available simulation frameworks are not optimized for fast computation. As a result, training complex models can be infeasible. In this contribution, we introduce *Cheetah*, a linear beam dynamics framework optimized for fast computations. We show that Cheetah outperforms existing simulation codes in terms of speed and furthermore demonstrate the application of Cheetah to a reinforcement-learning problem as well as the successful transfer of the Cheetah-trained model to the real world. We anticipate that Cheetah will allow for faster development of more capable machine learning solutions in the field, one day enabling the development of autonomous accelerators.

INTRODUCTION

In recent years, machine learning (ML) has proven to be a powerful solution to many problems in a variety of fields, including accelerator physics. The subfield of reinforcement learning (RL), in particular, promises solutions to many control and optimization problems encountered during accelerator operations, with previous works demonstrating the ability of RL to solve difficult high-stakes physics-based control problems [1].

In RL, intelligent agents – implemented for example as an artificial neural network (ANN) – are trained through experience to iteratively solve a problem by observing an environment $\mathscr{E}$ – for example representing an accelerator control problem – through observations o_t and applying actions a_t to it in order to maximize a *cumulative reward*, the sum of step-wise rewards r_t.

A major challenge in the field of RL remains the large amount of experience required to successfully train agents. While there is active research ongoing on improving the sample-efficiency of RL [2], solving problems of sufficient complexity continues to require in the order of 10^5 up to 10^9 samples. Due to physical limitations, such large amounts of experience are usually infeasible to acquire in the real world, as taking just a single sample can sometimes take from a second to a multiple minutes depending on the physical system one is hoping to solve. Accelerator physics are particularity constrained in terms of taking large numbers of real-word samples as beam time is a notoriously scarce resource.

The issue of gathering large numbers of samples in the real-world has given rise to a research direction in RL called *sim2real*, where agents are trained in a simulation of the real-world system and then transferred to the latter. With ever more efficient simulation codes and ever faster and increasingly parallel compute resources available, especially thanks to the rise of general purpose GPUs (GPGPUs), this approach has enabled the gathering of large amounts of samples in feasible time frames. A similar approach can be pursued when training RL agents for accelerator control, as a variety of capable simulation codes have been implemented for particle accelerators over the years. These include *ASTRA* [3], *elegant* [4], *MAD-X* [5] and *Ocelot* [6], just to name a few. Existing accelerator simulation codes have however been developed to be used during the design phase of accelerators and for finding new working points – applications where physical accuracy is often crucial and compute times of multiple seconds, minutes and sometimes even hours are acceptable. As a result, these simulation codes usually require infeasible amounts of compute time and resources when used to train RL agents. At the same time, recent work in the field of sim2real [7] has found that *dynamics randomization* – adding random disturbances to the dynamics of a simulation – during the training of an RL agent yields improved results over perfectly accurate simulations.

In this paper, we propose a new accelerator simulation code *Cheetah*[1] that trades accuracy for speed to achieve simulation compute times in the order of a few hundred microseconds on off-the-shelf PC hardware. To this end, we introduce Cheetah and its features, present benchmarks on its speed and accuracy as well as demonstrate the application of Cheetah to train an RL agent to solve an accelerator control problem.

FAST PYTORCH-BASED PARTICLE ACCELERATOR SIMULATION

The goal of Cheetah is to achieve fast iterations in simulation, if necessary at the cost of accuracy. To this end, we implement a linear beam transfer based on matrix multiplication with first-order transport matrices in six-dimensional phase space. Cheetah is implemented in *Python* and employs

* oliver.stein@desy.de

This work has in part been funded by the IVF project InternLabs-0011 (HIR3X) and the Initiative and Networking Fund by the Helmholtz Association (Autonomous Accelerator, ZT-I-PF-5-6).

[1] Source code available at https://github.com/desy-ml/cheetah

ISBN: 978-3-95450-227-1 ISSN: 2673-5490 doi:10.18429/JACoW-IPAC2022-WEPOMS037

MICROBUNCHING STUDIES FOR THE FLASH2020+ UPGRADE USING A SEMI-LAGRANGIAN VLASOV SOLVER

Ph. Amstutz* and M. Vogt
Deutsches Elektronen-Synchrotron DESY, Germany

Abstract

Precise understanding of the microbunching instability is mandatory for the successful implementation of a compression strategy for advanced FEL operation modes such as the EEHG seeding scheme, which a key ingredient of the FLASH2020+ upgrade project. Simulating these effects using particle-tracking codes can be quite computationally intensive as an increasingly large number of particles is needed to adequately capture the dynamics occurring at small length scales and reduce artifacts from numerical shot-noise. For design studies as well as dedicated analysis of the microbunching instability semi-Lagrangian codes can have desirable advantages over particle-tracking codes, in particular due to their inherently reduced noise levels. However, rectangular high-resolution grids easily become computationally expensive. To this end we developed SelaV$_{1D}$, a one dimensional semi-Lagrangian Vlasov solver, which employs tree-based domain decomposition to allow for the simulation of entire exotic phase-space densities as they occur at FELs. In this contribution we present results of microbunching studies conducted for the FLASH2020+ upgrade using SelaV$_{1D}$.

INTRODUCTION

In the injector and linac sections upstream of the undulators of an free-electron laser (FEL), collective interaction of the electrons in a bunch can – in combination with longitudinal dispersion in parts of the beamline – lead to the formation of substructures in the longitudinal phase-space density (PSD) of the bunch [1]. This so-called microbunching instability (MBI) can have significant impact on the efficacy of free-electron lasers, due to the resulting increase of the energy spread and enhanced irregularities in the longitudinal phase-space and in the current density [2]. Hence, during the design of new FEL injectors, care has to be taken to ensure the setup does not produce a microbunching gain beyond tolerable levels. While leading-order theories for the gain function of the MBI exist, simulations are still required to study the full dynamics of the instability and capture also non-linear effects. We present studies of the MBI for the FLASH2020+ upgrade project [3], conducted with SelaV$_{1D}$ [4], a semi-Lagrangian code in one degree of freedom, which employs tree-based domain decomposition to enable the simulation of an entire bunch on all relevant length scales [5]. The semi-Lagrangian approach yields a smooth solution [6] of the Vlasov equation and hence allows to efficiently study the MBI without the artificial shot-noise that is inherent to macroparticle simulation codes.

* philipp.amstutz@desy.de

COMPRESSION WORKING POINTS

The injector beamline of FLASH2020+ comprises two bunch compression stages in the form of C-shape magnetic chicanes with the corresponding upstream off-crest operated RF modules, shown in Figure 1. The nominal R_{56} of the two chicanes is 139.9 mm at a beam energy of around 145 MeV and 72.6 mm at around 550 MeV, respectively. Acceleration

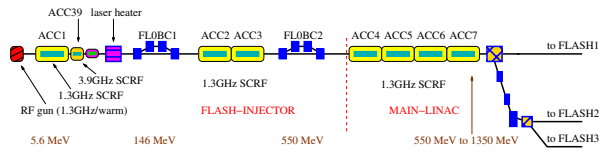

Figure 1: Layout of the injector and linac beamline of FLASH2020+.

is provided by seven accelerating modules ACC1 to ACC7, which, together with the 3.9 GHz linearizer module ACC39, yield a maximum energy of 1.35 GeV. In the focus of this

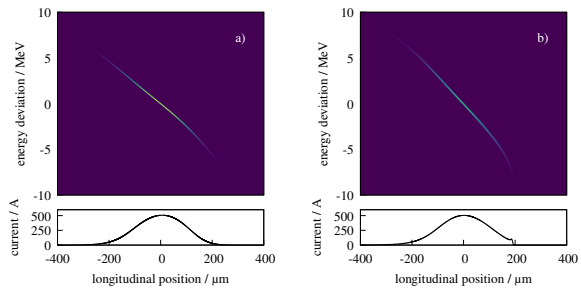

Figure 2: Longitudinal PSD and current profiles after the second chicane for a) WP1 and b) WP2.

study are two compression working points which are especially suited for the Echo-Enable Harmonics Generation (EEHG) seeding scheme, which will be employed in the FLASH1 beamline. An intermediate peak current of about 500 A is projected for EEHG operation in FLASH1. For EEHG it is particularly desirable for the electron bunch to feature a longitudinal PSD that has as small of a curvature in the central part of the bunch as possible.

To this end, two compression working points, WP1 and WP2, were chosen, as shown in Table 1. Both provide compression of a 400 pC bunch to a final current of 500 A. The final longitudinal phase-space has negligible non-linear covariance in the central part up to third order, shown in Figure 2. WP1 assumes the bunch to leave the gun with a peak current of $I_0 = 31.25$ A, which is then compressed by a factor 4 in each compression stage. For WP2 a reduced initial current of $I_0 = 20$ A is assumed, requiring stronger subse-

ISBN: 978-3-95450-227-1 ISSN: 2673-5490 doi:10.18429/JACoW-IPAC2022-WEPOMS039

ANALYSIS OF Xcos SIMULATION MODEL FOR INTENSITY AT THIRD AND FIFTH HARMONICS UNDULATOR RADIATION

H. Jeevakhan, Department of Applied Science Education, National Institute of Technical Teachers' Training and Research, Bhopal, India
G. Mishra, School of Physics, Devi Ahilya University, Indore, India
K. Kushwaha, M. Syed, Jabalpur Engineering college, Jabalpur, India

Abstract

Xcos simulation model is analysed for the intensity of planar undulator radiation at the third and fifth harmonics. The Xcos model is designed by using the numerical approach. The results obtained from the simulation model are compared with the analytical method. The model can also be utilized for observing the effect of energy spread on radiation by numerical approach.

INTRODUCTION

Free electron laser (FEL) is a coherent and tuneable light source available with high brightness up to order of 10^{13} [1]. In FEL systems, a relativistic electron beam is undulated in presence of periodic magnetic field i.e. undulator, to bring out a coherent electromagnetic radiation. The spectral properties of out-coming coherent electromagnetic radiation and the transfer of energy from electron beam to radiation and vice versa depends on the trajectory of electrons in an undulator [2-4]. Various simulation software like Genesis, EURA, SPECTRA are used for realization of FEL systems. SCILAB is an open-source numerical computation software [5] and tool boxes available with SCILAB, are used for model-based simulation of FEL systems [6-7].

The present work corresponds to develop model based SCILAB Xcos simulation model for numerical solutions of electron trajectory equations and radiation intensity equation in Harmonic undulator. The intensity at third and fifth harmonics of harmonic undulator radiation has been computed by varying the contributions of additional harmonic field component. In this analysis, the results are compared with the reported analytical results obtained from the method of generalized Bessel Functions. The present work will be helpful to find the intensity and small signal gain of harmonics in novel scheme by numerical method.

HARMONIC UNDULATOR FIELD AND TRAJECTOTRY

Harmonic undulator magnetic field considered for simulation is

$$\overrightarrow{B_H} = [0, B_y, 0] \quad (1)$$

Where, $B_y = A_0 B_0 \sin(k_u z) + A_1 B_0 \sin(k_h z)$

With $k_u = {}^{2\pi}/_{\lambda_u}$ and $k_h = {}^{2\pi}/_{\lambda_h}$ are wave number and harmonic wave number respectively, λ_u and $\lambda_h = h\lambda_u$ are undulator wave length and harmonic undulator wave length respectively. The value of h can be 3,5,7…. corresponding to odd harmonics. A_0 and A_1 are the amplitudes of main undulator field and additional harmonic field respectively and also the ratio of additional harmonic field to main undulator field is represented as 'Δ'.

The acceleration along 'x' and 'z' directions are deduced by using Lorentz force on electron [2-4]

$$\ddot{x} = \frac{eA_0B_o}{m_0\, c\gamma} v_z[\sin(\Omega_u t) + \Delta \sin(h\Omega_u t)] \quad (2)$$

$$\ddot{z} = -\frac{eA_0B_o}{m_0\, c\gamma} v_x[\sin(\Omega_u t) + \Delta \sin(h\Omega_u t)] \quad (3)$$

The velocity and trajectories of relativistic free electrons along 'x' and 'z' direction can be evaluated by integrating Eq. 2 and 3 and read as,

$$\beta_x = -\frac{K}{\gamma}\left[\cos(\Omega_u t) + \frac{\Delta}{h}\cos(h\Omega_u t)\right] \quad (4)$$

$$\beta_z = \beta_* - \frac{K^2}{4\gamma^2}cos(2\Omega_u t) - \frac{\Delta^2 K^2}{4h^2\gamma^2}\cos(2h\Omega_u t) - \frac{\Delta K^2}{2\gamma^2 h}\cos((1+h)\Omega_u t) - \frac{\Delta K^2}{2\gamma^2 h}\cos((1-h)\Omega_u t) \quad (5)$$

$$x = -\frac{K}{\gamma\Omega_u}\left[\sin(\Omega_u t) + \frac{\Delta}{h}\sin(h\Omega_u t)\right] \quad (6)$$

$$z = \beta_* t - \frac{K^2}{8\gamma^2\Omega_u}\sin(2\Omega_u t) - \frac{\Delta^2 K^2}{8h^3\gamma^2\Omega_u}\sin(2h\Omega_u t) - \frac{\Delta K^2}{2\gamma^2 h\Omega_u(1+h)}\sin((1+h)\Omega_u t) - \frac{\Delta K^2}{2\gamma^2 h\Omega_u(1-h)}\sin((1-h)\Omega_u t) \quad (7)$$

Where, $\Omega_u = k_u c$ is undulator frequency, $K = \frac{eA_0B_o}{m_0\, c\Omega_u}$ is undulator parameter and $\beta_* = 1 - \frac{1}{2\gamma^2}\left(1 + \frac{K^2 + K^2\frac{\Delta^2}{h^2}}{2}\right)$

Initial values of the velocity and trajectories are

$$x_{\,t=0} = 0\,, \quad z_{\,t=0} = 0$$

$$\beta_{x\,,t=0} = -\frac{K}{\gamma}\left(1 + \frac{\Delta}{h}\right) \text{ and}$$

$$\beta_{z\,,t=0} = \beta_* - \frac{K^2}{4\gamma^2} - \frac{\Delta^2 K^2}{4h^2\gamma^2} - \frac{\Delta K^2}{\gamma^2 h}$$

For numerical calculation of trajectories, with $z = \beta_* t$ Eq. 2 and 3 and rewritten as,

$$\ddot{x} = \frac{K}{\gamma}\Omega_u v_z[\sin(\Omega_u\, \beta_* t) + \Delta \sin(h\Omega_u\, \beta_* t)] \quad (8)$$

$$\ddot{z} = -\frac{K}{\gamma}\Omega_u v_x[\sin(\Omega_u\, \beta_* t) + \Delta \sin(h\Omega_u\, \beta_* t)] \quad (9)$$

The Intensity of radiation 'I' of electromagnetic radiation per unit solid angle '$d\Omega$' per unit frequency range '$d\omega$' of frequency 'ω' from accelerating electron of charge 'e' given by Lienard - Wiechart integral and read as [8],

ISBN: 978-3-95450-227-1 ISSN: 2673-5490 doi:10.18429/JACoW-IPAC2022-WEPOMS042

THE HOMEN MODEL: AN ESTIMATOR OF HIGH ORDER MODES EVOLUTION IN AN ENERGY RECOVERY LINAC

S. Samsam*[1], M. Rossetti Conti, A.R. Rossi, A. Bacci, V. Petrillo[2], M. Opromolla[2], M. Ruijter[1], D. Sertore, A. Bosotti, R. Paparella and L. Serafini, INFN - Sezione di Milano, Milano, Italy and LASA, Segrate (MI), Italy
A. Passarelli, M. R. Masullo, INFN - Sezione di Napoli, Napoli, Italy
[1]also at Università Sapienza, Roma, Italy
[2]also at Università degli Studi, Milano, Italy

Abstract

Energy recovery linacs represent the new frontier of energy sustainability in the field of particle accelerators while providing remarkable performance in terms of high average current and average brightness. Operating superconducting radio-frequency cavities in continuous wave make high repetition rates (GHz-class) affordable and allow the construction of light sources such as FEL or Compton based characterized by high flux. This study originates in the context of the design study of BriXSinO, an ERL based on the two-pass two-way scheme à la Maury Tigner in which the cavities are traveled by the beam in both directions, the first time in the accelerating phase and the second time in the decelerating phase. The code HOMEN was conceived as a model to simulate the evolution of high order modes on long time scales in high Q cavities of machines of this kind and monitor their effects on the beam.

INTRODUCTION

After 57 years of being discovered, Energy-recovery linacs (ERLs) became one of the most convenient technologies for electron accelerators, due to their ability to generate high-average current beams by operating in continuous wave (CW) mode with high brightness and small emittance at small cost [1–3]. The idea of the mechanism behind the ERL belongs to Maury Tigner. He had it while looking for an advanced way to boost the current in a collider for high energy physics at Cornell university [4].

ERL technology allows to recover more than 90% of the energy during the deceleration process. This energy will then be used as a power source for the next accelerated beam so that the electron bunch will be re-injected into the linac at the appropriate time and phase for deceleration. This mechanism avoids to dump a fully energetic beam, which is a huge loss of power in case of traditional linear accelerators.

Going back in history, ERL was first developed in order to drive high power Free electron laser (FEL) for providing high peak power and allowing an emission of coherent radiation from a high energy electron beam [5].

ERL's role now is expanded to cover more applications involving short pulse radiation sources, fixed target experiments, electron cooling instruments and many others.

The type of ERL studied in this paper is a two-pass two-way (TPTW) scheme based on SRF (Superconducting radio-frequency) technology able to drive an Inverse Compton Scattering and FEL sources. Another interesting point is that the machine is also conceived to be both a demonstrator of the double acceleration scheme based on TPTW of MariX and of the TPTW ERL of BriXS [6–13]. In this work we first introduce the theory of our model for evaluating the impact of High Order Modes (HOM) in long time-scale on beam dynamics, and the approaches behind our simulations. The second part describes in detail the stabilization of the fundamental mode in both accelerating and decelerating phases, followed by an example of the effects of HOM on the particle beam inside a multi-cell cavity.

HOMEN MODEL

The idea of HOMEN (High Order Mode evolution based on Energy budget) was born mainly to investigate the effect of HOMs on beam dynamics (BD) in a long-time scale generally in superconducting (SC) cavities and precisely in BriXSinO [14, 15]. Another relevant point of our model is the possibility to check the beam stability considering also the high repetition rate and high average current in the machine.

A set of coupled differential equations were developed to study neatly the propagation of an electron bunch inside the cavity. We represent the electric field on the cavity axis as a composition of normal orthogonal modes. Here, for our cavity model with an even number of gaps, it is convenient to write the time dependence of the longitudinal electric field equation using the sine in preference to the cosine:

$$E_n(z,t) = A_n(t)\ e_n(z)\ \sin(\omega_n t + \phi_{n,i}) \qquad (1)$$

where n and i are the RF mode and the bunch number respectively. We classically model the bunches as N point-like charges propagating along the cavity axis. A_n is the mode oscillation amplitude and e_n is the spatial field distribution calculated by POISSON/SUPERFISH code [16].

The system of coordinates is chosen to have the beam trajectory along the positive z cavity axis (beam axis). To evaluate the fields triggered off by the electron bunch while crossing the cavity, we compute the stored energy in each individual mode since all modes can be treated separately. Our model is based on energy budget. We considered the variation of the stored energy as the sum of the following power contributions:

* sanae.samsam@mi.infn.it

ISBN: 978-3-95450-227-1 ISSN: 2673-5490 doi:10.18429/JACoW-IPAC2022-WEPOMS043

UFO, A GPU CODE TAILORED TOWARD MBA LATTICE OPTIMIZATION

M. Carlà*, M. Canals, ALBA-CELLS, Barcelona, Spain

Abstract

The complexity of multi-bend achromatic optics is such that computational tools performance has become a dominant factor in the design process a last generation synchrotron light source. To relieve the problem a new code (UFO) tailored toward performance was developed to assist the design of the ALBA-II optics. Two main strategies contribute to the performance of UFO: the execution flow follows a data parallel paradigm, well suited for GPU execution; the use of a just-in-time compiler allows to simplify the computation whenever the lattice allows for it. At the core of UFO lies a parallel tracking routine structured for parallel simulation of optics which differs in some parameters, such as magnet strength or alignment, but retains the same element order, reflecting the scenario found in optimization processes, or when dealing with magnetic or alignment errors. Such an approach allows to take advantage of GPUs which yield the best performance when running thousands of parallel threads. Moreover UFO is not limited to tracking. A few modules that rely on the same tracking routine allow for the fast computation of dynamic and momentum aperture, closed orbit and linear optics.

INTRODUCTION

Single particle tracking is at the base of many optimization tasks frequently encountered during the development and tuning of lattices for light sources. Dynamic and momentum aperture optimizations are typical examples that can take advantage of a fast single particle tracking routine. Other use cases that can also benefits from a fast tracking routine are closed orbit and linear optics function computation, required respectively for orbit correction and optics matching. Traditionally these optimization tasks are carried out on large computer clusters by means of parallel optimization algorithms such as MOGA [1, 2]. However in recent time, some projects [3, 4] moved the computational burden to dedicated arithmetic processors (GPU), providing competitive performances at reduced costs. While these projects aims to provide a rather general purpose optics tool in an easy to use environment, it is possible to improve substantially the performances by tailoring the code specifically toward the optimization of electrons ring lattices, renouncing to some flexibility and ease of use by taking advantage of two main points:

- Radiation damping limits the number of turns required for stable aperture computation to around 1000 turns
- The optimization procedure (e.g. MOGA) requires to compute several variation of the same optics, that can be computed in parallel on a GPU

* mcarla@cells.es

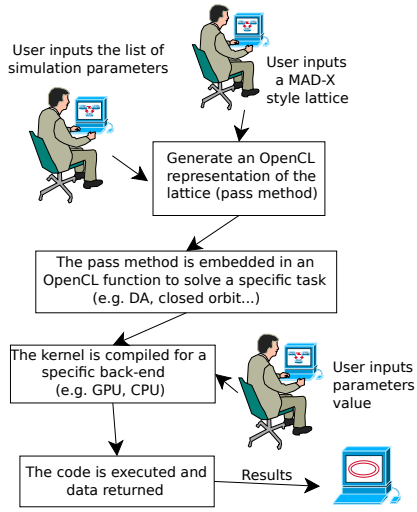

Figure 1: UFO working diagram.

Based on these assumption it was possible to develop an Utterly Fast 5D Optics code (UFO) [5] targeting electron rings optimization. The code was then characterized in terms of accuracy and performances by running simulations on a candidate multibend achromat lattice for ALBA2 [6] with alignment errors in each element.

EFFICIENT TRACKING ON GPU

The task of tracking thousands particles fits well the typical GPU architecture, where a single (or a small number) dispatch unit sends instructions to a group of computational units which therefore execute the same program in parallel. To ensure good performances code, no branching is allowed; otherwise different instruction flows would be required for each computational unit, a condition not allowed by the GPU architecture. In case of branching the different branches are executed sequentially resulting in performances penalties.

This requirement is easily met when tracking a bunch of particles through a lattice: every particle undergoes the same order of operation as any other, being the lattice identical for all of them. Also, when tracking particles through different variations of the same lattice, the condition is still met, as long as the order of the elements is maintained among the different lattice variations. The ability to simulate multiple lattices at the same time is of critical importance, in fact it would be difficult otherwise to keep a GPU with thousands of computational units under a high workload when dealing with a simulation of only 1000 particles for 1000 turns, as in the case of a typical electron dynamical aperture simulation.

Figure 1 shows the execution flow of UFO. The user is required to input a lattice (in a MAD style format) and a list of parameters (e.g. particle coordinates, magnet length, strength...). UFO generates an internal representation of

ISBN: 978-3-95450-227-1 ISSN: 2673-5490 doi:10.18429/JACoW-IPAC2022-WEPOMS045

MODELING AND MITIGATION OF LONG-RANGE WAKEFIELDS FOR ADVANCED LINEAR COLLIDERS*

F. Bosco[1†], M. Carillo[1], E. Chiadroni[2], L. Giuliano[1], A. Mostacci[1], L. Palumbo[1], M. Migliorati[1],
La Sapienza University of Rome, Rome, Italy
L. Faillace, A. Giribono, B. Spataro, C. Vaccarezza, INFN-LNF, Frascati, Italy
O. Camacho, A. Fukasawa, N. Majernik, J. Rosenzweig, UCLA, Los Angeles, California, USA
[1] also at INFN-Sez. Roma1, Rome, Italy
[2] also at INFN-LNF, Frascati, Italy

Abstract

The luminosity requirements of TeV-class linear colliders demand use of intense charged beams at high repetition rates. Such features imply multi-bunch operation with long current trains accelerated over the km length scale. Consequently, particle beams are exposed to the mutual parasitic interaction due to the long-range wakefields excited by the leading bunches in the accelerating structures. Such perturbations to the motion induce transverse oscillations of the bunches, potentially leading to instabilities such as transverse beam break-up. Here we present a dedicated tracking code that studies the effects of long-range transverse wakefield interaction among different bunches in linear accelerators. Being described by means of an efficient matrix formalism, such effects can be included while preserving short computational times. As a reference case, we use our code to investigate the performance of a state-of-the-art linear collider currently under design and, in addition, we discuss possible mitigation techniques based on frequency detuning and damping.

INTRODUCTION

Advanced experiments in the field of high energy particle physics rely on high luminosity electron/positron linear colliders working at the TeV scale. In the last decades, several conceptual facilities of such type have been investigated exploring techniques ranging from X-band (~ 12 GHz) rf-linacs to superconductivity and plasma acceleration [1–3]. A recent design proposed by SLAC [4] exploits advanced rf concepts to achieve high gradient performances relying on the mature and consolidated experience with C-band (5.712 GHz) technology [5, 6]. The design project, known as C^3 or the "Cool Copper Collider", allows to work with ~ 120 MeV/m accelerating gradients by means of state-of-the-art techniques such as distributed coupling [7] and cryogenic cooling of the accelerating structures [8, 9].

In all the above cases, the collective interaction among charged bunches constitutes a major concern since it can cause unstable motion due to *beam break-up* (BBU) effects [10, 11]. In particular, particles traveling off-axis in the accelerating structures excite parasitic dipole fields in the form of higher order modes (HOMs) supported by the structures themselves which deflect the trajectories of the trailing charges. In this paper we introduce a dedicated tracking code studying the long-range wakefield interaction caused by self-induced dipole modes in linacs and we exploit such a tool to investigate the C^3 machine. The code describes the bunches within the rf-pulse as a sequence of rigid macro-particles with no internal structure performing transverse oscillations in presence of an external focusing optics and acceleration. The combination of such fields in an alternating gradient FODO lattice with length L_c, average betatron function β_x and phase advance $\mu_x = L_c/\beta_x$ provides the following transfer map [12]

$$\begin{pmatrix} x \\ x' \end{pmatrix} \mapsto \sqrt{\frac{\gamma}{\gamma + \gamma' L_c}} \begin{pmatrix} \cos\mu_x & \beta_x \sin\mu_x \\ -\frac{1}{\beta_x}\sin\mu_x & \cos\mu_x \end{pmatrix} \begin{pmatrix} x \\ x' \end{pmatrix} \quad (1)$$

which is responsible for the adiabatic damping of the transverse oscillations and characterizes the motion in absence of collective effects.

THE PROCESS OF BEAM BREAK-UP

The interaction between two particles with time separation τ induced by a resonant mode with angular frequency ω_0, shunt impedance $R_\perp$ and quality factor Q is described by the dipole wake-function per unit length

$$w_\perp(\tau) = \frac{\omega_0 R_\perp}{Q} e^{-\alpha\tau} \sin(\omega_n \tau) \quad (2)$$

with $\omega_n = \omega_0\sqrt{1-(2Q)^{-2}}$ and $\alpha = \omega_0/2Q$ [13]. Deflected charges moving off-axis cause further excitation of the resonant mode intensifying the parasitic interaction. A quantitative analysis for such a process has been introduced by Mosnier [14] whose approach describes the bunch train as a sequence of point-like macro-particles accelerated inside a machine with uniform betatron function where the mutual interaction is due to a single dipole HOM which exhibits the same parameters in each cell of the linac. Such a model shows that the motion becomes highly unstable if the ratio of the HOM frequency and the bunch repetition rate is close to an integer so that the beam-mode interaction fulfills a resonant condition. Mitigation is possible by breaking the coherent interplay through a spread in frequency of the dipole modes [15, 16]. Indeed, it can be shown that frequency

* This work is supported by DARPA under Contract N.HR001120C0072, by DOE Contract DE-SC0009914 and DE-SC0020409, by the National Science Foundation Grant N.PHY-1549132 and by INFN through the project ARYA.
† fabio.bosco@uniroma1.it

ISBN: 978-3-95450-227-1 ISSN: 2673-5490 doi:10.18429/JACoW-IPAC2022-WEPOMS046

MACHINE LEARNING-BASED MODELING OF MUON BEAM IONIZATION COOLING

E. Fol*, D. Schulte, CERN, Geneva, Switzerland
C. Rogers, Rutherford Appleton Laboratory, Didcot, Oxfordshire, United Kingdom

Abstract

Surrogate modeling can lead to significant improvements of beam dynamics simulations in terms of computational time and resources. Application of supervised machine learning, using collected simulation data allows to build surrogate models which can estimate beam parameters evolution based on the provided cooling channel design. The created models help to understand the correlations between different lattice components and the importance of specific beam properties for the cooling performance. We present the application of surrogate modeling to enhance final muon cooling design studies, demonstrating the potential of such approach to be integrated into the design and optimization of other components of future colliders.

INTRODUCTION

In light of rising activities on the muon collider studies [1], the applied simulation tools, optimization of design parameters and overall software and data handling infrastructure gain more importance. Currently, one of the more active areas of the design study is the final cooling system. The reduction of the muon beam emittance is based on the concept of ionization cooling [2], where careful choice of the lattice and beam parameters is required. First results obtained from a prototype of an automatic optimization framework for the final cooling are presented in [3]. With the growing number of parameters and objectives to be considered in the design, the choice of initial simulation settings will become more challenging. Moreover, the required time and computational resources might become a bottleneck in optimization studies based on complex simulations. Applying supervised learning-based surrogate models promises a solution of both challenges. The results presented in this work first, demonstrate how optimization can be speeded up significantly by replacing tracking simulation with Machine Learning (ML) model prediction. Second, the application of inverted surrogate models is presented, allowing to obtain initial guess for optimization parameters, reducing the number of steps needed to reach an optimal solution.

Supervised Learning

Supervised learning methods allow to make predictions on unseen data, after learning a mapping function between input variables and output targets in the provided training samples. In this context, *supervision* is provided in the form of sets of data inputs with corresponding true output targets. While *learning* means adjusting parameters of the mapping function aiming to minimize the difference between prediction made by the model and true target values of the provided input-output pairs. The complexity of the mapping function depends on characteristics of the data and selected method, such that mapping between linearly related input and output variables can be built e.g. using linear regression models while for complex non-linear problems neural networks with various possible architectures are applied. Decision Trees, where each final node corresponds to a prediction of a single output target, are also widely used in supervised learning. Since decision trees are graphs, their predictions are easier to interpret than others such as deep neural networks. Combining several decision trees and making predictions by averaging the individual output helps to overcome the problem of over-fitting on training data and allows to make more reliable prediction on unseen data.

In this work, we apply the Random Forest algorithm [4], an ensemble method, where each tree in the ensemble is trained on different parts of the training data set. This is done in order to reduce the variance, usually causing a small increase of bias which is then mitigated by averaging the final prediction, allowing Random Forest to outperform a single decision tree.

MODELING BEAM DYNAMICS USING SUPERVISED LEARNING

Machine Learning concepts became a popular tool in various accelerator physics areas, ranging from operation and automatic control of machine parameters [5, 6] to beam instrumentation analysis to improve the quality of measurements data detecting anomalous signals [7]. While the advantages of unsupervised learning have been mostly demonstrated in online applications, supervised learning and in particular data-driven surrogate modeling is used also outside of operation, e.g. to model virtual diagnostics tools [8].

Also, solving optimization problems with the help of surrogate models brings the advantage of speeding up the optimization process by replacing measurements or slow-executable simulations with beam dynamics models. Such models can be built from measurements or simulations data to be used as training sets for supervised learning algorithms. The application of surrogate models for the optimization of existing accelerators and experiments planing has been demonstrated [9], however this approach did not find a wide application in the design of future facilities. Here we present the first results of improving the optimization of one of the most crucial components of the muon collider, the final cooling system with the help of supervised learning.

* elena.fol@cern.ch

ISBN: 978-3-95450-227-1 ISSN: 2673-5490 doi:10.18429/JACoW-IPAC2022-WEPOMS047

AUTOMATED DESIGN AND OPTIMIZATION OF THE FINAL COOLING FOR A MUON COLLIDER

E. Fol*, D. Schulte, CERN, Geneva , Switzerland
C. Rogers, Rutherford Appleton Laboratory, Didcot, Oxfordshire, United Kingdom
B. Stechauner, J. Schieck, Vienna University of Technology, Vienna, Austria

Abstract

The desired beam emittance for a Muon Collider is several orders of magnitude less than the one of the muon beams produced at the front-end target. Ionization cooling has been demonstrated as a suitable technique for the reduction of muon beam emittance. Final cooling, as one of the most critical stages of the muon collider complex, necessitates careful design and optimization in order to control the beam dynamics and ensure efficient emittance reduction. We present an optimization framework based on the ICOOL simulation code and application of different optimization algorithms, to automate the choice of optimal initial muon beam parameters and simultaneous tuning of numerous final cooling components.

INTRODUCTION

The proton-driven muon production leads to muon beams which initially occupy a large phase space. Cooling is required in order to reduce the beam emittance to satisfy the transverse and longitudinal acceptance requirements of the muon accelerator ring and to increase the luminosity of the collider, which is inversely proportional to the beam sizes [1]. An overview of the complete baseline design of the muon collider complex including different stages from proton injector to collider ring can be found in [2]. The 2.2 µs lifetime of muons makes ionization cooling [3, 4] the only possible technique to be applied to reduce the 6D emittance. In ionization cooling channels, muon beams are sent through absorber material placed at a focus. After losing energy through interaction with the absorber material, the beams pass through rf cavities which re-accelerate the particles.

In the past, extensive simulation studies have been conducted on the design of a final cooling system capable of achieving sufficiently small transverse emittance, at the cost of increasing the longitudinal emittance. The design presented in [5] aimed for transverse emittance reduction to 50 µm, while 55 µm have been achieved, increasing the longitudinal emittance from 1.5 to 70 mm at the end of the final cooling channel. However, latest studies show that transverse emittance below 25 µm is preferred [6]. Employing stronger solenoid fields and lower beam momenta will help to achieve lower emittances. This work focuses on the development of the infrastructure for design of the final stage of muon cooling, to improve the optimization process in terms of speed and usability of simulation tools.

* elena.fol@cern.ch

Simulation Tools for Ionization Cooling

Previous design studies of final cooling channel of a muon collider have been performed using either G4BEAMLINE code, which is based on GEANT4 libraries, or the simulation code ICOOL which has been developed specifically for 3-D tracking of particles in ionization cooling channels [7]. The cooling cells are defined as series of longitudinal regions with assigned configurations of different accelerating and magnet fields and material properties. The main advantage of these codes for the final cooling studies is that particle tracking takes into account decays and interactions of low energy muons in matter.

Motivation

Simple diagnostics such as calculation of emittances and optics functions are implemented in ICOOL, however the modification of text file-like input decks and evaluation of results imposes a big challenge to the users. Especially in a view of enlarging the muon collider study community, it is necessary to provide easily accessible, user-friendly software in order to reduce the effort of constructing and evaluating a large amount of simulation studies required to define an optimal design.

To achieve ideal matching between stages and various cooling channel configurations, a large parameter space needs to be explored. It is important to find an optimal trade-off between reduction of transverse emittance and longitudinal heating and transmission in order to provide beams with required properties to the next stages of muon collider complex. Apart from employing advanced optimization techniques, automation of the optimization and design is needed.

TOWARDS AUTOMATIC DESIGN

To improve the usability of the simulation framework for the final cooling, we extended it with an input handler and post-processing analysis both written in Python, which allows an easy integration of numerical optimization tools e.g. provided by the *scipy* library, but also the implementation of other advanced optimization techniques presented in the next section. The new components and their integration in the current version of optimization framework are presented in Fig. 1. The initial beam distribution and cooling channel properties are given in JSON format, which is well structured and can be easily modified manually or automatically during the optimization. The current value of a defined objective function is obtained by running ICOOL simulation

ISBN: 978-3-95450-227-1 ISSN: 2673-5490 doi:10.18429/JACoW-IPAC2022-WEPOMS048

A FLEXIBLE ONLINE OPTIMIZER FOR SPS *

T. Pulampong†, N. Suradet, Synchrotron Light Research Institute, Nakhonratchasima, Thailand

Abstract

Siam Photon Source (SPS) machine in Thailand has been operating for more than two decades with limited diagnostic systems. It is very challenging to efficiently tune and operate the machine. With online optimization, variables and objectives are required to tune for better solutions. It this work, a flexible optimizer was developed. Objectives and variables can be freely defined based on available hardware in the form of Process Variables (PVs). Several multi-objective and Robust Conjugated Direction Search (RCDS) algorithms are provided. The online optimizer was tested on the SPS machine to improved the injection efficiency. Due to its flexibility, the optimizer can also be used for other systems.

INTRODUCTION

Achieving the ultimate goals or objectives in a complex system is not simple. In practice, model based may not be sufficient due to higher order effects, non-linearities and noise. There are several subsystems in an accelerator. Parameters tuning requires immense experience and time. Sometimes the machine condition can also be affected by the environment which adds complexity to machine operation. In recent years, online optimization is gaining more popularity. This allows live parameters tuning to achieve the desired objectives. The usefulness of such optimization is obvious especially for a system with limited diagnostics like in SPS case. However setting up an optimization can be complicated. There are several factors that have to be taken into account: programming language, optimization algorithm, connection between the optimizer and hardware, etc.

An optimizer program, in this work, was developed to ease these difficulties. The optimizer acts as a box containing optimization tools and allows users to feed some inputs and acquire some output parameters and objectives.

OPTIMIZER

The optimizer was developed to provide flexibility and easy-to-use steps for users. Python, one of the most popular programming language providing several useful packages especially optimizer, was employed. Graphical User Interface (GUI) can also be created conveniently with Tkinter package. For hardware connection and control, Epics tools can be found in PyEpics package.

For an optimization, it starts from identifying the desired objectives and variables. Then the process follows the overall flow as shown in Fig. 1:

- A list of variables and objective functions should be prepared in text files in a form of process variable (PV). This allows easy connection between those parameters and the control. Upper and lower boundaries for the variables are also required to make effective and safe parameters tuning.
- An algorithm can be selected from the available list as shown in Fig. 2.
- Then the optimizer will check the input files and connection to the PVs. If there are some errors, user need to check the input files and PVs connection.
- If everything is ok, the optimization process will start and continue until the stopping criteria is met.
- The process stops when the stopping criteria is met. The maximum number of function evaluation can be set. Otherwise, the optimization can also be terminated by users any time because the data of the optimization is recorded during the process.

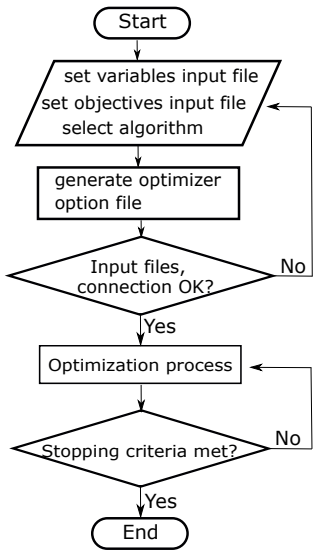

Figure 1: Overall program flow chart.

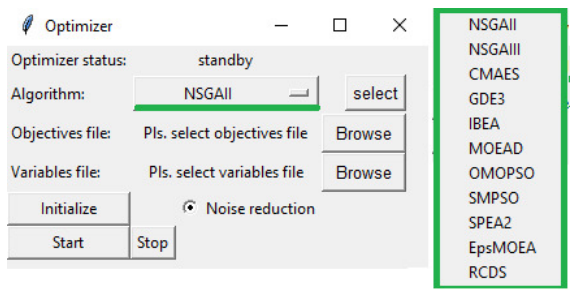

Figure 2: Optimizer user interface panel.

As shown in Fig. 2, the GUI was designed for user to set up an optimization in the described sequential steps from top to bottom. Browse buttons for objective and variable files selection are also provided. Moreover, to conveniently repeat the optimization, the optimizer will generate the required setting input files which can be executed again separately.

* Work supported by NSTDA
† thapakron@slri.or.th

ISBN: 978-3-95450-227-1 ISSN: 2673-5490 doi:10.18429/JACoW-IPAC2022-WEPOMS049

ESS RFQ ELECTROMAGNETIC SIMULATIONS USING CST STUDIO SUITE

E. Trachanas*, A. Bignami, N. Gazis, B. Jones, R. Zeng,
European Spallation Source, ESS-ERIC Lund, Sweden
P. Hamel, O. Piquet, CEA-IRFU, University Paris-Saclay, Gif-sur-Yvette, France
G. Fikioris, E. Gazis, A. Kladas, National Technical University of Athens, Athens, Greece

Abstract

The Radio Frequency Quadrupole (RFQ) of the European Spallation Source (ESS), operates at 352.21 MHz with an RF pulse length of 3.2 ms and repetition rate of 14 Hz. The RFQ focuses, bunches and accelerates the 62.5 mA proton beam from 75 keV up to 3.6 MeV. In an effort to study and compare the results from 3D electromagnetic codes, different models of the RFQ were simulated with CST Studio suite ®. This paper presents the selection of optimal parameters for simulation of the RFQ cavity voltage and comparison of the results with the RFQ design code Toutatis.

INTRODUCTION

The ESS RFQ was designed and manufactured by CEA-IRFU in France and installed at ESS site in 2019 [1]. Following a period of system installation and testing, RF power conditioning was successfully completed in summer 2021 and first proton beam injected in the RFQ in October of the same year. The cavity has a total length of 4.55 m divided in 5 segments (each $\sim 0.9m$ long) operating at the resonance frequency of 352.21 MHz. The vane type RFQ, achieves a voltage of 80 kV at the entrance and 120 kV at the high energy end. The RF power is delivered to the RFQ using two coaxial antenna couplers placed symmetrically 45 deg from the vertical axis equipped with ceramic windows that couple in total 1.1 MW of RF power during operation. In order to compensate for manufacturing errors that influence the resonant frequency of the cavity, 60 slug tuners are used and adjusted in fixed position during initial bead pull tuning of the cavity. Frequency detuning due to cavity thermal expansion (caused by RF power losses) is mitigated using water cooling circuits [2]. Main parameters of the ESS RFQ are presented in Table 1 whereas the 3D RFQ model with main interfaces is presented in Fig. 1.

3D electromagnetic (EM) simulation software possesses a prominent role in design and characterisation methodologies of a wide spectrum of accelerating cavities. Using designed and as-built models consists the most efficient way to investigate the impact of manufacturing and tuning errors on beam parameters incorporating simultaneously all EM effects [3-8]. Motivation for this study is the use of this approach in the frame of an integrated design methodology for RFQ design serving future ESS update projects. Towards that goal, benchmark of the cavity field results using different RFQ models, meshing techniques and electromagnetic solvers is considered essential.

* Emmanouil.Trachanas@ess.eu

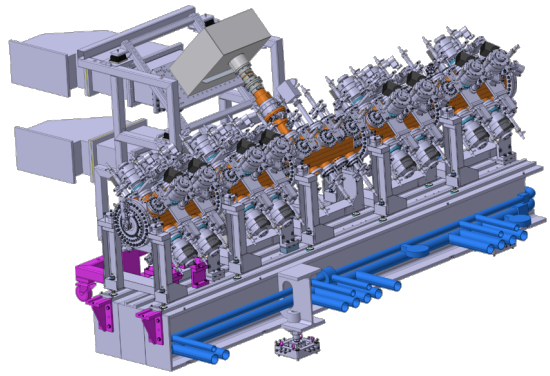

Figure 1: ESS Radio Frequency Quadrupole.

Table 1: ESS RFQ Main parameters

Requirement	Value
Operating Frequency	352.21 MHz
Vane-to-vane voltage	80-120 kV
Total Length	4.55 m
Input Energy	75 keV
Output Energy	3.6 MeV
RF Pulse Length	3.2 ms
Repetition Rate	14 Hz
Nominal RF power with beam	933 kW

ELECTROMAGNETIC SIMULATIONS

Simulations presented in the next sections have been performed with CST Studio suite®, a 3D EM analysis software package for designing, analyzing and optimizing electromagnetic components and systems [9]. For this analysis the in-built eigenmode solver was used. RFQ 3D models and geometries have been processed with CATIA® V6 CAD software to increase result accuracy, reduce computation time and respectively allocate memory footprint.

The goal of the simulations was the selection of the optimal parameters in an effort to reduce the error on resonant frequency calculation and increase resolution of the electric field distribution on the beam acceleration axis. Starting from the equation for obtaining the eigenvalues ω and eigenvectors $\vec{E}$:

$$\nabla \times \mu^{-1} \nabla \times \vec{E} = -j\omega^2 \left(\epsilon + \frac{\sigma}{j\omega}\right)\vec{E} \quad (1)$$

ISBN: 978-3-95450-227-1 ISSN: 2673-5490 doi:10.18429/JACoW-IPAC2022-WEPOMS051

SPIN MATCHING FOR THE EIC'S ELECTRONS*

M. G. Signorelli[1†], G. H. Hoffstaetter[1,2], J. Kewisch[2], J. A. Crittenden[1]
[1] Cornell University, Ithaca, NY, USA
[2] Brookhaven National Laboratory, Upton, NY, USA

Abstract

The Electron-Ion Collider (EIC) at Brookhaven National Laboratory will provide spin-polarized collisions of electron and protons or light ion beams. In order to maximize the electron polarization and require less frequent beam reinjections to restore the polarization level, the stochastic depolarizing effects of synchrotron radiation must be minimized via spin matching. In this study, Bmad was used to perform first order spin matching in the Electron Storage Ring (ESR) of the EIC. Spin matches were obtained for the rotator systems and for a vertical chicane, inserted as a vertical emittance creator. Monte Carlo spin tracking with radiation was then performed to analyze the effects of the spin matching on the polarization.

INTRODUCTION

The Electron-Ion Collider (EIC) at Brookhaven National Laboratory will explore a new frontier in nuclear physics experiments by allowing for spin-polarized collisions of electrons and light ions. The electron beam will be stored in a new ring, the electron storage ring (ESR) of the EIC; this lattice must be designed to give maximum longitudinal polarization at the interaction points (IPs) for various electron beam energies between 5-18 GeV. The Thomas-BMT equation, shown in Eq. (1), defines the spin dynamics of a charged particle moving relativistically through laboratory-frame magnetic fields, where $\vec{S}$ is a 3-vector of the spin expectation values in each direction [1–3].

$$\frac{d\vec{S}}{dt} = -\frac{q}{\gamma m}\left[(1+a\gamma)\vec{B}_{\perp} + (1+a)\vec{B}_{\parallel}\right] \times \vec{S} \tag{1}$$

The dynamics of this equation may be linearized in small phase space variables around the closed orbit, so that transfer through a lattice element is simply a multiplication of the original spin vector by some rotation matrix $R(\theta;\theta_0,\vec{z}_0)$ where θ_0 and θ are the initial and final azimuthal angles around the ring respectively and $\vec{z}_0$ is the initial 6-dimensional phase space coordinate. Thus, if on the closed orbit $\vec{z}_{\text{c.o.}}$, the periodic spin direction can be defined in Eq. (2) [4, 5].

$$\hat{n}_0 = R(\theta_0 + 2\pi;\theta_0,\vec{z}_{\text{c.o.}})\hat{n}_0 \tag{2}$$

The primary task in designing any polarized storage ring is ordering lattice elements so that $\hat{n}_0$ is rotated to point in the desired direction at each position, while also accounting for spin resonances. However, when designing a lepton ring, the stochastic emission of synchrotron radiation has several significant effects on polarization that must be accounted for; firstly, derivable from the Dirac equation, the Sokolov-Ternov effect is an asymmetrical spin flip of electrons during photon emission, with higher probability of flipping antiparallel to the magnetic field [6]. This phenomenon can be taken advantage of to improve the polarization in a ring, as over time most of the spins will align antiparallel to the vertical field. The second and not as convenient effect is that of spin diffusion; when an electron emits a photon in a dipole, it experiences a sudden quantum reduction in energy. This instantaneously changes the equilibrium orbit of the particle, thus exciting synchrobetatron oscillations around this new orbit. Because the spin precession is coupled with orbit motion, there is a diffusion of the spin from the stable spin direction. Finally, when there is photon emission without a spin flip, there will be an instantaneous increase in alignment of the spin with $\hat{n}_0$ - "kinetic polarization" [7].

Baier, Katkov, and Strakhovenko (BKS) derived expressions for the asymptotic polarization and build up time in a storage ring caused by the Sokolov-Ternov effect, and their work was then extended by Derbenev and Kondratenko (DK) to include spin diffusion and kinetic polarization [8–10]. Equation (3) gives the polarization time evolution from initial polarization P_0 to asymptotic P_{dk}, and Eq. (4) gives the time constant in terms of the polarization buildup and depolarization rates [11].

$$P(t) = P_{\text{dk}}\left(1 - e^{-t/\tau_{\text{dk}}}\right) + P_0 e^{-t/\tau_{\text{dk}}} \tag{3}$$

$$\tau_{\text{dk}}^{-1} = \tau_{\text{pol}}^{-1} + \tau_{\text{dep}}^{-1} \tag{4}$$

While the analytical forms exist, it is difficult to actually calculate accurate results for P_{dk} and τ_{dk}^{-1}. Thus, τ_{dep}^{-1} is best obtained by Monte Carlo spin tracking without spin-flip effects [12]. Analytically calculating P_{bks} and $\tau_{\text{pol}}^{-1} \approx \tau_{\text{bks}}^{-1}$, P_{dk} may then be sufficiently approximated with Eq. (5).

$$P_{\text{dk}} \approx P_{\text{bks}}\frac{\tau_{\text{bks}}^{-1}}{\tau_{\text{bks}}^{-1} + \tau_{\text{dep}}^{-1}} \tag{5}$$

Spin-orbit coupling, and dependence on energy, may be shown via a perturbative approach of the momentum deviation in the Thomas-BMT equation. To first order, the Thomas-BMT equation can be expressed as Eq. (6) in terms of the closed orbit spin precession $\vec{\Omega}_{\text{c.o.}}$ and the phase space dependent perturbative precession $\vec{\omega}$, where s is the longitudinal position, $\delta = \Delta p/p_0$, and K_y, K_1, $\tilde{K}_1$, and K_s are the normalized dipole, quadrupole, skew quadrupole, and

* This work was supported by the U.S. Department of Energy, Office of Science, Office of Workforce Development for Teachers and Scientists under the Science Undergraduate Laboratory Internships Program, and by Brookhaven Science Associates, LLC under Contract Nos. DE-SC0012704 and DE-SC0018370 with the U.S. Department of Energy.
† mgs255@cornell.edu

ISBN: 978-3-95450-227-1 ISSN: 2673-5490 doi:10.18429/JACoW-IPAC2022-WEPOMS052

IMPACTS OF AN ATS LATTICE ON EIC DYNAMIC APERTURE

J. Unger, G. H. Hoffstaetter, J. A. Crittenden CLASSE, Cornell University, Ithaca, 14850 NY, USA
D. Marx, Brookhaven National Laboratory, Upton 11973, NY

Abstract

The Electron-Ion Collider (EIC) project at Brookhaven National Laboratory has explored strategies for increasing the energy aperture of the Electron Storage Ring (ESR) to meet the goal of 1% for the 90 degree lattice at 18 GeV. Current strategies use a four sextupole family per arc correction scheme to increase the energy aperture and to keep the transverse aperture sufficiently large as well. A scheme called Achromatic Telescopic Squeezing (ATS), first introduced for the Large Hadron Collider, introduces a beta-beat into select arcs, allowing dynamic aperture optimizations with different sextupole strengths. The ATS scheme's mix of some higher beta-function and some lower sextupole strengths in the arcs has the potential to increase the energy aperture. Basic chromatic corrections and numeric optimizations were used to compare the ATS optics to a non-ATS scheme. In all cases, the ATS scheme performed similarly or better than the more common schemes. However, this increase in energy aperture from the ATS optics also has negative effects, such as an increase in emittance which poses complications for the current ESR design.

INTRODUCTION

The Conceptual Design Report (CDR) [1] for the Electron-Ion Collider (EIC) sets goals for the Dynamic Aperture (DA) of the ESR. For all configurations of the Electron Storage Ring (ESR), the on energy aperture requirements have been met. The energy aperture requirement of $\delta = 1\%$ has recently been met for the two Interaction Point (IP) configuration at 18GeV for the version 5.5 lattice, which operates with 90°cells in the arcs [2]. The previous version, 5.3, never achieved the energy aperture goal, which led to the exploration of alternative strategies. Under the current strategy, with phase trombones being used to set phases, a maximum of $\delta = 0.07\%$ was achieved. The optimization schemes being used largely consisted of four sextupole families per arc and adjustable phases going into each arc with a fixed overall tune. In simulations without synchrotron oscillations, the energy aperture could achieve the goal with little difficulty. The mechanism creating the difficulty in energy aperture optimization with synchrotron scillations have not yet been fully analyzed, however changes in the 5.5 lattice, including somewhat relaxed beta functions in the IP, improved this issue.

On the path from version 5.3 to 5.5 of the ESR, several strategies to optimize the DA were pursued. One of these was the Achromatic Telescopic Squeezing (ATS) scheme [3] presented here. The ATS scheme has promising features for optimizing the energy aperture of the ESR, however this was not the main objective of this scheme when it was conceived for the LHC. It's potential for the ESR therefore had to be evaluated in detail.

ATS SCHEME

The ATS scheme was first introduced at the LHC in order to fully utilize the existing large aperture in the arcs for luminosity optimization. Because the arc has to accommodate a lower energy beam at injection, it's aperture at high energy is unnecessarily large. The ATS scheme induces a β-beat in the arcs neighboring the IR which uses this available aperture, and this beta beat can reduce the cross section at the IP without strengthening the final focus quadrupoles. The ratio of the new peak β in the arc to the original one is called the telescopic ratio, which can be optimized for the lattice. A result of this, in a 90°lattice with four sextupole families, is that two of the families will be strengthened by an increase in β-function and two will be weakened by a decrease in β-function (which will be called the Strong and Weak families) [3]. This gives a different sextupole solution for the correction of chromaticities and chromatic beta beats. The different chromatic correction, although not the primary reason for the development of the ATS scheme in LHC, has possible advantages in DA optimization that can be beneficial to the EIC.

The possible advantages of the ATS scheme can be explained by looking at resonance driving terms that sextupoles excite. All terms that are first order in the sextupole strengths K scale as $K\beta^{3/2}$. In a simple estimate of the ATS scheme, these terms tend to decrease. As β_S, the β-function at the strong sextupole increases, their strength K_S proportionally decreases so that the chromaticities remains corrected, which go with $K\beta$.

If $\Delta\beta$ is the beta beat, then the increase in the driving term at the strong sextupole is proportional to $\sqrt{\beta + \Delta\beta}$ while it is proportional to $\sqrt{\beta - \Delta\beta}$ at the weak sextupoles. The average of these driving terms decreases with the beta beat, as it evaluates to $\sqrt{\beta}(1 - \frac{1}{4}(\Delta\beta/\beta)^2)$ in a second order expansion.

At second order, there are favourable and unfavourable terms, with some second order terms that could be greatly reduced if the weak sextupoles were turned off (This is true whether or not the ATS optics are used) [4]. This brings up the topic of interleaved versus non-interleaved sextupole schemes. The arcs in the ATS scheme are not fully non-interleaved if the weak sextupoles turned off, as the strong families will still be interleaved, this setup will be referred to as a partially interleaved sextupole scheme. The ATS scheme also has the benefit of reducing the effects of the remaining interleaved families due to the β-function being increased at only one family per plane. The usefulness of a partially interleaved system without the added benefit from the ATS optics was also tested, but yielded poor results.

ISBN: 978-3-95450-227-1 ISSN: 2673-5490 doi:10.18429/JACoW-IPAC2022-WEPOMS053

USING TAYLOR MAPS WITH SYNCHROTRON RADIATION EFFECTS INCLUDED

P. Nishikawa*, KEK, Tsukuba, Japan
D. Sagan, G. H. Hoffstaetter†, Cornell University, Ithaca, NY, USA

Abstract

Routinely, particle tracking in accelerators is done either by tracking element-by-element which is slow, or by using a transfer map that does not take into account radiation effects. Here we present a method for using Taylor maps that have radiation effects included. The mapping is divided into a radioactive part and a symplectic part. The radiative part produces the correct second order stochastic correlations between all phase-space dimensions. And the symplectic part is handled by partial map inversion, which eliminates non-symplectic effects due to the finite truncation of the Taylor series. This enables tracking simulations to use maps of lower order than what would otherwise be necessary leading to a speedup of the simulation.

INTRODUCTION

Particle tracking is an important and widely used simulation tool since it is the only technique that can accurately and reliably probe the nonlinear effects that can develop in particle beams over many turns [1].

Particle tracking generally is done either element-by-element or using maps which transport particles over many lattice elements. The element-by-element tracking is most reliable but slow, especially for large machines with sometimes tens of thousands of elements. Map tracking, which uses a set of truncated Taylor series expansions to represent large sections of the accelerator, can be orders of magnitude faster. However, such maps can introduce errors from truncating the power series, which are usually non-symplectic, and which disturb tracking especially at large amplitudes. Furthermore, such maps have historically not included radiation effects, which are often essential, especially in electron rings.

To partly remedy this, a map can be constructed which includes radiation effects. Denoting the orbital phase space coordinates with respect to some reference coordinates (generally the closed orbit) by ζ the map is written:

$$\vec{\zeta}^{\,f} = \vec{Z}\left(\vec{\zeta}^{\,i}\right) + S\,\vec{\xi} \tag{1}$$

Superscript i indicates initial coordinates at the beginning of the map, superscript f indicates final coordinates at the end of the map, and Z is a truncated Taylor series transport map at some order n_0 with radiation damping (the deterministic part of the radiation effect) included. It will be assumed that $\vec{Z}$ has no constant part: $\vec{Z}(\vec{0}) = \vec{0}$. In the above equation, $\vec{S}$ is a 6×6 matrix which represents the fluctuation (stochastic) radiation effect and $\vec{\xi}$ is a vector of six independent Gaussian distributed random numbers with unit sigma and zero mean. Here higher order terms in the stochastic fluctuations have been ignored.

Construction of maps of the form Eq. (1) have been implemented in the software package FPP/PTC [2, 3] and this code has been interfaced to the accelerator simulation code Bmad [4]. In this paper will be discussed how to avoid non-symplectic effects by partial map inversion.

For a truncated Taylor map, if $n_0 > 1$, by virtue of missing terms higher than n_0 in the expansion, there will be non-symplectic behavior that is more severe at larger amplitudes. One way to avoid this is to calculate $\vec{Z}$ at a large enough n_o so that the non-symplectic behavior at the maximum amplitude of tracked particles is not significant. This has the disadvantage in that it increases computation time, both in computing the map initially and during tracking when the map must be repeatedly evaluated. Another possibility is to add terms to $\vec{Z}$ of order higher than n_0 to counteract the non-symplectic effects. Unfortunately, adding terms may lead to nonphysical behavior. For example, if stochastic radiation effects are included in the simulation, one of the authors (P. Nishikawa) has observed vertical beam blow up due to slight nonphysical non-linear anti-damping.

Presented in this paper is a third way to remove non-symplectic behavior. This involves "symplectifying the map". This is done by first working on the jets via "symplectic restoration" and then tracking is done via "symplectification" using a generating function on the nonlinear symplectic part of the map.

SYMPLECTIC RESTORATION

Symplectic restoration involves a rewriting of the jet $\vec{Z}$ as a concatenation of 4 jets, dropping the cumbersome vector arrows:

$$Z = L_r \circ N_r \circ L_s \circ N_s \tag{2}$$

L_r is a linear map near the identity which is nonsymplectic since it contains the effects of the radiation, N_r is a purely nonlinear jet which contains effects of the radiation, L_s is a linear symplectic map, and lastly N_s is a purely nonlinear symplectic jet, the linear part of which is the identity.

In the absence of radiation, the map Z is simply the symplectic map $L_s \circ N_s$. To get this factorization, we first extract the linear part of Z denoted Z_1. This map is almost symplectic since it is assumed that the radiation effect is small. A contraction mapping due to Furman (see [5], p. 5351, denoted S_1) is used to produce a symplectic map near Z_1:

$$L_s = \lim_{k\to\infty} \underbrace{S_1\left(\,S_1\left(\,S_1\left(\cdots Z_1 \cdots\right)\right)\right)}_{k\ times} = S_1^k\left(Z_1\right) \tag{3}$$

* patrice.nishikawa@kek.jp
† Work supported in part by Department of Energy grant DE-SC0018370.

ISBN: 978-3-95450-227-1 ISSN: 2673-5490 doi:10.18429/JACoW-IPAC2022-WEPOMS055

CATHODE SPACE CHARGE IN Bmad*

N. Wang†, J. Crittenden, G. H. Hoffstaetter, D. Sagan
Cornell University (CLASSE), Ithaca, NY, USA
C. Gulliford, Xelera Research LLC, Ithaca, NY, USA
C. Mayes, SLAC National Accelerator Laboratory, Menlo Park, CA, USA

Abstract

We present an implementation of charged particle tracking with the cathode space charge effect included which is now openly available in the Bmad toolkit for charged particle simulations. Adaptive step size control is incorporated to improve the computational efficiency. We demonstrate its capability with a simulation of a DC gun and compare it with the well-established space charge code Impact-T.

INTRODUCTION

Space charge (SC) describes the interaction of electric charges in a charged particle bunch. It is an important effect especially in high brightness charged particle beams and especially when a beam has low-energy. The evolution of beam is complex when space charge and external fields are combined. Generally, numerical calculation methods are needed to incorporate space charge into particle simulations and this has been done with a number of programs including Impact-T [1], OPAL [2], GPT [3], ASTRA [4], etc. [5] Space charge methods have been incorporated in the Bmad toolkit for charged particle simulations [6, 7] but up to now the effect of space charge fields from a cathode have not been included.

When electrons are emitted from a cathode, image charges are formed inside the conductor. The space charge effect between bunch charges and image charges will modify the space charge field and this can be important close to the cathode especially with simulations of high brightness beams. Here, we report on the implementation of cathode space charge in the Bmad toolkit, describe the algorithm, and validate it by benchmarking with another well-established space charge code Impact-T [1].

CATHODE SPACE CHARGE EFFECT

The Bmad toolkit uses a stand-alone package called "Open Space Charge" (OpenSC) to calculate space charge fields from a bunch distribution [8]. OpenSC is an open-source software library developed by Robert Ryne and Christopher Mayes. OpenSC deposits charged particles on a 3D rectangular grid, calculates the space charge fields on this grid, and interpolates the field at any arbitrary point within its domain. The space charge fields are calculated in the local rest frame using integrated Green functions (IGFs), as described in [1], with fast Fourier transforms (FFT). Cathode image fields can be enabled in the code.

* This project was supported by Brookhaven Science Associates, LLC under Contract No. DE-SC0012704 with the U.S. Department of Energy.
† nw285@cornell.edu

Figure 1 illustrates the space charge field of a Gaussian bunch near the cathode at $z = 0$ using OpenSC. The cathode field is modeled as the space charge field from an equal and opposite image charge distribution inside the cathode. It attracts the bunch towards the cathode and modifies the overall field profile. This effect decays as the bunch moves away from the surface.

Bmad CATHODE SPACE CHARGE TRACKING

Cathode space charge tracking was implemented within Bmad by tracking a beam in a number time steps. At the beginning of a time step, the space charge field is calculated in the local rest frame using OpenSC. Particles are then tracked through the time step with a fourth-order Runge-Kutta time based integrator. Thus the space charge is applied smoothly during the time step.

Since the cathode space charge is most significant during emission from the cathode, an emission model was implemented with particles being "born" from the cathode over some time period. During a simulation, particles not yet emitted from the cathode do not contribute to the space charge calculation. Calculating the initial particle distribution is not part of Bmad but Bmad can read in appropriate data files generated externally. For this study, the initial particle distribution was generated by the code distgen [9].

ADAPTIVE STEP SIZE CONTROL

To improve the efficiency of the simulation, we implemented adaptive step size control. The algorithm tracks the bunch by a full step and two half steps and evaluates the difference. The error is the average difference between the two final bunches,

$$error = \frac{1}{N} \sum_{\text{particles}} |x_{\text{full}} - x_{\text{two halves}}|. \quad (1)$$

The scale of motion combines the bunch size and centroid position, and is defined as

$$scale = \sqrt{\frac{1}{N} \sum_{\text{particles}} x^2}. \quad (2)$$

The tolerance is controlled by two parameters, *rel_tol* and *abs_tol*

$$tol = rel\_tol * scale + abs\_tol \quad (3)$$

If $error < tol$ the step is accepted and the time period of the next time step duration will be 5 times the current step

ISBN: 978-3-95450-227-1 ISSN: 2673-5490 doi:10.18429/JACoW-IPAC2022-WEPOMS056

SPIN MATCHING AND MONTE-CARLO SIMULATION OF RADIATIVE SPIN DEPOLARIZATION IN e$^+$-e$^-$ STORAGE RINGS WITH BMAD*

O. Beznosov†, Los Alamos National Laboratory, Los Alamos, USA
J. A. Ellison, K. Heinemann, University of New Mexico, Albuquerque, USA
J. A. Crittenden, G. Hoffstaetter, D. Sagan, Cornell University (CLASSE), Ithaca, USA
D. P. Barber[1], DESY, Hamburg, Germany
[1] also University of New Mexico, Albuquerque, USA

Abstract

The *Bmad/Tao* software toolkit has been extended to estimate the rate of radiative spin depolarization in e^+-e^- storage rings. First estimates are made using the SLIM algorithm of linearized spin-orbit (s-o) motion. The extension implements the effects on s-o motion of stochastic photon emission using a Monte-Carlo tracking algorithm. Spins are tracked in 3-D along particle trajectories with the aid of Taylor expansions of quaternions provided by the Polymorphic Tracking Code (PTC). The efficiency of long-term tracking is guaranteed by the use of a sectioning technique that was exploited in previous-generation software (e.g. SLICKTRACK, SITROS). Sectioning is the construction of the deterministic s-o maps for sections between the dipoles during the initialization phase. Maps can be reused during the tracking. In a simulation for a realistic storage ring, the computational cost of initial map construction is amortized by the multi-turn tracking computational cost. The 1st-order terms in the quaternion expansions are used to construct the s-o coupling matrices in the matrices of the SLIM algorithm. These matrices are then available for an extension of the optimization facilities in *Bmad* to minimize depolarizing effects by spin matching.

INTRODUCTION

Relativistic electrons and positrons in storage rings emit synchrotron radiation and that can lead to a build up of spin polarization by the Sokolov-Ternov effect. At the same time noise is injected into the particle trajectories by the stochastic element of photon emission. The stochastic orbital variation couples via the T-BMT equation with the spin motion causing depolarization. The attainable equilibrium polarization results from the balance between the two effects. The rate of depolarization increases with beam energy much faster than the rate of polarization. Moreover the depolarization is enhanced near depolarizing resonances occurring when the closed-orbit spin tune ν_0 is close to an integer linear combination of the orbital tunes. See [1, 2] for details of these matters.

However it is highly desirable to have polarized beams at future high-energy rings like the proposed FCC-ee [3] and the CEPC [4, 5] as well as at the EIC [6] to extend the potential of the particle physics program as well as to provide a means of precise beam-energy calibration via resonant depolarization using radio-frequency transverse magnetic fields. Thus estimates of the attainable polarization are essential for guiding the design of a ring.

The attainable polarization can be estimated using perturbation theories to evaluate the terms in the Derbenev-Kondratenko (DK) formula [1, 2]. But the resulting formulas, describing the resonances, can be very complicated and the perturbation series might not converge. Moreover, at very high energy the so-called "uncorrelated resonance crossing" [7], whose effect is difficult to estimate with certainty, might dominate over the predictions of the DK formula. Thus it is better to rely on Monte-Carlo tracking simulations of the effects on spins of the magnetic and electric fields and of the stochastic photon emissions. An ideal modern framework for this is the *Bmad/Tao* software toolkit [8]. *Bmad/Tao* can handle nonlinear orbital motion, beam-beam forces and numerous phenomena in storage rings that go beyond standard spin-orbit tracking. Nevertheless, it always makes sense to begin with first-order perturbative analytical (SLIM) calculations to get a first impression of the situation. The SLIM formalism also provides structures for so-called spin matching, namely the method for minimizing depolarization at first order. This paper describes recent developments of *Bmad/Tao* spin simulation capabilities along with benchmarking with SLICKTRACK [1, 2].

RECENT DEVELOPMENTS IN BMAD/TAO SIMULATION TOOLKIT

Bmad/Tao has been extended to handle:

- Via the SLIM formalism [1, 2, 9] of linearized orbital and spin transport in terms of the 8×8 matrices which then can be analyzed using standard linear algebra techniques to deliver a first-order estimate of the rate of depolarization.
- Spin-orbit Monte-Carlo tracking with full 3-D spin motion implemented in a multi-turn/long-term tracking program which can employ many spin-orbit tracking backends: PTC [10], Bmad, One-turn Map, Multi-map with sectioning.
- Spin resonance strength calculations with energy scans implemented in a Python/PyTao script.

* Work supported by by the U.S. Department of Energy, Office of Science, Office of High Energy Physics, under Award Numbers DE-SC0018008 and DE-SC0018370
† obeznosov@lanl.gov

ISBN: 978-3-95450-227-1 ISSN: 2673-5490 doi:10.18429/JACoW-IPAC2022-WEPOMS057

SIMULATION STUDIES AND MACHINE LEARNING APPLICATIONS AT THE COHERENT ELECTRON COOLING EXPERIMENT AT RHIC*

W. Lin[1,†], M. A. Sampson[1], Y.C. Jing[2], K. Shih[3], G. H. Hoffstaetter[1,2], J. A. Crittenden[1]
[1]CLASSE, Cornell University, Ithaca, New York, USA
[2]Collider-Accelerator Department, Brookhaven National Laboratory, Upton, New York, USA
[3]Physics Department, Stony Brook University, New York, USA

Abstract

Coherent electron cooling is a novel cooling technique which cools high-energy hadron beams rapidly by amplifying the modulation induced by hadrons in electron bunches. The Coherent electron cooling (CeC) experiment at Brookhaven National Laboratory (BNL) is a proof-of-principle test facility to demonstrate this technique. To achieve efficient cooling performance, electron beams generated in the CeC need to meet strict quality standards. In this work, we first present sensitivity studies of the low energy beam transport (LEBT) section, in preparation for building a surrogate model of the LEBT line in the future. We also present preliminary test results of a machine learning (ML) algorithm developed to improve the efficiency of slice-emittance measurements in the CeC diagnostic line.

INTRODUCTION

The layout of the current CeC system is shown in Fig. 1. The electrons are generated from the superconducting radio frequency (SRF) gun with 1.5 nC of charge per bunch, and then bunched with a normal conducting RF cavity. The electron bunches are compressed ballistically in a long drift and accelerated to 14.5 MeV at the end of the low energy beam transport (LEBT) section [1]. To perform cooling, the accelerated electron beam travels through the dog-leg to interact with ions in the common section with RHIC. To evaluate electron beam quality, the transverse deflecting cavity (TDC) in the diagnostic line converts the electron beam's longitudinal distribution into a transverse distribution, which is measurable via YAG screens.

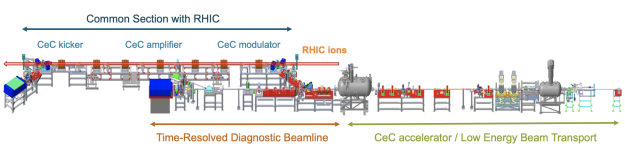

Figure 1: Current CeC system layout at BNL. Electron beams travel from right to left.

Electron beams need to meet strict requirements in the CeC accelerator and in the LEBT section to achieve efficient cooling performance in the common section with RHIC. Therefore, understanding how electron beam profiles are controlled and measured in the CeC system is crucial.

* Work supported by the U.S. National Science Foundation under Award PHY-1549132, and by Brookhaven Science Associates, LLC under Contract No. DEAC0298-CH10886 with the U.S. Department of Energy.
† wl674@cornell.edu

SENSITIVITY STUDIES OF LOW ENERGY BEAM TRANSPORT

A start to end (S2E) simulation of the low energy beam transport (LEBT) section was established using the beam dynamics code IMPACT-T [2]. There are three RF cavity systems (112 MHz SRF gun, 500 MHz buncher, and 704 MHz 5-cell SRF linac) and 6 solenoids (1 gun solenoid, 5 LEBT solenoids) in the LEBT beam line. The IMPACT-T simulation uses all components to optimize the electron beam profile at the end of the LEBT section, aiming for high peak current and low slice emittance for the core of the beam. The optimization results are summarized in [3].

To obtain core emittance measurements, the final electron beam from the IMPACT-T simulation is sliced longitudinally from the center by a Python script, and grouped into 20%, 50%, 80%, and 100% of the total particles. The script then calculates the normalized emittance for each group, and the emittance and current for each longitudinal slice, and plots all the results in an image. One sample image from the Python script is presented in Fig. 2.

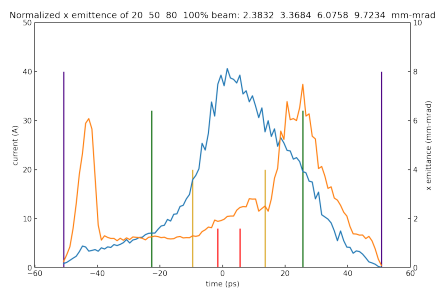

Figure 2: Slice current (blue) and slice emittance (orange) results for the electron beam at the end of the LEBT section. The emittances for the central 20% (red), 50% (yellow), 80% (green), and 100% (purple).

The end goal of the studies was to identify which control parameters are important to the beam behavior, so that they can be included in a neural network surrogate model for the LEBT section.

Table 1 lists the parameters considered in this project, and the value ranges within which they were changed. The SRF gun, gun solenoid, and the buncher are not included because the initial beam distribution used to run the studies in IMPACT-T already included effects from known displacement errors from the gun to the buncher.

In this work, sensitivity is defined as the effect a control parameter has on the core emittance of the electron beam,

ISBN: 978-3-95450-227-1 ISSN: 2673-5490 doi:10.18429/JACoW-IPAC2022-THOXGD1

ELENA - FROM COMMISSIONING TO OPERATION

L. Ponce*, L. Bojtar, C. Carli, B. Dupuy, Y. Dutheil, F. Freyermuth, D. Gamba, L. Joergensen, B. Lefort, S. Pasinelli, CERN, Geneva, Switzerland

Abstract

In 2021 the Extra Low ENergy Antiproton ring (ELENA) moved from commissioning into the physics production phase providing 100 keV antiprotons to the newly connected experiments paving the way to an improved trapping efficiency by one to two orders of magnitude compared to the AD era. After recalling the major work undertaken during the CERN Long Shutdown 2 (2019-2020) in the antiproton deceleration complex, details will be given on the ELENA ring and new electrostatic transfer line beam commissioning using an ion source. Subsequently, the progress from commissioning with ions to operation with antiprotons will be described with emphasis on the achieved beam performance.

INTRODUCTION

The Extra Low ENergy Antiproton ring (ELENA) is the new baby of the CERN Antimatter Factory complex. The small 30.4 m circumference synchrotron is complementing the 20 years old Antiproton Decelerator (AD) to further decelerate the antiprotons from 5.3 MeV kinetic energy down to 100 keV. The lower energy will allow for increased antiproton trapping efficiency in the experiments by up to two orders of magnitude, which was typically less than 1 % with the beam from AD. ELENA allows up to four bunches of equal intensity and emittance to be produced, which can be distributed to four different experiments at the same time. In the first phase of the project [1], the commissioning of the ring and a short transfer line was done successfully using a local ion source providing 100 keV H^- ions, as well as antiprotons coming from AD. At the end of 2018, just before the start of Long Shutdown 2 (LS2), decelerated beams with characteristics close to the design values were delivered to the first connected experiment (GBAR). Based on these results, the decision was taken to dismantle the old magnetic transfer lines from AD and to connect all the experiments to ELENA with new electro-static lines. Despite the unavailability of antiprotons during the LS2 (2019-2020), the ELENA ring could still be operated with beam from the local ion source, allowing the commissioning of the new transfer lines as well as the optimization of beam performance, including e-cooling.

BEAM COMMISSIONING OVERVIEW

The beam commissioning started mid-November 2016 with the injection into the ELENA ring of a 100 keV H^- ion beam coming from the local source through an electrostatic line. A few days later, beam was circulating for a few hundred turns. Due to the breakdown of the ion source isolation transformer, beam commissioning was stopped and resumed only in March 2017 with the source operated at 85 keV to minimize the risk of further breakdowns. ELENA commissioning with H^- was inefficient due to erratic injections, later traced back to strong fluctuations of the beam generated by the source. Thus, starting in June 2017, ELENA was also commissioned with antiprotons using typically three eight hours periods per week of AD beam time. The first antiprotons circulated in ELENA in August 2017. At the end of 2017, bunch to bucket transfer was operational and antiproton beams were decelerated almost to 100 keV.

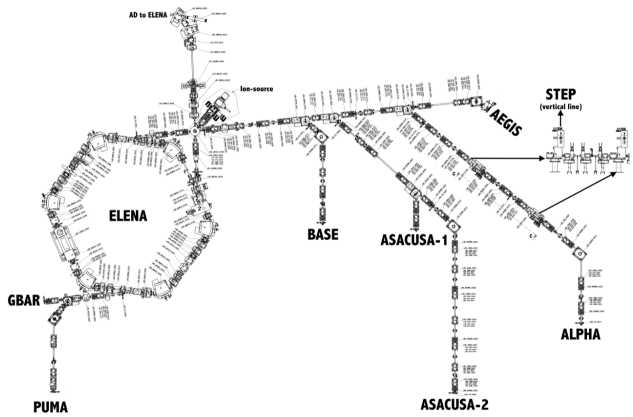

Figure 1: Layout of the ELENA ring and transfer lines.

Beam operation stopped again for a few months to complete the ELENA ring with the installation of its electron cooler. ELENA commissioning resumed end of April 2018. 2018 was an unfortunate year for AD with only 65% machine availability, affecting the physics run but also ELENA beam commissioning. Commissioning with the H^- ion beam was also perturbed by several breakdowns of the source which was not available from September onwards. End of May 2018, first antiproton beam was observed at 100 keV after tune and orbit corrections along the cycle, without beam cooling. Setting-up and conditioning of the e-cooler started end of May, and clear signs of longitudinal and transverse cooling at both energies were measured in July. Antiproton beam was observed at the entrance of the GBAR decelerator experiment at the end of July 2018. The remainder of the run was used to further commission many sub-systems (RF, beam instrumentation, electron cooler) and optimize the beam parameters to allow for a decision to be taken on the connection of all users to ELENA. Despite the little beam time available and issues with the ion source, by the end of 2018 it was possible to achieve beam parameters before extraction reasonably close to the design values [2].

During LS2, beam commissioning was interrupted for the time required to install the new electrostatic transfer lines and to consolidate the local ion source. Achieving reliable

* laurette.ponce@cern.ch

ISBN: 978-3-95450-227-1 ISSN: 2673-5490 doi:10.18429/JACoW-IPAC2022-THOXGD2

ELECTRON COOLING EXPERIMENT FOR PROTON BEAMS WITH INTENSE SPACE-CHARGE IN IOTA

N. Banerjee*, M.K. Bossard, J. Brandt, Y-K. Kim, The University of Chicago, Chicago, USA
B. Cathey, S. Nagaitsev[1], G. Stancari, Fermilab, Batavia, Illinois, USA
[1]also at The University of Chicago, Chicago, USA

Abstract

Electron cooling as a method of creating intense ion beams has a practical upper limit when it comes to the peak phase space density of ion beams which can be achieved in practice. We describe a new experiment to study electron cooling of 2.5 MeV protons at the intensity limit using the Integrable Optics Test Accelerator (IOTA), which is a storage ring dedicated to beam physics research at Fermilab. This system will enable the study of magnetized electron cooling of a proton beam with transverse incoherent tune shifts approaching -0.5 due to the presence of intense space-charge forces. We present an overview of the hardware design, simulations and specific experiments planned for this project.

INTRODUCTION

Electron cooling is the process of exchanging thermal energy between an ion beam and a co-propagating electron beam moving at the same average velocity. This method can be used to accumulate ions and reduce the emittance of the beam in storage rings and is especially important for future heavy-ion facilities [1–3] and cooling in an ion collider [4]. While its possible to generate very cold electron beams [5] to cool ions, the minimum emittance of ion beams achieved through electron cooling is limited by the additional heating processes of Intra-Beam Scattering (IBS) and resonance-driven transverse heating due to space-charge tune shifts. [6] In practice, this is observed as a minimum achievable beam size in a storage ring [7, 8] corresponding to transverse space-charge tune shifts of 0.1-0.2. We are developing an experiment to explore the interplay of electron cooling with space-charge and instabilities in a high-brightness high-intensity regime.

The Integrable Optics Test Accelerator (IOTA) which can store with a kinetic energy of 2.5 MeV is a suitable machine to explore electron cooling in the presence of intense space-charge forces. IOTA is a re-configurable 40 m storage ring which acts as a test facility at Fermilab dedicated to research on intense beams including the areas of Non-linear Integrable Optics (NIO), beam cooling, space-charge, instabilities and more. [9, 10] Here, we discuss the electron cooling experiment which forms a part of our electron-lens research program. [11]. We describe a setup capable of exploring the dynamics due to space-charge in the regime of large transverse tune shifts up to $\Delta\nu_{x,y} = -0.5$.

Table 1: Typical Operation Parameters for Protons in IOTA

Parameter	Value		Unit
Circumference (C)	39.96		m
Kinetic energy (K_b)	2.5		MeV
Emittances ($\epsilon_{x,y}$)	4.3, 3.0		μm
Momentum spread (σ_p/p)	1.32×10^{-3}		
	Coasting	**Bunched**	
Number of bunches	-	4	
Bunch length (σ_s)	-	0.79	m
Beam current (I_b)	6.25	1.24	mA
Bunch charge (q_b)	11.4	0.565	nC
Tune shifts ($\Delta\nu_{x,y}$)	-0.38, -0.50		
$\tau_{\mathrm{IBS,x,y,z}}$	6.4, 4.2, 8.1	8.7, 6.0, 23	s

In the next section, we detail the design specifications of the electron cooler setup at IOTA and list some of the relevant hardware. Then we show some simulations of the expected dynamics. In the last section, we discuss our simulation results and present plans for experiments.

ELECTRON COOLER SETUP

The design parameters of the electron cooler is dependent on the specific experiments to be performed and the proton beam parameters at IOTA. Table 1 shows some baseline operation parameters along with tune shifts and emittance growth times, in both coasting beam and bunched beam configurations. At the maximum design current corresponding to a vertical space-charge tune shift of -0.5, emittance growth times due to IBS are typically less than 10 seconds. Additionally, space-charge forces also create rapid emittance growth and beam-loss in the first few hundred turns after injection. We need a strong electron cooler to mitigate these effects. At beam currents 10 times smaller then the maximum, IBS is the dominant driver of emittance growth thus limiting beam lifetime and constraining other experiments which can be performed with proton beams at IOTA. Consequently a weaker electron cooler can compensate for the heating and is valuable for all research with proton beams in IOTA.

We have designed two separate electron cooler configurations for IOTA: a simple cooler configuration for cooling and performing beam manipulations at relatively small beam currents where space-charge forces are weak in the proton beam and a strong cooler configuration specifically for

* nilanjan@uchicago.edu

ISBN: 978-3-95450-227-1 ISSN: 2673-5490 doi:10.18429/JACoW-IPAC2022-THOXGD3

COMMISSIONING STATUS OF THE RAON SUPERCONDUCTING ACCELERATOR

H. J. Kim*, J. H. Jang, D. Jeon, H. C. Jin, J. I. Heo, B. S. Park, I. S. Hong, J. W. Kwon, G. D. Kim, S. H. Moon, E. H. Lim, D. M. Kim , M. J. Park, Y. H. Kim, Y. J. Choi, C. W. Son, S. I. Lee, Y. S. Chung, IBS, Daejeon, Korea

Abstract

The Rare isotope Accelerator Complex for ON-line experiments (RAON) has been proposed as a multi-purpose accelerator facility for providing beams of exotic rare isotopes of various energies. It can deliver ions from hydrogen (proton) to uranium. Protons and uranium ions are accelerated up to 600 MeV and 200 MeV/u respectively. It can provide various rare isotope beams which are produced by isotope separator on-line system. The RAON injector was successfully commissioned in 2021 to study the initial beam parameters from the main technical systems, such as the ECR ion source and RFQ, and to find the optimized LEBT and MEBT RF set-point and matching conditions. In this paper, we present the current commissioning status of the RAON injector in preparation for the upcoming SCL3 beam commissioning.

INTRODUCTION

The RAON accelerator has been planned to study a wide range of cutting edge science programs in atomic physics, material science, bio and medical science, nuclear astrophysics, nuclear science, and interdisciplinary science programs at the Institute for Basic Science (IBS). In order to meet the diverse demands, it can deliver various high intensity stable ions from protons to uranium atoms with a final beam energy, for example, 200 MeV/u for uranium and 600 MeV for protons, and with a beam current range from 8.3 pμA (uranium) to 660 pμA (protons) [1–3]. It can provide various rare isotope beams which are produced by isotope separator on-line (ISOL) system. The facility consists of three superconducting linacs of which superconducting cavities are independently phased and operating at three different frequencies, namely, 81.25, 162.5 and 325 MHz.

The accelerator facility is shown in Fig. 1. An injector system accelerates a heavy ion beam to 500 keV/u and creates the desired bunch structure for injection into the superconducting linac. The injector system comprises an electron cyclotron resonance ion source, a low-energy beam transport, a radio-frequency quadrupole, and a medium-energy beam transport. The superconducting driver linac accelerates the beam to 200 MeV/u. The driver linac is divided into three different sections, as shown in Fig. 2: a low-energy superconducting linac (SCL3), a post-accelerator to driver linac (P2DT) and a high-energy superconducting linac (SCL2). The SCL3 accelerates the beam to 18.5 MeV/u. The SCL3 uses two different families of superconducting resonators,

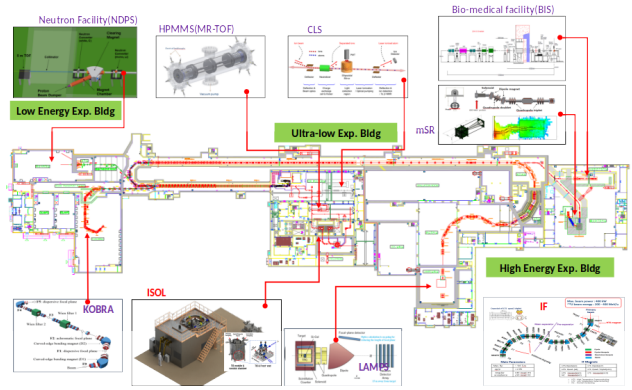

Figure 1: Layout of the RISP accelerator complex.

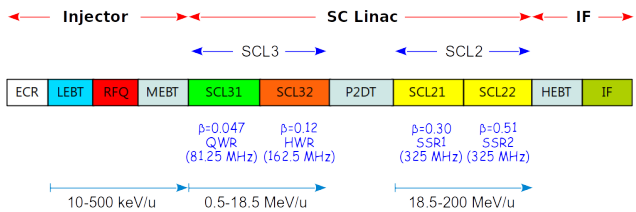

Figure 2: The RAON linear accelerator.

i.e., a quarter wave resonator (QWR) and a half wave resonator (HWR). It consists of a total of 22 QWR operating at 81.25 MHz of resonance frequency and 102 HWR operating at 162.5 MHz of resonance frequency. The SCL2 uses two different types of single spoke resonators (SSR1 and SSR2) and both types will operate at 325 MHz of resonance frequency. Both SCL3 and SCL2 adopts normal conducting quadrupole doublet focusing lattice in the warm section, where two quadrupole magnets are located between every cryomodules for beam focusing. The warm section also comprises a beam position monitor (BPM), a vacuum system, a beam loss monitor, and a dipole steering magnet integrated at the quadrupole magnet.

RAON INSTALLATION

As of November 2021, injector systems, 22 QWR cryomodules, 13 HWR type-A (2 cavities) cryomodules, and 19 HWR type-B (4 cavities) cryomodules were installed in the SCL3 tunnel, as shown in Fig. 3. The installation procedures are defined and well demonstrated, which take into account of a maintenance work including cryomodule disassembly from the beam line. The installation steps are as follows: (i) a warm section that consists of two quadrupole magnets, a beam position monitor, and a vacuum system is

* hjkim@ibs.re.kr

ISBN: 978-3-95450-227-1 ISSN: 2673-5490 doi:10.18429/JACoW-IPAC2022-THIXSP1

A NEW COMPACT 3 GeV LIGHT SOURCE IN JAPAN

N. Nishimori†, QST, Miyagi 980-8579, Japan

Abstract

A new 3 GeV light source with a circumference of 350 m and an MBA lattice is being constructed in north-eastern Japan. Aiming at stable and high-performance operations with an emittance of about 1 nm rad, various design and R&D activities are being performed: the four bend achromatic lattice using combined-function bend magnets; the compact RF system using a TM020 mode and in-cavity compact HOM absorbers; the in-vacuum off-axis injection scheme enabling stored beam oscillation-free injections with a small injection beam amplitude; the injector linac composed of a thermionic E-gun and C-band accelerators with a capability of extension to feed a future soft X-ray FEL driver, and so on. The installation of accelerator components is ongoing. The overall design of the light source, R&D results, and the latest construction status are presented.

INTRODUCTION

A new 3 GeV light source named NanoTerasu is under construction in Sendai, Japan [1]. The concepts of the light source are to build a highly brilliant compact soft X-ray (SX) source based on reliable and proven SPring-8 / SACLA accelerator technology, to be a complementary partner of SPring-8 to mainly cover the SX region, and to provide SX free-electron laser (SXFEL) in the future upgrade. The brilliance of the 3 GeV light source as a function of photon energy is represented by solid curves in Fig. 1 and those of SPring-8 by dotted curves. The main targets of NanoTerasu are EUV, SX and Tender X-ray regions where the brilliance is one to two orders of magnitudes higher than SPring-8. The target brilliance is 10^{21} photons/sec/mm^2/mrad^2/0.1% b.w. and coherent ratio of roughly 10 % for several keV photon energies. A multi-pole wiggler (MPW) serves as a hard X-ray source instead of a bending magnet. The above requirements can be satisfied with a beam energy of 3 GeV, stored current of 400 mA and horizontal beam emittance of 1 nm rad.

The initial portfolio of the first phase 10 beamlines under preparation was selected to meet the effective use of the low-emittance light source, needs of both academia and industry, and the complementary capability of other SR facilities in Japan. As shown in Fig. 2, there are two EUV/SX beamlines represented by orange, four SX by green, three Tender-X by purple and one HX by deep blue.

Polarization dependence in soft X-ray spectroscopy allows the investigation of electronic states in materials. In EUV/SX region, polarization is controlled by insertion devices such as APPLE-II because of the lack of polarizers. Resonant inelastic X-ray scattering will be used to probe charge, magnetic and orbital degrees of freedom on selected atomic species of various solid, liquid, and gas targets under various environments. Photoemission spectroscopy beamlines are used to measure the electronic structure of the materials to analyze the properties of catalysts, battery electrodes, and so on under the operating environment. X-ray magnetic circular dichroism beamline employs a four-segment APPLE-II crossed undulator for research of magnetic materials and devices [2], because fast and versatile control of polarization is feasible by phase shifters, and higher polarization up to 0.6 is obtained with four segments [3]. In addition, the generation of higher harmonic circular polarization is feasible by using high flux higher harmonic linear polarized light from APPLE-II.

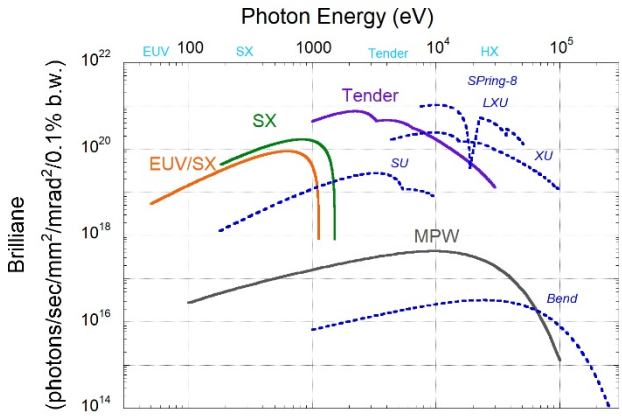

Figure 1: Brilliance as a function of photon energy.

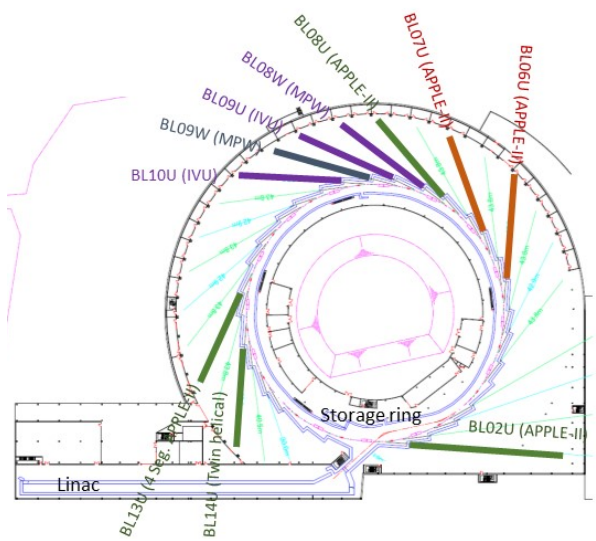

Figure 2: Layout of the 3GeV light source NanoTerasu.

In vacuum undulators (IVUs) and MPWs will be used as tender and hard X light sources above 2 keV. Hard X-ray photoemission spectroscopy and X-ray absorption fine structure (XAFS) will be used to investigate bulk

†nishimori.nobuyuki@qst.go.jp

ISBN: 978-3-95450-227-1 ISSN: 2673-5490 doi:10.18429/JACoW-IPAC2022-THOXSP2

BRIXSINO HIGH-FLUX DUAL X-RAY AND THz RADIATION SOURCE BASED ON ENERGY RECOVERY LINACS

I. Drebot*[1], A. Bacci[1], M. Bertucci[1], A. Bosotti[1], F. Broggi[1], F. Canella[4], S. Cialdi[2], M. Citterio[1], R. Ferragut[4], G. Galzerano[5], M. Giammarchi[1], D. Giannotti[1], D. Giove[1], S. Latorre[1], C. Meroni[1], P. Michelato[1], L. Monaco[1],M. Opromolla[2],B. Paroli[2], R. Paparella[1], V. Petrillo[2], F. Prelz[1], E. Puppin[4], M. Rossetti Conti[1], A. R. Rossi[1], L. Rossi[2], M. Ruijter[3], S. Samsam[3], L. Serafini[1], D. Sertore[1], M. Sorbi[2], M. Statera[1], E. Suerra[2], V. Torri[1]
INFN-Milano, 20133 Milano
M. P. Abbracchio[2], S. Altilia[2], S. Capra[2], D. Cipriani[2], C. Lenardi[2],
C. Pagani[2], A. Vanzulli[6], Universitá degli Studi di Milano,20122, Milano, Italy
A. Andreone[7], C. Koral[7], M. R. Masullo, Z. Mazaheri[7], G. Mettivier[7], G. P. Papari[7],
A. Passarelli, B. Piccirillo[7], A. Rubano[7], P. Russo[7], INFN-Napoli, 80126 Napoli, Italy
R. Calandrino, A. del Vecchio, IRCCS Ospedale San Raffaele, 20132, Milano, Italy
P. Cardarelli,G. Paternó[8], A. Taibi[8], INFN-Ferrara, 44122,Ferrara,Italy
A. Esposito, INFN-LNF, 00044,Frascati, Italy
D. Paparo, CNR -ISASI, 80078, Pozzuoli, Italy
A. Torresin[2], Polo Ospedaliero, DGWelfare, 20124, Milano, Italy
[1]also at INFN/LASA, 20090 Segrate (MI), Italy
[2]also at Università degli Studi, 20133, Milano, Italy
[3]also at Università degli Studi di Roma "La Sapienza", 00185,Roma ,Italy
[4]also at Politecnico di Milano, 20133, Milan, Italy
[5]also at CNR-IFN , 20133,Milan, Italy
[6]also at ASST Grande Ospedale Metropolitano Niguarda, 20162 Milan, Italy
[7]also at Universitá di Napoli Federico II,80126 Napoli, Italy
[8]also at Universitá degli Studi di Ferrara , 44122,Ferrara,Italy

Abstract

We present the conceptual design of a compact light source named BriXSinO. BriXSinO was born as demonstrator of the Marix project, but it is also a dual high flux radiation source Inverse Compton Source (ICS) of X-ray and Free-Electron Laser of THz spectral range radiation conceived for medical applications and general applied research. The accelerator is a push-pull CW-SC Energy Recovery Linac (ERL) based on superconducting cavities technology and allows to sustain MW-class beam power with almost just one hundred kW active power dissipation/consumption. ICS line produces 33 keV monochromatic X-Rays via Compton scattering of the electron beam with a laser system in Fabry-Pérot cavity at a repetition rate of 100 MHz. The THz FEL oscillator is based on an undulator imbedded in optical cavity and generates THz wavelengths from 15 to 50 micron.

INTRODUCTION

The increasing requests of complete autonomy of Research Infrastructures drive the research communities at developing sustainable accelerators for the frontiers of the High Energy Physics (HEP) and of the future applied researches. Energy Recovery Linacs (ERLs) [1] promise to be a keystone for future sustainable accelerators, providing a reasonable balancing between use of the beam and beam power waste/dissipation which is attractive not only to users oriented to radiation experiments, i.e. Free Electron Lasers (FEL), Inverse Compton Scattering (ICS), and synchrotron radiation, but also in the HEP scenario, as discussed in Ref. [2]. The main perspectives of ERLs include: to provide nearly linac quality/brightness beam at nearly storage ring beam powers, to mitigate intractable environmental/safety concerns since the beam can be dumped at low energy, to consider high power applications than would otherwise be unaffordable, looking at GW class beams. Main ERL paradigms worldwide are BNL-ERL [3] and CBETA [4]. The facility presented here, named BriXSinO [5], is inspired, on reduced scale, by the same philosophy of other more ambitious projects grown up around the MariX concept [6–11]. A newly conceived scheme of ERL with counter-propagating beams is proposed in BriXSinO: 5 mA of average electron beam current in CW mode with a time structure organized in a regular repetition rate up to 100 MHz, i.e. bunch spacing 10 ns. It is similar in parameters and dimensions to a storage ring, with the very much larger recovery of the 225 kW beam power (>90%). Moreover, the electron bunches in BriXSinO travel through the full orbit back-and-forth just one time, while, conversely, in a storage ring must electrons

* illya.drebot@mi.infn.it

ISBN: 978-3-95450-227-1 ISSN: 2673-5490 doi:10.18429/JACoW-IPAC2022-THOXSP3

PATH TO HIGH REPETITION RATE SEEDING: COMBINING HIGH GAIN HARMONIC GENERATION WITH AN OPTICAL KLYSTRON

G. Paraskaki*, E. Ferrari, L. Schaper, E. Schneidmiller
Deutsches Elektronen-Synchrotron DESY, Hamburg, Germany
E. Allaria, Elettra-Sincrotrone Trieste S.C.p.A., Trieste, Italy
W. Hillert, University of Hamburg, Hamburg, Germany

Abstract

External seeding in combination with harmonic generation has become a hot topic in the field of high gain free-electron lasers (FELs) since it allows delivery of superior FEL radiation characterized by, for example, full coherence and unprecedented shot-to-shot stability. At low repetition rate machines operating at few 10 Hz, novel experiments have been realized already, however, at superconducting machines, current laser technology does not support exploiting the full repetition rate available. One way to overcome this problem is to reduce the requirements in seed laser power: here, an optical klystron based high gain harmonic generation (HGHG) setup is proposed to reduce the laser peak power requirements by orders of magnitude, enabling operation at drastically increased repetition rates. We report simulation results based on the seeded beamline concept of the FLASH2020+ project. Among other topics, the effect of a linear electron beam energy chirp on this setup will be discussed.

INTRODUCTION

In the fast-moving world of high-gain FELs [1], the FEL facilities worldwide aim at improving the properties of the radiation to accommodate innovative experiments that depend on special features, such as short pulse duration, high average flux and small bandwidth, to name a few. One popular milestone in high-gain FELs is the generation of fully coherent radiation at a high repetition rate. With more and more facilities being able to generate electron bunches at high repetition rates, such as the already-under-operation FLASH [2] and the European XFEL [3], and the upcoming LCLS II [4] and SHINE [5], it is possible to generate partially longitudinally coherent FEL pulses at MHz repetition rates with techniques like the self-amplified spontaneous emission (SASE) [6, 7]. On the other hand, external seeding techniques provide fully coherent FEL pulses but depend on the limited repetition rate of available seed laser sources. The necessary high peak laser power, of tens to hundreds of MW at the interaction point, practically limits the repetition rate to tens of Hz when the wavelength of seeds spans the ultraviolet (UV) range.

To overcome this hurdle, it has been proposed [8, 9] to combine the high gain harmonic generation (HGHG) [10, 11] with another well-established scheme: the optical klystron (OK) [12]. Adding the optical klystron to the standard HGHG scheme allows us to reduce the required laser peak power allowing to operate at a higher repetition rate. In the following, we compare with three-dimensional and time-dependent simulations the output FEL pulses of a standard HGHG scheme and an OK-HGHG scheme and we verify the lower seed laser power required by the latter. In addition to these results, we investigate the impact of a linear correlation between the energy and longitudinal position of the electrons (linear energy chirp), which commonly exists at several FEL facilities as it is a fundamental ingredient for achieving short electron bunches. We present the key considerations to reoptimize the two setups under these conditions and we investigate whether such a linear energy chirp is detrimental to the FEL pulse properties.

THE LAYOUT

In standard HGHG, a modulator, a chicane and a radiator are required, as shown in Figure 1. The electron bunch interacts with the powerful seed laser along the modulator and, as a result, its energy is modulated. When traversing the chicane, higher-energy electrons take shorter paths and lower-energy electrons take longer paths, resulting in periodic longitudinal density modulations, quantified by the so-called bunching factor. If the energy modulation is sufficient, bunching at a harmonic of the seed laser wavelength can be obtained, resulting in fully coherent FEL pulses at that wavelength.

In OK HGHG, an additional modulator and chicane are required, as shown in Figure 2. The advantage here is that the seed laser power in the first modulator is much lower, as only a small energy modulation amplitude (in the order of the uncorrelated energy spread) is needed. With the assistance of chicane 1, microbunches are created with no need for harmonic content. In this way, the initially small energy modulation can be further self-amplified in modulator 2 and reach an amplitude that allows chicane 2 to induce bunching at harmonics of the seed laser wavelength.

SIMULATION RESULTS

To verify the efficiency of the OK HGHG scheme in comparison to the standard HGHG scheme, we simulated both of them with Genesis 1.3 [13] and optimized the simulations to generate the 15th harmonic of 300 nm seed laser wavelength (20 nm). For the beamline, electron beam, and laser parameters (see Table 1) we have based our study on the design parameters of FLASH2020+ [14], the upgrade project of FLASH. As a first step, we assumed an electron

* georgia.paraskaki@desy.de

ISBN: 978-3-95450-227-1 ISSN: 2673-5490 doi:10.18429/JACoW-IPAC2022-THIYGD1

WHITE RABBIT BASED BEAM-SYNCHRONOUS TIMING SYSTEMS FOR SHINE*

Y.B. Yan†, P.X.Yu, G.H. Chen, Q.W. Xiao, Shanghai Advanced Research Institute, Chinese Academy of Sciences, Shanghai, P.R. China
G.H. Gong, Y.M. Ye, Tsinghua University, Beijing, P.R. China
J.L. Gu, L. Zhao, Z.Y. Jiang, University of Science and Technology of China, Hefei, P.R. China

Abstract

Shanghai HIgh repetition rate XFEL aNd Extreme light facility (SHINE) is under construction. SHINE requires precise distribution and synchronization of the 1.003086 MHz timing signals over a long distance of about 3.1 km. Two prototype systems were developed, both containing three functions: beam-synchronous trigger signal distribution, random-event trigger signal distribution and data exchange between nodes. The frequency of the beam-synchronous trigger signal can be divided according to the accelerator operation mode. Each output pulse can be configured for different fill modes. A prototype system was designed based on a customized clock frequency point (64.197530 MHz). Another prototype system was designed based on the standard White Rabbit protocol. The DDS (Direct Digital Synthesis) and D flip-flops (DFFs) are adopted for RF signal transfer and pulse configuration. The details of the timing system design, laboratory test results will be reported in this paper.

OVERVIEW

Owing to the wide range of applications of X-rays in the research fields of physics, chemistry and biology, facilities with the ability to generate X-rays were developed continuously in the last century. The free electron laser (FEL) is a novel light source, producing high-brightness X-ray pulses. To achieve high-intensity and ultra-fast short wavelength radiation, several X-ray FEL facilities have been completed or under construction around the world [1].

The first hard X-ray FEL light source in China, the so-called Shanghai HIgh repetition rate XFEL aNd Extreme light facility (SHINE), is under construction. It consists of an 8 GeV continuous-wave (CW) superconducting RF Linac, 3 undulator lines, 3 following FEL beamlines, and 10 experimental end-stations. Main parameters are presented at Table 1.

SHINE timing system is design to provide precise clock pulses (Trigger) for drive laser, low-level RF, solid state amplifiers, kicker, beam and optical instruments, etc. It will ensure the electron beam is generated and accelerated to the design energy, to produce the free electron laser, while completing the beam and optical parameters measurement and feedback. The White Rabbit (WR) technology was evaluated and will be adopted.

Table 1: Main Parameters of the SHINE

Parameter	Value
Beam energy	8 GeV
Bunch charge	100 pC
Peak current	1500 A
Max repetition rate	1.003086 MHz
Photon energy	0.4 - 25 keV
Total length	3.1 km

ARCHITECTURE

SHINE timing system is composed of one master node, WR switches and more than 800 slave nodes. The master node receives reference signal from the femtosecond optical synchronization system. The switches distribute the clock to all the nodes in the network using a hierarchical architecture. The node basic functionality comes in the form of an IP Core called WR PTP Core. They can be standalone trigger fanout modules or FPGA Mezzanine Cards (FMC), which can be embedded in the beam signal processors for the beam position, beam length, arrival time, beam loss and charge measurement. The system architecture is shown in Fig. 1.

There are three functions designed: beam-synchronous trigger signal distribution, random-event trigger signal distribution and data exchange between multiple nodes. The frequency of the beam-synchronous trigger signal needs to be divided according to the accelerator operation mode. The output pulse needs to be configured according to the filling pattern.

SHINE project requires precise distribution and synchronization of the 1.003086 MHz (1300 MHz/1296) timing signals over a long distance of about 3.1 km. The beam-synchronous trigger signal distribution is the basic and priority function.

The standard White Rabbit network operates at 125/62.5 MHz clock. If the max repetition frequency of SHINE is 1.0 MHz, 1300 MHz RF reference signal can be divided to 10 MHz as the reference signal. The salve nodes output the trigger signals at the specified time, such as 1us, 2us, 5us, etc. But the repetition frequency is 1.003086 MHz, we need to find the new technical routes.

* Work supported by Shanghai Municipal Science and Technology Major Project (Grant No. 2017SHZDZX02).
† yanyingbing@zjlab.org.cn

ISBN: 978-3-95450-227-1 ISSN: 2673-5490 doi:10.18429/JACoW-IPAC2022-THOYGD1

EXPERIMENTAL VERIFICATION OF SEVERAL THEORETICAL MODELS FOR ChDR DESCRIPTION

K. Lasocha*, Institute of Physics, Jagiellonian University, Kraków, Poland
C Davut†, T. Lefevre, S. Mazzoni, C. Pakuza‡, E. Senes, A. Schloegelhofer§,
CERN, CH-1211 Geneva 23, Switzerland
P. Karataev, JAI, Royal Holloway, University of London, Egham, Surrey, UK

Abstract

In recent years the potential of using Cherenkov Diffraction Radiation (ChDR) as a tool for non-invasive beam diagnostics has been thoroughly investigated. Although several theoretical models of ChDR have been developed, differences in their assumptions result in inconsistent predictions. The experimental verification is therefore needed in order to fully understand ranges of validity of available models. In this contribution we present a detailed theoretical study of the radiation yield as a function of the beam-radiator distance. Following identification of beam parameters and frequency range for which differences between the model predictions are most prominent, we compare theoretical estimates with the results of a dedicated experiment.

INTRODUCTION

Beam diagnostics based on Cherenkov diffraction radiation (ChDR) [1] were intensively investigated over last few years, and require a good knowledge of the expected characteristics of the emitted radiation. Since the exact solutions of the electromagnetic problems are often not known, and detailed computer simulations require extensive time and resources, the properties of the radiation are often derived from simplified models, that assume specific assumptions on the radiator shape.

The first group of models can be labelled as *Stationary Models*. The name comes from the assumption that the radiator is infinitely long and uniform. As examples of the stationary models one can refer to the results obtained by Ulrich [2] for an infinitely wide and thick flat radiator, and the formulae provided by Olsen [3], which describe the ChDR emitted by a particle travelling through an infinite cylindrical tunnel excavated in an unbounded medium. Although such models will be clearly not suitable in cases when wavelength of the studied radiation is comparable to the radiator size, for most of the real case applications they would provide a good approximation for radiation emitted in the visible, ultraviolet and X-ray range. It is also worth mentioning a series of studies [4–8] that uses predictions of such models for the initial radiation yield, which is then modified based on the specific geometry of the radiator following the optical principles.

Alternatively, one might introduce some limitations on the longitudinal size of the radiator when calculating of the initial radiation yield. This approach distincts another group of models, namely *Non-Stationary Models* with a notable example, known as the Polarisation Current Approach (PCA) [9]. PCA describes ChDR emitted in various geometries of radiators, but, in this paper, we will focus on a result given for a flat, infinitely thick and transversely wide rectangular target [10], which is a geometry comparable to one described in the Ulrich model to allow a direct comparison between Stationnry and non-Stationary models. The latter include additional edge effects, such as diffraction radiation and transition radiation. In the case of short radiators these effects dominate the total radiation yield, but surprisingly PCA predictions differ from the stationary results even for arbitrarily long radiators.

Differences between the models can be illustrated by comparing spectral distributions of the energy radiated by a single electron as predicted by stationary and non-stationary models. Relevant spectra are presented in Fig. 1 assuming an electron beam energy of 200 MeV and a $\epsilon = 2.1$ radiator located 1 cm away from the beam. In the low frequency limit, where radiation wavelength λ is higher than the impact parameter h, all the models are compatible and their predictions follow the same dependence as Cherenkov radiation described by Frank-Tamm (F-T) formula [11]. Then, in the $\lambda < h < \gamma\lambda$ regime, stationary and non-stationary models diverge. While stationary results predict a decay proportional to freq^{-2}, according to PCA radiated energy stays at a constant level. Finally, at higher frequencies the intensity of radiation falls exponentially according to both models.

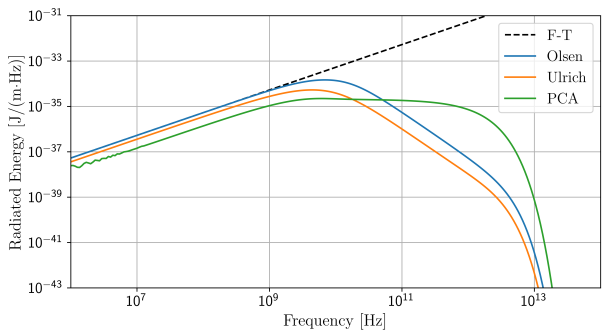

Figure 1: Spectral distribution of ChDR as predicted by different models.

* kacper.lasocha@doctoral.uj.edu.pl
† also at University of Manchester, Manchester, UK
‡ also at JAI and University of Oxford, Oxford, United Kingdom
§ also at TU Wien, Vienna, Austria

ISBN: 978-3-95450-227-1 ISSN: 2673-5490 doi:10.18429/JACoW-IPAC2022-THOYSP1

CONSTRUCTION AND MEASUREMENT OF A TUNEABLE PERMANENT MAGNET QUADRUPOLE FOR DIAMOND LIGHT SOURCE

A. R. Bainbridge*[1], A. Hinton[1], N. Krumpa, B. J. A. Shepherd[1], STFC Daresbury Laboratory, UK
I. P. S. Martin, W. Tizzano, Diamond Light Source, Oxfordshire, UK
[1]also at The Cockcroft Institute, UK

Abstract

Particle accelerator facilities around the world are becoming increasingly interested in permanent magnet (PM) technology as a replacement for traditional resistive electromagnets. This change is driven by the desire to save energy for both financial and environmental reasons. For fixed field systems the use of PMs is now established as a viable alternative to electromagnets however difficulties in using PMs remain where tuneability of field strength is a required feature. The ZEPTO project, a collaboration between CLIC and STFC, sought to address this by developing a system where PM blocks were moved inside fixed steel structures to allow field strength to be changed without sacrificing homogeneity. We discuss here the construction and measurement results to date of a magnet which will test this principle in reality by running on Diamond Light Source.

INTRODUCTION

The ZEPTO (ZEro Power Tuneable Optics) project is a long term magnet development activity conducted by the Accelerator Science & Technology Centre (ASTeC) based at STFC Daresbury Laboratory, UK, and was originally funded by the CLIC (Compact Linear Collider) collaboration at CERN [1]. The original purpose of the project was to reduce the power consumption of CLIC by replacing the electromagnets in the CLIC drive beam with permanent magnet (PM) alternatives which draw no power during normal operation.

Previous works have discussed the prior outputs of the ZEPTO project; two permanent magnet quadrupole designs (high strength [2] and low strength [3]), as well as an experimental dipole [4]. Whilst all these magnets were developed for CLIC, we aim to demonstrate that ZEPTO is a versatile technology concept that can be used as an energy saving replacement for electromagnets on accelerators ranging from existing light sources to new facilities such as XFELs. To this end we have developed a new ZEPTO quadrupole based on the design detailed in [3], but with a number of engineering and usability improvements over previous designs. This magnet is specifically designed to replace an existing electromagnetic quadrupole located on the booster-to-storage ring transfer line of Diamond Light Source (DLS), and is intended to demonstrate the principle of ZEPTO on a real accelerator for the first time, and provide us with valuable data on the long term reliability, field repeatability, and any issues with usability or assembly/installation procedures that may be useful in improving further iterations of the design. The replaced magnet typically operates at 14 T/m over 400 mm length, and the technology demonstrator is capable of operating at 22 T/m over 300 mm length.

In [5] we presented the design details of this technology demonstrator and described magnetic measurements as ongoing. Those measurements revealed a serious error in the construction of the magnet necessitating major modifications to the assembly frame. These modifications have now been made, the magnet has been reassembled and new measurements have been conducted. These measurements, combined with testing on DLS, will allow the ZEPTO concept to be refined in a real-world setting and create learning opportunities to help refine the engineering. Some important features requiring design changes for future iterations have already been revealed by the measurement of the prototype, particularly with regard to movement of the magnetic centre.

ASSEMBLY PROCESS

This magnet has advanced over previous iterations of ZEPTO quadrupoles by being symmetrically splittable such that it can be installed around an existing beam pipe without breaking vacuum conditions. To achieve this a dedicated assembly frame is required which was described in [5] and is shown in Figure 1. The steel yoke is split into two pre-assembled halves which attach to vertical brackets which are then slid along the frame symmetrically towards the carriages, driven by a ball screw turned manually by a handle. Once in the final position the top and bottom plates are bolted to lock components into position, and the frame detached and removed.

The magnetic forces acting on each half of the yoke as they approach the PM carriages are complex and non-linear. Numerous assembly trials were conducted, with the forces proving a challenge to manage. The forces were observed to cause slippage of components and twisting of load bearing brackets during assembly. The original frame used a single ball screw with manual handle to bring the magnet together. This has been adapted with a second linked ball screw on the opposite side, as well as a gearbox on the handle. Gas springs are employed to help manage the non-linear nature of the magnetic forces. It has also proven important to properly brace the assembly frame to the magnet pedestal to prevent minor movements that can cause the magnet halves to come together asymmetrically.

Figure 2 shows the simulated forces during assembly as the steel yokes are moved towards the magnet carriages. During the assembly a Hall probe was used to measure the flux

* alex.bainbridge@stfc.ac.uk

ISBN: 978-3-95450-227-1 ISSN: 2673-5490 doi:10.18429/JACoW-IPAC2022-THOYSP2

THE NEW EDDY CURRENT TYPE SEPTUM MAGNET FOR UPGRADING OF FAST EXTRACTION IN MAIN RING OF J-PARC

T. Shibata*, K. Ishii, S. Iwata, T. Sugimoto, H. Matsumoto, KEK, Tsukuba, Japan
K. Fan[1], HUST, Wuhan, China

Abstract

As part of the goal of increasing the beam power of the Main Ring for Fast eXtraction (FX) in J-PARC to 750 kW, we have been evaluating new FX low-field septa of induced eddy current type (Eddy-septum) since 2014. To reduce the leakage field in the circulating line of the eddy-septa, new pure iron duct-type magnetic shields were produced in July 2021, and in March 2022 we verified that the leakage field was greatly reduced . The construction of the two eddy-septa and their power supplies was completed in May 2022. Beam operation with a new 1.3-s cycle will be started in June 2022.

INTRODUCTION

The J-PARC proton accelerator experiment laboratory consists of a 400-MeV LINAC, a 3-GeV Rapid Cycling Synchrotron (RCS) and a 50-GeV Main Ring (MR). The MR is a proton synchrotron that receives the 3-GeV proton beam from the RCS, accelerates it to an energy of 30 GeV, and extracts it to the neutrino facility (NU) or the hadron facility. The present operation cycle is 2.48 s and the maximum beam power for fast extraction mode (FX) is 515 kW, which was achieved in March 2021 [1]. To realize the original design value of 750 kW, we are working towards operating the MR with a cycle of 1.3 s in June 2022 [2], referred to as "1 Hz operation". The cycle will also be reduced to 1.16 s to increase the beam power to 1.3 MW by 2028 (1.3 MW beam) [2]. The magnets for FX (FX magnets) in the MR, which are used for switching the direction of the proton beam to the NU or the abort dump (ABT), have been in the process of being upgraded for 1 Hz operation and 1.3 MW beam for a decade, and this will be completed by summer 2023. The FX magnets consist of five kickers, two low-field septa (LF-septa) and four high-field septa [3]. The upgrade includes an improvement of the power supply for the kickers and replacing the septa with new ones. During a long-term shutdown of the MR in 2021–2022, the two LF-septa was removed from the beam line and the new septa were installed. The construction of two sets of power supplies for the new septa was completed in May 2022. This article focuses on the upgrade of the LF-septa system.

FX LOW-FIELD SEPTUM MAGNET

The previous LF-septa, removed in 2021, had a conventional configuration with a thin septum coil. The typical gap field for the previous LF-septa was 0.3 T, and the applied current waveform had a time width of ~1.5 s, the same as that for the high-field septa. Each previous LF-septum consisted of two septa, located symmetrically with respect to the beam axis, one used for NU extraction and the other for ABT extraction, with a circulating beam passing through the space between the two septa. These septa were mounted in a vacuum chamber, because the extraction lines were not sufficiently separate from the circulating line, and there was no space to mount a beam duct.

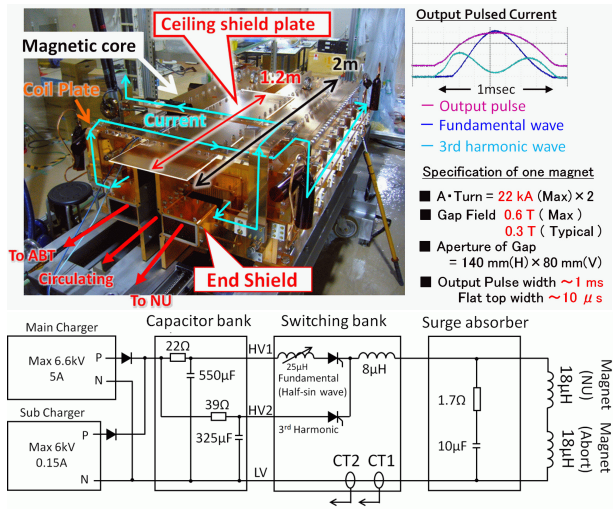

Figure 1: Photograph of eddy septum magnet (upper left), waveform of output pulsed current and specifications of eddy septum system (upper right), and circuit diagram of pulse power supply (lower).

The new LF-septa are induced eddy current type (eddy-septa) (Fig. 1) [4, 5]. We will use two eddy-septa, mounted in two vacuum chambers, as in the case of the previous LF-septa. The eddy-septa have developed in some electron and proton accelerators in the world except J-PARC: e.g., the injection/extraction of synchrotron SOLEIL [6, 7], the injection of SSRF storage ring [8, 9], the extraction of SPS in CERN [10]. The upstream and downstream eddy-septa are called Eddy-1 and Eddy-2, respectively. The most significant feature of an eddy-septum is that it can greatly reduce the leakage field compared to the previous LF-septa. Since the configuration of an eddy-septum is based on a C-type bending magnet, it does not have a septum coil but has a thin copper plate on the opening side of the magnetic core (septum plate). The applied current waveform for an eddy-septum is a short-pulse half-sinusoidal wave. When the short-pulse current is applied to the eddy-septum, the pulsed leakage field penetrates the septum plate, inducing an eddy current in the septum plate that cancels the leakage field. Other advantages of eddy-septa for high-power beam operation include: (1) a zero-Gauss leakage field during beam injection

* tatsunobu.shibata@j-parc.jp

ISBN: 978-3-95450-227-1 ISSN: 2673-5490 doi:10.18429/JACoW-IPAC2022-THPOST001

TEMPERATURE EFFECTS ON THE PETRA III TUNNEL STABILITY

M. Schaumann*, M. Bieler, J. Keil, J. Klute, L. Liao, R. Wanzenberg,
Deutsches Elektronen-Synchrotron DESY, Hamburg, Germany

Abstract

The tunnel of the synchrotron light source PETRA III is build from separate segments that are joint together every 24 m. The normal conducting magnets heat up the tunnel when operating, which leads to an expansion of the concrete walls and floor introducing movements between the tunnels segments. Especially during warm-up periods after shutdowns, this results in a drift of the accelerator elements that is transferred on the circulating beam over a duration of days, weeks or months according to the length of the cool-down period. This paper shows that not only inside temperature effects but also seasonal temperature changes are relevant.

INTRODUCTION

The third-generation light source PETRA III in Hamburg is operated since 2009, providing synchrotron light in the hard X-ray range to its users. The user demand for nanometrescale spectroscopy sets the requirements for the planned upgrade to PETRA IV. The upgrade will replace the old PETRA III ring with a ultra-low-emittance storage ring, aiming at vertical emittances lower than 10 pmrad.

A sketch of the PETRA III tunnel layout with its three experimental halls is shown in Fig. 1. The tunnel is made of individual segments of mostly 24 m length. Figure 2 (left) shows a photograph of the cross-section of one of this segments during the tunnel construction in 1976, when the PETRA tunnel was initially built to host an electron-positron collider. First the tunnel floor was poured in long pieces to obtain a continuous surface without gaps along the arcs. Then the tunnel walls and the roof were poured on the floor in segments of 24 m length, divided by rubber sealings. Later the tunnel floor developed cracks at the gaps between the segments, probably due to thermal stress. The main part of the tunnel is roughly 3-10 m underground, except when passing through the experimental halls, that are hosted in buildings on the surface.

In certain places and after heavy rain, water might leak into the tunnel. This indicates that the tunnel segments are moving against each other. As a result, the beamline elements, which are anchored to the tunnel floor, transmit this movements to the circulating beam. Since this movements are in general slow, they show up as continuous drifts of the beam orbit position that are in turn corrected by the orbit feedback in order to provide the required beam stability. A detailed analysis of the effect on the orbit can be found in Ref. [1]. If the disturbances become too large, the orbit correctors might reach their strength limit and thus an optimal orbit correction could no longer be guaranteed.

* michaela.schaumann@desy.de

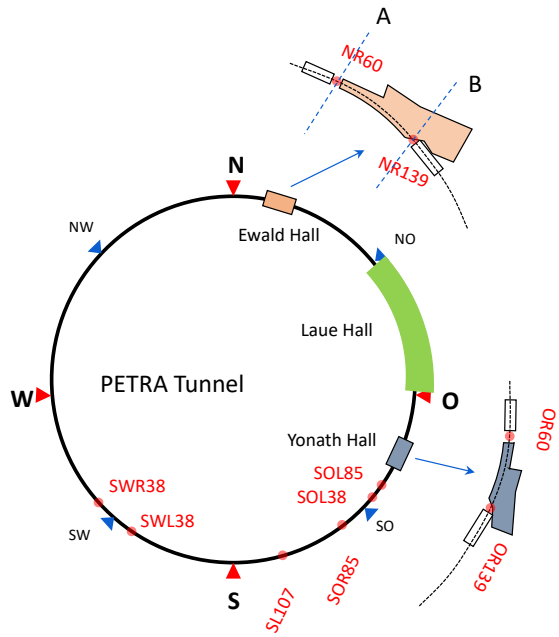

Figure 1: Overview of the PETRA III tunnel layout with its three experimental halls, indicating the locations of the mechanical measurement devices shown in Fig. 2 (right).

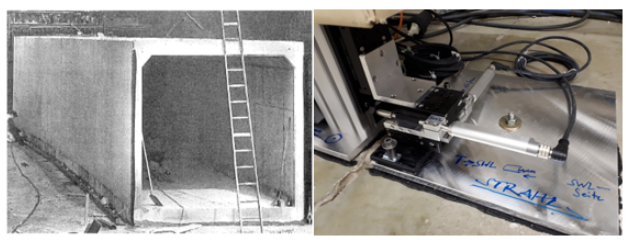

Figure 2: Left: Photograph of the tunnel segment cross-section during the construction of the PETRA III tunnel in 1976. Right: Mechanical measurement device as installed at ten positions around the PETRA circumference, measuring the vertical, horzontal and longitudinal tunnel motion.

The design of the planned upgrade to PETRA IV foresees to keep parts of the tunnel infrastructure and thus the described tunnel segment movements will remain. As part of the risk management strategy for PETRA IV, an understanding of long term tunnel movement and the therewith associated long term orbit stability is required.

TUNNEL TEMPERATURE

Since PETRA III is operated in topup mode with DESY II as a full energy injector, the PETRA III electromagnets are kept at a constant field. The high constant current in the magnets coils heats up the tunnel during operation, as can be

ISBN: 978-3-95450-227-1 ISSN: 2673-5490 doi:10.18429/JACoW-IPAC2022-THPOST003

COLLECTIVE EFFECTS ESTIMATES FOR THE DAMPING RING DESIGN OF FCC-*ee*

O. Etisken*[1], F. Antoniou, F. Zimmermann, CERN, Geneva, Switzerland
C. Milardi, A. Desantis, LNF-INFN, Frascati, Italy
[1] also at Kirikkale University

Abstract

The current injector complex design of the FCC-ee project consists of e^+/e^- linacs, which accelerate the beams up to 6 GeV, a damping ring at 1.54 GeV, a pre-booster ring, accelerating the beam up to 16 GeV and a booster synchrotron ring integrated in the collider tunnel accelerating the beams up to the collision energies. The purpose of the damping ring is to accept the 1.54 GeV beam coming from the linac-1, damp the positron/electron beams and provide the required beam characteristics for the injection into the linac-2. In this presentation the damping ring design is introduced and analytical calculations on various collective effect such as space charge, intra-beam scattering, longitudinal micro-wave instability, transverse mode coupling instability, ion effects, electron cloud and coherent synchrotron radiation, are presented.

INTRODUCTION

The Future Circular Collider (FCC) e^+e^- project is a design study of a high-luminosity, high-energy circular electron-positron collider to be installed in a new tunnel of around 98 km circumference. It is planned to be used as a high precision machine for the investigation of the Z, W, Higgs and top particles at center of mass energies varying between 91.2 and 365 GeV [1, 2].

The injector complex design of the FCC-e^+e^- consists of an e^+/e^- linac, which accelerates the beams up to 6 GeV, a pre-booster ring (PBR), accelerating the beams from 6 GeV to 16 GeV, and a booster synchrotron ring (BR), accelerating the beams up to the collision energy [3]. The pre-accelerator complex design (baseline) consists of an electron source, two linacs, a positron target and a damping ring. The 2-bunch and multi-bunches options have been discussed in the past months [4]. In this study, the collective effect estimates are done for the multi-bunches option. The ring has a racetrack shape consisting of 2 arcs and 2 straight sections; each arc has 50 FODO cells, whereas each straight section has two long damping wiggler magnets (17 m, 1.8 T) to reach short damping time [4]. The beam parameters for the multi-bunch DR design option are summarized in Table 1.

In this study, analytical estimates related to collective effects have been performed for the DR design as collective effects can be a limiting factor for the performance of an accelerator.

Table 1: Beam Parameters of the DR

Parameter	DR
Energy, E [GeV]	1.54
Circumference, C [m]	270.65
Geo. emit. (h), ϵ_x [nm·rad]	1.25
Bunch length, σ_z [mm]	3.19
Momentum sprd., σ_δ $(\times 10^{-2})$	0.074
Harmonic number, h	360
Mom. compac., α_c $(\times 10^{-3})$	1.49
Horizontal tune, Q_h	22.57
Vertical tune, Q_v	23.61
Synchrotron tune, Q_s	0.019
Energy loss/turn, U_0 [MeV]	0.47
Chamber radius, b [m]	0.01
Bunch pop., N_b $(\times 10^{10})$	2.13
Bunch spacing, ΔT_b [ns]	18
Number of bunches, n_b	50

COLLECTIVE EFFECT ESTIMATES

Space Charge

The Space Charge (SC) effect may apply undesired effects on the beam like intensity limitation, emittance growth, tune shift [5–7]. The incoherent tune shift by space charge effect can be estimated by an analytical expression for the incoherent SC tune shift for Gaussian bunches is given by [8–10]:

$$\delta Q_y^{\mathrm{inc}} = -\frac{N_b r_e C}{(2\pi)^{\frac{3}{2}}\beta^2\gamma^3\sigma_z\sqrt{\epsilon_y}}\left\langle \frac{\sqrt{\beta_y}}{\sqrt{\beta_x\epsilon_x + {D_x}^2{\sigma_\delta}^2} + \sqrt{\epsilon_y\beta_y}}\right\rangle, \quad (1)$$

where r_e is the electron radius, C the circumference and N_b the bunch population, ϵ_x and ϵ_y the geometrical transverse emittances, D_x the horizontal dispersion and $\beta_{x,y}$ the horizontal and vertical betatron functions, respectively.

The maximum value is computed after the beam reaches the equilibrium emittance values in all planes for electron and positron beams. For the case of electron beam, $\delta Q_y^{\mathrm{inc}} = -0.09$ while for the case of the positron beam $\delta Q_y^{\mathrm{inc}} = -0.01$. For the electron beam, the values are small and thus the SC is not expected to pose a limitation with respect to transverse emittance blow up or particle losses. For the positron case, the tune shift may cause issue due to resonance crossing. Thus, it should be taken into account on the working point choice.

* ozgur.etisken@cern.ch

ISBN: 978-3-95450-227-1 ISSN: 2673-5490 doi:10.18429/JACoW-IPAC2022-THPOST004

EIC'S RAPID CYCLING SYNCHROTRON SPIN TRACKING UPDATE

V.H.Ranjbar*, F. Meot, H.Lovelace III, Brookhaven National Laboratory, Upton, NY
F. Lin, ORNL RAD, Oak Ridge Tennessee

Abstract

The Electron Ion Collider (EIC) to be built will collide polarized electrons and ions up to 140 GeV center of mass with a time averaged polarization of 70% and luminosity up to 10^{34} cm^{-2} s^{-1}. The EIC's Rapid Cycling Synchrotron (RCS) will accelerate 2 polarized electrons bunches from 400 MeV to energies of 5, 10 and 18 GeV and inject them into the EIC's Electron Storage Ring. The design of the RCS has progressed to accommodate a larger magnet free section for the detectors and to meet the space requirements of the RHIC tunnel. We present progress on full 6D spin tracking studies of the RCS with the updated lattice using the Zgoubi code to include magnet misalignments, field errors and corrections as well as radiative effects.

INTRODUCTION

The Electron Ion Collider (EIC) to be built will collide polarized electrons and ions up to 140 GeV center of mass with a time averaged polarization of 70% and luminosity up to 10^{34} cm^{-2} s^{-1}. The EIC's Rapid Cycling Synchrotron (RCS) will accelerate 2 polarized electrons bunches from 400 MeV to energies of 5, 10 and 18 GeV and inject them into the EIC's Electron Storage Ring. To accommodate a longer magnet free section around the detectors we had to re-design the RCS's straight sections around 6 and 8 o'clock. The RCS is designed to accept four 7nC bunches from the pre-injector and merge them to achieve two 28nC bunches at injection energy and accelerate these two bunches to extraction energy.

The redesign made recovering the polarization and off-momentum dynamic aperture necessary to accelerate with the projected longitudinal emittance after the merge challenging. However as is detailed in another paper in these proceedings [1] a sufficient aperture and polarization transmission was achieved. In this paper we focus on the aspects of the polarization transmission for the new design. In particular we study the impact of misalignment and field errors.

IMPACT OF MISALIGNMENTS

Initial efforts with the new RCS lattice layout yielded optics which had very little beta-beat and a large off-momentum aperture. The estimated polarization loss at the level of 5 sigma also yielded polarization losses due to intrinsics less than 1%. In the past we would use an arbitrary metric of polarization transmission for a 1000 mm mrad rms emittance beam distribution. This of course was orders of magnitude higher than our physical aperture would permit. Previous lattices yielded intrinsic spin resonance induced polarization loss as estimated by DEPOL of under 5% at 1000 mm mrad. This initial lattice yielded transmissions of 15% at 1000 mm mrad, yet at the relevant operating emittances (40 mm mrad) we shouldn't have seen any polarization loss. However studying the effect of imperfection spin resonances driven by closed orbit distortions showed a lower threshold in terms of RMS orbit distortion for polarization loss. This of course is to be expected since it is well understood that the strength of both imperfection and intrinsic spin resonances are correlated due to their shared harmonic structure. Thus reducing the strength of the intrinsic spin resonances has the added benefit of reducing the strength of the average imperfection spin resonances. We revisited the RCS optics design and further pushed the intrinsic induced polarization losses to 8%, this did introduce some level of beta-beating however the overall off-momentum dynamic aperture was recovered and the sensitivity of the imperfections spin resonances to RMS orbit distortions was reduced as can be seen in Fig. 1.

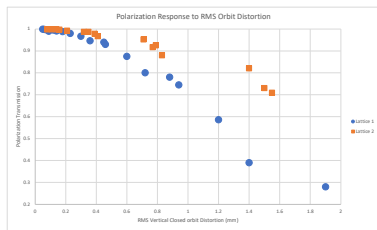

Figure 1: Comparison of polarization transmission due to imperfection spin resonances as function of RMS orbit distortion. Lattice 1, was our first RCS optics attempt with 15% intrinsic resonance induced losses at RMS emittance of 1000 mm mrad. Lattice 2 was our second and last RCS optics configuration with 8% losses at the same RMS emittance. This reduced imperfection spin resonance sensitivity as can be seen in the plot.

These results were confirmed using direct spin-orbit tracking in Zgoubi [2, 3] considering misalignments on the level of 0.6 mm RMS in the vertical plane and 0.3 mm RMS in the horizontal plane, as shown in Fig. 2.

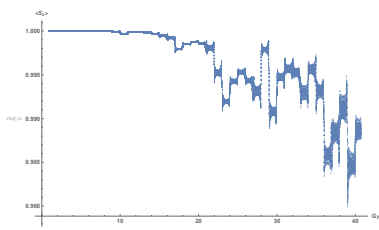

Figure 2: 13 particle tracking with 0.6 mm RMS vertical and 0.3 mm RMS horizontal closed orbit distortion.

* vranjbar@bnl.gov

ISBN: 978-3-95450-227-1 ISSN: 2673-5490 doi:10.18429/JACoW-IPAC2022-THPOST005

TRACKING DYNAMIC APERTURE IN THE iRCMS HADRONTHERAPY SYNCHROTRON*

François Méot†, Piyush Nanubhai Joshi, Nicholaos Tsoupas, BNL, Upton, NY, USA
Joseph Paul Lidestri, Manny Subramanian, Best Medical International, Springfield, VA, USA

Abstract

Dynamic aperture (DA) studies which are part of the ion Rapid Cycling Medical Synchrotron (iRCMS) lattice design have been undertaken. They are aimed at supporting ongoing plans to launch the production of the six magnetic sectors which comprise the iRCMS racetrack arcs. The main bend magnetic gap is tight (see Appendix), so allowing smaller volume magnets and resulting in a compact ring. The DA happens to be commensurate with the mechanical aperture, thus tracking accuracy is in order. In that aim, DA tracking uses the OPERA field maps of the six 60 degree magnetic sectors of the arcs. Simulation outcomes are summarized here.

INTRODUCTION

The 400 MeV/u Carbon iRCMS is a 2-periodic racetrack layout, its 180° arcs are achromats, comprised each of three 60° sectors separated by 1.14 m long drifts with include a quadrupole at their center (Fig. 1). Each sector is a BDH-BF-BD-BF-BDH combined function (CF) dipole series (Fig. 2, details in the Appendix), the dipole parameters are given in Table 1. One of the LSS accommodates two RF stations, sized for 15 Hz rapid-cycling. The other LSS accommodates the 8 MeV/u beam injection and the extraction systems. Five quadrupoles are installed in each of the two 13.75 m long straight sections (LSS) of the racetrack, they serve to set the tunes, nominally in the region $\nu_x = 4.8$, $\nu_y = 4.4$. Table 2 summarizes the optical parameters of the ring, Fig. 3 displays the optical functions.

One 60° sector prototype has been manufactured, at present under AC magnetic field measurements at the magnet division of Brookhaven National laboratory (BNL)[1].

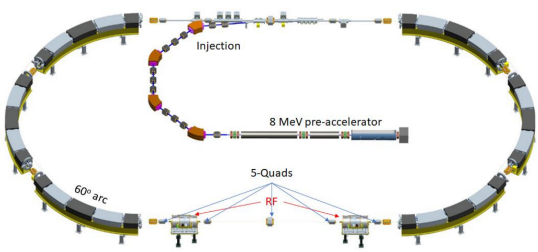

Figure 1: iRCMS ion ring.

A good agreement was found between the DC magnetic field measurements of the prototype 60° sector and the magnetic fields obtained from its OPERA model [1], confirming in particular magnetic lengths and focusing strength (Table 1). However, ray-tracing using the OPERA field maps showed that the 0.9 deg spacing (about 8 cm along the R=508 cm arc, see Appendix) between the magnets causes a 10 mm scalloping of the closed orbit around the R=508.022 cm reference along the sector [2]. This is not acceptable as it would eat up 20% of the ±2.5 cm horizontal aperture (Table 1) and 10 mm of a tight DA. As a consequence the sector has been re-designed, F and D-type dipole lengths have been re-optimized so that the former 0.9 deg spaces are filled with additional F and D-style laminations, leaving a marginal 0.034 deg spacing (3 mm along the R=508 cm arc), Fig. 2 [3]. In passing, this allowed salvaging the girder, main coil, and individual dipole tuning coils of the original design.

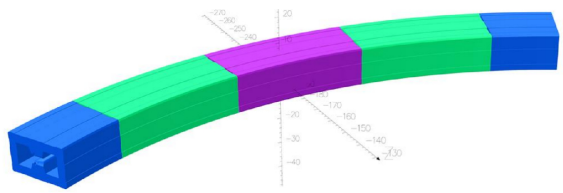

Figure 2: New design of the iRCMS 60 deg sector, with essentially null spacing between the CF dipoles, in order to ensure constant dipole field along the R=508.022 cm design arc and thus a circular reference orbit and maximal horizontal geometrical acceptance.

Table 1: Parameters of the CF Dipoles. Magnet current is of the form $I = I_{inj} + I_0 \sin(215t)$ for a 15 Hz cycling

Magnet	Arc-Length [deg]	Bend Angle [deg]	K1 [m^{-2}]	Comments	Hor. Apert. [cm]	Vert. Apert. [cm]
BDH	7.2	7.2	1.477	defocusing	±2.5	±1.75
BF	14	14	1.477	focusing	±2.5	±1.75
BD	14	14	1.477	defocusing	±2.5	±1.75
BF	14	14	1.477	focusing	±2.5	±1.75
BDH	7.2	7.2	1.477	defocusing	±2.5	±1.75

Regarding the RF system, two ferrite loaded cavities have been built; measured gap voltages is 15 kV over the full RF range of 0.6-3.35 MHz while sweeping at 15 Hz. These two single-gap RF stations therefore provide 30kV per turn, more than necessary; synchronous phase during acceleration is in 30 deg region. These are the typical parameter values liable to be considered for DA estimates.

* Work supported by a TSA agreement between Best Medical International and Brookhaven Science Associates, LLC under Contract No. DE-AC02-98CH10886 with the U.S. Department of Energy.
† fmeot@bnl.gov
[1] Under a Technical Scientific Agreement (TSA) with Best Medical International (BMI).

ISBN: 978-3-95450-227-1 ISSN: 2673-5490 doi:10.18429/JACoW-IPAC2022-THPOST006

SIMULATIONS OF THE SUITABILITY OF A DC ELECTRON PHOTOGUN AND S-BAND ACCELERATING STRUCTURE AS INPUT TO AN X-BAND LINAC

S. D. Williams*, R. P. Rassool, S. L. Sheehy[1], G. Taylor, M. Volpi
The University of Melbourne, 3010 Parkville, Australia
R. Auchettl, R. T. Dowd, AS - ANSTO, 3168 Clayton, Australia
[1]also at AS - ANSTO, 3168 Clayton, Australia

Abstract

Work has been underway for some time to design a compact electron beamline utilising X-band linear accelerating structures in the new Melbourne X-band Laboratory for Accelerators and Beams (X-LAB). The original design utilised an S-band RF photogun as an input to a pair of high gradient X-band linear accelerating structures, but we have been motivated to investigate an alternative starting section to allow for initial testing. This will utilise a DC photogun and S-band accelerating structure similar to those used at the Australian Synchrotron. Simulation results incorporating space charge of a beamline composed of a DC photogun, S-band accelerating structures, and two high gradient X-band structures will be presented. These simulation results will be optimised for minimum emittance at the end of the beamline.

INTRODUCTION

As part of the arrival of the X-Box test stand at the University of Melbourne we have been planning a beamline that can be installed in the University of Melbourne X-LAB accelerator hall utilising X-band RF accelerating cavities of a similar design to the structures used by the compact linear collider [1, 2].

For optimal beam capture and acceleration an RF photogun is planned as an injector, but in this document we investigate the possibility of integrating a relatively low-cost alternative for use during commissioning, that is a 100 keV DC photogun. However, the use of non-relativistic electrons ($\beta \approx 0.55$) will cause acceptance, capture, and acceleration issues as the X-band structures are matched to $\beta \approx 1$.

To alleviate this, we have investigated the possibility of using an S-band RF buncher available locally to increase the energy of the bunch to an satisfactory level for acceptance.

X-BAND RF ACCELERATING STRUCTURE ACCEPTANCE

The X-band structure in question is a TW X-band structure operating at 11.9942 GHz similar to the CLIC T24 structure [3]. Following simulation in CST Microwave Studio [4] its fieldmap is exported for further use in simulations, and can be seen in Figure 1. At this stage in Melbourne X-LAB planning it is estimated to be fed 20 MW of RF power, yielding an average accelerating gradient of 70 MW m^{-1}, with a maximum gain per structure of approximately 17.5 MeV.

To demonstrate the acceptance issues we shall show results from single particle tracking simulations using the code ASTRA [5]. We use single particle simulations for this section due to their simplicity, and ease of cross checking by numerical integration. Although we neglect whole bunch dynamics at this stage it is very unlikely for a whole bunch to pass through without issues if it a single particle can't.

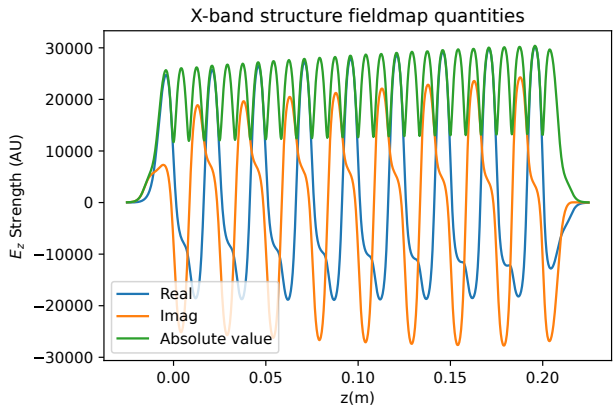

Figure 1: X-band structure fieldmap used.

To investigate acceptance we simulate a single on axis electron multiple times, for different initial Kinetic Energies (KE) and structure phases in increments of 1°. A particle is deemed to have passed though if it reaches the other end of the accelerating structure, and its longitudinal momentum p_z has not dropped below 200 keV c^{-1} (KE 37.75 keV). This threshold was chosen after inspection of multiple simulations to give good separation between simulations where the particle passes through or is brought to near halt.

In Figure 2 we present a combined plot showing the number of simulations deemed to have passed according the previous criteria for a given initial KE, and the maximum energy gain for a given initial KE. The range of phase acceptance (acceptable starting phases), in blue, is calculated by counting the number of simulations where a particle is transmitted for the given initial energy. We see that we need an initial energy of approximately 150 keV to have any phase range acceptable for transmission, and then as KE increases the entire phase range is allowed for transmission. We specifically note that this is for transmission only, not acceleration;

* scottdw@student.unimelb.edu.au

ISBN: 978-3-95450-227-1 ISSN: 2673-5490 doi:10.18429/JACoW-IPAC2022-THPOST007

SLOW-CONTROL LOOP TO STABILIZE THE RF POWER OF THE FLUTE ELECTRON GUN

M.-D. Noll*, N. Smale, A. Böhm, O. Manzhura, M. Schuh, R. Ruprecht, J. Jelonnek, A.-S. Müller,
Karlsruhe Institute of Technology, Karlsruhe, Germany
I. Kriznar, Paradigma-Tech, Senzana, Slovenia

Abstract

The linear accelerator FLUTE (Far Infrared Linac and Test Experiment) at KIT serves as a test facility for accelerator research and for the generation of ultra-intense coherent THz radiation.
To achieve stable THz photon energy and optimal beam trajectory, the energy of the electrons emitted from the RF photo-injector must be stable. The accelerating voltage of the RF cavity has been shown to be a significant influencing factor. Here, we report on the development of a slow closed-loop feedback system to stabilize the RF power and thus the accelerating voltage in the RF photo-injector cavity. With this closed-loop feedback system the relative standard deviation of the RF power in the cavity can be improved by 8.5 %.

INTRODUCTION

At FLUTE, the electron bunches are created and pre-accelerated to 7 MeV in the low-energy section, before being accelerated to 41 MeV by a traveling wave LINAC structure [1–3] (see Fig. 1).
The electron gun of the injector is of the RF photo injector type (see [4]) that uses a copper cathode where electrons are released when struck by UV laser pulses and a 2.5 cell standing wave RF cavity driven by a 2.9979 GHz low-level RF (LLRF) system, which currently does not correct for long-time drifts. Both for guidance along the beam pipe and scientific experiments, the electron energy is a key figure of the accelerator. To ensure proper operation it has to be kept constant over long periods of time (up to hours).

* marvin-dennis.noll@kit.edu

As the RF-induced E-field in the RF cavity has major influence on the electron energy, it has to be kept stable to achieve stable electron emission. Simulations showed the relative standard deviation of the RF power has to be less than 0.01 %. When measured with a pick-up inside one of the cavity cells for every pulse of the LLRF, apart from variations from one shot to another there are also slower disturbances of varying period and an even slower drift, see Fig. 2. Some sources of these slow variations have been identified in the past to be due to the power grid, the influence of which has already been mitigated in [5]. Other disturbances mainly originate from drifts of temperature or other parameters. These effects are hard to predict and to model.

Because of that, the slow-control approach described here needs no model or a-priori knowledge about the disturbances.

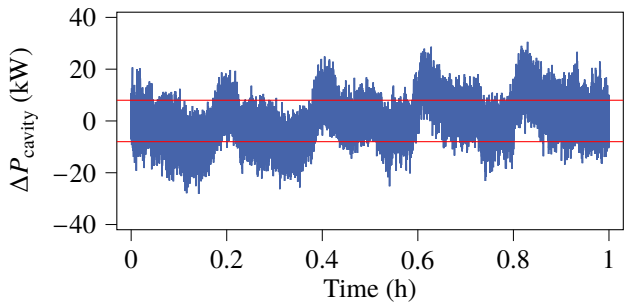

Figure 2: Deviation of the RF power as measured in the cavity from the target power $P_{\text{cavity}} = 9.5\,\text{MW}$; required maximum standard deviation in red.

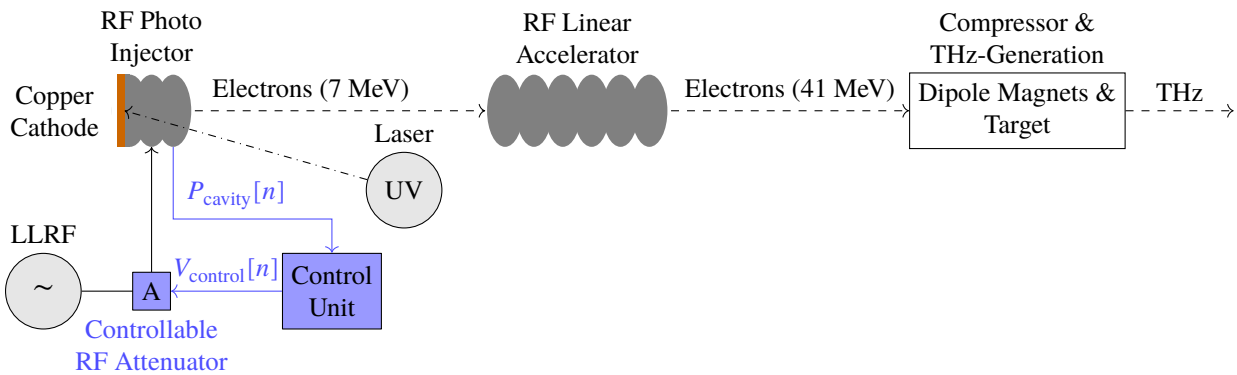

Figure 1: Simplified FLUTE architecture; components of the control system proposed here highlighted in blue (adapted from [1]).

ISBN: 978-3-95450-227-1 ISSN: 2673-5490 doi:10.18429/JACoW-IPAC2022-THPOST008

STATUS OF THE FLUTE RF SYSTEM UPGRADE

A. Malygin†, O. Manzhura, R. Ruprecht, M. Schuh, N. Smale, A.-S. Müller
Karlsruhe Institute of Technology, Karlsruhe, Germany

Abstract

FLUTE (Ferninfrarot Linac- Und Test-Experiment) is a compact versatile linac-based accelerator test facility at Karlsruhe Institute of Technology (KIT). Its main goal is to serve as a platform for a variety of accelerator studies and to generate intense ultra-short THz pulses for photon science. It will also serve as an injector for a Very Large Acceptance compact Storage Ring (VLA-cSR), which will be realized at KIT in the framework of the compact STorage Ring for Accelerator Research and Technology (cSTART) project. To achieve acceleration of electrons in the RF photo-injector and linac (from FLUTE) with high stability, it is necessary to provide stable RF power. For this goal, an upgrade of the existing RF system design has been proposed and is currently being implemented. This contribution will report on the updated RF system design and the commissioning status of the new RF system components.

INTRODUCTION

FLUTE [1] is an accelerator R&D facility that will allow the study of bunch compression with all related effects like space charge, coherent synchrotron radiation (CSR) as well as the systematic investigation of different generation mechanisms for coherent THz radiation in a comparison between experiment and theory. It will be used as a test bench for the development of new diagnostics and instrumentation for fs bunches. Furthermore, it will serve as an injector for the compact storage ring of the cSTART project [2], and to enable study for future compact, broadband accelerator-based THz user-facilities. All applications mentioned above will require, and strongly benefit from, a high stability of electron beam parameters (from 40 up to 90 MeV), low dark current, and a repetition frequency up to 50 Hz. In order to achieve these parameters, an upgrade of the FLUTE RF system has been proposed. In this contribution, an update on the new RF system will be presented. The main components of the new FLUTE RF system include: new RF photo-injector, two RF units (one for the new RF photo-injector and the other one for the linac). Also, two new RF waveguide systems for the RF photo-injector and the linac have been designed.

UPGRADE OF THE RF SYSTEM

In [1] the existing FLUTE layout is described. It consists of a 45 MW klystron where RF power is split between the RF photo-injector and the linac. The RF photo-injector gun used at FLUTE was designed and operated at CTF2, CERN [3]. It consists of 2.5 cells and was optimized for high charge beams (bunch trains with up to 13 nC per bunch). The energy of electrons that can be achieved with the existing FLUTE configuration at the end of the linac is up to 50 MeV. To increase the stability of the electron beam parameters and also increase the electron energy at the output of the linac, two new RF units will be utilized. Each RF unit consists of a modulator and a klystron. The first RF unit will provide RF power for the new RF photo-injector and the second for the linac. The first RF unit (K100) was already delivered by ScandiNova [4] and tested at FLUTE. The results of the site acceptance tests (SAT) for K100 RF unit are shown in Table 1. The RF unit (K300) that will provide RF power for the linac is presently being assembled by ScandiNova and will be delivered in the middle of 2022. The main design parameters of the K300 RF unit are presented in Table 2.

Table 1: K100 RF Unit SAT Results

Parameter	Value	Unit
RF power	10.6	MW
Frequency	3	GHz
Output voltage	177	kV
Output current	135	A
RF pulse top flatness	1	%
RF pulse length (top)	4.5	usec
Repetition rate	50	Hz
Pulse to pulse voltage stability	18	ppm

Table 2: K300 RF Unit Design Parameters

Parameter	Value	Unit
RF power	36.8	MW
Frequency	3	GHz
Output voltage	285	kV
Output current	315	A
RF pulse top flatness	1	%
RF pulse length (top)	4.5	usec
Repetition rate	50	Hz
Pulse to pulse voltage stability	20	ppm

New RF Photo-Injector

The new RF photo-injector has been designed and built by RadiaBeam [5]. It has 1.5 cells, electron energy up to 5.5 MeV (with 9.5 MW of RF power), exchangeable cathode and repetition rate of up to 50 Hz. It can operate in a wide range of bunch charges from 1 pC to 1 nC with a copper cathode. It has been successfully tested with low RF power during factory acceptance tests (FAT) and the results of the FAT as well as the main design parameters are presented in Table 3. High power RF tests at FLUTE are planned after delivery in the middle of 2022.

The RF photo-injector will be delivered with a new solenoid and an alignment stand for the RF photo-injector. The solenoid itself will be aligned on the existing motor-

† anton.malygin@kit.edu

ISBN: 978-3-95450-227-1 ISSN: 2673-5490 doi:10.18429/JACoW-IPAC2022-THPOST009

SIMULATION STUDY OF A BUNCH COMPRESSOR FOR AN ACCELERATOR-BASED THz SOURCE AT THE EUROPEAN XFEL

P. Boonpornprasert*, G.Georgiev, X. Li, M. Krasilnikov, A. Lueangaramwong
Deutsches Elektronen-Synchrotron DESY, Zeuthen, Germany

Abstract

The European XFEL has planned to perform pump-probe experiments using its X-ray pulses and THz pulses. A promising concept to provide the THz pulses with a pulse repetition rate identical to that of the X-ray pulses is to generate them using an accelerator-based THz source. The THz source requires a bunch compressor in order to manipulate the longitudinal phase space of the electron bunch to match with various options of THz radiation generation. This paper presents and discusses simulation study of the bunch compressor for the THz source.

INTRODUCTION

Research and development (R&D) of an accelerator-based THz source prototype for pump-probe experiments at the European XFEL are ongoing at the Photo Injector Test Facility at DESY in Zeuthen (PITZ). The R&D have been conducted in two parts. The first part is a proof-of-principle experiment to generate THz SASE FEL radiation by using an LCLS-I undulator driven by an electron bunch from the PITZ accelerator [1, 2]. The second part is conceptual design studies of an ideal accelerator-based THz source facility that can be established at the European XFEL site and used for the pump-probe experiments.

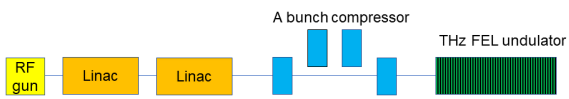

Figure 1: The basic concept layout of the ideal THz source.

A basic concept layout of the ideal THz source is shown in Figure 1. The layout consists of an RF electron gun, two identical RF linacs, a bunch compressor, and a THz FEL undulator. Models and locations of the RF gun and the first linac in the layout are identical to those at the PITZ facility with an additional linac downstream from the first one. The accelerators can produce an electron beam with an average beam momentum of up to 35 MeV/c, a bunch charge of up to 5 nC, and similar beam emittance values that are achievable at the PITZ facility [3, 4].

The ideal THz source has been designed to produce intense, tunable, and narrow-band THz radiation by means of a SASE FEL, a seeded FEL, and superradiant undulator radiation (SUR) as the proof-of-principle experiments are ongoing at the PITZ facility. The different means of THz radiation generation require different temporal shapes of the electron bunch. For example, a several-ps long electron bunch is required for the SASE FEL, a temporal-modulated bunch is necessary for the seeded FEL, and a sub-ps long bunch is essential for the SUR. Therefore, a bunch compressor between the second linac and the THz undulator is needed to manipulate the longitudinal phase space of the beam in order to achieve the required temporal shapes.

In this paper, we present simulation study of a bunch compressor that can provide an electron bunch with a sub-ps bunch length, which is required for the SUR, at its full compression. This bunch compressor can be used for the other required bunch shapes, a several-ps long electron bunch and a temporal-modulated bunch, which will be studied in future work. First, the beam requirements of the SUR are presented in the next section. Then, specifications of the bunch compressor which is based on BC0 of the European XFEL [5] are presented. After that, details of beam dynamics simulations for bunch compression of a 100 pC electron bunch with different beam momenta are presented and discussed. The OCELOT [6] was used for the simulations. Finally, a summary and outlook of this work are given.

BEAM REQUIREMENTS

SUR requires an electron bunch with a bunch length equal to or shorter than the fundamental wavelength of the undulator radiation, so the radiation is emitted coherently [7]. Specifications of an undulator for the SUR are assumed to be identical to those in [4]. The undulator is a helical undulator with a period length of 40 mm. The undulator parameter (K) is variable in a range of 0.26 to 1.90. Figure 2 shows the calculated fundamental wavelengths with $K = 0.26$ and $K = 1.90$ of the undulator radiation as a function of the electron beam momentum. The vertical range of 20 µm to 100 µm is the required range of the FEL wavelength in [4]. By considering the fundamental wavelength of 100 µm from the plots in Fig. 2, the rms bunch length up to 0.333 ps (100 µm/c) within a momentum range of 7.84 to 15.76 MeV/c is required for the SUR. This requirement will be used as a benchmark for beam dynamics simulations.

BUNCH COMPRESSOR FEATURES

The lattice configuration of the bunch compressor is shown in Figure 3. The configuration consists of two sets of quadrupole doublet and a magnetic chicane. The doublet Q1 & Q2 is used for matching the beam into the bunch compressor, while the doublet Q3 & Q4 is used for downstream transport and matching. Parameters of the chicane are based on the bunch compressor BC0 at the European XFEL [5], which are summarized in Table 1.

* prach.boonpornprasert@desy.de

ISBN: 978-3-95450-227-1 ISSN: 2673-5490 doi:10.18429/JACoW-IPAC2022-THPOST010

THE FRASCATI DAFNE LINAC AND THE BEAM TEST FACILITY (BTF) SETUPS FOR IRRADIATION *

C. Di Giulio†, A. B. Buonomo, F. Cardelli, D. Di Giovenale, L. G. Foggetta,
D. Moriggi on behalf of the eRAD project TEAM
INFN-LNF, Via E. Fermi 54, 00044 Frascati (RM), ITALY

Abstract

The Beam-Test Facility (BTF) of the DAΦINE accelerator complex in the Frascati laboratory of the Italian National Institute of Nuclear Physics (INFN) is devoted to the development and testing of particle detectors.

The LINAC and BTF irradiation setups are discussed in this work.

INTRODUCTION

In April 2020, the upgrade project of the facility with a new line for testing particle detector [1–3] aimed at improving the performance of the facility extending the range of application for the LINAC beam extracted to the BTF lines, in the directions of hosting irradiation test [4] and providing electron irradiation also for industrial users.

The original BTF line is in operation since 2002 [5, 6], and from 2004 operates in opportunistic mode [7] during the running of the Frascati electron-positron collider.

The Conceptual Design Report (CDR) presented in 2016 [8] and the commissioning of the new line are described in [9-11].

From 2022 both lines are available for the users. The main line of the line 1 is dedicated to the PADME experiment, the straight line of the dipole DHSTB002 (see Fig. 1) is dedicated to the irradiation test.

The irradiation test usually requires a non-opportunistic mode of operation of the LINAC, to manage the beam using all the possible range of pulse length, repetition rate and charge to fulfil the requirements of the users. All the possible value of the LINAC setup in dedicated mode are shown in Table 1.

THE DAFNE LINAC FOR IRRADIATION

The DAFNE LINAC could produce bunches of electrons and positrons for the Beam Test Facility. The BTF is used usually for single particle test of detectors but is authorized to receive up to 10^{10} particles per second, limit useful for the irradiation test.

The DAFNE LINAC working point could be deeply changed from the ordinary setup used for the DAFNE injection at 510 MeV.

To obtain low energy beam up to 165 MeV with a primary electron beam with enough pulse charge that fulfills irradiation test requirements, we need to modify the RF setup and manage the magnets to transfer this low energy beam in the BTF (see Figs. 2 and 3).

Table 1: The DAFNE LINAC Performances

	Design	Operational
Electron beam final energy	800 MeV	510 MeV
Positron beam final energy	550 MeV	510 MeV
RF frequency	2856 MHz	
Positron conversion energy	250 MeV	220 MeV
Beam pulse rep. rate	1 to 50 Hz	1 to 50 Hz
Beam macropulse length	10 nsec	1.4 to 300 nsec
Gun current	8 A	8 A
Beam spot on positron converter	1 mm	1 mm
norm. Emittance (mm. mrad)	1 (electron) 10 (positron)	< 1.5
rms Energy spread	0.5% (electron) 1.0% (positron)	0.5% (electron) 1.0% (positron)
electron current on positron converter	5 A	5.2 A
Max output electron current	>150 mA	500 mA
Max output positron current	36 mA	85 mA
Trasport efficiency from capture section to linac end	90%	90%
Accelerating structure	SLAC-type, CG, 2π/3	
RF source	4 x 45 MWp sledded klystrons TH2128C	

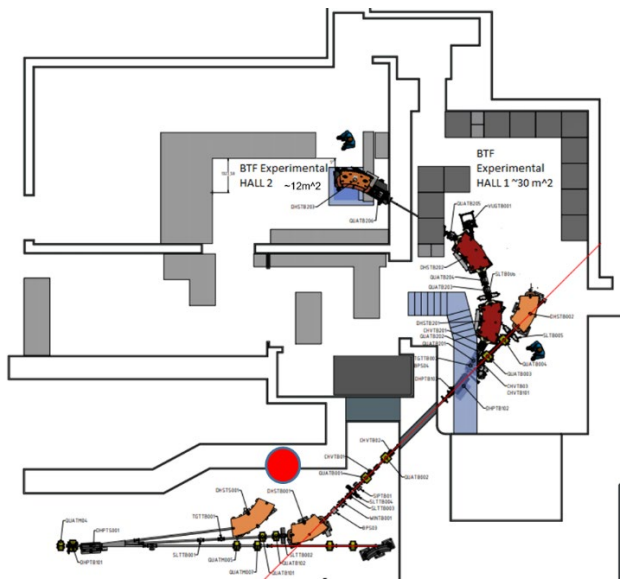

Figure 1: The BTF layout with the 2 lines.

* Work supported by Regione Lazio with the "Progetti Strategici 2019" public call, within POR-FESR 2014-2020 program
† claudio.digiulio@lnf.infn.it

ISBN: 978-3-95450-227-1 ISSN: 2673-5490 doi:10.18429/JACoW-IPAC2022-THPOST011

SuperKEKB ELECTRON POSITRON INJECTOR LINAC UPGRADE FOR HIGHER CHARGE AND LOWER EMITTANCE

K. Furukawa*, H. Ego, Y. Enomoto, N. Iida, T. Kamitani, M. Kawamura, S. Matsumoto, T. Matsumoto, T. Miura, M. Satoh, A. Shirakawa, T. Suwada, M. Yoshida,
High Energy Accelerator Research Organization (KEK), Tsukuba, Japan

Abstract

KEK electron positron injector LINAC has established simultaneous top-up injections in 2019 for 5 rings of SuperKEKB DR, LER, HER, PF ring and PF-AR as a base of the both elementary particle physics and photon science experiments even under a quite short beam lifetime. It improved the injection stabilities while the SuperKEKB broke the world record of the collision luminosity of the previous project KEKB. As the collision performance improves, the beam-beam effect makes the dynamic aperture shrink, and the beam lifetime reduces further. Thus, it became inevitable for the injector to be upgraded in order to resolve the contradictory improvements of higher charge and lower emittance of injection beams regarding beam wakefield till 2025. The upgrade plan is described including pulsed magnets, an energy compression system, accelerating structures, girders, positron generator and so on.

INTRODUCTION

The KEK electron positron injector LINAC [1, 2] established the simultaneous top-up injections in to 5 storage rings in 2019 in order to support both the SuperKEKB particle collider experiment with DR, LER and HER rings [3], and photon science experiment at PF ring and PF-AR as depicted in Fig. 1. It succeeded in improving the efficiency of the SuperKEKB collision experiment by 237% before and after the introduction of the simultaneous top-up injections [4]. This injection scheme became indispensable because the beam lifetime of the SuperKEKB ring is quite short, especially at the LER positron ring less than 10 minutes in 2021. Based on this operation arrangement, the injector LINAC gradually improves the injection performance and contributes to the achievement of the world record of collision luminosity of SuperKEKB [5].

It has been recognized that the dynamic aperture of the rings becomes small and the beam lifetime is shorter as the beam-beam interactions becomes noticeable. While expanding the storage and injection physical aperture, it is required to urge the injector to enhance the injection beam property. Straightforward multiplication of the LINAC beam may drastically increase the injection beam emittance by the wakefield effect in the accelerating structure. Therefore, it is necessary to reduce the emittance in parallel. We are planning to improve the performance of the injector in line with the progress of the improvement of collision performance in storage rings, and the outline the plan is presented including the modification and expansion of the equipment.

* kazuro.furukawa@kek.jp

INJECTOR IN KEK ACCELERATOR COMPLEX

In order to realize the advanced injection into SuperKEKB, we have been remodeling the injector since 2011 while maintaining the injection for the two light sources, PF ring and PF-AR. For a low emittance high charge electron beam, we have developed an RF electron gun that employs a combination of a quasi-travelling wave side-coupled cavity (QTWSC), an iridium-cerium alloy photocathode, and a high-power solid-state laser system, and promoted its stabilization [6].

The typical injection beam is limited up to 2 nC per bunch and 2 bunches at 50 Hz because of the emittance blow-up by wakefield effect in the downstream LINAC and coherent synchrotron radiation (CSR) effect in the beam transport. For the high current positron beam, a tungsten target is irradiated with the electron beam from a thermionic gun, and the positron is captured by the pulsed magnetic field of about 5 T in a flux concentrator (FC) and a long solenoid section with magnetic field of 0.5 T. After decelerating and bunching with a large-diameter S-band accelerating structure, the positron beam is accelerated to the damping ring (DR). Initially, there was concern that a discharge would occur in the 0.2 mm gap of FC, but the issue was solved by employing copper-nickel alloy [7].

In order to establish the simultaneous top-up injections with pulse-to-pulse modulation (PPM), various high-precision pulsed operation devices such as pulsed magnets [8] and beam instrumentation have been developed, and we have succeeded in realizing independent beam operation for each storage ring by developing the event-based wide-area synchronous beam control mechanism [9].

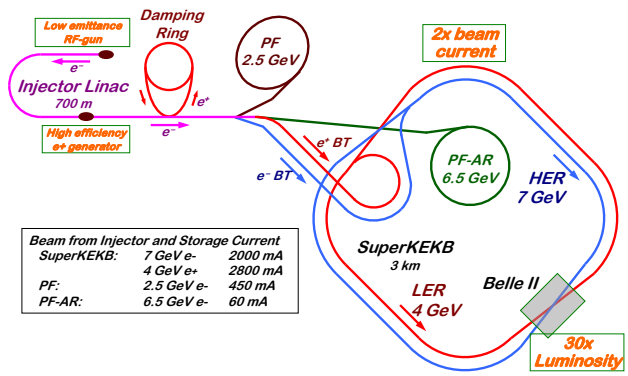

Figure 1: Layout of KEK electron/positron accelerator complex.

ISBN: 978-3-95450-227-1 ISSN: 2673-5490 doi:10.18429/JACoW-IPAC2022-THPOST012

ACHIEVEMENT OF 200,000 HOURS OF OPERATION AT KEK 7-GeV ELECTRON 4-GeV POSITRON INJECTOR LINAC

K. Furukawa*, M. Akemoto, D. Arakawa, Y. Arakida, H. Ego, Y. Enomoto, T. Higo, H. Honma, N. Iida, K. Kakihara, T. Kamitani, H. Katagiri, M. Kawamura, S. Matsumoto, T. Matsumoto, H. Matsushita, K. Mikawa, T. Miura, F. Miyahara, H. Nakajima, T. Natsui, Y. Ogawa, S. Ohsawa, Y. Okayasu, T. Oogoe, M.A. Rehman, I. Satake, M. Satoh, Y. Seimiya, T. Shidara, A. Shirakawa, H. Someya, T. Suwada, M. Tanaka, D. Wang, Y. Yano, K. Yokoyama, M. Yoshida, T. Yoshimoto, R. Zhang, X. Zhou, KEK, Tsukuba, Japan
Y. Bando, SOKENDAI, Tsukuba, Japan

Abstract

KEK electron positron injector LINAC initiated the injection operation into Photon Factory (PF) light source in 1982. Since then for 39 years, it has served for multiple projects, namely, TRISTAN, PF-AR, KEKB, and SuperKEKB. Its total operation time has accumulated 200 thousand hours on May 7, 2020. We are extremely proud of the achievement following continuous efforts by our seniors. The construction of the injector LINAC started in 1978, and it was commissioned for PF with 2.5 GeV electron in 1982. In parallel, the positron generator linac was constructed for the TRISTAN collider project. The slow positron facility was also commissioned in 1992. After the KEKB asymmetric-energy collider project was commissioned in 1998 with direct energy injections, the techniques such as two-bunch acceleration and simultaneous injection were developed. As the soft structure design of the LINAC was too weak against the great east Japan earthquake, it took three years to recover. Then the construction and commissioning for the SuperKEKB project went on, and the simultaneous top-up injection into four storage rings contributes to the both elementary particle physics and photon science.

INTRODUCTION

In the experimental particle physics research in the 1970s, there was growing expectation for the world-class Japanese domestic collider after the successes in the world-level theoretical research. On the other hand, in the field of synchrotron radiation science, there were demands for the establishment of a synchrotron radiation research institute with a dedicated accelerator. In order to realize both of those accelerator projects, a 400-m electron linear accelerator capable of 2.5 GeV direct energy injection was constructed in 1982.

Since then, the injector had been in operation for 38 years in 2020, supporting the consecutive accelerator projects of Photon Factory (PF), TRISTAN, KEKB, PF-AR, and SuperKEKB as depicted in Figs. 1, 3, 5 and 2. It has finally achieved 200,000 hours of operation in May 2020. The brief operation history would be given.

* kazuro.furukawa@kek.jp

2.5-GeV INJECTION FOR PF/TRISTAN

At the time of the initial construction since 1978, several university-based accelerator facilities had achieved research successes in Japan. It was fortunate that a new linear electron accelerator had been built to share resources for advanced scientific research in both particle physics and synchrotron radiation science, which were based on the accumulated experiences at universities. The situation might be similar to recent J-PARC's focus on both nuclear and particle physics, as well as neutron and muon science. It seems that there are not many accelerator projects in the world that have multiple disciplines from the beginning. Those Japanese accelerators are quite unique that deliver beams for multiple science fields.

While many researchers of synchrotron radiation research wanted the institute independent from particle physics, the accelerator science played a role as a bridge between those two. One hundred sixty of 2-m-long S-band traveling-wave accelerating structures with $2\pi/3$ mode quasi-constant gradient were installed, and driven by forty 20-MW klystrons to achieve 2.5 GeV electron and positron beams [1]. 2.5 GeV direct energy injection was made for PF and 2.5 GeV electron positron beams from the injector were accelerated through the TRISTAN synchrotron chain for the 32 GeV collision as depicted in Fig. 1.

When the synchrotron radiation facility, PF, was completed, there must be an enthusiastic response to the dedicated synchrotron radiation facility that would promote research in synchrotron radiation science. The TRISTAN project also began to take the lead in high-energy experimental physics, after Japanese theorist had contributed to

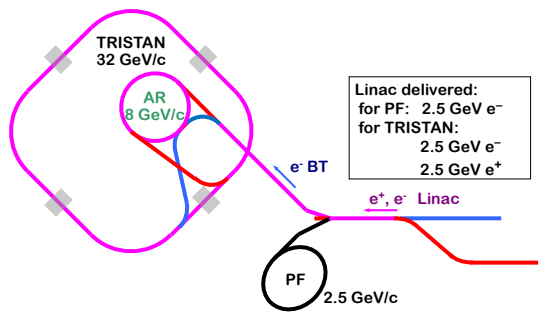

Figure 1: Injection for TRISTAN and PF.

ISBN: 978-3-95450-227-1 ISSN: 2673-5490 doi:10.18429/JACoW-IPAC2022-THPOST013

DEVELOPMENT OF A DETECTION SYSTEM FOR QUASI-MONOCHROMATIC THz PULSE BY A SPATIALLY MODULATED ELECTRON BEAM

K. Murakoshi†, Y. Koshiba, Y. Tadenuma, P. Wang, M. Washio,
WISE, Waseda University, Tokyo, Japan
K. Sakaue, Photon Science Center, The University of Tokyo, Tokyo, Japan
R. Kuroda, AIST, Bunkyo, Japan

Abstract

We have studied the generation of the broadband Terahertz (THz) pulse using a compact linear accelerator. The THz pulse is generated by control of an electron beam angle to Cherenkov radiation angle. In addition, we have succeeded in producing a quasi-monochromatic THz pulse by the spatially modulated electron beam by passing through a slit. This work aims to develop a detection system to elucidate the spectrum of the quasi-monochromatic THz pulse. To detect it stably in a noisy radiation environment, the stability of probe laser system for Electro Optic (EO) sampling and timing synchronization system are important. In this conference, the generation method of each THz pulses, the results of development of detection system, and future prospect will be reported.

INTRODUCTION

Terahertz (THz) wave is permeable like radio wave and travels in straight line like light because its frequency range lies between them. In addition, it has fingerprints spectrum originated from characteristic absorption peaks specific to the substances such as the excitation energy of intermolecular vibrations. These characteristics are expected for applied research, for instance, transmission imaging technology [1] and morphological change [2]. Accelerator-based THz light sources are attractive because they can produce the high intensity pulses needed for these applications. However, the small number of these facilities restrict opportunities to use them.

With the aim of improving this situation, we are trying to develop the compact monochromatic THz light source. The THz pulse have been generated by utilizing coherent Cherenkov radiation with electron beams of 4.8 MeV from a photocathode rf-gun. Furthermore, we have generated a quasi-monochromatic THz pulse from spatially modulated electron beam using a slit. However, the quasi-monochromatization of the THz pulse is only confirmed by using a few bandpass filters. Therefore, this study aims to reveal the spectral characteristics of quasi-monochromatic THz pulse.

THz PULSE GENERATION

Broadband THz Pulse from the Tilted Electron Bunch

We have utilized coherent Cherenkov radiation to generate a THz pulse. Coherent radiation is obtained when an electron bunch size is sufficiently smaller than the wavelength of the radiation, leading to the increase of the intensity from an electron bunch. We utilize the Cherenkov radiation by way of the THz pulse generation. When an electron travels faster than the phase velocity of light in the medium, the Cherenkov radiation occurs at the specific radiation angle, called the Cherenkov angle θ_c, which is as follows [3]:

$$\theta_c = \cos^{-1}\left(\frac{1}{n\beta}\right), \quad (1)$$

where $\beta(=v/c)$ is the relative velocity of the electron to the phase velocity of light and n is the refractive index of the medium. The tilt control of the electron bunch can match the phases of the radiations from each electron in an electron bunch. When the electron bunch is tilted to the Cherenkov angle, the coherent radiation depending on the beam size is obtained as shown in Fig. 1. The beam size of our electron bunch is typically about 300 μm, which corresponds to 1.0 THz band so we can generate the broadband THz pulse less than 1.0 THz.

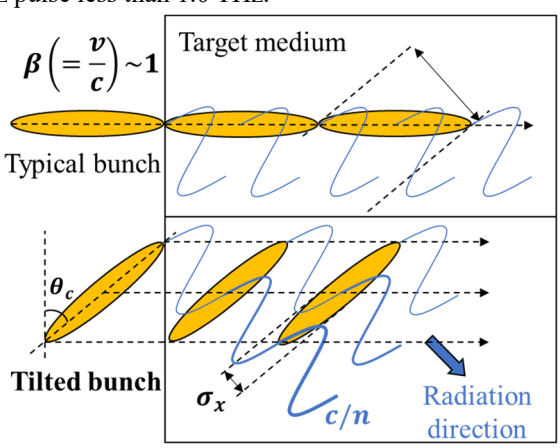

Figure 1: Schematic principle of THz pulse generation by coherent Cherenkov radiation.

† mura_koshi@akane.waseda.jp

ISBN: 978-3-95450-227-1 ISSN: 2673-5490 doi:10.18429/JACoW-IPAC2022-THPOST016

DEVELOPMENT PROGRESS OF HEPS LINAC*

C. Meng†, N. Gan, D. Y. He, X. He, Y. Jiao, J. Y. Li, J.D. Liu, X.H. Lu, Y. M. Peng, X.J. Nie, H. Shi, G. Shu, S. C. Wang, O. Z. Xiao, J. R. Zhang, Z.D. Zhang, Z.S. Zhou
Key Laboratory of Particle Acceleration Physics and Technology,
Institute of High Energy Physics, 100049, Beijing, China

Abstract

The High Energy Photon Source (HEPS) is a synchrotron radiation source of ultrahigh brightness and under construction in China. Its accelerator system is comprised of a 6-GeV storage ring, a full energy booster, a 500-MeV Linac and three transfer lines. The Linac is an S-band normal conducting electron linear accelerator with available bunch charge up to 10 nC. The Linac online equipment installation and vacuum connection in the tunnel has been finished at May 2022. The system joint debugging and device conditioning of the accelerating units, the power supplies, et al., are in progress. The beam commissioning will start in August 2022. This paper presents the status of the HEPS Linac and detailed introduction of the beam commissioning simulations and preparations.

INTRODUCTION

The High Energy Photon Source (HEPS) [1] is a 4th generation synchrotron light source based on a 6 GeV diffraction-limited storage ring [2] that is current under construction in northern China. The injector consists of a 500-MeV Linac [3], a full-energy booster [4], a low energy transfer line connecting the Linac and booster and two transfer lines transferring beams back and forth between the storage ring and booster [5]. The Linac is a normal conduction S-band linear accelerator and main parameters are show in Table 1. The Linac is composed of three subsystems includes an electron gun, a bunching system and the main accelerator. A thermal cathode electron gun is adopted and can provide larger than 10 nC electron beam per pulse. The baseline scheme of bunch structure is one bunch per pulse. However, based on the consideration of retaining certain TMCI charge threshold margin of booster, the Linac could be configured to provide three-bunches-per-pulse beams. So, the bunching system [6] includes two sub-harmonic bunchers (SHB), one pre-buncher (PBUN), one buncher (BUN) and one accelerating structure (AS). In the main Linac, there are eight accelerating structures driven by four klystrons and five triplets. The Linac layout is shown in Fig.1.

Table 1: Main Parameters of The Linac

Parameter	Unit	Value
RF frequency	MHz	2998.8
Energy	MeV	500
Max. Repetition frequency	Hz	50
Pulse charge	nC	0.5~7
Number of bunches per pulse	-	1 or 3
Bunch length (rms)	ps	~5
Energy spread (rms)	%	≤0.5
Emittance (rms)	nm	70

* Work supported by the High Energy Photon Source (HEPS) project, a major national science and technology infrastructure project and the Youth Innovation Promotion Association CAS (2019016)
† mengc@ihep.ac.cn

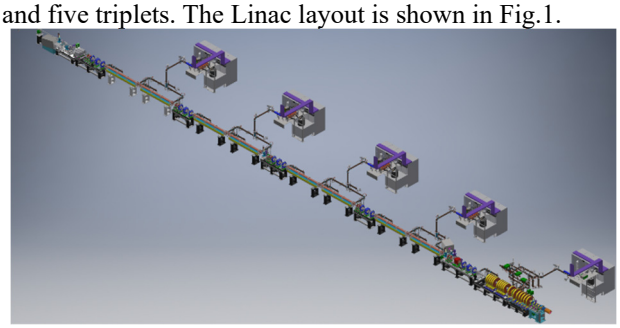

Figure 1: The layout of Linac.

The planed Linac beam commissioning will start in August this year. Before this, beam commissioning preparations should be completed. Now, the Linac equipment is being installed and vacuum connection in the tunnel has been finished. In this paper, beam commissioning simulation is presented in the second part and the status of Linac construction is presented at the third part.

BEAM COMMISSIONING SIMULATION

The main measured parameters of HEPS Linac are emittance, energy and energy spread. In order to suppress short longitudinal wakefield effect, the acceleration phase decreases as bunch charge increases. Phase scan method is adopted to obtain the offset between the physical phase and LLRF phase. In this part, the information of emittance measurement, energy and energy spread measurement, phase scan and orbit corrections are introduced. A new platform python accelerator physics application set (Pyapas) is under developing [7] to be used in the Linac beam commissioning and all the related commissioning applications based on Pyapas have been finished.

Emittance Measurement

The method used to measure the transverse emittance of beam is quadrupole scan [8] by measure the transverse beam size while changing the upstream quadruples. The beam size σ_i at measurement point location can express in matrix formulation by

$$\begin{pmatrix}\sigma_1^2\\ \sigma_2^2\\ \vdots\\ \sigma_n^2\end{pmatrix}_2 = \begin{pmatrix}R_{11} & R_{12} & R_{13}\\ R_{21} & R_{22} & R_{23}\\ \vdots & \vdots & \vdots\\ R_{n1} & R_{n2} & R_{n3}\end{pmatrix}\begin{pmatrix}\beta\varepsilon\\ \alpha\varepsilon\\ \gamma\varepsilon\end{pmatrix}_1 = \mathrm{R}\begin{pmatrix}\beta\varepsilon\\ \alpha\varepsilon\\ \gamma\varepsilon\end{pmatrix}_1 \quad (1)$$

$$\begin{aligned} R_{i1} &= m_{11}^2\\ R_{i2} &= -2m_{11}m_{12}\\ R_{i3} &= m_{12}^2 \end{aligned} \quad (2)$$

where "1" indicate the emittance measurement point and "2" indicate he beam size measurement point, and m_{ij} is

ISBN: 978-3-95450-227-1 ISSN: 2673-5490 doi:10.18429/JACoW-IPAC2022-THPOST017

PHYSICAL DESIGN OF A 10MeV HIGH SCANNING FREQUENCY IRRADIATION ELECTRON LINEAR ACCELERATOR*

S. Zhang[1†], J. R. Zhang, Z. S. Zhou, M. Iqbal, Z. D. Zhang, Y. L. Chi
Institute of high energy physics, Beijing, China
[1]also at University of Chinese Academy Science, Beijing, China

Abstract

A compact 10 MeV irradiation S-band electron linear accelerator has been proposed to carry out the electron radiation effect test of materials and devices. The Linac includes a standing wave pre-buncher, a traveling wave bunching accelerating structure and a traveling wave accelerating structure. The traveling wave accelerating structure uses a 5MW klystron as RF source, and provides electron beam energy 3.5-10MeV and average current 0.01-1mA. The required irradiation scanning frequency is very high, up to 100Hz and irradiation area is large (200mm×200mm). To meet the requirements, a novel beam scanning system, including one kicker for horizontal scanning and one magnet for vertical scanning, have been proposed. This paper presents the physical design of the 10 MeV electron Linac and beam dynamics simulation results.

INTRODUCTION

The beam irradiation generated by the electron linear accelerator has been applied to various fields of the national economy. For example, radiation sterilization and preservation of food, degradation of chemical pollutants; industrial radiation processing, customs inspection; disinfection and sterilization of medical equipment; Moreover, it can also be used to simulate the electronic environment of extraterrestrial space and conduct anti-radiation experiments. The 10 MeV high scanning is an important part of the comprehensive environment simulation system of "Space Environment Ground Simulation Device" [1-4].

The accelerator has high requirements in beam parameters, as shown in Table 1. Based on the scanning frequency requirements, the traditional scanning magnet method is improved, and a new method combining kicker and scanning magnet is proposed.

The structure design and simulation results of the linac from the electron gun to the beam transport line are presented.

PHYSICAL DESIGN AND DYNAMIC SIMULATION

The 10MeV electron linac is mainly composed of an electron gun, a microwave acceleration cavity, and a beam transport line (as shown in Figure 1). According to the requirements of the accelerator parameters (see Table 1), EGUN, PARMELA and ELEGANT are used to calculate the dynamics of the electron gun, accelerating structure and beam transport line respectively to meet the design requirements.

* Work supported by Institute of high energy physics, Beijing, China
† zhangshu@ihep.ac.cn

Table 1: 10MeV Accelerator Parameters

Parameters	Values
Beam energy (MeV)	3.5-10
Beam average current (mA)	0.01-1
Energy spread (10MeV)	≤2.5%
Beam pulse duration (us)	15
Emittance(6σ)/（mm·mrad）	≤30
Scan frequency (Hz)	100
Irradiation area (m·m)	0.2×0.2
Beam spot uniformity	≥90%
Repetition frequency (Hz)	500

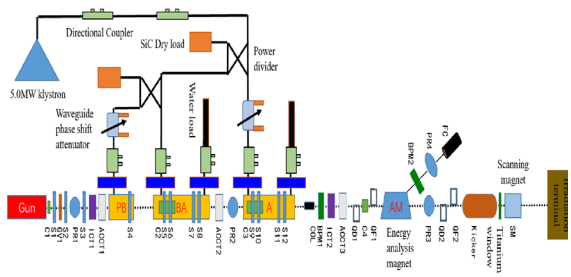

Figure 1: Layout of 10 MeV electron accelerator.

Electron Gun

After calculation, the beam current provided by the electron gun needs to be readjust within the range of 2-200mA to achieve beam average current. Using a three-pole grid controlled electron gun, the beam current can be controlled by changing the current emission density through the grid; and in order to improve the quality of beam emission, the horizontal (vertical) emittance is reduced as much as possible. The electron gun is designed in the EGUN program, and the calculation results of the beam dynamics at 2mA and 200mA are shown in Figure 2 and given in Table 2.

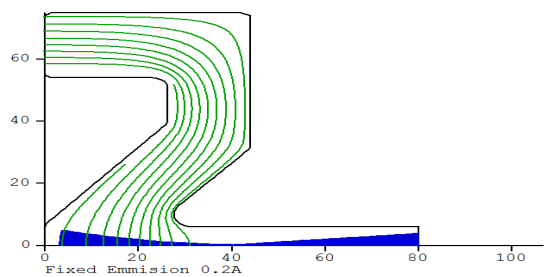

Figure 2: 200mA beam simulation results in EGUN.

ISBN: 978-3-95450-227-1 ISSN: 2673-5490 doi:10.18429/JACoW-IPAC2022-THPOST018

THE DESIGN OF A SECOND BEAMLINE FOR THE CLEAR USER FACILITY AT CERN

L.A. Dyks*[1], P.N. Burrows, P. Korysko[1], JAI, University of Oxford, Oxford, UK
R. Corsini, CERN, Geneva, Switzerland
[1]Also at CERN, Geneva, Switzerland

Abstract

The CERN Linear Electron Accelerator for Research (CLEAR) has been operating as a general user facility since 2017 providing beams for a wide range of user experiments. However, with its current optical layout, the beams available to users are not able to cover every request. To overcome this, a second experimental beamline has been proposed. In this paper we discuss the potential optics of the new line as well as detailing the hardware required for its construction. Branching from the current beamline, via a dogleg chicane that could be used for bunch compression, the new beamline would provide an additional in-air test stand to be available to users. The beamline before the test stand would utilise large aperture quadrupoles to allow the irradiation of large target areas or strong focusing of beams onto a target. In addition to this there would also be further in-vacuum space to install experiments.

INTRODUCTION

The CLEAR facility provides a flexible electron beam with a wide parameter range to its users [1–4]. The experiments performed at CLEAR have included the irradiation of electronics [5–8], studies into very-high energy electron (VHEE) radiotherapy and FLASH radiotherapy [9, 10], experiments into high-gradient X-band acceleration technology [11, 12], beam instrumentation [13], and research into novel accelerator technology such as the use of plasma lenses [14–16] and the generation of THz radiation [17, 18].

The beamline undergoes continuous improvement and consolidation [19] to expand the range of available beams, however, some limitations remain. Beams available to users on the in-air test stand have a transverse size between ~ 0.5 - 5.0 mm. The size can be increased by scattering the beam but this produces secondary particles that may be unwanted. The largest beam size is limited by the current optical arrangement of the beamline. Another optics based limitation is placed on the ability to perform strong focusing onto a target in-air. The strong focusing of electron beams is interesting to users working on VHEE radiotherapy and studies performing focusing within a water phantom have previously been done at CLEAR [20, 21]. However, it was only possible to focus the beam in one axis at a time due to the 40 mm diameter beam pipe placing a restriction on the maximum beam size before the final focus. Furthermore, with many proposed experiments and only two in-air test areas, often experimental set-ups have to be dismantled to make space for others, and reinstalled later to carry out further tests.

To improve the range of available beams and increase availability to users a new experimental beamline has been proposed. The new beamline will consist of a simple achromatic dogleg bend followed by an experimental beamline. By using larger aperture quadrupoles the maximum beam size in the new beamline could be expanded allowing the creation of larger beam sizes and the ability to perform increased focusing in both axes. The new beamline will also provide an additional in-air test stand and space for in-vacuum experiments, optimising the availability of testing slots. To reduce the cost of the new beamline, as many components as possible will be taken from the old CTF3 complex [22].

BEAMLINE DESCRIPTION

Table 1: List of Available Quadrupole Magnets

Name	Aperture	$g_{max.}$	Magnetic Length
QL3	40 mm	11.2 T/m	226 mm
QG8	100 mm	8.0 T/m	300 mm
QP	80 mm	12.7 T/m	350 mm
QTN	185 mm	5.33 T/m	385 mm

The present CLEAR beamline consists an RF photoinjector followed by three accelerating structures able to accelerate electron beams, of bunch charges up to 3 nC, to an energy between 60 - 220 MeV. There is an experimental beamline extending 18.4 m from the end of the third accelerating structure. At the end of the beamline there is a 0.9×1.2 m in-air test stand before a dump. There are three quadrupole triplets installed and one doublet, each using narrow aperture QL3 quadrupoles. Two MDX-type dipole magnets are installed on the beamline for use as both spectrometers and to direct the beam onto in-air test stands. One dipole is positioned before the in-air test stand at the end of the beamline. The other dipole is located 3.8 m after the end of the last accelerating structure and is used to direct beams onto the VESPER test stand. Along the beamline there are several diagnostics installed including, beam television screens (BTV) for beam profile measurements, inductive BPMs for beam position measurements, and an RF deflecting cavity to measure the longitudinal phase space of the bunch. The locations of all components installed on the present beamline are fully documented in the CLEAR lattice files [23].

The proposed layout for the new beamline in relation to the existing experimental beamline is shown in Figure 1, and the parameters of the available quadrupole magnets used

* luke.dyks@cern.ch

ISBN: 978-3-95450-227-1 ISSN: 2673-5490 doi:10.18429/JACoW-IPAC2022-THPOST019

GENERATION OF TRANSVERSELY UNIFORM BUNCHES FROM A GAUSSIAN LASER SPOT IN A PHOTOINJECTOR FOR IRRADIATION EXPERIMENTS

L.A. Dyks*[1], P.N. Burrows, JAI, University of Oxford, Oxford, UK
R. Corsini, A. Latina, CERN, Geneva, Switzerland
[1]Also at CERN, Geneva, Switzerland

Abstract

Beams of uniform transverse beam profile are desirable for a variety of applications such as irradiation experiments. The generation of beams with such profiles has previously been investigated as a method of reducing emittance growth. These methods, however, often use complicated optics setups or short, femtosecond laser pulse lengths. In this paper, we demonstrate that if ultra low emittance is not the target of the photoinjector, it is possible to produce transversely uniform beam profiles using a simple Gaussian laser, with a bunch length of a few picoseconds, utilising space-charge effects only.

INTRODUCTION

Irradiation facilities [1] around the world are used to investigate the effect of high-energy particle beams on electronics [2–4], to study the makeup of historical objects and art [5], and for medical applications, notably radiotherapy [6, 7]. Electron beams are used at several of these facilities, including the CLEAR user facility at CERN [8, 9]. Electron irradiation facilities typically consist of accelerators that produce beams with Gaussian beam profiles and direct them onto a target. Non-uniform transverse beam profiles can lead to uncertainty in the dose that is incident on the target. To increase the uniformity of the dose, the beam size is often increased to a significantly larger size than the target and often collimated, which reduces the total dose incident on the target and the maximum dose rate. If it was possible to generate an entirely uniform beam profile in the irradiation facility, then the total dose and dose rate could be increased.

Photoinjectors used in free electron lasers (FEL) are often designed to produce electron bunches that have 2D uniform beam profiles or have 3D uniform ellipsoid beam profiles in order to reduce the emittance of the beam and increase brightness [10]. 3D-uniform ellipsoids also have the added advantage in that the space-charge forces inside the bunch are linear. However, these photoinjectors commonly use extremely short laser pulses, often less than 100 fs, or laser pulses that are shaped in 3D [11, 12]. Such systems are complicated to set up and require regular maintenance, thus are not feasible for use in an irradiation facility. The ability to produce electron beams with uniform transverse beam profiles with Gaussian lasers with bunch lengths of a few picoseconds could potentially be useful in an irradiation facility and should, therefore, be investigated.

* luke.dyks@cern.ch

GENERATING UNIFORM BEAMS

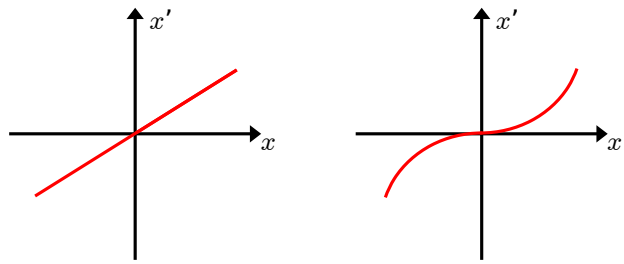

Figure 1: Transverse phase-space of a beam under the influence of linear and non-linear focusing forces.

Bunches produced in photoinjectors tend to exist in the space-charge regime, such that the interactions of particles within a bunch are dominated by the self field of the bunch. In the space-charge regime, non-linear space-charge forces cause the phase-space of the bunch to distort in the manner illustrated in Fig. 1. These space-charge forces cause bunches created in non-equilibrium to evolve towards stable states with a potential energy that is minimised. If a bunch is initially created with a Gaussian distribution then the space-charge forces will cause particles in the core to move towards the tails. If the space-charge forces present in the photoinjector are low, the beam will continue to have a transverse beam profile similar to a Gaussian. If the space-charge forces are increased, then the tails of the Gaussian begin to become more populated and the bunch will have a more uniform transverse beam profile. When the space-charge forces are too high, the beam becomes highly peaked around its centre, with a diffuse surrounding halo. In a photoinjector the evolution of the space-charge forces are determined by the bunch charge, the laser spot size, the laser pulse length, the strength of the RF field, the phase of the RF field, and the strength of solenoid field. It is, therefore, possible to control the space-charge driven evolution of the phase-space of a bunch by changing these parameters.

The photoinjector used at the CLEAR facility consists of a 2.5 cell RF gun operating at a frequency of 3 GHz. Electron bunches are produced by a UV laser with a Gaussian laser profile and 4.7 ps pulse length, incident upon a Cs_2Te photocathode [13]. The gun is surrounded by two solenoid magnets, one to focus the outgoing electron beam, and one to reduce the solenoid field to zero on the photocathode. By simulating a modified version of the CLEAR gun using

ISBN: 978-3-95450-227-1 ISSN: 2673-5490 doi:10.18429/JACoW-IPAC2022-THPOST020

VISUALISATION OF PARETO OPTIMAL SPACES AND OPTIMISATION SOLUTION SELECTION USING PARALLEL COORDINATE PLOTS*

S. Smith†, M. Southerby, S. Setiniyaz, R. Apsimon, G. Burt
Lancaster University, Cockcroft Institute, LA1 4YR Lancaster, United Kingdom

Abstract

In this paper, we build on previous work where multi-objective genetic algorithms were used to optimise rf cavities using non-uniform rational basis splines (NURBS) to improve the cavity geometries and reduce peak fields. [1] These optimisations can produce thousands of Pareto optimal solutions, from which a final cavity solution must be selected based on design criteria, such as accelerating gradient and power requirements. As all points are considered equally optimal, this can prove difficult without further analysis. Here we focus on the visualisation of the Pareto optimal points and the final solution selection process. We have found that the use of clustering algorithms and parallel coordinate plots (PCP's) provide the best way to represent the data and perform the necessary trade-offs between the peak fields and shunt impedance required to pick a final design.

INTRODUCTION

Multi-objective optimisation (MO) methods are employed when an optimisation must be performed that involves two or more conflicting objectives that must be optimized simultaneously, which is often the case in rf cavity design. Mathematically these types of problems can be summarized as follows:

$$\text{min/max } f_m(x), \quad m = 1, 2, ...M, \tag{1}$$

$$\text{subject to: } g_j(x) \geq 0, j = 1, 2, ...J, \tag{2}$$

$$x_{ilb} \leq x_i \leq x_{iub}, \quad i = 1, 2, ..., n \tag{3}$$

Where f_m are the objectives, g_j are the constraints and $x_{ilb/iub}$ are the bounds on the input parameters. As an example for cavity design, these may be the peak fields, a required operating frequency, and limits on some of the cavity dimensions, respectively. A single, unique, optimal solution to these MO problems does not exist, and instead a set is found that defines the trade-off between all the objectives. For complex optimisations with many inputs and objectives, these sets can contain thousands of solutions that are all considered equally optimal by the algorithm. These points can also have objective values that are very similar to each other, either because the algorithm has converged to a near continuous set, or in the case of rf design, due to numerical inaccuracies caused by meshing. This presents a difficulty to the designer who must then select a 'best' solution from this set to use for a final design based on some criteria. This paper explores methods that can be applied to these large sets in order to aid in the final solution selection process.

SINGLE CELL OPTIMISATION RESULTS

An optimisation was previously performed for a generic X-band (12 GHz), $\beta = 1$, $2\pi/3$ travelling wave cavity and the reader is referred to [1] for details. This optimisation produced a large Pareto optimal set of 5000 points which are shown in Fig. 1, with 2 objectives on the axis; shunt impedance per unit length (Z), and the peak electric field (E_{pk}/E_{acc}). The points are also colour coded with a third objective, the modified Poynting vector ($\sqrt{S_c}/E_{acc}$) [2].

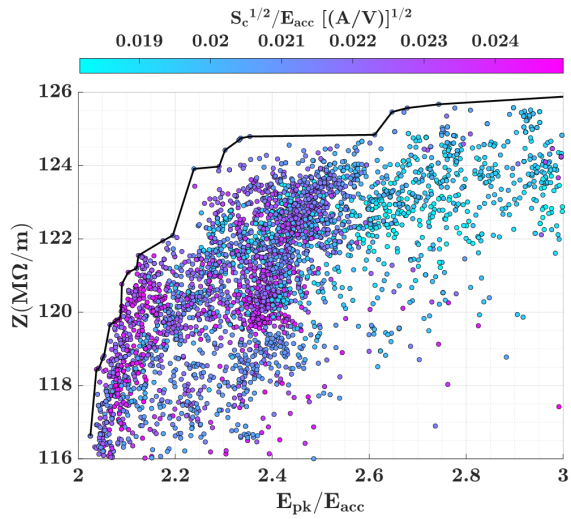

Figure 1: 2D scatter plot showing Pareto optimal set in the Z vs. E_{pk}/E_{acc} objective space, with $\sqrt{S_c}/E_{acc}$ in colour.

PARALLEL COORDINATE PLOTS

If there are only two objectives then selection can be relatively straightforward as the points can be plotted to create a 2D Pareto front as shown in black in Fig. 1. The designer can then easily select a point based on the trade off between the two objectives. If there are three objectives, then colour can be used to provide information about the third objective or a 3D plot could be used, however, as the number of objectives increases, it becomes significantly more difficult to visualise the data sets and select an individual final solution. A comprehensive list of appropriate visualisation techniques for Pareto optimal sets is given in [3] but we have found that the parallel coordinate plot (PCP) provides the best method for representing these sets, especially as the number of dimensions grows larger than four. PCP's display each solution as a piece-wise line that crosses equally

* Supported by Research Grant: ST/P002056/1
† s.smith26@lancaster.ac.uk

ISBN: 978-3-95450-227-1 ISSN: 2673-5490 doi:10.18429/JACoW-IPAC2022-THPOST021

BEAM DYNAMICS SIMULATIONS OF LINEAR ACCELERATOR FOR NATURAL RUBBER VULCANIZATION AT CHIANG MAI UNIVERSITY

J. Saisut[1†], N. Khangrang, S. Rimjaem[1], C. Thongbai[1], PCELL, PBP, Faculty of Science, Chiang Mai University, Chiang Mai, Thailand
M. Jitvisate, School of Physics, Institute of Science, Suranaree University of Technology, 111 University Avenue, Muang, Nakhon Ratchasima, 30000, Thailand
[1]also at ThEP Center, MHESI, Bangkok, Thailand

Abstract

The Linear accelerator system for natural rubber vulcanization has been developed at the Plasma and Beam Physics Research Facility, Chiang Mai University, Thailand. The main components of the accelerator system consist of a DC electron gun with a thermionic cathode, an RF linear accelerator, an RF system, a control system, and an irradiation system. The electron beam properties for natural rubber vulcanization are predicted from the beam dynamics simulation starting from a cathode to the titanium exit window. The electron beam generation and the particle in cell simulation inside the DC electron gun are performed using CST Studio Suite software. The electron distribution at the gun exit from the CST output is covered to be an input distribution of the ASTRA beam dynamics simulation program. The electron beam enters the linac and is accelerated by RF filed inside the linac. The ASTRA simulation code is used to track electron trajectories including the space-charge interaction and the simulation starts from the linac entrance to the exit windows. The electron beam properties for various conditions are evaluated and will be used for further simulations.

INTRODUCTION

A linear accelerator (linac) system for rubber vulcanization has been developed at the PBP-CMU Electron Linac Laboratory (PCELL), Plasma and Beam Physics (PBP) Plasma and Beam Physics Research Facility, Chiang Mai University, Thailand. The system consists of a Pierce-type DC gun with a thermionic cathode, a radio-frequency linear accelerator (RF linac), electron beam diagnostic instruments, and an irradiation system. The layout of the accelerator and irradiation system is shown in Fig. 1. The accelerator system is modified from a medical linac system model Mitsubishi ML-4M. The modified accelerator system is expected to generate beam energy from 1 to 4 MeV [1, 2] with a pulse current of 10 – 100 mA and a pulse repetition rate of 20 – 200 Hz. Some specifications of the accelerator system are listed in our published articles [1, 2].

In this paper, the beam dynamic simulation in the DC gun and the linac are reported and discussed. The electron beam generation and the particle in cell (PIC) simulation inside the DC electron gun were performed using CST Studio Suite software [3]. The results of this simulation were used as the input particle distributions for the beam dynamic simulation in the linac to the exit window using software A Space Charge Tracking Algorithm (ASTRA) [4]. The simulation results for an average beam energy of 1.20 MeV and 3.75 MeV which are close to the expected minimum and maximum beam energy respectively are presented and discussed. the contents of the template.

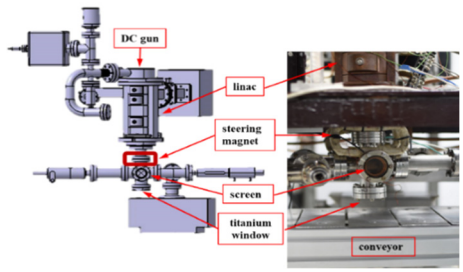

Figure 1: Layout of an accelerator unit.

ELECTRON BEAM DYNAMIC SIMULATION IN THE DC GUN

The simulations in the gun including electric field simulation, electron beam generation, and beam dynamic simulation were performed using CST Studio Suite 2022 software. The DC electron gun was taking a part for cathode and heating filament replacement, and dimension measurement. The simplified model of the DC gun for CST simulation is shown in Fig. 2 (a) which consists of a cathode, focusing electrode, and anode. The parallel gap between the focusing electrode and anode is 4.5 mm. For electric field simulation, the measured high voltage between two electrodes of 14.0 kV is applied since this value is normally used in machine operation. The simulated electric field is shown in Fig. 2 (b).

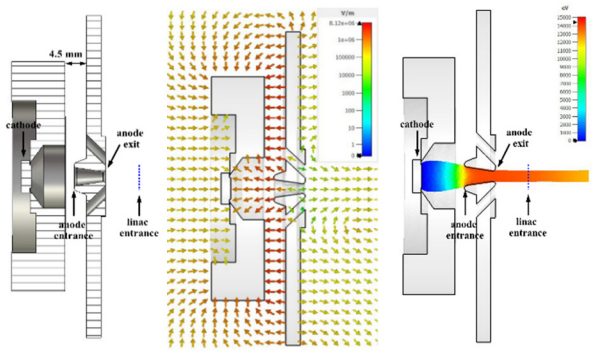

(a) (b) (c)

Figure 2: The DC electron gun: (a) the simplify model, (b) the simulated electric field, and (c) the electron beam trajectory.

†jatuporn.saisut@cmu.ac.th

ISBN: 978-3-95450-227-1 ISSN: 2673-5490 doi:10.18429/JACoW-IPAC2022-THPOST023

CURRENT STATUS OF THE FFA@CEBAF ENERGY UPGRADE STUDY*

R.M. Bodenstein†, J.F. Benesch, S.A. Bogacz, A.M. Coxe, K.E. Deitrick, B.R. Gamage, G.A. Krafft, K.E. Price, Y. Roblin, A. Seryi, Jefferson Lab, Newport News, VA, USA
J.S. Berg, S.J. Brooks, D. Trbojevic, Brookhaven National Lab, Upton, NY, USA
V.S Morozov, Oak Ridge National Lab, Oak Ridge, TN, USA
G. H. Hoffstaetter, Cornell University (CLASSE), Ithaca, NY, USA
D. Douglas, Douglas Consulting, York, VA, USA

Abstract

This work will describe the current status of the FFA@CEBAF energy upgrade feasibility studies. Technical updates are given, but more specific details are left to separate contributions. Specifically, this work will discuss improvements to the FFA arcs, a new recirculating injector proposal, and numerous modifications to the current 12 GeV CEBAF which will be required, such as the spreaders and recombiners architecture, splitters (time-of-flight chicanes), the extraction system, and the hall lines.

BACKGROUND OF PROPOSAL

Thomas Jefferson National Accelerator Facility must investigate paths forward for the post-12 GeV era of the laboratory. Approved and funded experiments will keep CEBAF's experimental schedule booked throughout this decade, at an operational pace of 32 weeks a year. Approved but yet-to-be funded experiments can keep CEBAF busy through the middle of the next decade. Once these experiments are completed, the lab must examine what can come next. One possible path forward involves increasing the energy of the CEBAF machine [1].

At IPAC21, we presented an initial proposal for an energy-doubling upgrade to CEBAF based on Fixed-Field, Alternating-Gradient (FFA) technology [2]. This proposal would upgrade the highest-energy recirculating arcs of CEBAF with permanent, FFA magnets, and allow for energies ranging from 20-24 GeV by recirculating the beam for several additional passes. Initial studies were presented, and we have made significant improvements based upon these optimization studies. This work will present the current state of the proposed upgrade, including a general description of the changes that have been made.

UPDATES TO BASELINE DESIGN

FFA Arcs

In the initial design, a single FFA arc on each side of the racetrack was considered. However, in order to reduce the required maximum magnetic fields for the permanent magnets, as well as decrease synchrotron radiation, two FFA arcs are now under consideration [3]. Figure 1 shows a generalized layout of the two-FFA option. In this case, the first three energy passes will remain in the current electromagnetic arcs, and FFA arcs will replace the two highest-energy arcs on both the east and west sides of CEBAF. In total, there will be 3 electromagnetic passes and 8 FFA passes, for a total of 11 passes in CEBAF.

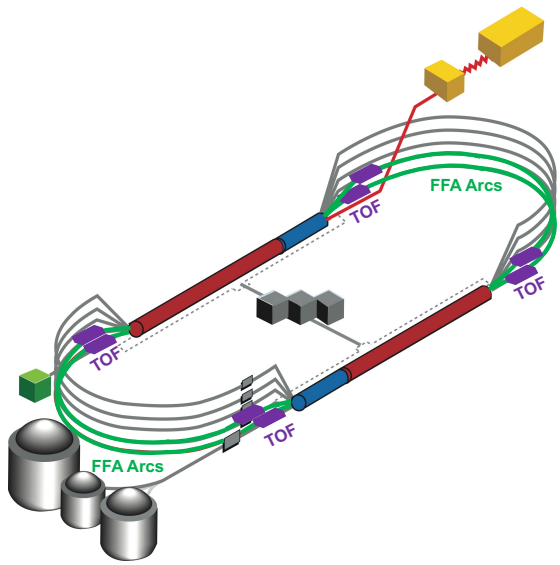

Figure 1: Overview schematic of 2-FFA CEBAF.

Table 1: Comparing 1 vs. 2 FFA Options

Option	**Max Field** [T]	**SR Loss** [MeV]
1 FFA	2.007	1211.48
2 FFA (4 + 4)	1.495	964.44
2 FFA (5 + 3)	1.489	935.30

Table 1 compares three options for the proposed upgrade: a single FFA option [2], a 2-FFA option with 4 passes in each of the new arcs, and a 2-FFA option with 5 passes in the first set of arcs and 3 passes in the second set of arcs. The 2-FFA options significantly reduce the maximum required field for the permanent magnets, and initial studies also show that SR loss is also decreased. The reduction in required fields has a further benefit of being more radiation hard. These options are all being weighed in terms of benefit and feasibility in terms of complexity and available space. Currently, the 2-FFA option with four passes in each set of

* Authored by Jefferson Science Associates, LLC under U.S. DOE Contract No. DE-AC05-06OR23177, Brookhaven Science Associates, LLC under Contract No. DE-SC0012704, and UT-Battelle, LLC, under contract DE-AC05-00OR22725 with the US Department of Energy (DOE).
† ryanmb@jlab.org

ISBN: 978-3-95450-227-1 ISSN: 2673-5490 doi:10.18429/JACoW-IPAC2022-THPOST025

OPERATIONAL EXPERIENCE WITH THE IMPROVED VSR DEMO COLLIMATING SHIELDED BELLOW IN BESSY II

H.-W. Glock†, V. Dürr, F. Glöckner, J. Knobloch[1], M. Ries, A. Velez[2]
Helmholtz-Zentrum Berlin für Materialien und Energie, Berlin, Germany
[1]also at University of Siegen, Siegen, Germany
[2]also at Technical University Dortmund, Dortmund, Germany

Abstract

The Collimating Shielded Bellow (CSB) is designed to serve both as a flexible beam pipe connection between two adjacent superconducting cavities as foreseen in VSR DEMO and as a synchrotron light collimator to shield the down-stream cavity from synchrotron radiation. A convoluted inner RF shield was applied to prevent fundamental mode heating of the stainless-steel-made bellow in the cryogenic environment, making the such captured inner volume very difficult to access for inspection and cleaning. A first version of the device (CSB1) was successfully tested as part of the beam pipe of the synchrotron light source BESSY II under regular operation for more than a year. It suffered from an unfavourable long outgassing commissioning. Therefore a detachable design, allowing for rigorous inner surface preparation and cleaning, was built and recently installed in BESSY II. CSB version 2 (CSB2) design and experimental outcomes are described in the paper. First results indicated a significantly improved vacuum commissioning performance, which was confirmed later on.

CSB FOR THE VSR DEMO MODULE

VSR Demo

VSR Demo, recently under construction at HZB, aims to demonstrate the technical feasibility of a beam-ready cryo-module [1] featuring two 1.5 GHz superconducting RF (SRF) cavities designed for strong bunch length modulation in the storage ring of the 3rd generation, 300 mA synchrotron light source BESSY II. This module will be used as a demonstrator for a later 4-cavity BESSY-VSR-module (Variable bunch length Storage Ring) [2], designed with two additional 1.75 GHz SRF cavities, which will allow to simultaneously offer long and short bunches in a fill pattern.

CSB Purpose, Development and Testing

In [3] the purpose and design of CSB1 as a flexible cryo-compatible beampipe connection between two SRF cavities in VSR, acting also as an actively cooled synchrotron light collimator, was explained in detail. In [4] the testing setup was described, which was used both to test CSB1 (Aug. ’19 to Dec. 2020) and later CSB2 (Jan. to May 2022). CSB1 tests were successful in general, but the initial vacuum conditioning took an unsatisfactory long time of about 80 days. Furthermore significant discolourations were found inside the bellow after destructive dismantling, as described in [5]. Both drawbacks were understood as a consequence of the very limited access to the captured volume between the coaxial shielding labyrinth and the bellow. Therefore a new design was developed, which incorporates a central flange, allowing to separate the device in two parts and to prepare, clean and inspect this inner volume (cf. Fig. 1). In order to be able to mount the screws for this central flange the downstream taper needed a length extension of 30 mm. Otherwise CSB2 fully resembles the inner design of CSB1, which in particular preserved the RF properties of the few localized electromagnetic eigenmodes (cf. [3]).

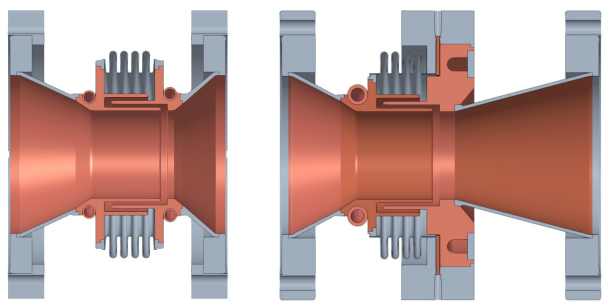

Figure 1: Cross sections of CSB1 (left) and CSB2 (right). Copper parts in red, stainless steel in grey, outer taper parts copper coated.

Manufacturing of CSB2 was delayed by a leaking brazing of the stainless-steel ring of the central flange to the new designed core copper part. It needed rebuilding of that part with careful adjustment of the brazing parameters like gap width, brazing material and temperature to resolve this issue. Therefore it was not possible to install CSB2 as originally planed during the 2021 summer shutdown of BESSY II, but only half a year later. CSB2 experienced wet ultrasound cleaning, 120 °C drying, clean room closing with particulate release control before its mounting in BESSY II in Dec’ 21, using a temporary local cleanroom.

* work supported by grants of the Helmholtz Association
† hans.glock@helmholtz-berlin.de

ISBN: 978-3-95450-227-1 ISSN: 2673-5490 doi:10.18429/JACoW-IPAC2022-THPOST026

DESIGN OF THE MAGNETIC SHIELD FOR VSR DEMO

H.-W. Glock†, P. Anumula, F. Glöckner, J. Knobloch[1], F. Pfloksch, A. Velez[2]
Helmholtz-Zentrum Berlin für Materialien und Energie, Berlin, Germany
[1]also at University of Siegen, Siegen, Germany
[2]also at Technical University Dortmund, Dortmund, Germany

Abstract

The VSR DEMO module, recently under development at Helmholtz-Zentrum Berlin (HZB), will house two 4-cell 1.5 GHz superconducting RF cavities with a particularly powerful HOM damping scheme based on five waveguide HOM absorbers per cavity. A magnetic shield made of high-permeable material is needed around the cavities in order to prevent the ambient magnetic field exceeding very few µT thereby causing considerable unwanted RF losses. The shield needs to accommodate the waveguides, the fundamental power coupler, two beam pipes, two He feed / return lines, the tuner and the support structures, whilst being manufacturable and mountable. The paper discusses those difficulties and presents the matured magnetic shield design. Numerical simulations are used to evaluate the efficacy of the shield.

THE VSR DEMO MODULE

VSR Demo

VSR Demo, recently under construction at HZB, aims to demonstrate the technical feasibility of a beam-ready cryo-module [1] (cf. Fig. 1) featuring two 1.5 GHz superconducting RF (SRF) cavities designed for strong bunch length modulation in the storage ring of the 3rd generation, 300 mA synchrotron light source BESSY II.

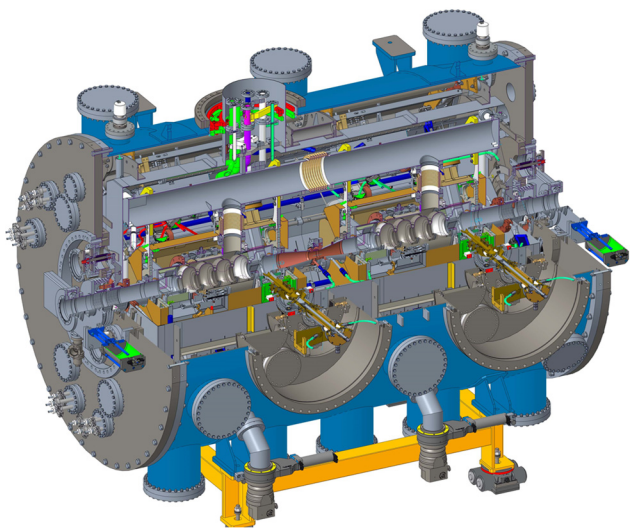

Figure 1: The VSR Demo module with two 4-cell 1.5 GHz SRF cavities.

This module will be used as a demonstrator for a later 4-cavity BESSY-VSR-module (Variable bunch length Storage Ring) [2], designed with two additional 1.75 GHz SRF cavities, which will allow to simultaneously offer long and short bunches in a fill pattern.

Main Properties Impacting the Shield Design

The high average beam current and its broad spectral distribution will cause a mean deposited wake power above 1 kW per cavity. In order to provide sufficient damping, each cavity will be equipped with five waveguides, terminated inside the cryo-module with specifically developed water-cooled HOM-absorbing loads [3]. Each cavity will be equipped with a coaxial fundamental power coupler (FPC) and an individual liquid helium (LHe) tank with a filling pipe and a gas-return pipe (GRP) connection on top. Together with the two beam pipe connections of each cavity a magnetic shield needs to accommodate in total 10 voids, most of them of significant size. That early revealed the need of at least two layers of magnetic shielding.

The LHe tank of each cavity is surrounded by a stepping-motor driven blade tuner, which allows to adjust the cavity's resonant frequency by extending its length by 0 … 1.2 mm. The inner shield, which for the reason of tuner accessibility needed to be mounted in between the tuner and the LHe tank, has to comply with such a length variation. A circumferential slit with coaxially overlapping parts, even though unfavourably reducing the shielding efficacy, was seen as the best engineering solution. The tuner stepping motor is considered as a potential source of permanent or low-frequency magnetic fields, therefore (and for easier access) it is placed outside the secondary magnetic shield.

In order to preserve the distance between the cavities during cool-down a set of four Invar-rods is used. Those are designed to attach the cavity supports and are placed around the cavity in parallel to the cavity axis. Invar is a special iron-nickel-alloy (Fe64Ni36) which experiences (almost) no thermal shrinkage. It is also a soft-magnetic material with a relative permeability μ_r found from supplier specification in a wide range of 1400…1800 [4] up to 4900 ... 12000 [5], very likely depending on the actual forming and annealing history of the samples; some rare measurements are given in [6], there a μ_r of 2420 was reported. The material is also known to be prone to non-negligible magnetic remanence, even though very few experimental data seem to be available [7].

* work supported by grants of the Helmholtz Association
† hans.glock@helmholtz-berlin.de

ISBN: 978-3-95450-227-1 ISSN: 2673-5490 doi:10.18429/JACoW-IPAC2022-THPOST027

FABRICATION OF ROBUST THERMAL TRANSITION MODULES AND FIRST CRYOGENIC EXPERIMENT WITH THE REFURBISHED COLDDIAG*

H. J. Cha†, D. Saez de Jauregui, A. Grau, N. Glamann, A.-S. Müller
Karlsruhe Institute of Technology (KIT), Eggenstein-Leopoldshafen, Germany

Abstract

Two sets of thermal transition modules as a key component for the COLDDIAG (cold vacuum chamber for beam heat load diagnostics) refurbishment were manufactured, based on the previous design study. The modules are installed in the existing COLDDIAG cryostat and tested with an operating temperature of approximately 50 K at both a cold bore and a thermal shield. This cool-down experiment is a preliminary investigation aiming at beam heat-load studies at the FCC-hh where the beam screens will be operated at almost the same temperature. In this contribution, we report the fabrication processes of the mechanically robust transition modules and the first thermal measurement results with the refurbished COLDDIAG in a cryogenic environment. The static heat load in the refurbished cryostat remains unchanged, compared to that in the former one (4-K cold bore and 50-K shield with thin transitions), despite the increase in the transition thickness. It originates from the identical temperature at the cold bore and the shield, which can theoretically allow the heat intakes by thermal conduction and radiation between them to vanish.

INTRODUCTION

At Karlsruhe Institute of Technology (KIT), the COLDDIAG (cold vacuum chamber for beam heat load diagnostics) was developed to mainly measure the beam heat loads in a cold-bore vacuum chamber, based on calibration methods with highly accurate temperature sensors [1-5]. It has been refurbished for more beam heat-load studies with different cryogenic temperatures and beam parameters [6]. Two thermal transitions between a cold bore (liner) and a thermal radiation shield are key components for the stable operation of the COLDDIAG. The former transitions for the liner at 4 K and the thermal shield at 50 K should have been as thin as possible to decrease the heat intake by conduction with considering the cooling power of a cryocooler. As a result, the transition with a thickness of several ten microns has been destroyed due to reasons related to its thermal contraction under an ultrahigh vacuum (UHV) [7].

The purpose of this investigation is to check out the mechanical robustness of new transitions for the stable operation and the possibility of practical applications with the refurbished COLDDIAG at the accelerator facilities. In this paper, we introduce the fabrication processes of a thermal transition module with a simple structure based on the previous design [6]. Especially, we consider the identical temperature at both the liner and the shield, which can increase the transition thickness to a mechanically rigid level (theoretically, infinity) from the following equation:

$$H = kA\frac{dT}{dx} \tag{1}$$

where H is a conductive heat intake, k a thermal conductivity, A a cross-sectional area of the thermal transition, dT a temperature difference between the liner and the shield, and dx a length of the transition [8]. A target temperature is 50 K for a preliminary beam heat-load study on beam screens of the future circular collider for hadron beams (FCC-hh), which is also reachable with the existing cryocooler used for the COLDDIAG [9]. The installation of the newly manufactured transition modules in the cryostat and the first cool-down testing with the refurbished COLDDIAG are described in the next section, which can evaluate the thermal and mechanical stabilities of the transitions. Finally, the beam power losses depending on possible beam heat-load sources in the COLDDIAG with the FCC-hh beams are estimated and the work is concluded with a summary and outlook.

FABRICATION OF THERMAL TRANSITION MODULES

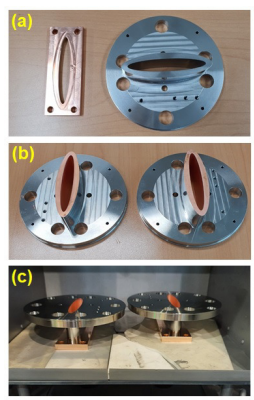

Figure 1: Fabrication processes of two thermal transition modules. (a) Machining of a Cu block and an SS component for a single transition module, (b) deposition of each thin Cu layer inside the SS components, and (c) formation of each permanent joint in a vacuum furnace.

The fabrication of a thermal transition module is based on the design parameters and the manufacturing scheme [6]. Firstly, as shown in Fig 1(a), the machining of an oxygen-free

* This work is supported by the BMBF project 05H18VKRB1 HIRING (Federal Ministry of Education and Research).
† hyuk.cha@kit.edu

ISBN: 978-3-95450-227-1 ISSN: 2673-5490 doi:10.18429/JACoW-IPAC2022-THPOST029

UPGRADE OF THE SLOW EXTRACTION SYSTEM OF THE HEIDELBERG ION-BEAM THERAPY CENTRE'S SYNCHROTRON

E. Feldmeier*, E. C. Cortés García, R. Cee, M. Galonska, Th. Haberer,
M. Hun, A. Peters, S. Scheloske and C. Schoemers, HIT, Heidelberg, Germany

Abstract

The Heidelberg Ion-Beam Therapy Centre HIT consists of a linear accelerator and a synchrotron to provide carbon ions, helium ions and protons for the clinical use as well as oxygen ions for experiments. The RF-KO slow extraction method is used to extract the particles from the synchrotron. To improve the spill quality of the extracted beam a new RF-signal was investigated which increases the R-value from 92.5% to 97.5% . The signal is a multiband RF signal broadened with a random BPSK at 3 frequency bands.

INTRODUCTION

The layout of the accelerator of the Heidelberg Ion Therapy Center HIT includes three ECR ion sources, an injector linac, a 6.5 Tm synchrotron and beam transport lines to deliver beam for the four target places: Two treatment rooms with a horizontally fixed beam-line, the heavy ion gantry and an experimental area.

The sources produces proton, helium and carbon beams for the medical treatment of localized tumors and oxygen beam for experiments.

The synchrotron accelerates the beam to an energy of up to 430 MeV/u for carbon ions, which corresponds to a penetration depth in water or human tissue of 30 cm.

RF Knock Out Slow Extraction

The beam is slowly extracted from the synchrotron by the radio frequency resonant knock out extraction method, the so called RF-KO extraction. A standard extraction time of 5 seconds with a constant intensity is used in this paper, in contrast to the raster point defined intensity modulation which is used in the routine operation described in [1].

SIGNAL GENERATION

The accelerator control system (ACS) provides the calculated set values from the data supply model in real time for the slow extraction. The Low-Level Radio Frequency (LLRF) signal is generated by a dedicated KO Direct Digital Synthesizer (KO DDS) and is delivered to the exciter by the broadband power amplifier (PA). The exciter generates the transverse electric field to excite the beam. The intensity feedback from [1] is delivered to the KO DDS to correct the pre-computed amplitude.

THE RF MULTIBAND SPECTRUM

The new RF KO spectrum consists of the sum of three single frequencies widened by a binary phase shift keying (BPSK) modulation. The two regions of interest found in the beam transfer function (BTF) signal [2, 3] near the betatron resonance were excited at the lower first harmonic and at the lower second harmonic. This is described in detail in WEPOTK022 on this conference [4].

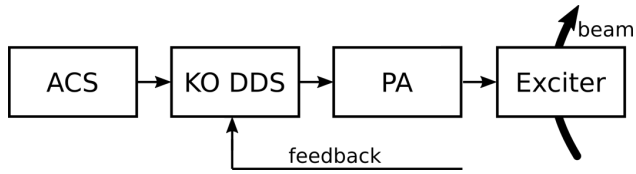

Figure 1: RF KO setup from the ACS, the Direct Digital Synthesizer (KO DDS), the power amplifier (PA) to the exciter, including the feedback for the intensity loop.

The central frequencies are calculated by

$$\begin{aligned} f_1 &= (2 - q_1) \cdot f_{\text{rev}} \\ f_2 &= (1 - q_0) \cdot f_{\text{rev}} \\ f_3 &= (1 - q_1) \cdot f_{\text{rev}} \end{aligned} \tag{1}$$

where q_0 is the fractional tune value of the nominal horizontal tune and q_1 represents the fractional tune value of the second peak found in the BTF signal at extraction conditions.

A signal of the form

$$U(t) = \cos\left(2\pi f_n t + \phi_{\text{BPSK}}\right), \qquad n \in \{1, 2, 3\} \tag{2}$$

was generated for each of the three central frequencies f_n, where the pseudo-random binary phase shift keying (BPSK) ϕ_{BPSK} is given by

$$\phi_{\text{BPSK}} = B \cdot \pi, \qquad B \in [0, 1]. \tag{3}$$

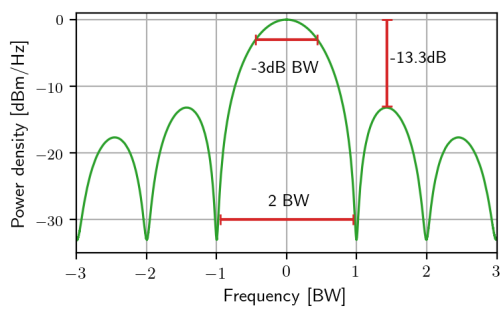

Figure 2: The symmetrical base band BPSK spectrum generated with a PRN has a -3 dB-bandwidth of BW = $f_{PRN,\text{clock}}$, the zeros of the spectrum are at n·BW and the first side band is suppressed by -13.3 dB.

* eike.feldmeier@med.uni-heidelberg.de

ISBN: 978-3-95450-227-1 ISSN: 2673-5490 doi:10.18429/JACoW-IPAC2022-THPOST030

LASER INSTRUMENTATION AND INSERTION DEVICE MEASUREMENT SYSTEM

Roma Khullar[1], Saif Mohd Khan, Ganeswar Mishra, Hussain Jeevakhan[2], Mona Gehlot[3]
Devi Ahilya Vishwavidyalaya, Indore, 452001, Madhya Pradesh, India
[1] Government College, Khategaon, Dewas, Madhya Pradesh, India
[2]NITTTR, Bhopal, Madhya Pradesh, India, [3]Max IV Lab, Lund, Sweden

Abstract

In this paper, we discuss the Hall probe, pulsed wire and stretched wire magnetic measurement systems indigenously developed and installed at the university laboratory at Devi Ahilya VishwaVidyalaya, Indore, India. The laser instrumentation such as position measuring detector, laser scanning micrometer, Wollaston interferometer and Michelson interferometer improves the Hall probe sledge alignment and magnet alignment in the undulator thus improves magnet measurement accuracy. The salient features with design specifics of the laser instrumentation along with magnetic measurement system parameters are described with context to some prototype undulators designed and developed in the laboratory.

INTRODUCTION

In recent years there exits interest in undulator design and development techniques. The undulator field strength B_0 scales with the undulator gap as $B(T) = 1.72 B_r \exp(-\pi g / \lambda_u)$ where g is the magnet-to-magnet gap and λ_u is the period. Therefore, a uniform gap undulator, the precise measurement of gap is crucial as a variation of the magnet-to-magnet gap introduces errors in undulator parameters along the length of the undulator. An error in the undulator parameter is the cause of the beam wander and line broaden. Hall Probe method is a point-to-point measurement. Pulsed wire and stretched wire are integral field measurement methods for characterization of the undulator field.

THE PULSED WIRE BENCH

The schematic of the pulsed wire and Hall probe magnetic measurement system is shown in Fig.1. A motorized linear translation stage with a Hall probe measures the magnetic field profile. The Hall probe is aligned by a position sensitive detector system. The undulator length is 500 mm with 20 mm period length. The accuracy of the Hall probe position during the motion along the undulator length is measured by a position sensitive measuring detector system. The vertical and horizontal offset of the Hall probe measured during the motion is less than 60 micron and 10 micron respectively as shown in Fig. 2. The pulsar in the pulsed wire bench is a 50V-12A High Current Voltage Source (HCVS). The V-I characteristics of the HCVS is shown in Fig. 3. Two wire diameters are used for the experiment. The 250µmwire is used with a current of 5A in the wire. The 125µmwire is used with 1.32A for the experiment.

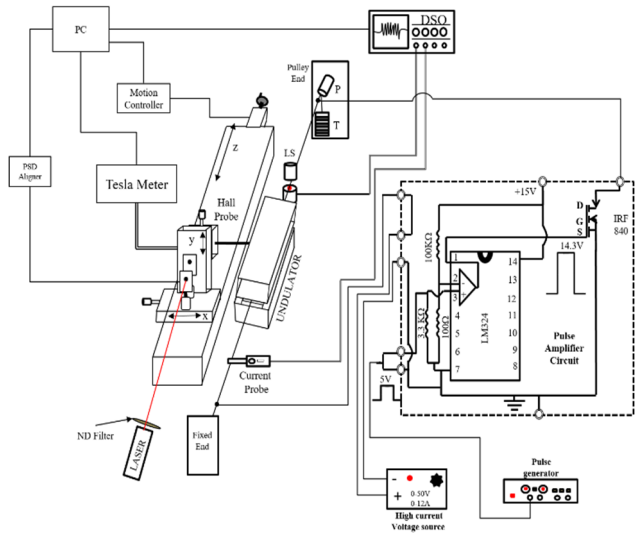

Figure 1: Schematic of the pulsed wire bench and Hall probe bench.

A current probe measures the current in the wire. We use Tektronix make, Model No A622 AC/DC current probe for the measurement. It is capable of measuring up to both 100A peak AC and DC current. We use Cu-Be wire for the experiment. The wire material parameter is $\mu = 4.1\times10^{-4}\,Kg/m$ for 250µmwire diameter and $\mu = 1.01\times10^{-4}\,Kg/m$ for 125µmwire diameter. The total wire length is 1660 mm and passes through the 500 mm length undulator on axis. The pulley end is 660 mm away from the undulator end. The fixed end is 500 mm away from the other undulator end. The wire length in the arrangement is kept at 3.32 times the length of the undulator i.e. $L \geq 3.32 L_u$, L_u is the length of the undulator. The issue of influence of end reflections on measurements is not observed. A laser-photodiode is used as the sensor. It is located near the undulator end at pulley side of the wire. Figure 4 shows the calibration curve of the sensor with no current in the wire. The experiment is conducted in the linear portion of the curve. The sensitivity is 6.5mV/µm and 6.0mV/µm for the two wires respectively. The transverse wire displacement propagates along the wire as a wave longitudinally along both the directions and is detected by a sensor located at the ends of the undulator. The shape of the pulse used for the study is close to rectangular. Both the long pulse and short pulse is shown in Figs. 5-8. The current falling is about 1.6% when the pulse length is 4ms. The current falling is 0.39% at 19.7µs.

ISBN: 978-3-95450-227-1 ISSN: 2673-5490 doi:10.18429/JACoW-IPAC2022-THPOST034

DEVELOPMENT OF MAGNETIC HARMONICS MEASUREMENT SYSTEM FOR SMALL APERTURE MAGNETS

Jongmo Hwang, Eun-San Kim, Jungbae Bahng,
Dept. of Accelerator Science, Korea University, Sejong, South Korea

Abstract

To achieve high brightness of x-ray light source by making beam size and beam emittance smaller and enlarging the beam intensity, the accelerator magnet has been improved to have a larger magnetic field gradient and complex function with small aperture size. Traditional field measurement methods such as hall probe and rotating loop have difficulties in measuring the harmonics of a magnet with a small aperture due to restrictions of physical sizes of the hall sensor and loop-card.

We are developing a well-known harmonics measurement system that uses thin wire, Single Stretched Wire magnetic field harmonics measurement bench, for 4th generation synchrotron radiation accelerator with small aperture(under 20 mm) magnet such as Ochang, Korea.

Not circular interpolation but, by adding a rotary stage to make an actual circular path using the additional stage, we are studying to combine a rotating loop method. In this paper, we are describing the development of the SSW system and the result of the performance test by using simple Halbach quadrupole magnet array.

INTRODUCTION

Prototype Single Stretched Wire field harmonics measurement system and simple Halbach quadrupole array were tested. With 3d printed part and permanent magnet, we developed python base operation GUI program. Since we used same driver and voltage measure unit, we could directly transplant the system to more precise linear stage without modification. To get a more stable result, data post-processing was performed. Three different types of wires were used and compared. Figure 1 shows schematic of prototype SSW bench.

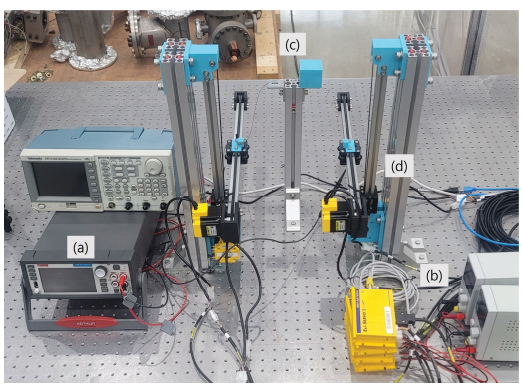

Figure 1: Schematic of Prototype SSW bench (a) Keithley 2450 (b) Driver and SMPS (c) Simple Halbach magnet array (d) 3D printed linear stage.

BASIC THEORY

At the regions where no current and no permeable materials, we could combine and express scalar potential V and vector potential A in to a one single complex representation. [1]

$$\overrightarrow{W}(x,y) = \vec{A}(x,y) + iV(x,y) \tag{1}$$

By expressing scalar potential V and vector potential A as a one single complex representation, we could derive a magnetic field from complex representation that is the solution of the homogeneous Poisson's equation, Laplace's equation.

Complex representation is a part of general solution of Laplace's equation that is an analytic function at $z = x + iy$. Let 2D magnetic field $\vec{B} = Bx + iBy$, then a complex conjugate of B, B* is given; [2]

$$\overrightarrow{B^*} = i\frac{d\overrightarrow{W}(z)}{dz} = i\left(\frac{\partial\overrightarrow{W}}{\partial x}\frac{dx}{dz} + \frac{\partial\overrightarrow{W}}{\partial y}\frac{dy}{dz}\right)$$
$$= i\left(\frac{\partial\overrightarrow{W}}{\partial x} + \frac{1}{i}\frac{\partial\overrightarrow{W}}{\partial y}\right) = \frac{\partial\overrightarrow{W}}{\partial y} + i\frac{\partial\overrightarrow{W}}{\partial x}$$

$$\text{Thus, we could get } B_x = \frac{\partial\overrightarrow{W}}{\partial y}, B_y = -\frac{\partial\overrightarrow{W}}{\partial x}$$

Let multiply C_n, a complex constant, to $z^n = (x+iy)^n$. Because of all the complex variable function always satisfy the Laplace's equation, $C_n(z)^n$ also satisfy the Laplace's equation. When the scalar potential and vector potential are constant values, Eq. (1) shows curves that can be expressed with $C_n(z)^n$. Also, real part of $W(z)$, vector potential $\vec{A}$ and imaginary par of $W(z)$, scalar potential V are orthogonal. So, we could get each other values by following the other one. This explains the induced voltages when measured by a wire that moves at the constant B field are perpendicular components of the moving wire path.

Measured integral voltage V and B field has a relation below [3].

$$V = \frac{d\Phi}{dt}$$
$$\phi = \text{total flux between wire movement}$$
$$\Phi = L_{eff}\int B(s)ds$$
$$\frac{d\Phi}{dt} = \frac{d\Phi}{ds}\frac{ds}{dt} = L_{eff}B(s)\frac{ds}{dt}$$
$$\therefore V = \frac{d\phi}{dt} = L_{eff}B(s)\frac{ds}{dt}$$

Wire moves at constant velocity and L_{eff} is constant at the same magnet. So, with constant coefficient C, we could set $B = C \times V$.

ISBN: 978-3-95450-227-1 ISSN: 2673-5490 doi:10.18429/JACoW-IPAC2022-THPOST035

STATUS OF THE ENGINEERING DESIGN OF THE IFMIF-DONES HIGH ENERGY BEAM TRANSPORT LINE AND BEAM DUMP SYSTEM*

D. Sánchez-Herranz†, University of Granada, Granada, Spain
O. Nomen, M. Sanmartí, B. K. Singh, IREC, Sant Adrià de Besós, Spain
F. Arranz, I. Podadera, C. Oliver, CIEMAT, Madrid, Spain
P. Cara, Fusion for Energy BA/IFMIF, Garching, Germany
V. Hauer, KIT, Eggenstein-Leopoldshafen, Germany
F. Ogando, UNED, Madrid, Spain

Abstract

IFMIF-DONES plant [1] (International Fusion Materials Irradiation Facility – DEMO Oriented Neutron Source) is currently being developed under the framework of a work package of the EUROfusion Consortium. It will be a facility located at the south of Spain in Granada. Its objective and main goal is the testing and qualification of fusion materials by the generation of a neutron flux with a broad energy distribution covering the typical neutron spectrum of a (D-T) fusion reactor. This is achieved by the Li(d,xn) nuclear reactions occurring in a liquid lithium target where a 40 MeV at 125 mA deuteron beam with a variable beam footprint between 200 mm x 50 mm and 100 mm x 50mm collides. The Accelerator Systems is in charge of providing such high energy deuterons to produce the required neutron flux. The High Energy Beam Transport line (HEBT) is the last subsystem of the IFMIF-DONES accelerator, and its main functions are to guide the deuteron beam towards the liquid lithium target and to shape it with the required rectangular reference beam footprints. The HEBT system includes a Beam Dump devoted to stop the beam during commissioning and start-up phases.

The present work details the present status of the HEBT engineering design, including beam dynamics, vacuum configuration, radioprotection, beam diagnostics devices and remote handling analyses performed detailing the layout and integration of required components throughout the beamline.

INTRODUCTION

The linear accelerator for the IFMIF-DONES facility [2] will produce a continuous wave deuteron beam of 125 mA, accelerated up to 40 MeV that will impinge on a liquid lithium target producing a fusion-like neutron flux for the assessment of materials damage in future fusion reactors. IFMIF-DONES linear accelerator is divided in seven subsystems: Injector, Radio Frequency Quadrupole, Medium Energy Beam Transport line, Superconducting RF LINAC, High Energy Beam Transport line, Radio Frequency Power and Accelerator Systems Ancillaries.

IFMIF-DONES accelerator is based on the design of LIPAC [3, 4], currently undergoing its commissioning phase.

This work has been carried out within the framework of the EUROfusion Consortium, funded by the European Union via the Euratom Research and Training Programme (Grant Agreement No 101052200 — EUROfusion). Views and opinions expressed are however those of the author(s) only and do not necessarily reflect those of the European Union or the European Commission. Neither the European Union nor the European Commission can be held responsible for them.
† dsherranz@ugr.es

The IFMIF-DONES High Energy Beam Transport Line and Beam Dump System (HEBT & BD) design has been developed considering as main requirements the ones shown in Table 1.

Table 1: Requirements HEBT&BD System

Requirement	Value
Particle Type	D+
Beam energy	40 MeV
Nom. beam peak current	125 mA
Nom. duty cycle	100%
Nom. transmission ratio	>99.8%
Beam dynamics length	48.8 m
Achromatic bending	9º
Beam footprint at target	20x5cm^2[10x5cm^2]
Beam Dump peak power	5 MW
Beam Dump avg. power	50 kW
RMS beam size BD cone	≈ 40 mm
Divergence at BD cone	14-16 mrad
Off axis	<3 mm
Pressure at SRF Linac	$<5\cdot10^{-6}$ Pa
Pressure at Li target	$>10^{-2}$ Pa

A preliminary design of the HEBT system was initiated following the requirements specified [5], establishing a first layout. It shall provide a continuous wave (CW) deuteron beam with adjustable rectangular footprint. Due to the development of the facility and its systems associated, multiple aspects have been either modified or developed for the HEBT main or beam dump transport lines. Next sections are devoted to give an overview of the current design and configuration updates. Main points of the HEBT engineering design which have been detailed from the previous preliminary design correspond to: Detailed design of magnets, recalculation of vacuum subsystem and adaptation to aluminium of beam facing components along the transport line, considering limiting factors for beam pipes the maximum outer diameter given by fixed aperture of magnets and minimum one due to beam envelope obtained in simulations. An important consequence of this material change to aluminium is the necessity to implement new type of flange connections, which is currently under-study. Figure 1 on the following page depicts configuration of all integrated components along the HEBT system.

ISBN: 978-3-95450-227-1 ISSN: 2673-5490 doi:10.18429/JACoW-IPAC2022-THPOST037

ANALYSIS WITH MECAMASTER ON THE CHAIN OF DESIGN TOLERANCES FOR THE TARGET SYSTEMS AT THE EUROPEAN SPALLATION SOURCE - ESS

A. Bignami†, N. Gazis, S. Ghatnekar Nilsson, ESS, Lund, Sweden
B. Nicquevert[1], CERN, Geneva, Switzerland
[1]also at ESS, Lund, Sweden

Abstract

The European Spallation Source - ESS, has achieved its major construction in Lund, Sweden and is currently continuing in parallel to commissioning its first systems. ESS is characterized by installing and commissioning the most powerful proton LINear ACcelerator (LINAC) designed for neutron production and a 5MW Target system for the production of pulsed neutrons from spallation. The highly challenging and complex design of the Target and Neutron Scattering System (NSS) requires an in-depth analysis of the impact of the stringent manufacturing requirements and tight design tolerances. A campaign of several MECAmaster simulations was performed by ESS Target Division (TD) and Engineering and Integration Support (EIS) Division, focusing on those components that successively come close to their installation and are known for their criticality in terms of achieving the final installation tolerances. The aim of this current study is to investigate and statistically list the possibilities of eventual criticality on the assembly and installation processes, allowing for potential design optimization, tooling implementation and adjustment of the installation procedures.

INTRODUCTION

The European Spallation Source – ESS in Lund undergoes currently its major manufacturing project phase with the aim to deliver Beam On Target (BOT), in the current decade and welcome the First Science results under the Start Of User Program (SOUP). In this context, the Engineering & Integration Support (EIS) division centralizes mechanical engineering expertise under the Mechanical Engineering & Technology (MET) section. Among the expert services of MET, special focus is given on the engineering reviews and tolerance stack-up analysis.

The different types of requirements for all ESS equipment pass through reviews and inspections that allow then for their mechanical design realization under the Single-Point-of-Truth in CAD [1]. Design standardization under ISO GPS plays a decisive role since there has been a tangible effort, including ESS resource investment, in the direction to improve the quality of drawings but also depict the detail level between the different kinds, i.e., drawings for conceptual, detailed, manufacturing and verification.

As part of the standardization, review and engineering training project, tolerance stack-up analysis was introduced on the ESS master model under MECAmaster [2] s/w. MECAmaster is a powerful tool on 3D CAD environment and fully integrated in CATIA V6 (official and central ESS CAD design tool), that allows for large assemblies' tolerance analysis, validation of installation procedures, study of assembly clearances and produce input for post-process kinematic calculations. One of the many unique features in use is the combined consideration of design tolerances with respect to the applicable alignment specifications.

† andrea.bignami@ess.eu

ESS MECAMASTER WAY OF WORKING

MECAmaster analysis is a great asset for big projects such as ESS, in which large and complicated assemblies are vastly present. To optimize the results, a Way of Working (WoW) has been implemented that foresees an exhaustive gathering of information through drawings and experts' contributions, the involvement of working package owners and the methodical implementation of tolerances and assembly procedures. The approach is the following: consider and then calculate the worst-case scenario, in which the max/min value of the tolerances are arithmetical added up and once the critical points are underlined, perform a statistical run (with uniform or gaussian distribution) to have the probability of the potential out-of-tolerance scenario or misalignment. In the following paragraphs the main ESS case studies analysed up-to-date are presented.

Pilot Case (Inner Shielding First Layer)

The first assembly taken into consideration is the first layer of the inner shielding of the Target [3] vessel. The inner shielding has been designed with a "pancake" configuration, with each layer correctly aligned and decoupled from the previous ones, to the most possible extend. Even with these precautions, the impact of the stack of tolerances is not negligible. For this reason, the positioning of the first layer on the bottom of the vessel and its correct alignment are crucial for reducing as much as possible its influence on the whole structure. Therefore, the analysis takes into account both the tolerances from the manufacturing and installation drawings and the whole assembly strategy, including the alignment process, with the intrinsic error, due to the resolution of the instrumentation and the human influence.

As depicted in Fig. 1, the inner shielding is made of three parts that are independently aligned. Once in position, special brackets are inserted in between, with the sole purpose of limiting the relative displacement in case of earthquake; there are not used as fixtures.

ISBN: 978-3-95450-227-1 ISSN: 2673-5490 doi:10.18429/JACoW-IPAC2022-THPOST038

ON-SITE TRANSPORT AND HANDLING TESTS OF CRYOMODULES FOR THE EUROPEAN SPALLATION SOURCE

F. Schlander*, A. Bignami, N. Gazis, European Spallation Source ERIC, Lund, Sweden

Abstract

The cryomodules for the superconducting Linac of the European Spallation Source ESS are now arriving in a steady stream and the long-distance transport requirements are well understood. For the on-site transportation, handling and storage, several challenges have risen, including the intermediate storage of cryomodules before testing and/or installation. In comparison to the long-distance transports, the cryomodule on-site transports and respective handling until installation take place with specialised and limited transport protection. This requires additional measures and tests of those handling steps with extended diagnostics, to make sure that handling and transport refrains from damages on the last mile. Those handling procedures and executed tests will be described in this contribution.

INTRODUCTION

The accelerator of the European Spallation Source will accelerate protons to 2.0 GeV at a pulse current of 62.5 mA. The main portion of the accelerator consists of in total 43 cryomodules containing superconducting cavities. For the lowest energy, 13 cryomodules, containing 2 double-spoke cavities each, are provided via in-kind by IJCLab in Orsay, France [1]. Further there are 9 medium-beta cryomodules, containing 4 6-cell elliptical cavities each, and 21 high-beta cryomodules, containing 4 5-cell elliptical cavities each. Those cryomodules are provided via in-kind from CEA Saclay IRFU, while the installed cavities are in-kind contributions from INFN LASA Milan for the medium-beta cavities, and the high-beta cavities from ASTeC, STFC Daresbury [2–4]. As cryomodules are very delicate objects, the transport and handling of those needs to be done with great care. For the road transport between the laboratories, lessons learned from other projects [5, 6] were taken into consideration and all of the approximately 15 transports to ESS up to now were successful. At ESS the cryomodules arrive at different locations for either temporary storage or testing. After this, the cryomodules will have at least another transport, although only on site, transport and handling tests with extensive diagnostics mounted on the cryomodules have been carried out, and the results with be described in the following sections. An overview of the different locations and routes on the ESS site is shown in Fig. 1.

MODULE PREPARATION

After the arrival at ESS the configuration of the elliptical cryomodules is changed from transport configuration to test and tunnel configuration. This results in removal of all transport protection (see Fig. 2 for explanation), which makes the contents of the cryomodules much more sensitive, as the cavity string, the thermal shield and the space frame are no longer blocked in their movement .

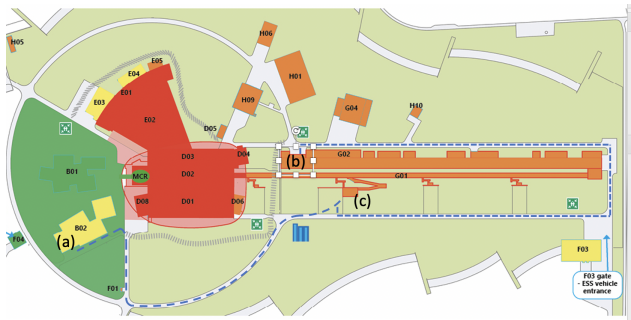

Figure 1: Site overview of ESS with cryomodule storage (a,b), test (b) and installation locations (c).

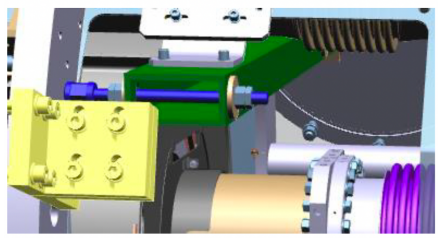

Figure 2: Transport protection inside the elliptical cryomodule. In green: a bar to block movement of the cavity string with respect to the space frame, in silver above: fixation of the thermal shield, yellow: blocking of the space frame fixed at the vacuum vessel.

The components mentioned and the installed diagnostics is shown in Fig. 3. For diagnostics, 4 enDAQ S3-D16 vibration sensors (shock loggers) and a combination of monoaxial (Mod. 602D01, 100 mV/g) and triaxial (Mod. 604B31, 100 mV/g) PCB piezo accelerometers have been used on the medium beta prototype cryomodule CM0 [7]as the test cryomodule.

For the spoke cryomodules no changes are done from the reception until the positioning in the tunnel. The diagnostics mounted are 2 PCB Mod. 356B18 and the locations are shown in Fig. 4

MEASUREMENTS

For the spoke and elliptical cryomodule transport tests different routes to the tunnel entrance were chosen according to their storage- or test location, as shown in Fig. 1.

* felix.schlander@ess.eu

ISBN: 978-3-95450-227-1 ISSN: 2673-5490 doi:10.18429/JACoW-IPAC2022-THPOST039

SPS BEAM DUMP SYSTEM (SBDS) COMMISSIONING AFTER RELOCATION AND UPGRADE

P. Van Trappen*, E. Carlier, L. Ducimetiere, V. Senaj, F. Velotti, N. Voumard, V. Namora
CERN, Geneva, Switzerland

Abstract

In order to overcome several machine limitations, the SBDS has been relocated from LSS1 (Long Straight Section 1) to LSS5 during LS2 (Long Shutdown 2) with an important upgrade of the extraction kicker installation. An additional vertical deflection kicker magnet (MKDV) was produced and installed while the high voltage (HV) pulse generators have been upgraded by changing gas-discharge switches (thyratrons and ignitrons) to semiconductor stacks operating in oil. Furthermore the horizontal sweep generators have been upgraded to allow for a lower kick strengths. The controls, previously consolidated during LS1, went through an additional light consolidation phase with among others the upgrade of the trigger & retrigger distribution system and the installation of a new fast-interlocks detection system. This paper describes the commissioning without and with beam and elaborates on the measured improvements and encountered problems with corrective mitigations.

PROJECT MOTIVATION

Relocation

As explained in [1], the pre-LS2 LSS1 internal high-energy absorber block (TIDVG) would not survive the nominal High-Luminosity Large Hadron Collider (HL-LHC) beam, due to an increased beam power and brightness, requesting an upgrade. Although multiple solutions have been investigated to try to design a completely external beam dump system for the SPS in view of the LIU operation, none of them was suitable for the improvements required within the technological limits. The retained solution is to displace the internal beam dump system from LSS1 to LSS5 since this location offers enough space to properly optimise the dump system to meet the activation, reliability and robustness requirements.

Upgrade

The SBDS was upgraded to increase its reliability and availability, with the main component being the addition of a third MKDV magnet to decouple the generators in case of a failure such as a magnet breakdown. Thanks to the upgrade from gas-tubes to semiconducter switches, the whole dynamic range of the SPS can be covered and there is no more need for two dump absorber blocks as in LSS1. Finally profiting of the displacement, several controls improvements were applied as described further in detail.

* pvantrap@cern.ch

ADDITIONAL MKDV MAGNET

Construction

The additional MKDV magnet has been built according to the original design. It is a delay-line type magnet of 2.5 m length, made of 5 cells, and enclosed in a vacuum vessel. It features a characteristic impedance of 2 Ω and a beam aperture of 83 mm horizontal and 56 mm vertical. The yoke is made of ferrite blocks and the decoupling capacitance consists of lump capacitor boxes built outside the vacuum vessel.

Tests and Conditioning

The HV tests and conditioning of the magnet is performed in three phases. First a DC conditioning is carried out where a positive voltage is progressively applied up to 33 kV, followed by a negative voltage up to −25 kV. The micro discharges and final leakage current are monitored and logged for future reference. The second stage is pulse conditioning with a reduced pulse length (about 2 μs), in order to minimise the spark energy in case of flashover into the magnet. The pulse forming network (PFN) voltage is progressively increased up to 38 kV by steps of 100 V and with up to 1000 pulses per steps at 10 s repetition period. At the end, the time interval between pulses is elongated up to 2 hours to reproduce the real operation scenario. Eventually the pulse conditioning is repeated with the full pulse length.

NEW MKDV GENERATOR

Upgrade

Originally the MKDV generator used a combo thyratron/ignitron switch to combine fast switching of thyratron and high current conduction capability of ignitron. This setup, although working reasonably well during decades, suffered from complex triggering and biasing, risk of approaching obsolescence and potential environmental risks due to the mercury contained in ignitrons. It was decided to replace this combo switch by fast GTO-like thyristors while accepting an inferior commutation performance. In view of required magnet field rise time of 1.1 μs this commutation speed reduction is considered as acceptable. A so-called ring gate topology GTO 5STH2045H0003 from ABB with 4.5 kV rating, 20 kA/μs anode current commutation speed and peak current capability of 80 kA was selected. To maximise its commutation speed, we used the maximum recommended triggering current of 2 kA with more than 4 kA/μs triggering current slew rate. Triggering of 12 GTO in series is ensured by a coaxial architecture triggering transformer developed

ISBN: 978-3-95450-227-1 ISSN: 2673-5490 doi:10.18429/JACoW-IPAC2022-THPOST040

COMMISSIONING OF AN X-BAND CAVITY FOR LONGITUDINAL PHASE SPACE LINEARIZATION AT UCLA PEGASUS LABORATORY *

P. Denham †, A. Ody, P. Musumeci
Department of Physics and Astronomy
University of California at Los Angeles, Los Angeles, CA, USA

Abstract

This paper discusses the commissioning of an X-band (9.6 GHz) linearizer cavity at the UCLA PEGASUS beamline. The photoinjector gun and booster linac operate at S-band (2.856 GHz) and the linearizer cavity can be used to compensate temporally correlated energy spread inherited by the use of relatively long (many ps) laser pulses at the photocathode. The cavity is comprised of 7 cells for a total length of a 9.45 cm, and is installed in the drift section between the gun and the linac. It can be used to remove higher order correlations and minimize the beam energy spread of 13 ps long beams to 10^{-4}.

INTRODUCTION

Linearizing the longitudinal phase space (LPS) of electron beams generated in RF-photoinjectors is essential for pushing the limits of ultrafast electron diffraction (UED) and ultrafast electron microscopy (UEM) [1]. UED sources that rely on velocity bunching benefit from having additional cavities because they can be utilized to remove higher-order distortions that show up at the ballistic focus, which can yield sub fs pulses. On the other hand, UEM sources favor ps long Cigar beams with low energy spread (<10^{-4}), as they have demonstrated an ideal compromise between temporal and spatial resolution (10 ps–10 nm) [2, 3].

Extensive work has been done, using multiple cavities of the same frequency for LPS linearization for both UED and UEM applications. Multi-objective optimizations of injectors with several cavities can feasibly generate attosecond pulses when operated in stroboscopic mode [4]. Alternatively, the pairing of an RF-gun and buncher LINAC has shown capable of linearizing either the bunching process or energy spread [5].

We focus on using a single higher harmonic X-band cavity for LPS linearization to reduce energy spread at the PEGASUS beamline. First, we provide design details and measurements of the X-band Cavity shunt impedance, then amplitude and phase stability. Then the LPS linearization procedure is described. Finally, we present results of energy spread minimization at the PEGASUS beam line that were obtained by using a high resolution (1.1 m dispersion) spectrometer.

* Work supported by DOE STTR grant No. DE-SC0013115 and by by the National Science Foundation under STROBE Science and Technology Center Grant No. DMR-1548924.
† pdenham@physics.ucla.edu

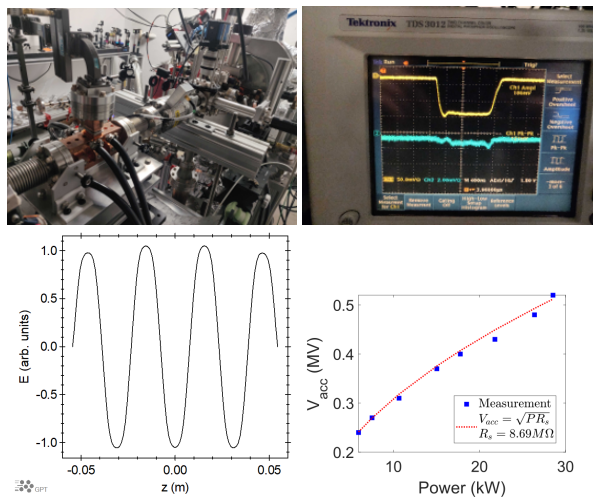

Figure 1: (a) X-band cavity installation at PEGASUS. (b) Forward and reverse power measurements. (c) Longitudinal Field profile. (d) Shunt Impedance measurement.

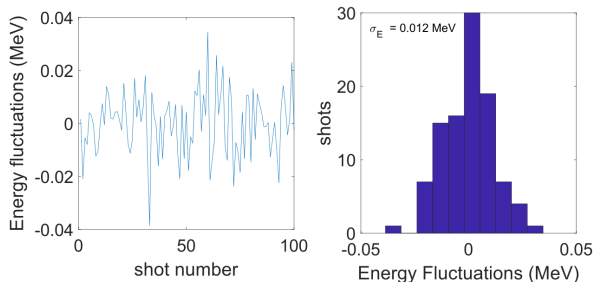

Figure 2: Measured central energy fluctuations at cavity zero crossing.

X-BAND CAVITY CHARACTERIZATION

The X-band linearizer is a 7 cell X-band (9.6 GHz) accelerating cavity that removes the higher order longitudinal phase space correlations and suppresses energy spread for ultra-fast electron microscopy. Each cell in the cavity is 13.492 mm (9.45 cm total length), and has a side-coupled geometry with noses. The Noses were added to increase accelerating voltage. The Beam pipe radius is 4 mm. The relative phase velocity of the structure is $\beta = 0.9922$ (ideally corresponding to a 3.5 MeV beam). There is a 30 MHz mode separation between accelerating and neighboring modes. The design shunt impedance is 90 MΩ/m. We installed the cavity 1.1 m

ISBN: 978-3-95450-227-1 ISSN: 2673-5490 doi:10.18429/JACoW-IPAC2022-THPOST041

CONSTRUCTION AND MANUFACTURING PROCESS OF SIAM PHOTON SOURCE II STORAGE RING GIRDER PROTOTYPE

S. Srichan†, O. Utke, K. Sittisard, M. Phanak, P. Pruekthaisong, S. Prabngulueam, S. Klinkhieo,
Synchrotron Light Research Institute, Nakhon Ratchasima, Thailand

Abstract

The Siam Photon Source II storage ring is designed with low emittance. This new machine requires a high-performance support system and a precise alignment capability. In order to meet these requirements, we have planned for construction of a half-cell components prototype. In the end of 2021, we completed the first girder prototype. This report will describe construction and manufacturing process.

INTRODUCTION

Siam Photon Source II (SPS-II) accelerator complex is the second synchrotron light source in Thailand. It consists of three main components: a 150 MeV injector linac, a 3 GeV full energy booster synchrotron, and a 3 GeV electron storage ring. The 3 GeV storage ring has a circumference of 321 m and the electron beam emittance of 0.9 nm-rad. The ring consists of 14 Double Triple Bend Achromat (DTBA) cells, resulting in 14 long and 14 short straights.

Since the DTBA cell consists of two mirrored halves only three different girders have to be designed. The beam height was set at 1.2 meters. There are 3 prototypes in different of top plate dimension (Table 1).

Table 1: Girder Top Plate Dimension

Girder1 [mm]	Girder2 [mm]	Girder3 [mm]
750x2750	750x2870	870x2240

GIRDER DESIGN

We developed a magnet girder system which uses wedgemount for precision alignment is based on 3-2-1 alignment method and requires three wedgemounts to control Z-direction, two weggemounts to control Y-direction and one wedgemount for X-direction (Fig. 1). The magnet alignment is based on mechanical tolerances. Therefore, the girder top plate is designed with precision surface with a flatness tolerance of 30 µm. [1]

Design Constraints

The design requirements are:

- The flatness of top plate is 30 µm.
- The allowable deflection is less than 20 µm.
- High vibration stability, design frequency above 35 Hz.

To evaluate the success of design, the first prototype construction has been started.

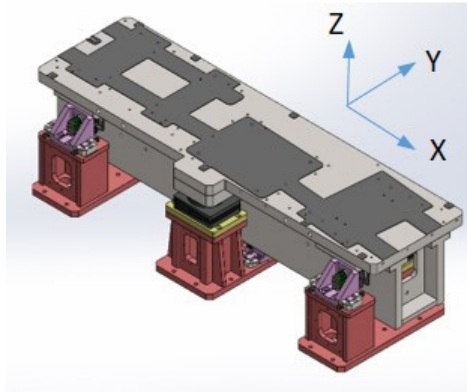

Figure 1: Girder system with three vertical support points.

Material Selection

ASTM A572 Steel Grade 50 was selected for girder construction. Its high strength property compatible with the design. And all of it available in domestic steel industry. The mechanical properties were shown in Table 2 [2].

Table 2: Material Properties

Item	Properties
Hardness, Rockwell B	74
Tensile strength, Ultimate	450 MPa
Tensile strength, Yield	345 MPa
Elongation at Break	18%
Shear Modulus	80.0 GPa

CONSTRUCTION

Because we have less experience for assembling the precision large support system, the girder assembly should be performed by ourselves. We separated the girder construction into two parts. We hired the manufacturing company for the production of some parts. For girder1, the production of girder consists of 2 parts.

Manufacturing Parts

- The top plate dimension 750x2750 mm
- The sub-parts of 3 pedestals.
- Adjustment structure parts.

Commercial Products

Table 3 lists the standard part.

ISBN: 978-3-95450-227-1 ISSN: 2673-5490 doi:10.18429/JACoW-IPAC2022-THPOST045

TEMPERATURE DEPENDENT EFFECTS ON RF SURFACE RESISTIVITY

G. E. Lawler*, A. Fukasawa, N. Majernik, J. B. Rosenzweig
UCLA, Los Angeles, California, USA

Abstract

A promising future for linear accelerators such as compact free electron lasers and electron positron colliders is higher gradient RF cavities enabled by cryogenic temperature operation. Breakdown rates have been shown empirically to be significantly reduced at low temperatures allowing for higher gradient. The surface physics associated with this observation is complicated and there many remain questions as to the exact phenomena responsible. One major figure of merit that can better inform the theory of breakdown is the RF surface resistivity which can be used to compute for example the RF pulse heating during operation. We then use techniques developed for previous X-band and S-band low power surface resistivity measurement by way of temperature dependent quality factor measurements to study C-band cavities. We first present a review of low temperature effects that may be responsible for the change in surface resistivity at low temperature. We then explain some of the initial measurements of these low power RF quality factor tests and compare them to a review some of the physical phenomena that could determine the low temperature surface effects.

INTRODUCTION

We are entering a new regime of cryogenic radiofrequency (RF) cavity operation especially for the future UC-XFEL and cool copper collider concepts [1, 2]. It is thus in our best interest to review the potential effects of temperature dependence on certain RF properties. The main figure of merit which we use is the RF surface resistivity. It is often calculated as the real component of the complex impedance of a cavity with respect to the RF field. In the classic sense this becomes the following in the normal skin effect regime.

$$R_s = Re(Z_s) = \sqrt{\frac{\omega\mu_0\rho}{2}} \tag{1}$$

Anomalous Skin Effect

Divergence from this occurs at low temperatures where surface resistivity is significantly higher than would classically be expected. The most cited theory used to explain this anomalous skin effect regime was originally derived by Reuter and Sondheimer in the 1950s [3]. Since then a number of different forms have been used to calculate the effects [4, 5]. Limits are usually taken to extreme high temperature and extreme low temperature and then patched together to generate a useful piecewise form [6]. We can thus see that the Reuter and Sondheimer explanation for ASE is independent of the bulk resistivity in the low temperature limit and only a function of frequency of resonance at low temperature.

In order to obtain the full temperature dependence of the Reuter and Sondheimer prediction we can use the simplest model for a temperature dependent resistivity: the Bloch-Gruneisen formulation given in integral form in Eq. 2. The simplest form uses $n = 5$ for a simple metal and a Debye temperature Θ_R that is independent of temperature.

$$\rho(T) = A\left(\frac{T}{\Theta_R}\right)^n \int_0^{\Theta_R/T} \frac{t^n}{(e^t - 1)(1 - e^{-t})} dt + C. \tag{2}$$

Putting this information all together we can calculate the surface resistivity by either rigorously computing the integrals in the initial Reuter and Sondheimer form or using the patching functions. To emulate a non ideal metal, a constant can be added to Eq. 2 to match experimental measurements in order to denote the nonzero residual resistivity ratio (RRR) found at low temperatures. We can can plot these calculations in Figure 1.

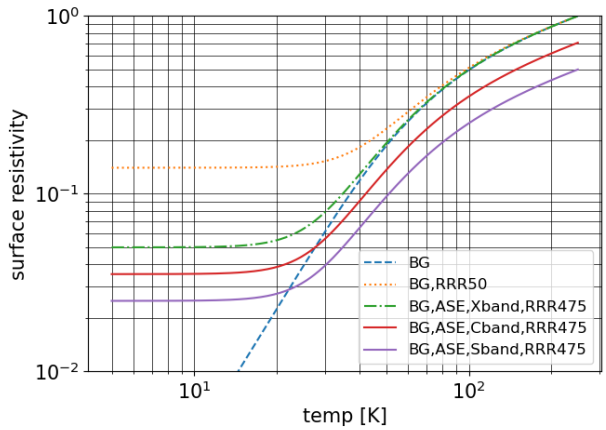

Figure 1: Chou formulation [6] of equation patching used to calculate surface resistivity from Reuter and Sondheimer using Bloch-Gruneisen temperature dependent bulk resistivity.

We can note several features of this formulation of ASE, in particular the main deficiency is that it does not replicate the local minimum empirically observed in certain surface resistivity measurements [7, 8].

BULK RESISTIVITY IMPROVEMENTS

In order to more fully understand the low temperature regime we first consider modifications and or improvements to the bulk resistivity. With respect to the forms often used there are some modifications that can be made.

* gelawler@physics.ucla.edu

ISBN: 978-3-95450-227-1 ISSN: 2673-5490 doi:10.18429/JACoW-IPAC2022-THPOST046

CRYOGENIC BRIGHTNESS-OPTIMIZED RADIOFREQUENCY GUN (CYBORG)

G. E. Lawler*, A. Fukasawa, N. Majernik, J. Parsons, Y. Sakai, A. Suraj, J. B. Rosenzweig
UCLA, Los Angeles, California, USA

Abstract

Producing higher brightness beams at the cathode is one of the main focuses for future electron beam applications. For photocathodes operating close to their emission threshold, the cathode lattice temperature begins to dominate the minimum achievable intrinsic emittance. At UCLA, we are designing a radiofrequency (RF) test bed for measuring the temperature dependence of the mean transverse energy (MTE) and quantum efficiency for a number of candidate cathode materials. We intend to quantify the attainable brightness improvements at the cathode from cryogenic operation and establish a proof-of-principle cryogenic RF gun for future studies of a 1.6-cell cryogenic photoinjector for the UCLA ultra compact XFEL concept (UC-XFEL). The test bed will use a C-band 0.5-cell RF gun designed to operate down to 45 K, producing an on-axis accelerating field of 120 MV/m. The cryogenic system uses conduction cooling and a load-lock system is being designed for transport and storage of air-sensitive high brightness cathodes.

INTRODUCTION

The primary motivational concept for much of the work at UCLA regarding cryogenic operation of normal conducting cavities is the 40 meter, ultra compact x-ray free electron laser [1]. It is based on the use of a combination of several novel technologies including, most notably, high gradient cryogenic C-band linac sections and photoinjector. We note that the photoinjector is a complex, novel device and so would be difficult to realize without a stepping stone.

As a prototype, we have thus designed and fabricated a 1/2-cell CrYogenic Brightness-Optimized Radiofrequency Gun (CYBORG) to serve as this stepping stone. It thus has three main functions. The first is as a general fabrication and RF test. We have examined in detail the beam dynamics for reentrant cavities with high spatial harmonics in simulation [2] but this is our first high gradient, cryogenic gun experiment. The second function is to serve as a development platform for infrastructure, especially in C-band RF and cryogenics.

The third function primarily refers to our collaboration within the National Science Foundation's Center for Bright Beams (NSF CBB). We are particularly interested in improving the brightness of electron bunches at the cathode [3]. Referring to a useful scaling law for the 1D beam brightness from equation 1, we expect to see improvements in the electron brightness that scale as the square of with the launch field and inversely with the cathode temperature, provided that we are near the photoemission threshold. Cooling also lowers the quantum efficiency so we have an incentive to employ more novel, high QE cathodes such as semiconductors for our brightness needs [4].

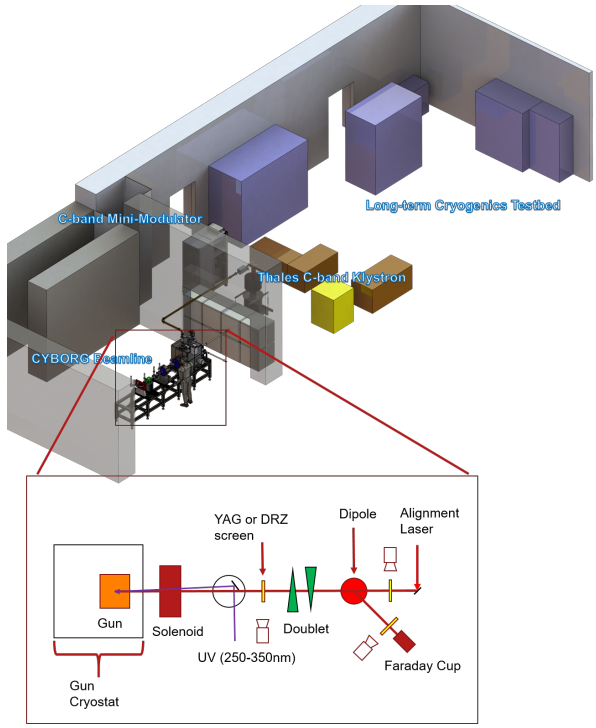

Figure 1: MOTHRA lab for developing CYBORG diagnostic beamline and general cryogenic and RF infrastructure.

$$B_{1d} \approx \frac{2ec\varepsilon_0}{k_B T_c} (E_0 \sin\varphi_0)^2 \quad (1)$$

Figure 1 shows a diagram of our lab space with an inset denoting the first phase of the CYBORG beamline. Our plan is to commission the beamline for eventual novel cathode testing but our first development phase will focus on the production and measurement of quantum efficiency (QE) and mean transverse energy (MTE) from a cryogenic copper cathode.

DESIGN

The device itself is composed of two half cavity pieces, brazed together, and a copper cathode backplane pressed into place. We initially considered a split in the y-z plane but the high machining tolerances in certain locations made it difficult to split. So the split for the braze joint was made in the x-y plane as shown. It is also worth noting that we use DESY/RIKEN UHV flanges on WR-187 waveguide.

* gelawler@physics.ucla.edu

ISBN: 978-3-95450-227-1 ISSN: 2673-5490 doi:10.18429/JACoW-IPAC2022-THPOST048

RHIC MACHINE PROTECTION SYSTEM UPGRADES*

M. Valette †, D. Bruno, K.A. Drees, P.S. Dyer, R. Hulsart, J.S. Laster, J. Morris,
G. Robert-Demolaize, J. Sandberg, C. Schultheiss, T. Shrey, G.M. Tustin,
Brookhaven National Laboratory (BNL) Collider-Accelerator Department, Upton, NY , USA

Abstract

In order to protect the future sPHENIX detector from spontaneous and asynchronous firing of one of the five RHIC abort kickers, mechanical relays were added to the triggering channel for each of them. The mechanical relays add several milliseconds to the delay between the detection of a failure or beam loss and the beam being safely disposed of. In order to account for this delay new inputs were included into the RHIC Machine Protection System to ensure detection of abnormal conditions as early as possible. These inputs include system diagnostics and beam measurements such as Beam Position Monitor signals. In this paper we detail the upgrades that will allow reliable operations with high intensity and high energy ion beams and the new detector as well as related operational challenges and how they were addressed.

INTRODUCTION

During the runs 2014 to 2017 of the Relativistic Heavy Ion Collider (RHIC) a number of pre-fires affected the beam abort system [1]. A pre-fire is a failure case where a thyratron spontaneously discharges a Pulse Forming Network (PFN) through one of the five abort kicker magnets [2], resulting in the beam being kicked partially into the accelerator aperture instead of the beam dump. These events are considered to be triggered by radiation and mostly happen at the end of the energy ramp-up [3]. In the past, pre-fires have been the cause of magnet quenches [4] as well as damage to the experimental detectors and to quench bypass diodes protecting superconducting magnets [5].

From 2023 onward, an upgraded experiment, sPHENIX [6], will be operating in the RHIC facility with the objective of measuring the collisions of a variety of ions circulating at an energy of 100 GeV per nucleon for ions and 255 GeV for protons. To protect this experiment from prefires, mechanical relays were added in series with thyratrons in order to veto an unwanted discharge [7]. Mechanical relays are considerably slower than the thyratrons and can take up to 6 milliseconds to be fully closed. In comparison, the thyratrons have a 0.9 microsecond ramping time and a 15 microsecond "flat" top, the shape of their discharge being responsible for painting the RHIC beam on the beam dump. To account for this extra time to abort the beam an upgrade of the Machine Protection System (MPS) was performed.

* Work supported by Brookhaven Science Associates, LLC under Contract No. DE-SC0012704 with the U.S. Department of Energy.
† mvalette@bnl.gov

OPERATION WITH SPHENIX

The PHENIX detector is being installed in IR8, upstream of collimators and one arc downstream from the Abort System on the Yellow ring. Pre-fires would cause partially kicked bunches to hit low-β IR magnets, particle showers would go through detectors and electronics, causing damage. This new Detector for nuclear physics, illustrated in Fig. 1, scheduled to run from 2023 to 2025 will feature the MVTX detector for vertex detection very close to the beam and will run with a crossing angle of 2 mrad which is the configuration where pre-fires could cause the most damage.

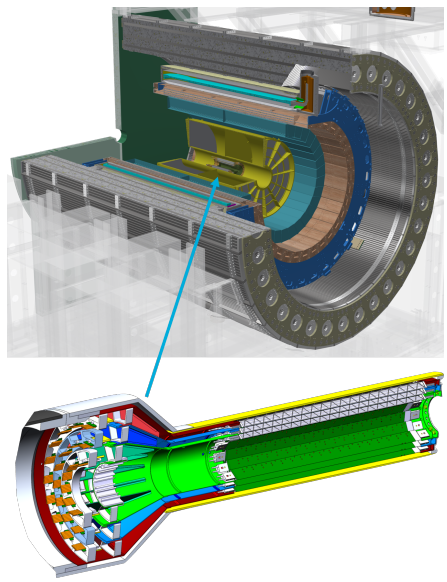

Figure 1: sPHENIX detector with MVTX vertex detector highlighted.

PRE-FIRES

A pre-fire is a degraded behavior of the Abort Kicker system where 1 out of 5 Abort Kicker modules discharges asynchronously, the timeline of a typical pre-fire is illustrated in Figure 2. Both Blue, clockwise, and Yellow, counter-clockwise, rings are affectd with around 10 events per year. Most events occur with beam in the last 20 s of the ramp (with voltages above 10.85 kV), they are assumed to be mostly a combination of high voltage and radiation. From Run 9 to Run 13, six occurrences of damage to both detectors were recorded. During Run 15, the PHENIX MPC detector was destroyed after two pre-fires. Such events must be avoided at all costs to ensure the safe operation of the sPHENIX detector.

ISBN: 978-3-95450-227-1 ISSN: 2673-5490 doi:10.18429/JACoW-IPAC2022-THPOPT001

ONLINE OPTIMIZATION OF THE ESRF-EBS STORAGE RING LIFETIME

N. Carmignani, L. R. Carver, L. Hoummi, S. Liuzzo, T. Perron, P. Raimondi, S. White,
ESRF, Grenoble, France

Abstract

In the first year of operation of the EBS storage ring, online nonlinear dynamics optimisations were performed to increase the Touschek lifetime. Several sextupole, octupole and skew quadrupole knobs have been studied in simulations and tested in the machine. A fast optimisation procedure has been defined and it is followed at each machine restart. The knobs and the optimisation procedure are described in the paper. As a result, up to 41 h Touschek lifetime in nominal multi-bunch mode have been achieved.

INTRODUCTION

The new ESRF storage ring has been successfully installed and commissioned in 2019 and 2020 [1] and it has been in operation with users since August 2020.

The lattice is a Hybrid Multi-Bend Achromat with 6 sextupoles per cell, divided in 3 families [2]. The two injection cells have 6 additional sextupole families used to correct the chromatic functions [3]. In addition to the 192 sextupoles, there are 64 octupole magnets, 2 per cell, grouped in a single family, used to reduce the horizontal tune-shift with amplitude.

All sextupoles and octupoles are powered with independent power supplies, so that any sextupole and octupole correction can be applied. Different ways to tune independently the sextupoles and the octupoles have been considered. The use of off-energy orbit response matrix to fit the sextupole setting and compute the sextupole corrections, like it has been successfully done at MAX-IV [4], is under study and some results are shown in [5]. In this paper we show how some sextupoles and octupoles knobs have been selected and are used to improve the lifetime.

The sum of the beam loss detectors (BLD) signal [6] is a very reliable quantity to use in nonlinear dynamics optimization. It is very fast to update, the signal is refreshed at 0.5 Hz, and the fluctuations are small enough to see the effect of a small change of lifetime due to a change of nonlinear magnet. The beam loss detectors signal has been used from early phase of the commissioning to precisely tune the 6 families of the injection cell. This method has then been used to find the optimum amplitude for a large number of sextupoles or octupoles knobs.

SIMULATION

Several hundreds sextupole, octupole and skew quadrupole knobs were tested in simulation to study their effect on the lifetime and on the dynamic aperture. The lattice used for the simulation is obtained fitting the measured orbit response matrix. The knobs are tested with the same maximum amplitude in the positive and negative direction. The knobs that have the strongest effect on the Touschek lifetime (reducing or increasing it) and with a small effect on the dynamic aperture were selected to be tested in the storage ring. The dynamic aperture and the Touschek lifetime for the lattices with the different knobs have been computed with matlab Accelerator Toolbox [7] on the ESRF computing cluster.

Pseudo Sextupolar Singular Vectors

Starting from the idea that the sextupoles can be used to correct the chromatic functions [4] [5], a list of *pseudo sextupolar singular vectors* has been obtained by SVD inversion of the derivative of the orbit response matrix (ORM) respect to quadrupole components inside the sextupoles.

$$J_{quad} = \frac{\delta ORM}{\delta K_{quad}} \tag{1}$$

$$K_{quad} \propto 2K_{sext}\eta_h \tag{2}$$

$$J_{sext} = J_{quad} \cdot 2\eta_h \tag{3}$$

where η_h is the horizontal dispersion function.

Each singular vector of J_{sext} has been tested in simulation to see its effect on the Touschek lifetime and DA. The effect of the first 96 vectors is shown in Fig. 1. Singular vectors number 9-10, 19-20 and 81-82 are the ones with the strongest effect.

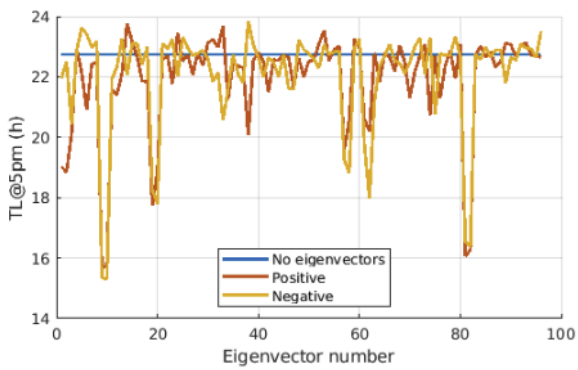

Figure 1: Effect of the off-energy optics correction singular vectors on the Touschek lifetime. The red and the yellow line are the lifetimes with a positive of negative knob applied to the sextupoles, the blue line is the lifetime without knobs.

The few singular vectors with an impact on chromaticity were excluded, for example number 1 and number 8 (Fig. 2).

Sine and Cosine Sextupolar and Octupolar Knobs

A second category of knobs tested in simulation is a sine or cosine wave with different frequencies added on the values

ISBN: 978-3-95450-227-1 ISSN: 2673-5490 doi:10.18429/JACoW-IPAC2022-THPOPT002

BEAM POWER DEPOSITION ON THE CRYOGENIC PERMANENT MAGNET UNDULATOR

L.R. Carver, C. Benabderrahmane, P. Brumund, N. Carmignani, J. Chavanne, G. Le Bec, R. Versteegen, S. White, ESRF, Grenoble, France

Abstract

The ESRF-EBS is currently delivering x-rays with a much higher brilliance and spatial coherence than its predecessor. Within the EBS, there are 5 cryogenic permanent magnet undulators (CPMUs). The magnet blocks for these undulators are operated at 80 K but in general they must be kept at room temperature (300 K) or less or they risk demagnetisation if heated excessively. In the event of a failure of the cryogenic pumps, the ambient magnet temperature increases and they can be further heated by the power induced within the device by the circulating beam. A simulation study was performed to determine the power deposition and temperature rise within the CPMU in order the help define an operational procedure in the event of a cooling failure.

INTRODUCTION

The ESRF-EBS has been commissioned and is currently in operation, delivering high brilliance and high spatial coherence x-rays to the users [1–3]. Within the EBS, there are currently 5 cryogenic permanent magnet undulators (CPMUs) installed and under operation. CPMUs are in-vacuum undulators (IVUs) that are cryogenically cooled to operating temperatures of 80 K. This cooling allows them to achieve higher peak undulator fields (resulting in an improved brilliance for photon energies above 50 keV), while being more resistant to radiation induced demagnetisation, a key feature needed when reducing the minimum gap during operation.

Heating of the magnet blocks can lead to permanent demagnetisation. If there is a failure of the cryogenic cooling during machine operation, the magnets will warm even further due to beam induced heating and could reach temperatures that exceed the safe limit for demagnetisation [4]. Computing the expected temperature rise is therefore an important parameter to be able to safely operate the CPMU.

The CPMU magnet blocks total 2 m in length, with a taper design upstream and downstream to match smoothly the apertures of the surrounding vacuum chamber to the CPMU which has a variable gap setting [6–8]. A photograph of the inside of a CPMU is shown in Fig. 1. The taper has been completely redesigned for the beginning of the EBS, as the previous design showed significant beam induced heating for low gap settings. This prior experience is a strong motivator for this study, as it is needed to confirm if the new taper design is sufficient. The new taper design is shown in Fig. 2.

The power deposited by the beam in the CPMU is a needed input for thermal simulations. To compute the power deposited in the CPMU by the beam a set of impedance simulations was performed in CST Particle Studio [9] and

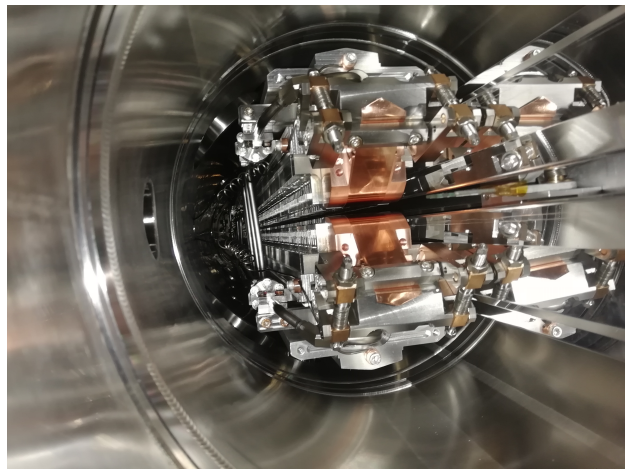

Figure 1: A view inside a CPMU during a bench measurement. A taper is connected at each end to smoothly match the vertical apertures.

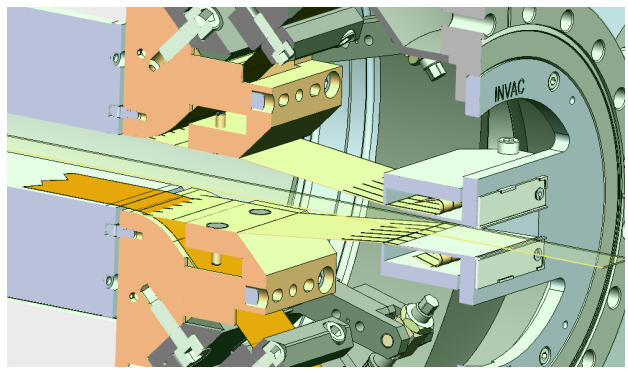

Figure 2: A view of the taper design, the RF fingers can also be seen [5].

Impedance Wake 2D (IW2D) [10]. The details of these impedance simulations will be given in the next section.

COMPUTING THE POWER DEPOSITION

The voltage deposition by a bunched beam in an impedance can be computed from the loss parameter [11,12]

$$\kappa_{\parallel}(\sigma) = \frac{1}{\pi}\int_0^{\infty} d\omega \mathrm{Re}[Z_{\parallel}(\omega)]h(\omega,\sigma), \quad (1)$$

where $Z_{\parallel}$ is the longitudinal impedance and h is the bunch power spectrum, computed from

$$\lambda(\omega) = \exp[-\frac{\omega^2\sigma_{\omega}^2}{2}], \quad (2)$$

where σ is the bunch length and therefore

$$h(\omega) = \lambda(\omega)\lambda^*(\omega). \quad (3)$$

ISBN: 978-3-95450-227-1 ISSN: 2673-5490 doi:10.18429/JACoW-IPAC2022-THPOPT003

A FIRST ATTEMPT AT IMPLEMENTING TRIBs IN BESSY III'S DESIGN LATTICE

M. Arlandoo*[1], P. Goslawski, M. Titze
Helmholtz-Zentrum Berlin für Materialien und Energie GmbH (HZB), Berlin, Germany
[1]Also at Humboldt-Universität zu Berlin (HU), Berlin, Germany

Abstract

At HZB's BESSY II and PTB's Metrology Light Source (MLS), resonances and islands in transverse phase space are exploited in a special operation mode usually referred to as Transverse Resonance Island Buckets (TRIBs). This mode provides a second stable orbit well separated from the main orbit and one of its applications in photon science is the ultra-fast switching of the helicity of circularly polarized light pulses. In the context of the conceptual design study of BESSY III, it is under investigation how this special optics mode can be implemented in an MBA structure and how it will impact the photon source parameters. In this paper we present a preliminary attempt at implementing TRIBs in BESSY III's design lattice, a multi-bend achromat, by breaking the symmetry of the lattice.

INTRODUCTION

The design work of BESSY III as BESSY II's successor started in 2020 [1] and it will be a 4th generation lightsource aiming for highest brilliance and an equilibrium emittance of 100 pm rad. It is well established that the state of the art solution for this requirement is a low-emittance multi-bend achromat (MBA) lattice. Two preliminary MBA lattice candidates have been proposed for BESSY III which we will name SF and CF and their respective lattice parameters are summarized in table 1.

Table 1: Global Parameters of the SF and CF Lattices

	SF	CF
Energy	2.5 GeV	2.5 GeV
Circumference	346 m	344 m
Natural emittance ε_0	99 pmrad	98 pmrad
Straight sections	16 × 5.6 m	16 × 5.6 m
Tune (Q_x, Q_y)	(44, 13)	(44, 13)
Mom. comp. factor α	10^{-4}	10^{-4}
Chromaticity (ξ_x, ξ_y)	(-94.7, -37.3)	(-83.1, -57.4)

The SF lattice contains homogeneous dipoles in the achromat and combined function dipoles in the matching cell and vice versa for the CF lattice. Both lattices were designed using the higher-order achromat (HOA) scheme [2, 3] which is robust against engineering tolerances such as misalignments and focusing errors. More details on the lattice development of BESSY III can be found in [4, 5]. The CF lattice is standard practice for MBA projects but in what follows, we will adopt the SF lattice as the baseline lattice [4] and its optics is shown in Fig. 1. The horizontal and vertical beta functions are β_x and β_y respectively and η_x is the horizontal dispersion. The only nonlinear elements present in the lattice are the chromatic sextupoles adjusted to correct the chromaticity to $(\xi_x, \xi_y) = (0, 0)$. All simulations were carried out in Elegant [6].

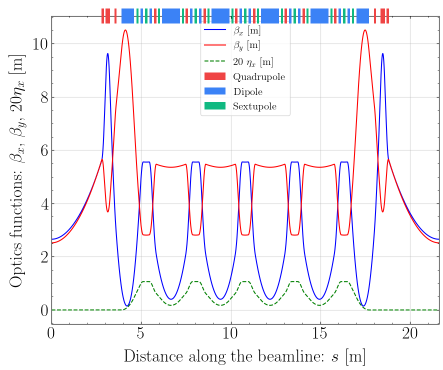

Figure 1: Superperiod of the SF lattice.

Timing mode experiments [7,8] are essential at BESSY II and the MLS and with TRIBs, a second stable orbit is operated together with the main one which can have a different fill pattern [9, 10]. This is beneficial to users because they can be provided light pulses with different repetition rates at the same beamline and a practical application at BESSY II in photon science is the fast switching of light polarization [11]. Due to its successful operation and benefits at BESSY II, the possibility of the TRIBs mode for BESSY III is appealing and worth investigating.

SYMMETRY BREAKING AND RESONANCES

Usually, storage rings are designed with repetitive/periodic structures, namely superperiods but engineering tolerances such as misalignments and focusing errors break the symmetry of the lattice and excite resonances. This also means that islands are always present in more realistic lattices (at least in principle) because they are resonance phenomena but since they are unwanted and considered to lie outside the dynamic aperture (stability region), working points are usually chosen to avoid them. As a first check, the SF ring was tuned to $(Q_x, Q_y) = (44.38, 13.2)$ using two quadrupoles in the triplet section to check whether islands in the horizontal (x, p_x) phase space can be established when the horizontal tune Q_x hits the third-order $(1/3)$ resonance.

* michael.arlandoo@helmholtz-berlin.de

ISBN: 978-3-95450-227-1 ISSN: 2673-5490 doi:10.18429/JACoW-IPAC2022-THPOPT004

DESIGN OF A COMPACT 180-DEGREE SINGLE-SHOT ENERGY SPECTROMETER BASED ON A HALBACH DIPOLE MAGNET

R. Bazrafshan[1,2], T. Rohwer[1], M. Fakhari[1], F. X. Kärtner[1,2,3], N. H. Matlis[1]
[1]Center for Free-Electron Laser Science, Deutsches Elektronen-Synchrotron, Germany
[2]Physics Department, Universität Hamburg, Germany
[3]The Hamburg Centre for Ultrafast Imaging, Universität Hamburg, Germany

Abstract

In the AXSIS project at DESY, we develop compact THz accelerating structures for a table-top x-ray source. Acceleration is achieved by passing the electron beam through a dielectric-loaded waveguide powered by multi-cycle THz radiation. The final electron energy strongly depends on THz-power injected into the LINAC and timing. Thus in first experiments we expect large energy fluctuations and a large range of energies to cover. Therefore, We designed an electron energy spectrometer for a wide range of final energies covering 5 to 20 MeV in a single-shot. Here, we present the design of an energy spectrometer which uses a compact dipole magnet based on the Halbach array concept to deflect the electron beam through a 180° path intercepted by a Fiber Optic Scintillator (FOS) mounted inside the vacuum perpendicular to the beam. The 180-degree bending geometry provides the possibility of having the focus point of all energies at the same distance from the magnet edge which makes the design simpler and more compact. It also removes the necessity of installing a safety dipole at the end of the accelerator. A slit system at the spectrometer entrance increases resolution to better than 0.2%.

INTRODUCTION

Particle energy analysis lies at the heart of numerous diagnostic and spectroscopic techniques in areas such as particle acceleration, electron diffraction and high-energy physics. Surface science alone relies on a host of methods that use electrons to probe matter and gain information regarding physical structure, composition and chemistry. In the AXSIS project, we develop a compact accelerator that leads to a highly optimized and compact THz-driven table-top x-ray source. A key aspect of the design principle is the use of single-cycle/multi-cycle to power an electron gun and multi-cycle terahertz pulses to power a dielectric-loaded metallic waveguide as a linear accelerator (LINAC. Since THz -pulse energy required has not been yet achieved, the design accounts for a wide range of final energies from 5 to 20 MeV which is then delivered through quadrupoles to a magnetic spectrometer in order to measure the energy of the accelerated electrons. THz-driven accelerators have shown significant progress over the past years, and have attracted considerable interest as the next generation linear accelerators. For the present LINAC, requirements placed on the electron spectrometer are somewhat different from those for conventional accelerators. A broad momentum acceptance with high resolution is critical. Most spectrometer implementations use a dipole magnet as a dispersive element and a collimator to control the instrumental resolution. Due to the expected varability in initial performance, the capability of single-shot measurement over the full range is desirable.

SPECTROMETER DESIGN

A novel 180° magnetic electron spectrometer having the distinct features of ultra-low fringe field, fully enclosed magnetic environment, compact design and wide energy range (5–20 MeV) is used as an energy analyser for the AXSIS project (Fig. 1). In order to realize a high energy resolution, a small slit width at the entrance of the spectrometer is necessary. The spectrometer uses a compact dipole magnet with a Halbach array concept to deflect the electron beam through 180°. The dispersion created by the magnet leads to an energy-dependent position then intercepted by a Fiber Optic Scintillating (FOS) screen mounted inside the vacuum perpendicular position to the beam to increase the resolution.

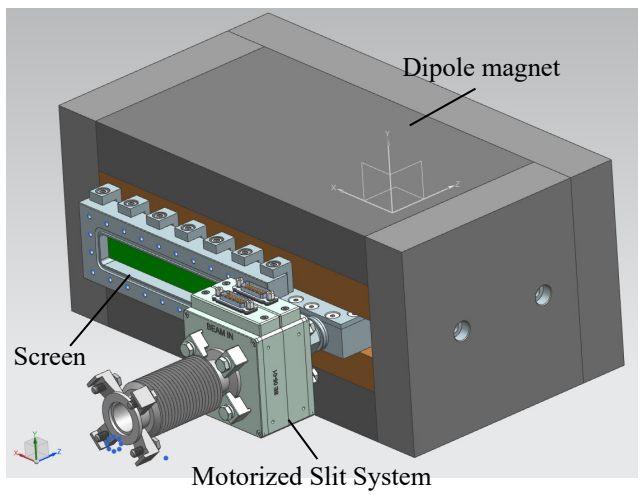

Figure 1: 180-degree bending spectrometer design.

Four synchronously triggered CCD cameras image a 16 cm screen, allowing simultaneous single-shot measurement of electrons from 5 to 20 MeV with a peak magnetic field of 0.6 T. To avoid damage from electrons hitting the CCD cameras directly, first-surface mirrors were used at 45° following the exit flanges, which separated fluorescent light from the electrons. The detector used in this system may be either a phosphor or any electron sensitive film. For our purposes a Fiber Optic Scintillating (FOS) screen proved most convenient since the image can be transferred from one end of the fiber to the other without any distortion. This layout generates excellent resolution, smaller than the thickness of the scintillating crystal [1].

ISBN: 978-3-95450-227-1 ISSN: 2673-5490 doi:10.18429/JACoW-IPAC2022-THPOPT005

FIELD ENHANCED, COMPACT S-BAND GUN EMPLOYING A PIN CATHODE

R. Bazrafshan[1,4], M. Fakhari[1], T. Rohwer[1], K. Flöttmann[2], N. H. Matlis[1] and F. X. Kärtner[1,3,4]
[1]Center for Free-Electron Laser Science, Deutsches Elektronen-Synchrotron DESY, Hamburg, Germany
[2]Deutsches Elektronen-Synchrotron DESY, Hamburg, Germany
[3]The Hamburg Centre for Ultrafast Imaging, Universität Hamburg, Germany
[4]Physics Department, Universität Hamburg, Germany

Abstract

S-band RF-guns are highly developed for production of low emittance relativistic electron bunches, but need powerful klystrons for driving. Here, we present the design and first experimental tests of a compact S-band gun, which can accelerate electrons up to 180 keV powered by only 10 kW from a compact rack-mountable solid-state amplifier. A pin-cathode is used to enhance the RF electric field on the cathode up to 100 MV/m as in large-scale S-band guns. An electron bunch is generated through photoemission from a flat copper surface on the pin excited by a UV laser pulse followed by a focussing solenoid producing a low emittance bunch with 0.1 mm mrad transverse emittance for up to 100 fC bunch charge. We are currently in the conditioning phase of the gun and first experiments show good agreement with simulations. The compact gun will serve three purposes: (i) it can be used directly for ultrafast electron diffraction; (ii) as an injector into a THz booster producing 0.3MeV to 2 MeV electron bunches for ultrafast electron diffraction; (iii) The system in (ii) serves as an injector into a THz linear accelerator producing a 20 MeV beam for the AXSIS X-ray source project.

INTRODUCTION

Photocathode rf guns have been proven to be an excellent electron source for very high-quality beams required for vacuum ultra-violet (VUV) and X-ray FELs [1]. In photocathode rf guns, electron beams are generated at the photocathode by the drive-laser pulses and accelerated immediately by the rf field. Since the electron bunches after emission from the photocathode are of very high intensity and have close to zero a velocity, high space charge forces quickly deteriorate beam quality. Thus, a high acceleration field at the cathode is of great importance for reaching a high electron beam quality. The beam quality can be further optimized by means of three-dimensionally (3D) shaped laser pulse with a well-defined profile [2]. The expansion and non-linearity of the electron bunch in the phase space can be minimized with the optimized initial electron distribution. The initial profile of the beam after extraction from the cathode undergoes a modification under the rf and the solenoid fields as well as the space charge force. Due to the strong accelerating field in the cavity, electrons can be field-emitted from the copper cavity surface and the photocathode. Any dusts on the front surface of the cathode may be a strong field emitter as well causing increased dark current. Dark current at the gun can be accelerated together with the electron bunch, thus the dark current dynamics must be investigated. During gun operation, multipacting peaks are found at the beginning and/or at the end of the rf pulse. The multipacting depends on the solenoid field profile. The amount of dark current and multipacting can be reduced by careful conditioning of the gun.

The concept of the AXSIS project at the Deutsches Elektronen-Synchrotron (DESY) is the development of a compact X-ray light source using terahertz acceleration [3]. Although the final AXSIS machine is expected to be powered exclusively by THz radiation, intermediate phases may resort to a radio-frequencies (RF), i.e. 3 GHz. S-band RF-guns are highly developed for production of low emittance relativistic electron bunches, normally need powerful klystrons which are bulky and expensive. Here, we present the design and first experimental tests of a compact electron source which can accelerate electrons up to 180 keV by only 10 kW from a compact rack mountable amplifier.

RF GUN DESIGN

The AXSIS RF gun is an S-band compact RF gun with a frequency of 2.998 GHz, combining both acceleration and compression of the electron bunch in a single device. By implementing a pin-shaped photocathode with a flat 0.8 mm tip [4,5], strong enhancement of the RF-field strength in the vicinity of the cathode is achieved which substantially reduces the power requirements, and hence the cost and complexity of the device. A solenoid is also used just after the gun to focus the electron beam transversely.

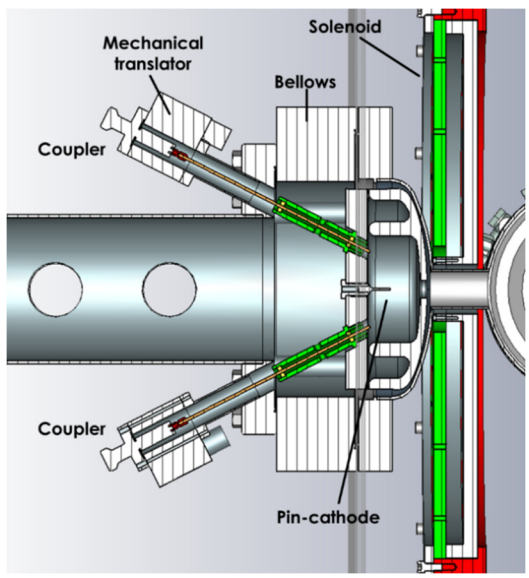

Figure 1: Sectional view of AXSIS RF gun (first prototype).

ISBN: 978-3-95450-227-1 ISSN: 2673-5490 doi:10.18429/JACoW-IPAC2022-THPOPT006

BEAM DYNAMICS OBSERVATIONS AT NEGATIVE MOMENTUM COMPACTION FACTORS AT KARA

P. Schreiber*, M. Brosi, B. Haerer, A. Mochihashi, A. I. Papash,
R. Ruprecht, M. Schuh, A.-S. Müller,
Karlsruhe Institute of Technology, Karlsruhe, Germany

Abstract

For the development of future synchrotron light sources new operation modes often have to be considered. One such mode is the operation with a negative momentum compaction factor to provide the possibility of increased dynamic aperture. For successful application in future light sources, the influence of this mode has to be investigated. At the KIT storage ring KARA (Karlsruhe Research Accelerator), operation with negative momentum compaction has been implemented and the dynamics can now be investigated. Using a variety of high-performance beam diagnostics devices it is possible to observe the beam dynamics under negative momentum compaction conditions. This contribution presents different aspects of the results of these investigations in the longitudinal and transversal plane.

INTRODUCTION

At the accelerator test facility KARA (Karlsruhe Research Accelerator) a new optics with negative momentum compaction factors α_c has been implemented in recent years. The aim is to investigate the effects of the negative sign of α_c on beam dynamics as well as to confirm the feasibility of using negative α_c optics in order to allow reduced sextupoles without incurring instabilities such as the head-tail instability. Previous publications showed effects of the switch in sign of α_c such as a shorter bunch length at negative α_c [1]. In this contribution the effect of changes to the sextupole magnet currents, and therefore the chromaticity, on the first and second order of α_c for the currently implemented optics at positive and negative α_c are explored. Furthermore, the transverse stability in regard to head-tail effects at negative α_c is investigated.

SECOND ORDER OF α_c

The negative α_c optics are operated with negative chromaticities and therefore reduced sextupoles. This reduction in sextupole magnets strengths affects higher order terms of the momentum compaction factor. When including higher orders α_c is a function of momentum

$$\alpha(\delta) = \alpha_0 + \alpha_1\delta + \alpha_2\delta^2 + \dots . \quad (1)$$

As an analysis of this the second order (first non-linear order) has been investigated by means of measurements of the synchrotron frequency f_s as function of accelerating frequency f_{RF} used as tuning knob for the energy offset. The

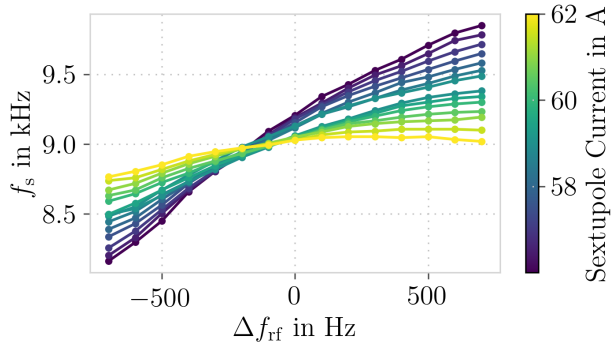

(a) positive α_c

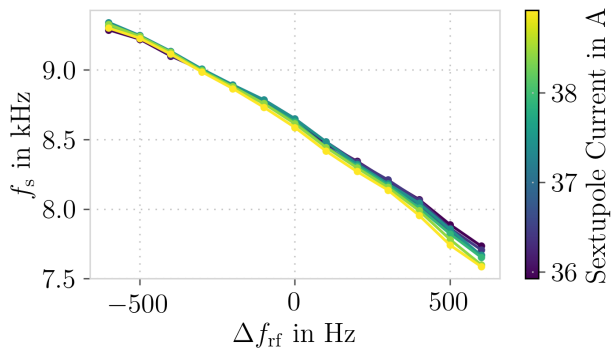

(b) negative α_c

Figure 1: Synchrotron frequency as function of the frequency of the RF system at positive and negative α_c for various sextupole magnet strengths.

synchrotron frequency in this case considering the first two orders of α_c is given as [2]

$$f_s = f_{rev}\sqrt{\frac{heV_{RF}\cos\psi_s}{2\pi\beta_0^2 E}}\cdot\sqrt{\frac{\alpha_0}{2}+\sqrt{\frac{\alpha_0^2}{4}-\alpha_1\frac{\Delta f_{RF}}{f_{RF}}}}, \quad (2)$$

where f_{rev} is the revolution frequency, h the harmonic number, V_{RF} the accelerating voltage, ψ_s the synchronous phase, $\beta_0 = \frac{v}{c}$ and E is the particle energy. From this equation the first and second order of α_c (α_0 and α_1) can be identified by fitting the equation to the mentioned measurements.

The synchrotron frequency has been measured at positive and negative α_c in order to allow comparison. In both cases the beam energy was set to 1.3 GeV. The measurements were done by using the RF system to vary f_{RF} and by using the BBB feedback system [3, 4] which calculates the beam spectrum from BPM data via a Fourier transformation. In this data the synchrotron frequency is then given as a

* patrick.schreiber@kit.edu

ISBN: 978-3-95450-227-1 ISSN: 2673-5490 doi:10.18429/JACoW-IPAC2022-THPOPT007

HIGH BUNCH CHARGES IN THE SECOND INJECTION BEAMLINE OF MESA

C. Stoll†, A. Kalamaiko, K. Aulenbacher, M.A. Dehn, S. Friederich
Institute of Nuclear Physics, Johannes Gutenberg University Mainz

Abstract

MESA (Mainz Energy-recovering Superconducting Accelerator) is an accelerator with two laser-driven electron sources (polarized and unpolarized) operating at 100kV, which is under construction at the Johannes Gutenberg University in Mainz.

The unpolarized electron source MIST (MESA Injector Source Two) allows producing highly charged electron bunches. This source and a double Mott polarimeter will be arranged on the same height above the MESA injector main beamline. A parallel shifting beamline was developed for transporting highly charged bunches from the source MIST to the main MESA beamline.

This report is dedicated to the design of the separation beamline which transports and compresses highly charged electron bunches from the electron source MIST to the first acceleration section of MESA.

INTRODUCTION

An important operation mode for MESA is using spin-polarized beam which will be covered by the STEAM electron source. STEAM will operate at a rather low potential of 100keV in order to maximize operational safety, in particular in view of the very sensitive NEA-photocathodes needed for spin-polarized beam. For the second, unpolarized, source at MESA, called MESA Injector Source Two (MIST), these restrictions do not apply in principle, however, in this paper we restrict ourselves to 100keV beam too. The MESA project aims at an average current of 10mA, which corresponds to a bunch charge of 7.7pC if MESA is operated CW at 1.3GHz. Hence, 100keV at 7.7pC are basic design objectives for this investigation. The goal is to design a separation beamline system which allows to compress and transport electron beam to the first acceleration section of MESA. This beamline should be operated in two different modes. The first mode should allow transporting the beam from the electron source STEAM [1] to the double scattering Mott polarimeter (DSMP). The second mode should allow injecting the beam from the second electron source MIST to the first acceleration section of MAMBO (Milliampere Booster) [2].

ELECTRON SOURCE

MIST is used as second photo electron source for the MESA project [3]. This source allows to produce unpolarized electron pulses from more robust materials. The design of this inverted electron source allows operating at up to 200keV but in this paper, we only consider 100keV which yields approximate values of the Lorentz-factor $\gamma = 1.2$ and $\beta = 0.548$).

The initial RMS length of produced electron bunch was set to 27ps. In the experiment this depends on length of laser-driver pulse and 27ps is a value which was already achieved with a compact laser diode [4]. The simulated bunch with 7.7pC charge has $2.7 \cdot 10^{-3}$ RMS energy spread.

SEPARATION BEAMLINE

MIST is potentially better suited for high bunch charge operation than STEAM. Since no spin polarization is foreseen, the complex and long spin rotation system of STEAM can be avoided. In contrast to STEAM no chopper system, must be foreseen since we believe that the hard limitation of longitudinal acceptance that the chopper produces gives an advantage only for the high precision spin polarized experiments, if a suitable synchronized laser is used. This concept was realized already at the Cornell photoinjector [5]. Moreover, as already mentioned, the source may be used in a later stage with higher potential which would allow for much high charges. On the other hand, the geometrical restrictions in the building require to inject the beam with large angle deflections which makes beam dynamics more complicated.

The electron source MIST and DSMP will be arranged on the same height above the MESA injector main beamline. Thus, it was necessary to develop a parallel shifting beamline in the vertical plane to transport the emitted electron beam.

This beamline has two different operation modes.

1. Transport the beam from the STEAM to the DSMP.
2. Transport the MIST beam to the first MAMBO acceleration section and compress this beam with a buncher which will be installed after the second dipole magnet (B2 in Fig. 1).

In order to fulfill both functions, the magnets must have three output ports. For 90 degree deflection this is difficult to realize with H-type magnets or the alpha-magnets which we have employed so far for low energy deflection. Therefore C-type magnets have been studied.

The optical structure of the proposed beamline consists of two quadrupole doublets and deflection arc. The dispersion function outside this deflection arc should be zero.

The scheme of the designed beamline is shown in Fig. 1.

Three types of optical schemes for the deflection arc were considered:

- Double bend achromat,
- 90° dogleg and
- 4 alpha magnets.

ISBN: 978-3-95450-227-1 ISSN: 2673-5490 doi:10.18429/JACoW-IPAC2022-THPOPT008

BEAM ORBIT SHIFT DUE TO BPM THERMAL DEFORMATION USING MACHINE LEARNING*

Kemin Chen, Faya Wang, Guanliang Wang, Zhe Wang, Masahito Hosaka, Wei Xu†
NSRL, University of Science and Technology of China, Hefei, Anhui, China
Lei Guo, Nagoya University, Furo, Chikusa, Nagoya, Aichi, Japan

Abstract

Stabilizing beam orbit is critical for advanced synchrotron radiation light sources. The beam orbit can be affected by many sources. To maintain a good orbit stability, global orbit feedback systems (OFB) has been widely used. However, the BPM thermal deformation would lead to BPM misreading, which can not be handled by OFB. Usually, extra diagnostics, such as position transducers, is needed to measure the deformation dependency of BPM readings. Here, an alternative approach by using the machine operation historic data, including BPM temperature, insertion device (ID) gaps and corrector currents, is presented. It is demonstrated at Hefei Light Source (HLS). The average orbit shift due to BPM thermal deformation is about 34.5 µm/°C (horizontal) and 20.0 µm/°C (vertical).

INTRODUCTION

Synchrotron radiation source has many advanced characteristics such as high brightness, transverse coherence, good time structure, etc, which is developed as one of the most powerful scientific tools over decades [1]. The beam orbit stability is required to be better than 10% of the beam size for modern light sources [2, 3]. Many sources could lead to beam orbit shifts. Global orbit feedback system has been widely used to suppress them. However, the BPM thermal deformation would lead to BPM misreading, instead of direct orbit disturbance, which could not be effectively corrected by OFB. Significant beam orbit shift due to BPM misreading has been observed in sources like APS [4], KEKB [5], and HLS [6].

Dedicated diagnostics is needed to measure and correct BPM thermal deformation, for example, the work carried out at HLS [6]. It is a straight forward method and generally provides good results. However, few downsides are there like the cost of hardwares and the need of machine study time, which actually make it difficult for wide implementation. In this paper, we will present an alternative approach by using machine learning, which is successfully demonstrated at HLS-II by predicting effective beam orbit shift accompanied by direct corrector current. It could be integrated to orbit feedback system to improve beam orbit stability.

In the following, we first introduce the theoretical model of beam orbit change due to BPM vacuum chamber thermal deformation, then a surrogate model built using a neural network (NN). Finally results from the surrogate model are presented.

THEORETICAL MODEL

Thermal effects from synchrotron radiation, parasitic heat induced by machine impedance and tunnel temperature variation can cause BPM vacuum chamber mechanical deformation, which leads to its geometric center shift in global reference coordinate and results in BPM misreading. BPM reading, $\vec{u}$, can be written as

$$\vec{u} = \vec{R} - \vec{r}, \tag{1}$$

where $\vec{r}$ and $\vec{R}$ are BPM center and beam position respectively in global coordinate.

In principle, BPM center shift does not affect beam orbit directly, except when OFB is functioning, where the beam experiences extra kicks from correctors. Accordingly, a BPM reading changes as,

$$\Delta\vec{u}_i = \Delta\vec{R}_i - \Delta\vec{r}_i = (\frac{\partial\vec{R}_i}{\partial\vec{r}_i} - \bar{\bar{I}}) \cdot \Delta\vec{r}_i, \tag{2}$$

where $\Delta\vec{r}_i$ is BPM center shift due to heating, $\Delta\vec{R}_i$, beam position change at BPM due to OFB, $\partial\vec{R}_i/\partial\vec{r}_i$, Jacobian matrix and $\bar{\bar{I}}$, a unit 2 by 2 tensor.

With an ideal OFB, beam orbit is corrected back to its original, it then yields

$$\Delta\vec{u} = (\Delta\vec{u}_1, ..., \Delta\vec{u}_N) = 0, \tag{3}$$

$$\Delta\vec{r} = \Delta\vec{R}|_{\Delta\vec{u}=0} = \mathcal{M} \cdot \Delta\Theta, \tag{4}$$

where $\Delta\Theta$ is corrector kick strength change, and $\mathcal{M}$ is machine orbit response matrix (ORM), which ideally depends only on machine optics and is given by

$$\mathcal{M}_{ik} = \frac{\partial u_i}{\partial\theta_k} = \frac{\sqrt{\beta_i\beta_k}}{2\sin\pi\nu}\cos[\nu(\phi_i - \phi_k + \pi)], \tag{5}$$

where (β_i, ϕ_i) and (β_j, ϕ_j) are the beta function and phase advance at position i and k and ν is the betatron tune.

The Θ only responses to the BPM readings, which depends on the beam reference orbit and real beam orbit change. The change of reference orbit is caused by the BPM misreading. The real beam orbit shift can be generated by the gap variation of IDs. The physics model of the corrector strength can be described as a function of the ID gaps and BPM temperature by

$$\Theta(\vec{g}, \vec{T}) \approx \Theta(\vec{g}, \vec{T}_0) + \frac{\partial\Theta}{\partial\vec{T}_0}\Delta\vec{T}, \tag{6}$$

* Work supported by the National Natural Science Foundation of China (No. 11975227)
† wxu@ustc.edu.cn

ISBN: 978-3-95450-227-1 ISSN: 2673-5490 doi:10.18429/JACoW-IPAC2022-THPOPT009

DEPENDENCY MEASUREMENT OF BPM READING IN THE HLS-II STORAGE RING*

G. Wang, K.M. Chen, Z. Wang, M. Hosaka, G. Feng, W. Xu†
NSRL, University of Science and Technology of China, Hefei, Anhui, China
S.W. Wang, Diamond Light Source, Oxfordshire, United Kingdom
L. Guo, Nagoya University, Furo, Chikusa, Nagoya, Aichi, Japan

Abstract

Beam orbit stability is essential for the operation of the storage ring based light sources. Orbit feedback systems are commonly adopted to maintain the beam on a reference orbit. Affected by its temperature, change of BPM reading leads to shift of the beam reference orbit. Online experiment is carried out in the HLS-II storage ring to measure the dependence of the BPM reading on the BPM temperature during top-off and decay operation. The result shows that the average change of BPM readings due to BPM temperature variation is about 147 µm horizontally and 47 µm vertically.

INTRODUCTION

Generally, beam orbit stability is required to be better than 10% of the beam size. With the help of the orbit feedback system, the beam is maintained on a reference orbit. However, factors that affect beam position monitor(BPM) reading lead to shift of this reference orbit, which greatly degrades the beam orbit stability.

Factors that affect BPM reading are found in many storage rings. In the Duke storage ring, the dependence of BPM reading on beam current is found to be caused by overloading BPM electronics with high peak voltage [1]. At DIAMOND, the dependency of beam current, filling pattern and enviornmental temprature is studied for the EBPM electronics [2]. At PLS, the BPM chamber movement due to the change of synchrotron radiation heat load and intensity dependence of BPM electronics is found to cause false BPM readings [3].

The button type BPM measures the shift between the beam and the electrode center through the induced charge on the button electrodes [4]. However, the electrode position changes with the movement and deformation of the BPM chamber caused by the parasitic heat load of machine impedances and synchrotron radiation. Therefore, change of BPM reading occurs in spite of an unchanged beam position.

In the HLS-II storage ring, the typical beam size at the middle of the long straight section is 742 µm in the horizontal plane and 76 µm in the vertical plane. Neglecting the change of the reference orbit, the overall beam orbit stability is better than 2 µm in both vertical and horizontal plane with the help of the orbit feedback system [5]. The reference orbit is determined using beam-based alignment(BBA) technique. Being the target of the orbit feedback system, the consistency of the reference orbit is critical for orbit stability.

* Work supported by the National Natural Science Foundation of China (No. 11975227)
† wxu@ustc.edu.cn

In this paper we present the on-line measurement of the de-pendence of BPM reading on the BPM temperature during top-off operation and decay operation.

TEMPERATURE DEPENDENCY OF BPM READING

In the HLS-II storage ring, the orbit feedback system is comprised of 32 BPMs and 32 correctors for each plane. To measure the BPM temperature, two temperature sensors are attached to the upper and lower outside surfaces of each BPM.

Change of BPM temperature occurs during top-off oper-ation after injection and decay operation. Because of the hysteresis of the mechanial movement due to thermal effect, the dependncy measurement is carried out in two operation modes, when the orbit feedback system is turned off. To minimize the disturbance to the beam orbit, the gaps of all insertion devices are kept unchanged.

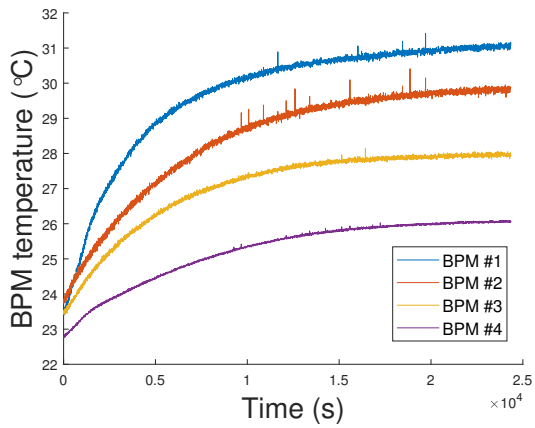

Figure 1: Measured BPM temperature during 400 mA top-off operation after injection.

MEASUREMENT FOR TOP-OFF MODE OPERATION

Before beam injection, the BPM temperature drops to the ambient temperature level of the storage ring tunnel. The measurement starts after the beam is injected to 400 mA with subsequent top-off operation while the orbit feedback system is turned off. During top-off operation, the BPM temperature increases due to the parasitic heat load of ma-

ISBN: 978-3-95450-227-1 ISSN: 2673-5490 doi:10.18429/JACoW-IPAC2022-THPOPT010

BEAM LOSS REDUCTION DURING ENERGY RAMP-UP AT THE SAGA-LS

Y. Iwasaki†, SAGA Light Source, Tosu, Japan

Abstract

The accelerator of the SAGA Light Source (SAGA-LS) consists of a 255 MeV injector linac and a 1.4 GeV storage ring. The energy of the electrons is ramped up to 1.4 GeV in 4.5 minutes in the storage ring. The electron beam current stored in the storage ring is about 300 mA. At the begging of the energy ramp-up, the electron beam was lost like step function. To understand the beam loss mechanism, we developed simultaneous image logging system of beam profile in addition to the beam current, the magnets power supplies, and the beam positions using National Instruments PXI. It was found that the vertical beam size was growing in the step-like beam loss process. The small perturbation of the output currents of the quadrupole power supplies caused the vertical beam size growth. By optimizing the ramp-up pattern of the quadrupole power supplies, sextupole power supplies, and the steering power supplies for the orbit control, we have achieved the reduction of the step-like beam loss and total time of the ramp-up.

INTRODUCTION

The accelerator of the SAGA Light Source (SAGA-LS) consists of a 255 MeV injector linac and a 1.4 GeV storage ring [1, 2]. Figure 1 shows the schematic view of the SAGA-LS accelerator. There are two 4T super-conducting wigglers [3], a planar undulator, and an APPLE-II undulator in the storage ring. The maximum electron beam current of the storage ring is about 300 mA. The energy of the electrons is raised up to 1.4 GeV in 4.5 minutes in the storage ring. The two 4T super-conducting wigglers are excited after beam acceleration. In the early stage of beam acceleration (the beam energy is lower than 400 MeV), the electron beam is lost like step function. The amount of beam loss is normally about 5 mA to 30 mA. In rare cases, total loss of the beam may occur. Although there is no clear threshold of the beam current, such step-like beam loss does not occur less than 200 mA of the beam current. In order to provide stable user operation, it was necessary to investigate the loss mechanism and reduce the amount of the beam loss.

It is expected that investigating the relationship between the growth of beam sizes and beam loss will lead to the identification of the cause of beam loss, since the blow-up of the beam sizes and beam loss occur only at low energy and high beam current. Therefore, we developed simultaneous measurement system of the images of the beam profiles and output values of magnet power supplies, which can be the cause of beam profile changing and beam shapes during ramp-up, and we performed time-series analysis of the beam shape changing and the output values of magnet power supplies during beam loss using National Instruments PCI eXtension for Instrumentation (PXI) based measurement system. The optics analyses of the storage ring from the measurement values of the power supplies were also performed using beam tracking code TRACY2 [4].

† iwasaki@saga-ls.jp.

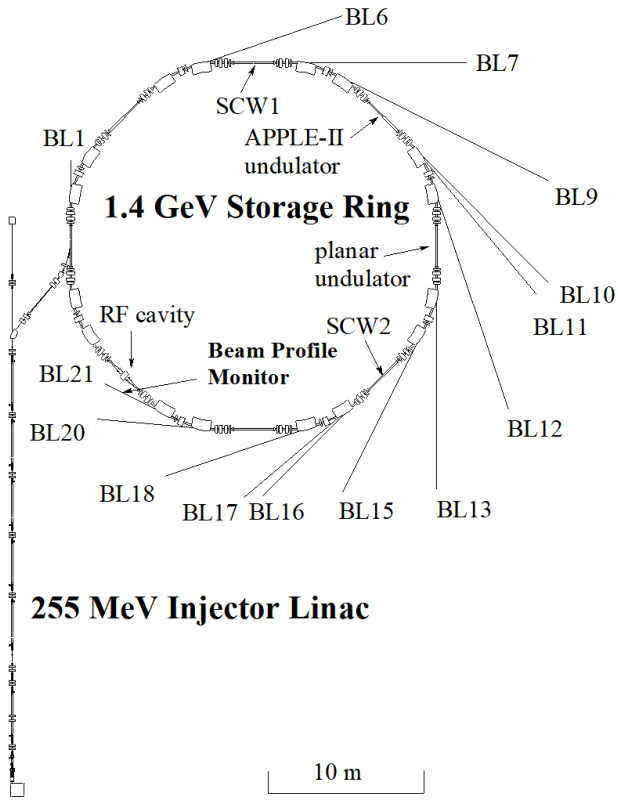

Figure 1: Schematic view of the SAGA-LS accelerator.

IMAGE AND DATA ACQUISITION SYSTEM

PC-based control system with the off-the-self remote I/O production, e.g., National Instruments Fieldpoint, YOKOGAWA PLC, are commonly adopted at the SAGA-LS accelerator [5]. The typical sampling rate of the monitoring system is from 0.5Hz to 2Hz. Originally, the beam loss occurred at the ramp-up was measured as a step like process by using this PC-based slow monitoring system. To analyse this phenomenon detail, we developed high-speed logging system of 250 kHz (PXIe-4300, 16bit ADC) for monitoring the beam current, beam positions, and output currents of the major power supplies of the storage ring magnets, using National Instruments PXI. In addition to acquiring these analogue parameters, image acquisition device (PXIe-1435, Frame Grabber) was set on this PXI system. Figure 2 shows the analogue data and image acquisition system for investigation of the beam loss. The typical sampling rate of the images is 60Hz. Beam profile images captured at accelerator beamline by CCD camera were translated to

ISBN: 978-3-95450-227-1 ISSN: 2673-5490 doi:10.18429/JACoW-IPAC2022-THPOPT013

EMITTANCE REDUCTION WITH THE VARIABLE DIPOLE FOR THE ELETTRA 2.0 RING*

A. Poyet†, Y. Papaphilippou, CERN, Geneva, Switzerland
M. A. Dominguez, F. Toral, CIEMAT, Madrid, Spain
E. Karantzoulis, Elettra-Sincrotrone, Trieste, Italy
R. Geometrante, KYMA, Trieste, Italy

Abstract

Elettra is a 2/2.4 GeV third-generation electron storage ring, located near Trieste, Italy. In view of a substantial increase of the machine performance in terms of brilliance, the so-called Elettra 2.0 upgrade is currently on-going. This upgrade is based on a 6-bends achromat, four dipoles of which having a longitudinally variable field. So far, those dipoles are foreseen to provide a field with a two step profile. The VAriable Dipole for the Elettra Ring (VADER) task, driven by the I.FAST European project, aims at developing a new dipole design based on a trapezoidal shape of the bending radius, which would allow for a further reduction of the horizontal emittance. A prototype of this magnet should be designed by the CIEMAT laboratory and built by KYMA company. This paper discusses the new dipole field specification and describes the corresponding optics optimization that was performed in order to reduce at best the emittance of the Elettra ring.

INTRODUCTION AND MOTIVATIONS

The present Elettra machine is a third-generation Italian light source, located in Trieste. Operating at two different energies of 2 or 2.4 GeV, Elettra presently delivers electron beams with an emittance of 7-10 nm.rad [1]. The Elettra 2.0 upgrade [2] aims mainly at reducing the emittance by at least one order of magnitude, while keeping the geometrical structure almost identical. The current plan for the machine upgrade is based on an enhanced 6-bend achromat (S6BA-E), relying on the use of longitudinal gradient (LG) dipoles to reach a bare horizontal emittance of about 210 pm-rad at 2.4 GeV. The dipolar field of those magnets varies longitudinally in the form of two steps, to reach 1.43 T (at 2.4 GeV) at the center.

It has been shown that hyperbolic profiles for the longitudinal evolution of the magnetic field could bring better performances in terms of emittance reach [3]. In that respect, this paper describes the different steps taken in order to replace the present LG dipoles by the so-called VADER (Variable Dipoles for the Elettra Ring). In a first part, it is shown how the longitudinal profile has been designed and implemented in MAD-X [4]. Then we will demonstrate how the VADER were included in the Elettra 2.0 lattice and how the optics were tuned in order to reach the best possible performance. Finally, we will show the first tracking results obtained with a new single particle tracking code being developed at CERN. In all those studies, we assume a beam energy of 2.4 GeV.

DESIGN OF A TRAPEZOIDAL PROFILE

The design of the longitudinal profile is highly inspired by the work presented in [3], where a longitudinally variable dipole was designed for the damping rings of the CLIC study [5]. The maximum field is reached at the center where consequently the bending radius is minimum. We want to design a trapezoidal profile in bending radius. The length of the central constant part in field is denoted L_1, while the length of the varying part of the magnet is denoted L_2. Moreover, the minimum bending radius - reached at the center - is denoted by ρ_1, and the maximum - reached at the edge of the dipole is denoted ρ_2. We can therefore define two ratios in terms of length L_i and bending radius ρ_i as:

$$\lambda = \frac{L_1}{L_2} \qquad \tilde{\rho} = \frac{\rho_1}{\rho_2}. \tag{1}$$

The design of the longitudinal profile is then determined using those two parameters and the definition of the bending angle provided by such a profile, as given in Eq. (2):

$$\theta_{\text{trap}} = \frac{L(\lambda(\tilde{\rho}-1)+\tilde{\rho}\ln\tilde{\rho})}{\rho_1(\tilde{\rho}-1)(1+\lambda)}. \tag{2}$$

Since the peak field of the dipole (2.3 T at 2.4 GeV), the total length L (0.8 m) and the dipole bending angle are determined by the original lattice and the technological constraints, we can choose λ and $\tilde{\rho}$ in order to optimize the emittance reduction. To do so, one can compute the emittance given by a Theoretical Minimum Emittance (TME) cell with a uniform dipole, and the one obtained with a trapezoidal profile. The emittance reduction factor is then defined as:

$$F_{TME} = \frac{\varepsilon_{\text{TME, uni}}}{\varepsilon_{\text{TME, trap}}}, \tag{3}$$

and the full expression can be found in the Appendix C of [3]. One can then parameterize the emittance reduction factor with λ and $\tilde{\rho}$, for combinations which conserve the magnet bending angle, as shown in Figure 1.

The best emittance reduction factor is found for $\lambda = 0.074$ and $\tilde{\rho} = 0.24$. Those parameters are then used to obtain the final longitudinal profile of the VADER dipole as displayed in Figure 2.

* Work supported by the I.FAST project
† axel.poyet@cern.ch

ISBN: 978-3-95450-227-1 ISSN: 2673-5490 doi:10.18429/JACoW-IPAC2022-THPOPT014

SIMULATION AND OPTIMIZATION OF SPS-II LINAC

T. Chanwattana†, S. Chunjarean, N. Juntong, S. Klinkhieo, K. Manasatitpong, P. Sudmuang
Synchrotron Light Research Institute, Nakhon Ratchasima, Thailand

Abstract

Siam Photon Source II (SPS-II), the new 3-GeV synchrotron light source project in Thailand, has been designed based on an accelerator system consisting of a 150-MeV injector linac, a full-energy booster synchrotron and a storage ring based on a Double Triple Bend Achromat (DTBA) lattice. A turn-key linac system has been used in an injection system of many synchrotron facilities, and thus it is considered for the SPS-II project. Preliminary beam dynamics simulation and optimization of the SPS-II linac are necessary for investigating achievable beam parameters which can be used for study of beam injection through a transfer line to the booster. Multi-objective genetic algorithm (MOGA) has been used in design and optimization of many accelerators including a linac system for synchrotron light sources, similar to the SPS-II linac. In this paper, results of beam dynamics simulation and MOGA optimization of the SPS-II linac are discussed.

INTRODUCTION

SPS-II project, is a project to build a new 3-GeV synchrotron light source in Thailand. The project aims to become a synchrotron facility to support synchrotron user community not only in Thailand but also in South East Asia. The SPS-II storage ring was designed based on DTBA lattice which provides moderately low beam emittance but double the number of straight sections per cell resulting in more than 20 straight sections for insertion devices (IDs) [1].

In the current design, an injection system of SPS-II was designed based on a conventional injection system consisting of a low-energy injector linac and a full-energy booster. This will allow the project to rely on conventional technologies, reduce the total project cost and increase the proportion of components developed and fabricated domestically. A 150-MeV injector linac has been adopted and tested recently at new synchrotron facilities such as TPS [2] and Sirius [3]. Thus, SPS-II plans to also adopt a 150-MeV injector linac based on a turn-key linac system [4]. However, the SPS-II storage ring and booster were designed based on RF system operating at RF frequency of 119 MHz [5] which is different from other modern storage rings. This leads to some design differences of the injector linac. Although the SPS-II linac will be a turn-key system, design and simulation of the linac have been done in order to study achievable beam parameters from the linac to be used in simulation of other parts of the machine, e.g. transfer lines and beam injection to the booster.

Design of the 150-MeV linac, and preliminary beam dynamics simulation and optimization of the SPS-II linac will be discussed in the following sections.

† thakonwat@slri.or.th

DESIGN AND MAIN PARAMETERS

The SPS-II injector linac has been designed [4] with main components as follows:

- Triode gun with 119-MHz voltage modulation at the grid level to produce a chopped beam
- Subharmonic prebuncher (SHB) operating at 476 MHz
- S-band buncher (BCH) operating at 2856 MHz
- Four S-band accelerating structures (ACC1-4).

The layout of the SPS-II linac for beam dynamics simulation and optimization in this work is shown in Fig. 1.

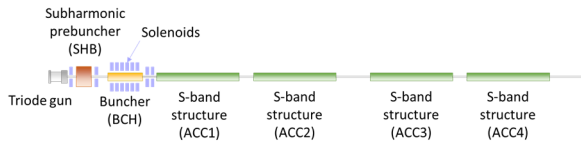

Figure 1: Schematic layout of the SPS-II linac.

The SPS-II linac aims to support beam injection for different operations of the storage ring, for example, normal user operation based on a uniform fill, and user request operations and machine developments based on other specialized filling patterns. Thus the linac should be able to operate in multi-bunch mode (MBM) and single bunch mode (SBM). Table 1 lists main parameters according to design specifications of the SPS-II linac.

Table 1: Main Parameters of the SPS-II Linac

Parameter	Value
Beam energy	150 MeV
Normalized emittance	≤ 50 mm·mrad
RMS energy spread	≤ 0.5%
Bunch train charge (MBM)	> 6 nC
Bunch charge (SBM)	≥ 1.5 nC
Bunch train duration (MBM)	150-600 ns
Bunch duration (SBM)	< 1 ns
Repetition rate range	1-5 Hz
Nominal repetition rate	2 Hz

SIMULATION AND OPTIMIZATION

Beam Dynamics Simulation

Multi-particle beam dynamics simulations of the SPS-II linac have been done with PARMELA [6]. Since the beam dynamics simulation is done starting from an electron gun at low beam energy, calculation of space-charge effects should be included in the simulations. In this work, beam dynamics simulations were performed by using a chopped beam from the triode gun as an initial beam distribution with uniform transverse and longitudinal distribution.

ISBN: 978-3-95450-227-1 ISSN: 2673-5490 doi:10.18429/JACoW-IPAC2022-THPOPT015

THE DESIGN OF THE FULL ENERGY BEAM EXPLOITATION (FEBE) BEAMLINE ON CLARA

A. R. Bainbridge, D. Angal-Kalinin, J. K. Jones, T. H. Pacey, Y. M. Saveliev, E. W. Snedden,
ASTeC, STFC Daresbury Laboratory, U.K.

Abstract

The CLARA facility at Daresbury Laboratory was originally designed for the study of novel FEL physics utilising high-quality electron bunches at up to 250 MeV/c. To maximise the exploitation of the accelerator complex, a dedicated full energy beam exploitation (FEBE) beamline has been designed and is currently being installed in a separate vault on the CLARA accelerator. FEBE will allow the use of high charge (up to 250 pC), moderate energy (up to 250 MeV), electron bunches for a wide variety of accelerator applications critical to ongoing accelerator development in the UK and international communities. The facility consists of a shielded enclosure, accessible during beam running in CLARA, with two very large experimental chambers compatible with a wide range of experimental proposals. High-power laser beams (up to 100 TW) will be available for electron-beam interactions in the first chamber, and there are concrete plans for a wide variety of advanced diagnostics (including a high-field permanent magnet spectrometer and dielectric longitudinal streaker), essential for multiple experimental paradigms, in the second chamber. FEBE will be commissioned in 2024.

INTRODUCTION

The Compact Linear Accelerator for Research and Applications (CLARA) is an ultra-bright electron beam test facility being developed at STFC Daresbury Laboratory. CLARA has been designed to test advanced Free Electron Laser (FEL) schemes that could be later implemented on existing and future short wavelength FELs, such as a UK XFEL.

CLARA is being constructed in stages: Phase 1 was completed in 2018 and consisted of the CLARA Front End: electron bunch production at 50 MeV, 100 pC at 10 Hz. Bunch charge up to 250 pC was achieved from the upgraded gun at 10 Hz with a hybrid Cu-photocathode. Design and commissioning of the CLARA Front End is detailed in Reference [1]. Phase 2 is currently under construction, and elevates the beam to 250 MeV/c, 250 pC at 100 Hz. A novel 100 Hz photo-injector gun [2] is currently being commissioned on the Versatile Electron Linear Accelerator (VELA)[3], situated adjacent to CLARA, and will be swapped over to the CLARA line when fully characterised. Phase 3 will allow installation of an FEL, seeding laser and modulators along with associated photon diagnostics. Phase 3 of CLARA is not yet funded.

During the construction of CLARA, in Phases 1 and 2, access to electron beams at ~35 MeV/c was made available to users from academia and industry. This enabled the testing of novel concepts and ideas in a wide range of disciplines, including development of advanced accelerator technology, beam diagnostics, medical applications and novel particle beam acceleration and deflection concepts [4]. Based on increasing user demand for access to the CLARA high brightness electron beam, a decision was made to design and build a dedicated beamline for user applications at the full CLARA beam momentum of 250 MeV/c.

The FEBE beamline is being built to transport 250 MeV/c beam to a dedicated hutch area, containing two experimental chambers, for user access. As a key component of the design, the hutch will be accessible without switching off the accelerator, allowing users to set up and access their experiments as required. The total beam power within the hutch is limited to ~6 W, which offers sufficient flexibility with available bunch charge (maximum 250 pC), bunch repetition rate (maximum 100 Hz) and beam momentum (up to 250 MeV/c).

The interaction of high-quality electron bunches with high instantaneous power laser light (>100 TW) is foreseen as a key component of any FEBE beamline exploitation, and will enable research in novel acceleration areas including LWFA, PWFA and dielectric laser acceleration (DLA). Beams accelerated inside the hutch can be accommodated up to 2 GeV/c.

FEBE DESIGN

The top-level overview of the CLARA and FEBE beamlines is shown in Fig. 1. The FEBE experiment hutch is a large (10x5.4x3m^3), shielded, and versatile area for performing electron beam exploitation experiments. Within the hutch, the beam transport is designed to deliver a strong focusing interaction point (IP) at two locations. Each IP is located within a large-volume (~2 m^3) vacuum experiment chamber.

A double-IP design is used to enable flexibility in experimental design and implementation, with most experiments having experimental apparatus situated in the first FEBE experimental chamber (FEC1) and diagnostics and other monitoring equipment situated in the second chamber (FEC2). A high power laser co-propagates with the electron beam to a common focus (IP1) in FEC1, with this capability included through a dedicated laser mirror box chamber (FMBOX1) upstream of the first experiment chamber, and a second mirror box (FMBOX2) between chambers to extract the laser following interaction.

The experimental hutch is connected to the main CLARA accelerator using a series of FODO arc cell structures optimised for minimal CSR emittance growth. The FEBE transverse offset is achieved using four 14° dipoles, which enables both sufficient space for an FEL seeding chicane, and fits within the existing CLARA shielding.

ISBN: 978-3-95450-227-1 ISSN: 2673-5490 doi:10.18429/JACoW-IPAC2022-THPOPT016

COMMISSIONING SIMULATIONS FOR THE DIAMOND-II UPGRADE

H.-C. Chao*, R. Fielder, J. Kallestrup, B. Singh, I. Martin, Diamond Light Source, Oxfordshire, UK

Abstract

The Diamond-II [1,2] storage ring, compared to Diamond, improves the natural emittance from 2.7 nm to 160 pm and the beam energy from 3 to 3.5 GeV. The number of straight sections is also doubled from 24 to 48 thanks to the modified hybrid six-bend-achromat lattice. To reduce the impact on the existing science program, the dark time period must be minimised. To assist in this aim, storage ring commissioning simulations have been carried out to predict and resolve possible issues. These studies include beam commissioning starting from on-axis first-turn beam threading up to beam based alignment and full linear optics correction with stored beam. The linear optics corrections with insertion devices are also included. The machine characterisations at different stages are compared. Considerations on realistic chamber limitations, error definitions and some commissioning strategies are also discussed.

INTRODUCTION

To predict and resolve possible problems during the storage ring commissioning, start-to-end beam commissioning simulations have been carried out. The simulations help to validate the specification and error tolerances defined for the machine components. The code Simulated Commissioning toolkit [3] based on the Accelerator Toolbox [4] which is well integrated with Matlab Middle Layer [5] scripts is chosen for the simulation. The commissioning of the storage ring can be divided into different phases:

1. Achieve a stored beam, starting with beam-threading and on-axis injection,
2. Achieve beam accumulation with off-axis injection,
3. Correct the linear optics, optimise the injection efficiency and the beam lifetime,
4. Commissioning of all insertion devices (IDs), harmonic cavity, etc.

The commissioning is simulated from the beam threading step to linear optics correction including all ID effects. Forty random machines are simulated to get the statistics.

The structure of this paper is organised as follows. Firstly, the error sources are defined. Then the early stage commissioning procedures including the beam threading and the RF tuning are described. Next is the linear lattice correction including the coupling correction and the alleviating of beta-beating caused by IDs. Finally a short conclusion is given.

* hung-chun.chao@diamond.ac.uk

ERROR DEFINITIONS

The error tolerences are developed in consultation with the Diamond-II Magnet and Engineering groups. They are tabulated in Table 1 and listed in Table 2. The systematic and random multipolar field errors are included up to 15-th order [1]. All the errors used here are populated in a normal distribution with truncation at two standard deviations.

Table 1: Magnet and Girder Errors

Element	Misalignment		Relative Field	
	Offset (μm)	Roll (μrad)	Main Field (%)	Secondary Field (%)
Girder	150/150§	150		
DL Magnet†	100	100	0.05	
Gradient Dipole	50	100	0.05	0.10
Anti-bend Quad	35	100	0.05	0.10
Pure Quad	35	100	0.10	
Sextupole	35	100	0.10	
Octupole	35	100	0.10	
CM	150	150	0.10	
CM‡				0.10
Skew Quad‡				0.50

§ Independent offsets at each end of the girder
† Longitudinal varying dipole
‡ Embedded in sextupole trim coils

Table 2: BPM, RF and Other Error Sources

BPM Errors		
Initial Offsets	500	μm
Roll	10	mrad
Calibration	5	%
Noise (Turn-by-Turn)	60	μm
Noise (Closed Orbit)	1	μm
RF Errors		
Frequency	100	Hz
Voltage	0.5	%
Phase Offset	90	°
Injected Beam Jitter		
Transverse Displacement	100	μm
Transverse Divergency	10	μrad
Energy Deviation	0.1	%
Phase Shifts	0.1	°
Other Errors		
Circumference	1	μm
Injection Pulsed Magnet Jitter	0.024	%

ISBN: 978-3-95450-227-1 ISSN: 2673-5490 doi:10.18429/JACoW-IPAC2022-THPOPT017

ORBIT STABILITY STUDIES FOR THE DIAMOND-II STORAGE RING

I.P.S. Martin, C.A. Abraham, D. Crivelli, H. Ghasem, B. Nicholson, T. Olsson, P. Sanchez-Navarro,
Diamond Light Source, Oxfordshire, U.K.

Abstract

The photon-beam stability relative to the beam size is a key performance parameter for storage ring light sources. The natural emittance of the Diamond-II ring will be lowered by a factor 16.7 compared to the existing facility [1], so the absolute stability requirement for the electron beam must reduce accordingly. In addition, advances in detector speed and resolution mean the tolerances are tighter compared to previous generations of storage rings, with a target of 3 % of beam size up to 1 kHz having been adopted for Diamond-II. In this paper we present studies of how the anticipated ground vibrations, girder motion, power supply ripple and RF noise will affect the electron beam stability as a function of frequency.

INTRODUCTION

To cope with advances in beamline detector speed and resolution, the target electron beam stability has been increased from 10% of beam size in the range 1-100 Hz for Diamond to 3% in the 1-1000 Hz bandwidth for Diamond-II. The new storage ring has an emittance of 162 pm.rad, corresponding to a factor ~5 reduction in horizontal beam size at the centre of the straights compared to the existing machine [1]. The vertical beam sizes at the source points are largely unchanged, as for both machines the β-functions are similar and the vertical emittance has been fixed at 8 pm.rad.

The increased stability requirements place strong demands on the facility design. To relieve the demands on the fast orbit feedback system, the storage ring components are being designed with their impact on electron beam stability considered from an early stage. Within the target bandwidth, the major contributors are expected to be ground vibrations, girder resonances, power supply ripple and RF noise. This paper contains a first analysis of how each of these sources are expected to contribute to the underlying electron beam stability. The target stability values for Diamond-II are given in Table 1.

Table 1: Required Electron Beam Stability (r.m.s.)

Location	Horizontal	Vertical
Long Straight	1.08 μm	0.16 μm
Standard Straight	0.87 μm	0.13 μm
Mid Straight	0.83 μm	0.11 μm

SOURCES OF DISTURBANCE

Ground Motion

Ground vibrations have been measured in the range 0.02 to 250 Hz using a combination of a Guralp seismometer and PCB seismic accelerometers [2]. In addition to the amplitude, the phase correlation of the ground motion has been measured along the vertical and North-South axes using two seismic accelerometers connected by a >100 m long cable [3]. The separation of the accelerometers was increased in steps and at each separation the amplitude and phase of the ground motion was recorded. This data was then used to extract the frequency at which the measured vibrations switch from being coherent to incoherent: motion with a phase deviation of below 45 degrees was defined to be in-phase (i.e. correlated) and anything greater than this was taken to be uncorrelated. Results are shown in Fig. 1.

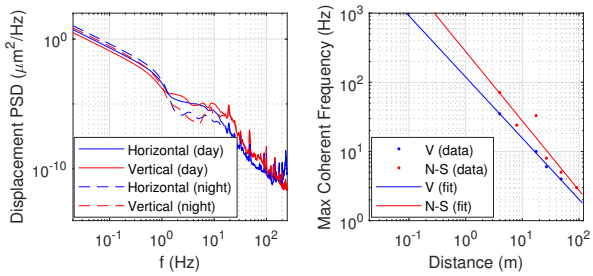

Figure 1: Left: Displacement power spectral density (PSD) for the Diamond tunnel. Right: Cross-over frequency when moving from correlated to uncorrelated motion.

An exponential fit was made to the correlation data to extract the general trend. The approximate scaling in each plane was found to be:

$$L_{coh,V} \approx \frac{222}{f^{1.1}}, \qquad L_{coh,N-S} \approx \frac{273}{f^{1.0}}. \tag{1}$$

From this analysis, for distances of up to ~10 m (corresponding to the length of a single girder or the BPM separation across an ID straight section), vibrations travelling through the storage ring floor will be coherent at frequencies up to around 15-25 Hz. That is to say, motion at these frequencies will be in-phase and everything supported by the slab will move as a single body.

The impact that ground motion has on electron beam stability has been analysed following a similar method to that described in [4]. Random displacements were calculated for the storage ring magnets over 100 seeds for a given correlation length. Ground-displacement to electron beam amplification factors could then be derived for each case by dividing the RMS closed orbit distortion at the source points by the amplitude of the ground motion and then averaging over the 100 seeds [1]. The results for that correlation length were then converted to excitation frequency using Eq. 1. Examples of the generated ground displacement for two correlation lengths are shown in Fig. 2.

ISBN: 978-3-95450-227-1 ISSN: 2673-5490 doi:10.18429/JACoW-IPAC2022-THPOPT018

APERTURE SHARING INJECTION FOR DIAMOND-II

J. Kallestrup*, H. Ghasem, I. P. S. Martin, Diamond Light Source, Oxfordshire, UK

Abstract

The planned Diamond-II storage ring will provide users with an increase in brightness of up to two orders of magnitude compared with the existing Diamond facility. The aim is to maintain excellent photon beam stability in top-up mode, which requires frequent injections. This paper introduces the aperture sharing injection scheme designed for Diamond-II. The scheme promises, through the use of short striplines equipped with high-voltage nano-second pulsers, a quasi-transparent injection while maintaining an approximately 100% injection efficiency.

INTRODUCTION

Traditionally, the injection process in storage ring-based synchrotron light sources has been driven by the use of transverse closed-orbit bumps created by pulsed dipole kickers in order to achieve off-axis accumulation. The inevitable non-closure of the orbit bumps, due to kicker imperfections or mis-match, leads to leakage of betatron oscillations to the remaining sections of the storage ring. These residual oscillations can create non-negligible photon beam perturbations for some beamlines, who may have to gate their detectors during the injection process, or attempt to schedule their measurements in the quiet-time between top-up cycles. Another option is to try to counteract the oscillations by means of a compensation kicker [1, 2]. With the new generation of synchrotron light sources based on multi-bend achromat (MBA) lattices, alternative injection schemes seek to conform with the relatively restricted dynamic- and momentum aperture while staying transparent (i.e., perturbation-free) to the users.

Diamond-II is the upgrade of the United Kingdoms national light source [3,4]. The new storage ring will be based on the Modified Hybrid Six-bend Achromat (M-H6BA), which includes ≈2.9 m straight section in the middle of the achromat ("mid-straights"), which can accommodate short insertion devices, cavities, injection elements etc.

The performance of several different injection schemes has been evaluated for top-up into Diamond-II. It was found that a single-bunch aperture sharing scheme provides the best compromise between reliability and transparency to the users, and will therefore be used during user operation. A combined thick- and thin septum situated in a single vacuum tank in the injection straight, inspired by developments for SLS 2.0 [5], is planned. A traditional four-kicker bump in the injection straight will be maintained for easy commissioning, fast multi-bunch filling and as a safe fall-back option. Furthermore, a static chicane is introduced in the injection straight to maximize flexibility [4].

* jonas.kallestrup@diamond.ac.uk

The remainder of this paper will describe the aperture sharing scheme, its expected performance and some key beam dynamics challenges.

SINGLE-BUNCH APERTURE SHARING

Top-up injections by single-bunch aperture sharing, to our knowledge initially proposed for the SLS 2.0 upgrade [6], is a bump-free injection scheme which uses short-pulse striplines to kick the injected beam towards the storage ring axis while simultaneously kicking the stored beam away from the axis. If the dynamic aperture is great enough, it is possible to kick the injected beam into the storage ring acceptance without kicking the stored beam out. The kicked bunches will then exhibit betatron oscillations around the closed orbit and are damped over time by synchrotron radiation emission.

The striplines must be fit into available space in the storage ring, and preferably at a phase advance equal to an odd multiple of $\pi/2$ after the exit of the septum magnet for the best possible compensation. The mid-straights in the H-M6BA lattice design can accommodate several striplines and has a reasonable phase advance when the effect of the non-linear magnets in the first half achromat is included. It was found that four striplines with 150 mm effective length will provide the best form factor while maintaining reasonable pulser requirements.

The position, angle and twiss parameters of the injected beam at the exit of the thin septum, together with the kick angle of the stripline kickers is optimized by numerically minimizing the horizontal RMS Courant-Snyder invariant of both the injected- and stored beam after the last stripline:

$$I_x = \frac{x^2 + (\alpha_x x + \beta_x x')^2}{\beta_x}, \quad (1)$$

where β_x and α_x are the twiss parameters after the last stripline. The optimum kick angle for each stripline is $\theta = -176\,\mu\text{rad}$.

A sketch of the aperture sharing implementation is shown in Fig. 1 together with the trajectory of the injected- and stored bunch centroids. The horizontal phase space of the two bunches during the first 50 turns is plotted in Fig. 2. Slightly more than 4 mm of DA is required, which is well-within what the storage ring is expected to deliver.

Robustness against Injection Mis-steering

A beam coming from the booster with the nominal parameters into an ideal storage ring is injected with 100% efficiency. Such a situation is too idealistic to evaluate the robustness of the injection scheme. Lattice and physical errors in storage ring will be present, and positional and angular errors due to mis-steering of the injected beam in the booster-to-storage ring transfer line, or jitter from the pulsed magnets involved

ISBN: 978-3-95450-227-1 ISSN: 2673-5490 doi:10.18429/JACoW-IPAC2022-THPOPT019

MULTI-ALKALI ANTIMONIDE PHOTOCATHODE DEVELOPMENT FOR HIGH BRIGHTNESS BEAMS

S. Mistry*, T. Kamps[1], J. Kühn, C. Wang [2],
Helmholtz-Zentrum Berlin für Materialien und Energie, Berlin, Germany
[1]also at Humboldt-Universität zu Berlin, Berlin, Germany
[2]also at Universität Siegen, Siegen, Germany

Abstract

Photocathode R&D at the Helmholtz-Zentrum Berlin (HZB) is driven by the motivation to produce high brightness electron beams for the SRF photoinjector test facility, Sealab/ bERLinPro. Multi-alkali antimonides are the choice photocathode material due to high quantum efficiency (QE) and low intrinsic emittance in the visible range. In this work a more robust alternative to the tried and tested Cs-K-Sb is considered. Na-K-Sb offers similar advantages to Cs-K-Sb including, high QE at green wavelengths but moreover, it offers excellent stability at elevated temperatures. This property could lengthen the cathode lifetime by enhancing the robustness of the photocathode inside the SRF gun. In this work, a status report showcasing first results towards the development of a growth procedure for Na-K-Sb is presented by means of spectral response and XPS measurements conducted in the HZB photocathode lab.

INTRODUCTION

The operation of a SRF photoinjector with a normal conducting photocathode has successfully been demonstrated at several research labs including BNL, HZB, HZDR and KEK, thanks to developments in photocathode integration technology [1]. Though significantly more challenging than using superconducting metals such as niobium or lead, integrating high QE semiconductor photocathodes enables the generation of high brightness beams and is therefore necessary for many applications.

At HZB, removable bi-alkali antimonide photocathodes will be used to drive the SRF photoinjector [2] to generate high brightness beams. For this, a non-contact, thermally insulated cathode insert design was developed to allow cathode cooling. Gun studies in the commissioning process revealed that the photocathode insert was damaged due to high thermal heat load from RF losses [3]. Consequently the insert design has been modified and tested to circumvent this issue [4]. Furthermore, we also consider the use of a more robust bi-alkali antimonide photocathode material, namely Na-K-Sb. Compared with Cs-K-Sb, there are relatively fewer studies on Na-K-Sb. Nevertheless, the aim is to develop a reproducible growth procedure for high QE Na-K-Sb photocathodes to provide a viable alternative to Cs-K-Sb for use in the Sealab/ bERLinPro SRF gun.

* sonal.mistry@helmholtz-berlin.de

EXPERIMENTAL SETUP

A "Work-Horse" Plug

To develop a growth procedure for Na-K-Sb photocathodes, the single use molybdenum plug substrate was traded in for a reusable all-molybdenum plug (see Fig. 1), or the so called "work-horse plug." The work-horse plug was prepared in-house from a single molybdenum block and surface polished using a series of diamond polishing paste solutions (6, 3, and finally 1 μ). Using the same substrate is advantageous in developing a growth procedure as this allows for direct comparison between the films. This is otherwise problematic if different substrates are used due to inconsistencies in surface preparation. Furthermore, reusing the sample substrate speeds up the turnaround time between growths. A substrate preparation procedure was devised to ensure a clean molybdenum surface is the starting point for each subsequent growth for this study.

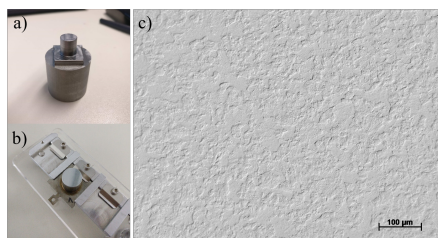

Figure 1: All-Mo plug with 10 mm diameter shown a) before, b) after polishing, and c) an optical microscope image of the polished surface.

Preparation and Analysis System

The preparation and analysis system is part of the infrastructure developed for the preparation, characterization and transport of photocathodes for the photoinjector. A full description of the system can be found in [5]. Multi-alkali antimonide films are grown in the preparation chamber under UHV conditions (base pressure 2×10^{-10} mbar) and XPS measurements are conducted in the adjoining analysis chamber. A spectral response set-up is attached to the preparation chamber to enable photocurrent measurements.

In the current configuration, one sample position is required for antimony deposition and another for alkali deposition; this chamber geometry therefore limits growth method options to either sequential or alkali co-evaporation onto an antimony layer, both of which are employed for the samples grown in this study.

ISBN: 978-3-95450-227-1 ISSN: 2673-5490 doi:10.18429/JACoW-IPAC2022-THPOPT020

STATUS AND PLANS FOR THE NEW CLS ELECTRON SOURCE LAB

X. Stragier, D. Betwistle, F. Le Pimpec, M. J. Boland,*[1]
Canadian Light Source, S7N 2V3 Saskatoon, Canada
[1]also at University of Saskatchewan, Department of Physics and Engineering Physics, S7N 5E2 Saskatoon, Canada

Abstract

The Canadian Light Source (CLS) has recently created a new Electron Source Lab (ESL) that can run independently from user operations. A section of the old Saskatchewan Accelerator Laboratory experimental nuclear physics tunnels has been rebuilt with new shielding and a separate entrance. The laboratory will be used to prepare an operational spare electron gun for the 250 MeV linac. In addition, there are plans to develop RF guns for a future branch line to inject into the linac and for possible short pulse production. This paper will give an overview of the ESL space and the first electron guns which plan to be installed.

INTRODUCTION

The CLS [1] has been in operation since 2005 and in 2018 suffered a major failure of the electron gun that brought down the facility for 7 months [2]. The gun dates from the 1970s and only a handful were built, hence very few spares are still available to repair it in case of another dramatic failure. To mitigate this risk, CLS has secured electron sources from other accelerator laboratories that can be used as replacements. The fastest way to come back into operation is to replace the present thermionic DC gun by another gun of the same energy. The DC voltage may require some tuning to match the beam dynamics at the exist of the gun to produce the appropriate bunches that can be transported and accelerated through the linac. Plans for such gun have been made with the help of a loan gun from MAX IV which is planned to be tested in the ESL. CLS has completed the construction of the ESL in a space in the basement which has separate and simultaneous access from the other linac tunnels, allowing for safe and flexible commissioning of electron sources and beams up to 100 MeV.

OVERVIEW OF ESL SPACE

The new bunker uses an existing location in the basement of the facility. The entire basement was used for nuclear research in the 1960s until the construction of the CLS ring. The area delimited in red, blue oval and black rectangle, see Fig. 1, were part of the Saskatchewan Accelerator Laboratory (SAL). Today the red part house the linac that feeds CLS; the blue oval has been decoupled from the linac tunnel for operation and for radiation protection and is home of the medical isotope production facility Canadian Isotope Innovation Corporation (CIIC) [3]. The area delimited in black is the location where the ESL will be installed (light blue area) including a reserved place where the local control room will be installed (dark blue area). The total area of the ESL is around 50 m^2.

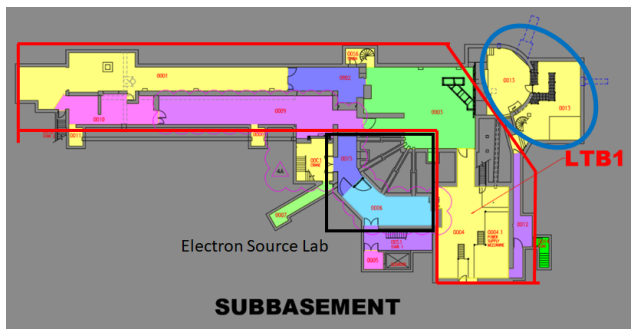

Figure 1: Location of the ESL in the CLS basement - next to the linac tunnel.

Like for the medical isotope production facility, new shielding, radiation protection system and interlocks have been installed to decouple the ESL operation from the linac operation. New operating license from the radiation regulator have been obtained that will allow the operation of ionizing radiation devices until 1 MeV. This phase has been achieved.

The second phase is to decouple the control room area from the experimental zone. Doors and radiation shielding are currently being installed. The experimental area can also be accessed via a side stairways with an elevator adjacent to it. The current door between the ESL and the stairways must be replaced by a lock with two doors, one is a fire resistant door the other is a radiation shielding door. Those doors are on order and the work regarding fire safety is ongoing including the needed paperwork as to certify that the construction comply to the construction code. It is expected that the infrastructure, water cooling, electricity, air conditioning, network, interlock system, fire safety system and city permit guaranteeing compliance to building code will be completed by end of March 2023.

Regarding radiation protection, the laboratory has been constructed and designed for operation up to 120 MeV electron beams by the CLS radiation protection authority. However, operation up to energy above 1 MeV will require new licensing from the Canadian radiation authority CNSC, which is also being taken care of at this moment.

* mark.boland@lightsource.ca

ISBN: 978-3-95450-227-1 ISSN: 2673-5490 doi:10.18429/JACoW-IPAC2022-THPOPT022

STUDY ON QE EVOLUTION OF Cs_2Te PHOTOCATHODES IN ELBE SRF GUN-II

R. Xiang†, A. Arnold, S. Ma[1], P. Michel, P. Murcek, J. Schaber[2], J. Teichert, A. Ryzhov, P. Zwartek,
Helmholtz-Zentrum Dresden Rossendorf, 01328 Dresden, Germany
[1] also at Univ. Hamburg, 20148 Hamburg, Germany
[2] also at TU Dresden, 01069 Dresden, Germany

Abstract

The quality of the photocathodes is critical for the stability and reliability of the photoinjector's operation. Thanks to the robust magnesium and Cs_2Te photocathodes, SRF gun-II at HZDR has been proven to be a successful example in CW mode for high current user operation.

In this contribution, we will present our observation of the QE evolution of Cs_2Te photocathodes during SRF gun operation. The variables including substrate surface, film thickness, Cs/Te stoichiometric, multipacting, RF loading and charge extract are considered in the analysis.

INTRODUCTION

As well known, the quality of photocathodes is a key factor to improve the stability and reliability of the photoinjectors [1]. For SRF guns developed at HZDR, metal cathodes (copper, magnesium) and semiconductor photocathode Cs_2Te are chosen as photocathode materials. Copper was used as commissioning cathode in SRF gun. But the work function of Cu (4.6 eV) is rather high and its quantum efficiency (QE) of 1×10^{-5} at 260 nm is too low for the regular beam production. For medium bunch charge mode, magnesium is a good photocathode candidate. Mg is a metal with low work function of 3.6 eV, and its QE can reach 0.5% after ps UV laser cleaning [2]. Although it has lower QE than Cs_2Te, Mg has the advantages of long life time, reliable compatibility and little risk of contamination to the niobium cavity.

Driven with UV laser the photocathode Cs_2Te (with band gap 3.3 eV + electron affinity 0.2 eV) has shown good QE and long life time in the ELBE SRF gun-I [3]. In 2017 we suffered the strong field emission and also thermal contact problem during SRF gun-II operation with three Cs_2Te cathodes (on molybdenum plug). An intensive study has been performed to understand the problem of overheating of those cathodes in SRF gun cavity. Then we decided to give up the Mo plug and apply OFHC as the plug material, though copper is not the friendliest substratum for the active Cs_2Te. Since then Cs_2Te on Cu plug has be prepared at HZDR and operated successfully in SRF gun-II for the THz user beam time.

CS_2TE CATHODES IN SRF GUN II

Since May 2020, seven Cs_2Te photocathodes have been used in the SRF gun-II. The average operation duration in gun is three months, providing 7-17 coulomb charge depending on the current request of the beam users. Cathodes would be exchanged when the gun warmed up during shutdown season and/or QE of the cathode in gun was not sufficient for the next beam time.

Preparation Process

The Cs_2Te photocathodes are prepared in the HZDR cathode lab and transported to the SRF gun in vacuum. The cathode plug is made of copper to ensure a high thermal conductivity for LN_2 cooling. The Cu plug is mirror polished or finished with diamond turning to a roughness in level of 10 nm. In our experiments, the Cs_2Te cathodes on the mechanical polished plugs and those on the diamond turning finished plugs show almost the same photoemission quality and also the same dark current in gun. The plugs are carefully treated in the clean room. The chemical cleaning, dry ice cleaning and 350°C baking in vacuum are applied to keep the surface free of any pollution.

During the preparation process, the plug is kept at 120°C with a halogen light. At first the tellurium and then cesium are deposited subsequently through a ϕ 4 mm mask onto the plug surface. Meanwhile, 260 nm and 340 nm LEDs are used to illuminate the cathode as the diagnostic light and the plug is -200 V biased. The cesium evaporation is stopped when the photocurrent at 260 nm reaches maximum, which actually leads to the Cs/Te ratio fluctuation from one cathode to another one.

The prepared cathodes are stored in the transport chamber with a vacuum around 5×10^{-11} mbar. Up to six photocathodes can be transported together from the photocathode lab to the SRF gun.

QE Dropping Due to RF Loading

During the cathode transport and insertion into gun, the QE can be very well preserved. However, a strong QE dropping did happen when the radio frequency power was started.

The QE tracking of the latest photocathode is shown in Fig. 1. This cathode was deposited with 6 nm Te and 37 nm Cs. From the photograph of the cathode, the coating was homogeneous with a narrow shadow of mask on the border. Note that QE measured in the transport chamber (red points) and the first QE value in SRF gun (first blue point) were almost the same, which means there was no QE lost during both transport and insertion activities. But soon after the pulsed RF was loaded, especially when the CW power was started, a strong QE degradation was observed.

† email address: r.xiang@hzdr.de

ISBN: 978-3-95450-227-1 ISSN: 2673-5490 doi:10.18429/JACoW-IPAC2022-THPOPT023

FLEXIBLE FEATURES OF THE COMPACT STORAGE RING IN THE cSTART PROJECT AT KARLSRUHE INSTITUTE OF TECHNOLOGY

A. I. Papash†, A. Bernhard, E. Bründermann, D. El Khechen, B. Härer, A.-S. Müller, R. Ruprecht, M. Schwarz, J. Schäfer, Karlsruhe Institute of Technology, Karlsruhe, Germany

Abstract

Within the cSTART project (compact storage ring for accelerator research and technology), a Very Large Acceptance compact Storage Ring (VLA-cSR) is realized at the Institute for Beam Physics and Technology (IBPT) of the Karlsruhe Institute of Technology (KIT). A modified geometry of a compact storage ring operating at 50 MeV energy range has been studied and the main features of the new model are described here. The new design, based on 45° bending magnets, is suitable to store a wide momentum spread beam as well as ultra-short electron bunches in the sub-ps range injected from a laser plasma accelerator as well as from the Ferninfrarot Linac- Und Test Experiment (FLUTE).

The DBA lattice of the VLA-cSR with different settings and relaxed parameters, split elements and higher-order optics of tolerable strength allows to improve dynamic aperture and momentum acceptance to an acceptable level. This contribution discusses the lattice features in detail, expected lifetime, injection, tolerances and different possible operation schemes of the ring.

INTRODUCTION

R&D on laser plasma acceleration is pursued with the aim to clear up key issues on the feasibility of a new generation of very compact sources of synchrotron radiation for future users [1]. Laser Plasma Accelerators (LPA) feature short bunch lengths and high peak currents combined with a small facility footprint. For wavelengths longer than the length of the emitting electron bunch, the photon emission becomes coherent [2]. Thus, the radiation intensity from the terahertz (THz) to the infrared range increases dramatically. The combination of a storage ring and a laser plasma accelerator might be a basis for a new generation of compact light sources and advancing user facilities to different commercial applications. [3].

Meanwhile, the post-LPA beam is not directly suitable for storage and accumulation in conventional light source facilities. The energy spread of post-LPA beams well exceed the values at existing light sources [4]. The initially ultra-short electron bunches will quickly be elongated in existing storage rings. Due to the expansion of electrons in the plasma "bubble" with large divergence and momentum spread the effective normalized beam emittance will grow significantly leading to an increase of bunch length due to synchro-betatron coupling in the dispersive sections of the storage ring [5].

A dedicated storage ring with adapted features is realized at KIT with the purpose to provide the experimental "proof of principle" of injection and storage of ultra-short electron bunches (sub-ps to tens of fs) as well as beam with large momentum spread of about 1% (rms) after laser plasma cell [6]. To test the ring's performance the compact linear accelerator FLUTE will serve as an injector of 50 MeV bunches [7].

FLEXIBLE LATTICE

Different geometries, lattices and operation modes of a compact storage ring have been extensively studies and the results have been reported at [2-4, 8-11]. The parameters of the facility and the electron beam are presented in Table 1. The ring footprint fits to the FLUTE experimental hall [7]. The highly non-linear lattice with flexible features and relaxed parameters is composed of four equal double bend achromat (DBA) sections (see Fig. 1).

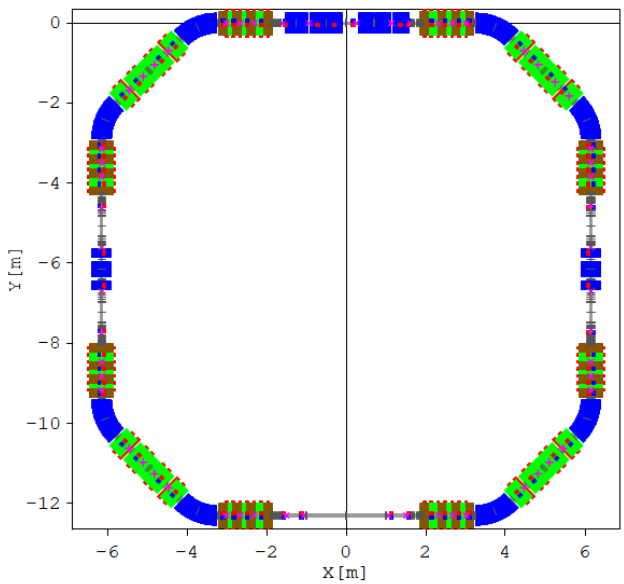

Figure 1: Layout of the cSTART ring.

Different operation modes to pursue accelerator R&D activities were described earlier [11]. The lattice of the cSTART storage ring satisfies contradictory features:

- The energy acceptance is increased to >5% to accommodate particles with large momentum deviation.
- The amplitude of the dispersion function is limited to keep a compact beam size in the bending sections.
- The dynamic aperture is large enough for stable storage of wide momentum spread beam.
- Additional sections for dedicated Accelerator Research and Development (ARD) experiments are included into the ring lattice.

†alexander.papash@kit.edu

ISBN: 978-3-95450-227-1 ISSN: 2673-5490 doi:10.18429/JACoW-IPAC2022-THPOPT024

MIST – THE MESA-INJECTOR SOURCE TWO*

M.A. Dehn[1], K. Aulenbacher[1,2,3], P.S. Plattner[1]
[1] JGU, Johannes Gutenberg-Universität Mainz, Germany
[2] HIM, Helmholtz-Institut Mainz, Germany
[3] GSI, Helmholtzzentrum für Schwerionenforschung, Darmstadt, Germany

Abstract

The new accelerator MESA (**M**ainz **E**nergy recovering **S**uperconducting **A**ccelerator) will provide an average CW electron beam current of up to 10 mA. Operating at 1.3 GHz, this corresponds to a bunch charge of 7.7 pC. The new DC-photoemission source MIST (the **M**ESA-**I**njector **S**ource **T**wo) is optimized for these requirements. A challenge is heating of the photocathode at high laser power. By a suitable mechanical construction and the use of specific materials, the heat can be dissipated during operation. Options for further improvements are discussed.

INTRODUCTION

MESA (**M**ainz **E**nergy recovering **S**uperconducting **A**ccelerator) will be able to operate with two different photoemission DC-electron sources at an extraction energy of 100 keV. The primary electron source STEAM (**S**mall **T**hermalized **E**lectron Source **A**t **M**ainz [1]) can provide spin-polarized electrons with an average beam current of 150 µA up to 1 mA [2]. The second source MIST can provide up to 10 mA unpolarized average beam current.

Laser intensities of 1 W or more are required to extract beam currents 10 mA from photocathodes. Most of this laser power is converted into thermal load within the cathode and has to be dissipated to avoid excessive heating of the device and thus a significant reduction in lifetime.

The MESA beam line in the low-energy range from STEAM up to the pre-accelerator booster consists of various elements, e.g. for spin manipulation or a chopper-buncher system [3]. Therefore, the beam line is too long for bunch charges higher than 1 pC in order to reach the booster as loss-free as possible [4, 5].

Due to the beam dynamics at high bunch charges, the distance between MIST and the pre-accelerator booster should be as short as possible in order to reach the booster as loss-free as possible. In a second beam line above the MESA injector main beam line MIST will be arranged together with a Mott polarimeter at a same height. A dogleg arrangement with two bending magnets was developed to enable both: transport high bunch charges from the source to the booster, or guide the spin polarized beam from STEAM to the Mott polarimeter [6].

DESIGN OF MIST

The design of MIST is based on the compact construction of the high voltage (HV) photoemission source CEBAF at Jefferson Laboratory [7]. The HV is provided by a R30 connector, the corresponding jack is a bakable Al2O3 insulator on a CF–200 flange. With a biased cathode at −100 kV, the anode and the whole vacuum chamber are grounded. The emission is in horizontal direction, allowing the source to be integrated into the accelerator along beam axis (see Fig. 1).

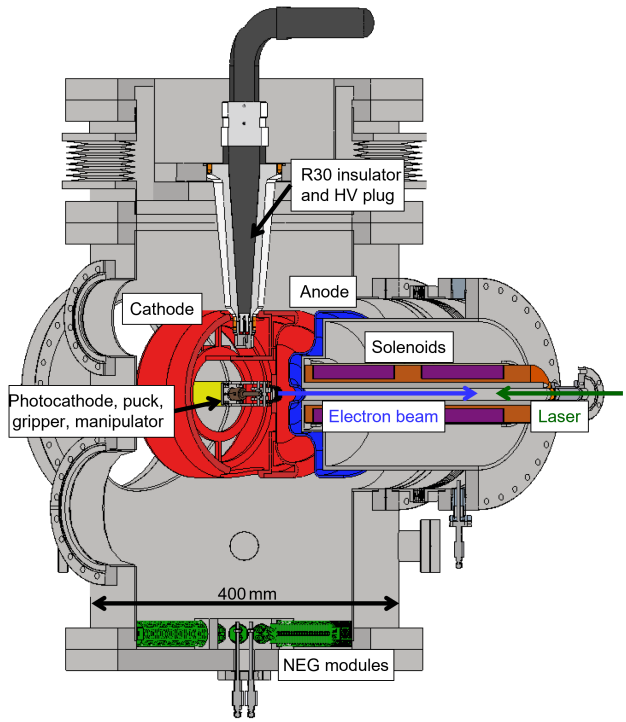

Figure 1: CAD model of MIST (MESA-Injector Source Two). A magnified view of the cathode (red) and anode (blue) region is given in Fig. 3.

An ion getter pump and NEG modules provide pressure conditions in the low UHV range. A load-lock system is directly connected to enable a photocathode change without breaking the source-vacuum.

Photocathode

MIST is planned as the high current electron source at MESA and will be operated with more robust and higher charge lifetime than GaAs-based photocathodes. The favored candidate is here the multi alkali K_2CsSb and can be produced in house. However, the photocathode is located in a so called puck. The thermal energy has to be transferred from the puck towards the boron nitride (BN) via the metallic gripper. The BN finally transports the heat towards compo-

* Work supported by the German science ministry BMBF through Verbundforschung within Projects 05K19UMA (CSBB) and 05K19UMB(BETH)

ISBN: 978-3-95450-227-1 ISSN: 2673-5490 doi:10.18429/JACoW-IPAC2022-THPOPT025

PHOTOCATHODE STRESS TEST BENCH AT INFN LASA

D. Sertore*, D. Giove, L. Monaco, INFN Milano - LASA, Segrate, Italy
A. Bacci, F. Canella, I. Drebot, D. Giannotti, L. Serafini, INFN Milano, Milano, Italy
G. Guerini Rocco[1], Università degli Studi di Milano, Segrate, Italy
[1]also at INFN Milano - LASA, Segrate, Italy
S. Cialdi, D. Cipriani, E. Suerra, Università degli Studi di Milano, Milano, Italy
G. Galzerano, CNR - Istituto di Fotonica e Nanotecnologie - Milano, Milano, Italy

Abstract

A UHV test bench based on a 100 kV DC gun and a 100 MHz repetition rate laser has been setup up at INFN LASA to test Cs_2Te photocathodes. This operation mode is the base for the BriXSinO project, currently in the design phase in our laboratory, and the qualification of the Cs_2Te photocathodes is a key issue. In this paper, we present the recent progress on the different components that are part of this R&D activity.

INTRODUCTION

High brightness electron sources are nowadays a key component for the most advance accelerators capable of generating intense X-ray beams. Free Electron Lasers (FELs), Energy Recovery Linacs (ERLs) and Inverse Compton Scattering (ICS) sources are some of the leading machines in this field.

To generate the electron beam with the required specifications, a laser-driven photocathode is exposed to very intense electric fields create either in an RF Gun or in High Voltage (HV) DC gun for promptly accelerate the emitted electrons.

Besides the many applications of these electron sources, the most challenging ones require average currents up to 100 mA in CW or nearly CW operation mode with bunch repetition rate of the order of GHz. To cope with these extreme requests, significant advancements are necessary both on the lasers and on the photocathodes.

Lasers need to provide train pulse at these high frequency guaranteeing, after all the manipulations necessary for providing the spatial and temporal profile needed to generate electron beams with the smallest emittances, the required energy per pulse necessary to photoemit the requested electrons.

On the photocathode side, operation at these very high repetition rates poses questions on the capability of the photoemissive film to sustain them. Moreover, the photocathodes are required to operate for long period to reduce the downtime of the accelerators.

In the context of advanced X-ray source based on accelerators, we are designing BriXSinO, an innovative accelerator whose aim is to operate as an ERL or a two-way accelerator feeding an ICS source and a THz FEL. It is within this framework that we are developing the key technologies necessary to its operation and two hot-topics are the development of a laser capable of operating at 100 MHz and a High Voltage (HV) testbench [1], coupled to the laser, for testing Cs_2Te photocathodes. The electron beam foreseen has an average current of 5 mA at 100 MHz repetition rate.

BriXSinO

BriXSino is a reduced scale demonstrator of the modified push-pull folded ERL scheme [2], capable of accelerating electrons up to a maximum energy of 50 MeV.

In this reduced scheme, only one cryogenic module, hosting three seven-cell 1.3 GHz superconducting cavities, will be used both for ERL operation but also for two-pass mode acceleration. In BriXSino, we will also test the compression of the beam in the recirculating loop. Moreover, in the loop, two experimental stations will be available for ICS and THz FEL. Figure 1 shows a functional layout of the machine.

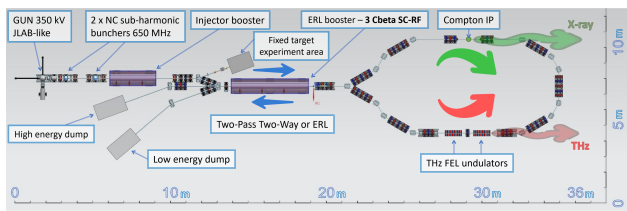

Figure 1: BriXSinO's functional layout.

The development of BriXSino's test facility (foreseen at INFN LASA in Milano) aims at maximum energy sustainability by investigating:

- best efficiency in accelerating a high-power electron beam (ERL operation)
- production of very high flux radiation beams (in THz spectral range by the FEL and in X-rays by ICS) for medical applications and applied research in general.

The Technical Design Report of BriXSinO is now available at [3] and a dedicated presentation at this conference is reporting the latest progress [4].

LASER SYSTEM

As previously anticipated, the laser plays a key role in the BriXSinO operation and, hence, we have an active R&D on this topic.

The scheme of the laser system is shown in Fig. 2. The main oscillator, model Orange from the Menlo Company, is a 1035 nm mode-locked Yb laser, with a 92.857 MHz repetition frequency. An internal amplification system guarantees

* daniele.sertore@mi.infn.it

ISBN: 978-3-95450-227-1 ISSN: 2673-5490 doi:10.18429/JACoW-IPAC2022-THPOPT026

ASSEMBLY AND CHARACTERIZATION OF LOW-ENERGY ELECTRON TRANSVERSE MOMENTUM MEASUREMENT DEVICE (TRAMM) AT INFN LASA

D. Sertore*, M. Bertucci, A. Bosotti, D. Giove, L. Monaco, R. Paparella
INFN Milano - LASA, 20054 Segrate, Italy
C. Pagani[1] and G. Guerini Rocco[1], Università degli Studi di Milano, 20054 Segrate, Italy
[1]also at INFN Milano - LASA, 20054 Segrate, Italy

Abstract

In the framework of high-brightness electron beam generation, thermal emittance is nowadays a key parameter. While alkali tellurides are extensively used in advanced electron sources, alkali antimonides photocathodes demonstrated high QE in the visible, thus making feasible CW operations for RF-based photoinjectors. The INFN LASA laboratory in Milan is fully equipped with dedicated production systems for photocathode preparation and optical setup for QE evaluation. In this paper, we describe a newly designed device dedicated to electron transverse momentum measurement (TRAMM). It will be connected to the main production chambers and will serve as an "emittance monitoring" system during photocathode growth. From the design phase, through the parameter estimate, assembly of the components, to the installation and first measurements, we describe the status of this project and its future developments.

INTRODUCTION

Laser-driven, visible light-sensitive photocathode based electron sources are crucial elements for the current 4th generation X-ray sources, namely Free Electron Lasers (FELs) and the upcoming and promising technology behind the Energy Recovery Linacs (ERLs).

The brightness of the electron beam generated at the photocathode strongly dictates the performance of all such systems. This parameter depends upon the cathode Quantum Efficiency (QE), i.e. the number of emitted electrons per incident photons, and the emittance of the source, ultimately limited by the thermal emittance. This last quantity determines the final capabilities of the machine.

At the LASA laboratories of INFN in Milano, we routinely produce high-yield photocathodes for high brightness RF guns. However, what we are missing is a diagnostic tool for the thermal emittance of our photocathodes at the production site. So, based on the idea developed at LBNL [1], we designed [2] and assembled a device for transverse momentum measurements that will be installed "in series" with our production system.

* daniele.sertore@mi.infn.it

PHYSICS PRINCIPLE

The physics principle of TRAMM is based on the conversion of the electron transverse velocity in a measurable displacement on a screen.

In fact, electrons are photoemitted by a suitable light beam from the surface of the photocathode located at position C in Fig. 1. A grid then accelerates the electrons to the kinetic energy of few keV, within a 100 ns order time given $t = g\sqrt{\frac{m_e}{2eV}}$ where g is the cathode-grid distance, m_e the electron mass, e the electron charge and V is the applied voltage.

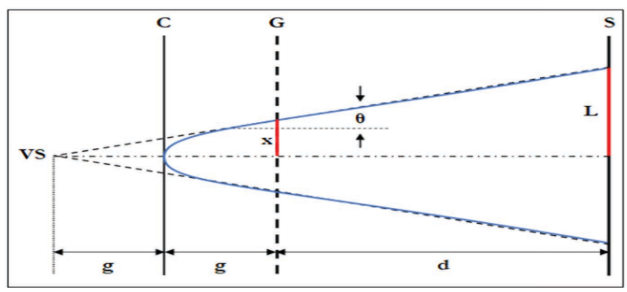

Figure 1: Schematics of the TRAMM experiment. Photocathode is placed at position C, grid in G and the screen at S.

From the grid onwards, electrons propagate freely with a transverse kinetic energy K_x and a deflection angle θ. On the screen S, the particles arrive with a transverse distance from the center L, corresponding to a transverse momentum:

$$\frac{p_x}{mc} = \frac{L}{2g+d}\sqrt{\frac{2eV}{mc^2}} \tag{1}$$

where d is the distance between the grid and the screen.

The accelerated electrons are collected on a screen composed of a phosphor and a CCD acquisition system. The acquired images are then processed to reconstruct the spatial distribution of the particle impinging on it. From the x-y function, we derive the mean square value $< p_x^2 >$ of the momentum distribution determined by the cathode density of states and electronic band structure.

Finally, we can evaluate the thermal emittance of the photocathode as a function of the laser wavelength:

$$\epsilon_n = \sigma_{x,y}\sqrt{\frac{< p_{x,y}^2 >}{mc}} \tag{2}$$

being $\sigma_{x,y}$ the r.m.s. spot size at the photocathode.

ISBN: 978-3-95450-227-1 ISSN: 2673-5490 doi:10.18429/JACoW-IPAC2022-THPOPT027

R&D ON HIGH QE PHOTOCATHODES AT INFN LASA

D. Sertore*, M. Bertucci, L. Monaco, INFN Milano - LASA, Segrate, Italy
G. Guerini Rocco[1], Università degli Studi di Milano, Segrate, Italy
[1]also at INFN Milano - LASA, Segrate, Italy
S. K. Mohanty, H. Qian, F. Stephan, DESY Zeuthen, Zeuthen, Germany

Abstract

We present the recent activities on antimonide and telluride alkali based photocathodes at INFN LASA. The R&D on Cs_2Te materials is focused on investigating effects of material thickness and growth procedures on the photocathodes performances during operation in RF guns. We aim to improve thermal emittance and long term stability of these films. The more recent work on alkali antimonide showed the need for substantial improvements in stability and QE during operation. We present here our recent achievements and plans for future activities.

INTRODUCTION

INFN LASA has a 30 years experience in producing telluride photocathodes for high brightness electron sources based on RF guns. The performances of Cs_2Te films (sensitive in the UV region of the e.m. spectrum) improved over the years, satisfying the major requests for their operation as laser triggered electron source, i.e. QE, QE uniformity, low dark current, and operative lifetimes as long as nearly 4 years in user facility operated 24h/7d [1].

These remarkable results have been achieved thanks to the long experience on photocathodes R&D, in their production and analysis after operation in RF guns. Moreover, the continuous improvement on diagnostic tools to be used during the deposition process (for example multiwavelenght diagnostic) has allowed a better understanding of photoemissive and optical properties of these films [2, 3] and, as a consequence, their improvement in term of operative performances.

Recently, the increasing interest in Continuos Wave (CW) machine moved us to start an activity on alkali antimonide films that are sensible to visible light. This properties allows reducing the requirements on the laser since there is no more need to generate the fourth harmonic, with a significant reduction in complexity of the system and with an increase of available power. R&D studies, still on-going, devoted to the development of a reproducible recipe of KCsSb films, bring us to built, in collaboration with DESY PITZ and European XFEL, a dedicated new production system at INFN LASA. With this system, we deposited three photocathodes in Summer 2021 that were later tested in the RF gun at PITZ (DESY-Zeuthen).

This paper presents and summarizes the main activities devoted to a deeper comprehension of photoemissive and optical properties of UV and green sensitive photocathodes. These studies are a key process towards developing reliable recipes that will guarantee reaching the always more challenging requirements needed for the operation of the photocathodes in the RF guns.

Cs_2Te PHOTOCATHODES

A deeper comprehension of the properties of Cs_2Te films is a key point to guarantee the requests coming from their users. The real-time multiwavelenght technique developed at LASA has been optimized during the years and applied both during the deposition of standard films (10 nm Te) and of films grown at different thicknesses. This technique allows studying the spectral responses at different wavelengths and provides a reliable tool to better control the photocathode growth process (limiting the Cs excess), to study the photoemissive energy threshold (E_g+E_a where E_g is the energy gap and E_a the electron affinity) formation, and also to study the optical properties during the deposition process.

The optical properties have been the subject of a recent study [4]. Indeed, we grew films at different thicknesses, by changing the initial Te film, respectively with 5, 10 and 15 nm of Te. A model has been developed to calculate the reflectivity at different wavelengths (from 239 to 436 nm) of a system composed by an optical polished Mo substrate and Cs_2Te with different thicknesses. The values for the refractive index of Mo have been measured in air at wavelengths ranging from 239 to 436 nm and varying angle between 10 to 85° as we reported in the following section, while Cs_2Te values are fitted from our experimental data.

Figure 1 shows preliminary simulation results for the reflectivity at different wavelengths versus the Cs_2Te thickness. The important feature is the flattening of the reflectivity for short wavelengths when the thickness of the photocathode is increased.

As deeply discussed in the before referred paper, the reflectivity presents minima and maxima that are related only to the amount of deposited Cs, i.e. the Cs_2Te thickness. To complete this analysis, our plan is to deposit a even more thick film (20 nm Te) that will allow us completing the analysis in view of better understanding the optical properties of these films.

PITZ colleagues performed emittance measurements on these three cathodes at different thicknesses finding an unexpected anticorrelation between thermal emittance and photocathode QE [5]. A model was developed based on the assumption that the negative correlation between the TMS (Transverse Momentum Spread) and the QE is potentially related to the excess of Cesium that could cause promotion

* daniele.sertore@mi.infn.it

ISBN: 978-3-95450-227-1 ISSN: 2673-5490 doi:10.18429/JACoW-IPAC2022-THPOPT028

DEPENDENCE OF CsK_2Sb PHOTOCATHODE PERFORMANCE ON THE QUALITY OF GRAPHENE SUBSTRATE FILM

L.Guo[1, †], K. Goto[1], H. Yamaguchi[2], M. Yamamoto[3] and Y. Takashima[1]
[1] Nagoya University, Nagoya, Aichi, Japan
[2] Los Alamos National Laboratory, Los Alamos, New Mexico, U.S.A.
[3] High Energy Accelerator Research Organization, Tsukuba, Ibaraki, Japan

Abstract

A high-performance photocathode is required to advanced accelerators and electron microscopes. In particular, the CsK_2Sb photocathode is of interest because it has features such as low emittance, excitability with visible light, and high quantum efficiency (QE). Generally, the CsK_2Sb photocathode is produced by depositing a cathode element on a substrate, so that the cathode performance strongly depends on the surface condition of the substrate. We have found graphene as reusable substrate, which has the property of being chemically inactive. In this study, graphene film quality dependence of CsK_2Sb photocathode performance was evaluated. Specifically, CsK_2Sb photocathode was deposited using different quality graphene film substrates and their QE values and uniformity were compared. The quality of graphene films was analyzed using X-ray Photoelectron Spectroscopy (XPS) and X-ray Absorption Spectroscopy (XAS). We found that the graphene film can be cleaned by heating at 500 deg. The QE of the cathode on a good quality graphene film was higher and more uniform than that on a poor quality graphene film.

INTRODUCTION

Cesium potassium antimonide (CsK_2Sb) is one of the highest performing alkali (multi) antimonide photocathodes, achieving quantum efficiency that exceeds 10% by a green laser (532 nm)[1,2]. It is also realized of record-high beam current of 60 mA in a DC injector with 30 hours 1/e lifetime[3].

Generally, CsK_2Sb photocathode is produced by depositing the cathode element on a substrate, so that the cathode performance strongly depends on the substrate material, including crystallinity[1,4], surface state (contamination, roughness, and surface orientation)[1,4-6] and dopant types[2]. If the substrate after cathode production is used again by heat cleaning, the performance of the reproduced cathode will drastically deteriorate. Therefore, since the cathode performance is prioritized, the substrates are generally not reusable. On the other hand, the exchange of substrate takes an enormous amount of time and labor. This hinders basic research and practical application of photocathodes. As an effectual method to deal with this problem, we have coated graphene on the substrate as a protective layer.[7]

In this study, we investigated the QE and its mapping using different quality graphene film substrates to understand the effect of graphene film quality on the photocathode performance. For this purpose, we used XPS and XAS to evaluate the quality of graphene films. The CsK_2Sb photocathode was fabricated onto them, and their performance was compared.

EVALUATION OF GRAPHENE QUALITY

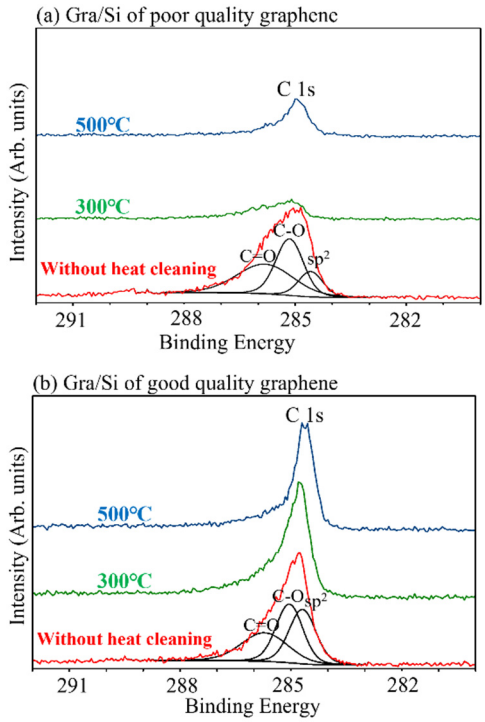

Figure 1: The XPS results of C 1s peaks for under different heat cleaning conditions. Red, green, and blue lines are for cleaning condition of without heat cleaning, 300°C, and 500°C, respectively. (a) is Gra/Si of poor quality graphene. (b) is Gra/Si of good quality graphene. The fitting for the sp^2, C-O, and C=O peaks are shown in the black lines below in the spectrum.

Graphene is produced on a Cu substrate by the chemical vapor deposition (CVD) method and transferred to Si substrate by a polymer support[8]. However, the Polymethyl methacrylate (PMMA) support remains on the graphene surface after transfer and must be removed. Considering the photocathode formation environment, the heat cleaning method under ultrahigh vacuum is used for the graphene-coated substrate.

We prepared two kinds of samples of graphene-coated Si substrate (Gra/Si), which one is Si coated with good quality graphene film, the other is Si coated with poor quality graphene film. They were analyzed of XPS and XAS under

† l.guo@nusr.nagoya-u.ac.jp

ISBN: 978-3-95450-227-1 ISSN: 2673-5490 doi:10.18429/JACoW-IPAC2022-THPOPT029

STUDY ON THE PERFORMANCE IMPROVEMENT OF ALKALI ANTIMONIDE PHOTOCATHODES FOR RADIO FREQUENCY ELECTRON GUNS

R. Fukuoka†, K. Ezawa, Y. Koshiba, M. Washio, WISE, Waseda University, Tokyo, Japan
K. Sakaue, UT-PSC, The University of Tokyo, Tokyo, Japan

Abstract

Semiconductor photocathodes such as Cs-Te and Cs-K-Sb are used as electron sources in accelerators to generate high brightness beams using radio frequency (rf) electron guns. Alkali antimonide photocathodes have a high QE of about 10%, and the excitation wavelength is in the visible light region (532 nm), which reduces the number of wavelength conversions and facilitates optical path adjustment, thus reducing the load on the optical system and increasing the amount of electric charge compared to Cs-Te. However, alkali antimonide photocathodes have a short lifetime and degrade under poor vacuum conditions, so it is beneficial to improve the durability by protective film coatings. Therefore, we are currently working on the fabrication of high QE alkali antimonide photocathodes that can withstand the QE reduction during coating. In this conference, we will report the results of the comparison between the fabricated alkali antimonide photocathode and Cs-Te photocathode, and future prospects.

INTRODUCTION

Recently, there is a growing demand for accelerator experiments such as energy recovery linac (ERLs) and free electron lasers (FELs) that require high-brightness electron beams. Photocathodes, which extract electrons by the photoelectric effect using laser irradiation, as an electron source for accelerators are mostly adopted to meet such requirements. Especially, alkali antimonide photocathodes (such as Cs-K-Sb and Cs-Sb), a type of semiconductor photocathode, have high QE and excitation wavelengths in the visible light region, and are being studied to fabricate photocathodes with performance that exceeds that of existing photocathodes.

However, despite these excellent characteristics, alkali antimonide photocathodes have some disadvantages like having a short lifetime of only a few weeks; the 1/e lifetime of Cs-Sb photocathodes were reported to be 20 to 500 hours under high-frequency electric fields [1].

Therefore, we fabricated and evaluated a Cs-Sb photocathode coated with CsBr, an alkali halide protective film for the higher performance photocathode with the higher QE and the longer lifetime. We also compared the results with those of our previous work in our laboratory on Cs-Te photocathodes coated with an alkali halide protective film [2].

† rinchan.00722@ruri.waseda.jp

EXPERIMENT

Experimental Equipment

The Cs-Sb photocathode and the coating of the CsBr protective film in this experiment were made in the vacuum evaporation chamber shown in Fig. 1. The pressure inside the chamber during the evaporation is about 10^{-7}~10^{-6}Pa, and the pressure inside the chamber during the lifetime measurement is about 5×10^{-8}Pa. This ultra-high vacuum was achieved by 6 vacuum pumps, a dry roots pump (Kashiyama: NeoDry30E), 2 turbo molecular pumps (PFEIFFER HiPace® 300 DN 100 CF-F EDWARDS STP-301), an ion pump (ULVAC: PST-100CX) and 2 NEG pumps (SAES Getters: CapaciTorr®), and the degree of vacuum during the experiment is monitored by a B-A vacuum gauge (Canon ANELVA: M-922HG).

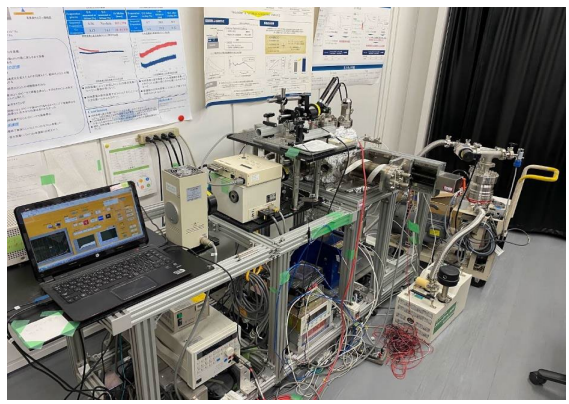

Figure 1: Appearance of the vacuum evaporation chamber.

Figure 2 shows the setup of the evaporation source holder (ESH) in this experiment. The ESH is equipped with a Cs dispenser (SAES Getters), which uses the principle of reduction reaction with chromium oxide, and Sb (Nilaco) and CsBr (Pier Optics) crystals in a tungsten basket. During the experiment, the total amount of material deposited on the surface of the cathode is measured in real time using a quartz crystal microbalance (QCM) thickness meter, which has a deposition rate of 0.1 Å/s and a resolution of 1 Å for the deposited film thickness.

ISBN: 978-3-95450-227-1 ISSN: 2673-5490 doi:10.18429/JACoW-IPAC2022-THPOPT030

DESIGN STUDY OF 30 MeV LINAC FOR A COMPACT THz RADIATION SOURCE*

S. Jummunt†, S. Chunjarean, N. Juntong, K. Manasatitpong, S. Klinkhieo
Synchrotron Light Research Institute, Muang District, Nakhon Ratchasima, Thailand

Abstract

A compact THz radiation source plays a possibility to achieve intense THz radiation at tunable frequencies between 0.5 and 5.0 THz, with a peak power of several MW and narrow bandwidth. This source requires essentially the reliable high gradient s-band linear accelerator (linac) to provide an electron beam energy up to 30 MeV with high bunch charge. In order to obtain a high gradient linac mentioned, the cell shape of cavity has been preliminary optimized and performed using the softwares Superfish and CST-MWS. The preliminary design of linac and beam dynamics study are presented in this paper.

THz SOURCE

The terahertz (THz) region of the electromagnetic spectrum in the range from 0.1 to 10 THz, is a rich zone and has attracted much attention in terms of new scientific and industrial applications. Nowadays, several types of efficient THz radiation sources are available as useful tools for producing high-power THz radiation to fulfill specific requirements. One effective way of producing this radiation is with an accelerator source based free-electron laser (FEL). The main goal is to achieve intense THz radiation at tunable frequencies of between 0.5 and 5.0 THz, with a peak power of several megawatts (MWs) and narrow bandwidth.

The proposed system consists of a 1.6-cell photocathode RF gun operated in the S-band of 2856 MHz to generate electrons with high brightness. The electron beam will then be focused and accelerated up to an energy of 10–30 MeV. To generate coherent radiation, the electron bunch length must be compressed to 100 fs by a chicane bunch compressor, before being passed to an undulator as shown the layout in Fig. 1. The details will be reported in Ref [1]. Based on the details reported, we can produce intense tunable THz radiation with narrow bandwidth in the frequency region of 0.5–5 THz to support a wide variety of applications.

Since FELs are the most powerful and wavelength-tunable radiation sources in the THz region, the facility generally needs a huge space with high cost in construction and operation. Therefore, a compact THz source considered will be based on super-radiant source or coherent radiation. It requires very good quality electron beams, corresponding to high brightness electron beams with 1 mm-mrad emittance, 1 nC bunch charge, and short bunch length in sub-picosecond. To be regarded as superradiance or coherent condition, the coherent superposition leads to a spectrally narrow and extremely intense THz beam. The radiation frequency in the range from 0.5 THz up to 5 THz can be covered, with the use of beam energies ranging from 10 to 30 MeV and magnetic field strength of undulator running up to 6.5. The spectral width is in the order of the inverse number of undulator periods. As a source of narrow-band THz radiation an undulator with 7 cm period length is foreseen.

In this paper, we focus on a preliminary design of high-gradient linac for a high-power THz FEL radiation source and present the beam dynamics required.

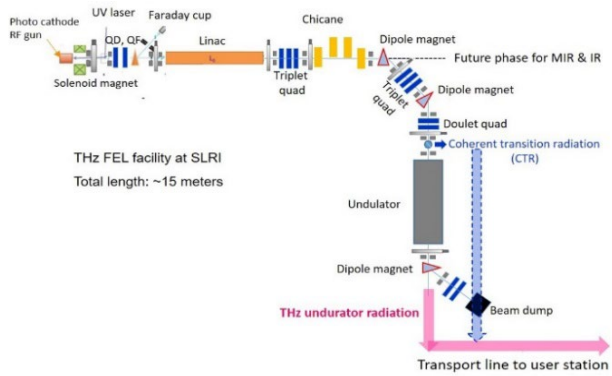

Figure 1: Layout of THz FEL source with the total length of 15 meters.

STUDY DESIGN OF LINAC

As mentioned about the short pulse required for THz source, in the process of accelerating the travelling-wave (TW) structures will achieve higher efficiency than that of standing wave (SW) structures because of providing smaller filling time and getting higher shunt impedance per unit length. For high efficiency, the high-gradient TW accelerating linac based on constant gradient structure with the mode TM010 fundamental electric field is considered with a phase advance per cell of $2\pi/3$ [2, 3].

In order to obtain a high gradient linac mentioned, the cell shape of cavity has been optimized and performed using the software tools Superfish [4] and CST-MWS [5]. The TW cells are optimized with having high shunt impedance, high quality factor, constant gradient field, and short filling time. For preliminary study, the aims of linac design are to provide the shunt impedance of higher than 60 MΩ/m, quality factor of higher than 14,000, filling time less than 1 μs, and the constant gradient field generated. Adjusting dimension of cell structure is the most important role to require attention. Figure 2 shows the model parameters for the linac cells optimization.

* Work supported by Synchrotron Light Research Institute, Thailand
† siriwan@slri.or.th

ISBN: 978-3-95450-227-1 ISSN: 2673-5490 doi:10.18429/JACoW-IPAC2022-THPOPT031

SUNDAE1: A LIQUID HELIUM VERTICAL TEST-STAND FOR 2m LONG SUPERCONDUCTING UNDULATOR COILS

B. Marchetti*, S. Abeghyan, J. Baader, S. Casalbuoni, M. Di Felice, U. Englisch,
V. Grattoni, D. La Civita, M. Vannoni, M. Yakopov, P. Ziolkowski
European XFEL GmbH, Schenefeld, Germany
S. Barbanotti, H.-J. Eckoldt, A. Hauberg, K. Jensch, S. Lederer,
L. Lilje, R. Ramalingam, T. Schnautz, R. Zimmermann
Deutsches Elektronen-Synchrotron, Hamburg, Germany
A. Grau
Karlsruher Institut fuer Technologie, Karlsruhe, Germany

Abstract

Superconducting Undulators (SCUs) can produce higher photon flux and cover a wider photon energy range compared to permanent magnet undulators (PMUs) with the same vacuum gap and period length. To build the know-how to implement superconducting undulators for future upgrades of the European XFEL facility, two magnetic measurement test-stands named SUNDAE 1 and 2 (Superconducting UNDulAtor Experiment) are being developed. SUNDAE1 will facilitate research and development on magnet design thanks to the possibility of training new SCU coils and characterizing their magnetic field. The experimental setup will allow the characterization of superconducting coils up to 2m in length. These magnets will be immersed in a Helium bath at 2K or 4K temperature. In this article, we describe the experimental setup and highlight its expected performances.

INTRODUCTION

The advancement of SCU technology has a strategic importance for the future development of the European XFEL facility. In the recent years, SCUs have been succesfully employed in synchrotron radiation sources [1, 2]. In a similar way of what happened with their application to synchrotrons, SCUs can potentially improve the performance and flexibility of advanced Free Electron Lasers (FELs). In particular by working at short undulator periods, superconducting magnet technology would allow reaching higher photon energies while keeping a wide range of tunability of the setpoint.

The extension of the energy range of the radiation towards higher values at European XFEL would fully exploit the high electron energy beam capability of the accelerator [3]. Moreover, this development can be considered complementary to the study on the upgrade of the XFEL linac for continuous wave (CW) operation [4]. CW operation at European XFEL is considered possible only with reduced electron beam energy. Specifically the electron beam energy will be limited to about 7 GeV, while the present maximum value is 17.5 GeV. The replacement of the existing PMUs beamline with SCUs having shorter undulator periods would enable the 7 GeV linac to cover the same photon energy range as the present accelerator.

* barbara.marchetti@xfel.eu

For all those reasons, a project for the realization of a SCU afterburner for the SASE2 line is being set-up. The main parameters and specifications for a pre-series prototype module (S-PRESSO) of such afterburner have been presented in [5].

The availability of equipment for the characterization of the magnetic coils of the undulator is a critical point to monitor the performances of the undulators that have been produced prior to the installation. For this reason two test-stands, SUNDAE1 and SUNDAE2 (Superconducting UNDulAtor Experiment 1 and 2) for the diagnostics of the novel SCUs are under realization in the DESY campus.

The test-stand SUNDAE1 will be dedicated to the training, tuning and characterization of new SCU coils by means of magnetic field measurements [6]. The cryostat of SUNDAE1 will have a vertical configuration and will be constituted by a liquid Helium bath in which the coils are immersed. SUNDAE2 will be used for the characterization of the final afterburner cryomodules [7]. This cryostat will have an horizontal configuration and the coils will be tested in their final cryostat. In this second test-stand the characterization of the module using the pulse-wire technique will also be foreseen [8, 9].

OVERVIEW OF SUNDAE1

Figure 1 shows the schematic drawing of SUNDAE1. The coils of the SCUs will be immersed in a liquid or superfluid Helium bath, at 4K or 2K respectively. Two Hall probes will be installed on a sledge driven by a Linear Motion System (LMS). The sledge will be able to move between the two coils constituting a SCU. The system will be able to characterize coils having a magnetic gap down to 5 mm. The coils are supported by a structure anchored on a plate of the lid. Several thermal shields guarantee a low heat load from the surroundings to the cryogenic vessel. The magnet is connected to the power supply outside the cryostat through current leads. Several feedthroughs at the lid allow the connection of diagnostics sensors (temperature sensors, voltage taps, Hall probes etc.) to the outside of the cryostat.

As illustrated in Fig. 1, the orientation of the Hall-probes allows the characterization of the y-component of the magnetic field of the coils, B_y. The resolution of the measure-

ISBN: 978-3-95450-227-1 ISSN: 2673-5490 doi:10.18429/JACoW-IPAC2022-THPOPT032

SUNDAE2 AT EuXFEL: A TEST STAND TO CHARACTERIZE THE MAGNETIC FIELD OF SUPERCONDUCTING UNDULATORS

J. E. Baader*, S. Abeghyan, S. Casalbuoni, D. La Civita, B. Marchetti, M. Yakopov, P. Ziolkowski, European XFEL GmbH, Schenefeld, Germany
H.-J. Eckoldt, A. Hauberg, S. Lederer, L. Lilje, T. Wohlenberg, R. Zimmermann, DESY, Hamburg, Germany
A. W. Grau, Karlsruhe Institute of Technology, Karlsruhe, Germany

Abstract

European XFEL foresees a superconducting undulator (SCU) afterburner in the SASE2 hard X-ray beamline. It consists of six 5m-long undulator modules with a 5 mm vacuum gap, where each module contains two 2m-long coils and one phase shifter. Prior to installation, the magnetic field must be mapped appropriately. Two magnetic measurement test stands named SUNDAE 1 and 2 (Superconducting UNDulAtor Experiment) are being developed at European XFEL. While SUNDAE1 will be a vertical test stand to measure SCU coils up to two meters with Hall probes in a liquid or superfluid helium bath, SUNDAE2 will measure the SCU coils assembled in the final cryostat. This contribution presents the development status of SUNDAE2 and its main requirements.

INTRODUCTION

European XFEL envisages the development of superconducting undulators (SCUs) technology as part of the facility development program. An SCU afterburner is proposed for the hard X-ray undulator beamline SASE2. This afterburner is composed of one pre-series prototype named S-PRESSO and five SCU modules [1,2]. The successful implementation of the SCUs has compelling benefits: First and foremost, it opens the possibility of lasing above 30 keV, which enables new types of experiments and opens the access to new scientific applications of FEL radiation. Also, SCUs can cover approximately the same photon energy range available from the presently installed PMUs (electron beam energy of 17.5 GeV), considering a continuous-wave (CW) operation mode.

The magnetic field characterization is an essential step in the design of high-quality undulators for storage rings and free-electron laser applications. Local field measurements (i.e., point-by-point) are commonly performed by Hall probes, while the flipping coil and moving wire systems are well known for field integral measurements. The pulsed wire method is an alternative method to map the local field. Although the pulsed wire technique is still not competitive with Hall probes in terms of accuracy, it has the potential to reconstruct space resolved magnetic fields for small-gap short-period long undulators (for which Hall probe-based measurements may be more difficult due to space constraints).

We are developing a test stand facility named SUNDAE2 (**S**uperconducting **UND**ul**A**tor **E**xperiment) to measure the SCU modules' magnetic field in the final cryostat. SUNDAE2 will be installed at DESY campus. It will operate three magnetic measurement techniques: two wire-based techniques (pulsed wire moving wire systems) and the Hall probe. This contribution presents the main features of the SCUs we aim to measure and the first steps taken towards developing SUNDAE2[1].

S-PRESSO MAIN PARAMETERS

S-PRESSO will be the first module to be delivered and characterized. It will be 5m-long, as the presently installed permanent magnet undulators. The magnetic period will be 18 mm and the on-axis peak magnetic field 1.82 T (K = 3.06). The maximum first and second field integrals allowed for both transversal field components are 4×10^{-6} Tm and 1×10^{-4} Tm^2, respectively. The vacuum gap of S-PRESSO will be 5 mm.

VACUUM CHAMBERS OF SUNDAE2

SUNDAE2 will be composed of three main vacuum chambers connected to each other. Each chamber consists of a welded vacuum tank with CF flanges and mounted equipment (e.g., blank flanges, electrical feed throughs, viewports, etc.). Figure 1 shows the design of the vacuum chambers of SUNDAE2. The main features of each vacuum chamber (named Chamber 1, Chamber 2, and Chamber 3 for convenience) are shown in Table 1.

Table 1: Main Dimensions of Chambers 1, 2, and 3

Parameter	Ch. 1	Ch. 2	Ch. 3
Longitudinal length (m)	2.8	1.0	1.3
Transversal length in x (m)	0.6	0.1	0.6
Transversal length in y (m)	0.6	0.1	0.6
Tube diameter (mm)	306	38	306

Vacuum and ion pumps will be connected to the lower flanges of Chambers 1 and 3 shown in Fig. 1. All the required electrical feed throughs will be placed on the opposite side of the lateral viewports of Chambers 1 and 3 illustrated in Fig. 1. Support structures (not shown in Fig. 1) will keep

* johann.baader@xfel.eu

[1] SUNDAE1 will be a vertical test stand capable of performing magnetic measurements and training of superconducting coils up to 2 m [3,4].

ISBN: 978-3-95450-227-1 ISSN: 2673-5490 doi:10.18429/JACoW-IPAC2022-THPOPT033

PERFORMANCE CHARACTERISATION AT DARESBURY LABORATORY OF Cs-Te PHOTOCATHODES GROWN AT CERN

L.A.J. Soomary[1], C.P. Welsch[1], The University of Liverpool, Liverpool, United Kingdom
L.B. Jones[1], T.C.Q. Noakes[1], H.M, Churn[1], C. Benjamin[2], STFC ASTeC, Daresbury, United Kingdom
H. Panuganti, E. Chevallay, M. Himmerlich, V. Fedosseev, E. Granados, CERN, 1211 Geneva 23, Switzerland
[1]also at Cockcroft Institute of Accelerator Science, Daresbury, United Kingdom
[2]also at The University of Warwick, Warwick, United Kingdom

Abstract

The search for high-performance photocathodes is a priority in the field of particle accelerators. The surface characteristics of a photocathode affect many important factors of the photoemission process including the photoemission threshold, the intrinsic emittance and the quantum efficiency. These factors in turn define the electron beam quality, which is measurable using figures of merit like beam emittance, brightness and energy spread.

We present characterisation measurements for four caesium telluride photocathodes synthesized at CERN. The photocathodes were transported under ultra-high vacuum (UHV) and analysed at STFC Daresbury Laboratory, using ASTeC's Multiprobe [1] for surface characterisation via XPS and STM, and Transverse Energy Spread Spectrometer (TESS) [2] for Mean Transverse Energy (MTE) measurements. The transverse energy distribution curves were measured at both cryogenic and room temperatures and the respective MTE values extracted at each illumination wavelength. We discuss correlations found between the chemical composition and MTE values.

INTRODUCTION

The intrinsic emittance of a photocathode is governed by multiple physical factors such as surface roughness, crystallographic face, cleanliness, work function and the QE. As the intrinsic emittance defines the achievable lower limit for the electron beam emittance within a linear accelerator, it is important to understand the effects that changing a photocathode surface has on these characteristics [3]. Minimising the mean transverse energy (MTE) of an electron beam is crucial, as total emittance cannot be reduced by using electrostatic or magnetic lenses as described by the Liouville theorem, thus motivating photocathode R&D to minimise MTE at the cathode surface to achieve low-emittance electron beams [4].

Caesium telluride (Cs-Te) has been used in accelerators as a photocathode for high bunch charge, high repetition rate superconducting radiofrequency photoinjectors, which are an essential technology for the current state of the art energy recovery linacs and high-power free electron lasers [5, 6]. The value of Cs-Te, as a photocathode source, stems from its balanced properties of high quantum efficiency (QE), its robustness to chemical contamination (in comparison to other semiconductor photocathodes such as GaAs [7]) and hence long operational lifetime. The main challenges of Cs-Te photocathodes, however, lie in the growth of the photoemissive layer as small variations in the growth conditions can significantly affect the composition and performance of the cathode, highlighting the complexity in the mechanism behind the chemical reaction between caesium and tellurium [8, 9].

In a collaboration between the STFC Daresbury Laboratory and CERN, caesium tellurium (Cs-Te) photocathodes were manufactured at the CERN photoemission laboratory [10] using the co-deposition method, and then transported overland in a UHV suitcase to the STFC Daresbury Laboratory. The photocathode surfaces were first performance characterised using the TESS to obtain their transverse energy distribution curves (TEDC) [11, 12], before being transferred to the Multiprobe system for surface characterisation. In this paper we present the results of MTE measurements for three of the four Cs-Te photocathodes, their atomic composition, and a discussion on the effect of surface composition on photoemissive performance.

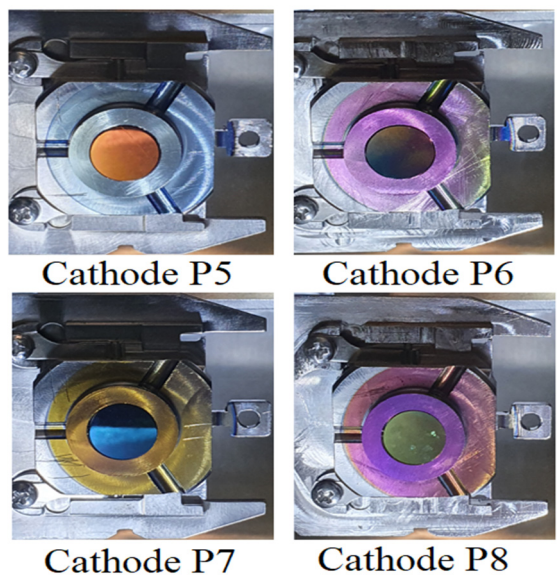

Figure 1: Photographs of the 4 Cs-Te photocathodes taken with the same lighting conditions and camera settings during transfer from the vacuum suitcase into the Photocathode Preparation Facility.

ISBN: 978-3-95450-227-1 ISSN: 2673-5490 doi:10.18429/JACoW-IPAC2022-THPOPT034

CONTROLLED DEGRADATION OF A Ag PHOTOCATHODE BY EXPOSURE TO MULTIPLE GASES

L.A.J. Soomary[1†], C.P. Welsch[1], The University of Liverpool, Liverpool, United Kingdom
L.B. Jones[1], T.C.Q. Noakes[1], STFC ASTeC, Daresbury, United Kingdom
[1]also at Cockcroft Institute of Accelerator Science, Daresbury, United Kingdom

Abstract

The search for high performance photocathode electron sources is a priority in the accelerator science community. The surface characteristics of a photocathode define many important factors of the photoemission process including the work function, the intrinsic emittance and the quantum efficiency of the photocathode. These factors in turn define the ultimate electron beam quality, which is measurable as normalised emittance, brightness and energy spread. Strategies for improving these parameters vary, but understanding and influencing the relevant cathode surface physics which underpin these attributes is a primary focus in this area of accelerator research [1].

We present performance data for a Ag polycrystalline cathode under illumination at 266 nm subjected to progressive degradation through exposure to O_2, CO_2, CO and N_2 in which we use our Transverse Energy Spread Spectrometer (TESS) instrument [2] to measure the mean transverse energy (MTE) of the photoemitted electrons with data at room and cryogenic temperatures. Crucially the data shows the effect of progressive degradation in photocathode performance [3] as a consequence of exposure to controlled levels of O_2 and that exposing an oxidized Ag surface to CO can drive a partial recovery in QE.

INTRODUCTION

The intrinsic emittance of a photocathode is governed by multiple physical factors such as surface roughness, crystallographic face, surface contaminants, work function and the quantum efficiency (QE). The ultimate achievable emittance in a linear accelerator is limited by its electron source, so a deep understanding of the factors which affect the performance of the photocathode is crucial to optimise the performance of accelerators [4]. Minimising the mean transverse energy (MTE) of a beam is crucial as total emittance cannot be reduced by using electrostatic or magnetic lenses, which leads the photocathode community to minimise MTE at the cathode surface to achieve low-emittance electron beams [5].

Naturally, the state of the vacuum in which the photocathode resides and operates is important. Residual gases within the vacuum system may react with the cathode surface causing the formation of new composites [6-8]. An inferred reduction of QE caused by gas adsorption may be observed, and such behaviour has been confirmed in previous work on alkali and semiconductor-based cathodes [3,9], and our work on an Ag (100) cathode [10].

The TESS experimental facility [2] measures the transverse energy distribution curve (TEDC) of a photocathode, and this data is analysed to extract the MTE [2,11]. The TESS is connected to a Photocathode Preparation Facility (PPF) [12] which supports in-vacuum photocathode transfer and storage, and provides thermal and atomic hydrogen photocathode cleaning. Investigations into the factors which affect photocathode performance require a multitude of diagnostic tools, and the Multiprobe system supports this work by providing a suite of complementary surface characterisation techniques [13].

EXPERIMENTAL DETAILS

Experiments were performed on a 6 mm diameter Ag polycrystalline cathode with an average roughness of 5 nm, as measured with our interferometric microscope. The sample holder was degreased in an ultrasonic acetone bath for 20 minutes before the sample was mounted. Once loaded into our Multiprobe system the photocathode underwent cycles of Ar+ ion bombardment for 20 minutes followed by annealing to 500°C via electron bombardment for 1 hour. This process was repeated until we observed a clean XPS survey spectrum without the presence of oxygen or carbon. The cathode was then transferred under XHV conditions in a vacuum suitcase from the Multiprobe to the PPF before performance was characterised in the TESS. TEDC measurements were taken under illumination at 266 nm, as described in previous publications [2,11].

Prior to gas admission, the chamber base pressure was measured and an initial photoemission image recorded using the previously mentioned parameters. With the chamber base pressure monitoring enabled, gas was admitted into the chamber and the photocathode subjected to progressive degradation. Pairs of photoemission data and dark background images were taken, both with an exposure time of 30 seconds. During each degradation experiment at both room and cryogenic temperatures, the leak valve was adjusted to maintain a constant gas pressure. With knowledge of the initial base pressure, an absolute value was determined for the cumulative level of gas exposure experienced by the photocathode during the experiments, and the consequent evolution of the MTE was determined from the photoemission images.

ISBN: 978-3-95450-227-1 ISSN: 2673-5490 doi:10.18429/JACoW-IPAC2022-THPOPT035

A SECOND GENERATION LIGHT SOURCE AIMING AT HIGH POWER ON THE GIANT DIPOLE RESONANCE

X. Buffat*, L.L. Cuanillion and E. Kneubuehler, CERN, Geneva, Switzerland

Abstract

We propose an alternative to nuclear waste transmutation and energy amplification using a second generation light source rather than a high power proton beam. The main parameters of the ring and insertion devices are estimated, targeting a photon beam power of 1 GW with a spectrum that maximizes the potential for nuclear reactions via the Giant Dipole Resonance. The synergies with technologies developed for high energy physics, in particular within the Future Circular Collider study (FCC), are highlighted.

INTRODUCTION

The usage of high power proton beams for the transmutation of nuclear waste from conventional reactors as well as for waste-less nuclear energy production is an active field of research since its initial proposal [1, 2]. Here we study an alternative approach based on a conventional light source of the second generation, with an insertion consisting of a high field superconducting dipole magnet. Nuclear fission and neutron emission are induced via the Giant Dipole Resonance (GDR) [3]. In the next section, we will determine the beam energy and insertion magnet properties that maximises the radiated power on the GDR. We then describe the design of a synchrotron that operates on this optimum. To conclude, the construction cost and the technologies that could lower it are discussed.

RADIATION SPECTRUM

Let us consider a beam of electrons with a current I_e and an energy E_e. We place a short dipole magnet with field B_i and magnetic length L_i on the beam trajectory. The photon beam power emitted is given by [4]:

$$P_i = I_e L_i \frac{e}{6\pi\epsilon_0}\frac{\beta_r^4\gamma_r^4}{\rho_i^2}, \tag{1}$$

with e the elementary charge, ϵ_0 the vacuum permittivity and β_r,γ_r the electrons's relativistic factors. The bending radius in the insertion magnet is given by:

$$\rho_i = \frac{m_e\gamma_r\beta_r c}{B_i e}, \tag{2}$$

with m_e the electron mass and c the speed of light. Defining the critical energy as:

$$E_c = \frac{3\hbar c}{2}\frac{\gamma_r^3}{\rho_i} \tag{3}$$

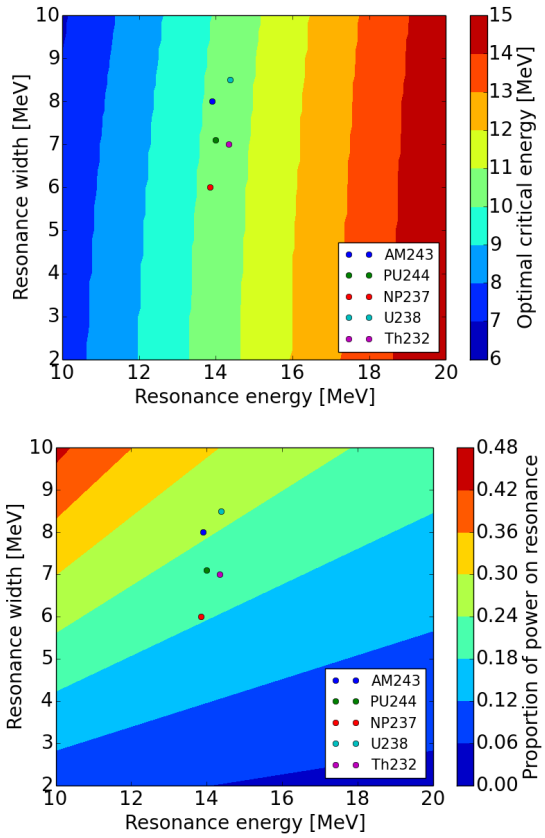

Figure 1: Optimal critical energy (top) and the corresponding proportion of the photon spectrum on the GDR (bottom) as a function of the resonance properties. The values corresponding to the main GDR of a few actinides are shown for reference.

with Planck's constant $\hbar$, we can write the power spectral density:

$$\frac{dP_i}{d\theta} = \frac{9\sqrt{3}}{8\pi}P_\gamma\theta\int_\theta^\infty K_{5/3}(x)dx. \tag{4}$$

$K_{5/3}$ is a modified Bessel function and the scaled photon energy is defined by $\theta \equiv E_\gamma/E_c$. This spectrum is rather wide, we are interested in maximising the fraction of the power on the GDR which is roughly given by:

$$\eta_r = \frac{1}{P_i}\int_{\theta_r-\frac{\Delta\theta_r}{2}}^{\theta_r+\frac{\Delta\theta_r}{2}}\frac{dP_i}{d\theta}d\theta, \tag{5}$$

with θ_r the resonance energy and $\Delta\theta_r$ its width scaled by the critical energy. Figure 1 shows the optimal critical energy and the corresponding fraction on the GDR for various

* xavier.buffat@cern.ch

ISBN: 978-3-95450-227-1 ISSN: 2673-5490 doi:10.18429/JACoW-IPAC2022-THPOPT036

NEW MICROWAVE THERMIONIC ELECTRON GUN FOR APS UPGRADE: TEST RESULTS AND OPERATION EXPERIENCE*

S. V. Kutsaev†, R. Agustsson, A. Araujo, R. Berry, O. Chimalpopoca, A. Murokh, M. Ruelas, A. Yu. Smirnov, S. Thielk, RadiaBeam LLC, Santa Monica, CA, U.S.A.
J. Hoyt, W. Jansma, A. Nassiri, Y. Sun, G. Waldschmidt, Argonne National Laboratory, Lemont, IL, U.S.A.

Abstract

Recently, RadiaBeam has designed and built a robust thermionic RF gun with optimized electromagnetic performance, improved thermal engineering, and a robust cathode mounting technique. This gun allows to improve the performance of existing and future light sources, industrial accelerators, and electron beam driven terahertz sources. Unlike conventional electrically or side-coupled RF guns, this new gun operates in π-mode with the help of magnetic coupling holes. Such a design allows operation at longer pulses and has negligible dipole and quadrupole components. The gun prototype was built, then installed and tested at the Advanced Photon Source (APS) injector. This paper presents the results of high power and beam tests of this RF gun, and operational experience at APS to this moment.

INTRODUCTION

The Advanced Photon Source (APS) at Argonne National Laboratory (ANL) is a national synchrotron-radiation light source research facility that utilizes a thermionic cathode RF gun system capable of providing beam to the APS linac [1]. The previously used RF gun was a 1.6-cell side-coupled structure operating at 2856 MHz frequency. Typically, the RF gun was powered with ~3.0 MW pulsed power but could sustain up to 7 MW via an end-coupled waveguide. The cathode used was a barium-tungsten dispenser cathode with a diameter of 6 mm. The gun could produce peak beam kinetic energies of up to 4.5 MeV and peak macro pulse currents of up to 1.3 A. Normal operating RF pulse parameters were ~1 μs at a repetition rate up to 30 Hz. More details of the previous gun parameters may be found in [2]. Three generations of RF guns have been used as injectors at the APS since 1997.

APS procured three RF guns in 2001 [3] and recorded a mixed experience with these systems' performance. Two RF guns failed in 2010 due to excess reflected power. Further failures of the last spare gun would limit capabilities and suspend APS operations. Inspection of the RF gun design revealed that most of the problems came from the distortion of the mating surfaces of the gun back plate and the cathode.

To solve these problems, RadiaBeam has developed and built a new reliable and robust thermionic RF gun with the parameters specified in Table 1. This RF gun for synchrotron light sources offers substantial improvements over existing thermionic RF guns and allow stable operation with up to 1 A of beam peak current at a 100 Hz pulse repetition at 3μs RF pulse length rate and up to 5 μs at a reduced repetition rate. More details about the gun design can be found in [4-6].

Table 1: Comparison of the Developed and Existing Thermionic RF Guns Parameters

Gun	Old	New
Mode	π/2	π
Mode separation, MHz	48	22
Shunt impedance (β=0.999), MΩ/m	62.5	60
Q-factor	16000	15000
Max pulse length, μs	1.5	3.0
Max repetition rate, Hz	10	100

The gun prototype was installed at the APS injector in February 2021. The gun was RF conditioned, the thermionic cathode activated, and electron beam extracted. The beam was sent through the APS linac and tuned to achieve 100% injection efficiency to the Particle Accumulator Ring (PAR). The gun has been running well supporting APS operations since then with a 150 mA current in the past 15 months.

RF CONDITIONING

After the gun was installed, the water temperature was set to 111 °F per the LLRF measurement of resonate temperature, performed at APS. This is different from design resonant temperature which is 105°F due to a minor detuning. The water station set up for the RF gun is shown in Fig. 1. Prior to the RF conditioning, the cathode heater was set to 9.2 W at equilibrium to keep the cathode warm and clean during the RF conditioning. As the heater is turned on, a gun vacuum spike is observed as expected.

The RF conditioning went smoothly. Gun vacuum was kept below 1×10^{-7} torr during the conditioning process. Over 70 minutes, the gun was conditioned to 3 MW at 6 Hz repetition rate with an RF pulse length of 1.05 μs. The forward and reflected RF waveform of the gun are plotted in Fig. 2.

* This work was supported by the U.S. Department of Energy, Office of Basic Energy Science, under contracts DE-SC0015191 and DE- AC02-06CH11357
† kutsaev@radiabeam.com

ISBN: 978-3-95450-227-1 ISSN: 2673-5490 doi:10.18429/JACoW-IPAC2022-THPOPT037

CERAMICS EVALUATION FOR MW-POWER COAXIAL WINDOWS, OPERATING IN UHF FREQUENCY RANGE*

S.V. Kutsaev†, R. Agustsson, P. Carriere, N. G. Matavalam, A.Yu. Smirnov, S. Thielk
RadiaBeam LLC, Santa Monica, CA, U.S.A.
W. Hall, D. Kim, J. Lyles, K. Nichols, Los Alamos National Laboratory, Los Alamos, NM, U.S.A.
A. Haase, SLAC National Accelerator Laboratory, Menlo Park, CA, U.S.A.

Abstract

Modern accelerator facilities require reliable high-power RF components. The RF vacuum window is a critical part of the waveguide couplers to the accelerating cavities. It is the point where the RF feed crosses the vacuum boundary and thus forms part of the confinement barrier. RF windows must be designed to have low power dissipation inside their ceramic, be resistant to mechanical stresses, and free of discharges. In this paper, we report on the evaluation of three different ceramic candidates for high power RF windows. These materials have low loss tangents, low secondary electron yield (SEY), and large thermal expansion coefficients. The acquired materials were inspected, coated, and measured to select the optimal set.

INTRODUCTION

Conventional RF vacuum windows are made from ceramics, such as BeO or 96-99% Al_2O_3, or plastics such as Rexolite that are then brazed or otherwise joined to a pillbox cavity [1]. The use of ceramics presents several major challenges and issues that limit the performance of the existing RF windows. First, the fabrication and machining of large ceramics discs can be challenging. For example, at 400 MHz frequency, the size of waveguide is 11.5×23 inches, which means that discs of >13'' must be fabricated. Size also increases ceramic-to-metal brazing process complexity due to temperature differentials and residual stress.

Another set of problem is related to operational conditions of the RF windows. First, since high-power accelerators for accelerator facilities require transmission of multi-MW RF power at ~10% duty-factors, the transmitted power level reach hundreds of kW and dielectric losses present a serious issue [2]. For example, the losses at this frequency are defined by the loss factor ($\varepsilon \cdot \tan\delta$), which is typically $>1-2\cdot10^{-3}$. This about an order of magnitude higher than novel low-loss dielectrics [3,4]. Besides net losses in the dielectric, its thermal conductivity should be considered. Materials with low thermal conductivity, such as rexolite, suffer from internal heating and thermo-mechanical stresses gradients that can lead to stress fractures. Finally, the electric discharges due to static charge build-up or multipactor discharges play a great role in the reliability of RF windows [5,6]. Coatings such as titanium nitride are needed to suppress multipacting, requiring careful process control to uniform thickness over a large area.

In response to this problem, we surveyed several readily available dielectrics, such as high-purity alumina, sapphire, aluminum nitride, Si3N4, sapphal, MgTi, and others, and identified the optimal candidates for high-power RF windows.

MATERIAL SELECTION CRITERIA

The critical material properties of the dielectric include RF, thermal, and mechanical considerations, along with manufacturing related requirements such as commercial availability, machinability, capability for brazing, and SEY reducing coating [7]. The important RF properties include a low loss tangent (tan δ) to avoid high-power dissipation in the window, a low secondary electron emission coefficient to suppress multipacting, a low dielectric constant (ε) to simplify impedance matching and a high dielectric strength to withstand breakdown. High thermal conductivity (κ) is desirable to conduct the dissipated power through the braze joint into the actively cooled metal body. A meaningful figure of merit of a ceramic is the ratio of thermal conductivity to loss tangent times permittivity, FOM = κ/(ε* tanδ). This FOM captures that for every watt of loss in the ceramic (tan δ), the materials thermal conductivity (k) must allow that power to be removed by the temperature differential caused by the active cooling. Note that a high FOM is desirable.

Mechanical strength capable of withstanding differential pressure associated with the vacuum barrier is also required. High fracture toughness is desirable, as this makes the material more robust against fracture from fabrication, operation, or cyclic loading (vacuum, thermal, transport). Another important property of the dielectric is the capability for brazing, either by metallization or the use of active braze alloys. Materials with low outgassing characteristics are important, implying that the material is easily cleaned and vacuum conditioned. Toxicity of the dielectric is also a concern, causing high-performing materials such as beryllium oxide to be phased out.

These parameters must be considered within a practical engineering context. First and foremost: the dielectrics must be commercially available in large sizes with limited development and realistic lead times. Procuring and qualifying expensive capital equipment (presses, furnaces, etc.) to fabricate parts at scale should not be the objective of a RF window assembly manufacturer and is best left to organization with proven ceramics expertise. Additional issues such as variability in material properties, both within the part and part-to-part, impact the design safety margins. The capability to accurately shape and finish the ceramic

* This work was supported by the U.S. Department of Energy, Office of Basic Energy Science, under SBIR grant DE- SC0021552
† kutsaev@radiabeam.com

ISBN: 978-3-95450-227-1 ISSN: 2673-5490 doi:10.18429/JACoW-IPAC2022-THPOPT038

SIRIUS INJECTION OPTIMIZATION

X. R. Resende*, M. B. Alves, F. H. de Sá, L. Liu, A. C. S. Oliveira, J. V. Quentino
Brazilian Synchrotron Light Laboratory (LNLS/CNPEM), Campinas, Brazil

Abstract

SIRIUS is the new 3 GeV storage ring (SR)-based 4th generation synchrotron light source built and operated by the Brazilian Synchrotron Light Laboratory (LNLS) located in the CNPEM campus, in Campinas. The foreseeable move to a top-up injection scheme demands improvement of injection efficiency and repeatability levels. In this work we report on the latest efforts in optimizing the SIRIUS injection system.

INTRODUCTION

The SIRIUS injector is comprised of a 150 MeV linac with 3 GHz RF structures and 500 MHz sub-harmonic buncher, a full-energy booster (BO) that shares the tunnel with the storage ring (SR) and low and high energy transport lines, LTB and BTS respectively. BO and SR are served by the same RF master frequency generator. See Table 1 for relevant SIRIUS parameters.

Table 1: Relevant SIRIUS Parameters

Parameter	Value	Units
RF frequency	499.67	MHz
BO harmonic number	828	
SR harmonic number	864	
BO revolution time	1.657	µs
SR revolution time	1.729	µs
BO repetition rate	2	Hz
BO natural emittance	3.6	nm rad
BO residual coupling	0.6	%
EGun multi-bunch charge	3.0	nC

The SR is currently operating in decay mode, with fill-ups to 100 mA current values twice a day. SIRIUS is planned to move to top-up mode before the completion of SIRIUS Phase-I, scheduled for 2024 [1]. For this new injection scheme to become feasible, accelerator teams have been putting considerable effort in the past year on improving the injection efficiencies at various stages, aiming at reduced required injection times and radiation doses from high energy beam losses.

Low-level RF linac parameters, such as sub-harmonic buncher and klystron phases and amplitudes, have been constantly optimized during the past months, as well as BO injection, ramp and extraction to the SR. In particular, we discuss in the next sections two of the major developments in this direction, both related to the BO: girder realignment and an emittance exchange implemented in the energy ramp. We also describe some of the pending injection issues we are yet to tackle in the next months, before top-up operation.

* ximenes.resende@lnls.br

Table 2: Efficiency for Each Stage in the Injector (1 nC/pulse)

Accelerator	Efficiency [%]
Linac	> 95
LTB	> 95
Booster	~ 70
BTS	> 95
SR Injection	~ 95

The current status of SIRIUS injection efficiencies after the improvements described in this work is shown in Table 2. The overall efficiency is around 60% and most of the losses happen in low energies, at the booster injection. For higher electron gun (EGun) charges the efficiency can drop, as discussed below, but the injector still can provide 1 nC/pulse to the SR, a conservative charge value for the envisaged top-up scheme.

BOOSTER REALIGNMENT

In the beginning of 2022, a major BO realignment was performed for a better match between the on-energy revolution time of the BO at low energies and the corresponding value in the SR, since both accelerators share RF frequency. All BO girders were moved inwards by 158 µm, corresponding to a reduction of 1 mm in circumference. This realignment was requested in order to reduce the off-energy orbit of the injected beam at low energy at the BO. Before the realignment, the off-energy orbit was estimated to be −0.88 mm, according to BPM-averaged orbit readouts. After realignment this average was reduced to −0.34 mm (Fig. 1). As dispersion function at BPMs is 22 cm, these horizontal position averages corresponds to −0.40 % and −0.15 % off-energy errors, respectively.

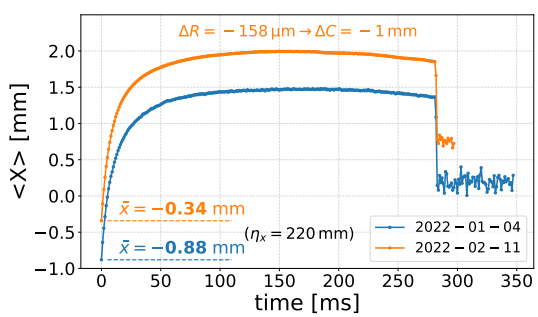

Figure 1: Effect of booster realignment on the average horizontal position. BPM acquisition at 1 kHz.

ISBN: 978-3-95450-227-1 ISSN: 2673-5490 doi:10.18429/JACoW-IPAC2022-THPOPT039

PERFORMANCE REPORT OF THE SOLEIL MULTIPOLE INJECTION KICKER

R. Ollier*, P. Alexandre, R. Ben El Fekih, A. Gamelin, N. Hubert,
M. Labat, A. Nadji, L. S. Nadolski, M.-A. Tordeux,
Synchrotron SOLEIL, L'Orme des Merisiers, Saint-Aubin, France

Abstract

A Multipole Injection Kicker (MIK) was installed in a short straight section of the SOLEIL storage ring and successfully commissioned in 2021. A small horizontal orbit distortion in the micrometer range was achieved outperforming the standard bump-based injection scheme installed in a 12 m long straight section. Refined studies have been conducted to fully understand and further improve the performance of the device. Indeed, a novel generation of the MIK will be the key element for the injection scheme of the SOLEIL Upgrade. We report simulation studies and the latest MIK experimental performance. Both injected and stored beam-based measurements were performed using new types of diagnostics with turn-by-turn capability (Libera Brillance+ BPM, KALYPSO: 2x1D imaging). The residual perturbations on the beam positions and sizes were measured; the magnetic field of the MIK device was reconstructed. An unexpected kick was detected in the vertical plane and an active correction implemented to cancel the resulting perturbation.

INTRODUCTION

After the successful commissioning of the Multipole Injection Kicker (MIK) at Synchrotron SOLEIL in the first half of 2021 [1], a finer tuning of the MIK has achieved unprecedented performance well below the tolerances which define transparent Top-Up injections: closed orbit distortions (CODs) lower than 2 to 3% of the rms stored beam size. Newly commissioned state-of-the-art diagnostics were required to measure such low COD levels. Beam position monitors (BPMs) connected to the improved Libera Brillance Plus electronics (LBP) [2] and the ultra-fast camera KALYPSO [3] provided turn-by-turn measurements of the transverse beam positions and sizes with high resolution. Turn-by-turn loss maps were also measured with the advanced beam loss monitors (BLMs) [4, 5]. The measurements were correlated to the simulation data computed with the refined Accelerator Toolbox (AT) [6] model of the storage ring.

We report the latest performance of the MIK, both from the simulation and experimental point of view, as well as a presentation of the new high-performance diagnostics.

* randy.ollier@synchrotron-soleil.fr

TOP-UP OPERATION AT SOLEIL

Top-Up Injection in the SOLEIL Storage Ring

SOLEIL is a 3rd generation storage ring-based synchrotron light source implementing a 110 MeV linear accelerator, a full energy booster injector and a 354 m long storage ring. The latter is based on a modified Chasman-Green lattice providing a 3.9 nm rad horizontal emittance at 1% coupling (see Table 1), in which a 2.75 GeV electron beam is stored. It provides synchrotron radiation, from infrared to hard X-rays, to 29 beamlines surrounding the storage ring. In the perspective of achieving sub-micrometer stability of the stored beam position, the Top-Up mode has been operated since 2009. Top-Up injection relies on a four kicker bump-based scheme installed in a 12 m long straight section [1]. Despite many efforts devoted to tuning the four kicker magnets to avoid residual CODs [7, 8], intrinsic design limitations prevent transparent injections. Thus, in the scope of R&D purposes, a single MIK was commissioned successfully in 2021 in order to prove it could be an alternative solution to the standard injection scheme [1].

Table 1: Main Parameters of the SOLEIL Storage Ring

Parameter	Value
Energy (GeV)	2.75
Circumf./Rev. period (m/μs)	354.1 /1.18
Harmonic number	416
RF Frequency/Voltage (MHz/ MV)	352.2 / 2.8
Natural emittance (nm rad)	3.9
Energy spread (%)	1.016×10^{-3}
Hor./Vert. betatron tunes	(18.156, 10.228)
Corrected hor./vert. chromaticities	(1.2, 2.4)

Innovative Injection Scheme for Top-Up Operation

The MIK was developed and built by SOLEIL in the scope of collaboration with MAX IV (2012-2017) [9, 10]. Its design was inspired by the non-linear kicker developed by BESSY [11]. The mechanical and magnetic design of the MIK as well as its assembly and integration into the SOLEIL storage ring are detailed in [1] while its main characteristics are recalled in Table 2.

After the installation of the MIK, the airflow around its vacuum chamber and the heat load dissipation had to be improved by adding extra air turbines [12]. Following the improvement of its cooling system, the MIK quickly reached the expected injection performance. Among the major achievements, we reached a maximum of 97% injection efficiency

ISBN: 978-3-95450-227-1 ISSN: 2673-5490 doi:10.18429/JACoW-IPAC2022-THPOPT040

INJECTION USING A NON-LINEAR KICKER AT THE ESRF

S. White, T. Perron, ESRF, Grenoble, France

Abstract

The ESRF injection consists in a standard four kickers bump off-axis injection. Although this scheme is very robust and reliable it is known to disturb users during injections and may represent a severe limitation in case frequent injections are required. The non-linear kicker injection scheme provides a possible solution to this problem by acting only on the injected beam. This paper reports on the potential integration of a non-linear kicker injection scheme at the ESRF. A layout and specifications for the kicker are proposed and simulations are provided to evaluate the performance and limitations of such scheme.

INTRODUCTION

The standard four kicker bump injection scheme used on the previous machine [1, 2] was adopted for the ESRF-EBS as a low risk solution for the commissioning of the new machine. This option also allowed to recuperate existing hardware from the previous machine such as the septum magnets or the kickers power supplies. 80 % injection efficiency could be achieved in user service mode (USM) with this scheme [3]. Nevertheless, the normalized residual injection perturbations are approximately an order of magnitude larger than for the previous machine due to the beam size reduction. Even though new slow kicker power supplies combined with feed-forward corrections [4] allowed for a major reduction, experiments with beam lines indicated that an additional factor 2 reduction was necessary [5]. Some small incremental improvements are still possible but the present systems are now showing their limits to achieve the ultimate goal of transparent injection with 100 % efficiency and alternative schemes have to be considered. Advanced injection schemes were proposed in recent years to solve this problem such as: single non-linear kicker [6–8],swap-out injection [9–11],longitudinal on-axis injection [12–14] or shared oscillations using a fast kicker [15]. This report concentrates on the non-linear kicker (NLK) option that is the only one capable of providing fully transparent injection with multiple bunches as demonstrated in [16].

INTEGRATING THE NLK DOWNSTREAM THE INJECTION POINT

This solution was proposed in [17], it consists in placing the NLK downstream the injection point where there is free space such as a straight sections or available drift spaces in the arcs. This scheme allows to preserve the present injection systems and allows staggered integration and commissioning of the new ones without disrupting the operation of the storage ring. However, large transverse oscillations will occur between the injection point, located in straight section 4, and the NLK that may deteriorate the injected beam properties and consequently the injection efficiency. To evaluate this effect we consider four possible locations: 2 drifts spaces in cell 5 ($ARC5_{1,2}$) and the straight sections of cells 6 and 8 (ID6 and ID8). All are realistic candidates with space available for the installation of the NLK, however, the arc drift spaces are only approximately 0.4 m. Integrating a complex device in such short space may be challenging.

Table 1: Injection Efficiency Considering Different Types of Kickers at Different Location in the Ring (x_0=6 mm Corresponds to the Present Off-axis Injection)

	Kicker type		
	Dipole	**Octupole**	**Oct. + Sext.**
x_0=6 mm	99.9%	99.9 %	99.9%
$ARC5_1$	99.4%	36.9%	95.0%
$ARC5_2$	99.5%	38.5%	96.5%
ID6	94.0%	31.3%	72.5%
ID8	76.5%	15.4%	50.1%

The first and second columns of Table 1 summarizes the results of the tracking simulations done using a pure dipole kicker for which all particles receive the same kick and an octupole kicker to model the case of a realistic NLK for which particle will receive a kick that depends on their transverse amplitude. The simulations were performed using an ideal storage ring lattice (no errors) and the following injection beam parameters: $\epsilon_{x,y} = 45$ nm, $\sigma_s = 20$ mm, $\sigma_p = 0.0012$. These correspond to the present conditions assuming the booster beam is extracted on the coupling resonance. For all cases, the initial angle and twiss parameters were optimized to give to largest efficiency. Cases are ordered by increasing distance with respect to the injection point and the present off-axis injection is represented by $x_0 = 6$ mm. The dipole kicker simulations allow to evaluate the impact of the large transverse oscillations between the injection point and the kicker. It is seen that as the distance to the injection point increases the performance degrades and the situation becomes unacceptable in ID8. For the more realistic case of the octupole kicker the field needs to vary from zero to the design kick of approximately 1.5 mrad in 3-4 mm. Unfortunately, the field variations are too strong across the transverse beam extension and a large part of the injected beam is kicked out of the acceptance. There are 2 possibilities to solve this issue: reduce the injected beam size or cancel the kicker field gradient at the amplitude of the injected beam. The latter was demonstrated and used in [4] where it was shown that multipoles of different order can be used to cancel the field gradient at any given amplitude. In this report, we will use an additional sextupole component, that can be generated by either the proper coil arrangement or with a compensation

ISBN: 978-3-95450-227-1 ISSN: 2673-5490 doi:10.18429/JACoW-IPAC2022-THPOPT041

COMMISSIONING OF NEW KICKER POWER SUPPLIES TO IMPROVE INJECTION PERTURBATIONS AT THE ESRF

S. White, N. Carmignani, L. Carver, M. Dubrulle, L. Hoummi, M. Morati,
T. Perron, B. Roche, ESRF, Grenoble, France

Abstract

The ESRF-EBS storage ring resumed operation in 2020. Due to the reduced lifetime, top-up injection is required for all operation modes. Perturbations on the stored beam introduced by the pulsed injection elements represent a significant disturbance to the beam lines that need to run experiments across injection. In order to reduce these perturbations, new kicker power supplies with slower ramping times and better shot-to-shot reproducibility were developed at ESRF to improve the efficiency of the feed-forward compensation scheme. This paper reports on the design, commissioning and first experimental validation of these new power supplies.

INTRODUCTION

Off-axis injection with a closed injection bump generated by 4 pulsed kicker magnets was used in the previous ESRF storage ring [1, 2]. It was then adopted during the design of the ESRF-EBS storage ring as it was considered a low risk solution for the commissioning of the new machine and would allow to recuperate some of the existing hardware components such as the injection kickers power supplies based on thyratron technology. With these systems, the injection efficiency in User Service Mode (USM) with gaps closed is of the order of 80 % for a fully optimized machine [3], 10 % below design expectation of 90 %. Off-axis injection is unfortunately known to introduce large perturbations on the stored beam during injections that can affect beam lines experiments. Based on past experience, the injection perturbations compensation methods and systems presented in [4] were successfully applied to the ESRF-EBS storage ring. Nevertheless, the normalized residual injection perturbations are approximately an order of magnitude larger than for the previous machine due to the beam size reduction. This paper reports on the implementation and commissioning of new kickers power supplies featuring slower ramping times to facilitate feed-forward corrections and improve the injection perturbations.

POWER SUPPLIES DESIGN

The main limitation of the feed-forward system is to achieve large deflections at high frequency in order to affect the bunches individually. Increasing the bandwidth of the present feed-forward system was not possible, new kicker power supplies with slower ramping times were therefore designed to improve the injection perturbations and other aspects of the pulsers. Their characteristics are shown in Table 1. The proposed solution, based on IGBT (Insulated Gate Bipolar Transistor) technology significantly increases

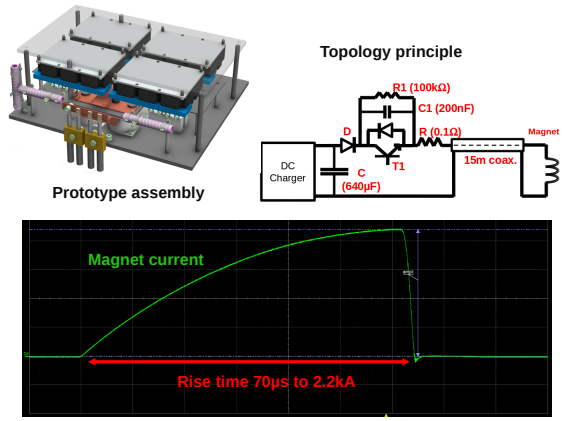

Figure 1: New kicker power supply assembly, topology and pulse shape.

the ramping time of the kicker pulses and improves by a factor 4 the pulse-to-pulse jitter, thereby reducing the random fluctuations that cannot be corrected with a feed-forward system. The fall time is presently set to approximately 2.2 µs slightly lower than one storage ring turn but could be increased further depending on the horizontal tune working point. It should be noted that the detrimental effect from eddy currents flowing in the Titanium coating of the ceramic chambers is also mitigated by slower ramping times. The implementation of these new power supplies therefore allowed to increase the Titanium thickness and reduce the beam induced heating on the ceramic chamber without degrading the injection performance.

Table 1: Comparison Between the Present Thyratron and the New Design

	Thyratron	New design
Voltage rating	30 kV to 40 kV	600 V
Max. current	2200 A	2200 A
Flat-top	1 µs	No flat-top
Rise/fall time	450 ns / 800 ns	70 µs / 2.2 µs
Pulse-to-pulse jitter	±0.2 %	±0.05 %

Figure 1 shows the new kicker power supplies assembly, topology and pulse shape. The design and assembly are done in-house. 2 prototypes were built and characterized in the laboratory before installation, demonstrating the parameters shown in Table 1 and showing excellent identity between the 2 systems, which is essential to minimize bump non-closure. However, the field experienced by the beam depends also on other parameters such as the magnet geometry and alignment

ISBN: 978-3-95450-227-1 ISSN: 2673-5490 doi:10.18429/JACoW-IPAC2022-THPOPT042

STUDIES FOR A LASER WAKEFIELD DRIVEN INJECTOR AT ELSA

K. Kranz*, K. Desch, D. Elsner, M. Switka
Physics Institute, University of Bonn, Germany

Abstract

At the University of Bonn, electron beams with energies up to 3.2 GeV can be extracted from the storage ring ELSA to hadron physics and novel detector testing experiments. We study the feasibility of replacing the current 26 MeV Linac injector with a laser plasma wakefield accelerator (LPWA). For this, contemporary achieved parameters from current LPWA setups at other laboratories are assumed and matched to the acceptance of the facility's synchrotrons. Moreover, a conceptional draft of a potential LPWA setup is created. This takes into consideration the influence of building conditions such as available floor space and building vibrations to estimate a setup of a plasma generating high power laser system and beamline to the plasma cell.

INTRODUCTION

The Physics Institute of the University of Bonn operates the three staged **EL**ectron **S**tretcher **A**nlage (ELSA) accelerator facility. It can accelerate spin-polarized or unpolarized electron beams up to energies of 3.2 GeV using a synchrotron ring design capable of quasi-continuous electron beam extraction to three experimental stations. The injector system consists of a linear accelerator, pre-accelerating the electrons to energies of 26 MeV, and a booster synchrotron. This combined-function synchrotron accelerates the electrons to a typical energy of 1.2 GeV. With a rate of 50 Hz and an average charge of 2 nC the electrons are injected into the storage ring, where the beam is accumulated up to 25 mA (~ 15 nC), accelerated up to 3.2 GeV and extracted via resonance extraction over several seconds to external experimental stations with a mean current of 1 nA.

It is of great interest, whether the implementation of a novel injector based on LPWA technology is possible, which ideally would form a redundant pre-accelerator to the current Linac. A potential setup with a plasma driving high power laser system, plasma cell assembly and energy compressor is sketched in Fig. 1.

INJECTION REQUIREMENTS

An LPWA could be used to inject directly into the stretcher ring or into the booster synchrotron as an intermediate injector, whose requirements on charge and beam energy are more relaxed. The different requirements for both synchrotrons are given in Table 1.

As typical pulse lengths of LPWAs are in the order of femtoseconds, but contemporary pulse repetition rates are in the order of a few Hertz with pulse charges of a few hundred pico-coulombs [1], it is difficult to satisfy all the conditions required for a direct injection into the storage ring, which

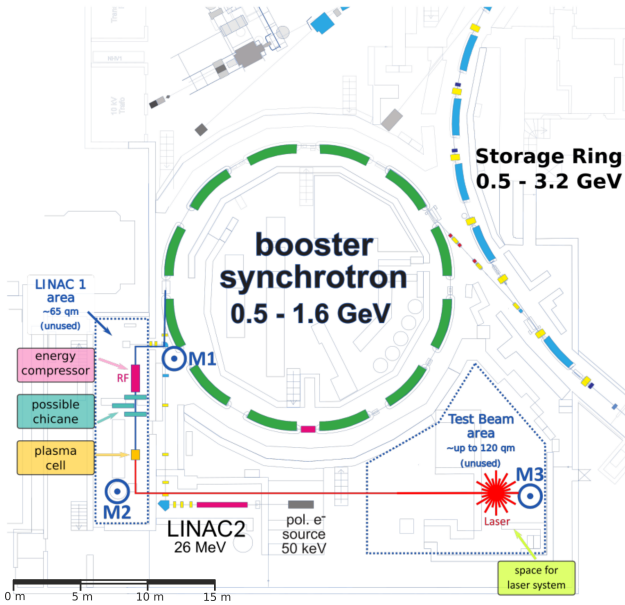

Figure 1: Injector area of the ELSA facility showing currently unused floor space (dashed) which is available for an LPWA injector setup. A high power laser system with multi-square-meter footprint can be installed at the former test beam area whereas the plasma cell and the subsequent beamline including an energy compressor system can be set up at the former LINAC 1-area.

Table 1: Injection Requirements of Both Synchrotron Rings of the ELSA Facility

Injection Requirement	Storage Ring	Booster
Energy	>1 GeV	15-30 MeV
Beam charge	15 nC	2 nC
Buckets	274	116
Rev. period	548 ns	232 ns
Inj. duration	0.5 s	1 µs
Emittance	$2.5{\cdot}10^{-6}$ m rad	$3{\cdot}10^{-6}$ m rad
Energy spread	0.3 %	0.5 %

requires a homogeneous filling of ~15 nC within a short injection duration of <1 s. Alternatively, an LPWA injector could be used to fill the booster synchrotron with an MeV electron beam, ideally with a total charge of 2 nC at 50 Hz repetition rate. Transverse LPWA beam properties (emittance ~1 μmmrad) tend to suffice the booster requirements. However, the momentum spread, usually in the order of some percent at MeV beam energies, and the very short pulse durations have to be adjusted to fit the requirements.

* kranz@uni-bonn.de

ISBN: 978-3-95450-227-1 ISSN: 2673-5490 doi:10.18429/JACoW-IPAC2022-THPOPT043

INJECTION DESIGN OPTIONS FOR THE LOW-EMITTANCE PETRA IV STORAGE RING

M. A. Jebramcik*, I. Agapov, S. A. Antipov, R. Bartolini, R. Brinkmann, D. Einfeld, T. Hellert, J. Keil, G. Loisch, F. Obier, Deutsches Elektronen-Synchrotron (DESY), Hamburg , Germany

Abstract

The proposed PETRA IV electron storage ring that will replace DESY's flagship synchrotron light source PETRA III will feature a horizontal emittance as low as 20 pm based on a hybrid six-bend achromat lattice. Such a lattice design leads to the difficulty of injecting the incoming beam into an acceptance that is as small as 2.6 µm. In contrast to earlier lattice iterations based on a seven-bend achromat lattice, the latest version allows accumulation, i.e., the off-axis injection of the incoming beam. In this contribution, the effects of deploying different septum types, namely a pulsed or a Lambertson septum, on the injection process as well as the injection efficiency are presented. This analysis includes the effects of common manipulations to the injected beam, e.g., beam rotation and aperture sharing, on the injection efficiency. Furthermore, the option of a nonlinear kicker and its optimization (wire positions, wire current, optics functions) are presented since a nonlinear kicker could provide an alternative to the rather large number of strip-line kickers that are necessary to generate the orbit bump at the septum.

SEPTUM CHOICE

The PETRA IV [1, 2] injection process is highly critical since the dynamic aperture (DA) in modern multi-bend achromat lattices tend to be small with PETRA IV being no exception, i.e., the acceptance is expected to be $A_x \leq 2.6\,\mu\text{m}$ in realistic machine conditions [3]. While an off-axis injection (accumulation) was ruled out for the initial seven-bend achromat lattice initially, the recent change of the baseline to a six-bend achromat lattice allows accumulation. In order to exploit the available acceptance as much as possible, a large horizontal beta function β_x at the septum and a thin septum blade is required. A pulsed septum may feature the possibility of a 1-mm-thick septum blade as envisaged by the SLS 2. A Lambertson septum could feature a 2-mm-thick blade; however, additional vacuum pipes may cause the effective blade thickness to reach 3 mm. While the pulsed septum would deflect the beam in the horizontal plane, a Lambertson septum would kick the beam vertically. The current transfer-line design features both an XFEL type Lambertson septum [4] as well as a SLS 2 type 1-mm-thick pulsed septum [5, 6] and an XFEL type 3-mm-thick Lambertson septum in a distance of less than 0.5 m (Lambertson septum acts as a pre-septum). This arrangement allows to offset the potential R&D risks if the pulsed septum is not operational at startup of PETRA IV since the sole Lambertson septum may suffice for the injection into PETRA IV without significant alterations of the transfer line. Figure 1 shows the injection section of PETRA IV with the septum location and the orbit bump generated by 16 strip-line kicker modules [7, 8] required for bringing the stored beam close to the septum blade. At the location of the septum, the β_x function reaches $\beta_x = 46$ m. In the following, the options of having a sole pulsed[1] and a sole Lambertson septum for the injection process is investigated.

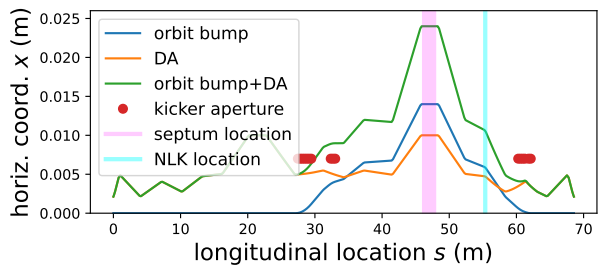

Figure 1: Orbit bump generated by strip-line kicker modules to enable the PETRA IV injection.

INJECTION-EFFICIENCY STUDY

Injection Scenarios

The injected beam is usually not matched to the optics functions of the stored beam at the septum. Emittance and optics manipulations are eventually carried out to enhance the injection efficiency. Throughout the analysis, four different injection scenarios are analyzed: a) Nominal injection, b) coupled beam (equally large horizontal and vertical emittances), c) rotated beam (exchange of emittances via three skew quadrupoles in the transfer line), d) aperture sharing (detuning of the last kicker of the orbit bump at septum causes the residual oscillation to be shared between the stored and the injected beam). It is important to note that while aperture sharing may lead to an improved injection efficiency in a single-particle model, the excitation of wakefields may lead to beam losses and has to be studied. The horizontal β_x function is optimized to better follow the curvature of the acceptance in all four injection scenarios (uses an modified version of the equation given in Ref. [9]). The separation between the injected and the stored beam Δx depends on the septum type, the optimized horizontal $\beta_{x,\text{opt}}$ function of the injected beam and whether aperture sharing is applied.[2] The separation takes a 2 mm error margin, the (effective) blade thickness, three times the

* marc.andre.jebramcik@desy.de

[1] The scenario of a sole pulsed septum covers the envisaged case of deploying the pulsed septum as a pre-septum for the DC Lambertson septum.

[2] For the aperture-sharing scenario, the separation of the beam at the last kicker has to be back propagated to the septum location.

ISBN: 978-3-95450-227-1 ISSN: 2673-5490 doi:10.18429/JACoW-IPAC2022-THPOPT044

THE ALKALI-METAL PHOTOCATHODE PREPARATION FACILITY AT DARESBURY LABORATORY: FIRST CAESIUM TELLURIDE DEPOSITION RESULTS

H. M. Churn[1*], C. Benjamin[2], L. B. Jones[1], T. C. Q. Noakes[1],
ASTeC, STFC Daresbury Laboratory, Warrington, UK
[1]also at The Cockcroft Institute, Daresbury Laboratory, Warrington, UK
[2]also at University of Warwick, Coventry, UK

Abstract

Fourth generation light sources require high brightness electron beams. To achieve this a photocathode with a high quantum efficiency and low intrinsic emittance is required, which is also robust with a long operational lifetime and low dark current. Alkali-metal photocathodes have the potential to fulfil these requirements, so are an important research area for the accelerator physics community.

STFC Daresbury Laboratory are currently commissioning the Alkali-metal Photocathode Preparation Facility (APPF) which will be used to grow alkali photocathodes. Photocathodes produced by the APPF will be analysed using Daresbury Laboratory's existing Multiprobe system and the Transverse Energy Spread Spectrometer (TESS). Multiprobe can perform a variety of surface analysis techniques while the TESS can measure the Mean Transverse Energy of a photocathode from its Transverse Energy Distribution Curve over a large range of illumination wavelengths.

We present an overview on our current progress in the commissioning and testing of the APPF, the results from the first Cs-Te deposition and detail the work planned to facilitate the manufacture of Cs_2Te photocathodes for the CLARA accelerator.

INTRODUCTION

X-ray free electron lasers (FELs), a type of 4th generation light source, require high brightness electron beams. The beam brightness, a key factor in FEL cost and performance [1], depends on the beam current, which should be maximised, and beam emittance, which should be minimised [2]. To achieve this, a photocathode with high quantum efficiency (QE) and low intrinsic emittance is required. Caesium Telluride, Cs_2Te, photocathodes fulfil these requirements, demonstrating measured levels of QE as high as 20 % at 266 nm and a low intrinsic emittance, all while being sufficiently robust to survive inside a electron gun [3]. As such, they are currently used in accelerator facilities around the world [4, 5].

The photocathode research group at Daresbury Laboratory currently operates two experimental systems: Multiprobe and the Transverse Energy Spread Spectrometer (TESS). Multiprobe is equipped for surface preparation and characterisation and is able to measure important photocathode performance properties such as quantum efficiency and work function [6]. TESS can measure the transverse energy distribution curve of a photocathode across a range of illumination wavelengths. From this, the mean transverse energy (MTE) can be extracted [7], which is related to the photocathode intrinsic emittance.

Daresbury Laboratory have constructed, commissioned and are in the final stages of calibrating a new machine, the Alkali-metal Photocathode Preparation Facility (APPF), which, when combined with Multiprobe and TESS, will enable the growth and extensive characterisation of Cs_2Te photocathodes. The design, construction and ongoing commissioning of the APPF is discussed below.

SYSTEM OVERVIEW

The APPF consists of a loading chamber and a deposition chamber. The loading chamber has a base pressure of 3×10^{-9} mbar and allows samples to be quickly loaded from atmosphere via a fast–entry port, or under UHV conditions via a vacuum suitcase. The deposition chamber is shown in Fig. 1. Pumping to the deposition chamber is provided by an ion pump (Fig. 1a.i) and a turbo-molecular pump (Fig. 1b.iv). This combination yields a base pressure of approximately 5×10^{-10} mbar. Residual gases can be monitored using an MKS Instruments Residual Gas Analyser (RGA) (Fig. 1a.vii).

The APPF deposition chamber is equipped with a UHV Design goniometer (Fig. 1a.vi) designed for compatibility with INFN-style photocathode pucks. Currently an adapter is installed to support initial work with Omicron 19 mm flag-style sample plates (Fig. 2i). The goniometer provides 3–axis translation, $-180\,^\circ$ to $+180\,^\circ$ rotation and sample tilt from $-5\,^\circ$ to $+50\,^\circ$ for alignment with particular instruments in the system. An yttria coated tantalum foil heater is used to heat the sample up to approximately 400 °C. The sample is electrically–isolated so can support a DC bias or drain current measurement using a RBD Instruments picoammeter (Fig. 1b.v). A mask assembly (Fig. 1b.vi, Fig. 2.iii) protects the goniometer during deposition, and limits the exposed region of the photocathode substrate.

A PSP ISIS 3000 Ion Source (Fig. 1b.i, Fig. 2.vii) is fitted approximately 100 mm from the sample and allows the sample to be cleaned using argon ion bombardment. The ion energy is typically 2 keV, with an available range of 100 to 3000 eV, and the drain current is between 12 and 18 μA.

The APPF is equipped with a RBD Instruments Cylindrical Mirror Analyser (CMA) (Fig. 1b.iii, Fig. 2v). This

* hugh.churn@stfc.ac.uk

ISBN: 978-3-95450-227-1 ISSN: 2673-5490 doi:10.18429/JACoW-IPAC2022-THPOPT045

OPAL SIMULATIONS OF THE MESA INJECTION SYSTEM

S. Friederich[1]*, C.P. Stoll[1], K. Aulenbacher[1,2,3],
[1]Institut für Kernphysik, Johannes Gutenberg-Universität Mainz, Germany
[2]Helmholtz Institut Mainz, Germany
[3]GSI Helmholtzzentrum für Schwerionenforschung, Darmstadt, Germany

Abstract

The MESA injection system will produce the spin-polarized electron beam for the upcoming accelerator MESA in Germany. The photoemission electron source (STEAM) will deliver 150 µA of spin-polarized electrons from GaAs-based photocathodes for the P2 experiment. Afterwards the low-energy beam transportation system (MELBA) can rotate the spin using two Wien filters and a solenoid for polarization measurements and to compensate for the spin precession in MESA. A chopper and buncher system prepares the phase space for the first acceleration in the normal-conducting pre-booster MAMBO. First OPAL simulation results of MELBA were presented at IPAC'21. Meanwhile these simulations have been extended by a 270-degree-bending alpha magnet as well as the electrostatic and magnetostatic fieldmaps of the Wien filters. Furthermore the fieldmaps of the 4 modules of the pre-accelerator MAMBO have been implemented. Hence, the complete MESA injection system could be simulated in OPAL and the results will be shown.

INTRODUCTION

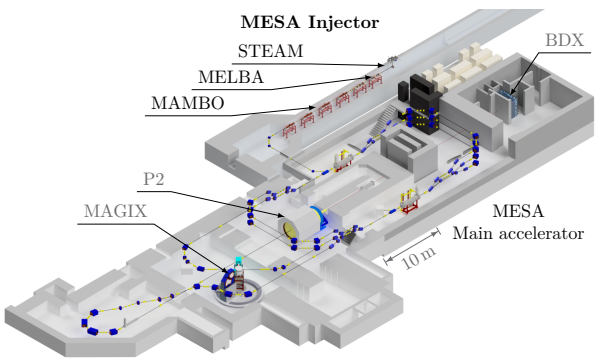

Figure 1: Scheme of MESA with its three experiments: P2, MAGIX and Beam dump experiment (BDX).

Figure 1 shows a scheme of the Mainz Energy-recovering Superconducting Accelerator (MESA) [1]. Operating at $f = 1.3$ GHz it will provide 150 µA of longitudinally spin-polarized electrons for the long-run parity violation experiment P2 at an energy of 155 MeV. The main tasks of the MESA injector are to emit the spin-polarized electrons, align the spin direction and prepare the phase space for the main accelerator.

* sifriede@uni-mainz.de

THE MESA INJECTOR

The MESA injector consists of three parts: The Small Thermalized Electron Source At Mainz (STEAM) [2], the MESA Low-energy Beam Apparatus (MELBA) [3] and the Milliampere Booster (MAMBO) [4].

The DC photoemission source STEAM operates at 100 kV and emits longitudinally spin-polarized electrons from GaAs-based photocathodes illuminated by infrared laser light into MELBA. An alpha magnet bends the vertically emitted beam by 270° into the horizontal accelerator plane where the beam passes MELBA's spin rotation system.

The electron spin experiences a total precession of 638° when passing through the three recirculations of MESA until it hits the P2 target [5]. A Wien filter is used to compensate for the precession by rotating the spin clock-wise by 82°. The electron spin can be flipped by changing the helicity of the laser, yet an additional solenoid in the spin system allows to flip the spin independently and, hence, offers further instrumentation serving the control of systematic errors. But this method also requires a second Wien filter to rotate the spin before entering the solenoid by 90°. As the solenoid has to be operated at about 15 mT ($\int B_z dz = 1.75$ mT m) that leads to a strong focus. Therefore, in this operation mode it is challenging to keep up the beam quality and the spin solenoid is turned off in the presented simulations. Yet, to investigate their influence, both Wien filters are fully excited.

Further downstream the beam enters the chopper system, which consists of two deflecting cavities, two solenoids and a movable collimator. The first chopper cavity deflects the beam circularly over the collimator and the solenoids focus it back onto the reference orbit where the second cavity cancels out the superimposed transverse momenta. Hence, this system chops the electron bunch head and tail that may not fit into the phase space acceptance of the main accelerator. Further down the MELBA beam line, the buncher cavities focus the beam longitudinally into the first section of MAMBO. All of its four modules accelerate the electrons up to 5 MeV. In-between all these main devices, quadrupole singlets, doublets or triplets as well as double solenoids, i. e., split solenoids with identical field amplitudes $|B_\parallel|$ yet alternating orientation in order to avoid further spin precession, guide the beam through the MESA injector.

The following simulations promoted the design process of the injector. The aim was to see if the beam can travel 9 m through the different devices and small apertures of MELBA, see Fig. 2, without a significant amount of beam loss. That would lead to gas desorption, to vacuum pressure degradation and, hence, to a reduced photocathode lifetime.

ISBN: 978-3-95450-227-1 ISSN: 2673-5490 doi:10.18429/JACoW-IPAC2022-THPOPT047

A DOUBLE DIPOLE KICKER FOR OFF AND ON-AXIS INJECTION INTO ALBA-II

G. Benedetti, M. Carlà, M. Pont
ALBA-CELLS Synchrotron, Cerdanyola del Vallès, Barcelona, Spain

Abstract

Injection into the ALBA-II storage ring will be performed off-axis in a 4 meters straight section with a single multipole kicker. We present a novel topology for the coils of the injection kicker, named double dipole kicker (DDK). The resulting magnetic field is the superposition of two opposite dipoles, generated by four inner and four outer conductor rods. When the eight rods are powered, the dipole term cancels and the remaining multipole field is used for off-axis injection. Alternatively, when the four inner rods are switched off, an almost pure dipole is produced, that is useful for on-axis injection during the commissioning. A prototype of DDK is presently under design to be installed and tested in the existing ALBA storage ring. The positioning of the rods is calculated in order to maximize the kick efficiency in mrad/kA and minimise the disturbance to the orbit and the emittance of the stored beam. A metallic coating with optimised thickness along the inner ceramic vacuum chamber should provide compensation for the eddy currents induced field in order to minimize the disturbance to the stored beam while ensuring sufficiently low heat dissipation by the beam image currents.

INTRODUCTION

ALBA started to study a pulsed multipole kicker for single turn off-axis injection in the previous years [1–3]. The proposed design was a so called non-linear kicker (NLK), whose coils topology was first conceived at BESSY-II [4] and then adopted and tested in other machines [5, 6]. The studies initiated in 2020 for the ALBA upgrade to a new low emittance ring have lead to a different design of the kicker which fits better the new needs of the injection into a ring with a smaller physical aperture and a very compact arrangement of the magnets. In the kicker presented in this paper, the coils have a different topology consisting of four inner rods and four outer rods which produce two opposite dipole fields cancelling each other along the longitudinal axis of the magnet and a non-linear field off axis [7]. The novel pulsed magnet, named double dipole kicker (DDK), has two important advantages: first, despite the small vertical aperture, the peak of the non-linear field can be generated at the position of the injected beam, and second, switching on either the inner or the outer coils an almost pure dipole is produced, that is very useful for on-axis injection in the first turn commissioning of the upgrade ring. In this paper the magnetic concept of the DDK and the parameters to design the prototype to be installed and tested in the existing ALBA storage ring are presented.

DOUBLE DIPOLE KICKER TOPOLOGY

We propose a new idea for the topology of the kicker coils. The topology designed in [1, 3] is changed to a different one shown in Fig. 1.

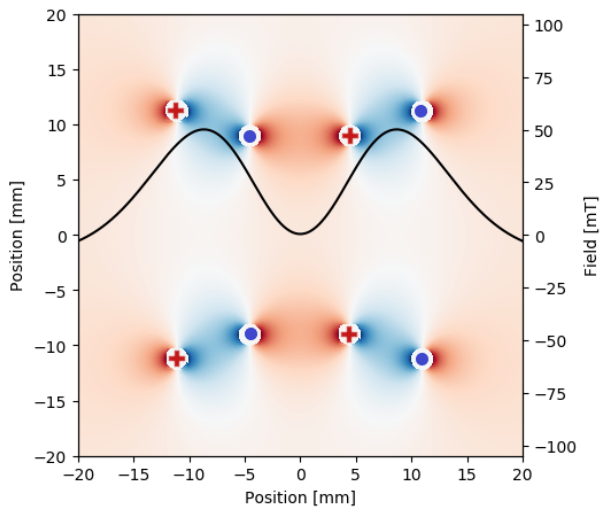

Figure 1: Cross section of the coils topology for the proposed DDK prototype for the ALBA storage ring (the red cross and the blue circle represent the direction of the current carried by the rods) and 2-D magnetic field (colour code) and the field along the horizontal mid plane (black solid line). The coils geometry produces a null field at the center where the stored beam is passing through. The minimum vertical aperture among the rods is ± 9 mm and the field reaches its peak value at the injected beam position $x = 8.7$ mm.

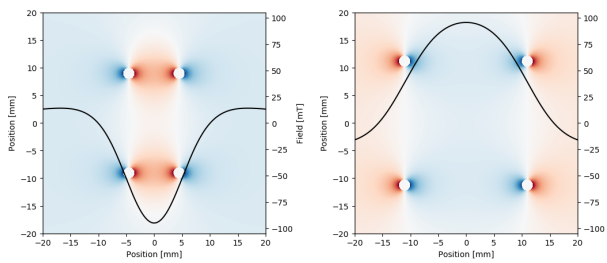

Figure 2: In the DDK, when either the four outer (left plot) or inner (right plot) rods are switched off, a dipole field is produced around the center.

The main difference of this field profile with respect to that of the NLK previously designed is that it results in a narrower plateau and a non zero crossing. On the other hand, the attractive feature of the DDK is that by switching off

ISBN: 978-3-95450-227-1 ISSN: 2673-5490 doi:10.18429/JACoW-IPAC2022-THPOPT048

IMPACT OF IDs ON THE DIAMOND STORAGE RING AND APPLICATION TO DIAMOND-II

R. Fielder†, B. Singh, Diamond Light Source, Oxfordshire, UK

Abstract

When investigating the effect of insertion devices (IDs) on storage ring operations, it is not possible to simulate all of the large number of gap, phase and field settings that are available. This can be of particular concern for transient effects in IDs that are moved frequently, or APPLE-II devices which may use many different polarisation states. We therefore present measurements of the impact of selected IDs on various parameters in the current Diamond storage ring including orbit distortion, tunes, chromaticity and emittance, and assess the expected impact when applied to the Diamond-II lattice.

INTRODUCTION

IDs cause a closed orbit distortion (COD) when changing gap due to non-zero field integrals through the device. Dipole trim coils are installed at the ends of each ID to provide a local orbit correction through feed-forward tables. Diamond-II [1] will use many similar IDs, some of which are already present in the operational Diamond ring. Due to the difficulty in simulating the large number of variations in ID settings, it is useful to assess the impact of selected IDs in the current ring and project what the effect of the same devices would be in Diamond-II.

By looking at the resulting COD at the location of the IDs, it is also possible to assess how effective existing correction schemes are at improving photon beam stability as well as the electron beam.

CLOSED ORBIT EFFECTS

The COD caused by a selection of IDs installed in the existing Diamond storage ring [2] was measured with and without the trim correction applied. Due to differences between types of ID, these have been grouped into three different classes: in-vacuum cryogenic permanent magnet undulator (CPMU), APPLE-II, and multipole wigglers (MPW). Two kicks, one at each end of the ID, could then be fitted for each type of ID in the accelerator model in Accelerator Toolbox [3] for Matlab, using the I03 CPMU, I05 APPLE-II undulator in horizontal and circular polarisations, and I20 MPW IDs as examples. These kicks were then applied in the Diamond-II model to calculate the total orbit distortion anticipated during operation.

Results

The projected COD in Diamond-II for each ID type is shown in Fig. 1. The MPW and circularly-polarised APPLE-II devices cause significant orbit distortions, especially in the vertical plane, which are well corrected by the local trim correctors. Horizontal polarisation for the APPLE-II is much less disruptive, as is the CPMU. The corresponding RMS values of the orbits are shown in Table 1.

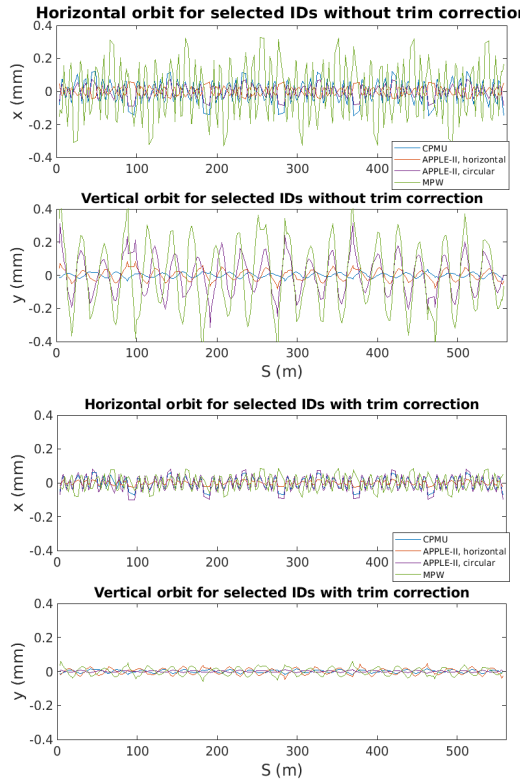

Figure 1: Simulated closed orbit distortion in Diamond-II for selected IDs. Without local trim correction (top), with trim correction (bottom).

Table 1: Simulated RMS Closed Orbit Distortion in Diamond-II for Different ID Types in Horizontal and Vertical Planes After Local Correction

	Uncorrected		Corrected	
ID Type	**H (um)**	**V (um)**	**H (um)**	**V (um)**
CPMU	63	13	32	8
APPLE-II (horizontal)	24	33	10	18
APPLE-II (circular)	38	121	43	4
MPW	165	219	16	13

Motion Timescale

The time taken for IDs to move ranges from seconds to minutes depending on the type of ID and the range of gap motion. CPMUs and other in-vacuum IDs have a relatively small range of movement, usually between 4-30 mm, and so can move their full range in 25 seconds. APPLE-IIs and other ex-vacuum IDs have a larger range of movement, up

† richard.fielder@diamond.ac.uk

ISBN: 978-3-95450-227-1 ISSN: 2673-5490 doi:10.18429/JACoW-IPAC2022-THPOPT049

BEAM DYNAMICS STUDIES FOR THE DIAMOND-II INJECTOR

I.P.S. Martin, R.T. Fielder, J. Kallestrup, T. Olsson, B. Singh,
Diamond Light Source, Oxfordshire, U.K.
J.K. Jones, B. Muratori, ASTeC, STFC Daresbury Laboratory, U.K.

Abstract

The replacement, low-emittance booster for the Diamond-II project will have a racetrack structure consisting of 36 unit and 4 matching cells [1]. In this paper we report on how the design and performance characterisation of the booster has recently developed; this includes an increase in the injection energy from 100 to 150 MeV, a modified circumference to match to the storage ring RF frequency, and a new nominal tune point to improve the performance and to enable emittance exchange. The influence of the vacuum chamber impedance and intra-beam scattering on the electron bunch parameters during the ramp are presented, along with the necessary changes to the transfer line layouts.

INTRODUCTION

With the aim of providing transparent top-up injection, a single-bunch aperture sharing injection scheme [2] has been selected for the Diamond-II storage ring [3, 4]. Successful implementation of this method relies on upgrading the existing booster to provide the required electron bunch parameters, as described in [1]. The new booster has a racetrack structure to match the existing tunnel, with two arc sections consisting of alternating focussing and defocussing combined-function dipoles to provide almost a factor 8 reduction in the extracted beam emittance despite the higher extraction energy. The bunch length has also been reduced to allow a better match to the storage ring RF bucket. A key feature of the vacuum chamber design was to have low impedance, as this will enable high-charge bunches to be accelerated without degradation in extracted bunch properties.

In this paper we describe the recent changes to the Diamond-II injector design. The performance of the booster is analysed both in terms of its robustness to errors and the impact of collective effects during the energy ramp. Finally, changes to the linac-to-booster (LTB) and booster-to-storage ring (BTS) transfer lines are summarised.

BOOSTER-II LATTICE

The fundamental design of the booster remains unchanged since the status presented in [1]. However, a number of design choices elsewhere in the facility and an evolution of the engineering design have necessitated a number of modifications to the booster lattice.

The most significant change to the design is the decision to raise the linac energy from 100 MeV to 150 MeV. This is expected to have a number of benefits [1], particularly around improving capture and transfer efficiency through the booster ramp. The increase in linac energy will be achieved by replacing the two 5.2 m long structures with three 3.1 m structures and operating them with higher gradient. This allows 150 MeV to be reached without extending the linac footprint and minimises the changes needed in the LTB. Replacing the linac also allows the S-band operating frequency to be matched to the storage ring (6×499.511 MHz).

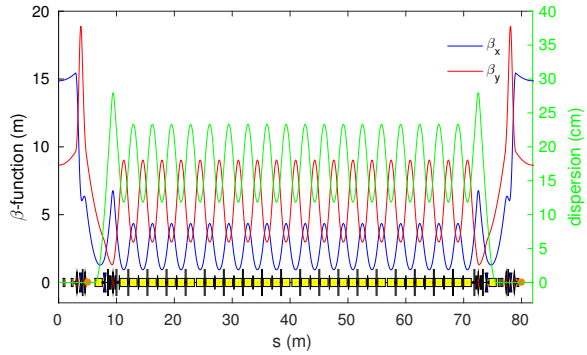

Figure 1: Twiss parameters and dispersion function for one super-period (half of the new booster).

Table 1: Booster Parameters and Beam at Extraction

Parameter	Present Booster	New Booster
Energy Range	0.1-3.0 GeV	0.15-3.5 GeV
# Cells	22	36 + 4
Circumference	158.4 m	163.847043 m
Harmonic Number	264	273
Betatron Tunes	[7.18, 4.27]	[12.41, 5.38]
Nat. Chromaticity	[-9.7, -6.3]	[-13.7, -12.3]
Mom. Comp. Factor	0.0252	0.0057
Natural Emittance	134.4 nm.rad	17.4 nm.rad
Energy Spread	0.073 %	0.087 %
Nat. Bunch Length	99.3 ps	38.9 ps
Loss per Turn	0.58 MeV	0.95 MeV

The next alteration to the design is a change in booster circumference, again to match the operating frequency to the storage ring RF. This necessitated lengthening the straight sections by 279 3.4 µm each and changing the harmonic number from 272 to 273.

The final change to the design is a shift in nominal tune from [12.20, 5.36] to [12.41, 5.38]. The primary reason for the change was to bring the working point closer to the coupling resonance to enable emittance exchange [5]. Subsequent studies of injection into the storage ring indicated emittance exchange would not be beneficial for the present optics; however, given the new tune point was also found to provide increased dynamic aperture it was retained for the combined-function magnet designs.

ISBN: 978-3-95450-227-1 ISSN: 2673-5490 doi:10.18429/JACoW-IPAC2022-THPOPT050

DEVELOPMENT AND CONSTRUCTION OF CRYOGENIC PERMANENT MAGNET UNDULATORS FOR ESRF-EBS

C. Benabderrahmane†, P. Brumund, J. Chavanne, D. Coulon, G. Le Bec, B. Ogier, R. Versteegen,
ESRF, Grenoble, France

Abstract

The ESRF Extremely Brilliant Source (ESRF-EBS) is on operation for Users since August 2020 after 20 months of shutdown. This first of a kind fourth generation high energy synchrotron is based on a Hybrid Multi-Bend Achromat lattice. The main goal of the ESRF-EBS is to reduce the horizontal emittance, which leads to a significant increase of the X-ray source brilliance. To cover the intensive demand of short period small gap undulators at ESRF-EBS, a new design for a 2 m Cryogenic Permanent Magnet Undulator (CPMU) has been developed. Six CPMUs will be installed in the next years; the first two CPMUs have been constructed and actually used on ID15 and ID16 beamline, the third one is under constructing. An intensive refurbishment work has been done on the existing insertion devices to adapt them to the new accelerator which has shorter straight section and closer dipoles to the IDs than in the old one.

This contribution will review the development, construction and commissioning of the new CPMUs, and the refurbishment work done on the existing ones to adapt them to the new accelerator.

INTRODUCTION

The European Synchrotron Radiation Facility (ESRF) is an intense X-ray source located in Grenoble, France. It is a centre of excellence for fundamental and innovation-driven research. ESRF owes its success to the international cooperation of 22 partners. A major upgrade project known as ESRF-EBS was launched in 2015 and achieved in 2020. It aims to reduce the horizontal emittance from 4 nm.rad down to less than 140 pm.rad. The brilliance of ESRF-EBS is increased by a factor of 30 compared to the precedent one, mainly due to this drastic decrease of the horizontal emittance. The Double Bend Achromat lattice is replaced with a Hybrid Multi Bend Achromat one [1,2].

Permanent magnet undulator are composed of permanent magnets whose direction of magnetization rotates between one magnet and the next magnet by 90° creating an almost sinusoidal magnetic field along the undulator axis [3]. The permanent magnets are installed on two girders separated by an air gap in which the electron beam circulates in a vacuum chamber. A variant of this technology consists in replacing certain permanent magnets by poles made of soft magnetic materials in order to increase the magnetic peak field in the air gap.

Undulators are able to produce very intense and concentrated radiation in a narrow energy band. The spectrum is made up of several harmonics, the fundamental resonant harmonic depends of the electron beam characteristics and the undulator deflection parameter $K = 0.934\ \lambda_u[\text{cm}]\ B[\text{T}]$, where λ_u is magnetic period, and B is the magnetic peak field. In-vacuum undulators eliminate the limitation of reducing the magnetic air gap due to the presence of the vacuum chamber by installing the two magnetic girders directly in a large vacuum chamber. The reduction of the air gap (5-6 mm for ESRF) results in a significant increase of the magnetic peak field. The period can be shortened to reach greater number of periods for a given length, which leads to a significant increase of the undulator performances in terms of brightness. CPMUs take benefit from improved magnetic properties of in-vacuum undulator permanent magnet at low temperature [4,5], the remanence B_r is increased leading to higher magnetic field, than shorter period to enhance farther the brightness of the undulator.

CPMU DESIGN

Permanent Magnet Grade

Praseodymium Iron Boron ($Pr_2Fe_{14}B$), Neodymium Iron Boron ($Nd_2Fe_{14}B$) and mixed Praseodymium and Neodymium ($Pr_{0.8}Nd_{0.2})_2Fe_{14}B$ are suitable grades for CPMUs. The use of ($Nd_2Fe_{14}B$) grade is limited to 130 K because of the magnet Spin Re-orientation Transition phenomenon (SRT) [6]. However, the two other grades are not limited by this phenomenon, the remanence continue to increase when lowering the temperature at least to the liquid nitrogen one [7]. Figure 1 shows the variation of the $(Pr_{0.8}Nd_{0.2})_2Fe_{14}B$ remanence versus temperature. The remanence increases from 1.41 T at 300 K to 1.62 T at 80 K, and the coercivity increases from 2 T at 300 K to 7 T at 80 K. This permanent magnet grade provided by Magsound-Konit is used for the construction of U18 and U20.5 new CPMUs.

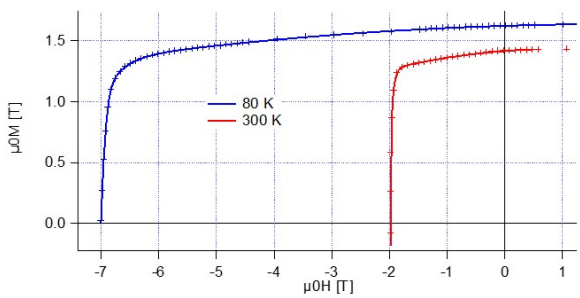

Figure 1: Magnet remanence versus temperature.

Magnetic Design

The magnetic design of the CPMUs is done with Radia [8] software as shown in Figure 2. The pole is in Fe-Co material with a Nickel coating. The permanent magnet of

† bchams@esrf.fr

ISBN: 978-3-95450-227-1 ISSN: 2673-5490 doi:10.18429/JACoW-IPAC2022-THPOPT052

THE STATUS OF THE IN-VACUUM APPLE II UNDULATOR IVUE32 AT HZB / BESSY II*

J. Bahrdt†, J. Bakos, S. Gaebel, S. Gottschlich, S. Grimmer, C. Kuhn, S. Knaack, F. Laube, A. Meseck, C. Rethfeldt, E. Rial, A. Rogosch-Opolka, M. Scheer, P. Volz
Helmholtz-Zentrum Berlin, 12489 Berlin, Germany

Abstract

At BESSY II, two new beamlines for RIXS and for X-Ray-microscopy need a short period variably polarizing undulator. For this purpose, the first in-vacuum APPLE II undulator worldwide is under construction. The parameters are as follows: $period\ length\ \lambda_0 = 32mm$, $\#\ periods = 78$, $minimum\ gap = 7mm$. The design incorporates a force compensation scheme as proposed by two of the authors at the SRI 2018. All precision parts of the drive chain are located in air. New transverse slides for the transversal slit adjustment have been developed and tested. Optical micrometers measure the gap and shift positions, similar to the system of the CPMU17 at BESSY II. They provide the signals for motor feedback loops. A new UHV-compatible soldering technique, as developed with industry, relaxes fabrication tolerances of magnets and magnet holders and simplifies the magnet assembly. A 10-period prototype has been setup for lifetime tests of the new magnetic keeper design. The paper summarizes the status of the undulator IVUE32.

INTRODUCTION

Photon beams with variably polarized light were already produced and used by the users in the 1980s at BESSY, the predecessor of BESSY II. BESSY II is a dedicated machine for soft X-ray photon production of arbitrary polarization with specific undulators. The low electron-beam energy of 1.7 GeV limits the fundamental photon energy range, and requires the usage of higher harmonics, e.g.: the 3rd harmonic for the transition metals and the 5th harmonic for the rare earth M-edges. Shorter periods lower the harmonic number and thus, enhance the brightness and the degree of polarization. Therefore, HZB launched the development of an in-vacuum APPLE II several years ago and published the design considerations and the mechanic layout at the IPAC 2018 [1].

The IVUE32 will serve two beamlines: A RIXS-beamline will use vertical linearly polarized photons in the range of 250-1000 eV for an efficient suppression of angle dependent optical effects. An X-ray microscope will operate in the range of 250-2500 eV, utilizing all polarization modes and the undulator harmonics 1–7.

In this paper, we focus on the new parts of the device and refer to [1] for the general design and the strategies, which did not change significantly. Meanwhile, the cast iron pieces and all components for the gap and phase motion are already fabricated. The bellows dimensions permit an inclined mode operation, which requires a longitudinal range of ±16 mm. Besides the inclined operation, the larger phase range (in the elliptical mode only ±8 mm are required) bears more flexibility in the design of the RF-shielding system.

TRANSVERSE SLIDES

After the IPAC 2018, we added transverse slides for the horizontal adjustment of the in-vacuum sub-girders. The slides employ two functions: i) the correction of geometric fabrication errors, ii) the correction of systematic field errors, where both errors may stay in relation, respectively. The slide adjustment provides an accuracy of $20\mu m$ over a range of a few 0.1mm. The slides consist of two halves, which are preloaded with spherical washers. Adjustment plates with a specific thickness define the final position. A Dicronite-coating (http://www.dicronite.de/) guarantees a smooth sliding.

Only recently, we did a thorough analysis of systematic field errors and related phase errors of the IVUE32, and derived the tolerances of the in-vacuum girder bending. The analysis prooved the viability of the slides for a precise horizontal slit adjustment [2].

In many cases, an analytic derivation of the phase error from a sytematic field error is simple [2-4]. Usually, the probability distribution $P(\Phi)$ of a systematic phase error is non-Gaussian. In many cases an analytic evaluation of this distribution for a strictly monotonic function is possible [5]. As an example, we illustrate the procedure for a linear taper, where s is the longitudinal coordinate and Φ^{-1} the inverse function of Φ:

$$\Phi(s) = s^2 \qquad s = \Phi^{-1}(\Phi) = \sqrt{\Phi}$$
$$P(\Phi) = \partial\ (\Phi^{-1}(\Phi))/\partial\ \Phi = 1/\left(2\sqrt{\Phi}\right)$$

If the phase function $\Phi(s)$ is not strictly monotonic, it can be split in piece-wise strictly monotonic segments $\Phi_i(s)$, which can be treated with the procedure above, and a weighted sum of the contributions $P_i(\Phi_i)$ yield $P(\Phi)$. Figure 1 gives a few examples for $\Phi(s)$ and the related probability function $P(\Phi)$.

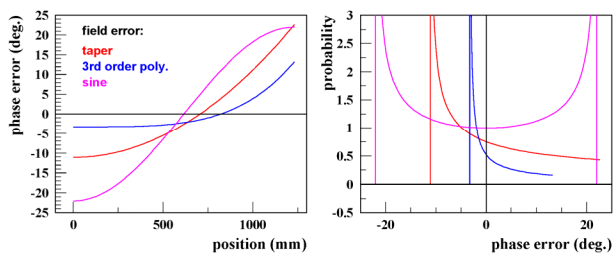

Figure 1: Examples of various systematic phase errors and their probability distributions as discussed in [2].

* Work supported by ATHENA, a project of the Helmholtz Association.
† johannes.bahrdt@helmholtz-berlin.de

ISBN: 978-3-95450-227-1 ISSN: 2673-5490 doi:10.18429/JACoW-IPAC2022-THPOPT053

GOUBAU-LINE SET UP FOR BENCH TESTING IMPEDANCE OF IVUE32 COMPONENTS

P. Volz*, A. Meseck, HZB, Berlin, Germany

Abstract

The worldwide first in-vacuum elliptical undulator, IVUE32, is being developed at Helmholtz-Zentrum Berlin. The 2.5 m long device with a period length of 3.2 cm and a minimum gap of about 7 mm is to be installed in the BESSY II storage ring. It will deliver radiation in the soft X-ray range to several beamlines. The proximity of the undulator structure to the electron beam makes the device susceptible to wakefield effects which can influence beam stability. A complete understanding of its impedance characteristics is required prior to installation and operation, as unforeseen heating of components could have catastrophic consequences. To understand and measure the IVU's impedance characteristics a Goubau-line test stand is being designed. A Goubau-line is a single wire transmission line for high frequency surface waves with a transverse electric field resembling that of a charged particle beam out to a certain radial distance. A concept optimized for bench testing IVUE32-components will be discussed, microwave simulations will be presented together with first measurements from a test stand prototype.

INTRODUCTION

BESSY II is a third generation synchrotron light source with an electron beam energy of 1.7 GeV. There are 32 dipole magnets and 13 undulators supplying 48 beam lines with radiation ranging from infrared to soft X-ray. In September of 2018 the first in-vacuum undulator (IVU) CPMU17 [1] was installed in BESSY II to provide hard X-rays for the Energy Materials In-Situ Laboratory (EMIL) [2]. As described in previous proceedings [12,13] IVUs require shielding foils between their magnets and the accelerator beam. The second IVU for BESSY II, IVUE32 [10], is currently under development. The APPLE II configuration poses even greater design challenges than the planar CPMU17. IVUE32 features four individually movable magnet rows which requires a longitudinal slit in the shielding foils. The split shielding foils further complicate the design of the transition taper between the beam pipe and the undulator magnets.

Motivation

Without a vacuum chamber wall between the beam and the undulator magnets, both CPMU17 and IVUE32 change their geometry from a collimator to a cavity over the entire gap range. This has an impact on wakefield characteristics and beam dynamics. The impact on beam stability is difficult to simulate. Beam based impedance measurements using orbit bump and tune shift methods have been done for the already installed CPMU17 with different gap settings [3]. Grow-damp and drive-damp methods have been utilized as well by M. Huck *et al.* [4].

The novel design of IVUE32 brings even more challenges as the shielding foil is split in the middle longitudinally to accommodate the different polarization settings. Therefore the impact on beam stability and accelerator operation are difficult to simulate and predict. Being able to measure impedance outside of the running accelerator is desirable to avoid complicated down time.

As introduced in [12] a Goubau-line test stand is a possible way to measure impedance of insertion devices. Designed by Georg Goubau in 1950 [5] based on the work of Sommerfeld from 1899 [6], a Goubau-line is a transmission line that uses a single wire to transmit surface waves. Its transverse electric field can be used to mimic that of a charged particle beam. Goubau-line set ups have been successfully used to measure the impedance of accelerator components, for example at Argonne APS [7] or at Bergoz Instrumentation [8]. Studies of CPMU17s impedance suggest that the fill pattern at BESSY II induces effects up to a frequency of 20 GHz which is significantly higher than the aforementioned test stand examples.

The following sections will show CST [11] simulations of the proposed Goubau-line design and discuss design parameters.

THEORETICAL CONSIDERATIONS

The main parts making up a Goubau-line are a transmitter, a receiver and a dielectrically coated wire. Horn antennas are used as transmitter and receiver shown in Fig. 1. The

Figure 1: Schematic of the Goubau-line modeled in CST consisting of two conical horn antennas and a dielectrically coated wire.

Horn antennas translate the signal coming from a coaxial cable to a surface wave on the dielectrically coated wire. Figure 2 shows the orientation of electric and magnetic fields along the coated wire. The electric and magnetic Fields are described by cylinder functions and their derivation is shown in Goubau's original paper [5] and in a modern revision by B. Vaughn *et al.* [9]. The radial electric field E_r is proportional to $1/r$ close to the coated wire and can therefore be used to emulate a charged particle beam before falling off exponentially at greater distances from the wire. In previous proceedings we discussed the wire parameters of the Goubau-line test stand by considering field extension and characteristic impedance [12, 13]. A 1 mm diameter copper wire with a 500 nm coating with a dielectric constant of $\varepsilon_r = 4$ was chosen. Extensive CST simulations have been

* paul.volz@helmholtz-berlin.de

ISBN: 978-3-95450-227-1 ISSN: 2673-5490 doi:10.18429/JACoW-IPAC2022-THPOPT056

EMITTANCE EXCHANGE AT SIRIUS BOOSTER FOR STORAGE RING INJECTION IMPROVEMENT

J. V. Quentino, M. B. Alves*, F. H. de Sá
Brazilian Synchrotron Light Laboratory (LNLS), 13083-100, Campinas, Brazil

Abstract

SIRIUS is the new 4th generation storage ring based synchrotron light source built and operated by the Brazilian Synchrotron Light Laboratory (LNLS) at the Brazilian Center for Research in Energy and Materials (CNPEM). Currently, the efficiency of the horizontal off-axis injection system of the storage ring is still not suitable for top-up operation due to a smaller than expected horizontal dynamic aperture. In this work, we report the simulations and experimental results of transverse emittance exchange (TEE) performed at SIRIUS booster by crossing a coupling difference resonance during energy ramp, with the goal of decreasing the injected horizontal beam size and improve the off-axis injection efficiency.

INTRODUCTION

The injection system for SIRIUS storage ring (SR) was designed since early stage for beam accumulation with off-axis injection using a single non-linear kicker (NLK) [1]. With this injection scheme, a small horizontal beam size is beneficial to minimize the sampling of non-linear fields at NLK and to allow for high injection efficiency. Thus, SIRIUS booster was designed to achieve a small horizontal emittance of 3.5 nm rad at extraction energy of 3 GeV [2].

The SIRIUS NLK was designed to have a peak field at $x_p \approx -9.0$ mm and no field at $x = 0$ mm, close to the stored beam. Injection dynamics studies indicated that this field profile would perform the injection with 99% of efficiency for a beam reaching the NLK at $x_0 = -8.5$ mm [1].

However, dynamic aperture measurements revealed a horizontal aperture of about -8.5 mm, which is worse than the -9.5 mm value predicted by the nominal model [3] and is strictly close to the planned injection position, obliging us to move the injection position to $x_0 = -8.0$ mm. As a consequence, even with the booster delivering a beam with small transverse sizes and the booster-to-SR transport line optics being optimized for partially compensate the defocusing effect made by nonlinear fields, the horizontal spread induced by the NLK in the actual injection position is sufficient to reduce the injection efficiency to about 86 %, with a large pulse-to-pulse variation [4]. Despite being an acceptable efficiency level, it is insufficient for operation in top up mode, which is planned to be implemented still this year.

One possible improvement in this scheme is to apply a transverse emittance exchange (TEE) at the SIRIUS booster, delivering the beam at NLK with an lower horizontal beam size to reduce the non linear fields sampling and attend the dynamic aperture restrictions.

* murilo.alves@lnls.br

The use of TEE for injection efficiency improvement was first proposed in Ref. [5] by different methods, such as modifying the booster quadrupoles ramp to cross the coupling difference resonance a few turns before beam extraction, applying a pulsed skew gradient field on the beam, or using a special arrangement of skew quadrupoles in the transfer line.

The first approach was chosen to be implemented in SIRIUS booster, since this method was already successfully applied in other synchrotron facilities, for example SLS [6] and ESRF-EBS [7], and it does not require any new accelerator component to be implemented.

This contribution will present the process of implementation of TEE in the SIRIUS booster, from simulations to the experimental results and its impact on the SR injection efficiency.

SIMULATIONS

A key concept regarding TEE in electron synchrotrons is the adiabaticity of the process, which can be described by the following scaling parameter [8, 9]:

$$S = \frac{\dot{\Delta}}{|C|^2}, \tag{1}$$

where $\dot{\Delta}$ is the tune crossing velocity in units of 1/turns and $|C|$ is the coupling coefficient modulus [10]. If the process is too fast such that it is non-adiabatic, the exchange will not be fully executed. On the other hand, if the process is too slow, radiation damping effects will push the emittances towards their initial equilibrium parameters, therefore reducing the emittance exchange efficiency as well [8, 11]. To investigate the behavior of emittance exchange with different coupling and crossing speed parameters, simulations with the booster model were carried out and the results are shown in Fig. 1.

The simulations started with the nominal booster fractional tunes difference $\Delta_0 = \mathrm{frac}(\nu_{x0}) - \mathrm{frac}(\nu_{y0})$, where $\mathrm{frac}(x) \coloneqq x - \lfloor x \rfloor$, and ran until $\Delta_{\mathrm{end}} = -\Delta_0$, crossing the resonance $\Delta = 0$ in the middle of the process. The results were obtained by tracking the beam envelope [12] for a number of turns in a range of 62 to 8000 revolutions, changing turn-by-turn the quadrupole strengths and updating the one-turn map and diffusion matrices to simulate the TEE process.

The TEE quality can be expressed by the R parameter, defined by [8]:

$$R(\epsilon_x) = 1 - \frac{\epsilon_x - \epsilon_{y0}}{\epsilon_{x0} - \epsilon_{y0}}, \tag{2}$$

where ϵ_{x0} and ϵ_{y0} are the horizontal and vertical initial emittances, and ϵ_x is the horizontal emittance at beam extraction

ISBN: 978-3-95450-227-1 ISSN: 2673-5490 doi:10.18429/JACoW-IPAC2022-THPOPT058

STATUS AND POWERING TEST RESULTS OF HTS UNDULATOR COILS AT 77 K FOR COMPACT FEL DESIGNS*

S. C. Richter†, [1], A. Ballarino, T. H. Nes, D. Schoerling, CERN, Geneva, Switzerland
A. Bernhard, A.-S. Müller, Karlsruhe Institute of Technology (KIT), Karlsruhe, Germany
[1]also at Karlsruhe Institute of Technology (KIT), Karlsruhe, Germany

Abstract

The production of low emittance positron beams for future linear and circular lepton colliders, like CLIC or FCC-ee, requires high-field damping wigglers. Just as compact free-electron lasers (FELs) require high-field but as well short-period undulators to emit high energetic, coherent photons. Using high-temperature superconductors (HTS) in the form of coated ReBCO tape superconductors allows higher magnetic field amplitudes at 4 K and larger operating margins as compared to low-temperature superconductors, like Nb-Ti.

This contribution discusses the development work on superconducting vertical racetrack (VR) undulator coils, wound from coated ReBCO tape superconductors. The presented VR coils were modularly designed with a period length of 13 mm. Powering tests in liquid nitrogen of multiple vertical racetrack coils were performed at CERN. The results from the measurements are presented for three VR coils and compared with electromagnetic simulations.

INTRODUCTION

Undulator magnets play a major role in accomplishing the next generation of compact and highly brilliant light sources, as they are used in synchrotrons and free-electron lasers as the main photon source with energies up to hard x-rays. When making the facilities more compact, short periods and high field undulators are crucial for delivering the needed high energetic photons for lower beam energies.

To achieve higher magnetic flux densities on the beam axis, the low-temperature superconductor (LTS) Nb-Ti was used to replace permanent magnets. An improvement of the resulting brilliance of high energy x-rays made it the state-of-the-art technology for superconducting undulators, e.g. Nb-Ti undulators operate successfully in KARA at KIT and at Argonne National Laboratory [1-3], whereas permanent magnet wigglers are used to lower the beam emittance, e.g. in PETRA III at DESY [4]. The CLIC wiggler design (3 T, 12 mm gap, 50 mm period) benefits from LTS as demonstrated with a Nb-Ti prototype at KARA, KIT [5]. An HTS version might be able to deliver around 4 T peak fields [6].

Consequently, employing high-temperature superconductors (HTS) like ReBCO (rare-earth barium copper oxide), to superconducting undulators is an attractive choice for the next upgrade. First, operations with larger temperature margins or at higher temperatures than 4 K would relax cryogenic requirements, thus reducing costs compared to LTS technologies. Second, a significant enhancement of the parameter space in terms of B_0, λ_u and gap could be shown in previous studies due to the ReBCO's high B_{c2} field at low temperatures (e.g., YBCO: $B_{c2,\perp}(4.2\,\mathrm{K}) \approx 100\,\mathrm{T}$) [7-9].

Other studies have already shown that ReBCO may be feasible for HTS undulator coils with $\lambda_u = 16$ mm to reach high current densities in the order of 2 kA/mm^2 at 4.2 K [10]. Yet, undulator periods smaller than 15 mm and quench protection stay challenging for these high currents. With our dry-wound, non-insulated (NI) design, we always give the current the option to circumvent normal conducting zones.

This paper presents and discusses the latest powering test results at 77 K of our three HTS VR undulator coils and briefly compares them to electromagnetic simulations, performed with Opera and J_c fits done at CERN [11-13].

EXPERIMENTAL SETUP

CERN and KIT are both contributing to the EU-financed CompactLight (XLS) study that explores feasibilities for a compact FEL, hence high on-axis fields for a given λ_u of 13 mm are part of the investigations [14]. Consequently, we decided to adopt this value to our modular coil design. All three presented VR undulator coils were wound with a 4 mm wide coated ReBCO tape superconductor onto a D-shaped copper winding body with an iron core (see Fig. 1). For VR coils #1 and #2, we used tape from Bruker HTS with a total thickness of 100 µm, including a 50 µm substrate and a total copper stabilizer thickness of 45 µm. For VR coil #3, 45 µm thick tape from SuperPower Inc. with a 30 µm substrate and a total copper stabilizer of 10 µm was used.

Each VR coil represents one period and thus consists of two sub-coils and two iron poles. The voltage was monitored via voltage taps on the inner- and outermost turn of each sub-coil. Two Hall probes were placed in a fixed position at a distance $d = 3.5$ mm from the iron pole face as displayed in Fig. 2. More design-related aspects can be found in Table 1. The complete design and manufacturing process were already described in previous work [15].

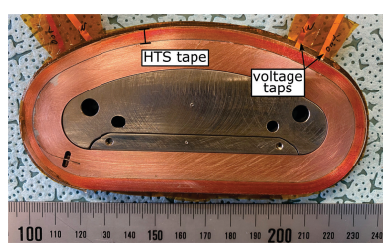

Figure 1: VR coil #3 with its four voltage taps. Scale in mm.

* This work has been supported by the Wolfgang Gentner Program of the German Federal Ministry of Education and Research.
† sebastian.richter@cern.ch

ISBN: 978-3-95450-227-1 ISSN: 2673-5490 doi:10.18429/JACoW-IPAC2022-THPOPT059

DEVELOPMENT OF A TRANSFER LINE FOR LPA-GENERATED ELECTRON BUNCHES TO A COMPACT STORAGE RING

B. Haerer*, E. Bründermann, D. El Khechen, A. Papash, S. C. Richter, R. Ruprecht, J. Schäfer, M. Schuh, C. Widmann, A.-S. Müller, KIT, Karlsruhe, Germany
L. Jeppe, A. Maier, P. Messner, J. Osterhoff, E. Panofski, DESY, Hamburg, Germany

Abstract

The injection of LPA-generated beams into a storage ring is considered to be one of the most prominent applications of laser plasma accelerators (LPAs). In a combined endeavor between Karlsruhe Institute of Technology (KIT) and Deutsches Elektronen-Synchrotron (DESY) the key challenges will be addressed with the aim to successfully demonstrate injection of LPA-generated beams into a compact storage ring with large energy acceptance and dynamic aperture. Such a storage ring and the corresponding transfer line are currently being designed within the cSTART project at KIT and will be ideally suited to accept bunches from a 50 MeV LPA prototype developed at DESY. This contribution presents the foreseen layout of the transfer line from the LPA to the injection point of the storage ring and discusses the status of beams optics calculations.

INTRODUCTION

Synchrotron light sources are among the most prominent applications of particle accelerators as they build the foundation for a huge set of user experiments in various scientific fields such as material science, biology, or chemistry. The combination of a short pulse injector with a storage ring would, as long as the short bunch length can be maintained either on a regular basis or at a certain position of the ring, allow the users observations at much shorter time scales with high repetition rate. Laser-plasma accelerators (LPAs) are promising candidates to revolutionize injectors for light sources [1]. They provide ultra-short bunches and easily reach accelerating field strengths orders of magnitude larger than those available from conventional RF-based injectors leading to a compact, lab-scale infrastructure footprint. The LPA community has shown dramatic progress over the past few years: Beam energies up to 8 GeV [2], continuous 30 h operation [3], and few-fs pulse length from a laser-plasma accelerator [4] have been demonstrated bringing LPAs closer to applications.

In order to reach the ambitious goal to demonstrate the very first injection of LPA beams into a storage ring, DESY and KIT formed a collaboration [5]: DESY will design, setup and operate an LPA injector with stable, reproducible high quality electron beams, while KIT will devise the no less challenging transfer line and high acceptance storage ring.

* bastian.haerer@kit.edu

LPA Injection into the cSTART Storage Ring

The aim of the KIT project cSTART is to investigate non-equilibrium beam dynamics of bunches of femto-second length with high repetition rate in a storage ring and provide the first study of LPA injection into a ring-based light source. Therefore, the lattice of the storage ring has been specifically designed to offer large momentum acceptance of $\delta = \pm 5.5\%$ and large dynamic aperture $\Delta x = \pm 15$ mm in the horizontal plane and $\Delta y = \pm 10$ mm in the vertical plane as presented in [6–10]. The storage ring will have a circumference of 43.2 m and is designed for a beam energy of 50 MeV. Two different injectors are foreseen: On the one hand the linac-based test facility FLUTE [11], which provides conventionally accelerated electron bunches, and on the other hand the LPA injector. All three accelerators will be housed in the same experimental hall. FLUTE is located at the ground floor, while the LPA and the cSTART storage ring will be installed at a level of about 3.5 m. Figure 1 shows an artificial view of FLUTE and the cSTART storage ring including the first design of the transfer line that lifts the electron bunches produced by FLUTE up to the height of the storage ring and re-compresses them to ultra-short bunch lengths [8, 12]. The LPA will be driven by a TW laser system installed in a clean room next to the experimental hall. The plasma cell will be positioned such that the LPA electron beam line will intersect the transfer line coming from FLUTE at the end of the long straight section and share the last Double-Bend Achromat (DBA) cell and the injection section as illustrated in Figure 2.

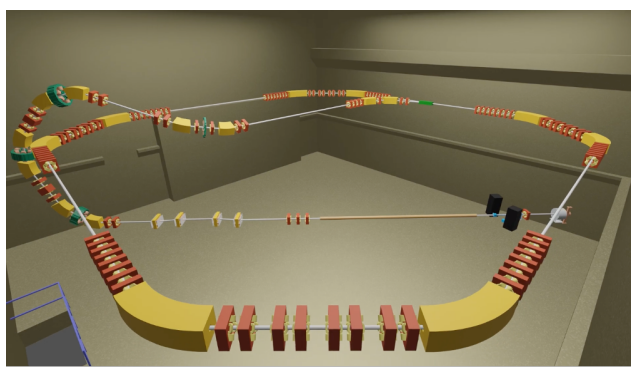

Figure 1: Artificial view of the cSTART storage ring, the injector FLUTE and the transfer line, in which the transfer line coming from the LPA will be incorporated (Courtesy J. Schäfer). The diameter of the storage ring is 12.5 m.

The commercial laser system has been delivered to the ready-to-use clean room at KIT. Plasma cell and target cham-

ISBN: 978-3-95450-227-1 ISSN: 2673-5490 doi:10.18429/JACoW-IPAC2022-THPOPT060

TOLERANCE STUDY ON THE GEOMETRICAL ERRORS FOR A PLANAR SUPERCONDUCTING UNDULATOR

V. Grattoni*, S. Casalbuoni, B. Marchetti, European XFEL, Schenefeld, Germany

Abstract

At the European XFEL, a superconducting afterburner is considered for the SASE2 hard X-ray beamline. It will consist of six undulator modules. Within each module, two superconducting undulators (SCU) 2 m long are present. Such an afterburner will enable photon energies above 30 keV. A high field quality of the SCU is crucial to guarantee the quality of the electron beam trajectory, which is directly related to the spectral quality of the emitted free-electron laser (FEL) radiation. Therefore, the effects of the SCU's mechanical imperfections on the resultant magnetic field have to be carefully characterized. In this contribution, we present possible mechanical errors affecting the undulator structure, and we perform an analytical study aimed at determining the tolerances on these errors for our SCUs.

INTRODUCTION

European XFEL considers the development of superconducting undulators a strategic field of research for future facility upgrades. European XFEL plans the installation of a superconducting afterburner downstream the permanent undulators of the SASE2 hard X-ray beamline. The afterburner consists of a series of six modules. Each module accommodates two 2 m long superconducting undulators (SCU) interleaved by a phase shifter [1]. The intersection between consecutive modules resembles the one between the permanent magnet undulators of the SASE2 beamline. Presently, we have specified a pre-series module named S-PRESSO and assigned its contract to the company Bilfinger Noell GmbH [2].

Errors in the field of the SCU can degrade the FEL performance. Deviations in the pole height or width, groove width and a vertical shift in the winding package cause errors in the magnetic field B and in the undulator period length λ_u. Consequently, also the undulator strength K is affected as it depends linearly on the undulator field and period length: $K \simeq 0.934 B[\mathrm{T}]\lambda_u[\mathrm{cm}]$.

The strategy used in our study is the following: we quantify the impact on the undulator strength of the identified errors individually. Then, we perform a Montecarlo simulation to generate several undulator fields with all the errors types to investigate how the undulator strength is affected. Finally, we compare the $\Delta K/K$ resulting from the defined mechanical tolerances with the $\Delta K/K$ found to keep the FEL power degradation below 5% of the emitted power in absence of undulator errors for an SCU line with $\lambda_u = 15$ mm.

This study integrates our previous one published in [3] including an undulator period $\lambda_u = 15$ mm. This time we have considered a $\lambda_u = 18$ mm, which is the final wavelength chosen for the SCU afterburner modules.

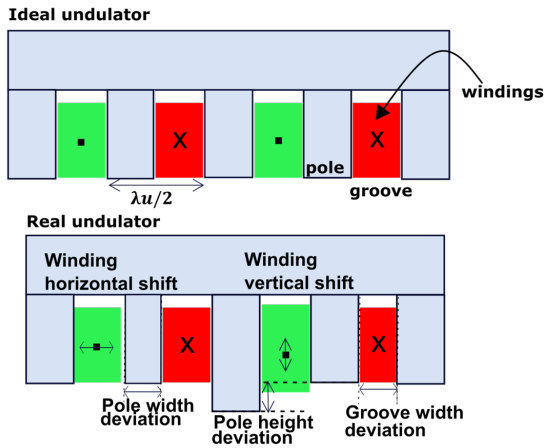

Figure 1: Top: ideal undulator. Bottom: undulator with mechanical deviations.

MECHANICAL ERRORS ON THE SCU

The yoke of an SCU has ferromagnetic poles interleaved by grooves that are wound using a superconducting wire, in this case, NbTi (see Fig. 1 top). The wire is wound with alternating direction in consecutive grooves. Two consecutive poles and the grooves following the poles define the undulator period length λ_u. The machining of the yoke introduces deviations from the design value of the pole height or width and on the groove width. The error on the pole or groove width causes a deviation from the nominal period length. In addition, the winding packages can result in a vertical or horizontal shift of their centre of mass, as shown in Fig. 1 bottom.

We have performed simulations in FEMM [4] to characterize the effect of each single error type on the magnetic field. We have considered an undulator with 15 periods and calculated the signature for each error type [5]. We define the signature as:

$$\Delta B = \tilde{B} - B_0 \quad (1)$$

where B_0 is the ideal field and $\tilde{B}$ is the field where only one of the errors at the time has been applied. We have calculated both fields with FEMM [4].

Characterization of the Signatures

Depending on the error type, different functions have been used to fit the signatures. In the following list, we present the considered analytic signature functions:

- a sinusoidal function has been used to fit the error on the groove width and on the pole width (Fig. 2(a))

* vanessa.grattoni@xfel.eu

ISBN: 978-3-95450-227-1 ISSN: 2673-5490 doi:10.18429/JACoW-IPAC2022-THPOPT061

EUROPEAN XFEL UNDULATORS - STATUS AND PLANS

S. Casalbuoni*, S. Abeghyan, J. E. Baader, U. Englisch, V. Grattoni, S. Karabekyan, B. Marchetti, H. Sinn, F. Wolff-Fabris, M. Yakopov, P. Ziolkowski, European XFEL GmbH, Schenefeld, Germany

Abstract

European XFEL has three undulator lines based on permanent magnet technology: two for hard and one for soft X-rays. The planar undulators can be tuned to cover the acceptance in terms of photon beam energy of the respective photon beamlines: 3.6-25 keV (SASE1/2) and 0.25-3 keV (SASE3) by changing the electron energy range between 8.5 GeV and 17.5 GeV and/or the undulator gap. In order to obtain different polarization modes, as required by the soft X-ray beamlines, a helical afterburner consisting of four APPLE X undulators designed by PSI has been installed at the downstream end of the present SASE3 undulator system. The European XFEL plans to develop the technology of superconducting undulators, which is of strategic importance for the facility upgrade. In order to extend the energy range above 30 keV a superconducting undulator afterburner is foreseen to be installed at the end of SASE2. This contribution presents the current status and the planned upgrades of the undulator lines at European XFEL.

INTRODUCTION

European XFEL has three undulator lines: two for hard and one for soft X-rays. The two hard X-ray lines SASE1 and SASE2 consist of 35 undulators cells each, while the soft X-ray line SASE3 of 21. The undulator system as built and commissioning of SASE1 are described in Ref. [1]. By changing the electron energy between 8.5 GeV and 17.5 GeV and/or the undulator gap, the undulator lines can be tuned to cover the acceptance in terms of photon beam energy of the respective photon beamlines: 3.6-25 keV (SASE1/2) and 0.25-3 keV (SASE3). The undulators have been specified and characterized to work in the range of the undulator parameter K values indicated in Table 1.

All undulators installed in the tunnel are planar and generate horizontally polarized radiation. In order to obtain different polarization modes, as required by the soft X-ray beamlines, a helical afterburner consisting of four APPLE X undulators has been installed downstream with resepct to the present SASE3 undulator system [2].

In all undulator lines it is in principle possible to extend the photon energy range of the fundamental to harder X-rays by further decreasing the undulator parameter K. In SASE1/2 it is possible to reach about 70 keV by working at larger undulator magnetic gaps up to 40 mm (K~ 0.33) and at 17.5 GeV. At this working point, the efficiency of the FEL is low because the coupling strength between electron beam and the emitted photons is proportional to the undulator parameter K. It is therefore foreseen to exploit these higher photon energies by increasing the FEL process efficiency and energy per pulse output with a superconducting undulator (SCU) afterburner [3]. This is planned to be installed after the present SASE2 line, which is already built with an X-ray optics transporting up to about 65 keV photon beams. The photons per pulse produced by the SCU afterburner ($\gtrsim 10^{10}$ for photon energies above 30 keV) are expected to be more than two orders of magnitude higher than the ones available at the diffraction limited storage rings as ESRF-EBS and APS-U, in pulses more than 5000 times shorter.

PLANAR PERMANENT MAGNET UNDULATORS

The main parameters of the planar permanent magnet undulators (PMUs) in the three lines are shown in Table 1. All installed planar PMUs are made of neodymium-iron-boron (NdFeB) and cobalt-iron poles. They all have the same support structure and mechanical drive. The beam vacuum chamber is made of extruded aluminium-magnesium and has an elliptical beam stay clear of 15 mm (horizontal) and 8.6 mm (vertical). The outer vertical height of the beam vacuum chamber is 9.6 mm. The undulator lines must be segmented. Each undulator is 5 m long. This is a compromise to maximise the number of periods along the line, by still having economic manufacturable lengths of the support structure to keep the magnetic forces and reasonable measurement benches.

Table 1: Main Parameters of the Planar Permanent Magnet Undulators [1]

	SASE1/2	SASE3
Period length (mm)	40	68
Operational K range	1.65–3.9	4–9
Magnetic length (mm)	4980	4998
Max. phase jitter (°)	≤ 8	≤ 8
Max. $I_{1x,y}$ (T mm)	±0.15	±0.15
RMS $I_{2x,y}$ (T mm^2)	< 100	< 210(y)100(x)

Each undulator is followed by a so-called intersection. This is 1.1 m long, equipped with air coil correctors, a quadrupole, an absorber to screen the following undulators from synchrotron radiation, a phase shifter, a cavity beam position monitor (BPM) with sub-micrometer resolution [4], and a beam loss monitor [5]. Air coil correctors at the entrance and exit of each undulator are used to compensate the vertical and horizontal first and second field integrals, so that the undulators are transparent to the electron beam. The maximum values of the first field integrals reported in Table 1 are to be further reduced with the air coil correctors to $I_{1x,y} < 0.02 - 0.03$ T mm, where the lower value refers to an electron beam energy of 10 GeV and the higher

* sara.casalbuoni@xfel.eu

ISBN: 978-3-95450-227-1 ISSN: 2673-5490 doi:10.18429/JACoW-IPAC2022-THPOPT063

DESIGN OF SCILAB Xcos SIMULATION MODEL FOR PULSED WIRE METHOD DATA ANALYSES

H. Jeevakhan, Department of Applied Science Education, National Institute of Technical Teachers' Training and Research, Bhopal, India
S. M. Khan, G. Mishra, School of Physics, Devi Ahilya University, Indore, India

Abstract

Pulsed wire method (PWM)is used for undulator characterisation. SCILAB Xcos simulation model is designed for the analyses of data obtained by PWM. The data obtained from PWM is given as input to the model and its output gives the magnetic field of the undulator.

INTRODUCTION

The performance of free electron laser and synchrotron radiation source depends on the quality of magnetic field of undulator. In an ideal case the on axis magnetic field of undulator is sinusoidal, such that the trajectory of relativistic electron which is injected along the axis is sinusoidal in the plane of oscillation. Any deviation in the trajectory from ideal sinusoidal trajectory produces phase error, which results in reduction of brightness of undulator radiations. It is therefore important to characterize the field quality of undulator. The magnetic field measurement by Hall probe method based on the principle of measuring the Hall voltage which is developed across one face of semiconductor say Indium Arsenide (InAs) crystal, on applying magnetic field and constant current across the other two perpendicular faces respectively. Different methods have been used to evaluate quickly the magnetic field characteristics, they are rotating coil and flipping coil methods, stretched wire measurement system. In recent years there exist interests in Pulsed wire method (PWM) magnetic field measurements of undulators/ wigglers for synchrotron radiation and free electron laser applications, which is proposed by R Warren [1]. In this method a thin wire is stretched along the undulator axis. A current pulse is passed through the wire produces a force on the wire proportional to the local transverse magnetic field. The force initiates a travelling wave that propagates in both the direction. An optical switch connected to an oscilloscope located at a place along the wire captures the traveling wave. A longer pulse returns a signal that approximates the second integral of the undulator field. For a short current pulse, the returned signal represents the first integral of the undulator magnetic field.

PWM is useful for in-vacuum insertion devices, as it can give magnetic profile of undulator with very small gap [2]. Recent studies on improvements in PWM shows its usefulness in measuring the magnetic field of planar, hybrid and superconducting undulators [3-6]. SCILAB is an open source software for numeric computation [7]. SCILAB's Xcos simulation model-based design is used for determining the trajectory of electrons in real undulator, by using the magnetic field of proposed superconducting undulator by RADIA codes [8].

The present work corresponds to develop SCILAB Xcos model for analysis of the experimental data measured from PWM. Xcos blocks are used to double differentiate the PWM data. The advantage of using model-based design over other methods is that we can visualise the output instantaneously and does not need any separate plotting software. The present model helps to visualise the filter used for elimination of noise from the signal. In present analyses, the magnetic field data of Hybrid undulator (U20) developed at DAVV lab Indore is utilised for the execution of the designed model. The details of the undulator is given in next section.

HYBRID UNDULATOR AT DAVV LAB

U20 undulator is a variable gap hybrid type undulator [4] made up of NdFeB magnets and M35 Grade Cobalt Steel poles. The undulator consists of 25 number of periods and each period is 20 mm long and each period have two magnets and two poles, thus the total length of the U20 undulator is 500 mm. There are 98 regular magnets and 98 regular poles. The regular magnets are 6.25 mm wide, 6.25 mm high and 50 mm long and regular poles are 3.75 mm wide, 4.7 mm high and 50 mm long. The U20 end magnet and end pole dimensions are 3.75 mm x 6.25 mm x 50 mm and 1.87 mm x 4.7 mm x 50 mm respectively. The gap between the jaws of undulator can be varied with the help of manually driven ball screw system from 9mm to 20 mm. The peak magnetic field range from 0.24 T to 0.05 T with respect to gap of the undulator.

PULSED WIRE METHOD SET UP

In the PWM, the second integral equation read as [1]

$$I_2 = x.\frac{2v^2\mu}{I_0} \quad (1)$$

Where,

x is displacement of wire in meter
v is the velocity in m/s
μ is linear density of wire in kg/m
I_0 is current in wire in Ampere

In the present PWM set up, beryllium-copper wire of 250 micron is used, having linear density 4.1 x10-4 g/m, I0 is 5.08 A, tension in wire is 26.26 N, hence velocity is 253.12 m/s. By inserting these values in Eq. 1 the multiplication factor comes out to be 10.34.

ISBN: 978-3-95450-227-1 ISSN: 2673-5490 doi:10.18429/JACoW-IPAC2022-THPOPT064

HALL PROBE MAGNETIC MEASUREMENT OF 50 mm PERIOD PPM UNDULATOR

S. M. Khan†, G. Mishra, Devi Ahilya VishwaVidyalaya (DAVV), Indore, India
M. Gehlot, MAX IV Laboratory, Lund, Sweden
H. Jeevakhan, NITTTR, Bhopal, India

Abstract

In this paper, we present theHall Probe magnetic measurement of the integrated multipoles of 50 mm period undulator.The ongoing activity on asymmetric undulator is discussed.

INTRODUCTION

The Hall probe is the most versatile magnetic measurement system for the undulators. The field integral and phase error [1,2] of the undulator are directly computed from the field mapping. The field integrals compute the angle and position offset of the electron at the undulator end. The phase error indicates the undulator quality through reduction of photon flux and small signal free electron gain. The multipole components of the undulator indicate the effects of the undulator on the propagating electron beam [3].

HALL PROBE MEASUREMENT BENCH

The schematic of the Hall probe bench is illustrated in Fig. 1. The Hall probe measurement bench uses a F.W. Bell make, Model No- 8030 Tesla meter and F.W. Bell make 3-axis probe Model No- ZOA83-3208-10. The cylindrical 3-axis probe stem is 205 mm in length and have 8 mm diameter. The probe is attached in specially designed indigenously made probe holder having measurable angle adjustment. The probe is fixed in a cylindrical tube of 20 mm inner diameter having 5 mm thickness attached inside the probe mount with the help of a coaxial cylinder, both the cylinders are covered with the mount case fixed with Allen screws. There is a knob in the bottom of probe mount for coarse adjustment and micrometer given on the side for fine adjustment of the angle of hall probe. The design of the hall probe holder presented in Fig. 2. The probe holder having M6 slot is mounted on a xy-stage; 50 mm travel distance each and moves on a motorized z-linear translation stage of 2000 mm length. A stepper motor with a single axis motion controller drives the hall probe assembly unit on the z-linear translation stage capable to move forward and backward. The motion controller operated with control software capable to record multiple Teslameter channels is programmed to control the speed and direction of the travel, delay time and step length of measurement defined by the user. The control software allow the linear translation stage to move distance range from 2 µm to 2000 mm both in forward and reverse directions with allowed speed ranging up to 20 mm/s and a delay time between the data capture range from 0ms to 9999 ms can be given to measurement system.

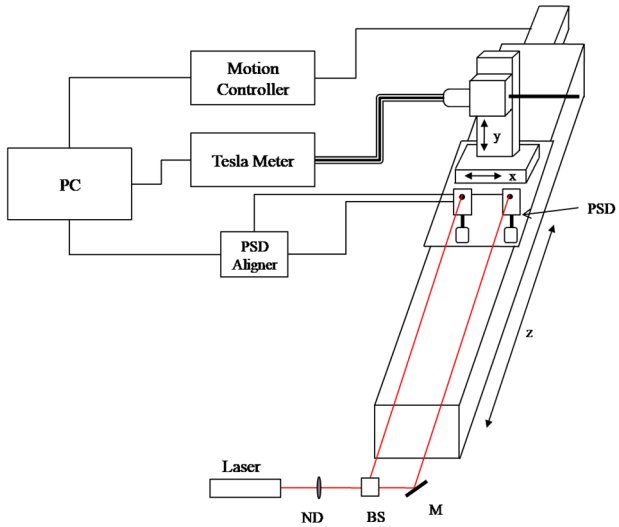

Figure 1: Hall probe bench.

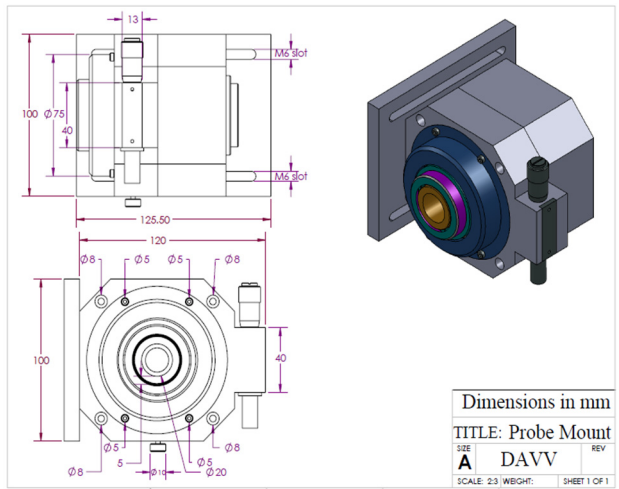

Figure 2: Design of Hall probe mount.

The 2D position sensing detector based position measuring system previously used for different setup [4] to align the Hall probe in both vertical and horizontal directions implemented on new 2000 mm long translation stage.

MAGNETIC MEASUREMENTS

Straightness and flatness of the travel of Hall probe measurement assembly shown in Fig. 3. The undulator is 1m long having 20 periods, each period is 50 mm in length. The motion of Hall probe is observed throughout

† saiffukhan@gmail.com

ISBN: 978-3-95450-227-1 ISSN: 2673-5490 doi:10.18429/JACoW-IPAC2022-THPOPT065

OPERATION OF X-RAY BEAM POSITION MONITORS WITH ZERO BIAS VOLTAGE AT ALBA FRONT ENDS

J. Marcos*, U. Iriso, V. Massana, R. Monge, D. Yépez
ALBA Synchrotron, Cerdanyola del Vallès, Spain

Abstract

Blade-type X-ray Beam Position Monitors (XBPMs) are customarily operated with a negative bias voltage applied to the blades in order to prevent the transference of photoelectrons between the blades, and hence to maximize the signal at each blade and to avoid cross-talk. This was the selected approach at ALBA since the start of its operation for users in 2012. However, over the years the insulation provided by the ceramic pieces separating the blades from the support structure has degraded progressively, giving rise to an ever-increasing leakage current not related with the photon beam to be monitored. On 2020 the level of these leak currents had already become comparable to the photocurrents generated by the photon beam itself, making the readings from many of the XBPMs unreliable. Following the example from other facilities, we decided to remove the bias voltage from the blades and to test the performance of the XBPMs under these conditions, with such good results that we apply this method also for the new, non degraded, XBPMs. In this paper we present the approach used at ALBA to analyse XBPM data, and our experience operating them with zero bias voltage.

INTRODUCTION

The general layout of the Front Ends (FEs) for Phase-I beamlines at ALBA was described in Ref. [1]. In particular, each FE is equipped with one blade-type XBPM in order to monitor the position of the photon beam at a distance of 7–10 m from the source point. Monitors were manufactured by FMB-Berlin [2] according to the designs developed by K. Holldack at BESSY [3]. Each XBPM makes use of four narrow blades which intercept the edges of the photon beam distribution. The photoelectrical currents generated at each blade are measured using a low current monitor, and combined in order to get an on-line estimation of the horizontal and vertical position of the centre of the beam

SIGNAL PROCESSING

The difference-over-sum of the current of right/left and top/bottom blades are used to define the raw position parameters associated to the XBPM:

$$X = \frac{(I_1 + I_3) - (I_2 + I_4)}{I_1 + I_2 + I_3 + I_4}, \quad Y = \frac{(I_1 + I_2) - (I_3 + I_4)}{I_1 + I_2 + I_3 + I_4}. \tag{1}$$

These dimensionless parameters are related to the real displacement of the photon beam with respect to the centre of the XBPM, X_{pos} and Y_{pos}. For convenience, at ALBA we assume that this relationship is linear. More precisely, the coordinates of the photon beam position X_{pos} and Y_{pos} are related with the output of the XBPM in terms of X and Y through the expressions:

$$X \simeq C_{xx}X_{\mathrm{pos}} + C_{xy}Y_{\mathrm{pos}}\,, \quad Y \simeq C_{yx}X_{\mathrm{pos}} + C_{yy}Y_{\mathrm{pos}}\,, \tag{2}$$

where C_{xx} and C_{yy} are the typical sensitivity coefficients which give the response of the XBPM to a given displacement of the beam along horizontal and vertical directions, respectively; the two additional coefficients, C_{xy} and C_{yx}, characterize any source of cross-talk between the two planes. These cross-talks can be due to either an improper alignment of the XBPM blades or to a lack of symmetry of the photon beam footprint.

In a practical situation, the X and Y parameters are obtained from the photocurrents measured at the XBPM through Eq. (1), and the photon beam position is determined by inverting Eq. (2):

$$\begin{aligned} X_{\mathrm{pos}} &\simeq \frac{C_{yy}X - C_{xy}Y}{C_{xx}C_{yy} - C_{xy}C_{yx}} \\ Y_{\mathrm{pos}} &\simeq \frac{-C_{yx}X + C_{xx}Y}{C_{xx}C_{yy} - C_{xy}C_{yx}}\,. \end{aligned} \tag{3}$$

In the particular case with zero cross-talk between planes, $C_{xy} = C_{yx} = 0$, the expected result $X_{\mathrm{pos}} = X/C_{xx}$ and $Y_{\mathrm{pos}} = Y/C_{yy}$ is recovered.

It has to be taken into account that all four coefficients C_{xx}, C_{xy}, C_{yx}, and C_{yy} in Eq. (2) depend on the characteristics of the photon beam distribution delivered by the source; therefore, in the case of Insertion Devices (IDs) those factors are a function of all the parameters defining their emission of radiation: the gap opening for planar devices, the phase displacement for APPLE-type undulators etc.

The calibration procedure to determine the sensitivity coefficients for a given configuration of the ID is based in introducing a known displacement of the XBPM with respect to the photon beam (change in X_{pos} and Y_{pos}) and recording the change in the output parameters (X and Y). The displacement is introduced by means of a two-axes linear stage at the base of the vacuum vessel that contains the XBPM. During the calibration the delivered photon beam is kept as steady as possible by means of the accelerator's orbit feedback, and the XBPM is displaced with respect to it over a rectangular grid. The resulting pairs of $(X_{\mathrm{pos}}, Y_{\mathrm{pos}})$ and (X, Y) data points are fitted according to Eq. (2) around the position where $X = Y = 0$, allowing to derive the value of the sensitivity factors. Such a measurement is carried out for a representative number of configurations of the ID, giving as a result a set of look-up tables for the sensitivity coefficients.

* jmarcos@cells.es

ISBN: 978-3-95450-227-1 ISSN: 2673-5490 doi:10.18429/JACoW-IPAC2022-THPOPT066

HELICAL WIGGLER DESIGN FOR OPTICAL STOCHASTIC COOLING AT CESR*

V.A. Khachatryan[1†], M.B. Andorf[1], I.V. Bazarov[1], W.F. Bergan[2], J.A. Crittenden[1], S.J. Levenson[1], J.M. Maxson[1], D.L. Rubin[1], J.P. Shanks[1], S.T. Wang[1]
[1]CLASSE, Cornell University, Ithaca, NY, USA
[2] Brookhaven National Laboratory, Upton, NY, USA

Abstract

A helical wiggler with parameter K_{und} = 4.35 has been designed for the Optical Stochastic Cooling (OSC) experiment in the Cornell Electron Storage Ring (CESR). We consider four Halbach arrays, which dimensions are optimized to get the required helical field profile, as well as, to get the best Dynamic Aperture (DA) in simulations. The end poles are designed with different dimensions to minimize the first and second field integrals to avoid the need of additional correctors for the beam orbit. The design is adapted to minimize the risk of demagnetization of the magnet blocks. To quantify the tolerances, we simulated the effects of different types of geometrical and magnetic field errors on the OSC damping rates. In addition, to understand the challenges for the construction, as well as, to validate the model field calculations, a prototype wiggler with two periods has been constructed. The prototype field is compared to the model, and the results are presented in this work.

INTRODUCTION

Optical Stochastic Cooling is considered one of the most promising methods for cooling stored particle beams. A key aspect of OSC is a pair of wigglers. The so called pickup wiggler radiates at optical frequencies. The kicker wiggler couples the radiation emitted by the pickup back into the beam at a phase that effects cooling. The idea was proposed in 1993 by A.A. Mikhailichenko and M.S. Zolotorev [1] and later refined by Zololotorev and Zholents into transit time OSC [2]. A high gain OSC demonstration in the Cornell Electron Storage Ring is an experimental aimed at developing.

For the demonstration of OSC at CESR the plan is to use a pair of identical helical wigglers for pickup and kicker. For compatibility with an optical amplifier based on a Ti:Sapphire gain medium, the wigglers are designed to radiate at a wavelength of 780 nm, corresponding to parameter K_{und}=4.35 for a beam energy of 1 GeV. The energy kick in the 14-period long kicker, which is the result of the interaction between the radiated wave-packet and the electron beam, is estimated to be 420 meV. The details about OSC simulations at CESR can be found in articles [3–5]. The focus of this work is the design of the wigglers based on permanent magnets. Nowadays, widely available Neodymium magnets give excellent opportunity to build more affordable wigglers compared to similar electromagnets, which have more complicated geometry, need separate power supplies and cooling subsystems.

HELICAL WIGGLER DESIGN

The configuration of magnetic material and shaping steel that generates a helical magnetic field has been defined and demonstrated. The dimensions of the components have been optimized for field quality. The end poles have been modified to tune the fringe fields. In addition, dependencies on geometrical errors and temperature variation have been investigated. Calculation of the forces between the magnet-steel arrays have been completed.

The coordinate system: Z axis is the beam direction, X and Y axes are horizontal and vertical directions respectively.

Geometry and Magnet Definition The wiggler geometry and the following field calculations are performed using the OPERA3D package [6]. The idea is to define four Halbach hybrid arrays [7] (top-left, top-right, bottom-left and bottom right), which can form two planar wigglers diagonally (top-left with bottom right, and top-right with bottom-left). The helical field can be achieved by giving a quarter period offset to one of the diagonal combination (see Fig. 1). As for magnet blocks, the best choice for such projects are Neodymium Ferrite Boron (NdFeB) magnets, as those are the strongest type of permanent magnets available commercially.

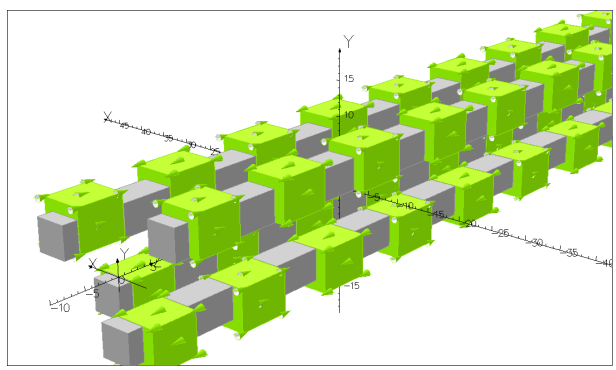

Figure 1: Permanent magnet based helical wiggler Opera-3D model. The green blocks are magnet blocks, the arrows show their magnetization orientation, the gray blocks are steel.

* Work supported by NSF award PHY-1549132 and DGE-1650441
† vk348@cornell.edu

ISBN: 978-3-95450-227-1 ISSN: 2673-5490 doi:10.18429/JACoW-IPAC2022-THPOPT067

PROPAGATION OF GAUSSIAN WIGNER FUNCTION THROUGH A MATRIX-APERTURE BEAMLINE*

B. Nash, D. T .Abell, P. Moeller, I. V. Pogorelov†
RadiaSoft LLC, Boulder, Colorado, USA
N. B. Goldring, STATE33 Inc., Portland, Oregon, USA

Abstract

We develop a simplified beam propagation model for x-ray beamlines that includes partial coherence as well as the impact of apertures on the beam. In particular, we consider a general asymmetric Gaussian Schell model, which also corresponds to a Gaussian Wigner function. The radiation is thus represented by a 4×4 symmetric second-moment matrix. We approximate rectangular apertures by Gaussian apertures, taking care that the loss in flux is the same for the two models. The beam will thus stay Gaussian through both linear transport and passage through the apertures, allowing a self-consistent picture. We derive expressions for decrease in flux and changes in second moments upon passage through the aperture. We also derive expressions for the coherence lengths and analyze how these propagate through linear transport and Gaussian apertures. We apply our formalism to cases of low emittance light source beamlines and develop a better understanding about trade-offs between coherence length increase and flux reduction while passing through physical apertures. Our formulae are implemented in RadiaSoft's Sirepo Shadow application allowing easy use for realistic beamline models.

GAUSSIAN WIGNER FUNCTION

Transverse coherence properties of partially coherent light at a given distance from the source can be described by means of the cross-spectral density (CSD) function, $\Gamma(\mathbf{r}_1, \mathbf{r}_2; t)$ in the time domain or $\tilde{\Gamma}(\mathbf{r}_1, \mathbf{r}_2; \omega)$ in the frequency domain [1–3]. An equivalent description can be effected in terms of the Wigner function (WF), $W(\mathbf{r}, \boldsymbol{\theta})$, related to the CSD $\tilde{\Gamma}(\mathbf{r}_1, \mathbf{r}_2; \omega)$ via the Fourier transform w.r.t. the pair of variables $\mathbf{r}_1 - \mathbf{r}_2$ and $\boldsymbol{\theta}$. Thus, one can choose to track either the CSD or the corresponding WF when modeling the propagation of partially coherent x-ray light through the beamline. One useful property of the WF is that it can be used just as a regular phase space density distribution for computing the moments with respect to the phase space variables. When the dynamics in the horizontal and vertical trace spaces are decoupled, both the WF and the CSD are separable, so that one is faced with a much simpler task of tracking functions of 2D phase space variables.

In the frequently encountered case where the radiation source is adequately described by the Gaussian Schell model, the corresponding Wigner function at the source is known to be Gaussian. As such, it is fully described by specifying its covariance matrix Σ, whose elements are the second-order moments, *viz.*, $\sigma_{xx} = \langle x^2 \rangle$, etc. Specifically, denoting the the vector of the 4D phase space variables $\vec{z} \equiv (\vec{x}, \vec{\theta})^T \equiv (x, y, \theta_x, \theta_y)^T$, the normalized Gaussian WF is given by

$$W(\vec{x}, \vec{\theta}) = \frac{1}{2\pi\sqrt{\det \Sigma}} \exp\left(-\frac{1}{2}\vec{z}^T \Sigma^{-1} \vec{z}\right) . \tag{1}$$

When x and y trace spaces are decoupled, we denote the 2D phase space variables (x, θ), and write for the Σ matrix and the rms emittance ϵ

$$\Sigma = \begin{pmatrix} \sigma_{xx} & \sigma_{x\theta} \\ \sigma_{x\theta} & \sigma_{\theta\theta} \end{pmatrix} \tag{2}$$

and

$$\epsilon = \sqrt{\sigma_{xx}\sigma_{\theta\theta} - \sigma_{x\theta}^2} = (\det \Sigma)^{1/2} , \tag{3}$$

respectively. For convenience, we also introduce the quantities α, β and γ (similar to the Twiss parameters used in accelerator physics):

$$\epsilon\beta = \sigma_{xx}, \quad \epsilon\gamma = \sigma_{\theta\theta}, \quad \epsilon\alpha = -\sigma_{x\theta}, \tag{4}$$

which are constrained by the identity

$$\beta\gamma - \alpha^2 = 1 . \tag{5}$$

The inverse of Σ is then given in the 2D phase space case by

$$\Sigma^{-1} = \frac{1}{\det \Sigma} \begin{pmatrix} \sigma_{\theta\theta} & -\sigma_{x\theta} \\ -\sigma_{x\theta} & \sigma_{xx} \end{pmatrix} = \frac{1}{\epsilon} \begin{pmatrix} \gamma & \alpha \\ \alpha & \beta \end{pmatrix} , \tag{6}$$

and for the Gaussian WF we have these parametrized expressions:

$$\begin{aligned} 2\pi\sqrt{\det \Sigma} W(x, \theta) \\ = \exp\left[-\frac{1}{2 \det \Sigma}(\sigma_{\theta\theta}x^2 - 2\sigma_{x\theta}x\theta + \sigma_{xx}\theta^2)\right] \\ = \exp\left[-\frac{1}{2\epsilon}(\gamma x^2 + 2\alpha x\theta + \beta\theta^2)\right] . \end{aligned} \tag{7}$$

As long as the WF stays Gaussian, its evolution is fully captured by tracking its moments through the second order (*i.e.*, tracking the elements of the 4×4 coupled Σ matrix or a pair of or 2×2 matrices in the uncoupled case). This closely parallels tracking the moments of the phase space distribution function in the particle beam dynamics setting. If the dynamics of the space space variables over a section of the beamline are linear and described by a transport matrix

* This work is supported by the US Department of Energy, Office of Basic Energy Sciences under Award Number DE-SC0020593.
† ilya@radiasoft.net

ISBN: 978-3-95450-227-1 ISSN: 2673-5490 doi:10.18429/JACoW-IPAC2022-THPOPT068

LINEAR CANONICAL TRANSFORM LIBRARY FOR FAST COHERENT X-RAY WAVEFRONT PROPAGATION*

Boaz Nash, Dan Tyler Abell, Paul Moeller, Ilya V. Pogorelov,
RadiaSoft LLC, Boulder, Colorado
Nicholas Burke Goldring, STATE33 Inc., Portland, Oregon, USA

Abstract

X-ray beamlines are essential components of all synchrotron light sources, transporting radiation from the stored electron beam passing from the source to the sample. The linear optics of the beamline can be captured via an ABCD matrix computed using a ray tracing code. Once the transport matrix is available, one may then include diffraction effects and arbitrary wavefront structure by using that same information in a Linear Canonical Transform (LCT) applied to the initial wavefront. We describe our implementation of a Python-based LCT library for 2D synchrotron radiation wavefronts. We have thus far implemented the separable case and are in the process of implementing algorithms for the non-separable case. Rectangular apertures are also included. We have tested our work against corresponding wavefront computations using the Synchrotron Radiation Workshop (SRW) code. LCT vs. SRW timing and benchmark comparisons are given for undulator and bending magnet beamlines. This algorithm is being included in the Sirepo implementation of the Shadow ray tracing code. Finally, we describe our plans for application to partially coherent radiation.

INTRODUCTION

Linear Canonical Transforms (LCTs) [1, 2] are a class of integral transforms with applications in optics, quantum mechanics and signal processing. In the optical context, given an *ABCD* matrix representing a linear transformation in ray optics, the corresponding LCT transforms a coherent wavefront through that same optical system.

X-ray beamlines in synchrotron light sources transport the radiation from source to sample. Modeling with full wave optics and ray tracing is common during the design phase of a beamline, but less common during everyday operation. In order to develop a fast, simplified beamline model that one may use in combination with diagnostic measurements, we present the theory and implementation of the linear canonical transform. Although, true synchrotron radiation is only partially coherent, a coherent mode decomposition [3] may be performed and each mode propagated independently. We also work within a simplified framework we refer to as a *matrix-aperture beamline* [4]. Finally, we note that although many references describe fast LCT implementations, there exist, to our knowledge, no publicly available software libraries. Thus, our interest in developing such a library and herein documenting this work.

* This work is supported by the US Department of Energy, Office of Basic Energy Sciences under Award Number DE-SC0020593 and the Office of High Energy Physics under award number DE-SC0020931.

We start by presenting the theory and implementation of the 1D LCT, followed by the 2D separable case, constructed out of the 1D case. The non-separable 2D case remains for further development.

LINEAR CANONICAL TRANSFORMS IN ONE DEGREE OF FREEDOM

The *Linear Canonical Transform*, or LCT, of a function $f(u)$ is defined by the rule [1]

$$\mathcal{L}_M[f](v) = \mathrm{e}^{-\mathrm{i}\pi/4}\sqrt{\beta}\int_{-\infty}^{\infty} f(u)\,\mathrm{e}^{-\mathrm{i}\pi(\alpha v^2 - 2\beta uv + \gamma u^2)}\,\mathrm{d}u. \tag{1}$$

The properties of a particular LCT are determined by the associated 2×2 symplectic matrix

$$M = \begin{pmatrix} A & B \\ C & D \end{pmatrix} = \begin{pmatrix} \gamma/\beta & 1/\beta \\ \alpha\gamma/\beta - \beta & \alpha/\beta \end{pmatrix}, \tag{2}$$

which describes the ray optics of an arbitrary beamline.

One may represent many of the well-known integral transforms as special cases of the general LCT. These include the Fourier transform, the fractional Fourier transform, the Fresnel transform, chirp multiplication, and scaling (or magnification). Moreover, LCTs obey the very important *group property*

$$\mathcal{L}_{M_2} \circ \mathcal{L}_{M_1} = \mathcal{L}_{M_2 \cdot M_1}. \tag{3}$$

As a consequence, one may compute a given LCT as a composition of simpler LCTs: First decompose the matrix M defining a given LCT into a product of simpler symplectic matrices, each of which defines one of a few specific special cases: scaling, Fourier transform, or chirp multiplication. Then compose those transformations.

The *scaling* operation corresponds to the matrix

$$M_m = \begin{pmatrix} m & 0 \\ 0 & 1/m \end{pmatrix}, \tag{4}$$

with the corresponding LCT given by

$$\mathcal{M}_m[f](u) = \frac{1}{\sqrt{m}} f\Big(\frac{u}{m}\Big). \tag{5a}$$

For numerical work, we use the equivalent form

$$\mathcal{M}_m[f](m\cdot u) = \frac{1}{\sqrt{m}} f(u). \tag{5b}$$

If $m < 0$, then one must introduce a factor of i.

The *Fourier transform* corresponds to the matrix

$$F_{\mathrm{LC}} = \begin{pmatrix} 0 & 1 \\ -1 & 0 \end{pmatrix}, \tag{6}$$

ISBN: 978-3-95450-227-1 ISSN: 2673-5490 doi:10.18429/JACoW-IPAC2022-THPOTK001

VARIABLE PERMANENT HYBRID MAGNETS FOR THE BESSY III STORAGE RING

J. Völker*, V. Dürr, P. Goslawski, A. Jankowiak, M. Titze
Helmholtz Zentrum Berlin, Berlin, Germany

Abstract

The Helmholtz Zentrum Berlin (HZB) is working on the conceptual design of a successor source to BESSY II, a new BESSY III facility, designed for a beam energy of 2.5 GeV and based on a multi-bend achromat (MBA) lattice for a low emittances of 100 pm−rad. Bending and focusing magnets in the MBA cells should consist of permanent magnets (PM), to allow for a competitive and compact lattice, to increase the magnetic stability and to decrease the electric power consumption of the machine. However, using pure permanent magnet systems would result in a completely fixed lattice. Therefore, we are developing Variable Permanent Hybrid Magnets (VPHM), combining PM materials like NdFeB with a surrounding soft iron yoke and additional electric coils. This design can achieve the same field strength and field quality as conservative electromagnets, with only a small fraction of the electric power consumption, and a ca. 10% variability in the field amplitudes. With this magnet concept the power consumtion of the BESSY III storage ring can be reduced by more than 0.5 MW. In this paper, design and first optimization results of the magnets will be presented.

MAGNETS FOR BESSY III

The lattice of BESSY III is currently being optimized fulfilling the requirements for a fourth-generation light source with a kinetic beam energy of 2.5 GeV. For the current versions of arc lattices, the overall storage ring needs a circumference of ca. 340 m. Further beam parameter can be seen in Table 1 and in [1–5]. The fixed defined beam energy and the optimized lattice solution resulting in a narrow parameter range for all bending and focusing magnets. Based on the required high magnetic fields and the large number of magnets, the overall power consumption for the storage ring can be estimated to ≈ 750 kW for the magnetic systems in case of conservative electromagnets. Integrated over the 7000 hours beam operation per year, one gets an energy consumption of > 5 GWh per year.

Here, Permanent Magnets (PMs) are a real alternative not only for bending magnets like described in [6] or [7], but also for Quadrupole (QP) magnets, for a sustainable storage ring with a decreased energy consumption of up to 80% for the magnetic system. However, the PM based QP magnets should be adjustable in the range of ±10% of the maximum gradient, to assist the later commissioning and to have the option for small corrections. To build almost all linear magnets with PMs produces a high number of PM based magnets for the BESSY III storage ring (see Table 1)

Table 1: Important BESSY III Parameter

Parameter	Value
MBA lattice	6BA
# of arcs	16
circumference	340 m
kin. energy	2.5 GeV
emittance	≈ 100 pm rad
magnet aperture radius	12.5 mm
# of dipol magnets	96
# of quadrupole magnets	≈ 250
# of sextupole magnets	≈ 250

with a strong impact on the tooling and the handling of the PMs and the final magnets. Therefore, a general magnet and PM design is necessary to simplify PM tests as well as construction and tooling of the magnets.

PM DESIGN

The general idea is that the PM design in all magnets has to be as similar as possible. A promising technique is the magnetic bridge where the PM blocks are installed between the return yoke and pole shoes together with an Aluminum framework. Such a geometry is visualized in Fig. 1. The

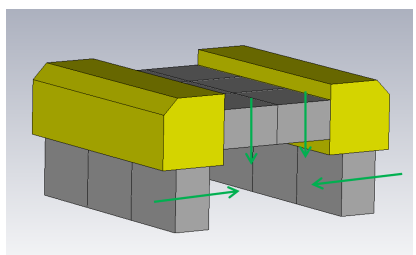

Figure 1: General design of magnetic bridge for all magnets. The PM blocks (grey) with shown magnetization axis (easy-axis = green) and aluminum holders (yellow).

Aluminum framework is used for the mechanical connection, the PM alignment as well as an option for later trimming and shimming of the PM blocks. Less individual PM blocks geometries and less equipment for the tooling and PM block tests will be necessary. This design was used for numerical calculations and optimizations of several concepts for dipole and quadrupole magnets.

CACULATION TOOLS

For the calculation of the PM based bending and focusing magnets three different 3d field solver tools were tested:

* jens.voelker@helmholtz-berlin.de

ISBN: 978-3-95450-227-1 ISSN: 2673-5490 doi:10.18429/JACoW-IPAC2022-THPOTK002

MAGNET DESIGN FOR THE PETRA IV STORAGE RING

I. Agapov, A. Aloev†, R. Bartolini, H.-J. Eckoldt, D. Einfeld, B. Krause,
A. Petrov, M. Thede, M. Tischer, DESY, Hamburg, Germany
J. Chavanne, ESRF, Grenoble, France

Abstract

The proposed PETRA IV electron storage ring that will replace DESY's flagship synchrotron light source PETRA III will feature a horizontal emittance as low as 20 pmrad. It is based on a hybrid six-bend achromat lattice. In addition to the storage ring PETRA IV, the Booster Synchrotron and the corresponding transfer line will be renewed.

Overall about 4000 magnets will be manufactured. This contribution presents the electromagnetic design of the magnets for the storage ring.

INTRODUCTION

DESY is currently producing the Technical design for the PETRA IV upgrade [1] with the aim of replacing the existing PETRAIII ring with a new ultra-low emittance storage ring based on a modified H6BA lattice [2]. The new storage ring will be built in the same tunnel 2.3 km long with the eight octants structure of the original PETRA collider. The nominal emittance of 20 pm is achieved by a using a H6BA cell structure repeated nine times per octant and the extensive use of damping wigglers in five of the eight octants of the ring. The basic cell is based on a quadrupole triplet at each end to control the optics function at the straight sections, on six combined function bending magnets and two dispersions bumps at π degrees phase advance to control the chromaticity correction. Octupoles are used to control the nonlinear beam dynamics. In total each cell hosts two longitudinal combined-function dipoles, four combined-function dipoles, 17 quadrupoles, 6 sextupoles, and 7 correctors. A layout of the H6BA cell with the location of the magnet is shown in Fig. 1

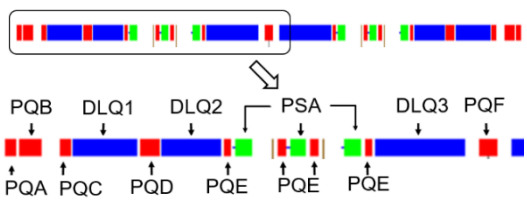

Figure 1: location of the magnetic element in the H6B cell: quadrupoles (red), sextupoles (green), dipoles (blue).

The dipoles will be built with permanent magnets while all the other magnets will be resistive. That reduces overall power consumption of the magnets to 1.2 MW. In this paper we report the current status of the design of the main magnetic elements highlighting the main challenges.

NORMAL CONDUCTING MAGNETS

Quadrupole Magnets

The PETRA IV lattice requires relatively high gradient quadrupoles to control the optics function in particular at the triplet of the straight sections. The main parameters of the quadrupoles are reported in Table. 1 with the corresponding field quality specifications provided by beam physics simulations. Significant effort has been put not only in providing the required field quality at high gradients, but also in minimising the power consumption.

The PQA, PQB, PQD and PQE quadrupole families would be unfeasible with conventional yoke material, such as Armco, due to the yoke saturation, caused not only by high gradients, but also by short magnet lengths. In order to reach the required gradient values and to reduce power consumption, these magnets were designed with pole tips, made of high permeability material (Vacoflux 50) and the rest of the yoke with Armco. This approach had been implemented and tested in APS-U magnets [3].

Table 1: Parameters of Designed PETRA IV Quadrupoles

Type	PQA	PQB	PQC	PQD	PQE	PQF	PQH
Gradient, T/m	115	112	86	97	91	83	86
Magnetic length, mm	169	345	161	280	110	250	300
Aperture radius, mm	11.0	11.0	12.5	12.5	12.5	12.5	12.5
Pole to pole clearance, mm	8.8	8.8	10.0	11.0	10.0	10.0	10.0
GFR, mm	6.5	6.5	7.9	7.9	7.9	7.9	7.9
Field harmonics $\sqrt{\Sigma b_n^2}$	$< 5\times10^{-4}$						
Operational gradient range, %	± 5 %						
Power, kW	0.9	1.4	0.7	1.6	0.7	0.9	1.2
Quantity	128	128	128	144	576	86	14

Even with the high-permeability pole tips, the PQA and PQB aperture radius had to be reduced from 12.5 to 11.0 mm. PQB quadrupole power loss would be 2.4 kW with laminated Powercore 1400 yoke and is only 1.4 kW with Vacoflux 50 pole tips.

Yoke geometries were optimised to maximise the gradients and the field quality and at the same time to minimise volume of the high-permeability poles. Due to short length of the magnets, transverse cross-sections were optimised

† alexander.aloev@desy.de

ISBN: 978-3-95450-227-1 ISSN: 2673-5490 doi:10.18429/JACoW-IPAC2022-THPOTK003

OPTIMIZATION OF MASS RESOLUTION PARAMETERS COMBINED WITH ION COOLER PERFOMANCE

M. Cavenago*, C. Baltador, L. Bellan, M. Comunian, E. Fagotti, A. Galatà,
M. Maggiore, A. Pisent, C. Roncolato, M. Rossignoli, A. Ruzzon, INFN-LNL, Legnaro, Italy
V. Variale, INFN-BA, Bari, Italy; G. Maero[1], M. Romé[1], Univ. Studi di Milano, Milano, Italy
[1]also at INFN-MI, Milano, Italy

Abstract

High resolution mass spectrometers (HRMS) for separation of exotic ion species in nuclear physics experiments request a low emittance and small energy spread (with ΔE the peak-to-peak value, and σ_E the rms value) for the input beam, so that ion cooler devices, as Radio Frequency Quadrupole Coolers (RFQC), are typically envisioned. The SPES (Selective Production of Exotic Species) project at LNL requests $M/\Delta M \cong 20000$, rms normalized emittance ϵ_x^N in the order of 2 nm (see definitions later), and in the case of 160 keV ions, $\sigma_E \cong 1$ eV. The relevant collisional data are reviewed, in particular for Cs^+ against He, whose pressure ranges from 3 Pa to 9 Pa, in Milan test bench optimization. Practical consideration on gas pumping, voltage stability σ_{Va} and magnet design are also included. Typical limits of RFQC and HRMS performances are discussed, and relevant formulas are implemented in easy reference tools.

INTRODUCTION

Cooling [1,2] of secondary beams is often necessary to accelerator based nuclear and sub-nuclear physics, with beams ranging from exotic nuclei ions (like $^{132}Sn^{1+}$), as in the SPES (Selective Production of Exotic Species [3,4]) project at LNL, to positrons e^+, muons $\mu^\pm$ [5] and antiprotons, for the respective collider facilities. In the latter cases, emittance reflects the phase space necessary to decay and/or efficient production reactions; so transverse momentum is large, also exceeding the MeV/c range. In SPES project a conveniently limited H^+ primary beam (from a cyclotron) induces fission reactions in a hot target, with products first stopped into the target, then diffused and singly ionized in sources IS of several kinds [6,7], which have to cope with the heat and radiation produced by the primary beam; so source voltage and ion kinetic energy K_i are limited, say $K_i \cong 40$ keV. Emittance and rms energy spread σ_{E1} of the secondary beam depend on source kind; we consider the worst case of plasma sources: we have $\sigma_{E1} \cong 5$ eVrms (so much smaller than $\mu^\pm$ one), which allows beam transport to a (less-shielded) re-accelerator; total current can be reduced to < 25 nA by a suitable Wien filter. Anyway, this beam still contains many nuclear species, so that most experiments require a High Resolution Mass Spectrometer (HRMS) [8], whose design relies on colder beams, as obtained in so-called coolers, for example a Radio Frequency Quadrupole (RFQ) Cooler (RFQC) [2], see Fig. 1.a.

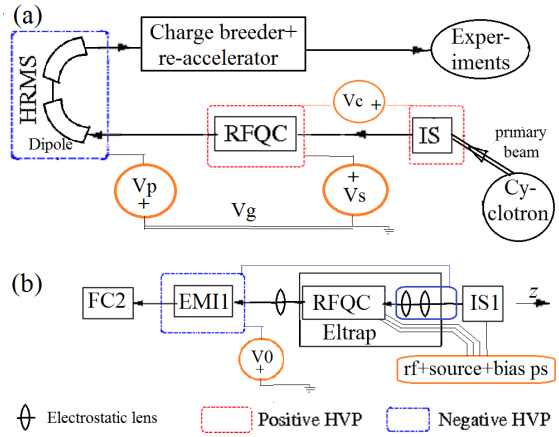

Figure 1: Block diagrams (not to scale) of: (a) interdependence of ion source IS, cooler and HRMS, as a zoom in the SPES project; (b) ion source IS1, cooler and emittance meter EMI1 in the Eltrap machine; beam stops at Faraday cup FC2. Some power supplies (ps) are sketched.

Cooling of particles X (that is the reduction of the momentum variance of ion population) is accomplished with two opposing processes, one involving collisions where particles X exchange energy and momentum with a colder beam [9] or gas, the other is a reacceleration, where all X particles receive an equal additional energy (by small bias voltages V_i^s in our case). A condition for cooling is that faster X particles loose more energy than slower ones in collisions; to obtain this, careful design, simulations and experimental verification of coolers are required.

OVERVIEW OF MAJOR COMPONENTS

In an RFQC [10–12], which is a kind of linear ion trap, ions are decelerated, and enter inside a gas cell, typically filled with He at a pressure from $p_g = 3$ Pa to 9 Pa, which contains an RFQ with rods divided in N sections; so ions are slowed down by this buffer gas and are confined by the RFQ voltages; the RFQC is usually enclosed in a box, at a voltage V_s with respect to ground, to maintain the gas pressure. By applying adequate drift voltages V_i^s (from 10 V to 100 V, respect to that box) to the RFQC sections $i = 1, \ldots, N$, ions are reaccelerated to one box end, where they are extracted. A previous LNL RFQ test prototype (with $N = 10$ sections [2,6]) was installed into the Eltrap facility (a Penning-Malmberg trap with a 1.5 m long solenoid) at Milan University, see Fig 1.b, to study the combined confinement

* cavenago@lnl.infn.it

ISBN: 978-3-95450-227-1 ISSN: 2673-5490 doi:10.18429/JACoW-IPAC2022-THPOTK004

THE REDUCTION OF THE LEAKAGE FIELD OF THE INJECTION SEPTUM MAGNET IN MAIN RING OF J-PARC

T. Shibata*, N. Matsumoto, K. Ishii, T. Sugimoto, H. Matsumoto, KEK, Tsukuba, Japan

Abstract

A new injection septum magnet 1 (Inj-SM1) was installed in the Main Ring (MR) of J-PARC in 2016 as an upgrade. We confirmed that the leakage field upstream from the circulating duct of Inj-SM1 was sufficiently smaller than that for the previous Inj-SM1. Nevertheless, we attempted to further reduce the leakage field by using a new magnetic shield to achieve a higher proton beam intensity. In 2017, the first version of the new magnetic shield was produced and installed. The strength of the leakage field with the shield was ≈30% of that without the shield; however, the magnetic field of a quadrupole magnet (QM) upstream of Inj-SM1 was reduced to below the permissible limit, ≈0.1% of the total field integral of the QM, from the point of view of beam optics. Consequently, the first version failed. A second shield, for which the defects of the first version were fixed, was produced in 2018. The strength of the leakage field of Inj-SM1 with the second shield was reduced to ≈30% of that without the shield, while that of the QM was maintained. Thus, we decided to use the second shield for beam operation starting in November 2019. We confirmed that the impact of the leakage field on the circulating beam was 1/20 of that of the previous Inj-SM1.

INTRODUCTION

The J-PARC Main Ring (MR) provides a high-intensity proton beam with an energy of 30 GeV to the neutrino facility [1] or the hadron facility [2]. The present operation cycle is 2.48 s and the maximum beam power to the neutrino facility is 515 kW, which was achieved in March 2021 [3]. To realize the original design value of 750 kW, we will start the operation of the MR with a cycle of 1.3 s in June 2022; this is referred to as 1-Hz operation. The cycle will be further reduced to 1.16 s by 2028 to increase the beam power to 1.3 MW [4]. Over the last decade, the injection magnets in the MR have also been upgraded for 1-Hz operation and a 1.3-MW beam. The high-field injection septum magnet 1 (Inj-SM1), which has a typical field strength of 1.4 T, is used for injecting the proton beam from the rapid cycling synchrotron into the circulating orbit in the MR. The first Inj-SM1 started operation in 2008 (start of the J-PARC MR) and was replaced with the new septum magnet for 1-Hz operation in 2016 [5, 6]. The replacement of the magnet was conducted because it was extremely difficult to further reduce the leakage field of ≈20 gauss around the entrance and exit of the circulating beam duct beside the septum plate. The reduction of the leakage field is an important target for the new septum magnet.

* tatsunobu.shibata@j-parc.jp

MEASURES AGAINST LEAKAGE FIELD IN 2015-2016

To minimize the leakage field, magnetic shields, vacuum chambers made of magnetic stainless steel [7], or an eddy current can be used to cancel the leakage field [8–10]. To reduce the leakage field of Inj-SM1, we applied several magnetic shields made of pure iron. The most significant contribution to the leakage field is from an end coil at the beam exit because it is located very close by the circulating beam line. To reduce the leakage field, we covered the entire end coil by a magnetic shield made of silicon-steel (field clamp) (Fig. 1 (top)). This reduced the leakage field to a few gauss [5, 6]. The second most significant contribution is the leakage field that passes through the septum plate. An ideal septum magnet has zero leakage on the outside of the septum plate; however, an actual septum magnet has a small leakage with an order of magnitude that is 0.1% of the gap field. For example, for a gap field of 1.4 T, the strength of the leakage field is ≈14 gauss. Therefore, we covered the circulating duct beside the septum plate by two magnetic shields made of pure iron (outer shields 1 and 2) (Fig. 1 (bottom)). Furthermore, we fabricated a 5-mm-thick circulating duct made of pure iron, which had a dc permeability of ≈8000 emu, in March 2016 [6] (Fig. 1 (bottom)), We measured the time-dependent field integral (BL) of the leakage field along the beam axis in the circulating duct with an applied current of 2,700 A, which is close to the optimal current for beam operation (2,590 A). The maximum value of BL during 0.2 s from the start of beam acceleration was 2 gauss·m. The bend angle of the circulating beam caused by the leakage field was then measured with the 3-GeV circulating beam in December 2016. Based on the measured angle, we obtained a BL value of ≈2.5 gauss·m, which is consistent with the field measurement [6]. The BL of the leakage field of the first Inj-SM1 was ≈30 gauss·m [11], which is 10 times greater than that of the second Inj-SM1. Because our ultimate target for the leakage field is zero gauss·m, we attempted to further reduce the leakage field.

REDUCTION OF LEAKAGE FIELD IN 2017

There was a leakage field of ≈9 gauss upstream from the pure iron circulating duct, where no shield was mounted and the circulating ducts were made of non-magnetic stainless steel [6] (Fig. 2). The origin of the field was the end coil at the injection beam entrance of Inj-SM1. Unfortunately, it was impossible to cover the end coil by a field clamp because of a lack of space. In addition, we could not cover the stainless steel circulating ducts by a magnetic shield because the magnetic field in the circulating ducts includes not only the field of Inj-SM1 but also that of a quadrupole magnet (QM)

ISBN: 978-3-95450-227-1 ISSN: 2673-5490 doi:10.18429/JACoW-IPAC2022-THPOTK005

THE NEW HIGH FIELD SEPTUM MAGNET FOR UPGRADING OF FAST EXTRACTION IN MAIN RING OF J-PARC

T. Shibata*, K. Ishii, S. Iwata, T. Sugimoto, N. Matsumoto, H. Matsumoto, KEK, Tsukuba, Japan
K. Fan[1], HUST, Wuhan, China

Abstract

The upgrade of the beam power of J-PARC Main Ring to 750 kW by reducing the cycle from 2.48 s to 1.3 s is underway, and the upgrade of the four high-field (HF) septa will be completed by summer of 2023. The operation test of one HF septum, SM31, was conducted in 2020. First trial was 1 Hz operation test, and we confirmed the joule heating at the magnetic coil was lower than limit. Second was magnetic field measurement. We obtained a good linearity between the applied current and the gap field without saturation. The field integral of the gap field was measured to estimate the optimal current for beam extraction, and we found it is 3,400 A. We compared the gap field between in the neutrino line and that in the beam abort line, then we found the longitudinal distributions have a small discrepancy but it was acceptable. The large leakage field was observed around the end-fringes, therefore, in order to reduce the leakage field, we produced an additional duct shield for mounting in the circulating duct in 2022. We verified that the additional duct shield reduced the leakage field to ≈2% of unshielded leakage field. The new SM31 and other two HF septa have been installed in MR by end of May 2022. The beam operation with the new HF septa will be started in June 2022.

INTRODUCTION

The J-PARC Main Ring (MR) provides the high-intensity proton beam with an energy of 30 GeV to the neutrino facility (NU) or the hadron facility. The present operation cycle is 2.48 s and the maximum beam power for Fast eXtraction mode (FX) is 515 kW which was achieved in March 2021 [1]. To realize original design value of 750 kW, we are going to start operation of MR with the cycle of 1.3 s, it is referred to as "1 Hz operation"; moreover, the cycle will be shorten to 1.16 s for increasing the beam power to 1.3 MW by 2028 (1.3MW beam) [2]. The magnets for FX in MR, which are used for switching the proton beam direction to NU or abort dump (ABT) [3], also have been upgrading for 1 Hz operation and 1.3 MW beam, and will be completed by summer of 2023. The four high-field septum magnets (SM) with magnetic field of above 1 T are used, and these magnets are called SM30, SM31, SM32 and SM33 from upstream. To upgrade, the replacement of these septa with new ones is underway. We produced the new septa in 2015, and conducted the operation test of the new SM30 and measured its magnetic field at first in 2018-2019 [3, 4]. Next, we conducted the test operation of the new SM31 in autumn 2020. The aim of the operation test was 1 Hz operation and measurement of the gap field and leakage field. After operation test, two large-sized vacuum flanges made of pure Titanium were weld to the vacuum ducts of the new SM31 in November 2020. In 2021, we produced two additional duct shields which can be mounted in the circulating duct of the new SM30 and SM31 in order to reduce the leakage field further. Regarding the new SM32, unfortunately, the installation in MR was postponed because of a fatal defect in the magnetic coil found in 2021. The new SM33 have been reconstructed with the new beam ducts and removed magnetic cores of SM32 and SM33. The installation of the new SM30, SM31 and SM33 in MR have been completed in May 2022 (Fig. 1). The beam operation with new cycle is going to be started in June 2022. This article focuses on the new SM31. The new SM31 is a bipolar septum magnet as same as the new SM30 [4]. Figure 2 shows the photograph, the specification and applied pattern current of the new SM31. The detail of the operation test in 2020 and the reduction of the leakage field by using the additional duct shield in 2022 will be described.

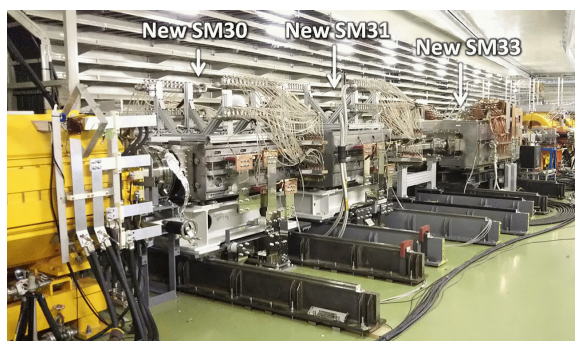

Figure 1: The high-field septa installed in MR in May 2022.

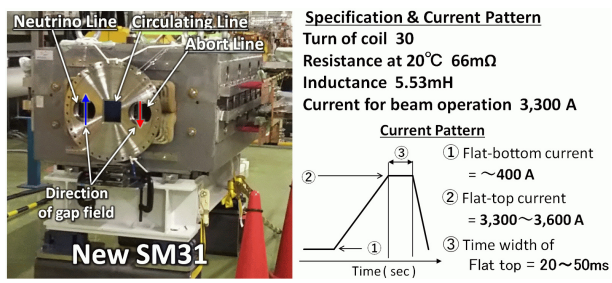

Figure 2: The photograph, the specification and the applied pattern current of the new SM31.

1 Hz OPERATION TEST

In the 1 Hz operation test, the operation cycles which we tested were 1.32 s, 1.28 s and 1.16 s, and the flat-top current

* tatsunobu.shibata@j-parc.jp

ISBN: 978-3-95450-227-1 ISSN: 2673-5490 doi:10.18429/JACoW-IPAC2022-THPOTK007

MAGNET SYSTEMS FOR KOREA 4GSR LIGHT SOURCE*

D. E. Kim†, Y. G. Jung, H. S. Suh, H. G. Lee, G. Hahn, T. G. Ha, J. Lee, S. S. Shin,
Pohang Accelerator Laboratory, POSTECH, Pohang, KyungBuk, Republic of Korea

Abstract

A 4th generation storage ring based light source is being developed in Korea since 2021. It features < 100 pm rad emittance, about 800 m circumference, 4 GeV e-beam energy, full energy booster injection, and more than 40 beamlines which includes more than 24 insertion device (ID) beamlines. This machine requires about 1000 magnets including dipole, longitudinal gradient dipole, transverse gradient dipole, sextupoles, and correctors. The apertures are small and the lattice space requirements are very tight. In this report, a preliminary design of the each magnet is presented with detailed plan for the future.

INTRODUCTION

Third generation storage ring based light sources have been used as a bright light source for many years. Recently multi-bend achromat (MBA) lattice presents a further decrease in the electron beam emittances and becoming a new standard for next generation light source like MAX-IV in Swden, ESRF-EBS in France, SIRIUS in Brazil. Many other laboratories are also preparing their own version of 4th generation light sources. In this context, Korea is trying to build a 4th generation light source (Korea-4GSR) based on modified hybrid multi-bend achromat lattice (MHMBA). The Korea fourth-generation storage ring (Korea-4GSR) adopt H7BA considering better nonlinear beam dynamics compared to the conventional 7BA and lower emittance compared to MH6BA [1].

We reiterate simple representation of magnet higher order components to evaluate the calculated magnetic field. Using Habach convention [2], for 2-dimensional magnet which has a longer magnetic length compared to the gap, we can write the complex potential $F = A + iV$ and expand it as a series of $z = x + iy$ as

$$F = A(x,y) + iV(x,y) = \sum_{n=1}^{\infty} c_n \frac{z^n}{r_0^n} = \sum_{n=1}^{\infty} c_n \frac{(x+iy)^n}{r_0^n}. \quad (1)$$

Here, A is a vector potential, and V is a scalar potential for the magnetic field satisfying Cauchy-Riemann conditions. Using the complex potential, transverse magnetic field can be expressed as

$$B_x - iB_y = i\frac{dF}{dz} = \sum_{n=1}^{\infty} \frac{inc_n}{r_0}\left(\frac{z}{r_0}\right)^{n-1} = \sum_{n=1}^{\infty} \frac{inc_n}{r_0}\left(\frac{x+iy}{r_0}\right)^{n-1} \quad (2)$$

We can write $c_n = a_n + ib_n$, where b_n is the skew components of the magnet, while a_n is a normal component of the magnet.

In terms of a polar coordinate $z = x + iy = re^{i\theta}$, we can express the $B_y(\theta)$ along the radius r as

$$B_y(r,\theta) = \sum_{n=1}^{\infty} \frac{-na_n}{r_0}\left(\frac{r}{r_0}\right)^{n-1} \cos((n-1)\theta) \quad (3)$$

Please note that in this indexing scheme, $n = 1$ is dipole, $n = 2$ is quadrupole, $n = 3$ is a sextupole components. In analyzing a magnet, we calculate the B_y along a circle at a slice (usually 1 mm thick) and decompose it according to Eq. (3) to analyze the longitudinal dependence of a multipole content.

MAGNET SYSTEM

Longitudinal Gradient Magnet

In most types of 4GSR based light sources, longitudinal gradient magnet is routinely used to achieve low bending field in high dispersion area. APS-U [3] tried a continuous gap longitudinal gradient magnet, and also stepped field and finally opted for stepped magnetic field distribution. There are two options in achieving the design stepped field. One option can be a permanent magnet (PM) based distribution like ESRF-EBS [4], and other option can be electromagnetic magnet excitation. PM excitation has an advantage of compact magnet size, and nearly zero operating energy costs. However, there is a possibility of long term degradation (although small) due to the radiation damage, higher manufacturing costs, and lack of tunability. ESRF-EBS is adopting Sm_2Co_{17} for their longitudinal gradient magnet which shows minimal radiation damage. APS-U design is based on the electromagnetic excitation. It has advantages in simpler construction, lower construction costs, and tunability. We opted for electromagnet excitation for our baseline

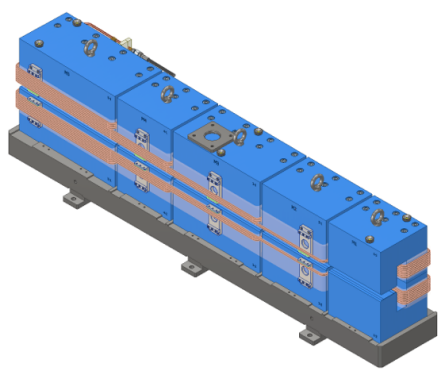

Figure 1: L3D design of LGBM1 magnet.

design considering the advantages. The 2D optimization is calculated using simple trapezoidal shims, and integrated uniformity for each segment is calculated to estimate the

* Work supported by MOST of Korea
† dekim@postech.ac.kr

ISBN: 978-3-95450-227-1 ISSN: 2673-5490 doi:10.18429/JACoW-IPAC2022-THPOTK009

DESIGN OF A PERMANENT MAGNET BASED DIPOLE QUADRUPOLE MAGNET*

A. G. Hinton†, B. J. A. Shepherd, STFC Daresbury Laboratory, Warrington, UK
A. Shahveh, Diamond Light Source, Oxfordshire, UK
M. Kokole, T. Milharcic, Kyma Srl, Trieste, Italy

Abstract

Permanent magnet technology can facilitate the design of accelerator magnets with much lower power consumption than traditional resistive electromagnets. By reducing the power requirements of magnets, more sustainable accelerators can be designed and built. At STFC, as part of the I.FAST collaboration, we are working to develop sustainable technologies for future accelerators. As part of this work, we have designed a permanent magnet based dipole-quadrupole magnet with parameters suited to meet the requirements of the proposed Diamond-II upgrade. We present here the magnetic design, which is based on a single sided dipole-quadrupole. The design includes the shaping of the pole tips to reduce multipole errors as well as methods of providing thermal stabilisation and field tuning. The mechanical design of the magnet is being undertaken by colleagues at Kyma and a prototype of the magnet will soon be built and tested.

INTRODUCTION

The I.FAST collaboration [1] aims to boost innovation in the particle accelerator community. A core theme of the collaboration is the development of more sustainable concepts and technologies. Magnets provide one of the largest sources of power consumption in modern accelerators. For instance, the dipoles and quadrupoles for the proposed Compact Linear Collider (CLIC) would dissipate an estimated 29.4 MW due to electrical resistance alone [2]. Therefore, if traditional electromagnets can be replaced by permanent magnets, future accelerators may be made to require less power and be more sustainable.

Table 1: Summary of Magnetic Design Requirements

Parameter	Value	Units
Central Dipole	-0.6951033	T
Central Gradient	32.3974035	T m^{-1}
Good Field Radius	7	mm
Field Quality ΔB/B	$5x10^{-4}$	
Gradient Quality ΔG/G	$1x10^{-3}$	
Integrated Dipole	0.6047	T.m
Integrated Gradient	28.1857	T
Integrated Multipoles	$<10^{-3}$	

The proposed Diamond-II upgrade will utilise multibend-achromat technology and an increase in electron beam energy to achieve gains in the brightness and coherence of the synchrotron radiation produced by the facility [3]. The lattice design relies upon the use of combined function dipole-quadrupole (DQ) magnets with high gradients to simultaneously bend and focus the beam. An electromagnetic DQ has been previously designed to meet the Diamond-II requirements. However, an alternative design, using permanent magnets as the main source of magnetic field (PMDQ) has been designed to demonstrate how the same magnetic field requirements can be met at reduced power consumption. The main magnetic requirements are summarised in Table 1.

DESIGN OVERVIEW

The design of the PMDQ is based on a single-sided electromagnetic combined function magnet [4]. This single sided design has been shown to produce larger gradients than traditional gradient dipole designs and is more efficient than an offset quadrupole [4]. Given the high field gradient that is required, a gradient dipole design would not have been suitable. A labelled image of the magnetic model of the PMDQ, generated using Opera 3D simulation software [5], is shown in Fig. 1. The different colours represent different materials and parts of the design. The thick black arrows indicate the direction of magnetisation of the permanent magnets.

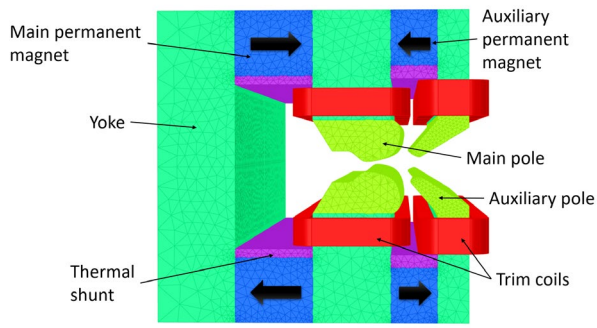

Figure 1: Labelled image of Opera 3D PMDQ model.

The primary source of the fields are permanent magnets, rather than current carrying coils. Therefore, the power and cooling requirements of the magnet can be greatly reduced.

The large magnet blocks shown in Fig. 1 will be split into carriages containing arrays of smaller magnets in order to ease the handling of the permanent magnet material. The blocks will be arranged with the magnetisation axes aligned horizontally in order to generate the desired combined function field in the bore.

The material and grade of magnet used in the design was Neodymium Iron Boron (NdFeB) grade 40EH from ZHmag [6]. The magnet grade was chosen to have a high

* Work supported by funding from the I.FAST collaboration
† alex.hinton@stfc.ac.uk

ISBN: 978-3-95450-227-1 ISSN: 2673-5490 doi:10.18429/JACoW-IPAC2022-THPOTK010

DEVELOPMENT OF A SHORT PERIOD SUPERCONDUCTING HELICAL UNDULATOR*

A.G. Hinton†, B.J.A. Shepherd, N. Thompson, STFC Daresbury Laboratory, Warrington, UK
J. Boehm, L. Cooper, B. Green, T. Hayler, P. Jeffery, C. Macwaters, B. Matthews,
STFC Rutherford Appleton Laboratory, Didcot, UK
S. Milward, Diamond Light Source, Oxfordshire, UK

Abstract

Superconducting undulators (SCUs) with short period and small magnetic gap have the potential to generate larger magnetic fields than alternative technologies. Implementing SCUs on future x-ray free electron laser (XFEL) facilities will allow a broader range of photon wavelengths to be generated. At STFC, we have undertaken work to design and build a prototype helical superconducting undulator (HSCU) module with parameters suitable for use within a future XFEL facility. This work includes the design of an undulator with 13 mm period and 5 mm magnetic bore diameter, as well as the supporting cryogenic and vacuum systems required for operation. Mechanical tolerances on the HSCU have been simulated to investigate the effect on the performance of the undulator. The fields produced by prototype undulators will soon be measured using a Hall sensor system to verify that the wound formers are within acceptable tolerances.

INTRODUCTION

At STFC, we are developing the design of a superconducting helical undulator with 13 mm period and 5 mm magnetic bore gap aimed at producing photons in the energy range 8-16 keV from a 5.5 GeV electron beam from a peak on-axis field of 1.09 T [1]. The use of high performance HSCUs and the corresponding parameters were defined to maximise the photon energy and peak FEL brilliance for an electron beam energy lower than those available at current FEL facilities [2].

The performance of an XFEL facility using this HSCU design is partly limited by the field quality produced by the undulators [3]. Errors in the field will reduce the radiated output power of the facility. The field quality will be limited by the mechanical tolerances on the manufacture and winding of the HSCU. An Opera 3D [4] model of the HSCU has been used to simulate how these mechanical tolerances affect the field quality.

Methods for manufacturing the magnet formers and winding the superconducting wire have been advanced to reduce the tolerances in order to improve the undulator field quality and FEL performance.

TOLERANCE MODELLING

There are two main mechanisms by which the undulator performance can be degraded that have been considered: the trajectory errors of the electron beam through the undulator and the root mean square (rms) peak-to-peak field deviation. Numerical simulations using Genesis 1.3 [5] have been used to define how the trajectory wander and field deviation will affect the degradation of the FEL output power for a 5.5 GeV electron beam generating 16 keV photons from a self-amplified spontaneous emission (SASE) line [3] comprised of HSCUs.

Trajectory Errors

In an ideal undulator, the electron beam will travel parallel to, and centred on, the axis of the undulator. This will ensure the radiation produced in the undulator overlaps the electron beam so that the two can interact via the SASE process and produce bright synchrotron radiation. If the radiation and electron beams overlap poorly then the process is weaker and the radiated power from the undulator will be reduced. Genesis simulations indicate that the power loss caused by trajectory errors can be kept below 10% if the trajectory error is less than 5 μm.

Local field errors in the undulator can result in the field integrals being non-zero. This will manifest as trajectory errors through the undulator. These errors can come as a result of manufacturing or winding tolerances. However, the trajectory of an electron through a non-ideal undulator can be influenced by dipole correction coils at either end of the undulator. It has been shown that correction coils will be required at either end of the undulator to correct for the kick to the electron beam caused by the wire turnaround periods [1]. These coils can also be used to correct for trajectory errors through the undulator caused by local field errors.

The first and second field integrals through an undulator are directly proportional to the exit angle and displacement, respectively, of an electron that has travelled through the device [6]. If the measured first and second field integrals through an undulator are non-zero, the corrector coils currents can be set to minimise the field integrals. This results in the exit angle and displacement of the electron beam being minimised, but also reduces the trajectory error significantly by minimising any net kick to the electron beam. Figure 1 shows an example of this. The plot shows the modelled trajectory of a single electron in the vertical plane through a 1.1 m long HSCU with a ±50 μm tolerance on the pitch and groove depth of the former (black). The trajectory error is larger than the specified 5 μm. However, with the corrector coils activated, the trajectory error is maintained within a 2 μm window of the axis (red). This has been shown for multiple models with former manufacturing tolerances up to ±50 μm. As this is a considerably larger tolerance than can be achieved, it has

* Work supported by funding from STFC
† alex.hinton@stfc.ac.uk

ISBN: 978-3-95450-227-1 ISSN: 2673-5490 doi:10.18429/JACoW-IPAC2022-THPOTK011

PERMANENT MAGNETS FOR THE CEBAF 24 GeV UPGRADE*

S.J. Brooks†, Brookhaven National Laboratory, Upton, NY, USA
S.A. Bogacz, Thomas Jefferson National Accelerator Facility, Newport News, VA, USA

Abstract

An upgrade of the CEBAF facility to double its present energy of 12 GeV has been proposed [1, 2]. To provide double the number of linac passes using the existing five stacked arc beamlines, some beamlines are replaced by fixed-field accelerator (FFA) arcs, allowing multiple energies to pass through the same magnets. A solution is presented in which two of the existing electromagnetic beamlines are replaced with permanent magnet non-scaling FFA arcs, as demonstrated at CBETA [3–5]. The two-stage design reduces peak magnetic field and synchrotron radiation loss compared to using a single stage. FFAs do not pulse their magnets, making permanent magnets a promising and power-efficient technology option. However, the magnetic field requirements are still at the high end of accelerator permanent magnets produced thus far (1.6 T peak on beam), while the magnets must also be combined-function, having a gradient with a dipole offset. Designs using a novel oval aperture and open midplane within an adapted Halbach magnet are presented.

ENERGY RANGES AND STAGES

The 1090 MeV energy gain of the present CEBAF linacs is not increased in this study, although the injector energy is assumed to be upgraded from 123 MeV to 650 MeV. This is because the same set of linac quadrupoles focusses all transmitted beam energies, so the ratio of maximum-to-minimum beam energy in the first linac should not get too large. The easiest way to do this is to raise the injector energy; it may be done by running the present injector at 110 MeV and adding a two-pass conventional loop through three 90 MeV RF modules, giving $110 + 2 \times (3 \times 90) = 650$ MeV. This is a simplification of the option explored previously in [1].

CEBAF at present has five stacked 180° electromagnetic arcs on either side of the oval-shaped facility and this paper explores replacing either one or two of the highest energy lines by FFA arcs. Limited vertical space in the CEBAF tunnel makes it difficult to add a sixth line of any sort, so each multi-pass FFA removes an electromagnetic line. To double the energy, the total arc passes on each side of the machine is increased from 5 to 11, remembering the final linac pass after all the arcs boosts the energy by an additional 'half turn' (~1 GeV) and the synchrotron radiation loss at higher energy removes about the same. The resulting numbers of arc passes and energy ranges are given in Table 1.

There is significant overlap between the FFA1 and FFA2 energy ranges because CEBAF physics requires a continuously-tunable energy range. In the electromagnetic lines this is accomplished by scaling the magnet currents with the linac energy gain. The FFAs are made of permanent magnets, so must accommodate any energy from any linac setting. Letting the linac energy range from 925–1090 MeV provides enough adjustment that the lowest possible energy of one FFA turn always coincides or overlaps with the highest energy of the previous turn, but this lowers the lowest energy of the FFA2 arc to below the FFA1 maximum.

Table 1: Energy Ranges of Electromagnetic and FFA Lines

Number of FFA Stages	E/M passes	FFA1 passes	FFA2 passes
None (current)	5	—	—
One	4	7	—
Two (4+4)	3	4	4
Two (5+3)	3	5	3
Energy ranges (GeV)			
None (current)	1.2–11	—	—
One	1.5–9.4	8.9–23	—
Two (4+4)	1.5–7.2	7.1–16	14–23
Two (5+3)	1.5–7.2	7.1–18	16–23

ARC CELL CONSTRAINTS

An optimisation was performed to try and find arc cells with minimal maximum field on any energy's closed orbit centroid. The constraints are given in Table 2.

Table 2: Constraints on FFA Arc Cell Optimisation

Parameter	Value	Unit
Cell angle	2	° clockwise
Radius of curvature	80.6	m
⇒ Cell length	2.81347	m
Both drift lengths	0.1	m
⇒ Packing factor	0.929	
Maximum tune	0.425	cycles/cell
Minimum tune	0.025	in either plane

The cell lattice is BF-O-BD-O using combined function magnets in all cases. The allowable cell tune range is generous to allow the full energy range from linac adjustment.

ARC CELL LATTICES

The parameters of the resulting optimised lattices, for all three options (and both FFAs for the options that have two FFAs), are shown in Table 3. The 'reference energy' implies a beam rigidity ($B\rho$) that can be used to derive the central dipole field given each magnet's bend angle and length.

* Work supported by Brookhaven Science Associates, LLC under Contract No. DE-SC0012704 with the U.S. Department of Energy.
† sbrooks@bnl.gov

ISBN: 978-3-95450-227-1 ISSN: 2673-5490 doi:10.18429/JACoW-IPAC2022-THPOTK013

COLD TEST RESULTS OF THE FAIR SUPER-FRS FIRST-OF-SERIES MULTIPLETS AND DIPOLE

A. Chiuchiolo, P. Kosek, F. Greiner, A. Beaumont, K. Sugita, E. Cho, H. Mueller, M. Michels, Y. Xiang, F. Wamers, C. Roux, V. Velonas, M. Winkler, H. Simon, GSI, Darmstadt, Germany
H. Allain, A. Madur, V. Kleymenov, CEA-Saclay, Gif-sur-Yvette, France

Abstract

Within the collaboration between GSI and CERN, a dedicated cryogenic test facility has been built at CERN (Geneva, Switzerland) in order to perform the site acceptance tests of the 56 Superconducting FRagment Separator cryomodules before their installation at the Facility for Antiproton and Ion Research (Darmstadt, Germany).

Two of the three benches of the CERN test facility were successfully commissioned with the powering tests of the first-of-series multiplets and dipole. The long multiplet, with a warm bore radius of 192 mm, is composed of nine magnets of different type (quadrupole, sextupole, steering dipole and octupole) assembled with Nb-Ti racetrack and cosine-theta coils, mounted in a cold iron yoke and in a common cryostat.

This work presents the first results of the cold powering tests at 4.5 K during which dedicated measurements have been implemented for the magnetic characterization of the single magnets up to nominal current (300 A for a long quadrupole) and the study of their crosstalk effects.

The results of the acceptance tests will be presented together with the challenges and lessons learnt during the facility commissioning.

INTRODUCTION

For the Superconducting FRagment Separator (Super-FRS) under construction at the Facility for Antiproton and Ion Research (FAIR) in Darmstadt, large acceptance superconducting magnets are currently under test at the European Organization for Nuclear Research (CERN) cryogenic test facility for their final validation before installation [1, 2].

In total 199 magnets grouped in 56 cryomodules will be tested: more specifically 32 multiplets and 24 main dipole magnets [3]. The multiplets, of different lengths (from 2.4 to 7 m), are composed of minimum two up to maximum nine magnets of different type (long and short quadrupoles, sextupoles, octupoles, steering dipoles) and positioned at 250 mm distance from each other. The magnets, with the Nb-Ti racetrack and cos-theta coils inside their cold iron yokes, are aligned along the beam pipe within a single common cryostat. Furthermore, the octupoles are nested inside the short quadrupoles.

Since 2019, cold tests started on First of Series short multiplet (FoS SM), First of Series long multiplet (FoS LM) and the FoS bending dipole magnet. The FoS SM is composed by a sextupole (SE) and a short quadrupole (SQ), while the FoS LM is composed by one long quadrupole (LQ), two short quadrupoles (SQ), two octupoles (OCT), three sextupoles and one steering dipole (St.Dip). Figure 1 shows the FoS installation at the CERN test facility on the reception area and on the test benches.

This work presents the FoS testing strategy and the main achievements with a particular attention given to the multiplets results before entering the series testing phase. The results of the FoS dipole magnet, presently under test, will be presented in future works.

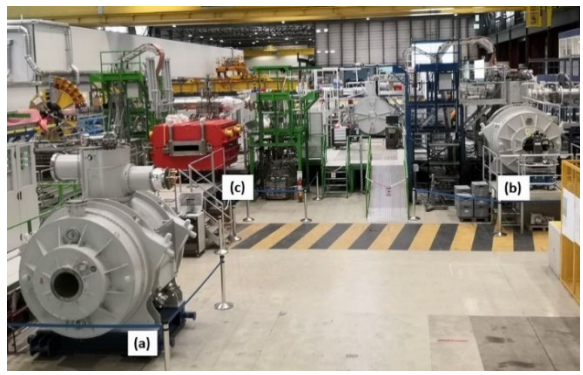

Figure 1: FoS short multiplet (a), the FoS long multiplet (b) and the FoS dipole (c) at the CERN test facility.

FOS TESTING GOAL AND STATUS

The objective of the FoS testing plan is the validation of the magnets design and performances at room and cold temperatures and the reproducibility of the results after thermal cycling.

The qualification of the magnetic field performances, with the required strength and homogeneity, is the most important part of the cold tests. Therefore, extended measurements plan has been followed. Different magnetic measurement methods have been employed and compared in order to optimize the series testing campaign [4].

The FoS tests had also the goal to commission the CERN test facility, comprising the cryogenic infrastructure and control systems, power converts, energy extraction and quench protection systems, as well as the magnetic measurement devices. For this reason, within the FoS test plan, dedicated powering tests and heat load measurements have been performed [5].

After the commissioning of two of the three test benches, the optimization of the cryomodule interface with the facility, the full characterization of the measurement devices and the successful testing campaign, on February 2022, the FoS SM was delivered to GSI. It will be followed by the FoS LM in July 2022 while the FoS dipole tests are continuing.

ISBN: 978-3-95450-227-1 ISSN: 2673-5490 doi:10.18429/JACoW-IPAC2022-THPOTK014

100 keV ELECTRON SOURCE DESIGN FOR THE NEW 3 GeV SYNCHROTRON FACILITY IN THAILAND

K. Manasatitpong*, S. Bootiew, T. Chanwattana, Ch. Dhammatong, S. Jummunt, N. Juntong, K. Kittimanapun, W. Phacheerak
Synchrotron Light Research Institute, Nakhon Ratchasima, Thailand

Abstract

The Synchrotron Light Research Institute (SLRI) is developing a new synchrotron light source with an electron beam energy of 3 GeV. The DC thermionic electron gun was chosen because it is simple and less cost. The design process is well known. The operation is more stable compared to the RF gun. The cathode Y-646B was considered because it had already been used at the old synchrotron machine and the possibility of sharing the stock outweighs other disadvantages. Moreover, it is used in many synchrotron facilities, so it is easy to find references. The present of the focusing electrode was discussed. The focusing electrode will increase the complexity of the gun, but it is necessary to get a high-quality beam from the gun. The designed electron gun can produce 1.1 A beams current with the normalized emittance of 0.910π mm mrad, which satisfied the requirement of the linac injector. The design and study results will be discussed in this report.

INTRODUCTION

The Synchrotron Light Research Institute (SLRI) is developing a new synchrotron light source with electron beam energy of 3 GeV. A DC thermionic electron gun was considered as an electron source for the new synchrotron. This is considering its simple design and less fabrication cost. The DC gun is part of the 150 MeV linac pre-injector to the 3 GeV booster ring. This gun is a conventional triode electron gun, which is a gridded gun with a thermionic cathode. The gun structure will be designed to fit the cathode-grid assembly Y-646B manufactured by EIMAC. It is used in many synchrotron facilities, so it is easy to find reference [1–3]. This cathode has a circular area of 0.5 cm^2, which is equivalent to 10 mm in diameter. It has a grid cathode spacing of 0.15 mm. This paper presents the structure design of the DC gun to fit this cathode.

The DC electron gun will be used to generate the electron beam for the injector of the new synchrotron. Therefore, the requirements and constraints from downstream systems like storage ring, booster ring, linear accelerators, and bunching system, will be considered thoughtfully. They are from both beam parameters and technical limitation. The gun will operate at 1100 °C temperature of cathode. It requires a focusing electrode for focusing the electron through the gun exit. Maximum potential between cathode and anode is 100 kV. The target electron beam current is 1 A. This gun should be able to operate at lower beam current. It should be optimized to get emittance of 1 mm mrad at the exit. It should produce the beam that can further be accelerated by downstream accelerators.

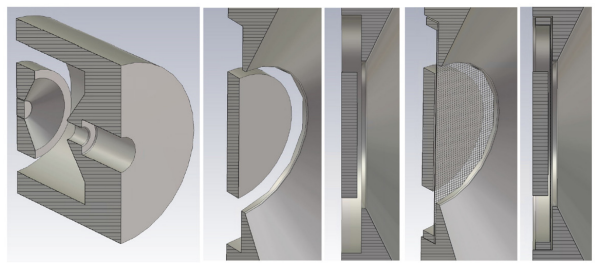

Figure 1: The model of electron gun in CST with (a) a complete model, (b) a gun-without-grid model, and (c) a gun-with-grid model.

DESIGN WORKFLOW

Usually, the DC electron gun has cylindrical symmetry which allow 2-dimensional (2D) simulation. 2D simulation is fast and accurate. The popular software in accelerator community is EGUN [4]. However, with the inclusion of the rectangular grid with the Y-646B cathode, the cylindrical symmetry broke. Therefore 3-dimensional (3D) software will be used. CST Studio Suite ®(CST) [5], which can solve electromagnetic field and particle trajectory will be used. The CST equips with many modules, electrostatic and tracking solver of the particle studio module will be used for designing the DC gun. The following workflow was done for the design process.

Firstly, modelling the gun with CAD software to check the integrity of the model. Solidworks [6] is used to cooperate easily with engineers. After the integrity check, model of the gun is constructed in CST according to the model from Solidworks. It is known that imported model can create inconsistency from different software. So, the model is not imported directly from Solidworks. The model in CST can be fully parametrized for further optimization.

Secondly, the simulation setup with the background set as vacuum. The gun parts is set as perfect electrical conductor (PEC). The potential of the gun parts will be set according to the requirement. Anode is fixed to ground potential, while the focusing electrode and the grid is floated at 100 kV. The cathode potential is referenced to the grid potential. It can be modified with a bias and pulse voltage. The source of the particle will be created at the cathode surface. Thermionic emission model is used with a maximum temperature of

* keerati@slri.or.th

ISBN: 978-3-95450-227-1 ISSN: 2673-5490 doi:10.18429/JACoW-IPAC2022-THPOTK015

SOLID-STATE PULSED POWER SUPPLY FOR A 100 keV ELECTRON SOURCE OF THE NEW SYNCHROTRON FACILITY IN THAILAND

W. Phacheerak*, S. Bootiew, T. Chanwattana, Ch. Dhammatong, N. Juntong,
K. Kittimanapun, K. Manasatitpong
Synchrotron Light Research Institute, Nakhon Ratchasima, Thailand

Abstract

The new synchrotron light source project in Thailand will utilize a thermionic DC electron gun. The maximum operation of the gun is 100 keV, which requires a pulsed power supply of 100 kV. The present synchrotron machine uses a conventional design of the gun power supply. To improve the high voltage pulsed quality, the solid-state design of the gun power supply is utilized. The output pulse width can be adjusted easily and the droop is less compared to the conventional design. The designed output of 100 kV amplitude with 5 µs pulsed width can be achieved with this design. It also produces a less droop of 1.8%. The design process and results will be presented.

INTRODUCTION

The Synchrotron Light Research Institute (SLRI) is developing a new synchrotron light source with electron beam energy of 3 GeV. Injector is a conventional linac and booster ring. The 150 MeV linac is utilized with the 3 GeV booster ring. A DC thermionic electron gun was considered as an electron source for the 150 MeV linac. Thus, SLRI need to develop knowledge and expertise of staff and techniques related to the injector. The 100 keV electron gun [1] is developed to serve this purpose. The pulsed high voltage power supply to the electron gun is also planned for the research and development. These activities will be a platform to train and practise staff of electron beam injector.

The DC thermionic electron gun with a maximum beam energy of 100 keV requires the high power DC pulsed power supply that can supply a 100 keV pulsed with adjustable pulsed width. Conventional pulse modulator is utilized normally for the second generation light source injector. These modulators use pulse transformers to obtain the required pulse energy. However, it requires a huge amount of subsystems and pulse-forming networks (PFN's) to drive the pulse transformer. This make the large physical size of modulator systems. The PFN of a conventional modulator normally operates at high voltage. It is driven by high voltage capacitors. Working with high voltage requires an experienced engineers and technicians.

A conventional pulse modulator has a PFN which comprised of several inductors (L) and capacitors (C) as in the simplified diagram in Figure 1. This PFN is charged rapidly to a range of 10 to 40 kV. Output of the PFN is connected to the primary winding of a pulse transformer by a high voltage switch. This switch is typically a hydrogen thyratron tube. It will deliver half the charging voltage to the pulse transformer. The transformer is typically a voltage step-up transformer with the turns ratio of the transformer, a primary winding to a secondary winding, is N:1.

The PFN discharges will extract energy from the capacitors (C) and feed this energy into the pulse transformer. The load will get energy from the pulse transformer as a rectangular voltage pulse, with a fast rise time to peak, a relatively flat pulse top, and a relatively fast fall time. A high-voltage capacitors and a high voltage switch are required in the PFN structure. So, this makes it a large physical size, and there are high electrical and thermal stress applied to its components, at high voltage. The PFN structure requires complex tuning. This makes the design and implementation of a reliable PFN a major challenge.

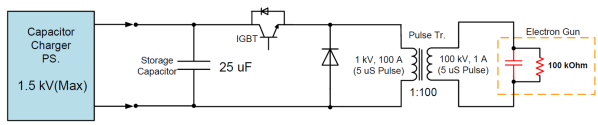

Figure 1: Simplified schematic diagram of a conventional modulator.

MODULATOR DESIGN

The modulator for electron gun is developed based on the new solid state type, CLW system [2, 3]. This is for the benefit of pulse energy, pulse width, rise time, fall time and pulse flatness, in which the solid state type is superior that the conventional type. The conceptual design diagram of the solid state type modulator is shown in Figure 2.

Major difference from the conventional modulator is the high voltage switch. The solid-state switches, such as IGBT-switches, are used in the solid state power modulator. The IGBT (Insulated-Gate Bipolar Transistor) switch is a solid-state switch. These switches can be turned on and turned off electronically. This is in contrast to thyristor switches, which can only be turned on electronically. The IGBT-switches eliminate the need for PFNs and high voltage capacitors in the modulator.

The modulator uses an energy storage capacitors connected to electronically on/off switches. Each capacitor is individually connected to the pulse transformer by a respective switch. Energy from the energy storage capacitors are transferred through the switches to the load through the pulse transformer for a specified time, and are then turned off electronically. The voltage droop-compensating circuit

* wiwek@slri.or.th

ISBN: 978-3-95450-227-1 ISSN: 2673-5490 doi:10.18429/JACoW-IPAC2022-THPOTK019

COLLIDER NICA POWER SUPPLY MAGNET SYSTEM

V. N. Karpinsky, R. M. Ahmadrizyalov, S. A. Arefev, A. V. Butenko, A. V. Karavaev, S. V. Kirov, A. V. Kopchenov, A. A. Kozlykovskaya, T. A. Kulaeva, M. I. Kuznetsov, A. L. Osipenkov, A. V. Sergeev, A. A. Shurygin, E. M. Syresin†, V. G. Tovstuha, N. V. Travin,
Joint Institute for Nuclear Research, Dubna, Russia

Abstract

A power supply system for Collider structural magnets is considered, which consists of precision current sources, energy evacuation devices for superconducting elements, additional sources, and control and monitoring equipment. The status of the equipment and the plan of its placement in Collider bldg. 17 are presented.

INTRODUCTION

The NICA (Nuclotron-based Ion Collider fAcility) project is a new acceleration and storage complex that is currently under construction at JINR [1]. The Collider is the main installation of NICA.

The power supply system of the Collider's structural superconducting magnets should provide:

- formation of magnetic fields in accordance with the required cycle,
- set ranges of variation and accuracy of currents in groups of structural magnets,
- reliable operation of superconducting magnets in the event of a normal zone.

The main parameters of the Collider's structural magnets are: inductance of 36 mH for dipole magnets and 4.6 mH for focusing and defocusing lenses, magnet current of 10.4 kA, and field/current stability of $2{\cdot}10^{-5}$ on a plateau and $2{\cdot}10^{-4}$ in other modes.

The working cycle of the magnetic field is shown in Fig. 1.

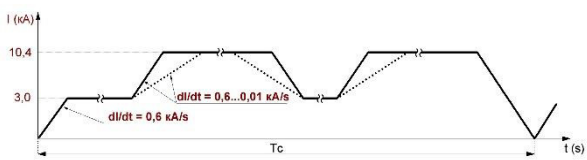

Figure 1: Current cycle of Collider magnets.

BASIC CIRCUIT OF THE POWER SUPPLY SYSTEM

The Collider consists of 2 independent rings of structural superconducting magnets. Each ring has its own power system. The power supply circuit of the first Collider ring is shown of Fig. 2.

The main powerful PS1 source of the power supply system generates the required current with a given field growth rate in all sequentially connected structural magnets. The PS2 source of lower power allows one to simultaneously change the field gradient in the focusing and defocusing lenses, and the PS3 is only for the defocusing lenses.

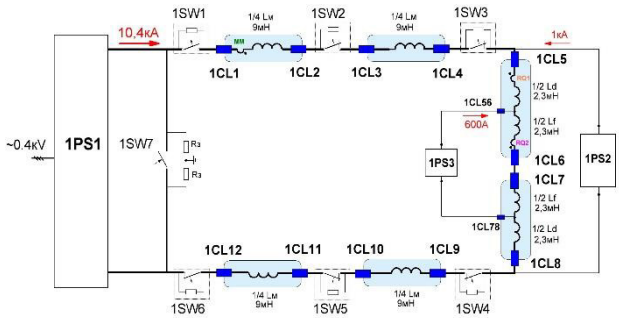

Figure 2: Schematic diagram of the power supply.

To evacuate the energy stored in magnets in the event of a breakdown of superconductivity, SW1…6 switches connected in series with a chain of magnets are used. They are controlled by an external signal from the detection system for the appearance of a normal phase in a superconductor. When a signal occurs, the energy evacuation switches (SWs) open, and the energy stored in the magnets is dissipated in the field quenching resistors connected in parallel to the switches. The SW7 shunts the power supply at the energy evacuation (EE).

Table 1: Parameters of the Main Current Sources

	PS1 PIT 11-50	PS2 PIT 01-40	PS3 PIT 0.6-30
Supply voltage Un	3f~50 Hz 380/220 V		
Peak power, kW	600	45	25
Source voltage, VDC	+/−50	+/−40	+/−30
Maximal current, kADC	11	1	0.6
Current stability at dI/dt not equal to zero	$2{\cdot}10^{-4}$		
Minimal duration of the rise/fall of the field, s	18		
Current stability at dI/dt=0	$2{\cdot}10^{-5}$		
Maximal duration of the field table, hour	24		

† email address: esyresin@jinr.ru

ISBN: 978-3-95450-227-1 ISSN: 2673-5490 doi:10.18429/JACoW-IPAC2022-THPOTK020

RECENT EXPERIENCE FROM THE LARGE-SCALE DEPLOYMENT OF POWER CONVERTERS WITH MAGNET ENERGY RECOVERY

K. Papastergiou, European Laboratory for Particle Physics, Geneva, Switzerland
G.L. Godec, European Laboratory for Particle Physics, Geneva, Switzerland
V. Montabonnet, European Laboratory for Particle Physics, Geneva, Switzerland

Abstract

A new powering solution was deployed at CERN for transfer lines in the injector complex as part of the LHC injectors upgrade. The new powering uses regenerative power converters to recycle the magnet energy between physics operations. This work gives an overview of the developed technology, the way it is used in the accelerators complex and some results of first period of operation with beam.

INTRODUCTION

The consolidation and upgrade projects that are performed, approximately, every four years at CERN are important for the performance improvement of the particle accelerators. In addition, recent developments on the climate front, imply new requirements for sustainable operation and energy consumption reduction.

A new power converter family named Sirius [1] has been developed to improve the magnet current regulation stability (half-hour) and 24-hours reproducibility precision from more than 100 parts per million (ppm) to under 20ppm. Additionally, new requirements were set for a faster transition of the magnet field from one accelerator user to the next. These requirements imply new faster and more precise magnetic pre-functions in transfer lines such as the TT2, guiding particles from PS to the SPS accelerator.

This paper discusses some of the powering requirements in the injector's complex and presents the features of the new Sirius converter family and the associated tools to monitor and maintain the new converter farms.

The last section presents the results of measurements performed recently after commissioning of the East Area facility [2]. As a flagship energy saving project for CERN, East Area now operates with a 94% energy economy in comparison to the pre-upgrade operation. The impact of this optimisation exercise on the electrical network infrastructure opens the way for other self-funded projects in the accelerator facilities.

FACILITY DESCRIPTION

Three key facilities at CERN benefited from the consolidation and renovation programmes to renew their powering architecture; a total of 140 power converters were installed in the TT2 Transfer line between the PS and the SPS, in the Booster Transfer line from the Booster to PS and to ISOLDE and finally in all transfer lines from PS to the new East Experimental Area. An example of the diverse magnet loads that are powered by the new converter family is illustrated in Fig. 1.

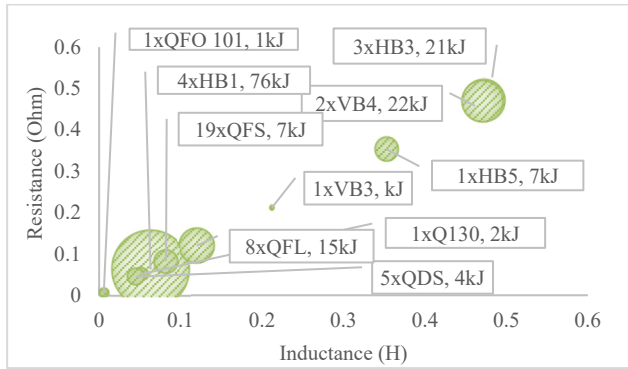

Figure 1: Inductance and resistance value of the magnet loads in the TT2 transfer line. Bubble size corresponds to the energy stored by the magnet.

The first challenge that is a consequence of the different electrical characteristics of magnets is the wide variation of the recyclable energy (stored in the magnetic field) that varies from as low as few kJ to almost 100kJ.

An additional challenge for the new power converters design was related to the wide voltage requirements due to the fast cycling needed under so different load inductance values.

The development of a standard powering system for such a diverse user environment required significant modularisation of the design. Furthermore, in certain cases a double powering scheme has been applied where two smaller power converters are used, instead of a larger one, to power separately the two coils of a single electromagnet. This allows reuse members of the Sirius converter family, instead of developing dedicated converter for specific magnets, to benefit from a standardisation effort and from a more cost-effective large-scale manufacturing.

POWER CONVERTERS

A new power converter family, called Sirius, was designed in the laboratory and mass produced in industry. The power converter is modular with up to four power bricks and each brick has a rated output of 450A peak and 450V. The topology used is an H-bridge IGBT converter operating at 6.5kHz with a front-end diode rectifier with a boost regulator operating at 13kHz for the dc-link voltage regulation.

The power converter, see conceptual drawing in Fig. 2, recycles the magnet's field energy using the DC-link capacitors as energy storing units. To account for the very diverse load size and energy requirements the power

ISBN: 978-3-95450-227-1 ISSN: 2673-5490 doi:10.18429/JACoW-IPAC2022-THPOTK022

CRYOGENIC INFRASTRUCTURE FOR THE MAINZ ENERGY-RECOVERING SUPERCONDUCTING ACCELERATOR (MESA)*

T. Stengler†, D. Simon, K. Aulenbacher, F. Hug, P. S. Plattner, Johannes Gutenberg-Univ. Mainz
(KPH) Fachbereich Physik Institut für Kernphysik, Mainz, Germany

Abstract

The 'Mainz Energy-Recovering Superconducting Accelerator' (MESA), currently under construction at the Institute of Nuclear Physics, Johannes Gutenberg University Mainz, Germany, requires a cryogenic infrastructure for its superconducting components. Prior to the start of the project, a helium liquefier was purchased that is capable of supplying the existing infrastructure of the Institute for Nuclear Physics, as well as the SRF test facility of the Helmholtz Institute. The liquefier has already been purchased in such a way that nitrogen pre-cooling can be integrated and can be upgraded for the operation of MESA. In addition to the superconducting accelerator modules, all components of the P2 experiment, i.e. solenoid, target and polarimeter (Hydromøller), must also be supplied with liquid helium. Therefore, besides the upgrade of the liquefier, it is necessary to extend the system with a dedicated cryogenic supply for the P2 target. This paper presents the current status of the cryogenic supply of the MESA accelerator, the future modifications and additions.

GENERAL OVERVIEW OVER THE CRYOGENIC INFRASTRUCTURE FOR MESA

The MESA accelerator ('Mainz Energy-Recovering Superconducting Accelerator'), which is currently under construction, has several cryogenic components that need to be integrated into an existing cryogenic circuit. The existing circuit previously served experiments by Dewar filling and the test stand for SRF research at the Helmholtz-Insititut Mainz by a 200 m transfer line [1]. These consumers, as well as the new MESA components, must continue to be supplied after the upgrade.

General Layout of MESA

Figure 1 illustrates the MESA layout. The cryogenic elements to be supplied are marked. MESA is designed as an energy-recovering linear accelerator. A normal conducting pre-accelerator injects a 5 MeV electron beam into the main accelerator. Two superconducting accelerator modules of the ELBE/Rossendorf type [2] provide the acceleration and deceleration in the recirculating main accelerator. MESA serves three experiments to precisely measure the limits of the standard model, MAGIX [3], darkMESA (BDX) [4] and P2 [5]. From these, only the P2-experiment needs to to be integrated into the cryogenic cycle containing three elements to be cooled.

First, the superconducting solenoid of the experiment will be cooled by liquid Helium, which comes from the MESA cryoplant. In addition, since the measurement uncertainty of the experiment includes the measurement uncertainty of the spin polarisation of the electron beam, a high-precision cryogenic Møller polarimeter (Hydromøller) [6] was forseen, which demands liquid Helium for cooling as well. Due to the sanctions imposed by the Federal Republic of Germany on Russian suppliers, it is currently impossible to continue the project. Therefore, a conventional Møller polarimeter that does not require a cryogenic supply is to be provided in the first expansion stage of the accelerator. For later upgrades, however, the possibility to upgrade the circuit to supply the Hydromøller with liquid helium has to be considered.

The third device of P2 to be cooled is the liquid Hydrogen target. This target will be cooled by gaseous Helium of a temperature of 15 K coming from an additional cryoplant which does not affect the amount of liquid Helium needed for the accelerator. Nevertheless, this additional circuit needs to be taken into account for the planning of the cryogenic piping under limited space constraints.

MESA can be operated in two modes. In the energy-recovering mode, the electron beam is recirculated up to two times to a beam energy of up to 105 MeV and then sent into the internal target MAGIX. After the interaction with the experiment, the non-interacted part of the electron beam will return to the main accelerator and decelerated via a phase shift of 180° in order to recuperate the energy for the accelerating beam.

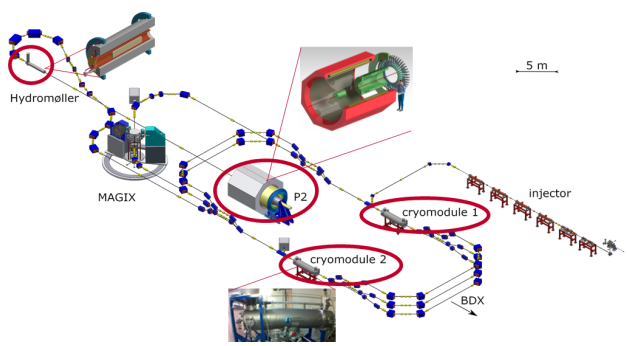

Figure 1: Lattice of MESA. The recirculating main linac is fed by a normal conducting injector. The main accelerator is driven by two superconducting ELBE-/Rossendorf-type cryomodules. The accelerator will serve three experiments, MAGIX, P2 and BDX (darkMESA). Only P2 will have cryogenic components, namely a solenoid and a hydrogen target.

* Work supported by the German Research Foundation (DFG) under the Cluster of Excellence "PRISMA+" EXC 2118/2019
† stengler@kph.uni-mainz.de

ISBN: 978-3-95450-227-1 ISSN: 2673-5490 doi:10.18429/JACoW-IPAC2022-THPOTK023

FERRITE SPECIFICATION FOR THE Mu2e 300 kHz AND 4.4 MHz AC DIPOLE MAGNETS

K. P. Harrig, E. Prebys, University of California Davis Physics Dept., Davis, USA,
L. Elementi, C. Jensen, H. Pfeffer, D. Still, I. Terechkine, S. J. Werkema, M. Wong-Squires
Fermilab National Accelerator Laboratory, Batavia, USA

Abstract

The Mu2e experiment at Fermilab will measure the rate for neutrinoless-conversion of negative muons into electrons with never-before-seen precision. This experiment will use a pulsed 8 GeV proton beam with pulses separated by 1.7 µs. To suppress beam induced backgrounds to this process, a set of dipoles operating at 300 kHz and 4.4 MHz have been developed that will reduce the fraction of out-of-time protons at the level of 10^{-10} or less. Selection of magnetic ferrite material for construction must be carefully considered given the high repetition rate and duty cycle that can lead to excess heating in conventional magnetic material. A model of the electromagnetic and thermal properties of candidate ferrite materials has been constructed. Magnetic permeability, inductance, and power loss were measured at the two operating frequencies in toroidal ferrite samples as well as in the ferrites from which prototype magnets were built. Additionally, the outgassing rates of the ferrite material was measured to determine vacuum compatibility. The outcome of this work is a detailed specification of the electrical and mechanical details of the ferrite material required for this application.

INTRODUCTION

The Mu2e experiment aims to observe conversion to an electron of a muon that has been captured by an aluminium nucleus. This process violates charged lepton favor number and is forbidden by the standard model. A conclusive result, null or otherwise, would shed light on beyond the standard model physics. The Mu2e collaboration aims to improve on the sensitivity of previous measurments of this process by four orders of magnitude. Specifically, the experiment will measure the ratio of the coherent neutrinoless conversion in the field of a nucleus of a negatively charged muon into an electron to the muon capture process.

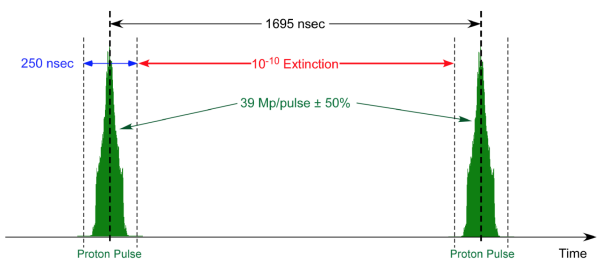

Figure 1: Longitudinal structure of the proton beam after exiting the Delivery Ring [2].

$$R_{\mu e} = \frac{\mu^- + A(Z,N) \rightarrow e^- + A(Z,N)}{\mu^- + A(Z,N) \rightarrow \nu_\mu + A(Z,N)} \quad (1)$$

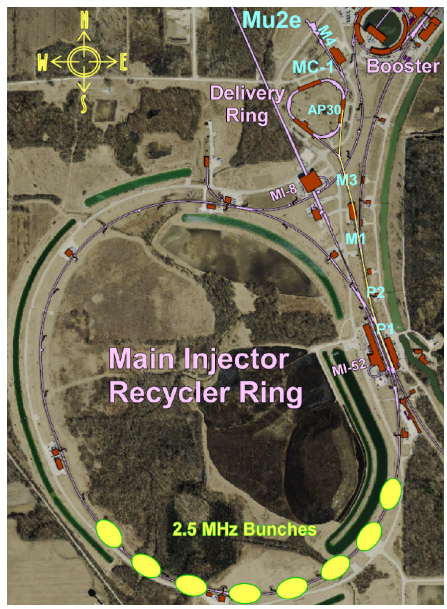

Figure 2: Fermilab accelerator complex.

The first search for a muon to electron conversion took place in 1955 [1]. However, more recent experiments placed a 90% CL limit on the process of 4.6×10^{-12}, and 7×10^{-13} [1]. A key component to the increase in sensitivity is the longitudinal structure of the proton beam shown in Fig. 1. Specifically, the experiment hopes to achieve $R_e = 6 \times 10^{-17}$ at 90% CL limit. The muons will be created via the decay of pions created by 800 GeV protons impinging on a tungsten target. The out-of-time protons will be eliminated using the extinction system located on the M4 beam line just before the tungsten target. The muons will then be captured on an aluminium nucleus and the resulting electrons will be detected [1]. A diagram of the accelerator complex is shown in Fig. 2. The proton pulses are 250 ns wide and spaced 1.7 µs apart. Each pulse contains 39×10^6 protons. The experimental signature of the process will include a large background from muons decaying in the orbit of the nucleus before capture can occur.

EXTINCTION

The ratio of out of time protons to total number of protons in a pulse is defined as the extinction. The goal is to obtain a

ISBN: 978-3-95450-227-1 ISSN: 2673-5490 doi:10.18429/JACoW-IPAC2022-THPOTK025

HEAT LOADS MEASUREMENT METHODS FOR THE ESS ELLIPTICAL CRYOMODULES SAT AT LUND TEST STAND

N. Elias†, X.T. Su, ESS, Lund, SWEDEN
W. Gaj, P. Halczynski, M. Sienkiewicz, F.D. Skalka, IFJ-PAN, Kraków, POLAND

Abstract

The Site Acceptance Testing, SAT of all ESS elliptical cryomodules is done at the Lund Test Stand. Determining cryogenic heat loads (static and dynamic) is an essential part of the acceptance criteria. We present complementary measurement methods for evaluating the cryogenic heat loads and discuss a qualitative comparison between them. We also present a summary of the results of these methods for one of the cryomodules.

INTRODUCTION

The ESS accelerator is currently under construction in Lund, Sweden [1]. Thirty elliptical cryomodules (CM) distributed in 2 families: 9 Medium-Beta and 21 High-Beta, will go through SAT at the Lund test Stand, TS2 [2, 3]. Each CM integrates four superconducting radio-frequency cavities made of niobium immersed in a superfluid helium bath at 2 K. An important portion of the acceptance tests consists of verifying the proper working behaviour of the superconducting cavities and other cryomodule components at nominal working conditions [4].

Another important part of the cryomodule acceptance tests is the measurement of cryogenic static heat loads and RF-induced dynamic heat loads. This paper describes a set of methods used to evaluate these parameters.

THE CM CRYOGENICS AT TS2

The cold test takes place inside the radio-protection bunker where the CM is connected to various auxiliary systems, such as: radiofrequency distribution, beam vacuum, isolation vacuum, water cooling and cryogenic distribution.

The TS2 cryomodule cryogenics system is designed and constructed such that the nominal operating conditions for the accelerating cavities can be achieved. It also allows to safely go through a series of operating modes [5] necessary for example for the cool down, warm up or response to accidental states.

Simplified Cryogenics Layout

At the TS2 a dedicated cryogenic plant, TICP [6] and distribution system, CDS [7] supplies refrigeration to the cryomodule at conditions similar to those present in the accelerator tunnel where each single cryomodule operates together with a dedicated valve box (VBox) and can be operated independently from other CM.

At the interface between the CM and the VBox there are four cold process lines. Two of these lines are for the thermal shield cooling, TS (supply and return), whilst the other two lines are for the cold mass helium supply and vapour return. Figure 1 below shows a very simplified scheme of the cryogenic system at TS2 with selected relevant equipment.

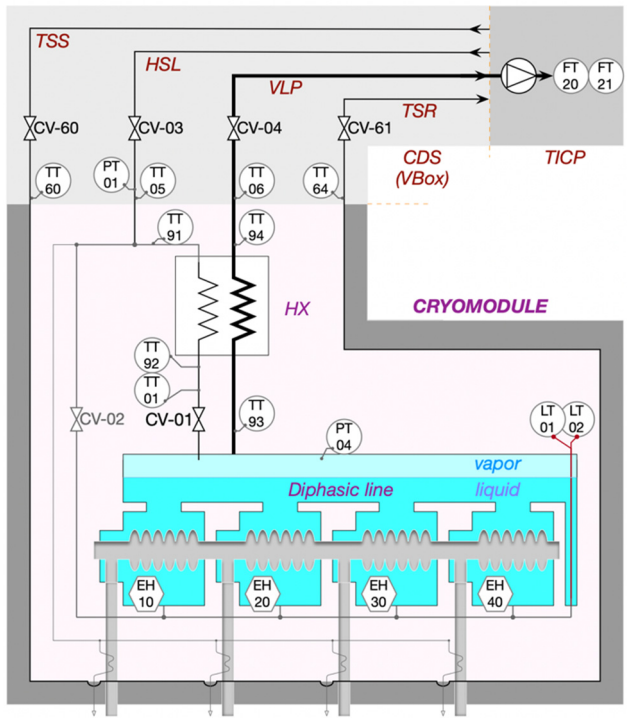

Figure 1: Simplified scheme of the cryogenic system.

The high-pressure (HP) supercritical helium is supplied at 3 bar and 5.3 K. It first passes through a heat exchanger (HX), where it is pre-cooled by heat exchange with the low-pressure (LP) evaporated vapours from the 2 K bath.

The pre-cooling of the HP line allows to recover the available frigories from the LP line and significantly enhance the efficiency of the "Joule-Thomson" (JT) expansion valve feeding the 2 K bath.

The typical thermodynamic conditions at the TS2 interface between Vbox and CM are shown Table 1.

Table 1: Conditions at the CM interface with VBox

Circuit name	Pressure, Temperature
Thermal shield supply, TSS	13.8 bar, 33 K
Thermal shield return, TSR	13.3 bar, 36 K
Helium supply line, HSL	3 bar, 5.3 K
Vapour return line, VLP	31 mbar, -

Under nominal conditions, the superconducting cavities operate fully immersed in the superfluid liquid helium bath, with the helium level stabilized inside the diphasic line which interconnects the four helium tanks at the top.

The level of the helium bath is measured by two redundant level gauges, LT-01 and LT-02, and it is controlled by

† nuno.elias@ess.eu

ISBN: 978-3-95450-227-1 ISSN: 2673-5490 doi:10.18429/JACoW-IPAC2022-THPOTK026

DEVELOPMENT AND TEST OF A PROGRAM FOR AUTOMATIC CONDITIONING OF ROOM TEMPERATURE CAVITIES

K. Kümpel†, H. Podlech, A. Rüffer, M. Märcz, C. Wagner, S. Wagner, Institut für Angewandte Physik (IAP) at Goethe-University Frankfurt am Main, Frankfurt am Main, Germany

Abstract

The conditioning of room temperature cavities is a time-consuming process that can take several weeks and requires the supervision of experienced experimenters. To simplify this process for future cavities, a program is currently being developed at the IAP Frankfurt that will simplify the experimenter's work and eventually will take it over completely. This paper describes the basic setup of the program as implemented so far, as well as the tests performed on different cavities. In addition, an outlook for the next development steps and their application is given.

INTRODUCTION

Conditioning is the process of slowly increasing the power injected into the cavity until the power levels necessary to create the electric fields required by the beam dynamics are reached.

During the conditioning process, undesirable effects can occur within the cavity, with multipacting, outgassing and discharges being among the most common. These undesirable processes not only disrupt the conditioning process, but also pose the risk of permanent damage or destruction to the cavity itself or the measuring equipment used. [1]
Therefore, conditioning should only be carried out extremely carefully and by trained personnel.

During conditioning, as is usually carried out at the IAP Frankfurt, the forward power P_f, the reflected power P_r and the transmitted power P_t are monitored by the experimenter in addition to the pressure p inside the cavity, while the conditioning can be controlled by the level of the forward power P_f and its frequency *f*.

Typically, conditioning takes between a few days and several weeks, whereby the required conditioning times can vary greatly even for structurally similar cavities.
In order to be able to reduce this large amount of time for the experimenter in future conditioning, a program should be written that supports the experimenter.

PROGRAM

The new program is based on a LabView-based readout software that was developed as part of a master's thesis at the IAP Frankfurt and has already been successfully used to condition cavities for the MYRRHA project. [2]

Several functions should be added to this program:

Emergency Stop

The most important function for the safety of the cavity and the connected measuring equipment is the implementation of an emergency stop, which completely shuts down the conditioning.

Since the measured values for the pressure p and the reflected power *Pr* increase during problems that occur during conditioning, these values are particularly suitable to be used for the emergency stop.

In its present form, the program can be given limit values for the pressure *p* and the ratio of P_r/P_f during operation, and if these are exceeded, the conditioning is immediately terminated.

For this purpose, an interface between the program and the signal generator used has been implemented in order to be able to switch off the forward power here, while another interface with which the amplifier can be switched off directly is conceivable, but has not yet been implemented.

Frequency Adjustment

Due to thermal effects, the frequency can change with the level of transmitted power P_t, which is indicated in an increase in reflected power P_r, while the pressure *p* usually shows little to no change.

The necessary adjustment of the frequency is achieved within the program by a simple algorithm that searches for a minimum of the ratio P_r/P_f in a predefined number of iteration steps. Of course, it must be considered that this frequency adjustment does not lead to success in all cases. Especially with larger deviations, this method is still too slow.

Automatic Conditioning

The automatic conditioning builds up from a gradual increase of the forward power P_f, checking the pressure p and the ratio P_r/P_f at fixed intervals. Two limits can be set for each of these measured values, defining three ranges. In the first range, where both values are below the lower limit, P_f is increased further. If at least one value is between the two limits, the program waits for another measuring cycle before measuring again. This range is used to "wait" until the values normalise while there is still no danger to the cavity and the equipment used.

As soon as one of the values is above the second limit, the conditioning is aborted and the forward power P_f is switched off.

ISBN: 978-3-95450-227-1 ISSN: 2673-5490 doi:10.18429/JACoW-IPAC2022-THPOTK027

TEMPERATURE DEPENDENT EFFECTS ON QUALITY FACTOR IN C-BAND RF CAVITIES

Jake Parsons, Gerard Lawler, Atsushi Fukasawa, Nathan Majernik, James Rosenzweig
University of California, Los Angeles, CA, USA

Abstract

Cryogenic operation and associated skin effects are promisng fields of study for increasing RF gradients within cavities and decreasing the required size for linear accelerators and their applications, such as free electron lasers [1–6]. Notably, a cavity's RF quality factor Q, the ratio of the outgoing RF signal power to the input power, is theoretically multiplied by over 4 when subjected to cryogenic temperatures [7, 8]. Precise measurements of this Q factor require defining a cryostat unit, which consists of a high vacuum chamber, a coldhead, and multi-layered insulation (MLI) shielding. We optimized the cryostat by running several cool down tests at high vacuum, incorporating different geometries of MLI shielding to achieve the lowest possible temperatures. We then performed a low power C-band test after installing a cylindrical copper RF cavity to measure the Q factor. Finally, we improved stability and amplification within the chamber by installing edge welded bellows to the coldhead to reduce vibrations. These measurements provide a basis for the development of cryogenic infrastructure to sustain a cryogenic temperature environment for future RF applications.

CRYOGENIC THEORY

Skin effects govern the atypical behavior of resonating C-band radiation within these RF cavities at cryogenic temperatures [7, 8]. Namely, the anomalous skin effect theory, developed by Reuter and Sondheimer, predicts that, as the temperature of an RF conducting cavity decreases, the electron free mean path length shrinks to the order of the skin depth of the conductor. This results in the surface conductivity scaling both to a non-zero value at cryogenic temperatures as well as inversely to the quality factor of the RF cavity: the ratio of outgoing power of RF radiation to the input signal power. We expect an increase of the quality factor on the order of 3-4.5 times at temperatures less than 40 K [6,7]. Given the radius, a, and the height, h, of a cylindrical cavity of conductivity σ, Equation 1 demonstrates how to evaluate the Q factor from geometry and material considerations alone [8]:

$$Q = \frac{\sqrt{2a\eta\sigma\chi_{01}}}{\left(1 + \frac{a}{h}\right)}, \tag{1}$$

where $\eta = \sqrt{\frac{\mu_0}{\epsilon_0}}$ and χ_{01} is a constant proportional to the resonant frequency ω_0 given by the relation:

$$\omega_0 = \chi_{01}\frac{c}{a}. \tag{2}$$

CRYOSTAT OVERVIEW

The cryostat, shown in Figure 1, is a rectangular stainless steel vacuum chamber, a 1 phase helium cooled cryocooler coldhead and necessary vacuum and cooling components to ensure a high vacuum seal and temperatures consistently below 90 K. The cavity is mounted on 80/20 aluminum rods that are insulated by polyether ether ketone (PEEK) material. MLI shielding surrounds the cavity and the coldhead to shrink the effective size of the chamber and minimize heat leaks. Edge welded bellows have been implemented to reduce vibrations from the coldhead, thereby diminishing heat transfer and chamber instability from vibrations. The coldhead is a 1 phase cryocooler with a copper plated tip that allows for a copper thermal braid to join the cavity to the coldhead in thermal contact [8].

Figure 1: View of internal cryostat components, including MLI wrapping, 80/20 supports, coldhead, and thermal braid connection.

Cavities

The cavity itself is a 14.7 cm diameter cylindrical brazed copper cavity of height 7.3 cm with an RF port on top and coupling sites for thermal braid connections. It is designed to run low-level radio frequency (LLRF) room temperature and cryogenic c-band tests. A secondary cylindrical copper cavity, fabricated by Comeb, will be tested in future applications. See also Figure 2.

ISBN: 978-3-95450-227-1 ISSN: 2673-5490 doi:10.18429/JACoW-IPAC2022-THPOTK029

ROLE OF SURFACE CHEMISTRY IN CONDITIONING OF MATERIALS IN PARTICLE ACCELERATORS

G. Sattonnay†, S. Bilgen, B. Mercier, D. Longuevergne, S. Della-Negra, I. Ribaud
Université Paris-Saclay, CNRS/IN2P3, IJCLab, Orsay, France

Abstract

For the vacuum scientists and the accelerator community, finding solutions to mitigate pressure rises induced by electron, photon and ion desorption, and also beam instabilities induced by ion and electron clouds is a major issue. Along the time, changes in the surface chemistry of vacuum chambers are observed during beam operations, leading to modifications of: outgassing rates, stimulated desorption processes and secondary emission yields (SEY).

To understand the role of the surface chemistry of air exposed materials in the electron conditioning process, typical air exposed materials used in particle accelerators : thin film coatings (NEG, i.e a Ti-Zr-V alloy, and carbon), copper (and its oxides Cu_2O and CuO) and niobium were conditioned by low energy electron irradiation for a better understanding of electron-cloud effect. First, SEY was measured to understand the changes of surface conditioning upon particle irradiation; then, surface chemistry evolution after electron irradiation was investigated by both XPS orTOF-SIMS analyses using the ANDROMEDE facility at IJCLab. Finally, the relationship between the surface chemistry and the conditioning phenomenon will be discussed.

INTRODUCTION

Electron emission is a major phenomenon involved in the formation of the electron-cloud (EC) in the LHC. EC effects have been identified among the major performance limitations for the Large Hadron Collider (LHC). The EC is induced by the electron multipacting process related to the secondary electron yield (SEY) of the surfaces exposed to electron irradiation. The SEY depends strongly on the nature of materials and on the surface chemistry, and consequently the EC formation is determined by the surface properties. Nevertheless, electron bombardment of the inner surface of the beam pipes is also responsible for a beneficial effect called “surface conditioning” (or the “scrubbing effect”) leading to a reduction of SEY and therefore inducing a mitigation of the multipacting process and electron cloud build up.

The aim of this study was first to validate the set-up developed in our laboratory and devoted to SEY measurements, by reproducing the results that exist elsewhere for Cu and Nb for instance. Then, we proposed an alternative method for the analysis of the surface chemistry to the X-ray Photoelectron Spectroscopy which is traditionally used: Time-of-Flight Secondary Ion Mass Spectrometry with high energy gold nanoparticles to probe the surface. We investigated the conditioning of copper beam screen induced by electron bombardment and identified the role played by the modifications of the surface chemistry in this phenomenon.

EXPERIMENTAL DESCRIPTION

The experimental set up for SEY measurements is an in-house build set-up developed at IJCLab. It consists of a single UHV chamber (base pressure: $7x10^{-10}$ mbar) equipped with an electron gun providing a pulsed electron beam (with a pulse length of 30 ms) in the energy range 10 to 4000 eV, with an intensity from few nanoamperes to 50 µA. The sample is carried by a single manipulator allowing for a precise positioning of the sample in the chamber.

The SEY was measured by the sample bias method that is a two-step SEY measurement. First, the primary current I_p is acquired for each primary electron energy E by applying a positive sample bias (V=+50 V). In this case, the current measured on the sample is $I_M(+50V) = I_P$. The emitted secondary electrons (SE) are trapped and recaptured by the sample. The sample polarity is then switched to a negative value (V=-20 V) and I_M is acquired while shooting with the electron gun on the sample with the same energy settings as during I_p acquisition. The SE current (I_{SE}) is given by:

$$I_{SE} = I_p - I_M(-20V) \quad (1)$$

The SEY δ is then obtained by:

$$\delta = \frac{I_{SE}}{I_p} = \frac{I_p - I_M(-20V)}{I_p} = 1 - \frac{I_M(-20V)}{I_M(+50V)} \quad (2)$$

In the present work, we used the ANDROMEDE facility [1] to analyse samples of copper beam screen. 12-MeV Au_{400}^{4+} ion beams are accelerated by a NEC Pelletron® 4MV electrostatic accelerator to bombard samples. The emitted secondary ions (both positive and negative ions) are analysed with the ToF spectrometer EVE In this set-up, it is possible to record a mass spectrum with only one single ion impact. Consequently, the secondary ion emission yield is strongly enhanced and the sensitivity of chemical surface analysis is improved. A high detection efficiency for molecules deposited in very small quantities on metal surfaces (lower than the monolayer) is reached. Moreover, the limited number of primary ions (about 107 nanoparticles/cm2) required to analysis the samples prevents excessive damage of the surface. Only the extreme surface (i.e. the molecules deposited on the surface and the materials surface corresponding to a depth of ≈10 nm) is analysed.

The experimental system used for XPS analysis in the present work is the K-ALPHA system from Thermo-Fisher, equipped with a monochromatic Al kα X-ray source (hν=1486.6 eV) and an Ar^+ ion gun for XPS sputter depth profiling. For each analysis, a full energy spectrum

†sattonnay@ijclab.in2p3.fr

ISBN: 978-3-95450-227-1 ISSN: 2673-5490 doi:10.18429/JACoW-IPAC2022-THPOTK032

A VACUUM SYSTEM FOR THE MILLIAMPERE BOOSTER*

R. Heine, C. Lorey
Institut für Kernphysik, Johannes Gutenberg-Universität Mainz,
D-55099 Mainz, Germany

Abstract

The Milliampere Booster (MAMBO) is the injector linac for the Mainz Energy-recovering Superconducting Accelerator MESA. MESA is a multi-turn energy recovery linac with beam energies in the 100 MeV regime currently designed and built at Institut für Kernphysik (KPH) of Johannes Gutenberg-Universität Mainz [1]. The main accelerator consists of two superconducting Rossendorf type modules [2–4], while the injector MAMBO [5] relies on normal conducting technology. The four MAMBO radio frequency cavities are bi-periodic $\pi/2$ structures [6,7] that are about 2 m long, each. In this paper we present the results of Molflow+ [8] simulations of several setups of the vacuum system for MAMBO that differ in number of pumps, pumping speed and diameter of the pumping ports that are connected to the DN40 beam pipe.

INTRODUCTION

The MESA facility is a few turn recirculating electron linac that can be operated in two modes. The first mode is called external mode where a beam of polarised electrons at $T = 155$ MeV and up to $I = 150\,\mu$A ($Q = 0.12$ pC) is lead onto the target of the P2-experiment [9] and dumped afterwards. The second mode is the energy recovery mode for the MESA gas internal target experiment (MAGIX) [10]. Here a beam of $I = 1$ mA ($Q = 0.77$ pC) of non polarised electrons is recovered from $T = 105$ MeV to injection energy ($T = 5$ MeV) after interaction with the target. For MESA stage-II the beam current delivered to MAGIX will be increased to 10 mA ($Q = 7.7$ pC).

Two main components of MESA are quite susceptible to high vacuum pressure: the superconducting cavities of the main linac and the photo cathodes of the particle sources. Therefore it was agreed to have stainless steel chambers with ConFlat (CF) flanges to achieve ultra high vacuum (UHV). The beam pipe diameter was set to DN40.

MAMBO comprises of four copper cavities of approx. 2 m length that are connected by three drifts of 1 m length that contain ion getter pumps (IGP). The first cavity has 37 cells, the other three have 33 cells. The cells are separated by copper webs that incorporate two coupling slots and the beam port. In a bi-periodic structure there are two types of cells, a long one that accelerates the beam and a short one that couples the field. The later one being about 10 % of $\lambda_{RF}/2$ long, and the first one $\approx 0.9\lambda_{RF}/2$. The cavities are pumped by the drifts via the beam ports. The cavities are expected to act like a differential pumping stage. Because of their geometry, analytical vacuum calculations are complicated and therefore numerical simulations with the Molflow+ code [8] were carried out.

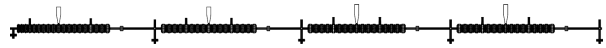

(a) One IGP per drift with DN40 pipes on LUMOs (in total five IGPs).

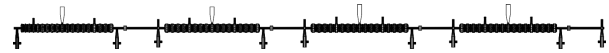

(b) Two IGPs per drift with DN63 pipes on LUMOs and a T-crosses (in total nine IGPs).

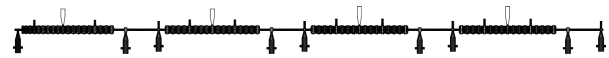

(c) Two IGPs per drift with DN100 pipes on LUMOs and PIMOs (in total nine IGPs).

Figure 1: Examples of vacuum geometries used for the Molflow+ simulations. Beam direction is from left to right.

VACUUM SETUPS

Initially vacuum pumps at the entrance of each cavity were foreseen. From the analytical formulas (e.g. [11]), it was expected that the DN40 beam pipe would limit pumping and therefore a pumping speed of $S_0 \approx 35$ L/s would be sufficient.

This starting point was expanded to three IGP sizes ($S_0 =$ 35 L/s, 60 L/s and 90 L/s) and three sizes of pumping ports (CF40, CF63 and CF100). The pumps were connected to the beam pipe at a spare CF40 flange of a screen monitor (LUMO) acting as a T-chamber followed by a 150 mm straight chamber (see Fig. 1(a)) or one that tapers from DN40 to DN63 or DN100, respectively.

Further configurations with two IGPs comparable to the one shown in Fig. 1(b) were investigated. Those setups allow pumping of the cavities from both beam ports, but one would have to sacrifice either a pair of steerer magnets or the phase intensity monitor cavity (PIMO) needed for finding the correct accelerating phase. Because of the high bunch charge of MESA stage-II increasing the length of the drifts is not an option.

The two pump setups then were altered so that the PIMO has a DN40 pumping port (see Fig. 1(c)). This port is screened by a sieve (compare Fig. 2), so there is no evanescent field leaking into the pipe. This maintains the radio frequency (RF) properties of the resonator and protects the IGP from RF.

SIMULATION & RESULTS

For the simulations baked surfaces of the stainless steel chambers of the beam pipe and the stub to the IGP are as-

* Work supported by DFG Cluster of Excellence "PRISMA+"

ISBN: 978-3-95450-227-1 ISSN: 2673-5490 doi:10.18429/JACoW-IPAC2022-THPOTK034

VACUUM SYSTEM PERFORMANCE OF THE 3 GeV ELECTRON STORAGE RING AT MAX IV LABORATORY

M. Grabski†, E. Al-Dmour, S. M. Scolari, MAX IV Laboratory, Lund University, Lund, Sweden

Abstract

The 3 GeV electron storage ring at MAX IV laboratory is the first synchrotron light source with compact multi-bend achromat (MBA) magnet lattice to achieve ultra-low emittance. The vacuum system of the accelerator is fully coated with non-evaporable getter (NEG) thin film to ensure low gas density. The storage ring started commissioning in August 2015 and currently delivers photon beams from insertion devices (IDs) to 9 beamlines that are in user operation or commissioning. After over 6 years of operation, the NEG coated vacuum system continues to be reliable, is conditioning well and do not pose any limitation to the accelerator operation. The average dynamic pressure is lower than the design value (below 3×10^{-10} mbar) and is reducing with the accumulated beam dose. The vacuum beam lifetime is greater than 39 Ah, and the total beam lifetime is above the design value of 5 Ah - thus is not limited by the residual gas density. Several successful interventions to install new vacuum components were performed on few achromats in the storage ring during shutdowns. Some of them were done utilizing purified neon gas to vent the vacuum system, thus avoiding the need of re-activation of the NEG coating and saving intervention time without compromising the storage ring performance.

INTRODUCTION

MAX IV laboratory consists of 1.5 GeV and 3 GeV storage rings and a full-energy linear accelerator that injects electrons at 3 GeV to the rings and drives short-pulse facility. The injector operates at repetition rate of 10 Hz.

The 1.5 GeV storage ring has delivery beam current of 400 mA, with average total beam lifetime approximately 20 h and delivers photon beams from Insertion Devices (IDs) to 5 beamlines.

The 3 GeV storage ring operates at beam current of 300 mA and deliver photons through IDs to nine beamlines. The electron injection to the ring is done with top-up every 10 minutes. Typical total beam lifetime is 16 h.

3 GEV STORAGE RING VACUUM SYSTEM LAYOUT

The vacuum system of the 3 GeV storage ring follows the geometry of the seven-bend achromat magnet lattice, having 20 fold symmetry. There are 20 long straight sections from which 19 are available for IDs and one is devoted to injection. The main accelerator parameters are listed in Table 1. The detailed design of the vacuum system is described in detail in [1].

† marek.grabski@maxiv.lu.se

Table 1: 3 GeV Storage Ring Main Parameters

Parameter	Value
Energy	3 GeV
Design beam current	500 mA
Horizontal natural emittance	328 pm rad
Circumference	528 m
Number of achromats	20
ID straight section length	4.5 m

3 GeV Storage Ring Layout

The layout of the storage ring is presented in Fig. 1.

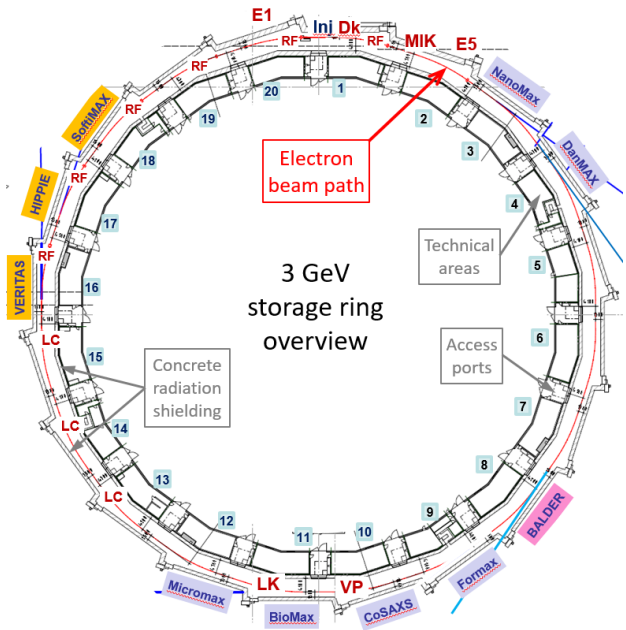

Figure 1: 3 GeV storage ring layout, with marked insertion device/beamline names and main accelerator systems: Inj - Injection straight; Dk - Dipole kicker; MIK - Multipole Injection Kicker; E1, E5 - Diagnostic beamlines for emittance measurement; RF - 100 MHz RF cavities, LC - 300 MHz Landau RF cavities, LK - Longitudinal kicker cavity; VP - Vertical Pinger.

Currently there are 10 insertion devices installed in straight sections (9 of them are delivering photons to beamlines) as indicated in Fig. 1:

- 3 Elliptically Polarized Undulators (EPU) Veritas, Hippie, Softimax.
- 6 In Vacuum Undulators (IVU): Nanomax, Danmax, Formax, Cosaxs, Biomax, Micromax (first light to be delivered in 2022),
- 1 In Vacuum Wiggler (IVW): Balder.

ISBN: 978-3-95450-227-1 ISSN: 2673-5490 doi:10.18429/JACoW-IPAC2022-THPOTK035

THERMO-MECHANICAL MODELING AND THERMAL PERFORMANCE ANALYSIS OF BEAM VACUUM LINE INTERCONNECTIONS AND COLD WARM TRANSITIONS IN HL-LHC LONG STRAIGHT SECTION MAGNETS

J. Harray*, V. Petit, C. Garion, CERN, Geneva, Switzerland

Abstract

The HL-LHC upgrade, aiming at increasing the LHC levelled luminosity by a factor five, relies on novel superconducting magnets requiring a new beam vacuum system. Along with the challenges related to magnet design, the beam optic configuration exposes this new equipment to stringent conditions for vacuum and cryogenic performance. Both cold warm transitions and magnet interconnections appear to be delicate components that are crucial for the thermal heat transfer between diverse subsystems. The proposed study aims at assessing the heat loads to the cryogenic system and the temperature fields in the vacuum system. A nonlinear static thermal analysis is first performed. A thermo-mechanical approach is developed to capture additional thermal resistance arising from contact between components and their behaviour during cool-down. The system is then studied under dynamic operations when beams are circulating and colliding. A thorough analysis of beam-induced heat loads under ultimate conditions highlights the different relevant contributions. Finally, the transient response of the systems is computed to assess thermal time constants.

CONTEXT

High Luminosity

The High Luminosity Large Hadron Collider (HL-LHC) is the ongoing CERN project aiming at multiplying the integrated luminosity of the LHC by a factor 10 [1]. Superconducting insertion magnets in the vicinity of ATLAS (IR1) and CMS (IR5) need to be replaced [2, 3]. Conservative beam-induced heat loads are derived according to the HL-LHC optics v1.5 [4] where the beam operates at $L_0 = 7.5\,10^{34}$ cm^{-2}·s^{-1} ultimate levelled instantaneous luminosity target and at 7 TeV nominal energy [5].

The study focuses on the thermo-mechanical design of magnet interconnections (IC) and magnet transitions to the ambient referred as cold warm transitions (CWT). Four different CWTs of interest are identified in the experimental insertion area: (i-ii) the two extremities (Q1/D1) of the inner triplet (IT) and (iii-iv) both ends of the stand-alone D2 recombination dipole (IP/NIP). One IC (Q2B/Q3) is investigated and defined as a representative baseline.

Cryogenics and Vacuum

The exposition to highly energetic debris from collision requires the design of shielded beam screens [6, 7]. The operating temperature of the aperture needs to be in accordance with its required thermodynamic behavior for vacuum integrity [8]. Associated required cooling is of prior interest to draw a rigorous and complete heat budget for the insertion area [9].

Sequence

The analysis studies the system at equilibrium at its cryogenic temperature referred as the stand-by configuration. At this stage, heat transfer mechanisms are either static losses to the ambient or internal exchanges between cryogenic systems. When beam operates, cryogenic regimes are adapted to further extract beam-induced heat loads and reach its ultimate equilibrium. The dynamic transition from stand-by to ultimate configurations is finally assessed.

MODELING

Methods

A multiphysics numerical model is defined in COMSOL Multiphysics©. Thermal conduction equations are derived under a non linear formulation using temperature-dependent properties [10]. Solid mechanics is coupled to heat transfer in one-way. Isotropic and elastic material behavior is considered. Models are meshed in 3D with approximately 250k linear tetrahedron elements. Surface coatings and thin components are modeled under a thin layer approximation with shell elements for computational efficiency.

Mechanical results are computed with a fully coupled direct PARDISO stationary solver. Static thermal results are computed with a direct segregated PARDISO stationary solver. The dynamic behavior is solved with an iterative GMRES transient solver and a time step $\Delta t = 1$ min.

Thermal Contact

The joint conductance h_c of contact interfaces is modeled with nonlinear thermo-mechanical contact and the empirical Cooper-Mikic-Yovanovich (CMY) correlation given as [11]:

$$h_c = 1.25 k_c \frac{m_{\text{asp}}}{\sigma_{\text{asp}}} \left(\frac{p}{H_c} \right)^{0.94} \quad (1)$$

with p the contact pressure, k_c the harmonic mean of the contacting surface conductivities, σ_{asp} and m_{asp} respectively the RMS value of the average height and slope of surface asperities and H_c the Vickers microhardness of the softer material.

* jerome.harray@cern.ch

ISBN: 978-3-95450-227-1 ISSN: 2673-5490 doi:10.18429/JACoW-IPAC2022-THPOTK036

DETERMINATION OF PUMPING AND DYNAMIC VACUUM PROPERTIES OF CONDUCTIVE QUATERNARY ALLOY OF TiZrVAg NON-EVAPORABLE GETTER

R. Valizadeh, A. Hannah, O.B. Malyshev
ASTeC Vacuum Science Group, UKRI/STFC Daresbury Laboratory, Warrington, Cheshire, UK
G.Y. Hsiung, NSRRC, Hsinchu, Taiwan
N .Tagdulang[1,2], M. Pont[1], J. O'Callaghan[2]
[1]ALBA Synchrotron, Barcelona, Spain
[2]CommSensLab, UPC, Barcelona, Spain

Abstract

Non Evaporable Getter (NEG) coating has been employed extensively in the particle accelerator especial-ly where the vacuum conductance of the vessel is se-verely restricted and ultra-high vacuum condition is required. NEG coating will significantly reduce the outgassing rate and provides active pumping surface for H_2, CO and CO_2. In addition, it has been proven that NEG coated surfaces have a very low secondary electron yield, as well as low photon and electron stimulated desorption yields. However, the existing NEG film increases the RF surface resistance of the beam pipe.

In order to increase NEG coating conductivity, at ASTeC, in the past several years, the alternative NEG composition have been studied by adding more con-ductive element such as Cu, Au, Al and Ag. In this study, we report on the photon stimulated desorption, activation temperature and surface resistance from room temperature to cryogenic temperature for a new NEG quaternary alloy of TiVZrAg as function of the film composition.

INTRODUCTION

Non-evaporable getter (NEG) coating, originally invented at CERN, is already used in many accelerators [1-5] due to three main properties:

1. In a dense structure, it acts as barrier between a vacuum chamber material and an inner vacuum hence even in non-activated state it provides lower residual gas pressure.
2. In a columnar structure, it has a large surface area, hence, a fully coated vacuum chamber has large distributed pumping speed, the benefit of this is essential for the narrow vessels with a limited vacuum conductance.
3. In activated state, the NEG coating has low secondary electron (SEY) yield that helps to supress electron multipacting and electron cloud in high intensity accelerators.

Over recent years, ASTeC Vacuum Solutions Group made a good progress in further development of NEG coatings. New quaternary alloy coating which, can be activated at 140 °C, it is 40 °C lower than for an original invention [6, 7]. A good progress was achieved in reducing photon and electron induced desorption [8, 9]. There are two main challenges in further NEG coating optimisation: (1) the beam impedance in the NEG coated chamber, which related to beam parameters and NEG coating RF surface resistance, this is a problem for short-bunch machines [10, 11]; (2) coating with NEG on narrow tubes with a diameter less than 10 mm, this is a problem for small aperture machines like a future UK-XFEL.

In this report we will concentrate mostly on solution of decreasing NEG surface RF resistance while keeping the integrity of its main three properties.

SAMPLE PREPARATION

Two type of samples was used in this set of experiment: tubular sample that, is the best geometry for evaluation of the pumping properties and flat samples for surface analysis and surface resistance. For the tubular sample a 316 LN stainless steel tube of inner diameter of 38 mm and the length of 0.5 m equipped with two CF40 flanges at either end was deposited with TiZrVAg. The film was deposited using a coaxial cylindrical magnetron configuration with an external magnetic field provided by a solenoid. The deposition method and apparatus is described in our previous publications [6]. The target was a single 3-mm diameter NEG alloy wire of TiZrV specially made for ASTeC, with 1-mm diameter Ag wire raped around the NEG wire. The concentration of Ag is controlled by the number of turn used within the 0.5 m length of the tube. The deposition was done at 10^{-2} mbar and with DC sputtering mode. The flat samples were produced by placing different size of Ag wire in a 3" planar magnetron target. The deposition condition was kept the same as one chosen for tubular deposition.

PSD MEASUREMENT

The PSD was carried out at Taiwan National Synchrotron Radiation Research centre, beam line TLS-BL19B of 1.5 GeV beamline. The PSD experimental system contains a turbo-molecular pump (TMP), a conductance-limited long aluminium pipe, RGA, and two gauges, that connected the NEG-Tube for carrying out the measurement. The whole experimental system with the NEG-coated tube was performed the vacuum baking and the NEG-activation and then achieve the ultimate pressure of 2×10^{-10} mbar.

ISBN: 978-3-95450-227-1 ISSN: 2673-5490 doi:10.18429/JACoW-IPAC2022-THPOTK037

MEASUREMENT OF THE PHOTON STIMULATED DESORPTION FOR VARIOUS VACUUM TUBES AT A BEAM LINE OF TLS

G. Y. Hsiung†, C. M. Cheng, NSRRC, Hsinchu, Taiwan
R. Valizadeh, ASTeC Vacuum Science Group, STFC Daresbury Laboratory, Warrington, Cheshire, UK

Abstract

For most light sources, the synchrotron radiation (SR) hit on the beam ducts or absorbers results in higher pressure-rise and the consequent higher radiation level through the commissioning stage. Various surface treatments, e.g. chemical cleaning, oil-free machining, NEG-coating, etc., for the beam ducts or absorbers have developed worldwide for mitigating the yield of Photon Stimulated Desorption (PSD). A beam line, BL19B, of 1.5 GeV Taiwan Light Source (TLS) have modified to measure the PSD-yield of the vacuum tubes. The white light of BL19B covers the critical length at 2.14 keV is suitable for generating higher yield of the photo-electrons (PEY) and the consequent PSD-yield to be measured can be resolved wide range of $10^{-2} \sim 10^{-7}$ molecules/photon. The PSD-outgas, measured by RGA, contains the typical H_2, CO, CO_2, hydrocarbons (C_xH_y), and the Kr from NEG-coating, the alcohol from ethanol-machined surface in some cases. The effect of beam cleaning reflects the PSD-molecules generated from the SR-irradiated surface. This paper will describe the results about PSD-measurement for various vacuum tubes.

INTRODUCTION

The beamline BL19B(PSD) of the 1.5 GeV Taiwan Light Source (TLS) has been constructed since 1999 and dedicated to measure the photon stimulated desorption (PSD) from the samples at UHV for inspecting the qualities of the surface cleaning. The TLS, at the critical photon energy of 2.14 keV, has routinely operated at 362 mA top-up mode that delivered an angular power of 7.35 W/mrad. The yield of PSD was obtained via the throughput method that measures the pressure rise near the sample converted to the outgassing rate and divided by the photon flux. The outgas molecules desorbed from the surface irradiated by the synchrotron radiation (SR) reflects the concentration of the atoms out of the absorbed or residual molecules on the surface or oxide layers. In this paper, the sample tubes including the aluminum (AL), provided by NSRRC, and the titanium (Ti), stainless steel (SS) with NEG-coating, provided by ASTeC were measured. Selection of the tube-materials considered the application as the beam ducts for most of the accelerators that the results of the PSD experiment must be interesting to be a reference.

EXPERIMENTAL

The experiment was carried out by introducing the horizontal photon span of 2.53 mrad, confined by the XY-Slits, from the TLS-BL19B beamline [1]. A machined Reducer Flange (tilted-angle: 3°) was inserted between the beamline and the sample tubes (38 mm I.D., 0.5 m length) that spreads the photon beam on the inner side of tube uniformly. Figure 1 and Fig. 2 show the photographs and the layout of the BL19B (PSD) beamline respectively. In Fig. 2, P1 and P2 indicate the pressures measured closed to the sample tube and the end of beamline, respectively. An aluminum pipe, I.D. 20×68 mm and Long 0.8 m, possesses a conductance (label "C" in Fig. 2) of 10 l/s for the throughput-measurement [2]. A residual gas analyser (RGA) installed near the P1-gauge measures the outgas species dominantly from the tube.

Figure 1: The BL19B (PSD) beamline at TLS.

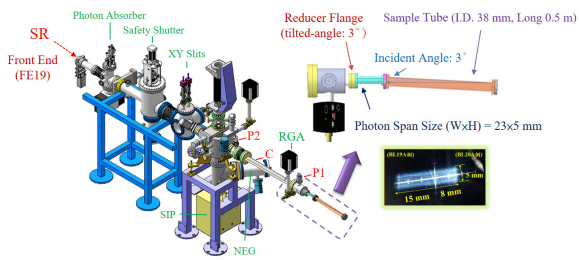

Figure 2: Layout of the experimental system at BL19B.

The four sample tubes for the measurement are listed in Table 1. The AL-1 and AL-2 tubes were machined inside with ethanol (Eth), then AL-2 tube was further cleaned with ozonied water (O_3W: 10 ppm, 30 min) [3]. The Ti-3 tube was originally cleaned via standard proceedure of ASTeC [4], and cleaned with O_3W at NSRRC prior to the experiment. The SS-4 (NEG) tube was prepared and coated the Dual-NEG, TiZrV column and dense, film at ASTeC. All the tubes except the SS-4 were in-situ baked at 150°C, 24 h to the UHV at the ultimate pressure under 2×10^{-10} Torr (2.7×10^{-8} Pa) at the beamline prior to the experiment. While the SS-4 tube was first baked at 80°C, 24 h, only for inspecting the PSD without NEG-activation within a short exposure beam dose (< 0.8 Ah), and then activated the NEG at 180°C, 24 h for another PSD measurement with long exposure dosage afterwards.

† hsiung@nsrrc.org.tw

ISBN: 978-3-95450-227-1 ISSN: 2673-5490 doi:10.18429/JACoW-IPAC2022-THPOTK038

ELECTRON STIMULATED DESORPTION FROM TITANIUM TUBE

O.B. Malyshev†, R. Valizadeh, STFC Daresbury Laboratory, Warrington, UK

Abstract

Titanium is one of the materials that used for production of accelerator vacuum chamber and components. In this paper we report the results of vacuum properties evaluation measurements of titanium vacuum chamber. The sample was produced from 40-mm inner diameter tube made of titanium and equipped with CF40 flanges at both ends. The electron stimulated desorption (ESD) was measured after 24-h bakeout to 80, 150, 180 and 250 °C. H_2 and CO initial sticking probabilities were measured after bakeout before the ESD measurements. After ESD measurements, the initial H_2 and CO sticking probabilities were measured again together with CO sorption capacity. These measurements provide the results for ESD as a function of electron dose baked to different temperatures and demonstrate the efficiency of electron stimulated activation of titanium vacuum chamber.

INTRODUCTION

Titanium and its alloys were investigated in the past as materials for accelerator vacuum chamber that can provide low thermal, photon, electron and ion stimulated desorption yields [1-3]. However, the information on the desorption yields after different treatments and for different conditions is still very limited.

Ti is a well-known getter material which is used in sputter ion pumps (SIP) and evaporable getter (titanium sublimation pumps – TSP). Our earlier studies of non-evaporable getter films demonstrated that a Ti film with a columnar structure shows pumping properties after heating to ≥ 200 °C for 24 hours. Dense Ti structures would require higher activation temperature.

The aims of this work were: (1) to check is any pumping properties of pure Ti material would be measured after heating to 150-300 °C (typical range of temperatures applied for vacuum chamber bakeout), (2) to measure ESD yield from non-baked Ti and after bakeout to 150, 180 and 250 °C, (3) to check if there are effects of electron bombardment stimulated activation similar to one for NEG coatings [4, 5].

SAMPLE

The sample is a tube with an inner diameter of 40 mm and a length of 50 cm, and was produced from titanium tube welded to CH40 flanges made of 316 LN stainless steel at Scanwel Ltd. (Bala, Gwynedd, UK).

The received sample was cleaned at Daresbury Laboratory following standard cleaning procedure [6].

† oleg.malyshev@stfc.ac.uk

ESD FACILITY

A facility for ESD measurement from tubular samples is described in [5]. This facility provides electron bombardment from a hot Thoria coated filament placed along the tube axis. The filament is heated with a current (up to I_f=8 A) from the floating power supply, biasing the filament is possible up to 6.5 kV allowing electron incident energies in the range $0 \le E_e \le 6.5$ keV. The experiments described in this paper were performed with the electron incident energy of E_e = 500 eV and the electron current in the range of $1 < I_e < 30$ mA. The sample temperature was maintained at room temperature. The gas injection line allows the injection of H_2, CH_4, CO, CO_2 and N_2 for RGA calibration, sticking probability, pumping speed and capacity measurements.

EXPERIMENTAL PROCEDURE

After installing the Ti tubular sample on the ESD measurement facility, the test vacuum chamber was pumped out and, after 12 hours pumping, set for a bakeout. In this study, to minimise a possible contamination of the Ti sample, the bakeout procedure was the same as used for the NEG coated samples [1].

The Run 1 procedure consists of the following steps:

a. Initially, all parts of test chamber were heated to 200 °C with exception of the Ti tube heated to 80 °C.
b. After the 24-h bakeout all other parts of test chamber were cooled to 150 °C, while Ti tube remains heated to 80 °C.
c. Thoria filament switched on and degassed, then extractor gauge and RGAs switched on and degassed.
d. After that all parts of test chamber including the sample were cooled to room temperature.
e. The ESD measurement were started after ~12 hours at room temperature.
f. Pumping properties were checked before irradiation started and after irradiation completed.
g. Venting to air for 30 minutes.

The Ti sample temperature of 80 °C is a compromised value allowing us to minimise two effect: it should be sufficiently high to avoid re-condensation of gas species desorbed from other parts of test chamber during their bakeout and, from another side, it should be low in comparison to usual bakeout temperatures (150-300 °C) and it should be sufficiently low to avoid activation of the Ti as a getter material.

The Run 2-4 procedure was different and consists of the following steps:

a. Initially, same as in Run 1, all parts of test chamber were heated to 200 °C with exception of the Ti tube heated to 80 °C.

ISBN: 978-3-95450-227-1 ISSN: 2673-5490 doi:10.18429/JACoW-IPAC2022-THPOTK039

THE EFFECT OF ACTIVATION DURATION ON THE PERFORMANCE OF NON-EVAPORABLE GETTER COATINGS

E. Marshall†, O. B. Malyshev, R. Valizadeh
ASTeC Vacuum Solutions Group, STFC Daresbury Laboratory, Warrington, Cheshire WA4 4AD, UK

Abstract

Non-evaporable getter (NEG) coatings can be activated at temperatures as low as 140°C. However, better pumping properties are achieved using higher temperatures, between 150-300 °C. This paper investigates whether using an increased activation *duration* can improve the NEG properties obtained using lower activation temperatures, and so decrease the energy and temperature requirement. This could allow a greater range of materials to be used in particle accelerator systems. Our findings have shown that increasing activation duration from 24 hrs to 1 week at 160 °C produces an improvement in the NEG pumping properties.

INTRODUCTION

With the aim of increasing the sustainability and efficiency of particle accelerators, non-evaporable getter (NEG) coatings have been increasingly used within their vacuum chambers, allowing tubes with larger aspect ratios (length over diameter) to be used, as their limited conductance is overcome by the distributed pumping provided by the NEG coating [1-5]. This reduces the need for external pumps, and decreases the required baking temperature to reach UHV, thereby decreasing the energy requirement of accelerators.

NEG coatings create a diffusion barrier in the inner walls of vacuum chamber for gas atoms, therefore reducing desorption from the walls. In addition, they absorb residual gas molecules desorbed from uncoated walls, resulting in lower pressures through which a beam can travel. NEG coating structure and composition can be varied to maximise certain properties, such as diffusivity and sorption capacity.

NEG-coated tubes must be activated following installation; a process done by heating to temperatures between 150 and 300 °C [2]. The activation process allows the gasses absorbed onto the surface of the NEG to either be desorbed and pumped away with an external pump (ex.: H_2, Ar, C_xH_y) or diffuse into its bulk (ex.: CO and CO_2), changing the surface state from oxide to metallic, allowing the NEG to absorb residual gases in the vacuum system. This activation process must be repeated in the case when NEG coated surface is saturated with CO, O_2 and CO_2.

Some level of activation has been shown to occur at levels as low as 140 °C [6]. However the lowest activation temperature depends on coating morphology, structure, composition, number of previous activations, etc.

In most previous studies, the NEG coating activation is performed for 24 hrs. However, it is well known for getter pumps that activation temperature can be reduced (within some limits) by increasing a duration of heating. As NEG coating utilises the same materials as these pumps, it is reasonable to expect similar effect take place. Therefore, with the effort to decrease the required activation temperature, this paper investigates the effect of a longer activation duration on NEG coating properties, to see if similar properties can be achieved as compared with 24 hrs at higher temperatures.

SAMPLE PREPARATION

The cylindrical magnetron deposition facility used at Daresbury Laboratory is described in detail in [7]. For each deposition, an alloy TiVZr wire target was used.

For this study, two samples were coated: a copper tube (S-Cu) with inner diameter ID = 20 mm, and an aluminium tube (S-Al) with ID = 36 mm. Both samples were 50 cm in length, and cleaned using a standard Daresbury Laboratory procedure [2] before deposition.

The deposition parameters used to coat each tube are summarised in Table 1. The pressure and power supply were varied with the aim to create different structures in the NEG coating. Pulsed DC was used to create dense coatings, which act as good barriers between the bulk wall material and the vacuum, and so a desirable to prevent degassing. Meanwhile, columnar coatings were created with DC power, along with an order of magnitude higher pressure. Columnar structures provide a larger surface area, and smaller grains, hence more grain boundaries which lead to better diffusivity and greater NEG capacity [6].

Deposition parameters were set with the aim to create a dense coating on S-Al, and a dual coating of dense and columnar layers on S-Cu.

Table 1: Deposition Parameters of NEG Coated Samples

Parameter	S-Cu	S-Al
Gas	Kr	Kr
Target	TiVZr	TiVZr
Layers	Dense/Columnar	Dense
Duration	2hrs 20m + 3 hrs 45m	5 hrs
Power Supply	Pulsed DC/DC	Pulsed DC
Pressure	10^{-2} – 10^{-1} mbar	10^{-3} mbar
Power	70 W	70 W

The structure and composition of the coatings were characterised with scanning electron microscopy (SEM) and Energy Dispersive X-Ray Analysis (EDX).

† eleni.marshall@stfc.ac.uk

ISBN: 978-3-95450-227-1 ISSN: 2673-5490 doi:10.18429/JACoW-IPAC2022-THPOTK040

FEW-NANOSECOND STRIPLINE KICKERS FOR TOP-UP INJECTION INTO PETRA IV

G. Loisch*, V. Belokurov, F. Obier,
Deutsches Elektronen-Synchrotron DESY, Hamburg, Germany

Abstract

PETRA IV is the planned ultralow-emittance upgrade of the PETRA III synchrotron light source at DESY, Hamburg. The current baseline injection scheme is an off-axis, top-up injection with few-nanosecond stripline kickers, which would allow for accumulation and least disturbance of experiments during injection. Besides the requirements on kick-strength, field quality, pulse rise-rate, and heat management, two mechanical designs with different apertures are necessary, as the devices will be used for injection and the transverse multi-bunch feedback system. In this contribution we will present the current status of 3D finite element simulations of electromagnetic fields as well as the mechanical design and first pulse electronics tests.

INTRODUCTION

Several major lightsources have recently been upgraded or are currently undergoing an upgrade to so-called 4th generation light sources, which approach the diffraction limit of the produced synchrotron light with ultra-low emittances in the range of a few 10 pm to 150 pm. One difficult aspect of the beam optics of such low-emittance storage rings is a very limited dynamic aperture. This hinders top-up injection of bunches into the machine and has led to the choice of a full-charge swap-out injection scheme in most designs.
The PETRA IV project aims at upgrading the PETRA III 6 GeV synchrotron radiation facility into a 4th generation light source [1]. Simulations indicate that in PETRA IV top-up injection is nevertheless possible and it is currently pursued as the baseline injection scheme. To limit the impact of an injection event on the stored beam, the kickers in PETRA IV are designed to have a kick duration equal to the target bunch separation of 2 ns. This is only achievable with short stripline kickers, which are being developed for this purpose at DESY. First simulations of the electromagnetic design of these devices have been presented before [2]. In this contribution we will give an update on the kicker magnet requirements for single-bunch top-up injection, show the updated electromagnetic design, and go into some details of the mechanical design and pulse electronics development.

INJECTION KICKER REQUIREMENTS

The stripline design had to be adjusted to the new baseline top-up injection scheme from the original swap-out injection of 80 ns bunch trains. To not constrain the dynamic aperture of the storage ring, the free aperture of the striplines has to be at least 16 mm in diameter. Stripline length and high voltage (HV) pulse duration define the kick strength on neighbouring bunches, which are not being injected into. This residual kick shall be minimised for least disturbance of user experiments during injection. On the other hand, shortening the striplines also reduces the absolute kick strength of one kicker module and ultimately results in a very large number of modules, making injection increasingly complicated. Additionally, the length of every kicker module should be used efficiently. Figure 1 shows analytical calculations for all these criteria. In Fig. 1 (a) half of the assumed, time-symmetric input HV pulses is depicted for several assumed pulse lengths. The absolute kick angle for different lengths is shown in Fig. 1 (b). Efficiency of length usage is judged upon by the relation between actual kick angle and the maximum possible kick angle at a certain voltage and stripline length, which is shown in Fig. 1 (c). Finally, the kick strength on a neighbouring bunch at 2 ns separation relative to the nominal kick strength is shown in Fig. 1 (d).
Based on these calculations, a stripline length of 0.35 m with a flat top pulse length of 2 ns was chosen. The assumed rise and fall times are 0.5 ns.
With these theoretical parameters a total of 16 stripline kicker modules (plus 4 spare modules) would be required for a 4-kicker bumped orbit at the Lambertson-type injection septum in the current lattice design. Pulse voltage has to be adjustable within a range of (8-14) kV in order to provide the required kick strength at the four different positions as well as a certain adjustment range and redundancy.

ELECTROMAGNETIC DESIGN

Simulations of the electromagnetic behaviour of the striplines are performed using CST Microwave Studio. The simulations have been integrated into a Bayesian optimisation routine to allow complex geometry optimisation [2]. The cross-section geometry is shown in the lower right of Fig. 2. A symmetric aperture of 16 mm in diameter is kept free between the stripline blades and the side fenders, which are introduced to reduce capacitive coupling between the blades. The same cross-section geometry is also planned to be used for the striplines of the transverse multi-bunch feedback system of PETRA IV.
In the end sections of the stripline blades, not only the optimal electromagnetic design has to be taken into account, but also constraints as e.g. possibilities for mechanical adjustment of the stripline positions have to be considered. A first optimisation of this has been performed for a prototype of the PETRA IV injection kickers. Simulated reflected pulses at the rising and falling edge of the input current of this prototype exhibit a maximum of 4 % of the incoming

* gregor.loisch@desy.de

ISBN: 978-3-95450-227-1 ISSN: 2673-5490 doi:10.18429/JACoW-IPAC2022-THPOTK041

DEVELOPMENT OF PROGRAMMABLE BIPOLAR MULTI kHz KICKER DRIVERS FOR LONG PULSE SUPERCONDUCTING ELECTRON LINACS

J. L. Teichgräber*, W. Decking, J. Kahl, F. Obier,
Deutsches Elektronen-Synchrotron DESY, Notkestr. 85, Hamburg, Germany

Abstract

Superconducting cavities allow for long RF-pulses, which enable the acceleration of thousands of electron bunches within one RF-pulse. Due to transient effects, e.g. coupler kicks, eddy currents, wakefields or gun properties the beam trajectory can change along the pulse train. To compensate for this, kicker systems based on high-current operational amplifiers (OA) have been developed for the free electron lasers European XFEL and FLASH at DESY in Hamburg. Here, we present the layout of the kicker system, the setup of the pulse electronics and operational results with beam.

INTRODUCTION

During the commissioning the European XFEL used 500 bunches per train [1]. It was later shown that the full specified 2700 bunches in a 600 µs bunch train can be produced at 10 Hz repetition rate. Due to the architecture of the current photo injector laser only completely filled bunch trains can be generated. If the machine is set up with 4.5 MHz bunch repetition rate but an experiment needs a reduced repetition rate the unwanted bunches need to be dumped after the accelerator section. This leads to a high firing rate of the six dump kickers. The continuous use of the dump kickers leads to an accumulation of orbit deviation along the bunch train. This is probably caused by eddy currents in the six simultaneously used stripline kickers [2]. The horizontal orbit deviation leads to the reduction of the SASE intensity after each change in dump kicker repetition rate. A solution to this problem has been successfully tested using programmable bipolar multi kHz kicker drivers with the air coil kickers.

PROBLEM DESCRIPTION

The orbit deviation already showed up during commissioning. In Fig. 1 a deviation of 25 µm is observed for a 100 µs bunch train. The steep curve on the left can be explained by the fact that a large number of bunches was dumped before the shown bunches were used. Then the eddy currents decline due to the reduced dump kicker repetition rate. One solution to this problem could be the transverse intra bunch train feedback system. But using this expensive high bandwidth system for this purpose in addition to correcting various other orbit errors would be increasingly difficult and might bring it to its limit. In this paper a system is presented that uses a commercially available OA to directly drive the air coil kickers shown in Fig. 2.

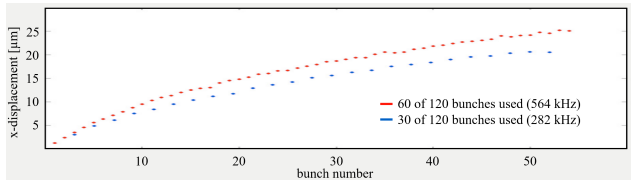

Figure 1: Orbit Deviation in the undulator section of SASE 1. The machine is set up with 1128 kHz repetition rate. The first block of the bunch train is dumped completely. This figure shows the comparison between dumping every second bunch and dumping three of four bunches.

Figure 2: One meter long air coil around the ceramic beam pipe for horizontal correction.

SYSTEM DESCRIPTION

The location of the error source is known and it was decided to do the correction as close to the source as possible. In addition, two kickers are placed in such a way that amplitude and phase in the horizontal plane can be corrected independently. One is placed before and one behind the dump kicker section. The kicker compensation relies on BPM readings from the SASE section.

In the current state the system consists of several different components. The actual kicker is a 1-meter long air coil made of copper strand and a durable polymer. The kicker is built around the ceramic vacuum tube with a thin sputtered metal layer. The kicker magnets are identical to the long pulse beam distribution kickers. The connection from the pulser to the kicker is realized by ten parallel approximately fifteen meter long RG213 cables to reduce resistance and inductance of the connection while having standard connectors. The current towards the kickers flows through the inner conductor while the cable shield is used as the return path. A simplified schematic is shown in Fig. 3. The pulser is basically a powerful OA by Apex Microtechnology [3] which is connected to the pulser output and used as a variable current source. The return current of the kicker is connected to a shunt resistor and the resulting voltage is fed into the negative input of the amplifier. Thus the output current is determined by the voltage applied to the positive amplifier input. To decouple the signal source from the pulser an instrumentation amplifier AD8421 is used at the input of the pulser. A differential input was implemented for increased

* jan.lukas.teichgraeber@desy.de

ISBN: 978-3-95450-227-1 ISSN: 2673-5490 doi:10.18429/JACoW-IPAC2022-THPOTK042

NON-LINEAR PHENOMENA STUDIES IN HIGH-GRADIENT RF TECHNOLOGY FOR HADRONTHERAPY AT IFIC*

P. Martinez-Reviriego†, D. Esperante, N. Fuster-Martínez, B. Gimeno,
D. Gonzalez-Iglesias, P. Martín-Luna, J. Fuster, C. Blanch,
Instituto de Fisica Corpuscular (IFIC), Paterna, Spain
University of Valencia (UV), Valencia, Spain

Abstract

High-Gradient accelerating cavities are one of the main research lines in the development of compact linear colliders. However, the operation of such cavities is currently limited by non-linear effects that are intensified at high electric fields, such as dark currents and radiation emission or RF breakdowns. A new normal-conducting High Gradient S-band Backward Travelling Wave accelerating cavity for medical application (v=0.38c) designed and constructed at CERN is being tested at IFIC. In this paper, we present experimental measurements and simulation of such non-linear effects. The main goal of these studies is to establish the viability of using these techniques in linear accelerators, in order to improve our understanding in such effects. The main goal of these studies is to determine the viability of techniques in linear accelerators for hadrontherapy treatments in hospitals.

THE IFIC HIGH-POWER S-BAND FACILITY

The design of High-Gradient (HG) accelerating cavities is a key issue in the development of compact linear accelerators. The Compact Linear collaboration [1] developed accelerating cavities capable of reaching accelerating gradients of the order of 100 MV/m compared with the 20-30 MV/m achieved by traditional technology.

Continuous efforts are made to apply this technology for medical and industry applications. In particular, the use of the HG technology is being investigated to develop compact linear accelerators for hadrontherapy. Currently, circular accelerators are used for hadrontherapy due to their compactness. However, linear accelerators have the advantage of a fast energy modulation which could be of great interest for 3D dose painting and to treat moving organs.

Nevertheless, the intense electromagnetic fields in HG technology lead to undesirable non-linear effects, i.e., electrons emission from the cavity walls due to field emission, also called dark currents, and vacuum discharges, known as RF breakdowns. These effects, in addition lead to beam instabilities and high radioactive dose emission, preventing the cavities from reaching straightaway the designed gradient. Thus, an RF conditioning treatment is needed for this kind of structures in order to work at high gradients under an acceptable confidence level of performance. The breakdown rate (BDR), defined as the number of breakdowns per pulse and unit length increases as:

$$BDR \propto E_{acc}^{30} \cdot \tau^5, \quad (1)$$

where E_{acc} is the accelerating gradient and τ the pulse length.

At the Instituto de Fisica Corpuscular (IFIC) a High-Power S-Band (3 GHz) Radio-Frequency laboratory was built to condition and characterize HG cavities as well as to investigate the mechanism of vacuum arcs and RF breakdowns. This laboratory works at a central frequency of 2.9985 GHz. The laboratory at IFIC was designed to reach a peak power of 15 MW with pulses of 5 μs length and it is capable of performing the conditioning of two structures at 200 Hz simultaneously or one structure at 400 Hz.

THE BTW S-BAND CAVITY

A new design for a HG Backward Travelling Wave (BTW) cavity for low energy protons was developed and manufactured at CERN for the TUrning LInac for Protontherapy (TULIP) [2]. The main parameters of the cavity summarized in Table 1 and a picture of the cavity is shown in Fig. 1.

Table 1: BTW RF Accelerating Cavity Main Parameters

Parameter (unit)	Value
Frequency (GHz)	2.9985
Phase advance per cell (rad)	$5\pi/6$
Phase velocity	0.38c
Pulse width (μs)	2.5
Average accelerating gradient (MV/m)	50
Number of cells	12
Structure length (mm)	189.9
Quality factor (first/last cell)	6954/7415
Normalised shut impedance (MΩ/m)	51.5/54.6
Filling time (ns)	224
Group velocity (first/last cell) (%c)	0.39/0.21
Peak input power (MW)	20.6
Max S_c/E_a^2 (A/V)	3.1×10^{-4}
Max E_s (MV/m)	219

In Fig. 2 the Modified Poynting Vector of one coupling cell is shown [3]. It is maximum in the iris, due to the high surface electric field, and also in the upper coupling hole, because of the high magnetic field.

* Work supported by Ministerio de Universidades (Gobierno de España) under grant number FPU19/00585 and Generalitat Valenciana CDEIGENT/2021/012
† pablo.martinez.reviriego@ific.uv.es

ISBN: 978-3-95450-227-1 ISSN: 2673-5490 doi:10.18429/JACoW-IPAC2022-THPOTK043

MITIGATION OF HIGH VOLTAGE BREAKDOWN OF THE BEAM SCREEN OF A CERN SPS INJECTION KICKER MAGNET

M.J. Barnes, W. Bartmann, M. Díaz, L. Ducimetière, L. Feliciano,
T. Kramer, V. Namora, D. Standen, T. Stadlbauer, P. Trubacova, F. Velotti, C. Zannini
CERN, Geneva, Switzerland

Abstract

The SPS injection kicker magnets (MKP) were developed in the 1970's, before beam induced power deposition was considered an issue. These magnets are very lossy from a beam impedance perspective: this is expected to be an issue during SPS operation with the higher intensity beams needed for HL-LHC. A design, with serigraphy applied to an alumina carrier, has been developed to significantly reduce the broadband beam coupling impedance and hence mitigate the heating issues. During high voltage pulse testing there were electrical discharges associated with the serigraphy. Detailed mathematical models have been developed to aid in understanding the transiently induced voltages and to reduce the magnitude and duration of electric field. In this paper, we discuss the solutions implemented to mitigate the electrical discharges while maintaining an adequately low beam-coupling impedance. In addition, the results of high voltage tests are reported.

INTRODUCTION

In CERN's Super Proton Synchrotron (SPS), a fast kicker system (MKP) is used for injection of the beam into the accelerator [1]. Two different types of the MKP magnets are used - the MKP-S and MKP-L. The MKP-S has an aperture of 100 mm wide by 61 mm high and the MKP-L aperture is 141.5 mm wide by 54 mm high: the width is the distance between the high voltage (HV) and return conductors. The two apertures are used to both meet optics requirements and provide the required deflection, within the constraints of available length and voltage and current demands on the pulse generators. The MKP magnets are transmission line type, constructed of multiple cells and operated in machine vacuum: the MKP-L has 22 cells.

As a result of the difference in the aperture dimensions, between the MKP-S and MKP-L modules, the real part of the beam coupling impedance of the MKP-L is generally significantly higher than that of the MKP-S [2]. Figure 1 shows temperature and pressure measurements, during March 2022, for an MKP-S and an MKP-L: the measured temperature rise of the MKP-L module is a factor of 3 to 4 times higher than for the MKP-S. The relatively large temperature rise of the MKP-L is attributable to its high beam coupling impedance. The temperature probes are mounted on the MKP side plate, which is at ground potential. Hence, the ferrite temperature will be higher than measured during beam induced heating [3]. The measured pressure in the MKP-L tank is considerably higher than for the MKP-S tank. The pressure consists of both a static component (without beam) and a dynamic component (i.e. due to Electron cloud). The static pressure (the envelope of the base of the pressure) reaches a maximum of $\sim 5 \times 10^{-7}$ mbar for the MKP-L – this is mainly due to the heating of the ferrite: during the scrubbing, to avoid damage to the MKP-L modules, the measured temperature was purposefully limited to 70°C, and thus limited scrubbing [4]. The dynamic pressure, which is the difference between the envelope of the peak pressure and the static pressure, is also significant for the MKP-L.

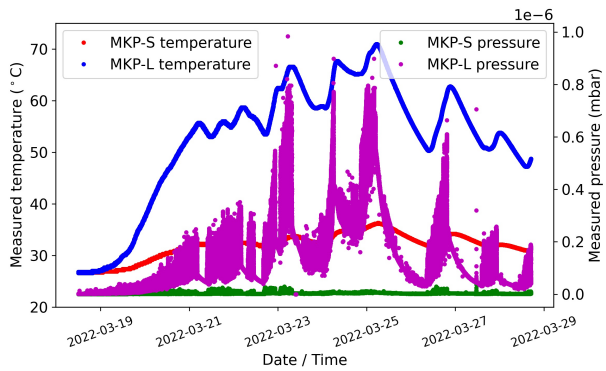

Figure 1: Temperature and pressure measurements, during March 2022, for an MKP-S module and an MKP-L module.

With the advent of higher bunch intensities for High Luminosity LHC, higher beam induced heating is expected in the ferrite yoke of the MKP-L, and will result in its Curie point being reached and unacceptably high static pressure. A design that mitigates the high heat load, which uses serigraphy, has been developed [2, 5, 6]. However, during high-voltage (HV) pulse testing, issues were encountered with the design: thus, it was necessary to re-optimise the design of the serigraphy for both beam impedance and HV behaviour.

SERIGRAPHY DESIGN

The cells of the MKP-L module are too short to apply serigraphy directly to the ferrite yoke [2]. Hence, a carrier is required to mechanically support the serigraphy in the aperture: alumina has been chosen for this purpose. The alumina will reduce the aperture available to the beam in the MKP-L's. Hence, a detailed model of the injection region has been constructed and subsequent aperture studies carried out [7]. These studies defined both the required beam aperture and good field regions at the entrance and exit of the MKP-L magnet [7], and hence defined the maximum thickness of the alumina.

During HV pulse conditioning a Pulse Forming Network (PFN), which is charged to a positive voltage, is discharged

ISBN: 978-3-95450-227-1 ISSN: 2673-5490 doi:10.18429/JACoW-IPAC2022-THPOTK044

ULTRA-FAST GENERATOR FOR IMPACT IONIZATION TRIGGERING*

A. A. del Barrio Montañés†[1], V. Senaj, T. Kramer, Y. Dutheil, CERN, Geneva, Switzerland
M. Sack, Karlsruhe Institute of Technology, Karlsruhe, Germany
[1] also at Karlsruhe Institute of Technology, Karlsruhe, Germany

Abstract

Impact ionization triggering can be successfully applied to standard thyristors, thus boosting their dI/dt capability by up to 1000x. This ground-breaking triggering requires applying significant overvoltage on the anode-cathode of a thyristor with a slew rate > 1 kV/ns. Compact pulse generators based on commercial off-the-shelf (COTS) components would allow the spread of this technology into numerous applications, including fast kicker generators for particle accelerators.

In our approach, the beginning of the triggering chain is an HV SiC MOS with an ultra-fast super-boosting gate driver. The super boosting of a 1.7 kV rated SiC MOS allows to reduce the MOS rise time by a factor of > 26 (datasheet tr = 20 ns vs. measured tr < 800 ps), resulting in an output voltage slew rate > 1 kV/ns and an amplitude > 1 kV.

Additional boosting is obtained by a Marx generator with GaAs diodes, reaching an output voltage slew rate > 11 kV/ns. The final stage will be a Marx generator with medium size thyristors triggered in impact ionization mode with sufficient voltage and current rating necessary for the triggering of a high power thyristor.

This paper presents the impact ionization triggering of a small size thyristor.

INTRODUCTION

In beam transfer facilities for particle accelerators, magnets generally require multi kV/kA pulse generators. Presently this is achieved using thyratrons. However, these devices present several disadvantages such as erratic firing, their need of complex triggering and biasing electronics, their rarity, approaching obsolescence and high cost. These factors are driving their replacement by semiconductor switches.

Recent investigations have shown that switching semiconductors using impact ionization mode is a viable option to replace thyratrons. Impact ionization is achieved when a high dU/dt creates an ionization wavefront in the semiconductor structure. This ultra fast switching technique is even feasible in cheap commercially available thyristors [1]. Thyristors are cheaper and faster than thyratrons (when triggered in impact ionization mode), and offer a higher current density compared to thyratrons.

The following conditions are necessary to achieve impact ionisation on a thyristor:

- A voltage applied by the triggering circuit on the anode-cathode of the thyristor more than double the static breakdown voltage
- Said triggering voltage requires a slew rate of >1 kV/ns in order to create the right conditions in the semiconductor structure
- All this while providing enough current to charge the parasitic capacitance of the thyristor with the required dU/dt.

In this paper, we present a Marx generator based topology that achieves impact ionization triggering in a small size (D2PAK) thyristor.

METHODOLOGY

Traditionally, as seen in [2], the triggering generators for impact ionization used drift step recovery diodes (DSRD) and semiconductor opening switch (SOS) diodes. Generators based on both of these components are bulky, require relatively long pre-charging and more importantly, DSRD and SOS themselves are not commercially available. This is why we propose an alternative approach, based on three main stages.

The first stage has been described in [3] and [4]: ultra-fast MOSFET triggering based on the upgraded gate boosting technique outlined by M. Hochberg *et al*. [5]. M. Azizi *et al* presented in [6] a gate-boosting driving method optimized for a SiC MOSFET to reduce its turn-on time. Our SiC MOSFETs were more aggressively gate-boosted, resulting in an acceleration of their rise time by a factor of >26, depending on the device.

In order to more aggressively boost the MOS device, as per the depicted method in [4], we developed a driver that can deliver 430 V/ns onto a 50 Ω load, with a maximum output voltage >300 V. The resulting output voltage is presented in Fig. 1, indicated by the blue lines.

This SiC MOSFET, the second stage of the series, was tested onto a 50 Ω load (by mistake up to 2.1 kV, and survived) at the nominal voltage of 1.3 kV and it produced a 1.2 kV/ns slew rate, as seen in Fig. 2. Once these parameters are achieved, we can use this pulse generator for impact ionization triggering in the third stage.

The third stage is an ultra-fast Marx generator with GaAs diodes switched in impact ionization mode acting as switches. As seen in Fig. 3, this generator is made up of multiple stages of 900 V rated GaAs diodes [7]; their number depends on the required output voltage amplitude. The triggering of this Marx generator is conducted by a super-boosted SiC MOSFET (Infineon IMBF170R450M1), thanks

* This work has been sponsored by the Wolfgang Gentner Programme of the German Federal Ministry of Education and Research
† alicia.ana.del.barrio.montanes@cern.ch

ISBN: 978-3-95450-227-1 ISSN: 2673-5490 doi:10.18429/JACoW-IPAC2022-THPOTK045

BRANCH MODULE FOR AN INDUCTIVE VOLTAGE ADDER FOR DRIVING KICKER MAGNETS WITH A SHORT CIRCUIT TERMINATION*

J. Ruf†, M.J. Barnes, Y. Dutheil, T. Kramer, CERN, Geneva, Switzerland
M. Sack, KIT, Karlsruhe, Germany

Abstract

For driving kicker magnets terminated in a short circuit, a branch module for an inductive voltage adder has been designed and assembled. The module has been designed for a maximum charging voltage of 1.2 kV and an output current of 200 A considering the current doubling due to the short circuit termination. It features three consecutive modes of operation: energy injection, freewheeling, and energy extraction. Therefore, the topology of the branch module consists of two independently controlled SiC MOSFET switches and one diode switch. In order not to extend the field rise time of the kicker magnet significantly beyond the magnet fill time, the pulse must have a fast rise time. Hence, the switch for energy injection is driven by a gate boosting driver featuring a half bridge of GaN HEMTs and a driving voltage of 80 V. Measurements of the drain source voltage of this switch showed a fall time of 2.7 ns at a voltage of 600 V resulting in a voltage rise time of 5.4 ns at the output terminated with a resistive load. To meet both the rise time and current requirements, a parallel configuration of four SiC MOSFETs was implemented.

INTRODUCTION

At present, installations at CERN, for driving kicker magnets equipped with a short-circuit termination, comprise pulse generators based on transmission lines [1]. For some of these transmission-line based generators, a future replacement by an inductive voltage adder is currently under investigation. The inductive voltage adder comprises branch modules which are paralleled in layers for sharing the load current and stacked for adding up the voltage. The inductive voltage adder usually feeds into a matched load. Thereby, the match between the power to be fed into the load impedance and the power delivered by one module is made by an appropriate selection of the number of modules per layer and the number of stacked layers.

When driving a transmission line type kicker magnet terminated in a short circuit, with a low impedance source like an inductive adder, the following mode of operation can be used to deal with the reflections from the termination [2]. Initially, the generator outputs a voltage that travels as a wave along the connecting cable and the transmission line type kicker magnet. The wave is reflected at the short circuit termination and travels back to the pulse generator, causing a doubling of the current. Thereby, energy is fed into the system comprising the connecting cable and the kicker magnet and is stored as magnetic energy. Once the reflected wave reaches the pulse generator, the generator stops feeding energy into the system. Hence, the voltage over the output of the pulse generator settles to zero, disregarding losses. Finally, at the end of the pulse, the energy is extracted from the load.

CIRCUIT TOPOLOGY OF THE BRANCH MODULE

In order to implement the functionality described above, the branch modules of the inductive voltage adder need to be equipped with an appropriate circuitry. Figures 1 and 2 show a simplified schematic with an appropriate arrangement of MOSFET switches, and a capacitor C_{pulse} to store initial energy. The circuit elements in Figs. 1 and 2 can each represent multiple paralleled components.

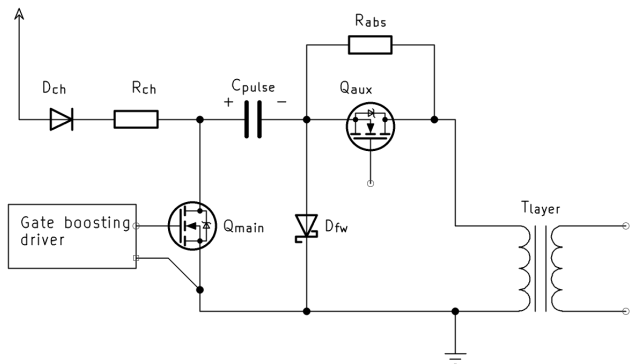

Figure 1: Simplified circuit diagram of one branch module with a resistor R_{abs} for dissipating the energy. (R_{abs} = 10 Ω; Q_{main} = 25µF; Q_{main}: 4 × G3R160MT17J; Q_{aux}: 2 × C2M0045170P; D_{fw}: 2 × GB25MPS17-247).

Initially, the capacitor is charged via the circuit elements D_{ch}, R_{ch}, and D_{fw}. Thereby, D_{ch} prevents undesired discharging. To transfer energy from the capacitor to the load, consisting of the cable and the kicker magnet, both MOSFET switches Q_{main} and Q_{aux} are closed. Thereby, the transformer T_{layer} is part of the inductive adder and serves for combining the current originating from the branch modules of one layer. The output wave from T_{layer} travels through the kicker magnet to the short circuit. When the wave reflected from the short circuit reaches the module, switch Q_{main} opens, and the current commutates into the freewheeling diode D_{fw}. For extracting the energy at the end of the pulse switch Q_{aux} opens, and the energy stored in the load dissipates in the resistor R_{abs}. Alternatively, in order to recuperate the extracted energy back into the capacitor C_{pulse} a diode D_{rec}

* This work has been sponsored by the Wolfgang Gentner Programme of the German Federal Ministry of Education and Research.
† johannes.ruf@cern.ch

ISBN: 978-3-95450-227-1 ISSN: 2673-5490 doi:10.18429/JACoW-IPAC2022-THPOTK048

RADIATION LOAD STUDIES FOR THE FCC-ee POSITRON SOURCE WITH A SUPERCONDUCTING MATCHING DEVICE*

B. Humann†[1], A. Lechner, Y. Zhao, A. Latina, CERN, Geneva, Switzerland
B. Auchmann, J. Kosse, PSI, Villingen, Switzerland
I. Chaikovska, S. Ogur, CNRS/IN2P3, Orsay, France
[1]also at TU Wien, Vienna, Austria

Abstract

For an electron-positron collider like the Future Circular Collider lepton machine (FCC-ee), the production of positrons plays a crucial role. One of the design options considered for the FCC-ee positron source employs a superconducting solenoid made of high temperature superconductor coils as an adiabatic matching device. The solenoid, which is placed around the production target, is needed to capture positrons before they can be accelerated in a linear accelerator. A superconducting solenoid yields a higher peak field than a conventional normal-conducting matching device, therefore increasing the achievable positron yield. In order to achieve an acceptable positron production, the considered target is made of tungsten-rhenium, which gives also a significant flux of unwanted secondary particles, that in turn could generate a too large radiation load on the superconducting coils. In this study, we assess the feasibility of such a positron source by studying the heat load and long-term radiation damage in the superconducting matching device and surrounding structures. Results are presented for different geometric configurations of the matching device.

INTRODUCTION

The Future Circular Collider lepton machine (FCC-ee) is one option for a new collider at CERN [1]. With a circumference of around 91 km it is meant to store and collide electrons and positrons with different beam energies ranging from 45.6 GeV to 182.5 GeV. The different operation modes enable precision measurements over a wide energy range, spanning from the Z pole to the $t\bar{t}$ threshold. Operation relies on the production of high-intensity and low-emittance positron beams, both for filling the collider when empty and for top-up injection. [2]. Positron sources typically use an adiabatic matching device for capturing positrons from a heavy target before they can be accelerated in a first linear accelerator. The baseline solution considered for FCC-ee assumes a classical magnetic matching device consisting of a tapered normal-conducting solenoid downstream of the target [3]. The entire assembly is further enclosed by bridge coils. A similar solution is already used for the positron source at SuperKEKB [4]. As a novel alternative for FCC, a superconducting solenoid made of YBCO tapes is considered. Using a superconducting matching device allows for higher magnetic field, which in turn enables a higher positron yield. A demonstrator of such a high-temperature superconductor (HTS)-based positron source, called P^3, will be built at the SwissFEL facility at PSI [5].

Although a superconducting matching device is beneficial for the positron yield, it exhibits a higher sensitivity to radiation. In this paper, we present first radiation load studies for a FCC-ee positron source with HTS coils. The studies were carried out with the FLUKA Monte Carlo code [6–8], which is commonly used for shielding calculations. We consider two different configurations with different coil and beam apertures, one being similar to the P^3 experiment [5], whereas the second layout has a larger vacuum chamber. For both configurations, we quantify the instantaneous power deposition and the cumulative radiation damage. The results are scaled to collider operation at the Z pole (45.6 GeV), which requires the highest positron intensity [1]. The assumed electron drive beam has an energy of 6 GeV and a beam spot size of 0.5 mm rms at the target. The repetition rate lies at 200 Hz, with a electron bunch charge of 1.43 nC and two bunches per pulse, which leads to a drive beam power of 3.43 kW [9]. This beam power is needed when refilling the collider when empty, but is around one order of magnitude less during top-up injection [1].

SIMULATION SETUP

In this study, a conventional target configuration is considered (see Fig. 1), where the electron drive beam directly impacts on a disk made of tungsten-rhenium alloy. When the electrons enter the target, they emit electromagnetic radiation in the form of Bremsstrahlung photons. The produced photons are then subject to electron-positron pair production. These two processes happen in form of a cascade, as long as the energy is high enough. After the target, photons, electrons and positrons can be found. An alternative production scheme under consideration for the FCC-ee is based on a hybrid setup [3], where the electron beam first generates photons through coherent interaction with a crystal; the photons then impact on a target, where positrons are produced. However, this alternative scheme is not considered here. The target thickness is selected to be $5X_0$ (17.5 mm), with X_0 being the radiation length. The target thickness has been optimised for the positron yield in a separate study [10]. The engineering and cooling design of the target, as well as the target integration inside the cryostat are beyond the scope of this paper. We therefore consider a simple stationary disk.

In the following, two different versions of the matching device are discussed (see Fig. 2), that have similar gross

* Work supported by FCC.
† barbara.humann@cern.ch

ISBN: 978-3-95450-227-1 ISSN: 2673-5490 doi:10.18429/JACoW-IPAC2022-THPOTK049

IRRADIATION OF LOW-Z CARBON-BASED MATERIALS WITH 440 GeV/c PROTON BEAM FOR HIGH ENERGY & INTENSITY BEAM ABSORBERS: THE CERN HiRadMat-56-HED EXPERIMENT

P. Andreu-Muñoz†, E. M. Farina, F-X. Nuiry, A. Krainer, J. Maestre, A. Lechner, M. Calviani, R. Seidenbinder, C. Torregrosa, P. Simon, N. Charitonidis, CERN, Geneva, Switzerland

Abstract

The beam stored energy and the peak intensity of CERN Large Hadron Collider (LHC) will grow in the next few years. The former will increase from max. of 320 MJ for Run2 (2015-2018) to almost 555 MJ during Run3 (2022 onwards) and 709 MJ during the HL-LHC era, putting stringent requirements on beam intercepting devices, such as absorbers and dumps. The HiRadMat-56-HED (High-Energy Dumps) experiment performed in Autumn 2021 executed at CERN HiRadMat facility employed the Super Proton Synchrotron accelerator (SPS) 440 GeV/c proton beam to impact different low-density carbon-based materials targets to assess their performance to these higher energy beam conditions. The study focused on advanced grades of graphitic materials, including isostatic graphite, carbon-fibre reinforced carbon and carbon-SiC materials in addition to flexible expanded graphite. Some of them precisely tailored in collaboration with industry to specific properties. The objectives of this experiment are: (i) to assess the performance of existing and potentially suitable advanced materials for the currently operating LHC beam dumps and (ii) to study alternative materials for the HL-LHC main dump or for the Future Circular Collider dump systems. This contribution will detail the R&D phase during design, the execution of the experiment, the pre-irradiation tests as well as the first post irradiation examination of the target materials. Lessons learnt and impact on operational devices will also be drawn.

INTRODUCTION

The LHC operates with a Beam Dumping System (LBDS) that is critical for its safe operation. The LBDS [1] is based on a fast beam extraction system made of a series of kicker and septum magnets used to deviate the two counter-rotating beams from the LHC ring towards two extraction lines. Each one of these extraction lines finishes on a different Target Dump External (TDE) unit.

The LHC TDE beam absorbing core is composed of six blocks of isostatic graphite (SGL Sigrafine® 7300), two 50 mm extruded graphite plates (SGL Sigrafine® HLM) and 1630 sheets, each 2 mm thick, of flexible expanded graphite (SGL Sigraflex® L20012C). The TDE core is designed to dilute and diffuse the energy of the beam [2]. The stored energy of the LHC beam during Run3 (2022-2025) will be higher than original LHC ultimate design values (523 MJ) [3].

The operational challenges encountered in LHC Run2 (2015-2018) on the two LHC TDE units were solved during Long Shut Down 2 (LS2) by a thorough programme of upgrades on the TDE spare units, which then became the main in-operation units [4, 5]. Nevertheless, experimental results from HiRadMat-43 (2018) [6], highlighted the importance of finding low-density Carbon-based alternatives to be used within the TDE core. During this experiment (HRMT-43), four Sigraflex® sheets received 440 GeV/c proton beam impacts to assess their performance to Run3 peak energy density values (2.35 kJ/g - 2.5 kJ/g). These sheets delaminated, bursting within their bulk, and causing permanent deformations of up to 250 µm on both sheet sides [6,7]. As options for the TDE low-density region [8], Carbon-Fibre-Reinforced-Carbon (CC) grades were considered due to their low density, good mechanical and thermo-mechanical properties and their non-fragile behaviour [9]. Moreover, HiRadMat-56-HED experiment included CCs currently implemented in two LHC beam extraction absorbers (TCDQ [10] and TCDS [11]). Finally, the design and material choices for the FCC-ee dumping system spoiler were assessed [12]. To fulfil all the experiment objectives a R&D campaign was carried out.

EXPERIMENT R&D

The HiRadMat [13, 14] beam (extracted from the SPS) was not capable of delivering by default the peak energy densities expected during Run3 and HL-LHC (> 2.5 kJ/g) on the targets, this triggered thorough R&D studies. The temperature and thermal strain fields obtained for HiRadMat-56 samples simulations had to represent the conditions calculated for the HL-LHC operational cases. To approach the experiment results to simulations, a deep R&D campaign was performed where beam diluters (used to increase the peak energy density on targets), specific targets and beam optics were designed for the HMRT-56 experiment and installed inside an Aluminium tank [8].

The proposed target design (Fig. 1 – (a)) features three disks of CC stacked together, inside an aluminium hollow cylinder. These targets axis is collinear with the beam trajectory, allowing to send four beam pulses at their centre. CC disks are axially constrained with Sigraflex® washers, contact springs and Titanium bolts.

Figure 1: CC Target model (a) & Diluter model (b) [10].

† pablo.andreu.munoz@cern.ch

ISBN: 978-3-95450-227-1 ISSN: 2673-5490 doi:10.18429/JACoW-IPAC2022-THPOTK050

CFD STUDIES OF THE CONVECTIVE HEAT TRANSFER COEFFICIENTS AND PRESSURE DROPS IN GEOMETRIES APPLIED TO WATER COOLING CHANNELS OF THE CROTCH ABSORBERS OF ALBA SYNCHROTRON LIGHT SOURCE

S. Grozavu*, G. Raush†,
Terrassa School of Industrial, Aerospace and Audiovisual Engineering (ESEIAAT), Terrassa, Spain
J.J. Casas‡, C. Colldelram§, M. Quispe¶, ALBA-CELLS Synchrotron, Cerdanyola del Vallés, Spain

Abstract

Currently, the storage ring vacuum chambers of ALBA are protected by 156 crotch absorbers made of copper and Glidcop. After more than 10 years of operation as a third-generation light source, the ALBA II project arose, aiming to transform this infrastructure into a fourth-generation synchrotron. This introduces new challenges in terms of the thermal and mechanical design of the future absorbers.

The absorbers' cooling channels consist of a set of 8-mm-diameter holes parallel to each other and drilled in the body of the absorbers. In each hole, there is a 6x1 mm stainless steel concentric inner tube coiled in spiral wires, whose aim is to enhance the heat transfer. The convective heat transfer coefficients used for the original design of the absorbers come from experimental correlations from the literature, and are applied as a global value for the whole system.

In this work, Heat Transfer-Computational Fluid Dynamics (HT-CFD) studies of the convective heat transfer coefficients and pressure gradients in three different cooling channel geometries are carried out, aiming at leading the way of designing the cooling systems toward the CFD simulations rather than applying global experimental values. This information will be useful for the sizing of the new absorbers for the ALBA II project.

INTRODUCTION

Modern synchrotron light sources widely utilize crotch absorbers to protect the vacuum chambers from synchrotron radiation, and their proper refrigeration is essential for their optimal functioning since they are exposed to very high power densities [1]. The impact of the geometry of the refrigeration capacity of their cooling channels has not been properly reported, and there is little information in the specific literature.

The aim of this research is to perform HT-CFD studies of the fluid inside different refrigeration channel geometries, in order to better understand the heat transfer phenomenon and quantify how conservative or optimistic experimental correlations from the literature are.

* grozavustefania@gmail.com
† gustavo.raush@upc.edu
‡ jcasas@cells.es
§ ccolldelram@cells.es
¶ mquispe@cells.es

METHODOLOGY

The methodology followed for the obtainment of the presented results has been designed in order to set a rigorous foundation above which increased difficulty of simulation could be reliable despite the complex geometry of the problem.

Geometry

This methodology consists in three blocks distinguished by the cooling channels' geometry (depicted in Fig. 2):

1. *Stage 1*: Conventional circular section channel. Simulation of the fluid flow inside a 8 mm diameter channel of 500 mm length.
2. *Stage 2*: Concentric channels. Simulation of the fluid flow along concentric channels formed between the 8 mm diameter orifice and a 6x1 mm pipe inserted inside, leaving a 4 mm length free end where the reversing of the flow occurs.
3. *Stage 3*: Concentric channels with spiral wire. The geometry is equivalent to the latter stage, except for the addition of a 0.9 mm diameter spiral wire wrapped around the exterior of the interior pipe.

Meshing

O-grid structured mesh has been employed for the cylindrical portions and along all the wall boundaries inside the fluid, inflation layers had been introduced for a smooth transition of the mesh until reaching a $y^+ \approx 1$ [2], essential for the proper implementation of $k - \omega$ and SST viscous models. For the complex fluid zones, tetrahedrons have been employed. These characteristics can be observed in Fig. 1.

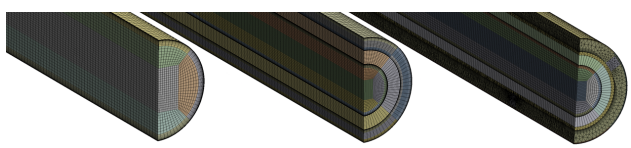

Figure 1: Finest meshes detail of (from left to right): Stage 1 (2.5 M), Stage 2 (5.7 M), and Stage 3 (9.0 M).

Also, a grid convergence study of three levels of mesh refinement has been performed, implementing the 'convergence' Python program provided as a part of the NASA Examining Spatial (Grid) Convergence tutorial [3].

ISBN: 978-3-95450-227-1 ISSN: 2673-5490 doi:10.18429/JACoW-IPAC2022-THPOTK051

CORROSION OF COPPER COMPONENTS IN THE DEIONIZED WATER COOLING SYSTEM OF ALBA SYNCHROTRON LIGHT SOURCE: CURRENT RESEARCH STATUS AND CHALLENGES

M. Quispe†, E. Ayas, J.J. Casas, C. Colldelram, Ll. Fuentes, J. Iglesias, ALBA – CELLS Synchrotron, Cerdanyola del Vallès, Spain
A. Garcia, La Romanica, Sabadell, Spain

Abstract

Currently, the ALBA Synchrotron Light Source is carrying out studies on corrosion in copper components of the deionized water cooling circuit. The preliminary studies, based on Scanning Electron Microscopy (SEM), Energy Dispersive X-Ray Spectroscopy (EDS), and X-Ray Diffraction (XRD) have shown the presence of intergranular, pitting, and generalized corrosion in the analysed copper samples. The purpose of this paper is to present new advances in the field of this research, such as: the study of the influence of low velocity water flow in the cooling circuit on the current high dissolved oxygen content (> 6500 ppb), the results of corrosion products found in the cooling circuit, the description of the improper operation of the cooling circuit as a closed loop, and FEA studies of copper components in order to redefine the water flow velocity design criteria to values lower than 3 m/s and thus minimize corrosion by erosion. Finally, in order to attenuate the corrosion rate, preventive solutions are presented such as the viability to install an oxygen content degassing plant, new instrumentation for water quality monitorization, and installation of degassing equipment at strategic positions of the cooling circuit.

BACKGROUND

The requirement of deionized water (DIW) for cooling in Accelerators has brought an added problem: an increase in the rate of corrosion of the copper components. This particularity has an impact on the lifetime, as well as on the operation of the Accelerators. This problem has been extensively studied [1-7], and there is a consensus on the alternative to attenuate its effect, according to which, following the experimental correlation pH vs concentration of dissolved oxygen (DO) [8], it is advisable to fix the properties of the water in the "low-oxygen alkaline region" of regime 1 (see Fig. 1). Although the corrosion rate in regime 2 is similar to that of regime 1, however, to be in regime 2 it would be necessary to increase the pH above 7.6. On the other hand, for values of DO content < 10 ppb and with pH values from 7.2, we would easily be in regime 1. This last option is the most feasible technical solution, and has been applied by most of the Accelerators.

In the case of ALBA, the quality of the DIW has been very irregular. Based on the evolution of the pH reported since 2012 [9], our water quality has oscillated between regimes 3, 4 and 5. Currently our goal is to work in regime 1. This would allow reducing the corrosion rate to a range between 4 to 10 times lower compared to our current situation.

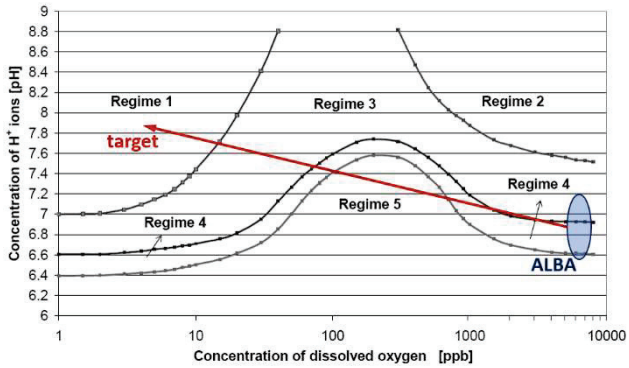

Figure 1: Copper corrosion rates. Regimes 1 and 2: < 0.1 µg/(cm^{2}y), regime 3: 0.1-0.4 µg/(cm^{2}y), regime 4: 0.4-1 µg/(cm^{2}y) and regime 5: > 1.0 µg/(cm^{2}y).

FIRST STUDIES

The visual inspections of the first samples taken during the years 2018, 2019 and 2020, have confirmed the first evidences of corrosion in ALBA after more than 10 years of operation. A common pattern has been found in all the samples: surfaces with moderate to high roughness, such as the examples of cases (b), (c) and (d) of Fig. 2, corresponding to pieces of the masks of the Front Ends BL11 and BL13 and the radiofrequency cavity of the Storage Ring (SR), respectively.

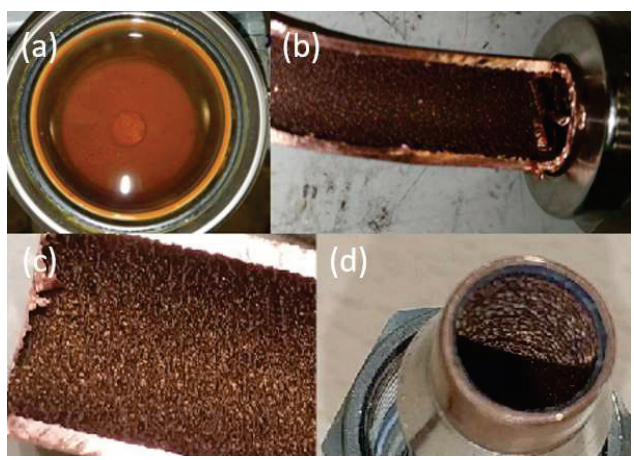

Figure 2: Visual signs of corrosion in ALBA. (a) Copper oxide particles; (b, c, and d) Pieces of the masks in BL11 and BL13 and of the radiofrequency cavity of the SR.

†mquispe@cells.es

ISBN: 978-3-95450-227-1 ISSN: 2673-5490 doi:10.18429/JACoW-IPAC2022-THPOTK052

MUON COLLIDER GRAPHITE TARGET STUDIES AND DEMONSTRATOR LAYOUT POSSIBILITIES AT CERN

F. J. Saura*, R. Franqueira†, D. Calzolari, M. Calviani, A. Lechner,
R. Losito, D. Schulte, A. M. Krainer, CERN, Geneva, Switzerland
C. Rogers, STFC Rutherford Appleton Laboratory, Harwell Oxford, Didcot, OX11 0QX, UK

Abstract

Muon colliders offer enormous potential for research of the particle physics frontier. Leptons can be accelerated without suffering large synchrotron radiation losses. The International Muon Collider Collaboration is considering 3 and 10 TeV (CM) machines for a conceptual stage. In the core of the Muon Collider facility lays a MW class production target, which will absorb a high power (1 and 3 MW) proton beam to produce muons via pion decay. The target must withstand high dynamic thermal loads induced by 2 ns pulses at 5-50 Hz. Also, operational reliability must be guaranteed to reduce target exchanges to a minimum. Several technologies for these systems are being studied in different laboratories. We present in this paper the results of a preliminary feasibility study of a graphite-based target, and the different layouts under study for a demonstrator target complex at CERN. Synergies with advanced nuclear systems are being explored for the development of a liquid metal target.

BEAM PARAMETERS

In the framework of the Muon Collider project, the Muon Accelerator Program (MAP) [1] studies previewed the target working parameters. According to these studies, a 5 GeV/c proton round beam will impact the target with an intensity of $3.76 \cdot 10^{14}$ protons per bunch with a repetition rate of 5 Hz. The bunch length considered is 2 ns and, therefore, the total average beam power reaches 1.5 MW.

TARGET CONCEPT

The initial concept for the present study has been the CERN Neutrinos to Gran Sasso (CNGS) target [2]. This target operated at max. power of 520 kW, but it was capable of accepting up to 750 kW. It is thought that, with a careful design optimisation and R&D, this concept could potentially withstand 1.5-1.7 MW. The target is placed after the proton driver, and has the function of producing pions, which subsequently will decay in muons. Past studies optimized the pion production on a graphite target [3].

The Muon Collider target is currently conceived as an 80 cm long isostatic graphite rod inserted in an aluminum internal vessel which provides an isolated confinement of the target. It is filled with static helium gas (at 1 bar) which prevents graphite from sublimating [4] due to high temperatures (≈ 1800 °C), and promotes heat dissipation via natural convection. The inner vessel is finned to enhance the heat exchange between helium and water which will flow (3 m/s) between the internal vessel and an aluminum external vessel.

The whole assembly will be surrounded by a tungsten shielding to shield the pion capture solenoid from the high radiation [5]. This shielding is also water cooled to evacuate the heat from the energy deposited in it, which accounts for 34 % of the total beam power. The full concept is shown in Figure 1.

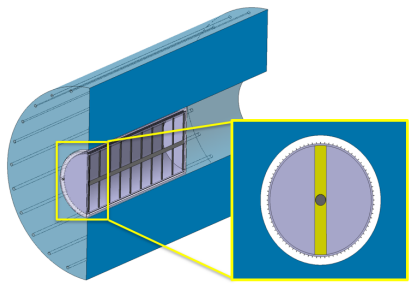

Figure 1: Current Muon Collider target 3D concept.

Figure 2 schematically details the bodies, dimensions and materials of the current proposal.

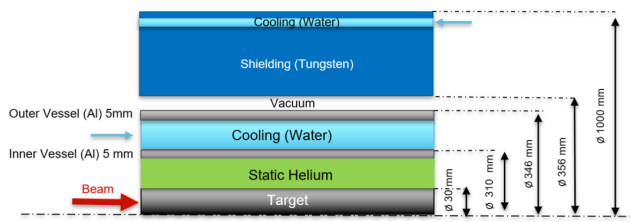

Figure 2: Muon Collider target schematic concept (not to scale).

PARAMETRIC ANALYSIS

Energy Deposition

The conceptual design strategy consisted in studying the thermal behaviour of the target rod under different load cases. A parametric study along five different beam sigma and four working frequencies has been developed. Rod radius has been kept proportional to three times the beam sigma size. The length has been kept fixed to 80 cm equal to 1.79 nuclear lengths. FLUKA [6] studies have been conducted to produce the energy deposition map in the target.

* f.saura@cern.ch
† rui.franqueira.ximenes@cern.ch

ISBN: 978-3-95450-227-1 ISSN: 2673-5490 doi:10.18429/JACoW-IPAC2022-THPOTK053

FOILED AGAIN: SOLID-STATE SAMPLE DELIVERY FOR HIGH REPETITION RATE XFELs

N. Majernik*, N. Inzunza, P. Manwani, J. B. Rosenzweig, UCLA, Los Angeles, CA, USA
A. Halavanau, C. Pellegrini, SLAC, Menlo Park, CA, USA
R. Ash, U. Bergmann, N. Welke, University of Wisconsin-Madison, Madison, WI, USA
R. Agustsson, A. Moro, Radiabeam Technologies, Santa Monica, CA, USA

Abstract

XFELs today are capable of delivering high intensity pulse trains of x-rays with up-to MHz to sub-GHz frequency. These x-rays, when focused, can ablate a sample in a single shot, requiring the sample material to be replaced in time for the next shot. For some applications, especially serial crystallography, the sample may be renewed as a dilute solution in a high speed jet. Here, we describe the development and characterization of a system to deliver solid state sample material to an XFEL nanofocus. The first application of this system will be an x-ray laser oscillator operating at the copper Kα line with a ~30 ns cavity.

INTRODUCTION

Early x-ray free electron lasers, e.g. LCLS, permitted relatively slow replenishment of sample material between shots. But, as noted by [1], "supplying pristine material has not been an issue at first-generation XFELs running at up to 120 Hz, it becomes a question of the utmost importance at megahertz repetition-rate XFELs, where the jet speed needs to be much higher and extremely carefully controlled to ensure that pristine sample is supplied within time delays as short as 0.22–1 μs between X-ray pulses". For samples which can be delivered as a liquid solution, this problem may be addressed by high speed jets, but this approach is not without potential problems [2], *e.g.* limited viscosity. However, for solid-state samples, it was previously adequate to raster scan the samples using motion stages [3], but at MHz rep rates, this is not a practical approach. In this work, we discuss the requirements and design of a high speed, solid-state sample delivery system for use with high rep rate XFELs based on a spinning disk.

The first version of this sample delivery system is designed to enable an x-ray laser oscillator (XLO). An XLO, as envisioned by [4], is a means of using an x-ray free electron laser (XFEL) to pump gain medium in a Bragg crystal optical cavity to generate high power, fully coherent, transform-limited hard x-ray pulses with improved stability when compared to XFEL pulses. Presently, an effort to demonstrate the first XLO is underway [5]. This proof-of-concept XLO will operate at the copper $K\alpha_1$ line, 8.05 keV, pumped by 9 keV XFEL pulses from LCLS. In this configuration, the LCLS will deliver a train of pump pulses, spaced at ~30 ns, a timing equivalent to the round trip of the cavity. In each subsequent pass, the LCLS pulse will excite the copper gain medium to population inversion, permitting amplification of the circulating ASE. A schematic overview of the experiment is provided in [4].

A crucial hurdle in this experiment is to ensure that fresh gain medium is present for each pulse since the ultra-high intensity x-ray pulses will transform any target material to a hot and rapidly expanding plasma. Early efforts focused on the development of high speed water jets, doped with copper nitrate [6]. At 200 m/s, the jet moves by 6 µm every 30 ns, enough to replace the gain medium in time for the next pulse. This approach was originally preferred due to the option to achieve very high speeds and the intrinsically self-healing nature of the medium. However, solid targets are appealing since they offer a much higher number density of the target atomic species while having effectively no other elements present to absorb the pump pulse. In particular, it was experimentally determined that the manageable concentration of the copper nitrate is limited to 4 molar, which corresponds to a number density of about 2 copper atoms per cubic nanometer, while solid copper has a number density of 80 atoms per cubic nanometer. The latter fact reduces the pump pulse intensity requirements, therefore decreasing the heat load on the in-coupling crystal, while maintaining the same photon yield. In addition to the high speeds required, there are many additional constraints which influence the design of a solid-state target for an x-ray laser oscillator.

SYSTEM REQUIREMENTS

The physics needs of the experiment will impose a number of requirements on the design of the sample and delivery system including:

- Sample speed – The target must deliver a fresh sample for each x-ray pulse. The required sample speed is therefore dictated by the XFEL repetition rate and the crater size left by the x-rays. For the XLO, the crater diameter left by the nanofocus in the copper foil is approximately 10 µm, with pulses arriving every 30 ns. If the nanofocus spot is small compared to the crater, the target must advance at least (crater radius)/(pulse period) = 170 m/s. We note that the exact copper foil damage mechanism is a topic of active research in various groups around the world, so the final velocity requirements will be established during the experiment [7].
- Sample thickness and tolerance – The target's thickness must be selected to optimally interact with the incoming x-ray pulse while not overly attenuating the signal. For

* NMajernik@g.ucla.edu

ISBN: 978-3-95450-227-1 ISSN: 2673-5490 doi:10.18429/JACoW-IPAC2022-THPOTK054

PROPOSAL OF A VHEE LINAC FOR FLASH RADIOTHERAPY *

L. Giuliano†[1],F. Bosco[1], M. Carillo[1], D. De Arcangelis[1],L. Ficcadenti[1],D. Francescone[1],
A. De Gregorio[1], G. Franciosini[1], M. Migliorati[1], A. Mostacci[1], L. Palumbo[1], V. Patera[1],A. Sarti[1],
Sapienza University, Rome, Italy
[1]also INFN-Roma, Rome, Italy
D. Alesini, M. Behtouei, L. Faillace , A. Gallo, B. Spataro,A. Vannozzi, INFN-LNF, Frascati, Italy
P. Cirrone, G. Cuttone, G.Torrisi, INFN-LNS, Catania,Italy
M. G. Bisogni, J. H. Pensavalle, INFN-Pisa, Pisa, Italy
F. Di Martino, Azienda Ospedaliera Pisana, Pisa , Italy
V. Favaudon, S. Heinrich, A. Patriarca, Curie Institute, Orsay, France

Abstract

Translation of electron FLASH radiotherapy in clinical practice requires the use of high energy accelerators to treat deep tumours and Very High Electron Energy (VHEE) could represent a valid technique to achieve this goal. In this scenario, a VHEE FLASH linac is under study at the University La Sapienza of Rome (Italy) in collaboration with the Italian Institute for Nuclear Research (INFN) and the Institut Curie (France). Here we present the preliminary results of a compact C-band system aiming to reach an high accelerating gradient and an high pulse current necessary to deliver high dose per pulse and ultra-high dose rate required for FLASH effect. We propose a system composed of a low energy high current injector linac followed by a modular section of high accelerating gradient structures. CST code is used to define the required LINAC's RF parameters and beam dynamics simulations are performed using TSTEP and ASTRA.

INTRODUCTION

In 2014 Favaudon *et al.* [1] discovered a new effect, called FLASH, that can change the scenario of the radiotherapy. Several pre-clinical studies demonstrated that a high dose per pulse (1-10 Gy) with ultra high dose-rate ($> 10^6$ Gy/s) and a total irradiation time < 100 ms, decreases dramatically the toxicity in the healthy tissue while keeping the same efficacy in cancer cure [2]. The technology of the accelerators actually used in the radiotherapy does not allow to explore this novel approaches in terms of dose and dose-rate, therefore a new low energy LINAC (7 MeV) [3,4] has been developed by our team in collaboration with S.I.T. - Sordina IORT Technologies S.p.A. [5] and has been installed at Institut Curie (Orsay-France) in August 2020, in order to investigate the FLASH effect. A strong interest has also grown on high energy machines (60-150 MeV) able to treat deep tumours. Recent studies [6–8] have investigated the potential of the VHEE for clinical applications, showing that 60–150 MeV beams could become an alternative modality in radiotherapy. The proposed VHEE source is based on a C-band LINAC, working at the frequency of 5.712 GHz, which allows more compactness compared to the traditional S-band cavities. The irises of the cavities have been designed with a radius such to get a high accelerating gradient and at the same time ensure a good transmission efficiency of electrons, necessary to transport the high peak current required for the high dose and dose rate in the FLASH irradiation.

The whole system is thought to be realize in two successive phases (phase 1 and phase 2) as show in Fig. 1. In phase 1, we use an injector (standing wave LINAC) and two traveling wave accelerating structures 90 cm long. The injector accelerates, at an energy of 10 MeV, a current of 200 mA generated by a pulsed DC gun. The RF design of the C-band injector is essentially based on the experience gained with above mentioned S band low energy LINAC, scaling properly the whole geometry. The electron beam is injected into a compact traveling wave (TW) C-band structure characterized by a high accelerating gradient (~ 40 MeV/m without the beam) able to bring the energy of the electron beam up to about 60 MeV. In phase 2, with two addition accelerating structures the system can reach an energy up to 130 MeV. The injector is powered by a C-band klystron of 5 MW, upstream of a circulator necessary to prevent reflected waves from the accelerating structure that can damage the klystron itself. A 50 MW klystron, foreseen for phase 1, feeds the first two accelerating structures. The power is split such to feed two LINACs by means of a waveguide network. A second 50 MW C-band klystron provides power to the other two LINACs for the phase 2.

RF DESIGN OPTIMIZATION

The RF accelerator design is performed by using CST 3D code [9] with eigen and frequency domain solver. The electrons are emitted from a triode electron gun with spherical emission area (see Fig. 2) with a diameter of about 6 mm. The nominal operation energy is around 12 keV adjustable up to 30 keV. The first cavity of the injector is composed of a half cell with an input plate required to adapt the electric field from the gun to the linac (Fig. 3). The first linac is a Standing Wave (SW) bi-periodic structure, working in $\pi/2$mode with a frequency of operation of 5.712 GHz. The first part of the linac is composed of three SW cavities called bunching section, aimed to generate the bunches and maximize the beam charge capture which results to be around 45%, corresponding to 225 mA.

* Work supported by FRIDA, INFN call.
† lucia.giuliano@uniroma1.it

ISBN: 978-3-95450-227-1 ISSN: 2673-5490 doi:10.18429/JACoW-IPAC2022-THPOTK057

ESS RFQ EXPERIMENTAL MODAL ANALYSIS

E. Trachanas*, A. Bignami, N. Gazis, B. Jones
European Spallation Source ESS-ERIC, Lund, Sweden

Abstract

The European Spallation Source-ESS, which is currently under construction and commissioning at Lund, Sweden is a neutron source that consists of a 2 GeV linear accelerator (LINAC) accelerating a proton beam to a solid Tungsten (W) target. The proton beam is produced by the Ion Source (ISRC) and transported through the Low Energy Beam Transport (LEBT) to the Radio Frequency Quadrupole (RFQ) that will then focus, bunch and accelerate it to 3.6 MeV. The RFQ beam commissioning started in October 2021, following the RF conditioning phase in summer 2021. This current work presents an experimental modal analysis performed on the RFQ including the comparative analysis with the modal finite element simulation using the ANSYS ® software suite. Measurements were performed using accelerometer sensors connected to a data acquisition system excited with an impact hammer. Geophones were used in parallel to the modal measurements in order to monitor the seismic background of the accelerator tunnel. Acquired data were post-processed and analyzed with dedicated software, juxtaposed with simulated results in order to determine the resonance frequencies, structural deformation patterns (mode shapes) and error margin between experimental and simulated results.

INTRODUCTION

The ESS RFQ designed and built by CEA-IRFU in France, was delivered to the ESS site in 2019. Following a period of system installation and testing, RF power conditioning commenced in summer 2021 and first proton beam was injected in the RFQ in October of the same year. The RFQ cavity is installed between the Low Energy Beam Transport (LEBT) and Medium Energy Beam Transport (MEBT) sections. It has a total length of 4.55 m divided in 5 segments operating at the resonant frequency of 352.21 MHz. Respectively, the RF power is delivered to the RFQ using two coaxial antenna couplers placed symmetrically 45 deg from the vertical axis equipped with ceramic windows that couple in total 1.1 MW of RF power during operation . Frequency detuning due to manufacturing errors and cavity thermal expansion caused by RF power losses is mitigated using 60 slug tuners and water cooling circuits [1]. Experimental modal analysis is the method to evaluate the dynamic response of the RFQ under external excitations in the final installation configuration in view of identifying the modal profile and vibrational response of this operationally critical component [2-6].

TEST SETUP & METHODOLOGY

In order to measure cavity response caused by external excitation, five (5) accelerometers were installed on the same side of each segment of the RFQ. The sensing devices used, were high sensitivity triaxial accelerometers from PCB Piezoelectronics® (Model 356B18) that were fixed with threaded studs on the cavity ensuring adequate response in higher frequencies.

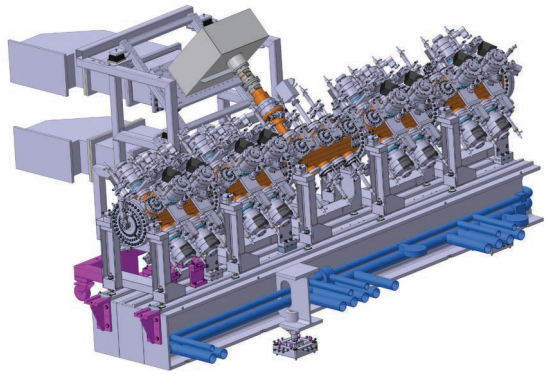

Figure 1: ESS Radio Frequency Quadrupole.

Moreover, two geophones were used for background vibration measurements placed on the accelerator tunnel floor and RFQ girder. The 6TD broadband type from Güralp ® with integrated digitizer and output sensitivity 2400 V/ms^{-1} and measurement range from 0.03 Hz to 100 Hz was used. An impact hammer with a medium hardness tip was chosen to excite the cavity in five (5) equally spaced points at the center of each segment with ten (10) strikes per point for acquired data averaging. The accelerometers were connected to the 16-analog channel sensor data acquisition system SIRIUS® from Dewesoft®. Each analog channel can achieve a dynamic range of 160 dB in time and frequency domain with a sampling rate of 200 kHz enabling high quality, low-error measurements.

Data analysis and post-processing was performed with MEscopeVES® software from Vibrant Technologies® in order to extract the resonant frequencies from frequency response functions, damping factors and mode shapes. The results and vibrational patterns were plotted and compared with the results from the finite elements analysis using ANSYS®. Figure 2 presents an example of an accelerometer sensor installation on the RFQ main body and on the right part the data acquisition system with the five (5) sensors connected and the impact hammer.

DATA ANALYSIS

A simplified meshed RFQ geometry with assigned measurement and impact points was created in the in-built SIRIUS® software with input from the detailed 3D CAD model. During measurements, data blocks that correspond to the response of accelerometers to impact hammer exci-

* Emmanouil.Trachanas@ess.eu

ISBN: 978-3-95450-227-1 ISSN: 2673-5490 doi:10.18429/JACoW-IPAC2022-THPOTK058

CERN's EAST EXPERIMENTAL AREA: A NEW MODERN PHYSICS FACILITY

S. Evrard†, D. Banerjee, J. Bernhard, F. Carvalho, S. Danzeca, M. Lazzaroni, B. Rae, G. Romagnoli,
CERN, Geneva, Switzerland

Abstract

CERN's East Area has hosted a variety of fixed-target experiments since the 1950s, using four beamlines from the Proton Synchrotron (PS). Over the past 4 years, the experimental area – CERN's second largest – has undergone a complete makeover. New instrumentation and beamline configuration have improved the precision of data collection, and new magnets and power convertors have drastically reduced the area's energy consumption. This article will summarize the major challenges encountered for the design of the renovated beamlines and for the preparation and test of the components. The infrastructure was carefully fitted resulting in a very smooth beam commissioning, the details of which will also be presented along with the restart of physics in the second half of 2021. With the return of the beams in the accelerator complex, the East Area's experiments have taken physics measurements again and the facility's central role in the modern physics landscape has been restored.

INTRODUCTION

The East Hall, which hosts all the primary areas, the secondary beamlines, the Cosmic Leaving Outdoor Droplets (CLOUD) experiment [1], IRRAD and CHARM facilities, as well as the T09 and T10 test beam areas as shown in Fig. 1, has been renovated during the Long Shutdown 2 of the LHC (2019-2021).

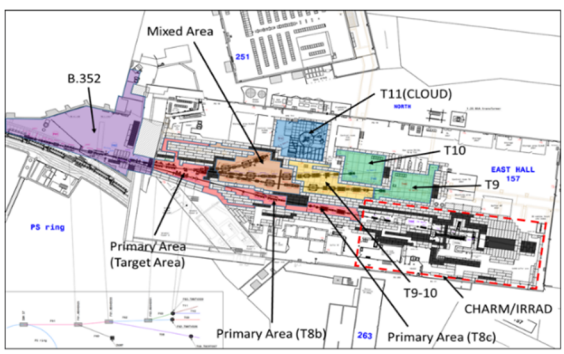

Figure 1: New facility layout.

To ensure the long-term operation of the PS East experimental area and to reduce the energy consumption of the facility by means of power converters with energy recovery option were the two main key drivers for the upgrade. Practically, this was achieved by implementing a new beamline layout, a new cycled powering scheme, and thoroughly refurbishing the associated infrastructure. To be able to change from a continuous to a pulsed power supply, the yokes of the magnets needed to be laminated. In addition, over the last years of operation, the maintainability of the magnets has been a critical issue, mainly because of long cooldown and repair times and the lack of spares for some magnet families. These two reasons drove the complete renovation of the magnets with laminated yokes and of fewer families.

INFRASTRUCTURE UPGRADE

To comply with the power consumption reduction, some services such as AC powering and the cooling network were downsized and renewed according to lower operation requirements [2]. Moreover, the shielding of the primary area was completely modified to satisfy radioprotection requirements, and to reduce the time needed to open it in case any equipment needs to be replaced. The access system was adapted to the new configuration and the size of the high activation areas was reduced to limit the exposure of workers during maintenance. The building envelope was completely refurbished to eliminate asbestos and improve greatly its thermal insulation.

Figure 2: New power converter farm.

Major refurbishment also took place in the neighbouring service buildings where the new power converters are located as shown in Fig. 2. They are now served by new systems such as demineralized water-cooling circuits and HVAC. With regards to the experimental areas (T09, T10, and T11), most of the services were upgraded and include new control rooms, gas distribution, and dedicated areas for detector/experiment set-up. Undoubtedly the upgrade turned out to be a unique opportunity to bring the facility up to the modern safety standards in terms of radioprotection by implementing dynamic air confinement in the primary area and separating the cooling circuits between activated and non-activated water. On the conventional safety

† sebastien.evrard@cern.ch

ISBN: 978-3-95450-227-1 ISSN: 2673-5490 doi:10.18429/JACoW-IPAC2022-THPOTK059

LASER SYSTEM FOR SuperKEKB RF GUN IN PHASE III COMMISSIONING

R. Zhang†, X. Y. Zhou, M. Yoshida KEK/SOKENDAI, Tsukuba, Japan
H. Kumano, N. Toyotomi, Mitsubishi Electric System & Service Co., Ltd, Tsukuba, Japan

Abstract

In order to generate high quality electron beam with high charge in Phase III commissioning of SuperKEKB, some improvements have been done in Ytterbium doped fiber and Neodymium doped YAG (Nd:YAG) hybrid laser system. Spatial reshaping part for the 4th harmonic laser beam at 266 nm has been adopted to realize low emittance electron beam. In addition, for achieving continuous and stable laser operation, position feedback system has also been used to improve the pointing stability of laser beam. In 2021c commissioning of SuperKEKB, stable 2 nC electron beam is generated for HER injection. Meanwhile, we achieved the best emittance results at B-sector of linac injector and BT line for comparable low injection background and higher injection efficiency. With the aim of generating higher charge electron beam with good quality in the following commissioning, a perspective towards the next step update for current laser system is also introduced.

INTROCUTION

SuperKEKB phase III commissioning has been being operated from 2018. Highest luminosity achieved in 2022a commissioning is almost two times of KEKB luminosity record [1]. Study about the bunch number of fill pattern and the bunch current has been being done for achieving higher luminosity and more physics run before long short down 1.

From SuperKEKB phase II commissioning, RF gun has been used for electron beam generation source. The Ytterbium (Yb)/Neodymium (Nd) hybrid laser system is built for high charge electron beam generation. By using of two lasers injection method, 2.3 nC electron beam was generated for SuperKEKB high energy ring (HER) injection. Meanwhile, the highest generation charge was 5.3 nC under the full laser energy input case [2]. Basing on the operation experiences of Phase I and II, the Yb/Nd hybrid laser system is also used for the phase III commissioning after upgrading for the higher quality electron beam generation.

In order to generate low emittance electron for phase III commissioning, the laser spatial distribution should be reshaped from Gaussian distribution into flat-top distribution [3]. Diffractive optics element (DOE) has been introduced into the UV laser part before injection into the RF gun. Thanks to the contribution of DOE, the best emittance results have been measured by wire scanner method at B-sector of SuperKEKB linac under 2 nC electron charge condition. In addition, the discharge induced by the laser injection decreased dramatically thanks to the application of DOE.

Furthermore, the laser beam pointing stability affected the electron beam stability during phase II commissioning. Due to the long distance from ground laser hut to the tunnel optics system and RF gun, it is found that the temperature fluctuation affected the laser pointing stability. We designed a laser position monitor and made a feedback system by piezo mirror mounts for the stabilization of laser beam. It has been demonstrated that the laser pointing fluctuation has been suppressed to one-fifth of the previous value without this stabilization system.

Beside these, electron charge feedback system has been also developed for stable and continuous 2 nC electron beam generation. All of these improvements ensure our phase III operation smoothly from 2019. In this proceeding, all the improvements mentioned above will be introduced in details.

IMPROVEMENTS IN LASER SYSTEM FOR HIGH CHARGE & STABLE ELECTRON BEAM GENERATION

The ability has been demonstrated to generate high charge electron beam for our Yb/Nd hybrid laser system and RF gun in SuperKEKB commissioning phase II [2]. In order to realize more stable and effective injection in phase III, the high-quality electron beam with low emittance and high stability under high charge condition is necessary. Some research and development have been done for improving the current laser system. The details and latest operation results are introduced in this part.

Introduction of Current Yb/Nd Hybrid Laser System

The current Yb/Nd hybrid laser system is almost the same as the laser system used in Phase II. The overall layout of it is shown in Fig. 1. Two commercial mode-lock oscillators are used for smooth commissioning, both of them are synchronized with the 114 MHz. One 2*1 MEMS switch is applied to select one oscillator for the laser system operation. After one stage of Yb doped single mode fiber (SMF) amplifier and grating stretcher, one semi-conductor optical amplifier (SOA) is used. Meanwhile, the repetition rate is changed into 10.38 MHz. An electric-optical module (EO) is used as a pulse picker to reduce the repetition rate into 25 Hz (1-25 Hz available). At the end of the fiber part, a half waveplate and a polarizer divide the seed laser into two equal parts, one is for the first Nd:YAG rod amplifier line, the other one is for the second line, both of them have 5 stages of Nd:YAG rod amplifier.

† rui.zhang@kek.jp

ISBN: 978-3-95450-227-1 ISSN: 2673-5490 doi:10.18429/JACoW-IPAC2022-THPOTK061

MACHINE LEARNING APPROACH TO TEMPORAL PULSE SHAPING FOR THE PHOTOINJECTOR LASER AT CLARA

A.E. Pollard*, W. Okell, D. Dunning, E. Snedden
ASTeC, Cockcroft Institute, STFC Daresbury Laboratory, UK

Abstract

The temporal profile of the electron bunch is of critical importance in accelerator areas such as free-electron lasers and novel acceleration. In FELs, it strongly influences factors including efficiency and the profile of the photon pulse generated for user experiments, while in novel acceleration techniques it contributes to enhanced interaction of the witness beam with the driving electric field. Work is in progress at the CLARA facility at Daresbury Laboratory on temporal shaping of the ultraviolet photoinjector laser, using a fused-silica acousto-optic modulator. Generating a user-defined (programmable) time-domain target profile requires finding the corresponding spectral phase configuration of the shaper; this is a non-trivial problem for complex pulse shapes. Physically informed machine learning models have shown great promise in learning complex relationships in physical systems, and so we apply machine learning techniques here to learn the relationships between the spectral phase and the target temporal intensity profiles. Our machine learning model extends the range of available photoinjector laser pulse shapes by allowing users to achieve physically realisable configurations for arbitrary temporal pulse shapes.

INTRODUCTION

In photoinjector systems, control over the longitudinal properties of the electron bunch can be achieved through temporal shaping of the laser pulse temporal profile [1]. Following the temporal shaping concept presented in [2], we have developed an apparatus for temporally shaping the photoinjector laser pulses at CLARA, shown schematically in Fig. 1. The input laser pulse is spectrally dispersed by a transmission grating. A concave mirror one focal length away from the grating collimates the spectrum and focuses the laser pulse to a line focus, along which the laser wavelength varies approximately linearly. A fused-silica AOM is placed at the position of the focus, and a transducer driven with an RF waveform at 200 MHz central frequency generates an acoustic wave in the AOM, which propagates along the line focus of the laser. The laser pulses are diffracted from the induced refractive index modulation, and the spectral components are recombined using a second concave mirror and transmission grating.

To shape the laser pulse temporally, the spectral phase can be adjusted by varying the temporal phase of the acoustic wave via the temporal phase of the RF drive wave. The laser pulses can also be shaped temporally by varying the temporal amplitude of the acoustic wave; however, as this approach is lossy, it is necessary to carry out all shaping using

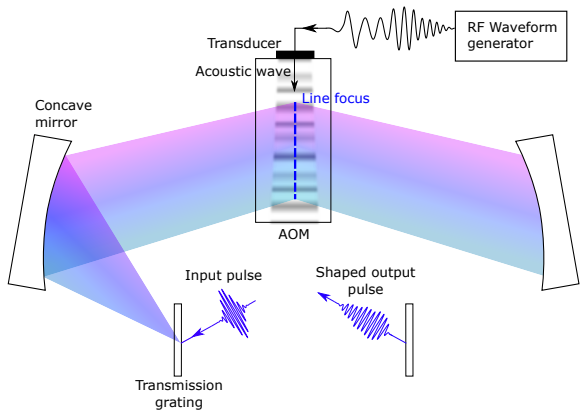

Figure 1: Schematic of the temporal pulse shaper at CLARA.

only the phase. In order to produce a particular target pulse temporal intensity profile, we need to find a suitable spectral phase mask to apply to the shaper. This is non-trivial for arbitrary shapes, as we require both the phase and amplitude in either the spectral or temporal domain to fully define the pulse. However we know only the temporal intensity and the spectral intensity, leaving the temporal and spectral phase as unknowns with many potential solutions. The complexity of real experimental systems poses additional challenges, for example, there are limitations imposed by the physical characteristics of the AOM. Modulating the spectral phase by modulating the temporal phase of the RF wave broadens the RF spectrum. The AOM has a finite acoustic bandwidth, and the RF spectrum must remain within this bandwidth for spectral phase modulations to be physically realisable.

Machine learning approaches excel for complex non-linear problems such as this. In particular, deep neural networks are known to be capable of approximating any function[3], and recent work has demonstrated that such networks can be used to learn and manipulate spectral, temporal, and shape properties of laser pulses[4, 5]. Recent research has explored encoding physical laws into machine learning models with partial differential equations as priors[6] to reduce the data requirements of these otherwise data-intensive approaches. This approach has come to be known as Physically Informed Neural Networks (PINNs) and can be used to constrain the outputs of deep neural networks within physical reality, by encoding properties such as conservation of energy *a priori*.

In this paper, we present a PINN for finding the spectral phase mask required to produce a target temporal intensity profile in our photoinjector laser pulse shaper, subject to the physical limitation of the AOM bandwidth. Our approach both reduces the data requirements of our model and con-

* amelia.pollard@stfc.ac.uk

ISBN: 978-3-95450-227-1 ISSN: 2673-5490 doi:10.18429/JACoW-IPAC2022-THPOTK062

THERMAL MODELING AND BENCHMARKING OF CRYSTALLINE LASER AMPLIFIERS*

D. T. Abell, D. L. Bruhwiler, P. Moeller, R. Nagler, B. Nash, I. V. Pogorelov
RadiaSoft LLC, Boulder, CO, USA
Q. Chen, C. G. R. Geddes, C. Tóth, J. van Tilborg, LBNL, Berkeley, CA, USA
N. B. Goldring, STATE33 Inc., Portland, OR, USA

Abstract

Ti:sapphire crystals constitute the lasing medium of a class of lasers valued for their wide tunability and ultra-short, ultra-high intensity pulses. When operated at high power and high repetition rate (1 kHz), such lasers experience multiple effects that can degrade performance. In particular, thermal gradients induce a spatial variation in the index of refraction, hence thermal lensing [1]. Using the open-source finite-element code FEniCS [2], we solve the relevant partial differential equations to obtain a quantitative measure of the disruptive effects of thermal gradients on beam quality. We present thermal simulations of a pump laser illuminating a Ti:sapphire crystal. From these simulations we identify the radial variation in the refractive index, and hence the extent of thermal lensing. In addition, we present analytic models used to estimate the effect of thermal gradients on beam quality. This work generalizes to other types of crystal amplifiers.

INTRODUCTION

Titanium-doped sapphire (Ti:sapphire) crystals constitute the lasing medium of a class of lasers valued for their wide tunability and capacity to produce ultra-short, ultra-high intensity pulses. But when operating at high power with a high repetition rate (1 to 10s of kHz), multiple natural/thermal/mechanical effects can degrade the performance of Ti:sapphire crystal laser amplifiers.

For example, during steady-state operation, *i.e.* with a crystal amplifier operating in equilibrium, thermal gradients induce both a positional variation in the index of refraction and mechanical stresses. The changes in the index of refraction can lead to thermal lensing. And stresses in an anisotropic, uniaxial crystal such as Ti:sapphire can modify the crystal's birefringent characteristics and further degrade the beam.

THERMAL MODELS AND TIME SCALES

The heat equation derives from conservation of energy and the Fourier law. In the context of heat flow in a solid, one may express conservation of energy in the form

$$\rho \frac{\partial u}{\partial t} = -\nabla \cdot \vec{q} + f, \tag{1}$$

where ρ denotes the mass density of the solid, u the internal energy per unit mass, $\vec{q}$ the local heat flux, and f a source term that represents the rate of external heat deposition per unit volume. This equation expresses the rate of change of the local energy density as a sum of the local heat loss, $-\nabla \cdot \vec{q}$, and the local heat deposition, f. The Fourier law,

$$\vec{q} = -K_c \nabla \Theta, \tag{2}$$

describes the local heat flux as proportional to and in the direction opposite the local temperature gradient, $\nabla\Theta$, with the proportionality given by K_c, the thermal conductivity. One may relate energy density and temperature via the *specific heat*, $c_p = \partial u / \partial \Theta$. This relation allows one to write

$$\dot{u} = \frac{\partial u}{\partial \Theta}\frac{\partial \Theta}{\partial t} = c_p \dot{\Theta}, \text{ and } \nabla u = \frac{\partial u}{\partial \Theta}\nabla\Theta = c_p \nabla\Theta. \tag{3}$$

In the very simplest case—ρ, K_c, and c_p experience negligible variation over the temperature range of interest—one may use the above results to derive the linear heat equation:

$$\dot{\Theta} = \frac{K_c}{\rho c_p}\nabla^2\Theta + \frac{f}{\rho c_p} = \alpha \nabla^2 \Theta + g, \tag{4a}$$

where α denotes the *thermal diffusivity*, $K_c/(\rho c_p)$, and $g = f/(\rho c_p)$. More generally, however, the quantities K_c and c_p—and, to a much smaller extent, ρ—do vary with temperature; and one cannot then convert the heat deposition term f to a "temperature deposition" term so simply as dividing by ρc_p. In this case it simplifies matters to work with u in preference to Θ. If we may treat ρ as constant, then we instead derive the heat equation in the nonlinear form [3]

$$\dot{u} = \nabla \cdot (\alpha(u)\nabla u) + f/\rho. \tag{4b}$$

When necessary, one may convert between u and Θ by means of the (monotonically increasing) specific heat capacity.

Time Scales for Thermal Relaxation

For now we focus on the linear form Eq. (4a) of the heat equation. If the source term vanishes—except for possibly a brief pulse that defines the initial condition—and we assume azimuthal symmetry, one may use separation of variables to identify the essential functional form of the solution:

$$J_0(\nu r)[\cos(kz) + \beta \sin(kz)]e^{-\alpha(\nu^2+k^2)t}. \tag{5}$$

A complete solution, written as a linear combination of these functions, is determined by the boundary conditions, with

* This work is supported by the US Department of Energy, Office of High Energy Physics under Award Numbers DE-SC0020931 and DE-AC02-05CH11231.

ISBN: 978-3-95450-227-1 ISSN: 2673-5490 doi:10.18429/JACoW-IPAC2022-THPOTK063

OPEN SOURCE SOFTWARE TO SIMULATE Ti:SAPPHIRE AMPLIFIERS*

D. L. Bruhwiler, B. Nash, D. T. Abell, G. Khalsa, RadiaSoft LLC, Boulder, CO, USA
J. van Tilborg, Q. Chen, C. Tóth, C. G.R. Geddes, LBNL, Berkeley, CA, USA
N. B. Goldring, STATE33 Inc., Portland, Oregon, USA

Abstract

The design of next-generation PW-scale fs laser systems, including scaling to kHz rates and development of new laser gain media for efficiency, will require parallel multiphysics simulations with realistic errors and nonlinear optimization. There is currently a lack of broadly available modeling software that self-consistently captures the required physics of gain, thermal loading and lensing, spectral shaping, and other effects required to quantitatively design such lasers [1]. We present initial work towards an integrated multiphysics capability for modeling pulse amplification in Ti:Sa lasers. All components of the software suite are open source. The Synchrotron Radiation Workshop (SRW) [2–6] is being used for physical optics, together with Python utilities. The simulations are being validated against experiments.

EXPERIMENTS

Pump-probe experiments of Ti:Sa thermal lensing have been performed at the HTU line of the BELLA Center [7], with a schematic and photo seen in Fig. 1. The 532 nm Gaussian pump beam from a kHz Revolution laser has a FWHM diameter of 1.2 mm, a FWHM pulse duration of 500 ns, and an averaged power of 19.6 W (35 mJ per pulse).

This beam pumps and heats a 1 cm diameter, 2.5 cm long Ti:Sa crystal, which has its c-axis parallel to the optical table and is water cooled. The thermal lensing effects were diagnosed with probe beams from the kHz rep rate 800 nm Coherent FrontEnd Laser System, with a FWHM pulse duration of 300 ps. The transmitted pump wavefronts were measured using a HASO wavefront sensor (WFS). A DG535 is used to control the relative delay between the pump and probe to sub-microsecond levels. Waveplates are used to tune the polarization of both pump and probe beams.

SIMULATION AND OPTICS

The software development uses operator splitting, where the laser pulse and crystal are sliced in a manner that enables robust and rapid 2D computations, leveraging the SRW code. The software is in a GitHub repository [8]. Figure 2 shows the WFS image pair, each 32x32 pixels. The intensity and phase data is used to construct real and imaginary electric fields of the longitudinally integrated wavefront, with no need to include the rapid variation in space and time. These fields are used to construct a native SRW wavefront object, which can be propagated with full physical optics. The phase distribution is essentially flat, to within measurement uncertainties.

* Work supported by the US Department of Energy, Office of High Energy Physics under Award Nos. DE-SC0020931 and DE-AC02-05CH11231.

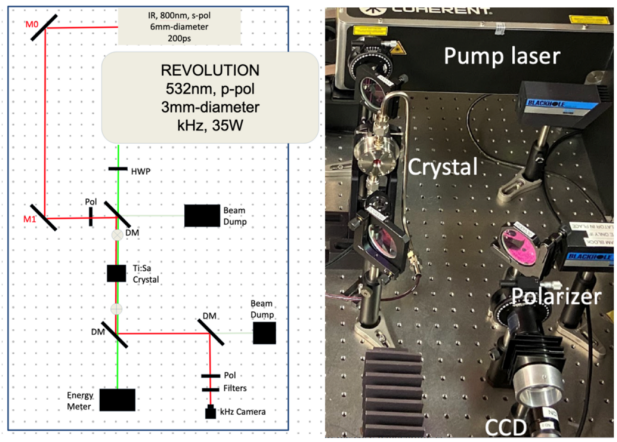

Figure 1: Design (left) and implementation (right) of the thermal lensing measurements. The pump laser deposits up to 35mJ per pulse in the Ti:Sa crystal at 1 kHz. The 800 nm, 300 ps probe pulse is synchronized with the pump. A wavefront sensor (not shown) is used to measure any effects.

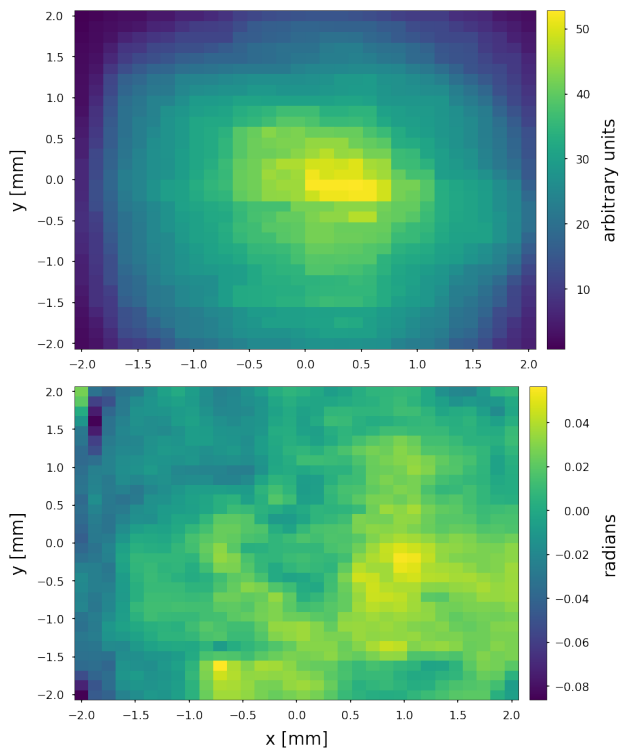

Figure 2: Wavefront sensor (WFS) measurements of a 0.8 nm probe pulse after propagating through an unpumped crystal; the intensity (upper) and phase (lower) are obtained simultaneously. This is the initial condition for SRW simulations. The low resolution is characteristic of WFS data.

ISBN: 978-3-95450-227-1 ISSN: 2673-5490 doi:10.18429/JACoW-IPAC2022-THPOMS001

TURBO: A NOVEL BEAM DELIVERY SYSTEM ENABLING RAPID DEPTH SCANNING FOR CHARGED PARTICLE THERAPY

J. S.L. Yap*, S. L. Sheehy[1], University of Melbourne, Melbourne, Australia
R.B. Appleby[2], H X.Q. Norman[2,3], A. F. Steinberg[2,3] , University of Manchester, Manchester, UK
[1]also at Australian Nuclear Science and Technology Organisation (ANSTO), Australia
[2]also at Cockcroft Institute, Warrington, UK
[3]also at University of Melbourne, Melbourne, Australia

Abstract

Charged particle therapy (CPT) is a well-established modality of cancer treatment and is increasing in worldwide presence due to improved accelerator technology and modern techniques. The beam delivery system (BDS) determines the overall timing and beam shaping capabilities, but is restricted by the energy variation speed: energy layer switching time (ELST). Existing treatment beamlines have a ±1% momentum acceptance range, needing time to change the magnetic fields as the beam is delivered in layers at various depths across the tumour volume. Minimising the ELST can enable the delivery of faster, more effective and advanced treatments but requires an improved BDS. A possibility for this could be achieved with a design using Fixed Field Alternating Gradient (FFA) optics, enabling a large energy acceptance to rapidly transport beams of varying energies. A scaled-down, novel system – Technology for Ultra Rapid Beam Operation (TURBO) – is being developed at the University of Melbourne, to explore the potential of rapid depth scanning. Initial simulation studies, beam and field measurements, project plans and clinical considerations are discussed.

INTRODUCTION

The use of charged particle beams as a therapeutic modality has several recognised advantages over conventional treatments as the characteristic 'Bragg Peak' enables a precise amount of radiation to be delivered with a greater radiobiological effect. High facility capital costs are prohibitive and new developments in delivery techniques, accelerators and related technologies, along with improved clinical and biological outcomes can better exploit CPT benefits and treatment accessibility. The emergence of methodologies such as ultra-high dose rate 'FLASH' [1], Arc [2] and multi-ion [3] therapies also place greater demands on the capabilities of the BDS: significant improvements are needed to overcome existing technical limitations [4].

Although there are many factors which contribute to the delivery process and treatment time, the ELST is a bottleneck constraint and this deadtime whilst waiting for magnetic field adjustments to transport different beam energies has several implications, impacting treatment efficiency and efficacy [5]. As most facilities offer state-of-the-art treatments with active pencil beam scanning, the ELSTs accumulate and longer beam delivery times translate to higher costs, lower patient throughput and can decrease treatment quality: physical uncertainties and sensitivities with motion cause inferior dosage i.e. 'interplay effects' [6]. Numerous mitigation approaches [7] currently used in the clinic to manage uncertainties can be complex to apply and further extend treatment times. Shorter ELSTs, thus faster delivery with the possibility of improved dosimetric quality and robust plans are also particularly beneficial for treating mobile sites [8].

The need for better immobilisation has led to upright treatments being revisited [9] and could offer practical and clinical benefits, notably enabling fixed beamline: gantryless treatments [10]. This presents the opportunity of not only added cost reduction [11], but in combination with a large energy acceptance BDS with fast ELST, can further improve the effectiveness of standard pencil beam scanning and accommodate new delivery techniques. The applicability for heavier ions could be even greater than for protons given the impracticality of a gantry due to the complexities and infrastructure cost; the increased radiobiological factor may also favour fewer fields and fractions [12]. The clinical advantages and requirements will direct the development of TURBO as a scaled-down, proof-of-concept demonstrator to de-risk these concepts and explore the feasibility of a large energy acceptance BDS for CPT.

TURBO

TURBO comprises several interchangeable modules (A–F as shown in Fig. 1) adapted for the UniMelb low energy ion '*Pelletron*' accelerator [13] (0.5–3.5 MeV protons & He at 100's nA to several μA). The FFA section will be curved to accommodate the system requirements for a clinical setting, followed by a fast scanning system downstream to replicate active pencil beam scanning. A self-developed control system will manage all component operation, where precision and synchronicity is required to enable rapid beam delivery.

Initial measurements and beam characterisation studies have been initiated to establish the suitability of the Pelletron for TURBO. Two NEC helical wire beam profile monitors [14] (BPM1,2) and Faraday cups are situated together with the upper and lower slits. These BPMs measure both the horizontal and vertical beam distributions simultaneously but do not give the beam centre position. To determine the beam profile and position, a UniBEaM fibre scanner system [15, 16] was integrated into the beamline ~2.10 m downstream of the lower slits. A single motorised (200 μm diameter) op-

* jacinta.yap@unimelb.edu.au

ISBN: 978-3-95450-227-1 ISSN: 2673-5490 doi:10.18429/JACoW-IPAC2022-THPOMS002

GANTRY BEAMLINE AND ROTATOR COMMISSIONING AT THE MEDAUSTRON ION THERAPY CENTER

M. T. F. Pivi*, L. Adler, G. Guidoboni, C. Kurfürst, C. Maderböck, D. A. Prokopovich, V. Rizzoglio, I. Strasik, EBG MedAustron, Wiener Neustadt, Austria
M. G. Pullia, CNAO Foundation, Pavia, Italy
M. Pavlovič, Slovak University of Technology in Bratislava, Bratislava, Slovakia
G. Kowarik, GKMT Consulting, Vienna, Austria

Abstract

The MedAustron Particle Therapy Accelerator located in Austria delivers proton beams in the energy range 60-250 MeV and carbon ions 120-400 MeV/n for tumour treatment in three irradiation rooms. Proton beams up to 800 MeV are also provided to a separate room dedicated to research. Over the last two years, in parallel to clinical operations, we have completed the installation and commissioning of the proton gantry beamline with the first patient treated in May 2022. In this paper, we provide an overview of the gantry beamline commissioning including the world-wide first "rotator" system used to match the slowly extracted asymmetric beams to the coordinate system of the gantry. Using the rotator, all beam parameters at the location of the patient become independent from the gantry rotation angle. The presented overview of the beamline commissioning includes technical solutions, main results and the first rotator measurements.

INTRODUCTION

The MedAustron accelerator delivers proton and carbon ion beams for cancer treatment to three irradiation rooms with the goal of treating 800 patients per year.

Figure 1: Bird view of the MedAustron gantry laying in the horizontal position. The gantry entrance is in the lower-right corner of the picture.

The center also provides infrastructure installations for external research institutes internationally. Following the commissioning of the gantry beamline, shown in Figure 1, all rooms at MedAustron are now operational. Since the first patient in 2016, about 1400 patients have been treated with protons and carbon ions using approximately 35,000 single fractions with a weekly machine uptime during clinical operation > 96%. Accelerator parameters are defined by requirements for clinical treatment and research. Accelerator and beam parameters for the fixed beamlines are shown in Table 1.

Table 1: MedAustron Accelerator and Beam Parameters

Parameter	Value
Synchrotron circumference	77.6 m
Energy range for protons	62.4÷252.7 (800) MeV
Energy range for carbon ions	120÷402.8 MeV/n
Spot size FWHM: at the isocenter	p: 7÷21 mm C^{6+}: 6.5÷9.5 mm
Number of particles/spill (max)	p: 2×10^{10} C^{6+}: 1.5×10^{9}
Spill length carbon/proton	4 s / 10 s
Irradiation field at the patient	20 cm × 20 cm

HEBT AND GANTRY LAYOUT

The MedAustron accelerator design originates from the Proton Ion Medical Machine Study (PIMMS) and National Centre for Oncological Hadrontherapy (CNAO) as described in [1, 2].

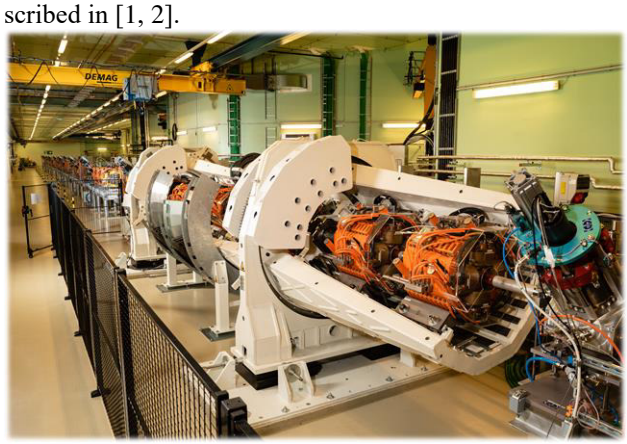

Figure 2: World-wide first rotator system (white structure) in the high energy beam transfer line. Seven quadrupoles (orange) are mounted on the structure and rotated synchronously with the gantry located downstream. With a rotator, the beam parameters at the gantry isocenter become independent from the gantry rotation angle.

The High Energy Beam Transfer line (HEBT) transports the beam from the synchrotron into four irradiation rooms:

*mauro.pivi@medaustron.at

ISBN: 978-3-95450-227-1 ISSN: 2673-5490 doi:10.18429/JACoW-IPAC2022-THPOMS003

UPGRADE OF A PROTON THERAPY EYE TREATMENT NOZZLE USING A CYLINDRICAL BEAM STOPPING DEVICE FOR ENHANCED DOSE RATE PERFORMANCES

E. Gnacadja*, C. Hernalsteens[1], N. Pauly, R. Tesse, E. Ramoisiaux, M. Vanwelde
Service de Métrologie Nucléaire, Université libre de Bruxelles, Brussels, Belgium
[1]also at CERN, Geneva, Switzerland

Abstract

Proton therapy is a well established treatment method for ocular cancerous diseases. General-purpose multi-room systems which comprise eye-treatment beamlines must be thoroughly optimized to achieve the performances of fully dedicated systems in terms of depth-dose distal fall-off, lateral penumbra, and dose rate. For eye-treatment beamlines, the dose rate is one of the most critical clinical performances, as it directly defines the delivery time of a given treatment session. This delivery time must be kept as low as possible to reduce uncertainties due to undesired patient movement. We propose an alternative design of the Ion Beam Applications (IBA) Proteus Plus (P+) eye treatment beamline, which combines a beam-stopping device with the already existing scattering features of the beamline. The design is modelled with Beam Delivery SIMulation (BDSIM), a Geant4-based particle tracking and beam-matter interactions Monte-Carlo code, to demonstrate that it increases the maximum achievable dose rate by up to a factor 3 compared to the baseline configuration. An in-depth study of the system is performed and the resulting dosimetric properties are discussed in detail.

INTRODUCTION

The use of proton beams to treat ocular tumors is well established [1–3]. The optimization of high energy multi-room proton therapy systems to allow ocular tumors treatment poses many challenges compared to dedicated low energy facilities. The key point of the design of such systems is the trade-off that must be found between a small depth-dose distal fall-off [1] (DFO, typically below 2 mm) and a high dose rate (often required to be at least equal to 15 Gy/min) in order to minimize treatment delivery time. Indeed, as eye tumors depths often vary from 5 to 35 mm, the beam nominal energy of high energy systems must be reduced from 250 MeV to 70 MeV or less prior to additional range shifting inside of a dedicated eye nozzle. As this energy degradation unevitably leads to a significant energy spread, momentum slits must be positioned at a location of high dispersion to intercept the more energetic particles and reduce the DFO of the dose deposition profiles. Such particles interception directly affects the transmission of the beamline, leading to a huge limitation on the dose rate performances of the system.

The Ion Beam Applications (IBA) eye treatment beamline, so-called "eyeline", is an example of such a high energy system, in which the beam is produced at a nominal energy of 230 MeV. The IBA eyeline has been previously designed [4] and experimentally optimized with an energy of 105 MeV at the nozzle entrance [5], leading to a maximum dose rate of 30 Gy/min, but with a DFO of only 3.2 mm. More recently, the different steps toward a numerical optimization for a smaller DFO (below 2 mm) has been presented in detail in [6], using Beam Delivery SIMulation (BDSIM) [7]. BDSIM is a geant4 based particle tracking and beam-matter interactions simulation code, that has already proven its ability to model low energy proton therapy systems [8]. This smaller DFO requirement forced the reduction of the nominal energy at the nozzle entrance from 105 to 80 MeV, leading to a smaller maximum achievable dose rate. Table 1 summarizes the clinical performances required during the optimization presented in [6].

Table 1: The clinical requirements (minimum range (R_{min}), maximum range (R_{max}), DFO, Flatness, Lateral Penumbra (LP) and Dose Rate (DR)) imposed on the dosimetric properties of the IBA passive scattering eyeline.

R_{min} (mm)	R_{max} (mm)	DFO (mm)	Flatness (%)	LP (mm)	DR (Gy/min)
5	35	< 2	< 2	< 1.5	> 15

As discussed in [6], two designs of the IBA eyeline were studied. The first design only uses the scattering and range shifting features of the system to optimize the nozzle, with at the end a maximum achievable dose rate of 17 Gy/min. The second, alternative design combines a cylindrical, lead material beam stopper, with the scattering features of the nozzle to achieve a transversally flat dose profile. Figure 1 illustrates the BDSIM model of the nozzle as designed with this cylindrical beam stopping device.

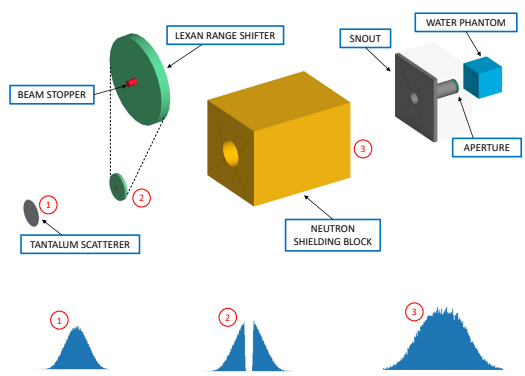

Figure 1: BDSIM model of the IBA eye treatment nozzle as designed with a cylindrical beam stopping device.

* eustache.gnacadja@ulb.be
[1] The distal fall-off is defined as the difference between the 20 % and 80 % dose points on the distal side of the Bragg peak: DFO = $R_{80} - R_{20}$.

ISBN: 978-3-95450-227-1 ISSN: 2673-5490 doi:10.18429/JACoW-IPAC2022-THPOMS004

ACHROMATIC GANTRY DESIGN USING FIXED-FIELD SPIRAL COMBINED-FUNCTION MAGNETS

R. Tesse*, C. Hernalsteens[1], E. Gnacadja, E. Ramoisiaux, N. Pauly, M. Vanwelde
Université libre de Bruxelles, Brussels, Belgium
[1] also at CERN, Geneva, Switzerland

Abstract

Arc-therapy and flash therapy are promising proton therapy treatment modalities as they enable further sparing of the healthy tissues surrounding the tumor site. They impose strong constraints on the beam delivery system and rotating gantry structure, in particular in providing high dose rate and fast energy scanning. Fixed-field achromatic transport lattices potentially satisfy both constraints in allowing instant energy modulation and sufficient transmission efficiency while providing a compact footprint. The presented design study uses fixed-field magnets with spiral edges respecting the FFA scaling law. The cell structure and the layout are studied in simulation and integrated in a compact gantry. Results and further optimizations are discussed.

INTRODUCTION

The treatment of cancer is a major societal challenge for which numerous treatment techniques are actively developed. Novel proton therapy treatment modalities, such as flash and arc therapy, aim at increasing the clinical efficiency and reducing the treatment time. These techniques pose new challenges for the accelerators and beam delivery systems as they require tighter control of the beam spot sizes at the isocenter, better control of beam losses and higher beam currents [1–3]. Gantry designs providing achromatic transport with fixed-field magnets meet these challenges and allow arbitrarily fast energy scanning. We report on a preliminary design of the CASPRO ("Compact Achromatic System for Proton Therapy") project, for an achromatic proton gantry in the energy range 70-230 MeV using normal conducting magnets. The objective is to retain the reduced footprint of modern variable-field compact gantries, such as the IBA Proteus One [4] or the ProNova SC360 superconducting gantry [5]. The adopted strategy is to divide the system into three distinct blocks. The proposed block diagram, presented in Fig. 1, is as follows. A proton beam with an energy of 230 MeV enters the first block that consists of a fixed dipole that deflects the beam and is sent on an energy degrader mounted directly on the gantry, to make the system more compact. The beam transport line following the degrader follows a straight scaling fixed-field lattice design. The second block, detailed in this paper, bends the beam towards the isocenter and is at the heart of the design to reduce the footprint by providing a small bending radius and achromatic properties across the entire energy range. The studied concept is based on Fixed-Field Alternating Gradient (FFAGs) cells using normal conducting magnets. The starting point is the spiral FFAG cells of the RACCAM design [6–9]. The third block is composed of the scanning magnets that are positioned downstream of the last cell to limit the opening of the FFA magnets.

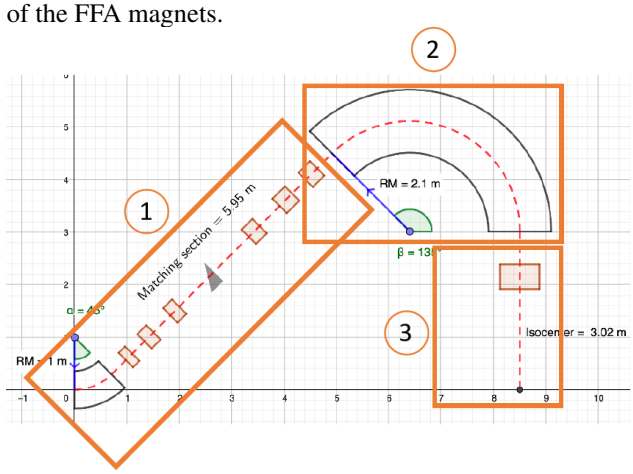

Figure 1: The proposed structure for the CASPRO achromatic gantry. The three main blocks are highlighted in orange.

SPIRAL FFA CELL

We adapt the design of the RACCAM original cell aiming to minimize the size of the magnets. The parameters before and after optimisation are presented in Table 1. An additional constraint arise from the the fact the gantry design uses downstream scanning magnets to scan the beam at isocenter. To minimize the required in-plane aperture of the scanning magnets, the orbit excursion with energy has to be minized. The aim is to keep the excursion span over the full energy range below 20 cm.

Table 1: Periodic Cell Parameters of the RACCAM Design and the Preliminary Design of the Gantry Cell

Parameters (units)	RACCAM	CASPRO
Mean radius R_0 (m)	3.48	2.1
Angle (degrees)	45	45
Field index	4.415	6.0
Spiral angle (degrees)	50.36	65
Field at R_0 (T)	1.5	1.6
Gap (cm)	3	3

The simulations are performed with the ray-tracing code Zgoubi [10, 11] using the Zgoubidoo Python interface [12]. Zgoubidoo provides many additionnal functionalities, such

* robin.tesse@ulb.be

ISBN: 978-3-95450-227-1 ISSN: 2673-5490 doi:10.18429/JACoW-IPAC2022-THPOMS005

LAB-INDUSTRY COLLABORATION: INDUSTRIALISATION OF A NOVEL NON-INTERCEPTIVE TURN-KEY DIAGNOSTIC SYSTEM FOR MEDICAL APPLICATIONS

S. Srinivasan†, H. Bayle, E. Touzain, Bergoz Instrumentation, Saint-Genis-Pouilly, France
D. Bisiach, M. Cargnelutti, K. Roskar, Instrumentation Technologies, Solkan, Slovenia
P. A. Duperrex, Paul Scherrer Institut, Villigen, Switzerland

Abstract

A novel non-interceptive beam current monitor prototype was successfully developed to measure the ultra-low beam currents (0.1-10 nA) with a 1 Hz measurement bandwidth at the Paul Scherrer Institute's (PSI's) proton radiation therapy facility, PROSCAN. The monitor resonance frequency is tuned to a harmonic of the beam pulse repetition rate, enabling a larger signal-to-noise ratio compared to those of broadband systems. Since the tuned frequency certainly differs for other facilities, such a system requires customisation. To enhance the application of the monitor to a turn-key system, a fast digitiser solution allowing (1 kHz data rate) streaming of measurements to various control systems is of importance as well. In this paper, we report on the industrial challenges associated, such as quality, reliability, repeatability and customisability, online monitoring, turn-key system, etc. in manufacturing a working novel prototype from a research environment. A fruitful collaboration between PSI, Bergoz Instrumentation, and Instrumentation Technologies is foreseen to make it happen, from a first-of-a-kind industrialised product to be tested in the lab, to a product line in a catalogue.

INTRODUCTION

In proton therapy facilities such as at PSI [1], monitoring of low beam currents (0.1-10 nA) with high accuracy and precision is of crucial importance as it is directly related to the delivered dose and its related errors. Ionisation chambers (IC) are typically used in such facilities [2, 3] for beam current measurements but with strict regulations during therapy. As a potential alternative, a non-interceptive beam current monitor was successfully developed and tested at PSI. Here, we report on the prototype development and validation at PSI, industrialisation of the turn-key diagnostic system, and challenges associated with the process.

PROTOTYPE DEVELOPMENT AND VALIDATION AT PSI

A non-interceptive beam current monitor (BCM) working on the principle of electromagnetic resonance was developed [4, 5] at PSI (shown in Figure 1) as part of an EU Horizon 2020 project from the Optimisation of Medical Accelerators (OMA) network. The BCM operates at the fundamental mode of resonance which is tuned at the second harmonic of the beam repetition rate i.e. 145.7 MHz. It has been tested successfully with beam currents in the range of 0.1-10 nA for energies 230-70 MeV [5–7] and the resolution achieved was 0.05 nA. The beam current response is highly position-independent (0.03 %/mm up to 60 % of the beam pipe aperture) and beam-size-independent [5]. This was achieved using a 1 Hz measurement bandwidth digital system developed by PSI [8].

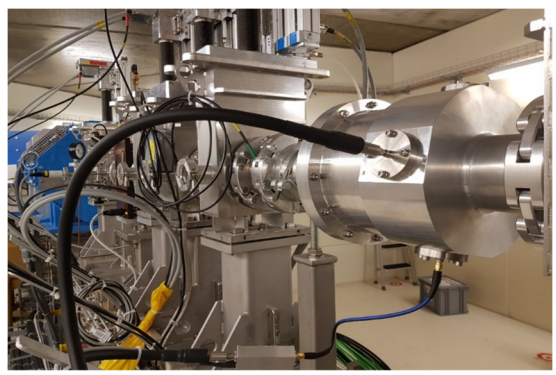

Figure 1: Prototype dielectric-filled re-entrant cavity resonator (BCM) installed at PROSCAN.

To take advantage of the BCM's fast response, a low-noise and wide-dynamic range digitiserr with a wider measurement bandwidth and various interfaces for the user and Control System integration purposes, the Libera Digit 500 provided by Instrumentation Technologies, was identified and customised. Digital down-conversion (I/Q demodulation) of the digitised signal was implemented in its FPGA. The resonator response as a function of beam current measured with the Libera Digit 500 (with 1 kHz refresh rate) is shown in Figure 2. The response is linearly proportional to beam currents higher than 0.5 nA with the same beam current resolution as before.

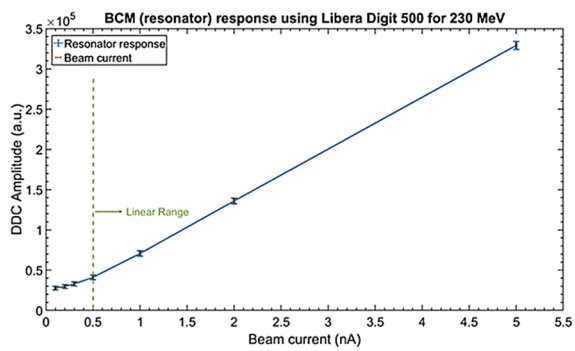

Figure 2: Prototype BCM response (in arbitrary units) measured by the customised Libera Digit 500. The beam current reference is measured using an IC.

† s.srinivasan@bergoz.com

ISBN: 978-3-95450-227-1 ISSN: 2673-5490 doi:10.18429/JACoW-IPAC2022-THPOMS006

A CARBON MINIBEAM IRRADIATION FACILITY CONCEPT

M. Mayerhofer[1]*, V. Bencini[2], M. Sammer[1] and G. Dollinger[1]
[1]Universität der Bundeswehr München, Neubiberg, Germany
[2]University of Oxford, Oxford, United Kingdom

Abstract

In minibeam therapy, the sparing of deep-seated normal tissue is limited by transverse beam spread caused by small-angle scattering. Contrary to proton minibeams, helium or carbon minibeams experience less deflection, which potentially reduces side effects. To verify this potential, an irradiation facility for preclinical and clinical studies is needed. This manuscript presents a concept for a carbon minibeam irradiation facility based on a LINAC design for conventional carbon therapy. A quadrupole triplet focuses the LINAC beam to submillimeter minibeams. A scanning and a dosimetry unit are provided to move the minibeam over the target and monitor the applied dose. The beamline was optimized by TRAVEL simulations. The interaction between beam and these components and the resulting beam parameters at the focal plane is evaluated by TOPAS simulations. A transverse beamwidth of < 100 µm (sigma) and a peak-to-valley (energy) dose ratio of > 1000 results for carbon energies of 100 MeV/u and 430 MeV/u (~ 3 cm and 30 cm range in water) whereby the average beam current is ~ 30 nA. Therefore, the presented irradiation facility exceeds the requirements for hadron minibeam therapy.

INTRODUCTION

Compared to proton or heavy ion radiotherapy, minibeam radiation therapy has the potential to further spare normal tissue [1, 2]. The dose required for tumor control is applied through minibeams with an inital transverse width in the submillimetre range. Pencil or planar minibeams are arranged in a grid or an array with a center-to-center distance (ctc) of a few millimeters [3, 4]. The resulting transverse dose distribution with dose minima between minibeam channels spares normal tissue compared to broad beams, reducing side effects. The lateral width of the beams increases with penetration depth due to small-angle scattering. With a suitable ctc, the individual minibeams superimpose in the tumor resulting in a homogeneous dose [5]. The potential of minibeam therapy has been confirmed by preclinical experiments for protons [1, 2, 6–9]. However, it has been shown that the normal tissue sparing decreases with increasing transverse beam width [8]. Therefore, especially the sparing of the deeper normal tissue is limited due to the spreading of the proton beam. In comparison, heavier hadrons such as helium or carbon are less affected by small-angle scattering, which offers the possibility to enhance normal tissue sparing [5, 10, 11]. To evaluate the potential of heavy ions for minibeam therapy in (pre)clinical studies, an irradiation facility needs to be established. Here, we focus on a carbon minibeam facility that could easily be adapted to a helium minibeam facility. Thereby the following requirements should be fulfilled: 1. a carbon ion range in water from 3 cm to 30 cm. 2. a beam current > 1 nA to allow single-session treatments. 3. a transverse beam width of 100 μm and a peak-to-valley dose ratio (PVDR) of > 540 which causes no normal tissue reaction for proton minibeams [8] 4. a possibility for beam scanning up to X=Y=$\pm$ 15 mm that would be sufficient for preclinical experiments as well as for first clincial trials. This manuscript shows a LINAC-based concept for a carbon (helium ion) minibeam irradiation facility that fulfils these requirements.

HADRON MINIBEAM IRRADIATION FACILITY CONCEPT

Figure 1 shows the concept we suggest for a hadron minibeam irradiation facility. It is based on a bent carbon LINAC concept currently being developed at CERN and funded by the CERN Knowledge Transfer Office as part of the NIMMS project [12, 13]. This LINAC concept consists of 5 substructures. A TwinEBIS source [14, 15] delivers $^{12}C^{6+}$ -ions. The ions are initially accelerated and transferred to a subsequent RFQ accelerator by the Low Energy Beam Transport (LEBT). The RFQ accelerates the carbon ions to 5 MeV/u [16]. It operates at a frequency of 750 MHz, allowing a bunch-to-bunch injection into the subsequent 3 GHz bent LINAC structure which can be divided into two parts. The fixed energy section accelerates the ions to 100 MeV/u and does not allow an energy variation due to the dipole magnets in the "arc part". The subsequent variable energy section allows an energy variation of the carbon ions from 100 MeV/u to 430 MeV/u at a mean beam current of 30 nA. The advantage of a bent accelerator over a straight accelerator chain is the reduced space required for future irradiation facilities. For (pre)clinical minibeam application, several components are added downstream of the bend-Linac which have already been designed similarly for a proton minibeam irradiation facility [17, 18]: To focus the beam to a transverse width in the submillimeter range (minibeams) on the target (F in Fig. 1), a quadrupole triplet is used (see #4, Fig. 1). To scan the minibeam over the target, a scanning unit (see #3, Fig. 1) is placed upstream of the quadrupole triplet. It consists of two steerer magnets which first deflect the beam in X- and Y-direction (SX1 and SY1) and two steerer magnets to bend the beam back in the opposite direction (SX2 and SY2). This arrangement allows the beam to pass the quadrupole triplet as close as possible to the optical axis, minimizing abberations. The beam extraction to air is achieved via a 25 µm thick Kapton

* michael.mayerhofer@unibw.de

ISBN: 978-3-95450-227-1 ISSN: 2673-5490 doi:10.18429/JACoW-IPAC2022-THPOMS007

BEAM DIAGNOSTICS FOR FLASH RT IN THE VARIAN PROBEAM SYSTEM

M. Schedler, S. Busold
Varian Medical Systems Particle Therapy GmbH & Co. KG, Troisdorf, Germany
M. Bräuer, Siemens Healthcare GmbH, Erlangen, Germany

Abstract

FLASH RT is a novel ultra-high dose rate radiation therapy technique with the potential of sparing radiation induced damages to healthy tissue while keeping tumor control unchanged. Recent studies indicate that this so-called FLASH effect occurs when applying high doses of several Grays in a fraction of a second only, and thus significantly faster than with conventionally available radiation therapy systems today.

Varian's ProBeam system has been enabled to deliver ultra-high beam currents for FLASH treatments at 250 MeV beam energy. The first clinical trial is currently conducted at Cincinnati Children's Hospital Medical Center and all involved human patients have been successfully irradiated at FLASH dose rates, operating the system at cw cyclotron beam currents of up to 400 nA. With these modifications, treatment times could be reduced down to less than a second.

First automated switching between conventional and FLASH operation modes has been demonstrated in non-clinical environment, including switching of the dose monitor system characteristics and all involved beam diagnostics. Furthermore, for an improved online beam current control system with full control over dose rate in addition to dose Varian has demonstrated first promising results that may improve future applications.

FLASH RT

In conventional IMPT[1], three-dimensional dose distribution in the patient target volume is applied and controlled by the radiotherapy system. With pencil-beam scanning technique, a treatment plan is a set of energy layers, each containing a set of individual spots, defined by 2D beam position at isocenter plane and accumulated proton beam charge. Typical treatment times for a single treatment fraction vary in the range of 30 s up to several minutes.

Recent studies discovered a sparing effect of radiation induced damage to healthy tissue under influence of ionizing radiation at ultra-high dose rates of $> 40\,\mathrm{Gy\,s^{-1}}$ [1], approximately two orders of magnitude above conventional dose rates. This effect is refered to as FLASH effect. The resulting treatment time of a single treatment field is reduced to < 1 s.

The pencil-beam dose rate $\dot{D}_{\mathrm{PB}}$ can be defined based on the stopping power $-\frac{\mathrm{d}E}{\mathrm{d}x}\big|_{\mathrm{water}}$ of the pencil beam on a circular detector of radius r for a given particle flux $\dot{n}$ as

$$\dot{D}_{\mathrm{PB}} = -\frac{\mathrm{d}E}{\mathrm{d}x}\Big|_{\mathrm{water}} \frac{\dot{n}\left(1 - \mathrm{e}^{-\frac{r^2}{2\sigma^2}}\right)}{\pi r^2} \quad (1)$$

assuming a gaussing beam shape with a standard deviation of σ. For the Varian ProBeam system, this yields to nozzle dose rates of up to $2400\,\mathrm{Gy\,s^{-1}}$ at maximum beam energy and current.

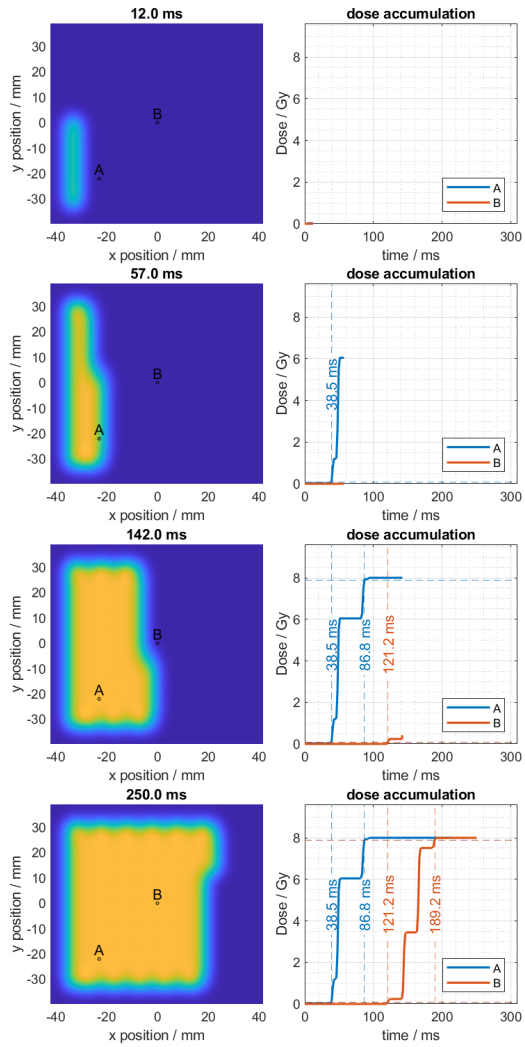

Figure 1: Dose accumulation in a clinical 2D FLASH treatment field calculated for four different time slices. Detailed dose accumulation dynamics is shown for two voxels *A* and *B*.

[1] IMPT: **I**ntensity **M**odulated **P**roton **T**herapy

ISBN: 978-3-95450-227-1 ISSN: 2673-5490 doi:10.18429/JACoW-IPAC2022-THPOMS008

PHYSICS DESIGN OF ELECTRON FLASH RADIATION THERAPY BEAMLINE AT PITZ

X.-K Li*, H. Qian, Z. Aboulbanine[1], Z. Amirkhanyan[2], M. Gross, M. Krasilnikov, A. Lueangaramwong, G. Loisch[3], R. Niemczyk, F. Obier[3], A. Oppelt, S. Philipp, M. Schmitz[3], F. Stephan, Deutsches Elektronen-Synchrotron DESY, Zeuthen, Germany,
[1]on leave from University Mohammed V in Rabat, Rabat, Morocco,
[2]on leave from CANDLE Synchrotron Research Institute, Yerevan, Armenia,
[3]Deutsches Elektronen-Synchrotron DESY, Hamburg, Germany

Abstract

The Photo Injector Test facility at DESY in Zeuthen (PITZ) is preparing an R&D platform for electron FLASH radiotherapy, very high energy electron (VHEE) radiotherapy and radiation biology based on its unique beam parameters: ps scale bunches with up to 5 nC bunch charge at MHz bunch repetition rate in bunch trains of up to 1 ms in length repeating at 10 Hz. This platform is called FLASHlab@PITZ. The PITZ beam is routinely accelerated to 22 MeV, with a possible upgrade to 250 MeV for VHEE radiotherapy in the future. The 22 MeV beam will be used for dosimetry experiments and studying biological effects in thin samples in the next years. A new beamline to extract and match the beam to the experimental station is under physics design. The main features include: an achromatic dogleg to extract the beam from the PITZ beamline; a sweeper to scan the beam across the sample within 1 ms for tumor painting studies. In this paper, the beam dynamics with bunch charges from 10 pC to 5 nC in and the preparation of the new beamline will be presented.

INTRODUCTION

The FLASH radiation therapy (FLASH-RT) has drawn worldwide attention in recent years for its reduced damage to healthy issues [1, 2]. FLASH-RT usually uses an ultra-high peak dose rate (>40 Gy/s), that is two orders of magnitude higher than that in conventional radiotherapy and thus needs much shorter treatment time. While the underlying biological mechanisms are still not fully understood, a broad parameter space study will help to define the optimal working window for FLASH-RT. Therefore, the Photo Injector Test facility at DESY in Zeuthen (PITZ) has proposed an R&D platform for electron FLASH-RT as well as very high energy electron (VHEE) radiotherapy and radiation biology. This platform, called FLASHlab@PITZ, will take advantage of the unique beam parameters at PITZ. The PITZ accelerator runs in the RF burst mode, with an RF pulse length up to 1 ms and a repetition rate at 1-10 Hz. The electron bunches in the RF pulse repeat at a frequency of 1 MHz, making a bunch train of 1000 at maximum. Meantime, the bunch charge can be tuned from sub-pC to 5 nC. The 22 MeV beam will be used for dosimetry experiments and studying biological effects in thin samples in the next years [3]. The very flexible electron beam parameters and widely tunable dose distributions and rates are summarized in Table 1. In this paper, we report the beam dynamics studies performed at a few typical bunch charges up to 5 nC.

Table 1: Parameter Space Summary for FLASHlab@PITZ

Parameters	Low dose case	High dose case
Energy	22 MeV	22 MeV
Charge	0.1 pC	5 nC
Single bunch or train	single bunch	bunch train 1 ms × 1 MHz
RF pulse rep. rate	1 Hz	10 Hz
Dose per bunch	0.0002 Gy	10 Gy
Peak dose rate within train	-	1×10^7 Gy/s
Avg. dose rate	0.0002 Gy/s	1×10^5 Gy/s

* Assuming e-beam in water with 1 cm^3 irradiation volume.

DESIGN OF FLASH-RT BEAMLINE

The PITZ photoinjector consists of an L-band RF gun with a CsTe semiconductor photocathode, a cut-disk-structure (CDS) booster accelerator and various transport and diag-nostic devices, e.g., momentum spectrometers, phase space scanner, steerer and quadrupole magnets. The gun runs at a gradient ≤ 60 MV/m, providing a maximum beam energy of 6.2 MeV. After acceleration in the booster, the beam energy can reach as high as 22 MeV. Then the beam will travel a long way before being sent to a downstream undulator in the tunnel annex (~25 m downstream the photocathode) for the generation of THz radiations, as shown in Fig. 1.

The new FLASH-RT beamline will be installed in the tunnel annex, in parallel with the THz free electron laser (FEL). The electron beam will be translated by ~22 m with a dogleg, which consists of two dipole magnets which deflect the beam in opposite directions with bending angles of 60 degrees and two pairs of quadrupole magnets. To remove dispersive effects at the dogleg exit, the strengths of quadrupoles in the dogleg should be properly chosen. This can be done with transfer matrix method, as implemented in the software Elegant [4]. By making it achromatic (i.e., $\eta_x = 0$, $\eta'_x = 0$), the beam quality degradation due to energy dispersion is minimized, which is especially critical at high

* xiangkun.li@desy.de

ISBN: 978-3-95450-227-1 ISSN: 2673-5490 doi:10.18429/JACoW-IPAC2022-THPOMS010

HEATING AND BEAM IMPACT OF HIGH INTENSITY EXIT WINDOWS FOR FLASHLAB@PITZ

Z. Amirkhanyan[†,1], M. Schmitz[2], Z. Aboulbanine[3], X. Li, H. Qian, M. Gross, M. Krasilnikov, A. Oppelt, R. Niemczyk, S. Philipp, T. Kuhl, F. Stephan, DESY Zeuthen, Germany
[1]on leave from CANDLE Synchrotron Research Institute, Yerevan, Armenia
[2]DESY, Hamburg, Germany
[3]on leave from University Mohammed V in Rabat, Rabat, Morocco

Abstract

The high-brightness electron beam at the Photo Injector Test facility at DESY in Zeuthen (PITZ) is being prepared for dosimetry experiments and radiation biology studies in thin samples. These are the main missions of the FLASH-lab@PITZ, an R&D platform for FLASH and very high energy electron (VHEE) radiation therapy and radiation biology at DESY. These studies require precise information on the electron beam parameters downstream of the exit window, such as the scattering angle and the energy spectrum of the particles as well as the thermal load on the exit window. A Titanium window is compared with a DESY Graphite window design. Heat deposition in the window by a single 22 MeV / 1nC electron bunch of various sizes, its scattering and energy spectrum due to passage through the window are calculated by means of FLUKA Monte Carlo simulations. Time resolved temperature profiles, as induced by the passage of 1ms long electron pulse trains with up to 4500 single pulses, each of them between 0.1 and 60 ps long, were calculated with a self-written finite element method (FEM) code.

INTRODUCTION

Electron beams generated from linear accelerator are used in fundamental nuclear physics, particle physics as well as in applied sciences such as medical applications [1,2]. The Photo-Injector Test Facility at DESY in Zeuthen (PITZ) is starting an R&D project aiming to explore the potential of electron beams in the FLASH dose rate regime for radiation therapy and radiation biology experiments [3]. A wide and unique electron beam parameter range is going to be used for this purpose. An extraction of the electron beam from the vacuum is there-fore needed to irradiate a target placed in air and located at a certain distance from the accelerator exit window. Key parameters of the electron beam, mainly its spot size but also the electron bunch length, the repetition rate and the energy of the electron beam are influencing the heat distribution on the exit window [4,5]. Damages induced by high repetition rate electron beams crossing the exit window might lead to vacuum leaks or in the worst case to a complete collapse of the vacuum/air barrier. In this work, simulations and numerical investigations were carried out in order to estimate the scattering effect on the electron beam crossing an exit window and the resulting heat load under extreme and achievable electron beam parameters at the PITZ facility.

MONTE CARLO SIMULATIONS

Beam Scattering Effect

The interaction of the electron beam with the exit window involves variations of important beam properties, mainly the transverse spatial distribution, the angular distribution and the energy spectrum. For radiation therapy and radiation biology, each of the previous quantities should be precisely identified in the air. In addition, the thermal stability of the exit window should be investigated in order to avoid any vacuum failure or leakage. A FLUKA [6] Monte Carlo model was used to calculate the energy deposition map in the window and its dependence on the electron beam parameters. In this section, we consider two types of exit windows: first one is made of 50 µm thick Titanium, the second one is based on Graphite consisting of a 500 µm carbon fiber reinforced graphite (CF-C, 1.5 g/cm^3) carrier material, coated on one side with less than 50 µm layer of Pyrolytic graphite (PyC, 2 g/cm^3) to make the porous substrate leak tight. Figure 1 shows the distribution of electron scattering angles (left) and energy spectrum (right) at the exit windows generated by a bunch of electrons with an energy of 22 MeV for the Titanium and Graphite window. A Gaussian fit, defines the RMS angle of the electrons at the window exit 17.2 mrad for 50 µm titanium and 20.7 mrad for 550 µm graphite. On the other hand, the analytical estimation of the electron scattering in a thin layer is carried out using the theory of multiple Coulomb scattering. Namely, the Moliere angle is determined as [7]

$$\theta_{RMS} = \frac{13.6MeV}{\beta cp}\sqrt{\frac{x}{X_0}}\left(1 + 0.038 \ln\left(\frac{x}{X_0}\right)\right) \quad (1)$$

where β is the ratio of the electron velocity to the speed of light c, p is the electron momentum, X_0 the radiation length and x is the material. Numerical estimation using Eq. 1 is defined as Moliere angle 16.8 mrad for 50 µm titanium and 21.01 mrad for 550 µm graphite, which is consistent with the simulation results.

The titanium generates less secondary particles and leads to a reduced contribution in the low energy component compared to the Graphite window. The RMS of the angular distribution for the Titanium window is slightly lower with respect to the graphite (Fig. 1).

† zohrab.amirkhanyan@desy.de

ISBN: 978-3-95450-227-1 ISSN: 2673-5490 doi:10.18429/JACoW-IPAC2022-THPOMS011

BEAM OPTICS STUDIES FOR A NOVEL GANTRY FOR HADRON THERAPY*

E. Felcini†, G. Frisella, A. Mereghetti, M. G. Pullia, S. Savazzi, CNAO Foundation, Pavia, Italy
M. T. F. Pivi, EBG MedAustron, Wr. Neustadt, Austria
E. Benedetto, SEEIIST, Geneva, Switzerland

Abstract

The design of smaller and less costly gantries for carbon ion particle therapy represents a major challenge to the diffusion of this treatment. Here we present the work done on the linear beam optics of possible gantry layouts, differing for geometry, momentum acceptance, and magnet technology, which share the use of combined function superconducting magnets with a bending field of 4 T. We performed parallel–to–point and point–to–point optics matching at different magnification factors to provide two different beam sizes at the isocenter. Moreover, we considered the orbit distortion generated by magnet errors and we introduced beam position monitors and correctors. The study, together with considerations on the criteria for comparison, is the basis for the design of a novel and compact gantry for hadrontherapy.

INTRODUCTION

In the context of the European project HITRI*plus* [1], the study and design of a novel superconducting gantry has been undertaken. Following up the studies performed by the TERA Foundation on superconducting gantries [2, 3], a wide explorative study on dozens of gantry layouts and optics configurations was performed [4, 5]. This manuscript presents the assumptions made and methods used to analyse and compare the different optics solutions. Furthermore, the two most promising layouts are described in more detail.

GANTRY DESIGN CHOICES

Before entering in the details of the optics studies, it is important to highlight the design choices that defined the perimeter of the explored parameters space. The first fundamental choice was to position the scanning magnets after the last bending section. Although this approach poses relevant challenges on the design of the scanning magnets, it allows to operate with standardized dipoles in the whole gantry, avoiding an increase of aperture in last bending section.

The second fundamental choice was the selection of the bending field. While state of the art gantries operate with fields up to 3.5 T [6–8], we decided to push toward 4 T superconducting dipoles [9], aiming for a further reduction of the gantry weight. Depending on the layouts, these dipoles may need a superimposed gradient that can be obtained through an asymmetric assembly of the coils [10]. Even if it would be possible to wind the magnet with separate circuits for dipole and quadrupole (nested magnets), this option was discarded in the context of this study to favor the easiness of construction and operation of the superconducting magnets. To standardize the comparison between the different gantry layouts, two options were considered for the magnet aperture: 70 mm and 90 mm in diameter. Optics layouts that require an aperture larger than 90 mm are considered not suitable for the proposed study. In the same way, two options were considered for the dipoles angle length: 30 ° and 45 °.

GANTRY BEAM OPTICS

The main constraints to the beam optics of the gantry, resulting from the continuous interaction with medical doctors and physicist of CNAO (Italian National Center for Oncological Hadron Therapy) and MedAustron (Center for Ion Therapy and Research, Austria), were identified:

- operation with $^{12}C^{6+}$ up to 430 MeV/u kinetic energy, equivalent to 31 cm of range in water;
- beam characteristics at the isocenter independent on the angle of rotation;
- two different beam sizes at the isocenter: 8 mm and 12 mm (FWHM) at the minimum extraction energy;
- global achromaticity to avoid distortion of beam size and position due to the beam momentum spread.

A more thorough and detailed list of medical constraints and requirements is reported in [5].

Matching Procedures at the Isocenter

In order to obtain a beam size independent of the gantry angle, two different types of telescopic matching were implemented between the coupling point and the isocenter [11]:

- "point–to–point" matching, where particles with the same initial position in (x, y) end up in the same position independently of the initial divergence (x', y'). In this case, an input round beam in (x, y) maintain its size at the isocenter independently from the gantry rotation angle;
- "parallel–to–point" matching, where particles with the same initial divergence (x', y') end up in the same position independently of the initial position (x, y). In this case, an input round beam in (x', y') maintain its size at the isocenter independently from the gantry rotation angle.

For both matching methods, it is possible to impose a magnification factor (MF), i.e. the factor by which the input beam size is increased to obtain the output beam size at the end of the beam line.

* This study was (partially) supported by the European Union Horizon 2020 research and innovation program under grant agreement no. 101008548 (HITRI*plus*).
† enrico.felcini@cnao.it

ISBN: 978-3-95450-227-1 ISSN: 2673-5490 doi:10.18429/JACoW-IPAC2022-THPOMS012

EXPLORATIVE STUDIES OF AN INNOVATIVE SUPERCONDUCTING GANTRY*

M. G. Pullia†, M. Donetti, E. Felcini, G. Frisella, A. Mereghetti, A. Mirandola, A. Pella, S. Savazzi, CNAO Foundation, Pavia, Italy
L. Dassa, M. Karppinen, D. Perini, D. Tommasini, M. Vretenar, CERN, Geneva, Switzerland
C. Kurfürst, M. T. F. Pivi, M. Stock, EBG MedAustron, Wr. Neustadt, Austria
E. De Matteis, S. Mariotto[1], M. Prioli, L. Rossi, INFN–Milano, LASA Laboratory, Segrate, Italy
L. Sabbatini, A. Vannozzi, INFN–LNF, Frascati, Italy
L. Piacentini, A. Ratkus, T. Torims, J. Vilcans, Riga Technical University, Riga, Latvia
E. Benedetto, SEEIIST, Geneva, Switzerland,
S. Uberti, Università di Brescia, Brescia, Italy
[1]also at University of Milan, Milan, Italy

Abstract

The Heavy Ion Therapy Research Integration plus (HITRI*plus*) is an European project that aims to integrate and propel research and technologies related to cancer treatment with heavy ion beams. Among the ambitious goals of the project, a specific work package includes the design of a gantry for carbon ions, based on superconducting magnets. The first milestone to achieve is the choice of the fundamental gantry parameters, namely the beam optics layout, the superconducting magnet technology, and the main user requirements. Starting from a reference 3 T design, the collaboration widely explored dozens of possible gantry configurations at 4 T, aiming to find the best compromise in terms of footprint, capital cost, and required R&D. We present here a summary of these configurations, underlying the initial correlation between the beam optics, the mechanics and the main superconducting dipoles design: the bending field (up to 4 T), combined function features (integrated quadrupoles), magnet aperture (up to 90 mm), and angular length (30° – 45°). The resulting main parameters are then listed, compared, and used to drive the choice of the best gantry layout to be developed in HITRI*plus*.

INTRODUCTION

In the framework of the Heavy Ion Therapy Research Integration plus (HITRI*plus*) project [1], a new design of a gantry for carbon ions is being developed, based on superconducting (SC) magnets. The new design shall represent the next generation of gantries for hadrontherapy, targeting small dimensions, an affordable cost and a credible time scale for construction.

An international panel gathering experts in accelerator design and clinicians at the forefront of research in hadrontherapy suggested [2] to start the development from a recent gantry design proposed by a joint TERA–CERN team [3]. The reviewers put particular emphasis on reviewing and confirming the clinical requirements with the clinical staff of the hadrontherapy centers participating to the project and on decreasing the overall dimensions and weight of the gantry. For this reason, the panel suggested to push the field on the bending magnets beyond the state of the art of normal [4] and superconducting [5, 6] carbon–ion gantries up to 4 T. Prototyping the magnets was also indicated as a key achievement, in order to prove the feasibility of the design.

Starting from the clinical requirements, this contribution presents the main layout and optics solutions identified during a first exploratory phase of the development; key parameters are compared and the two most promising layouts are chosen for further development. Details on the chosen optics can be found at Ref. [7].

CLINICAL REQUIREMENTS

The clinical requirements were extensively discussed with medical physicists and doctors at CNAO [8] and MedAustron [9]. The most relevant ones are:

- the beam with the largest magnetic rigidity is $^{12}C^{6+}$ at 430 MeV per nucleon kinetic energy, corresponding to 6.62 Tm and 31 cm of range in water;
- the scanned area shall be as large as possible, indicatively 350 mm × 350 mm, at least 200 mm × 300 mm; the larger dimension is parallel to the gantry rotation axis. The minimum scanning speed shall be 20 m/s;
- the minimum set of beam sizes at the isocenter shall be 8 mm and 12 mm (FWHM) at the minimum extraction energy; at larger energies, the beam size will reduce following the adiabatic damping of the beam emittance;
- a source–to–axis distance (SAD) of at least 2 m – 2.5 m;
- possibly 360° rotation, minimum 220°;
- volumetric imaging at the isocenter.

LAYOUT EXPLORATION

All the layouts are based on the following assumptions:

- scanning magnets located downstream of the last bending section, to relax constraints on the aperture of the SC magnets;

* This study was (partially) supported by the European Union Horizon 2020 research and innovation program under grant agreement no. 101008548 (HITRI*plus*).
† marco.pullia@cnao.it

ISBN: 978-3-95450-227-1 ISSN: 2673-5490 doi:10.18429/JACoW-IPAC2022-THPOMS013

ELECTRON GUN SYSTEM DESIGN FOR FLASH RADIOTHERAPHY*

H. Lee†, G. Jang, J. Koo, D. Yu, H. Seo, H. Shin, VITZRONEXTECH Co., Ltd, Ansan, Korea
G. B. Kim, D. H. An, K. U. Kang, J. H. Kim, S. H. Chai,
Korea Institute of Radiological & Medical Sciences, Seoul, Korea
Y.-G. Son, Pohang Accelerator Laboratory, Pohang, Korea

Abstract

An electron gun is a device that emits electron beams used in an electron accelerator, an electron beam welder, an x-ray generator, etc. This device can be broadly divided into three components: a cathode, a grid, and an anode. A medical electron gun, which is a sub-system of an electron accelerator for FLASH radiotherapy, requires a high current. The electron gun was designed to obtain a peak current up to 15A using EIMAC Y824 cathode. We would like to introduce the structure of the electron gun and the required power supply system. In this paper, we will describe the optimization process of the electron gun structure design, the Marx-type power supply providing 200 kV pulse voltage, and the grid pulse power supply ranging from 1ns to 1.5 μs.

INTRODUCTION

Cancer treatments, in general, heavily rely on three main modalities of systemic therapy: surgery, radiation therapy, and chemotherapy. Radiation therapy (RT) is a cost-effective cancer treatment with an approximately 50% survival, when used alone or in combination with other cancer therapies [1]. A new radiation treatment maximizes the removal of a tumor while minimizing the damage to healthy tissues surrounding the tumor, thus reducing the side effects of treatment. FLASH electron beam radiation therapy is a promising treatment that delivers therapeutic doses at a high dose rate (>40 Gy/s) in less than 1 second (example:90 ms) [2-4]. Most FLASH RT studies are performed using electron beams generated from linear accelerators [5, 6] with energy of 4–6 MeV or energy-modified clinical linear accelerators. The clinical linear accelerators were modified with energy levels up to 20 MeV and successfully generated electron beams at ultra-high dose rates [7,8]. However, the inability of the beam to penetrate to the desired location remains problematic due to the limitations in the clinical energy level range (4-22 MeV). Dosimetric studies were also conducted using electron beams with energy level up to 50 MeV. The studies conducted with a 50 MeV electron beam concluded that the beam could reach deep tumors and enable FLASH radiation therapy for umors 10-15 cm deep with ultra-high dose rate electron beams [9].

With reference to the data, we are developing an electron gun system consisting of a cathode, an anode and a grid, for use in a 50 MeV FLASH electron accelerator that provides a high current. A pulse voltage of 200 kV is applied between the cathode and the anode of the electron gun to obtain a high current. The ceramic section of the electron gun is designed to be assembled with the oil tank to prevent discharge. In this paper, the beam physics design, structural design and analysis of the electron gun, and the power supply design are explained.

ELECTRON GUN DESIGN

The electron gun used in the 50 MeV FLASH electron linear accelerator is designed based on Eimac's Y-824 dispenser cathode. The characteristics of this cathode are explained in Table 1, and the external shape is shown in Fig. 1. The shape of the cathode and the anode electrodes was optimized using CST simulation program to generate a current of 15 A when 200 kV was applied to the electron gun. The shape of the node and the shape of the electron beam are shown in Fig. 2. In addition, the size of the current emitted from the electron gun and the size of the electron beam were calculated through simulation when a voltage of 150 kV was applied between the cathode and the anode. The results are shown in Table 2.

Table 1: Specification of the Cathode

Item	Specification
Model	Y824
Type	Dispenser
Cathode area	2 sq. cm
Emission	15A @$E_c = 200V$
Conflat size	2-3/4”

Figure 1: Eimac's Y-824.

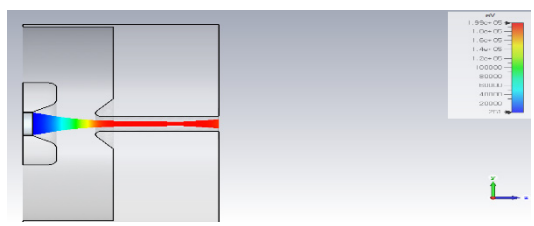
Figure 2: Simulation results with CST PS Studio.

*Work was supported by a grant of the Korea Institute of Radiological ar Sciences(KIRAMS), funded by Ministry of Science and ICT(MSIT), Rep (50572-2022)
†pallhs@vitzrotech.com

ISBN: 978-3-95450-227-1 ISSN: 2673-5490 doi:10.18429/JACoW-IPAC2022-THPOMS015

NEW DESIGN OF CYCLOTRON FOR PROTON THERAPY

O. Karamyshev†, JINR, Dubna, Russia

Abstract

An innovative approach to a design of cyclotron allows to produce cheaper and more power efficient cyclotrons for medical and industrial application is presented. A 230 MeV cyclotron for proton therapy, using this design scheme is presented. The cyclotron is one of the line of cyclotrons from 15 to 230 MeV, that uses same magnet field level and RF frequency and utilises many identical solutions within the line-up to make it cheaper to produce and run. The design suits for FLASH therapy as is it able to produce larger beam current then existing accelerators for proton therapy.

INTRODUCTION

The proposed design follows the same concept, described in the [1]. Currently two types of cyclotrons are successfully operated for proton therapy: IBA C235 [2] and Varian Proscan [3]. More recently developed synchrocyclotrons such as IBA S2C2[4] and Mevion [5] were looking as a superior option in terms of compactness and price before an innovative technique, called FLASH [6] has been discovered, which requires higher beam currents then existing accelerators for proton therapy produce.

In order to achieve high beam current (over 10 micro-Amperes) the cyclotron should have good acceleration rate and low magnetic field to ensure efficient extraction.

In this paper the cyclotron project for proton therapy using similar approach is described. Unlike a 10-70 MeV cyclotrons [7], a 230 MeV proton therapy accelerator requires a 4-sector structure. Acceleration at the 6 harmonic mode is possible when four accelerating cavities operate in push-pull mode, meaning that opposite cavities operate in the same phase, and the other two cavities have to operate with 180deg phase shift. It can be achieved by having a capacitance coupling in the central region.

Such configuration is beneficial for both magnet and RF design, as the magnet, while having necessary average magnet field is being very efficient (has small number of A*turns), high frequency RF system is very compact and power-efficient, despite its high frequency due to high Q factor. The number of A*turns in this project is 80000 per coil, so coil has rather small cross-section 240*120 mm^2. Compared to the IBA C235 cyclotron with resistive coils, which is widely used in the proton therapy, has the number of A * turns of 250000 per coil and, as a result, its coil dimension is about 500x350mm^2, and as a result the yoke of the magnet is much larger, although the pole diameter is smaller. Minimizing coil cross-section leads to significant reduction of the overall dimensions (see Table 1). As the result, the proposed design requires just 2.7 Tons of copper, which is about 8 times less than for IBA C235 and overall price of copper wire is much cheaper than cryogenics equipment, required for superconducting coil.

Computer model of the cyclotron (see Fig. 1, Fig. 2) was build in CAD and simulated in CST studio [8].

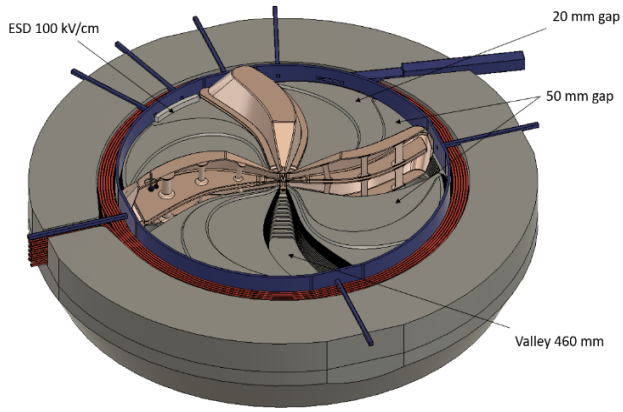

Figure 1: 3D computer model of the cyclotron.

Table 1: Parameters of the Cyclotron

Accelerated particles	protons
Final energy	232 MeV
Ion source	Internal, PIG
Extraction scheme	1 ESD, 2 correctors
Magnet Power Consumption	95 kW
RF power consumption	80 kW (wall losses)
Dimensions	3850x3850x2000 mm^3
Beam current	Up to 100 micro Ampers

MAGNET SYSTEM OF THE CYCLOTRON

In order to minimize the A-turns number the design of the magnet is following the rule: maximize the amount of steel inside the cyclotron.

Magnet sectors consist of two parts:

1. wide-aperture part with a vertical distance of 50 mm and low helicity
2. small-aperture part with a vertical distance of 25 mm and high helicity.

This structure makes it possible, firstly, to place the deflector between the sectors in the wide-aperture part, while retaining the valleys for placing the resonators, and, secondly, to ensure isochronous growth and vertical focusing due to the small-aperture part of the sector.

Two Coils consists 6 double pancakes of square 19x19mm^2 hollow conductor (Luvata 8171) with 10 mm in diameter hole. Length of each pancake is 105 meters. Parameters of the magnet are presented in Table 2.

† olegka@jinr.ru

ISBN: 978-3-95450-227-1 ISSN: 2673-5490 doi:10.18429/JACoW-IPAC2022-THPOMS016

A NEW DESIGN OF PET CYCLOTRON

O. Karamyshev†, JINR, Dubna, Russia

Abstract

An innovative approach to a design of cyclotron allows to produce cheaper and more power efficient cyclotrons for medical and industrial application. 15 MeV cyclotron for PET (and other) isotopes production are widely used and in very high demand. In this paper a design of a very compact and cheap to build and to run cyclotron is presented.

INTRODUCTION

Demand for cyclotrons, delivering 10-70 MeV proton (mostly) beams for medical isotopes production such as PET, SPECT isotopes and 200-250MeV proton beams for hadron therapy rapidly is growing. All around the world scientists and engineers are looking into ways to make such cyclotrons more compact, and less costly. The modern trend is to apply superconducting coils to increase magnetic field strength of the cyclotron in order to make the accelerator more compact, and thus reduce the overall cost of the cyclotron setup. Nowadays superconducting cyclotrons and synchrocyclotrons are successfully operating not just for proton therapy (Varian Proscan[1], S2C2 (IBA) [2], Mevion [3]) but also for isotope production (Ionetix [4]). Some of them appeared quite recently, and some work for years and have proved their effectiveness. However, the majority of the cyclotrons still use resistive coils due to it's low cost and reliability.

Here are the reasons why the author believes that cyclotrons with resistive coils are still a good choice for medical applications:

- There are opportunities for optimization, examples are presented further in the paper.
- Compared to superconducting cyclotrons, power consumption and dimensions are not necessarily higher, but in some cases could be lower, as cryocoolers consume power, and occupy space around the magnet.
- Low magnet field is easier to shim, the isochronizing requirements are lower.
- As accelerating system remains resistive, water cooling is required, therefore costly infrastructure of water preparation system can be used also for coil cooling.

A NEW 15 MeV CYCLOTRON

Usually, cyclotrons dedicated for isotope production accelerate H^- ions to get use from extraction by stripping on the foil. Extraction by stripping has about 100% efficiency, low energy H^- ions has only one disadvantage, high vacuum is required. The presented cyclotron is accelerating H^- ions.

† olegka@jinr.ru

Concept

The cyclotron needs to be compact, cheap, reliable and to have a low power consumption. Concept RC3/6 has been published on Cyclotrons 2019 conference, has been modified, magnet field and RF frequency increased, so RF frequency is placed in 144-146 MHz range, which is dedicated for amateur use. This ensures that there should be no issues with legal use of the frequency. This leads us to more efficient design of the cyclotron than typical four-sector accelerator. What is the essence and specific feature of the concept 3/6? The three-sector cyclotron operating at the 6 harmonic mode of acceleration allows to have an effective magnetic system due to wide sectors providing higher mean field and narrow valleys sufficient for placing resonators corresponding to 6^{th} harmonic of acceleration (see Fig. 1). The sectors of the magnet are 90 degrees azimuthal width, and valleys are about 30 degrees. In such case the 6^{th} harmonic mode is optimal for acceleration and the resonance frequency must be 145 MHz for magnetic field equal to 1.55 T.

Such configuration is beneficial for both magnet and RF design, as the magnet, while having necessary average magnet field is being very efficient (has small number of A*turns), high frequency RF system is very compact.

Resistive coils and rather big pole diameter reduce the effort and cost of producing this machine.

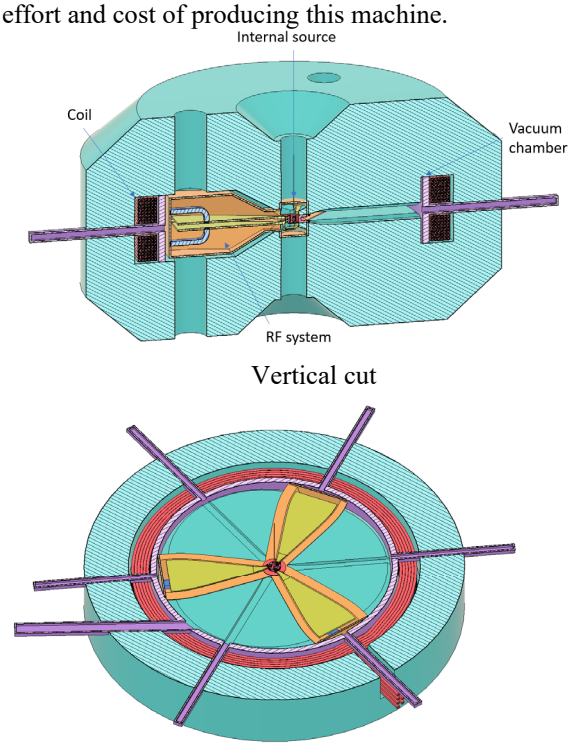

Figure 1: Layout of the 3D computer model of the cyclotron.

ISBN: 978-3-95450-227-1 ISSN: 2673-5490 doi:10.18429/JACoW-IPAC2022-THPOMS017

MSC230 SUPERCONDUCTING CYCLOTRON FOR PROTON THERAPY

K.S. Bunyatov, V.A. Gerasimov, S. Gurskiy, O. Karamyshev†, G.A. Karamysheva, I.D. Lyapin, V. Malinin, M.S. Novikov, D. Nikiforov, D. Popov, V.M. Romanov, A.A. Sinitsa, G.V. Trubnikov, G. Shirkov, S.G. Shirkov, G.G. Hodshibagijan, S.Yakovenko, JINR, Dubna, Russia

Abstract

Superconducting cyclotron MSC230 is intended for acceleration of the proton beam to 230 MeV for medico-biological research. MSC230 [1,2] is an isochronous four-sector compact cyclotron with a 1.7 T magnetic field in the centre. Acceleration is performed at the fourth harmonic mode of the accelerating radio-frequency (RF) system consisting of four cavities located in the cyclotron valleys. The accelerator will use an internal Penning type source with a hot cathode. Extraction is carried out by an electrostatic deflector located in the gap between sectors and two passive magnetic channels. The current status of the project is discussed.

INTRODUCTION

Many years of practical experience in the treatment of cancer patients with proton beams at the Medical Technical Complex (MTC) of Joint Institute for Nuclear Research (JINR) [3,4] creates a unique environment for the development of innovative technologies in the field of proton therapy. Recent studies of a promising new method, called FLASH [5-7], have shown that it has great potential for expanding the use of proton therapy on tumors that previously could not be treated with protons, at the same time significantly improving the quality of treatment. The FLASH method decreases the number of irradiation procedures, and, therefore, decreases the cost of treatment, making it more affordable for an ordinary patient. The necessary equipment to study the method is available with the medical beam of the MTC DLNP, where conformal irradiation of tumors is possible. The task of the FLASH research makes relevant the creation of a research and innovation center equipped with a modern proton accelerator, a beam delivery system and laboratory equipment for biomedical research.

Table 1: Parameters of the Cyclotron

Accelerated particles	protons
Magnet type	Compact, SC coil, warm yoke
Number of sectors	4
Number of RF cavities	4
Harmonic number Frequency, MHz	4 106.5
Ion source	Internal, PIG
Final energy, MeV	230
Number of turns	500

This article is devoted to the project of a cyclotron aimed at obtaining an intense proton beam. In the coming years, it is planned to create a cyclotron and equipment for studying the FLASH-irradiation method. Main parameters of MSC230 cyclotron are presented in Table 1. Computer model of the cyclotron is seen in Fig. 1.

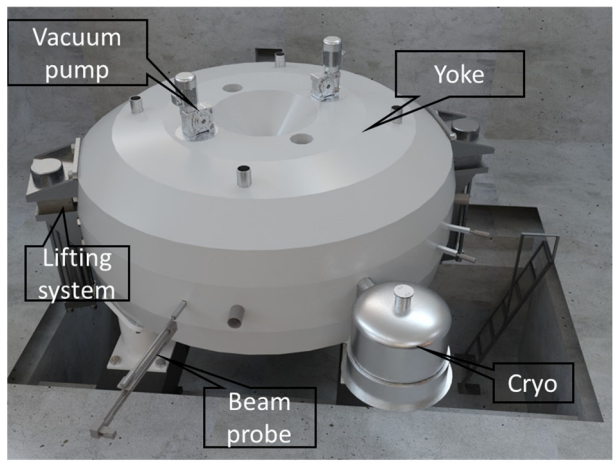

Figure 1: View of the cyclotron's 3D computer model.

MAGNET SYSTEM

The MSC230 magnet is composed of a superconducting (SC) solenoid and an iron yoke. The technology with the use of a hollow composite SC cable, proposed at JINR and well-proven in the magnets of the Nuclotron synchrotron, was chosen as the basis for the manufacture of the solenoid. JINR has a base for the production of such a cable, which requires only the modernization of the existing equipment.

To achieve high intensity of the beam it is necessary to provide an intense source of ions and minimize losses at all stages of acceleration. It is easier to ensure a high transmission coefficient in a cyclotron with a lower magnetic field, so we chose the value of the magnetic field in the centre equal to 1.7 T. Simulations of the magnet and accelerating systems were performed in CST studio [8] (see Fig. 2).

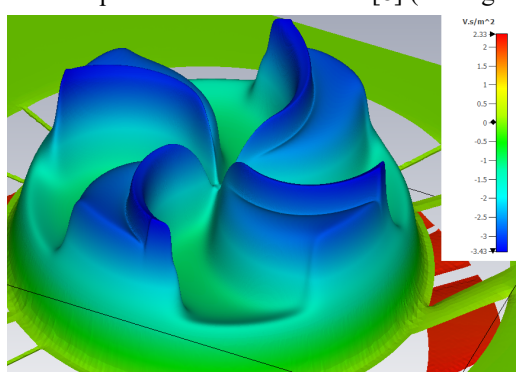

Figure 2: Magnetic field distribution.

† olegka@jinr.ru

ISBN: 978-3-95450-227-1 ISSN: 2673-5490 doi:10.18429/JACoW-IPAC2022-THPOMS018

STUDY OF COIL CONFIGURATION AND LOCAL OPTICS EFFECTS FOR THE GaToroid ION GANTRY DESIGN*

Ewa Oponowicz†, Luca Bottura, Yann Dutheil, Ariel Haziot, CERN, Geneva, Switzerland
Alexander Gerbershagen[1], CERN, Geneva, Switzerland
[1]also at Particle Therapy Research Center (PARTREC), Department of Radiation Oncology, University Medical Center Groningen, University of Groningen, The Netherlands

Abstract

GaToroid, a novel gantry configuration for hadron therapy, is based on superconducting coils that generate a toroidal magnetic field to deliver the beam to the tumour location. Designing the complex GaToroid coils requires careful consideration of the local beam optical effects.

We present a Python-based tool for charged particle transport in complex electromagnetic fields. The code implements fast tracking in arbitrary three-dimensional field maps, and it does not require a definition of specific or regular reference trajectories, as is generally the case for accelerator physics codes. The tool was used to characterise the beam behaviour inside the GaToroid system: to automatically determine the reference trajectories in the symmetry plane and analyse three-dimensional beam dynamics around these trajectories. Beam optical parameters in the field region were compared for various magnetic configurations of GaToroid.

This paper introduces the new tracker and shows the benchmarking results. Furthermore, first-order beam optics studies for different arrangements demonstrate the main code features and serve for the design optimisation.

INTRODUCTION

A number of well-established codes for beam tracking studies are widely available [1, 2]. However, most of them are typically designed for long magnets of small aperture, i.e., magnetic configurations generating conventional fields or superposition of such, which can be easily represented with multipole expansion theory. Beam optics studies in complex magnetic fields are either not implemented, or require complex post-processing [3].

The development of a fast and compact code for particle tracking in arbitrary magnetic (or electric) field was motivated by the beam optics studies of GaToroid, a novel gantry for hadron therapy [4, 5]. The GaToroid concept is based on an axis-symmetric toroidal fixed-field magnet which, in combination with an upstream vector magnet, is capable of delivering the beam onto the patient. Characterisation of the local beam dynamics properties of this system is required to optimise its design. This work demonstrates the transport of carbon ions (C^{6+} of kinetic energy in the range 120 – 430 MeV/u) through several examples of GaToroid configurations.

* Project co-supported by the CERN Budget for Knowledge Transfer to Medical Applications.
† ewa.oponowicz@cern.ch

METHOD

Coil Geometry

The principle of GaToroid is based on two parts: the main toroidal magnet to bend the beam onto the patient (Fig. 1) and an upstream *vector magnet* (VM, modelled here as single kick) for beam steering. The angular kicks imposed at the VM are polar, depending on the beam kinetic energy, and/or azimuthal, determined by the desired irradiation direction. The azimuthal variations are discrete and limited to the number of coil pairs constituting the toroid. For a given irradiation angle, the beam passes in between a set of two coils tilted symmetrically around the toroid axis (Fig. 1a). Due to the periodic axis symmetry, beam dynamics studies concentrate on the region bounded by two coils forming the "beam channel".

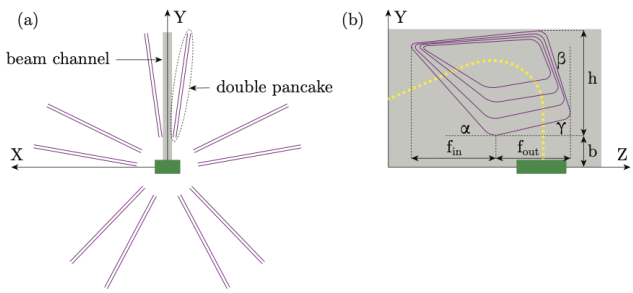

Figure 1: Schematic drawings of GaToroid with patient (green rectangle) in the axis of the toroid (treatment position), and the conductor windings (purple curves): (a) projection of a full gantry consisting of 5 beam channels; each channel is the space between two adjacent coils, (b) projection of the single coil geometry onto the bending plane together with and example beam trajectory (yellow dashed curve). f_{in} - entrance leg length, f_{out} - exit leg length, , h - maximum coil height, b - bore radius, α - entrance face angle, β - back leg angle, γ - exit face angle. The configuration consists of 4 coil grades.

The geometry of the coil (Fig. 1b) substantially impacts beam dynamics. In a typical toroidal configuration, the magnetic field decreases with the radius of the coil; higher energy particles require a larger kick at VM and hence experience a lower magnetic field and their bending is weaker. For treatment purposes this defocusing effect must be compensated to ensure it is an achromatic system. The field profile is modified by so called grading, i.e., introducing spacing between the coil winding in the coil for an appropriate distribution of

ISBN: 978-3-95450-227-1 ISSN: 2673-5490 doi:10.18429/JACoW-IPAC2022-THPOMS019

SLOW EXTRACTION MODELLING FOR NIMMS HADRON THERAPY SYNCHROTRONS*

R. Taylor†, CERN, Geneva, Switzerland & Imperial College London, UK
E. Benedetto, M. Sapinski, SEEIIST, Geneva, Switzerland
J. Pasternak, Imperial College London & STFC Rutherford Appleton Laboratory, Didcot, UK

Abstract

The Next Ion Medical Machine Study (NIMMS) is an umbrella R&D programme for CERN accelerator technologies targeting advanced accelerator options for proton and light ion therapy. In collaboration with the European programme HITRIplus, one area of study is slow extraction which is required to deliver a uniform beam spill for radiotherapy treatment. Several techniques use the third-order resonance to extract hadrons; these include betatron core driven extraction and radiofrequency knock-out. Flexible simulation tools using these techniques were prepared and initially benchmarked with results from the literature that used the Proton-Ion Medical Machine Study (PIMMS) design. The limits of the current PIMMS design were then pushed to evaluate its compatibility to deliver > 10× higher intensity ion beams, and using increased extraction rates.

MOTIVATIONS

Flexible modelling techniques have been developed to facilitate the design of NIMMS [1]. The NIMMS study has a variety of designs available including normal and superconducting options [2]; all aiming to provide a variety of light ion beams for clinical treatment and radiobiological research.

Resonant slow extraction is used to ensure a continuous and stable dose delivery during treatment. It is performed by setting the horizontal tune of the machine close to the third-order resonance (Q_x =1.666) which is excited with strong resonant sextupole magnets. The particles are then driven to the resonance via excitation methods, leave the stable triangle phase-space and are extracted at the electrostatic septum (ES).

Simulations of slow extraction were used to assess if the PIMMS [3, 4] design, as utilized by CNAO and MedAustron therapy facilities, can be adapted to suit advanced accelerator options. The feasibility study was performed, first by modelling the PIMMS lattice, then changing excitation methods to ensure it can be upgraded to meet two requirements: adapting to extract higher emittance beams, and providing the option of increased extraction rates.

Higher Emittance Multi-Energy Extraction (MEE) uses multiple flat-tops for each required treatment energy, rather than having one energy per magnet duty cycle. This technique decreases wait-time during delivery of different energies, and was proposed and implemented at the NIRS HIMAC center [5].

To deliver a dose of 2 Gy to a 1-liter tumour within one cycle of MEE, the synchrotron must store 1 to 2 × 10^{10} carbon ions [2], which is 20× higher than what current European hadron therapy synchrotrons can deliver. With an ion source of 600 µA, a multi-turn injection method of 30 turns needs to be performed to achieve this higher intensity, assuming 50% injection efficiency. This method would consequently generate a horizontal, normalised rms emittance increase of $\varepsilon_{x\mathrm{rms}} < 6\,\pi \cdot \mathrm{mm} \cdot \mathrm{mrad}$. Slow-extraction studies have been performed to assess the fesibility of extracting a beam with these larger emittances.

Increased extraction rates Treating with dose delivery rates of 50-100 Gy s^{-1} reduces toxicities to healthy tissue compared to conventional radiotherapy [6]. This technique is known as FLASH therapy. With a suggested threshold dose of 10 Gy, the beam should be provided within 100 ms [7]. The NIMMS synchrotron should provide a hadron beam which can meet the recommended dose within this time frame. The PIMMS revolution frequency for high-energy carbon is 2.8 MHz [4] so 100 ms requires 280,000 turns. This is a challenge compared to nominal slow extraction which delivers over millions of turns. This study will observe whether a high quality beam spill can be provided within this increased extraction rate.

METHOD

Simulations were performed to reproduce slow extraction results from the existing PIMMS synchrotrons, then these were adapted to meet the two advanced options. The lattice was implemented into MAD-X [8] and matched for the extraction conditions for two excitation methods: betatron core and radiofrequency knock-out (RKFO).

The main lattice parameters relevant to slow extraction are horizontal and vertical tune Q_x, Q_y, chromaticity Q'_x, virtual sextupole strength S_{virt} and beam momentum spread $\frac{\Delta p}{p}$, shown in Table 1 for both methods.

Table 1: Lattice Extraction Parameters

	Q_x	Q'_x	Q_y	S_{virt}	$\Delta p/p$
Betatron	1.666	-4.041	1.720	28.4	0.4%
RFKO 1ε_x	1.675	-0.004	1.695	32.1	0.1%
RFKO 6ε_x	1.680	-0.007	1.695	32.1	0.1%

* This study was partially supported by the European Union's Horizon 2020 research and innovation programme under grant agreement no. 101008548 (HITRIplus).
† rebecca.taylor@cern.ch

ISBN: 978-3-95450-227-1 ISSN: 2673-5490 doi:10.18429/JACoW-IPAC2022-THPOMS020

BEAM OPTICS STUDY FOR A POTENTIAL VHEE BEAM DELIVERY SYSTEM

C. S. Robertson*, P. N. Burrows, M. Dosanjh[1], University of Oxford, Oxford, UK
A. Latina, CERN, Geneva, Switzerland
A. Gerbershagen[1], PARTREC, UMCG, University of Groningen, Netherlands
[1]also at CERN, Geneva, Switzerland

Abstract

VHEE (Very High Energy Electron) therapy can be superior to conventional radiotherapy for the treatment of deep seated tumours, whilst not necessarily requiring the space and cost of proton or heavy ion facilities. Developments in high gradient RF technology have allowed electrons to be accelerated to VHEE energies in a compact space, meaning that treatment could be possible with a shorter linac. A crucial component of VHEE treatment is the transfer of the beam from accelerator to patient. This is required to magnify the beam to cover the transverse extent of the tumour, whilst ensuring a uniform beam distribution. Two principle methodologies for the design of a compact transfer line are presented. The first of these is based upon a quadrupole lattice and optical magnification of beam size. A minimisation algorithm is used to enforce certain criteria on the beam distribution at the patient, defining the lattice through an automated routine. Separately, a dual scattering-foil based system is also presented, which uses similar algorithms for the optimisation of the foil geometry in order to achieve the desired beam shape at the patient location.

INTRODUCTION AND BACKGROUND

Current Modalities of Radiotherapy

Radiotherapy (RT) is an essential component of cancer treatment, required by 50% of patients [1]. In RT, a treatment beam is used to damage the DNA of the tumour cells and cause cell death. The main goal of RT is to cause as much damage to the tumour as possible, whilst reducing dose to any surrounding healthy tissue. This is known as increasing the "Therapeutic Window". This is most critical when the tumour is seated deep within a patient, as organs particularly susceptible to radiation may be traversed. The dose deposition profile from an RT beam is dependent on the particle used for treatment [2]. Modern techniques in conventional (X-ray) RT have been developed to reduce dose to healthy tissues longitudinally and laterally [3]. Hadron beams can provide more precise treatments with less dose to healthy tissues than conventional RT due to the Bragg peak [2]. They can also be manipulated directly with magnets to allow scanning of the beam across the tumour. As such, they are very well suited for the treatment of deep-seated tumours. Hadron treatment facilities are however much larger and more expensive than conventional RT facilities [4]. This is due to the requirement for cyclotrons or synchrotrons for acceleration rather than the small LINACs used for conventional RT, extended shielding requirements as well as the much larger gantries for bending the higher rigidity hadron beams.

VHEE

A promising modality for RT is VHEE (Very High Energy Electron) therapy. These are defined as electron beams with energies above 50 MeV, and would be capable of reaching deep-seated tumours [5]. There is evidence that VHEE beams would be less sensitive to inhomogeneities in the patient tissues than hadron beams. With the implementation of scanning and/or focusing, VHEE beams could also provide superior tumour conformity and avoidance of healthy tissues compared to conventional RT [6, 7]. Two crucial advantages that VHEE would have over hadron therapy are the required cost and space. A 200 MeV electron beam would require weaker magnets and/or a more compact gantry for delivering treatment. Developments in high gradient X-band RF-technology have also allowed the possibility of electrons being accelerated to VHEE energies in a very compact LINAC [8]. This would require less space than the circular accelerators used for hadron therapy.

Aim

The aim of this work is to design a transfer line for a 100 MeV VHEE beam from acceleration to the patient, using a simple model. This is an exploration and verification of the methodology for this design process, rather than a fully practical implementation. The beam should meet certain requirements for treatment whilst also being compact and efficiently designed to minimise associated costs.

Initial Conditions and Beamline Geometry

The gantry was based upon a "Riesenrad" style gantry, consisting of a beamline with a single dipole [9]. This gantry would be rotated along with the patient couch to allow irradiation from multiple angles, shown in Fig. 1. The initial beam was assumed to have a uniform transverse distribution with a radius of 1 mm, an angular divergence of 1 mrad, and a momentum spread of 0.25%. It was required to be magnified to the radius of a large tumour - here taken to be between 50 mm and 100 mm. Furthermore, the beam was required have a uniform transverse distribution to ensure an even dose across the tumour. The study of scanned and focused beam delivery was left for future work. Achromaticity of the beamline whilst desirable for symmetry in both

* cameron.robertson@physics.ox.ac.uk

ISBN: 978-3-95450-227-1 ISSN: 2673-5490 doi:10.18429/JACoW-IPAC2022-THPOMS022

PRODUCTION OF RADIOISOTOPES FOR CANCER IMAGING AND TREATMENT WITH COMPACT LINEAR ACCELERATORS*

M. Vretenar†, A. Mamaras, CERN, Geneva, Switzerland
G. Bisoffi, INFN-LNL, Legnaro, Italy and CERN, Geneva, Switzerland
P. Foka, GSI, Darmstadt, Germany

Abstract

Accelerator-produced radioisotopes are widely used in modern medicine, for imaging, for cancer therapy, and for combinations of therapy and diagnostics (theragnostics). Clinical trials are well advanced for several radioisotope-based treatments that might open the way to a strong request of specific accelerator systems dedicated to radioisotope production.

While cyclotrons are the standard tool in this domain, we explore here alternative options using linear accelerators. Compared to cyclotrons, linacs have the advantage of modularity, compactness, and reduced beam loss with lower shielding requirements. Although in general more expensive than cyclotrons, linacs are competitive in cost for production of low-energy proton beams, or of intense beams of heavier particles.

After a review of radioisotopes of potential interest, in particular produced with low-energy protons or helium, this paper presents two linac-based isotope production systems. The first is a compact RFQ-based system for PET (Positron Emission Tomography) isotopes, and the second is an alpha-particle linac for production of alpha-emitters. The accelerator systems are described, together with calculations of production yields for different targets.

INTRODUCTION

In the last decades, the use of radioisotopes for applications in medicine that include both diagnostics and therapy has shown a significant increase, generating a clear demand for novel solutions to produce standard and new radioisotopes with low-cost, easy-to-use, accelerators possibly located close to the hospitals where they are used.

At present, several hospitals are equipped with small proton cyclotrons at energy between 10 and 25 MeV, supplying radioisotopes which, via chemical purification and biological manipulations, are then transformed into radiopharmaceuticals and quickly provided to local patients.

Although cyclotrons are fairly small, the required massive shielding around accelerator and target imposes serious limitations to their installation in hospitals. Moreover, the costs related to the frequent and expensive maintenance required by commercial cyclotrons can be prohibitive for small hospitals. In this respect, linear accelerators (linacs) might provide a viable alternative to cyclotrons, because thanks to their well-defined beam optics up to the production target they are not affected by the large beam loss, particularly at extraction, leading to the sensitive activation levels of cyclotrons. In a linac, nearly all particles produced by the ion source impinge on the target, which is the only element that requires substantial radiation shielding: a linac can be hence operated in a simple radiation-controlled area with only the target placed inside a shielding casing. Linacs are lighter in weight than cyclotrons (they do not need large magnets), which makes them easier to handle and install and are very reliable, with few moving or high voltage components.

The first part of this paper reports calculations of the doses that can be produced at saturation with currents and energies achievable with a compact linac. In the second part, two linac configurations are presented, the first for production of Positron Emission Tomography (PET) imaging radiotracers ^{18}F or ^{11}C via low energy protons, and the second for production of ^{211}At for Targeted Alpha Therapy (TAT) via alpha particles.

PRODUCTION YIELDS

A numerical calculation method to estimate the production yields of two PET (^{18}F, ^{11}C) and one TAT (^{211}At) radioisotopes was developed [1], and after benchmarked to existing data [2-4], was applied for dose calculation at different conditions (energy, current), where no data were available. ^{18}F is produced via the nuclear reaction ^{18}O(p,n)^{18}F, ^{11}C via ^{14}N(p,α)^{11}C and ^{211}At via ^{209}Bi(α,2n)^{211}At. Yields were calculated for protons in the energy range 3÷15 MeV and for alphas in the energy range 21÷30 MeV.

Production Yields for ^{18}F and ^{11}C

The ^{18}F saturation yields, calculated via the numerical calculation method, are reported in Fig. 1. The corresponding PET doses are also shown, knowing that an average dose of ^{18}F-FDG is ~400 MBq for a patient of 80 kg, based on literature data and routine experience of a hospital [1, 5, 6].

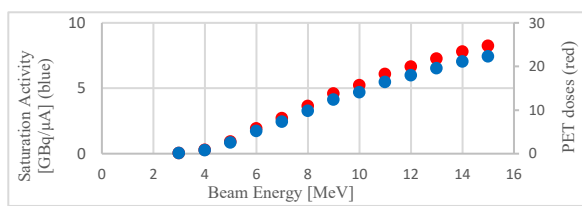

Figure 1: Saturation yield of ^{18}F (blue) and PET doses (red) as a function of E_b (saturation time of 3.5 $T_{1/2}$= 6.4 h).

* This project has received funding from the European Union's H2020 R&I programme under Grant Agreement No 730871 (Project ARIES)
† maurizio.vretenar@cern.ch

ISBN: 978-3-95450-227-1 ISSN: 2673-5490 doi:10.18429/JACoW-IPAC2022-THPOMS023

DESIGN OF THE 590 MeV PROTON BEAMLINE FOR THE PROPOSED TATTOOS ISOTOPE PRODUCTION TARGET AT PSI

M. Hartmann†[1], D. Kiselev, D. Reggiani, J. Snuverink, H. Zhang, M. Seidel[1]
Paul Scherrer Institut, 5232 Villigen PSI, Switzerland
[1]also at École Polytechnique Fédérale de Lausanne (EPFL), Lausanne, Switzerland

Abstract

IMPACT (Isotope and Muon Production with Advanced Cyclotron and Target Technologies) is a proposed initiative envisaged for the high-intensity proton accelerator facility (HIPA) at the Paul Scherrer Institute (PSI). As part of IMPACT, a radioisotope target station, TATTOOS (Targeted Alpha Tumour Therapy and Other Oncological Solutions) will allow the production of terbium radionuclides for therapeutic and diagnostic purposes. The proposed TATTOOS beamline and target will be located near the UCN (Ultra Cold Neutron source) target area, branching off from the main UCN beamline. In particular, the beamline is intended to operate at a beam intensity of 100 µA, requiring a continuous splitting of the main beam via an electrostatic splitter. Realistic beam loss simulations to verify safe operation have been performed and optimised using Beam Delivery Simulation (BDSIM), a Geant4 based tool enabling the simulation of beam transportation through magnets and particle passage through the accelerator. In this study, beam profiles, beam transmission and power deposits are generated and studied.

INTRODUCTION

The High Intensity Proton Accelerator (HIPA) at the Paul Scherrer Institute (PSI) is at the forefront of the high intensity frontier of particle accelerators delivering a 590 MeV continuous wave proton beam with currents of up to 2.4 mA (1.4 MW beam power) [1].

IMPACT (Isotope and Muon Production using Advanced Cyclotron and Target technologies) is a proposed initiative envisaged for HIPA [2]. As part of IMPACT, a radioisotope target station, TATTOOS (Targeted Alpha Tumour Therapy and Other Oncological Solutions) will allow the production of unprecedented quantities of terbium radionuclides for therapeutic and diagnostic purposes. The TATTOOS beamline is intended to operate at a beam intensity of 100 µA (60 kW beam power), requiring a continuous splitting of the high-powered beam via an electrostatic splitter [3].

A realistic model of the complete TATTOOS beamline from splitter to target was established for the first time in Beam Delivery Simulation (BDSIM) [4], a Geant4 [5] based tool enabling simulation of beam transportation through magnets and particle tracking in electromagnetic fields. BDSIM allows electromagnetic fields to be attached to user-built elements such as the splitter.

The splitter has to withstand significant power deposition and the beam losses due to scattering are a major aspect of the concept that must be evaluated. Indeed, in both the design and operational phases of high intensity accelerators it is critical to minimise beam losses to avoid damage and activation of components, while at the same time maintaining high transmission. In this paper, beam profiles, beam transmission to the target and power deposits are simulated and studied.

PROTON BEAMLINE

Overview of the HIPA Facility

An overview of the HIPA facility with the TATTOOS installation is illustrated in Fig. 1 [2].

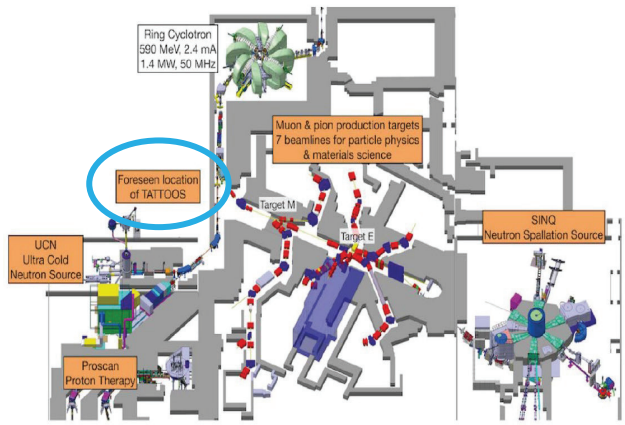

Figure 1: PSI's proton accelerator facility HIPA and the proposed TATTOOS installation circled in blue.

The proton beam is extracted from the Ring Cyclotron and transported to two target stations, Target M (TgM) and Target E (TgE) where secondary particles are produced for user experiments.

The proton beam also feeds two spallation sources, Swiss Spallation Neutron Source (SINQ) [6] and Ultra Cold Neutron source (UCN) [7], the latter running concurrently to the targets. A fast kicker magnet diverts the full intensity beam towards UCN via macro-pulsed kicks. Finally, the splitter located downstream from the kicker magnet can peel off a small portion of the main beam and send it to the UCN target. The elements of the TATTOOS beamline are described in detail in the following section.

TATTOOS Beamline Description

The simplest way of including the proposed TATTOOS beamline within the present framework is to split off part of the proton beam needed for TATTOOS by means of the splitter, use the existing magnetic septum magnet (ABS) to divert the peeled beam to the UCN beamline

† marco.hartmann@psi.ch

ISBN: 978-3-95450-227-1 ISSN: 2673-5490 doi:10.18429/JACoW-IPAC2022-THPOMS024

A NOVEL INTENSITY COMPENSATION METHOD TO ACHIEVE ENERGY INDEPENDENT BEAM INTENSITY AT THE PATIENT LOCATION FOR CYCLOTRON BASED PROTON THERAPY FACILITIES*

V. Maradia[1], D. Meer, D. C. Weber[2], A. J. Lomax1, S. Psoroulas
Paul Scherrer Institute, Villigen, Switzerland
[1]also at ETH Zurich, Switzerland
[2]also at University hospital Bern and University hospital Zurich, Switzerland

Abstract

In cyclotron-based proton therapy facilities, an energy selection system is typically used to lower the beam energy from the fixed value provided by the accelerator (250/230 MeV) to the one needed for the treatment (230-70 MeV). Such a system has the drawback of increase beam emittance and introducing an energy-dependent beam current at the patient location, resulting in energy dependent beam intensity ratios of about 10^3 between high and low energies. This complicates treatment delivery and challenges patient safety systems. As such, we propose the use of a dual energy degrader method that can reduce beam intensity for high-energy beams. The first degrader is made of high Z material and the second is made of low Z material and are placed next to each other. For high energies (190-230 MeV), we use only the first degrader to increase beam emittance after the degrader and thus lose intensity in the emittance selection collimators. For intermediate energy beams (110-190 MeV) we use the combination of both degraders, whereas for low energy beams (70-110 MeV), only the second degrader limits the increase in emittance. With this approach, energy-independent beam intensities at the patient location can be achieved, whilst localizing beam losses around the degrader.

INTRODUCTION

Proton therapy provides better dose distribution conformity and also better spares healthy tissues when compared with equivalent photon plans. Therefore, proton therapy has become a credible option in radiotherapy to treat certain types of cancers.

In proton therapy, based on the size and location of the tumor, proton beams with different energies are required to deliver the dose in the target volume. The energy required for patient treatments is typically in the range of 70-230 MeV.

Most proton therapy facilities use a cyclotron. Since a cyclotron produces beams of fixed energy (250 MeV for the PSI COMET cyclotron [1]), to modulate the energy of the beam, a degrader with an adjustable thickness is required. Unfortunately, beam scattering in the energy degrader increases the beam size, divergence, and energy spread beyond the beamline and gantry acceptance. It is unavoidable to use one or more collimator systems and an energy selection system (ESS) to cut these quantities to those that fit in the acceptance of the following beam transport system, to prevent unwanted beam losses along the beamline. This limited acceptance depends on the energy, the geometrical layout of the beam transport system, and the setting of the magnets in the beamline. At PSI, for example, for the highest energies (200-230 MeV), transmission through the beamline is about 30%. However, for the lowest energies (70-100 MeV), transmission through the beamline is below 0.1% [2-5].

The beam intensity at the patient would be strongly dependent on beam energy, due to this energy-dependent transmission. It may result in significant change in beam current at patient location and could have consequences for safety, due to a limitation of reaction times. Therefore, an intentional beam loss for higher energies is necessary to obtain the similar beam intensity for all energies.

This can be done by adjusting the intensity in the cyclotron, but one could also design a beamline setting with energy-dependent controlled beam losses at dedicated collimators in the beam-transport system.

In this study, we report a new way to do intensity compensation for high-energy beams using two degraders made of different materials. For the proof of principle simulation study, by using two degraders, we tried to achieve the similar transmission from the cyclotron to the end of the ESS beamline.

METHODS AND MATERIALS

Dual Energy Degrader Method

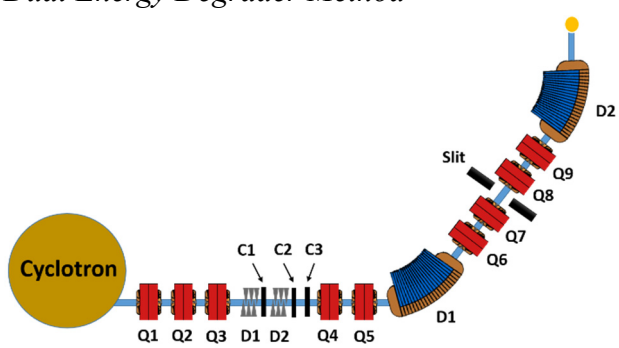

Figure 1: Schematic of the ESS beamline. (Q1-Q9: Quadrupole magnets, D1-D2: Dipole magnets, D1-D2: Degraders C1-C3 collimators).

To intentionally lose the intensities of the high energy beams, we designed an ESS beamline using two degraders (As shown in Fig. 1). We used two degraders made of different materials, Aluminium (D1) and Carbon (D2).

ISBN: 978-3-95450-227-1 ISSN: 2673-5490 doi:10.18429/JACoW-IPAC2022-THPOMS025

A NOVEL METHOD OF EMITTANCE MATCHING TO INCREASE BEAM TRANSMISSION FOR CYCLOTRON BASED PROTON THERAPY FACILITIES: SIMULATION STUDY*

V. Maradia†,[1], D. Meer, D. C. Weber[2], A. J. Lomax[1], J. M. Schippers, S. Psoroulas,
Paul Scherrer Institute, Villigen, Switzerland
[1]also at ETH Zurich, Switzerland
[2]also at University hospital Bern and University hospital Zurich, Switzerland

Abstract

In proton therapy, high dose rates can reduce treatment delivery times, allowing for efficient mitigation of tumor motion and increased patient throughput. With cyclotrons however, high dose rates are difficult to achieve for low-energies as, typically, the emittance after the degrader is matched in both transversal planes using circular collimators, which does not provide an optimal matching to the acceptance of the following beamline. Transmission can however be substantially improved by transporting maximum acceptable emittances in both orthogonal planes, but at the cost of gantry angle-dependent beam shapes at isocenter. Here we demonstrate that equal emittances in both planes can be recovered at the gantry entrance using a thin scattering foil, thus ensuring gantry angle-independent beam shapes at the isocenter. We demonstrate in simulation that low-energy beam transmission can be increased by a factor of 3 using this approach compared to the currently used beam optics, whilst gantry angle-independent beam shapes are preserved. We expect that this universal approach could also bring a similar transmission improvement in other cyclotron-based proton therapy facilities.

INTRODUCTION

Brought into clinical practice at Paul Scherrer Institute (PSI) in the 1996, pencil beam scanning (PBS) is nowadays the standard beam delivery technique in proton therapy[1], [2]. However, current challenges of PBS particle therapy are the dosimetric uncertainties in treatment of moving targets and the relatively long treatment times involved. The dosimetric uncertainty can be minimized through the use of motion mitigation techniques, which aim to mitigate the interplay effect between the motions in the patient and the beam delivery; the most common motion mitigation techniques are breath-hold [3], rescanning [4], and gating [5]. For all these techniques, it is also desirable to have shorter treatment delivery times [6,7]. One way to reduce the treatment delivery time for PBS proton therapy is to increase the intensity of the low-energy beams by improving the transmission of the beam from the cyclotron to the isocenter (patient position), thereby reducing beam-on time (the time required to deliver the dose) during treatment delivery.

Most of the proton therapy facilities use a cyclotron. Since a cyclotron produces beams of a fixed energy, to modulate the energy of the beam, an energy selection system (ESS), consisting of a degrader with an adjustable thickness followed by momentum selection, is required. However, due to scattering in the degrader, for low-energy beams, the emittance after the degrader is in the range of a few hundreds of π*mm*mrad. Therefore, to minimize beam losses in the beamline, it is necessary to use beam emittance selection collimators after the degrader to restrict the emittance to the requirement of the following beamline or gantry. Currently, all cyclotron-based proton therapy facilities transport a maximum emittance of 30 π*mm*mrad through the beamline (in this work, beam sizes, divergences, and emittances are expressed as 2σ values), which limits the transmission of low-energy beams. At PSI for example, for the lowest energies (70-100 MeV), transmission through the beamline is below 0.1% [8]. Such low transmission for these low energies causes an increase in beam-on time.

One way to achieve higher intensity beams at the isocenter is to transport a higher emittance through the following beamline and gantry [8-11]. At our facility, we can transport a maximum of ~ 65 π*mm*mrad in X-plane and ~ 139 π*mm*mrad in Y-plane. These will increase the beam transmission significantly compared to conventional 30 π*mm*mrad emittance transport in both planes, at the cost of an asymmetric emittance at the gantry entrance, leading to gantry angle dependent beam shapes at the isocenter. To achieve gantry angle independent beam shape at the isocenter, it is necessary to have same emittance at the entrances of the gantry.

In this study, we report on the use of a thin scattering foil, placed in the beamline between the ESS and gantry coupling point, to achieve equal emittances in both planes, whilst maintaining a high transmission through the beamline and gantry, a method also used in several synchrotron-based ion beam therapy facilities [12,13]. In this work, all simulation investigations were performed with 70 MeV beam as our goal was to increase the transmission for low energy beams.

METHODS AND MATERIALS

Emittance Matching with Scattering Foil

To increase the emittance in the X-plane to a similar value as the Y-plane emittance, but with minimally effect on the emittance in the Y-plane, the following boundary conditions have been applied: (as expressed schematically in Fig. 1).

* Work supported by the PSI's CROSS funding scheme
† vivek.maradia@psi.ch

ISBN: 978-3-95450-227-1 ISSN: 2673-5490 doi:10.18429/JACoW-IPAC2022-THPOMS026

MONTE CARLO SIMULATION OF ELECTRON BEAM IN PHANTOM WATER FOR RADIOTHERAPY APPLICATION

P. Apiwattanakul*[1], S. Rimjaem†[2], J. Saisut[2], C. Phueng-ngern,
PCELL, PBP, Faculty of Science, Chiang Mai University, Chiang Mai, Thailand
P. Nimmanpipug, CSML, faculty of Science and I-ANALY-S-T, Chiang Mai University, Chiang Mai, Thailand
P. Lithanatudom, Faculty of Science, Chiang Mai University, Chiang Mai, Thailand
[1] also at Master Program in Physics, Chiang Mai University, Chiang Mai, Thailand
[2] also at ThEP Center, MHESI, Bangkok, Thailand

Abstract

Radiotherapy (RT) is an effective treatment that can control the growth of cancer cells. There is a hypothesis suggests that secondary electrons with an energy of a few eV produced from RT play an important role on cancer's DNA strand break. In this study, the Monte Carlo simulation of electron beam irradiation in phantom water is performed to investigate the production of low-energy electrons. Electron beams produced from an radio-frequency linear accelerator (RF linac) are used in this study. The accelerator can generate the electron beam with adjustable energy of up to 4 MeV and adjustable repetition rate of up to 200 Hz. With these properties, the electron dose can be varied. We used ASTRA software to simulate the electron beam dynamics in the accelerator and GEANT4 toolkit for studying interactions of electrons in water. The energy of electrons decreases from MeV scale to keV-eV scale as they travel in the water. From simulations, the dose distribution and depth in phantom water were obtained for the electron dose of 3, 5, 10, 25, and 50 Gy. Further study on effect of low-energy electron beam with these dose values on cancer DNAs will be performed with GEANT4-DNA simulation.

INTRODUCTION

The main propose of radiotherapy (RT) technique is to kill tumour cell by inducing the damages on the DNA while sparing normal cells [1]. The particle irradiating onto the cells would lead to two actions on DNAs, which are direct and indirect actions. In direct action the ionized electrons directly deposit their energy to the DNA strand while OH radicals are generated then give the damages to the DNA strand in indirect action. Theses damages can be occurred in the form of single strand breaks (SSBs) and double strand breaks (DSBs). The DSBs are more complex than the SSBs, which lead to less opportunity for the cell to repair itself and result in cell death [2].

To investigate the effect of electron irradiation on the cell samples, the RF linac at the PBP-CMU electron Linac laboratory (PCELL) is used to generate the electron beam for this experiment. This linac can produce electron beam with energy in a range of 0.5 - 4 MeV with adjustable repetition rate of up to 200 Hz [3].

To estimate the electron absorbed dose in liquid sample, GEANT4 Monte Carlo toolkit [4] is used. From the simulation results, we can design the experimental setup to detect some interesting parameters, for example; number of electrons after passing through the material or the electron absorbed dose in material. To generate input electrons for GEANT4 simulation, we use the ASTRA software [5] and to track electron in 3D magnetic field obtained from CST simulation [6]. Since phantom water can offer the excellent agreement with irradiation experiment on human anatomy, it therefore widely used to estimate the absorbed dose in human tissue [7]. In this work, the phantom water (soft tissue [8]) is considered as the representation of the cell sample. The aim of this work is to find the most appropriate position for electron beam irradiation as well as the irradiation time that can provide the electron absorbed dose of 3, 5, 10, 25, and 50 Gy in the sample.

Table 1: The Percentage of Phantom Water Components Used in GEANT4 Simulation [8]

Material	Component	Percentage
Phantom water(soft tissue)	Hydrogen	10.4472
	Carbon	23.2190
	Nitrogen	2.4880
	Oxygen	63.0238
	Sodium	0.1130
	Magnesium	0.0114
	Phosphorus	0.1130
	Sulfur	0.1990
	Chlorine	0.1340
	Potassium	0.1990
	Calcium	0.0230
	Iron	0.005
	Zinc	0.0030

SIMULATION METHOD

The simulation in this work was divided into two sections for acceleration and irradiation. The simulation layout and details of components in simulation setup are demonstrated in Fig. 1.

* pittaya_ap@cmu.ac.th
† sakhorn.rimjaem@cmu.ac.th

ISBN: 978-3-95450-227-1 ISSN: 2673-5490 doi:10.18429/JACoW-IPAC2022-THPOMS028

PERFORMANCE STUDY OF THE NIMMS SUPERCONDUCTING COMPACT SYNCHROTRON FOR ION THERAPY WITH STRONGLY CURVED MAGNETS

H. X.Q. Norman*[1,2], R. B. Appleby[1], University of Manchester, Manchester, UK
S. L. Sheehy[3], University of Melbourne, Melbourne, Australia
E. Benedetto, SEEIIST Association, Geneva, Switzerland
M. Karppinen, CERN, Geneva, Switzerland
H. L. Owen[1], STFC Daresbury Laboratory, Warrington, UK
[1]also at Cockcroft Institute, Warrington, UK
[2]also at University of Melbourne, Melbourne, Australia
[3]also at Australian Nuclear Science and Technology Organisation (ANSTO), Australia

Abstract

Delivery of heavy ion therapy currently utilises normal conducting synchrotrons. For the future generation of clinical facilities, the accelerator footprint must be reduced while adopting beam intensities above 1×10^{10} particles per spill for more efficient, effective treatment. The Next Ion Medical Machine Study (NIMMS) is investigating the feasibility of a compact (27 m circumference) superconducting synchrotron, based on 90° alternating-gradient, canted-cosine-theta magnets to meet these criteria. The understanding of the impact of the higher order multipole fields of these magnets on the beam dynamics of the ring is crucial for optimisation of the design and to assess its performance for treatment. We analyse the electromagnetic model of a curved superconducting magnet to extract its non-linear components. Preliminary assessment is performed using MADX/PTC. Further scope, involving cross-referencing with other particle tracking codes, is discussed.

INTRODUCTION

The Next Ion Medical Machine Study (NIMMS) is a CERN-based initiative for the development of accelerators and supporting technology for future hadron therapy facilities. A compact synchrotron design, based on 90° superconducting (SC) alternating-gradient, canted-cosine-theta (AG-CCT) magnets has been proposed [1]. Due to the coil geometry of the magnets, one can achieve high quality, combined-function dipole and quadrupole fields by nesting quadrupole layers within each dipole magnet [2]. This reduces the circumference of the accelerator to ≈ 27 m, as shown in Fig. 1.

The design motivation is for delivery of carbon ion therapy (energies ranging from 100 MeV/u to 430 MeV/u), which is not widely available despite clinical benefits compared with proton therapy and x-ray radiotherapy [3]. By employing AG-CCT magnets in the four bending sections (operating at $B_{\mathrm{dip}} = 3.5$ T), the size and weight of the accelerator is reduced, as well as building and operation costs. The configuration achieves strong focusing, reducing maximum dispersion to 2.5 metres. To realise the design for future facilities, a detailed magnet model is needed, subject to clinical and technical requirements of the accelerator. An electromagnetic (EM) AG-CCT model is anticipated.

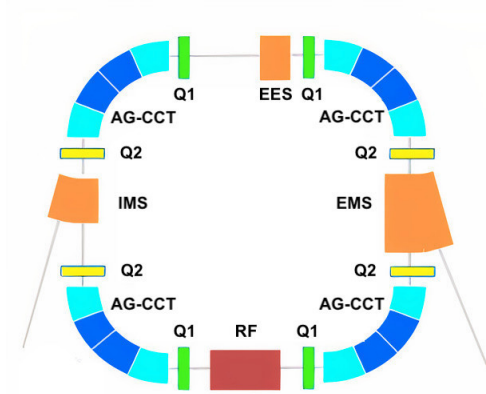

Figure 1: 27 m circumference superconducting synchrotron. The elements are: AG-CCT magnets (blue, outer corners of the ring, dark blue quadrupole layers centered); injection and extraction septa (IMS, EES, EMS) (orange, left-middle, right-middle and top-centre); RF cavity (red, bottom-centre); tuning quadrupoles (yellow and green, either side of the AG-CCT magnets, septa and RF). Modified from [1].

In this study, we develop the numerical analysis tools needed to extract multipole fields from the prospective AG-CCT magnet to understand their impact on the performance of the NIMMS synchrotron. We first analyse a complementary cosine-theta (CT) magnet model; numerical methods are used to extract multipole fields from simulated magnetic field maps, which are then incorporated into the accelerator lattice for beam dynamics simulations using MAD-X [4]. The analysis tools developed during this study will be applied to a future AG-CCT EM model to assess the effect of its multipole fields on the beam dynamics of the ring, and if it is clinically suitable.

* hannah.norman@manchester.ac.uk

ISBN: 978-3-95450-227-1 ISSN: 2673-5490 doi:10.18429/JACoW-IPAC2022-THPOMS029

TESTING THE PROPERTIES OF BEAM-DOSE MONITORS FOR VHEE-FLASH RADIATION THERAPY

J. J. Bateman*, P. N. Burrows, M. Dosanjh[1], L. A Dyks[1], P. Korysko[1],
JAI, University of Oxford, Oxford, UK
R. Corsini, W. Farabolini, A. Gerbershagen[3], N. Heracleous, S. Morales, F. Murtas,
V. F. Rieker, B. Salvachua, M. Silari, G. Zorloni, CERN, Geneva, Switzerland
[1]also at CERN, Geneva, Switzerland
[2] also at PARTREC, University of Groningen, Groningen, Netherlands

Abstract

Very High Energy Electrons (VHEE) of 50 - 250 MeV are an attractive choice for FLASH radiation therapy (RT). Before VHEE-FLASH RT can be considered for clinical use, a reliable dosimetric and beam monitoring system needs to be developed, able to measure the dose delivered to the patient in real-time and cut off the beam in the event of a machine fault to prevent overdosing the patient. Ionisation chambers are the standard monitors in conventional RT; however, their response saturates at the high dose rates required for FLASH. Therefore, a new dosimetry method is needed that can provide reliable measurements of the delivered dose in these conditions. Experiments using 200 MeV electrons were done at the CLEAR facility at CERN to investigate the properties of detectors such as diamond beam loss detectors, GEM foil detectors, and Timepix3 ASIC chips. From the tests, the GEM foil proved to be the most promising.

INTRODUCTION

The most widely used modality of RT is external beam therapy with high energy photons (6 - 15 MV) and low energy electrons (3 - 25 MeV). However, the maximum dose that can be delivered to the tumour is limited by the dose that the surrounding healthy tissue can tolerate. This is a particular challenge as these X- rays deliver their maximum dose at 1.5 - 3.0 cm depth in water-equivalent tissue and then have a near-exponential attenuation. Recent research suggests that delivering the prescribed dose to the patient's tumour at ultra-high dose rates (UHDR) elicits a larger differential response between the tumour cells and the healthy tissues, known as the FLASH effect [1]. The entire prescribed dose is delivered within less than a second at a mean dose rate of ≥ 100 Gy/s; compared to ≤ 0.03 Gy/s used in conventional RT. Due to recent advances in particle accelerator technology such as high gradient electron acceleration cavities, e.g. the ones developed as part of the CLIC study [2], it may be possible to treat deep-seated tumours with Very High Energy Electrons (VHEE) with energies of 50 - 250 MeV due to their increased longitudinal range and sharper lateral penumbra in comparison to current clinical electron beams [3]. Ionisation chambers have been the standard for electron beam dosimetry, however, studies have shown that at the ultra high dose rates required for FLASH-RT the response of the ionisation chamber suffers from non-linearities due to ion recombination within the cavity volume [4]. Therefore, new detectors and monitoring systems will need to be developed and tested in order to achieve accurate and reliable measurements of the delivered dose at UHDR for FLASH irradiations in both pre-clinical experiments to verify the FLASH effect, and for the eventual clinical implementation of FLASH-RT [5]. The requirements on such a system are:

- A response that does not saturate at the ultra-high dose rates of $\geq$100 Gy/s that are required for FLASH.
- A temporal resolution which is high enough to resolve individual bunches or trains.
- A response time that is fast enough to trigger a safety interlock in between pulses.
- Minimal perturbation on the beam.

The aim of the experiments described in this work is to understand the characteristics of the response of the detectors tested to the electron beam parameters at the CLEAR facility [6] and whether they exhibit any of the characteristics that suggest they would meet the criteria required for real-time dosimetry of VHEE at UHDR.

PCVD DIAMOND DETECTOR

The first detector tested was a B2-HV pCVD diamond beam loss detector which is currently employed as a fast beam loss monitor (BLM) at the LHC [7]. The diamond detector consists of a 10 mm × 10 mm × 0.5 mm pCVD diamond substrate coated on each side with a 200 nm thick gold electrode with a size of 8 mm × 8 mm. In the LHC, the detector is used alongside an AD-DC splitter and a 2 GHz amplifier, however for the FLASH dosimetry experiments only the detector was used since the beam intensity does not need amplification. This detector was considered due to its known ability to have a quick response time and resolve individual bunches when used as a BLM. However, since its primary usage is as a BLM and hence it is not directly installed in the path of the beam center, it has been expected that the detector response would reach saturation at FLASH rates.

Setup

The diamond detector was installed at the In-Air Test Stand at CLEAR, at approximately 25 cm away from the end of the beam pipe, and was aligned such that the pCVD

* joseph.bateman@physics.ox.ac.uk

ISBN: 978-3-95450-227-1 ISSN: 2673-5490 doi:10.18429/JACoW-IPAC2022-THPOMS030

UPDATES, STATUS AND EXPERIMENTS OF CLEAR, THE CERN LINEAR ELECTRON ACCELERATOR FOR RESEARCH

P. Korysko[1*], M. Dosanjh, L.A. Dyks[1], J.J. Bateman, C. Robertson, University of Oxford, Oxford, UK
R. Corsini, W. Farabolini, A. Gilardi, CERN, Meyrin, Switzerland
K. N. Sjobak, V. Rieker[1], University of Oslo, Oslo, Norway
[1]Also at CERN, Geneva, Switzerland

Abstract

Operating since 2017, the CERN Linear Electron Accelerator for Research (CLEAR) is a user facility providing electron beams for a large and varied range of experiments. The electron beam is produced from a Cs_2Te photocathode and is accelerated between 60 MeV and 220 MeV in a 20 m long linear accelerator (LINAC). The accelerated beam is then transported to an experimental beamline, in which experiments such as irradiations on electronics, irradiations for medical applications, plasma-lens experiments and beam-diagnostics development are performed. In this paper, the status, the upgrades of the beamline and the recent and future experiments are presented.

INTRODUCTION

The CLEAR facility offers to its users an electron beam with a large range of parameters [1–4]. They are shown in Table 1 and in Fig. 1. A diagram of the beamline is shown in Fig. 2. Two in-air test areas area available. The first is mostly used for VESPER (Very energetic Electron facility for Space Planetary Exploration missions in harsh Radiative environments) while the second In-Air Test Area is for more general use. In practice, both areas can be used for medical applications studies like Very High Energy Electron (VHEE) radiotherapy, the sterilisation of personal protective equipment research studies [5, 6] and irradiations of electronics [7–10], including components of ESA's JUpiter ICy moons Explorer (JUICE). These and other in-vacuum test areas are also used for experiments with in-beam instrumentation [11] and novel accelerator technology studies like plasma lenses [12–14].

CLEAR is a fully independent installation and doesn't require any other accelerators from the CERN Accelerator Complex to run. Thus, the machine can run during LHC's long shutdowns and upgrades. The beam schedule is very flexible: a usual beam access is scheduled on Monday mornings to install the experiment of the week and the machine can run from 8 to 12 hours per day, 5 days a week, depending on the needs of the users. The machine ran for 38 weeks in 2019, 34 and 35 weeks during the 2020 and 2021 COVID-19 crisis. In September 2020 the CERN Council approved the CERN Medium Term Plan which extends CLEAR operation until 2025.

* pierre.korysko@cern.ch

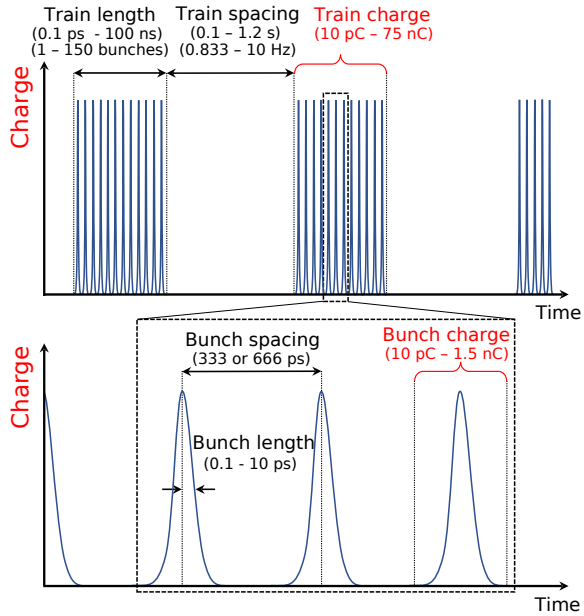

Figure 1: CLEAR beam time structure and charge parameters at the end of the beam line in 2022.

Table 1: Updated List of CLEAR Beam Parameters

Parameter	Value
Beam Energy	60 – 220 MeV
Beam Energy Spread	< 0.2% rms (< 1 MeV FWHM)
Bunch length rms	0.1 – 10 ps
Bunch frequency	1.5 or 3.0 GHz
Bunch charge	0.005 – 1.5 nC
Norm. emittance	1 – 20 μm
Bunches per pulse	1– ~ 150
Max. pulse charge	75 nC
Repetition rate	0.8333 – 10 Hz

OPERATION AND PERFORMANCE

During the 2021/2022 winter shutdown several modifications were done to the CLEAR beamline: the CLIC Cavity BPMs and the CLIC structure were removed from the beam line for repairs and diagnostics studies. This leads to a larger beam pipe aperture at these locations and results in a better beam transport at the end of the line.

A new quadrupole (QDD0920) was installed on the In-Air test stand, 1400 mm downstream of the final doublet. The alignment of this last quadrupole has been verified and corrected by the survey group. This quadrupole is used

ISBN: 978-3-95450-227-1 ISSN: 2673-5490 doi:10.18429/JACoW-IPAC2022-THPOMS031

VHEE HIGH DOSE RATE DOSIMETRY STUDIES IN CLEAR

V. F. Rieker*, W. Farabolini, R. Corsini, CERN, Geneva, Switzerland
J. J. Bateman[1], P. Korysko[1], L.A. Dyks[1], University of Oxford, Oxford, United Kingdom
[1]also at CERN, Geneva, Switzerland

Abstract

The 200 MeV electron beam of the CERN Linear Accelerator for Research (CLEAR) user facility at CERN has been intensively used to study the potential use of Very High Energy Electrons (VHEE) in cancer radiotherapy. In particular, irradiation tests have been performed in the high dose rate regime, which has gained a lot of interest for the so called FLASH biological effect, in which cancer cells are damaged while healthy tissue is largely spared. High dose rate dosimetry, though, poses a number of challenges: to validate standard or new methods of passive dosimetry, like radiochromic films and alanine pellets, and especially to develop new methods for real-time dosimetry since the normally used ionization chambers suffer from non-linear effects at high dose rates. In this paper we describe the results of experimental activities at CLEAR aimed at developing solid, high-dose rate dosimetry standards adapted to VHEE beams.

INTRODUCTION

Real-time dosimetry methods used in radiotherapy are generally not well adapted for the high dose-rate regime. Both conventional ionisation chambers and solid-state detectors suffer from nonlinear saturation effects due to recombination at very-high dose-rates [1, 2]. For ionisation chambers, the charge collection efficiency has been reported to drop from more than 90 % for standard radiotherapy dose rates (in the order of tens of mGy/pulse) to less than 10 % for the Ultra-High Dose-Rates (UHDR, in the order of 10 Gy/pulse) used for FLASH. However, it could in theory be possible to mitigate such effects through careful calibration or a re-design of the detector geometry [3].

To this point, dosimetric measurements for UHDR have thus been performed using passive methods such as radiochromic films as their response is thought to be almost independent of dose rate. However as these require post-irradiation processing for reading the deposited dose, they are impractical for use in a medical facility [4]. Alternatives such as novel solid state detectors and calibrated dosimetry based on beam diagnostics are thus currently being investigated as potential real-time dosimetry solutions at CLEAR.

An important part of this development is the establishment of efficient, systematic and reproducible methodologies for testing and verification of the new developments using reliable methods, such as films. It is also essential to validate and obtain statistics on the response of the films under the particular conditions for which we aim to test new dosimeters, in particular for methods involving calibration against films. In this context, there have been developments in terms of a robot facilitating remote sample handling without manual interventions, as well as procedures for scanning and processing films.

VHEE FLASH AT CLEAR

Table 1: CLEAR Machine Parameters for Dosimetry Studies

Energy	200 MeV
Bunch charge	0.05 nC - 3 nC
Bunch frequency	1.5 GHz / 3 GHz
Bunches per pulse	1 - 150
Pulse repetition rate	0.8 Hz - 10 Hz

A list of beam parameters for the CLEAR facility is shown in Table 1. VHEE UHDR dosimetry studies are performed at CLEAR at an energy of 200 MeV [5, 6]. By varying the charge, train length and number of trains, one may operate at both conventional dose rates and the UHDR required to access the FLASH effect for various target doses [7]. The beamline is equipped with Yttrium Aluminium Garnet (YAG) scintillator screens linked to cameras, allowing observation of the beam size, position, and intensity distribution in real time. They exhibit excellent time and spatial resolution and do not suffer from non-linearities at high dose-rates. These screens play an integral part in the parametric high dose-rate dosimetry studies, aimed at correlating beam diagnostics with passive dosimetry.

SAMPLE HANDLING AND PROCESSING

C-Robot

A robot has been developed by the CLEAR team in order to facilitate the efficient irradiation of multiple samples, and reduce the number of accesses [8, 9]. It consists of a grabber, able to move in 3D, which can move samples from a slotted sample container, able to hold 24 standardised sample holders, to the path of the beam. It is possible to install a water phantom in the beam area. The robot is controlled using an open-source GUI [10]. The sample holders are 3D printed to ensure that they match the grabber and sample container, and can be adapted to various types of samples, such as films and Eppendorf tubes.

Radiochromic Films

Radiochromic films change colour macroscopically due to polymerisation caused by ionising radiation, with the change in colour related to the accumulated dose. The films are processed post-irradiation to read the dose. The films

* vilde.rieker@cern.ch

ISBN: 978-3-95450-227-1 ISSN: 2673-5490 doi:10.18429/JACoW-IPAC2022-THPOMS032

ADVANCES IN THE OPTIMIZATION OF MEDICAL ACCELERATORS*

C. P. Welsch†, University of Liverpool/Cockcroft Institute, Liverpool, UK

Abstract

Between 2016 and 2020, 15 Fellows have carried out collaborative research within the 4 M€ Optimization of Medical Accelerators (OMA) EU-funded innovative training network. Based at universities, research and clinical facilities, as well as industry partners in several European countries, the Fellows have successfully developed a range of beam and patient imaging techniques, improved biological and physical models in Monte Carlo codes, and also helped improve the design of existing and future clinical facilities. This paper presents three selected OMA research highlights: the use of Medipix3 for dosimetry and real-time beam monitoring, studies into the technical challenges for FLASH proton therapy, recognized by the European Journal of Medical Physics' 2021 Galileo Galilei Award, and research into novel monitors for in-vivo dosimetry that emerged on the back of the OMA network.

INTRODUCTION

The OMA network was built around 15 early stage researchers (ESRs) working on dedicated projects to maximize the benefits of the use of particle beams for cancer treatment [1]. The network consists of an international consortium of 41 partner organizations working in this field. It has provided a cross-sector interdisciplinary environment for beyond state-of-the-art research, researcher training, and new collaborations. The network has pushed technologies and simulation techniques significantly beyond the state-of-the-art and developed solutions that are now applied in clinical practice. OMA has also established a comprehensive and unique postgraduate training concept that can also be applied to other research areas and that was presented to educators at national and international learning and teaching events. The Fellows have benefited from a well-rounded training and successfully completed their projects within the network. This paper illustrates some of the research outcomes in the network.

SELECTED RESEARCH RESULTS

OMA has significantly advanced knowledge in proton/ion beam therapy and related key technologies. Research within the network was carried out by the Fellows across three closely interlinked work packages: Beam Imaging and Diagnostics, Treatment Optimization, and Facility Design and Optimization. A roughly equal number of Fellows has their main research focus on each work package, but there are also many collaborative links between the individual projects and work packages so that an overall optimization of ion beam therapy was achieved. The following sections present selected research highlights obtained across OMA.

Studies with MiniPIX-TimePIX Detectors

Recent advancements in accelerator technology have led to a rapid emergence of particle therapy facilities worldwide, affirming the need for enhanced characterization methods of radiation fields and radiobiological effects. The Clatterbridge Cancer Centre (CCC) operates a 60 MeV proton facility to treat ocular cancer and facilitates studies into proton-induced radiobiological responses [2, 3].

The Medipix3 is a hybrid pixel detector able to count individual protons with millisecond time resolution at clinical flux with near instant readout and count rate linearity. The system has previously demonstrated use in medical and other applications, showing wide versatility and potential for particle therapy.

OMA Fellows Jacinta Yap and Navrit Bal, together with their co-workers, have carried out measurements of the Medipix3 detector in the 60 MeV ocular proton therapy beamline at the CCC [4]. The beam current and lateral beam profiles were evaluated at multiple positions in the treatment line and compared with EBT3 Gafchromic film. The recorded count rate linearity and temporal analysis of the beam structure was measured with Medipix3 across the full range of available beam intensities, up to 3.12×10^{10} protons/s. The measurements allowed them to explore the capacity of Medipix3 to provide non-reference measurements and its applicability as a tool for dosimetry and beam monitoring for CPT. This is the first time the performance of the Medipix3 detector technology has been tested within a clinical, high proton flux environment.

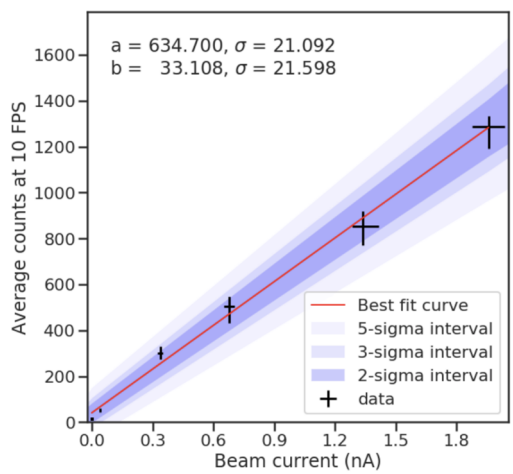

Figure 1: Count rate linearity over all active pixels recorded at 10 frames per second for 6 beam currents [4].

Figure 1 shows that the detector has a linear response across the entire tested range of beam currents from 0.012 to 1.97 nA. There is relatively large uncertainty of the

* This project has received funding from the European Union's Horizon 2020 research and innovation programme under the Marie Sklodowska-Curie grant agreement No 675265.
† c.p.welsch@liverpool.ac.uk

ISBN: 978-3-95450-227-1 ISSN: 2673-5490 doi:10.18429/JACoW-IPAC2022-THPOMS033

DESIGN AND OPTIMISATION OF A STATIONARY CHEST TOMOSYNTHESIS SYSTEM WITH MULTIPLE FLAT PANEL FIELD EMITTER ARRAYS: MONTE CARLO SIMULATIONS AND COMPUTER AIDED DESIGNS*

T. G. Primidis[1,2†], C. P. Welsch[1], University of Liverpool, Liverpool L69 3BX, United Kingdom
V. Y. Soloviev, S. G. Wells, Adaptix Ltd, Oxford OX5 1PF, United Kingdom
[1]also at The Cockcroft Institute, Warrington WA4 4AD, United Kingdom
[2]also at King's College London, London SE1 7EU, United Kingdom

Abstract

Digital tomosynthesis (DT) allows 3D imaging by using a ~30° range of projections instead of a full circle as in computed tomography (CT). Patient doses can be ~10 times lower than CT and similar to 2D radiography but diagnostic ability is significantly better than 2D radiography and can approach that of CT. Moreover, cold-cathode field emission technology allows the integration of 10s of X-ray sources into source arrays that are smaller and lighter than conventional X-ray tubes. The distributed source positions avoid the need for source movements and Adaptix Ltd has demonstrated stationary 3D imaging with this technology in dentistry, orthopaedics, veterinary medicine and non-destructive testing. In this work we present Monte Carlo simulations of an upgrade to the Adaptix technology to specifications suited for chest DT and we show computer aided designs for a system with various populations of these source arrays. We conclude that stationary arrays of cold-cathode X-ray sources could replace movable X-ray tubes for 3D imaging and different arrangements of many such arrays could be used to tailor the X-ray fields to different patient size and diagnostic objective.

INTRODUCTION

Adaptix Ltd have demonstrated veterinary and human cadaver extremity digital tomosynthesis (DT) with the devices shown in Fig. 1. Both are small and light enough to be carried by hand and have been operated safely in clinics and exhibitions globally. Demonstrated applications also include dental DT with human cadavers and non-destructive testing of electronics and composites [1].

Adaptix DT systems use a compact flat panel source (FPS) with a square array of emission positions. The FPS comprises electron field emitters etched on a silicon wafer in square arrays as shown in Fig. 2. In this design, all electron emitters turn on simultaneously with a 60-70 kV potential, but an electron beam steering module ensures only one electron beam at a time enters its respective collimator aperture to reach the X-ray target. The rest are absorbed in the bulk of the collimator. The FPS is coupled to a flat panel detector (FPD) to create the full DT system and both FPS and FPD remain stationary.

* Work funded by the Accelerators for Security, Healthcare and Environment Centre for Doctoral Training by the United Kingdom Research and Innovation Science and Technology Facilities Council; ID: ST/R002142/1.
† thomas.primidis@gmail.com

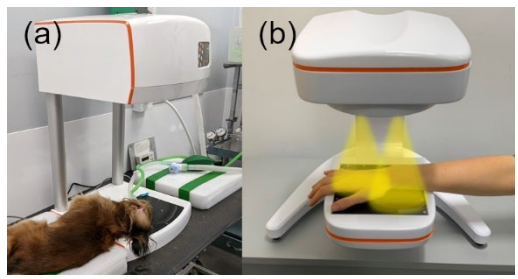

Figure 1: Adaptix (a) veterinary and (b) extremity DT systems. Reproduced with permission from Adaptix Ltd.

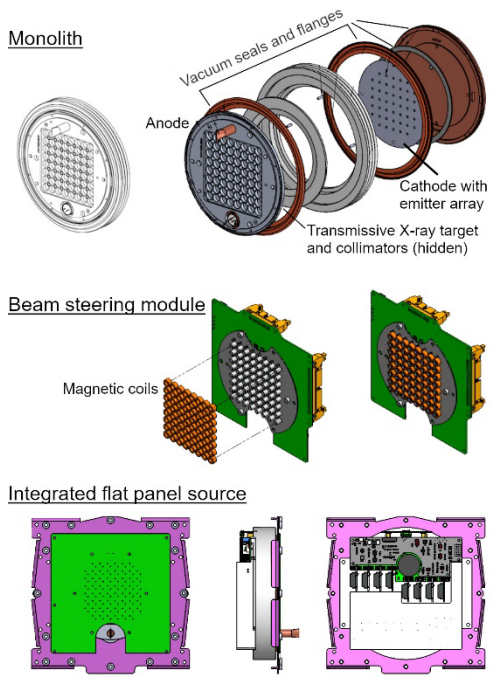

Figure 2: Schematics of the Adaptix FPS. Reproduced with permission from Adaptix Ltd.

DT uses a limited (~30°) angular range of projections instead of half-, full- or multi-circle scans used in computed tomography (CT) [2]. DT is a 3D X-ray imaging modality with a cost and dose comparable to 2D radiography but with image quality that can approach that of CT and literature suggests DT could be an alternative to both modalities on specific occasions [3-5].

The most requested X-ray exam is for the chest. In 2020-21 in England, 2D chest and 3D chest or abdomen X-ray imaging amounted to 80% (7.3 million) of all imaging

ISBN: 978-3-95450-227-1 ISSN: 2673-5490 doi:10.18429/JACoW-IPAC2022-THPOMS035

FIRST PRODUCTION OF ASTATINE-211 AT CROCKER NUCLEAR LABORATORY AT UC DAVIS*

E.J. Prebys†, M.R. Backfish, D.A. Cebra, R.B. Kibbee, L.M. Korkeila and K.S. Stewart
UC Davis, Davis, CA, USA

Abstract

There is a great deal of interest in the medical community in the use of the alpha-emitter ^{211}At as a therapeutic isotope. Among other things, its 7.2 hour half life is long enough to allow for recovery and labeling, but short enough to avoid long term activity in patients. Unfortunately, the only practical technique for its production is to bombard a ^{209}Bi target with a 29 MeV alpha beam, so it is not accessible to commercial isotope production facilities, which all use fixed energy proton beams. The US Department of Energy is therefore supporting the development of a "University Isotope Network" (UIN) to satisfy this need. As part of this effort, we have developed an ^{211}At production facility using the variable-energy, multi-species cyclotron at Crocker Nuclear Lab the University of California, Davis. This effort relies on a beam probe which has been modified to serve as an internal ^{209}Bi target, to avoid problems with alpha particle extraction efficiency. We have recently performed the first production and recovery run, in which we recovered on the order of 50 μCi of ^{211}At in solution. Now that production has been demonstrated, we plan to increase capacity to 10s of mCi per run for use in local research.

INTRODUCTION

The detailed motivation for this project was discussed IPAC19 [1], but it is summarized here for completeness.

Radionuclides are an important component of medical diagnosis and therapy. Broadly speaking, they fall into two categories: positron (β^+) emitters to be used for PET scans and α or β emitters to be used for treatment. α emitters are particularly attractive for treatment, because all of the energy is deposited in close proximity to the update site. In this context, there has recently been a great deal of interest in ^{211}At as a therapeutic α-emitter. Unfortunately, sources of ^{211}At are limited, because the only practical method that has been demonstrated for production is to bombard a ^{209}Bi target with α particles of roughly 29 MeV kinetic energy to produce ^{211}At through the reaction

$$^{209}\mathrm{Bi}(\alpha, 2\mathrm{n})^{211}\mathrm{At}$$

Most medical isotope production facilities rely on either nuclear reactors or proton accelerators, with low energy (10-40 MeV) proton cyclotrons being the most common commercial production tool. Such cyclotrons are designed to accelerate only protons to a fixed energy, as designing them for variable energy and/or multiple species acceleration would increase the cost and complexity, threatening their commercial viability. Thus, they are unable to produce the α beam necessary to create ^{211}At.

We have been funded to develop the capability to produce ^{211}At at the Crocker Nuclear Laboratory cyclotron at the University of California Davis [2]. This is a research cyclotron built in the mid-1960s, which can accelerate protons, deuterons, helions ($3He^{++}$), or alpha particles to variable energies, with a maximum energy of 67 MeV for protons.

EXPERIMENTAL TECHNIQUE

An excellent overview of ^{211}At production can be found in reference [3]. Its production cross section is a strong function of the energy of the α beam incident on the ^{209}Bi; however, care must also be taken to avoid the the production of ^{210}At, because that decays to ^{210}Po, which poses a serious health risk. The production rates for both are shown in Fig. 1 (See Figs. 2.3.2 and 2.4.3 in [4]). We see that while the production rate for ^{211}At peaks at about 31 MeV, that is above the turn-on threshold for ^{210}At, so we will plan to use a beam of about 28-29 MeV, a point at which production is still significant.

UC Davis is uniquely positioned to provide such a service. The Crocker Nuclear Cyclotron has been used to produce isotopes in the the past [5], and has demonstrated the currents required. Figure 2 shows the layout of the cyclotron. Extracted beam goes through a switch magnet, where it can be directed to one of 7 beam lines. Three of these are internal to the cyclotron vault and four go to three external caves, as shown in. The external lines are limited to 100 nA for radiation safety reasons, while currents can go to at least 100 μA inside the vault.

Historically, isotopes were produced in “line 0", as indicated in the figure; however, while high currents have been demonstrated in the cyclotron, the efficiency of extraction is

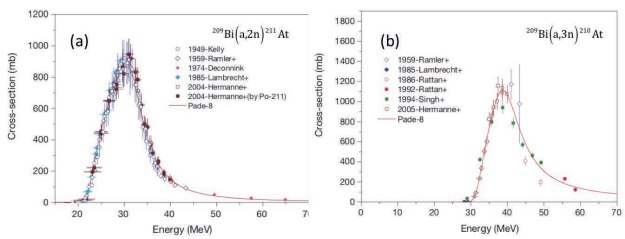

Figure 1: Production cross-section as a function of beam energy for (a) ^{209}Bi(α,2n)^{211}At and (b) ^{209}Bi(α,3n)^{210}At. (Cyclotron Produced Radionuclides: Physical Characteristics and Production Methods, Technical Reports Series Number 468, International Atomic Energy Agency: Vienna, 2009, pp. 33-40 with permission from the IAEA)

* This work supported by Department of Energy grant DE-SC0020407
† eprebys@ucdavis.edu

ISBN: 978-3-95450-227-1 ISSN: 2673-5490 doi:10.18429/JACoW-IPAC2022-THPOMS036

HERACLES: A HIGH AVERAGE CURRENT ELECTRON BEAMLINE FOR LIFETIME TESTING OF NOVEL PHOTOCATHODES

M.B. Andorf*, J.K. Bae, A.C. Bartnik, L. Cultrera, J.M. Maxson, I.V. Bazarov
Cornell University, Ithaca, NY, USA

Abstract

We report on the building and commissioning of a high current beamline dedicated to testing novel photocathodes for high current and spin-polarized electron applications. The main features of the beamline are a 200 keV DC electron gun and a beam dump capable of handling 75 kW of beam power. In this report, a Cs3Sb photocathode is used to demonstrate the facilities high current capabilities.

INTRODUCTION

Numerous accelerator techniques and applications require the ability to produce high-average current ($\geq$ 1 mA) bright electron beams from a photoinjector. Electron-based strong hadron cooling techniques may require average currents as high as 100 mA. A high current Electron Recovery Linac (ERL) is envisioned for LHeC[1]. For EUV lithography with an ERL, 10 mA beam current is needed[2], while it has been estimated that medical isotope production with an ERL requires 100 mA[3]. High average-current spin-polarized electron production is highly desirable for a number of nuclear physics facilities[4, 5] and for polarized positron production[6]. The realization of these applications will push the boundary of what is state-of-the-art in accelerator physics technology; however, ultimately the viability of their use depends on the reliability of the electron source.

Semiconductor based photocathodes are a proven way to generate high average current electron beams. They have quantum efficiencies (QE) on the order of 10% at convenient visible or near infared wavelengths where commercial high power laser sources are available. A major complication of a semiconductor based photocathode is they are extremely sensitive to the vacuum environment and degrade with use more rapidly than metal photocathodes. In particular at high current, in addition to vacuum poisoning, ion back-bombardment[7–10] from the ionization of residual gas in the gun and thermal desorption[11] from exposure to an intense laser beam limit the cathodes operation lifetime.

The High ElectRon Average Current for Lifetime ExperimentS (HERACLES) at Cornell has been recently commissioned at 200 keV with up to 10 mA average beam current. In close proximity to the Photocathode Laboratory at Cornell, HERACLES is a dedicated beamline aimed at improving the robustness of photocathodes operated at high current.

FACILITY

HERACLES Beamline

The start of the HERACLES beamline is a DC electron gun[12] originally designed and fabricated for Cornell's ERL program where it was used to achieve a record high average current from a photoinjector of 65 mA[13]. Currently we operate the gun at 200 keV. The beamline is shown in Fig.1. Outside the gun, the beamline has two solenoids, three independent horizontal/vertical corrector coils, three BeO pneumatically controlled viewscreens, a faraday cup for low current ($\approx$ 100 nA) measurements, a quadrant detector for beam positioning information at high currents. The beamline includes an EMS system which has not been recommissioned[14]. The beamdump is designed for up to 75 kW of beam power. It is cooled via a closed loop heat exchanger. The same heat exchanger also cools the gun's power supply and the main drive laser, a Coherent gas Argon laser. In this work, the laser was operated with a single line at 488 nm. Trapped ions[15] outside the gun are removed by two clearing electrodes. In addition to contributing to cathode damage via ion back-bombardment, trapped ions can cause beam loss leading to a trip off of the machine[16].

Cathodes are transported in HERACLES via a vacuum port. The port interfaces with a vacuum suitcase which is used to transport cathodes grown in the photocathode laboratory. During transport the suitcase is pumped with two non-evaporative getter (NEG) pumps combining in approximately 400 liter/s of pump speed. The vacuum port is pumped with a single 100 liter/s NEG. After attaching the suitcase, it typically takes 20 hours for the vacuum port to pump down to approximately 5×10^{-9} Torr. Given that moving the cathdoe through the vacuum port takes only a few seconds, this vacuum is sufficiently low to avoid degradation from vacuum poisoning.

CATHODE GROWTH AND TRANSPORT

For a high-current demonstration, a Cs_3Sb cathode was grown off center with a Molybdenum puck. After annealing at 500 C for 48 hours, the puck was cooled to 120 C. A metallic mask screens the puck from the Cs and Sb sources, allowing the active area to be grown off center. The active area shape is circular with a radius of approximately 2 mm. An off centered cathode is used to reduce damage from ion back-bomardment[17].

During the growth, initially only Cs was deposited until the QE peaked at which point we started to deposit Sb. A Quartz Microbalance (QCM) was used to monitor the Sb

* mba83@cornell.edu

ISBN: 978-3-95450-227-1 ISSN: 2673-5490 doi:10.18429/JACoW-IPAC2022-THPOMS037

RIPPLE PATTERN FORMATION ON SILICON CARBIDE SURFACES BY LOW-ENERGY ION-BEAM EROSION*

Divya Gupta† and Sanjeev Aggarwal, Ion Beam Centre, Department of Physics, Kurukshetra University, Kurukshetra 136119, India
G.R. Umapathy, Inter University Accelerator Centre (IUAC), New Delhi 110001, India
Rahul Singhal, Malviya National Institute of Technology (MNIT), Jaipur, Rajasthan 302017, India

Abstract

A versatile experimental facility air insulated high current medium energy 200 kV Ion Accelerator, with the terminal voltage in the range of 30-200 kV has been running successfully at Ion Beam Centre, KUK for carry out multifarious experiments in material science and surface physics. This system offers single charge state, switching magnet with five exit ports and large area irradiation/implantation using hollow cathode ion source.

Ion beam induced structures on the surfaces of semiconductors have potential applications in photonics, magnetic devices, photovoltaics, and surface-wetting tailoring etc. In this regard, silicon carbide (SiC) is a fascinating wide-band gap semiconductor for high-temperature, high-power and high-frequency applications. In this work, fabrication of ripple patterns is carried out on the SiC surfaces using 80 keV Ar^+ ion beam for different fluences at oblique incidence of 50^0. AFM study demonstrates that ripple wavelength and amplitude, ordering and homogeneity of these patterns vary linearly with argon ion fluence. The formation of such surface structures is attributed to the preferential sputtering of silicon in comparison to carbon. The evolution of high degrees of order is explained with the help of existing formalisms of coupling between surface topography and preferential sputtering.

INTRODUCTION

Oblique angle sputter erosion (OASE) is a versatile and cost effective tool for patterning and structuring solid surfaces at the nanoscale level [1-3]. This is a scalable method that fabricates a myriad of patterns in a single technological step and is applicable to most solid materials, ranging from metals to semiconductors, and from organic to inorganic materials [1-9].

Considering the stochastic nature of OASE at micro- to nano-scopic scales, the spontaneous formation of patterns by this technique is a highly non-trivial process, and has long drawn attention due to its potential applications in surface technology and applied sciences [1-4].

In this regard, a versatile experimental facility 200 kV Ion Accelerator with ion beams having energy in the range of 30–200 keV is running successfully at Ion Beam Centre, KUK for carry out patterning and structuring the surfaces of different classes of materials. This system offers single charge state, switching magnet with five exit ports and large area irradiation/implantation using hollow cathode ion source [7].

For binary compounds, non-stoichiometric sputtering of one element in comparison to other occurs. This preferential sputtering determines the degree of patterning and structuring by oblique angle sputter erosion. Hence, it becomes extremely vital to have detailed knowledge of the composition modulation as a result of non-stoichiometric sputtering [8, 9].

In this paper, we address the study of the temporal evolution of SiC surfaces with the aim of characterizing the features as a function of ion dose. This type of quantitative and qualitative analysis is required for designing large-scale ordered nanostructures on the sputtered surfaces.

MATERIALS AND METHODS

Silicon Carbide (SiC) thin films were deposited on Si(111) substrates employing RF sputtering method. These SiC thin films were then irradiated with 80 keV argon ions by 200 kV Ion Accelerator Facility available at Ion Beam Center, Kurukshetra University, Kurukshetra, India under a vacuum of 3.2 x 10^{-7} Torr. Argon ion fluence of 1×10^{18}, 2×10^{18} and 3×10^{18} ions cm^{-2} has been used at fixed incident angle of 50^0 [7].

Surface morphological evolution of these RF sputtered and argon irradiated SiC surfaces was profoundly evaluated by Atomic Force Microscopy (AFM) utilizing Bruker HR Mutlimode-8 available at Ion Beam Centre, Kurukshetra University, Kurukshetra. In order to get a better statistics, at least 5 AFM scans on each sample were performed.

RESULTS AND DISCUSSION

Figure 1 ((a)-(d)) shows the AFM images of RF sputtered SiC over Si(111) and SiC surfaces bombarded using 80 keV Ar^+ ions at fixed incident angle of 50^0 with fluences of 1×10^{18}, 2×10^{18} and 3×10^{18} ions cm^{-2} respectively. The corresponding Fast Fourier Transforms (FFT) is shown in insets of these micrographs.

Figure 1 (a) reveals that globular type particles of SiC can be easily distinguished. These particles are uniform in size, with a lateral dimension of about 30-40 nm. FFT image depicts the random nature of the SiC particles after RF sputtering.

* The work has been supported by the Department of Science and Technology (DST) by funding major research project for utilizing 200 kV Ion Accelerator and related characterization facilities. Authors are highly grateful to the MHRD for RUSA 2.0 grants for Centre for Advanced Material Research (CAMR) to Kurukshetra University.
† divyagupta2017@kuk.ac.in

ISBN: 978-3-95450-227-1 ISSN: 2673-5490 doi:10.18429/JACoW-IPAC2022-THPOMS038

SPALLATION TARGET OPTIMIZATION FOR ADS BY MONTE CARLO CODES

M. Mumyapan, M. Ghergherechi, D. H. Ha, H. Namgoong, J. S. Chai†, Department of Electrical and Computer Engineering, Sungkyunkwan University, Suwon, Gyeonggi-do, Korea

Abstract

Accelerator Driven Systems are advanced systems for the use of Thorium as fuel, aiming to reduce nuclear waste through transmutation. The spallation target, which is responsible for producing neutrons, is one of the main parts of the ADS system. In this research, neutronic parameters of spallation targets consisting of several materials LBE, Mercury, and Lead, on the cylindrical, box, and conic shapes using Monte Carlo codes (FLUKA, PHITS, MCNPX) were investigated. Energy Deposition and spallation neutron yield of spallation target with different shapes and dimensions have been calculated to optimization of the target. According to the results, the neutron yield values from MCNPX and PHITS are similar and it's close to the experimental result. On the other hand, the error rate of the values in Fluka is higher.

INTRODUCTION

Accelerator Driven Systems (ADS) are up-and-coming tools that provide reliable energy and transmute long-lived radioactive waste. The simultaneous operation of ADS's passively safe subcritical core and accelerator distinguishes it from conventional fission reactors. So, the unique feature of this system is that the reaction stops shortly after the proton beam from the accelerator is turned off. In this way, it provides safety that will significantly reduce the risk of nuclear accidents. In addition, nuclear waste is a big problem for which no solution can be found [1]. ADS aims to transmute long-lived radioactive waste like Pu, and Np isotopes [2]. Thus, it can figure out this problem and contribute to the sustainability of nuclear energy [3].

Powerful particle accelerators with high proton beam energy, spallation target, and sub-critical system are the main components of ADS [4]. The particle accelerator continuously delivers a dense beam of accelerated particles toward the target. As a result, these neutrons can be multiplied in the subcritical nuclei enclosing the target [5].

The spallation target is the part that connects the accelerator and the subcritical reactor. Therefore, the spallation target design has a key point for ADS design. There are some difficulties for design spallation target; selecting the most suitable material, heat removal, radiation damage, and distribution of power density. To handle these issues, subjects such as neutronic analysis, and energy deposition are required for spallation target design [6].

† jschai@skku.edu

The neutron yield per incident proton is the principal data that has been used in the ADS study [7]. Neutron yield calculation with MCNPX has been investigated by several researchers [8-10]. However, a comparison of neutron yield with different Monte Carlo codes such as FLUKA and PHITS was not well reported.

Three well-proved Monte Carlo codes (FLUKA, PHITS, and MCNPX) were used to calculate and compare the neutron yield to determine the most suitable material and select the optimum size and shape for the spallation target.

MATERIALS AND METHODS

In this paper, by using FLUKA, PHITS, and MCPNX, the neutron yield of the cylindrical target was calculated according to different proton beam energies and this process was repeated for 4 different target materials (LBE, Mercury, Lead, and Tungsten). The fixed cylinder target with a radius of 20 cm and height of 80 cm was chosen based on the literature [10]. To compare the different shapes, the dimensions of the Conical target were selected the same (Fig. 1). Proton beam (2.35 mm spatial FWHM) with energies ranging from 600 to 1500 MeV, in the z-direction (0, 0, -2) injected into the target.

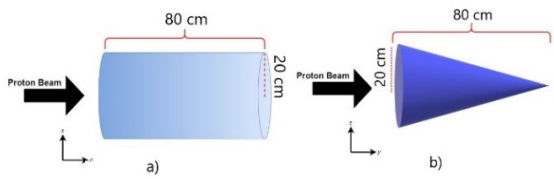

Figure 1: Fixed cylindrical and conical spallation target.

To determine the optimum target shape and dimensions, the neutron yield of the cylindrical target as well as the conical target were calculated and repeated for different materials (Tungsten, LBE, Mercury, and Lead) and dimensions. The length of the cylindrical target has been changed to 20,40,60,80 and 100 cm, and then the radius of the target has been changed to 5,10,15,20,25, and 30 cm. Conical target length has been varied from 40, 60, 80,100 cm and radius 10,20,30,40, and 50 cm. Equation 1 is used to calculate the neutron yield per incident proton [11]. Proton beam energy, target material, shape, and dimensions of the target are the factors affecting the neutron yield. Sp is the number of primary protons and Sn is the number of primary neutrons.

$$Spallation\ neutron\ yield\ per\ proton \quad Yn/p = \frac{Sn}{Sp} \quad (1)$$

ISBN: 978-3-95450-227-1 ISSN: 2673-5490 doi:10.18429/JACoW-IPAC2022-THPOMS039

INVESTIGATION ON INTERMOLECULAR INTERACTIONS LIQUIDS IN IONIC USING ACCELERATOR-BASED THz TRANSITION RADIATION

P. Nanthanasit*,[1], S. Rimjaem†,[2], PCELL, PBP, Faculty of Science, Chiang Mai University, Chiang Mai, Thailand
N. Chattrapiban, Quantum Simulation Research Laboratory, Faculty of Science, Chiang Mai University, Chiang Mai, Thailand
P. Nimmanpipug[2], CSML, Faculty of Science and I-ANALY-S-T, Chiang Mai University, Chiang Mai, Thailand
M. Jitvisate[2], School of Physics, Institute of Science, Suranaree University of Technology, Nakhon Ratchasima, Thailand
[1]also at Ph. D. Program in Physics (International Program), Chiang Mai University, Chiang Mai, Thailand
[2]also at ThEP Center, MHESI, Bangkok, Thailand

Abstract

Ionic liquids (ILs) are interesting material that can be used in many applications. Spectroscopic measurement using accelerator-based terahertz transition radiation (THz TR) is one of potential techniques to investigate their intermolecular interactions by observing the vibrational bands in the terahertz region due to TR's exceptional properties: coherent, broadband, and high intensity. This work aims to study intermolecular interactions of ILs using the THz TR produced from an electron beam at the PBP-CMU Electron Linac Laboratory. The THz TR with the frequency range of 0.3-2.5 THz can be produced from electron beam of energy 10-25 MeV. This radiation is produced and transported to the experimental area, where it is used as the coherent and polarization selective light source for the Fourier transform infrared (FTIR) spectrometer. The absorption spectrum in the THz region of the ILs is then measured. In addition, to explain the experimental results deeply, theoretical calculations using the density functional theory are performed. In this contribution, we present the results from experiment and computational calculation that can be used together to describe the intermolecular interactions in ILs.

INTRODUCTION

Ionic liquids (ILs) are room temperature liquids comprised entirely of cations and anions [1-2]. Originated from their molecular structures and strong Coulombic interactions, ILs possess a collection of properties that are of technological interest, e.g., extremely low vapor pressure, modest intrinsic ionic conductivity, high thermal and chemical stability, and can dissolve a wide range of chemical species [3-4]. These properties can be tuned by changing the choice of cation and anion, whose variety is large and can form countless combinations. As a consequence of this unusual range of properties, ILs are significantly promising for several applications, such as electrochemical energy storage devices, materials for nano-lubrication, high temperature and/or vacuum phase materials synthesis, semiconductor and superconductor gating applications, and novel self-assembly media [5].

To apply ILs in each application effectively, insight knowledge about their properties, structures, dynamics, and reactions is greatly important. Special intermolecular interactions such as hydrogen bonds can somehow strongly affect these properties [6]. The vibration of this hydrogen bonding is in the terahertz (THz) region and can be studied with the spectroscopic techniques such as terahertz Fourier transform infrared (THz FTIR) spectroscopy and terahertz time-domain spectroscopy (THz TDS) with the high intensity accelerator-based coherent terahertz transition radiation (THz TR) produced at the PBP-CMU Electron Linac Laboratory (PCELL). We expect to be able to study properties of ILs with better signal to noise ratio and lower sample volume compared with the conventional THz source.

ACCELERATOR-BASED THZ TRANSITION RADIATION

The THz TR can be generated from the accelerator system at PCELL. Schematic diagrams of the system for generation of THz TR are shown in Fig. 1-2. From these figures, the electron bunches with energy in the range of 2-2.5 MeV are obtained from a thermionic cathode radio frequency (RF) electron gun. These electron bunches are compressed to have a bunch length in the order of femtosecond using an alpha magnet. After that, they travel through the travelling-wave linear accelerator (linac) and are accelerated to have the beam energy in the range of 10-25 MeV [7-8]. In the THz TR station, an aluminium foil is used as a radiator. It is tilted by 45° with respect to the electron beam direction. When the electron bunches from the linac travel from vacuum to conductor, the backward TR is emitted perpendicular to the electron beam path. This radiation is collimated using a first-surface gold coated parabolic mirror to obtain a parallel ray. Finally, this collimated THz radiation is transported through a high-density

* panat_14@hotmail.com
† sakhorn.rimjaem@cmu.ac.th

ISBN: 978-3-95450-227-1 ISSN: 2673-5490 doi:10.18429/JACoW-IPAC2022-THPOMS040

PRESENT STATUS OF LINEAR ACCELERATOR SYSTEM FOR NATURAL RUBBER VULCANIZATION AT CHIANG MAI UNIVERSITY

C. Thongbai[1,2] *, S. Rimjaem[1,2], J. Saisut[1,2], P. Jaikaew[1], N. Khangrang[1], E. Kongmon[1], P. Wongkummoon[1], M.W. Rhodes[2]
[1] Plasma and Beam Physics Research Facility, Department of Physics and Materials Science, Faculty of Science, Chiang Mai University, Chiang Mai 50200, Thailand
[2] Thailand Center of Excellence in Physics, Ministry of Higher Education, Science, Research and Innovation, Bangkok 10400, Thailand

Abstract

At the Plasma and Beam Physics (PBP) Research Facility, Chiang Mai University (CMU), an electron beam accelerator system for natural rubber irradiation has been under development and is currently under the commissioning. The research project is carried out with the aim to modify an old medical linac, retired from the clinical operation, for rubber latex vulcanization and materials irradiation using electron beams. The accelerator system consists of a DC-thermionic cathode electron gun, a standing-wave RF linear accelerator, an RF system, a control system, beam diagnostic systems, and an irradiation system. The components were completely assembled, and the RF system was tested. The RF processing has been performed and some of the electron beam properties have been measured. This contribution presents some experimental results while developing and testing the various sub-systems of this accelerator. The present status of development and some vulcanization results will also be reported in this contribution.

INTRODUCTION

The radio-frequency (RF) linear accelerator (linac) system for natural rubber vulcanization has been developed and is currently under the commissioning at the Plasma and Beam Physics Research Facility, Chiang Mai University, Thailand [1]. The system aims to generate electron beams for induction of cross-linking in natural rubber latex at room temperature as an alternative to a conventional sulfur vulcanization. Not only does the sulfur vulcanization require high temperature, but it also needs some chemical for activation and acceleration of crosslink reaction [2,3]. Moreover, the rubber vulcanization using an electron beam has high potential to reduce extractable proteins which is possible to cause allergy to the consumers [4].

The accelerator system was constructed using parts from the 4 MeV medical electron linac system model Mitsubishi ML-4M [5], retired from clinical operation at Maharaj Nakorn Chiang Mai Hospital. The main components of the accelerator system are a DC gun, an RF linear accelerator, a magnetron with waveguide components, a modulator system, a control unit, and irradiation system as the diagram shown in Fig. 1. The layout of the system is illustrated in Fig. 2.

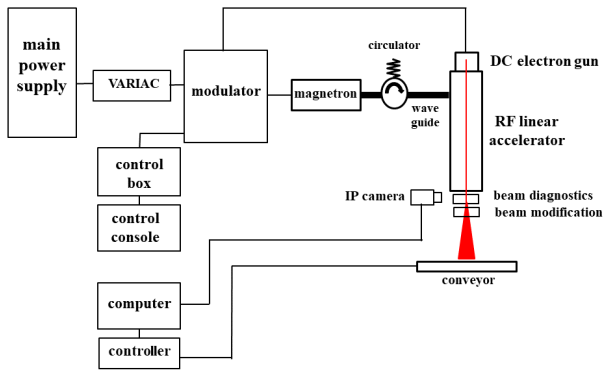

Figure 1: Diagram of the RF-linac system for natural rubber vulcanization at Chiang Mai University.

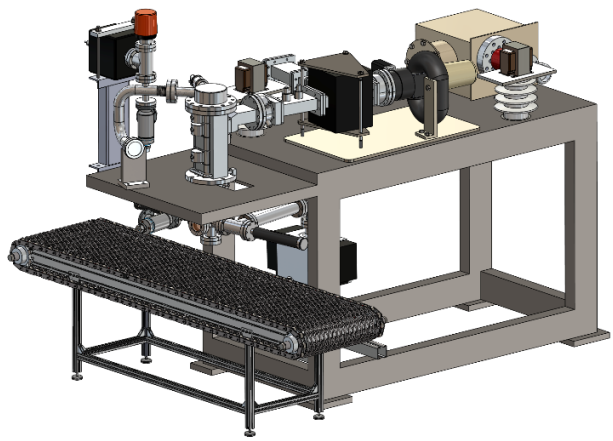

Figure 2: Layout of the accelerator system consisting of a DC-gun, a linac, a magnetron and a conveyor under the beamline.

RF AND ACCELERATOR SYSTEMS

The RF system consists of a modulator unit, a magnetron, and waveguide components. Within the modulator unit, there are a pulse forming network (PFN), a pulse transformer, a trigger board, and a thyratron switch. The modulator provides high voltage pulses for the DC electron gun, and for the magnetron. A variac (VAR) was added to the RF system, as shown in the diagram in Fig.1, to control the charging voltage for the PFN. Having linear relation to the output RF power, the magnetron RF power can then be adjusted via the VAR adjustment. From the RF

* chitrlada.t@cmu.ac.th

ISBN: 978-3-95450-227-1 ISSN: 2673-5490 doi:10.18429/JACoW-IPAC2022-THPOMS041

DESIGN AND PARAMETERIZATION OF ELECTRON BEAM IRRADIATION SYSTEM FOR NATURAL RUBBER VULCANIZATION

P. Wongkummoon [1, *], C. Thongbai [1, 2, †], J. Saisut [1, 2], S. Rimjaem [1, 2], N. Kangrang [1], M.W. Rhodes [2]
[1] Plasma and Beam Physics Research Facility, Department of Physics and Materials Science, Faculty of Science, Chiang Mai University, Chiang Mai, Thailand
[2] Thailand Center of Excellence in Physics, Ministry of Higher Education, Science, Research and Innovation, Bangkok, Thailand

Abstract

Electron beam irradiation is a process to modify or improve the properties of materials with less chemical residue. In natural rubber vulcanization, a proper electron absorbed dose is about 50 - 150 kGy. In this study, the experimental station is designed to investigate the deposition of the electron beam in natural rubber. Electron beams generated from an RF linac are used in this study. This accelerator can generate the beam with energies in the range of 1 - 4 MeV and an adjustable repetition rate of up to 200 Hz. We can optimize these parameters to maximize the throughput and uniformity of electron dose in the vulcanization. The simulation results from GEANT4 were used to narrow down the appropriate parameters in the experiment. In the early stage of the study, water was used as a sample instead of natural rubber. The dose distribution was obtained by placing a B3 film dosimeter under a water chamber. The water depth was varied from 0.5 to 2.0 cm. The simulation results provide the dose distribution to compare with the experimental results. In a further study, the beam irradiation in natural rubber with these optimal parameters and vulcanization tests will be performed.

INTRODUCTION

The electron radio-frequency linear accelerator (RF-linac) with an irradiated station for rubber vulcanization has been developed at the Plasma and Beam Physics Research Facility, Chiang Mai University, Thailand [1]. The electron beams generated from this RF-linac have energies in the range of 1 - 4 MeV. Difference electron beam energies provide different absorbed doses along penetration depths in the material. In the case of rubber vulcanization, the suitable absorbed dose is in the range of 50 - 150 kGy. The main objective of the work is to design the irradiation station for rubber vulcanization. The throughput is aimed to be maximum and uniform in quality. In the early stage, water is employed instead of rubber latex to set up a proper depth dose study for further rubber vulcanization experiments. In this study, the water depths were varied to investigate the absorbed dose in the water volume along with the Monte Carlo simulations.

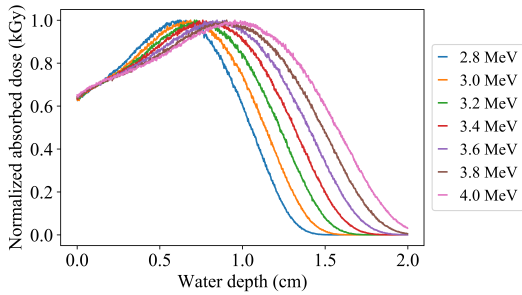

Figure 1: Normalized depth dose distributions in water volume thickness of 2 cm using monoenergetic point source of 3 - 4 MeV beams.

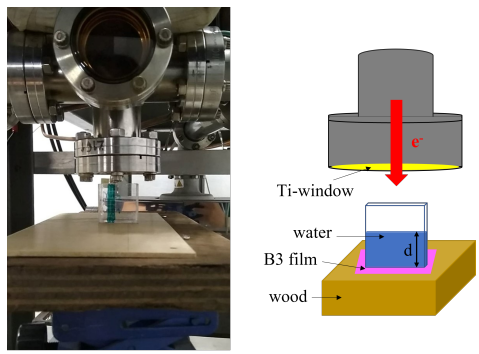

Figure 2: Dose deposition experimental set up for rubber vulcanization at the Plasma and Beam Physics Research Facility, Faculty of Science, Chiang Mai University.

DOSE DEPOSITION MEASUREMENT

Performance of an irradiation system is determined by the electron absorbed dose in water (sample) volume and related directly to the electron beam parameters. To demonstrate the effect of beam energy, different depth dose distributions in water volume using monoenergetic point source beams of 3 - 4 MeV are illustrated in Fig. 1. To prepare for vulcanization experiments, the experimental station for dose deposition was set up by placing the water container downstream of the accelerator system, after the Ti-window, as shown in Fig. 2. The electron absorbed dose was measured using B3 radiochromic film from GEX cooperation [2] so the B3 film was placed under the water c ontainer. The water container and the B3 film were then placed on a wood

* wongkummoonpitch@gmail.com
† chitrlada.t@cmu.ac.th

ISBN: 978-3-95450-227-1 ISSN: 2673-5490 doi:10.18429/JACoW-IPAC2022-THPOMS042

DEVELOPMENT OF A CYCLOTRON BASED EXTERNAL BEAM IRRADIATION SYSTEM FOR ELEMENTAL ANALYSIS

P. Thongjerm*, S. Wonglee, W. Pornroongruengchok, A. Ngamlamiad and K. Tangpong
Thailand Institute of Nuclear Technology, Thailand

Abstract

We present the studies carried out at the cyclotron facility at the Thailand Institute of Nuclear Technology (TINT, Nakhon Nayok, Thailand). The cyclotron accelerates up to 30 MeV proton with a maximum beam current of 200 µA. In addition to radioisotope production, the R&D beamline equipped with a five-port switching magnet allows further extension for multidisciplinary research and experiments. The first station of the research vault is dedicated to non-destructive and multi-elemental analysis using particle-induced x-ray (PIXE) and particle-induced gamma (PIGE) techniques. For this purpose, the beam is extracted through an exit foil to the air. The beam size is then shaped by a beam nozzle before reaching a sample. However, the range of the protons in air and the attenuation of x-rays may deteriorate. Therefore, the external irradiation system, including energy degrader foil, collimator and detector arrangement, are evaluated in Geant4 to optimise the proton beam quality and improve detection efficiency.

INTRODUCTION

The cyclotron (MCC30/15) can accelerate protons and deuterons. It is primarily used for radioisotope production. The energy of the beam is adjustable between 15-30 MeV. The related parameters of the cyclotron are listed in Table 1 [1]. However, the beam energy and current are not compatible with elemental analysis applications. The purpose of this study is to design an external irradiation system for elemental analysis.

Table 1: Main Parameters of the TINT Cyclotron

Parameter	Value
Type of ions:	
accelerated	H-/D-
issued	H+/D+
Accelerated ion energy	
- Proton	15-30 MeV
- Deuteron	9-15 MeV
Beam current	
- Proton	200 µA
- Deuteron	50 µA
Number of beam line	3

When a charged particle or proton interacts with the target material, the energy of the particle gradually decreases due to Coulomb interaction. Therefore, it is possible to reduce the beam energy when adding material, with a certain thickness, in between the system exit window and the target. The mean rate of the energy loss of charged particles is given by the Bethe-Bloch formula:

$$-\frac{dE}{dx} = \rho K \frac{Z}{A}\frac{z^2}{\beta^2}\left[ln\frac{2m_e c^2\gamma^2\beta^2}{I} - \beta^2 - \frac{\delta}{2} - \frac{C}{Z}\right],$$

where $K = 4\pi N_A r_e^2 m_e c^2$, N_A is Avogadro's number, r_e is the electron radius, m_e is the mass of an electron, ρ is the density of the medium, z is the atomic number of the beam particle, Z is the atomic number of the absorber, β=v/c is the speed of the particle relative to c and I is the mean excitation energy of the medium.

An appropriate for the construction of an energy degrader is considered based on several material properties including transverse dispersion, energy deviation and secondary radiation yield. The determination of degrader materials using SRIM [2] and FLUKA [3] were also carried out in other studies.

ELEMENTAL ANALYSIS SYSTEM

In the R&D vault, the beamline consists of a five-port switching magnet, beam diagnostic device, triplet quadrupole lens, niobium exit window and irradiation station. It is also equipped with a camera, for visual inspection of the sample during the analysis, and a laser positioning system for proper alignment. However, the last section of the system is under installation as shown in Fig. 1. The setup of the external irradiation station enables a multi-elemental analysis and near-surface structural characterisation of samples. The sample analysis can be carried out non-destructively without the limitation of the sample size. Figure 2 shows the detectors setup of the system.

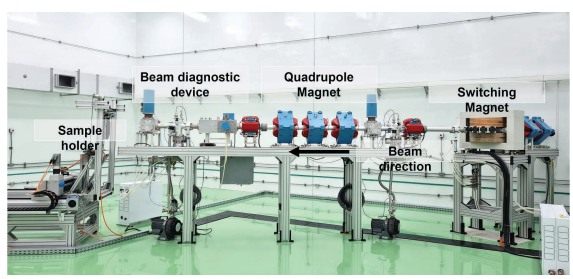

Figure 1: The current setup of R&D beam line consists of a five-port switching magnet, a set of quadrupole magnets, a beam diagnostic device and a sample holder.

In PIXE analysis, a Si(Li), 30 mm^2 active area, with 8 µm Be entrance window, is used for detecting low-energy x-ray

* piyanud@tint.or.th

ISBN: 978-3-95450-227-1 ISSN: 2673-5490 doi:10.18429/JACoW-IPAC2022-THPOMS043

Mu*STAR: SUPERCONDUCTING ACCELERATOR DRIVEN SUBCRITICAL MOLTEN SALT NUCLEAR POWER PLANTS

Mary Anne Clare Cummings†, Rolland P. Johnson, J.D. Lobo, Robert Abrams, Thomas J. Roberts,
Muons, Inc., Batavia, IL, USA

Abstract

The Mu*STAR Nuclear Power Plant (NPP) is a transformational and disruptive concept using advances in superconducting accelerator technology to consume the fertile content in spent nuclear fuel (SNF) from light water reactors (LWRs) and to eliminate need for uranium enrichment. One linac drives multiple Mu*STAR Small Modular Reactors (SMR) using subcritical molten salt fueled reactors with an internal spallation neutron target. Neutrons initiate fission chains that die out in the subcritical core. That means intrinsic immunity to criticality accidents. This new way to make nuclear energy employs continuous online removal of all fission products from molten salt fuel volatiles removed by helium purge gas. This reduces chance of accidental release. Non-volatiles removed by vortex separators, allowing complete burning of SNF.

INTRODUCTION

The Mu*STAR Accelerator-Driven System includes a 500 MWt subcritical, graphite-moderated, thermal-spectrum, molten-salt fueled, reactor design that was described in the Handbook of Nuclear Engineering in 2010 [1]. The reactor parameters are larger by a factor of 4 in linear dimension than the ORNL 8 MWt Molten Salt Reactor Experiment (MSRE) [2] done in the late 1960s. The reactor operates subcritically, with additional neutrons generated by an internal spallation target that is driven by a superconducting RF (SRF) linear proton accelerator, similar to that in the ORNL Spallation Neutron Source (SNS). Unlike the SNS, the target is not subjected to shock from the beam, which in Mu*STAR is rastered over the face of a solid uranium target that is cooled by molten salt fuel. Muons, Inc. and its collaborators have simulated engineering solutions to combine the accelerator and reactor with an internal uranium spallation target that is cooled by the MS fuel.

In 2017, Muons, Inc. was awarded a GAIN voucher award [3] with ORNL, INL, and SRNL to design and cost a facility to convert LWR SNF into molten salt (MS) fluoride fuel suitable for use in Mu*STAR. Our expectations are that such a facility will be relatively small and inexpensive enough to consider building one at each of the existing reactor sites in the US and abroad wherever SNF is stored.

CONCEPTS AND INNOVATIONS

Our concept is to install Mu*STAR accelerator-driven subcritical systems at existing light-water reactor (LWR) sites, transform the LWR spent nuclear fuel (SNF) using on-site technology developed under our GAIN award into molten salt fuel, and to burn it to produce electricity for at least 200 years. The concept is shown in Fig. 1. The additional neutron flux provided by the accelerator permits a much deeper burn such that several times more energy can be produced from the SNF than was generated by the LWR. The limit is reached when the accelerator cannot economically overcome the neutron absorption by fission products. Schemes for reducing those products are described below. This innovative and disruptive concept eliminates the need for uranium mining, fuel enrichment, fuel rod manufacture, SNF off-site storage and transport, and encourages local communities to consider consent-based storage of SNF combined with continued operation of their power utility using Mu*STAR when their LWR is retired.

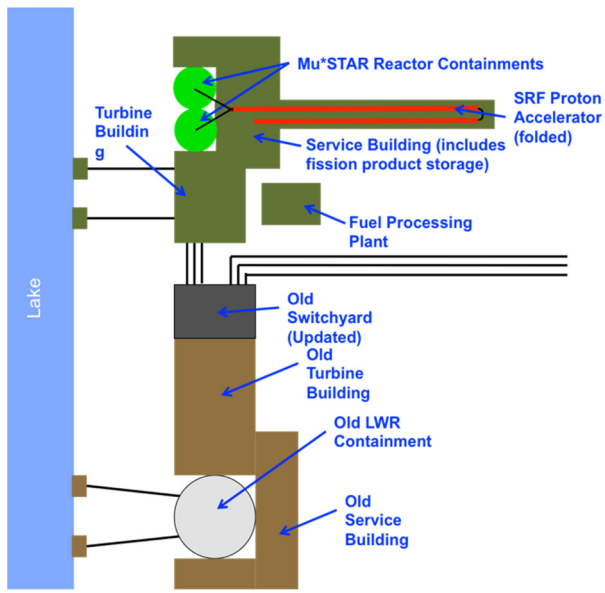

Figure 1: Mu*STAR installed at an old LWR site.

Leaving the SNF on the site where it was produced solves many problems that have long confounded the US government that is legally required to eventually take title to the SNF.

Two important consequences of the Mu*STAR are: 1) the conversion of the SNF to MS does not require fission products to be removed by chemical reprocessing and 2) the accelerator neutrons allow a deeper burn to extract as much as seven times as much energy from the SNF than was extracted by the LWR. Normalized to the energy produced, the amount and toxicity of the SNF will be reduced by more than a factor of 7 over the course of a few centuries of operation.

The reactor design since its inception has been concerned with development of self-cleaning technologies that simultaneously recover valuable nuclear materials along with neutron poisons reduction, and reduction of reactor-

† macc@muonsinc.com

ISBN: 978-3-95450-227-1 ISSN: 2673-5490 doi:10.18429/JACoW-IPAC2022-THPOMS046

GENERATION OF FLAT-LASER COMPTON SCATTERING GAMMA-RAY BEAM IN UVSOR

H. Ohgaki, K. Ali, T. Kii, H. Zen
Institute of Advanced Energy, Kyoto University, Gokasho, Uji, Kyoto, Japan
T. Hayakawa, T. Shizuma, Tokai, Quantum Beam Science Center,
National Institutes for Quantum Science and Technology, Ibaraki, Japan
M. Fujimoto, Y. Taira, UVSOR-III Synchrotron Facility, Institute for Molecular Science,
National Institutes of Natural Sciences, Okazaki, Japan

Abstract

Flat-Laser Compton Scattering Gamma-ray beam (F-LCS), which has a flat distribution in the energy spectrum and the spatial distribution with a small beam size, has been developed to study an isotope selective CT Imaging application in the beamline BL1U in UVSOR. We propose generation of an F-LCS beam by using a circular motioned electron beam, which can be generated by a helical undulator installed in a storage ring, and collision with an intense laser beam. A simulation study on the LCS beamline BL1U in UVSOR shows a weak magnetic field (K=0.2) can generate an F-LCS beam. A demonstration experiment has been carried out in UVSOR with the APPLE-II undulator. The spectra of the LCS beams were measured by using a 120% Ge detector. As a result, the energy bandwidth of the LCS peak was observed. The energy bandwidth measured in the energy spectra and the distribution map agreed with the EGS5 simulation.

INTRODUCTION

Flat-Laser Compton Scattering Gamma-ray beam (F-LCS), which has a flat distribution in the energy spectrum and the spatial distribution, has been developed to study an isotope selective CT Imaging application. We have successfully demonstrated a three-dimensional (3D) isotope-selective CT image of an enriched ^{208}Pb sample inserted into an aluminium cylindrical holder with isotope enriched ^{206}Pb by using a conventional LCS beam to excite Nuclear Resonance Fluorescence (NRF) [1]. However, for obtaining a good image resolution in CT, the small beam size of the incident LCS beam is required, which makes it challenging to excite different isotopes at the same time because of the narrow energy bandwidth of the LCS beam. In addition, the energy spectrum of the LCS beam has a scattering angle dependence which makes that the energy spectrum of the LCS beam has a spatial dependency. Therefore, we have proposed the F-LCS beam which has broader energy bandwidth with a small beam size and a spatially uniform energy spectrum, which can be generated by using a helical undulator such as the APPLE-II undulator installed at the BL1U beamline in the UVSOR synchrotron facility [2] to excite a circular motion of the electron beam circulating in the storage ring. In this paper, we briefly explain the concept of generation of an F-LCS beam, EGS5 [3] simulation result, and the demonstration experiments carried out in 2021 and 2022.

PRINCIPLE OF F-LCS BEAM GENERATION

LCS beams are generated by the collision between a relativistic electron beam and an intense laser beam [4]. The backscattering laser photon, whose energy is E_p, has a scattered angle (θ_γ) - energy dependency as described in the following formula [4],

$$E_\gamma = \frac{E_p\left(1+\beta cos\theta_p\right)}{1-\beta cos\theta_\gamma + \frac{E_p}{E_e}\left(1-cos\theta_s\right)},$$

where E_γ is the energy of the backscattered laser photon, E_e is the electron energy, β is the electron velocity relative to the speed of light, θ_p is the incident laser angle, and θ_s is the angle between the incident laser photon and the scattered photon.

By using a small collimator to define the scattering angle, we can generate a narrow bandwidth LCS beam described as

$$\frac{\sigma_{E_\gamma}}{E_\gamma} = \sqrt{\left(\frac{\sigma_\theta}{E_\theta}\right)^2 + \left(\frac{\sigma_\gamma}{E_\gamma}\right)^2 + \left(\frac{\sigma_L}{E_L}\right)^2 + \left(\frac{\sigma_\varepsilon}{E_\varepsilon}\right)^2},$$

where the terms in the right-hand side correspond the contribution to the bandwidth of the LCS beam from the collimator, the electron energy spread, the laser bandwidth, and the electron beam emittance, respectively [5].

To reduce the angle dependence, it is obvious to use a large energy spread and/or a large emittance electron beam. However, in general, LCS facilities use an electron beam circulating in a storage ring whose energy spread is small ($<10^{-3}$) with low unnormalized emittance (<1 μmrad).

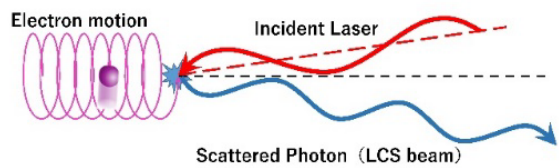

Figure1: Conceptual drawing of F-LCS beam generation.

ISBN: 978-3-95450-227-1 ISSN: 2673-5490 doi:10.18429/JACoW-IPAC2022-THPOMS047

DESIGN OF RADIATION SHIELDING FOR THE PBP-CMU ELECTRON LINAC LABORATORY

P. Jaikaew*[1], N. Khangrang, S. Rimjaem†[2], PCELL, PBP, Faculty of Science,
Chiang Mai University, Chiang Mai, Thailand
M. Jitvisate[2], School of Physics, Institute of Science, Suranaree University of Technology,
Nakhon Ratchasima, Thailand
[1]also at Master Program in Physics, Chiang Mai University, Chiang Mai, Thailand
[2]also at ThEP Center, MHESI, Bangkok, Thailand

Abstract

The local radiation shielding is designed for the electron linear accelerator beam dump at the PBP-CMU Electron Linac Laboratory (PCELL) with the aim to control the annual ambient dose equivalent during the operation. The study of radiation generation and design of radiation shielding is conducted based on the Monte Carlo simulation toolkit GEANT4. The study results include an annual ambient dose equivalent map and design of local shielding for the first beam dump downstream the linac section. With this design, the leaking radiation outside the accelerator hall is completely blocked and the average annual ambient dose equivalent on the rooftop of the hall is within the IAEA safety limit for the supervised area. The shielding model will then be used as a guideline for the construction in the near future.

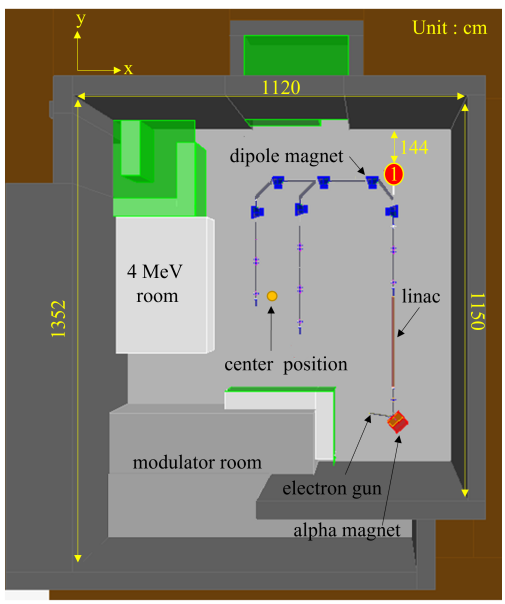

Figure 1: The top view of GEANT4 3D drawing of the PCELL accelerator hall based on the actual dimension. The linear accelerator (linac) can be seen as a red pipe housed inside the hall. The red circle with number 1 marks the position where the electron beam is dumped into a Faraday cup [1].

* phanthip_jai@cmu.ac.th
† sakhorn.rimjaem@cmu.ac.th

INTRODUCTION

Operation of an electron linear accelerator can possibly produce unwanted ionizing radiations such as high energy photons and neutrons, with the fluence depending on the electron beam energy and charge. Our previous studies have shown that an electron beam with energy in the range of 10-25 MeV and the bunch charge of 60-80 pC is optimized for the generation of the aimed terahertz transition radiation (THz-TR), mid-infrared free-electron laser (MIR-FEL), and terahertz free electron laser (THz-FEL) at our facility [2–4]. Based on these energy and bunch charge ranges, we apply the Monte Carlo method for studying the radiation produced in the accelerator hall and the surrounding area. The local radiation shieldings are then designed for the case with highest radiation dose, which is the 25 MeV electron beam with a bunch charge of 60 pC hitting the beam dump. The aim of this study is to obtain the shielding design that can control the radiation to be below 6 mSv/year for the supervised area according to the annual ambient dose equivalent, $AADE$ [5–7].

METHODOLOGY

Simulation setup

The accelerator hall with the accelerator system was constructed in the GEANT4 software as shown in Fig. 1. Beam dump No.1, which is the main focus of this study, is the first beam dump located downstream the linac structure. The concerned position of the radiation generated in this work is at the Faraday cup inside the beam dump No.1. The Faraday cup is a hallow copper tube with 10.35 cm of outer diameter and 5.74 cm of inner diameter. The vacuum tube with 5.74 cm of diameter is connected between the dipole beam dump chamber and the Faraday cup with the bending angle of 60°. The primary electrons were injected along the center line of this vacuum tube at the starting position of 25 cm directing to the Faraday cup. In the simulation, 1000 million primary electrons per task was suggested to prevent the empty bin for radiation fluence collection [1]. However, it would require enormous simulation time. Due to the time limitation, we took the advantage from the theory of sampling distribution of the mean, which states that the mean of the sampling distribution is approximately to the population mean [8]. Thus, we simulated ten times of 100 million primary electrons for one set of simulation. By using this method, the simulation

ISBN: 978-3-95450-227-1 ISSN: 2673-5490 doi:10.18429/JACoW-IPAC2022-THPOMS048

CHALLENGE BASED INNOVATION "ACCELERATORS FOR THE ENVIRONMENT"*

N. Delerue†, IJCLab IN2P3/CNRS, Orsay, France
P. Burrows, University of Oxford, Oxford, UK
B. Holland, L. Rinolfi, European Scientific Institute, Archamps, France
E. Métral, M. Vretenar, CERN, Geneva, Switzerland

Abstract

We present an initiative to foster new ideas about the applications of accelerators to the Environment. Called "Challenge Based Innovation" (CBI) this initiative will gather four teams each of six master-level students each coming from different academic backgrounds. As part of the EU-funded I.FAST project (Innovation Fostering in Accelerator Science and Technology), they will gather during 10 days in Archamps near CERN to receive high level lectures on accelerators and the environment and to brainstorm on possible new applications of accelerators for the environment. At the end of the gathering, they will present their project at CERN to a jury made of experts.

MOTIVATION

Sometimes taking a fresh look at an issue can help find new solutions. This is the idea underlying a Challenge Based Innovation (CBI) event called the I.FAST-CBI which is task 2.3 of the I.FAST project [1]. The I.FAST-CBI (hereafter called the challenge) stems from the historic collaboration between the European Scientific Institute (ESI) [2], CERN and others partners to run the Joint Universities Accelerator School (JUAS). This new collaboration has been inspired by the success of CERN's IdeaSquare CBI program [3] but with a much shorter duration. For this challenge, 24 students from different countries will spend nine days at ESI in Archamps near Geneva exploring ways in which accelerators and related technologies could be used to meet a societal challenge related to one of the Horizon Europe missions [4]. The choice for the 2022 challenge is "Accelerators for the environment". These students will form strongly multidisciplinary teams with students coming from law, environmental studies and, of course, physics and engineering. Working together in teams they will develop an innovative way to address the challenge using accelerators. On the tenth day, they will be invited to spend a day at CERN and present their work in front of a jury.

STUDENTS APPLICATIONS

A call for application and a poster (shown on Fig. 1) were circulated in December 2021 through various networks, including the "Accelerating News" newsletters [5] and the ESI/JUAS network of universities.

Figure 1: I.FAST CBI poster.

To apply students had to submit a form online and write short texts on their interest for particles accelerators and the applications of accelerators to the environment (which for most of them required some background reading). The application deadline was February 28^{th}.

A total of 187 applications were received, 85 % of which were from I.FAST participant countries (Figure 2 shows the country of affiliation of students coming from the European Union or the UK). The country of affiliation of the selected participants reflects this diversity (see Fig. 3).

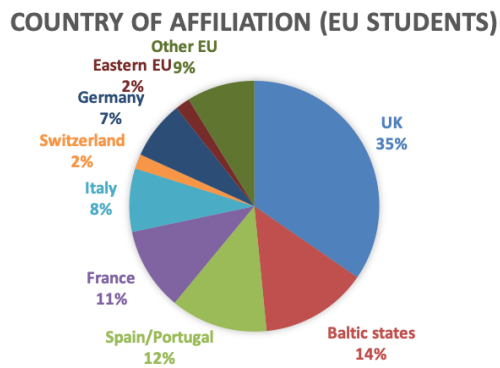

Figure 2: Country of affiliation of students coming from an University located in the European Union or the UK.

A good diversity of fields of studies was achieved (see Fig. 4): most of these applications were from engineering (39 %) and physics (37 %), but there were also 20 applications (11 %) from environmental sciences and 9 from other scientific fields. There were 6 applications from law students, 5 from management/business students, 3 from humanities students and 2 from medicine students.

* This project has received funding from the European Union's Horizon 2020 Research and Innovation programme under Grant Agreement No 101004730.
† nicolas.delerue@ijclab.in2p3.fr

ISBN: 978-3-95450-227-1 ISSN: 2673-5490 doi:10.18429/JACoW-IPAC2022-THPOMS049

ENERGY COMPARISON OF ROOM TEMPERATURE AND SUPERCONDUCTING SYNCHROTRONS FOR HADRON THERAPY

G. Bisoffi[1], E. Benedetto[2], M. Karppinen, M. Reza Khalvati, R. van Weelderen, M. Vretenar, CERN, Geneva, Switzerland,
M.G. Pullia, G. Venchi, CNAO Foundation, Pavia. Italy
L. Rossi, M. Sorbi, Universita' degli Studi di Milano and INFN, Milano, Italy
R. U. Valente, Università La Sapienza, Rome, Italy
M. Sapinski[2], PSI, Villigen, Switzerland
[1] on leave of absence from INFN-LNL, Legnaro, Italy
[2] also at SEEIIST Association, Geneva, Switzerland

Abstract

The yearly energy requirements of normal conducting (NC) and superconducting (SC) magnet options of a new hadron therapy (HT) facility are compared. Special reference is made to the layouts considered for the proposed SEEIIST facility. Benchmarking with the NC CNAO HT centre in Pavia (Italy) was carried out. The energy comparison is centred on the different synchrotron solutions, assuming the same injector and lines in the designs. The beam current is 20 times higher than present generation facilities: this allows efficient multi-energy extraction (MEE), which shortens the therapy treatment and is needed especially in the SC option, because of the slow magnet ramping time. Hence, power values of the facility in the traditional mode were converted into MEE ones, for a fair comparison between NC and SC magnets. cryocoolers (c.c.) and a liquefier are also compared, for synchrotron refrigeration. This study shows that a NC facility in MEE mode requires the least average energy, followed by the SC synchrotron solution with a liquefier, while the most energy intensive solution is the SC one with c.c.

INTRODUCTION

Radiotherapy is a fundamental component of effective cancer treatment. Radiation therapy with protons and other ions, also called hadron therapy (HT), offers several advantages over the classical RT with X-rays. Nowadays, HT has reached the time of transitioning from a limited number of specialized institutions to many particle therapy centres worldwide. In 2018, the conceptual study of a new ion therapy and research facility in Southeast Europe was proposed [1]. It consists in an advanced version of the PIMMS design [2], accelerating beams of p (up to 250 MeV), $^{4}He^{2+}$, $^{12}C^{6+}$ and heavier nuclei (up to 430 MeV/u), with 20 times more beam current than present generation machines. It will work in MEE mode [3], with the possibility of a single-turn extraction (10^{10} ions in ~1 us) to perform FLASH therapy [4]. For the SEEIST facility, the gantry is assumed to be superconducting (SC) [5], while for the synchrotron both the room temperature (RT) and superconducting (SC) versions are studied. A SC synchrotron is certainly more compact than a RT one (see Fig. 1 and Table 1). This paper provides a first evaluation of the average power required by the whole SEEIIST facility, comparing the RT and SC synchrotron cases.

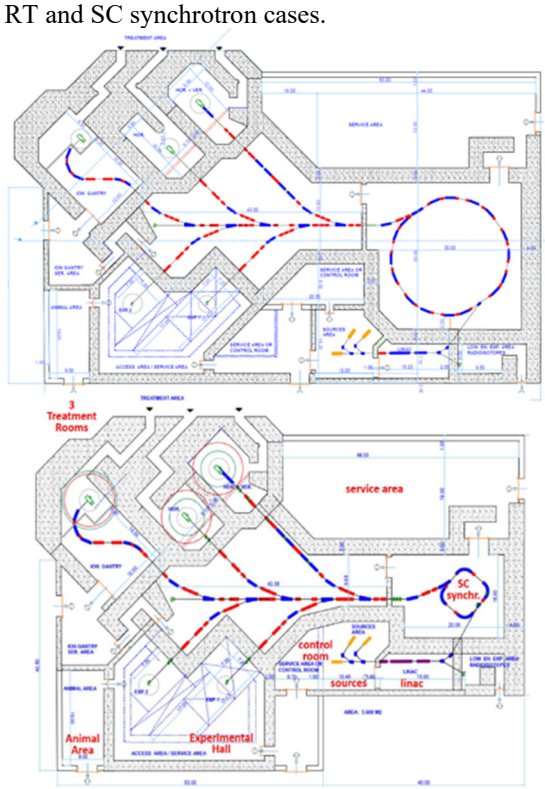

Figure 1: Layout of the SEEIST RT facility (16 dipole synchrotron, left) and the SC one (4 dipoles).

Table 1: Main Specifications of the RT and SC Synchrotrons (for $^{12}C^{6+}$)

	RT synchrotron	SC synchrotron
Energy	430 MeV/u	430 MeV/u
Circumference	70 m	27 m
$(B\rho)_{max}$	6.62 Tm	6.62 Tm
B_{max}	1.5 T	3.5 T
ρ	4.23 m	1.89 m
Ramp rate	2.4 T/s	1 T/s

ISBN: 978-3-95450-227-1 ISSN: 2673-5490 doi:10.18429/JACoW-IPAC2022-THPOMS050

DESIGN OF LINAC BASED NEUTRON SOURCE

N. Upadhyay, S. Chacko, University Department of Physics, Mumbai University, Mumbai, India
A. Deshpande, T. Dixit, R. Krishnan, Society for Applied Microwave Electronics Engineering and Research (SAMEER), Mumbai, India

Abstract

Neutron sources are of great utility for various applications, especially in the fields of nuclear medicine, nuclear energy and imaging. At SAMEER, we have designed a linear electron accelerator based neutron source via photo-neutron generation. The accelerator is a 15 MeV linac with both photon and electron mode and is capable of delivering high beam current to achieve beam power of 1 to 2 kW. Efforts are in place to achieve further higher beam powers. 15 MeV electrons are incident on a bremsstrahlung target followed by a secondary target to achieve neutrons. To further optimize and enhance the neutron yield, backing material is provided. In this paper, we present the simulation of (e, γ) and (γ, n) processes using the Monte Carlo code FLUKA. The optimization of Tungsten as the convertor target whereas of the Beryllium as the neutron target is discussed in detail. We have explored various backing materials in order to optimize the total neutron yield as well as the thermal neutron yield. The simulation results have been considered for the finalisation of all material parameters for the set-up of this neutron source activity.

INTRODUCTION

Neutrons have a wide range of applications, especially in the areas of imaging and medical isotope generation. Though reactors are the largely used method for neutron generation, using electron accelerators can be very efficient due to the low cost and compact size of the set-up. In this method, bremsstrahlung photons are generated when an electron beam irradiates a metal target. These photons then interact with a neutron source secondary target to generate neutrons via photo-nuclear reaction. The secondary target material has a threshold energy lower than that of the bremsstrahlung photons to produce neutrons [1].

At SAMEER, we have designed a linear electron accelerator based neutron source via photo-neutron generation. The accelerator is a 15 MeV linac with both photon and electron mode and is capable of delivering high beam current to achieve beam power of 1 to 2 kW.

To simulate the photo-nuclear interaction, we have used FLUKA which is a Monte Carlo code that can simulate transport and interaction of electromagnetic and hadronic particles in any target material over a wide energy range [2]. For imaging purposes, a high count of thermal neutrons is desired. So, we have studied the energy spectra of the photo-neutrons produced and based on that, we have explored various backing materials that can be used to further optimize the total neutron yield as well as thermal neutrons. Also, appropriate shielding has been applied to keep the doses within the radiation safety limits during operation.

ACCELERATOR AND TARGET DESIGN

The linac designed is a standing wave, side coupled structure operating at π/2 mode at 2998 MHz frequency [3]. The RF power comes from a Klystron with 6 μs pulse width operating at 0.1% duty cycle. Efforts are ongoing to enhance the duty cycle to 0.4%. When operating at maximum duty, the linac will be able to achieve a 15 MeV electron beam with an average current of about 350 μA at the exit [4]. The electron gun is a diode type gun with pulsed injection voltage of 20 kV. We have achieved high shunt impedance structure and demonstrated 15 MeV energy with 1 kW beam power. For the proposed neutron source, we are replacing the Klystron and modulator to achieve 0.004 duty cycle thus enhancing the beam power by a factor of four. The linac is already designed as per the high repetition rate operation and is thermally suitable to accept high average power from the source. The line type modulator developed in-house is being replaced by solid state modulator capable of high repetition rate with longer pulse width operation. The new RF system is under testing and once received we will initiate the beam trials. The linac is shown in Fig. 1 and the parameters are shown in Table 1.

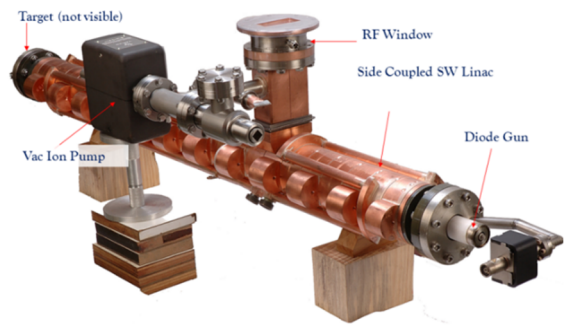

Figure 1: SAMEER made 15 MeV linac tube.

In a photo-neutron process, the neutrons are produced via (e, γ) and (γ, n) reaction. 15 MeV electrons are made incident on a bremsstrahlung target to produce photons which then interact with a suitable neutron target to generate neutrons through photo-nuclear reactions. The bremsstrahlung tungsten target is followed by a neutron source target along with a backing material which further optimizes the neutron yield. The backing material also

ISBN: 978-3-95450-227-1 ISSN: 2673-5490 doi:10.18429/JACoW-IPAC2022-THPOMS051

STUDY ON CONSTRUCTION OF AN ADDITIONAL BEAMLINE FOR A COMPACT NEUTRON SOURCE USING A 30 MeV PROTON CYCLOTRON

Y. Kuriyama*, M. Hino, Y. Iwashita, R. Nakamura, H. Tanaka
Institute for Integrated Radiation and Nuclear Science, Kyoto University, Kumatori, Japan

Abstract

The Institute for Integrated Radiation and Nuclear Science, Kyoto University (KURNS) has been actively using neutrons extracted from the research reactor (KUR) for collaborative research. Since the operation of KUR is scheduled to be terminated in 2026 according to the current reactor operation plan, the development of a general-purpose neutron source using the 30 MeV proton cyclotron (HM-30) installed at KURNS for Boron Neutron Capture Therapy (BNCT) research has been discussed as an alternative neutron source. In this presentation, we report on the conceptual design of an additional beamline for a compact neutron source using this cyclotron.

INTRODUCTION

At the Institute for Integrated Radiation and Nuclear Science, Kyoto University (KURNS), a medium-sized neutron source, neutrons extracted from a research reactor (KUR) with a maximum thermal power of 5 MW has been actively used for joint use. However, due to the deadline for the return of spent fuel, the KUR is not expected to continue operation after 2026, so there is an urgent need to construct a neutron source to replace the KUR.

Since 2007, Kyoto University has been developing a Boron Neutron Capture Therapy (BNCT) system using a proton cyclotron (HM-30), an average beam current of 1 mA and extraction beam energy of 30 MeV [1]. This system consists of HM-30 and a target station that moderates neutrons generated from Be targets to an energy suitable for BNCT [2, 3].

In 2019, HM-30 was transferred to Kyoto University, therefore, the consideration to use HM-30 as a proton accelerator for the KUR alternative neutron source had been started. Figure 1 shows KUR, Kyoto University Critical Assembly (KUCA), and Innovation Research Laboratory (Innovelab).

Figure 1: Appearance of KUR, KUCA and Innovelab in KURNS.

* kuriyama.yasutoshi.6n@kyoto-u.ac.jp

ACCELERATORS INSTALLED IN INNOVELAB AT KURNS

Innovelab at KURNS is equipped with four ring accelerators and one linear accelerator. Among these accelerators, the 150MeV FFAG main-ring (MR) and its injector [4], the 11MeV linear accelerator (linac) and HM-30 are currently in operation.

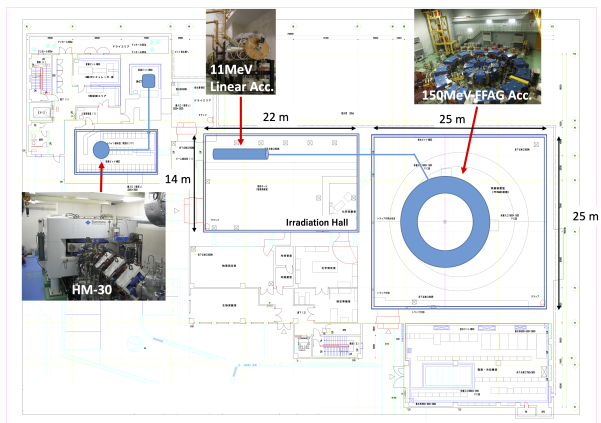

Figure 2: Layout of accelerators in Innovelab building at KURNS.

The Innovelab is divided into a medical building and an experimental building. HM-30 is located on the first floor of the medical building, and MR and linac are on the first floor of the experimental building. Figure 2 shows the layout of the accelerators in the Innovelab.

To make a room for a neutron generation target station in the irradiation hall (left-side of the experimental building), the linac has to move to the MR room (rigth side of the experimental building).

30MeV PROTON CYCLOTRON (HM-30) AT KURNS

30MeV proton cyclotron (HM-30), manufactured by Sumitomo Heavy Industories, had been installed for BNCT research in Innovbelab medical building in 2008. Figure 3 shows HM-30, and Table 1 shows the main specifications of the HM-30 [1].

For BNCT research, a 30 kW proton beam is extracted from the HM-30 and transported to the target station by 90-degree beam transport, as shown in Fig. 2.

ISBN: 978-3-95450-227-1 ISSN: 2673-5490 doi:10.18429/JACoW-IPAC2022-THPOMS052

MAGNETIC FIELD SHIELD FOR SC-CAVITY WITH THIN Nb SHEET

Y. Iwashita, Y. Kuriyama, KURNS, Kyoto University, Kumatori, Osaka, Japan
H. Tongu, ICR, Kyoto University, Uji, Kyoto, Japan
Y. Fuwa, JAEA/J-PARC, Tokai, Ibaraki, Japan

Abstract

While superconducting accelerating cavities can generate high electric fields with a small amount of high frequency power, they require a shield against faint environmental magnetic field. Because the material niobium is a type-II superconductor, it traps the environmental magnetic flux in the material during the superconducting transition, which results in loss during operation. This makes it essential to shield from faint magnetic field. However, high magnetic permeability magnetic materials for very low temperatures are expensive, not easy to handle, and increase costs. We are researching magnetic shields that utilize the diamagnetism of superconducting materials, rather than the magnetic flux absorption phenomenon caused by high magnetic permeability materials.

INTRODUCTION

Superconducting accelerating cavities have become popular because of their low RF power consumption. Almost all of these cavities are made of niobium, which is a type-II superconductor, and trap the environmental magnetic flux in the material during the superconducting transition. When the trapped flux is shaken by RF electromagnetic field on the inner wall of the cavity, it generates heat and increases power load on the cryogenic system. This effect becomes more pronounced as the Q value of the cavity increases. This makes it essential to shield from faint magnetic field. However, high magnetic permeability magnetic materials for very low temperatures are expensive, not easy to handle, and increase costs. Furthermore, their permeabilities decrease at very low temperature and also low magnetic field. On the other hand, superconductors have perfect diamagnetism and can be complementary to the high permeability materials. Among the easy-to-handle superconducting materials, niobium has the highest transition temperature of pure metals (see Table 1). The transition temperature of Pb is the second highest, but the availability of sufficiently high purity may not be clear, and Pb is a restricted material such as RoHS (Restriction of Hazardous Substances). On these circumstances, niobium is the first choice as a shielding material, except that it can trap flux.

Table1: Superconducting Transition Temperatures of Pure Metals

Material	In	Sn	Hg	Ta	V	La	Pb	Nb
Temperature [K]	3.4	3.7	4.2	4.5	5.3	5.9	7.2	9.2

In recent years, it has become clear that the expulsion of magnetic flux is induced by making a superconducting transition of the cavity under a temperature gradient [1-4]. If the shield can be cooled with a sufficient temperature gradient before the cavity reaches the transition temperature, it may function as a weak magnetic field shield that complements a normal shield [5]. Since the cavity wall is about 3 mm thick for mechanical strength, it has a larger heat capacity than a thin niobium sheet of about 0.5 mm, for example. Figure 1 shows the possible shapes of the cell's Nb sheet cover [7]. The full cell on the right is covered with a pillbox-shaped hollow shield, and the unshielded left half-cell is shown for comparison. The flux component normal to the wall Bnormal in the shielded cell is less except at the iris region, where the Bnormal has less effect.

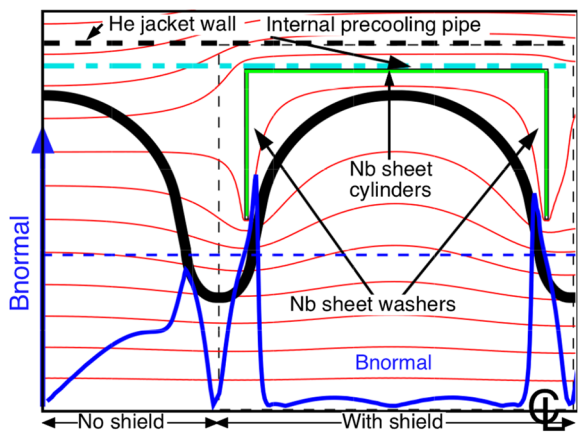

Figure 1: Possible geometry for the magnetic field shield with superconducting sheet.

This example of calculation includes one and a half cells with and without the shield cover, respectively. Since the effects from the adjacent cells would be small, both geometries are calculated in one calculation. A shield cover consists of one niobium sheet cylinder and two washers (thick green line). The leftmost half-cell does not have a shield. Black thick line shows the cavity wall, which has no effect on the magnetic field calculation. Red thin lines show calculated flux lines when immersed in a uniform magnetic field along the axis. The shielding effect is simulated by setting the permeability to 0.0001. The magnetic component normal to the cavity surface Bnormal is also plotted, which is a relative value to the immersed field. The thin broken line shows the immersed field level. The location of the He jacket wall is shown by the broken line and the possible location of the internal precooling pipe is shown by the chained line. The precooling pipe should contact all shield covers.

ISBN: 978-3-95450-227-1 ISSN: 2673-5490 doi:10.18429/JACoW-IPAC2022-THPOMS053

PROTON BEAM IRRADIATION SYSTEM FOR SPACE PART TEST*

H.-J. Kwon†, H.-S. Kim, J.-J. Dang, S. Lee, S.-P. Yoon,
W.-H. Jung, Y.-G. Song, K-R. Kim, K. Kim
Korea Multipurpose Accelerator Complex,
Korea Atomic Energy Research Institute, Gyeongju, South Korea

Abstract

A proton beam irradiation system for space part test has been developed at Korea Multipurpose Accelerator Complex (KOMAC) based on 100 MeV proton linac. It consists of a thermal vacuum chamber, a beam diagnostic system and a control system in the low flux beam target room. The thermal vacuum chamber accommodates the capacity for proton beam irradiation in addition to temperature control in vacuum condition. The beam diagnostic system is newly installed to measure the lower dose rate than existing one. In this paper, the proton beam irradiation system for space part test including a thermal vacuum chamber, newly installed beam diagnostic system is presented.

INTRODUCTION

In recent days, commercially available off the shelf (COTS) are tried to be used in many parts of the satellite in order to reduce cost [1]. The COTS which is going to be used as a space part should be confirmed its hardness to space radiation. Until now, many single event effect (SEE) tests have been done by using a 100-MeV proton accelerator at KOMAC. But most of them has been driven by a few major companies and there were no systematic test procedures for the beginners in this field. A program called "Development of Evaluation Technology for Space Parts" has started to develop the space irradiation environment, improve the test conditions and setup test procedures based on 100-MeV proton accelerator in 2021. In this paper, the low flux beam line is briefly introduced, design of the thermal vacuum chamber and beam diagnostic system for the space part test are discussed.

LOW FLUX BEAM LINE

The low flux beam line at KOMAC started its operation 2017. The specification of the low flux beam line is shown in Table 1. To reduce the beam intensity by more than three orders of magnitude, we installed a locally shielded collimator. Two octupole magnets were installed to provide a uniform beam with a uniformity better than 10 % in a 100 mm by 100 mm area at the sample position [2]. The low flux beam can be further collimated by using an in-air collimator to restrict the irradiation to a specific sample position. The target room of the low flux beam line is shown in Figure 1. The beam comes from the left side through the beam window. Beam shutter, beam current monitor and beam profile monitor are installed. The sample is installed at the right side. The reference dose rate monitoring system is also installed at the target position. Ion chamber is used as a reference dosimeter. The beam profile at the sample position is shown in Figure 2. We can reliably provide a proton beam with an intensity as low as 10^6 proton/cm^2/sec. Even a lower intensity was possible from the accelerator, precise dose monitoring was difficult up to now. But we apply another tool to decrease the possible intensity, which will be discussed in later section.

Table 1: Low Flux Beam Line Specification

Parameters	Values
Energy at target	20~100 MeV
Max. average power at collimator	800 W
Max. average beam power at target	1 W
Quality assurance beam size at target	100 mm × 100 mm
Beam uniformity at target	< 10 %

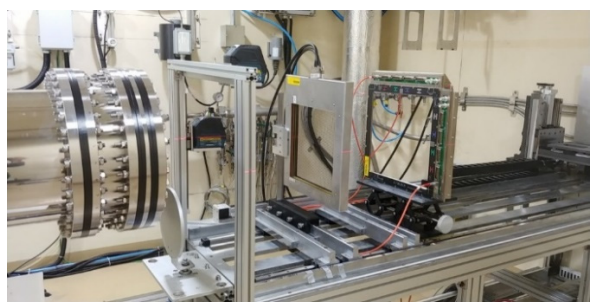

Figure 1: Low flux beam line target room. The proton beam comes from the left through the beam window. Beam shutter, beam current monitor, beam profile monitor are installed.

SPACE SIMULATION CHAMBER

Major difference between the common thermal vacuum chamber and the space simulation chamber is capability of high energy proton beam irradiation in the space simulation chamber case. Therefore, we should take the proton beam irradiation into consideration in designing the space simulation chamber [3, 4]. The basic requirements of the space simulation chamber are summarized in Table 2.

* Work supported by the Nuclear Research and Development Program (2021M2D1A1045615) through the National Research Foundation of Korea
† hjkwon@kaeri.re.kr

ISBN: 978-3-95450-227-1 ISSN: 2673-5490 doi:10.18429/JACoW-IPAC2022-THPOMS054

BEAM LINES AND STATIONS FOR APPLIED RESEARCH BASED ON ION BEAMS EXTRACTED FROM NUCLOTRON

G. Filatov, A. Slivin, A. Agapov, A. Baldin, A. Butenko, A. Galimov, S. Kolesnikov, K. Shipulin, E. Syresin†, G. Timoshenko, A. Tuzikov, A. Vorozhtsov, Joint Institute for Nuclear Research, Dubna, Russia
T. Kulevoy, Y. Titarenko, Institute for Theoretical and Experimental Physics of National Research Centre "Kurchatov Institute", Moscow, Russia
D. Bobrovskiy, A. Chumakov, Specialized Electronic Systems (SPELS) and National Research Nuclear University (NRNU) "MEPHI", Moscow, Russia
A. Kubankin, D. Firsov, Yu. Kubankin, Vacuum systems and technologies, Belgorod, Russia
P. Chernykh, S. Osipov, E. Serenkov, Ostec Enterprise Ltd, Moscow, Russia
I. Glebov, V. Luzanov, LLC "GIRO-PROM" (GIRO-PROM), Dubna, Russia
S. Antoine, W. Beeckman, X. Guy Duveau, J. Guerra-Phillips, P. Jehanno, SIGMAPHI S.A., Vannes, France

Abstract

New beamlines and irradiation stations of the Nuclotron-based Ion Collider fAcility (NICA) are currently under construction at JINR. These facilities for applied research will provide testing on capsulated microchips (ion energy range of 150-500 MeV/n) at the Irradiation Setup for Components of Radioelectronic Apparatus (ISCRA) and space radiobiological research (ion energy range 400-1100 MeV/n) at the Setup for Investigation of Medical Biological Objects (SIMBO). In this note, the technical details of the SIMBO and ISCRA stations and their beamlines are described and discussed.

INTRODUCTION

The NICA (Nuclotron-based Ion Collider fAcility) project is a new acceleration and storage complex that is currently under construction at JINR [1]. The project includes both fundamental and applied research.

Beams of ions from the Nuclotron accelerator will be used to simulate cosmic rays within applied research at NICA. The applied research assumes construction of new stations and beam lines to irradiate targets. These setups with special equipment help assess the risks of space radiation to human and equipment during space trips.

In this note SIMBO and ISCRA stations, their beamlines technical details are described and discussed [2-4].

PURPOSES

Safety space exploration requires studies of risks of cosmic radiation. Space equipment and biological samples can be irradiated by simulated cosmic rays on the Earth before a space mission. Existing and new setups in frame of the NICA applied research program will be used for these aims.

So, risks of cosmic radiation posed to space missions due to galactic cosmic rays can be simulated and studied on the Earth at NICA.

For these purposes ion beams extracted from the Nuclotron with varying species types and energies (Table 1) and equipment of SIMBO and ISCRA setups with different irradiation forming and measurement methods help to determine and measure radiation influence on the biological and electronics targets.

Table 1: Parametres of Ion Beams Extracted From the Nuclotron for SIMBO and ISCRA

Parameter	SIMBO	ISCRA
Ion type	$^{12}C^{6+}$, $^{40}Ar^{18+}$, $^{56}Fe^{26+}$, $^{84}Kr^{36+}$, $^{131}Xe^{54+}$, $^{197}Au^{79}$	
Ion energy, Mev/nucleon	400-1100	150-500
Extracted beam intensity, ion/spill	10^6-3×10^9	3×10^4-10^8
Beam emittances (95%), $\varepsilon_x/\varepsilon_y$, π·mm·mrad	3-10/8-15	5-17/13-25
Spill time, sec	2-20	

BEAM LINES

New beam lines will be constructed and integrated into the existing VP-1 transfer line, to transport the beams from Nuclotron to SIMBO and ISCRA stations. The SIMBO and ISCRA beam lines are 17 m and 22 m long respectively include two existing dipole magnets SP-94, which bend the ion beams to its station (Fig.1).

The scanning and non-scanning operating modes will be used to provide different beam spot sizes at the station targets. The SIMBO and ISCRA stations can operate in both modes. The parameters of the magnets and their positions in the transfer lines were defined by beam dynamics simulation using the MAD-X code [3, 5]. One of the main requirements at sample irradiation is the homogeneity of the beam distribution at the target area.

† esyresin@jinr.ru

ISBN: 978-3-95450-227-1 ISSN: 2673-5490 doi:10.18429/JACoW-IPAC2022-THPOMS055

COMMISSIONING OF THE SOCHI APPLIED STATION BEAM AND BEAM TRANSFER LINE AT THE NICA ACCELERATOR COMPLEX

A. Slivin, A. Agapov, A. Baldin, A. Butenko, D. Donets, G. Filatov, A. Galimov, K. Shipulin, E. Syresin†, A. Tikhomirov, A. Tuzikov, V. Tyulkin
Joint Institute of Nuclear Research, Dubna, Russia
T. Kulevoy, Y. Titarenko, National Research Centre Kurchatov Institute, Moscow, Russia
D. Bobrovskiy, A. Chumakov, S. Soloviev, Specialized Electronic Systems (SPELS) and National Research Nuclear University (NRNU) "MEPHI", Moscow, Russia
A. Kubankin, Belgorod State University, Belgorod, Russia
I. Glebov, V. Luzanov, LLC "GIRO-PROM" (GIRO-PROM), Dubna, Russia

Abstract

The SOCHI (Station of CHip Irradiation) station was constructed at the NICA accelerator complex for single event effect testing of decapsulated microchips with low-energy ion beams (3.2 MeV/n). The peculiarity of microchip radiation tests in SOCHI is connected with the pulse beam operation of the heavy ion linear accelerator (HILAc) and a restriction on the pulse dose on the target. The SOCHI station construction, the equipment and the results of the first beam runs are discussed.

INTRODUCTION

During the development of the space industry the electronics used in spacecraft is becoming more complex and small-sized. In order to ensure the long-term operation of spacecraft, there is an urgent need to test electronics for radiation hardness. One of the methods for predicting, evaluating and controlling the radiation hardness of microelectronic products to the effects of charged particles is based on conducting tests on ion accelerators. The SOCHI applied station (Fig. 1) was created as part of the NICA accelerator complex [1].

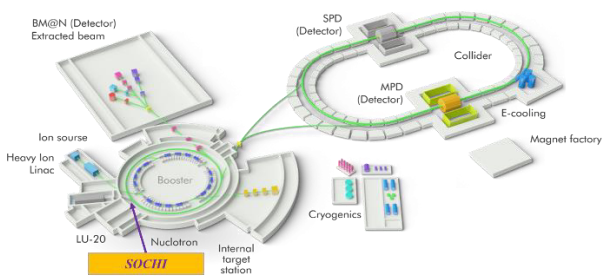

Figure 1: Area 1 infrastructure layout.

SOCHI BEAM TRANSFER LINE

The SOCHI beam transfer line is integrated into the existing HILAc-Booster beam line. The description of the SOCHI beam transfer line as well as its beam optics is given in [2].

The technical specification for the magnets is presented in Table 1.

Table 1: Technical Specification for the Magnets

Dipole magnet	
Type of power source	Pulse
Effective length, m	0.65
Max. magnetic field, T	1
Gap, mm	45
Quadrupole lenses	
Type of power sources	Pulse
Effective length, m	0.29
Max. gradient, T/m	10
Gap (diameter), mm	95

The integration of the SOCHI station at a pressure of 10^{-3} Pa into the HILAc-Booster channel at a pressure of 10^{-6} Pa requires the following vacuum equipment: cryogenic trap, pulsed diaphragm, and turbomolecular pumps. This equipment should prevent the ingress of heavy gases into the existing HILAc-Booster transfer line and in the Booster, where the pressure is 10^{-9} Pa. According to the results of the vacuum tests in November-December 2021, it was confirmed that the developed and manufactured vacuum system of the SOCHI station and beam transfer line meet these requirements. Figure 2 shows the signal of the Microvision 2 mass-spectrometric gas analyzer at measurements of the composition of the residual gas in the transfer line after its connection to the SOCHI station.

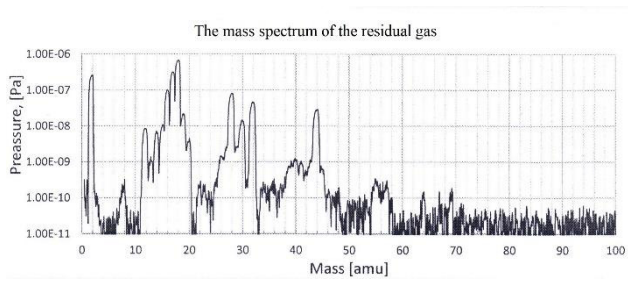

Figure 2: Total mass spectrum of residual gases at the end of the vacuum tests.

As shown in Fig. 2, the residual gas pressure (less than 10^{-6} Pa) behind the dipole magnet is lower than the pressure in the HILAc-Booster channel (10^{-6} Pa, before dipole magnet).

†esyresin@jinr.ru

ISBN: 978-3-95450-227-1 ISSN: 2673-5490 doi:10.18429/JACoW-IPAC2022-THPOMS056

AN OVERVIEW OF THE APPLICATIONS OF MIR AND THz SPECTROSCOPY IN ASTROCHEMISTRY STUDIES*

C. Suwannajak†[1], W. Jaikla[1], M. Jitvisate[5], U. Keyen[1], A. Leckngam[1], P. Nimmanpipug[3], S. Pakluea[2], T. Phimsen[4], S. Rimjaem[2,6], N. Tanakul[1], P. Wongkummoon[2],
[1]National Astronomical Research Institute of Thailand, Chiang Mai, Thailand
[2]Plasma and Beam Physics Research Facility, Department of Physics and Materials Science, Faculty of Science, Chiang Mai University, Chiang Mai, Thailand
[3]Department of Chemistry, Faculty of Science, Chiang Mai University, Chiang Mai, Thailand
[4]Synchrotron Light Research Institute, Nakhon Ratchasima, Thailand
[5]School of Physics, Suranaree University of Technology, Nakhon Ratchasima, Thailand
[6]also at Thailand Center of Excellence in Physics, Ministry of Higher Education, Science, Research and Innovation, Bangkok, Thailand

Abstract

Interstellar complex molecules can be found in molecular clouds throughout our galaxy. Some of these molecules are thought to be precursors of bio-molecules. Therefore, understanding the formation processes of those interstellar complex molecules is crucial to understanding the origin of the building blocks of life. There are currently more than a hundred known complex molecules discovered in interstellar clouds. However, the formation processes of those molecules are not yet well understood since they occur in very extreme conditions and very short time scale. Ultrafast spectroscopy can be applied to study those processes that occur in the time scales of femtoseconds or picoseconds. In this work, we present an overview of the applications of MIR and THz pump-probe experiments in astrochemistry studies. An experimental setup to simulate space conditions that mimic the environments where the interstellar complex molecules are formed is currently being developed at the PBP-CMU Electron Linac Laboratory. Then, we present our development plan of the experimental station and its current status.

INTRODUCTION

Stars, planets, and everything around us are all originated from the interstellar medium, which is the matter in the space between stars. The interstellar medium can be found in the form of molecular clouds, which contain simple molecules such as H_2 and CO in gas phase and micron-size solid dust grains. When those molecular clouds collapse due to their own gravity to form stars and planets, relatively more complex molecules can be formed. Certain species of the complex molecules are thought to be the precursors of bio-molecules such as sugars and amino acids. These molecules can be later transported to planets through asteroid and meteoroid bombardments during the process of planet formation and thus, provide the planets with the building blocks of life.

During the collapse of a molecular cloud, the density of the cloud increases. This allows gas molecules to stick onto a solid dust grain, forming ice layers, which further allow the formation of relatively more complex molecules to occur on the ice surface under extremely cold temperature. The process usually be referred to as grain surface chemistry. It is currently accepted that complex molecules found in interstellar clouds are formed through this process. In addition, the increased density of the cloud also shield the grains from external stellar radiation, preventing the newly formed molecules from being photo-dissociated. When the temperature of the cloud increase due to the newly formed star inside the cloud, the molecules can be desorbed into gas phase. This allow them to be observed from the earth through their rotational spectra.

Currently, there are more than a hundred known species of complex molecules identified in molecular clouds [1]. Organic molecules such as ribose and related sugars were also found in a meteorite [2]. However, the formation pathways of those molecules and the conditions that those complex molecules prefer are not yet well understood. Here we present the development of Thailand's first astrochemistry laboratory to study the processes of complex molecule formation under extreme interstellar conditions. The work includes the current progress, the development plan, and the experiments and applications.

DESIGN OF THE EXPERIMENTAL CHAMBER

With the goal to study the processes of complex molecule formation under interstellar cloud conditions, an experimental chamber needs to be constructed to simulate such extreme conditions. This includes an ultrahigh vacuum with pressure as low as 10^{-10} mbar and a temperature of about 77 K or below similar to those of the molecular clouds. In addition, a vacuum UV source is also needed to irradiate the sample inside the chamber to trigger chemical processes similar to the cosmic ray-induced UV inside the interstellar clouds [3].

Figure 1 shows the design of the experimental chamber and its side-view schematic. The chamber will be con-

* Work supported by The National Astronomical Research Institute of Thailand (NARIT) and the PBP-CMU Electron Linac Laboratory (PCELL)
† chutipong@narit.or.th

ISBN: 978-3-95450-227-1 ISSN: 2673-5490 doi:10.18429/JACoW-IPAC2022-THPOMS057

USING CO-MOVING COLLISIONS IN A GEAR-CHANGING SYSTEM TO MEASURE FUSION CROSS SECTIONS*

E. Nissen†, Thomas Jefferson National Accelerator Facility, Newport News, VA, USA

Abstract

In this work we look at a possible use for a system that collides beams moving in the same direction using a gear-changing synchronization method as a means of measuring low energy phenomena, such as fusion cross sections. Depending on the energies used this process will allow for interactions for any desired charge state of the target nuclei. Earlier concepts for low energy interactions to study focused on beams crossing at an angle to give the low energy interactions, as well as general investigations of comoving collisions. This proposal would use gear-changing, a method involving two different harmonic numbers of bunches in each collider ring, to have the same types of collisions, with a luminosity equal that of a head-on machine. In this work we detail the design considerations for such a machine, leveraging experimental experience with a co-moving, gear-changing system.

INTRODUCTION

This work will leverage research done on Gear-changing done using the low energy ion machine DESIREE (Double ElectroStatic Ion Ring ExpEriment) at Stockholm University [1-3]. This machine generally performs zero energy mergers of low energy ion beams to study neutralization reactions like those found in the interstellar medium. We were able to use it to demonstrate gear-changing, which is a collider synchronization system where each ring has a different harmonic number. In this case we've shown a 4 on 3 gear changing system where the 3 bunch system moves at 4/3 the velocity of the slow bunches. These collisions occur in a moving reference frame which opens up new possibilities for research.

Having the bunches collide in a moving reference frame leads to a large reduction in the center of mass energy when compared to a head on or fixed target collision. This provides an opportunity to perform low center of mass energy collisions, while preserving the control benefits of higher energy ion beams. An excellent use for these types of collisions would be studying nuclear fusion interactions [4].

The center of mass kinetic energy ranges involved in most fusion reactions are of the order of 100s of keV. One advantage that a comoving system would have is that it could study these interactions at different ionization states, which are generally not attainable using fixed target facilities. Such a system, if properly designed, can also perform research on the effects of spin polarization on these interactions. Finally, with the right reactants this could be used to create a "neutron accelerator" which could be used to create a high energy neutron beam.

In this work we will review some of the initial design considerations for such a machine, and apply them to two possible experimental machine designs. While gear-changing was the basis for this research there are situations where coasting beam systems might be more useful.

CENTER OF MASS ENERGY

The center of mass energy is actually easy to calculate, we can use the total center of mass energy from [5] with θ=π to calculate it, and simply subtract out the rest masses. The equation is:

$$E_{cm} = \sqrt{2E_1E_2 + ((m_1c^2)^2 + (m_2c^2)^2) + 2 * P_1P_2Cos(\theta)}$$

We can then determine the required energies for a given center of mass energy, and starting kinetic energy of one of the atoms. The plot would look like Fig. 1. For a given atom type there is an answer where the other beam is either faster or slower than the first beam. While they don't scale linearly, they do scale with the mass ratio of the two ion species. If we are looking at a system where gear-changing is necessary then we will also have to look at the relative velocities, an example of such is shown in Fig. 2.

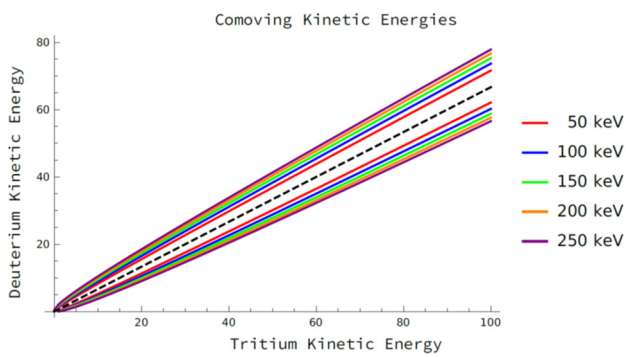

Figure 1: The kinetic energies of the Tritium and Deuterium beams for a variety of center of mass kinetic energies. Two possible energies for each center of mass energy will be given, one where the deuteron is faster, one where it's slower. The dashed line is the mass ratio.

*Authored by Jefferson Science Associates, LLC under U.S. DOE Contract No. DE-AC05-06OR23177. The U.S. Government retains a non-exclusive, paid-up, irrevocable, world-wide license to publish or reproduce this manuscript for U.S. Government purposes.
† nissen@jlab.org

ISBN: 978-3-95450-227-1 ISSN: 2673-5490 doi:10.18429/JACoW-IPAC2022-THPOMS060

DEVELOPMENT OF ANALYTICAL LIGHT SOURCE FOR CONSTRUCTION OF FEMTOSECOND PULSE RADIOLYSIS SYSTEM USING ER FIBER LASER

Y. Kaneko†, M. Sato, Y. Koshiba, M. Washio, WISE, Waseda University, Tokyo, Japan
K. Sakaue, UT-PSC, The University of Tokyo, Tokyo, Japan

Abstract

The initial processes in radiation chemistry occur from the ultrafast time scale (sub-femtosecond timescale) and are the dominant factor for the subsequent reaction. It is important to elucidate the initial process of the radiation chemical reaction. One of the methods to elucidate the initial process is pulse radiolysis. In pulse radiolysis, a substance is irradiated with ionizing radiation and at the same time irradiated with analytical light, and the absorption spectrum of the light is observed, which allows us to track the short-lived intermediate species. There are several requirements required for analytical light. We aimed to use the supercontinuum light generated by the second harmonic of the Er fiber laser as analytical light. In this conference, we report on the status of the development of this supercontinuum light and the prospects.

INTRODUCTION

Our research is aimed at elucidating the initial processes of radiation chemical reactions. Radiation chemical reactions are chemical reactions that occur due to the interaction between radiation and electrons in materials. To understand the whole picture of radiation chemical reactions, it is important to elucidate the interaction, i.e., the initial process. The interaction occurs in ultrafast time (sub-femtosecond timescale). Therefore, special techniques must be used to observe the interaction.

One of the methods for elucidating initial processes is pulse radiolysis. In pulse radiolysis, a material is irradiated with an electron beam and simultaneously allowed to pass through an analysing light to measure its absorbance, enabling temporal tracking of reaction intermediates that are formed and disappear in an ultrashort time range derived from bunch length of electron beam and pulse width of analyzing light. A conceptual diagram of pulse radiolysis is shown in Fig. 1.

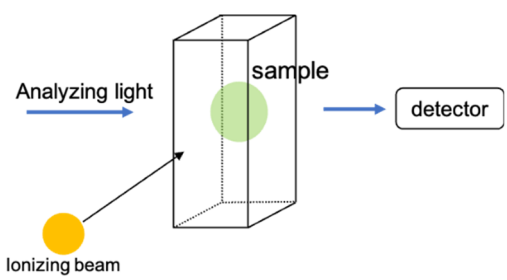

Figure 1: Diagram of pulse radiolysis.

† yutaka.lucky.k@ruri.waseda.jp

There are three major requirements for analytical light. Firstly, it must have ultrashort pulse width. This is because the initial processes of radiation chemical reactions occur in the ultrafast time range, and pulse radiolysis systems need to have the same high temporal resolution. Secondly, wavelength is broadband. If the wavelength is broadband, a single pulse radiolysis system can observe many substances that absorb in that wavelength band. Thirdly, the intensity is high. A certain level of intensity is necessary so that the spectra of absorption wavelengths are not buried in noise, making it difficult to observe the spectra of absorption wavelengths. We aimed to use a supercontinuum (SC) light as the analysis light that satisfies the above three conditions. Supercontinuum light is broadband light generated by nonlinear optical effects in a nonlinear medium, which maintains the properties of the ultrashort laser pulse. We have constructed an optical laser system to generate this SC light.

In a previous study, a supercontinuum light with a spectral width of 750-1030 nm had been successfully generated by injecting a Yb laser (wavelength: 1030 nm) into a photonic crystal fiber (PCF) [1]. Figure 2 shows a spectral diagram of the generated supercontinuum light [1].

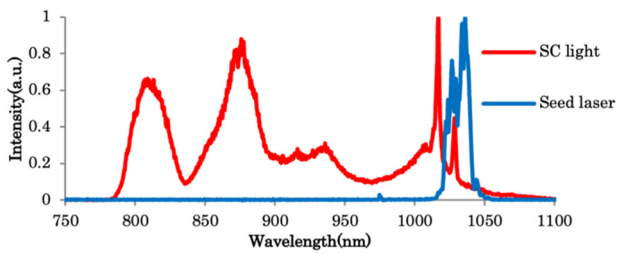

Figure 2: Spectral diagram of the generated supercontinuum light [1].

Figure 2 shows that the wavelength extends toward the short wavelength side with respect to the incident laser wavelength. On the other hand, active species observed in chemical radiation reactions seem to be absorbed in the visible wavelength region [2]. The SC light produced in previous studies does not cover this visible light region. Therefore, we have attempted to generate SC light that includes the visible light region by injecting the second harmonic (775 nm) of Erbium (Er) fiber laser (1550 nm) into a PCF, thinking that the wavelength of the laser injected into the PCF should be closer to the visible light region.

ISBN: 978-3-95450-227-1 ISSN: 2673-5490 doi:10.18429/JACoW-IPAC2022-FRIXGD1

STATUS AND PROSPECTS IN FAST BEAM-BASED FEEDBACKS

W. Höfle*
CERN, Geneva, Switzerland

Abstract

Fast beam-based Feedback systems play an important role in circular accelerators to mitigate instabilities and reduce the impact of injection oscillations and perturbations on beam quality, both in the longitudinal and transverse planes. The status and prospects of such beam-based feedback systems for circular accelerators are reviewed. This includes progress towards the fundamental limits in noise and feedback gain and the possibilities of modern digital systems to extract large amounts of data that can be used to characterise beam properties. The talk concentrates on machines with hadrons and gives an outlook on possible developments for future accelerator projects under study.

INTRODUCTION

Modern synchrotrons are designed to have a low machine impedance in order to increase the beam intensity threshold above which instabilities will occur. Despite these efforts in the design and due to the ever increasing desire for more beam current, accelerators are still suffering from instabilities both of coupled bunch type, and intra-bunch instabilities characterized by motion within the bunch. Transverse feedback systems have been used since the early days of accelerator design as a means of actively mitigating instabilities. These systems detect with beam position monitors any beam movement and feed back an amplified signal to a deflecting structure applying kicks with the correct phase and timing with respect to the circulating beam in order to counteract the motion. Feedback changes the dynamics of the motion and renders the beam stable [1].

RECAP OF TRANSVERSE FEEDBACK SYSTEMS IN OPERATION

The CERN hadron accelerator chain is an excellent example of the different challenges faced by transverse instabilities for which feedback systems are deployed for mitigation [2]. Table 1 shows some of the parameters of the feedback systems in the CERN Proton Booster Synchrotron (four rings), the CERN Proton Synchrotron (PS) and the Super Proton Synchrotron (SPS) [3, 4]. All these feedback systems underwent upgrades as part of the LHC Injector Upgrade project to increase the intensity delivered to the LHC and hence the luminosity of LHC itself. The last of these upgraded systems, the CERN PS transverse feedback was fully commissioned in 2021 and consisted both in an upgrade of the power system increasing the maximum kick strength as well as new digital signal processing as already deployed in the CERN SPS and PSB [5, 6]. The LHC transverse feedback system came into operation in 2010 [7] and beyond a feedback system, evolved into a versatile tool for diagnostics and beam manipulations [2].

Similar feedback systems are deployed in hadron accelerators worldwide, including ion synchrotrons currently under construction for the FAIR facility in Germany [8], NICA in Russia [9] and HIAF in China [10].

At CERN, after successfully completing the LHC transverse damper (ADT), and demonstrating its use during the entire cycle of LHC from injection through acceleration and with colliding beams during the LHC run 1 [2], research and development has shifted to explore

- possible upgrades to the LHC transverse damper in particular to further reduce the noise in the bunch position detection [11] and to fully exploit the breadth of data available from the feedback systems for characterisation of the beam [12–14]
- develop and test an intra-bunch feedback as part of a possible mitigation of electron-cloud and impedance driven high frequency instabilities leading to transverse motion within the bunches [15, 16]
- research on proposals for HL-Lumi LHC [17] and the future hadron collider (FCC-hh) at CERN [18].

FULL EXPLOITATION OF THE LHC ADT SYSTEM

From the originally envisaged possible upgrade paths for the LHC ADT system [3], increase in kick strength, increase in gain towards 20 MHz (half the bunch repetition frequency) and improved signal-to-noise ratio, all but the first were realised [11, 19]. An increase in kick strength was not necessary as the deployed strength permitted feedback operation, injection damping and beam excitation for measurement purposes beyond expectation [2]. Concerning the increase in gain towards full bunch-by-bunch operation, digital signal processing techniques were deployed during run 1 of LHC and fully used for run 2 for the nominal bunch spacing of 25 ns [19, 20]. The improvement of the signal-to-noise ratio of the beam detection has been achieved through

- increasing the number of pick-ups per beam and plane from two to four [3, 11]
- extensive research and development for the best RF receiver technique for the beam position detection [11]
- many small improvements to eliminate interference and adapt gains to the bunch intensity to optimally use the dynamic range available.

* Wolfgang.Hofle@cern.ch

ISBN: 978-3-95450-227-1 ISSN: 2673-5490 doi:10.18429/JACoW-IPAC2022-FROXGD1

A METHOD FOR OBTAINING 3D CHARGE DENSITY DISTRIBUTION OF A SELF-MODULATED PROTON BUNCH

T. Nechaeva*, P. Muggli, L. Verra[1,2], Max-Planck-Institute for Physics, Munich, Germany,
G. Zevi Della Porta, CERN, Geneva, Switzerland
(the AWAKE Collaboration)
[1] also at CERN, Geneva, Switzerland
[2] also at Technical University Munich, Munich, Germany

Abstract

The Advanced Wakefield Experiment (AWAKE) at CERN is the first plasma wakefield accelerator experiment to use a proton bunch as driver. The long bunch undergoes seeded self-modulation (SSM) in a 10 m-long plasma. SSM transforms the bunch into a train of short micro-bunches that resonantly drive high-amplitude wakefields. We use optical transition radiation (OTR) and a streak camera to obtain time-resolved images of the bunch transverse charge density distribution in a given plane. In this paper we present a method to obtain 3D images of the bunch by scanning the OTR across the entrance slit of the streak camera. Reconstruction of the 3D distribution is possible because with seeding self-modulation is reproducible. The 3D images allow for checking the axi-symmetry of SSM and for detecting the possible presence of the non-axi-symmetric hosing instability (HI).

INTRODUCTION

Plasma-based acceleration is a promising alternative to conventional one, as plasma can sustain accelerating fields several orders of magnitude higher than the RF cavities. Acceleration of electron bunches up to 8 GeV [1] and 42 GeV [2] has already been demonstrated in laser wakefield and beam-driven wakefield experiments, respectively.

The Advanced Wakefield Experiment (AWAKE) uses a long relativistic proton bunch as driver. This long bunch, propagating in plasma, undergoes self-modulation instability (SMI). SMI transforms the bunch into a train of short micro-bunches that drive high-amplitude wakefields. In order to control SMI we use a relativistic ionization front (RIF) or a short electron bunch preceeding the proton bunch that creates initial seed wakefields. When seeded, self-modulation (or SSM) yields reproducible outcome [3, 4].

Seeding of the self-modulation that is an axi-symmetric process with the electron bunch relies on the alignment of the electron and proton bunches with respect to each other. When misalignment is present, SSM is accompanied by the non-axi-symmetric hosing instability (HI). HI occurs in the plane of misalignment and, in case this plane is different from the main plane of observation, additional diagnostic is required in order to detect this instability.

In this paper we present a method that allows simultaneous observation of the proton bunch evolution in two perpendicular planes and, by extension, in any plane. We use a streak camera that yields time-resolved images of slices of the proton bunch charge density distribution [5, 6]. From the slices we obtain a 3D charge density distribution, which gives the possibility to detect whether HI is present in the plane perpendicular to the main plane of observation.

OPTICAL SETUP

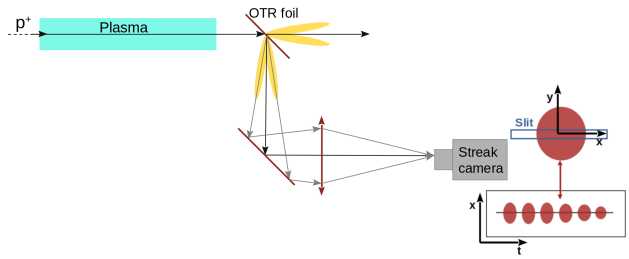

Figure 1: Simplified schematic of OTR transport line.

After exiting the Rubidium (Rb) vapor source, where plasma is created, the proton bunch propagates through a 280 μm-thick Silicon waver coated with 1 μm mirror-finished Aluminium foil, see Fig. 1 [6]. The emitted backwards optical transition radiation (OTR) contains information of the spatio-temporal proton bunch charge distribution. It is collected and guided in free-space using optical relay imaging to the streak camera room, where it is imaged onto the slit of the streak camera. The field of view of the imaging system is ~ ± 4 mm [7]. The streak camera yields light intensity distribution as a function of time and position.

The streak camera can operate with various slit widths and in different time windows. The choice of these parameters affects the temporal resolution of the resulting images. We measure the time resolution in two time windows, 73 ps and 210 ps respectively, and in the range of slit widths from 10 μm to 200 μm, using a 120 fs-short laser pulse. We define time resolution as the standard deviation in time of the intensity of the measured much shorter signal. The optimal resolution value is obtained with the slit width of 20 μm with minimum loss of signal, therefore this width is used in all the measurements. In the measurement presented below we use 1 ns time window in order to capture the full proton bunch charge density distribution. Corresponding time resolution value is ~ 4.79 ps.

The spatial resolution of the imaging system is measured using a 1951 USAF resolution target illuminated with the

* tatiana.nechaeva@cern.ch

ISBN: 978-3-95450-227-1 ISSN: 2673-5490 doi:10.18429/JACoW-IPAC2022-FROXGD3

INJECTION BEAM MEASUREMENT USING SYNCHROTRON RADIATION MONITOR AT THE SuperKEKB ELECTRON RING

H. Ikeda[1,2], G. Mitsuka[1,2], T. Mitsuhashi[1],
[1] High Energy Accelerator Research Organization (KEK), Tsukuba, Japan
[2] SOKENDAI, Tsukuba, Japan

Abstract

We upgraded the diamond mirror of the SuperKEKB electron ring to extract the good quality synchrotron light in 2020 summer. As a result, the accuracy of profile measurement for each bunch using a gate camera has improved dramatically, and it has become possible to measure the incident beam for each turn. The electron beam was injected with single turn injection mode to measure the properties of the beam and measured turn by turn after injection. In order to convert the measurement results into beam size, convolution by diffraction effect and absolute value calibration using real images were performed. We report the behaviour of the injection beam during normal operation of SuperKEKB.

INTRODUCTION

SuperKEKB is a collider with 7 GeV electron and 4 GeV positron. Aiming for the highest luminosity in world, we have adopted a nanobeam scheme and have just recorded a peak luminosity twice that of KEKB [1].

Beam size measurement is very important for collision tuning to improve luminosity. SuperKEKB mainly uses synchrotron radiation X-rays for beam size measurement and visible light for beam size measurement and other behaviour measurements.

One example is the turn-by-turn measurement of the injection beam [2, 3]. For stable beam operation, the stability of the beam injection from the injector linac is significant. When the injection efficiency becomes unstable, it becomes difficult to accumulate the beam and the background to the detector increases, which hinders physics experiments. Therefore, it is important to observe how the injection beam turn in the ring usually and prepare for the measurement of difference with worth efficiency injection beam.

SYNCHROTRON RADIATION MONITOR

The setup of SuperKEKB visible light monitor consist of extraction mirror, optical window, transfer mirrors and optical system. An extraction mirror of visible light is made of diamond. Since it is a high current machine from KEKB, it was a problem to suppress the thermal deformation of the extraction mirror for visible light. At the beginning of SuperKEKB, we have developed a single crystal diamond mirror and made efforts to suppress the current dependence of thermal deformation, but the mirror had not only the current dependence of the deformation at high currents, but also some deformations made during manufacturing [4]. Therefore, we made a new thick polycrystalline diamond mirror that is not easily deformed by heat and installed it in 2020 [5]. Resistance to thermal deformation is similar to single crystal. In addition, the reflectance is high because the coating is changed from gold to platinum. At the result, it became possible to obtain a sufficient amount of light for beam profile measurement for each bunch, and it became possible to measure the injection beam for each turn.

A diamond mirror is inserted into the antechamber type light extraction chamber as shown in Fig. 1 and pass into the optical window made of silica quartz on the opposite side of the chamber. Extraction chamber is set up to downstream 23 m of source bend magnet. At the downstream of the chamber, five mirrors are used to relay light to the above-ground SRM hat about 30 m downstream. An optical system for beam measurement, a gated camera, streak camera etc. are installed in the SRM hat on the ground. Figure 2 is an incident optical system for measuring an injection beam. Object system which designed for corona graph is used to measure the injection beam [6].

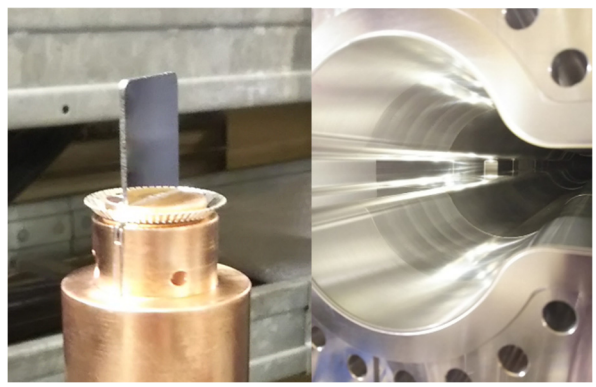

Figure 1: (Left) Diamond mirror mounted on the holder. (Right) Mirror inserted inside the chamber.

INJECTION BEAM MEASUREMENT

The standard injection beam measurement was performed with a single turn injection using stable injection parameters at electron ring. Each injection bunch kicks out the previous injected bunch. Then the ring always has only one bunch.

The gate width of the gated camera is one turn, in other words, 10μs. The trigger was applied at the injection timing, and after finding the first turn, the beam behaviour was observed turn by turn by shifting the timing. Figure 3 shows the examples of first turn to 10^{th} turn after injection. It can be seen that the beam just after the injection repeatedly oscillation. Since SuperKEKB operating tune is close to a half-integer, it can be seen that the bunch moves left and right at every turn. The beam size does not shrink monotonically, but shrinks while repeating oscillation.

ISBN: 978-3-95450-227-1 ISSN: 2673-5490 doi:10.18429/JACoW-IPAC2022-FRIXSP1

LOW-EMITTANCE COMPACT RF ELECTRON GUN WITH A GRIDDED THERMIONIC CATHODE

T. Asaka†, QST, Miyagi 980-8579, Japan

Abstract

A new type of rf electron gun has developed to generate a stable electron beam with a low-emittance of less than 2 mm mrad, that can be injected into Soft-x ray free electron laser (SX-FEL) and (Diffraction-limited storage ring) DLSR, without using a large ultraviolet laser system nor an ultra-high voltage pulsers. This electron gun consists of a 50 kV pulsed gun equipped with a commercially available thermionic cathode with grid and a 238-MHz acceleration cavity driven by a 42-kW solid-state amplifier. The system is simple, stable, robust, and easy-maintenance. To obtain a "grid-transparent" condition, the cathode voltage and the control grid voltage are optimized not to distort the electric field near the grid. To avoid the emittance growth due to the space charge effect, the gun and a special magnetic lens are embedded in the 238-MHz cavity at the shortest distance, and the beam energy is immediately accelerated to 500 keV. The first model of this electron gun has been operated as the 1 GeV injector of the NewSUBARU storage ring. The same electron gun will also be used in the injector linac of the 3 GeV light source under construction in Japan. This paper presents an overview of the rf electron gun system and our proof-of-performance experimental results.

INTRODUCTION

Gridded thermionic guns are used as electron sources for accelerator facilities because of their reliability, easy maintainability and long lifetime. Commercially available thermionic cathodes with a radius of 4 mm have a normalized emittance of larger than 10 mm mrad [1-4], but x-ray and soft x-ray free electron laser (XFEL and SXFEL) requires an order-of-magnitude smaller emittance of less than 2 mm mrad. The low-emittance electron sources developed for XFELs fall into two principal categories: photocathode radio-frequency (rf) guns [5, 6] and high voltage thermionic guns [7]. The photocathode rf guns have been used in many facilities as they provide a smaller and homogeneous emittance and have a more compact size. The photocathode however requires a complex drive laser system at ultraviolet wavelength, which demands laser specialists to maintain stable and reliable operations of the rf guns. The high voltage thermionic gun is nearly maintenance free, but it requires a high voltage pulse modulator to generate a microsecond 500 keV beam. In addition, an electromagnetic chopper system needs to be installed downstream of the gun not only to cut a short pulse of 1ns from the microsecond beam, but also to preserve the low electron beam emittance [8].

As a third type of low-emittance electron gun, we developed an rf gun using a gridded cathode, which provides a sufficiently small beam emittance with pulse length shorter than 0.7 ns and offers the prime advantage of the thermionic gun while not requiring the complex high voltage pulse modulator and chopper systems [9]. Our system features a 50-kV thermionic gun connected to a 238-MHz rf cavity in order to immediately increase the beam energy to 500 keV or even higher. This system uses a commercially available gridded cathode that provides an electron pulse shorter than 1ns, which assures high capture efficiency for the subsequent rf acceleration cavity. The electron bunch from the present electron source will be compressed by velocity bunching system consisting of 476-MHz and S-band rf cavities and two magnetic bunch compressors, similarly to SACLA [8]. The bunched beam will be accelerated to 3 GeV by a C-band acceleration system. Our simulation study shows generation of 3 GeV electron beam with peak current greater than 2 kA and a normalized slice emittance below 2 mm mrad is feasible with our 3 GeV linear accelerator system design.

An initial concern about our schema was how to suppress the emittance growth that resulted from the distorted electric potential (lens effect) near the grid mesh next to cathode. The lens effect originates from a mismatch between grid and gun high voltages, which forms the unnecessary electric field to transversally kick the electrons passing the grid. The lens effect is considered to be controllable by adjusting the grid voltage to compensate the distortion of the electric potential given by a gun high voltage of 50 kV [10]. To confirm this approach, we used computer simulations to determine the optimum conditions for making the grid transparent for the extracted beam in terms of the achieving a small emittance value. Based on the simulation results, we designed an electron gun system with a gridded thermionic cathode and built a gun test stand to verify the beam performance.

LOW EMITTANCE BEAM GENERATION IN ELECTRON GUN

The electron gun system comprises a 50-kV electron gun with a gridded thermionic cathode, magnetic lens, a 238-MHz rf cavity, and a beam collimator. The gun generates low-energy, short-pulsed, and homogeneous cylindrical electron beams with an initial normalized emittance of about 1 mm mrad with optimum grid voltage. Then, an axially symmetric magnetic lens focuses the beam so as not to spread it widely over the minimized distance to the downstream rf cavity. The 238-MHz rf cavity immediately accelerates the extracted beam to 500 keV to suppress emittance growth. The collimator just after the cavity adjusts the beam charge depending on the purpose of injecting electron beams into a storage ring or driving FELs.

† asaka.takao@qst.go.jp

ISBN: 978-3-95450-227-1 ISSN: 2673-5490 doi:10.18429/JACoW-IPAC2022-FROXSP1

20-YEAR COLLABORATION ON SYNCHROTRON RF BETWEEN CERN AND J-PARC

C. Ohmori*, K. Hasegawa, Y. Morita, H. Okita, M. Shirakata, Y. Sugiyama, F. Tamura, M. Yoshii, J-PARC, Tokai, Ibaraki, Japan
M. Paoluzzi, M. Brugger, M. Brucoli, H. Damerau, S. Danzeca, C. Rossi
CERN, Geneva, Switzerland

Abstract

In 2002, KEK/J-PARC and CERN started the collaboration on the RF systems of Low Energy Ion Ring to use magnetic alloy loaded cavities for heavy ion collision program at LHC. It was an exchange of our expertise on the wideband cavities and high-power solid-state amplifiers. This paper summarizes the 20-year collaboration which includes many synchrotrons at both facilities: J-PARC rapid cycling synchrotron (RCS) and main ring (MR), CERN Proton Synchrotron, PS Booster, Antiproton Decelerator, Extra Low Energy Antiproton ring, and MedAustron. With the improvements of cavity core by the magnetic annealing, field gradient and compactness of cavity were improved to fulfill the needs of the LHC Injector Upgrade (LIU) program. Radiation-hard and compact high-power solid-state amplifiers were also developed for LIU and future accelerator improvements.

INTRODUCTION

In a synchrotron, particles circulate on the fixed orbit. Therefore, the magnetic field of bending, quadrupole and other magnets are ramped according to the variation of particle momentum. The variation in particle velocity is significant in hadron and proton synchrotrons, although it remains negligible in electron synchrotron. On the resonant-type cavity technology for hadron beam acceleration, it has been an issue how we change the resonant frequency of the RF cavity. When synchrotrons were invented as a weak-focusing machine in the 1950s, a large amounts of ferrite rods and blocks were used for the cavity [1]. To change the permeability of the ferrite material, a large biasing current was applied on so-called Figure-of-Eight loop which surrounded ferrite materials. In strong focusing machines invented in the late 1950s, the ferrite rings became much smaller than the ferrite bricks of weak focusing machines [2, 3]. The ferrite cavity technology made the energy of these synchrotrons higher. However, the tuning circuit was still inevitable. A large frequency swing was an issue on this scheme to apply for heavy-ion synchrotron because it required a large variation of permeability. In the 1980s, a new approach to extend the frequency bandwidth of RF cavity was tried in Saclay, France. A magnetic alloy, amorphous, material was used as a cavity core instead of ferrite [4]. However, the tuning circuit was still applied to change the resonant frequency because of the large frequency swing.

In the mid-1990s, an iron-based nano-crystalline material, Finemet® [5], was tested as the cavity material in Japan [6]. The material exhibited three significant characteristics: thermal stability, stable shunt impedance on high voltage and a very large permeability [7]. The saturation magnetic flux density B_s of Finemet® (~1.2 T) was higher than that of ferrite (~0.3 T). Therefore, the material has stable shunt impedance to use for ordinary accelerators. Our measurement shows it is stable up to 200 mT as a RF flux density. This was an important feature for a high intensity proton machine. The cavity exhibited wideband characteristics, indicating that cavity tuning circuit was not needed.

In the late 1990s, the first beam test was carried out at HIMAC in National Institutes for Quantum Science and Technology, Japan [8]. It was the first demonstration to show that ion beam acceleration was possible by a compact RF cavity without tuning. This is because magnetic alloys including nano-crystalline and amorphous materials have much higher permeability than ferrites. As a result, $\omega L \sim R$, and $Q \sim 1$, assuming the magnetic alloy cavity system as a paralell LCR circuit. In case of ferrite cavity system, $\omega L < R$, and typically $Q \sim 100$. The ferrite cavity system, therefore, exhibits narrowband characteristics and needs a tuning circuit to sweep the resonant frequency for acceleration. In many proton-ion medical synchrotrons, the cavity system based on the magnetic alloys is adopted because of its simple structure without a tuning circuit and easier beam acceleration [9, 10].

At J-PARC, the cavity bandwidth was controlled. A cut-core technique was used to obtain narrow-band cavity for MR [11]. For RCS, Alexander Schnase used an external inductor to adjust bandwidth for beam acceleration and the 2nd harmonics [12]. Using these technologies, J-PARC succeeded in accelerate the beam at the RCS in 2005 and at the MR in 2006. And, the beam intensity of the RCS reaches 1 MW, which is the design value and the MR delivers 515 kW for T2K long-baseline neutrino experiments.

LOW ENERGY ION RING (LEIR)

Our collaboration between CERN and KEK began in March 2002 to develop the LEIR wideband cavities and high-power solid-state amplifiers of J-PARC. The LEIR is a Pb-ion accelerator converted from the Low Energy Antiproton Ring (LEAR) [13, 14]. It is the first ring in the ion-beam injection chain for Pb-ion collision in the LHC. An RF system was required to accelerate Pb-ion beam by a single cavity. Another RF system was installed as a backup. They

* chihiro.ohmori@kek.jp

ISBN: 978-3-95450-227-1 ISSN: 2673-5490 doi:10.18429/JACoW-IPAC2022-FROXSP2

DEMONSTRATION OF GRADIENT ABOVE 300 MV/m IN SHORT PULSE REGIME USING AN X-BAND SINGLE-CELL STRUCTURE

J. Shao[1,*], X. Lin[2], M. Peng[1,2], H. Chen[2], S. Doran[1], G. Ha[1], C. Jing[1,†], W. Liu[1], J. Power[1], J. Shi[2,‡], C. Whiteford[1], E. Wisniewski[1], H. Zha[2]
[1]Argonne National Laboratory, Lemont, IL, USA
[2]Tsinghua University, Beijing, China

Abstract

High gradient acceleration is one of the critical technologies required by future linear colliders, free-electron lasers, and compact linac-based applications. Among decade-long effort to break state-of-the-art gradient limitation of ~100 MV/m in normal conducting structures, using RF pulses shorter than 20 ns is a promising approach based on theoretic analysis and experimental observation. In this study, we demonstrated high gradient above 300 MV/m using an X-band 11.7 GHz single-cell travelling-wave structure with 6 ns FWHM RF pulses generated by a power extractor. In comparison, a scaled 11.424 GHz structure only reached below 150 MV/m driven by 30-100 ns RF pulses from a klystron with pulse compression. The experimental results and the suggested new mechanism of beam acceleration in the Breakdown Insensitive Acceleration Regime (BIAR) are presented in this manuscript.

INTRODUCTION

Gradient is a key figure of merit of linear accelerators to increase energy gain while maintaining facility footprint. Over the past decades, worldwide effort has been devoted to X-band normal-conducting accelerating structures driven by the challenging requirements of TeV-scale linear colliders. To date, ~120 MV/m and ~150 MV/m accelerating gradient have been respectively achieved in multi-cell and single-cell structures owing to continuous improvements of geometry optimization, high precision machining, high quality surface preparation, and understanding of RF breakdown. However, further breakthrough of gradient may rely on advanced acceleration concepts.

Acceleration using RF pulses shorter than 20 ns is a promising approach as predicted by the empirical scaling law of breakdown rate (BDR) [1] as well as proved in recent experiments by two-beam acceleration [2] and collinear wakefield acceleration [3]. In this study, we directly demonstrate the effectiveness of this approach where at least two-fold improvement of gradient has been obtained by shortening the RF pulses from 30-100 ns to 6 ns. Encouraged by the results, we propose the BIAR scheme in which the transmitted RF pulse and the accelerated beam remain intact even when RF breakdown occurs.

* Now at Institute of Advanced Facilities, Shenzhen, China
† jingchg@anl.gov
‡ shij@tsinghua.edu.cn

STRUCTURE DESIGN

The X-band metallic disk-loaded single-cell travelling-wave accelerating structure (Fig. 1(a)) has been optimized for high transient gradient with 6 ns FWHM RF pulses (3 ns rising time, 3 ns flat-top, and 3 ns falling time) generated by power extractors available at Argonne Wakefiele Accelerator facility (AWA) [2, 4–6]. The transient gradient is defined as the one seen by an ultra-relativistic witness beam,

$$G(t_0) = \frac{\int_{l_1}^{l_2} E(z,t)dt}{l_2 - l_1}|_{t=t_0+z/c} \quad (1)$$

where E is the on-axis field, t_0 is the injection moment of the witness beam, and $l_{1,2}$ are the longitudinal boundaries.

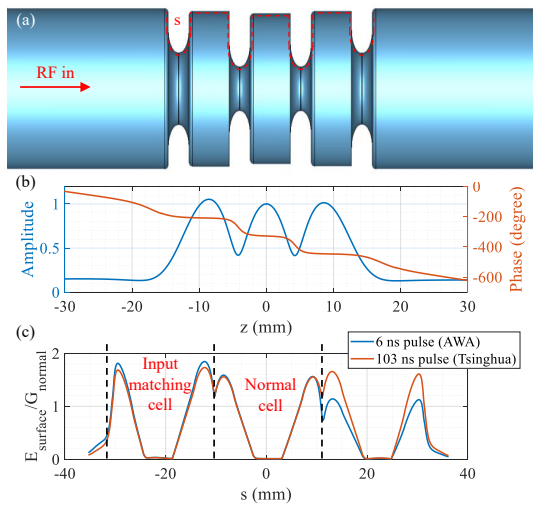

Figure 1: The X-band single-cell travelling-wave structure (a), the on-axis field (b), and the surface field along the contour (c).

The optimized structure consists of a normal cell and two matching cells designed by Kroll's method [7]. The resultant on-axis and surface field of the input matching cell are slightly higher than the normal one, therefore making it more vulnerable to RF breakdown, as illustrated in Fig. 1(b-c).

The simulated transient accelerating gradient is illustrated in Fig. 2. Using 6 ns FWHM RF pulses, the maximum transient accelerating gradient of the normal cell (denoted as $G_{normal,short}$) and the input matching cell (denoted as $G_{matching,short}$) reaches 80% and 92% of the theoretical steady value calculated from RF properties of the normal cell

ISBN: 978-3-95450-227-1 ISSN: 2673-5490 doi:10.18429/JACoW-IPAC2022-FROXSP3

FIRST OPERATION OF A KLYSTRON FITTED WITH A SUPERCONDUCTING MgB_2 SOLENOID

N. Catalan-Lasheras, M. Boronat, G. McMonagle, I. Syratchev, CERN, Geneva, Switzerland
A. Baig, A. Castilla-Loeza, Cockcroft Institute, Lancaster, UK
T. Kimura, P. Kolda, Communication & Power Industries, Palo Alto, California, USA
S. Michizono, A. Yamamoto, KEK, Ibaraki, Japan

Abstract

As part of the effort to reduce the energy consumption of large research facilities using accelerators, high efficiency klystrons are being developed by CERN. However, a large fraction of the wall-plug power required to operate these klystrons is used in the focusing magnetic elements around the klystron in the form of normal conducting solenoids. In 2019, a prototype solenoid made of MgB_2 was manufactured as a joint venture from CERN, Hitachi and KEK with the aim of reducing the power consumption by a factor ten using higher temperature superconductors. The characteristics of the magnet were measured upon manufacture and checked after the transport across the world. In 2020, the MgB_2 magnet was integrated around one of the klystrons in the X-band facility at CERN and put into operation in the beginning of 2021. We present in this paper the final performance of the klystron when fitted with the new superconducting (SC) solenoid and compare it with the standard normal conducting solenoid system.

INTRODUCTION

Originally motivated by the possibility to power the CLIC low energy stage using klystrons as RF power source, CERN led a strong initiative to improve the efficiency of the existing commercial tubes from 40% to about 65% [1]. This gain in efficiency could save 10.6 kW average power in a single klystron operated at 50 MW peak power, 2.2 µsec pulse length, and 100 Hz repetition rate. In a facility that comprise about 5500 klystrons, this corresponds to a saving in average power of 58.3 MW.

With the same motivation in mind, we turned our attention to the solenoid electromagnet required to focus and confine the electrons in the klystron RF channel. For the same pulsed 50 MW klystron, the electromagnet uses about 20 kW wall plug power which represents about 30% of the overall wall-plug power consumption of each klystron-modulator system. A collaboration between CERN, KEK, and Hitachi [2] was established to build a prototype solenoid based on MgB_2 superconductor designed to fit the X-band, 50 MW pulsed klystron manufactured by Communication & Power Industries (CPI) currently in use in the X-band facility at CERN [3]. The final solenoid was built and tested at the manufacturer premises [4, 5] demonstrating that it could be operated in very stable conditions and with a total plug-power of <3 kW for cryo-cooler operation, significantly below the conventional magnet. The main characteristics of the magnet are shown in Table 1.

After the delivery to CERN, the magnet was cooled down and subjected to magnetic measurements to confirm the integrity of the magnet. Magnetic measurements were also done in the conventional magnet to establish the reference field necessary for the klystron. After installation in the test facility and in coordination with the klystron manufacturer, we adjusted the magnetic circuit to recover the original performance at the factory.

Table 1: Main Parameters of the Super-Conducting Solenoid Prototype

Parameter	Specification	
SC material	MgB_2	
Nominal Field	0.8	T
Coil maximum field	1.06	T
Nominal current	57.1	A
Coil inner diameter	337	mm
Coil outer diameter	379	mm
Inductance	7.23	H
Operating temperature	< 20	K
Load factor (@20K)	45	%
Power (for cryo-cooler	< 3	kW
Total weight	600	kg

INTEGRATION

The new solenoid was built to be installed around the VKX-8311A klystron manufactured by CPI and operated at two of the CERN X-band test benches. The inner and outer diameter, and the length match the electromagnet shipped originally with the klystron.

The two MgB_2 coils forming the solenoid can be unbalanced with an additional power supply to shape the magnetic field. They are housed in a vacuum volume and cooled by conduction below 20 K. The cryostat partly made of iron doubles also as return yoke for the magnetic field. A large volume on the side of the magnet houses the current leads, a cold head, vacuum feeds, and the feedthroughs for instrumentation. The cold head connects a Cu thermal link to a 3 kW commercial cryocooler compressor. The solenoid (green) and the 50 MW klystron (yellow), installed on the modulator of the X-band test facility at CERN, are shown in Fig. 1. Special care needed to be taken during transport and installation due to the unbalanced weight of the group.

Unlike a traditional solenoid, the SC magnet requires a vacuum system and an ion pump (red in the picture) capable of maintaining a good insulating vacuum. It does not require however a cooling water system whose interlock needs to be strapped in the modulator side.

ISBN: 978-3-95450-227-1 ISSN: 2673-5490 doi:10.18429/JACoW-IPAC2022-FRPLYGD1

TOWARDS EFFICIENT PARTICLE ACCELERATORS - A REVIEW*

M. Seidel†, Paul Scherrer Institut, 5232 Villigen PSI, Switzerland
and École Polytechnique Fédéderale Lausanne, Switzerland

Abstract

Sustainability has become an important aspect of all human activities, and also for accelerator driven research infrastructures. For new facilities it is mandatory to optimize power consumption and overall sustainability. This presentation will give an overview of the power efficiency of accelerator concepts and relevant technologies. Conceptual aspects will be discussed for proton driver accelerators, light sources and particle colliders. Several accelerator technologies are particularly relevant for power efficiency. These are utilized across the various facility concepts and include superconducting RF and cryogenic systems, RF sources, energy efficient magnets, conventional cooling and heat recovery. Power efficiency has been a topic in the European programs EUCARD-2, ARIES and the ongoing I.FAST project and the documentation of these programs is a related source of information.

INTRODUCTION

The environmental sustainability of research infrastructures (RI) has many aspects and includes not only energy consumption, but also issues such as water and helium consumption or the use of critical materials and life cycle management of components. For many accelerator-driven facilities, energy consumption and efficiency are the most important topics. In this paper the important aspects and power drivers will be reviewed for the classes of proton driver accelerators, lights sources and particle colliders. Technologies that are relevant for efficiency, for example RF power sources or superconducting (s.c.) resonators, are discussed where appropriate.

First of all we note that the purpose of all accelerator driven RIs is to produce secondary radiation for research. This can be tailored photon radiation in light sources or FELs, it can be neutrons and muons, or even exotic particles generated in the collisions of particle colliders. The power flow in all facilities can be divided in two main conversion processes. The first one uses grid power and converts it to the power of a primary beam, of course with properties that are dictated by the specific application. In a second step the primary beam power is converted into the desired secondary radiation. For certain facilities, including neutron-, muon-, neutrino-sources or lepton colliders, the performance is rather directly coupled to the beam power via the conversion chain. In these cases it is important to maximize the grid-to-beam conversion efficiency. For other facilities like hadron collider rings with superconducting magnets or pulsed free electron lasers with low beam power, the grid consumption depends less on the beam power and may be dominated by auxiliary systems. For all types of facilities it is often possible to improve the performance per grid power significantly by implementing an optimized scheme for generating the secondary radiation. This can be a low beta insertion for colliders, a low emittance lattice for light sources, a seeding scheme for an FEL or advanced target and moderator assemblies for neutron sources. A generic power flow for accelerator facilities is shown in Fig. 1.

PROTON DRIVER ACCELERATORS

Proton drivers are utilized for neutron, muon or neutrino sources for condensed matter research or particle physics. Often high beam intensity is needed and the conversion efficiency from grid to beam power is an important parameter. Today three megawatt-class proton driver accelerators operate worldwide which utilize different accelerator concepts: the J-PARC facility with a rapid cycling synchrotron, the superconducting linear accelerator of the spallation neutron source SNS and the PSI cyclotron based HIPA accelerator. In 2016 efficiency aspects of these facilities were discussed at a workshop [1] and a summary has been published at IPAC'17 [2]. The choice of concept depends primarily on the application. Here the perspective for high CW beam intensity operation of s.c. linacs will be discussed to show the potential of this technology. S.c. resonators operate with small losses, characterised by high quality factors Q_0. The dissipated power P_{dissip} in the cavity and the power transferred to the beam ΔP_{beam} are calculated using:

$$P_{\mathrm{dissip}} = \frac{U_a^2}{\left(\frac{R}{Q}\right) Q_0}, \; \Delta P_{\mathrm{beam}} = U_a I_b. \qquad (1)$$

Here U_a is the cavity voltage, I_b the beam current and Q_0 the quality factor of the cavity. As an example, typical values for the high energy section of the planned PIP-II linac [3] are given in Table 1. Compared to normal conducting structures, the dissipated power is small, in fact three orders of magnitude lower than the power transferred to the beam. This fact supports the notion of s.c. technology being efficient. However, these few watts of heat are deposited at cryogenic temperatures and the cooling is quite inefficient at 1.8 K. As s.c. technology is increasingly used for magnets and resonators, it is worth to address cooling efficiency here.

Table 1: Parameters of HB650 s.c. Cavities for PIP-II

U_a	(R/Q)	Q_0	I_b	P_{dissip}	P_{beam}
20 MV	609 Ω	$2 \cdot 10^{10}$	2 mA	33 W	40 kW

* Work supported by the European Union's Horizon 2020 Research and Innovation programme under GA No 101004730.
† mike.seidel@psi.ch

ISBN: 978-3-95450-227-1 ISSN: 2673-5490 doi:10.18429/JACoW-IPAC2022-FRPLYGD2

ACCESS TO EFFECTIVE CANCER CARE IN LOW-MIDDLE INCOME COUNTRIES REQUIRES SOPHISTICATED LINEAR ACCELERATOR BASED RADIOTHERAPY

M. Dosanjh, CERN, Geneva, Switzerland
also at John Adams Institute, University of Oxford, U.K.
International Cancer Expert Corps, Washington DC, USA

Abstract

There are substantial and growing gaps in cancer care for millions of people in Low- Middle- Income countries (LMICs) and for geographically remote settings in High-income countries (HICs), often indigenous populations. Assessing the cancer care shortfall led to understanding the essential gap, that of a radiation therapy machine that can reliably and effectively provide the appropriate first-rate cancer treatments within the challenging environments.

More than 10,000 electron linear accelerators (linacs) are currently used worldwide to treat patients. However only 10% of patients in low-income and 40% in middle-income countries who need radiotherapy have access to it.

The idea to address the need for a novel medical linac for challenging environments has led to the creation of the STELLA project (Smart Technology to Extend Lives with Linear Accelerators) project. STELLA is multidisciplinary international collaborative effort to design and develop an affordable and robust yet technically sophisticated linear accelerator-based radiation therapy treatment (RTT) in LMICs. Here we describe Project STELLA.

INTRODUCTION

The incidence and number of deaths from cancer has been rising for many years in Low-Middle Income Countries (LMICs) [1] as has the gap in available cancer care. Despite a 2011 declaration by the UN General Assembly regarding the importance of addressing the non-communicable diseases (NCDs) as well as the infectious diseases - which are the primary focus of global health - investment in cancer care remains minimal.

There has been a surge in interest addressing the gap in radiation therapy punctuated in 2015 by Atun et al in the report of the Global Task Force for Radiotherapy for Cancer Control (GTFRCC) supported by the Lancet Oncology Commission [2]. Through modelling, this report demonstrated how radiation therapy is not only cost effective but also positive for the economy. A growing interest in global health projects by radiation oncology trainees in the US and Europe raised the exposure of the chronic shortage. Yet, the gap in the number of radiation therapy (RT) machines needed, estimated to be approximately 5,000 by the GTFRCC and possibly twice that by 2035 remained steady. Consequently, a number of experts in global health, cancer care, radiation therapy, accelerator physics & engineers sought a deeper understanding of why this gap persisted and, more importantly, how the gap can be closed.

The need for adequate cancer care for all is obvious yet the chronic lack of improvement perhaps becoming a self-fulfilling expectation of a problem "too hard" to solve. Completely new paradigms are clearly needed. Herein, the various strings of the problem are weaved together: the various channels of technology development, in depth understanding of the on-the-ground problems, health system shortcomings and opportunities, career tracks, concerns of misuse of high activity radiation sources and global agency efforts. These challenges provide the opportunity to investigate potentially disruptive innovative approaches to make a serious impact on the shortage of effective cancer care. Figure 1 shows the variation in RT capacity across Africa [3, 4].

MULTI-LEVEL ANALYSIS OF THE SHORTAGE

Improved Data Sources

The commonly used data sources to address global cancer use a combination of data from surveys and projections of need based on population data. These data are useful for the macroscopic assessment and readily visible demonstrations of shortage as illustrated below. More detailed data are available from the International Atomic Energy Agency (IAEA) [3] that demonstrate the heterogeneity of distribution of resources. However, the essential data for program building and providing the necessary resources and support require detailed site-based data as seen in the ICEC surveys of Africa and Eastern Europe [4, 5, 6]. The act of conducting the survey engages those working on-the-ground who understand the breadth and depth of the issues and can serve as local champions to provide solutions they see as necessary to drive the change.

Engaging Expertise with Commitment to a Solution

The magnitude of the cancer care gap often leads to an overwhelming sense of a problem "to big" to solve. Indeed, it is often suggested by experts in global health that for cancer care only prevention is appropriate in such resource-limited settings. The critical lack of access to cancer care treatment, including radiotherapy, in LMICs and geographically isolated populations in HICs is increasing, and there are few, if any, scalable solutions to address the global cancer crisis. The challenge is so enormous it is perceived as impossible. In 2014, at the ICTR-PHE physics component of the meeting in Geneva, a presentation delivered by Dr. Norm Coleman highlighted